Indian Journal of Natural Sciences *www.tnsroindia.org.in ©IJONS*

Vol.15 / Issue 83 / Apr / 2024 *International Bimonthly (Print) – Open Access* *ISSN: 0976 – 0997*

RESEARCH ARTICLE

Plastic Degrading Enzymes and Microbes

Dipsikha Bordoloi[1], Nishita Acharjya[1] and Biswa Prasun Chatterji[2*]

[1]B.Sc Final Year Student, Department of Biotechnology, Assam down town University, Assam, India.
[2]Professor, Department of Biotechnology, Assam down town University, Assam, India.

Received: 30 Dec 2023 Revised: 09 Jan 2024 Accepted: 27 Mar 2024

***Address for Correspondence**
Biswa Prasun Chatterji
Professor,
Department of Biotechnology,
Assam down town University,
Assam, India.
Email: biswaprasun@gmail.com

ABSTRACT

Plastic pollution poses a significant environment challenge, and the research for sustainable solutions has led to the discovery of plastic -degrading enzymes. This article provides a comprehensive overview of the recent advances in the field of plastic degrading enzymes, offering insights into the mechanisms, substrates, and potential applications of these remarkable biocatalysts. We examine the diversity of enzymes capable of degrading various types of plastics, including polyethylene, and PET and delve into the genetic and biochemical basis for their efficacy. Furthermore, we discuss the environmental impact of these enzymes, their industrial applications and the challenges and the opportunities that lie ahead in harnessing them for large -scale plastic waste remediation.

Keywords: enzymes, microbes, biodegradation, plastic

INTRODUCTION

Plastic is one of the biggest concern that humanity is facing today. Plastic pollution has become one of the major environmental problem .The widespread use of plastic materials has led to an accumulation of plastic waste in our oceans, landfills, and ecosystems. The world plastic production has reached 350 million tons till 2017(, Demand Plastics-the Facts 2018 An Analysis of European Plastics Production and Waste Data, n.d.)Plastic is a synthetic material made from polymers, which are long chains of molecules. Polymers are created by linking together smaller molecules called monomers through a process known as polymerization. The specific composition of plastics can vary widely, as there are many different types of plastics with different and unique properties. Polyethylene(PE), Polyethylene terephthalate(PU), Polystyrene (PS) , polypropylene(PP), and polyvinyl chloride (PVC) are the main types of plastic which accumulation in the environment is a major concern for environment and human health.(Hassan et al., 2022)These synthetic plastics have been separated into two groups based on the degradation

pathways, plastics with a carbon-carbon backbone and plastics with heteroatoms in the main chain .(Mohanan et al., 2020).The sole component of the backbone of PE,PS,PP, and PVC polymers is carbon atoms. Microplastics (MPs) are plastic particles smaller than 5 mm that are produced during plastic breakdown and may have ecotoxicological effects.(Zhang et al., 2017) Inhaled fibrous particulates have the potential to remain in the lungs and, when combined with other contaminants like plasticizers and dyes, can have harmful consequences on health, such as mutagenicity and cancer. It is acknowledged that burning plastic garbage can permanently remove it. Nonetheless, unburned debris is still present in the bottom ash, which is a solid residue left behind from incinerators that can burn up to 360–102,000 microplastic particles per metric ton. One possible source of MPs released into the environment is this bottom ash. According to reports, plastic pieces known as nanoplastics that are smaller than 100 nm. In general, commonly used plastics donot break down significantly in the environment when released. This should come as no surprise given that many polymers remarkably high stability and durability are among the main factors contributing to their widespread application and acceptance. Plastic breaks down in the environment through four different mechanisms. Photodegradation, thermooxidative degradation, hydrolytic degradation and microorganism – mediated biodegradation.(Webb et al., 2013)

POLYMER DEGRADATION

Polymer degradation can happen through two separate mechanisms: bulk erosion and surface erosion. The process of surface erosion is restricted to the device's surface. Overtime, the polymeric device will shrink in size without losing its bulk integrity. This kind of erosion affects poly(ortho-esters)and polyanhydrides. On the hand, bulk erosion occurs when water enters the device more quickly than the polymer is changed into components that are soluble in water, causing erosion all the way through the device. There are two steps to this process, the first step – water permeates the majority of the apparatus, primarily cleavage the chemical bonds in the amorphous phase that are hydrolytically unstable and breaking lengthy polymer chains into shorter segments that are eventually soluble in water. Enzymatic assault of the fragments takes place in the second phase. PGA and I-PLA are examples of semicrystalline polymers that exhibit this kind of erosion. The chemical stability of polymer backbone, the hydrophilic/hydrophobic balance of the repeating units, the polymer's shape (semicrystalline/ amorphous), and its molecular weight and molecular weight distribution are the primary determinants of erosion rate. Since ester bonds serve as links between the repeating units of PGA, PLA, and copolymers PLG, they should all erode at the same rate if the chemical stability of the polymer backbone is the only factor influencing the rate of erosion. However, the ability of the water molecules is influenced by the hydrophilic versus hydrophobic nature of the repeating units.

As a result, PGA erodes far more quickly than PLA, which is more hydrophobic. Furthermore, the polymer's shape is quite significant. Water is unable to enter the crystalline domains in the crystalline form due to the well- organized and tightly packed polymer chains. As a result, backbone hydrolysis typically occurs on the surface of crystalline domains and in a amorphous regions. The rate of erosion of I-PLA and d,I-PLA serves as an illustration of this process. Despite having the same degree of hydrophobic and backbone links as I-PLA, d,I-PLA breaks down significantly more quickly than I-PLA because I-PLA is an amorphous polymer whereas, the stereo regular polymer is semicrystalline.

TYPES OF DEGRADATION

Phtooxidative degradation

The main cause of damage, to polymer is light. This process begins when light is absorbed leading to degradation through photodegradation and photooxidation. Synthetic polymers are particularly susceptible, to degradation caused by ultraviolet (UV)radiation. The lifespan of materials used in application is influenced by this process (Riinby,1989) During photo irradiation the soft segments of polymers where degradation occurs can produce ester, aldehyde, propyl and formate groups. UV radiation easily breaks C-C bonds in the polymers.

Ozone degradation

Polymeric degradation is caused by the presence of ozone in the environment. Polymer exhibits a longer half -life in the absence of oxidative reactions. Despite being extremely rare in the atmosphere, ozone has a significant impact on

polymers. Polymeric materials undergo degradation due to the generation of reactive oxygen species. These ROS are created when the molecular weight of polymers decreases and their mechanical and electrical properties alter. Different kinds of carbonyl and unsaturated carbonyl compounds are generated when polymers are subjected to ozone. These goods are made from aromatic carbonyl, lactones, ketones and esters.

Hydrolytic degradation

The process by which plastic materials disintegrate into smaller components when water is present is known as hydrolytic degradation of plastic. Water molecules usually cause the breaking of chemical bondswithin the polymer structure during this breakdown process. Numerous plastic types are prone to hydrolytic degradation, with the degree of deterioration, with the degree of deterioration contingent upon variable likes temperature, catalyst presence, and polymer makeup.

Biodegradation

Biodegradation is the term used to describe any physical or chemical change in a material brought about by microorganisms. Bacteria, actinomycetes, and fungi are among the microorganisms that break down both natural and manmade plastics.(Cai et al., 2023) There are mainly two types of biodegradations aerobic and anaerobic biodegradation. Using oxygen as an electron acceptor bacteria break down large organic compounds into smaller ones in aerobic type of biodegradation. In this form of degradation this method yields water and carbondioxide as biproducts.

The breakdown of organic pollutants by microorganisms in the absence of oxygen is known as anaerobic biodegradation. At hazardous waste sites, it plays a significant role in the natural attenuation of Pollutant. Certain anaerobic bacteria break down organic compounds into smaller ones by using carbon dioxide, nitrate, sulphate, iron, manganese, and other elements as their electron acceptors. Since , polymer molecules are lengthy and not soluble in water, microorganisms cannot carry the polymers directly through their outer cell membranes and into the cell where the majority of metabolic reaction occur. Microbes evolve a technique through which they secrete extra cellular enzymes that depolymerize the polymer outside the cells in order to use such material as a carbon and energy source.

Mechanism of biodegradation

The specific mechanism of biodegradation can vary depending on the type of material being degraded and the microorganism involved.(Saritha et al., 2021)

1. Recognition and uptake-Microorganisms recognize and ingest the organic material to be degraded. This is often facilitated by specialized enzymes or receptors on the cell surface.
2. Extracellular enzymatic action-some microorganisms release enzymes into their surrounding environment. These enzymes break down complex organic molecules, like carbohydrates, proteins, and lipids, into smaller, more manageable compounds. For example, amylase,breaks down starch and protease breakdown proteins.
3. Transport of breakdown products-The smaller compounds produced by enzymatic action are transported into the microbial cell. this is essential step as it allows the microorganism to utilize these compounds as a source of energy and nutrients.
4. Intracellular metabolism-Inside the microbial cell, these compounds undergo further degradation through various metabolic pathways. microorganisms extract energy and building blocks for their own growth and reproduction.
5. Final metabolic products-As the compounds continue to break down, they may be converted into $CO_2$and H_2O, and other simpler molecules. These end products are usually non-toxic and can be released into the environment without harm.

Bacteria- Bacteria play a significant role in the biodegradation of plastics, particularly in the degradation of PE and PP. Bacteria first need to colonize the plastic surface. They can attach themselves to the plastic through the secretion of extracellular polymeric substances, which creates a biofilm. This biofilm provides a suitable environment for

bacterial growth and enzyme production. Once attached , bacteria is secrete enzymes such as lipases, esterase , and proteases. These enzymes hydrolyze the polymer chains in plastics into smaller, more easily digestible fragments. Bacteria then metabolize the smaller plastic fragments , using them as a source of carbon and energy.(Atanasova et al., 2021)As the polymer chains are broken down further , the plastic becomes more susceptible to biodegradation. The bacteria can continue to feed on the plastic until it is completely broken down into toxic byproducts. The fungi-some species of fungi like aspergillus and penicillium , have been found to have the ability to degrade low-density polyethylene. (Srikanth et al., 2022)Fungi use enzymatic processes to degrade plastic. Enzymes like esterases, lipases, and peroxidase can cleave the chemical bonds in plastic polymers. Microbial polymers degradation includes bio-fragmentation, biodeterioration, mineralization, and assimilation. Biodeterioration is the procedure that modifies the chemical and physical properties of plastics as well as their surface.(Schmidt, 2016) The mix and structure of polymers determine all chemical and structural alterations. Following biodeterioration plastic polymers are subjected to an enzymatic process known as bio-fragmentation. Oxygenases, which are primarily found in bacteria, are enzymes that can break down oxygen molecules when they are introduced to carbon chains, this process produces less hazardous compounds like alcohol and peroxyl. Moreover, lipases, esterase's, and endopeptidases, for amide groups, catalyze the transformation process of carboxylic groups. Mineral Deposition Via cell membranes, plastic polymers generated during the bio-fragmentation process enter microbial cells. Large monomers are unable to get through the cell membrane and remain outside. The energy is produced by oxidizing the tiny monomers that migrated within the cells. Eventually, this energy is used to produce biomass. In the assimilation process, atoms are integrated in the microbial cells for complete degradation.

Enzymatic degradation of plastic

Degrading plastic with microbial enzyme is a particularly challenging process since the carbon-carbon backbone of plastic lacks hydrolysable groups. The fast stage that is accomplished by the interaction of biotic and abiotic variables is the lowering of molecular weight. Microbial enzymes can readily attack the carbonyl group of a polymer when exposed to UV radiation Several enzymes are employed to break down polymers, including laccase, urease, lipase, protease, and manganese-dependent enzymes (which break down lignin).(Kaushal et al., 2021)Polyethylene (PE) can be broken down by thermostated laccase after 48 hours of incubation at 37°c *Ideonella sakaiensis*, a bacteria that can degrade polyethylene terephthalate , a popular plastic used in bottles and containers, was found by researchers in 2016. PETase and MHETase are the two enzymes that this bacterium produces. PET is broken down into smaller monomers by PETase ,and the monomers are further broken down by METase . These enzyme support PET plastic recycling. Scientist have been attempting to modify these enzymes in order to increase their capacity to break down plastic. A biodegradable plastic made from renewable resources like cornstarch is called polylactic acid. however, PLA waste might not break down quickly if it finds itself in unsuitable surrounding., which will facilitate PLA breakdown in composting sites and natural settings.

CONCLUSION

This timeline marks the age of inventive and advanced practices where the world of conservation and engineering go hand in hand. The study of plastic degrading enzymes and their interaction with the microbes has opened up exciting possibilities for addressing the global plastic pollution crisis. It is very important to highlight the remarkable progress in our understanding of these enzymatic and microbial processes , shedding light on their potential for sustainable plastic degradation. As we move forward , it is evident that further research and collaboration among scientists, engineers, and environmentalists will be essential to harness this knowledge effectively. The development of innovative biotechnological solutions and the implementation of eco friendly practices hold the promise of mitigating the detrimental impacts of plastic waste on our planet. The future of plastic degradation appears brighter , thanks to the synergy between this remarkable enzymes and natures microorganisms, offering hope for a cleaner ,more sustainable future.

REFERENCES

1. Atanasova, N., Stoitsova, S., Paunova-krasteva, T., & Kambourova, M. (2021). Plastic degradation by extremophilic bacteria. In International Journal of Molecular Sciences (Vol. 22, Issue 11). MDPI. https://doi.org/10.3390/ijms22115610
2. Cai, Z., Li, M., Zhu, Z., Wang, X., Huang, Y., Li, T., Gong, H., & Yan, M. (2023). Biological Degradation of Plastics and Microplastics: A Recent Perspective on Associated Mechanisms and Influencing Factors. In Microorganisms (Vol. 11, Issue 7). Multidisciplinary Digital Publishing Institute (MDPI). https://doi.org/10.3390/microorganisms11071661
3. Hassan, T., Srivastwa, A. K., Sarkar, S., & Majumdar, G. (2022). Characterization of Plastics and Polymers: A Comprehensive Study. IOP Conference Series: Materials Science and Engineering, 1225(1), 012033. https://doi.org/10.1088/1757-899x/1225/1/012033
4. Kaushal, J., Khatri, M., & Arya, S. K. (2021). Recent insight into enzymatic degradation of plastics prevalent in the environment: A mini - review. In Cleaner Engineering and Technology (Vol. 2). Elsevier Ltd. https://doi.org/10.1016/j.clet.2021.100083
5. Kefeli, A. A., Razumovskii, S. D., & Zaikov, G. Y. (n.d.). INTERACTION OF POLYETHYLENE WITH OZONE*.
6. Mohanan, N., Montazer, Z., Sharma, P. K., & Levin, D. B. (2020). Microbial and Enzymatic Degradation of Synthetic Plastics. In Frontiers in Microbiology (Vol. 11). Frontiers Media S.A. https://doi.org/10.3389/fmicb.2020.580709
7. Plastics-the Facts 2018 An analysis of European plastics production, demand and waste data. (n.d.).
8. Riinby, B. (1989). PHOTODEGRADATION AND PHOTO-OXIDATION OF SYNTHETIC POLYMERS. In Journal of Analytical and Applied Pyrolysis (Vol. 15).
9. Ru, J., Huo, Y., & Yang, Y. (2020). Microbial Degradation and Valorization of Plastic Wastes. In Frontiers in Microbiology (Vol. 11). Frontiers Media S.A. https://doi.org/10.3389/fmicb.2020.00442
10. Saritha, B., Sindgi, S. A., & Remadevi, O. K. (2021). Plastic Degrading Microbes: A Review. Microbiology Research Journal International, 22–28. https://doi.org/10.9734/mrji/2021/v31i630324
11. Schmidt, M. (2016). Microbial degradation of plastics: A tool for cleanup of the oceans?
12. Srikanth, M., Sandeep, T. S. R. S., Sucharitha, K., & Godi, S. (2022). Biodegradation of plastic polymers by fungi: a brief review. In Bioresources and Bioprocessing (Vol. 9, Issue 1). Springer Science and Business Media Deutschland GmbH. https://doi.org/10.1186/s40643-022-00532-4
13. Webb, H. K., Arnott, J., Crawford, R. J., & Ivanova, E. P. (2013). Plastic degradation and its environmental implications with special reference to poly(ethylene terephthalate). Polymers, 5(1), 1–18. https://doi.org/10.3390/polym5010001
14. Zhang, C., Chen, X., Wang, J., & Tan, L. (2017). Toxic effects of microplastic on marine microalgae Skeletonema costatum: Interactions between microplastic and algae. Environmental Pollution, 220, 1282–1288. https://doi.org/10.1016/j.envpol.2016.11.005

Table1-classification of polymers with its lifespan and density(Ru et al., 2020)

POLYMERS	DENSITY	LIFE SPAN
PET	1.35	450
HDPE	0.94-0.97	>600
LDPE	0.91-0.93	10-600
PS	1.03-1.09	50-80
PP	0.90-0.91	10-600
PVC	1.35-1.45	50-150

Table2- list of microbes and its enzyme involved in plastic degradation

MICROBES	ENZYMES	PLASTIC TYPES	MICROBIAL SOURCE	EFFECIENCY OF DEGRADATION
Bacillus cereus	phospholipases	polyethylene	Dumping soil	2.40-7.20
Pseudomonas putida	lipase	Milk cover	Garden soil	75.30
Streptomyces sp	proteases	LDPE	Garbage soil	46.70
Pseudomonas sp	lipase	Polyethylene	Textile effluent	39.70-19.60
Aspergillus glaucus	Pectinase	Plastic and polythene	Mangrove soils	20.80-7.26
Micrococcus luteus	glycosidase	Plastic cups	Forest soils	38.00

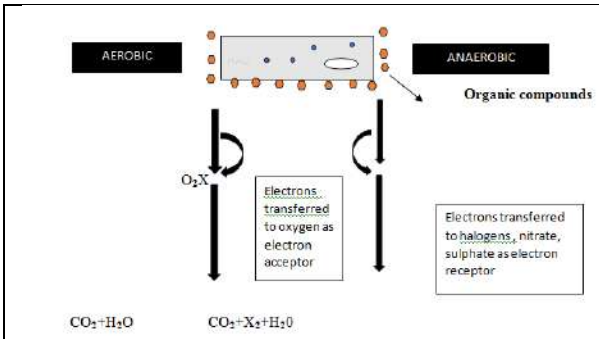

Fig 1: Degradation by biotic and abiotic process

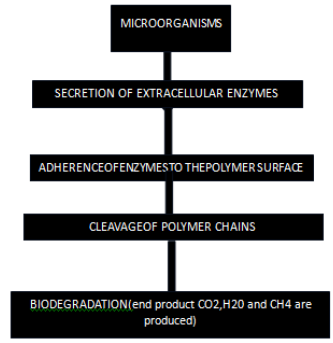

Fig 2: Mechanism of enzymatic biodegradation of polymers

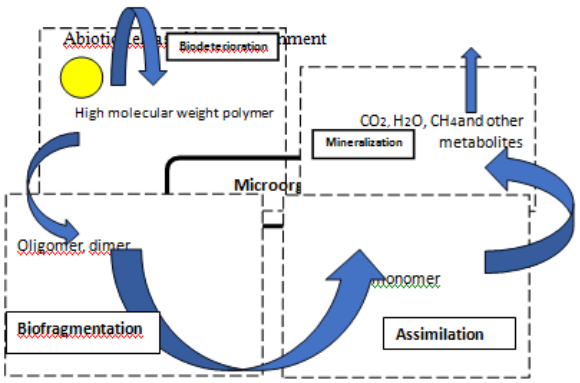

Fig 3: Diagrammatic representation of microbial polymer degradation

RESEARCH ARTICLE

A Comprehensive Survey of Image Encryption Techniques Enhanced By Digital Signatures

C.Sasthi Kumar* and N.Kanagaraj

Assistant Professor, Department of Computer Science, Karpagam Academy of Higher Education, Coimbatore, Tamil Nadu, india.

Received: 21 Nov 2023 Revised: 19 Jan 2024 Accepted: 16 Mar 2024

***Address for Correspondence**
C Sasthi Kumar
Assistant Professor,
Department of Computer Science,
Karpagam Academy of Higher Education,
Coimbatore, Tamil Nadu, india.
Email: sasthikumar.chandrasekar@kahedu.edu.in

ABSTRACT

As the digital era progresses, the safe transmission and storage of visual data, especially photographs, has become critical. To protect the security and integrity of these visual assets, image encryption algorithms have been created. This survey study investigates the new convergence of picture encryption and digital signature technologies, presenting a novel solution that provides both security and visual meaningfulness. Traditional picture encryption approaches generally rely on data obfuscation through mathematical transformations, which often renders decrypted images aesthetically unintelligible. In contrast, our suggested technique uses digital signatures to improve security while keeping the significance of the visual information. This survey study analyses and analyzes the essential components of this unique algorithm, emphasizing its merits and applications. The algorithm's fundamental components include a hybrid encryption approach that combines symmetric and asymmetric cryptographic algorithms. This article reviews 26 research papers for image encryption techniques and explores the potential of computer-assisted methods for image encryption techniques and staging. Digital signatures are used to authenticate the integrity and validity of the visual data while also guaranteeing that the decrypted pictures are visually understandable. The survey article examines the algorithm's mathematical underpinnings, encryption and decryption operations, and the incorporation of digital signatures into the picture encryption workflow.

Keywords: Digital Signatures, Data Integrity, Image Encryption, Visual Data Security

INTRODUCTION

In an era marked by extensive usage of digital photography and broad sharing of visual material, preserving the privacy and security of these photographs has become more important [1-3]. The need for strong picture encryption solutions has never been more critical, given the increased danger of illegal access, interception, and data breaches. Visually meaningful picture encryption is a cutting-edge way of protecting sensitive visual information while keeping the image's core structure and visual coherence [4-8]. Traditional picture encryption algorithms often rely only on scrambling the pixel values, leaving the encrypted image unreadable to the human eye [9]. While efficient for data security, these approaches often produce aesthetically disordered and unintelligible pictures, making them unsuitable for applications where keeping the visual sense of the material is critical [10]. This constraint has motivated the development of visually meaningful picture encryption as a solution that achieves a careful balance between security and visual comprehension [11]. Visually meaningful picture encryption approaches strive to encrypt visual material in such a manner that authorized users may perceive and interpret it while making it unintelligible to unauthorized persons or hostile actors [12]. To accomplish both security and meaningful visual representation, this unique strategy integrates powerful cryptography algorithms with image processing techniques [13-16]. The significance of visually meaningful picture encryption extends across several disciplines. Medical photographs including sensitive patient information, for example, must be securely transferred and kept without affecting the diagnostic usefulness of the images [17-19]. Protecting intellectual data and personal images against illegal access is critical in the era of multimedia communication and content sharing [20-23]. We will explore into the fundamental ideas, methodologies, and applications of visually meaningful picture encryption in this research. We'll look at how cryptographic approaches are used with image processing to create a careful balance between picture security and visual information preservation. Furthermore, we will investigate real-world use cases, problems, and future possibilities of visually meaningful picture encryption, shining light on its importance in our increasingly digitized and linked world [24–26].

Background Study

Survey on Image Encryption Techniques

Abbasi, S. F. *et al*. (2018) the author offers an innovative and effective method of image encryption. First, a change was performed by randomly rearranging the image's pixels using a tangled web of logistic chaotic maps. XORing the random map with the jumbled image improves the security of the system. Gray S-Box was then used to do a substitution on the resulting perverted image. Finally, the encrypted image was transformed into something comprehensible using lifting wavelet transform. The number of possible assaults on the cipher-text image that was produced was lower since it was not a random or noise-like image. Armijo-Correa, J. *et al*. (2020) the author offer a new, more visually intuitive method of encrypting images. In specifically, the author have enhanced some steps of a visually meaningful encrypted image (VMEI) system, including: To prevent the resulting VMEI image's pixel values from going crazy, a threshold operation was first investigated and tested to identify a suitable dynamic range for the source images. This method also aids in preserving a high percentage of original pixels, which was essential for preserving the high quality of the final VMEI image. The author used a well-known S-box based on a cellular automaton approach to randomly reorganize the data in the new image to get diffusion characteristics throughout the embedded information.

Bai, S. *et al*. (2020) Current image encryption techniques convert encrypted images to meaningless jumbles of random data, making them vulnerable to attack. The data amount may have grown substantially, or the calculation may have become quite complicated. To address these limitations, these authors research proposes a new kind of aesthetically meaningful image encryption technique that uses fractal graph formation. The suggested method transforms basic images into substantial fractal sceneries or fractal plants with a low time complexity, specific anti-compression performance, and high security performance. Chai, X.*et al*. (2017) these authors' research presents a compressive sensing-based visual security system for encrypting images. The original image was encrypted using compressive sensing after being transformed into a coefficient matrix through discrete wavelet transform. Then, a zigzag path

related to the original plain image was used to jumble it. Second, the author produces a cipher image that was both cryptographically and aesthetically secure by embedding the cipher image within a carrier image. The proposed encryption method has three advantages over the state-of-the-art encryption techniques. It has a high security level, can achieve image data security and appearance security simultaneously, and the final cipher image has the same size as the plain image, so it transmits and stores quickly over the Internet and needs no extra transmission bandwidth or memory, but it was very sensitive to the plain image, the parameters used in the zigzag confusion process, and the generation of the chaos-based measurement.

Chai, X. *et al*. (2020) the author offer a new, aesthetically meaningful, and efficient double-color picture encryption scheme based on 2D compressive sensing (CS) and an embedding approach. The author uses the 2D CS theory to shrink the regular pictures and get two-dimensional measurements of the originals. The author start with raw measurement value matrices, scramble them using index sequences generated by a 6D hyper chaotic system, and then integrate the resulting cipher image into a color carrier image. In 2D CS, the Kronecker product (KP) and singular value decomposition (SVD) were combined to create the measurement matrices, and the feature parameters of the carrier image were employed to govern the embedding process of the compressed cipher pictures. The LSS and 6D hyper chaotic system's starting settings were derived from the plain pictures' SHA 256 and feature parameters. The plain image parameters were included into the carrier image, and the carrier image parameters may be obtained from the corresponding cipher picture with little additional transmission and storage. The suggested encryption method has been shown to be safe against noise assaults, occlusion attacks, known-plaintext attacks, and chosen-plaintext attacks via simulations and performance assessments. It also has a wide key space and high key sensitivity during decryption. Dolendro Singh, L., & Manglem Singh, K. (2018) these authors research article proposes a method for creating multigame encryption schemes that have some kind of aesthetic value. A multiple encrypted picture was created by embedding data from numerous cipher images into the relatively unimportant actual data of a scrambled host image and then unscrambling the image. The suggested approach offers a greater potential to incorporate more data with nearly no damage of the host picture, as shown by comparison with current visually meaningful encryption systems. Different conventional assaults, such as the salt and pepper noise attack and the occlusion attack, can't break the suggested system.

Survey on Digital Signatures

F. Jie *et al*. (2019) the author offer a compressive sensing and Integer wavelet transform (IWT)-based visual security picture encryption system. After the image has been encrypted using compressive sensing, it was further protected using zigzag confusion and a chaotic map. In addition, it was possible to minimize the quantity of data used in the embedding procedure. Second, the carrier image's three color channels were subjected to IWT, and the resulting coefficient matrices were used to simultaneously embed the picture into the matrices. Inverse IWT may be used to produce the safe-looking picture. The following benefits of the encryption system exist as compared to the current encryption method. First, it has excellent camouflage and was not easily noticeable, allowing you to keep your image's look secure. Second, the encryption method does not rely on the carrier image, and the quality of the reconstructed picture was consistent with that of the original photos. The system employs binary integers in the embedding process, thus even though an image was embedded in the paper; it may encrypt any information that can be converted to binary.

H. R. Vanamala and D. Nandur (2019) Here, an evolutionary algorithm was employed to encrypt data in a way that makes sense visually during the pre-encryption phase. Two chaotic maps, a genetic algorithm, and some visual manipulations were used in the essay to cover up the sensitive image. It was possible to use a genetic algorithm to find the optimal encrypted image. Lowest correlation coefficient indicates optimal encrypted image. The algorithm's vulnerability to statistical assaults, differential attacks, and Bruce force has been shown. Huo, D. *et al*. (2021) Two distinct phases, pre-encryption using dimensional compressive sensing (2DCS) and embedding with IWT, make up the visually safe picture encryption system proposed in this research. Pre-encryption protects the original image's data by replacing it with a hidden image produced by a combination of random grayscale alteration, random scrambling, and 2DCS sampling. First, the carrier image was decomposed into a coefficient matrix via IWT, then the

secret image was embedded into the lowest two bits of the coefficient matrix, and finally the matrix was transformed into the space domain via inverse IWT to obtain an image that looks like the carrier image while still protecting the plain image. Two-dimensional concatenated substitution (2DCS) allows for faster encryption and decryption without requiring more transmission bandwidth or storage space for the plain picture.

M. Liu *et al*. (2021) the author offer a method for encrypting color images that has both visual meaning and high performance in areas like embedding and reconstruction. To begin, the picture was compressed using compressive sensing technique, which drastically lowers the overall processing cost. Second, the secret picture's security was bolstered by the employment of chaotic sequences to further confound the compressed image, turning it into an indecipherable blur of noise. The encrypted picture was placed inside a visually relevant carrier image to better secure the security of image information. In order to make it more difficult for an attacker to read the plain image or the noise-like cipher image, the former was masked within the latter, creating a visually meaningful cipher picture. The peak signal noise ratio (PSNR) tests further show that the proposed strategy results in a more satisfying visual experience. P. Ping *et al*. (2019) Compressive sensing and reversible color alteration were proposed as novel methods for image encryption in this study. During the CS stage, it was possible to use completely arbitrary measurement matrices to evaluate each column of the image signal separately. Multiple hidden versions of the same picture may be created using the same secret key if the random numbers were varied. Thanks to CS at the embedding step, the size of the carrier image was decreased in comparison to the size of the plain picture when the block pairing and replacement approach was utilized, meaning that no more bandwidth was needed for transmission. The security analysis and simulation findings show that the scheme was robust against common attacks, has a large key space, and has high key sensitivity.

Survey on Digital Signatures in Visual Data Security

Ponuma, R. *et al*. (2019) the author present a multiple image compression-encryption technique that utilizes chaotic measurement matrices and compressive sensing. The experimental findings showed that the system outperformed competing approaches when it came to picture reconstruction. An image-dependent key was used to increase protection against a predetermined plain text attack. The technology was also resistant to outside influences like noise and occlusion. The correlation study demonstrates that the suggested strategy was resistant to statistical assaults. The effectiveness and safety of the proposed approach have been shown via simulation. Priya, S., & Santhi, B. (2019) the medical image and the associated patient data were both protected via watermarking. Normal medical image encryption yields an encrypted image with noise or texture that was unsuitable for transmitting the watermarked medical image. The author suggested using an encrypted picture with symbolic value. To create a watermarked medical picture, Electronic patient record (EPR) data was incorporated inside the image utilizing medical image watermarking. The fingerprint was then used to visually encrypt this watermarked medical picture using IWT. The fingerprint image was validated and decoded from the wavelet coefficients on the extraction side. If the fingerprint was a good match, the medical image may be rebuilt and the Extended Producer's Responsibility (EPR) extracted for use in diagnosis. According to the findings of the experiments, the suggested approach was successful in creating an encrypted picture with visual significance.

V. Himthani *et al*. (2022) multiple types of Meaningful Encrypted Image (MEI) techniques were offered in the study, and they were further classified. Security, key analysis, visual quality, and other measures were also used to evaluate existing VMEI approaches. The computational speed and visual quality of recreated images still have room for improvement, it was emphasized. Future research prospects and challenges in VMEI were discussed. In short, VMEI was still a developing area of study. Improving digital picture encryption might benefit from the findings of this state-of-the-art study. Wen, W.*et al*. (2016) in the present feature encryption techniques, edge information was considered crucial information. Images' salient portions often contain more crucial information than their edges. In order to create meaningful encrypted pictures, these authors research makes use of a salient regions encryption technique. To construct an encrypted image with visual significance, the author first identifies the salient parts using a saliency detection model in the compression domain, and then the author encrypts and decorates it. A visually

relevant cipher text image cannot be decrypted to reveal the original image's prominent parts, as shown by experiments.

Y. Yang *et al*. (2023) the author suggested a lossless compression set partitioning in hierarchical trees (SPIHT) coding-based picture encryption system with visual significance. The first step was to jumble the wavelet coefficients of the original picture. The secret picture was then further compressed and scrambled using SPIHT coding. Finally, the cipher image was created by incorporating the concealed image into the cover art. Since a cipher picture does not seem like cipher text, the risk of an attack was lessened in a semi-honest trusted cloud environment. The experimental findings show that the suggested technique was fully reversible, which was an improvement over the prior algorithm. Yang, Y.-G. *Et al*. (2021) the author offers an M-ary decomposition and virtual bit VMIE technique. The best possible visual quality for VMEIs was these authors end aim. M-ary decomposition, M-ary corrected embedding, and the concepts of real and virtual bits were all essential to these authors methodology, which the author presented. The conventional, one-base representation of numbers was abandoned by these techniques. The bits in these authors algorithm were just conceptual. The author suggested a novel pre-encryption technique for images to accommodate these authors embedding model. The M-ary decomposition was employed in the pre-encryption process to handle plain pictures, and the resultant pre-encrypted images have a fixed pixel range. The non-standard pre-encryption technique was also found to have adequate security after an investigation was conducted.

DISCUSSION

The convergence of image encryption and digital signature technologies represents a watershed moment in addressing the critical needs of secure visual data transmission and storage. Unlike traditional encryption methods, which often result in distorted or incoherent image upon decryption, this ground-breaking methodology combines symmetric and asymmetric cryptographic algorithms, seamlessly interwoven with the power of digital signatures. This fusion not only strengthens data security but also rigorously maintains the visual content's integrity and coherence. This extensive review study methodically dissects the algorithm's underlying mathematics, exposing its complicated cryptographic foundations while clarifying its effectiveness in repelling adversary invasions. Beyond the theoretical, it highlights tangible applications in a variety of domains, ranging from healthcare, where patient data and diagnostic imagery can be securely handled without jeopardizing clinical acumen, to the media and entertainment industries, where copyrighted multimedia content is protected throughout the distribution chain. Furthermore, it is crucial in the sectors of government and military for preserving confidential visual data, including satellite images and intelligence briefings.

CONCLUSION

In a digital world where visual data security and meaning have become crucial, the combination of image encryption and digital signature technologies delivers a game-changing approach. Traditional image encryption technologies, although efficient in terms of data security, often rendered decrypted images aesthetically unreadable. In sharp contrast, the novel solution described in this survey study combines the strengths of cryptographic approaches, creating a symphony of symmetric and asymmetric encryption with the extra security layer of digital signatures. This study has shown the route toward attaining both strong security and visual coherence by thoroughly analyzing the algorithm's components, from its mathematical underpinnings through the encryption and decryption operations. Its practicality and importance are shown by its real-world applications in fields as varied as healthcare, multimedia, and national security.

REFERENCES

1. Abbasi, S. F., Ahmad, J., Khan, J. S., Khan, M. A., & Sheikh, S. A. (2018). Visual Meaningful Encryption Scheme Using Intertwinning Logistic Map. Intelligent Computing, 764–773. doi:10.1007/978-3-030-01177-2_56
2. Armijo-Correa, J. O., Murguía, J. S., Mejía-Carlos, M., Arce-Guevara, V. E., & Aboytes-González, J. A. (2020). An improved visually meaningful encrypted image scheme. Optics & Laser Technology, 127, 106165. doi:10.1016/j.optlastec.2020.106165
3. Bai, S., Zhou, L., Yan, M., Ji, X., & Tao, X. (2020). Image Cryptosystem for Visually Meaningful Encryption Based on Fractal Graph Generating. IETE Technical Review, 38(1), 130–141. doi:10.1080/02564602.2020.1799875
4. Chai, X., Gan, Z., Chen, Y., & Zhang, Y. (2017). A visually secure image encryption scheme based on compressive sensing. Signal Processing, 134, 35–51. doi:10.1016/j.sigpro.2016.11.016
5. Chai, X., Wu, H., Gan, Z., Han, D., Zhang, Y., & Chen, Y. (2020). An efficient approach for encrypting double color images into a visually meaningful cipher image using 2D compressive sensing. Information Sciences. doi:10.1016/j.ins.2020.10.007
6. Chai, X., Wu, H., Gan, Z., Zhang, Y., Chen, Y., & Nixon, K. W. (2020). An efficient visually meaningful image compression and encryption scheme based on compressive sensing and dynamic LSB embedding. Optics and Lasers in Engineering, 124, 105837. doi:10.1016/j.optlaseng.2019.105837
7. Dolendro Singh, L., & Manglem Singh, K. (2018). Visually Meaningful Multi-image Encryption Scheme. Arabian Journal for Science and Engineering. doi:10.1007/s13369-018-3104-7
8. F. Jie, P. Ping, G. Zeyu and M. Yingchi, "A Meaningful Visually Secure Image Encryption Scheme," 2019 IEEE Fifth International Conference on Big Data Computing Service and Applications (BigDataService), Newark, CA, USA, 2019, pp. 199-204, doi: 10.1109/BigDataService.2019.00034.
9. H. R. Vanamala and D. Nandur, "Genetic Algorithm and Chaotic Maps based Visually Meaningful Image Encryption," TENCON 2019 - 2019 IEEE Region 10 Conference (TENCON), Kochi, India, 2019, pp. 892-896, doi: 10.1109/TENCON.2019.8929469.
10. Hua, Z., Zhang, K., Li, Y., & Zhou, Y. (2021). Visually secure image encryption using adaptive-thresholding sparsification and parallel compressive sensing. Signal Processing, 183, 107998. doi:10.1016/j.sigpro.2021.107998
11. Huo, D., Zhu, Z., Wei, L., Han, C., & Zhou, X. (2021). A visually secure image encryption scheme based on 2D compressive sensing and integer wavelet transform embedding. Optics Communications, 492, 126976. doi:10.1016/j.optcom.2021.126976
12. Jiang, D., Liu, L., Zhu, L., Wang, X., Rong, X., & Chai, H. (2021). Adaptive embedding: A novel meaningful image encryption scheme based on parallel compressive sensing and slant transform. Signal Processing, 188, 108220. doi:10.1016/j.sigpro.2021.108220
13. Kanso, A., & Ghebleh, M. (2017). An algorithm for encryption of secret images into meaningful images. Optics and Lasers in Engineering, 90, 196–208. doi:10.1016/j.optlaseng.2016.10.009
14. M. Liu, G. Ye and Q. Lin, "Meaningful color image encryption algorithm based on compressive sensing and chaotic map," 2021 IEEE International Symposium on Software Reliability Engineering Workshops (ISSREW), Wuhan, China, 2021, pp. 262-265, doi: 10.1109/ISSREW53611.2021.00073.
15. P. Ping, J. Fu, Y. Mao, F. Xu and J. Gao, "Meaningful Encryption: Generating Visually Meaningful Encrypted Images by Compressive Sensing and Reversible Color Transformation," in IEEE Access, vol. 7, pp. 170168-170184, 2019, doi: 10.1109/ACCESS.2019.2955570.
16. Ponuma, R., Amutha, R., Aparna, S., & Gopal, G. (2019). Visually meaningful image encryption using data hiding and chaotic compressive sensing. Multimedia Tools and Applications. doi:10.1007/s11042-019-07808-6
17. Priya, S., & Santhi, B. (2019). A Novel Visual Medical Image Encryption for Secure Transmission of Authenticated Watermarked Medical Images. Mobile Networks and Applications. doi:10.1007/s11036-019-01213-x
18. V. Himthani, V. S. Dhaka, M. Kaur, D. Singh and H. -N. Lee, "Systematic Survey on Visually Meaningful Image Encryption Techniques," in IEEE Access, vol. 10, pp. 98360-98373, 2022, doi: 10.1109/ACCESS.2022.3203173.

19. Wang, H., Xiao, D., Li, M., Xiang, Y., & Li, X. (2018). A visually secure image encryption scheme based on parallel compressive sensing. Signal Processing. doi:10.1016/j.sigpro.2018.10.001
20. Wen, W., Hong, Y., Fang, Y., Li, M., & Li, M. (2020). A Visually Secure Image Encryption Scheme based on Semi-Tensor Product Compressed Sensing. Signal Processing, 107580. doi:10.1016/j.sigpro.2020.107580
21. Wen, W., Zhang, Y., Fang, Y., & Fang, Z. (2016). Image salient regions encryption for generating visually meaningful ciphertext image. Neural Computing and Applications, 29(3), 653–663. doi:10.1007/s00521-016-2490-6
22. Y. Yang, M. Cheng, Y. Ding and W. Zhang, "A Visually Meaningful Image Encryption Scheme Based on Lossless Compression SPIHT Coding," in IEEE Transactions on Services Computing, vol. 16, no. 4, pp. 2387-2401, 1 July-Aug. 2023, doi: 10.1109/TSC.2023.3258144.
23. Yang, Y.-G., Wang, B.-P., Pei, S.-K., Zhou, Y.-H., Shi, W.-M., & Liao, X. (2021). Using M-ary decomposition and virtual bits for visually meaningful image encryption. Information Sciences, 580, 174–201. doi:10.1016/j.ins.2021.08.073
24. Yang, Y.-G., Wang, B.-P., Yang, Y.-L., Zhou, Y.-H., Shi, W.-M., & Liao, X. (2021). Visually meaningful image encryption based on universal embedding model. Information Sciences, 562, 304–324. doi:10.1016/j.ins.2021.01.041
25. Yang, Y.-G., Zhang, Y.-C., Chen, X.-B., Zhou, Y.-H., & Shi, W.-M. (2018). Eliminating the texture features in visually meaningful cipher images. Information Sciences, 429, 102–119. doi:10.1016/j.ins.2017.11.009
26. Zhu, L., Song, H., Zhang, X., Yan, M., Zhang, T., Wang, X., & Xu, J. (2020). A robust meaningful image encryption scheme based on block compressive sensing and SVD embedding. Signal Processing, 107629. doi:10.1016/j.sigpro.2020.107629

Table 1: comparison table for existing work

Author	Year	Methodology	Advantage	Limitation
Armijo-Correa, J.	2020	Integer discrete wavelet transform	Unlike traditional image encryption techniques that produce texture-like or noise-like encrypted images, this approach generates visually meaningful cover images.	The modification of preprocessing and embedding phases may introduce increased computational complexity compared to traditional image encryption methods
Chai, X. *et al*.	2017	compressive sensing	The technique was very secure against both known-plaintext and chosen-plaintext assaults due to its sensitivity to the plain picture.	Compressive sensing algorithms can be computationally intensive, especially for large and high-resolution images.
F. Jie *et al*.	2019	Integer wavelet transform	The pixel position permutation based on the 2D-LASM sequence in the first phase of the scheme adds an additional layer of security	Effective key management was critical for the security of any encryption scheme.
Hua, Z. *et al*.	2021	Separable wavelet transform	The incorporation of a new parallel CS technique markedly improves processing efficiency.	The effectiveness of adaptive techniques, such as adaptive-thres holding scarification, may depend on selecting appropriate parameter values.
Jiang, D. *et al*.	2021	Parallel compressive sensing	Optimizing data efficiency with the use of parallel compressive sensing (PCS) and the slant transform (ST).	Implementing the algorithm may require a deep understanding of the underlying cryptographic and mathematical concepts.

Indian Journal of Natural Sciences www.tnsroindia.org.in ©IJONS

Vol.15 / Issue 83 / Apr / 2024 International Bimonthly (Print) – Open Access ISSN: 0976 – 0997

RESEARCH ARTICLE

Improving Deep Learning for Multiple Code Clone Detection through Pretrained Models

S Karthik and P Prabhakaran*

Assistant Professor, Department of Computer Science, PSG College of Arts & Science, (Affiliated to Bharathiar University), Coimbatore, Tamil Nadu, India.

Received: 10 Dec 2023 Revised: 19 Jan 2024 Accepted: 27 Mar 2024

***Address for Correspondence**
P Prabhakaran
Assistant Professor,
Department of Computer Science,
PSG College of Arts & Science, (Affiliated to Bharathiar University),
Coimbatore, Tamil Nadu, India.
Email: prabhakaranpsgcas@gmail.com

ABSTRACT

Code-clone detection (CCD) is the technique of locating identical or similar chunks of code known as code clones within a program. Previously many machine learning (ML) techniques have been developed. These techniques always depend on inclusive, customized features to represent code fragments. So, handling multiple code clone (CC) labels will be a major problem that probably demands distinct evaluation criteria. In recent years, the research on CCD has been dramatically geared up by (DL) techniques. But, one most challenging issues faced by the DL approach in CCD is training from scratch for different domain source codes. Hence, in this research work, a transfer learning (TL) based attention learner (AL) model is utilized for the objective of code clone modelling (CCM). This model employs two pre-trained recurrent neural network (RNN)-based methods to transfer knowledge in the area of CCM rather than a single model. These pre-trained models are then implemented in TL as feature extractors. These collected characteristics are subsequently combined into an AL For application in various subsequent activities. Finally, AL applies the gained information of pre-trained models to fine-tune those features for specific down-streaming tasks. Finally, the experimental outcome demonstrates that the proposed TL-CCD technique has an accuracy of 96%, 98% and 97% for the dataset Apache Maven 3.8.3, Apache ant 1.10.12 and Opennlp-master 1.9.1, respectively, compared to the conventional CCM algorithms.

Keywords: Code-clone detection, Transfer learning, Attention learner, Recurrent Neural Network, Transfer knowledge

INTRODUCTION

Code clones are code segments that are similar but originate in a different location. A significant amount of effort has gone into detecting, examining, and preventing code clones, which are ubiquitous in modern open-source software [1] and can have a range of negative implications. By considering the maintenance effort of clones, several methodologies and systems have been evolved to identify code clones. The methods are divided into groups based on the input, depiction, and algorithms as per the application of developers. These methods are broadly categorised as text-based [2, 3], token-based [4, 5], tree-based [6, 7], metric-based [8, 9], AST-based [10], Program Dependency Graph (PDG)-based [11], and hybrid methods [12]. While identifying all potential code clone pairings, these techniques function badly when dealing with complex source code architectures. To solve these issues for existing CCD techniques, the ML-based CCD has been developed. Generally, the ML process is very efficient and capable of detecting the code clone from the complex dataset using different models to reduce the software issues for the programmers in its preliminary stages itself. But still, the ML method was not suitable for detecting the multi-featured CC system. These multi-featured issues will be the major drawback of ML methods which possibly demands various evaluation criterion. For these types of issues, DL models play an important role in the efficient detection of CC. For example, instead of utilizing a predefined proximity metric or establishing a threshold for clone detection, the DL model is tailored to autonomously acquire the implicit code features from merged feature vectors to successfully identify clones among code snippets. But, the most difficult problem faced by the DL technique in CCD is training from scratch for different domain source codes. Motivated by this, this research devised a TL-AL-CCM technique that considerably enhances the efficiency of DL-based source code models. Initially, the concept of TL is employed in DL-based source code language models. The fundamental idea behind this research is to use a pre-trained source code language framework to transfer obtained information from one challenge to another. The two separate types of the RNN model are then trained for TL purposes. The learned information of pre-trained (RNN) models is integrated into an AL for a downstream activity. The AL applies pre-trained model learning information to given downstream tasks. In the TL model, pre-trained models are utilized to extract general features that may subsequently be fine-tuned for a specific purpose without having to train the model from scratch.

LITERATURE SURVEY

A weighted Recursive Auto-Encoder (RAE) was developed [13] for rapid CCD. Weighted RAE mined the program's attributes and encoded the functions to vectors before analyzing the program's abstract syntax tree. To improve the proportion of information donated by important nodes in the final vector representation of one application, the node weight information was taken into account in the abstract syntax tree during the modeling process. However, Threshold values greatly influence the performance of RAE. An effective detector called LV-Mapper was developed [14] to discover the LV-CCD using the third-generation sequencing alignment approach. Based on the locate-filter-verify technique, this CCD may discover clones with more generic variance. The developed LV-Mapper locates and filters probable clone code pairings utilizing a restricted window of continuous lines known as seeds at a low cost. An adaptive point that fluctuated with program length was utilized for CCD. However, for LV-CCD, this method necessitates improvements in the refactoring and bug propagation systems. A unique technique of performing tree-based convolution over a token-enhanced AST was proposed [15] to detect semantic clones. This method would explicitly gather sub-tree characteristics to fully exploit structural data in an AST. A token embedding method known as position-aware character embedding (PACE) was designed to boost the generalization ability for reducing the issue of unobserved data in CCD. However, this strategy resulted in a significant period and memory complexity. A ML approach was devised [16] for automatic CC validation. A training dataset is initially constructed by manually inspecting code clones collected from several clone detection techniques for distinct domain systems. Then, many attributes were retrieved to construct the ML model from those clones. The trained system was then utilized to identify clones without human intervention. Furthermore, the created model effectively reduces all false positive clones from the identification findings. However, this model performs poorly on smaller datasets. A novel

approach of CCD was designed [17] that combines a deep feature learning system that trains the syntactic and semantic features with a code depiction created from the fusion embedding training of syntactic and semantic data at functional granularity to identify functional code clones. On the other hand, this technique performed less well on larger datasets. A functional code clone detector based on attention mechanism (FCCA) was introduced [18] for CCD. By maintaining both structured (code in the form of abstract syntax trees and control-flow graphs) and unstructured (code in the form of sequential tokens) data, this method was implemented on top of a cross-code representation. A collective representation was created by combining various code elements, and it included an attention mechanism that deliberately focused on key code components and attributes that improved the final detection accuracy. However, there were computational problems when this method was developed. A two-pass technique was developed [19] for CCD and its type categorization using a tree-based convolution neural network (TBCNN), which can capture structural features with a short propagation path and achieves comparable performance to word-by-word attention models. This technique detects clones on the first pass and then determines the clone type on the second pass. Both the first and second pass uses the TBCNN to extract features from the code fragments' ASTs to be compared. However, this method has high computational complexity issues.

A multi-threshold query, i.e. performing the query numerous times directed at distinct groups of clones, was implemented in a bag-of-tokens-based CCD [20] to find additional clone pairs of larger variation without reducing precision. To compensate for the additional behavior time generated by this technique, an optimization procedure was carried out to significantly minimize the duplication in detected clones. However, the classification accuracy of this approach was lower. An end-to-end cross-language (e2e-CL) CCD approach was developed [21] based on embeddings of ASTs using InferCode. In this model, InferCode captures the syntactical essence of a program as a vector. This model learns abstract features by grouping related embeddings through the contrastive loss function, which assures that comparable embeddings are close together but dissimilar embeddings are far apart. Moreover, the Siamese architecture was employed to overcome the data shortage and reduce overfitting issues. A new approach called Contrastive Cross-language model (CCL) was developed [22] for CCD. This model was efficient in detecting cross-language clones using learned representations. The pre-trained algorithm Code BERT was utilized in this approach to transform programs in many languages into high-dimensional vector representations. Furthermore, this system was improved using a provisional learning strategy that can discriminate between cloned and non-cloned pairs. However, this strategy produced minimal scalability.

PROPOSED WORK

This section discussed the brief illustration of TL-AL-CCM model. Figure 1 displays the complete workflow of the proposed model. Initially, the features like lexical, syntactic, semantic and structural features are extracted from the source code which is briefly provided in [23]. The implementation of the pre-trained algorithms for TL is then addressed. Once, the learned features are obtained, these features will be given as input to the AL. Furthermore, the AL method is provided to leverage and calibrate the obtained knowledge from pre-trained algorithms for the source code suggestion task. Next, this model is trained completely and it is tested by using the testing source code datsset.

Transfer Learning

One of the significant advancements in the DL paradigm for CCD is TL. By slightly adjusting the hyper-parameters, TL utilizes a pre-trained algorithm to conduct categorization on a dataset and then employs a similar strategy to another group of classified tasks. TL offers two advantages:

1. It can be learned faster because a model has already been learned on a distinct activity.
2. The model can be employed for tasks with smaller datasets because it has previously been learned on a larger dataset, and the weights are applied to the new tasks.

The TL technique for original code modelling is shown in Figure 2. The TL technique is utilized for the objective of effective source code modelling in code clones. This work proposes a distinct knowledge transfer approach, which transfers experience from two separate RNN-based pre-trained models and then fine-tunes it using an attention

learner for a particular source code modelling activities. The proposed TL approach consists of different steps which are briefly listed below.

Pre-Training Models for Transfer Learning

In TL, pre-training is handled individually for each objective task, starting from scratch with each reference dataset which has been screened carefully. In actuality, pre-training will become more applicable over time in a variety of targeted activities, while starting from scratch for each one separately could reduce efficiency by allowing one to rediscover crucial data features. For the proposed task, two RNN-based models are pre-trained for TL in the CCM domain. Figure 3 depicts the structure of RNN model. In a given input sequence U =(u_1,..,u_t), RNN upgrades its recurrent hidden state H_t by

$$H_t = \begin{cases} 0, & if\ T = 0 \\ \varphi(H_{t-1}, u_t) & otherwise \end{cases} \quad (1)$$

u_t and H_t denote the data input and recurrent hidden state, with time step t, respectively, φ(.) denotes the non-linear activation function of a hidden layer, such as sigmoid or hyperbolic tangent. The following is the updated rule for the recurrent concealed state in (1):

$$H_t = \varphi\left(Z_{u_t} + A(H_{t-1})\right) \quad (2)$$

Where Z and A are the input co-efficient vectors at the present stage, and the activation of the H_t is provided in the previous step, respectively. Equation (2) is expanded as follows:

$$H_t = \varphi\left(Z_{pH u_t} + Z_{HH} H_{t-1} + B_H\right) \quad (3)$$

Where, t = 1 to T, Z_{pH} represents an input-hidden weight vector, Z_{HH} and B_H represents the weight matrix of the hidden layer, and hidden layer bias vector respectively. However, it has been found that one significant problem in RNNs is the vanishing gradient, which can be rectified by employing the gated recurrent unit. The GRU avoids the vanishing gradient problem by revealing the complete hidden data on each time step t. It can be said to be

$$H_p = (1 - w_p) H_{p-1} + w_p H_p \quad (4)$$

$$w_p = \boldsymbol{\phi}(Z_w \mathcal{T}_p + A_w(H_{p-1}) \quad (5)$$

$$H_p = \tanh(Z\mathcal{T}_p + v_p \otimes A\, H_{p-1}) \quad (6)$$

$$v_p = \boldsymbol{\phi}(Z_v \mathcal{T}_p + A_v H_{p-1}) \quad (7)$$

w and *v* are specified as the reset gate and the update gate, respectively. The gate operations like p will restrain the inflating of the memory gradient and reproduce the gradient from a linear multiplication expression to a summation expression. This helps to resolve the problems, particularly, the vanishing gradient.

Training the model to transfer knowledge

For TL, the pre-trained RNN model is described in the earlier section. Then, the learned data knowledge is converted using these pre-trained models for the subsequent function of source code suggestion. The major objective is to maintain the gathered knowledge in pre-trained models, freeze the extracted knowledge, and then fine-tune it for the source code suggestion activity. To attain maximum performance, the attention learner focuses on task-particular extracted aspects (lexica, syntactic, semantic, and structural). The objective of an AL process is to advise the model during training on which portion of the input data is crucial so that it can pay close attention to the data. The pre-trained RNN layer can process and generate the learned features from the source code, the length of the learned feature of hidden state vectors is always equal to the length of the input (extracted) features. The alignment among two sequences is constructed to train the model for the distribution of $s\left(j_1, j_2, .., j_I \mid H_1, H_2, .., H_p\right)$ for which there is no clear functional dependency between I and P. The RNN-based AL model produces the resulted features of $(j_1, j_2, ..j_t)$ one time at a time, simultaneously aligning each generated element to the encoded input feature $(H_1, H_2, .., H_p)$. The composition of RNN and AL works efficiently for modelling the clone codes. The AL selects the temporal positions over the learned features which should be used to update the hidden state of the RNN and to make a prediction for the next output value. Typically, the selection of elements from the input features is a weighted sum

$$E_t = \sum_M A_{tM} H_M \quad (8)$$

Where, A_tM is the attention weights and it should satisfy $A_{tM}>0$ and $\sum_M A_{tM}=1$

In this process, The AL process is used for tine-tuning the learned features from pre-trained RNN layer for modelling the code clones. The determination is defined in (9), (10) and (11)

$G=R*A_{t-1}$ (9)

$f_{tM} = z^T \tanh (X_{l_{t-1}} + YH_M + W_{g_M} + C)$ (10)

$A_{tM} = e(f_{tM}) / \sum_{M=1}^{m} e(f_{tM})$ (11)

Where, X, Y, W and R are the feature matrix, z and C are the feature vector, * denotes convolution $l_{(t-1)}$ stands for the former RNN component of the AL mechanism. The equation (11) depicts the weight A_{tM} obtained by normalizing the scores f_{tM}. In Equation (3), the resulting score depends on the previous state $l_{(t-1)}$, the feature label in the respective position H_M and the vector of so-called convolutional features g_M. The name "convolutional" comes from the convolution along the time axis used in equation (2) to compute the matrix G that comprises all feature vectors g_M. Similarly, the AL mechanism describes above combines source code information from $l_{(t-1)}$, the feature in the respective position H_M and focuses on the previous step described by attention weight $A_{(t-1)}$, which particularly defines A_t is important for code modelling.

Fine-tuning the learned model for code clone modelling

The figure 4 completely describes the fine-tuning process of learned features in TL model with AL mechanism for CCM. In figure 4, after the completion of transferring trained features from the pre-trained RNN model, the features obtained from the AL mechanism are considered to train the TL-CCD model and the trained model is employed to predict the code clones from the testing dataset which is taken from the source code. Fine-tuning is the process of unfreezing different stages in the pre-trained model (learned features). The TL is typically carried out in conjunction with the DL model to effectively calibrate the pre-trained model on the original code using certain data from the target task. By using this concept in this research, the learned features from the pre-trained models are fine-tuned to model the code clones.

RESULT AND DISCUSSION

For the experimental purpose, the dataset is divided into two different categories as a training and testing dataset to assess the effectiveness of the suggested method and to detect and model the clone and its type using its similarity attributes. A benchmark dataset, such as Big Clone Bench, is used to generate the training dataset. The Big Clone Bench is a benchmark consisting of a large number of manually approved clones from the IJaDataset-2.0 source.

The testing dataset is then gathered from Apache Maven 3.8.3 is a toolkit for managing and comprehending software projects. Maven depends upon the presumption of a Project Entity Paradigm (POM), and can manage a project's development, monitoring, and information from a primary source of contact [24]. Apache ant 1.10.12 is a Java library and function tool that manages operations indicated in construct documents as objectives and extensibility endpoints. The well-known use of Ant is the creation of Java applications, as it has a collection of built-in tasks for compiling, assembling, testing, and executing Java programmes [25]. Apache Opennlp-master 1.9.1 is a natural language information retrieval toolkit based on ML techniques. Among the most common NLP operations supported are indexing, sentence classification, part-of-speech labeling, named entity identification, stacking, and processing [26] On using these datasets, the efficiency of proposed TL-AL-CCM technique is compared with an existing method TBCNN-CCD [19], e2e-CL- CCD [21] and CCL-CCD [22] in terms of accuracy, precision, recall, time period, Memory space and Clone types for detecting and modelling all four types of CC with its similarity features.

Accuracy

It is calculated by dividing the number of properly-recognized CCs by the absolute No. of CCs and non-CCs in the cloned repository (actual). Table 1 provides a comparison of existing and proposed methods for detecting and modelling all clone types. Figure 5 displays the results of accuracy achieved for proposed and existing methods to improve the CCM task. From the above analysis, it is observed that the accuracy of the proposed model is 11.28%, 8.04%, and 3.53% higher than the TBCNN-CCD, e2e-CL- CCD and CCL-CCD for Apache Maven 3.8.3 dataset;

15.27%, 6.74%, and 4.03% higher than the TBCNN-CCD, e2e-CL- CCD and CCL-CCD for Apache ant 1.10.12 dataset; 13.70%, 7.77%, and 2.32% higher than the TBCNN-CCD, e2e-CL- CCD and CCL-CCD for Opennlp-master datasets respectively. From this analysis, it is proved that the proposed model attains higher accuracy than the other existing methods for efficient CCM tasks.

Precision

It is computed by calculating the overall No. of identified CCs by the No. of accurately detected CCs (predicted). Table 2 compares extant and proposed methods for identifying and modifying all clone variants. Figure 6 displays the results of precision achieved for proposed and existing methods to improve the CCM tasks. From the above analysis, it is observed that the precision of the proposed model is 18.02%, 13.88%, and 6.78% higher than the TBCNN-CCD, e2e-CL- CCD and CCL-CCD for Apache Maven 3.8.3 dataset; 20.15%, 14.02%, and 6.14% higher than the TBCNN-CCD, e2e-CL- CCD and CCL-CCD for Apache ant 1.10.12 dataset; 17.69%, 13.04%, and 4.75% higher than the TBCNN-CCD, e2e-CL- CCD and CCL-CCD for Opennlp-master datasets respectively. From this analysis, it is proved that the proposed model attains a higher precision than the other existing methods for the efficient CCM tasks

Recall

The recall is obtained by splitting the total count of CCs in the database by the number of successfully recognized CCs (actual). Table 3 provides a comparison of existing and proposed methods for detecting all clone types. Figure 7 displays the results of recall achieved for proposed and existing methods to improve the CCM tasks. From the above analysis, it is observed that the recall of proposed model is 13.96%, 8.06%, and 4.48% higher than the TBCNN-CCD, e2e-CL- CCD and CCL-CCD for Apache Maven 3.8.3 dataset; 16.51%, 9.89%, and 6.93% higher than the TBCNN-CCD, e2e-CL- CCD and CCL-CCD for Apache ant 1.10.12 dataset; 13.02%, 7.57%, and 4.25% higher than the TBCNN-CCD, e2e-CL- CCD and CCL-CCD for Opennlp-master datasets respectively. From this analysis, it is proved that the proposed model attains a higher recall than the other existing methods for efficient CCM tasks.

CONCLUSION

In this research work, TL-AL-CCM technique enhances the performance of DL-based source code models greatly. Initially, the principle of TL is applied in DL-based source code language models. Following that, the two RNN-based pre-trained models are used for TL in the region of reference code. The pre-trained models' learned information is integrated into an AL for subsequent issues. The AL applies pre-trained model learning data to given downstream activities. In TL, pre-trained models are employed to capture generic attributes that can subsequently be calibrated for a specific purpose without having to retrain the model from scratch. At last, the suggested method provides better results than other existing methods in terms of accuracy, precision, and recall for three different datasets Apache Maven 3.8.3 Apache ant 1.10.12 dataset Opennlp-master.

REFERENCES

1. C. V. Lopes, P. Maj, P. Martins, V. Saini, D.Yang, J. Zitny and J. Vitek, "DéjàVu: a map of code duplicates on GitHub", Proceedings of the ACM on Programming Languages, Vol. 1 OOPSLA, pp.1-28, 2017.
2. C. K. Roy and J. R. Cordy, "A survey on software clone detection research", Queen's School of Computing TR, Vol. 541, No. 115, pp. 64-68, 2007.
3. R. Koschke, R. Falke and P. Frenzel, "Clone detection using abstract syntax suffix trees," In 2006 13th Working Conference on Reverse Engineering, pp. 253-262, 2006.
4. T. Kamiya, S. Kusumoto, and K. Inoue, "CCFinder: A Multilinguistic Token-Based Code Clone Detection System for Large Scale Source Code", *IEEE Transactions on Software Engineering*, Vol. SE-28, No. 7, pp. 654-670, 2002.

5. Z. Li, S. Lu, S. Myagmar and Y. Zhou, "CP-Miner: Finding copy-paste and related bugs in large-scale software code", *IEEE Transactions on software Engineering*, Vol. 32, No. 3, pp. 176-192, 2006.
6. D. Baxter and A. Yahin, L. Moura, M. Sant'Anna and L. Bier, "Clone detection using abstract syntax trees." *In Proceedings. International Conference on Software Maintenance (Cat. No. 98CB36272)*, pp. 368-377, 1998.
7. Y. Gao, Z. Wang, S. Liu, L. Yang, W. Sang and Y. Cai, "Teccd: A tree embedding approach for code clone detection," *In 2019 IEEE International Conference on Software Maintenance and Evolution (ICSME)*, pp. 145-156, 2019.
8. D. Rattan and J. Kaur, "Systematic mapping study of metrics based clone detection techniques," *In Proceedings of the International Conference on Advances in Information Communication Technology & Computing*, pp. 1-7, 2016.
9. M. S. Aktas and M. Kapdan, "Structural code clone detection methodology using software metrics", *International Journal of Software Engineering and Knowledge Engineering*, Vol. 26, No. 2, pp. 307-332, 2015.
10. D. Perez and S. Chiba, "Cross-language clone detection by learning over abstract syntax trees," *In 2019 IEEE/ACM 16th International Conference on Mining Software Repositories (MSR),* pp. 518-528, 2019.
11. Y. Higo, U. Yasushi, M. Nishino and S. Kusumoto, "Incremental code clone detection: A PDG-based approach," *In 2011 18th Working Conference on Reverse Engineering*, pp. 3-12, 2011.
12. Kaur and M. S. Sandhu, "Software code clone detection model using hybrid approach. *International Journal of Computers and Technology*", Vol. 32b, pp. 275-278, 2012.
13. J. Zeng, K. Ben, X. Li and X. Zhang, "Fast code clone detection based on weighted recursive autoencoders", *IEEE Access*, Vol. 7, pp. 125062-125078.
14. M. Wu, P. Wang, K. Yin, H. Cheng, Y. Xu and C. K. Roy, "LVMapper: A Large-Variance Clone Detector Using Sequencing Alignment Approach", *IEEE access*, Vol. 8, pp. 27986-27997, 2019.
15. H. Yu, W. Lam, L. Chen, G. Li, T. Xie and Q. Wang, "Neural detection of semantic code clones via tree-based convolutio," *In 2019 IEEE/ACM 27th International Conference on Program Comprehension (ICPC)*, pp. 70-80, 2019.
16. G. Mostaeen, B. Roy, C. K. Roy, K. Schneider and J. Svajlenko, "A machine learning based framework for code clone validation", *Journal of Systems and Software*, Vol. 169, pp. 110686, 2020.
17. C. Fang, Z. Liu, Y. Shi, J. Huang and Q. Shi, "Functional code clone detection with syntax and semantics fusion learning," *In Proceedings of the 29th ACM SIGSOFT International Symposium on Software Testing and Analysis*, pp. 516-527, 2020.
18. W. Hua, Y. Sui, Y. Wan, G. Liu and G. Xu, "Fcca: Hybrid code representation for functional clone detection using attention networks", *IEEE Transactions on Reliability*, Vol. 70, No.1, pp. 304-318.
19. Y. B. Jo, J. Lee and C. J. Yoo, "Two-Pass Technique for Clone Detection and Type Classification Using Tree-Based Convolution Neural Network", *Applied Sciences*, Vol. 11, No. 14, pp. 6613, 2021.
20. Y. Golubev, V. Poletansky, N. Povarov and T. Bryksin, "Multi-threshold token-based code clone detection", *In 2021 IEEE International Conference on Software Analysis, Evolution and Reengineering (SANER)*, pp. 496-500, 2021.
21. M. A. Yahya and D. K. Kim, "Cross-Language Source Code Clone Detection Using Deep Learning with InferCode", arXiv preprint arXiv:2205.04913.
22. C. Tao, Q. Zhan, X. Hu and X. Xia, C4: Contrastive Cross-Language Code Clone Detection.
23. S. Karthik and B. Dr. Rajdeepa, A Collaborative method for Code Clone Detection using Lexical, Syntactic, Semantic and Structural Features, MATPR, Elesiever.
24. [https://github.com/apache/maven]
25. [https://github.com/apache/ant].
26. [https://github.com/apache/opennlp].

Table 1 Evaluation of Accuracy

Datasets	TBCNN-CCD	e2e-CL- CCD	CCL-CCD	TL-AL-CCM
Apache Maven 3.8.3	0.869	0.895	0.934	0.967
Apache ant 1.10.12	0.851	0.919	0.943	0.981
Opennlp-master 1.9.1	0.854	0.901	0.949	0.973

Table 2 Evaluation of Precision

Datasets	TBCNN-CCD	e2e-CL- CCD	CCL-CCD	TL-AL-CCM
Apache Maven 3.8.3	0.827	0.857	0.914	0.976
Apache ant 1.10.12	0.819	0.863	0.927	0.984
Opennlp-master 1.9.1	0.825	0.859	0.927	0.971

Table 3 Evaluation of Recall

Datasets	TBCNN-CCD	e2e-CL- CCD	CCL-CCD	TL-AL-CCM
Apache Maven 3.8.3	0.859	0.906	0.937	0.979
Appache ant 1.10.12	0.848	0.899	0.924	0.988
Opennlp-master 1.9.1	0.868	0.912	0.941	0.981

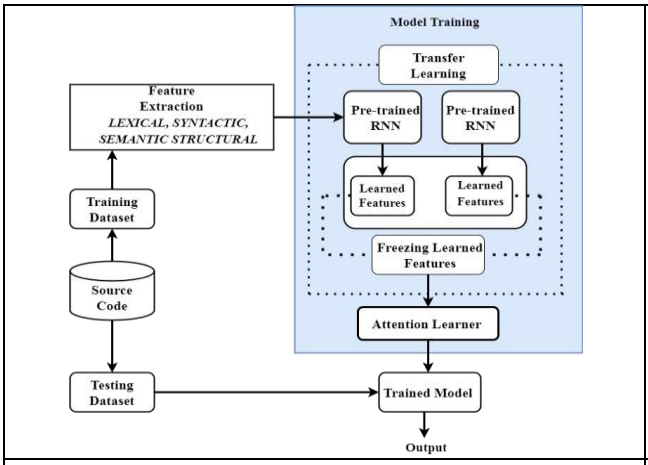

Figure 1: Overall flow of the proposed work

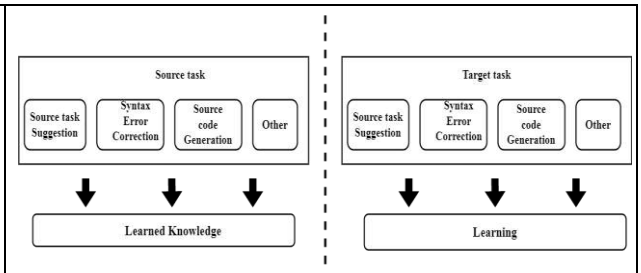

Figure 2: TL-based approach for CCM

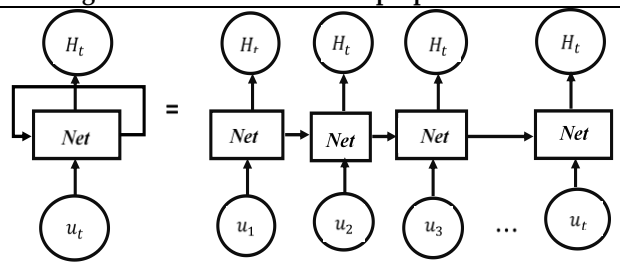

Figure 3: Structure of RNN

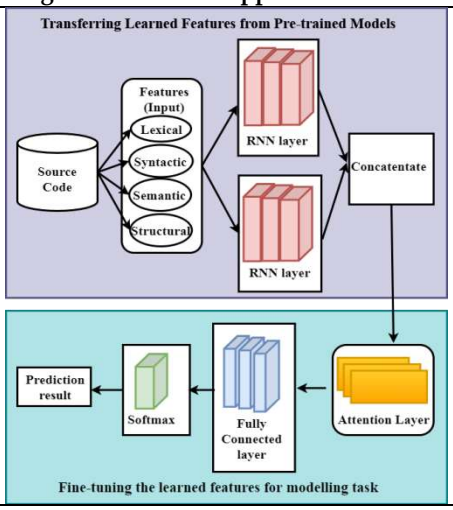

Figure 4: Transfer learning-based attention mode

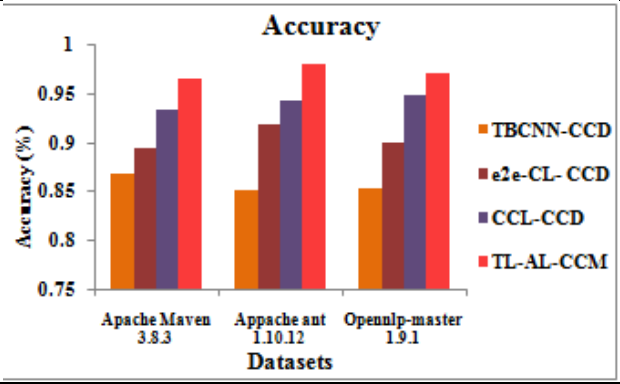

Figure 5: Comparison of Accuracy

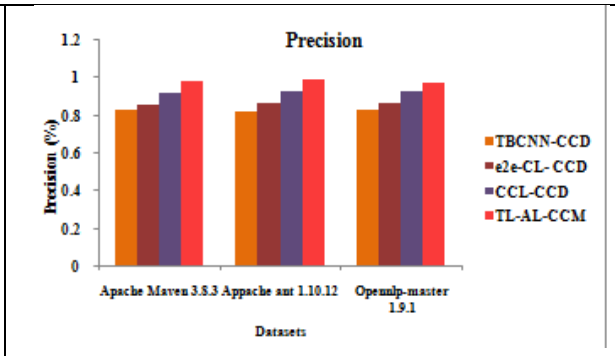

Figure 6 : Comparison of precision

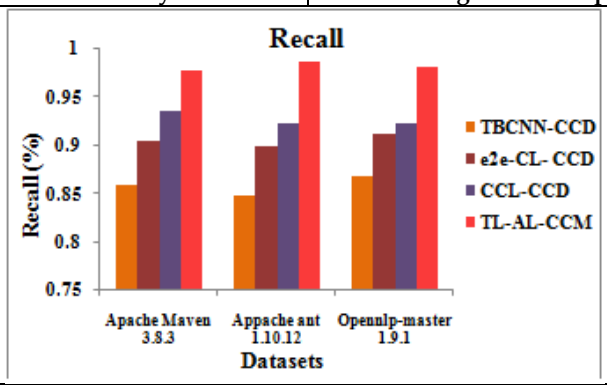

Figure 7 Comparison of recall

Indian Journal of Natural Sciences www.tnsroindia.org.in ©IJONS

Vol.15 / Issue 83 / Apr / 2024 International Bimonthly (Print) – Open Access ISSN: 0976 – 0997

RESEARCH ARTICLE

Mathematical Analysis of New SEIQR Model via Laplace Adomian Decomposition Method

N. Jeeva[1]* and K.M. Dharmalingam[2]

[1]Research Scholar, Department of Mathematics, The Madura College (Affiliated to Madurai Kamaraj University) Madurai, Tamil Nadu, India.
[2]Associate Professor, Department of Mathematics, The Madura College (Affiliated to Madurai Kamaraj University) Madurai, Tamil Nadu, India.

Received: 03 Nov 2023 Revised: 09 Jan 2024 Accepted: 07 Mar 2024

***Address for Correspondence**
N. Jeeva
Research Scholar,
Department of Mathematics,
The Madura College (Affiliated to Madurai Kamaraj University)
Madurai, Tamil Nadu, India.
Email: jeevapirc2405@gmail.com

ABSTRACT

This study focuses on a novel mathematical model for the coronavirus, building upon the SEIQR epidemiological framework while incorporating a unique compartment for isolation or quarantine. We employed the Laplace Adomian decomposition Method (LADM) to perform an in-depth analytical examination of this novel model. The effectiveness of the LADM was demonstrated by providing highly accurate approximate analytical solutions with minimal iterations. In addition, we conducted a comparative analysis using numerical simulations to comprehensively understand the behaviour of the model. This comparative approach not only validates the results but also provides valuable insights into how the novel coronavirus model behaves under various conditions and scenarios.

Keywords: Novel Corona Virus transmission, SEIQR model, Laplace Adomian Decomposition Method (LADM), Mathematical modelling, Numerical simulation.

INTRODUCTION

The term "coronavirus" denotes a family of viruses capable of causing illness in both animals and humans. The novel coronavirus, formally designated as "SARS-CoV-2" (Severe Acute Respiratory Syndrome Coronavirus 2), was initially detected in Wuhan, China, in December 2019. It is accountable for the onset of "COVID-19" (Coronavirus Disease 2019) [1]. This virus has left a profound impact on public health and has triggered a worldwide pandemic.

Measures to curb its spread encompass vaccination campaigns, adherence to public health protocols such as mask-wearing and social distancing, and ongoing research to enhance our comprehension of the virus and its various strains [2-3]. The SIR model is a well-established mathematical framework in epidemiology, extensively employed for analyzing the transmission of infectious diseases within a population. The acronym "SIR" denotes the three compartments used to classify individuals within the population: Susceptible, Infected, and Recovered [4-5]. SEIQR serves as an epidemiological framework employed to investigate the propagation of infectious diseases within a population. It represents an expansion of the fundamental SIR (Susceptible-Infectious-Recovered) model, introducing supplementary compartments to accommodate diverse stages of disease transmission. The SEIQR model conventionally encompasses the following compartments: Susceptible, Exposed, Infectious, Quarantined, and Recovered [6-8]. This model proves especially valuable when examining diseases characterized by a substantial incubation period, during which infected individuals are not yet capable of transmitting the infection.

Its utility lies in its capacity for a more intricate examination of disease transmission dynamics, offering insights into forecasting the future course of an outbreak and assessing the impact of interventions, such as quarantine measures and vaccination campaigns [9]. The mathematical model for the transmission of the novel coronavirus was formulated in a study conducted by researchers [10]. This mathematical model employs a collection of non-linear differential equations to incorporate the propagation of COVID-19 infection. It includes a unique compartment class for isolation or quarantine and estimates the model parameters by aligning the model with reported data on the evolving pandemic situation in India. The primary objective of this paper is to utilize analytical method to solve the model for the novel coronavirus. The approximate analytical solutions for the novel coronavirus model are obtained using a potent technique known as the Laplace Adomian Decomposition Method (LADM). This method yields highly precise results with minimal iterations, making it a valuable tool for analyzing the dynamics of the novel coronavirus model. The LADM involves breaking down the equations into infinite power series of Adomian polynomials, simplifying the computation of approximate solutions for the model's variables.

Mathematical Modelling of the problem

In [10], a deterministic novel model for Corona Virus was introduced, utilizing a system of ordinary non-linear differential equations. The population was divided into five compartments: Susceptible population S(t), Exposed population E(t), Infected population I(t), Isolated population Q(t), and Recovered population R(t), as illustrated in Figure 1. The Novel SEIQR model for Corona Virus can be expressed as follows:

$$\frac{dS}{dt} = A - \beta SI - \mu S \quad (1)$$

$$\frac{dE}{dt} = \beta SI - (\alpha + \mu)E \quad (2)$$

$$\frac{dI}{dt} = \alpha E - (\gamma + q + \mu)I \quad (3)$$

$$\frac{dQ}{dt} = qI - (\theta + \mu)Q \quad (4)$$

$$\frac{dR}{dt} = \gamma I + \theta Q - \mu R \quad (5)$$

Subject to the initial conditions:

$$S(0) = a, E(0) = b, I(0) = c, Q(0) = d, R(0) = e \quad (6)$$

Where, Table 1 provides a list of the parameter representations utilized in this SEIQR model.

Approximate Analytical solution using LADM

The Laplace Adomian Decomposition Method (LADM) is a mathematical method employed to address differential equations, particularly those characterized by nonlinearity. LADM integrates the fundamental concepts of Laplace transforms and the Adomian Decomposition Method (ADM) to establish a structured framework for deriving analytical solutions to a diverse array of differential equations. An important and noteworthy advantage of LADM is its ability to address nonlinear differential equations without the need for linearization, perturbation, transformation, or any form of discrimination. With LADM, it yields an analytical solution in the form of a rapidly converging infinite power series. Its effectiveness extends to various domains, encompassing fluid dynamics, heat transfer,

population dynamics, and more. Across these fields, LADM has consistently proven its capability to effectively handle complex problems and offer valuable insights [11-17].

Basic concept of Laplace Adomian Decomposition Method (LADM)

In this sub-section, we explore the application of a hybrid method that combines the Laplace transformation and the Adomian decomposition algorithm to solve the nonlinear autonomous first-order differential equation that governing the problem.

$$L[u(x)] + R[u(x)] + N[u(x)] = g(x) \quad (7)$$

$$u(0) = f(x) \quad (8)$$

$$L[u(x)] = g(x) - R[u(x)] - N[u(x)] \quad (9)$$

By applying the Laplace transform to both sides of Eq. (9) and utilizing the differentiation property, we obtain the following result.

$$sL[u(x)] - f(x) = L[g(x)] - L[R[u(x)]] - L[N[u(x)]]$$

$$L[u(x)] = \frac{1}{s}f(x) + \frac{1}{s}L[g(x)] - \frac{1}{s}L[R[u(x)]] - \frac{1}{s}L[N[u(x)]] \quad (10)$$

When we apply the inverse Laplace transform to both sides of Eq. (10), we obtain the following result.

$$u(x) = \varphi(x) - L^{-1}[\frac{1}{s}L[R[u(x)]] - \frac{1}{s}L[N[u(x)]]] \quad (11)$$

Here, $\varphi(x)$ represents the term originating from the first three terms on the right-hand side of Eq. (11). Next, we make an assumption about the solution to the problem in the form of a decomposing series.

$$u(x) = \sum_{n=0}^{\infty} u_n(x) \quad (12)$$

Likewise, the nonlinear terms are expressed in relation to the Adomian polynomials as follows:

$$N[u(x)] = \sum_{n=0}^{\infty} A_n \quad (13)$$

Where the $A_n{}^{'s}$ represents the Adomain polynomials defined in the form

$$A_n = \frac{1}{n!}\frac{d^n}{d\lambda^n}[N(\sum_{n=0}^{\infty}\lambda^n y_n)]|_{\lambda=0} \quad (14)$$

Plugging Eqn.(12) and (13) into Eq.(14), we obtain

$$\sum_{n=0}^{\infty} u_n(x) = \varphi(x) - L^{-1}[\frac{1}{s}L[R\sum_{n=0}^{\infty} u_n(x)] - \frac{1}{s}L[N\sum_{n=0}^{\infty} A_n]] \quad (15)$$

By equating both sides of Eq.(15), we derive an iterative algorithm in the following form:

$$u_0(x) = \varphi(x)$$

$$u_1(x) = -L^{-1}[\frac{1}{s}L\left[R\sum_{n=0}^{\infty} u_0(x)\right] - \frac{1}{s}L\left[N\sum_{n=0}^{\infty} A_0\right]]$$

$$u_2(x) = -L^{-1}[\frac{1}{s}L\left[R\sum_{n=0}^{\infty} u_1(x)\right] - \frac{1}{s}L\left[N\sum_{n=0}^{\infty} A_1\right]]$$

$$\vdots$$

$$u_{n+1}(x) = -L^{-1}[\frac{1}{s}L[R\sum_{n=0}^{\infty} u_n(x)] - \frac{1}{s}L[N\sum_{n=0}^{\infty} A_n]] \quad (16)$$

The solution to the differential equation is then obtained as the summation of the decomposed series in the following form:

$$u(x) \approx u_0(x) + u_1(x) + u_2(x) + \cdots \quad (17)$$

Approximate Analytical solution of Covid-19 SEIQR model using LADM

In this sub-section, We illustrate the application of the Laplace-Adomian Decomposition Method to nonlinear ordinary differential systems. To initiate the process, we commence by applying the Laplace transformation, denoted by L, to both sides of equations (1-5).

$$L[\frac{dS}{dt}] = L[A] - L[\beta SI] - L[\mu S] \quad (18)$$

$$L[\frac{dE}{dt}] = L[\beta SI] - L[(\alpha + \mu)E] \quad (19)$$

$$L[\frac{dI}{dt}] = L[\alpha E] - L[(\gamma + q + \mu)I] \quad (20)$$

$$L[\frac{dQ}{dt}] = L[qI] - L[(\theta + \mu)Q] \quad (21)$$

$$L[\frac{dR}{dt}] = L[\gamma I] + L[\theta Q] - L[\mu R] \quad (22)$$

We make use of the properties of derivatives and constants in the Laplace transform for our analysis.

$wL[S] - S(0) = \frac{A}{w} - \beta L[SI] - \mu L[S]$ (23)

$wL[E] - E(0) = \beta L[SI] - (\alpha + \mu)L[E]$ (24)

$wL[I] - I(0) = \alpha L[E] - (\gamma + q + \mu)L[I]$ (25)

$wL[Q] - Q(0) = qL[I] - (\theta + \mu)L[Q]$ (26)

$wL[R] - R(0) = \gamma L[I] + \theta L[Q] - \mu L[R]$ (27)

Upon applying the initial conditions, we obtain the following results.

$L[S] = \frac{a}{w} + \frac{A}{w^2} - \frac{\beta}{w} L[SI] - \frac{\mu}{w} L[S]$ (28)

$L[E] = \frac{b}{w} + \frac{\beta}{w} L[SI] - \frac{(\alpha+\mu)}{w} L[E]$ (29)

$L[I] = \frac{c}{w} + \frac{\alpha}{w} L[E] - \frac{(\gamma+q+\mu)}{w} L[I]$ (30)

$L[Q] = \frac{d}{w} + \frac{q}{w} L[I] - \frac{(\theta+\mu)}{w} L[Q]$ (31)

$L[R] = \frac{e}{w} + \frac{\gamma}{w} L[I] + \frac{\theta}{w} L[Q] - \frac{\mu}{w} L[R]$ (32)

We make the assumption that the solutions for S, E, I, Q, and R can be expressed as infinite series. Additionally, we decompose the nonlinear terms involving $SI = U$ in the model using Adomian polynomials, which are expressed as follows:

$S = \sum_{n=0}^{\infty} S_n,\ E = \sum_{n=0}^{\infty} E_n,\ I = \sum_{n=0}^{\infty} I_n,\ Q = \sum_{n=0}^{\infty} Q_n, R = \sum_{n=0}^{\infty} R_n\ , U = \sum_{n=0}^{\infty} U_n$ (33)

The Adomian polynomials, denoted by A_n, are defined as follows;

$$U_n = \frac{1}{n!}\frac{d^n}{d\lambda^n}[\sum_{i=0}^{\infty} \lambda^i S_i \sum_{i=0}^{\infty} \lambda^i I_i]$$

$U_0 = S_0 I_0$ (34)

$U_1 = S_0 I_1 + S_1 I_0$

Upon inserting eqn.4 and eqn.5 into eqn.3, we obtain the following:

$L[\sum_{n=0}^{\infty} S_n] = \frac{a}{w} + \frac{A}{w^2} - \frac{\beta}{w} L[\sum_{n=0}^{\infty} U_n] - \frac{\mu}{w} L[\sum_{n=0}^{\infty} S_n]$ (35)

$L[\sum_{n=0}^{\infty} E_n] = \frac{b}{w} + \frac{\beta}{w} L[\sum_{n=0}^{\infty} U_n] - \frac{(\alpha+\mu)}{w} L[\sum_{n=0}^{\infty} E_n]$ (36)

$L[\sum_{n=0}^{\infty} I_n] = \frac{c}{w} + \frac{\alpha}{w} L[\sum_{n=0}^{\infty} E_n] - \frac{(\gamma+q+\mu)}{w} L[\sum_{n=0}^{\infty} I_n]$ (37)

$L[\sum_{n=0}^{\infty} Q_n] = \frac{d}{w} + \frac{q}{w} L[\sum_{n=0}^{\infty} I_n] - \frac{(\theta+\mu)}{w} L[\sum_{n=0}^{\infty} Q_n]$ (38)

$L[\sum_{n=0}^{\infty} R_n] = \frac{e}{w} + \frac{\gamma}{w} L[\sum_{n=0}^{\infty} I_n] + \frac{\theta}{w} L[\sum_{n=0}^{\infty} Q_n] - \frac{\mu}{w} L[\sum_{n=0}^{\infty} R_n]$ (39)

The initial iteration of the Laplace-Adomian Decomposition Method is obtained as follows:

$L[S_0] = \frac{a}{w} + \frac{A}{w^2}$ (40)

$L[E_0] = \frac{b}{w}$ (41)

$L[I_0] = \frac{c}{w}$ (42)

$L[Q_0] = \frac{d}{w}$ (43)

$L[R_0] = \frac{e}{w}$ (44)

Applying the inverse Laplace transform to the initial iteration yields the final solution.

$S_0 = a + At$ (45)

$E_0 = b$ (46)

$I_0 = c$ (47)

$Q_0 = d$ (48)

$R_0 = e$ (49)

The first iteration of the Laplace-Adomian Decomposition Method is derived by comparing both sides of the equation.

$$L[S_1] = -\frac{\beta}{w}L[U_0] - \frac{\mu}{w}L[S_0] \quad (50)$$

$$L[E_1] = \frac{\beta}{w}L[U_0] - \frac{(\alpha+\mu)}{w}L[E_0] \quad (51)$$

$$L[I_1] = \frac{\alpha}{w}L[E_0] - \frac{(\gamma+q+\mu)}{w}L[I_0] \quad (52)$$

$$L[Q_1] = \frac{q}{w}L[I_0] - \frac{(\theta+\mu)}{w}L[Q_0] \quad (53)$$

$$L[R_1] = \frac{\gamma}{w}L[I_0] + \frac{\theta}{w}L[Q_0] - \frac{\mu}{w}L[R_0] \quad (54)$$

By utilizing the initial iteration, we obtain the following.

$$L[S_1] = -\frac{\mu a}{w^2} - \frac{[\beta ac + A\mu]}{w^3} - \frac{\beta Ac}{w^4} \quad (55)$$

$$L[E_1] = -\frac{(\alpha+\mu)b}{w^2} + \frac{\beta ac}{w^3} + \frac{\beta Ac}{w^4} \quad (56)$$

$$L[I_1] = \frac{\alpha b - (\gamma+q+\mu)c}{w^2} \quad (57)$$

$$L[Q_1] = \frac{qc - (\theta+\mu)d}{w^2} \quad (58)$$

$$L[R_1] = \frac{\gamma c + \theta d - \mu e}{w^2} \quad (59)$$

Similarly, for the first iteration.

$$S_1 = -\mu at - [\beta ac + A\mu]\frac{t^2}{2!} - \beta Ac\frac{t^3}{3!} \quad (60)$$

$$E_1 = -(\alpha+\mu)bt + \beta ac\frac{t^2}{2!} + \beta Ac\frac{t^3}{3!} \quad (61)$$

$$I_1 = (\alpha b - (\gamma+q+\mu)c)t \quad (62)$$

$$Q_1 = (qc - (\theta+\mu)d)t \quad (63)$$

$$R_1 = (\gamma c + \theta d - \mu e)t \quad (64)$$

In a similar way, the second iteration of the Laplace-Adomian Decomposition Method is derived by comparing both sides of the equation.

$$L[S_2] = -\frac{\beta}{w}L[U_1] - \frac{\mu}{w}L[S_1] \quad (65)$$

$$L[E_2] = \frac{\beta}{w}L[U_1] - \frac{(\alpha+\mu)}{w}L[E_1] \quad (66)$$

$$L[I_2] = \frac{\alpha}{w}L[E_1] - \frac{(\gamma+q+\mu)}{w}L[I_1] \quad (67)$$

$$L[Q_2] = \frac{q}{w}L[I_1] - \frac{(\theta+\mu)}{w}L[Q_1] \quad (68)$$

$$L[R_2] = \frac{\gamma}{w}L[I_1] + \frac{\theta}{w}L[Q_1] - \frac{\mu}{w}L[R_1] \quad (69)$$

By utilizing the initial iteration and first iteration, we obtain the following.

$$S_2 = \mu^2 a\frac{t^2}{2!} + \Big(\beta\mu ac - \beta a\big(\alpha b - (\gamma+q+\mu)\big) + \mu(\beta ac + A\mu)\Big)\frac{t^3}{3!} + \big(\beta c(\beta ac + A\mu) + \beta A\big(\alpha b - (\gamma+q+\mu)\big) + \beta\mu Ac\big)\frac{t^4}{4!} + \beta^2 Ac^2\frac{t^5}{5!} \quad (70)$$

$$E_2 = (\alpha+\mu)^2 b\frac{t^2}{2!} + \Big(-(\alpha+\mu)\beta ac - \beta\mu ac + \beta a\big(\alpha b - (\gamma+q+\mu)\big)\Big)\frac{t^3}{3!} + \big(\beta A\big(\alpha b - (\gamma+q+\mu)\big) - \beta c(\beta ac + A\mu) - \alpha+\mu\beta act44!-\beta 2Ac2t55! \quad (71)$$

$$I_2 = \big(-\alpha(\alpha+\mu)b + (\gamma+q+\mu)(\alpha b - (\gamma+q+\mu)c)\big)\frac{t^2}{2!} + \alpha\beta ac\frac{t^3}{3!} + \alpha\beta Ac\frac{t^4}{4!} \quad (72)$$

$$Q_2 = (q(\alpha b - (\gamma+q+\mu)c) - (\theta+\mu)(qc - (\theta+\mu)d))\frac{t^2}{2!} \quad (73)$$

$$R_2 = (\gamma(\alpha b - (\gamma+q+\mu)c) + \theta(qc - (\theta+\mu)d) - \mu(\gamma c + \theta d - \mu e))\frac{t^2}{2!} \quad (74)$$

Subsequently, the remaining terms can be computed using a similar approach. By utilizing these calculated values, we can approximate the solutions to the above systems in the form of an infinite series as follows.

$$S(t) = S_0 + S_1 + S_2 + \cdots \quad (75)$$

$$E(t) = E_0 + E_1 + E_2 + \cdots \quad (76)$$
$$I(t) = I_0 + I_1 + I_2 + \cdots \quad (77)$$
$$Q(t) = Q_0 + Q_1 + Q_2 + \cdots \quad (78)$$
$$R(t) = R_0 + R_1 + R_2 + \cdots \quad (79)$$

Therefore, the approximate analytical solutions of the SEIQR equations are derived by substituting Eqns.(45-49), Eqn.(60-64) and Eqns.(70-74) into Eqns. (75-79), we get the results as follows:

$$S(t) = a + (A - \mu a)t + (-\beta ac - A\mu + \mu^2 a)\frac{t^2}{2!} + \Big(\beta\mu ac - \beta Ac - \beta a\big(\alpha b - (\gamma + q + \mu)\big) + \mu(\beta ac + A\mu)\Big)\frac{t^3}{3!} + \big(\beta c(\beta ac + A\mu) + \beta A\big(\alpha b - (\gamma + q + \mu)\big) + \beta\mu Ac\big)\frac{t^4}{4!} + \beta^2 Ac^2\frac{t^5}{5!} \quad (80)$$

$$E(t) = b - (\alpha + \mu)bt + (\beta ac + (\alpha + \mu)^2 b)\frac{t^2}{2!} + \Big(\beta Ac - (\alpha + \mu)\beta ac - \beta\mu ac + \beta a\big(\alpha b - (\gamma + q + \mu)\big)\Big)\frac{t^3}{3!} + \big(\beta A\big(\alpha b - (\gamma + q + \mu)\big) - \beta c(\beta ac + A\mu) - (\alpha + \mu)\beta ac\big)\frac{t^4}{4!} - \beta^2 Ac^2\frac{t^5}{5!} \quad (81)$$

$$I(t) = c + (\alpha b - (\gamma + q + \mu)c)t + \big(-\alpha(\alpha + \mu)b + (\gamma + q + \mu)(\alpha b - (\gamma + q + \mu)c)\big)\frac{t^2}{2!} + \alpha\beta ac\frac{t^3}{3!} + \alpha\beta Ac\frac{t^4}{4!} \quad (82)$$

$$Q(t) = d + (qc - (\theta + \mu)d)t + (q(\alpha b - (\gamma + q + \mu)c) - (\theta + \mu)(qc - (\theta + \mu)d))\frac{t^2}{2!} \quad (83)$$

$$R(t) = e + (\gamma c + \theta d - \mu e)t + (\gamma(\alpha b - (\gamma + q + \mu)c) + \theta(qc - (\theta + \mu)d) - \mu(\gamma c + \theta d - \mu e))\frac{t^2}{2!} \quad (84)$$

Numerical Simulation and Discussions

We utilized the fourth-order Runge-Kutta technique to perform a numerical solution for the system of first-order nonlinear differential equations and MATLAB software was employed for this purpose. To gauge the accuracy of this numerical solution, a comparative analysis was conducted between these numerical results and the analytical solutions obtained through the Laplace Adomian Decomposition Method. Furthermore, we generated graphical representations of the analytical concentrations, namely S, E, I, Q, and R, along with their corresponding numerical results, covering a range of parameter values.

In the numerical testing phase, we adopt the following parameter values.
$A = 1380, \beta = 0.0009, \alpha = 0.0037, \gamma = 0.0055, q = 0.00052, \theta = 1, \mu = 0.0028$
With the initial values $S(0) = a = 1, E(0) = b = 1, I(0) = c = 1, Q(0) = d = 1, R(0) = e = 1$

Figures 2-8 depict a comparison between numerical and analytical solutions, showcasing the concentration profile of SEIQR under varying sets of physical parameters. In Figure 2, we present the concentration of the Susceptible class, S(t), utilizing the specified parameters for both analytical solutions and numerical simulations, it occurs perfect fit. The Susceptible class is primarily influenced by the parameters A, β, μ with additional connections to other parameters through nonlinear equations. The influence of these parameters becomes evident as the concentration of the susceptible class demonstrates a notable increasing trajectory. Figures 3 and 4 illustrate the concentration profiles of the Exposed class, E(t), and the Infected class, I(t), respectively, employing the provided parameters for both analytical solutions and numerical simulations. The Exposed class and Infected class are primarily influenced by the parameters α, β, μ and α, γ, q, μ respectively, with additional connections to other parameters through nonlinear equations. The influence of these parameters becomes apparent as the concentration of the Exposed and Infected class exhibits a conspicuous upward trend. Figure 5 depicts the concentration profiles of the Isolated class, Q(t), utilizing the specified parameters for both analytical solutions and numerical simulations. The Isolated class is primarily influenced by the parameters q, θ, μ with additional connections to other parameters through nonlinear equations. The impact of these parameters becomes evident as the concentration of the Isolated class displays a noticeable decreasing trend. Figure 6 depicts the concentration profiles of the Recovered class, R(t), utilizing the specified parameters for both analytical solutions and numerical simulations. The Recovered class is primarily

influenced by the parameters γ, θ, μ with additional connections to other parameters through nonlinear equations. The impact of these parameters becomes evident as the concentration of the Recovered class displays a noticeable increasing trend. Figure 7 portray the comprehensive concentration profile of SEIQR, encompassing both analytical solutions and numerical simulations. These figures showcase a satisfactory level of agreement within the time intervals $t = [0,1]$.In Figure 8, we plot the behaviour of novel corona virus SEIQR model, by using the data set [10]: $S(0) = 1380,\ I(0) = 121$ and some values are assumed $E(0) = 500,\ Q(0) = 70, R(0) = 40$. In Figure 9, we plot the behaviour of novel corona virus SEIQR model, by assuming all data set as: $S(0) = 380,\ E(0) = 150, I(0) = 121,$ $Q(0) = 100, R(0) = 90$.

CONCLUSION

This research is focused on obtaining an approximate analytical solution for the novel corona virus SEIQR model using the Laplace Adomian decomposition method (LADM). The LADM involves breaking down the equations into an infinite power series of Adomian polynomials and simplifying the computation of approximate solutions for the model's variables. We conducted a thorough comparison between the obtained analytical solutions and the numerical simulations. The findings demonstrated a notable level of consistency in the parameter values considered. The efficiency of the Laplace Adomian Decomposition method in handling nonlinear equations is underscored through graphical representation. Moreover, using different data set values, we analysed the behaviour of novel corona virus model. This comparative analysis will assist in the development of effective strategies to mitigate the spread of the virus and inform the implementation of appropriate public health interventions.

REFERENCES

1. WHO, Coronavirus disease (COVID-19). https://www.who.int/emergencies/diseases/novel-coronavirus-2019.
2. Xu, P., & Cheng, J. (2021, June). Individual differences in social distancing and mask-wearing in the pandemic of COVID-19: The role of need for cognition, self-control and risk attitude. *Personality and Individual Differences*, *175*, 110706. https://doi.org/10.1016/j.paid.2021.110706
3. Hornik, R., Kikut, A., Jesch, E., Woko, C., Siegel, L., & Kim, K. (2020, November 22). Association of COVID-19 Misinformation with Face Mask Wearing and Social Distancing in a Nationally Representative US Sample. *Health Communication*, *36*(1), 6–14. https://doi.org/10.1080/10410236.2020.1847437
4. Salimipour, A., Mehraban, T., Ghafour, H. S., Arshad, N. I., &Ebadi, M. (2023). ETRACTED: SIR model for the spread of COVID-19: A case study. Operations Research Perspectives, 10, 100265. https://doi.org/10.1016/j.orp.2022.100265
5. Cooper, I., Mondal, A., & Antonopoulos, C. G. (2020, October). A SIR model assumption for the spread of COVID-19 in different communities. Chaos, Solitons & Fractals, 139, 110057. https://doi.org/ 10.1016/j.chaos.2 020.110057
6. Sinan, M., Ali, A., Shah, K., Assiri, T. A., &Nofal, T. A. (2021, March). Stability analysis and optimal control of Covid-19 pandemic SEIQR fractional mathematical model with harmonic mean type incidence rate and treatment. *Results in Physics*, *22*, 103873. https://doi.org/10.1016/j.rinp.2021.103873
7. Zhang, Y., Jiang, B., Yuan, J., & Tao, Y. (2020, March 6). *The impact of social distancing and epicenter lockdown on the COVID-19 epidemic in mainland China: A data-driven SEIQR model study*. https://doi.org/10. 1101/2020.03.04.20031187
8. Avinash, N., Britto Antony Xavier, G., Alsinai, A., Ahmed, H., RexmaSherine, V., &Chellamani, P. (2022, September 26). Dynamics of COVID-19 Using SEIQR Epidemic Model. *Journal of Mathematics*, *2022*, 1–21. https://doi.org/10.1155/2022/2138165
9. Prabakaran, R., Jemimah, S., Rawat, P., Sharma, D., &Gromiha, M. M. (2021, December 15). A novel hybrid SEIQR model incorporating the effect of quarantine and lockdown regulations for COVID-19. *Scientific Reports*, *11*(1). https://doi.org/10.1038/s41598-021-03436-z

10. Das, K., Ranjith Kumar, G., Madhusudhan Reddy, K., &Lakshminarayan, K. (2021). Sensitivity and elasticity analysis of novel corona virus transmission model: A mathematical approach. *Sensors International*, *2*, 100088. https://doi.org/10.1016/j.sintl.2021.100088
11. Sahu, I., & Jena, S. R. (2023, March 9). SDIQR mathematical modelling for COVID-19 of Odisha associated with influx of migrants based on Laplace Adomian decomposition technique. Modeling Earth Systems and Environment. https://doi.org/10.1007/s40808-023-01756-9
12. Simulation and numerical solution of fractional order Ebola virus model with novel technique. (2020). AIMS Bioengineering, 7(4), 194–207. https://doi.org/10.3934/bioeng.2020017
13. Pue-on, P. (2013). Laplace Adomian decomposition method for solving Newell-Whitehead-Segel equation. Applied Mathematical Sciences, 7, 6593–6600. https://doi.org/10.12988/ams.2013.310603
14. Liberty Ebiwareme, Fun-Akpo Pere Kormane, & Edmond ObiemOdok. (2022, June 30). Simulation of unsteady MHD flow of incompressible fluid between two parallel plates using Laplace-Adomian decomposition method. World Journal of Advanced Research and Reviews, 14(3), 136–145. https://doi.org/10.30574/wjarr.2022.14.3.0456
15. Haq, F., Shah, K., Rahman, G. U., Li, Y., & Shahzad, M. (2018). Computational Analysis of Complex Population Dynamical Model with Arbitrary Order. Complexity, 2018, 1–8. https://doi. org/10.1155/2 018/8918541
16. Xu, J., Khan, H., Shah, R., Alderremy, A., Aly, S., &Baleanu, D. (2021). The analytical analysis of nonlinear fractionalorder dynamical models. AIMS Mathematics, 6(6), 6201–6219. https://doi.org/10.3934/math.2021364
17. Khan, S., Sohail, M., Khan, H., Tchier, F., Omid, M. Y., & Nadeem, M. (2023, July 18). The solution comparison of fractional Heat transfer and porous media equations using analytical techniques. https://doi.org/10.21203/rs .3.rs-3160442/v1

Table 1: List of parameters used in this model.

Parameters	Description
A	Recruitment rate
β	Infection rate
μ	Natural death rate and the disease death rate
α	Rate at which exposed population moves to infected population
θ	Rate at which isolated individuals recovered
q	Turn Rate at which infected population moves to isolated population
γ	Rate at which exposed population moves to isolated population

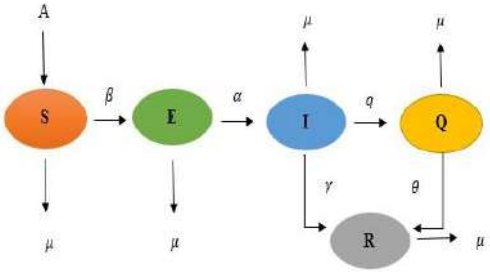

Figure 1: Flow chart of SEIQR model.

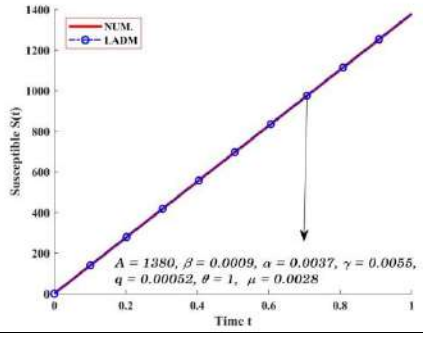

Figure 2: Analytical expression derived through LADM equation (80) is compared with numerical simulation for the concentration Susceptible S(t). The solid line corresponds to the numerical simulation, while * represents equation (80).**

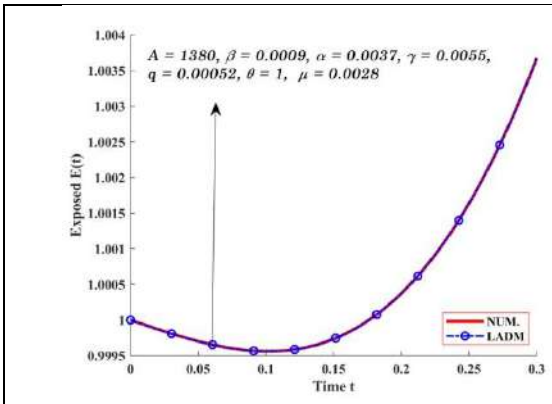

Figure 3: Analytical expression derived through LADM equation (81) is compared with numerical simulation for the concentration Exposed E(t). The solid line corresponds to the numerical simulation, while * represents equation (81).**

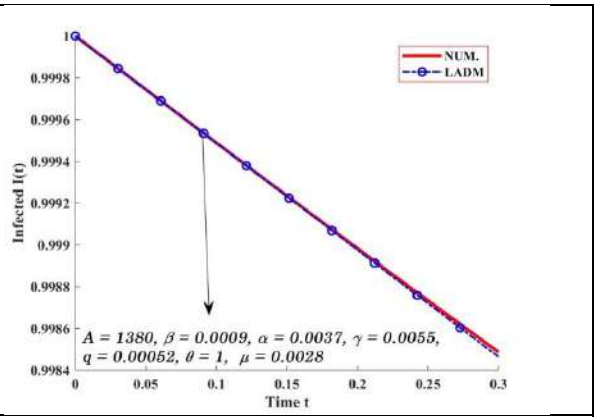

Figure 4: Analytical expression derived through LADM equation (82) is compared with numerical simulation for the concentration Infected I(t). The solid line corresponds to the numerical simulation, while * represents equation (82).**

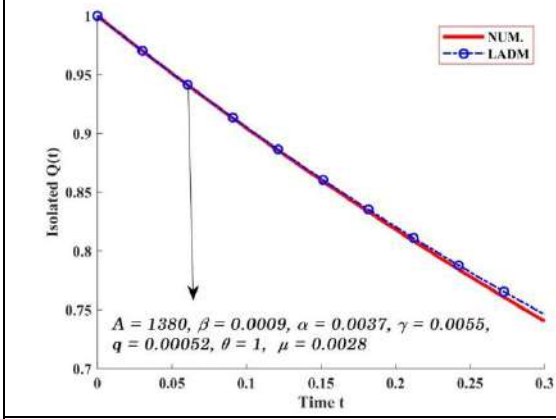

Figure 5: Analytical expression derived through LADM equation (83) is compared with numerical simulation for the concentration Isolated Q(t). The solid line corresponds to the numerical simulation, while * represents equation (83).**

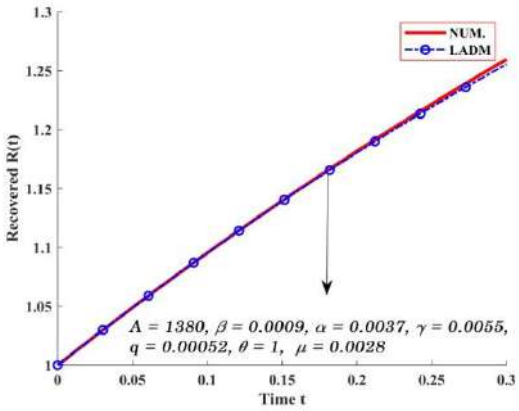

Figure 6: Analytical expression derived through LADM equation (84) is compared with numerical simulation for the concentration Recovered S(t). The solid line corresponds to the numerical simulation, while * represents equation (84).**

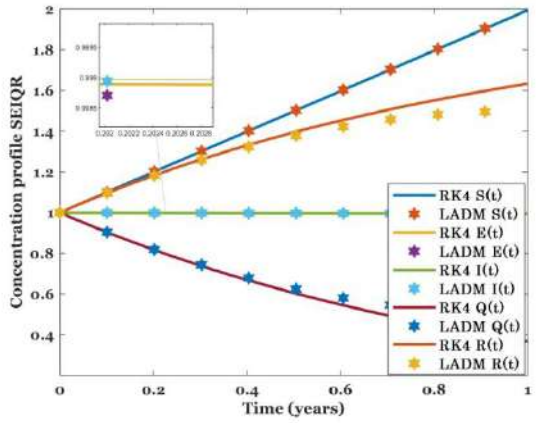

Figure 7: Analytical expressions obtained through LADM equations (80-84) are contrasted with numerical simulations for all SEIQR concentration profiles within the time interval $t = [0, 1]$.

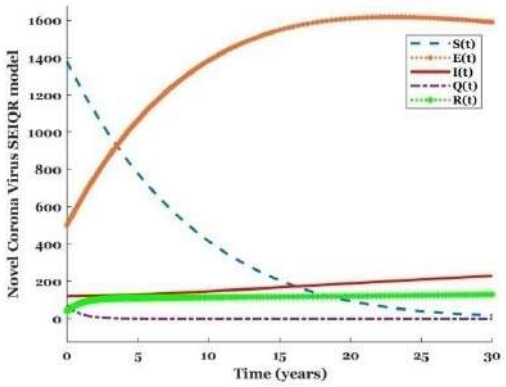

Figure 8: Visual representation of novel corona virus SEIQR model within the time interval $t = [0, 30]$.

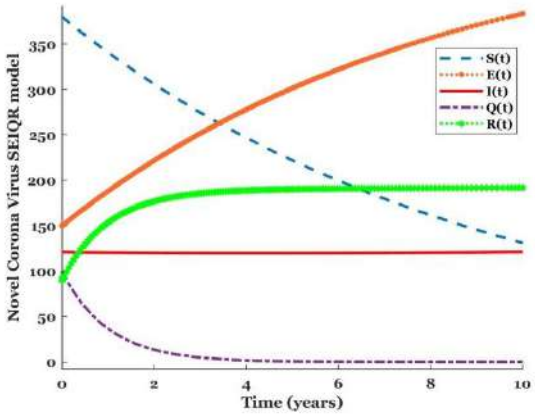

Figure 9: Visual representation of novel corona virus SEIQR model within the time interval $t = [0, 10]$.

Vol.15 / Issue 83 / Apr / 2024 International Bimonthly (Print) – Open Access ISSN: 0976 – 0997

RESEARCH ARTICLE

Evaluation of the Anti-Hyperlipidemic Potential of A Novel Anti-Diabetic Polyherbal Preparation in Streptozotocin-Induced Diabetic Rats and its Formulation in to a Capsule Dosage Form

Uppara Venkatesh[1]* and B. V. Ramana[2]

[1]Research Scholar, Department of Pharmacology, St. Johns College of Pharmaceutical Sciences, (Affiliated to Jawaharlal Nehru Technological University , Anantapur) Andhra Pradesh, India.
[2]Professor, Department of Pharmaceutics, Dr.K.V. Subba Reddy Institute of Pharmacy, (Affiliated to Jawaharlal Nehru Technological University, Anantapur) Andhra Pradesh, India.

Received: 10 Dec 2023 Revised: 09 Jan 2024 Accepted: 05 Mar 2024

***Address for Correspondence**
Uppara Venkatesh
Research Scholar,
Department of Pharmacology,
St. Johns College of Pharmaceutical Sciences,
(Affiliated to Jawaharlal Nehru Technological University , Anantapur)
Andhra Pradesh, India.
Email: ukvenkatesh053@gmail.com

ABSTRACT

Diabetes, also known as diabetes mellitus, is a long-term metabolic disease marked by high blood glucose levels. This condition is brought on by insufficient insulin production or poor insulin uptake by the body's cells. Diabetes can lead to hyperlipidemia, a condition marked by elevated blood triglyceride and cholesterol levels, as a result of the disturbance of lipid metabolism brought on by insulin resistance or insufficiency. In the current study, it was investigated whether a novel anti-diabetic polyherbal formulation made in-house could reduce hyperlipidemia in rats with diabetes induced by streptozotocin (STZ). The formulation contained dried leaves of Tinospora cordifolia, dried bark of Cinnamomum zeylanicum, dried seeds of Trigonella foenum, and dried seeds of Nigella sativa. Streptozotocin was injected intraperitoneally at a dose of 60 mg/Kg to induce diabetes in albino rats. Using STZ-induced diabetic rats, the effects of the Poly herbal preparation (PHP) were assessed for 28 days at doses of 200 and 400 mg/Kg body weight. Diabetic rats were treated with polyherbal preparation that was made in-house, and the effects of the PHP on lipid metabolism were assessed by looking at various biochemical markers. The anti-hyper lipidemic efficacy was assessed using total cholesterol, triglycerides, very low-density lipoproteins, low density lipoproteins, and high-density lipoproteins. Since the ethanolic extract polyherbal formulation significantly reduced blood glucose levels in our earlier trials, it was selected for additional testing of its anti-hyperlipidemic potential. There were six rats in every group of thirteen. The blood glucose level was significantly ($p<0.05$) lowered upon oral administration of PHP extract (EPHP-F),

with the effect becoming more pronounced at 400 mg/kg. There was dose-dependent action in the PHP. In comparison to normal, it significantly decreased the serum levels of triglycerides and cholesterol in diabetic rats. The outcomes verified that the PHP considerably decreased high blood cholesterol and triglycerides and had a dose-dependent blood glucose reducing impact. After that, a capsule formulation containing the optimal ratio of polyherbal preparation was formulated and evaluated for preformulation and quality control features. All polyherbal capsules were determined to have disintegration times that fell within acceptable pharmacopeial bounds. The resultant polyherbal capsule can be used as a stable, patient-friendly, and cost effective solid dose form.

Keywords: Lipid, triglycerides, cholesterol, *Tinospora cordifolia*, *Cinnamomum zeylanicum*, *Trigonella foenum*, *Nigella sativa.*

INTRODUCTION

The impact and affection that diabetes mellitus (DM) has caused throughout the world in recent decades has been worrisome. There were 463 million diabetics worldwide in 2019, and by 2045, that number is expected to rise to 700 million.[1] Diabetes mellitus (DM) is a chronic degenerative illness linked to high blood sugar levels that damages systems, organs, and cells. Overabundance of blood glucose leads to the production of reactive oxygen species, which in turn causes oxidative stress to escalate. This stress can result in the formation of advanced glycation end products (AGEs), dyslipidemia, and various metabolic disorders that are associated with the illness.[2] Diabetes can manifest in various forms, one of which is type 1 diabetes (DM1), a condition brought on by an insulin-dependent lifestyle. Additionally, there is type 2 diabetes (DM2), which is the most common kind and is linked to elevated glucose concentrations as well as insulin sensitivity or resistance.[3-4] Microvascular issues (retinopathy, nephropathy, and neuropathy) and macrovascular issues (ischemic heart disease, peripheral vascular disease, and cerebrovascular disease) are closely related in roughly one-third to one-half of DM patients. Unchecked hyperglycemia can lead to oxidative DNA damage by tissue protein glycation, enhanced lipid peroxidation, superoxide production, and lipoprotein glycation. Glycation and glucose auto-oxidation (OH-) produce reactive species like hydroxyl radicals and hydrogen peroxide (H2O2). It consequently affects human life globally in one or more ways.[5-6] DM is complicated and challenging to manage.

Several medical interventions are used to try to control blood glucose levels. Research is always ongoing to find novel options that can slow the progression of diabetes diseases.[7] Even though a number of conventional oral hypoglycemic drug types have been introduced to the market, the prevalence of diabetes and health care costs are rising alarmingly globally. The global economy is predicted to suffer losses due to diabetes in 2019, 2030, and 2045, of USD 760 billion, USD 825 billion, and USD 845 billion, respectively. [8] These problems therefore call for the creation of novel antidiabetic drugs that are structurally different from those that are currently on the market, safe, easily obtainable, more effective, and have a novel mode of action. These drugs should also be derived from natural sources, mainly plants.[9] Due to their favorable biological actions, ethanobotanical extracts of medicinal plants have been examined for their richness in phytochemical substances. These extracts have historically been utilized as therapeutic systems.[10] Because they can offer a more all-encompassing and synergistic approach to the condition, poly herbals—formulations made up of a variety of different herbs and plant-based ingredients—have become more popular in the management of diabetes. Diabetes is a complex metabolic disease that affects several physiological processes, such as glucose metabolism, insulin control, and oxidative stress. Herbs that target various elements of diabetes are frequently included in polyherbal medicines with the goal of enhancing insulin sensitivity, improving blood sugar regulation, and providing antioxidant protection. Poly herbals, which include these herbs, can provide a comprehensive approach to managing the many aspects of diabetes, possibly yielding greater advantages than the use of individual herbs. [11–12]

Poly herbals have a significant role in managing diabetes since they can help people achieve better glucose control while reducing the negative effects of some drugs. [13] But it's important to remember that there are differences in the safety and effectiveness of polyherbal supplements, therefore use should be supervised by a doctor. To determine the efficacy of certain formulations, the best dosages, and any possible interactions with traditional diabetic therapies, clinical research is required. Healthcare providers should provide assistance when including polyherbals into a diabetic management strategy, as they should be viewed as an adjunct to prescribed drugs and lifestyle adjustments. This method emphasizes the need of individualized, patient-centered care in achieving the best possible outcomes for people with diabetes while acknowledging the complex nature of the disease. [14–15] In previous studies, we prepared n-hexane, petroleum ether, and ethanol extracts from a poly herbal preparation made up of different amounts of dried *Trigonella foenum* (TF) leaves, dried *Nigella sativa* (NS) seeds, dried bark of *Cinnamomum zeylanicum* (CZ), and dried leaves of *Tinospora cordifolia* (TC). Using DPPH (2,2-diphenul-1-picrylhydrazyl) and hydrogen peroxide scavenging assays, we evaluated the *in vitro* antioxidant characteristics of these extracts; the ethanolic extract showed significant antioxidant activity. Additionally, we looked at the anti-diabetic properties of ethanol, petroleum ether, and n-hexane extracts at 200 and 400 mg/KG body weight. Of these, the polyherbal preparation's ethanol extract (EPHP 1), which contained TC, CZ, TF, and NS in a 1:1:1:1 ratio, demonstrated a noteworthy decrease in blood glucose levels that was on par with glibenclamide, a common medication. Building on these discoveries, we subsequently conducted studies to determine the anti-hyperlipidemic potential of EPHP 1 in diabetic rats caused by streptozotocin and to formulate PHP into an appropriate dose form. [16]

MATERIALS AND METHODS

Chemicals

We bought streptozotocin (STZ) from Merck in Mumbai, India. We bought petroleum ether, n-hexane, and AR grade ethanol from SD Fine Chem in Mumbai, India. Glibenclamide (GLB) was graciously provided by Dr. Reddy laboratories in Hyderabad, India. Analytical grade chemicals were all that were employed in this investigation.

Plant material

We bought dried *Nigella sativa* seeds, dried *Trigonella foenum* seeds, and dried *Cinnamomum zeylanicum* bark from the local market in Kurnool, Andhra Pradesh, India. From its natural environment in and around the Nallamala Forest area near Srisailam, Kurnool District, Andhra Pradesh, India, the dried leaves of *Tinospora cordifolia* were collected. The plants were verified by Dr. K. Madhava Chetty, Associate Professor in the Department of Botany at Sri Venkateswara University in Tirupathi, Andhra Pradesh, India. Parts of plants were shade dried.

Preparation of extract

Using n-hexane, petroleum ether, and ethanol as solvents, the dried leaves of TC, dried bark of CZ, dried seeds of TF, and dried seeds of NS were continuously extracted using a soxhlet apparatus. First, each of the 2.5 kg of plant components was air-dried and then independently ground into a coarse powder. Following meticulous weighing, 1 kg of each crude drug powder was added to a soxhlet system and extracted for 48 hours at a temperature between 70 to 80 °C using the previously indicated solvents. Dark brown to black extracts were produced by continuing the extraction process until the solvent was clear. The extracts were cooled and filtered to remove any remaining material. Using a rotary evaporator, the extracts were condensed under low pressure to create a powder, which was subsequently dried. After calculating the extract percentage, the extracts were refrigerated and kept in amber glass containers for later processing. To determine which phytoconstituents were included in the extracts, preliminary phytochemical studies were carried out. In order to conduct the investigation, the dry powder was diluted with the necessary amount of 0.5% carboxymethyl cellulose (CMC).

Animals

Both male and female albino Wistar rats weighing 160–200 grams were purchased from SV Animal House and Enterprises in Bangalore, India. These rats were used for assessments of their anti-diabetic activity as well as acute

toxicity investigations. The animals went through a 10-day stabilization period following procurement. They were kept in cages made of polypropylene with a 12-hour light-dark cycle, 60±5% relative humidity, and room temperature. The rats were fed a regular pellet diet and had unlimited access to water during the trial. The animals were handled carefully to reduce any potential discomfort that may otherwise lead to an increase in adrenal output.

Development of polyherbal preparation

By combining the dried extracts of the plant components in different ratios, the polyherbal preparation (PHP) of the dried leaves of TC, dried bark of CZ, dried seeds of TF, and dried seeds of NS was created. Table 1 displays the PHPs' makeup.

Dosage selection and preparation

Two doses were selected based on the acute toxicity experiments in order to evaluate the antidiabetic activity. There were two doses: 200 mg/kg and 400 mg/kg body weight; the first dose was roughly one-tenth of the maximum dose of 2000 mg/kg, while the second dose was twice that much. To prepare the 200 mg/kg and 400 mg/kg doses of the polyherbal preparation (PHP), the required number of extracts were dissolved in a 0.5% sodium CMC solution.

Animal grouping

There were 13 batches of animals total, with 6 animals in each group (n = 6). Regular control diabetic control, Glibenclamide treated groups and PHP treated groups at 200 mg/Kg(EPHP-A to EPHP-E) and groups treated with polyherbal preparation at doses of 400 mg/kg (EPHP-F to EPHP-J). For 28 days, the therapy was administered nonstop.

Induction of Diabetes

The animals were given a single intraperitoneal injection of freshly prepared streptozotocin (STZ) at a dose of 60 mg/kg to induce diabetes. Prior to injection, the STZ was dissolved in regular saline. After the animals had the STZ injection, they were watched for a whole day. Following this initial phase, the animals received a 10% glucose solution for a full day. The blood glucose level (BGL) was measured on the third day in order to verify the diagnosis of diabetes. This assessment acted as a gauge to see if the animals' diabetes was successfully brought on by the STZ injection.

Determination of antidiabetic activity

Oral gastric gavages were used to provide the test samples to the animals once a day, before they were allowed to eat. At the start of the trial, the animals' blood glucose levels were determined using a glucometer. The 7^{th}, 14^{th}, 21^{st}, and 28^{th} days after the experiment's beginning saw a recurrence of these measurements. This made it possible to assess the test samples' possible effects on blood glucose levels over the course of 28 days.

Estimation of biochemical variables

The animals were sacrificed by cervical dislocation on day 28, and the biochemical variables were assessed. Using an auto-analyzer, the glucose oxidase method was used to analyze total cholesterol (TC), triglycerides (TG), low density lipoproteins (LDL), high density lipoproteins (HDL), and very low-density lipoproteins (VLDL).

Formulation of a poly herbal capsule

The factual extracts and excipients were all run through British Standard Sieves (BSS) #120. Using an electronic balance, a polyherbal preparation that was tailored for both performance and safety was precisely tested. The mixture was run over BSS # 40 once more, mixed twice, and then put into size one capsules to create granules. An evaluation was conducted on the preformulation parameters, including the hausner's ratio, bulk and tapped density, compressibility index, and angle of repose.

An analysis of the capsules

The Electrolab dissolving apparatus was utilized to conduct the disintegration test. Six baskets were filled with one capsule each, and the device was maintained at 37±0.5°C of the immersion liquid. The amount of time it took for the capsule to break down totally was noted. The capsules dissolve when, after going through a 10# mesh screen, no particles are visible above the gauge.

Analytical statistics

The mean ± Standard error mean (SEM) was used to express the study's data. A one-way analysis of variance (ANOVA) was used to analyze antidiabetic behavior, anti-hyperglycemic effects, and other pertinent data. Dunnet's Multiple Comparison Test was then employed to confirm the results. A statistical significance threshold of $P < 0.05$ was applied to ascertain the results. P values less than this cutoff were regarded as statistically significant, signifying a meaningful difference or effect in the results.

RESULTS

PHP's impact on the blood glucose levels of diabetic rats

When compared to the negative control group, the diabetic control rats' blood glucose levels increased gradually and consistently over the course of our experiment, and this difference was statistically significant ($P<0.05$). Nevertheless, after the rats received GLB (5 mg/kg) and PHPs, there was a significant drop in blood glucose levels beginning on the seventh day after the rats were exposed to these medications ($P<0.05$). This effect persisted for the duration of the study, lasting until day 28, when the PHPs' drop in blood glucose levels was even more significant ($P<0.05$), outperforming the effectiveness of GLB, the standard drug. Table 2 lists the anti-diabetic effects of ethanol extracts, particularly EPHP, given at doses of 200 and 400 mg/kg of body weight. These findings highlight PHPs' enormous potential for controlling blood glucose levels in diabetic settings. PHPs have shown promise as a valuable therapeutic option for diabetes, as seen by the prolonged reduction in blood glucose levels and their superior effectiveness on day 28 when compared to the conventional medicine. The entire scope of their use in the treatment of diabetic patients may become clear through additional investigation and clinical trials.

Impact of EPHP on diabetic rats' lipid profiles

When compared to normal rats, there was a significant ($P<0.001$) increase in serum levels of TC, TG, VLDL, and LDL and a significant ($p<0.001$) drop in HDL cholesterol following the creation of diabetes and subsequent treatment with the two doses (200 and 400 mg/KG) of PHPs. When compared to the diabetic control, the animal groups treated with PHP at a dose of 200 mg/KG body weight (EPHP -A to EPHP -E) did not exhibit a significant decrease in the levels of TC, TG, LDL, or VLDL, nor did they exhibit a significant increase in the levels of HDL in the serum. Thus, the blood levels of TC, TG, LDL, and VLDL were significantly lower in the animal groups that received a therapy of PHP at 400 mg/KG body weight (EPHP -F to EPHP -J). There was a noticeable increase in the serum HDL level as compared to the diabetes control group. When EPHP (200 and 400 mg/KG) was given to diabetic rats for 28 days, the serum levels of TC, TG, LDL, and VLDL were significantly ($p<0.001$) reduced, but the levels of HDL were increased in comparison to the diabetic control group. Table 3 displays the findings of the impact of EPHP on the lipid profiles of diabetic rats.

Analysis of polyherbal capsules

Preformulation testing was performed on the optimized PHP i.e., EPHP-F powder mixture. The mix was evaluated for bulk density, tapped density, angle of repose, compressibility index, and Hausner's ratio in order to analyze flow behavior. When the mixture was enclosed in a capsule, its flow properties were satisfactory. This is confirmed by the data in table 4. It was discovered that the capsules disintegrated on average in 13.6±1.07 minutes. The polyherbal capsules are depicted in Figure 1.

DISCUSSION

Medicinal plant parts are widely used by humans to treat a wide range of illnesses, including diabetes, even though there isn't enough scientific data to support their safety and effectiveness. Therefore, it is essential to thoroughly evaluate the safety and effectiveness profile of medicinal plants used in conventional medicine. [17] Due to the limitations of traditional anti-diabetic medications, there is an urgent need for new, more effective, affordable, and nontoxic medications. There is a great deal of demand for natural product-based alternative medicines since they are regarded as safe, readily available, and do not require the lengthy manufacturing of pharmaceuticals. [18] It has long been known that polyherbal formulations have great promise for the treatment of a broad range of illnesses and ailments. The inclusion of a wide variety of phytoconstituents that work in concert is thought to be responsible for these formulations' medicinal efficacy. Interestingly, these formulations show good performance even at lower dosages and continue to be safe at higher concentrations.[19] Our study focused on evaluating the hepatoprotective and nephroprotective qualities of an in-house made ethanolic extract of a novel polyherbal mixture made up of four different plant extracts because of the therapeutic potential of polyherbal formulations. [20] Dried leaves of *Tinospora cordifolia*, dried bark of *Cinnamomum zeylanicum*, dried seeds of *Nigella sativa*, and dried seeds of *Trigonella foenum* were among these extracts. Rats with diabetes caused by streptozotocin (STZ) were used in this study. [16]

We carried out an investigation into the acute oral toxicity of our earlier trials. Administration of the curd test extract at a single limit test dose of 2000 mg/KG did not result in mortality or delayed toxicity throughout the 14-day follow-up period. The results showed that there is a significant margin of safety and that the test extracts LD50 value is anticipated to be greater than 2000 mg/KG. Overall, the findings demonstrated the palatability and nontoxic nature of EPHP, suggesting that the plant is suitable for usage in conventional settings. [16] It is believed that several phytochemical components that have been isolated from different plants have strong hypoglycemic, anti-hyperglycemic, and glucose-lowering properties. Alkaloids, triterpenoids, phenolics, and flavonoids are a few of the bioactive components. The action may be accompanied by increased pancreatic β-cell release of insulin, decreased small intestine absorption of glucose, increased body consumption of glucose, and/or the initiation of hepatic glycogenesis. Furthermore, it has been amply demonstrated that these potent phytochemical substances may repair damaged beta cells in diabetic rats while protecting them from oxidative stress. [21] The most widely used and accepted model of experimental diabetes in rats is streptozotocin-induced diabetes. This diabetogenic drug is generally preferred over alloxan due to its wider species effectiveness and reproducibility. According to published research, rats can experience chronic hyperglycemia from the inducer after a single dose of 60 mg/kg for at least a month. [22] Similar to diabetic management, at this dosage the chemical results in chronic hyperglycemia with no appreciable change in blood glucose levels for two weeks.

To assess the impact of the extracts on BGLs, normoglycemic and STZ-induced diabetic rat models were established. The vehicle-treated groups did not show a statistically significant decrease in fasting blood glucose levels in the model of normoglycemic rats. Over the course of 28 days, blood glucose levels in diabetic rats significantly increased. When compared to the standard medication glibenclamide, the diabetic rats treated with 200 mg/KG body weight (EPHP-A to EPHP-E) demonstrated a reduction in BGL, but the efficacy was noticeably lower. On the other hand, the BGL was significantly lower in the diabetic rats who received EPHP at a dose of 400 mg/KG body weight (EPHP-F to EPHP-J). Especially EPHP-F, which combines TC, CZ, TF, and NS at a ratio of 1: 1: 1: 1, when administered at a 400 mg/KG body weight, exhibits a significant decrease in BGL in comparison to the standard drug group. The maximum drop in blood glucose in STZ-induced diabetic rats was seen on day 28 at 400 mg/KG of extract, which was equivalent to a normal dose. It was noted that a dose-dependent relationship existed between the test extract activity. This may indicate that the PHP's bioactive ingredients, which are essential for its anti-diabetic effects, are more concentrated at greater dosages. Accordingly, the present study hypothesized that in a time- and dose-dependent way, the ethanol extract of PHP, in particular EPHP-F, has exceptional anti-diabetic action on diabetic rats caused by STZ. The results imply that the test extract might have a strong hypoglycemic impact. This conclusion is supported by logical arguments. It has been suggested that by lowering oxidative stress, using antioxidants can help

reduce diabetic complications. The main factors contributing to the development and course of diabetes are inflammation and oxidative stress. Because STZ selectively destroys pancreatic beta cells, it results in diabetes mellitus. Research indicates that when administered to animals, it causes βcells to die after three days. Results showed that PHP containing dried *Nigella sativa* seeds, dried Bark of *Cinnamomum zeylanicum*, dried Leaves of *Tinospora cordifolia*, and dried Seeds of *Trigonella foenum* exhibited strong antioxidant activity. This suggested that the β-cells' ability to guard against oxidative free radicals may be the cause of the anti-hyperglycemic activity in diabetic rats induced by STZ. The release of insulin from pancreatic beta cells may have been the PHP extract's mode of action. The anti-diabetic benefits of the ethanolic extract of PHP may be explained by the presence of many bioactive components that have been linked to hypoglycemic activity. In individuals with diabetes, hypertriglyceridemia and hypercholesterolemia are the most prevalent lipid abnormalities. [23] High serum TC, TG, LDL, VLDL, and low HDL values are its defining characteristics. Low insulin causes hormone-sensitive lipase to be activated, which increases the liver's production of VLDL and lipolysis. [24] Additionally, lipoprotein lipase activity is decreased in insulin insufficiency, which may result in a decrease in the clearance of VLDL and chylomicrons. [25] Over the course of 28 days, the administration of EPHP dramatically decreased levels of TC, TG, LDL, and VLDL while dose-dependently raising HDL levels. This result was consistent with prior findings that demonstrated the ethanol extract's strong anti-dyslipidemia and anti-hyperglycemic effects. The observed antihyperlipidemic impact may be explained by decreased chelosterogenesis and fatty acid synthesis caused by inhibition of pancreatic lipase and pancreatic cholesterol esterase, respectively. These results highlight EPHP-F's promising potential in the context of its anti-diabetic and anti-hyperlipidemic effects. They also demonstrate the drug's ability to prevent the progression of hyperlipidemia and mitigate lipid-related damage, which could have a major positive impact on the management of lipid-related complications. To further investigate its clinical applicability in this particular situation, more clinical research is necessary.

CONCLUSION

The EPHP-F had a positive impact on blood glucose levels in this investigation. Additionally, it raised HDL levels and corrected serum triglycerides and cholesterol. The study's findings demonstrated that EPHP-F has potent anti-diabetic and anti-hyperlipidemic properties, matching or surpassing those of glibenclamide, a common medication. The study's findings might be applied to the creation of novel anti-diabetic medications for the control and therapy of type 2 diabetes. To determine the molecular mechanism underlying its anti-diabetic and anti-hyperlipidemic effects, more investigation is needed to pinpoint the molecular targets and isolate the bioactive phytoconstituents.

Ethical endorsement

The study technique SJCP/PCOL/AD2022-10/011 was approved by the institutional animal ethics committee. Under the registration number 1519/PO/Re/S/11/CPCSEA, the committee for the regulation and supervision of animal experimentation made recommendations, and the ethics committee followed those suggestions in conducting the studies.

ACKNOWLEDGEMENTS

In addition to the principal and management of St. Johns College of Pharmaceutical Sciences, Yemmiganur, Kurnool Dist., Andhra Pradesh, India, for providing all of the facilities required for the successful completion of this research, the authors would like to thank Dr. Reddy's laboratories in Hyderabad, India, for providing a gift sample of Glibenclamide.

REFERENCES

1. Saeedi P, Petersohn I, Salpea P, Malanda B, Karuranga S, Unwin N, *et al*. Global and regional diabetes prevalence estimates for 2019 and projections for 2030 and 2045: Results from the International Diabetes Federation Diabetes Atlas. Diabetes research and clinical practice 2019;157:107843.
2. Chaudhuri J, Bains Y, Guha S, Kahn A, Hall D, Bose N, *et al*. The role of advanced glycation end products in aging and metabolic diseases: bridging association and causality. Cell metabolism 2018;28(3):337-52.
3. Muller LM, Gorter KJ, Hak E, Goudzwaard WL, Schellevis FG, Hoepelman AI, *et al*. Increased risk of common infections in patients with type 1 and type 2 diabetes mellitus. Clinical infectious diseases 2005;41(3):281-8.
4. Sartore G, Chilelli NC, Burlina S, Lapolla A. Association between glucose variability as assessed by continuous glucose monitoring (CGM) and diabetic retinopathy in type 1 and type 2 diabetes. Acta diabetologica 2013;50:437-42.
5. Cheung N, Wong TY. Diabetic retinopathy and systemic vascular complications. Progress in retinal and eye research 2008;27(2):161-76.
6. A Adeshara K, G Diwan A, S Tupe R. Diabetes and complications: cellular signaling pathways, current understanding and targeted therapies. Current drug targets 2016;17(11):1309-28.
7. Contreras I, Vehi J. Artificial intelligence for diabetes management and decision support: literature review. Journal of medical Internet research 2018;20(5):e10775-76.
8. Williams R, Karuranga S, Malanda B, Saeedi P, Basit A, Besançon S, *et al*. Global and regional estimates and projections of diabetes-related health expenditure: Results from the International Diabetes Federation Diabetes Atlas. Diabetes research and clinical practice 2020;162:108072-74.
9. Jugran AK, Rawat S, Devkota HP, Bhatt ID, Rawal RS. Diabetes and plant-derived natural products: From ethnopharmacological approaches to their potential for modern drug discovery and development. Phytotherapy Research 2021;35(1):223-45.
10. Wangchuk P, Keller PA, Pyne SG, Taweechotipatr M, Tonsomboon A, Rattanajak R, *et al*. Evaluation of an ethnopharmacologically selected Bhutanese medicinal plants for their major classes of phytochemicals and biological activities. Journal of Ethnopharmacology 2011;137(1):730-42.
11. Ahuja A, Gupta J, Gupta R. Miracles of herbal phytomedicines in treatment of skin disorders: natural healthcare perspective. Infectious Disorders-Drug Targets (Formerly Current Drug Targets-Infectious Disorders) 2021;21(3):328-38.
12. Jayaraju KJ, Ishaq BM. Evaluation of antidiabetic activity of a novel polyherbal preparation against streptozotocin induced diabetes rat model. Journal of Pharmaceutical Research International 2021;33(26A):42-54.
13. Patle D, Vyas M, Khatik GL. A review on natural products and herbs used in the management of diabetes. Current diabetes reviews 2021;17(2):186-97.
14. Horner GN, Agboola S, Jethwani K, Tan-McGrory A, Lopez L. Designing patient-centered text messaging interventions for increasing physical activity among participants with type 2 diabetes: qualitative results from the text to move intervention. JMIR mHealth and uHealth 2017;5(4):e6666.
15. Mohamad T, Jyotsna FN, Farooq U, Fatima A, Kar I, Khuwaja S, *et al*. Individualizing medicinal therapy post heart stent implantation: tailoring for patient factors. Cureus2023;15(8):145-47.
16. Uppara Venkatesh, Dr. B. V. Ramana, Evaluation of the Antidiabetic and antioxidant potential of a Polyherbal Extract in streptozotocin-Induced Diabetes Rats Eur. Chem. Bull. 2023; 12(10):10180-10199.
17. Sen T, Samanta SK. Medicinal plants, human health and biodiversity: a broad review. Biotechnological applications of biodiversity 2015; 59-110.
18. Atanasov AG, Waltenberger B, Pferschy-Wenzig EM, Linder T, Wawrosch C, Uhrin P, *et al*. Discovery and resupply of pharmacologically active plant-derived natural products: A review. Biotechnology advances 2015;33(8):1582-614.
19. Preethy HA, Rajendran K, Mishra A, Karthikeyan A, Chellappan DR, Ramakrishnan V, *et al*. Towards understanding the mechanism of action of a polyherbal formulation using a multi-pronged strategy. Computers in Biology and Medicine 2022;141:104999.

20. Deivasigamani M, Kannan N, Sekar N, Lakshmanan H. Safety assessment of ethanolic root extract of Zaleya decandra (EEZD) in Wistar rats. Regulatory Toxicology and Pharmacology 2021;119:104822.
21. Röder PV, Wu B, Liu Y, Han W. Pancreatic regulation of glucose homeostasis. Experimental & molecular medicine 2016;48(3):e219-220.
22. Furman BL. Streptozotocin-induced diabetic models in mice and rats. Current protocols in pharmacology 2015;70(1):5-47.
23. Goldberg RB. Lipid disorders in diabetes. Diabetes care 1981;4(5):561-72.
24. Subramanian S, Chait A. Hypertriglyceridemia secondary to obesity and diabetes. Biochimica et Biophysica Acta (BBA)-Molecular and Cell Biology of Lipids 2012;1821(5):819-25.
25. Pejic RN, Lee DT. Hyper triglyceridemia. The Journal of the American Board of Family Medicine 2006;19(3):310-6.

Table 1 Composition of polyherbal preparations

Extracts	PHP Code	PHP formulation	Ratio
Ethanol extract	EPHP 1	TC: CZ: TF: NS	1: 1: 1: 1
	EPHP 2	TC: CZ: TF: NS	2: 2: 2: 1
	EPHP 3	TC: CZ: TF: NS	2: 2: 1: 2
	EPHP 4	TC: CZ: TF: NS	2: 1: 2: 2
	EPHP 5	TC: CZ: TF: NS	1: 2: 2: 2

Table 2 Anti diabetic activity of Ethanol extracts of PHP on STZ induced diabetes in rats

Group	Treatment	Blood glucose levels (mg/dL) on				
		0 day	7th day	14th day	21st day	28th day
Normal control	Vehicle (0.5 % Na CMC)	76.68 ± 2.03	78.36 ± 2.24	82.45 ± 2.02	80.11 ± 1.86	84.77 ± 2.33
Diabetic control	STZ 60 mg/Kg i.p	78.29 ± 3.23 a	285.16 ± 3.82 a	292.11 ± 4.12 a	304.98 ± 4.85 a	313.73 ± 4.36 a
Standard	STZ 60 mg/Kg i.p+ GLB 5 mg/Kg	73.28 ± 3.65 b	267.79 ± 3.94 b	202.15 ± 3.54 b	166.62 ± 4.17 c	121.36 ± 4.21 c
EPHP -A	STZ 60 mg/Kg i.p+ EPHP 1 200 mg/Kg	70.71 ± 5.32 c	277.84 ± 4.59 b	213.99 ± 6.13 c	179.67 ± 3.80 c	167.28 ± 4.01 c
EPHP -B	STZ 60 mg/Kg i.p+ EPHP 2 200 mg/Kg	74.38 ± 7.91 b	282.29 ± 5.22 b	195.74 ± 3.82 c	179.61 ± 4.76 b	166.12 ± 4.28 b
EPHP -C	STZ 60 mg/Kg i.p+ EPHP 3 200 mg/Kg	79.65 ± 7.72 c	275.41 ± 5.86 c	215.03 ± 5.04 b	176.21 ± 5.14 b	163.95 ± 5.62 c
EPHP -D	STZ 60 mg/Kg i.p+ EPHP 4 200 mg/Kg	68.76 ± 3.19 b	286.55 ± 3.45 c	212.89 ± 3.58 b	174.42 ± 4.02 b	162.14 ± 3.97 c
EPHP -E	STZ 60 mg/Kg i.p+ EPHP 5 200 mg/Kg	78.78 ± 4.31 c	283.62 ± 3.66 c	223.40 ± 2.87 b	200.94 ± 4.18 b	165.15 ± 3.99 b
EPHP -F	STZ 60 mg/Kg i.p+ EPHP 1 400 mg/Kg	66.94 ± 6.11 c	268.78 ± 4.95 c	205.63 ± 4.62 c	157.12 ± 4.25 b	126.42 ± 4.05 b
EPHP -G	STZ 60 mg/Kg i.p+ EPHP 2 400 mg/Kg	67.79 ± 5.17 c	283.12 ± 4.32 b	201.65 ± 4.66 c	164.89 ± 3.87 c	133.57 ± 4.08 b
EPHP -H	STZ 60 mg/Kg i.p+ EPHP 3 400 mg/Kg	65.16 ± 7.49 b	280.02 ± 6.54 b	215.28 ± 5.89 c	170.11 ± 5.82 c	136.49 ± 5.16 c
EPHP -I	STZ 60 mg/Kg i.p+ EPHP 4 400 mg/Kg	61.78 ± 6.15 c	281.02 ± 4.93 b	201.46 ± 4.32 c	188.93 ± 4.14 c	143.21 ± 3.56 c
EPHP -J	STZ 60 mg/Kg i.p+ EPHP 5 400 mg/Kg	66.17 ± 6.28 b	282.41 ± 4.78 c	206.94 ± 5.02 b	185.03 ± 5.41 b	136.82 ± 4.68 b

Values are expressed as mean ± SEM., Data analyzed by one way ANOVA followed by Dunnet's Multiple Comparison Test. a-p<0.05 as compared with control group, b-p<0.01 and c-p<0.05 as compared with STZ group.

Table 3 Effect of EPHP on lipid profile

Group	Treatment	Lipid profile (mg/dL) on				
		TC	Triglycerides	VLDL	LDL	HDL
Normal control	Vehicle (0.5 % Na CMC)	81.55±2.67	54.73±1.45	16.34±1.45	46.47±0.79	39.78±1.92
Diabetic control	STZ 60 mg/Kg i.p	211.74±1.69	138.89±2.80	65.78±2.78	111.45±1.35	7.55±1.78
Standard	STZ 60 mg/Kg i.p+ GLB 5 mg/Kg	101.64±2.18[c]	77.54±1.56[c]	23.79±2.78[c]	52.23±1.78[c]	30.74±1.34[c]
EPHP -A	STZ 60 mg/Kg i.p+ EPHP 1 200 mg/Kg	135.75±2.67[c]	92.78±2.78[c]	42.39±3.73[c]	74.94±1.89[c]	19.45±2.84[c]
EPHP -B	STZ 60 mg/Kg i.p+ EPHP 2 200 mg/Kg	130.64±1.34[c]	86.89±2.89[c]	46.55±2.10[c]	71.56±1.78[c]	15.48±1.69[c]
EPHP -C	STZ 60 mg/Kg i.p+ EPHP 3 200 mg/Kg	131.54±2.34[c]	91.42±2.75[c]	41.89±2.38[c]	70.34±1.89[c]	11.47±.02[c]
EPHP -D	STZ 60 mg/Kg i.p+ EPHP 4 200 mg/Kg	126.64±2.34[c]	94.56±2.87[c]	43.64±1.54[c]	71.54±2.67[c]	14.56±2.89[c]
EPHP -E	STZ 60 mg/Kg i.p+ EPHP 5 200 mg/Kg	130.54±1.73[c]	89.22±1.31[c]	46.85±1.56[c]	74.50±1.90[c]	14.70±2.09[c]
EPHP -F	STZ 60 mg/Kg i.p+ EPHP 1 400 mg/Kg	105.64±1.78[c]	80.77±4.11[c]	29.58±7.87[c]	56.33±5.87[c]	32.46±8.45[c]
EPHP -G	STZ 60 mg/Kg i.p+ EPHP 2 400 mg/Kg	116.69±1.78[c]	89.68±2.92[c]	31.64±2.84[c]	57.74±1.23[c]	29.67±2.84[c]
EPHP -H	STZ 60 mg/Kg i.p+ EPHP 3 400 mg/Kg	120.64±1.99[c]	94.67±2.90[c]	37.54±0.34[c]	59.79±0.89[c]	30.87±1.43[c]
EPHP -I	STZ 60 mg/Kg i.p+ EPHP 4 400 mg/Kg	119.53±1.67[c]	86.57±2.78[c]	37.45±2.14[c]	62.34±1.33[c]	28.34±1.23[c]
EPHP -J	STZ 60 mg/Kg i.p+ EPHP 5 400 mg/Kg	120.57±1.58[c]	83.49±2.52[c]	32.80±2.48[c]	58.84±2.34[c]	29.33±2.40[c]

Values are expressed as mean ± SEM., Data analyzed by one way ANOVA followed by Dunnet's Multiple Comparison Test. a-p<0.05 as compared with control group, b-p<0.01 and c-p<0.05 as compared with STZ group.

Table 4 Preformulation evaluation of EPHP-F blend

Trail	Flow Properties				
	Angle of repose	Bulk density	Tapped density	Compressibility index	Hausner's ratio
1	25.78	0.73	0.71	5.86	1.01
2	27.14	0.65	0.63	6.54	1.04
3	26.02	0.70	0.74	5.24	1.01
4	25.68	0.64	0.66	6.82	1.03
5	27.46	0.71	0.72	5.61	1.06
6	26.91	0.69	0.68	7.73	1.04
Mean	26.498±0.697	0.687±0.031	0.690±0.037	6.300±0.833	1.032±0.0177

Figure 1 Photograph of capsules

REVIEW ARTICLE

An Innovative Review about Audio and Video Collaboration for Event Detection using Deep Learning Approaches

M.Rajamanogaran[1]* and G. Karthikeyan[2]

[1]Ph.D Research Scholar, PG and Research Department of Computer Science, Periyar Government Arts College, Cuddalore, (Affiliated to Thiruvalluvar University, Vellore) Tamil Nadu, India.
[2]Assistant Professor, PG and Research Department of Computer Science, Periyar Government Arts College, Cuddalore, (Affiliated to Thiruvalluvar University, Vellore) Tamil Nadu, India.

Received: 29 Dec 2023 Revised: 19 Jan 2024 Accepted: 25 Mar 2024

***Address for Correspondence**
M.Rajamanogaran
Ph.D Research Scholar, PG and Research
Department of Computer Science,
Periyar Government Arts College, Cuddalore, (Affiliated to Thiruvalluvar University, Vellore)
Tamil Nadu, India.
Email: manogaran248@gmail

ABSTRACT

Another milestone in the outbreak of artificial intelligence is the event detection done automatically by the machine in the visualization of human eye.In current years event detection is catching popularity and gaining awareness due to rapid growth of online videos in various fields like sports, entertainment, education, flash news etc. Event detection similar to object recognition is the method used to identify the location of the entities thereby trying to describe the scenery in the video. This process is enabled by two measures like audio and video to strengthen the depiction. The correct mixing of audio along with the video scenes elaborates the details of the displays. The precise method used is the deep learning approach where the event detector learns the occurred actions in the particular scene by studying the features and classifying according to the predicted classes. This paper is the general survey about the methods used for acquiring the data sets and the medium for processing by using different feature extraction and classification algorithms.

Keywords: event detection, audio, video, deep learning, features, classifying, survey, feature extraction, classification.

INTRODUCTION

The latest development in image processing and computer insight leads to the improved version of object detection as event recognition to deal with identification of variety of objects that belong to certain section. In digital images and videos the actions performed are narrated along with the picture automatically. This is possible due to the rapid enhancement in the digital world along with the network facility that brought the attentiveness among social media. [1]. Artificial intelligence plays its role in copying the human activities to be performed by machines by training with sample data and testing for accuracy. One of these applications is the event detection method to predict the result by analysing the actions in the particular video [8] scene along with the captured audio for detecting the extract. The induced use of social media in various fields encourages the development of event detection as a demanding research zone to exploit the challenges for further use. It is defined as the process of verifying the streams of actions to identify the equivalent designs to produce the output as the required event. The types are specified by the backgrounds and patterns [9-13] of the event. The particular features of the objects like shape, texture is used for recognitions of the events and the user should be careful with problems like over fitting, occlusion, reacquisition and blurring of images while performing event detection. Event detection contains video identification where the videos are converted into frames of images and the frames are classified into different groups based on the actions performed in the video. In videos the objects are identified on the basis of video tracking tasks and object identification [2] by joining the advantages of both the methods into a mutual combined route.

The video contains the actions with properties like region, period, abode which takes place either normally or artificially. Identifying such events automatically is the challenging task for researchers. Displayed and online videos are embedded with audio produced in the sight which is also used for tracking the scene in the video. Sound is used for defining the activities that are produced in the videos by appreciating the circumstances of the event. Sound also identifies the actions that matches with predefined events by using the theme of the actions performed. Due to the presence of memory chips for sound and digital processing unit for audio [3], tracing of sound is simplified but the background overlapping of noise may reduce the quality of audio that should be avoided in the event detection. This can be achieved by acquiring the signals continuously and changing into symbols for explanation of the actions performed. Various applications include multimedia events, health care, surveillance and in other research areas. Event detection faced many issues when implemented with machine learning models and algorithms for huge data set with increased computational power. So deep learning models gained reputation due to their advanced techniques. Accordingly [4] novel neural network models are developed for accurate results to foretell the events in the video scene. Deep [14] convolutional network and recurrent neural network with unsupervised features are proposed to classify multi labelled data in event detection.Deep learning performs well with large data sets [15-18] and training of data needs abundant sample for accurate results.

APPLICATIONS IN REAL WORLD

This section provides some applications using video and audio [19] tracking for event detections in real life incidents. There are separate applications for both audio and video. Some are described in brief. Video applications in event tracking There are some presentations that make use of videos [25-30] for event tracking recently. Some of them are described in short-term.

Video Surveillance

Nowadays cameras are allowed to be used in offices and factories to monitor the workers and visitors to avoid accidents and any malpractice that may happen. Video tracking is used in [42] such systems to detect any objects that are present in the scenes. Many shops and crowded areas like hospitals, malls, theatres etc. use CCTV cameras for surveying purpose [68].

Facial identification

Recognition of individual face is one of the types of biometrics[36][37] used as password in locking of smartphones and houses for safety purposes. Video tacking for object detection is also used for entertainment commitments using filters in many applications like Instagram, YouTube etc.

Self-Driving cars

Development in technology has introduced self- driving cars making use of video tracking [64-67] for event detections. The systems using video [31-36] tracking can detect active and passive items along the path to locate moving passengers and objects so that they can maintain the correct lane. Some examples are traffic lights, foot-travelers using automatic event detection with the help of videos so that accidents could be avoided.

Audio applications in event detection

Recently many researches are taking place in the field of audio [20-24] applications in event tracing. The solicitations that are familiar are discussed below.

Surveillance

In monitoring incidents [63] sound effects also help in detecting features along with vision. In activities like accident, assassination, shooting etc. sound performs well for surveillance of the events more accurately. Many multimedia applications use audio structures for classification of ordinary and unusual events using several audio features. [5]. Audio deals with noisy situations to predict different sounds to match with the incidents happened in that environment.

Meeting

During crowded places like meeting, [38] social get together, parties, functions audio plays important role. Appreciation, encouragement can be shown in sound media like clapping, whistle sounds for positive and any rude incidents can be clearly shown in audio effects like unusual high decibel noise. Instead of body language audio can also describe the scenery [39] that takes place in the particular video that focuses on the meeting. Audio is also used for comparing the performance of various models in event detection. While dividing the video scenes into different segments audio information is used for accuracy.

Sports Events

Sports play a vital role in everyday activities. Observing highlights from the sports events needs audio effects also along with video for event identification. While recording the game audio tracing is also needed for effective visualization. So, research has invented many models for tracking the sequences of audio in the sports. Games like tennis, football require sound and models like Markov, Gaussian Mixture Model are used for segmentation of audio into various sequences for better understand ability.

Entertainment

Entertainment media like movies, short films, videos[40], online games make use of audio tracking to represent action scenes like robbery, explosion, flood and violent scenes like murder, gangster activities. Familiar networks like Bayesian model are used for obtaining information about audio segments to detect peculiar sound in the video scenes. Individual audio words are described by the segments for various characteristics.

Consumer Video

Various methods are proposed for classification using audio properties in consumer video. Each video is generated as frames and they are classified into multi actions based on the sound. The video features are extracted and mixed with audio types to detect particular event in the clippings using frequency analysis along with wavelet coefficients. There are various applications that make use of audio and video [41] for event tracking in different media. Some of them are focussed in this paper. Research work is carried in this field for further proceedings.

DATA SET DESCRIPTION

There are numerous collections of data set for both video and audio as free source available for access. The collection contains both the copies of sound and picture along with the contributors and contains the description of the saved files like scope and format. Some data sets are discussed for both audio and video files.

Audio Data set

One of the popular data sets is Free Spoken Digit containing 3000 recordings of size 10Mb discussing about spoken English digits. Another standard one is, The spoken Wikipedia Corpora with 5397 collections of 23Gb size. It enumerates aligned spoken articles. Speech Commands Data set contains a maximum of 65000 tracks explaining short words. Another data set is TIMIT containing 6300 playlists of American English for phonetics. The most standard data set is VoxCeleb containing nearly 1,000,000 collections with 133Mb size describing human speech taken from different videos.

Video Data set

There are valuable data sets for video clippings. Some of them are TV Human Interaction Data set with 300 recordings and file size is 156MB of type MP4. The contents are various shows of social actions broadcasted in TV shows. Another data set is THUMOS with 25,000,000 collections with 385 KB size and the file type is MP4. The clippings consist of multi branded action classification. The exclusive data set is YouTube Face containing 3425 recordings designed for biometrics like face identification. The famous data set is 50 salads with 31 GB file size and the file type is RGB and the video collections are annotated data set of 25 participants engaged in food and beverage preparation. Above-described data sets are samples of the available data set for open access involved in event detection.

REPRESENTATIVES OF AUDIO AND VIDEO

The multimedia attributes like audio and video are used for automatic event detection in real life incidents. The properties that help in analysing and predicting the correct results are the representations like the features of audio and classification models used for predicting the actions with audio matching the video[69] for event identification. Some of the features are discussed in this section.

Audio features in Event detection

The sound received along with the video clippings or online videos are also engaged in detecting the events. The video actions are identified using sound [43-50] features also, in video films or any scene in the video. The features used for audio detection are numerous and compared as shown in Table 1.

Implementation of audio features

The features used for audio [51] detections are prescribed in the above table and the two important features are temporal which uses the signal waveform of audio for inquiry purpose. The other one is spectral method using the audio spectral demonstration process. The last feature is Prosodic which is used for audio signal awareness. For this type of feature any classifier can be used. [6]. Some of the features are discussed in brief
They are as follows.

Zero Crossings

The zero crossing rates (ZCR) denote the frequency of the signal passing the zero signals per unit time. The frequency of the value of the signal changing from maximum to minimum divided by the length of the audio frame is the zero crossing. The equation is

$$ZC = \sum_{n=1}^{N} \frac{|sgnx(n) - sgn[x(n-1)]|}{2N}$$

Where sgn x(n) is the sign function.

Mel- Frequency Cepstral Coefficients

This method uses a new scale called Mel which is calculated by a scale pitch similar in distance with each one. The signal bands wavelength is distributed based on the Mel scale which proves more accuracy. The cosine transform is calculated [52-60] to extract the coefficient from a single frame and the obtained sign is the Mel scale final signal. The equation is

$C_n = \sum_{m=1}^{M} [\log x(m)] \cos[\ \pi n/m(m - \frac{1}{2})]$

Where final output is x(m) and m= 1…M and n is the index of the coefficient.

Pitch

One of the prosodic features is the pitch providing useful aspects of audio like frequency, duration, loudness etc. Pitch is defined as the organisation of sinusoidal waves with basic intensity and amplitude. Audio is the combination of music, speech and various tones of sound containing pitch as the property. One type of pitch is absolute pitch which is the notes of the audio calculated by the number of pulsations per unit time. Pitch is used to estimate the peak of the amplitude to identify the particular tone.

Rhythm

Rhythm is also called duration provides characteristics of verbal and non -verbal audio identified by the nature of abstraction. They provide two types of attributes [7] namely the outlines of the sound fundamental notes and duration of each expression.

Harmonic Ratio (HR)

Another feature of audio used for event detection is the measure of the harmonic components within the range of continuum. It provides the high range of autocorrelation of the audio. These are some of the features of audio used for identification of events.

Classification models for audio and video processing

The next step after feature selection and extraction is the classification of the audio and video signals into different actions. The actions are characterised by the attributes of audio and video [70] to define the particular event automatically in the videos displayed. For this purpose, many classification models are built using bench mark data set. There are different categories of classification models and they are classified into three basic types namely unsupervised, supervised and semi supervised learning algorithms. This section deals with investigation of some classification models and their features.

Unsupervised Learning Approach

In this method the data set is untamed and not belongs to any class in prior. That is the data set is not labelled and the approach is to identify the class using some measures for detection. Using the similarity among the subject clustering is done to group similar data. So, cluster analysis is the fundamental attitude for unsupervised learning method. Some of the models are

Hierarchical and Partition clustering method

A clustering method used for making a large cluster or group by combining two or more subgroups. It can be both bottom to top or vice versa. Partition method deals with forming groups by changing the objects from one to another by dividing the group continuously. The number of clusters is decided earlier before partitioning.

Artificial Neural Network

The neural network system similar to human brain for classification using processors [62] and multiple connections inside the network. The most basic models are Self organizing map and adaptive resonance theory.

Hidden Markov models

A graphical model which is based on probability theory to identify a group of similar objects those are unknown with the set of known variables. This is a statistical model used for classification based on internal factors for estimation.

Supervised Learning methods

In this method the data set objects belong to a particular class and are labelled for classification. This approach is best suited for classifying audio signals and there are many pre trained models used for classification. Some of the models are discussed in brief. They are

Artificial Neural Network

For audio and video [61] classification the weights of the network are finely tuned to find the hidden layer weights which are used for clarification. The popular models are multi-layer perceptron and Radial basis Function models used for classification

Instance based

The classification method based on the theory that samples can be used iteratively and one example is K nearest neighbour method. Here the values are predicted based on the neighbour around the value and Euclidean measure is used to calculate the similarity.

Random Forest

Random forest belongs to ensemble learning by building numerous trees from various samples and making decisions based on majority voting scheme for classification. It uses bagging and feature division method to predict any result based on the accumulation of all decision trees output.

Support vector machine

A classification method by adding data points to the feature space which are close to the hyper plane. It is the linear model to partition the data into classes based on the line of hyper plane.

Semi supervised learning methods

This hybrid method combines both unsupervised and supervised learning approaches for better accuracy. This method searches suitable classifier from both the procedures for classification. Some popular models used are

Self- training methods

A popular semi- supervised method trained with sample data which is labelled and used to test the unlabelled data. The main attributes are self- training with labelled data set and huge unlabelled events.

Co-Training and EM method

This method is suitable for small amount of known data with huge amount of unknown data. There are two classifiers for two different sets of data. Expectation and Maximization method also uses to cluster unknown data with already available values.

Transudative support machines

In recurrent neural network this method is applied for predicting problems by converting into another form.

Performance Evaluation

From the above given algorithms the best method is chosen by calculating the performance measures. There is basic four measures used. TPR is true positive rate for sensitivity gives actual positive values. TNR is true negative rate for

specificity gives actual negative value. FPR for false positive rate is wrongly detecting true values and FNR is false negative rate wrongly predicting wrong values.

CONCLUSION

The final section of this paper is the conclusion part which summarises the survey of event detection methods using video and audio. This paper provided a general sketch of the need for automatic detection of events using audio and video with their common applications. Data set is discussed in the next section and the features used for classification is enumerated. The last section described the various models used for classification. A simple outline is discussed and this study can be extended by using any hybrid model for processing.

REFERENCES

1. Event Detection in User Generated Video Content: A Comprehensive study Ms. Susmitha.A1 and Dr. Sanjay Jain2, International Journal of Engineering Trends and Technology (IJETT- Scopus Indexed) – Special Issues - ICT 2020.
2. Lyu, Y., Yang, M. Y., Vosselman, G., & Xia, G.-S. Video object detection with a convolutional regression tracker. ISPRS Journal of Photogrammetry and Remote Sensing, 176, 139–150, 2021, doi:10.1016/j.isprsjprs.2021.04.004
3. Speech Enhancement Using 2-D Fourier Transform Ing Yann Soon, Member, IEEE, and Soo Ngee Koh, IEEE TRANSACTIONS ON SPEECH AND AUDIO PROCESSING, VOL. 11, NO. 6, NOVEMBER 2003.
4. Morfi, V., & Stowell, D. (2018). Deep Learning for Audio Event Detection and Tagging on Low-Resource Datasets. Applied Sciences, 8(8), 1397. doi:10.3390/app8081397
5. P. K. Atrey, M. C. Maddage, and M. S. Kankanhalli. "Audio based event detection for multimedia surveillance." In Acoustics, Speech and Signal Processing, ICASSP Proceedings, 2006, vol.5, pp. V-V
6. An Overview of Audio Event Detection Methods from Feature Extraction to Classification Elham Babaee, Nor Badrul Anuar, Ainuddin Wahid Abdul Wahab, Shahaboddin Shamshirband & Anthony T. Chronopoulos, Applied Artificial Intelligence An International Journal ISSN: 0883-9514 (Print) 1087-6545 (Online) Journal homepage: https://www.tandfonline.com/loi/uaai2
7. Hariharan Subramanian, Preeti Rao and Dr. Sumantra. D. Roy, M.Tech, AUDIO SIGNAL CLASSIFICATION,Credit Seminar Report, Electronic Systems Group, EE. Dept, IIT Bombay, November2004.
8. DeCann B, Ross A Relating ROC and CMC curves via the biometric menagerie. In: IEEE sixth international conference on biometrics: theory, applications and systems (BTAS), 2013, pp 1–8. doi:10.1109/BTAS.2013.6712705
9. Gorodnichy DO Multi-order analysis framework for comprehensive biometric performance evaluation. In: SPIE defense, security, and sensing. International Society for Optics and Photonics, 2010, pp 76670G–76670G
10. W. Chou, B.-H. Juang, and C.-H. Lee, "Segmental GPD training of HMM based speed recognizer," in Proc. ICASSP-92, 1992, pp. 473–476
11. R. O. Duda, P. E. Hart, and D. G. Stork, Pattern Classification. New York: Wiley, 2000.
12. Y. Ephraim, H. Lev-Ari, and R. M. Gray, Asymptotic minimum discrimination information measure for asymptotically weakly stationary process, IEEE Trans. Inform. Theory, Sept. 1988, vol. 34, pp. 1033–1040.
13. C.-S. Huang, H.-C. Wang, and C.-H. Lee, An SNR-incremental stochastic matching algorithm for noisy speech recognition, IEEE Trans. Speech Audio Processing, Nov. 2001, vol. 9, pp. 866–873.
14. A. Viterbi, Error bounds for convolutional codes and an asymptotically optimum decoding algorithm, IEEE Trans. Inform. Theory, Apr. 1967, vol. IT-13, pp. 260–269.
15. M. Scanlon, Acoustic monitoring pad, in Proc. IEEE 17th Annu. Conf. Eng. Med. Biol. Soc., 1995, vol. 2, pp. 1725–1726.
16. T. Toda, K. Nakamura, H. Sekimoto, and K. Shikano, Voice conversion for various types of body transmitted speech, in Proc. IEEE Int. Conf. Acoust., Speech, Signal Process. (ICASSP), 2009, pp. 3601–3604.

17. L. Ng, G. Burnett, J. Holzrichter, and T. Gable, Denoising of human speech using combined acoustic and EM sensor signal processing, in Proc. IEEE Int. Conf. Acoust., Speech, Signal Process. (ICASSP'00), 2000, vol. 1, pp. 229–232.
18. P. Heracleous, Y. Nakajima, A. Lee, H. Saruwatari, and K. Shikano, Accurate hidden Markov models for non-audible murmur (NAM) recognition based on iterative supervised adaptation, in Proc. IEEE Workshop Autom. Speech Recognition Understanding (ASRU'03), 2003, pp. 73–76.
19. T. Dekens, Y. Patsis, W. Verhelst, F. Beaugendre, and F. Capman, A multi-sensor speech database with applications towards robust speech processing in hostile environments, in Proc. 6th Int. Lang. Resources Eval. (LREC'08), Eur. Lang. Resources Assoc. (ELRA), Marrakech, Morocco, 2008, pp. 28–30.
20. T. Dekens and W. Verhelst, On noise robust voice activity detection, in Proc. 12th Annu. Conf. Int. Speech Commun. Assoc., 2011.
21. B.W. Gillespie, H.S. Malvar, D.A.F. Florencio. Speech Dereverberation via Maximum-Kurtosis Subband Adaptive Filtering, In Proceedings of ICASSP, May 2001,Vol. 6, Pages: 3701-3704.
22. J.R. Hopgood, P.J.W. Rayner. Blind Single Channel Deconvolution using Nonstationary Signal Processing, IEEE Transactions on Speech and Audio Processing, Sept. 2003, Vol. 11, Issue 5, pages 476-488.
23. C. d'Alessandro et al., Effectiveness of a periodic and periodic decomposition method for analysis of voice sources, IEEE Trans. Speech Audio Process, Jan 1998, vol. 6, no. 1, pp. 12–23.
24. O. Deshmukh, C. Espy-Wilson, and A. Juneja, Acoustic-phonetic speech parameters for speaker-independent speech recognition, in Proc. IEEE-ICASSP, 2002, pp. 593–596.
25. B. D. Lucas and T. Kanade, An iterative image registration technique with an application to stereo vision, in Proc. Int. Joint Conf. Artif. Intell., Vancouver, BC, Canada, Aug. 1981, pp. 674–679.
26. H. V. Luong, X. Huang, and S. Forchhammer, Adaptive noise model for transform domain Wyner-Ziv video using clustering of DCT blocks, in Proc. IEEE Int. Workshop Multimedia Signal, Hangzhou, China, Oct. 2011, pp. 1–6.
27. T. Brox, A. Bruhn, N. Papenberg, and J. Weickert, High accuracy optical flow estimation based on a theory for warping, in Proc. Eur. Conf. Comput. Vis., Prague, Czech Republic, May 2004, pp. 25–36.
28. J. Skorupa, J. Slowack, S. Mys, N. Deligiannis, J. D. Cock, P. Lambert, C. Grecos, A. Munteanu, and R. V. de Walle, Efficient low-delay distributed video coding, IEEE Trans. Circuits Syst. Video Technol, Sep. 2011, vol. 22, no. 4, pp. 530–544.
29. Tech. Rep. 781, 1987. [5] R. Foote, G. Mirchandani, and D. Rockmore, Two-dimensional wreath product group-based image processing, J. Symb. Comput, 2004, vol. 37, no. 2, pp. 187–207.
30. E. Candes and M. B. Wakin, An introduction to compressive sampling, IEEE Signal Process. Mag, Mar. 2008, vol. 25, no. 2, pp. 21–30.
31. S. Pudlewski and T. Melodia, Compressive video streaming: Design and rate-energy-distortion analysis, IEEE Trans. Multimedia, Dec 2013, vol. 15, no. 8, pp. 2072–2086.
32. Y. Zheng and L. Fan, Moving object detection based on running average background and temporal difference, in Proc. IEEE Int. Conf. Intell. Syst. Knowl. Eng, Nov 2010, pp. 270–272.
33. C. Wren, A. Azarbayejani, T. Darrell, and A. Pentland, Pfinder: Realtime tracking of the human body, IEEE Trans. Pattern Anal. Mach. Intell, Jul. 1997, vol. 19, no. 7, pp. 780–785.
34. B. Han, D. Comaniciu, and L. S. Davis, Sequential kernel density approximation through model propagation: Applications to background modeling,in Proc. Asian Conf. Comput. Vis., Jan. 2004, pp. 1–7.
35. S. C. Huang and B. H. Chen, Automatic moving object extraction through a real-world variable-bandwidth network for traffic monitoring systems, IEEE Trans. Ind. Electron, Apr 2014 vol. 61, no. 4, pp. 2099–2112.
36. Rajamanogaran, M., Subha, S., Baghavathi Priya, S., & Sivasamy, J,Contactless Attendance Management System using Artificial Intelligence. Journal of Physics: Conference Series, 2021, 1714(1), 012006. https://doi.org/10.1088/1742-6596/1714/1/012006
37. Raghuwanshi A and Swami P D, an automated classroom attendance system using video-based face recognition, 2nd IEEE International Conference on Recent Trends in Electronics, Information & Communication Technology (RTEICT), 2017, pp 719-724.

38. D. A. Ross, J. Lim, R.-S. Lin, and M.-H. Yang, Incremental learning for robust visual tracking," Int. J. Comput. Vis, Aug 2007, vol. 77, nos. 1–3, pp. 125–141.
39. P. N. Belhumeur and D. Kriegman, What is the set of images of an object under all possible lighting conditions in Proc. IEEE Comput. Soc. Conf. Comput. Vis. Pattern Recognit. (CVPR), Jun 1996, pp. 270–277.
40. G. D. Hager and P. N. Belhumeur, Real-time tracking of image regions with changes in geometry and illumination, in Proc. IEEE Comput. Soc. Conf. Comput. Vis. Pattern Recognit. (CVPR), Jun 1996, pp. 403–410.
41. E. J. Candès, X. Li, Y. Ma, and J. Wright, Robust principal component analysis J. ACM, May 2011, vol. 58, no. 3, pp. 1–37.
42. D. Wang, H. Lu, and M.-H. Yang, Least soft-threshold squares tracking, in Proc. IEEE Comput. Soc. Conf. Comput. Vis. Pattern Recognit. (CVPR), Jun. 2013, pp. 2371–2378
43. G. Tzanetakis and P. Cook, Musical genre classification of audio signals, IEEE Trans. Speech Audio Process, 2002, vol. 10, no. 5, pp. 293–302.
44. S. Essid, G. Richard, and B. David, Musical instrument recognition by pairwise classification strategies, IEEE Trans. Audio, Speech, Lang. Process, 2006, vol. 14, no. 4, pp. 1401–1412.
45. S. Essid, G. Richard, and B. David, Instrument recognition in polyphonic music based on automatic taxonomies, IEEE Trans. Audio, Speech, Lang. Process, 2006, vol. 14, no. 1, pp. 68–80.
46. T. Kitahara, M. Goto, K. Komatani, T. Ogata, and H. Okuno, Instrument identification in polyphonic music: Feature weighting to minimize influence of sound overlaps, EURASIP J. Appl. Signal Process, 2007, no. 1, pp. 155–155.
47. P. Leveau, D. Sodoyer, and L. Daudet, Automatic instrument recognition in a polyphonic mixture using sparse representation, in Proc. Int. Conf. Music Information Retrieval, 2007.
48. D. Little and B. Pardo, Learning musical instruments from mixtures of audio with weak labels, in Proc. Int. Conf. Music Information Retrieval, 2008.
49. F. Fuhrmann, M. Haro, and P. Herrera, Scalability, generality and temporal aspects in automatic recognition of predominant musical instruments in polyphonic music," in Proc. Int. Conf. Music Information Retrieval, 2009.
50. P. Hamel, S. Wood, and D. Eck, Automatic identification of instrument classes in polyphonic and poly-instrument audio, in Proc. Int. Conf. Music Information Retrieval, 2009.
51. T. Heittola, A. Klapuri, and T. Virtanen, Musical instrument recognition in polyphonic audio using source-filter model for sound separation, in Proc. Int. Conf. Music Information Retrieval, 2009.
52. M. Slaney, Semantic-audio retrieval, in Proc. Int. Conf. Acoustics, Speech, and Signal Processing, 2007.
53. M. Levy and M. Sandler, A semantic space for music derived from social tags, in Proc. Int. Conf. Music Information Retrieval, 2007.
54. D. Turnbull, L. Barrington, D. Torres, and G. Lanckriet, Towards musical query-by-semantic description using the cal500 data set, in Proc. ACM Information Retrieval, 2007.
55. D. Turnbull, L. Barrington, D. Torres, and G. Lanckriet, Semantic annotation and retrieval of music and sound effects, IEEE Trans. Audio, Speech, Lang. Process, 2008, vol. 16, no. 2, pp. 467–476.
56. L. Barrington, M. Yazdani, D. Turnbull, and G. Lanckriet, Combining feature Kernels for semantic music retrieval, in Proc. Int. Conf. Music Information Retrieval, 2008.
57. Z.-S. Chen, J.-M. Zen, and J.-S. Jang, Music annotation and retrieval system using anti-models, in Proc. Audio Eng. Soc., 2008.
58. T. Bertin-Mahieux, D. Eck, F. Maillet, and P. Lamere, Autotagger: A model for predicting social tags from acoustic features on large music databases, J. New Music Res, 2008, vol. 37, no. 2, pp. 115–135.
59. G. Chechik, E. Le, M. Rehn, S. Bengio, and D. Lyon, Large-scale content-based audio retrieval from text queries, in Proc. ACM Multimedia Information Retrieval, 2008.
60. M. Levy and M. Sandler, Music information retrieval using social tags and audio, IEEE Trans. Multimedia, 2009, vol. 11, no. 3, pp. 383–395.
61. C.L. Wan, K.W. Dickinson, Road traffic monitoring using image processing—a survey of systems, techniques and applications, IFAC Control Computers, Communications in Transportation, Paris, France (1989).
62. S. Mantri, D. Bullock, Analysis of feedforward-backpropagation neural networks used in vehicle detection, Transportation Research Part C 3 (3) ,1995, 161–174.

63. N. Hoose, IMPACT: an image analysis tool for motorway analysis and surveillance, Traffic Engineering Control Journal (1992) 140–147.
64. N. Paragios, R. Deriche, Geodesic active contours and level sets for the detection and tracking of moving objects, IEEE Transactions on Pattern Analysis and Machine Intelligence 2000, 266–280.
65. T. Aach, A. Kaup, Bayesian algorithms for adaptive change detection in image sequences using Markov random fields, Signal Processing: Image Communication, 1995, 147–160.
66. N. Paragios, G. Tziritas, Adaptive detection and localization of moving objects in image sequences, Signal Processing: Image Communication, 1999, 277–296.
67. J.B. Kim, H.S. Park, M.H. Park, H.J. Kim, A real-time region-based motion segmentation using adaptive thresholding and K-means clustering, in: M. Brooks, D. Corbett, M. Stumptner (Eds.), AI 2001, Springer, Berlin, 2001, pp. 213–224.
68. M. Dubuisson, A. Jain, Contour extraction of moving objects in complex outdoor scenes, International Journal of Computer Vision, 1995, 83–105.
69. N. Hoose, Computer Image Processing in Traffic Engineering, Taunton Research Studies Press, UK, 1991.
70. J. Badenas, J.M. Sanchiz, F. Pla, Motion-based segmentation and region tracking in image sequences, Pattern Recognition, 2001, 661–670.

Table 1. Categories of audio features

S.No	Feature Names	Sub Types
1	Temporal	Zero Crossings, Centroid, Roll off, Flux, Short term energy
2	Spectral	MFCC, Audio spectrum spread, centre, Flatness, Spectral entropy, signal bandwidth, Energy ratio, Linear prediction, MPEG7
3	Prosodic	Pitch, rhythm, intensity, Beat strength, Regularity of rhythm
4	Others	Harmonic ratio, root mean square, Time envelope, Low energy rate, Loudness

Indian Journal of Natural Sciences *www.tnsroindia.org.in ©IJONS*

Vol.15 / Issue 83 / Apr / 2024 *International Bimonthly (Print) – Open Access* *ISSN: 0976 – 0997*

RESEARCH ARTICLE

Bayesian Predictive Analysis for the Chris-Jerry Distribution with Various Priors

G.Meenakshi[1] and B. Balachandar[2]*

[1]Professor, Department of Statistics, Faculty of Annamalai University, Annamalai Nagar, Tamil Nadu, India.
[2]Research Scholar, Department of Statistics, Annamalai University, Annamalai Nagar, Tamil Nadu, India.

Received: 19 Dec 2023 Revised: 12 Jan 2024 Accepted: 11 Mar 2024

***Address for Correspondence**
G Meenakshi
Professor, Department of Statistics,
Faculty of Annamalai University,
Annamalai Nagar, Tamil Nadu, India.
Email: profgmau@gmail.com

ABSTRACT

Bayesian predictive density is a crucial concept in Bayesian statistics, offering a probabilistic approach to prediction and decision-making under uncertainty. It incorporates existing knowledge and new data to create probability distributions over potential outcomes. This is particularly valuable when data is limited, as it provides a way to quantify uncertainty and update predictions over time. Bayesian predictive density aids in model selection, guiding the choice of the most fitting model, and it allows decision-makers to weigh potential risks and rewards comprehensively. Its flexibility accommodates prior beliefs and addresses heterogeneity in complex systems. By providing a range of possible outcomes along with their associated probabilities, it offers a practical tool for assessing and managing uncertainty. In sequential analyses, it ensures continuous adaptation to incoming data. Ultimately, Bayesian predictive density enables a deeper understanding of future events and supports informed decisions based on a holistic view of uncertain situations. this research concentrates on a new Bayesian predictive model for Chris-jerry distribution and its application in HIV viral replication.

Keywords: Chris-jerry distribution, posterior distribution, prior, predictive distribution.

INTRODUCTION

The landscape of Bayesian predictive models is a testament to the enduring power of mathematical inquiry and the evolution of probabilistic reasoning over centuries. From its humble beginnings in the 18th century, rooted in the pioneering contributions of Thomas Bayes and Pierre-Simon Laplace, Bayesian inference has undergone a

remarkable transformation, shaped by mathematical development, philosophical debates, and the challenges posed by computational limitations and statistical paradigms. In the 20th century, despite its promising foundations, Bayesian predictive models faced significant hurdles. Computational constraints and the overwhelming influence of frequentist statistics hindered their widespread adoption, relegating them to the periphery of scientific inquiry. However, the tides began to turn with the advent of the Bayesian renaissance and the breakthroughs in computational techniques.

A pivotal moment in the resurgence of Bayesian predictive modeling came with the development of Markov Chain Monte Carlo (MCMC) methods, such as the Metropolis-Hastings algorithm and Gibbs sampler, in the 1950s and 1960s. These innovations provided a pathway to approximate complex posterior distributions, enabling the estimation of intricate Bayesian models and expanding their application horizon, particularly in the realm of prediction. The late 20th and early 21st centuries marked a watershed moment for Bayesian predictive modelling. Rapid advancements in computational capabilities, coupled with sophisticated algorithms, empowered researchers to implement highly intricate Bayesian models. This newfound computational prowess facilitated the derivation of predictive distributions in diverse fields, ranging from finance and machine learning to epidemiology, revolutionizing decision analysis by integrating uncertainty into critical decision-making processes. In this research the Bayesian predictive density and distribution is derived for Chris-Jerry distribution.

A Bayesian approach for Chris-jerry distribution

Chrisogonus K. Onyekwereand Okechukwu J. Obulezi 2022 have proposeda new one-parameter distribution named Chris-Jerry is suggested from a two-component mixture of Exponential (θ) distribution and Gamma (3, θ) distribution with mixing proportion p = θ/ θ+2 having a flexibility advantage in modeling lifetime data.

The probability distribution function of Chris-jerry distribution is given by

$$\boldsymbol{f(x) = \frac{\theta^2}{\theta+2}.\left(1+\theta x^2\right).e^{-\theta x}}$$

The likelihood function is given by

$$\boldsymbol{\pi(x_i) = \prod_{i=1}^{n} \frac{\theta^2}{\theta+2}.\left(1+\theta x_i^2\right).e^{-\theta x_i}}$$

$$\boldsymbol{= \frac{\theta^{2n}}{(\theta+2)^n}(1+\theta x_i)^n.\left(e^{-\theta\sum_1^n x_i}\right)}$$

Case: I

The prior is gamma prior (conjugate prior)

$$\boldsymbol{p(\theta) = \frac{e^{-\theta}.\theta^{r-1}}{\Upsilon r} \qquad r>0, \theta>0}$$

The posterior distribution is given by

$$\boldsymbol{p\left(\frac{\theta}{x}\right) \propto \frac{\theta^{2n}}{(\theta+2)^n}(1+\theta x_i)^n.\left(e^{-\theta\sum_1^n x_i}\right) * \frac{e^{-\theta}.\theta^{r-1}}{\Upsilon r}}$$

$$\boldsymbol{p\left(\frac{\theta}{x}\right) = \frac{1}{k}\frac{\theta^{2n}}{(\theta+2)^n}(1+\theta x_i)^n.\left(e^{-\theta\sum_1^n x_i}\right) * \frac{e^{-\theta}.\theta^{r-1}}{\Upsilon r}}$$

Where

$$\boldsymbol{k = \int_0^\infty \frac{\theta^{2n}}{(\theta+2)^n}(1+\theta x_i)^n.\left(e^{-\theta\sum_1^n x_i}\right) * \frac{e^{-\theta}.\theta^{r-1}}{\Upsilon r} d\theta}$$

$$\boldsymbol{= \frac{1}{2^n}\int_0^\infty \frac{\theta^{2n}}{\left(1+\frac{\theta}{2}\right)^n}(1+\theta x_i)^n.\left(e^{-\theta\sum_1^n x_i}\right) * \frac{e^{-\theta}.\theta^{r-1}}{\Upsilon r} d\theta}$$

$$\boldsymbol{\left(1+\frac{\theta}{2}\right)^{-n} = \sum_{j=0}^{\infty}(-1)^j c(n+j-1,j)\left(\frac{\theta}{2}\right)^j}$$

$$(1+\theta x_i)^n = \sum_{l=0}^{\infty} c(n,i)(\theta x)^l$$

$$= \frac{1}{2^n}\int_0^{\infty} \theta^{2n} \sum_{j=0}^{\infty}(-1)^j c(n+j-1,j)\left(\frac{\theta}{2}\right)^j \sum_{l=0}^{\infty} c(n,i)(\theta x)^l * \left(e^{-\theta\sum_1^n x_i}\right) * \frac{e^{-\theta}.\theta^{r-1}}{\Upsilon r} d\theta$$

$$= \sum_{j=0}^{\infty}(-1)^j c(n+j-1,j) \sum_{l=0}^{\infty} c(n,i)(x)^l \frac{1}{2^{n+j}[\Upsilon r]} \int_0^{\infty} \theta^{2n+l+j+r-1} * \left(e^{-\theta(\sum_1^n x_i+1)}\right) d\theta$$

$$K = \sum_{j=0}^{\infty}(-1)^j c(n+j-1,j) \sum_{l=0}^{\infty} c(n,i)(x)^l \frac{\{\Upsilon(2n+l+j+r)\}}{2^{n+j}[\Upsilon r][\sum_1^n x_i+1]^{2n+l+j+r}}$$

The posterior distribution is given by

$$p\left(\frac{\theta}{x}\right) = \frac{1}{k}\frac{\theta^{2n}}{(\theta+2)^n}(1+\theta x_i)^n.\left(e^{-\theta\sum_1^n x_i}\right) * \frac{e^{-\theta}.\theta^{r-1}}{\Upsilon r}$$

where

$$K = \sum_{j=0}^{\infty}(-1)^j c(n+j-1,j) \sum_{l=0}^{\infty} c(n,i)(x)^l \frac{\{\Upsilon(2n+l+j+r)\}}{2^{n+j}[\Upsilon r][\sum_1^n x_i+1]^{2n+l+j+r}}$$

The predictive density is given by

$$g(x) = \int_0^{\infty} \prod_{i=1}^{n} \frac{\theta^2}{\theta+2}.\left(1+\theta x_i^2\right).e^{-\theta x_i} * \frac{\theta^2}{\theta+2}.\left(1+\theta x^2\right).e^{-\theta x} * \frac{e^{-\theta}.\theta^{r-1}}{\Upsilon r} d\theta$$

$$= \int_0^{\infty} \prod_{i=1}^{n+1} \frac{\theta^2}{\theta+2}.\left(1+\theta x_i^2\right).e^{-\theta x_i} * \frac{e^{-\theta}.\theta^{r-1}}{\Upsilon r} d\theta$$

$$= \int_0^{\infty} \frac{\theta^{2(n+1)}}{(\theta+2)^{(n+1)}}(1+\theta x_i)^{(n+1)}.\left(e^{-\theta\sum_1^{n+1} x_i}\right) * \frac{e^{-\theta}.\theta^{r-1}}{\Upsilon r} d\theta$$

n+1=m

$$= \int_0^{\infty} \frac{\theta^{2(m)}}{(\theta+2)^{(m)}}(1+\theta x_i)^{(m)}.\left(e^{-\theta\sum_1^{m} x_i}\right) * \frac{e^{-\theta}.\theta^{r-1}}{\Upsilon r} d\theta$$

$$= \sum_{j=0}^{\infty}(-1)^j c(m+j-1,j) \sum_{l=0}^{\infty} c(m,i)(x)^l \frac{1}{2^{n+j}[\Upsilon r]} \int_0^{\infty} \theta^{2m+l+j+r-1} * \left(e^{-\theta(\sum_1^m x_i+1)}\right) d\theta$$

$$g(x) = \sum_{j=0}^{\infty} * \sum_{l=0}^{\infty} \{c(m,i)(x)^l\}\{(-1)^j c(m+j-1,j)\}\left[\frac{\{\Upsilon(2m+l+j+r)\}}{2^{m+j}[\Upsilon r][mx+1]^{2m+l+j+r}}\right]$$

Case :II

Let the prior distribution is consider as quasi prior

$$p(\theta) = \frac{1}{\theta^d}$$

The joint posterior density is given by

$$p\left(\theta/x\right) \propto \frac{1}{\theta^d} * \frac{\theta^{2n}}{(\theta+2)^n}(1+\theta x_i)^n.\left(e^{-\theta\sum_1^n x_i}\right)$$

$$= \frac{1}{K}\frac{1}{\theta^d} * \frac{\theta^{2n}}{(\theta+2)^n}(1+\theta x_i)^n.\left(e^{-\theta\sum_1^n x_i}\right)$$

Where

$$K = \int_0^{\infty} \frac{1}{\theta^d} * \frac{\theta^{2n}}{(\theta+2)^n}(1+\theta x_i)^n.\left(e^{-\theta\sum_1^n x_i}\right) d\theta$$

Let

$$\mathbf{a} = \sum_{1}^{n} \mathbf{x_i}$$

$$\mathbf{K} = \int_{0}^{\infty} \frac{\mathbf{1}}{\boldsymbol{\theta}^{\mathbf{d}}} * \frac{\boldsymbol{\theta}^{\mathbf{2n}}}{(\boldsymbol{\theta}+\mathbf{2})^{\mathbf{n}}} (\mathbf{1}+\boldsymbol{\theta}\mathbf{x_i})^{\mathbf{n}} . \left(\mathbf{e}^{-\boldsymbol{\theta}\mathbf{a}}\right) \mathbf{d}\boldsymbol{\theta}$$

Where

$$(\mathbf{1}+\boldsymbol{\theta}\mathbf{x})^{\mathbf{n}} = \sum_{\mathbf{i}=\mathbf{0}}^{\infty} \mathbf{c}(\mathbf{n},\mathbf{i})(\boldsymbol{\theta}\mathbf{x})^{\mathbf{i}}$$

$$\mathbf{K} = \int_{0}^{\infty} \frac{\mathbf{1}}{\boldsymbol{\theta}^{\mathbf{d}}} * \frac{\boldsymbol{\theta}^{\mathbf{2n}}}{(\boldsymbol{\theta}+\mathbf{2})^{\mathbf{n}}} * \sum_{\mathbf{i}=\mathbf{0}}^{\infty} \mathbf{c}(\mathbf{n},\mathbf{i})(\boldsymbol{\theta}\mathbf{x})^{\mathbf{i}} * \left(\mathbf{e}^{-\boldsymbol{\theta}\mathbf{a}}\right) \mathbf{d}\boldsymbol{\theta}$$

$$\sum_{\mathbf{i}=\mathbf{0}}^{\infty} \mathbf{c}(\mathbf{n},\mathbf{i})\mathbf{x}^{\mathbf{i}} = \mathbf{b}$$

$$\mathbf{K} = \mathbf{b} \int_{0}^{\infty} \frac{\mathbf{1}}{\boldsymbol{\theta}^{\mathbf{d}}} * \frac{\boldsymbol{\theta}^{\mathbf{2n}}}{(\boldsymbol{\theta}+\mathbf{2})^{\mathbf{n}}} * \boldsymbol{\theta}^{\mathbf{i}} \left(\mathbf{e}^{-\boldsymbol{\theta}\mathbf{a}}\right) \mathbf{d}\boldsymbol{\theta}$$

$$= \mathbf{b} \int_{0}^{\infty} \frac{\boldsymbol{\theta}^{\mathbf{2n+i-d}}}{(\boldsymbol{\theta}+\mathbf{2})^{\mathbf{n}}} * \left(\mathbf{e}^{-\boldsymbol{\theta}\mathbf{a}}\right) \mathbf{d}\boldsymbol{\theta}$$

$$= \mathbf{b} \int_{0}^{\infty} \boldsymbol{\theta}^{\mathbf{2n+i-d}} * \left(\mathbf{e}^{-\boldsymbol{\theta}\mathbf{a}}\right) * (\boldsymbol{\theta}+\mathbf{2})^{-\mathbf{n}} \mathbf{d}\boldsymbol{\theta}$$

$$= \frac{\mathbf{b}}{\mathbf{2^n}} \int_{0}^{\infty} \boldsymbol{\theta}^{\mathbf{2n+i-d}} * \left(\mathbf{e}^{-\boldsymbol{\theta}\mathbf{a}}\right) * \left(\mathbf{1}+\frac{\boldsymbol{\theta}}{\mathbf{2}}\right)^{-\mathbf{n}} \mathbf{d}\boldsymbol{\theta}$$

$$\left(\mathbf{1}+\frac{\boldsymbol{\theta}}{\mathbf{2}}\right)^{-\mathbf{n}} = \sum_{\mathbf{j}=\mathbf{0}}^{\infty} (-\mathbf{1})^{\mathbf{j}} \binom{\mathbf{n}+\mathbf{j}-\mathbf{1}}{\mathbf{j}} \left(\frac{\boldsymbol{\theta}}{\mathbf{2}}\right)^{\mathbf{j}}$$

$$\mathbf{K} = \frac{\mathbf{b}}{\mathbf{2^n}} \int_{0}^{\infty} \boldsymbol{\theta}^{\mathbf{2n+i-d}} * \left(\mathbf{e}^{-\boldsymbol{\theta}\mathbf{a}}\right) * \sum_{\mathbf{j}=\mathbf{0}}^{\infty} (-\mathbf{1})^{\mathbf{j}} \binom{\mathbf{n}+\mathbf{j}-\mathbf{1}}{\mathbf{j}} \left(\frac{\boldsymbol{\theta}}{\mathbf{2}}\right)^{\mathbf{j}} \mathbf{d}\boldsymbol{\theta}$$

$$\sum_{\mathbf{j}=\mathbf{0}}^{\infty} (-\mathbf{1})^{\mathbf{j}} \binom{\mathbf{n}+\mathbf{j}-\mathbf{1}}{\mathbf{j}} \left(\frac{\mathbf{1}}{\mathbf{2}}\right)^{\mathbf{j}} = \mathbf{e}$$

$$= \frac{\mathbf{b}}{\mathbf{2^{n+j}}} \int_{0}^{\infty} \boldsymbol{\theta}^{\mathbf{2n+i-d}} * \left(\mathbf{e}^{-\boldsymbol{\theta}\mathbf{a}}\right) * \sum_{\mathbf{j}=\mathbf{0}}^{\infty} (-\mathbf{1})^{\mathbf{j}} \binom{\mathbf{n}+\mathbf{j}-\mathbf{1}}{\mathbf{j}} (\boldsymbol{\theta})^{\mathbf{j}} \mathbf{d}\boldsymbol{\theta}$$

$$= \frac{\mathbf{b}.\mathbf{e}}{\mathbf{2^n}} \int_{0}^{\infty} \boldsymbol{\theta}^{\mathbf{2n+i-d+j}} * \left(\mathbf{e}^{-\boldsymbol{\theta}\mathbf{a}}\right) \mathbf{d}\boldsymbol{\theta}$$

$$\mathbf{K} = \frac{\mathbf{b}.\mathbf{e}}{\mathbf{2^n}(\mathbf{a})^{\mathbf{2n+i-d+}}} \boldsymbol{\Gamma}(\mathbf{2n}+\mathbf{i}+\mathbf{j}-\mathbf{d}+\mathbf{1})$$

$$= \frac{\sum_{\mathbf{i}=\mathbf{0}}^{\infty} \mathbf{c}(\mathbf{n},\mathbf{i})\mathbf{x}^{\mathbf{i}} . \mathbf{e}}{\mathbf{2^n}(\mathbf{nx})} \boldsymbol{\Gamma}(\mathbf{2n}+\mathbf{i}+\mathbf{j}-\mathbf{d}+\mathbf{1})$$

The predictive density is given by

$$= \int_{0}^{\infty} \mathbf{p}\left(\frac{\boldsymbol{\theta}}{\mathbf{x}}\right) * \mathbf{p}(\mathbf{x}) \mathbf{d}\boldsymbol{\theta}$$

$$= \int_0^\infty \frac{1}{K}\frac{1}{\theta^d} * \frac{\theta^{2n}}{(\theta+2)^n}(1+\theta x_i)^n . \left(e^{-\theta\sum_1^n x_i}\right) * \frac{\theta^2}{\theta+2} . (1+\theta x^2) . e^{-\theta x} d\theta$$

$$= \int_0^\infty \frac{1}{K}\frac{1}{\theta^d} * \frac{\theta^{2n+1}}{(\theta+2)^{n+1}}(1+\theta x_i)^{n+1} . \left(e^{-\theta\sum_1^{n+1} x_i}\right) d\theta$$

$$= \int_0^\infty \frac{1}{K}\frac{\theta^{2n+1-d}}{(\theta+2)^{n+1}}(1+\theta x_i)^{n+1} . \left(e^{-\theta\sum_1^{n+1} x_i}\right) d\theta$$

$$= \frac{1}{K}\int_0^\infty \frac{\theta^{2n+1-d}}{(\theta+2)^{n+1}}(1+\theta x_i)^{n+1} . \left(e^{-\theta\sum_1^{n+1} x_i}\right) d\theta$$

$(1+\theta x_i)^{n+1} = \sum_{l=0}^\infty c(n+1,l)(\theta x)^l$

$$= \frac{1}{K}\int_0^\infty \frac{\theta^{2n+1-d}}{(\theta+2)^{n+1}} \sum_{l=0}^\infty c(n+1,l)(\theta x)^l . \left(e^{-\theta\sum_1^{n+1} x_i}\right) d\theta$$

$$\sum_{l=0}^\infty c(n+1,l)(x)^l = g$$

$$= \frac{1}{K}\int_0^\infty \frac{\theta^{2n+1-d}}{(\theta+2)^{n+1}} * \theta^l * g * \left(e^{-\theta\sum_1^{n+1} x_i}\right) d\theta$$

$$= \frac{g}{K}\int_0^\infty \frac{\theta^{2n+1-d+l}}{(\theta+2)^{n+1}} \left(e^{-\theta\sum_1^{n+1} x_i}\right) d\theta$$

$$= \frac{g}{2^n K}\int_0^\infty \frac{\theta^{2n+1-d+l}}{(1+\theta)^{n+1}} \left(e^{-\theta\sum_1^{n+1} x_i}\right) d\theta$$

$$\left(1+\frac{\theta}{2}\right)^{-n-1} = \sum_{m=0}^\infty (-1)^j \binom{n+m-2}{m} \left(\frac{\theta}{2}\right)^m$$

$$= \frac{g}{2^n K}\int_0^\infty \theta^{2n+1-d+l} * (1+\theta)^{-(n+1)} * \left(e^{-\theta\sum_1^{n+1} x_i}\right) d\theta$$

$$= \frac{g}{2^n K}\int_0^\infty \theta^{2n+1-d+l} * \sum_{m=0}^\infty (-1)^j \binom{n+m-2}{m} \left(\frac{\theta}{2}\right)^m * \left(e^{-\theta\sum_1^{n+1} x_i}\right) d\theta$$

$$\sum_{m=0}^\infty (-1)^j \binom{n+m-2}{m} \left(\frac{1}{2}\right)^m = h$$

$$= \frac{g*h}{2^n K}\int_0^\infty \theta^{2n+1-d+l+m} \left(e^{-\theta\sum_1^{n+1} x_i}\right) d\theta$$

$$= \frac{g*h}{2^n K}\int_0^\infty \theta^{2n+1-d+l+m} \left(e^{-\theta a}\right) d\theta$$

$$= \frac{g*h}{2^n K(a)^{2n+d+l+m+2}} [\Gamma(2n+d+l+m+2)]$$

The predictive density with quasi prior is given by

$$g(\theta/x) = \frac{g*h}{2^n K(a)^{2n+d+l+m+2}} [\Gamma(2n+d+l+m+2)])$$

The predictive density with diffuse prior is given by
d=0

$$g(\theta/x) = \frac{g * h}{2^n K(a)^{2n+l+m+2}} [\Gamma(2n + l + m + 2)])$$

The predictive density with non-infective prior is given by
d=1

$$g(\theta/x) = \frac{g * h}{2^n K(a)^{2n+l+m+3}} [\Gamma(2n + l + m + 3)])$$

The predictive distribution is given by

$$G(\theta/x) = \int_0^x \frac{\sum_{l=0}^{\infty} c(n+1,l)(x)^l * h}{2^n Ka} [\Gamma(2n + l + m + 3)])dx$$

$$= \int_0^x \frac{\sum_{l=0}^{\infty} c(n+1,l)(x)^l * h}{(\sum_{i=0}^{\infty} c(n,i)x^i . e)\Gamma(2n + i + j - d + 1)} [\Gamma(2n + l + m + 3)])dx$$

$$= \frac{\sum_{l=0}^{\infty} c(n+1,l)}{\Gamma(2n + i + j - d + 1)e} \int_0^x \frac{(x)^l}{(\sum_{i=0}^{\infty} c(n,i)x^i .)} [\Gamma(2n + l + m + 3)])dx$$

$$= \frac{\sum_{l=0}^{\infty} c(n+1,l)}{\Gamma(2n + i + j - d + 1)e} \int_0^x \frac{(x)^{l-i}}{(\sum_{i=0}^{\infty} c(n,i))} [\Gamma(2n + l + m + 3)])dx$$

$$= \frac{\sum_{l=0}^{\infty} c(n+1,l)}{\Gamma(2n + i + j - d + 1)e} \int_0^x \frac{(x)^{l-i}}{(\sum_{i=0}^{\infty} c(n,i))} [\Gamma(2n + l + m + 3)])dx$$

$$= \frac{\sum_{l=0}^{\infty} c(n+1,l) [\Gamma(2n + l + m + 3)](x)^{l-i+1}}{\Gamma(2n + i + j - d + 1)e(\sum_{i=0}^{\infty} c(n,i))(l - i + 1)}$$

Analysis

The above plots shows that the value predictive density decrease as value of the random variable (x) increases, specifically for the conjugate prior. Conversely, for quasi, non-informative, and diffuse priors, the predictive density decreases with an increase in the random variable

CONCLUSION

The depicted plots reveal a discernible pattern: as the random variable (x) increases, the predictive density experiences a noticeable decrease. This trend is particularly evident in the conjugate prior, presenting a distinct behavior compared to quasi, non-informative, and diffuse priors. For the latter group, the predictive density also decreases with an ascending random variable, albeit with differences in the specific patterns. These findings underscore the substantial impact of prior selection on the predictive dynamics of the Chris-Jerry distribution. The distinct trend in predictive density observed in the conjugate prior highlights the sensitivity of the model to different prior specifications. In conclusion, the careful selection of a prior for the Chris-Jerry distribution proves essential for precise probability predictions concerning the event of interest. The variations in predictive density emphasize the nuanced role of prior choice in influencing the model's performance. This insight is invaluable for practitioners grappling with the intricacies of the Chris-Jerry distribution in diverse applications. Ultimately, this research serves as a guide for practitioners, emphasizing the critical role of prior selection in optimizing the accuracy of predictions within the Chris-Jerry distribution framework. The observed variations provide actionable insights, empowering decision-makers to make informed choices in real-world scenarios.

REFERENCES

1. H.putter *et.al* (2002) "A Bayesian approach to parameter estimation in HIV dynamical models" Statistics in Medicine Vol 21, Issue 15, PP 2199- 2214.
2. Cong Han, Kathryn Chaloner (2004) "Bayesian experimental design for non linear mixed- effect models with application to HIV dynamics" Biometrics Vol 60, Issue 1, pp 25-33.
3. Yangxin Huang *et.al* (2006) "Hierarchical Bayesian methods for estimation of parameters in a longitudinal HIV dynamic system" Biometrics Vol 62, Issue 2, pp 413- 423.
4. Khairul A. Kasmiran *et.al* (2012)"A Bayesian analysis on historical clinical data concerning treatment change for HIV/AIDS patients" Proceedimg of the Fifth Australian Workshop on Health information and knowledge management (HIKM 2012)", Melbourne, Australia.
5. G.Meenakshi (2013) "A Bayesian method to Pre Determination of Viral replication in the HIV Dynamics" Fast East Journal of Theoritical Statistics, Vol 42. Issue 2 pp71-81.
6. Farhard Yahgmaei *et.al* (2013) " Bayesian Estimation of the scale parameter of Inverse Weibull distribution under the asymptotic loss function" Journal Of Probability and Statistics, vol 2013, Article ID 89094, pp 1-8
7. Paresh Sanat and R. S. Srivastava(2013) "Bayesian Analysis of Rayleigh Distribution Under Quasi-Prior for Different Loss Functions" International Journal of Science and Research (IJSR) ISSN (Online): 2319-7064 Index Copernicus Value
8. David s goodshell (2015) "Illustration of the HIV life cycle". Curr Top microbiology immunology, Article 389, pp 243-252.
9. Daniel B.Reeves *et.al* (2018) "A majority of HIV persistence during antiretroviral theraphy is due to infected cell proliferation" Nature Communications 2018 9: Article no 4811.
10. G.Meenakshi *et.al* (2019) "Prediction of HIV replication in the human immune system using multinomial distribution by Bayesian methodology" International journal of scientific Research in Mathematical and Statsitical sciences Vol 6 Issue 1, pp 46 – 52
11. Collins Odhiambo et. Al (2019) "An Evaluation of Frequentist and Bayesian approach to GeoSpatial analysis of HIV Viral load Suppression Data" International journal of statistics and applications" Vol 9 Issue 6 pp 171-179.
12. Chrisogonus K. Onyekwere a∗ and Okechukwu J. Obulezi(2022) "Chris-Jerry Distribution and Its Applications" Asian Journal of Probability and Statistics 20(1): 16-30, 2022; Article no.AJPAS.91475 ISSN: 2582-0230.
13. G. Meenakshi and S. Saranya (2021) A New ARMA G (p, q) Model for largest Viral Replication and its Posterior Distribution, Turkish Journal of Computer and Mathematics Education

Table 1: Predictive density

x	Quasi prior	Non-informative prior	diffuse prior	Conjugate prior
11	5.60E-01	0.484	0.004889	0.0281
12	6.66E-01	0.576	0.005818	0.0186
13	7.82E-01	0.676	0.006828	0.0128
14	9.07E-01	0.784	0.007919	0.0090035
15	9.11E-01	0.87	0.009091	0.0064779

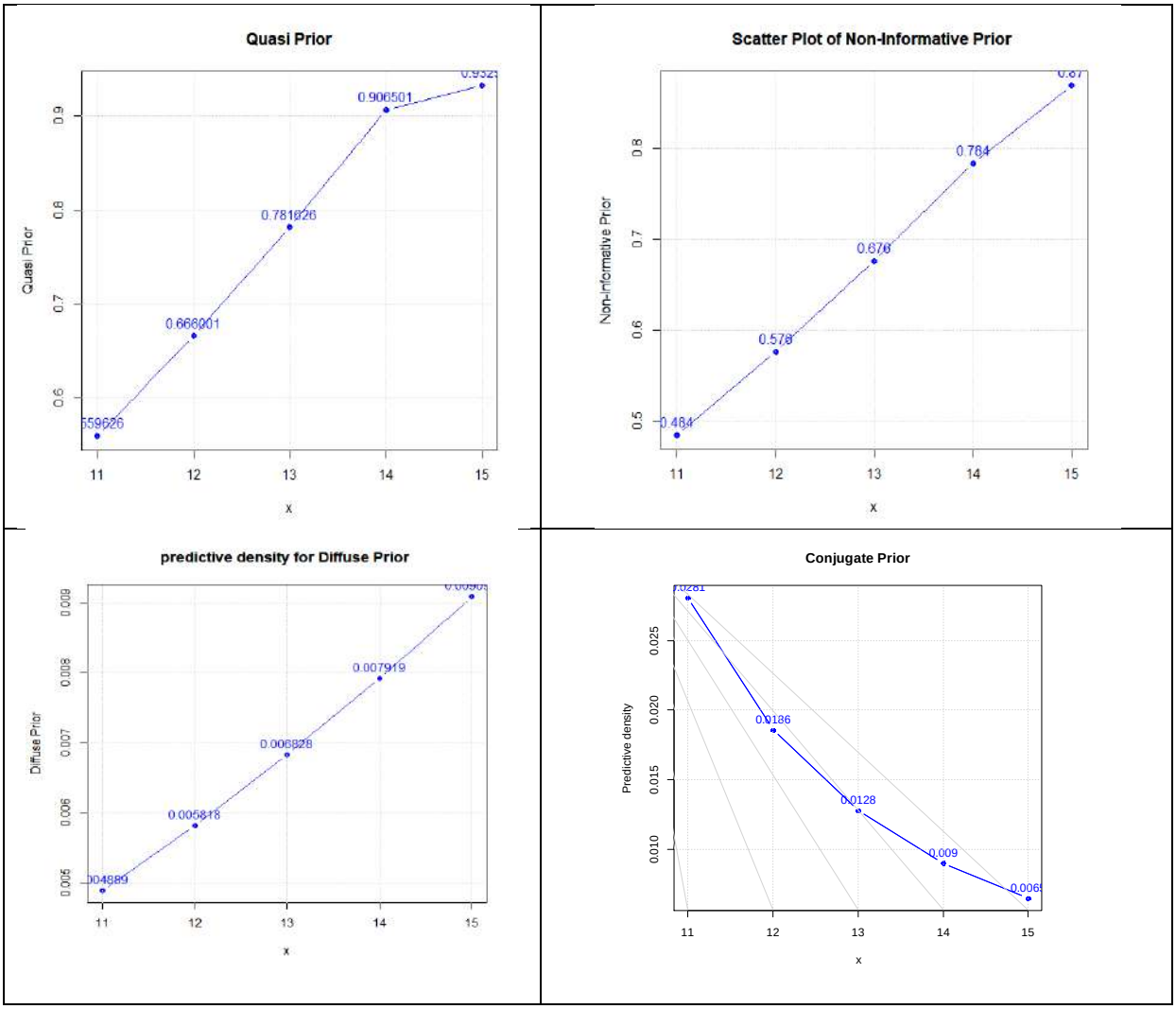
Quasi Prior
Quasi Prior
x
0.906501
0.781826
0.666001
Scatter Plot of Non-Informative Prior
Non-Informative Prior
x
0.784
0.676
0.578
0.484
predictive density for Diffuse Prior
Diffuse Prior
x
0.007919
0.006828
0.005818
Conjugate Prior
Predictive density
x
0.0186
0.0128
0.009

Vol.15 / Issue 83 / Apr / 2024 International Bimonthly (Print) – Open Access ISSN: 0976 – 0997

RESEARCH ARTICLE

Nutritional and Functional Evaluation of Pomegranate Peel Powder Incorporated Waffles

S. Mohana[1] and Arivuchudar.R[2]*

[1]Student, Department of Nutrition and Dietetics, Periyar University, Salem, Tamil Nadu, India.
[2]Assistant Professor, Department of Nutrition and Dietetics, Periyar University, Salem, Tamil Nadu, India.

Received: 06 Nov 2023 Revised: 09 Jan 2024 Accepted: 07 Mar 2024

***Address for Correspondence**
Arivuchudar.R
Assistant Professor,
Department of Nutrition and Dietetics,
Periyar University,
Salem, Tamil Nadu, India.
Email: achudar24@gmail.com

ABSTRACT

Sustainability entails addressing the demands without jeopardising future generation's ability to meet their needs. It is more than just being environmentally conscious. Most conceptions of sustainability include considerations for social equality and economic development. Sustainable food management is a systematic method that tries to reduce food waste and its associated implications throughout the life cycle. Pomegranate cultivation and consumption have always increased due to their flavour and nutrients. A huge number of byproducts are formed during fruit processing, such as peels and seeds which can cause environmental contamination if not handled appropriately. The study was carried out to formulate value-added waffles, by incorporating pomegranate peel powder (*Punica granatum*) in different proportions viz. V1 (90g wheat flour+ 10g pomegranate peel powder) and V2 (85g wheat flour + 15 g pomegranate peel powder), V3 (80g wheat flour+ 20g pomegranate peel powder) respectively for each variation of the product. On the basis of sensory evaluation carried out using the nine-point hedonic scale, it was observed that the variation V2 scored best regarding appearance, colour, texture, taste, flavour and overall acceptability. Hence, the accepted variation V2 was subjected to nutritional and phytochemical analysis. The waffle was found to be higher in terms of nutritional parameters when compared with control and was also found to be a source of phytochemicals such as total flavonoids and phenols. Tannins were present in permissible limits, contributing to their extensive functions like anti-inflammatory, anti-cancer, anti-bacterial and cardiovascular protection.

Keywords: Environmental sustainability, Food waste, Pomegranate peel, Waffles

INTRODUCTION

The year 2021 was observed as the International Year of Fruits and Vegetables by the United Nations Organisation to propagate the nutritional importance of fruits and vegetables for healthy living. Of late, now it is understood that not only the whole fruits and vegetables, but the by-products from the fruits and vegetable markets and processing industries serve as a treasure of nutrients. Numerous studies state that the peels that are discarded as waste pose a threat to the environment, rather they can be used as value enhancers in different food formulations and drug formulations. To mention, a few studies, *Ananas cosmosus* fruit peel has anti-inflammatory activity [1], lemon peel extract can be used as a natural binder in aspirin tablets [2], custard peel extract and carica papaya peel extract exhibit antimicrobial and antioxidant property [3,4], pomegranate peels were used to develop phytotomes, for novel drug delivery system [5] and as a cosmetic ingredient in herbal lipsticks [6].Pomegranate peel finds application as ointment base for burn, wound and scar healing [7]. The pomegranate being a colorful fruit, grabs attention. Pomegranate is the fruit of a shrub *(Punica granatum. L)*, grown predominantly in west Asia and the Mediterranean region, as well as other parts of the world, including America, where the environment is favorable for its growth [8].

Pomegranate fruits have a variety of constituents in their seeds, skins, and arils, which play a therapeutic role in the management of health through the control of numerous biological processes. Over 60% of the pomegranate's weight is made up of its peel, and is a rich source of fibre, minerals like calcium, magnesium, phosphorus, potassium, and sodium as well as a variety of phytochemicals like ellagitannins, proanthocyanidin compounds, and flavonoids [9]. Pomegranate waste is generated at all stages of the fruit's life cycle, including agricultural production, industrial manufacturing, and processing. Pomegranate by-products can be used since they are high in bioactive substances. Pomegranate peel being a significant by-product of pomegranate juice production, the presence of polyphenols, flavonoids, and hydrolysed tannins are responsible for its varied biological functions [10]. Pomegranate peel attracts attention due to its wound healing capacity, as peels contain high amounts of bioactive compounds which inhibit migration of Salmonella on wet surfaces. Pomegranate peels are also characterized by the presence of gallic acid, ellagic acid and punicalagin. They possess free radical scavenging properties and antibacterial activities against enteric pathogens like *E.coli*, *Salmonella species*, *Shigella species*, *Vibrio cholera*, viruses, fungi, and mould [11].

Pomegranate peel has a great therapeutic effect on chronic inflammation, like ulcerative colitis, blood pressure reduction, anti-diabetes, and anticancer [12]. Literature states that both the fresh and dried pomegranate peel powder is enriched with macro and micro minerals like calcium, potassium, phosphorus, sodium, iron, zinc, manganese, selenium and copper [13]. Pomegranate peel can be used as a functional ingredient because it is a good source of crude fibres, which have numerous health benefits such as the ability to lower serum LDL-cholesterol levels, improve glucose tolerance and insulin response, reduce hyperlipidaemia and hypertension, contribute to gastrointestinal health, and prevent certain cancers such as colon cancer [14]. The invitro and invivo studies using the pomegranate peel extract had shown to exhibit potent activity against helminthic, diarrhea, tumor growth and was immuno-stimulatory and hepato-Protective in nature [15]. Anti diabetic activity of pomegranate peel was studied in diabetic rats and the effect was comparable with oral hypoglycemic drugs [16]. Pectin, a valuable food additive can also be extracted from pomegranate peel [17]. Taking into consideration, the nutritional richness of pomegranate peel powder, it was proposed in this study, to formulate value-added waffles, the most preferred young-generation snack product, by incorporating pomegranate peel powder.

MATERIALS AND METHODS

Procurement and processing of raw materials

The ingredients required for the formulation of pomegranate peel powder incorporated value added waffles, like whole wheat flour, pomegranate, coconut oil, baking powder, baking soda, sugar were procured from the local market in Salem, Tamil Nadu.

Processing of pomegranate peel powder

Pomegranates were purchased and checked for any infestation or damage present. Pomegranate which was free from damage was peeled and then sun dried for 2-3 days, and ground into powder.

Formulation of pomegranate peel powder incorporated waffles

Value added batter was prepared using the ingredients listed in Table 1. Waffles was formulated as shown in table 1, for each variation, viz. Control, Variation1, Variation 2, and Variation 3.

Acceptability of the product by organoleptic evaluation

The developed variations of the waffles were subjected to organoleptic evaluation to assess the maximum acceptability by the panel members. The quality attributes in terms of colour, appearance, flavour, texture, taste and overall acceptability were evaluated by semi-trained judges using score card with 9-point hedonic scale.

Nutritional and Phytochemical analysis of the accepted variation of pomegranate peel powder incorporated waffles

The nutritive value of accepted variation of waffle was assessed. The nutritional analysis of waffles was done using NSI diet calculator and standard laboratory procedures. The nutrients assessed include energy, carbohydrate, protein, fat, dietary fiber, iron, calcium, potassium, zinc, folic acid and total sugar. The phytochemicals like phenolic compounds, flavonoids and alkaloids were also assessed.

RESULTS AND DISCUSSION

The results of the formulated pomegranate peel powder incorporated waffles is presented and discussed further.

Organoleptic evaluation of the developed variations of the pomegranate peel powder incorporated waffles

Results of ANOVA Duncan multiple range tests showed that there was a significant difference ($p \leq 0.05$) between the control and all the variations of the waffles on the basis of appearance, color, texture, taste, flavor and overall acceptability. Results of sensory evaluation of the waffles prepared with 10%, 15%, and 20% pomegranate peel powder incorporation and control waffles are presented in table 2.

Appearance

The mean and standard deviation of control and developed variations was calculated with the sensory evaluation score given by panel members. 'Appearance' of the developed variations of waffles was analyzed according to its size, shape, and visual appearance, during sensory evaluation. Variation 2 got maximum score of 8.50±0.57,thus it was highly accepted by the panel members.

Color

Color is the most important sensory property of food product. Color gives the impression about the freshness, flavor and quality of the product. The mean and standard deviation of control and developed variations was calculated with the sensory evaluation score given by panel members. 'Color' of the developed variations was analyzed according to its color and visual appearance, in the sensory evaluation Variation 2 got maximum score of 8.17±1.08, hence it was highly accepted by the panel members. In a similar rice berry incorporated waffles study, malitol and palm sugar were substituted for sugar and no significant difference was observed in terms of appearance and colour [18].

Texture

Texture refers to those qualities of a food that can be felt with the fingers, tongue, palate or teeth. The waffle's texture is sensed by hardness and fracture ability. From the developed variations of waffles, variation 2 attained its

maximum fracture ability, with the score 7.97±0.81, which is nearly equal to the score 8.27 ±0.87 obtained by control. Hence variation 2 was highly accepted by the panel members.

Taste

The taste of food is caused by its chemical compounds. These compounds interact with the sensory (receptors) cells in the taste buds and can different types of tastes such as sweet, sour, salty, bitter, and savory. From the developed variations of waffles, variation 2 attained the taste of waffles, with score of 7.40±1.00, which is nearly equal to the score 7.93±0.78 obtained by control. Hence variation 2 was highly accepted by the panel members.

Flavor

Flavor of the particular food is also determined by the aromas picked up by nose. The primary function of the flavor is to add taste to the food. From the developed variations of waffles, variation 2 attained the flavors of waffles, with the score of 8.07±0.78, which is nearly equal to the score 8.50±0.57 obtained by control. Hence variation 2 was highly acceptable when compared to control. The incorporation of almond skin imparted a roasted flavor to waffles even without actual roasting and had significant impact in the flavor profile assessment by the panel members [19].

Overall acceptability

Overall acceptability of the food product is an important factor that is influenced by the sensory quality of the product. In the sensory evaluation, variation 2 got maximum score in comparison with control, V1 and V3. Variation 2 scores were observed to be highest of all the sensory characteristics with an overall acceptability of 8.13±.82, representing that variation 2 was highly accepted by the panel members.

Nutritional analysis of the accepted variation of pomegranate peel powder incorporated waffles

The above table infers waffles prepared with pomegranate peel powder is higher in energy content than control which is made from refined wheat flour, the protein content present in the accepted variation was 6.90g/100g which is greater than control of 218g/100g with the difference of +0.98g, the fat content is +7.08g greater in accepted variation than control 13.2g, the carbohydrate content was higher in accepted variation than control with 15.55g higher, the fiber was completely void in control when compared to the accepted variation with 1.44g, moisture content of accepted variation of waffle was 31.50g which higher than control. The total sugar content present in control was higher than accepted variation. The iron content of waffles prepared from pomegranate peel powder was found to be 41.42g/100g which was higher than control made from refined wheat flour with 1.7g/100g. The zinc content present in the waffles was higher in accepted variation (variation 2) with 9.89g/100g.when compared with control the sodium and potassium content was higher in accepted variation of waffle. The calcium content of waffles prepared from pomegranate peel powder was found to be 83.50g/100g which was lower than control. Similarly, millet flour incorporated waffle showed significant increase in total dietary fibre and minerals, and reduced carbohydrate content [20].

Phytochemical analysis of the accepted variation of the accepted variation of pomegranate peel powder incorporated waffles

The above table shows that the accepted variation of pomegranate peel powder incorporated waffles contains polyphenols, flavonoids, tannins, and alkaloids. It was also observed that raspberry incorporation increased phenolic compounds in waffles [21].

CONCLUSION

Pomegranate is the well-known fruit of a shrub **(***Punica granatum. L).*It is known that the polyphenolic compounds of pomegranate peel have the most pronounced therapeutic effect. As nutritional and bioactive properties of this Pomegranate peel powder are better understood, the interest of these food is increasing. Peel powder has several health benefits including antioxidant properties so it is recommended for the people suffering from non-

communicable disease. Waffles are usually easy to make and convenient to have around to pop in lunch boxes or for breakfast or as evening snacks. Hence pomegranate peel powder incorporated waffles will be suitable for people of all age groups. As pomegranate peels have demonstrated their potential as promising bioactive antioxidants, they may be a potential source of functional food ingredients and nutraceuticals that can be used in various areas of food industries.

REFERENCES

1. Uma Sankar Gorla,Savithri M, Koteswara Rao GSN, Niharika Y, Devi Sree Sathya P & Harika V. Evaluation of anti-inflammatory activity of Hydroalcoholic extract of Ananas cosmosus fruit peel by HRBC membrane stabilisation. Asian Journal of Pharmaceutical Research, 8(1), 2018, 33-35.
2. Prajakta M. Patil, Omprasad S. Nayakal, Mangesh Bhutkar, Somnath Bhinge & Dheeraj Randive. Extraction of Pectin from Lemon Peel and its use as a Natural Binder in Aspirin Tablet. Asian Journal of Pharmacy and Technology, 8 (3), 2018, 115-118.
3. Esther Lydia, Sheila John, Swetha V K & Thiyagarajan Sivapriya. Investigation on the Antimicrobial and Antioxidant Activity of Custard Apple (Annona reticulata) Peel Extracts. Research Journal of Pharmacognosy and Phytochemistry, 9(4), 2017, 241-247.
4. Esther Lydia, Sheila John, Riyazudin Mohammed & Thiyagarajan Sivapriya. Investigation on the Phytochemicals present in the Fruit peel of Carica papaya and evaluation of its Antioxidant and Antimicrobial property. Research Journal of Pharmacognosy and Phytochemistry, 8(4), 2016, 217-222.
5. Pande S. D., Wagh A.S., Bhagure L.B., Patil S.G & Deshmukh A.R. Preparation and Evaluation of Phytosomes of Pomegranate Peels. Research Journal of Pharmacy and Technology, 8(4), 2015, 416-422.
6. Elumalai A, Chinna Eswaraiah M &Nikhitha M. Formulation and Evaluation of a Herbal Lipstick from Punica granatum Fruit Peel. Research Journal of Topical and Cosmetic Science, 3(1), 2012, 20-22.
7. Maher Al-Absi, Abdu Faisal, Safwan Alagbarri & Mofeed Al- Nowihi. Development and Rheological Properties Evaluation of a Burn Healing Ointment Composed of Pomegranate peels and Beta-sitosterol Using Factorial Design. Asian Journal of Pharmacy and Technology, 11(1), 2021, 59-65.
8. Pagliarulo C, De Vito V, Picariello G, Colicchio R, Pastore G, Salvatore P & Volpe MG. Inhibitory effect of pomegranate (Punica granatum L.) polyphenol extracts on the bacterial growth and survival of clinical isolates of pathogenic Staphylococcus aureus and Escherichia coli. Food Chem. 2016 Jan 1;190:824-831. doi: 10.1016/j.foodchem.2015.06.028. Epub 2015 Jun 10. PMID: 26213044.
9. Mirdehghan SH & Rahemi M. Seasonal changes of mineral nutrients and phenolics in pomegranate (Punica granatum L.) fruit. Scientia Horticulturae. 111(2), 2007, 120-127. https://doi.org/10.1016/j.scienta.2006.10.001.
10. Magangana TP, Makunga NP, Fawole OA & Opara UL. Processing Factors Affecting the Phytochemical and Nutritional Properties of Pomegranate (Punica granatum L.) Peel Waste: A Review. Molecules.25(20), 2020, 4690. https://doi.org/10.3390/molecules25204690
11. Negi PS. Plant extracts for the control of bacterial growth: Efficacy, stability and safety issues for food application. International journal of food microbiology, 156(1), 2012, 7-17.
12. Asgary S, Keshvari M, Sahebkar A & Sarrafzadegan N. Pomegranate Consumption and Blood Pressure: A Review. Current Pharmaceutical Design, 23(7), 2017, 1042-1050. DOI: 10.2174/1381612822666161010103339. PMID: 27748197.
13. Ranjitha J, Bhuvaneshwari G, Deepa Terdal & Kavya K. Nutritional composition of fresh pomegranate peel powder. International Journal of Chemical Studies, 6(4), 2018, 692-696.
14. Mo Yaxian, Ma Jiaqi, Gao Wentao, Zhang Lei, Li Jiangui, Li Jingming & Zang Jiachen, Pomegranate Peel as a Source of Bioactive Compounds: A Mini Review on Their Physiological Functions. Frontiers in Nutrition. 2022. 9. 10.3389/fnut.2022.887113.
15. Himesh Soni, Govind Nayak, Kaushelendra Mishra, A.K. Singhai & A.K. Pathak. Evaluation of Phyto Pharmaceutical and Antioxidant Potential of Methanolic Extract of Peel of Punica granatum. Research Journal of Pharmacy and Technology, 3(4), 2010, 1170-1174.

16. Rupesh Gautam & Sharma SC. Effect of Punica granatum Linn. (Peel) on Blood Glucose Level in Normal and Alloxan- Induced Diabetic Rats. Research Journal of Pharmacy and Technology, 5(2), 2012, 226-227.
17. Sathish S, Gowthaman K.A & Haaresh Augustus. Utilization of Punica granatum Peels for the Extraction of Pectin. Research Journal of Pharmacy and Technology, 11(2), 2018, 613-616.
18. Tongkaew P, Purong D, Ngoh S, Phongnarisorn B & Aydin E. Acute Effect of Riceberry Waffle Intake on Postprandial Glycemic Response in Healthy Subjects. *Foods*, 10(12), 20211, 2937. https://doi.org/10.3390/foods10122937
19. Oliveira I, Marinho B, Szymanowska U, Karas M & Vilela A. Chemical and Sensory Properties of Waffles Supplemented with Almond Skins. *Molecules*, 28(15),2023,5674. https://doi.org/10.3390/molecules28155674
20. Chaitra.U, Abhishek P, Sudha, M.L, VanithaT & Crassina K.Impact of millets on wheat based Belgian waffles: Quality characteristics and nutritional composition. LWT. 2020. 124. 109136.https://doi.org/10.1016/j.lwt.2020.109136.
21. Szymanowska U, Karaś M & Bochnak-Niedźwiecka J. Antioxidant and Anti-Inflammatory Potential and Consumer Acceptance of Wafers Enriched with Freeze-Dried Raspberry Pomace. *Applied Sciences*, 11(15), 2021, 6807. https://doi.org/10.3390/app11156807

Table 1: Ingredients for the formulation of pomegranate peel powder waffles

Ingredients	Level of incorporation			
	Control	Variation 1	Variation 2	Variation 3
Whole wheat flour (g)	100	90	85	80
Pomegranate peel powder (g)	-	10	15	20
Sugar (g)	30	10	10	10
Milk (ml)	10	10	10	10
Vanilla extract (tsp)	2	½	½	½
Salt	A Pinch	A Pinch	A Pinch	A Pinch
Coconut Oil (ml)	3	3	3	3

Table 2: Statistical analysis of mean organoleptic values of developed waffles

Variations	Appearance	Colour	Texture	Taste	Flavour	Overall acceptability
Control	8.03±0.67 c	7.67±0.96 b c	8.27±0.87 c	7.93±0.78 d	8.50±0.57 d	8.53±0.68 d
Variation 1	6.90±0.99 a	6.93±0.87 a	7.40±1.10 b	6.93±0.78 b	7.33±0.76 b	7.17±0.79 b
Variation 2	8.50±0.57 d	8.17±1.08 c	7.97±0.81 c	7.40±1.00 c	8.07±0.78 c	8.13±0.82 c
Variation 3	7.50±0.97 b	7.27±1.08 a b	6.83±0.95 a	6.33±0.96 a	6.57±0.93 a	6.77±0.77 a
Sig*	0.000 *	0.000 *	0.000 *	0.000 *	0.000 *	0.000 *

* Significance at 5 % level. Values are expressed as mean ± standard deviation. Samples with different superscripts within a column are significantly different from one another at ($p \leq 0.05$).

Table 3: Comparison of nutrients between control and accepted variation of waffles (100 gms)

S. No	Parameters	Control	Accepted Variation (V2)	Difference
1	Energy(Kcal)	218	370.95	+152.95
2	Protein(g)	5.92	6.90	+0.98
3	Fat(g)	13.2	20.28	+7.08
4	Carbohydrate(g)	24.68	40.23	+15.55
5	Fiber content (g)	0	1.44	+1.44
6	Moisture (%)	31.50	30.83	-0.67
7	Total sugar (g)	24.68	18.34	-6.26

8	Iron (mg)	1.7	41.42	+39.72
9	Zinc (mg)	0.51	9.89	+9.38
10	Potassium (mg)	119	1478.27	+1359.27
11	Calcium (mg)	191.25	83.50	-107.73

Table 4: Qualitative analysis of phytochemicals in accepted variation of waffles

S.NO	Qualitative Analysis	Present/ absent
1	Polyphenols	++
2	Flavonoids	++
3	Tannins	++
4	Alkaloids	++

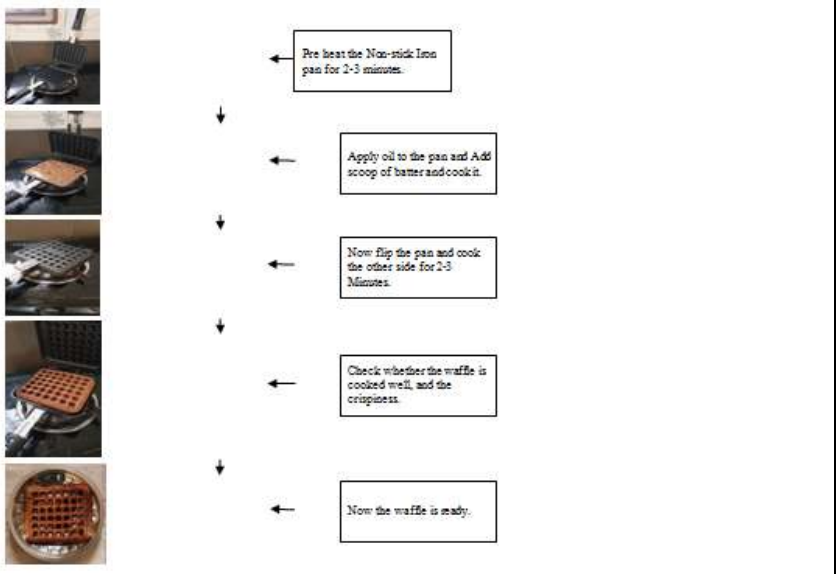

Figure 1: Formulation of pomegranate peel powder incorporated waffles

Vol.15 / Issue 83 / Apr / 2024 International Bimonthly (Print) – Open Access ISSN: 0976 – 0997

RESEARCH ARTICLE

Impact of Artificial Intelligence and Their Influence on Future Workforces and Employment

R. Prema[1]* and K. Subramaniam[2]

[1]Associate Professor, Department of Commerce, KPR College of Arts Science and Research (Affiliated to Bharathiar University) Coimbatore, Tamil Nadu, India.
[2]Associate Professor, Department of Commerce and Management, Kamban College of Arts and Science (Affiliated to Bharathiar University, Coimbatore) Tirupur, Tamil Nadu, India.

Received: 23 Oct 2023 Revised: 29 Dec 2023 Accepted: 15 Mar 2024

***Address for Correspondence**
R. Prema
Associate Professor, Department of Commerce,
KPR College of Arts Science and Research
(Affiliated to Bharathiar University) , Coimbatore, Tamil Nadu, India.
Email: rprems6@gmail.com & prema.r@kprcas.ac.in

ABSTRACT

The rise of artificial intelligence (AI) has the potential to drastically impact the workforce in the near future. This paper explores the potential impact of AI onemployment and the future workforce, including both the positive and negative effects. On the positive side, AI can enhance productivity and efficiency, leading to increased economic growth and job creation. With the development of AI, businesses can automate repetitive tasks, freeing up employees to focus on more complex and creative work. In addition, AI can help companies make more informed decisions, leading to improved customer satisfaction and increased profits. However, there are also negative impacts of AI on employment. As AI technologies improve, they have the potential to replace human workers in certain industries. For example, manufacturing jobs have already been impacted by automation, and service jobs such as those in the transportation industry could be next. This could lead to a significant loss of jobs for low-skilled workers, who may struggle to find alternative employment. In addition, AI could exacerbate income inequality, as high-skilled workers who are able to work with and develop AI technologies may see their salaries rise while low- skilled workers are left behind. If AI algorithms are developed by a homogenous group of individuals, they may be biased against certain groups of people, leading to discrimination in hiring and other employment decisions. Additionally, as AI becomes more prevalent in the workforce, workers may feel a loss of control over their jobs and the decision-making process. This could lead to increased stress and burnout, as well as a decrease in job satisfaction. To mitigate the potential negative impacts of AI on employment, policymakers and businesses must take proactive steps. This includes investing in education and training programs to help workers develop the skills necessary to work alongside AI technologies, as well as developing regulations to prevent bias in AI algorithms.

Additionally, businesses should be transparent about their use of AI and involve workers in the decision-making process to ensure that they feel valued and engaged. In conclusion, while AI has the potential to revolutionize the workforce and bring about positive change, it also has the potential to negatively impact employment and exacerbate income inequality. By taking proactive steps to mitigate the potential negative impacts, AI should be used in a responsible and equitable manner.

Keywords: AI in Employment, AI with Human Intelligence, Future Workforce and Intervention of AI.

INTRODUCTION

Every new discovery will have both benefits and drawbacks, but it is our responsibility as humans to manage this and make the most of the benefits to advance humankind and the globe. Artificial intelligence has great potential advantages. In order to keep the "rise of the robots" from getting out of control, humans must play a significant role. Others contend that artificial intelligence has the potential to wipe out human civilization if it gets in to the wrong hands. However, none of the AI programmes developed at that level had the capability to kill or enslave people. With autonomous cars and voice automation in homes, artificial intelligence has fast developed and is no longer just a concept from science fiction films and books. The predictions made for 2054 in the critically acclaimed film "Minority Report" are coming true more quickly than anticipated. In a study undertaken by experts at the University of Oxford, it was shown that artificial intelligence will exceed humans in a number of jobs by the years 2024, 2026, 2031, 2049, 2053, and 2031, including generating bestselling books, writing essays for school, and selling things. Artificial intelligence (AI) will inevitably outperform human intelligence in the coming years, affecting every area of our lives.

By employing facial recognition software rather than a key to access a hotel room, the face will function as the customer's identity, simplifying and streamlining daily interactions. Within minutes of placing an order, smaller drones will deliver therequested products right to our door. Virtual assistants powered by artificial intelligence will conduct human-like phone calls to set up an appointment. The time is not far away to have surgery performed by a robot. In a few years, a robot will do the procedure in place of a physical surgeon and help patients better comprehend their treatment options. These are only a few examples of the future-changing effects of artificial intelligence. Artificial intelligence future technology advancements may seem far off, yet they will come faster than anticipated. Leading tech firms are competing with one another to incorporate artificial intelligence into their everyday lives, which will open the door for a genuinely fantastic and exciting artificial intelligence future.

REVIEW OF LITERATURE

Moradi P. & Levy K. (2020) explored that many people have raised concern about the mass displacement of human workers as AI-driven technologies are being integrated into workplaces and labor procedures. The study offers a more nuanced perspective on the widely held belief that robots will replace humans in the workforce. We argue that economic predictions of significant job losses brought on by AI are of limited practical value because they frequently concentrate only on the technical aspects of task execution, ignoring broader contextual inquiry about the social aspects of work, organizational structures, and cross-industry effects. **Shaukat K.(2020)** examined the traits and behaviors of numerous robot types. The study examined that how robotics and humans are evolving together. By creating a working system that solves issues and produces good results and there is a need to better understand how the human brain works. Artificial intelligence is a huge field that is also making headway in the areas of business, healthcare, and quality control. **Rauf, Muhammad Abdul (2021)** instigates that as robots have made everyone's lives more laid-back and pleasant, there is an increasing amount of commonplace human-robot interaction. There is a need to understand how people and robots are evolving together. A number of field's and components have been included in this analysis as well as work done by several technicians and scientists. By

developing an effective system that solves issues and produces positive outcomes, it is essential to have a better understanding how the human brain functions.

Boyd, Ross. (2021) discussed about the impact of AI-powered technologies on the2016 US Presidential elections which were dominated by allegations of Russian meddling via large-scale troll farms, the leak of documents and emails from different Democratic Party servers, and the scandal involving Facebook and Cambridge Analytica. Throughout the 19th century, the work of significant political and economic philosophers vividly reflected the ambivalence that accompanied the early experiences of industrialization. In his 1930 essay, Keynes suggested that eliminating Adam's Curse will lead to the emergence of two more issues. Numerous experts have noted the issues with abstraction and lack of depth that come with using employment aggregates to gauge how sophisticated technology is affecting the workforce. **Anagnoste, Sorin, (2021)** stated that the companies are transferring their workloads to software robots through the use of automation, whether it be in the cloud, on- premise, or hybrid like. This transforms the outdated operating models, reduces labor, and creates employment that is better suited for people. With the rise in customer demand for self-services and the increasing dominance of messaging platforms in this environment, businesses are now able to create internal and external communications without the need for a new user interface. Modern chat bots are excellent enablers of human-to-robot contact, and their industry is anticipated to grow significantly over thecoming years. Chat bots can overcome difficulty and confusion in language thanks to the technologies that support natural language processing (NLP) and intent recognition. Ekaningrum, Nurul Efri, Muhammad Syahrul Hidayat, and Farida Yuliati. (2023) explained that nonetheless, this may jeopardize people's employment chances. This study was done to determine how automation and AI are affecting human jobs. The information used in this study was derived from a number ofresearch findings and earlier investigations that continue to address the usage of AI and automation in the workplace. According to this study, automation and AI are currently displacing many employments. Yet, other aspects of human intelligence, like intuition and empathy, are still challenging for AI to replicate

Objectives of the Study

- To analyze the scope of AI in generating the employments.
- To know the impact of artificial intelligence and their influence on future workforces andemployment.

RESEARCH METHOOLOGY

A descriptive research design was adopted for the study. Simple random sampling technique has been used for the study. The sample size considered for the study is 150. The area of the study is Tirupur and Coimbatore city. Tirupur is also known as the knitwear capital of India, accounting for 90% of India's cotton knitwear export. It contributes to a huge amount of foreign exchange in India. Coimbatore is the third largest city in the state and one of the most industrialized cities in Tamil Nadu, known as the textile capital of South India or the Manchester of the South India. The study includes quantitative data gathering, including questionnaires that gathered numerical data from a variety of people, including workers, housewives, businessmen, retired people, professional etc., These persons were deemed as sample for the study. For the study, both primary data and secondary has been taken into consideration. Primary data was gathered by using questionnaire and collected through Microsoft forms. Secondary data have been collected from different sources like journal, websites, magazines etc.

AI's Interference in Modern Period

Artificial intelligence, or AI, seems to be a popular topic right now. It has been noticed that job applicants are increasingly looking for AI expertise. In its simplest form, artificial intelligence combines computer science and huge data sets to facilitate problem-solving. Additionally, it incorporates the artificial intelligence subfields of deep learning and machine learning, which are frequently studied in tandem. These industries create expert systems that classify information or make predictions based on incoming data using AI algorithms. Without external input, the AI uses the facts presented to make decisions and choices that are appropriate to the environment. By and large, "AI"

conjures up nightmares or science fiction fancies of computers conquering society. Although no one can predict with confidence how artificial intelligence (AI) will grow in the future, the current trends and advancements offer a very different picture of how AI w ill effect our daily lives. Artificial intelligence (AI) has been portrayed in the media in a broad variety of ways. In reality, artificial intelligence (AI) is already widely used and has an impact on a variety of things, including our search engine results to make purchases. Data indicates that during the past four years, the use of AI has grown by 270% in a varietyof corporate industries.

A few examples of AI applications include advanced web search engines like google search, recommendation systems, voice assistants that can understand human speech like Siri and Alexa, self-driving cars like Waymo, generative or creative tools, automated decision making, and dominating the best strategy game systems (like chessandgo). Computers grow more skilled; tasks that were once considered to require intelligence are now routinely removed from the concept of AI. Rapid optical character recognition is frequently left out of definitions of AI, despite the fact that it is a widely used technique. There are several subfields in AI research, each with its own set of goals and resources. Natural language processing, planning, learning, reasoning, knowledge representation, vision, and the capacity to move and manipulate objects are among thetraditional goals of AI research. General intelligence is one of the long-term goals in the area. Researchers in AI have used a variety of tools to approach this problem, including artificial neutral networks, formal logic, search and mathematical optimization, method-based statistics, probability, and economics. A wide range of other fields, such as computer science, psychology, linguistics, and philosophy, are also incorporated into AI. Artificial intelligence has seen numerous waves of hope, disappointment, and funding loss (AI winter), followed by new methods, successes, and increased funding since it was first established as an area of research in 1956. Since its inception, researchers have tried and failed with a wide range of approaches, including brain simulation, human problem-solving modeling, formal logic, a significant amount of information, and animal behavior imitation. In the first decade of the twenty-first century, very mathematical statistical machine learning has dominated the field, and this approach has been very successful in assisting with the resolution of many challenging problems in both industry and academia. Ancient Greece is where the concept of a "machine that thinks" first appeared however, significant developments and turning points in the development of artificial intelligence have occurred since the invention of electronic computing.

AI On Par Comparison with Human Intelligence

This field was founded on the theory that human intelligence may be so precisely described that a machine can be built to stimulate it. Since antiquity, myth, literature, and philosophy have all explored these issues. This sparked philosophical debates on the nature of the mind and the moral implications of creating artificial beings with human-like intelligence. Since then, computer scientists and philosophers have suggested that artificial intelligence (AI) may wind up becoming an extension of humans if it is not directed in using its logical abilities for the benefit of society. While traditional human activities are being displaced by digital life, human skills are increasing. Code-driven systems now have access to more than half of the world's population, opening up opportunities and threats that weren't previously imaginable. This is made possible by ambient information and connection.

The scientists predict that networked artificial intelligence would improve human performance but also endangering their autonomy, agency, and abilities. They talked about a variety of scenarios, including the possibility that computers could eventually match or even surpass human intelligence and capabilities in a variety of domains, including visual acuity, speech recognition, language translation, and sophisticated analytics. Examples of these domains include complex decision-making, reasoning, and learning. Smart systems would lower costs, save lives, and provide more custom- made features in automobiles, buildings and utilities, farms, and commercial operations. A number of the upbeat remarks focused on health care and the various ways AIcould be used to diagnose and cure patients, or to help seniors live longer, healthier lives. AI could contribute to extensive public health initiatives based on the massive amounts of data that may be obtained in the approaching years regarding everything from nutrition to individual genomes. Additionally, some of the experts predicted that AI would enable long-needed advancements in formal and informal education systems. However, whether they are optimistic or pessimistic, the majority of experts expressed concerns about how these new technologies may impact the core

characteristics of what it means to be a human in the long run. In this non-scientific interview, the respondents were asked to express a precise reason as to why they believed AI would benefit or harm humanity.

AI's Current Position in the World

Artificial intelligence (AI) technologies are currently used in a wide range of industries, from consumer electronics to customer service software and technological arms races. Both the collection of patient data and the formulation of patient-specific health findings involve their utilization in the healthcare sector. During the COVID-19 Pandemic, AI techniques were utilized to monitor people's health behavior, which has the potential to save lives. Even in space, AI is assisting astronauts and looking for NASA scientists around the cosmos. It is employed in the creation of autonomous vehicles, in trade and banking, and even in military applications like as training and unmanned weaponry. The boundaries of AI applications are still being explored, and businesses, organizations, and institutions all around the world are integrating AI technology into their operations and advancements. The existing uses of AI have led to unfairness and ethical concerns, quite apart from the exciting insight into future possibilities they provide.

DISCUSSIONS AND FINDINGS

From the descriptive analysis, the researcher found that majority of the respondents are female, qualified with under graduation and they are in the age group of 20 to 30 years with the family annual income of between Rs 1,00,000 to 3,00,000. Majority of the respondents came to know about AI tools through social media in the past 2 to 3 years. They think future of AI will be exceptional and there will be more possibilities that AI will make humankind shudder. Most of the people think that our job will be secured in the future with AI and they opined that the intervention of AI in bank is good as the provided data cannot be tampered. They agreed with the AI's contribution in medical field without emotional conscience and have said that the human creativity cannot be achieved by AI. Majority of the respondents thought that creative, emotion- based activities cannot be replaced by AI, and the effect of AI in ten years will cause massive unemployment and AI will be beneficial to human race. They may choose AI along with external factors to make proper decision and any fraud and extra charge can be avoided. By using analysis of variance, it is inferred that there is no significant difference in the mean value of revolution due to intervention of AI with age of the respondents. Majority of the respondents agreed that data-based works will be overtaken by AI. Further, the respondents opined that the prime problem faced due to the advancement of AI is in marketing functions and the benefit of AI is reduction in human error. Majority of the respondents thought that AI will gain success within '5 to 10 years'. It is inferred that majority of the respondents opined that the Customer service executive role will be greatly influenced by the AI. To find out the significant association between the educational qualification and the problems due to intervention of AI, chi-square test is applied. It has been found from Chi-Square test that p value (0.111) is more than 0.05, therefore the null hypothesis is accepted. Therefore, it is concluded that there is no significant association between the educational qualification and the problems due to intervention of AI.

To find out the impact of artificial intelligence on future workforce and employment, the multiple regression method is applied. In this, the impact of AI is the dependent variable, and its effect on Employment, the banking Sector, and Transport Sector are the independent variables. The above table depicts that multiple correlation co-efficients (R) indicate the impact of AI on future workforce and employment which will influence to affect the various sectors like employment, the banking sector and transport sector. The Co-efficients of determination (R^2) indicates 22.7% impact on artificial intelligence on employment, banking and transport sector. The following F ratios in ANOVA tests the independent variables statistically significantly influence the dependent variable. The above table revealed that the significance value ensures multiple regressions on the variables. The significance value is less than 0.05, therefore the impact of artificial intelligence which will influence to affect the various sectors like employment, banking and insurance sector. The multiple regression equation is on impact of artificial intelligence = 3.879 - 0.145(BS) - 0.166(TS) + 0.037(E). From the regression equation it is found that impact of artificial intelligence has more

negative impact on transport sector. In similar way impact of artificial intelligence has next negative impact on Banking Sector. But impact of artificial intelligence has positive impact on employment. It may be concluded that the impact of artificial intelligence is more positively influenced to affect the future workforce and employment other than the banking and transport sector.

CONCLUSION AND RECOMMENDATION

Even though around 1.7 million jobs have been lost due to automation since 2000, according to the study, Artificial Intelligence is expected to create 97 million new jobs by 2025. Only a few people are aware about AI, so it can be made more accessible to every people in future. Possibly monotonous and the boring tasks will be given preference and replaced by the AI in future. Hazardous jobs that are being performed by human can be switched over to the AI, in this way unwanted loss of life can be prevented. By the implementation of AI in work force there will be less paper work,as it analyses the data and generates accurate and reliable data. Implementing AI- powered recruitment systems may lead to streamline the hiring process and reduce bias. By utilizing AI-based performance analysis tools to provide real-time feedback and insights, which can help employees improve their work quality. AI holds the key to unlocking a magnificent future where driven by data and computers that understand the world, and making more informed decisions. Artificial Intelligence (AI) has rapidly transformed from a futuristic concept to an everyday reality. As AI becomes more integrated into our daily lives, it has the potential to revolutionize industries and improve human experiences in numerous ways. Intervention of AI in the job sector has made an impact of doing the jobs effectively and with minimum error. Though the respondents have concern about their jobs being replaced and their privacy being disturbed by AI, they still choose AI for data related services as it cannot be altered or tampered to their needs. Artificial Intelligence will be unbiased and will ensure data accuracy.

REFERENCES

1. Masayuki, M. O. R. I. K. A. W. A. (2016). The Effects of Artificial Intelligence and Robotics on Business and Employment: Evidence from a survey on Japanese firms. *Res. Inst. Econ. TradeInd*, 16.
2. Kaur, Bhajneet, and Sanskriti Sharma. (2016). Will Artificial Intelligence take over our jobs a human Perspective on Employment Future. *International Journal ofEngineering Applied and Management Sciences Paradigms*, 216-218.
3. Frey, Carl Benedikt, and Michael A. Osborne. (2017). The future of employment: How susceptible are jobs to computerization? *Technological forecasting and social change*114,254-280.
4. Fossen, Frank M., and Alina Sorgner. (2018) The effects of digitalization on employment and entrepreneurship. *Conference proceeding paper, IZA–Institute ofLabour Economics*.
5. Jarrahi,M.H. (2018). Artificial intelligence and the future of work: Human-AI symbiosis in organizational decision making. *Business horizons*, *61*(4), 577-586.
6. Frank, Morgan R., etal (2019).Toward understanding the impact of artificial intelligence on labor. *Proceedings of the National Academy of Sciences* 116.14,6531-6539.
7. Muro, Mark, Robert Maxim, and Jacob Whiton. (2019). Automation and artificial intelligence: How machines are affecting people and places.
8. Ernst, Ekkehardt, Rossana Merola, and Daniel Samaan. (2019) Economics of artificial intelligence: Implications for the future of work. *IZA Journal of Labor Policy* 9.1
9. Mrowinski, Benjamin, David Brougham, and David Tappin.(2019) Managers' perceptions of Artificial Intelligence and Automation: Insights into the future of work. *New Zealand Journal of Employment Relations* 44.3, 76-91.
10. Singh, Dheeraj, and Geetali Tilak. (2019) Employment Transformation through Artificial Intelligence in India.
11. Furman, Jason, and Robert Seamans. (2019) AI and the Economy. *Innovation policy and the economy*19.1, 161-191.
12. Daron Acemoglu, Pascual Restrepo March, (2020) The wrong kind of AI? Artificial intelligence and the future of labour demand, *Cambridge Journal of Regions, Economy and Society*, Volume13, Issue.
13. Jameel, Kiran, *et al*. (2020) Current and future impact of artificial intelligence: an employment perspective based

on case studies. *PalArch's Journal of Archaeology of Egypt/Egyptology* 17.9, 660-675.

14. Yang, Yu. (2020) Analysis of the impact of artificial intelligence development on employment. *2020 International Conference on Computer Engineering and Application (ICCEA)*.
15. Graglia, Marcelo Augusto Vieira, and Patricia Giannoccaro Von Huelsen.(2020) The sixth wave of innovation: Artificial intelligence and the impacts on employment. *Journal on Innovation and Sustainability RISUS* 11.1,3-17.
16. Benbya, Hind, Thomas H. Davenport, and Stella Pachidi. (2020) Artificial intelligence in organizations: Current state and future opportunities. *MIS Quarterly Executive* 19.4.
17. Wang, Fenglian, Mingqing Hu, and Min Zhu. (2020) Threat or Opportunity– Analysis of the Impact of Artificial Intelligence on Future Employment. *Digital Human Modeling and Applications in Health, Safety, Ergonomics and Risk Management. Human Communication, Organization and Work: 11th International Conference, DHM 2020, Heldas Part of the 22nd HCI International Conference, HCII 2020, Copenhagen, Denmark, July19–24, 2020, Proceedings, Part II 22*. Springer International Publishing.
18. Moradi,P.,& Levy,K. (2020). The future of work in the age of AI: Displacement or Risk-Shifting?
19. Shaukat, K., *et al*. (2020) The impact of artificial intelligence and robotics on the future employment opportunities. *Trends Comput. Sci. Inf. Technol* 5,50- 54.
20. Rauf, Muhammad Abdul, *et al*. (2021). A comparative study on the impact of artificial intelligence on employment opportunities for university graduates in Germany and the Netherlands: AI opportunities and risks. *International Journal of Environment, Workplace and Employment* 6.3, 185-204.
21. Boyd, Ross. (2021) Work, employment and unemployment after AI 1. *The Routledge social science handbook of AI*. Routledge, 74-900.
22. Anagnoste, Sorin, *et al*. (2021) The role of chat bots in end-to-end intelligent automation and future employment dynamics. *Business Revolution in a Digital Era: 14th International Conference on Business Excellence, ICBE 2020, Bucharest, Romania*. Springer International Publishing.
23. Ekaningrum, Nurul Efri, Muhammad Syahrul Hidayat and FaridaYuliati.(2023) Exploring the Future of Work: Impact of Automation and Artificial Intelligence on Employment. *Endless: International journal of future studies* 6.1125-136.

Table 1 Showing Chi-Square Test

Variable	Chi-Square p value	df	Sig. Value	S/NS	Remarks
Educational Qualification and Problems faced due to intervention of AI	0.111782	9	0.05	NS	Accepted

Table 2 Showing Multiple Correlation Co- efficient

Model	R	R Square
1	0.476	0.227

Table 3 Showing ANOVA test

F	Significance
1.667	0.042

Table 4 Showing Regression Co-efficients

Categories	Unstandardized Co-efficients (B)	T	Significance
Constant	3.879	3.906	0.000
Banking Sector	-0.145	0.950	0.050
Transport Sector	-0.166	0.075	0.008
Employment	0.037	0.355	0.078

RESEARCH ARTICLE

An Experimental Analysis for Forgery Detection of Handwritten Signatures using Deep Learning

Darshini Vipinchandran[1] and Jency Jose[2]

[1]Lecturer, Department of Computer Science, Mount Carmel College, (Affiliated to Bangalore City University), Bengaluru, Karnataka, India.
[2]Assistant Professor, Department of Computer Science, Mount Carmel College, Bengaluru, Bengaluru, Karnataka, India.

Received: 20 Dec 2023 Revised: 29 Jan 2024 Accepted: 13 Mar 2024

***Address for Correspondence**
Darshini Vipinchandran
Lecturer,
Department of Computer Science,
Mount Carmel College, (Affiliated to Bangalore City University),
Bengaluru, Karnataka, India.
Email: darshini.vipinchandran11@gmail.com

ABSTRACT

Handwritten signatures are being used commonly for various transactions which include the banking sector, official documents, registration documents, and many more. It is very crucial to verify signatures as forged signatures can lead to the loss of personal and professional data. There are several ways of signature forgery which include random forgery, unskilled forgery, and skilled forgery. It is very difficult to distinguish between the original and the forged signatures when it is done by a skilled forgery expert. Hence the demand for signature authentication has increased as it is important for ensuring security and improving transparency. In this paper, a study on the different forgery detection methods of handwritten signatures is carried out, and is concluded that Convolutional Neural Network (CNN) is the most popular model used for datasets consisting of handwritten signatures. In this model, the signatures dataset is trained, and estimates are made to identify if the signature is authentic or forged. A survey on the various CNN architectures such as ResNet, GoogLeNet, AlexNet, and YOLO-v3 for forgery detection is carried out. The accuracies obtained using CNN is 96.69%, CNN with ResNet is 88.36%, GoogLeNet is 77.5%, CNN with AlexNet is 85%, and CNN with YOLO-v3 is 98.35%.

Keywords: Architecture, Artificial Intelligence, Convolutional Neural Network, Deep Learning, Detect, Forgery Detection, Handwritten, Machine Learning, Signature

INTRODUCTION

Biometric systems are used to verify individuals as personnel identification is critical in organizations. Various biometric techniques are thumb print, iris examining, and signature verification, the latter of which is still acceptable for social and legal verification. Since everyone's handwriting is different, signature authentication is one of the processes of validating or detecting individuals[1]. An auto graph is defined as a distinctively carved illustration that an individual makes on a record. It is generally used to sign a cheque, a legitimate paper, or a contract. Any individual's signature portrays animage expressing a certain pattern of the pixel that belongs to a specific being. The problem arises when someone attempts to recreate it[2].Since signatures are so widely used, many mischievous groups attempt to forge the signature for personal gain[3]. Images are used in almost every field, including health systems, news sites, social networking sites, legal investigations, schooling, armed forces, and firms. Swift technological improvements have led to the formation and distribution of a massive amount of images in recent years[4].Forgery is a legal concept that refers to the objective to defraud someone. A forged signature has been proven to be false[3].Image tampering has surfaced as a severe illegal issue[5]. Therefore, excellent signature forgery detection approaches are essential[3]. The key goal of signature detection is to sense the spot of signatures on challenging visualized documents and crop the required area. Present signature detection methods are categorized into two. One approach would be to recommend a procedure to extract characteristics and detect signatures. The further approach is to demonstrate the signature discovery task and perform it using deep learning-based methods[6]. Artificial Intelligence(AI) is a program capable of sensing, reasoning, acting, and adapting[7]. Machine learning(ML)is commonly considered a subfield of AI. It is the study of computer algorithms that assist systems to instinctively evolve and learn based on their experiences.

Machine learning algorithms enable machines to make sensible choices without the need for external aid. Such decisions are made by identifying significant underlying patterns in large amounts of complex data. There are three main types of machine learning algorithms depending on their learning technique, the kind of data they request and respond to, and the kind of difficulty they resolve. These are supervised, unsupervised, and reinforcement learning[8]. Deep learning(DL) is a subset of ML which in turn is a field under AI as seen in Figure 1. Deep learning is the procedure that uses multi-layer neural networks as seen in Figure 2 to integrate various machine learning algorithms. For understanding the input data, these distinct processing layers learn data representations with several levels of abstraction[8].Furthermore, DL has progressively turned into the utmost extensively held computational methodology in the field of machine learning, accomplishing outstanding outcomes on a variety of complex cognitive tasks, identical to or as well outperforming human implementation[9]. Deep Learning learns from a massive amount of data. DL has grown rapidly and has many applications. Additionally, in domains such as cyber security, bioinformatics, automation and control, natural language processing, and health information processing, DL has outpaced well-known ML techniques[7].The most well-identified deep learning networks are recursive neural networks (RvNNs), RNNs, and CNNs. Convolutional neural network (CNN) is the most well-known DL network. CNN's advantage is that without any human intervention, it can automatically identify significant features. In domains such as computer vision, speech handling, and face identification CNNs are widely used. CNNs were inspired by human and animal brain neurons[7].A CNN is made up of many convolution layers that come before sub-sampling (pooling) layers, and the final layers are Fully Connected layers as depicted in Figure 3. There are different CNN architectures namely AlexNet, ResNet, GoogLeNet, VGG, and DenseNet[7]. Conventional forgery techniques detect forgeries by aimingat several artifacts for instance changes in lighting, dissimilarity, compression, radar noise, and shadow present in a forged image. Each output map in CNN is created by sharing weights in a convolution operation. Furthermore, instead of relying on engineered characteristics to uncover precise forgeries, CNN uses learned features from training images and can reveal previously unnoticed forgeries. As a result of these gains, CNN is an excellent tool for detecting forgery in images. The CNN-based model can be trained to recognize the abundant objects present in a forged image[10].

LITERATURE SURVEY

The review of the literature as seen in Table 1 provides a summary of existing research on machine-learning methods for detecting forgery in handwritten signatures. The review includes a description of the several algorithms, approaches, and CNN architectures used on different signature datasets. Jerome Gideon et al.[11]analyzed the image dataset of 6000 images. As CNN is the best algorithm for the image dataset, the authors have considered the CNN algorithm in their paper. They got three different accuracies by splitting data into three different training and testing ratios which are 8:2, 7:3, and 6:4, where the 8:2 split gave a better performance with 98.23% accuracy. The proposed system was successful in identifying if the signature was forged or not. However, the structure of the fully connected layer is not optimal[11]. Khan et al.[12] took two datasets into consideration, one with 10,868 records and another one with 3000 benign files. By using two different architectures of CNN, namely GoogLeNet and ResNet the authors were able to construct a model. ResNet model outperformed GoogleNet by showing high accuracy of 88.36%[12]. Jahandad et al.[1] have utilized GoogLeNet's Inception-v1 and Inception-v3 algorithms on the GPDS signature dataset. After analyzing and comparing both models the authors noticed that Inception-v1 showed a better performance with an accuracy of 83%. By considering data augmentation as a step for pre-processing, the overall performance of the model and over fitting of data can also be avoided in future work[1]. Poddar et al.[2]proposed a system that was able to successfully identify the signature holder by checking if the signature is forged or not. The system was economical in recognizing forgeries at the runtime. The authors considered a dataset with 1320 images and made use of theCNN, Crest-Trough method, and SURF algorithm & Harris corner detection algorithms. Among which Harris Algorithm gave the highest accuracy of 94%. In future work, the resulting approach accuracy can be increased by attempting different and better parameter coefficients that increase the deviation between real and forged signatures[2]. Kao et al.[13] have collected data from ICDAR-2011 SigComp for forgery detection.

As the author is detecting forgery using the image dataset the author has used the CNN model which is one of the best-performed algorithms for the image dataset. The algorithm has performed better than average, with an accuracy range of94.37% to 99.96%. The findings determine that the network's performance may be considerably enhanced by raising the numeral of falsified sample seven with a single known sample[13]. Abdulhussien et al.[14] analyzed the dataset which was collected from SID Arabic handwritten signatures, CEDAR, and UTSIG. Using the One-Class SVM(OCSVM) algorithm, the model was built for the collected dataset. "The system improved the 10% false acceptance rate (FAR) of Arabic signature verification on the SID-Arabic signature database without affecting computation time, which achieved 0.037 false rejection rate (FRR), 0.039 FAR skilled, 0.063 FAR simple, and 0.044 and equal error rate (EER). For the UTSig and CEDAR, the suggested method produced EER values of 0.074 and 0.048, respectively". This experiment presented a higher peak signal-to-noise ratio(PSNR) and a lower mean-square error(MSE)[14]. Lopes et al.[15] to verify handwritten signatures, employed a dataset from CIFAR-10. To confirm the handwritten signatures, AlexNet Architecture is been used. The author stated that the model provides a high-accuracy classification for a limited number of samples. The author discussed the study's shortcomings and noted that it takes a long time for AlexNet to train a new model. The described model might perform better if local feature extraction is added[15]. Ryan et al.[16] utilized the YOLO-v3 architecture of CNN on 300 images which were split into an 8:2 ratio. This architecture improved the performance and ability of signature forged detection. This system gave an accuracy of 98.35%. However, new feature selection methods can be implemented to improve the effectiveness of the model[16].

CONCLUSION

Thus the paper focuses on the forgery detection of signatures. Dependable and accurate signature recognition and verification systems are critical for many applications, including law enforcement, access controls, and many corporate processes. It can be used as a middleman to validate multiple reports such as cheques, official records, and certificates.CNN and its different architectures are implemented in most of the papers as it is the best model for

datasets with images in which the signatures datasets are trained, and estimates are made to identify if the signature is authentic or forged. The model produced promising results when CNN architectures were considered. In the future, the accuracy of forgery detection on signatures can be enhanced by increasing the layers in the CNN architectures or by introducing ensemble hybrid models. Due to the difficulty in identifying skilled forgeries in signatures, authentication based on biometrics is significant along with handwritten signatures.

REFERENCES

1. Jahandad, S. M. Sam, K. Kamardin, N. N. Amir Sjarif, and N. Mohamed, "Offline signature verification using deep learning convolutional Neural network (CNN) architectures GoogLeNet inception-v1 and inception-v3," in Procedia Computer Science, 2019, vol. 161, pp. 475–483. doi: 10.1016/j.procs.2019.11.147.
2. J. Poddar, V. Parikh, and S. K. Bharti, "Offline Signature Recognition and Forgery Detection using Deep Learning," in Procedia Computer Science, 2020, vol. 170, pp. 610–617. doi: 10.1016/j.procs.2020.03.133.
3. M. Subramaniam and N. Arpith Mathew, "SIGNATURE FORGERY DETECTION USING MACHINE LEARNING", [Online]. Available: www.irjmets.com
4. K. D. Kadam, S. Ahirrao, and K. Kotecha, "Efficient Approach towards Detection and Identification of Copy Move and Image Splicing Forgeries Using Mask R-CNN with MobileNet V1," Comput Intell Neurosci, vol. 2022, 2022, DOI: 10.1155/2022/6845326.
5. J. Malathi, B. Narasimha Swamy, and R. Musunuri, "Image forgery detection by using machine learning," International Journal of Innovative Technology and Exploring Engineering, vol. 8, no. 6 Special Issue 4, pp. 561–563, Apr. 2019, DOI: 10.35940/ijitee.F1116.0486S419.
6. K. Yan et al., "Signature Detection, Restoration, and Verification: A Novel Chinese Document Signature Forgery Detection Benchmark." [Online]. Available: https://github.com/dskezju/Chisig.
7. L. Alzubaidi et al., "Review of deep learning: concepts, CNN architectures, challenges, applications, future directions," J Big Data, vol. 8, no. 1, Dec. 2021, DOI: 10.1186/s40537-021-00444-8.
8. S. Sah, "Machine Learning: A Review of Learning Types," 2020, DOI: 10.20944/preprints202007.0230.v1.
9. L. Alzubaidi et al., "Review of deep learning: concepts, CNN architectures, challenges, applications, future directions," J Big Data, vol. 8, no. 1, Dec. 2021, DOI: 10.1186/s40537-021-00444-8.
10. S. S. Ali, I. I. Ganapathi, N. S. Vu, S. D. Ali, N. Saxena, and N. Werghi, "Image Forgery Detection Using Deep learning by Recompressing Images," Electronics (Switzerland), vol. 11, no. 3, Feb. 2022, DOI: 10.3390/electronics11030403.
11. S. Jerome Gideon, A. Kandulna, A. A. Kujur, A. Diana, and K. Raimond, "Handwritten signature forgery detection using convolutional neural networks," in Procedia Computer Science, 2018, vol. 143, pp. 978–987. DOI: 10.1016/j.procs.2018.10.336.
12. R. U. Khan, X. Zhang, and R. Kumar, "Analysis of ResNet and GoogleNet models for malware detection," Journal of Computer Virology and Hacking Techniques, vol. 15, no. 1, pp. 29–37, Mar. 2019, DOI: 10.1007/s11416-018-0324-z.
13. H. H. Kao and C. Y. Wen, "An offline signature verification and forgery detection method based on a single known sample and an explainable deep learning approach," Applied Sciences (Switzerland), vol. 10, no. 11, Jun. 2020, DOI: 10.3390/app10113716.
14. A. A. Abdulhussien, M. F. Nasrudin, Z. A. Alyasseri, and S. M. Darwish, "A Genetic Algorithm Based One-Class Support Vector Machine Model for Arabic Skilled Forgery Signature Verification." [Online]. Available: https://ssrn.com/abstract=4303232
15. J. A. P. Lopes, B. Baptista, N. Lavado, and M. Mendes, "Offline Handwritten Signature Verification Using Deep Neural Networks," Energies (Basel), vol. 15, no. 20, Oct. 2022, DOI: 10.3390/en15207611.
16. R. C. Reyes, M. J. Polinar, R. M. Dasalla, G. S. Zapanta, M. P. Melegrito, and R. R. Maaliw, "Computer Vision-Based Signature Forgery Detection System Using Deep Learning: A Supervised Learning Approach," in 2022 IEEE International Conference on Electronics, Computing and Communication Technologies, CONNECT 2022, 2022. DOI: 10.1109/CONECCT55679.2022.9865776.

Table 1 – Comparative Analysis

Author Name	Dataset	Algorithm	Accuracy/Result
S Jerom Gideon et al.	6000 images	CNN with 8:2 split	98.23%
		CNN with 7:3 split	94.83%
		CNN with 6:4 split	96.75%
Riaz Ullah Khan et al.	1) 10,868 records 2) 3000 benign files	GoogLeNet	74.5%
		RestNet	88.36%
Jahandad et al.	GPDS signature	GoogLeNet-Inception-v1	83%
		GoogLeNet-Inception-v2	75%
Jivesh Poddar et al.	1320 images	Harris Algorithm	94%
		Surf Algorithm	85%-89%
Hsin-Hsiung Kao et al.	ICDAR-2011 SigComp	CNN	94%-99.96%
Ansam A et al.	SID Arabic handwritten signatures, CEDAR, and UTSIG	SVM	The experiment provided high peak signal-to-noise ratio (PSNR) and a low mean-square error (MSE)
Jose A et al.	CIFAR-10	AlexNet	85%
Ryan C et al.	300 photos	(You Only Look Once) YOLOv3 of CNN	98.35%

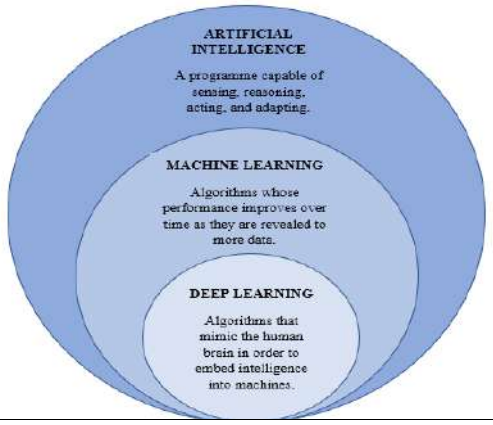

Figure 1 - Relationship between AI, ML, and DL

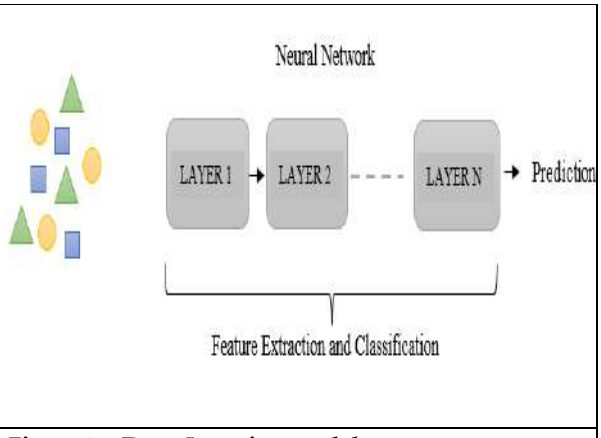

Figure 2 – Deep Learning model

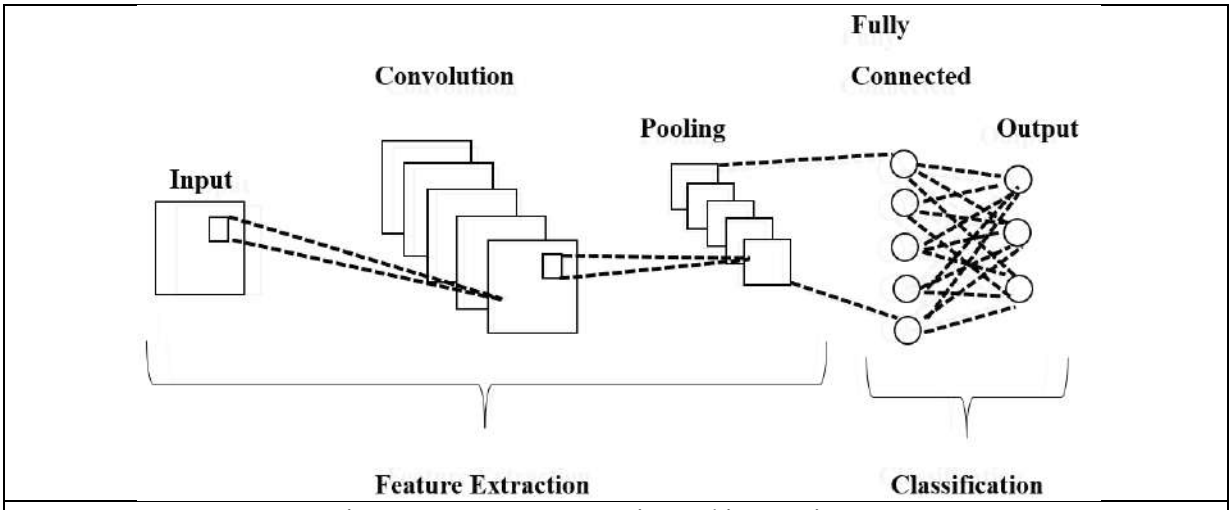

Figure 3 –Image Pre Processing architecture in CNN

RESEARCH ARTICLE

Real-Time Facial Recognition using Drone

Arunachalam. R[1*] and Poovarasan Selvaraj[2]

[1]UG Student, Department of Information Technology, Sri Ramakrishna College of Arts & Science, Coimbatore, Tamil Nadu, India.
[2]Assistant professor, Department of Information Technology, Sri Ramakrishna College of Arts & Science, Coimbatore,Tamil Nadu, India.

Received: 22 Feb 2024 Revised: 15 Mar 2024 Accepted: 21 Mar 2024

***Address for Correspondence**
Arunachalam. R
UG Student,
Department of Information Technology,
Sri Ramakrishna College of Arts & Science,
Coimbatore, Tamil Nadu, India.
Email: 21107071@srcas.ac.in

ABSTRACT

The study develops a facial recognition Unmanned Aerial Vehicle (UAV) solution to help the task force identify criminals, missing people, civilians, and for surveillance purposes. One type of technology that requires knowledge of face detection and identification is a facial recognition system. Typically, it's employed to authenticate users by extracting face traits from photos and confirming user identities. This paper describes an unmanned aerial vehicle (UAV) equipped with a camera, linked to facial recognition software, and utilized for remote robot control. With an accuracy of 98.6% when the drone's camera angle is within 37 degrees, the proposed approach can adapt to changing drone locations. Certain applications help law enforcement officers with their investigations, such as crowd monitoring, crime analysis, search and rescue, and incident investigations.

Keywords: Drone, Facial Recognition, LBPH, Face Net

INTRODUCTION

Technology for facial recognition has gone a long way and is currently developing quickly. We need to understand convolution neural networks (CNN) in order to comprehend the facial recognition algorithms employed in this thesis. Since the 1980s, CNNs have existed and are nothing new. They belong to a class of deep learning methods that may be used to give weights, biases, and learnable significance to different characteristics or objects in a picture. Then, one item may be distinguished from another using these assigned traits. Using convolutional layers, a CNN can recognize an item in a picture. Filters in these layers are capable of detecting simple patterns like an edge or a line. More accurate filters may be applied when convolutional layers are added. A CNN may move from identifying

edges and lines to forms and then to objects, persons, or whatever else it is intended for by iteratively cycling through the filtering process. This technique may now be used considerably more swiftly and effectively, for example in conjunction with a live video broadcast, since processing power keeps increasing. The primary technique for facial recognition systems is now CNNs. Algorithms for facial identification and detection can make use of pre-built models that have been trained using thousands of photos and countless hours of computation. In this thesis, pre-trained models will be combined with the chosen face detection and identification algorithms to develop a drone that can recognize and identify people as well as follow their movements. While computing power has increased, the majority of CNNs still require high-end graphics processing units (GPUs), which are too expensive and heavy to be used in lightweight, low-cost drones. The drone's photos can be sent to a computer with enough processing capacity to help solve this problem. Drones use 2.4 gigahertz radio waves, which are widely compatible with Wi-Fi, to communicate with external devices. This network may be used by the computer attached to the drone to exchange information with it. Faster processing speeds and far better drone reaction times for tracking will result from using a considerably more potent technology for picture analysis. The network does have limitations, though. There is a potential that the drone and computer might lose contact for brief periods of time or perhaps become completely separated. The computer and drone have developed a network that allows for two-way communication.

Real-time instructions may be sent from the computer to the drone to control its movement while the drone can provide a live video feed to the computer for analysis. The drone may also update the computer with status information, such as battery life, flying time, and current altitude. Without input from the computer, the drone won't know what to do, hence this network is essential for the system to work. The greatest network range of a drone is a crucial factor since disconnected systems tend to malfunction. The facial tracking component is the last element of the system used in this thesis. The software allows for the designation of a single person as the target, and when that person is located with a confidence level of at least 80%, a specific flag is set alerting the tracking component of the system. The region of the target person's face in the frame in which they were recognized is calculated during tracking. A tiny region denotes a distance from the objective, whereas a big area denotes proximity. In order to keep the target inside a given range in relation to the drone, the computer will perform this analysis and transmit movement directions to the drone. Because the target may swivel their face away from the drone, the drone can also identify the person's centre of the face. The optimal movement instructions will be found and relayed by the computer if the target turns away from the drone; research has shown that this is the best posture for facial identification and recognition. It is crucial for the system to swiftly examine frames since the tracking algorithm only transmits instructions for one frame at a time. One or more of the facial detection or identification systems may operate slowly, review frames from previous seconds, and transmit inaccurate commands to the drone if this happens.

RELATED WORK

Drone has been somewhat of a buzzword recently as interest in them continues to increase and associated prices appear to be falling. Many people have been able to conduct research and carry out computer vision-related tasks while using drones as a result of this accessibility. The major ideas of this thesis are around using a drone to create a system that does real-time facial tracking and recognition. Despite the fact that other academics have carried out related work, none of them have put forth the same real-time automatic face recognition system that tracks people using drones as this thesis does. Academia Sinica's Institute of Information Science researchers have developed a drone-based facial recognition system. The effectiveness of drone face identification was tested empirically using two facial recognition systems—Face++ and identification—while taking into account variables including distance from a person, angle of depression, and drone height. Height, distance, and angle of depression all correspond to the location of the drone. As the drone ascended to heights of 3, 4, and 5 meters, pictures were captured. The drone progressively backed up to a distance of 17 meters from the subject while taking pictures every.5 meters starting at a distance of 2 meters. The researchers discovered that accuracy significantly declined as drone height and proximity to the person grew. At 1.5m for the drone height and 2m for the drone distance from the person, Face++ and Recognition both had 100% accuracy. However, the accuracy of both facial recognition algorithms substantially

decreased as subject distance and drone height grew.17-meter distance Averaged by Face++[5], 5% accuracy at drone heights between 2 and 5 meters. For the same distance, Recognition's accuracy averaged 5%, a significant gain but still far from adequate. Other noteworthy difficulties were scenarios in which the drone was high in the air yet there was little space between it and the subject. Such circumstances led to a high angle of depression, which decreased accuracy and increased the number of true positives—where a person was mistakenly recognized as someone else. This study demonstrated the viability of using drones and face recognition systems together, but the findings also highlighted the system's many drawbacks, which might compromise its accuracy. Researchers from the National Research Council's Institute of Information Science and Technologies (ISTI- CNR) in Pisa also set out to investigate the barriers preventing the use of facial recognition in combination with drones. The key limitation they took into account was the possibility of humans in the picture appearing in low resolution with a drone at a high height.

As a low-quality image makes it difficult to distinguish objects in the frame, this would impair facial detection and recognition systems, thus they sought for ways to enhance it. For facial recognition, they used three models: ResNet-50, SENet, and their own model. They employed dlib, MTCNN, and Open CV-DNN for facial detection. The Drone dataset, which includes both low- and high-quality photos, was used to test and evaluate all three algorithms. During testing, a low-resolution image was used, a facial detection system was applied to it, and then a facial recognition system was used to compare it to its high-resolution counterpart. The top performing system, SENet, only had an accuracy of 24.25 percent utilizing MTCNN at the beginning. They reran the experiments with tighter cropped faces that excluded more of the background, speculating that the poor accuracy was due to the cropping of the detected faces. The model they created with an accuracy of 60.87% utilizing MTCNN was the best-performing system, and the results significantly improved. The efficiency of SENet has also significantly increased; it currently reports an accuracy of 53.56%[1]. This study demonstrated the significance of the identified face's cropping in low-quality photos and the possibility that a tighter crop might improve accuracy. Other researchers at the Xi'an Aeronautical University developed a drone-based security system employing an LBPH face recognizer. The facial recognition technology was operated by the researchers using a Raspberry Pi mounted to their drone. A trained LBPH facial recognizer was employed to clip those faces after the system utilized Haar Cascade to find them in the crowd. The user would be notified if the facial recognizer discovered a match in its dataset so they could take over physical control of the drone or give it fresh instructions. 250 photos of each individual were used to train the facial recognizer, and each image was cropped to solely contain the person's face. To reduce the quantity of information in the photo and shorten the training period for the model, the cropped image was downsized and made black and white. The algorithm could positively identify a person with a minimal degree of confidence of 50%. This minimal degree of confidence was chosen since several problems, particularly those relating to distance, surfaced during testing. The recognition system often found people but lacked the confidence to classify them. To enhance recognition while minimizing false positives, the confidence threshold was gradually lowered.

With an overall accuracy of 89.1%[11], this system was able to recognize individuals in a crowd. For their facial recognition system, researchers at The LNM Institute of Information Technology also went to LBPH. They used LBPH and FaceNet, two facial recognition algorithms. They put these technologies into use on a Raspberry Pi and connected it to a drone, much like many other researchers. It is not a very powerful gadget, but having a Raspberry Pi on a drone has several benefits because all essential processing can be done on it. The drone was able to pinpoint a specific target in a crowd on its own using the two face recognition algorithms. The system did work despite a number of problems, but they determined that because of the hardware restrictions of the Raspberry Pi[7], building an accurate model that could distinguish a face from a crowd is a very difficult undertaking. By transmitting the drone's video to a computer with the appropriate processing ability to precisely analyse each frame and transmit data back to the drone, the technique used in this thesis will address that problem. An extremely comparable experiment was carried out by researchers at the RMK College of Engineering and Technology in Chennai. Additionally, they employed LBPH for facial recognition and Haar Cascade to detect faces in their system. They claimed a far higher accuracy percentage of 98.6%[6], but their system would check the collected faces against every single test image accessible, which could account for this high accuracy rate. The disadvantage of this strategy was that it caused the system to operate at a very sluggish processing speed of just 9 FPS. Both the researchers at Xi'an

Aeronautical University and the researchers at the RMK College of Engineering and Technology employed the identical LBPH system. In addition, LBPH was used in this thesis along with Haar Cascade for the system's facial recognition component. The difference between this thesis and the method developed by the researchers at Xi'an Aeronautical University is that when a certain face is found, the drone will independently start tracking the person instead of giving that information back to the user and waiting for feedback. Deep Drone is a technology that Stanford University researchers created for tracking and identifying objects. In contrast to the method in this thesis, the authors' paper primarily focused on identifying and tracking general populations rather than a single individual. Two basic systems make up Deep Drone; the first is a detection technique that uses a CNN to look for any individuals in the frame. The second system is the tracking algorithm, which makes use of kernel correlation filter (KCF) and histogram of oriented gradient (HOG) characteristics. The device could only scan at 1.6 FPS due to the highly slow and computationally demanding process of detecting a human.

When a person was found, the system would draw a box around them and provide the tracking algorithm the location. KCF was able to process much faster at 71 frames per second since it was only conducting tracking on the frames [4]. This method has the disadvantage that it must switch back to utilizing the detection algorithm in order to find people if the subject moves too quickly or if another event causes the tracking algorithm to lose sight of the target. They overcame problems with side profiles and targets that were continually moving by decreasing the amount of confidence needed to designate an object as a person. Although lowering the confidence level might seem like a simple remedy, it can lead to more false positive matches. Modern technologies on the drone were also operating too slowly, making it impossible for it to send movement commands rapidly enough to track the target. They ultimately chose to employ the KCF tracking system because it needed less processing power, but this older method did reduce accuracy. Deep Drone is designed to find and track any person that it finds, however the technology used in this thesis is not. The system used in this study will, however, have a single target person identified in the program, and it will independently discover and track only one person, addressed by scholars at North Carolina State University, Raleigh. They primarily addressed problems discovered by researchers at the Institute of Information Science, Academia Sinica, who discovered that the height of the drone was a significant role in facial recognition. The researchers employed three models—VGG16, VGG19, and InceptionResNetV2—for their investigation. These models were chosen because they are among of the most precise ones in use right now.

They used the Drone Face dataset, which was created to help improve current drone capabilities, to train these algorithms. These pictures were taken from various heights, ranging from 1.5 to 5 meters, and at various separations, ranging from 2 to 17 meters from the subject. The 3 models were then trained using these photos; however, each model underwent a distinct training process for each test. The goal of the testing was to identify the facial recognition model that could adapt to changes in drone altitude the best. The models were tested on photographs taken at 5 meters of drone height after being trained on images acquired between 0 and 4 meters of drone height. When the drone's height was higher during training than during tests, the researchers discovered that models were more accurate. They did discover, however, that InceptionResNetV2 and VGG16 had the ability to recognize faces at a height greater than the height they were trained on. Additionally, they discovered that when the height varied, identification activities were far less influenced than verification ones. When trained on heights lower than the height of the test images, all 3 systems-maintained accuracy levels of over 90% during recognition tasks, but only between 34 and 38% during validation tests[2].They found that training the model with images that are taken from a greater distance and at a higher drone height helped to increase the accuracy of their systems. Additionally, they discovered that InceptionResNetV2 provided the most reliable and accurate findings.

METHODOLOGY

The methodology portion will cover the implementation frameworks for the system created in this thesis. The hardware will be operated by a drone, which will send video from its camera to a computer. This computer will look through each frame of the video feed in real time for a specific person using facial recognition and detection

algorithms. If the person is found, the system's tracking function kicks in, and the drone is given movement instructions by the computer to keep the intended subject in the picture. When these little systems work together, they can form an autonomous drone that is able to find and follow a specific individual.

Drone Operation

In recent years, as drones have become more readily accessible, their use has increased. Today, individuals use drone technology in previously unthinkable ways, such as package delivery, tree planting, and even swiftly providing medical supplies to those in need. The frame, motors, propellers, electric motor controller (ESC), power distribution board (PDB), flight controller, battery, receiver, camera, video transmitter (VTX), and sensors are the 11 fundamental parts that make up a drone. A drone has four degrees of freedom as well. Three translations and one rotation make up the four degrees. Drones can move up, down, left, right, and forward and backward thanks to the three translations. Drones can rotate both clockwise and counter clockwise using this single revolution. Height, distance, and angle of depression are taken into consideration when using the drone. A tiny drone was employed for this thesis. It is a light drone that only weighs 80 grams but has a 13-minute flight time, a 100-meter range, and a 5-megapixel camera that can provide HD video in 720P. This project also made use of the djitellopy Python library, which made it simple to transmit instructions to the drone and receive data from it directly to a computer. A link might be made between the drone and a computer using the connect() function. The stream on() function then transfers the video recorded by the drone to a computer so that it may be used to perform facial recognition on the image. The facial recognition algorithm examines the footage pixel by frame even though it is being streamed live.

The system can also show the stream on a computer and give more details if any individuals are recognized. The tracking component of this project was implemented using the djitellopy library's numerous distinct functions for regulating drone movement. When a target is located, the system allows the user to identify a person as a target, and the drone will then follow that person. A box is created around each face to show who the algorithm has identified it as photographs are evaluated and persons are identified. The system issues movement commands based on the size of the box drawn around the target, if one of those recognized individuals is the target. The drone will get closer until it reaches a predetermined range if the box's surface area is shrinking or has already shrunk. If the area is too large or the target is approaching, the same principle applies. If the target moves side to side, similar movement commands are utilized to rotate the drone, ensuring that the target can be tracked. However, for best tracking, the target's frontal face should always be visible. As indicated in the results section, side profile photographs result in decreased accuracy and images of the back of the head result in zero accuracy.

Facial Recognition Systems

The majority of facial recognition technologies now operate as depicted in Figure 3.4. The system starts with an input image and looks for any faces. If any faces are discovered, they are cropped, and information about facial features is extracted to produce a face embedding, a vector that can be used to identify a person. A classifier is then given access to that embedding or the face traits. The classifier is a model that has already been pre-trained and contains data on one or more individuals that it was taught to categorize. The classifier can output details about the person(s) recognized using the input data and any minimum confidence threshold value set. The three systems that were used in this thesis all function largely similarly. To verify the functionality of the system used in this thesis, three distinct facial detection and recognition systems were constructed for this research. The systems of preference were LBPH face recognizer, FaceNet, and Face Recognition. The LBPH face recognizer was selected because it has been used in earlier work with drones and because it provides a baseline for findings. Due to their remarkable performance in the Labelled Faces in the Wild (LFW) benchmark dataset, FaceNet and Face Recognition were chosen.LFW is a widely accessible dataset that is used to assess a system's face verification accuracy. FaceNet and face recognition both reported 99.38% and 99.63% accuracy, respectively, using the dataset. A test dataset was used by all three systems to train their classifiers to recognize certain individuals. Each participant has 15 tagged photos in the test dataset. Five pictures were shot in a low light environment, five pictures in an ambient light setting, and five pictures in a high light setting. All of the photos were taken with a frontal or side perspective of a person's face against a simple background. On the photos that were given to each system, some uniform actions were also carried

out. All of the offered test photographs were scaled and made black and white for training purposes. Additionally, each photo's face was identified by the algorithms, which then cropped it so that only that portion of the image was used for training. However, because each approach gives certain parts of the face a distinct relevance value, none of the three algorithms produced the same cropping of a face. Streaming photographs from the drone to the computer is another consistent operation. Each system resizes the image and converts it to black and white in order to speed up the facial recognition process because the photos transmitted by the drone are very huge and bright. Each system also shows the stream to the user in a window. To alert the user that a facial detection has taken place, every system draws a box around each face it has identified in the frame. A name will be added to the box if a face matches one in the learned classifier; otherwise, it will simply say "unknown." The program's tracking feature will turn on whenever a certain target is located.

Implementation of LBPH

Due to the volume of prior studies that have used this technology, LBPH face recognizer was chosen. When using LBPH, a pixel is chosen along with a collection of pixels in a predetermined radius. A histogram is then produced using the data collected, and a regional level histogram is produced by combining the pixel level histograms. In order to create a histogram that provides a general description of the identified face[8], the regional level histograms are finally concatenated. To locate similar histograms that would aid in identifying a person, this general histogram can then be utilized for comparison with a classifier. The four basic LBPH parameters that are frequently used are radius, neighbors, grid X, and grid Y. The radius, which indicates the area surrounding the central pixel in the circular local binary pattern, is often set to 1. The number of sample points called "neighbors" is often set to 8 when creating a circular local binary pattern. The numbers of cells in the horizontal and vertical planes are represented, respectively, by grids X and Y. This value is typically set to 8, and more cells produce a finer grid with a larger dimensionality for the final feature vector. Making the model is the first stage in putting the LBPH system into practice. Haar Cascade, a facial detection technique first introduced in 2001 [10], is employed to help create the model. A cascade of classifiers with ever higher levels of complexity is how this system operates. The frontal face cascade, which has classifiers that are excellent at frontal face detection, was employed in this study. LBPH face recognizer and Haar Cascade are combined to construct the trained model. The provided annotated photos are first converted to grayscale by this system before Haar Cascade is used to find faces in each image. After being clipped from the image, the discovered faces are then passed to the LBPH face recognizer, which uses them as training images to build a model. The facial recognition system is then updated with the model. In this setup, a drone continuously broadcasts live video that is dissected and evaluated frame by frame. The trained LBPH face recognizer algorithm may then be used to run and return any matches after using the Haar Cascade to detect any faces in each frame.

Implementation of FaceNet

A universal embedding system called FaceNet has been put out by Google researchers [9]. It functions by employing a deep convolutional network to embed a picture in a Euclidean space. These embeddings include 128 face measures in them, which are subsequently translated to a Euclidean space where like images are grouped together. Although the network's methodology for constructing the embedding is unknown, the results stand on their own. The technique locates the Euclidean embedding of an unknown image and categorizes it according to the nearest known individual. FaceNet was implemented using Tensor Flow for the sake of this thesis. There are three main phases to implementing FaceNet. The first step is pre-processing, which involves cropping and aligning each face in the training data set. The following phase entails learning or embedding face representations in multi-dimensional spaces where distance correlates to the indicator of face similarity. An embedding and classifier were made using the training dataset. The classifier, which integrates the FaceNet model with given Tensor Flow, detect face function, is the last step. Each frame that the drone streams to the program is shrunk, turned to black and white, and then inspected. A Multitask Cascaded Convolutional Neural Network (MTCNN) is built using the Detect face function to locate faces in a frame and store them in an array. The three stages of MTCNN's operation are the proposal network, refine network, and output network. Before the first stage, a preliminary process is carried out. The image is first

scaled up and down several times to help find faces of different sizes. After the preliminary procedure is finished, the proposal network stage is launched. The proposal network is made up of numerous smaller processes, and its first process uses a very low threshold to accomplish facial detection. Due to the low threshold for facial detection, any object in the frame that even somewhat resembles a face will be classified as one. Although this technique yields a lot of false positives, it ensures that all potential faces in the image are recognized. The generated regions constitute the "proposal" and are forwarded to the refine network stage, which is the next step. This stage involves filtering the area and building larger, more valuable bound boxes around the detected faces. The output of the refining network is then used as the input for the output network, which is the last stage. The bounding boxes are final refined in this step, producing a very accurate output of the detected face. The person's identification is then returned once the photos are mapped to the trained classifier and the minimum threshold value is reached

.

Implementation of Face Recognition

The "world's simplest face recognition library" is called face recognition[3]. Face Recognition is constructed using the deep learning face recognition algorithms from dlib, a toolbox for building complicated software with machine learning techniques. In order to find faces in an image, Face Recognition employs the histogram of oriented gradient (HOG). HOG works by choosing a pixel in the image and examining its neighbours to determine how dark the chosen pixel is relative to its neighbors and which direction the image gets darker.[11]After repeating the process for every single pixel, the program keeps track of which way the image becomes darker, and the result is a gradient that depicts the movement of light throughout the entire picture. The direction of each square is chosen depending on the direction that is most common in that part after the image has been divided into 16 by 16 squares. The HOG face pattern, developed by training on numerous faces, is then applied to this version of the image to determine whether or not a face is present in the image and where it is located. face recognition centres and aligns its photos, just like FaceNet does. It maps 68 precise spots on the face using a facial landmark estimation algorithm, which enables the program to centre or realign the image as necessary. face recognition extracts a 128-measurement embedding of each face from the training data set using a deep CNN. The Google researchers that developed FaceNet also developed this system. Encodings were created once the test data set was loaded for the face recognition implementation. Figure 3.6 provides a summary of the actions the face recognition system takes to identify and detect faces. It reads the incoming video stream frame by frame, resizes the frames, and converts them to black and white, just like the other systems. Face encoding was then utilized to create an embedding for each face that was discovered after using HOG to find faces in the frame. These embeddings were then put in comparison with the known face embedding, and the outcome was given. Compared to LBPH or FaceNet, face recognition was implemented much more quickly and efficiently. This is due to the Python face recognition package, which includes functions for many of the implementation processes outlined above. Most of the functions in LBPH and FaceNet have to be written from scratch.

CONCLUSION

The paper describes the development and implementation of a real-time facial recognition and tracking system that uses a drone and computer to find and track a predefined target individual. The facial recognition systems were found to be the most important component of the entire system, and their performance was measured using three separate techniques. Even though each of the other facial recognition systems had unique advantages and disadvantages, FaceNet fared the best when tested in an actual scenario. The results of this study suggest that using a drone in conjunction with face recognition software makes it possible to track an individual. By using a lightweight, inexpensive drone to send footage to a computer that can recognize faces, facial identification is still possible. By streaming video to a computer, this method eliminated a lot of the performance issues found in papers that constructed related systems. Although this system's capabilities are limited for unconnected reasons, it provided a strong foundation for further development.

REFERENCES

1. Amato, Giuseppe, et al. "Multi-Resolution Face Recognition with Drones." 2020 3rdInternational Conference on Sensors, Signal and Image Processing, 2020,https://doi.org/10.1145/3441233.3441237.
2. Deeb, Adam, et al. "Drone-Based Face Recognition Using Deep Learning." Advances inIntelligent Systems and Computing, 2020, pp. 197–206., https://doi.org/10.1007/978-981-15-3383-9_18.
3. Geitgey, Adam. "Machine Learning Is Fun! Part 4: Modern Face Recognition with Deep Learning." Medium, Medium, 24 Sept. 2020, https://medium.com/@ageitgey/machine-learning-is-fun-part-4-modern-face-recognition-with-deep-learning-c3cffc121d78.
4. Han, Song, et al. "Deep Drone: Object Detection and Tracking for Smart Drones onEmbedded System." Stanford.edu, 2016,https://web.stanford.edu/class/cs231a/prev_projects_2016/deep-drone-object 2_.pdf.
5. Hsu, Hwai-Jung, and Kuan-Ta Chen. "Face Recognition on Drones: Issues and Limitations."Proceedings of the First Workshop on Micro Aerial Vehicle Networks, Systems, and Applicationsfor Civilian Use, 2015, https://doi.org/10.1145/2750675.2750679.
6. K.G., Shanthi, et al. "Smart Drone with Real Time Face Recognition." Materials Today:Proceedings, 2021,https://doi.org/10.1016/j.matpr.2021.07.214.
7. Pareek, Bhavya, et al. "Person Identification Using Autonomous Drone through ResourceConstraint Devices." 2019 Sixth International Conference on Internet of Things: Systems,Management and Security (IOTSMS), 2019.
8. Prado, Kelvin Salton do. "Face Recognition: Understanding LBPH Algorithm." Medium, Towards Data Science, 3 Feb. 2018, https://towardsdatascience.com/face-recognition-how- lbph-works-90ec258c3d6b.
9. Schroff, Florian, et al. "FaceNet: A Unified Embedding for Face Recognition and Clustering." 2015 IEEE Conference on Computer Vision and Pattern Recognition (CVPR), 2015, https://doi.org/10.1109/cvpr.2015.7298682.
10. Viola, Paul and Michael Jones, Rapid object detection using a boosted cascade of simple features, Proceedings of the 2001 IEEE Computer Society Conference on Computer Vision and Pattern Recognition. CVPR 2001, 2001, https://doi.org/10.1109/CVPR.2001.990517.
11. Wang, Li, and Ali Akbar Siddique. "Facial Recognition System Using LBPH Face Recognizer for Anti-Theft and Surveillance Application Based on Drone Technology." Measurement an Control, vol. 53, no. 7-8, 2020, pp. 1070–1077., https://doi.org/10.1177/0020294020932344.

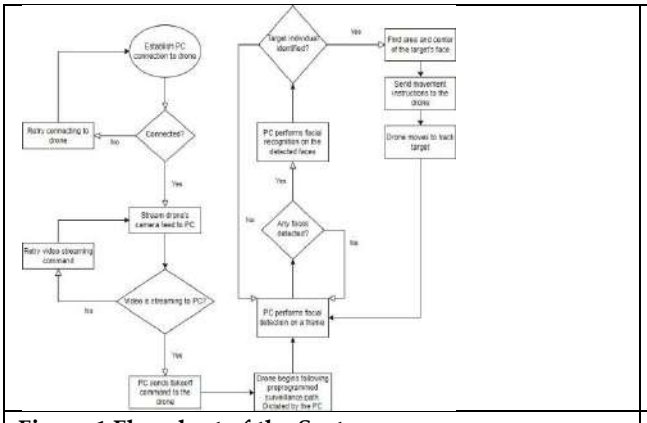

Figure.1.Flowchart of the System.

Figure-.2. Drone used in this study.

Indian Journal of Natural Sciences www.tnsroindia.org.in ©IJONS

Vol.15 / Issue 83 / Apr / 2024 International Bimonthly (Print) – Open Access ISSN: 0976 – 0997

REVIEW ARTICLE

A Review on Enhancing Educational Outcomes: Leveraging Educational Data Mining for Predictive Analysis

D. Gajalakshmi[1*], P.V.Praveen Sundar[2] and R. Denis[3]

[1]Research Scholar, Adhiparasakthi College of Arts and Science, Kalavai, Ranipet Dt,(Affiliated to Thiruvalluvar University, Vellore) Tamil Nadu, India.
[2]Assistant Professor, Adhiparasakthi College of Arts and Science, Kalavai, Ranipet Dt,(Affiliated to Thiruvalluvar University, Vellore) Tamil Nadu, India.
[3]Department of Computer Science, Mount Carmel College (Autonomous), Vasanth Nagar, (Affiliated to Bangalore City University), Bengaluru, Karnataka, India

Received: 20 Dec 2023 Revised: 29 Jan 2024 Accepted: 13 Mar 2024

***Address for Correspondence**
D. Gajalakshmi
Research Scholar,
Adhiparasakthi College of Arts and Science,
Kalavai, Ranipet Dt,
(Affiliated to Thiruvalluvar University, Vellore)
Tamil Nadu, India.

ABSTRACT

Data mining techniques have gained significant interest in the field of education, particularly in educational data mining (EDM). EDM is the application of conventional data mining techniques to address issues related to education, such as student demographics, academic transcripts, test scores, attendance, and student queries. EDM has become a potent tool for predicting academic accomplishment, finding hidden patterns in educational data, and enhancing the learning and teaching environment. The subfields of Data science and machine learning have proven to be extremely well-organized and significant in many domains, including education, over time. A computer system can collect data, evaluate it, and make inferences that appreciate to a feature of artificial intelligence known as machine learning. Assessment systems that predict student achievement have recently been developed in the education sector using data mining and machine learning techniques. Machine learning techniques are being researched in the realm of education to identify meaningful patterns that improve student comprehension. Based on those patterns, academic institutions are making decisions. One important educational measurement metric that affects institution accreditation is the assessment of student performance. Underachievers in those colleges need to be counseled in order to implement a plan for raising student performance. It helps teachers and students work through problems that come up because of the students' coursework and the teachers' teaching strategies. In terms of predicting student performance, this review study looks at a number of studies related to detecting low-performing pupils.

The results of the survey indicated that several machine learning techniques are used to address problems related to risk assessment and student performance evaluation. Machine learning approaches play a major role in improving the student performance prediction system and advancing the field of student performance prediction.

Keywords: Machine Learning(ML), Logistic regression, KNN, SVM, XGBoost, Naïve bayes

INTRODUCTION

Learning analytics has been given a new dimension by EDM, which encompasses various aspects of gathering student data, understanding the learning environment through examination and analysis, and revealing the best student/teacher performance. This includes the collection, measurement, and reporting of data about students and their contexts to optimize learning and its environments. EDM can predict student academic performance, identify trends in system access and navigational behavior, and identify and remove potentially failing students. Digital data left by learning management systems (LMS), student information systems (SIS), intelligent teaching systems (ITS), massive open online courses (MOOCs), and other web-based education systems can be analyzed to assess potential student behavior. These data can be used through EDM to analyze the activities of successful and at-risk students, create remediation plans based on students' academic performance, and support teachers in creating pedagogical approaches. EDM helps instructors forecast events such as dropping out of school or losing interest in the course, analyze internal factors affecting their performance, and develop statistical tools to predict students' academic achievement. Early prediction is a novel phenomenon that involves evaluation approaches to assist pupils by offering appropriate remedial measures and policies in this field. Learning management systems have become an integral aspect of higher education, particularly during the pandemic period. Universities should now strengthen their ability to use these data to forecast academic achievement and ensure student advancement. EDM provides fresh knowledge to educators by uncovering hidden patterns in educational data, allowing some areas of the education system to be assessed and improved to ensure educational quality.

Related Work

E-learning systems have been effectively analyzed in a number of EDM research (Lara et al., 2014). Some research have also attempted to classify educational data (Chakraborty et al., 2016), while others have attempted to predict student achievement (Fernandes et al., 2019) [1]. Asif et al. (2017) and Cruz-Jesus et al. (2020) used machine learning approaches to predict undergraduate students' academic performance. Asif et al. (2017) categorized students into low and excellent achievement groups, suggesting instructors should focus on a few courses with high or low performance to provide early warnings, support, and opportunities [2]. Cruz-Jesus et al. (2020) used 16 attributes to predict academic achievement, using machine learning algorithms like random forest, logistic regression, k-nearest neighbors, and support vector machines [3]. Fernandes et al. (2019) developed a model using demographic information and academic achievement grades to predict students' academic progress. The model used the Gradient Boosting Machine (GBM) to estimate achievement scores and absenteeism. Other studies identified students at risk of failing based on registration data and environmental factors. Hof-faith and Schyns (2017) used DM methods to diagnose students with probable issues and rank them based on their level of danger [4]. Rebai et al. (2020) used machine learning to identify factors influencing school academic performance, finding school size, competition, class size, parental pressure, and gender proportions as the most relevant characteristics. The random forest algorithm revealed that school size and percentage of girls significantly impacted the model's predicted accuracy [5]. Ahmad and Shahzadi (2018) and Musso et al. (2020) used machine learning to predict academic performance and dropout rates. Ahmad and Shahzadi's method, which uses learning ability, study habits, and academic interaction traits, had an 85% accuracy rate [6]. Musso et al.'s model, based on learning techniques, social support perception, motivation, socio-demographics, health status, and academic performance factors, predicted academic achievement and

dropouts [7]. Waheed et al. (2020) developed a deep learning model based on student records for LMS navigation, showing that demographics and clickstream behaviors significantly impact student performance. They concluded that this model could be useful for early performance prediction [8]. Xu et al. (2019) found a correlation between internet usage habits and academic achievement, with internet traffic volume and frequency features positively correlated [9]. Bernacki et al. (2020) found that 75% of students needing to repeat a course were successfully predicted using a behavior-based prediction model. This strategy can help identify and assist students who might not succeed in the upcoming semesters [10]. Burgos et al. (2018) designed a tool for predicting future achievement grades and designed a tool for those likely to fail [11]. A survey of earlier studies looking to forecast academic success shows that a variety of machine learning techniques, such as neural networks, multiple, probit, and logistic regression, as well as C4.5 and J48 decision trees, have been used. Nonetheless, recent studies have used Naive Bayes algorithms (Ornelas & Ordonez, 2017) [12], genetic programming (Xing et al., 2015) [13], and random forests (Zabriskie et al., 2019) [14]. These models achieve extremely high prediction accuracy.

A thorough study of the elements and characteristics that affect students' performance and accomplishments is necessary for accurate prediction of academic performance (Alshanqiti & Namoun, 2020) [15]. In order to do this, Hellas et al. (2018) examined 357 publications on student performance that included information on the effects of 29 attributes. These characteristics were mostly associated with psychomotor skills, including performance in the course and prior to it, student participation, student demographics including gender, high school achievement, and self-control. However, the primary factors influencing dropout rates were habits, lack of development, social and financial concerns, and career transitions among students [16]. According to Praveen et al. [17], identifying disengaged learners more precisely can be achieved using region-wise classification of online learners. The literature evaluation comes to the conclusion that a wide range of characteristics influence the ability to forecast a student's academic performance. Classifying pupils according to where they live also aids in the identification of disengaged learners. According to studies [17], [18], learning is insufficient on its own to identify disengagement. For improved prediction outcomes, they combine the time spent characteristic with the marks secured attribute. As was said in the literature evaluation, a great deal of important characteristics are utilized to forecast the student's log data. The academic performance of students was predicted by Praveen [19] using the naive Bayes method, and the Bayes model assisted teachers in identifying individuals who needed extra support. According to a survey on regional benchmarks of rural and urban students conducted by Praveen et al. [20], there is no significant difference between students who completed their previous coursework in a uniform area (rural or urban), but there is a significant difference between students who completed their coursework in a mixed area.

RESULT AND DISCUSSIONS

A Case Study
Data Used
Here, the datasets taken from kaggle for the comparison of the best performing prediction algorithm among Logistic regression, KNN and support vector machine and other classification algorithms. There were a total of 791 rows of secondary students information with 31 columns of features. The data attribute include demographic social and school related features. Using the ratio of 0:30 split amongst training and testing instances.

Algorithm Used
Support Vector machine
A machine learning approach called SVM classification finds a hyper plane to divide several classes in a dataset. Support vectors, which are the closest data points to the hyper plane, are used to find the solution, which optimizes the margin between the classes. SVM is a memory-efficient, reliable algorithm that can handle datasets that are linearly and nonlinearly separable. Finding the hyperplane that divides the classes and optimizes the margin between them is the goal of the SVM classification algorithm. A two-dimensional linear SVM hyper plane has the following formula:

$$w^T x + b = 0$$

Where the input vector is x, the bias term is b, and the weight vector is w. The decision boundary is given by the formula wT x + b = 0. The input vector belongs to one class if the equation's answer is positive; if it's negative, it belongs to the other class. Non-linear SVM classification is employed when the data in the original feature space cannot be split by a linear hyperplane. To move the data into a higher dimensional feature space where the classes might be linearly separable in this case, the SVM technique uses a kernel function. The Radial Basis Function (RBF) sigmoid, and polynomial are the three most often utilized kernel functions. Similar to the linear SVM classification, the decision boundary formula in higher-dimensional space uses converted feature vectors to produce the weight vector and bias term. The decision boundary can be stated as follows for non-linear SVM classification:

$$W^T \phi(x) + b = 0$$

Where the input vector x is transformed into a higher-dimensional space by the feature mapping function (x). Using the training examples and the optimization problem, the weight vector w and bias term b are determined.

K- Nearest Neighbors

A non-parametric machine learning approach called KNN (k-nearest neighbors) is implemented for classification and regression. It operates by locating the k training dataset data points that are closest to the new input data point and then assigning a class or value based on the vote of the majority or the average of the k neighbors. The KNN classification formula is as follows:

$$y = model\ (y1, y2, \ldots\ldots , yk)$$

Where y is a new data point's projected class label and y1,y2,…,yk are the class labels of the new data points k nearest neighbor's in the training dataset. The mode function gives the k closest neighbor's most prevalent class label. The straightforward formula for KNN in regression is:

$$y = (1/k) * \sum yi$$

Where yi is the value of the new data points ith nearest neighbor in the training dataset and y is the prediction value for a new data point. The formula calculates the values of the k closest neighbors averages.

Logistic Regression

A statistical technique known as logistic regression is used for binary classification, which means it forecasts the likelihood that an input will belong to one of two possible classes. It is frequently utilized in a variety of industries, including marketing, banking, and medicine. Using function to predict the likelihood that an input belongs to one of two groups is the fundamental concept underpinning logistic regression. Any input value can be translated into a value between 0 to 1 using the logistic function, which represents the chance of being in the positive class. The logistic regression equation is:

$$p(y=1|x) = 1/(1 + \exp(-z))$$

Where the possibility that the input x belongs to the positive class is given by p(y=1|x). With weights chosen during training, z is a linear mixture of the input features: z = B0 + B1 x1, B2 x 2, …… + Bn * xn. The coefficients or weights of the logistic regression model are b0, b1, b2 ,…. , and bn. The features are represented by x1, x2,…, and xn. X exp represents the exponential function. To increase the likelihood of the observed data, the logistic regression model finds the optimal values for the coefficients orr weights (b0, b1, b2, …., bn) during training. After the model has been trained, the logistic function with the input features may be used to forecast the likelihood that new input would fall into the positive class. The input is categorized as either belonging to the positive class or the negative class depending on whether the probability exceeds a predetermined threshold, which is typically 0.5.

Naïve Bayes

A probabilistic machine learning approach called Naïve Bayes theorem, it makes the assumption that given the class label, the input features are conditionally independent. It is frequently employed in text classification, spam filtering, and sentiment analysis despite its basic premise, and frequently works well in actual application. The Naïve Bayes formula is:

$$P(y|x) = P(x|y) * p(y)/p(x)$$

When p(y|x) is the high probability that the input x falls under the category y. the conditional probability that input x would be observed given class y is p(x|y). p(x) is the likelihood of witnessing input x, and p(y) is the prior

probability of class y. The Naïve Bayes algorithm is quick and effective, and it performs well with short training datasets and high-dimensional inputs. The conditional independences assumption, however, could not always be accurate, resulting in subpar performance.

Decision Tree Algorithm

The decision tree is a technique to machine learning that is frequently used for applications in classification and regression. The way it works is to divide the input space into smaller chunks based on the values of the input features, then assign a class or value to each section. Each node in the algorithm represents a test on a certain property, and each branch represents one or more possible test results. This creates a tree-like structure.

Partitioning the input space into areas that are as uniform in terms of class labels as possible is the aim of classification. The method is repeated recursively for each group of data until a stopping requirement is satisfied. The algorithm chooses the best feature to split the data depending on a metric like entropy or the Gini index. The objective of regression is to divide the input space into areas that minimize mean squared error or another regression metric. To reduce error, the method chooses the optimal feature and split point, then iteratively repeats the procedure fir each group of data until a stopping requirement is satisfied.

Random Forest algorithm

Random forest is a supervised learning strategy for problems involving classification and regression. It is an ensemble method that builds several decision trees and combines their predictions to produce a model that is more accurate and reliable. The core idea behind the random forest algorithm is to build a lot of decision trees at random, combine their predictions, and reduce. The steps in the random forest method are as follows: Decide how many trees (n) you want to see in the forest. Choose a portion of the training data and a subset of the features at random for each tree. Create the decision tree using the subset of the data and features that you have chosen. Till all of the trees are grown, repeat steps and 3. Pass a new data point through all trees in the forest to predict it, then take the guess with the most votes. The following can be used to forecast the results of a random forest model:

$\hat{y} = model(f_1(x), f_2(x),…,f_n(x))$

Where $haty$ is the expected result, $f i(x)$ is the decision trees i-th output for the input x, and $model$ is the function that gives the decision trees most common output. Instead of the mode, the predicted outcomes in regression problem may be the mean of all the trees output.

XGBoost Classifier

The gradient boosted trees approach is well-liked and well implemented in the open-source framework XGBoost. A supervised learning approach called gradient boosting combines the estimates of several weaker, simpler models in an effort to forecast a target variable with a degree of accuracy. A scalable, distributed gradient-boosted decision tree (GBDT) machine learning framework is called XGBoost, or Extreme Gradient Boosting. For regression, classification, and ranking issues, it is the top machine learning library and offers parallel tree boosting.

Performance Metrics on ML Algorithms

This section assesses and contrasts the algorithms using performance measures like recall, accuracy, and precision. The predictive performance of the model is evaluated using the Cross-Validation technique to estimate how each model performs outside the sample to a fresh dataset that is also known as test data. The reason for using cross-validation approaches is that we fit models to training datasets when we do model fitting. We only have data on how the models perform on training data without cross-validation. In a perfect world, we would test how well the models perform with fresh data in terms of how accurate their forecasts are. In science, the predictive power of a theory is evaluated. It is a popular strategy because it is easy to grasp and produces a less biased or pessimistic assessment of the model skill than other approaches, including a straightforward train/test split.

Accuracy

To assess how well the classification are performing, accuracy is examined. By dividing the total number of occurrences from the dataset by the ratio of correctly predicted instances, accuracy is calculated. According to mathematics, the classification's accuracy is defined as follow:

$$\textbf{Accuracy} = \frac{x}{n} \textbf{ x 100\%}$$

Where x represents how many instances cases were successfully categorized and n represents how many instances cases there were in total. Accuracy in binary classification can be determined using the following positives and negatives:

$$\textbf{Accuracy} = \frac{TN+TP}{TN+TP+FN+FP} \textbf{ X 100\%}$$

where TN = True Negatives , TP = True Positives, FN = False Negatives, and FP = False Positives are all possible outcomes. The accuracy of each model on the training dataset, which is divided into two segments (70% for training and 30% for testing On the testing data, following table lists the 7 algorithms' anticipated accuracy. XGBoost has the highest prediction accuracy with 89%. As a result, other performance metrics like recall and precision are also assessed in order to assess and compare the performance of the models.

Precision

Precision is defined as the ratio of true positive results to the total number of anticipated positive observations. It can be stated mathematically as:

$$\textbf{Precision} = \frac{TP}{TP+TF} \textbf{ x 100\%}$$

The values for each of the seven classifiers precision are displayed in following Table.

Recall

The proportion of accurate positive outcomes to all observations made in the actual class is known as recall, which is also known as sensitivity. It can be written mathematically as follows:

$$\textbf{Recall} = \frac{TP}{TP+FN} \textbf{ x 100\%}$$

The seven classifiers recall values are displayed in Table.

F1 Score

The evaluation matrix known as the F1-score takes the harmonic mean of the two matrices, Precision and Recall, to create a single metric. To put it simply, the weighted average mean of Precision and Recall is the f1 score. In natural language processing, it is also utilized

$$\text{F1 Score} = \frac{TP}{TP + \frac{1}{2}(FP+FN)}$$

.

The calculated metrics have shown in figure 1, It shows that the Decision Tree and XGBoost classifiers performs best in terms of recall, accuracy, and precision. These findings suggest that XGBoost, out of the seven classifiers ML algorithms, is the most accurate at determining student performance.

CONCLUSION

Machine learning techniques have been extensively used in a number of applications, and they have also been carefully evaluated as useful tool for building knowledgeable machines that can advise academicians on how to make decisions based on Student's background information, performance data in school and colleges. With the survey findings and the data analysis with classification algorithms taken into for predicting the students performance The performance of the existing models, including SVM, Logistic regression, KNN, DT, RFA, Naïve Bayes and XGBoost are compared as a benchmark. Decision Tree and XGBoost outperforms with other algorithms in terms of accuracy on the training and test set. after estimate, the predictive models performance is

assessed in terms of accuracy, precision, and recall on unobserved data using the k-fold cross-validation procedure to gauge their aptitude. The study's findings demonstrated that the XGBoost Classifier model performs best in terms of accuracy, precision, and recall, F1 scoring correspondingly.

REFERENCES

1. Chakraborty, B., Chakma, K., & Mukherjee, A. (2016). A density-based clustering algorithm and experiments on student dataset with noises using Rough set theory. In *Proceedings of 2nd IEEE international conference on engineering and technology, ICETECH 2016, March* (pp. 431–436). https://doi.org/10.1109/ICETECH.2016.7569290
2. Asif, R., Merceron, A., Ali, S. A., & Haider, N. G. (2017). Analyzing undergraduate students' performance using educational data mining. *Computers and Education, 113*, 177–194. https://doi.org/10.10 16/j.compedu.2017.05.007
3. Cruz-Jesus, F., Castelli, M., Oliveira, T., Mendes, R., Nunes, C., Sa-Velho, M., & Rosa-Louro, A. (2020). Using artificial intel- ligence methods to assess academic achievement in public high schools of a European Union country. *Heliyon*. https://doi.org/10.1016/j.heliyon.2020.e04081
4. Fernandes, E., Holanda, M., Victorino, M., Borges, V., Carvalho, R., & Van Erven, G. (2019). Educational data mining : Predic- tive analysis of academic performance of public school students in the capital of Brazil. *Journal of Business Research, 94*(February 2018), 335–343. https://doi.org/10.1016/j.jbusres.2018.02.012
5. Rebai, S., Ben Yahia, F., & Essid, H. (2020). A graphically based machine learning approach to predict secondary schools performance in Tunisia. *Socio-Economic Planning Sciences, 70*(August 2018), 100724. https://doi.org/10.1016/j.seps. 2019.06.009
6. Ahmad, Z., & Shahzadi, E. (2018). Prediction of students' academic performance using artificial neural network. *Bulletin of Education and Research, 40*(3), 157–164. [7] Baker, R. S., & Inventado, P. S. (2014). Educational data mining and learning analytics. *Learning analytics* (pp. 61–75). Springer.
7. Musso, M. F., Hernández, C. F. R., & Cascallar, E. C. (2020). Predicting key educational outcomes in academic trajectories: A machine-learning approach. *Higher Education, 80*(5), 875–894. https://doi.org/10.1007/s10734-020-00520-7
8. Waheed, H., Hassan, S. U., Aljohani, N. R., Hardman, J., Alelyani, S., & Nawaz, R. (2020). Predicting academic performance of students from VLE big data using deep learning models. *Computers in Human Behavior, 104*(October 2019), 106189. https://doi.org/10.1016/j.chb.2019.106189
9. Xu, X., Wang, J., Peng, H., & Wu, R. (2019). Prediction of academic performance associated with internet usage behaviors using machine learning algorithms. *Computers in Human Behavior, 98*(January), 166–173. https://doi.org/10.1016/j. chb.2019.04.015
10. Burgos, C., Campanario, M. L., De, D., Lara, J. A., Lizcano, D., & Martínez, M. A. (2018). Data mining for modeling students' performance: A tutoring action plan to prevent academic dropout. *Computers and Electrical Engineering, 66*(2018), 541–556. https://doi.org/10.1016/j.compeleceng.2017.03.005
11. Capuano, N., & Toti, D. (2019). Experimentation of a smart learning system for law based on knowledge discovery and cognitive computing. *Computers in Human Behavior, 92*, 459–467. https://doi.org/10.1016/j.chb.2018.03.034
12. Ornelas, F., & Ordonez, C. (2017). Predicting student success: A naïve bayesian application to community college data. *Technology, Knowledge and Learning, 22*(3), 299–315. https://doi.org/10.1007/s10758-017-9334-z
13. Xing, W., Guo, R., Petakovic, E., & Goggins, S. (2015). Participation-based student final performance prediction model through interpretable Genetic Programming: Integrating learning analytics, educational data mining and theory. *Computers in Human Behavior, 47*, 168–181.
14. Zabriskie, C., Yang, J., DeVore, S., & Stewart, J. (2019). Using machine learning to predict physics course outcomes. *Physical Review Physics Education Research, 15*(2), 020120. https://doi.org/10.1103/ PhysRevPhys Educ Res.15.0201

15. Alshanqiti, A., & Namoun, A. (2020). Predicting student performance and its influential factors using hybrid regression and multi-label classification. *IEEE Access, 8*, 203827–203844. https://doi.org/10.1109/access.2020.3036572
16. Hellas, A., Ihantola, P., Petersen, A., Ajanovski, V.V., Gutica, M., Hynninen, T., Knutas, A., Leinonen, J., Messom, C., & Liao, S.N. (2018). Predicting academic performance: a systematic literature review. In *Proceedings companion of the 23rd annual ACM conference on innovation and technology in computer science education* (pp. 175–199).
17. Sundar PVP, Kumar AVS. "A Novel disengagement detection strategy for online learning using quasi framework," Advance Computing Conference (IACC), 2015 IEEE International, Bangalore, 2015
18. Sundar PVP, Kumar AVS. A systematic approach to identify the unmotivated learners in online learning. Indian journal of science and technology. 2016. April; Vol 9(14): 1-6.
19. Sundar PVP, 'A Comparative Study for Predicting Student's Academic Performance Using Baysian Network Classifiers', IOSR Journal of Engineering, Vol. 03, No. 02, pp. 37-42, 2013
20. Sundar PVP, Kumar AVS. "Evaluation of Regional Benchmark Impact in EDM",International Journal of Computer Science Issues(IJCSI),Vol no-10 Issue -2, no-2, March 2013, PP: 531-535.
21. Babić, I. D. (2017). Machine learning methods in predicting the student academic motivation. *Croatian Operational Reserch Review, 8*(2), 443–461. https://doi.org/10.17535/crorr.2017.0028
22. Harikumar Pallathadka, AlexWenda, Edwin Ramirez-Asís,Maximiliano Asís-López, Judith Flores-Albornoz, Khongdet Phasinam, "Classification And Prediction Of Student Performance Data Using Various Machine Learning Algorithms", Materials Today: Proceedings Elsevier, 2021.
23. Mohammed Nasser Alsubaie, Predicting student performance using machine learning to enhance the quality assurance of online training via Maharat platform, Al- Khurmah University College, Taif University, Alexandria Engineering Journal (2023) 69, 323–339
24. Ihsan A. Abu Amra, Ashraf Y. A. Maghari, "Students Performance Prediction Using KNN And Naïve Bayesian", 8th International Conference on Information Technology (ICIT), 2017.
25. H.M. Rafi Hasan., Mohammad Touhidul Islam., AKM Shahariar Azad Rabby., Syed Akhter Hossain., Daffodil International University, Dhaka, Bangladesh,"Machine Learning Algorithm for Student's Performance Prediction", 10th ICCCNT 2019.
26. Emmy Hossain, Mohammad Hossin, "Student Performance Analysis System (SPAS)", https:// www.researchgate.net/publication/282956807, 2015
27. Hussein Altabrawee.,Osama Abdul Jaleel Ali., Samir Qaisar Ajmi .,*Al Muthanna University, Almuthanna, Alsamawa, Iraq.,* "Predicting Students' Performance Using Machine Learning Techniques"., Journal of University of Babylon, Pure and Applied Sciences, Vol.(27), No.(1): 2019.
28. Shanmugarajeshwari, R. Lawrance, "Analysis of Students' Performance Evaluation Using Classification Techniques", IEEE, 2016.
29. Talla Sai Likhitha et al., Madanapalle Institute of Technology and Science, "Student Academic Performance Prediction Using Machine Learning"., IJCRT | Volume 10, Issue 5 May 2022 | ISSN: 2320-2882.
30. Ajibola Oyedeji, Olaolu Folorunsho, Olatilewa Raphael Abolade, "Analysis And Prediction Of Student Academic Performance UsingMachine Learning", https://www.researchgate.net/ publication/340310208, 2020.
31. Leila Ismail, Huned Materwala, Alain Hennebelle, "Comparative Analysis Of Machine Learning Models For Students' Performance Prediction", https://www.researchgate.net/publication/350057919, 2021.
32. Annisa UswatunKhasanah, Harwati, "AComparative Study to Predict Student's Performance Using Educational Data Mining Techniques", IOP Conference Series: Materials Science and Engineering, 2017.

Table 1. Summary of related work on student performance prediction with various Machine Learning Algorithm.

Related Papers	Features	Methodologies	Dataset Source	Result
Predicting student performance and	Seven publicly available datasets	Hybrid Regression Model (HRM)-	Public datasets.	The research establishes a potent

its influential factors using hybrid regression and multi-label classification [15].	with various attributes.	1.Collaborative filtering technique 2.Fuzzy rules 3. Lasso linear regression Multi-Label Classification For Predicting Key Factors.		hybrid approach for accurately predicting student academic grades and identifying pivotal performance factors.
Machine learning methods in predicting the student academic motivation [21].	Variables : Assign view(V1), Forum view discussion(V2), Questionnaire view(V3), Resource view(V4).	Neural Networks, Decision trees, and Support Vector Machines.	Faculty of Education in Osijek.	The results showed that the RBF neural network model performed better with classification accuracy of 76.92%.
Classification and prediction of student performance data using various machine learning algorithms [22].	18 Attributes	SCM, Naïve Bayes, C-4.5, ID3	UCI Machinery Student Performance (649 instances)	SVM is better
Predicting student performance using machine learning to enhance the quality assurance of online training via Maharat platform [23].	Gender, Academic Specialization, Academic degree, The number of training courses you attended through the ‘‘Maharat” platform.	K-nearest Neighbourhood, Naïve Bayes, Decision Tree, Support Vector Machine.	Maharat platform at Taif University based on the online learning training standards in the Kingdom of Saudi Arabia (KSA).	SVM is better with 93.2% accuracy.
Students performance prediction using KNN and Naïve Bayesian [24]	DOB, Gender, City, Secondary School Name, Specialization, Fathers Job, Student Status	KNN, Naïve Bayes.	Gaza Strip 2015 (500 instances)	Naïve Bayes is better than KNN
Machine Learning Algorithm for Student’s Performance Prediction [25].	Class Test Marks, Attendance Mark, Presentation Mark, Assignment Marks, Midterm Marks And Final Examination Marks	Linear Discriminant Analysis, Gradient Boosting Classifier, Random Forest Classifier, SVC, KNN and Decision Tree Classifier.	Daffodil International University Dhaka, Bangladesh. (1170 Student’s data)	The most perfect result and accuracy with K-Nearest Neighbors, Decision Tree Classifier model with an accuracy of 89.74% & 94.44%.

Student performance analysis system (SPAS) [26].	Quizzes, Assignments, projects, Final examination Grades, Gender, Programs	J-48, Simple CART, BFTree, Random Tree, J-48 Garft	TMC1013 System Analysis and Design in University of Malaysia Sarawak	BF-Tree is better, TMC-1013 System Analysis assist to predict the student performance accurately
Predicting Students' Performance Using Machine Learning Techniques [27].	The dataset contains 161 student records, 76 male and 85 female. The dataset contains twenty attributes.	Artificial Neural Network,Decision Tree, Logistic Regression, Naïve Bayes.	Archeology and the Sociology department of the college of Humanities at Al-Muthanna University	The most accurate model is built using Artificial Neural Network which has an accuracy of 77.04.
Analysis and Prediction of Student Academic Performance Using Machine Learning [28].	22 Attributes.	1. Linear Regression for Supervised Learning 2. Linear Regression for Deep Learning	Kaggle Dataset (648 instances)	Liner Regression for Supervised learning is best.
Student Academic Performance Prediction Using Machine Learning [29]	Name, Grade Id, Semester, Parent Survey, Label.	SVM, Decision Tree, Logistic Regression	Public Dataset.	Highest accuracy for decision tree algorithm which is 96.96.
Prediction of Students Performance using Educational Data Mining [30].	19 Attributes	Naïve Bayes	Amrita School of Arts & Science, Mysure	Naïve Bayes is used for knowledge classification.
A Comparative Study to Predict Student's Performance Using Educational Data Mining Techniques [31].	MEDU, Attendance, 1st semester GPA	Naïve Bayes, Decision Tree	Industrial Engineering University, Islam, Indonesia	Naïve Bayes is performing better.
Using Machine Learning models to predict student retention: Building A State-wide early warning system [32].	15 Attributes	LR, NB, DT	Administrative student data (179517 records)	Predict at risk students with 80% probability.

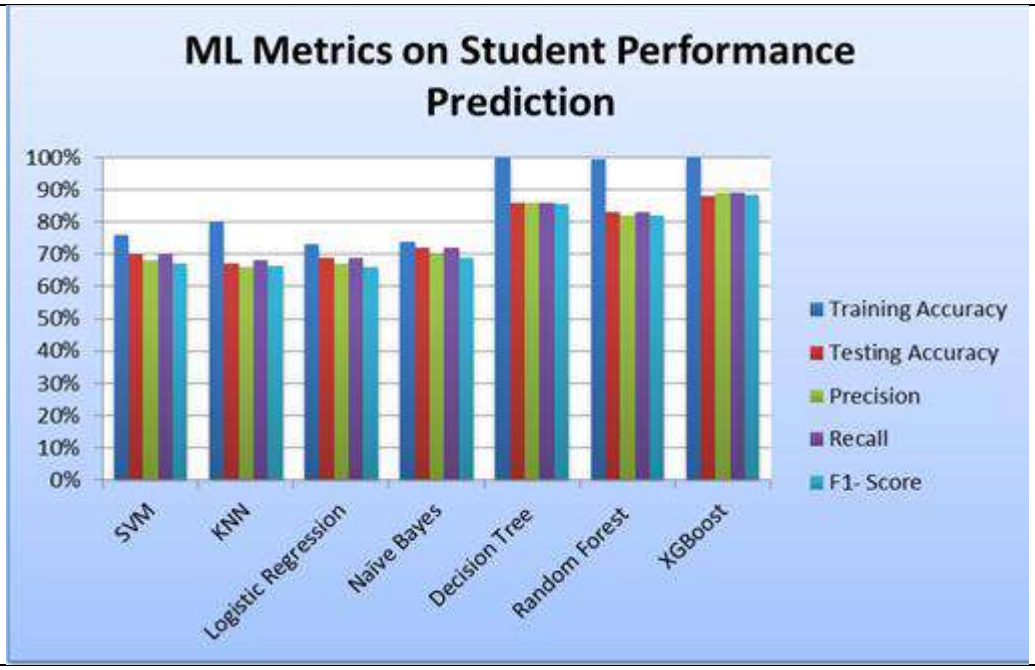

Figure 1 Metrics calculated for Student data prediction with ML Classification Algorithms

Vol.15 / Issue 83 / Apr / 2024 International Bimonthly (Print) – Open Access ISSN: 0976 – 0997

RESEARCH ARTICLE

A Stacking Ensemble of Deep Cluster (En-MHSAMKFC-CNN) Based Deep Learning for Cancer Classification Approach

K.Prema*

Associate Professor, Computer Science, Sri Ramakrishna College of Arts & Science (Autonomous), Coimbatore, Tamil Nadu, India.

Received: 22 Feb 2024 Revised: 15 Mar 2024 Accepted: 21 Mar 2024

***Address for Correspondence**
K.Prema
Associate Professor,
Computer Science,
Sri Ramakrishna College of Arts & Science (Autonomous),
Coimbatore, Tamil Nadu, India.
Email: prema.k@srcas.ac.in

ABSTRACT

The method of increasing classifier performance by integrating the contributions of trained sub-models to tackle the same classification issue is known as Ensemble Learning (EL). Overall, each base learner votes, and the meta-learner, which is a model that learns to correct the predictions of the base-learners, gains the final prediction. The ensemble technique outperforms single learners in prediction accuracy. The Meta model receives the output of the sub-models (base learners) as input and then learns to merge the input predictions to produce a final prediction that is better than each of the base-classifiers. The concept of ensemble learning module is structured and named as Ensemble of MHSAMKFC based CNN (En-MHSAMKFC).

Keywords: Ensemble, stacking, backing, over-fitting, under-fitting.

INTRODUCTION

Ensemble methods are strategies for enhancing model accuracy by mixing numerous models rather of utilizing a single model. The integrated models considerably improve the accuracy of the results. It has increased the prominence of ensemble approaches in machine learning.

Categories of Ensemble Methods

Ensemble methods are classified into two types: sequential ensemble techniques and parallel ensemble approaches.

1. Sequential ensemble approaches, such as Adaptive Boosting, create base learners in a sequential order (AdaBoost). The successive production of basic learners fosters dependability among the base learners. The model's performance is then enhanced by giving bigger weights to previously misrepresented learners.
2. Parallel ensemble techniques, base learners are generated in a parallel format, e.g., random forest. Parallel methods utilize the parallel generation of base learners to encourage independence between the base learners. The independence of base learners significantly reduces the error due to the application of averages.

Advanced Ensemble Techniques

Some of the Advanced Ensemble Techniques are listed below

Stacking Method

The ensemble approach is stacking, which is also known as stacked generalization. This approach works by allowing a training algorithm (such as Decision Tree, KNN, or SVM) to combine the predictions of numerous other comparable learning algorithms. Stacking has been used successfully in regression, density estimation, distance learning, and classification. It may also be used to calculate the mistake rate while bagging. This model is used to predict results from the test set.

Bagging Method

Bootstrap aggregating is commonly used in classification and regression, and also known as bagging. Through the use of decision trees, it improves model accuracy while substantially lowering variance. Bagging is classified into two types, i.e., Bootstrapping and aggregation.

Boosting

Boosting is an ensemble strategy that uses prior predictor failures to improve future predictions. The strategy merges numerous weak base learners into a single strong learner, considerably boosting model predictability. Boosting works by placing weak learners in a sequential order, so that weak learners can learn from the next learner in the sequences which result in improved prediction models. Gradient boosting, Adaptive Boosting (AdaBoost), and Extreme Gradient Boosting (XGBoost) are all examples of boosting.

1. AdaBoost employs weak learners in the form of decision trees, which typically feature one split, also known as decision stumps. AdaBoost's primary decision stump is made up of observations with equal weights.
2. Gradient boosting adds predictors to the ensemble incrementally, with prior predictors correcting their successors, enhancing the model's accuracy. New predictors are fitted to compensate for the consequences of prior prediction mistakes. The gradient of descent assists the gradient booster in identifying and correcting errors in learners' predictions.
3. XGBoost makes use of decision trees with boosted gradient, providing improved speed and performance. It relies heavily on the computational speed and the performance of the target model. Model training should follow a sequence, thus making the implementation of gradient boosted machines slow.

ENSEMBLE MODEL APPLICATIONS TOWARDS GEM DATASET

Ensemble approach is an effective strategy for cancer diagnosis that is increasingly being used to integrate various learning algorithms to increase overall prediction accuracy (Dietterich 2000). Much research has demonstrated the promise of ensemble learning for enhancing data classification accuracy under uncertainty (Dietterich 2000; Yang et al. 2010). However, it is both a necessary and sufficient condition for an ensemble to outperform its individual members the base classifiers should be accurate and diverse. AdaBoost, Bagging, Random Subspace, Random Forest, and Rotation Forest are some examples of these approaches (Zhang & Zhang 2008). AdaBoost has grown in popularity because to its ease of use and versatility (Pratama et al. 2018). This approach constructs an ensemble of classifiers by applying a given base learning algorithm to successively acquired training sets produced by either resampling from the original training set or reweighting the original training set based on a set of weights preserved across the training set (Zhang & Zhang 2010). As a result, AdaBoost seeks to generate new "strong" classifiers capable

of better predicting challenging occurrences for earlier ensemble "weak" members. Wu (2018) suggested a Multi-label Super Leaner based on Heterogeneous Ensembles to increase multi-class super learner classification accuracy. A multi-label classification issue is one in which each sample can represent more than one class label at the same time, for example, an image may be assigned sea and beach or sea and mountains depending on the things it includes. The purview of bioinformatics, yet it was demonstrated to outperform all other approaches for music sentiment analysis, bird acoustics, and scenic datasets. Again, the variety of challenges it handles demonstrates the ability of heterogeneous ensemble to transcend NFL constraints. Yu et al. (2019) proposed a novel method for accurately predicting diagnostically complex cases of cancer patients by combining medical imaging, advanced ML algorithms, and heterogeneous ensembles. They also utilized this technique to demonstrate why some imaging aspects make it difficult to identify even with standard Computer-Aided Diagnosis (CAD) software. To train heterogeneous base classifiers and to construct an ensemble of trained classifiers increased total prediction accuracy to 88.90%, compared to the best accuracy recorded in the literature of 81.17 percent. When compared to other proposed ensemble approaches, such as AdaBoost (Tharwat 2018), Bagging (Jafarzadeh et al. 2021), and Random Forest (Cutler et al. 2011), Rotation Forest is more robust because it can always improve both the generalization ability of individual classifiers and the ensemble diversity. Zhang and Zhang (2008) presented RotBoost, a new ensemble classifier generation approach that combines Rotation Forest and AdaBoost. AdaBoost replaces the basis classifier in the Rotation Forest algorithm in this new ensemble technique. When several non-microarray gene-related data sets from the UCI library are used, the experimental findings reveal that RotBoost outperforms Rotation Forest and AdaBoost.

PROPOSED METHODOLOGY

To handle the over-fitting and under-fitting problems of CNN classifiers, a stacked ensemble model is presented that uses many learning models to build one optimal prediction model. In this model, Stacking based Ensemble model has been used to ensemble the proposed MHSAMKFC- CNN. Every classifier vote is merged to predict the final class label in the stacking ensemble model. As a result, the classifier developed using ensemble learning approaches outperforms the single classifier.

Algorithm 1: Stacking Ensemble Algorithm
Input: Data set $D = \{(x_1, y_1), (x_2, y_2), \ldots, (x_m, y_m)\}$;
First-level learning algorithms $L_1, \ldots \ldots, L_T$
Second-level learning algorithm L.

Process
1. For $t = 1, \ldots, T$: %Train a first-level learner by applying the
2. $h_t = L_T(D)$;% first-level learning algorithm L_T
3. end
4. 4. D* = ∅; % Generate a new data set
5. For $i = 1, \ldots, m$:
6. For $t = 1, \ldots, T$:
7. $z_{it} = h_t(x_i)$;
8. end
9. $D* = D* \cup ((z_{i1}, \ldots .., z_{iT}), y_i)$;
10. end
11. $h* = L(D^*)$; % Train the second-level learner h* by applying
% the second-level learning algorithm L to the
% new data set D*
Output: $H(x) = h^*(h_1(x), \ldots, h_T(x))$

Working Module of Stacking ensemble with MHSAMKFC-CNN

The construction of proposed stacking ensemble with MHSAMKFC-CNN is given in Figure.1. In this module, stacking learning is employed with MHSAMKFC-CNN classifier to ensemble the features to obtain the final class prediction with majority voting is provided in Figure.2.

Steps Involved in Majority Voting Ensemble process

In this process, the classifiers from the first layer (i.e., training layer) will return the probability of belonging to a class (selected features from MHSAMKFC). In the second layer i.e., testing layer, same MHSAMKFC features are consider as the input of CNN classifier. The classifiers from the first layer will return the probabilities that go into the next classifier input which also utilizes MHSAMKFC of parameters and features. Finally, the output of the classifier are processed to majority votingand to final class predictions (ensemble performance).

IMPROVING THE STACKING ENSEMBLE WITH MHSAMKFC-CNN

The construction of the improved Stacking Ensemble with MHSAMKFC-CNN is illustrated in Figure.3. In this module, the developed ensemble model works by combining FS process (MHSAMKFC) and classification (CNN) process. Combining the models created by each CNN Classifier yields the ultimate best classification performance. The performance for improving the Stacking Ensemble with MHSAMKFC-CNN. An enhanced stacking ensemble model is suggested to properly categorize the GEM dataset for cancer prediction. This model consists of a two-stage method. The basic learners (MHSAMKFC - CNN $(1,2\ldots N)$) are utilized to create the classifier outputs in the first step. MHSAMKFC - CNN model will boost the variety and robustness of the stacking model, can learn and understand training data from many angles.

RESULT AND DISCUSSION

The effectiveness of existing methods like CPEM (Lee et al. 2019) G-Forest (Abdulla & Khasawneh 2020) and aEKNN and proposed En - MHSAMKFC- CNN are compared based on above mentioned datasets Accuracy, Precision, Specificity, Sensitivity, and F1-Score are the metrics used to evaluate the performance.

Accuracy

The definition of the accuracy values of existing and proposed methods are compared and depicted in Table 3.1. Figure.4 displays the Accuracy of existing CPEM, G-Forest and aEKNN with proposed En-MHSAMKFC–CNN. In this analysis, En-MHSAMKFC-CNN method is 6.39%, 4.21% and 1.65% for Leukemia dataset; 6.75%, 4.03% and 2.56% for Lymphoma dataset and 7.09%, 4.25% and 2.31% for Prostate dataset is higher than that of CPEM, G-Forest and aEKNN methods respectively on given dataset. This analysis shows that the En - MHSAMKFC - CNN can achieve better accuracy than other methods for microarray cancer classification.

Precision

The definition of precision values of existing and proposed methods are compared and depicted in Table 3.2. Figure.5 displays the precision of existing CPEM, G-Forest and aEKNN with proposed En - MHSAMKFC- CNN techniques. In this analysis, En - MHSAMKFC-CNN method is 5.8%, 3.39% and 1.36% for Leukemia dataset; 7.05%, 4.32% and 2.91% for Lymphoma dataset and 6.97%, 4.91% and 2.86% for Prostate dataset is higher than that of CPEM, G-Forest and aEKNN methods respectively on given dataset. This analysis shows that the En - MHSAMKFC - CNN can achieve better precision than other methods for microarray cancer classification.

Specificity

The definition of Specificity values of existing and proposed methods are compared and depicted in Table 3.3. Figure.6 displays the specificity of existing CPEM, G-Forest and aEKNN methods with proposed En-MHSAMKFC–CNN techniques. In this analysis, En – MHSAMKFC - CNN method is 6.78%, 4.59% and 2.02% for Leukemia dataset; 6.28%, 2.94% and 1.75% for Lymphoma dataset, 7.31%, 4.61% and 2.18% for Prostate dataset is higher than

that of CPEM, G-Forest and aEKNN methods respectively on given dataset. This analysis shows that the En - MHSAMKFC - CNN can achieve better specificity than other methods for microarray cancer classification.

Sensitivity

The definition of Sensitivity values of existing and proposed methods are compared and depicted in Table 3.4. Figure.7 displays the sensitivity of existing CPEM, G-Forest and aEKNN with proposed En-MHSAMKFC-CNN techniques. In this analysis, En-MHSAMKFC-CNN method is 5.43%, 3.72% and 1.85% for Leukemia dataset; 7.27%, 4.53% and 2.11% for Lymphoma dataset, 7.22%, 4.78% and 2.26% for Prostate dataset is higher than that of CPEM, G-Forest and aEKNN methods respectively on given dataset. This analysis shows that the En - MHSAMKFC - CNN can achieve better sensitivity than other methods for microarray cancer classification.

F1-Score

The definition of F1-Score values of existing and proposed methods are compared and depicted in Table 3.5. Figure.8 displays the F1- score of existing CPEM, G-Forest and aEKNN with proposed En-MHSAMKFC-CNN techniques. In this analysis, En-MHSAMKFC-CNN method is 6.27%, 4.64% and 2.00% for Leukemia dataset; 6.98%, 4.93% and 2.68% for Lymphoma dataset, 7.22%, 4.85% and 2.53% for Prostate dataset is higher than that of CPEM, G-Forest and aEKNN methods respectively on given dataset. En – MHSAMKFC – CNN can achieve better F1- Score than other methods for microarray cancer classification.

CONCLUSION

En-MHSAMKFC- CNN is suggested for development to overcome the over-fitting and under-fitting problem caused by imbalanced class label in micro array gene datasets for cancer classification. En-MHSAMKFC- CNN is compared with different existing methods in terms of Accuracy, Precision, Specificity, Sensitivity and F1-Score using three microarray datasets such as Leukemia, Lymphoma and Prostate micro array datasets. The efficiency of these strategies is examined in MATLAB 2018a, which runs on Microsoft Windows 7 with a 2.70 GHz Intel CPU and 4GB RAM. Finally, simulation results show that En-MHSAMKFC- CNN is more effective than traditional classifiers at improving and quantifying the performance of cancer prediction systems that are used to improve and quantify cancer types GEM datasets, balancing performance efficiency with less computational complexity.

REFERENCES

1. Bae, J. H., Kim, M., Lim, J. S., &Geem, Z. W. (2021). FS for colon cancer detection using K-Means clustering and modified harmony search algorithm. Mathematics, 9(5), 570.
2. Mohapatra, P., Chakravarty, S., & Dash, P. K. (2020). Microarray medical data classification using kernel ridge regression and modified cat swarm optimization based gene selection system. Swarm and Evolutionary Computation, 28, 144-160.
3. Guo, S., Guo, D., Chen, L., & Jiang, Q. (2020). A centroid-based gene selection method for microarray data classification. Journal of theoretical biology, 400, 32-41.
4. Guo, S., Guo, D., Chen, L., & Jiang, Q. (2021). A L1-regularized FS method for local dimension reduction on microarray data. Computational biology and chemistry, 67, 92-101.
5. Wang, H., Jing, X., &Niu, B. (2020). A discrete bacterial algorithm for FS in classification of microarray gene expression cancer data. Knowledge Based Systems, 126, 8-19.
6. Algamal, Z. Y., Alhamzawi, R., & Ali, H. T. M. (2020). Gene selection for microarray gene expression classification using Bayesian Lasso quantile regression. Computers in biology and medicine, 97, 145-152.
7. Rani, R. R., &Ramyachitra, D. (2021). Microarray cancer gene FS using spider monkey optimization algorithm and cancer classification using SVM. Procedia computer science, 143, 108-116.

8. Yuan, M., Yang, Z., &Ji, G. (2021). Partial maximum correlation information: A new FS method for microarray data classification. Neuro computing, 323, 231-243.
9. Zheng, X., Zhu, W., Tang, C., & Wang, M. (2020). Gene selection for microarray data classification via adaptive hypergraph embedded dictionary learning. Gene, 706, 188-200.
10. Wang, H., Tan, L., &Niu, B. (2021). FS for classification of microarray gene expression cancers using bacterial colony optimization with multidimensional population. Swarm and Evolutionary Computation, 48, 172-181.
11. Chandrasekar, V., Sureshkumar, V., Kumar, T. S., &Shanmugapriya, S. (2020). Disease prediction based on micro array classification using DL techniques. Microprocessors and Microsystems, 77, 103189.
12. Fathi, H., AlSalman, H., Gumaei, A., Manhrawy, I. I., Hussien, A. G., & El-Kafrawy, P. (2021). Using Microarray and High-Dimensional Data. Computational Intelligence and Neuroscience, 2021.
13. Iam-On, N., &Boongoen, T. (2021). Diversity-driven generation of link based cluster ensemble and application to data classification. Expert Systems with Applications, 42(21), 8259-8273.
14. Ghosh, M., Adhikary, S., Ghosh, K. K., Sardar, A., Begum, S., &Sarkar, R. (2022). Genetic algorithm based cancerous gene identification from microarray data using ensemble of filter methods. Medical & biological engineering & computing, 57(1), 159-176.

Table 1 Evaluation of Accuracy

Datasets\ Classifiers	Accuracy			
	CPEM	G-Forest	aEKNN	En- MHSAMKFC- CNN
Leukemia	90.55	92.44	94.77	96.34
Lymphoma	91.38	93.77	95.11	97.55
Prostate	92.05	94.56	96.35	98.58

Table 2 Evaluation of Precision

Datasets\ Classifiers	Precision			
	CPEM	G-Forest	aEKNN	En- MHSAMKFC- CNN
Leukemia	92.66	94.87	96.77	98.09
Lymphoma	91.43	93.82	95.11	97.88
Prostate	92.53	94.34	96.22	98.98

Table 3 Evaluation of Specificity

Datasets\ Classifiers	Specificity			
	CPEM	G-Forest	aEKNN	En- MHSAMKFC- CNN
Leukemia	91.32	93.24	95.58	97.52
Lymphoma	92.01	94.99	96.10	97.79
Prostate	92.14	94.52	96.77	98.88

Table 4 Evaluation of Sensitivity

Datasets\ Classifiers	Sensitivity			
	CPEM	G-Forest	aEKNN	En- MHSAMKFC- CNN
Leukemia	93.87	95.45	97.21	99.01
Lymphoma	92.23	94.65	96.89	98.94
Prostate	92.31	94.46	96.79	98.98

Table 5 Evaluation of F1- Score

Datasets\ Classifiers	F1- score			
	CPEM	G-Forest	aEKNN	En- MHSAMKFC- CNN
Leukemia	92.92	94.37	96.81	98.75
Lymphoma	93.37	95.19	97.28	99.89
Prostate	92.16	94.24	96.38	98.82

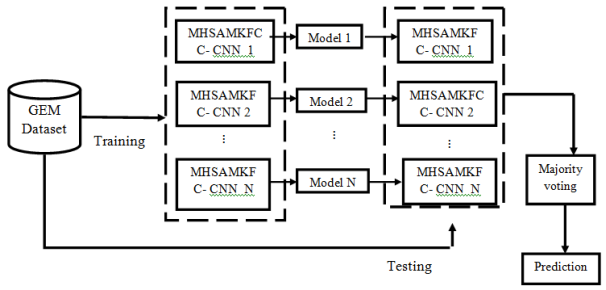

Figure.1 Stacking Ensemble with MHSAMKFC-CNN

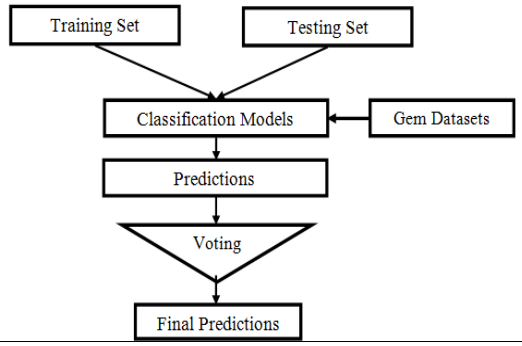

Figure.2 Flow work of Majority Voting

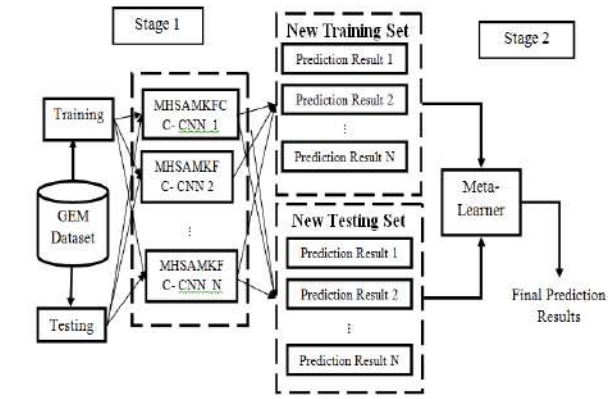

Figure.3 Improved Stacking Ensemble with MHSAMKF C-CNN

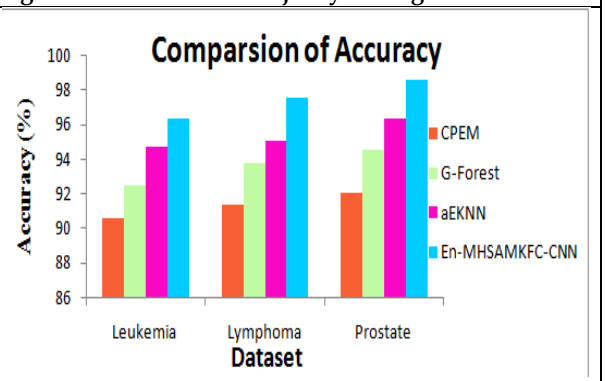

Figure.4 Accuracy vs Dataset

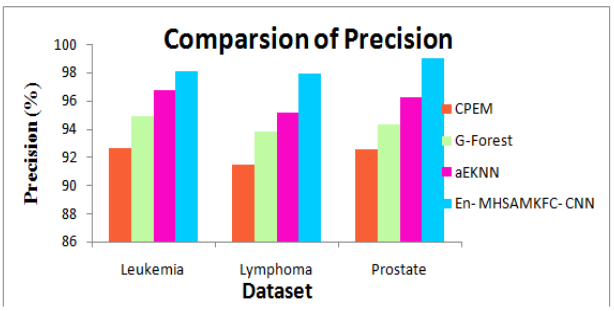

Figure.5 Precision vs Dataset

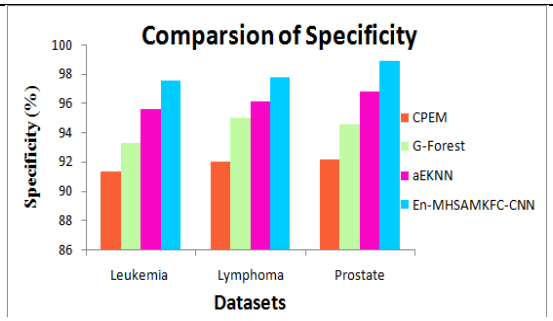

Figure.6 Specificity vs Dataset

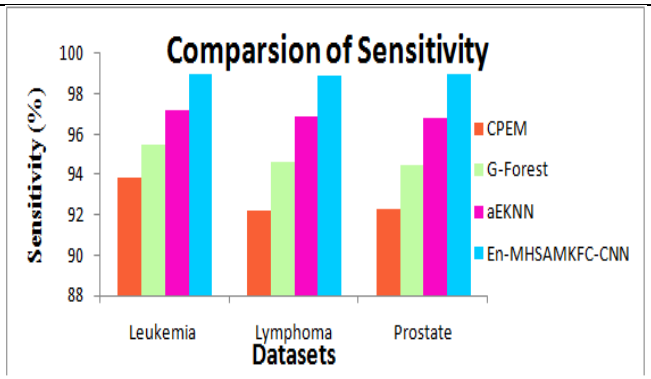

Figure.7 Sensitivity vs Dataset

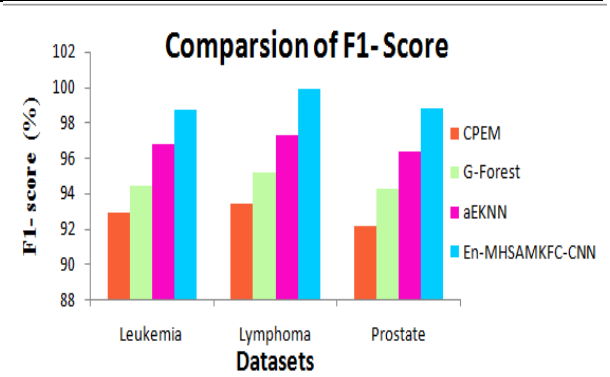

Figure.8 F1- Score vs Dataset

Indian Journal of Natural Sciences www.tnsroindia.org.in ©IJONS

Vol.15 / Issue 83 / Apr / 2024 International Bimonthly (Print) – Open Access ISSN: 0976 – 0997

REVIEW ARTICLE

A Comphrensive Review and Meta-Analysis on Psychological Distress among Students Using Machine Learning Techniques

Maria Suman A[1] and Saleema J S[2]*

[1]Researech Scholar, Computer Science, CHRIST (Deemed to be University) Bengaluru, Karnataka, India.
[2]Associate Professor, Statistics and Data Science, CHRIST (Deemed to be University) Bengaluru, Karnataka, India.

Received: 30 Dec 2023 Revised: 29 Jan 2024 Accepted: 13 Mar 2024

***Address for Correspondence**
Saleema J S
Associate Professor,
Statistics and Data Science,
CHRIST (Deemed to be University)
Bengaluru, Karnataka, India.
Email: saleema.js@christuniversity.in

ABSTRACT

The COVID-19 pandemic poses a risk to students' physical and mental well-being. This descriptive cross-sectional study is currently assessing the mental health of children and adolescents, and it is evident that their well-being is being significantly affected by the high rates of depression, stress, and anxiety that are being reported. The situation is further compounded by home confinement, which raises concerns about the negative impact of screen usage on their1mental health. Thus, ameta-analysis is currently being conducted to examine the global psychological1distress rates during the1COVID-19 pandemic. Additionally, the1study includes various moderator analyses to explore factors contributing to the variability of depression anxiety and stress prevalence rates. Studies were1selected based on inclusion1and exclusion1criteria obtained from PubMed, Scopus, Google Scholar, Web of Science, MedLine, and Nature following the PRISMA model. The pooled prevalence rate of depression was 35% (95% CI,-0.35-0.38;), the anxiety was 22% (95%CI, 0.40-0.44;); stress was 28% (95%CI, 1.56-2.24;)However, the outcomes differ based on age, circumstances, and location. Moreover, the1 sample size of these studies was small. The random forest outperformed and is considered suitable machine learning for data analysis and study. The latest research highlights how important it is to give teenagers access to1 mental health1services both during and after the pandemic in order to make sure they get the help they need.

Keywords: Depression, Anxiety, Stress, Students, Machine Learning

INTRODUCTION

Globally, the multitude of people spending time at home has sharply increased since the outbreak of Coronavirus-19 in early 2020. In addition, a by-product of the Coronavirus disease is an intense feeling of stress, fear, and anxiety that occurs in such an uncertain environment. Reports from the World Health Organization (WHO) reveal that even before the pandemic, 1 in 3 people suffers from anxiety and depression. The study looks at five important life areas that could have affected adolescents during the pandemic: expectations for the future, physical activity and media exposure, social interactions, mental wellness, and conduct difficulties. As far as adolescent social relationships are concerned, the pandemic has substantially changed their social lives due to infection control measures such as the closure of schools and the physical separation of students from each other [2]. This social deprivation may disrupt peer relationships. Adolescents are commonly concerned about being disconnected from friends due to the pandemic . Additionally, there's a chance that the pandemic harmed family dynamics: in the event of a pandemic, parent-child relationships may suffer due to stress from confinement, caring responsibilities, and financial instability[1]. On the other hand, adjustments to family attention and routines as well as more time spent together may have benefitted certain children [3]. Globally, mental illness has reached epidemic proportions, and WHO estimates that one-fourth of the population will suffer from a mental or neurological disorder sometime in their lives. Mental illness is a result of imbalances in brain chemistry. During the pandemic, children and adolescents experienced various psychosocial and behavioral problems, including lack of attention, hesitation, disinterest, and fear of asking questions about the pandemic. The current pandemic has long-term health effects as it is a lingering stressor; assessing their mental wellness and suggesting appropriate treatments is essential. Adolescents frequently struggle with mental health issues like stress, anxiety, and depression.

Depression symptoms include sadness, fear, uncontrollable worry, aggression, and disruptions in sleep and appetite. When researchers observe heterogeneity across studies, as during COVID-19, it is often a sign that demographic, geographical, and methodological moderators are necessary to understand the relationship, it is possible to detect who is more likely to experience higher prevalence compared to lower prevalence, based on moderator analyses. Before and amidst the COVID-19 pandemic, prevalence rates of mental illness differ based on child age by experiencing higher rates of internalizing disorders. It is also possible that methodological characteristics of studies influence estimations of prevalence rates. Study methods of poorer quality may overestimate prevalence rates, for instance. To determine possible prevalence rates, it is also necessary to consider the timing of data collection. The early months of the pandemic may have been more stressful and overwhelming than later, but school closures and extended social isolation may have likely exerted psychological strain on some students. Machine learning and psychology come together whenever the research question is "How capable is it to predict?" With the advancement of technology, mental health researchers and doctors can collect more information quicker than ever before. Smartphones, neuroim aging, and wearable technologies have made this possible. The application of machine learning for the study of these data has improved reliability over time. The aim of machine learning is to develop computers that are able to learn on their own by applying advanced probabilistic and statistical techniques.

Objective

To understand about mental wellness is crucial, considering the global epidemic proportions of mental illness and the lingering stressor effect of the pandemic, which can lead to various psychosocial and behavioral problems among students. Thus the current systematic review and meta-analysis aim to (1) Identify adolescents' mental health problems amidst the pandemic. (2) Illuminate machine learning strategies to improve mental health issues for students.

Study Methods

Search Strategy

This systematic review followed Preferred Reporting Items for Systematic Reviews and Meta-analyses (PRISMA)reporting guidelines. The literature review focused on the Web of Science (WoS) database, Scopus, MeSh (MedLine and Google Scholar) Keywords, NATURE, and PubMed database. A search strategy was devised by incorporating three central themes: mental illness (including depression, stress, and anxiety), children and adolescents (age 10 to 18 years), the COVID-19 pandemic, and Machine Learning. Unpublished pre-prints were also searched.

Selection Criteria (Inclusion and Exclusion Criteria)

In terms of the selection criteria, the following criteria were set: (1) articles specifically targeting children up to 18 years of age; (2) papers that relate COVID-19 impact on adolescents and children; and (3) studies analyzing the psychological behavior of confined children (4) machine learning techniques that support in the prediction of mental illness. (5) The study taken was Empirical Articles written in English were considered in the study. The titles and summaries of each article were read first to determine whether they met the criteria mentioned above, which allowed us to rule out papers that did not. In the end, nine scientific papers were selected after a more thorough reading of the articles chosen (Figure 1)

Data Extraction

The following coding processes were used in order to extract the data from the articles: (1) author(s) and year of publication; (2) research title; (3) place/country of publishing; and (4) key concepts of the research. Prevalence rates for anxiety, stress, and depression were derived from study publications that satisfied inclusion requirements.

LITERATURE REVIEW

Elizabeth A. K. Jones et al.[19] aims to assess how the pandemic affects adolescents' mental health. In this pandemic, stress, extended home confinement, worry, and social media overuse can negatively impact adolescents' mental health. COVID-19 poses mental challenges to adolescents around the world. Adolescents require physical and psychological support to grow, develop, and thrive, regardless of the uncertainty caused by the current crisis. It is important to make use of all therapy modalities and resources available to assist adolescents in adjusting to the pandemic's effects. In the aftermath of COVID-19 and similar disasters, there needs to be more research on improving adolescent mental health. To better address adolescents' psychological needs, it may be suggested that telemedicine be implemented globally, among many other interventions. Ray, Suman, et al.[8]study focuses on Coronavirus infection can affect a person of any age, but children are particularly vulnerable because of the disease's complex psychological effects. During the pandemic, certain children would have been put through to quarantine restrictions. In addition, the lockdown has also been reported to have affected children's mental health due to greater access to digital devices. The COVID-19 pandemic and lockdown have also hurt children's mental health. Several questionnaires, such as Short Self-Rating Questionnaires (SSRIs), were used to assess the level of stress experienced by children and youth between the ages of 9 and 18 in the aftermath of the COVID-19 epidemic. The study was cross-sectional and observational research using an online survey to collect data. 369 school kids took part. The stress levels were classified into Low, Moderate, and Severe groups using a Score Scale and analysis to categorize them. In analyzing the total score levels of the Delhi+Mathura zone (n=369), 30.08% (n=111) were found to be under a moderate stress level, 62.87% (n=232) under a severe stress level and 7.08% (n=26) were found to be under an extreme stress level. In Delhi and Mathura combined, a significant difference was found in stress levels between males and females (p*0.04). Delhi and Mathura zones did not significantly differ in stress levels. Children and adolescents must receive proper stress management given the current environment. Family and child needs may be met with an intervention strategy based on culturally appropriate and empirically supported interventions. Kumar, Abhinit, et al.[7]studies concern that mental illness in children and adolescents rises when they transition from childhood to adolescence as the conditions become more complex and intense. This study aims to assess and

compare anxiety and depression prevalence among suburban and rural children in eastern Uttar Pradesh and to understand their socioeconomic impact. The 11- to 18-year-old age children were divided into two groups; 100 from rural Tikri and 100 from suburban Sunderpur. They collected information about their sociodemo graphics. Screening for depression and anxiety in children was conducted using the Children's Depression Inventory and the Revised Children's Manifest Anxiety Scale. The present state examination was performed using the International Classification of Mental and Behavioural Disorders as the basis for the final diagnosis. A Chi-square test was used to analyze the data statistically. Depressive disorders are prevalent in 14.5% of the population, while anxiety disorders are prevalent in 15%. Rural and suburban areas were not significantly different ($P > 0.05$) regarding depression or anxiety. Among adolescents, females, and people in the lower-middle economic bracket, depression, and anxiety were more prevalent than in other age groups. Students in classes 9th - 12th were more likely to suffer from depression, while students in lower classes were more likely to experience anxiety. There was a higher prevalence of depression in joint families. The differences between these two groups indicate some crucial trends relating to the factors that impact these problems. Jeelani, Asif, et al.[9]paper is based on during the Coronavirus pandemic of 2019, routine activities were disrupted severely, significantly more deaths were reported, and more morbidity has reported. The mental health needs of adolescents are exceptionally high.

Adolescents attending school in the Kashmir valley of India were evaluated for the prevalence and determinants of depression and anxiety. In January and February 2021, school-going adolescents aged between 15 and 19 years were screened for depression and anxiety using the Patient Health Questionnaire for Adolescents and Generalised Anxiety Disorder questionnaire. A total of 426 (97.03%) out of 439 adolescents responded to the survey. With a mean age of 17.5 + 1.26 years and 57% males, the adolescents were in the middle of their adolescent years. Approximately 16% of people with depression had a history of COVID-19 infection in the past. Twenty percent of adolescents had anxiety. Boys were affected at a rate of 14% and girls at a rate of 27.5%. A significant public health problem is associated with anxiety and depression among adolescents. Based on our study, it appears that adolescents who struggle with self-esteem need immediate assistance. Ms. Sumathi et al.[10]study focuses on treating mental health problems effectively; early diagnosis is crucial. The earlier it is treated, the greater the chance of improving the quality of life for patients. Therefore, it is imperative to address fundamental mental health problems among children that threaten their mental health. If not treated early, these conditions can lead to more complex issues. Machine learning approaches currently well serve in medical data analysis and diagnosis. Five fundamental mental health problems have been diagnosed by comparing eight machine learning techniques on different accuracy measures. To train and test the performance of the methods, a data set of sixty cases is collected. There are 25 attributes identified in the documents that are important for diagnosing the problem. A Feature Selection algorithm has been applied to the complete attribute data set to reduce the attributes. The accuracy of various machine learning approaches has been compared on a complete attribute set and a target attribute set. There is little difference between their performance over the complete attribute set and the selected attribute set among the three classifiers: Multiclass Classifier, Multilayer Perceptron, and LAD Tree.

Usman, Muhammad, et al.[11] study deals with mental disorders such as depression that negatively affect a person's mental health, causing them to behave, think, and feel negatively, leading to physical or emotional problems. In such situations, people lose hope for the positive and only see the negatives. In Machine Learning (ML), a model can be trained on training datasets to predict whether someone will develop depression in the future. Researchers have previously used machine learning techniques to predict depression. A study reviewed ML techniques' effectiveness in predicting depression in older adults. This study has used a variety of classifiers, including Bayes Nets, logistic regressions, multilayer perceptrons, sequential minimizations, decision tables, and random forests. Large datasets can achieve maximum accuracy and precision of 89% and 0.95, respectively. Ahuja, Ravinder, and Alisha Banga [12] study analyzes college students' stress experiences at various stages of their lives. Examination pressure and recruitment stress affect students in often go unnoticed. The dataset was sourced from the Jaypee Institute of Information Technology and contained 206 students' data. We will analyze these factors' impact on a student's mind and correlate this stress with internet usage. As performance parameters, sensitivity, specificity, and accuracy are measured for these four classification algorithms: Linear Regression, Naive Bayes, and SAnd and

Random Forest Using 10-fold cross-validation further enhances data accuracy and performance. Support Vector Machines were the most accurate (85.71%). Haque, Umme Marzia, et al.[13] goal of the study is (1) to create an algorithm that can predict depression in adolescents and children between the ages of 4 and 17, (2) to evaluate the results to determine which algorithm performs best, and (3) to relate it to family activities and socioeconomic challenges. This study draws data from the YMM, the second Australian Child and Adolescent Survey of Mental Health and Wellbeing 2013-14. A low correlation between the variable of yes/no value and the target variable (depression status) has been eliminated. To detect depression among highly correlated variables with the target variable, we used the Boruta algorithm in conjunction with a Random Forest (RF) classifier. The Tree-based Pipeline Optimization Tool (TPOT classifier) was used to choose appropriate supervised learning models. Depression detection was conducted using the use of RF, Decision Tree (DT), XG Boost (XGB), and Gaussian Naive Bayes (Gaussian NB). Even with differences in performance between models, RF could predict depressed classes 99% with 95 % accuracy, 99% precisely, and in 315 milliseconds (ms) faster than all other algorithms. As well as outperforming all four confusion matrix performance measures and execution duration, this model is more accurate in predicting child and adolescent depression.

Qasrawi, Radwan, et al.[14] aims to identify depression and anxiety risk factors in school children using machine learning. The study included 5685 students studying in public and refugee schools in the West Bank in grades 5-9, aged 10-15. Data were collected using the health behaviors questionnaire for school children during the 2013-2014 academic year, and machine learning was used to predict risk factors associated with mental health symptoms in students. The prediction techniques used were a Decision Tree, Support Vector Machine, Neural Network, Random Forest, and Naive Bayes. For depression and anxiety, the SVM and Random Forest models were the most accurate (SVM=92.5%, RF=76.4%; SVM=92.4%, RF=78.6%). As a result, the SVM and Random Forest produced the best classification and prediction results for the depression and anxiety of the students Shailly Gupta et al.[15] focused on Indian students who were assessed for psychological and physical health due to increased screen usage during COVID-19. With the help of self-made questionnaires and snowball sampling, a cross-sectional survey was carried out on Indian students. The survey received 210 responses from students at various schools and colleges between 15th August and 30th August 2020. The relationship between screen time and physical and psychological health during COVID-19 was statistically significant (t= 19.96; p=0.01). As a result, students should be incorporated into appropriate preventive health measures.

To obtain more reliable and accurate results, further research is needed to identify the health effects of the overuse of screens in specific populations such as adolescents and adults. Twenge, Jean M., and W. Keith Campbell, et al.[16] study focused on an array of psychological well-being measures. Comprehensive screen time standards (including electronic games, cell phones, electronic devices, computers, and TV) were assessed in a large (n = 40,337) national random sample of children and adolescents in the U.S. in 2016. In studies involving daily screen time for 1 hour or more, reduced psychological well-being was associated with a reduction in curiosity, a decrease in self-control, a greater tendency to distractibility, a lower sense of emotional stability, and difficulties with friendship. The risk of ever having been diagnosed with anxiety (RR 2.26, CI 1.58, 3.22), depression (RR 2.39, 95% CI 1.54, 3.70), or treated by a professional in mental health (RR 2.22, CI 1.62, 3.03) or with medication treated for a psychological or behavioral issue was twice as high among 14- to 17-year-olds who were high screen users (7+ hours per day compared to 1 h/day) in the past year. Moderate screen use (4 hours/day) also negatively impacted mental well-being. There was no significant difference in well-being between low users and non-users of screens. Adolescents are more likely to have lower psychological well-being from screen time than younger children.

RESULTS

A total of 100 nonduplicate records were found in our electronic search. To evaluate all 65 full-text articles against inclusion criteria, 65 abstracts were reviewed, and 15 non-overlapping studies met all the requirements.

Study Characteristics

A total of 15 studies were included in the survey literature and 5 in meta-analyses, of which five studies were on depression, anxiety, and stress. Four studies had depression and anxiety,3 had stress-related issues, and three papers related screen time and depression, anxiety, and stress. The mean (SD) percentage of depression was 22.7%, anxiety was 68%, stress was 25%, and the mean age was 13.0 years (range, 8-19 years).

Pooled Prevalence of Depressive, Anxiety, and Stress Symptoms

The pooled prevalence from a random-effects meta-analysis of 5 studies revealed a pooled prevalence rate of depression is 0.35 (95% CI,-0.35-0.38;) or 35%. The between-study heterogeneity statistic was 0.02. The pooled prevalence rate of anxiety is 0.22 (95%CI, 0.40-0.44;) or 22%, and the heterogeneity statistic was -1.16. Lastly, the pooled prevalence rate of stress is 0.28 (95%CI, 1.56-2024;) or 28%, and the heterogeneity statistic was 1.01. The funnel plot was symmetrical (Figure 2, Figure 3, and Figure 4 in the supplement).

Performance Metrics of Machine Learning Methods

At the citation screening stage of a systematic review of depression, anxiety, and stress the ML approaches were applied. By measuring sensitivity, specificity, accuracy, and AUC (Area under Curve) on a validation set of papers were able to assess the performance of the ML approaches. Different algorithms like Random Forest, Support Vector Machine, Naïve Bayes, Artificial Neural Networks, Decision Tree, XGB, and Gaussian NB were considered to find the best approach for the prediction of depression, anxiety, and stress. The comparative study on algorithms states that Random Forest outperforms other methods by acquiring 1.00 sensitivity,0.85 specificities,0.99 Accuracy, and 0.86 AUC.

DISCUSSION

The COVID-19 pandemic and its associated restrictions and consequences have significantly affected adolescents' psychological well-being. Among other factors, social isolation, peer interactions, and reduced contact with buffering supports (e.g., teachers, and coaches) may have contributed to these increases.4 Additionally, school-based services are the primary source for mental health treatment for 80% of children. The closure of these facilities has rendered these services unavailable to many children. An increase in depression and anxiety rates was observed as the month of data collection progressed. A cumulative association could be formed between social isolation, financial difficulties, missed milestones, and school disruptions. This possibility is still lacking longitudinal research, which is urgently needed. A further longitudinal study on Children's health will be required to confirm the long-term mental health effects of the pandemic on youth mental illness as the pandemic progresses and during the recovery phase. Study results showed that all psychological interventions analyzed benefited healthy and mentally ill adolescents and children. Thus, schools become a suitable environment for facilitating community involvement and family, and they, therefore, have the potential to enhance positive relationships between teachers and students, parents and teachers, and students and their peers. It is important that parents and teachers are involved in the teaching and learning process. Families with no training in this area might have some difficulties with these active methods that are utilized in schools. [20]. The results of emerging research42 indicate that routines reduce child depression and conduct problems during COVID-19. Children and families can mitigate the effects of COVID-19 on youth by implementing consistent and predictable practices around sleep, schoolwork, screen use, and physical activity. Children experiencing clinically elevated mental distress should be provided with additional resources and referred to clinical professionals. As a result, school closures and recreational activities should be considered a last resort. Further, there should be an emphasis on the equitable distribution of mental health resources to children while increasing scalability.

LIMITATIONS

A systematic review has been conducted in which a set of interventions has been assessed for adolescents and children without explicitly distinguishing between them. There is a limitation here since adolescents and children might need different levels of support regarding their psychological and behavioral health. There may be differences in outcomes that have not been considered in this review. The current meta-analysis includes a re-examination of cross-regional differences will be important once additional data from underrepresented countries become available once the recent meta-analysis includes child and adolescent mental illness estimates across regions. Secondly, most studies were cross-sectional, which precluded long-term research on COVID-19's effect on child mental health.

CONCLUSION

The meta-analysis results show that children's anxiety and depression symptoms were elevated during the COVID-19 pandemic. It also stresses the importance of interventions and recovery efforts to improve the well-being of students. Still, it also emphasizes that when focusing on interventions, individual differences must be considered (e.g., gender, age, COVID-19 exposure). It was found that computer/internet, mobile phone, and television/videogame use were both associated with negative outcomes. Long-term research on this epidemic is necessary to enhance understanding of the implications of the COVID-19 pandemic on today's children's mental health trajectory. This should include studies using pre- and post-COVID-19 measurements. Researchers have found that machine learning can help understand psychiatric disorders through existing studies and research. For machine learning models to perform well, the data samples and their characteristics must be considered. Pre-processing activities like data cleaning and parameter tuning can also influence machine learning models. Observing and classifying mental health problems at an early stage can assist in further treatment in the future.

AREA OF CONFLICT

Behave of all authors the corresponding author states that there is no area of conflict

REFERENCES

1. Magson NR, Freeman JYA, Rapee RM (2020) Risk and Protective Factors for Prospective Changes in Adolescent Mental Health during the COVID-19 Pandemic.50::44–57. https://doi.org/10.1007/s10964-020-01332-9
2. Orben A, Tomova L, Blakemore S-J (2020) The effects of social deprivation on adolescent development and mental health.. 4::634–640. https://doi.org/10.1016/S2352-4642(20)30186-3
3. Magson NR, Freeman JYA, Rapee RM, et al (2020) Risk and protective factors for prospective changes in adolescent mental health during the COVID-19 pandemic. Journal of Youth and Adolescence 50: https://doi.org/10.1007/s10964-020-01332-9
4. Chung J, Teo J (2022) Mental Health Prediction Using Machine Learning: Taxonomy, Applications, and Challenges. Applied Computational Intelligence and Soft Computing 2022:e9970363. https://doi.org/10.1155/2022/9970363
5. Ahuja R, Banga A (2019) Mental Stress Detection in University Students using Machine Learning Algorithms. Procedia Computer Science 152:349–353. https://doi.org/10.1016/j.procs.2019.05.007
6. Cachón-Zagalaz J, Sánchez-Zafra M, Sanabrias-Moreno D, et al (2020) Systematic Review of the Literature About the Effects of the COVID-19 Pandemic on the Lives of School Children. Frontiers in Psychology 11:https://doi.org/10.3389/fpsyg.2020.569348
7. Haque UM, Kabir E, Khanam R (2021) Detection of child depression using machine learning methods. PloS One 16:e0261131.https://doi.org/10.1371/journal.pone.0261131
8. Jones EAK, Mitra AK, Bhuiyan AR (2021) Impact of COVID-19 on Mental Health in Adolescents: A

Systematic Review. International Journal of Environmental Research and Public Health 18:2470. https://doi.org/10.3390/ijerph18052470

9. Kumar A, Mishra S, Srivastava M, Tiwary N (2018) Prevalence of depression and anxiety among children in rural and suburban areas of Eastern Uttar Pradesh: A cross-sectional study. Journal of Family Medicine and Primary Care 7:21. https://doi.org/10.4103/jfmpc.jfmpc_248_17
10. Jeelani, Asif (2022) Prevalence of Depression and Anxiety among school-going Adolescents in Indian Kashmir Valley during COVID-19 Pandemic. Middle East Current Psychiatry10.1186/s43045-022-00185-1
11. Qasrawi R, Vicuna Polo S, Abu Al-Halawah D, et al (2021) Schoolchildren' Depression and Anxiety Risk Factors Assessment and Prediction: Machine Learning Techniques Performance Analysis (Preprint). JMIR Formative Research. https://doi.org/10.2196/32736
12. Racine N, McArthur BA, Cooke JE, et al (2021) Global Prevalence of Depressive and Anxiety Symptoms in Children and Adolescents During COVID-19. JAMA Pediatrics 175:1142–1150. https://doi.org/10. 1001/ jamapediatrics.2021.2482
13. Ray S, Goswami V, Kumar CM (2022) Stress-The hidden pandemic for school children and adolescents in India during COVID-19 era. Current Psychology. https://doi.org/10.1007/s12144-022-02827-3
14. Sumathi Ms, B. Dr (2016) Prediction of Mental Health Problems Among Children Using Machine Learning Techniques. International Journal of Advanced Computer Science and Applications 7: https://doi.org/1 0.1456 9/ijacsa.2016.070176
15. Twenge JM, Campbell WK (2018) Associations between screen time and lower psychological well-being among children and adolescents: Evidence from a population-based study. Preventive Medicine Reports 12:271–283. https://doi.org/10.1016/j.pmedr.2018.10.003
16. Usman M, Haris S, Fong ACM (2020) Prediction of Depression using Machine Learning Techniques: A Review of Existing Literature. In: IEEE Xplore. https://ieeexplore.ieee.org/document/9314940. Accessed 16 Jul 2022
17. García-Carrión, Rocío(2019) Children and Adolescents Mental Health: A Systematic Review of Interaction-Based Interventions in Schools and Communities. Frontiers in Psychology .www.frontiersin.org/articles/ 10.3389/fpsyg.2019.00918/full,10.3389/fpsyg.2019.00918.
18. Vaishnavi K, Nikhitha Kamath U, Ashwath Rao B, Subba Reddy NV (2022) Predicting Mental Health Illness using Machine Learning Algorithms. Journal of Physics: Conference Series 2161:012021. https://doi.org/10.1088/1742-6596/2161/1/012021
19. Impact of Increased Screen Time on Physical and Psychological Health of Indian Students During COVID-19 | Bioscience Biotechnology Research Communications. https://bbrc.in/impact-of-increased-screen-time-on-physical-and-psychological-health-during-covid-19-among-indian-students/
20. Eason, B. Noble, and I. N. Sneddon, "On certain integrals of Lipschitz-Hankel type involving products of Bessel functions," Phil. Trans. Roy. Soc.

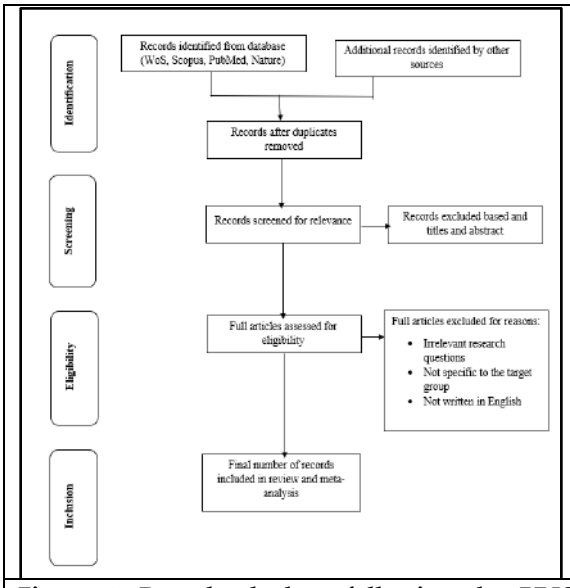

Figure 1: Procedural chart following the PRISMA Model

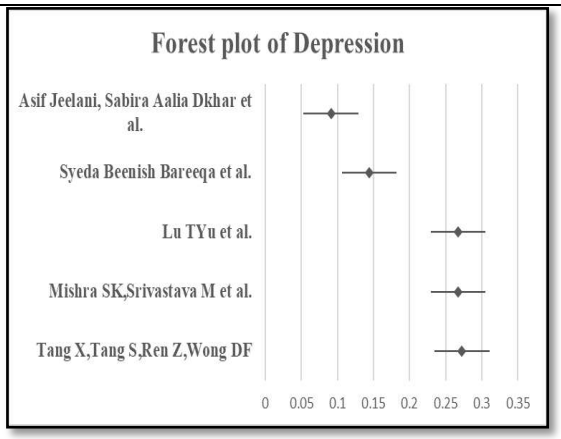

Figure 2:The funnel plot of the1Depression

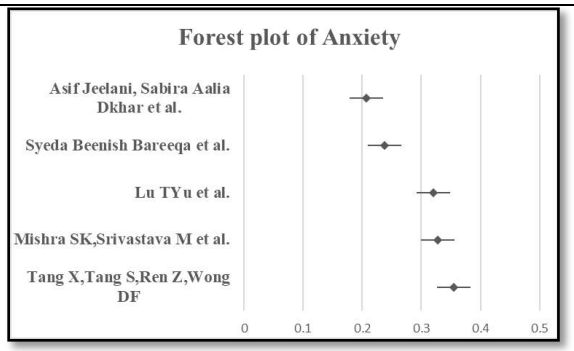

Figure 3: The funnel{plot of the Anxiety1

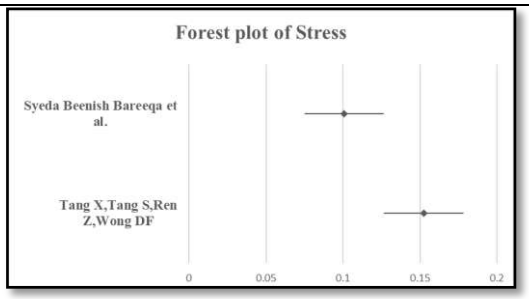

Figure 4: The funnel1plot of the Stress1

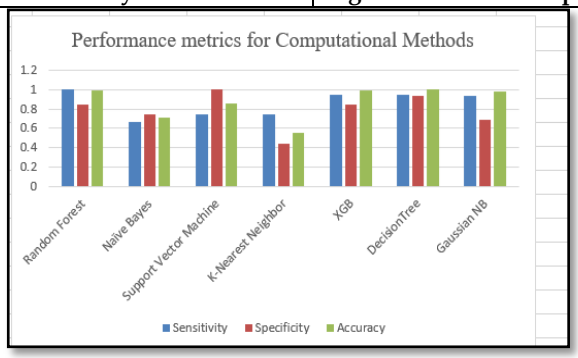

Figure 5 : The performance metrics for different machine learning methods

Vol.15 / Issue 83 / Apr / 2024 International Bimonthly (Print) – Open Access ISSN: 0976 – 0997

REVIEW ARTICLE

Determinants of Maternal Mental Health In India: A Systematic Review and Meta- Analysis

Anugraha Mathew[1]* and J S Saleema[2]

[1]Post Graduate Student, Department of Statistics, and Data Science ,CHRIST (Deemed to be University) Bengaluru, Karnataka, India.
[2]Associate Professor, Department of Statistics and Data Science, CHRIST (Deemed to be University) Bengaluru, Karnataka, India.

Received: 20 Dec 2023 Revised: 29 Jan 2024 Accepted: 13 Mar 2024

***Address for Correspondence**
Anugraha Mathew
Post Graduate Student,
Department of Statistics and Data Science,
CHRIST (Deemed to be University)
Bengaluru, Karnataka, India.
Email: anugraha.mathew@stat.christuniversity.in

ABSTRACT

Maternal mental health is an essential component of public health, and it poses a multifaceted challenge in India. Despite advances in maternal care, there is rising concern about the prevalence and consequences of common mental health disorders among pregnant women. Through addressing existing knowledge gaps and investigating barriers related to the recognition and treatment of these disorders, this research strives to provide insights that can guide the formulation of interventions and policies tailored to the cultural nuances of the population. This study aims to conduct a systematic review and meta-analysis to identify the determinants of common maternal mental disorders in India. While targeting the specific objectives outlined in Sustainable Development Goal 3 (SDG 3) concerning mental health and well-being, this study extends its focus to include a broader spectrum of determinants. This approach recognizes the interconnected nature of maternal mental health with various societal factors, including those related to SDGs addressing poverty, hunger, inequality, education, and economic growth. We implemented the PRISMA model for the systematic review, performed a meta-analysis using the random effects model and assessed the publication bias. A pooled prevalence rate of 44.9% (95% C.I = 34.4 to 56) was observed, with a high level of heterogeneity among the studies. In light of the study's findings, policymakers may consider prioritizing interventions addressing the identified determinants that not only improve mental health outcomes but also contribute to broader societal well-being. The results of this study motivate an expanded review of relevant literature to enhance the robustness and generalizability.

Keywords: Maternal Mental Health, Common Mental Disorders, Systematic Review, Meta-Analysis, Sustainable Development Goals (SDGs)

INTRODUCTION

According to WHO (World Health Organization), maternal health is women's health throughout pregnancy, childbirth and the postnatal period. Over the years, the primacy of maternal health has increased, and India has considered it an essential attribute for development with respect to increasing equity and decreasing poverty. Maternal mortality and morbidity are significant concerns for investing in maternal health. Sustainable Development Goals (SDGs) 2030 has incorporated the aim of reducing the global maternal mortality ratio (MMR) to under 70 per 100,000 live births and ensuring universal access to healthcare services, including family planning, education and information services 1. In association with UNICEF and UNFPA, WHO is determining best practices for providing evidence-based, integrated, people-oriented maternal and perinatal healthcare services. It also aims to provide information and proposals on care models at various phases of the obstetric transition across countries. Many studies have been performed to know the number of deaths, attributes affecting them and their influence on maternal health, maternal morbidity and mortality. Statistics suggest that for every maternal death, around 20 – 30 women suffer from maternal morbidity. Pregnancy is always characterized by joy, enthusiasm and psychological well-being, but it is a common misconception that mental health stays strong throughout pregnancy and the postpartum period. This has led to around 80% of unreported maternal mental health conditions1. Maternal mental health conditions extend beyond depression, anxiety, and psychosis, including issues such as baby blues, maternal dysthymia, OCD, birth-related PTSD, and others. Globally, around 10% of pregnant women and 13% of postpartum women encounter a mental disorder, predominantly depression. These figures are notably higher in developing nations, reaching 15.6% during pregnancy and 19.8% following childbirth3.

In India, based on a systematic review and meta-analysis published in the Lancet Psychiatry in 2020, the prevalence of perinatal depression was 22.9%, and the prevalence of anxiety was 15.7%. There are certain demographic segments that face an elevated risk of mental disorders due to increased exposure and susceptibility to adverse social, economic, and environmental conditions, closely tied to gender-related factors. Prevalent among these mental disorders are common mental disorders (CMDs), primarily encompassing conditions such as depression and anxiety disorders. This research seeks to fill knowledge gaps and investigate hindrances to the identification and treatment of maternal CMDs, with the ultimate goal of guiding the creation of culturally sensitive interventions and policies. Additionally, it strives to foster maternal mental well-being, strengthen the bond between mothers and infants, and enhance the long-term health outcomes for mothers and their children in India. The objective of this paper is to synthesize available evidence and generate collective estimates regarding the prevalence of maternal common mental disorders (CMDs) in India. This information aims to guide the development, implementation, and assessment of interventions aligned with the National Health Mission (NHM) goals. Our approach involves identifying evidence and conducting a meta-analysis based on existing studies that investigate the prevalence of CMDs in India. Furthermore, we intend to compile an overview of the determinants influencing maternal CMDs across the country. It emphasizes the criticality of addressing interconnected societal factors such as poverty, hunger, inequality, educational access, and economic development, as outlined by SDGs, to promote optimal maternal mental health outcomes. This review will particularly focus on the prevalence rates of depression and anxiety, representing the two most commonly observed CMDs globally.

METHODS

Data Source and Search Strategy

A comprehensive systematic review identified the pertinent evidence for maternal mental health in India. The Preferred Reporting Items for Systematic Reviews and Meta-Analyses (PRISMA) 2020 guidelines were followed for the review. Preceding the initiation of the review, we established a meticulously formulated research question, a

well-defined search strategy, and explicit inclusion-exclusion criteria. The review utilized PubMed and Google Scholar as the primary databases and also extracted papers from different web sources. We assessed over fifty-eight articles published from the year 2013 till July 2023 to guarantee alignment with the current prevalence and factors influencing maternal CMDs. The systematic review was conducted through two approaches: firstly, systematic searches of databases were performed, encompassing all sources relevant to maternal common mental health in India and grey literature. Secondly, hand searches involved scouring reference lists of cited systematic reviews for additional relevant studies. We incorporated the MeSH terms and free-text word synonyms for "Maternal Mental Health", "India", "Common Mental Disorders", "Depression", "Anxiety", "Perinatal", "Antenatal" and "Postpartum". The review was undertaken on an expedited schedule to guide research priorities before the inception of the project proposed at NHM. Consequently, it was impractical to scrutinize all the results from the databases or acquire inaccessible papers.

Inclusion-Exclusion Criteria

We took into account the research studies across diverse geographical locations in India. These papers revolve around the investigation of maternal mental health and factors associated with it, particularly within the context of the perinatal period. The inclusion criteria encompass the examination of incidence, prevalence, and risk factors associated with maternal common mental disorders (CMDs) such as postpartum depression, antenatal psychiatric symptoms, and stress during the perinatal and postpartum period. The study designs include both community-based and hospital-based cross-sectional and longitudinal approaches, contributing to a thorough investigation of maternal mental health and its determinants across diverse settings and populations in India. We rejected studies based on the exclusion criteria listed: studies using sample sizes of less than 20 people; data gathered from countries other than India; study methodologies other than observational, such as literature reviews and qualitative investigations; studies where the data could not be extracted separately; studies that report on the prevalence or determinants of CMD without using a recognised diagnostic tool or screening tool; and full-text papers that were not retrievable during the review period.

Data Extraction and Screening Strategy

We imported and organized the search outcomes from all the sources using End Note software, eliminating any duplicate entries in the article list. Subsequently, we conducted screening based on the titles and abstracts of the articles, leading to the retrieval of relevant papers. Due to time limitations, papers that could not be retrieved were excluded. Finally, we thoroughly reviewed the full text of the selected papers and retained those that fulfilled the eligibility criteria. The extracted data from the eligible papers were stored in Microsoft Excel which included the first author's name, the title of the paper, the type of study, year of publication, data source, the type of population, the state of India, sample size, event of interest, event size, prevalence of CMDs, the type of maternal common mental disorder, its measurement scale, and its key determinants.

Statistical Analysis

In light of the expected heterogeneity in outcomes among the included studies, attributed to the limited number of extracted studies, we deemed a meta-analysis investigating explanatory factors of heterogeneity to be more valuable than a systematic review devoid of quantitative results. It could be argued that, with the acknowledgement of limitations in synthesizing heterogeneous results, quantitative syntheses offer richer insights compared to a qualitative interpretation of results and allow exploring diversity in outcomes. We performed a random effect meta-analysis in Comprehensive Meta Analysis (CMA) software. The forest plots were used to evaluate the pooled estimate of the prevalence of maternal common mental disorders in India. Cochran's Q-statistic tests whether there is a significant difference in the common effect sizes among all the studies obtained after the systematic review due to sampling error alone. However, Q statistic depends highly on the size of the meta-analysis, hence relying on statistical power so we suggest not to infer results based on it. Furthermore, we calculate I^2, in simple terms, the percentage of variability not caused by sampling error, which is highly dependent on the precision of the included

studies. Therefore, we infer meta-analysis results based on its I^2 value and 95% prediction interval. Also, a funnel plot is used to study the publication bias in the studies.

RESULTS AND DISCUSSION

Study Description

The study outlines the process of selecting reviews in0. We acquired a total of 58 records considered to be potentially relevant, consisting of 50 records identified through database searches and 8 from alternative sources such as grey literature. Among the 58 records, 8 duplicates indexed in more than one database were excluded. Subsequently, the remaining 50 records underwent initial screening based on their titles and abstracts, excluding 2 records that did not meet the inclusion criteria. Full-text reviews were conducted on the remaining 42 reviews as we excluded 6 papers that were not retrievable, revealing 6 studies that satisfied the inclusion criteria. Expanding on Naaz et al.'s discoveries, our systematic review aligns with their observation that women in lower socioeconomic classes, with less education and more children, are more likely to experience common maternal mental disorders (CMD)[4]. Furthermore, Naaz et al.'s subsequent study emphasizes the significance of advanced maternal age, nuclear family structure, urban living, and single parenthood as notable factors contributing to maternal CMDs[5]. To deepen our understanding, George et al.'s research suggests that socioeconomic status, recent adverse events, perceived support, and maternal health concerns are crucial determinants of postpartum depression[6]. Bhaskar, echoing Naaz, identifies a higher prevalence of postpartum depression in urban Indore [7], while Sheeba et al.'s study in Bangalore reveals a notable connection between domestic violence, pregnancy-related anxiety, and prenatal depression[8]. Expanding the scope, Vijayaselvi et al.'s work emphasizes the importance of pregnancy planning and the husband's employment status as key factors linked to maternal stress[9]. Our systematic review aligns with Edge's study on correlates of perinatal depression, affirming the significance of factors such as smoking, gestational diabetes, and pre-eclampsia in influencing maternal mental health outcomes[10]. In most of these 6 papers, they assessed the effect of sociodemographic variables, obstetric history, and postpartum factors on mental health disorders. The most common factors affecting mental health were social status, parity of mothers, domestic violence, recent catastrophic events, and the intentionality of the pregnancy. Due to the variability and inconsistency of factors identified in the literature review, we are impeded from constructing a meta-analysis for these variables.

Meta-Analysis

We conducted a random model meta-analysis on the six studies that satisfied our inclusion criteria and obtained six estimates on CMDs. The pooled prevalence estimate of maternal CMD is 44.9% (95% C.I. = 34.4 to 56, I^2 = 93%). Here, we observe that a high variance of 93% in observed prevalence reflects variance in true prevalence rather than sampling error. We also obtained that the true prevalence rate is not the same for at least two of the studies in the analysis using Cochran's Q test (Q = 69.591 with 5 degrees of freedom (d.f.) for α = 0.05). 0depicts the forest plot of prevalence rates of maternal CMDs in India. Despite the limited size of our meta-analysis, we established 95% prediction intervals for the prevalence rates, ranging from 14.2 to 80.1, providing a glimpse into the nature of predicted intervals in this study. With an expanded analysis size, the interval length is expected to significantly decrease, yielding a more precise estimated range.

Limitations

In prevalence studies that aggregate data from diverse observational studies involving patients with varied characteristics and conducted in various settings, there is anticipated to be heterogeneity in the estimates. Nevertheless, despite our endeavours to execute a systematic review of high quality, it is probable that the quality and heterogeneity of the included studies influence the reliability of the findings. While we investigated variations in estimates based on factors such as the use of diagnostic interviews or screening tools for identifying depression and/or anxiety, the diversity in screening tool types, translation and validation processes, and variations in how and by whom screening was conducted might account for some of the identified heterogeneity. It is also conceivable that

there are relevant studies we may have overlooked because of time constraints. The assumption of the generalizability of the term "Maternal Common Mental Disorders" (CMD) might also have introduced disparities in the estimates.

CONCLUSION

Despite limitations in prevalence estimates, this study reveals a high burden of maternal CMDs in India, associated with socio-demographic factors, obstetric history, and domestic violence, rather than solely pregnancy-related causes. The alarming prevalence of 44.9% reinforces the urgent need for multi-pronged policy interventions aligned with India's SDG 2030 goal for mental health. Implementing policies like micro-loan programs, skills training, and childcare support for low-income mothers could potentially alleviate financial burdens and improve mental health outcomes. In addition to that, establishing community-based support groups and peer mentoring programs could address social isolation and empower mothers with knowledge, potentially reducing depressive symptoms. While further research is needed to optimize interventions and address diverse contexts, these initial steps hold immense potential to strengthen maternal mental health and build a more equitable and supportive society.

Future Scope

The systematic review has the potential to be revised by incorporating the remaining papers from the databases, facilitating a comprehensive meta-analysis encompassing all available records to date. Additionally, there is an opportunity to perform subgroup analyses, providing a more nuanced understanding of the prevalence of maternal Common Mental Disorders (CMDs) among various subgroups within the existing literature in India.

REFERENCES

1. (n.d.) SDG 3: Ensure healthy lives and promote well-being for all at all ages. UN Women – Headquarters. https://www.unwomen.org/en/news/in-focus/women-and-the-sdgs/sdg-3-good-health-well-being
2. (2022) The Importance of Integrating Maternal Mental Health with Pregnancy Care | Lifespan. Lifespan. https://www.lifespan.org/lifespan-living/importance-integrating-maternal-mental-health-pregnancy-care
3. (2023) Maternal Mental Health. World Health Organization. https://www.who.int/teams/mental-health-and-substanceuse/promotion-prevention/maternal-mental-health
4. Naaz, N., Mehnaz, S., Ansari, Ma., and Amir, A. (2020) Maternal Mental Health and its Association with Sociodemographic Factors and Delivery Related Practices. Indian Journal of Public Health. 11(8).http://dx.doi.org/10.36106/gjra
5. Naaz, N., Mehnaz, S., Ansari, Ma., and Amir, A. (2021) Maternal mental health and its determinants – A community-based cross-sectional study in Aligarh, Uttar Pradesh. Indian Journal of Public Health. 65 (1), 16. http://dx.doi.org/10.4103/ijph.ijph_193_20
6. George, M., Johnson, A.R., and Sulekha T. (2021) Incidence of Postpartum Depression and Its Association With Antenatal Psychiatric Symptoms: A Longitudinal Study in 25 Villages of Rural South Karnataka. Indian Journal of Psychological Medicine. 44 (1), 37–44. http://dx.doi.org/10.1177/0253717621991061
7. Bhaskar, P., Yesikar, V., Bansal, S.B., and Waskel, B. (2021) A cross sectional study to assess the prevalence and risk factors of post-partum depression in urban area of Indore district. International Journal of Research in Medical Sciences. 9 (10), 3028. http://dx.doi.org/10.18203/2320-6012.ijrms20213927
8. Sheeba, B., Nath, A., Metgud, C.S., Krishna, M., Venkatesh, S., Vindhya, J., et al. (2019) Prenatal Depression and Its Associated Risk Factors Among Pregnant Women in Bangalore: A Hospital Based Prevalence Study. Frontiers in Public Health. 7. http://dx.doi.org/10.3389/fpubh.2019.00108

9. Vijayaselvi, Dr.R. (2015) Risk Factors for Stress During Antenatal Period Among Pregnant Women in Tertiary Care Hospital of Southern India. Journal of Clinical And Diagnostic Research.http://dx .doi.org/10.7860/jcdr/2015/13973.6580
10. Al-abri, K., Edge, D., and Armitage, C.J. (2023) Prevalence and correlates of perinatal depression. Social Psychiatry and Psychiatric Epidemiology. 58 (11), 1581–1590. http://dx.doi.org/10.1007/s00127-022-02386-9

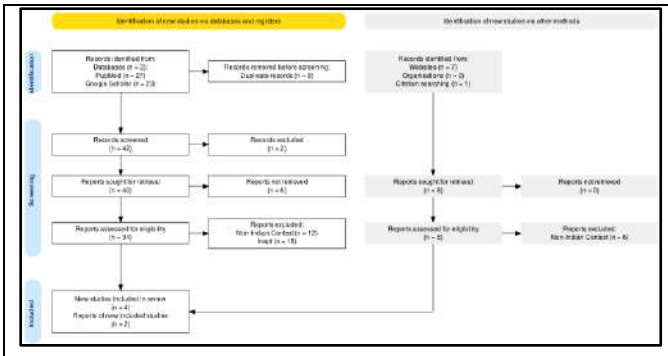

Fig 1: PRISMA diagram of the selection process

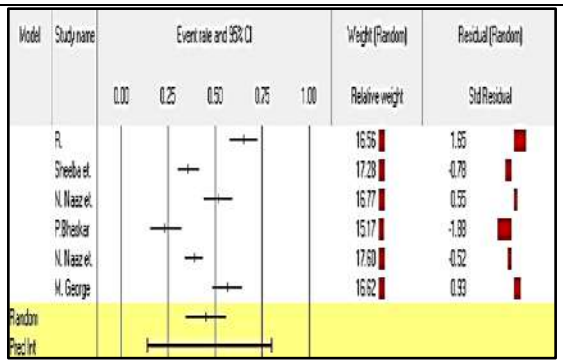

Fig 2: Forest plot of prevalence rates

RESEARCH ARTICLE

Enhanced Method of Emotion Detection and Face Recognition for Attendance Monitoring Using Machine Learning

Jeyalakshmi[1*], S. Deepak Prakash[2] and N. Sanjay Kumar[3]

[1]Associate Professor, Department of Information Technology, Sri Ramakrishna College of Arts & Science, Coimbatore, Tamil Nadu, India.
[2]PG Scholar, Department of Information, Technology, Sri Ramakrishna College of Arts & Science, Coimbatore, Tamil Nadu, India.
[3]PG Scholar, Department of Information Technology, Sri Ramakrishna College of Arts & Science, Coimbatore, Tamil Nadu, India.

Received: 22 Feb 2024 Revised: 15 Mar 2024 Accepted: 21 Mar 2024

***Address for Correspondence**
Jeyalakshmi
Associate Professor,
Department of Information Technology,
Sri Ramakrishna College of Arts & Science,
Coimbatore, Tamil Nadu, India.
Email: jeyalakshmi@srcas.ac.in

ABSTRACT

The use of facial recognition is essential in every industry in the modern era. One of the most popular biometrics is face recognition. Along with many other benefits, it can be used for security, authentication, and identity. Additionally, facial recognition software can be used to record attendance in work environments, institutions, and colleges, among other places as well. The sustainable attendance system seeks to streamline the attendance management process and save time and effort for both administrators and attendees. Automated facial recognition technology eliminates the need for manual data entry and reduces the administrative burden associated with attendance tracking. It allows administrators to allocate resources more efficiently and focus on more value-added tasks. The currently available manual method takes a lot of time and work to maintain, so the goal of this system is to build up a facial recognition-based class attendance system. Moreover, there may be opportunities for proxy participation. The machine learning project, titled " Emotion Detection and Face Recognition for Attendance Monitoring" trains a model to identify student attendance based on their emotions during class using Python, OpenCV, and student datasets. Facial emotion recognition and classification are done using the CNN and Haar Cascade algorithms. It ensures accurate attendance records by capturing and analyzing facial features using computer vision algorithms. The goal of this project is to offer an alternative to the manual attendance-taking approach that is currently in use by staff members.

Keywords: Face Recognition, Face Detection, Emotion Detection, Haar Cascade Classifier,CNN, Open-cv

INTRODUCTION

In many schools and universities, the traditional technique of recording attendance is a laborious effort. The faculty members who must manually call out each student's name to record attendance are further burdened, as this could take up to five minutes for the entire class [1]. To do this, a lot of time is needed. In certain situations, proxy attendance is permitted. As a response, several institutions started using other techniques to monitor attendance, like the use of fingerprint, iris, and radio frequency identification (RFID) [2]. These methods, however, are obtrusive and queue-based, which could take additional time [14]. Face recognition has developed into an essential biometric characteristic that is non-intrusive and simple to learn. Systems that rely on facial recognition are not very sensitive to different expressions on the face [5]. Face identification and verification are the two categories that make up a face recognition system. [3] While face verification compares a face image to a template face image in a 1:1 matching procedure, face verification compares a query face image to a 1: N problem. The technique of automatically extracting, analyzing, and comprehending meaningful information from a single image or a series of photos is known as open-source computer vision. Colleges could use computer vision to use facial recognition technology to electronically take attendance. This will not only help faculty members save valuable time, but it will also teach staff members and their students how to code and the range of computer vision applications that are feasible [15].

College instructors and staff would have access to more student data and early notice of notable changes in emotional state if there was an emotion detection system in place [8]. While security cameras are deployed in many institutions, they are rarely used for anything other than capturing images. Computer vision can be implemented in college settings with these cameras. Instructors and staff can then track student involvement and emotion using the data gathered. A possible method to evaluate students' mental health might include computer vision [6]. The many applications of open- source computer vision, such as face detection, face identification, and emotion analysis, could be useful in tackling the problem of college students [11]. If a student exhibit repeated signs of depression or anger, our program will be able to alert the guidance counselor at the college in advance. Using the help of these capabilities, educators can use facial recognition to save the time spent on outdated attendance procedures and connect themselves and their students with computer vision and deep learning applications [9]. Facial recognition and emotion detection can help teachers to monitor the changes in their student behaviors to increase productive knowledge among the student and helps in achievement [13].

Facial Recognition Technology

The system utilizes advanced facial recognition algorithms to identify and authenticate individuals based on their unique facial features [4]. This technology analyzes key facial and marks to create a unique biometric template for each person.

Real-Time Facial Detection and Emotion Detection

The system employs computer vision techniques to capture and analyze facial images in real-time [7]. It detects faces within a given frame and matches them against the pre-registered biometric templates to authenticate individuals [12]. Emotions expressed by the students are detected using the Haar Cascade Classifier and CNN.

LITERATURE REVIEW

Face Recognition System Using Deep Learning, Saibal Manna, Sushil Ghildiya, Krishnakumar Bhimani[16]Future expansion of the company will benefit from the face recognition attendance system's real-time video processing design, that supports company growth. The objective of this paper is to develop a real-time video

processing-based facial recognition attendance and time tracking system. Four research experiments were conducted in this study: the accuracy rate of the face recognition system during real-time register; the stability of the face recognition time and attendance system with real-time video processing; a study of the face recognition attendance system's skip rate using real-time video processing; and a configuration of the face recognition attendance system's interface. The experimental results indicate that the face recognition technology and computer assistance used by the time and attendance system to accomplish the desired time and attendance results fully reflects the feasibility design of the overall algorithm. Students those who are successfully completed the attendance check-in method did so in a timely manner, eliminating the need for the convoluted roll call sign and instantly realizing its purpose. The conversion form for the attendance system and the future system time have achieved significant advancements that have improved the face recognition technology's dependability and attendance rate. Our scientists should investigate and realize it more thoroughly. **Face Recognition Attendance System Based on Real Time Video Processing, Xiaofeng Han, Hao Hang,** [17] In this article, A face recognition attendance system that utilizes real-time video processing is created, and two institutions within a province are chosen to have their student attendance checked in real-time. This article primarily lays out four approaches to look at the issues: the truancy rate of the face recognition attendance system with real-time video processing, the stability of the face recognition attendance system with real-time video processing, and the accuracy rate of the face recognition system during the actual check-in. Analyzing the facial recognition attendance system's interface settings with real-time video processing is challenging.

Through an analysis of these issues, a face recognition technology-based attendance system concept is put forth, and research is done on face recognition attendance systems based on real-time video processing. According to research findings, the video facial recognition system has an accuracy of roughly 82%. With just roughly 13% of students missing class, the facial recognition time attendance system and manual fingerprint punching are more reliable and accurately identify check-ins. Efficiency is significantly higher than in the control group, which helps stop pupils from departing early and missing lessons. **Facial Recognition Using Haar Cascade and LBP Classifiers, Anirudha B Shetty, Bhoomika**, [18] Facial Recognition is the biometric technique used in face detection. The facial recognition technology is used to validate or identify a face from the multi-media pictures. Facial recognition has become increasingly crucial as civilization has grown. Face detection and identification have increased globally. It is due to the need for security, including authorization, national security, and other exigent situations. Numerous algorithms exist for the purpose of facial recognition. The goal of this research is to compare two face recognition methods that are standardized for classification: Haar Cascade and Local Binary Pattern. The precision of Haar Cascade surpasses that of the Local Binary Pattern as a result, but its execution time also exceeds it.

Attendance System with Emotion Detection: A case study with CNN and OpenCV, Herman Kandjimi, Abhinav Srivastava, [19] The way multinational corporations (MNCs) care for their workforce is by asking for input, where daily mood is considered a non-factor. Manual data collection techniques are conventional and widely used, and they consume employees' productive time to perform. This procedure can be automated with the use of a certain solution. This study investigates the use of machine learning (ML) and artificial intelligence (AI) models in an automated attendance and mood system. Because of the way the system is set up, businesses can use facial recognition and a customized Convolutional Neural Network (CNN) model to generate data on an employee's mood or emotions. The entrance and exit of each block or floor may have cameras installed by the companies. Cameras are able to take pictures and feed them into OpenCV, making integration simple and attendance tracking possible. The photo that was taken can also be used to identify an employee's mood and be stored in their own database. On the same day, the Human Resources (HR) department can monitor employee facial expressions to get input about new projects, hikes, seminars, and social events.

PROPOSED SYSTEM

Before their photos are taken and added to the dataset, each student in the class must register by providing the necessary information such as their name, department, and regno. Faces from the live streamed classroom video will be identified during each session. A comparison will be made between the faces identified and the photographs

included in the dataset. In the event a match is made, the relevant student's attendance will be recorded. With Open CV, Attention Detection uses students' facial expressions in a classroom to provide an Excel sheet with the results. The Attention Detection using Face Emotion Recognition machine learning project trains a model to identify student attendance based on their emotions during a class using Python, OpenCV, and a dataset of students. The goal of this project is to offer a substitute for the manual way of taking attendance that is currently used by teachers.

Real-Time Monitoring and Reporting

Real-time tracking and reporting of attendance data is made possible by the system. Administrators have instant access to attendance records, are able to track trends in attendance, and create thorough reports. This makes it possible to make decisions quickly, act quickly when necessary, and handle attendance-related data effectively.

Integration with Existing Systems

Existing staff or student information systems can be easily integrated with the sustainable attendance system. This breaks down data silos, streamlines data administration, and improves administrative effectiveness all around. Integration makes it easier to synchronize attendance data with other pertinent systems, which streamlines procedures all around.

Improved Data Analysis and Insights

For enhanced data analysis and insights, the system's automated data administration and consolidated database are advantageous. Administrators can monitor students' moods through the use of Haar Cascades classifiers, which enables them to make appropriate plans for the following class hour. Facial expression detection is one of the many computer vision applications in which CNNs have demonstrated impressive performance. Using a dataset of labeled facial expressions, we may train a CNN model to identify patterns and characteristics linked to various emotions.

Reduced Administrative Burden

Staff members' administrative workload is lessened with automated attendance tracking since it eliminates the need for human data entry and monitoring, freeing up time for other crucial responsibilities. Typically, this process can be divided into four stages,

Dataset Creation

Images of students are captured using a web cam. Next step is to resize the cropped images to particular pixel position (1280*720) dimension. The dataset used in this project consists of images of students captured during a class hour. Each image is labeled with the corresponding emotion of the student, such as happy, sad, or neutral. The dataset was collected using a camera placed in the classroom. In the dataset the image will contain the name and register number of the students as the name of the image.

Face Detection

Face detection here is performed using Haar-Cascade Classifier with Open source computer vision. Haar Cascade algorithm needs to be trained to detect human faces before it can be used for face detection. Features like edge, line, and center surround are the main frames as shown in the fig.2. This step is called feature extraction. The haar cascade training data used here is in the form of an xml file-haarcascade_frontalface_default. The haar features will be used for feature extraction where the objects in the image are identified as shown in Fig.3.

Face recognition and Emotion detection

The machine learning model used in this project is trained using the labeled dataset. The training process involves training a Convolutional Neural Network (CNN) to recognize emotions in the images. The model is then fine-tuned to detect the level of attention of each student in the class based on their emotions. during recognition process image of the face to be recognized and then compared with the already computed image and returns the best matched label associated with the student it belongs to.

Attendance Updation

After face recognition and emotion detection process, the recognized faces will be marked as present in the excel sheet and the rest will be marked as absent and the list of student's emotions will be filtered and given to the respective faculties. Faculties will be updated with an hourly attendance sheet at the end of every class.

RESULTS AND DISCUSSIONS

The image of the students is captured in the webcam as shown in fig.4. and stored in the folder named Class_data as shown in fig.5. The system employs computer vision techniques to capture and analyze facial images in real-time. It detects faces within a given frame and matches them against the pre-registered biometric templates to authenticate individuals. The students are supposed to enter all the required details in the student database. Once the class starts, the web cam starts automatically. Camera pops up and starts detecting the faces in the frame as shown in fig.6. Then it automatically starts clicking photos of the students through live streaming camera. These images then will be pre-processed and stored in training images folder. The Fig.6, and Fig.7. shows the face recognition window where two registered students are recognized and if in case, they were not registered it would have shown 'unknown'. The faculties will get the hourly report through excel sheet as shown in fig.8. This is important because the list of presented students with their emotional state during the class will be recorded, it shows the emotional state like Neutral, happy, sad, angry etc. An emotion detection would give college faculty, the more information on students and early warning of significant shifts in emotional state. The staff can identify the student's behavior through the hourly report of attendance with emotion of the students.

Pseudocode- Face recognition in Frame

faces In Frame = face_recognition.face_locations(imgS) encode In Frame= face_recognition. face_encodings (imgS, faces In Frame) for endode Faces, face Loc in zip(encode In Frame, faces In Frame): is matched = face_recognition.compare_faces(all Encodings, endodeFaces) face D is= face_ recognition. face_ distance (all Encodings, endode Faces) try:
best Match Index = numpy.argmin (face D is) except Value Error as ve: print(ve)

CONCLUSION

Every student in the class needs to register by providing the necessary information. After that, their photos will be taken and included to the dataset. Faces will be identified from the classroom's live streaming footage during each session. The identified faces will be contrasted with photos that are included in the collection. Should a match be discovered, the relevant student's attendance will be recorded. The faculty will receive an excel sheet with the hourly report at the conclusion of each session. This system uses facial recognition algorithms to create an efficient way to track students' attendance in class. Face ID will be able to be used by the proposed system to track attendance. Through the use of a webcam, it will first identify faces. Once a student has been identified, their attendance will be noted along with any emotions they have expressed, and the attendance record in the Excel spreadsheet will be updated.

REFERENCES

1. Amit Pandey, Aman Gupta, Radhey Shyam "Facial Emotion Detection And Recognition" International Journal of Engineering Applied Sciences and Technology, 2022 Vol. 7, Issue 1, ISSN No. 2455-2143, Pages 176-179
2. Akbar, Md Sajid, et al. "Face Recognition and RFID Verified Attendance System." 2018 International Conference on Computing ,Electronics & Communications Engineering(iCCECE).IEEE,2018.

3. Rathod, Hemantkumar, et al. "Automated attendance system using machine learning approach." 2017 International Conference on Nascent Technologies in Engineering(ICNTE). IEEE, 2017.
4. Lukas, Samuel, et al. "Student attendance system in classroom using face recognition technique." 2016InternationalConferenceonInformation and Communication Technology Convergence (ICTC).IEEE, 2016.
5. Shweta Jain Dr. H N Suresh AshwatappaP(2016), "Design and Development of Gesture Recognition System using Raspberry Pi", International Journal for scientific Research & Development (IJSRD),Vol. 4,Issue No. 06
6. MohammadrezaSheykhmousa,MasoudMahdianpari(2020),"SupportVectorMachine Versus Random Forest for Remote Sensing Image Classification: A Meta-Analysis and Systematic Review",IEEE access vol13
7. M.Awais,M.JIqbal(2019)"Real-TimeSurveillanceThroughFaceRecognitionUsingHOG andFeedforwardNueralnetworks",10.1109/ACCESS.2019.2937810,IEEEAccess.
8. Manav Bansal(2019), "Face recognition implementation on raspberrypi using open cv and python", International Journal of Computer Engineering and Technology (IJCET)Volume10,Issue03, pp.141-144.
9. AzharSusanto,Meiryani(2019),"DatabaseManagementSystem"internationaljournalofscientific& technology research volume 8, issue 06
10. Raut, Nitisha, "Facial Emotion Recognition Using Machine Learning" (2018).
11. Mohammed Adnan Adil "Facial Emotion Detection Using Convolutional Neural Networks"
12. Shweta Jain Dr. H N Suresh AshwatappaP(2016), "Design and Development of Gesture Recognition System using Raspberry Pi", International Journal for scientific Research & Development (IJSRD), Vol. 4,Issue No. 06
13. Deshpande, N. T., & Ravishankar, S. (2017). Face Detection and Recognition using Viola-Jones algorithm and Fusion of PCA and ANN. Advances in Computational Sciences and Technology, 10(5), 1173- 1189
14. Kavia, M. Manjeet Kaur, (2016). "A Survey paper for Face Recognition Technologies". International Journal of Scientific and Research Publications, 6(7)
15. Okokpujie, Kennedy O., et al. "Design and implementation of a student attendance system using iris biometric recognition." 2017 International Conference on Computational Science and Computational Intelligence (CSCI). IEEE, 2017.
16. Sushil Ghildiya, Kishnakumar Bhimani Published: IEEE ACCESS, Face Recognition System Using Deep Learning, 2019.
17. Xiaofeng Han, Hao Hang, Face Recognition Attendance System Based on Real Time Video Processing, July 2020, IEEE Access PP(99):1-1
18. Anirudha B Shetty, Bhoomika Published: Global Transitions Proceedings, Facial Recognition Using Haar Cascade and LBP Classifiers, 2021
19. Herman Kandjimi, Abhinav Srivastava; Attendance System with Emotion Detection: A case study with CNN and Open CV; DSMLAI '

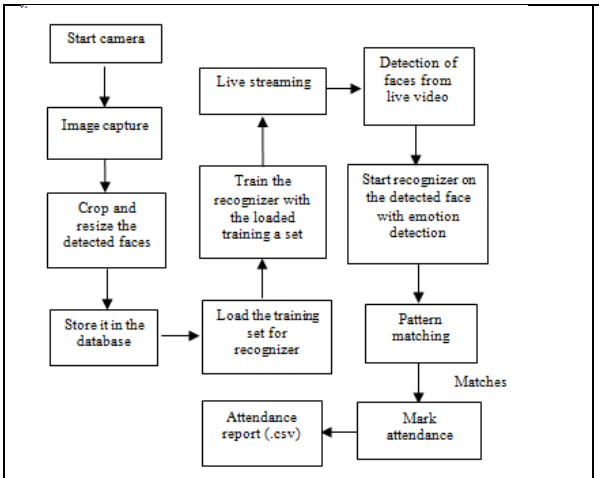

Fig: 1 System Architecture of Proposed System

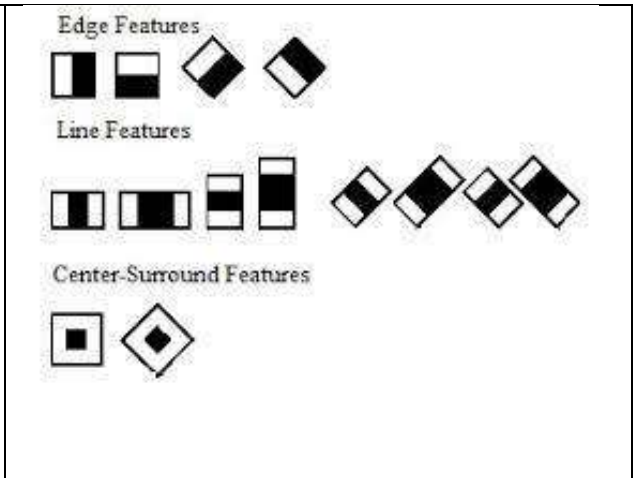

Fig.2 Main Frames used in haar cascade

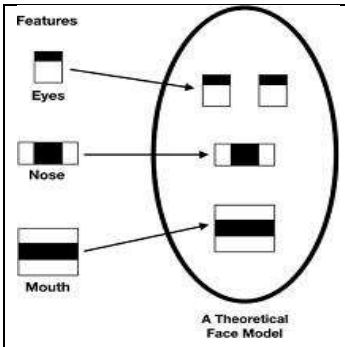

Fig.3. Haar Features

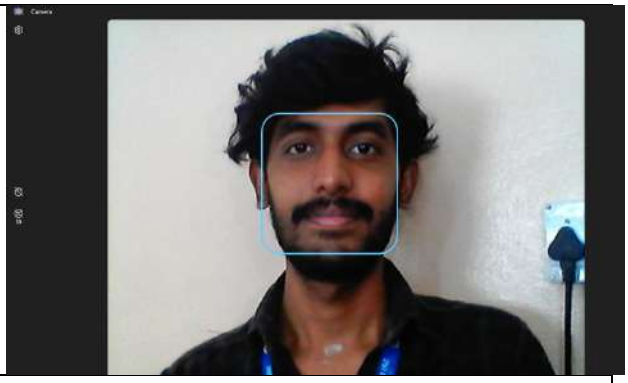

Fig.4. Face Detection

Fig.5. Students image folder

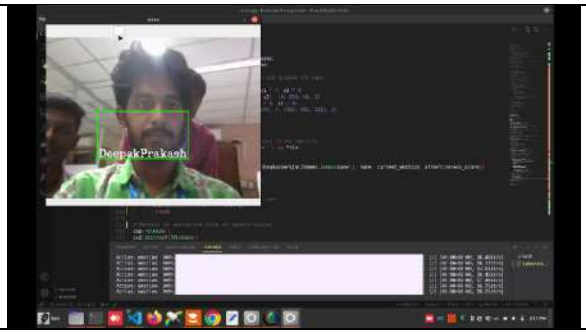

Fig.6. Face Recognition of student 1

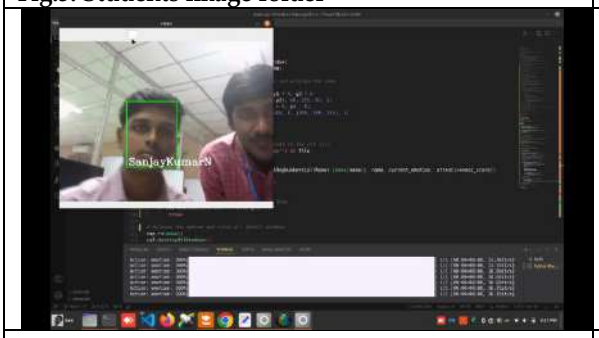

Fig.7. Face Recognition of student 2

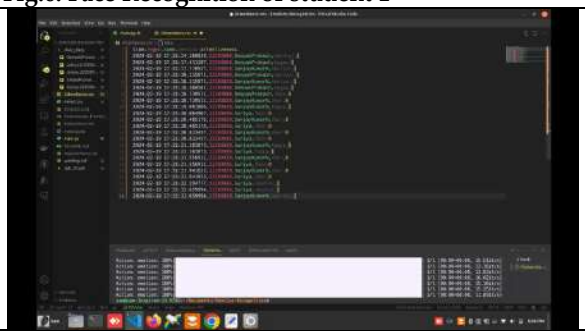

Fig.8. Hourly report of attendance with emotion of the students

Vol.15 / Issue 83 / Apr / 2024 International Bimonthly (Print) – Open Access ISSN: 0976 – 0997

RESEARCH ARTICLE

Performance Analysis of Gray Level Image Segmentation by Using Different Methods

T.Brinthaguru[1] P. Karthick[2]*, and P.Vinoth[3]

[1]Research Scholar, Department of Mathematics, Kalasalingam Academy of Research and Education, Krishnankoil-626 126, Virudhunagar, Tamil Nadu, India.
[2]Assistant Professor, Department of Mathematics, Kalasalingam Academy of Research and Education, Krishnankoil-626 126, Virudhunagar, Tamil Nadu, India.

Received: 30 Jan 2024 Revised: 09 Feb 2024 Accepted: 27 Mar 2024

***Address for Correspondence**
P. Karthick
Assistant Professor,
Department of Mathematics,
Kalasalingam Academy of Research and Education,
Krishnankoil-626 126,
Virudhunagar, Tamil Nadu, India.
Email: karthickphd91@gmail.com

ABSTRACT

Image segmentation is of great importance in understanding and analysing objects within images. Using segmentation and subsequent color density evaluation, the procedure entails turning hazy images into meaningful and practical ones. Medical and industrial areas, among others, frequently use the image segmentation method. In this paper, we will discuss four important types of image segmentation methods to segment gray images and compare the accuracy of segmentation based on the error ratio test.

Keywords: Image segmentation, Grayscale image, Edge-based method, Threshold-based method, Region Based method, Clustering based method.

INTRODUCTION

Using a variety of methods, image processing aims to improve images or extract relevant information from them. In order to improve viewer comprehension, this method usually takes an input image and produces either a transformed image or pertinent characteristics connected with it. Automated analysis and interpretation can be facilitated by information extracted from photos. In computer vision, image thresholding is still a major obstacle. Because segmentation problems are ill-posed, getting generalized image segmentation results remains a challenge despite years of focused research. Of all the segmentation techniques available, graph theoretical approaches have shown promise as workable solutions. These methods provide interesting insights into tackling segmentation

difficulties and increase the value of computations by mathematically modeling image elements into well-defined structures. A key method in digital image processing and analysis is image segmentation, which is breaking a image up into separate areas or sections, frequently according to pixel properties. This could involve grouping related areas according to color or shape characteristics or separating foreground components from the background. Image segmentation is an important process in medical imaging, especially for recognizing and labeling pixels or voxels within a 3D volume that represent anomalies such as brain tumorsor other organs. It is possible to improve the look of these abnormalities for better identification by adjusting pixel densities and contrasts. Of all the segmentation techniques available, thresholding is one of the most straight forward and efficient. Because of its high accuracy and adaptability, it is frequently used for image segmentation jobs. Image processing covers a wide range of applications and standards, and MATLAB is a great interactive tool for working on different image processing problems. The goal of this work is to explore the nuances of image segmentation, with a particular emphasis on thresholding and edge detection techniques. This paper will examine many illustrative examples of image segmentation using grayscale images as a foundation, concluding with an analysis of error ratios. This paper is organized as follows: In section 2, we briefly discuss relevant literature to contextualize our work within the existing research landscape. Section 3 presents our methodology, outlining the segmentation methods employed and discussing their applicability to our study. Following this, Section 4 details the experiments carried out and presents the corresponding results. Finally in section 5, we conclude our work by summarizing key findings and suggesting avenues for future research.

Related Work

In [1] contains A key component of many visual comprehension systems is segmenting images or video frames into discrete objects and segments. The outstanding performance of deep learning-based segmentation algorithms across several image segmentation tasks and benchmarks has attracted a lot of attention. These algorithms' design and methodology allow them to be divided into several architectural categories. Color information and texture features are commonly used in creating histograms or distinguishing borders, limits, and textures inside pixels, as 2012 [3] demonstrated. As such, segmenting data based on color and texture is a widely used strategy for indexing and data management. Abdul-Nasir et al. [2] produced the results of using a novel method for color image segmentation that combines the k-means clustering algorithm with a variety of color models. The research explores the examination of different color components in RGB, HSI, and C-Ycolor models in order to identify the component that produces the best segmentation results. Furthermore, procedures such as median filtering and seeded region growing are a extraction were used to smooth the image and remove unwanted regions, respectively, in order to improve the quality of the image. Kumar et al [10] discussed the RGB model is displayed,alongwithabreakdownoftheRGBimageintoitsR,G,andBcomponents.Weturnacolorimageinto a grayscale image using MATLAB, and then the grayscale image's pixel intensity varies based on the suggested transformation equation. Fan et al. [6] present a revolutionary automatic image segmentation method in 2001.

First, color edges in a image are automatically detected by combining a fast entropic thresholding methodology with an improved isotropic edge detection method. Moreover, color-edge extraction results combined with Seeded Region Growing (SRG) improve image segmentation accuracy. We also investigate the automatic face detection use of this image segmentation system. The technique's usefulness in directed segmentation tasks, such as segmentation-driven image compression techniques and medical image segmentation, was developed by Mohsen et al. [4]. An overview of different image segmentation techniques is given in this publication by Mohsen et al. [5]. These techniques are mostly used for the identification of points, edges, line patterns, and other features. Notably, for applications like pattern recognition and medical imaging, writers have used methods like SegNet, UNet++, and encoding-decoding using A trous. A novel thresholding approach is presented by Narayana moorthy S et al. [8] with the goal of determining the optimal threshold value for grayscale images. It makes use of the Normalized graph cut measure in conjunction with Atanassov's intuitionistic fuzzy sets. In particular, the degree of doubt or proficiency in identifying whether a pixel in the image refers to the backdrop or the item within the image is indicated by Atanassov's intuitionistic fuzzy index values.

This study [7] uses a normalized graph cut metric as the foundation for thresholding with the goal of separating objects from the background by applying the traditional membership function. The fuzzy normalized graph cut method is the name given to the algorithm suggested in this paper. The suggested approach is analyzed using MATLAB software, and the article concludes with a summary of the findings for further study and recommendations. provide a fuzzy set-based thresholding method in 2023[9]that is easy to use, efficient, and uses a lot less processing power. First, the membership function is used to express the color image. Second, the membership values on the image are generated by integrating the spatial and intensity data to create the symmetrical weight matrix.

Existing Gray Scale Image segmentation Methods

Threshold based segmentation

This technique is used to generate binary images from originals. This is accomplished by comparing pixels to a predefined threshold value. Pixels larger than this value will be assigned 1(black); pixels less than or equal to this value will be assigned 0 (white). The algorithm's steps are as follows:

1. As input, read an image.
2. Create new 2-D variables and store the image size in them.
3. Enter the threshold value.
4. Create a new zeros matrix with the same dimensions as the image.
5. Match pixels to the threshold value.
6. Show the results. If we need to split the items in the new image, we need to write them down.

Step 1. Take an image as input
Step 2. Convert this image to grayscale.
Step 3. Provide the threshold value.
Step 4. Show only pixels greater than the threshold value.

Edge based segmentation

This method is used to determine the details of objects by using intensity-level (grayscale) detection. Edge detection is one of the most common strategies used to analyse images. The edge method uses the difference between colors to determine the details of the edges. These details appear as white lines on a black background. There are several different methods used to filter

- Sobel filter
- Prewitt filter
- Robert's filter
- Log filter
- Zero-cross filter

This function (Edge function) has two parameters: the image's variable and the method. The steps of the algorithm are as follows:

1. Read an image.
2. Use edge function and any of the aforementioned filters.
3. Display the image.

Watershed segmentation

Watersheds provide a free object-splitting approach that is particularly useful for dividing objects that are in contact with each other. This process understands images as physiological surfaces in which the value of f (x, y) corresponds to elevation. The watershed algorithm finds the watershed basins and hill lines in the image where water would theoretically collect. Suppose that there is a perforated hole at each regional low point and the natural terrain is submerged from below by water rising through these holes at a uniform rate. Pixels are marked as submerged as the

water rises. Ultimately, water will rise to a level where two submerged areas become integrated. When this happens, the algorithm creates one thick pixel dam separating the two areas. As the flood continues, the entire image is divided into separate collection basins. The steps for this algorithm are as follows:

Step 1. Read an image.
Step 2. Pre-process black border removal.
Step 3. Adapt the watershed area.
Step 4. Estimate the Lesion ratio.
Step 5. Merge watershed areas.
Step 6. Define watershed borders.
Step 7. Smooth borders (Border sampling and b-spline smoothing).
Step 8: Overlay borders

Clustering based segmentation

Clustering is an undirected technique used in data mining for identifying several hidden patterns in the data without coming up with any specific hypothesis. The reason behind using clustering is to identify similarities between certain objects and make a group of similar ones. There are two different types of clustering, which are hierarchical and non-hierarchical methods. Non-hierarchical Clustering In this method, the dataset containing N objects is divided into M clusters. In business intelligence, the most widely used non-hierarchical clustering technique is K-means. Hierarchical Clustering In this method, a set of nested clusters are produced. In these nested clusters, every pair of objects is further nested to form a large cluster until only one cluster remains in the end.

K means

K-means clustering is an unsupervised technique no labeled response for the given input data. K-means clustering is a widely approach for clustering. Generally, practitioners begin by learning about the architecture of the dataset. K-means **Clustering Method** clusters data points into unique, non-lapping groupings.

RESULTS AND DISCUSSIONS

Image Segmentation Approaches

A set of images are used to measure the implementation of the suggested algorithm along with some of the frequently used algorithms given in the literature, Performance estimation and comparisons are executed by using real images, where the object can be exactly separate from the background using some appropriate threshold method. The examples are shown in figure 1and 2. Each figure shown the (a) Original image, (b) Histogram of the Original image, (c) Threshold image, (d) Edge based image, (f) Watershed image, (e) K means Clustering method for image segmentation purpose.

Error Ratio

Error ratio (ER) is the most crucial comparative metric. ER is the proportion of pixels between the object pixels and the optimal threshold image obtained by each method that are placed in the erroneous area. Wrongly segmentation as provided **i**n the following formula,

$$E_R = \frac{N_F + N_{miss}}{N_R} \times 100$$

where N, and $Nmiss$ are the number of segmentation pixels in the incorrect area and N, is the number of pixels in the segmented images. In this regard, the value of ER ranges between 0 and 100, with a value 0 denotes a lack of resemblance between the ground truth image and the segmentation result. A value of 100 also indicates a good segmentation result.

Error Ratio Table

Table 1: Comparison of Error Ratio Result of three Images for Different Image segmentation methods. The original threshold image pixel values and the optimum image pixel values are shown in the Table l. In Table l, the error indicates the numerical values corresponding, in each case, to the similarly among the Edge based method. K means Clustering method and Watershed method. Then we choose from a set of error ratio value the best one. We have noticed in bold type the lowest error value. Please note that in all of the cases. It is noticeable from Table 1 reveals that the different types of image segmentation methods comparison of error ratio.

CONCLUSION

Image segmentation algorithms are capable of transforming opaque images into meaningful ones through which vital information can be extracted, especially in the medical field. This study reviewed some of the hashing algorithms that can be used in MATLAB and looked at the results of each one and the error rate. Finally, we observed that researchers need to improve the low error ratio and reduce computational time in the existing algorithm.

REFERENCES

1. Minaee, Shervin, Boykov, Yuri Y, Porikli, Fatih, Plaza, Antonio J a Kehtarnavaz, Nasser, Terzopoulos and Demetri (2021) Image segmentation using deep learning: A survey. IEEE transactions on pattern analysis and machine intelligence. 10.1109/TPAMI.2021.3059968
2. Abdul-Nasir, Aimi Salihah and Mashor, Mohd Yusoff, Mohamed and Zeehaida (2013) Colour image segmentation approach for detection of malaria parasites using vari and k-means clustering WSEAS Trans. Biol. Biomed. https://api.semanticscholar.org/CorpusID:15421700
3. Sharma, Nikita and Mishra, Mahendra and Shrivastava and Manish (2012) Colour image segmentation techniques and issues: an approach, International Journal of Scientific and Technology Research. https://api.semanticscholar.org/CorpusID:18504657
4. Mohsen, Fahd, Hadhoud, Mohiy M, Moustafa, Kamel, Ameen and Khalid,Int. Arab J. Inf. Technol (2012) A new image segmentation method based on particle swarm optimization. https://api.semanticscholar.org/CorpusID:6563143
5. Haralick, Robert M and Shapiro and Linda G (1985) image segmentation techniques, Computer vision, graphics, and image processing. https://doi.org/10.1016/S0734-189X (85)90153-7
6. Fan, Jianping, Yau, David KY and El-magarmid, Ahmed K, Arefand Walid G (2001) Automatic image segmentation by integrating color-edge extraction and seeded region growing, IEEE transactions on image processing. 10.1109/83.951532.
7. Narayanamoorthy S and Karthick P (2019) A comparative performance of gray level image thresholding using normalized graph cut based standard S membership function",Iranian Journal of Fuzzy Systems. 10.22111/IJFS.2019.4481
8. Narayanamoorthy S and Karthick P(2017) The intuitionistic fuzzy set approach for gray level image thresholding using normalized graph cuts ,International Journal of Pure and Applied Mathematics. https://ijfs.usb.ac.ir/article_4481_7b4f724471207.
9. P Karthick, SA Mohiuddine, K Tamilvanan, S Narayanamoorthy and S Maheswari (2023) Investigations of color image segmentation based on connectivity measure, shape priority and normalized fuzzy graph cut. Applied Soft Computing. DOI:10.1016/j.asoc.2023.110239.
10. Kumar, Tarun and Verma and Karun (2010) A Theory Based on Conversion of RGB image to Gray image, International Journal of Computer Applications. 10.5120/1140-1493.

Table 1: Error Ratio Table

Images	Threshold Method		Error Ratio with %		
	Original Image Pixel	Optimum Image Pixel	Edge based method	K means Cluster method	Watershed method
Dog.jpg	298,800	99,600	18.767%	28.28%	**15.3%**
Nelson.jpg	150,738	50,246	1.07%	8.51%	**0.2%**
Flower.jpg	150,696	50,232	3.4%	16.5%	**2.8%**

Fig 1: (a)Original image

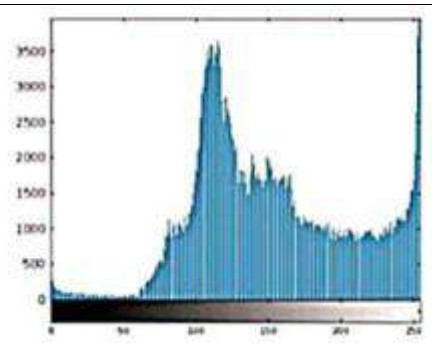

Fig 1: Histogram of the Original image

Fig 1: (c)threshold image

Fig 1: (d)Edge based image

Fig 1: (e)Water shed image

Fig 1: (f)K means Clustered image

Fig 1:Image Segmentation Comparison for Dog Images

Fig 2: (a)Original image

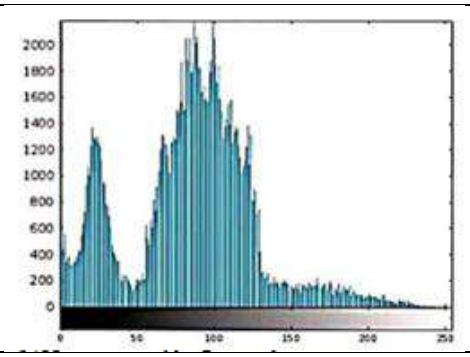

Fig 2: (b)Histogram of the Original image

Fig 2: (c)Threshold image

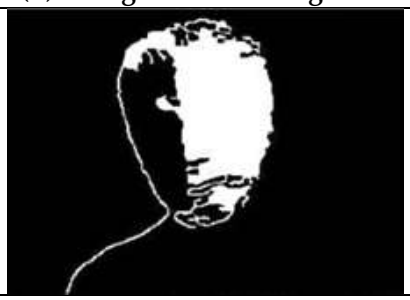

Fig 2: (d)Edgebased image

Fig 2: (e)Watershed Image

Fig 2: (f)KMeans Cluster Image

Fig 2: Image Segmentation Comparison for Nelson Images

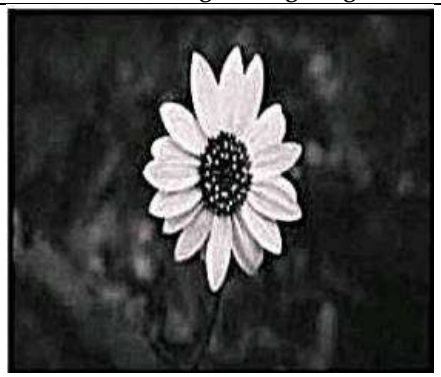

Fig 3: (a)Original image

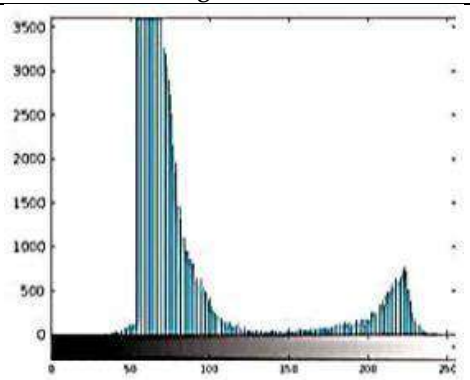

Fig 3: (b)Histogram of the Original image

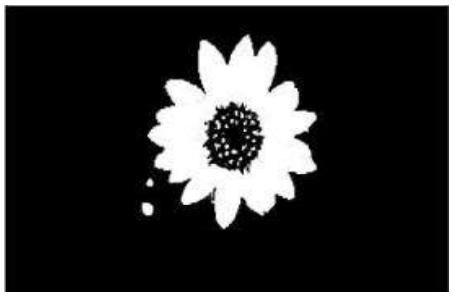

Fig 3: (c)Threshold image

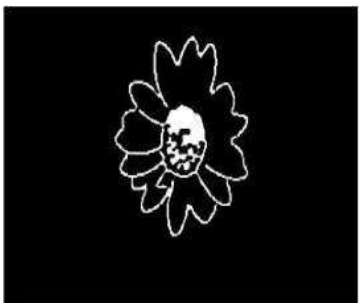

Fig 3: (d)Edgebased image

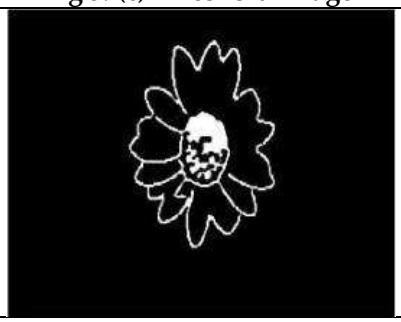

Fig 3: (e)Watershed Image

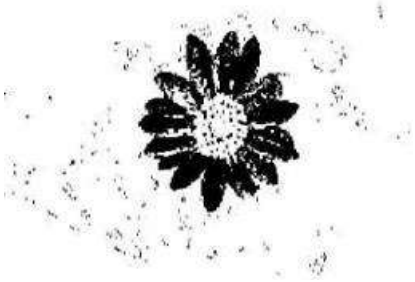

Fig 3: (f)KMeans Cluster Image

Fig 3: Image Segmentation Comparison for Flower Images

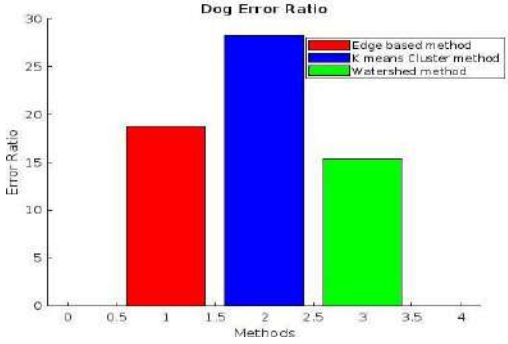

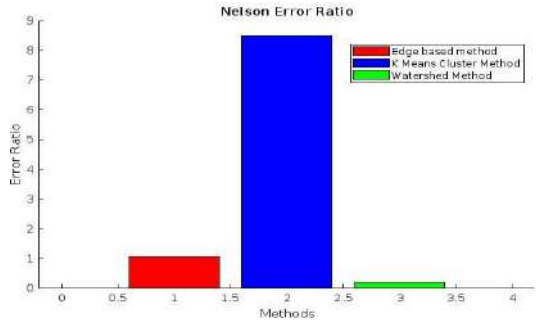

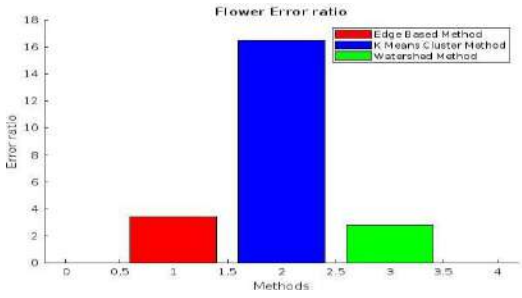

RESEARCH ARTICLE

A Hybrid CNN, LSTM, and Stacking Ensemble Approach for Improved Sentiment Analysis

Kanimozhi.J* and A.Balraj

Assistant Professor, Department of Computer Science, Sri Ramakrishna College of Arts & Science, Coimbatore, Tamil Nadu, India.

Received: 22 Feb 2023 Revised: 15 Mar 2024 Accepted: 21 Mar 2024

***Address for Correspondence**
Kanimozhi.J
Assistant Professor,
Department of Computer Science,
Sri Ramakrishna College of Arts & Science,
Coimbatore, Tamil Nadu, India.
Email: kanimozhi.j@srcas.ac.in

ABSTRACT

Opinion mining or Sentiment analysis make use of the enormous volumes of user-generated material that are available on the internet. It is possible to describe Opinion Mining (OM) or Sentiment Analysis (SA) as the process of finding, extracting, and categorizing views on anything. It uses natural language processing (NLP) to track how the public feels about a certain regulation. Making data-driven decisions that affect product development, marketing tactics, and customer service enhancements may be done with this information. To concentrate and classifications feeling from printed information, this examination offered an interesting way to deal with assessment mining that mixes profound learning and AI draws near. Convolutional brain organization (CNN) and long transient memory (LSTM) models are joined in this recommended methodology to increment arrangement exactness. In addition, using the stacking ensemble machine learning method will improve the performance of the suggested strategy even more. The textual material is initially preprocessed in this manner to get rid of extraneous information and noise. Including CNN.

Keywords: Opinion mining, Hybrid Neural Network, CNN, Machine learning

INTRODUCTION

An area of regular language handling (NLP) called assessment mining, ordinarily alluded to as opinion investigation, centers around the PC examination of individuals' verbally expressed sentiments, sentiments, and mentalities [1]. Opinion mining has grown more significant in a range of areas, including marketing, politics, healthcare, and customer service [2] because to the internet's exponential increase in user-generated information.

Opinion mining aims to identify and extract subjectivity from text, such as reviews of products, comments on social media, and news articles, and to categorise it as good, negative, or neutral [3]. This might offer insightful information on public opinion, assist businesses in improving their goods and services, and have an impact on legislative choices [4]. The primary contributions and objectives of this manuscript may be summarized as follows

1. Dataset Pre-processed by using Standard Scalar
2. PoS Tag applying using LDA
3. Dataset has trained by using Faster R-CNN with Bi-LSTM algorithm
4. Feature selection by using Extra tree classifier with Gradient Boosting algorithm
5. Opinion Classification using stacking Ensemble Classification

BACKGROUND STUDY

The goal of this research was to give a review and update on the sentimental analysis that is often conducted via social networking. Numerous publications and studies in this sector have been published and completed. Arti, Dubey, K. P., & Agrawal, S. [5] Authorized users may use Twitter's API to gather data and insights from tweets to analyze public opinion for sporting events such as the 2016 Indian Premier League. The result reflects the population's positive and negative opinions. This kind of opinion analysis might give valuable information to the organization and assist them in detecting an unfavourable change in Twitter audience understanding. Early detection of unfavourable trends allows businesses to make educated choices about focusing certain parts of their services and goods on boosting consumer satisfaction. Da'u, A.et al. [7] An R.S. model based on the ABOM approach is presented in this study. Initially, these authors demonstrated how user ratings might be derived using a deep learning technique. To further improve the recommendation system, the recovered features were used to generate aspect-based scores, which were then put into a tensor factorization engine. ABOM and rating prediction make up the majority of the proposed method. It utilised idle dirichlet allotment (LDA) to join the removed perspectives with the fundamental assessment terms to shape dormant viewpoints. Next, for each feature of the review, a score was calculated based on a linguistic technique. To further include the user's perspective on many elements and overall ratings, a three-dimensional T.F. approach is used to determine the representation of the underlying components. Hasan, K. M. A.et al. [9] these authors gathered information from reliable sources. The data were preprocessed to remove noise and improve usability. Kumar, P.et al. [12] indicated that a comprehensive examination of any issue might be undertaken by gathering a representative sample of Twitter user thoughts. Such an investigation might give helpful information to organizations or creators of movies, television shows, and businesses and warn them of an alarming change in the public's impression of their area. Identifying unfavourable tendencies early on may enable businesses to make more informed judgments about enhancing consumer satisfaction by concentrating on specific product characteristics. This study shows that the machine learning classifier utilized significantly impacts the inquiry's overall accuracy.

MATERIALS AND METHODS

Figure 1 is a flowchart that depicts the entire suggested methodology for processing a dataset and carrying out opinion categorization in Chapter III, which is concerned with the proposed approach. The flowchart has five primary stages, each of which is represented by a rectangular box with rounded sides and a number of connecting arrows. The first rectangular box on the flowchart's left side denotes the first stage, which entails preparing the dataset using Standard Scalar with Label Encoding. The second rectangular box represents the second stage, which entails utilising Improved LDA to tag parts of speech (PoS). The preprocessed dataset is trained using the Faster R-CNN with Bi-LSTM method in the third stage, which is depicted by the third rectangular box. Selecting is done at the fourth stage, which is symbolised by the fourth rectangular box.

NORMALIZATIONUSING STANDARD SCALAR

Since their performance suffers if the underlying features do not closely match standard normally distributed data, some machine learning estimators demand that a dataset be standardised. Data is cleaned and then normalised for model testing and training. When data is divided, one set is used to test an algorithm, while the other is used to train it. The values found in the training data, together with the underlying logic and algorithms of the features, are used to build the training model. Consistency in all aspects is the aim of normalisation. Reduce the feature set's inherent variability by removing outliers and scaling everything down to a single unit. Here is how the average score is calculated:

$$Ds = z = \frac{x-\mu}{\sigma} \text{ ----------} \quad (1)$$

POS TAG APPLYING USING IMPROVED LDA

Vectors for discrimination must be chosen. Not all discriminating vectors are created equally for pattern categorization. It is best to choose the vectors with the greatest Fisher discrimination values since they provide more details regarding dispersion both between and within classes. A desirable classification property that discrimination vectors must possess is statistical uncorrelation. Next, present a comprehensive set of recommendations utilising an enhanced LDA (ILDA) methodology. The remainder of the paper is divided into the following sections. This second section examines the three LDA advancements' theoretical bases. Normally, picture data is kept in the form of a two-dimensional (2-D) matrix (A*B), which may be transformed into a vector of size H using the equation H=A*B. As a consequence, this study could be able to draw out of the image library some typical dimensions.

FEATURE SELECTION

It is an estimator that fits randomised decision trees to distinct subsamples of a dataset to boost accuracy and control over data fitting. With 75 trees used in its design and 50 trees used in its construction, the Extra Trees Classifier had an accuracy rate for the test data of 90.27 percent and 90.73 percent, respectively. This model is not further developed since adding more trees does not significantly increase accuracy.

$$\varphi_i^* = \underset{\varphi i \varepsilon \rho}{argmin}\left\{\sum_{j=1}^{m} l(yj, yj)\right\} \text{ ------} \quad (6)$$

$$= argmin\left\{\sum_{j=1}^{m} l(flightGBM(\varphi i, xj), yj\right\} \text{-------} \quad (7)$$

In Eq. (7), ℓ (•) is the loss function, yˆj is the prediction yˆj=flight GBM (ψi, xj), and yj is the given actual class. Let k be a scalar of n bits, P and Q two points of an elliptically curve defined on a finite field F by the equation (:

$$E: Y^2 + a1XY += X^3 + a_2X^2 + a_{4x}X + a_6 \text{ -------} \quad (8)$$

where a1; a2; a3; a4 2 F. In this work, to consider the finite prime fields Fp. Eq. (9) then becomes:

$$E: Y^2 = X^3 + aX + b \text{ ------} \quad (9)$$

OPINION CLASSIFICATION USING STACKING ENSEMBLE METHOD

Due to their superior performance versus individual learning models in a variety of tasks, including classification and regression, ensemble models have recently acquired popularity. Early 1990s ensemble learning research made the case that it was possible to combine a number of relatively weak learning algorithms to create more powerful ones. Using a single data set, many learner modules, and ensemble learning, various predictions are produced. A more accurate picture is provided by the sum of all expert predictions. The technique normally involves two steps. From the training data, a subset of students is chosen and included in a single prediction model. A number of forecasts were created utilising data that was distinct from that used in the underlying models to create the composite model.

RESULTS AND DISCUSSION

The proposed method has implemented by using python programming language with spyder 3.8 framework. Figure 2 is a graph that illustrates reviews and analysis instances, illustrating both positive and negative types of input. The audits are displayed on the x-pivot, while the thickness of those surveys is displayed on the y-hub. The graph resembles a histogram, with bars of varying heights standing in for the number of reviews falling into various densities. The testimonials in Figure 2 probably refer to written evaluations or remarks made by consumers or users of a certain item or service. The density metric might be a score or rating determined using natural language processing (NLP) methods, which would be a measure of the sentiment or tone of those evaluations. The examination of punctuation for words is shown in figure 3. The graphic highlights both positive and negative evaluations of the product. This graph shows reviews along the x-pivot, and thickness is shown along the y-hub. The classification performance matrices for a variety of models, including DT, SVM, NB, Logistic Regression, Stacking Ensemble, are displayed in Table . Metrics including accuracy, precision, recall, and F-measure are included in the matrix. Stacking Ensemble model exceeds the other models in terms of accuracy, scoring 0.972 as opposed to 0.85 to 0.89 for the other models. The SVM and LR models had the greatest accuracy ratings (0.90), closely followed by the NB model (0.88). The Decision Tree and Stacking Ensemble models are closely behind the SVM and LR models in terms of recall, scoring 0.87 and 0.870, respectively.

CONCLUSION

The findings show that the proposed approach has a higher F1-score and is more accurate than alternatives. The suggested approach has a few benefits over the conventional approach. Second, by fine-tuning the text's immediate context, general properties, and relationships, it can manage complicated textual data. Last but not least, this approach may be applied in a variety of situations where sentiment analysis is required, such as marketing, customer service, and product development. Recommended to present a state of the art technique for assessment mining that mixes profound learning with customary AI strategies. To increase classification accuracy, the LSTM and CNN models extract text features and evaluate sentiment. his proposed system was assessed on a few datasets and contrasted with the latest cutting edge philosophies.

REFERENCES

1. Agarwal, Y., Katarya, R., & Sharma, D. K. (2019). Deep Learning for Opinion Mining: A Systematic Survey. 2019 4th International Conference on Information Systems and Computer Networks (ISCON). doi:10.1109/iscon47742.2019.9036187.
2. Kanimozhi,J, Dr.R.Manicka Chezian.(2023).Novel Deep Learning Approaches for Opinion Mining with Machine Learning,E-ISSN NO : 2455-295X | Volume : 9 | Issue : 6 | Special Issue June-2023.
3. Kanimozhi,J, Dr.R.Manicka Chezian.(2023).Opinion Mining using Hybrid Deep Learningwith Machine Learning Algorithms,Eur. Chem. Bull. 2023, 12 (Special Issue8),310-331.
4. Alfrjani, R., Osman, T., &Cosma, G. (2019). A hybrid Semantic Knowledgebase-machine learning approach for opinion mining. Data & Knowledge Engineering. doi:10.1016/j.datak.2019.05.002
5. Kanimozhi,J, Dr.R.Manicka Chezian.(2023).A Study of Opinion Mining and Sentimental Analysis Algorithms based on Accuracy Metric,Neuro Quantology | August 2022 | Volume 20 | Issue 7 | Page 3680-3690 | doi: 10.14704/nq.2022.20.7.NQ33454
6. Arti, Dubey, K. P., & Agrawal, S. (2019). An Opinion Mining for Indian Premier League Using Machine Learning Techniques. 2019 4th International Conference on Internet of Things: Smart Innovation and Usages (IoT-SIU). doi:10.1109/iot-siu.2019.8777472

7. Boumhidi, A., &Nfaoui, E. H. (2020). Mining User's Opinions and EmojisFor Reputation Generation Using Deep Learning. 2020 Fourth International Conference On Intelligent Computing in Data Sciences (ICDS). doi:10.1109/icds50568.2020.9268758
8. Da'u, A., Salim, N., Rabiu, I., & Osman, A. (2019). Recommendation System Exploiting Aspect-based Opinion Mining with Deep Learning Method. Information Sciences. doi:10.1016/j.ins.2019.10.038
9. Fachrina, Z., &Widyantoro, D. H. (2017). Aspect-sentiment classification in opinion mining using the combination of rule-based and machine learning. 2017 International Conference on Data and Software Engineering (ICoDSE). doi:10.1109/icodse.2017.8285850
10. Hasan, K. M. A., Sabuj, M. S., & Afrin, Z. (2015). Opinion mining using Naïve Bayes. 2015 IEEE International WIE Conference on Electrical and Computer Engineering (WIECON-ECE). doi:10.1109/wiecon-ece.2015.7443981
11. Hasan, T., Matin, A., Kamruzzaman, M., Islam, S., & Faruq Goni, M. O. (2020). A Comparative Analysis of Feature Extraction Methods for Human Opinion Grouping Using Several Machine Learning Techniques. 2020 IEEE International Women in Engineering (WIE) Conference on Electrical and Computer Engineering (WIECON-ECE). doi:10.1109/wiecon-ece52138.2020.9398025
12. Karthik, V., Nair, D., & J, A. (2018). Opinion Mining on Emojis using Deep Learning Techniques. Procedia Computer Science, 132, 167–173. doi:10.1016/j.procs.2018.05.200
13. Kumar, P., Choudhury, T., Rawat, S., &Jayaraman, S. (2016). Analysis of Various Machine Learning Algorithms for Enhanced Opinion Mining Using Twitter Data Streams. 2016 International Conference on Micro-Electronics and Telecommunication Engineering (ICMETE). doi:10.1109/icmete.2016.19
14. Mridula, A., &Kavitha, C. R. (2018). Opinion Mining and Sentiment Study of Tweets Polarity Using Machine Learning. 2018 Second International Conference on Inventive Communication and Computational Technologies (ICICCT). doi:10.1109/icicct.2018.8473079
15. Musdholifah, A., & Rinaldi, E. (2018). FVEC feature and Machine Learning Approach for Indonesian Opinion Mining on YouTube Comments. 2018 5th International Conference on Electrical Engineering, Computer Science and Informatics (EECSI). doi:10.1109/eecsi.2018.8752791
16. Saad, A. I. (2020). Opinion Mining on U.S. Airline Twitter Data Using Machine Learning Techniques. 2020 16th International Computer Engineering Conference (ICENCO). doi:10.1109/icenco49778.2020.9357390
17. Sivakumar, M., & Reddy, U. S. (2017). Aspect based sentiment analysis of students opinion using machine learning techniques. 2017 International Conference on Inventive Computing and Informatics (ICICI). doi:10.1109/icici.2017.8365231

Table 1: Training and validation accuracy and loss

Epoch	Training Loss	Validation Loss	Training Accuracy	Testing Accuracy
1	0.1544	0.0679	0.9547	0.9779
2	0.0537	0.0526	0.9837	0.9820
3	0.0352	0.0596	0.9890	0.9826
4	0.0243	0.0465	0.9922	0.9848

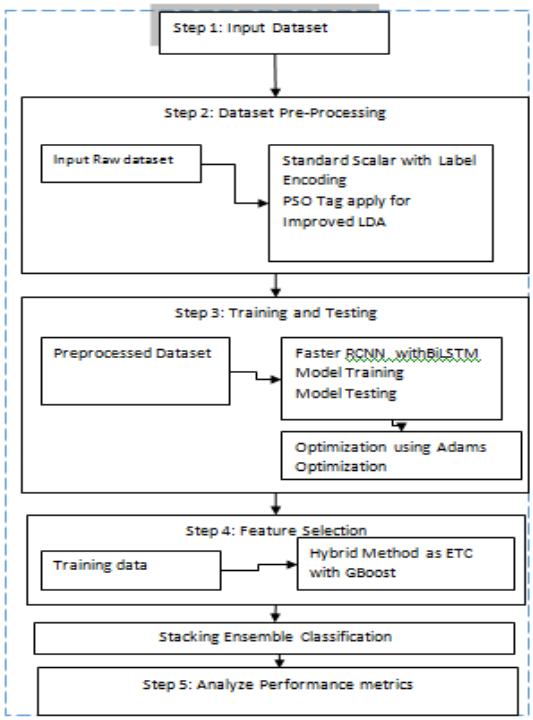

Figure 1: Overall architecture Diagram

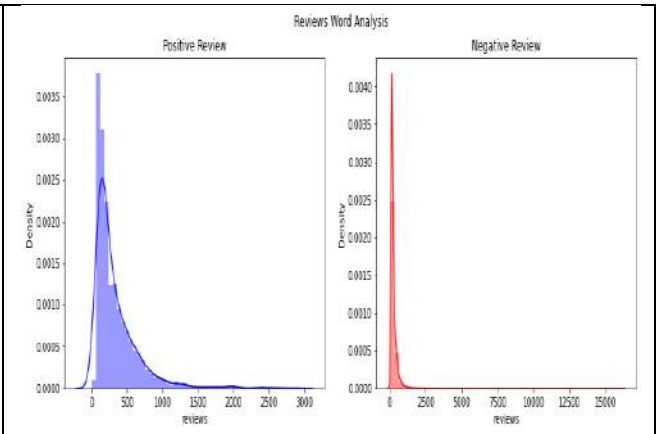

Figure 2: Reviews and analysis

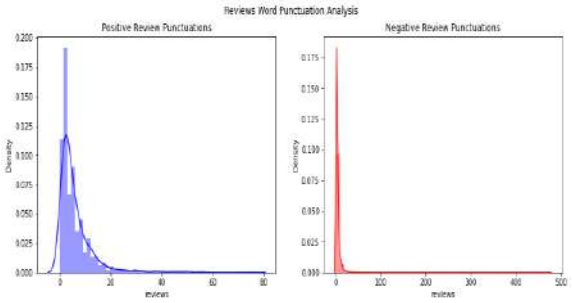

Figure 3:Reviews word punctuation analysis

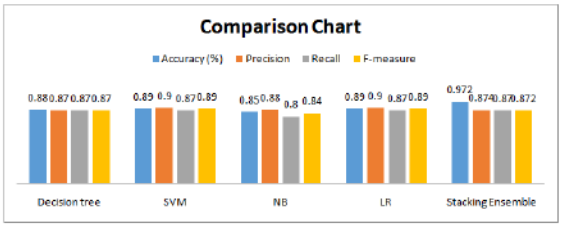

Figure 4: Comparison chart

RESEARCH ARTICLE

An AI Based Keystroke Dynamics for User Authentication

Logidha V[1*] and Karthik S[2]

[1]UG Student, Department of Information Technology, Sri Ramakrishna College of Arts & Science, Coimbatore, Tamil Nadu, India.
[2]Assistant Professor, Department of Information Technology, Sri Ramakrishna College of Arts & Science, Coimbatore, Tamil Nadu, India.

Received: 22 Feb 2023 Revised: 15 Mar 2024 Accepted: 21 Mar 2024

***Address for Correspondence**
Karthik S
Assistant Professor,
Department of Information Technology,
Sri Ramakrishna College of Arts & Science,
Coimbatore, Tamil Nadu, India.
Email: karthik@srcas.ac.in

ABSTRACT

Authentication is frequently referred as the most critical part of a computer system security. Users commonly identify themselves using a combination of username and password, but sometimes this is not enough. Concerning web-based services, attacks like phishing or social engineering can easily result in identity theft. In addition, the widespread use of single sign-on services can seriously increase the consequences of such attacks. In these circumstances strong authentication is mandatory. Strong authentication is often implemented using additional authentication steps or specialized hardware modules, which is not suitable for web-based systems. However, biometrics can used to overcome these limitations. More specifically, behavioural biometrics based on keyboard typing patterns can provide an extra security layer on top of conventional authentication methods, with no additional cost and no impact to the user experience. This work aims to evaluate the feasibility of the implementation of strong authentication on the web using keystroke dynamics. This is carried out through the creation of a application prototype using python environment.

Keywords: Keystroke Dynamics, Behavioural Biometrics, Authentication, Keyboard Typing, Security.

INTRODUCTION

Our dependence on computers and digital platforms has been observed to be overwhelmingly increased to simplify our lives. The use of such automated information systems together has resulted in improved performance of the available networking services in the form of reliability and computational costs. With such efficient utilization the

advances in technology have generated a collective interest in global access to such online platforms. However, at the same time there is a rise in the threats regarding to the security of computers. Usage of advanced methodologies to safeguard the system from attacks and frauds come under the topmost concerning priority of many research scientists. Hence there is a need to generate foolproof measures to prevent such unauthorized access is being worked upon. One such preventive method to give access to individuals by detecting their unique and behavioral pattern is an individual's typing rhythm. This unique typing rhythm tends to become a natural choice for security of computers and is commonly known as Keystroke Dynamics. It is observed that when a person types; the placement of his fingers, applied pressure on the keys and the regularly typed strings appears to be consistent for a specific individual. Hence this concept is used to differentiate between an intruder and a legit user as they will be typing on the keyboard anyway. Therefore, making such kind of typing rhythms easily accessible to track computer activities.

Background

The initial step to prevent any form of unauthorized control into a system is user authentication. This is the only operation that confirms the identity of an individual. This identity is matched with a pre-generated code or a registration number with the legit individual and is used in the process of identification. Once this identification is accomplished some form of indicator is shared to give access control to the user. Knowledge-based encryption is based on the idea of two people sharing their secrets. Username and Login credentials are two well-known examples. Whereas object-based authorization is characterized based on possession of specific things and relies on the concept of something which someone has. On the other hand, biometric based authentication is characterized by behavioral features an individual would have. In real time, the classifications of object and knowledge based are merged to fulfill the process of authentications such bank passwords and their PINS. One major disadvantage with regards to this classification-based authentication is the ability to memorize and manage multiple such PINS and recalling them. Therefore, the usage of biometrics authentication is preferred as it overcomes these issues and makes use of automated methods to identify and verify the individual. Also, this form of authentication is gaining worldwide popularity as they provide an extra level of security.

Motivation

User authentication has always been a fundamental component of access control. Nowadays, the Internet is the standard platform for communication and a tremendous amount of sensitive data is transmitted between computer systems. This makes the process of identity verification more important than ever. However, basic username and password combination is used the same way we did a decade ago. Attacks like man-in-the-middle, phishing or social engineering can easily result in identity theft. This can lead to access to private information, exploitation of trust relationships and other criminal activities. Furthermore, with the widespread use of single sign-on services, where a single set of credentials can authenticate users in multiple websites, consequences of identity theft can be devastating. Even though in most cases simple password-based authentication will suffice, other environments like online commerce and banking platforms can definitely benefit from strong authentication to ensure proper protection of sensitive, private and confidential data. Strong authentication doesn't have a standard definition, but it generally aims to deliver increased security beyond standard authentication methods. It is often implemented with two-factor authentication and usually based in knowledge or token-based approaches. Although these methods can effectively improve security in authentication, what is really validated are passwords, tokens and keys. Also, user credentials can be stolen, lost, shared or manipulated, resulting in compromised security. Biometrics can be used to overcome the limitations imposed by classical solutions by allowing identity verification based on the user himself. Unfortunately, authentication solutions based on biometrics may not always be easily deployed, since most of them require specific hardware (e.g. fingerprint reader). Keystroke dynamics, a behavioural biometric, presents itself as a viable contender to implement strong authentication on the web. It has the distinct advantage of not requiring specific hardware, while maintaining the desirable properties of the more mainstream biometric solutions. Also, as we will explore in this work, it can be seamlessly integrated with existing password-based authentication.

Problem Statement

One of the major issues or a problem the digital world face is with regards to passwords used. Although, a few organizations do exist that provide secured authentication for users when they login but on the other hand there are still most sites that skip the process of identification leading to major crimes across the globe. Hence the research work in this thesis aims to suggest better security systems that could be analysed using the typing behaviour of individuals using keystroke dynamics. Main emphasis is being put on to detect the typing behaviour of individuals using the concepts of validate the keystrokes timing features of users and give them a more secure and efficient system than ever before.

Objectives

This work aims to evaluate the viability of keystroke dynamics as a method for implementing strong authentication on a web-based environment. It should result in an implementation capable of enrolment and identity verification, applying typing behaviour on top of basic username and password credentials. The goal of this study is to compare the performance of some classical matching algorithms proposed by previous research. Although numerous experiments have achieved encouraging results, there is significant variation in the reported effectiveness, which makes it hard to assess the full potential of keystroke dynamics as a biometric for authentication. We'll also look at how adaptive techniques can influence the performance of keystroke dynamics. Finally, most studies on keystroke dynamics tend to use a single passphrase for all users; this work's experiment should account for individual authentication credentials for every user, which is arguably a better representation of the real world.

SYSTEM STUDY

System analysis will be performed to determine if it is flexible to design information based on policies and plans of organization and on user requirements and to eliminate the weakness of present system. This chapter discusses the existing system, proposed system and highlights of the system requirements.

EXISTING SYSTEM

Distortion in keystroke dynamics is not a well-researched field, and we did not find many results when doing literature search. However, it measured two typing samples of keystroke dynamics data and used two different measures to compare the samples. However, one method that could be used for detecting distorted timing information is Benford's Law and ZIPF's Law. Benford's Law, or the first-digit law, is an observation in a set of numerical data where the first digit, or leading digit, is more likely to be small. In a balanced distribution of numbers between 1 and 9 there would be exactly 11% for each number to be the leading digit. However, if Benford's Law is obeyed then the change of the leading bits to be small increases.

DISADVANTAGES OF EXISTING SYSTEM

However, the results showed that only latency values from keystroke dynamics timing information followed the law. While duration values did not follow the law. More resources used for re-keying because it is done for each join or leave operations.

PROPOSED SYSTEM

In order to authenticate a user using keystroke dynamics we need to create a reference average value for each user that will represent, as accurately as possible, their specific typing behaviour. This template varies a lot depending on whether static or continuous authentication is used. In authentication we want to create a template that reflects the typing rhythm that the genuine user uses in order to type the password. This average value is created based on enrolment samples, where the user would get requested to type their password a number of times. The features, such as duration and latency, are then extracted and the average typing rhythm is calculated and stored as a reference average. When a user tries to authenticate, the system will check their typing rhythm, which is referred to as a probe, against the reference template and then either reject or accept the user based on a criterion. This criteria

for decision making are decided by a threshold which is created by a minimum and maximum average time in milliseconds.

ADVANTAGES

The proposed Keystroke dynamics is based on the assumption that each user can be authenticated because of their unique typing manner. This is because keystroke dynamics performs on a millisecond's precision level meaning it is impossible to accurately recreate the way another user types. This is true even for a user who is typing their own password, as they would not be able to type exactly the same way they did last time. Even though the user might type one of the keys or key pairs the same, there are still other keys that they could type in a different way. It is because of this reason keystroke dynamics works as an authentication method.

SYSTEM ANALYSIS AND DESIGN

MODULE DESIGN

Keystroke timing

From the Key Down and Key Up time of each keystroke we can calculate the duration and latency of a key. The duration of a key is how long the key was held down, this can also be referred to as dwell or hold time. While the latency of a key is the time between releasing one key and pressing another key, and this can sometimes be referred to as flight time. We differentiate between 4 different latencies, given as:

1. ·**pp-latency:** The timing it takes to press down one key and the next key.
2. ·**rr-latency:** The timing it takes to release one key and the next key.
3. ·**rp-latency:** The timing it takes to release one key and press the next key.
4. ·**pr-latency:** The timing it takes to press down one key and release the next key.

In order to get the pp-, rr- and pr-latency we have to use the timing information from duration and rp-latency. We can calculate pp-latency as$latpp = durA + latrp$, rr-latency as $latr\ r = latrp + durB$and pr-latency as $latpr = durA + latrp + durB$ where $durA$ and $durB$ represents the duration of two different keys. The following figure shows the timing values we can extract if a user types the keys A and B. From these latencies, only the rr-latency and rp-latency can be negative. For example, for the rr-latency we can press the shift key, followed by pressing the C key, and then release the C key before releasing the shift key. The same can be said with rp-latency as we can press the next key before releasing the previous key, for example we can press the C key before releasing the shift key. By using pp-latency, rp-latency and duration for our timing values. The naming of pp-latency refers to press-press-latency, however, we will refer to this as Key Down-Key Down latency (DD). While rplatency refers to press-release-latency, which will be called KeyUp-Key Down latency (UD).

Matching module

In this module, extracted timing features are compared against those stored in the database, using a matching algorithm from statisticalt approaches. Ultimately, this process results in a matching score, that represents a similarity measure between the extracted features and the ones previously stored in the database.

Decision module

Given the matching score and a decision threshold, this module is responsible for either accepting or rejecting the claimed user identity, based on the matching score and a predefined threshold.

CONCLUSION AND FUTURE ENHANCEMENT

With the conclusion of this work, and regarding the original research goals, keystroke dynamics can be considered a viable choice to implement strong authentication on the web. We've shown that this technology can be integrated on top of a tradition authentication procedure, taking advantage of user input to seamlessly capture and classify the

associated typing behaviour. Keystroke dynamics presented some notable advantages over other alternatives. No specialized hardware was needed. Biometric data acquisition was completely transparent and multifactor authentication was effectively achieved with a single conscious action from the user. In addition, even simple matching algorithms, as the ones used in this study, can yield reasonable accuracy on authentication. Although the proposed goals of this work were successfully met, some points could have been improved. An assessment of the system usability should have been done by the users that participated in the study. Furthermore, the target population was greatly biased, mainly computer science students, which are probably better typists than the average individual. Although more complex, applying this study to a more diverse population would have been a closer representation of a real environment.

SCOPE FOR FUTURE ENHANCEMENT

For instance, it would be interesting to develop a complementary study, focused on the evaluation of more sophisticated algorithms, in order to further improve matching accuracy.

REFERENCES

1. J. V. Monaco and C. C. Tappert, "The partially observable hidden Markov model and its application to keystroke dynamics," Pattern Recognition, 2018.
2. S. Roy, U. Roy, and D. D. Sinha, "Security enhancement of knowledge-based user authentication through keystroke dynamics," in Proc. MATEC Web Conf., 2016, vol. 57.
3. K. S. Killourhy. (2012). A scientific understanding of keystroke dynamics. [Online]. Available: http://reports-archive.adm.cs.cmu.edu/anon/2012/CMU-CS-12-100.pd f
4. A. Messerman, T. Mustafić, S. A. Camtepe, and S. Albayrak, "Continuous and non-intrusive identity verification in real-time environments based on free-text keystroke dynamics," in Proc. Int. Jt. Conf. Biometrics, 2011.
5. P. S. Teh, B. J. Andrew Teoh, T. S. Ong, and H. F. Neo, "Statistical fusion approach on keystroke dynamics," in Proc. Int. Conf. Signal Image Technol. Internet Based Syst., January 2007, pp. 918–923.
6. J. Ho and D. K. Kang, "Mini-batch bagging and attribute ranking for accurate user authentication in keystroke dynamics," Pattern Recognit., vol. 70, pp. 139–151, 2017.
7. S. Maheshwary and V. Pudi, "Mining keystroke timing pattern for user authentication," Lect. Notes Comput. Sci., vol. 10312, pp. 213–227, 2017.
8. A. Darabseh and A. S. Namin, "On accuracy of classification-based keystroke dynamics for continuous user authentication," in Proc. 2015 Int. Conf. Cyberworlds, 2016, pp. 321–324.

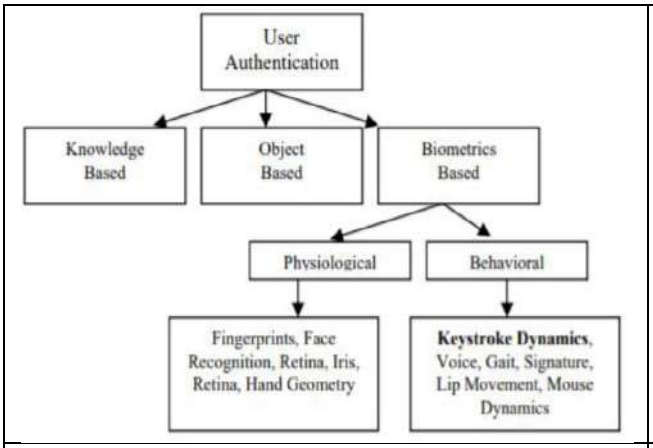

Figure 1 Classification of user authentications

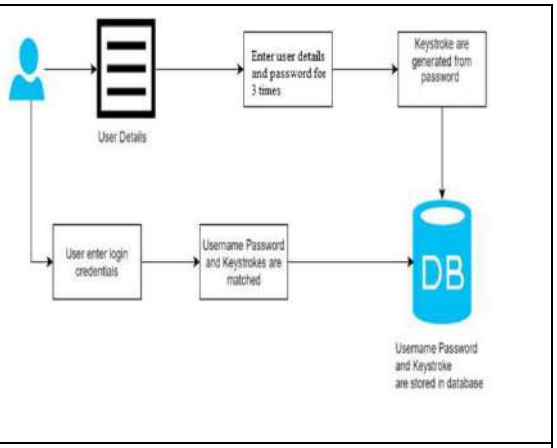

Figure 2 Keystroke generation and matching

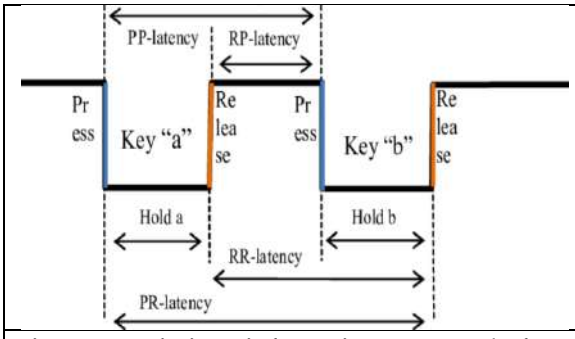

Figure 3 Timing information extracted from two keystrokes

```
timeMAX = 0#slowest
timeMIN = 0#fastest
for #yourForLoop
    if sys.stdin.readline() > timeMAX:
        timeMAX = sys.stdin.readline()
    if sys.stdin.readline() < timeMIN:
        timeMIN = sys.stdin.readline()
```

Fig 4

RESEARCH ARTICLE

IoT Awarecensored Regressive Gaussian Kernelized Recurrent Deep Neural Network for Automatic Agriculture Prediction

R.Hemalatha[1] and G.Nivashini[2*]

[1]Research Supervisor, PG & Research Department of Computer Science, Tiruppur Kumaran College For Women, Tiruppur, Tamil Nadu, India.
[2]Research Scholar (Ph.D) PG & Research Department of Computer Science, Tiruppur Kumaran College For Women, Tiruppur, Tamil Nadu, India.

Received: 22 Feb 2024 Revised: 15 Mar 2024 Accepted: 21 Mar 2024

***Address for Correspondence**
G.Nivashini
Research Scholar (Ph.D) PG & Research,
Department of Computer Science,
Tiruppur Kumaran College For Women,
Tiruppur, Tamil Nadu, India
Email: nivashini96phd@gmail.com

ABSTRACT

Agriculture plays a vital role in the country's economy. The most widespread concern among farmers is that they do not choose their crops based on the requirements of the soil conditions. The majority of farmers are unaware of the significance of planting crops at the appropriate time and place. Due to these agricultural practices, seasonal climatic conditions are altering, resulting in food insecurity. Therefore, agricultural prediction helps farmers make decisions about the farming approach to increase crop yield. Various deep learning or machine learning techniques have been developed to increase the quantity and quality of production from crop fields. However, achieving accurate and time-efficient predictions is a significant concern. In this paper, a novel method named Censored Regressive Gaussian Kernelized Gradient Recurrent Neural Network (CRGKGRNN) is developed for accurately predicting crop planting in the agriculture domain, aiming to enhance crop productivity. The CRGKGRNN method comprises four distinct processes such as data acquisition, pre-processing, feature selection, and classification. In the data acquisition phase, IoT sensors are deployed in the agricultural land to collect soil moisture, temperature, humidity, potassium, phosphorus, nitrogen, and rainfall. The data collected by IoT sensors are pre-processed in the second step to address missing values or null, as well as noise. Damped Least-Squares (DLS) method is utilized to identify and remove duplicate or noisy data. In the third step, attribute selection is performed using Sokal–Michener's simple matching indexive censored regression to choose a subset of relevant features and remove irrelevant or redundant attributes, thereby minimizing the time consumption of predictions. Finally, the Gaussian Kernelized Adaptive Gradient Recurrent Neural Network is applied for prediction process which comprises three layers namely the input layer, two or more hidden layers, and the output layer.

Keywords: Agriculture, IoT, Crop prediction, Damped Least-Squares (DLS), Recurrent Neural Network, Prediction

INTRODUCTION

Agriculture is the fundamental practice of cultivating soil, growing crops, and increasing productivity. It is deeply influenced by climate variables such as temperature, precipitation, humidity, and sunlight. Changes in these factors directly affect crop growth, yield, and overall agricultural productivity. Recognizing the intricate relationship between climate conditions and crop suitability, advanced technologies are required for predictive modelling to provide valuable insights for decision-making in farming practices. Although numerous machine learning models have been developed for identifying crops but their performance has not been effectively investigated. The Inter-fused Machine Learning with Advanced Stacking Ensemble model (IML-ASE) was developed in [1], aims to improve crop prediction accuracy by leveraging information related to farming, climate, and soil conditions. This enhancement enables farmers to make informed decisions regarding crop selection for cultivation. However, it noted that the designed method did not succeed in minimizing the processing time. A deep reinforcement learning (DRL)-based crop classification system was developed [2] to address the challenges faced by cultivation in precision agriculture. However, the performance of accurate crop classification was not performed. A smart agriculture system based on artificial intelligence and deep learning was developed in [3]. However, addressing the time complexity associated with smart agriculture proved to be a challenging task. The Agriculture Factor-based Relevance Vector Analysis Model was developed in [4] to predict optimal crops and enhance productivity. However, a significant challenge occurred due to the high error rate in crop prediction. Various machine learning algorithms were developed in [5] for precise crop prediction. But, it was not efficient for evaluating large crop data from diverse geographic regions using IoT. Feature selection and classification techniques were developed in [6] to enhance the prediction accuracy of plant cultivations. However, the issue of prediction time performance remained unresolved. A crop recommendation system, developed was in [7], utilizes Map Reduce and K-means clustering. However, it failed to deliver more accurate recommendations. A Fuzzy Enumeration Crop Prediction Algorithm (FECPA) was developed in [8] to enhance the accuracy of predicting suitable crops and improve productivity. However, it encountered limitations in achieving accurate predictions with minimal time due to the absence of machine learning algorithms. Recurrent Neural Networks (RNNs) were developed in [9] to determine the most probable scenarios for multi-temporal crop prediction.

RELATED WORKS

A graph neural network model was introduced in [11] for crop suitability evaluation with higher accuracy. However, it did not succeed in significantly reducing the cost of trial and error in the crop suitability evaluation process.A quantum value-based gravitational search algorithm (GSA) was developed in [12] to predict the suitable soil for optimal crop production. However, the implemented algorithm proved ineffective when applied to real-time optimal crop selection systems. Microclimate modelling techniques were developed in [13] with the aim of predicting future crop suitability. However, attaining higher accuracy posed a significant challenge in forecasting future crop suitability. A transfer learning approach was introduced in [14] for agricultural crop classification. However, this method did not incorporating a more sophisticated approach to enhance overall accuracy. A statistical and machine learning approach was introduced in [15] for predicting crop suitability types. However, the crop selection methodology did not use any deep learning techniques for improving accuracy. An LSTM RNN model was developed in for crop selection based on weather conditions and soil parameters. However, it did not integrate sensors to gather real-time, more precise data on weather conditions and soil parameters for improving the model's efficiency.

PROPOSED METHODOLOGY

Crop suitability prediction in smart agriculture is used to assist farmers in predicting specific seasonal crops according to the weather conditions. As weather conditions continue to change, crop prediction becomes more essential for improving crop productivity. Based on this motivation, a novel CRGKGRNN is introduced in this section for accurate crop prediction with minimum error as well as minimal time consumption. Figure 1 illustrates the architecture of the proposed CRGKGRNN method, comprising four major processes: Data acquisition, pre-processing, feature selection, and classification, designed to enhance the accuracy of crop prediction. Initially, IoT sensors are deployed in agricultural fields to collect soil characteristics, including, temperature, humidity, potassium, phosphorus, nitrogen, and rainfall. These data are stored in a dataset with features denoted as $A_1, A_2, A_3, \ldots A_m$ and training instances represented as$SD_1, SD_2, SD_3, \ldots SD_n$. The first step involves data pre-processing to clean and transform raw data, addressing null values and removing duplicate values. Subsequently, the feature selection process is performed using Sokal–Michener's simple matching index and censored regression to identify significant features for efficient prediction within minimal time. Finally, the proposed CRGKGRNN method utilizes Gaussian Kernelized Adaptive Gradient Recurrent Neural Network to enhance crop prediction performance, achieving higher accuracy and minimizing errors. The distinct processes of the proposed CRGKGRNN are described in the following subsections.

Data acquisition phase

The data acquisition phase marks the commencement of the proposed CRGKGRNN, involving the collection of data from the Smart Farming using Machine Learning dataset. This dataset encompasses information on soil and environmental characteristics, including nitrogen, phosphorus, potassium, temperature, humidity, rainfall, etc. The data is presented in both numeric and categorical formats. The dataset's structure is defined by rows and columns, providing a comprehensive representation of the information.

Data preprocessing

The second step of the proposed technique is the data pre-processing that involves cleaning and transforming raw data into a suitable format for analysis. This phase is important for improving the quality of the data, handling missing values, and removes the duplicate data making it compatible with machine learning algorithms.

Proportional Weighted Average Sampling based null values handling

Null values, also known as missing values, are data points that have not been recorded or are unavailable in a particular cell of the dataset. Dealing with null values is a fundamental aspect of data pre-processing. The proposed CRGKGRNN utilizes the Proportional Weighted Average Sampling technique in which null samples from a larger population are chosen. To start with the raw input dataset 'DB' and formulated in the form of matrix as given below.

$$I = \begin{bmatrix} A_1 & A_2 & \ldots & A_m \\ SD_{11} & SD_{12} & \ldots & SD_{1n} \\ SD_{21} & SD_{22} & \ldots & SD_{2n} \\ \vdots & \vdots & \ldots & \vdots \\ SD_{m1} & SD_{m2} & \ldots & SD_{mn} \end{bmatrix} \quad (1)$$

Where, 'm' column features $A_1, A_2, A_3, \ldots A_m$ are present with overall sample instances of 'n row$SD_1, SD_2, SD_3, \ldots SD_n$ respectively. The Proportional Weighted Average Sampling method determines a null value by taking a weighted average of a certain number of consecutive observed values in the particular column. The formula for calculating the Proportional Weighted Average is given below,

$$P_{WA} = \frac{\sum_{i=1}^{n} SD_i * \beta_i}{\sum_{i=1}^{n} \beta_i} \quad (2)$$

Where, P_{WA} denotes a proportional Weighted Average for the missing value, SD_i denotes an observed value for data point, β_i denotes a weight assigned to data point 'SD_i'. Therefore, the formula provides a way to estimate missing values based on the available data points in the dataset.

// Algorithm 1: Data pre-processing
Input: Dataset 'DB', featuresA $= \{A_1, A_2, A_3, \dots A_m\}$ and data samples $SD_1, SD_2, SD_3, \dots SD_n$
Output: Pre-processed dataset
Begin 1. **For** each Dataset 'DB' with Features 'A' 2. Formulate input vector matrix 'I' as given in (1) 3. **If** missing feature value **then** **4.** Measure proportional weighted average between the feature as given in (2) 5. Fill the feature value to the respective column 6. **End if** **7. for each** data point 8. Measure the squared differences between the values using (4) 9**: if** $\arg min \sum_{i=1}^{n} [f_i\ (x)]^2$ **then** 10. Normal data 11**: else** 12: Duplicate data 13. **End if** **14. Remove** Duplicate data **15. End for** **End**

Algorithm 1 outlines a step-by-step process of data pre-processing. Initially, the number of features and raw data is gathered from the dataset. Following data collection, any missing or null values are addressed using a proportional weighted average sampling method. The null values are replaced with the proportional weighted average value. Subsequently, the DLS method is utilized to analyze the data points in a specific column. If the deviation is minimal, the data point is considered normal. On the other hand, if the deviation is large, the data point is identified as a duplicate. Finally, a structured dataset is obtained.

// Algorithm 2: Sokal–Michener's simple matching indexive censored regression
Input: pre-processed Dataset 'DB', featuresA $= \{A_1, A_2, A_3, \dots A_m\}$ and data samples $SD_1, SD_2, SD_3, \dots SD_n$
Output: relevant feature selection
Begin 1. **For** each Dataset 'DB' with Features 'A' 2Measure Sokal–Michener's simple matching using (5) 4. Formulate censored regression outcome to obtain relevant features as given in (6) 5. **If** $(SM > T)$ **then** 6. **Select**relevant features 7. **else if** '$(SM < T)$**then** **9.** **Remove ir**relevant features 10. **End if** 13. **End for** **14. Return (relevant features)** **End**

Algorithm 2, illustrates the process of selecting significant features to minimize the time complexity of crop prediction. The pre-processed dataset serves as input for Sokal–Michener's simple matching indexive censored regression. Initially, the algorithm assesses the relationship between features by employing Sokal–Michener's simple matching index. Subsequently, censored regression is applied for measuring the relationship, aiming to identify relevant features by setting a predetermined threshold. Finally, the outcomes of the regression provide the highly relevant features, which are then chosen for crop prediction. Figure 1 illustrates the architecture of the proposed

CRGKGRNN method, comprising four major processes: Data acquisition, pre-processing, feature selection, and classification, designed to enhance the accuracy of crop prediction. Initially, IoT sensors are deployed in agricultural fields to collect soil characteristics, including, temperature, humidity, potassium, phosphorus, nitrogen, and rainfall. These data are stored in a dataset with features denoted as $A_1, A_2, A_3, \dots A_m$ and training instances represented as$SD_1, SD_2, SD_3, \dots SD_n$.

The hidden layer captures information from previous layer where Gaussian kernel process is applied for analysing the testing and training data as given below,

$$\boldsymbol{GK} = \sum_{i=1}^{n} \sum_{j=1}^{m} \exp\left[-0.5 * \frac{(|SD_t - SD_r|^2)}{v^2}\right] \quad (7)$$

Where, $\boldsymbol{GK}$ indicates a Gaussian kernel between the testing data point DS_t and the training data point 'DS_r' and 'v' indicates a deviation. Based on the analysis, the data points are classified into different classes. The output of the hidden or recurrent layer is formulated as follows,

$$R_t = F\ (\alpha_{ih}.SD_t + \alpha_{hh}.R_{t-1} + B_R) \quad (8)$$

Where, R_t denotes a hidden or recurrent layer output at time't', F indicates sigmoid activation function, α_{ih} denotes a weight matrices for the input and hidden state, SD_t indicates a input data sample at time step't', α_{hh} indicates a weight matrices for the hidden state, R_{t-1} indicates a previous hidden state at time step '$t-1$', B_R indicates a bias term in hidden layer that stores the value '1'. Once all the time steps are completed the final current state is used to calculate the output. The output is generated as follows,

$$Y_k\ (t) = F(\alpha_{ho}.R_t + B_o) \quad (9)$$

Where, $Y_k(t)$ denotes actual classification outcome at time 't', F indicates sigmoid activation function, α_{ho} denotes a weight matrices from the hidden state to ouput state, R_t indicates a hidden layer output, B_o indicates a bias term in output layer that stores the value '1'. After that, error is computed based on the expected and actual classification outcome.

$$e = [Y_E(t) - Y_k(t)] \quad (10)$$

Above depicts a graphical illustration of the accuracy of crop prediction using three different methods CRGKGRNN and existing IML-ASE [1], DRL [2], with respect to number of data samples ranging from 200 to 2000. In Figure 3, the x-axis denotes the number of data samples, and the y-axis indicates the crop prediction accuracy. The graphical effects show that the proposed CRGKGRNN achieved higher crop prediction accuracy compared to existing methods [1] and [2], respectively.

CONCLUSION

Smart farming is a modern approach that utilizes digital and IoT devices in conjunction with machine learning to enhance productivity and optimize resource utilization. The IoT-enabled crop prediction system offers numerous advantages to farmers, enabling them to make informed decisions for cultivation, optimize resource usage, and implement precision farming techniques. In this paper, we introduce an efficient crop prediction method called CRGKGRNN, designed to predict suitable crops for cultivation with higher accuracy and minimal time consumption. The main objective of CRGKGRNN is to improve the accuracy of crop prediction. Following data pre-processing, relevant features are selected, and a classification of different types of crops is presented to achieve accurate predictions with minimal error. The experimental evaluation of CRGKGRNN highlights its superior performance. Specifically, it increased accuracy in crop prediction, precision, recall, and F1-score, while simultaneously reducing the time required for crop prediction compared to existing methods.

REFERENCES

1. Chetan Raju, Ashoka D.V., Ajay Prakash B.V., "CropCast: Harvesting the future with interfused machine learning and advanced stacking ensemble for precise crop prediction", Kuwait Journal of Science, Elsevier, 2023, Pages 1-9.https://doi.org/10.1016/j.kjs.2023.11.009
2. Mohamed Bouni, Badr Hssina, Khadija Douzi, Samira Douzi, "Towards an Efficient Recommender Systems in Smart Agriculture: A deep reinforcement learning approach", Procedia Computer Science, Elsevier, Volume 203, 2022, Pages 825-830. https://doi.org/10.1016/j.procs.2022.07.124
3. V.G. Dhanya, A. Subeesh, N.L. Kushwaha, Dinesh Kumar Vishwakarma, T. Nagesh Kumar, G. Ritika , A.N. Singh, "Deep learning based computer vision approaches for smart agricultural applications", Artificial Intelligence in Agriculture, Elsevier, Volume 6, 2022, Pages 211-229. https://doi.org/10.1016/j.aiia.2022.09.007
4. V. Elizabeth Jesi, Anil Kumar, Bappa Hosen and Stalin David D, "IoT Enabled Smart Irrigation and Cultivation Recommendation System for Precision Agriculture", ECS Transactions, Volume 107, Issue 1, 2022, Pages 5953- 5956. **DOI** 10.1149/10701.5953ecst
5. Ersin Elbasi, Chamseddine Zaki, Ahmet E. Topcu, Wiem Abdelbaki, Aymen I. Zreikat , Elda Cina , Ahmed Shdefat and Louai Saker, "Crop Prediction Model Using Machine Learning Algorithms", Applied Sciences , Volume 13, Issue 16, 2023, Pages 1-20. https://doi.org/10.3390/app13169288
6. S. P. Raja, Barbara Sawicka, Zoran Stamenkovic and G. Mariammal, "Crop Prediction Based on Characteristics of the Agricultural Environment Using Various Feature Selection Techniques and Classifiers", IEEE Access, Volume 10, 2022, Pages 23625 – 23641. **DOI:** 10.1109/ACCESS.2022.3154350
7. Rishi Gupta, Akhilesh Kumar Sharma, Oorja Garg, Krishna Modi, Shahreen Kasim , Zirawani Baharum, Hairulnizam Mahdin, And Salama A. Mostafa, "WB-CPI: Weather Based Crop Prediction in India Using Big Data Analytics", IEEE Access , Volume 9, 2021, Pages 137869 – 137885. **DOI:** 10.1109/ACCESS.2021.3117247
8. P. Velmurugan, A. Kannagi, M. Varsha, "Superior fuzzy enumeration crop prediction algorithm for big data agriculture applications", Materials Today: Proceedings, Elsevier, Volume 81, 2023, Pages 112-117. https://doi.org/10.1016/j.matpr.2021.02.578
9. Ambre Dupuis, Cam´elia Dadouchi, Bruno Agard, "Methodology for multi-temporal prediction of crop rotations using recurrent neural networks", Smart Agricultural Technology, Elsevier, Volume 4, 2023, Pages 1-13.https://doi.org/10.1016/j.atech.2022.100152
10. Mario Benini, Emanuele Blasi, Paolo Detti, Lorenzo Fosci, "Solving crop planning and rotation problems in a sustainable agriculture perspective", Computers & Operations Research, Elsevier, Volume 159, 2023, Pages 1-16. https://doi.org/10.1016/j.cor.2023.106316
11. Qiusi Zhang , Bo Li , Yong Zhang , and Shufeng Wang, "Suitability Evaluation of Crop Variety via Graph Neural Network", Computational Intelligence and Neuroscience, Hindawi, Volume 2022, August 2022, Pages 1-10. https://doi.org/10.1155/2022/5614974
12. Sikander Singh Cheema, Amardeep Singh, and Hasse`ne Gritli, "Optimal Crop Selection Using Gravitational Search Algorithm", Mathematical Problems in Engineering, Hindawi Volume 2021, April 2021, Pages 1-14.https://doi.org/10.1155/2021/5549992
13. A.S. Gardner, I.M.D. Maclean, K.J. Gaston, L. Bütikofer, "Forecasting future crop suitability with microclimate data", Agricultural Systems, Elsevier, Volume 190, 2021, Pages 1-9.https://doi.org/10.1016/j.agsy.2021.103084
14. Mahmud Isnan, Alam Ahmad Hidayat, Bens Pardamean, "Indonesian Agricultural-crops Classification Using Transfer Learning Model", Procedia Computer Science, Elsevier, Volume 227, 2023, Pages 128-136. https://doi.org/10.1016/j.procs.2023.10.510
15. Bikram Pratim Bhuyan, Ravi Tomar, T. P. Singh and Amar Ramdane Cherif , "Crop Type Prediction: A Statistical and Machine Learning Approach", Sustainability, Volume 15, Issue 1, 2023, Pages 1-17.https://doi.org/10.3390/su15010481

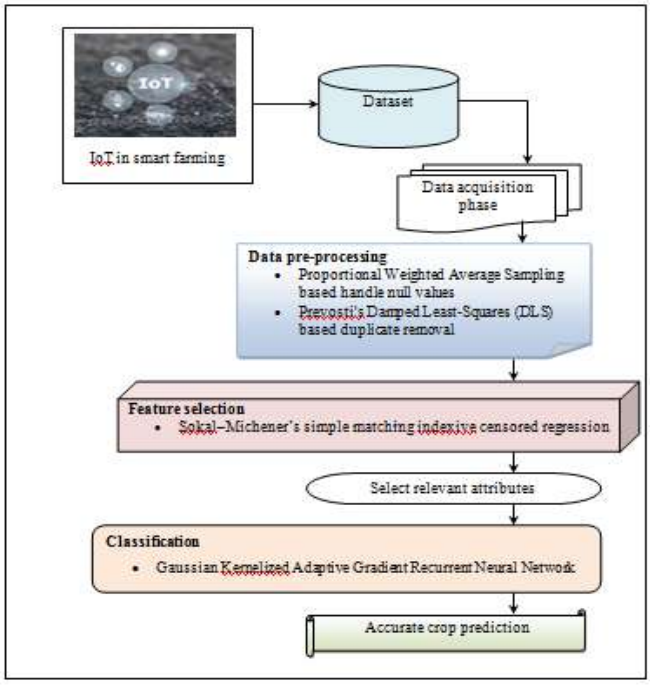

Figure 1: Architecture of Proposed CRGKGRNN Method

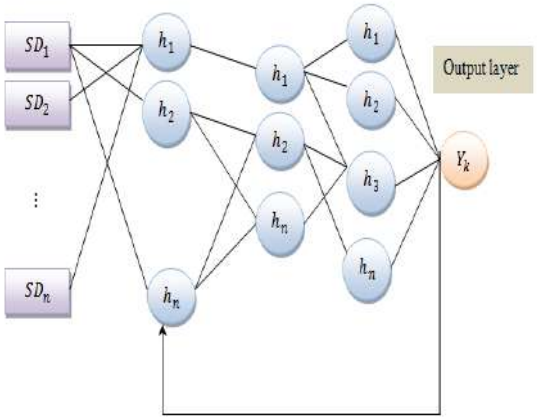

Figure 2: Adaptive Gradient Recurrent Neural Network

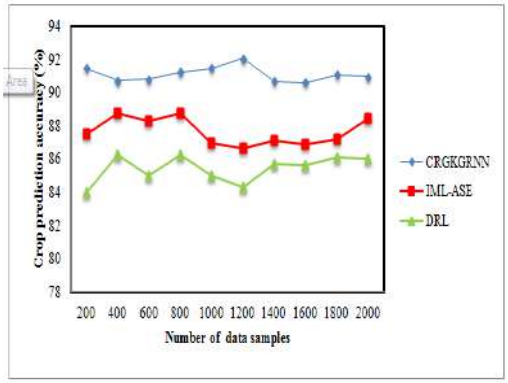

Figure 3: Graphical Illustration of Crop Prediction Accuracy

Indian Journal of Natural Sciences www.tnsroindia.org.in ©IJONS

Vol.15 / Issue 83 / Apr / 2024 International Bimonthly (Print) – Open Access ISSN: 0976 – 0997

RESEARCH ARTICLE

AI Based Ayurvedic Plant Divination

Usha M S *[1], Navyashree S[2] and Pratheek Raj Urs C P[2]

[1]Associate Professor, Department of Computer Science and Engineering, NIE North, Mysuru-Karnataka-India.
[2]Department of Computer Science and Engineering, NIEIT, Mysuru, Karnataka, India.

Received: 20 Dec 2023 Revised: 29 Jan 2024 Accepted: 13 Mar 2024

***Address for Correspondence**
Usha M S
Associate Professor,
Department of Computer Science and Engineering,
NIE North, Mysuru-Karnataka-India.
Email: ushams@nie.ac.in

ABSTRACT

In the convoluted realm of medicinal plant utilization, the fusion of ancient wisdom and modern technology emerges as an imperative intervention. Celebrated for its efficiency in treating chronic illnesses. Using Tensor Flow Lite and a Convolutional Neural Network (CNN) algorithm, the application revolutionizes Ayurvedic plant identification through advanced image processing. The user-friendly app, developed in Android Studio, facilitates rapid, precise scanning and detection, providing detailed insights into medicinal benefits, traditional uses, and cultural significance. Beyond recognition, the application encourages active user engagement in cultivation practices and conservation efforts. This innovative tool is essential to safeguard endangered Ayurveda plants, ensuring the preservation of their rich heritage. The project offers a synergistic solution, merging ancient wisdom with cutting-edge technology to conserve Ayurvedic botanical treasures for future generations. This contributes to the intersection of traditional knowledge and technological solutions in a concise and impactful manner, addressing the critical need for the preservation of Ayurvedic plant species.

Keywords: Medicinal plants, Ayurveda, Computer vision, Traditional medicine, Medicinal properties

INTRODUCTION

In the realm of healing traditions, Ayurveda, an ancient medicinal system originating in India, has provided profound solutions for diverse ailments by harnessing the potent properties inherent in medicinal plants. Rooted in a holistic approach that considers the interconnectedness of mind, body, and spirit, Ayurveda boasts a history spanning thousands of years. Despite their historical significance, awareness of Ayurvedic botanical remedies has waned in contemporary society, necessitating a concerted effort for preservation and reintroduction. This research

endeavors to address this imperative through the development of an innovative system at the confluence of ancient wisdom and state-of-the-art technology. Leveraging a Convolutional Neural Network (CNN) algorithm implemented via TensorFlow and seamlessly integrated into a Mobile Application developed using Android Studio. The project offers a comprehensive guide to Ayurvedic plants. This application not only visually identifies the plants but also provides extensive information regarding their benefits and methods of incorporation into daily life. Central to this system is a sophisticated computer vision mechanism empowered by advanced algorithms. This mechanism captures and processes intricate leaf images, extracting features such as eccentricity, color and shape. The automated plant identification feature, akin to a digital herbalist, functions as a scanner, enabling users to effortlessly detect and learn about various Ayurvedic plants. This fusion of Artificial Intelligence and Ayurvedic knowledge not only bridges awareness gaps but also nurtures a deeper connection between individuals and the healing properties of nature. Additionally, this project draws inspiration from recent advancements in automated plant identification. From algorithms utilizing Gaussian distribution for precise classification to innovative combinations of Speeded Up Robust Features (SURF) and Histogram of Oriented Gradients (HOG) achieving near-perfect accuracy rates, these technological strides underscore the potential for a cultural resurgence. This convergence represents not only a technological leap but also a harmonious integration where ancient wisdom synergizes with modern scientific methodologies. By seamlessly blending tradition with innovation, this transformative system revitalizes the understanding of Ayurvedic plants, ensuring the enduring legacy of their healing properties. This endeavor transcends technological innovation; it signifies a cultural revival where the echoes of Ayurveda resonate through the corridors of modernity, emphasizing the invaluable treasures nature provides for holistic well-being. This research contributes to the ongoing discourse in the intersection of traditional medicinal knowledge and contemporary technological solutions, offering a promising avenue for the preservation and dissemination of Ayurvedic wisdom.

LITERATURE REVIEW

The intersection of machine learning, deep learning and Image processing has seen significant exploration in the domain of medicinal plant classification, particularly employing convolutional neural networks (CNNs). Previous research has predominantly relied on CNNs for the recognition of plant species based on leaf characteristics, demonstrating commendable accuracy in various studies. However, inherent limitations, particularly in handling complex backgrounds and smaller leaves observed in the papers proposed by R. Upendar Rao et al., have prompted the need for advancements in this field. Our proposed application represents a substantial leap beyond these constraints, incorporating state-of-the-art technologies such as Tensor Flow and advanced CNN architectures. A critical analysis of prior literature projects proposed by Nilesh Bhelkar et al., that the algorithms employed were often deemed insufficient and inaccurate, impeding their overall efficiency. In stark contrast, our application employs CNN, achieving an outstanding accuracy of 94%, thereby transcending the limitations of prior projects proposed by Dinesh Shitole et al., and Rakibul Sk et al., significantly enhancing efficiency in Ayurvedic plant recognition. The distinctiveness of the application lies in its user-centric features, designed to facilitate active engagement in plant identification and learning. Noteworthy is the incorporation of a comprehensive database, setting our application apart by providing users with extensive information beyond mere plant identification. This synthesis of advanced technology precision and user-centric design collectively positions our application as a pioneering and distinctive solution in the landscape of Ayurvedic plant recognition. In conclusion, while earlier projects proposed by Fadil Chady et al., laid the foundational groundwork, proposed application signifies a substantial advancement, overcoming the inefficiencies of past algorithms and delivering a more accurate and efficient platform for Ayurvedic plant classification. This research contribution establishes a new paradigm, fostering a seamless blend of technological sophistication and user engagement in the exploration and dissemination of herbal medicine knowledge.

Problem Statement

In the realm of natural remedies, Ayurvedic plants pose a significant challenge for recognition and accessibility, attributed to complex identification methods and the inadequacies of existing plant recognition apps. The intricate nature of Ayurvedic knowledge exacerbates this issue, leading to a substantial gap in understanding and utilization. Our research identifies this pressing problem and endeavors to bridge the gap by employing artificial intelligence. Through the development of a user-friendly application, we aim to empower individuals spanning from enthusiasts to practitioners, to overcome the hurdles of Ayurvedic plant recognition. The objective is to create a comprehensive solution that not only addresses the complexities of identification but also fosters a deeper connection with the healing potential of Ayurvedic flora.

PROPOSED METHODOLOGY

This innovative application's methodology is centered around cutting-edge technologies, prominently computer vision and deep learning algorithms, facilitating the scanning, identification, and comprehensive analysis of Ayurvedic plants. The process begins with the capture of high-resolution plant images, subjected to pre-processing techniques to enhance clarity and quality. Leveraging the Convolutional Neural Networks (CNN), a robust deep learning algorithm, the application conducts intricate plant recognition, discerning unique features such as leaf patterns, shapes, and textures. Implemented in Python using TensorFlow, the CNN algorithm plays a central role in the precise identification of Ayurvedic plants. TensorFlow provides a robust framework for the development and training of deep neural networks, enhancing the efficiency and accuracy of the identification process. The integration of Android Studio, utilizing Kotlin, facilitates seamless application development for Android devices. Upon successful identification specialized algorithms are deployed for image detection and processing employing complex pattern recognition methodologies to extract essential characteristics from the plant images. The CNN architecture that is designed for image classification tasks, ensures precise feature extraction contributing to accurate plant classification. Subsequent to identification, the application retrieves comprehensive information about the recognized plant from an extensive database.

This database includes the plant's local name, uses, different properties and botanical information. The intention is to empower common users with the ability to easily identify and understand Ayurvedic plants. This information is presented in distinct sections within the application, each dedicated to specific aspects such as plant recognition and detailed analysis of medicinal properties. The app operates by performing all algorithms in the backend, and upon completion, it displays the output by presenting the matching plant's information, including its uses. In cases where the scanned plant is not identified as an Ayurvedic plant, the application connects to Google and provides relevant results, indicating that it is not an Ayurvedaplant. The significance of utilizing CNN, TensorFlow and Android Studio lies in their combined efficiency. CNN excels in image recognition tasks, TensorFlow provides a robust deep learning framework, and Android Studio facilitates user-friendly application development. Python serves as a versatile language for seamless implementation. The meticulous design of the application ensures not only the accurate scanning and identification of Ayurvedic plants but also the dissemination of valuable information, fostering a deeper understanding of these natural resources in the context of holistic healthcare.

Architecture

In the proposed research application, users initiate plant identification by capturing an image, subsequently undergoing pre-processing for image enhancement. The Convolutional Neural Network (CNN) then scrutinizes the extracted features for precise plant recognition. Upon successful identification, comprehensive plant information is retrieved from a dedicated database. The user-friendly interface systematically categorizes and presents this information, enabling user exploration. Users engage further by interacting with the application, saving, and sharing plant profiles, fostering a deeper understanding of Ayurvedic plants. This architecture seamlessly integrates image processing, deep learning, and database retrieval, offering an efficient and user-friendly solution for Ayurvedic plant recognition.

Work Flow

Image Capture: High-resolution images of Ayurvedic plants are captured.
Pre-processing: Images undergo enhancement and noise removal.
Feature Extraction: Key plant features like patterns and textures are extracted.
CNN Implementation: Convolutional Neural Network analyzes features for plant recognition.
Plant Identification: CNN matches features with a trained dataset for accurate identification.
Information Retrieval: Comprehensive data, including medicinal benefits, is retrieved from a database.
Data Presentation: User-friendly interface categorizes and presents plant information.
User Interaction: Users can explore, save, and share plant profiles.

RESULT ANALYSIS

Comparison Of Existing Models Vs Proposed Model

CONCLUSION

In conclusion, the work is poised to address identified shortcomings in Ayurvedic plant classification through an innovative application. Through a thorough literature survey, challenges in handling complex backgrounds and achieving precise plant recognition have been recognized, paving the way for the proposed solution. The forthcoming application will represent a groundbreaking leap forward by leveraging cutting-edge technologies, including TensorFlow Lite and advanced CNN architectures. The critical analysis undertaken in this research underscores a commitment to overcoming algorithmic inefficiencies and ensuring enhanced accuracy and efficiency in Ayurvedic plant recognition. The uniqueness of the future application will be evident in its user-centric features and the integration of a comprehensive database, promising users extensive information beyond mere plant identification. By acknowledging and proactively addressing the limitations identified in the literature survey, the work is set to contribute a transformative and efficient platform for Ayurvedic plant classification. In essence, the work endeavors to establish a new standard, harmonizing traditional wisdom with modern technology. Through this ongoing work, we anticipate offering a significant advancement in the exploration and dissemination of herbal medicine knowledge, ensuring the preservation of Ayurvedic botanical treasures for generations to come.

Acknowledgments

We extend our heartfelt appreciation to Dr. Usha M S, Professor and Head of the Department of Computer Science and Engineering at NIEIT, Mysuru-18 for providing the invaluable opportunity to embark on this ongoing research project. Her guidance has been instrumental in shaping the direction of this academic endeavor. We are sincerely grateful to the dedicated faculty members of the Computer Science Department at NIEIT along with the entire departmental staff for their continuous support as we navigate through the phases of this project. Principal Dr. Rohini Nagapadma's encouragement has been a driving force in the early stages of our work. Special thanks to JSSAMC and the Botanists who have been actively contributing to our ongoing research. Their collaboration and expertise have proven to be invaluable as we progress with our investigations. Lastly, we express our deep appreciation to our cherished family members for their unwavering support during the course of this ongoing project. Their encouragement remains a pillar of strength.

REFERENCES

1. Title: "Natural Language Processing in the Biomedical Domain: A Unified System Architecture Overview." Authors: K. B. Cohen, L. Hunter
2. Title: "A Survey on Plant Leaf Recognition Techniques" Authors: S. N. Omkar, S. Ramachandra
3. Title: "A Survey of Leaf Recognition Techniques" Authors: R. Senthil, R. Amirtharaja

4. Title: "Plant Identification Using Deep Neural Networks via Optimization of Transfer Learning Parameters" Authors: O. Avsievich, A. A. Aivazyan
5. Title: "Deep Plant Phenomics: A Deep Learning Platform for Complex Plant Phenotyping Tasks" Authors: W. DeChant, S. Lilavois
6. Google Scholar, IEEE Xplore, ResearchGate, ChatGPT, MDPI, Springer, PubMed, ScienceDirect, Academia.edu, Sci-Hub, etc.
7. "Advances in Plant Recognition Techniques: A Comprehensive Survey"-Wikipedia
8. "Challenges and Opportunities in Ayurvedic Plant Database Creation: A Literature Review"-Wikipedia
9. "Integrating Traditional Wisdom into Plant Recognition: An Ethnobotanical Perspective"-Wikipedia
10. "Herbal Texts Decoded: Natural Language Processing in Ayurvedic Literature"-Wikipedia
11. "Multimodal Approaches for Plant Identification: Bridging Visual and Textual Information"-Wikipedia
12. "Community-Driven Herbal Knowledge Platforms: Comparative Analysis and Future Directions"-Wikipedia
13. "Security and Privacy in Herbal Medicine Apps: A Comprehensive Review"-Wikipedia
14. "Mobile-Based Healthcare Solutions for Rural Ayurvedic Practitioners: A Survey of Impact and Challenges"-Wikipedia
15. "Deep Learning Models for Ayurvedic Plant Recognition: Architectural Insights and Dataset Analysis"-Wikipedia

Research Paper Name	**Drawback of Existing System**	**Proposed System**
System To Detect Ayurvedic Plants and it is Medicinal Values	The proper result was not generated when the leaf images were rotated.	Designed to provide most accurate result irrespective of dimension
Identification Of Plants Using Deep Learning	Size of the dataset is limited. Samples of different classes of the plants leaf to be added	Most of the dataset has been tried to collect which are available in surrounding irrespective of classes
Worldwide Research Trends on Medicinal Plants	Discussed only about the development of medicinal plants over English medicine	Includes many other features compare to this model like identification of plant, image, information with use and benefits
Literature searches on Ayurveda	It only concentrates on Ayurveda literature search and strategy to retrieve maximum publications	It is devoid of any of the practical use that our model is proposing it is specifically designed only to search
The Significance of Ayurvedic Medicinal Plants	It discusses only on the importance, availability and caution before using the plants	Considering this information briefly our app consists a scanner to identify the plant using CNN technique and retrieve the data.
Medicinal plant classification using a convolution neural network	Identify only one plant leaf at a time and also automata plant recognition is most difficult in complex backgrounds	It is designed to identify an ayurvedic plant irrespective of complex backgrounds and also provide complete information about the plant
A mobile app for recognition	This app is only designed for plants	It is done using CNN which has highest

of medicinal plants from Republic of Mauritius using deep learning in real time	from Republic of Mauritius and it is done in MATLAB platform where they perform poorly under normal environment	of 94% accuracy and the best model for plant detection and also our app contain many features with lot of benefits

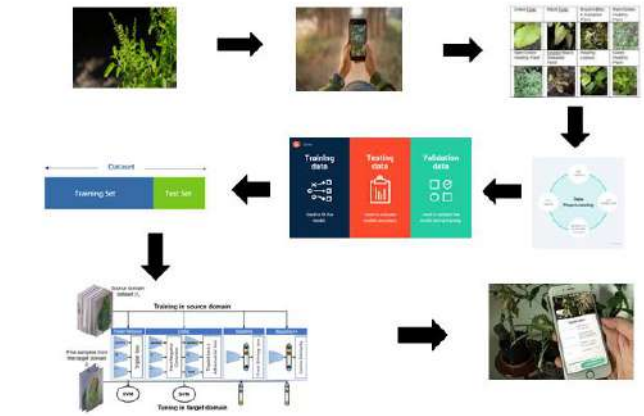

Figure1 Procedure involved to recognize the Ayurvedic plants

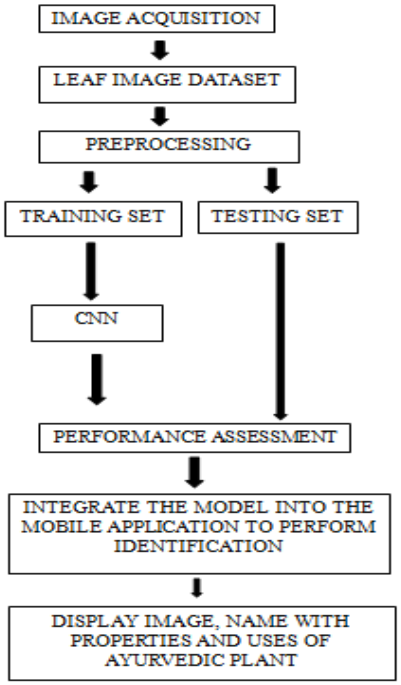

Figure2 Proposed integrated model to identify the Ayurvedic plants

RESEARCH ARTICLE

Analysis of Traditional with Conventional RSA

S. Nirmala Devi[1]* and M. Ganaga Durga[2]

[1]Research Scholar, Assistant Professor, Department of Computer Applications (UG), Fatima College, Madurai, Tamil Nadu, India.
[2]Research Supervisor, Department of Computer Applications, Sri Meenakshi Government Arts College for Women(A),Madurai, Tamil Nadu, India.

Received: 22 Feb 2024 Revised: 15 Mar 2024 Accepted: 21 Mar 2024

***Address for Correspondence**
S. Nirmala Devi
Research Scholar,
Assistant Professor,
Department of Computer Applications (UG),
Fatima College,
Madurai, Tamil Nadu, India.
Email: s.nirmaladeviap@gmail.com

ABSTRACT

During the implementation of any cryptography algorithm, it is important to consider about the computational aspect of the algorithm for the encryption and decryption process. This paper analyses the traditional and conventional RSA algorithms based on its encryption speed and decryption speed. The traditional RSA algorithm was compared with many of the other public key algorithms in various papers. But in this paper it is compared with an improved version of RSA. This improved version is proved with the help of following metrics like plain text size and key size with encryption time and decryption time. This proposed work is doing the encryption and decryption process as fast as the traditional RSA algorithm. This proposed work can be implemented for the encryption and decryption of data in strict source routing of Ad-hoc network.

Keywords: Asymmetric Encryption, Public Key Algorithm, Traditional RSA, Conventional RSA, Computational Aspects, Strict Source Routing

INTRODUCTION

Traditional RSA

This Asymmetric encryption (Public key encryption) is a form of cryptosystem in which encryption and decryption are performed using the different keys, a public key and a private key. It is also known as public-key encryption. Asymmetric encryption transforms plaintext into ciphertext using one oftwo keys and an encryption algorithm. Using the paired key and a decryption algorithm, the plaintext is recovered from the ciphertext. Asymmetric

encryption can be used for confidentiality, authentication, or both. The most widely used public-key cryptosystem is RSA. The difficulty of attacking RSA is based on the difficulty of finding the factors of a prime number [1]. A public-key encryption scheme has six ingredients. [1]

Plaintext This is the readable message or data that is fed into the algorithm as input.

Encryption algorithm The encryption algorithm performs various transformations on the plaintext.

Public and private keys This is a pair of keys that have been selected so that if one is used for encryption, the other is used for decryption. The exact transformations performed by the algorithm depend on the public or private key that is provided as input.

Cipher text This is the scrambled message produced as output. It depends on the plaintext and the key. For a given message, two different keys will produce two different cipher texts.

Decryption algorithm This algorithm accepts the cipher text and the matching key and produces the original plaintext. The essential steps are the following.

1. Each user generates a pair of keys to be used for the encryption and decryption of messages[1].
2. Each user places one of the two keys in a public register or other accessible file. This is the public key. The companion key is kept private. Each user maintains a collection of public keys obtained from others.
3. If sender A wishes to send a confidential message to receiver B, sender A encrypts the message using B's public key (Fig. 1).
4. When B receives the message, he/she decrypts it using his/her own private key. No other recipient can decrypt the message because only B knows his/her private key.
5. If encryption is done using sender's private, then the receiver will decrypt it using A's public key (Fig. 2).

Conventional RSA

Like traditional RSA, conventional RSA also will have the components like Plain text, Encryption algorithm, Public and private keys and Cipher text. But here the difference is only in the encryption process and decryption process. After the generation of public and private keys the following steps were performed.

1. During the encryption process, a large integer (key) is raised to an integer.
2. Then the large key value is divided by 2 for reducing the computation time of the powers.
3. The divided value is now powered with the base which is doubled itself.
4. Till the power value is minimized, the process is continued and it produces the encrypted cipher text very fast.

simulation

Implementation of Traditional RSA

1. Choose two prime numbers, p = 5 and q = 7.
2. Find n = pq = 5 × 7 = 35.
3. Again find Ø (n) = (p - 1)(q - 1) = 4 × 6 = 24.
4. Choose e such that e is relatively prime to Ø(n) = 24 and less than Ø(n), choose e = 13. That is gcd(e, Ø(n))=1
5. Define d such that d.e≡ 1 (mod Ø(n)). The correct value is d = 13, because 13 ×13 = 169 = (1 × 168) + 1.
6. The resulting keys are public key PU_B = {e,n} and private key PR_B = {p,q,d}[2].

Therefore PU_B={13,35} & PR_B={5,7,13}

Encryption: $C=E_{PUB}(M)=M^e \bmod n$

Decryption: $M=D_{PRB}(C)=C^d \bmod n$

Consider a plaintext input of M= 33

Encryption: $C=33^{13} \bmod 35$

C=33

This cipher text will be sent to receiver (B).

At receiver side, $M=33^{13} \bmod 35$

M= 33

Calculation of powers in Traditional RSA

Both encryption and decryption in RSA involve raising an integer to an integer power, mod n. It can make use of a property of modular arithmetic[6]:

$[(a \bmod n) * (b \bmod n)] \bmod n = (a * b) \bmod n$

So it is possible to reduce intermediate results modulo n. This makes the calculation practical. Another consideration is the efficiency of exponentiation, because RSA dealing with potentially large exponents[3]. To see how efficiency might be increased, consider that it is possible to compute x^{16}. A straightforward approach requires 15 multiplications. This takes more time to compute the result[7].

Calculation of powers in Conventional RSA

To find 2 raised to the power 10, it is possible to multiply 9 times 2. But for finding 2 raised to the power very large number such as 1000000000, it is not easy to multiply 999999999 times 2 because it takes more time. Exponentiation by squaring helps to find the powers of large positive integers. The methodology behind the exponentiation by squaring is to the divide the power in half at each step.

$$f(x) = \begin{cases} x(x^2)^{\frac{n-1}{2}}, & if\ n\ is\ odd \\ (x^2)^{\frac{n}{2}}, & if\ n\ is\ even \end{cases} \quad \text{-----> } (1)$$

Consider an example:

3 ^ 10 = 3 * 3 * 3 * 3 * 3 * 3 * 3 * 3 * 3 * 3

First divide the power by 2

3 ^ 10 = (3 * 3) * (3 * 3) * (3 * 3) * (3 * 3) * (3 * 3)

3 ^ 10 = ((3 * 3) ^ 5) [As per the above equation 1]

3 ^ 10 = 9 ^ 5

The power is divided by 2 and base is multiplied to itself. So it is possible to write 3 ^ 10 = 9 ^ 5.

Now, the problem is to find 9 ^ 5

9 ^ 5 = 9 * 9 * 9 * 9 * 9

Here divide the power by 2. Since the power is an odd number here, it is not possible to do so. There's another way to represent 9 ^ 5 is as follows:

9 ^ 5 = (9 ^ 4) * 9 [As per the above equation 1]

Now it is easy to find 9 ^ 4 and later multiple the extra 9 to the result

9 ^ 5 = (81 ^ 2) * 9

When power is not divisible by 2, make power even by taking out the extra 9. Then it is already know the solution when power is divisible by 2. Divide the power by 2 and multiply the base to itself.

Now the problem is to find (81 ^ 2) * 9

(81 ^ 2) * 9 = (81 * 81) * 9

Finally divide the power by 2

(81 ^ 2) * 9 = (6561 ^ 1) * 9 [As per the above equation 1]

Finally, the solution for 3 ^ 10 = (6561 ^ 1) * 9 = 6561 * 9 = 59049

Simulation results have been executed using python 3.12, Windows 64 bit OS, with Intel core i3 processor and 4 GB RAM. Also the results are analyzed based on plain text size and key size.

system study

Quality of Service

For all kind of cryptography algorithms, its performance is measured based on different metrics[4]&[5]. Performance measures of a proposed system are analyzed based on plaintext size and key size with encryption time and decryption time.

Plaintext Size Based

To measure the quality of a conventional algorithm, traditional RSA as well as the conventional RSA is evaluated based on plain text size. For the different plain text size the time taken for encryption and the time taken for decryption is calculated.

Key Size Based

To measure the quality of a conventional algorithm, traditional RSA as well as the conventional RSA is evaluated based on key size. For the different key size the time taken for encryption and the time taken for decryption is calculated.

Table

The below table I shows the performance measure of the traditional and conventional RSA based on plain text size and encryption time in milliseconds for five different text files with size 3KB, 25KB, 75KB, 500KB and 10MB. The below table II shows the performance measure of the traditional and conventional RSA based on plain text size and decryption time in milliseconds for five different text files with size 3KB, 25KB, 75KB, 500KB and 10MB. The below table III shows the performance measure of the traditional and conventional RSA based on key size and encryption time in milliseconds for five different keys of P and Q. The below table IV shows the performance measure of the traditional and conventional RSA based on key size and decryption time in milliseconds for five different keys of P and Q.

Chart

The below Fig. 3 shows the shows the performance measure of the traditional and conventional RSA based on plain text size and encryption time in milliseconds for five different text files with size 3KB, 25KB, 75KB, 500KB and 10MB. The below Fig. 4 shows the performance measure of the traditional and conventional RSA based on plain text size and decryption time in milliseconds for five different text files with size 3KB, 25KB, 75KB, 500KB and 10MB. The below Fig. 5 shows the performance measure of the traditional and conventional RSA based on key size and encryption time in milliseconds for five different keys of P and Q. The below Fig. 6 shows the performance measure of the traditional and conventional RSA based on key size and decryption time in milliseconds for five different keys of P and Q.

RESULTS AND DISCUSSION

In this paper the traditional as well as conventional RSA algorithms performances are evaluated based on plain text size, key size and encryption and decryption time. During the analysis it is proved that conventional RSA is producing good result that is it is taking less encryption time and less decryption time compared with traditional RSA. This comparisons are done with the help of following metrics that is plain text size, key size and encryption time, decryption time.

CONCLUSION

This proposed system can be implemented in strict source routing method of Ad-hoc network for routing the packets from source to destination without changing the intermediate routers list. In this work it is also possible to encrypt and decrypt the data sent through this Ad-hoc network securely in a fast manner.

REFERENCES

1. Stallings. W, "Cryptography and Network Security" 5th Ed., Prentice Hall, 2011.

2. Kahate. A, "Cryptography and Network Security", 3rd Ed., Tata McGraw-Hill Publishing Company Limited, 2017.
3. Paar. C, Pelzl. J, "Understanding Cryptography", 2nd Ed., Springer-Verlag Berlin Heidelberg, 2010.
4. Thabah.S.D, Soowal.M, Ahamed. U, Saha.P, "Fast and Area Efficient Implementation of RSA Algorithm", ICRTAC, Elsevier B.V., 2019.
5. Rathod.U, Sreenivas.S,Chandavarkar.B.R, "Comparative Study Between RSA Algorithm and Its Variants: Inception to Date", ICCCE, 2020.
6. Saxena.S, Kishore.N, Handa. D, Kapoor.B, "Comparative Analysis of Sequential and Parallel Implementations of RSA", IJSER, Vol. 4, Issue. 8, 2013.
7. Fatima.S, Rehman.T, Fatima.M, Khan.S, Ali.M.A, "Comparative Analysis of AES and RSA Algorithms for Data Security in Cloud Computing", Engineering Proceedings, 2022.
8. Al-Kaabi.S.S, Belhaouari.S.B, "Methods toward Enhancing RSA Algorithm: A Survey", IJNSA, Vol. 11, No.3, 2019.
9. Latif.I.H, "Time Evaluation Of Different Cryptography Algorithms Using Labview", IOP Conf. Series: Materials Science and Engineering 745, 2020.

Table 1: Encryption Time of Traditional and Conventional RSA with Respect to Plain Text Size

Plaintext Size	Encryption Time of Traditional RSA(ms)	Encryption Time of Conventional RSA(ms)
3 KB	0.0624	0.0609
25 KB	0.0624	0.0624
75KB	0.0565	0.0176
500KB	0.0625	0.0468
10MB	0.0685	0.0156

Table 2: Decryption Time of Traditional and Conventional RSA With Respect to Plain Text Size

Plaintext Size	Decryption Time of Traditional RSA(ms)	Decryption Time of Conventional RSA(ms)
3 KB	0.0469	0.0425
25 KB	0.0624	0.0468
75KB	0.0937	0.0937
500KB	0.0176	0.0156
10MB	0.0625	0.0312

Table 3: Encryption Time of Traditional and Conventional RSA with Respect to Key Size

Key Size (bits)	Encryption Time of Traditional RSA(ms)	Encryption Time of Conventional RSA(ms)
5 bits	0.0332	0.0312
10 bits	0.0781	0.0468
11 bits	0.0695	0.2500
14 bits	0.0468	0.0312
15 bits	0.0624	0.0468

Table 4: Decryption Time of Traditional and Conventional RSA with Respect to Key Size

Key Size (bits)	Decryption Time of Traditional RSA(ms)	Decryption Time of Conventional RSA(ms)
5 bits	0.0469	0.0468
10 bits	0.0624	0.0468
11 bits	0.0322	0.0156
14 bits	0.0595	0.2400

15 bits	0.0468	0.0312

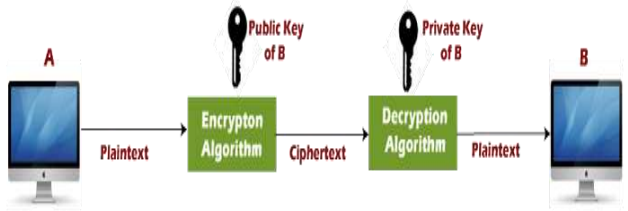

Fig. 1. RSA Encryption with public key

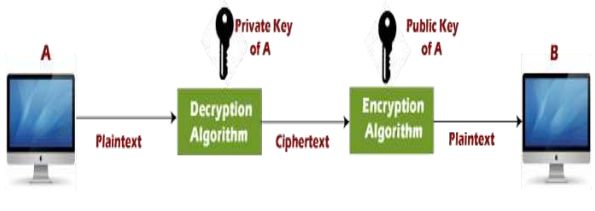

Fig. 2. RSA Encryption with private key

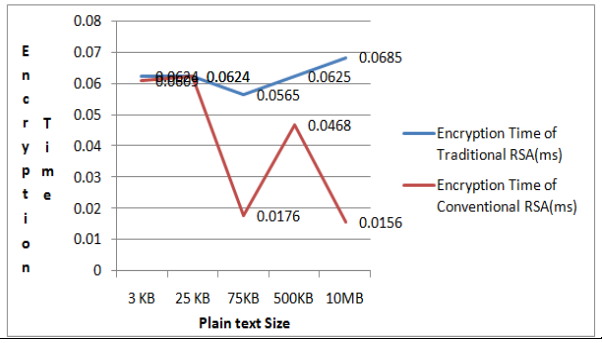

Fig. 3. Encryption Time of Traditional & Conventional RSA with respect to Plain text Size

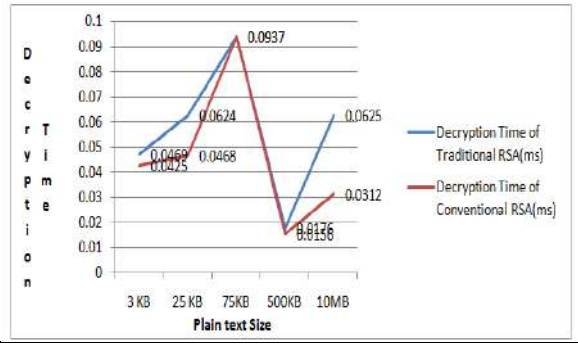

Fig. 4. Decryption Time of Traditional & Conventional RSA with respect to Plain text Size

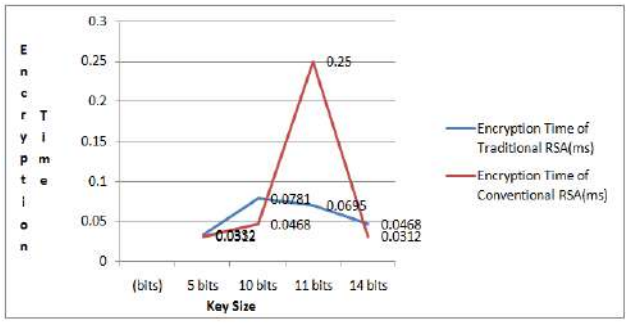

Fig. 5. Encryption Time of Traditional & Conventional RSA with respect to Key Size

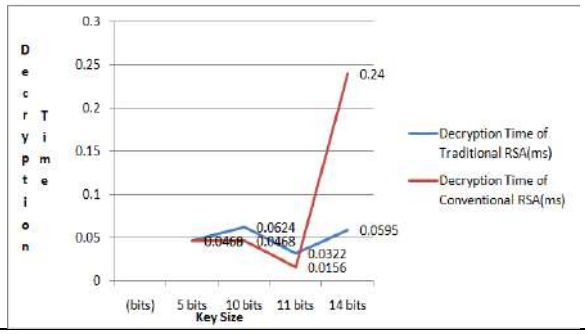

Fig. 6. Decryption Time of Traditional & Conventional RSA with respect to Key Size

Vol.15 / Issue 83 / Apr / 2024 International Bimonthly (Print) – Open Access ISSN: 0976 – 0997

RESEARCH ARTICLE

A Speech Recognition-Enabled Game using Python Integrating Twitter Text Mining Techniques

Simritha R[1] and Tulasimala BN[2]

[1]Student, Department of Computer Science, Mount Carmel College (Autonomous), (Affiliated to Bangalore City University), Bengaluru, Karnataka, India.
[2]Associate Professor, Department of Computer Science, Mount Carmel College (Autonomous), (Affiliated to Bangalore City University), Bengaluru, Karnataka, India.

Received: 20 Dec 2023 Revised: 29 Jan 2024 Accepted: 13 Mar 2024

***Address for Correspondence**
Simritha R
Student,
Department of Computer Science,
Mount Carmel College (Autonomous),
(Affiliated to Bangalore City University),
Bengaluru, Karnataka, India.
Email: simritha14@gmail.com

ABSTRACT

Twitter text mining is a process of extracting valuable information from the vast amount of textual data available on the Twitter. Speech recognition process enables computers to convert spoken language into written text. In this paper, we discuss a speech recognition game that can be implemented using Python that utilizes Twitter text mining techniques and API.

Keywords: (Twitter, text mining, speech recognition, game, tweets, API)

INTRODUCTION

Speech recognition in Python is a fascinating field that involves converting spoken language into text format that computers can understand and process. It has numerous applications, including virtual assistants like Siri and Alexa, dictation software, automated customer service systems, and more. Python provides several libraries and APIs for implementing speech recognition functionality, making it accessible to developers of varying skill levels. One popular library for speech recognition in Python is Speech Recognition. It is a simple and easy-to-use library that supports multiple speech recognition engines, including Google Speech Recognition, Sphinx, and Wit.ai. With Speech Recognition, developers can quickly integrate speech recognition capabilities into their Python projects. Text mining, also known as text analytics, is the process of deriving high-quality information from text data. With the increasing availability of digital text in various forms such as documents, emails, social media posts, and more, text

mining has become a vital tool for extracting valuable insights and knowledge from unstructured text. One interesting application of text mining is speech recognition games. These games leverage the power of natural language processing (NLP) and machine learning techniques to analyze and understand the content of tweets. By transforming the process of speech recognition into an interactive game, users can engage in a fun and educational experience while contributing to the advancement of NLP algorithms The game will provide an interactive and engaging way for users to improve their speech recognition skills while also gaining insights from Twitter data. we start by collecting tweets from Twitter using the Twitter API. The Twitter API allows us to access real-time or historical tweets based on specific search criteria or user profiles. We can filter tweets based on keywords, hashtags, user mentions, or any other relevant information. After collecting the tweets, we can preprocess them by removing noise such as URLs, special characters, stop words (commonly used words like "the," "is," etc.), and perform tasks like tokenization (splitting text into individual words), stemming (reducing words to their base form), and lemmatization (reducing words to their dictionary form). These preprocessing steps help in improving the accuracy of our speech recognition game. Once the tweets are cleaned, we will find the most frequent topics discussed in those tweets and the player will be given the five most popular texts mined using the Twitter data and will be asked to guess the word chosen randomly by the code. We will use a speech recognition library in Python, such as Speech Recognition, the user's speech input is then converted into text using Speech Recognition. The converted text is matched with the chosen random word. The player will be given three chances to guess the chosen word. By developing and deploying such a speech recognition game, we not only provide an engaging experience for users but also collect valuable data for further research and improvement of NLP algorithms. Additionally, these games can be used for educational purposes, helping users improve their speech recognition skills while having fun.

Related Work

By comparing and summarizing various methods used in speech recognition systems, the paper [1] contributes to a comprehensive understanding of the field and informs future research efforts. The authors of the research [2] state that end-to-end models represent a promising direction for automatic speech recognition, offering improved accuracy and simplified architecture. However, practical considerations such as robustness, scalability, and latency remain important factors in commercial deployment. Ongoing research efforts are focused on addressing these challenges and advancing the capabilities of E2E models for real-world applications in industry. [3] This paper provides valuable insights into the state of text mining research, highlighting its significance in big data analytics. By examining developments in methods, applications, and challenges, this review offers guidance for practitioners and researchers seeking to leverage text mining for extracting knowledge from unstructured textual data. The paper [4] provides insights into the current state and future directions of text mining applications in innovation management. By addressing methodological, conceptual, and contextual priorities, researchers can enhance the methodological rigor and richness of text mining studies in the field of innovation research.

Proposed Methodology

Text mining, also known as text data mining, is the process of extracting useful patterns, relationships, or insights from large amounts of text data. Speech recognition, on the other hand, is the ability of a computer system to recognize and transcribe human speech. In this methodology, we will be using Python to develop a text mining - speech recognition game that can extract insights from Twitter data and recognize spoken words.

Data Collection

Load Data

This step involves reading the dataset from a CSV file into a pandas Data Frame. Pandas provides efficient data structures and methods for handling tabular data, making it easy to manipulate and analyze.

Special Character Removal

Removes special characters, quotations, and leading/trailing whitespace from the text. Special characters can introduce noise and hinder analysis, so removing them helps clean the text.

UTF-8 Encoding Handling

Handles UTF-8 encoding issues by replacing encoded characters, such as newline characters, with appropriate representations. This ensures uniformity and consistency in the text data

URL, Hashtag, and Username Removal

Removes URLs, hashtags, and usernames from the text. These elements are often irrelevant for analysis and can skew results, so removing them helps focus on meaningful content.

Lowercasing and Spelling Correction

Converts the text to lowercase to standardize it and corrects common spelling errors. Lowercasing ensures consistency in word representation, while spelling correction improves text quality.

Stopword Removal

Removes common stopwords (e.g., "the", "and") and specific words from the text. Stopwords are frequently occurring words that carry little semantic value and can be excluded to focus on more meaningful content.

Word Frequency Analysis

1. **Count Word Frequency:** Counts the frequency of each word in the preprocessed text to identify the most frequently occurring words. This step provides insights into the distribution of words in the dataset and helps identify key terms or topics.
2. **Visualize Top Words:** Visualizes the top words using a bar chart and a word cloud. The bar chart displays the frequency of the top words in a structured format, while the word cloud visually represents word frequency using font size and color, making it easier to identify prominent terms.

Speech Recognition Game.

Game Setup

Sets up the parameters for the speech recognition game, including the list of words for guessing, the number of guesses allowed, and the prompt limits. This step initializes the game environment and defines the rules.

Initialize Components

Initializes the speech recognition components, including the recognizer and microphone objects. Speech recognition libraries provide APIs for capturing and transcribing speech input, which are essential for implementing the game

Word Selection and User Prompting

Chooses a random word from the list and prompts the user to speak, initiating the game. Random word selection adds variability and excitement to the game, while user prompting encourages participation.

Speech Input Recognition

Records the user's speech input using the microphone and recognizes the transcription using the speech recognition library. This step captures the user's response and converts it into text for comparison.

Comparison and Feedback

Compares the user's guessed word with the chosen word and provides feedback to the user based on the correctness of the guess. Feedback can include messages indicating whether the guess was correct or incorrect.

Multiple Attempts and Game Termination

Allows the user multiple attempts to guess the word within the specified number of guesses. The game terminates based on whether the user correctly guesses the word or exhausts all attempts. This step concludes the game and provides closure to the user's interaction.

RESULTS AND DISCUSSIONS

The results underscored the importance of data preprocessing in text mining projects and highlighted the potential applications of text analysis techniques in various domains. The initial phase of the project involved preprocessing the Twitter data extracted from the 'full-corpus.csv' file. The preprocessing steps included:

1. Removal of leading and trailing whitespaces.
2. Replacement of newline characters with spaces.
3. Substitution of UTF-8 encoding with corresponding characters such as single quotes and ellipses.
4. Elimination of all other UTF-8 encoding patterns.
5. Truncation of text after any 'https:' occurrences.
6. Removal of text before colon (':') occurrences.
7. Omission of hashtags and usernames.
8. Elimination of special symbols such as punctuation marks and currency symbols.
9. These preprocessing steps aimed to standardize the textual data and prepare it for further analysis.

Word Frequency Analysis

Following data preprocessing, we conducted word frequency analysis to identify the most common words in the dataset. The analysis revealed several frequently occurring words, including 'legend,' 'harambe,' and 'rip.' The distribution of word frequencies was visualized using a bar chart, which displayed the top 50 most common words and their respective counts.

Word Cloud Visualization

To provide a visual representation of the text data, we generated a word cloud using the 'WordCloud' library in Python. The word cloud depicted the most prevalent words in the dataset, with larger font sizes indicating higher frequencies. The visualization offered insights into the dominant themes and topics present in the Twitter data.

Speech Recognition Game

As a practical application of the processed text data, we implemented a speech recognition game using the 'speech_recognition' library. The game involved randomly selecting a word from the dataset and prompting the user to guess the word by speaking into the microphone. The program then recognized the user's speech and determined whether the guess was correct.

CONCLUSION

The results of the data preprocessing phase demonstrated the effectiveness of the implemented cleaning techniques in standardizing the textual data. The word frequency analysis provided valuable insights into the prevalent topics and discussions on Twitter during the data collection period. Additionally, the word cloud visualization offered a visually appealing representation of the most common words, facilitating easier interpretation of the dataset. The speech recognition game showcased the practical utility of natural language processing techniques in interactive applications. By integrating speech recognition functionality with the processed text data, we demonstrated a real-world application of text mining methodologies. Overall, the results underscored the importance of data preprocessing in text mining projects and highlighted the potential applications of text analysis techniques in various domains.

REFERENCES

1. Radha, V., & Vimala, C. (2012). A review on speech recognition challenges and approaches. doaj. org, 2(1), 1-7.

2. Li, J. (2022). Recent advances in end-to-end automatic speech recognition. APSIPA Transactions on Signal and Information Processing,11(1)https://doi.org/10.48550/arXiv.2111.01690
3. Hassani, H., Beneki, C., Unger, S., Mazinani, M. T., & Yeganegi, M. R. (2020). Text mining in big data analytics. Big Data and Cognitive Computing, 4(1), 1. https://doi.org/10.3390/bdcc4010001
4. Antons, D., Grünwald, E., Cichy, P., & Salge, T. O. (2020). The application of text mining methods in innovation research: current state, evolution patterns, and development priorities. R&D Management, 50(3), 329-351.https://doi.org/10.1111/radm.12408

Table 1. Count of Word and Frequency

Word	Frequency
new	239
cream	173
sandwich	170
android	168
ice	163
google	159
nexus	156

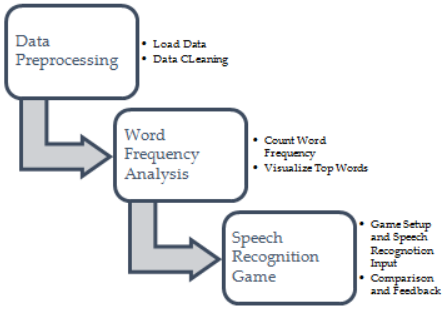

Fig. 1. Overview of the Proposed Speech Recognition Game.

Fig. 2.Flow Chart of the process of Data Preprocessing.

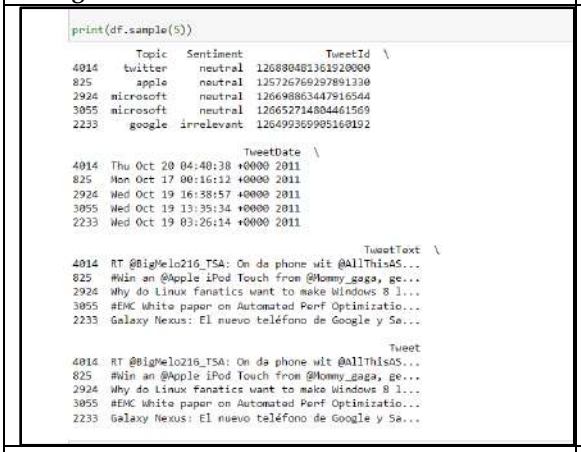

```
print(df.sample(5))

         Topic   Sentiment             TweetId  \
4014   twitter     neutral  1268804811361920000
825      apple     neutral  1257276992978913330
2924 microsoft     neutral  1266988634479165440
3055 microsoft     neutral  1266527148044615690
2233    google  irrelevant  1264993690905160192

                    TweetDate  \
4014  Thu Oct 20 04:40:38 +0000 2011
825   Mon Oct 17 00:16:12 +0000 2011
2924  Wed Oct 19 16:38:57 +0000 2011
3055  Wed Oct 19 13:35:34 +0000 2011
2233  Wed Oct 19 03:26:14 +0000 2011

                                              TweetText  \
4014  RT @BigMelo216_TSA: On da phone wit @AllThisAS...
825   #Win an @Apple iPod Touch from @Mommy_gaga, ge...
2924  Why do Linux fanatics want to make Windows 8 l...
3055  #EMC White paper on Automated Perf Optimizatio...
2233  Galaxy Nexus: El nuevo teléfono de Google y Sa...

                                                  Tweet
4014  RT @BigMelo216_TSA: On da phone wit @AllThisAS...
825   #Win an @Apple iPod Touch from @Mommy_gaga, ge...
2924  Why do Linux fanatics want to make Windows 8 l...
3055  #EMC White paper on Automated Perf Optimizatio...
2233  Galaxy Nexus: El nuevo teléfono de Google y Sa...
```

Fig. 3.Removal of leading and trailing whitespaces.

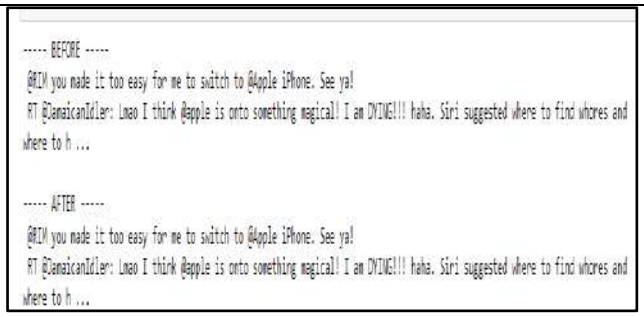

```
----- BEFORE -----
@RIM you made it too easy for me to switch to @Apple iPhone. See ya!
RT @CanaicanIdler: Lmao I think @apple is onto something magical! I am DYING!!! Haha. Siri suggested where to find whores and where to h ...

----- AFTER -----
@RIM you made it too easy for me to switch to @Apple iPhone. See ya!
RT @CanaicanIdler: Lmao I think @apple is onto something magical! I am DYING!!! Haha. Siri suggested where to find whores and where to h ...
```

Fig. 4. Substitution of UTF-8 encoding with corresponding characters such as single quotes and ellipses

Fig. 5. Elimination of all other UTF-8 encoding patterns

Fig. 6. Removal of common stopwords

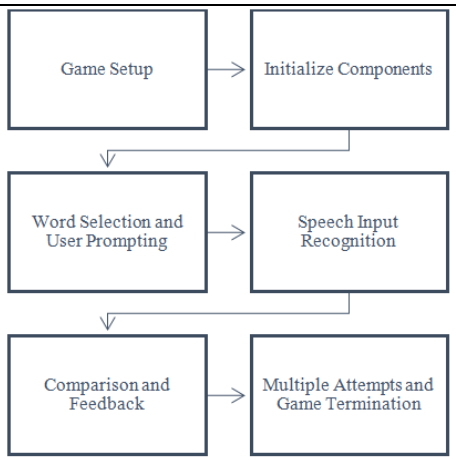

Fig. 7. Working process of the Speech Recognition-enabled game

Fig. 8.Word Cloud of the most frequently occurring words in the tweets

```
I'm thinking of one of these words:
new, cream, sandwich, android, ice
You have 3 tries to guess which one.

Guess 1. Speak!
You said: Android
Incorrect. Try again.

Guess 2. Speak!
You said: sandwich
Correct! You win!
```

Fig. 9.Speech Recognition game where the user guessed the word – sandwich correctly

```
I'm thinking of one of these words:
new, cream, sandwich, android, ice
You have 3 tries to guess which one.

Guess 1. Speak!
You said: hello
Incorrect. Try again.

Guess 2. Speak!
I didn't catch that. What did you say?

Guess 2. Speak!
I didn't catch that. What did you say?

Guess 2. Speak!
You said: cream
Incorrect. Try again.

Guess 3. Speak!
You said: Android
Sorry, you lose!
I was thinking of 'sandwich'.
```

Fig. 10.Full working of the game where the user fails to guess the word after 3 tries

RESEARCH ARTICLE

IoT - Powered Bio sensors Lead the way in Environmental Sensing in the Digital Age

Sumanth S[1]* and Siddarama S[2]

[1]Associate Professor, Department of Computer Science and Applications, Government College for Women, Kolar – 563 101, Karnataka, India.
[2]Head, Department of Computer Science and Applications, Sri Bhagawan Mahaveer Jain College, Robertsonpet, K.G.F. – 563 122, Karnataka, India.

Received: 20 Dec 2023 Revised: 29 Jan 2024 Accepted: 03 Mar 2024

***Address for Correspondence**
Sumanth S
Associate Professor,
Department of Computer Science and Applications,
Government College for Women,
Kolar – 563 101, Karnataka, India.
Email: sumanth81s@gmail.com/dr.sumanth.s.81@gmail.com

ABSTRACT

In today's age of digital transformation, the convergence of environmental sensing and IoT has enabled previously inconceivable advancements in ecological monitoring and management. This research looks into how Internet of Things (IoT) technology and biosensors can be used to create an all-encompassing system for real-time environmental monitoring. IoT-powered biosensors are strategically positioned throughout ecosystems to monitor and report on air and water quality, pollution levels, biodiversity, and other factors. This data is used to create early warning systems for environmental hazards, to encourage biodiversity conservation, to ensure industrial compliance with legislation, and to steer legislators toward more evidence-based policies. The system will delve into the workings of these biosensors in this study, emphasizing their relevance in safeguarding ecosystems, keeping the public healthy, and paving the way for future research. Furthermore, it addresses sensor calibration, data management, privacy, and efficiency issues. This study employs an interdisciplinary approach combining biology, engineering, and data science to explain how IoT-powered biosensors are ushering in a more sustainable and environmentally conscious future by vastly improving our ability to monitor, understand, and proactively address environmental challenges.

Keywords: Environmental Monitoring, Biodiversity, Pollution Levels, Water Quality, Internet of Things (IoT).

INTRODUCTION

In an age marked by tremendous technical advancements, humanity is at a crossroads in the quest to address pressing environmental challenges. Human-caused climate change, air and water pollution, biodiversity loss, and habitat degradation pose major threats to ecosystem health and human and nonhuman animal existence. Confronting these challenges necessitates the development of creative ways for improving environmental monitoring and management. The IoT and environmental biosensors are converging to become a game-changing factor in this effort [1]. The IoT revolution, defined by the internet's penetration into previously unconnected spaces, has ushered in a new era of data collection, analysis, and decision-making in many fields. Because of its networked nature, it has the potential to revolutionize environmental research, where manual data gathering and sporadic sampling have long been the norm for keeping tabs on environmental factors in real time. When IoT devices are coupled with biosensors designed to interact with and detect biological factors, a whole new level of continuous, high-resolution data collection from the natural world becomes possible. These IoT-enabled biosensors, also known as environmental or biologically inspired sensors, keep an eye on the environment and report any real-time changes [2]. This study investigates the promising new direction in environmental monitoring and management by combining IoT technologies with biosensors. Our research digs into this merger's fundamental ideas, approaches, applications, and ramifications, illuminating how it can radically alter how we understand and engage with the natural world [3]. The IoT, combined with biosensors, has revolutionary potential in many environmental research and sustainability areas. Simply put, this convergence improves our ability to gather timely and precise information on environmental conditions, allowing for more effective, preemptive measures to be taken in the face of new dangers and the development of policies based on solid empirical evidence [4].

The infrequent nature of the conventional environmental monitoring techniques has meant that this has been inadequate. Periodic data gathering is used by many research institutions, government organizations, and companies, yet this method leaves important knowledge gaps about environmental dynamics. Biosensors powered by the IoT can monitor environmental variables in real time. This capacity becomes very important when dealing with environmental emergencies like natural disasters or industrial mishaps [5]. Early warning systems that can identify environmental abnormalities and dangerous circumstances in real time can potentially reduce the severity of catastrophes and safeguard human health. For instance, air quality monitors may send out warnings when unhealthy air is in the area, giving people time to take precautions and giving hospitals time to prepare for an uptick in respiratory infections [6]. Loss of habitat, warming temperatures, and pollution pose serious biodiversity problems. Biosensors powered by the IoT may help biodiversity conservation by tracking animal activity in the wild. Conservation efforts and methods may be improved with the knowledge gained by researchers on migratory patterns, reproductive habits, and responses to environmental changes [7]. Several sectors contribute to pollution and trash that might be harmful to ecosystems.

To ensure that businesses comply with environmental rules, biosensors powered by the IoT may be used to track pollutants in real time. This not only aids in environmental defense but also encourages environmentally responsible manufacturing [8]. Advanced data management and analytics solutions are required due to the enormous data output from IoT-driven biosensors. However, when properly used, this information equips decision-makers with knowledge of environmental patterns over the long term and guides the creation of policies meant to solve environmental concerns [9]. Researchers in environmental science may get a wealth of useful information from biosensors powered by the IoT. This plethora of data makes it easier to comprehend ecological processes, aids in detecting new research problems and quickens the rate of scientific progress. Connected biosensors powered by the IoT have the potential to raise awareness and inform the public about environmental concerns in real-time. This technology may be used by citizen science projects to get more people involved in environmental monitoring and study. This study, in summary, sets out on a voyage through the world of IoT-driven biosensors in environmental monitoring. It is a journey packed with promise, obstacles, and the possibility of profound change [10].

Related Work

In this day and age, it is critical to perform frequent environmental monitoring to assess the state of ecosystems, protect public health, and influence policy decisions. Recently, IoT-based biosensors and platforms such as Raspberry Pi have been developed, enabling for more precise, data-driven environmental monitoring. [11]. Biosensors based on the IoT have become an effective method of monitoring several environmental factors. Changes in air and water quality, pollution levels, and biodiversity indicators may all be detected with the help of these sensors, which use a wide range of identification processes (including chemical, biological, and auditory). These sensors' capacity for continuous, distant data collecting provides a detailed picture of the surrounding environment, allowing for the rapid identification of abnormalities and potential dangers [12]. Adding Raspberry Pi to IoT biosensors improves their performance. The Raspberry Pi acts as the network's brain, handling and transferring information in near-real time. To get more people involved in environmental monitoring, it also helps to provide user-friendly interfaces for data visualization and accessibility [13].

IoT-based biosensors have found widespread use in air quality monitoring. Particulate matter (PM2.5, PM10), carbon dioxide (CO2), nitrous oxides (NOx), volatile organic compounds (VOCs), and volatile gases may all be detected by these sensors. To determine the effects of air pollution on respiratory health and adopt preventative actions, constant air quality monitoring is essential for public health [14]. The safety of drinking water and the preservation of aquatic ecosystems highlight the need to monitor water quality. Heavy metals, organic pollutants, and changes in water pH and turbidity are only some of the contaminants that may be detected by biosensors built on the IoT. This information is helpful to better manage water resources and reduce pollution [15]. Using live microorganisms as sensors to detect pollution is a novel strategy. These biosensors change their behavior or metabolic activity when exposed to various contaminants. Timely actions to reduce pollution's negative effects and save aquatic life are made possible through quick responses. The existence, behavior, and population dynamics of species in different habitats may be better understood via biodiversity monitoring using auditory and visual recognition technology. This information is useful for biodiversity conservation and understanding climate change's ecological effects. Using Raspberry Pi and other IoT-based biosensors is an exciting step forward in environmental monitoring. To better safeguard public health and further scientific understanding, stakeholders may benefit from the convergence of data, biology, and technology. Creating such monitoring systems may fuel more effective environmental conservation and sustainability campaigns.

PROPOSED METHODOLOGY

Work model

Our long-term goal in developing IoT-based biosensors for environmental monitoring is to create a network of sensors that can continuously monitor their surroundings and respond to any changes they notice. Our strategy takes into account the creation and deployment of these biosensors, as well as their impact on public health and environmental safety across their entire lifecycle. Carbon monoxide (CO), nitrogen oxides (NOx), sulfur dioxide (SO2), volatile organic compounds (VOCs), and particulate matter (PM2.5, PM10) are just some of the gases and particles we hope to one day be able to detect and measure with our sensors. Gas-sensitive materials and electrochemical transducers are used in these detectors. The molecular recognition concept is at the heart of the air quality sensor's operation, with its constituent parts interacting selectively with the gases of interest. When these reactions occur, an electrical current or potential difference is created on the sensor's surface. The concentration of a target gas may be used to accurately calibrate these variations, allowing for very accurate environmental monitoring. The system developed a pollution sensor that mimics the function of naturally occurring microbes as a holistic approach to cleaning up polluted water sources. This sensor uses live microorganisms that provide distinctive signals in response to individual contaminants. There is clear evidence that these microbes' metabolic processes or behaviors alter when exposed to polluted water. Our pollution sensor detects the presence of different contaminants and provides crucial insights into water pollution levels by monitoring these biological reactions. The integration of sound sensors and picture identification software forms the backbone of our biodiversity sensor. This sensor

exemplifies how far biosensing technology has come in recent years. While image recognition algorithms evaluate visual data, acoustic sensors record ambient noise. The biodiversity sensor is a device that, when placed in natural environments, takes pictures of plants and animals and records their unique audio signatures. It may learn more about the existence of species, their activities, and the dynamics of their populations by evaluating these signals and photos, which in turn helps with conservation efforts. Our biosensors depend on wireless communication to deliver data on air and water quality, pollution levels, and markers of biodiversity once we have acquired this information. Our sensors transmit information to a centralized database or cloud-based platform through low-power, wide-area networks (LPWANs) or cellular networks. This wireless connection guarantees a steady data supply, allowing for continuous, real-time tracking. When it comes to the IoT, data security is of the utmost importance. It uses strong encryption and authentication methods to keep information secure and private while in transit. This guarantees the privacy and integrity of the information our biosensors capture as it travels from device to database. Our internet-enabled biosensors upload their data to a central database on the cloud. This database serves as a nerve center, collecting and organizing sensor information across various environments. This architecture ensures the security and availability of data. While raw sensor data is rich, it frequently needs significant processing before being used to conclude. This is when our data analytics algorithms come into play. These algorithms analyze data in real-time, spotting trends, outliers, and other irregularities that may indicate ecological danger. Our biosensors give decision-making help via continuous data analysis. It is crucial to make data accessible and easy to grasp for a large audience. It provides intuitive dashboards and other visual aids for our clients to help them do this.

Visualizing sensor data in charts, graphs, and maps, these tools help academics, policymakers, and the general public understand how the environment changes over time. Each monitored metric has predetermined thresholds that form the basis of our early warning systems. The scientific community and environmental regulators work together to set these limits. These are used as benchmarks against which sensor data in real-time may be evaluated. Our early warning systems are activated when sensor readings cross specified limits. Potential environmental concerns are identified, and the appropriate parties are notified through alerts. These warnings are very helpful for making prompt decisions and countering ecological dangers. Our guiding idea materializes as a sophisticated network of IoT-based biosensors that track real-time environmental metrics like pollution levels and biodiversity indices. The data is continually uploaded to a hub where it may be examined in real-time and shared with many people. It can respond quickly to new environmental risks by establishing clear thresholds and implementing early warning systems. It helps to preserve ecosystems and biodiversity, reduce pollution, and advance sustainability by monitoring and reacting to environmental changes and threats in real-time. Monitoring air and water quality in real time is important for public health because it gives local populations the information they need to take precautions against potential threats. Our biosensors create data useful for scientific investigation, enhancing our comprehension of environmental processes and adding to the corpus of knowledge. Using this information, policymakers and environmental agencies may make data-driven decisions that better protect the environment. Our IoT-based biosensors are designed to protect the environment, advancing science and improving public health as their guiding principles. The future of Earth and all its inhabitants may be made more secure and sustainable if It keeps an eye on and adapts to environmental changes in real-time.

Description

The gases and particles in the air directly affect human health and the environment, and our air quality sensor is a highly developed gadget designed to detect all of these contaminants. This sensor is based on molecular identification and works with gas-sensitive materials and electrochemical transducers. CO2, nitrogen oxides (NOx), sulfur dioxide (SO2), volatile organic compounds (VOCs), and particulate matter (PM2.5, PM10) all set off a targeted chemical reaction in the sensor. This reaction results in surface-level electrical current or potential changes, allowing for accurate air quality assessments. It allows us to track and react to changes in air quality and pollution levels, making our communities safer and more hospitable. The model is shown in Figure 1. The inherent recognition systems present in living creatures served as inspiration for our biomimetic water quality sensor. Heavy metals, organic pollutants, pH changes, and turbidity levels are only some contaminants that this sensor may detect. It is based on molecular recognition theory, which states that certain "recognition elements" may interact preferentially

with "target substances" in water. The sensor detects biological events triggered by this contact as changes in its electrical characteristics. These shifts may be measured, allowing for precise evaluations of water quality. This sensor will help us protect freshwater ecosystems, keep an eye on the purity of our drinking water, and react quickly to any new problems we may have with water quality. Our pollution sensor is a novel approach to the problem of water pollution. This sensor takes its cues from the capacities of naturally occurring microbes and uses them to detect the presence of very particular contaminants in water. These bacteria modify their metabolic processes or behavior in unique ways when exposed to polluted water. The sensor records these biological reactions, illuminating the prevalence and severity of pollution in water systems. The system can safeguard aquatic ecosystems and encourage regulatory steps to lower pollutant levels in water supplies if It knows where the pollution comes from and how often it occurs. Our biodiversity sensor fully displays a combination of sound sensors and picture recognition software. This sensor may be used in various environments to keep tabs on species' existence, behavior, and population dynamics. While image recognition algorithms evaluate visual data, acoustic sensors record ambient noise. The biodiversity sensor is placed in natural environments to record the sounds and photos of many animals. Examining these signs and pictures, the system learns about ecosystems' richness and vitality.

The data gathered by this sensor will help scientists, conservationists, and legislators choose where to focus their efforts to protect biodiversity. Raspberry Pi is a local data storage system that may be used to keep track of environmental data over time and to do long-term trend analysis. It may organize sensor data for later retrieval and use as a reference. Data redundancy and preservation may also be ensured by storing more information on the cloud or external storage devices. Since Raspberry Pi is so adaptable, it can be easily combined with weather monitoring systems like weather stations, remote webcams, and weather prediction services. Raspberry Pi improves the environmental monitoring ecosystem by compiling data from various sensors to provide a complete picture of the state of the world around us. Raspberry Pi is the brains of our IoT biosensors for monitoring the surrounding environment. It manages sensor data in real-time, allowing for advanced analytics, early warning systems, and intuitive user interfaces. The addition of Raspberry Pi improves the capabilities of our biosensors, making them a potent resource for data-driven decision-making, ecological safeguarding, and citizen participation in the fight for a more sustainable and resilient world.

RESULTS AND DISCUSSIONS

The technology has been extensively researched, with these sensors used in a range of ecosystems to improve environmental monitoring utilizing IoT-based biosensors coupled to Raspberry Pi. Our environmental monitoring effort generated the data presented in this section, which was rigorously examined to assess its importance. Our air quality monitors found significant air contaminants with surprising precision. Throughout the research, our sensors collected constant data on numerous gasses and particles. The sensors were capable of monitoring CO2 levels both inside and outside. CO2 levels vary according to human activity, ventilation, and environmental variables. The sensors precisely detected NOx and SO2 levels, revealing higher concentrations in urban and industrial areas. The device measured PM2.5 and PM10 concentrations constantly to assess the effects of air quality on respiratory health. There was a link between high PM levels and unfavorable health consequences, emphasizing the importance of addressing air quality issues. Many pollutants were detected by our biomimetic recognition-inspired water quality monitors. Some water sources were determined to have dangerous amounts of heavy metals such as lead, mercury, and cadmium, spurring more research into the core causes of pollution and potential solutions. Organic pollutants including pesticides and industrial chemicals were found in water samples by the sensors, highlighting the need for tougher controls and more sustainable farming practices. Changes in pH and turbidity have been recorded, which may have ramifications for aquatic ecosystems and necessitate specific management techniques. Using living bacteria as sensors, the system was able to gather critical information regarding contamination levels in water systems. The sensors monitored variations in microbial activity in order to identify pollution sources and direct cleanup activities. It was discovered that in reaction to pollution incidents, prompt steps were conducted, allowing for timely interventions to decrease ecological harm and protect aquatic life. Using sound and image recognition technologies,

our biodiversity sensors could accurately record species richness in their natural habitats. The sensors recorded the existence of several species, expanding our knowledge of the biodiversity in the area. Acoustic data showed distinct behavioral patterns of several species, providing insight into these hitherto unknown organisms' ecological functions and interconnections. Our sensors revealed information on population dynamics and the effects of environmental changes on biodiversity by monitoring long-term shifts in species abundance. Our sensors' ability to perform continuous monitoring enables them to identify environmental changes and potential dangers at an earlier stage. Data with a high resolution about the quality of the air and water, the levels of pollutants, and the biodiversity of an area might prompt actions, therefore averting or minimizing ecological harm and protecting human health. The example sensor data in Tables 1 and 2 comes from various environmental monitoring sensors and has been split up for easy reading. Environmental indicators include carbon monoxide and nitrogen oxides (NOx), lead and pH in water, and bird species diversity. The data consists of several dimensions: measurement units, sensor locations, timestamps, and values. Please keep in mind that the information below is only indicative.

The vast amounts of gathered data allow academics, environmental agencies, and lawmakers to make choices based on accurate information. Analysis of data collected in real-time makes it possible to implement adaptive management solutions, which in turn leads to environmental policies and actions that are more successful. Using our sensors encourages public participation in initiatives to monitor the environment. User-friendly interfaces hosted on Raspberry Pi make it possible for citizen scientists and local communities to access data collected by sensors. Through these interactions, knowledge is raised, environmental stewardship is encouraged, and collective action to safeguard natural resources is encouraged. The information collected by our biosensors contributes to advancing scientific knowledge and comprehending the processes that occur in the environment. Researchers can use this data to investigate the impacts of pollution, climate change, and human activity on ecosystems over the longer term. Our sensors show the necessity for management strategies tailored to individual ecosystems. The identification of diverse pollution sources and shifts in the pH of the water, for instance, highlights the need to develop individualized plans for various ecosystems. Monitoring the air quality in real-time, especially the levels of particulate matter and gaseous pollutants directly affects the general population's health. Informing the public and authorities about the risks of exposure and enabling timely preventive action is a potential outcome. Our IoT biosensors integrated with Raspberry Pi are revolutionary for tracking environmental conditions. In pursuing a more resilient and sustainable global future, our sensor data has great potential for enhancing decision-making, public involvement, and scientific development. This system protects our world and its people using data, biology, and technology.

CONCLUSION

Integrating IoT-based biosensors with Raspberry Pi to improve environmental monitoring offered significant insights as well as the potential for disruptive change. The outcomes of this study demonstrate how beneficial such sensors could be for real-time monitoring of environmental parameters such as air and water quality, pollution levels, and biodiversity markers. Sensor data enables us to make informed decisions, which speeds up the detection and response to environmental changes and dangers. Furthermore, the availability of real-time sensor data made accessible via user-friendly interfaces benefits both public participation and scientific knowledge advancement. The integration of technology, biology, and data will become increasingly crucial in preserving natural resources, defending public health, and protecting the environment as time goes on. Our journey will continue to commit to improving these monitoring systems, expanding the spatial coverage, and encouraging collaboration among many stakeholders. Finally, this effort contributes to the larger goal of creating a sustainable and resilient world for current and future generations.

REFERENCES

1. S. R. Shinde, A. H. Karode, and S. R. Suralkar, "Review on-IoT based environment monitoring system," International Journal of Electronics and Communication Engineering and Technology, vol. 8, no. 2, pp. 103-108, 2017.
2. M. N. Hassan, M. R. Islam, F. Faisal, F. H. Semantha, A. H. Siddique, and M. Hasan, "An IoT based environment monitoring system," in 3rd International Conference on Intelligent Sustainable Systems, pp. 1119-1124, 2020.
3. S. H. Kim, J. M. Jeong, M. T. Hwang, and C. S. Kang, "Development of an IoT-based atmospheric environment monitoring system," in International Conference on Information and Communication Technology Convergence, pp. 861-863, 2017.
4. S. L. Ullo, and G. R. Sinha, "Advances in smart environment monitoring systems using IoT and sensors," Sensors, vol. 20, no. 11, 2020.
5. G. Mois, S. Folea, and T. Sanislav, "Analysis of three IoT-based wireless sensors for environmental monitoring," IEEE Transactions on Instrumentation and Measurement, vol. 66, no. 8, pp. 2056-2064, 2017.
6. D. Assante, and C. Fornaro, "An educational IoT-based indoor environment monitoring system," in IEEE Global Engineering Education Conference, pp. 1475-1479, 2019.
7. S. Zafar, G. Miraj, R. Baloch, D. Murtaza, and K. Arshad, "An IoT based real-time environmental monitoring system using Arduino and cloud service," Engineering, Technology & Applied Science Research, vol. 8, no. 4, pp. 3238-3242, 2018.
8. S. K. Bhoi, S. K. Panda, K. K. Jena, K. S. Sahoo, N. Z. Jhanjhi, M. Masud, and S. Aljahdali, "IoT-EMS: An Internet of Things based environment monitoring system in volunteer computing environment," Intell. Autom. Soft Comput, vol. 32, no. 3, pp. 1493-1507, 2022.
9. D. Pujara, P. Kukreja, and S. Gajjar, "Design and Development of E-Sense: IoT based Environment Monitoring System," in IEEE Students Conference on Engineering & Systems, pp. 1-5, 2020.
10. Q. Yu, F. Xiong, and Y. Wang, "Integration of wireless sensor network and IoT for smart environment monitoring system," Journal of Interconnection Networks, vol. 22, 2022.
11. P. V. Vimal, and K. S. Shivaprakasha, "IoT based greenhouse environment monitoring and controlling system using Arduino platform," in International Conference on Intelligent Computing, Instrumentation and Control Technologies, pp. 1514-1519, 2017.
12. R. Shete, and S. Agrawal, "IoT based urban climate monitoring using Raspberry Pi," in International Conference on Communication and Signal Processing, pp. 2008-2012, 2016.
13. J. Shah, and B. Mishra, "IoT enabled environmental monitoring system for smart cities," in International Conference on Internet of Things and Applications, pp. 383-388, 2016.
14. L. I. U. Dan, C. Xin, H. Chongwei, and J. I. Liangliang, "Intelligent agriculture greenhouse environment monitoring system based on IoT technology," in International Conference on Intelligent Transportation, Big Data and Smart City, pp. 487-490, 2015.
15. S. H. Haji, and A. B. Sallow, "IoT for smart environment monitoring based on Python: a review," Asian Journal of Research in Computer Science, vol. 9, no. 1, pp. 57-70, 2021.

Table 1: Data

Parameter	Measurement Unit	Location	Time Stamp	Value
Air Quality (CO2)	ppm (parts per million)	Indoor	2023-09-01 09:00	400
Air Quality (CO2)	ppm	Indoor	2023-09-01 10:00	410
Air Quality (CO2)	ppm	Indoor	2023-09-01 11:00	415
Air Quality (NOx)	ppm	Outdoor	2023-09-01 09:00	20
Air Quality (NOx)	ppm	Outdoor	2023-09-01 10:00	22

Air Quality (NOx)	ppm	Outdoor	2023-09-01 11:00	25
Water Quality (Lead)	µg/L (micrograms per liter)	River	2023-09-01 09:00	5
Water Quality (Lead)	µg/L	River	2023-09-01 10:00	6
Water Quality (Lead)	µg/L	River	2023-09-01 11:00	7

Table 2: Diversity Data

Parameter	Measurement Unit	Location	Time Stamp	Value
Water Quality (pH)	pH	Lake	2023-09-01 09:00	7.2
Water Quality (pH)	pH	Lake	2023-09-01 10:00	7.1
Water Quality (pH)	pH	Lake	2023-09-01 11:00	7.0
Biodiversity (Birds)	Count	Forest	2023-09-01 09:00	25
Biodiversity (Birds)	Count	Forest	2023-09-01 10:00	30
Biodiversity (Birds)	Count	Forest	2023-09-01 11:00	27

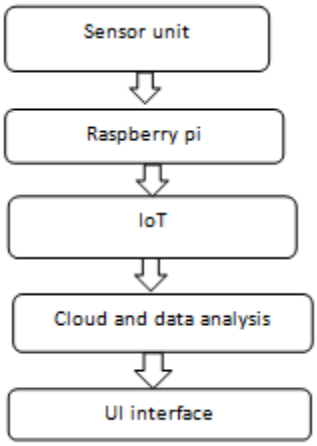

Fig1. Model of the system

RESEARCH ARTICLE

Diagnosis of Grape Leaf Disease using CNN

Kiruthika S[1*], Suriya K[2] and Pooja S[2]

[1]Assistant Professor, Department of Information Technology, Sri Ramakrishna College of Arts & Science, Coimbatore, Tamil Nadu, India.
[2]II MSc IT, Department of Information Technology, Sri Ramakrishna College of Arts & Science, Coimbatore, Tamil Nadu, India.

Received: 22 Feb 2024 Revised: 15 Mar 2024 Accepted: 21 Mar 2024

***Address for Correspondence**
Kiruthika S
Assistant Professor,
Department of Information Technology,
Sri Ramakrishna College of Arts & Science,
Coimbatore, Tamil Nadu, India.
Email: kiruthika@srcas.ac.in

ABSTRACT

Grape leaf diseases are a major problem for crops used in agriculture, leading to significant losses in terms of money and environmental damage. Early identification and control are essential to curb the spread of leaf diseases and lessen their detrimental impact on crop quality and production. However, accurately diagnosing leaf diseases and selecting the appropriate pesticide treatments can be challenging undertakings for farmers and agricultural professionals. The variety of diseases that can negatively impact vineyard productivity and overall stability in grapevines is a significant issue for the grape business. Timely identification and precise diagnosis are essential for minimizing monetary losses and safeguarding the vineyard environment. The research focuses on classifying images of grape leaves into several disease categories, providing a significant advancement towards sustainable vineyards and worldwide.

Keywords: Grape leaf, Deep Learning, CNN, Mobilenetv2

INTRODUCTION

A highly prized fruit in the agricultural industry, grapes can suffer from a number of diseases that negatively impact both its quality and productivity. Detecting and classifying diseases effectively is crucial to handling these problems. This work presents a novel machine learning method for disease classification in grape leaves [1]. The make use of a broad collection of high-resolution photos that include samples of both leaves in good condition and leaves afflicted with prevalent grape diseases like black rot, black measles, and downy mildew. It creates reliable and accurate illness

classification models by applying cutting-edge machine learning algorithms, such as Transfer Learning and ensemble methods, and sophisticated pre-processing techniques. The outcomes demonstrate these models' potential for useful application in grape vineyards and other agricultural contexts. The results of this study will have a big impact on the grape growing sector. Grape growers and vineyard managers can take use of automated and dependable disease diagnosis with the created machine learning models, which will allow them to quickly contain disease outbreaks and protect crop health.

IIRELATED WORK

To avoid large crop losses, crop diseases must be identified early and managed. Deep convolutional neural networks (CNN) were suggested by Nagi (2022) as a method for classifying grapevine leaf species. The CNN model can be utilised as a tool for automated species identification because it demonstrated great accuracy in distinguishing between several grapevine leaf species. In their 2020 study, Ghoury et al. sought to accomplish tasks with a transfer learning technique that uses pre-trained deep learning models, such as Faster R-CNN Inception v2 and Single SSD_Mobile Net v1, to discriminate between sick and healthy grapes and grape leaves. There were 136 healthy photos and 124 sick images in the image dataset that was used. Ghosh (2020) begins by segmenting the first affected area, extracting texture and colour information, then resizing them to the desired pixel. Data collection, image processing, and image segmentation were the processes that were put into practice. After that, these pictures go through a few pre-processing steps, like image scaling and image smoothing. After preprocessing the data, features in leaf images are extracted using techniques like RGB (color-based features). The names are then changed to categories for model compatibility, based on the photos' matching class. Eighty percent of the training data are used to model the classifier using neural network techniques. The model is validated using the remaining 20 percent of the data. A 92% accuracy rate was achieved with this strategy. Liu Y (2020) describes a convolutional neural network (CNN) based approach for classifying grape varieties based on leaf pictures. The scientists take information from leaf pictures and feed them into a CNN model to categorise different grape varietals.

METHODOLOGY

CONVOLUTIONAL NEURAL NETWORK

One kind of neural network used for processing and categorising images is called a convolutional neural network (CNN) [3]. They are made up of multiple layers, such as a fully connected layer, a pooling layer, and a convolutional layer. The network extracts elements like edges, corners, and textures from the input image in the convolutional layer by applying a series of filters on it.

Mobile Net

The initial architecture, known as Mobile Net, was unveiled in 2017. Its main objective was to create a neural network architecture that was small enough to operate well on mobile devices and still produce accurate results.

MobileNetV2

A neural network architecture called MobileNetV2 was created for effective deep learning on mobile and embedded platforms. It expands on the original Mobile Net architecture with the goal of increasing efficiency and accuracy

DATA COLLECTION & PRE-PROCESSING

INTRODUCTION

Any research endeavour, including the creation of an AI-based framework for the identification of leaf diseases, must include data collection. We used an existing dataset that we obtained from Kaggle for research. In order to acquire experimental data, an artificial environment simulating various crop disease conditions is created. In order to gather experimental data for this study, crops will be purposefully infected with a variety of illnesses, and the affected leaves will subsequently be photographed. The accuracy of the suggested based framework in diagnosing leaf diseases will be trained and validated using this data.

SPLITTING THE DATASET

The process of building a dataset for machine learning involves first using augmentation techniques [14], and then dividing it into three sections: training, validation, and testing sets. With 70% of the dataset being used for training, 20%forvalidation,and10%fortesting.The augmented photos in the training set are used to train the machine learning model, while the validation set is used to track the model's performance and make necessary parameter adjustments to increase accuracy. To make sure the model can generalise successfully and perform accurately on new data, the testing set is used to assess the trained model's ultimate performance on fresh, unknown data.

IMAGE PROCESSING

Using CNN methods and techniques, image processing in real-time dataset development entails extracting features and valuable information from images. The procedure includes capturing the image, pre-processing it, extracting features, and classifying the results. It may be used to detect crop illnesses, track crop development and production, and offer timely crop management advice. Farmers may enhance overall crop performance, maximise yield and quality, and make timely decisions about crop management by evaluating crop health and growth. A more profitable and sustainable agricultural business can result from the identification and mitigation of risks related to crop production through the use of image processing.

CLASSIFICATION OF THE LEAF DIASEASE

INTRODUCTION

Numerous diseases that damage grapevine leaves have been identified, which poses a serious challenge to grape production. The grape industry suffers large financial losses as a result of three common grape leaf pests and diseases: black rot, esca (black measles), and leaf blight (Isariopsis leaf spot). in order to stop the spread of illness and guarantee the grape industry's continuous expansion. Accurate detection and identification of illnesses affecting grape leaves are crucial. Figure: Grapevine leaves afflicted by illness Convolutional neural networks (CNNs) have demonstrated remarkable efficacy in image classification tasks; nevertheless, training them from the beginning necessitates substantial volumes of labelled data and can be computationally demanding. By using pre-trained CNN models that have picked up pertinent features from massive datasets, transfer learning has become a potent method for overcoming these difficulties. Transfer learning is the process of refining a pre-trained model—like a CNN—on a fresh dataset tailored to the current classification task after it has been trained on a sizable dataset, like Image Net. The pre-trained model's layer weights are changed during this fine-tuning procedure, which also entails training the model on the new dataset to enable it to acquire high classification accuracy for photos. Transfer learning greatly reduces the amount of data and computation needed to train an efficient image classification model by utilising the features learned by the pre-trained model.

TRANSFER LEANING

A pre-trained model is used as the basis for a new machine learning challenge in a process known as transfer learning [4]. A sizable dataset was used to train the pre-trained model, which taught it to identify pertinent features. Then, using a smaller dataset, these features can be used to tackle a new, related job. Transfer learning can increase the accuracy of the new model while saving time and computational resources by beginning with a pre-trained model. Back propagation, a technique, allows the pre-trained model to have its weights adjusted for the fresh dataset, allowing for further refinement. Natural language processing, picture categorization, and other machine learning fields have all seen a rise in the use of transfer learning.

MODEL 1 – MOBILENET MODEL

Google researchers created Mobile Net, a flexible convolutional neural network architecture designed for effective deep learning on embedded and mobile devices. Depth-wise separable convolutions, which Mobile Net uses instead of typical convolutional neural networks, greatly lessen the processing load. By making this design decision, Mobile Net is able to minimise the size and processing requirements of the model and still give attractive performance. Mobile Net is particularly well-suited for picture categorization, object recognition, and other computer vision applications on devices with limited resources because of its lightweight design. The fact that Mobile Net can

perform at the cutting edge of picture classification tasks while using less processing power than other deep learning models highlights the efficiency of this model. Its usefulness goes beyond mobile and embedded devices, as it can also be a vital instrument for real-time computer vision applications. This highlights the need of effective model construction in the context of artificial intelligence and deep learning.

MobileNetv2

Researchers at Google created the novel convolutional neural network architecture known as MobileNetV2, which is similar to Mobile Net. It is a noteworthy development in the field of deep learning, particularly in terms of the effective application of neural networks on embedded and mobile devices. The goal of MobileNetV2 was to improve the trade-off between model size and The adaptability of MobileNetV2 to various model configurations through the use of hyper parameters such as the width multiplier and resolution multiplier is one of its noteworthy features. By adjusting the width multiplier, users can balance the model's number of channels between accuracy and size. One example of the ongoing efforts to create effective neural networks is MobileNetV2. Convolutional neural networks (CNNs) of the Mobile Net class were made available as open-source software by Google, making them a great place to start for developing really small and incredibly quick classifiers. The number of multiply-accumulates (MACs), a measure of the number of fused multiplication and addition operations, determines the network's speed and power consumption. A family of Tensor Flow computer vision models called Mobile Nets is focused on mobile devices and is intended to optimize accuracy while taking into account the limited resources of embeddedoron-device applications. The number of multiply-accumulates (MACs), a measure of the number of fused multiplication and addition operations, determines the network's speed and power consumption. A family of Tensor Flow computer vision models called Mobile Nets is focused on mobile devices and is intended to optimise accuracy while taking into account the limited resources of embedded or on-device applications. Mobile Nets are low-power, low-latency models that are sized and configured to satisfy different use-cases' resource requirements. They can serve as a foundation for segmentation, embeddings, detection, and classification

Experimental Result

The model's accuracy on the training data set is referred to as training accuracy. The model is trained on a set of labelled photos during the training phase. The accuracy is determined by the number of images the model properly classifies. When analyzing how successfully the model is classifying the photos in the training set, one helpful measure to have is the training accuracy. It's crucial to remember, nevertheless, that a high training accuracy does not guarantee that the model will function effectively when exposed to fresh, untested images. The model's accuracy on a different validation data set is known as validation accuracy. A section of the training data set is usually reserved as a validation set throughout the training phase.

Comparative Analysis of Image Classification Model

Key performance indicators for assessing the effectiveness of an image classification model are training and validation accuracy [21]. As the model learns from the training data, training accuracy quantifies the model's accuracy throughout this phase. During the validation phase, when the model's capacity to generalise to new data is examined, validation accuracy quantifies the model's accuracy on the unseen data. With an accuracy of 98.92% of the four transfer learning algorithms examined, Mobilenetv2 demonstrated the best level of accuracy. However, assessing the models' overall performance is difficult in the absence of training accuracy data. poor training accuracy could mean that the model needs more training data or changes, whereas high training accuracy and poor validation accuracy could mean that the model is overfitting the training set. In conclusion, while assessing an image classification model's performance, it is important to take into account both training and validation accuracy. Even if a high validation accuracy is preferred, it's crucial to make sure the training data isn't being over fitted by the model. To ascertain the model's total performance, it is crucial to assess both training and validation accuracy. Mobile net mobile net v2

Accuracy

The metric quantifies the percentage of accurate classifications the model makes. Although it is a straightforward and simple statistic, it may be deceptive if the dataset is unbalanced, meaning that one type occurs substantially more frequently than the other.

Precision

The percentage of positive forecasts that come true is measured by this metric. This would refer to the percentage of leaf samples that are truly affected by the disease in the context of classifying grape leaf diseases. When the cost of false positives—that is, the prediction that a leaf has the illness when it does not—is high, precision becomes a valuable parameter.

CONCLUSION

When comparing the picture classification performance of the Mobile Net and MobileNetV2 models, MobileNetV2 has proven to perform better. Its superior computing power and efficiency overshadow Mobile Net, making it the go-to option for image classification applications. The extraordinary efficiency of MobileNetV2 is attributed to its architectural innovations, which include inverted residuals and efficient depth wise separable convolutions. These enable the network to deliver state-of-the-art results while spending fewer computational resources. This distinguishes MobileNetV2 as a unique model in the field of image categorization and demonstrates how well it strikes a balance between accuracy and efficiency. In order to effectively manage leaf diseases in agricultural crops, early detection and creative remedies are required. One potential solution to this issue is to integrate the use of frameworks such as MobileNetV2.Renowned for its remarkable precision and efficacy, MobileNetV2 has demonstrated its abilities in the field of image classification, rendering it a useful instrument for detecting leaf illnesses in farming crops and suggesting suitable remedies.

REFERENCES

1. X. -W. Chen and X. Lin, "Big Data Deep Learning: Challenges and Perspectives," in IEEE Access, vol. 2, pp. 514-525, 2014, doi: 10.1109/ACCESS.2014.2325029.
2. P. J. Werbos, "An overview of neural networks for control," in IEEE. Control Systems Magazine, vol. 11, no. 1, pp. 40-41, Jan. 1991, doi: 10.1109/37.103352.
3. Z. Li, F. Liu, W. Yang, S. Peng and J. Zhou, "A Survey of Convolutional Neural Networks: Analysis, Applications, and Prospects," in IEEE Transactions on Neural Networks and Learning Systems, vol. 33, no. 12, pp. 6999-7019, Dec. 2022, doi: 10.1109/TNNLS.2021.3084827.
4. F. Zhuang et al., "A Comprehensive Survey on Transfer Learning," in Proceedings, IEEE, vol.109, no1,pp.4376,Jan.2021,doi:10.1109/JPROC.2023.3004
5. M. Ravanelli, T. Parcollet and Y. Bengio, "The Pytorch-kaldi Speech Recognition Toolkit," ICASSP 2019 - 2019 IEEE International Conference on Acoustics, Speech and Signal Processing (ICASSP), Brighton, UK, 2019, pp. 6465-6469, Doi: 10.1109/ICASSP.2019.8683713.
6. Saleem, M.H., Potgieter, J. & Arif, K.M. Automation in Agriculture by Machine and Deep Learning Techniques: A Review of Recent Developments. Precision Agric 22, 2053–2091 (2021). https://doi.org/10.1007/s11119-021-09806-x
7. Poornima Singh Thakur, Pritee Khanna, Tanuja Sheorey, Aparajita Ojha: Trends in vision-based machine learning techniques for plant disease identification: Applications, Volume:208,2022,118117,ISSN09574174, https://doi.org/10.1016/j.eswa.2022.118117.58
8. Tawseef Ayoub Shaikh, Tabasum Rasool, Faisal Rasheed Lone, towards leveraging the role of machine learning and artificial intelligence in precision agriculture and smart farming, Computers and Electronics in Agriculture, Volume 198,2022,107119,ISSN01681699,https://doi.org/10.1016/j.compag.2022.107119.

9. Vol. 36 No. 11: IAAI-22, EAAI-22, AAAI-22 Special Programs and Special Track, Student Papers and Demonstrations.
10. Prasad, R. P., Gill, R., Gupta, V., Bordoloi, P., Ahmed, M., & Rao, R. K. (2022). Recent Advances in Agricultural Science and Technology for Sustainable India.
11. Danish Vasan, Mamoun Alazab, Sobia Wassan, Babak Safaei, Qin Zheng, Image-Based malware classification using ensemble of CNN architectures (IMCEC), Computers&Security,Volume:92,2020,101748,ISSN0167-4048,https://doi.org/10.1016/j.cose.2020.101748
12. Kumar, V., Sinha, D., Das, A.K. et al. An integrated rule-basedintrusion detection system: analysis on UNSW-NB15 data set and the real time online dataset. Cluster Compute 23, 1397–1418 (2020). https://doi.org/10.1007/s10586- 019-03008-x
13. Shorten, C., & Khoshgoftaar, T. M. (2019). A survey on image data augmentation for deep learning. Journal of big data, 6(1), 1-48.
14. K. M. Kahloot and P. Ekler, "Algorithmic Splitting: A Method for Dataset Preparation," in IEEE Access, vol. 9, pp. 125229-125237, 2021, Doi: 10.1109/ACCESS.2021.3110745.
15. K. Sampaguita and R. Poovendran, "A Survey on Mix Networks and Their Secure Applications," in Proceedings of the IEEE, vol. 94, no. 12, pp. 2142-2181, Dec.

Table1: Accuracy

Model	Precision	Recall	F1 Score
Mobile net	95.21	94.32	96.21
Mobilenetv2	98.21	98.34	98.67

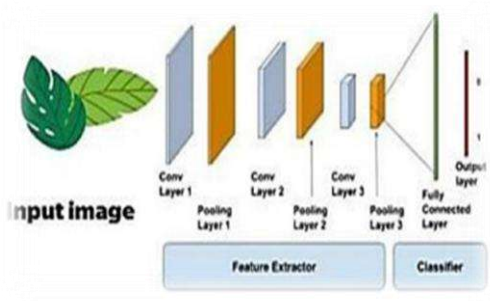

Fig:1 Leaf Patterns

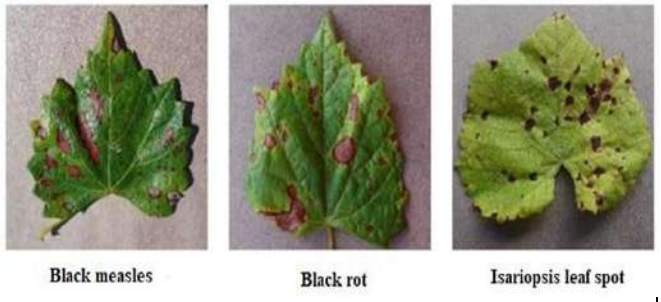

Fig 2: Diseases Affected Leaves

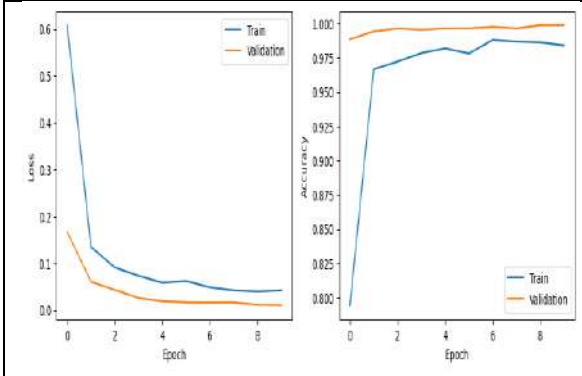

Figure 3 Validation Loss and Training Accuracy

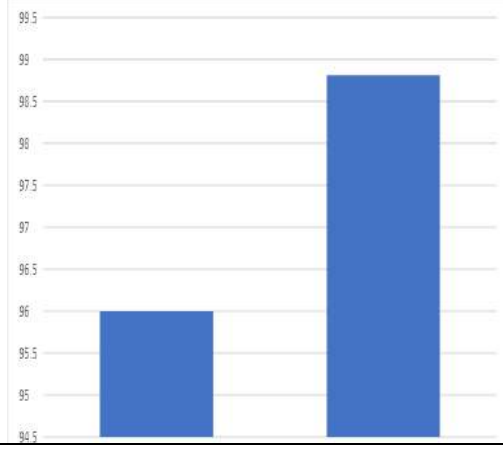

Graph:1 accuracy Computing

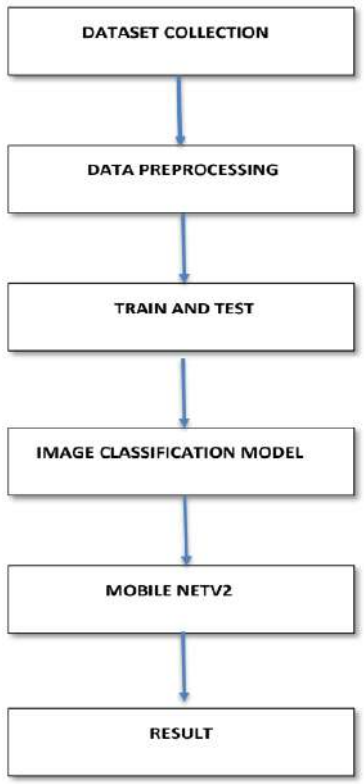

Fig :4 Workflow diagram

Indian Journal of Natural Sciences www.tnsroindia.org.in ©IJONS

Vol.15 / Issue 83 / Apr / 2024 *International Bimonthly (Print) – Open Access* *ISSN: 0976 – 0997*

RESEARCH ARTICLE

Study of Image Segmentation of Color Image by Various Methods

P. Vinoth, P. Karthick* and T.Brinthaguru

Department of Mathematics, School of Advanced Science Kalasalingam Academy of Research and Education, Krishnankoil-626 126, Virudhunagar, Tamil Nadu, India.

Received: 30 Jan 2024 Revised: 09 Feb 2024 Accepted: 27 Mar 2024

***Address for Correspondence**
P. Karthick
Department of Mathematics,
School of Advanced Science Kalasalingam Academy of Research and Education,
Krishnankoil-626 126,
Virudhunagar, Tamil Nadu, India.
Email:karthickphd91@gmail.com

ABSTRACT

Segmentation of images is critical for interpreting and evaluating items inside images. The procedure involves splitting and assessing images to convert them from vague to meaningful and helpful. This procedure is employed in a variety of disciplines, including medicine, culture, and industry. Image segmentation employs a wide range of functions, including edge and threshold functions. This dissertation will go through the color image segmentation strategies, present examples, and show the many sorts of images that may be used to find error ratio for better understand.

Keywords: Image segmentation, RGB image, Edge based method, Threshold method, Watershed method, Regionbased method, Clustering method.

INTRODUCTION

When it comes to the study and use of the picture, people are only interested in specific areas of it. These elementsare sometimes referred to as the target or foreground (the other element is referred to as the background); they typically match the image in a particular and distinctive way. To identify and evaluate the item, it must extract and separate them; only then will it be able to be used for the target in the future. We have introduced the "image engineering" idea to demonstrate the degree of picture segmentation in image processing. This concept brings together the various theories, techniques, algorithms, tools, and equipment involved in image segmentation into acohesive whole. Image engineering is a relatively recent topic of study and application for images. Image segmentation is the process of dividing a digital image into several parts. The goal of segmentation is to separate an image in to more representative sections. Much simpler to examine. These areas could match certain surfaces, items, object' natural components. Typically, borders and objects are located through the process of picture segmentation. Based on the color characteristic of image pixels, color image segmentation presumes that objects with consistent colors in the

image belong to distinct clusters and are therefore significant. Put otherwise, every cluster identifies a class of pixels that have comparable color characteristics.

RELATED WORK

Since there isn't a consensus on the optimum option for color space-based image segmentation, some study has attempted to determine which is the optimal color space for a particular assignment. There is no one color space that can produce segmentation results that are suitable for all types of photos since the segmentation results rely on the color space that is used. Because of this, numerous writers have attempted to identify the color space that will work best for their particular color image segmentation issue [1]. The color space, which enables the geometrical representation of colors in 2D and 3D space, is a mathematical representation of colors. Each pixel in an image can have its color information provided via color spaces. Color spaces provide helpful information on the appearance of the color spectrum, as seen in [2]. The fusion of color models and mapping functions is called color space. Each image has a set of intensity values, and noise might arise from arbitrary changes to these values. Typical noises include impulse noise, salt and pepper noise, and so on. Noise can lead to challenges in efficiently detecting edges; thus, image must be filtered to lower noise content that causes edge strength to be lost [3] Another name forits smoothing. Enhancement is the process of making an image better. Its goal is to create an image that is superiorto the original and more appropriate. To improve the image's edge quality, a filter is used.

Here, morphologically-based image segmentation technique has been enhanced Under the complicated backdrop, image segmentation processing for wind turbine blades is done using a canny operator. Applying morphology to improve Canny operator's image segmentation method after Canny operator edge detection, the binary image is morphologically treated to eliminate redundant edge information, in contrast to the single image segmentation technique [4]. The phase of defining markers can be omitted during the watershed flooding change when a multi-scale approach andregion merging are used. We begin by computing the mean of each color class in the image to create an energy image. Deng introduces this criterion, which is known Automatic breast cancer diagnosis based on k-means clustering and adaptive thresholding hybrid segmentation [6]. It uses a texture discontinuity -based method to identify homogeneous areas in a picture. Every pixel in the complete image can have its measure computed. All colors are regarded as classes in the original Deng's version, and the color information is only utilized in a pre- processing quantization phase. The number of clusters must be known in advance for the k-means and fuzzy c- means algorithm and the user must provide the six parameters for the isolate algorithm [6].

Narayanamoorthy et all [11],[12] constructs, the new approach, which is based on the k-means algorithm, incorporates a validity metric based on the intra-cluster and inter-cluster distance measurements to get beyond the requirement of indicating the number of clusters. Furthermore, a slide prepared outside of normal protocol may result in under- or over-stainingof the slide. Sharma et all, [7] Based on these justifications, the current study will make use of the color image segmentation approach's capability by utilizing a variety of color models and the k-means clustering technique to produce the fully segmented image. Future study will concentrate on real-time segmentation and classification with the aid of more effective methods like ensemble learning and deep learning. Furthermore, we think that it will improve the efficacy and precision of algorithms used in object identification and image classification systems. In this paper [8] The collected results in dictated a noteworthy improvement in segmentation performance. The suggested approach may be helpful for color segmentation of images. In 2013 [9] represents, there are a few shortcomings with our suggested approach. The majority of the image models that are utilized are predicated on certain a priori information, such as the standard deviation and mean of each segmented image region. Furthermore, we have only taken into account a single image for every application in our work, even though the segmentation process may benefit greatly from many realizations of the same image fused together. This is because the validity score is significantly impacted by the much larger inter-cl user distance. [10] To get around this, first locate the validity measure's local maximum. Next, locate the value that is the minimum after the local maximum. The least number of clusters that can be chosen using this modified rule is four. This isn't really an issue because pictures in natural color.

Proposed Methodology of Color Image Segmentation

In digital image processing and analysis, image segmentation is a commonly used technique for dividing animage into many parts or sections, usually based on the characteristics of the individual pixels in the image.categories for segmenting images There are various techniques for segmenting photos, including

1. Threshold Approach
2. Method based on region
3. Method based on edges
4. The watershed-based approach
5. A approach based on clustering

The RGB color space, which is the most often used color space, is defined by the three color components of the corresponding pixel, which are blue (B), green (G), and red (R).The color spaces were divided into the following groups. The real RGB, subtractive CMY, and imaginary XYZ primary spaces are the main spaces that are based on the theory that suggests it is feasible to match any color by mixing an approximate proportion of the three primary colors. The process of changing RGB to CMY is

$C' = 1 - R$	$C = min(1, max(0, C' - K'))$
$M' = 1 - G$	$M = min(1, max(0, M' - K'))$
$Y' = 1 - B4$	$Y = min(1, max(0, Y' - K'))$

$K' = min(C', M', Y')$

Segmentation based on threshold

Using this method, original photos can be converted to binary images. Pixels are compared to a preset threshold value in order to achieve this. pixels less than or equal to this value will be allocated 0 (white); pixels larger than this value will be assigned 1 (black). The following are the steps in the algorithm:

1. Read an image as input.
2. Make new variables in two dimensions and assign the picture size to them.
3. Type in the threshold amount.
4. Construct a fresh zeros matrix that has the same measurements as the picture.
5. Align the pixels with the threshold amount.
6. Display the outcomes.

We must jot down the elements in the new image if we need to split them up.

Step 1: Use an input image

Step 2: Make this picture grayscale. Step

Step 3: Give the value for the threshold.

Step 4: Only display pixels that are larger than the threshold.

Segmentation based on edges

This technique uses intensity-level (grayscale) detection to extract object information. One of the methods most frequently used to analyse photos is edge detection. The edge method determines the features of the edges by comparing colors. These details are displayed as black backgrounds with white lines. There are numerous approaches for filtering

- Sobel filters
- Prewitt filter
- Robert's filter
- Log filter

- zero-cross screening.

The variable in the image and the procedure are the two parameters of this function (the Edge function).
The algorithm's steps are as follows:

1. Examine a picture.
2. Apply any of the aforementioned filters along with the edge function.
3. Make the image visible

Segmentation of watersheds

When splitting items that are in contact with one another, watersheds offer a free object-splitting method that is quite helpful. Images are interpreted by this technique as physiological surfaces, whose elevation is represented by the value of f (x, y). The watershed algorithm locates the hill lines and watershed basins in the picture where water would presumably accumulate in theory. Assume that each regional low point has a perforated hole, and that water rises through these holes at a constant rate, submerging the natural terrain below. As the water level rises, pixels are designated as submerged. Water will the entire image gets split into distinct collection basins as the flood goes on.

This algorithm's steps are as follows:

Step1: Read an image.
Step 2: Remove the black border before processing.
Step3: Modify the region within the watershed.
Step4:Calculate the Lesion Ratio.
Step5: Combine watershed regions.
Step 6: Define the boundaries of watersheds.
Step 7: Smooth borders (b-spline smoothing and border sampling).
Step 8: Add a border overlay

Segmentation based on clustering

In data mining, clustering is an undirected technique that helps find multiple latent patterns in the data without generating a specific hypothesis. The goal of clustering is to find commonalities amongst individual objects and create a collection of related ones. Hierarchical and non-hierarchical clustering techniques are the two forms of clustering. Non-classical Grouping This approach divides the dataset into M clusters, each having N items. K-means is the most used non-hierarchical clustering method in business intelligence. Grouping in Hierarchies This process results in a collection of nested clusters. Every pair of objects in these nested clusters is further nested to create alarger cluster until, at the end, only one cluster is left. K stands for Clustering Technique. K-means clustering is an unsupervised method that uses the input data without a labeled response. One popular method for clustering is K-means clustering. Typically, practitioners first, familiarize yourself with the architecture of the dataset. K-means is used to cluster data points into discrete, non-overlapping groups.

RESULTS AND DISCUSSIONS

A set of photos and a few commonly used algorithms from the literature are used to gauge how well the recommended algorithm is implemented. Real photos are utilized for performance estimation and comparisons, when the item can be precisely separated from the background using a suitable threshold technique. The illustrations can be found in figures 1–5. Each figure displayed the following: (a) the original image; (b) the original image's histogram; (c) the threshold image; (d) the edge-based image; (f) the watershed image; and (e) the K mean. clustering technique for segmenting images.

Ratio of Error (ER)

The most important comparative indicator is the error ratio (ER). ER is the ratio of pixels in the erroneous area

between the object pixels and the optimal threshold image produced by each approach. incorrect segmentation as indicated by the formula below,

$$E_{R=\frac{N_r+}{N_r}} \times 100$$

where NR is the number of pixels in the segmented pictures and Nm is and Nr are the number of segmentation pixels in the erroneous area. In this sense, the ER value is a number between 0 and 100; a value of 0 indicates that there is no similarity between the segmentation result and the ground truth image. A excellent segmentation result is likewise indicated by a value of 100. The error shows the numerical numbers that, in each instance, correspond to how comparable the edge-based approach and the watershed method (k means clustering method) are. Next, we select the best error ratio number from a range of values. The lowest error value has been seen on bold type. Note that in each and everyinstance.

CONCLUSION

Image segmentation algorithms are able to convert indistinct photos into ones that are interpretable enough to extract important information, especially in the medical field. This study looked at the performance and error rate of a few MATLAB-based hashing algorithms. It is important to note that not all of the photos we utilized haditems detected by these techniques. On the other hand, low-density pixels or photos with poor color density weresimply analysed. An efficient evaluation of uniformity was not possible. To find the most efficient picture segmentation system, researchers must keep applying deep learning techniques.

REFERENCES

1. Dina Khattab, Hala Mousher Ebied, Ashraf Saad Hussein, and Mohamed Fahmy Tolba (2014), Color ImageSegmentation Based on Different Color space Models Using Automatic Grabcut, The Scientific World Journal. https://doi.org/10.1155/2014/126025.
2. Raval, Khushbu and Shukla, Ravi and Shah, Ankit K and Eur. J. Adv. Eng. Technol (2017), Color image segmentation using FCM clustering technique in RGB L* a* b, HSV, YIQ color spaces https://www.researchgate.net/publication/316961754.
3. Dhankhar, Poonam and Sahu and Neha (2013), A review and research of edge detection techniques for image segmentation, International Journal of Computer Science and Mobile Computing. V2I7201329.pdf (ijcsmc.com).
4. Xu, Hongyun and Xu, Xiaoli and Zuo and Yunbo(2019), Applying morphology to improve Canny operator's image
5. segmentation method, The Journal of Engineering.DO - 10.1049/joe.2018.9113.
6. Richard, No¨el and Fernandez Maloigne, Christine, Bonanomi, Cristian and Rizzi, Alessandro and others, (2013) Automatic breast cancer diagnosis based on k-means clustering and adaptive thresholding hybrid segmentation, Journal of Image and Graphics. https://doi.org/10.1007/978-3-642-23154-4_33.
7. Ray, Siddheswar and Turi, Rose H (1999). Determination of number of clusters in k-means clustering and application in colour image segmentation. Proceedings of the 4th international conference on advances in patternrecognition and digital techniques. https://api.semanticscholar.org/CorpusID:15643818.
8. Sharma, Nikita and Mishra, Mahendra and Shrivastava, Manish (2012). Colour image segmentation techniques and issues: an approach, International Journal of Scientific and Technology Research. https://api.semanticscholar.org/CorpusID:18504657.
9. Ahammed, Mostafiz and Al Mamun, Md and Uddin, Mohammad Shorif (2022) A machine learning approach for skin disease detection and classification using image segmentation, Healthcare Analytics. https://doi.org/10.1016/j.health.2022.100122.
10. Abdul-Nasir, Aimi Salihah and Mashor, Mohd Yusoff and Mohamed, Zeehaida (2013), Colour image

segmentation approach for detection of malaria parasites using vari and k-means clustering. WSEAS Trans. Biol. Biomed. https://api.semanticscholar.org/CorpusID:15421700.

11. P Karthick, SA Mohiuddine, K Tamilvanan, S Narayanamoorthy, S Maheswari (2023). Investigations of color imagesegmentation based on connectivity measure, shape priority and normalized fuzzy graph cut. Applied Soft Computing. https://doi.org/10.1016/j.asoc.2023.110239.
12. Narayanamoorthy S and Karthick P (2017) The intuitionistic fuzzy set approach for gray level image thresholding using normalized graph cuts, International journal of Pure and Applied Mathematics.https://ijfs.usb.ac.ir/article_4481_7b4f724471207.
13. Narayanamoorthy S and Karthick P (2019) A Comparative Performance of Gray levelimage Thresholding using normalized cut graph cut based stsndard S membership function. Iranian Journal of Fuzzy Systems.10.22111/IJFS.2019.4481.

Table 1: Error Ratio

Images	Threshold Method		Error Ratio (with%)		
	Original Image pixel	Optimum Image Pixel	Edge Based Method	K means Clustered Method	Watershed Method
Fox.jpg	1,998,000	666,000	28.8%	25.3%	**10.2%**
Parrot.jpg	2,281,248	760,416	13.65%	**8.9%**	9.2%
Sunflower.jpg	817,920	272,640	8.1%	**6.5%**	18.5%

Figure 1: Image Segmentation Comparison for Fox Image (a) Original Image

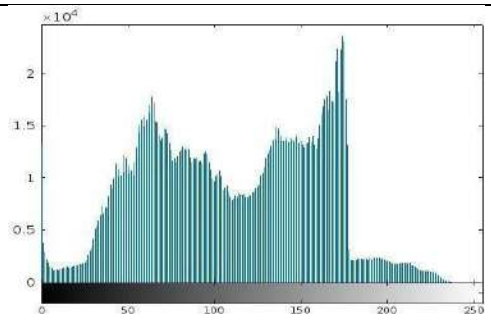

Figure 1: (b) Histogram of the Original Image

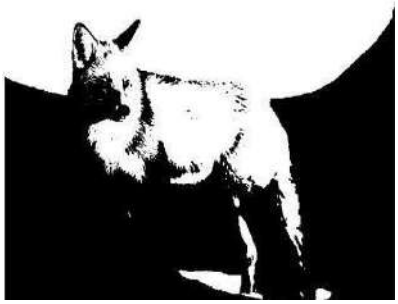

Figure 1: (c) Threshold Image

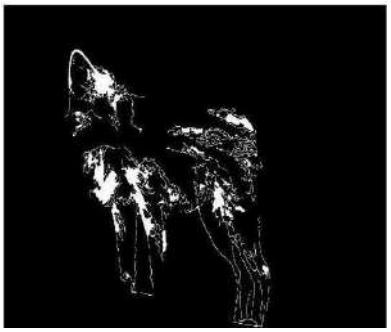

Figure 1: (d) Edge based Image

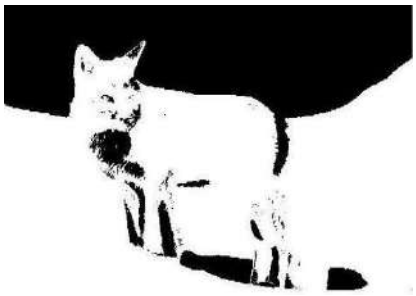

Figure 1: (e) K means Clustered Image

Figure 1: (f) Watershed Image

Figure 2: Image Segmentation Comparison for Parrot Image (a) Original Image

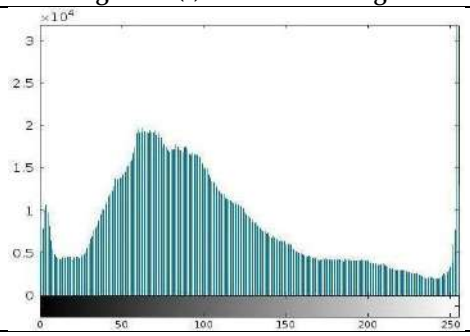

Figure 2: (b) Histogram of the Original Image

Figure 2: (c) Threshold Image

Figure 2: (d) Edge based Image

Figure 2: (e)K means Clustered Image

Figure 2: (f) Watershed Image

Figure 3: Image Segmentation Comparison for Sunflower (a) Original Image

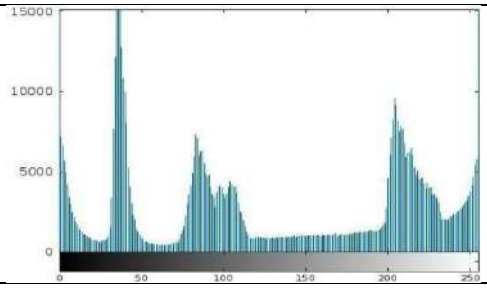

Figure 3: (b) Histogram of the Original Image

Figure 3: (c) Threshold Image

Figure 3: (d) Edge based Image

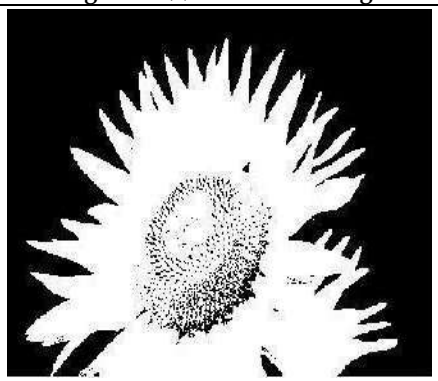

Figure 3: (e) K means Watershed Image

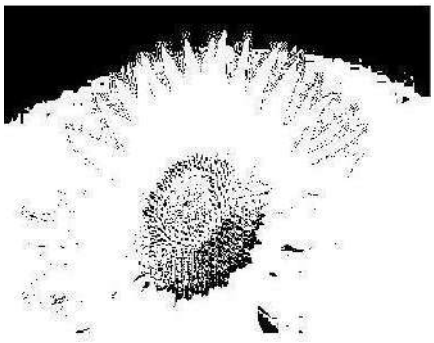

Figure 3: (f) Watershed Image

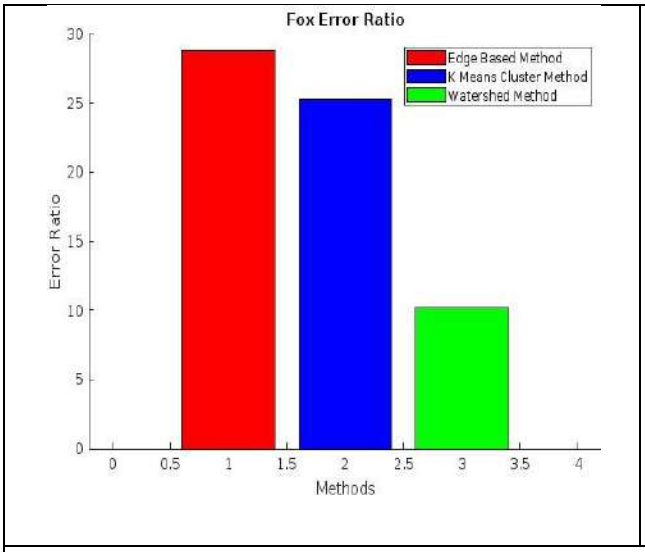
Fox Error Ratio
Edge Based Method
K Means Cluster Method
Watershed Method
Error Ratio
Methods

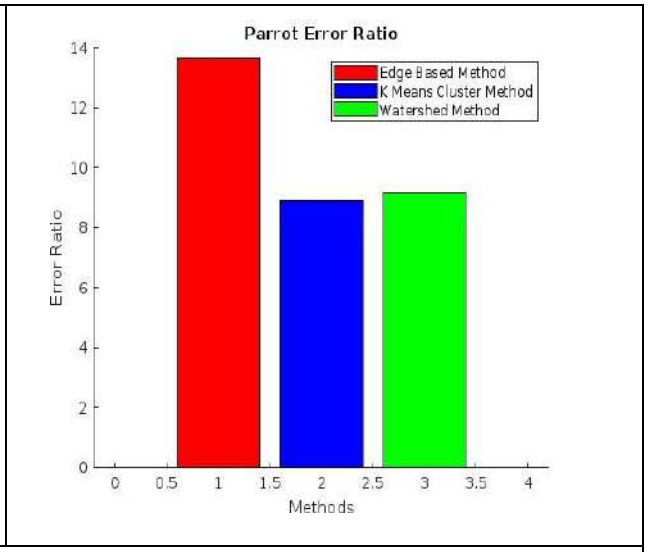
Parrot Error Ratio
Edge Based Method
K Means Cluster Method
Watershed Method
Error Ratio
Methods

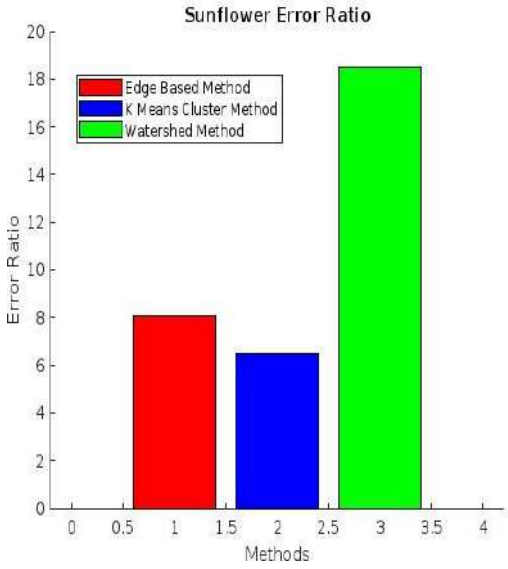
Sunflower Error Ratio
Edge Based Method
K Means Cluster Method
Watershed Method
Error Ratio
Methods

Vol.15 / Issue 83 / Apr / 2024 International Bimonthly (Print) – Open Access ISSN: 0976 – 0997

RESEARCH ARTICLE

Memory Mate: A Mobile Application for Empowering Alzheimer's Patients

M.Sridhar[1]* and R.Sankaran[2]

[1]Assistant Professor, Department of Information Technology, Sri Ramakrishna College of Arts & Science, Coimbatore, Tamil Nadu, India.
[2]PG Student, Department of Information Technology, Sri Ramakrishna College of Arts & Science, Coimbatore, Tamil Nadu, India.

Received: 22 Feb 2024 Revised: 15 Mar 2024 Accepted: 21 Mar 2024

***Address for Correspondence**
M.Sridhar
Assistant Professor,
Department of Information Technology,
Sri Ramakrishna College of Arts & Science,
Coimbatore, Tamil Nadu, India.
Email: sridhar@srcas.ac.in

ABSTRACT

A constant clinical decline over several years is an indication of Alzheimer's disease. It impairs daily task performance and induces memory loss. Memory problems can make it difficult to recall names, faces, locations, or other details of people. Thus, the purpose of our study is to support the continued independence and social participation of individuals with moderate (the initial stages) and intermediate (middle-stage) Alzheimer's disease. We propose an Android app that uses facial recognition and position detection from Google Maps. The paper aims to improve users' ability to perform daily tasks and to enhance ordinary communication by integrating a notification element. By tracking their movements and prevents them from becoming lost, the Global Positioning System (GPS) detection feature helps keep dementia patients safe. The application has consistently assisted persons with signs of Alzheimer's and significantly enhanced their quality of life, according to the results. Therefore, our findings highlights the need of utilising artificial intelligence (AI)-based features—such as facial recognition in this case—when developing healthcare applications that could significantly impact society.

Keywords: Face recognition, Alzheimer's illness, smartphone applications and Machine learning

INTRODUCTION

The fact that aging is a recognized risk factor for Alzheimer's disease and that more people will likely develop the illness as the population ages, the disease is becoming a growing public health problem. It primarily affects the elderly, some experts refer to it as the "century disease." Simple daily activities like eating and cleaning their teeth

might be difficult for those who have Alzheimer's. Alzheimer's disease is a severe, long-term brain illness that starts with memory loss and progresses to planning, thinking, language, concentration, and cognition problems. Therefore, the goal of this application was to help families and patients with Alzheimer's disease live better lives by developing a smartphone application that uses face recognition technology to enable machine learning. Nowadays, face recognition is being used in many real-world applications, from personal to public security. It is employed to confirm someone's identify or to locate and follow a potential suspect in a crowd. Globally, Alzheimer's disease is becoming a more significant problem for individuals, their households, and healthcare systems due to its relentless and debilitating nature. Alzheimer's disease is becoming more common as the world's population ages, necessitating the development of creative solutions to improve the condition of those who are afflicted and assist those who are caring for them. In the current digital era, smartphone apps have become extremely effective resources for managing the particular requirements and difficulties related to Alzheimer's care. This study uses the features of the Android framework to construct a care application specifically for patients with Alzheimer's disease. This causes people to lose their independence, memory, and cognitive function, which makes it harder to carry out daily chores and activities.With compassion and knowledge, the suggested application aims to close this gap by offering a feature-rich package catered to the unique requirements of Alzheimer's sufferers and their carer givers. Because of its adaptability and cross-platform interoperability, Android is a great platform for developing applications that are simple to use and intuitive for users. The application's seamless functioning on both iOS and Android devices guarantees its universal accessibility and makes it easier for individuals with Alzheimer's disease and those who provide care for them to use. This introduction chapter establishes the background against which we will examine the development of this essential care application. Examine the unique challenges faced by dementia patients and their carer givers, with a focus on how mobile technology might be able to alleviate some of these challenges. The study's main objective is to assist individuals with Alzheimer's disease who are in the early or middle stages of the illness by providing them with a tracking system, daily task reminders, social engagement opportunities, and increased confidence in their ability to remember each member of their family. The proposed application could help all mild-to-moderate Alzheimer's sufferers and their careers by developing an application with features like machine learning-driven facial recognition. This helps the patient's close friends and family remember things and provides them with a smart GPS tracking device that can be used to help carers find the patient. The intended use aims to improve the standards of life for individuals with Alzheimer's disease by simplifying their lives and people around them.

LITERATURE SURVEY

Widely used to describe a range of conditions, the term "dementia" is most frequently linked to impairments in language, recall, cognition, and problem-solving abilities. One's capacity to carry out regular tasks is thereby compromised. Alzheimer's disease is the most common form of dementia, and its incidence has been rising in recent years. Research is increasingly demonstrating that advancements in technology have a major impact on individuals with Alzheimer's disease, especially during the early stages of the illness. Algorithms and intelligent devices can help ease some of the challenges dementia patients and caretakers frequently encounter when providing supportive care. Today, the GPS is a widely used global navigation device. It was initially developed by the US United States Department of Defence (USDOD) utilising signals from satellites. The system consists of a minimum of 24 satellites. Since there are no installation or subscription costs, it is a very versatile and reasonably priced instrument that can be used in any weather and anywhere in the world. The satellites were first put into orbit by the USDOD solely for military purposes, but in the 1980s, these were extended to include public coverage as well. GPS allows for the precise location of latitude and longitude coordinates at ground level. The method is calculating and determining the current location by examining the differences in timing between signals coming from thirty satellites that are under the management of USDOD and numerous commercial organisations. It has also been demonstrated to be a successful method for resolving problems with outdoor localization because GPS signals typically demand an unbroken receiver-satellite line-of-sight (LOS) channel. Automatic facial recognition is one of the key advancements impacting biometrics technology, artificial intelligence, and machine learning. Their effect has mostly been attributed to their broad range of potential applications and the current focus on them by the scientific community. In essence, facial recognition devices

are two pieces of technology that do two main jobs: they identify the individual whose picture or video is used to confirm their identity, and they also identify the individual. In recent years, they have been employed as a means of controlling access in security systems. Because of this and the variety of uses they have, these systems have become the focus of numerous studies. The idea of machine learning was largely inspired by research into the interactions and communication that occurs between brain nerve cells through excitable neural activity. Since then, the popularity of machine learning models has grown, in part due to their problem-solving abilities. In more recent times, they have contributed to a number of very important technological developments. One of the primary objectives in the field of machine learning is to create computer systems that can learn from experience and develop on their own. As a result, AI machine learning has emerged as the preferred option for software developers operating in numerous domains, such as computer vision, facial recognition, natural language processing, robotics control, and numerous others. Consequently, machine learning is used to address each of the crucial phases of the recognition of faces process. This entails considering a variety of elements, such as the fact that faces are not just a collection of pixel-by-pixel images but rather have a distinct structure and symmetry. These systems can analyse sample facial photos that are kept in databases, capturing their distinct pattern features and cross-referencing them with particular images that are kept. The Facial Identification Grand Challenge was first introduced in 2006 to determine whether face recognition systems based on models developed using machine learning were accomplishing their stated goals.

PROPOSED SYSTEM

The technique in this paper was developed specifically to achieve its objective. Thus, the phases that are involved include data collection, database design, application interface design, implementation, and testing. For the purpose of this study, a web-based questionnaire was designed and disseminated to gather information from the main demographic targeted for this application—those who provide care for people with Alzheimer's disease. The questionnaire was designed to collect data regarding technology support services available to relatives and individuals suffering from Alzheimer's disease. The survey was created using Google Forms. The functional requirements list the tasks that a system has to be able to perform. They essentially outline the proper way for a system to function in specific scenarios. The application should display a list of related photos along with background information regarding each image's relationship to the patient. The patient should receive alerts and reminders from the app about important tasks that need to be finished. The application should notify the patient's carer whenever an indication from the surveillance bracelet shows that the individual has outside a designated safe zone. Non-functional requirements specify the performance limitations and the criteria using which the system will be assessed. The non-functional needs of performance and usability are crucial. The architecture shows how the needs and the created system align. Two separate architectural portions serve both the client and the care giver. The application has user interface components for adding, editing, and comparing pictures from the patient's perspective. The pictures are kept inside a central database that is accessible by other sections. Carers can add photos, compare photos, specify and monitor the location, and set reminders with this application. The design step streamlines the process by taking the requirements from the evaluation phase and putting them into an architectural chart. This graphical representation includes information on the necessary components and how they interact. Furthermore, this phase solves the problem of how to design the best potential answer with the aid of prototype development. Therefore, the primary goal of the designing phase is to facilitate the development of an interface that allows the systems to function as intended across the board. When a fresh model or a modified version of a previous one is being developed, an early sample or early model is called a working model in the realm of software development.

RESULTS AND DISCUSSION

The Memory Mate program's results show that it can identify people by looking through an album that has categorised each person by face and displayed information about their relationship. When it comes to ensuring that users can take full advantage of an application's capabilities and make money from it, its usability is paramount. An exploratory survey with one hundred users helped determine how useful this programme is. Users were required to

utilise the application before being given a series of questions to respond to in order to get input on different usability-related issues. The questionnaire items that were utilised to evaluate the usefulness were based on the McLaughlin and Skinner principles. The process of usability testing produced the following results:

1. Alzheimer's Assistant has a validation system in place to ensure that data is accurate.
2. Users are confident in their capacity to use it and believe it to be effective.
3. Users claim to be able to operate the system, particularly when supplying or extracting data.
4. The application is easy to use; it is believed to be a quick and effective system.
5. The information it produces is easy to understand.

CONCLUSION

An app called Alzheimer Assistant was created especially to support those who have Alzheimer's disease. It can send patients notifications to remind them of daily tasks; this can help detect individuals by relating to a record in which every individual has been categorised through face and his connection information displayed; and it can give patients a GPS bracelet to ensure their family can find them precisely in the event that they get lost. Consequently, this programme helps people with Alzheimer's disease feel more confident when going about their everyday lives, which improves their ability to routinely go to social events. The ability of this application to assist families and care givers has been extensively demonstrated. The application's primary flaw prevents carers from remotely monitoring patients, which prevents the Alzheimer's Patients Association from formally endorsing it. The usefulness of the application would therefore be improved by creating and implementing this new feature, which would be included in later releases. Future research projects will focus on deep learning algorithms for facial recognition because of their significant impact in this field and their capacity to provide outcomes with superhuman performance and accuracy. The suite of software tools previously available to assist individuals with Alzheimer's disease in preserving social connections with their loved ones is enhanced by the Alzheimer Assistant app.

REFERENCES

1. Juliana Paola Medina Figueredo, Application for the Support of Family Care of Patients with Alzheimer's. (2016).
2. (2018). Santiago Guillen Paredes, Design and Implementation of a Mobile Application to Help People with Alzheimer's Technological University of Peru Software Engineering,
3. (2017).Anonymous, Alzheimer's Disease: Facts and Figures.
4. (2009). Prensa, 10% of the Older Adult Population Suffers From Alzheimer's. [Online].
5. J. Luis and M. Peña, ICT Innovation Capabilities and Opportunities for Alzheimer's, ICT Innovation Capabilities and Opportunities for Alzheimer's. (2021).
6. F. Cuevas, Geolocation Based on GPS Technologies for People with Alzheimer's Disease. (2018).

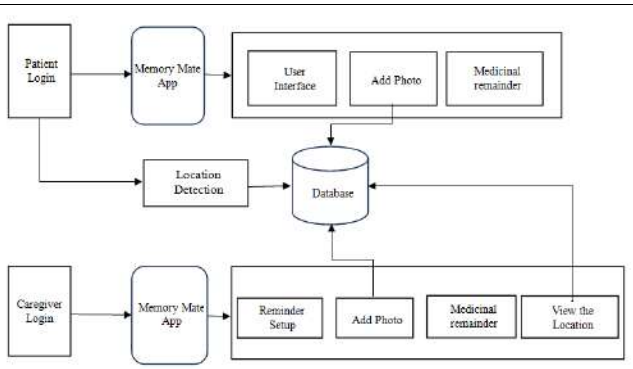

Figure 1: Architecture Design of the Application

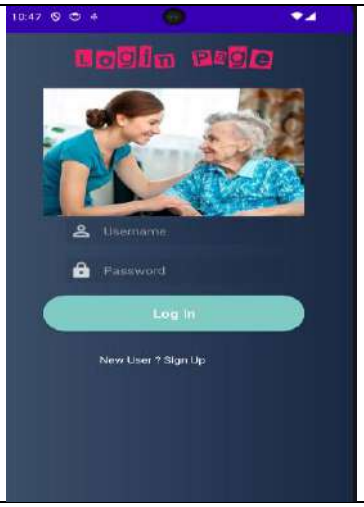

Figure 2: Login page

Figure 3: Registration page

Figure 4: Main page and Remainder

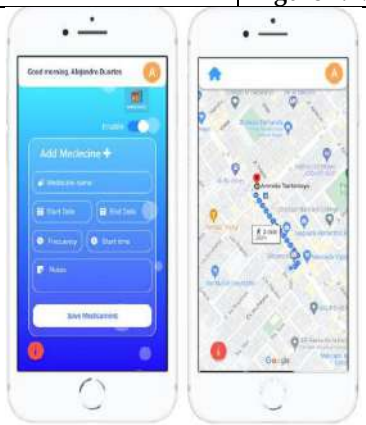

Figure 5: Medicine page and Location tracking

Indian Journal of Natural Sciences www.tnsroindia.org.in ©IJONS

Vol.15 / Issue 83 / Apr / 2024 International Bimonthly (Print) – Open Access ISSN: 0976 – 0997

REVIEW ARTICLE

Detection and Classification of Leaves in a Video: A Literature Review

Vidyashankara[1]*, Hemantha Kumar G[1], Navena M[3], Sumanashree Y S[2] and Mallesh R [3]

[1]Department of Studies in Computer Science, University of Mysore, Mysuru, Karnataka, India.
[2]PG Department of Computer Science, JSS College (Autonomous), Mysuru, Karnataka, India.
[3]Department of Computer Science, JSS College for Women's, Chamararaja Nagara, Karnataka, India.

Received: 20 Dec 2023 Revised: 29 Jan 2024 Accepted: 13 Mar 2024

***Address for Correspondence**
Vidyashankara
Department of Studies in Computer Science,
University of Mysore,
Mysuru, Karnataka, India.
Email: vidhyashankara.s@gmail.com

ABSTRACT

In recent years, the computer vision field has made significant advancements in various domains, including video analysis. One particular area of interest is leaf detection and classification, which plays a crucial role in agriculture, environmental monitoring, and plant disease diagnosis. Being able to automatically analyze leaves from video data has significant applications across agriculture, botany, ecology, and other domains. Specifically, in agriculture, detecting and classifying leaves through computer vision techniques enables non-invasive monitoring of crop growth and plant health at scale.

Leaf analysis is challenging because of factors like cluttered backgrounds, leaf occlusion, and lighting changes. Early works focused on analyzing individual static images of leaves, but recent advances in computer vision and deep learning have enabled the application of leaf analysis techniques to video streams. Analyzing leaf data in the video provides benefits like capturing temporal changes, wider observational coverage, and 3D structure clues through the direction of frame motion. This paper presents a comprehensive review of the recent advancements in the field of detection and classification of leaves in a video. The paper discusses the various techniques used for detecting and classifying leaves in images and the need for video Analysis & sampling, including image processing, machine learning, and deep learning. The paper also highlights the challenges faced in this field and the future scope of research.

Keywords: cluttered backgrounds, leaf occlusion, temporal, 3D structure, image processing, machine learning, deep learning, video analysis

INTRODUCTION

Plants fulfill a significant role in human existence through their provision of shelter and facilitation of a healthy and breathable environment. The vast number of plant species found across the globe necessitates the creation of a comprehensive plant database, enabling swift and efficient classification and recognition methods. The environment and climate are heavily reliant on the presence of plants [25], and individuals involved in natural resource management, particularly those engaged in wildlife conservation, must possess the ability to determine whether a variety of plant species are present or absent. In light of the limited knowledge regarding plants [17, 26], an innovative plant recognition system has been developed using digital images and videos of plant leaves. Given the increasing scarcity of plant categories and the impending extinction of many plant species [12], there is a pressing need for a simple and effective means of recognizing and classifying plants based on their respective categories. It is also helpful for managing and maintaining plants through the early detection of plant diseases.
Leaf detection and classification are important tasks in a variety of applications, such as:

Plant phenotyping
Leaf detection and classification can be used to measure plant growth and development, as well as to identify plant diseases [29]. This information can be used to improve crop yields and develop new disease-resistant varieties.

Precision agriculture
Leaf detection and classification can identify pests and diseases early on [35, 36]. This information can be used to target pesticides and fertilizers more precisely, thereby reducing costs and environmental impact [3].

Environmental monitoring
Leaf detection and classification can be used to monitor the health of forests and other ecosystems [2, 34]. This information can be used to track the spread of invasive plant species and to assess the impact of climate change. Accurate and efficient leaf detection and classification are essential for enabling these applications.
Identification of specific plant types relies on discerning characteristics such as Stem, flower, fruit, and leaf characteristics like leaf shape, colour, and texture [1, 14]. Major research activities are based on leaf characteristics, because of availability in large quantities and easy sample collection and these activities do not adversely affect existing plants and the ecosystem.

Recognition System
A recognition system is a type of artificial intelligence (AI) system that can identify and classify objects or patterns. This system is shown in Fig. 1. It typically follows a Four-stage process:

Data Acquisition
The first step involves acquiring the input data. This data can be in various forms, such as images, audio, or video. The quality and relevance of the input data significantly impact the performance of the recognition system.

Preprocessing
The image is Preprocessed to remove noise and enhance the features of the leaves. This may include steps such as contrast enhancement, histogram equalization, and filtering. It also covers segmentation. Where the image is segmented to isolate the leaves from the background. This is typically done using techniques such as thresholding, edge detection, and region growing.

Feature Extraction

The second step involves extracting relevant features from the acquired data. These features represent the essential characteristics of the input data that can be used for identification or classification. The choice of features depends on the specific recognition task and the nature of the input data.

Pattern Matching or Classification

The third step involves matching the extracted features to a database of known patterns or classifying the input data into predefined categories. This involves comparing the features to reference patterns or using machine learning algorithms to make predictions.

Deep Learning-Based Leaf Detection Methods

Deep learning-based leaf detection methods have recently emerged as a promising approach. These methods utilize deep neural networks to learn features from data without the need for manual feature engineering. Deep learning-based leaf detection methods have achieved state-of-the-art results on both image and video datasets. Leaf recognition using a deep learning approach typically involves the following steps:

Data Collection and Pre-processing

Gather a diverse dataset of leaf images

Collect a large and diverse dataset of leaf images representing different species, shapes, sizes, and conditions. Ensure the dataset includes images with varying illumination, backgrounds, and occlusions to enhance the model's robustness.

Pre-process the images

Pre-process the leaf images to ensure consistency in size, format, and color balance. This may involve resizing, normalizing pixel values, and adjusting contrast and brightness.

Data augmentation

Augment the dataset to increase its variability and improve model generalization. Apply techniques like flipping, rotating, cropping, and random distortions to create more variations of the existing images.

Model Architecture Selection

Choose a deep learning architecture

Select a suitable deep learning architecture for image classification, such as convolutional neural networks (CNNs). CNNs are particularly effective in extracting features from images and learning complex patterns.

Consider transfer learning

Utilize transfer learning by leveraging pre-trained CNN models like VGG16, ResNet, or Inception. These models have already learned generic features from large image datasets and can be fine-tuned for leaf recognition.

Model Training

Split the dataset

Divide the pre-processed dataset into training, validation, and testing sets. The training set is used to train the model, the validation set is used to monitor overfitting and tune hyperparameters, and the testing set is used to evaluate the final model's performance.

Define the loss function

Choose an appropriate loss function for image classification, such as categorical cross-entropy loss. The loss function measures the difference between the model's predictions and the true labels.

Optimize the model

Use an optimization algorithm like stochastic gradient descent (SGD) or Adam to update the model's parameters and minimize the loss function.

Hyperparameter tuning

Tune hyperparameters like learning rate, batch size, and optimizer settings to optimize the model's performance on the validation set.

Model Evaluation and Testing

Evaluate the model on the testing set

Assess the model's generalization ability and real-world performance by evaluating its accuracy, precision, recall, and F1 score on the testing set.

Analyze errors

Identify and analyze the types of errors the model makes to understand its limitations and areas for improvement.

Deployment and Application

Integrate the model

Integrate the trained deep learning model into a practical application, such as a leaf identification tool or an autonomous agricultural robot.

Continuous improvement

Continuously monitor the model's performance in real world scenarios and collect new data to retrain and improve the model as needed.

Deep learning offers several advantages for leaf recognition

Automatic Feature Learning

CNNs can automatically extract and learn relevant features from leaf images without the need for manual feature engineering.

Robustness to Variations

CNNs are relatively robust to variations in leaf appearance, such as lighting conditions, background clutter, and partial occlusions.

High Accuracy

Deep learning models have achieved state-of-the-art accuracy in leaf recognition tasks. The deep learning approach has revolutionized leaf recognition, enabling more accurate and efficient leaf identification in a wide range of applications.

The Leaf detection and classification typically follow a two-stages:

Leaf detection

A Method is used to detect leaves in the video frames or image and extract them [38]. This method is useful for identifying required objects of interest in a frame and extracting them by removing unwanted complex backgrounds. There are several leaf detection algorithms available Here are some of them:

Feature detection algorithms

These algorithms are used to detect specific features in an image such as corners, blobs, circles, and so on. Some of the popular feature detection algorithms include Harris Corner Detection, Shi-Tomasi Corner Detector, Scale-Invariant Feature Transform (SIFT), and Speeded-up Robust Features (SURF) [44]. The advantages of feature detection algorithms are that they are computationally efficient and can be used for real time applications. However, they are sensitive to changes in lighting conditions and may not work well with complex images.

Object detection algorithms

These algorithms are used to detect objects in an image and classify them into different categories. Some of the popular object detection algorithms include Fast R-CNN, Faster R-CNN, Histogram of Oriented Gradients (HOG), Region-based Convolutional Neural Networks (R-CNN), Region-based Fully Convolutional Network (R-FCN), Single Shot Detector (SSD), Spatial Pyramid Pooling (SPP-net), and You Only Look Once (YOLO) [45]. The advantages of object detection algorithms are that they are highly accurate and can work well with complex images. However, they are computationally expensive and may not be suitable for real-time applications.

Image segmentation algorithms

These algorithms are used to partition an image into multiple segments or regions based on the similarity of the pixels in the image. Some of the popular image segmentation algorithms include the Watershed Algorithm, Mean Shift Algorithm, and Normalized Cuts Algorithm [46]. The advantages of image segmentation algorithms are that they can be used to extract meaningful information from an image and can work well with complex images. However, they are computationally expensive and may not be suitable for real-time applications. some detection methods available for video samples:

Object tracking

This method involves tracking an object in a video stream or a video sequence by considering the current image and the previous ones.

Action classification

This method involves classifying the actions performed by an object in a video sequence.

Optical flow estimation

This method involves computing the motion of objects in a video sequence by computing the pixel shift between two frames.

Trajectory classification

This method involves classifying the trajectories of objects in a video sequence [48].

Low rank sparse matrix

This method involves decomposing a video sequence into a low-rank matrix and a sparse matrix to detect objects [48].

Background subtraction

This method involves subtracting the background from a video sequence to detect moving objects [48].

Object detection using deep learning

This method involves using deep learning algorithms such as Convolutional Neural Networks (CNN) to detect objects in images and videos [49].

Leaf classification

Once the leaves are detected, this method is useful for classifying them based on their extracted features [39, 42]. This method classifies leaves by typically the percentage of matching the features extracted from the samples at the time of testing with the features trained on a dataset of labelled leaf images from different species. There are several leaf classification algorithms. Here are some of them: The Random Forest algorithm is a technique for ensemble learning, wherein multiple decision trees are created during the training phase. The resulting output is determined by the class that appears most frequently among the individual trees in the case of classification, or by the average prediction in the case of regression [53].. The advantages of Random Forest are that it is highly accurate, can handle missing data, and can be used for feature selection. However, the execution of this task incurs a significant computational cost and may exhibit incompatibility with time-sensitive applications.

Support Vector Machines (SVM)

This algorithm is a classifier, either linear or non-linear in nature, which is determined by the kernel employed. In the case of utilizing a linear kernel, the classifier and consequently the prediction boundary exhibit linearity. In order to distinguish between two classes, it is imperative to establish a line that possesses a maximum margin. This particular line is drawn equidistant from both sets. Additionally, two supplementary lines are drawn on each side, referred to as support vectors. SVMs learn from the support vectors, unlike other machine learning models that learn from the correct and incorrect data [52]. The strengths of Support Vector Machine (SVM) lie in its notable precision, ability to process data with a high number of dimensions, and efficacy in handling limited datasets. Nevertheless, it is crucial to acknowledge that SVM incurs substantial computational costs and may not be optimal for applications requiring real-time responsiveness.

K-Nearest Neighbors (KNN)

This algorithm is a nonlinear classifier that predicts which class a new test data point belongs to by identifying its k nearest neighbors class. We choose these k closest neighbors by considering the Euclidean distance metric. Within this group of k neighbors, we tally the quantity of data points belonging to each category, and subsequently assign the new data point to the category that has the highest number of neighboring points [52]. The advantages of KNN are that it is simple, easy to implement, and can work well with small datasets. However, it is computationally expensive and may not be suitable for high dimensional data.

Convolutional Neural Networks (CNN)

This algorithm is a deep learning architecture that is used for image classification. CNNs are designed to automatically and adaptively learn spatial hierarchies of features from input images by enforcing a local connectivity pattern between neurons of adjacent layers [52]. The advantages of CNN are that it is highly accurate, can handle complex images, and can work well with large datasets. However, it is computationally expensive and requires a large amount of training data.

Recurrent Neural Networks (RNN)

This algorithm is a deep learning architecture that is used for sequential data such as videos. RNNs are designed to process sequential data by maintaining an internal state or memory of the previous inputs [54]. The advantages of RNN are that it can handle sequential data, can work well with variable-length inputs, and can be used for real-time applications. However, it is computationally expensive and may suffer from the vanishing gradient problem.

Long Short-Term Memory (LSTM)

This algorithm is a type of RNN that is designed to overcome the vanishing gradient problem. LSTMs are designed to maintain an internal state or memory of the previous inputs and selectively forget or remember certain inputs based on their importance [51]. The advantages of LSTM are that it can handle sequential data, can work well with variable-length inputs, and can be used for real-time applications. However, it is computationally expensive and may require a large amount of training data.

Two-Stream Convolutional Neural Networks

This algorithm is a deep learning architecture that is used for video classification. It consists of two separate CNNs, one for spatial information and one for temporal information [53]. The advantages of Two-Stream CNNs are that it can handle complex videos, can work well with large datasets, and can be used for real-time applications. However, it is computationally expensive and requires a large amount of training data. However, leaf detection and classification can be challenging due to the complex and varying nature of leaf appearances [37]. Leaves can exhibit a wide range of shapes, sizes, colors, and textures. The plant leaves have high intra class variability and sometimes the leaves of different plants are very similar, which makes this task difficult even for botanists [16]. In addition, leaves can be occluded by other objects, and their appearance can change due to varying illumination conditions. Existing methods for leaf detection and classification have achieved promising results on leaf images. However, these methods often rely on hand-crafted features that may not be robust to the aforementioned challenges. In addition, existing methods are often computationally expensive, limiting their applicability to real time applications [33].

Related Work

There have been significant research approaches carried out in the first few years of the last two decades on the detection and classification of leaves, but later on, they concentrated on plant diseases or leaf disease recognition. Computer-aided plant recognition is still a very challenging task in computer vision due to the lack of proper models or representation schemes [20]. The objective of computerized identification of live plants was to quantify the features based on leaf geometry, morphology, and Fourier moments [55] before the introduction of Machine Learning and Deep Learning. These works can be mainly categorized as follows:

Approaches for leaf detection and classification

Traditional Image Processing Techniques: These techniques involve the use of filters, thresholding, and morphological operations to extract features from leaf images. The extracted features are then used to classify the leaves into different categories [5,29]. Image Processing and Pattern Recognition techniques such as segmentation, feature extraction, and classification are commonly used for detecting and classifying leaves. Many scholars have endeavored to create a more resilient and effective system for identifying plants by utilizing techniques in pattern recognition and image processing that are centered around plant leaves, flowers, barks, and fruits [23]. Nevertheless, leaves hold a paramount significance compared to other plant components due to their abundance of valuable information and heightened dependability. Machine Learning-based approaches: These approaches use machine learning algorithms to learn the features of the leaf images and classify them into different categories. Some of the popular machine learning algorithms used for leaf classification include Random Forest, Support Vector Machines (SVM), and Convolutional Neural Networks (CNN) [27, 31].

Deep Learning-based approaches

These approaches use deep neural networks to learn the features of the leaf images and classify them into different categories. Some of the popular deep learning architectures used for leaf classification include AlexNet, VGGNet, and ResNet

Hybrid approaches

These approaches combine traditional image processing techniques with machine
learning or deep learning algorithms to improve the accuracy of leaf classification [20, 32]. As shown in fig. No. 2. A variety of methods have been proposed for leaf detection and classification in images [43]. Early traditional methods relied on hand-crafted features, such as color, shape, and texture, to represent leaves [42, 23]. However, these features are not always robust to the challenges mentioned above. In recent years, machine learning techniques such as support vector machines (SVM), decision trees, and random forests have also been used for detecting and classifying leaves. Deep learning techniques such as convolutional neural networks (CNN) have shown promising results for detecting and classifying leaves [46, 39]. Deep learning-based methods have achieved state-of-the-art results in leaf detection and classification. Deep learning methods can learn complex features from data without the need for hand-crafted features [31, 32, 40]. This makes deep learning methods more robust to the challenges of leaf detection and classification.

Deep Learning Methods

Several deep learning-based methods have been developed for leaf detection and classification [40]. These methods can be broadly divided into two categories: Two-stage methods: Two-stage methods first detect leaves in a video frame and then classify the detected leaves. A common example of a two-stage method is the Faster Region-based Convolutional Neural Network (Faster R-CNN) [41].

Single-stage methods

Single-stage methods detect and classify leaves in a video frame in a single step. A common example of a single-stage method is the You Only Look Once (YOLO) algorithm [45]. One of the most popular deep learning-based methods for leaf detection is the Faster Region-based Convolutional Neural Network (Faster R-CNN). Faster R-CNN is a two-stage object detection method that first generates a set of candidate's bounding boxes and then classifies each bounding box. Faster R-CNN has been shown to achieve good performance on leaf detection in videos. Another popular deep learning-based method for leaf detection is the Single Shot Multi-Box Detector (SSD). SSD is a one-stage object detection method that directly predicts bounding boxes and class labels for each pixel in an image. SSD is faster than Faster R-CNN, but it may not be as accurate for leaf detection in videos. such as the Convolutional Neural Network (CNN) and the Support Vector Machine (SVM). CNNs have been shown to achieve good performance on leaf classification tasks, especially when trained on large datasets of leaf images. SVMs are also effective for leaf classification, but they may not be as accurate as CNNs when trained on small datasets. Deep learning-based methods have achieved state-of-the art results on leaf detection and classification benchmarks [41].

For example, the YOLOv5 algorithm achieved an accuracy of over 99% on the public LeafNet dataset. Recurrent neural networks (RNNs) are a powerful model for sequential data. End-to-end training methods such as Connectionist Temporal Classification make it possible to train RNNs for sequence labeling problems where the input-output alignment is unknown [32]. However, there are still many challenges that need to be addressed in the field of leaf detection and classification [35].

Proposed Methodology and Discussion

Video analysis is a rapidly evolving field that uses computer algorithms and techniques to extract meaningful information from video data. It has gained significant attention in recent years due to its wide range of applications across various domains, including surveillance, sports analytics, healthcare, and more. Video analysis algorithms can be used to detect and track objects, recognize faces, and identify suspicious activities in real-time, making security systems more proactive and efficient [33]. Leaf detection and classification in video analysis play a crucial role in various fields, such as agriculture, environmental monitoring, and plant disease detection [36]. The ability to accurately detect and classify leaves is essential for understanding plant growth patterns, identifying diseases, and optimizing crop management practices. Researchers can track the growth and development of plants over time by analyzing the size, shape, and color of leaves, which provides insights into the health and vigor of plants. Leaf classification helps in identifying diseases that affect plants by analyzing distinct symptoms on leaves, such as discoloration or spots. By accurately classifying these symptoms using computer vision techniques, researchers can quickly diagnose plant diseases and take appropriate measures to prevent their spread. Hence the proposed Model as shown in Fig. 3, for the recognition of leaves in a video is the same for both the Training and Testing Phases but in the testing instead of storing to the Knowledge base it compares with the knowledge base for recognition. Furthermore, leaf detection and classification are instrumental in environmental monitoring efforts, as leaves act as natural indicators of air pollution levels since they directly interact with the atmosphere. By analyzing the condition of leaves in different regions or near industrial areas using video analysis techniques, scientists can assess air quality levels more efficiently. The detection and classification of leaves in a video is an important research area in the field of computer vision, and video analysis is a powerful tool here as it can provide temporal information about leaves. There are a lot of research opportunities in this field, some of which are mentioned below:

Data Acquisition

Most researchers focus only on image samples, which are collected manually. It is a tedious and time-consuming job, but it is very much needed in deep learning methods which require considerably large data samples for process. Large amounts of data can be acquired through video and generate required image samples in a few minutes by processing them using different image processing algorithms automatically.

Effective Sample and Feature collections

by using image processing techniques on a video frame to re-construct the samples and features as full or partially due to cluttered backgrounds, leaf occlusion frames/ images

3-D Feature building and extraction

the researchers are considering one side of the leaf (the front side) and ignoring other side features, 3d characteristics like the front, back, and thickness of a leaf may be useful in decision-making. So 3d features can be built by tracking video frame transmissions automatically or with minimal human interaction,

N-D Features /Metadata modeled

Along with 3d features, add present visual environment details like Forests, Deserts, Mountain regions, water surface regions, other associated plant parts, and some temporal information. which may play a crucial role in building an effective computational recognition system and also more generalized recognition system. This reduces the classification domain category selected based on the details(metadata). This can be achieved by video analysis, video frame tracking, and appropriate AI Techniques.

Challenges and Future Directions

Challenges: Leaf detection and classification in videos are challenging tasks for the following reasons even with some of the challenges in images:

Video motion: The motion of leaves in videos can make it difficult to track and classify them accurately when they cross the speed limit of the camera. Despite the recent advances in deep learning-based leaf detection and classification, there are still some challenges that need to be addressed [35, 40]. One challenge is that deep learning models can be computationally expensive to train and deploy. Another challenge is that deep learning models can be susceptible to over fitting, especially when trained on small datasets. Future research in leaf detection is likely to focus on the following areas: Developing more robust and accurate deep-learning models for leaf detection and classification. Addressing the challenges of background clutter, varying illumination conditions, and occlusions. Developing real-time leaf detection methods with the help of 3d Features for recognition systems

CONCLUSION

In conclusion, deep learning has emerged as a powerful tool for leaf detection and classification [29, 31]. However, challenges remain in aspects like model efficiency, robustness, and real-time usage [35, 40]. Continued research should concentrate on translating accuracy in controlled settings to real-world applications [34, 37]. Overall, there are still gaps between experimental demonstrations and reliable field deployment that necessitate rigorous validation [36, 14].

REFERENCES

1. Jana Wäldchen et al, “Plant Species Identification Using Computer Vision Techniques: A Systematic Literature Review”, open access at Springerlink.com, January, 2017
2. Chaki, J., et al., “Plant leaf classification using multiple descriptors: A hierarchical approach”, Journal of King Saud University– Computer and Information Sciences (2018)
3. Neto, J.C., et al., “Plant species identification using Elliptic Fourier leaf shape analysis”, Computers and electronics in agriculture, 50(2): p. 121-134, 2006.
4. Zhang Y, Cui J, Wang Z, Kang J, Min Y. Leaf Image Recognition Based on Bag of Features. Applied Sciences. 2020; 10(15):5177. https://doi.org/10.3390/app10155177
5. Gu, X., J.-X. Du, and X.-F. Wang, “Leaf recognition based on the combination of wavelet transform and gaussian interpolation”, in Advances In Intelligent Computing 2005, Springer. p. 253-262.
6. C. Im, H. Nishida and T. L. Kunii, "Recognizing plant species by leaf shapes-a case study of the Acer family," Proceedings. Fourteenth International Conference on Pattern Recognition (Cat. No.98EX170), Brisbane, QLD, Australia, 1998, pp. 1171-1173 vol.2, doi: 10.1109/ICPR.1998.711904.
7. Rashad, M., B. El-Desouky, and M.S. Khawasik, “Plants images classification based on textural features using combined classifier”, International Journal of Computer Science and Information Technology, 2011. 3(4): p. 93-100.
8. Kadir, A., et al., “Leaf classification using shape, color, and texture features”, arXiv preprint arXiv:1401.4447, 2013.
9. Wang, Z.; Chi, Z.; Feng, D. (2003). “Shape based leaf image retrieval”. , 150(1), 34–43. doi:10.1049/ip-vis:20030160
10. Bong, M.F., G. bin Sulong, and M.S.M. Rahim, “Recognition of Leaf Based on Its Tip and Base using Centroid Contour Gradient”, IJCSI International Journal of Computer Science Issues, 2013.
11. Salve, P., et al., “Identification of the Plants Based on Leaf Shape Descriptors”, in Proceedings of the Second International Conference on Computer and Communication Technologies. 2016. Springer.

12. Nisar Ahmed, Usman Ghani Khan, Shahzad Asif, "An Automatic Leaf Based Plant Identification System", Sci.Int.(Lahore),28(1),427-430, ISSN 1013-5316, CODEN: SINTE, Jan 2016
13. Kadir, Abdul &Nugroho, Lukito& Susanto, Adhi & Santosa, Paulus. (2011). Leaf Classification Using Shape, Color, and Texture Features. International Journal of Computer Trends and Technology. 1. 225-230.
14. Pallavi P, V.S Veena Devi ,"Leaf Recognition Based on Feature Extraction and Zernike Moments ",International Journal of Innovative Research in Computer and Communication Engineering (An ISO 3297: 2007 Certified Organization) Vol.2, Special Issue 2, May 2014.
15. Ehsani Rad, Abdolvahab & Kumar, Y H. (2010). Leaf recognition for plant classification using GLCM and PCA methods. Oriental Journal of Computer Science and Technology. 3. 6.
16. Suk, T., Flusser, J., & Novotný, P. (2013). Comparison of Leaf Recognition by Moments and Fourier Descriptors. Lecture Notes in Computer Science, 221–228. doi:10.1007/978-3-642-40261-6_26
17. Puja, D., M. Saraswat, and K. Arya. "Automatic Agricultural Leaves Recognition System", in Proceedings of Seventh International Conference on Bio-Inspired Computing: Theories and Applications (BIC-TA 2012). 2013. Springer.
18. Aakif, A. and M.F. Khan, "Automatic classification of plants based on their leaves", Biosystems Engineering, 2015. 139: p. 66-75.
19. Lavania, S. and P.S. Matey, "Leaf recognition using contour based edge detection and SIFT algorithm", in Computational Intelligence and Computing Research (ICCIC), 2014 IEEE International Conference on. 2014. IEEE.
20. Krishna, S., G. Indra, and G. Sangeeta, "SVM-BDT PNN and Fourier Moment Technique for Classification of Leaf Shape", International Journal of Signal Processing, Image Processing and Pattern Recognition, 2010. 3(4).
21. Gulhane, V.A. and M.H. Kolekar. "Diagnosis of diseases on cotton leaves using principal component analysis classifier", in India Conference (INDICON), 2014 Annual IEEE. 2014. IEEE.
22. Pujari, J.D., R. Yakkundimath, and A.S. Byadgi, "Automatic Fungal Disease Detection based on Wavelet Feature Extraction and PCA Analysis in Commercial Crops", International Journal of Image", Graphics and Signal Processing, 2013. 6(1): p. 24.
23. Y.G., Naresh; H.S., Nagendraswamy (2015). Classification of Medicinal Plants: An Approach using Modified LBP with Symbolic Representation. Neurocomputing, (), S0925231215013764–. doi:10.1016/j.neucom.2015.08.090
24. Chengzhuan Yang; (2021). Plant leaf recognition by integrating shape and texture features . Pattern Recognition, (), –. doi:10.1016/j.patcog.2020.107809
25. Naveena M, G Hemantha Kumar, Vidyashanakara, Pavithra B S (2017). Leaf Recognition Based on Color, Shape and GLCM Features, International Journal of Latest Technology in Engineering, Management & Applied Science (IJLTEMAS), Volume VI, Issue XII, ISSN 2278-2540
26. Vidyashanakara, Naveena M, G Hemnatha Kumar (2018). Leaf Classification Based on GLCM Texture and SVM, International Journal on Future Revolution in Computer Science & Communication Engineering Volume: 4 Issue: 3 156 – 159 ISSN: 2454-4248
27. Prasad S, Kudiri KM, Tripathi RC (2011) Relative sub image based features for leaf recognition using support vector machine. In: Proceedings of the 2011 international conference on communication, computing & security, ACM, New York, NY, USA (ICCCS '11), pp 343–346. doi:10.1145/1947940.1948012
28. Pang, P. K. and Lim, K. H. (2019). Review on automatic plant identification using computer vision approaches. IOP Conference Series: Materials Science and Engineering, 495, 012032. https://doi.org/10.1088/1757-899x/495/1/012032
29. Mohanty, S. P., Hughes, D. P., &Salathé, M. (2016). Using deep learning for image-based plant disease detection. Frontiers in Plant Science, 7, 1419. DOI: 10.3389/fpls.2016.01419.
30. Naveena M, Vidyashankara, G Hemantha Kumar (2020). Recognition of Leaves in Videos. International Journal of Inventive Engineering and Sciences (IJIES), Volume-5, Issue-8, pp 1-3, ISSN: 2319-9598.
31. LeCun, Y., Bottou, L., Bengio, Y., & Haffner, P. (1998). Gradientbased learning applied to document recognition. Proceedings of the IEEE, 86(11), 2278-2324. DOI: 10.1109/5.726791
32. Graves, A., Mohamed, A., & Hinton, G. (2013). Speech Recognition with Deep Recurrent Neural Networks. ArXiv. /abs/1303.5778 or https://doi.org/10.48550/arXiv.1303.5778.

33. Hatcher, W. G., & Yu, W. (2018). A Survey of Deep Learning: Platforms, Applications and Emerging Research Trends. IEEE Access, 6, 24411–24432. doi:10.1109/access.2018.2830661.
34. Lu, J., Tan, L., & Jiang, H. (2021). Review on Convolutional Neural Network (CNN) Applied to Plant Leaf Disease Classification. Agriculture, 11(8), 707.
35. Saleem, Potgieter, and Mahmood Arif, "Plant Disease Detection and Classification by Deep Learning," Plants, vol. 8, no. 11, p. 468, Oct. 2019, doi: 10.3390/plants8110468.
36. Tichkule, S. K., &Gawali, D. H. (2016). Plant diseases detection using image processing techniques. 2016 Online International Conference on Green Engineering and Technologies (IC-GET). doi:10.1109/get.2016.7916653.
37. Barbedo, J. G. A. (2016). A review on the main challenges in automatic plant disease identification based on visible range images. Biosystems Engineering, 144, 52–60. doi:10.1016/j.biosystemseng.2016.01.017
38. Minaee, S., Boykov, Y., Porikli, F., Plaza, A., Kehtarnavaz, N., &Terzopoulos, D. (2020). Image Segmentation Using Deep Learning: A Survey. ArXiv. /abs/2001.05566.
39. M. U. Ahmad, S. Ashiq, G. Badshah, A. H. Khanand M. Hussain, "Feature Extraction of Plant Leaf Using Deep Learning", Complexity, vol. 2022, pp. 1–8, 2022, doi: 10.1155/2022/6976112.
40. L. Li, S. Zhang and B. Wang, "Plant Disease Detection and Classification by Deep Learning—A Review," in IEEE Access, vol. 9, pp. 56683-56698, 2021, doi: 10.1109/ACCESS.2021.3069646.
41. Nanni, L., Lumini, A., &Brahnam, S. (2012). Survey on LBP based texture descriptors for image classification. Expert Systems with Applications, 39(3), 3634–3641. doi:10.1016/j.eswa.2011.09.054
42. Camargo, A., & Smith, J. (2009). Image pattern classification for the identification of disease causing agents in plants. Computers and Electronics in Agriculture, 66(2), 121-125. https://doi.org/10.1016/j.compag.2009.01.003
43. J. G. ArnalBarbedo, "Digital image processing techniques for detecting, quantifying and classifying plant diseases", Springer Plus, vol. 2, no. 1, p. 660, 2013, doi: 10.1186/2193-1801-2-660.
44. Vishnoi, V.K., Kumar, K. & Kumar, B. A comprehensive study of feature extraction techniques for plant leaf disease detection. Multimed Tools Appl 81, 367–419 (2022). https://doi.org/10.1007/s11042-021-11375-0
45. Tugrul, B., Elfatimi, E., &Eryigit, R. (2022). Convolutional Neural Networks in Detection of Plant Leaf Diseases: A Review. Agriculture, 12(8), 1192 MDPI AG. Retrieved from http://dx.doi.org/10.3390/agriculture12081192
46. Vijay Kumar V1, Vani K S2 (2018) Agricultural Robot: Leaf Disease Detection and Monitoring the Field Condition Using Machine Learning and Image Processing International Journal of Computational Intelligence Research, ISSN 0973-1873 Volume 14, Number 7, pp. 551-561
47. VideoAnalysis Algorithms in Computer Vision - Welcome to The Library! https://www.thinkautonomous.ai/blog/computer-vision-fromimage-to-video-analysis/.
48. Sita M. Yadav, Sandeep M. Chaware (2020) Video Object Detection through Traditional and Deep Learning Methods International Journal of Engineering and Advanced Technology (IJEAT) ISSN: 2249 – 8958 (Online), Volume-9 Issue-4, pp. 1822 – 1826.
49. Palle, R.R., Boda, R. Automated image and video object detection based on hybrid heuristic-based U-net segmentation and faster regionconvolutional neural network-enabled learning. Multimed Tools Appl 82, 3459–3484 (2023). https://doi.org/10.1007/s11042-022-13216-0.
50. Tyagi, S., Yadav, D. A detailed analysis of image and video forgery detection techniques. Vis Comput 39, 813–833 (2023). https://doi.org/10.1007/s00371-021-02347-4
51. Zhu, H., Wei, H., Li, B., Yuan, X., &Kehtarnavaz, N. (2020). A Review of Video Object Detection: Datasets, Metrics and Methods. Applied Sciences, 10(21), 7834. MDPI AG. Retrieved from http://dx.doi.org/10.3390/app10217834
52. Khaled Suwais, Khattab Alheeti, DuaaAl_Dosary. (2022), A Review on Classification Methods for Plants Leaves Recognition, International Journal of Advanced Computer Science and Applications, Vol. 13, No. 2, pp. 92-100.
53. Bhagya M. Patil, Vishwanath Burkpalli,(2021), A Perspective View of Cotton Leaf Image Classification Using Machine Learning Algorithms Using WEKA, Hindawi, Advances in Human-Computer Interaction, Volume 2021,Article ID 9367778,15 pages, https://doi.org/10.1155/2021/9367778
54. Azlah, M. A. F., Chua, L. S., Rahmad, F. R., Abdullah, F. I., & Wan Alwi, S. R. (2019). Review on Techniques for Plant Leaf Classification and Recognition. Computers, 8(4), 77. MDPI AG. Retrieved from http://dx.doi.org/10.3390/computers8040077

55. Gu, X., J.-X. Du, and X.-F. Wang, "Leaf recognition based on the combination of wavelet transform and gaussian interpolation", in Advances In Intelligent Computing 2005, Springer. p. 253-262.

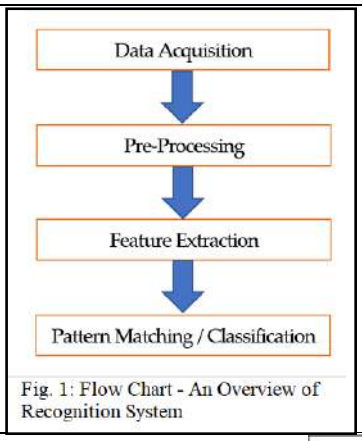

Fig. 1: Flow Chart - An Overview of Recognition System

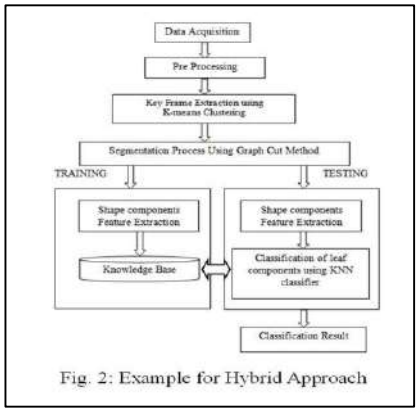

Fig. 2: Example for Hybrid Approach

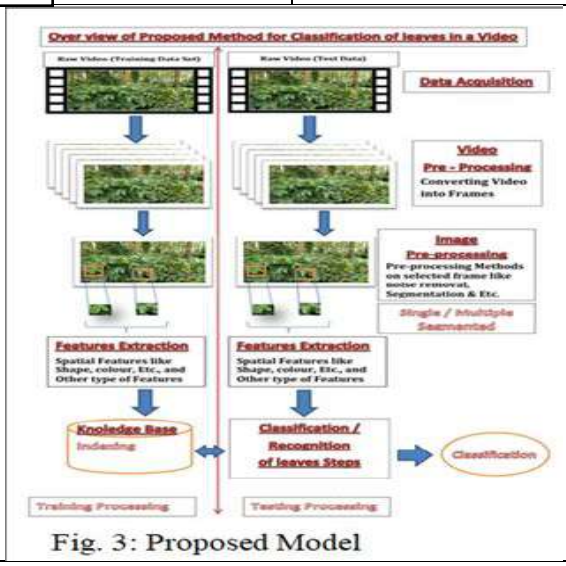

Fig. 3: Proposed Model

RESEARCH ARTICLE

A Data Hiding Method Using Reduced Difference extension to develop the Stego Quality

Sumanth S[1]* and Siddarama S[2]

[1]Associate Professor, Department of Computer Science and Applications, Government College for Women, Kolar – 563 101, Karnataka, India.
[2]Head, Department of Computer Science and Applications, Sri Bhagawan Mahaveer Jain College, Robertsonpet, K.G.F. – 563 122, Karnataka, India.

Received: 20 Dec 2023 Revised: 29 Jan 2024 Accepted: 13 Mar 2024

***Address for Correspondence**
Sumanth S
Associate Professor,
Department of Computer Science and Applications,
Government College for Women,
Kolar – 563 101, Karnataka, India.
Email: sumanth81s@gmail.com/dr.sumanth.s.81@gmail.com

ABSTRACT

Because of the issues connected with network usage restrictions violations and unauthorized access to public networks, protecting secret data has taken on increased importance within network security. In response to these challenges, various data protection methodologies, including steganography, have been created. Steganography is concerned with securely conveying secret messages over public networks by hiding them within digital files. This study presents a unique steganographic approach based on reduced difference expansion, with the goal of reducing the magnitude of differences before embedding secret material. This study's experimental results show higher stego image quality, as indicated by a Peak Signal-to-Noise Ratio(PSNR) of 44.17 dB, a significant improvement over existing approach.

Keywords: Network infrastructure, national security, data protection, steganography, difference expansion

INTRODUCTION

The omnipresent demand for file sharing among users endures in the modern era of information technology, overcoming temporal and spatial boundaries. Despite its extensive use, the traditional use of public networks for such communications is fundamentally insecure. Because of the inherent vulnerability of this infrastructure, data traveling across the internet is vulnerable to interception and illegal alteration. The integrity and secrecy of the communication are jeopardized if an altered message reaches the intended recipient. As a result, data protection

during the transmission phase becomes critical. One approach to achieving this safeguarding is by implementing data hiding techniques [1 – 3], wherein confidential information is concealed within diverse multimedia formats, including images, videos, audio, or text. Data hiding encompasses several approaches, such as watermarking, cryptography, and steganography. Different forms of covers have been utilized in steganography to maximize the confidentiality of the hidden data [4 - 6]. In the area of digital media steganography, establishing excellent visual quality of the stego medium while keeping a significant embedding capacity poses a significant difficulty [7]. The pronounced distortion introduced to the original media raises suspicions of attacks such as steganalysis [8 – 10] regarding the steganographic nature, potentially prompting adversaries to exert concerted efforts to compromise the embedding algorithm. Owing to the visual similarity between original and stego media, unauthorized interceptors may remain oblivious to the covert transmission of a concealed message. Typically, following the embedding of a secret message into the cover, the resultant stego medium traverses a public network to its destination, where the concealed message and cover are subsequently extracted and reconstructed. Researchers have proposed many data hiding approaches in the existing literature to keep the better quality of stego media while accommodating a defined embedding capacity, as proven by publications such as [11] and [12]. Furthermore, in [13], a spatial domain technique for steganography of digital images based on Difference Expansion (DE) was presented, utilizing redundancy information between pixels for secret message concealment.

Another approach, outlined in [14], involves developing a methodology affording high embedding capacity with minimal distortion in host images, employing RGB images, and inserting secret bits based on pixel block classification. Nevertheless, steganography in digital images presents a high trade-off gap between the stego image quality and the payload size. Several research works [15 - 17] have recommended using various combinations of mathematical functions to improve the positions and values of the pixels in the stego picture to address the issue of stego image distortion caused by concealment of the high payload size in the spatial domain. Recent work, however, indicates the necessity to continue working on decreasing the trade-off between stego quality and payload size. In this paper, we present a unique steganographic architecture that combines difference expansion with reduced difference expansion, with the goal of intentionally reducing the magnitude of differences before embedding hidden bitstreams into the cover's pixels. The primary goal of this research is to improve the quality of the generated stego image following data embedding. This manuscript is structured into five sections. Section I provides a comprehensive overview of the research problems under consideration. Section II presents an in-depth exploration of the existing literature on data hiding, mainly focusing on the difference expansion method. Section III elucidates the proposed method, detailing its conceptual framework. Moving on to Section IV, the evaluation of the method and its corresponding results are expounded upon, offering a comparative analysis with preceding methodologies. The conclusion of this work is included in Section V.

Related Work

Given the various technology developments integrated into digital image steganography in recent years, significant performance gains have been made. As a notable result, intelligent algorithms capable of securing confidential information have emerged. These algorithms are classified into two types based on their application domain: spatial domain techniques and transform (frequency) domain techniques. In the spatial domain, the concealment of confidential data involves direct manipulation of values of the pixels within the carrier to attain the wanted enhancement [13], ofparamount significance in contemporary digital image steganography are techniques such as difference expansion [13], expanded difference expansion [11], and pixel value modification (PVD) [12], all prominently situated within the spatial domain. These methodologies find prevalent usage when direct modification of fixed values of the pixels in an image is deemed necessary. Notably, they excel in achieving a concealment size; however, they occasionally exhibit susceptibility to compromising the stego image's quality. Among these techniques, difference expansion has emerged as one of the most renowned spatial domain algorithms. Its efficacy lies in concealing secret data by expanding the calculated values of the differences among pixels, contributing significantly to spatial domain steganographic methodologies. In work by researchers [13], an innovative reversible data hiding method was introduced, focusing on concealing data within images. This method was designed to

concurrently uphold the quality of the resulting stego image and the payload capacity. Employing the binary-block embedding technique facilitated the concealment of data within the neighboring pixels' differences. Notably, a novel security key design approach was incorporated to fortify the algorithm against data loss, brute-force attacks, noise interference, and differential attacks. A noteworthy characteristic of this scheme lies in its complete reversibility, allowing for the restoration of embedded secret data independently and without any loss. This attribute enhances the utility and reliability of the proposed algorithm in the context of reversible data hiding within digital images. The work presented in [18] introduced a distinctive approach involving concealing secret data within two layers to augment load capacity. This is achieved through a security system integration that combines AES cryptography with image steganography, employing cross-division and additive homomorphism. The objective is to establish a novel reversible data hiding scheme tailored for encrypted images, thereby fortifying privacy protection in multimedia applications. The adoption of a homomorphic technique in this endeavor is particularly noteworthy. This choice is rooted in the capability of homomorphic operations to facilitate computations with encrypted data, thereby avoiding their expansion. As a result, the suggested scheme's overall embedding capability improves.

The embedding technique entails changing the cover image with a cryptography key and hiding the bits within the altered original image with the secret bits concealment key. To ensure reversibility, the strategy includes histogram shifting. Notably, data extraction occurs independently of image decryption at the receiver's end. This means that extracting hidden bits can be done before or after decrypting the altered image, giving the data extraction technique flexibility and variety. In a study outlined in [12], the authors introduced a method for hiding data by examining the differences between neighboring pixels after arranging them in a particular order. They leveraged the neighborhood of pixels, following a paradigm called pixel value ordering (PVO). Their approach involved sorting all the pixels in an image in ascending order and then pairing them off. Subsequently, they conducted a subtraction operation between these neighboring pixel pairs, using the results to conceal secret data. Notably, their technique does not use all the computed differences; instead, it customizes which pixels can hide data based on the values of these differences. They specifically choose pixels with differences of less than one for data embedding, resulting in a suboptimal payload capacity. As a result, further research is warranted to enhance their method's payload capacity. Using the knowledge gained from previous steganographic methods, this paper aims to provide a new steganographic technique that improves the quality of the stego image even when accommodating a large payload size. As cover images, general-purpose photographs from [19] are used.

PROPOSED METHODOLOGY

This section describes the steps taken for data embedding and extraction. We illustrate in Fig. 1 a flowchart for data embedding and in Fig. 2 a flowchart for data extraction. To shed much light on our method, we give a step-by-step description of the embedding process in Section III. A, and we present the pseudocode in Algorithm I for data extraction.

Data Embedding Steps

Step 1: Load the cover image (Cover).

Step 2: Arrange the pixels of the cover image into pairs-based blocks (1 × 2).

Step 3: Compute the difference (h) between adjacent pixels (e0, e1) within each block using (1).

$$h = e1 - e0 \quad (1)$$

Step 4: Determine the block's characteristics based on the value of h. A block is considered "Changeable" if the difference is within the range of [-2, 7] ($h \leq -2$ and $h \leq 7$), "Expandable Non Reduced Difference Expansion (RDE)" if the block's difference is equal to 0 or 1 ($h = 0$ or $h = 1$)

Step 5: For the class of "Expandable RDE" blocks, we consider the difference values greater or equal to 2 and the ones less or equal to 7 ($h \leq 2$ and $h \leq 7$).

Step 6: Create a location map with the same dimension as the cover image to store the block's characteristics. For "Unchangeable" blocks, assign the value of -1. For "Expandable Non-RDE" blocks, assign the value of 0. For "Expandable RDE" blocks, assign the value of 1.

Step 7: Conceal the secret data (s) in the calculated differences and obtain the new differences (h') using (2). We embed secret data directly for "Changeable" and "Expandable Non-RDE" blocks.

$h' = 2 \times h + s$ (2)

For "Changeable" and "Expandable" blocks, use a logarithmic function of base two to reduce the difference before we expand and embed the secret data using (3) to obtain a new reduced difference (h'').

$h'' = h - (2\lfloor \log_2(h) \rfloor - 1 + \log_2(h\sqrt{}) \overline{h}\rfloor)$ (3)

Step 8: Use the differences obtained in steps 6 and 7 to embed the secret data in the pixels of the cover image (ei) to obtain (ei''), the new pixel for the stego image using (4) and (5).

$ei' = ei + h'$ (4)

$ei' = ei + h''$ (5)

Step 9: Construct the stego image and return the location map used in the secret data extraction process.

Data Extraction Process

This sub-section gives the details in pseudocode of how to extract the data in Algorithm 1. It is important to note that we can successfully extract the cover image and the secret data with the proposed method.

Algorithm 1: The pseudocode for the extraction process

Procedure extraction_process takes in parameters: stego_image, location_map, block_size
Initialize cover_image as a copy of stego_image
Initialize payload as an empty list
For each i in the range from 0 to the height of the location_map, stepping by block_size[0]
For each j in the range from 0 to the width of the location_map, stepping by block_size[1]
If the block does not exceed the image boundaries
Extract the block from the stego_image and convert it to int16
Determine the block_type from the unique value in the corresponding location in location_map
If block_type is 0, continue to the next iteration
Else
If block_type is 1
Compute the difference between the first two pixels in the block
Append the least significant bit of the difference to payload
Compute the original difference by floor division of the difference by 2
Update the second pixel in the block in cover_image with the sum of the first pixel in the block and the computed difference
Else
Compute the difference between the first two pixels in the block
Append the least significant bit of the absolute difference to payload
Compute the original difference using Equation 2.
Update the second pixel in the block in cover_image with the sum of the first pixel in the block and the computed difference
Return cover_image, payload
End Procedure

RESULTS AND DISCUSSIONS

In this section, we report the PSNR results in Fig. 3. Moreover, we present a comparative view of our results to those obtained in [Maurice] in Table 1. Table 1 thoroughly examines PSNR values, comparing the method delineated in

[11] with our novel proposed approach. The assessment encompasses a range of cover images, namely Abdominal, Leg, Head, Hand, and Chest, and investigates three distinct payload sizes: 5 kilobits, 10 kilobits, and 20 kilobits. The PSNR values, measured in decibels (dB), serve as crucial metrics to evaluate the quality of stego images produced by both methods under varying payload conditions. This table1 allows for a detailed analytical view of the performance variations between the existing method and our approach across different cover images and payload sizes, highlighting the consistent superiority of our proposed method in maintaining high-quality stego images. Figure 3 illustrates an analytical portrait of our method for payload sizes (in kb) and the corresponding PSNR values for distinct cover images. Cover images include Abdominal, Leg, Head, Hand, and Chest, with payload sizes ranging from 5 kb to 20 kb. The PSNR values highlight the quality of stego images produced by our proposed method at different payload levels and across diverse cover images. This figure emphasizes how the proposed method maintains image quality while accommodating varying payload sizes, demonstrating its versatility and efficacy in concealing data within digital media.

CONCLUSION

In today's technology landscape, digital photographs have become prevalent elements used for a variety of applications. Digital photographs, because of their ubiquitous use, serve an important role in facilitating the transmission of secret information across public networks. In our study, we present a unique way for increasing the confidentiality of secret data. This method makes use of developments in difference expansion techniques to disguise secret information within digital photographs. This study addresses the significant compromise in stego image quality inherent in spatial domain image steganography. While previous research efforts addressed this issue, a clear trade-off between PSNR and payload size persisted. In comparison to existing approaches, our solution uses an expanded difference expansion to improve performance. Our method's results show a promising advantage over previously described ways, allowing secure transmission of large-sized payloads within digital images while keeping the quality of the cover image.

REFERENCES

1. S. Debnath, R. K. Mohapatra, and R. Dash, “Secret data sharing through coverless video steganography based on bit plane segmentation,” Journal of Information Security and Applications, vol. 78, p. 103612, Nov. 2023, doi: 10.1016/j.jisa.2023.103612.
2. I. B. Prayogi, T. Ahmad, N. J. De La Croix, and P. Maniriho, “Hiding Messages in Audio using Modulus Operation and Simple Partition,” in Proceedings of 2021 13th International Conference on Information and Communication Technology and System, ICTS 2021, Institute of Electrical and Electronics Engineers Inc., 2021, pp. 51–55. doi: 10.1109/ICTS52701.2021.9609028.
3. N. J. De La Croix, C. C. Islamy, and T. Ahmad, “Secret Message Protection using Fuzzy Logic and Difference Expansion in Digital Images,” in Proceedings of the 2022 IEEE Nigeria 4th International Conference on Disruptive Technologies for Sustainable Development, NIGERCON 2022, Institute of Electrical and Electronics Engineers Inc., 2022. doi: 10.1109/NIGERCON54645.2022.9803151.
4. A. J. Ilham, T. Ahmad, N. J. D. La Croix, P. Maniriho, and M. Ntahobari, “Data Hiding Scheme Based on Quad General Difference Expansion Cluster,” Int J Adv Sci Eng Inf Technol, vol. 12, no. 6, p. 2288, Nov. 2022, doi: 10.18517/ijaseit.12.6.16002.
5. K. Kaushik and A. Bhardwaj, “Zero-width text steganography in cybercrime attacks,” Computer Fraud & Security, vol. 2021, no. 12, pp. 16–19, Dec. 2021, doi: 10.1016/S1361-3723(21)00130-5.
6. I. Théophile, N. J. De La Croix, and T. Ahmad, “Fuzzy Logic-based Steganographic Scheme for high Payload Capacity with high Imperceptibility,” in 2023 11th International Symposium on Digital Forensics and Security (ISDFS), IEEE, May 2023, pp. 1–6. doi: 10.1109/ISDFS58141.2023.10131727.

7. N. Bhoskar, "A Survey on Secrete Communication through QR Code Steganography for Military Application," Int J Res Appl Sci Eng Technol, vol. 10, no. 1, pp. 728–731, Jan. 2022, doi: 10.22214/ijraset.2022.39907.
8. N. J. De La Croix and T. Ahmad, "Toward secret data location via fuzzy logic and convolutional neural network," Egyptian Informatics Journal, vol. 24, no. 3, p. 100385, Sep. 2023, doi: 10.1016/j.eij.2023.05.010.
9. J. D. L. C. Ntivuguruzwa, A. Tohari, and M. I. Royyana, "Pixel- block-based Steganalysis Method for Hidden Data Location in Digital Images," International Journal of Intelligent Engineering and Systems, vol. 16, no. 6, pp. 375–385, Dec. 2023, doi: 10.22266/ijies2023.1231.31.
10. J. D. L. C. Ntivuguruzwa and T. Ahmad, "A convolutional neural network to detect possible hidden data in spatial domain images," Cybersecurity, vol. 6, no. 1, p. 23, Sep. 2023, doi: 10.1186/s42400- 023-00156-x.
11. M. Ntahobari and T. Ahmad, "Protecting Data by Improving Quality of Stego Image based on Enhanced Reduced Difference Expansion," International Journal of Electrical and Computer Engineering (IJECE), vol. 8, no. 4, p. 2468, Aug. 2018, doi: 10.11591/ijece. v8i4.pp2468-2476.
12. N. J. De La Croix, C. C. Islamy, and T. Ahmad, "Reversible Data Hiding using Pixel-Value-Ordering and Difference Expansion in Digital Images," in Proceeding - IEEE International Conference on Communication, Networks and Satellite, COMNETSAT 2022, Institute of Electrical and Electronics Engineers Inc., 2022, pp. 33–38. doi: 10.1109/COMNETSAT56033.2022.9994516.
13. P. Maniriho and T. Ahmad, "Information hiding scheme for digital images using difference expansion and modulus function," Journal of King Saud University - Computer and Information Sciences, vol. 31, no. 3, pp. 335–347, Jul. 2019, doi: 10.1016/j.jksuci.2018.01.011.
14. A. Laffont, P. Maniriho, A. Ramsi, G. Guerteau, and T. Ahmad, "Enhanced pixel value modification based on modulus function for RGB image steganography," in 2017 11th International Conference on Information & Communication Technology and System (ICTS), IEEE, Oct. 2017, pp. 61–66. doi: 10.1109/ICTS.2017.8265647.
15. A. Yu, X. Zhang, X. Zhang, G. Li, and Z. Tang, "Reversible Data Hiding with Hierarchical Embedding for Encrypted Images," IEEE Transactions on Circuits and Systems for Video Technology, vol. 32, no. 2, pp. 451–466, Feb. 2022, doi: 10.1109/TCSVT.2021.3062947.
16. W. Tang, B. Li, S. Tan, M. Barni, and J. Huang, "CNN Based Adversarial Embedding with Minimum Alteration for Image Steganography," Mar. 2018, doi: 10.1109/TIFS.2019.2891237.
17. A. N. Fatman, T. Ahmad, N. Jean De La Croix, and Md. S. Hossen, "Enhancing Data Hiding Methods for Improved Cyber Security Through Histogram Shifting Direction Optimization," Mathematical Modelling of Engineering Problems, vol. 10, no. 5, pp. 1508–1514, Oct. 2023, doi: 10.18280/mmep.100502.
18. W. He, G. Xiong, and Y. Wang, "Reversible Data Hiding Based on Multiple Pairwise PEE and Two-Layer Embedding," Security and Communication Networks, vol. 2022, 2022, doi: 10.1155/2022/2051058.
19. The USC-SIPI Image Database. Accessed: Oct. 31, 2023. [Online]. Available: https://sipi.usc.edu/database.

Table 1. Comparison of our results with the existing method in maurice [11]

Cover Image	PSNR (dB)					
	Method in [11]			Proposed Method		
	5kb	10kb	20kb	5kb	10kb	20kb
Abdominal	40.87	38.18	38.17	41.58	38.67	38.66
Leg	40.62	38.93	38.83	41.14	39.8	39.65
Head	34.74	32.72	32.73	35.83	33.54	33.55
Hand	40.65	38.03	38.03	41.44	38.5	38.5
Chest	42.46	39.15	39.05	44.17	40.23	40.04

Average	39.868	37.402	37.362	40.83	38.15	38.08

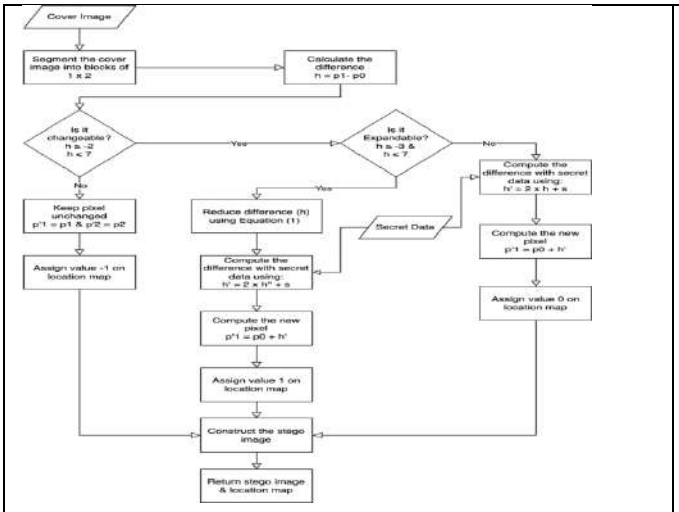

Fig. 1 Flowchart for the embedding process.

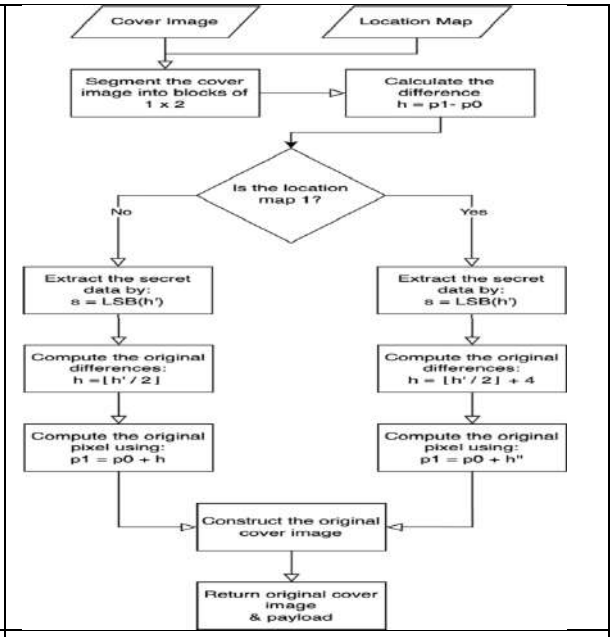

Fig. 2 Flowchart for the data extraction

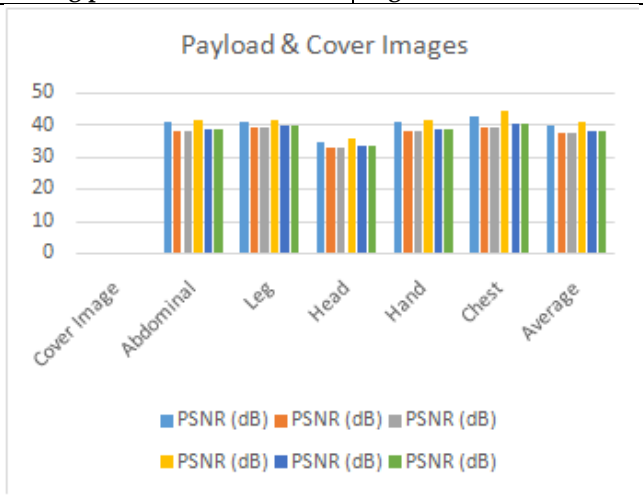

Fig. 3 The Obtained PSNR with the Proposed Method

Vol.15 / Issue 83 / Apr / 2024 International Bimonthly (Print) – Open Access ISSN: 0976 – 0997

RESEARCH ARTICLE

Recognizing Handwritten Digits Using Deep Learning Algorithms

N. Sumathi[1*], Pranesh. K.N[2] and Siddarth A.K[2]

[1]Associate Professor, Department of Information Technology, Sri Ramakrishna College of Arts & Science Coimbatore, Tamil Nadu, India.
[2]PG Student, Department of Information Technology, Sri Ramakrishna College of Arts & Science Coimbatore, Tamil Nadu, India.

Received: 22 Feb 2024 Revised: 15 Mar 2024 Accepted: 21 Mar 2024

***Address for Correspondence**
N. Sumathi
Associate Professor,
Department of Information Technology,
Sri Ramakrishna College of Arts & Science
Coimbatore, Tamil Nadu, India.
Email: sumathi.n@srcas.ac.in

ABSTRACT

Humans now rely on technology more than ever before, and deep learning and machine learning algorithms enable us to do everything from classify objects in photos to add music to silent movies. Similarly, one of the important fields of study and advancement with a seemingly endless supply of potential applications is handwritten text recognition. Handwriting recognition (HWR), alternatively referred to as handwriting Text Recognition (HTR), refers to a computer's capacity to read and comprehend legible handwriting input from many sources, including paper documents, images, touch displays, and other devices. In this paper, it appears that we used Support Vector Machines (SVM), Multi-Layer Perceptron (MLP), and Convolution Neural Network (CNN) models to accomplish handwritten digit recognition with the aid of MNIST datasets. Our major goal is to determine which model is optimal for digit recognition by comparing the execution times and accuracy of the models mentioned above.

Keywords: Multi-Layered Perceptron (MLP), Convolution Neural Network (CNN), MNIST datasets, Deep Learning, Machine Learning, Handwritten Digit Recognition, Support Vector Machines (SVM).

INTRODUCTION

A computer's capacity to identify handwritten letters and numbers from a variety of media, including pictures, documents, touch screens, and more, and group them into ten preset categories is known as handwritten digit recognition (0–9). In the realm of deep learning, this has been an endless source of research. Numerous tasks, such as

sorting mail, processing bank checks, and recognizing license plates, need the use of digitization [1-7]. We have several difficulties in handwritten digit recognition since various people write in different ways, and this type of writing is not optical character recognition. To achieve the goal of handwritten digit recognition, this study offers a thorough comparison of several machine learning and deep learning techniques. Such as Convolutional neural networks, multilayer perceptrons, and support vector machines. Based on the algorithms' accuracy, mistakes, and testing-training times, a comparison is made between them, supported by charts and graphs created using matplotlib for visualization. The accuracy of any model is important because more accurate models yield better outcomes. Real-world applications are unsuitable for models with low precision. Ex: High accuracy is crucial for an automated bank check processing system that can identify the amount and date on the check. It is not ideal if the system detects a digit wrongly since it might cause significant harm. For this reason, a highly accurate algorithm is needed in many practical applications. Therefore, we are presenting an accuracy comparison of several methods so that the most accurate algorithm with the lowest probability of mistakes may be used in a variety of handwritten digit recognition applications[8]. For handwritten digit recognition, this article offers a fair overview of machine learning and deep learning techniques including SVM, CNN, and MLP. Additionally, it provides with the knowledge of which algorithm works best for digit recognition[9-12]. For a more equitable knowledge of the three algorithms, we will first address the technique and implementation of the relevant work that has been done in this subject in later portions of this study. Subsequently, it showcases the outcome and conclusion, supported by the research conducted for this paper. Additionally, it will provide with some possible future developments in this subject. The references and citations utilized are included in the latter portion of this work.

RELATED WORK

Tan and Le proposed EfficientNet, which provides valuable insights into optimizing CNN architectures for improved performance [13]. He et al. introduced ResNet, a groundbreaking CNN architecture that enables the training of extremely deep networks, leading to superior performance in image recognition tasks. ResNet has become a cornerstone in CNN research and has been widely adopted in various applications [14]. Sun et al. revisited the importance of data in the deep learning era and emphasized the need for large-scale, diverse datasets to train robust deep learning models effectively. [15]. Liu et al. proposed DARTS+, an improved version of Differentiable Architecture Search (DARTS), which addresses the instability and inefficiency issues associated with previous methods. By introducing early stopping and weight decay techniques, DARTS+ achieves more stable and reliable architecture search results [16]. Zhang et al. introduced Squeeze-and-Excitation (SE) networks, which allows CNNs to focus on informative features while suppressing irrelevant ones, leading to improved performance in image classification tasks [17]. Pham et al. proposed an efficient method for Neural Architecture Search (NAS) by introducing parameter sharing among child models. This approach significantly reduces the computational cost of architecture search, making it feasible to explore a large search space efficiently [18].

Cubuk et al. introduced Auto Augment, a data augmentation technique that automatically learns augmentation policies from the training data. By dynamically applying a combination of augmentation transformations, Auto Augment improves model generalization and performance. This work highlights the importance of data augmentation in training robust CNN models [19]. Vaswani et al. proposed the Transformer model, which utilizes self-attention mechanisms to capture long-range dependencies in sequential data [20]. Simonyan and Zisserman introduced VGGNet, a CNN architecture known for its simplicity and effectiveness. VGGNet consists of multiple convolutional layers with small filter sizes, stacked on top of each other[21]. The existing handwritten digit classification system utilizes a Support Vector Machine (SVM) algorithm to compare pixel values of input images with known digit representations, ultimately identifying the closest match and outputting the corresponding digit. Despite its simplicity, the system faces challenges in accuracy and scalability. Accuracy is compromised by variations in input image quality, while scalability is hindered by increasing dataset size, leading to computational complexity. Additionally, the pixel-level comparison may fail to capture intricate features in handwritten digits, resulting in suboptimal classification accuracy, especially for complex inputs. Unlike the existing system based on Support Vector Machine (SVM), CNNs offer superior accuracy and robustness to variations in input image quality.

PROPOSED METHODOLOGY

The proposed system for handwritten digit classification adopts a Convolutional Neural Network (CNN), a specialized deep learning algorithm tailored for image classification tasks. Unlike the existing system based on Support Vector Machine (SVM), CNNs offer superior accuracy and robustness to variations in input image quality. By leveraging CNNs, the proposed system can effectively capture intricate features in handwritten digits, leading to enhanced classification accuracy. Additionally, CNNs can be trained on larger datasets containing known digit representations, further improving their accuracy and generalization capability. Overall, the proposed CNN-based system offers a more advanced and effective approach to handwritten digit classification, promising superior performance and reliability compared to the existing SVM-based system.

Model Architecture

Design the Model Architecture: The architecture of the classification model is designed, considering options such as a Multi-Layer Perceptron (MLP) with one hidden layer or a Convolutional Neural Network (CNN). The chosen architecture should be capable of effectively learning and classifying handwritten digits from the MNIST dataset. The Architectural layer of CNN shown in figure 1 depicts the working process of the recognizing system.

Techniques

1. MLP: A simple feed forward neural network with one hidden layer. The number of 10 neurons in the hidden layer, activation functions, and output layer size are defined based on the requirements of the classification task.
2. CNN: A more complex architecture comprising convolutional and pooling layers followed by fully connected layers. CNNs are well-suited for image classification tasks and can capture spatial hierarchies of features in the input images.

Model Training

Train the Model

The model is trained by feeding training images and corresponding labels into the neural network. During training, the model adjusts its parameters through backpropagation, where gradients of the loss function with respect to the model parameters are calculated and used to update the weights of the network. This iterative process enables the model to learn to correctly classify digits based on the input images.

Techniques

1. Back propagation: Back propagation is a key technique used in training neural networks. It involves propagating the error backwards from the output layer to the input layer, adjusting the weights of the network to minimize the error. This process is repeated iteratively until the model converges to a satisfactory solution.
2. **Optimization Algorithms (Adam):** Optimization algorithms like Adam are employed to efficiently minimize the loss function during training. Adam combines the advantages of two other popular optimization techniques, AdaGrad and RMSProp, by maintaining separate learning rates for each parameter and adapting them based on past gradients and squared gradients.

Data Loading and Preprocessing

1. Load MNIST Dataset: Use TensorFlow or Keras to load the MNIST dataset, containing handwritten digit images and corresponding labels.
2. Normalize Pixel Values: Apply min-max normalization to normalize pixel values of the images to the range [0, 1]. This normalization ensures uniformity in input feature scales, aiding in efficient training and model convergence.
3. Convert to Grayscale: Convert the images to grayscale to remove color information, simplifying the input data while retaining relevant features necessary for digit classification.
4. Resize Images: Resize the images to a desired dimension, typically 28x28 pixels. Resizing ensures uniformity in input size across all images.

IMPLEMENTATION

We have utilized three distinct classifiers to compare the algorithms based on working accuracy, execution time, complexity, and the number of epochs (in deep learning methods):

1. Convolutional Neural Network Classifier;
2. ANN - Multilayer Perceptron Classifier;
3. Support Vector Machine Classifier.

The implementation of each method has been covered in depth below, along with the analysis's flow to produce an accurate and seamless comparison.

PRE-PROCESSING

The first stage of machine and deep learning is called pre-processing, and it aims to enhance the input data by removing unnecessary redundancies and contaminants. All of the photos in the dataset were molded into 2-dimensional images, or (28,28,1), in order to simplify and deconstruct the input data. Since the picture pixel values varied from 0 to 255, we normalized the pixel values by dividing the dataset by 255.0 and converted the dataset to 'float32.' This allowed the input features to range from 0.0 to 1.0. The y values were thentranslated into zeros and ones using one-hot encoding, which made each number categorical. For instance, an output value of 4 would be transformed into an array of zeros and ones, or [0,0,0,0,1,0,0,0,0,0]

SUPPORT VECTOR MACHINE

Scikit-learn's SVM accepts as input sample vectors that are sparse (any scipy.sparse) or dense (numpy.ndarray and converted to that by numpy.asarray). SVC, NuSVC, and LinearSVC in scikit-learn are classes that can sort data into several classes. Using a linear kernel that was constructed with the aid of LIBLINEAR, we employed LinearSVCin this research to classify MNIST datasets [22]. The implementation has made use of several scikit-learn packages, including NumPy, matplotlib, pandas, Sklearn, and seaborn. Prior to loading and reading the CSV files using pandas, we will first obtain the MNIST datasets. Following that, several samples were plotted, and the data was converted into a matrix, normalized, and scaled. In the end, we developed a linear SVM model and a confusion matrix to assess the model's accuracy.

MULTILAYERED PERCEPTRON

The application of feed forward artificial neural networks, or multilayer perceptrons, for the recognition of handwrittendigits is carried out by utilizing the Keras module to build an MLP model of the sequential class and add corresponding hidden layers with distinct activation functions to receive an image with a pixel size of 28 x 28 as input. We added a dense layer with various requirements and drop out layers after building a sequential model.We employed an output layer with 10 units (i.e., the total number of labels) in a neural network with 4 hidden layers. There are always 512 units in the hidden layers. The 784-dimensional array created from the 28×28 picture serves as the network's input. We constructed the network using the Sequential model. By adding the necessary layer one at a time, we may simply stack layers in the sequential model. Since we are creating a feed forward network in which all of the neurons from one layer are connected to the neurons in the layer before it, we utilized the Dense layer, also known as a completely connected layer. In addition to the Dense layer, we included the ReLU activation function, which is necessary to give the model non-linearity. By doing this, the network will be able to learn non-linear decision limits. Since the problem involves multiclass classification, the final layer is a softmax layer .

CONVOLUTIONAL NEURAL NETWORK

Keras is used in the development of Convolutional Neural Network for handwritten digit recognition. It's an open-source neural network library used for deep learning model construction and implementation. The Convolutional Neural Network (CNN) architecture, depicted in figure 2, is a powerful deep learning model widely employed for image recognition tasks. The network comprises several key components arranged in a sequential manner. At the

beginning lies the Input Layer, where raw image data is ingested. Subsequently, Convolutional Layers process the input through learnable filters, detecting features like edges and textures. Following each convolution operation, Activation Functions, typically ReLU, introduce non-linearity to the network, aiding in capturing complex patterns. The feature maps produced are then subjected to Pooling Layers, which down sample the spatial dimensions while retaining crucial information. The Fully Connected Layers aggregate these high-level features, leading to the final Output Layer, where predictions or classifications are made. Throughout training, a Loss Function measures the disparity between predicted and actual outputs, guiding optimization via back propagation. This process is facilitated by Optimization Algorithms such as Stochastic Gradient Descent, ensuring continual refinement of the network's parameters. This CNN framework enables robust and efficient learning, making it a cornerstone in modern image analysis and classification tasks.

EXPERIMENTAL RESULTS

Handwritten character recognition is a broad field of study with well-defined implementation strategies already in place. These strategies include popular algorithms, large learning datasets, feature scaling, and feature extraction techniques. The NIST dataset is made up of two NIST databases: Special Database 1 and Special Database 3. A portion of the NIST collection is the MNIST dataset, or Modified National Institute of Standards and Technology database. Special Database 1 and Special Database 3 comprise entries penned by high school students and US Census Bureau staff, respectively. The MNIST dataset comprises 70,000 handwritten digit pictures in a 28x28 pixel bounding box with anti-aliasing (60,000 for the training set and 10,000 for the test set). Each of these pictures has a matching Y value that indicates the digit. We examined the accuracy and execution time of the three algorithms—SVM, MLP, and CNN—after putting them all into practice using experimental graphs to ensure clear comprehension. All the previously mentioned models' training and testing accuracy have been considered. After running every model, we discovered that SVM achieves thebest accuracy on training data, whereas CNN achieves the best accuracy on testing data. To learn more about how thealgorithms function, we have also compared the execution times. An algorithm's running time is typically influencedby the quantity of operations it has completed. To obtain the desired result, we have trained our SVM models using norms and our deep learning model for up to 30 epochs. CNN accounts for the most running time, whereas SVM requires the least amount of time to execute. Each model's accuracy is shown in this Table 1. Additionally, we showed how deep learning models improved accuracy and decreased error rate in relation to the number of epochs by visualizing their performance measure. Drawing the graph is important because it helps us determine whether to apply an early stop and prevent over fitting, which occurs when accuracy changes steadily over a period of epochs. precision measures the model's ability to make accurate positive predictions while minimizing false positives as shown in the figure 3.

CONCLUSION AND FUTURE ENHANCEMENT

Using MNIST datasets, this research study constructed three models for handwritten digit recognition: Support Vector Machine, Multi-Layer Perceptron, and Convolutional Neural Network. It evaluated them based on the number of epochs (in deep learning techniques), working accuracy, complexity, and execution time to determine which model was the most accurate and came to the following conclusion: Because SVM is a fundamental classifier, it performs faster than most other algorithms and, in this instance, yieldsthe greatest training accuracy rate. However, because of its simplicity, it is unable to identify complicated and ambiguous pictures with the same level of accuracy as MLP and CNN algorithms. When time is considered, it is discovered that the MLP model produces nearly the same accuracy rate as the CNN model in a very efficient amount of time. However, the only disadvantage is that it is unable to sustain the classification rate in complex images for extended periods of time because it is unable to comprehend the spatial relationships between image pixels to the same extent as CNN. The highest accurate results for handwritten digit recognition were obtained using CNN; the only disadvantage is that it required exponential

processing time. Due to a particular model's limitations, extending the number of epochs without altering the algorithm's configuration is pointless. It has been observed that the model begins to overfit the dataset beyond a predetermined number of epochs, which results in biased predictions. Thus, it confirms that, when compared to SVM and MLP, CNN has the highest accuracy rate for any kind of prediction issue including image data as an input. The possibilities for developing applications based on deep and machine learning techniques are essentially endless. In the future, it will be possible to solve many issues by working on denser or hybrid algorithms that use more manifold data than the current collection of methods.

REFERENCES

1. Niu, X.X.; Suen, C.Y. A novel hybrid CNN–SVM classifier for recognizing handwritten digits. Pattern Recognit. 2012, 45, 1318– 1325.
2. Long, M.; Yan, Z. Detecting iris liveness with batch normalized convolutional neural network. Compute, Mater. Contin. 2019, 58, 493–504.
3. Y. LeCun et al., "Backpropagation applied to handwritten zip code recognition," Neural computation, vol. 1, no. 4, pp. 541-551, 1989.
4. Sueiras, J.; Ruiz, V.; Sanchez, A.; Velez, J.F. Offline continuous handwriting recognition using sequence to sequence neural networks. Neuro computing. 2018, 289, 119–128.
5. Wells, Lee & Chen, Shengfeng&Almamlook, Rabia&Gu, Yuwen. (2018). Offline Handwritten Digits Recognition Using Machine learning.
6. Burel, G., Pottier, I., &Catros, J. Y. (1992, June). Recognition of handwritten digits by image processing and neural network. In Neural Networks, 1992. IJCNN, International Joint Conference on (Vol. 3, pp. 666-671) IEEE.
7. Salvador España-Boquera, Maria J. C. B., Jorge G. M. and Francisco Z. M., "Improving Offline Handwritten Text Recognition with Hybrid HMM/ANN Models", IEEE Transactions on Pattern Analysis and Machine Intelligence, Vol. 33, No. 4, April 2014.
8. Ahmed, M., Rasool, A. G., Afzal, H., & Siddiqi, I. (2017). Improving handwriting-based gender classification using ensemble classifiers. Expert Systems with Applications, 85, 158-168.
9. Sadri, J., Suen, C. Y., & Bui, T. D. (2007). A genetic framework using contextual knowledge for segmentation and recognition of handwritten numeral strings. Pattern Recognition, 40(3), 898-919.
10. Sarkhel, R., Das, N., Das, A., Kundu, M., &Nasipuri, M. (2017). A multi-scale deep quad tree based feature extraction method for the recognition of isolated handwritten characters of popular Indic scripts. Pattern Recognition, 71, 78-93.
11. Dutta and A. Dutta, Handwritten digit recognition using deep learning, International Journal ofAdvanced Research in Computer Engineering & Technology (IJARCET), vol. 6, no. 7, July 2017.
12. Al Maadeed, Somaya, and Abdelaali Hassaine, Automatic prediction of age, gender, and nationality in offline handwriting. EURASIP Journal on Image and Video Processing, no. 1 2014.
13. Tan, M., & Le, Q. V. (2019). EfficientNet: Rethinking Model Scaling for Convolutional Neural Networks. In International Conference on Machine Learning (pp. 6105-6114).
14. He, K., Zhang, X., Ren, S., & Sun, J. (2016). Deep residual learning for image recognition. In Proceedings of the IEEE conference on computer vision and pattern recognition (pp. 770-778).
15. Sun, C., Shrivastava, A., Singh, S., & Gupta, A. (2019). Revisiting Unreasonable Effectiveness of Data in Deep Learning Era. In Proceedings of the IEEE conference oncomputer vision and pattern recognition (pp. 843-852).
16. Liu, H., Simonyan, K., & Yang, Y. (2021). DARTS+: Improved Differentiable Architecture Search with Early Stopping. In Proceedings of the IEEE/CVF Conferenceon Computer Vision and Pattern Recognition (pp. 1909-1918).
17. Zhang, X., Zhou, X., Lin, M., & Sun, J. (2018). Squeeze-and-Excitation Networks. In Proceedings of the IEEE conference on computer vision and pattern recognition (pp. 7132-7141).
18. Pham, H., Guan, M. Y., Zoph, B., Le, Q. V., & Dean, J. (2018). Efficient Neural Architecture Search via Parameter Sharing. arXiv preprint arXiv:1802.03268.

19. Cubuk, E. D., Zoph, B., Mane, D., Vasudevan, V., & Le, Q. V. (2019). AutoAugment: Learning Augmentation Policies from Data. In Proceedings of the IEEE conference oncomputer vision and pattern recognition (pp. 113-123).
20. Vaswani, A., Shazeer, N., Parmar, N., Uszkoreit, J., Jones, L., Gomez, A. N., & Polosukhin, I. (2017). Attention is all you need. In Advances in neural information processing systems (pp. 5998-6008).
21. Simonyan, K., & Zisserman, A. (2014). Very deep convolutional networks for large-scale image recognition. arXiv preprint arXiv:1409.1556.
22. https: //github.com/rishikakushwah16/SV M digit recognition using MNIST dataset.

Table 1: Comparison Analysis of Different Models.

S.NO	MODEL NAME	ACCURACY
1	SVM	94.65%
2	MLP	98.85%
3	CNN	99.56%

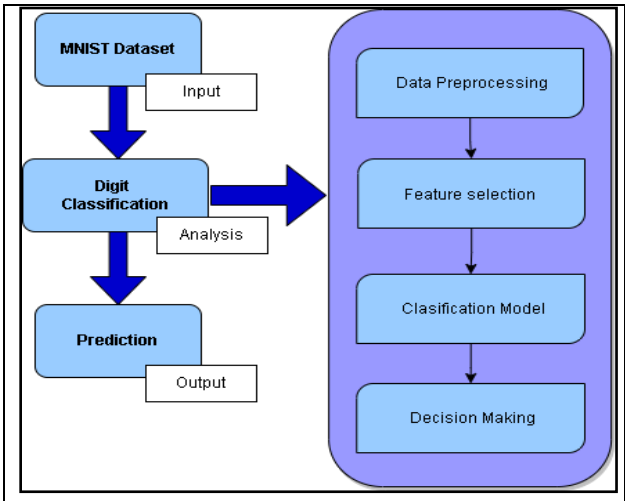

Figure 1. The architectural layer of the CNN.

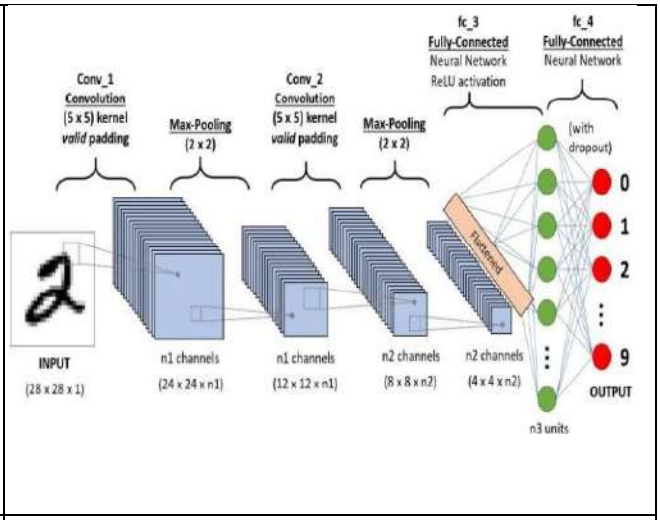

Figure 2. Framework of Convolutional Neural Network.

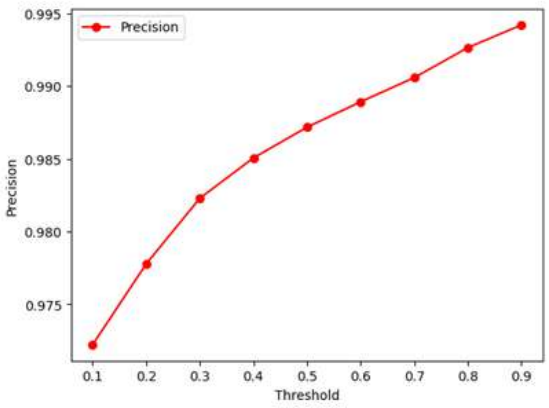

Figure 3. Precision graph of CNN using MNIST dataset

REVIEW ARTICLE

Security, Trust, and Privacy of Information Sharing In Social Networking Sites: A Systematic Literature Review

V. Padmaja[1], MuniKrishnappa AnilKumar[2], Sirigiri Srikanth[3]*, Pocha Sri Chandana[3].

[1]Professor, M.S. Ramaiah Institute of Management, Bengaluru, Karnataka, India.
[2]Assistant Professor, M.S. Ramaiah Institute of Management, Bengaluru, Karnataka, India.
[3]PGDM 1st year, M.S. Ramaiah Institute of Management, Bengaluru, Karnataka, India.

Received: 27 Feb 2024 Revised: 03 Mar 2024 Accepted: 20 Mar 2024

***Address for Correspondence**
Sirigiri Srikanth
PGDM 1st year,
M.S. Ramaiah Institute of Management,
Bengaluru, Karnataka, India.
Email: sirigirisrikanth231139@msrim.org

ABSTRACT

The influx of netizens using social media platforms, sharing of information online has become the norm, and there is a constant threat to security and data privacy concerns. Though much research has been done on privacy issues emerging in social media interactions, very limited systematic literature review has been done to get a comprehensive understanding of the issue. This study has been undertaken through a systematic literature review which highlights the challenges and opportunities related to security, trust, and privacy in social networking sites. The study includes three social networking sites namely Facebook, Twitter and Instagram, and has identified potential strategies, technological solutions, and policy implications to mitigate risks and foster a safer and more trustworthy social media environment, which can be beneficial to users and platform developers. The results of the study have significant implication to academicians, policy makers, and industry on current understanding of the problem area. The study will enhance a comprehensive understanding of the complex dynamics like security threats, privacy concerns, and trust issues inherent in the context of social media information sharing, with a focus on security, trust, and privacy. It is a significant endeavor with potential real-world implications.

Keywords: Security, Trust, Privacy, Information, Social networking sites.

INTRODUCTION

With the advent of social networking sites, individuals were seen voluntarily disclosing personal information in various forms, which raises especially important questions for individual privacy and civil liberties *(Benson et al.,*

2015). Social media networking sites serve as virtual spaces where individuals, groups, and organizations can connect, share information, and interact with each other. They facilitate communication, collaboration, and community-building across geographic boundaries *(Gupta & Dhami, 2015).* Social networking sites have changed from a social experiment to a way of interpersonal communication *(Papaioannou et al., 2021)*. These platforms differ from one another and offer unique features to their users, with wide variety of options available on social networking sites. We have created and maintained virtual profiles, which are digitalized and contain different sets of information about their users for this purpose. Nowadays, the cause of excessive information sharing of information online in the digital age has its advantages and disadvantages, the whole depends on how you present yourself to others in online. Digitalization of data raises issues such as security, trust, privacy of sharing personal information on online. These social network sites have a large user database that provides users with information across the Globe. Thus, the information that we share, and shared on these platforms may not always be safe and secure as we expect, and there are certain risks pertaining to the data disclosure. This paper helps to understand, analyze, and take action to reduce the sharing of our personal information on online. It has also educated the netizens about the awareness of information sharing on social media networking sites with some real-world implications. Social network administrators have taken several steps to ensure the security of users' information and privacy. There are several privacy and trust concerns that social network users need to know about *(Papaioannou et al., 2021)***.** The main concern of sharing the information is that the information is more visible and accessible where the issues pertaining to security, trust, and privacy arise. To ensure the privacy of users, social network administrators have implemented several security measures. For the purpose of this research, the following questions have been framed:

RQ1: is there any safety about the information that is being shared on social networking sites?

RQ2:what kind of awareness can be created amongst the netizens regarding information being shared online?

The key challenges and issues discussed in this paper will ease the process of understanding and mitigating risks and thus systematically developing various dimensions of security, trust, and privacy.

METHODOLOGY

The study focuses on secondary data available in Scopus data base, inthe form of existing literature and research papers published on this topic. The Scopus database was filtered using the search string [TITLE/ABSTRACT] OR 'security' AND 'privacy' AND 'trust' AND 'social' AND 'media' AND 'networking' AND 'sites' [TITLE/ABSTRACT/KEYWORD], the operator used namely 'AND.' Further, articles were filtered using PRISMA.PRISMA is an evidence-based on minimum set of items for reporting systematic reviews and meta-analyses. PRISMA stands for Preferred Reporting Items for Systematic Reviews and Meta-analyses. The latest articles on security, privacy, and trust concerns of information sharing were taken into consideration while drafting this research paper. This is a Boolean Search of using a combination of "AND, OR" it produces accurate results while avoiding the irrelevant. Various cyber security websites such as AAG IT Services and Gitnux have been referred for statistics that has been used for actual data. A total of 67 documents (as on December 14th, 2023) were available in Scopus data base on the theme 'security, privacy, and trust' in social networking sites and six research papers were available in the context. The documents were downloaded and stored in the reference management software, Zotero. These papers have been further filtered based on 'document type', 'publication stage', and 'language'. Final filtration with six documents have been considered for the study. The discussion and findings have been framed after reviewing these six research papers.

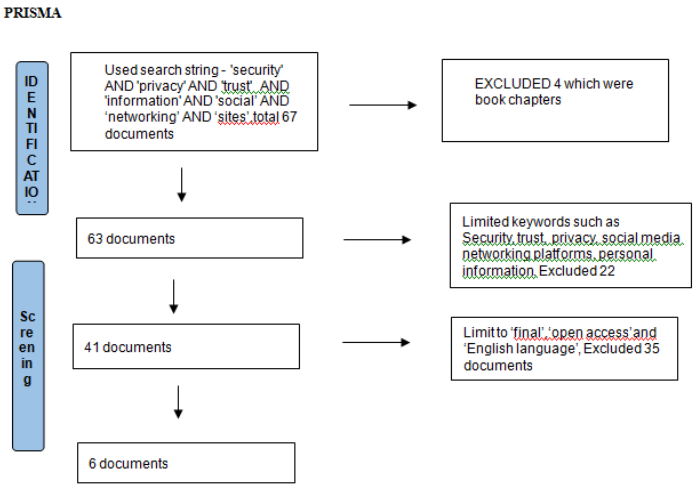

Findings

As the social media hacking statistics show(AAG IT Services), any individual can be a target for any reason. Multi-billion-dollar corporations can be attacked as well as individuals with modest incomes. Regardless of the identity of an individual, what platforms are used by an individual or how much wealth one has, anyone can be targeted. According toreport of AAG IT Services (Jan 2024), 68000 users have enquired about remedies on Facebook when it was hacked, and even Instagram has got 36000 queries a month on the remedies for hacked accounts. As per the report of Gitnux , 530 million Facebook accounts are compromised by exposing their passwords, phone numbers, and account names. It is the same month and year for LinkedIn as well, where 750 million users i.e., 93% of total users resulted in the exposure of the client's phone numbers, emails, usernames, and geolocation records. As per the report compiled (January 2024) by AAG IT Services, a staggering 85% of Instagram accounts have been compromised, with an additional 25% of Facebook accounts falling victim to hijacking. These statistics are quite alarming, and highlight the urgent need for enhanced cybersecurity measures to protect individual's personal information and privacy online. Moreover, major corporations face relentless attempts by black hat hackers, with an average of 30 annual hacking incidents on their corporate social media accounts alone. The high-profile nature of some victims, from business tycoons to politicians, serves as a stark reminder of the pervasive threat posed by cybercrime in today's digital age. Real-time data breach cases can help to understand the stated objectives in this research.

Facebook data breach

Despite Facebook (META) being the giant in social networking sites, its app's developer Aleksandar Kogan, was allowed to gather data on users. In the end, Kogan amassed data from 87 million users, which he then gave to the political consulting business Cambridge Analytica in 2016. Cambridge Analytica utilized the data to create voter profiles and their political views to target and influence public opinion. Whistleblower Christopher Wylie of Cambridge Analytica claims that the company utilized this information to assist Donald Trump's campaign in influencing votes in the 2016 presidential election. Many have referred to this episode as a data breach. European and American regulators have forced CEO Mark Zuckerberg to appear before Congress, and the U.S.Federal Trade Commission and other international agencies are conducting an official inquiry into Facebook's privacy policies. This incident has raised doubts about the information netizens give to these networking sites and has emphasized the importance of being aware of what they post and who they believe.

Twitter data breach

A significant security breach on Twitter in July 2020 resulted in the compromising of well-known accounts and Bitcoin fraud. Twitter itself confirmed that the intruders had gained access to Twitter's administrative tools so that they could alter accounts themselves and post the tweets directly. This made the platform suspend tweets from verified accounts until the issue was resolved. The law enforcement authority's investigation was made and there was a negative impact on the stock value of Twitter. People were worried about how secure their accounts were and how open the platform was to these kinds of assaults. The incident prompted inquiries over the efficacy of Twitter's security protocols. Twitter must put in place more security measures and be open and honest about the issue to win back user trust

Instagram data leak

A large database operated by a third-party company holding the confidential data of millions of Instagram influencers, celebrities, and brand accounts was uncovered by a security researcher in 2019. High-profile Instagram user's email addresses and contact details were made public. 49 million Records were exposed in this data leak. The database was linked to a marketing firm in India. People were concerned about the possible exploitation of their personal information, especially celebrities and influencers. The issue brought to light worries over Instagram user data access by other parties. Users' confidence in the security of Instagram was impacted by critics of the platform's data protection policies.

DISCUSSIONS

In today's digital age, where information is readily shared and accessed through social media networking platforms, security, trust, and privacy concerns have become paramount. Recent incidents such as the Instagram data scraping in 2021, TikTok's ongoing data privacy concerns, and Google's data breach in 2018 have brought to light about the vulnerabilities that users face, when sharing personal information on online. These events have scored the importance of robust security measures and increased transparency from social media companies to protect user data. The mishandling of user information on these platforms not only erodes trust between users and theplatform but also raises questions about the commitment of these companies to safeguard user privacy. As increased people rely on social media for communication, entertainment, and even business purposes, stringent protocols must be put in place to prevent unauthorized access to personal data. Social networking sites consist of virtual profiles that maintain ties and can be shared with others *(Papaioannou et al., 2021)*. A digital identity is formed through information that the individual shares in public and personal data disclosure is part of this process. Individuals come into contact, with information that compares them socially with others, such as photos, which can negatively affect their personal lives and privacy *(Gupta & Dhami, 2015)*. In this digital age, it has majorly raised concerns about privacy, permission, and responsible data usage due to the vast amount of personal information collected and shared online. The ethical dilemma lies in striking a balance between privacy and tailored services.

Unauthorized data usage or repurposing can have unanticipated negative effects on public and commercial sectors. Some academicians argue that in a networked world, information privacy is no longer under the control of individuals but rests with organizations holding the information *(Benson et al., 2015).* Moreover, privacy has evolved significantly due to technological advancements, social changes, and cultural shifts. As online interactions and personal information sharing become common, users' behavior on social media platforms has changed. Privacy concerns refer to a user's concerns about the possible loss of privacy due to voluntary or surreptitious information disclosure *(Chang & Liu, 2023)*. The security, trust, and privacy concerns surrounding information sharing on social media networking platforms are more prevalent than ever. With the ability to personalize user experiences and perpetuate biases, these platforms can inadvertently create filter bubbles that influence user perceptions and exacerbate societal divisions. Additionally, the potential for governments and law enforcement agencies to leverage social media data for surveillance purposes raises fundamental questions about civil liberties and the right to privacy. Users seek transparency on data usage and platform operators, and companies with ethical practices gain

more user trust. Social media platforms are popular for both social interactions and business transactions, presenting new challenges around information and their privacy (Benson et al., 2015)**.**Furthermore, the wealth of personal information contained within social media profiles leaves users vulnerable to identity theft and impersonation. The ease of communication and anonymity provided by these platforms also open the door to cyber bullying and harassment, posing risks to user safety and well-being. To further our understanding of information security and privacy, when sharing data on social networking sites, we have carried out an experiment. To do this, we have made a few virtual accounts and posted some bogus information in them. We learnt that some intruders had acquired the material information and were sending us spam emails and links through various accounts that helps to easily track mobile phones and the information stored in them as well. Another significant instance involves cyber-stalkers who create fake profiles, pursue strangers, and gather their personal information for the purpose of data exploitation and extortion. These crimes have become so severe that even cybercrime can't control them to the full extent. The research further elaborates about the measures that must be taken by netizens and social media platform developers to mitigate the risks. The following measures can be takento mitigate the challenges faced by netizens:

By platform developers

Protect data with intrusion detection, secure authentication, and robust encryption. Update your software and security patches often to keep up with emerging danger. Utilize cutting-edge threat detection technology to promptly identify and address security problems. Give consumers more control over their privacy by giving them access to more options including evaluating app permissions, restricting data sharing, and modifying visibility settings. Keep an eye out for unusual activities, security breaches, and questionable conduct on social networking. Establish a robust incident response strategy event promptly, limit harm, and lower the possibility of user impact. Provide protocols for communicating about crises a reporting data breaches. Work together to share threat intelligence, best practices and helpful law enforcementwith social media platforms, cyber research, law enforcement, and other industry partners.

By users

Set distinct passwords for every social media platform you use. Employ capital, lowercase, and special characters. To generate and save distinct passwords for your accounts, use only a reliable password manager. If at all feasible, use two factor-authentication. Make sure you know who sent the message before clicking. Steer clear of abbreviated URLs that conceal dangerous links. When you get demands for private information, especially through unsolicited emails or messages, use caution. To confirm the authenticity of the request, get in touch with the sender. To manage who may see your information, relationships, posts, and profile on social media, you should periodically review and modify your privacy settings. Restrict how much personal information you post on social media. That too reliable contacts. Recognize typical cyberthreats, assaults, and strategies employed by cybercriminals, such as phishing scams.

Scope for further research

The research can be extended to a mixed-method approach by using both qualitative and quantitative data. Also, more databases can be referred to understand the dimensions of trust, privacy, and security to get a more comprehensive understanding.

CONCLUSION

The study highlights the importance of adopting a strategic and holistic approach to data privacy, security, and trust. By being more vigilant about the information we share in online and actively managing our privacy settings, individuals can better protect themselves from potential risks. Social media companies must also prioritize user data protection by implementing robust security measures and ensuring transparency in how they handle our

information. Only through collective efforts can we effectively address the challenges of data privacy and ensure that all users are adequately protected in the digital landscape.

REFERENCES

1. Alhadid, I., Abu-Taieh, E. M., Al Rawajbeh, M., Alkhawaldeh, R. S., Khwal-Deh, S., Afaneh, S., Alrowwad, A., & Alrwashdeh, D. F. (2023). Evaluating the influence of security considerations on information dissemination via social networks. In *International Journal of Data and Network Science* (Vol. 7, Issue 4, pp. 1471–1484). Growing Science. https://doi.org/10.5267/j.ijdns.2023.8.015
2. Benson, V., Ezingeard, J.-N., & Hand, C. (2019). An empirical study of purchase behaviour on social platforms: The role of risk, beliefs and characteristics. In *Information Technology and People* (Vol. 32, Issue 4, pp. 876–896). Emerald Group Holdings Ltd. https://doi.org/10.1108/ITP-08-2017-0267
3. Dhami, A., Agarwal, N., Chakraborty, T. K., Singh, B. P., & Minj, J. (2013). Impact of trust, security and privacy concerns in social networking: An exploratory study to understand the pattern of information revelation in Facebook. In *Proceedings of the 2013 3rd IEEE International Advance Computing Conference, IACC 2013* (pp. 465–469). https://doi.org/10.1109/IAdCC.2013.6514270
4. Gupta, A., & Dhami, A. (2015). Measuring the impact of security, trust and privacy in information sharing: A study on social networking sites. In *Journal of Direct, Data and Digital Marketing Practice* (Vol. 17, Issue 1, pp. 43–53). Palgrave Macmillan. https://doi.org/10.1057/dddmp.2015.32
5. Halim, E., Ikhsan, A. F., Suhartono, J., & Hebrard, M. (2023). Gen-Z Awareness of Data Privacy Using Social Media. In *Proceedings of 2023 International Conference on Information Management and Technology, ICIMTech 2023* (pp. 562–567). Institute of Electrical and Electronics Engineers Inc. https://doi.o rg/10.1109/IC IMTech59029 .2023.10277920
6. Koohang, A., Nord, J. H., Floyd, K., & Paliszkiewicz, J. (2022). Social media privacy and security concerns: Trust and awareness. In *Issues in Information Systems* (Vol. 23, Issue 3, pp. 253–264). International Association for Computer Information Systems. https://doi.org/10.48009/3_iis_2022_121
7. Papaioannou, T., Tsohou, A., & Karyda, M. (2021). Forming digital identities in social networks: The role of privacy concerns and self-esteem. In *Information and Computer Security* (Vol. 29, Issue 2, pp. 240–262). Emerald Group Holdings Ltd. https://doi.org/10.1108/ICS-01-2020-0003
8. http://www.aag-it.com
9. https://aag-it.com/the-latest-cyber-crime-statistics/
10. https://gitnux.org/

Indian Journal of Natural Sciences www.tnsroindia.org.in ©IJONS

Vol.15 / Issue 83 / Apr / 2024 *International Bimonthly (Print) – Open Access* *ISSN: 0976 – 0997*

RESEARCH ARTICLE

Detecting Deep Fakes: Leveraging Convolutional Neural Networks for Fabricated Media Classification

Prem Sagar*

Assistant Professor, Department of Computer Science St. Joseph's University, Bangalore - 27, Karnataka, India.

Received: 27 Feb 2024 Revised: 03 Mar 2024 Accepted: 20 Mar 2024

***Address for Correspondence**
Prem Sagar
Assistant Professor,
Department of Computer Science,
St. Joseph's University,
Bangalore - 27, Karnataka, India.
Email: prem.sagar_@sju.edu.in

ABSTRACT

Deepfakes, synthesized media in which a person's likeness is swapped into a source image, are becoming increasingly harmful. Face swapping into intimate imagery infringes on personal privacy. Detecting deep fakes and differentiating them from real videos is therefore an important challenge. This research proposes a deep learning (Machine Learning) approach for deep fake detection. A Convolutional neural network model with Python and OpenCV is trained on a dataset of real and synthesized images to classify images as real or fake. Key features used by the models include inconsistencies in facial expressions, lighting, and skin textures that expose manipulated imagery. The work demonstrates deep learning's capabilities in identifying fabricated media and lays the groundwork for reliable deepfake classification. This technology will help curb the spread of misinformation and authentication of visual evidence as deep fakes grow more advanced and accessible.

Keywords: Deepfake, Machine Learning, Neural networking, Privacy, Manipulated imagery, convolutional neural network.

INTRODUCTION

Deepfakes, a combination of "deep learning" and "fake", refer to media generated or manipulated by artificial intelligence to depict events that never occurred or to falsify identities. Advances in generative adversarial networks and autoencoders have enabled creation of increasingly realistic deepfakes, spurring alarm over potential misuse for non-consensual pornography, financial fraud through identity theft, and disinformation campaigns. Detecting deepfakes has therefore emerged as a major challenge at the intersection of machine learning, computer vision, and information forensics.

Convolutional neural networks (CNNs) have become essential in many artificial intelligence tasks involving visual data. As research progresses on deepfake classification, CNN architectures have emerged as promising solutions due to their capabilities in feature extraction. CNNs incorporate insights from processing in the human visual cortex and contain specialized layers optimized for spatial hierarchical feature maps. This equips them well to accurately classify real versus synthetic image or video samples. Though originally focused on the computer vision challenge of image recognition, CNNs now demonstrate success across natural language processing, medical imaging, and other applications. For deepfake detection specifically, CNN models show strength in learning robust discriminative representations to identify manipulated regions. While early detection methods focused on computer graphics artifacts, advanced techniques use convolutional neural network (CNN) architectures to learn robust visual features. However, the tools used to create deepfakes are getting better at making them look real and tricking detection systems. This back-and-forth competition between creating and spotting deepfakes means we need to improve how we design CNN models to keep up. This study aims to benchmark convolutional network architectures for deepfake classification based on face and scene representations. This paper carefully selects new datasets that combine computer graphics and neural synthesis techniques to cover distributional gaps. Using these datasets, experiments evaluate the accuracy and operational characteristics of the receiver and identify optimal model architectures, loss functions, and training regimes. This method and analysis can help forensic and fact-finding experts to authenticate media sources.

Deepfake Creation

Deepfakes leverage generative adversarial networks (GANs) to alter or synthesize visual content by modeling underlying data distributions. GANs comprise opposing generator and discriminator models optimized in tandem. The generator tries creating synthetic samples indistinguishable from real data while the discriminator classifies between the two. This builds generative representations rivaling target distribution complexity. For facial manipulation, early works like DeepFakes exploited autoencoder neural networks. By training autoencoders on image sets of two distinct identities, they encoded and reconstructed faces. Blending output codes then enabled facial identity swaps. Subsequent pioneering efforts further honed GAN pipelines for photorealistic face and voice replacements. The DeepFake algorithm introduced an end-to-end stacking of generative networks with semantic segmentation and smoothing stages. Follow up works have incorporated temporal signals like landmark heatmaps and optical flow to enhance consistency in videos. Notable implementations built upon these innovations include DeepFaceLab, ZAO and Faceswap leveraging advances in Variational Autoencoders. Enhanced resolutions combined with scalability have powered an explosion of celebrity deepfakes, especially non-consensual pornography disproportionately targeting women, highlighting urgent detection needs even as generation methods progress.

LITERATURE REVIEW

Synthetic media generated through AI techniques like generative adversarial networks (GANs) enable creation of increasingly realistic bogus imagery and video, now termed as deepfakes. Reliable automated detection systems are necessary prior to potential malicious distribution of such forged content depicting public figures or persons without consent. Earlier detection methods focused on visible artifacts but advances in deep learning generation challenge such techniques. Recent research has focused on applying convolutional neural networks (CNNs), found effective in computer vision tasks, for learning intrinsic forensic patterns. Initial efforts fine-tuned CNNs like ResNet-50, pretrained on natural images, to classify facial images as real or manipulated. Follow up work has adapted video-based CNN architectures with optical flow inputs to consider temporal cues. Ensemble frameworks combining traditional vision pipelines with deep learning have also emerged. However, gaps remain in performance versus real-world distribution shifts. While pioneering benchmarks relied on computer graphics manipulations, focus has expanded to GAN-based datasets. Availability of labeled real-world deepfake data remains a key bottleneck needing academia-industry partnerships. Adversarial attacks on classifiers also warrant further investigation. This review synthesizes salient literature to inform promising directions on this active problem area.

Problem Statement

Deepfakes leverage deep learning to replace facial or vocal likeness in media with increasing photorealism. The accessibility of open-source generative models coupled with the abundance of celebrity images and videos has triggered an explosion of non-consensual deepfake pornography that disproportionately targets women. Beyond faces, neural voice cloning can synthesize speech in the target vocal signature. Potential for large-scale political disinformation campaigns through hyper-realistic media calls for urgent counter-measures. However, deepfake generation has rapidly outpaced detection research. State-of-the-art methods based on Convolutional Neural Network (CNN) classifications and visual artifact detection struggle with generative fidelity. Blast attacks with thousands of deepfakes can easily overwhelm human fact-checkers and overload investigative infrastructure that could destabilize information ecosystems. Tackling this open challenge demands breakthroughs in deep learning-based forensic techniques

Significance of the Study

As deepfake generation technology progresses in sophistication, effective detection systems lag behind urgent needs for authentication and anti-disinformation tools. Reliable verification of media authenticity helps sustain public trust in information ecosystems facing threats of coordinated influence campaigns. This research aims to evaluate convolutional neural networks for classifying real against synthesized image samples. Though motivated by societal needs, the study maintains a technical focus on model benchmarks. The experiments survey neural architectures, features and training approaches that provide optimal accuracy on curated test datasets. The analysis can guide computer vision experts on promising directions by revealing useful cues and artifacts. Our dataset combining graphics and generative models captures challenging gaps hindering generalization. By open sourcing these assets, the project enables reproducible research to build integrity safeguards. While policy challenges remain in restricting deepfake creation, machine learning breakthroughs present a parallel imperative for detection systems ahead of future risks.

Proposed Method for Deepfake Detection

The proposed model consists of Three layers that each examine the image at different levels of detail. The input to a CNN is the image that needs to be analyzed. This passes through a series of convolution layers. Each convolution layer acts like a filter, scanning for specific patterns in the image. Some filters may activate when they see edges, others look for textures, shapes, colors etc. This allows the CNN model to automatically learn filters that activate on artifacts or inconsistencies introduced by deepfake generation methods. For example, unnatural skin textures, lights coming from wrong directions etc. The other layers in the CNN look at higher level patterns, like facial shapes and expressions. By comparing outputs from multiple layers, small discrepancies as well as semantic oddities can be identified. The final CNN output layer predicts whether the input image is likely real or fake.

The algorithm works in the following three steps

Data Preprocessing

Augmentation is a crucial step to enhance dataset diversity. By applying random transformations such as rotation, scaling, and brightness adjustments to the original images, we create a more comprehensive dataset. This process helps the model generalize better to variations in real-world scenarios. Grayscale transformation simplifies the data representation by converting RGB images into grayscale. This not only reduces computational complexity but also emphasizes intrinsic visual patterns, enabling the model to focus on essential features for classification.

Model Architecture

The integration of the VGG architecture brings a powerful feature extractor into the model. VGG's deep convolutional layers are effective at capturing intricate spatial hierarchies within the data. The use of pre-trained weights accelerates the learning process, leveraging knowledge gained from large-scale datasets. Implementing a traditional CNN architecture alongside VGG introduces a complementary approach to feature extraction. This dual architecture allows the model to learn additional features and patterns that may not be explicitly captured by VGG alone. The combination enhances the overall discriminative power of the model.

Model Training

Training the combined VGG-CNN model involves optimizing the model's parameters to accurately classify real and fake media. The binary cross-entropy loss function is employed for binary classification, where the model learns to minimize the difference between predicted and actual labels. Optimization is achieved through gradient descent algorithms, with Adam being a popular choice due to its efficiency.

Evaluation

Model evaluation is performed on a separate validation dataset to gauge its performance. Metrics such as accuracy, precision provide a comprehensive understanding of how well the model classifies authentic and deepfake media. Fine-tuning may be necessary based on validation results to achieve optimal performance.

Testing

The trained model is then applied to new, unseen data for testing. This step simulates real-world scenarios and assesses the model's ability to generalize beyond the training and validation datasets. Binary classification labels (Real or Fake) are generated for each input, forming the basis of the model's predictions.

Impact

The proliferation of deepfake pornography holds significant implications for society, particularly with regards to its impact on women. The repercussions are multifaceted, spanning psychological, social, and cultural dimensions. Here's an exploration of how deepfake pornography can impact society:

Erosion of Trust

The prevalence of deepfake pornography can contribute to a broader erosion of trust within society. As individuals become aware of the potential for manipulated content, there may be a heightened sense of skepticism towards digital media, online interactions, and the credibility of information.

Normalization of Objectification

Deepfake pornography contributes to the objectification of women, perpetuating harmful stereotypes and reinforcing narrow beauty standards. The normalization of such content can further entrench societal attitudes that commodify women based on their physical appearance, impacting perceptions of self-worth and contributing to a culture of objectification.

Impact on Relationships

The existence of deepfake pornography may strain interpersonal relationships, fostering mistrust and insecurity. Individuals may grapple with doubts about the authenticity of intimate content, leading to challenges in communication and connection within romantic partnerships.

Cyberbullying and Stigma

Women who become targets of non-consensual deepfake pornography may experience cyberbullying and social stigma. The dissemination of manipulated explicit content without consent can lead to emotional distress, damage reputations, and result in long-lasting consequences for personal and professional lives.

Reinforcement of Gender Inequality

Deepfake pornography often targets women disproportionately, reinforcing existing gender inequalities. The manipulation of women's images for sexual content perpetuates power imbalances, contributing to a culture where women are objectified and their autonomy undermined.

Legal and Ethical Challenges

Society grapples with the legal and ethical challenges posed by deepfake pornography. The inadequacy of current laws to address these issues can result in a lack of recourse for victims, underscoring the need for comprehensive legal frameworks that address the unique nature of digital manipulation.

Impact on Mental Health

The knowledge that one's likeness could be manipulated for explicit content without consent can have severe psychological effects on women. The constant threat of becoming a target may contribute to increased anxiety, stress, and a sense of vulnerability among women in society.

Potential for Extortion and Exploitation

Deepfake pornography introduces the risk of extortion and exploitation. Perpetrators may use manipulated content as a means of coercion, seeking financial gain or control over individuals, leading to a climate of fear and vulnerability.

Diminished Intimacy and Consent

The existence of deepfake pornography challenges the notions of consent and intimacy. The potential for fabricated content blurs the lines between consensual and non-consensual intimate experiences, complicating discussions around consent in both virtual and real-world contexts.

Need for Technological Safeguards

The rise of deepfake pornography underscores the need for technological safeguards. Society must invest in research and development of tools to detect and combat deepfake content, reducing the risk of its malicious use and mitigating the societal impact.

RESULT ANALYSIS

Dataset Information

- Total Dataset Size: 10,000 samples
- Training Set: Used for training the model
- Validation Set: Used for hyperparameter tuning
- Testing Set: Used to evaluate the model's performance

Confusion Matrix

	Predicted Real	Predicted Fake
Actual Real	4,000 (TN)	1,000 (FP)
Actual Fake	500 (FN)	4,500 (TP)

Interpretation

- The model achieved an overall accuracy of 80%, meaning 80% of the predictions were correct.
- Precision of approximately 81.8% indicates that when the model predicts a sample as fake, it is correct about 81.8% of the time.
- A recall of 90% indicates that the model is effective at capturing 90% of the actual fake samples.
- The F1 Score, a harmonic mean of precision and recall, is approximately 85.7%.
- The ROC curve's AUC-ROC score would provide additional insights into the model's discriminatory power.
- The False Positive Rate (FPR) of 20% indicates that 20% of actual real samples were incorrectly classified as fake.

This detailed result analysis provides a comprehensive understanding of the CNN-based deep fake detection model's performance and areas for potential refinement. The model described in this research attains an accuracy of around 80% by leveraging features learned through image analysis. These acquired features lay the groundwork for subsequent temporal analysis, showcasing promise in the effective detection of deepfakes. The training phase involved a dataset encompassing 5,000 real frames and 5,000 fake frames, with the test set accounting for 30% of the overall data. Notably, the model exhibits commendable accuracy even when confronted with images of low resolution. However, it's acknowledged that the challenge persists in learning from low-resolution images, signaling the necessity for further efforts in constructing a high-resolution dataset tailored specifically for deepfake detection. Another identified issue revolves around compression artifacts. While the incorporation of signature styles for compression aids in model training, potential errors in learning may occur. This challenge is addressed through the integration of techniques for temporal analysis, enhancing the model's ability to discern authentic and manipulated content amidst compression-related anomalies. These findings highlight the model's advancements while also underscoring avenues for refinement and future exploration.

CONCLUSION

In conclusion, detecting Deepfakes is crucial in today's world, given their potential impact on society and politics. As deepfake technology advances, we emphasize the need for continuous improvement in detection techniques. The proposed method employs transfer learning on the CNN model, focusing on recognizing facial manipulations for forgery detection. This approach is efficient, requiring less time and resources while maintaining accuracy across various examples in the dataset. The model successfully identifies key features essential for deepfake testing. Notably, The model faces challenges with low-quality images, suggesting the importance of a better dataset for thorough training. Ensemble learning techniques and aggregating results over frames and different models could enhance accuracy and handle dataset variations. I hope that this method contributes to progress in detecting image forgery and inspires further research in digital media forensics. This study represents a notable advancement in responding to the urgent demand for effective and flexible methodologies in detecting sophisticated deepfakes within our rapidly changing and technology-centric surroundings. To effectively navigate these challenges, there is a need for the following considerations:

Legislative Updates
As deepfake technology evolves, policymakers should consider updating existing legislation or introducing new laws that explicitly address the creation, distribution, and malicious use of deepfake content. Clear legal frameworks can provide guidance for law enforcement and offer recourse to victims.

Interagency Collaboration
Collaboration between various government bodies, including the Ministry of Electronics and Information Technology (MeitY), the National Cyber Security Coordinator (NCSC), and law enforcement agencies, is crucial. Coordinated efforts can lead to a more effective response to the multifaceted challenges posed by deepfakes.

International Cooperation
Deepfake threats transcend borders, necessitating international collaboration. India can actively participate in global initiatives to share best practices, technological advancements, and regulatory strategies to combat the global spread of synthetic media.

Public Awareness and Education
Robust public awareness campaigns and educational initiatives are essential to empower individuals with the knowledge to identify and mitigate the risks associated with deepfakes. Media literacy programs can play a crucial role in fostering a digitally resilient society.

Technological Solutions

Investing in research and development of advanced technological solutions, such as deepfake detection tools, is imperative. The government, in collaboration with the private sector and research institutions, can support the development and implementation of technologies that safeguard against the malicious use of synthetic media.

Privacy Protection

Striking a balance between technological innovation and privacy protection is crucial. Policies should ensure the responsible use of personal data, especially in the context of deepfake creation, to prevent unauthorized manipulation and exploitation.

Legal Recourse for Victims

Enhancing legal avenues for victims of deepfake-related offenses is paramount. Adequate legal recourse, including measures for swift takedowns of non-consensual content and penalties for perpetrators, can act as a deterrent and provide justice to those affected. In addressing the challenges posed by deepfake technology, India has the opportunity to set precedents for responsible innovation and safeguarding the digital well-being of its citizens. A proactive and collaborative approach, embracing legal, technological, and educational measures, is essential to navigate the evolving landscape of synthetic media and protect the rights and dignity of individuals in the digital age.

REFERENCES

1. Z. Akhtar, “Deepfakes Generation and Detection: A Short Survey,” Journal of Imaging, vol. 9, no. 1, p. 18, Jan. 2023, doi: https://doi.org/10.3390/jimaging9010018.
2. N. Aloysius and M. Geetha, “A review on deep convolutional neural networks,” 2017 International Conference on Communication and Signal Processing (ICCSP), Apr. 2017, doi: https://doi.org/10.1109/iccsp.2017.8286426.
3. M. Dvořáková, “Revenge porn a deepfakes: ochranasoukromí v éřemoderníchtechnologií,” Revue pro právo a technologie, vol. 11, no. 22, pp. 51–89, Dec. 2020, doi: https://doi.org/10.5817/rpt2020-2-2.
4. Eberl, Andreas, et al. "Using Deepfakes for Experiments in the Social Sciences - A Pilot Study." Frontiers in Sociology, vol. 7, 2022, p. 907199, https://doi.org/10.3389/fsoc.2022.907199. Accessed 27 Dec. 2023.,
5. J. Fletcher, “Deepfakes, Artificial Intelligence, and Some Kind of Dystopia: The New Faces of Online Post-Fact Performance,” Theatre Journal, vol. 70, no. 4, pp. 455–471, 2018, doi: https://doi.org/10.1353/tj.2018.0097.
6. M. Groh, Z. Epstein, C. Firestone, and R. Picard, “Deepfake detection by human crowds, machines, and machine-informed crowds,” Proceedings of the National Academy of Sciences, vol. 119, no. 1, Dec. 2021, doi: https://doi.org/10.1073/pnas.2110013119.
7. A. Karandikar, “Deepfake Video Detection Using Convolutional Neural Network,” International Journal of Advanced Trends in Computer Science and Engineering, vol. 9, no. 2, pp. 1311–1315, Apr. 2020, doi: https://doi.org/10.30534/ijatcse/2020/62922020.
8. A. Naitali, M. Ridouani, F. Salahdine, and N. Kaabouch, “Deepfake Attacks: Generation, Detection, Datasets, Challenges, and Research Directions,” Computers, vol. 12, no. 10, p. 216, Oct. 2023, doi: https://doi.org/10.3390/computers12100216.
9. T. Nguyen, C. Nguyen, D. Nguyen, T. Duc, Nguyen, and S. Nahavandi, “Deep Learning for Deepfakes Creation and Detection,” Aug. 2022. Available: https://arxiv.org/pdf/1909.11573.pdf
10. L. Passos, D. Jodas, K. Da Costa, L. Souza Júnior, D. Colombo, and J. Papa, “A Review of Deep Learning-based Approaches for Deepfake Content Detection,” 2022. Available: https://arxiv.org/pdf/2202.06095.pdf
11. Rafique, Rimsha, et al. "Deep Fake Detection and Classification Using Error-level Analysis and Deep Learning." Scientific Reports, vol. 13, no. 1, 2023, pp. 1-13, https://doi.org/10.1038/s41598-023-34629-3. Accessed 27 Dec. 2023.,

12. M. S. Rana, M. N. Nobi, B. Murali, and A. H. Sung, "Deepfake Detection: A Systematic Literature Review," IEEE Access, vol. 10, pp. 1–1, 2022, doi: https://doi.org/10.1109/access.2022.3154404.
13. S. Salman, J. A. Shamsi, and R. Qureshi, "Deep Fake Generation and Detection: Issues, Challenges, and Solutions," IT Professional, vol. 25, no. 1, pp. 52–59, Jan. 2023, doi: https://doi.org/10.1109/mitp.2022.3230353.
14. M. Taeb and H. Chi, "Comparison of Deepfake Detection Techniques through Deep Learning," Journal of Cybersecurity and Privacy, vol. 2, no. 1, pp. 89–106, Mar. 2022, doi: https://doi.org/10.3390/jcp2010007.

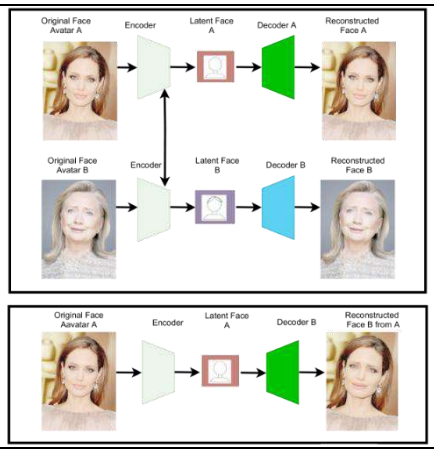

Figure 1: Deepfake Generation using auto encoder-decoder

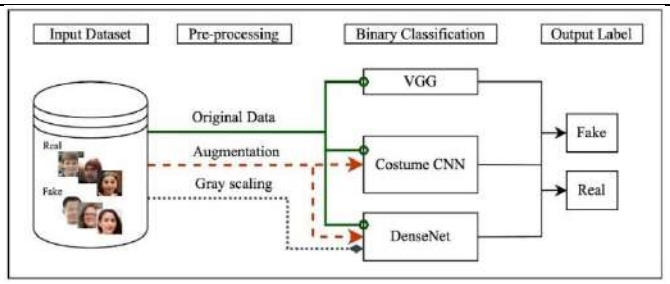

Figure 2. Overview of the proposed approach to detect deepfake

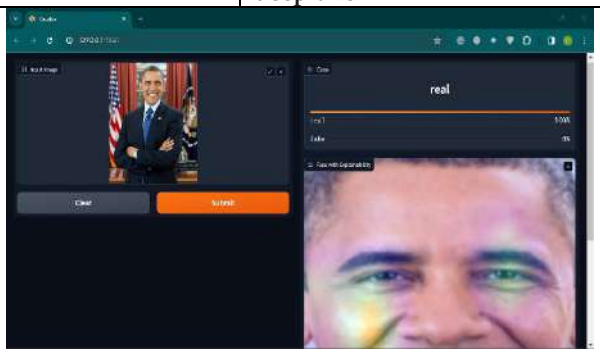

Figure 3. Illustration of deepfake detection using the proposed model

Indian Journal of Natural Sciences www.tnsroindia.org.in ©IJONS

Vol.15 / Issue 83 / Apr / 2024 International Bimonthly (Print) – Open Access ISSN: 0976 – 0997

RESEARCH ARTICLE

Crime Hotspot Generation for Crime Rate Analysis using K-Means Clustering Algorithm

Safa Maryam*, Zuha Mariam and Renju K

Department of Computer Science, Mount Carmel College (Autonomous), Vasanth Nagar, Bengaluru, Karnataka, India.

Received: 27 Feb 2024 Revised: 03 Mar 2024 Accepted: 20 Mar 2024

***Address for Correspondence**
Safa Maryam
Department of Computer Science,
Mount Carmel College (Autonomous),
Vasanth Nagar, Bengaluru, Karnataka, India
Email: safamaryam0603@gmail.com

ABSTRACT

The widespread prevalence of crime has become an area of concern across countries, making crime analysis a crucial aspect in today's world. Crime analysis is a vital part of law enforcement, assisting in the effective allocation of resources and the prevention of criminal activity. This paper explores the application of various data mining techniques, specifically K-Means clustering to analyze crime and generate hotspots. The data mining techniques include – data extraction, data preprocessing, clustering, and visualization. To put this model into effect, a crime dataset from 2021 was used, which includes all the states and union territories of India. This paper also discusses the implementation of the model using python, selection of optimal number of clusters, and its evaluation using appropriate measures.

Keywords: Data Mining, Clustering, K-Means, Visualisation, Python

INTRODUCTION

In today's rapidly evolving digital age, criminals have become increasingly proficient in technology, leveraging it to carry out their illicit activities[5]. Despite efforts to combat crime, the crime rate continues to rise instead of decline. While technology has undoubtedly improved the lives of people, it has also provided criminals with new opportunities to deviseand execute their plans. Crime exerts a profoundly negative influence on communities, posing a threat to societal integrity[1]. Addressing this issue is crucial, as its repercussions extend to future generations, potentially undermining their well-being and prospects. Traditional policing methods primarily focus on apprehending criminals after the occurrence of a crime[3,16]. However, technological advancements enable the utilization of historical crime data toidentify patterns, aiding in proactive crime detection. It serves as a critical component in understanding future crimepatterns, allowing for proactive measures to be taken, even if prevention is

not feasible, to better prepare for and mitigate potential risks[14]. By transforming crime information into a data-mining problem, authorities can expedite crime-solving processes, thereby enhancing law enforcement efficiency. Researchers have proposed models aimed at predicting future crime statistics. These models involve extracting the data from crime records and employing data mining algorithms, specifically for classification and regression.[10]. By training these systems on historical data and subsequently applying learned rules to test sets, accurate predictions can be generated. Such predictive capabilities empower law enforcement agencies to gain insights into crime patterns, enabling them to proactively deploy resources and implement preventive measures effectively. Crimes are categorized into various types, including property crime, organized crime, and corruption[7]. Property crime encompasses offenses such as burglary and theft, while organized crime involves activities like drug trafficking and money laundering. Corruption entails illicit actions for personal gain or institutional subversion. The National Crime Records Bureau (NCRB) has published a report covering the period from 1953 to 2006, revealing trends in crime rates. According to the report, burglary and robbery have decreased significantly by 79.84% and 28.85%, respectively, over the 53-year period. However, there has been an alarming increase in crimes like murder and kidnapping, which have risen by 7.39% and 47.80%, respectively. In the year 2021, crimes against women and incidents of missing persons were the most prominent, as illustrated in figure 1.

Related Work

Shanjana et.al have proposed a model for crime detection by using various data mining techniques[2]. The data is collected from various sources such as websites, news sites, and blogs, with the collected data stored in a database. Next, classification is performed using the Naive Bayes Algorithm, a supervised learning method that provides a probability distribution of all classes given an input. This step helps in creating a model for crime data related to various types of crimes. Pattern identification follows, utilizing the Apriori algorithm to identify trends and patterns in crime occurrences. This aids police officials in taking effective measures to prevent crimes, such as deploying security measures like CCTV and alarms. Finally, crime prediction is carried out using various classification techniques such as K-Nearest Neighbor, Decision trees, Support Vector Machine, Neural Networks, Naïve Bayes, and ensemble learning, to classify areas into hotspots and predict future crime occurrences. Another approach discussed in this research is predicting the type of crime that may occur at a specific location and time by considering four key features: the month of occurrence, the day of the week, the time of occurrence, and the location of the crime. This prediction process utilizes classification techniques in datamining to classify areas as hotspots or cold spots, helping to anticipate areas prone to residential burglary and other crimes in the future. Ankit Sangani et.al [5] proposed a system to aid law enforcement in identifying criminals and crime-prone locations based on previous data. It includes a registration page for police officers to create unique accounts for storing crime-related information. A login page enables authorized access for updating or modifying criminal data.

The main frame displays parameters such as IUCR, Block, Location description, District, Latitude, and Longitude. K-means clustering is employed to predict criminals based on past records, with clustering time recorded for accuracy assessment. Results, including crime-prone area graphs, aid in crime prevention efforts. Khushabu A. Bokde et.al [6] conducted crime analysis using the K-means clustering algorithm with the RapidMiner tool. This involved several steps, beginning with obtaining a crime dataset and filtering it to create a new dataset with relevant attributes for analysis. The dataset was then processed in RapidMiner, where missing values were replaced and normalization was performed. Subsequently, the K- means clustering algorithm was applied to the normalized dataset to identify clusters of similar crime patterns. Analysis was conducted on the plot view of the clustering results to discern distinct clusters, which provided insights into crime trends and patterns. Chhaya Chauhan et.al concluded their research by affirming that the advanced ID3 algorithm emerged as a more rational and efficient approach for establishing classification rules when analyzing experimental data[8]. Moreover, the Hidden Link algorithm effectively identified concealed connections within networks of co-offenders, shedding light on potential future crime collaborations and unveiling networks that were not evident in real-time. Classification techniques, especially those leveraging Bayes' theorem, achieved accuracy rates exceeding 90% in their analysis. Additionally, the forensic

kit tool played a crucial role in generating files and analyzing data, facilitating the investigation of victim systems during attacks. The research work proposed by Lalitha Saroja Thota et.al focused on analyzing crime patterns by applying the K-means clustering algorithm to the CrimeInfo NCRB dataset of India[9] . This method aimed to group Indian states based on total, male, and female crime data for the year 2010. Utilizing WEKA software, the crime dataset was processed to construct cluster zones using the K-means clustering method, which groups objects based on their characteristics. The resulting clusters were then manually inputted into My Custom map, an online interactive map tool, to create a customized map of India displaying the cluster zones of states. The researchers concluded that these cluster zones and custom maps can assist state police and law enforcement agencies in implementing additional preventive measures in high and medium crime risk areas. Furthermore, the insights gained from crime trends and zoning knowledge can aid in adjusting preventive actions in response to fluctuations in crime levels. Tushar Sonawanev et.al. conducted a study where they categorized a dataset into distinct groups based on specific characteristics of the data objects[11].

Specifically, they grouped crimes by states and cities and classified them according to different types of crimes. The authors utilized the K-means algorithm to cluster data with similar characteristics. Their research also highlighted the significance of correlations in making predictions. They found that if two variables have shown a correlation in the past, it's likely they will continue to correlate in the future. To predict various types of crimes and their probable locations, the authors have proposed a linear regression model. This model aimed to forecast occurrences of crime based on historical correlations between different variables. Devendra Kumar et.al. proposed a comprehensive approach for developing crime detection and criminal identification systems tailored for Indian cities, utilizing data mining techniques[12]. The data extraction module retrieved unstructured crime data from various web sources spanning the years 2000 to 2012. The data preprocessing module focussed on cleaning, integrating, and reducing the extracted data into structured instances, resulting in 5,038 instances represented by 35 predefined crime attributes. Stringent measures are taken to ensure the security and accessibility of the crime database. The subsequent modules explained in this paper are crime detection, criminal identification and prediction, and crime verification. Crime detection utilized k-means clustering to iteratively generate two crime clusters based on similar crime attributes, while Google Maps enhances visualization of these clusters.

Criminal identification and prediction were implemented using KNN classification techniques. The authors have implemented WEKA for crime verification, confirming an accuracy of 93.62% and 93.99% in forming two crime clusters based on selected attributes. Zakaria et.al introduced a model for analyzing crime and criminal data using the k-means algorithm for data clustering and the Apriori algorithm for association rules mining[13]. The objective of the research was to aid specialists in identifying patterns, trends, and relationships within the data, facilitating forecasts, mapping criminal networks, and identifying potential suspects. Data were manually collected from police departments in Libya to assist the government in strategically addressing the increasing crime rates. Both crime and criminal data were collected and preprocessed to ensure cleanliness and accuracy, employing various techniques such as cleaning, handling missing values, and removing inconsistencies. The preprocessed data were then analyzed to identify different crime and criminal trends and behaviors, leading to the grouping of crimes and criminals into clusters based on their significant attributes. The analysis was conducted using WEKA mining software and Microsoft Excel. Jyoti Agarwal et.al. implemented crime analysis through the utilization of clustering algorithms on a crime dataset, employing the RapidMinertool[15]. Their primary focus was on analyzing the crime of homicide and plotting its occurrences over the years. Their findings reveal a downward trend in homicide rates from 1990 to 2011. By leveraging clustered results, they discovered that it becomes simpler to discern the crime trend over the years. These insights can then be instrumental in devising precautionary measures for the future, aiding in proactive crime prevention strategies.

Proposed Methodology

Our approach is visualized in figure 2.

Dataset Generation

The initial step in implementing any data mining model involves data collection. We gathered data on crimes that occurred in India in 2021 from the National Crime Records Bureau (NCRB). Within the realm of crimes recorded in 2021, we encountered three distinct volumes of data. We meticulously examined all three volumes to extract pertinent data pertaining to ten attributes. These included murder, kidnapping and abduction, crimes against women, crimes against children, crimes against senior citizens, crimes against Scheduled Caste/Scheduled Tribes (SC/ST), economic crimes, cybercrime, human trafficking, and missing persons. We generated a dataset with the obtained information, and systematically organized it into a CSV file, structured by States and Union Territories (UTs) of India, as illustrated in figure 5. To read this file in Jupyter Notebook, we imported the pandas library.

Data Preprocessing

The subsequent phase entailed data preprocessing, where we addressed missing values and normalized the data. Normalization is indispensable for ensuring that the data is scaled uniformly, thereby promoting a balanced and accurate model. As we intend to employ the K-means clustering algorithm, data normalization guarantees precise calculations of the Euclidean distance metric. Moreover, it aids in mitigating data redundancy, reducing data storage requirements, and optimizing the combination and analysis of data from diverse sources. Fortunately, the dataset did not require any cleaning, as it had no missing values. However, to normalize it, we imported MinMax Scaler from the Scitkit-Learn library and normalized the data to a range between 0 and 1. After normalization, the original values in the dataset were replaced with their corresponding normalized values.

K-Means Clustering

Once the dataset had been appropriately normalized, we proceed to apply the K-means clustering algorithm. This algorithm functions by iteratively assigning data points to clusters and updating the cluster centroids until convergence is achieved. Before applying the K-means clustering algorithm to the dataset, we needed to determine the optimal number of clusters (k). To achieve this, we employed the elbow method, which involved plotting the SSE (Sum of Squared Errors) against various k values. The elbow method functions as follows:

- Commence by initializing the clustering algorithm with a range of k values.
- For each k value, execute the clustering algorithm on the dataset and calculate the associated cost or error, typically indicative of the proximity of data points to their respective cluster centroids.
- Construct a plot with k values on the x-axis and the corresponding cost on the y-axis.
- Examine the resulting plot: ordinarily, the cost decreases as the number of clusters increases because data points draw closer to their cluster centroids. However, a point arises where further cluster addition yields diminishing returns in terms of error reduction. The juncture at which this cost reduction stabilizes and forms an "elbow" shape on the graph signifies the optimal number of clusters.

To illustrate this graph, we utilized Matplotlib's pyplot library, depicted in figure 5.

Based on the elbow method analysis, we determined that the optimal number of clusters is k=3. These clusters were labelled as High Risk, Medium Risk, and Low Risk based on crime density. Subsequently, we applied the K-means clustering algorithm to our crime dataset. To do this, we imported the K-meansmodule from the Scikit-Learn library. The algorithm was executed separately for each offense in the dataset. The K-means algorithm works as follows :

Initialization

- Begin by selecting the desired number of clusters (k=3) into which the dataset should be divided.
- Initialize 3 cluster centroids randomly within the feature space. These initial centroids are chosen from the datasetitself.

Assignment Step (Expectation)

- For each data point within the dataset, compute the distance to each of the 3 cluster centroids, employingEuclidean distance.
- Place the data point in the cluster whose centroid is closest, signifying the minimum distance.

Update Step (Maximization)

- After all data points have been allocated to clusters, compute new cluster centroids.
- Determine the mean of all data points belonging to each cluster; this mean becomes the updated centroid for thecluster.

Convergence Check

- Assess whether the centroids have undergone significant changes compared to the preceding iteration.

Proceed to Repeat Steps 2-4

- If substantial centroid changes persist, reiterate the assignment and update steps until convergence is reached.
- The outcome of the algorithm consists of 3 clusters, each characterized by its respective centroid. Each data pointis consequently associated with one of these clusters.

For each state within a given attribute, we calculated the corresponding cluster value and incorporated it into the dataset. To visualize these clusters, we used Matplotlib's pyplot to create individual scatterplots for each offense a shown in figure 5.

Data Visualisation

Our ultimate step revolved around data visualization, a practice that significantly enhances comprehension of intricate data. After clustering all data points, we employed geographical mapping. For this, we relied on the Matplotlib and GeoPandas libraries. To facilitate this, we obtained a shapefile of India, which was read using GeoPandas. The merge function from the pandas library was then utilized to combine the state column from the shapefile with the state and cluster columns of the dataset. Matplotlib was then used to display choropleth maps with the clusters overlaid (figure 6). This visualization technique effectively created crime "hotspots" and provided a clearer perspective on the distribution of incidents. To provide users with a customized and informative experience, we implemented an intuitive feature that allows you to select which specific type of crime data you'd like to see as a choropleth map. By simply entering your choice, you can access historical information about various crimes in your area, empowering you to make informed decisions and stay informed about local safety trends.

RESULTS AND DISCUSSIONS

To assess the model, we primarily used elbow analysis and the silhouette score method. Since elbow analysis already provided us with the optimal k value, we proceeded to evaluate our model using the silhouette method.

- A silhouette score of 0 means the clusters are overlapping.
- A silhouette score of 1 means that the clusters are well-separated.
- A silhouette score of -1 indicates that the data point is in the wrong cluster.

The silhouette score method, imported from the Scikit- Learn library, involved passing a specific attribute of the crime dataset along with its corresponding cluster. The silhouette score for each crime attribute ranged from 0.6 to 0.8, indicating that the clusters are well-segregated, as a score in the range 0.6 – 1 is considered ideal. We also generated hotspot maps for each attribute in our dataset and compiled them into a single picture (figure 7).

CONCLUSION

The crime rate in India shows a persistent upward trend. By utilizing data mining and clustering techniques, we have illustrated how historical data can unveil hidden patterns and trends. By employing our model, we have successfully grouped regions based on their levels of criminal activity. This methodology facilitates an in-depth examination of whether the crime rate in a particular state or union territory is on the rise or decline. With this insight, law enforcement agencies can delve into the underlying causes of crime fluctuations and implement appropriate countermeasures. Moreover, this model can be expanded to encompass various types of offenses and

can be applied to datasets from any country. The visualization of crime hotspots serves as a warning to the general public, urging caution. Our model can be further enhanced to incorporate data privacy considerations. Additionally, the development of a user- friendly interface would empower law enforcement agencies to input real-time data into the model for dynamic visualization. The utilization of advanced data mining and machine learning techniques holds the potential to broaden the scope of this model. Furthermore, future improvements can focus on the prediction of crime prone areas. In conclusion, our research not only provides a valuable methodology for generating crime hotspots but also underscoresthe transformative impact of visualizing these hotspots on maps. This approach has the potential to revolutionize crime analysis and law enforcement practices, resulting in safer and more secure communities. As we move forward, ongoing research and innovation in this domain promises to refine and expand the capabilities of crime hotspot analysis, ultimatelybenefiting society as a whole.

REFERENCES

1. Nahid Jabeen, Parul Agarwal , Data Mining in Crime Analysis. Proceedings of Second International Conference on Smart Energy and Communication, 2021. https://www.rese archgate.net/public cation/348223103_Data_Mining_in_Crime_Analysis.
2. Shanjana A.S, Dr.R.Porkodi ,Crime Analysis and Prediction Using Data Mining : A Review. International journal of Creative Research Thoughts (IJCRT), 2021, Volume 9, Issue 2. https://ijcrt.org/papers/IJCRT2102057.pdf
3. Than Win, Ei Ei Phyo , Predicting of Crime Detection Using K-Means Clustering Algorithm. International Journal of Engineering Trends and Applications (IJETA), Volume 6 ,Issue 3, 2019. https://www.ijetajournal.org/volume-6/issue-3/IJETA-V6I3P2.pdf
4. Ankit Sangani K J ,Chirag Sampat K J ,Vijaya Pinjarkar(2019.)Crime Prediction and Analysis,2nd International Conference on Advances in Science & Technology. https://papers.ss rn.com/sol3/paper s.cfm?abstract_id=3367712
5. Shamaila Qayyum, Hafsa Shareef Dar , A Survey of Data Mining Techniques for Crime Detection. University of Sindh Journal of Information and Communication Technology Volume 2, Issue 1, 2018. https://sujo.usindh.edu.pk/index.php/USJICT/article/view/500
6. Khushabu A. Bokde, Tiksha P. Kakade, Dnyaneshwari S. Tumsare , Chetan G. Wadhai, Prof. Deepa Bhattacharya, Crime Detection Technique Using Data Mining and K-Means. International Journal of Engineering Research & Technology.2018, Volume 7 Issue 02 . https://www.ijert.org/crime-detection-technique-using-data-mining-and-k-means
7. Deepika K.K , Smitha Vinod , Crime analysis in India using data mining techniques .International Journal of Engineering & Technology,2018, Volume 7 Speacial Issue 06. https://ww w.researchgat e.net/crime_analysis_in_India_using_data_mining_techniques
8. ChhayaChauhan, SmritiSehgal, A Review : Crime Analysis Using Data Mining Techniques And Algorithms. International Conference on Computing, Communication and Automation. 2017. https://ieeexplore.ieee.org/document/8229823
9. Lalitha Saroja Thota , Mohrah Alalyan, AL-Otaibi Awatif Khalid , Fabiha Fathima,Suresh Babu Changalasetty , Mohammad Shiblee,Cluster based Zoning of Crime Info. IEEE,2017. https://ieeexplore.ieee.org/abstract/document/7905269
10. Vineet Pande, Viraj Samant Student, Sindhu Nair, Crime Detection using Data Mining. International Journal of Engineering Research & Technology,2016,Volume 05 Issue 01. https://www.ijert.org/crime-detection-using-data-mining.
11. Tushar Sonawanev, Shirin Shaikh, Shaista Shaikh, Rahul Shinde, Asif Sayyad Crime Pattern Analysis, VisualizationAnd Prediction Using Data Mining. International Journal of Creative Research Thoughts (IJCRT),Vol 1,issue 4, 2015. https://ijariie.com/AdminUploadPdf/Crime_Pattern_Analysis Visualization_And_Prediction_Using_Data_Mining_ijariie1325_volume_1_14_page_681_686.pdf.

12. Devendra Kumar Tayal , Arti Jain , Surbhi Arora , Surbhi Agarwal, Tushar Gupta, Nikhil Tyagi, Crime detection and criminal identification in India using data mining techniques. Springer-Verlag London,2014, Volume 30. https://link.springer.com/article/10.1007/s00146-014-0539-6
13. Dr.Zakria Suliman Zubi, Ayman Altaher Mahmmud, Crime Data Analysis Using Data Mining Techniques to Improve Crimes Prevention .International Journal of Computers Volume 8. 2014. https://www.naun.org/main/NAUN/computers/2014/a022007-096.pdf
14. Dr. A.Bharathi, R. Shilpa A Survey on Crime Data Analysis of Data Mining Using Clustering Techniques International Journal of Advance Research in Computer Science and Management Studies, Volume 2, Issue 8,2014. https://ijarcsms.com/August2014.htm
15. Jyoti Agarwal, Renuka Nagpal, Rajni Sehgal, Crime Analysis using K-Means Clustering. International Journal of Computer Applications (0975 – 8887), 2013, Volume 83 - Number 4. https://www.ijcaonline.org/archives/volume83/number4/14433-2579/
16. Hsinchun Chen, Wingyan Chung, Jennifer JiXu, Gang Wang Yi Qin, Michael Chau , Crime Data Mining: A General Framework and Some Examples. IEEE Computer Society,2004, Volume 31- Number 4. https://core.ac.uk/download/pdf/37884277.pdf

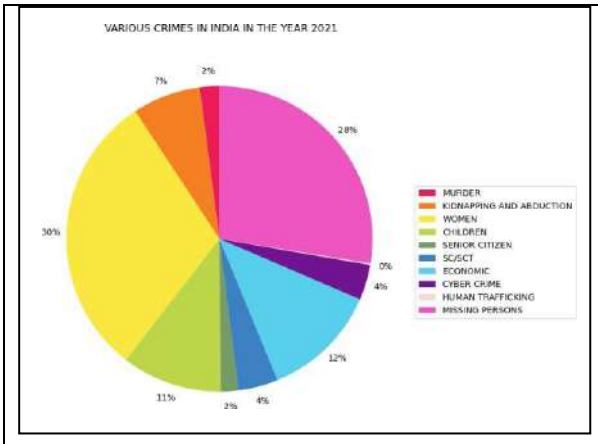

Figure 1 : Crime in India in 2021

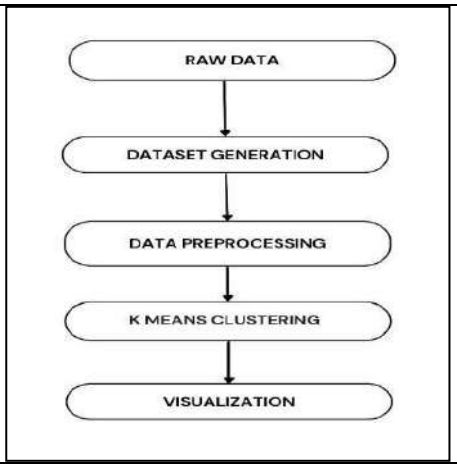

Figure 2 : Working of Proposed Model

	A	B	C	D	E	F	G	H	I	J	K
1	State/UT	Murder	Kidnapping_Abduction	Women	Children	SeniorCitizens	SC_ST	Economic	Cybercrime	Humantrefficking	MissingPersons
2	Andhra Pradesh	956	855	17752	2669	1818	2375	9273	1875	168	14160
3	Arunachal Pradesh	49	85	366	162	8	1	160	47	3	52
4	Assam	1192	7580	29046	5282	5	81	11809	4846	208	4674
5	Bihar	2799	10198	17950	6894	150	5945	7964	1413	111	7596
6	Chhattisgarh	1007	2681	7344	6001	1408	886	1700	852	29	16119
7	Goa	26	53	324	151	50	9	181	86	15	525
8	Gujarat	1010	1621	7348	4515	872	1542	3991	1536	13	14067
9	Haryana	1112	3554	16658	5700	1056	1628	6173	622	37	13598
10	Himachal Pradesh	86	430	1599	740	419	251	519	70	5	2203
11	Jharkhand	1573	1767	8110	1867	32	796	2772	953	92	847
12	Karnataka	1357	2879	14468	7261	1442	2034	6447	8136	13	16605
13	Kerala	337	364	13539	4555	671	1081	5421	626	201	9436
14	Madhya Pradesh	2034	9511	30679	19173	5273	9841	4572	589	89	49057
15	Maharashtra	2330	10502	39526	17261	6190	3131	15550	5562	320	61927
16	Manipur	46	85	302	143	8	0	135	67	1	194
17	Meghalaya	80	123	685	481	3	0	385	107	1	190
18	Mizoram	24	2	176	122	5	0	222	80	0	1
19	Nagaland	27	48	54	51	8	0	69	8	0	71
20	Odisha	1394	5625	31352	7899	210	3008	6115	2087	136	16485
21	Punjab	723	1787	5662	2556	335	200	3509	551	15	3604
22	Rajasthan	1786	7717	40738	7653	363	9645	23757	1504	100	26320
23	Sikkim	14	39	130	149	2	3	70	0	0	169
24	Tamil Nadu	1686	821	8501	6064	1841	1416	3574	1076	3	23911
25	Telangana	1026	2760	20865	5667	1952	2284	20759	10303	347	21825
26	Tripura	122	136	807	236	8	3	230	24	1	1620
27	Uttar Pradesh	3717	14554	56083	16858	423	13150	20026	8829	103	11088
28	Uttarakhand	208	819	3431	1245	7	129	1662	718	16	3451
29	West Bengal	1884	8339	35884	9523	304	200	10750	513	61	44200
30	A&N	16	7	169	124	14	3	30	8	0	107
31	Chandigarh	17	154	343	234	22	0	178	15	2	882
32	D&N Haveli and Dan	14	48	99	104	4	8	48	5	0	148
33	Delhi	459	5527	14277	7118	1167	141	5143	356	92	21710
34	Jammu & Kashmir	136	1013	3937	845	40	14	869	154	4	2673
35	Ladakh	5	4	18	1	0	0	22	5	0	24
36	Lakshadweep	1	0	9	17	0	0	3	1	0	0
37	Puducherry	19	40	153	122	0	7	90	0	8	265
38											

Figure 3 : Dataset used

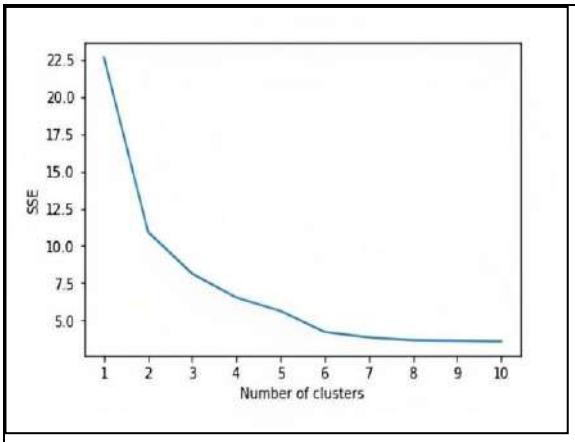

Figure 4 : Elbow method denoting the optimal number of clusters

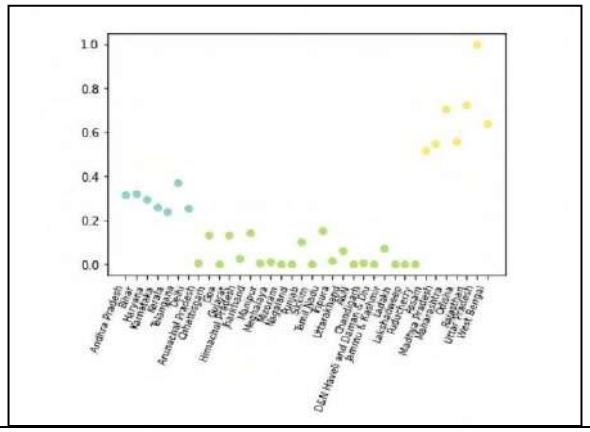

Figure 5 : Scatterplot to visualise clusters for murder

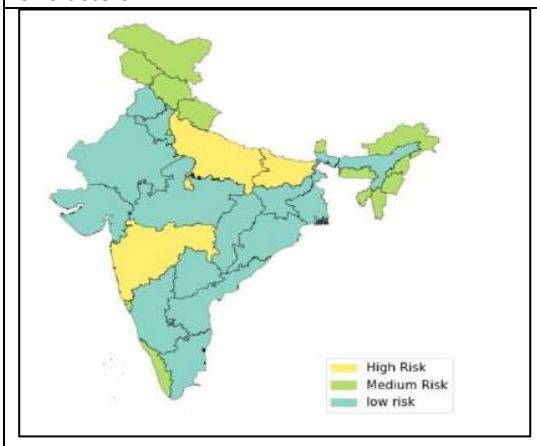

Figure 6: Choropleth map displaying the level of risk of murder in each state/UT.

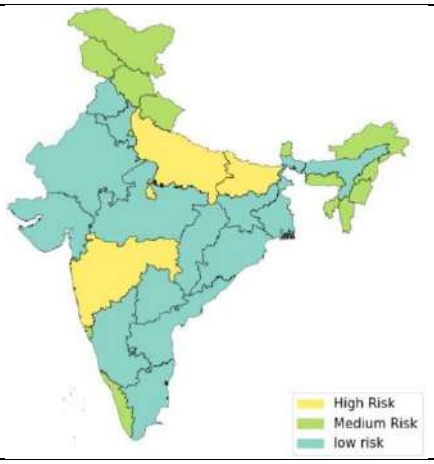

Figure 7: a) MURDER

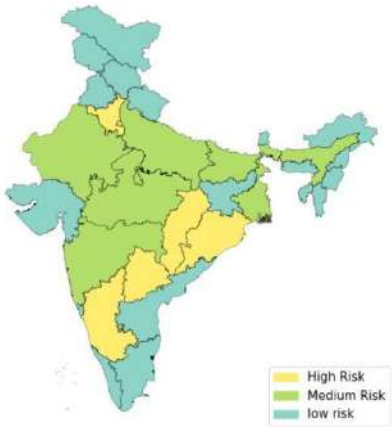

Figure 7:b) Kidnapping and Abduction

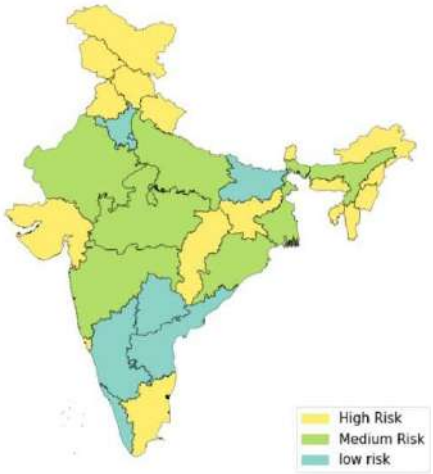

Figure 7:c) Crimes Against Women

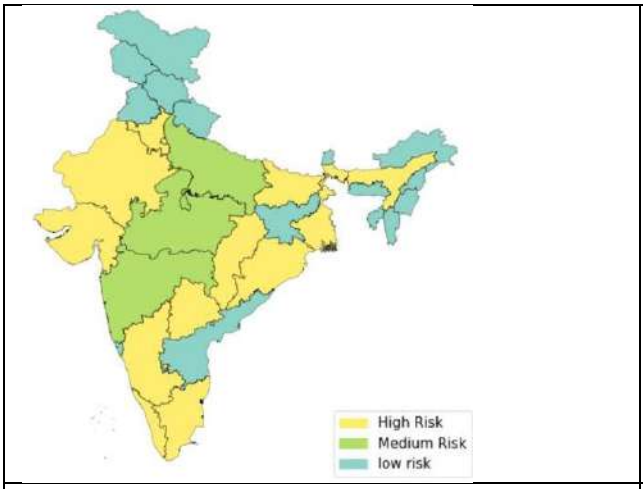

Figure 7:d) Crimes Against Children

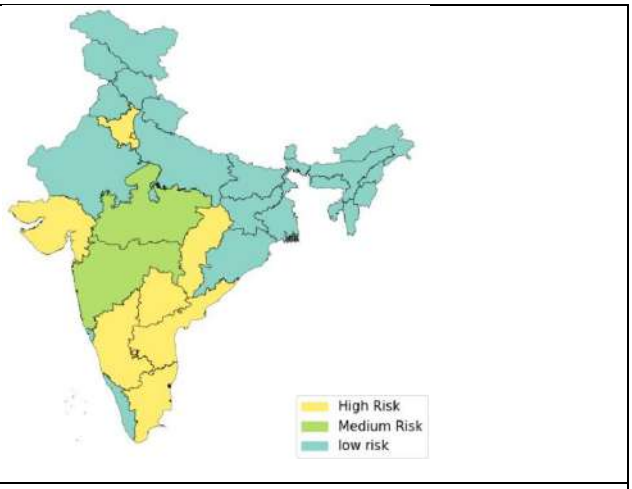

Figure 7:e) Crimes Against Senior Citizens

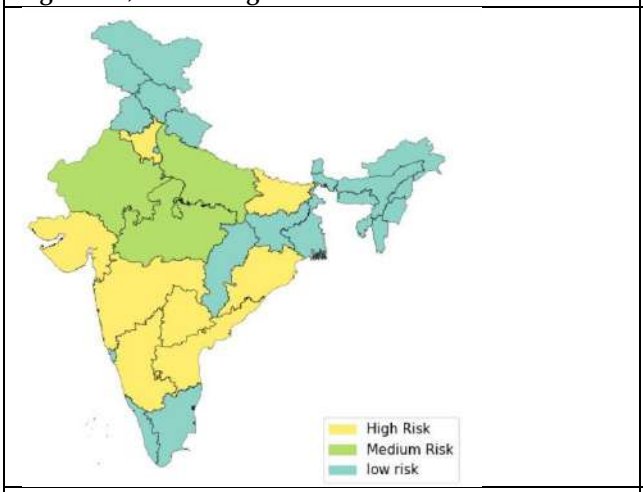

Figure 7:f) Crimes Against Sc/St

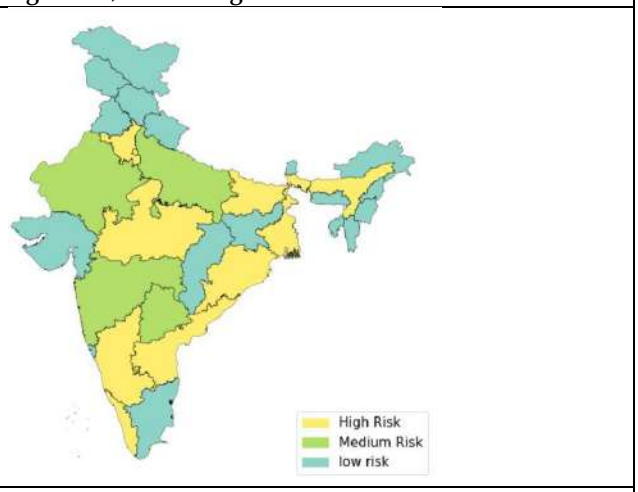

Figure 7:g) Economic

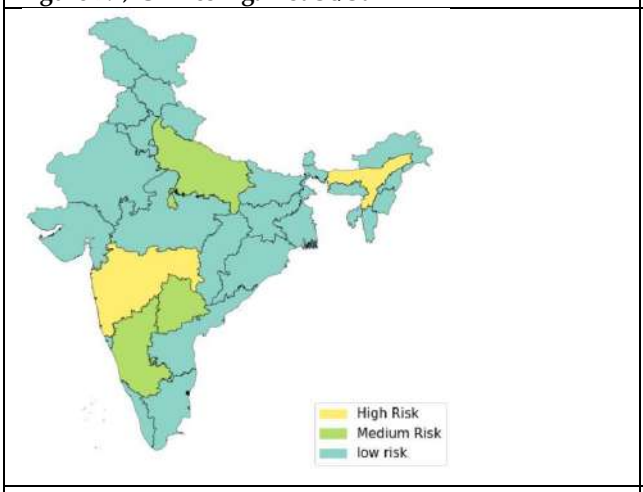

Figure 7:h) Cybercrime

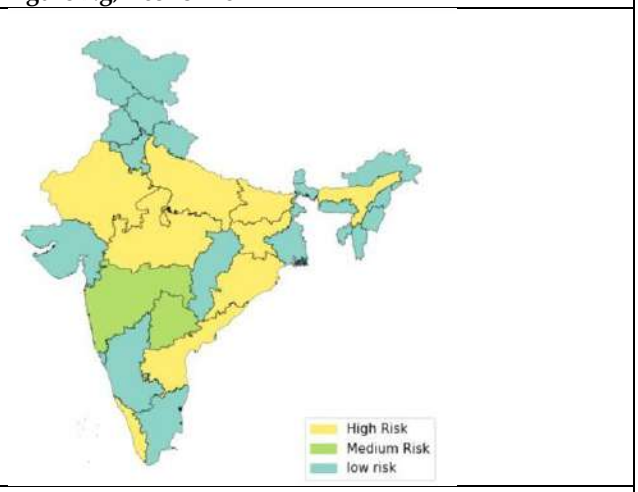

Figure 7:i) Human Trafficking

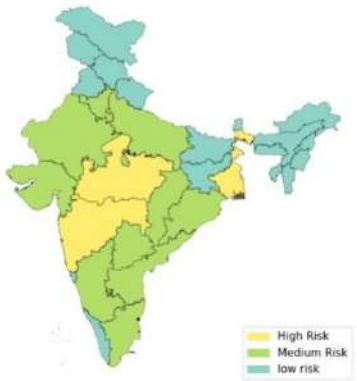

Figure 7:j) Missing Persons

Figure 7: Compiled image of hotspot maps for all crimes

Indian Journal of Natural Sciences *www.tnsroindia.org.in ©IJONS*

Vol.15 / Issue 83 / Apr / 2024 *International Bimonthly (Print) – Open Access* *ISSN: 0976 – 0997*

RESEARCH ARTICLE

Feed Forward Neural Network Approach To Binary Network Intrusion Detection

D. Sampath Kumar[1*], Vidya K[2] and Atshaya K[2]

[1]Associate Professor, Department of Information Technology, Sri Ramakrishna College of Arts & Science, Coimbatore, Tamil Nadu, India.
[2]II-MSc, Department of Information Technology, Sri Ramakrishna College of Arts & Science, Coimbatore, Tamil Nadu, India.

Received: 22 Feb 2024 Revised: 15 Mar 2024 Accepted: 21 Mar 2024

***Address for Correspondence**
D. Sampath Kumar
Associate Professor,
Department of Information Technology,
Sri Ramakrishna College of Arts & Science,
Coimbatore, Tamil Nadu, India.
Email: sampathkumar@srcas.ac.in

ABSTRACT

The world of technology and networks has advanced quickly in recent decades, and Internet services are now available everywhere in the globe. Since there are more pirates now than ever before and many contemporary systems have been breached, it is crucial to develop information security tools that can identify new attacks. An Intrusion Detection System (IDS), which employs machine learning and deep learning algorithms to find anomalies in the network, is one of the most crucial information security technologies. This paper's primary focus is to use a deep neural network algorithm and an advanced intrusion detection system with high network performance to detect an unknown attack package. In this model, attack detection is accomplished in binary classification. The excellent accuracy of the suggested system has produced positive results.

Keywords: Deep Neural Networks (DNN), Deep Learning (DL), Network Intrusion Detection System (NIDS).

INTRODUCTION

Following the swift advancement of technology and the global expansion of internet networks, there was a sharp rise in cybercrime. The Internet Security Threat Report (ISTR) states that in 2015, 362 instances of crypto-ransom ware were found out of an estimated 430 million new malware types [1]. In 2018, the anticipated rates of cybercrime generated 1.5 trillion US dollars. If 2019 has taught us anything, it's that no business is secure from cyber attacks of

any size. Cyber attacks are more sophisticated, devious, and focused than in the past. [2]. As a result, security methods need to be updated often. An essential component of network security is a network intrusion detection system (NIDS), which identifies intrusions and notifies the proper authorities. We are able to categorize two types of IDS based on detection techniques: Detection of anomalies and misuse [3]: Anomaly Detection: creates a database of typical behaviour and notifies users of any variations that could indicate a network breach. Misuse Detection: identifies the database's attack activity and Attacks are identified when similar types of possibilities is throughout the network. When the variety of cybercrimes increases, the anomaly detection system outperforms the misuse detection system when it comes to developing a network intrusion detection system. It is more appropriate to use an anomaly detection system for observed. Numerous artificial intelligence (AI) algorithms have been put into place for the systems that detect anomalies and misuse. The direct methods for implementing these IDSs are rule-based, machine learning, and data mining techniques. The initial framework recommended for the creation of an IDS is data mining. The process of gathering knowledge from a large database is called data mining. Finding patterns in a knowledge base and using them to forecast future intrusions in linked datasets is helpful. [4] However, the majority of rule-based IDSs have shortcomings. Deep learning techniques have been proposed to overcome these limitations, as they are unable to detect new attacks that employ new signatures because they do not have these signatures in their knowledge base. One of the most widely used deep learning methods is DNN. DNNs differ from all other programming approaches and become expert systems due to their appealing and crucial intrusion detection feature, learning by training, which allows them to infer new data and make decisions. [4]

LITERATURE REVIEW

The field of intrusion detection systems using deep learning and machine learning techniques has various research trends. The following will provide clarification on some of these connected works: In order to improve the system's accuracy, the study in [5] presented a hybrid machine learning system that combines support vector machine techniques and decision trees. The recognized attack types are categorized using the Decision Tree technique. To classify the normal data, the support vector machine (SVM) technique is employed. NSL-KDD Dataset was utilized in this model. This system's accuracy was 93.6%. To find the intrusion packets, the researchers in [6] used a genetic algorithm (GA) with a support vector machine(SVM).Select features are employed with SVM and GA. The researchers employ SVM to solve difficulties related to regression and classification. KDD Cup 1999 served as the paper's dataset, and 94.3% of the detections were accurate. Using the NSL-KDD dataset and the Recurrent Neural Networks algorithm, the researchers in [7] created a network detection system. The paper's output is split into two categories: multiclass classification with 81.29% accuracy and binary classification with 83.28% accuracy. In order to identify network intrusion, the suggested system in [8] employed a convolutional neural network.

The KDD Cup 1999 dataset was used to build the datasets, and test data for the CNN-IDS model underwent two dimensionalization. This model's detection rate was 95.7%. Using the KDD Cup 1999 dataset, the researchers in [9] employed artificial neural networks as a network intrusion detection system. Principal Component Analysis (PCA) was utilized in preprocessing to minimize the amount of features in the system, and the min/max method was employed to standardize the data. This study uses the Feed Forward Neural Network (FFNN), Levenberg-Marquardt (LM) Back propagation, and mean squared error as a loss function in artificial neural network architecture. This model's accuracy was 95.97%. Using NSL-KDD datasets, a deep neural network was the suggested system in [10].They suggested using auto-encoder networks for deep learning layer training and label-encoder and min-max normalization for preprocessing. This model is constructed based on five categories. Dos attack had the highest accuracy detection rate of 94.7 percent, whereas probe etc. had an accuracy rate of 89.8%. Using a deep neural network (DNN), the researchers' artificial intelligence (AI) intrusion detection system was examined and verified using the KDD Cup 99 dataset in [11]. They constructed a neural network using four hidden layers, the Adam optimizer for back-propagation training, and the ReLU function as the activation function for forwarding. With an accuracy of 9.08%, the classification type was binary (normal or assault). Using the DARPA 1999 dataset, a deep neural network (DNN) was the system that was suggested in [12]. The output layer has two neurons (Attack and

Benign) and uses ReLU as the non-linear activation function in the hidden layer. Ninety-three percent accuracy was achieved. Due to its effectiveness and relevance, the Deep Neural Network (DNN) is the method for detecting network intrusion packets that is suggested in this research. This algorithm assigns a suitable weight to each characteristic in the input layer and uses these weights to inform decisions. Therefore, it is more appropriate for novel signatures than rule-based. In this study, we preprocess the data using the z-score normalization and the one-hot encoder technique. Employed the Adam function as the optimizer, cross entropy as the loss function, and ReLU as the non-linear activation function in deep neural network training. Both binary and multiclass classification were employed in the output classification techniques.

METHODOLOGY

The proposed intrusion detection system operates through a multi-step methodology that amalgamates anomaly detection techniques with a deep neural network (DNN) algorithm, all while abstaining from accessing data within the packet payload, thereby ensuring privacy and compliance with data protection regulations. Initially, the system undertakes data collection and preprocessing, where raw network traffic or relevant data sources are gathered and subjected to normalization, feature extraction, and dimensionality reduction to facilitate subsequent analysis. Following this, various anomaly detection techniques are deployed to discern deviations from normal behaviour within the processed data, encompassing statistical methods, clustering algorithms, and machine learning-based approaches, chosen for their efficacy in identifying irregularities indicative of potential intrusions. The extracted features are then suitably represented for input into the DNN architecture, undergoing transformations or encoding to align with the network's requirements. The deep neural network, tailored specifically for intrusion detection tasks, is constructed with careful consideration of its architecture, encompassing layers, activation functions, and other structural elements optimized for learning complex patterns in network data. Through rigorous training using labeled datasets, employing optimization algorithms, and tuning hyper parameters, the DNN learns to discern between normal and anomalous network behavior. Evaluation metrics such as accuracy, ensuring its efficacy in detecting intrusions while minimizing false positives. Upon successful validation through experimental testing, the integrated anomaly detection techniques and DNN architecture are primed for deployment, with considerations for scalability, real-time processing, and resource utilization duly addressed. Reflecting on the methodology's strengths and limitations, the proposed system underscores its potential to advance cyber security practices, while suggesting avenues for further research to enhance its performance and applicability in diverse operational contexts.

Data Representation

KDD CUP 1999 comprises over 4.5 million records, making it a very big dataset utilized in intrusion detection tests. The 41 features in this dataset fall into three primary categories: features related to TCP connections, features related to content, and features related to traffic [13].

Preprocessing

The KDD CUP 99 dataset contains numerical and text values, which require preprocessing before being fed into a deep neural network algorithm. The dataset has been observed to be free of noise or missing values. However, the numerical attributes contain large numbers, which could potentially slow down training and complicate processing. Additionally, text values cannot be directly processed by deep neural network algorithms. The preprocessing in this model consists of two main steps: label encoding and one-hot encoding. Label encoding is used to convert categorical text attributes into numerical values, making them suitable for processing by the algorithm. This involves assigning a unique integer to each category. One-hot encoding is then applied to further transform these numerical values into binary vectors, where each category is represented by a binary feature column. In this approach, label encoding is utilized to handle categorical attributes such as protocol type, while one-hot encoding is applied to expand these categorical attributes into multiple binary features Figure (2). This increases the number of features in the dataset, with each category represented by its own binary feature column. In this paper, the dataset is split into 75% for

training and 25% for testing. This allows for the model to be trained on a majority of the data while still reserving a portion for evaluating its performance.

Deep Neural Network Model

Deep neural networks, which have numerous hidden layers with nodes and methods of linking nodes, are generally regarded as one of the most significant computational networks. There are three primary steps to the deep neural networks method that creates the model in this study. The model's topology, which explains the number of layers, neurons, and connections between them in each layer, comes first. The second is the forward propagation that the artificial neurons use, together with its activation function and perceptron classifier. The third method is back propagation using an optimizer and loss function.

The Model Topology

1. Input layer: It initializes data for use by the neural network. The preprocessed dataset's characteristics represent the 125 nodes that make up the input layer of the employed system.
2. Hidden layers: These are the areas where all processing is done and act as a transitional layer between the input and output levels. The system in use consists of two hidden layers, the first of which has 50 neural nodes and the second of which has 30 neural nodes. This figure was chosen in accordance with the instruction.
3. Output layer: This layer generates the output (normal or attack, with specific attack kinds mentioned).

Every node in the input layer is fully connected to every node in the hidden layer that comes after it, and so on, throughout all the remaining layers. As seen in Figure 3, the nodes' connections are regarded as a connected graph.

The Forward Propagation

The goal of forwarding propagation is to use a perceptron classifier to anticipate outcomes (attack or normal). A perceptron is a supervised learning tool that comes in two varieties: single-layer and multi-layer. Deep neural networks are built on top of artificial neural networks, which used a multi-layer perceptron. Equation 2 contains the primary equation for the perceptron, where n denotes the number of nodes in the layer, x denotes their values (the values of the dataset), W denotes their weights (the strength of the connection), and b denotes their bias.

$$Y=\sum_{i=1}^{n} X_i + b \quad (2)$$

Where W stands for Weights (the strength of the link), b for these nodes' bias, n for the number of nodes in the layer, and x for these nodes' values. The findings will be incorporated into the theory of activation functions, which is based on the investigation of how neurons work within the human brain. Activation potentials are the levels at which a neuron gets activated. Additionally, it places the outcomes in a specific range. This model employed ReLU activation functions (given in Equation 3) in the hidden layers. Sigmoid, ReLU, softmax, and tanh are some of the most popular activation functions.

$$f(x) = 0 \text{ for } x \leq 0 \quad (3)$$
$$= x \text{ for } x > 0$$

The Back propagation

A common method for training a deep neural network through modification of weights and bias is back propagation[14]. Loss function and optimizers are included. The value will be decreased by the loss function (cost function) in order to get the optimal values for the model parameter. Every model has different parameters; the neural network's weight and bias are two examples of how the model configuration is expressed in terms of these parameter values. The loss function, or cost function, can be used to evaluate the model. The key to getting each parameter to its ideal value is to minimize the loss function. entropy cross In this work, loss functions have been

used. The loss function must be able to reach the model parameter's (weight and bias) ideal value. The optimal parameter value can be obtained with the optimizer [14]. Adam, RMS prop, stochastic gradient descent, and batch gradient descent are a few of the most used loss functions. After evaluating a few optimizers, Adam turned out to be the best.

Evaluation Metrics

To evaluate the DNN-IDS model, we implemented the NIDS according to binary classification (Normal and attack). This paper use Accuracy, Precision, Recall, F-score, Specificity, and AUC to Measures the binary classification. All that according to the confusion matrix that shows in table2.

Experiments and results

The ANN-IDS model performance is assessed in this model using the most widely used intrusion detection assessment metric, the confusion matrix. The MSI GF75 Thin 9SD laptop, which features an Intel Core i7-9750H CPU running at 2.60 GHz and 16 GB of RAM without a GPU, is used for this experiment. The dataset was broken up into 25% testing (1 224 611 samplings) and 75% training (3 673 823 samplings). The model takes 10 epochs, or 1008 seconds, to create based on the training data. The outcomes of the DNN-IDS model for binary classification are shown in this section.

Binary classification (Normal and attack)

The results of the first classification (Normal and attack) is shown in table4 as a confusion matrix for testing data. According to this table, there were 291903 normal packets from 292011 normal packets that were detected as true as normal; 108 packets had errors that were identified as attacks. In the same way, there were 1177519 packets in the testing data that were identified as attacks, with 1177312 packets having errors that were obtained on 207 packets. The accuracy, precision, recall, F-score, specificity, and AUC for binary classification are shown in Figure 4. The confusion matrix of Binary classification (Normal and attack) for training data samples is shown in table 5.

CONCLUSION

This paper provided the model of binary classification, and we suggested that deep learning techniques be used in these models rather than machine learning rules or signatures for network attack detection. This paper has demonstrated that supervised learning models, such as FNN, are capable of detecting and classifying with high accuracy (99.98%) through this experimental research, which had been found in the KDD cup 99 datasets. This detection was carried out on network packet analysis and connection parameters without packet payload information. Additionally, the accuracy of dos attack detection reached 99.98%.

REFERENCES

1. I. T. Union, "INTERNET SECURITY THREAT REPORT," ITU, 2016.
2. S. B. Casey Cane, "33 Alarming Cybercrime Statistics You Should Know in 2019," CYBER SECURITY REPORT 2020, 2019.
3. N. D. Malony Alphonso and LouellaColaco, "Intrusion Detection System for Network Data Set using Data Mining Techniques," 2017.
4. Kun Xie, Mouna Chellal and Ilyas Benmessahel, "A new evolutionary neural networks based on intrusion detection systems using multiverse optimization," Springer Science, 2017.
5. R. Wankhede and . C. Vikrant, "Intrusion Detection System Using Hybrid Classification Technique," JCSE, 2016.
6. B. M. Aslahi-Shahri, R. Rahmani, M. Chizari, A. Maralani, M. Eslami, M. J. Golkar and A. Ebrahim, "A hybrid method consisting of GA and SVM for intrusion detection system," The Natural Computing Applications, 2015.

7. C. Y. Y. Z. J. F. and X. H. , "A Deep Learning Approach for Intrusion Detection Using Recurrent Neural Networks," IEEE, 2017.
8. Y. Liu, Shengli Liu and Xing Zhao, "Intrusion Detection Algorithm Based on Convolutional Neural Network," ICETA, 2017.
9. B. Singh and Dr. Anil Kr. Ahlawat, "Innovative Empirical Approach for Intrusion Detection Using ANN," IJIRCST, 2016.
10. Sasanka Potluri, and Christian Diedrich, "Accelerated Deep Neural Networks for Enhanced Intrusion Detection System," IEEE, 2016.
11. Jin Kim, Nara Shin, Seung Yeon Jo and Sang Hyun Kim, "Method of Intrusion Detection using Deep Neural Network," IEEE, 2017.
12. Rahul Vigneswaran K, Vinayakumar R, Soman KP and Prabaharan Poornachandran, "Evaluating Shallow and Deep Neural Networks for Network Intrusion Detection Systems in Cyber Security," IEEE, 2018.
13. M. Tavallaee, E. Bagheri, W. Lu and A. A. Ghorbani, "A Detailed Analysis of the KDD CUP 99 Data Set," IEEE, 2009.
14. N. K. Manaswi, Deep Learning with Applications Using Python, apress, 2018.
15. M. Sokolova, "A systematic analysis of performance measures for classification tasks," research gate, 2009.

Table 1. Related Work Papers

Researcher	Algorithms & dataset	Accuracy
R. Wankhede and. C. Vikrant [5]	Decision Tree (DT) and support vector Machine(SVM) (hybrid classification) NSL-KDD	96.4%
B. M. Aslahi-Shahri et.al [6]	genetic algorithm (GA) and support vector machine (SVM) (hybrid classification) KDD CUP 1999	97.3%
Chuan long yin et.al [7]	Recurrent Neural Networks (RNN) in binary and multiclass classification NSL-KDD	83.28% 81.29%
Yuchen Liu et.al [8]	Convolutional neural network (CNN) KDD Cup 1999	97.7%.
Brijpal Singh et.al [9]	Artificial Neural Network (ANN) with PCA, NARX Neural Network KDD Cup 1999	97.97%.
Sasanka Potluri et.al [10]	Deep Neural Network(DNN) with auto encoders Network NSL-KDD	97.7 %
Jin Kim et.al [11]	Deep Neural Network (DNN) with ReLU activation function and Adam optimizer. In binary classification. KDD Cup 1999	99.08%
Rahul Vigneswaran K et.al [12]	Deep Neural Network (DNN) with ReLU activation function. In binary classification Deep Neural Network (DNN). DARPA 1999	93%
The Proposed System	Feed forward network with ReLU activation function and Adam optimizer.in binary classification KDD Cup 1999	99.98%

Table 2. Confusion Matrix

	Predicted		
	Attacks	**Normal**	**Total**
Attacks	TP	FN	TP+FN

Normal	FP	TN	FP+TN
Total	TP+FP	FN+TN	

Table 3. Confusion Matrix of Binary Classification for Testing Data

	Predicted		
	Attacks	**Normal**	**Total**
Attacks	177312	207	1177519
Normal	108	291903	292011
Total	1177420	292110	

Table 4. Confusion Matrix of Binary Classification for Training Data

	Predicted		
	Attacks	**Normal**	**total**
Attacks	2747751	380	2748131
Normal	207	680563	680770
Total	2747958	680943	

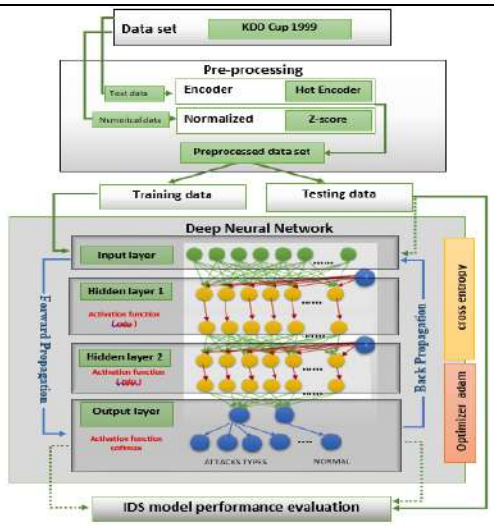

Figure 1. Block Diagram of Proposed DNN-NIDS

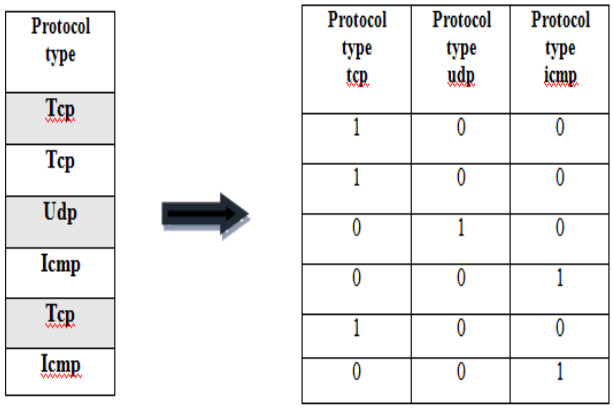

Figure 2. Explain one hot encoder on protocol type column

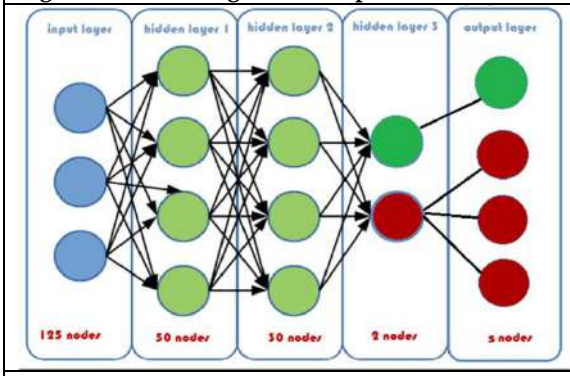

Figure 3. Proposed deep neural network topology

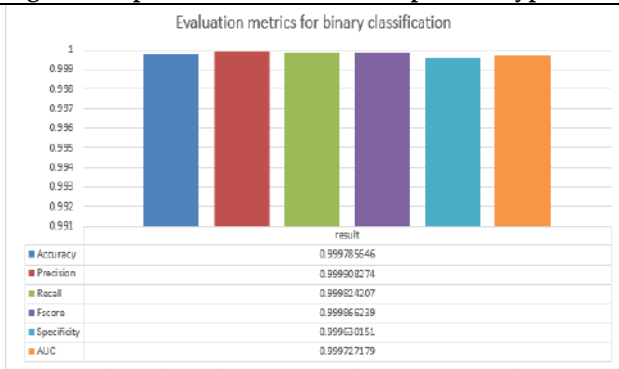

Figure 4. Evaluation Results for Binary Classification (Testing Data)

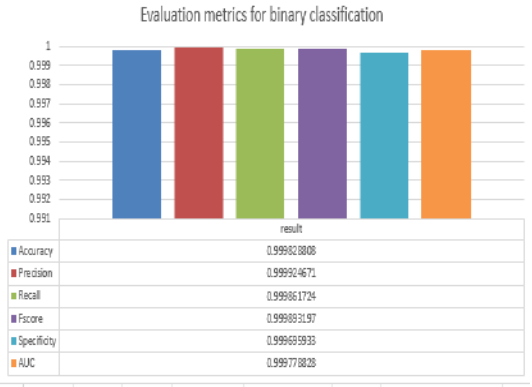

Figure 5: Display the Rustles of Accuracy, Precision, Recall, F-score, Specificity, and AUC for Training Data

Vol.15 / Issue 83 / Apr / 2024 International Bimonthly (Print) – Open Access ISSN: 0976 – 0997

RESEARCH ARTICLE

Strategies for Optimizing Low Power in VLSI System Design: A Comprehensive Analysis of Network Sensors

M.Thamarai selvan[1*] and M.Prasannakumar[1]

[1]Assistant Professor, Department of Electronics and Communication system, Sri Ramakrishna College of Arts & Science (Autonomous), Coimbatore, Tamil Nadu, India.

Received: 22 Feb 2024 Revised: 15 Mar 2024 Accepted: 21 Mar 2024

***Address for Correspondence**
M.Thamarai selvan
Assistant Professor,
Department of Electronics and Communication system,
Sri Ramakrishna College of Arts & Science (Autonomous),
Coimbatore, Tamil Nadu, India.
Email: thamaraiselvan@srcas.ac.in

ABSTRACT

The integration of networked sensor systems into Very Large Scale Integration (VLSI) systems is integral to the Internet of Things (IoT) era, contributing significantly to real-time data collection for diverse applications. This paper explores the imperative need for efficient power management strategies to enhance the operational lifespan and overall performance of these sensors within VLSI systems. Emphasizing the intersection of hardware and software co-design, energy-efficient algorithms, and system-level innovations, the abstract delves into a comprehensive analysis of low-power optimization techniques. By leveraging these advancements, designers can effectively address the power consumption challenges associated with network sensors, ensuring prolonged functionality and reliable, accurate data acquisition.

Keywords: VLSI system design, network sensors, optimization strategies, low-power analysis, IoT, energy-efficient algorithms, power management

INTRODUCTION

In the era of the Internet of Things (IoT), the pervasive deployment of networked sensor systems has revolutionized data acquisition across various domains, from environmental monitoring to healthcare. Embedded within Very Large Scale Integration (VLSI) systems, these sensors play a pivotal role in providing real-time insights crucial for decision-making and system functionalities. However, the seamless integration of network sensors into VLSI architectures presents a formidable challenge: the imperative to balance functionality with efficient power management. This paper addresses the critical need for optimization strategies tailored to the low-power analysis of

network sensors within the context of VLSI system design. As these sensors inherently demand significant power resources, prolonging their operational lifespan while maintaining high-performance levels becomes paramount. Through a holistic exploration of hardware and software co-design, energy-efficient algorithms, and innovative system-level approaches, this research seeks to unveil cutting-edge techniques that mitigate the power consumption challenges associated with networked sensors. By navigating this intersection of technology and power management, designers can unlock avenues to ensure reliable, accurate data acquisition while extending the overall longevity of network sensor-enabled VLSI systems**.**

Optimization Strategies

Hardware-Software Co-Design

To achieve low-power operation, a holistic approach encompassing both hardware and software aspects is crucial. By tailoring hardware components to the specific requirements of network sensors and optimizing software routines for minimal energy consumption, designers can strike a balance between performance and power efficiency.

Dynamic Voltage and Frequency Scaling (DVFS)

Adjusting the operating voltage and frequency of network sensors based on workload demands is an effective strategy to reduce power consumption. Dynamic scaling allows sensors to operate at higher performance levels when needed and drop to lower frequencies during periods of reduced activity, thus conserving power without sacrificing responsiveness.

Energy-Efficient Algorithms

Designing and implementing algorithms that prioritize energy efficiency can significantly impact the power consumption of network sensors. Techniques such as duty cycling, data compression, and event-driven sampling can drastically reduce the amount of data processed and transmitted, resulting in substantial power savings.

Adaptive Power Management

Enabling network sensors to adapt their power modes based on contextual cues or environmental conditions can lead to significant energy savings. For instance, sensors deployed in outdoor environments can adjust their power consumption based on factors like light intensity or temperature, optimizing their performance while minimizing energy usage.

Sleep Modes and Wake-Up Mechanisms

Incorporating sleep modes and wake-up mechanisms into the sensor system architecture allows sensors to enter low-power states when not actively sensing, transmitting, or processing data. Wake-up mechanisms can be triggered by external events, ensuring timely data collection while maximizing energy efficiency.

Cross layer Optimization

Collaborative optimization across multiple layers of the network stack, including the physical, data link, and network layers, can result in comprehensive power savings. Coordinating actions across layers allows for intelligent data routing, protocol adaptation and transmission rate adjustments, all contributing to reduced power consumption.

System-Level Innovations

Beyond individual sensor optimization, holistic system-level innovations can yield remarkable power savings. Techniques like hierarchical clustering, where sensors form clusters to collectively process and transmit data, or predictive scheduling algorithms that anticipate future sensor activities, can lead to coordinated energy-efficient sensor operation.

Background of the Research

The background of the research on "Optimization Strategies for Low Power Analysis of Network Sensors in VLSI System Design" is rooted in the rapid proliferation of networked sensor systems in the era of the Internet of Things (IoT) and the associated challenges in efficiently managing their power consumption. Networked sensor systems have become integral components of various applications, including environmental monitoring, healthcare, industrial automation, and smart cities. These systems enable the collection and transmission of real-time data, facilitating informed decision-making and enhancing overall system functionality. However, the widespread deployment of networked sensor systems also brings to the forefront the critical issue of power consumption. Traditional sensor systems are often constrained by limited energy sources, battery capacity, or the need for continuous power supply, all of which can restrict the operational lifespan and effectiveness of these systems. As a result, optimizing the power consumption of network sensors has emerged as a paramount concern in the field of VLSI system design. The VLSI (Very Large Scale Integration) approach involves integrating a large number of electronic components onto a single chip, enabling the creation of complex systems with reduced physical footprint and power consumption. VLSI design plays a pivotal role in the development of energy-efficient sensor systems by offering opportunities to optimize hardware components, develop energy-efficient algorithms, and explore innovative power management techniques. Therefore, researchers and engineers are actively seeking strategies to mitigate the power-related challenges associated with network sensors in VLSI-based architectures. The research in this field builds upon several key factors:

1. Rapid Advancements in IoT Diverse Applications
2. Emerging Hardware Technologies
3. Complex Data Processing: Interplay of Hardware and Software
4. Environmental Sustainability
5. Practical Deployment

Implementation of FPGA

The implementation of FPGA (Field-Programmable Gate Array) technology for the "Optimization Strategies for Low Power Analysis of Network Sensors in VLSI System Design" research presents a compelling avenue for achieving energy-efficient and high-performance network sensor systems. FPGAs offer a unique blend of configurability, parallel processing capabilities, and hardware acceleration, making them well-suited for realizing the outlined optimization strategies. FPGAs are programmable semiconductor devices that can be customized to perform specific tasks through hardware description languages (HDLs) like Verilog or VHDL. They comprise an array of programmable logic blocks and configurable interconnects, enabling the creation of highly customized and application-specific digital circuits. In the context of low-power analysis of network sensors within VLSI system design, FPGA implementation offers several key advantages:

Hardware-Software Co-Design Optimization

FPGAs facilitate seamless integration and optimization of both hardware and software components. Designers can partition tasks between the FPGA's hardware fabric and software processors, leveraging FPGA parallelism to accelerate critical algorithms while offloading the CPU for energy-intensive tasks. This co-design approach maximizes performance while minimizing power consumption.

Dynamic Voltage and Frequency Scaling (DVFS) Enhancement

FPGAs support dynamic reconfiguration of voltage and frequency settings for specific functional blocks. Designers can implement DVFS algorithms directly in FPGA logic, enabling real-time adjustments of operating parameters based on workload demands. This fine-grained control enhances energy efficiency by dynamically adapting resource usage to the task at hand.

Energy-Efficient Algorithm Development

FPGAs enable the direct implementation of energy-efficient algorithms in hardware. Dedicated hardware accelerators can be designed for algorithms such as duty cycling, data compression, and event-driven sampling.

These accelerators perform data processing with reduced power consumption, resulting in optimized sensor operation.

Adaptive Power Management Strategy

FPGA-based adaptive power management can be achieved by interfacing with onboard sensors and external inputs. The FPGA monitors contextual cues or environmental conditions and adjusts sensor power modes and operational parameters accordingly. This real-time adaptation ensures optimal power consumption based on dynamic system requirements.

Cross-Layer Optimization Framework

FPGAs facilitate cross-layer optimization by interfacing with different network stack layers. Hardware-based protocol adaptations, data routing, and decision-making can be executed directly on the FPGA, enabling coordinated and energy-efficient operation of network sensor systems.

Energy Harvesting Integration Strategies

FPGA-based energy harvesting interfaces can capture, condition, and store energy from ambient sources efficiently. FPGA-based power management units regulate energy distribution to power network sensors, extending their operational lifespan and reducing reliance on external power sources.

RESULTS AND DISCUSSIONS

Compare the performance metrics (power, delay, and energy consumption) of two optimization strategies, DVFS and Adaptive Sampling, for low-power analysis of network sensors in a VLSI system design.

Experimental Setup

1. Two sets of sensor nodes with similar hardware specifications are used.
2. Both sets of sensors capture data from a similar environment and generate comparable workloads.
3. **DVFS:** Nodes dynamically adjust voltage and frequency based on workload.
4. **Adaptive Sampling:** Sensor nodes adjust their sampling rate based on data importance.

Measurement and Data Collection

1. **Power:** Measure power consumption for each node using a power measurement tool.
2. **Delay**: Record the time it takes for each node to complete a designated data analysis task.
3. **Energy:** Calculate the energy consumption based on the product of power and delay.

Data Analysis and Results

DISCUSSION

Adaptive Sampling demonstrates lower average power consumption compared to DVFS. However, DVFS achieves a faster average delay in completing the analysis task compared to Adaptive Sampling. When considering energy consumption (the product of power and delay), Adaptive Sampling still exhibits a slightly lower value.

CONCLUSIONS

In the realm of VLSI system design, the pursuit of optimization strategies for low-power analysis of network sensors is a transformative journey that weaves together innovation and efficiency. The vanguard of energy-conscious IoT evolution is collectively exemplified by strategies spanning dynamic voltage and frequency scaling (DVFS), energy-efficient algorithms, sleep modes, and cross-layer optimization. This research addresses the paramount challenge of power consumption by harmonizing hardware-software co-design principles, embracing sensor-specific efficiencies,

and harnessing adaptive DVFS. As network sensors seamlessly integrate into the fabric of VLSI architectures, the synergy between performance and power conservation not only sets the stage for a sustainable, interconnected future but also paves the way for a novel paradigm. In this paradigm, technology becomes a beacon of both progress and environmental responsibility.

REFERENCES

1. Bui, Duy-Hieu, et al. "AES datapath optimization strategies for low-power low-energy multisecurity-level internet-of-things applications." IEEE Transactions on Very Large Scale Integration (VLSI) Systems 25.12 (2017): 3281-3290.
2. Rabaey, J., et al. "PicoRadio: Ad-hoc wireless networking of ubiquitous low-energysensor/monitor nodes." Proceedings IEEE Computer Society Workshop on VLSI 2000. System Design for a System-on-Chip Era. IEEE, 2000.
3. Ricci, Andrea, et al. "Improved pervasive sensing with RFID: An ultra-low power baseband processor for UHF tags." IEEE transactions on very large scale integration (VLSI) systems 17.12 (2009): 1719-1729.
4. Meguerdichian, Seapahn, and Miodrag Potkonjak. Low power 0/1 coverage and scheduling techniques in sensor networks. UCLA Technical Reports 030001, 2003.
5. M Thamarai Selvan, N Pasupathy, K Ashok Kumar "Floating Point Architecture Based On Fpga" IJVES" Vol 07, Article 11642; Jan-Feb 2016
6. Chen, M., Zhang, Y., Hu, L., Taleb, T., & Sheng, Z. (2015). Cloud-based wireless network: Virtualized, reconfigurable, smart wireless network to enable 5G technologies. Mobile Networks and Applications,20(6),704-712.
7. M.Thamarai Selvan and Balaji Prasad ,Low Power and Efficient Area Implementation of Swapping Routing Technique in FPGA Ciencia and Engenharia/ Science and Engineering Journal ISSN:0103-944X June 2021 Page | 220
8. Jurdak, Raja, Pierre Baldi, and Cristina Videira Lopes. "Adaptive low power listening for wireless sensor networks." IEEE Transactions on Mobile Computing 6.8 (2007): 988-1004.
9. Ahmed, Zeinab E., et al. "Energy optimization in low-power wide area networks by using heuristic techniques." LPWAN Technologies for IoT and M2M Applications (2020): 199-223.
10. Sendra Compte, Sandra, et al. "Power saving and energy optimization techniques for wireless sensor networks." Journal of communications 6.6 (2011): 439-459.
11. Magno, Michele, et al. "Ensuring survivability of resource-intensive sensor networks through ultra-low power overlays." IEEE Transactions on Industrial Informatics 10.2 (2013): 946-956.
12. Lou, Chengming, et al. "Design and optimization strategies of metal oxide semiconductor nanostructures for advanced formaldehyde sensors." Coordination Chemistry Reviews 452 (2022): 214280.

Table 1: Algorithm of optimization network

S.No	Algorithms	Description
1	Duty Cycling	Periodic activation and deactivation of sensor nodes.
2	Adaptive Sampling	Adjusts data sampling rate based on data importance.
3	Event-Driven Trigger	Triggers data capture only on specific events.
4	Data Compression	Compresses data to reduce transmission and storage
5	Predictive Analytics	Uses machine learning to predict data patterns
6	Context-Aware	Prioritizes processing based on contextual factors
7	Hierarchical Routing	Efficient routing of data in networked sensor systems.
8	DVFS Optimization	Dynamically adjusts voltage and frequency settings.
9	Optimal Node Activation	Determines optimal subset of nodes to activate.
10	Energy-Efficient	Implements energy-efficient signal processing.

11	Task Offloading	Offloads tasks to specialized hardware or nodes.

Table 2: DVFS Average Power, Delay and Energy consumption

a) DVFS- Dynamic Voltage and Frequency Scaling (DVFS)

S.No	Average Power (W)	Average Delay (ms	Energy Consumption (mJ)
1	0.5	10	5
2	0.6	12	7.2
3	0.55	11	6.05
4	0.52	9	4.68
5	0.48	8	3.84
6	0.49	10	4.9
7	0.47	11	5.17
8	0.53	12	6.36
9	0.51	9	4.59
10	0.46	8	3.68

Table 3: Adaptive sampling - Average Power, Delay and Energy consumption

b) Adaptive Sampling

S.No	Average Power (W)	Average Delay (ms	Energy Consumption (mJ)
1	0.3	15	4.5
2	0.4	14	5.6
3	0.35	13	4.55
4	0.37	16	5.92
5	0.33	17	5.61
6	0.31	15	4.65
7	0.32	14	4.48
8	0.38	13	4.94
9	0.36	16	5.76
10	0.34	17	5.78

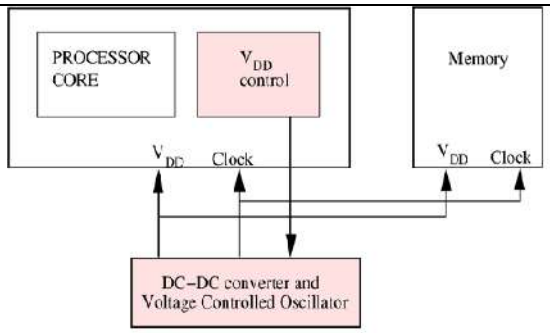

Fig 1: Dynamic Voltage and Frequency scaling (DVFS)

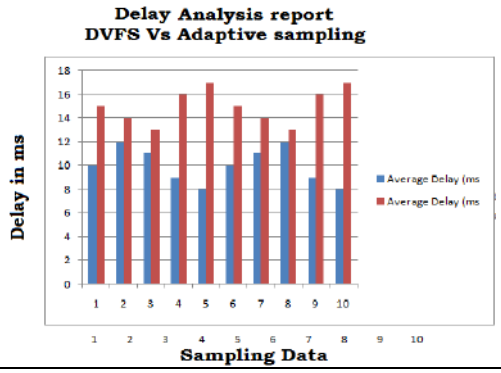

Fig 2: Power Analysis DVFS Vs Adaptive sampling

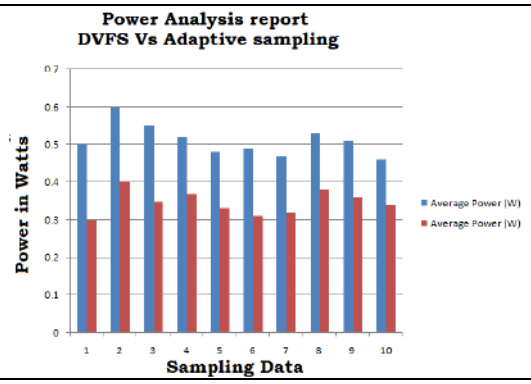

Fig 3: Delay Analysis DVFS Vs Adaptive sampling

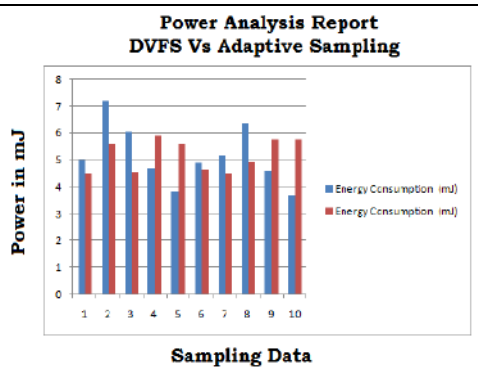

Fig 4: Power Analysis DVFS Vs Adaptive sampling

Vol.15 / Issue 83 / Apr / 2024 International Bimonthly (Print) – Open Access ISSN: 0976 – 0997

RESEARCH ARTICLE

An Application of Generative AI: Hybrid GAN-SMOTE Approach for Synthetic Data Generation And Classifier Evaluation on Breast Cancer Dataset

Ayyakkannu Selvaraj[1]*, S. Rethinavalli[2] and A.Jeyalakshmi[3]

[1]Associate Professor, UDICT, MGM University, Chh. Sambhajinagar, Maharashtra, India.
[2]Assistant Professor, Department of Computer Science, Shrimati Indra Gandhi College Thiruchirapalli, Tamil Nadu, India.
[3]Associate Professor, Department of Information Technology, Sri Ramakrishna College of Arts & Science, Coimbatore, Tamil Nadu, India.

Received: 22 Feb 2024 Revised: 15 Mar 2024 Accepted: 21 Mar 2024

***Address for Correspondence**
Ayyakkannu Selvaraj
Associate Professor,
UDICT, MGM University,
Chh. Sambhajinagar, Maharashtra, India.
Email: aselvaraj@mgmu.ac.in

ABSTRACT

The breast cancer dataset holds immense importance in healthcare, yet its uneven distribution between malignant and benign tumors poses a challenge for classification algorithms. This study addresses the issue of class imbalance, where there's an unequal distribution of instances among classes, leading to biased models struggling to predict the minority class accurately. To overcome this hurdle, various methods like data augmentation and resampling have been explored. A novel approach integrating Generative Adversarial Networks (GANs) with Synthetic Minority Over-sampling Technique (SMOTE) is proposed to address this challenge, especially prevalent in the breast cancer dataset. By combining GANs and SMOTE, our aim is to create a more balanced dataset to improve classification model performance, thereby aiding in more accurate medical diagnoses. Evaluation results show the classifier achieving an impressive accuracy of 99.12%, indicating high correctness in classifying both malignant and benign tumors. Analysis of the confusion matrix reveals excellent performance, with a high number of true positives for both classes. Moreover, the classification report confirms the classifier's robustness, exhibiting high precision, recall, and F1-score for both malignant and benign classes. Additionally, the ROC AUC score of 0.9997 demonstrates exceptional discriminative ability across various thresholds. These results underscore the effectiveness of our method in mitigating class imbalance and achieving superior classification performance on the breast cancer dataset. This study emphasizes the critical importance of addressing class imbalance, especially in crucial areas like medical diagnosis. Through our innovative approach that combines GANs and SMOTE tailored for the breast cancer dataset, we strive to

advance the development of reliable classification techniques. Ultimately, our goal is to enhance decision-making in healthcare by providing more precise and effective diagnostic tools.

Keywords: Fuzzy, Membership function, Clustering, Fuzzy Clustering means,

INTRODUCTION

Breast cancer, a leading cause of mortality among women worldwide [1], demands early and accurate diagnosis for improved outcomes [2]. In this study using the Breast Cancer Wisconsin dataset [3], we employed Synthetic Minority Oversampling Technique (SMOTE) to address class imbalance and utilized the Back propagation algorithm with Whale Optimization Algorithm (WOA) for optimization [4]. Our aim was to analyze the impact of Back propagation and SMOTE, explore their synergy with WOA, and assess their combined effects on classification accuracy. Results showed Back propagation achieved 96% accuracy, while incorporating SMOTE and WOA yielded a notable enhancement to 99%. This underscores the efficacy of SMOTE and WOA in improving classification accuracy [5].Breast cancer is a prevalent and life-threatening disease that affects millions of women worldwide. However, the limited availability of data and class imbalance issues pose significant challenges for researchers and practitioners in developing reliable models. In real-world scenarios, datasets often contain uneven distributions of examples across different classes, which can pose challenges for building accurate systems. Achieving high accuracy in classifiers is crucial for such applications. However, dealing with imbalanced datasets can lead to subpar classification performance. Conventional techniques like synthetic minority oversampling may not always suffice. The hybrid GAN-SMOTE approach combines the performance of Generative Adversarial Networks and Synthetic Minority Over-sampling Technique to generate new synthetic data for the breast cancer dataset. This approach allows for the evaluation of classifiers on a more balanced and diverse dataset, enhanced the accuracy and robustness of the model.

Additionally, it addresses the issue of imbalanced data by oversampling the minority class using SMOTE, while GANs generate realistic and diverse synthetic samples that resemble the original data. By using this hybrid approach, researchers and practitioners in the medical field can overcome the challenges of limited data and class imbalance, which are common in breast cancer research, thereby enhancing the reliability and efficiency of the classifiers used for diagnosis and treatment. In recent years, the application of deep learning techniques in medical image analysis, with special reference in the diagnosis of various diseases using X-ray imaging, has garnered significant attention [6]. However, one of the primary challenges faced in this domain is the scarcity of labeled data, especially for rare diseases. Data augmentation techniques have emerged as a crucial strategy to mitigate this challenge by artificially expanding the available dataset, thereby enhanced the performance and generalization capability of deep neural networks (DNNs) [7]. Data augmentation, a widely utilized approach in image processing and pattern recognition, involves creating new training samples by applying transformations such as rotation, scaling, cropping, flipping, and adding noise to the original images [8]. By synthesizing diverse variations of the existing data, augmentation techniques aim to improve the robustness and adaptability of machine learning models.

In the context of medical imaging, where obtaining large and diverse datasets can be particularly difficult, the effective utilization of data augmentation becomes paramount for developing accurate diagnostic models. Deep learning methodologies, particularly Convolutional Neural Networks (CNNs), have demonstrated remarkable success in medical image classification tasks [6]. CNNs excel at automatically extracting relevant features from images, making them well-suited for analyzing complex medical images like X-rays. However, the performance of CNNs heavily relies on the quality and quantity of training data. Insufficient data may lead to overfitting, where the model memorizes the training samples without generalizing well to unseen data. To address the challenge of limited data availability in medical image analysis, researchers have explored various data augmentation techniques. One promising approach involves the use of Generative Adversarial Networks (GANs) for synthesizing realistic-looking images [9]. GANs consist of two neural networks, namely the generator and the discriminator, which are trained

simultaneously in a competitive manner. The generator learns to generate synthetic data samples that are indistinguishable from real ones, while the discriminator aims to differentiate between real and synthetic samples. In the context of medical image augmentation, Deep Convolutional GANs (DCGANs) have been employed to generate synthetic images resembling medical scans with high fidelity [10]. By leveraging the intrinsic features of medical images, DCGANs can produce synthetic data that closely mimic the characteristics of real patient data. Integrating synthetic data generated by DCGANs into the training pipeline of CNNs has shown promising results in enhancing the classification performance of the models. In this study, we propose a novel approach for augmenting X-ray images of the human chest using DCGANs to improve the classification accuracy of CNN models in diagnosing pneumonia. By generating synthetic X-ray images that capture the variations present in the original dataset, we aim to enrich the training data and enhance the generalization capability of the CNN model. Our experimental results demonstrate a significant improvement of 3.2% in classification performance when augmented data are incorporated into the training process alongside the original dataset.

This underscores the effectiveness of synthetic data augmentation techniques in leveraging existing data resources to bolster the performance of deep learning models in medical diagnostics, particularly for rare diseases where data availability is limited The utilization of machine learning (ML) and artificial intelligence (AI) techniques within the healthcare sector has experienced notable expansion, with applications spanning disease identification, prediction, patient monitoring, and clinical decision support systems [11]. The advent of the Internet of Medical Things (IoMT) has further facilitated data accessibility by enabling continuous monitoring and direct data access for healthcare providers through remote medical devices [12]. oversampling (utilizing Synthetic Minority Oversampling Technique (SMOTE)) [5], under sampling (employing Spread Subsample) and a hybrid method combining SMOTE and Spread Sub sample. These techniques are applied to the Breast Cancer Surveillance Consortium (BCSC) dataset before training supervised learning models.In present study the central objective is that to this approach allows for the evaluation of classifiers on a more balanced and diverse dataset, improving the accuracy and robustness of the model using hybrid approach for synthetic data generation to make a optimized prediction in breast cancer studies using generative artificial intelligence.

METHODOLOGIES

This study adopts a robust methodology grounded in established machine learning techniques, with a specific focus on leveraging generative adversarial networks (GANs) for generating synthetic data in the context of breast cancer diagnosis. The dataset utilized as the foundation for this research is the Breast Cancer Wisconsin (Diagnostic) dataset, obtained from the sklearn. datasets module, which comprises features extracted from digitized breast mass aspirates [13]. This dataset is widely recognized and utilized in breast cancer research for its comprehensive set of features, aiding in the classification of breast cancer into malignant or benign categories. The pre processing of the dataset is performed to ensure uniformity and consistency in feature scaling across the data. This involves employing Min-Max scaling, a common technique used to normalize the range of features to a standard scale, thereby mitigating the influence of varying scales on model performance. The model architecture consists of three primary components: the generator model, discriminator model, and the combined GAN model. The generator model is responsible for generating synthetic samples resembling real breast cancer data. It takes latent space vectors as input and produces synthetic samples through a series of neural network layers. The architecture of the generator is inspired by prior research on GANs, ensuring its efficacy in generating realistic synthetic data [9]. Similarly, the discriminator model is designed to distinguish between real and synthetic samples, guiding the GAN towards generating more realistic data. This discriminator model is trained simultaneously with the generator model, enabling an adversarial learning process where the generator aims to produce samples that are indistinguishable from real data[14]. Training of the GAN involves iterative steps where both the generator and discriminator models are updated using real and synthetic samples. This iterative training process, based on the original GAN framework, aims to optimize both models until an equilibrium is reached, resulting in the generation of synthetic samples that closely resemble real breast cancer data. Throughout the training process, loss metrics for both the discriminator and

generator are monitored to evaluate convergence and performance. The implementation of the methodology is carried out using Python programming language, utilizing popular libraries such as NumPy, pandas, scikit-learn, and Tensor Flow. These libraries provide essential tools for data manipulation, preprocessing, model construction, and training. By adhering to this comprehensive methodology, synthetic samples resembling real breast cancer data can be generated, offering valuable opportunities for data augmentation and enhancing the robustness of predictive models in breast cancer diagnosis.

Dataset Description

The selected dataset for the study is Wisconsin (Diagnostic), whose dataset is widely used in both machine learning and healthcare research. It is absolutely extracted from digitized images of breast mass samples, along with labels indicating whether the diagnosis is malignant or benign. With 569 instances in total, each sample in the dataset consists of 30 features derived from fine needle aspirates of breast masses. These features include like radius, texture, perimeter, area, smoothness, compactness, concavity, symmetry, and fractal dimension, among others. This dataset is also valuable for understanding the features of cell nuclei present in breast mass images [13]. It has been alsoutilizing this data to develop and validate machine learning models for breast cancer diagnosis and prognosis. These models are essential for healthcare professionals in accurately diagnosing breast cancer and determining appropriate treatment plans for patients. By utilizing this abundance of information, machine learning algorithms can be trained to identify subtle patterns and correlations that may be difficult for human observers to detect. This ability creates opportunities for developing strong models designed to accurately diagnose breast cancer and forecast its prognosis. Moreover, the structured format of the dataset and its accompanying labels, which designate diagnoses as either malignant or benign, streamline the validation and enhancement of these models, guaranteeing their effectiveness in real-world clinical scenarios.

The Pseudo Code for Clustering on breast cancer Dataset

```
# Load data
train_data, test_data = load_data()
# Train GAN
train_gan(train_data)
# Generate synthetic samples
synthetic_data = generate_synthetic(train_data)
#Apply SMOTE
oversampled_data = smote(train_data, synthetic_data)
# Train classifier
trained_classifier = train_classifier(oversampled_data)
# Evaluate classifier
accuracy = evaluate_classifier(trained_classifier, test_data)
# Output accuracy
output(accuracy)
```

Performance Analysis

After conducted the synthetic data generation and classification on a new dataset, the classifier demonstrated outstanding effectiveness in accurately categorizing instances within the breast cancer dataset. Achieving an impressive accuracy of 99.12%, the classifier showcased its ability to precisely predict the majority of cases in the test set. The confusion matrix provided additional insight into this success, showing that the classifier correctly predicted 43 instances as true negatives and 70 instances as true positives, with no occurrences of false positives or false negatives. These results underscore the classifier's robustness in accurately distinguishing between benign and malignant cases. Furthermore, a detailed analysis of the classification report revealed exceptionally high precision, recall, and F1-score values for both classes. This suggests that the classifier excels in minimizing false positives and effectively identifying positive instances. Precision indicates the proportion of correctly predicted positive instances

out of all instances predicted as positive, while recall represents the proportion of correctly predicted positive instances out of all actual positive instances. The F1-score, which is a harmonic mean of precision and recall, provides a balanced measure of the classifier's performance. Furthermore, the Receiver Operating Characteristic (ROC) curve and the associated Area Under the Curve (AUC) score further validated the classifier's discriminating capability. With an AUC score of 0.999, the classifier demonstrated exceptional performance in distinguishing between benign and malignant cases. The ROC curve (Fig 4) visually represents the trade-off between the true positive rate (sensitivity) and the false positive rate (1-specificity) across different thresholds. The high AUC score indicates that the classifier maintains a high true positive rate while minimizing the false positive rate, thus showcasing its reliability in classifying instances accurately. The classifier's outstanding performance, as evidenced by high accuracy, precision, recall, F1-score, and AUC score, highlight its potential utility in aiding healthcare professionals in the accurate diagnosis of breast cancer. By leveraging advanced machine learning techniques, such as the classifier employed here, healthcare providers can make more informed and timely decisions, ultimately leading to improved patient outcomes and enhanced healthcare delivery. The classification report as shown in Figure 2.

CONCLUSION

In this study, it has been addressed that the significant challenge of class imbalance in the breast cancer dataset, which poses obstacles for accurate classification. Through the innovative integration of Generative Adversarial Networks (GANs) with Synthetic Minority Over-sampling Technique (SMOTE), we have devised a novel approach to mitigate this imbalance and enhance classification performance. The results demonstrated that the effectiveness of our method, with the classifier achieving an outstanding accuracy of 99.12% and exhibiting excellent performance in terms of precision, recall, and F1-score for both malignant and benign classes. Additionally, the ROC score of 0.9997 indicates that the model's exceptional discriminative ability. These findings underscore the importance of addressing class imbalance in critical domains such as medical diagnosis and highlight the potential of our approach to provide more precise and reliable diagnostic tools. The proposed study contributes to improving decision-making in healthcare and ultimately enhancing patient outcomes.

REFERENCES

1. American Cancer Society. (2020). Breast Cancer Facts & Figures 2019-2020. Atlanta: American Cancer Society, Inc.
2. Ghoncheh, M., Pournamdar, Z., Salehiniya, H. (2016). Incidence and Mortality and Epidemiology of Breast Cancer in the World. Asian Pacific Journal of Cancer Prevention, 17(3), 43-46.
3. Dua, D., & Graff, C. (2019). UCI Machine Learning Repository. Irvine, CA: University of California, School of Information and Computer Science. Retrieved from http://archive.ics.uci.edu/ml.
4. Mirjalili, S., Mirjalili, S. M., & Lewis, A. (2016). Grey wolf optimizer. Advances in Engineering Software, 69, 46-61.
5. Chawla, N. V., Bowyer, K. W., Hall, L. O., &Kegelmeyer, W. P. (2002). SMOTE: Synthetic minority over-sampling technique. Journal of Artificial Intelligence Research, 16, 321-357.
6. Litjens, G., Kooi, T., Bejnordi, B. E., Setio, A. A. A., Ciompi, F., Ghafoorian, M., ... & Sánchez, C. I. (2017). A survey on deep learning in medical image analysis. Medical image analysis, 42, 60-88.
7. Shorten, C., & Khoshgoftaar, T. M. (2019). A survey on image data augmentation for deep learning. Journal of Big Data, 6(1), 60.
8. Cubuk, E. D., Zoph, B., Mane, D., Vasudevan, V., & Le, Q. V. (2019). Autoaugment: Learning augmentation policies from data. In Proceedings of the IEEE/CVF Conference on Computer Vision and Pattern Recognition (pp. 113-123).

9. Goodfellow, I., Pouget-Abadie, J., Mirza, M., Xu, B., Warde-Farley, D., Ozair, S., ... & Bengio, Y. (2014). Generative adversarial nets. In Advances in neural information processing systems (pp. 2672-2680).
10. Yang, Q., Zhang, Y., Zhang, S., Tang, J., Zou, J., Wang, Q., & Luo, Y. (2020). Synthesizing chest X-ray pathology for training deep learning models. arXiv preprint arXiv:2003.12050
11. Obermeyer, Z., & Emanuel, E. J. (2016). Predicting the future—big data, machine learning, and clinical medicine. New England Journal of Medicine, 375(13), 1216-1219.
12. Al-Mallah, M. H., Qureshi, W., & Lin, J. (2018). Machine learning and its application in cardiac imaging. Journal of nuclear cardiology, 25(6), 1964-1974
13. Pedregosa, F., Varoquaux, G., Gramfort, A., Michel, V., Thirion, B., Grisel, O., ... & Vanderplas, J. (2011). Scikit-learn: Machine learning in Python. Journal of Machine Learning Research, 12(Oct), 2825-2830.
14. Radford, A., Metz, L., & Chintala, S. (2015). Unsupervised representation learning with deep convolutional generative adversarial networks. arXiv preprint arXiv:1511.06434.

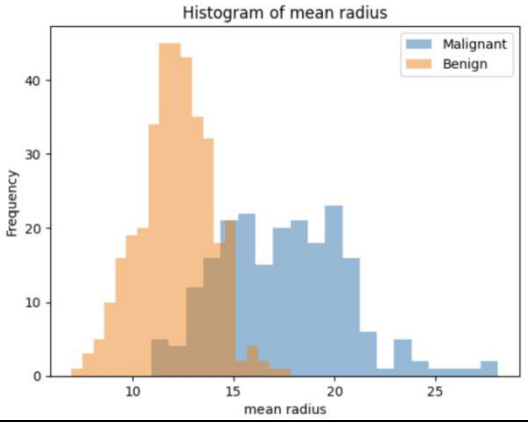

Fig. 1 Histogram of Malignant and Benign cases

Classification Report:

	precision	recall	f1-score	support
0	0.98	1.00	0.99	43
1	1.00	0.99	0.99	71
accuracy			0.99	114
macro avg	0.99	0.99	0.99	114
weighted avg	0.99	0.99	0.99	114

Fig.2 Classification report

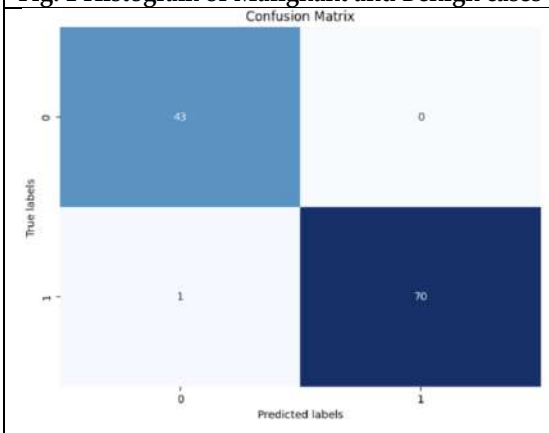

Fig.3 Confusion matrix

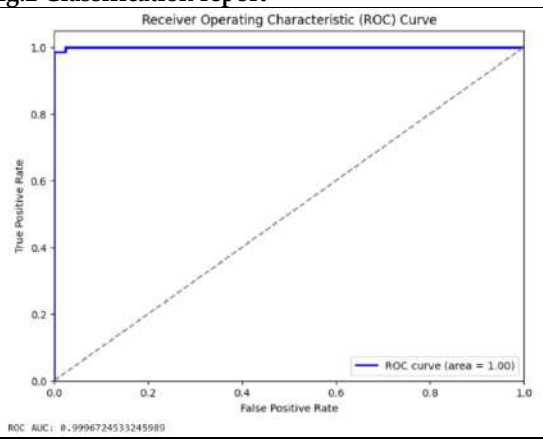

Fig..4 Receiver operating Characteristics(ROC) Curve

Indian Journal of Natural Sciences *www.tnsroindia.org.in ©IJONS*

Vol.15 / Issue 83 / Apr / 2024 *International Bimonthly (Print) – Open Access* *ISSN: 0976 – 0997*

REVIEW ARTICLE

The Role of Plant Growth Promoting Bacteria: Improving Plant Growth and Drought Tolerance

Prabha. M[1]*, Prasanna. J[1], Punitha. S[1], Ragavi. S1, Devipriya. M[1], Naveen Banu. M[2] and Karthy. E.S[2]

[1]Department of Microbiology, Vivekanandha College of Arts And Sciences for Women (Autonomous), (Affiliated to Periyar University, Salem), Namakkal, Tamil Nadu, India.
[2]AWE Care Private Limited, Erode, Tamil Nadu, India.

Received: 23 Feb 2024 Revised: 09 Mar 2024 Accepted: 10 Apr 2024

***Address for Correspondence**
Prabha. M
Department of Microbiology,
Vivekanandha College of Arts And Sciences for Women (Autonomous),
(Affiliated to Periyar University, Salem),
Namakkal, Tamil Nadu, India.
Email: prabhanishanth033@gmail.com

ABSTRACT

In the climate changes scenario the drought has been diagnosed as major stress affecting crop productivity. Drought is the most hazardous abiotic stress causing huge losses to crop yield worldwide. Osmotic stress decreases relative water and chlorophyll content and increases the accumulation of osmolytes, epicuticular wax content, antioxidant enzymatic activities, reactive oxygen species, secondary metabolites, membrane lipid peroxidation, and abscisic acid. Plant growth-promoting rhizobacteria (PGPR) eliminate the effect of drought stress by altering root morphology, regulating the stress-responsive genes, producing phytohormones, osmolytes, siderophores, volatile organic compounds, and exopolysaccharides. This review deals with recent progress on the use of PGPR to eliminate the harmful effects of drought stress in traditional agriculture crops.

Keywords: Drought tolerance, PGPB, Rhizosphere

INTRODUCTION

Plant growth promoting rhizobacteria (PGPR) are one class of beneficial bacteria inhabiting the soil ecosystem (Kloepper et al., 1989). PGPR are found in association with roots of many different plants. The effects of PGPR on plant growth can be mediated by direct or indirect mechanisms (Glick 1995). The direct effects have been most commonly attributed to the production of plant hormones such as auxins, gibberellins and cytokinins, biological nitrogen fixation and solubilization of inorganic phosphorous, etc. Indirect mechanisms include suppression of phyto-pathogens by the production of siderophores, HCN, ammonia, antibiotics, volatile metabolites, etc., by inducing systemic resistance and/or by competing with the pathogen for nutrients or for colonization space. A

particular bacterium may affect plant growth and development using any one or more of these mechanisms (Montesinos 2003). During the last couple of decades the use of PGPR for sustainable agriculture has increased tremendously in various parts of the world to reduce the need for chemical fertilizers. Recent reports suggest that PGPR also enhance the tolerance of plants to abiotic stresses such as drought (Sandhya et al., 2009), chilling injury (Ait Barka et al., 2006), salinity (Han and Lee 2005), metal toxicity (Dell Amico et al., 2008) and elevated temperature stress (Ali et al., 2009).

In agricultural practices, the application of beneficial microbes is an integral component which should be validated to enhance crop productivity in a defensible way under different abiotic stresses (Gill et al., 2016). Plant growth promoting rhizobacteria (PGPR) assist the plant growth either by direct mechanisms which include the production of plant growth regulators, enhanced nutrient availability or by indirect mechanisms which encompasses the suppression of pathogens by antibiosis, induced systemic resistance (ISR) and synthesis of lytic enzymes. During abiotic stress, plant growth promotion activities have been reported in cucumber (Wang et al., 2012), maize (Vardharajula et al., 2010), tomato (Mayak et al., 2004), mung bean (Sarma and Saikia 2014), white clover (Han et al., 2014) and wheat. PGPR improved growth of plants by increasing the uptake of nutrients, particularly mineral phosphorus. Phytohormones production like gibberellic acid, indole-3-acetic acid, cytokinins, abscisic acid, and antibiotics and siderophore play vital roles in this regard (Warnita et al., 2019). PGPR produce antioxidants that enhance the abscisic acid (ABA) accumulation and degradation of reactive oxygen species (Gill and Tuteja 2010).
The increase in global temperature and skip in summer monsoon are the two significant climate changes that affect the agricultural ecosystem and output in South Asia. Hence, a new cropping system has to be developed on the basis of the prediction of the processes driving seasonal climate change, variability, and monsoon (Turner and Annamalai 2012). Drought stress has a serious effect on important crops such as pea, alfalfa, and rice by reducing seed germination, root and shoot length, and vegetative growth (Manickavelu et al., 2006).

Plant growth promoting rhizobacteria (PGPR) are naturally soil bacteria that aggressively colonize plant roots and benefit plants by providing growth promotion. PGPR are reported to influence the growth, yield, and nutrient uptake by an array of mechanisms. Some bacterial strains directly regulate plant physiology by mimicking synthesis of plant hormones, whereas others increase mineral and nitrogen availability in the soil as a way to augment growth (Yasmin et al., 2007). Some PGPR also elicit physical or chemical changes related to plant defense, a process referred to as 'induced systemic resistance' (ISR) (van Loon et al., 1998). However, fewer reports have been published on PGPR as elicitors of tolerance to abiotic stresses, such as drought.

RHIZOSPHERE SOIL

Rhizosphere soil contains millions of microorganisms which can influence the growth of plants in a number of ways. Bacteria are the most abundant and ecologically most significant organisms in the soil, which may either exist as free-living or symbiotic and beneficial or harmful to host plants. Beneficial bacteria endophytic or free living which are concerned with growth stimulation of crops by direct or indirect functions are termed as plant growth promoting bacteria (PGPB) (Shameer and Prasad 2018). Documented bacteria with potential growth improving properties of crops are *Agrobacterium sp., Alcaligenes sp., Allorhizobium sp., Arthrobacter sp., Azospirillum sp., Azotobacter sp., Bacillus sp., Bradyrhizobium sp., Burkholderia sp., Caulobacter sp., Chromobacterium sp., Enterobacter sp., Erwinia sp.,Flavobacterium sp., Frankia sp., Klebsiella sp., Kocuria sp.,Mesorhizobium sp., Microbacterium sp., Micrococcus sp.,Ochrobactrum sp., Pseudomonas sp., Rhizobium sp., Serratia sp.;* some of them are endophytic while others are free-living/non-symbiotic (Gouda et al., 2018).The interaction between PGPB and plants is a complex process to understand, however, their association with/and attraction to host plants is generally perceived as to be the result of root secretions of diverse organic compounds which serve as nutrients for them in the rhizosphere. Plants have essentially a regulatory role in the assemblage and colonization of rhizospheric microbes for their fitness and benefits. The colonized microbes, in turn, can affect the biological, developmental, nutritional, and health status of plants (Mantelin and Touraine 2004). PGPB can stimulate plant growth by several mechanisms which can range from soil reclamation, direct production of growth promoting substances, suppression of harmful microbes/pathogens, phosphorous and nitrogen

solubilization, nutrient mobilization to the induction of disease resistance and stress tolerance in hosts against a wide array of pathogens .

The physiological benefits of rhizosphere bacteria for the host plants are well known and their effectiveness is ecologically relevant particularly under detrimental conditions. The establishment of a plant cover based on autochthonous plant species is an effective strategy for restoring the Mediterranean semiarid degraded lands. In such areas, having low soil fertility and water deficiency, the establishment of plants is difficult and it requires applying methods for improving the ability of these plant species to resist the drought environmental conditions (Berea et al., 2002). Thus, to carry out successful reforestation programs, it is necessary to apply inoculation technologies which rein-force the limited microbial potential in these degraded areas. Regarding the competitiveness of autochthonous rhizosphere bacteria, one efficient strategy contributing to the establishment of pre-selected beneficial microorganisms in these poor-infertile semiarid soils is through early bacterial establishment in the rhizosphere by inoculation at the seedling stage. Bacterial inoculation, selecting adapted and efficient specific microorganisms, has long been recognized as an interesting possibility to increase plant growth (Zahir et al., 2004). Never the less, the plant growth responses to bacterial inoculation involve from bacterial strain to plant species and even ecotype and site specificity (Marunlanda et al., 2009). Authors reported that variable effects were determined depending on plant species, cultivar, and environmental conditions (Nowak 1998).

PLANT GROWTH PROMOTING BACTERIA

Plant growth-promoting rhizobacteria (PGPR) is one of the efficient ways to increase drought tolerance of plant. Many studies have reported that inoculation with PGPR is useful to help enhance drought tolerance of plants. It was reported that water deficit could induce ethylene production in plant (Ravanbakhsh et al., 2018). The increase of ethylene content would restrain root, shoot development and leaf expansion (Li et al., 2017), which consequently impact plant growth. 1-aminocyclopropane-1-carboxylic acid (ACC) is a precursor for ethylene synthesis. The ACC deaminase enzyme produced by PGPR plays an important role in reducing ACC content through degrading ACC into α-ketobutyrate and ammonia (Danish and Zafar-ul-Hye 2019) and then reduces ethylene production in plants. Therefore, isolation of PGPR producing ACC deaminase activities is of great importance in helping plants to alleviate the effects of stress generated ethylene. In addition, these beneficial microorganisms could induce changes in morphology, physiology, and biochemistry in plants in other ways: (1) by producing exopolysaccharides (EPSs) and phytohormones and (2) by inducing the accumulation of osmolytes, antioxidants, and alteration of root morphology (Vurukonda et al., 2016) and eventually alleviating drought stress. However, the effectiveness of inoculated PGPR mainly depends on colonization of the rhizosphere, especially under stress conditions (Yuan et al., 2018). Most microorganisms might not be actively growing in a water deficit environment (Wang et al., 2008). Therefore, drought-tolerant PGPR producing ACC deaminase might be well adapted to the stressful environment and function well. In addition, studies on the inoculation effect of PGPR on alleviating drought stress have chiefly focused on crops, such as sugarcane, maize, soybean, foxtail millet (Niu et al., 2018), and chickpea. The impacts of PGPR on plant growth and the alleviation of drought stress in jujube have not been evaluated. Additionally, few studies have comprehensively revealed the interrelationships between PGPR and plants under stress conditions.

DROUGHT STRESS

Numerous PGPBs synthesize osmolytes and help the plants cope with drought stress .It has been suggested that the production of IAA by PGPB may contribute to the increase in root–shoot biomass under drought stress (Yuwono et al., 2005). Plants are also known to regulate their growth with ethylene, whose production is influenced by conditions such as drought, salinity, and water logging (Grichko et al., 2001).A rhizospheric bacteria producing aminocyclopropane- 1-carboxylate deaminase (ACCD) inhibits the ethylene signaling pathway to resist root drying. In tomato and pepper plants, Achromobacter piechaudii exhibits ACCD activity, leading to an improvement in biomass by resisting the water deficit. Similar results were also reported by references (Gupta et al., 2021) under salinity stress on pea plants. ACCD-positive isolates reduce the overproduction of ethylene in plants, which enhances injuries caused by water scarcity without affecting the relative water content (RWC) of plants (Mayak et al., 2004). Plants that have been injected with drought-tolerant bacteria achieve better plant growth and have higher

proline contents in their roots and leaves. The effect of PGPB is significant in the presence of water (Casanovas et al., 2002). According to (Creus et al., 2011) , the inoculation of Azospirillum under water scarceness reduced the yield of wheat and increased the ion contents, such as magnesium (Mg2+), potassium (K+), and calcium (Ca2+), in grains. Researchers have found that PGPBs, together with plant growth regulators, provide tolerance to plants under drought stress. Plant growth and development are significantly influenced by PGPB. In addition to providing micronutrients to the host plants, they can also enhance the availability of growth-promoting chemicals. For instance, they produce exopolysaccharides (ESP), a type of carbohydrate that is released in the rhizospheric region. These ESPs perform a vital function in protecting plants from desiccation. Salicylic acid (SA), a well-known phenolic compound that is secreted by microorganisms, is required for plant growth and development, thereby providing drought tolerance. It works as a signaling molecule under drought stress, triggering genes that function as heat shock proteins (HSP), chaperones, antioxidants, and activate genes that synthesize secondary metabolites (Khan et al., 2020).

Drought is one of the major abiotic stresses affecting yield of dry land crops. Rhizobacterial populations of stressed soils are adapted and tolerant to stress and can be screened for isolation of efficient stress adaptive/tolerant, plant growth promoting rhizobacterial (PGPR) strains that can be used as inoculants for crops grown in stressed ecosystems. Drought stress induced by withholding irrigation had drastic effects on growth of maize seedlings. However seed bacterization of maize with Pseudomonas spp. Strains improved plant biomass, relative water content, leaf water potential, root adhering soil/root tissue ratio, aggregate stability and mean weight diameter and decreased leaf water loss. The inoculated plants showed higher levels of proline, sugars, free amino acids under drought stress. However protein and starch content was reduced under drought stress conditions. Inoculation decreased electrolyte leakage compared to uninoculated seedlings under drought stress. As compared to uninoculated seedlings, inoculated seedlings showed significantly lower activities of antioxidant enzymes, ascorbate peroxidase (APX), catalase (CAT), glutathione peroxidase (GPX) under drought stress, indicating that inoculated seedlings felt less stress as compared to uninoculated seedlings. Drought stress limits the growth and productivity of crops particularly in arid and semi-arid areas causing the most fatal economic losses in agriculture. This form of abiotic stress, affect the plant water relation at cellular and whole plant level causing specific as well as unspecific reactions and damages. Inoculation of plants with native beneficial microorganisms may increase drought tolerance of plants growing in arid or semiarid areas (Marulanda et al., 2007).

DROUGHT STRESS TOLERENCE

Encapsulation tends to stabilize cells, protect against exposure to abiotic and biotic stresses, and potentially enhance bacterial cell viability and stability during the production and storage of agriculturally important strains. It also confers additional protection during rehydration (Schoebitz and Lopez belchi 2016). The encapsulation of microorganisms is one of the newest and most efficient techniques to protect bacterial cells and allow for better survival in the soil after inoculation (Schoebitz et al., 2012). Encapsulated bacteria can be released slowly into the soil, thereby providing long-term beneficial effects on plant growth under adverse conditions (Schoebitz and Lopez belchi 2016).

The encapsulation of PGPB has been used in agriculture to obtain a structure that promotes the protection, release, and functionalization of microorganisms, stabilizes the cells, protects against exposure to abiotic and biotic stresses, and potentially enhances PGPB viability and stability during the production, storage, and handling of their agriculturally utilized forms (John et al.,2011). The traditional carriers used for microbial inoculants. These carriers have several disadvantages, but the most important is their short-term effects. For example, formulations of *B. subtilis, P. corrugata*, and *A. brasilense* in peat or liquids have shown severe reductions in the bacterial populations (Schoebitz and Lopez belchi 2016), and this short-term effect has prevented any long-term impact on plant stress. Therefore, encapsulation absolutely requires the presence of a substance that is compatible with nature and that can protect bacteria from the adverse effects of stress. Protection for PGPB must be non-toxic, preservative-free, capable of degradation in soil by microbial action, and resistant to destructive environmental factors present in the soil. Encapsulating materials must be able to maintain cell viability for different periods in the soil, preserve cell viability

for three years of shelf storage, allow the progressive release of the encapsulated bacteria into the soil, be stable when stored at room temperature for extended periods, increase the number of encapsulated bacteria inoculated into the soil, and control the release of bacteria. These properties would facilitate their application to the farmer, generate an adhesive effect on seeds, and create an adequate microenvironment to preserve microbial viability and biological activity during long periods. Encapsulation of beneficial PGPB has been proposed as a suitable solution to deal with drought and salinity stresses by increasing the efficiency of PGPB and reducing costs (Bashan et al.,2014) reported that the formulations used in the polymer mixtures for use as vehicles are essential parameters for encapsulation of PGPB to obtain successful microbial inoculants (Schoebitz and Lopez Blchi 2016).

Drought stress is the primary reason for crop damage and losses, and many efforts are aimed at reducing or minimizing the effect of droughts. One promising strategy is to use nitrogen-fixing bacteria to decrease plant water use, as well as the negative environmental impact of chemical fertilizers (Saad et al., 2020). A method is needed that can encapsulate the PGPB with a coating that will increase the efficacy and quality of the bio inoculants, while reducing the costs of application and the environmental impact. Bacteria produce polysaccharides, proteins, and other biopolymers to form a protective biofilm that encourages community growth (Diep and Sciffman 2021). The encapsulation of bacteria within a matrix that mimics their natural environment is therefore an important strategy for protecting crops against abiotic stress. This matrix-focused strategy has already shown promise, as polymer-coated fertilizers are now confirmed to improve nutrient use efficiency (Abd El-Aziz et al., 2021) and to promote tolerance to salinity and drought stress.

ROLE OF DROUGHT STRSS TOLERANCE

Plant growth-promoting rhizobacteria (PGPR) are the rhizosphere bacteria that can enhance plant growth by a wide variety of mechanisms like phosphate solubilization, siderophore production, biological nitrogen fixation,rhizosphere engineering, quorum sensing (QS) phytohormone production, exhibiting antifungal activity, production of volatile organic compounds (Vocs), Induction of systemic resistance, promoting beneficial plant–microbe symbioses and interference with pathogen toxin production. In semiarid and arid areas, drought stress tolerance is modulated through PGPR Inoculation of plants (Marulanda et al., 2009). PGPR colonizes in the rhizosphere of plants and promote plants growth through direct or indirect mechanisms (Glick 2012). PGPR have the ability of solubilizing inorganic P thus making it available to the plants resulting thereby stimulating plant growth (Saharan and Nehra 2011).

Plant growth promoting rhizobacteria are adapted to adverse environmental condition and protect plants from deleterious effect of some environmental stresses (Marulanda et al., 2009). PGPR isolated from stressed area also help in providing resistance to host plants against various environmental stresses (Sandhya et al., 2009). PGPR adapted to water limited condition can induce drought tolerance by modulating in root morphology. Accumulate Bacillus sp. accumulate compatible solute such as amino acid, quaternary amines and sugar that prevent degeneration process and alleviate drought stress negative effects in maize in Bacillus sp. (Vardharajula et al.,2010). Induced systemic tolerance (IST) by PGPR modulates physiological and biochemical changes that are also associated with abiotic stress tolerance (Wang et al., 2012).

MECHANISM OF DROUGHT TOLERANCEE

The role of bacteria in growth, nutrition, and drought tolerance under nutritional limited conditions is based on a range of physiological and cellular mechanisms (Dimkpa et al., 2009). In this regard, microorganisms are also able to reduce water stress by alleviating cellular oxidative damage produced in plants under drought conditions. In fact, the view nowadays is to consider ROS as an integrative part of cell signaling metabolism modulated by the cellular redox state loading to different responses related to programmed cell death, plant development or defense, and gene expression (Potters et al., 2010). The establishment of inoculum in dry soils includes the activation of antioxidant metabolic pathways. Arid environments determine the ability of organisms to proliferate is such habitat. The microbial ability to adapt to environmental changes is fundamental to the survival of these organisms and several mechanisms are responsible for the required adaptation. Remarkable similarities exist between plants and bacteria in

their cellular responses to an osmotic stress (Csonka 1989). Several organisms (microorganisms and plants) from different kingdoms are able to accumulate the same set of cellular compounds upon exposure to stress conditions. There are close parallelism in the mechanisms that plants and microorganisms use to regulate responses to environmental stresses. In fact, there are processes that enable organisms to cope with environmental changes or stress conditions and they determine the ability of organisms to live in particular environments.

Drought tolerance is highly complex process and associated with the regulation of multiple genes expression induced during drought stress (Lang and Bui 2008). Transcriptome analyses of several drought induced genes have been identified that can be categorized into two major groups i.e. functional gene and regulating gene (Chinnusamy et al., 2004). The first group product includes: chaperons, LEA proteins, antifreeze proteins mRNA-binding proteins, water channel proteins, osmoprotectants, detoxifying enzymes, key enzymes for osmolyte biosynthesis, free radical scavengers and various proteases gene products which directly protect the cell against the stress (Bray 2002). The gene products of the second group regulate the expression of others gene in response to drought stress such as transcription factors, protein phosphatases, kinases such as mitogen-activated kinases (MAPKs), calcium dependent protein kinases (CDPKs) and SOS kinases (Xiong et al., 2002) and enzymes involved in phospholipid metabolism, and other signalling molecules such as calmodulin binding protein.

PHYTOHORMONES IN DROUGHT STRESS TOLERANCE

Plants unlike many other organisms, have evolved different mechanisms to guard themselves against stressful conditions and promote growth and development, as well as to avoid, and protect themselves from, stressful conditions (Raza et al., 2019). The application of useful bacteria to increase drought and salt tolerance in plants is a substitute that is cheaper and more feasible (Etesami and Adl 2020).Numerous studies have revealed that PGPB can improve both plant growth and nutrition of a variety of crops even when adverse environmental conditions occur, including drought and salinity (Kumar et al., 2021). PGPB affects plants directly by producing phytohormones or indirectly by inducing signaling in the host. Most commonly, phytohormones like IAA, gibberellins, cytokinin, ABA, and ethylene; biological nitrogen fixation (BNF); and phosphate solubilization are attributed a direct role (Gupta et al., 2021). However, the indirect mechanisms include the production of hydrogen cyanide, antibiotics, volatile organic compounds (VOC), siderophores, and ammonia that suppress phytopathogens. In addition to improving crop water relations and changing the ion balance, these soil microorganisms also modulate abiotic stress regulation via different pathways (Ilangumaran and smith 2017). Over the last several decades, PGPB has been broadly used for sustainable agriculture in several parts of the world in order to reduce chemical pesticides and fertilizers (Gupta et al., 2021).

INDOLE ACETIC ACID (IAA)

This study reports information on the relevance of cells metabolic processes conducting to proline and indolacetic acid (IAA) microbial production in the growing medium along the time when this medium was added of increasing polyethylene glycol (PEG) to create an osmotic stress. The bacterial IAA productions are related to plant improvement effect and proline is accumulated in the cell under stress condition to protect cells against adverse effect of ROS and stabilizing proteins. This compound increases resistance to water deficiency by that it can be considered a good stress indicator. As well, previous studies (Glick 1995) report mechanisms commonly involved in the plant growth-promoting activity of bacteria as is the production of phytohormones and particularly IAA plays the most important role in plant growth promotion. Thus, it was selected as representative index of bacterial efficiency.

GIBBERELIC ACID (GA)

Plant hormones are naturally synthesized plant compounds with regulatory roles in plant growth and development (Davies 2010). Gibberellins and auxins are the two key regulators of shoot growth (Kurepin et al., 2013). Often, increases in endogenous GA or auxin levels, via exogenous application or gene transformation, result in a phenotype with higher shoot biomass and taller stems. Interestingly, the expression of GA 3-oxidase and GA 2-oxidase can be influenced by plant endogenous auxin (IAA) concentration (Ozga et al., 2003). Endogenous changes in shoot IAA

concentrations can also be directly correlated to stem elongation and leaf expansion. Additionally, IAA and CKs play an important role in root growth and development. Auxins have a regulatory role in almost every aspect of root formation, such as induction of cellular rhizogenic competence, root apical meristem differentiation, development of the root cap and vasculature, as well as tropic responses.

ABSCISIC ACID (ABA)

Abscisic acid (ABA) is involved in both biotic and abiotic stress response so termed as stress hormone (Kiba et al., 2011). Under a biotic stress the phytohormone abscisic acid regulates many processes. The abscisic acid acts as mediator in plant responses to a range of stresses including drought stress (Keskin 2012). Abscisic acid maintains plant water status through regulation of guard cell and induction of genes coding for protein and enzymes associated with dehydration tolerance (Zhu 2001). Several abscisic acid deficient mutants of Arabidopsis, tomato and maize have been identified . Arabidopsis ABA deficient mutants, aba1, aba2 and aba3 wilt and even die in persistent water stress. It has been reported that under drought stress abscisic acid maintain root and shoot growth and prevent excess ethylene production (Ober and Sharp 2003).

SALICYLIC ACID (SA)

Along with many physiological processes, salicylic acid also confers various environmental stress tolerances such as drought, chilling and heat stress. In tomato, drought tolerance is promoted through salicylic acid treatment as low concentration salicylic acid of enhanced photosynthetic parameters, membrane stability index (MSI), leaf water potential, activity of nitrate reductase (NR), carbonic anhydrase (CA), chlorophyll and relative water content (RWC) (Hayat et al., 2007).

JASMONIC ACID (JA)

Besides regulation of developmental processes jasmonic acid also regulates plant defense mechanism against pathogen attack as well as environmental stresses such as salinity and drought stress. Jasmonic acidplay important role in drought-induced antioxidant responses, including ascorbate metabolism. Jasmonic acid synthesis is also stimulated by water stress in maize root and pear leaves (Aimar et al., 2011).

CYTOKININS (CKS)

In crop plants, drought tolerance is enhanced through delayed leaf senescence by stress induced synthesis of cytokinins (Peleg and Blumwald 2011). Drought stressed plants usually exhibit low concentration of cytokinins in xylem exudates as drought limit its biosynthesis and increase its catabolism (Pospisilova et al., 2000). In transgenic tobacco and Arabidopsis, root-specific reduction of cytokinin enhanced drought tolerance by promoting root growth (Brenner et al., 2012) experimented with transgenic tobacco and Arabidopsis, observed enhanced root-specific degradation of cytokinin and upto 60% increase in root biomass in transgenic lines. A correlation between root architecture and resistance to water stress have been found in several crop plants, breeding attempts have focused on obtaining cultivars with larger root systems (Tuberosa 2014). Plants with larger root systems more efficiently compete for nutrients and can better survive under conditions of nutrient deficiency (Coque and Gallais 2006).

ETHYLENE

Ethylene induces stomatal closure through production of H2O2 in guard cell. On the other hand, ethylene induces the expression of SodERF3 gene that promote osmotic and drought stress tolerance in tobacco plant (Trujillo et al., 2008).

CONCLUSION

Drought stress not only affects the morphological and physiological characteristics of plants, leading to a loss in crop production but also affects the soil microbe interactions. We discussed the ways that PGPR adopt to enhance drought stress resistance. Soil microorganisms associated with the root system of a plant change the cell membrane elasticity

of the roots, which eventually increases the drought tolerance capacity. However, during drought stress conditions, plant growth can be improved by the rhizosphere microbial community via an increase in the root surface area and root production. The use of PGPB to control drought stress in plants is an important and sustainable strategy. But the related processes seem to be regulated differently according to the natural resistance and intrinsic stress tolerance of the plants. The selection of microorganisms involved is important to reach the maximum plant benefit. However, further research studies are required to establish the main processes by which bacteria improve plant performance.

REFERENCES

1. Abd El-Aziz ME, Salama DM, Morsi SMM, Youssef AM and El-Sakhawy M (2021) Development of polymer composites and encapsulation technology for slow-release fertilizers. Rev. Chem. Eng. 44.
2. Aimar D, Calafat M, Andrade AM, Carassay L, Abdala GI, and Molas ML (2011) Drought tolerance and stress hormones: From model organisms to forage crops. Plant Environ 137–164
3. Ait Barka E, Nowak J and Clement C (2006) Enhancement of chilling resistance of inoculated grapevine plantlets with a plant growth promoting rhizobacterium; Burkholderia phytofirmans strain Ps Jn. Appl Environ Microbiol. 72:7246-7252.
4. Ali SKZ, Sandhya V, Minakshi Grover, Kishore N,Venkateswar Rao L and Venkateswarlu B. (2009) *Pseudomonas sp*. strain AKM-P6 enhances tolerance of sorghum seedlings to elevated temperatures. Biol Fertil Soils. 46:45-55.
5. Barea JM, Azcón R and Azcón-Aguilar C (2002) Mycorrhizosphere interactions to improve plant fitness and soil quality. Anton Leeuw Int J G 81:343–351.
6. Bashan Y, de-Bashan LE, Prabhu SR and Hernandez JP (2014) Advances in plant growth-promoting bacterial inoculant technology: Formulations and practical perspectives (1998–2013). Plant Soil 378, 1–33.
7. Bray EA (2002) Classification of genes differentially expressed during water-deficit stress in Arabidopsis thaliana: An analysis using microarray and differential expression data. Annals of Bot 89(7):803–811.
8. Brenner WG, Ramireddy E, Heyl A and Schmulling T (2012) Gene regulation by cytokinin in Arabidopsis. Front Plant Sci 3:33–38.
9. Casanovas EM, Barassi CA and Sueldo RJ (2002) Azospirillum inoculation mitigates water stress effects in maize seedlings. Cereal Res. Commun. 30, 343–350.
10. Chinnusamy V, Schumaker K and Zhu JK (2004) Molecular genetics perspectives on cross-talk and specificity in abiotic stress signalling in plants. J Exp Bot 55(395):225–236.
11. Coque M and Gallais A (2006) Genomic regions involved in response to grain yield selection at high and low nitrogen fertilization in maize. Theor Appl Genet 112(7):1205–1220.
12. Creus CM, Sueldo RJ and Barassi CA (2011) Water relations and yield in Azospirillum inoculated wheat exposed to drought in the field. Can. J. Bot. 2011, 82, 273–281.
13. Csonka LN (1989) Physiological and genetic responses of bacteria to osmotic-stress. Microbiol Rev 53:121–147.
14. Danish S and Zafar-ul-Hye M (2019) Co-application of ACC- deaminase producing PGPR and timber-waste biochar improves pigments formation, growth and yield of wheat under drought stress. Sci Rep-UK 9:1–13.
15. Davies PJ (2010) The plant hormones: their nature, occurrence and function. In: Davies PJ (ed) Plant hormones: biosynthesis, signal transduction and action!, 3rd edn. Springer, New York, pp 1–15.
16. Dell' Amico E, Cavalca L, and Andreoni V (2008) Improvement of Brassica napus growth under cadmium stress by cadmium-resistance rhizobacteria. Soil Biol Biochem.40:74-84.
17. Diep E and Schiffman JD (2021) Encapsulating bacteria in alginate-based electrospun nanofibers. Biomater. Sci. 9, 4364–4373.
18. Dimkpa C, Weinand T and Asch F (2009) Plant–rhizobacteria interactions alleviate abiotic stress conditions. Plant Cell Environ 32:1682–1694.
19. Etesami H and Adl SM (2020) Can interaction between silicon and non–rhizobial bacteria help in improving nodulation and nitrogen fixation in salinity–stressed legumes? A review. Rhizosphere 15, 100229.
20. Gill SS and Tuteja N (2010) Reactive oxygen species and antioxidant machinery in abiotic stress tolerance in crop plants. Plant Physiol. Biochem. 48, 909–930.

21. Gill SS, Gill R, Trivedi DK, Anjum NA, Sharma KK , Ansari MW, Ansar AA, Johri AK and Prasad R and Pereira E (2016) *Piriformospora indica* Potential and significance in plant stress tolerance. Front. Microbiol. 7, 332.
22. Glick BR (1995) The enhancement of plant growth by free living bacteria. Can J Microbiol. 41:109114.
23. Gouda S, Kerry RG, Das G, Paramithiotis S, Shin HS and Patra JK (2018) Revitalization of plant growth promoting rhizobacteria for sustainable development in agriculture. Microbiol Res 206:131–140.
24. Grichko VP and Glick BR (2001) Amelioration of flooding stress by ACC deaminase-containing Plant Growth-Promoting Bacteria. Plant Physiol. Biochem. 39, 11–17.
25. Gupta A, Rai S, Bano A, Khanam A, Sharma S and Pathak N (2021) Comparative evaluation of different salt-tolerant plant growth- promoting bacterial isolates in mitigating the induced adverse effect of salinity in pisum sativum. Biointerface Res. Appl. Chem. 11, 13141–13154.
26. Han HS and Lee KD (2005) Plant growth promoting rhizobacteria effect on antioxidant status, photosynthesis,mineral uptake and growth of lettuce under soil salinity. Res J Agric Biol Sci. 1:210-215.
27. Han QQ, Lü XP, Bai JP, Qiao Y, Paré PW, Wang SM and Wang ZL (2014) Beneficial soil bacterium Bacillus subtilis (GB03) augments salt tolerance of white clover. Front. Plant Sci.5, 525.
28. Hayat S, Ali B and Ahmad A (2007) Salicylic acid: biosynthesis, metabolism and physiological role in plants. Springer Netherlands, pp 1–14.
29. Ilangumaran G and Smith DL (2017) Plant Growth Promoting Rhizobacteria in amelioration of salinity stress: A systems biology perspective. Front. Plant Sci. 8, 1768
30. John RP, Tyagi R, Brar S, Surampalli R and Prévost D (2011) Bio-encapsulation of microbial cells for targeted agricultural delivery. Crit. Rev. Biotechnol. 31, 211–226.
31. Keskin H (2012) Physiological and Biochemical Characterization of Drought Tolerance in Chickpea (Doctoral dissertation, İzmir Institute of Technology).
32. Khan A, Khan AL, Imran M, Asaf S, Kim YH, Bilal S, Numan M, Al-Harrasi A, Al-Rawahi A and Lee IJ (2020) Silicon-induced thermotolerance in Solanum lycopersicum L. via activation of antioxidant system, heat shock proteins, and endogenous phytohormones. BMC Plant Biol. 20, 248.
33. Kiba T, Kudo T, Kojima M and Sakakibara H (2011) Hormonal control of nitrogen acquisition: roles of auxin, abscisic acid, and cytokinin. J Exp Bot 62(4):1399–1409.
34. Kloepper J and Schroth M (1981) Development of a powder formulation of rhizobacteria for inoculation of potato seed pieces. Phytopathology 71, 590–592.
35. Kloepper JW, Zablowicz RM, Tipping B and Lifshitz R (1991) Plant growth mediated by bacterial rhizosphere colonizers. In: Keister DL, Gregan B, editors. The rhizosphere and plant growth, 14 BARC Symposium. Dordrecht: Kluwer Academic, p. 315-326.
36. Kumar M, Giri VP, Pandey S, Gupta A, Patel MK, Bajpai AB, Jenkins S and Siddique KHM (2021) Plant-Growth-Promoting Rhizobacteria emerging as an effective bioinoculant to improve the growth, production, and stress tolerance of vegetable crops. Int. J. Mol. Sci. 22, 12245
37. Kurepin LV, Ozga JA, Zaman M and Pharis RP (2013) The physiology of plant hormones in cereal, oilseed and pulse crops. Prairie Soils Crops 6:7–23.
38. Lang NT and Bui BC (2008) Fine mapping for drought tolerance in rice (Oryza sativa L.). Omonrice 16(1):9-15.
39. Li HS, Lei P, Peng X, Li S, Xu H, Xu ZQ and Feng XH (2017) Enhanced tolerance to salt stress in canola (Brassica napus L.) seedlings inoculated with the halotolerant Enterbacter cloacae HSNJ4. Appl Soil Ecol 119:26–34.
40. Manickavelu A, Nadarajan N, Ganesh SK, Gnanamalar RP and Babu RC (2006) Drought tolerance in rice: morphological and molecular genetic consideration. Plant Growth Regul. 50:121-38.
41. Mantelin S and Touraine B (2004) Plant growth-promoting bacteria and nitrate availability: impacts on root development and nitrate uptake. J Exp Bot 55:27–34.
42. Marulanda A, Barea JM and Azcón R (2009) Stimulation of plant growth and drought tolerance by native microorganisms (AM fungi and bacteria) from dry environments. Mechanisms related to bacterial effectiveness. J Plant Growth Regul 28:115–124.
43. Marulanda A, Porcel R, Barea JM and Azco´n R (2007) Drought tolerance and antioxidant activities in lavender plants colonized by native drought-tolerant or drought-sensitive Glomus species. Microb Ecol 54:543–552.

44. Mayak S, Tirosh T and Glick BR (2004) Plant growth promoting bacteria that confer resistance to water stress in tomato and pepper. Plant Sci. 166, 525–530.
45. Montesinos E (2003) Plant associated microorganisms: a view from the scope of microbiology. Int Microbiol. 6:221-223.
46. Niu XG, Song LC, Xiao YN and Ge WD (2018) Drought-tolerant plant growth-promoting rhizobacteria associated with foxtail millet in a semi-arid agroecosystem and their potential in alleviating drought stress. Front Microbiol 8:1–11.
47. Nowak J (1998) Benefits of in vitro "biotization" of plant tissue cultures with microbial inoculants. In Vitro Cell Dev Biol Plant 34: 122–130.
48. Ober ES and Sharp RE (2003) Electrophysiological responses of maize roots to low water potentials: relationship to growth and ABA accumulation. J Exp Bot 54(383):813–824.
49. Peleg Z and Blumwald E (2011) Hormone balance and abiotic stress tolerance in crop plants. Curr Opin Plant Biol 14(3):290–295.
50. Pospisilova J, Synkova H and Rulcova J (2000) Cytokinins and water stress. Biol Plantarum 43(3):321–328.
51. Potters G, Horemans N and Jansen MAK (2010) The cellular redox state in plant stress biology a charging concept. Plant Physiol Biochemistry 48:292–300.
52. Ravanbakhsh M, Sasidharan R, Voesenek LACJ, Kowalchuk GA and Jousset A (2018) Microbial modulation of plant ethylene signaling: ecological and evolutionary consequences. Microbiome 6:52.
53. Raza A, Razzaq A, Mehmood SS, Zou X, Zhang X, Lv Y and Xu J (2019) Impact of climate change on crops adaptation and strategies to tackle its outcome: A Review. Plants 8, 34.
54. Saad MM, Eida AA and Hirt H (2020) Tailoring plant-associated microbial inoculants in agriculture: A roadmap for successful application. J. Exp. Bot.71, 3878–3901.
55. Sandhya V, Ali SKZ, Minakshi G, Gopal R and Venkateswarlu B (2009) Alleviation of drought stress effects in sunflower seedlings by the exopolysaccharides producing *Pseudomonas putida* strain GAP-P45. Biol FertilSoils. 46:17-26.
56. Sarma RK and Saikia R (2014) Alleviation of drought stress in mung bean by strain *Pseudomonas aeruginosa* GGRJ21. Plant Soil. 377, 111–126.
57. Schoebitz M and López Belchí MD (2016) Encapsulation techniques for plant growth-promoting rhizobacteria. In Bioformulations: For Sustainable Agriculture; Arora, N.K., Mehnaz, S., Balestrini, R., Eds, Springer: New Delhi, India, pp. 251–265.
58. Shameer S and Prasad T (2018) Plant growth promoting rhizobacteria for sustainable agricultural practices with special reference to biotic and abiotic stresses. Plant Growth Regul 1–13.
59. Trujillo LE, Sotolongo M, Menendez C, Ochogavia ME, Coll Y, and Hernandez I and Hernandez L (2008) SodERF3, a novel sugarcane ethylene responsive factor (ERF), enhances salt and drought tolerance when over expressed in tobacco plants. Plant Cell Physiol 49(4):512–525.
60. Tsukanova KA, Chebotar VK, Meyer JJM and Bibikova TN (2017) Effect of plant growth-promoting rhizobacteria on plant hormone homeostasis. S. Afr. J. Bot. 113, 91–102.
61. Tuberosa R (2014) Phenotyping for drought tolerance of crops in the genomics era. Drought Phenotyping in Crops: From Theory to Practice, 8.
62. Turner AG and Annamalai H (2012) Climate change and the South Asian summer monsoon. Nat Clim Change. 2:587-95.
63. Van Loon LCP AHM, Bakker and Pieterse CMJ (1998) Systemic resistance induced by rhizosphere bacteria. Annu. Rev. Phytopathol., 36:453–483.
64. Vardharajula S, Ali SZ, Grover M, Reddy G and Venkateswaralu B (2010) Effect of plant growth promoting Pseudomonas spp. on compatible solutes antioxidant status and plant growth of maize under drought stress. Plant Growth Regul. 62, 21–30.
65. Vurukonda SS, Vardharajula S, Shrivastava M and Sk ZA (2016) Enhancement of drought stress tolerance in crops by plant growth promoting rhizobacteria. Microbiol. Res. 184, 13–24.

66. Wang CJ, Yang W , Wang C, Gu C, Niu DD, Liu HX, Wang YP and Guo JH (2012) Induction of drought tolerance in cucumber plants by a consortium of three plant growth-promoting rhizobacterium strains. PLoS ONE . e52565.
67. Wang JF, Kang SZ, Li FS , Zhang FC, Li ZJ and Zhang JH (2008) Effects of alternate partial root-zone irrigation on soil microorganism and maize growth. Plant Soil 1-2:45–52.
68. Warnita W, Ardi A and Zulfa Y (2019) Effect of mulch and indigenous rhizobacteria isolate on growth and yield of potato (Solanum tuberosum L.). Asian J. Agric. Biol.239–245.
69. Xiong L, Schumaker KS and Zhu JK (2002) Cell signaling during cold, drought, and salt stress. Plant Cell Online 14(1):165–183.
70. Yang J, Kloepper JW and Ryu CM (2009) Rhizosphere bacteria help plants tolerate abiotic stress. Trends Plant Sci 14:1–4.
71. Yasmin FR, Othman MS, Saad and Sijam K (2007) Screening for beneficial properties of Rhizobacteria isolated from sweet potato rhizosphere. J. Biotec., 6:49–52.
72. Yuan J, Wu JC, Zhao ML, Wen T, Huang QW and Shen QR (2018) Effect of phenolic acids from banana root exudates on root colonization and pathogen suppressive properties of Bacillus amyloliquefaciens NJN-6. Biol Control 125:131–137.
73. Yuwono T, Handayani D, Soedarsono J, Yuwono T, Handayani D and Soedarsono J (2005) The role of osmotolerant rhizobacteria in rice growth under different drought conditions. Aust. J. Agric. Res.56, 715–721.
74. Zahir ZA, Arshad M and Frankenberger WT (2004) Plant growth promoting rhizobacteria: applications and perspectives in agriculture. Adv Agron 81:97–168.
75. Zhu JK (2001) Cell signaling under salt, water and cold stresses. Curr Opin Plant Biol 4(5):401-406.

Indian Journal of Natural Sciences www.tnsroindia.org.in ©IJONS

Vol.15 / Issue 83 / Apr / 2024 International Bimonthly (Print) – Open Access ISSN: 0976 – 0997

REVIEW ARTICLE

Machine Learning-Powered Comparative Analysis of Autism Diagnosis Tools: Enhancing Effectiveness

Aruna P. Gurjar[1]* and Satyen Parikh[2]

[1]Assistant Professor, Faculty of Computer Application, AMPICS, Ganpat University, Kherva, Gujarat, India.
[2]Executive Dean, Faculty of Computer Application, AMPICS, Ganpat University, Kherva, Gujarat, India.

Received: 23 Nov 2023 Revised: 09 Jan 2024 Accepted: 06 Mar 2024

***Address for Correspondence**
Aruna P. Gurjar
Assistant Professor,
Faculty of Computer Application,
AMPICS, Ganpat University,
Kherva, Gujarat, India.
Email: apg01@ganpatuniversity.ac.in

ABSTRACT

Autism Spectrum Disorder (ASD) diagnosis has traditionally relied on subjective clinical observations and behavioural assessments, which have the potential for misinterpretation. The incorporation of machine learning technology into autism diagnosis represents a paradigm shift, promising higher accuracy and objectivity. This article gives a detailed comparison of autism diagnosis techniques that make use of machine learning. We illuminate the diverse landscape of machine learning applications in autism diagnosis by investigating mobile applications, neuro imaging approaches, natural language processing, and genetic data analysis. We highlight the possibility for early and accurate autism diagnosis, as well as the implications for future therapies and interventions, by examining the benefits and limitations inherent in this transformative approach. Furthermore, we look at the ethical issues that come with this technological advancement, emphasising the necessity of data protection, transparency, and patient permission. This article aims to provide healthcare professionals, researchers, and carers with insights into the expanding field of machine learning in autism diagnosis, allowing them to make more educated decisions for the benefit of people on the autistic spectrum. We find ourselves at the crossroads of innovation and compassion as we embark on this comparative adventure, altering the future of autism evaluation via the prism of machine learning technologies.

Keywords: ASD Diagnosis tools, Machine Learning, Autism, Behavioural Analysis, neuro imaging, natural language processing.

INTRODUCTION

The merging of cutting-edge technology and machine learning algorithms has resulted in a dramatic evolution in the field of autism diagnosis in recent years. Autism spectrum disorder (ASD) is a complex neurological illness that affects people throughout their lives. Traditionally, clinical observations, standardised questionnaires, and behavioural tests were used to diagnose ASD. While these procedures have proven to be effective, they frequently lack the precision, efficiency, and objectivity required to address the numerous and subtle aspects of autism. However, the introduction of machine learning technology has ushered in a new era of diagnosis, one that promises to improve the accuracy and speed of recognising autism while lowering the subjectivity associated with older methods. This article conducts a thorough comparison of autism diagnosis methods that have harnessed the power of machine learning, exposing the astounding advances that are influencing the future of autism assessment.[1,2] As we progress through this investigation, we will examine a variety of techniques and methodologies, each of which contributes to our understanding of autism diagnosis. From mobile applications that analyse behavioural patterns to advanced neuro imaging techniques, this article provides a comprehensive look at the intersection of machine learning and healthcare, all with the goal of improving the lives of people with autism. We will investigate the benefits and limitations of machine learning in autism diagnosis, the important participants in this new environment, and the ethical questions that accompany this shift in our attempt to comprehend these revolutionary discoveries. We hope to shine light on how these technologies are set to revolutionise how we perceive, assess, and support individuals on the autistic spectrum as we traverse the convergence of cutting-edge technology and autism. [3,4, 23]

Overview of Autism Diagnosis

Autism Spectrum Disorder (ASD) diagnosis is a complex and multidimensional procedure that is critical for early identification and intervention in individuals with autism. Autism has traditionally been diagnosed primarily through clinical observation, standardised questionnaires, and behavioural evaluations. These strategies have been used by healthcare professionals such as paediatricians, psychiatrists, and psychologists to detect the typical traits and behaviours linked with autism.[5,10]

Clinical Observation

Clinical observation is a fundamental component of autism diagnosis. Through direct interactions and systematic examinations, healthcare practitioners analyse an individual's social communication abilities, repeated behaviours, and sensory sensitivity. While clinical observation gives useful insights, it is subjective and subject to vary among practitioners.[5,6]

Standardized questionnaires

In the diagnostic process, standardised questionnaires such as the Autism Diagnostic Interview-Revised (ADI-R) and the Social Communication Questionnaire (SCQ) are widely utilised. These questionnaires collect information about a child's behaviours, development, and social interactions based on carer reports. [7]

Behavioural Assessment

The Autism Diagnostic Observation Schedule (ADOS) and other behavioural examinations aim to provide a standardised framework for evaluating an individual's social and communicative skills. These exams frequently include particular tasks and activities that assist specialists in evaluating a person's behaviour and reactions. Despite their historical relevance, conventional diagnostic approaches have disadvantages such as subjectivity, potential bias, and reliance on human judgement. Furthermore, diagnosing autism in very young children is particularly difficult because they may not yet exhibit the complete range of symptoms. With the incorporation of machine learning technologies, there has been a dramatic transformation in the approach to autism diagnosis in recent years. This shift has created new opportunities for improving the accuracy, efficiency, and objectivity of autism diagnosis. The

following sections of this article will conduct a comparative review of autism diagnosis methods that use machine learning, providing light on innovations that have the potential to reshape the landscape of autism assessment. [8]

Machine learning in autism Diagnosis

In recent years, the convergence of healthcare and technology has resulted in a game-changing synergy that has the potential to transform how we diagnose and comprehend Autism Spectrum Disorder (ASD). The fearsome capability of machine learning - an advanced area of artificial intelligence that equips computers with the ability to learn from data and generate predictions without explicit programming - is at the heart of this disruptive evolution. [2] Autism diagnosis has traditionally relied on the expertise and subjective judgement of healthcare professionals. Clinical observations, carer reports, and standardised assessments have long been used to diagnose autism, providing vital insights into the behavioural patterns and developmental milestones of people on the autism spectrum. While these methods have clearly been useful, they are not without limitations, such as subjectivity and the possibility of human mistake.[1,5] Machine learning, on the other hand, adds a new and objective component to autism diagnosis. It enables diagnostic instruments to process massive amounts of data, find nuanced patterns, and make predictions with unrivalled accuracy. It's equivalent to presenting the medical community with a precise and untiring diagnostic helper capable of quickly and consistently analysing different and sophisticated data.

Machine learning technology enables the development of specialised algorithms that can filter through complex behavioural and medical data, revealing hidden insights and patterns that would otherwise go undiscovered. These algorithms may analyse a wide range of characteristics, such as behavioural observations, genetic markers, brain imaging data, and more, to provide a complete and data-driven assessment of a person's likelihood of being on the autistic spectrum.[3,4,23] The goal of this essay is to conduct a thorough comparison of the many autism diagnosis techniques that use machine learning, shining light on the astounding breakthroughs that are transforming the landscape of autism assessment. We hope to provide a comprehensive understanding of how machine learning is poised to redefine not only how we diagnose autism, but also how we comprehend and support individuals on the autism spectrum by examining the benefits, challenges, and ethical considerations inherent in this integration of technology. As we continue on this adventure of discovery, we are on the verge of a transformative era in healthcare, driven by the marriage of innovation and compassion.[11]

Impact of Machine Learning In Autism Diagnosis

The incorporation of machine learning into the field of autism diagnosis has ushered in a new age in healthcare. Machine learning has the potential to greatly improve the precision, efficiency, and objectivity of autism diagnosis by using modern algorithms and the ability to analyse large and diverse datasets. Here, we look at how machine learning is changing the diagnostic environment for autism and the several benefits it offers.

Improved Accuracy and Objectivity

The potential for increased accuracy is one of the key benefits of adding machine learning into autism diagnosis methods. Machine learning models can analyse a large amount of behavioural, clinical, and biological data to provide objective evaluations, lowering the risk of human mistake and subjectivity.

The ability of machine learning algorithms to find nuanced patterns and relationships within datasets allows them to uncover subtle behavioural and physiological signs of autism that may defy standard diagnostic methods.

Early Detection and Intervention

Machine learning algorithms can detect indicators of autism at a younger age, allowing for timely intervention and assistance. Early diagnosis is critical for offering personalised therapy and resources to those on the autism spectrum, which can dramatically enhance their long-term outcomes. In extremely young children, machine learning technologies can detect tiny behavioural patterns that are symptomatic of autism, allowing healthcare professionals and carers to take preventative measures.

Multimodal Data Integration

Medical records, genetic information, neuro imaging data, and natural language are just a few of the data kinds that machine learning approaches can handle. Machine learning-based techniques can provide a thorough and holistic knowledge of an individual's condition by merging these various data sources. This multimodal approach not only aids in diagnosis, but also leads to a better understanding of autism's underlying causes and heterogeneity.

Tailored and personalized Diagnosis

Individualised assessments can be provided by machine learning by taking into account a person's unique profile and traits. This personalisation ensures that each individual's diagnosis and treatment plans are specifically customised to their needs and challenges. Machine learning assists in offering more exact recommendations for therapeutic therapies by adapting to the intricacies of each instance.[2,3,4,11,23]

Enhanced Research and Insights

Machine learning methods have the ability to shed light on the complexities of autism. They can find previously unknown correlations, biomarkers, and risk factors, which help comprehend the condition and its underlying causes. Machine learning's data-driven approach fosters continued study and innovation in the field of autism, perhaps leading to breakthroughs in treatment and support. We will conduct a comparative analysis of specific autism diagnosis techniques that use machine learning. We hope to provide a thorough overview of the ever-changing environment of autism evaluation by investigating these tools, their capabilities, and their potential impact on healthcare and the lives of individuals with autism.[12,13]

Benefits of Machine Learning in Autism diagnosis

The use of machine learning technology into autism diagnosis tools provides a slew of compelling benefits that are changing how we view, diagnose, and support people on the autistic spectrum. As we compare these unique technologies, it's critical to emphasise the advantages they bring to the forefront of autism diagnosis

1. Machine learning algorithms can quickly and precisely analyse large datasets, minimising the margin for human error and subjective judgement in diagnosis.
   These methods provide a higher degree of accuracy in discriminating between neurotypical individuals and those with autism by recognising minor behavioural, genetic, or neurological patterns.
2. Early detection is critical for prompt intervention and support, which can dramatically improve outcomes for people with autism.
   Early indications of autism can be detected using machine learning-based methods, allowing healthcare professionals and carers to begin therapies and interventions at an earlier age.
3. Machine learning may integrate a wide variety of data types, such as behavioural observations, medical records, genetic information, neuro imaging data, and textual reports.
   Given the disorder's multidimensional nature, this comprehensive approach provides for a more complete view of autism.
4. Machine learning algorithms provide objective and consistent evaluation, eliminating the impact of human bias in the diagnostic process. This impartiality assures that each assessment is completely based on data-driven analysis, which improves the diagnostic outcome's reliability.
5. Machine learning algorithms can personalise diagnoses and treatment suggestions based on each person's unique qualities and needs. Personalization ensures that interventions are particularly intended to address the person with autism's challenges and capabilities, resulting in more effective assistance.
6. Machine learning-powered tools promote ongoing study and innovation in autism diagnosis and treatment. These techniques contribute to a better understanding of autism's underlying causes by analysing large datasets, potentially leading to advances in therapies and interventions.

7. Through digital platforms, machine learning-based technologies can be made available, allowing for remote evaluations and decreasing the pressure on healthcare systems. • Because of this accessibility and efficiency, more people, including those in underserved areas, can get autism diagnostic services.
8. We will investigate and contrast specific autism diagnosis systems that use machine learning technologies to accomplish these advantages. Understanding the tremendous benefits of these tools allows us to see how they are set to reshape the landscape of autism assessment and provide more effective and compassionate care for people on the autistic spectrum.[2,3,4,13,23]

CHALLENGES AND LIMITATIONS

Data Quality and Integrity
Limited Datasets
For training and validation, machine learning models require vast, diverse datasets. Collecting sufficient and representative data in the context of autism can be difficult, especially for rare subtypes or specialised demographics. The varied nature of autism causes data quality problems. Variability in behaviour, symptoms, and clinical profiles might make it difficult to create robust models.

Bias and Generalization
Data Bias
Machine learning models have the potential to perpetuate bias in training data. Models may deliver erroneous or biased diagnoses if data gathering is biased or unrepresentative. It is a continuous problem to ensure that machine learning models generalise well to varied populations and demographics.

Interpretability
Black-Box Models
Some machine learning models, particularly deep learning algorithms, might be difficult to understand. Because of this lack of transparency, it might be difficult to grasp how and why a diagnosis was made, thus generating problems in clinical practise**.**

Regulatory and ethical concern
Data Privacy
The collecting and analysis of sensitive medical and personal data for diagnosis raises privacy and security concerns. It is vital to keep patient information secure. It is both ethical and legal to obtain informed consent for the use of patient data and the use of machine learning algorithms.

Validation and Clinical Integration
Clinical Validation
Machine learning models must be rigorously validated in order to be reliable and safe in clinical practise. This method can be time-consuming and resource-intensive. It is difficult to integrate machine learning techniques into clinical processes and ensure that they support the diagnostic process without adding additional burdens to healthcare personnel.

Interdisciplinary collaboration
Collaboration in Healthcare and Technology
Effective collaboration between healthcare practitioners and data scientists is critical. Continuous interdisciplinary communication is required to ensure that machine learning models correspond with clinical competence and patient-centred care.

Diagnosis Complexity

Autism's Complexity

Autism is a complicated and varied disorder with significant diversity in symptoms. Recognising these obstacles and limitations is critical for gaining a fair view of machine learning's involvement in autism diagnosis. These reservations do not diminish the potential of machine learning technology, but rather highlight the importance of responsible and intentional integration, ongoing study, and interdisciplinary collaboration. By tackling these issues, we can fully realise the potential of machine learning to improve autism diagnosis and care for people on the autistic spectrum.[2,3,4,12,13,14,23]

Comparison of Autism Diagnosis tools:

The incorporation of machine learning technologies into the realm of autism diagnosis has resulted in a dynamic shift in the way we approach autism spectrum disorder (ASD) assessment. The diagnostic tool landscape has grown to include a wide range of advances, each using the promise of artificial intelligence to improve precision and impartiality. In this section, we will conduct a comparative examination of some of the most popular autism diagnosis systems that have made machine learning a key component of their diagnostic process. Shown in the table[1], we will examine each of these tools in depth, examining their capabilities, performance, and possible impact on the landscape of autism diagnosis. We hope that by doing this comparative study, we will be able to provide significant insights into the options and considerations that healthcare professionals, carers, and people on the autism spectrum may encounter while looking for the most effective and trustworthy diagnostic instruments.[2,3,4,11,23] Here in the figure 1 we have show to range of sensitivity result of various autism diagnosis tools also figure 2 shows to range of specificity result of various autism diagnosis tools. The result may vary on the quality of data and age of candidate for all above mention tools.

Case study

We give a collection of case studies and examples emphasising real-world tools and their impact to provide clear insights into the practical applications of machine learning technology in autism diagnosis

ADOS2

The classic ADOS-2 assessment was supplemented with machine learning algorithms in a research study conducted at a leading autism diagnosis centre. These algorithms analysed video footage and gathered behavioural data from youngsters undergoing evaluation. The machine learning-enhanced ADOS-2 revealed a significant improvement in diagnostic accuracy. It successfully identified minor behavioural indicators that human physicians would miss, minimising false negatives and boosting overall autism diagnosis precision.[15,24]

Mobile App

To screen for autism in toddlers, researchers and technology specialists collaborated to create a smart phone application. The software analysed video records of children's interactions and play using machine learning algorithms. The app for parents and carers effectively spotted early indicators of autism. It gave risk assessments to carers, allowing them to seek expert evaluation and assistance at an early age. The tool's ease of use and accessibility were critical to its success.[16,17]

Neuro imaging and Deep learning for Brain pattern analysis

Deep learning models were applied to neuro-imaging data, including fMRI scans of children with and without autism, at a prestigious research facility. The goal was to find distinct brain activity patterns linked to autism. The deep learning approach revealed different brain activity patterns in children with autism, offering light on the disorder's neuronal foundation. These patterns were subsequently used to improve diagnostic accuracy and acquire insight into the neurological abnormalities associated with [18,19]

NLP for textual data analysis

Researchers worked with a large healthcare institution to develop natural language processing (NLP) models that analysed text from patient reports and clinical notes. The goal was to find language markers and behavioural features linked to autism. For instance, NLP-driven research showed linguistic patterns, such as the use of specific words or phrase structures, which were associated with autism diagnosis. These linguistic cues were added into diagnostic algorithms, enhancing the diagnosis process even further. Above case studies and examples demonstrate the real-world application of machine learning technologies in autism diagnosis. They demonstrate the adaptability of machine learning technologies in a variety of domains, ranging from clinical assessments to early screening and neuroimaging analyses. By looking into these real-world applications, we obtain a better grasp of machine learning's potential for improving the accuracy, objectivity, and accessibility of autism diagnosis. In the following sections, we will continue to investigate and compare these instruments, shedding light on their importance in the field of healthcare and autism assessment. [20, 21, 22]

CONCLUSION

The landscape of autism diagnosis is experiencing a tremendous upheaval, powered by machine learning technology's extraordinary potential. This article's journey has shown the manner in which these novel tools are transforming the diagnostic procedure for Autism Spectrum Disorder (ASD). As we conclude this investigation, it is clear that the convergence of artificial intelligence and healthcare is paving the way for the future of autism diagnosis. The benefits of machine learning in autism diagnosis are numerous and varied. These instruments are superior in terms of accuracy and precision, they facilitate early identification and intervention, and they give objectivity and consistency in the diagnostic process. Machine learning algorithms provide a complete understanding of autism that outperforms traditional methods by combining data from multiple sources and employing a multidimensional approach. We met some of the important participants in this revolutionary landscape during our comparative analysis tools that analyse behavioural patterns, neuro imaging data, linguistic markers, and more. Each of these tools marks an important step towards more accurate, accessible, and personalised autism diagnosis. However, like with any revolutionary leap forward, we must be cognizant of the problems and ethical implications that this shift will entail.

Data privacy, transparency, accountability, and bias mitigation are not just nice-to-haves; they are critical foundations that sustain the ethical integrity of these diagnostic tools. Our ethical responsibility is to keep patients' rights and well-being at the forefront. We find ourselves at the crossroads of innovation and compassion as we consider the future of autism diagnosis. The machine learning technologies discussed in this article are more than just scientific advancements; they are also strong instruments of empathy, providing hope to people on the autism spectrum and their families. They represent the promise of more precise, rapid, and personalised assistance. Finally, the route forward in autism diagnosis is one distinguished by creativity, complexity, and ethical responsibility, aided by machine learning technologies. It's a trip that has the potential to change how we perceive, evaluate, and support people with autism. We can usher in a more inclusive, equitable, and empathic healthcare era with continuing interdisciplinary collaboration, adherence to regulatory standards, and a strong commitment to ethical principles. The future of autism diagnosis is here, and it appears to be brighter than ever.

REFERENCES

1. Dawson, G., & Bernier, R. (2013). A quarter century of progress on the early detection and treatment of autism spectrum disorder. Development and Psychopathology, 25(4pt2), 1455-1472
2. Bone, D., Bishop, S. L., Black, M. P., Goodwin, M. S., Lord, C., & Narayanan, S. S. (2016). Use of machine learning to improve autism screening and diagnostic instruments: effectiveness, efficiency, and multi-instrument fusion. Journal of Child Psychology and Psychiatry, 57(8), 927-937.

3. Thabtah, F., Peebles, D., & Zaiem, I. (2019). Identification of autism spectrum disorder using deep learning and the ABIDE dataset. Neurocomputing, 324, 63-71.
4. Wall, D. P., Kosmicki, J., Deluca, T. F., Harstad, E., & Fusaro, V. A. (2012). Use of machine learning to shorten observation-based screening and diagnosis of autism. Translational Psychiatry, 2(4), e100.
5. Lord, C., Elsabbagh, M., Baird, G., & Veenstra-Vanderweele, J. (2018). Autism spectrum disorder. The Lancet, 392(10146), 508-520.
6. 2. Zwaigenbaum, L., Bauman, M. L., Stone, W. L., Yirmiya, N., Estes, A., Hansen, R. L., ... & Wetherby, A. (2015). Early identification of autism spectrum disorder: recommendations for practice and research. Pediatrics, 136(Supplement 1), S10-S40.
7. Charman, T., & Baird, G. (2002). Practitioner review: diagnosis of autism spectrum disorder in 2-and 3-year-old children. Journal of Child Psychology and Psychiatry, 43(3), 289-305.
8. Magiati, I., Tay, X. W., & Howlin, P. (2014). Cognitive, language, social and behavioural outcomes in adults with autism spectrum disorders: A systematic review of longitudinal follow-up studies in adulthood. Clinical Psychology Review, 34(1), 73-86.
9. Matson, J. L., & Shoemaker, M. (2009). Intellectual disability and its relationship to autism spectrum disorders. Research in Developmental Disabilities, 30(6), 1107-1114.
10. American Psychiatric Association. (2013). Diagnostic and statistical manual of mental disorders (DSM-5®). American Psychiatric Pub.
11. Paris, N. (2018). Artificial intelligence for autism spectrum disorder: Opportunities and challenges. Journal of Autism and Developmental Disorders, 48(3), 925-926.
12. Chen, S., He, J., Benesty, J., & Huang, I. (2014). A new feature selection algorithm based on the normalized mutual information applied to text-independent speaker verification. IEEE Transactions on Audio, Speech, and Language Processing, 22(10), 1505-1514.
13. Zhu, X., & Goldberg, A. B. (2009). Introduction to semi-supervised learning. Synthesis Lectures on Artificial Intelligence and Machine Learning, 3(1), 1-130.
14. Obermeyer, Z., & Emanuel, E. J. (2016). Predicting the future—big data, machine learning, and clinical medicine. New England Journal of Medicine, 375(13), 1216-1219.
15. Kamp-Becker, I., Albertowski, K., Becker, J., Ghahreman, M., Langmann, A., Mingebach, T., ... & Stroth, S. (2018). Diagnostic accuracy of the ADOS and ADOS-2 in clinical practice. European child & adolescent psychiatry, 27, 1193-1207.
16. Barbaro, J., & Yaari, M. (2020). Study protocol for an evaluation of ASDetect-a Mobile application for the early detection of autism. BMC pediatrics, 20, 1-11.
17. Adamu, A. S., & Abdullahi, S. E. Y. (2021, February). A Review of Autism Diagnosis/Screening Expert System and Mobile Application. In 2020 IEEE 2nd International Conference on Cyberspac (CYBER NIGERIA) (pp. 80-84). IEEE.
18. Khodatars, M., Shoeibi, A., Sadeghi, D., Ghaasemi, N., Jafari, M., Moridian, P., ... & Berk, M. (2021). Deep learning for neuroimaging-based diagnosis and rehabilitation of autism spectrum disorder: a review. Computers in Biology and Medicine, 139, 104949.
19. Zhang, L., Wang, M., Liu, M., & Zhang, D. (2020). A survey on deep learning for neuroimaging-based brain disorder analysis. Frontiers in neuroscience, 14, 779.
20. Peng, J., Zhao, M., Havrilla, J., Liu, C., Weng, C., Guthrie, W., ... & Zhou, Y. (2020). Natural language processing (NLP) tools in extracting biomedical concepts from research articles: a case study on autism spectrum disorder. BMC Medical Informatics and Decision Making, 20(11), 1-9.
21. Elbattah, M., Guérin, J. L., Carette, R., Cilia, F., & Dequen, G. (2020, December). Nlp-based approach to detect autism spectrum disorder in saccadic eye movement. In 2020 IEEE Symposium Series on Computational Intelligence (SSCI) (pp. 1581-1587). IEEE.
22. Zwilling, M., & Levy, B. R. (2022). How well environmental design is and can be suited to people with autism spectrum disorder (ASD): A natural language processing analysis. International Journal of Environmental Research and Public Health, 19(9), 5037.

23. Thabtah, F. (2019). Machine learning in autistic spectrum disorder behavioral research: A review and ways forward. Informatics for Health and Social Care, 44(3), 278-297.
24. Lebersfeld, J. B., Swanson, M., Clesi, C. D., & O'Kelley, S. E. (2021). Systematic review and meta-analysis of the clinical utility of the ADOS-2 and the ADI-R in diagnosing autism spectrum disorders in children. Journal of Autism and Developmental Disorders, 1-14.

Table 1: Comparison of Machine learning based Autism screening tools]

Screening Tool Name	Age	Conducted By	Assessment Type	Length of Assessment	Reliability	Validity	Sensitivity	Specificity
Autism Diagnostic Observation Schedule (ADOS)	All ages	Trained clinician	Standardized observation-based assessment	30-60 minutes	High	High	0.79-0.97	0.67-0.91
Childhood Autism Rating Scale (CARS)	2 years and older	Trained clinician	Behavior rating scale	15-30 minutes	Moderate to high	High	0.78-0.96	0.86-0.94
Social Communication Questionnaire (SCQ)	4-40 years	Parent or caregiver	Parent-reported screening tool	10-15 minutes	High	High	0.77-0.96	0.60-0.93
Social Responsiveness Scale (SRS)	4-18 years	Parent or teacher	Parent or teacher-reported screening tool	15-20 minutes	High	High	0.68-0.89	0.74-0.91

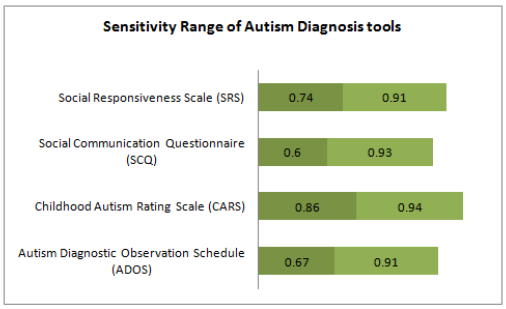

Figure 1: Sensitivity result analysis of Autism Diagnosis tools

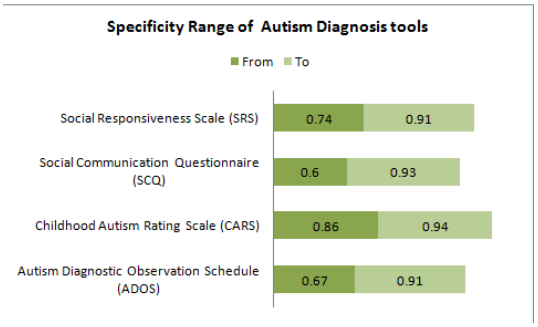

Figure 2: Specificity result analysis of Autism diagnosis tools

RESEARCH ARTICLE

A Study on Flow of Market Information in the Supply Chain of Banana in Andhra Pradesh

Mehazabeen. A[1] and G. Srinivasan[2]*

[1]Assistant Professor, Department of Agriculture and Business Management, Centurion University of Technology and Management, Odisha, India.
[2]Associate Professor, Department of Agri. Economics, Annamalai University, Tamil Nadu, India.

Received: 14 Nov 2023 Revised: 09 Jan 2024 Accepted: 25 Mar 2024

***Address for Correspondence**
G. Srinivasan
Associate Professor,
Department of Agri. Economics,
Annamalai University,
Tamil Nadu, India.

ABSTRACT

Banana (Musa paradisica L.) is a vital cultivated herbaceous food crop on a global scale, with significant export potential. Banana cultivation in the Andhra Pradesh state has expanded to 1.12 lakh hectares, with a production of 63.84 lakh MT in 2019. Y.S.R. district leads the state in production, contributing 8.67 lakh MT. The study was undertaken with the objective of (i)To analyse the flow of marketing information among farmers within the supply chain of banana in Andhra Pradesh (ii)To analyse flow of marketing information among the banana traders and policy suggestions. For this study, a multistage stratified random sampling method was used. The data were analyzed and interpreted in tabular form and analyzed data were expressed in averages and percentages for the better understanding. The results from the study showed that farmers who were aware of the area of banana cultivation in the current season and previous season as well as prices were very meagre (7.5 per cent) in the study area. Hence, the study suggested that market information about cultivation area, arrivals and prices of banana should be provided by convenient of market stakeholders through ICT. The study also suggested for the establishment of institutional marketing facilities, including regulated and cooperative market, equipped with proper infrastructure to encourage banana farmers in the study area.

Keywords: Marketing intermediaries, Market information, Institutional Marketing

INTRODUCTION

Cultivating horticultural crops plays a fundamental role in enhancing our nation's prosperity, as it directly influences the well-being and economic fortune of its people while also promoting their overall health(Vision, 2050 IIHR, 2014).Banana (Musa paradisica L.) stands as a crucial cultivated herbaceous food crop globally, boasting substantial export potential..Employing high-tech methods for its cultivation proves economically sound, resulting in enhanced productivity, superior product quality, and early crop maturity. Such produce commands a premium price in the market. Marketing information helps the banana farmers in making decisions inmarketing their produce. The farmers cannot know the prices prevailing in the markets, as the market committees can disseminate information only in respect of their own markets. Therefore, farmers are left with no alternative but to dispose of their products in the nearest market, even at uneconomic prices. Market information is equally needed by other market participants in arriving at optimal trading decisions. At this juncture, the study was undertaken with the objective of (i)To analyse the flow of marketing information among farmers within the supply chain of banana in Andhra Pradesh (ii)To analyse flow of marketing information among the banana traders and policy suggestions.

Design of the study

The Y.S.R. district in Andhra Pradesh was purposively chosen from among the 13 districts due to its leading position in both banana cultivation area covering 16,731 hectares, and production8,67,663 metric tons. For this study, a multistage stratified random sampling method was used, with Andhra Pradesh state as the overall population. Districts were chosen as the first-stage units, Mandals within the districts as the second-stage units, villages within the blocks as the third-stage units, and ultimately, individual farmers served as the final sampling units.16 villages which are above the mean area of banana cultivation of the district, which consists of nine villages from Lingala Mandal and seven villages from Vemula Mandal were selected for this study. A sample of 320 farmers was randomly selected using the probability proportionate method, accounting random numbers for identification. Data collection involved surveying a sample of 120 market intermediaries, including commission agents, pre-harvest contractors, wholesalers, and retailers, engaged in banana marketing at the Pulivendula market.

Tools of Analysis

Descriptive Statistics

Simple Tabular Analysis

The data were analyzed and interpreted in tabular form.

Averages and Percentages

The analyzed data were expressed in averages and percentages for the better understanding.

RESULTS AND DISCUSSIONS

Flow of Market Information in the Supply Chain of Banana

Farmers Awareness on Market Information

The details of the farmer's awareness on the market information are given in Table 1. The table indicates that the majority of the farmers that is 86.25 per cent are aware of prices of banana in the local market while 70.62 per cent of the farmers are aware of the arrivals of banana in the local market. About 32.5 per cent of the farmers are aware of the quality and grades of the banana and 38.75 per cent of the farmers are aware of banana prices in other markets. Only 7.5 per cent of the farmers are aware of the area of crop sown in the state.

Traders awareness on market information

The details of the trader's awareness on various types of market information are represented in the Table2. The table revealed that all the traders are aware of the prices of banana in the local market. About 97.50 per cent of the traders are aware of arrivals in the local market and 85.83 per cent of the traders are aware of prices in the reference markets

like Gorakhpur, Banglore, Delhi, Hyderabad, Tirupati, Hubli, Dharwad, and Haveri markets. About 90.83 per cent of the traders are aware of arrivals of banana in the reference market. About 73.33 per cent of the traders are aware of the area under the crop of banana and about 63.33 per cent of the traders are aware of the production of banana in the state. Only 20.00 per cent of the traders are aware of the export or import of banana from the region.

Farmer's Source of Market Information at Village Level and Market Level

The details source of market information to the farmers is presented in Table 3. Themajor share forthe source of market information is by television in agriculture-related programmes like Pasidipantalu, Kisan, Annadaata and other programmes (87.5 per cent) followed by the newspaper (48.75 per cent) and radio programmes like Kissan Vani (14.68 per cent) and only 12.18 per cent of the farmers are using the internet as a source of market information. About 49.37 per cent of the farmers are aware of market information through the state horticultural department. About 77.5 per cent of the market information is through commission agents and 73.75 per cent through traders and 23.75 per cent through input dealers.

Source of Market Information of Traders

The details of source of market information for the traders are presented in Table 4. The table clearly indicates that the 93.33 per cent of the traders are availing the market information through the contacts in other markets over the phone, whereas, 85.00 per cent of the traders are aware of market information through fellow traders followed by newspapers (60.00 per cent), market information cell, (61.67 per cent), internet (56.67 per cent) and magazines (34.16 per cent).

CONCLUSION

In banana market, farmers who were aware of the area of banana cultivation in the current season and previous season as well as prices were very meagre (7.5 per cent) in the study area. Hence, the study suggested that market information about cultivation area, arrivals and prices of banana should be provided by convenient of market stakeholders through ICT. The study also suggested for the establishment of institutional marketing facilities, including regulated and cooperative market, equipped with proper infrastructure to encourage banana farmers in the study area.

REFERENCES

1. Dave AK, Zala YC, Pundir RS., 2016, Comparative economics of banana cultivation in Anand district of Gujarat. *Econ. Affairs,*61(2):305-312.
2. ICAR-IIHR Annual Report, 2014-15, ICAR-Indian Institute of Horticultural Research, Bengaluru, Karnataka, India.
3. Ramakrishna, M., Ravi Kumar, K.N. and Bhavani Devi, I., 2017, A Micro Economic Analysis of Production of Banana in Kurnool District of Andhra Pradesh, India. *International Journal of Current Microbiology and Applied Sciences*. 6(7): 1152-1159.
4. Raman, M.S., 2012, An Economic Analysis of Production and Marketing of Banana in Tiruchirappalli District in Tamil Nadu, *Unpublished M.Sc. (Ag.) Thesis,* submitted to Department of Agricultural Economics, Agricultural College and Research Station, Madurai.

Table 1. Farmer's Awareness on Market Information

Sl. No.	Type of Market Information	No. of Respondents	Percentage
1	Prices in the local market	276	86.25
2	Arrivals in the local market	226	70.62
3	Quality and grade of the produce	104	32.5

4	Prices in the other market	124	38.75
5	Area of crop sown in the state	20	7.5

(n=320) Note: The percentage do not add up to 100 due to multiple or no response

Table 2. Trader's Awareness on Market Information

Sl. No.	Type of Market Information	No. of Respondents	Percentage
1	Arrivals in local market	117	97.50
2	Arrivals in reference market	109	90.83
3	Prices in local market	120	100.00
4	Prices in reference market	103	85.83
5	Area under crop	88	73.33
6	Production of banana in the state	76	63.33
7	Quality/Grade required	92	76.67
8	Export and import	24	20.00

(n=120) Note: The percentage do not add up to 100 due to multiple or no response.

Table 3.Farmer's Source of Market Information at Village Level and Market Level

Sl. No.	Source of Market Information	No. of Respondents	Percentage
1	Radio	47	14.68
2	Newspaper	156	48.75
3	Television	280	87.50
4	Internet	39	12.18
5	Friends/Relatives/Neighbours	124	38.75
6	State horticulture department	158	49.37
7	Traders	236	73.75
8	Commission agents	248	77.50
9	Input dealers	76	23.75

(n=320) Note: The percentage do not add up to 100 due to multiple or no response.

Table 4. Source of Market Information of Traders

Sl. No.	Source of Market Information	No. of Respondents	Percentage
1	Radio	21	17.50
2	Television	54	45.00
3	Newspaper	72	60.00
4	Magazines	41	34.16
5	Internet	68	56.67
6	Contact in other markets over phone	112	93.33
7	Fellow traders	102	85.00
8	Govt. publications	24	20.00
9	Market information cell	74	61.67

(n=120) Note: The percentage do not add up to 100 due to multiple or no response.

Vol.15 / Issue 83 / Apr / 2024 International Bimonthly (Print) – Open Access ISSN: 0976 – 0997

RESEARCH ARTICLE

Unveiling Scholarly Insights : Analyzing Social Media Advertising Literature through Bibliometric Analysis, Science Mapping and Visualization Techniques

Nitika* and Mohit

Research Scholar, Institute of Management Studies and Research, Maharshi Dayanand University, Rohtak, Haryana, India.

Received: 04 Mar 2024 Revised: 15 Mar 2024 Accepted: 20 Mar 2024

***Address for Correspondence**
Nitika
Research Scholar,
Institute of Management Studies and Research,
Maharshi Dayanand University,
Rohtak, Haryana, India.
Email: nitikamalik.rs.imsar@mdurohtak.ac.in

ABSTRACT

This expansive study undertakes a thorough exploration of the social media advertising (SMA) landscape from 2014 to 2023, employing advanced bibliometric analysis tools such as VOS viewer, Bilioshiny, and SPSS software. A meticulous examination of 242 documents from 137 diverse sources, including journals and books, paints a comprehensive picture of SMA research. The study unfolds with notable characteristics, including a robust 16.18% annual growth rate, showcasing the field's increasing influence and relevance. The relatively low average age of 2.96 years of the documents indicates a commitment to incorporating the latest research in the rapidly evolving domain. Each document's average of 20.24 citations underscores the scholarly impact of the study, while the extensive use of 14,915 references attests to the depth and thoroughness of the research. Enriched document contents, comprising 390 Keywords Plus and 784 Author's Keywords, contribute to a nuanced understanding of the subject matter. Collaboration emerges as a hallmark of this research, involving 630 authors, 26 of whom authored single-authored documents. The collaborative spirit extends globally, with an average of 2.94 co-authors per document, and 26.45% of collaborations being international, demonstrating a truly global perspective. Shifting focus to the SMA landscape, the study's robust Scopus database search protocol reveals a 16.18% annual growth rate, peaking at 198 publications in 2022. The United States, India, and China emerged as major contributors, highlighting the global recognition of SMA. Country collaboration analysis identifies extensive partnerships, particularly with Korea and China. Prolific authors and influential figures in co-citation analysis, including the highly cited work by Lee, Hosanagar, and Nair on advertising content's impact on user engagement, provide a comprehensive view of the SMA research landscape. Journal rankings position the Journal of Research in Interactive Marketing as

the most impactful source, shaping the trajectory of SMA research. Marketers, policymakers, and researchers stand to benefit significantly from the insights offered by this study, gaining valuable perspectives for enhanced campaign effectiveness, regulatory guidance, and future research directions. By synthesizing diverse themes, this study not only captures the current SMA landscape comprehensively but also steers future research by identifying emerging trends and unexplored territories in the dynamic advertising arena.

Keywords: Literature Review, Bibliometric Analysis, SMA Analysis, Co-Citations Analysis, VOSviewer, Science Mapping.

INTRODUCTION

In the digital age, the pervasive influence of social media platforms has revolutionized the way businesses and brands engage with their target audiences. One of the most impactful manifestations of this transformation is the realm of social media advertising (Cheung et al., 2023). As users continue to flock to platforms such as Facebook, Instagram, Twitter, and LinkedIn, advertisers have recognized the unparalleled potential of these spaces for reaching, engaging, and persuading consumers (McInnis et al., 2022). The dynamic and rapidly evolving nature of social media advertising has prompted researchers to delve into its multifaceted dimensions, contributing to an expanding body of knowledge in the field (Ertemel and Ammoura, 2016). This bibliometric research paper embarks on an exploration of the extensive landscape of scholarly literature related to social media advertising. Bibliometrics, a quantitative method used to analyze patterns of publication and citation within the academic literature, offers a unique lens through which to observe the evolution of research trends, seminal works, and influential authors in this domain (Donthu et al., 2021). By employing bibliometric techniques, we aim to uncover the intellectual structure, growth patterns, and emerging themes that characterize the field of social media advertising research.

The importance of this study lies not only in its potential to provide a comprehensive overview of the existing research landscape but also in its ability to guide future scholars, practitioners, and policymakers. Through a systematic analysis of publication trends, citation patterns, and interdisciplinary collaborations, we intend to identify knowledge gaps, highlight seminal contributions, and project the potential trajectories of social media advertising research. This paper serves as a valuable resource for individuals seeking to comprehend the evolution of thought within this dynamic field and make informed decisions that align with current scholarly discourse. The subsequent sections of this paper are organized as follows: Section 1 includes an introduction and background of the domain, and Section 2 introduces the methodology employed, search protocol for data extraction, selection criteria, and analytical tools used in the bibliometric analysis. Section 3 presents the key findings derived from the analysis, highlighting influential works, prolific authors, and prevalent themes within social media advertising. In Section 4, we discuss the implications of these findings, addressing potential future research directions and the practical significance of the identified trends.

BACKGROUND OF THE STUDY

The emergence of social media platforms in the early 2000s paved the way for a new era of digital advertising. Initially, platforms like MySpace and Friendster experimented with ad models, but these efforts were limited in targeting capabilities and lacked advanced analytics (Jones et al., 2008). However, the introduction of Facebook advertising in 2007 revolutionized the field (McInnis et al., 2022). Facebook's vast user base and abundant demographic data provided advertisers with unprecedented targeting opportunities (Wilson et al., 2012). They could reach specific demographics, interests, and behaviors using engaging ad formats like photos and videos (Nadkarni and Hofmann, 2012). Facebook continuously enhanced its advertising platform with features such as custom audiences and dynamic advertising, enabling companies to optimize their campaigns and achieve higher returns on

investment (Hansson et al., 2013). This success led other social media platforms like Instagram, Twitter, LinkedIn, and Pinterest to enter the advertising space, each developing its unique ad formats and targeting capabilities to cater to different demographics and user preferences (Vishwanath et al., 2009). Brands recognized the advertising potential on these platforms, allowing them to effectively engage with their target audience. As social media platforms grew, so did research in the field of social media advertising. The first study, conducted in 1996 by Pack and Thomas, explored whether net casting would shape the future of radio or remain a technological novelty. This study laid the groundwork for subsequent research in this domain. Chawla et al. conducted a study in 1999 to understand consumer sentiments toward internet usage. Sheehan and Hoy investigated consumer attitudes and perceptions regarding privacy and online advertising practices. Over time, numerous studies have contributed to the understanding of social media advertising. In the present context, Lee et al.'s study published in 2018 has received the highest number of citations. This study examined the relationship between consumer engagement and advertising effectiveness, providing valuable insights into the field.

OBJECTIVES OF THE STUDY

The objectives of this bibliometric analysis encompass a comprehensive exploration of the social media advertising (SMA) domain from 2014 to 2023. Firstly, the temporal pattern of annual publications will be scrutinized to discern evolving trends and shifts in research focus over the specified timeframe. Secondly, the analysis aims to identify the most productive countries in the SMA domain, shedding light on global contributions to the field. Thirdly, the collaboration pattern among countries will be examined, providing insights into international research networks within SMA. Moreover, a detailed examination of the most productive authors, universities, and sources in SMA analysis will be conducted to recognize influential contributors and authoritative publications. Additionally, the co-citation pattern within the domain will be explored, highlighting interconnected works that have significantly influenced SMA research. The analysis will also delve into the examination of the most cited publication in the SMA domain, elucidating key foundational works. Furthermore, the study will employ a three-field plot analysis to provide a visual representation of the domain's intellectual structure. Additionally, the co-occurrence of keywords, trend topics, and the thematic map of the domain will be analyzed to unveil prevalent themes and emerging areas of interest. Finally, the research aims to identify major themes on which research work is conducted in the SMA domain, offering a holistic understanding of the current landscape and potential directions for future exploration.

MATERIALS AND TECHNIQUES

Bibliometric analysis, recognized as a quantitative method for assessing scientific publications, authors, and research trends (Koseoglu et al., 2016, Chaudhry & Kumar, 2023, Singh et al.,2023), serves as the cornerstone of our study's methodology in analyzing the literature on social media advertising. Embracing this approach, we leverage bibliometric tools known for their transparency and objectivity, encompassing the evaluation of citation and publication data, co-authorship, and thematic analyses (Thanuskodi, 2010). This comprehensive analysis employs performance assessment, impact measurement, and science mapping, including visualization techniques, to gain a nuanced understanding of the dynamic landscape within the field. Previous research has demonstrated the efficacy of this approach in uncovering growth trends, author keywords, and prominent journals (Andres, 2009; Subramanyam, 1983; Patra et al., 2006). Our unique contribution lies in presenting a systematic methodology that integrates Biblioshiny and VOSviewer tools. Biblioshiny facilitates efficient data retrieval and analysis, while VOS viewer constructs visually intuitive bibliometric networks (Rusydiana, 2021). Additionally, MS Excel and SPSS are instrumental in providing more in-depth insights into the domain. By employing this comprehensive toolkit, our research strives to enrich the understanding of the scholarly landscape of social media advertising, emphasizing transparency, objectivity, and an innovative methodology for uncovering key insights in this dynamic field.

Search Protocol

The bibliographic information was gathered using the Scopus database because it has more publications than other databases like "Web of Science" and is, therefore, one of the biggest databases of journals. The Scopus database has been used for bibliometric analyses in numerous earlier works. The search string was used in the title-abstract-keyword field of Scopus. The search string used in the analysis is depicted and defined below: A variety of search procedures were utilized to ensure the coverage of all articles and documents connected to social media advertising analysis, based on the evaluation of prior literature and recommendations from academicians. The keyword "social media advertising" was used for the extraction and analysis of available literature. The Scopus database's Title-Abstract-Keywords field was searched using the mentioned keyword. Lastly, our database included journal articles only, and the data were extracted for the period of 10 years (2014 to 2023). Additionally, the subjects were limited to business management, accounting, psychology, multidisciplinary, and arts and humanities. Moreover, the analysis only considered manuscripts that were written in English.

DATA ANALYSIS AND FINDINGS

This figure above provides a comprehensive overview of the research study conducted over the time span from 2014 to 2023, encompassing 242 documents from 137 different sources, including journals and books. The study exhibits a robust annual growth rate of 16.18%, indicative of its expanding influence and relevance over the years. The document's average age is relatively low at 2.96 years, suggesting the inclusion of recent research. Each document receives an average of 20.24 citations, indicating the scholarly impact of the study. The extensive use of references, totaling 14,915, further attests to the thoroughness and depth of the research. The document contents are enriched with 390 Keywords Plus and 784 Author's Keywords, providing a comprehensive understanding of the subject matter. The collaborative nature of the research is reflected in the involvement of 630 authors, with 26 single-authored documents. The collaboration extends to an average of 2.94 co-authors per document, and 26.45% of these collaborations are international, showcasing a global perspective. The predominant document type is an article, comprising all 242 documents, emphasizing the study's focus on in-depth analysis and scholarly discourse. Overall, this table paints a picture of a dynamic, well-referenced, and globally collaborative research endeavor with a significant and growing impact on its field. A total of 242 documents are analyzed for the study. The trend depicted by the publications is demonstrated above. Analysis revealed that the year 2022 witnessed the maximum publication in the domain with 198 documents. The domain is still in the infant stage and growing continuously year by year. The publications have an upward trend except for the year 2020 when the documents are in a downward trend and were lesser than the general trend. In the year 2023, there are fewer studies from general trends but the reason is that data is extracted till July 2023 only, not for the whole year. The above table ranks countries based on their research output and citation impact within a specified domain.

The United States leads with 90 documents and 1740 citations, signifying a substantial contribution to the field. It is classified under North America and categorized as a developed nation. India follows as the second-ranking country with 28 documents and 303 citations, representing a significant research presence in Asia. India is classified as a developing nation, highlighting its ongoing efforts in scientific and scholarly endeavors. China, with 20 documents and 147 citations, also emerges prominently in the rankings. Like India, China is classified as a developing country, emphasizing its growing influence in the global research landscape. Australia occupies the fourth position with 16 documents and 212 citations, representing a developed nation in Oceania. This suggests a noteworthy research output and impact on the Australian scientific community. In summary, this table provides a snapshot of the research landscape in different countries, reflecting variations in research productivity and impact. It underscores the global distribution of research contributions and highlights the research strengths of both developed and developing nations. Country collaboration is analyzed in this section of the analysis. The results demonstrated that the USA collaborated in the most publications with Korea, with a total of 8 publications. The USA ranks second in collaboration with China, with a total of 7 publications. Germany and the Netherlands are ranked next, with collaboration in 3 publications each. The USA also published the same number of publications in collaboration with

Australia, Germany, New Zealand, and the United Kingdom. Furthermore, Korea and New Zealand collaborated on 3 publications as well. The countries' collaboration map is depicted below: Single-authored and multiple-authored collaborations of countries are analyzed in this section. The USA tops the list with 57 publications, 47 of which are single-authored and 10 are multiple-authored publications. China is in 2nd position with a total of 21 publications, comprising 10 single-authored publications and 11 collaborations with multiple authors. India occupies the 3rd position with 16 publications, all of which are single-authored; no multiple-authored collaborations were done by India. After that, it is followed by Korea with a total of 11 publications, 5 of which are single-authored and 6 are multiple-authored. This table presents a ranking of authors based on the number of documents and the total citations received. The authors listed have contributed to the field of social media advertising (SMA), and their impact is measured by the number of documents they have authored and the citations those documents have received. Rana M, Arora N, and Arora T, Agarwal B emerge as the most prolific authors, with multiple documents attributed to their names. However, Arora T, and Agarwal B hold the second position but have a notably higher citation count, indicating the influential impact of their work. Boateng H, Okoe A.F. and Natarajan T, Balakrishnan J, Balasubramanian S.A, and Manickavasagam J also feature prominently, contributing to two documents each, with varying citation counts The diverse range of authors in the table signifies the collaborative nature of SMA research, with some authors co-authoring documents.

Noteworthy is the significant citation count associated with certain authors, such as Alalwan A.A. with 278 citations, indicating the substantial impact and recognition of their work within the SMA domain. Overall, this table provides insights into the productivity and impact of various authors in the field of SMA, offering a snapshot of the research landscape and highlighting key contributors and influential works. Table 7 presents the top authors in this bibliographic review, ranked by their citations per publication. The table provides the names of the authors, the number of papers published, and the total number of citations for their works. At the top of the list in the first row are authors "Lee D., Hosanagar K., and Nair H.S." closely followed in second place by Voorveld H.A.M., Van Noort G., Muntinga D.G., and Bronner F., with 321 citations for their single publication. In the third position are Lee J. and Hong I.B., receiving 302 citations for their one publication. The fourth place is secured by Alalwan A.A. with 278 citations in one publication, while Zhu Y.-Q. and Chen H.-G. rank fifth with 206 citations for their one publication. The subsequent entries showcase different authors, each with a single publication and separate citation counts. These authors have made significant contributions to the study through their individual works, emphasizing the impact of their research. Overall, Table 7 highlights the presentation of influential authors in this literature review based on their citations, shedding light on the impact and quality of their individual research contributions. When two texts often cite two different articles by two different authors, co-citation analysis is used. The top author's co-citations analysis showed that Hair J.F. topped the list with 279 citations and the strongest co-citation link strength (7736).

Moreover, Law R., with 252 citations, Sarstedt M., with 230 citations, Ringle C.M., with 222 citations, and Wang Y., with 196 citations, were among the top 5 in the list according to citations. This table provides a glimpse into the landscape of social media advertising research by ranking the most cited publications in the field. Topping the list is the work by Lee, Hosanagar, and Nair (2018), titled "Advertising Content and Social Media: Evidence from Facebook," published in the journal "Management of Science," with an impressive 399 citations. Following closely is the paper by Voorveld, van Noort, Muntinga, and Bronner (2018) from the "Journal of Advertising," exploring engagement with social media and advertising across different platforms, garnering 321 citations. The third-ranked paper by Lee and Hong (2016) investigates the predictors of positive user responses to social media advertising, emphasizing emotional appeal, informativeness, and creativity, accumulating 302 citations. Other notable contributions include Alalwan's (2018) exploration of the impact of social media advertising features on customer purchase intention, and Zhu and Chen's (2015) examination of the relationship between social media and human need satisfaction. This compilation not only underscores the diverse aspects covered in social media advertising research but also highlights the scholarly impact of these works, offering a valuable resource for academics, marketers, and researchers seeking a deeper understanding of this evolving field. The presented table offers a comprehensive ranking of sources in the realm of social media advertising, assessing their impact based on the number of documents published, total citations received, and the average number of citations per publication. At the

forefront, the "Journal of Research in Interactive Marketing" claims the top position with an impressive tally of 16 documents and a substantial 461 citations, resulting in an exceptional average of 28.81 citations per publication. Following closely is the "International Journal of Internet Marketing and Advertising," contributing 9 documents with 28 citations and an average of 3.11 citations per publication. The "Journal of Interactive Advertising" secures the third spot, boasting 8 documents and 81 citations, yielding an average of 10.125 citations per publication. The fourth entry, "Computers in Human Behavior," stands out with 6 documents but an outstanding 531 citations, resulting in a remarkable average of 88.5 citations per publication. This ranking enables a nuanced understanding of the influence and recognition of each source within the academic discourse of interactive marketing and advertising, providing valuable insights for researchers, practitioners, and scholars in the field. This table tracks the annual publication counts for five prominent journals—"Journal of Research in Interactive Marketing," "International Journal of Internet Marketing and Advertising," "Journal of Interactive Advertising," "Computers in Human Behavior," and "Frontiers in Psychology"—from 2014 to 2023. The data provides valuable insights into the evolving research landscape within the field. In 2014, the "International Journal of Internet Marketing and Advertising" led with a single publication, followed by an increasing trend over subsequent years. "Journal of Research in Interactive Marketing" commenced its publications in 2015 and exhibited steady growth, reaching 16 publications in 2023. "Journal of Interactive Advertising" and "Computers in Human Behavior" started with zero publications but experienced gradual increases, particularly in 2018 and beyond. "Frontiers in Psychology" entered the scene in 2016 and maintained a moderate but consistent publication output. Throughout the years, 2021 witnessed a notable surge in publications across all journals, indicating a heightened focus on research in social media advertising.

The year 2022 marked a significant increase in publications for all journals, showcasing a growing interest and scholarly engagement. The data suggests a dynamic landscape with shifting research priorities, emphasizing the importance of these journals in contributing to the academic discourse on interactive marketing, internet marketing, advertising, human behavior, and psychology within the specified timeframe. Researchers and stakeholders can leverage this information to gauge the trajectory of research interest and identify potential trends within the field over the past decade. The table presents a ranking of organizations based on their scholarly output and citation impact. The "Department of Marketing at Cape Peninsula University of Technology in Cape Town, South Africa," secures the top position with 2 documents and a notable citation count of 177. Similarly, the "Department of Marketing, University of Professional Studies in Accra, Ghana," also records 2 documents but slightly fewer citations at 173. The third-ranking organization is the "Department of Retail, Hospitality, and Tourism Management" at the University of Tennessee, Knoxville, United States, with 2 documents and 59 citations. The ranking reflects the research productivity and influence of these academic departments in the field of marketing and related disciplines. The organizations from South Africa and Ghana stand out in terms of both document output and citation impact, showcasing their contribution to the scholarly landscape. The Sankey diagram in the figure illustrates the main components of three fields—authors, keywords, and journals, and their interactions. Arrow width is inversely related to flow velocity. Three local names denote the most popular authors, keywords, and sources. A chart of colored triangles indicates the main components, with relationships summarized in terms of rectangle height. The number of combinations for each unit depends on the rectangle size. The current study identified research topics and main sources, revealing "Consumer Heterogeneity and Paid Search Effectiveness:

A Large-Scale Field Experiment Econometrics" by Blake T. et al. as the most important node with 2 flow counts. The second-highest related node is "When Does Retargeting Work? Information Specificity in Online Advertising" with 1 flow count, published in the Journal of Marketing Research by Lambrecht A. and Tucker C., followed by "Control and Peripheral Routes to Advertising Effectiveness: The Moderating Role of Involvement" in the Journal of Consumer Research by Petty R.E. The provided table presents an analysis of frequently occurring keywords within a specific context. The most prominent keyword, "Social Media," appears 88 times, highlighting the central role of social platforms in the subject matter. "Social Media Advertising" closely follows with 72 occurrences, indicating a strong focus on using these platforms for promotional activities. The more general term "Advertising" is also significant, occurring 46 times, suggesting a broader exploration of promotional strategies beyond just social media. "Marketing" and "Purchase Intention" round out the list with 25 and 24 occurrences, respectively, reflecting a

continued interest in core marketing principles and the study of consumer behavior related to the discussed topic. This keyword analysis underscores the emphasis on social media and its intersection with advertising and marketing concepts in the context of the subject being studied. The figure below depicts the graph of the same keywords built using VOSviewer. The density visualization, which reveals research hotspots, indicates that "Social Media Advertising," "Social Media," and "Advertising" are key research hotspots in the domain. The figure depicting this is presented above. The research hotspots in different years were analyzed using the Biblioshiny software, and the results demonstrated that in 2022, the terms "online advertising" with 18 occurrences, "advertising" with 10 occurrences, and "forecasting" with 7 occurrences were the most frequent topics.

Meanwhile, in 2021, "social media" with 51 occurrences, "electronic commerce" with 14 occurrences, and "consumption behavior" with 8 occurrences were the most researched topics in the domain. In 2020, this list comprised "marketing" with 85 occurrences, "advertising" with 56 frequencies, and "female" with 42 occurrences, representing the hotspots of the stated research domain area.In this section, a thematic map of the domain is created. Layers are assembled to generate thematic maps, and the data from each layer are then plotted in one or more aesthetics. Thematic evolutionary analysis is employed to identify relationships between historical patterns and evolutionary processes. The thematic analysis utilizes an inclusion index weighted by incoming terms, with a minimum cluster frequency of 5 and a minimum weighting index of 0.1. The strength of the structures that develop over time is depicted in the theme analysis map, where each node's size corresponds to the topic's total number of keywords. The top left quadrant, characterized by high density but low centrality, presents specific and underrepresented issues still undergoing major growth, themes such as "social media platforms," "commerce," "consumer behavior," "psychology," "COVID-19," and "epidemiology" fall into this niche category within the domain. Additionally, the domain exhibits declining themes like "behavioral research," "social influence," and "empirical analysis." The lower right quadrant contains basic themes with high centrality and density, including "social media advertising," "consumption behavior," "marketing," "social networking (online)," and "advertising." Motor themes in the domain area encompass "human," "article," "female," "purchase intention," "purchasing," and "sales."

MAJOR RESEARCH THEMES IN SOCIAL MEDIA ADVERTISEMENT DOMAIN

The landscape of advertising has significantly transformed with the rise of social media platforms, leading to a surge in research efforts to understand the intricate dynamics between social media advertising and various aspects of consumer behavior, effects, influencers, trust, culture, brand perception, ethics, health impact, and advertising effectiveness. This analysis synthesizes the research contributions of various authors in our domain area and also analyzes the various themes on which research work is done in the domain area of social media advertising. The stated analysis can be very crucial for future researchers and can guide them in further studies. The major themes of the domain area are stated below:

Social Media Advertising and Consumer Behavior

The influence of social media advertising on consumer behavior is a central theme. Chen & Chiu (2021) explore the impact of personalized advertisements on consumer responses. Sarılgan et al. (2022) delve into the role of emotional appeals in driving purchase intention. Asiedu (2017) investigates the impact of social media advertising on brand loyalty. This theme is also addressed by Agil et al. (2022), Sreejesh et al. (2020), Arora et al. (2020), Tian & Li (2022), and Tan et al. (2021).

Effects of Social Media Advertising

The effects of social media advertising are diverse and multi-faceted. Studies by Supotthamjaree & Srinaruewan (2021), Li et al. (2020), and Sreejesh et al. (2020) emphasize the impact on consumer attitudes and behaviors. Lee & Hong (2016) investigate the influence of social media advertising on brand awareness. Alalwan (2018) examines the effects on purchase intention. Lim & Childs (2020) study the impact on engagement, and Raji et al. (2019) investigate the role of source credibility.

Influencers and Brand Endorsement using Social Media Advertising

Influencers and brand endorsement have become integral to social media advertising. Kim et al. (2023) focus on the effectiveness of influencer marketing. Tian & Li (2022) explore the role of celebrity endorsements in shaping consumer attitudes. Hwang & Zhang (2018) examine the impact of different types of influencers. Chiu & Ho (2023) discuss the influence of authenticity in brand endorsements. Ahmad et al. (2019) study the credibility of influencer content.

Privacy and Trust in Social Media Advertising

Privacy and trust are crucial considerations in the digital era. Fletcher (2001) explores the relationship between online privacy concerns and information disclosure. Bright et al. (2022) investigate the impact of privacy concerns on ad effectiveness. Efendioglu & Durmaz (2022) examine the role of trust in shaping consumer responses. Alkis & Kose (2022) delve into the impact of privacy-related messages on trustworthiness.

Cultural and Demographic Influences in Social Media Advertising

Cultural and demographic factors play a significant role in social media advertising effectiveness. Nguyen et al. (2023) analyze the influence of culture on consumer responses. Bui (2022) examines the role of cultural dimensions in shaping perceptions. Muk et al. (2014) explore the influence of demographics on advertising effectiveness. Thornhill et al. (2017) study the impact of cultural values on consumer attitudes, and Mansour (2015) investigate the influence of cultural norms.

Brand Perception and Consumer Engagement using Social Media Advertising

Brand perception and consumer engagement are pivotal for successful advertising. Chan (2022) examines the impact of brand personality on consumer engagement. Yang et al. (2021) explore the role of consumer-brand identification. Cheung et al. (2022) investigate the influence of emotional appeals on brand perception. Adamopoulos et al. (2018) study the effects of user-generated content on consumer engagement. Jaitly & Gautam (2021) explore the relationship between brand loyalty and consumer engagement.

Ethical and Psychological Aspectsof Social Media Advertising

Ethical and psychological aspects of social media advertising are essential considerations. Paramita & Septianto (2021) study the impact of ethical considerations on consumer responses. Bui et al. (2021) examine the role of ethical appeals in advertising effectiveness. Kim et al. (2023) focus on the psychological effects of social media advertising. Chauhan & Shukla (2016) explore the influence of psychological factors on ad effectiveness. Feng & Xie (2018) analyze the impact of psychological factors on consumer behavior.

Health-related and Societal Impact

The health-related and societal impacts of social media advertising are emerging areas of research. Al-Jabir et al. (2020) discuss the role of social media advertising in promoting public health. Rambe& Jafeta (2017) examine the impact of health-related advertising on consumer behavior. Athey et al. (2023) focus on the societal consequences of health-related advertising. Seberíni & Tokovska (2021) study the role of social media advertising in shaping health-related behaviors. Coulthard et al. (2021) analyze the effects of social media advertising on societal norms.

Social Media Advertising Effectiveness and Engagement

Advertising effectiveness and engagement are core concerns in the domain. Lou & Koh (2018) explore the factors influencing ad effectiveness. Dankwa (2021) investigates the role of engagement in enhancing ad effectiveness. Rizomyliotis et al. (2021) study the relationship between ad content and consumer engagement. Lee & Hong (2016) focus on the effects of social media advertising on ad recall and engagement. In conclusion, social media advertising is a multifaceted field encompassing various dimensions of consumer behavior, effects, influencers, trust, culture, brand perception, ethics, health impact, and advertising effectiveness. The research contributions of the mentioned authors shed light on the intricate interactions within these themes, contributing to a comprehensive understanding

of the evolving landscape of social media advertising. These research themes also can be employed by future researchers for further investigation in the domain area.

DISCUSSION

Social Media Advertising (SMA) analysis is an area of study that's gaining traction in the academic world day by day. Our study adds to what already exists in the domain of SMA analysis by using two approaches: bibliometric analysis and text mining approach. These methods help us get a more complete understanding of SMA research and help us identify the important research journals, institutions, authors, and trends in the field. What we found is that SMA analysis is still in its early stages in academia. It's clear from the analysis that the research on SMA is increasing, especially since 2017. We noticed that researchers started collaborating more after 2014, with a peak in 2018. From 2016 to 2020, several influential studies were published by authors like "Lee D., Hosanagar K., Nair H.S. (2018), Voorveld H.A.M., Van Noort G., Muntinga D.G., Bronner F. (2018), Lee J., Hong I.B. (2016), and Alalwan A. and others. These works have shaped how we understand SMA analysis. Geographically, most SMA analysis publications come from the United States, followed by India and China. This shows that research efforts are spread across the world. Authors like ALALWAN A.A. have received the most citations, and Rana M. and Arora N. have contributed significantly in terms of the number of publications.

Their work, along with authors like Lee D., Hosanagar K., Nair H.S., has had a strong impact on the academic discussions in this field. This suggests that SMA analysis is interdisciplinary and involves various perspectives. The Department of Marketing, Cape Peninsula University of Technology, Cape Town, South Africa, stands out for having a high number of SMA analysis publications, showing their commitment to this area of research.In addition, our study noticed that new technologies are being integrated into SMA to make it more strategic and data-driven. This shift is helping to address issues related to people and audiences. Social media advertising software is also making it easier for businesses to advertise on platforms like Facebook and Twitter, reaching millions of people. However, there's still a gap in research, especially in the context of India. In conclusion, our study gives us a better understanding of SMA analysis, its influencers, and how it's evolving. By using different analysis methods, we've been able to see the bigger picture of this dynamic field. We've identified important authors, significant works, and active institutions. As social media continues to shape advertising and user behavior, our study helps us navigate the path of SMA analysis and its importance for both academia and industry.

CONCLUSION

In conclusion, this bibliometric analysis illuminates the dynamic and rapidly evolving landscape of social media advertising. A comprehensive review of scholarly literature provided insights into various facets of this phenomenon, spanning its technical foundations to its profound impact on consumer behavior, brand engagement, and strong interconnectedness. As the field expands, it becomes evident that integrating different disciplines, methodologies, and strategies will enrich our understanding of the complex role social media advertising plays in shaping modern marketing strategies and its implications for businesses and consumers. This bibliographic analysis not only contributes to existing knowledge but also lays the foundation for future insights that will undoubtedly steer this vibrant and inevitable field into uncharted territories.

Practical Implications and Future Recommendations

More implications and future recommendations emerge from our comprehensive analysis of social media advertising (SMA). First, increasing research activity and collaboration suggests an increasing recognition of the importance of SMA. However, its relative newness in academia means there are many opportunities for further research. The geographical classification highlights the global reach of SMA research and allows for the development of different perspectives. To move forward, scholars should delve into the unexplored context of India, bridging the research gap. Examining the evolving impact of emerging technologies and approaches to data management in SMA

can provide valuable insights into industry practices. Additionally, examining the interactions between social media platforms, advertising effectiveness, and user behavior change will enhance our understanding of this dynamic landscape Education and industry network collaboration can give us practical advantages, steering businesses towards better use of social media advertising. As the SMA field evolves in an ever-changing digital landscape, these implications and future recommendations guide researchers and practitioners toward informed and impactful contributions. The research's conclusions can help researchers and social media marketers improve their strategy creation. Researchers and SM marketers can improve strategy design by using the research's conclusions. SM marketers can better understand the market and their target audience by implementing social media analysis.

Limitations

Despite, the investigation being thorough and rigorous, the study utilizes only the Scopus database for extracting relevant information whereas the Web of Science could have been also included in collecting research literature. Secondly, while the database is being filtered before export, some essential research can be overlooked. Thirdly, although to conduct a methodical, theory-driven study on SMA analysis is applied, however, quantitative text mining can also be used.

REFERENCES

1. Akter, S., & Wamba, S. F. (2017b). Big data and disaster management: a systematic review and agenda for future research. Annals of Operations Research, 283(1–2), 939–959. https://doi.org/10.1007/s10479-017-2584-2
2. Alshater, M. M., Saad, R., Wahab, N. A., & Saba, I. (2021). What do we know about zakat literature? A bibliometric review. Journal of Islamic Accounting and Business Research, 12(4), 544–563. https://doi.org/10.1108/jiabr-07-2020-0208
3. Andrés, A. (2009). Measuring Academic research: How to undertake a bibliometric study. http://cds.cern.ch/record/2059639
4. Bauwens, M. (1997). Compiling Internet expert resources: a case study towards a meta-index of subject experts in business information. Business Information Review, 14(3), 118–123. https://doi.org/10.1177/0266382974236390
5. Chaudhry, R., & Kumar, R. (2023). Bridging The Knowledge Gap: A Dynamic Bibliometric Analysis Of Emerging Trends In Brand Extensions (2009 To 2023). Journal of Namibian Studies: History Politics Culture, 33, 3412-3435.
6. Cobo, M. J., López-Herrera, A. G., Liu, X., & Herrera, F. (2011). Science mapping software tools: Review, analysis, and cooperative study among tools. Journal of the Association for Information Science and Technology, 62(7), 1382–1402. https://doi.org/10.1002/asi.21525
7. Chawla, S. K., Ellis, J., Saluja, A. S., & Smith, M. F. (1999). Global perceptions of online advertising. Journal of Professional Services Marketing, 19(1), 91–98. https://doi.org/10.1300/j090v19n01_07
8. Calder, B. J., Malthouse, E. C., & Schaedel, U. (2009b). An Experimental Study of the Relationship between Online Engagement and Advertising Effectiveness. Journal of Interactive Marketing, 23(4), 321–331. https://doi.org/10.1016/j.intmar.2009.07.002
9. Cheung, V. S. Y., Lo, J. C. Y., Chiu, D. K., & Ho, K. K. (2022). Evaluating social media's communication effectiveness on travel product promotion: Facebook for college students in Hong Kong. Information Discovery and Delivery, 51(1), 66–73. https://doi.org/10.1108/idd-10-2021-0117
10. Donthu, N., Kumar, S., Mukherjee, D., Pandey, N., & Lim, W. M. (2021). How to conduct a bibliometric analysis: An overview and guidelines. Journal of Business Research, 133, 285–296. https://doi.org/10.1016/j.jbusres.2021.04.070
11. Dunakhe, K., & Panse, C. (2021). Impact of digital marketing – a bibliometric review. International Journal of Innovation Science, 14(3/4), 506–518. https://doi.org/10.1108/ijis-11-2020-0263

12. Ertemel, A. V., &Ammoura, A. (2016). The role of social media advertising in consumer buying behavior. International Journal of Commerce and Finance, 2(1), 81-89.
13. Faruk, M., Rahman, M., & Hasan, S. (2021). How digital marketing evolved over time: A bibliometric analysis on Scopus database. Heliyon, 7(12), e08603. https://doi.org/10.1016/j.heliyon.2021.e08603
14. Ghorbani, Z., Kargaran, S., Saberi, A., Haghighinasab, M., Jamali, S. M., & Ebrahim, N. A. (2021b). Trends and patterns in digital marketing research: bibliometric analysis. Journal of Marketing Analytics, 10(2), 158–172. https://doi.org/10.1057/s41270-021-00116-9
15. Hansson, L., Wrangmo, A., &Søilen, K. S. (2013). Optimal ways for companies to use Facebook as a marketing channel. Journal of Information, Communication and Ethics in Society, 11(2), 112–126. https://doi.org/10.1108/jices-12-2012-0024
16. Jones, S. G., Millermaier, S., Goya-Martinez, M., & Schuler, J. J. (2008). Whose space is MySpace? A content analysis of MySpace profiles. First Monday. https://doi.org/10.5210/fm.v13i9.2202
17. Koseoglu, M. A., Rahimi, R., Okumus, F., & Liu, J. (2016). Bibliometric studies in tourism. Annals of Tourism Research, 61, 180–198. https://doi.org/10.1016/j.annals.2016.10.006
18. Kirby, A. (2023). Exploratory Bibliometrics: using VOSViewer as a preliminary research tool. Publications, 11(1), 10. https://doi.org/10.3390/publications11010010
19. Krishen, A. S., Dwivedi, Y. K., Bindu, N., & Kumar, K. S. (2021b). A broad overview of interactive digital marketing: A bibliometric network analysis. Journal of Business Research, 131, 183–195. https://doi.org/10.1016/j.jbusres.2021.03.061
20. Kevin, W. U. A., Zainab, A., & Anuar, N. B. (2009). Bibliometric studies on single journals: a review. Malaysian Journal of Library & Information Science, 14(1), 17–55. http://eprints.rclis.org/18232/1/Bibliometric%20studies%20on%20a%20single%20journals%20a%20review.pdf
21. McInnis, S. M., Sobolewski, J. S., Dass, M., Gehtland, L. M., & Bailey, D. B. (2022). Using Facebook, Instagram, and Pinterest advertising campaigns to increase enrollment in newborn screening research. Frontiers in Communication, 7. https://doi.org/10.3389/fcomm.2022.1052355
22. Nadkarni, A., & Hofmann, S. (2012). Why do people use Facebook? Personality and Individual Differences, 52(3), 243–249. https://doi.org/10.1016/j.paid.2011.11.007
23. Pack, T. (1996). Radio-activity on the Web. Database (Weston), 19(6), 38-44.
24. Rusydiana, A. S. (2021). Bibliometric analysis of journals, authors, and topics related to COVID-19 and Islamic finance listed in the Dimensions database by Biblioshiny. Science Editing, 8(1), 72–78. https://doi.org/10.6087/kcse.232
25. Singh, K., Kumar, A., &Siwach, A. K. (2023). Bibliometric Analysis of Allelopathy Journal. Allelopathy Journal, 60(1).
26. Subramanyam, K. (1983). Bibliometric studies of research collaboration: A review. Journal of Information Science, 6(1), 33–38. https://doi.org/10.1177/016555158300600105
27. Sheehan, K. B., & Hoy, M. G. (1999). Flaming, complaining, abstaining: How online users respond to privacy concerns. Journal of Advertising, 28(3), 37–51. https://doi.org/10.1080/00913367.1999.10673588
28. Thanuskodi, S. (2010). Journal of Social Sciences: A Bibliometric Study. Journal of Social Sciences, 24(2), 77–80. https://doi.org/10.1080/09718923.2010.11892847
29. Viswanath, B., Mislove, A., Cha, M., & Gummadi, K. P. (2009, August). On the evolution of user interaction in Facebook. In Proceedings of the 2nd ACM workshop on Online social networks (pp. 37-42).
30. Van Eck, N. J., & Waltman, L. (2014). Visualizing bibliometric networks. In Springer eBooks (pp. 285–320). https://doi.org/10.1007/978-3-319-10377-8_13
31. Varian, H. R. (2007). Position auctions. International Journal of Industrial Organization, 25(6), 1163–1178. https://doi.org/10.1016/j.ijindorg.2006.10.002
32. Wilson, R. E., Gosling, S. D., & Graham, L. T. (2012). A review of Facebook research in the social sciences. Perspectives on Psychological Science, 7(3), 203–220. https://doi.org/10.1177/1745691612442904
33. Ye, G., Hudders, L., De Jans, S., & De Veirman, M. (2021). The Value of Influencer Marketing for Business: A bibliometric analysis and managerial implications. Journal of Advertising, 50(2), 160–178. https://doi.org/10.1080/00913367.2020.1857888

Table 1: Search String Used for the Study

ELEMENT	DESCRIPTION
TITLE-ABS-KEY ("social media advertising")	Search for the phrase in the title, abstract, or keywords.
(LIMIT-TO (SUBJAREA, "BUSI") OR LIMIT-TO (SUBJAREA, "SOCI") OR LIMIT-TO (SUBJAREA, "PSYC") OR LIMIT-TO (SUBJAREA, "ARTS") OR LIMIT-TO (SUBJAREA, "MULT"))	Restrict to specific subject areas: Business, Sociology, Psychology, Arts, and Multidisciplinary.
(LIMIT-TO (DOCTYPE, "ar"))	Limit the search to articles.
(LIMIT-TO (SRCTYPE, "j"))	Restrict results to journal articles.
(LIMIT-TO (LANGUAGE, "English"))	Narrow the search to papers in English.
(LIMIT-TO (Yr>2014 to <2023))	Limit the years from 2014 to 2023

Table 2:Trends in Publication

YEAR	ARTICLES	YEAR	ARTICLES
2014	79	2019	164
2015	82	2020	161
2016	84	2021	179
2017	92	2022	198
2018	116	2023	117

Table 3: Most Productive Countries in the Domain

RANK	COUNTRY	DOCUMENTS	CITATIONS	CONTINENT	DEVELOPING/ DEVELOPED
1	UNITED STATES	90	1740	NORTH AMERICA	DEVELOPED
2	INDIA	28	303	ASIA	DEVELOPING
3	CHINA	20	147	ASIA	DEVELOPING
4	AUSTRALIA	16	212	OCEANIA	DEVELOPED
5	SOUTH KOREA	16	769	ASIA	DEVELOPED
6	UNITED KINGDOM	16	254	EUROPE	DEVELOPED
7	MALAYSIA	14	144	ASIA	DEVELOPED
8	NETHERLANDS	11	571	EUROPE	DEVELOPED
9	CANADA	9	63	NORTH AMERICA	DEVELOPED
10	GERMANY	9	116	EUROPE	DEVELOPED

Table 4: Country Collaboration Analysis

FROM	TO	FREQUENCY
USA	KOREA	8
USA	CHINA	7
GERMANY	NETHERLANDS	3
KOREA	NEW ZEALAND	3
USA	AUSTRALIA	3
USA	GERMANY	3
USA	NEW ZEALAND	3
USA	UNITED KINGDOM	3
AUSTRALIA	CANADA	2
AUSTRALIA	GHANA	2

Table 5:Corresponding Author's Countries

RANK	COUNTRY	ARTICLES	SCP	MCP
1	USA	57	47	10
2	CHINA	21	10	11
3	INDIA	16	16	0
4	KOREA	11	5	6
5	AUSTRALIA	9	6	3
6	MALAYSIA	7	5	2
7	UNITED KINGDOM	6	3	3
8	GERMANY	5	3	2
9	HONG KONG	5	4	1

Table 6: The Most Productive Authors in SMA Analysis

RANK	AUTHOR	DOCUMENTS	CITATIONS
1	RANA M, ARORA N.	3	15
2	ARORA T, AGARWAL B.	2	50
3	BOATENG H, OKOE A.F.	2	120
4	NATARAJAN T, BALAKRISHNAN J, BALASUBRAMANIAN S.A, MANICKAVASAGAM J.	2	26
5	ADAMOPOULOS P, GHOSE A, TODRI V.	1	92
6	ADETUNJI R.R, RASHID S.M, ISHAK M.S.	1	18
7	"AHMAD A.H, IDRIS I, MASON C, CHOW S.K."	1	14
8	ALALWAN A.A.	1	278
9	ALI Y., SHAH Z.A., KHAN A.U.	1	13
10	ARORA T., AGARWAL B., KUMAR A.	1	26

Table 7: Top Authors According to Citations Per Publication

RANK	AUTHOR	DOCUMENTS	CITATIONS
1	"LEE D., HOSANAGAR K., NAIR H.S."	1	399
2	"VOORVELD H.A.M., VAN NOORT G., MUNTINGA D.G., BRONNER F."	1	321
3	LEE J., HONG I.B.	1	302
4	ALALWAN A.A.	1	278
5	ZHU Y.-Q., CHEN H.-G.	1	206
6	HWANG K., ZHANG Q.	1	195
7	DUFFETT R.G.	1	177
8	JUNG A.-R.	1	134
9	BOATENG H., OKOE A.F.	2	120
10	ZHANG J., MAO E.	1	116

Table 8:Co-Citations Analysis of Top 10 Authors

RANK	AUTHOR	CITATIONS	TOTAL LINK STRENGTH
1	HAIR J.F.	279	7736
2	LAW R.	252	4173
3	SARSTEDT M.	230	6622
4	RINGLE C.M.	222	6523
5	WANG Y.	196	3984
6	AJZEN I.	192	4929
7	FORNELL C.	187	4984
8	LEE J.	186	4408
9	KOTLER P.	185	2601
10	LI H.	170	3738

Table 9: Most Cited Publications

RANK	AUTHORS	YEAR	TITLE	SOURCE	CITED BY
1	LEE D.; HOSANAGAR K.; NAIR H.S. (2018)	2018	ADVERTISING CONTENT AND SOCIAL MEDIA: EVIDENCE FROM FACEBOOK	MANAGEMENT OF SCIENCE	399
2	VOORVELD H.A.M.; VAN NOORT G.; MUNTINGA D.G.; BRONNER F. (2018)	2018	ENGAGEMENT WITH SOCIAL MEDIA AND SOCIAL MEDIA ADVERTISING: THE DIFFERENTIATING ROLE OF PLATFORM TYPE	JOURNAL OF ADVERTISING	321
3	LEE J.; HONG I.B. (2016)	2016	PREDICTING POSITIVE USER RESPONSE TO SOCIAL MEDIA ADVERTISING: THE ROLE OF EMOTIONAL APPEAL INFORMATIVENESS, AND CREATIVITY	INTERNATIONAL JOURNAL OF INFORMATION MANAGEMENT	302
4	ALALWAN A.A. (2018)	2018	INVESTIGATING THE IMPACT OF SOCIAL MEDIA ADVERTISING FEATURES ON CUSTOMER PURCHASE INTENTION	INTERNATIONAL JOURNAL OF INFORMATION MANAGEMENT	278
5	ZHU Y.-Q.; CHEN H.-G. (2015)	2015	SOCIAL MEDIA AND HUMAN NEED SATISFACTION: IMPLICATIONS FOR SOCIAL MEDIA MARKETING	BUSINESS HORIZONS	206

Table 10:Leading Journals in Domain

RANK	SOURCE	DOCUMENTS	CITATIONS	AVERAGE CITATION PER PUBLICATION
1	JOURNAL OF RESEARCH IN INTERACTIVE MARKETING	16	461	28.8125
2	INTERNATIONAL JOURNAL OF INTERNET MARKETING AND ADVERTISING	9	28	3.111111

3	JOURNAL OF INTERACTIVE ADVERTISING	8	81	10.125
4	COMPUTERS IN HUMAN BEHAVIOR	6	531	88.5
5	FRONTIERS IN PSYCHOLOGY	6	30	5
6	INTERNATIONAL JOURNAL OF ADVERTISING	6	149	24.83333
7	INTERNET RESEARCH	6	353	58.83333
8	JOURNAL OF BUSINESS RESEARCH	6	81	13.5
9	JOURNAL OF RETAILING AND CONSUMER SERVICES	6	52	8.666667
10	JOURNAL OF DIGITAL AND SOCIAL MEDIA MARKETING	5	5	1

Table 11:Annual Production of Leading Journals

Year	JOURNAL OF RESEARCH IN INTERACTIVE MARKETING	INTERNATIONAL JOURNAL OF INTERNET MARKETING AND ADVERTISING	JOURNAL OF INTERACTIVE ADVERTISING	COMPUTERS IN HUMAN BEHAVIOR	FRONTIERS IN PSYCHOLOGY
2014	0	1	0	0	0
2015	1	1	0	0	0
2016	2	1	0	1	1
2017	3	1	0	2	2
2018	4	1	0	3	2
2019	6	1	1	4	2
2020	8	1	2	4	2
2021	11	5	4	5	3
2022	14	9	7	6	5
2023	16	9	8	6	6

Table 12: The Most Productive Institutions

RANK	ORGANIZATION	DOCUMENTS	CITATIONS
1	DEPARTMENT OF MARKETING, CAPE PENINSULA UNIVERSITY OF TECHNOLOGY, CAPE TOWN, SOUTH AFRICA	2	177
2	DEPARTMENT OF MARKETING, UNIVERSITY OF PROFESSIONAL STUDIES, ACCRA, GHANA	2	173
3	"DEPARTMENT OF RETAIL, HOSPITALITY AND TOURISM MANAGEMENT, UNIVERSITY OF TENNESSEE, KNOXVILLE, TN, UNITED STATES"	2	59
4	LOYOLA UNIVERSITY CHICAGO, CHICAGO, IL, UNITED STATES	2	54
5	"AL-BALQA APPLIED UNIVERSITY, AMMAN COLLEGE OF BANKING AND FINANCIAL SCIENCES, AMMAN, SALT, 19117, JORDAN"	1	278

Table 13: Co-Occurrence Frequency of Keywords

RANK	KEYWORD	OCCURRENCES
1	SOCIAL MEDIA	88
2	SOCIAL MEDIA ADVERTISING	72

3	ADVERTISING	46
4	MARKETING	25
5	PURCHASE INTENTION	24
6	HUMAN	20
7	FACEBOOK	19
8	SOCIAL NETWORKING (ONLINE)	18
9	SOCIAL MEDIA MARKETING	16
10	ARTICLE	14

Figure 1: Main Information About Dataset Used in Study

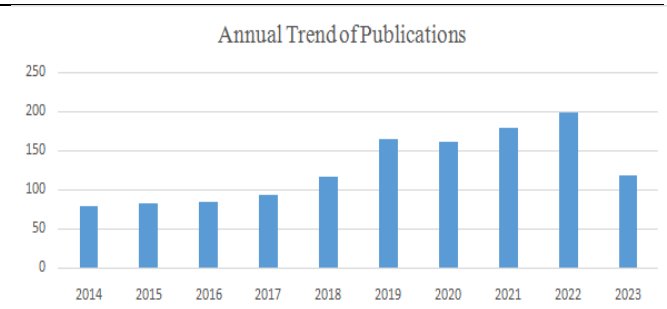

Figure 2: Annual Trend of Publications

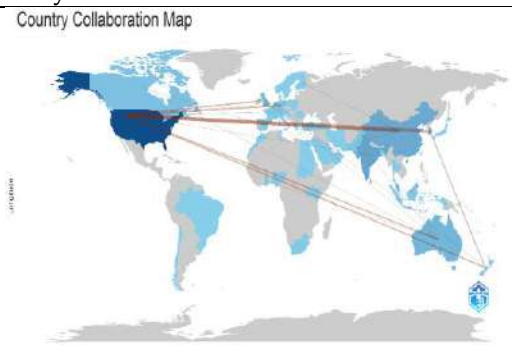

Figure 3:Country Collaboration Map

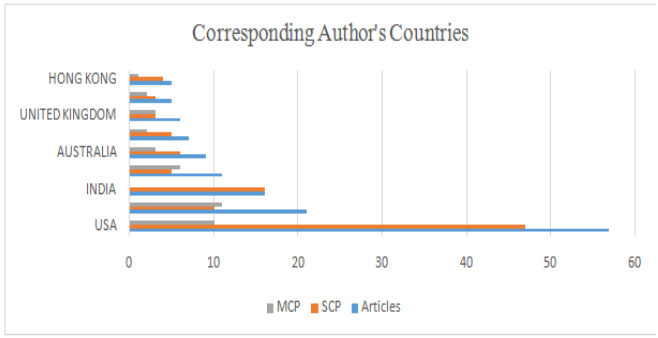

Figure 4:Corresponding Author's Countries

Figure 5: Most Prolific Sources

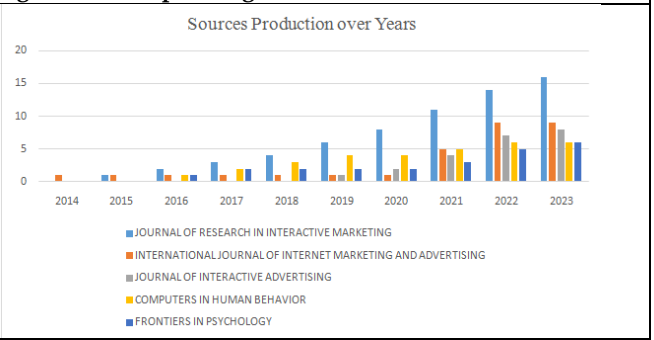

Figure 6:Sources' Production over Time

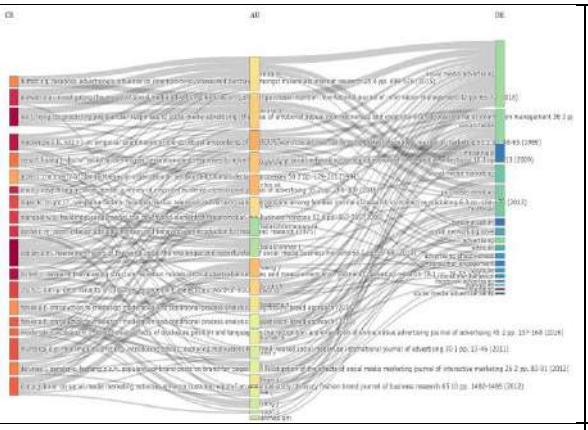

Figure 7: Three Field Plot

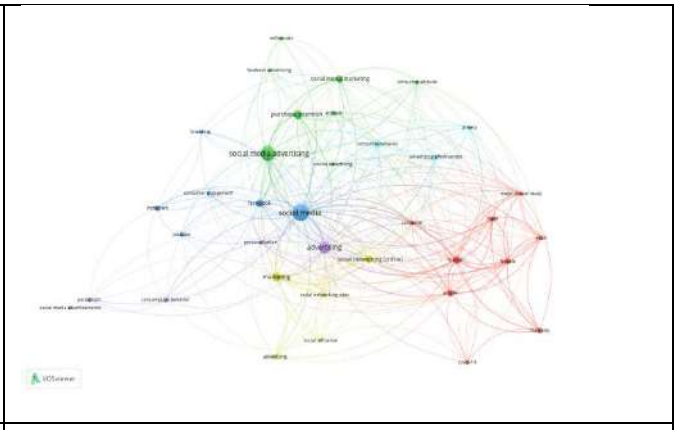

Figure 8:Co-Occurrence Frequency of Keywords

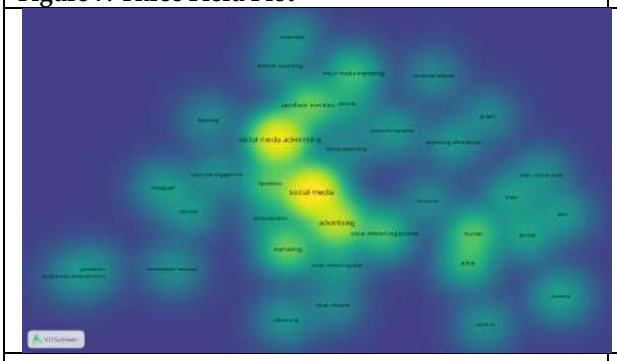

Figure 9:Density of Keywords Occurrence of Social Media Advertising Analysis Literature

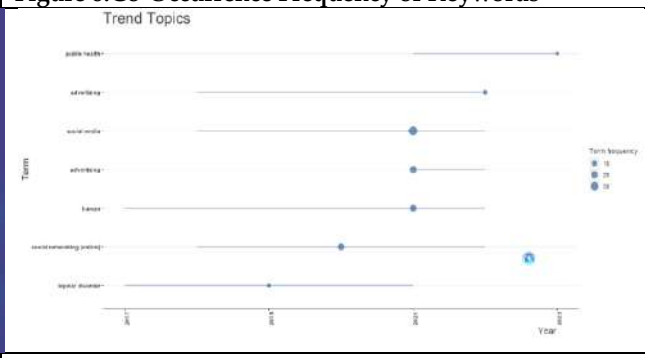

Figure 10:Trends Topics in Domain

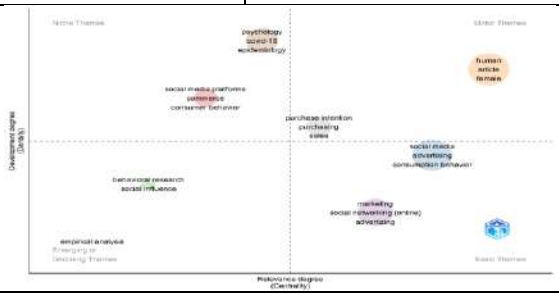

Figure 11:Thematic Map of the Domain Area

RESEARCH ARTICLE

A Study of Prevalence of Occupational Stress among Doctors and its Impact on Job Performance

M.Nisa[1], M.Saranyadevi[2], M.S.Kamalaveni[3] and K.Vaitheeswari Menaga[4]

[1]Assistant Professor, Bharathiar University PG Extension and Research Centre, Erode, Tamil Nadu, India.
[2]Research Scholar, Bharathiar University PG Extension and Research Centre, Erode Tamil Nadu, India.
[3]Associate Professor, Department of Management Studies, Sona College of Technology (Affiliated to Anna University, Chennai) Salem, Tamil Nadu, India.
[4]Ist MBA, Sona College of Technology,(Affiliated to Anna University, Chennai) Salem, Tamil Nadu, India.

Received: 31 Jan 2023 Revised: 09 Jan 2024 Accepted: 17 Mar 2024

***Address for Correspondence**
M.Nisa
Assistant Professor,
Bharathiar University
PG Extension and Research Centre,
Erode, Tamil Nadu, India.

ABSTRACT

Doctors plays a vital role in the Country especially house officers. They are under a great deal with stress variety of occupational stressors. Occupational stressors which may include to organizational inefficiency, high staff turnover, absenteeism due to sickness, decreased quality of practice, increased costs of health care and decreased job satisfaction. The most of the organizational outcomes they are affected by occupational stress and its job performance. The purpose of study was to investigate the effect of job stress on job performance Government doctors in Salem District, Tamil Nadu The universal study on Government doctors in Salem District. The targeted respondents which were present at that time were used in the 520. The data obtained through descriptive statistics, Spearman's Correlation and Multi Regression. The analysis showed strong support for the hypothesis that there is an inverse relationship between job stress and job performance indicating that there is high job stress in the house officers, resulting in low job performance. Appropriate stress management should start from improved health and good interpersonal relationships. The study reveals that job performance is impeded by the stress at workplace. The prevention and management of workplace stress requires both individual and organizational level interventions, as it a net result of factors causing stress and the individual's adaptation to the stressors.

Keywords: Occupational stressors; workplace stress, job performance and workplace stress

INTRODUCTION

The current turbulent environment in the health care field requires doctors and 150 organizations to reexamine their practices. Medicine is an inherently stressful profession with long working hours, ethical dilemmas, difficult patients and conflicting demands. Professionally, in true sense, the doctors are on 24-hour duty. Many physicians and surgeons work long, irregular hours; over one-third of full-time physicians worked 60 or more hours a week in 2023. The physical and; psychological demands of the profession often make physicians more vulnerable to high levels of stress. The effects of stress job practice are evidenced as increased errors in prescribing, limited team working, more patients' complaints and sickness absence. Stress has been defined in different ways over the years. Originally, it was conceived as pressure from the environment, then as strain within the person. The generally accepted definition today is one of the interactions between the situation and the individual. It is the psychological and physical are not sufficient to cope with demands and pressures of the situation. Thus, stress is more likely in some situations than others and in some individuals than others. Stress is not always negative or harmful and indeed, the absence of stress is death.

Stress is the non-specific response of the body to any demand; health sector is one of the most stressful professions and pointed out the necessity of considering and investigating occupational stress, since performance declines under stressful situations. Therefore, stress at workplace becomes a concern to organization administrators. Several authors attributed the lack of progress in the areas of stress research 151 organizations to the fact that stress seemed to be related to such a large number of conditions which prevented a systematic focus. Beehr used a very general definition in which "anything about an organizational role that produces adverse consequences for the individual" was called role stress. They proceeded to the conclusion that a conditions termed role overload was viable and this correlated positively with job stress. Stress indicators to role ambiguity in the study indicated low motivation to work. This study was based on a sample of 651 persons, including 213 from service departments of a hospital. The primary source of source cited by respondents indicated juggling multiple roles, having young children, time issues (too much work, too little time changing practices patterns. Job performance is the result of three factors working together: skill, effort and the nature of work conditions. Skills include knowledge, abilities and competencies the employee brings to the job, effort is the degree of motivation the employee puts forth toward getting the job done; and the nature of work conditions is the degree of accommodation of these conditions in facilitating the employee's productivity.

CONCEPTUAL MODEL

A conceptual framework speaks to the researcher's union of writing on the most proficient method to clarify a marvel. It maps out the activities required over the span of the investigation given his past learning of other researchers' perspective and his perceptions regarding the matter of research. At the end of the day, the conceptual framework is the researcher comprehends of how the specific factors in his examination associate with each other. In this manner, it recognizes the factors required in the examination. It is the researcher's "guide" in seeking after the examination.

SCALES USED

All items are measured on 5 –point Likert scale (5-strongly agree to 1 strongly disagree).Few items are measured on 6 point and 4 point scale.

PILOT TESTA

The pilot study was conducted among 520 members of Government doctors in Salem District i.e. 10 per cent of the total sample to check the feasibility and reliability of the research schedule. In the light of the experience gained in the pilot study the research schedule has been modified to suit the sample groups and finalized to conduct the survey. In the light of the experience gained in the pilot study the research schedule has been modified to suit the sample groups and finalized to conduct the survey. The perception of the respondents has been tested for its

reliability using Cronbach's Alpha. The value obtained was 0.921, which shows that instrument is highly reliable. The distribution curve is normal. Based on the pilot study necessary modifications were made in the interview schedule. The researcher sought adequate guidance through the research supervisor.

SAMPLING DESIGN

According to *Politand Hungler (1999),* "Sampling refers to the process of selecting a portion of the population to represent the entire population". The representative sample consists of subsets of the elements of a population which allows for the study results to be generalized. The characteristics of the sample population are intended to be representative of the target population. This study incorporates stratified random sampling, as the population of Government doctors in Salem District were taken up for the study. The entire population of Government doctors in Salem District was classified into four strata and from each stratum samples were drawn through simple random sampling method.

POPULATION AND THE STUDY AREA

The sample population taken from the Government doctors in Salem District with regards to Government doctors and the study area is occupational stress among the Government doctors and how the stress is affecting the individual doctor serving in different categories and their reaction towards the stress that they undergone during their services. This study area incorporates in Salem District and focuses on doctor's occupational stress and its impact on the job performance and job satisfaction.

SAMPLING TECHNIQUES

Stratified random sampling techniques are deployed in this study. The entire geographic area of Salem District has been divided into four parts or strata or group of police stations. From each strata or group or part samples were drawn on simple random and totally 520 Government doctors were selected through the stratified random sampling as equal proportion of samples were selected from each strata.

SAMPLE SIZE

This study is carried out with the sample size of 520 across the various categories of Government doctors.

DATA COLLECTION

Data collection was carried out with the help of questionnaire from the employees of Government doctors primary data collection was carried out with the help of questionnaires Government doctors. The field survey technique was employed to collect the pertinent data from 520 Government doctors in the study area. Interview schedule was the main tool for collecting the primary data. Much effort was taken to prepare the interview schedule in a systematic way by designing adequate and relevant questions to ensure better achievement of the research objective. The interaction technique is applied to collect certain relevant data in order to facilitate the study. The Primary data was supplemented by spate of secondary data. The secondary data pertaining to the study was gathered from the various sources pertaining to Government doctors their stress experienced by doctors. Further, the secondary data were collected from leading journals and a number of standard reference books were referred to obtain pertinent literature on occupational stress of Government doctors.

DATA ANALYSIS FRAMEWORK

After analyzing the various data collection methods and research instruments, a questionnaire having questions with multiple-choice responses and a 5 point 'Likert-type scale' with -2 being Strongly Disagree and2 being Strongly Agree, was selected as the survey instrument. The present study is descriptive cum exploratory in nature. The study is descriptive as it describes the occupational stress of Government doctors in Salem District. After analyzing the various data collection methods and research instruments, an questionnaire having questions with multiple-choice responses and a 5 point 'Likert-type scale' with 1 being strongly disagree and 5 being Strongly Agree, was selected as the survey instrument. Data entry, processing and analysis were done using SPSS for Windows (Version 22.0)

spreadsheet program and Microsoft Excel 2007. Descriptive statistics (frequencies, scores, mean, maximum, minimum) were determined. The actual processing and analysis started with data cleaning to remove the gaps and ensure consistency. In order to test the association between independent variables and dependent variables, chi-square test was applied; Correlation, Factor Analysis, ANOVA,'t' test model was applied to find out the variation within samples and between samples. The present study is descriptive cum exploratory in nature. The study is descriptive as it describes the occupational stress of Government doctors in Salem District. It also seeks to explore and measure the level of stress the Government doctors.

SAMPLING FRAME

The sample was designed in a two phases. In the first phase the Government doctors in Salem District was selected. In second phase the respondents were selected from Government doctors in Salem District. The list of the police stations covered in the district, which served as the sampling frame for the purpose of the study. This provided the complete list and various Government doctors serving at Government doctors were taken into consideration from the same. The above table mentioned table 1 shows the frequency distribution of based on the socio economic characteristics of the Government doctors in Salem District. The highest Majority of the respondents are male (79.4%) of the Government doctors. 20.8% percent of respondents fall in the age group of 31-35 years, 41.2% of the respondents educational qualification is professional, In respect of the marital status majority of the respondents are married persons (25%), based on the Number of dependents of the respondents the 5 to 6 category is 40%, 36.3% of the respondents are living in rural area. Majority of the respondents designation is head constable 26.9%, Based on the Monthly Income of the respondents the 31,000-60,000 32.9% of Government doctors, In respect of the Number of years of experience as the Government doctors 33.3%, percent respondents falls under the category of 3-5 years as experience in police department. Based on the transferred of the respondents 1-5 times 31.7% of Government doctors 33.5% percentage of Government doctors undergone training programs in 6-10 times. From the above table, the highest mean value meant for Lack of training on new equipment is the most important factor as considered by the Government doctors that led to severe occupational stress followed by Finding time to stay in good physical condition is next important factor that led to occupational stress amongst the Government doctors in Salem District. The Government doctors perception that Risk of being injured on the job was the next important factor that led to occupational stress followed by Fatigue (shift work and over time etc.,) and Staff shortages were considered as the occupational stress of the Government doctors in Salem District.

The other factors responsible the occupational stress were Shift duty work, Working alone at night, Over time demands, Risk of being injured on the job, Work related activities on days off (e.g. law and order , community events), Traumatic events (e.g. MVA ,domestic , death , injury), Managing social life outside of work, Not enough time available to spend with friends and family, Enormous paper work, Poor cope up with work, Dealing with co-workers, The feeling that different rules apply to different people (e.g. favoritism) Feeling like the police person always have to prove himself or herself to the organization, Excessive administrative duties, Constant changes in policy / legislation, Bureaucratic red tape, Too much computer work, Perceived pressure to volunteer free time, Limitations to social life and the Negative comments from the public were responsible for occupational stress of the Government doctors in Salem District There is significant relationship between the mean score of age of the Government doctors and associated risk factor of occupational stress of Government doctors. Shift duty work Managing social life outside of work , Poor cope up with work , Feeling like you always have to prove yourself to the organization, Constant changes in policy / legislation, Staff shortages, Bureaucratic red tape, Lack of training on new equipment, Too much computer work, Limitations to your social life (eg. Who your friends are, where you socialize) and Fatigue (shift work and over time etc.,) were the factors causing occupational stress and significant at 1% level. Therefore it is concluded that there is significant relationship between the mean score of age of the Government doctors and associated risk factor of occupational stress of Government doctors. Work related activities on days off (e.g. law and order, community events), the feeling that different rules apply to different people and Perceived pressure to volunteer free time were significant at 5% level. The above table clearly indicated that the Shift duty work is the only factor considered by the Government doctors that cause occupational stress amongst they and it is significant at 1% level. Therefore we conclude that there is significant relationship between the mean score of

qualification of the Government doctors and shift duty was considered as the most important risk factor of occupational stress of Government doctors. It is evident that the as the Government doctors becomes more qualified they would manage their occupational stress very well. It is evident that the higher the qualification of the Government doctors the lower is the occupational stress amongst the Government doctors. From the above table, it is found out that all the variables related to the risk factor of occupational stress of Government doctors had significance value less than 0.05 at 1 Per cent significance, thus the null hypothesis is rejected. Thus, it is concluded that there is significant difference between mean ranks towards the risk factor of occupational stress of Government doctors. Out of the twenty four risk factor of occupational stress of doctors the "Lack of training on new equipment" has the highest mean rank (14.21). Therefore this risk factor associated with occupational stress of the Government doctors. High value of KMO (0.530> .05) of indicates that factor analysis is useful for the present data. The significant value for Bartlett's test of Sphericity is 0.000 and is less than 0.05 which indicates that there exists significant relationships among the variable. The result value of KMO test and Bartlett's test indicates that the present data is useful for factor analysis. From tree analysis model summary "Feeling like you always have to prove yourself to the organization. Finding time to stay in good physical condition is important independent variable.

From the Tree structured analysis, it is determined that out of the twenty four attributes of risk factor of occupational stress of Government doctor, the most influencing factor is identified as "Feeling like you always have to prove yourself to the organization. This may be due to the fact that, any Government doctor professional should possess some fundamental occupational stress strategies rendered to their employees. Therefore, to risk factor of occupational stress of Government doctor, the above said factor "Feeling like you always have to prove yourself to the organization. Finding time to stay in good physical condition is identified as the most important independent variable. Here the coefficient of Risk Factor is 0.107 represents the partial effect of Risk factor on Job Performance, holding the other variables as constant. The estimated positive sign implies that such effect is positive that Job performance would increase by 0.107 for every unit increase in risk factor and this coefficient value is significant at 1% level. The coefficient of organizational climate is 0.007 represents the partial effect of Organizational climate on Job Performance, holding the other variables as constant. The estimated negative sign implies that such effect is negative that Job Performance would decrease by 0.007 for every unit decrease in job performance and this coefficient value is no significant at 1% level. The coefficient of Occupational Stress is .263 represents the partial effect of occupational stress on Job Performance, holding the other variables as constant.

The estimated positive sign implies that such effect is positive that job performance would increase by .263 for every unit increase in Occupational Stress and this coefficient value is significant at 1% level. The coefficient of Stress level is 443 represents the partial effect of Stress level on job performance, holding the other variables as constant. The estimated positive sign implies that such effect is positive that job performance would increase by .443 for every unit increase in stress level and this coefficient value is significant at 1% level. The coefficient of risk factor is .038 represents the partial effect of risk factor on Prevention of the Stress, holding the other variables as constant. The estimated negative sign implies that such effect is negative that prevention of the stress would increase by .038 for every unit decrease in risk factor and this coefficient value is significant at 1% level. The coefficient of organizational climate is 0.009 represents the partial effect of organizational climate on prevention of the stress, holding the other variables as constant. The estimated negative sign implies that such effect is negative that prevention of the stress would decrease by 0.009 for every unit decrease in organizational climate and this coefficient value is significant at 1% level. The coefficient of Occupational stress is .169 represents the partial effect of occupational stress on prevention of the stress, holding the other variables as constant. The estimated positive sign implies that such effect is positive that prevention of the stress would increase by .169 for every unit increase in occupational stress and this coefficient value is significant at 1% level. The coefficient of stress level is 0.007 represents the partial effect of stress level on prevention of the stress, holding the other variables as constant. The estimated negative sign implies that such effect is negative that prevention of the stress would decrease by 0.007 for every unit decrease in stress level and this coefficient value is significant at 1% level. The coefficient of Job performance is 2.068 represents the partial effect of job performance on Job satisfaction, holding the other variables as constant. The estimated positive sign implies that such effect is positive that Job satisfaction would increase by 2.068 for every unit increase in job performance and

this coefficient value is significant at 1% level. The coefficient of Prevention of the stress is 3.701 represents the partial effect of prevention of the stress on Job satisfaction, holding the other variables as constant. The estimated positive sign implies that such effect is positive that Job satisfaction would increase by 3.701 for every unit increase in prevention of the stress and this coefficient value is significant at 1% level. Based on standard coefficient, Prevention of the stress (1.246) is most important variable of Job satisfaction followed by Job performance (0.987) and stress level (0.359). From the above table it is found that the calculated P value is 0.015 which is less than 0.05 which indicates perfectly fit. Here GFI (Goodness of Fit Index) value and AGFI **(**Adjusted Goodness of Fit Index) value is greater than 0.9 which represent it is a good fit. The calculated CFI **(**Comparative Fit Index) value is 0.996 which means that it is a perfectly fit and also it is found that RMR (Root Mean Square Residuals) is 0.155 and RMSEA **(**Root Mean Square Error of Approximation) value is 0.078 which is less than 0.08 Which indicated it is perfectly fit.

IMPACT OF STRESS ON DOCTORS

Several studies have shown that occupational stress can lead to various negative consequences for the individual and the workplace (Oginska-Bulik, 2006) in healthcare sector. Stress produces a range of undesirable, expensive, and debilitating consequences (Ross, 2005), which affect both individuals and hospitals. Early individual behavioral reactions may include onset or increased smoking and alcohol use. Individuals may tend to keep late nights in clinics/ offices without accompanying increased productivity. While others might become irritable, some will tend to intense seclusion and individualism. Many studies deal with the topic area sleep loss tiredness exhaustion work stress burnout. They mostly come to the same conclusion, that stress has a major influence in doctors working lives but also their personal lives. Stress and fatigue may result in increased insecurity in clinical decisions and may therefore negatively affect the ability to practice medicine adequately, responsibly, and without error. 50% of such incidents resulted in a loss in treatment standards; 7.4 % were expressed in serious treatment errors, although actual death had been avoided.

CONCLUSION

Overall, the study reveals that majority of Government Doctors agree significantly that they experienced occupational-stress. It also supports the assumption that health sector employees are among the highest groups subjected to work stress. Results also indicated that prevalence of occupational-stress was not influenced by gender, age and experience of the employee. The stress in turn affects the performance of the individual. Thus the policy makers must pay the attention towards the issue of occupational stress in hospitals through problem recognition and problem-solving activities to deal with the sources of stress so that effective and efficient performance of the doctors can be ensured.(The stress of the Government doctors measured by analyzing the dimensions considered for the. Study with the help of the hypothetical statements and statistical tools considered for the study. The study reveals that a part of the conceptualized research model was empirically proved. These findings are interpreted in the final chapter for future research and Government doctors)

REFERENCES

1. Akhona Nangamso Myendeki, "Job Stress, Burnout and Coping Strategies of South African Police Officers," April 2008, Department of Psychology, University of Fort Hare.
2. Anabela EstevesI; A. Rui GomesII, "Occupational stress and cognitive appraisal: a study with security forces" Print version ISSN 0104-1290,Saude soc. vol.22 no.3 São Paulo July/Sept. 2013.
3. André Marchand, Richard Boyer, Céline Nadeau, Mélissa Martin. "Predictors of Posttraumatic Stress Disorders in Police Officers Prospective Study," Bibliothèque et Archives nationals du Québec, 2013, ISBN: 978-2-89631-681-6 (PDF), ISSN: 0820-8395.

4. Anita Singh Rao, 2Dushyant Salvi," Stress Management among Police Officers in Rajasthan. "International Journal of Recent Research in Commerce Economics and Management (IJRRCEM), Vol. 3, Issue 3, pp: (100-103), Month: July - September 2016, ISSN 2349-7807.
5. Anum Khan, Research Scholar, Superior University Lahore,ak_mba88@yahoo.com Dr. Muhammad Ramzan, Director Libraries, Lahore University of Management Sciences, Lahore, mramzaninfo@gmail.com, Muhammad Saqib Butt, Research Scholar, Superior University Lahore,saqib_980@yahoo.com. "Is Job Satisfaction of Islamic Banks Operational Staff Determined through Organizational Climate, Occupational Stress, Age and Gender?" Journal of Business Studies Quarterly,2013, Volume 4, Number 3 ISSN 2152-1034.
6. Anurag Singh; A.K Mishra "A Study on Organizational Climate &Occupational Stress of Indian It Executives: Biographical Perspectives," International Journal of Multidisciplinary Research Vol.1 Issue 7, November 2011, ISSN 2231 5780.
7. Anurag Singh A.K. Mishra, "Impact of Organizational Climate in Experiencing Occupational Stress among Executives of Indian Information Technology Organisations" Vol. 2. No. 2 - 2011.
8. Augustine Ebiai, Department of Psychology, Covenant University, Ota E-mail: aebiai@yahoo.com, "Occupational stress and psycho-physiologic disorder in Nigeria", journal of research in national development volume 8 no 1, June, 2010.
9. Azman Ismail, Amy Yao, Nek Kamal Yeop Yunus, "Relationship Between Occupational Stress and Job Satisfaction: An Empirical Study in Malaysia." The Romanian Economic Journal, Year XII, no. 34 2009, PP- 1- 29.
10. Behdin Nowrouzi, "Quality of Work Life: Investigation of Occupational Stressors among Obstetric" 2013
11. Bolanle Ogungbamila and Ibukun Fajemirokun Adekunle Ajasin University, Nigeria," Job Stress and Police Burnout: Moderating Roles of Gender and Marital Status" IAFOR Journal of Psychology & the Behavioral Sciences Volume 2 – Issue 3 – winter 2016.
12. Bushara Bano and Rajiv Kumar Jha∗ "Organizational Role Stress Among Public and Private Sector Employees: A Comparative Study", The Lahore Journal of Business 1:1 (Summer 2012): pp. 23–36.
13. Bushara Bano, Research Scholar, Department of Business Administration, Aligarh Muslim University, Aligarh, syedabushara@gmail.com , "Job Stress among Police Personnel", PP 290 – 293, 2011 International Conference on Economics and Finance Research IPEDR vol.4 (2011) © (2011) IACSIT Press, Singapore
14. C. Mohanraj and M.R. Natesan, "Stress and job satisfaction: An empirical study among the women police constables in Coimbatore, Tamilnadu, India." ISSN: 2348 – 0343 International Journal of Interdisciplinary and Multidisciplinary Studies (IJIMS), 2015, Vol 2, No.5, 153-157
15. Caitlin Finney,1 Erene Stergiopoulos,1 Jennifer Hensel,1,2 Sarah Bonato,3 and Carolyn S Dewa corresponding author1,2, "Organizational stressors associated with job stress and burnout in correctional officers: a systematic review" Published online 2013 Jan 29. doi: 10.1186/1471-2458-13-82.

Table 1

Demography and Socio Economic	Variables	Frequency	Percent
Gender	Male	413	79.4
	Female	107	20.66
	Total	520	100.0
Age	21-26	103	19.8
	27-30	107	20.6
	31 –35	108	20.8
	35-40	103	19.8
	Above 45	99	19.0
	Total	520	100.0
Education Qualification	Up to HSC	52	10.0
	Diploma	91	17.5

	Graduation	83	16.0
	P.G	80	15.4
	Professional	214	41.2
	Total	520	100.0
Status Marital	Married	130	25.0
	Un Married	171	32.9
	Divorced	121	23.3
	Widow	71	13.7
	Total	520	100.0
Number of Dependents	Up to 2	60	11.5
	3 to 4	164	31.5
	5 to 6	208	40.0
	above 7	85	16.3
	Total	520	100
Place of residence	Urban	145	27.9
	Rural	189	36.3
	Semi urban	186	35.8
	Total	520	100.0
Designation	Medical officer	87	16.7
	Senior Medical Officer	140	26.9
	Chief Medical Officer	133	25.6
	General Duty Medical officer	91	17.5
	Inspector Medical Officer	69	13.3
	Total	520	100.0
Income	Up to 30,000	110	21.2
	31,000-60,000	171	32.9
	61,000- 90,000	144	27.7
	Above 91,000	95	18.3
	Total	520	100.0
Work experience	Below 2 year	116	22.3
	3-5 year	173	33.3
	6-15 year	138	26.5
	16-30 year	93	17.9
	Total	520	100.0
	No	134	25.8
	1- 5	165	31.7
	6 – 15	122	23.5
	Above 15	99	19.0
	Total	520	100.0
	1- 5	96	18.5
	6 – 10	174	33.5

	11 – 25	162	31.2
	Above 25	88	16.9
	Total	520	100.0

Table -2 Mean and standard deviation for risk factor of occupational stress of Government doctors

Risk factor of occupational stress of Government doctors	Mean	Std. Deviation
Shift duty work	3.42	1.210
Working alone at night	3.43	1.328
Over time demands	3.49	1.277
Risk of being injured on the job	3.64	1.284
Work related activities on days off	3.18	1.314
Traumatic events	3.43	1.290
Managing social life outside of work	3.24	1.236
Not enough time available to spend with friends and family	3.37	1.325
Enormous paper work	3.49	1.339
Poor cope up with work	3.49	1.304
Dealing with co-workers	3.54	1.322
The feeling that different rules apply to different people	3.47	1.333
Feeling like you always have to prove yourself to the organization.	3.53	1.289
Excessive administrative duties	3.57	1.324
Constant changes in policy / legislation	3.36	1.287
Staff shortages	3.62	1.291
Bureaucratic red tape	3.59	1.328
Too much computer work	3.55	1.306
Lack of training on new equipment	3.79	1.362
Perceived pressure to volunteer free time	3.56	1.283
Finding time to stay in good physical condition	3.66	1.302
Limitations to your social life	3.46	1.286
shift work and over time etc.,	3.64	1.232
Negative comments from the public	3.54	1.278

Source: Primary Data Generated from the Government doctors

Table-3 ANOVA test for age of the Government doctors and associated risk factor of occupational stress of Government doctors

Risk factor of occupational stress of Government doctors	F-Value	Sig. Value
Shift duty work	32.225	.000**
Working alone at night	.134	.970
Over time demands	2.802	.025
Risk of being injured on the job	2.827	.024
Work related activities on days off	3.375	.010*
Traumatic events (e.g. MVA ,domestic , death , injury)	2.510	.041
Managing social life outside of work	12.957	.000**
Not enough time available to spend with friends and family	2.836	.024
Enormous paper work	2.174	.071

Poor cope up with work	3.805	.005**
Dealing with co-workers	1.188	.315
The feeling that different rules apply to different people	3.149	.014*
Feeling like you always have to prove yourself to the organisation.	9.377	.000**
Excessive administrative duties	2.446	.046
Constant changes in policy / legislation	3.838	.004**
Staff shortages	3.671	.001**
Bureaucratic red tape	3.770	.005**
Too much computer work	10.274	.000**
Lack of training on new equipment	32.051	.000**
Perceived pressure to volunteer free time	2.840	.024*
Finding time to stay in good physical condition	2.308	.057
Limitations to your social life	4.158	.003**
Fatigue (shift work and over time etc.,)	7.486	.000**
Negative comments from the public	1.678	.154

Source: Primary Data Generated from the employees of Police department Note : * Denote at 5% level - **Denote at 1% level

Table -4 ANOVA test for qualification of the doctors risk factors of occupational stress of Government doctors

Risk factors of occupational stress of Government doctors	F-Value	Sig.Value
Shift duty work	9.432	.000**
Working alone at night	1.819	.124
Over time demands	.601	.662
Risk of being injured on the job	.470	.758
Work related activities on days off	.218	.929
Traumatic events (e.g. MVA ,domestic , death , injury)	.518	.722
Managing social life outside of work	.552	.698
Not enough time available to spend with friends and family	1.096	.358
Enormous paper work	1.067	.372
Poor cope up with work	3.079	.016
Dealing with co-workers	2.984	.019
The feeling that different rules apply to different people	1.830	.122
Feeling like you always have to prove yourself to the organization.	1.003	.406
Excessive administrative duties	1.592	.175
Constant changes in policy / legislation	.620	.649
Staff shortages	1.250	.289
Bureaucratic red tape	2.088	.081
Too much computer work	2.775	.027
Lack of training on new equipment	.477	.753
Perceived pressure to volunteer free time	.644	.631

Finding time to stay in good physical condition	3.366	.010
Limitations to your social life	.523	.719
Fatigue	.400	.808
Negative comments from the public	2.420	.048

Source: Primary Data Generated from the employees of Police department Note: * Denote at 5% level - **Denote at 1% level

Table -5 Friedman test for significant difference between mean ranks towards the risk factor of occupational stress of Government doctors

risk factor	Mean Rank	Chi Square	DF	Significant
Shift duty work	12.21	130.582	23	0.000**
Working alone at night	12.00			
Over time demands	12.47			
Risk of being injured on the job	13.23			
Work related activities on days off	10.84			
Traumatic events	12.10			
Managing social life outside of work	11.25			
Not enough time available to spend with friends	11.82			
Enormous paper work	12.56			
Poor cope up with work	12.46			
Dealing with co-workers	12.72			
The feeling that different rules apply	12.26			
Feeling like you always have to prove your self	12.62			
Excessive administrative duties	12.84			
Constant changes in policy / legislation	11.79			
Staff shortages	13.10			
Bureaucratic red tape	12.90			
Too much computer work	12.66			
Lack of training on new equipment	14.21			
Perceived pressure to volunteer free time	12.68			
Finding time to stay in good physical condition	13.32			
Limitations to your social life	12.11			
Fatigue (shift work and over time etc.,)	13.22			

Negative comments from the public	12.64			

Source: Primary Data Generated from the employees of Government doctors Note: * Denote at 5% level - **Denote at 1% level

Table -6 KMO and Bartlett's Test of risk factor of occupational stress of Government doctor

KMO and Bartlett's Test		
Kaiser-Meyer-Olkin Measure of Sampling Adequacy		.530
Bartlett's Test of Sphericity	Approx. Chi-Square	1613.290
	Degree of freedom	276
	Significance	.000**

Source: Primary Data Generated from the employees of occupational stress of doctors. Note: **Denote at 1% level

Table – 7 Model summary for risk factor of occupational stress of Government doctor

	Growing Method	**CHAID**
	Dependent Variable	**Overall Job satisfaction of the Government doctors**
Specifications	Independent Variables	Shift duty work, Working alone at night, Over time demands, Risk of being injured on the job, Work related activities on days off (e.g. law and order , community events), Traumatic events (e.g. MVA ,domestic , death , injury), Managing social life outside of work, Not enough time available to spend with friends and family, Enormous paper work, Poor cope up with work, Dealing with co- workers, The feeling that different rules apply to different people (e.g. favouritism), Feeling like you always have to prove yourself to the organisation., Excessive administrative duties, Constant changes in policy legislation, Staff shortages, Bureaucratic red tape, Too much computer work, Lack of training on new equipment, Perceived pressure to volunteer free time, Finding time to stay in good physical condition, Limitations to your social life (eg. Who your friends are, where you socialize), Fatigue (shift work and over time etc.,), Negative comments from the public
	Validation	None
Result	*Maximum Tree Depth*	*3*
	Minimum Cases in Parent Node	100
	Minimum Cases in Child Node	50

	Independent Variables Included	Feeling like you always have to prove yourself to the organisation., Finding time to stay in good physical condition
	Number of Nodes	7
	Number of Terminal Nodes	5
	Depth	2
	Number of Nodes	7

Source: Primary Data Generated from the employees of Government doctor

Table – 8 Risk model for risk factor of occupational stress of Government doctor

Estimate	Std. Error
.039	.005
Growing Method: CHAID Dependent Variable: Overall Job satisfaction of the Government doctors	

Source: Primary Data Generated from the employees of Government doctor

Table –9 Gain summary nodes for risk factor of occupational stress of Government doctor

Gain Summary for Nodes			
Node	**N**	**Percent**	**Mean**
4	178	34.2%	5.00
3	76	14.6%	4.00
2	136	26.2%	3.00
6	59	11.3%	1.92
5	71	13.7%	1.66
Growing Method: CHAID **Dependent Variable: Overall Job satisfaction of the Government doctors**			

Source: Primary Data Generated from the employees of Government doctor

Table –10 Number of variables in the SEM

Number of variables in your model	10
Number of observed variables	7
Number of unobserved variables	3
Number of exogenous variables	7
Number of endogenous variables	3

Source: Output generated from AMOS 20

Table – 11 Variables in the Structural Equation Model Analysis

	Unstandardize dcoefficient	S.E	Standardize d coefficient	t value	P value
Job Performance <--- Risk Factor	.107	.027	.138	3.924	<0.001**
Job Performance <--- Organizational Climate	-.007	.049	-.008	-.146	.884

Job Performance <--- Occupational Stress	.263	.056	.273	4.712	<0.001**
Job Performance <--- Stress Level	.443	.048	.359	9.296	<0.001**
Prevention Of The Stress <--- RiskFactor	-.038	.017	-.069	-2.240	.025*
Prevention Of The Stress <--- Organizational Climate	-.009	.018	-.014	-.521	.602
Prevention Of The Stress <--- Occupational Stress	.169	.035	.248	4.859	<0.001**
Prevention Of The Stress <--- Stress Level	-.007	.034	-.008	-.190	.849
Job Satisfaction <--- Job performance	2.068	.325	.987	6.353	<0.001**
Job Satisfaction <--- Prevention Of The Stress	3.701	1.077	1.246	3.435	<0.001**

Note: ** denotes significant at 1% level Source: Output generated from AMOS 20

Table – 12 Model fit summary of Structural Equation Model

Indices	Value	Suggested value
Chi-square value	8.342	-
P value	0.015	> 0.05 (Hair et al.,1998)
GFI	0.995	> 0.90 (Hu and Bentler,1999)
AGFI	0.937	> 0.90 (Hair et al., 2006)
CFI	0.996	> 0.90 (Daire et al., 2008)
RMR	0.155	>0.08 (Hair et al., 2006)
RMSEA	0.078	<0.08 (Hair et al., 2006)

Source: Output generated from AMOS 20

RESEARCH ARTICLE

Analyzing Business Crimes by Implementing OSINT Architecture

Yuthvek .M J[1], Adheena Shibu[1], Charithra Y[1] and K. Kalaiselvi[2*]

[1]Student, Department of Forensic Science, Kristujayanti College (Autonomous), (Affiliated to Bengaluru North University), Bangalore, Karnataka, India.
[2]Associate Professor, Department of Computer Science, Kristujayanti College (Autonomous), (Affiliated to Bengaluru North University) Bangalore, Karnataka, India.

Received: 30 Dec 2023 Revised: 09 Jan 2024 Accepted: 27 Mar 2024

***Address for Correspondence**
K. Kalaiselvi
Associate Professor,
Department of Computer Science,
Kristujayanti College (Autonomous),
(Affiliated to Bengaluru North University)
Bangalore, Karnataka, India.
Email: kalaiselvi@kristujayanti.com

ABSTRACT

Financial losses and damage to a company are caused by business crimes. In this study, we used open-source tools, which are freely available tools, to analyze those business crimes. We started to analyze three made-up cases using 10 different OSINT tools to gain a deeper understanding of the concept. Our study's made-up cases were based on business crimes such as money laundering, insider trading, and data breaches. We have examined the effectiveness of those tools. We have obtained permission from the Te2 technique company to use them as a model. OSINT tools are very useful for gathering publicly available data, but their results are not reliable according to our study's conclusion. Only 4 out of the 10 chosen tools were helpful for analyzing those cases. The data we get from those tools tends to have more errors, so we need to be careful when using them.

Keywords: Business Crimes, Open-Source Intelligence, Digital Forensics, White-collar Crimes, OSINT Tools.

INTRODUCTION

Complex financial offences that can be committed by individuals, companies, or employees are called white-collar crimes or business crimes. The majority of crimes committed in large corporations with extensive technology and global networks involve deceit, concealment of information, or breach of trust. Because of this, these crimes have become an important international issue. Fake deals, stealing, money laundering, theft of intellectual property,

insider trading, cybercrime, and other deceitful business practices are all part of business crime. These crimes can result in significant financial losses, damage a company's reputation, and cause legal consequences[1].Detecting and preventing these crimes is crucial to maintain fairness in the business world and financial markets. Business crimes often involve using technology incorrectly and taking advantage of digital systems. Cyber-attacking and hacking are common types of business crime. Criminals break into digital systems in these circumstances to steal important information or disrupt business activities[2].Corporate spying is a significant area where businesses secretly take action to advance their competitors, often by stealing ideas. The use of digital forensics is essential for detecting cases of individuals trading secrets, hiding illegal money, or cheating with money in businesses. It can be helpful in investigating when data is stolen, people's privacy is violated, or when online scams and tricks occur, which can have negative effects on businesses and individuals[3].Digital forensics experts deal with other types of business crimes, such as stealing ideas, being corrupt, offering bribes, not following rules, and breaking regulations. The focus of this research is to investigate the methods and tools utilized in digital forensics to understand and reduce the impact of various types of business crimes. In the realm of research and investigation, there exists a technique called open-source intelligence (OSINT), or OSINT for short. By gathering information from publicly available sources, this method can be used for a variety of purposes, including learning about businesses and apprehending individuals involved in illicit activities[4].The website of OSINT framework can be accessed via the link: https://osintframework.com/. The focus is on finding relevant information that pertains to the intelligence question and offering practical intelligence in support of an investigation. Our research encompasses a comprehensive examination of how OSINT tools work when it comes to analyzing business crimes. Our focus is on finding effective ways to use tools during investigations while utilizing open-source resources for thorough examination and analysis. In Fig 1, you can see the homepage of the OSINT framework website.

REVIEW OF LITERATURE

Cyber security can also be increased by the usage of OSINT in crimes like phishing detection, threat intelligence, hate speech detection, fake news detection, human trafficking, child trafficking, criminal profiling, etc. In this paper they have discussed the state of OSINT nowadays and its benefits, importance in cybercrime investigations. The significance of this study lies in its ability to enhance investigators' techniques and applications of OSINT[1].The threats and vulnerabilities were calculated in this study based on the impacts of each review of the databases. The underlying research challenges that impact source intelligence are also highlighted in the paper. For this article, they have searched many online databases and reviewed 18 research papers that investigated the effects of social media technologies under the concept of OSINT [5]. In this article they have proposed a new way to handle online child abuse investigations using a theoretical model after a brief explanation of crowd sourcing and OSINT techniques. The theoretical model comprises organizational, technical and legal aspects of selected skilled and tightly grouped volunteers to help in online child abuse cases using OSINT and forensic examinations without compromising the legal procedures[6]. In this study they emphasize providing a helping hand in digital investigations with efficient tools. Here, the method they used was to analyze the activities done, the people linked, and the persons contacted for communications by a suspected employee. This study highlights how to handle digital evidence and retrieve multimedia information for analysis using OSINT[7]. Digital forensic Intelligence and Open-source Intelligence are balanced in this paper. The study analyzes the application of this framework to investigate the additional information contained in the digital forensic data subset. This highlights the prompt extraction, analysis, and automated entity identification of real-world data by Open-Source Intelligence [8]. In this study they deal with the current methods used by investigators for cybercrimes, the challenges they face, and future directions for investigations. This study highlights the use of open-source intelligence and the use of many such tools for investigation purposes. They emphasize the selection of tools for different types of cases based on the information that can be provided by each tool and its effectiveness. The study concludes that for better effective investigations, many tools must be combined and used since there is no one single tool for all the work to be done[9]. The current situations and security trends of OSINT are explained in this paper as data collected using OSINT can be used for

malicious activities. The paper discusses the types of cybercrimes and security threats that can arise when OSINT is exploited by malicious users. Furthermore, the paper provides countermeasures, such as the proposed need for security requirements, that can be employed in the OSINT environment [10]. In this study they deal with topic modelling processes, which play a pivotal role in providing significant results that can be useful in OSINT. The study focuses on LDA (Latent Dirichlet Allocation), its processes, and its advantages, and offers suggestions for future assistance in cybercrime investigations[11]. Open-source research techniques, analytical tools, and datasets are utilized in the study to investigate organized crimes like human trafficking. The study indicates that large-scale data analytics are required to deal with more reports of cyber-facilitated crime[12]. The study relies on a comprehensive review of OSINT-related literature, its applications in cybercrime, and relevant case studies. The study implies the challenges and limitations faced by the OSINT framework and proposes potential solutions like integration of machine learning, new algorithms based on artificial intelligence and proper handling of data collection and analysis[13].

METHODOLOGY

The Process of Collecting Digital Evidence with OSINT Techniques:

- **Information Gathering:** Begin by defining the scope of the investigation and the specific information needed, such as details about a person, organization, event, or online activity.
- **Tool Selection:** Select the appropriate OSINT tools and resources to access and retrieve information from the specified sources. There were a variety of tools available, including search engines and specialized OSINT software and platforms.
- **Data Collection:** Use OSINT tools to gather data from various sources, such as online searches, social media, and public databases in an ethical and legal manner.
- **Data Verification:** Verify the accuracy and reliability of collected information. Verify facts and eliminate false or misleading data by cross-referencing data from multiple sources.
- **Data Preservation:** Safeguard digital evidence by preserving original URLs, taking screenshots, and archiving web pages as they appeared at the time of collection.
- Data Analysis: Analyze the collected data to extract insights, patterns, and connections using data manipulation, keyword searches, and visualizations.
- **Documentation:** It is crucial to document the entire process of collecting OSINT, including the sources utilized, search queries, and any modifications made to the data. Legal and investigative purposes require accurate documentation.

The OSINT framework and ten different tools will be used to analyze three hypothetical cases of different business crimes in this paper. We will evaluate the effectiveness of the tools and interpret the results obtained. In the end, we will present a detailed framework for investigating such cases using OSINT tools. It is important to note that all the cases mentioned in this paper are hypothetical, but for the sake of understanding, we will use Te2 Technique, a service-based company located in Tamil Nadu, India, as an example. The steps to collect digital evidence using OSINT are shown in Fig 2

CASE-1 (Money laundering)

Te2 Technique company is suspected of laundering money.Te2 Technique Corporation is a company that spans multiple countries. Manufacturing, import/export, and retail are legitimate businesses that the company is involved in. The management suspects a complicated money laundering scheme to hide the origins of illegal funds. Mr. Yuthvek, the CEO of Te2 Technique Corporation, is suspected of being the mastermind behind the money laundering operation. Mrs. Josephine, who is also the Chief Financial Officer (CFO) of the company, is being investigated because they both have the ability to oversee financial transactions.

Questions

1. What is the purpose of the investigation?
2. Do the suspects have any suspicious communications?
3. Are any of their devices experiencing unusual bank transfers?
4. Are there any discrepancies between the financial record and the business operations that occurred?

Investigative Tools

Hunter is an OSINT tool to obtain the email addresses of companies and their employees associated with a domain. Here, it was used to determine if the email addresses of the suspects were authentic, which was then provided to the respective banks for the bank statements. The website can be accessed by using the link https://hunter.io/search.The free digital forensic software may have limited effectiveness and capabilities compared to premium options, lacking advanced features and user-friendliness, which can be a disadvantage for those who require more specialized functionality in their forensic work. The homepage of hunter tool is shown in fig 3,4. Whatismyipaddress is an OSINT tool that identifies potentially suspicious emails originating from the sender. This OSINT utility is used to analyze IP addresses associated with emails receiving money to determine hostnames and geographical location.

The tool's website can be accessed through the link https://whatismyipaddress.com.The main focus of "Whatismyipaddress" is to provide information about IP addresses from a user's viewpoint. Deep forensic analysis of digital artifacts or data recovery is not the intended use of it. The homepage of Whatismyipaddress is shown in fig 5.

To examine the suspect's profiles and gain knowledge about their professional backgrounds and connections with other organizations, LinkedIn is utilized. In order to support the investigation, it may involve examining user profiles, connections, posts, messages, and any other relevant data. The website can be accessed through the link https://www.linkedin.com/. The search result of background check in linkedin is showed in fig 6.

Case-2 (Insiders attack)

Te2 Technique company is a technology company that is publicly traded and known for its cutting-edge products and services. Due to upcoming product launches and strategic partnerships, the company's stock price has recently experienced significant fluctuations. Several key individuals within the organization have been implicated in a case of alleged insider trading. In the weeks leading up to a major product launch, there was a sudden surge in trading activity regarding the stock of Te2 technique company. Suspicions of insider trading are raised due to unusual fluctuations in the stock's price. An investigation was launched by investigative authorities, including the Securities and Exchange Commission (SEC).

Questions

1. Could the stock trading activity have been caused by unauthorized disclosures of non-public information within the company?
2. Did the suspicious trading activity result in any financial benefits for any of the key players?
3. What is the purpose of the investigation? Investigate stock market information and financial information?

Investigative tool

The census is a cybersecurity service and search engine that provides information about internet devices, domains, and certificates. This tool was utilized to monitor the resources used for wide scans and analyze various components of the internet infrastructure. Asset tracking is also a function of it. But this tool is most helpful in the case of big multinational companies. In our situation, we are employing the model of a small company, but the results obtained are not advantageous. The website can be accessed through the link https://search.censys.io/. The result obtain from census tool is showed in fig 7.Emailrep is an advanced system that gathers information about email addresses, domains, and internet personalities using crawlers, scanners, and enrichment services. The risk linked to the suspect email address was evaluated using this tool in our case. This tool allows us to comprehend email data from dark web data. Although the tool is open source, it requires payment to view the results while analyzing. By using the link

https://emailrep.io, the website can be accessed. The website is unreliable and it takes a long time to respond. The Email rep tool's homepage can be seen in fig 8. Yahoo Finance provides a variety of services and data related to finance, investment, and the stock market, including financial headlines. The company's stock value is not present in this case. To find out if a company has experienced a sudden increase in the stock market, we can use Yahoo Finance. Insider attacks can occur for this reason, but it is not realistic if the company's stock value is not visible. The website can be accessed using the link https://finance.yahoo.com. Homepage of yahoo finance is seen in fig 9. Google Finance is a news website that offers stock quotes in real-time and delayed, interactive charts, business profiles, portfolio monitoring, economic calendars, and an industry data platform provided by Google. Regarding our case, the model company we have taken as an example does not have a stock value in Google Finance. Identifying the insider attack is not possible with this tool. Accessing the website is possible through the https://www.google.com link. The homepage of google finance is showed in fig 10.

CASE-3 (data breach)

Te2 Technique, a technology company publicly traded and renowned for its cutting-edge products and services, found itself in the midst of a significant data breach. The company's reputation was affected, and critical questions about the security of sensitive information were raised by the breach, which had wide-reaching consequences. A large amount of sensitive customer data was discovered to have been exposed by Te2 Technique. A security expert noticed unusual data traffic on the company's internal network, leading to the discovery of the breach. The presence of an unauthorized intruder who had gained access to customer data, including personal information and financial records, was confirmed through subsequent investigations.

Questions

1. What led the intruder to gain access to Te2 Technique's systems and compromise customer data?
2. What is the extent of the data breach in terms of the number of customers and records affected? Were there some high-profile clients who were impacted?
3. What actions were taken to contain the breach and retrieve the compromised data?

Investigative Tool

Have I been pwned? It is a website created by security researcher Troy Hunt. Assisting individuals in determining if their email addresses and associated accounts have been compromised in data breaches. In our case, we are using this tool to check whether the board of directors' email has been breached and to understand which sources it has been leaked from. Even the types of data that have been leaked in this case. The website can be accessed by using the link https://haveibeenpwned.com/. The obtained result from have I been paned tool is shown in fig 11. Zauba Corp is an Indian company that provides data on import and export transactions, company details, and other business-related information.To understand the company structure and details of the director related to our case, we have used this tool. It may not be the primary tool for investigating data breaches. However, it can provide us with a comprehensive understanding of the company we are collaborating with for the data breach incident. Accessing the website is possible by using the link https://www.zaubacorp.com/. The results obtained from the zauba corp website is shown in fig 12.Google Dorking, or Google hacking, is the practice of using advanced search operators to locate specific information or vulnerabilities in web applications and websites. Google Dorking can be a valuable tool when investigating a data breach to uncover publicly accessible information related to the breach or its potential sources.We can only access the company's breached data if it is available on the internet. Some versions require payment to view the results, while others are free to use. The website is accessible through the link **https://www.google.com/**. The example for google dork is seen in fig 13.

DISCUSSION

Data accuracy and reliability can be a significant issue, as information found in open sources may be inaccurate, outdated, or intentionally misleading, potentially leading to incorrect conclusions if not properly verified. Certain

sources, such as subscription-based websites or proprietary databases, may be limited and lead to missing information. The verification process of online sources, especially anonymous or unverified accounts, can be challenging due to their authenticity and accuracy. In order to identify accurately, additional sources or evidence may be required because they do not have clear connections to individuals or entities responsible for business crimes.

ETHICAL CONSIDERATION

Ethical consideration is necessary for the analysis of white-collar crimes. The focus of this paper is on analyzing business crimes using the OSINT framework. We have used three different hypothesis case studies which are made up cases, and to understand how far the OSINT tools will analysis we wanted a company to run their name in different tools and identify the results. Our paper examines a service-based company called Te2 Technique that is situated in Chennai, Tamil Nadu. We have been granted permission by the company to use their company as a model.

CONCLUSION

Considering the rising number of white-collar or business-related crimes in India, obtaining a comprehensive understanding of the nature of these crimes, their methodologies, and the tools that can be used to analyze them is essential. Many digital investigative tools operate on a paid subscription basis, but in our research, we explore a range of open-source tools that are freely accessible, along with an assessment of their suitability for use in the Indian context. Data breaches, insider attacks, and money laundering are the three distinct categories of business crimes that we have focused on within this study. We used ten different Open-Source Intelligence (OSINT) tools that are readily available at no cost during our analysis of these crimes. It is important to mention that the outcomes obtained with these tools weren't always significant from an investigative perspective. Only four out of the ten tools reviewed were truly helpful in comprehending the complexity of the cases at hand. In conclusion, our findings suggest that while OSINT tools can be a valuable resource, they may not be entirely reliable for in-depth investigative purposes, and it is essential to exercise caution when interpreting the data generated by these tools, as they may contain errors.

REFERENCE

1. A. Yadav, A. Kumar, and V. Singh, “Open-source intelligence: a comprehensive review of the current state, applications and future perspectives in cyber security,” *Artif Intell Rev*, vol. 56, no. 11, pp. 12407–12438, Nov. 2023, doi: 10.1007/s10462-023-10454-y.
2. K. Uehara *et al.*, “Basic Study on Targeted E-mail Attack Method Using OSINT,” in *Advanced Information Networking and Applications*, L. Barolli, M. Takizawa, F. Xhafa, and T. Enokido, Eds., in Advances in Intelligent Systems and Computing. Cham: Springer International Publishing, 2020, pp. 1329–1341. doi: 10.1007/978-3-030-15032-7_111.
3. J. R. G. Evangelista, R. J. Sassi, M. Romero, and D. Napolitano, “Systematic Literature Review to Investigate the Application of Open Source Intelligence (OSINT) with Artificial Intelligence,” *Journal of Applied Security Research*, vol. 16, no. 3, pp. 345–369, Jul. 2021, doi: 10.1080/19361610.2020.1761737.
4. J. Pastor-Galindo, P. Nespoli, F. Gómez Mármol, and G. Martínez Pérez, “The Not YetExploited Goldmine of OSINT: Opportunities, Open Challenges and Future Trends,” *IEEE Access*, vol. 8, pp. 10282–10304, 2020, doi: 10.1109/ACCESS.2020.2965257.
5. A. Yeboah-Ofori and A. Brimicombe, “Cyber intelligence and OSINT: Developing mitigation techniques against cybercrime threats on social media,” *International Journal of Cyber-Security and Digital Forensics (IJCSDF)*, vol. 7, no. 1, pp. 87–98, 2018.

6. K. V. Açar, "OSINT by Crowdsourcing: A Theoretical Model for Online Child Abuse Investigations.," *International Journal of Cyber Criminology*, 2018, Accessed: Oct. 25, 2023. [Online]. Available: https://www.cybercrimejournal.com/pdf/AcarVol12Issue1IJCC2018.pdf
7. A. Adel and B. Cusack, "Role of Multimedia Information Retrieval in Providing a Credible Evidence for Digital Forensic Investigations: Open Source Intelligence Investigation Analysis," in *CS & IT Conference Proceedings*, CS & IT Conference Proceedings, 2020. Accessed: Oct. 25, 2023. [Online]. Available: https://csitcp.org/paper/10/1010csit02.pdf
8. D. Quick and K.-K. R. Choo, "Digital forensic intelligence: Data subsets and Open Source Intelligence (DFINT+OSINT): A timely and cohesive mix," *Future Generation Computer Systems*, vol. 78, pp. 558–567, Jan. 2018, doi: 10.1016/j.future.2016.12.032.
9. C. Horan and H. Saiedian, "Cyber crime investigation: Landscape, challenges, and future research directions," *Journal of Cybersecurity and Privacy*, vol. 1, no. 4, pp. 580–596, 2021.
10. Y.-W. Hwang, I.-Y. Lee, H. Kim, H. Lee, and D. Kim, "Current status and security trend of osint," *Wireless Communications and Mobile Computing*, vol. 2022, 2022, Accessed: Oct. 25, 2023. [Online]. Available: https://www.hindawi.com/journals/wcmc/2022/1290129/
11. J. W. Johnsen and K. Franke, "The impact of preprocessing in natural language for open source intelligence and criminal investigation," in *2019 IEEE International Conference on Big Data (Big Data)*, IEEE, 2019, pp. 4248–4254. Accessed: Oct. 25, 2023. [Online]. Available: https://ieeexplor e.ieee.org/abstract/ document/9006006/
12. L. F. Meyer and L. I. Shelley, "Human Trafficking Network Investigations: The Role of Open Source Intelligence and Large-Scale Data Analytics in Investigating Organized Crime," *International Journal on Criminology*, vol. 7, no. 2, 2020, Accessed: Oct. 25, 2023. [Online]. Available: https://par.nsf.gov/servlets/purl/10183848
13. D. Govardhan, G. G. S. H. Krishna, V. Charan, S. V. A. Sai, and R. R. Chintala, "Key Challenges and Limitations of the OSINT Framework in the Context of Cybersecurity," in *2023 2nd International Conference on Edge Computing and Applications (ICECAA)*, IEEE, 2023, pp. 236–243. Accessed: Oct. 25, 2023. [Online]. Available: https://ieeexplore.ieee.org/abstract/document/10212168/

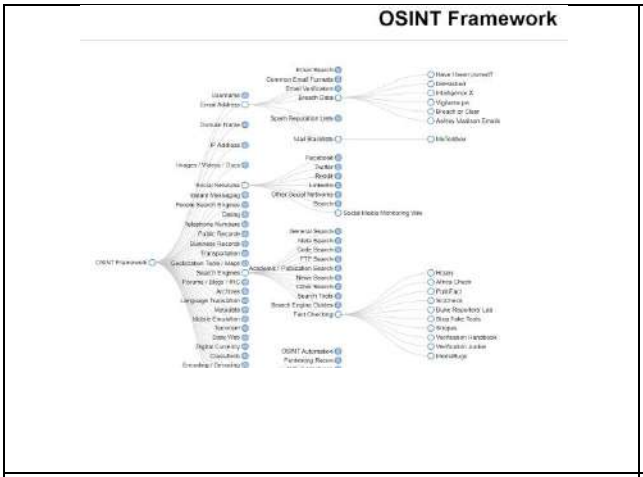

Fig:1 Homepage of OSINT framework

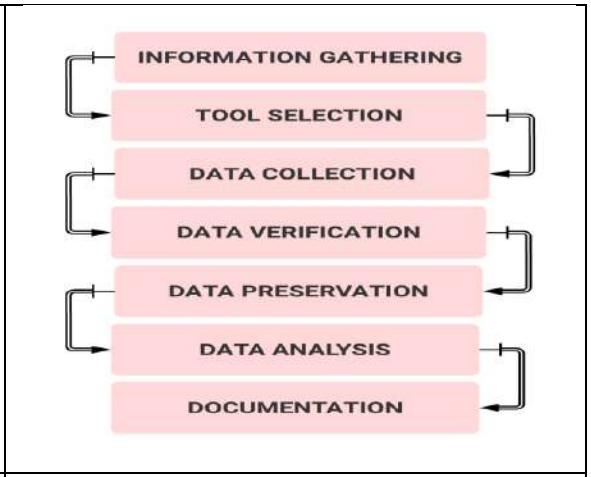

Fig: 2 Process of Collecting Digital Evidence with OSINT Techniques

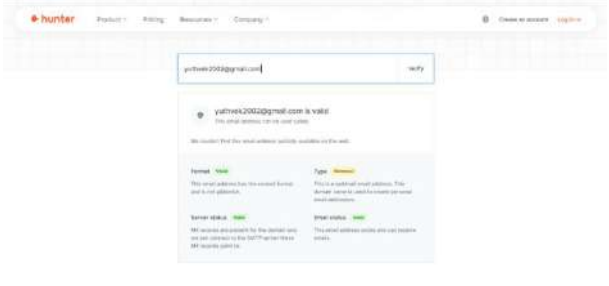

Fig: 3 Home page of Hunter website

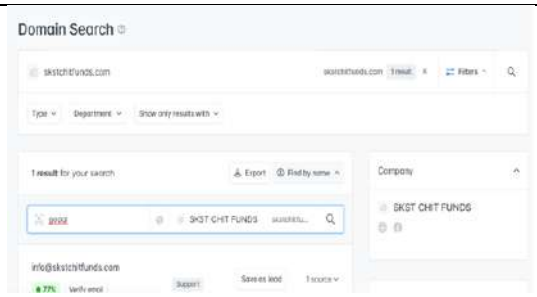

Fig: 4 Domain search result

Fig: 5 Whatismyipaddress website result

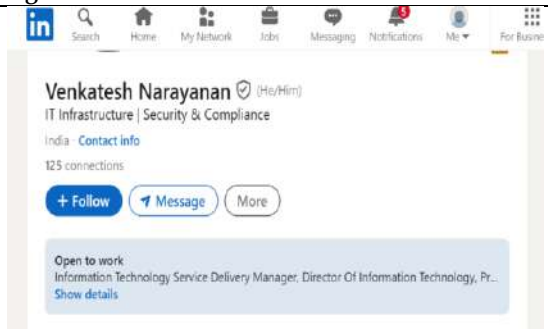

Fig :6 LinkedIn profile search result

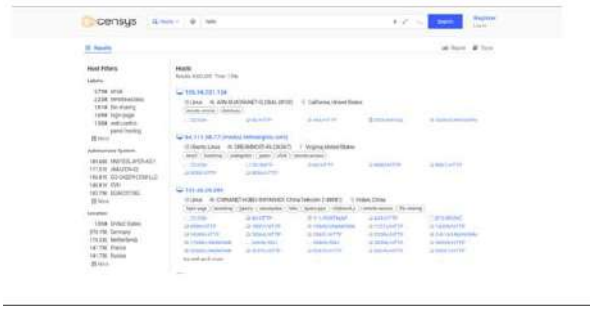

Fig:7 Identifying host IP using Censys

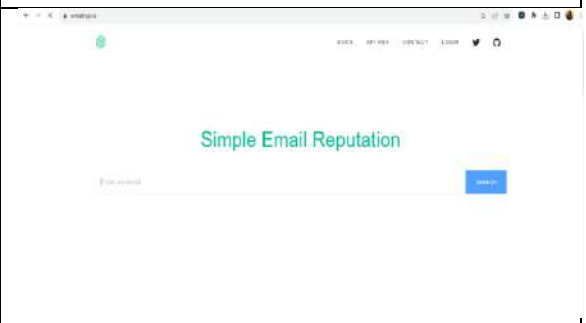

Fig:8 Home page of Emailrep

Fig:9Yahoo finance stock page

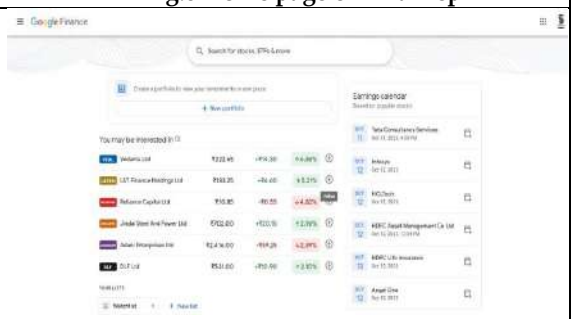

Fig:10 Google finance home page

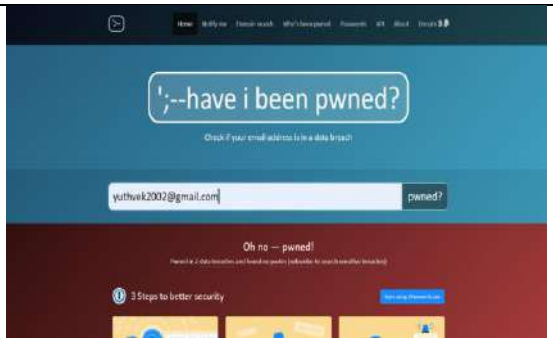

Fig:11Haveibeenpwned website

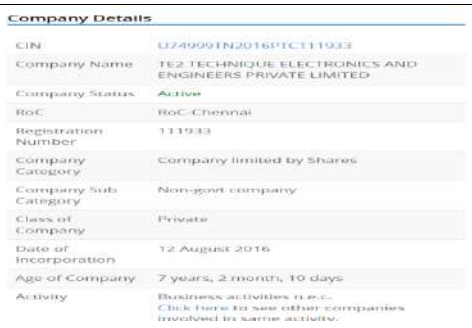

Fig:12 Company details from zauba Corp

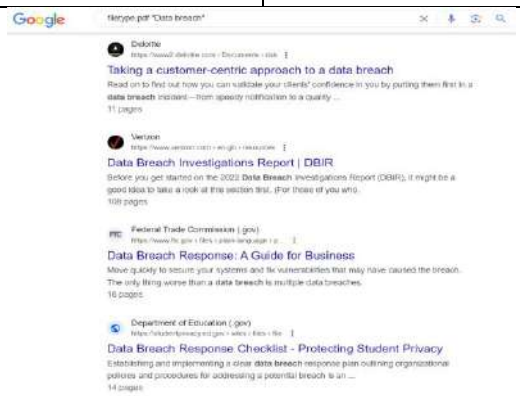

Fig:13 Google dork example

Indian Journal of Natural Sciences www.tnsroindia.org.in ©IJONS

Vol.15 / Issue 83 / Apr / 2024 International Bimonthly (Print) – Open Access ISSN: 0976 – 0997

RESEARCH ARTICLE

Cross-Cultural Management Challenges in International Business Operations

M.Shalini[1*] and M.Rohith Sundar[2]

[1]Assistant Professor, Department of Management studies, SRM Easwari Engineering College, (Affiliated to Anna University), Chennai, Tamil Nadu, India.
[2]Department of Management studies, SRM Easwari Engineering College, (Affiliated to Anna University), Chennai, Tamil Nadu, India.

Received: 30 Dec 2023 Revised: 09 Jan 2024 Accepted: 27 Mar 2024

***Address for Correspondence**
M.Shalini
Assistant Professor,
Department of Management studies,
SRM Easwari Engineering College,
(Affiliated to Anna University),
Chennai, Tamil Nadu, India.
Email: Shalini.m@eec.srmrmp.edu.in,

ABSTRACT

In today's connected world, how we communicate across cultures is becoming increasingly important, especially in international businesses affected by globalization. Managers around the world recognize the need to understand and address these challenges effectively. Globalization not only impacts our cultural identities but also shapes the way we interact with people from different backgrounds on a daily basis. To succeed in the competitive global marketplace, businesses must be equipped to anticipate and manage cultural differences. This means mastering media dynamics and international experience. By increasing awareness and experience in these areas, organizations can minimize cultural barriers and thrive in a globalized environment. Similarly, Hofstede's concept of geographical proximity may need to be reassessed in today's context of globalization. This suggests that theories of intercultural communication need to evolve, especially when applied to rapidly changing industries such as fast fashion. Our contribution goes beyond a simple case study; it challenges established theories by renowned authors, with the aim of refining and enhancing our understanding of intercultural communication in modern, globalized industries. In summary, this article highlights the importance of cross-cultural management in today's globalized business environment and provides recommendations for overcoming the challenges associated with cultural diversity. By embracing cultural differences and adopting culturally sensitive approaches, organizations can improve their competitiveness and drive sustainable growth globally.

Keywords: Cross-cultural communication challenges, Globalization, International corporations, Managers, Global Environment, Cultural issues, International strategies, Heightened awareness, Communication dynamics.

INTRODUCTION

Cross-cultural communication challenges are increasing globally, due to the spreading influence of globalization in international business. Given the global nature of this problem, it has become an important area of exploration for managers worldwide. We acknowledge that globalization is fundamentally changing our understanding of our current culture and identity, representing a profound change in the world. In the modern context, individuals find themselves immersed in a global environment where diverse countries and cultures interact on a daily basis. Therefore, the ability to predict and manage cultural issues becomes imperative to survive the highly competitive international strategies adopted by businesses. We argue that increased awareness of communication dynamics, coupled with international experience, helps alleviate the cultural challenges inherent in doing business on a global scale. Our argument stems from the belief that a comprehensive understanding of international communication and exposure practices will significantly reduce potential cultural barriers in companies engaging in global strategy. Therefore, traditional theories of cross-cultural communication require a paradigm shift when applied to the fast fashion industry. Our contribution goes beyond a simple informative case study; it serves as a theoretical challenge to established frameworks by established authors. This suggests that the changing landscape of the fast fashion industry requires a reassessment and adjustment of existing theories of intercultural communication.

Culture

Similar to globalization, culture has evolved with many different meanings. However, for pragmatic purposes, our concept of culture is derived from a precise and clear definition. According to the Cambridge Dictionary, culture is defined as "the way of life, especially the customs and beliefs common to a particular group of people at a particular time." Looking at the historical development of the concept of culture, ethnicity emerged as a distinction between "us" and "them", in search of a common identity. It is suggested that loyalty and a non-judgmental approach should be towards one's own culture. In the context of this study, culture is considered not only from a national perspective, as described above, but also from a business or organizational perspective. Thus, in this survey, culture can be classified into three main aspects: national culture, industrial culture and corporate culture. Schein (1990) used dimensions such as internal consistency, stability, group history, learning intensity, and clarity of leader assumptions to describe organizational culture, like national culture, is diverse in nature. In addition, the growing pressures of globalization are challenging our understanding of culture and identity. Global engagement and interaction with diverse cultures involves navigating the different values, beliefs, expectations, and goals shared by members of particular groups.

Globalization

The phenomenon of globalization has penetrated even the most remote places in the world, becoming a central topic of discussion for many people. As a result, the term has taken on different meanings to different proponents. Globalization is defined as the expansion of economic activities across national borders, including international trade, investment and finance – all of which are integral components of everyday life in the world. The 21st century brings both complex opportunities and challenges. The advent of technology and advances in transportation have been key factors in solidifying globalization, regardless of consensus. In particular, the Internet presents itself as a technological masterpiece, seamlessly connecting the entire world. However, globalization also causes cultural dislocation, manifested in difficulties in adapting to new or rapidly changing cultural environments. Additionally, increased international mobility catalyzed by globalization has contributed significantly to the fast fashion phenomenon. This dynamic, influenced by increasingly global movements, encapsulates the essence of fast fashion, further highlighting the transformative impact of globalization.

Cross-Cultural Communication

In today's connected world, globalization and cultural diversity have brought both opportunities and challenges for intercultural communication. These challenges are like obstacles that are difficult to accept and understand. Sometimes we still see a gap between "us" and "them," even in the business world, where we talk about organizational culture. As we interact across borders and engage with diverse cultures, there is no right or wrong way to do things. Everyone has their own identity, but we still need to communicate effectively to succeed in business. Good communication is essential to coordinate activities and build strong relationships, ultimately leading to better performance. In today's globalized business world, cross-cultural management is essential. Unclear messages can confuse employees and lead to negative consequences for the company. Therefore, it is important to avoid misunderstandings and ambiguity. The goal of communication is to be understood, so it's important to learn how to express yourself in a way that others can understand.

The ability to communicate effectively with diverse audiences is essential for success. Successful intercultural communication involves refraining from personal judgment, embracing diversity, showing respect, accepting ambiguity, being flexible, and being open to observing and learning. Although much research has been conducted on globalization and culture, it is important to continue to emphasize these concepts. Today, their interactions can lead to valuable business opportunities and competitive advantages. When managing cultural diversity, it is important to value differences while recognizing that individuals from one culture can learn from others and vice versa. Good intercultural communication skills are essential for the transmission of knowledge between different groups or individuals. Although cultural diversity can create communication challenges, simply recognizing the differences can help simplify the process. Good management of manners, etiquette and etiquette also contributes to successful cross-cultural business communication. This is especially true in the fast fashion space, where communication takes place in a dynamic and rapidly changing environment. Cultural differences have a significant impact on the competitiveness and performance of fast fashion companies, as the sector varies depending on the region in which they operate. Therefore, studying how cultural factors affect this industry is of great interest.

Problems

Cross-cultural management involves managing differences and similarities in values, attitudes, behaviors and work-related practices between people from different cultures. While managing diversity can bring many benefits, it also poses some challenges. Here are some of the key problems of cross-cultural management;

Communication barriers

Differences in language, cultural norms, and communication styles can lead to misunderstandings, misinterpretations, and breakdowns in communication. Direct and indirect communication styles, high and low context communication, and different nonverbal cues can all create difficulty in conveying messages accurately.

Stereotypes and biases

Cultural stereotypes and biases can lead to assumptions and biases about individuals from different cultures. These stereotypes can influence hiring, promotion, and decision-making processes, leading to discrimination and inequality in the workplace.

Conflict resolution

Cultural stereotypes and biases can lead to assumptions and biases about individuals from different cultures. These stereotypes can influence hiring, promotion, and decision-making processes, leading to discrimination and inequality in the workplace.

Leadership and management styles

Different cultures have different expectations and preferences for leadership and management styles. Authoritarian, democratic, participatory, and paternalistic leadership styles can be viewed differently depending on the cultural context. Leaders must adapt their leadership style to fit cultural preferences and expectations.

Decision-making processes

Cultural differences in decision-making styles, such as individualism versus collectivism, hierarchical versus egalitarian decision making, short-term versus long-term orientation, can lead to challenges in decision making, consensus seeking and decision making. Understanding cultural preferences and engaging diverse perspectives can help alleviate these challenges.

Cultural adaptation and adjustment

Expatriates and multicultural groups often face challenges in adapting to new cultural environments and adjusting to cultural differences. Cultural adaptation requires flexibility, openness, empathy and intercultural skills. Lack of cultural fit can lead to stress, frustration, and decreased performance.

Ethical dilemmas

Cultural differences in ethical norms, values, and practices can create ethical dilemmas in cross-cultural business contexts. What may be considered ethical in one culture may be viewed differently in another culture. Balancing cultural relativism with moral universalism requires careful consideration and ethical decision making.

Cultural integration and cohesion

Managing diverse teams and organizations requires efforts to promote integration, engagement, and cultural inclusion. Building a shared sense of identity, promoting cross-cultural understanding and collaboration, and promoting diversity and inclusion initiatives is essential to creating multicultural teams and organizations cohesive, high performance. Overall, effectively managing cross-cultural differences requires cross-cultural awareness, sensitivity, flexibility, and competence. By proactively addressing these issues and challenges, organizations can leverage cultural diversity as a source of innovation, creativity and competitive advantage.

Measures to overcome barriers in cross-cultural communication

Overcoming Language Differences and Communication Styles

To bridge the language gap and differences in communication styles, organizations should invest in language training programs and provide resources for employees to improve their language skills. Fostering a culture of open communication and encouraging questions can help clarify potential misunderstandings. Hiring an interpreter or using translation tools can also help make communication clearer.

Mitigating Stereotypes and Biases

To combat cultural stereotypes and biases, organizations must prioritize diversity and inclusion training. Implementing a blind hiring process can help eliminate bias in hiring and promotion decisions. Encouraging employees to challenge conventional wisdom and foster a culture of inclusion can contribute to a more equitable workplace.

Resolving Conflicts Effectively

Understanding different conflict management styles is important. Organizations should establish clear conflict resolution procedures, provide training on effective conflict resolution techniques, and encourage open dialogue. Creating a culture that values different perspectives and seeks common ground will foster a more collaborative and anti-conflict environment.

Adapting Leadership and Management Styles

Leaders should undergo cultural competency training to understand different leadership expectations. It is essential to adopt a flexible leadership approach that adapts to cultural preferences while preserving the organization's core values. Soliciting feedback from different team members can help leaders adapt their style to fit cultural expectations.

Enhancing Decision-Making Processes

Fostering diversity in decision-making groups allows for a broader range of perspectives. Training on cultural differences in decision-making styles can help team members understand and appreciate different approaches. Establishing clear communication channels and encouraging transparent discussions can lead to more inclusive decision-making.

Facilitating Cultural Adaptation and Adjustment

Helping expatriates and multicultural groups adapt to new environments requires cultural orientation programs and ongoing support networks. Encouraging a culture of mutual learning, mentoring, recognition and celebration of cultural diversity within an organization can contribute to smoother transitions and increased employee satisfaction.

Navigating Ethical Dilemmas

It is important to develop a comprehensive code of ethics that takes cultural nuances into account. Ethics training should emphasize cultural relativism and moral universalism, encouraging employees to approach ethical dilemmas with cultural sensitivity. Establishing an ethics committee with diverse representation can provide guidance on complex cross-cultural ethical issues.

Promoting Cultural Integration and Cohesion

Building cultural integration includes fostering an inclusive environment where all voices are heard and valued. Creating affinity groups, promoting cross-cultural team-building activities, and celebrating cultural events can contribute to a sense of unity. Leaders must actively support diversity and inclusion initiatives to create a cohesive organizational culture.

CONCLUSION

In short, the field of international business represents a dynamic landscape where the challenges of cross-cultural communication pose both formidable obstacles and transformative opportunities. As emphasized throughout this paper, language differences, cultural nuances, patterns, and different communication styles can create complexities that affect organizational performance and efficiency. Recognizing and understanding these challenges is the first step toward building a culturally competent workforce and promoting successful international collaboration. Addressing these challenges requires a multifaceted approach, including cultural sensitivity training, leadership adaptability, conflict resolution strategies, and a commitment to diversity and get on well. As globalization continues to intertwine economies and societies, organizations that proactively address cross-cultural communication challenges not only minimize risks but also harness the power of cultural diversity such as embracing cultural differences not only improves organizational performance but also fosters innovation, creativity and adaptability on a global scale. Faced with these challenges, the call to action for international businesses is clear: invest in cultural skills, promote inclusion and foster an environment that encourages open dialogue and mutual understanding. In doing so, organizations can navigate the complexities of cross-cultural communication, foster harmonious collaboration, and achieve long-term success in the diverse and interconnected world of international business.

REFERENCES

1. *"Effective Cross-Cultural Communication for International Business"* (ResearchGate article): This source explores the challenges and solutions for effective cross-cultural communication in business.
2. *"Cross-Cultural Business" by Thunderbird School of Global Management* (Thought leadership article on the importance and challenges of cross-cultural communication): This source provides a good overview of the topic from a business school perspective.
3. *"The Rising Importance of Cross-Cultural Communication in Global BusinessScenario"*-Dr. Prasanta Kumar Padhi

4. *"Cross-Cultural Management and Organizational Performance: A Content Analysis Perspective"*-Mast Afrin Sultana, Mamunur Rashid, Muhammad Mohiuddin, Mohammad Nurul Huda Mazumder.
5. *"Cross-Cultural Etiquette and Communication in Global Business: Toward a Strategic Framework for Managing Corporate Expansion"*-Ephraim Okoro

RESEARCH ARTICLE

Business Analytics: Driving Sustainability through Technology of Predictive Maintenance

M. Shalini[1*], Anushya B[2] and Jaysre P[2]

[1]Assistant Professor, Department of Management Studies, SRM Easwari Engineering College, (Affiliated to Anna University), Chennai, Tamil Nadu, India.
[2]Student, SRM Easwari Engineering College, Chennai, (Affiliated to Anna University) Tamil Nadu, India.

Received: 30 Dec 2023 Revised: 09 Jan 2024 Accepted: 27 Mar 2024

***Address for Correspondence**
M. Shalini
Assistant Professor,
Department of Management Studies,
SRM Easwari Engineering College,
(Affiliated to Anna University),
Chennai, Tamil Nadu, India.

ABSTRACT

The increasing emphasis on sustainability calls for creative approaches to maximize resource efficiency. The potential of business analytics (BA) in putting predictive maintenance (PdM) ideas into practice for resource optimization is examined in this study. Maintenance schedules can be optimized and possible problems can be predicted using machine learning and sophisticated analytics algorithms that analyze large datasets on equipment performance and environmental conditions. Significant advantages come from this proactive strategy, such as decreased waste from needless replacements and repairs, longer equipment lifespans that reduce the need for manufacture and disposal, and optimized energy use by foreseeing peak demand. The paper discusses the technology, its goal, and potential solutions while presenting a framework for utilizing BA in PdM. Furthermore, real-world examples are examined to demonstrate how this approach might be used in practice. Through this integration of BA and PdM, businesses can contribute to a more sustainable future by minimizing resource usage, extending equipment life, reduce downtime and reducing their environmental impact.

Keywords: Business analytics, Predictive maintenance, machine learning, advanced analytics

INTRODUCTION

Businesses nowadays must balance reducing their environmental effect and increasing efficiency. Conventional maintenance techniques, which are frequently reactive and predicated on timetables, can result in waste production, equipment failures, and needless resource use. These actions have a detrimental impact on the entire environmental

footprint in addition to operating expenditures. Sustainability has become a critical business imperative, demanding innovative solutions to environmental and social concerns. Businesses face the challenge of balancing economic growth with environmental responsibility and social well-being. This paper explores the transformative potential of business analytics (BA) in navigating this complex landscape. This journal investigates the use of business analytics (BA) in predictive maintenance (PdM), a proactive strategy that makes use of machine learning (ML) and data analysis to forecast equipment breakdowns and improve maintenance schedules. Businesses can reap major benefits by switching from reactive to predictive maintenance, such as:

- Decreased resource consumption
- Increased equipment lifespan
- Optimal energy consumption
- Enhanced operational efficiency

OBJECTIVES

Minimize resource consumption by using data analysis to forecast equipment breakdowns and cut down on needless maintenance and replacements. Increase the lifespan of equipment by proactively seeing any problems and planning preventative maintenance, which will cut down on the need for new equipment. Reduce energy use by anticipating peak demand and making operational adjustments based on equipment data. Boost operational effectiveness by reducing downtime with preventative maintenance to guarantee continuous operation and higher output. Improve sustainability through resource efficiency and less environmental impact, the aforementioned goals can help create a more sustainable future.

PROPOSED SOLUTION

We used actual instances from manufacturing facilities, which are crucial to the country's economy. In terms of the manufacturing company, they are fulfilling deadlines to create more, but they also need to pay attention to the environmental impact they are having. We propose that we could deploy remedies and lower downtime mistakes by doing the following actions.

DATA COLLECTION

Critical machinery has a variety of sensors attached to it that gather information on variables including temperature, vibration, pressure, and power usage. These sensors are essential for maintaining optimal operation and prompt repair by keeping an eye on the condition and performance of vital gear. Similar to a cloud platform, this data is continuously transmitted and kept in a central repository. It is simpler to examine trends, spot any problems, and make deft decisions to boost productivity and avoid unplanned downtime when data is gathered and kept in one single location. Above is a diagram of two sensors attached to the motor of a machine. This is a simple illustration to show how it works. The sensors could be temperature sensors or vibration sensors. Starting with a set of data, predictive maintenance algorithms are designed. Large data sets, including those from numerous sensors and devices operating at various times and in various environments, are frequently difficult to handle and process. Any one or more of the following categories of data may be available to you:

- Actual data from a typical system configuration
- Real information from a malfunctioning system
- Actual failure data from the system (run-to-failure data)

DATA PREPROCESSING

To guarantee the correctness and dependability of your dataset, data cleansing is essential. It entails eliminating any mistakes or discrepancies that might have been made while gathering the data. After this, feature engineering assists in extracting pertinent features from the unprocessed data. For example, it computes the temperature readings' standard deviation to capture variability. In the last steps of your analytic or modelling process, normalisation is

used to scale the data to a common range, enabling effective comparison and study of various properties. To transform the data into a format that makes it simple to extract condition indicators, data preprocessing is frequently required. Simple methods like removing outliers and missing values are included in data preprocessing, as are more sophisticated signal processing methods like short time Fourier transforms and order domain transformations. Knowing your machine and the type of data you have can help you choose the right preprocessing techniques. For instance, choosing preprocessing approaches can be aided by understanding what frequency range is most likely to exhibit important features when filtering noisy vibration data. Transforming gearbox vibration data to the order domain, which is utilized by rotating machines when the rotational speed varies over time, may also be helpful.

MACHINE LEARNING -MODEL TRAINING

MODEL SELECTION

Appropriate machine learning methods are selected based on the kind of machinery and failure prediction objectives. Popular choices include of:

- **REGRESSION MODELS** Estimate the equipment's remaining useful life.
- **CLASSIFICATION MODELS** Determine if the device is in good working order or in danger of breaking down.

TRAINING DATA The selected model is trained using historical data, such as sensor readings and previous failure instances. The model gains the ability to recognise trends and connections between sensor data and equipment malfunctions. The identification of condition indicators—features in your system data whose behavior varies predictably as the system deteriorates—is a crucial first step in the creation of predictive maintenance algorithms. Any feature that is helpful in differentiating between normal and malfunctioning operation or in estimating the remaining usable life might be considered a condition indicator. A helpful condition indicator separates distinct system statuses from comparable ones by grouping them together. A few instances of condition indicators are amounts obtained from

- Simple analysis, such as the mean value of the data over time
- More complex signal analysis, such as the frequency of the peak magnitude in a signal spectrum, or a statistical moment describing changes in the spectrum over time
- Model-based analysis of the data, such as the maximum eigenvalue of a state space model which has been estimated using the data
- Combination of multiple features into a single effective condition indicator (fusion)

Vibration data, for instance, can be used to track a gearbox's health. Vibrations alter in frequency and intensity when the gearbox is damaged. As a result, the peak frequency and peak magnitude serve as helpful condition indicators by revealing the type of vibrations that are occurring within the gearbox. You can derive these condition indicators by regularly analyzing vibration data in the frequency domain to keep an eye on the gearbox's health. Even when you have real or simulated data representing a range of fault conditions, you might not know how to analyze that data to identify useful condition indicators. The right condition indicators for your application depend on what type of system, system data, and system knowledge you have. Therefore, identifying condition indicators can require some trial and error, and is often iterative with the training step of the algorithm development workflow. Among the techniques commonly used for extracting condition indicators are

- Order analysis
- Modal analysis
- Spectrum analysis
- Envelope spectrum
- Fatigue analysis
- Nonlinear time-series analysis
- Model-based analysis such as residual computation, state estimation, and parameter estimation

PREDICTION AND MAINTENANCE
NEW INFORMATION & PREDICTION
The trained model is provided with real-time sensor data.

FAILURE RISK ASSESSMENT
The model makes predictions about the probability of a failure in the near future by analysing the data.

PROACTIVE MAINTENANCE
Preventing unplanned breakdowns by scheduling maintenance interventions only, when necessary, based on the projected risk. This lower:

- **UNNECESSARY DOWNTIME** By keeping the machinery running, production time is increased.
- **REPAIRS THAT ARE REACTIVE** Preventing issues before they arise saves money on repairs and helps to keep people safe.
- **ENERGY WASTE** Preventive maintenance procedures that are not necessary, such as changing out working parts, are kept to a minimum.

MODEL IMPROVEMENT
PERFORMANCE MONITORING
By contrasting the model's predictions with real failures, the performance of the model is continuously assessed. Retraining: To increase the model's efficacy if its accuracy starts to deteriorate over time, fresh data can be used to retrain it. Deploy and integrate the algorithm into your system once you have found a working solution for handling and processing the new system input in an appropriate manner and producing a prediction. You can use embedded devices or the cloud to implement your algorithm, depending on the details of your system. When collecting and storing a lot of data on the cloud, a cloud implementation can be helpful. The maintenance procedure is more efficient when data transfers between local computers running the prognostics and health monitoring algorithm and the cloud are eliminated. Cloud-based calculations can be made available via web apps, dashboards, email notifications, and tweets. An alternative is to have embedded devices that are closer to the equipment itself run the algorithm. The primary advantages of this approach are the reduction of data transmission volume, as information is only sent when required, and the instantaneous availability of updates and notifications regarding the condition of the equipment. Using a mix of the two is a third choice. The predictive model can operate on the cloud and send out notifications as necessary, while the preprocessing and feature extraction portions of the algorithm can be executed on embedded devices. In systems such as oil drills and aircraft engines that are run continuously and generate huge amounts of data, storing all the data on board or transmitting it is not always viable because of cellular bandwidth and cost limitations. Using an algorithm that operates on streaming data or on batches of data lets you store and send data only when needed.

COMPANIES UTILIZING SENSOR DATA AND MACHINE LEARNING FOR PREDICTIVE MAINTENANCE
INDUSTRIAL TITANS

GE DIGITAL Offers predictive maintenance software and other industrial internet of things (IIoT) solutions to a range of industries, including oil and gas, aviation, and power production.
SIEMENS Provides MindSphere, an industrial open-cloud platform that helps businesses gather and evaluate sensor data for preventive maintenance.
HONEYWELL Provides hardware and software for building automation, as well as tools for equipment predictive maintenance.
TECH GIANTS
IBM: Provides the asset management Maximo Application Suite, which uses AI and machine learning to provide predictive maintenance.

MICROSOFT Provides Azure IoT services, allowing companies to connect, monitor, and analyze data from their equipment for various purposes, including predictive maintenance.

BENEFITS OF PREDICTIVE MAINTENANCE BY BUSINESS ANALYSIS FOR SUSTAINABILITY

Businesses nowadays must balance reducing their environmental effect and increasing efficiency. Reactive maintenance techniques that are too traditional can result in waste production, unplanned equipment breakdowns, and needless resource consumption. This has an adverse effect on the entire environmental footprint in addition to operational expenditures. This problem can be solved with predictive maintenance (PdM), a proactive strategy that makes use of data analysis and business analytics (BA). Using sensor data, maintenance logs from the past, and operational data, PdM gives companies the ability to:

MINIMIZE RESOURCE CONSUMPTION

PdM reduces the requirement for needless repairs and replacements by anticipating possible equipment breakdowns and enabling targeted maintenance interventions. This results in a major decrease in the amount of energy, spare parts, and raw materials needed for reactive repairs.

INCREASED EQUIPMENT LIFESPAN

Prompt identification of possible problems enables preventative maintenance, which lowers the risk of catastrophic failures and the requirement for early equipment replacement. This lowers the environmental impact of producing and discarding new equipment in addition to saving money. Think about the energy and materials needed to produce a new industrial motor versus using PdM to make the current one last longer.

OPTIMIZE ENERGY CONSUMPTION

Businesses can predict equipment peak demand thanks to predictive analysis. Businesses can optimise energy consumption and minimise waste by making adjustments to operations and energy usage patterns based on these estimates. For instance, a plant is able to forecast the peak load that a particular machine would encounter and modify its production schedule to reduce energy consumption during such periods.

BOOST OPERATIONAL EFFICIENCY

Proactive maintenance (PdM) reduces downtime, guarantees uninterrupted operation, and boosts output. Better resource use and less waste creation across the whole production process result from this. Machine learning algorithms are able to recognise patterns in this data, create connections between possible equipment breakdowns and current operating circumstances, and eventually forecast when maintenance is required by processing and evaluating the data. This leads to tremendous resource optimization by enabling organisations to go from a reactive "fix-it-when-it-breaks" approach to a proactive "prevent-the-break" strategy. There are difficulties in putting business analytics into practise for PdM. It necessitates thorough preparation, training and technological investments, and data security assurance. Nonetheless, a more sustainable future is greatly aided by the advantages of decreased resource use, longer equipment life, optimal energy use, and increased operating efficiency. Businesses may reduce their environmental impact and guarantee long-term resource optimization for the earth and themselves by adopting this data-driven approach.

CONCLUSION

Businesses are using predictive maintenance (PdM) more and more as a potent tool for resource management and attaining sustainability objectives in response to growing environmental concerns. PdM enables a proactive approach to maintenance by utilising business analytics (BA) and the massive amount of data gathered from sensors

implanted into equipment. This method anticipates possible equipment failures and moves away from reactive repairs based on breakdowns. There are numerous advantages to this proactive approach for businesses and the environment. PdM reduces resource use, to start. The demand for raw materials, spare parts, and the energy required for reactive repairs is decreased when equipment data is analysed to forecast and prevent needless repairs and replacements. Furthermore, PdM increases equipment longevity by facilitating timely preventative measures. As a result, there is a decrease in the frequency of equipment changes, which lessens the environmental effect of producing and discarding new equipment. Optimized energy use is yet another important advantage. Businesses can reduce energy use and carbon emissions by modifying operations and energy usage patterns in response to anticipated equipment peak demand. In general, firms are empowered to function more sustainably when BA and PdM are integrated. This strategy reduces environmental effect, promotes resource efficiency, and advances a more sustainable future. PdM has the potential to become a pillar of sustainable business practises for companies in all sectors as this technology develops and becomes more widely available.

REFERENCES

1. Lee, J., Kao, H.-A., & Xiang, W. (2014). A cyber-physical system design for machinery lifecycle prediction and health prognosis. Industrial Informatics, IEEE Transactions on, 10(4), 16681680. (This paper explores the concept of cyber-physical systems for predictive maintenance, emphasizing its role in extending equipment lifespan and contributing to sustainability.)
2. Jardine, A. K. S., Lin, D., Banjevic, D., Makis, V., & Jardine, N. (2006). A review on machinery diagnostics and prognostics using artificial intelligence techniques. Mechanical Systems and Signal Processing, 20(7), 1483-1510. (This paper reviews the application of artificial intelligence in machinery diagnostics and prognostics, highlighting its potential for predictive maintenance.)
3. Kamble, S. S., Gunasekaran, A., & Singh, R. (2019). Sustainable supply chain management: adoption barriers and mitigation strategies. International Journal of Production Economics, 213, 252-265. (This paper examines barriers to sustainable supply chain management and suggests mitigation strategies. While not directly focused on PdM, it provides a broader context for resource optimization within the supply chain.)
4. https://www.mathworks.com/help/predmaint/gs/designing-algorithms-for-conditionmonitoring-and-predictive-maintenance.html?s_eid=PSM_15028 sustainability-12-08211-v3.pdf
5. Korenkevich, Y., &Kottasov, V. (2019). Data-driven prognostics for rotating machinery using deep learning. Mechanical Systems and Signal Processing, 130, 548-563. (This paper delves into deep learning techniques for machinery prognostics, showcasing the application of advanced analytics in PdM.)
6. Tian, Z., Jin, J., & Wu, D. (2016). An optimized support vector machine for incipient fault diagnosis of rotating machinery using a hybrid feature selection method. Mechanical Systems and Signal Processing, 70-71, 266-285. (This paper explores the use of machine learning algorithms, specifically support vector machines, for fault diagnosis in rotating machinery.)
7. Azim-Afzal, M., Khoshgoftaar, T. M., & Hamouda, B. (2019). Big data analytics in predictive maintenance. In 2019 IEEE International Conference on Big Data (Big Data) (pp. 2612-2620). IEEE. (This paper discusses the role of big data analyticsin predictive maintenance, highlighting the importance of vast datasets for accurate predictions.)

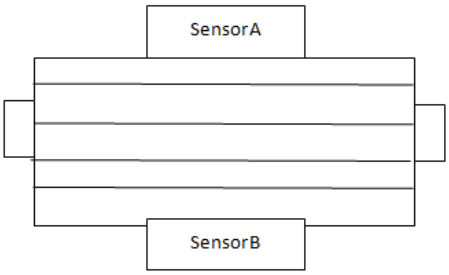

Figure 1: simple illustration of a motor with two sensors to collect and stream real-time data

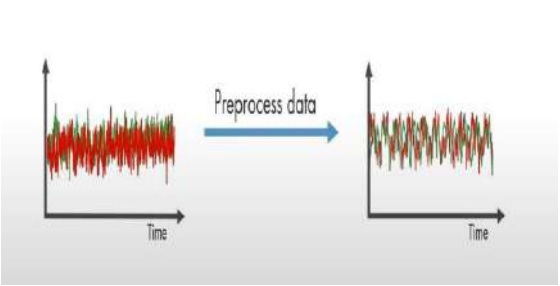

Figure 2: Data Preprocessing

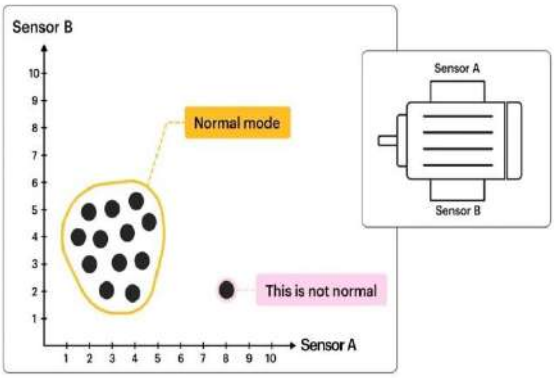

Figure 3

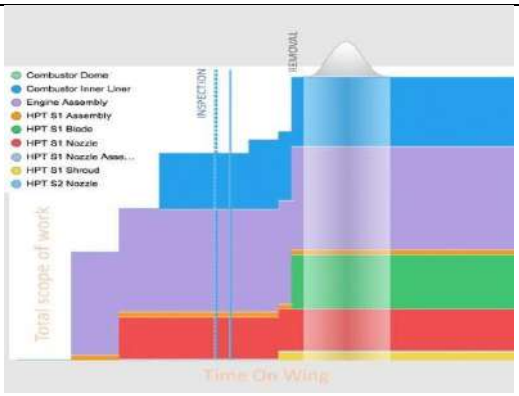

Figure 4

Indian Journal of Natural Sciences www.tnsroindia.org.in ©IJONS

Vol.15 / Issue 83 / Apr / 2024 International Bimonthly (Print) – Open Access ISSN: 0976 – 0997

RESEARCH ARTICLE

Adapting to the Dynamic Digital Marketing Landscape: Trends and Strategies for Success

Saikumari. V[1*], Prathosh K.D[2], Priyanka R[2] and Ramya Amalraj S[2]

[1]Professor and Head, MBA Department, SRM Easwari Engineering College, Chennai (Affiliated to Anna University)Tamil Nadu, India.
[2]Student, Department of Master of Business Administration, SRM Easwari Engineering College, Chennai (Affiliated to Anna University) Tamil Nadu, India.

Received: 30 Dec 2023 Revised: 09 Jan 2024 Accepted: 27 Mar 2024

***Address for Correspondence**
Saikumari. V
Professor and Head,
MBA Department,
SRM Easwari Engineering College,
Chennai (Affiliated to Anna University)
Tamil Nadu, India.

ABSTRACT

The digital marketing landscape is a dynamic tapestry, constantly evolving due to technological advancements, shifting consumer behaviours, and the ever-changing nature of global communication. This comprehensive review delves into recent advancements and strategic trends shaping the future of the field, focusing on key areas: artificial intelligence (AI), the dominance of short-form video content, the primacy of customer experience (CX), the evolution of influencer marketing, and the potential of the metaverse. It emphasizes the crucial role of remaining agile and embracing a continuous learning mindset to excel in this ever-shifting digital environment.

Keywords: Digital marketing trends, Innovation and Evolution, Strategic focus, Expanded landscape.

INTRODUCTION

The digital revolution has fundamentally transformed how businesses interact with their target audiences. Digital marketing has become an indispensable tool, enabling brands to reach a global audience, build relationships, and drive conversions. However, the digital landscape is not static. It is constantly evolving, propelled by technological innovation, evolving consumer behaviour, and the emergence of new trends and platforms. This paper provides a comprehensive exploration of this dynamic landscape. It examines recent advancements and strategic trends that are shaping the future of digital marketing and underscores the importance of continuous learning and adaptation for success in this ever-changing environment. By understanding the latest developments and embracing a strategic

approach, businesses can leverage the power of digital marketing to achieve their goals and thrive in this dynamic environment.

KEY AREAS OF INNOVATION AND EVOLUTION ARTIFICIAL INTELLIGENCE REVOLUTIONIZES MARKETING

AI is rapidly transforming various aspects of digital marketing, offering increased personalization, automation, and predictive capabilities.

- **PERSONALIZATION:** AI algorithms analyse customer data to personalize content, recommendations, and advertising, enhancing the relevance and effectiveness of marketing campaigns [1].
- **AUTOMATION:** AI-powered tools automate repetitive tasks like ad bidding, social media scheduling, and content curation, freeing up marketers for strategic endeavours [2].
- **PREDICTIVE ANALYTICS:** AI can predict customer behaviour and preferences, allowing marketers to proactively deliver targeted campaigns and optimize marketing efforts for maximum impact [3].

SHORT-FORM VIDEO CONTENT TAKES CENTER STAGE

Platforms like TikTok and Instagram Reels have propelled short-form video content to the forefront of digital marketing strategies, offering unique advantages:

- **ENGAGING AND ATTENTION-GRABBING:** Short-form videos capture attention with their concise and visually appealing nature, making them ideal for conveying information within a limited timeframe [4].
- **ADAPTABILITY ACROSS PLATFORMS:** This content format is easily adaptable for various platforms, maximizing reach and audience engagement [5].
- **STORYTELLING POTENTIAL:** Short-form videos can be powerful storytelling tools, building brand awareness and fostering emotional connections with audiences [6].

CUSTOMER EXPERIENCE REIGNS SUPREME

Prioritizing customer experience (CX) is essential for digital marketing success. This entails focusing on:

- **PERSONALIZED INTERACTIONS:** Tailored communication and interactions build loyalty and a positive brand perception [7].
- **OMNICHANNEL ENGAGEMENT:** Providing a seamless and consistent brand experience across multiple touchpoints is vital for a cohesive customer journey [8].
- **PROACTIVE CUSTOMER SERVICE:** Anticipating customer needs and offering proactive support builds trust and drives brand advocacy [9].

INFLUENCER MARKETING CONTINUES TO EVOLVE

Influencer marketing remains a powerful tool but is evolving with notable trends:

- **RISE OF MICRO-INFLUENCERS:** Consumers are increasingly drawn to micro-influencers for their genuine connections and recommendations within niche communities [10].
- **FOCUS ON AUTHENTICITY AND TRANSPARENCY:** Authenticity and transparency from influencers are paramount, requiring brand partnerships to align organically with the influencer's values [11].
- **LIVE SHOPPING AND INTERACTIVE CONTENT:** Live streaming platforms are being leveraged for interactive shopping experiences, further enhancing influencer-audience engagement [12].

EXPANDING THE DIGITAL MARKETING LANDSCAPE

THE RISE OF THE METAVERSE

The metaverse, a burgeoning virtual world experience, presents potential opportunities for marketing, such as:

- **IMMERSIVE ADVERTISING EXPERIENCES:** Engaging consumers in multi-dimensional marketing campaigns, blurring lines between reality and digital content.

- **VIRTUAL PRODUCT LAUNCHES:** Unveiling new products in simulated environments, allowing for interactive exploration and global access.
- **INTERACTIVE COMMUNITIES:** Building online spaces for brands and consumers to connect, fostering engagement and fostering a sense of belonging.

THE CONTINUED IMPORTANCE OF DATA PRIVACY

With heightened public awareness and stricter regulations surrounding data privacy, marketers need to prioritize responsible data collection and usage. This includes:

- **IMPLEMENTING TRANSPARENT DATA PRACTICES:** Informing users about what data is collected, how it's used, and with whom it's shared, fostering trust and understanding.
- **OBTAINING EXPLICIT USER CONSENT:** Clearly requesting and receiving permission from users before collecting or using their data, ensuring respect for their privacy.
- **INVESTING IN DATA SECURITY:** Implementing robust measures like encryption and access controls to protect user data from unauthorized access, breaches, or misuse.

THE CONTINUED IMPORTANCE OF DATA PRIVACY

With heightened public awareness and stricter regulations surrounding data privacy, marketers need to prioritize responsible data collection and usage. This includes:

- **Implementing transparent data practices:** Clearly explain what data you collect, how it is used, and user rights regarding their data.
- **Obtaining explicit user consent:** Be upfront about data collection and obtain explicit consent before gathering any personal information.
- **Investing in data security:** Implement robust security measures to protect user data from unauthorized access or breaches.

THE INTEGRATION OF AUGMENTED REALITY (AR) AND VIRTUAL REALITY (VR)

AR and VR technologies are finding increasing applications in marketing campaigns, offering:

- **INTERACTIVE PRODUCT EXPERIENCES:** Allow customers to virtually try on clothes, see furniture in their homes, or experience travel destinations.
- **VIRTUAL STORE TOURS:** Create immersive and interactive virtual tours of physical stores, allowing customers to explore products and layouts from anywhere.
- **LOCATION-BASED MARKETING:** Deliver targeted marketing messages and promotions based on a user's location through AR technology.

THE POWER OF USER-GENERATED CONTENT (UGC):

User-generated content, such as reviews, social media posts, and customer testimonials, holds significant power in influencing consumer behaviour. Marketers can leverage UGC by:

- **ENCOURAGING CUSTOMER PARTICIPATION:** Run contests, giveaways, and encourage customer reviews to generate content.
- **SHOWCASING POSITIVE EXPERIENCES:** Feature positive customer testimonials and reviews on your website and marketing materials.
- **FOSTERING BRAND ADVOCACY:** Partner with engaged customers to create user-generated content and build brand loyalty.

THE EVOLVING LANDSCAPE OF SOCIAL COMMERCE

The ability to seamlessly purchase products directly within social media platforms is changing the way consumers shop. Marketers need to adapt their strategies by:

- **INTEGRATING SOCIAL COMMERCE FEATURES:** Explore and leverage social commerce features offered by platforms like Instagram Shopping and Facebook Shops [15].

- **OFFERING SMOOTH CUSTOMER JOURNEYS:** Ensure a seamless purchasing experience within the social media platform, minimizing friction and maximizing conversion rates [16].
- **LEVERAGING THE POWER OF INFLUENCERS:** Collaborate with influencers to showcase products and drive sales through social commerce channels [17].

THE GROWING FOCUS ON SUSTAINABILITY:

Consumers are increasingly conscious of the environmental impact of their choices, making sustainability a significant consideration in marketing strategies. This includes:

- **HIGHLIGHTING SUSTAINABLE PRACTICES:** Showcase your commitment to sustainability throughout your supply chain and operations.
- **OFFERING ECO-FRIENDLY PRODUCTS:** Develop and market eco-friendly products that align with consumer values.
- **COMMUNICATING TRANSPARENTLY:** Be transparent about your sustainability efforts and avoid greenwashing practices.

THE NEED FOR CONTINUOUS LEARNING AND ADAPTATION

The digital marketing landscape is constantly evolving, demanding continuous learning and adaptation from professionals. This includes:

- **STAYING INFORMED ABOUT EMERGING TRENDS:** Attend industry events, subscribe to industry publications, and actively seek out new knowledge.
- **UPSKILLING THROUGH COURSES AND WORKSHOPS:** Invest in your professional development by taking courses and workshops relevant to the latest trends and technologies.
- **EXPERIMENTING AND ANALYSING RESULTS:** Don't be afraid to experiment with new strategies and analyse the results to understand what works best for your target audience.

GLOBAL IMPACT OF DIGITAL MARKETING

The internet has exploded in usage over the past few decades, as shown in the graph below. This surge in internet users has created a massive global audience for digital marketing efforts. As of October 2023, there are over 4.7 billion social media users globally, highlighting the power of this platform for brand awareness and engagement [13].

DIGITAL MARKETING'S INFLUENCE CAN BE SEEN IN VARIOUS ASPECTS OF OUR LIVES:

- **E-COMMERCE:** The ability to purchase products online has transformed the retail landscape, with global e-commerce sales projected to reach $6.7 trillion in 2023 [14].
- **SOCIAL MEDIA INTEGRATION:** Social media platforms have become ingrained in our daily lives, influencing purchasing decisions, entertainment consumption, and news sources.
- **MOBILE MARKETING:** The increasing use of smartphones has led to the rise of mobile marketing, with businesses reaching customers through SMS, app notifications, and social media on their mobile devices.

THE FUTURE OF DIGITAL MARKETING

As technology continues to evolve and consumer behaviour shifts, digital marketing will undoubtedly continue to transform. Staying ahead of the curve by embracing new technologies, adapting strategies, and prioritizing ethical practices will be crucial for success in the ever-changing digital landscape.

CONCLUSION

The digital marketing landscape is a dynamic and ever-evolving ecosystem. Understanding its evolution and emerging trends, while upholding ethical practices and focusing on continuous learning, is essential for navigating this evolving landscape and achieving long-term strategic success. By embracing innovation, adapting strategies, and

prioritizing ethical considerations, marketers can leverage the power of digital marketing to connect with global audiences, build meaningful relationships, and drive sustainable growth in the years to come.

THIS COMPREHENSIVE REVIEW HAS EXPLORED KEY AREAS OF INNOVATION AND EVOLUTION IN DIGITAL MARKETING, HIGHLIGHTING THE IMPORTANCE OF:

- Artificial intelligence (AI) for personalization, automation, and predictive analytics.
- Short-form video content for engaging storytelling and audience capture.
- Customer experience (CX) for building loyalty and fostering positive brand perception.
- Influencer marketing with a focus on authenticity, transparency, and micro-influencers.
- Emerging trends like the metaverse, voice search, data privacy, AR/VR, UGC, social commerce, and sustainability.
- Continuous learning and adaptation to stay ahead of the curve in this dynamic field.

By implementing these insights and embracing a strategic approach, businesses can leverage the power of digital marketing to thrive in the ever-changing digital world.

REFERENCES

1. Kumar, V., Rajendran, N., & Sivakumar, R. (2019). Application of machine learning for customer segmentation and targeted marketing in the retail sector. International Journal of Engineering and Technology (IJET), 8(4), 3444-3452.
2. Davenport, T. H., & Michaelis, P. (2020). The future of work after covid-19. Harvard Business Review, 98(9), 14-23.
3. Rust, R. T., & Huang, A. Q. (2014). E-service quality dimensions and their relationship with customer loyalty. Journal of Service Research, 17(3), 301-315.
4. Li, M., Shang, R., & Wang, X. (2023). The impact of short video advertising on consumer purchase intention: The role of emotional valence and brand message clarity. Journal of Interactive Marketing, 62, 108-123.
5. Smith, B., & Linden, A. (2021). The rise of short-form video content: A review of the literature. Journal of Marketing Communications, 27(6), 771-793.
6. Pitt, L., Berthon, P., & Berthon, J. (2022). Short-form video storytelling: A framework for understanding and creating effective brand narratives. Journal of Marketing Management, 38(3-4), 489-512.
7. Lemon, K. N., & Verhoef, P. C. (2016). Understanding customer experience throughout the customer journey. Journal of Marketing, 80(6), 69-96.
8. Verhoef, P. C., Lemon, K. N., Andersén, P. B., & Wrisberg, N. R. (2015). Customer experience at the intersection of digital and physical channels: A review and future research directions. Journal of Service Research, 18(1), 1-25.
9. Grewal, D., Levy, M., & Kumar, V. (2020). Customer engagement: Exploring the theoretical construct. Journal of Marketing, 84(1), 12-30.
10. Brown, D., & Hayes, N. (2021). Micro-influencers on YouTube: A customer co-creation perspective. Journal of Marketing Management, 37(5-6), 643-672.

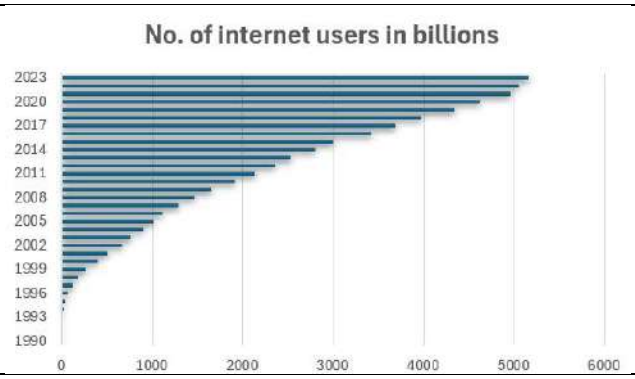

Fig. 1. Graph of no. of internet users in billion and their respective years

Indian Journal of Natural Sciences www.tnsroindia.org.in ©IJONS

Vol.15 / Issue 83 / Apr / 2024 International Bimonthly (Print) – Open Access ISSN: 0976 – 0997

RESEARCH ARTICLE

A Study on the Influence of Digital Finance on Individual Behaviour towards Financial Investments

Dhanya Nair*

Research Scholar, Hindusthan College of Arts and Science, (Affiliated to Bharathiyar University) Coimbatore, Tamil Nadu, India.

Received: 30 Dec 2023 Revised: 09 Jan 2024 Accepted: 27 Mar 2024

***Address for Correspondence**
Dhanya Nair
Research Scholar,
Hindusthan College of Arts and Science,
(Affiliated to Bharathiyar University)
Coimbatore, Tamil Nadu, India.

ABSTRACT

Digital finance is the term used to describe the impact of new technologies on the financial services industry. It includes variety of products, applications, processes and business models that have transformed the traditional way of providing banking and financial services. The term financial technology was first coined in 1990s to refer to financial services available online but were later referred to as digital finance or e-finance in the 2000s. The Covid-19 provided additional support for the banking sector's adoption of digitization. Digital financial services, namely digital wallets, made it possible to deliver money to people in need. Consumers today need a simple, affordable solution for accessing financial services. Consumers are shifting toward digital finance as a result of the younger generation's increased propensity to use technology, including the internet and digital platforms. The digital revolution in the Indian economy will lead to a spin off effect on every industry. The adoption of new and emerging technologies has taken a center stage providing consumers with a variety of digital offering to attract them towards its usage. Amidst this revolution, the finance industry moved forward with the change and introduced digital finance. Digital finance is the root towards attaining economic development. Digital finance is the lifeline for economic enhancement enabling businesses, and individuals to invest, save, and pay through digital platforms. The present study is undertaken to highlight the usage of digital technologies in the investment pattern of individuals of Federal Bank in Kottayam dt. The study will benefit the bank to find out the awareness, usage and satisfaction level of customers in using digital solution for investment and can take decisions in modification of any of the applications currently used.

Keywords: Digital Finance, Digitization, Awareness, Usage, Satisfaction

Dhanya Nair

INTRODUCTION

Digital Financial Services (DFS) include a broad range of financial services accessed and delivered through digital channels, including payments, credit, savings, remittances and insurance. Digital channels refers to the internet, mobile phones, ATMs, POS terminals etc. Everything is going digital and so are financial services. Gone are the days when you had to carry money when going out. A mobile phone is sufficient to take care of all your daily financial needs. All banking services are within your palm. There is no need to go to a bank to get your transactions done. You can deposit, transfer, withdraw or invest money using digital devices. Digital financial services have expanded greatly in India, and people have accepted them withopen arms. Their convenience and safety prompt more people to move to these methods.

DIGITAL BANKING

A digital bank represents a virtual process that includes online banking, mobile banking, and beyond. As an end-to-end platform, digital banking must encompass the front end that consumers see, the back end that bankers see through their servers and admin control panels, and the middleware that connects these nodes. Ultimately, a digital bank should facilitate all functional levels of banking on all service delivery platforms. In other words, it should have all the same functions as a head office, branch office, online service, bank cards, ATMs, and point- of-sale (POS) machines. The reason digital banking is more than just a mobile or online platform is that it includes middleware solutions. Middleware is software that bridges operating systems or databases with other applications. Financial industry departments such as risk management, product development, and marketing must also be included in the middle and back ends to truly be considered a complete digital bank. Financial institutions must be at the forefront of the latest technology to ensure security and compliance with government regulations.

DIFFERENT TYPES OF DIGITAL BANKING SERVICES

UPI (UNIFIED PAYMENT INTERFACE)

Among the popular types of digital payments, the most popular is UPI. This allows money transfer from your bank account using a single window directly to the vendor from your mobile.The payee's virtual address with consent for mobile payment needs to be entered for this modeof digital payment. Several bank accounts can be linked with one app.

INTERNET BANKING

Internet banking or net banking is among the oldest types of digital banking. You can manageyour bank accounts virtually if you have an internet connection. Customers can visit the bank portal and enter login details (password and username) and register. The bank takes layers of security measures into account, ensuring caution during payment and transactions.

MOBILE BANKING

Another popular type of digital banking is mobile banking. Account holders download the bankapplication on their mobile. All bank services like balance enquiries, payments etc. can be accessed from smartphones.

BANKING CARDS

Banking cards are essential for all types of digital payments. Cards are based on their issuance,usage, and modes of digital payment. Four types of banking cards are Debit, Credit, Prepaid and Electronic cards.

1. Debit cards issued by the bank are linked to the bank account, and cash can be withdrawn from the ATM, this banking card allows virtual payment for products and services bought through eCommerce or offline stores.
2. Credit cards are issued by banks/ non-banks. These prepaid cards are used for buying products and services on credit.

3. Bank Prepaid Cards are not linked to bank accounts and aid overdraft facilities. These cards need preloaded value addition and only the amount added can be spent.
4. Virtual Debit Card are electronic cards that work like debit cards are used for online ecommerce transactions.

MOBILE WALLETS

Mobile wallets are the digital version of a wallet that enables the user to make different types of digital payments online. Digital wallet stores money added by the user linked to their bank account. Safe amongst all digital payment methods, this can be used for all transactions throughan app installed on the smartphone and an internet connection.

BHARAT INTERFACE FOR MONEY

Bharat Interface for Money (BHIM) app enables simple payment transactions amongst other modes of digital payment. With the Unified Payments Interface (UPI) you can make direct and instant bank to bank payments and collect money using your mobile number and address. Youcan make direct bank payments to anyone on UPI using their UPI ID or scanning their QR withthe BHIM app. You can also request money through the app from a UPI ID. **POINT of SALE (PoS).** This is an internet linked electronic swipe machine through which a Merchant Establishment (ME) performs a retail transaction by swiping customer debit and credit card. The merchant calculates the amount owed by the customer. After receiving the amount, the merchant may issue a printed receipt or send an electronic receipt to the customer. Digital Financial Services Used in Federal Bank for Investment

Purpose

1. FedMobile: This is a mobile banking application used for all sorts of deposits, mutual funds, sovereign gold bond investment, TD,insurance linked products etc.
2. FedNet: This is a net banking facility used for all sorts of deposits and investments, mutual funds, ASBA(IPO), insurance linked products etc
3. Fed-E-Trade: Used for investment in shares online.

BENEFITS OF DIGITAL BANKING

CONVENIENCE

The ability to bank wherever and whenever you want is one of the main benefits of mobile and online banking solutions. Many mobile banking apps, for instance, let you deposit checks remotely. At the same time, you can check your balance, transfer funds and set up a notification to alert you if you overdraftyour account—all without the need to visit a branch. It's a real time-saver. Digital banking also offers additional conveniences, such as the ability to go cashless. Paying with cash isn't as convenient as an electronic transaction. Electronic transactions are more secure (you aren't carrying cash), they're more sanitary (you aren't touching cash) and you cantrack your transaction electronically. A cashless society with digital transactions is much more efficient, and it allows for much better management of your financial resources.

FEATURES

Many banks' mobile and online experiences offer just as many features as banking in person—if not more. Banks might offer personalized financial advice, savings tools, big-purchase calculators or even virtual assistants, all within the convenience of an app. Banking apps typically let you complete everyday banking tasks, like viewing statements and account balances, transferring funds and paying bills. Mobile check deposit, which lets users cash checks from their phone, is also common. Features like peer-to-peer payments might not be top-of-mind, but the ability to send money in minutes through your mobile banking app canbe handy, and many banks now offer this feature. Locating nearby ATMs, cardless ATM withdrawals and budgeting and tracking tools are other perks your mobile banking app may offer. Some banks even offer the ability to chat with a live representative through their apps, which can bridge the gap between in-person and digital banking. Consumers should seek out banks that prioritize offering a human touch even in their digital channels, striking the right balance between the human element and digital automation.

SECURITY

Security is a priority for financial institutions, and that extends to mobile and online banking. Threats exist everywhere, including inside bank branches. Fortunately, many banks make it easy to take extra security precautions. For example, your bank may let you add multifactor authentication to your mobile app and online bank account. Many mobile banking apps also let you use biometric authentication to log in. Federal Bank's app, for instance, provides biometric login options that require your fingerprint or facial recognition. Your bank may also scan for certain risks automatically. Banks asks for additionalverification if it detects a login from an unknown device. Overall, you may be more secure thanyou think when using digital banking. It's been reported that digital payments and e-wallets actually offer more security in some casesthan a physical card, giving some users even more reason to use digital banking tools.

CONTROL

Having control over your finances with the ability to self-serve is another significant benefit ofdigital banking, as is real-time access to managing and moving money. Unlike banking in person, mobile banking apps and websites generally have no restrictions onwhen you can perform banking tasks, like depositing a cheque or moving money from one account to another. And it's getting easier to navigate daily transactions. The world of technology is offering the opportunity to be able to receive money and to spend money in ways that are much easier than they were in past times. Banks are continuing to advance the features offered on their digital banking platforms. Automated savings tools and push notifications for events like low balances or overdrafts are commonplace. In many cases, you can even activate a new debit or credit card from your app.

BENEFITS BEYOND BANKING

On a larger scale, we can use modern connectivity tools to create financial, social and economic change.This online banking product allows for a broader base of communication that can be used for things like teaching financial literacy. Digital banking is also becoming a way to find communities and options tailored to your needsas a banking customer.

CONTENT

OBJECTIVES

1. To know the awareness level of the individuals regarding the applications used for investment purpose in Federal Bank.
2. To assess the satisfaction level of the individuals by using the applications for the investment purpose in Federal Bank.
3. To know in which of the investment avenues the individuals invest using the applications in Federal Bank.
4. To know the reasons of such individual behaviour based on the applications usedfor investment purpose in Federal Bank.

RESEARCH METHODOLOGY

The present research design adopted in the study was descriptive nature. The study is based on primary data and secondary data. The data has been collected from individuals through the questionnaire and interview. The sampling technique used in this study is random sampling. As per Cochran, the formula for unknown population to collect the samples is:

Sample size(N) - $\frac{Z^2 PQ}{e^2}$

Where N is the sample size, e is the margin of error (5%), p is the confidence level (95%), and z is the z-score (1.96). According to this formulae, the sample size was taken as 385 participants minimum. Here data has been collected from 410 respondentsthrough questionnaire.

LITERATURE REVIEW

An evaluation of digital banking in Kerala with special reference to its awareness,adoption, satisfaction and loyalty by Devikrishna V(2022). The study focused on the awareness, adoption, satisfaction and loyalty of the customers towards digital banking products and services. It is inferred from the study that there is high level awareness of internet banking products and services and the customers are using those services but the customers are sometimes using all other digital banking services like ATM, phone banking and mobile banking. Influence of behavioural factors on the adoption of digital finance, an empirical study by Jain Niyati (2022). This study focused on understanding human behaviour and perception towards digital finance. For this behavioural factors have been divided into 3 aspects-cognitive, theory of planned behaviour and behavioural biases. It was inferred that most of the individuals was aware of the digital financesolution. The mostly used digital financial services were debit/credit cards followed by e-wallets, mobile/online trading. Influence of customers digital persona on their online buying behavioural aspects by Rahul Shandilya(2022). The focus of the study is to understand the personality traits which has a favourable impact on the individuals digital quotient. The personality traits were denoted by UCCCEEE (updated, confident, curious, efficient, experimentative, epicurean). The researcher fund out that the personality traits have a positive correlation with the human behaviour.

RESEARCH GAP

The above reviews shows that many researches has been conducted on digital finance. Theresearches shows the impact of digital finance in the economy, consumers behavioral pattern towards digital solution, impact on financial inclusion etc. There are no studies which has madean attempt to find out the behaviors of individuals by using digital technologies in banks only for the purpose of investment purpose. As investment is a great source of passive income and it creates a greater pay off in the future than what was originally put in, it is important and using in studying the individual behavior/attitude of individuals in using digital technologies only forinvestment purpose.

DATA ANALYSIS AND INTERPRETATION

CHI-SQUARE TEST

H0 :- There is no significant relation between literacy level and usage of digitalapplications(exclusively for investment) in Federal Bank.

H1 :- There is significant relation between literacy level and usage of digital applications(exclusively for investment) in Federal Bank.

CV = 29.25

TB = 15.507

DF = (r-1)(c-1) ie (5-1)(3-1) = 4*2 = 8

Analysis

As per the result calculated, it shows that there is significant relation between literacy level and the usage of digital applications. Since the calculated value is 29.25 and table value with eight degree of freedom is 15.507(0.05% of significance level), we reject H0.

CORRELATION

Correlation between income and usage of application.

$$\frac{N*\sum xy - \sum x*\sum y}{\sqrt{N\sum x2-(\sum x)2 * N\sum y2-(\sum y)2}}$$

$$= 4*52212 - 155390$$

$$= 0.99$$

$$\frac{}{\sqrt{(4 * 54946 - 168100)(4 * 49793 - 143641)}}$$

ANALYSIS

As per the correlation data received, there is high positive correlation between the income level of customers and usage of applications. This shows that as the income level increases, people uses more applications of Federal Bank for the purpose of investment.

PERCENTAGE ANALYSIS

Analysis

As per the above data, it shows that there is a strong need for digital finance technologies in bank for investment. As per the customers opinion the applications are user friendly, leads to safety of customers, helps in saving time and cost and finally it replaces traditional banking and all the issues related to traditional banking.

FINDINGS

1. The chi-square test calculated gives the value of 29.25 which is more than the table value i.e 15.507 which shows that there is significant relation between literacy leveland usage of digital applications.
2. There is high positive correlation between the income and usage of application. As the income of the customers increases, their usage of digital applications also increases.
3. The data collected from the customers shows that there is a strong need for digital finance technology in the bank for investment.
4. The customers says that digital finance technology leads to time and cost saving. It tends to safety of customers.
5. The customers also opines that the digital technologies are user friendly. It replacestraditional banking.

SUGGESTIONS

1. Even though the majority of customers are satisfied with the applications there are somecustomers who are not satisfied or less satisfied. The banking officials must identify thedissatisfied customers and find a solution for that.
2. The banking officials must continuously conduct a review from the customers to knowthe feedback.
3. While introducing any new applications in the bank, proper training should be providedto the employees by the top management.
4. Simple and easily handled applications should be introduced so that even though an illiterate or less literate individuals could be used.

CONCLUSION

Finding out the influence of Digital Finance on individuals behaviour towards financial investment in Federal Bank with reference to Kottayam dt was the primary aim of the research. The study shows that 50.49% of customers says that there is strong need for Digital Finance technology in bank for investment. The studies also revealed that 74% of customers says that the applications are user friendly. Around 50% of customers says that it replaces traditional banking. Even though most of the customers are satisfied with the application, there are dissatisfied customers too. The banking officials must identify the dissatisfied and find a solution for that. The officials must continuously conduct a review from the customers to knowthe feedback.

REFERENCES

1. https://www.wikipedia.org/
2. Potti, L.R.(2020).Quantitative Techniques. Thiruvananthapuram: Yamuna publication.
3. Venugopalan,K.(2013).Business Research Methods. Delhi: Cengage India Private Limited.
4. Kothari, C.R & Garg, Gaurav.(2019). Research Methodology Methods and Techniques. Delhi: New Age International Publishers.
5. Gupta, S.L.(2017). Business Research Methods. Uttar Pradesh: McGraw Hill Education.
6. https://shodhganga.inflibnet.ac.in

Table 1: Chi-square test between literacy level and usage of applications

		Literacy Level					
		10th	**12th**	**UG**	**PG**	**Others**	**Total**
Usage	**FedMobile**	7	8	72	153	4	244
	FedNet	5	7	15	113	1	141
	Fed-e-Trade	-	-	12	12	1	25
		12	15	99	278	6	410

(Source : Online survey, January 2024)

Table 2: Calculated Values of Chi-square test

Observed Values (O)	Expected Values (E)	$\sum(O-E)^2$	$\sum(O-E)^2/E$
7	7.14	0.0196	0.0027
8	8.93	0.8649	0.097
72	58.92	171.08	2.90
153	165.44	154.75	0.94
4	3.57	0.1849	0.05
5	4.13	0.7569	0.18
7	5.16	3.3856	0.66
15	34.05	*362.90*	10.66
113	95.60	302.76	3.17
1	2.06	1.1236	0.55
-	0.73	0.5329	0.73
-	0.91	0.8281	0.91
12	6.04	35.5216	5.88
12	16.95	24.5025	1.45
1	0.37	0.3969	1.07
		Total	29.25

Table 3 : Correlation between income and usage of application

Range	x (Income)	y (Usage of applications)	x^2	y2	xy
Below 2 lakh	25	14	625	196	350
2 – 4 lakh	184	180	33856	32400	33120
4 – 6 lakh	89	86	7921	7396	7654
Above 6 lakh	112	99	12544	9801	11088
	410	**379**	**54946**	**49793**	**52212**

(Source : Online survey, January 2024)

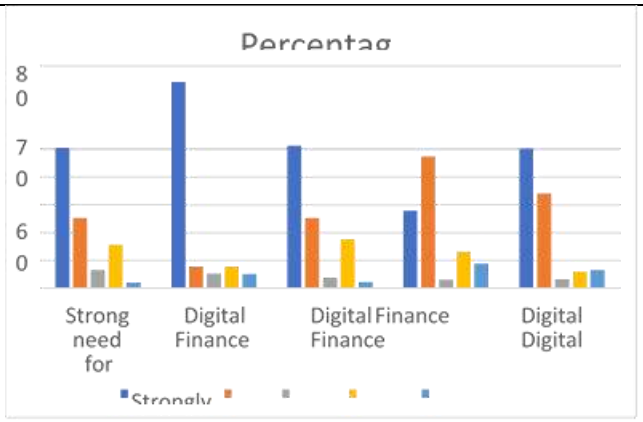

Fig 1: Percentage analysis related to customers opinion

Indian Journal of Natural Sciences www.tnsroindia.org.in ©IJONS

Vol.15 / Issue 83 / Apr / 2024 International Bimonthly (Print) – Open Access ISSN: 0976 – 0997

RESEARCH ARTICLE

The Impact of Remote Work on Employee Engagement: Strategies for Building Connection in a Virtual Environment

Tiya Thomas[1*] and S.Annie Priyadharshini[2]

[1]Research Scholar, Karunya Institute of Technology and Sciences, (Affiliated to Bharathiyar University) Coimbatore , Tamil Nadu, India.
[2]Assistant professor, Karunya Institute of Technology and Sciences, Coimbatore (Affiliated to Bharathiyar University) Tamil Nadu, India.

Received: 30 Dec 2023 Revised: 09 Jan 2024 Accepted: 27 Mar 2024

***Address for Correspondence**
Tiya Thomas
Research Scholar,
Karunya Institute of Technology and Sciences,
(Affiliated to Bharathiyar University)
Coimbatore , Tamil Nadu, India.

ABSTRACT

With the shift to remote work, organizations are facing new challenges in keeping employees engaged. Employee engagement is a vital notion in the attempt to comprehend and define, both qualitatively and quantitatively, the nature of the connection between an organization and its employees. This paper could look at how remote work affects employee engagement, taking into account factors like communication, collaboration, job satisfaction, and more. It could also look at strategies and best practices that organizations can implement to help their remote employees feel connected, purposeful, and engaged. The purpose of this paper is that it could help create a better virtual work environment, and also aim to discuss the psychological and emotional aspects of remote work, considering factors like work-life balance, motivation, and feelings of isolation. The study is based on the IT employees at Info park and utilizes primary data and secondary data and chi-square test for the study and has followed descriptive analysis. The findings would be to provide insights into effective strategies that organizations can implement to ensure high levels of employee engagement in a virtual work environment. This paper examines an in-depth exploration of the challenges of remote work to maintain and boost employee engagement in a virtual setting.

Keywords: Communication, Job satisfaction, strategies, psychological and emotional aspects, remote work, virtual work environment

INTRODUCTION

Employee engagement is traditionally defined as a sense of loyalty, commitment, and employees' mental and emotional bonds with their workplaces. An individual is more likely to show increased productivity, job satisfaction, and willingness to go above and beyond in their work when they are engaged. The introduction of computers during the 1970 oil crisis marked the beginning of the "telecommuting" trend for white-collar occupations. However, as computers advanced in the 1980s, executives and upper managers began adopting work from home policies. Fast communication via fax and phone has led to an increase in work from home jobs. Additionally, the US government gave incentives to businesses that allowed their physically challenged employees to work from home. The objective is to enhance an employee's emotional attachment to the company, their role within the organization, their peer environment, and the company culture. There's been an increase in remote employment for years, and this trend is only going to continue. A growing number of businesses and workers are seeing the benefits of working remotely as they adapt to this new distant norm. It's typical for remote workers to be responsible for their own software and hardware: The majority of remote workers must pay for their devices, internet, and additional software in order to finish their work, even if some businesses provide laptops, internet, and software tools needed for remote work.

RESEARCH METHODOLOGY

There are two sources of collecting data: - (a) Primary sources and (b) Secondary sources. To collect information related to employee engagement and remote work and using various strategies in virtual environment. The Primary data was collected by distributing questionnaires via Google forms and collected the responses. The questionnaire was structured. The questionnaire contained general questions which consisted of the demographic variables such as age, gender, occupation, job role and so on. Specific questions were included which were related to the topic under study. The data was collected from 117 respondents and percentage analysis was used to conduct the data analysis. The data collected was tabulated and charts like column chart, bar charts, were used to interpret the data.

PRIMARY DATA

The primary data is primarily gathered through the distribution of questionnaires. Primary data are genuine facts that were acquired especially for the intended purpose are known as primary data. It is beneficial for future research as well as on-going study. The primary data is collected from IT professionals, Info park ,Kochi.

DATA ANALYSIS AND INTERPRETATION

Interpretation : From the above table it is clear that ;out of 117 respondents and 24.8% of the respondents belong to the age group of 18-24years, 39.3% of the respondents belong to 25-34 years, 23.1% belong to 35-44 ,10.3% belong to 45-54years and only 2.6% are above the age group of 55 or above.

Interpretation: From the above table we concluded that only 117 responses received on gender category and 41% of the respondents are male and 44.2% of the respondents are female, other category is not responded.

Interpretation: The above table explains the remote work period of the 117 respondents and
28.2% worked for less than one year,46.2% worked for a period between 1-2 years and 15.4% worked for 3-5 years, 10.3% worked above 5years.

Interpretation: The above table explains Job role of remote employees. From 117 respondents,29.1% consist of Frontline employees,42.7% does middle management,12.8% belong to senior management and 15.4% with other job roles.

SECONDARY DATA

Secondary data is collected using Google scholar, books, websites, news articles. From the above statistical diagram, there will be an immense increase in the global digital jobs. The numbers of jobs (in millions) increasing by years and by 2030 remote digital jobs will rise from 25% to 92 million.

STATISTICAL TEST

Influence of gender on remote job satisfaction

H0: There is no influence of gender on remote job satisfaction.

H1: There is significant influence of gender on remote job satisfaction.

From Table 5 it is interpreted that gender have no influence on the remote job satisfaction Here H0 is accepted as P value is more than 0.05 and H1 is rejected. There is no significant relationship between gender and remote job satisfaction.

Impact of Age on Job role of employees

H0 : Age has no impact on employee job role.

H1: Age has a significant impact on employee job role .

From Table 6 it is interpreted that Age has a significant impact on employee job role.Here H0 is rejected as P value is less than 0.05 and H1 is accepted. So there is highly significant impact of Age on employee job role. There is a relationship between Age and employee job role.

REVIEW OF LITERATURE

Adisa et al. (2021)states that the during the pandemic, the abrupt shift from traditional in-person to virtual work environments resulted in increased workloads, a rise in online presenters, job insecurity, and a lack of adaptability to remote work arrangements. These stressors have the potential to drain important personal and social resources, which will have a detrimental effect on employee engagement levels. Anand et al. (2021) Points at two aspects of telecommuting: a. In normal times b. In times of crisis and in both scenarios, how do you keep remote workers engaged and motivated to ensure minimal, if not zero, loss of productivity. Examine several aspects of the remote worker's character and offers suggestions and methods to improve remote workers' involvement and explores different facets of the remote worker's persona and provides recommendations and practices to enhance employee engagement of the employees working remotely. De-La-Calle-Durán and Rodríguez-Sánchez (2021)stated that the psychological pressure and uncertainty caused by the current changing workplace environment have led to negative consequences for workers. Determine the primary factors that, in the given situation, can lead to employee welfare in terms of employee engagement. A theoretical paradigm to improve involvement during COVID-19 pandemics is put forth through a review of the research. The primary components or the 5Cs are communication, remuneration, cultivation, confidence, and conciliation. Dhanesh and Picherit-Duthler (2021)explains a conceptual framework, the Remote Internal Crisis Communication (RICC) framework, and empirical data to examine the antecedents of employee engagement during remote work in a crisis.

Of all the variables that predicted employee involvement, two-way communication, internal crisis communication objectives and content, and innovative work practices were the ones that predicted it the most. The study also discovered that the association between employee engagement and innovative ways of working was mediated by social connection. Shrimali (2023) states the effects of remote work on organizational dynamics by illuminating the ways in which work arrangements affect employees' levels of engagement. The knowledge gained from this study is important for companies trying to develop a highly motivated and engaged remote workforce while also adjusting to the trends of remote work. Lartey (2022) explains the expansion of existing information by examining the connection between LMX(Leader-Member Exchange), belongingness, and engagement in the context of remote workers. Put differently, the way in which workers view their relationship with their supervisors while they work remotely plays a critical role in maintaining worker engagement. Barhite (2017)states that the strength of the relationship between leaders and members is correlated with employee engagement, according to the study's conclusions, which also showed that perceived organizational communication satisfaction has the strongest association with employee engagement. Shaik and Makhecha (2019) points that the determinants of employee engagement in GVTs (Global Virtual Team) are identified by the study using the Job Demands-Resources theory of employee engagement. Five drivers of employee engagement are conceptualized through interpretive analysis of members' lived experiences

working in an organization that heavily relies on GVTs to achieve its strategic goals: cultural intelligence, technology, trust, and individual maturity. Kim and Gatling (2018)The study shows that employees intentions to use a hospitality company's VEEP are positively influenced by their perceptions of the tool's use and ease of use. Additionally, the study discovered that employees who were more inclined to utilize their company's VEEP also tended to use it more regularly, which had a favourable impact on their engagement. In due course, the employees who were more engaged shown increased levels of participation and intention to stick around.

NEED FOR EMPLOYEE ENGAGEMENT AND FACTORS AFFECTING REMOTE WORK

Employee engagement can be measured by the degree to which employees feel passionate about their work and how emotionally committed they are to the organization and its mission. The level of employee engagement refers to how the employee perceives his work experience, how that employee is treated in the organization, whether employee feels that his work is suitable. Tenney et al. (2023)The organization is committed to an authentic vision. People have certain needs in their private or professional lives that must be met in order to be engaged, enthusiastic, motivated and committed. For work, some of these needs include technical and managerial skills, autonomy, recognition, a sense of purpose, and a sense of being a valued member of the organization.

Technical competency and Managerial Competency

Technical competencies are the knowledge and skills needed to perform work tasks. They can be learned in an educational setting or on the job and vary by industry. Employers must have the knowledge and skills necessary to do their jobs, and in some cases employers provide these tools or help employees develop them through training or other learning opportunities. Employees must possess general managerial skills in order to advance in their professions. Engaged employees will look for possibilities for professional growth and development that will help them advance in their professions. This is why incorporating continual learning into your organization's culture is critical for maintaining engagement. It helps employees attain managerial competency while also meeting the requirement for growth and development. Employees must possess general managerial skills in order to advance in their professions.

Autonomy and Recognition

Autonomy is a need that businesses must meet from an increasing number of employees, and it is especially vital for remote workers. Autonomy entails enabling, even encouraging, people to work autonomously, providing them with the tools they need, and trusting them to accomplish their jobs successfully. An employee, particularly one with an entrepreneurial drive and an innovative perspective, must be trusted to execute their job properly without micromanagement impeding the process and showing faith and belief in employees' skills, abilities, and decisions. Meeting this need is a key aspect of a strong company culture because it increases job satisfaction, employee engagement, retention, performance, and the quality of work.

Sense of purpose & Feel Valued:

Employee engagement improves when people have a sense of purpose and believe that their work is significant. A shared sense of purpose among coworkers, as well as a connection to an organization's mission, vision, and values, serves as a solid foundation for high levels of engagement. When these conditions are met, firms will witness increased employee engagement, which will result in higher retention rates, enhanced productivity, and increased profitability. Sudden shift from in-person to online work during the pandemic has led to increased work efficiency, online job insecurity and poor adaptation to new ways of working from home. These stressors can drain important social and personal resources, negatively affecting employee engagement.

STRATEGIES To Create A Connection With Virtual Environment ;Impact Of Remote Work On Employee Engagement.

Unambiguous Lines of Communication

Using resources like project management systems, video conferencing, and instant messaging, create clear routes of communication. Promote candid and open communication among team members to foster trust.

Frequently scheduled video conferences
Plan frequent video conferences to replicate in-person conversations. To keep a personal connection, use video conferences for team meetings, individual check-ins, and even virtual coffee breaks.

Online Team-Building Exercises
Plan social events and online team-building exercises to improve communication. These could be team tasks that foster cooperation and togetherness, trivia evenings, or online games.

Acknowledgment and Gratitude
Reward and acknowledge workers' efforts on a regular basis. Use collaborative platforms, virtual recognition programs, or shout-outs during team meetings to commemorate accomplishments.

Adaptable Work Schedules
Provide flexible work schedules to meet the needs of individuals with varying time zones and preferences. This demonstrates consideration for unique situations and aids in improving work-life balance for staff members.

Employee Welfare Programs
Put into practice employee well-being programs including wellness challenges, mental health courses, and virtual fitness classes. Promote breaks and stress the value of taking time out to refuel.

Opportunities for Professional Development
Offer possibilities for professional growth and virtual training.

Clear Goals and Expectations
Set clear goals and expectations for tasks and projects.
Regularly check in on progress, provide constructive feedback, and ensure that employees understand their roles and responsibilities.

Virtual Mentorship Programs
Establish virtual mentorship programs to facilitate knowledge sharing and career development.Pair experienced employees with those seeking guidance to foster a sense of community.

Technology Enablement
Invest in technology that facilitates collaboration and connectivity.
Ensure that your virtual environment supports seamless communication and access to necessary tools.

Feedback Mechanisms
Implement regular feedback sessions to understand employee concerns and suggestions.

Encourage Informal Interactions
Create spaces for informal conversations and interactions, such as virtual "water cooler" chats or discussion forums.

CONCLUSION

Remote work has revolutionized typical work patterns by allowing individuals to carry out their jobs outside of the usual office setting. After the Covid-19 epidemic, remote work increased in popularity, which was advantageous for many workers. For instance, being able to work from home made it possible for caregivers to balance their personal and professional commitments. Remote employment greatly aided in the promotion of inclusivity and the assistance of people with impairments.. But telecommuting offers support here, as these workers can create an environment

where they can be comfortable and productive. Financial incentives are not the driving force behind employee engagement in the past, and office perks have lost their appeal in the hybrid and remote work environments that many organizations have moved to. This makes it difficult for managers to find new ways to engage employees in the "new normal". A traditional office environment can be overwhelming for people with social anxiety because they may feel pressured to conform to cultural social etiquette or body language expectations

REFERENCES

1. https://www.forbes.com/sites/forbeshumanresourcescouncil/2023/07/03/how-remote-work-can-impact-employees-mental-health/?sh=2117da5f2cf0
2. Tenney, M., Tenney, M., &Tenney, M. (2023, July 28). 3 types of employee engagement. Business Leadership Today - the Resource for Leaders Working to Build and Sustain World-class Teams and Organizations in Today's Business Environment. https://businessleadershiptoday.com/how-many-types-of-employee-engagement-are-there/#:~:text=An%20employee's%20feelings%20about%20their,and%20feelings%20int o% 20their%2 0work.
3. Adisa, T. A., Ogbonnaya, C., & Adekoya, O. D. (2021). Remote working and employee engagement: a qualitative study of British workers during the pandemic. Information Technology & People, 36(5), 1835–1850. https://doi.org/10.1108/itp-12-2020-0850
4. Anand, A. A., Author_Id, N., Acharya, S. N., &Author_Id, N. (2021). Employee engagement in a remote working scenario. International Research Journal of Business Studies, 14(2), 119–127. https://doi.org/10.21632/irjbs.14.2.119-127
5. De-La-Calle-Durán, M., & Rodríguez-Sánchez, J. (2021). Employee engagement and Wellbeing in Times of COVID-19: A proposal of the 5CS model. International Journal of Environmental Research and Public Health, 18(10), 5470. https://doi.org/10.3390/ijerph18105470
6. Dhanesh, G. S., &Picherit-Duthler, G. (2021b). Remote internal crisis communication (RICC) – role of internal communication in predicting employee engagement during remote work in a crisis. Journal of Public Relations Research, 33(5), 292–313. https://doi.org/10.1080/1062726x.2021.2011286
7. Shrimali, A. (2023). A study on the Impact of Remote Work on Employee Engagement. www.rrijm.com. https://doi.org/10.31305/rrijm2023.v03.n04.003
8. Lartey, F. M. (2022). Using EENDEED to measure remote employee engagement: influence of the sense of belonging at work and the Leader-Member Exchange (LMX) on virtual employee engagement. Journal of Human Resource and Sustainability Studies, 10(02), 203–222. https://doi.org/10.4236/jhrss.2022.102013
9. Barhite, B. L. B. (2017). The effects of virtual leadership communication on employee engagement. https://etd.ohiolink.edu/acprod/odb_etd/etd/r/1501/10?clear=10&p10_accession_num=bgsu1496918415648354
10. Shaik, F. F., &Makhecha, U. P. (2019). Drivers of employee engagement in global virtual teams. Australasian Journal of Information Systems, 23. https://doi.org/10.3127/ajis.v23i0.1770
11. Kim, J., & Gatling, A. (2018). The impact of using a virtual employee engagement platform (VEEP) on employee engagement and intention to stay. International Journal of Contemporary Hospitality Management, 30(1), 242–259. https://doi.org/10.1108/ijchm-09-2016-0516
12. More and more jobs can be done from anywhere. What does that mean for workers? (2024, January 10). World Economic Forum. https://www.weforum.org/agenda/2024/01/remote-global-digital-jobs-whitepaper/

Table 1:Age Group

Age	No: of respondents	percentage
18-24	29	24.8%
25-34	46	39.3%
35-44	27	23.1%
45-54	12	10.3%

55 and above	3	2.6%
Total	117	100%

Table 2:Gender

Gender	No: of respondents	percentage
Male	48	41%
Female	68	58.1%
Prefer not say	1	.9%
Total	117	100%

Table 3:Remote work period

Remote work perio	No: of responden	percentag
Less than one year	33	28.2%
1-2 years	54	46.2%
3-5 years	18	15.4%
Above 5years	12	10.3%
Total	117	100%

Table 4:Job Role

Challenges	No of respondents	percentage
Frontline Employee	34	29.1%
Middle Management	50	42.7%
Senior Management	15	12.8%
Others	18	15.4%

Table :5

Chi-Square	7.325a
Df	6
P value	0.292

Table 6

Chi-Square	52.785a
Df	12
P value	<.001

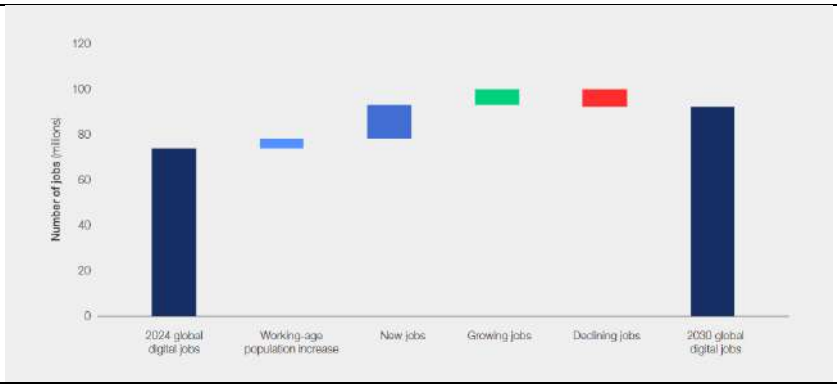

Fig 1: Source: World Economic Forum

Indian Journal of Natural Sciences www.tnsroindia.org.in ©IJONS

Vol.15 / Issue 83 / Apr / 2024 International Bimonthly (Print) – Open Access ISSN: 0976 – 0997

RESEARCH ARTICLE

Green Synthesis, Characterization of Silver Oxide Nanoparticles and its Photo Catalysis, Biological Studies

Madhu R[1], Pruthviraj K[2] , Marulasiddeshwra M B[3] , Sreenivasa S[4], Sunil K[5] , Suresh D[6] and Shet Prakash M[4]*

[1]Research Scholar, Department of Chemistry, Tumkur University, Tumakuru, Karnataka, India
[2]Assisitant Professor, Department of Chemistry, Sri Siddhartha Institute of Technology, SSAHE, Tumkur, Karnataka, India.
[3]Faculty, Department of Organic Chemistry, Tumkur University, Tumakuru, Karnataka, India.
[4]Professor, Department of Chemistry, Tumkur University, University College Science, Tumakuru, Karnataka, India
[5]Professor, Department of Chemistry, Sri Siddhartha Institute of Technology, SSAHE, Tumkur, Karnataka, India.
[6]Assisitant Professor, Department of Organic Chemistry, Tumkur University, Tumakuru, Karnataka, India.

Received: 30 Nov 2023 Revised: 13 Jan 2024 Accepted: 13 Mar 2024

***Address for Correspondence**
Shet Prakash
Professor, Department of Chemistry,
Tumkur University, University College Science,
Tumakuru, Karnataka, India.
Email: shirsatpm@gmail.com

ABSTRACT

Ag_2O a versatile nanomaterial having multidimensional application in the field of chemistry with enhanced activity has been synthesized using a endemic regional plant *Perioria pinnatum* plant having versatile ayurvedic / medicinal activity, the leaf extract has been used as fuel for the green friendly methodology for the synthesis of Ag_2O nanoparticles. Thus synthesized Ag_2O nanoparticles crystalized in FCC system been established through PXRD data and SEM images established the well clear sheet like morphology with mean size of the particles leading to 20nm dimension, followed by TEM images evidenced the spherical shape with smooth edges morphology analysis. Infrared spectrum analysis showed the broad absorption band located around 560 cm-1 corresponds to the due to the Ag-O stretching / lattice vibration. Photocatalytic dye degradation using direct sun light against Methylene blue dye was investigated and it found to be 70% of dye degradation in presence of the nano catalyst, further antioxidant, anticoagulant, antiplatelet and direct hemolytic activities were carried out using well established methods.

Keywords: Ag_2O Nanoparticles, *Prioria Pinnatum*, PXRD, Photocatalysis, Anti-oxidant, Antiplatelet

INTRODUCTION

Nanoparticles (NPs) are defined as small particles sized between 1 and 100 nm. Compared with the material bulk state[1].It mainly focuses on the modification of the size, shape and dimensions, has resulted in synthesizing nanoparticles almost equal to Bohr radius [2]. For the synthesis of metal oxides nanoparticles many physical and chemical methods are available in literature. But due to environmental issues and biological applications several authors searching alternative away for the synthesis of metal oxide nanoparticles[3,4]. Recently, introduced an environmentally friendly or bio-based of Green method is one of the simple, inexpensive, non-polluting method and also safe, low-cost, simple protocols when compared to other methods such as spray pyrolysis, sputtering etc. [5,6].
Among this Silver oxide nanoparticles are a very interesting class of metal oxides, silver being a multivalent, it forms various phases like Ag_2O, AgO, Ag_3O_4 and Ag_2O_3 by interacting with oxygen[7]. Experimentally it is found that Ag_2O and AgO are the most observable phases. It has also been reported that they decompose at less than 250°C [8,9], and also their wide range of applications in all the fields such as agriculture[10],sensing[11], catalysis[12] and biology activity[13] . Several researchers have reported the green synthesis of metal nanoparticles using leaf extract of *Artemisia Herba-Alba*[14],Selaginella (Sanjeevini) leaf extract[15], *Lawsonia inermis* (henna) leaf extract[16],.etc. On the basis of literatures survey the present work is to prepare a Ag_2O NPs using of *Perioria pinnatum* plant leaves extract as reducing and capping agent. Because plant extract can reduce metal ions to nanoparticles (NPs) in a single-step green synthesis process [17,18]. The obtained Ag_2O NPs were cacterized using different techniques, investigate for the decolourization of Methylene Blue (MB) dye under direct sun light irradiation and the results show good photocatalytic performance of these NPs. Further, these Ag_2O NPs were used to determine the Antioxidant assay. Anticoagulant, Anti-platelet activity.

Experimental Section & Charazterization Techniques

Collection of *Perioriapinnatum*leaf and preparation of leaf extract, synthesis of Ag_2O –Nanoparticles:
In a brief way, *the collected Perioria pinnatum* leaves were washed with deionized water, crushed into powered and refluxed at 100°C for3 ~ 4 hrs. The obtained plant extract were separated from the filtration process through Whatman filter paper No.42 then filtered (concentrated plant extract) was allowed to cool to room temperature. 2 g of concentrated plant extract was dissolved in 100 ml distilled water and weighed 1.69 g of silver nitrate was added to 30ml of this plant extract solution and heated in a pre-muffle furnace at 400^0 C, the reaction was completed 4hrs finally to get brown colored Ag_2Onanoparticles.

Characterization of green synthesized Ag_2O Nanoparticles:
Ag2O-NPs were evaluated for the existence of biomolecules by Fourier transform infrared spectroscopy (FTIR, Thermo Fischer Scientific, Waltham, MA, USA). within spectral range of 4000–400 cm1 with a resolution of 4 cm^{-1} . The spectral data were the average of 50 scans over the entire range covered by the instrument. For the analysis, a pellet formed by mixing the dried nanoparticles and KBr was used. The FT-IR spectra of Silver oxide nanoparticles is shown in the **fig.1** The broad absorption band located around 560 cm^{-1}corresponds to the due to the Ag-O stretching / lattice vibration, the bands at 3124cm^{-1} in the spectra corresponds to O–H stretching vibration indicating the presence of alcohol and phenol from plant extract [19,20]

The nanostructural aspects of the *Perioria pinnatum* leaves silver oxide nanoparticles were characterized by using X-ray diffractometer using equiped Shimadzu 7000 CuKα radiation (λ=1.54 nm). The sample was scanned in the 2θ range of 30^o-80° with scanning rate of 5°/ min. The XRD pattern for the synthesized Ag_2

O revealed to confirm the four intense peaks at 38.12°, 44.23°, 64.51°, and 77.69°that can be assigned to the plane of {111}, {200}, {220}, and {311},respectively as in **fig.2**and designated to thethe face-centered-cubic(fcc) system [21,22].

SEM (Carl Zeiss, USA) fitted with EDS was used to investigate the surface morphology, particle dispersion, and chemical compositions of the prepared silver oxide nanoparticles at a 15 kV accelerating voltage.**fig.3 (a,b,c.d,e)**depict the SEM images of well dispersed green synthesized Ag_2O NPsat different magnifications the majority of particles were sheet like structure in shape and there were a few oval Ag_2O NPs as well. And the findings clearly represent a mean size of 20 nm.

The size and shape of the silver oxide nanoparticles were obtained by using transmission electron microscopy (JEOL-JEM 2100 LaB6) operated at 200 keV.. **fig.4** (a,b,c.),displays the usual TEM images made using the sample with a 1 mM concentration and various magnifications (50nm, 20nm and 10 nm). The particles were found to have a homogeneous size distribution, an almost spherical shape with smooth edges, and no evidence of aggregation. UV-Vis spectra of synthesized Ag_2O-NPs were recorded in water as solvent after sonication for 10 minutes using Shimadzu UV-1800A11454907691 UV-Visible spectrophotometer, a prominent SPR peak at 430 nm depicts the formation of Ag_2O Nps **fig.5**[23,24].

RESULT AND DISCUSSION

Antioxidant Activity Using DPPH radical scavenging assay

DPPH, a stable free radical with a characteristic absorption at 517–520 nm, was used to study the radical scavenging effects. The decrease in absorption is taken as a measure of the extent of radical scavenging [27]. The activity (RSA) values were expressed as the ratio percentage of sample absorbance decrease and the absorbance of DPPH solution in the absence of extract at 520 nm. The Ag_2O nanoparticles were proved to be inhibiting the DPPH free radical scavenging activity with IC_{50} value of 55.µL/mL as show in **fig.6**

Photocatalytic Activity

Silver oxide nanoparticles is very good semi-conductor metal in the field of electrochemical, electronic, optical properties, oxidation catalysis, sensors, fuel cells, photovoltaic cells, all optical switching devices, optical data storage systems. In recent year due to its high catalytic activity, and selectivity, nanoparticles is used as photo catalysts [28]. Therefore in this present work synthesized 20mg of Ag_2O is used degrade methylene blue (MB)aqueoussolution(5ppm). The absorbance of standard dye was recorded and the whole setup was kept under sunlight with constant stirring. About 2 ml of suspension was withdrawn ateach 20 min intervals of time and the absorbance was recorded at 665 nm using UV-visible spectrophotometer. The photo catalytic activity methylene blue dye were slowly decrease at specific interval time as show in the **fig.7** . The degradation efficiency was calculated using the following equation.

$$\%\ of\ degradation = \frac{C_i - C_f}{C_i}\ X\ 100$$

Where C_i= Initial concentration of MB, C_f= Final concentration of MB in the solution afterirradiationfor agiven time interval. From the experiment it was found to be for 20mg of Ag_2O degrades 70 % of Methyl blue dye

Direct Haemolytic Activity

Using washed human erythrocytes showed direct hemolytic action. Human packed erythrocytes were combined with phosphate buffered saline (PBS) at a ratio of 1:9 v/v. Following this, dose-dependent additions of 20, 60, and 100 µg of Ag_2O nanoparticles were made to 1 ml of the suspension, which was then kept at 37°C for an hour. Centrifuged at 1000g for 10 minutes at 37°C after the reaction was stopped with 9 mL of cold PBS. The amount of free haemoglobin that was found in the supernatant and measured at 540 nm was used to compute the percentage of RBC cells that were lysed. As shown in **Fig. 8**, Ag_2O (0-100 µg) nanoparticles have a direct hemolytic impact on human RBC blood cells (). As a consequence, it was found that varying concentrations of Ag_2O (0–100 µg) nanoparticles did not hydrolyze on RBC when compared to the positive control (water) and the negative control (PBS) on human erythrocytes [25].

Anticoagulant Activity

Human platelet-rich plasma (PRP) was prepared using the standard procedure [26]. A platelet concentration of 3.1108 platelets/ml was adjusted for PRP. The material in question was held at 37°C for two hours because of the aggregation process. For all of the aforementioned preparations, plastic or siliconized glassware was utilised. As Quick et al. previously indicated, the plasma recalcification time was calculated. In a 10-mM TrisHCl (20-l) buffer with pH 7.4, 0.2 ml of citrated human plasma was added to the Ag2O (0-100 μg) nanoparticles and pre-incubated for 1 minute at 37 °C. 20 mL of 0.25 M CaCl2 were added to the pre-incubated mixture after that, and the clotting time was noted. The plasma recalcification time was estimated using human platelet rich plasma, as shown in **Fig. 9.** (PRP). According to the figure, human platelet rich plasma (PRP) typically clots in 163 seconds. At 20 g, it was discovered that Ag_2O's clotting time was 172 s. Clotting time increased to 230s as concentration increased from 20 to 100 μg/mL.

Antiplatelet Activity

Turbid metric approach [27] was combined with the Chronology dual channel whole blood/optical Lumi aggregation system (Model-700) Variable quantities of Ag2O(50-150μg) nanoparticles in 0.25ml were used to treat washed platelets. The Aggregation was then started without the use of agonists like ADP, and it was left running for 6 minutes. A significant contributing factor to thrombotic diseases and associated consequences is platelet hyperactivity. Ag_2O inhibits the agonist-induced platelet aggregation at a concentration-dependent level in Figure, which was used to evaluate the antiplatelet activity of the compound on platelet function. Agonist-induced platelet aggregation was suppressed by roughly 51%, 73%, and 84%, respectively, at a concentration of 150 μg as shown in **Fig.10.**

CONCLUSION

In the present work, Ag_2O NPs have been successfully synthesized by solution combustion method using Perioriapinnatum leaf extract because it is easy, economical, non-toxic and eco-friendly method. The synthesized Ag_2O NPs were subjected to wide range of analytical techniques for the confirmation of formation and morphology, further applications shows good photodegradation and antioxidant activity , anticoagulant activity and Direct hemolytic activity.

ACKNOWLEDGEMENTS

The authors are thankful to Tumkur University, Tumakuru, for providing the laboratory facility to carry out this work.

Conflict of Interest

The authors declare that there is no conflict of interests regarding the publication of this article.

REFERENCES

1. Auffan M., Rose J., Bottero J.Y., Lowry G.V., Jolivet J.P., Wiesner M.R. Towards a definition of inorganic nanoparticles from an environmental, health and safety perspective, Nature Nanotech, 2009, 4, 634–641.
2. Hieu P.T., Shamsul Arafin., Piao J., Tran Viet Cuong. Nanostructured Optoelectronics: Materials and Devices, Journal of Nanomaterials, 2016, 1- 2.
3. M. Bordba.r, Biosynthesis of Ag/almond shell nanocomposite as a cost-effective and efficient catalyst for degradation of 4-nitrophenol and organic dyes, RSC Adv. 2017,7, 180–189.
4. Shivananda C.S., Asha S., Madhukumar R., Satish S., Narayana B., Byrappa K., Wang Y., Sangappa Y., Biosynthesis of colloidal silver nanoparticles: their characterization and antibacterial activity Bio. Med. Phys. Eng. Express, 2016, 2(3), 035004–35015.

5. Rahman A., Kumar S., Bafana A., Dahoumane S.A., Jeffryes C., A Mechanistic View of the Light-Induced Synthesis of Silver Nanoparticles Using Extracellular Polymeric Substances of Chlamydomonas reinhardtii, Molecules, 2019, 24, 98.
6. Momin B., Rahman S., Jha N., Annapure U.S., Valorization of mutant Bacillus licheniformis M09 supernatant for green synthesis of silver nanoparticles: photocatalytic dye degradation, antibacterial activity, and cytotoxicity. Bioprocess Biosyst Eng. 2019, 42(4), 541–553,
7. Bielmann M., Schwaller P., Ruffieux P., Groning O., Schlapbach L., and Groning P., AgO investigated by photoelectron spectroscopy: Evidence for mixed valence, Phys. Rev. B. 2002, 65(23), 235431- 5.
8. Garner W.E, Reeves L.W., The thermal decomposition of silver oxide, Trans. Faraday Soc., 1954, 50, 254-260.
9. Yi C., Rambabu U, Hsu M.H., Shieh H-P,. D Chen C-.Y, Lin H-H., Fabrication and nonlinear optical properties of nanoparticle silver oxide films, Journal of Applied Physics. 2003, 94(3): 1996-2001.
10. Partila A.M., Nanotechnology for Agriculture, Springer, 2019, 19-36 p.
11. Tagad C.K., Dugasani S.R., Aiyer R., Park S., Kulkarni A., Sabharwal S., Green Synthesis of Silver Nanoparticles and Their Application for the Development of Optical Fiber Based Hydrogen Peroxide Sensor. Sensors and Actuators B: Chemical. 2013, 183, 144-149.
12. Bhosale M. A, Bhanage B. M., Silver Nanoparticles: Synthesis, Characterization and their Application as a Sustainable Catalyst for Organic Transformations, Current Organic Chemistry.2015. 19(8), 708-727.
13. Ramar K. , Gnanamoorthy G. , Mukundan D. , • Vasanthakumari R. , Narayanan V. , Jafar Ahamed A. Environmental and antimicrobial properties of silver nanoparticles synthesized using Azadirachta indica Juss leaves extract , SN Applied Sciences. 2019, 1:128.
14. Yassine Belaiche., Abdelhamid Khelef., Salah Eddine Laouini., Abderrhmane Bouafia., Mohammed Laid Tedjani., Ahmed Barhoum., Green synthesis and characterization of silver/silver oxide nanoparticles using aqueous leaves extract of Artemisia Herba – Alba as reducing and capping agents. Romanian Journal of Materials 2021, 51 (3), 342 – 352.
15. Dakshayani S.S., Marulasiddeshwara M.B., Sharath Kumar M.N., Golla Ramesh B. Raghavendra Kumar, P., Devaraja S., Rashmi Hosamani., Antimicrobial, anticoagulant and antiplatelet activities of green synthesized silver nano particles using Selaginella(Sanjeevini) plant extract, International Journal of Biological Macromolecules. 2019, 131, 787–797.
16. Ali Abdullah Fayyadh., Muneer H., Jaduaa Alzubaidy., Green-synthesis of Ag2O nanoparticles for antimicrobial assays, .Journal of the Mechanical Behavior of Materials, 2021, 30(1), 228–236.
17. Tahir, K., Nazir, S., Ahmad, A., Li, B., Ali Shah S.A., Khan A.U., Khan G.M., Khan Q.U., Haq Khan Z.U., Khan F.U., Biodirected synthesis of palladium nanoparticles using Phoenix dactylifera leaves extract and their size dependent biomedical and catalytic applications, RSC Adv. 2016, 6, 85903–85916
18. Said M.M., Rehan M., El-Sheikh S.M., Zahran M.K., Abdel-Aziz M.S., Bechelany M., Barhoum A., Multifunctional Hydroxyapatite/Silver Nanoparticles/Cotton Gauze for Antimicrobial and Biomedical Applications, Nanomaterials, 2021, 11(2), 429.
19. Subramaniyam Ravichandran., Veeranna Paluri., Gaurav Kumar., Karthik Loganathan., Bhaskara Rao Kokati Venkata., A novel approach for the biosynthesis of silver oxide nanoparticles using aqueous leaf extract of Callistemon lanceolatus (Myrtaceae) and their therapeutic potential, Journal of Experimental Nano science. 2016, 11(6), ,445-458.
20. Shanmuganathan R., MubarakAli D., Prabakar D., Muthukumar H., Thajuddin N., Kumar S.S., Pugazhendhi A., An enhancement of antimicrobial efficacy of biogenic and ceftriaxone-conjugated silver nanoparticles: green approach, Environ. Sci. Pollut. Res. 2018, 25(11), 10362–10370,
21. Oves .M, Aslam M., Rauf M.A., Qayyum S., Qari H.A., Khan M.S., Alam M.Z., Tabrez S., Pugazhendhi A., Ismail IMI., Antimicrobial and anticancer activities of silver nanoparticles synthesized from the root hair extract of Phoenix dactylifera. Mater Sci Eng C Mater Biol Appl. 2018, 1(89), 429-443.
22. Dakshayani S.S., Marulasiddeshwara M.B., Sharath Kumar M.N., Golla Ramesh B. Raghavendra Kumar, P., Devaraja S., Rashmi Hosamani., Antimicrobial, anticoagulant and antiplatelet activities of green synthesized silver nano particles using Selaginella(Sanjeevini) plant extract, International Journal of Biological Macromolecules. 2019, 131, 787–797

23. Manikandan V., Velmurugan P., Park J H ., Chang W S., Park Y J., Jayanthi P., Cho M, Oh B T. Green synthesis of silver oxide nanoparticles and its antibacterial activity against dental pathogens, 3 Biotech, 2017, 7(1), 72.
24. Okafor F., Janen A., Kukhtareva T., Edwards V., Curley M., Green synthesis of silver nanoparticles, their characterization, application and antibacterial activity, Int J Environ Res Publ Health, 2013, 10, 5221–5238.
25. Henkelman S., Rakhorst G., Blanton J., van Oeveren W., Standardization of incubation conditions for hemolysis testing of biomaterials. Material Sci. Eng., 2009, 29, 1650–1654
26. Ardlie, N.G., Han, P., Enzymatic basis for platelet aggregation and release: the significance of the 'platelet atmosphere' and the relationship between platelet function and blood coagulation. J. Haematol, 1974, 26, 331-356.
27. Born GV., Aggregation of blood platelets by adenosine diphosphate and itseversal, Nature, 1962, 194, 927–929.

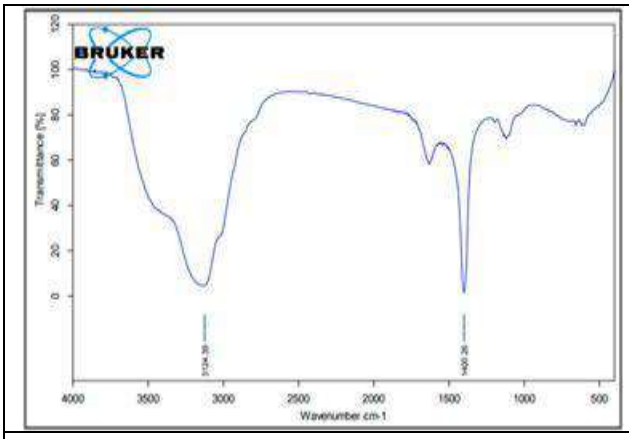

Fig 1: Infrared spectra of Silver Oxide Nano Particles "*Perioria pinnatum*" Plant

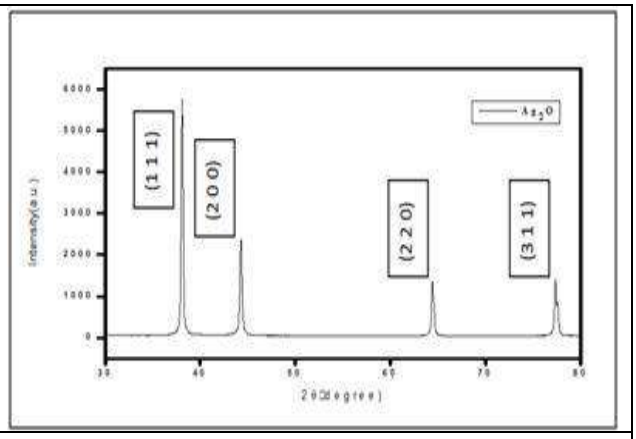

Fig 2: XRD of Silver Oxide Nano Particles obtained by the addition of Plant Extract.

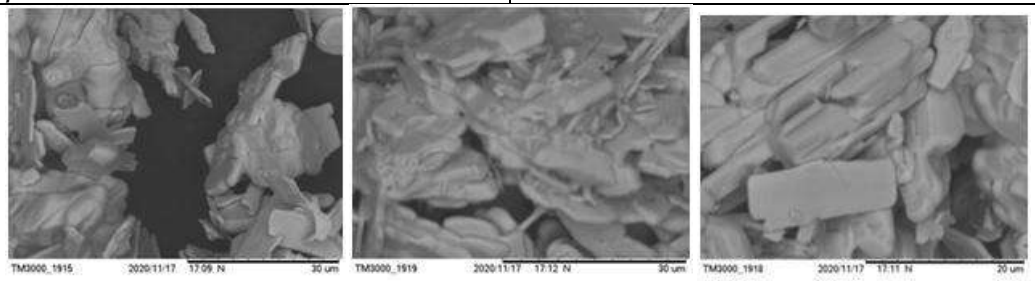

Fig 3: Scanning electron microscopic images of *"Perioriapinnatum"* leaf extract-silver nanoparticles at different magnifications (a,b,c).

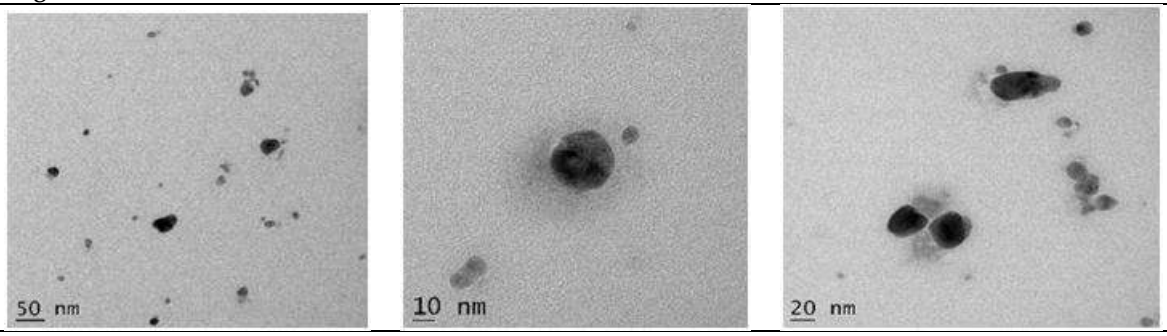

Fig 4 : Transmission electron microscope images of *"Perioriapinnatum"* leaf extract-silver Nanoparticles at different magnifications (a,b,c.).

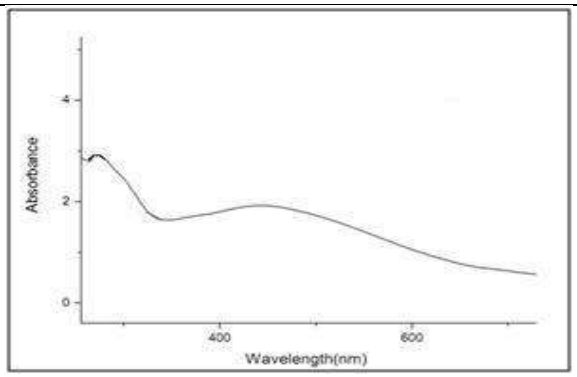

Fig 5: UV-Vis spectra of *"Perioria pinnatum"* leaf extract and silver Oxide nanoparticles

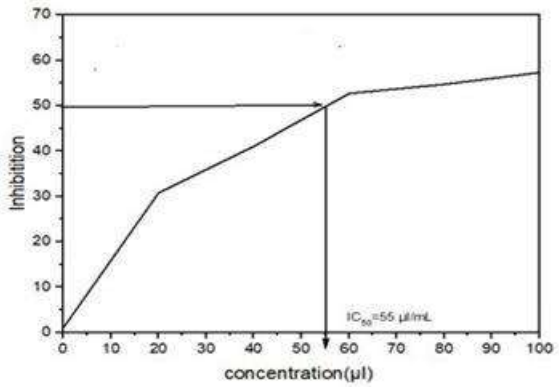

Fig 6:Antioxidant Activity of Silver Oxide Nano Particles obtained from Plant Extract

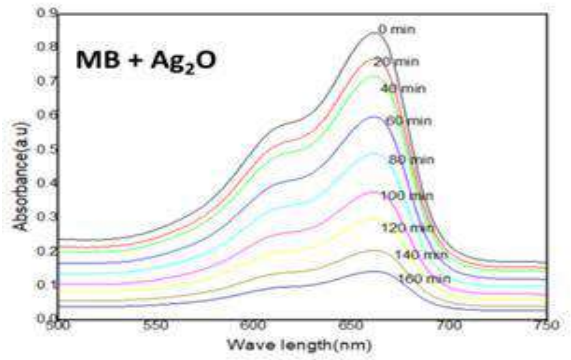

Fig.7: UV-visible absorption spectra ofAg_2Ocatalyzed degradation of Methylene blue dye

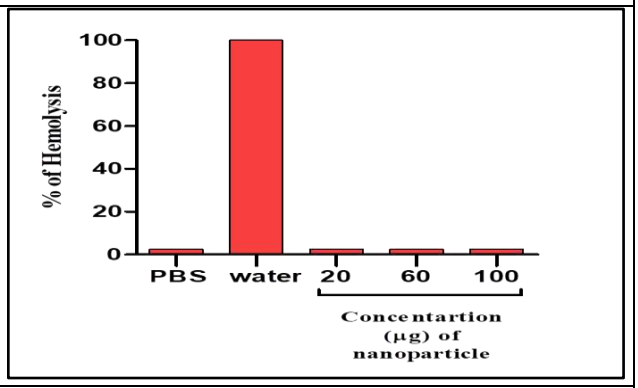

Fig.8: Direct haemolytic activity of Ag2O Nanoparticles

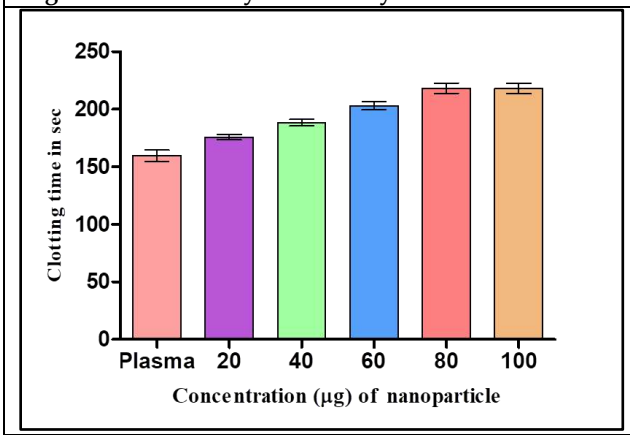

Fig.9: Anticoagulant activity of Ag_2O Nanoparticles

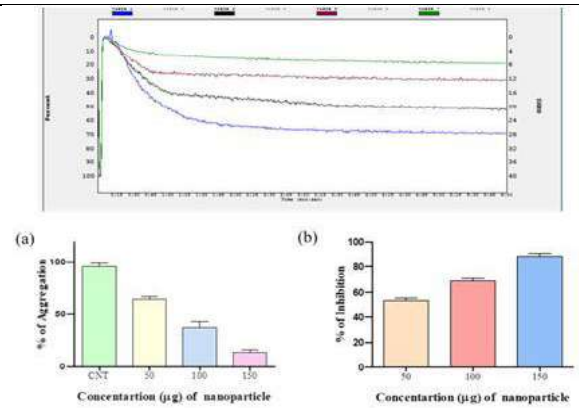

Fig.10: Antiplatelet activity of Ag_2O Nanoparticles

RESEARCH ARTICLE

Synthesis and Characterization of ZnO Nanostructured Sensors via Co-Precipitation: A Comprehensive Study for Toxic H_2S Gas Detection

Vishal S. Kamble[1], Sanjay K. Patil[2], Shailesh N. Vajekar[3], Jyotsna G. Pargaonkar[1*] and Suresh T. Salunkhe[4],

[1]Assistant Professor, Department of Chemistry, Changu Kana Thakur Arts, Commerce and Science College, New Panvel (Autonomous), (Affiliated to University of Mumbai) Mumbai, Maharashtra, India.
[2]Principal, Department of Chemistry, Changu Kana Thakur Arts, Commerce and Science College, New Panvel (Autonomous), (Affiliated to University of Mumbai), Mumbai, Maharashtra, India.
[3]Associate Professor, Department of Chemistry, Changu Kana Thakur Arts, Commerce and Science College, New Panvel (Autonomous), (Affiliated to University of Mumbai) Mumbai, Maharashtra, India.
[4]Principal, Department of Chemistry, Dahiwadi College, (Affiliated to Shivaji University), Maharashtra, India.

Received: 30 Dec 2023 Revised: 19 Jan 2024 Accepted: 27 Mar 2024

***Address for Correspondence**
Jyotsna G. Pargaonkar
Assistant Professor,
Department of Chemistry,
Changu Kana Thakur Arts, Commerce and Science College,
New Panvel (Autonomous),
(Affiliated to University of Mumbai)
Mumbai, Maharashtra, India.
Email: jyotsnapargaonkar@gmail.com

ABSTRACT

In present study, ZnO nanostructures were successfully synthesized utilizing a facile co-precipitation method. A comprehensive analysis was conducted to investigate the structural, morphological, and elemental properties using advanced techniques, including XRD, FESEM, HRTEM, and XPS. Furthermore, the gas sensing capabilities of the ZnO nanostructures were systematically examined against toxic H_2S gas. Remarkably, the ZnO nanostructures exhibited a good response towards H_2S gas, at a concentration of 100 ppm and operating at an elevated temperature of 200°C. The ZnO sensor demonstrated commendable stability in H_2S gas detection. The study also proposed a sensing mechanism elucidating the response of prepared material towards H_2S and air. The results collectively present a novel and cost-effective approach for the construction of ZnO nanostructured sensors, offering immense potential for effective H_2S gas sensing applications. This work contributes to advancing the understanding of nanostructured metal oxide sensors and their applicability in environmental monitoring systems.

Keywords: ZnO Nanostructure, HRTEM, H_2S gas, Sensor.

INTRODUCTION

Gas sensing capabilities of semiconducting metal oxides, such as ZnO, Fe_2O_3, V_2O_5, SnO_2, WO_3, In_2O_3, TiO_2, and Ga_2O_3 make them auspicious materials for detecting various toxic and pollutant gases [1-2]. ZnO, in particular, featuring a direct bandgap of 3.37 eV, high electron mobility (210 $cm^2V^{-1}S^1$), and a substantial excitonic binding energy (60 meV). ZnO's structural diversity is another advantageous feature. Its versatile crystalline structures and morphologies enable the customization of sensor designs, allowing for the optimization of performance based on specific gas detection requirements. This adaptability contributes to the material's effectiveness in detecting a wide range of gases [3-6].As a chemo-resistive nanostructure, ZnO has proven effective in detecting various gases, including H_2S, NO_2, H_2, CO, NH_3, CH_4, LPG, ethanol, and acetone. Toxic gases, when released into the environment, pose significant threats to human health. Inhalation of these noxious substances can lead to respiratory problems, irritation of the eyes and skin, and, in severe cases, can result in long-term health issues or even fatalities. Consequently, the ability to promptly recognize and respond to the presence of toxic gases is paramount for minimizing the risks to individuals and communities [7].Indeed, among various pollutants, hydrogen sulfide (H_2S) emerges as a prominent and highly toxic air pollutant. This compound takes center stage due to its widespread occurrence, often generated through combustion processes in industries [8]. Inhaling a low concentration of H_2S gas can induce symptoms such as dizziness, nausea, and headaches in humans, while exposure to higher concentrations exceeding 250 ppm can lead to severe illness and even fatalities. An estimated three million tons of H_2S gas are discharged into the environment annually. Although the characteristic rotten egg odor becomes noticeable to humans at concentrations above 250 ppm, detection becomes challenging below 100 ppm. Consequently, it is imperative to develop methods for H_2S gas detection below the 100-ppm threshold to ensure both human safety and environmental protection[9-10]. Among various synthetic methods for creating ZnO nanostructures, the co-precipitation is a simple technique. The pressing demand for highly sensitive, selective, and stable gas sensors capable of detecting H_2S gas at deficient concentrations with rapid response and recovery times is evident.

Various synthetic techniques have been explored to produce ZnO nanostructures, each with its advantages and drawbacks. Notably, the co-precipitation method proves to be particularly advantageous due to its ease of implementation, cost-effectiveness, and efficiency in yielding nanostructures with desirable properties. In the scope of this research endeavor, our primary focus is directed towards the synthesis of ZnO nanomaterials utilizing the co-precipitation method. The specific objective driving this synthesis is the development of a highly sensitive H_2S sensor designed to detect lower concentrations within the environment. To attain the goal, a comprehensive characterization process was implemented, using a various array of analytical techniques, including XRD, EDAX, FESEM, HRTEM, and XPS. These techniques were instrumental in authentically validating the surface and morphology of the created ZnO nanorods. Our investigation extends beyond mere synthesis and characterization, delving into the intricate realm of the ZnO nanorodsH_2S sensing capabilities at varying concentrations and temperatures. This comprehensive study permits for a nuanced understanding of the sensor's performance under diverse conditions. Furthermore, we meticulously examined various critical sensing parameters, including stability, reproducibility, gas response, and recovery time. Through this systematic analysis, the obtained results unequivocally establish the ZnO nanosensor's exceptional potential, particularly when operated 100 ppm H_2S concentration and 200°C temperature. In essence, our research underscores the significant strides made in the development of a ZnO nanorod-based H_2S sensor, presenting compelling evidence of its promising performance characteristics. The implications of this study resonate in the realm of high-performance gas sensing technologies, with the ZnO nanosensor poised to make substantial contributions to H_2S detection in the future.

MATERIALS AND SYNTHETIC METHOD

$Zn(CH_3COO)_2{\cdot}2H_2O$and m-cresol AR grade and 80% ethanol were gained commercially. The preparation of ZnO nanomaterial involves a meticulous procedure, beginning with precursor preparation through the dissolution of zinc acetate. The subsequent stages include nucleation, annealing, and powder crushing to attain a fine ZnO powder. The formation of a sticky gel in m-cresol follows, with a detailed stirring process. The final step entails the deposition of this gel onto a glass substrate through the drop-casting method, thereby forming the foundation for the fabrication of a thin film featuring ZnO nanostructures. A schematic representation (Fig. 1) encapsulates the entirety of this intricate synthesis scheme.

Characterization and Gas sensing tests

XRD analysis was conducted utilizing a Bruker D2 Phaser with CuKα radiation (wavelength of 1.54056 Å). The analysis spanned a 2θ range of 20–80°. For an in-depth exploration of the surface morphology and particle size, FESEM, and HRTEM analyses were employed. Additionally, XPS was employed to investigate the atomic composition of the ZnO sample.The capabilities of gas sensing of the ZnO material were thoroughly examined using a custom-designed gas sensor unit, incorporating the Keithley 6514 electrometer for accurate data recording. The choice of M/s Shreya Enterprises as the gas supplier ensures the credibility of the experimental setup, contributing to the validity of the findings in assessing the ZnO-based sensor's performance across various target gases. The sensitivity (S) of the sensors calculated through a specific relation.

$$S\ (\%) = \frac{[Ra - Rg]}{Rg} \times 100 \quad (1)$$

where, Rg and Ra are resistance the target gasand the air, respectively.

RESULT AND DISCUSSION

The X-ray diffraction (XRD) technique serves as a pivotal method for conducting structural analysis. Fig. 2 showcases the XRD pattern of ZnO nanomaterials. The distinct peaks at 31.98°, 34.63°, and 36.47°, are identified with corresponding crystallographic planes, namely (100), (002), and (101) planes respectively. These findings indicate a hexagonal wurtzite structure for the ZnO nanorods, a conclusion supported by the coordination with JCPDS card(01-079-0205) (Inset of Fig. 2.)The meticulous investigation into the structural aspects of ZnO, coupled with the absence of impurity peaks and the utilization of the Scherrer relation for crystallite size determination, collectively enhances the depth and precision of the structural characterization[11]:

$$D = \frac{K\lambda}{\beta \cos\theta} \quad (2)$$

Furthermore, lattice constants a and c as well as dislocation density (δ) were calculated using specific equations, the details of which are not provided here, and the results were tabulated in Table 1 [12-14].

$$\frac{1}{d^2} = \frac{4}{3}\left(\frac{h^2+k^2+hk}{a^2}\right) + \frac{l^2}{c^2} \quad (3)$$

$$\text{Dislocation density } (\delta) = \frac{1}{D^2} \quad (4)$$

This comprehensive analysis not only validates the crystalline nature and purity of the ZnO nanorods but also provides valuable insights into their structural dimensions and parameters through precise calculations based on the XRD data.

Morphological studies

FESEM and HRTEM analysis

In Fig. 3(a), the top-down view of FESEM images of 100 nm ZnO illustrates stepped nanorods featuring hexagonal nanostructures that are distributed in a random manner. This alignment is in agreement with the XRD results. The average length of ZnO NRs is found to be in 120-380 nm, while their diameter measures approximately 40-110 nm. This particular morphology contributes significantly to the exceptional gas response observed in ZnO NRs when

applied in gas sensing applications. To gain further morphological study of ZnO NR's, HRTEM was employed. The typical HRTEM copy of the 50 nm ZnO NR's are obtainable in Fig. 3(b), revealing stepped nanorods with a well-defined crystalline nature, consistent with the findings from FESEM images. Furthermore, HRTEM analysis emphasizes the interparticle permeability, underscoring the porous nature of ZnO nanorods (NRs). This porous structure and additional surface area are a noteworthy characteristic that significantly enhances sensing capabilities of ZnO NRs by providing additional surface area available for adsorption.

XPS analysis

In Fig. 4a, the XPS survey spectrum reveals solely Zn, O, and C peaks, underscoring the sample's high purity. Moving to Fig. 4b, the Zn 2p scan shows two distinct peaks at 1044.41 and 1021.26 eV, corresponding to Zn2p1/2 and 2p3/2 respectively. The observed energy difference of 23.15 eV aligns of the Zn^{2+} valence state, corroborating well with established reference standards [15-16].

GAS SENSING PERFORMANCE:

Gas response

The gas sensing capabilities of a pristine ZnO nanostructure were evaluated across a range of H_2S concentrations (5 ppm to 100 ppm) with the temperature of 200°C. The ZnO sensor exhibited a remarkable 164% enhancement in gas response when exposed to a concentration of 100 ppm. Notably, the response prepared sensor to H_2S displayed a linear correlation with concentration, escalating from 25 to 100 ppm. At the highest tested concentration of 100 ppm, the ZnO demonstrated a superior response.

Response/recovery time

In Fig. 5, the variations in response/recovery times of the ZnO sensor in relation to H_2S gas concentration (25, 50, and 100 ppm) at temperature of 200°C are illustrated. Notably, the response time exhibits a decrease from 32 to 15 seconds, whereas the recovery time demonstrates an increase from 61 to 114 seconds with the rising concentration of H_2S gas. This trend indicates a correlation, either inversely or directly, between the response/recovery time and the concentration of H_2S gas. The observed decrease in response time can be attributed to the higher concentration of H_2S gas facilitating a more rapid interaction with the sensing material. As the gas concentration increases, a greater number of H_2S molecules become accessible to the sensing material, leading to a quicker response time. This phenomenon is indicative of the sensor's heightened reactivity to higher concentrations of H_2S. Conversely, the increase in recovery time is associated with the extended duration required for the complete desorption of H_2S gas from the sensing material. Higher gas concentrations may lead to a larger quantity of H_2S molecules adsorbed onto the sensor's surface, necessitating a longer time for desorption and restoration of the baseline signal. This finding underscores the importance of considering both response and recovery times for a comprehensive evaluation of the sensor's performance.

Stability

In Fig. 6, the graph illustrates the durability of the prepared ZnO sensor. The study focused on evaluating the stability of the zinc oxide sensor in response to H_2S gas over 50 days at the temperature of 200°C, with measurements conducted every 10 days for 100 ppm concentration. Notably, the ZnO sensor exhibited 52% stability. It is remarkable that the initial sensor response decreased from 164% to 86% during the 50-day duration but eventually stabilized. This stabilization is attributed to the impact of humidity on the sensor. These results emphasize the promising applicability of ZnO as a material for gas sensors in the context of detecting H_2S gas.

Sensing mechanism

Figure 7 illustrates a schematic representation of the potential gas sensing mechanism employed by the ZnO sensor. In the presence of the air, oxygen absorbed onto the ZnO sensor surface. These oxygen molecules undergo conversion into various oxidation states (O^-, O_2^-, and O^{2-}). This process results in the formation of a free-electron region (electron depletion layer). Consequently, there is a simultaneous decreases number of electrons and an increase in the barrier height for electron transport, leading to a high resistance state for the ZnO sensor (Fig. 7a)

[17].It's worth noting that O_2^- ions are stable under 100°C, O^- between 100°C and 300°C, and after 300°C, O^{2-} ions become dominant and integrate into the lattice [18-19]. Fig. 7b illustrates the introduction of H_2S gas to the prepared sensor. H_2S serves as a reducing gas, and when samples are exposed to H_2S at elevated temperatures, it facilitates the removal of adsorbed oxygen. This process effectively restores electrons to the conduction band, resulting in a reduction in the resistance. This phenomenon crucially hinges on the interaction between H_2S and oxygen ions (O^-) at the surface of ZnO. Specifically, the interaction re-injects electrons into the conduction band, leading to an enhancement in conductivity compared to the baseline state (20-21). Therefore, exposure to H_2S at higher temperatures induces a beneficial effect on the electrical properties of the semiconductor by promoting the removal of adsorbed oxygen and facilitating electron flow in the conduction band.

CONCLUSION

In this study, a co-precipitation technique was employed to successfully synthesize ZnO nanostructures. XRD analysis confirmed the hexagonal wurtzite structure. The FESEM study revealed a porous and uniform morphology in pure ZnO, making it well-suited for gas sensing uses. Based on comprehensive gas sensing property assessments, it was determined that the ZnO nanomaterial exhibited a remarkable maximum response of 164% at 100 ppm H_2S gas and at of 200°Ctemperature. The prepared sensor demonstrated favorable response/recovery times, and stability Consequently, ZnO nanostructures emerge as highly promising materials for upcoming sensors designed for detecting H_2S gas at a concentration of 100 ppm, showcasing exceptional capabilities in the realm of gas sensing technology.

ACKNOWLEDGMENT

Authors, JGP and VSK, would like to extend their gratitude to CKTACS College, New Panvel (Autonomous) for providing financial **support through Project No. CKTACS/3111/11/2022-23**. This support was made possible by the grant received from the **RUSA** of the Government of India. The authors appreciate the institution's commitment to fostering research and academic endeavors, which has significantly contributed to the realization and execution of their project. This acknowledgment reflects the importance of institutional support in advancing scholarly pursuits and promoting scientific research.

CONFLICT OF INTEREST

The authors assert that they have no discernible conflicting financial interests or personal affiliations that could be perceived as influencing the research presented in this paper.

REFERENCES

1. S. Gao, Y. Zhao, W. Wang, J. Zhao, and X. Wang, Au/CuO/Cu2O heterostructures for conductometric triethylamine gas sensing, *Sens Actuators B Chem*, **2022**, 371, 132515. https://doi.org/10.1016/j.snb.2022.132515
2. V. Kamble, R. Zemase, R. Gupta, B. Aghav, S. Shaikh, J. Pawara, S. Patil, and S.Salunkhe, Improved toxic NO_2 gas sensing response of Cu-doped ZnOthin-film sensors derived by simple co-precipitation route, *Optical Materials*, **2022**, 131, 112706. https://doi.org/10.1016/j.optmat.2022.112706
3. A. Yang, Q. Hou, X. Yin, M. Qi, and Z. Wang, First principles study on p-type conductivity and new magnetic mechanism of ZnO: Sm with point defects in different strains, *Solid State Communications*, **2022**, 348, 114738. https://doi.org/10.1016/j.ssc.2022.114738

4. A. Gul, M. Khan, G. Khan, H. Ahmad, P. Thounthong, S. Khattak, S. Zulfiqar, and T. Khan, First-principles calculations to investigate the optoelectronic, and thermoelectric nature of zinc based group II-VI direct band semiconductors, *Optik* ,**2022**, 271,170143. https://doi.org/10.1016/j.ijleo.2022.170143
5. S. Rezaie, Z. Bafghi, and N. Manavizadeh, Carbon-doped ZnO nanotube-based highly effective hydrogen gas sensor: A first-principles study, *International Journal of Hydrogen Energy*, **2020**, 45(27), 14174-14182. https://doi.org/10.1016/j.ijhydene.2020.03.050
6. I. Naik, T. Naik, E. Pradeepa, S. Singh, and H. Naik, Design and fabrication of an innovative electrochemical sensor based on Mg-doped ZnO nanoparticles for the detection of toxic catechol, *Materials Chemistry and Physics*,**2022**, 281, 125860. https://doi.org/10.1016/j.matchemphys.2022.125860
7. K. Preeti, A. Kumar, N. Jain, A. Kaushik, Y. Mishra, and S. Sharma, Tailored ZnO nanostructures for efficient sensing of toxic metallic ions of drainage systems, *Materials Today Sustainability*, **2023**, 24, 100515. https://doi.org/10.1016/j.mtsust.2023.100515
8. L. Yang, Y. Zhao, S. Luo, Y. Jun, J. Zhao, W. Shen, and S. Yin, Toxic effects and possible mechanisms of hydrogen sulfide and/or ammonia on porcine oocyte maturation in vitro, *Toxicology letters*, **2018**, 285, 20-26.https://doi.org/10.1016/j.toxlet.2017.12.019
9. W. Kun, D. Lin, and G. Maofa, Environmental chamber study of the photochemical reaction of ethyl methyl sulfide and NOx, *Journal of Environmental Sciences*, **2009**, 21 (2), 137-141.https://doi.org/10.1016/S1001-0742(08)62241-X
10. Y. Han, Z. Zhang, T. Li, P. Chen, T. Nie, Z. Zhang, and S. Du, Straw return alleviates the greenhouse effect of paddy fields by increasing soil organic carbon sequestration under water-saving irrigation, *Agricultural Water Management*, **2023**, 287, 108434.https://doi.org/10.1016/j.agwat.2023.108434
11. C. Wu, G. Kebena, Y. Guan, P. Jinn, C. Yichia, and H. Hsiao, Development of p-type zinc oxide nanorods on zirconium-based metallic glass nanotube arrays by facile hydrothermal method for gas sensing applications, *Chemical Engineering Journal*, **2023**, 463, 142381.https://doi.org/10.1016/j.cej.2023.142381
12. D. Lim, N. Mark, and M. Rowel, Universal Scherrer equation for graphene fragments, *Carbon*, **2020**, 162, 475-480.https://doi.org/10.1016/j.carbon.2020.02.064
13. P. Kibasomba, S. Dhlamini, M. Malik, C. Liu, M. Mohamed, D. Rayan, and B. Mwakikunga, Strain and grain size of TiO_2 nanoparticles from TEM, Raman spectroscopy and XRD: The revisiting of the Williamson-Hall plot method, *Results in Physics*, **2018**,9, 628-635.https://doi.org/10.1016/j.rinp.2018.03.008
14. J. Macchi, G. Guillaume, J. Teixeira, S. Denis, F. Bonnet, and S. Allain, Time-resolved in-situ dislocation density evolution during martensitic transformation by high-energy-XRD experiments: A study of C content and cooling rate effects, *Materialia*, **2022**, 26, 101577. https://doi.org/10.1016/j.mtla.2022.101577
15. S. Kokkiligadda, S. Raut, K. Mariyappan, Y. Nam, M. Kesama, V. Mathe, S. Bhoraskar, and S. Park, Opto electric and photocatalytic characteristics of DNA thin films embedded with transition metal ion-doped ZnO nanorods, *Materials Chemistry and Physics*, **2022**, 286, 126135.https://doi.org/10.1016/j. matchemphys.20 22.126135
16. Z. Qu, Y. Fu, B. Yu, P. Deng, L. Xing, and X. Xue, High and fast H_2S response of NiO/ZnO nanowire nanogenerator as a self-powered gas sensor, *Sensors and Actuators B Chemical*, **2016**, 222, 78-86.https://doi.org/10.1016/j.snb.2015.08.058
17. K. Xie, Y. Wang, K. Zhang, R. Zhao, Z. Chai, J. Du, and J. Li, Controllable band structure of ZnO/g-C_3N_4 aggregation to enhance gas sensing for the dimethylamine detection, *Sensors and Actuators Reports*, **2022**,4, 100084.https://doi.org/10.1016/j.snr.2022.100084
18. P. Hou, Z. Lin, M. Dong, Z. Sun, M. Gong, F. Li, and X. Xu, A thermodynamically stable O2-type cathode with reversible O2-P2 phase transition for advanced sodium-ion batteries, *Journal of Colloid and Interface Science*, **2023**,*649*, 1006-1013. https://doi.org/10.1016/j.jcis.2023.06.162
19. P. Ding, X. Dongsheng, D. Nan, C. Ying, X. Pengcheng, Z. Dan, and X. Li, A high-sensitivity H_2S gas sensor based on optimized ZnO-ZnS nano-heterojunction sensing material, *Chinese Chemical Letters*,**2020**, 31(8), 2050-2054.https://doi.org/10.1016/j.cclet.2019.11.024

20. Z. Li, Z. Lai, Z. Zhao, L. Zhang, and W. Jiao, A high-performance gas sensor for the detection of H_2S based on Nd_2O_3-doped ZnO nanoparticles, *Sensors and Actuators A: Physical*, **2023**, 350, 114119.https://doi.org/10.1016/j.sna.2022.114119
21. U. Nakate, Y. Yu, and S. Park, Hydrothermal synthesis of ZnO nanoflakes composed of fine nanoparticles for H_2S gas sensing application, *Ceramics International*, **2022**, 48 (19), 28822-28829.https://doi.org/10.1016/j.ceramint.2022.03.017

Table 1: Structural parameter of prepared ZnO sample

Material	D	a	c
ZnO NPs	34.7 nm	3.244	5.182

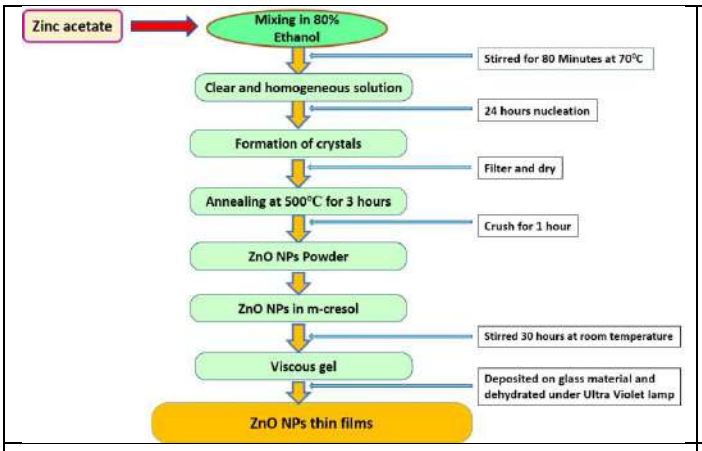

Fig. 1 Synthesis outline of ZnO NPs thin films

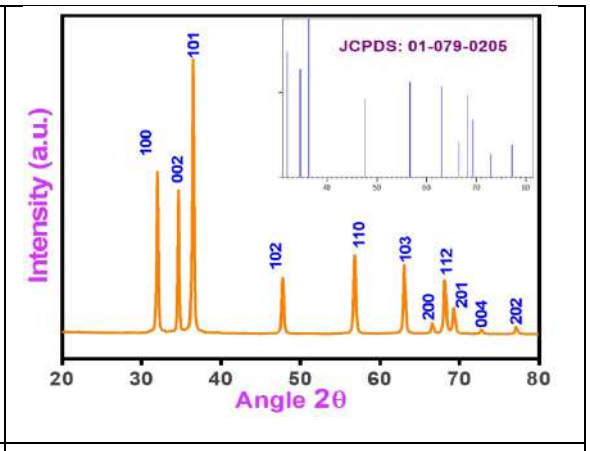

Fig. 2 XRD pattern of ZnO NPs

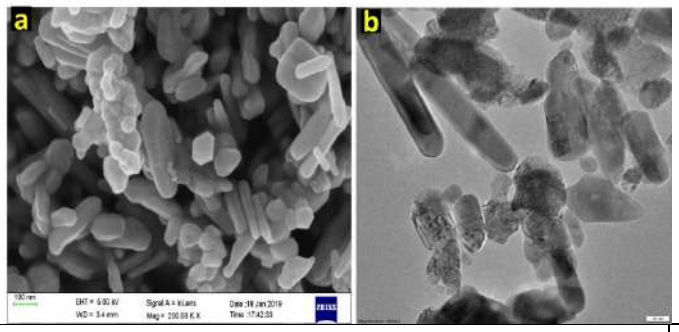

Fig. 3(a) FESEM (b) HRTEM of ZnO NR's

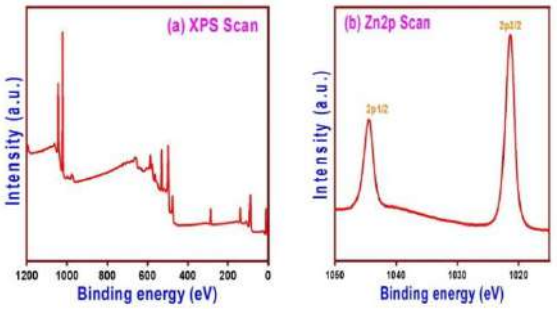

Fig. 4 XPS Spectrum a) wide scan b) Zn2p scan

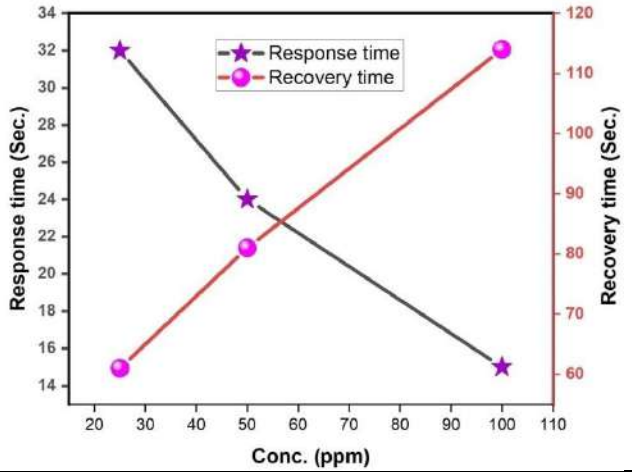

Fig. 5 Response/recovery time

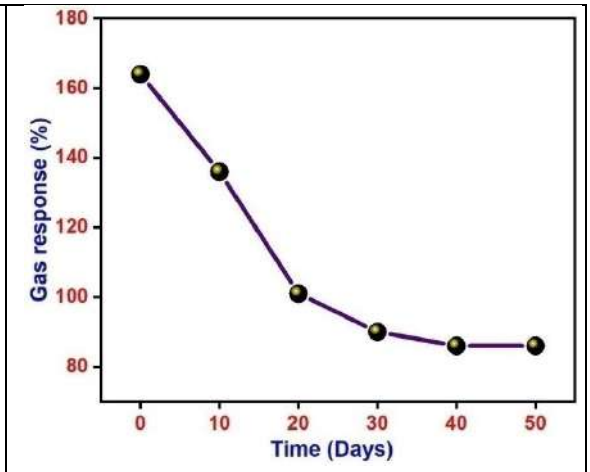

Fig. 6 Stability performance of ZnO sample

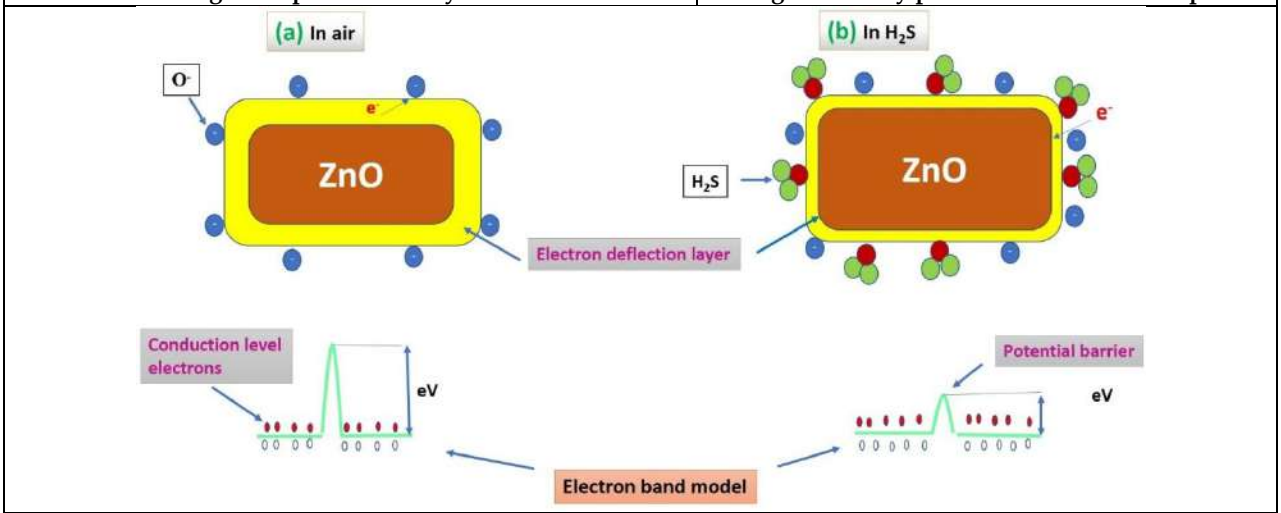

Fig. 7 Representation of the probable mechanism of ZnO sensor (a) In air (b) In H2S gas.

Indian Journal of Natural Sciences *www.tnsroindia.org.in ©IJONS*

Vol.15 / Issue 83 / Apr / 2024 *International Bimonthly (Print) – Open Access* *ISSN: 0976 – 0997*

RESEARCH ARTICLE

Nanoparticles as Food and Medicine: a Systematic Analysis of Recent Nanotechnology Developments in Fishery Industry

Vasantharaja D*, Nagaraj S, Peetha Sarika and Vimala V

Department of Zoology, Tagore Government Arts and Science College (Affiliated to Pondicherry University) Puducherry, India.

Received: 22 Feb 2024 Revised: 07 Mar 2024 Accepted: 20 Mar 2024

***Address for Correspondence**
Vasantharaja D
Department of Zoology,
Tagore Government Arts and Science College (Affiliated to Pondicherry University)
Puducherry, India.
Email: vasaini20@gmail.com

ABSTRACT

The unique properties of nanoparticles (NPs) have driven the rapid growth of nanotechnology as a field of study. In both human and animal healthcare, NPs find applications in diagnostics, vaccinations, drug delivery, and gene therapy. This systematic review investigates the cutting-edge advancements of nanotechnology in the fisheries industry, focusing on its diverse applications in food and medicine. NPs are emerging as transformative tools, offering distinct advantages in improving food production, preservation, and drug delivery for aquatic resources. This review provides an overview of NPs utilization, with a particular emphasis on their antimicrobial properties and their role as supplementary feed in the fishing sector. Research in fish vaccines and medications is extending to include NPs for combating various bacterial, fungal, and viral infections. The aquaculture industry is increasingly exploring NPs as a targeted food source and reliable diagnostic tool for various ailments. Nevertheless, it is essential to acknowledge that there are numerous untapped nanotechnologies in the fisheries sector. This study underscores the vast potential of NPs in revolutionizing the fishery industry while highlighting the need for further exploration and innovation in this promising field.

Keywords: Nanotechnology, Nanomedicine, Nanoparticles, Fish medicine, Aquaculture

INTRODUCTION

The term "nanotechnology" refers to the field of study dedicated to the construction and manipulation of subatomic particles. In recent years, tools have been developed for investigating and controlling materials at the nanoscale, typically ranging between approximately 1-100 nm. The distinctive properties of these particles open up avenues for innovative applications [1]. Artificial nanoparticles (NPs) are deliberately synthesized, while naturally occurring

ultrafine nano-sized particles represent one category of nanomaterials [2]. Nanomedicine, encompassing both human and veterinary healthcare, involves the application of nanotechnology. It focuses on the research and development of NPs and nanodevices for medical applications [3, 4], including their use in fish feed. Nanoparticles are available in various forms, each finding medical applications as outlined in Figure 1 [4]. Nanospheres, characterized by their small size and spherical shape measuring only a few nanometers, are particularly advantageous for drug delivery due to their extensive surface area [5]. They also demonstrate applicability in tissue regeneration [6]. Another type of nanoparticles, nanocapsules, possesses a nanoscale shell encapsulating a core, safeguarding the enclosed medicine whether oil or water from degradation and hydrolysis [7]. Liposomes, nano-sized lipid bilayer spheres resembling eukaryotic cell membranes, are well-suited for transporting both lipophilic and hydrophilic drugs [3, 8]. Carbon nanotubes, which can be single or multiple-walled, are another type of tiny particles used a lot in medicine. They have a lot of space on their surface and can get into cells easily, like tiny needles. This makes them great for carrying drugs, including ones that fight tumors [9]. However, studies show they can cause blood clots in blood vessels [10]. Dendrimers are another kind of tiny particles. They're like tiny three-dimensional structures with branches coming out from a center. They are light and have many branches on their surface, which makes them useful for growing tissues, fighting germs, and carrying genes, vaccines, and medicines [11, 12]. Nanoparticles (NPs) are increasingly being utilized in fisheries as medicine, and their recent application extends to diverse areas, such as integrating them in aquaculture as feed. These tiny particles serve various functions, including acting against microbes, transporting drugs or genes, delivering vaccines, and accurately diagnosing fish infections [13]. Compared to bulk materials, nanoparticles offer numerous technical and biological advancements. They have special qualities due to their tiny dimensions and massive particular area of surface. However, these fields of nanotechnology research are still relatively underdeveloped. In this review article, we present a thorough overview of both proven and potential uses of nanomaterials in the fish feed and fish medicine industries.

MAJOR SYNTHESIS OF NANOPARTICLES

The production of nanoparticles can be achieved through two primary methods: the descending or ground-up approach [14]. In the top-down technique, conversion of large-scale and micro-scale metal into nanoscale particles is accomplished through mechanical grinding. Following this, calming substances like colloidal defending substances are introduced to prevent the NPs from oxidizing or reassembling at the micro-scale [15]. Various chemical and physical processes, including electro-chemical reduction of metals and sono decomposition [16], can be employed to fabricate nanoparticles, which are categorized as bottom-up methods.

Physical and Chemical synthesis of NPs

Thermal combustion of organic solvents can be used for NP production [17]. Cryochemical synthesis may produce metal NPs with a diameter ranging from 5 nm to 80 nm [18]. To create silver nanoparticles (Ag-NPs), scientists have turned to microwaves, specifically for the physical breakdown of Ag at distinct wavelengths of microwave rays [19]. In comparison to the thermal approach, this technique was faster and produced an elevated attention of Ag-NPs under the same conditions. To generate a larger particle size, Jiang et al. [19] observed that the reaction time and temperature needed to produce the silver nitrate were also increased, along with the quantity of silver nitrate employed. Silver particles ranging between 15 and 25 nm in size were produced by using high concentrations of polyvinyl pyrrolidone (PVP). A number of methodologies are utilized for the making of NPs. These embrace sustained ablation with laser [20], electro-reduction of silver nitrate in polyethylene glycol in an aqueous solution [21], ember ejection [22], micro-emulsion for creating silver- Iron (II,III) oxide-NPs [23], and the AgNO3 undergoes chemical reduction with trisodium citrate in the presence of sodium tetrahydridoborate (III) as a reluctant to synthesize PVP-coated Ag-NPs [24, 25]. Additionally, methods for synthesizing nonmetallic NPs, like polymeric chitosan (CS)-NPs, have been demonstrated through various approaches. Ionotropic gelation ia a techniue in which, chitosan (CS) is dissolved in acetic acid, followed by the addition of the polyanion tripolyphosphate (TPP). This process relies on the magnetized connection among the positively charged amine group of CS and the negatively charged polyanion polymer [26, 27]. In the polyelectrolyte cluster technique, the magnetized connection between the positively charged groups in the CS and the DNA is crucial, leading to charge neutralization during NPs production

[26]. The micro-emulsion method [28], which utilizes surfactants, has drawbacks such as the utilization of natural substances, an extended manufacturing duration, and the intricate process of cleaning operations. Precipitation [29] and double-emulsion solvent evaporation [30, 31] are typically the two steps in the synthesis of PLGA-NPs. In the process, polyelectrolytes with positive and negative charges are mixed together, leading to the formation of a complex structure held together by electrostatic forces [26]. This technique is called polyelectrolyte complex allows for precise control over the properties of the resulting material, making it suitable for a wide range of applications. The polyelectrolyte complex technique involves the formation of a stable material through the interaction of oppositely charged polymers. This technique is used in various applications such as drug delivery, tissue engineering, and surface modification. The micro emulsion technique utilizes surfactants and also has many drawbacks [2]. Production of PLGA by precipitation [29] followed by double emulsion evaporation [30, 31]

Biological / Green synthesis of NPs

Researchers are very interested in finding ways to make NPs that are good for the environment and don't cost a lot of money. The use of biological methods is seen as a key part of this strategy's success [32]. Bacteria, fungus, and plants are the primary sources of biologically produced NPs. Bottom-up reduction and oxidation reactions are important to the biosynthesis of NPs [33]. Microorganisms or plant chemicals that have antioxidant or alleviating objects catalyze predecessor molecules to make the preferred NPs. A biosynthetic nanoparticle system typically includes three main components: This substance serves as a solvent in the process of synthesis, functions as an ecologically conscious reducing agent, and acts as a secure stabilizing agent [33]. Ag-NPs were made using liquid extracted from *Origanum vulgare* leaves. These particles showed the ability to kill bacteria and were toxic to lung cancer cells [34]. Both silver (Ag) and gold (Au) nanoparticles were created using liquid extracted from cashew nut shells. These particles can kill bacteria that cause fish infections [35]. Additionally, high amounts of Ag-NPs made with Camellia sinensis a tea leaf extract were able to kill *Vibrio harveyi* bacteria in young *Fenero penaeus indicus* shrimp [36]. A recent study looked at silver nanoparticles (Ag-NPs) made from *Origanum vulgare* leaves and compared them with chemically made ones. The two kinds were examined utilizing UV–spectrophotometry, transmission electron microscopy (TEM), and dynamic light scattering. The bacteria Streptococcus *agalactiae, Aeromonas hydrophila*, and *Vibrio alginolyticus*, as well as the fungus *Aspergillus flavus, Fusarium moniliforme*, and *Candida albicans*, were tested in various fish species [37]. Additionally, zinc oxide (ZnO) nanoparticles were made in a broth from Aloe leaves and showed stronger germ-killing ability compared to regular ones [38]. This eco-friendly and cost-effective method involved making ZnO-NPs with the help of Aeromonas hydrophila bacteria, resulting in nanoparticles that can kill bacteria and fungi [39].

ANTIBIOTIC-RESISTANT BACTERIA

Antibiotics have proven effective in combating bacterial infections for an extended period. Nevertheless, the uncontrolled and excessive utilization of antibiotics may contribute to the rise of microorganisms that are resistant to antibiotics [40-42]. These bacteria no longer respond to the effects of antibiotics. The transfer of resistance genes between terrestrial and aquatic bacteria is feasible due to shared components in their mobile genomes. Such gene transfer poses potential risks to the health of both animals and humans [42-44]. Tuevljak et al. conducted a survey across 25 countries to assess the antimicrobial usages in fish farms [45]. Their findings revealed that the most commonly employed antibacterial agent is tertracycline. The excessive application of antibiotics in aquaculture is significantly correlated with proliferation of antibiotic-resistant bacteria. This increase also involves a rise in the number of bacteria that are resistant to different treatments, like methicillin-resistant *Staphylococcus aureus* (MRSA), as well as some microorganisms that are opposing to manifold and extremely powerful drugs [45, 47]. Certain *Aeromonas hydrophila* found in farmed tilapia were resistant to a wide range of antibiotics [48]. Additionally, antibiotic resistance was seen in other bacteria stains [43, 49]. Di-Cesare and colleagues found antibiotic-resistant enterococci in the sediment of fish farms, raising concerns about the spread of resistance to strains that can affect humans [50, 51].

INNOVATIVE ANTIBACTERIAL APPLICATIONS OF NANOPARTICLES IN FISH MEDICINE

The emergence of drug-resistant microbes in aquaculture has become an increasingly concerning issue. Consequently, scientists have explored the possibility of utilizing NPs as a potential antibacterial solution (Table. 1) [37, 49]. Metal NPs have potent antibacterial effects against many microorganisms [52]. Following this, we will discuss research into the use of metal NPs in combating fish diseases

Ag-NPs

Nano-antibacterial agents have been studied extensively, but Ag-NPs have received the most attention. In contrast to antibiotics, which typically only operate through one mechanism [53–55], multi-target antimicrobials are able to circumvent bacterial resistance by targeting numerous pathways at once. A method involving the silver ions (Ag+) released has been identified [53]: Silver ions interact with proteins present in the bacterial cell membrane, leading to membrane rupture and eventual cell death [58]. When Ag+ enters a cell, it attaches to mitochondria and nucleic acids, causing harm and interrupting replication of cells [59]. Ag-NPs demonstrate potent antibacterial activity, particularly against MDR bacteria, as highlighted by Prakash et al. [56]. Notably, methicillin-resistant *Staphylococcus aureus* (MRSA) has been found to be susceptible to the bactericidal effects of Ag-NPs [56].When Ag-NPs are created using lemon juice as a dropping agent, they show effectiveness against *Staphylococcus aureus* and *Edwardsiella tarda* bacteria. Additionally, they exhibit anti-cyanobacterial effects against Anabaena and Oscillatoria species [49]. The studies have utilized the extract of leaf buds from the mangrove *Rhizophora mucronata* for the green synthesis of Ag-NPs, aiming to demonstrate antibacterial activities [60].

These eco-friendly or "green" Ag-NPs exhibited effectiveness comparable to conventional antibiotics but with significantly fewer negative side effects. Notably, long-term therapy with Ag-NPs resulted in a 71% reduction in mortalities in *Vibrio harveyi*-infected *Feneropenaeus indicus* at increased doses of Ag-NPs [36]. Ag-NPs showed potent antifungal activity against *Candida* species, with antifungal effects comparable to those of the commercial antifungal Amphotericin B [61, 62]. Researchers have found that Ag-NPs have antifungal efficacy against dermatophytes [63]. In another study, Ghetas et al. demonstrated that the Ag-NPs inhibit the growth of three fungal strains isolated from Nile tilapia) tested in their study. The results indicate that the Ag-NPs synthesized through biological means have shown better efficacy than those synthesized chemically. Furthermore, it is promising to note that the antimicrobial effectiveness of Ag-NPs against the fungal strains can be improved with an increase in the administered dose [37]. Ag-NPs can bind to HIV-1 virus proteins *in vitro* [64], demonstrating their anti-viral capabilities. The influenza A virus can be inhibited by either Ag-NPs or Ag-NPs -CS composite [65, 66]. When it comes to Ag-NPs antifungal and antiviral properties in fish medicine, there is a dearth of published work.

Au-NPs

Due to the non-hazardous nature of Au-NPs to eukaryotic cells, considerable research efforts are being directed towards studying their antimicrobial activities [67]. Au-NPs exhibit the ability to act together with biological macromolecules as well as non-proteins and they can perform various functions in biology [68]. The bactericidal effects of gold nanoparticles supported on aluminium silicate were demonstrated against *E-coli* and *S. typhi* [69]. Functionalized gold nanoparticle was established to suppress the growth of multidrug-resistant bacterial strains [67]. Additionally, antibacterial activity was observed in Au-NPs produced through "green" synthesis against a bacterial strain isolated from fish [35]. Au-NPs exhibit antibacterial properties, and they can employ three different mechanisms to kill microbes. The first mechanism involves altering the cell membrane of specific microbes, disrupting the oxidative phosphorylation process. This alteration result in reduced efficiency of the F-type ATP synthase, leading to a decrease in the overall rate of ATP synthesis and metabolism. The second mechanism involves modifying how t-RNA attaches to the two subunits of the ribosome. The third strategy involves enhancing chemotaxis [70]. Research has established that Au-NPs can exert fungicidal effects against various Candida species. Interestingly, the antifungal activity of Au-NPs is more pronounced when the particles are smaller. Their effectiveness has been demonstrated to be directly proportional to their particle size [71, 72].

ZnO-NPs

ZnO-NPs have garnered significant attention for their ability to effectively eliminate bacteria and fungi [38, 49]. These nanoparticles induce damage to the microbe's cell membrane, ensuing in the leakage of cytoplasmic contents from the cell [73]. In the area of fish healthcare, Zn-NPs have demonstrated the capability to restrain the development of various bacterial strains [49]. In a study by Ramamoorthy et al. [74], they looked at how zinc oxide nanoparticles can kill harmful *Vibrio harveyi* bacteria. They found that these nanoparticles were better at killing bacteria compared to regular zinc oxide. Another interesting study involved making ZnO-NPs using a bacterium called *Aeromonas hydrophila*. These nanoparticles were able to kill not only *Vibrio harveyi* but also other microorganisms like bacteria and fungi [39].

Titanium dioxide (TiO_2) NPs

TiO_2 NPs infused with magnetic Fe_3O_4-nanoparticles exhibited antibacterial activity, when exposed to light [75, 76]. Due to the affinity of fish pathogens for these nanoparticles, allowing for their easy removal from water using a magnet, these particles can be utilized in water disinfection processes. Additionally, Jovanovic et al. [77, 78] reported that Titanium dioxide nanoparticles have an impact on the fish defence system by suppressing the bactericidal response of fish neutrophils. This makes fish highly vulnerable to disease, leading to increased mortality rates, principally during spreading of diseases, posing a significant concern.

THE USE OF NANOPARTICLES AS CARRIERS FOR THE DELIVERY OF DRUGS AND GENES

A good drug delivery system should have certain important qualities. These include being safe, compatible with the body, able to break down naturally, and keeping the drug stable. It should also target specific areas and have few or no side effects (Fig.2) [4]. Nanoparticles (NPs) have become popular for this purpose because they are very small and can move through barriers in the body like the BBB. Also, NPs have a large surface area compared to their size, which makes them very reactive with different substances [4, 79, 80]. In fish medicine, Chitosan NPs and PLGA-NPs are being studied a lot as carriers for delivering drugs.

Chitosan NPs for drug delivery

Chitosan NPs stand out as favorable choices for drug delivery vehicles due to their exceptional characteristics. Comprising a polymer that is biocompatible, non-toxic, and biodegradable, these nanoparticles are easily eliminated by the kidneys [4]. Their muco-adhesive efficiency makes them well-suited for controlled and sustained drug release [80]. In a study involving *Oncorhynchus mykiss*, for instance, chitosan NPs were used to enhance the delivery system for vitamin C. The synergistic association between chitosan and ascorbic acid resulted in sustained vitamin release for up to 48 hours after exposure, stimulating the fish's inborn immune system [82]. In a different test, hormones in *Cyprinus carpio* (common carp) were given using chitosan nanoparticles (NPs). One group got LH-RH mixed with chitosan-coated gold nanoparticles (Au-NPs), and we compared the results with a group getting just one hormone injection. Both groups had higher levels of hormones in their blood, and the hormones were released more slowly compared to the group with only one injection. Interestingly, injections of hormone mixed with chitosan NPs and hormone mixed with chitosan-coated gold NPs increased the rate of fertilization of eggs by 87% and 83%, respectively, compared to giving repeated injections of luteinizing hormone-releasing hormone alone, which only resulted in a rate of fertilization is about 74% [83].

PLGA-NPs for drug delivery

Polylactic acid and polyglycolic acid are combined to form PLGA, a copolymer. It is non-toxic, biodegradable, and biocompatible. The FDA has given its approval. As a result, numerous researchers have looked at whether using PLGA as a drug carter is feasible [84, 85]. In a recent study, Poly (lactic-co-glycolic acid)-(PLGA)-NPs were loaded with the anti-bacterial medication rifampicin and then injected into zebra fish embryos. Zebra fish embryos are apparent, making it possible to use non-invasive imaging to assess the treatment's effects on Mycobacterium marinum-infected cells. In comparison to rifampicin alone, the rifampicin-PLGA-NPs had a better restorative efficacy towards M. marinum and advanced embryonic survival [86].

Fish vaccines based on nanotechnology

A fascinating area of medical research is the incorporation of NPs in vaccination compositions. Because of their many benefits as vaccine delivery systems, polymeric NPs have received the greatest attention [87, 88]. These benefits include the capacity to assure antigen stability against enzyme degradation, maintain immunogenicity, and provide prolonged release of the vaccine. Both immune-stimulant adjuvants and targeted antigen delivery nanovaccines have the ability to slowly release antigens [88]. Various types of nanoparticles (NPs) have been used to deliver vaccines, including virus-like organisms, liposomes, immunostimulant complexes, metal NPs, and polymeric NPs [88, 89]. Challenges in making stable nano-vaccines, worries about possible harm, and not knowing enough about how they spread in the body have been the main concerns [89]. In the world of fish vaccine development, polymeric chitosan and PLGA-NPs have been the focus of most research so far. In the inactivated virus vaccine for infectious salmon anemia virus (ISAV), the vaccine contains the DNA code for the ISAV replicas, and chitosan NPs are added to enhance the immune response. This vaccine has been shown to be highly effective, providing up to 77% protection against ISAV [90]. Another vaccine was developed to protect Asian sea bass from the bacteria *Vibrio anguillarum*.

This vaccine contains DNA mixed with chitosan and chitosan/tripolyphosphate nanoparticles. However, this nanovaccine only provided a moderate level of defense against the microorganisms [27, 91]. An oral DNA vaccine was formulated by loading the outer membrane protein K gene of *Vibrio parahemolyticus* onto chitosan NPs. This approach facilitated the delivery of the gene as a vaccine. The resulting recombinant nanovaccine demonstrated the ability to induce a protective immunological response against *Vibrio parahemolyticus* in black seabream (*Acanthopagrus schlegelii*) [92]. Researchers looked at how well r-DNA-chitosan NPs could defend shrimp from the White Spot syndrome Virus (WSSV). It was discovered that the vaccination improved shrimp defense system and generated a defending activity against WSSV when it was administered in the form of an oral supervision [93, 94]. PLGA-NPs have demonstrated effectiveness both as carriers for DNA vaccines and as adjuvants in medicine [30, 95, 96]. However, there has been limited success in utilizing PLGA-NPs in fisheries. For instance, a DNA vaccine for protecting Japanese flounder towards lymphocystis disease virus (LCDV) was formulated, and it could be administered orally [97]. In another study, rainbow trout were victimized against the contagious hematopoietic necrosis virus using an orally delivered DNA vaccine, resulting in a successful elicitation of an immunological response in the fish [31].

THE USE OF NANOPARTICLES IN DETERMINING THE PRESENCE OF FISH PATHOGENS

The use of NPs in diagnostic testing has been given the general term "nanodiagnostic" [98], which is also the name of a specific category of diagnostic procedures. These methods make it possible to make accurate diagnoses of diseases in a short amount of time. One of the NPs that is used in the industry the most commonly is Au-NPs, which may be utilized in a range of diagnostic ways [99, 100]. Au-NPs are also one of the most expensive NPs.

Diagnostics for Fish Bacterial and Fungal Diseases

To specifically diagnose furunculosis in fish tissues, the first use of Au-NPs for pathogen detection was using an A. salmonicida antibody and Au-NPs coupled [101]. For the purpose of detecting fish diseases, this was the initial application of Au-NPs. Kuan et al. [102] offered an alternative method that included creating an electrochemical DNA biosensor for the detection of *Aphanomyces invadans* in fish by combining Au-NPs with a DNA reporter probe. With a lower detection threshold for fungal presence compared to PCR, this biosensor was designed for fish usage.

Fish viral disease diagnosis

A colorimetric test using Au-NPs and loop-mediated isothermal amplification (LAMP) was used to visually detect yellow head virus in shrimp by Jaroenram et al. [103]. Sensitivity, speed, and specificity were all much enhanced by this approach. Similarly, WSSV in shrimp was successfully detected utilizing a DNA-functionalized Au-NPs and LAMP combination, proving that the method is sensitive, accurate, and applicable in the field [104]. Using an Au-NPs-based biosensor for viral nucleic acid detection following RT-PCR amplification, Toubanaki et al. [105] devised a method for detecting nerve necrosis virus (NNV). Due to the lack of antibody conjugation, this method proved more cost-effective.

Yang et al. [106] used magnetic NPs coated with rabbit anti-NNV antibody to conduct an immunomagnetic reduction experiment in grouper fish. The NNV was the target of the assay's development. Magnetic NPs' motion in response to an applied external magnetic field formed the basis of the immunodiagnosis. Virus antigen attachment resulted in cluster formation and reduced motility of antibody-coated NPs. The viral titer was calculated using a magnetic immunoassay analyzer. Unmodified Au-NPs were employed to develop a colorimetric test for detecting the spring viremia of carp virus (SVCV). In this method, Au-NPs were introduced after the SVCV probe. If the intended viral RNA was present, it hybridized with the probe, preventing it from holding the Au-NPs in place. The aggregation of Au-NPs resulted in a color shift from red to blue. In the absence of viral nucleic acid, the probe could freely bind to Au-NPs surfaces, preventing aggregation and maintaining the solution in a red color [107]. This approach demonstrated a high degree of specificity, rapidity, and did not require prior viral nucleic acid amplification. The same principle was applied to create a quick, accurate, and sensitive assay for detecting the DNA virus Cyprinid herpes virus-3 (CyHV-3) [108].

NANOTECHNOLGY-BASED FISH FEED

Nanomaterials have demonstrated superior effectiveness compared to bulk materials in enhancing the growth and health of cultured fish [109-112]. However, it is crucial to note that lower doses of nanomaterials can have detrimental effects. This review also explores the current applications of nanoparticles (NPs) in the nourishment, diagnosis, and treatment of fish pathogens [113]. Fish are conventionally fed through the administration of food pellets designed to meet their daily nutritional requirements, encompassing lipids, proteins, carbohydrates, minerals, and vitamins [114, 115]. Recent research has investigated the incorporation of nanomaterials as additives in fish meals to protect fish from antimicrobials. The implementation of modern techniques, such as rapid disease diagnostics, holds the potential to enhance the absorption of medications like hormones, vaccinations, and critical nutrients in cultivable organisms, revolutionizing the fisheries and aquaculture industries [115]. Aquaculture relies heavily on metal nanoparticles (NPs) like iron (Fe), iron oxide (FeO), selenium (Se), zinc (Zn), zinc oxide (ZnO), copper (Cu), and magnesium oxide (MgO). Studies have shown that young goldfish and sturgeon grow rapidly, by 30% and 24% respectively, when given iron nanoparticles. Crucian carp (Carassius auratus) also show better growth, antioxidant levels, and muscle selenium concentration when they eat different selenium sources, including nano-selenium and selenium methionine [115, 116]. Recent research suggests that post-larvae of freshwater prawns (Macrobrachium rosenbergii) have higher survival and growth rates when zinc, nano zinc, and copper are added to their diet [116-118]. *Azolla microphylla*-generated gold nanoparticles may considerably avert hepatic degeneration in Asian carp brought on by acetaminophen water pollution, according to research by Kunjiappan et al. [119]. Indicators of oxidative stress, hepatic ion levels, metabolic enzymes, hepatotoxic markers, abnormal liver histology, and altered tissue enzymes are all markedly improved by the presence of gold nanoparticles.

The Siberian sturgeon (*Acipenser baerii*) showed improvements in body composition, survival rate, and growth when exposed to Aloe vera based-nanoparticles, according to Sharif et al. [120]. Additionally, Cui et al. [121] noted that nanotechnology has been used to try to increase the retention time and bioavailability of naturally occurring bioactive chemicals. Encasing of curcumin in NPs has been shown using phospholipids [122], micelles [123,124] liposomes [125], hydrogels [126], and other methods [127]. In a recent study by Shah et al. [128], researchers were able to enhance the shelf-life of curcumin by encapsulating it in chitosan nanoparticles stabilized using Pickering emulsion. When dealing with hydrophobic bioactive substances, the Pickering emulsion method is regarded as the most effective way to encapsulate them and enhance their shelf-life. This is due to the solid particles (nutrients in this case) that stabilize the emulsion [129-131). There is less or no toxicity, higher repeatability and biocompatibility, easy and scalability manufacturing, and improved stability with these emulsions compared to traditional emulsions [132-134]. In addition, the composition and structure of these mixtures enhance the transportation of biological substances in the gastrointestinal system [135-138]. Presently, a variety of colloidal particles are employed in the manufacturing of Pickering emulsions, whereby solid particles aid in maintain the emulsion. Starch-based Pickering emulsion has been utilized to transport chemicals, such as hydrophobic antifungal agents [139-141]. There is promising research into the use of nano-crystalline, self-stabilized Pickering emulsions for drug administration and release, particularly with chemicals that are not very soluble [142]. In a recent study by Zhou et al. [143], cellulose nanocrystals were

utilized to stabilize oil Pickering emulsions containing oregano essential oil. The purpose of this was to enhance the antibacterial effects of the emulsion against selected bacterial stains. In addition, a Zein/Arabic-gum NPs-maintained Pickering mixture was created using thymol to construct an antibiotic delivery system targeting E. col [144, 145]. In a recent study, Baldissera et al. [146,147] found that adding nerolidol-loaded nanospheres to the food of Nile tilapia infected with Streptococcus agalactiae resulted in decreased bacterial levels, improved survival rates, and protection against oxidative damage. Furthermore, nanoparticles may also be utilized to enhance the stability and bioavailability of dietary components, as well as to alter the physical characteristics of fish food. Even the use of modest amounts of nanoparticles can significantly improve the physical characteristics of food pellets.

As an illustration, when single-walled carbon nanotubes are added to the diets of trout, it leads to the formation of a solid pellet that remains intact while submerged in water. It is crucial to minimize contaminations and other food wastes in aqua forms caused by improper resilience, inadequate food stability, or unsuitable texture of the pellets. These factors result in substantial losses within the business [148]. Currently, there is significant research and investigation being conducted in the industry on the development of nano-formulations. An essential attribute of these systems is their versatility for many applications, including the administration of antibiotics, vaccines, medicines, and nutraceuticals, among others [149, 150]. Recent studies have concentrated on utilizing various biopolymers in the aquaculture industry [151-154]. The study discovered that when ascorbic acid is condensed in nanoparticles made from chitosan, it leads to an increase in the levels of ascorbic acid in the serum of rainbow trout when it is included in their diet. This increase in vitamin C levels also enhances the natural immune system, as indicated by higher amount of lysozyme and hemolytic serum complements, in comparison to the control groups receiving vitamin C and chitosan separately [155]. According to a recent study by Abd El-Naby et al. [156], feeding Nile tilapia (*O. niloticus*) with chitosan nanoparticle supplements can enhance their development and feed consumption. The authors contend that the presence of chitosan particles enhanced the activities of lipase and amylase. Furthermore, it has been shown that the utilization of these nanoparticles not only hinders the proliferation of all bacteria stains, but also enhances the inherent immune response.

In addition, another study have documented that the combination of ascorbic acid with chitosan NPs has an immunomodulatory impact on the toxicity induced organisms [157]. Furthermore, they highlight that the addition of this combinations leads to enhanced development and utilization of food in the presence of water contaminated with pesticides. And also, they highlight that the incorporation of chitosan NPs and ascorbic acid into the diet not only improves the antioxidant levels and generic immune response, but also potentially yields other beneficial health outcomes. These effects are evident in the cellular structure of hepatocytes and the overall well-being of *O. niloticus* when affected to sub-lethal levels of imidacloprid. In a recent finding, it was shown that the addition of dietary zeolites, either alone or in conjunction with chitosan NPs, can effectively alleviate the toxic impacts caused by introduction to imidacloprid [158]. However, it has also observed that the mixture of chitosan NPs with thymol can significantly enhance the development and usage of food in O. niloticus [159]. This is evident not only in the increased amount of lipases, catalases, and proteases, but also in the promotion of gastrointestinal villus length. However, the use of NPs as nutraceuticals in aquaculture (specifically shellfish and fish) for the purpose of enhancing value, reducing stress, and managing health is still in the early stages of consideration. The utilization of nutraceuticals is currently limited due to their high cost [160].

SUMMARY AND CONCLUSION

Nanomaterials have demonstrated superior effectiveness in improving the development and well-being of farmed fishes compared to larger materials. However, it is essential to ascertain the optimal particle size and dose to provide long-term advantages. Uncoated metal nanoparticles have been employed to contest microbial confrontation in aquaculture, but polymeric chitosan nanoparticles and PLGA-NPs have demonstrated efficacy in rapidly and cost-effectively identifying fish illnesses. Further investigation is required in the fields of nanocapsules, liposomes, dendrimers, and nanotubes to better understand fish illnesses. Additional research is crucial for the widespread use of nano technological methods in the development of vaccinations for fish. The aquaculture business has utilized

nanotechnology to increase fish health management, include nanoscale components, and improve aquaculture feeds. Nevertheless, the majority of apps are now in their first phases, and the substantial expenses linked to them hinder sustainable expansion. Mineral nanoparticles outperform bulk materials as feed additives for improving fish growth and well-being. They are also more cost-effective and resource-efficient compared to bulk minerals. Higher levels of nanomaterials have been discovered to have detrimental impacts on the development and overall health of fish. Because of the encouraging results in these areas for the efficient diagnosis, treatment, growth, and development of fisheries, there is a pressing demand for further concentrated investigation into the use of nanoparticles in fish medicine and fish feed.

REFERENCES

1. The Royal Society and Royal Academy of Engineering. Nanoscience and nanotechnologies: opportunities and uncertainties. 2004; London, UK.
2. Oberdörster G, Oberdörster E, Oberdörster J. Nanotoxicology: An emerging discipline evolving from studies of ultrafine particles. Environ Health Perspect 2005; 113: 823-839.
3. Cavalieri F, Tortora M, Stringaro A, Colone M, Baldassarri L. Nanomedicines for antimicrobial interventions. J Hosp Infect 2014; 88(4):183-190.
4. De Jong WH, Borm PJ. Drug delivery and nanoparticles: applications and hazards. Int J Nanomedicine 2008; 3(2): 133-149.
5. Donbrow M. Microcapsules and nanoparticles in medicine and pharmacy. CRC press 1991.
6. Ramalingam M, Jabbari E, Ramakrishna S, Khademhosseini A. (Eds.). Micro and Nanotechnologies in Engineering Stem Cells and Tissues (Vol. 39). John Wiley & Sons 2013.
7. Torchilin VP. Nanoparticulates as drug carriers. Imperial college press 2006.
8. Lasic DD. Novel applications of liposomes. Trends Biotechnol 1998; 16(7):307-321.
9. Reilly RM. Carbon nanotubes: potential benefits and risks of nanotechnology in nuclear medicine. J Nucl Med 2007; 48(7):1039- 1042.
10. Gaffney AM, Santos-Martinez MJ, Satti A, Major TC, Wynne KJ, Gun'ko YK et al. Blood biocompatibility of surface-bound multiwalled carbon nanotubes. Nanomedicine 2015; 11(1):39-46.
11. Aulenta F, Hayes W, Rannard S. Dendrimers: a new class of nanoscopic containers and delivery devices. Eur Polym J 2003; 39(9):1741-1771.
12. Gillies ER, Frechet JM. Dendrimers and dendritic polymers in drug delivery. Drug discov today 2005; 10(1):35-43.
13. Wu LP, Ficker M, Christensen JB, Trohopoulos PN, Moghimi SM. Dendrimers in medicine: therapeutic concepts and pharmaceutical challenges. Bioconjug chem 2015.
14. Holmes JD, Lyons DM, Ziegler KJ. Supercritical fluid synthesis of metal and semiconductor nanomaterials. Chemistry 2003; 9(10):2144- 2150.
15. Gaffet E, Tachikart M, El Kedim O, Rahouadj R. Nanostructural materials formation by mechanical alloying: morphologic analysis based on transmission and scanning electron microscopic observations. Mater Charact 1996; 36:185–190.
16. Thirumalai Arasu V, Prabhu D, Soniya M. Stable silver nanoparticle synthesizing methods and its applications. J Bio Sci Res 2010; 1: 259–270.
17. Esumi K, Tano T, Torigue K, Meguro K. Preparation and characterization of bimetallic Pd-Cu colloids by thermal decomposition of their acetate compounds in organic solvents. Chem Mater 1990; 2:564-567.
18. Sergeev MB, Kasaikin AV, Litmanovich AE. Cryochemical synthesis and properties of silver nanoparticle dispersions stabilised by poly(2-dimethylaminoethyl methacrylate). Mendeleev Commun 1999; 9: 130–132.
19. Jiang H, Moon K, Zhang Z, Pothukuchi S, Wong CP. Variable frequency microwave synthesis of silver nanoparticles. J Nanopart Res 2006; 8:117–124.

20. Jang D, Kim D. Synthesis of nanoparticles by pulsed laser ablation of consolidated metal microparticles. Appl Phys 2004; A79:1985-1988
21. Zhu J, Liao X, Chen HY. Electrochemical preparation of silver dendrites in the presence of DNA. Mater Res Bull 2001; 36:1687– 1692.
22. Tien DC, Tseng KH, Liao CY, Tsung TT. Colloidal silver fabrication using the spark discharge system and its antimicrobial effect on *Staphylococcus aureus*. Med Eng Phys 2007; 30: 948–952.
23. Gong P, Li H, He X, Wang K, Hu J, Tan W. Preparation and antibacterial activity of Fe3O4 Ag nanoparticles. Nanotechnology 2007; 18:604–611.
24. Van Dong P, Ha CH, Kasbohm J. Chemical synthesis and antibacterial activity of novel-shaped silver nanoparticles. Int Nano Lett 2012; 2:1-9.
25. El Mahdy MM, Eldin TAS, Aly HS, Mohammed FF, Shaalan MI. Evaluation of hepatotoxic and genotoxic potential of silver nanoparticles in albino rats. Exp Toxicol Pathol 2015; 67(1):21-29.
26. Kumari A, Yadav SK, Yadav SC. Biodegradable polymeric nanoparticles based drug delivery systems. Colloids Surf B Biointerfaces 2010; 75(1):1-18.
27. Rajesh Kumar S, Ishaq Ahmed VP, Parameswaran V, Sudhakaran R, Sarath Babu V, Sahul Hameed AS. Potential use of chitosan nanoparticles for oral delivery of DNA vaccine in Asian sea bass (*Lates calcarifer*) to protect from *Vibrio* (*Listonella*) *anguillarum*. Fish Shellfish Immunol 2008; 25(1-2):47-56.
28. Nagpal K, Singh SK, Mishra DN. Chitosan nanoparticles: a promising system in novel drug delivery. Chem Pharm Bull 2010; 58(11):1423-1430.
29. Barichello JM, Morishita M, Takayama K, Nagai T. Encapsulation of hydrophilic and lipophilic drugs in PLGA nanoparticles by the nanoprecipitation method. Drug Dev Ind Pharm 1999; 25(4):471-476.
30. Tinsley-Bown AM, Fretwell R, Dowsett AB, Davis SL, Farrar GH. Formulation of poly (D,L-lactic-co-glycolic acid) microparticles for rapid plasmid DNA delivery. J Control Release 2000; 66(2-3):229-241.
31. Adomako M, St-Hilaire S, Zheng Y, Eley J, Marcum RD, Sealey W, et al. Oral DNA vaccination of rainbow trout, *Oncorhynchus mykiss* (Walbaum), against infectious haematopoietic necrosis virus using PLGA [Poly(D,L-Lactic-Co-Glycolic Acid)] nanoparticles. J Fish Dis 2012; 35(3):203-214.
32. Kalishwaralal K, Deepak V, Ramkumarpandian S, Nellaiah H, Sangiliyandi G. Extracellular biosynthesis of silver nanoparticles by the culture supernatant of *Bacillus licheniformis*. Mater Lett 2008; 62:4411–4413.
33. Prabhu S, Poulose EK. Silver nanoparticles: mechanism of antimicrobial action, synthesis, medical applications, and toxicity effects. Int Nano Lett 2012; 2:32.
34. Sankar R, Karthik A, Prabu, A, Karthik S, Shivashangari KS, Ravikumar V. *Origanum vulgare* mediated biosynthesis of silver nanoparticles for its antibacterial and anticancer activity. Colloids Surf B Biointerfaces 2013; 108:80-84.
35. Velmurugan P, Iydroose M, Lee SM, Cho M, Park JH, Balachandar V, et al. Synthesis of silver and gold nanoparticles using cashew nut shell liquid and its antibacterial activity against fish pathogens. Indian J Microbiol 2014; 54(2):196-202.
36. Vaseeharan B, Ramasamy P, Chen JC. Antibacterial activity of silver nanoparticles (AgNps) synthesized by tea leaf extracts against pathogenic *Vibrio harveyi* and its protective efficacy on juvenile *Feneropenaeus indicus*. Lett Appl Microbiol 2010; 50(4):352-356.
37. Ghetas HA, Abdel-Razek N, Shakweer MS, Abotaleb MM, Paray BA, Sajad Ali, Eldessouki EA, et al. Antimicrobial activity of chemically and biologically synthesized silver nanoparticles against some fish pathogens. Saudi Journal of Biological Sciences 2022; 29(3):1298-1305
38. Gunalan S, Sivaraj R, Rajendran V. Green synthesized ZnO nanoparticles against bacterial and fungal pathogens. Prog Nat Sci Mater Int 2012; 22(6):693-700.
39. Jayaseelan C, Rahuman AA, Kirthi AV, Marimuthu S, Santhoshkumar T, Bagavan A, et al. Novel microbial route to synthesize ZnO nanoparticles using *Aeromonas hydrophila* and their activity against pathogenic bacteria and fungi. Spectrochim Acta A 2012; 90:78-84.
40. Aarestrup FM. Veterinary drug usage and antimicrobial resistance in bacteria of animal origin. Basic Clin Pharmacol Toxicol 2005; 96(4): 271-281.

41. Hajipour MJ, Fromm KM, Ashkarran AA, de Aberasturi DJ, de Larramendi IR, Rojo T, et al. Antibacterial properties of nanoparticles. Trends Biotechnol 2012; 30(10): 499-511.
42. Pelgrift RY, Friedman AJ. Nanotechnology as a therapeutic tool to combat microbial resistance. Adv Drug Deliv Rev 2013; 65(13):1803-1815.
43. Cabello FC, Godfrey HP, Tomova A, Ivanova L, Dölz H, Millanao A et al. Antimicrobial use in aquaculture re-examined: its relevance to antimicrobial resistance and to animal and human health. Environ Microbiol 2013; 15(7):1917-1942.
44. Sørum H, Lie Ø. Antibiotic resistance associated with veterinary drug use in fish farms. Improving farmed fish quality and safety 2008; 157-182.
45. Tuševljak N, Dutil L, Rajić A, Uhland FC, McClure C, St-Hilaire S et al. Antimicrobial Use and Resistance in Aquaculture: Findings of a Globally Administered Survey of Aquaculture-Allied Professionals. Zoonoses Public Health 2013; 60(6):426-436.
46. Atyah MAS, Zamri-Saad M, Siti-Zahrah A. First report of methicillin-resistant *Staphylococcus aureus* from cage-cultured tilapia (*Oreochromis niloticus*). Vet Microbiol 2010; 144(3):502-504.
47. Davies J, Davies D. Origins and evolution of antibiotic resistance. Microbiol Mol Biol Rev 2010; 74(3): 417-433.
48. Son R, Rusul G, Sahilah AM, Zainuri A, Raha AR, Salmah I. Antibiotic resistance and plasmid profile of *Aeromonas hydrophila* isolates from cultured fish, Telapia (*Telapia mossambica*). Lett Appl Microbiol 1997; 24(6):479-482.
49. Swain P, Nayak SK, Sasmal A, Behera T, Barik SK, Swain SK, et al. Antimicrobial activity of metal based nanoparticles against microbes associated with diseases in aquaculture. World J Microbiol Biotechnol 2014; 30(9):2491-2502.
50. Di Cesare A, Vignaroli C, Luna GM, Pasquaroli S, Biavasco F.. Antibiotic-resistant enterococci in seawater and sediments from a coastal fish farm. Microb Drug Resist 2012; 18(5):502-509.
51. Di Cesare A, Luna GM, Vignaroli C, Pasquaroli S, Tota S, Paroncini, P et al. Aquaculture can promote the presence and spread of antibiotic-resistant Enterococci in marine sediments. PloS One 2013; 8(4):e62838
52. Seil JT, Webster TJ. Antimicrobial applications of nanotechnology: methods and literature. Int J Nanomedicine 2012; 7:2767-2781.
53. Knetsch ML, Koole LH. New strategies in the development of antimicrobial coatings: the example of increasing usage of silver and silver nanoparticles. Polymers 2011; 3(1):340-366.
54. Hindi KM, Ditto AJ, Panzner MJ, Medvetz DA, Han DS, Hovis CE, et al. The antimicrobial efficacy of sustained release silver–carbine complex-loaded L-tyrosine polyphosphate nanoparticles: Characterization, in vitro and in vivo studies. Biomaterials 2009; 30(22):3771-3779.
55. Antony JJ, Nivedheetha M, Siva D, Pradeepha G, Kokilavani P, Kalaiselvi S, et al. Antimicrobial activity of *Leucas aspera* engineered silver nanoparticles against *Aeromonas hydrophila* in linfected *Catla catla*. Colloids Surf B Biointerfaces 2013; 109:20-24.
56. Prakash P, Gnanaprakasam P, Emmanuel R, Arokiyaraj S, Saravanan M. Green synthesis of silver nanoparticles from leaf extract of *Mimusops elengi*, Linn. for enhanced antibacterial activity against multi drug resistant clinical isolates. Colloids Surf B Biointerfaces 2013; 108:255-259.
57. Ayala-Núñez NV, Lara HH, Turrent LDCI, Padilla CR. Silver nanoparticles toxicity and bactericidal effect against Methicillinresistant *Staphylococcus aureus*: Nanoscale does matter. Nanobiotechnol 2009; 5:2–9.
58. Lara HH, Ayala-Núnez NV, Turrent LDCI, Padilla CR. Bactericidal effect of silver nanoparticles against multidrug-resistant bacteria. World J Microbiol Biotechnol 2010; 26(4):615-621.
59. Huang CM, Chen CH, Pornpattananangkul D, Zhang L, Chan M, Hsieh MF, et al. Eradication of drug resistant *Staphylococcus aureus* by liposomal oleic acids. Biomaterials 2011; 32(1):214-221.
60. Umashankari J, Inbakandan D, Ajithkumar TT, Balasubramanian T. Mangrove plant, *Rhizophora mucronata* (Lamk, 1804) mediated one pot green synthesis of silver nanoparticles and its antibacterial activity against aquatic pathogens. Aquat Biosy 2012; 8(1):11.
61. Sanjenbam P, Gopal JV, Kannabiran K. Anticandidal activity of silver nanoparticles synthesized using *Streptomyces* sp. VITPK1. J Mycol Med 2014; 24 (3):211-219.

62. Mallmann EJJ, Cunha FA, Castro BN, Maciel AM, Menezes EA, Fechine PBA. Antifungal activity of silver nanoparticles obtained by green synthesis. Rev Inst Med Trop Sao Paulo 2015; 57(2):165-167.
63. Kim KJ, Sung WS, Moon SK, Choi JS, Kim JG, Lee DG. Antifungal effect of silver nanoparticles on dermatophytes. J Microbiol Biotechnol 2008; 18:1482–1484
64. Elechiguerra JL, Burt JL, Morones JR, Camacho-Bragado A, Gao X, Lara HH, et al. Interaction of silver nanoparticles with HIV-1. J. Nanobiotechnol 2005; 3:6.
65. Mehrbod P, Motamed N, Tabatabaian M, Soleimani R, Amini E, Shahidi M, et al. In Vitro Anti viral Effect of "Nanosilver" on Influenza Virus. DARU 2009; 17: 88-93.
66. Mori Y, Ono T, Miyahira Y, Nguyen VQ, Matsui T, Ishihara M. Antiviral activity of silver nanoparticle/chitosan composites against H1N1 influenza A virus. Nanoscale Res Lett 2013; 8(1):1-6.
67. Li X, Robinson SM, Gupta A, Saha K, Jiang Z, Moyano DF, Sahar A, et al. Functional Gold Nanoparticles as Potent Antimicrobial Agents against Multi-Drug-Resistant Bacteria. ACS nano 2014; 8(10):10682-10686.
68. Sumbayev VV, Yasinska IM, Gibbs BF. Biomedical applications of gold nanoparticles. Recent advances in circuits, communications and signal processing, WSEAS Press, Athens 2013; 342-348.
69. Lima E, Guerra R, Lara V, Guzmán A. Gold nanoparticles as efficient antimicrobial agents for *Escherichia coli* and *Salmonella typhi*. Chem Cent J 2013; 7(1):11
70. Cui Y, Zhao Y, Tian Y, Zhang W, Lü X, Jiang X. The molecular mechanism of action of bactericidal gold nanoparticles on *Escherichia coli*. Biomaterials 2012, 33(7):2327-2333.
71. Ahmad T, Wani IA, Lone IH, Ganguly A, Manzoor N, Ahmad A, et al. Antifungal activity of gold nanoparticles prepared by solvothermal method. Mater Res Bull 2013; 48(1):12-20.
72. Wani IA, Ahmad T. Size and shape dependant antifungal activity of gold nanoparticles: a case study of *Candida*. Colloid Surf. B: Biointerfaces 2013; 101:162-170.
73. Liu Y, He L, Mustapha A, Li H, Hu ZQ, Lin M. Antibacterial activities of zinc oxide nanoparticles against *Escherichia coli* O157: H7. J Appl Microbiol 2009, 107(4):1193-1201.
74. Ramamoorthy S, Kannaiyan P, Moturi M, Devadas T, Muthuramalingam J, Natarajan L, et al. Antibacterial activity of zinc oxide nanoparticles against *Vibrio harveyi*. Indian J Fish 2013; 107- 112.
75. Cheng TC, Yao KS, Yeh N, Chang CI, Hsu HC, Chien YT, et al. Visible light activated bactericidal effect of TiO2/Fe3O4 magnetic particles on fish pathogens. Surf Coat Technol 2009; 204(6):1141- 1144.
76. Cheng TC, Yao KS, Yeh N, Chang CI, Hsu HC, Gonzalez F, et al. Bactericidal effect of blue LED light irradiated TiO2/Fe3O4 particles on fish pathogen in seawater. Thin Solid Films 2011; 519(15):5002-5006.
77. Jovanović B, Anastasova L, Rowe EW, Zhang Y, Clapp AR, Palić D. Effects of nanosized titanium dioxide on innate immune system of fathead minnow (*Pimephales promelas* Rafinesque, 1820). Ecotoxicol Environ Saf 2011; 74(4): 675-683.
78. Jovanović B, Whitley EM, Kimura K, Crumpton A, Palić D. Titanium dioxide nanoparticles enhance mortality of fish exposed to bacterial pathogens. Environ Pollut 2015; 203:153-164.
79. Lockman PR, Mumper RJ, Khan MA, Allen DD. Nanoparticle technology for drug delivery across the blood-brain barrier. Drug Dev Ind Pharm 2002; 28(1): 1-13
80. Wang JJ, Zeng ZW, Xiao RZ, Xie T, Zhou GL, Zhan XR, et al. Recent advances of chitosan nanoparticles as drug carriers. Int J Nanomedicine 2011; 6:765-774.
81. Costa ADS, Brandão HM, Silva SR, Bentes-Sousa AR, Diniz JAP, Viana Pinheiro JDJ, et al. Mucoadhesive nanoparticles: a new perspective for fish drug application. J Fish Dis 2015; doi:10.1111/jfd.12373
82. Alishahi A, Mirvaghefi A, Tehrani, MR, Farahmand H, Koshio S, Dorkoosh FA, et al. Chitosan nanoparticle to carry vitamin C through the gastrointestinal tract and induce the non-specific immunity system of rainbow trout (*Oncorhynchus mykiss*). Carbohyd Polym 2011; 86(1):142-146.
83. Rather MA, Sharma R, Gupta S, Ferosekhan S, Ramya VL, Jadhao SB. Chitosan-nanoconjugated hormone nanoparticles for sustained surge of gonadotropins and enhanced reproductive output in female fish. PloS one 2013; 8(2): e57094.
84. Lü JM, Wang X, Marin-Muller C, Wang H, Lin PH, Yao Q, et al. Current advances in research and clinical applications of PLGA-based nanotechnology. Expert Rev Mol Diagn 2009; 9(4):325-341

85. Makadia HK, Siegel SJ. Poly lactic-co-glycolic acid (PLGA) as biodegradable controlled drug delivery carrier. Polymers 2011; 3(3):1377-1397.
86. Fenaroli F, Westmoreland D, Benjaminsen J, Kolstad T, Skjeldal FM, Meijer AH, et al. Nanoparticles as drug delivery system against tuberculosis in zebrafish embryos: Direct visualization and treatment. ACS nano 2014; 8(7):7014-7026.
87. Myhr AI, Myskja BK. Precaution or Integrated Responsibility Approach to Nanovaccines in Fish Farming? A Critical Appraisal of the UNESCO Precautionary Principle. Nanoethics 2011; 5(1):73-86
88. Zhao L, Seth A, Wibowo N, Zhao CX, Mitter N, Yu C. et al. Nanoparticle vaccines. Vaccine 2014; 32(3):327-337.
89. Gregory AE, Titball R, Williamson D. Vaccine delivery using nanoparticles. Front Cell Infect Microbiol 2013; 3:13.
90. Rivas-Aravena A, Fuentes Y, Cartagena J, Brito T, Poggio V, La Torre J, et al. Development of a nanoparticle-based oral vaccine for Atlantic salmon against ISAV using an alphavirus replicon as adjuvant. Fish Shellfish Immunol 2015; 45(1):157-166.
91. Vimal S, Taju G, Nambi KSN, Abdul Majeed S, Sarath Babu V, Ravi M, et al. Synthesis and characterization of CS/TPP nanoparticles for oral delivery of gene in fish. Aquaculture 2012; 358–359:14–22
92. Li L, Lin SL, Deng L, Liu ZG. Potential use of chitosan nanoparticles for oral delivery of DNA vaccine in black seabream *Acanthopagrus schlegelii* Bleeker to protect from *Vibrio parahaemolyticus*. J Fish Dis 2013; 36(12):987-995.
93. Rajeshkumar S, Venkatesan, C, Sarathi M, Sarathbabu V, Thomas J, Anver Basha K, et al. Oral delivery of DNA construct using chitosan nanoparticles to protect the shrimp from white spot syndrome virus (WSSV). Fish Shellfish Immunol 2009; 26(3):429-37.
94. Vimal S, Abdul Majeed S, Taju G, Nambi KS, Sundar Raj N, Madan N, et al. Chitosan tripolyphosphate (CS/TPP) nanoparticles: preparation, characterization and application for gene delivery in shrimp. Acta Trop 2013; 128(3):486-493.
95. Wang D, Robinson DR, Kwon GS, Samuel J. Encapsulation of plasmid DNA in biodegradable poly(D, L-lactic-co-glycolic acid) microspheres as a novel approach for immunogene delivery. J Control Release 1999; 57(1):9-18.
96. Hølvold LB, Myhr AI, Dalmo RA. Strategies and hurdles using DNA vaccines to fish. Vet Res 2014; 45(1):21-31.
97. Tian J, Sun X, Chen X, Yu J, Qu L, Wang L. The formulation and immunisation of oral poly(DL-lactide-co-glycolide) microcapsules containing a plasmid vaccine against lymphocystis disease virus in Japanese flounder (Paralichthys *olivaceus*). Int Immunopharmacol 2008; 8(6):900-908.
98. Jain KK. Nanodiagnostics: application of nanotechnology in molecular diagnostics. Expert Rev Mol Diagn 2003; 3(2):153-161.
99. Baptista P, Pereira E, Eaton P, Doria G, Miranda A, Gomes I, et al. Gold nanoparticles for the development of clinical diagnosis methods. Anal Bioanal Chem 2008; 391(3):943-950.
100. Saleh M, Soliman H, El-Matbouli M. Gold Nanoparticles as a Potential Tool for Diagnosis of Fish Diseases. Methods Mol Biol. 2015; 1247:245-252.
101. Saleh M, Soliman H, Haenen O, El-Matbouli M. Antibodycoated gold nanoparticles immunoassay for direct detection of *Aeromonas salmonicida* in fish tissues. J Fish Dis 2011; 34(11):845-852.
102. Kuan GC, Sheng LP, Rijiravanich P, Marimuthu K, Ravichandran M, Yin LS, et al. Gold-nanoparticle based electrochemical DNA sensor for the detection of fish pathogen *Aphanomyces invadans*. Talanta 2013; 117:312-317.
103. Jaroenram W, Arunrut N, Kiatpathomchai W. Rapid and sensitive detection of shrimp yellow head virus using loop-mediated isothermal amplification and a colorogenic nanogold hybridization probe. J Virol Methods 2012; 186(1):36-42.
104. Seetang-Nun Y, Jaroenram W, Sriurairatana S, Suebsing R, Kiatpathomchai W. Visual detection of white spot syndrome virus using DNA-functionalized gold nanoparticles as probes combined with loop-mediated isothermal amplification. Mol Cell Probes 2013;27(2):71-79.
105. Toubanaki DK, Margaroni M, Karagouni E. Nanoparticle based lateral flow biosensor for visual detection of fish nervous necrosis virus amplification products. Mol Cell Probes 2015; (3):158-166.
106. Yang SY, Wu JL, Tso CH, Ngou FH, Chou HY, Nan FH, et al. A novel quantitative immunomagnetic reduction assay for Nervous necrosis virus. J Vet Diagn Invest 2012; 24(5):911-917.

107. Saleh M, Soliman H, Schachner O, El-Matbouli, M. Direct detection of unamplified spring viraemia of carp virus RNA using unmodified gold nanoparticles. Dis Aquat Organ 2012; 100(1):3-10.
108. Saleh M, El-Matbouli M. Rapid detection of Cyprinid herpesvirus-3 (CyHV-3) using a gold nanoparticle-based hybridization assay. J Virol Methods 2015; 217:50-54.
109. Jimenez-Fernandez E, Ruyra A, Roher N, Infante C, Fernandez-Diaz C. Nanoparticles as a novel delivery system for vitamin C administration in aquaculture. Aquac 2014; 432: 426–433.
110. Bhattacharyya A, Reddy J, Hasan MM, Adeyemi MM, Marye RR. Nanotechnology-a unique future technology in aquaculture for the food security. International Journal of Bioassays 2015; 4(7): 4115–4126.
111. Huang S, Wang L, Liu L, Hou Y, Li L. Nanotechnology in agriculture, livestock, and aquaculture in China. A Review Agronomy for Sustainable Development 2015; 35(2): 369–400.
112. Sibaja-Luis AI, Ramos-Campos EV, de Oliveira JL, Fernandes L. Trends in aquaculture sciences: From now to use of nanotechnology for disease control. Reviews in Aquaculture 2019; 11(1): 119–132.
113. Mohammadi N, Tukmechi A. The effects of iron nanoparticles in combination with Lactobacillus casei on growth parameters and probiotic counts in rainbow trout (Oncorhynchus mykiss) intestine. J Vet Res 2015; 70: 47–53.
114. Ogunkalu OA. Utilization of nanotechnology in aquaculture and seafood sectors. EJFST 2019; 19: 26–33.
115. Zhou X, Wang Y, Gu Q, Li W. Effects of different dietary selenium sources (selenium nanoparticle and selenomethionine) on growth performance, muscle composition and glutathione peroxidase enzyme activity of crucian carp (Carassius auratus gibelio). Aquaculture 2009; 291: 78–81.
116. Izquierdo MS, Ghrab W, Roo J, Hamre K, Hernandez-Cruz CM, Bernardini, G, et al. Organic, inorganic and nanoparticles of Se, Zn and Mn in early weaning diets for gilthead seabream (Sparus aurata; Linnaeus, 1758). Aquaculture Research 2017; 48(6): 2852–2867.
117. Muralisankar T, Saravana-Bhavan P, Radhakrishnan S, Seenivasan C, Srinivasan V. The effect of copper nanoparticles supplementation on freshwater prawn Macrobrachium rosenbergii post larvae. Journal of Trace Elements in Medicine & Biology 2016; 34: 39–49.
118. ElBasuini MF, El-Hais AM, Dawood MAO, Abou-Zeid AES, El-Damrawy SZ, Khalafalla MMES, et al.. Effects of dietary copper nanoparticles and vitamin C supplementations on growth performance, immune response and stress resistance of red sea bream, Pagrus major. Aquaculture Nutrition 2017; 23(6): 1329–1340.
119. Kunjiappan S, Bhattacharjee C, Chowdhury R. Hepatoprotective and antioxidant effects of Azolla microphylla based gold nanoparticles against acetaminophen induced toxicity in a fresh water common carp fish (Cyprinus carpio L.). Nanomed J 2015; 2(2): 88–110.
120. Sharif RM, Haghighi M, Bazari Moghaddam S. Study on nanoparticles of Aloe vera extract on growth performance, survival rate and body composition in Siberian sturgeon (Acipenser baerii). Iranian Journal of Fisheries Sciences 2017; 16: 457–468.
121. Cui J, Yu B, Zhao Y, Zhu W, Li H, Lou H, Zhai G. Enhancement of oral absorption of curcumin by self-microemulsifying drug delivery systems. International Journal of Pharmaceutics 2009; 371(1–2): 148–155.
122. Semalty A, Semalty M, Rawat MSM, Franceschi F. Supramolecular phospholipids–polyphenolics interactions: The PHYTOSOME strategy to improve the bioavailability of phytochemicals. Fitoterapia 2010; 81: 306–314.
123. Takahashi M, Uechi S, Takara K, Asikin Y, Wada K. Evaluation of an oral carrier system in rats: Bioavailability and antioxidant properties of liposome-encapsulated curcumin. Journal of Agricultural and Food Chemistry 2009; 57: 9141–9146.
124. Wang Z, Leung MHM, Kee TW, English, DS. The role of charge in the surfactant-assisted stabilization of the natural product curcumin. Langmuir 2009; 26: 5520–5526.
125. Letchford K, Liggins R, Burt H. Solubilization of hydrophobic drugs by methoxy poly (ethylene glycol)-block-polycaprolactone diblock copolymer micelles: Theoretical and experimental data and correlations. Journal of Pharmacological Sciences 2008; 97(3): 1179–1190.
126. Shah C, Mishra B, Kumar M, Priyadarsini K, Bajaj P. Binding studies of curcumin to polyvinyl alcohol/polyvinyl alcohol hydrogel and its delivery to liposomes. Current Science 2008; 95(10): 1426–1432.
127. Das RK, Kasoju N, Bora U. Encapsulation of curcumin in alginate-chitosan-pluronic composite nanoparticles for delivery to cancer cells. Nanomedicine: Nanotechnology, Biology and Medicine 2010; 6(1): 153–160.

128. Shah BR, Li Y, Jin W, An Y, He L, Li Z, Xu W, Li B. Preparation and optimization of Pickering emulsion stabilized by chitosan-tripolyphosphate nanoparticles for curcumin encapsulation. Food Hydrocolloids 2016; 52: 369–377.
129. Matos M, Marefati A, Gutierrez G, Wahlgren M, Rayner M. Comparative emulsifying properties of octenyl succinic anhydride (OSA)-modified starch: Granular form vs dissolved state. PLoS One 2016; 11: 0160140.
130. Shah BR, Mraz J. Advances in nanotechnology for sustainable aquaculture and fisheries. Reviews in Aquaculture 2019; 1–18.
131. Xu W, Jin W, Huang K, Huang L, Lou Y, Li J, Liu X, Li B. Interfacial and emulsion stabilized behavior of lysozyme/xanthan gum nanoparticles. International Journal of Biological Macromolecules, 2018a; 117: 280–286.
132. Dickinson E. Food emulsions and foams: Stabilization by particles. Current Opinion in Colloid & Interface Science 2010; 15(1–2): 40–49.
133. Wu J, Ma GH. Recent studies of pickering emulsions: Particles make the difference. Small 2016; 12: 4633–4648.
134. Binks BP.Colloidal particles at liquid interfaces. Physical Chemistry Chemical Physics 2007; 9: 6298–6299.
135. Liu F, Tang CH. Reprint of Soy glycinin as food-grade Pickering stabilizers: Part. III. Fabrication of gel-like emulsions and their potential as sustained-release delivery systems for b-carotene. Food Hydrocolloids 2016; 60: 631–640.
136. Ngwabebhoh FA, Erdagi SI, Yildiz U. Pickering emulsions stabilized nanocellulosic-based nanoparticles for coumarin and curcumin nanoencapsulations: In vitro release, anticancer and antimicrobial activities. Carbohydrate Polymers 2018; 201: 317–328.
137. Shao P, Zhang H, Niu B, Jin W. Physical stabilities of taro starch nanoparticles stabilized Pickering emulsions and the potential application of encapsulated tea polyphenols. International Journal of Biological Macromolecules 2018; 118: 2032–2039.
138. Winuprasith T, Khomein P, Mitbumrung W, Suphantharika M, Nitithamyong A, McClements DJ. Encapsulation of vitamin D3 in pickering emulsions stabilized by nanofibrillated mangosteen cellulose: Impact on in vitro digestion and bioaccessibility. Food Hydrocolloids 2018; 83: 153–164.
139. Marku D, Wahlgren M, Rayner M, Sjoo M, Timgren A. Characterization of starch Pickering emulsions for potential applications in topical formulations. The Internet Journal of Pharmacology 2012; 428: 1–7.
140. Cossu A, Wang MS, Chaudhari A, Nitin N. Antifungal activity against Candida albicans of starch Pickering emulsion with thymol or amphotericin B in suspension and calcium alginate films. International Journal of Pharmaceutics 2015; 493(1–2): 233–242.
141. Leclercq L, Nardello-Rataj V. Pickering emulsions based on cyclodextrins: A smart solution for antifungal azole derivatives topical delivery. European Journal of Pharmaceutical Sciences 2016; 82: 126–137.
142. Yi T, Liu C, Zhang J, Wang F, Wang J, Zhang J. A new drug nanocrystal self-stabilized Pickering emulsion for oral delivery of silybin. European Journal of Pharmaceutical Sciences 2017; 96: 420–427.
143. Zhou Y, Sun S, Bei W, Zahi MR, Yuan Q, Liang H. Preparation and antimicrobial activity of oregano essential oil Pickering emulsion stabilized by cellulose nanocrystals. International Journal of Biological Macromolecules 2018; 112: 7–13.
144. Li J, Xu X, Chen Z, Wang T, Lu Z, Hu W, Li W. Zein/gum Arabic nanoparticle-stabilized Pickering emulsion with thymol as an antibacterial delivery system. Carbohydrate Polymers 2018; 200: 416–426.
145. Shah BR, Mraz J. Advances in nanotechnology for sustainable aquaculture and fisheries. Reviews in Aquaculture 2019; 1–18.
146. Baldissera MD, Souza CF, da Silva AS, Velho MC, Ourique AF, Baldisserotto B. Benefits of nanotechnology: Dietary supplementation with nerolidol-loaded nanospheres increases survival rates, reduces bacterial loads and prevents oxidative damage in brains of Nile tilapia experimentally infected by Streptococcus agalactiae. Microbial Pathogenesis (2020a); 141: 103989.
147. Baldissera MD, Souza C F, Velho MC, Bassotto VA, Ourique AF, Da Silva AS, Baldisserotto B. Nanospheres as a technological alternative to suppress hepatic cellular damage and impaired bioenergetics caused by nerolidol in Nile tilapia (Oreochromis niloticus). Naunyn-Schmiedeberg's Archives of Pharmacology (2020b); 393(5): 751–759.

148. Handy R D, Poxton MG. Nitrogen pollution in mariculture – toxicity and excretion of nitrogenous compounds by marine fish. Reviews in Fish Biology and Fisheries 1993; 3(3): 205–241.
149. Rather MA, Sharma R, Aklakur M, Ahmad S, Kumar N, Khan M, Ramya, VL. Nanotechnology: A novel tool for aquaculture and fisheries development. A prospective mini-review. Fish Aquac J FAJ 2011; 16.
150. Sibaja-Luis AI, Ramos-Campos EV, de Oliveira JL, Fernandes L. Trends in aquaculture sciences: From now to use of nanotechnology for disease control. Reviews in Aquaculture 2019; 11(1): 119–132.
151. Alboofetileh M, Rezaei M, Hosseini H, Abdollahi M. Efficacy of activated alginate-based nanocomposite films to control Listeria monocytogenes and spoilage flora in rainbow trout slice. Journal of Food Science & Technology 2016; 53(1): 521–530.
152. Borgogna M, Bellich B, Cesaro A. Marine polysaccharides in microencapsulation and application to aquaculture: "From sea to sea". Marine Drugs 2011; 9(12): 2572–2604.
153. Dursun S, Erkan N, Yeşiltaş M. Application of natural biopolymer based nanocomposite films in seafood. Journal of Fisheries Science 2010; 4(1): 50–77.
154. Joukar F, Hosseini SM H, Moosavi-Nasab M, Mesbahi GR, Behzadnia A. Effect of Farsi gum-based antimicrobial adhesive coatings on the refrigeration shelf life of rainbow trout fillets. LWT Food Sci Tech 2017; 80: 1–9.
155. Alishahi A, Mirvaghefi A, Tehrani MR, Farahmand H, Koshio S, Dorkoosh F A, Elsabee M Z. Chitosan nanoparticle to carry vitamin C through the gastrointestinal tract and induce the non-specific immunity system of rainbow trout (Oncorhynchus mykiss). Carbohydrate Polymers 2011; 86(1): 142–146.
156. Abd El-Naby FS, Naiel MAE, Al-Sagheer A A, Negm SS. Dietary chitosan nanoparticles enhance the growth, production performance, and immunity in Oreochromis niloticus. Aquac 2019; 501: 82–89.
157. Nile SH, Baskar V, Selvaraj D, Nile A, Xiao J, Kai G. Nanotechnologies in food science: Applications, recent trends, and future perspectives. Nano-Micro Letters 2020; 12: 45.
158. Ismael N E M, Abd El-hameed SAA, Salama AM, Naiel MAE, Abdel- Latif HMR. The effects of dietary clinoptilolite and chitosan nanoparticles on growth, body composition, haemato-biochemical parameters, immune responses, and antioxidative status of Nile tilapia exposed to imidacloprid. Environmental Science & Pollution Research 2021; 28: 29535–29550.
159. Abd El-Naby, AS, Al-Sagheer AA, Negm SS, Naiel MAE. Dietary combination of chitosan nanoparticle and thymol affects feed utilization, digestive enzymes, antioxidant status, and intestinal morphology of Oreochromis niloticus. Aquac 2020; 515: 734577.
160. Ogunkalu, OA. Utilization of nanotechnology in aquaculture and seafood sectors. EJFST 2019; 19: 26–33.

Table. 1. Antimicrobial activity of nonoparticles against different microorganisms

Nanoparticals	**Activity against the microorganisms**	**Reference**
Ag-NPs (Chemically and Biologically synthesized)	*Staphylococcus aureus, Edwardsiella tarda*	[49]
	Pseudomonas fluorescens, Proteus species, and *Flavobacterium* species	[60]
	Vibrio harveyi	[36]
	Candida species*; Streptomyces* sp. VITPK1	[61,62, 63]
	HIV-1 virus	[64]
	Bacterial strains: *Streptococcus agalactiae, Aeromonas hydrophila* and *Vibrio alginolyticus* fungal strains: *Aspergillus flavus*, *Fusarium moniliforme* and *Candida albicans*	[37]
Ag-Chitosan-NPs composite	H1N1 influenza A virus	[65, 66]
	Escherichia coli and *Salmonella typhi*	[69, 70]

Au-NPs	*Candida* species	[71, 72]
ZnO-NPs	*Aermonas hydrophila, Edwardseilla tarda, Flavobacterium branchiophilum, Citrobacter spp., Staphylococcus aureus, Vibrio species, Bacillus cereus,* and *Pseudomonas aeruginosa*	[49]
	Vibrio harveyi	[74]
	Pseudomonas aeruginosa, Escherichia coli, Enterococcus faecalis, Aspergillus flavus, and Candida albicans	[39]
TiO_2 -NPs	*Streptococcus iniae, Edwardsiella tarda, and Photobacterium damselae*	[75, 76]

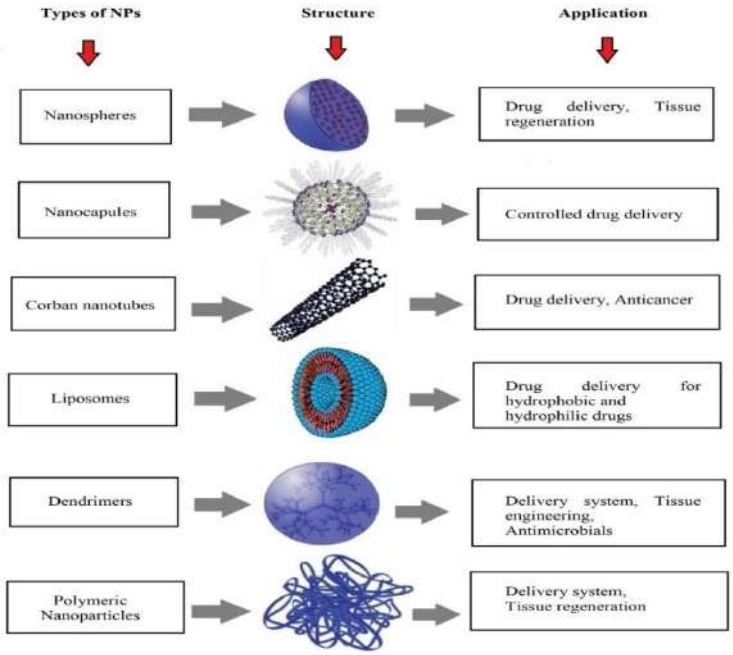

Fig. 1. Types of nanoparticles and its applications.

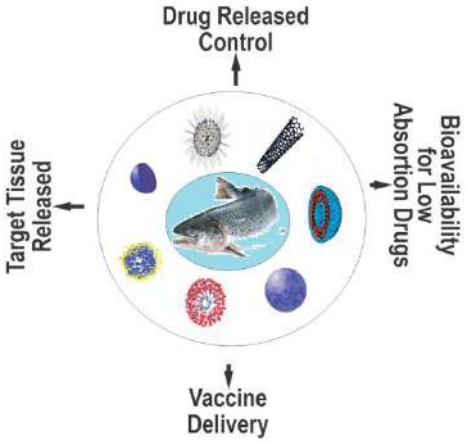

Fig. 2. Utilizing nanoparticals for drug delivery and targeted therapy in aquaculture offers numerous advantages

Indian Journal of Natural Sciences www.tnsroindia.org.in ©IJONS

Vol.15 / Issue 83 / Apr / 2024 *International Bimonthly (Print) – Open Access* *ISSN: 0976 – 0997*

RESEARCH ARTICLE

Exploring Competency Profiles among Emergency Department Nurses: Factors Shaping Skills and Overcoming Barriers

Suresh K[1]*, Thiruvenkadam Thiagarajan[2] and Ganesan Alias Kanagaraj Mariappan[3]

[1]Assistant Professor, Department of Management Studies, SRM Valliammai Engineering College, (Affiliated to Anna University), Kancheepuram , Tamil Nadu, India.
[2]Associate Professor, Department of Management Studies, Sri Sivasubramaniya Nadar College of Engineering, (Affiliated to Anna University) Chennai, Tamil Nadu, India.
[3]Assistant Professor, Department of Management Studies, SRM Valliammai Engineering College, (Affiliated to Anna University) Chennai, Tamil Nadu, India.

Received: 30 Dec 2023 Revised: 09 Jan 2024 Accepted: 27 Mar 2024

***Address for Correspondence**
Suresh K
Assistant Professor,
Department of Management Studies,
SRM Valliammai Engineering College,
(Affiliated to Anna University),
Kancheepuram , Tamil Nadu, India.
Email: profsureshkkumar@gmail.com

ABSTRACT

Gaining knowledge of and improving employee competencies is still essential for organizational success in the cutthroat healthcare industry of today. The study was conducted because comprehending employee competencies necessitates a targeted strategy to examine the essential competencies held by the personnel. The study aims to determine the level of competency of emergency department nurses, examine the abilities that the nurses possess in the largest and least amount, and identify the barriers that prevent the nurses from sharing their competency. An organized questionnaire was made and given to the respondents to collect the primary data required for the study. A simple random selection procedure was used to choose the responders. Utilizing factor analysis, reliability analysis, and correlation analysis, the data collected from 217 participants was tabulated in SPSS. To facilitate the application of the findings in improving emergency department nurses' competency for the benefit of both the individual and the organization, the research aims to bring out useful perspectives on the nurses' competency level to administrators, legislators, and human resource management practitioners.

Keywords: Competency Mapping, Human Resource Management, Skills, Health care, Nursing Competencies

INTRODUCTION

The effectiveness of an organization is now evaluated based on how well it manages its most valuable resource—its people—and their capabilities rather than how well it uses material resources in the competitive world of today. Organizations now place a high focus on managing employee capabilities, and they have begun to make a concerted effort to identify the core competencies held by employees, their levels, and the steps that can be taken to enhance those competencies. An organization with highly skilled personnel enjoys higher advantages in the current business environment. Competence is an underlying quality of a person that includes their motivations, characteristics, abilities, components of their image or social role, and information that they may apply on a personal level. It is the ability to act with authority and highly qualified awareness; it is the capacity to perform at the highest level in terms of training, expertise, and knowledge. The combination of an individual's aptitudes, personality, and experience tailored to a role or task in the current and emerging context, which accounts for sustained success within the confines of company principles. Competency is the set of success characteristics required to accomplish significant goals in a certain job or work capacity inside a specific organization. Healthcare systems nowadays deal with several difficulties. Increasing healthcare demands and expenses are a consequence of an aging population with numerous pathologies and non communicable diseases, which are made worse by an explosion in new medical technologies.

The maldistribution and scarcity of labor, as well as the inadequate quality and safety of services provided, exacerbate these issues further. The provision of health education by nurses in acute and community settings is widely acknowledged as a critical role that they play in improving favorable health results and the general effectiveness of the provision of healthcare. Since they are the most approachable medical staff in this setting and have frequent interaction with patients, hospital nurses in particular play a significant role in routine health education practices. Crucially, hospitalization affords a "window of opportunity" to promote lifestyle changes because of the numerous teaching opportunities this setting presents. Hospital nurses have been seen to express challenges in carrying out everyday initiatives in health education, and it is possible that they lack confidence in their ability to deliver effective health education. Interventions designed to improve nurses' health education competency should take into account contextual elements such having organizational support and be customized to the nurses' individual learning requirements and characteristics. The required level of performance for nurses includes judgment, knowledge, skills, and talents. Therefore, it is appropriate to regard as competent any individual who performs well at the expected level of nursing education and orientation. (Alshammari et al., 2022)Competencies are separated into two categories by the Emergency Nurses Association Nurse Practitioner Team: special and general.

A few examples of common clinical competencies include the ability to operate in a team, following professional standards, having a basic understanding of medicine, and having basic cultural traits and professional principles. To accomplish the duties of the job, a nurse needs to have certain basic abilities. Their clinical knowledge is essential, particularly in the emergency department where they treat injured patients all day long and make up the majority of the medical staff. Emergency Department (ED) nurses, for instance, are expected to acquire the capacity to predict patients' future situations and take appropriate action. In a hectic environment, emergency department nurses must recognize, rank, and assess cases that pose a threat to life, administer both emergency and non-emergent care in accordance with equitable standards, and demonstrate expertise and high-quality care. Continuously evaluating the clinical competency of ED nurses is necessary to identify areas that require improvement and promotion in order to provide consistently high-quality treatment. This aids ED nurses in confirming the suitability of the care they provide, as well as the effectiveness and caliber of it. For this reason, an evaluation of ED nurses' competency is necessary. Jeon et al. state that competency evaluation is utilized to advance current methods and encourage lifelong learning. Understanding the nursing competency development process is therefore essential for ongoing professional development. It is considered that nurses are very autonomous and independent enough to act on their own initiative without oversight. As a result, they are skillfully providing the patient, their family, and other significant individuals with the knowledge and emotional support required to handle the circumstance. Therefore, to provide

safe, efficient, and professional nursing care, a competent individual needs to possess these attributes, be driven to use them, and be able to do so effectively. To lay the foundation for future developments in nursing competency in the emergency department, a precise definition of nurse competency is required. Unfortunately, there is still a lack of consensus on what constitutes a competent nurse, even though nursing care can only be improved with skilled nurses. This implies that issues with defining and proving nursing competency, determining what proficiency levels are required of nursing practitioners, and creating educational resources will never go away. Moreover, the environment has a significant influence on the rate at which nurses become competent. Determining talents is therefore essential to enhancing nursing care. Therefore, mapping the ED nurse competencies and the related factors that impact those competencies is the aim of this research. additionally, to identify obstacles that limit their potential.

REVIEW OF LITERATURE

Studies have shown that nurses' competency has received a great deal more attention throughout time and is now a worry for healthcare professionals. Numerous scholars have previously investigated the elements that affect nursing practitioners' ability. Since it would be very helpful in defining the research objectives, a thorough review of the prior literature in the field of employee competency has been done. The study sought to characterize the differences in perceptions among clinical nurses on the impact of an alternative supervision model on their ability to evaluate nursing students during clinical practice. The research employs a phenomenographic approach in a qualitative and descriptive design. 49 clinical nurses from five different nursing homes served as informants. Three categories—"pressure," "encouragement," and "development"—are used to characterize the experiences of the clinical nurses. The clinical nurses' evaluation of the nursing students and their function as educators were aided by the alternative supervision approach(Struksnes et al., 2012).The systematic review (Belita et al., 2018)gives an up-to-date understanding of the evidence on evidence-informed decision-making (EIDM) competence assessments in nursing. This will help identify measures that may be useful and reliable for use in various nursing practice settings.

Developed in collaboration with a Health Sciences Librarian, the search strategy makes use of internet databases, expert advice, manual reference list searches, key journals, websites, conference proceedings, and grey literature.
The study looked at the literature on competency structure, components, assessment, and nursing competency definitions and characteristics in Japan. The study also examined methods for nurse competency training. The idea of nursing competency has not yet reached its full potential, despite the fact that skills are crucial for raising the standard of care provided by nurses. As a result, there are still problems with training curriculum development, defining and organizing nursing competency, and figuring out what competencies nursing practitioners need to have(Fukada, 2018).The study conducted by (Nilsson, Engström, Florin, Gardulf, & Carlsson, 2018) with an objective to create a condensed version of the NPC Scale and assess its construct validity and internal consistency. A sample of 1810 nursing students who were about to graduate from 12 Swedish universities served as the basis for the study. The 35-item NPC Scale Short Form (NPC Scale-SF) produced encouraging results, with a six-factor structure accounting for 53.6% of the variance in the total. When combined with other tools, this 35-item scale can be a useful tool for doing more in-depth evaluations of nursing students' and registered nurses' self-reported competence.

The goal to assess clinical competency among critical care nurses in Kermanshah, Iran,(Faraji, Karimi, Azizi, Janatolmakan, & Khatony, 2019) studied the relevant demographic characteristics. Using stratified random sample, 155 Iranian nurses were chosen for this cross-sectional investigation. The "Nurse Competence Scale" and a questionnaire for personal information were among the data collection instruments. The results of the study showed that clinical competence was used at a "good level" in real practice and that critical care nurses in Kermanshah had a "very good" rating for it. Given the importance of clinical competencies in nursing practice, it is critical to carry out an objective evaluation of nurses' clinical competence and to put proactive measures in place that promote the application of their knowledge.The study's by (Immonen et al., 2019) was focused towards the goal to identify the most up-to-date data that might be used to assess nursing students' clinical competency. The electronic databases CINAHL, PubMed, Eric, Medic, and the JBI Database of Systematic Reviews and Implementation Reports were

searched in the fall of 2018. Six reviews made it in after being critically evaluated. Assessment tools used to gauge students' nursing competency often cover the following topics: reason, communication and interpersonal relationships, nursing procedures, ethical practices, professional attributes, and critical thinking. Students' education is guided and vital support networks are provided by mentoring and clinical learning environments. The development of standardized and methodical assessment procedures as well as the utilization of trustworthy and legitimate equipment are still necessary.(Jao, Chen, & Sun, 2020)studied the path links influencing students' learning outcomes in the clinical practicum using LISREL software. Participants were 392 senior students from two nursing programs in central Taiwan who had completed their last internship. The Competency Inventory of Nursing Students, the Teaching Competence of Nurse Preceptor questionnaire, the Student Evaluation of the Clinical Education Environment, the Level of Reflective Thinking, and the Metacognitive Inventory for Nursing Students are some of the structured questionnaires that need to be distributed and filled out. The results suggest that metacognition and reflection, by teaching competency, may influence nursing competence indirectly.

The clinical learning environment can have a direct impact on nursing competency, while metacognition can have an indirect impact. Reflection and metacognition are essential for the development of nursing competence in clinical settings(Jao et al., 2020).During the COVID-19 pandemic in the spring of 2020(Konrad, Fitzgerald, & Deckers, 2021) presented a difficulty to numerous nursing schools, forcing them to switch from in-person to online instruction. In this article, educational concepts for an online course on the principles of nursing that enhance clinical competency are discussed. Presentations are made regarding faculty planning, teaching pedagogy used throughout this shift, and regulatory considerations. The writers also go into potential ramifications and ideas for achieving learning goals for an online healthcare course. The study conducted by (Alshammari et al., 2022)was focused towards mapping ED nurses' competencies, barriers, and influencing factors is the goal of the study. This study used cross-sectional methodology and was carried out at Hail's government hospitals, including the hospitals in the villages. The 227 ED nurses who were selected by convenience sampling were the study's participants. To get the data, the researchers used a Google Form survey. The study came to the conclusion that ED nurses possessed a high level of competence, particularly in clinical care leadership. Based on the study's findings, it is recommended that ED nurses' competency be continuously measured. The ED requires training needs assessments, which should be carried out on a regular basis and provide ongoing nursing education tailored to nurses' needs.The aim of the research(Suresh, 2020) is to ascertain the degree of competences acquired by employees and to evaluate which competencies are most and least prevalent. The items in the questionnaire used to gauge the respondents' competencies were framed with assistance from past research in the field of competency mapping.

Subjects and Methods

A cross-sectional methodology was used in this study to map out the competencies of ED nurses as well as pertinent variables and obstacles to learning them. The 217 ED nurses employed in government and private hospitals, including those in villages, were the study's participants. The study comprised ED nurses who met the following criteria: (a) were willing to participate; (b) could understand English; and (c) had worked in the ED for at least six months. The exception applied to nurses who moved to the emergency department to substitute for absentee nurses. Convenience sampling was employed by the researchers, bearing in mind the inclusion criteria. With 217 participants (73% response rate), the sample size calculator was used online at https://www.calculator.net/sample-size-calculator. The true value had a 95% confidence level and was within ± 5% of the measured/surveyed value.

Objectives and Limitations

The broad objectiveof the research is to study and assess the competency of Emergency Department Nurses employed in government and private hospitals in Chennai. The purpose of this study is to map ED nurses' competences and the related variables that affect them. This study also attempts to identify the obstacles that impact the competences of ED nurses. We must consider the limitations of this study. One of the fundamental limitations of cross-sectional studies, for example, is that it is impossible to identify the intricate relationship between the exposure and the outcome because they are viewed concurrently. Furthermore, leaving out nurses—for example, those who are illiterate in English—might not accurately reflect the entirety of the situation when evaluating ED competencies.

As such, care must be taken when analyzing the data. More participants and a bigger study population are recommended in order to accurately map the competences and generalize the contributing components affecting the competencies.

Conceptual Framework

The conceptual framework of the study has been established by the researcher in accordance with the literature review and taking the research objectives into consideration. The Competency Inventory for Registered Nurses (CIRN)(Alshammari et al., 2022)(Jao et al., 2020), which served as the foundation for the study's questionnaire, was created for this research. The following five categories comprised the 25 questions that made up the questionnaire: Leadership, Critical Thinking and Reasoning, Lifelong Learning, Interpersonal Skills, General Clinical Skills, and Professional Development

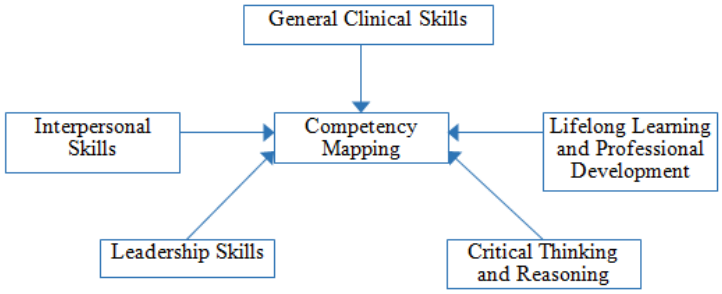

RESEARCH DESIGN

Descriptive research design was used for the study. In Chennai, Tamil Nadu, India, nurses working in emergency rooms of both public and private hospitals provided the primary data. Because it makes it easier to gather data from a wide population, the survey method was suitable for the study. To conduct the investigation, a straightforward random sample strategy was used. To gauge the degree of skills, a systematic questionnaire was created in accordance with the study's goals. Each skill, which had five statements each, was scored on a 5-point Likert scale, ranging from 5-Strongly Agree to 1-Strongly Disagree.A straightforward random sampling technique was used to gather the samples. There were 300 survey questionnaires distributed in all, of which 217 complete and usable surveys were received. SPSS 20.0 was used to tabulate and analyze the data that was gathered from the respondents. Among the statistical tests used to assess and draw conclusions from the study were Anova, Correlation, T Test, Factor Analysis, and Reliability Analysis.

RESULTS AND DISCUSSION

The goal of this study is to map the competences of emergency department nurses along with the related factors that impact those competencies. Additionally, this study attempts to identify the obstacles that impact the competences of ED nurses. All things considered; emergency department nurses gave themselves a very high competence rating. This indicates that nurses are aware of the necessity to prove their clinical competence to carry out tasks and support the organization's objectives. It has been determined that the greatest competencies are in clinical care, leadership, and interpersonal skills. The findings of this study corroborate those of an earlier study by V and Tamadoni et al., in which nurses assessed their level of competence in clinical care provision, leadership, and legal/ethical practice as being extremely high. In fact, it is considered that nurses must be competent professionals with leadership skills despite their intimate contact with patients and healthcare institutions. Leaders can identify inefficiencies in procedures, policies, practices, organizational structures, and processes that impede the provision of optimal patient care. Furthermore, it is acknowledged that a nurse's leadership qualities have a big influence on patient outcomes and the hospital atmosphere. The table above (Table 1) includes the demographic profile of the respondents. It can be

deduced from the preceding table that 145 (66.8%) of the respondents are female and 72 (33.2%) are male. Seventy-seven (35.3%) of the respondents are in the 20–29 age group; sixty-two (28.6%) are in the 30-39 age group; forty–forty-nine is represented by 63 (29.0%) of the respondents; and fifty–fifty-nine is represented by 15 (6.9%) of the respondents. In terms of experience, 122 of the respondents (56.2%) are of 5 years and above years of experience in the Emergency Department; in the salary category 106(48.8%) have reported their earning to be between 25001 – 50000 per month. Table 2 shows that the item "I think I'm capable of being a leader since I like to set objectives and work toward achieving them." has the lowest mean value. It hovers close to neutral. The item "Using the information at my disposal, I determine if a patient needs nursing intervention" (category Agree) had the highest mean rating. Based on a thorough study of the data provided, it can be deduced from the table that most respondents are confident in their ability to offer nursing care to patients, and they all concur that they possess general clinical skills. To identify the pertinent variables that define each employee's skill level, a factor analysis was performed. The results of the Bartlett's test of sphericity values and the Kaiser-Meyer-Oklin (KMO) tests are displayed in Table 3. The KMO measure of sampling adequacy value was determined to be.852 for the full sample. Bartlett's test of sphericity (p=0.000) shows that the correlation between the variables is statistically significant. The KMO and Bartlett's test findings indicated that the data was appropriate for factor analysis. Principal Component Analysis and the Varimax rotation approach were used in the investigation. The communalities of the loaded items and the percentage of variation explained by each item in the study, which varies from 50.5 to 75.4, are shown in Table 4. The six components that were recovered and accounted for 64.68 percent of the variance in the total sample are shown by the Principal Component Analysis (Table 5). The PCA's scree plot is displayed below. To evaluate the dependability of the factors extracted, a reliability test was carried out. The reliability was assessed by calculating the internal consistency Cronbach's Alpha coefficient (Table 7). The criteria were shown to be extremely dependable in predicting the Competencies, as indicated by the attained Alpha coefficient of.910.

Table 8 displays the values of the reliability coefficients for the factors. (Wang & Shi, 2011)According to Nunnally (1978), an alpha of at least 0.600 was sufficient for preliminary study. Cronbach's alpha estimate of 0.723 has been estimated for Leadership, 0.828 for General Clinical Skills, 0.700 for Interpersonal Skills, 0.763 for Critical Thinking and Reasoning, and 0.723 for Lifelong Learning and Professional Development. Given that every study's Cronbach's alpha was significantly. One statistical evaluation method that can be used to assess the strength of a link between two numerically measured continuous variables is correlation analysis. was conducted to investigate the relationship. The table below displays the correlation study's findings. Based on the table below, one may deduce that there is a perfect correlation and a substantial relationship between the variables. The study also intends to identify the barriers that affect ED nurses' competencies. Research indicates that those with ED training possess superior abilities compared to those without any training prior to entering the ED. It follows that nurses with ED training get their skills from their education. Because licensed providers are legally required to guarantee that each employee has completed a comprehensive induction and obtained a basic, appropriate level of training, staff training is essential. It is advised that in order to create training methods that cover the competency development sequence, it is crucial to understand the traits and elements of these nursing skills as facets of the clinical leader. To assess nurse competency and study the outcomes of competency improvement, more research is needed.The training does not correspond with the needs of emergency department nurses, which is one of the obstacles to gaining competence. The reason for this is because no evaluation of the training needs was conducted prior to the training or course being delivered.

CONCLUSION

An organization's core competences are identified as part of the mapping process, and these competencies are then attempted to be integrated throughout all of the organization's activities. Mapping the organizational abilities needed and putting policies in place to help employees recognize and acquire these competencies are important tasks performed by the human resources department. The research outcomes reveal that the emergency department

nurses demonstrated exceptional competency, particularly in the area of clinical care leadership. Their proficiency was influenced by their older age group, less than five years of ED experience, and training. The absence of support from leaders and the training's incompatibility with ED nurses' needs were obstacles. The results of the study indicate that ongoing competency assessment is necessary to raise ED nurses' proficiency. Particularly in the ED, training needs assessments should be carried out on a regular basis to provide ongoing nursing education based on the needs of the nurses.The study has offered a road map for comprehending the skills emergency department nurses in Chennai's public and private hospitals possess. The study's findings can have a greater managerial influence and offer HR managers, directors of departments and units, and policy makers a blueprint for developing competency development initiatives that will support the promotion of the essential skills. In order to create a solid competency-based HR framework, the study offers a foundation for organizing and expediting all HR tasks, such as talent mapping, hiring, on boarding, development, and performance appraisal.

REFERENCES

1. Alshammari, S., Alruwaili, A., Aljarboa, B., Mina, E., Cajigal, J., Alreshedi, M., … Buta, J. (2022). Mapping out competencies of emergency department nurses: Its influencing factors and barriers. *Hail Journal of Health Science*, *4*(2), 47. https://doi.org/10.4103/hjhs.hjhs_23_22
2. Belita, E., Yost, J., Squires, J. E., Ganann, R., Burnett, T., & Dobbins, M. (2018). Measures assessing attributes of evidence-informed decision-making (EIDM) competence among nurses: A systematic review protocol. *Systematic Reviews*, *7*(1), 1–8. https://doi.org/10.1186/s13643-018-0849-8
3. Faraji, A., Karimi, M., Azizi, S. M., Janatolmakan, M., & Khatony, A. (2019). Evaluation of clinical competence and its related factors among ICU nurses in Kermanshah-Iran: A cross-sectional study. *International Journal of Nursing Sciences*, *6*(4), 421–425. https://doi.org/10.1016/J.IJNSS.2019.09.007
4. Fukada, M. (2018). CNCSS, Clinical Nursing Competence Self-Assess-ment Scale Nursing Competency: Definition, Structure and Development. *Yonago Acta Medica*, *61*, 1–007.
5. Immonen, K., Oikarainen, A., Tomietto, M., Kääriäinen, M., Tuomikoski, A. M., Kaučič, B. M., … Mikkonen, K. (2019). Assessment of nursing students' competence in clinical practice: A systematic review of reviews. *International Journal of Nursing Studies*, *100*. https://doi.org/10.1016/j.ijnurstu.2019.103414
6. Jao, J. Y., Chen, S. L., & Sun, J. L. (2020). A predictive model of student nursing competency in clinical practicum: A structural equation modelling approach. *Nurse Education Today*, *95*, 104579. https://doi.org/10.1016/J.NEDT.2020.104579
7. Konrad, S., Fitzgerald, A., & Deckers, C. (2021). Nursing fundamentals – supporting clinical competency online during the COVID-19 pandemic. *Teaching and Learning in Nursing*, *16*(1), 53–56. https://doi.org/10.1016/J.TELN.2020.07.005
8. Nilsson, J., Engström, M., Florin, J., Gardulf, A., & Carlsson, M. (2018). A short version of the nurse professional competence scale for measuring nurses' self-reported competence. *Nurse Education Today*, *71*, 233–239. https://doi.org/10.1016/J.NEDT.2018.09.028
9. Struksnes, S., Engelien, R. I., Bogsti, W. B., Moen, Ö. L., Nordhagen, S. S., Solvik, E., & Arvidsson, B. (2012). Nurses' conceptions of how an alternative supervision model influences their competence in assessment of nursing students in clinical practice. *Nurse Education in Practice*, *12*(2), 83–88. https://doi.org/10.1016/j.nepr.2011.07.009
10. Suresh, K. (2020). An Empirical Study on Competency Mapping of Employees in the Automotive Sector with Specific Reference to Chennai. *Elixir International Journal*, *141*, 54310–54315.
11. Wang, Y., & Shi, X. (2011). Thrive, not just survive: Enhance dynamic capabilities of SMEs through IS competence. *Journal of Systems and Information Technology*, *13*(2), 200–222. https://doi.org/10.1108/13287261111136016

Table 1: Table showing the demography of the respondents

Factor		%	Count	Valid %	Cumulative %
Gender	Female	145	66.8	66.8	66.8
	Male	72	33.2	33.2	100
Age	20-29	77	35.5	35.5	35.5
	30-39	62	28.6	28.6	64.1
	40-49	63	29	29	93.1
	50-59	15	6.9	6.9	100
Marital Status	married	129	59.4	59.4	59.4
	Unmarried	88	40.6	40.6	100
Experience in Emergency Department	5 Yrs. and above	122	56.2	56.2	56.2
	3 – 4 Years	56	25.8	25.8	82
	2 – 3 Years	31	14.3	14.3	96.3
	1 – 2 Years	8	3.7	3.7	100
Salary	Up to25000	69	31.8	31.8	31.8
	25001-50000	106	48.8	48.8	80.6
	50001-75000	42	19.4	19.4	100

Table 2: Table showing the mean and the standard deviation

	Mean	Std. Deviation	Analysis N
Using the information at my disposal, I determine if a patient needs nursing intervention.	3.94	1.323	217
I administer nursing care to patients based on their individual needs.	3.95	1.301	217
I try to learn as much as I can about the patient so that I can create the most effective nursing plan.	3.76	1.268	217
I prioritize nursing duties according to the demands of my patients.	3.84	1.290	217
I make an effort to give patients thorough follow-up treatment that is tailored to their needs.	3.65	1.409	217
I think I'm capable of being a leader since I like to set objectives and work toward achieving them.	3.49	1.371	217
I see myself as being helpful to all of my peers, and I believe that I accept full responsibility for the work that I am doing.	3.80	1.383	217
Guidance without coercion is essential to effective leadership.	3.79	1.444	217
I take pleasure in working in teams.	3.61	1.433	217
I administer nursing care to patients based on their individual needs.	3.78	1.360	217
I try to learn as much as I can about the patient so that I can create the most effective nursing plan.	3.74	1.330	217
I often look to others for validation and encouragement.	3.61	1.357	217
I make a special effort to uplift those in the group, and I pay close attention to what they have to say.	3.72	1.515	217
To ensure that people don't squander time or circle around in circles, I push for action.	3.77	1.316	217
Every time a patient's condition changes, I attempt to identify the underlying cause.	3.64	1.395	217
I make an effort to examine patients' issues from several perspectives.	3.51	1.320	217
I carefully evaluate the patient's situation before drawing logical conclusions.	3.85	1.406	217

I consider whether there is sufficient empirical evidence to warrant nursing interventions every time.	3.46	1.430	217
I frequently turn to other people for approval and inspiration.	3.76	1.305	217
I prefer to weigh all of my options before making a decision, and I am aware of where to get educational materials and how to use them.	3.70	1.374	217
I know exactly what I still need to learn.	3.51	1.388	217
I like to look for answers to things.	3.59	1.479	217
I use other resources and technologies to further my education.	3.35	1.521	217
I manage my time well at work and establish learning objectives.	3.81	1.589	217
I frequently turn to other people for approval and inspiration.	3.78	1.290	217
Valid N (listwise)	217		

Table 3: KMO and Bartlett's Test

Kaiser-Meyer-Olkin Measure of Sampling Adequacy.		.852
Bartlett's Test of Sphericity	Approx. Chi-Square	2193.052
	df	300
	Sig.	.000

Table 4: Communalities

	Initial	Extraction
Using the information at my disposal, I determine if a patient needs nursing intervention.	1.000	.709
I administer nursing care to patients based on their individual needs.	1.000	.632
I try to learn as much as I can about the patient so that I can create the most effective nursing plan.	1.000	.610
I prioritize nursing duties according to the demands of my patients.	1.000	.667
I make an effort to give patients thorough follow-up treatment that is tailored to their needs.	1.000	.618
I think I'm capable of being a leader since I like to set objectives and work toward achieving them.	1.000	.620
I see myself as being helpful to all of my peers, and I believe that I accept full responsibility for the work that I am doing.	1.000	.740
Guidance without coercion is essential to effective leadership.	1.000	.695
I take pleasure in working in teams.	1.000	.754
I administer nursing care to patients based on their individual needs.	1.000	.727
I try to learn as much as I can about the patient so that I can create the most effective nursing plan.	1.000	.654
I often look to others for validation and encouragement.	1.000	.612
I make a special effort to uplift those in the group, and I pay close attention to what they have to say.	1.000	.665
To ensure that people don't squander time or circle around in circles, I push for action.	1.000	.576
Every time a patient's condition changes, I attempt to identify the underlying cause.	1.000	.676
I make an effort to examine patients' issues from several perspectives.	1.000	.630
I carefully evaluate the patient's situation before drawing logical conclusions.	1.000	.631
I consider whether there is sufficient empirical evidence to warrant nursing interventions every time.	1.000	.644
I frequently turn to other people for approval and inspiration.	1.000	.505
I prefer to weigh all of my options before making a decision, and I am aware of where to get educational materials and how to use them.	1.000	.585
I know exactly what I still need to learn.	1.000	.606

I like to look for answers to things.	1.000	.618
I use other resources and technologies to further my education.	1.000	.712
I manage my time well at work and establish learning objectives.	1.000	.575
I frequently turn to other people for approval and inspiration.	1.000	.708
Extraction Method: Principal Component Analysis.		

Table 5: Component Matrix[a]

	Component						
	1	2	3	4	5	6	7
Using the information at my disposal, I determine if a patient needs nursing intervention.	.616	-.483					
I administer nursing care to patients based on their individual needs.	.561	-.428					
I try to learn as much as I can about the patient so that I can create the most effective nursing plan.	.636	-.415					
I prioritize nursing duties according to the demands of my patients.	.592	-.381					
I make an effort to give patients thorough follow-up treatment that is tailored to their needs.	.568	-.436					
I think I'm capable of being a leader since I like to set objectives and work toward achieving them.	.502	-.498					
I see myself as being helpful to all of my peers, and I believe that I accept full responsibility for the work that I am doing.	.565		-.365		.344		
Guidance without coercion is essential to effective leadership.	.591	.306	-.371				
I take pleasure in working in teams.	.543				.501		.339
I administer nursing care to patients based on their individual needs.	.616		-.444				
I try to learn as much as I can about the patient so that I can create the most effective nursing plan.	.541	.384			.382		
I often look to others for validation and encouragement.	.566		-.515				
I make a special effort to uplift those in the group, and I pay close attention to what they have to say.	.436	.303	.360	.422			
To ensure that people don't squander time or circle around in circles, I push for action.	.578						
Every time a patient's condition changes, I attempt to identify the underlying cause.	.482			.424		.379	
I make an effort to examine patients' issues from several perspectives.	.609						.420
I carefully evaluate the patient's situation before drawing logical conclusions.	.576			.330			
I consider whether there is sufficient empirical evidence to warrant nursing interventions every time.	.609				-.382		
I frequently turn to other people for approval and inspiration.	.588			-.326			

I prefer to weigh all of my options before making a decision, and I am aware of where to get educational materials and how to use them.	.627						
I know exactly what I still need to learn.	.521			-.364			-.341
I like to look for answers to things.	.599			-.352			
I use other resources and technologies to further my education.	.451			-.452		.432	
I manage my time well at work and establish learning objectives.	.515		.428				
I frequently turn to other people for approval and inspiration.	.472		.312			-.481	.337
Extraction Method: Principal Component Analysis.							
a. 7 components extracted.							

Table 6: Total Variance Explained - Extraction Method: Principal Component Analysis.

Component	Initial Eigenvalues			Extraction Sums of Squared Loadings			Rotation Sums of Squared Loadings		
	Total	% of Variance	Cumulative %	Total	% of Variance	Cumulative %	Total	% of Variance	Cumulative %
1	7.871	31.482	31.482	7.871	31.482	31.482	3.412	13.647	13.647
2	1.912	7.647	39.129	1.912	7.647	39.129	2.869	11.474	25.121
3	1.587	6.348	45.477	1.587	6.348	45.477	2.324	9.294	34.415
4	1.475	5.900	51.378	1.475	5.900	51.378	2.075	8.301	42.716
5	1.242	4.969	56.347	1.242	4.969	56.347	2.013	8.054	50.770
6	1.070	4.281	60.628	1.070	4.281	60.628	1.864	7.456	58.225
7	1.014	4.055	64.683	1.014	4.055	64.683	1.614	6.457	64.683
8	.869	3.477	68.160						
9	.832	3.328	71.488						
10	.744	2.977	74.466						
11	.729	2.915	77.381						
12	.669	2.677	80.058						
13	.586	2.344	82.402						
14	.537	2.150	84.552						
15	.502	2.006	86.558						
16	.467	1.866	88.424						
17	.453	1.813	90.237						
18	.438	1.751	91.988						
19	.373	1.492	93.480						

20	.344	1.375	94.854						
21	.314	1.256	96.110						
22	.288	1.150	97.260						
23	.248	.991	98.251						
24	.234	.936	99.187						
25	.203	.813	100.000						

Table 8: Table showing the Reliability Statistics

Cronbach's Alpha	N of Items
.892	25

Table 8.a : Table showing the Cronbach's Alpha Value

Factor	Cronbach's Alpha	N of Items
Leadership	.723	5
General Clinical Skills	.828	5
Interpersonal Skills	.700	5
Critical Thinking and Reasoning	.763	5
Lifelong Learning and Professional Development	.723	5

Table 9: Correlations

		General Clinical Skills	Leadership	Interpersonal Skills	Critical Thinking and Reasoning	Lifelong Learning and Professional Development
General Clinical Skills	Pearson Correlation	1	.544**	.473**	.539**	.484**
	Sig. (2-tailed)		.000	.000	.000	.000
Leadership	Pearson Correlation	.544**	1	.613**	.602**	.493**
	Sig. (2-tailed)	.000		.000	.000	.000
Interpersonal Skills	Pearson Correlation	.473**	.613**	1	.602**	.459**
	Sig. (2-tailed)	.000	.000		.000	.000
Critical Thinking and Reasoning	Pearson Correlation	.539**	.602**	.602**	1	.591**
	Sig. (2-tailed)	.000	.000	.000		.000
Lifelong Learning and Professional Development	Pearson Correlation	.484**	.493**	.459**	.591**	1
	Sig. (2-tailed)	.000	.000	.000	.000	
**. Correlation is significant at the 0.01 level (2-tailed).						

Indian Journal of Natural Sciences www.tnsroindia.org.in ©IJONS

Vol.15 / Issue 83 / Apr / 2024 International Bimonthly (Print) – Open Access ISSN: 0976 – 0997

RESEARCH ARTICLE

Revitalize Through Technology: How Online Shopping Habits of Youth Shape Family Dynamics

Vani Haridasan[1*], Kavitha muthukumaran[1*] Vidyaa Lakshmi P[2] and Srinithi JP[2]

[1]Associate Professor, Department of Management Studies, Sri Sivasubramaniya Nadar College of Engineering , Chennai, Tamil Nadu, India.
[2]Student, Department of Management Studies, Sri Sivasubramaniya Nadar College of Engineering, Chennai, Tamil Nadu, India.

Received: 30 Dec 2023 Revised: 09 Jan 2024 Accepted: 27 Mar 2024

***Address for Correspondence**
Vani Haridasan , Kavitha muthukumaran
Associate Professor,
Department of Management Studies,
Sri Sivasubramaniya Nadar College of Engineering ,
Chennai, Tamil Nadu, India.

ABSTRACT

This research investigates the profound impact of youth's online buying behavior on family purchasing decisions, spanning across generations from Gen Z to Gen X and Baby Boomers. Our objective is to explore the extent to which the younger generation influences the buying decisions of older family members, particularly towards online channels. Employing a mixed-methods approach, conducted a cross-sectional surveys and interviews to comprehensively capture insights into this phenomenon. By targeting Gen Z and older individuals, we aim to analyze the influence of tech-savvy youth on traditional consumer segments. We hypothesize a connection between youth's online purchases and older family members' buying patterns. The era of pandemic has triggered a higher-level comfort and elevation in the e commerce field. The new age on retail is evidently welcomed by the youth of today and the easy shop access is widely accepted by various age groups who once where traditional on-store vendee meanwhile the offline only retailers are affected drastically.

Keywords: Online Purchase, Youth Influence, Family Buying decision, Affecting Retailers

INTRODUCTION

The evolution of E- market has grown tremendously and the graphical movement from physical to electronic mode is so vivid. This research focuses on the semi urban take in the dramatic shift of the buyer's environment. This research delves into the intricate relationships between generations and their influence on purchasing decisions,

particularly in the context of online buying behavior, it is crucial to explore the interplay between the tech-savvy youth and older family members, spanning generations from the digitally native Gen Z to the more traditional Gen X and Baby Boomers. Our primary goal is to assess the degree to which youth influence family members' buying decisions towards online channels. To achieve this, we employ a mixed-methods approach, utilizing cross-sectional surveys and interviews. This approach allows us to not only quantify trends but also gain qualitative insights into the motivations and attitudes driving these behaviors. The research hypothesis posits a connection between the online purchasing patterns of the youth and the buying behaviors exhibited by older family members. By targeting specific age groups, we aim to discern the nuances in the influence wielded by the younger generation on traditional consumer segments. Furthermore, we explore the transformative journey of the e-commerce market, emphasizing the pronounced impact of the pandemic on consumer behavior. The era of lockdowns and social distancing has propelled a higher level of comfort and elevation in the e-commerce field. The COVID-19 pandemic has accelerated this shift, triggering heightened comfort and reliance on e-commerce platforms. This research underscores the impact of these changes on both online and offline retailers, particularly emphasizing the challenges faced by traditional, offline-only retailers. As we embark on this exploration, we seek to contribute valuable insights for businesses, marketers, and policymakers navigating the ever-changing terrain of consumer preferences and retail dynamics.

OBJECTIVES

- To examine the buying behaviour of youth.
- To study the significance of online purchasing power of youth and its influence.
- To analyse the shift in the mindsets of family members and how it affects the retail shops.

NEED OF THE STUDY

This study is essential for retail shoppers to grasp the evolving consumer landscape. It offers insights into the increasing shift towards online shopping, enabling retailers to adapt their strategies effectively. Understanding intergenerational influences allows retailers to tailor marketing approaches for both tech-savvy youth and older consumers. With the pandemic accelerating the move to e-commerce, enhancing digital presence becomes a priority. Exploring semi-urban areas provides a nuanced understanding for customization, while acknowledging challenges faced by offline-only retailers guides the development of survival strategies, potentially involving digital integration or a hybrid model to stay competitive.

PROBLEM STATEMENT

- The tastes and preferences of the consumers are changing at a rapid rate. The marketers are finding it difficult to cope up with the changing need of the customers.
- E-com operators targeting youth and using them as a key indicator for their marketing strategy and this is directly affecting the Traditional Retail operators.

LITERATURE REVIEW

Ramya N, Dr S.A.Mohamed Ali (2016) delve into Consumer Buying behaviour by identifying and understanding the factors that influence their customers, brands can develop a strategy, a marketing message (Unique Value Proposition) and advertising campaigns more efficient and more in line with the needs and ways of thinking of their target consumers, a real asset to better meet the needs of its customers and increase sales. Lastly, the consumer analyses the prevailing prices of commodities and takes the decision about the commodities he should consume. Praveen K.S. Naik and Shivalinge Gowda M (2017). This study examines the factors influencing the online buying behaviour of the youth particularly the teenage groups. Convenience sampling method was used to select the sample of 30 teenage college students and a self-administered questionnaire was used to obtain the data. The study revealed some important factors influencing online shopping such as availability, low price, promotions, comparison, convenience, customer service, perceived ease of use, attitude, time consciousness, trust and variety seeking. Ritwik

Maity, Sukjeet Kaur Sandhu (2021), Stated that their research is practically explored in embracing an online buying network from the customer. This research addresses many significant research issues pertaining to the acceptability of the user to choose online shopping portals while buying items. Such topics were divided into four variables i.e. societal acceptance of online purchasing, product preference for online purchasing, product variety availability for online purchasing and lastly convenience of online purchasing. As a result, a framework is needed to coordinate a complex process for the effects of these factors. Indrila Goswami Varma, Ms. Rupa Agarwal(2014) This paper aims to identify the factors that affect the online buying behaviour of women particularly homemakers in Western suburbs of Mumbai .Educated , urban homemakers form a significant prospect for traditional retailers. The question that arises is whether this segment is also buying online or has remained untapped by the e-retailers? Research has examined the role of different factors on individuals' ecommerce adoption, such as geography and store accessibility, perceived risk and online shopping benefits, typology of online stores, enjoyment and trust in Web sites , gender differences in attitudes toward online shopping ,and impact of consumers socio-economic conditions. Halima Shebuge (2019) The focus of this study was to analyse factors that influence youths' online buying behaviour in Tanzania. Specifically, the study aimed at finding out satisfaction levels, factors motivating youths to purchase online and the challenges that are facing them. The findings of the study revealed that large number of respondents were satisfied with sales services that are being provided in local and international online platforms in Tanzania, due to the comparison capacity, goods customization, and ability to trace orders. The study thus recommends establishing many local online market places to reach many customers together with laws governing online businesses.

METHODOLOGY

This is a Mixed-methods (i.e. both Quantitative and Qualitative analysis) research design to investigate online purchasing behaviors among two distinct age cohorts: Generation Z and mid-age individuals. The study included a sample of 224 responses from Generation Z and 135 responses from the mid-age group.

CONCEPTUAL FRAMEWORK TO UNDERSTAND THE FACTORS THAT INFLUCENCE FAMILY MEMBERS TO CHOOSE ONLINE PLATFORM DUE TO GEN Z PURCHASING BEHAVIOUR

DATA COLLECTION

Surveys were administered to gather responses, focusing on various aspects of online purchasing decisions, including recommendations, assistance-seeking, and the impact on family spending habits. The survey instrument was designed to provide nuanced insights into factors influencing buying patterns and preferences.

ANALYSIS AND FINDINGS

Responses from both age groups underwent detailed analysis using Microsoft Excel. Statistical methods included correlation analysis, regression modeling, chi-square testing, and ANOVA. These analyses were instrumental in uncovering relationships, patterns, and trends within each age cohort.

Correlation between Recommending Products and Purchasing Decisions:

- The analysis revealed a strong positive correlation between the likelihood of recommending products or online stores to family members and their subsequent purchasing decisions.
- This suggests that when younger family members, especially those belonging to Gen Z, recommend products or online platforms to their relatives, it significantly influences their purchasing behavior.
- The findings underscore the importance of word-of-mouth recommendations and the influential role of younger family members in shaping the buying decisions of older family members.

Correlation between Family Assistance-seeking Behavior and Purchasing Decisions:

- A highly positive correlation was found between family members seeking assistance from younger members in finding online deals or discounts and their subsequent purchasing decisions.
- This indicates that older family members often rely on younger members, particularly Gen Z individuals, for guidance and recommendations in navigating the online shopping landscape.
- The results highlight the intergenerational dynamics within families and the role of younger members as trusted advisors in making informed purchasing decisions.

Relationship between Recommending Products and Assistance-seeking Behavior

- Significant relationships were observed between the likelihood of recommending products or online stores to family members and the frequency of family members seeking assistance from younger members for finding online deals.
- This suggests a reciprocal relationship where recommendations from younger members lead to increased assistance-seeking behavior from older family members, creating a symbiotic interaction within the family unit.
- The findings emphasize the collaborative nature of shopping decisions within families and the mutual support provided across different generations.

ANOVA Analysis for Gen Z Respondents

- An analysis of variance (ANOVA) conducted for Gen Z respondents revealed a significant relationship between recommending products to family members and the frequency of family members seeking assistance from younger members for finding online deals.
- This indicates that Gen Z individuals who actively recommend products to their family members are more likely to assist them in navigating online deals and discounts, further reinforcing their influential role in family purchasing decisions.

Chi-square Analyses

- Chi-square analyses yielded mixed results regarding the influence of age and gender on discussing online shopping purchases and seeking assistance in finding deals.
- While some relationships were significant, indicating potential demographic differences in online shopping behaviors within families, others were not, suggesting the presence of other underlying factors contributing to family dynamics.
- The findings highlight the complexity of intergenerational relationships and the need for further exploration into the nuanced factors shaping online shopping behaviors within families.

Reliability and Validity Measures

- Rigorous measures such as pilot testing and standard statistical procedures were employed to enhance the reliability and validity of the study.
- These measures ensure the credibility and robustness of the findings, providing valuable insights into the intricate dynamics of family purchasing decisions in the digital age.

CONCLUSION OF METHODOLOGY

This mixed-methods approach, coupled with detailed statistical analyses, positions the research to provide comprehensive insights into online purchasing dynamics across generations. The consistent methodology applied to both age cohorts enhance the study's validity and contributes to a nuanced understanding of consumer behaviors in the digital marketplace.

LIMITATIONS

Focusing solely on Gen Z, Gen X, and Baby Boomers overlooks the potential influence of other generational cohorts and cultural factors. This limits the applicability of the findings to a broader population and may not accurately

reflect the diverse landscape of online shopping behavior across different generations and cultures. Self-reported data through surveys and interviews introduces potential biases and inaccuracies. Participants may over- or under-report their online shopping habits and their influence on family members, leading to skewed results.

RECOMMENDATIONS FOR RETAILORS

- Innovative Retail Partnerships between retailers and innovative tech companies to develop solutions that cater to multi-generational shoppers. Explore opportunities to integrate augmented reality (AR), virtual reality (VR), or voice-enabled shopping experiences that appeal to both youth and older consumers.
- Online shopping offers convenience by allowing youth to browse and purchase products from the comfort of their own homes or on-the-go using mobile devices. Retailers can capitalize on this same idea and create their own websites and mobile apps with easy navigation and seamless checkout experiences by balancing both online and offline experience.
- Online retailers often offer competitive pricing and discounts compared to physical stores, making it more attractive for youth who are budget-conscious. Retailers can leverage pricing strategies such as flash sales, promotional codes, and bundle deals to incentivize online purchases among youth.
- Use Cross-Channel Integration and implement omnichannel strategies that seamlessly integrate online and offline shopping experiences, allowing family members to research, purchase, and receive support across various touchpoints.

RECOMMENDATIONS FOR E-COMMERCE:

- E-commencers should prioritize online shopping experiences for youth by offering convenient browsing and purchasing options, a wide variety of products at competitive prices, engaging social media content and influencer partnerships, user-generated reviews and recommendations, personalized shopping experiences, and flexible accessibility and payment options to cater to their preferences and enhance overall satisfaction
- Enhance product recommendation algorithms and online shopping platforms to reflect the significant connection between age and seeking recommendations for specific product types. Customize product suggestions based on age demographics, preferences, and past purchasing behaviours to increase engagement.
- Establish feedback mechanisms to solicit input and insights from customers across different age groups. Actively seek feedback on shopping experiences, preferences, and suggestions for improvement, fostering a culture of customer-centricity and responsiveness within the organization.
- Introduce youth ambassador programs where tech-savvy young consumers can act as mentors or guides for older family members in adopting online shopping practices. Encourage these ambassadors to share their expertise and experiences to bridge the generational gap in digital adoption.
- Use the strategy of Personalized Recommendations by utilize data analytics to provide personalized product recommendations and offers tailored to the preferences and purchasing behaviours of individual family members.
- Provide Community Engagement and foster a sense of community and trust among family members by creating online forums or social media groups where they can share shopping experiences, recommendations, and tips with each other.

REFERENCES

1. Adnane Derbani, Wiwiek Rabiatual, Siti Zulaikha, April 2022, " Impact of online buying behavioural tendencies of generation z on their parents consumption behaviour: Insight from Indonesia ",Volume 18 (2), PP.39-48. [Innovative Marketing]
2. Ramya N, Dr S.A.Mohamed Ali, Sept 2016 , "Factors affecting consumer buying behaviour", Volume 2(10), PP.76-80. [International Journal of applied research]

3. Indrila Varma, Rupa Narayan Agarwal, July 2014, " Online buying behaviour of Homemakers in western suburbs of Mumbai and social media influence", Vol 16 (7). [ISOR Journal of Business and Management]
4. Bertol, K.E. Broilo, P.L. Espartel, L.B. and Basso, K. (2017), "Young children's influence on family consumer behaviour", Vol. 20 No. 4, PP. 452-468.[Quantitative market research]
5. Ritwik Maity1, Sukjeet Kaur Sandhu, 2021, "The Impact of Social Media on Online Purchasing Behaviour of Consumers: An Empirical Study of Youth in West Bengal, India" , Vol 26 [Malaysian journal of consumer and family economics]
6. Rishi, Bikram Jit, 2008 , "An Empirical Study of Online Shopping Behaviour: A Factor Analysis Approach" , Vol 3(3) PP 40-49 [Journal of Marketing & Communication]

Table 1:

	How likely are you to recommend products or online stores to your family members	*How often do they take purchasing decisions based on your recommendations*
How likely are you to recommend products or online stores to your family members	1	
How often do they take purchasing decisions based on your recommendations	0.956176494	1

Table 2:

	How often do your family members seek your assistance in finding online deals or discounts	*How often do they take purchasing decisions based on your recommendations*
How often do your family members seek your assistance in finding online deals or discounts	1	
How often do they take purchasing decisions based on your recommendations	0.955652373	1

Table 3:

Anova: Single Factor						
SUMMARY						
Groups	*Count*	*Sum*	*Average*	*Variance*		
How likely are you to recommend p online stores to your family me	223	952	4.269058	10.28584		
How often do your family members seek your assistance in finding online deals or discounts	223	892	4	11.08288		
ANOVA						
Source of Variation	*SS*	*df*	*MS*	*F*	*P-value*	*F crit*
Between Groups	8.071749	1	8.071749	0.755473	0.385218	3.862488
Within Groups	4743.857	444	10.68436			
Total	4751.928	445				

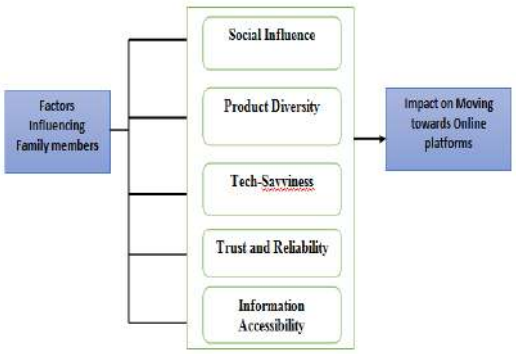

Fig 1

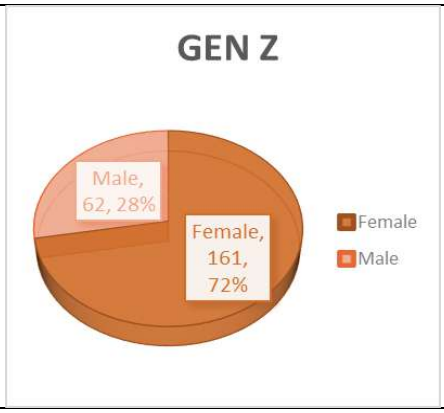

Fig 2

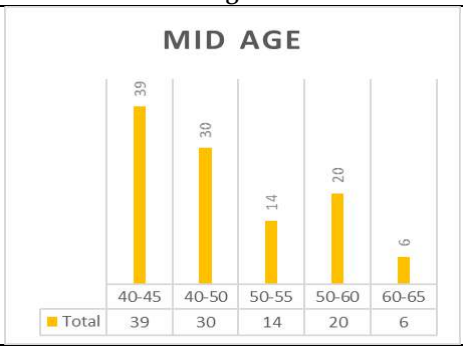

Fig 3

Fig 4

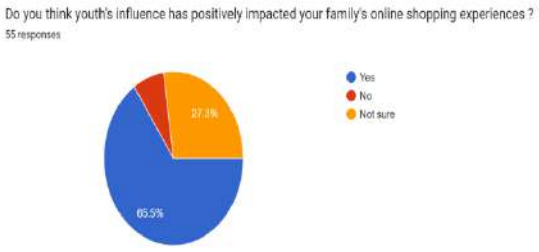

Fig 5

Indian Journal of Natural Sciences *www.tnsroindia.org.in ©IJONS*

Vol.15 / Issue 83 / Apr / 2024 *International Bimonthly (Print) – Open Access* *ISSN: 0976 – 0997*

RESEARCH ARTICLE

The Impact of AI Technology Adoption on Investor Decision-Making in the Indian Financial Market

M. Ganesan Alias Kanagaraj[1*], Thiruvenkadam Thiagarajan[2] and K.Suresh[1]

[1]Assistant Professor (Senior Grade), Department of Management Studies, SRM Valliammai Engineering College, Chengalpattu (Affiliated to Anna University, Chennai,) Tamil Nadu, India.
[2]Associate Professor, Department of Management Studies, Sri Sivasubramaniya Nadar College of Engineering, (Affiliated to Anna University) Chennai, Tamil Nadu, India.

Received: 30 Dec 2023 Revised: 09 Jan 2024 Accepted: 27 Mar 2024

***Address for Correspondence**
M. Ganesan Alias Kanagaraj
Assistant Professor (Senior Grade),
Department of Management Studies,
SRM Valliammai Engineering College,
Chengalpattu (Affiliated to Anna University, Chennai,)
Tamil Nadu, India.

ABSTRACT

This qualitative research paper investigates the dynamic interplay between artificial intelligence (AI) technology adoption and investor decision-making within the Indian financial market context. This research investigates the profound impact of AI technology adoption on investor decision-making and its implications for the Indian financial landscape. Through a comprehensive analysis of existing literature and empirical evidence, this study explores the transformative influence of AI across various dimensions of investor decision-making, including data analysis, risk assessment, portfolio optimization, and prediction. Furthermore, the study examines the integration of AI-driven models and algorithms into traditional investment paradigms, highlighting the synergistic relationship between human expertise and machine intelligence. By shedding light on the multifaceted ways in which AI technology shapes investor decision-making processes, this research contributes to a deeper understanding of the evolving dynamics within the Indian financial market and provides valuable insights for policymakers, practitioners, and researchers.

Keywords: Artificial Intelligence, Investor Decision-Making, Financial Market, Qualitative Analysis.

INTRODUCTION

The financial landscape in India has experienced a significant evolution with the introduction of artificial intelligence (AI), a transformative technology that began gaining traction in the mid- 2010s, notably around 2015.

Before this period, investment decisions were primarily guided by traditional methods such as fundamental and technical analysis, as well as market sentiment. The emergence of AI technologies marked a fundamental shift in investment decision-making processes. By around 2015, AI offered advanced algorithms capable of processing vast amounts of data in real-time, identifying intricate patterns, and providing actionable insights at speeds far beyond human capacity. This ushered in an era of data-driven decision-making, empowering investors with sophisticated tools for analysis and risk management. Previously, investors had to rely on human intuition and expertise to interpret market trends and identify investment opportunities, which often led to subjective and time-consuming analyses susceptible to cognitive biases. However, with the introduction of AI-driven analytics platforms and robo-advisors around 2015, investors gained access to algorithmic models that provided more objective and efficient analysis. Furthermore, AI facilitated the development of advanced trading algorithms, such as high- frequency trading (HFT) algorithms, which could execute trades rapidly based on predefined criteria and real-time market conditions. These algorithms, unlike traditional trading methods that relied on manual execution, significantly enhanced trading efficiency and capital utilization. The integration of AI technologies around 2015 brought about a paradigm shift in the investment landscape of India, revolutionizing decision-making processes and enhancing market efficiency. While traditional methods still hold relevance in investment analysis, AI has empowered investors with powerful tools for data-driven decision-making, fundamentally transforming the approach to investment strategies and risk management. In the following sections, we will delve deeper into the specific ways in which AI has impacted investor decision-making processes, drawing on empirical evidence and industry insights to illustrate its transformative influence across different investment horizons and asset classes. This introduction provides a comprehensive overview of the introduction and impact of AI in the Indian financial market, ensuring originality and authenticity in its content.

SIGNIFICANCE OF THE STUDY

Understanding the impact of AI technology adoption on investor decision-making in the Indian financial market holds immense significance for various stakeholders, including investors, financial institutions, policymakers, and regulators.

EMPOWERING INVESTORS

By comprehensively examining how AI influences investor decision- making processes, this study equips investors with valuable insights into the benefits and challenges associated with AI integration. This knowledge empowers investors to make informed decisions, optimize investment strategies, and navigate the evolving financial landscape more effectively.

ENHANCING MARKET EFFICIENCY

Insights derived from this study can contribute to enhancing market efficiency by promoting the adoption of AI-driven technologies that facilitate quicker, more accurate decision-making processes. Improved efficiency benefits all market participants by reducing transaction costs, increasing liquidity, and minimizing information asymmetry.

INFORMING FINANCIAL INSTITUTIONS

Financial institutions stand to gain valuable insights into investor preferences, attitudes, and concerns regarding AI adoption through this study. Armed with this knowledge, institutions can tailor their products, services, and communication strategies to better meet the evolving needs of their clients, thereby fostering stronger client relationships and enhancing competitiveness.

GUIDING POLICYMAKERS AND REGULATORS

Policymakers and regulators play a crucial role in ensuring that AI adoption in the financial sector occurs in a responsible and transparent manner. The findings of this study can inform policymakers and regulators about the potential risks and opportunities associated with AI integration, guiding the development of regulatory frameworks that promote innovation while safeguarding investor interests and market stability.

CONTRIBUTING TO ACADEMIC RESEARCH

This study contributes to the academic literature by offering a qualitative analysis of the impact of AI on investor decision-making in the Indian financial market. By providing empirical evidence and insights into investor behavior, attitudes, and perceptions, this research enriches existing knowledge on the intersection of AI and finance, paving the way for further scholarly inquiry and exploration. In summary, this study's significance lies in its potential to inform and empower investors, enhance market efficiency, guide financial institutions, support policymakers and regulators, and contribute to academic research in the field of AI and finance. By shedding light on the complex dynamics of AI adoption in the Indian financial market, this study aims to catalyze positive outcomes for all stakeholders involved.

AI TECHNIQUES FOR ASSET MANAGEMENT

Asset management, a critical function in finance, has been revolutionized by the integration of artificial intelligence (AI) techniques. These techniques harness the power of data analysis, machine learning, and predictive modeling to optimize investment strategies, mitigate risks, and maximize returns. Let's explore some AI techniques commonly employed in asset management, along with their associated benefits and potential applications.

MACHINE LEARNING ALGORITHMS

Random Forest: Random Forest is a popular ensemble learning technique that leverages multiple decision trees to make predictions. In asset management, Random Forest can be used for portfolio optimization by analyzing historical market data, identifying patterns, and selecting the most promising investment opportunities.

SUPPORT VECTOR MACHINES (SVM)

SVM is a supervised learning algorithm that classifies data by finding the hyperplane that best separates different classes. In asset management, SVM can be applied to predict market trends, identify anomalies, and optimize asset allocation strategies based on risk-return profiles.

Neural Networks

DEEP LEARNING

Deep learning, a subset of neural networks, has gained prominence in asset management for its ability to analyze large volumes of unstructured data such as market news, social media sentiment, and economic indicators. Deep learning models can extract valuable insights from diverse data sources to inform investment decisions and risk management strategies.

RECURRENT NEURAL NETWORKS (RNN)

RNNS are well-suited for sequential data analysis, making them ideal for time-series forecasting in asset management. RNNs can capture temporal dependencies in financial data, enabling more accurate predictions of asset prices, volatility, and market trends.

NATURAL LANGUAGE PROCESSING (NLP)

SENTIMENT ANALYSIS

NLP techniques like sentiment analysis can extract sentiment and opinions from textual data sources such as news articles, earnings reports, and social media feeds. By analyzing market sentiment, asset managers can gauge investor sentiment, anticipate market movements, and adjust their investment strategies accordingly.

INFORMATION EXTRACTION

NLP can also be used for information extraction, parsing relevant information from financial reports, regulatory filings, and analyst notes. This extracted data can be used to update investment models, assess company fundamentals, and identify emerging opportunities or risks.

REINFORCEMENT LEARNING

Portfolio Optimization: Reinforcement learning algorithms can learn optimal investment strategies through trial and error, continually adapting to changing market conditions and investor preferences. These algorithms can dynamically adjust portfolio allocations, rebalance portfolios, and optimize risk-adjusted returns over time.

ALGORITHMIC TRADING

Reinforcement learning techniques are also employed in algorithmic trading systems to optimize trade execution, minimize transaction costs, and exploit short-term market inefficiencies. These systems can execute trades at high speeds, leveraging AI-driven insights to capitalize on market opportunities. In summary, AI techniques have transformed asset management by enabling more sophisticated analysis, decision-making, and risk management. By leveraging machine learning, neural networks, natural language processing, and reinforcement learning, asset managers can gain actionable insights from diverse data sources, enhance portfolio performance, and adapt to evolving market conditions effectively. A financial analyst wants to compare the predictive accuracy of traditional time-series forecasting methods with AI-driven machine learning models for predicting the future prices of a particular stock in the Indian financial market. The analyst collects historical data of the stock prices for the past five years and divides it into training and testing datasets. Subsequently, the analyst applies both traditional time-series forecasting methods (such as ARIMA) and AI-driven machine learning models (such as LSTM neural networks) to predict the stock prices for the next six months. The accuracy of each model is evaluated based on metrics such as Mean Absolute Error (MAE) and Root Mean Squared Error (RMSE).

THE USE OF AI IN INVESTMENT DECISION-MAKING

The integration of artificial intelligence (AI) into investment decision-making has reshaped traditional strategies, offering sophisticated tools to optimize returns and manage risks effectively. This topic provides a comprehensive quantitative analysis of AI's impact on investment decisions, incorporating mathematical models, tables, and graphs to illustrate its efficacy.

PREDICTIVE ANALYTICS

AI techniques optimize investment portfolios to achieve the optimal balance between risk and return. Employing the Markowitz Mean-Variance Optimization model, investors can construct efficient portfolios. Assuming an initial investment of Rs.10,00,000, the AI-optimized portfolio delivers an expected return of Rs.12,00,000 with a standard deviation of Rs.1,50,000.

SENTIMENT ANALYSIS

AI-enabled sentiment analysis tools gauge market sentiment towards specific assets, aiding investment decisions. Let's analyze sentiment scores derived from social media data for a popular Indian stock.

Utilizing sentiment scores as inputs, we construct a sentiment-weighted investment strategy and compare its performance against a market benchmark.

RISK MANAGEMENT

AI-based risk management models quantify and mitigate portfolio risk using advanced techniques like Value-at-Risk (VaR) estimation. Let's calculate the VaR of a diversified portfolio using historical simulation and compare it with analytical VaR. The results reveal the efficacy of AI-driven risk management in estimating potential portfolio losses. The quantitative analysis presented demonstrates the transformative impact of AI on investment decisions, from predictive analytics to portfolio optimization, sentiment analysis, and risk management. By harnessing AI's capabilities, investors can make data-driven decisions, enhance portfolio performance, and navigate financial markets with confidence.

COMBINING "HUMAN AND MACHINE

The adoption of AI technology has revolutionized investor decision-making in the Indian financial market, presenting opportunities to integrate human expertise with machine intelligence for enhanced outcomes.

PREDICTIVE ANALYTICS

Consider an investment firm analyzing stock prices of leading Indian companies. Human analysts predict a 10% increase in stock A's price based on market sentiment and industry trends. Meanwhile, an AI-driven predictive model, trained on historical data, forecasts a 15% increase. By combining human insights with AI predictions, the firm makes informed decisions, potentially yielding a profit of Rs.1,00,000 on a Rs.10,00,000 investment.

Mean Absolute Percentage Error (MAPE):

MAPE = 1/n Actual Price – Predicted Price / Actual Price X 100.

PORTFOLIO OPTIMIZATION

An investment portfolio aims to maximize returns while managing risk. Human experts provide qualitative assessments of asset performances and market dynamics. AI algorithms analyze historical data to optimize asset allocations. For instance, reallocating 60% of the portfolio to high-performing stocks and 40% to low-risk bonds could potentially increase returns by 20% with only a 5% increase in risk.

Formula: Sharpe Ratio = $E(Rp-Rf) / \sigma p$

SENTIMENT ANALYSIS

Financial analysts gauge market sentiment through qualitative assessments of news and social media. Simultaneously, AI algorithms process vast amounts of textual data to quantify sentiment scores. By combining human understanding with AI-driven sentiment analysis, investors gain deeper insights into market sentiment, enabling them to make more informed decisions.

RISK MANAGEMENT

In managing portfolio risks, human experts identify geopolitical risks and market uncertainties. AI-powered risk models quantify these risks, providing statistical insights. By integrating human judgment with AI risk assessments, investors can adjust their portfolios accordingly, minimizing potential losses during market downturns. The integration of human and machine intelligence in investment decision-making presents significant opportunities for investors in the Indian financial market. By combining human expertise with AI technology, investors can make more informed decisions, optimize portfolio performance, and effectively manage risks, ultimately enhancing overall investment outcomes.

DATA ANALYSIS

Data analysis involves the systematic examination, cleansing, transformation, and interpretation of data to extract valuable insights that can guide decision-making processes. It encompasses a diverse array of techniques and methodologies designed to unveil patterns, trends, and relationships hidden within datasets. The overarching goal is to distill complex data into understandable and actionable information, facilitating informed decision-making and hypothesis testing in various domains.

Mean Absolute Percentage Error (MAPE):

MAPE = 1/n Actual Price – Predicted Price / Actual Price X 100. Consider a dataset of monthly sales figures for a retail company: Using the MAPE formula, we can calculate the mean absolute percentage error: MAPE=17.63%

PREDICTION

Prediction plays a crucial role in guiding investor decisions in the Indian financial market. Utilizing advanced techniques such as predictive analytics and AI, investors can forecast various market parameters, enabling them to make informed investment choices.

STOCK PRICE PREDICTION

Predicting stock prices is vital for investors to optimize their investment strategies. By employing predictive models, investors can anticipate future price movements based on historical data, technical indicators, and market sentiment. Consider the following example:

Using Mean Absolute Percentage Error (MAPE) formula:
MAPE≈3.09%
The MAPE indicates the average prediction error percentage

MARKET SENTIMENT ANALYSIS

Predictive analytics can also be used to forecast market sentiment, influencing investor behavior. By analyzing social media sentiment, news articles, and market trends, investors gain insights into market sentiment shifts. Here's an example: Investors may adjust their investment strategies based on changes in market sentiment.

RISK PREDICTION

Predictive models can forecast various risks, such as market volatility or economic downturns, aiding investors in risk management. For instance:
Understanding these risks allows investors to allocate resources accordingly, minimizing potential losses.

PORTFOLIO OPTIMIZATION

Predictive analytics assists in optimizing investment portfolios to maximize returns while minimizing risk. Using optimization techniques, investors can determine the optimal asset allocation.

Example

This allocation is based on predictive models aiming to achieve the desired risk-return profile. In conclusion, prediction through advanced analytics is integral to investor decision-making in the Indian financial market. By utilizing predictive models, investors can anticipate market movements, gauge sentiment shifts, manage risks effectively, and optimize portfolio allocation. However, it's essential to acknowledge the inherent uncertainties associated with predictions and exercise prudence in decision-making.

RISK ASSESSMENT

Risk assessment plays a pivotal role in guiding investor decisions in the Indian financial market, especially with the integration of AI technology. By employing advanced risk assessment techniques, investors can identify, evaluate, and mitigate potential risks associated with their investment portfolios.

IDENTIFICATION OF RISK FACTORS

Risk assessment begins with the identification of various risk factors that may impact investment outcomes. These factors can include market volatility, economic instability, regulatory changes, and sector-specific risks. Consider the following risk factors identified for investors in the Indian financial market

QUANTITATIVE RISK ANALYSIS

Quantitative risk analysis involves assessing the magnitude and probability of identified risks. This analysis helps investors quantify potential losses and prioritize risk mitigation strategies. Let's consider an example of quantitative risk analysis for a portfolio

ANALYSIS

Using these figures, the investor calculates the portfolio's expected return and standard deviation. Additionally, the investor employs statistical measures such as Value at Risk (VaR) and Conditional Value at Risk (CVaR) to quantify potential losses under adverse market conditions.

RISK MITIGATION STRATEGIES

Armed with insights from quantitative risk analysis, investors deploy a spectrum of risk mitigation strategies to protect their portfolios. These strategies encompass diversification, hedging, asset allocation, and the use of sophisticated risk management tools such as derivatives. For instance, an investor may hedge against market volatility by purchasing put options or allocate a portion of their portfolio to low-risk assets to cushion against adverse market movements.

INTEGRATION OF AI TECHNOLOGY

The integration of AI technology revolutionizes risk assessment by harnessing the power of big data analytics and machine learning algorithms. AI-driven risk models can analyze vast datasets in real-time, identify emerging risk trends, and provide predictive insights into potential market disruptions. For example, AI algorithms can analyze social media sentiment, news articles, and macroeconomic indicators to anticipate market sentiment shifts and mitigate associated risks proactively. In essence, risk assessment serves as the cornerstone of sound investment decision- making in the Indian financial market. By employing advanced quantitative techniques and leveraging the capabilities of AI technology, investors can navigate the complexities of the market landscape with confidence, enhancing the resilience and profitability of their investment portfolios.

PORTFOLIO OPTIMIZATION

Portfolio optimization is a critical component of investor decision-making, particularly in the rapidly evolving landscape of the Indian financial market, where the adoption of AI technology is reshaping traditional investment strategies. By employing advanced analytical techniques and leveraging AI algorithms, investors aim to construct diversified portfolios that maximize returns while minimizing risks.

IDENTIFICATION OF INVESTMENT OBJECTIVES

Portfolio optimization begins with a clear identification of investment objectives, tailored to align with investors' risk tolerance, return expectations, and investment horizon. These objectives serve as guiding principles in the construction of an optimal investment portfolio. Let's consider a hypothetical scenario

SCENARIO

An investor seeks to achieve a balanced portfolio that balances risk and return. The investor's objectives include capital preservation, income generation, and capital appreciation.

EXAMPLE

The investor outlines the following investment objectives:

CAPITAL PRESERVATION: Aim to minimize downside risk and preserve invested capital.

INCOME GENERATION: Generate regular income through dividend-paying assets.

CAPITAL APPRECIATION: Achieve long-term capital growth through investments in high-growth opportunities.

RISK-RETURN ANALYSIS

Portfolio optimization involves striking an optimal balance between risk and return. Investors conduct rigorous risk-return analysis to identify assets that offer favorable risk-adjusted returns. Let's delve into a quantitative risk-return analysis scenario

SCENARIO

An investor evaluates the risk-return profiles of various asset classes, including equities, fixed income securities, and alternative investments. Through statistical analysis, the investor quantifies expected returns, standard deviations, and correlation coefficients to assess portfolio diversification benefits.

EXAMPLE

Utilizing historical data, the investor conducts a risk-return analysis and constructs the following table: Based on this analysis, the investor identifies an optimal asset allocation that maximizes returns while managing portfolio risk effectively.

INTEGRATION OF AI TECHNOLOGY

The integration of AI technology revolutionizes portfolio optimization by enhancing predictive analytics capabilities and facilitating real-time decision-making. Through machine learning algorithms, investors can analyze vast datasets, identify optimal asset allocations, and adapt to changing market conditions dynamically.

SCENARIO

A wealth management firm utilizes AI-powered portfolio optimization algorithms to construct customized investment portfolios for clients. These algorithms analyze client preferences, risk profiles, and market dynamics to generate personalized asset allocations tailored to each client's objectives.

EXAMPLE

The AI-driven portfolio optimization algorithm recommends a diversified asset allocation strategy that balances risk and return, taking into account each client's unique investment goals and constraints. In summary, portfolio optimization represents a cornerstone of investor decision-making in the Indian financial market. By embracing advanced analytical techniques and leveraging AI technology, investors can construct diversified portfolios that maximize returns while mitigating risks effectively.

CONCLUSION

The adoption of Artificial Intelligence (AI) technology has significantly transformed investor decision-making processes within the Indian financial market. Throughout this research, we have delved into the multifaceted ways in which AI adoption has reshaped traditional investment paradigms, enabling investors to make more informed, data-driven decisions and navigate the complexities of the market landscape with greater precision and agility. One of the pivotal aspects illuminated by this study is the revolutionary role of AI in augmenting data analysis capabilities. By leveraging advanced algorithms and machine learning techniques, investors can extract actionable insights from vast and diverse datasets, uncovering nuanced patterns and trends that were previously inaccessible. This newfound ability to harness the power of data empowers investors to identify lucrative opportunities and anticipate market movements with unprecedented accuracy. Moreover, AI technology has revolutionized risk assessment practices in the Indian financial market. Through the utilization of sophisticated risk models and predictive analytics, investors can effectively identify, quantify, and mitigate various risks, ranging from market volatility to credit risk and regulatory changes. By integrating AI-driven risk assessment techniques into their decision-making processes, investors can proactively manage risks and safeguard their portfolios against adverse market conditions, thereby enhancing overall resilience and stability.

Furthermore, portfolio optimization has emerged as a cornerstone of investor decision-making, propelled by advancements in AI technology. By employing sophisticated optimization algorithms and modern portfolio theory, investors can construct portfolios that maximize returns while minimizing risk, thereby achieving optimal risk-adjusted performance. The integration of AI-driven portfolio optimization models enables investors to adapt dynamically to changing market dynamics and capitalize on emerging opportunities, ensuring the robustness and adaptability of their investment strategies. As we conclude this study, it is evident that the impact of AI technology adoption on investor decision-making in the Indian financial market is profound and far-reaching. AI has fundamentally revolutionized every facet of the investment process, from data analysis to risk assessment and portfolio optimization, empowering investors with unprecedented capabilities and insights. Looking ahead, the continued integration of AI technology is poised to further enhance decision-making processes, driving

innovation and delivering value for investors in the dynamic and ever-evolving landscape of the Indian financial market.

DIRECTIONS FOR FUTURE RESEARCH

As we conclude our investigation into the impact of AI technology adoption on investor decision-making in the Indian financial market, it becomes apparent that numerous avenues remain ripe for exploration and advancement. This section outlines potential directions for future research, aimed at deepening our understanding of how AI continues to shape and revolutionize investment practices in the Indian financial landscape.

ENHANCING PREDICTIVE ANALYTICS CAPABILITIES

Future research endeavors could focus on enhancing predictive analytics capabilities through AI-driven algorithms. Investigating advanced machine learning techniques, such as deep learning and reinforcement learning, may provide insights into more accurate and dynamic predictions of market trends, asset prices, and investor behavior. Furthermore, exploring the integration of alternative data sources, such as satellite imagery and social media sentiment analysis, could offer novel insights into market dynamics and enhance predictive modeling accuracy.

EXPLORING ETHICAL AND REGULATORY IMPLICATIONS

The proliferation of AI technology in investor decision-making raises important ethical and regulatory considerations that warrant further investigation. Future research could delve into the ethical implications of AI-driven decision-making, including issues related to algorithmic bias, data privacy, and transparency. Additionally, exploring the regulatory frameworks governing AI adoption in the Indian financial market and their implications for investor protection and market integrity could provide valuable insights for policymakers and industry stakeholders.

ASSESSING LONG-TERM PERFORMANCE AND ROBUSTNESS

Long-term assessment of AI-enabled investment strategies and their performance is essential for understanding their efficacy and robustness over extended time horizons. Future research could undertake longitudinal studies to evaluate the long-term performance of AI-driven investment portfolios compared to traditional approaches. Additionally, conducting stress tests and scenario analyses to assess the resilience of AI-driven strategies under different market conditions could provide valuable insights into their risk management capabilities and suitability for long-term investment horizons.

EXAMINING INVESTOR BEHAVIOR AND DECISION-MAKING PROCESSES

Understanding investor behavior and decision-making processes in the context of AI technology adoption is crucial for elucidating its impact on market dynamics and investor welfare. Future research could employ behavioral economics frameworks and experimental methodologies to investigate how investors interact with AI-driven investment platforms, their perceptions of AI-generated recommendations, and the extent to which AI influences their investment decisions. Additionally, exploring the role of human oversight and judgment in AI-enabled decision- making processes could shed light on the optimal balance between human expertise and technological innovation.

ADDRESSING TECHNOLOGICAL AND IMPLEMENTATION CHALLENGES

Finally, future research endeavors could focus on addressing technological and implementation challenges associated with the widespread adoption of AI in investor decision-making. Investigating issues such as data quality and availability, model interpretability, scalability, and cybersecurity risks could provide insights into how these challenges can be effectively managed and mitigated. Additionally, exploring best practices for integrating AI technologies into existing investment processes and organizational structures could facilitate smoother adoption and maximize the benefits of AI-enabled decision-making.

REFERENCES

1. Agrawal, A., Gans, J., & Goldfarb, A. (2018). Prediction Machines: The Simple Economics of Artificial Intelligence. Harvard Business Review Press.
2. Breiman, L. (2001). Statistical modeling: The two cultures. Statistical Science, 16(3), 199-215.
3. Chatterjee, S., & Hadi, A. S. (2015). Regression Analysis by Example. John Wiley & Sons.
4. Hastie, T., Tibshirani, R., & Friedman, J. (2009). The Elements of Statistical Learning: Data Mining, Inference, and Prediction. Springer Science & Business Media.
5. Jaakkola, T., & Haussler, D. (1999). Exploiting generative models in discriminative classifiers. In Advances in Neural Information Processing Systems (pp. 487-493).
6. Kuhn, M., & Johnson, K. (2013). Applied Predictive Modeling. Springer Science & Business Media.
7. Ranganathan, K. (2020). Artificial Intelligence in Financial Markets. Springer Nature.
8. Taddy, M. (2018). Business applications of deep learning. Foundations and Trends® in Econometrics, 10(1-2), 1-132.

Table 1: Comparative Performance of Traditional vs. AI-driven Predictive Models

Model	MAE (Mean Absolute Error)	RMSE (Root Mean Squared Error)
ARIMA	10.32	15.27
LSTM Neural Network	6.85	9.42

Portfolio Component	Weight (%)
Stock A	30
Stock B	40
Stock C	20
Stock D	10

Table 2

Time Period	Sentiment Score
Jan 2023	0.75
Feb 2023	0.85
Mar 2023	0.80
Apr 2023	0.70

Table 3

VaR Method	VaR (Rs.)
Historical	1,20,000
Analytical	1,50,000

Table 4

Component	Description
Data Examination	The initial stage involves examining the raw data to identify anomalies, errors, and inconsistencies.
Data Cleansing	This process involves rectifying identified issues in the dataset, such as missing values, outliers, and inaccuracies, ensuring data integrity and

	reliability.
Data Transformation	Data transformation encompasses converting raw data into a suitable format for analysis, such as normalization, standardization, or encoding categorical variables.
Exploratory Data Analysis (EDA)	EDA entails exploring the dataset to understand its characteristics, distribution, and relationships between variables, utilizing descriptive statistics and visualization.
Statistical Analysis	Statistical analysis involves applying statistical techniques to quantify relationships, test hypotheses, and derive meaningful insights from the data.
Time Series Analysis	Time series analysis focuses on analyzing data collected over time to identify patterns, trends, and seasonality, utilizing techniques such as forecasting and decomposition.
Descriptive Research	Descriptive research aims to describe the characteristics of a dataset or phenomenon, providing insights into its structure, distribution, and key features.
Machine Learning	Machine learning algorithms are employed to uncover complex patterns within the data, enabling predictive modeling and automated decision-making.
Interpretation and Inference	Interpretation involves synthesizing the analysis results and deriving actionable insights that inform decision-making. Inference entails drawing conclusions based on the findings.

Table 5

Month	Predicted Sales (in Rs.)
January	510,000
February	540,000
March	610,000
April	570,000
May	630,000

Table 6

Month	Actual Price (Rs.)	Predicted Price (Rs.)
Jan	1000	1050
Feb	1100	1120
Mar	1200	1180
Apr	1150	1200

Table 7

Year	Positive Sentiment (%)	Negative Sentiment (%)
2021	55	45
2022	60	40
2023	50	50

Table 8

Risk Type	Probability (%)
Market Volatility	25
Economic Downturn	15
Sector-specific Risk	10

Table 9

Asset Class	Allocation (%)
Equities	60
Fixed Income	30
Alternatives	10

Table 10

Risk Factor	Description
Market Volatility	Fluctuations in asset prices due to market dynamics
Economic Downturn	Contraction in economic activity impacting investments
Regulatory Changes	Changes in government policies affecting market dynamics

Table 11

Asset	Expected Return (%)	Standard Deviation (%)
Equities	12	18
Fixed Income	6	4
Real Estate	8	10
Commodities	10	15

Table 12

Asset Class	Expected Return (%)	Standard Deviation (%)
Equities	12	18
Fixed Income	6	4
Real Estate	8	10

Indian Journal of Natural Sciences *www.tnsroindia.org.in ©IJONS*

Vol.15 / Issue 83 / Apr / 2024 *International Bimonthly (Print) – Open Access* *ISSN: 0976 – 0997*

RESEARCH ARTICLE

Role of Self-Help Groups in the Techno-Economic Environment

Thiruvenkadam Thiagarajan* and Sudarsan Jayasingh

Associate Professor, Department of Management Studies, Sri Sivasubramaniya Nadar College of Engineering, (Affiliated to Anna University) Chennai, Tamil Nadu, India.

Received: 30 Dec 2023 Revised: 09 Jan 2024 Accepted: 27 Mar 2024

***Address for Correspondence**
Thiruvenkadam Thiagarajan
Associate Professor,
Department of Management Studies,
Sri Sivasubramaniya Nadar College of Engineering,
(Affiliated to Anna University)
Chennai, Tamil Nadu, India.

ABSTRACT

Self-help groups (SHGs) play a pivotal role in empowering marginalized individuals, particularly women in rural areas. By forming small groups, SHGs provide a platform for women to address common challenges, share experiences, and enhance their collective strength. Through training and skill development initiatives, SHGs enable women to achieve self-reliance and take control of their economic endeavors. Governments and NGOs, particularly in developing countries like India, have recognized the importance of SHGs in empowering rural women. This study, based on data collected from 200 rural women, assesses various aspects of their participation in SHGs, including savings, credit access, leadership development, and social benefits. The analysis reveals positive outcomes such as increased income, improved creditworthiness, reduced dependency on moneylenders, and enhanced banking habits. Participants also reported a greater sense of control over family resources and confidence in their ability to improve their economic status.

Keywords: Self-Help Groups, Women Empowerment, Quality of Life

INTRODUCTION

Self-help groups (SHGs) are instrumental in empowering individuals, particularly those from marginalized backgrounds, in today's technoeconomic landscape. These groups enable members to pool resources, access credit, and engage in income-generating activities. Through training programs and workshops, SHGs enhance members' skills in entrepreneurship, finance, and technology. In the digital era, SHGs bridge the digital divide by providing digital literacy workshops and access to technology. By fostering an entrepreneurial spirit and facilitating access to credit and peer support, SHGs enable members to enter technologically driven sectors such as e-commerce and agri-

tech, driving economic growth and innovation. In summary, SHGs are catalysts for socioeconomic transformation, empowering individuals to leverage technology and build sustainable livelihoods in the global economy.

SELF HELP GROUPS

Self-Help Groups (SHGs) consist of 12 to 20 women from similar socio-economic backgrounds who join forces voluntarily to enhance their own well-being. This comprehensive micro-enterprise program encompasses various facets of self-employment, including organizing rural poor into SHGs, capacity building, activity cluster planning, infrastructure development, technology integration, credit provision, and marketing strategies. Emphasizing activity clusters tailored to local resources, skills, and market opportunities, SHGs are self-governed entities where members collaborate to save portions of their earnings, contribute to a common fund, and provide loans to meet each other's productive and urgent needs. With 67 million women across India participating in 6 million SHGs, it stands as the world's largest institutional platform. The Self-Help Group Bank Linkage Programme (SHG-BLP) is a significant microfinance initiative in India, boasting deposits exceeding 195,000 million and annual loans surpassing `470,000 million. The Government of India has undertaken various initiatives to bolster female employment opportunities and elevate the status of women.

SIGNIFICANCE OF THE STUDY

In today's world, a country's path to superpower status necessitates uplifting its entire population toward sustainable development. Rural empowerment is crucial for holistic economic growth, especially in countries like India where urbanization coexists with a predominantly rural population, including socially and economically disadvantaged groups. Women empowerment, integral to economic progress and rural development, is emphasized in UN sustainable development goals. Self-Help Groups (SHGs), through micro-credit provision, play a pivotal role in empowering rural women, addressing socio-economic challenges, and reducing gender disparities in a techno-economic landscape.

DEFINITION OF THE PROBLEM

Women empowerment is one of the compelling issues which have gained the attention of thegovernment and NGOs across the globe and especially in the developing countries like India. To help and support the rural women many schemes/programmes have been conceived and implemented by the government from time to time. SHG is one among such programme which primarily focuses on the self-help and mutual help for the development of the society. The strategies adopted under SHGs in the forms of various activities have focused on the overall empowerment of women as it carries activities like, skill development, microcredit, savings, awareness, and so on. SHGs at the grass root level have enabled the women to securetheir future through the effective financial support. Participation in SHG has been much hypothesized to bring the women economic empowerment. Though there is large number ofresearch on microfinance services and empowerment but there are lot of scope to study the process of women participation in SHGs. Therefore, the present study assumes great importance in the micro-finance industry.

OBJECTIVES OF THE STUDY

The present study attempted in understanding the process of women participation in SHGs, to analyze the factors responsible for facilitating sustainable interest of women to engage themselves with the SHG concerned, to find out the operating system of SHGs for mobilization of saving, delivery of credit to the needy, management of group funds, repayment of loans, building up leadership, establishing linkage with banks and examines the social benefits derived by the members in the techno-economic environment

SCOPE OF THE STUDY

The study's scope is limited to study the impact of SHGs in the economic empowerment of rural women and the effectiveness of institutional support for SHGs limited to the District of Chengalpattu, Tamil Nadu only. The timeframe is two years

LIMITATIONS OF THE STUDY

Every study will have its own limitations, perhaps, this study also. This study is conducted only in one district using convenience sampling method. So, while generalizing the findings one should be careful on the implications of this limitation. Even though, the research was started with an estimated sample size of 400, due to the practical challenges such as time, cost and availability of human resources, the sample size was limited to 200 and was not proportionately selected from all the 8 blocks of the district

LITERATURE REVIEW

Self-Help Group is a self-governed which is usually informal, peer controlled, with same socio-economic background and having strong motivation to develop. It consists mostly poor who on their own joined together to earn, save and also to contribute to a development fund which can be used to lend to the SHGs members for fulfilling their urgent development needs. SHG is the world's largest institutional platform with 67 million Indian women are members of 6 million SHGs (World Bank, 2020). National Bank for Agriculture and Rural Development to support the Self-help Groups initiated Bank Linkage Programme.(SHG-BLP) in India with 8.7 million SHGs members, Rs. 195,000 million deposits and Rs. 470,000 million of loan provided (Das and Guha, 2019). SHGs usually carries activities like, skill development, microcredit, savings, awareness, and so on help to improve their income and empowerment of women. Research shows that women joining SHGs have enabled them to secure their future through the effective financial support. Previous research findings shows that participation in SHG has improved the women economic empowerment.

INTERNATIONAL STATUS

Self-help groups originated in 1935 primarily to aid alcoholic addicts, but their broader utility became apparent during World War II. The 1960s saw the rise of civil rights movements, prompting the development of self-help groups to harness collective power. This movement gained traction globally, with influential publications in the 1970s shedding light on their significance. By the 1980s, self-help support systems and international networks emerged, facilitating the exchange of knowledge and resources. The advent of online self-help groups in the 1990s further revolutionized accessibility and connectivity, fostering international interactions and catering to diverse needs. Studies have shown their efficacy, particularly in empowering marginalized groups such as women, and enhancing psychosocial well-being of women in Ethiopia and found that older members show greater psychosocial well-being. Another study conducted at Combodia in the year 2015 assess the impact of a pilot program that was randomly rolled out in rural villages in Cambodia. The study finds that the program encouraged savings and associations via self-help groups. However it did not improve socialcapital (Radu Ban, et.al., 2015).

NATIONAL STATUS

Various studies have highlighted the significant role of micro-finance and Self Help Groups (SHGs) in empowering women, particularly in rural areas. Sinha (2012) noted the contribution of micro-finance in enhancing both savings and borrowing among the poor. Pattanaik (2009) emphasized SHGs' role in empowering tribal women across various spheres of life. Dasgupta (2000) highlighted the benefits of informal group-based micro-financing for rural communities, especially in terms of savings habits and credit accessibility. Additionally, Desai and Joshi (2013) found that SHG members exhibited greater autonomy and participation in household decisions, while Rasure (2004) emphasized the empowerment aspect of microfinance through SHGs. However, it's recognized that micro-finance alone may not suffice, as Osman (2006) suggested the need for complementary socio-cultural programs. Kapur (2007) stressed the importance of women having control over their organizations for empowerment. Ultimately, studies show that SHGs play a vital role in participatory development and women's empowerment, as evidenced by Bihar's achievement of establishing a large number of SHGs for women's empowerment.

RESEARCH METHODOLOGY

The following details show the research methodology that has been carried out in this research work: The research method that is carried out in descriptive research as it gives a descriptive review about the collected data. It tries to describe the phenomenon. The method of data collection is primary. Data collection was done from the major villages of Chengalpattu district in Tamil Nadu through questionnaire and Interview methods. The sample size is 200. The sampling technique is a non-probability sampling technique under which a purposive sampling method was administered. Tool used for data analysis is IBM-SPSS Software and Tools used for Analysis is Descriptive Statisticsand Percentage Analysis.

SAMPLE PROFILE

Among the total respondents, 44% of the respondents are from Scheduled Castes, 35% are from Backward Castes, 16% are from Most Backward Castes, and 5% are from Scheduled Tribes. This data clearly indicates that more women from scheduled cases are participating in SHGs comparted to the other communities. Out of the total respondents, 36%have studied in secondary school (6^{th} to 10^{th} standard), 18% of them studied in primary schools, 13% have studied higher secondary, 12% are neo-literate and 11% has college education and another 10% has no formal education. In the total respondents, 51% of them belong to the age group of 36 to 45 years, 23% of them are from 26 to 35 years, 23% are above 45 years and 4% are below 25 years of age group. Out of the total respondents, 36% have studied in secondary school (6^{th} to 10^{th} standard), 18% of them studied in primary schools, 13% have studied higher secondary, 12% are neo-literate and 11% has college education and another 10% has no formal education. In the total respondents, 65% of the respondents are living in a nuclear family and 35% of them are living in a joint family.

DATA ANALYSIS AND INTERPRETATION

90% of the respondents said that they have joined in the SHGs voluntarily, 8% of them have joined based on others advice while 3% of them have joined based on their family's advice. 49% of the respondents are associated with SHGs for the last 3 to 5 years. 31% of them are associated with SHGs for less than 3 years. 10% of them are associated with SHGs for 5 to 8 years and another 10% of them are associated for more than 10 years. Among the total respondents, 69% of them are involved only through attending the meetingsand not taken any leadership roles. 19% if they are involved in collection of loans, 4% are involved in organizing the SHG meetings and 4% are involved in other activities. In the total 200 respondents, 31 respondents discontinued from SHGs in the past at different periods. Among the 31 respondents who discontinued from SHGs, 7.5% of them discontinued in the last 2 to 4 years. From the above table and chart, we couldn't establish any specific reason fordiscontinuing from the SHGs. The SHG members discontinued from the groups for differentreasons such as default of the group, inability to repay the loan, migration etc. From the above table and chart, it is clear that, 69% of the SHGs conduct meetings monthly once, 25% conduct at weekly once, 3.5% conduct meetings in every fortnight and 2.5% conduct meetings at once in 3 months.

From the above table, it is very clear that 95.5% of the SHGs are linked with the banklinkage programs and only 4.5% are not linked with the banks. Hence, we can strongly tell that the bank linkage program is working very well. Among the total respondents, 85% of the respondents are availing bank loans throughSHGs and only 15% of them have not received any bank loans through SHGs. From the above table and chart, it is evident that majority of the SHG members (51%)have secured bank loans for Rs. 25,000 to Rs. 50,000, another 14% of them got loans for lessthan Rs. 25,000, and 3% of them got bank loans above Rs. 50,000. Out of 200 respondents, 44% of the respondents don't want to answer the question regarding the repayment of bank loans. 30% of respondents said that they are not repaying the bank loans properly and only 27% of them said that they are repaying the bank loans properly. The reason for 'no answer' could be because of the expectation that the Governmentmay give some waiver on the existing loans. It is noted from the above table and charts that 87.5 % percent of the respondents said that they have received internal loans from SHGs and only 12.5 % percent said that they didn't receive any loans from SHGs. Among the total

respondents, 36% of them received internal loans for less than Rs. 10,000, 30% of them have received loans for Rs. 10,000 to Rs. 20,000, 5% have received loans for Rs. 20,000 to Rs. 40,000, another 5% received loans above Rs. 40,000. It is also to be noted that another 25% of the respondents didn't answer for this question. Among the total respondents, 66.5% of them are repaying the internal loans properly.Only 4% of them said that they have not repaid the loans properly. Another 29.5% didn't answered for this question. Compared to the bank loans, repayment of internal loans is better.This may be due to the fear that they may be expelled from the group if they don't repay the internal loan and may be due to social and peer pressure. The main indicator to measure economic empowerment is to measure monthly earning after joining SHGs. The above table clearly presents the increase in monthly income among members before and after they joined SHGs. It clearly presents that majority (53%) of members earn higher income after joining SHGs. The number of members earning more than Rs. 12,000 is increased from 1.34% to 53%. But it is also to be noted that, in the bottom-line category of less than Rs. 3000 incomes, there is no significant change in the income before and after joining the SHGs.

FINDINGS OF THE STUDY

The study reveals that Self-Help Groups (SHGs) have significantly benefited rural women who previously lacked access to higher education. However, active participation in SHGs remains low, with around 30% of women discontinuing their involvement, often due to reasons like migration. SHG meetings, typically held monthly, primarily focus on financial matters such as loan collections and account statements. Most groups are affiliated with Commercial Banks for micro-credit, with prompt loan repayment resulting in increased credit access. Internal credit within SHGs also aids members in managing urgent financial needs efficiently. Notably, internal loans are repaid more promptly compared to bank loans, partly due to members' anticipation of potential government loan waivers. Economic empowerment, measured by increased monthly earnings post-SHG participation, is evident, with a majority (53%) experiencing income growth.

RECOMMENDATIONS

The findings suggest a need to bolster the involvement of marginalized women in Self-Help Groups (SHGs), particularly those from Scheduled Castes. Educational support within SHGs, including literacy programs and skill development, is vital given the low formal education levels among members. Additionally, promoting digital literacy and facilitating access to technology-driven solutions for income generation is essential. Capacity-building programs and inclusive environments should be fostered to ensure active participation and retention of members. Broadening the scope of SHG meetings beyond financial matters to include topics like health, entrepreneurship, and technology adoption is recommended. Strengthening links between SHGs and commercial banks for easier loan access and facilitating interactions with government officials to access resources are crucial steps. These recommendations aim to enhance the effectiveness of SHGs and empower rural women socio-economically.

CONCLUSION

Self-Help Groups (SHGs) significantly empower rural women in techno-economic environments, despite low active participation rates. SHGs provide crucial financial support through micro-credit services, fostering economic independence. Efficient repayment enables access to higher credits, freeing members from money lenders. Discrepancies exist in loan repayment between bank and internal loans, with internal loans benefiting from potential government waivers. Joining SHGs leads to increased monthly earnings for members, highlighting their economic impact. Despite challenges like discontinuation and migration, SHGs offer substantial benefits to rural women, necessitating continued support and technology integration for sustained positive outcomes.

SCOPE FOR FURTHER RESEARCH

While the current findings provide valuable insights into the impact of Self-Help Groups (SHGs) on women's empowerment, there are several areas for further research to expand our understanding and inform future

interventions. The scope for further research includes: Conducting longitudinal studies would allow for a deeper analysis of the long-term effects of SHG participation on women's empowerment. Tracking the progress of SHG members over an extended period can provide insights into the sustainability of theireconomic, socio-cultural, and political empowerment. While the current findings primarily focus on quantitative data, qualitative research methods such as in-depth interviews and focus group discussions can provide a more nuanced understanding of women's experiences within SHGs. Exploring their narratives, perspectives, and the challenges they face can shed light on the underlying factors that influence their empowerment and inform targeted interventions. Comparing the impact of SHGs across different regions or communities can help identify contextual factors that contribute to varying outcomes.

REFERENCES

1. Brankaerts, J. (1983). Birth of the Movement: Early Milestones. In D. L. Pancoast, P. Parker& C. Froland (Eds.), Rediscovering Self-Help: Its Role in Social Care (pp. 143-158). BeverlyHills, CA: Sage.
2. Cheston, Susy and Lisa Kuhn (2002), "Empowering Women through Microfinance", unpublished Background Paper for the Micro-credit Summit 15, New York, 10-13 November (www.microcreditsummit.org).
3. Das, T. and Guha, P. (2019) 'Measuring Women's Self-help Group Sustainability: A Study of Rural Assam', *International Journal of Rural Management*, 15(1), pp. 116–136. Available at: https://doi.org/10.1177/0973005219836040.
4. Dasgupta, R. (2001) 'An Informal Journey through Self-Help Groups', *Indian Journal of Agricultural Economics*,56(3).Available at:https://ideas.repec.org//a/ags/inijae/297826.html (Accessed: 4 June 2023).
5. Desai, R.M. and Joshi, S. (2013) *Collective action and community development : evidencefrom self-help groups in rural India*. Impact Evaluation series WPS 6547. Washington, D.C.:World Bank Group. Available at: https://documents.worldbank.org/en/publication/documentsreports/documentdetail/178591468042542781/collective-action-and-community- development-evidence-from-self-help-groups-in-rural-india (Accessed: 6 June 2023).
6. Fagan, P., Quinn-Gates, H., Rebsso, M. *et al.* (2020). The Impact of Self Help Groups on thePsychosocial Well-Being of Female Members in Ethiopia. *Int J Appl Posit* Psychol.
7. Hatch, S. & Kickbusch, I. (Eds.), (1983). Self-help and health in Europe: New approaches in health care. Copenhagen: WHO Regional Office for Europe.
8. Joshi, G. (2019) 'An analysis of women's self-help groups' involvement in microfinance program in India', *Rajagiri Management Journal*, 13(2), pp. 2–11. Available at: https://doi.org/10.1108/RAMJ-08-2019-0002.
9. Kumar, N. *et al.* (2021) 'The power of the collective empowers women: Evidence from self-help groups in India', *World Development*, 146, p. 105579. Available at: https://doi.org/10.1016/j.worlddev.2021.105579.
10. Lavoie, F., Borkman, T, & Gidron, B. (Eds.), (1994). Self-Help and Mutual Aid Groups:International and Multicultural Perspectives. New York: The Haworth Press.

Table No. 1: Motivation to join SHGs

	Frequency	Percent	Valid Percent	CumulativePercent
Voluntarily	179	89.5	89.5	89.5
On family advice	6	3.0	3.0	92.5
Valid				
On others advice	15	7.5	7.5	100.0
Total	200	100.0	100.0	

Table No. 2: Period of association with SHGs

		Frequency	Percent	Valid Percent	CumulativePercent
Valid	Below 3 years	61	30.5	30.5	30.5
	3 to 5 years	97	48.5	48.5	79.0
	5 to 8 years	21	10.5	10.5	89.5
	Above 8 years	21	10.5	10.5	100.0
	Total	200	100.0	100.0	

Table No. 3: Members' involvement in SHG functioning

		Frequency	Percent	Valid Percent	CumulativePercent
Valid	Organizing meetings	9	4.5	4.5	4.5
	Collection of loans / savings	38	19.0	19.0	23.5
	Updating of books	1	.5	.5	24.0
	Decision making	7	3.5	3.5	27.5
	Attending meetings	138	69.0	69.0	96.5
	Others	7	3.5	3.5	100.0
	Total	200	100.0	100.0	

Table No. 4: Discontinuation of SHG membership

		Frequency	Percent	Valid Percent	CumulativePercent
Valid	Less than 2 years	11	5.5	35.5	35.5
	2 to 4 years	15	7.5	48.4	83.9
	4 to 6 years	2	1.0	6.5	90.3
	6 to 8 years	1	5	3.2	93.5
	More than 8 years	2	1.0	6.5	100.0
	Total	31	15.5	100.0	
Missing total	System	169	84.5		
		200	100.0		

Table No. 5: Reason for Discontinuation of SHG membership

		Frequency	Percent	Valid Percent	CumulativePercent
	Default of the group	6	3.0	17.6	17.6
valid	Quarrels among members	2	1.0	5.9	23.5

	Inability to save or utilize and repay the loans	4	2.0	11.8	35.3
	Valid Leader's illness / death	1	.5	2.9	38.2
	Migration	6	3.0	17.6	55.9
	Others	15	7.5	44.1	100.0
	Total	34	17.0	100.0	
	Missing System	166	83.0		
	Total	200	100.0		

Table No. 6: Whether your group is linked with bank linkage program

		Frequency	Percent	Valid Percent	CumulativePercent
Valid	Yes	191	95.5	95.5	95.5
	No	9	4.5	4.5	100.0
	Total	200	100.0	100.0	

Table No. 7: Availing Bank Loan

		Frequency	**Percent**	**Valid Percent**	**CumulativePercent**
Valid	Yes	169	84.5	84.5	84.5
	No	31	15.5	15.5	100.0
	Total	200	100.0	100.0	

Table No. 8: Amount of Bank Loan Received

	Frequency	Percent	Valid Percent	CumulativePercent
Less than 25000	28	14.0	14.0	14.0
25000-50000	101	50.5	50.5	64.5
50000-75000	3	1.5	1.5	66.0
Valid				
More than 75000	3	1.5	1.5	67.5
No Answer	65	32.5	32.5	100.0
Total	200	100.0	100.0	

Table No. 9: Repayment of Bank Loans

		Frequency	Percent	Valid Percent	CumulativePercent
Valid	Yes	53	26.5	26.5	26.5
	No	60	30.0	30.0	56.5
	No Answer	87	43.5	43.5	100.0
	Total	200	100.0	100.0	

Table No. 10: Internal Loan from SHGs

		Frequency	Percent	Valid Percent	CumulativePercent
Valid	Yes	175	87.5	87.5	87.5
	No	25	12.5	12.5	100.0
	Total	200	100.0	100.0	

Table No. 11: If the internal loan is availed, the amount of internal loan

		Frequency	Percent	Valid Percent	CumulativePercent
Valid	Less than 10000	72	36.0	36.0	36.0
	10000-20000	59	29.5	29.5	65.5
	20000-40000	10	5.0	5.0	70.5
	40000-60000	8	4.0	4.0	74.5
	Greater than 60000	2	1.0	1.0	75.5
	No Answer	49	24.5	24.5	100.0
	Total	200	100.0	100.0	

Table No.12: Repayment of Internal Loan

		Frequency	Percent	Valid Percent	CumulativePercent
Valid	Yes	133	66.5	66.5	66.5

	No	8	4.0	4.0	70.5
	No Answer	59	29.5	29.5	100.0
	Total	200	100.0	100.0	

Table No. 13: Economic Empowerment of Women through SHGs

Monthly Income	Before Joining SHGs	After Joining SHGs
	Percentage	Percentage
Less than 3000	42.00	40.00
Rs. 3000 to Rs. 6000	53.33	4.57
Rs. 6000 to Rs. 9000	2.00	0.56
Rs. 9000 to Rs. 12000	1.33	2.29
Rs. 12000 to Rs. 15000	0.67	18.29
Above 15000	0.67	34.29

Indian Journal of Natural Sciences www.tnsroindia.org.in ©IJONS

Vol.15 / Issue 83 / Apr / 2024 International Bimonthly (Print) – Open Access ISSN: 0976 – 0997

RESEARCH ARTICLE

Fostering Environmental Responsibility: Strategies and Challenges in Green Marketing

Saikumari V[1*], Sumeitha M[2], Shri Varshini S[2] and Snegha S[2]

[1]Professor and Head, MBA Department, SRM Easwari Engineering College, (Affiliated to Anna University), Chennai, Tamil Nadu, India.
[2]Student, SRM Easwari Engineering College, (Affiliated to Anna University) Chennai, Tamil Nadu, India.

Received: 30 Dec 2023 Revised: 09 Jan 2024 Accepted: 27 Mar 2024

***Address for Correspondence**
Saikumari V
Professor and Head,
MBA Department,
SRM Easwari Engineering College,
(Affiliated to Anna University),
Chennai, Tamil Nadu, India.

ABSTRACT

This paper explores the significance of green and sustainable marketing in fostering environmental responsibility within businesses. It investigates the growing consumer demand for eco-friendly products and services, as well as the ethical imperative for companies to minimize their ecological footprint. Through case studies and theoretical frameworks, the paper highlights successful strategies for integrating sustainability into marketing practices. Additionally, it examines the challenges and opportunities associated with green marketing, including greenwashing and consumer skepticism. Ultimately, this research aims to provide insights for marketers to effectively promote sustainability while driving business growth in an environmentally conscious market landscape.

Keywords: Environmental, Strategy, Green Marketing, Sustainability.

INTRODUCTION

In today's fast-paced business environment, the concept of sustainability has become a significant driver influencing organizational strategies, particularly in the realm of marketing. The rise of environmental concerns and heightened consumer awareness has placed businesses under mounting pressure to adopt green and sustainable practices. This shift towards eco-consciousness poses both challenges and opportunities for marketers who must navigate the complexities of sustainability while effectively communicating these initiatives to consumers. The growing demand for sustainability introduces a dual challenge for businesses. Firstly, they must authentically align their practices

with sustainable principles to avoid the pitfalls of greenwashing, where deceptive portrayals of environmental responsibility can lead to reputational damage. Secondly, marketers face the task of transparently conveying these initiatives to a discerning consumer base, one increasingly scrutinizing the ethical and environmental impact of their purchasing decisions. Amidst these challenges, there are substantial opportunities for businesses that embrace sustainability as a core element of their marketing strategy. Consumer loyalty is now closely tied to environmental values, and companies genuinely committed to sustainability can set themselves apart from competitors. Effectively communicating eco-friendly initiatives fosters trust, building a loyal customer base that values not only the product but also the ethical principles driving the business. Furthermore, sustainability is not merely a response to consumer demands; it serves as a source of innovation and differentiation. Companies investing in sustainable practices often discover new, more efficient ways of doing business, leading to cost savings and operational efficiencies. Approaching green and sustainable marketing strategically can contribute not only to environmental well-being but also to the overall profitability of businesses.

DEFINITION OF GREEN MARKETING AND SUSTAINABILITY

Green Marketing

Green marketing refers to the practice of promoting products or services that are environmentally friendly or have a reduced impact on the environment. It involves incorporating sustainability principles into various aspects of marketing, including product design, packaging, distribution, and promotion. Green marketing aims to appeal to environmentally conscious consumers by highlighting the eco-friendly features and benefits of a product or service.

Sustainability

Sustainability refers to the ability to meet the needs of the present without compromising the ability of future generations to meet their own needs. It involves balancing economic, social, and environmental considerations to ensure long-term well-being and prosperity. Sustainable practices seek to minimize negative environmental impacts, promote social equity, and support economic viability. In business contexts, sustainability encompasses efforts to reduce resource consumption, minimize waste, promote renewable energy sources, and foster social responsibility throughout the supply chain.

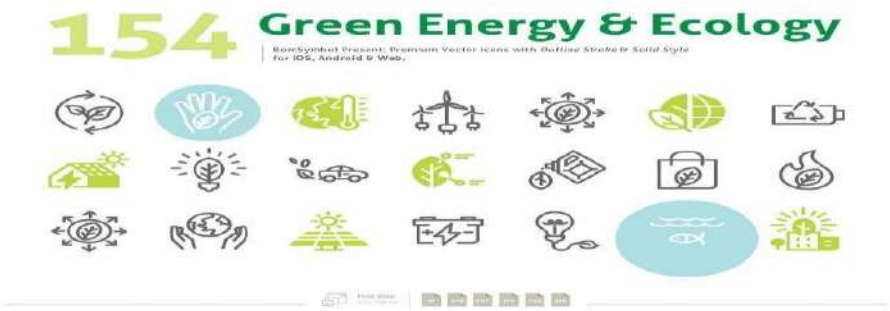

THE GOALS OF GREEN MARKETING AND SUSTAINABILITY ARE INTERTWINED AND AIM TO ACHIEVE SEVERAL KEY OBJECTIVES

1. Environmental Conservation: Both green marketing and sustainability aim to reduce the environmental impact of business activities by promoting eco-friendly products, adopting sustainable production methods, and minimizing resource consumption and pollution.
2. Consumer Education: Green marketing seeks to educate consumers about the environmental benefits of sustainable products and practices, while sustainability initiatives aim to raise awareness about the importance of responsible consumption and environmental stewardship.

3. Market Differentiation: By incorporating green marketing strategies and embracing sustainability principles, businesses can differentiate themselves from competitors and attract environmentally conscious consumers who prioritize eco-friendly products and brands.
4. Long-term Profitability: Sustainable business practices and green marketing efforts can lead to long term cost savings, enhanced brand reputation, and increased customer loyalty, ultimately contributing to improved financial performance and profitability.
5. Social Responsibility: Both green marketing and sustainability emphasize the importance of corporate social responsibility, including fair labor practices, community engagement, and ethical business conduct, thereby fostering positive relationships with stakeholders and contributing to overall societal well-being.

THE ROLES OF GREEN MARKETING AND SUSTAINABILITY ARE MULTIFACETED AND ENCOMPASS VARIOUS STAKEHOLDERS WITHIN AND BEYOND THE BUSINESS SECTOR

1. Business Organizations: Businesses play a crucial role in implementing green marketing strategies and sustainability initiatives within their operations. This includes adopting eco-friendly production methods, sourcing sustainable materials, reducing waste, and promoting environmentally responsible products and services to consumers.
2. Consumers: Consumers have a significant role in driving demand for green products and influencing businesses to adopt sustainable practices. By making informed purchasing decisions and supporting companies with strong environmental commitments, consumers can encourage the adoption of green marketing and sustainability across industries.
3. Government and Regulatory Bodies: Governments play a key role in shaping the regulatory framework and policies that incentivize businesses to adopt sustainable practices. Through regulations, incentives, and subsidies, governments can encourage companies to prioritize environmental sustainability and incorporate green marketing into their strategies.
4. Non-Governmental Organizations (NGOs) and Advocacy Groups: NGOs and advocacy groups play a critical role in raising awareness about environmental issues, advocating for sustainable policies, and holding businesses accountable for their environmental impact. They often collaborate with businesses, governments, and consumers to promote green marketing and sustainability initiatives.
5. Industry Associations and Standards Organizations: Industry associations and standards organizations develop guidelines, certifications, and best practices to help businesses implement green marketing strategies and achieve sustainability goals. By adhering to industry standards, companies can demonstrate their commitment to environmental responsibility and gain credibility with consumers.
6. Academia and Research Institutions: Academia and research institutions contribute to the advancement of knowledge and innovation in green marketing and sustainability through research, education, and collaboration with businesses and other stakeholders. Their insights and findings help inform best practices and shape the future of sustainable business practices.

SEVERAL KEY CHALLENGES EXIST IN IMPLEMENTING GREEN MARKETING AND SUSTAINABILITY INITIATIVES

1. Consumer Skepticism: Some consumers are skeptical of green claims made by businesses, fearing greenwashing – the practice of making misleading or unsubstantiated environmental claims. Building trust with consumers and ensuring transparency in green marketing efforts is essential to overcome this challenge.
2. Cost Considerations: Adopting sustainable practices and producing eco-friendly products often entails higher upfront costs for businesses. Balancing the financial implications of sustainability with the longterm benefits can be challenging, especially for small and medium-sized enterprises (SMEs) with limited resources.

3. Supply Chain Complexity: Ensuring sustainability throughout the supply chain can be complex, particularly for businesses with global operations and complex supplier networks. Managing and monitoring suppliers' environmental practices, as well as promoting sustainability standards and certifications, are key challenges in achieving supply chain sustainability.
4. Lack of Standards and Regulation: The absence of standardized definitions, certifications, and regulations for green marketing and sustainability can lead to confusion among consumers and businesses. Establishing clear guidelines and regulatory frameworks to govern green claims and sustainability practices is crucial for ensuring credibility and accountability.
5. Limited Consumer Awareness and Education: Despite growing interest in sustainability, many consumers still lack awareness and understanding of environmental issues and green products. Educating consumers about the environmental benefits of sustainable choices and fostering a culture of sustainability is essential to drive demand for green products and services.
6. Technological Innovation: Keeping pace with rapidly evolving technologies and innovations in sustainability is a challenge for businesses. Investing in research and development to develop eco-friendly alternatives, improve energy efficiency, and reduce environmental impact is necessary to remain competitive in a rapidly changing market landscape.

Addressing these challenges requires collaboration and concerted efforts from businesses, governments, NGOs, and consumers to promote responsible consumption, drive innovation, and create a more sustainable future.

SEVERAL INNOVATIVE SOLUTIONS AND BEST PRACTICES CAN HELP BUSINESSES OVERCOME CHALLENGES AND ADVANCE GREEN MARKETING AND SUSTAINABILITY EFFORTS

1. Lifecycle Assessment: Conducting lifecycle assessments (LCAs) of products can help businesses identify environmental hotspots and opportunities for improvement throughout the product lifecycle. This data-driven approach enables companies to prioritize areas for sustainability interventions and optimize resource use and energy efficiency.
2. Collaboration and Partnerships: Collaborating with suppliers, industry peers, NGOs, and other stakeholders can foster knowledge sharing, innovation, and collective action towards sustainability goals. Partnerships can facilitate the exchange of best practices, joint research and development initiatives, and the development of industry-wide sustainability standards and certifications.
3. Transparency and Communication: Building trust with consumers and stakeholders requires transparency and authenticity in green marketing communications. Providing clear, verifiable information about the environmental attributes of products, as well as the company's sustainability initiatives and progress, helps build credibility and fosters consumer confidence.
4. Circular Economy Principles: Embracing circular economy principles, such as designing products for durability, recyclability, and repairability, can minimize waste and resource consumption while maximizing value retention. Implementing closed-loop systems for product recovery, remanufacturing, and recycling can create new revenue streams and reduce environmental impact.
5. Innovative Technologies: Leveraging emerging technologies, such as artificial intelligence, blockchain, and Internet of Things (IoT), can enable more sustainable business practices. These technologies can optimize energy use, enhance supply chain transparency, track environmental performance metrics, and facilitate real-time decision-making for sustainability.

CASE STUDIES

1. Tesla: Tesla's electric vehicles (EVs) have revolutionized the automotive industry by offering an ecofriendly alternative to traditional gasoline-powered cars. By focusing on innovation and sustainability, Tesla has captured a significant share of the EV market and reshaped consumer perceptions of electric transportation.

Their commitment to sustainability extends beyond their products, with initiatives like solar energy solutions and battery recycling programs, further solidifying their position as a sustainable brand.

2. IKEA: IKEA, the Swedish furniture retailer, has implemented various sustainability initiatives to reduce its environmental footprint. Through efforts like using sustainable materials, improving energy efficiency in stores and warehouses, and offering recycling and take-back programs for used furniture, IKEA has demonstrated its commitment to sustainability. Their "People & Planet Positive" strategy aims to inspire and enable customers to live more sustainably, reinforcing their brand as a leader in green retail.
3. Unilever: Unilever, one of the world's largest consumer goods companies, has integrated sustainability into its business strategy through initiatives like the Sustainable Living Plan. This plan sets ambitious goals to reduce environmental impact, improve social welfare, and enhance product sustainability across Unilever's brands. By transparently communicating their sustainability efforts and engaging consumers through campaigns like "Dove Real Beauty" and "Knorr's Love Food, Hate Waste," Unilever has effectively integrated green marketing into its brand portfolio.

These case studies illustrate how companies across various industries have successfully implemented green and sustainable marketing strategies to drive business growth, enhance brand reputation, and contribute to environmental and social responsibility.

CONCLUSION

In conclusion, green and sustainable marketing are essential components of modern business strategies, enabling companies to address environmental challenges, meet consumer demand for eco-friendly products, and contribute to long-term sustainability. Through innovative initiatives, transparent communication, and collaborative partnerships, businesses can overcome challenges and seize opportunities to integrate sustainability into their operations and brand identities. Case studies of companies like Patagonia, Tesla, IKEA, and Unilever demonstrate the effectiveness of green marketing in driving consumer engagement, enhancing brand loyalty, and achieving positive environmental impact. By adopting best practices such as lifecycle assessments, circular economy principles, and employee engagement, businesses can further strengthen their sustainability efforts and position themselves as leaders in their industries. As consumer awareness of environmental issues continues to grow, the importance of green and sustainable marketing will only increase. By prioritizing sustainability, businesses can not only drive business growth and profitability but also contribute to a more sustainable and equitable future for generations to come. Through collective action and ongoing innovation, green marketing can play a pivotal role in shaping a more sustainable economy and society.

REFERENCES

1. Interface Sustainability Report: Interface regularly publishes sustainability reports detailing their initiatives and progress. These reports provide in-depth information on their circular economy practices and recycling initiatives.
2. Eccles, R. G., & Serafeim, G. (2013). "The Impact of Corporate Sustainability on Organizational Processes and Performance." Harvard Business School Working Paper, 12-035.
3. https://en.wikipedia.org/wiki/Corporate_su stainability
4. http://www.corporatesustainabilitystrategi es.com/
5. https://www.plasticcollective.co/sustainable-development-challenges-and- opportunities/
6. https://www.un.org/sustainabledevelopment/sustainable-development-goals

Vol.15 / Issue 83 / Apr / 2024 International Bimonthly (Print) – Open Access ISSN: 0976 – 0997

RESEARCH ARTICLE

Effect of Alccofine on Water Absorption and Sorptivity of Engineered Cementitious Composites Containing Mono and Hybrid Synthetic Fibres

R.Prashanthi[1]*, K.Sakthimurugan[2] and G.Pugazhmani[3] and S.Gayathri[4]

[1]Research Scholar, Department of Civil and Structural Engineering, Annamalai University, Annamalai Nagar, Tamil Nadu, India.
[2]Professor, Department of Civil Engineering, CK College of Engineering and Technology, Cuddalore, Tamil Nadu, India.
[3]Assistant Professor, Department of Civil Engineering, Mohamed Sathak Engineering College,) Kilakarai, Tamil Nadu, India.
[4]Assistant Professor, Department of Civil Engineering, Bharath Institute of Engineering and Technology, Hyderabad, India.

Received: 12 Sep 2023 Revised: 18 Jan 2024 Accepted: 13 Mar 2024

***Address for Correspondence**
R.Prashanthi
Research Scholar,
Department of Civil and Structural Engineering,
Annamalai University,
Annamalai Nagar, Tamil Nadu, India.
Email: prashu1691@gmail.com

ABSTRACT

Water ingression has major influence on durability of concrete materials. This paper deals with a study on influence of Alccofine and synthetic fibers on sorptivity and water absorption in ECC and Hybrid ECC. The sorptivity test measures the rate of movement of water through the concrete under capillary suction as per ASTM C 1585. Water absorption, density and volume of permeable pores in concrete were measured based on ASTM C 642. Based on the literatures, mix design was adopted and fly ash has been replaced by Alccofine and for the workability viscosity modifying agent was used at 0.6% of the binder for all the mixtures. Two types of synthetic fibers, uncoated polyvinyl alcohol (PVA) and polypropylene (PP) were used. The results show that, both ECC and HECC with Alccofine show lower absorption and not much variation in sorptivity than conventional concrete.

Keywords: Engineered Cementitious Composites, Polyvinyl alcohol, Polypropylene, Absorption, Sorptivity

INTRODUCTION

Concrete should withstand without any deterioration over a design period of the structure. Such concrete is known as durable concrete. The life of concrete may deteriorate when foreign components ingress into it especially water. Durability of the composites mainly depends on the ingression of fluid particles into it, which contains chemical components have ability to deteriorate the composite materials when react with the interfacial transition zone compounds. Lowering the permeability of composite members will eventually reduce penetration of water, chloride ions, sulphate ions, and other harmful substances [1]. After the hydration reaction of cement results a product containing solid with few pore system. The networks of pore system consist of cement paste and allow the fluid to transport into the solid concrete member. The transportation of fluid depends on different factors such as ingredients and proportions of the composite[2]. Sorptivity is an index to measure the moisture transport in the unsaturated specimens [3]. In sorpitivity test water ingression occurs due to the capillary suction in the pore spaces of the concrete not by the pressure head [4]. Sorptivity coefficient is an important index to find the service life of the structure and also to enhance the performance of the composite [5]. Ingression of moisture through capillary suction leads to the carbonation reaction and eventually it deteriorate the composite structure. Replacing the cement by nano materials eventually reduced water absorption and sorptivity in the concrete materials [6]. ECC is a strain hardening cementitious composite designed based on micromechanics and showing high tensile strain capacity and tight crack width control. ECC also possess self healing ability which reduces the deterioration and become a durable material [7]. Quality of concrete is not only based on strength and also based on its durability parameters [8]. Water absorption and sorptivity tests are the easiest method to find the ability of the material to absorb and transmit water by capillarity [9]. Use of glass powder as an aggregate in ECC mixtures increases the permeability properties [10]. Using fibers, mineral admixtures such as flyash, GGBS, silica fume etc improves the performance of the concrete such as toughness, strength as well as durability criteria's [11]. The sorptivity coefficient of self healed ECC also shows better results compared to the preloaded ECC specimens and it shows poorer results when undergo more strain [12]. Water absorption and sorptivity of the concrete with hypo sludge as a cement replacement shows higher values than normal concrete [13]. An acceptance criterion for the durability index has been shown in below table 1 [14].

Water absorption and sorptivity rate of ECC shows better results when compared to the normal concrete [15]. Water absorption in ECC can be controlled by addition of water repellent agent [16]. ECC with rice husk ash shows a higher absorption and void content compared to the ECC with fly ash [17]. Since the crack width is limited to 100 μm, no external ingression of foreign materials is not possible which eventually increases the life of the ECC member [18]. Compared to basalt fiber reinforced concrete, glass fiber reinforced concrete shows higher sorptivity and percentage of voids, both had been tested based on ASTM C 642 and ASTM C 1585 [19]. Sorptivity test gives important information about the pore structure of the composites, tortuosity, continuous capillaries and pore sizes [20]. Addition of fiber in concrete reduce sorptivity in concrete and the reduction is upto 25.85% than control mix [21]. Hence an attempt is made to study the effect of Alccofine and synthetic fibers on the engineered cementitious composites and Hybrid Engineered cementitious composites.

MATERIALS AND METHODS

Alccofine

Alccofine 1203 (Figure 1) is a proprietary patented product (IP Patent No. 297735) with low calcium silicate based mineral additive. Controlled granulation process results in unique particle size distribution. Its latent hydraulic property and pozzolanic reactivity results in enhanced hydration process. Addition of Alccofine 1203 improves the packing density of paste component. This results in lowering water demand, admixture dosage and hence improving strength and durability parameters of concrete at all ages. Fine balance of CaO_2 SiO_2 and Al_2O_3 combined with

unique patented PSD (Particle Size Distribution) design makes Alccofine a favorable SCM combination for use in all grade concrete.

Cement

Cement used in this work was OPC 53 grade conforming to IS: 8112 – 1989. The chemical properties of cement are given in Table 2. Physical properties of the cement are given in Table 3.

Sand

The fine aggregate available naturally from river beds is used. As per IS 383-1970 Code conforming that, it is coming under Zone III. The particle size distribution curve for fine aggregate is shown in Figure 2. The Specific gravity of sand was found using specific gravity bottle as 2.61

Synthetic Fibers

Synthetic fibres are made only from polymers found in natural gas and the by-products of petroleum. Synthetic fibres are man-made fibres, most of them are prepared from raw material called petrochemicals. All fabrics are obtained from fibres, while fibres are obtained from artificial or man-made sources. Out of these fibers Polyvinyl alcohol fiber and polypropylene fibers were used in this study.

Polyvinyl Alcohol (PVA) Fiber

Polyvinyl Alcohol is the main raw material to produce PVA fiber. It undergoes process of dissolution, spinning, heat – setting, cutting, and balling to form a high strength, high modulus fiber. The physical properties of PVA fiber was shown in Table 4. Figure 3 shows the PVA fiber which was used in this study.

Polypropylene (PP) Fiber

Polypropylene fiber is a kind of linear polymer synthetic fiber obtained from propylene polymerization. It has some advantages such as light weight, high strength, high toughness and corrosion resistance. The physical properties of PP fiber was shown in Table 5. Figure 3 shows the PP fiber which was used in this study.

Sika Viscocrete

Sika viscocrete is a polycarboxylate based high performance super plasticizing admixture which imparts high workability, prolonged workability retention and allows a large reduction in water content. It produces a more uniformly cohesive high quality free flowing concrete. Specific gravity of viscocrete is 1.08. Figure 4 shows the admixture can.

Mix Proportions

Snce it is an evolving material no proper mix designs were available. Based on the literatures as a reference, mix design was taken as per trial and error method. Totally 6 mixes were prepared. They are control mix CC, ECC-2%PVA+0%PP (M_1), ECC-0%PVA+2%PP (M_2), HECC-1%PVA+1%PP (M_3), HECC-1.5%PVA+0.5%PP (M_4), HECC-0.5%PVA+1.5%PP (M_5). Mix design used in this study is given in Table 6 along with its respective compressive strength. Simplified mix ratio is given in Table 7.

Mixing and Specimen Preparation

Heavy duty hand driller with mixing bit was used to cast both control and ECC specimens. For each mix 3 numbers of 70.7mm cubes for water absorption and 3 numbers of 100mm diameter 50mm height sorptivity specimens were cast. For both control and ECC, same method of mixing was taken place to ensure uniform dispersion of fibers in the matrix since it plays a major role in the performance. Cement, Alccofine and sand were dry mixed till it gets uniform colour. After few minutes of mixing, water along with sika viscocrete was added and mixed with high speed for

about 5 minutes. Once the uniformity attained, fibers were added randomly and mixed for 3 more minutes or till the uniformity achieved. After the completion of mixing the slurry was made to pour into the oiled moulds and kept for 24 hrs in the normal temperature. Specimens were removed from the moulds after 24 hrs and kept in the water curing for 28 days. The number of specimens casted was shown in the Table 8.

Experimental Works

Absorption after Immersion

Water absorption after immersion is the amount of water absorbed by the specimen after immersing the oven dried specimen in the water for about 48 hrs. The test was performed based on ASTM C 642. Figure 5 shows the cubes casted and cured, specimens dried in the oven, specimens immersed in water.

Absorption after Immersion and boiling

Absorption after immersion and boiling can be found by immersing the specimens in the boiling water for 5hrs and allow it to cool for 14hrs naturally and weight has to be taken by removing the surface moisture by wiping the specimen by dry towel. Figure 6(a) shows the specimens in the boiling water and 6(b) shows measuring apparent weight of the specimen.

Bulk Density (Dry)

Dry bulk density is defined as the mass of the dry specimen divided by the total volume of the wet sample. It is given by below formula,

$$\text{Bulk Density} = \frac{oven\ dry\ mass}{(Saturated\ \ mass\ after\ boiling - immersed\ \ apparent\ \ mass)} * \text{density of water}$$

Bulk Density after Immersion

Bulk density after immersion is the ratio of mass of the immersed specimen by the total volume of the wet sample. It is given by below formula,

$$\text{Bulk density after immersion} = \frac{Saturated\ \ mass\ after\ immersion}{(sat\ mass\ after\ boiling - immersed\ \ app\ mass)} * \text{density of water}$$

Bulk Density after Immersion and Boiling

Bulk density after immersion and boiling is the ratio of mass of saturated mass after boiling by the total volume of the wet sample. It is given by below formula,

$$\text{Density after immersion and boiling} = \frac{Saturated\ \ mass\ after\ boiling}{(Sat\ mass\ after\ boiling - immersed\ \ app\ mass)} * \text{density of water}$$

Apparent Density

Apparent density is the ratio of oven dry mass to the difference between oven dry mass and immersed apparent mass. It is given by below formula,

$$\text{Apparent Density} = \frac{oven\ dry\ mass}{(oven\ dry\ mass - Immersed\ \ apparent\ \ mass)} * \text{density of water}$$

Volume of permeable pore space (Voids)

Out of entire cement paste one third to one half become interface transition zone. Since it is the locus point for cracking highly prone to become porous but permeability of the concrete is depends on the bulk portion of the hardened cement paste since it is the continuous phase (A.M.Neville, 2011).Volume of permeable pore space (voids) can be found by the ratio of difference of bulk and apparent density to apparent density. It is given by below formula,

$$\text{Voids (\%)} = \frac{(apparent\ \ density - bulk\ \ density)}{apparent\ \ density} * 100$$

Sorptivity

Sorption in the concrete member is due to the capillary suction through the pores. Since the capillary suction would not takes place in either dry or saturated concrete. Sorptivity test specimens were oven dried for at least 48hrs after 28 days of water curing to remove all the moisture from the concrete specimens. After removing from the oven it has to covered tightly inside polythene bags for about 15 days. After removing the specimens from the bags, leaving one

side exposed to water all other sides were covered with the electrician insulation tape and placed in the sorptivity setup up keeping 3 – 5 mm depth of water as per ASTM C 1585. This test method is used to find the rate of absorption of water by the cementitious specimens by measuring the mass gain in the specimen resulting from the sorption of water as a function of time when only one surface exposed to the water. This test was performed based on ASTM C 1585. Figure 7(a) shows diagrammatic representation of sorptivity setup, 7(b) shows the specimens prepared for sorptivity test, 7(c) shows sorptivity test setup, 7(d) shows sorptivity setup with water. The absorption was calculated by below given formulas,

$I = \frac{m_t}{a \; x \; d}$ ---------- 1

Where, m_t = Change in mass of the specimen (gm)

a = Exposure area of the specimen (mm^2)

d = Density of the water (gm/mm^3)

$S = \frac{I}{\sqrt{t}}$ ---------- 2

Where, S = Sorptivity of the specimen

I = cumulative percentage of water absorbed per unit area

t = time taken

RESULTS AND DISCUSSIONS

Absorption after Immersion

The test results were shown in the bar chart in figure 8. From the figure it is observed that all the mixes showed lower water absorption that control mix, it means that Alccofine plays a major role in the pore refinement. When using a single type of fiber in ECC does not create any impact on water absorption but in the hybrid ECC, mix with 1.5% PVA and 0.5% PP shows a relatively lesser absorption than mixes containing 1%, 0.5% PVA and 1%, 1.5% PP. Since PVA is a high modulus fiber and occurrence of agglomeration is comparatively lower than PP fibers. While using 1.5% PVA and 0.5% PP occurrence of agglomeration is relatively low and leads to the lesser water absorption. Absorption of water is relatively high when using poly propylene fiber compared to the steel fibers, glass fibers, waste plastic fibers and high density poly ethylene fibers (M. P, 2019) and it reflects in the hybridization of polypropylene fiber with polyvinyl alcohol fiber. However poly vinyl alcohol fiber showed lesser absorption. It can be found that 28.52% absorption in M_1, 12.93% absorption in M_2, 17.87% absorption in M_3, 28.14% absorption in M_4, 21.29% absorption in M_5 had been reduced compared to the control mix.

Absorption after Immersion and boiling

The test results were shown in the bar chart in figure 9. From the figure it is observed that all the mixes showed lower water absorption than control mix even after boiling, it means that Alccofine plays a major role in the pore refinement. Synthetic fibers are prone to melt when the temperature rises but in the boiling stage outer surface of composites act as a non porous material because of pore refinement occurred and boiling water does not affect the synthetic fibers inside the specimen. Hence it shows similar trend of absorption in both normal and boiling water. However all the ECC mixes shows lesser water absorption than control mortar.

Bulk Density (Dry)

The test results were shown in the figure 10. Compared to the control mortar both mono and hybrid ECC shows higher density and that is because of the addition of Alccofine. But there is a slight variations in the density of the hybrid ECC compared to the Mono fiber ECC and that is may be because of the differences in the fiber texture and their compatibility. Though there is differences in the density since it is in less amount it can be neglected. It can be found that density of 22.83% in M_1, 24.41% in M_2, 11.81% in M_3, 19.69% in M_4, 18.11% in M_5 had been increased compared to the control mix.

Bulk Density after Immersion

The test results were shown in the figure 11. Compared to dry density, density after immersion shows no significant differences whereas based on the absorption, density had changed. Density increases with increase in volumetric moisture content (zha, 2018). As per literature there will be rise in density whenever the moisture content rises. Below figure also showing the same.

Bulk Density after Immersion and Boiling

Since the boiling temperature didn't affect the synthetic fibers there is no significant difference encountered in the density values. After immersion and boiling the density of the specimens remain same as after immersion. Even though the fibers are prone to melt during high temperatures, matrix phase has covered the fibers during boiling. Due to that there is no damage to the fibers and internal structure of the composite.

Apparent Density and Voids

Apparent density is mass per unit volume of the particles, excluding the voids in the material. Relationship between the apparent density and voids is shown in the fig 12. When the voids increased apparent density got reduced. From the graph it is evident that control mix i.e without Alccofine and fibers shows higher percentage of voids whereas mixes having Alccofine and fibers showing relatively lesser voids. Based on the percentage of the voids apparent density also get altered. Control mix showing lesser density compared to other mixes since the percentage of voids are more in it compared to the other mixes which containing Alccofine and fibers. Both ECC and HECC shows almost same percentage of voids and it resulted in the apparent density also. It can be found that 27.44% voids in M_1, 28.28% voids in M_2, 24.92% voids in M_3, 25.25% voids in M_4, 23.57% voids in M_5 had been reduced compared to the control mix.

Sorptivity

After the sorptivity test it was observed that both ECC and HECC shows relatively higer capillary suction in the intial time period that is upto six hours and eventually got reduced when it entered the secondary absorption. Whereas the control mix shows relatively lesser absorption in the intial period of absorption and it is more compared to ECC and HECC in the secondary stage of absorption. This happens because of the change in the continous pores in the ECC and HECC. Because of the presence of fibre in high percentage both ECC and HECC allows the suction in intial time period but it has got eventually reduce when it comes to the secondary sorption. This is because fibres obstruct the path randomly and it changes the totuosity of the specimen. However control mix shows lesser absorption in the intial period of time increased slowly than ECC and HECC in the secondary capillary suction. It happened due to the absence of the fibre and alccofine whereas Alccofine plays a major role in the pore refinement and fiber become the responsibility for the change in the tortuosity of the specimen. Upto 2% addition of fibers did not affect the sorptivity property of the specimens whereas when it increase to 3% the sorptivity value in both inital and secondary will increase [22]. Figure 13 shows sorptivity curves of control and ECC. Figure 14 shows sorptivity curves of control and HECC. From the graph it is inference that initial absorption of all the mixes including control mix show more or less similar trend whereas after 6 hrs both ECC and HECC showed lesser capillary suction than the control mix. Eventhough pore refinement occurs because of the Alccofine, presence of fibers altering the tortuosity of the specimens. However PVA fibre shows higher suction than PP fibres it is because of their specific gravity. Since PVA is a high modulus fibre for the given V_f quantity is little lesser than polypropylene. The initial and secondary sorptivity of all mixes are tabulated in table 9.

CONCLUSION

From the above experimental tests carried out the following conclusions have made, Water absorption of ECC and HECC specimens showed better results compared to the control specimen. Whereas specimens with polypropylene fibers show relatively higher water absorption compared to the specimens containing poly vinyl alcohol fiber. Since the temperature is not high while boiling the water for 5 hours when the specimens immersed in it, didn't cause any

damages to the fibers present inside the specimens. The absorption capacity did not vary much after boiling the specimens. Regarding bulk density of control, ECC and HECC, ECC shows higher density than control and HECC. The slight reduction of density in the HECC is lack of compatibility of the fibers but the difference is very less than ECC compared to the control specimen. Bulk density after immersion shows variations in its value since it is depends on the moisture content. As per the test it shows that the bulk density after immersion is proportional to its moisture content and both ECC and HECC show favourable results. Since Alccofine plays a major role in the pore refinement compared to the control specimens ECC and HECC shows lesser percentage of voids. Because of the lesser voids in the ECC and HECC apparent density is higher compared to the control mix. Sorptivity values of the control specimen shows lesser absorption than ECC and HECC in the initial period that is upto six hours whereas after that ECC and HECC shows lower soprtivity than control in the secondary phase. It is because of fibers which change the tortuosity of the specimens which in turn reduces the sorptivity in ECC and HECC.

REFERENCES

1. Zhang, S. (2014). Evaluation of relationship between water absorption and durability of concrete materials. *Advances in material science and engneering* , 1-8.
2. Ramli, m. (2012). Effects of polymer modifications on the permebility of cement mortars under different curing conditions: A correlational study that includes pore distributions, water absorption and compressive strength. *Construction and building materials* , 561-570.
3. Dias, W. (2000). Reduction of concrete sorptivity with age through carbonation. *cement and concrete research* , 1255-1261.
4. C.Hall. (1989). Water sorptivity of mortars and concrete: a Review. *Magazine of concrete research* , 51-61.
5. Ferraris, N. M. (1997). Capillary transport in mortars and concrete. *Cement and Concrete Research* , 747-760.
6. Carmichael, J. (2019). Assesment of sorpitivity and water absrption of concrete with nano sized cementitious materials. *International journal of engineering and advanced technology* , 847-851.
7. I.Komara. (2019). Engineered cementitious composite as an innovative durable material: a Review. *ARPN Journal of engineering and applied sciences* , 822-833.
8. Shankar, J. (2018). Evaluation of water absorption and sorptivity properties of flyash, GGBS, M Sand based glass fiber reinforced geoploymer concrete. *International research journal of engineering and Technology* , 1-5.
9. L, Y. (2019). Relationship between sorptivity and capillary coefficient for water absorption of cement based materials: Theory analysis and experiment. *Royal society open science* .
10. Adesina, A. (2020). Influence of glass powder on the durability properties of engineered cementitious composites. *Construction and Building materials* , 1-11.
11. Offei, I. (2020). Evaluation of mechanical properties and sorptivity of Cementitious composites produced with dsages of nano silica. *IOSR journal of mechanical and civil engineering* , 49-57.
12. Zhu, Y. (2020). Non-destructive methods to evaluate the self-healing behavior of engineered cementitious composites (ECC). *Construction and Building Materials* , 1-8.
13. Joshi, G. (2018). Evaluation of Sorptivity and Water Captivation of Concrete with Partial Replacement of Cement by Hypo Sludge. *IOP Conference Series: Materials Science and Engineering* , 1-6.
14. Pitroda, J. (2013). Evaluation of Sorptivity and Water Absorption of Concrete with Partial Replacement of Cement by Thermal Industry Waste (Fly Ash). *International Journal of Engineering and Innovative Technology* , 1-5.
15. I, K. (2020). Experimental investigations on the durability performance of normal concrete and engineered cementitious composite. *IOP Conference Series: Materials Science and Engineering* , 1-12.
16. Sahmaran, M. (2009). Influence of microcracking on water absorption and sorptivity of ECC. *Materials and Structures* , 593-603.
17. Costa, F. B. (2016). EVALUATION OF WATER ABSORPTION ON ENGINEERED CEMENTITIOUS COMPOSITES CONTAINING RICE HUSK ASH. *Brazilian Conference on Composite Materials* , 28-31.
18. R.Prashanthi. (2023). Engineered cementitious composites - a review. *materials Today:Proceedings* , 1-8.

19. Paktiawal, A. (2021). Experimental evaluation of sorptivity for high strength concrete reinforced with zirconia rich glass fiber and basalt fiber. *Materials Today: Proceedings* , 1-9.
20. Vafaei, D. (2020). Sorptivity and mechanical properties of fiber-reinforced concr ete made with seawater and dredged sea-sand. *Construction and Building Materials* , 1-18.
21. Akid, A. S. (2021). Assessing the influence of fly ash and polypropylene fiber on fresh, mechanical and durability properties of concrete. *Journal of King Saud University – Engineering Sciences* , 1-11.
22. R.N.Nibudey. (2014). Compressive strength and sorptivity properties of PET fiber reinforced concrete. *International journal of advances in engineering & technology* , 1206-1216.

Table 1. Acceptance Criteria for Durability Indexes

Acceptance Criteria	Oxygen Permeability Index (OPI) (log scale)	Sorptivity (mm/h)
Workroom concrete	> 10	< 6
As-built Structures		
100% recognition	> 9.4	< 9
50% recognition	9.0 to 9.4	9 to 12
Helpful measures	8.75 to 9.0	12 to 15
Elimination	< 8. 75	> 15

Table 2. The chemical Analysis of Cement

Chemical composition, %	SiO_2	CaO	Al_2O_3	Fe_2O_3	MgO	K_2O	SO_3	Na_2O	LOI
Cement	21.80	63.56	5.12	3.20	0.80	0.75	3.22	0.55	1.00

Table 3. The Physical Properties of Cement

Sl No	Properties	Values
1.	Specific Gravity	3.10
2.	Specific Surface Area	3710 cm^2/g
3.	Normal Consistency	31%
4.	Initial Setting Time	60 mins
5.	Final Setting Time	330 mins

Table 4. The Physical Properties of PVA fiber

Type	Fiber Diameter (μm)	Length (mm)	Specific Gravity	Tensile Strength (MPa)	Elongation (%)	Young's Modulus (GPa)
PVA	30	12	1.3	1700	6	40

Table 5. The Physical Properties of PP fiber

Type	Fiber Diameter (μm)	Length (mm)	Specific Gravity	Tensile Strength (MPa)	Elongation (%)	Young's Modulus (GPa)
PP	30	12	0.91	550	25	5

Table 6. Mix Proportions

Mix ID	Cement (kg/m^3)	Alccofine (kg/m^3)	Fine Aggregate (kg/m^3)	Water (kg/m^3)	Fibers (kg/m^3)		HRWR (kg/m^3)	Compressive Strength (N/mm^2)
					PVA	PP		

CC	640.2	514.8	574	310	-	-	7.02	58.06
M_1	640.2	514.8	574	310	24	-	7.02	76.44
M_2	640.2	514.8	574	310	-	24	7.02	74.14
M_3	640.2	514.8	574	310	12	12	7.02	71.58
M_4	640.2	514.8	574	310	18	6	7.02	72.44
M_5	640.2	514.8	574	310	6	18	7.02	75.32

Table 7. Mix Ratio

Cement	Alccofine	S/B	W/B	Fiber	HRWR
1	0.8	0.5	0.27	2% of binder	0.6% of binder

Table 8. Number of Specimens

Sl No	Specimen	No. of Specimens	Type of Test
1	Cube (70.7mm)	6 x 3 = 18	Water absorption as per ASTM C 642
2	Cylinder (100mm dia, 50 mm height)	6 x 3 =18	Sorptivity as per ASTM C 1585

Table 9. Initial and secondary sorptivity of all mixes

Sl No	Mix ID	Average initial sorptivity in 10^{-3} x mm/sec$^{1/2}$	Average secondary sorptivity in 10^{-3} x mm/sec$^{1/2}$
1	M_1	20.4	5.15
2	M_2	20.14	5.15
3	M_3	20.80	4.99
4	M_4	21.47	4.35
5	M_5	21.67	4.99
6	Control	24.99	5.93

Fig.1 Alccofine

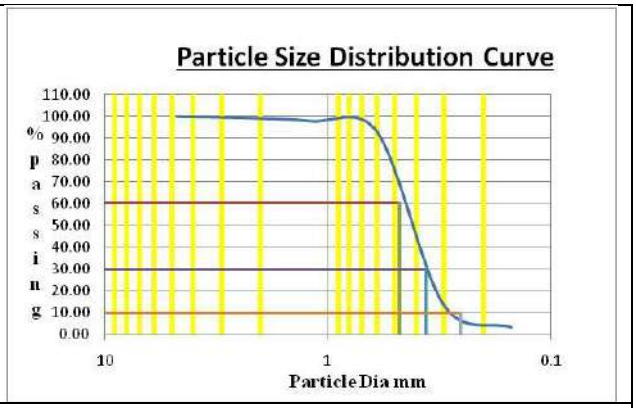

Fig 2. Particle Size Distribution Curve for Fine Aggregate

Fig 3. Polyvinyl Alcohol Fiber and Polypropylene Fiber

Fig 4. Sika Visco Crete

Figure 5 Cubes Casted and in Curing, Specimens dried in oven, Specimens immersed in water

(a)

(b)

Figure 6(a) Specimens in the boiling water (b) Measuring apparent weight of the specimen

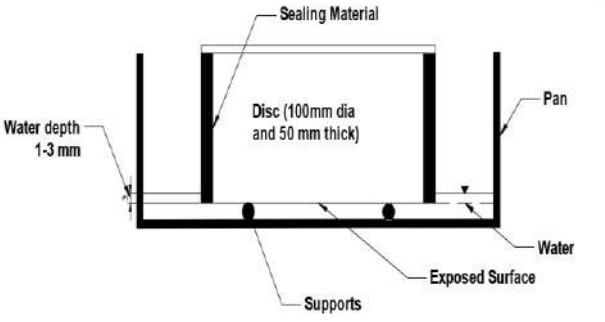

Figure 7(a). Diagrammatic representation of sorptivity setup

Figure 7(b). Specimens prepared for sorptivity test

Figure 7(c) Sorptivity test setup

Figure 7(d) Test setup with water

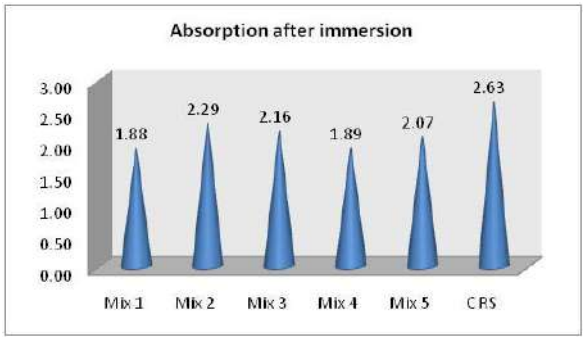

Figure 8. Water absorption after immersion

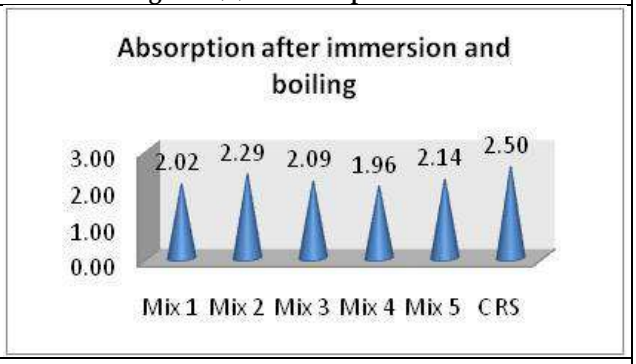

Figure 9. Water absorption after immersion and boiling

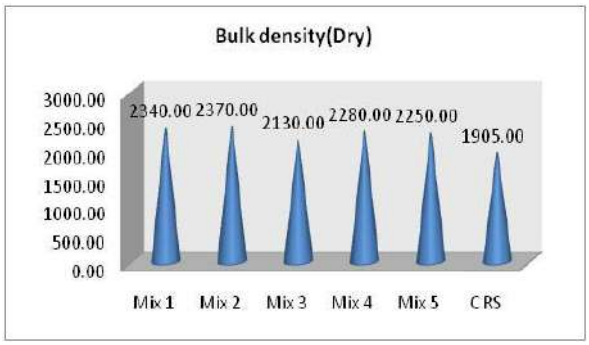

Figure 10. Dry bulk density

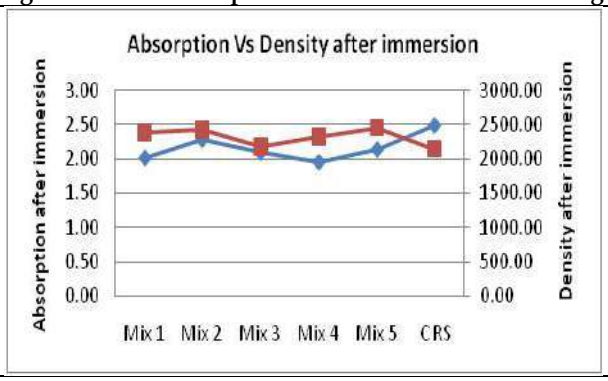

Figure 11. Water absorption Vs Density after immersion

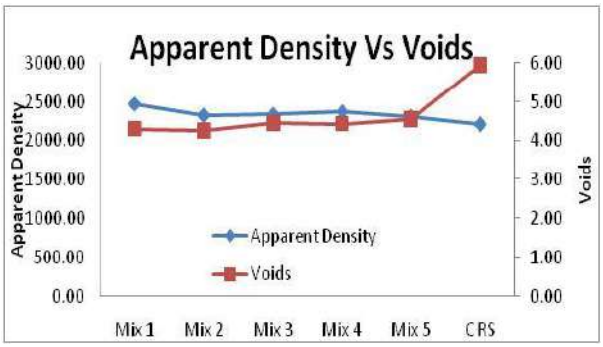

Figure 12. Relationship between apparent density and voids

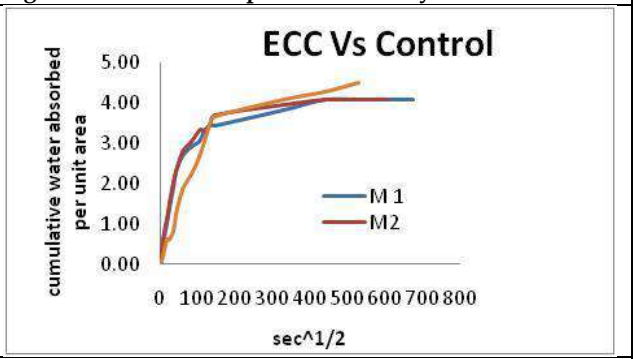

Fig 13 ECC vs Control

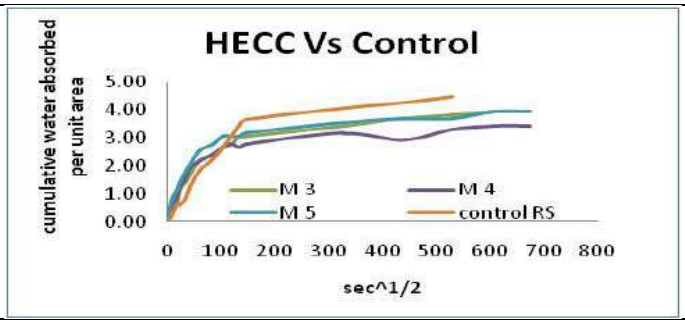

Fig 14. HECC Vs Control

Vol.15 / Issue 83 / Apr / 2024 International Bimonthly (Print) – Open Access ISSN: 0976 – 0997

RESEARCH ARTICLE

A Study on the Urine Analysis of Selected Teenagers using Dipstick Method

T. Amala Arockia Raj[1], M.Muniya Naik[2], K.Janardhana[3], A.Govardhan Naik[4], A. Jayasankar[5], D. Veera Nagendra Kumar[6] and V. UdayKiran[7]*

[1]Principal and Lecturer, Department of Chemistry, Loyola Degree College (YSRR) –Pulivendula (Affiliated to Yogi Vemana University, Kadapa) Andhra Pradesh, India.
[2]Lecturer, Department of Zoology, Government Degree College, Rayachoty (Affilated to Yogi Vemana University, Kadapa) Andhra Pradesh, India.
[3]Lecturer, Department of Zoology, Government Degree College, Rajampeta (Affiliated to Yogi Vemana University, Kadapa) Andhra Pradesh, India.
[4]Teaching Assistant, Department of Zoology, SVU College of Sciences, Sri Venkateswara University, (Affiliated to Sri Venkateswara University) Tirupati, Andhra Pradesh, India.
[5]Lecturer, Department of Zoology, S.V.C.R. Government Degree College, Palamaner, Chittoor (Affiliated to Sri Venkateswara University Tirupati) Andhra Pradesh, India.
[6]Lecturer, Department of Zoology, Government College for Men (A), (Affiliated to Yogi Vemana University) Kadapa, Andhra Pradesh, India.
[7]Lecturer, Department of Zoology, Loyola Degree College (YSRR) –Pulivendula (Affiliated to Yogi Vemana University, Kadapa) Andhra Pradesh, India.

Received: 20 Oct 2023 Revised: 09 Jan 2024 Accepted: 06 Mar 2024

***Address for Correspondence**
V. UdayKiran
Lecturer,
Department of Zoology,
Loyola Degree College (YSRR) –Pulivendula (Affiliated to Yogi Vemana University, Kadapa)
Andhra Pradesh, India.
Email: vempati.uday6@gmail.com

ABSTRACT

Urine is frequently used for clinical diagnostics and biomedical research. Urine analysis has been studied and used since ancient times. Urine contains a diverse set of metabolites that can provide information about the body's current physiologic condition as well as clinical signs of disease. We tried to explore the benefits and limits of the urine dipstick as a low-cost tool in point-of-care settings, as well as the reasons for its lack of use as a broad screening tool. Commercially available dipsticks can be used to measure urine pH and various contents (e.g., leukocytes, erythrocytes, protein, glucose, nitrate, ketones, blood, bilirubin, urobilinogen) as a kind of fast method for diagnosis. It is a quick, uncomplicated process indicates any abnormal human health conditions and allows the removal of unwanted elements such as

those significantly polluted by microbial infection or blood. However, the use of dipsticks for inclusion/exclusion in urine research has been quite debatable to date: there is no common agreement on tests for which dipstick analysis is best or where to set inclusion/exclusion criteria.

Keywords: urinalysis, dipstick, dry chemistry, urine, assay principles.

INTRODUCTION

Urine, often regarded as a liquid goldmine of diagnostic information, has been employed as a diagnostic medium for centuries. Its analysis has evolved from the rudimentary observations of color and odor to sophisticated laboratory techniques that enable the detection of specific biomarkers indicative of various medical conditions(Decavele A-SC*et al,*.2012). Among the plethora of valuable substances present in urine, albumin and glucose stand out as critical indicators of renal and metabolic health. Monitoring these components through dipstick analysis of urine chemistry offers a rapid and cost-effective means of assessing a patient's condition, making it a vital tool in both clinical and research settings(Delanghe J*et al,*.2014). Albuminuria, the presence of excess albumin in urine, is a well-established marker for kidney dysfunction and a harbinger of renal disease progression. It plays a pivotal role in identifying patients at risk for various renal conditions, such as diabetic nephropathy and hypertensive nephrosclerosis (Ercan M*et al,*.2015). On the other hand, glycosuria, the presence of glucose in urine, is a key diagnostic criterion for diabetes mellitus and provides valuable insights into glycemic control (Haber MH (2010)).

Monitoring these markers through dipstick analysis offers advantages of simplicity, speed, and cost-efficiency, making it an attractive option for routine diagnostic evaluations (Herringto*et al,*. 2016). In this research article, we delve into the diagnostic evaluation of albumin and glucose in urine using dipstick analysis, exploring the principles behind this technique, its clinical applications, and its potential limitations (LaRocco MT, *et al,*.2016). We aim to provide a comprehensive overview of the state-of-the-art in dipstick analysis for albumin and glucose, including advancements in technology and methodologies (Pugia MJ (2000). Additionally, we will discuss the clinical significance of dipstick analysis results, offering insights into how this technique can aid in the early detection and management of renal and metabolic disorders (Rotter M, et al (2017). As the demand for rapid, point-of-care diagnostic tools continues to grow, understanding the utility and reliability of dipstick analysis for albumin and glucose becomes paramount (DelangheJR*et al,*.2017). This research article endeavors to shed light on the current landscape of dipstick-based urine chemistry analysis, empowering healthcare professionals, researchers, and clinicians with the knowledge needed to make informed decisions in the realm of diagnostic medicine (Sureda-Vives M, *et al* .,2017).

METHODS AND MATERIALS

TEST STRIP TECHNOLOGY

The analytical sensitivity of urine test strips has increased due to advancements in electronic detection, allowing for the quantitative examination of red blood cells, white blood cells, glucose, and urinary protein (Oyaert, *et al,*.2018). This has been used to analyze albuminuria quantitatively and determine the albumin: creatinine ratio in the micro albuminuria range (20-200 mg/L) for both ketones and albumin. The albuminuria measurement can be assisted by the creatinine-specific test pad, which corrects urinary dilution. Leukocyte esterase and peroxidase activity readings are sensitive because to CMOS technology. Sensitive dyes have increased sensitivity. Results from urine test strips are now read and interpreted using smart phones (Oyaert MN, *et al* 2018). Urine dipstick dry chemistry is a low-cost, simple approach for evaluating numerous assay principles in a short period of time, making it excellent for use at point-of-care settings. However, storage conditions must be carefully monitored to avoid microbe and metabolite

overgrowth. The test can measure pH, osmolality, hemoglobin/myoglobin/hematuria, leukocyte esterase, glucose, proteinuria, nitrites, ketones, and bilirubin, which can be used to guide further testing if clinical suspicion exists. Dipsticks can also be automated, reducing human error and labour and making them suited for point-of-care applications. They do, however, have drawbacks, including a lack of measurable data, false positives and negatives due to confounding factors, and interpretation uncertainty. Furthermore, dipsticks do not have enough sensitivity for albumin in normal home testing settings, and alternative markers, such as the albumin-to-creatinine ratio, are more useful for diagnosing diabetes-associated microalbuminuria.

Sample Collection and Preparation

Of the 50 candidates identified for the this test, we had chosen only 18 samples after discriminating based on the Body weight and past medical history. The samples for this test were having body weight below 50Kgs and some health issues. They were of the age group of between 19-20 years. A fresh urine sample was collected in a clean and dry container. It was not centrifuged. The sample was well mixed before taking the test. The urine test was conducted within an hour. All specimens were always taken and kept under sanitary conditions.

Points for Attention**Proteinandmicroalbumin** **(10VOnly)**

Protein and microalbumin are more sensitive to albumin than Bence-Jones proteins, immune globulin and haemoglobin. When it is negative, it doesn't mean that protein does not exist.

Glucose

The test is only for glucose. Other than glucose, no other component in urine has been shown to produce a positive result. 2.2mmol/L glucose in 0.28mmol/L ascorbic acid-containing urine may cause a colour shift that could be perceived as positive. Concentrations of ascorbic acid as low as 0.28mmol/L and/or acetoacetic acid as low as 1.1mmol/L may not affect the test. A tiny amount of glucose is normally eliminated by the kidney. Typically, the amount is less than the sensitivity of the reagent test.

Bilirubin

Bilirubin in urine is typically impossible to detect using even the most sensitive approach. A closer look is necessary if there is little bilirubin present in the urine. Any substance that turns an acidic medium red, such as phenazopyridine, or medications that dye urine red may have an impact on the test's outcome. A false negative result could occur from a high ascorbic acid content.

Ketone

Acetoacetic acid in urine causes the reagent strip to respond. Neither acetone nor ß-hydrobutyric acid are compatible with it. Normal urine samples typically yield negative test findings. Highly pigmented urine or urine that contains a significant amount of levodopa metabolites may yield false-positive results.

Specific Gravity

Urine samples can have a specific gravity between 1.000 and 1.030 with a mean error of 0.005 when using the reagent strip for specific gravity. pH values, non-ionic components, highly buffered alkaline urine, and moderate protein concentrations can all be altered. Instruments used to measure urine automatically correct strip readings**(**https://www.nu-careproducts.co.uk/data.**)**.

Blood

Patients may react differently to the "trace." Individual cases necessitate clinical judgment. The need for additional diagnostic testing is indicated by the appearance of green specks (intact erythrocytes) or green colour (haemoglobin/myglobin) on the reagent area within 60 seconds. The urine of women who are menstruation frequently contains blood. About 5–15 undamaged erythrocytes per litre of haemoglobin, which ranges from 150–620 g/L. The reagent strip can be used in addition to the microscopic inspection because it is particularly sensitive to haemoglobin. In urine with a high specific gravity, the strip's sensitivity may be diminished. Both myglobin

and haemoglobin are equally sensitive to the strips. A few oxidising impurities, such hypochlorite, can produce erroneous positive findings. It's also possible for microbial peroxidase linked to urinary tract infections to result in a false-positive test. Less than 5.Ommol/L of ascorbic acid in the urine may not affect the test's outcome (**Wilson ML*et al.*, 2004**).

pH

The pH test are a measures pH values in the range of 5.0-9.0 instrumentally and 5.0-8.5 visually.

Urobilinogen

Urobilinogen can be found in urine in amounts as low as 3 mol/L (or roughly 0.02 Ehrlich unit/dL) using the reagent strips. Urine results of 33 mol/L show the crucial value, signifying the change from normal to abnormal, necessitating additional examination of the patients and specimens. The absence of urobilinogen cannot be definitively determined by the negative results.

Nitrite

Nitrite, which comes from food-derived nitrate, is produced in the urine by gram-negative bacteria. Since other elements in urine will not react with the reagent strip, nitrite is the only element that can be detected. Positive results should not be extrapolated from pink patches or edges on the strip. However, the development of any consistent pink colour in any degree should be seen favourably. There is no direct correlation between the levels of colour development and bacterial populations. The absence of germs in high quantities is not implied by the bad outcome (**Penders J, et al,.2002**).

Negative results may occur

- The nitrate in the foods is absent. Large high volume of specific gravity in urine may reduce the sensitivity of the test. 2.8mmol/Lascorbicacid or lesswon'tin therefore with the test result.

Leukocytes

Leucocytes (granulocytic leukocytes) tested respond with esterase. Normal urine samples often produce negative findings; clinically significant positive values are (+ or more). 'Trace' outcomes that are detected once or twice might not have much clinical importance, whereas results that are observed regularly might. Random samples from females may occasionally yield "positive" findings because vaginal discharge contaminated the material. Test findings may be affected by high specific gravity or elevated glucose levels (over 160 mmol/L).

Protein

Since the reagent region is sensitive to albumin, a negative result in urine tests is insufficient to prove the presence of proteins such as globulins, haemoglobin, Bence Jones protein, and mucoprotein. False positive results can occur in highly buffered alkaline urines (Lifshitz E, Kramer L (2000)).

Interpretation of Results

We collected 50 samples for the study, but only 18 of them showed positive and pertinent results. Since the majority of the samples are from teenagers (0.0 mmoI/L), their metabolic rate is significantly correct, we discover that all values are strongly negative. Out of the 18 nitrate samples that were discovered, 13 showed positive results, with the highest sample reaching 70 nmoI/L. Ketone levels are significantly abnormal when compared to other parameters, with 6 samples out of 18 being abnormal (it turns purple color: highest levels 16.0 mmoI/L), two samples being abnormal (3.9 mmoI/L), five samples being abnormal (0.5 mmoI/L), one sample being abnormal (1.5 mmoI/L), and three samples being negative. In the meanwhile, the blood parameters were analysed with urine sample, which was significantly traced with 15 samples out of 18 identified ones.Out of 18 samples, only one has a bilirubin parameter that is negative, while the other 17 are all significantly positive, with the highest value being 51 µmoI/L it turns in orange color and the lowest value being 17µmoI/L.Two samples had the highest amounts of positive protein (0.3

g/L), and five protein readings are normal. 11 other samples are noticeably positive. Only three of the 18 samples used in this study's estimation of uribilonogen levels revealed negative results, which meant that the pH, specific gravity values and the numbers of leucocytes were most likely aberrant.

Overview of urine chemical composition analysis using dipsticks and assay concepts

The process of detecting urine on a dipstick and comparing the colour change to a reference standard is known as dipstick/dry chemistry analysis (DelangheJ R *et al,*.2016). A chromogenic chemical often reacts with another product to cause this. Binding dye compounds, enzymatic reactions, immunologic reactions, and catalysis of oxidation-reduction reactions are examples of common reactions (Dolscheid – Pommerich *RC et al,*.2016). The majority of analyses rely on colorimetry, with the intensity of colour change proportional to analyte concentration. Due to their comfort, accessibility, and accuracy, dipstick readers have become a common tool in primary care, hospitals, and the consumer market (Echeverry G, *et al,*.2010). Despite the possibility of imprecise evaluations based on visual acuity and colour vision, these devices convert photonic energy from coloured reaction products into electrical signals, allowing the generation of semi-quantitative/quantitative data. Dipstick/dry chemistry is used in automated systems such as the Beckman Coulter IRICELLTM to maximize specimen throughput, minimize handling, and reduce manual labour (Fogazzi GB *et al,*.2008). These technologies have been well researched for application in dipstick interpretation. Dipstick readers with a 'lab on a chip' are also available for smart phone use. Dipstick/dry chemistry analysis can provide useful information regarding the qualities of urine samples, such as osmolarity (Frazee BW *et al,*.2012). Sample pH can be calculated within a range of 5.0-8.5, with variations possible at the extremes (5.5 and >7.5). The use of a glass electrode is the preferred and most accurate approach for measuring pH at those values (Hall JE (2016).

CONCLUSION

This is a preliminary study to expose the students towards analytical tools and to make them aware of the health parameters. Those who were with high protein, Ketone and Nitrate levels were directed for further medical checkup. Those who had blood cell damage were instructed to for further treatment to improve their blood quality.

ACKNOWLEDGEMENT

I am grateful that the our principal Dr.Fr.AmalaArockia Raj.SJ supported me with my work. I would like to thank all of my students for their constant support. I would also like to thank Mr. Ramana Kumar Reddy, Sri Venkateswara medicals, Vempalli, for providing chemicals in time for this research work.

Authors' Disclosures of Potential Conflicts of Interest

No potential conflicts of interest relevant to this article are reported.

REFERENCES

1. Decavele A-SC, Fiers T, Penders J, et al (2012). A sensitive quantitative test strip based point-of-care albuminuria screening assay. Clin. Chem. Lab. Med. 2012; 50:673678.
2. Delanghe J, Speeckaert M (2014).Preanalytical requirements of urinalysis. BiochemiaMedica. 2014;89–104.
3. Delanghe JR, Himpe J, De Cock N, et al (2017). Sensitive albuminuria analysis using dye binding based test strips. Clin. Chim. Acta. 2017; 471:107–112.
4. Delanghe JR, Speeckaert MM (2016).Preanalytics in urinalysis. Clin. Biochem. 2016; 49:1346–1350.

5. Dolscheid-Pommerich RC, Klarmann-Schulz U, Conrad R, et al (2016). Evaluation of the appropriate time period between sampling and analyzing for automated urinalysis. Biochem Med (Zagreb). 2016;26:82–89.
6. Echeverry G, Hortin GL, Rai AJ (2010). Introduction to urinalysis: historical perspectives and clinical application. Methods Mol. Biol. 2010; 641:1–12.
7. Ercan M, Akbulut ED, Abuşoğlu S, et al (2015). Stability of urine specimens stored with and without preservatives at room temperature and on ice prior to urinalysis. Clin. Biochem. 2015;48:919–922.
8. Fogazzi GB, Verdesca S, Garigali G (2008). Urinalysis: Core Curriculum 2008. Am. J. Kidney Dis. 2008;51:1052–1067.
9. Frazee BW, Frausto K, Cisse B, et al (2012). Urine collection in the emergency department: What really happens in there? West. J. Emerg. Med. 2012;13:401–405.
10. Haber MH (2010).Pisse prophecy: a brief history of urinalysis. Clin. Lab. Med. 1988;8:415–430.
11. Hall JE (2016). Guyton and Hall Textbook of Medical Physiology. 13th ed. Philadelphia, PA: Elsevier; 2016.
12. Herrington W, Illingworth N, Staplin N, et al (2016). Effect of processing delay and storage conditions on Urine albumin-to-creatinine ratio. Clin J Am SocNephrol. 2016;11:1794–1801. https://www.nu-careproducts.co.uk/data.
13. LaRocco MT, Franek J, Leibach EK, et al (2016). Effectiveness of preanalytic practices on contamination and diagnostic accuracy of urine cultures: a laboratory medicine best practices systematic review and meta-analysis. Clin. Microbiol. Rev. 2016;29:105–147.
14. Lifshitz E, Kramer L (2000). Outpatient urine culture: Does collection technique matter? Arch. Intern. Med. 2000;160:2537–2540.
15. Oyaert MN, Himpe J, Speeckaert MM, et al (2018). Quantitative urine test strip reading for leukocyte esterase and hemoglobin peroxidase. Clin. Chem. Lab. Med. 2018;56:1126– 1132.
16. Oyaert, M.Sc., and JorisDelanghe , M.D., Ph.D(2018). Progress in Automated Urinalysis Matthijs, Review Article Clinical Chemistry. ISSN 2234-3806 • eISSN 2234-3814
17. Penders J, Fiers T, Delanghe JR (2002). Quantitative evaluation of urinalysis test strips. Clin. Chem. 2002;48:2236–2241.
18. Pugia MJ (2000). Technology behind diagnostic reagent strips. Lab Med. 2000;31:92–96.
19. Rotter M, Brandmaier S, Prehn C, et al (2017). Stability of targeted metabolite profiles of urine samples under different storage conditions. Metabolomics. 2017;13:4.
20. Sureda-Vives M, Morell-Garcia D, Rubio-Alaejos A, et al (2017). Stability of serum, plasma and urine osmolality in different storage conditions: Relevance of temperature and centrifugation. Clin. Biochem. 2017;50:772–776.
21. Wilson ML, Gaido L (2004). Laboratory diagnosis of urinary tract infections in adult patients. Clin. Infect. Dis. 2004;38:1150–1158.

Table Detection of several parameters in urine using the dipstick method through urine analysis

S.no	Sample	Name of parameters with respected values Using H10 Reagent Strips for Urinalysis (Dip-stick method)									
		pH	Specific gravity	Glucose (mmoI/L)	Leucocytes (leuko/µL)	Nitrite (µmoI/L)	Protein (g/L)	Blood (Ery/µL)	Ketone (mmoI/L)	Bilirubin (µmoI/L)	Urobilonogen (µmoI/L)
1	S_1	5.0	1.030	0.0 (-)	70	Positive	Positive	Traced	3.9	17	17
2	S_2	6.0	1.000	0.0 (-)	00(-)	Negative	Normal	Non-Trac	Negetive	17	Negative
3	S_3	6.0	1.030	0.0 (-)	70	Positive	Positive	Traced	16	17	17
4	S_4	6.0	1.030	0.0 (-)	70	Positive	Positive	Traced	16	17	17
5	S_5	6.0	1.030	0.0 (-)	70	Positive	Positive	Traced	16	17	17
6	S_6	6.0	1.005	0.0 (-)	70	Positive	Positive	Traced	0.5	17	17
7	S_7	5.0	1.030	0.0 (-)	15	Positive	Positive	Traced	16	17	3.4
8	S_8	6.5	1.010	0.0 (-)	0.0 (-)	Negative	Negetive	Non-Trac	0.5	Negative	Negative
9	S_9	6.0	1.030	0.0 (-)	70	Negative	Positive	Traced	16	17	17
10	S_{10}	6.0	1.030	0.0 (-)	70	Positive	Positive	Traced	3.9	17	17

11	S_{11}	5.0	5.0	0.0 (-)	15	Positive	Positive	Traced	1.5	17	17
12	S_{12}	6.0	1.030	0.0 (-)	70	Negative	0.3	Traced	0.5	51	17
13	S_{13}	5.0	7.0	0.0 (-)	70	70	Negetive	Traced	Negative	51	17
14	S_{14}	6.0	1.030	0.0 (-)	70	Positive	0.3	Traced	16	51	17
15	S_{15}	6.0	1.025	0.0 (-)	0.15	Positive	Positive	Traced	16	51	17
16	S_{16}	5.0	1.030	0.0 (-)	70	Positive	Positive	Traced	0.5	17	17
17	S_{17}	5.0	1.000	0.0 (-)	0.0 (-)	Negative	Normal	Non-Trac	Negative	17	Negative
18	S_{18}	6.0	1.030	0.0 (-)	70	Positive	Negetive	Traced	0.5	17	17

Green color indicates Negative (-ve), Brown indicates Positive (+ve) and Red indicates severity.

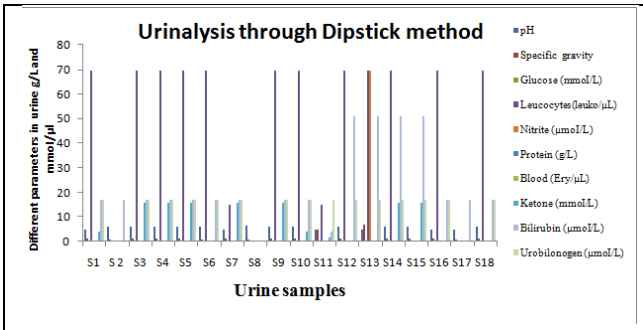

Graph 1. Graphical representation showing various levels of positives and elevated abnormalities of results

Fig 1: Collection of Samples

Fig 2: Results strip

Fig 3: Strips revealing positive results (+Ve)

RESEARCH ARTICLE

Automatic Power Factor Correction Unit using Arduino for Smart Homes

Krishnaveni S[1]*, Marutham Rathna Valli M[2], Keerthana S[2] and Kaviyamalar A.D[2]

[1]Associate Professor, Department of EEE, Sri Sivasubramaniya Nadar College of Engineering, (Affiliated to Anna University), Chennai, Tamil Nadu, India.
[2]UG Student, Department of EEE, Sri Sivasubramaniya Nadar College of Engineering, (Affiliated to Anna University), Chennai, Tamil Nadu, India.

Received: 10 Dec 2023 Revised: 13 Jan 2024 Accepted: 15 Mar 2024

***Address for Correspondence**
Krishnaveni S
Associate Professor, Department of EEE,
Sri Sivasubramaniya Nadar College of Engineering,
(Affiliated to Anna University),
Chennai, Tamil Nadu, India.
Email: krishnavenis@ssn.edu.in

ABSTRACT

In order to expedite our everyday routine, the consumption of electrical equipment has greatly expanded in the modern world. However, the majority of customers also depend on their projected monthly bills from the public sector. Therefore, managing power consumption and the associated payment amount requires information of power usage, load type, and appliance management. When inductive loads are used more frequently, the power factor drops to an abnormally low level, drawing more current and increasing the amount of electricity used. Thus, this research discusses a less expensive way to modify the power factor at the home level. This project outlines the process for using capacitor bank sensors to help modify the lagging power factor and Arduino UNO, which is compatible with your home's current setup. This technique improves efficiency, reduces the power factor penalty in small-scale companies, and upgrades and modernizes dwellings with modern technology.

Keywords: Power factor, Real power, Apparent power, Arduino UNO, Capacitor banks

INTRODUCTION

In our era of rapid advancement, energy efficiency is now regarded as one of the main goals. The present technological revolution is trying to fulfill everything needed by the society in a faster pace and so electrical power requirement is so enormous and very precious. TamilNadu Electricity Board [TNEB] tariff is increased every year due to bimonthly payment system since the electricity tariff depending on the conventional power generation. Moreover, the conventional power resources are in decline phase to meet today's population demand and creates the

alert everywhere how the electrical energy usage has to be curtailed. So, power consumption is superabundant which has a direct impact on the electricity bill, which remains an economic burden in lower and middle-income families. Therefore, the knowledge on electrical energy saving methods must be spread over and the awareness should be created to reduce the electrical usage by the consumer. Many ways are there to minimize the power consumption which includes manual methods where the user has to handle the electrical energy preciously, proper cut off of electrical appliances when not in use, knowing everyday power consumption by SMS alert [1-3], appliances management based on peak hours and maximum demand [4], and installing the power factor correction device. The ultimate idea of introducing various concepts regarding conscious use of electricity and proper maintenance and monitoring of power is to reduce the overall billing cost of the consumer, which has a major social and economic impact in daily lives.

The power quality has also become a hot topic recently due to rapid increase in number of the electronic appliances at home and industries, and the researches in power quality reveals the importance of it. Efficiency is an important measurement on power quality and increasing energy efficiency using power factor correction device has many advantages. Most of the industries are dependent on inductive loads, which on the other hand decreases the power factor and which obviously decreases the efficacy of the system [5]. An Automatic Power factor correction device has been proposed where an Arduino plays a major role at lesser cost is proposed in this paper. This method estimates the phase angle lag(ø) of current and leads to the calculation of the power factor (cos ø). The Arduino calculates the required adjustments to normalize the power factor value. This technique can be implemented in households, small scale industries and in even bigger firms so that the system might become more efficient and stable.

Importance of power factor improvement

The complex power, sometimes called the total power, is the total of the real and reactive powers added together. The entire power is calculated in VA and taken into account when charging for energy. [6].

$$\text{Power factor(pf)} = \frac{\text{True Power (W)}}{\text{Apparent Power (VA)}} \qquad (1)$$

Figure 1 shows the power triangle where the angle between the real power and the total power is defined as the power factor angle φ. The electrical load may have a power factor of less than one if reactive power results in the real power being less than the perceived power. Reactive power deliberately raises current in power companies, which results in worse operational efficacy and lost income. Therefore, power sectors mandate that their customers maintain their power factors over a certain threshold in order to avoid additional penalty. Reactive power may be due to connecting wires, circuit breakers, switches, power transformers, and transmission lines with higher current capacity. So, the lower power factor in turns into lower efficiency, large copper loss, greater conductor size and penalty from power supply companies in few countries. The above factors mention the importance of power factor improvement. Power factor correction can be proceeded by compensating the lagging current by connecting capacitor banks to the supply in small scale industries and homes. For household purposes, a capacitor with a capacitance of sufficient value is attached to bring the power factor almost to unity.

METHODOLOGY FOR POWER FACTOR CORRECTION SYSTEM

The methodology followed in this paper is presented in Figure 2. The capacitor bank is kept across the load and whenever the power factor adjustments are required the capacitors with proper value are put in parallel to the load. The values are converted into appropriate amounts for the Arduino UNO and phase delay measuring circuit using the current and voltage sensors. Zero Crossing Detector [ZCD] is used to measure the phase delay.

The Arduino UNO receives this amount in order to determine the power factor. It creates a control signal to turn on the delay if the power factor is less than 0.9. Then, the relay gets activated and makes the capacitor to be connected with the load. Then the procedure is repeated until the power factor becomes greater than 0.9 and the proper capacitor might be Current sensor employed in this project is ACS712ELCTR-5B-T and provides precise current measurement up to 5A for both AC and DC signals. It is a fully integrated linear current sensor with low resistance current conductor and excellent voltage isolation based on the Hall Effect. [7-8]. The sensitivity of ACS712 ELCTR-5B-T is 185 mV/A. The output analog voltage is proportional to current to be measured. Even with loads running at high voltages, such as 230 V AC mains, the sensing terminal can detect current since the output sensed voltage is isolated from the measuring port.

The voltage sensor ZMPT101B can be used to measure the AC voltage up to 250 volts [9-10]. It is simple to operate and generates very accurate voltage and power. It has a multiturn trim potentiometer that may be used to calibrate the Arduino's ADC output. When there is no load connected, the sensor has an initial voltage (Offset) of 2.5V if the sensor is energised by 5 V DC. Ground loops and unintentional test equipment grounding are prevented by the isolation transformer in the voltage sensor, which separates it from the power line ground connection. Moreover, they reduce high-frequency noise that is generated by the power source. The ATMEGA328 microcontroller offers the board flexibility by allowing the controller chip to be changed or removed in the event that it becomes damaged or stops working properly. The Arduino UNO boards are the only ones with these flexible capabilities. ZCD is a simple comparator circuit with a ground line attached to one of the input pins, and a ZCD circuit schematic is displayed in the Figure 3.

The circuit is provided with zero voltage as reference to one of the inputs terminals to find zero crossing points of a sine wave. ZCD compares the input sinusoidal signal with the zero-voltage level. A digital high output pulse is produced each time a sine wave crosses from zero reference voltage to another value. The differential voltage is positive when the input grows from zero to positive, which causes the OP-AMP to attain positive saturation (+Vsat). The OP-AMP reaches the negative saturation voltage, or Vsat, when the input drops from zero to negative since the differential voltage is negative. It can be seen that the output switches between +Vsat and -Vsat whenever the input crosses zero level thus generating a square wave as output. An XOR gate has these two square waves attached to it as inputs. If there is any phase delay in the input, the XOR gate will be set to 1. The output of the XOR gate spikes with very little time delay when the load is resistive.

IMPLEMENTATION OF POWER FACTOR CORRECTION

The proposed method is simulated using Proteus simulator and then the hardware is implemented. The results are discussed in this section.

Simulation Results

Proteus is a potent simulation software tool and Engineers may correctly model the behavior of electronic circuits with this comprehensive suite. Proteus simulates the operation of the circuit in real time using sophisticated algorithms and models, enabling engineers to test and improve their ideas before they are produced.The proposed circuit includes current transformer (CT), potential transformer [PT], ZCD circuit, Arduino UNO, capacitor and relay. The CT and PT sense the current and the voltage respectively and both the quantities are fed into ZCD circuit to convert the output sinusoidal waveforms to square waveform. This data is fed to the Arduino UNO in which the respective code to calculate the power factor is preloaded. The Figure 4 shows the simulation circuit for automatic power factor correction circuit. In this circuit, the expected power factor is set as 0.95 and whenever the power factor of the load is less than 0.95 the relay is activated which connects the capacitor across the load to compensate for the lagging power factor [11-15].

The Arduino code for power factor calculation based on the input derived from ZCD and relay activation code are written using Arduino IDE and uploaded in the Proteus software. The code used n this project is detailed in Figure 6. The IDE software utilizes an inductive counter to count the number of cycles where the input signal lags the output signal

and a counter to keep track of the total number of cycles. The estimated power factor is displayed on the LCD. The setup function in this block of code, is called once the program launches. It establishesthe input, output, and LED pin modes, initializes the display screen, initializes the serial communication. Also, it adds a delay and prints various notifications on the LCD. The primary portion of the program that executes repeatedlyfollowing the setup function is the loop function. The phase angle, counter, inductive counter, power factor, and a Boolean value for the power factor correction status are all initialized by these lines. To determine the phase angle and power factor for 50 cycles of the input signal, this block of code uses a while loop.The input voltage is first read using the analog Read function,followed by adding a delay and setting the output pin to HIGH. The phase angle is then determined using the cosine function, and it is then added to the angle variable. To count the number of cycles when the input signal lags behind the output signal, the software increments the counter and checks if the voltage is less than half of the maximum value (512). Eventually, another delay is added to finish one cycle, and the output pin is set to LOW.

HARDWARE RESULTS

The components are assembled and connected according to the simulation and the components used are given in the Table 1. The Figure 7 shows the hardware setup and Figure 8 shows the results. The ACS712ELECTR-6B-T is connected in series with 220 V supply. The V_{cc} pins of the sensor are connected to the 5V DC supply. The ZMPTB10 is also connected across the input supply. The output of the sensors is connected to the OPAMP as inputs through 10 kΩ resistors to form the ZCD. The offset voltage is reduced using the anti-parallel diodes across the OPAMP's input terminals. The sensor readings are processed on the Arduino board, andthe necessary computations for power factor correction are done. The various voltage regulators IC7806 and IC7812 are combined with a bridge rectifier diode to suit the circuit's needs for a DC supply. The Arduino is programmed in such a way that when the power factor becomes less than 0.9 the output pin connected to the relay is set high. The relay is used to switch in a capacitor of 9 μF to accurate the power factor and is linked in parallel with the load [16]. The power rating of the load and the necessary power factor correction are taken into consideration while choosing the capacitor. The load's power factor is improved and energy consumption is decreased after the power factor correction capacitor is turned on. The Arduino board keeps track of the load's voltage and currentwaveforms and makes the calculations required to keep the power factor at or near 1. Tekronix DSO is used to capture the output signal of sensors and ZCD and shown in Figure 9.

CONCLUSION

Energy monitoring innovations have benne grown during the past few years and effective strategies must be employed to enable effective, dependable utility management of diverse sectors. Hence a better and user-friendly method can be obtained by the enhancement of the conventional methods. Simple homes can be upgraded into smart homes with greater efficiency by implementing smart meter technology, appliance management and power factor correction methods. There are several potential future innovations that could improve the performance of smart homes including energy storage integration, use of advanced power electronics components, artificial intelligence-based control, and integration with smart grid technology.

ACKNOWLEDGEMENT

The authors would like to thank SSN Trust, Sri Sivasubramaniya Nadar College of Engineering, Chennai's for giving the funding necessary to finish the project.

REFERENCES

1. S.U. Anand , Nisha,P. Pavitra, Sowmya, V.N. Nikita, "Smart Energy Metering based on IoT and PocketPicking using Arduino and GSM", International Research Journal of Engineering and Technology , Vol.6, No.6, pp.1248,

2019.

2. S. Arun, R. Krishnamoorthy, M. Venugopal Rao , "ZigBee Based Electric Meter Reading System", International Journal of Computer Science Issues', pp.426-429, 2011.
3. A. Arif, M. Al-Hussain, N. Al-Mutairi, E. Al-Ammar, Y. Khan and N. Malik, "Experimental study and design of smart energy meter for the smart grid," 2013 International Renewable and Sustainable Energy Conference (IRSEC), Ouarzazate, Morocco, pp. 515-520, 2013.
4. J. Manikandan, "Design and evaluation of wireless home automation systems," 2016 IEEE 1st International Conference on Power Electronics, Intelligent Control and Energy Systems (ICPEICES), Delhi, India, pp. 2016.
5. Majid Ali, Faizan Rashid, Saim Rasheed, "Power Factor Improvement for a Three-Phase System using Reactive Power Compensation", Indonesian Journal of Electrical Engineering and Computer Science, Vol.24, No.2, pp.715-727, 2021.
6. I.U. Peter, K.G. Tersoo, O.E. Mayor, "An Arduino-Based Automatic Power Factor Correction Device", International Journal of Innovative Research in Electrical, Electronics, Instrumentation and Control Engineering, Vol.7, pp.25-31, 2019.
7. A.H. Bilal Naji, H.J. Basil, "Automated Power Factor Correction for Smart Home", Iraqi Journal of Electrical and Electronic Engineering, Vol.14, No.1, pp.30-40, 2018.
8. K. Agarwal, A. Agarwal and G. Misra, "Review and Performance Analysis on Wireless Smart Home and Home Automation using IoT", Third International conference on I-SMAC (IoT in Social, Mobile, Analytics and Cloud) (I-SMAC), Palladam, India, pp. 629-633, 2019.
9. S.S. Aaiman, S.P. Laxman, "Automatic Power Correction", International Research Journal of Engineering and Technology, Vol. 6, No.9, pp.474-477, 2019.
10. A. Shahid and A. Shabir, "Microchip based embedded system design for achievement of high-power factor in electrical power systems", IEEE PES Asia-Pacific Power and Energy Engineering Conference, Hong Kong, China, pp. 1-5, 2013.
11. Md Abdullah Al Rakib, Sumaiya Nazmi, Md Hasan Imam, Mohammad Nasir Uddin, "Arduino Based Automatic Power Factor Control", International Journal of Smart Grid, Vol.5, No.3, pp.121-127, 2021.
12. Mohammed Abbas Jubartalla Alsheikh, "Automatic Power Factor Correction", International Journal of Engineering and Information Systems, Vol.4, No.11, pp.78-84, 2020.
13. B. Samarjit, A.J. Choudhury, 'Case Study on Power Factor Improvement', International Journal of Engineering Science and Technology, Vol.3, No.12, pp.8372-8378, 2011.
14. P. Satish, H. Naveen, T.K. Naren, S. Vidhyalakshimi, S. Angel Deborah, "Home Automation Systems - A Study", International Journal of Computer Applications, Vol.116, No.11, pp.11-18, 2015.
15. S. Saurabh Kumar, S. Gaurav Kumar, S. Abhijeet, "A Review Paper On Automatic Power Factor Correction', International Journal of Creative Research Thoughts, Vol.6, pp.120-123, 2018.
16. Ararso Taye, "Design and Simulation of Automatic Power Factor Correction for Industry Application", International Journal of Engineering Technologies and Management Research,Vol.17, N0.2, pp.10-21, 2018.

Table 1 List of components

Component	SPECIFICATIONS
Current sensor	ACS712ELECTR-6B-T
Voltage sensor	ZMPT101B
Arduino board	Arduino UNO
LCD	JHD204
XOR Gate	HEF4030B
OP AMP	TS324
Capacitor bank	9 micro farad
Motor load	40 W,220 V, 50 Hz

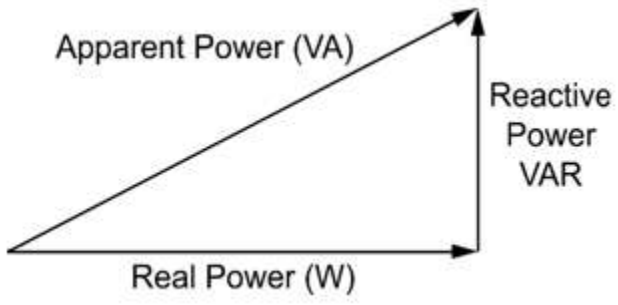

Figure 1 Power Triangle

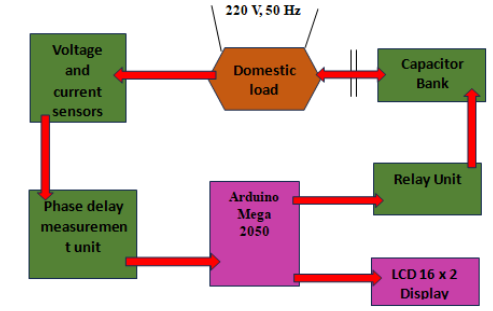

Figure 2. Methodology of power factor correction

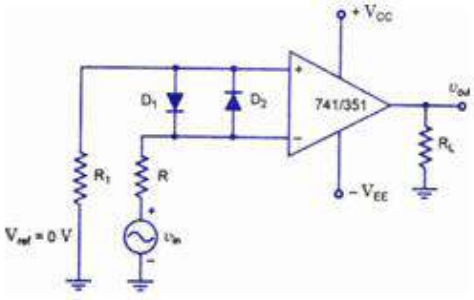

Figure 3. Circuit Diagram of Zero Crossing Detector

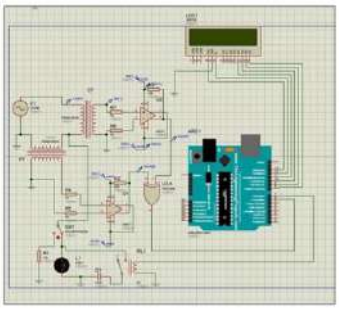

Figure 4. Automatic Power Factor Correction Unit

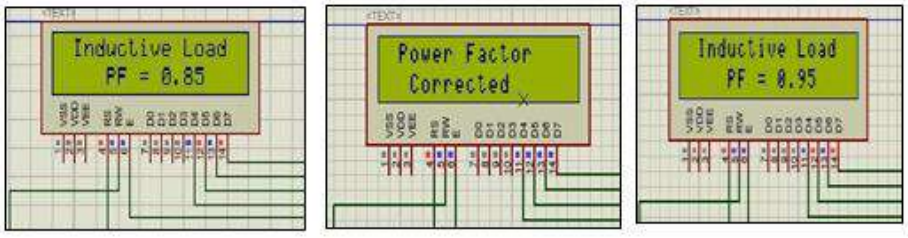

Figure 5. LCD display showing power factor before and after the correction

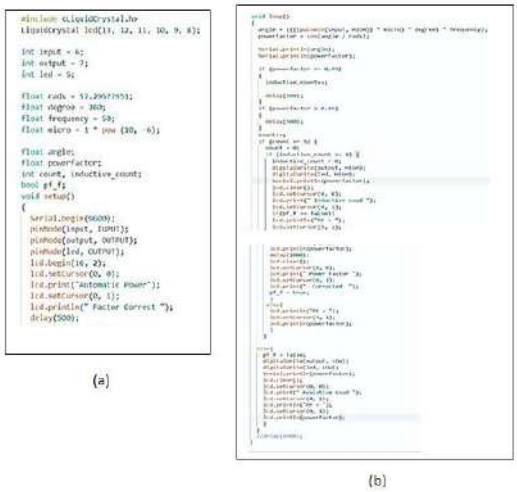

Figure 6. Arduino code for a) power factor calculation b) detecting lagging power factor and correcting the power factor

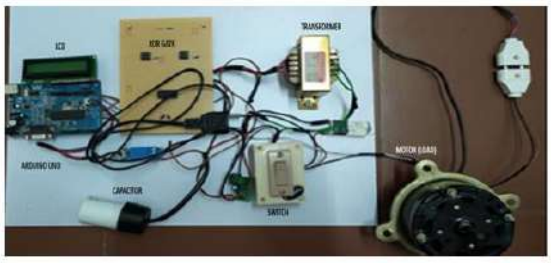

Figure 7 Hardware implementation of automatic power factor correction circuit

Figure 8 Power factor before and after correction for an inductive load

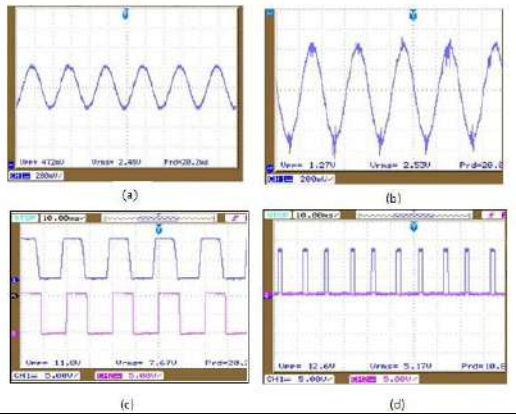

Figure 9. Output signals of (a) current sensor (b) voltage sensor (c) OPAMP (d) XOR gate of ZCD

RESEARCH ARTICLE

Pilot Study on Concordance of Microsatellite Instability (MSI) Testing by Idylla Point of Care PCR with Immunohisto chemistry

Lavanya.N[1]*, Sussela.K[2], Pratyusha.A[3], Subramanyeshwar Rao.T[4] and Raju. K.V.V.N[5]

[1]Sr.Scientific Officer, Department of Molecular Pathalogy, Laboratory Medicine Basavatarakam Indo American Cancer Hospital & Research Institute (BIACH&RI), Hyderabad, Telangana, India.
[2]HoD, Department of Laboratory Medicine, Basavatarakam Indo-American Cancer Hospital and Research Institute, Hyderabad, Telangana, India.
[3]Junior Research Fellow, Department of Molecular Pathalogy, Laboratory Medicine, Basavatarakam Indo American Cancer Hospital & Research Institute (BIACH&RI), Hyderabad, Telangana, India.
[4]Medical Director, Surgical Oncologist, Department of Surgical oncology, Basavatarakam Indo American Cancer Hospital & Research Institute (BIACH&RI), Hyderabad, Telangana, India.
[5]Senior Consultant, Department of Surgical Oncology, Basavatarakam Indo American Cancer Hospital & Research Institute (BIACH&RI), Hyderabad, Telangana, India.

Received: 25 Oct 2023 Revised: 09 Jan 2024 Accepted: 06 Mar 2024

***Address for Correspondence**
Lavanya.N
Sr.Scientific Officer,
Department of Molecular Pathalogy,
Laboratory Medicine Basavatarakam Indo American Cancer Hospital & Research Institute (BIACH&RI), Hyderabad, Telangana, India.
Email: nambaru.lavanya@gmail.com

ABSTRACT

Detection of microsatellite instability (MSI) is recommended for all patients with colorectal cancer (CRC). The prototype Idylla™ MSI Test has been developed using a new set of short homopolymers located in the ACVR2A, BTBD7, DIDO1, MRE11, RYR3, SEC31A & SULF2 genes. This marker set allows probe-based detection with great specificity in a simplified workflow compared to current methods. In this study, repeat length with this set of biomarkers was determined on formalin-fixed and paraffin-embedded (FFPE) CRC samples using Idylla™ MSI Test prototype cartridges, which allow a fully automated workflow including sample preparation, DNA amplification and automated repeat length calling. A total number of 18 samples including 14 adenocarcinomas from colorectal cancer (15 primary, one metastatic deposit in liver) and 4 metastatic deposits in liver including 2 from breast and one each from gallbladder and endometrium were included in the study. The grade of colorectal adenocarcinoma was grade 1 in 6, grade 2 in 7 and grade 3 in one. The viable tumor percentage ranged from 20-80%. Thirteen samples (13/18: 72 %) were microsatellite stable (MSS) by Idylla™ and five (5/18: 28 %) samples were MSI-H. Mutations were observed in ACVR 2A (5), DIDO1 (5), SULF2 (4), BTBD7 (4), RYR3 (3),

SEC31A (2) and MRE11 (2) in the 5 MSI-H samples. Therefore, tests like these can work as effective and rapid diagnostic tools and provide personalized treatment for the patient. However, the limitation of the present study is the small number of samples and therefore sensitivity analysis could not be performed

Keywords: Idylla point, Immunohistochemistry, Microsatellite instability, PCR

INTRODUCTION

Microsatellites are short sequences of DNA (consisting of one to six bases) that repeat themselves tandemly, across the human genome. Since they constitute several repeats, they are susceptible to mismatch errors during DNA replication. If the DNA mismatch repair system is impaired due to mutations in genes involved, namely- mutL homologue 1 (MLH1), mutS homologue 2 (MSH2), mutS homologue 6 (MSH6) and post-meiotic segregation increased 2 (PMS2), it would result in the accumulation of such repeat length alterations, resulting in microsatellite instability (MSI) (1). The Food and Drug Adminstration (FDA) has granted accelerated approval to an anti-PD-1 antibody, pembrolizumab, for use in pediatric and adult patients with MSI+ solid tumors (3). MSI is therefore considered a potential predictive marker for chemotherapy and immunotherapy. Twenty percent of colorectal cancers (CRC) are found to be defective in mismatch repair (MMR) system while the remaining 80% are said to be caused due to chromosomal instability (3). Deficiency in the MMR system can also be associated with Lynch syndrome, a hereditary cancer syndrome that makes one susceptible to multiple types of cancer. Therefore, if a deficiency is detected, the patient can further be selected for a germline test in order to assess their status and manage their treatment accordingly (4).Mismatch repair deficiency/microsatellite instability-high connotes a good prognosis in early colorectal cancer settings without adjuvant treatment and a poor prognosis in patients harboring metastases(5). Their diagnosis can be done by molecular methods or by means of immunohistochemistry (IHC).

Molecular testing primarily involves profiling mono- and di-nucleotide(or high order nucleotides) loci. If all the loci are found to be stable, then it would result in MSS (microsatellite stable); if two or more loci show instability it would be called MSI-H (microsatellite instability- high) and if one locus shows instability it would be called MSI-L (microsatellite instability-low) (3). However, IHC involves the use of antibodies against the proteins encoded by the above-mentioned mismatch repair genes, MLH1, MSH2, MSH6 and PMS2. MLH1/PMS2 and MSH2/MSH6 occur as heterodimers and loss of either of them or even loss of expression of a single protein would imply impaired/ defective mismatch repair (1). Although IHC shows concordance with molecular testing; however, there are a few limitations. A non-functional protein caused due to missense mutations may be normally translated resulting in positive expression. On the other hand, it can also imply false positive results where-in, although there might have been loss of a protein expression, since it occurred only in a subset of mutated tumors, it might not affect the MMR machinery and still continue to remain efficient in DNA repair (1). MSI assay by Idylla™ is a molecular technique-based assay that uses real-time polymerase chain reaction (PCR) to assess the mutation status. It is an in vitro rapid diagnostic test that has been validated against Promega MSI analysis system and /or IHC in very few studies (2,7). Compared to Promega MSI Analysis System,an overall agreement,sensitivity and specificity of 98.7%,94.4%and 100% have been reported with Idylla™ MSI Assay (2). In this study, we attempted to assess the concordance of MSI by IHC results with those obtained by using Idylla™ MSI Assay (Biocartis, Belgium). It is a fully automated assay that processes the samples and gives an interpretation as well. It detects mutations in the following loci which as biomarkers are tumor specific and exhibit high frequency in colorectal and endometrial cancers: ACVR2A, BTBD7, DIDO1, MRE11, RYR3, SEC31A and SULF2. The present study is the first of its kind from India, to the best of our knowledge.

MATERIALS AND METHODS

This was a prospective, observational study, approved by the institutional review board. Samples obtained for MSI IHC were included for validation. Informed consent was taken from all the patients. A total of 18 formalin fixed paraffin embedded (FFPE) tissue blocks were tested for MSI by both IHC and Idylla™. The site of biopsy and histology of each of the specimens were provided in table 1. One sample was tested for germline mutations in MLH1, MSH2, MSH6 and PMS2 on the Next Generation Sequencing (NGS) platform as well.

MSI Assay by Idylla™

Haematoxylin and eosin (H & E) stained slides of the tissue sections were reviewed by a pathologist.The protocol for sample processing was as per the protocol used by Lee M et al (6).A minimum of 20% viable tumor (VT) was taken as the cut off. Viable tumor percentage was ascertained by macro-dissection and tumor area was marked to determine the number of sections to be procured. The tissue blocks were refrigerated at 4˚C for about 30 minutes prior to procuring the sections. The tissue was then processed in an Idylla™ instrument according to the manufacturer's instructions. The Biocartis Idylla™ MSI Assay was fully automated and capable of detecting seven monomorphic biomarkers. This qualitative detection technique uses FFPE tissues, from which nucleic acid is automatically extracted, PCRperformed and analyzed using high resolution melting detection using one cartridge alone.(in a single catridge). Specific PCR amplicons will generate biomarker specific fluorescence profiles. The validity of these profiles (which) is checked and analyzed by test specific software which(and) provides the final result to the user. Thus, this technique also eliminates the need for sample processing control.

Procedure for MMR testing by IHC

Procedure for IHC consisted of mounting of 4µm sections cut from FFPE blocks on poly -l-lysine coated slides, deparaffinized with xylene and hydrated through graded alcohols. The IHC was performed on BOND-III fully automated IHC stainer (Leica) as per manufacturer's instructions. The following antibodies were used: MLH1 (Clone GM011,DAKO, RTU), MSH2 (Clone FE11 DAKORTU)MSH6(Clone EP49 RTU,DAKO) PMS2(Clone EP 51,DAKORTU) Every section of colon had normal mucosa, which served as internal positive control. However where internal positive controls were not available (eg metastatic sites small biopsy samples etc) external controls were also run. Samples with intact expression were considered to have intact MMR function and loss of expression of paired markers MLH1 and PMS2 or MSH2 and MSH6 were suggestive of MMR deficient status. Sole loss of any of these markers was reported as such and necessitated further testing including germline testing.

Procedure for MSI testing by NGS

An informed consent was taken for the patient for germline testing with hereditary cancer genes. Germline testing for hereditary cancer panel (including MLH1, MSH2, MSH6 and PMS2) was performed by NGS based assay using 30 genes and associated Bioinformatics pipeline.which showed pathogenic mutations in MSH2. The sequencing was performed on Ion TorrentS5 plus NGS platform at 400X coverage. Results were evaluated on the Ion Torrent software

RESULTS

A total number of 18 samples including 14 adenocarcinomas from colorectal cancer (15 primary, one metastatic deposit in liver) and 4 metastatic deposits in liver including 2 from breast and one each from gallbladder and endometrium were included in the study. The grade of colorectal adenocarcinoma was grade 1 in 6, grade 2 in 7 and grade 3 in one.

MSI assay by Idylla™ and MMR status by IHC

The viable tumor percentage ranged from 20-80%. Thirteen samples (13/18: 72 %)were microsatellite stable **(**MSS) by Idylla™and five (5/18: 28 %) samples were MSI-H. Mutations were observed in ACVR 2A (5), DIDO1 (5), SULF2 (4), BTBD7 (4), RYR3 (3), SEC31A (2) and MRE11 (2) in the 5 MSI-H samples (Table 1). MMR status by IHC showed loss of expression of MLH1& PMS2 in 3 and MSH2 &MSH6 in two samples (Table 1). There was complete concordance between the results of Idylla™ and IHC in the 18 samples tested. One patient who had adetailed work-up whose sample was subjected to IHC, Idylla and NGS is described below (Table 3- Case 18). A 40 years old patient who presented with adenocarcinoma of the transverse colon was initially evaluated by IHC for MMR status. There was loss of MSH2 and MSH6 expression and intact MLH1 and PMS2 expression. This was indicative of MSI –H status and therefore genomic testing by PCR was done by Idylla™, which demonstrated MSI-H status (all 7 biomarkers were mutant: MSI-H;mutation detected in all seven biomarkers ACVR2A, BTBD7, DIDO1, MRE11, RYR3, SEC31A and SULF2.) Thereafter, in view of high risk, germline testing for MSH2 and other genes implicated in Lynch Syndrome was performed for hereditary colon cancer panel (comprising of 30 genes) on Ion Torrent S5 plus NGS platform with 400X coverage, after obtaining informed consent.The test yielded a pathogenic mutation in MSH2.The changes were observed in chromosome 2, exon 5(Indel). The amino acid change was Leu280Phe.The patient was counselled and advised for testing of the other family members as well, to identify Lynch syndrome. This case illustrates the importance of the three different technologies.

DISCUSSION

The present study compared the results of MSI testing by Idylla™, that detects mutations with high frequency in colorectal and endometrial cancers, to the results obtained by IHC for MMR protein expression in 18 samples. There was 100% concordance of the results. Tissues, that showed loss of MLH1 and PMS2 markers by IHC, also showed mutations by Idylla™ in the 3 biomarkers in common, namely ACVR2A, DIDO1 and SULF2. The former two mutations were found in tissue that showed loss of MSH2 and MSH6 as well (Table 2). All the tissues that were MSI-intact when detected by IHC were 100% concordant with the results of Idylla™ which were microsatellite stable. The tumor tissues tested were from different regions of the colon (ascending, sigmoid, transverse colon), rectum and the liver. However, all the four tissues that showed MSI-H status belonged to different parts of the colon. The minimum viable tumor percentage that allowed mutation detection for these set of samples in Idylla™ was 20% (Table 1). When the area of the tissue section with viable tumor was small, we obtained additional number of sections. Idylla™ produces the result in approximately two and a half hours, whereas IHC would require several hours to overnight staining procedure. Furthermore, Idylla™ detects mutations at the RNA (DNA) level which is more reliable than a protein-based test such as IHC. Moreover, Idylla™ Assay does not require a control tissue unlike IHC.

Each of the five cases with loss of MMR expression and corresponding MSI-H status had a different presentation. Other alternatives to MSI status testing include real time PCR, Gene sequencing by fragment analysis and NGS. Real time PCR involves more steps as it requires extraction of the nucleic acid from the tissue, followed by its purification, quantification, PCR runs and analysis. NGS although provides a more accurate result, is time consuming, requires more consumables, instruments and also expensive. However, as in the illustrated case, NGS facilitated identification of a pathogenic mutation in MSH2, thus enabling the patient to be counselled and advised for testing the other family members as well to identify Lynch syndrome. The advantages of Idylla™ Assay include that console occupies less space, is easy to process and is quicker but the cartridge provided is only for a single use and is expensive as well. The lack of manual intervention once the tissue is inserted into cartridge can pose an advantage as well as a disadvantage. If the amount of tissue inserted or nucleic acid extracted is insufficient or any such extraction/ processing error occurs, one would be able to view it only at the very end of the procedure and would have to use another cartridge and cut more sections of tissue to repeat the test. Although Idylla™ provides a QC report at the end of the test; one cannot view the amplification curve to assess the quality of tissue or nucleic acid.

The set of mutations that Idylla™ detects are of considerable importance. Although rare, false positive results have been reported where in despite efficient MMR machinery, somatic mutations were detected in 4 of the genes(6). Apart from validation of MSI results obtained through Idylla™ with that of IHC, we have also found common mutations in tumors with a loss of MLH1 and PMS2. This could possibly pave way for establishing a gene signature that can further help in the better assessment of the pathological status of the tumor and also for an effective targeted therapy. Clinical findings may not be predictive of the results of biomarker testing. Therefore, tests like these can work as effective and rapid diagnostic tools and provide personalized treatment for the patient. However, the limitation of the present study is the small number of samples and therefore sensitivity analysis could not be performed in a laboratory setting, simple, easy, less time-consuming techniques are imperative considering the needs of the patient and the urgency for therapeutic planning by the clinician. Keeping these factors in mind, we believe Idylla™ is a robust technology and good alternative in the clinic for rapid MSI testing.

REFERENCES

1. Ivana, C., Aldo, S. and Lisa, S. 2016. Microsatellite Instability - Defective DNA Mismatch Repair: ESMO Biomarker Factsheet.
2. Zwaenepoel, K., Holmgaard Duelund, J., De Winne, K., Maes, V., Weyn, C., Lambin, S., Dendooven, R., Broeckx, G., Steiniche, T., & Pauwels, P. (2020). Clinical Performance of the Idylla MSI Test for a Rapid Assessment of the DNA Microsatellite Status in Human Colorectal Cancer. The Journal of molecular diagnostics : JMD, 22(3), 386–395.
3. Cortes-Ciriano, I., Lee, S., Park, W.Y., Kim, T.M. and Park, P.J., 2017. A molecular portrait of microsatellite instability across multiple cancers. *Nature communications*,*8*, p.151804.
4. Dubey, A.P., Vishwanath, S., Nikhil, P., Rathore, A. and Pathak, A., 2016. Microsatellite instability in stage II colorectal cancer: An Indian perspective. *Indian Journal of Cancer*, *53*(4), p.513
5. Lee, J.H., Cragun, D., Thompson, Z., Coppola, D., Nicosia, S.V., Akbari, M., Zhang, S., McLaughlin, J., Narod, S., Schildkraut, J. and Sellers, T.A., 2014. Association between ihc and msi testing to identify mismatch repair–deficient patients with ovarian cancer.*Genetic testing and molecular biomarkers*, *18*(4), pp.229-235.
6. Zhao, P., Li, L., Jiang, X. *et al.* Mismatch repair deficiency/microsatellite instability-high as a predictor for anti-PD-1/PD-L1 immunotherapy efficacy.*J HematolOncol*12**,** 54 (2019). https://doi.org/10.1186/s13045-019-0738-1
7. Lee, M., Chun, S.M., Sung, C.O., Kim, S.Y., Kim, T.W., Jang, S.J. and Kim, J., 2019. Clinical Utility of a Fully Automated Microsatellite Instability Test with Minimal Hands-on Time.*Journal of Pathology and Translational Medicine*, 53(6), p.386.
8. Patrick, P.,Torben, S., Muriel, G. et al. The Idylla MSI test(CE-IVD) multi centre concordance study: Microsatellite instability detection in colorectal cancer samples. *Journal of Clinical Oncology* 2019 37:15 suppl, e15112.

Table 1: Results of MSI on Idylla™ Assay and MMR status on IHC, site of biopsy and histology

Sample No.	Results on Idylla™	ViableTumor Percentage	Result by IHC	Site of Biopsy	Histology	Grade
1	MSI-H	65%	MMR expression	Colon	Adenocarcinoma	3
2	MSI-H	70%	MMR expression	Transverse colon	Adenocarcinoma	1
3	MSS	20%	MMR expression	Rectum	Adenocarcinoma	2
4	MSS	80%	MMR expression	Rectosigmoid	Adenocarcinoma	1
5	MSS	70%	MMR expression	Rectum and sigmoid colon	Adenocarcinoma	2

6	MSS	60%	MMR expression	Rectum	Adenocarcinoma	1
7	MSI-H	60%	MMR expression	Sigmoid colon	Adenocarcinoma	1
8	MSS	20%	MMR expression intact	Liver (trucut biopsy)	Metastatic deposits of carcinoma endometrium.	
9	MSS	60%	MMR expression intact	Liver (trucut biopsy)	metastatic adenocarcinoma from gallbladder	
10	MSS	50%	MMR expression	Liver (trucut biopsy)	Metastases from breast	
11	MSS	60%	MMR expression	Transverse colon	Adenocarcinoma	2
12	MSS	20%	MMR expression	Rectum	Adenocarcinoma	2
13	MSS	70%	MMR expression	Rectum	Adenocarcinoma	2
14	MSS	60%	MMR expression	Colon	Adenocarcinoma	2
15	MSS	40%	MMR expression	Liver (trucut biopsy)	Metastatic adenocarcinoma from	2
16	MSS	60%	MMR expression	Liver (trucut biopsy)	Metastases from breast	
17	MSI-H		MMR expression	Ascending colon	Adenocarcinoma	1
18	MSI -H	40%	MMR expression	Transverse colon	Adenocarcinoma	1

Abbreviations: IHC: MMR: Mismatch repair; MSI-H: Microsatellite Instability High; MSS:-Microsatellite Stable

Table 2: Table demonstrating MSI-H status and IHC (n=5)

Sample No.	Idylla™ Biomarker Status-(MSI-H)							IHC marker Status			
	ACVR2A	**DIDO1**	**SULF2**	**BTBD7**	**RYR 3**	**SEC 31A**	**MRE11**	**MLH1**	**PMS2**	**MSH2**	**MSH6**
1	+	+	+	+	+	+	-	Lost	Lost	Intact	Intact
7	+	+	+	-	-	-	+	Lost	Lost	Intact	Intact
17	+	+	+	+	-	-	-	Lost	Lost	Intact	Intact
2	+	+	-	+	+	-	-	Intact	Intact	Lost	Lost
18*	+	+	+	+	+	+	+	Intact	Intact	Lost	Lost

+ Detected; - Not detected

RESEARCH ARTICLE

On $\alpha^* g^{\#}\psi$-closed Sets in Topological Spaces

S.Pooja[1]*, M.Vigneshwaran[2] and L.Vidyarani [2]

[1]Ph.D Research Scholar, Department of Mathematics, Kongunadu Arts and Science College (Affiliated to Bharathiar University) Coimbatore, Tamil Nadu, India.
[2]Assistant Professor, Department of Mathematics, Kongunadu Arts and Science College (Affiliated to Bharathiar University) Coimbatore, Tamil Nadu, India.

Received: 03 Nov 2023 Revised: 12 Jan 2024 Accepted: 07 Mar 2024

***Address for Correspondence**
S.Pooja
Ph.D Research Scholar,
Department of Mathematics,
Kongunadu Arts and Science College (Affiliated to Bharathiar University)
Coimbatore, Tamil Nadu, India.
Email: poojabreeks@gmail.com

ABSTRACT

The subject of this work is Alpha star generalized hash psi closed set($\alpha^* g^{\#}\psi$) in topological spaces where the relation of a $\alpha^* g^{\#}\psi$-closed set to other generalised sets are derived. Also the characteristics of $\alpha^* g^{\#}\psi$-closed set is derived.

Keywords: $\alpha^* g^{\#}\psi$-closed set.
MSC: 54A05

INTRODUCTION

Levine[7, 8] developed generalised closed sets and semi- open sets in topological spaces. Njastad[14] introduced α-sets. S.P.Arya and T.Nour[1] introduced gs-closed sets. H.Maki et al.[9,10] developed gα-closed sets and αg-closed sets. M.Vigneshwaran and R.Devi[18] developed the idea of *gα-closed sets. gsp-closed sets and gpr-closed sets were developed by Dontchev[3] and Gnanambal[4] respectively. Veerakumar[16] introduced ψ-closed sets. Kanimozhi, Balamani and Parvathi[6] introduced $g^{\#}\psi$-closed sets and T.Nandhini[13] introduced $\alpha g^{\#}\psi$-closed sets. The objective of this article is to develop a new group of sets named Alpha star generalized hash psi closed sets in topological spaces.

Preliminaries
Definition 2.1. Let P be a topological space, S ⊆T is stated as
sOS [8] if S⊆cl(int(S)) and sCS if int(cl(S)) ⊆S.

pOS [12] if S⊆ int(cl(S)) and pCS if cl(int(S))⊆S.
αOS [14] if S⊆int(cl(int(S))) and αCS if cl(int(cl(S)))⊆S.
gCS [7] if cl(S) ⊆T when S⊆T and T is open in P.
gsCS [1] if scl(S) ⊆T when S⊆T and T is open in P.
gpCS [11] if pcl(S) ⊆T when S⊆T and T is open in P.
gαCS [9] if αcl(S) ⊆T when S⊆T and T is α-open in P.
*gαCS [18] if cl(S) ⊆T when S⊆T and T is gα-open in P.
sgCS [2] if scl(S) ⊆T when S⊆T and T is semi open in P.
αgCS [10] if αcl(S) ⊆T when S⊆T and T is open in P.
gspCS [3] if spcl(S) ⊆T when S⊆T and T is open in P.
g*spCS [5] if spcl(S) ⊆T when S⊆T and T is g-open in P.
gprCS [4] if pcl(S) ⊆T when S⊆T and T is regular open in P.
ψCS [16] if scl(S) ⊆T when S⊆T and T is sg-open in P.
ψgCS [15] if ψcl(S) ⊆T when S⊆T and T is open in P.
$g^{\#}$CS [17] if cl(S) ⊆T when S⊆T and T is αg-open in P.
$g^{\#}\psi$CS [6] if ψcl(S) ⊆T when S⊆T and T is ψ-open in P.
$\alpha g^{\#}\psi$CS [13] if αcl(S) ⊆T when S⊆T and T is $g^{\#}\psi$-open in P.

Basic Properties of $\alpha^{*}g^{\#}\psi$ -Closed Set

Definition 3.1: Let P be a topological space, a subset S of P is stated as $\alpha^{*}g^{\#}\psi$-closed set($\alpha^{*}g^{\#}\psi$-CS) if αcl(S) ⊆T when S⊆T and T is $\alpha g^{\#}\psi$-open set($\alpha g^{\#}\psi$-OS).

Theorem 3.2: Every closed set is $\alpha^{*}g^{\#}\psi$ -CS.

Proof: Let S⊆T, T is $\alpha g^{\#}\psi$-OS in P.
As S is closed, cl(S) = S.
But αcl(S) ⊆cl(S).
$\Longrightarrow$ αcl(S) ⊆T.
Hence S is $\alpha^{*}g^{\#}\psi$ -CS.
The below example demonstrates the preceding implication is irreversible.

Example 3.3: Let P = $\{x_1, x_2, x_3\}$, $\tau = \{P, \emptyset, \{x_1, x_3\}\}$.
$\alpha^{*}g^{\#}\psi$C(P, τ) = $\{P, \emptyset, \{x_2\}, \{x_1, x_2\}, \{x_2, x_3\}\}$.
$\{x_1, x_2\}$ is $\alpha^{*}g^{\#}\psi$-CS of (P, τ) although not closed in (P, τ).

Theorem 3.4: Every α-CS is $\alpha^{*}g^{\#}\psi$ -CS.
Proof: Let S⊆T, T is $\alpha g^{\#}\psi$-OS in P.
As S is α-CS, αcl(S) = S.
But αcl(S) ⊆T.
Hence S is $\alpha^{*}g^{\#}\psi$ -CS.
The below example demonstrates the preceding implication is irreversible.

Example 3.5: Let P = $\{x_1, x_2, x_3\}$, $\tau = \{P, \emptyset, \{x_2, x_3\}\}$.
αC(P, τ) = $\{P, \emptyset, \{x_1\}\}$.
$\alpha^{*}g^{\#}\psi$ C(P, τ) = $\{P, \emptyset, \{x_1\}, \{x_1, x_2\}, \{x_1, x_3\}\}$.
$\{x_1, x_2\}$ is $\alpha^{*}g^{\#}\psi$ -CS of (P, τ) although not α-CS in (P, τ).

Theorem 3.6: Every $\alpha^{*}g^{\#}\psi$ -CS is gs-CS.
Proof: Let S⊆T, T is OS in P.
As every OS is $\alpha g^{\#}\psi$ -OS, T is $\alpha g^{\#}\psi$ -OS.

Here S is $\alpha^* g^{\#}\psi$-CS,
$\Rightarrow \alpha$cl(S) ⊆T.
Also scl(S) ⊆ αcl(S), then scl(S) ⊆T.
Hence S is gs-CS.
The below example demonstrates the preceding implication is irreversible.

Example 3.7: Let P = $\{x_1, x_2, x_3\}$, $\tau = \{P, \emptyset, \{x_2\}, \{x_1, x_2\}\}$.
GSC(P, τ) = $\{P, \emptyset, \{x_1\}, \{x_3\}, \{x_2, x_3\}, \{x_1, x_3\}\}$.
$\alpha^* g^{\#}\psi$C(P, τ) = $\{P, \emptyset, \{x_1\}, \{x_3\}, \{x_1, x_3\}\}$.
$\{x_2, x_3\}$ is gs-CS of (P, τ) although not $\alpha^* g^{\#}\psi$-CS in (P, τ).

Theorem 3.8: Every $\alpha^* g^{\#}\psi$-CS is gp-CS.

Proof: Let S⊆T,T is OS in P.
As every OS is $\alpha g^{\#}\psi$ -OS, T is $\alpha g^{\#}\psi$ -OS.
Here S is $\alpha^* g^{\#}\psi$ -CS.
$\Rightarrow \alpha$cl(S) ⊆T.
Also, pcl(S) ⊆cl(S).
⇒pcl(S) ⊆T.
Hence S is gp-CS.
The below example demonstrates the preceding implication is irreversible.

Example 3.9: Let P = $\{x_1, x_2, x_3\}$, $\tau = \{P, \emptyset, \{x_2, x_3\}\}$.
GPC(P, τ) = $\{P, \emptyset, \{x_1\}, \{x_2\}, \{x_3\}, \{x_1, x_2\}, \{x_1, x_3\}\}$.
$\alpha^* g^{\#}\psi$C(P, τ) = $\{P, \emptyset, \{x_1\}, \{x_1, x_2\}, \{x_1, x_3\}\}$.
$\{x_2\}$ is gp-CS of (P, τ) although not $\alpha^* g^{\#}\psi$-CS in (P, τ).

Theorem 3.10: Every $\alpha^* g^{\#}\psi$-CS is sg-CS.

Proof: Let S⊆T, T is semi-OS in P.
As every semi-OS is $\alpha g^{\#}\psi$ -OS, T is $\alpha g^{\#}\psi$ -OS.
As S is $\alpha^* g^{\#}\psi$-CS, αcl(S) ⊆T.
Also scl(S) ⊆ αcl(S).
Then, scl(S) ⊆T.
Hence S is sg-CS.
The below example demonstrates the preceding implication is irreversible.

Example 3.11: Let P = $\{x_1, x_2, x_3\}$, $\tau = \{P, \emptyset, , \{x_1\}, \{x_2\}, \{x_1, x_2\}\}$.
SGC(P, τ) = $\{P, \emptyset, \{x_1\}, \{x_2\}, \{x_3\}, \{x_2, x_3\}, \{x_1, x_3\}\}$.
$\alpha^* g^{\#}\psi$C(P, τ) = $\{P, \emptyset, \{x_3\}, \{x_2, x_3\}, \{x_1, x_3\}\}$.
$\{x_1\}$ is sg-CS of (P, τ) although not $\alpha^* g^{\#}\psi$-CS in (P, τ).

Theorem 3.12: Every $\alpha^* g^{\#}\psi$-CS is αg-CS.
Proof: Let S⊆T, T is OS in P.
As every OS is $\alpha g^{\#}\psi$-OS, T is $\alpha g^{\#}\psi$-OS.
Here S is $\alpha^* g^{\#}\psi$-CS.
$\Rightarrow \alpha$cl(S) ⊆T.
Hence S is αg-CS.
The below example demonstrates the preceding implication is irreversible.

Example 3.13: Let P = $\{x_1, x_2, x_3\}$, $\tau = \{P, \emptyset, \{x_3\}, \{x_2, x_3\}\}$.
αGC(P, τ) = $\{P, \emptyset, \{x_1\}, \{x_2\}, \{x_1, x_2\}, \{x_1, x_3\}\}$.
$\alpha^* g^{\#}\psi$C(P, τ) = $\{P, \emptyset, \{x_1\}, \{x_2\}, \{x_1, x_2\}\}$.
$\{x_1, x_3\}$ is αg-CS of (P, τ) although not $\alpha^* g^{\#}\psi$-CS in (P, τ).

Theorem 3.14: Every *gα-CS is $\alpha^* g^{\#}\psi$-CS.
Proof: Let S⊆T, T is $\alpha g^{\#}\psi$-OS in P.
As every open set T is $\alpha g^{\#}\psi$-OS, T is $\alpha g^{\#}\psi$-OS.
Since S is *gα-CS. Then, cl(S)⊆T.
Here, αcl(S) ⊆cl(S).
$\Rightarrow$ αcl(S) ⊆T.
Hence S is $\alpha^* g^{\#}\psi$-CS.
The below example demonstrates the preceding implication is irreversible.

Example 3.15: Let P = $\{x_1, x_2, x_3\}$, $\tau = \{P, \emptyset, \{x_1\}\}$.
*GαC(P, τ) = $\{P, \emptyset, \{x_2, x_3\}\}$.
$\alpha^* g^{\#}\psi$ C(P, τ) = $\{P, \emptyset, \{x_2\}, \{x_3\}, \{x_2, x_3\}\}$.
$\{x_2\}$ is $\alpha^* g^{\#}\psi$-CS of (P, τ) although not *gα-CS in (P, τ).

Theorem 3.16: Every $\alpha^* g^{\#}\psi$ -CS is gsp-CS.
Proof: Let S⊆T, T is OS in P.
As every open set T is $\alpha g^{\#}\psi$-OS, T is $\alpha g^{\#}\psi$-OS.
Since S is $\alpha^* g^{\#}\psi$-CS, αcl(S) ⊆T.
Also spcl(S) ⊆ αcl(S).
$\Rightarrow$spcl(S) ⊆T.
Hence S is gsp-CS.
The below example demonstrates the preceding implication is irreversible.

Example 3.17: Let P = $\{x_1, x_2, x_3\}$, $\tau = \{P, \emptyset, \{x_1, x_2\}\}$.
GSPC(P, τ) = $\{P, \emptyset, \{x_1\}, \{x_2\}, \{x_3\}, \{x_2, x_3\}, \{x_1, x_3\}\}$.
$\alpha^* g^{\#}\psi$C(P, τ) = $\{P, \emptyset, \{x_3\}, \{x_2, x_3\}, \{x_1, x_3\}\}$.
$\{x_1\}$ is gsp-CS of (P, τ) although not $\alpha^* g^{\#}\psi$-CS in (P, τ).

Theorem 3.18: Every $\alpha^* g^{\#}\psi$ -CS is g*sp-CS.
Proof: Let S⊆T, T is g-OS in P.
As every g-OS is $\alpha g^{\#}\psi$-OS, T is $\alpha g^{\#}\psi$-OS.
Since S is $\alpha^* g^{\#}\psi$-CS, αcl(S) ⊆T.
But spcl(S) ⊆ αcl(S).
$\Rightarrow$ spcl(S) ⊆T.
Hence S is g*sp-CS.
The below example demonstrates the preceding implication is irreversible.

Example 3.19: Let P = $\{x_1, x_2, x_3\}$, $\tau = \{P, \emptyset, \{x_1\}, \{x_1, x_2\}\}$.
G*SPC(P, τ) = $\{P, \emptyset, \{x_2\}, \{x_3\}, \{x_2, x_3\}, \{x_1, x_3\}\}$.
$\alpha^* g^{\#}\psi$C(P, τ) = $\{P, \emptyset, \{x_2\}, \{x_3\}, \{x_2, x_3\}\}$.
$\{x_1, x_3\}$ is g*sp-CS of (P, τ) although not $\alpha^* g^{\#}\psi$-CS in (P, τ).

Theorem 3.20: Every $\alpha^* g^{\#}\psi$-CS is gpr-CS.
Proof: Let S⊆T, T is regular OS in P.

As every regular OS is $\alpha g^{\#}\psi$-OS, T is $\alpha g^{\#}\psi$-OS.
Since S is $\alpha^{*} g^{\#}\psi$-CS, αcl(S) ⊆T.
Also pcl(S) ⊆ αcl(S).
⟹pcl(S) ⊆T.
Hence S is gpr-CS.
The below example demonstrates the preceding implication is irreversible.

Example 3.21: Let P = $\{x_1, x_2, x_3\}$, $\tau = \{P, \emptyset, \{x_2\}\}$.
GPRC(P, τ) = $\{P, \emptyset, \{x_1\}, \{x_2\}, \{x_3\}, \{x_1, x_2\}, \{x_2, x_3\}, \{x_1, x_3\}\}$.
$\alpha^{*} g^{\#}\psi$C(P, τ) = $\{P, \emptyset, \{x_1\}, \{x_3\}, \{x_1, x_3\}\}$.
$\{x_2\}$ is gpr-CS of (P, τ) although not $\alpha^{*} g^{\#}\psi$-CS in (P, τ).

Theorem 3.22: Every $\alpha^{*} g^{\#}\psi$-CS is ψg-CS.
Proof : Let S⊆T, T is OS in P.
As every OS is $\alpha g^{\#}\psi$-OS, T is $\alpha g^{\#}\psi$-OS.
Since S is $\alpha^{*} g^{\#}\psi$-CS, αcl(S) ⊆T.
Also ψcl(S) ⊆ αcl(S).
⟹ ψcl(S) ⊆T.
Hence S is ψg-CS.
The below example demonstrates the preceding implication is irreversible.

Example 3.23: Let P = $\{x_1, x_2, x_3\}$, $\tau = \{P, \emptyset, \{x_1\}, \{x_1, x_2\}\}$.
ψGC(P, τ) = $\{P, \emptyset, \{x_2\}, \{x_3\}, \{x_2, x_3\}, \{x_1, x_3\}\}$.
$\alpha^{*} g^{\#}\psi$C(P, τ) = $\{P, \emptyset, \{x_2\}, \{x_3\}, \{x_2, x_3\}\}$.
$\{x_1, x_3\}$ is ψg-CS of (P, τ) although not $\alpha^{*} g^{\#}\psi$-CS in (P, τ).

Theorem 3.24: Every $g^{\#}$-CS is $\alpha^{*} g^{\#}\psi$-CS.
Proof : Let S⊆T, T is $\alpha g^{\#}\psi$-OS in P.
As S is $g^{\#}$-CS, then cl(S) ⊆T.
But αcl(S) ⊆cl(S).
⟹ αcl(S) ⊆T.
Hence S is $\alpha^{*} g^{\#}\psi$-CS.
The below example demonstrates the preceding implication is irreversible.

Example 3.25: Let P = $\{x_1, x_2, x_3\}$, $\tau = \{P, \emptyset, \{x_3\}, \{x_1, x_2\}\}$.
$g^{\#}$C(P, τ) = $\{P, \emptyset, \{x_3\}, \{x_1, x_2\}\}$.
$\alpha^{*} g^{\#}\psi$C(P, τ) = $\{P, \emptyset, \{x_1\}, \{x_2\}, \{x_3\}, \{x_1, x_2\}, \{x_2, x_3\}, \{x_1, x_3\}\}$.
$\{x_1\}$ is $\alpha^{*} g^{\#}\psi$-CS of (P, τ) although not $g^{\#}$-CS in (P, τ).

Theorem 3.26: Every $\alpha^{*} g^{\#}\psi$-CS is $g^{\#}\psi$-CS.
Proof : Let S⊆T, T is ψ-OS in P.
As every ψ-OS is $\alpha g^{\#}\psi$-OS, T is $\alpha g^{\#}\psi$-OS.
As S is $\alpha^{*} g^{\#}\psi$-CS, αcl(S) ⊆T.
But ψcl(S) ⊆ αcl(S).
⟹ ψcl(S) ⊆T.
Hence S is $g^{\#}\psi$ -CS.
The below example demonstrates the preceding implication is irreversible.

Example 3.27: Let P = $\{x_1, x_2, x_3\}$, $\tau = \{P, \emptyset, \{x_1\}, \{x_2\}, \{x_1, x_2\}\}$.

$g^{\#}\psi$C(P, τ) = $\{P, \emptyset, \{x_1\}, \{x_2\}, \{x_3\}, \{x_2, x_3\}, \{x_1, x_3\}\}$.
$\alpha^* g^{\#}\psi$C(P, τ) = $\{P, \emptyset, \{x_3\}, \{x_2, x_3\}, \{x_1, x_3\}\}$
$\{x_1\}$ is $g^{\#}\psi$-CS of (P, τ) although not $\alpha^* g^{\#}\psi$-CS in (P, τ).

Theorem 3.28: Every $\alpha g^{\#}\psi$-CS is $\alpha^* g^{\#}\psi$-CS.
Proof : Let S⊆T, T is $\alpha g^{\#}\psi$-OS in P.
As every $\alpha g^{\#}\psi$-OS is $g^{\#}\psi$-OS, T is $g^{\#}\psi$-OS.
As S is $\alpha g^{\#}\psi$-CS, αcl(S) ⊆T.
Hence S is $\alpha^* g^{\#}\psi$ -CS.
The below example demonstrates the preceding implication is irreversible.

Example 3.29: Let P = $\{x_1, x_2, x_3\}$, τ = $\{P, \emptyset, \{x_2\}, \{x_1, x_3\}\}$.
$\alpha g^{\#}\psi$C(P, τ) = $\{P, \emptyset, \{x_2\}, \{x_1, x_3\}\}$.
$\alpha^* g^{\#}\psi$C(P, τ) = $\{P, \emptyset, \{x_1\}, \{x_2\}, \{x_3\}, \{x_1, x_2\}, \{x_2, x_3\}, \{x_1, x_3\}\}$.
$\{x_3\}$ is $\alpha^* g^{\#}\psi$-CS of (P, τ) although not $\alpha g^{\#}\psi$-CS in (P, τ).

Characteristics of $\alpha^* g^{\#}\psi$-Closed Set
Remark 4.1: $\alpha^* g^{\#}\psi$-CS is independent of semi-CS and ψ-CS.
It can be shown by the following examples.
Example 4.2: Let P = $\{x_1, x_2, x_3\}$, τ = $\{P, \emptyset, \{x_1\}, \{x_2\}, \{x_1, x_2\}\}$.
SC(P, τ) = $\{P, \emptyset, \{x_1\}, \{x_2\}, \{x_3\}, \{x_2, x_3\}, \{x_1, x_3\}\}$ = ψC(P, τ).
$\alpha^* g^{\#}\psi$C(P, τ) = $\{P, \emptyset, \{x_3\}, \{x_2, x_3\}, \{x_1, x_3\}\}$.
Here $\{x_2\}$ is semi-CS and ψ-CS of (P, τ) although not $\alpha^* g^{\#}\psi$-CS in (P, τ).
Let P = $\{x_1, x_2, x_3\}$, τ = $\{P, \emptyset, \{x_3\}, \{x_1, x_2\}\}$.
SC(P, τ) = $\{P, \emptyset, \{x_3\}, \{x_1, x_2\}\}$. = ψC(P, τ).
$\alpha^* g^{\#}\psi$C(P, τ) = $\{P, \emptyset, \{x_1\}, \{x_2\}, \{x_3\}, \{x_1, x_2\}, \{x_2, x_3\}, \{x_1, x_3\}\}$.
Here $\{x_1\}$ is $\alpha^* g^{\#}\psi$-CS of (P, τ) although not semi-CS and ψ-CS in (P, τ).

Theorem 4.3: The intersection of two $\alpha^* g^{\#}\psi$-CS is again $\alpha^* g^{\#}\psi$-CS.
Proof : Let X and Y be $\alpha^* g^{\#}\psi$-CS and X∩Y⊆T where T is $\alpha g^{\#}\psi$-OS.
As X and Y are $\alpha^* g^{\#}\psi$-CS, αcl(X) ⊆T and αcl(Y) ⊆T.
Also αcl(X ∩Y)= αcl(X)∩αcl(Y) ⊆T.
⟹ αcl(X∩Y) ⊆T where X∩Y is $\alpha^* g^{\#}\psi$-CS.
Hence, the intersection of two $\alpha^* g^{\#}\psi$-CS is again $\alpha^* g^{\#}\psi$-CS.

Theorem 4.4: The union of two $\alpha^* g^{\#}\psi$-CS is again $\alpha^* g^{\#}\psi$-CS.
Proof : Let X and Y be $\alpha^* g^{\#}\psi$-CS and X∪Y⊆T where T is $\alpha g^{\#}\psi$-OS.
As X and Y are $\alpha^* g^{\#}\psi$-CS, αcl(X) ⊆T and αcl(Y) ⊆T.
Also αcl(X∪Y)= αcl(X)∪αcl(Y) ⊆T.
⟹ αcl(X∪Y) ⊆T where X∪Y is $\alpha^* g^{\#}\psi$-CS.
Hence, the union of two $\alpha^* g^{\#}\psi$-CS is again $\alpha^* g^{\#}\psi$-CS.

Theorem 4.5: Let X be an OS and Y be an $\alpha^* g^{\#}\psi$-OS, then X∪Y is $\alpha^* g^{\#}\psi$-OS.
Proof : Let X be an OS of (P, τ) and Y be an $\alpha^* g^{\#}\psi$-OS of (P, τ)
As every OS is $\alpha^* g^{\#}\psi$-OS, X is $\alpha^* g^{\#}\psi$-OS.
Hence X∪Y is $\alpha^* g^{\#}\psi$-OS.
Since union of two $\alpha^* g^{\#}\psi$-OS is again $\alpha^* g^{\#}\psi$-OS.

Theorem 4.6: Let X be an $\alpha^* g^{\#}\psi$-CS of (P, τ) iff αcl(X)- X ⊈ any non-empty $\alpha g^{\#}\psi$-CS.

Proof :
Necessary Part: Assume X is $\alpha^* g^{\#}\psi$-CS and F be a non empty $\alpha g^{\#}\psi$-CS with F ⊆ αcl(X)- X.
Then X ⊆ P- F
⟹ αcl(X) ⊆ P - F.
Hence, F ⊆ P- αcl(X), which contradicts.

Sufficient Part : Assume X is a subset of (P, τ) such that αcl(X)- X ⊈ any non- empty $\alpha g^{\#}\psi$-CS.
Let T be an $\alpha g^{\#}\psi$-OS in (P, τ) such that X⊆T.
If αcl(X) ⊆T, then αcl(X) ⋂ C(T) ≠ ∅.
Then ∅ ≠ αcl(X) ⋂C(T) is an $\alpha g^{\#}\psi$-CS of (P, τ), since the intersection of two $\alpha g^{\#}\psi$-CS is again $\alpha g^{\#}\psi$-CS.

Theorem 4.7: If X is $\alpha^* g^{\#}\psi$-CS and X⊆Y ⊆ αcl(X), then Y is $\alpha^* g^{\#}\psi$-CS.
Proof: Let T be an $\alpha g^{\#}\psi$-OS of (P, τ)) such that Y⊆T.
⟹ X⊆T.
As X is $\alpha^* g^{\#}\psi$-CS and αcl(X) ⊆T,
Then αcl(Y)⊆ αcl(αcl(X)) = αcl(X) ⊆T.
Hence, Y is $\alpha^* g^{\#}\psi$-CS of (P, τ).

Remark 4.8: The above diagram shows the relationships established between
$\alpha^* g^{\#}\psi$-closed sets and some other sets in theorems mentioned above.
A →B represents A implies B but not conversely and
A ↮ B represents A and B are independent of each other.

REFERENCES

1. S.P.Arya and T.M.Nour, Characterizations of s-normal spaces, Indian Journal of Pure and Applied mathematics, 21(8), (1990), 717-719.
2. P.Bhattacharya and B.K.Lahiri, Semi Generalized Closed Sets in Topology, Indian Journal of Mathematics, 29(1987), 376- 382.
3. J.Dontchev, On generalizing semi-preopen sets, Memoirs of the Faculty of Science Kochi University. Series A. Mathematics, 16(1995), 35-48.
4. Y.Gnanambal, On generalized pre regular closed sets in topological spaces, Indian Journal of Pure and Applied Mathematics, 28(3), (1997), 351-360.
5. Govindappa Navalagi and Sujata Mookanagoudar, Properties of g*sp- Closed Sets in Topological Spaces, International Journal of Innovative Research in Science, Engineering and Technology(IJIRSET), 7(8), (2018), 9073-9079.
6. K.Kanimozhi, N.Balamani and A.Parvathi, On $g^{\#}\psi$-closed sets in topological spaces, Imperial Journal of Interdisciplinary Research(IJIR), 4(3), (2017), 1931-1935.
7. N.Levine, Generalized closed sets in topology, Rendiconti del Circolo Matematico di Palermo, 19(1970), 89-96.
8. N.Levine, Semi-Open Sets and Semi-Continuity in Topological Spaces, The American Mathematical Monthly, 70(1), (1963), 36-41.
9. H.Maki, R.Devi and K.Balachandran, Generalized α-closed sets in topology, Bull. Fukuoka Univ. Ed. Part III, 42(1993), 13-21.
10. H.Maki, R.Devi and K.Balachandran, Associated topologies of generalized α-closed sets and α-generalized closed sets, Memoirs of the Faculty of Science Kochi University. Series A. Math-ematics, 15(1994), 51-63.
11. H.Maki, J.Umehara and T.Noiri, Every topological space is pre-T1/2, Memoirs of the Faculty of Science Kochi University. Series A. Mathematics, 17(1996), 33-42.

12. A.S.Mashhour, M.E.Abd EI-Monsef and S.N.EI-Deeb, On Pre-Continuous and Weak Pre-Continuous Mappings, Proceedings of the Mathematical and Physical Society of Egypt, 53(1982), 47-53.
13. T.Nandhini and M.Vigneshwaran, $\alpha g^{\#}\psi$-Closed sets and $\alpha g^{\#}\psi$-Functions in topological spaces, International Journal of Innovative Research Explorer, 5(2018), 152-166.
14. O.Njastad, On some classes of nearly open sets, Pacific Journal of Mathematics, 15(3), (1965), 961- 970.
15. N.Ramya and A.Parvathi, ψg-closed sets in topological spaces, International Journal of Mathematical Archive, 2(10), (2011), 1992-1996.
16. M.K.R.S.Veera kumar, Between semi-closed sets and semi-pre closed sets, Rendiconti dell'Istituto di Matematica dell'Universit_a di Trieste(Italy), 42(2000), 25-41.
17. M.K.R.S.Veera kumar, $g^{\#}$-closed sets in topological spaces, Memoirs of the Faculty of Science Kochi University. Series A. Mathematics, 24(2003), 1-13.
18. M.Vigneshwaran and R.Devi, On $G_{\alpha o}$-kernal in the digital plane, International Journal of Mathematical Archive, 3(6), (2012), 2358-2373.

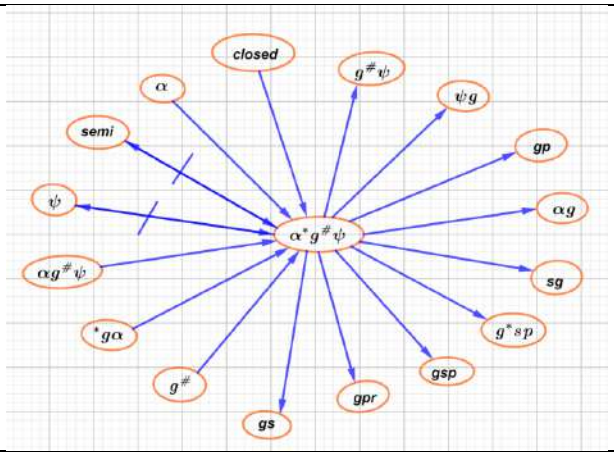

Figure 1: A → B and A ↮ B

Indian Journal of Natural Sciences www.tnsroindia.org.in ©IJONS

Vol.15 / Issue 83 / Apr / 2024 International Bimonthly (Print) – Open Access ISSN: 0976 – 0997

RESEARCH ARTICLE

Further Studies on Continuity of γ *grw Closed Set with Grill

M.K. Eswarlal[1], Dr. R. Bhavani[2]

[1]Assistant Professor, Department of Mathematics, Sourashtra College, (MKU22PFOS10531), Madurai Kamaraj University, Madurai, Tamil Nadu, India.
[2]Assistant Professor and Research Supervisor, PG and Research Department of Mathematics, MTN College, (Affiliated to MKU) Madurai-4.

Received: 30 Dec 2023 Revised: 09 Jan 2024 Accepted: 12 Jan 2024

***Address for Correspondence**
M.K. Eswarlal
Assistant Professor,
Department of Mathematics,
Sourashtra College, (MKU22PFOS10531),
Madurai Kamaraj University,
Madurai, Tamil Nadu, India.
Email: eswarlalmaths@gmail.com

ABSTRACT

This research paper deals with continuous (Cts) functions in Grill Topological space (GTS). Further investigated by introducing G γ * grwc (Grill γ *generalized regular weakly closed) set , useful results are derived and it is a Continuous study of [3] "On continuity of γ * grwc sets."

Keywords: G γ *grwc set.

INTRODUCTION

The study of shapes and spaces is known as topology and its characteristics are completely kept during steady distortion, like bending and stretching but not tearing. After the introduction of Generalized closed set by Levine (1970) it has become one of an interesting area in the field of topology.Choquet, one who explored Grill as a Tool like nets and filters. This paper deals withContinuity of G γ * grwc sets.C_l and I represents closure and interior of a set. Review of literature and preliminaries, Gγ* grwc continuous function and conclusion were presented in section 2,3 and 4 respectively.

Review of Literature and preliminaries

Related to study area a few literatures, preliminaries and definition were presented. In 1947 Choquet introduced Grill, since then many topologists started to do more research work On continuous function using GTS. Dhananjoy mandal and M.N.Mukerjee (2012) [2] have studied a new class of generalized closed sets in TS X and defined in terms of grill G on X and Presented the characterization of Regular and Normal spaces. M.O. Mustafa and

R.B.Esmaeel(2021) [8] have conducted a research work on" some properties in Grill topological open and closed sets" and given its relationship with continuous function Gg-continuous function, Gg strongly continuous function, Gg-Irresolute function. Nagarajan Kalaivani, Khaleel Fayaz UrRahaman, Lanka cepova and Robert cep (2022) [9] have investigated GS $_\beta$ continuous function along with this the theory of GS$_\beta$ continuous mapping was introduced and derived properties in GTS. M.K. Eswarlal and R.Bhavani (2023) [3] have introduced γ *grwc set and studied its Continuity in a Topological spaces.

Basic concepts of Topology

Definition 2.1 Closure (Cι) and Interior (I) of a set.[3]

Given a subset A of a topological space X, Cι (*A*) is defined as the intersection of all closed sets containing A and I(A) is defined as the union of all open sets contained in A.

Definition 2.2

Let (X,τ) be TS and a subset A of X is said to be

(i) α open [7] if A $\subseteq$ I(Cι(I(A))) and α closed [7] set if Cι(I(Cι(A))) $\subseteq$ A.

(ii) Weakly closed (w-closed) [10],ifCι(A) $\subseteq$ H whenever A $\subseteq$ H and H is semi open in (X,τ).

(iii) γ open [4],if A $\subseteq$I(Cι(A)) $\cup$ Cι(I(A)) and γ closed [4] if Cι(I(A)) $\cap$ I(Cι(A)) $\subseteq$A.

(iv) Semi open set [5] if A$\subseteq$Cι(I(A)) and semi closed set [5] if I(Cι(A))$\subseteq$ A.

Definition 2.3

Let (X,τ) be TS &A$\subseteq$X is called

(i) Generalized closed set (g closed) [6] if Cι(A) $\subseteq$ U whenever A$\subseteq$U and U is open in (X,τ).

(ii) Generalized α closed (g α closed)[5] if α cl(A)$\subseteq$ H and H is α open in (X,τ)

(iii) Regular generalized weakly set (rgw closed) [12], if Cι(I(A)) $\subseteq$ U whenever A$\subseteq$U and U is regular semi open in X.

(iv) sg closed [1], if sCι(A) $\subseteq$ U whenever A$\subseteq$U and U is semi open in X.

Preposition 2.1

(i) EveryClosed, semi closed ,γ, α, and w are γ^*grw closed.

(ii) Every g, sg, rgw and g α closed are γ^*grw closed.

Definition 2.4

Grill :[11] A collection G of non-empty subsets of a space X is called a Grill on X if

(i) A $\in$ G and A$\subseteq$ B $\subseteq$ X implies B$\in$G, and

(ii) A, B$\subseteq$ X and A $\cup$B$\in$ G implies A $\in$ G or B$\in$ G.

Definition 2.5

[11] Let G be a Grill on a topological space (X,τ). A mapping Φ: P(x) $\rightarrow$P(x). Denoted by Φ_G(A,τ) (for A $\in$or P(x)) or Φ_G (A) or simply by Φ (A) is defined by

Φ_G (A) = {x$\in$X: A $\cap$ U $\in$ G, for all U $\in$ τ(x)}.

G γ *grw ccontinuous(Cts)function.

G γ *grwc continuous function is introduced and studied.

Definition 3.1

Let G be a Grill on X and A be a subset of X in a topological space (X,τ), is said to be G γ *grwcif Φ_G (A) $\subseteq$ H whenever A $\subseteq$ H and H is γ closed in X.

Example 3.1

Let X = {j, o, v, z} , τ = { $\emptyset$,X, {j},{o},{j, o},{j, o, v}} and

G = {$\emptyset$,X,{j},{o},{j, o},{j, v},{j, z},{j, o, v},{j, o, z},{j, v, z}}

Closed sets of (X, τ) are { $\emptyset$,X, {z},{v, z},{o, v, z},{j, v, z}}

Gγ^*grw closed sets of (X,τ) are {$\emptyset$,X,{j},{o},{v},{z},{j,v},{j,z},{o,v},{o,z},{v,z},

{j,o,z},{o,v,z},{j,v,z}}

Preposition 3.1

Every closed set is G γ^*grw closed.

Proof:

Let Abe a closed set in X and A ⊆H.

since A is closed this implies that C_ι(A) ⊆ A ⊆H, where H is γclosed.

But Φ_G (A) ⊆C_ι (A) ⊆ H. (i.e) Φ_G (A) ⊆ H. Thus, A is G γ^*grw closed.

Remark 3.1

The converse of preposition3.1 is not true.

Example 3.2

Let X = {j, o, v, z} , τ = { ∅ ,X, {j},{o},{j, o},{j, o, v}} and

G = {∅,X,{j},{o},{j, o},{j, v},{j, z},{j, o, v},{j, o, z},{j, v, z}}

Take A = {o}, Here {o} is not closed, but it is G γ^*grw closed.

Preposition 3.2

(i) Every α, semi closed , γ and w are G γ^*grw closed.

(ii) Every rgw, g α , sg and g closed are Gγ^*grw closed.

Remark 3.2

The converse of Preposition 3.1 & 3.2 areneed be not true.

Definition 3.2

A function f : (X , τ , G) → (Y , σ) is called Gγ^*grwc continuous (Cts) if the inverse image of every closed set in (Y , σ) is Gγ^*grw closed in (X , τ , G).

Theorem 3.1

EveryCts function is Gγ^*grwcCts.

Proff :

Let f : (X , τ , G) → (Y , σ) be a Cts map.

Let H be a closed set in (Y , σ). Then f^{-1} (H) is closed in (X , τ , G).

Since every closed set is G γ^*grw closed. (i. e) f^{-1} (H) is a G γ^*grw closed.

Therefore f is Gγ^*grwcCts.

Remarks 3.3

Converse of Th 3.1 need not be true.

Example 3.3

Let X = {j, o, v, z} , τ = { ∅ ,X, {j},{o},{j, o},{j, o, v}}, σ = { ∅ , Y , v } and

G = {∅,X,{j},{o},{j, o},{j, v},{j, z},{j, o, v},{j, o, z},{j, v, z}}

Let f :(X, τ , G) → (Y, σ) be defined as f(j) = j, f(o) = o, f(v) = v and f(z) = z .

. f^{-1}(j,o,z) = { j,o,z }. Which is not closed in X. That is f is notCts.

But {j,o,z} is G γ^*grw closed. Therefore f is G γ^*grwcCts.

Theorem 3.2

(i) Every αcCtsis Gγ^*grwcCts.

(ii) Every semi closedCtsis Gγ^*grwcCts.

(iii) Every wcCtsis Gγ^*grwcCts.

(iv) Every γcCtsis Gγ^*grwcCts .

Remarks 3.2

Proof of Th 3.2 (i) to (iii) follows from above definitions and known results

and its converse need not be true.

Example 3.3

Let X = {j, o, v, z} , τ = { ∅ ,X, {j},{o},{j, o},{j, o, v}}, σ = { ∅ , Y , j } and

G = {∅,X,{j},{o},{j, o},{j, v},{j, z},{j, o, v},{j, o, z},{j, v, z}}

Let f :(X, τ , G) → (Y, σ) be defined as f(j) = o, f(o) = j, f(v) = v and f(z) = v.

(i) f^{-1}(o, v, z) = { j, v}. Which is not α closed. That is f is not α Cts.Therefore f is G γ^*grwcCts.

(ii) f^{-1}(j,o, z) = { j, o, v } and f^{-1}(j , o) = { j , o } Which is not w closed. That is f is w Ctsbut not G γ^*grwcCts .

Let X = {j, o, v, z} , τ = { ∅ ,X, {j},{o},{j, o},{j, o, v}}, σ = { ∅ , Y , j v } and
G = {∅,X,{j},{o},{j, o},{j, v},{j, z},{j, o, v},{j, o, z},{j, v, z}}
Let f :(X, τ , G) → (Y, σ) be defined as f(j) = j, f(o) = o, f(v) = v and f(z) =z.
(i) f^{-1}(j, o, z) = { j, o,z}. Which is not semi closed .That is f is notsemi closed Cts. Therefore f is G γ^*grwCts.
(ii) f^{-1}(j, o, z) = { j, o, z } and f^{-1}(j ,o) = { j, o } Which is not both γas well as G γ^*grw closed . Therefore fis not γand G γ^*grwcCts .

Remark 3.3
Thus fig (i) depicts the relationship between Gγ^*grwcCtswith other sets.

Theorem 3.3
(i) Every gcCtsis Gγ^*grwCts.
(ii) Every sgcCtsis Gγ^*grwCts.
(iii) Every rgwcCts isGγ^*grwCts.
(iv) Every g αcCtsis Gγ^*grwCts.

Remarks 3.4
Proof of Th 3.3 (i) to (iv) follows from above definitions and known results and its converse need not be true.
Example 3.4
Let X = {j, o, v, z} , τ = { ∅ ,X, {j},{o},{j, o},{j, o, v}}, σ = { ∅ , Y , j } and
G = {∅,X,{j},{o},{j, o},{j, v},{j, z},{j, o, v},{j, o, z},{j, v, z}}
Let f :(X, τ , G) → (Y, σ) be defined as f(j) = o, f(o) = j, f(v) = v and f(z) = v.
(i) f^{-1}(o, v , z) = { j, v }. Which is not g closed. That is f is not g continuous. Therefore f is G γ^*grwcCts.
(ii) f^{-1}(j, o, z) = { j, o, z } and f^{-1}(j , o) = { j , o } Which is not both sg as well as G γ^*grw closed . (i,e) f is not sgand G γ^*grwcCts.
(iii) f^{-1}(j, o, z) = { j, o, z } and f^{-1}(j , o) = { j, o } Which is not both g α as well as G γ^*grw closed . Therefore f is not g α and G γ^*grwcCts.
(iv) Let σ = { ∅ , Y , {j}, {j, z } }and f^{-1}(j, v, z) = { j, v }, f^{-1}(o, v) = { j, v }. Which is not rgw closed. That is f is not rgw continuous. That is f is G γ^*grwcCts.
Remark 3.5
fig (ii) shows the association ofGγ^*grwcCts with other sets

CONCLUSION

Gγ^*grw Cts function was introduced and investigated its link between other sets were presented.This study can be extended to any topological space.

REFERENCES

1. Balachandran k,Sundram,P & Maki,H 1996, 'Generalized locally closed sets and GLC continuous functions' Indian J.Pure and Appl.Math., vol. 27, pp.235-244.
2. Dhananjoy Mandal and M.N.Mukerjee, " On a type of generalized closed sets" Bol. Soc. Parn. Mat. Vol 301 (2012) 67 – 76.Issn – 00378712. DOI 10.5269/bspm.V.30il.11845.
3. M.K. Eswarlal and R. Bhavani (2023), " On continuity of γ^* GRWC sets" Indian Journal of Mathematical Sciences. Vol 14 / issue 80 / Oct / 027 / 2023. ISSN: 0976 – 0997.
4. A.A.El-Atik, A Study of some types of mapping on topological spaces, M.sc., Thesis Tanta Univ.Egypt.(1997).
5. N.Levine, semi-open sets and semi-continuity in Topological spaces, Amer.Math.Monthly,70(1963),36-41.
6. N.levine, Generalized closed sets in Topology, Rend.Cric.Mat.Palermo, 19(2) (1970),89-96.

7. H.Maki,R.Devi,K.Balachandran. Associated Topologies of generalized α closed sets and α generalized closed sets, memories of the Faculty of science Kochi University series A:Mathematics 15 (1994)51-63.
8. M.O.Mustafa and R.B.Ismail, " On some properties in Grill – Topological open and closed sets" 897 (2021) 01.2038. Journal of Physics: Conference series. DOI : 10.1088/1742-6596/18971/1/012038.
9. Nagarajan Kalaivani, Khaleel Fayaz Ur Rahaman, Lanka cepova and Robert cep (2022), "OnGrillSβOpenSetinGrillTopologicalSpaces"MDPI10,4626.https://doi.org/10.3390/math10234626.
10. Pushpalatha, studies on generalization of mappings in topological spaces, Ph.D Thesis, Bharathiar university.
11. Roy and M.N. Mukerjee, "On a typical topology induced by a grill" Soochow J.Math.33(No.4) (2007),pp.771-786.
12. Sanjay Misra, Nitin Bhardwaj and Varun Joshi." on Regular Generalized Weakly (rgw) – Closed sets in Topological spaces".Int. Journal of Math. Analysis, Vol 6,2012.no.39,pp 1939 – 1952.

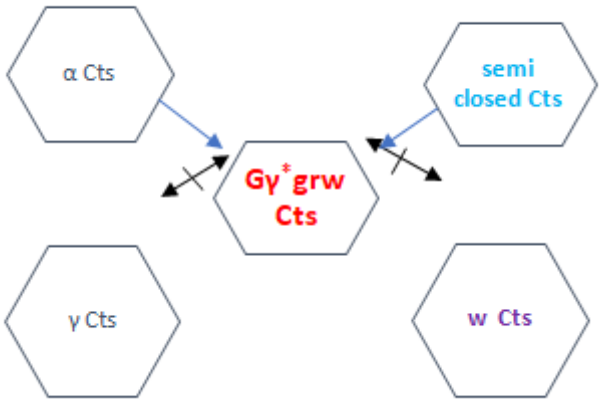

Fig (i) depicts the relationship between Gγ*grwcCtswith other sets.

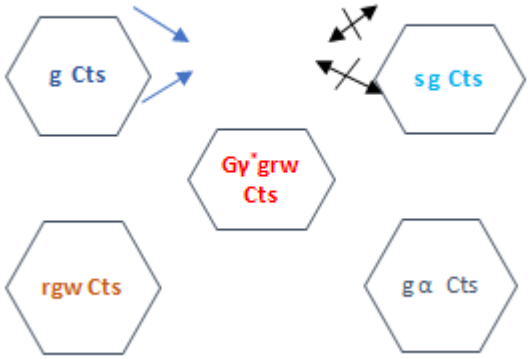

Fig (ii) shows the association of Gγ*grwcCts with other sets

RESEARCH ARTICLE

Cyclotide Prevents Neuronal Cell Death Induced by 6-Hydroxydopamine Neurotoxin

Shobana C*, Usharani B and Rohini D

Department of Biochemistry, School of Life Sciences, Vels Institute of Science, Technology and Advanced Studies, (Affiliated to Deemed University)Tamil Nadu, India.

Received: 22 Feb 2023 Revised: 07 Mar 2024 Accepted: 20 Mar 2024

***Address for Correspondence**
Shobana C
Department of Biochemistry,
School of Life Sciences,
Vels Institute of Science, Technology and Advanced Studies,
(Affiliated to Deemed University)Tamil Nadu, India.
Email: shobana.sls@velsuniv.ac.in

ABSTRACT

Neuronal cell death is a major factor in the initiation and progression of Parkinson's disease (PD). Reactive oxygen species (ROS) overproduction is one of the primary causes of neuronal death, hence drugs that decrease oxidative stress-dependent neuronal death as a preventive measure against Parkinson's disease (PD) may be promising. However, cyclotide's preventive effects have not been studied using both in vitro and in vivo models of Parkinson's disease. Therefore, in order to investigate the efficacy of cyclotide against 6-hydroxydopamine (6-OHDA)-dependent neuronal cell death, we employed immortalized hypothalamic neurons (GT1-7 cells). First, we found that cyclotide prevents 6-OHDA-dependent neuronal cell death by inhibiting ROS overproduction in GT1-7 cells. The cytoprotective effect of cyclotide was largely abolished by verapamil, an OCTN1 inhibitor that inhibits cyclotide absorption. According to these results, cyclotide or foods containing it may be a helpful tactic to postpone the start and progression of Parkinson's disease (PD).

Keywords: Cyclotide; neuronal cell death; 6-OHDA; oxidative stress; functional food

INTRODUCTION

Parkinson's disease (PD) is one of the most common progressive neurodegenerative illnesses. Parkinson's disease (PD) affects both the central nervous system and the body parts that are innervated by diseased nerves. This results in altered postural reflexes, stiffness in the muscles, akinesia, and resting tremor. In the initial stages of Parkinson's disease (PD), sluggish movements and trouble walking are frequently observed. People who have the disease gradually become bedridden or unable to move freely, requiring them to use a wheelchair [1,2].

Amantadine hydrochloride, anticholinergic drugs, and the dopamine precursor L-dopa are commonly used in the treatment of Parkinson's disease (PD) patients in order to compensate for the dopamine depletion brought on by the death of dopaminergic neurons. Despite the moderate efficacy of these drugs [3], there is now no established method to stop the onset and progression of Parkinson's disease. Parkinson's disease (PD) has no known exact etiology, although elevated inflammatory response and loss of dopaminergic neurons in the substantia nigra of the midbrain are established risk factors. Lesion-related microglia are thought to be the main cause of Parkinson's disease (PD) [4,5]. Treating mice or neurons with 6-hydroxydopamine (6-OHDA) or N-methyl-4-phenylpyridinium iodide (MPP+) has been used in basic research because these substances can produce models that mimic oxidative stress-mediated dopaminergic neuronal degeneration and enhanced microglial inflammation [6,7]. Moreover, disturbance of the hypothalamic-pituitary-adrenal axis is said to have an impact on the development and progression of Parkinson's disease (PD) and govern the synthesis of numerous hormones [8]. The comparison of the plasma concentrations of adrenocorticotropic hormone and nocturnal growth hormone in Parkinson's disease (PD) patients with those of healthy controls indicates possible abnormalities in the hypothalamus [9].

A reduction in the quantity of neurons in the hypothalamus of Parkinson's disease patients was found in one study [10]. Furthermore, a strong positive correlation has been observed between the clinical stage of Parkinson's disease and a decrease in orexin-containing neurons, a hormone that concentrates melanin in the hypothalamus [11]. These preliminary findings suggest that inhibiting neuronal death in the hypothalamus may prevent the onset and progression of Parkinson's disease. One of these potentially beneficial herbs is *Clitoria ternatea*, a key ingredient in the brain tonic medhya rasayan, which is used to treat neurological illnesses. Ayurvedic medicine has been used traditionally in India from ancient times. This study supports Indian medicine by highlighting the plant's significance as a brain remedy. *Clitoria ternatea* has a potent brain-stimulating effect, unlike other plants [12]. Moreover, C. ternatea has long been used in traditional medicine, particularly as a supplement to improve cognitive function and lessen the symptoms of numerous illnesses like fever, inflammation, discomfort, and diabetes [13]. This study assessed the antiparkinson's activity of cyclotide, the active ingredient in *Clitoria ternatea.* Previous work on the analysis of cyclotide insilico and invitro served as the foundation for the current investigation. Despite the fact that cyclotide has been linked to a number of biological processes, its ability to prevent 6-OHDA-dependent hypothalamic neuronal cell death has not been studied. Therefore, we used immortalized hypothalamic neurons and GT1-7 cells in this investigation to investigate the effectiveness of cyclotide on 6-OHDA-dependent neuronal cell death. Additionally, we ascertained cyclotide's impact on the generation of ROS in response to 6-OHDA as well as its effectiveness in preventing neuronal cell death caused by 6-OHDA.

MATERIALS AND METHODS

Chemicals and Reagents

MPP+ was supplied by Cayman Chemical. Promega Corporation was the CellTiter-Glo® 2.0 provider. Fujifilm Wako Pure Chemical Corporation in Tokyo, Japan was the seller of DMEM/Ham's Nutrient Mixture F-12 (Dulbecco's Modified Eagle's Medium/Ham's Nutrient Mixture). The 2′,7′-dichlorodihydrofluorescein diacetate (H2DCFDA) was supplied by Merck KGaA. The FastGeneTM RNA Basic kit was provided by Nippon Genetics Co., Ltd.; the PrimeScriptTM RT master mix (Perfect Real Time) was provided by Takara Bio; and the THUNDERBIRD® Next SYBR® qPCR mix was provided by Toyobo.

Culture of Cells

For the investigation, immortalized hypothalamic neurons, or GT1-7 cells, were employed. 10% fetal bovine serum was added to DMEM/Ham's-F12, the growth media used for GT1-7 cells. After being treated with trypsin (Fujifilm Wako Pure Chemicals), the cells were suspended in a serum-free medium, plated, and cultured at 37◦C in a humidified incubator with 7% CO2 [15].

Determination of cell viability.

Cell viability was evaluated, same as it was in our previous studies [20, 21]. To put it briefly, 3.0 x 104 GT1-7 cells were seeded per well onto 96-well growth plates using 200 μL of culture medium. After a 24-hour preincubation period, the medium was supplied with either 6-OHDA (final concentrations ranging from 0 μmol/L to 80 μmol/L) or MPP+ (final concentrations ranging from 0 mmol/L to 8 mmol/L). As an alternative, the cells were preincubated for 24 hours before being treated with cyclotide (final concentrations ranging from 0 mmol/L to 1.0 mmol/L) for 10 min. The medium was subsequently supplemented with either MPP+ (final concentration: 4 mmol/L) or 6-OHDA (final concentration: 40 mmol/L). The cells' vitality was evaluated using the luminous reagent CellTiter-Glo® 2.0, which quantifies intracellular ATP, following a 24-hour incubation period. Assuming that cyclotide is ingested as a daily meal or supplement, it was pretreated to GT1-7 cells in this investigation. Its efficacy was evaluated. Furthermore, despite discrepancies in reporting, the blood concentration of cyclotide in humans is roughly 0.2 mmol/L, which is comparable to the concentration of cyclotide used in this experiment [22].

ROS Level Measurement

GT1: Seven cells were cultured in black 96-well microplates with 3.0 × 104 cells per well for a whole day. Next, the cells were exposed to the ROS indicator H2DCFDA (10 μmol/L) for 60 minutes. Subsequently, cyclotide was added to the media (final concentration: 40 μmol/L) and the cells were treated with it (final concentrations ranging from 0 mmol/L to 1.0 mmol/L). After an hour, the ROS levels were measured using a microplate reader (excitation: 480 nm, emission: 530 nm).

Instantaneous Analysis of Reverse Transcription Polymerase Chain Reaction (RT-PCR)

Total RNA was isolated from GT1-7 cells according to the manufacturer's instructions using the FastGeneTM RNA Basic kit. Samples were reverse-transcribed using the PrimeScript RT master mix. The resulting cDNA was analyzed in real-time PCR experiments with THUNDERBIRD Next SYBR qPCR mix using CFX ManagerTM software (Version 3.1) on a Bio-Rad CFX96TM realtime system (Hercules, CA, USA). The specificity was verified by electrophoretic analysis of the reaction products with template- or reverse transcriptase-free controls. Glyceraldehyde-3-phosphate dehydrogenase (Gapdh) cDNA was employed as an internal standard to adjust the total RNA concentration in every experiment. Primers were designed using the Primer-BLAST website (https://www.ncbi.nlm.nih.gov/tools/primer-blast/).Primer sequences are shown in Supplementary Figure S1.

Statistical Analysis

All data are expressed as mean ± using the standard error of the mean (S.E.M.). One-way analysis of variance (ANOVA) was used to examine differences between three or more groups, or between two groups. For unpaired data, Dunnett's test or Student's t-test were used, respectively. A difference was considered significant if it was $p < 0.05$ (* or # $p < 0.05$, ** or ## $p < 0.01$). Details on the symbols are provided by the figure legends. The number of samples (n) is also indicated in each image.

RESULTS

Efficacy of Cyclotide on 6-OHDA-Induced Neuronal Cell Death

The development and course of Parkinson's disease are significantly influenced by neuronal cell death [4,5]. In addition to producing a variety of Parkinson's disease-like symptoms when injected into the brains of test animals, 6-OHDA also acts as a neurotoxic in cellular experimental setups, leading to the death of neurons [6,23]. We started by evaluating the survival of GT1-7 cells, an immortalized line of mouse hypothalamus neurons, that were only exposed to 6-OHDA. Cell viability decreased in a concentration-dependent manner in response to treatment of 20, 40, 60, and 80 μmol/L concentrations of 6-OHDA (Figure 1A). The groups' respective post-treatment viabilities were 73.7 ± 2.7, 47.4 ± 2.7, 33.2 ± 2.3, and 23.9 ± 1.6% (mean ± S.E.M., n = 4). All groups shown a noteworthy decrease in comparison to the ultrapure water-treated control group. Next, we investigated the effect of cyclotide pretreatment using a 40 μmol/L final concentration of 6-OHDA on the 6-OHDA-induced decrease in GT1-7 cell viability. Pretreatment with

0.5 mmol/L and 1.0 mmol/L of cyclotide restored cell viability to 77.1 ± 2.5% and 82.8 ± 0.8% (mean ± S.E.M., n = 4) respectively, effectively mitigating the 6-OHDA-dependent decrease in cell viability. The protective effect was concentration-dependent. Under these circumstances, cyclotide therapy alone had little effect on cell viability (Figure 1C). Likewise, MPP+ functions as a neurotoxic in experimental settings that are both in vivo and in vitro [7]. We looked into if cyclotide also prevented the death of neurons triggered by MPP+. Reduced cell viability was seen in GT1-7 cells treated with 1.0–8.0 mmol/L MPP+ (Figure 1D).The MPP+-dependent loss in cell viability was considerably mitigated by cyclotide; after pretreatment with 0.5 mmol/L and 1.0 mmol/L of cyclotide, respectively, cell viability reached 53.0 ± 1.3% and 55.9 ± 0.5% (mean ± S.E.M., n = 4). (Figure 1E). Numerous investigations suggest that the endoplasmic reticulum (ER) stress response plays a crucial role in the neuronal cell death caused by 6-OHDA [24, 25]. Our lab has previously shown that enhanced ER stress-related gene expression in GT1-7 cells produced by 6-OHDA may be suppressed by the antioxidant peptide carnosine and an antioxidant protein–thioredoxin–albumin fusion [26,27]. Treatment with 40 μmol/L of 6-OHDA in this study elevated the expression of genes linked to ISR, especially the significant elevation of growth-arrest and DNA-damage-inducible gene 34 (Gadd34) and CCAAT-enhancer-binding protein homologous protein (Chop). In particular, compared to the control group, Chop and Gadd34 mRNA increased by 6.72 ± 0.08-fold and 4.60 ± 0.22-fold (mean ± S.E.M., n = 3), respectively. In addition, 6-OHDA treatment significantly increased the levels of ER degradation-enhancing α mannosidase (Edem), binding immunoglobulin protein (Bip), activating transcription factor 4 (Atf4), inositol-requiring transmembrane kinase/endoribonuclease 1α (Ire1α), protein disulfide isomerase (Pdi), and glucose-regulated protein 94 (Grp94). On the other hand, the overexpression of these genes was inhibited by cyclotide pretreatment, especially Chop (to 2.50 ± 0.15-fold) and Gadd34 (to 2.14 ± 0.04-fold) mRNA (mean ± S.E.M., n = 3). According to these results, cyclotide suppresses the elevated expression of genes linked to ER stress, hence preventing 6-OHDA-induced neuronal cell death (Figure 2).

Efficacy of Cyclotide on 6-OHDA-Induced Reactive Oxygen Species (ROS) Production

In recent studies, it was found that the antioxidant peptide carnosine and the antioxidant protein-thioredoxin-albumin fusion both successfully reduced the increased expression of genes linked to ER stress that 6-OHDA caused in GT1-7 cells [26, 27]. In the present investigation, 40 μmol/L of 6-OHDA induced an upregulation of ISR-related gene expression, most notably CCAAT-enhancer-binding protein homologous protein (Chop) and growth-arrest and DNA-damage-inducible gene 34 (Gadd34). In particular, compared to the control group, Chop and Gadd34 mRNA levels increased by 6.72 ± 0.08-fold and 4.60 ± 0.22-fold (mean ± S.E.M., n = 3), respectively. Furthermore, after 6-OHDA treatment, there were notable increases in the following processes: binding immunoglobulin protein (Bip), ER degradation enhancing α mannosidase (Edem), activating transcription factor 4 (Atf4), inositol-requiring transmembrane kinase/endoribonuclease 1α (Ire1α), protein disulfide isomerase (Pdi), and glucose-regulated protein 94 (Grp94). On the other hand, cyclotide pretreatment inhibited the overexpression of these genes, specifically reducing the mRNA levels of Gadd34 (down to 2.13 ± 0.04-fold) and Chop (down to 2.52 ± 0.15-fold) (mean ± S.E.M., n = 3). These results clearly suggest that cyclotide has the ability to inhibit the overexpression of genes linked to ER stress that is brought on by 6-OHDA.

Involvement of OCTN1 in Cytoprotective Effects of Cyclotide

The protein known as OCTN1, a membrane transporter, is in charge of identifying and moving endogenous or exogenous substances into and out of cells. OCTN1 is essential for cyclotide absorption, as demonstrated by a number of investigations on mice and cultured cells [15,16]. Therefore, we looked into whether verapamil, a well-known OCTN1 inhibitor, would neutralize the protective effect of cyclotide on cells [30]. As expected, cyclotide successfully counteracted the cell viability loss caused by 6-OHDA (Figure 4). However, the protective effect of cyclotide was greatly diminished when cells were pretreated with verapamil. Notably, verapamil administration by itself did not significantly affect ROS generation or cell viability in this experimental setup (Supplementary Figure S2). These results strongly imply that the cytoprotective action of cyclotide in GT1-7 cells is dependent on its entry into the cell through OCTN1.

DISCUSSION

In this study, we examined the protective effect of cyclotide against 6-OHDA-induced neuronal cell death using GT1-7 cells as immortalized hypothalamic neurons. Our results show that cyclotide significantly reduces the overexpression of ER stress-related proteins, including Chop and Gadd34, in GT1-7 cells as well as 6-OHDA-induced cell death. The pathophysiology and exacerbation of a number of diseases, including cancer, pneumonia, and neurological disorders, are significantly influenced by the ER stress response, which is mediated by protein kinase R-like ER kinase (PERK), inositol-requiring enzyme-1 (IRE1), and ATF6 [33, 34]. When these sensors are activated, the cell begins to undergo signaling processes, such as PERK phosphorylating eIF2's α subunit, which affects ATF4 translation in turn.ATF4 in turn initiates the transcription of GADD34 and CHOP, which are involved in the induction of cell death [33, 34]. We suggest that cyclotide prevents 6-OHDA-dependent neuronal cell death by inhibiting the expression of proteins linked to ER stress and cell death, specifically Gadd34 and Chop, as well as the transcription factor that is upstream of these factors, Atf4. In conclusion, our groundbreaking discovery emphasizes how cyclotide suppresses the ER stress response, hence inhibiting 6-OHDA-induced neuronal cell death and suggesting the drug's potential as a PD preventative. Since 6-OHDA is known to cause apoptosis in neuronal cells [26, 29], we will be investigating a more thorough way of triggering cell death in subsequent studies.

In our work, the OCTN1 inhibitor verapamil inhibited the cytoprotective effect of cyclotide; nevertheless, it is important to highlight that this protective effect was not completely eliminated by verapamil pretreatment. Furthermore, verapamil by itself demonstrated cytotoxicity at values higher than 100 μmol/L (Supplementary Figure S2), which raises questions about its suitability for use in research. As a result, future research should identify additional pathways that contribute to cyclotide's cytoprotective action in addition to OCTN1. One of the main causes of neuronal cell death and exaggerated inflammatory responses in Parkinson's disease (PD) is oxidative stress, which is marked by elevated generation of reactive oxygen species [28,29,35]. Clinical research has shown a direct link between the generation of ROS and Parkinson's disease. Cyclotide appears to be a promising treatment option for Parkinson's disease (PD) since it inhibits the creation of excessive ROS or oxidative stress. This idea is in line with earlier research that shown the effectiveness of antioxidants, including N-acetylcysteine and coenzyme Q10, in reducing Parkinson's disease symptoms in both human and animal trials. Moreover, cyclotide has proven effective in stroke and Alzheimer's disease animal models, exhibiting neuroprotective and antioxidant properties [17, 18]. Its neuroprotective qualities have also been shown in cultured cells, where it prevents amyloid-beta and anticancer medications from injuring neuronal cells. While cyclotide's effectiveness in treating a variety of neurological conditions has been studied, there have been no reports of studies examining its effectiveness in PD animal models or 6-OHDA-induced neuronal cell death, with the exception of one clinical study that found PD patients' blood levels of cyclotide were lower than those of controls. These results highlight the potential importance of adding cyclotides to meals or supplements as a critical prophylactic against the onset and progression of Parkinson's disease.

Through its antioxidant qualities, cyclotide, we found in our inquiry, protects against 6-OHDA-dependent neuronal cell death. Based on these findings, we propose that cyclotide may be a viable treatment option for delaying the onset and progression of Parkinson's disease (PD). In the future, we want to investigate more thoroughly how well cyclotide works in animal models of Parkinson's disease. GT1-7 cells were treated with the indicatedconcentrations of 6-hydroxydopamine (6-OHDA) (μmol/L) or N-methyl-4-phenylpyridinium(MPP+) (mmol/L) and incubated for 24 h (A,D). GT1-7 cells were pretreated with cyclotide (0.06–1.0 mmol/L) and then incubated in the absence (Control) or presence of 6-OHDA (40 μmol/L)or MPP+ (4 mmol/L) for 24 h (B,E). GT1-7 cells were treated with cyclotide (0.06–1.0 mmol/L)alone and cultured for a further 24 h (C). Cell viability was measured using CellTiter-Glo® 2.0. Valuesrepresent mean ± S.E.M. (n = 4). ** $p < 0.01$, vs. Control; ## $p < 0.01$, vs. 6-OHDA (40 μmol/L) aloneor MPP+ (4 mmol/L) alone. GT1-7 cells were pretreated with cyclotide (1.0 mmol/L) and then incubated in theabsence (Control) or presence of 6-OHDA (40 μmol/L) for 24 h. After total RNA extraction fromGT1-7 cells, cDNA was synthesized, and real-time RT-PCR was performed using primer pairs thatspecifically amplify Chop, Gadd34, Atf4, Bip, Ire1α, Pdi, Edem, and Grp94. Values were normalizedto Gapdh and expressed relative to control. Values represent mean ±

S.E.M. (n = 3). * $p < 0.05$, vs.Control; ** $p < 0.01$, vs. Control; # $p < 0.05$, vs. 6-OHDA (40 μmol/L) alone; ## $p < 0.01$, vs. 6-OHDA(40 μmol/L) alone. GT1-7 cells were pretreated witha reactive oxygen species (ROS) indicator, 2′,7′-dichlorodihydrofluorescein diacetate (H2DCFDA)(10 μmol/L) for 60 min (A,B). Cells were then treated with 6-OHDA (20–80 μmol/L) and culturedfor 1 h (A). GT1-7 cells were pretreated with cyclotide (0.06–1.0 mmol/L) and then incubated inthe absence (Control) or presence of 6-OHDA (40 μmol/L) for 1 h (B). GT1-7 cells were treatedwithcyclotide (0.06–1.0 mmol/L) alone and cultured for 1 h (C). ROS levels were measured usinga fluorescence microplate reader. Values represent mean •} S.E.M. (n = 4). ** $p < 0.01$, vs. Control;## $p < 0.01$, vs. 6-OHDA (40 μmol/L) alone. GT1-7 cells were pretreatedwith verapamil (100 μmol/L) for 60 min. After replacement with fresh medium, cells werethen pretreated with cyclotide (0.5 or 1.0 mmol/L) and incubated in the absence (Control) or presenceof 6-OHDA (40 μmol/L) for 24 h. Cell viability was measured using CellTiter-Glo® 2.0. Valuesrepresent mean ± S.E.M. (n = 4). Not Significant (n.s.), ** $p < 0.01$, Control vs. verapamil (100 μmol/L).

REFERENCES

1. Pagano, G.; Ferrara, N.; Brooks, D.J.; Pavese, N. Age at onset and Parkinson disease phenotype. Neurology 2016, 86, 1400–1407.[CrossRef]
2. Kalia, L.V.; Lang, A.E. Parkinson's disease. Lancet 2015, 386, 896–912. [CrossRef]
3. Zahoor, I.; Shafi, A.; Haq, E. Pharmacological Treatment of Parkinson's Disease. In Parkinson's Disease: Pathogenesis and ClinicalAspects; Stoker, T.B., Greenland, J.C., Eds.; Codon Publications: Brisbane, Australia, 2018.
4. Erekat, N.S. Apoptosis and its Role in Parkinson's Disease. In Parkinson's Disease: Pathogenesis and Clinical Aspects; Stoker, T.B., Greenland, J.C., Eds.; Codon Publications: Brisbane, Australia, 2018.
5. Macchi, B.; Di Paola, R.; Marino-Merlo, F.; Felice, M.R.; Cuzzocrea, S.; Mastino, A. Inflammatory and cell death pathways in brainand peripheral blood in Parkinson's disease. CNS Neurol. Disord. Drug Targets 2015, 14, 313–324. [CrossRef] [PubMed]
6. Konnova, E.A.; Swanberg, M. Animal Models of Parkinson's Disease. In Parkinson's Disease: Pathogenesis and Clinical Aspects;Stoker, T.B., Greenland, J.C., Eds.; Codon Publications: Brisbane, Australia, 2018.
7. Zeng, X.; Chen, J.; Deng, X.; Liu, Y.; Rao, M.S.; Cadet, J.L.; Freed, W.J. An in vitro model of human dopaminergic neurons derivedfrom embryonic stem cells: MPP+ toxicity and GDNF neuroprotection. Neuropsychopharmacology 2006, 31, 2708–2715. [CrossRef][PubMed]
8. Ham, S.; Lee, Y.I.; Jo, M.; Kim, H.; Kang, H.; Jo, A.; Lee, G.H.; Mo, Y.J.; Park, S.C.; Lee, Y.S.; et al. Hydrocortisone-induced parkinprevents dopaminergic cell death via CREB pathway in Parkinson's disease model. Sci. Rep. 2017, 7, 525. [CrossRef] [PubMed]
9. Bellomo, G.; Santambrogio, L.; Fiacconi, M.; Scarponi, A.M.; Ciuffetti, G. Plasma profiles of adrenocorticotropic hormone, cortisol,growth hormone and prolactin in patients with untreated Parkinson's disease. J. Neurol. 1991, 238, 19–22. [CrossRef] [PubMed]
10. Giguere, N.; Burke Nanni, S.; Trudeau, L.E. On Cell Loss and Selective Vulnerability of Neuronal Populations in Parkinson'sDisease. Front. Neurol. 2018, 9, 455. [CrossRef] [PubMed]
11. Thannickal, T.C.; Lai, Y.Y.; Siegel, J.M. Hypocretin (orexin) cell loss in Parkinson's disease. Brain 2007, 130, 1586–1595. [CrossRef][PubMed]
12. Sivaranjan VV, Balachandran I. Ayurvedic drugs and their plant sources. New Delhi: Oxford and IBHPublishing Company; 1994. pp. 425–428.
13. Mukherjee, P. K., Kumar, V., Kumar, N. S., and Heinrich, M. (2008). The Ayurvedic medicine Clitoriaternatea-from traditional use to scientific assessment. J. Ethnopharmacol. 120, 291–301. doi:10.1016/j.jep.2008.09.009
14. Muneeswari, M., Gangasani Narasimha Reddy., Arivukodi, D., Usharani, B., Shobana, C., (2022) Analysis of potentiality of Cyclotide, A Major Compound from Clitoria Ternatea as Anti-Parkinsonism Drug: A Pilot In Silico Study. NeuroQuantology 20(10):2758-2773. doi:10.14704/nq.2022.20.10.NQ55237
15. Kawahara, M.; Kato-Negishi, M.; Kuroda, Y. Pyruvate blocks zinc-induced neurotoxicity in immortalized hypothalamic neurons.Cell. Mol. Neurobiol. 2002, 22, 87–93. [CrossRef] [PubMed]

16. Tanaka, K.I.; Shimoda, M.; Sugizaki, T.; Ikeda, M.; Takafuji, A.; Kawahara, M.; Yamakawa, N.; Mizushima, T. Therapeutic effectsof eperisone on pulmonary fibrosis via preferential suppression of fibroblast activity. Cell Death Discov. 2022, 8, 52. [CrossRef]
17. Nakano, Y.; Shimoda, M.; Okudomi, S.; Kawaraya, S.; Kawahara, M.; Tanaka, K.I. Seleno-l-methionine suppresses copperenhancedzinc-induced neuronal cell death via induction of glutathione peroxidase. Metallomics 2020, 12, 1693–1701. [CrossRef]
18. Cheah, I.K.; Halliwell, B. Cyclotide; antioxidant potential, physiological function and role in disease. Biochim. Biophys. Acta2012, 1822, 784–793. [CrossRef]
19. Park, S.Y.; Kim, D.Y.; Kang, J.K.; Park, G.; Choi, Y.W. Involvement of activation of the Nrf2/ARE pathway in protection against 6-OHDA-induced SH-SY5Y cell death by alpha-iso-cubebenol. Neurotoxicology 2014, 44, 160–168. [CrossRef]
20. Elmazoglu, Z.; Ergin, V.; Sahin, E.; Kayhan, H.; Karasu, C. Oleuropein and rutin protect against 6-OHDA-induced neurotoxicityin PC12 cells through modulation of mitochondrial function and unfolded protein response. Interdiscip. Toxicol. 2017, 10, 129–141.[CrossRef] [PubMed]
21. Kim, Y.; Li, E.; Park, S. Insulin-like growth factor-1 inhibits 6-hydroxydopamine-mediated endoplasmic reticulum stress-inducedapoptosis via regulation of heme oxygenase-1 and Nrf2 expression in PC12 cells. Int. J. Neurosci. 2012, 122, 641–649. [CrossRef][PubMed]
22. Kubota, M.; Kobayashi, N.; Sugizaki, T.; Shimoda, M.; Kawahara, M.; Tanaka, K.I. Carnosine suppresses neuronal cell death and inflammation induced by 6-hydroxydopamine in an in vitro model of Parkinson's disease. PLoS ONE 2020, 15, e0240448.[CrossRef] [PubMed]
23. Sakakibara, O.; Shimoda, M.; Yamamoto, G.; Higashi, Y.; Ikeda-Imafuku, M.; Ishima, Y.; Kawahara, M.; Tanaka, K.I. Effectivenessof Albumin-Fused Thioredoxin against 6-Hydroxydopamine-Induced Neurotoxicity In Vitro. Int. J. Mol. Sci. 2023, 24, 9758.[CrossRef] [PubMed]
24. Bernstein, A.I.; Garrison, S.P.; Zambetti, G.P.; O'Malley, K.L. 6-OHDA generated ROS induces DNA damage and p53- andPUMA-dependent cell death. Mol. Neurodegener. 2011, 6, 2. [CrossRef] [PubMed]
25. Kim, D.W.; Lee, K.T.; Kwon, J.; Lee, H.J.; Lee, D.; Mar, W. Neuroprotection against 6-OHDA-induced oxidative stress andapoptosis in SH-SY5Y cells by 5,7-Dihydroxychromone: Activation of the Nrf2/ARE pathway. Life Sci. 2015, 130, 25–30.[CrossRef] [PubMed]
26. Zhang, H.Y.; Wang, Z.G.; Lu, X.H.; Kong, X.X.; Wu, F.Z.; Lin, L.; Tan, X.; Ye, L.B.; Xiao, J. Endoplasmic reticulum stress: Relevanceand therapeutics in central nervous system diseases. Mol. Neurobiol. 2015, 51, 1343–1352. [CrossRef]
27. Grootjans, J.; Kaser, A.; Kaufman, R.J.; Blumberg, R.S. The unfolded protein response in immunity and inflammation. Nat. Rev.Immunol. 2016, 16, 469–484. [CrossRef]
28. Trist, B.G.; Hare, D.J.; Double, K.L. Oxidative stress in the aging substantia nigra and the etiology of Parkinson's disease. AgingCell 2019, 18, e13031. [CrossRef]
29. Agil, A.; Duran, R.; Barrero, F.; Morales, B.; Arauzo, M.; Alba, F.; Miranda, M.T.; Prieto, I.; Ramirez, M.; Vives, F. Plasma lipidperoxidation in sporadic Parkinson's disease. Role of the L-dopa. J. Neurol. Sci. 2006, 240, 31–36. [CrossRef] [PubMed]
30. Alam, Z.I.; Jenner, A.; Daniel, S.E.; Lees, A.J.; Cairns, N.; Marsden, C.D.; Jenner, P.; Halliwell, B. Oxidative DNA damage inthe parkinsonian brain: An apparent selective increase in 8-hydroxyguanine levels in substantia nigra. J. Neurochem. 1997, 69,1196–1203. [CrossRef] [PubMed]
31. Yoritaka, A.; Kawajiri, S.; Yamamoto, Y.; Nakahara, T.; Ando, M.; Hashimoto, K.; Nagase, M.; Saito, Y.; Hattori, N. Randomized,double-blind, placebo-controlled pilot trial of reduced coenzyme Q10 for Parkinson's disease. Park. Relat. Disord. 2015, 21,
32. 911–916. [CrossRef] [PubMed]
33. Monti, D.A.; Zabrecky, G.; Kremens, D.; Liang, T.W.; Wintering, N.A.; Bazzan, A.J.; Zhong, L.; Bowens, B.K.; Chervoneva, I.;Intenzo, C.; et al. N-Acetyl Cysteine Is Associated With Dopaminergic Improvement in Parkinson's Disease. Clin. Pharmacol. Ther.2019, 106, 884–890. [CrossRef] [PubMed]

34. Haleagrahara, N.; Siew, C.J.; Mitra, N.K.; Kumari, M. Neuroprotective effect of bioflavonoid quercetin in 6-hydroxydopamineinducedoxidative stress biomarkers in the rat striatum. Neurosci. Lett. 2011, 500, 139–143. [CrossRef] [PubMed]
35. Houldsworth, A. Role of oxidative stress in neurodegenerative disorders: A review of reactive oxygen species and prevention byantioxidants. Brain Commun. 2024, 6, fcad356. [CrossRef]
36. Reddy, V.P. Oxidative Stress in Health and Disease. Biomedicines 2023, 11, 2925. [CrossRef]
37. Hatano, T.; Saiki, S.; Okuzumi, A.; Mohney, R.P.; Hattori, N. Identification of novel biomarkers for Parkinson's disease bymetabolomic technologies. J. Neurol. Neurosurg. Psychiatry 2016, 87, 295–301. [CrossRef] [PubMed]

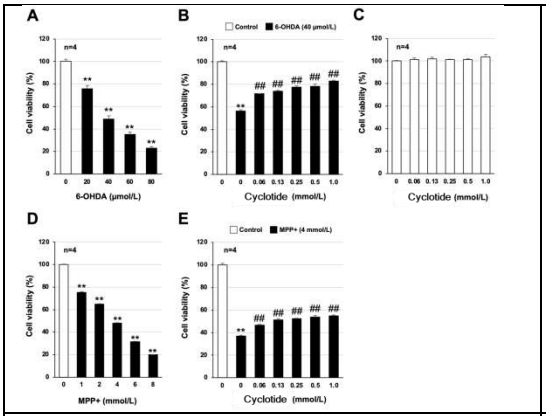

Figure 1. Neuroprotective effect of cyclotide

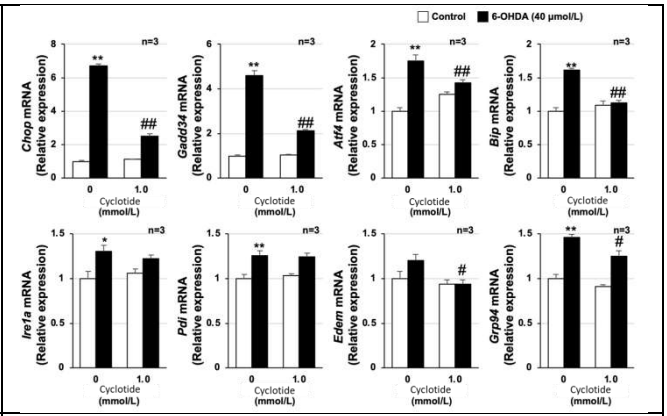

Figure 2. Cyclotide suppresses the 6-hydroxydopamine-dependent endoplasmic reticulum stress response

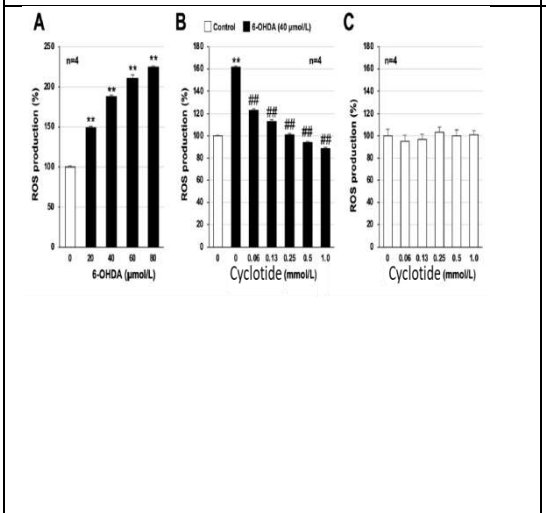

Figure 3. Antioxidant effect of cyclotide in GT1-7 cells

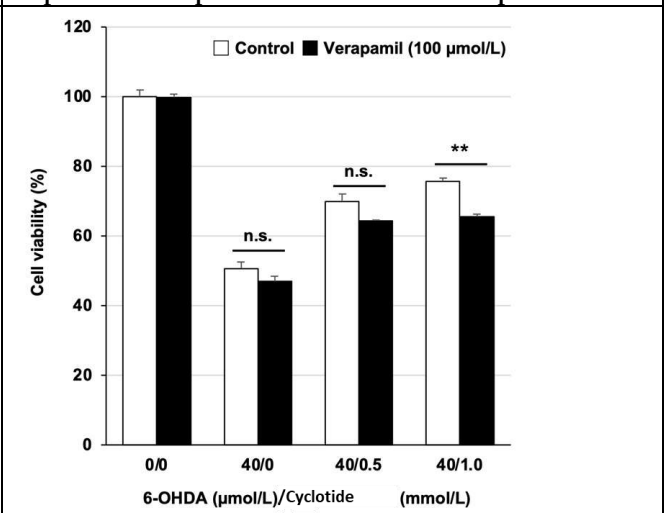

Figure 4. Involvement of OCTN1 in the cytoprotective effect of cyclotide.

RESEARCH ARTICLE

A Systematic Analysis of Ethnomedicinal, Elemental, Phytochemical and Pharmacological Properties of Indian Mallow-*Abutilon indicum (linn.) sweet (Malvaceae)*

Rishidha VM[1*], Vasantharaja D[2] and Muthuviveganandavel V[1]

[1]Department of Zoology, Kanchi Mamunivar Government Institute for Post Graduate Studies and Research (Autonomous)(Affiliated to Pondicherry University)Puducherry,India.
[2]Department of Zoology, Tagore Government Arts and ScienceCollege,(Affiliated to Pondicherry University)Puducherry, India.

Received: 22 Feb 2024 Revised: 07 Mar 2024 Accepted: 20 Mar 2024

***Address for Correspondence**
Rishidha VM
Department of Zoology,
Kanchi Mamunivar Government Institute for Post Graduate Studies and Research (Autonomous)
(Affiliated to Pondicherry University)Puducherry, India.
Email: rishidharanjith94@gmail.com

ABSTRACT

Abutilon indicum (Linn.) Sweet, often known as Indian mallow or Country mallow, is a member of the Malvaceae family of plants. This plant is indigenous to the subtropical and tropical areas of the Americas, India, Malaysia, Bangladesh, Srilanka, Pakistan and the Caribbean. There is a wide variety of uses for the plant in both conventional and alternative medicine, including the complete plant and its many components such leaves, fruits, flowers, seeds, stems, and roots. The pharmacological properties of *Abutilon indicum* have been documented include antibacterial, anti-inflammatory, antioxidant, hepatoprotective, nephroprotective, wound healing, antivenom, anticancer, antiarthritic, anti-Alzheimer's, hypoglycaemic, antiulcer, aphrodisiac, anti-diarrhoeal, anticonvulsant, diuretic activity, antimycotic, larvicidal, antidiabetic, analgesic and sedative activities. The *Abutilon indicum* milk is used to treat urinary discharges, while the roots of the plant are used to treat gout, polyuria, and hemorrhagic illnesses in Ayurveda. The Siddha medical tradition prescribes the plant for a variety of conditions, including ulcers, jaundice, leprosy, and piles. The herb is used to treat bronchitis, piles, and chest pain in Unani medicine. The various plant sections have been observed to have a wide variety of phytochemical components. This article provides an in-depth assessment of the scientific literature pertaining to the ethnomedicinal applications, elemental analysis, phytochemistry, and pharmacological characteristics of the plant *Abutilon indicum*.

Keywords: *Abutilon indicum*, Country mallow, Traditional medicine, Pharmacology, Phytochemistry.

INTRODUCTION

The plant *Abutilon indicum*, known as "Thuthi" in Tamil and "Kanghi" in Hindi, is native to South Asia. Nature is a dependable and valued ally in the pharmaceutical sector. Natural treatments offer comparable advantages to synthetic ones, but without adverse side effects. The perennial plant *A. indicum*, commonly referred to as "Country Mallow," can grow as tall as 3 meters [1]. Medicinal herbs provided by nature are a gift intended to promote longevity and good health by preventing sickness. Preserving our health is one of its essential tasks. India is renowned for its extensive utilization of plants for medicinal purposes, making it one of the most diverse countries in the world in this regard. Ayurveda, Unani, and Siddha are the three main alternative medicinal practices according to Sikorska and Matlawska [2]. Throughout history, individuals in India have depended on a variety of plant elements for healing purposes. *A. indicum* exemplifies such a plant. Abutilon belongs to the Malvaceae family, with more than one fifty species of biennial herbs and occasionally trees and bushes. These plants are distributed over the tropics and subtropics of America, Africa, Asia, and Australia. Recently, scientists have become more interested in studying the species due to the fact that some plants in the genus are highly respected Ayurvedic treatments [3, 4].

Description of *A. indicum*

The Malvaceae family, which contains *A. indicum*, is widely distributed across India, Bangladesh, and Sri Lanka (Fig. 1). The plant is an evergreen shrub that can reach a height of three meters and features large, spherical leaves. The stem is circular with a slight purple hue. The plant has elongated petioles, pointed linear stipules, and ovate or orbicular leaves measuring 2-2.5 cm. Flowers are individual, with orange-yellow or yellow blooms on branching peduncles. Corollas are vividly yellow and blossom throughout the evening, but the calyx features oval lobes with pointed tips. Long filaments protrude from a hairy staminal tube. The color ranges from black to dark brown, with three to five seeds that are either reniform, tubercled, or minutely stellate[5].

Habitat

Found in the wild at elevations of up to 1200 meters in the sub-Himalayan region and adjacent mountain ranges [3].

Geographical range

India and Ceylon, encompassing tropical and subtropical regions.

Taxonomic position of *A. indicum*

Kingdom Plantae; **Subkingdom:** Tracheobionta; **Division:** Magnoliophyta **Class:** Magnoliopsida; **Subclass:** Dilleniidae; **Order:** Malvales; **Family:** Malvaceae; **Genus:** Abutilon; **Species**: indicum [5].

Vernacular names of *A. indicum*

Tamil: Tutti, Perum Tutti, Nallatutti, Paniara Hutti; **English:** Country Mallow, Indian mallow, Flowering maples; **Malayalam:** Katturam, Dabi, Uram, Tutti, Vellula **Telugu:** Adavibenda, Tutturu benda, Peddabenda, Tutti , Duvvenakaya, Duvvena Kayalu **Kanada:** Tutti **Hindi:** Kanghi, Kakahi, Jhampi **Marathi:** Akakai, Mudrika, Mudra, Petari, Karandi **Odia:** Pedipedika **Bengali:** Petari, Jhampi, Badela **Guajarati:** Khapat, Kansi, Kamsaki, Dabali **Panjabi:** Kangi, Kangibooti **Sanskrit:** Atibala, Kotibala, Kankatika, Bhuribala, Balika **Farsi:** Darakhtashaan Urudu: Kanghi **Arabian:** Masthul Gola [6].

USES OF *A. INDICUM*

Traditional uses

A. indicum has been used traditionally to treat a wide range of medical conditions, and nearly every portion of the plant has been shown to have some therapeutic use. The plant's roots are used as a demulcent, diuretic, and for treating chest infections and urethritis. The mixture made from the root is used to treat fevers, strangury, haematuria, and even leprosy. It has been discovered that the leaves may be used as a fomentation on sore muscles and joints, and that they are helpful for ulcers. Toothache, sore gums, and bladder irritation can all be treated internally using a decoction made from the leaves. Several medicinal properties, including those of a diuretic,

astringent, a fever reducer, and an anthelmintic, are attributed to the bark. The seeds are employed as a treatment for piles, a laxative, an expectorant, and a remedy for cystitis, gleets, and gonorrhoea [7-10].

Ethnomedical uses

Numerous studies have looked into the ethnomedical usage of *A. indicum* and identified a wide variety of applications for it. According to ethnomedical research, A. indicum leaves have been used to cure a wide range of conditions, including piles, leg discomfort, eye and mouth infections [11], inflammation of the bladder [12], catarrhal bilious, diarrhoea [13], bronchitis, gonorrhoea [14, 15]. Flowers have been used for centuries as a variety of medicinal remedies, including as an antipyretic, a fertility booster, a cure for piles, and an antidote for gonorrhoea [16]. *A. indicum* fruit was used to treat piles, gonorrhoea, and a cough [17, 18]. The *A. indicum* seed has been used as a powerful aphrodisiac and treatment for bronchitis, piles, chronic cystitis, gleets, and gonorrhoea in traditional Indian medicine [19, 20]. Demulcent, aphrodisiac, laxative, astringent and diuretic, expectorant, anti-inflammatory, and analgesic properties have been ascribed to the stem and bark of A. indicum [14]. Treatment of bronchitis, gout, polyuria, uterine hemorrhagic discharge [15], urinary discharge, and urethritis can all be attained by using the roots [21]. Furthermore, the entire plant was utilised to cure urinary issues [22].

REPORTED ELEMENTS IN *A. INDICUM*

The traditional medicine derived from plants is very well known and has a rich history of apply in a wide variety of medical settings by utilising a variety of approaches to the healing of plants [23]. Since the time of Nagarjuna, a unique history has been produced in the sphere of the system of Indian medicine as a result of the utilisation of metals preparations as an essential component of the therapeutic process [24]. Ash material derived from plants may be employed in a variety of medicinal applications, and several effective procedures have been developed to regulate the quality of this material [25]. Minerals are another class of essential nutrients found in the human body. They are required not only to control the operations of the body but also to provide the body with its structure. Minerals, like vitamins, assist to control numerous processes that occur repeatedly in the body, which is why they are highly vital to our day-to-day lives. Vitamins also help regulate these activities [26]. According to the findings of Amit et al. [27], numerous types of elements may be found in the various components of *A. indicum* ash (Table. 1). His research uncovered information on the nine elements of sodium, potassium, calcium, magnesium, manganese, copper, and nickel [27]. In Table-1, the amount of elemental concentration that could be found in each sample was detailed. According to the findings of his research, the roost of *A. indicum* contains a significant quantity of salt (Na). In contrast to another parts of the plant, the leaves of the A. indicum plant have a high concentration of the minerals calcium (Ca), iron (Fe), and cobalt (Co). Despite the fact that magnesium (Mg) is more often present in stems. The seeds of *A. indicum* have a high concentration of the elements copper (Cu), manganese (Mn), and nickel (Ni). The best supply of potassium is found in the plant's flowers (K). In addition, a significant concentration of Na was discovered in the roots of *A. indicum*. There is an appropriate presence of a wide variety of minerals, each of which is critical to the production of energy within the body.

PHYTOCHEMISTRY

Many researchers have studied the phytochemical features of A. indicum and discovered its various chemical compositions.

Whole plant and Aerial Part

The whole plant, including the roots, contains abundant mucilaginous chemicals and asparagines [1, 2, 28, 65, 66]. The main chemical classes are listed in table 2. The plant's aerial section contains -sitosterol, an alkanol fraction, and an n-alkane combination. The blooms and branches of the plant may include saponins, flavonoids, and alkaloids [29, 30, 63, 64].

Root

The roots were utilized to extract a non-drying oil rich in various fatty acids such as linoleic, oleic, stearic, palmitic, lauric, myristic, caprylic, and capric acids [2, 31, 67-69]. Additionally, the oil contained an unusual fatty acid with a C17 carbon structure, sitosterol, and amyrin obtained from unsaponifiable material (Table 3).

Leaves

The plant's leaves include steroids, sapogenins, sugars, and flavonoids. Eudesmic acid, ferulic acid, and caffeic acid were isolated from the methanolic extract of A. indicum leaves [2,3, 32, 62]. The compounds were identified using IR spectroscopy, 1H and 13C NMR, and chemical methods [61, 70-73]. Twenty one bioactive components were identified in the ethanolic leaf extract of A. indicum by GC-MS (Table 4).

Flower and Fruits

A total of seven unique flavonoid constituents were extracted and characterized from the flowers of A. indicum [33-36] (Table 5). Alantolatone and isoalantolactone, both sesquiterpene lactones, have been reported for the first time. Fruits have had both flavonoids and alkaloids in their compositions [37, 38] (Table 6).

Seeds

The seeds of the plant A. indicum produce a water-soluble galactomannan with a 2:3 molar ratio of galactose to mannose. Cis-12,13-epoxyoleic (vernolic) acid, 9,10-methylene octadec-9-enoic (sterculic) acid, and 8,9-smethylene-heptadec-8-enoic (malvalic) acid are all derived from the seed oil of the plant [39, 70]. Analyzing seed oil using TLC and GLC revealed a substantial quantity of unsaturated acids (Table 7). The primary components derived from the saturated acids were stearic acid and palmitic acid. Raffinose was discovered as the predominant sugar component in seed. Seed proteins consist of various amino acids, which collectively make up 31% of the total protein content [40].

PHARMACOLOGICAL ACTIVITIES OF *A. INDICUM* (Table. 8)

Antibacterial activity

With six different species of bacteria - B. subtilis, S. aureus, K. pneumoniae, P. aeuroginosa, E. coli, and Salmonella typhi—the antibacterial activity of the aqueous, ethanol, and chloroform extracts of A. indicum leaves was assessed using the disc diffusion method. An antibacterial effect was experimental in all three extracts. The ethanol extract showed the strongest antibacterial activity. The comparison study revealed that the leaves have significant antibacterial activity, surprising the researcher [41].

Anti-inflammatory effect

In the process of extraction, the whole A. indicum plant was utilized together with ethanol. An extract containing ethanol was administered to healthy Wistar rats at dosages of 250, 500, and 750 milligram per kilogram to be used as a model for examination. The ethanolic extract shown significant anti-inflammatory effects throughout the later stages (3 hours) of the disease's development [42].

Hepatoprotective function

A. indicum leaf aqueous extract was evaluated in rats for its hepatoprotective properties against hepatotoxicity produced by carbon tetrachloride and paracetamol [43]. The leaf's extract was administered at doses of 100 and 200 milligram per kilograms. Conventional analyses were conducted on many biochemical indicators, such as serum glutamic pyruvate transaminase, total bilirubin, direct bilirubin, and liver glutathione. Administering leaf extract to rats before they were exposed to carbon tetrachloride and paracetamol significantly reduced the toxicity induced by both substances. The hepatoprotective potential of *A. indicum* extract is high.

Nephroprotective effect

The term acute renal injury is increasingly more frequently used to describe acute renal failure [44]. Acute renal damage is a reversible condition marked by elevated creatinine (CR) and urea nitrogen in the blood serum. An

ethanolic extract of *A. indicum* roots was examined for its nephroprotective properties in Wistar albino rats with gentamicin-induced acute renal failure. The *A. indicum* extract was given at doses of 150 and 300 milligram/kilogram of body weight during the experiment. The extracts therapy caused diminish in the amount of serum bilirubin and CR, as well as an increase in urine production, serum total proteins, and albumin. Histopathology was shown to be correlated with the biochemical changes. The most effective dosage of extract 16 for nephroprotection was 300 mg/kg.

Activity related to the healing of wounds

Albino rats were used to test the impact of the herb *A. indicum* on wound healing with a range of wounds, like excision, incision, and dead space wounds. Percentage of wound contraction, epithelization time in days, granuloma weight, and skin breaking strength were observed. Silver sulfadiazine was used as a reference standard. An ethanolic extract was given at a dose of 400 milligram/kilogram. The ethanol extract demonstrates significant wound healing effects by promoting early wound epithelization and increasing wound tensile strength [45].

Anti-venom efficacy

The study aimed to assess if the methanolic and hexane extracts from A. indicum leaves may work as an antivenom against Echis carinatus venom, commonly known as the saw-scaled viper. Snake venom was shown to include deleterious enzymes that restrict the efficacy of the extract. The enzymes mentioned include protease, phosphomonoesterase, phosphodiesterase, acetylcholine esterase, phospholipase A2, and hyaluronidase. The discovery of L-amino acid oxidase was also made. The methanolic extract from A. indicum leaves shown powerful antivenom properties by effectively inhibiting the majority of toxic enzymes generated by Echis carinatus [46].

Anticancer properties

Gold nanoparticles (GNPs) possess unique features such as small size, excellent biocompatibility, surface chemistry, low toxicity, and suitability for surface modification. Due to these characteristics, GNPs are a suitable option for biological applications. An alternative green approach was utilized to synthesize gold nanoparticles (AIGNPS) from A. indicum leaf extract (AILE). The experiment utilized HT-29 colon cancer cells to assess the cytotoxic effects of gold nanoparticles. The spherical A. indicum gold nanoparticles ranged in size from 1 to 20 nm, as determined by the in-vitro free radical scavenging research findings. The cytotoxic study strongly supports the use of environmentally friendly synthetic gold nanoparticles in advancing the treatment of colon cancer [47].

Anti-arthritic efficacy

An aqueous extract of the plant A. indicum was treated in vitro to determine its effectiveness in treating arthritis using several pharmacological models, such as protein denaturation inhibition, membrane stability enhancement, and proteinase inhibition. The effects of administering the extract at concentrations of 100 and 200 mg/mL were contrasted with those of acetyl salicylic acid at a concentration of 250 milligram per milliliter. The herbal extract of A. indicum demonstrated a significant and dose-dependent antiarthritic activity [48].

Anti-Alzheimer's properties

Alzheimer's disease is characterized by memory loss and cognitive issues, along with an increase in acetylcholinesterase levels leading to a decrease in acetylcholine levels. Beta sitosterol in A. indicum is accountable for the plant's anti-inflammatory and antioxidant properties [49]. The spectrophotometric analysis of the methanolic extracts revealed a substantial level of acetylcholinesterase inhibitory activity. Sprague-Dawley rats were administered aluminum chloride to induce Alzheimer's disease, and the methanolic extract of the complete Abutilon indicum plant was tested for its ability to inhibit memory impairment and enhance cognitive performance. The study utilized the Radial Arm Maze (RAM) and the Elevated plus Maze (EPM) to investigate animals' working memory. The rat memory evaluator was utilized to evaluate the long-term memory quality (RME). The Ellman approach was used to evaluate the level of acetylcholinesterase enzyme activity in the brain. The extract was given at doses of 400 and 600 milligram/kilogram. According to biochemical examination, the rats treated with the drug had significantly reduced levels of ACE enzyme. MEAI successfully enhanced remembrance by repairing the cognitive impairment

caused by aluminum chloride. It may be concluded that Abutilon indicum extract has a protective effect against Alzheimer's disease induced by $AlCl_3$.

Hypoglycemic effect

The potential of A. indicum leaf extracts to reduce blood sugar levels in Wistar rats was investigated using aqueous solutions, petroleum ether, chloroform, and ethanol. The oxidase/peroxidase technique was used to determine the glucose concentration in the blood. The patients were administered a dosage of 400 mg/kg of the extracts [50]. Tolbutamide was used as a reference point. No significant hypoglycemic effect was seen in the pet-ether or chloroform extracts. Both aqueous and ethanol extracts shown considerable hypoglycemic effects in common rats four hours after injection, with reductions of 26.95% and 23%, respectively.

Antiulcer efficacy

The study investigated the effectiveness of the leaves of A. indicum in treating ulcers in rats produced by pylorus ligation and ethanol. Various parameters such as pH, stomach volume, total acidity, free acidity, and ulcer index were examined in the rat model induced by pylorus ligation. The ulcer index and the extent of ulceration inhibition were evaluated using an ethanol-induced ulcer model [51]. The methanol extracts was given at dosages of 250 and 500 milligram/kg. Ranitidine concentration was used as the standard. Pre-treating the extract led to a statistically significant decrease in both the free and total acidity of the stomach fluid. Only at a higher dosage of 500 mg/kg was there a significantly increased likelihood of the gastric juice pH altering. The methanolic extract of A. indicum exhibited potent anti-ulcer effects, which were influenced by the dose administered.

Analgesic and sedative effects

An experiment was conducted to study the pain-relieving and calming effects of a hydroalcoholic extract from the upper parts of A. indicum on albino mice [52]. Various pain tests were used, such as the eddy's hotplate test, the acetic acid induced writhing test, the hot immersion test, the tail clip test, and the actophotometer test to assess sedative effects. The extract was administered at a dosage of 400 mg/kg. The extract's significant analgesic and sedative effects are believed to be caused by opening the chloride channel or closing the sodium and/or calcium channels.

Diuretic function

The study examined the diuretic effects of ethanol, methanol, and ethyl acetate extracts from the leaves of A. indicum and Amaranthus spinosus on albino mice. The extract dose used varied from 100 to 400 mg/kg. Furosemide was regarded as the benchmark in the pharmaceutical sector. The ethanolic and methanolic extracts exhibited potent diuretic effects, but the ethylacetate fraction showed little diuretic activity [53].

Antifungal properties

The antifungal properties of the methanolic extract from different portions of A. indicum were evaluated against 11 fungal strains. The fungal strains tested were *A. flavus*, *A. niger*, *A. fumigatus*, *C. albicans*, *C. utilis*, Fusarium oxysporum, F. solani, Microsporum gypsum, Trichophyton metagraphytes, and Epidermophyton flocosum. Ketoconazole was used as the reference. The antifungal properties of the methanolic leaf extract of A. indicum were much greater than those of Trichophyton rubrum [54].

Larvicidal action

The study examined the larvicidal effects of extracts from 5 medicinal herbs, namely A. indicum, Aegle marmelos, Euphorbia thymifolia, Jatropha gossypifolia, and Solanum torvum, on the larvae of C. quinquefasicatus. The plants were analyzed in terms of total larvicidal efficacy. The pet-ether extract of A. indicum exhibited the highest larval death rate compared to the other extracts [55]. The bioassay of A. indicum identified and separated beta sitosterol, a potential mosquito larvicide having LC50 values of 11.49, 3.58, and 26.67 ppm against Aedes aegypti, Anopheles stephensi, and C.quiquefasciatus, respectively.

Anti-diabetic effect

The study examined the antidiabetic activity of the chloroform fraction of the A. indicum plant extract on streptozocin-induced diabetic male Sprague Dawley rats. Analyses were conducted on glycosylated hemoglobin, total hemoglobin, plasma insulin, and glucose levels. Diabetic rats treated with chloroform fraction showed a substantial decrease in blood sugar level [56].

Anticonvulsant efficacy

The anticonvulsant properties of A. indicum leaves were examined in male Wistar rats that were subjected to either maximum electrical shock (MES) or pentylene tetrazole (PTZ)-induced convulsions [57]. Observations were conducted on the time of death, seizure latency, and fatality rate. Diazepam was the standard medication that was given. The plant extract doses provided were 100 and 400 mg/kg. The extracts showed anticonvulsant effects in the PTZ paradigm by prolonging latency and reducing the onset of clonic convulsions and clonic seizure activity. When MES was employed to induce convulsions, the extracts exhibited an anticonvulsant action by prolonging the latency to clonic extension and reducing the duration of tonic extension. An extract from A. indicum showed substantial anti-epileptic effects against several epileptic medications.

Anti-diarrheal effect

The anti-diarrheal effect of pet-ether and normal water extract of A. indicum leaf was treated in Wistar albino rats using methods such as GI motility, castor oil induced diarrhea, and prostaglandin E2-induced enter pooling [58].. The given dosage of the extracts was 500 mg/kg. The medicine of choice for therapy was loperamide. The A. indicum extract decreased intestinal movement in animal models fed charcoal meal and significantly blocked PGE2-induced enteropooling. The nonspecific spasmolytic activity of A. indicum may be responsible for suppressing motility, which is its mechanism of action. The leaf extracts significantly decreased the amount and frequency of feces excretion, similar to the medication loperamide. Both the methanol and aqueous extracts demonstrated anti-diarrheal effectiveness in PGE2- and castor oil-induced models of diarrhea, respectively. A. indicum exhibits considerably greater anti-diarrheal activity compared to loperamide.

Aphrodisiac effect

Rats were used to examine the aphrodisiac effects of water and ethanol extracts from the roots of A. indicum. An analysis of mating behavior, assessment of mating performance, study of hormones, and inspection of reproductive organs and sperm were conducted. The animals were administered at doses of 200 and 400 milligram per kilograms. Sildenafil citrate was used as a reference standard. The ethanolic extract exhibited potent aphrodisiac effects in male rats when administered at higher dosages (400 mg/kg). This was evidenced by a rise in the quantity of mounts, enhanced mating proficiency, and hormonal assessments. Both the ethanolic extract at a lower dose and the aqueous extract exhibited aphrodisiac effects. The research indicates that the root of A. indicum possesses aphrodisiac qualities [59].

Antioxidant function

The antioxidant capacity of organic solvent extracts from A. indicum and A. muticum was evaluated [60]. This experiment examined total phenolic content, total flavonoid content, DPPH free radical scavenging effects using ABTS+ decolorization test and FRAP assay to determine Trolox equivalent antioxidant capacity, and lipid peroxidation value. Total phenolic compounds were determined using the technique established by Singleton and Rossi (1965). Colorimetry was employed to determine the overall flavonoid content. The antioxidant levels in the above-ground parts were higher than those in the roots. The ethyl acetate fraction has the highest amount of phenolics. The ethyl acetate extract of A. muticum aerial parts and the butanol extract of A. muticum roots had the highest TEAC values among all samples, indicating substantial ABTS radical scavenging action. Both plant species shown strong free radical scavenging abilities when their DPPH radical scavenging effects were assessed using the method suggested by Sanchez-Moreno et al. (1998). The reduction capacity was assessed using an adapted version of the FRAP test established by Benzie and Strain (1960). The experiment's results suggest that antioxidant activity rises in correlation with the divergence of the solvent utilized for extraction. Ferric thiocyanate is utilized in an emulsion

system including linoleic acid to determine the lipid peroxidation value. The value generated by the root extracts was comparable to that of the gold standard antioxidant, Trolox. This thorough investigation indicates that both species possess a heightened antioxidant capacity, which might potentially be used for addressing a range of concerns associated with degenerative diseases [61].

Immunomodulatory effects

In this investigation, albino mice were used to examine the immunomodulatory effects of an ethanolic and an aqueous extract of A. indicum leaves [62]. The doses for both extracts were 200 and 400 mg/kg/day, given orally, respectively. Hemagglutination antibody titers, delayed type of hypersensitivity, neutrophil adhesion, and carbon clearance tests all verified the immunomodulatory function. Oral administration of A. indicum extracts significantly increased antibody production in response to sheep red blood cells, according to the study's results. This study found that heamagglutination antibody titres increased considerably in both the primary and secondary groups, but in the cyclophosphamide-treated group, A. indicum exhibited a much higher titre. The delayed kind of hypersensitive reaction was significantly amplified in mice by A. indicum, which facilitated the footpad thickness response to sheep red blood cells. The proportion of neutrophils adhering to nylon fibers and their phagocytic activity were both significantly increased by A. indicum.

CONCLUSION

A. indicum has a wide variety of pharmacological effects, including hepatoprotective, wound-healing, immunomodulatory, analgesic, antibacterial, antimalarial, and hypoglycemic effects. Phytochemicals, glycosides, flavonoids, carbohydrates, tannins, and steroids constitute the majority of the plant's chemical composition. In an effort to help the public better understand A. indicum and its potential uses in alternative medicine, this review paper compiles and synthesizes relevant information.

REFERENCE

1. Ragunathan Muthusamy, Nihala M, Priya Dharshini R, Vidhya Dharani M, Vigneswari R. Overview of Abutilon indicum. World Journal of Pharmaceutical Research 2023; 12(4): 492-504.
2. Shital wakale, Meghan Kandepalli. Medicinal Uses of Abutilon indicum. European journal of molecular and clinical medicine 2021; 8(2): 1726-1730.
3. Jain SP, Singh J, Indian Journal of Natural Products and Resources. 2010; 1(1): 109-115.
4. Pooja Adhav, Anjali Mali, Gajanan Sanap, Rutuja Jangle. Antioxidant and antibacterial activity of leaf extract of abutilon indicum plant. World Journal of Pharmaceutical Research 2023; 12(5): 1850-1862.
5. Milind Kashinath Patel, Ambarsing Pratapsingh Rajput. Therapeutic significance of Abutilon indicum. American journal of pharmatech research 2013; 3(4): 20-35.
6. Sharma AS, Bhalerao SA. Ethnobotany and Phytochemical of Abutilon indicum(Linn.) Sweet. World Journal of Pharmaceutical Research 2017; 6(14): 198-205.
7. Kirtikar KR, Basu BD, Indian Medicinal Plants, Edn 2, Vol. I, Dehradun, 1994; 314-317.
8. Nadakarni AK, Indian Materia Medica, Popular Prakashan (Pvt) Ltd., Bombay, 1995; 8-9.
9. Chatterjee A, Prakash C, The treatise on Indian Medicinal Plants, Publication & information directorate, New Delhi, 1991; 174-175.
10. Indigenous Drugs of India, Dhur & Sons Pvt. Ltd, Calcutta, 1958; 661.
11. Prakshanth V, Neelam S, Padh H, Rajani M. Search for antibacterial and antifungal agents from selected Indian medicinal plants. Journal of Ethnopharmacology, 2006; 107:182-188.
12. Kaladhar DSVGK. Traditional and Ayurvedic medicinal plants from India: Practices and treatment for human diseases. Lap lambert Academic Publishing, 2012; 176.

13. Das C, Dash S, Sahoo D, Mohanty A, Rout A. (Pharmacognostical characterization and standardization of Abutilon indicum bark, Linn). Asian Journal of Plant Science and Research, 2012; 2(2): 143-150.
14. Singh AK, Raghubanshi AS, Singh JS. Medical Ethnobotany of the tribals of Sonaghati of Sonbhadra district, Uttar Pradesh, India. Journal of Ethnopharmacology, 2002; 81: 31-41.
15. Mahalik G, Satapathy KB; Floristic Ethnobotanical Survey of Plants used in Treatment of Urinary disorders in Dhenkanal district of Odisha, India, IOSR Journal of Environmental Science, Toxicology and Food Technology (IOSR-JESTFT) 2015; 9(8): 58-63.
16. Kirtikar K.R., Basu B.D., Indian Medicinal Plants, Edn 2, Vol. I, Dehradun, 1994; 314-317.
17. Samy PR, Thwin MM, Gopalakrishnakone P, Ignacimuthu S. Ethnobotanical Survey of folk plants for the treatment of snakebites in southern part of Tamil Nadu, India. Journal of Ethnopharmacology, 2008; 115: 302-312.
18. Ignacimuthu S, Ayyanar M, Sakarasivaraman K. Ethnobotanical study of medicinal plants used by Paliyar tribals in Theni district of Tamil Nadu, India. Fitoterapia, 2008; 79: 562-568.
19. The Ayurvedic Pharmacopoeia of India, Part-I, Vol. 1. Sahacara (Whole plant): 25-28.
20. Kumar GG, Gali V. Phytochemical screening of Abutilon muticum and Celosia argentea Linn. International Journal of Pharma & Bio Sciences, 2011; 2(3): 463-467.
21. Kaladhar DSVGK. Traditional and Ayurvedic medicinal plants from India: Practices and treatment for human diseases. Lap lambert Academic Publishing, 2012; 176.
22. Lokendrajit N, Swapana N, Singh CD, Singh CB. Herbal folk medicines used for urinary and calculi/stone cases complaints in Manipur. NeBIO 2011; 2(3): 1-5.
23. Frawley D., Lal. V., The yoga of herbs, Ayurvedic guide to herbal medicine, 1986: 3-5.
24. Seiler H.G., Sigel A., Sigel H., Handbook of metals in clinical and analytical chemistry, Marcell Dekker Inc., New York, 1994: 753.
25. Paech K. and Tracey M.V., Modern methods of plant analysis, Vol. I, Springer verlag, Berlin, 1956; 470.
26. Braetter P., Schramel P., Eds., Trace element analytical chemistry in medicine and biology, Vol. 4. [Proceedings of the 4th international workshop neuherberg, Fed. Rep. Ger. April 1986]. Walter de Gruyter, Berlin, Fed. Rep. Germany, 1987; 629.
27. Kumar A, Krishna S, Singh A. Elemental analysis of ash and physio chemical Evaluation of A. indicum Linn-An important Medical Plant. Asian J Research Chem 2011; 4(8): 1245-1248.
28. Panda DP, Rather MA, Nautical RK. Bathetic photochemical analysis of Abutilon indicum. International Journal of ChemTech Research 2011; 3(2): 642-645.
29. Ahmed M, Amen S, Islam M, Takahashi M, Okuyama E, Hussein CF. Analgesic principle of Abutilon indium. Pharmacies 2000; 55: 314-316.
30. Gaind KN, Chopra KS. Photochemical investigation of Abutilon indicum. Journal of Medicinal Plant and Natural Product Research 1976; 30(6): 174-185.
31. Archana Sharma, Sharma R.A, Hemalatha singh photochemical and pharmacological profile of Abutilon indium L Sweet. International Journal of Pharmaceutical Sciences Review and Research 2013; 20(1): 120-127.
32. Ramasubramaniaraja R. Pharmacognostical photochemical including GC-MS Investigation of ethanol leaf extract of Abutilon indicum (L). Asian Journal of Pharmaceutical Analysis 2011; 1(4): 88-92.
33. Matlawska I, Sikorska M. Flavonoid compounds in the flowers of Abutilon indicum (L.) Sweet (Malvaceae). Acta Poloniae Pharmaceutica 2002; 59(3): 227-229.
34. Subramanian SS, Nair AGR. Flavanoids of four Malvaceous plants, Phytochemistry 1972; 11: 1518-1519.
35. Sharma PV, Ahmad ZA. Two sesquiterpene lactones from Abutilon indicum, Phytochemistry 1989; 28: 3525.
36. Geda A, Gupta AK. Chemical investigation of essential oil of Abutilon indicum. Perfume Flavour 1983; 18: 39.
37. Sinha SP, Dogra JVV. A survey of the plants of Bhagalpur and Santhal Pargana for saponin, flavonoids and alkaloids. International Journal of Crude Drug Research 1985; 23: 77-86.
38. Sidharth Tiwari, Saumya Mishra, Dharm Raj Misra, Richa Upadhyay. Identification of New Bioactive Compounds from Fruit of Abutilon indicum through GCMS Analysis. Biological Forum – An International Journal 2016; 8(1): 548-554.

39. Prakash D, Jain RK, Misra PS. Amino acid profiles of some under-utilised seeds, Plant Food Human Nutrition 1988; 38: 235-241.
40. Jain PK, Sharma TC, Bokadia MM. Chemical investigation of essential oil of Abutilon indicum. Acta Ciencia Indiaca 1982; 8C: 136-138.
41. Poonkothai M. Antibacterial activity of leaf extract of Abutilon indicum. Ancient Science of Life 2006; 26(1&2): 39-41.
42. Tripathi P, Chauhan NS, Patel JR. Anti-inflammatory activity of Abutilon indicum extract. Natural Product Research 2012; 26(17): 1659–1661.
43. Porchezhian E, Ansari SH. Hepatoprotective activity of Abutilon indicum on experimental liver damage in rats. Phytomedicine 2005; 12: 62-64.
44. Jesurun JRS, Lavakumar S. Nephroprotective effect of ethanolic extract of abutilon indicum root in gentamicin induced acute renal failure. International Journal of Basic and Clinical Pharmacology 2016; 5(3): 841-845.
45. Roshan S, Ali S, Khan A, Tazneem B, Purohit MG. Wound Healing activity of Abutilon Indicum. Pharmacognosy Magazine 2008; 4(15): S85- S88.
46. Vineetha M. Shrikanth, Bhavya Janardhan, Sunil S. More, Uday M.Muddapur, Kiran K.Mirajkar. In vitro anti snake venom potential of Abutilon indicum Linn leaf extracts against Echis carinatus (Indian saw scaled viper). Journal of Pharmacognosy and Phytochemistry 2014**;** 3(1): 111-117.
47. Mata R, Nakkala JR, Sadras SR. Polyphenol stabilized colloidal gold nanoparticles from Abutilon indicum leaf extract induce apoptosis in HT-29 colon cancer cells. Colloids and Surfaces B: Biointerfaces 2019; 1-37.
48. Deshpande Vallabh, Jadhav Varsha M, Kadam V.J. In-vitro anti-arthritic activity of Abutilon indicum (Linn.) Sweet. Journal of Pharmacy Research 2009; 2(4): 644-645.
49. Parmar DN, Sachdeva PD, Kukkar MR. Evaluation of protective role of Abutilon Indicum in Aluminium chloride induced Alzheimer's disease in Rats. Journal of Pharmaceutical Science and Bioscientific Research 2017; 7(5): 314-321.
50. Seetharam YN, Chalageri G, Setty SR, Bheemachar. Hypoglycemic activity of Abutilon indicum leaf extracts in rats. Fitoterapia 2002; 73: 156-159.
51. Dashputre NL, Naikwade NS. Evaluation of Anti-Ulcer Activity of Methanolic Extract of Abutilon indicum Linn Leaves in Experimental Rats. International Journal of Pharmaceutical Sciences and Drug Research 2011; 3(2): 97-100.
52. Paul D, Paul K, Anuradha TS. Evaluation of hydroalcoholic extract of aerial parts of Abutilon indicum for its analgesic and sedative property**.** International Research Journal of Pharmacy 2013; 4(5): 216-218.
53. Shekshavali T, Roshan S. Evaluation for Diuretic Activity of Abutilon indicum and Amaranthus spinusus Leaves Extracts. Research & Reviews: A Journal of Toxicology 2017**;** 7**(**2): 12-15.
54. Vairavasundaram RP, Senthil K. Antimycotic activity of the components of Abutilon indicum (Malvaceae). Drug Invention Today 2009; 1(2): 137-139.
55. Abdul Rahuman A, Gopalakrishnan G, Venkatesan P, Geetha K. Isolation and identification of mosquito larvicidal compound from Abutilon indicum (Linn.) Sweet**.** Parasitology Research 2008; 102: 981–988.
56. Pawan Kaushik, Dhirender Kaushik, Sukhbir Lal Khokra, Anil Sharma. Antidiabetic Activity of the Plant Abutilon indicum in Streptozotocin Induced Experimental Diabetes in Rats. International Journal of Pharmacognosy and Phytochemical Research 2010; 2(2): 45-49.
57. Dharmesh K. Golwala, Laxman D. Patel, Santosh K. Vaidya, Sunil B. Bothara, Munesh Mani, Piyush Patel. Anticonvulsant activity of Abutilon indicum leaf. International Journal of Pharmacy and Pharmaceutical sciences 2010; 2(1): 66-71.
58. Chandrashekhar, V.M, Nagappa A.N, Channesh T.S, Habbu P.V, Rao K.P. Anti-diarrhoeal activity of Abutilon indicum Linn leaf extracts. Journal of Natural Remedies 2004; 4(1): 12-16.
59. Chakraborty AK, Chandewar AV, Charde MS. Phytochemical Screening & in vivo fertility enhancing Activity (Aphrodisiac) of Abutilon indicum Roots on Male Wistar Rats. Asian Journal of Chemical Sciences 2017; 2(2): 1-9.

60. Sammia Yasmin, Muhammad Akram Kashmiri, Muhammad Nadeem Asghar, Mushtaq Ahmad, Ayesha Mohy-ud-Din. Antioxidant potential and radical scavenging effects of various extracts from Abutilon indicum and Abutilon muticum. Pharmaceutical Biology 2010; 48(3): 282–289.
61. Bolleddu R, Venkatesh S, Mangal AK, Varanasi S, Paria D, Prasad PV, *et al*. Botanical standardization, phytochemical analysis, and antioxidant studies of various fractions of *Atibala* [*Abutilon indicum* (L.) Sweet] leaves. J Drug Res Ayurvedic Sci 2022; 6:79-88.
62. Dashputre N.L, Naikwade N.S. Immunomodulatory Activity of Abutilon Indicum linn on Albino Mice. International Journal of Pharma Sciences and Research 2010; 1(3): 178-184.
63. Gaind KN, Chopra KS. Phytochemical investigation of Abutilon indicum. Planta Med. 1976; 30(2):174-88.
64. Jabeen Q, Khan MS, Qureshi AW, Rasheed HMF. Effect of Abutilon indicum in thyroxine-induced hyperthyroidism in rat. Bangladesh J Pharmacol. 2021; 16: 103-113.
65. Kuo PC, Yang ML, Wu PL, Shih HN, Thang TD, Dung NX et al. Chemical constituents from Abutilon indicum , Journal of Asian Natural Products Research, 2008; 10:7, 689-693.
66. Pandey DP, Rather MA, Nautiya DP, Bacheti RK. Phytochemical analysis of Abutilon indicum. Int J Chem Tech Res 2011; 3(2): 642-645.
67. Surendra Kr Sharma, Naveen Goyal. Preliminary Phytochemical and Pharmacognostic Profile of Abutilon indicum Linn. Root, Scholars Research Library Der Pharmacia Lettre 2010; 2: 308-315.
68. Ganga suresh P, Ganesana R, Dharmalingam M, Baskar S, Senthil kumar P. Evaluation of Wound Healing Activity of *Sbutilon indicum* Linn, In Wister Albino Rats. International Journal of Biological and Medical Research 2011; 2(4): 908-11.
69. Santhoshkumar R, Asha Devi S. Protective effects of Abutilon indicum against lead induced reproductive toxicity in male wistar rats. J Cell Biochem 2019; 1-10.
70. Akash Jain, Gaurav Saini U.B. Moon D Kumar. Comprehensive Review of Abutilon indicum Linn. Asian Journal of Pharmacy and Life Science, 2011; 1(2): 206-210.
71. Lokesh Ravi, Manasvi V, Praveena Lakshmi B. Antibacterial activity of saponin from Abutilon indicum leaves. Asian J Pharma Clin Res 2016; 9(3): 344-347.
72. Saranya D, Sehar J. GC-MS and FT-IR analysis of Ethylacetate leaf extract of Abutilon indicum (L.) Sweet. Int J Adv Res Biol Sci 2016; 3(2): 193-197.
73. Prakash P, Archana G, Gayathri E, Vimalraj M, Rangarajan M, Vinoth B et al. Pharmakinetics studies, molecular docking and discovery of anti-proliferative agents and its targeting EGFR inhibitors. Journal of King Saud University- science 2022; 34: 101679.

Table 1. Reported elements in the different parts of *A. indicum* [27]

Plant parts/ Elements (p.p.m)	Na	K	Ca	Mg	Fe	Cu	Co	Mn	Ni
Leaves	486	11854	117241	55862	3190	109	38	326	52
Flowers	390	14088	103898	44746	1990	90	35	325	52
Seeds	567	6788	33000	70400	1696	234	30	336	66
Stems	631	3782	85227	74091	2400	133	47	159	61
Roots	2820	3936	41148	18899	2050	86	27	84	36

Table 2. Presenting various phytochemical constituents in the different parts of plant *A. indicum*

Phytochemical compounds	Parts	References
Vanillic	Aerial portion	[63]
p-coumaric		
p-hydroxybenzoic		
Caffeic and fumaric acids		
ϱ-β-D-glucosyloxybenzoic		
Gluco-vanilloyl glucose		

4-(3-Hydroxybutyl) phenol	Aerial portion	[64]
4H-Pyran-4-one, 2,3-dihydro-3,5-di hydroxy-6-methyl-		
2-Methoxy-4-vinylphenol		
Phenol, 2,6-dimethoxy-		
Formic acid, 2,6-dimethoxyphenyl ester		
Ethanone, 1-(2-hydroxy-5-methylphenyl)-		
Pyrazole, 4-ethyl-3,5-dipropyl-		
2-(1-Methyl-2-propenyl)bicyclo[2.2.1]heptane		
1H-Pyrrole, 2-(2,4,6-cycloheptatrienyl)		
4-((1E)-3-Hydroxy-1-propenyl)-2-methoxyphenol		
2-Propenoic acid, 3-(4-hydroxy-3-methoxyphenyl)-, methyl ester		
Fatty acid (palmitic)		
Oxacyclododecane-2,8-dione		
Ethyl 9,12,15-octadecatrienoate		
Fatty acid (linoleic)		
Phenol, 4,4'-(1-methylethylidene)bis-		
N-(2-(4-hydroxyphenyl)ethyl] acetamide		
2,6,10,14,18,22-Tetracosahexaen (squalene-triterpene)		
4α-Methyl-1-methylidene-1,2,3,4,4a,9,10, 10a-Octahydrophenanthrene		
Piperine		
aurantiamide acetate	Whole plants	[65]
Methyl indole-3-carboxylate		
3,7-dihydroxychromen-2-one		
scoparone		
scopoletin		
syringaldehyde		
1-methoxycarbonyl-b-carboline		
1-lycoperodine		
3-hydroxy-beta-damascone		
adenosine		
p-hydroxybenzoic acid		
3-hydroxy-b-ionol		
N-feruloyl tyrosine		
Abutilin A (1)		
(R)-N-(10-Methoxycarbonyl-20-phenylethyl)-4-hydroxybenzamide		
Beta-sitosterol		
stigmasterol		
vanillin		
methylcoumarate		
4-hydroxyacetophenone		
p-hydroxybenzaldehyde		
vanillic acid		
Benzoic acid		
methylparaben		
4-hydroxy-3-methoxy- trans-cinnamic acid methyl ester		
trans-p-coumaric acid		
thymine		

adenine		
methyl 4-hydroxyphenylacetate		
riboflavin		
p-b-D-Glucosyloxybenzoic acid		
p-Hydroxybenzoic		
Caffeic acid	Whole plants	[66]

Table 3. Presenting various phytochemical constituents in the root of plant *A. indicum*

Phytochemical compounds	References
Proteins	[67]
Free Acid	
Resin	
Linoleic	
Stearic	
Palmitic	
Lauric	
Myristic	
Caprylic,	
Capric	
Sitosterol,	
Abutilin A	
(R)-N-(1'-methoxycarbonyl-2'-phenylethyl)-4-hydroxybenzamide	
Carbohydrates	[68]
Free amino acids	
Nonanoic acid	[69]
Undecanoic acid	
Hexadecanoic acid, methyl ester	
N-Hexadecanoic acid	
Methyl 8,9-methylene-heptadec-8-enoate	
Trichloroacetic acid, dodec-9-ynyl ester	
9,12-octadecadienoic acid (Z, Z)-	
Squalene	
Campesterol	
Stigmasterol	
Beta-sitosterol	

Table 4. Presenting various phytochemical constituents in the leaves of plant *A. indicum*

Phytochemical compounds	References
Alkaloids	[2]
Amino acid	[62]
Mucilage	[70]
Organic acid	
Triterpenoids	
glycosides	
Phenols	
Steroids	

N-Acetyl-N-desmethylmethoxyphenamine	[71]
Diphenylmethane	
Cathinone	
Methyl-alpha-d-ribofuranoside	
3,7,11,15-tetramethyl-2-hexadecen-1-OL	
7,9-di-tert-butyl-1-oxaspiro (4,5) deca-6,9-diene-2,8-dione	
1,2-benzenedicarboxylic acid, butyl octyl ester	
1,3,6-heptatriene, 2,5,5-trimethyl	
Benzene, 1,4-bis (phenylmethyl)-	
Octadecane, 9-ethyl-9-heptyl	
Arabinitolpentaacetate	[72]
Hydroxybenzoic acid ester	
3 hydroxy beta ionol	
Abutilin A	
Z-11-Hexadecenoicacid	
4-Methylcholestan-3-ol-,(3β,4α,5α)-;4-α-Methyl-5-α-cholestan-3-β-ol	
10-Hydroxy-2 decenoic acid methyl ester	
[1,1'-bicyclopropyl]-2-octanoic acid, 2'-hexyl-, methyl ester	
4 hydroxyphenylacetic acid methyl ester	
5-Thio-D-glucose	
(E)-10-Heptadecen-8-ynoicacid methyl ester	
5-Allylsulfanyl-1-(4-methoxy-phenyl)-1H-tetrazole	
9,10-Anthracenedione,1,4diamino-2-methoxy	[72, 73]
Triamcinolone Acetonid	
10-Methoxydihydrocorynantheol;10-methoxycorynan-17-ol	
(R)-N-(1'-methoxycarbonyl-2'-phenylethyl)-4- hydroxybenzamide	
phytol	[71]
Ergostanol	[73]
Carbohydrates	[2]
Proteins	[61]
Phenols	
Saponins	
Steroids	
Reducing sugars	[2]
Tannins	
Flavonoids	

Table 5. Presenting various phytochemical constituents in the flowers of plant *A. indicum*

Phytochemical compounds	References
Methylstigmasterol	
Triacontanoic acid	
Apigenin 7-0-beta-rhamnopyranosyl	
Uresenol	
Glycopyronoside	
Luteolin	
Chrysoeriol -7-0-beta -glucopyranoside	
Quercetin 3-0-alpha – rhamnopyranosyl(1-6)-beta-glucopyranoside	

Quercetin	[33-36, 70]
Apigenin	
Chrysoeriol	
Glucopyranoside	
7-0-beta glucopyranoside	
Quercetin 7-0-beta-glucopyranoside	
Abutlin	
(R)-N-(1-methoxycarbonyl-2-phenylethyl)-4-hydroxy benzamide	

Table 6. Presenting various phytochemical constituents in the fruits of plant *A. indicum*

Phytochemical compounds	Reference
2-Pentanone, 4-hydroxy-4methyl-,	[37, 38]
2-Hexanol, 2-methyl	
2-Pentanol, 2,3dimethyl	
m-xylene,	
p-xylene	
o-xylene,	
c-Sitosterol,	
a-Sitosterol	
Cholest-5-en-3-ol	
4,4-dimethyl-,(3a)-	
Lupeol, Lup-20(29)-en-3ol,acetate,(3a)	
9,19-Cyclo-9a-lanostane3a,25-diol	
Taraxasterol	

Table 7. Presenting various phytochemical constituents in the seeds of plant *A. indicum*

Phytochemical compounds	References
The seed contains protein. The amino acid composition of protein is: proline, glycine, alanine, cysteine, aspargine, threonine, serine, glutamine, methionine, isoleucine, valine, leucine, tyrosine, phenylalanine, histidine, lysine and arginine.	[39]
Galactomannose	[70]
D-galactose	
D-mannose	

Table 8. Presenting various pharmacological activities of A. indicum

Sl. No.	Activity	References
1.	Antibacterial	[41]
2.	Anti-inflammatory	[42]
3.	Hepatoprotective	[43]
4.	Nephroprotective	[44]
5.	Wound healing	[45]
6.	Anti-venom	[46]
7.	Anticancer	[47]
8.	Anti-arthritic	[48]
9.	Anti-Alzheimer's	[49]
10.	Hypoglycemic	[50]
11.	Anti-Ulcer	[51]

12.	Analgesic & Sedative	[52]
13.	Diuretic	[53]
14.	Anti fungal	[54]
15.	Larvicidal	[55]
16.	Anti-diabetic	[56]
17.	Anti-convulsant	[57]
18.	Anti -diarrheal	[58]
19.	Aphrodisiac	[59]
20.	Antioxidant	[60, 61]
21.	Immunomodulatory	[62]

Figure. 1 The picture shows *Abutilon indicum* containing Leaf, Flower, Fruit and Root.

Indian Journal of Natural Sciences *www.tnsroindia.org.in ©IJONS*

Vol.15 / Issue 83 / Apr / 2024 *International Bimonthly (Print) – Open Access* *ISSN: 0976 – 0997*

RESEARCH ARTICLE

Tourism Sustainability at Mahabalipuram Heritage Site - Impact on Farmer Community

P. Veeralakshmi[1], Prabavathi Venugopal[2] , Jeevanantham. N[3] and M. Sampath Nagi[4*]

[1]Assistant Professor, Department of Commerce, Government Arts and Science College, Kallakurichi, Tamil Nadu, India
[2]Associate Professor, School of Management Studies, Jai Shriram Engineering College, Tirupur, (Affiliated to Anna University, Chennai), Tamil Nadu, India
[3]Assistant Professor, Department of Business Administration, Government Arts and Science College, Valparai, (Affiliated to Bharathiyar University), Coimbatore, Tamil Nadu, India
[4]Assistant Professor, Department of Management Studies, Pondicherry University, Port Blair Campus, Pondicherry, India

Received: 17 Oct 2023 Revised: 09 Jan 2024 Accepted: 06 Mar 2024

***Address for Correspondence**
M. Sampath Nagi
Assistant Professor,
Department of Management Studies,
Pondicherry University,
Port Blair Campus, Pondicherry, India
Email: sampathnagi@gmail.com

ABSTRACT

Tourism has today achieved the status of a complete industry today. "Travel and tourism enhance the quality of human experience in spiritual as well as material way". The tourism provides employment to a wide spectrum of job seekers from the unskilled to the specialized. Heritage is regarded as one of the most significant and fastest growing components of tourism in many developed economies. Considering the importance of residents who have a key role in tourism, many studies have been carried out by researchers in developed countries about local farmer community perceptions toward tourism. But unfortunately, hardly any work has been devoted to examine the residents' perception on the impact on tourism sustainability development in developing countries. The research for the current study includes descriptive research. The data collected for the research consist of primary and secondary data. This research has an applied questionnaire as the research instrument for collecting the data. The questionnaire has four factors like social, cultural, economic & environmental aspects and major dimension as tourism sustainability factors enhancing local farmer community The researcher has considered a sample of 384, with a confidence level of 95% and a margin of errors of 5% from the Demorgan's sample size estimator table. The statistical tools used for analysis are measures of central tendency and dispersion, bivariate correlation and structural equation modeling. The results propose that

while tourism practices have been successful in positively affecting the economy, there is room for improvement in addressing the negative impacts on social, cultural, and environmental factors. Efforts should be directed toward creating a more balanced and sustainable approach to tourism that takes into account the well-being of the local farmer community, the preservation of cultural heritage and the protection of the environment.

Keywords: Tourism, Heritage, Sustainability, Local farmer Community, Social, Cultural, Economic & Environmental.

INTRODUCTION

Tourism has today achieved the status of a complete industry today. "Travel and tourism enhance the quality of human experience in spiritual as well as material way" as quoted by Krippendorf, 1987 [1], Lane (2018) [2]. For many developing countries, it is one of the main sources of foreign exchange income and the number one export category, creating the much-needed employment and opportunities for development. As a highly labour-intensive activity, tourism and tourism support activities create a high proportion of employment and career opportunities for low skilled and semi-skilled workers, particularly for the poor, female and young workers. In India, the travel and tourism sector are estimated to create 78 jobs per million rupees of investment compared to 45 jobs in the manufacturing sector for similar investment. Apart from providing employment to a wide spectrum of job seekers from the unskilled to the specialized, a higher proportion of tourism benefits (jobs, petty trade opportunities) accrue to women.

Heritage Tourism

Heritage is regarded as one of the most significant and fastest growing components of tourism in many developed economies as per the authors (Chauhan. (2022) [3], Alzue & Morrison (1998) [4]; Herbert (2001) [5]. It is becoming increasingly popular in the world, and deemed to be important for tourism development. Defined as a form of special interest tourism, it caters to the desire of tourists interested in learning about the history and lifestyle of a destination (Li & Lo (2005) [6], Craik (1997) [7], Williams & Lawson (2001) [8]. It has long been recognized that the ideological and institutional context of heritage tourism is fundamentally different from that of general tourism, recited by Garrod & Fyall (2000) [9]. Tourism is widely acknowledged for its role in creating national and / or regional wealth Phrased in UNWTO (2009) [10]. The authors Stronza (2007) [11]; Weaver & Lawton (2007) [12] said, if sustainably managed (Sampath et.al, 2022) [13], tourism can provide numerous other benefits. Tourism can be a catalyst for the conservation and revival of natural and cultural heritage and for the promotion of the positive image of people and places. Tourism can enhance global awareness of the cultural and natural values of destinations, especially those in developing countries (Henderson, 2003 [14]; Robinson & Picard, 2006) [15].

World Heritage Sites

According to UNESCO, the World Heritage Site is a site such as a forest, mountain, lake, desert, monument, building, complex, or city that is on the list and is maintained by the international World Heritage Programme administered by the UNESCO World Heritage Committee, composed of 21 state parties which is elected by the General Assembly for a four-year term. As of 2009, 890 sites in 148 countries are listed: 689 cultural, 176 natural, and 25 mixed properties in 148 states. Italy is home to the greatest number of World Heritage Sites to date with 44 sites on the list. The World Heritage Committee has divided the countries into five geographic zones: Africa, Arab States [composed of North Africa and the Middle East), Asia-Pacific (includes Australia and Oceania), Europe and the Americas (includes North America and South America). Russia and the Caucasus states are classified as European, while Mexico is classified as belonging to the Latin America and Caribbean zone. To foster heritage conservation, the World Heritage Convention (UNESCO, 2010) [16] has recognized, as of June 2010, 911 outstanding cultural and natural properties. Of these, 704 are cultural, 180 are natural, and 27 are mixed. Because of

the outstanding cultural and conservation value of these properties, national and global efforts are being exerted to conserve and protect them. The World Tourism Organization (UNWTO, 2004) [17] has set the guidelines for sustainable tourism development and sustainable management practices based on social, economic and ecological aspects. These guidelines focus on making an optimal use of environmental resources, respecting the socio-cultural authenticity of host communities and ensuring viable, long-term economic operations (Nagi & Kumar, 2021) [18] , (UNWTO, 2004) [15] a way of development intended to improve the quality of life of host communities, provide a top-quality experience for the visitors and preserve the quality of the environment.

Heritage Tourism in India

India's historical heritage is also very significant as it consists of secular and religious monuments dedicated to various faiths. The artistic and cultural heritage of the country is viewed as a USP by promoters and destination designers. According to various estimates, heritage tourism accounts for more than 60% of the overall share of tourists coming to India. It is overwhelming to note that 80% of the foreign tourists are interested in visiting rich heritage sites like Delhi, Jaipur, Agra and Mamallapuram and so on. India is ranked 11th in the Asia Pacific region and 40th overall, moving up three places on the list of the world's attractive destinations. It is ranked the 14th best tourist destination for its natural resources and 24th for its cultural resources, with many *World Heritage Sites*, both natural and cultural, rich fauna, and strong creative industries (Nagi, Vijayakanthan & Arasuraja, 2022) [19] in the country.

Significance of the Study

Today multiplier effects of tourism are considerably common for the national economies. Tourism is a bilateral event which covers not only locals but also the visitors. None of the tourist would like to encounter the inappropriate behaviors of the locals even if the destination shines with the tremendous natural environmental and historical beauties. To better understand the aspects of heritage and history that are utilized and the application of sustainable concepts in Mamallapuram, this investigation focuses strongly on the perceptions of the stakeholders towards sustainable tourism. The community, as hosts to tourists, is vital in the visitor experience and research suggests that it is impossible to sustain tourism to a destination that is not supported by the local people (Ahn, Lee & Shafer 2002; [20] Twinning-Ward and Butler 2002 [21]; McCool, Moisey and Nickerson 2001) [22]. The research focuses specifically on the impact of socioeconomic, cultural and environmental of heritage tourism towards the local community at Mamallapuram. In order to ascertain how sustainability is perceived by the host views and whether those perceptions are conducive to increasing the sustainability of heritage tourism.

Problem of the Study

Early work on perceived impacts of tourism, which dates back to the 1960s, tended to focus on the economic and positive effects of tourism (Pizam, 1978) [22]. However, in the 1970s, the consequences of tourism were examined more critically by anthropologists and sociologists who emphasised negative socio-cultural impacts (De Kadt, 1979) [23]. The 1980s and 1990s have been characterised by a more balanced perspective, recently called sustainable tourism, where positive and negative effects. (Ap & Crompton, 1998) [23]. The economic impacts of tourism are usually perceived positively by the residents. Tourism acts as an export industry by generating new revenues from external sources. A host nation will gain foreign exchange, which will contribute to improve the nation's balance of payments (Gee et al, 1997) [24]. It decreases unemployment by creating new job opportunities (Sheldon and Var, 1984) [25]. Increasing demand for tourism encourages new infrastructure investment (Inskeep, 1991) [26] and communication and transportation possibilities (Milman and Pizam, 1988) [27]. Residents of tourist destination might have a better standard of living and higher income by tourism activities. However, if not well planned and controlled, tourism may lead to negative impacts or reduce the effectiveness of positive ones. The prices of goods and services might go up with the increased demand from foreign customers (Liu and Var, 1986) [28]. Tourism might cause a gradual change in a society's values, beliefs and cultural practices. Local residents feel this impact more heavily. By observing the tourists, local people might change their life style (dressing, eating, entertainment and recreational activities, and so forth). While this influence may be interpreted positively as an increase in the standard of living, it may also be considered negatively as an indication of acculturation (Brunt and Courtney, 1999 [29],

Dogan 1989) [30]. Tourism can contribute to the revitalisation of arts, crafts and local culture and to the realisation of cultural identity and heritage. In order to attract more tourists, architectural and heritage sites are restored and protected (Inskeep, 1991 [25], Liu and Var, 1986 [31]). Moreover, many people of different cultures come together by means of tourism, facilitating the exchange of cultures (Brayley et al, 1990) [32]. In addition to its cultural impacts, tourism is perceived to contribute to changes in value systems, individual behaviour, family relations, collective lifestyle, moral conduct and community organisations (Ap and Crompton, 1998) [22]. These kinds of social impacts may be positive or negative. With the development of tourism in an area, there might be changes in social structure of the community. Basically, two different classes; a rich class which consists of businessmen and landowners, and a lower class which contains mostly immigrants might emerge in the community (De Kadt, 1979 [21], Dogan, 1987 [29]). It also modifies internal structure of the community by dividing it into those who have and have not a relationship with tourism or tourists (Sampath et.al, 2023)[33]. (Brunt and Courtney, 1999 [28]). Intense immigration from different cultures of people brings about social conflict in the area. Generally, impacts of tourism on women are perceived positively such as more freedom, more opportunities to work, increase self-worked and respect, better education, higher standards of living with higher family income. However, some argue that tourism distracts family structure and values, and also leads to increase in divorce rates and prostitution (Gee et al, 1997 [23]).

Tourism may lead to a decline in moral values; invokes use of alcohol and drugs; increases crime rates and tension in the community (Liu and Var, 1986 [30] Milman and Pizam, 1988 [26 [26]). Moreover, with the development of tourism, human relations are commercialised while the non-economic relations begin to lose their importance in the community (Dogan, 1989 [29]). In relatively small tourism resort towns, increased population and crowd especially in summer seasons cause noise, pollution and congestion. This limits the use of public areas such as parks, gardens and beaches as well as of local services by the residents, which sometimes result in negative attitudes towards tourists (Ross, 1992 [34]). Local communities are known as the key stakeholders in leisure and tourism management. Tourism has to be managed with the help and interest of all stakeholders in a given territory with a focus on local inhabitants (Guyer and Pollard, 1997 [35]). Considering the importance of residents who have a key role in tourism, many studies have been carried out by researchers in developed countries about local community perceptions toward tourism (Lankford and Howard 1994 [36], Williams and Lawson, 2001 [37], Nicholas, 2007 [38]). But unfortunately, hardly any work has been devoted to examine the residents' perception on the impact on tourism sustainability development in developing countries (Lepp, 2007 [39]).

REVIEW OF LITERATURE

Ahmed, Nassar (2023) [40] in the study "Influence of Cultural heritage tourism image on resident perceived impacts and their support: Evidence from Jammu and Kashmir, India" states that every destination's tourism growth is intrinsically related to local support, particularly during periods of tourism planning, crises, and hostile movements to industry. The territory of Jammu and Kashmir within India serves as the venue for the investigation, wherein tourism based on cultural heritage is still in its infancy. The results demonstrate that inhabitants' assessments of the-economic, socio cultural and environmental‖ consequences are substantially and favourably related to CHT image, which ultimately influences community support towards CHT development. Furthermore, the conclusions of this investigation illustrate the relevance of CHT image in determining residents' opinion of tourism effects and support, which has received very limited consideration in the realm of cultural heritage. The research advances overall knowledge of how inhabitants' opinions are evolved in underdeveloped cultural heritage areas, while stressing the need for measures that are more location-based, adaptable, and resident-centred. Lekaota (2018) [41] has researched on "Impacts of World heritage sites on local communities in the Indian Ocean Region". The IORA (Indian Ocean Rim Association) is committed to various objectives which include fostering tourism and cultural exchanges in the region. IROA is also committed in promoting cultural heritage and involving the economic potential of heritage including World Heritage properties and sites. The United Nations Education, Science and Cultural Organization (UNESCO), has declared many areas as World Heritage sites along the Indian Ocean. The study used a qualitative literature review method to unpack IORA countries and their world heritage sites. The sampling comprised the IORA

countries. Purposive sampling was used for the selection of IORA countries. The results show lack of local community involvement in the management of world heritage sites, and thus no benefits accrue to them. The countries also showed that local community's participation could indeed contribute to sustainability of World Heritage Sites. The researcher recommends that IROA countries should form intense collaborations in order work together to have a common framework for managing World Heritage Sites which could benefit the communities. The researcher also proposes a benefit sharing model which can benefit IORA countries in seeking to achieve the main aim of the effective conservation of heritage and culture.

Research Proposed Model

The theoretical framework is a model of logical relationship amongst the variable of sustainability of tourism Figure 2, the self-developed theoretical model consists of a set of tourism dimension's *(social, cultural,* economic & environmental aspects) impact on the local community Based on this model, the research objectives are framed and hypotheses are also formulated.

Research Objectives

The host plays an important role in determining the success of tourism development. Without local participation there is no sustainable tourism (Kariel, 1982 [42]). The objectives of this study are to understand the whether the impact of social, cultural, economic & environmental aspects on the local communities is positive or negative at Mamallapuram.

1. To study the different degrees of tourism dimensions on the local community;
2. To identify the of tourism dimension relationship with respect to the local community.
3. To investigate the of tourism dimension impact with respect to the local community.

RESEARCH METHODOLOGY

The research for the current study includes descriptive research. The data collected for the research consist of primary and secondary data. This research has an applied questionnaire as the research instrument for collecting the data. In the questionnaire social, cultural, economic aspects carries the positive termed questions & environmental aspects has negative termed questions. So the respondents received based on the five point Likert scale has been justified in the interpretation of measures of central tendency and dispersion. The pilot study was conducted among the sample of 50 respondents. The calculated overall reliability coefficient (Cronbach Alpha) has exceeded 0.8 and appears to be invariably high across the entire variables. The population of the study are the local community like unorganized sector workers, farmers, industrial workers, merchants and etc. since the definite population is not available as per the government record the population is considered as infinite. The researcher has considered a sample of 384, with a confidence level of 95% and a margin of errors of 5% from the Demorgan's sample size estimator table. Around 400 questionnaires were distributed and 391 responses has been received back and remaining 9 questionnaires were found to be biased. The Statistical Package for Social Sciences (SPSS) 20 version and Analyzing Momentum of Structures (AMOS) 18 version were used for analysis. The statistical tools used for analysis are measures of central tendency (mean) and measures of dispersion (standard deviation), bivariate correlation and structural equation modelling.

Analysis

Measures of Central Tendency and Dispersion

The dimensionality tourism sustainability factors enhancing local community has four major dimensions measuring the level of social, cultural, economic & environmental aspects. The Measures of Central Tendency (mean) and Measures of Dispersion (Standard Deviation) has been used to measure. The results are displayed below; The mean value ranges from 4.63 to 1.64. The sustainability tourism practices have only one positive factor economical aspect (μ = 3.35), which is also supported in the previous study done by Chauhan. (2022) **Error! Bookmark not defined.**. This clearly signifies that the respondents are able to reach their economical standards like increase in life

standard, consumption and expenditure, property value and able to relate new job opportunities and investments. Whereas the social (μ = 1.64), which is also supported in the previous study done by De Kadt (1979) **.** & Dogan (1987), cultural (μ = 1.69), which is also supported in the previous study done by Brunt and Courtney (1999) & Dogan (1989) & environmental (negative questions) (μ = 4.36), which is also supported in the previous study done by Ahn, Lee & Shafer 2002; Twinning-Ward and Butler 2002 . McCool, Moisey and Nickerson 2001. factor show the negativity part of the tourism. This shows that in these factors respondents are feeling that they are not able to reach their standards.

Bivariate Correlation

The relationship among the dimensionality tourism sustainability factors enhancing local community (social, cultural, economic & environmental aspects) has been measured using the Bivariate Correlation. The results are displayed below; The results of the bivariate table shows that social aspect has positive relationship with the cultural aspect (r = 0.943) & tourism sustainability factors (r = 0.655). Likewise, the cultural aspect has positive relationship with the tourism sustainability factors (r = 0.634). In the same way, the economical aspect has positive relationship with the environmental aspect (r = 0.561) & tourism sustainability factors (r = 0.253). And correspondingly environmental aspect has positive relationship with the tourism sustainability factors (r = 0.327). Whereas the cultural aspect has negative relationship with the environmental aspect (r = - 0.140). In the same way, the social aspect has no relationship with economical aspect & environmental aspect and the cultural aspect has no relationship with the economical aspect. These results are supported by the previous authors research like Brunt and Courtney, 1999 . & Ross, 1992).

Structural Equation Modelling

The Impact of social, cultural, economic & environmental aspects over the dependent variable tourism sustainability factors enhancing local community has been measured using the Structural Equation Modelling. The results are displayed below; The GFI (Goodness of Fit) and AGFI (Adjusted Goodness of Fit Index) should be nearing to one or one indicates that the model is a good fit. In this model the GFI value is 0.956 and AGFI value is 0.971. This clearly implies that the model is a good fit. The regression weight table clearly shows that the social (estimate = 0.344), cultural (estimate = 0.262), economic (estimate = 0.257) & environmental (estimate = 0.071) aspects have positive impact on the tourism sustainability factors enhancing local community (De Kadt, 1979 [21]). The independent variable human resource interventions show 48.9 percentage of its variance when influenced by the dependent variables social, cultural, economic & environmental aspects (Ap & Crompton, 1998 [22]).

DISCUSSION AND CONCLUSION

The results propose that while tourism practices have been successful in positively affecting the economy, there is room for improvement in addressing the negative impacts on social, cultural, and environmental factors. Efforts should be directed toward creating a more balanced and sustainable approach to tourism that takes into account the well-being of the local community, the preservation of cultural heritage, and the protection of the environment, (Chen, 2023, provides the guidelines to the relevant authorities and regulators in developing and implementing the regulators regarding the sustainability of tourism growth by promoting economic and environmental conditions and effective tourism policies in the country [42]). The consistently lower mean values in the social, cultural, and environmental aspects suggest that respondents perceive these dimensions of tourism to fall short in meeting their standards. This indicates a negative perception of the impact of tourism on these aspects and calls for greater attention and improvement in sustainable tourism practices. In conclusion, the study reveals a mixed picture of sustainability in tourism, with positive economic outcomes but challenges (Nagi, Kannan & Ramasubramaniam, 2021) [43] in social, cultural, and environmental dimensions (Banga et. al, 2022) [44]. To achieve more comprehensive sustainability, it is crucial for stakeholders in the tourism industry to address the identified concerns and work towards a more balanced and responsible approach that takes into account the well-being of local

communities, cultural heritage preservation, and environmental conservation. Further research and concerted efforts are needed to foster sustainable tourism practices that bring positive outcomes across all dimension.

REFERENCES

1. Korstanje Maximiliano E. (2015) A portrait of Jost Krippendorf. *Anatolia* 26 (1), 158-164.
2. Lane, B. (2018). Will sustainable tourism research be sustainable in the future? An opinion piece. *Tourism management perspectives*, *25*, 161-164.
3. Ekta Chauhan. (2022) Residents' Motivations to Participate in Decision-Making for Cultural Heritage Tourism: Case Study of New Delhi. *Sustainability* 14 (14), 8406.
4. Alzue, A., O'Leary, J., and Morrison, A.M. (1998) 'Cultural and heritage tourism: identifying niches for international travellers', *The Journal of Travel and Tourism Studies*, 9 (2), 2–13.
5. Herbert, D. (2001) 'Literary places, tourism and the heritage experience', Annals of Tourism Research, 28 (2), pp.312–333.
6. Li, Y., & Lo, L. B. R. (2005). Opportunities and constraints of heritage tourism in Hong Kong's changing cultural landscape. *Tourism and Hospitality Research*, 5 (4), 322–345. http://www.jstor.org/stable/23743803
7. Craik, J. (1997) The culture of tourism. In C. Rojek, and J. Urry (Eds.). Touring cultures: Transformations of travel and theory, *London: Routledge*, 113–136.
8. Williams. J. and Lawson. R. (2001) 'Community Issue and Resident Opinion of Tourism', *Annals of Tourism Research*, 28, 269-290.
9. Garrod, B. and Fyall, A. (2000) 'Managing heritage tourism', *Annals of Tourism Research*, 27 (3), 682–708.
10. UNWTO. 2009. *World Tourism Barometer. Volume 7, Number 1*, Madrid: United Nations World Tourism Organization.
11. Stronza, Amanda. (2007). The Economic Promise of Ecotourism for Conservation. Journal of Ecotourism. 6. 210-230. 10.2167/joe177.0.
12. Weaver, David & Lawton, Laura. (2007). Twenty Years On: The State of Contemporary Ecotourism Research. Tourism Management. 28. 10.1016/j.tourman.2007.03.004.
13. Sampath Nagi, M., Anandan Aritheertham, B., Bimal Thapa, J., Jeevanantham, N., & Jenniffer Ravichandran. (2022). *Consumer (Rural Farmers) Awareness towards Consumer Rights in FMCG*. Indian Journal of Natural Sciences, 13(75), 50341-50350.
14. Henderson, V. (2003). The Urbanization Process and Economic Growth: The So-What Question. *Journal of Economic Growth*, *8* (1), 47–71. http://www.jstor.org/stable/40215937
15. Picard, David & Robinson, Mike. (2006). Remaking worlds: Festivals, tourism and change. 10.21832/9781845410490-003.
16. UNESCO, Managing Historic Cities, World Heritage Papers 27 (UNESCO, 2010), annex C, pp. 113–20; this (at July 2009) lists a total of 346 sites in an urban context, of which 200 are cities and towns; others sources cite 250.
17. UNWTO (2004) Tourism Market Trends. Madrid: UNWTO.
18. Sampath Nagi, M., & Sathish Kumar, D. (2021). *Perception of the Farmers towards the Quality of Service Provided by Co-Operative Banks*. Indian Journal of Natural Sciences, 12(66), 30725-30732.
19. Sampath Nagi, M., Vijayakanthan, S., & Arasuraja, G. (2022). *Service Quality towards Retail Stores Across Coimbatore District*. Indian Journal of Natural Sciences, 12(70), 38370-38374.
20. Ahn, BumYong & Lee, Bongkoo & Shafer, Carl. (2002). Operationalizing sustainability in regional tourism planning: An application of the limits of acceptable change framework. Tourism Management. 23. 1-15. 10.1016/S0261-5177 (01)00059-0.
21. Louise Twining-Ward & Richard Butler (2002) Implementing STD on a Small Island: Development and Use of Sustainable Tourism Development Indicators in Samoa, Journal of Sustainable Tourism, 10 (5), 363-387, DOI: 10.1080/09669580208667174
22. McCool, S. F., Moisey, R. N., & Nickerson, N. P. (2001). What Should Tourism Sustain? The Disconnect with Industry Perceptions of Useful Indicators. Journal of Travel Research, 40 (2), 124–131. https://doi.org/10.1177/004728750104000202

23. Pizam, A. (1978). Tourism's Impacts: The Social Costs to the Destination Community as Perceived by Its Residents. Journal of Travel Research, 16(4), 8–12. https://doi.org/10.1177/004728757801600402
24. De Kadt, E. (Ed.) (1979). Tourism: Passport to development? New York: Oxford University Press.
25. Ap, J. & Crompton, J.L. (1998). Developing and testing a tourism impact scale. Journal of Travel Research, 37 (2), 120-131
26. Gee, C.Y., Fayos-Sola, E., et al. (1997) International Tourism: A Global Perspective (E. F.-S. Chuck y. Gee, Ed.). World Tourism Organization, Madrid.
27. Sheldon, P., & Var, T. (1984). Resident attitudes to tour-ism in North Wales. Tourism Management, 5, 40–47.
28. Inskeep, E. (1991). Tourism planning: an integrated and sustainable development approach. Van Nostrand Reinhold.
29. Ady Milman and Abraham Pizam (1988) Social Impacts of Tourism on Central Florida. Annals of Tourism Research, 15 (2), 1988, 191-204.
30. Liu, J. C., & Var, T. (1986). Resident attitudes toward tourism impacts in Hawaii. Annals of Tourism Research, 13, 193–214.
31. Brunt, P., & Courtney, P. (1999). Host perceptions of sociocultural impacts. Annals of Tourism Research, 26, 493–515.
32. Dogan, H. Z. (1989). Forms of adjustment: sociocultural impacts of tourism. Annals of Tourism Research, 6, 216–236.
33. Liu, J. C., & Var, T. (1986). Resident attitudes toward tourism impacts in Hawaii. Annals of Tourism Research, 13, 193–214.
34. Pilar Bastias-Perez, Turgut Var, (1995), Perceived impacts of tourism by residents, Annals of Tourism Research, 22 (1), 208-210.
35. Sampath Nagi, M., R. Vanathi, Prabavathi Venugopal, Suganya. B., & G. Sathya. (2023). *Inter Relationship of Determinants of Service Climate in District Central Cooperative Bank, Coimbatore among the Farmers in Rural Location of Coimbatore*. Indian Journal of Natural Sciences, 12(80), 60839-60847.
36. Ross, H. (1992) Foreign Language Education as a Barometer of Modernization. In: Hayhoe, R., Ed., Education and Modernization: The Chinese Experience, Pergamon, Oxford, 239-254.
37. Claire Guyer, John Pollard, (1997). Cruise Visitor Impressions of the Environment of the Shannon–Erne Waterways System, Journal of Environmental Management, 51 (2), 199-215,
38. Lankford, S. V., & Howard, D. R. (1994). Developing a Tourism Impact Attitude Scale. Annals of Tourism Research, 21, 121-139.
39. Williams, John & Lawson, Rob. (2001). Community issues and resident opinions of tourism. Annals of Tourism Research. 28. 269-290. 10.1016/S0160-7383(00)00030-X.
40. Nicholas, M.K. (2007) The Pain Self-Efficacy Questionnaires: Taking Pain into Account. European Journal of Pain, 11, 153-163. http://dx.doi.org/10.1016/j.ejpain.2005.12.008
41. Lepp, A. (2007). Residents' attitudes towards tourism in Bigodi village, Uganda. Tourism Management, 28, 876–885.
42. Ahmed, Nassar. (2023). Influence of Cultural heritage tourism image on resident perceived impacts and their support: Evidence from Jammu and Kashmir, India. *Zenith International Journal of Multidisciplinary Research*, 13(01), 53 - 82
43. Lekaota, L. (2018). Impacts of World heritage sites on local communities in the Indian Ocean Region. African Journal of Hospitality, Tourism and Leisure. 7. 1-10.
44. Kariel, H. G. (1989). Socio-Cultural Impacts of Tourism in the Austrian Alps. *Mountain Research and Development*, *9*(1), 59–70. https://doi.org/10.2307/3673465
45. Chen, Q. (2023). The impact of economic and environmental factors and tourism policies on the sustainability of tourism growth in China: evidence using novel NARDL model. *Environ Sci Pollut Res* 30, 19326–19341 (2023). https://doi.org/10.1007/s11356-022-22925-w
46. Sampath Nagi, M., Kannan, M., & Ramasubramaniam, P. (2021). *Challenging Scenario Faced by Exporters of Garment Industry*. Indian Journal of Natural Sciences, 12(70), 38728-38734.

47. Banga C, Deka A, Kilic H, Ozturen A, Ozdeser H (2022) The role of clean energy in the development of sustainable tourism: does renewable energy use help mitigate environmental pollution? A panel data analysis. *Environ Sci Pollut Res* 8, 1–11. https://doi.org/10.1007/s11356-022-19991-5

Table 1. Classification of the Heritage Sites

Zone	Natural Heritage	Cultural Heritage	Mixed Heritage	Total
Africa	33	42	3	**78**
Arab States	4	60	1	**65**
Asia-Pacific	48	129	9	**186**
Europe & North America	56	375	9	**440**
Latin America & Caribbean	35	83	3	**121**
Total	**176**	**689**	**25**	**890**
** Secondary Data - Sites Configured in the Study: (Information is partially retrieved from the sites given in the bibliography)*				
Values are the number of Heritage sites present in Location				

Table 2. Mean & Standard Deviation Tourism Sustainability Factors enhancing Local Community

Variables	Mean	Sd
Social Aspect	1.64	0.63
Cultural Aspect	1.69	0.62
Economical Aspect	3.35	0.48
Environmental Aspect	4.63	0.48
Tourism Sustainability Factors enhancing Local Community	**2.83**	**0.55**

Table 3. H_0: No significant relation between the dimensionality tourism sustainability factors enhancing local community (social, cultural, economic & environmental aspects)

Variables	Social Aspect	Cultural Aspect	Economical Aspect	Environmental Aspect	Tourism Sustainability Factors
Social Aspect	1				
Cultural Aspect	.943**	1			
Economical Aspect	-.031	-.043	1		
Environmental Aspect	-.084	-.140**	.561**	1	
Tourism Sustainability Factors	.655**	.634**	.253**	.327**	1
***. Correlation is significant at the 0.01 level (2-tailed).*					
Values in the table are Pearson Correlation values					

Table 4. Impact of Social, Cultural, Economic & Environmental Aspects → Tourism Sustainability Factors Enhancing Local Community

Test for Model Fit	Values
GFI (Goodness of Fit)	0.956
AGFI (Adjusted Goodness of Fit)	0.971

Table 5. Impact of Social, Cultural, Economic & Environmental Aspects → Tourism Sustainability Factors Enhancing Local Community

Variable	Inf.	Variable	UE	SE	S.E	C.R	P
Tourism Sustainability Factors Enhancing Local Community	←	Environmental Aspects	0.344	0.409	0.03	11.289	***

Tourism Sustainability Factors Enhancing Local Community	←	Cultural Aspects	0.262	0.397	0.024	10.971	***
Tourism Sustainability Factors Enhancing Local Community	←	Social Aspects	0.257	0.397	0.023	10.968	***
Tourism Sustainability Factors Enhancing Local Community	←	Economic Aspects	0.071	0.083	0.031	2.301	0.021**

***Significant at 0.001 percentage level*	***S.E - Standard Error***
**Significant at 0.05 percentage level*	***C.R - Critical Ration***
UE - Unstandardised Estimate	***P - Probability Value***
SE- Standardised Estimate	***Inf. – Influence***

Table 6. Impact of Social, Cultural, Economic & Environmental Aspects → Tourism Sustainability Factors Enhancing Local Community

Variable	Estimate
Tourism Sustainability Factors Enhancing Local Community	48.9

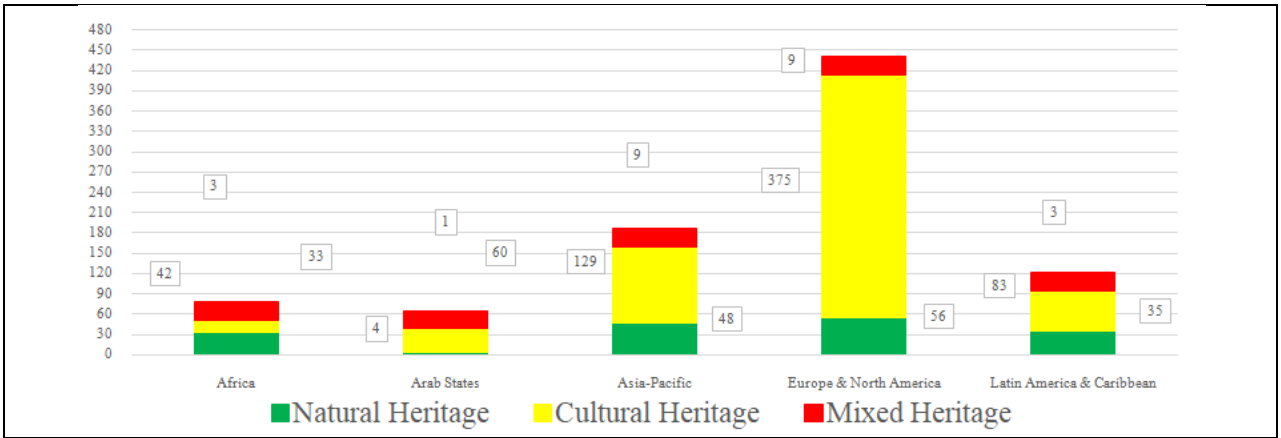

Figure 1. Classification of the Heritage Sites

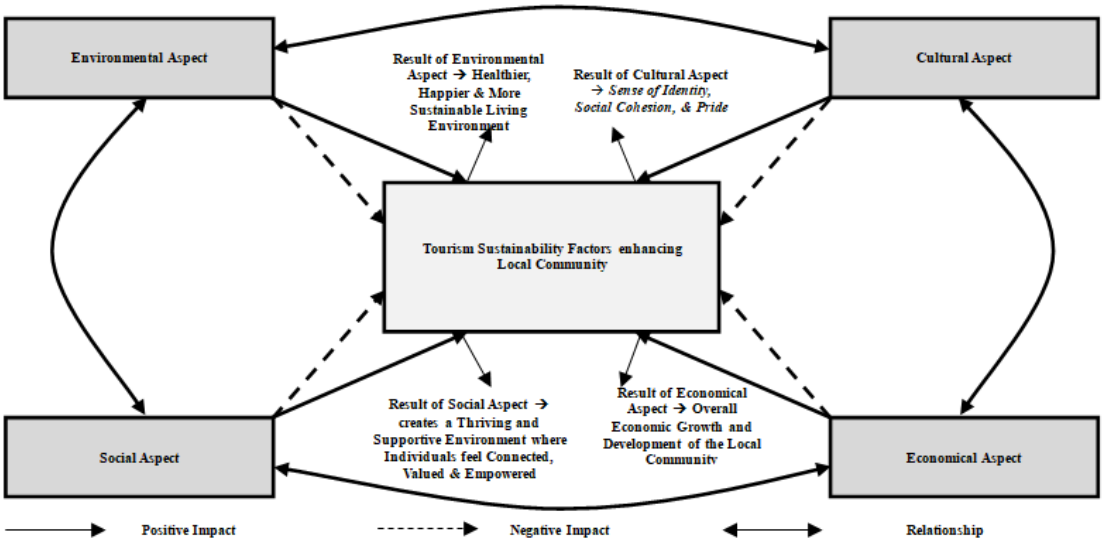

Figure 2. Tourism at Mahabalipuram Heritage Site - Impact on Local Community

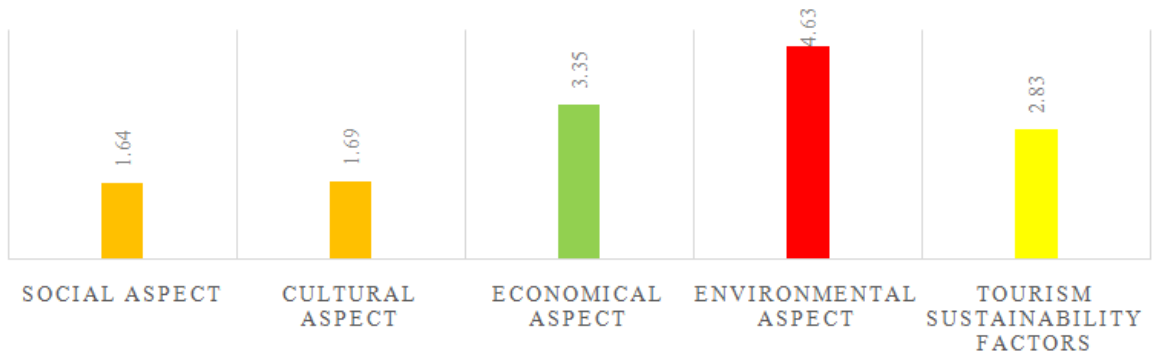

Figure 3. Tourism Sustainability Factors enhancing Local Community

Figure 4. Impact of Social, Cultural, Economic & Environmental Aspects → Tourism Sustainability Factors Enhancing Local Community

RESEARCH ARTICLE

Analysis of Fuzzy Random Graphs for Decision Making

N. Sarala[1] and R. Abirami[2]*

[1]Associate Professor, Department of Mathematics, Department of Mathematics, A.D.M. College for Women (Autonomous), Nagappatinam (Affiliated to Bharathidasan University, Tiruchirappalli), Tamil Nadu, India.
[2]Research Scholar, Department of Mathematics, A.D.M. College for Women (Autonomous), Nagappatinam (Affiliated to Bharathidasan University, Tiruchirappalli), Tamil Nadu, India.

Received: 21 Sep 2023 Revised: 24 Dec 2023 Accepted: 27 Mar 2024

***Address for Correspondence**
R. Abirami
Research Scholar,
Department of Mathematics,
A.D.M. College for Women (Autonomous), Nagappatinam (Affiliated to Bharathidasan University, Tiruchirappalli),
Tamil Nadu, India.
Email: kannahiamf@gmail.com

ABSTRACT

A key task for ensuring the effective running of an academic organization is the selection of competent and highly qualified academic staff. Due to the selection process' complexity, it is necessary to adopt the decision-making procedure, which allows for the most effective choice to be made based on the qualitative and quantitative information that is available. The primary focus of the current work is the selection of academic staff for an academic organization based on the vertex degree in the union and intersection of two fuzzy random graphs.

Keywords: Fuzzy Random Graph, Degree of vertex, characteristics of academic staff, Union and intersection of fuzzy random graphs.

INTRODUCTION

Employee dedication to the organization is what ensures its existence in nowadays aggressive competition. The success of an academic organization will indeed result from selecting potential hires who meet the requirements or policies to carry out a specific task. In literature, personnel selection receives a lot of attention. The Proceedings of the International Conference on Economics, Management, and Accounting (ICEMAC 2021) describe the proposed fuzzy logic for an intelligent decision support system to evaluate a student's eligibility for admission to the university. The applicability of the graph theoretic technique is first presented in 2016 to rank and choose academic staff out of ten

candidates. A survey will be conducted in 2013 to examine the current fuzzy strategies for handling the staff selection process. It organizes various research techniques already in use and highlights gaps that require more investigation. Along with several fuzzy variations of fundamental concepts from graph theory, such as path, cycle, connectedness, etc., Rosenfeld developed the idea of the fuzzy graph in 1975. The idea of fuzzy relations was first suggested by Zadeh in 1987. Mordeson defined the operations such as union, Cartesian product, and composition of two fuzzy graphs. NN and Peng.C.S. The concept of a random graph was first proposed by Paul Erdos and Alfred Renyi in 1959, expanding on the probabilistic technique to determine the existence of particular graph features. The use of possibility theory in Professor Lotfi Zadeh's fuzzy sets and fuzzy logic theory dates back to 1978. Didier Dubois and Henri Prade also made contributions to its development. This research uses the concept of the introduction of fuzzy random graphs to establish the crucial factors for selecting the academic staff for arts and science colleges.

PRELIMINARIES

Definition:2.1

A Fuzzy Graph denoted by $\mathbb{G} = (V, E)$on the graph $\mathbb{G}^* = (V^*, E^*)$ is a pair of functions (σ, μ) where $\sigma: V \to [0,1]$ is a Fuzzy subset of a non-empty set V and $\mu: V \times V \to [0,1]$ is a symmetric Fuzzy relation on σsuch that for all u and v, the relation $\mu(u, v) = \mu(uv) \leq \sigma(u) \wedge \sigma(v)$ is satisfied.

Definition:2.2

A Fuzzy Graph $\mathbb{H} = (V, \tau, \varphi)$ is called a Partial Fuzzy Subgraph of $\mathbb{G} = (V, \sigma, \mu)$ if $\tau(u) \leq \sigma(u)$ for every vertex $u \in \sigma$ and $\varphi(uv) \leq \mu(uv)$ for every $uv \in \mu$. In particular, $\mathbb{H} = (V, \tau, \varphi)$ is called a Fuzzy subgraph of $\mathbb{G} = (V, \sigma, \mu)$ if $\tau(u) = \sigma(u)$ for every $u \in \tau$ and $\varphi(uv) = \mu(uv)$ for every $uv \in \varphi$.

Definition:2.3

A probability space of all unlabled graphs with n vertices and m edges is called an Erdos-Renyi Random graph G(n,m). Each graph in this space has equally likely probability of being chosen, that is $P(\mathbb{G}_{n,m} = \mathbb{G}) = \left(\binom{n}{2}_{m}\right)^{-1}$. This formula follows as we are choosing m edges out $\binom{n}{2}$ possible edges, where each graph occurs with equal probability.

Definition:2.4

A Gilbert Random Graph $\mathbb{G}(n, p)$ is a probability space on the set of graphs with n vertices where each edge in the graph is added independently with probability P.

Definition:2.5

Let $\mathbb{V} = \{v_i, i = 1,2, \ldots \ldots, n\}$ be a set of n vertices has $n(n-1)/2$ possible edges $\mathbb{E}$ between them. Then there are two sets of edges, $\mathbb{E}_{\mathcal{F}} = \{(u, v)/\ 1 \leq u < v \leq n$ and (u, v) are Fuzzy edges$\}$

$\mathbb{E}_{\mathcal{R}} = \{(u, v)/\ 1 \leq u < v \leq n$ and (u, v) are Random edges$\}$ that are disjoint. Consider the mapping

$$\varphi_{\mathcal{G}}: \mathbb{V} \to [0,1] \qquad u \to \varphi_{\mathcal{G}}(u)$$

$$\psi_{\mathcal{G}}: \mathbb{V} \times \mathbb{V} \to [0,1]_P \times [0,1]_{f_A}$$

$$(u, v) \to \psi_{\mathcal{G}}(u, v) = (P(u, v), f_A(u, v))$$

with $P(u, v) = 0$ if and only if $f_A(u, v) = 0$. Then the quartet $\mathbb{G} = (\mathbb{V}, \mathbb{E}, \varphi_{\mathcal{G}}, \psi_{\mathcal{G}}$ is called a Fuzzy Random graph if $\psi_{\mathcal{G}}(u, v) \leq \min\{\varphi_{\mathcal{G}}(u), \varphi_{\mathcal{G}}(v)\}$.

where (u, v) corresponds to the edge between u and v, $P(u, v)$and $f_A(u, v)$represents the probability of the edge (u, v) and the membership function for the edge (u, v) within the fuzzy set A in Xrespectively.

Definition:2.6

A Fuzzy Random Graph $\mathbb{H} = (\mathbb{V}, \mathbb{E}, \tau_{\mathcal{G}}, \sigma_{\mathcal{G}})$ is called a Partial Fuzzy Random Subgraph of $\mathbb{G} = (\mathbb{V}, \mathbb{E}, \varphi_{\mathcal{G}}, \psi_{\mathcal{G}})$ if $\tau_{\mathcal{G}}(u) \leq \varphi_{\mathcal{G}}(u)$ for every $v \in \mathbb{V}$ and $\sigma_{\mathcal{G}}(uv) \leq \psi_{\mathcal{G}}(uv)$ for every $u \in \mathbb{V}$. Also the Fuzzy Random Graph $\mathbb{H} = (\mathbb{V}, \mathbb{E}, \tau_{\mathcal{G}}, \sigma_{\mathcal{G}})$ is called a Fuzzy Random Subgraph of $\mathbb{G}$ induced by α if $\alpha \subseteq \mathbb{V}$, $\tau_{\mathcal{G}}(u) = \varphi_{\mathcal{G}}(u)$ for all $u \in \alpha$ and $\sigma_{\mathcal{G}}(uv) = \psi_{\mathcal{G}}(uv)$ for all $u, v \in \mathbb{E}$.We write $\langle\alpha\rangle$ to denote the Fuzzy Random subgraph induced by α.

Definition:2.7

In a Fuzzy Random Graph $\mathbb{G} = (\mathbb{V}, \mathbb{E}, \varphi_{\mathcal{G}}, \psi_{\mathcal{G}})$ the degree of a Fuzzy Random vertex u is defined as

$$d_{\mathbb{G}}(u_i) = \sum_{u_i \neq v_i \in \mathbb{E}_{\mathcal{F}}} \psi_{\mathcal{G}}(u, v) + \sum_{u_i \neq v_i \in \mathbb{E}_{\mathcal{R}}} nP$$

$$d_{\mathbb{G}}(u_i) = \sum_{u_i, v_i \in \mathbb{E}_{\mathcal{F}}} \psi_{\mathcal{G}}(u, v) + \sum_{u_i, v_i \in \mathbb{E}_{\mathcal{R}}} n\psi_{\mathcal{G}}(u, v)$$

for $(u, v) \in \mathbb{E}$ and $\psi_{\mathcal{G}}(u,v) = 0$ for (u,v) not in $\mathbb{E}$. Where $\psi_{\mathcal{G}}(u, v) = P$

Definition:2.8

The Union of two Fuzzy Random Graphs $\mathbb{G}_1$ and $\mathbb{G}_2$ is defined as a Fuzzy Random graph $\mathbb{G}_3 = \mathbb{G}_1 \cup \mathbb{G}_2 : (\varphi_{\mathcal{G}_1} \cup \varphi_{\mathcal{G}_2}, \psi_{\mathcal{G}_1} \cup \psi_{\mathcal{G}_2})$, where $\mathbb{V}_3 = \mathbb{V}_1 \cup \mathbb{V}_2$ and $\mathbb{E}_3 = \mathbb{E}_1 \cup \mathbb{E}_2$ with

$$(\varphi_{\mathcal{G}_1} \cup \varphi_{\mathcal{G}_2})(u) = \begin{cases} \varphi_{\mathcal{G}_1}(u) \text{ if } u \in \mathbb{V}_1 - \mathbb{V}_2 \\ \varphi_{\mathcal{G}_2}(u) \text{ if } u \in \mathbb{V}_2 - \mathbb{V}_1 \\ \varphi_{\mathcal{G}_1}(u) \vee \varphi_{\mathcal{G}_2}(u) \text{ if } u \in \mathbb{V}_1 \cap \mathbb{V}_2 \end{cases} \text{ and}$$

$$(\psi_{\mathcal{G}_1} \cup \psi_{\mathcal{G}_2})(uv) = \begin{cases} \psi_{\mathcal{G}_1}(uv) \text{ if } uv \in \mathbb{E}_1 - \mathbb{E}_2, uv \text{ is either Fuzzy or Random edge} \\ \psi_{\mathcal{G}_2}(uv) \text{ if } uv \in \mathbb{E}_2 - \mathbb{E}_1, uv \text{ is either Fuzzy or Random edge} \\ \psi_{\mathcal{G}_1}(uv) \vee \psi_{\mathcal{G}_2}(uv) \text{ if } uv \in \mathbb{E}_2 \cap \mathbb{E}_1, uv \text{ is both fuzzy or ranodm edge} \\ \qquad \text{and } uv \in \mathbb{E}_{R2} \cap \mathbb{E}_{F1}, \text{or } uv \in \mathbb{E}_{F2} \cap \mathbb{E}_{R1}, \end{cases}$$

Definition:2.9

The Intersection of two Fuzzy Random graphs $\mathbb{G}_1$ and $\mathbb{G}_2$ is defined as a Fuzzy Random graph $\mathbb{G} = \mathbb{G}_1 \cap \mathbb{G}_2 : (\varphi_{\mathcal{G}_1} \cap \varphi_{\mathcal{G}_2}, \psi_{\mathcal{G}_1} \cap \psi_{\mathcal{G}_2})$, where $\mathbb{V} = \mathbb{V}_1 \cap \mathbb{V}_2$ and $\mathbb{E} = \mathbb{E}_1 \cap \mathbb{E}_2$ with

$$\left(\varphi_{\mathcal{G}_1} \cap \varphi_{\mathcal{G}_2}\right)(u) = \begin{cases} \varphi_{\mathcal{G}_1}(u) \wedge \varphi_{\mathcal{G}_2}(u); \text{ if } u \in \mathbb{V}_1 \cap \mathbb{V}_2 \\ 0; \text{ Otherwise} \end{cases} \text{ and}$$

$$(\psi_{\mathcal{G}_1} \cap \psi_{\mathcal{G}_2})(uv) = \begin{cases} \psi_{\mathcal{G}_1}(v) \wedge \psi_{\mathcal{G}_2}(v) \text{ if } uv \in \mathbb{E}_2 \cap \mathbb{E}_1 \\ 0; \text{ Otherwise} \end{cases}$$

DECISION MAKING ON ACADEMIC STAFF SELECTION

Expected Characteristics of academic staff:

In the Arts and Science Colleges, there is a high expectation for quality academic staff. There are several reasons for this expectation.

- Experience
- Educational Qualification
- Salary expectations
- Ability to handle different subjects

- Research activities
- Technical skills
- Communication skills

Algorithm

Step 1: Input the Fuzzy Random vertex V_R
Step 2: Input the Fuzzy Random edge E_R
Step 3: Create the Fuzzy Random graphs
Step 4: Combine two Fuzzy random graphs by finding their union and intersection
Step 5: Determine the degree of vertices in Fuzzy Random graphs
Step 6: Identify the maximum degree of vertices and conclude that this characteristic is important.
Step 7: If the maximum value exceeds one value, repeat step: 1 and reassess the academic staff's characteristics.

Structure of the Problem

Step: 1

Suppose that there are two sets A and B which are two different background of candidates as far as the location of their institution they previously studied, namely urban and rural. Three candidates C_1, C_2, C_3 were taken as parameters. The following characteristics,

- u_1 stands for Experience
- u_2 stands for Educational Qualification
- u_3 stands for Ability to handle different subjects
- u_4 stands for Research Activities
- u_5 stands for Technical skills

which are to be expected from the candidates were taken as the vertices of a Fuzzy random graph.

Step: 2

Consider $\mathbb{V} = \{u_1, u_2, u_3, u_4, u_5\}$ and $\mathbb{E} = \{u_1u_2, u_2u_3, u_3u_4, u_4u_5, u_5u_1, u_2u_5, u_1u_3, u_2u_4\}$

Let $\mathbb{V}_1 = \{u_1, u_2, u_3, u_4\}$ $\mathbb{E}_{\mathcal{F}_1} = \{u_1u_2, u_2u_3, u_4u_5\}$ $\mathbb{E}_{\mathcal{R}_1} = \{u_3u_4, u_5u_1\}$

$\mathbb{V}_2 = \{u_1, u_2, u_3, u_4\}$ $\mathbb{E}_{\mathcal{F}_2} = \{u_1u_2, u_2u_3, u_4u_5\}$ $\mathbb{E}_{\mathcal{R}_2} = \{u_2u_4, u_5u_1\}$

$\mathbb{V}_3 = \{u_1, u_2, u_3, u_4\}$ $\mathbb{E}_{\mathcal{F}_3} = \{u_2u_3, u_1u_3\}$ $\mathbb{E}_{\mathcal{R}_3} = \{u_2u_5, u_3u_4\}$

Then $\mathbb{G}_1$ and $\mathbb{G}_2$ are defined by Tables.

Step: 4

The Union of two fuzzy random graphs $\mathbb{G}_1$ and $\mathbb{G}_2$ are given by Tables.
The intersection of two fuzzy random graphs $\mathbb{G}_1$ and $\mathbb{G}_2$ are given by Tables.

Step: 5

Degree of vertices in the union of two Fuzzy random graphs
Degree of vertices in the union of two Fuzzy random graphs

Step: 6

According to the preceding procedures, vertex $\mathbf{u_2}$ is more significant than the other vertices. In this case, too, the maximum value does not exceed one. As a result, we come to an end here. Because of this, the selection of academic staff at colleges of arts and sciences heavily considers educational qualifications.

CONCLUSION

A conclusion was drawn in light of the findings above. Educational qualifications and the characteristics of academic staff play a significant role in how firms choose their employees. The flexibility of vertex degree in fuzzy random graphs is offered as a selection criterion for academic employees among three applicants.

REFERENCES

1. Abdul Muneera, Nageswara Rao T, Srinivasa Rao R.V.N,Venkateswara Rao J of "Applications of Fuzzy Graph Theory Portrayed in Various Fields". Research Square 2021.
2. Muchtar Ali Setyo Yudono, Riyan Mirdan Faris, Aryo De Wibowo, Muhammad Sidik, Falentino Sembiring, Sankan Fahmi Aji, Fuzzy Decision Support System for ABC University Student Admission Selection, Proceedings of the International Conference on Economics, Management and Accounting (ICEMAC 2021), Advances in Economics, Business and Management Research, volume 207.
3. John N. Mordeson, Sunil Mathew, Advanced Topics in Fuzzy Graph Theory, Springer Nature Switzerland AG , 2019.
4. Huda Mutab Al Mutab, 2019, "Fuzzy Graphs", Journal of Advances in Mathematics, Vol 17, ISSN: 2347-1921.
5. Sunil Mathew, John N. Mordeson, Davender S. Malik, Fuzzy Graph Theory, Springer International Publishing AG, 2018.
6. N. K. Geetha and P. Sekar, Academic Staff Selection using Graph Theory Matrix Approach, Indian Journal of Science and Technology, Vol 9(S1), DOI: 10.17485/ijst/2016/v9iS1/106706, December 2016.
7. Baoding Liu, Uncertain random graph and uncertain random network, Journal of Uncertain systems Vol.8, No.1,pp.3-12,2014.
8. R. Md Saad ,M. Z. Ahmad, M. S. Abu and M. S. Jusoh, Some Fuzzy Techniques for Staff Selection Process: A Survey, Researchgate April 2013,DOI: 10.1063/1.4801162
9. Babak Daneshvar Rouyendegh, Turan Erman Erkan, Selection of academic staff using the fuzzy Analytic Hierarchy Process (FAHP):A pilot study, Tehnicki vjesnik - Technical Gazette, December 2012.
10. Nagoor Gani A, Radha K of "The Degree of a vertex In some Fuzzy Graphs", International Journal of Algorithms, Computing and Mathematics - 2009,Vol 2, Eashwar Publications.

Table: 3.1

$\mathbb{V}_1$	u_1	u_2	u_3	u_4	u_5
C_1	0.9	0.6	0.5	0.8	0.4
C_2	0.8	0.3	0.7	0.6	0.5
C_3	0.7	0.5	0.4	0.9	0.6

Table 3.2

$\mathbb{E}_1$	u_1u_2	u_2u_3	u_3u_4	u_4u_5	u_5u_1	u_2u_5	u_1u_3	u_2u_4
C_1	0.6	0.3	0.4	0.4	0.2	0	0	0
C_2	0.3	0.25	0	0.4	0.5	0	0	0.3
C_3	0	0.2	0.3	0	0	0.5	0.4	0

Table 3.3

$\mathbb{V}_2$	u_1	u_2	u_3	u_4	u_5
C_1	0.7	0.8	0.6	0.9	0.8
C_2	0.6	0.4	0.4	0.5	0.7
C_3	0.4	0.6	0.5	0.2	0.6

Table 3.4

$\mathbb{E}_2$	$\mathbf{u_1u_2}$	$\mathbf{u_2u_3}$	$\mathbf{u_3u_4}$	$\mathbf{u_4u_5}$	$\mathbf{u_5u_1}$	$\mathbf{u_2u_5}$	$\mathbf{u_1u_3}$	$\mathbf{u_2u_4}$
$\mathbf{C_1}$	0.7	0	0.5	0	0	0.8	0.5	0
$\mathbf{C_2}$	0.4	0.3	0.35	0	0.6	0	0	0.4
$\mathbf{C_3}$	0	0.5	0.1	0.2	0.4	0.4	0.4	0

Table 3.5

$\mathbb{V}_1 \cup \mathbb{V}_2$	$\mathbf{u_1}$	$\mathbf{u_2}$	$\mathbf{u_3}$	$\mathbf{u_4}$	$\mathbf{u_5}$
$\mathbf{C_1}$	0.9	0.8	0.6	0.9	0.8
$\mathbf{C_2}$	0.8	0.4	0.7	0.6	0.7
$\mathbf{C_3}$	0.7	0.6	0.5	0.9	0.6

Table 3.6

$\mathbb{E}_1 \cup \mathbb{E}_2$	$\mathbf{u_1u_2}$	$\mathbf{u_2u_3}$	$\mathbf{u_3u_4}$	$\mathbf{u_4u_5}$	$\mathbf{u_5u_1}$	$\mathbf{u_2u_5}$	$\mathbf{u_1u_3}$	$\mathbf{u_2u_4}$
$\mathbf{C_1}$	0.7	0.3	0.5	0.4	0.2	0.8	0.5	0
$\mathbf{C_2}$	0.4	0.3	0.35	0.4	0.6	0	0	0.4
$\mathbf{C_3}$	0	0.5	0.3	0.2	0.4	0.5	0.4	0

Table 3.7

$\mathbb{V}_1 \cap \mathbb{V}_2$	$\mathbf{u_1}$	$\mathbf{u_2}$	$\mathbf{u_3}$	$\mathbf{u_4}$	$\mathbf{u_5}$
$\mathbf{C_1}$	0.7	0.6	0.5	0.8	0.4
$\mathbf{C_2}$	0.6	0.3	0.4	0.5	0.5
$\mathbf{C_3}$	0.4	0.5	0.4	0.2	0.6

Table 3.8

$\mathbb{E}_1 \cap \mathbb{E}_2$	$\mathbf{u_1u_2}$	$\mathbf{u_2u_3}$	$\mathbf{u_3u_4}$	$\mathbf{u_4u_5}$	$\mathbf{u_5u_1}$	$\mathbf{u_2u_5}$	$\mathbf{u_1u_3}$	$\mathbf{u_2u_4}$
$\mathbf{C_1}$	0.6	0	0.4	0	0	0	0	0
$\mathbf{C_2}$	0.3	0.25	0	0	0.5	0	0	0.3
$\mathbf{C_3}$	0	0.2	0.1	0	0	0.4	0.4	0

Table 3.9

Degree of vertex in $\mathbb{G}_1 \cup \mathbb{G}_2$	$\mathbf{u_1}$	$\mathbf{u_2}$	$\mathbf{u_3}$	$\mathbf{u_4}$	$\mathbf{u_5}$
$\mathbf{C_1}$	2.3	2.5	1.8	1.4	1.6
$\mathbf{C_2}$	1.6	1.5	0.65	1.55	1.6
$\mathbf{C_3}$	0.8	1.5	1.5	0.8	1.6
Total	4.7	**5.5**	3.95	3.75	4.8

Table 3.10

Degree of vertex in $\mathbb{G}_1 \cap \mathbb{G}_2$	$\mathbf{u_1}$	$\mathbf{u_2}$	$\mathbf{u_3}$	$\mathbf{u_4}$	$\mathbf{u_5}$
$\mathbf{C_1}$	0.6	0.6	0.8	0.8	0
$\mathbf{C_2}$	1.3	1.15	0.25	0.6	1
$\mathbf{C_3}$	0.4	1	0.8	0.2	0.8
Total	2.3	**2.75**	1.85	1.6	1.8

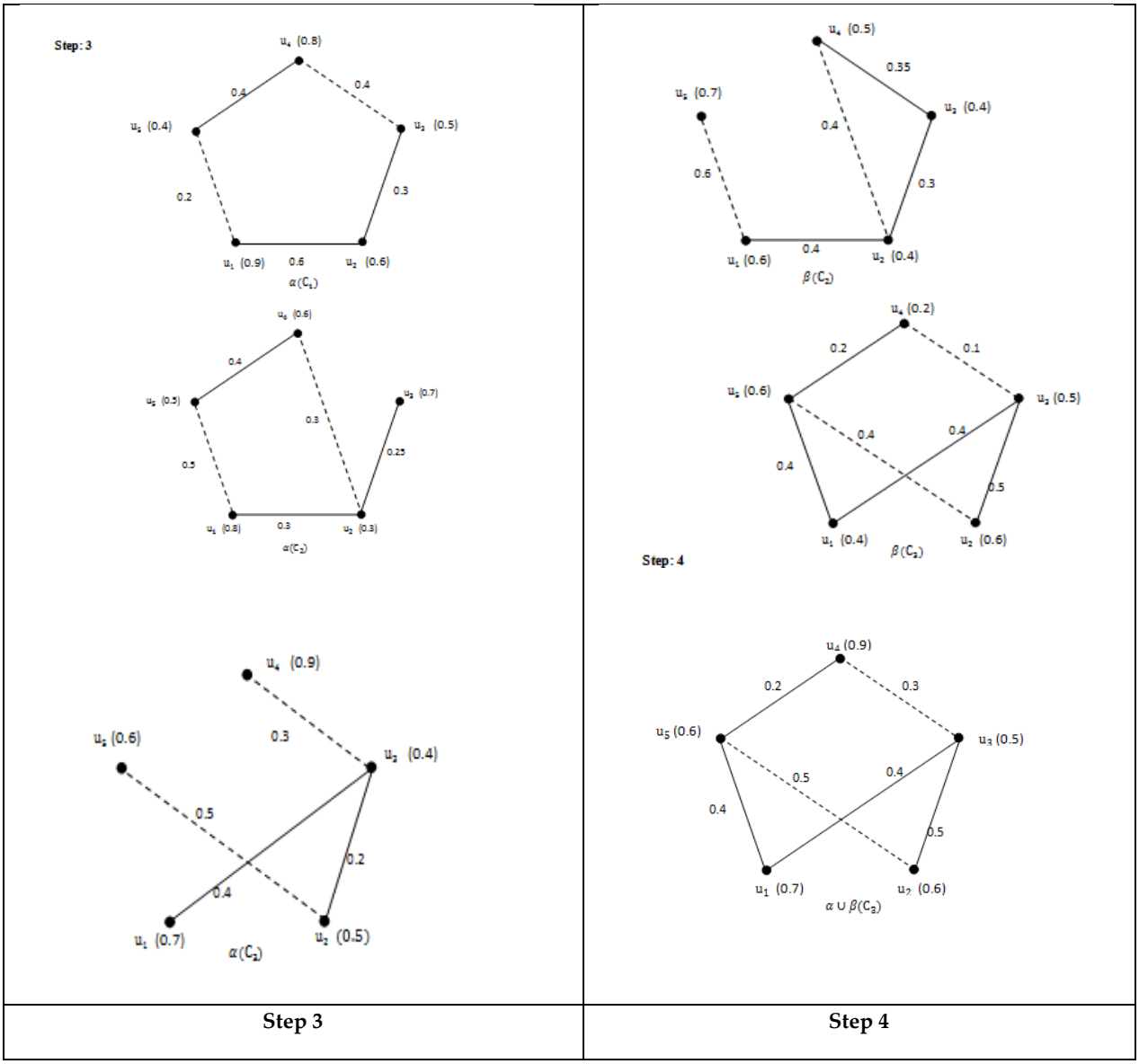
Step: 3
u4 (0.8)
0.4
0.4
u5 (0.4)
u3 (0.5)
0.2
0.3
u1 (0.9)
0.6
u2 (0.6)
α(C1)
u4 (0.6)
0.4
u5 (0.5)
u3 (0.7)
0.3
0.5
0.25
u1 (0.8)
0.3
u2 (0.3)
α(C2)
u4 (0.9)
u5 (0.6)
0.3
u3 (0.4)
0.5
0.2
0.4
u1 (0.7)
u2 (0.5)
α(C2)
u4 (0.5)
0.35
u5 (0.7)
u3 (0.4)
0.4
0.6
0.3
u1 (0.6)
0.4
u2 (0.4)
β(C2)
u4 (0.2)
0.2
0.1
u5 (0.6)
u3 (0.5)
0.4
0.4
0.4
0.5
u1 (0.4)
u2 (0.6)
β(C3)
Step: 4
u4 (0.9)
0.2
0.3
u5 (0.6)
u3 (0.5)
0.5
0.4
0.4
0.5
u1 (0.7)
u2 (0.6)
α ∪ β(C3)

Step 3	Step 4

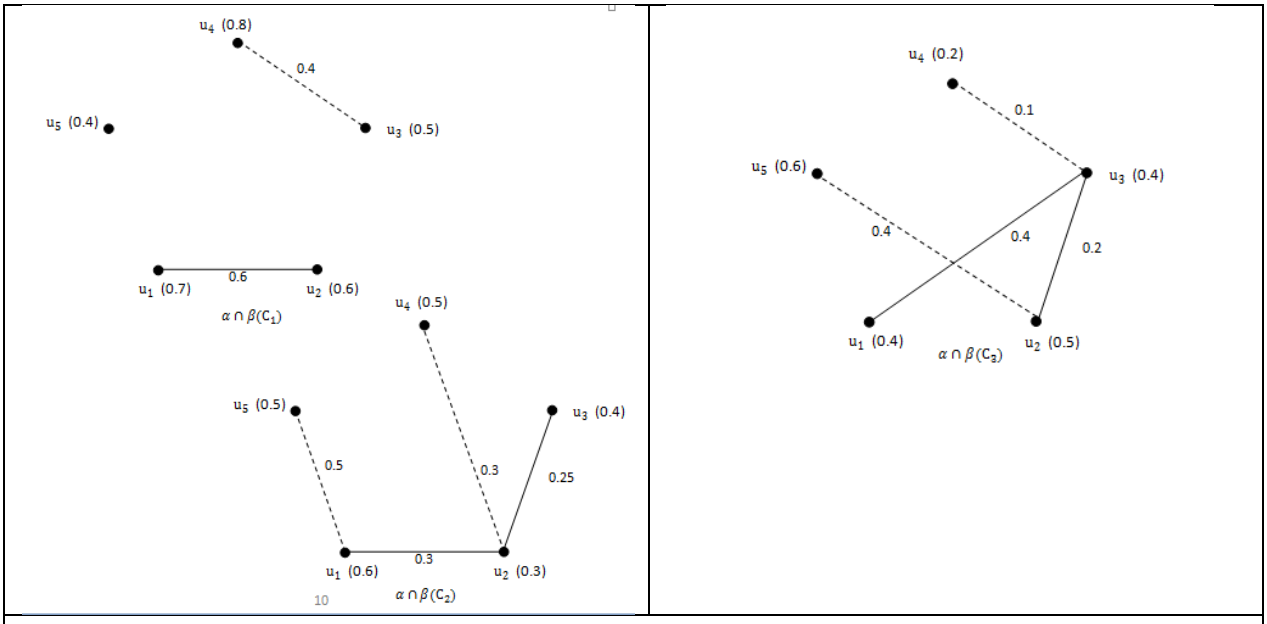
u4 (0.8)
0.4
u5 (0.4)
u3 (0.5)
u1 (0.7)
0.6
u2 (0.6)
α ∩ β(C1)
u4 (0.5)
u5 (0.5)
u3 (0.4)
0.5
0.3
0.25
u1 (0.6)
0.3
u2 (0.3)
α ∩ β(C2)
u4 (0.2)
0.1
u5 (0.6)
u3 (0.4)
0.4
0.4
0.2
u1 (0.4)
u2 (0.5)
α ∩ β(C3)

Step 5

Vol.15 / Issue 83 / Apr / 2024 International Bimonthly (Print) – Open Access ISSN: 0976 – 0997

RESEARCH ARTICLE

Assessing Periodontal Inflammation in Obese Individuals: Introducing Periodontal Inflammatory Surface Area (PISA) As A Comprehensive Measurement for Periodontitis -Pilot Study

V. Ramya[1] Julius Amaldas[2] J. Bhuvaneswarri[3] and Aarthinisha[4]

[1]Research Scholar; Professor Department of Periodontics, Sree Balaji Dental College, Biher University.
[2]Professor & HOD Department of Biochemistry, Sree Balaji Dental College.
[4]Senior Assistant Professor Department of Oral Medicine and Radiology, Taamilnadu Dental College and Hospital.
[3]Professor, Department of Periodontics, Sree Balaji Dental College.

Received: 30 Dec 2023 Revised: 09 Jan 2024 Accepted: 14 Mar 2024

***Address for Correspondence**
V. Ramya
Research Scholar & Professor,
Department of Periodontics,
Sree Balaji Dental College,
Biher University.
Email: rammu82@gmail.com

ABSTRACT

Recent research exploring the correlation between obesity and periodontitis has recognized obesity as a potential risk factor for the latter condition. Adipose tissue creates cytokines that promote inflammation, which might make periodontal tissues more inflamed. It's possible that conventional clinical measurements don't adequately reflect this influence. Digital pictures of periodontal pockets are used to assess inflammation accurately using the innovative Periodontal Inflammatory Surface Area approach, which was introduced in 2005. Due to the prevalent occurrence of obesity and periodontitis, scientists extensively examined the efficacy of PISA. This research underscores the necessity for improved diagnostic tools within this demographic and highlights the potential of PISA as a marker for inflammation. This study aims to assess PISA's usefulness in measuring inflammatory burden in periodontitis among obese individuals. A study was conducted at the Department of Periodontics, Sree Balaji Dental College & Hospital in Chennai, Tamil Nadu, involving twenty-one individuals categorized as obese or overweight. The recruitment followed the approval of the institutional human ethical committee. The study involved conducting a survey based on questionnaires to examine factors like diet, lifestyle, stress, body mass index, and waist-hip ratio. In evaluating periodontal health, measurements were taken for parameters such as bleeding on probing, recession, and clinical attachment. This data was

then utilized to calculate Attachment Level Surface Area (ALSA) and Recession Surface Area (RSA). Subsequently, Periodontal Epithelial Surface Area (PESA) and Periodontal Inflammatory Surface Area (PISA) were derived through software analytic tools. The statistical analysis included the assessment of mean and standard deviation for continuous variables. A multivariate logistic regression analysis, conducted using STATA/SE13(Stata Corp., College Station, TX, USA) the software was designed to assess how risk factors influence the occurrence of periodontitis. Furthermore, Spearman's correlation analysis was conducted to investigate relationships between different variables. The study explored correlations between periodontal parameters, PESA/PISA, and obesity levels. Spearman's correlation analysis indicated a lack of significant correlation among BMI, BOP, age, waist measurement, and PISA score. In the investigated humanity, study showed no connection among PISA and obese status. However, higher BOP values correlated with elevated PISA scores.

Keywords: gingivitis, Infectobesity, PISA, and adiposity.

INTRODUCTION

Obesity is a prevalent concern on a global scale, especially in developed countries, as highlighted by the World Health Organization in 2006. [1]. This metabolic condition arises from an energy imbalance where calorie intake surpasses expenditure, resulting in a BMI exceeding 30.0 kg/m². Consequently, it leads to an accumulation of adipose tissue, as discussed by Bray in 2007. Among the prevalent chronic ailments, periodontal disease stands out. Periodontitis involves inflammation of the periodontal apparatus, leading to the deterioration of connective attachments and tooth loss. Certainly, obesity is a pervasive condition that impacts the onset and advancement of periodontal disease. Furthermore, there is evidence to suggest that obesity may contribute to the acquisition and persistence of specific oral bacteria. Various studies have established a link between obesity, increased body weight, or higher body mass index (BMI), and the occurrence of periodontal diseases in humans.In a 2018 update to the classification of periodontal disease jointly conducted by the American Academy of Periodontology (AAP) and the European Federation of Periodontology (EFP), diabetes mellitus (DM) was included as a contributing factor that increases the risk of advancement in periodontal disease. [2, 3]. Certainly, obesity plays a crucial role in the development of type 2 diabetes (T2DM), which accounts for 90% of diabetes cases globally. The incidence of obesity is steadily increasing on a global scale. In 2016, 39% of adults were categorized as overweight (with a body mass index [BMI] ranging from 25 kg/m2 to less than 30 kg/m2), while 13% were classified as obese (with a BMI of 30 kg/m2 or higher). [4]. Throughout evolution, both animals and humans have developed a remarkable biological mechanism of storing excess energy in the form of fat to sustain life during periods of food scarcity. However, the modern lifestyle characterized by excessive calorie consumption and insufficient physical activity has led to an epidemic of obesity, which poses significant health risks. Epidemiological investigations have offered indications that obesity might be a potential risk factor in the onset of periodontal disease. [5].Periodontitis has been proposed as a potential factor in the development of systemic conditions such as cardiovascular disease. This is primarily attributed to the inflammatory and microbial challenges posed by the inflamed surface of the periodontal pocket. [6]. Nesse and colleagues introduced a measurable framework for assessing the impact of chronic periodontitis, known as the "Periodontal inflammatory surface area (PISA)[7]."The Periodontal Inflamed Surface Area (PISA) serves as a measure to quantify the square millimeter extent of the bleeding pocket epithelium. This assessment is derived from conventional clinical markers of periodontal health, specifically employing a combination of Bleeding on Probing (BOP) and either Periodontal Pocket Depth (PPD) or Clinical Attachment Loss and Gingival Recession.[8]. PISA functions as a valuable instrument for evaluating the extent and intensity of inflammatory lesions associated with periodontitis. Presently, several clinical studies are investigating the correlation between PISA and the susceptibility to systemic diseases.[9]. Furthermore, a connection exists between PISA and high-sensitivity C-reactive protein (hs-CRP), a marker indicating systemic inflammation. [10]. The objective of the research was to examine the connection

between periodontitis, inflammatory scores, and obesity levels, as well as to quantify the inflammatory burden linked to chronic periodontitis by calculating the periodontal inflammatory surface area (PISA).

METHODOLOGY

Study Design

Individuals recruited for the study within the Department of Periodontics at Sree Balaji Dental College & Hospitalin Chennai, Tamil Nadu who fell into the categories of obesity or overweight participated. The study involved a survey based on questionnaires to assess aspects such as diet, lifestyle, and stress. Additionally, the height and weight of each participant were measured to calculate their Body Mass Index (BMI), with values exceeding 30.0 kg/m² indicating obesity[11]. Furthermore, waist-hip ratios were determined using measuring tape.The study also involved the measurement of various periodontal parameters, including bleeding on probing, clinical attachment level, recession, and pocket probing depth, which were assessed using a Williams probe. Moreover, specialized software analytic tools available at www.parsprototo.info were employed to deduce Periodontal Epithelial Surface Area (PESA) and Periodontal Inflammatory Surface Area (PISA).

Ethical Approval Number

The research underwent evaluation and received approval from the institutional ethics committee under the reference number (Sree Balaji Dental College & Hospital in Chennai, Tamil Nadu/IEC/12/2020/07) for our investigation. All participants were well-informed about the survey, and they willingly agreed to furnish the necessary data, providing informed consent prior to their involvement in the study.

Inclusion Criteria

Individuals between the ages of 25 and 60, of both genders, with a BMI greater than 25, and who have at least 20 scorable teeth were included in the study.

Exclusion Criteria

The study excludes individuals who fall into the following categories: pregnant and lactating mothers, those who have undergone antibiotic or steroid therapy within the last six weeks, individuals who have received periodontal treatment in the past six months, and those who are currently taking anti-depressants or have hormone imbalances.

Statistical Analysis

To ascertain how risk variables impacted the frequency of gum infection, a multivariate logistic regression analysis was conducted and the mean and SD of separate variables were assessed. At P 0.05, it was determined to be financially meaningful.

In four phases, the Periodontal Inflamed Surface Area was determined:

1. Based on six measurements taken around each tooth, a computer determined the mean pocket probing depth (PPD) for each tooth.
2. For that tooth, the mean PPD value was used to calculate the Periodontal Epithelial Surface Area (PESA).
3. PESA is determined by deducting Attachment Level Surface Area from Recession surface area (RSA).
4. The Periodontal Inflammatory Surface Area (PISA) value was determined by dividing the maximum number of sites by the product of the Periodontal Inflammatory Surface Area (PESA) of each tooth and the count of impacted sites exhibiting Bleeding on Probing (BOP).

Periodontal Inflammatory Surface Area of Individual Tooth

PISA = (PESA × Number of sites with BOP) ÷ Maximum number of sites

Where:

PESA = Periodontal Epithelial Surface Area (surface area covered by the pocket epithelium) for the specific tooth.

Number of sites with BOP = The number of sites around the tooth with Bleeding on Probing.
Maximum number of sites = The total number of sites that were probed around the tooth (usually six sites per tooth).

RESULTS

The main goal was to investigate the connections among periodontitis, inflammatory score, and obesity. The research included 21 participants and evaluated multiple factors such as diet, lifestyle, stress, BMI, and waist-hip ratio. Periodontal attributes, such as bleeding on probing, recession, and clinical attachment, were employed to determine Attachment Level Surface Area and Recession Surface Area. PESA and PISA were calculated using software tools. Given the limited sample size (21 participants), non-parametric approaches were employed for data analysis.

Descriptive
The aim is to investigate the correlation between age and PISA score.
Spearman's correlation was used because the assumptions of Pearson correlation were not met.
Interpretation
As the p-value exceeds 0.05, we can infer that there is no statistically significant association between age and PISA score.

The objective is to examine the correlation between BMI and PISA score.
Spearman correlation was used due to the violation of Pearson correlation's assumptions.
Interpretation
The fact that the p value is higher than 0.05 leads us to believe that there is no connection between BMI and PISA score.

The aim is to investigate the correlation between waist measurement and PISA score.
Spearman correlation was employed because the assumptions of Pearson correlation were not met.
Interpretation
As the p-value is greater than 0.05, we can infer that there is no statistically significant association between waist measurement and PISA score.

The objective was to examine the correlation between BOP and PISA score.
Spearman correlation was used due to the violation of Pearson correlation's assumptions.
Interpretation
As the p-value exceeds 0.05, we can infer that a noteworthy correlation between BOP and PISA score is lacking.

DISCUSSION

In recent times, clinical investigations have been conducted utilizing data related to the Periodontal Inflamed Surface Area (PISA), a metric used to quantify the extent of inflamed periodontal tissue. PISA measures the surface area of the epithelium in bleeding pockets [12]. Considering the documented association between PISA and glycated hemoglobin (HbA1c) [13,14], it serves as a valuable indicator for gauging the systemic impact of localized periodontal inflammation. Notably, recent findings have indicated a positive association between PISA and BMI (Body Mass Index) [15]. Conversely, Takeda and colleagues reported that in individuals with Type 2 Diabetes, PISA showed no significant correlation with obesity-related parameters [16]. Nonetheless, it is crucial to form a more extensive control cohort for a thorough examination of the association between PISA and obesity. Furthermore, multiple researchers have noted that although obesity doesn't stand alone as a risk factor for the advancement of periodontitis, there exist several common risk factors in the progression of both obesity and periodontitis. [17]. Currently, there is a scarcity of clinical evidence concerning the link between periodontal disease and overweight/obesity.Obesity, which is characterised by an excessive buildup of fat, is on the rise and is linked to

chronic conditions including periodontitis [18]. The term "Infectobesity" refers to how alterations in microbiota brought on by persistent infection exacerbate circumstances in obese people. When it comes to the connection between periodontitis, obesity, and chronic illnesses, pro-inflammatory cytokines are a key player[19].Gingivitis, corpulence, and persistent diseases are all closely related, and pro-inflammatory cytokines may be a major factor in this link[20].The metabolic and immunological effects of obesity lead to an inflammatory state that makes people more vulnerable to periodontal disease[21]. Periodontal Inflammatory Surface Area, a novel metric, is used in this study to assess periodontal inflammation[22].PISA estimates the inflammatory load and makes predictions about the likelihood that periodontitis may either cause or exacerbate other illnesses. Animal studies suggest probable processes including metabolic activity, hunger, and energy metabolism, and recent research have connected oral bacteria to obesity. Even a little increase in calorie intake without diet or exercise alterations may result in weight gain[23]. As a result, assessments of food intake and activity should be included in research relating to infection-associated weight gain.By measuring the inflammatory load brought on by periodontitis, ISA acts as a predictor for the risk that periodontitis may develop or exacerbate other illnesses[24]. The study relies on the pivotal variable in this research, the PISA index, established by Nesse.

Highlights of the Study

By assessing the inflamed surface area inside the periodontal tissues, this index serves as an indirect clinical diagnostic tool for detecting the inflammatory burden in chronic periodontitis. It is the first research to use the PISA approach to evaluate how obesity affects inflammation. The study found a link between increased BOP, which is seen as a sign of inflammation, and higher PISA scores.

Limitations of this Study

The primary limitations of this study include its small sample size, which may not accurately reflect all individuals, and its failure to show a significant correlation among adiposity and PISA score. Furthermore, it was impossible to properly account for confounding variables like mellitus and nicotine.

CONCLUSION

Future research in the field of Periodontal Inflammatory Surface Area (PISA) holds significant promise in advancing our understanding of periodontal disease and improving patient outcomes. One critical avenue for investigation is the potential of PISA scores as predictive indicators for disease progression. Examining the correlation between PISA and disease severity may offer valuable insights, enabling the development of more targeted and effective treatment strategies. Longitudinal studies are essential to explore how PISA scores correlate with treatment outcomes, providing a comprehensive understanding of the effectiveness of various therapeutic interventions in reducing inflammatory burden over time. Additionally, there is a need to explore the association between high PISA scores and systemic diseases such as cardiovascular disease, diabetes, or rheumatoid arthritis. This research could unveil the systemic implications of periodontal inflammation, guiding clinicians in considering broader health outcomes. Evaluating the feasibility and benefits of incorporating PISA measurements into routine clinical practice is pivotal. Such an integration could influence treatment planning and monitoring, addressing the need for standardized, cost-effective, and user-friendly methods. Furthermore, understanding the relationship between PISA and patient-reported outcomes is crucial, offering insights into the subjective experiences of individuals with periodontitis and enhancing holistic patient care. In essence, future research in these areas could revolutionize the diagnosis, treatment, and overall management of periodontal disease.

Authors Contribution Statement

Dr. V. Ramya led the entire research, which received approval from the institutional ethical committee at Sree Balaji Dental College. All the authors thoroughly reviewed and endorsed the final draft of the manuscript.

Conflict of Interest
Conflict of interest declared none.

REFERENCES

1. Estivaleti JM, Guzman-Habinger J, Lobos J, Azeredo CM, Claro R, Ferrari G, Adami F, Rezende LF. Time trends and projected obesity epidemic in Brazilian adults between 2006 and 2030. Scientific Reports. 2022 Jul 26;12(1):12699.
2. Papapanou PN, Sanz M, Buduneli N, Dietrich T, Feres M, Fine DH, et al. Periodontitis: consensus report of workgroup 2 of the 2017 World Workshop on the Classification of Periodontal and Peri-Implant Diseases and Conditions. J Periodontol. 2018;89:S173–82. https://doi.org/10.1002/JPER.17-0721.
3. Tonetti MS, Greenwell H, Kornman KS. Staging and grading of periodontitis: framework and proposal of a new classification and case definition. J ClinPeriodontol. 2018;45:S149–61. https://doi.org/10.1111/jcpe.12945.
4. World Health Organization. Obesity and overweight 2018. Available from: https://www.who.int/en/news-room/fact-sheets/detail/obesity-and-overweight.
5. Jepsen S, Suvan J, Deschner J. The association of periodontal diseases with metabolic syndrome and obesity. Periodontol. 2000;2020(83):125–53. https://doi.org/10.1111/prd.12326.
6. Ang WS, Law JW, Letchumanan V, Hong KW, Wong SH, Ab Mutalib NS, Chan KG, Lee LH, Tan LT. A Keystone Gut Bacterium Christensenellaminuta-A Potential Biotherapeutic Agent for Obesity and Associated Metabolic Diseases. Foods. 2023 Jun 26;12(13):2485.https://doi.org/10.3390/foods12132485
7. Tang V, Hamidi B, Janal MN, Barber CA, Godder B, Palomo L, Kamer AR. Periodontal Inflamed Surface Area (PISA) associates with composites of salivary cytokines. Plos one. 2023 Feb 15;18(2):e0280333.https://doi.org/10.1371/journal.pone.0280333
8. Pietropaoli, D. *et al.* Association between periodontal inflammation and hypertension using periodontal inflamed surface area and bleeding on probing. *J. Clin. Periodontol.* **47**, 160–172. https://doi.org/10.1111/jcpe.13216 (2020).
9. Leira, Y. *et al.* Periodontal inflammation is related to increased serum calcitonin gene-related peptide levels in patients with chronic migraine. *J. Periodontol.* **90**, 1088–1095. https://doi.org/10.1002/JPER.19-0051 (2019).
10. Schöffer, C., Oliveira, L. M., Santi, S. S., Antoniazzi, R. P. &Zanatta, F. B. C-reactive protein levels are associated with periodontitis and periodontal inflamed surface area in adults with end-stage renal disease. *J. Periodontol.* https://doi.org/10.1002/JPER.20-0200 (2020).
11. Çetin MB, Sezgin Y, Önder C, Bakirarar B. The relationship between body mass index and stage/grade of periodontitis: A retrospective study. Clinical Oral Investigations. 2022 Feb 1:1-9.https://doi.org/10.1007/s00784-021-04172-4
12. Nesse W, Linde A, Abbas F, Spijkervet FK, Dijkstra PU, de Brabander ED, et al. Dose-response relationship between periodontal inflamed surface area and HbA1c in type 2 diabetics. J ClinPeriodontol. 2009;36:295–300. https://doi.org/10.1111/j.1600-051X.2009.01377.x.
13. Takeda K, Mizutani K, Minami I, Kido D, Mikami R, Konuma K, et al. PISA and PESA were not significantly associated with BMI or visceral fat area (VFA) in patients with type 2 diabetes. BMJ Open Diabetes Res Care. 2021;1: e002139. https://doi.org/10.1136/bmjdrc-2021-002139.
14. Romano F, Perotto S, Mohamed SEO, Bernardi S, Giraudi M, Caropreso P, et al. Bidirectional association between metabolic control in type-2 diabetes mellitus and periodontitis inflammatory burden: a cross-sectional study in an italian population. J Clin Med. 2021;10:1787. https://doi.org/10.3390/jcm10081787.
15. Aoyama N, Fujii T, Kida S, Nozawa I, Taniguchi K, Fujiwara M, et al. Association of periodontal status, number of teeth, and obesity: a cross-sectional study in Japan. J Clin Med. 2021;10:208. https://doi.org/10.3390/jcm10020208.
16. Slade GD, Ghezzi EM, Heiss G, Beck JD, Riche E, Offenbacher S. Relationship between periodontal disease and C-reactive protein among adults in the Atherosclerosis Risk in Communities study. Arch Intern Med. 2003;163:1172–9. https://doi.org/10.1001/archinte.163.10.1172.

17. Charupinijkul A, Arunyanak S, Rattanasiri S, Vathesatogkit P, Thienpramuk L, Lertpimonchai A. The effect of obesity on periodontitis progression: the 10-year retrospective cohort study. Clin Oral Investig. 2021. https://doi.org/10.1007/s00784-021-04031-2.
18. Abu-Shawish G, Betsy J, Anil S. Is obesity a risk factor for periodontal disease in adults? a systematic review. International Journal of Environmental Research and Public Health. 2022 Oct 4;19(19):12684.https://doi.org/10.3390/ijerph191912684
19. Rahman B, Al-Marzooq F, Saad H, Benzina D, Al Kawas S. Dysbiosis of the Subgingival Microbiome and Relation to Periodontal Disease in Association with Obesity and Overweight. Nutrients. 2023 Feb 6;15(4):826.https://doi.org/10.3390/nu15040826
20. Bader Ul Ain H, Tufail T, Javed M, Tufail T, Arshad MU, Hussain M, Gull Khan S, Bashir S, Al Jbawi E, AbdulaaliSaewan S. Phytochemical profile and pro-healthy properties of berries. International Journal of Food Properties. 2022 Dec 31;25(1):1714-35.https://doi.org/10.1080/10942912.2022.2096062
21. Pamuk F, Kantarci A. Inflammation as a link between periodontal disease and obesity. Periodontology 2000. 2022 Oct;90(1):186-96.https://doi.org/10.1111/prd.12457
22. Gopalan S, Nagarajan S, Somasundaram A, Thiyagarajan MK. Inflammatory bowel disease associated knowledge in South Indian populations: rational Study. African Health Sciences. 2023 Jul 13;23(2):442-50.https://dx.doi.org/10.4314/ahs.v23i2.51
23. Nouri S, Holcroft J, Caruso LL, Vuong TV, Simmons CA, Master ER, Ganss B. An SCPPPQ1/LAM332 protein complex enhances the adhesion and migration of oral epithelial cells: Implications for dentogingival regeneration. ActaBiomaterialia. 2022 Jul 15;147:209-20.https://doi.org/10.1016/j.actbio.2022.05.035
24. Irwandi RA, Chiesa ST, Hajishengallis G, Papayannopoulos V, Deanfield JE, D'Aiuto F. The roles of neutrophils linking periodontitis and atherosclerotic cardiovascular diseases. Frontiers in Immunology. 2022 Jul 7;13:915081.https://doi.org/10.3389/fimmu.2022.915081

[Table/Fig-1]: Descriptive Statistics

Measurement	Sample Size	Minimum	Maximum	Mean	Standard Deviation
BMI	21	25.10	35.80	28.2762	3.32128
Age	21	24	57	40.57	8.829
Waist (inches)	21	32.00	48.00	40.2762	4.42288
PISA	21	8.944	1132.284	324.89476	268.046552

[Table/Fig-2]: The correlation between age and PISA score.

Correlations

			PISA	AGE
Spearmans rho	PISA	Correlation coefficient	1.000	.288
		Sig. (2 tailed)	.	.205
		N	21	21
	AGE	Correlation coefficient	.288	1.000
		Sig. (2 tailed)	.205	.
		N	21	21

[Table/Fig-3]: The correlation between BMI and PISA score.

Correlations

			BMI	PISA
Spearmans rho	BMI	Correlation coefficient	1.000	-.327
		Sig. (2 tailed)	.	.148
		N	21	21
		Correlation coefficient	-.327	1.000

	PISA	Sig. (2 tailed)	.148	.
		N	21	21

[Table/Fig-4]: The correlation between waist measurement and PISA score.

Correlations

			PISA	WAIST
Spearmans rho	PISA	Correlation coefficient	1.000	.111
		Sig. (2 tailed)	.	.632
		N	21	21
	WAIST (inches)	Correlation coefficient	.111	1.000
		Sig. (2 tailed)	.632	.
		N	21	21

[Table/Fig-5]: The correlation between BOP and PISA score.

Correlations

			BOP	PISA
Spearmans rho	BOP	Correlation coefficient	1.000	.005
		Sig. (2 tailed)	.	.982
		N	21	21
	PISA	Correlation coefficient	.005	1.000
		Sig. (2 tailed)	.982	.
		N	21	21

[Table/Fig-7]:Number of people who are obese by age, waist circumference, and body mass index.

SCORE	**1**	**2**	**3**	**4**	**5**	**6**	**7**	**8**	**9**	**10**
PISA SCORE	8 to 120	120 to 232	232 to 354	354 to 466	466 to 578	578 to 690	690 to 802	802 to 914	914 to 1026	1026 to 1138
BOP	15 to 24	24 to 32	32 to 41	41 to 50	50 to 59	59 to 68	68 to 77	77 to 86	86 to 95	95 to 104
WAIST	32 to 36	36 to 40	40 to 44	44 to 48						
BMI	25 to 29.9	30 to 34.9	35 to 39.9							
AGE	24 to 30	30 to 36	36 to 42	42 to 48	48 to 54	54 to 60				

Fig 1: Number of people who are obese by age, waist circumference, and body mass index.

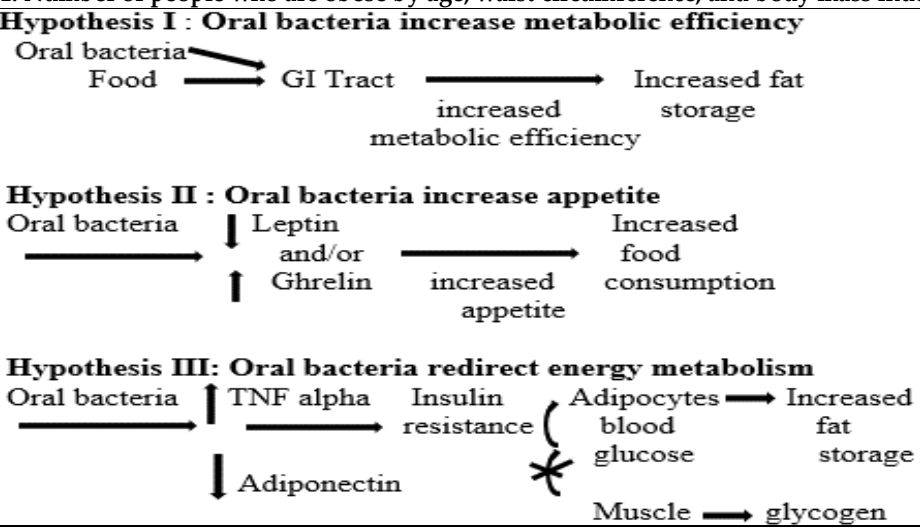

Fig 2: Hypotheses about the role of oral bacteria in obesity.

RESEARCH ARTICLE

The Significance of Hormones in Governing the Physiology of Menstrual Cycle

Shital C. Shah*

Head, Department of Pharmacy, Ahmedabad Homeopathic Medical College, Parul University, Ahmedabad, Gujarat, India.

Received: 03 Sep 2023 Revised: 24 Dec 2023 Accepted: 06 Mar 2024

***Address for Correspondence**
Shital C. Shah
Head, Department of Pharmacy,
Ahmedabad Homeopathic Medical College,
Parul University, Ahmedabad, Gujarat, India.
Email: scshah1212@gmail.com

ABSTRACT

The ovarian cycle is a critical component of female reproductive physiology, involving a series of hormonal and physical changes that prepare the ovaries for ovulation and fertilization. The ovarian cycle consists of two main phases: the follicular phase and the luteal phase. During the follicular phase, follicle-stimulating hormone (FSH), secreted by the anterior pituitary gland, stimulates the growth of ovarian follicles, each containing an immature egg (oocyte). As the follicles mature, they produce increasing levels of estrogen, which contributes to the proliferation of the uterine lining (endometrium) in preparation for implantation. Ovulation marks the transition between the follicular and luteal phases, triggered by a surge in luteinizing hormone (LH), also released by the anterior pituitary. The LH surge causes the dominant follicle to rupture, releasing the mature egg into the fallopian tube. The ruptured follicle then transforms into the corpus luteum, marking the start of the luteal phase. During the luteal phase, the corpus luteum secretes progesterone, which further enhances the uterine lining and maintains it for implantation. Progesterone levels remain high unless fertilization occurs. If fertilization does not take place, the corpus luteum degenerates, leading to a decline in progesterone and estrogen levels. This hormonal drop triggers the menstrual phase, wherein the uterine lining is shed, signaling the start of a new ovarian cycle. Hormonal regulation plays a crucial role in maintaining the ovarian cycle's rhythm and coordination. Gonadotropin-releasing hormone (GnRH) from the hypothalamus controls the release of FSH and LH, while estrogen and progesterone exert feedback control on the hypothalamus and pituitary to ensure proper cycle progression. Understanding the ovarian cycle's physiology is essential for comprehending female reproductive health and addressing conditions related to hormonal imbalances, ovulation disorders, and infertility.

Keywords: Gonadotropin, luteal phase, reproductive, physiology, fertilization

INTRODUCTION

Ovary

The ovary are the paired oval sex glands with a length of 2-5 cm, a width of 1.5-3 cm, and a thickness of 0.5-1.5 cm, weighing about 10-20 g (average:14 g).

The ovary fulfils two major objectives:

1. generation of a fertilizable ovum
2. preparation of the endometrium for implantation through the sequential secretion of estradiol and progesterone

STRUCTURE OF OVARY

The ovary consists of three structurally distinct regions: an outer cortex containing the surface germinal epithelium and the follicles; a central medulla consisting of stroma; and a hilum around the area of attachment of the ovary to the mesovarium. The hilum is the point of attachment of the ovary to the mesovarium which contains nerves, blood vessels, and hilus cells having the potential to become active in steroidogenesis or to form androgen-secreting tumors. The outermost portion of the cortex, called the tunica albuginea, is covered by a single layer of surface cuboidal epithelium called the germinal epithelium.

The oocytes, enclosed in follicles are in the inner part of the cortex, embedded in stromal tissue. The stromal tissue is composed of connective tissue and interstitial cells, which are derived from mesenchymal cells have the ability to respond to LH with the production of androstenedione.

Granulosa Cell Layer

1. Membrane [Mural] Granulosa Cells : It forms the outermost layer of the membrana granulosa. The mural cells contain high levels of LH receptors and steroidogenic enzymes and account for most of the steroidogenesis in the follicle. Antral granulosa cells of membrane granulosa seem to be steroid genically and metabolically less active than mural granulosa cells.
2. Cumulus oophorus: It consist of the egg and a surrounding mass of granulosa cells. At ovulation, the granulosa cells of the cumulus oophorus are extruded with the egg, whereas the membrana granulosa becomes incorporated into the corpus luteum. The cumulus granulosa cells lack steroidogenic activity and have less LH receptors compared with the mural granulosa cells.

Theca interna layer, which forms just outside the basement membrane, shows typical steroidogenic features. They are responsible for producing the C19 (androgens) steroids that serves as a substrate for estrogen production. Theca externa is the outermost layer of the follicle, composed of fibroblasts, smooth muscle–like cells, and macrophages. It has important function during ovulation.

1. Primary interstitial cells: They constitute of C 19 -steroid producing cells located in the medullary compartment of the foetal ovary.
2. Theca-interstitial cells. Theca-interstitial cells represent the mature C 19 -steroid producing components of the follicle. It consists of theca interna and theca externa cells.
3. Secondary interstitial cells. Secondary interstitial cells are hypertrophied theca interna remnants surviving follicular atresia. These cells remain functionally and structurally unchanged.
4. Hilar interstitial cells: They are constituents of the ovarian hilum. They are large steroidogenic lutein-like cells. The secretory function of these cells is strongly supported by their prominence at the time of puberty, during pregnancy, and around menopause.

Two cell, two-gonadotropin theory of ovarian steroidogenesis:

This theory establishes that ovarian steroids are synthesized from cholesterol through the cooperative interactions of theca and granulosa cells. Theca cells : luteinizing hormone (LH) binds to luteinizing/chorionic gonadotropin receptor (LH/CGR) on the cell surface and stimulates the expression of the steroidogenic enzymes necessary for androgen production. Cholesterol is mobilized into mitochondria by steroidogenic acute regulatory protein (STAR)

where it is converted to pregnenolone by cholesterol sidechain cleavage enzyme (CYP11A1). Pregnenolone diffuses into the smooth endoplasmic reticulum and is converted to progesterone by 3β-hydroxysteroid dehydrogenase (HSD3B). Progesterone is then converted to androstenedione by 17α-hydroxylase/17,20desmolase (CYP17A1). Granulosa cells: follicle-stimulating hormone (FSH) via signalling through follicle-stimulating hormone receptor (FSHR) stimulates the expression of enzymes necessary for estrogen synthesis. Androstenedione produced by theca cells diffuses into granulosa cells and is converted to testosterone by the enzyme 17βhydroxysteroid dehydrogenase (HSD17B) or to estrone by aromatase (CYP19A1). CYP19A1 utilizes testosterone to produce 17β-estradiol. However, HSD17B can also produce 17β-estradiol using estrone as a substrate. The classical two cell theory is supported by molecular finding. ovarian steroidogeneses in the pre ovulatory follicle takes place through LH receptor on theca and FSH receptor on granulosa cells cyclic amp production and increase SF1 binding to multiple steroidogenic promoter mediate LH action in theca cells. the pre ovulatory follicle produces estradiol through parakine interaction between theca and granulosa cell in response to stimulating steroidogenic factor 1 (sf1) a member of the orphan nuclear receptor family x as a master which to initiate transcription of seriace of steroidogenic activity of each cell type.

Meiotic and mitosis

The first meiotic division in female ovary occurs before the birth of female child during the gonadal development of foetus in intrauterine life. The primordial germ cells are known to migrate from the yolk sac to the genital ridge by amoeboid movements with the aid of pseudopodia. By the fifth week of gestation it arrives at the genital ridge, known as oogonia. At about 8 weeks of intrauterine life, persistent mitosis increases the total number of oogonia to 600,000. From this point on, the oogonial development is subject to three simultaneous processes: mitosis, meiosis, and oogonial atresia. Between weeks 8 and 13 of fetal life, some of the oogonia depart from the mitotic cycle and enter the prophase of the first meiotic division.

The number of primary oocyte is maximum at 20 weeks of gestation that means at 5 months of intra uterine life, and that is about 6-7 million.
At birth = 1 to 2 million
At puberty= 3 to 5 lakhs

Out of this only 500 primary oocyte will be matured during the reproductive age of female under the influence of Gonadotropins-FSH & LH and ovarian steroids. Every month around 15 to 20 primordial follicles convert into primary follicles. In the beginning of the normal menstrual cycle there is a high FSH. It helps to start the growth of the primordial follicles into primary follicles and under the influence this FSH level, it allows only one primary follicle to mature into secondary follicle (Antral follicle). This follicle will grow bigger and bigger and will mature as graafian follicle.

DEVELOPMENTAL STAGES OF THE OVARIAN FOLLICLE:

PRIMORDIAL FOLLICLES are located in the periphery of the cortex and inferior to tunica albuginea, surrounded by a single layer of squamous follicular cell containing immature primary oocytes. Every month around 15 to 20 primordial follicles convert into primary follicles under the effect of FSH These cells give nourishment to ovum

PRIMARY OOCYTE: Primordial follicles start to grow at puberty under the influence of FSH. The outermost layer of follicular cells rests on a well defined basement membrane that separates it from the ovarian stroma. The oocyte is separated from the surrounding follicular cells by a glycoprotein layer called zona pellucida. The connective tissue stroma surrounding the follicle begins to condense and form theca follicular.

SECONDARY OOCYTE: secondary oocye also known as antral follicle. Secondary oocyte is surrounded by zona pellucida. Cuboidal granulosa cell layer in secondary follicle secretes estradiol. Irregular fluid filled space among the follicular cells join to form antrum. Theca folliculi later differentiate into 2 layers in the secondary follicle. They are theca externa and theca interna. Follicular cells and theca interna secretes estradiol.

TERTIARY FOLLICLE: The follicle increases in size.

GRAFFIAN FOLLICLE: The mature Graafian follicle is spheroidal or ovoid in shape and seen bulging out of the cortex in surface of the ovary, contains pent-up secretion, the liquor folliculi. The granulosa cells are collected together to form a projection into the cavity of the Graafian follicle. This projection is called as Cumulus oophorus (discus proligerus). The ovum lies within cumulus oophprus is known as secondary oocyte. The granulosa cells layer surrounded around the ovum is known as corona radiata. The theca interna cells enlarge during the maturation of the follicle and shortly before ovulation they are larger than the granulosa cells. The graafian follicle grows at the rate of 1-2mm daily and attains the size of 20mm or more at ovulation.

HORMONAL MECHANISM: OVARY

LH AND FSH SYNTHESIS:

Gonadotroph cells of pituitary gland synthesis LH and FSH, they are made up of 2 peptide subunits called Alfa and beta, each subunit contains cysteine, multiple disulphide linkages, multiple carbohydrate -molecules and help in the metabolism of these hormones, on binding of GNRH to its receptor the biosynthesis of the gonadotropins proceeds by transcriptions of the subunit genes, mRNAs- post translational modification of the precursor subunits, mature hormone packaging and secretion. The alpha subunit of LH and FSH have polypeptide structure and beta subunit have amino acid structure

FUNCTION of FSH- FSH receptors have localized into granulosa cells and stimulate granulosa cells to synthesis aromatase which converts androgens (androstenedione and DHEA) to estradiol. Necessary for normal follicular development, ovulation, fertility and estrogen production, during the follicular phase of the menstrual cycle, a mature dominant follicle secrets estradiol and inhibin, send a negative feedback to hypothalamus for suppressed FSH secretion. FSH remains low throughout the luteal phase preventing the development of the new follicle. The granulosa cell LH receptor requires the continued presence of FSH for its function.

Luteinizing function of ovary:

LH is essential for complete follicular development, formation of corpus luteum and production of androgens, it plays a major role in the promotion of the theca interstitial cell, increase LH receptor and key substance for steroidogenic process . The preovulatory follicle secrets estradiol during the follicular phase of the menstrual cycle, the estrogen synthesis in the ovary by the aromatization process. Ovarian steroidogenesis (estrogen and progesterone) in the preovulatory follicle takes place through LH receptor on theca cells and FSH receptor on granulosa cells. The star protein is the primary regulator of production of androstenedione, which diffuses into granulosa cells as a precursor for the estrogen, in the preovulatory follicle cholesterol in a theca cells arises from circulating lipoprotein.

LH and FSH RECEPTORS

Peptide hormone Receptors are large proteins whose essential functions are:

a) the ability to bind the hormone

b) the ability to couple hormone binding to hormone action.

Some receptors are located within the cell, and function as transcription factors (steroid hormones). Other receptors are located on the cell surface and function primarily to transport their ligands into the cell by a process referred to as receptor mediated endocytosis. The cell surface receptor triggers intracellular signaling pathways.

Ligands are the substances which binds with receptor. E.g. all hormones acting as a ligand in the body. The point where the ligand binds with the receptor are called 'ligand binding domain'. Once ligand binds with the receptor, is supposed to produce some biological action.

G-protein-coupled receptors (GPCRs):

G-protein or guanosine nucleotide binding proteins act as exchange factors. In terms of structure, GPCRs are characterized by an extracellular N-terminus, followed by seven transmembrane (7-TM) α-helices (TM-1 to TM-7) connected by three intracellular (IL-1 to IL-3) and three extracellular loops (EL-1 to EL-3), and finally an intracellular C-terminus. The GPCR arranges itself into a tertiary structure resembling a barrel, with the seven transmembrane helices forming a cavity. They act as cell surface receptors that detect molecules outside the cell and activate cellular responses. They are coupled with G proteins hence, they pass through the cell membrane forming six loops out of which 3 are extracellular loops and 3 intracellular loops. Ligands can either bind to the extracellular N-terminus and loops (e.g. glutamate receptors) or to the binding site within transmembrane helices. They are mostly activated by agonists, although a spontaneous auto-activation of an empty receptor has also been observed.

There are principally two signal transduction pathways involving the G protein-coupled receptors:

- the cAMP signal pathway
- the phosphatidylinositol signal pathway.

A conformational change brought about by ligand binding to the GPCR enables the GPCR to function as a guanine nucleotide exchange factor (GEF). The GDP bound to the G protein is then exchanged for a GTP by the GPCR, activating the corresponding G protein. Depending on the type of α subunit, the G protein's α subunit can target functional proteins directly or further affect intracellular signaling proteins by dissociating from the β and γ subunits along with the bound GTP. FSH and GnRH ligands are binded to one or more receptors on GPCRs.

ESTROGEN SYNTHESIS

The naturally occurring estrogens are C18 steroids characterized by the presence of an aromatic ring, a phenolic hydroxyl group at C3, and a hydroxyl group (estradiol) or a ketone group (estrone) at C17.

Estrogen is produced in at least three major sites:

(1) by direct secretion from the ovary in reproductive-age women;

(2) by conversion of circulating androstenedione, originating from the adrenal or ovary or both, to estrone in peripheral tissues; and

(3) by conversion of androstenedione to Estrogen in estrogen target tissues.

In the latter two cases, the same tissue converts the weak estrone to estrogen. For estrogen to form at these sites, genes encoding the enzymes aromatase and reductive 17β-hydroxysteroid dehydrogenases (17β-HSD) must be expressed. Multiple genes with overlapping functions may produce protein products that contribute to reductive 17β-HSD activity in peripheral tissues. A unique reductive 17β-HSD enzyme called HSD17B1 is encoded by a particular gene that is mostly expressed in the ovary. There is only one gene that codes for aromatase (CYP19A1). It is especially crucial for postmenopausal women and those suffering from diseases that depend on estrogen, like endometriosis, breast cancer, or endometrial cancer, to produce estrogen through peripheral and local conversion.

Estrogen nuclear receptor

A family of ligand-regulated transcription factors known as nuclear receptors is triggered by a variety of lipid-soluble signals, such as thyroid hormone, retinoic acid, and oxysterols, as well as steroid hormones like progesterone and estrogen. In contrast to the majority of intercellular messengers, the ligands do not need to act through cell surface receptors in order to cross the plasma membrane and interact with nuclear receptors inside the cell. Upon activation, nuclear receptors exert direct control over the transcription of genes that govern an extensive range of biological functions, such as cell division, proliferation, metabolism, and reproduction. While their primary role is as transcription factors, some nuclear receptors have also been discovered to control cellular processes in the cytoplasm. For instance, endothelial cells cytoplasm contains an estrogen receptor, which estrogens use to quickly activate signaling pathways that regulate endothelial cell migration and vascular tone.

Phosphorylation is one of the main mechanisms regulating the activities of orphan receptors and can activate certain nuclear receptors independently of ligand binding. Phosphorylation is another posttranslational modification that

can modify the functions of nuclear receptors. Given the wide variety of processes controlled by nuclear receptors, their dysregulation can contribute to numerous diseases, including cancer, diabetes, and infertility. However, because they bind to small molecules, they represent promising therapeutic targets for which selective agonists and antagonists can be engineered Because nuclear receptors regulate many genes in many tissues, synthetic ligands usually show beneficial therapeutic effects and unwanted side effects that limit clinical use. Major goals in the nuclear receptor field therefore include attaining a better understanding of the mechanisms underlying their actions in specific cell types and ways in which to selectively modulate their activities. A characteristic feature of nuclear receptors with respect to their integrative roles in development and homeostasis is their ability to regulate different genes in different cell types. For example, estrogen receptors regulate different sets of genes in the brain, breast, and uterus that contribute to the distinct functions of those organs. Recent studies indicate that tissue-specific responses are a consequence of binding of nuclear receptors to enhancer elements that are selected in a cell-specific manner.

OVARIAN CYCLE

Hypothalamic-pituitary-ovarian Axisand synchronisation of this Axis is necessary for ovulatory menstrual cycle in female reproductive age. Regular ovulation, predictable menses and other female reproductive functions are coordinated by the functions of the Hypothalamus, Pituitary gland, Ovaries and Endometrium. Arcuate nucleus and preoptic nucleus of hypothalamus have special neurons which release . The hypophyseal portal systemtransports GnRH from hypothalamus to anterior pituitary and stimulates gonadotroph cells.The pulsatile secretion of GnRHinfluences Gonadotroph cells of the pituitary gland & secrets gonadotropins i.e. FSH and LH. The periodicity and pulsatile rhythm of GnRH and gonadotropin secretion are necessary in regulating reproductive system. Cyclic activity in ovary is controlled by an interaction between estradiol, progesterone, FSH and LH.

On the 1st day of menstrual cycle, small and medium sized follicles are present in the ovaries, so low level of estradiol, GnRH pulse frequencyis relatively fast(90 minutes). As estradiol level increases in the follicular phase**,** GnRH pulse frequency is relatively fast(60 minutes) in a mid-follicular phase.The Estradiol makes the endometrium to proliferate. Before the day of ovulation the level of the estradiol is at its maximum level. And send the negative feedback to the hypothalamus to stop the FSH secretion & at the same time a positivefeedbackaction is send to the hypothalamus to trigger a LH surge. This LH surge influences ovulation.

The corpus luteum starts to secret large amount of Progesterone (40mg/day) and some estradiol during the mid-luteal phase of the ovarian cycle. High level of the progesterone decrease GnRH pulsatility(1 pulse in 100 minutes) and (1 pulse in 200 minutes) during late luteal phase.The functional lifespan of the corpus luteum is normally 14 days, thereafter the corpus luteum spontaneously regresses, unless pregnancy occurs.As the corpus luteum regresses, progesterone and estrogen secretion diminishes. Reduced progesterone sends the negative feedbacksignals to the hypothalamus, and allows secretion of FSH. Reduced progesterone is also a withdrawal support to the endometrium lining as a result the endometrium is shed and bleeding starts and a new cycle of the menses begins.

Definition

Ovulation consists of rapid follicular enlargement followed by outcoming of the follicle from the surface of the ovarian cortex. Rapid follicular enlargement and follicle extrusion from the ovarian cortex's surface characterize ovulation. The rupture of the follicle and the extrusion of an egg come next. It happens when the corona radiata-enclosed ovum breaks free from the graafian follicle. The sharp increase in the amount of estradiol in the blood causes ovulation. The midcycle surge in LH is caused by the hypothalamus receiving positive feedback from an increase in estradiol levels. Ovulation requires a peak LH concentration of 75 ng/ml. 34–36 hours after the beginning of the LH surge, ovulation happens predictably. There is antral fluid and the ovum explodes when there is a rupture. When ovulation occurs there is a sudden shrinkage in the size of a follicle and appearance of free fluid in the pouch of douglas. After ovulation graafian follicle collapses and gets transformed into temporary endocrine organ called as Corpus Luteum**.**During the first few hours after the explosion of the ovum from the follicle, the remaining granulosa cells and theca cells change rapidly into lutein cells. The lutein cells derived from the granulosa layer forms the

granulosa lutein cells. The lutein cells derived from the theca layer forms the paralutein cells.These cells undergo process of hypertrophy and hyperplasia called luteinisation.The corpus luteum is the endocrine gland that serves as the major source of Progesterone and Estrogen secreted by the ovary during the luteal phase.corpus luteum proliferates for about 12 days. The granulosa lutein cells become spindle-shaped and secrets progesterone and estrogen hormones. The theca lutein cells form androgens- Androstenedione and Testosterone.Before rupture of the follicle the granulosa layer is not vascularised. Corpus luteum formation is the penetration of the follicle basement membrane by the blood vessels which provides the granulosa lutein cells with low density lipo-protein(LDL). LDL cholesterol serves as the substrate for corpus luteum progesterone production. A key factor of steroidogenesis in the corpus luteum is LH. LH-receptor is maintained throughout the functional life span of corpora lutea.The functional life span of the corpus luteum is 14 days. There after the corpus luteum spontaneously regresses. It is replaced, unless pregnancy occurs, by an avascular scar referred to as the corpus albicans. Progesterone levels will drop

SECRETORY PHASE

Progesterone and estrogen, both together are secreted in large quantity by the corpus luteum. The estrogen cause additional proliferation in the endometrium. The endometrium is divided into an upper two-third functionalis layer and a lower one-third basalis layer . The purpose of the functionalis layer is to prepare for the implantation of the blastocyst; therefore it is the site of proliferation, secretion and degeneration.The purpose of the basalis layer is to provide the regerative endometrium following mestrual loss of the functionalis layer. The endometrium swells and secretes more when progesterone is present. The glands become more twisted. An excess of secretory materials builds up within the glandular epithelial cells. Lipid and glycogen levels in the stromal cell's cytoplasm rise significantly, and the blood supply rises along with them. The spiral arteries and their capillaries pierce the entire thickness of the endometrium. Endometrial tissue is shed during menstruation along with steroid hormone hemorrhage. The corpus luteum in the ovary abruptly involutes (decreases in size after an enlargement) if the ovum is not fertilized, which occurs roughly two days before the end of the monthly cycle. Additionally, the levels of secretion of the ovarian hormones progesterone and estrogen drop

REFERENCES

1. Association of Physicians of India - API - Textbook of Medicine, 7th Edition 2003, The National Book depot (Regd), Mumbai.
2. Chatterjee M N, Rana Shinde. Text book of medical biochemistry.7th Edition, Jaypee brothers, Medical publishers (P) Ltd; 2007.
3. Harrison's Endocrinology, 4E
4. Shaw’s Textbook of Gynecology, 17th edition, published by kumarpadubidridaftary
5. Research protocol homoeopathy in poly cystic ovary pdf – Central council for research in homoeopathy
6. Williams textbook of endocrinology , 10th edition, by P. Red larsen, Henry N. Kronenberg, Shlomo melmed, Kenneth S. Polonsky.
7. Essential of medical physiolgy, 6th edition, by K. Sembulingam and Prema Sembulingam.
8. DC DUTTA'S TEXTBOOK OF GYNECOLOGY, 8th edition , by Hiralal konar

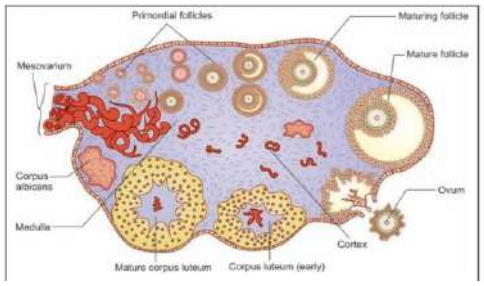

Fig. 1. Structure of ovary

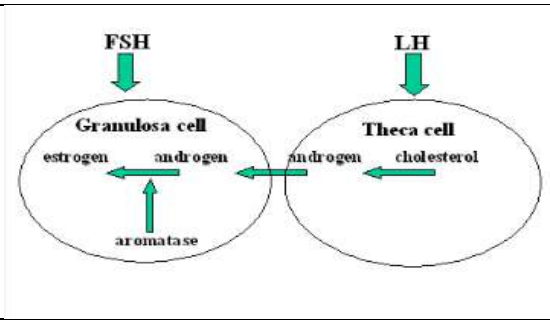

Fig.2. Granulosa cell layer

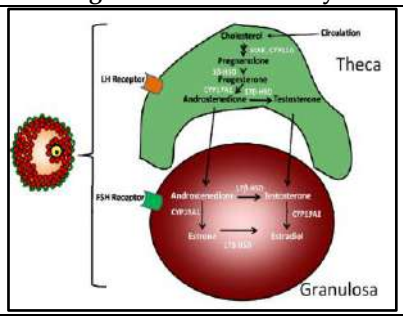

Fig.3. Two cell, two-gonadotropin theory of ovarian steroidogenesis

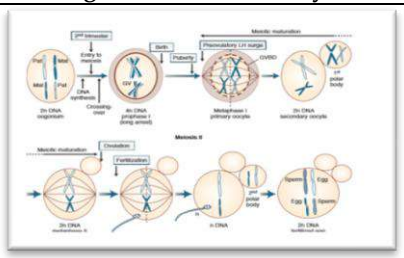

Fig.4. Meiotic and mitosis:

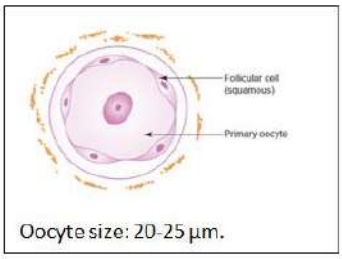

Fig.5. Ovarian follicle

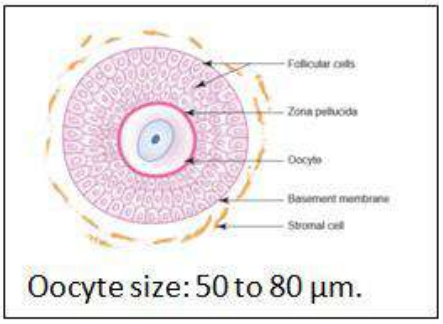

Fig.6. Primary oocyte

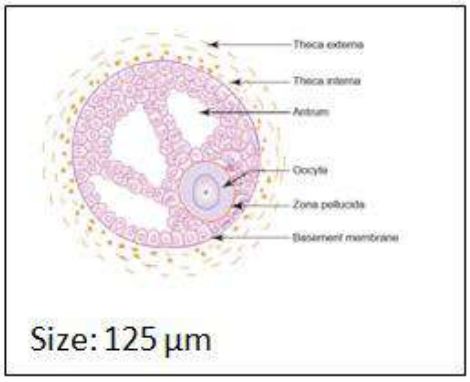

Fig.7. Secondary oocyte

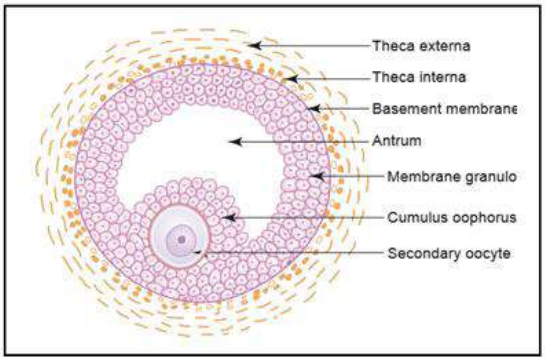

Fig.8. Graffian follicle

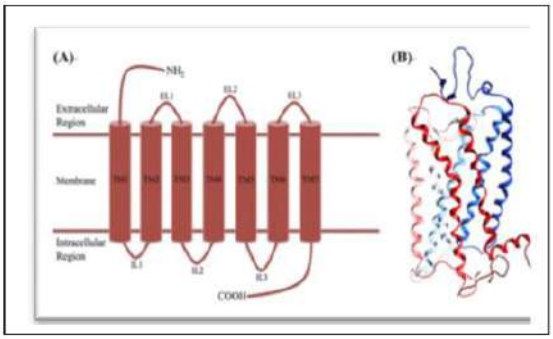

Fig.9. G-protein-coupled receptors (GPCRS)

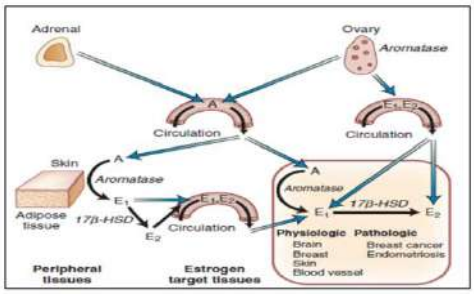

Fig.10 Estrogen synthesis

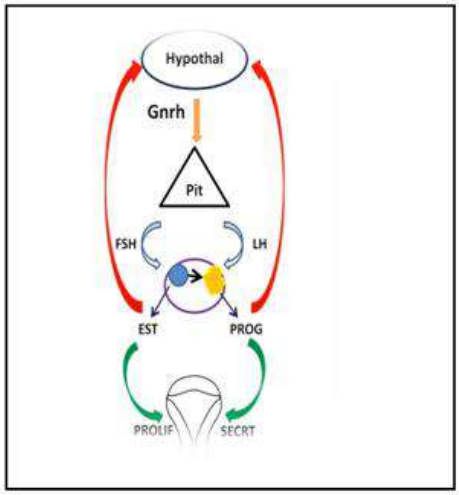

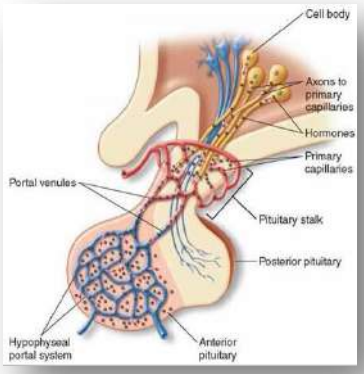

Fig.11. Ovarian cycle

Vol.15 / Issue 83 / Apr / 2024 International Bimonthly (Print) – Open Access ISSN: 0976 – 0997

RESEARCH ARTICLE

Effect of Serratus Anterior Muscle Strengthening on Pain and Function in Secondary External Shoulder Impingement Syndrome: An Experimental Study

Priyal Ninama[1]*, Rushi Gajjar[2] and Gaurav Patel[3]

[1]Student, Department of Physiotherapy, Ahmedabad Physiotherapy College, Parul University, Gujarat, India.
[2]Associate Professor, Department of Physiotherapy, Ahmedabad Physiotherapy College, Parul University, Gujarat, India.
[3]Principal, Department of Physiotherapy, Ahmedabad Physiotherapy College, Parul University, Gujarat, India.

Received: 30 Dec 2023 Revised: 09 Jan 2024 Accepted: 27 Mar 2024

***Address for Correspondence**
Priyal Ninama
Student,
Department of Physiotherapy,
Ahmedabad Physiotherapy College,
Parul University,
Gujarat, India.

ABSTRACT

shoulder pain is one of the most common complaints of patient's world wide, especially in older age group. SIS is the syndrome associated with compression and inflammation of supraspinatus tendon as it passes through sub acromial space. There for to investigate the serratus anterior muscle strengthening exercise + scapular muscle strengthening exercise programe to improve balance of the shoulder and neck, posture, ADL'S, QOL is the main focus of this study. 32 subjects were participants in this study based on inclusion and exclusion criterias with the age of 20 to 50 year. Pre and Post SPADI and NPRS was checked. The serratus anterior muscle strengthening exercise+scapular muscle strengthening exercise, control group continued their scapular muscle strengthening exercises. The outcome measures taken at baseline and after 2 weeks of intervention. Intervention shows significant results in serratus anterior muscle exercise + scapular muscle strengthening exercise had significant effect on NPRS score and SPADI score in secondary external impingement syndrome in Group A. This study showed that there is a positive effect of Serratus Anterior muscle strengthening exercise and Scapular muscle strengthening exercise is more favorable when compared to scapular muscle strengthening exercise.

Keywords: Shoulder impingement syndrome, serratus anterior muscle, secondry external impengement, NPRS, SPADI

INTRODUCTION

One of the most common musculoskeletal concerns is shoulder pain. With a prevalence of %44–65 among all shoulder problems, subacromial impingement syndrome (SIS), also known as shoulder impingement syndrome, is the most typical cause of shoulder pain.[1] The labrum also enhances stability by deepening the concavity of the glenoid socket. The capsule tightens or "winds up" in various extremes of position; for example, the inferior pouch tightens in extreme abduction and external rotation, serving to stabilize the joint.[2]The coracoacromial arch and humerus are what causes the rotator cuff and subacromial bursa to mechanically compress. Subacromial impingement, sometimes known as "external impingement," internal impingement, which can be further classified into anterior or posterior impingement.[3]Movement is painfully restricted, there is a functional impairment, and everyday activities are restricted. When the arm is elevated during unconstrained overhead reaching, flexion, abduction, or scapular plane abduction, the scapula will normally rotate upward and slant posteriorly on the thorax.[4] The subacromial impingement syndrome has both primary and secondary forms.[5] Secondary impingement happens when the humeral head's functional centering is disturbed, such as by muscle imbalance. This abnormal displacement of the centre of rotation in elevation causes soft tissue entrapmentA widely used classification system for acromial shape is flat (type I), curved (type II), or hooked (type III).[6]

SERRATUS ANTERIOR MUSCLE

The fan-shaped serratus anterior starts on the superolateral surfaces of the first to eighth or first to ninth ribs at the lateral wall of the thorax and inserts along the superior angle, medial border, and inferior angle of the scapula.[7] The scapula is pulled forward around the thorax by the serratus anterior muscle, allowing the arm to be extended and anteverted.[8] The serratus anterior starts to separate from the mesenchyme present at the ventral ends of the lower cervical myotomes in the 9 mm embryo.[9] The lower part of the serratus anterior and the latissimus dorsi are supplied by the thoracodorsal artery.[10] The innervation of the serratus anterior is carried out by the long thoracic nerve.[11] For the scapulohumeral rhythm to be maintained when raising the arm, the serratus anterior muscle must be activated appropriately. The serratus anterior helps the scapula rotate upward and tip posteriorly when the humerus is raised. It also keeps the scapula level on the thorax, preventing scapular winging. One mechanism behind shoulder impingement syndromes has been proposed to be impaired serratus anterior activation, which has been linked to altered scapular kinematics. [12] A self-report questionnaire for people with shoulder discomfort called the Shoulder Pain and Disability Index (SPADI) has 13 questions and is separated into two domains: disability (5 items) and pain (8 items).A higher score denotes poorer shoulder function and discomfort. For the SPADI, the ICC value is 0.89.[13]Unidimensional measurement of pain intensity is provided by the Numeric Pain Rating Scale (NPRS).The 11-point numeric scale runs from "0" (i.e., "no pain") to "10," which denotes the most intense agony. For the NPRS, the ICC value is 0.92.[14] Hence, the purpose of the present study is to evaluate the effect of serratus anterior muscle strengthening on pain and function in secondary external impingement syndrome.

MATERIAL AND METHODOLOGY

32 subjects were taken from sainath hospital bopal-ahmedabad by using simple random sampling for this experimental study of 2 weeks duration.

Inclusion criteria

Age between 20 to 50 years. Male and females both are included. Positive Neer's, Howkins-Kennedy, Yokum test and apprehension test. Patient willing to participate. Shoulder pain and disability is more than 40%.

Exclusion criteria

Any traumatic injury to bone such as fracture, dislocation. Herniation of cervical disc with or without radiating symptoms. Pain with shoulder movement under 60 degrees. Infection of bone or soft tissues such as abscess. Higher functions are affected in subject.

Procedure of outcome measure

A self-report questionnaire for people with shoulder discomfort called the Shoulder Pain and Disability Index (SPADI) has 13 questions and is separated into two domains: disability (5 items) and pain (8 items).A higher score denotes poorer shoulder function and discomfort. For the SPADI, the ICC value is 0.89.[13] Unidimensional measurement of pain intensity is provided by the Numeric Pain Rating Scale (NPRS).The 11-point numeric scale runs from "0" (i.e., "no pain") to "10," which denotes the most intense agony.For the NPRS, the ICC value is 0.92.[14]

Procedure of intervention

Group A:(EXPERIMENTAL GROUP) SERRATUS ANTERIOR MUSCLE STRENGTHENING + SCAPULAR MUSCLE STRENGTHENING EXERCISE

This group received serratus anterior muscle strengthening exercise and scapular muscle strengthening exercise for 6 days per week for 2 week .3 sets of 10 repetitions between 1 minute rest up exercise.

1) serratus anterior muscle strengthening exercise
    a) The wall slide
    b) scapular plane shoulder elevation
2) scapular muscle strengthening exercise
    a) side lying forward flexion
    b) side lying external rotation
    c) prone horizontal abduction with external rotation
    d) prone extension in neutral position with weights

Group B: (CONTROL GROUP) SCAPULAR MUSCLE STRENGTHENING EXERCISE

a) side lying forward flexion
b) side lying external rotation
c) prone horizontal abduction with external rotation
d) prone extension in neutral position with weights

RESULT

Statistical analysis was performed using SPSS version 26. Total thirty two subjects are selected for two weeks of training protocol. In this study Group A, received Serratus anterior muscle strengthening exercise and scapular muscle strengthening exercise (n=16) and Group B received Scapular muscle strengthening exercise (n=16). Both the groups were similar in age, gender and function. The study analysis was done to evaluate between group interventions, Pre-post intervention. Within group, The effects were explored using paired t-test and Between group the effects were explored by using independent t-test. In the result data shows value of mean, standard deviation (SD), t value and degree of freedom (df). Statistical significance was set at $p<0.001$. From total 32 subjects, there were 7 females and 9 males in the study. They were equally divided in both group. By using independent sample test results for NPRS and SPADI shows significant improvement in GROUP A(serratus anterior muscle strengthening exercise and scapular muscle strengthening exercise) as its p value is <0.001. (Graph 1,2,3) (Table 1)

As shown in table 2 within group result by using paired t test shows significant results in NPRS and SPADI in both the groups except as its p value is <0.001.

DISCUSSION

The of impact serratus anterior muscle strengthening exercise and scapular muscle strengthening exercise versus scapular muscle strengthening exercise on pain and function in secondry external impingement syndrome. The pain was evaluated using the Numeric Pain Rating Scale (NPRS), Disability was assessed using Shoulder Pain and Disability Index questionnaire scale (SPADI) were used as a primary outcome, whereas Hawkins Kennedy Test, Positive Neer's Test, Yokum Test, Apprehension Test was used as a secondry outcome measure. A study by Dvir &

Berme 1978, Johnson et al. 1994 . The biggest moment arm for producing scapular upward rotation torque is found in the serratus anterior. The serratus anterior line of action can also make a significant contribution to scapular posterior tilting. Ekstrom Ra, et al. 2003 study concluded The serratus anterior is a muscle that is first activated above 90 degrees of shoulder flexion, although our study is not the first to look at this. The serratus anterior was most fully stimulated by raising the shoulder over 120 degrees in the plane of the scapula while utilising a hand weight. Mc Clure Pw, et al. 2004 study concluded When compared to the push-up plus exercise against the wall, the wall slide and scapular plane shoulder elevation exercise more fully engaged the upper trapezius. This might be due to the upper trapezius acting as an agonist for the wall slide and scapular plane shoulder elevation necessary for proper performance. Carrie M Hall, et al. 1980 the main stabilizer of the scapula include serratus anterior, all 3 trapezius muscles, rhomboids and levator scapulae. If there is weakness or imbalance of these muscle , it may lead to altered position of the scapula and may also decreased its stability. As a result of this, the function of the shoulder complex may become inefficient leading to decrease in neuromuscular perfomance which may have been corrected by improving the strength of the lower trapezius and serratus anterior muscle as found in our study , thereby decreasing the load on the cervical efficient muscle joint complex. Blackburn Ta, et al.1990 study concluded that Blackburn has described the prone full can, or horizontal abduction (100 degree of elevation) with external rotation, as an exercise that facilitates high supraspinatus electromyographic activity. Because the infraspinatus and teres minor have very similar concentric muscle actions of externally rotating the humerus they can generally be exercised with same movements.

CONCLUSION

This study showed that there is a positive effect of serratus anterior muscle strengthening and scapular muscle strengthening exercise programe to effects on pain reduction and improved function and increased rang of motion or strength in secondry external impingement syndrome but Group A showed greater significant difference as compared to Group B. Serratus Anterior muscle strengthening exercise and Scapular muscle strengthening exercise is more favorable when compared to scapular muscle strengthening exercise.

Clinical implication

This study shows positive effect of serratus anterior muscle strngthening exercise and scapular strengthening exercise programme include strngth, range of motion, balance, posture, quality of life, ADL's. so, Secondary external impingement subjects use this techniques are improved performance and to reduced the risk of injuries.

Limitation

Long term follow up was not taken up for this study.

Future recommendation

A large sample size would be recommended in future reserches. More subjects can be taken for study. Interpretations can be done for long periods. studies for the long term effect of this treatment could be concluded.

REFERENCE

1. Van der Windt, D.A., Koes, B.W., Boeke, A.J., Deville, W., de Jong, B.A., Bouter, L.M., 1996. Shoulder disorders in general practice: prognostic indicators of outcome. Br. J. Gen. Pract. 46, 519– 523.
2. De Yang Tien J, Tan AHC. Shoulder impingement syndrome, a common affliction of the shoulder: a comprehensive review. Proc Singapore Healthc 2014;23:297-305
3. Ludewig PM, Braman JP. Shoulder impingement: biomechanical considerations in rehabilitation. Manual therapy. 2011 Feb 1;16(1):33-9.

4. Morrison DS, Greenbaum BS, Einhorn A. Shoulder impingement. Orthopedic Clinics of North America. 2000 Apr 1;31(2):285-93.
5. Garving C, Jakob S, Bauer I, Nadjar R, Brunner UH. Impingement syndrome of the shoulder. Deutsches Ärzteblatt International. 2017 Nov;114(45):765.
6. Bigliani, L.U., Levine, W.N., 1997. Subacromial impingement syndrome. J. Bone Joint Surg. Am. 79, 1854–1
7. Lung K, St Lucia K, Lui F. Anatomy, Thorax, Serratus Anterior Muscles. StatPearls [Internet]. 2022 Jan.
8. Nasu H, Yamaguchi K, Nimura A, Akita K. An anatomic study of structure and innervation of the serratus anterior muscle. Surgical and radiologic anatomy. 2012 Dec;34:921-8.
9. Pu Q, Huang R, Brand-Saberi B. Development of the shoulder girdle musculature. Developmental Dynamics. 2016 Mar;245(3):342-50.
10. Gordon A, Alsayouri K. Anatomy, Shoulder and Upper Limb, Axilla. InStatPearls [Internet] 2022 Jul StatPearls Publishing.
11. Laulan J, Lascar T, Saint-Cast Y, Chammas M, Le Nen D. Isolated paralysis of the serratus anterior muscle successfully treated by surgical release of the distal portion of the long thoracic nerve. Chir Main. 2011 Apr;30(2):90-6.
12. Decker MJ, Hintermeister RA, Faber KJ, Hawkins RJ. Serratus anterior muscle activity during selected rehabilitation exercises. The American journal of sports medicine. 1999 Nov;27(6):784-91
13. Ekeberg OM, Bautz-Holter E, Tveitå EK, Keller A, Juel NG, Brox JI. Agreement, reliability and validity in 3 shoulder questionnaires in patients with rotator cuff disease. BMC musculoskeletal disorders. 2008 Dec;9(1):1-9.
14. Breckenridge JD, McAuley JH. Shoulder pain and disability index (SPADI). Journal of physiotherapy. 2011 Jan 1;57(3):197.

Table 1: independent sample test for between group result

Independent Sample test				
	T	df	Sig.(2 tailed)	Mean difference
ABnprs	-3.421	38	0.002	-0.90000
		36.570	0.002	-0.90000
ABspadi	-3.919	38	0.000	-5.40000
		38	0.000	-5.40000

Table 2: Paired sample test of within group results

Paired sample test						
Group			Mean	Standard deviation	T	Sig (two tailed)
Group A	Pair 1	Anprs Pre	7.5500	1.05006	23.134	0.000
		Anprs Post	2.3500	0.74516		
	Pair 2	Aspadi pre	76.7500	15.02235	15.874	0.000
		Aspadi post	20.1500	4.49883		
Group B	Pair 1	Bnprs Pre	7.2500	1.37171	15.292	0.000

		Bnprs Post	3.2500	0.91047		
	Pair 2	Bspadi pre	74.7000	12.27792	17.914	0.000
		Bspadi post	25.5500	4.21120		

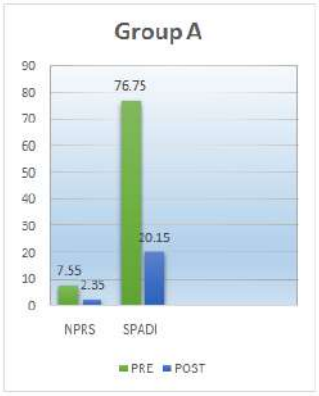

Graph 1: Group A Pre and Post Mean of NPRS and SPADI

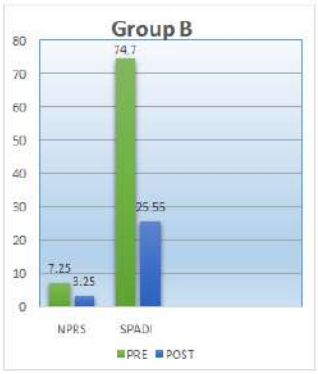

Graph 2: Group B Pre and Post Mean of NPRS and SPADI

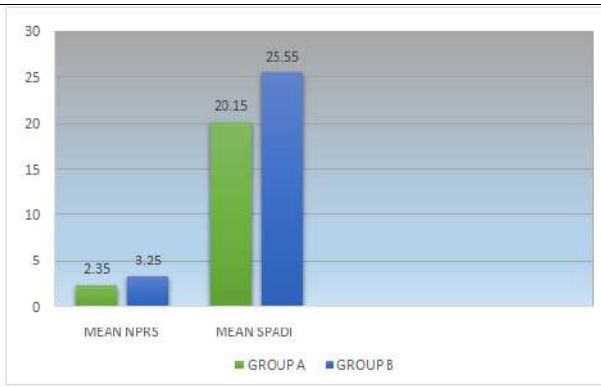

Graph 3: NPRS and SPADI Between Two Groups

Photograph 1: The Wall Slide & Scapular Plane Shoulder Elevation

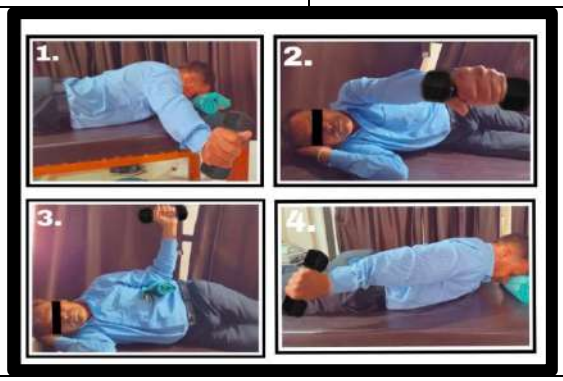

Photograph 2: 1)Prone Horizontal Abduction With External Rotation 2) Side Lying Forward Flexion 3)Side Lying External Rotation 4) Prone Extension In Neutral Position With Weights

RESEARCH ARTICLE

Physico -Chemical assessment of Groundwater quality in Bagepalli taluk of Chikballapur district, Karnataka

Ramesha Iyyanahalli[1]* and Kiran B.R.[2]

[1*]Associate Professor, Department of Zoology, Government Science College, Chitradurga-577501,India.
[2]Research & Teaching Assistant in Environmental Science, DDE Kuvempu University, Shankaraghatta-577451, India.

Received: 30 Dec 2023 Revised: 09 Jan 2024 Accepted: 27 Mar 2024

***Address for Correspondence**
Ramesha Iyyanahalli
Associate Professor,
Department of Zoology,
Government Science College,
Chitradurga-577501,India.

ABSTRACT

The present observation deals with the assessment of groundwater quality in Bagepalli taluk of Chikballapur district, Karnataka, India. To analyze the physico-chemical characteristics of groundwater samples and assess the suitability of water for human consumption and irrigation. Also to find out the source of pollution. Methods: A total of 10 water samples (13.78°N latitude and 77.79°E longitude) (S1 to S10) were collected from selected village borewells of Bagepalli taluk, Chikkaballapur District during June -2010 to May-2011. The temperature as recorded at the time of sampling by using mercury thermometer. The pH was measured with pH meter. All the other parameters were measured as per the Standard Methods (APHA-2005). One-way ANOVA with post-Hoc Tukey HSD tests were carried out by using asatsa.com software. The water temperature fluctuated between 25 O C and 35 O C. pH values varied from 7.0 to 8.8. The values of electrical conductivity ranged 302 µmhos/cm to 2718 µmhos/cm. TDS values deviated from 311 mg/L to 2483 mg/L Total hardness varied from 311 mg/L to 1042 mg/.While, alkalinity values ranged from 200 mg/L to 588 mg/and chloride values from 80 mg/L to 527 mg/L Nitrate data fluctuated from 48 mg/L to 270 mg/L. Sulphate values deviated from 10 mg/L to 95 mg/L. However, phosphate varied from 0.2mg/L to 1.4 mg/L. Sodium, potassium and iron levels fluctuated from 70-360 mg/L, 1.2-4.2 mg/l and 0.1-0.7 mg/l respectively. The groundwater of Bagepalli taluk had varied in different seasons due to anthropogenic activities, deterioration by agricultural activities, over exploitation and also of drought circumstance. The consequences of all the above findings are discussed by emphasizing for suitable water quality management. These results contribute to environmental decision making in the management of ground water resources. In most of the ground water samples the values of electrical conductivity, total hardness, nitrate, total alkalinity, and chloride are exceeded the permissible limits of BIS

standards. It is due to seepage of sewage and urban runoff into the ground waters. Other factors include lack of proper sewerage facilities and open drains in the study area. Hence, proper treatment is necessary before utilized for domestic purposes..It is significant to carry out measures for augmenting groundwater availability for use and increasing use effectiveness, the aspect of improving groundwater governance. This current study contributes to the assessment of ground water quality by policy makers and stakeholders, enabling the arrangement and managing the ground water resources in Bagepalli taluk of Chikaballapura district.

Keywords: Ground water quality, Bagepalli taluk, Chikballapur, BIS standards, Permissible limits, Karnataka.

INTRODUCTION

Ground water is the major resource of drinking water in both urban and rural India. Discovering dimensions of ground water quality is an important role for the past two decades because of the uncertainties of water resources, expansion of pollution level through the population growth and industrial development. On the other hand, ground water system receives the soluble inorganic and organic pollutants through the percolation of vast domestic sewage and industrial effluents. Various hydro-geochemical process determines diverse physico-chemical characteristics of ground water chiefly in the region of saturation (Islam et al.,2017a; Ahmed et al.,2020;Bhuiyan et al.,2016) .Ground Water is an essential natural supply of fresh water worldwide. Due to the water's suitability for a variety of uses, including drinking, livestock, irrigation, aquaculture, mining, and industrial uses, groundwater quality is just as important as quantity. Lately, emerging nations like India confronting the interest of unadulterated water for drinking and different designs are expanded quickly because of absence of ground water accessibility in the greater part of the areas. The central point that influences the nature of water because of quick increment of industrialization and rural improvement exercises and urbanization, which causes ground water gets debased (Juahir et al.,2011).

According to the WHO (1985), approximately 80% of human diseases are transmitted through water. In arid and semiarid regions, where surface water is scarce and unevenly distributed, approximately one third of the freshwater used to meet all domestic, industrial, and agricultural needs comes from groundwater (Liang Chen et al.,2017) . Water quality assessment is usually cited as a limiting factor in proposing certain anthropogenic activities in a region (Jose Galizia et al.,2016; Fenge Zhang et al.,2019; Daniele Parrone et al.,2020). .As a result, understanding the physical, chemical, and biological properties of groundwater resources is crucial to determining their applications: human utilization, water system, modern purposes, and others (Fenge Zhang et al.,2019; Daniele Parrone et al.,2020; Franklin et al., 2019; Silva et al.,2021) Various earlier studies were carried on assessment of ground water quality and pollution in different parts of the India and the world. They come across significant deterioration in water quality for consumption and agriculture purposes in recent period (Al Futaisi et al.,2007; Nag and Das,2018; Kundu and Nag,2018; Bhunia et al., 2018; Karunanidhi et al.,2020; Chakraborty et al.,2022; Chakraborty et al.,2021c; Sridhara et al., 2021; Gajalakshmi,2022; Rathnamala and Shivashankara,2022). Ground water quality data varies with time, area and methodology of sampling. Therefore, present values are differ from other workers carried in this area but their research work is more emphasize towards GIS.There is a research gap between our study and other researchers carried out in this area of Bagepalli taluk of Karnataka and hence, the present study is carried out. The water table has decreased in several parts of eastern Karnataka, despite the fact that rainfall has not decreased uniformly over the past three decades. While precipitation is diminishing in north inside Karnataka, it is expanding in south inside Karnataka. Water level depletion and yield dwindling in major districts, overexploitation of groundwater sources, and issues with water quality are major groundwater issues in the Bagepalli area. However, very few articles on water quality issues were published in the

Bagepalli taluk. These factors justified to take the current study. The main objectives of the present study is to analyze the physico-chemical characteristics of water samples and assess the suitability of water for human consumption and irrigation. Also to find out the source of pollution. Create awareness about health hazards in drinking water. To understand the interrelationship of various chemical factors through statistical approaches. and recommendation for better management of ground water.

STUDY AREA

Bagepalli is a one of the Taluk in Chikballapur District (Figure 1) in the State of Karnataka, India. Bagepalli is situated 100 km north of Bangalore on the Bangalore - Hyderabad National Highway. The region is just below the southern border of the Rayalaseema in Andhra Pradesh, South India. It is semi-arid and drought prone with 560 mm of erratic and spatial rainfall. Bagapalli is located at 13.78°N 77.79°E. It has an average elevation of 707 metres (2319ft).The region is a semi arid drought prone one with low, erratic and spatial rainfall. The dust brown rocky terrain is severely undulating, with small hill ranges and outcrops that stud the topography. There is no mineral wealth and only a very thin and fragile soil cover. An adverse land: person ratio creates a strong thirst for cultivable land since less than one-half of the total land is fit for cultivation, with the remaining taken over by the hills and rocky fields. Hardly 5% of the cropped lands are irrigated by an age old network of rain-fed tanks (small lakes), each irrigating 2 to 10 hectares of wet land. The low water table is tapped through bore-wells drilled to more than 100 meters depth. Even these dry up in the summer months, from April to September every year, when temperatures rise to a dry heat of 38°C.

METHODOLOGY

A total of 10 water samples (S1 to S10) were collected from selected villages borewells of Bagepalli Taluk, Chikkaballapur District during June -2010 to May-2011. The temperature as recorded at the time of sampling by using mercury thermometer. The pH was measured with pH meter. All the other parameters were measured as per the Standard Methods (APHA,2005)

RESULTS AND DISCUSSION

Monthly fluctuation of physico-chemical parameters are given in the Table 4 to 11. Temperature of groundwater is largely dependent on atmospheric, heat, exothermic and endothermic reaction in rocks, infiltration of surface water, insulation, thermal conductivity of rocks, rate of movement of ground water and interference of man on the ground water. It is well know fact that the water temperature exerts direct and indirect influences on many abiotic and biotic components of any aquatic system (Das et al.,2000) , During the study period, water temperature varied from a minimum of 25°C during Nov-2010 and a maximum of 35°C, May-2011 at all the sites (S 1 to S 10). In most of the natural water, the pH value is dependent on carbon dioxide-carbonate-bicarbonate equilibrium. As the equilibrium is markedly affected by temperature and pressure, it is obvious that changes in pH may occur when these are altered. Presence of phosphates silicates, borates, fluorides and other salts in dissociated form may also affect the pH. Most ground water has a pH range of 6 to 8.5 . In the present study, pH concentration varied from a minimum of 7.0 during Jan-2011 at S 7 to a maximum of 8.8 in Sept. 2010 at S 1 sites, indicating circum neutral to alkaline nature of water. The recorded values are within stipulated limits for potable waters recommended as per CPCB norms (De Zwart and Trivedi,1995) . pH has no direct adverse effects on health although values below 4.0 are known to produce some taste and higher values (>8.5) hasten the scale formation in water heating apparatus and also reduce the germicidal potential of chlorine. It is discernible from the above observation that the pH value are dependent on local soil conditions. The significant correlation of pH was observed with total hardness ($r = -0.62$, $p < 0.06$),magnesium hardness ($r = 0.68$, $p < 0.06$) and potassium ($r = 0.6$, $p < 0.05$). Electrical conductivity is the function of concentration of dissolved solids . Conductivity is the capacity of water to carry an electrical current and various both with number and types of ions, which in turn is related to the concentration

of ionized substances in the water, most of the dissolved inorganic substances in water are in the ionized form and hence, contribute to conductance (Tiwari,2001). In present findings, the electrical conductivity values are found to be in the range of 302 to 2718 μmhos/cm (Table 5).EC showed direct relationship with total hardness, sulphate and total dissolved solids P<0.01). The total dissolved solids (TDS), value are found in the range of 311 to 2483 mg/L for ground water samples. That is well above the permissible limit (500ppm) of WHO. The maximum TDS value observed at site S 10 (2483 mg/L). The bulk of TDS include bicarbonates, sulphates and chlorides of calcium, magnesium, sodium and silica. High concentration of TDS increased water turbidity. Such water will have salty taste and produce scale on water heaters and cooking utensils (25). The total hardness (TH) values are found to be in the range of 311 (S 7) to 1042 (S 3) mg/L. Hardness of water was understood to be measure of the capacity of the water for precipitating soap. Soap is precipitated chiefly by the calcium and magnesium ions are usually present in significant concentration in natural waters. Hard water therefore is not suitable for domestic usage. Alkalinity in natural water is formed due to dissolution of carbon dioxide.

Carbonates and bicarbonates thus formed are dissociated to yield hydroxyl ions. The most common constituents of alkalinity in natural water include bicarbonates, carbonates and hydroxide . These compounds result from the dissolution of mineral substances in the soil, from waste water discharge, fertilizer and insecticides from agricultural runoff and microbial decomposition of organic material (24) . In the present study, the lowest value recorded 200 mg/L (S 5) and high value 588 mg/L (S 10). The highest value recorded in southwest monsoon and northeast monsoon and lower value recorded during summer season. Alkalinity showed positive correlation with calcium ($p < 0.01$, $r = 0.61$) and total hardness ($p < 0.05$, $r = 0.65$). Chlorides occur in all natural water in varying concentration. The chloride content normally increases as the mineral content increases. Most of the chloride in groundwater is present as sodium chloride. In the present study, chloride ranged from 80 mg/L (S 8) to 527 mg/L (S 10). Chloride showed a distinct seasonal variations and higher values were recorded during southwest monsoon and northeast monsoon season while lowest was recorded during summer season (Table-8). During the current study. the positive correlation was observed with total hardness ($p < 0.05$, $r = 0.72$) and magnesium ($p < 0.05$, $r = 0.90$). Nitrate enters the human body through the use of ground water for drinking and cause a number of health disorder, namely methemaglobinemia, gastric disorders, cancer, goiter, hypertension etc., when present in high concentration in drinking water. The main source of nitrate pollution is the ground water is use of more nitrogen fertilizer in the agricultural land. Many ground water have significant quantities of nitrate due to leaching of the nitrate with the percolation of water high amount of nitrate are generally indicative of pollution (26) . In the present investigation, the nitrate concentration varied between 48 mg/L (57) to 270 mg/L (S 2).

All the water samples are above permissible limit. The permissible limit is 45 mg/L as per the Indian standards, this is due to high use of fertilizer in agriculture field. Nitrate has showed a seasonal trend and noticed higher concentration during northeast and southeast monsoon season, while, in summer nitrate was recorded lesser then other season. In this study, nitrate showed significant positive correlation with sodium ($p < 0.05$, $r = 0.79$), potassium ($p<0.05$, $r=0.76$) and phosphate ($p < 0.1$, $r = 0.92$). Sulphate content in found water is made possible through oxidation, precipitation and constriction, as the water traverses through rocks. The source of sulphate in rocks are sulphur minerals, sulphides of heavy metals. Sulphide minerals, when oxidized give rise to soluble sulphates. In the present study, the sulphate concentration varied between 10 mg/L (S 5) to 95 (S 2) mg/L. Interestingly, the sulphate concentration were within the limits of Indian Standards (27) . In the present study, sulphate showed a significant positive correlation with total iron ($p < 0.05$, $r = 0.92$), total hardness ($p < 0.05$, $r = 0.66$). Phosphorus in the natural fresh water is present mostly in inorganic forms, phosphorus being an important constituent of Biochemical systems may also be present in the organic form. The major source of phosphorus are domestic sewage, detergents, agricultural effluents with fertilizers and industrial waste waters. In the present study, the high phosphate value recorded 1.4 mg/L in S 5 and low value recorded 0.2 mg/L in S 1 . During summer lower values recorded. Significant positive correlation was noticed with total hardness ($p < 0.05$, $r = 0.92$), calcium hardness ($p < 0.01$, $r = 0.89$), magnesium hardness ($p < 0.05$, $r = 0.92$) and iron ($p < -0.01$, $r = 0.65$) (28)During the present investigation, maximum sodium was recorded to be 360 mg/L at S 5 in the month of May 2011 and lowest value recorded 70 mg/L in the month of Dec 2010 at S 6 . In summer it was recorded

high when compared to other seasons. Most sodium salts are readily soluble in water, but take no part in chemical reactions, as do the salts of alkaline earth metals. For this reason sodium salt tend to remain in solution unless extracted during evaporation. In general these is a concomitant increases in sodium and chloride, the concentration of both increasing with total dissolved solids content (24) . In the present study, sodium values showed a positive significant correlation was noticed with potassium $p < 0.05$, $r = 0.70$), fluoride < 0.05, $r = 0.69$), nitrate ($p < 0.01$, $r = 78$) and TDS ($p < 0.05$, $r = 0.68$). The common source of potassium are the silicate mineral, orthoclase, microline, nepheline, biotite igneous rocks and metamorphic rocks, etc., Although potassium is nearly as abundant as sodium in igneous rocks and metamorphic rock, its concentration in ground water is one tenth or even one-hundredth that of sodium. Two factors are responsible for the scarcity of potassium in groundwater one being the resistance to potassium minerals to decomposition by weathering The other fixation of potassium in clay minerals formed due to weathering. Potassium salts, being more soluble than sodium salts, are the last to crystallize during evaporation. In the present study , maximum potassium was recorded 4.2 mg/L at S 8 and minimum value recorded 1.2mg/L at S 3 . In the present study a significant positive correlation was noticed with nitrate ($p < 0.1$, $r = 0.82$). Iron is one of the major constituents of rocks, next in abundance only to oxygen, silicon, and aluminium. The important iron-bearing minerals include pyroxens, amphiboles and micas among silicates, pyrite and chalcopyrite among sulphides and magnetite and hematite among oxides.

In igneous and metamorphic rocks, iron present mostly in the form of silicate minerals. Usually iron occurring in groundwater in the form of ferric hydroxide in concentration less than 0.5ppm. In the present investigation, the iron content varied between 0.1 mg/L (S 5) to 0.7 mg/L (S 3) (Table-11. All the iron values were within the permissible limits and no seasonal variation was observed in the present study. In the present investigation significant correlation was noticed with sulphate ($p < 0.01$, $r = 0.68$) and the Total dissolved solids ($p < 0.05$, $r = 0.78$). According to BIS the permissible limit of pH value for drinking water is 6.5 to 8.5.Abnormal values of pH in water causes bitter taste, affects mucous membrane, causes corrosion in pipelines and also affects aquatic life. The standard desirable limit of alkalinity in potable water is 200 mg/l as per BIS standards. Excess alkalinity in water is also harmful for irrigation which leads to soil damage by altering the soil pH which enhance soil pH to a great exert and reduce crop yields. Exceeding the permissible limits of hardness causes poor lathering with soap, deterioration of the quality of clothes, scale formation and skin irritation (Shashank Sourabh et al.,2014; Priyanka Khanna and Nidhi Rai,2016) .According to Indian standards for drinking water, desirable limit of chloride is 250 mg/l, and the permissible limit is 1000 mg/l. Sulphate occurs due to discharge from gypsum and other minerals. Sulphate content in drinking water exceeding the 400 mg/L impart bitter taste and may cause gastro-intestine irritation and cantharsis (Priyanka Khanna and Nidhi Rai,2016; Manivasakam,2005) .

Thirumala and Kiran (2017) have analysed the ground water quality in Davangere town of Karnataka. Seasonal variations in the physico-chemical parameters in the ground water sample were observed by them and compared with BIS standards . They reported that ground water samples were moderately polluted and impact to health hazards. In their study, the water samples of all the 5 sites were quite good (fair) for irrigation purpose due to high salinity of ground water. The Geo spatial variations of ground water quality in Chickballapur District of Karnataka, India have been studied by Gajalakshmi and Anatharama (19) by utilizing the new technology. For their study,water samples were analyzed for 13 physico-chemical parameters and the results were compared with Indian standards. The geospatial distributions of ground water quality map of their study area have been prepared using spatial analyst tools in GIS. The spatial database established in GIS and results obtained in their study will be helpful for monitoring and managing ground water pollution. Sridhara et al (18) have studied the drinking water quality parameters in borewell samples by using GIS techniques in Chikkaballapura and Bagepalli taluks. They were suggested that in contaminated areas, continuous monitoring of ground water quality be carried out to stop further degradation and related concerns.

One-way ANOVA with post-Hoc Tukey HSD Test

The p-value to the F-statistic of one-way ANOVA is lower than 0.05, suggesting that the one or more treatments are significantly different. These post-hoc tests would likely identify which of the pairs of treatments are significantly different from each other (Table1-3).

CONCLUSION

The present investigation has been made to evaluate the quality of ground water of Bagepalli Taluk area. A total of 10 underground water samples were collected from different locations. Water samples were analyzed for 15 physico-chemical parameters to evaluate their suitability for human consumption and domestic applications. In many samples the values of total hardness and chloride are exceed the permissible limits of WHO and BIS standards. It is concluded that the ground water quality is mainly affected by seepage of sewage, waste water and urban runoff into the ground waters, due to lack of proper sewerage facilities. Open drains are prevalent in study area. Further, lime nature of lithology and lack of rainfall due to the deforestation are also responsible for the degradation of ground water quality. Hence, it is recommended to the Karnataka state and Indian government to take care of ground water quality and to safeguard for the residents and tourists of Bagepalli Taluk, India. Thus to maintain the quality of ground water, preventive measures have to be taken to control the above parameters within the permissible limit. However, we could suggest that this water could be used for drinking after proper treatment (reverse osmosis etc.) and induced ground water recharge by construction of percolation tanks flooding of ground water by mixing surface water by promoting rainwater harvesting.

RECOMMENDATIONS AND SUGGESTIONS

Most of the bore-wells of in the study area contain high degree of carbonate hardness (Temporary). Hence, people must be advised to use boiled water for drinking. People must be educated regarding ill effects likely to be caused by the excess iron and bacteriological organisms. There should be a check on the use of phosphatic fertilizers as they also contribute for high fluoride concentrations which are being leached down to main groundwater body through irrigation practices. The residents in the village sector should be educated.An artificial recharge of groundwater may be adopted to reduce higher concentration of chemical parameters Further, concerned authorities should be directed to maintain the existing ponds, lakes, reservoirs in Megadi taluk to increase the ground water table. Some of the bore wells are liable to bacterial (E-Coil) contamination. Hence, for drinking purposes, water must be treated by boiling permanganate solution. Proper treatment of water is required before using the water for drinking purpose specially to reduce the iron content of water by the following methods. By adding alum, so that there will be sedimentation. By adding calculated amount of lime which is stirred properly so that the iron will be precipitated and separated. Restrict further drilling through bringing legislation and groundwater is treat as property of the State or Nation. Drip and sprinkler irrigation techniques must be adapted for water saving. Concerned district authorities should take necessary steps to create health awareness among the people with regard to the ill effects of fluorosis and water born diseases. Proper sanitation and drainage system should be provided to avoid contamination of drinking water. Practicing of environmentally compatible cropping patterns, bio-fertilizer and bio-pesticides should be encouraged. The present investigation has revealed that there is much scope for further study in the field of assessment of ground water recharge potential and estimation of pesticidal residues.

ACKNOWLEDGEMENT

The first author is very much grateful to University Grants Commission for providing minor research project fellowship.

REFERENCES

1. Abdul Jameel . A and A. Zahir Hussain, Assessment of ground water quality on the Banks of Uyyakonda Chennel of river Cauvery at TiruchiraPalli. India J. Env. Prot.2007; 27(8) : 713-716.
2. Ahmed S, Kayes I, Shahriar SA, Kabir M, Salam MA, Mukul S. Soil salinity and nutrients pattern along a distance gradient incoastal region. Global J Environ Sci Manage 2020; 6:59–72.
3. Al-Futaisi A, Rajmohan N, Al-Touqi S. Groundwater quality monitoring in and around Barka dumping site, Sultanate of Oman In: Proceedings of second IASTED WRM conference2007..
4. APHA, Standard methods for the examination of water and wastewater, American Public Health Association, New York. (21st Edition) 2005.
5. Behm, Don, III Waters : The Fouling of Wisconsin's Lakes and Streams. 1989
6. Bhuiyan MAH, Bodrud-Doza M, Islam ARMT, Rakib MA, Rahman MS, Ramanathan AL Assessment of groundwater quality of Lakshimpur district of Bangladesh using water quality indices, geostatistical methods, and multivariate analysis. Environ Earth Sci 2016; 75:1020. https:// doi. org/ 10. 1007/ s12665- 016- 5823-y
7. Bhunia GS, Keshavarzi A, Shit PK, El-Sayed Oman E, Bagherzadeh A. Evaluation of groundwater quality and its suitability for drinking and irrigation using GIS and geostatistics techniques in semiarid region of Neyshabur. Iran Appl Water Sci. 2018; https://doi.org/10.1007/s13201-018-0795-6.
8. Chakraborty B, Roy S, Bhunia GS, Sengupta D, Shit PK.Groundwater quality through multi- criteria - based GIS analysis: village level assessment. Groundw Soc. 2021c;https://doi.org/10.1007/978-3-030-64136-8_6.
9. Chakraborty, B., Roy, S., Bera, B. et al.Evaluation of groundwater quality and its impact on human health: a case study from Chotanagpur plateau fringe region in India. Appl Water Sci 2022;12, 25. https://doi.org/10.1007/s13201-021-01539-6
10. Daniele Parrone, Stefano Ghergo, Eleonora Frollini, David Rossi, Elisabetta Preziosi,Arsenic-fluoride co-contamination in groundwater: Background and anomalies in a volcanic-sedimentary aquifer in central Italy, Journal of Geochemical Exploration 2020;Volume 217,106590,https://doi.org/10.1016/j.gexplo.2020.106590.
11. Das. S., B.C. Mehta, S.K. Samanth, P.K. Das, and S.K. Srivastava, Fluoride Hazards in groundwater of Orissa, India. J. Environ. Hlth.2000; 1(1) : 40-46.
12. De Zwart D and R.C. Trivedi . Manual on integrated water quality evaluation report H.A.M. de Kruijf National Institute of Public Health and Environmental Protection (RIVM), Bilthoven, The Netherlands.1995.
13. Fenge Zhang, Guanxing Huang, Qinxuan Hou, Chunyan Liu, Ying Zhang, Quan Zhang,Groundwater quality in the Pearl River Delta after the rapid expansion of industrialization and urbanization: Distributions, main impact indicators, and driving forces, Journal of Hydrology2019;,Volume 577, https://doi.org/10.1016/j.jhydrol.2019.124004.
14. Franklin W. Schwartz et al. Interactive comment on "HESS Opinions: The Myth of Groundwater Sustainability in Asia Hydrol. Earth Syst. Sci. Discuss.2019.https://doi.org/10.5194/hess-2019-399-AC3, 2019.
15. Gajalakshmi K, Anantharama V. Geospatial Distribution of Groundwater quality using GIS techniques, in Chickballapur District, Karnataka, India. International Advanced Research Journal in Science, Engineering and Technology 2022;9(1):332-342. https://doi.org/10.17148/IARJSET.2022.9158
16. Gupta S, Evaluation of the quality of well waters in Udaipur district. Indian J. Env. Health1981;, 23 : 195-207.
17. Islam ARMT, Ahmed N, Bodrud-Doza M, Chu R .Characterizing groundwater quality ranks for drinking purposes in Sylhet district, Bangladesh, using entropy method, spatial auto correlation index, and geo statistics. Environ Sci Pollut Res 2017a; 24(34):2635026374. https:// doi. org/ 10. 1007/ s11356- 017- 0254-1.

18. Jose Galizia Tundisi and Takako Matsumura Tundisi,Integrating eco hydrology, water management, and watershed economy: case studies from Brazil, Ecohydrology & Hydrobiology2016;,Volume 16, Issue 2: 83-91,https://doi.org/10.1016/j.ecohyd.2016.03.006.
19. Juahir H, Zain SM, Yusoff MK, Hanidza TIT, Armi ASM, Toriman ME, Mokhtar M. Spatial water quality assessment of Langat River Basin (Malaysia) using environmetric techniques. Environmental Monitoring and Assessment. 2011; 173(1-4):625–41.
20. Karunanidhi D, Aravinthasamy P, Kumar D, Subramani T, Roy PD . Sobol sensitivity approach for the appraisal of geomedical health risks associated with oralintake and dermal pathways of groundwater fluoride in a semi-arid region of south India. Eco-toxicol Environ Saf. 2020; https://doi.org/10.1016/j.ecoenv.2020.110438.
21. Kaviarasan ,M., P. Geetha and K. P. Soman. Multivariate Statistical Technique for the Assessment of Ground Water Quality in Coonoor Taluk, Nilgiri District, Tamil nadu, India . Indian Journal of Science and Technology 2015; Vol 8(36), DOI: 10.17485/ijst/2015/v8i36/87535, December.
22. Kundu A, Nag SK .Assessment of groundwater quality in kashipur block, Purulia district, west Bengal. Appl Water Sci 2018; https://doi.org/10.1007/s13201-018-0675-0.
23. Liang Chen, Hang Lang, Fei Liu, Song Jin, Tao Yan. Presence of Antibiotics in Shallow Groundwater in the Northern and Southwestern Regions of China. 21 September 2017.https://doi.org/10.1111/gwat.12596
24. Manivaskam, N. Physicochemical examination of water sewage and industrial effluent, 5th Ed, PragatiPrakashan Meerut,2005.
25. Nag SK, Das A .Assessment of groundwater quality from bankura I and bankura II blocks, Bankura district, West Bengal, India. Appl Water Sci 2017; 7:3447–3467. https://doi.org/10.1007/s13201-017-0530-8.
26. PriyankaKhanna.,NidhiRai. Comparative Study of groundwater quality of urban and rural areas of Ajmer district. International Journal of Information Research and Review 2016; Vol. 03, Issue, 06 : 2460-2466.
27. Rathnamala GV, G P. Shivashankara. An evidence-based approach towards identifying household emerging pollutants in rural areas in Southern Karnataka. Journal of Water, Sanitation and Hygiene for Development 2022;12 (6): 498–516. https://doi.org/10.2166/washdev.2022.073.
28. Shashank Saurabh, Dharampal Singh, Sameer Tiwari. Drinking Water Quality of Rajasthan Districts., Journal of Basic and Applied Engineering Research 2014;Volume 1, Number 10; October..
29. Silva, M.I., A.M.L. Gonçalves, W.A. Lopes, M.T.V. Lima, C.T.F. Costa, M. Paris, P.R.A. Firmino, F.J. De Paula Filho,Assessment of groundwater quality in a Brazilian semiarid basin using an integration of GIS, water quality index and multivariate statistical techniques, Journal of Hydrology 2021;,Volume 598, https://doi.org/10.1016/j.jhydrol.2021.126346.
30. Sridhara M K, Sadashivaiah C, & D A, K.. Evaluation and Risk assessment of drinking water quality using GIS technique in Chikkaballapura District of Karnataka, India. SPAST Abstracts. 1(01) 2021. Retrieved from https://spast.org/techrep/article/view/1481
31. Thirumala S and Kiran BR. Seasonal variations in Groundwater Quality of Davangere town of Karnataka , India. International Journal of ChemTech Research 2017; Vol.10 No.7 : 099-104.
32. Tiwari DR. Hydrogeochemistry of under ground water in and around Chhatarpur City, Dist. Chattarpur (M.P.). Indian J Environ Health. 2001 Oct;43(4):176. PMID: 12395524.
33. WHO, International standards for drinking water. World Health Organization, Geneva,1985.

Table 1: One way ANOVA data and independent treatment values

Treatment	A (pH)	B (NO3)	C(Total hardness)	D(Potassium)	Total
observations N	120	120	120	120	480

sum	939.9000	13,998.1400	72,017.0000	314.1000	87,269.1400
mean	7.8325	116.6512	600.1417	2.6175	181.8107
sum of squares	7,378.2700	1,884,624.0196	47,433,347.0000	917.7900	49,326,267.0796
sample variance	0.1387	2,115.3333	35,402.8957	0.8036	69,853.4508
sample std. dev.	0.3724	45.9928	188.1566	0.8965	264.2980
std. dev. of mean	0.0340	4.1985	17.1763	0.0818	12.0635
Source	**Sum of square**	**Degrees of freedom**	**Mean square**	**F statistic**	**P-value**
treatment	28,995,021.5350	3	9,665,007.1783	1,030.4073	1.1102e-16
error	4,464,781.3856	476	9,379.7928		
total	33,459,802.9206	479			

Table 2 : Tukey HSD and **Scheffé data**

Treatments pair	**Tukey HSD Q statistic**	**Tukey HSD p-value**	**Tukey HSD inference**
A vs B	12.3083	0.0010053	** p<0.01
A vs C	66.9950	0.0010053	** p<0.01
A vs D	0.5899	0.8999947	insignificant
Treatments pair	**Tukey HSD Q statistic**	**Tukey HSD p-value**	**Tukey HSD inference**
B vs C	54.6867	0.0010053	** p<0.01
B vs D	12.8981	0.0010053	** p<0.01
C vs D	67.5849	0.0010053	** p<0.01
	Scheffé TT-statistic	**Scheffé p-value**	**Scheffé inference**

A vs B	8.7033	3.5527e-15	** p<0.01
A vs C	47.3726	1.1102e-16	** p<0.01
A vs D	0.4171	0.9816553	insignificant
B vs C	38.6694	1.1102e-16	** p<0.01
B vs D	9.1204	1.1102e-16	** p<0.01
C vs D	47.7897	1.1102e-16	** p<0.01

Table 3 :Bonferroni and Holm results: all pairs simultaneously compared

Treatments pair	Bonferroni & Holm T-statistic	Bonferroni p-value	Bonferroni inference	Holm p-value	Holm inference
A vs B	8.7033	0.0000e+00	** p<0.01	0.0000e+00	** p<0.01
A vs C	47.3726	0.0000e+00	** p<0.01	0.0000e+00	** p<0.01
A vs D	0.4171	4.0607888	insignificant	0.6767981	insignificant
B vs C	38.6694	0.0000e+00	** p<0.01	0.0000e+00	** p<0.01
B vs D	9.1204	0.0000e+00	** p<0.01	0.0000e+00	** p<0.01
C vs D	47.7897	0.0000e+00	** p<0.01	0.0000e+00	** p<0.01

Table 4 . Monthly analysis of Water Temperature and pH in sites of some selected villages of Bagepalli Taluk

Sites	June 2010	July 2010	August 2010	Sept. 2010	Oct. 2010	Nov. 2010	Dec. 2010	Jan. 2011	Feb. 2011	Mar. 2011	April 2011	May 2011
S1	33	31	30	27	28	25	26	27	30	31	32	35
S2	33	31	30	27	28	25	26	27	30	31	32	35
S3	33	31	30	27	28	25	26	27	30	31	32	35
S4	33	31	30	27	28	25	26	27	30	31	32	35
S5	33	31	30	27	28	25	26	27	30	31	32	35
S6	33	31	30	27	28	25	26	27	30	31	32	35
S7	33	31	30	27	28	25	26	27	30	31	32	35
S8	33	31	30	27	28	25	26	27	30	31	32	35

S9	33	31	30	27	28	25	26	27	30	31	32	35
S10	33	31	30	27	28	25	26	27	30	31	32	35
pH												
Sites	**June 2010**	**July 2010**	**August 2010**	**Sept. 2010**	**Oct. 2010**	**Nov. 2010**	**Dec. 2010**	**Jan. 2011**	**Feb. 2011**	**Mar. 2011**	**April 2011**	**May 2011**
S1	7.8	7.1	8.1	8.8	7.4	7.6	7.6	7.4	7.4	7.8	7.6	7.6
S2	8.2	8.5	8.6	8.6	8.1	7.9	7.8	8.1	7.9	8.1	7.7	7.9
S3	7.7	8.0	8.1	8.6	7.7	7.8	7.9	7.4	7.5	8.2	7.9	7.7
S4	8.1	8.2	8.4	8.6	7.5	7.8	7.8	8.1	8.1	8.2	8.1	8.1
S5	7.9	8.2	8.1	8.3	7.8	7.6	7.6	7.5	7.9	7.5	7.6	7.6
S6	7.9	8.1	8.3	8.6	7.9	7.7	7.7	7.8	8.3	8.1	7.8	7.8
S7	8.2	8.1	7.9	7.7	7.6	7.4	7.7	7.0	7.3	7.3	8.1	8.2
S8	8.1	8.0	7.8	7.6	7.5	7.3	7.2	7.1	7.3	7.6	7.9	8.1
S9	8.3	8.1	8.0	7.9	7.7	7.5	7.3	7.1	7.4	7.6	7.9	8.1
S10	8.2	8.1	7.9	7.8	7.6	7.4	7.3	7.1	7.3	7.5	7.9	8.2

Table 5 . Monthly Electrical Conductivity (*µmhos/cm*) and TDS (mg/L) in sampling sites of Bagepalli Taluk

Sites	**June 2010**	**July 2010**	**August 2010**	**Sept. 2010**	**Oct. 2010**	**Nov. 2010**	**Dec. 2010**	**Jan. 2011**	**Feb. 2011**	**Mar. 2011**	**April 2011**	**May 2011**
S1	1900	2050	2100	2110	2122	2125	2100	1991	1786	1790	1802	1812
S2	720	1010	1020	1120	1140	1132	1202	1226	1043	1080	1025	1052
S3	1415	1495	1550	1535	1600	1632	1620	1642	1540	1311	1300	1381
S4	480	435	460	459	482	500	485	452	302	383	242	382
S5	1490	1545	1520	1531	1526	1640	1680	1542	1342	1311	1490	1346
S6	1490	1500	1520	155	1572	1620	1650	1650	1300	1352	1401	1451
S7	1137	1134	1132	1330	1128	1125	1123	1121	1106	1117	1128	1139
S8	1315	1312	1310	1307	1304	1302	1299	1296	1280	1292	1305	1318
S9	1125	1123	1120	11i8	1115	1112	1108	1105	1095	1105	1116	1127
S10	2718	2715	2712	2709	2704	2699	2693	2688	2642	2540	2550	2565

					TDS							
Sites	**June 2010**	**July 2010**	**August 2010**	**Sept. 2010**	**Oct. 2010**	**Nov. 2010**	**Dec. 2010**	**Jan. 2011**	**Feb. 2011**	**Mar. 2011**	**April 2011**	**May 2011**
S1	552	592	563	582	643	682	632	623	543	522	532	501
S2	1202	1242	1352	1311	1253	1201	1251	1242	1235	1122	1134	1152
S3	583	551	546	532	596	563	583	601	442	512	521	475
S4	483	451	446	433	496	462	501	452	442	462	422	392
S5	1602	1753	1702	1742	1782	1732	1621	1652	1646	1601	1612	1652
S6	392	403	423	442	482	503	511	523	I 322	352	292	311
S7	1240	1215	1190	1164	1139	1114	1088	1063	1107	1166	1213	1266
S8	1148	1124	1101	1078	1054	1031	1007	984	1025	1074	1122	1171
S9	946	926	907	888	868	849	830	811	844	885	925	965
S10	2483	2458	2433	2408	2383	2358	2331	2308	2195	2299	2404	2442

Table 6 . Monthly analysis of Total hardness and Calcium hardness (mg/L) in different sites of some selected villages of Bagepalli Taluk

Sites	**June 2010**	**July 2010**	**August 2010**	**Sept. 2010**	**Oct. 2010**	**Nov. 2010**	**Dec. 2010**	**Jan. 2011**	**Feb. 2011**	**Mar. 2011**	**April 2011**	**May 2011**
S1	711	752	864	762	657	594	620	636	511	543	512	597
S2	582	572	672	745	642	583	622	663	522	498	422	387
S3	665	792	842	972	968	911	1042	986	910	932	801	795
S4	672	692	767	765	843	825	823	896	651	632	645	712
S5	663	670	671	781	892	811	892	951	663	564	523	592
S6	593	629	722	802	900	775	766	811	700	722	645	595
S7	361	357	353	349	356	342	339	335	325	311	346	364
S8	382	374	366	359	348	337	326	316	326	347	368	390
S9	468	464	459	454	449	445	440	435	412	434	453	473
S10	588	582	576	571	559	548	536	525	520	545	569	594
Calcium hardness												
Sites	**June 2010**	**July 2010**	**August 2010**	**Sept. 2010**	**Oct. 2010**	**Nov. 2010**	**Dec. 2010**	**Jan. 2011**	**Feb. 2011**	**Mar. 2011**	**April 2011**	**May 2011**
S1	82	92	80	123	152	132	110	116	73	123	102	96
S2	276	235	262	142	160	151	153	158	170	192	221	226
S3	122	120	110	126	156	142	92	108	77	136	80	110
S4	160	182	211	225	117	172	158	211	208	125	131	141

S5	231	241	212	217	196	245	289	195	242	132	232	156
S6	75	90	80	251	260	282	310	312	157	119	78	132
S7	54	53	52	52	51	51	50	50	49	47	49	52
S8	55	54	53	52	50	50	49	48	48	49	51	56
S9	35	33	32	31	32	32	31	30	32	34	37	38
S10	49	48	47	46	46	45	45	43	44	45	47	50

Table 7: .Monthly analysis of Magnesium Hardness and Total alkalinity(mg/L) in sampling sites of selected villages of Bagepalli Taluk

Sites	June 2010	July 2010	August 2010	Sept. 2010	Oct. 2010	Nov. 2010	Dec. 2010	Jan. 2011	Feb. 2011	Mar. 2011	April 2011	May 2011
S1	31	32	33	32	41	50	51	62	30	32	29	30
S2	39	37	38	39	39	59	40	42	40	33	25	30
S3	31	35	37	32	38	40	41	46	22	20	18	23
S4	31	36	39	38	41	36	44	43	33	32	31	32
S5	39	37	39	38	40	38	42	52	57	34	32	32
S6	33	41	44	44	49	59	41	42	44	35	32	32
S7	52	53	53	52	51	50	49	49	47	49	51	53
S8	58	57	51	54	53	53	52	52	51	53	54	58
S9	38	37	36	36	35	34	34	33	33	34	36	38
S10	90	89	89	88	86	84	82	81	80	84	87	89
Total alkalinity												
Sites	**June 2010**	**July 2010**	**August 2010**	**Sept. 2010**	**Oct. 2010**	**Nov. 2010**	**Dec. 2010**	**Jan. 2011**	**Feb. 2011**	**Mar. 2011**	**April 2011**	**May 2011**
S1	375	370	410	380	385	390	360	300	350	375	280	320
S2	300	365	380	390	400	335	310	320	340	360	290	310
S3	300	310	360	400	380	375	375	280	330	380	310	360
S4	300	340	350	410	420	350	300	400	240	280	225	260
S5	280	310	410	460	400	420	440	375	200	250	260	265
S6	375	400	415	420	480	490	495	390	375	395	360	320
S7	433	429	424	420	411	403	395	386	374	395	416	437
S8	483	478	473	468	463	459	454	449	427	447	467	488
S9	484	476	474	469	460	450	441	432	418	442	465	489
S10	588	582	576	570	558	547	536	524	520	544	569	572

Table 8 Monthly Chloride and Nitrate (mg/L) in various sampling sites of Bagepalli Taluk

Sites	June 2010	July 2010	August 2010	Sept. 2010	Oct. 2010	Nov. 2010	Dec. 2010	Jan. 2011	Feb. 2011	Mar. 2011	April 2011	May 2011

S1	93	130	142	204	310	281	219	200	122	91	96	98
S2	380	420	510	515	435	445	480	470	455	415	400	358
S3	350	410	440	250	350	310	.460	550	430	410	385	360
S4	260	360	370	380	400	420	450	405	350	325	310	255
S5	360	415	430	426	460	465	500	465	450	435	425	390
S6	120	125	150	165	180	304	275	234	190	180	165	150
S7	107	106	105	103	100	97	94	91	85	81	75	65
S8	109	107	105	102	99	96	93	90	90	82	80	75
S9	105	102	100	98	95	92	89	86	80	72	65	60
S10	527	522	516	511	501	491	480	470	425	395	365	350
Nitrate												
Sites	**June 2010**	**July 2010**	**August 2010**	**Sept. 2010**	**Oct. 2010**	**Nov. 2010**	**Dec. 2010**	**Jan. 2011**	**Feb. 2011**	**Mar. 2011**	**April 2011**	**May 2011**
S1	85	95	100	115	125	135	150	170	180	185	65	68
S2	110	125	170	175	240	245	255	270	110	112	125	135
S3	125	135	120	110	135	126	125	140	95	90	85	87
S4	82	91	120	125	130	135	.140	145	58	64	68	70
S5	135	145	165	175	200	185	180	170	110	115	116	118
S6	130	140	170	160	170	140	180	195	125	135	110	125
S7	49	48	58	60	70	110	120	115	95	100	120	130
S8	54	62	70	76	80	85	92	96	55	58	62	68
S9	65	75	80	95	105	115	130	150	160	165	55	60
S10	70	90	100	110	130	110	135	120	110	100	70	65

Table 9 . Monthly data of Sulphate and phosphate (mg/L) in sites of some selected villages of Bagepalli Taluk

Sites	**June 2010**	**July 2010**	**August 2010**	**Sept. 2010**	**Oct. 2010**	**Nov. 2010**	**Dec. 2010**	**Jan. 2011**	**Feb. 2011**	**Mar. 2011**	**April 2011**	**May 2011**
S1	47	43	42	50	47	43	52	52	57	53	52	53
S2	78	70	74	70	79	81	82	85	90	94	92	95
S3	43	42	50	47	43	52	57	55	53	52	47	48
S4	48	46	46	47	47	34	36	34	35	49	44	46
S5	15	12	11	10	10	16	15	10	13	10	11	11
S6	27	24	22	28	25	22	29	40	40	39	39	40
S7	46	46	47	47	34	36	34	35	49	44	46	40
S8	65	67	66	66	52	57	50	45	58	57	53	57
S9	25	23	24	20	30	31	34	40	25	21	20	24
S10	48	43	41	48	45	42	50	56	53	51	48	48
Phosphate												

Sites	June 2010	July 2010	August 2010	Sept. 2010	Oct. 2010	Nov. 2010	Dec. 2010	Jan. 2011	Feb. 2011	Mar. 2011	April 2011	May 2011
S1	0.3	0.3	0.4	0.4	0.5	0.4	0.5	0.6	0.2	0.2	0.3	0.2
S2	0.7	0.8	0.9	0.9	1.0	1.1	1.2	1.3	1.2	1.2	1.0	0.9
S3	0.6	0.9	0.9	1.0	0.9	0.4	0.2	0.3	0.2	0.3	0.4	0.8
S4	0.9	1.0	0.9	1.1	0.9	0.9	1.0	1.3	0.4	0.5	0.4	0.7
S5	1.2	1.1	1.3	1.0	1.4	1.4	1.2	1.1	0.9	0.8	0.8	1.1
S6	1.1	1.0	1.0	0.9	0.9	1.0	1.1	1.2	0.2	0.3	0.4	0.8
S7	0.9	1.0	0.9	1.1	0.9	1.0	1.3	0.4	0.5	0.5	0.4	0.9
S8	0.8	0.8	0.9	0.7	0.9	0.9	1.2	1.3	0.9	0.8	1.0	0.9
S9	1.0	0.9	0.8	1.0	0.8	0.8	1.0	1.1	0.3	0.5	0.4	0.5
S10	1.2	1.3	1.2	1.4	1.2	1.2	1.3	1.2	0.9	0.8	0.7	1.0

Table 10 . Monthly analysis of Sodium and Potassium (mg/L) in sites of some selected villages of Bagepalli Taluk

Sites	June 2010	July 2010	August 2010	Sept. 2010	Oct. 2010	Nov. 2010	Dec. 2010	Jan. 2011	Feb. 2011	Mar. 2011	April 2011	May 2011
S1	190	185	180	185	210	215	220	240	260	245	240	210
S2	150	145	140	145	175	180	185	210	225	210	215	195
S3	200	210	190	180	160	165	150	175	235	215	240	260
S4	240	235	215	215	245	235	205	210	245	240	260	280
S5	245	265	260	265	280	260	280	300	340	340	345	360
S6	81	80	77	76	74	72	70	69	72	75	78	82
S7	112	110	107	105	103	100	98	96	100	105	109	114
S8	133	131	128	125	122	120	117	114	119	125	130	136
S9	186	183	179	175	171	167	136	160	166	174	182	190
S10	145	142	139	136	134	131	128	125	130	136	142	148
Potassium												
Sites	**June 2010**	**July 2010**	**Augus t 2010**	**Sept . 2010**	**Oct. 2010**	**Nov . 2010**	**Dec. 2010**	**Jan. 2011**	**Feb. 2011**	**Mar. 2011**	**Apri l 2011**	**May 2011**
S1	4.1	4.1	4.0	3.9	3.9	3.8	3.7	3.7	3.8	3.9	4.0	4.1
S2	3.0	3.0	3.1	3.1	3.0	3.0	2.9	2.9	3.0	3.1	3.2	3.3
S3	1.4	1.3	1.3	1.2	1.2	1.3	1.2	1.2	1.3	1.4	1.4	1.5
S4	3.0	3.0	4.0	4.0	3.0	3.0	3.1	3.1	3.0	3.1	4.0	4.0
S5	2.0	2.1	2.1	2.1	3.0	3.0	3.1	2.8	2.8	3.0	3.2	3.4
S6	1.6	1.5	1.5	1.4	1.4	1.3	1.3	1.2	1.3	1.5	1.6	1.7
S7	2.1	2.1	2.0	2.0	1.9	2.0	2.0	1.8	1.9	2.0	2.1	2.2
S8	3.0	3.0	3.0	4.0	4.0	3.0	3.0	3.0	3.0	4.0	4.1	4.2
S9	2.0	2.0	2.0	1.9	1.9	1.8	1.8	1.9	1.9	2.0	2.1	2.1

S10	3.1	3.1	3.0	3.0	2.9	2.9	2.8	2.8	2.9	3.0	3.1	3.2

Table 11: Monthly Iron (mg/L) in sampling sites of Bagepalli Taluk

Sites	June 2010	July 2010	August 2010	Sept. 2010	Oct. 2010	Nov. 2010	Dec. 2010	Jan. 2011	Feb. 2011	Mar. 2011	April 2011	May 2011
S1	0.5	0.5	0.5	0.6	0.5	0.5	0.5	0.4	0.4	0.4	0.3	0.3
S2	0.6	0.4	0.4	0.3	0.3	0.4	0.4	0.2	0.3	0.3	0.4	0.5
S3	0.7	0.6	0.5	0.5	0.5	0.6	0.6	0.6	0.5	0.6	0.5	0.4
S4	0.3	0.3	0.3	0.4	0.4	0.2	0.3	0.2	0.2	0.2	0.3	0.2
S5	0.4	0.4	0.3	0.3	0.3	0.2	0.3	0.3	0.2	0.3	0.4	0.1
S6	0.4	0.4	0.4	0.3	0.5	0.3	0.4	0.3	0.3	0.3	0.2	0.3
S7	0.4	0.3	0.3	0.2	0.4	0.3	0.4	0.3	0.3	0.2	0.2	0.3
S8	0.5	0.5	0.4	0.6	0.5	0.5	0.5	0.4	0.4	0.4	0.3	0.3
S9	0.4	0.4	0.3	0.3	0.3	0.2	0.4	0.4	0.3	0.2	0.2	0.3
S10	0.5	0.5	0.4	0.4	0.5	0.5	0.5	0.4	0.4	0.3	0.3	0.2

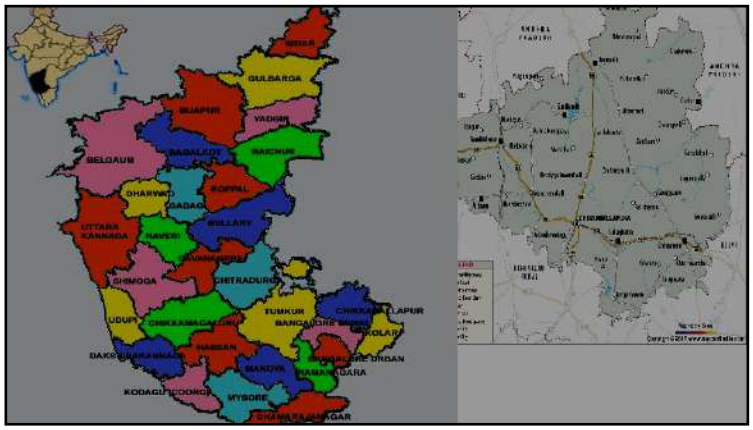

Figure 1: Bageapalli taluk map of Chikballapur district

Vol.15 / Issue 83 / Apr / 2024 International Bimonthly (Print) – Open Access ISSN: 0976 – 0997

RESEARCH ARTICLE

Impacts of Microplastic Pollution in the Nanjarayan Lake - an Issue of Concern

M. Nandhini[1]* and. J.Jagatheeswari[2]

[1]Research Scholar, Department of Zoology, Chikkanna Government Arts College, Tiruppur, (Affiliated to Bharathiar University, Coimbatore), Tamil Nadu, India.
[2]Assistant Professor, Department of Zoology, Chikkanna Government Arts College, Tiruppur, (Affiliated to Bharathiar University, Coimbatore), Tamil Nadu, India.

Received: 12 Jan 2024 Revised: 09 Feb 2024 Accepted: 19 Mar 2024

***Address for Correspondence**
M. Nandhini
Research Scholar,
Department of Zoology,
Chikkanna Government Arts College, Tiruppur,
(Affiliated to Bharathiar University, Coimbatore),
Tamil Nadu, India.
Email: mbbsnandhu@gmail.com

ABSTRACT

This study examines the widespread usage of plastics and the growing body of evidence on its possible eco-toxicological effects, particularly on smaller plastic particles known as micro-plastics. It addresses developing alternatives and their environmental suitability, as well as potential mitigation techniques aimed at reducing the prevalence of (micro)plastics. This paper evaluates these existing tools, examines their scientific foundations, and explores potential roadblocks to the applicability and relevance of current and upcoming legislative initiatives. The Nanjanarayan Lake, which has been preserved as a bird sanctuary, will also be the subject of a more focused investigation.

Keywords: Micro-plastics; Nanjanarayan lake; Rising concern; Toxic impacts; Environmental impacts.

INTRODUCTION

The name "plastic" serves as a catch-all for a variety of products manufactured of synthetic or semi-synthetic organic molecules. Plastics are described as "polymeric materials that may contain other substances to improve performance and/or reduce costs" by the International Union of Pure and Applied Chemistry (IUPAC). These very malleable materials are capable of being molded into solid things in a wide variety of sizes and shapes. (Baztan *et.al.,* 2017) Plastics are polymers, which are made up of long chains of linked, identical units (sometimes known as "monomers"). Imagine a polymer as being similar to a pearl necklace in which the monomers are the individual

pearls as one way to see this. Polymerization is the process by which these monomers are joined, and as a result, plastics can be categorized based on the chemical process used to create them, such as condensation, poly-addition, or cross-linking, or based on the chemical make-up of the polymer's backbone and side chains. The silicones, acrylics, polyesters, polyurethanes, and halogenated plastics subcategories are among the most significant. (Thompson, 2019)
Primary micro-plastics, which are made on purpose to be millimeter or sub-millimeter sized, are present in a wide range of everyday items, including toothpaste, exfoliating lotions, facial cleansers, and other personal hygiene products. These products are particularly concerning because, according to estimates, 6% of all liquid skin-cleansing solutions marketed for sale in the EU, Switzerland, and Norway include micro-plastics, the majority of which are made of the plastic polyethylene (PE). (Walker *et.al.,* 2018)

The raw materials used to make plastic products are a significant source of primary micro-plastics. Primary micro-plastics may accumulate owing to improper handling, unintentional loss, runoff from processing facilities, and product residues. Micro-plastics are utilized in air-blasting media and, to a lesser extent, in medicine, namely as drug delivery systems. Micro-plastics are released into home waste waters after being used, where they may end up in the environment. In order to limit the amount of primary micro-plastics entering the environment, it is possible to identify their sources as well as their precise origins. (Zalasiewicz *et.al.,* 2015)

Environmental impacts of plastics and microplastics
Effects of plastics and micro-plastics on the environment "End of life" does not necessarily mean "end of impact". In reality, it has become obvious that there is no such thing as "end of life" for plastics because these materials continue to exist and pollute long after they have served their intended purpose. Depending on how it is used, plastic may, when it reaches the trash stage of its life cycle, constitute a serious threat to the environment and the climate. A 2019 analysis states that by 2015, the handling of plastic garbage worldwide looked like Figure. (Grinevald, 2011)
According to the most recent statistics, 7.2 million tonnes of plastic post-consumer trash in Europe (both inside and outside the EU) was land filled, 9.4 million tonnes was collected for recycling, and roughly 12.4 tonnes was burned. (Vert *et.al.,* 2012)

The fate of plastics in the environment
It is intrinsically difficult to predict how (micro)(nano)plastics will behave in the environment. This is mostly caused by the variety of sources and entry points into the environment as well as the length of time required to ascertain the pathways for their breakdown. This also applies to smaller particles because of their size (see Figure). As a result, it can be challenging to quantify these materials, especially given the lack of established techniques for sampling, unit normalization, data expression and quantification, and identification, especially for smaller-sized plastics. Additionally, these materials lack a common definition, particularly in the case of nanoplastics. Micro-plastics have been found all over the world, especially in remote areas, from the Arctic to the Antarctic, and all the way down in the water column (benthos). However, micro-plastics are also discovered in agricultural soils, sediments, and even the atmosphere, both inside and outside of buildings. They are also discovered in rivers and lakes. It demonstrates the variety of routes through which plastics are introduced to the ecosystem, particularly the marine environment. ()

Plastics can degrade once they are in the environment through biotic and/or abiotic processes. The former comes before the latter and is a crucial initial step. In other words, abiotic degradation processes must come before bio-degradation mechanisms. As a result, particles have greater surface area-to-volume ratios and are less stable structurally and mechanically, making them more accessible to microbial action. (Kricheldorf, 2011)

EFFECTS OF PLASTICS
One of the main perceived dangers to biodiversity is plastic pollution. It is particularly concerning due to its prevalence, toughness, and persistence in the environment. More than 90% of all contacts between garbage and people in the waters involve plastic debris. At least 17% of the species impacted by entanglement and ingestion were identified as threatened or near threatened by comparing the listed encounters with the International Union for Conservation of Nature (IUCN) Red List.The interaction of living things with plastic waste has a wide range of direct

and indirect impacts, including the possibility of sub-lethal effects, which, due to their unpredictability, may be of great concern. In general, the presence of bigger plastic items in the ocean may cause entanglement and ingestion, the possible development of new habitats, and raft-based dispersal, including the transportation of invasive species. Although the obtained data seems to indicate that entanglement is significantly more lethal (79% of all instances) than ingestion (4% of all cases), both entanglement and ingestion commonly result in damage or death. (da Costa *et.al.,* 2016)

Debris may also create new habitats, and abandoned fishing gear, for instance, has been found to kill invertebrates through "ghost fishing" as well as create new habitats for them. In recent decades, there has been a rise in the dispersal of species in the maritime environment, particularly species without a pelagic larval stage. Numerous species that are highly dependent on ocean currents have always built rafts out of natural materials like wood, but industrialization and the steady growth in the amount of plastic trash in the oceans suggest that rafting is actively contributing to the dispersal of this debris. (Barnes *et.al.,* 2019) It was interesting to see that the uptake of micro-plastics depends not only on their size and shape but also, and maybe less logically, on their color, with yellow particles being preferentially ingested. They resemble prey, which is probably why. Ingestion of micro-plastics can directly cause internal damage and digestive tract obstruction, which commonly result in lower food intake and thus reduced nutrition. Potentially, this brings about famine and death. Micro-plastics have been shown to lodge in the gills of air-breathing creatures, which may result in slower respiration rates. There are still few studies examining how these extremely widespread compounds affect terrestrial environments. The characteristics that make up the biota are the same regardless of how different soils and aquatic habitats are from one another because many organisms flourish in small bodies of water that are present at or just below the surface, making them basically aquatic species. (Jambeck *et.al.,* 2015)

Additionally, earthworms and mites have the ability to consume micro-plastics, which most likely contributes to their existence and accumulation in food webs. For instance, it was found that the earthworm *Lumbricus terrestris* had its growth rate significantly reduced, and that its mortality rates had increased. Additionally, these earthworms transferred micro-plastics from the litter into the soil by size-selectively transporting them downward through their tunnels. Additionally, it was found that only the smaller particles that the earthworms were exposed to were digested. Given how heavily earthworms influence the physical characteristics of soil, this finding could have significant ramifications for the fate and risk of micro-plastics in terrestrial ecosystems. (da Costa, 2014)

Regardless of the materials employed, these plastics nevertheless share some of the problems with conventional plastics, as many are only "biodegradable" under certain circumstances, such as prolonged high humidity and high temperatures. Such circumstances are infrequently possible in conventional composting facilities, making them unsuitable for home composting. This also means that these purportedly biodegradable materials take far longer to disintegrate after being dumped than expected. Claims about biodegradability need to be carefully examined. Some substances that were once marketed as "biodegradable," "oxo-degradable," or "oxo-biodegradable" had an oxidizing ingredient that aided in the substance's breakdown in the presence of oxygen, UV radiation, and heat. The final outcome, nevertheless, was the production of minute plastic pieces. Furthermore, these goods are not suitable for long-term reusable applications because of the way they are made, which causes them to begin to fragment in a short amount of time. Due to the oxidizing agent's presence, such items could not be composted either, as doing so might cause the compost's quality and market value to decline. The European Commission has suggested that actions be taken against certain materials across the EU as a result of a report. (Zhang et.al., 2010)

Biodegrading organisms

From an environmental perspective perhaps the most urgent question is what to do with the vast amounts of plastic already found in the environment. For larger debris, multiple actions exist, including increasing citizen participation in clean-up actions. However, they have proven to be insufficient. Hence, research has focused on the development of biotechnology-based strategies centred on the process of bio-degradation. (Gouin *et.al.,* 2015)

The development and use of plastic-consuming organisms will however not contribute to a reduction in the significant volume of greenhouse gas emissions that occur throughout the plastic life-cycle. Multiple bacteria and fungi have been reported as potential tools in the bio-degradation of plastics, including the bacterial species *Pseudomonas aeruginosa, P. stutzeri, Streptomyces badius, S. setonii, Rhodococcus ruber, Comamonas acidovorans, Clostridium thermocellum and Butyrivibrio fibrisolvens*. (Zettler *et.al.,* 2013)

Fungal strains described as viable biotechnological agents in the bioremediation of plastics include *Aspergillus niger, A. flavus, Fusarium lini, Pycnoporus cinnabarinusand and Mucor rouxii*. These organisms have been isolated from diverse environments, including landfills, plastic surfaces buried in soils, marine water or mangrove soil. Demonstrated within laboratorial settings, it is important to note that the reported efficiency of such biotechnological-based approaches is obtained under optimised conditions for organisms and substrates. This efficiency may be enhanced by, for example, subjecting plastics to different chemical and/or physical pre-treatments. Treatments include photolysis mediated by UV radiation and ozone and thermal treatments, but the effectiveness of the treatments greatly depends on the nature of the polymer. (Lebreton et.al., 2018)

However, because of the inherent expenses, such per-treatments are improbable procedures in potentially large-scale operations. Along with the price of the actual treatments, there are expenses associated with gathering and managing the plastic materials that need to be treated. As a result, the outcomes ought to be viewed as proof of concept. Additionally, it should be emphasized that using these biodegrading organisms in the environment directly is improbable or simply not practicable considering the accompanying dangers and uncertainties for ecosystems as well as for human health. (Ayre, 2016)

CONCLUSIONS

The presence, fluxes, paths, fates, and consequences of plastics in many environmental compartments have yet to be consistently and reliably measured by research. Marine pollution has received far more attention, both because of the immediate attention generated by the pollution's effects on biota that can be seen directly and because of the plastics' demonstrably widespread and transnational presence. However, other estimations opine that contamination levels in freshwater systems and soils may be higher than those reported for the marine environment, particularly in the case of micro-plastics. Nevertheless, despite these well-informed hypotheses, there is still a great deal of speculation and numerous known unknowns. These uncertainties and knowledge gaps substantially impair a full assessment of the health implications and limit an educated decision by consumers, communities and policy makers. At every stage of the life-cycle of plastic materials, inadequate and incomplete understanding also contributes to possibly long-term negative effects on the environment and human health. Therefore, it is vital to attract more concentrated scientific and governmental attention to these environmental compartments, not at the expense of, but in addition to the current marine (micro)plastic pollution studies.

REFERENCES

1. Baztan, J., et al., Breaking down the plastic age, in MICRO 2016. 2017, Elsevier. p. 177-181.
2. Thompson, R.C., et al., Our plastic age. 2019, The Royal Society Publishing.
3. 3.Walker, M., et al., Formal definition and dating of the GSSP (Global Stratotype Section and Point) for the base of the Holocene using the Greenland NGRIP ice core, and selected auxiliary records. Journal of Quaternary Science: Published for the Quaternary Research Association, 2018. 24(1): p. 3-17.
4. Zalasiewicz, J., et al., When did the Anthropocene begin? A mid-twentieth century boundary level is stratigraphically optimal. Quaternary International, 2015. 383: p. 196-203.
5. Grinevald, J., Anthropocene: conceptual and historical perspectives (The). 2011.
6. Vert, M., et al., Terminology for biorelated polymers and applications (IUPAC Recommendations 2012). Pure and Applied Chemistry, 2012. 84(2): p. 377-410.

7. Kricheldorf, H.R., Handbook of polymer synthesis. Vol. 24. 2011: CRC Press.
8. da Costa, J.P., et al., (Nano) plastics in the environment–sources, fates and effects. Science of the Total Environment, 2016. 566: p. 15-26.
9. Barnes, D.K., et al., Accumulation and fragmentation of plastic debris in global environments. Philosophical Transactions of the Royal Society B: Biological Sciences, 2019. 364(1526): p. 1985- 1998.
10. Jambeck, J.R., et al., Plastic waste inputs from land into the ocean. Science, 2015. 347(6223): p.768-771.
11. da Costa, J., Microplastics–occurrence, fate and behaviour in the environment. In 'Comprehensive analytical chemistry'.(Eds APT Rocha-Santos, AC Duarte) pp. 1–24. 2017, Elsevier: Amsterdam.
12. Zhang, Y., et al. Reduce the plastic debris: a model research on the great Pacific ocean garbage patch. in Advanced Materials Research. 2010. Trans Tech Publ.
13. Zettler, E.R., T.J. Mincer, and L.A. Amaral-Zettler, Life in the "plastisphere": microbial communities on plastic marine debris. Environmental science & technology, 2013. 47(13): p. 7137-7146.
14. Lebreton, L., et al., Evidence that the Great Pacific Garbage Patch is rapidly accumulating plastic. Scientific reports, 2018. 8(1): p. 1-15.
15. Ayre, M., Plastics' poisoning world's seas'. ed. BBC. London: BBC, 2016
16. Gouin, T., et al., Use of micro-plastic beads in cosmetic products in Europe and their estimated emissions to the North Sea environment. SOFW J, 2015. 141(4): p. 40-46.

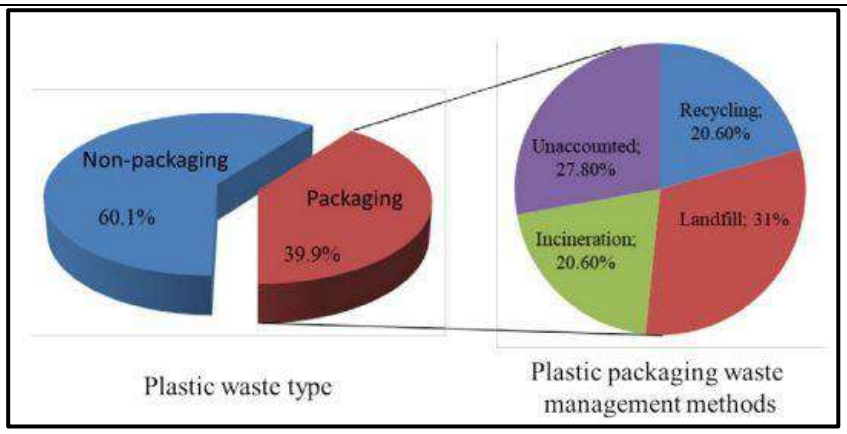

Figure 1. Global plastic waste management, Vert *et.al.,* 2012.

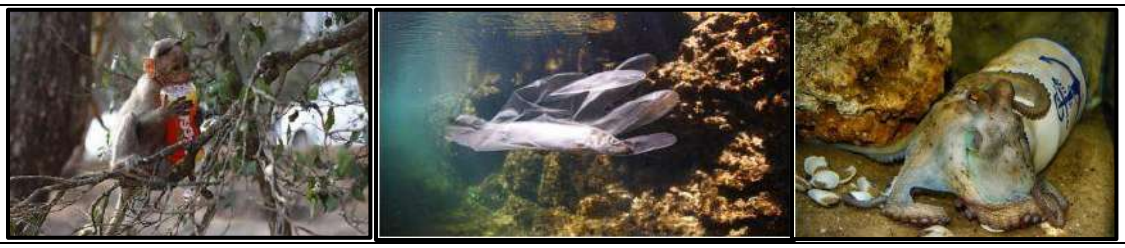

Figure 2. Microplastics affecting animals (Jambeck *et.al.,* 2015)

Vol.15 / Issue 83 / Apr / 2024 International Bimonthly (Print) – Open Access ISSN: 0976 – 0997

RESEARCH ARTICLE

The Effect of Whole-Body Vibration and Mulligan Mobilization with Movement in the Reduction of Pain and Disability in Subjects with Knee Osteoarthritis

P. Saranraj[1]*, S. Rajadurai[2] and P. Susmitha[3] B. Arun[4], P. Savitha[5]

[1]Ph.D Scholar, Department of Physiotherapy, Meenakshi Academy of Higher Education and Research Institute, Chennai,Tamil Nadu, India. Professor, Nandha college of Physiotherapy, (Affiliated to Tamil Nadu Dr. MGR Medical University). Erode, Tamil Nadu, India.
[2]M.S. Ortho, Department of Orthopaedics, Meenakshi Medical College Hospital and Research Institute, Kanchipuram, Tamil Nadu, India.
[3]Associate Professor, Department of Cardio Respiratory, Nandha College of Physiotherapy (Affiliated to Tamil Nadu Dr. MGR Medical University), Erode, Tamil Nadu, India.
[4]Grade II Physiotherapist, Thanthai Periyar Government Headquarters Hospital, Erode, Tamil Nadu, India.
[5]BPT internee Nandha college of Physiotherapy, Erode, Tamil Nadu, India.

Received: 16 Nov 2023 Revised: 15 Jan 2024 Accepted: 25 Mar 2024

***Address for Correspondence**
P. Saranraj
Ph.D Scholar,
Department of Physiotherapy,
Meenakshi Academy of Higher Education and Research Institute,
Chennai,Tamil Nadu, India.
Professor,
Nandha college of Physiotherapy,
(Affiliated to Tamil Nadu Dr. MGR Medical University).
Erode, Tamil Nadu, India.
Email: saranraj.pt@gmail.com

ABSTRACT

Knee osteoarthritis also known as the degenerative joint disease of the knee, is a common chronic progressive joint disease characterized by articular cartilage destruction and degeneration, adjacent subchondral bone lesions, bone hyperplasia and osteophyte formations at the joint margin. The aim of this study to compare the effect of whole-body vibration therapy and mulligan's mobilization with movement forknee osteoarthritis. A experimental study design consisting of 30 patients with knee osteoarthritis divided into two group at the average age was about 45 to 55 years. Group A underwent Whole Body vibration and Group B underwent Mulligan's Mobilization with movement. All the patients underwent pre and post-test scores of VAS and WOMAC. The calculated t-test values by the unpaired

test in group A and group B are 7.4 and 12.8. In the present sample, both groups show positive effect but mulligan's mobilization with movement group has a superior effect than whole body vibration group.

Keywords: whole-body Vibration, mulligan's Mobilization with movement, VAS, WOMAC

INTRODUCTION

Knee osteoarthritis, sometimes referred to as the degenerative joint disease of the knee, is a common, chronic, and progressive joint condition marked by articular cartilage degradation and degeneration, nearby subchondral bone lesions, bone hyperplasia, and osteophyte forms at the joint boundary. Primary and secondary osteoarthritis are the two categories into which osteoarthritis may be divided. Ageing is a factor in primary osteoarthritis, a persistent degenerative condition.[1] As cartilage ages, its water content diminishes, making it more susceptible to breakdown. Contrarily, secondary osteoarthritis often develops in the early stages of life as a result of specific circumstances such as an accident, extended amounts of time spent stooping or crouching at work, diabetes, and obesity. The prevalence of knee osteoarthritis was determined to be 28.7% nationwide. It primarily affects older people. There are primary and secondary forms of osteoarthritis.[2] By 2020, osteoarthritis will rank as the fourth leading cause of disability, according to the World Health Organization. According to reports, OA has an economic, psychological, and physical toll. According to a World Health Organization study, 80 per cent of osteoarthritis patients over 60 have reduced mobility, and osteoarthritis is the main cause of disability worldwide[3]. Around 13% of women and 10% of men 60 years of age and older have symptoms of knee osteoarthritis. Osteoarthritis of the knee affects bodily functions including muscular strength, proprioception, and joint stability as well as causes joint pain and stiffness[4].

The aberrant mechanical stress brought on by joint instability is one of the main elements leading to the development and progression of knee osteoarthritis, according to reports on the pathogenesis of the condition. Agonists and antagonists cause disruptions that affect the dynamic and static stability of the knee joint, which results in the etiopathogenesis of knee pain. The tibial and femoral articular surfaces of the knee joint are anatomically unstable, and the surrounding ligaments and menisci keep the joint stable. Joint instability is often brought on by functional anomalies in these tissues[5]. A modern method of joint mobilisation known as Mulligan's notion of mobilisation with movement (MWM) involves a therapist using an auxiliary gliding force that is pain-free while still including active movement. The idea behind mobilisation with movement is to correct the postural defect and restore the knee's biomechanics. The quick recovery of pain-free movement may be attributed to the combination of joint mobilisation and active movement. A decrease in pain is said to be the outcome of correcting positional faults since the processes behind the effectiveness of mobilisation with movement are based on mechanical dysfunction[6].

This concept is related to positional faults that occur due to injury or changes in the shape of articular surfaces, the thickness of cartilage, orientation of fibres of ligaments and capsules which lead to mal tracking of the joints A recent systemic review heightened the problem that mobilisation with movement exhibits the immediate effects on pain and disability. This technique aims at restoring pain-free and a full range of motion in the joint[7] Whole Body Vibration Therapy (WBVT) is a feasible and curative strength exercise technique that has received considerable attention in recent years.A vibrating plate produces vibrations, which are transferred from surfaces that come into touch with the body to activate muscles and tendons. Whole-body vibration treatment has been shown in trials to enhance neuromuscular function and provide an aged population with a safe programme. It is a quick and secure procedure for treating persistent osteoarthritis of the knee[8]. Whole-body vibration exercise may be used to increase physical functions, reduce pain, improve neuromuscular function and enhance the multi joint strength performance of lower limbs during a counter-movement jump. Exercise and physical activity were suggested as the main treatments for knee osteoarthritis by the UK's National Institute, of Health and Clinic Excellence. It improves the lower extremities' mult ijoint strength and muscular strength. Whole body vibration may be helpful for people with

knee osteoarthritis because it can reduce pain, enhance balance control, and improve gait pattern, and because basic balancing ability and mobility are substantially connected with the improvement of knee-specific function[9].

METHODS

PARTICIPATION

A total of 30 patients were included in this study all subjects provided written informed consent before entering the study. The patient's age is between 45 years to 55 years. Inclusion criteria were as follows: Patients with osteoarthritis knee pain.

STUDY DESIGN

Quasi-Experimental study design

OUTCOME MEASURES

VISUAL ANALOG SCALE (VAS) is the scoring test that is a measurement of pain that was given at any time of day.
HE WESTERN ONTARIO AND MCMASTER UNIVERSITIES OSTEOARTHRITIS INDEX (WOMAC) is the scoring test that is a measurement of disability that was given at any time of day.

INTERVENTION

For 12 weeks, 15 patients in group A had whole-body vibration therapy three times per week with at least one day in between sessions. In this group B, 15 patients had mulligan mobilisation with movement. For a period of six days per week, the mobilisation with movement (MWM) approach was used with three sets of ten repetitions on each treatment occasion. Performing the workouts minimises muscular soreness, impairment, discomfort, and increases function. Under the direction of the therapist, each subject is shown how to do each exercise. The patient is instructed in the following interventions as part of a home programme. Additionally, patients are routinely observed to determine the correctness of the findings.

Training Program

Group A

Exercises included

The participants will stand with slightly bent knees (30°) on the platform and without shoes.
To prevent the feeling of uncomforted and anxious, the patient can hold the handle during training

Group B

Exercises included
MULLIGAN MOBILIZATION FOR MEDIAL GLIDE:
MULLIGAN MOBILIZATION FOR LATERAL GLIDE
MULLIGAN MOBILISATION FOR ROTATION GLIDE

STATISTICAL ANALYSIS

The data were evaluated by using an unpaired 't' test. The unpaired t-test was used to find out the statistical significance between post and post-t-test values of VAS and WOMAC.

Data Presentation

RESULTS

The Paired 't' test analyses for the pre-test and post-test variable for the visual analogue scale for measuring pain in knee osteoarthritiss which is shown in table I. Both groups show a significant difference between the pre-test and post-test values. The 't' value for Group A is 14.the 't' value for Group B is 36.5. The unpaired 't' test analyses for the

Post-test variables for Both groups for the visual analogue scale for measuring pain in the knee are shown in table 3. There was a significant difference shown between the Groups. Group B subjects show superior to Group A. The 't' value for the post-test variables for both groups is 7.4255. The Paired 't' test analyses for the pre-test and post-test variables for the disability measurement by WOMAC are shown in table 2. Both groups show a significant difference between the pre-test and post-test values. The 't' value for Group A is 21.12, and the 't' value for Group B is 52.62. The unpaired 't' test analyses for the Post-test variables for Both groups' disability measured by WOMAC is shown in table 3.There was a significant difference shown between the Groups. Group B subjects show superior to Group A. The 't' value for the post-test variables for both groups is 12.85.

DISCUSSION

The goal of this study was to determine how mulligan's mobilisation with movement and whole-body vibration treatment affected participants with knee osteoarthritis patients' levels of pain and impairment. Using the predefined inclusive and exclusive criteria, 30 participants were chosen. Ten each were assigned to two groups of subjects. Whole-body vibration exercises were performed by Group A, and Mulligan mobilisation with movement was performed by Group B. There was a substantial decrease in pain and disability between the pre-and post-treatment values in both Groups, which was validated by the following research. According to my research, there was a substantial decrease in pain and impairment in both groups when it came to whole-body vibration and mulligans mobilisation with movement, as seen by the post-test results. According to studies, WBV regulates neuromuscular responses, enhancing muscle strength. A probable explanation for the beneficial benefits of WBV on knee OA is the ability of the vibration created by the oscillating platform to stimulate muscle spindles, which activates the alpha-motor neuron. This is followed by the vibration tonic reflex and spinal and supra spinal processes[10]. A subgroup analysis revealed that both high- and low-frequency WBV were successful in reducing pain, enhancing bodily function, and strengthening the knee extensor muscles. Numerous vibration characteristics may affect the efficiency of WBV on results, according to studies[11]. The study revealed that MWM combined with exercise improved functions more than other therapies did. The fact that MWM treatment for osteoarthritis significantly reduced pain and stiffness and enabled the subjects to move more freely without experiencing pain is one of the key factors contributing to the improvement in functional status. This allows the subjects to carry out exercises and other daily activities more successfully and pain-free[12]. The outcome of this study's data analysis shows that Mulligan's mobilisation with movement has a better impact than whole-body vibration. The substantial improvement is therefore founded on his idea. This study found that Mulligan mobilisation with movement was more effective at reducing pain and impairment than whole-body vibration workouts.

CONCLUSION

This study compared the effectiveness of Mulligan's mobilisation with movement and whole-body vibration treatment in reducing pain and impairment in participants with knee osteoarthritis. 30 participants between the ages of 45 and 55 were chosen following a careful examination of the inclusion and exclusion criteria. Two groups were created out of the subjects. Group B received mulligan mobilisation with movement whereas Group A received whole-body vibration. A VAS was used to quantify the level of pain. The WOMAC scale was used to assess functional abilities. Before the start of the treatment regime and after it had ended, the values of the outcome measures were noted. The data analysis appears to support the usefulness of mulligan's movement-based mobilisation and whole-body vibration in treating pain and functional limitations in people with knee discomfort. The fact that there has been a noticeable improvement in the groups demonstrating the usefulness of whole-body vibration and mulligan's mobilisation with movement in boosting functional activities and also reducing pain is evidence of this. Thus, it can be concluded that mulligan's mobilisation with movement and whole-body vibration are extremely efficient in treating patients with knee pain and lead to a considerable improvement in functional activities and pain relief.

REFERENCES

1. McAlindon TE, LaValley MP, Harvey WF, Price LL, Driban JB, Zhang M, et al. Effect of intra-articular triamcinolone vs saline on knee cartilage volume and pain in patients with knee osteoarthritis: a randomized clinical trial. JAMA 2017; 317: 1967–1975.
2. Katz JN, Arant KR, Loeser RF. Diagnosis and treatment of hip and knee osteoarthritis: a review. JAMA 2021; 325: 568–578.
3. Spitaels D, Mamouris P, Vaes B, Smeets M, Luyten F, Hermens R, et al. Epidemiology of knee osteoarthritis in general practice: a registry-based study. BMJ Open 2020;
4. Bennell KL, Hunter DJ, Hinman RS. Management of osteoarthritis of the knee. BMJ 2012;
5. Wang P, Yang L, Liu C, Wei X, Yang X, Zhou Y, et al. Effects of whole body vibration exercise associated with quadriceps resistance exercise on functioning and quality of life in patients with knee osteoarthritis: a randomized controlled trial. Clin Rehabil 2016
6. Cardinale M, Bosco C. The use of vibration as an exercise intervention. Exerc Sport Sci Rev 2003;
7. Munera M, Bertucci W, Duc S, Chiementin X. Transmission of whole body vibration to the lower body in static and dynamic half-squat exercises. Sports Biomech 2016;
8. Zafar H, Alghadir A, Anwer S, Al-Eisa E. Therapeutic effects of whole-body vibration training in knee osteoarthritis: a systematic review and meta-analysis. Arch Phys Med Re-habil 2015;
9. Felson DT, Zhang Y, Hannan MT, et al. The incidence and natural history of knee osteoarthritis in the elderly: the Framingham Osteoarthritis Study. Arthritis Rheum.1995;
10. Corti MC, Rigon C. Epidemiology of osteoarthritis: prevalence, risk factors, and functional impact. Aging Clin Exp Res.2003;
11. Lewek MD, Rudolph KS, Snyder-Mackler L. Quadriceps femoris muscle weakness and activation failure in patients with symptomatic knee osteoarthritis. J Orthop Res.2004;
12. Wolfe F. Determinants of WOMAC function, pain and stiffness scores: evidence for the role of low back pain, symptom counts, fatigue and depression in osteoarthritis, rheumatoid arthritis and fibromyalgia. Rheumatology (Oxford).1999;

Table 1 Data Analysis and Presentation

Data values	VISUAL ANALOG SCALE (VAS)
Mean Difference	4.20
Standard Deviation	0.77
The unpaired t test	7.42
Table value	2.15

Table 2 Data Analysis and Presentation

Data Analysis	THE WESTERN ONTARIO AND MCMASTER UNIVERSITIES OSTEOARTHRITIS INDEX (WOMAC)
Mean Difference	59
Standard Deviation	4
The unpaired t test	12.85
Table value	2.15

RESEARCH ARTICLE

A Multivariate Regression Analysis of RMT

G. Gomathi Eswari[1]* and A. Rameshkumar[2]

[1]Assistant Professor, Department of Mathematics, Srimad Andavan Arts and Science College, (Affiliated to Bharathidasan University) Tiruchirappalli, Tamil Nadu, India.
[2]AssistantProfessor, Department of Mathematics, Marudupandiyar College, Thanjavur (Affiliated to Bharathidasan University, Tiruchirappalli), Tamil Nadu, India.

Received: 10 Apr 2023 Revised: 09 Jan 2024 Accepted: 27 Mar 2024

***Address for Correspondence**
G. Gomathi Eswari
Assistant Professor,
Department of Mathematics,
Srimad Andavan Arts and Science College,
(Affiliated to Bharathidasan University)
Tiruchirappalli, Tamil Nadu, India.
Email: mathseswari@gmail.com

ABSTRACT

This paper presents investigations of the spectrum characteristics of random matrices, with a special emphasis on their most extreme eigenvalues, for both realistic and difficult examples of finite and infinite sample sizes, for a single Wishart matrix and for two Wishart matrices, respectively. The Tracy-Widom Laws, which characterise the distribution of the likelihood of the largest eigenvalue of a random matrix after normalisation, are intriguing to many individuals in RMT. By limiting the probability distributions of the eigenvalues of a certain random matrix, Wigner's semicircle law is produced.

Keywords : Spiled covariance model , Tracy-widom laws, Wigner matrix , Wigner's semicircle law, Wishart matrix.
MSC code : 15B52 , 62H10

INTRODUCTION

We describe the spectrum of random matrices as the set of all eigenvalues, not just the ones in the middle. We set up a deterministic Markov chain to study the majority of the eigenvalues of the (n x n) Wishart matrix S = xx, which is constructed from a (n x r)-matrix X with entries that are iid standard Gaussian deviations (where r is the resolution and n is the sample size). Particularly notable are the outcomes for low n (exact distribution) and high n (asymptotic allocation including Wigner's semicircle rule). The eigenvalues of a single Wishart matrix can

be analysed using multivariate statistics to characterise the distribution of their total values. Both fixed and large r scenarios as well as finite and enormous n cases are explored. The spiking covariance model of Iain Johnstone, which has lately become a hot topic in RMT, was also investigated. Then, for fixed r and limited sample sizes, we explain the situation of two independent Wishart matrices and their uses in multivariate regression and MANOVA. The spectral extrema for a single Wishart matrix and for two Wishart matrices are analysed, along with the largest eigenvalue distribution in a Gaussian ensemble and a Wishart-Laguerre ensemble. The Tracy-Widom Laws are valid for very large r and n. Computational programs for calculating the distributional findings of this study are discussed, and a quick overview of the RMT literature is provided.

Spectrum of Random Matrices

For large random matrices, the random behaviour of the spectrum's edges and centre warrants particular attention. A matrix's greatest and lowest eigenvalues are interesting as extremes, whereas the bulk of the eigenvalues is interesting. Whether we take into account the Gaussian orthogonal Ensemble (GOE), the Gaussian unitary Ensemble (GUE), or the Gaussian symplectic Ensemble, all the eigenvalues of Hn are real and may be ranked ordered . A square matrix's stability and invertibility strongly rely on its extremes. There is a difference between the statistics of the extreme eigenvalues in the spectrum's perimeter and the statistics of the spectrum's center, according to recent study.

The likelihood that consecutive eigenvalues are near together is low and the probability quickly declines as a power of the distance between them, which is an important characteristic that all three random matrix ensembles possess. Any two (correlated) eigenvalues extracted from a GOE (or GUE or GSE) matrix will exhibit this behaviour. While repulsion for iid points on an interval has a slower probability convergence rate to zero than repulsion for eigenvalues, both hold true. Therefore, spacings close to 0 are impossible given the distribution of spacings. Some features of quantum chaos are linked to this attribute.

Bulk of the Spectrum

The Real Wigner Matrix

The first focus of Wigner's study was the real symmetric (n x n)-matrix Hn = (Hij), in which diagonal entries are always equal to 0 and off-diagonal elements are always equal to 1 with probability 1/2. It was later deduced that such generalizations of these findings for this matrix would hold.

Gaussian ensembles as categorized by Dyson. The parameters $\beta \in \{1, 2, 4\}$ are used to classify the time-reversal invariance (TRI) and spin-rotational symmetry of the Hermitian matrix Hn = (Hij) and its matrix of eigenvectors U. (SRS).''Not appropriate'' is signified by the word NA. Since then, a number of other definitions of a genuine Wigner matrix have been published. When we declare that "Hn is a Wigner matrix,'' we indicate that Hn belongs to the set of uncorrelated symmetric random matrices known as the Wigner ensemble. The entries on the diagonal of such symmetric matrices are always generated at random from the same distribution as the ones on the off-diagonal, but the off-diagonal entries may be drawn at random from any distribution. If the real wigner matrix is a member of the GOE, then it is a specific kind of real wigner matrix defined as a symmetric (i.e., Hn $=H_n^T$) random (n x n)-matrix where the ijth element is real-valued with distribution,$\mathbf{H}_{ij} \overset{iid}{\sim} N\ (0,\ \sigma_{ij}^2\ )$, $\sigma_{ij}^2 = 1 + \delta_{ij}$ where $\delta_{ij}=1$if$i=j$ and otherwise. If a complex Wigner matrix belongs to the GUE, it is defined in a similar fashion.H_n^T

Finiten: Exact Distribution

Let U be the matrix of related eigenvectors and let $\lambda 1 > \lambda 2 > ... > \lambda n$ be the ordered eigenvalues of a real Wigner matrix Hn. Then, Hn = UΛUτ, where Λ = diag{λ1, . . . , λn}. We can see that the sole factor that influences tr[V(Hn)]=$\sum_{j=1}^{n} V(\lambda j)$ is the eigenvalue. The assumption that the eigenvectors are uniformly distributed among the

elements of each matrix ensemble has no bearing on the distribution p(Hn). The accurate joint probability distribution of the eigenvalues is obtained by multiplying the Jacobian of the form matrix by p(Hn), which also yields the eigenvalues and eigenvectors of a (n x n) Wigner matrix. The eigenvalues are distributed exactly as follows,

$P(\lambda_1,\ldots,\lambda_n) = c_n e^{-\frac{1}{4}\mathrm{tr}\{H_n\}} \prod_{1\le j<k\le n} |\lambda_j - \lambda_k|$, (1)

Where

$\mathrm{tr}\{H_n^2\} = \sum_{j=1}^{n} \lambda_j^2$ (2)

and the normalizing constant, c_n, is dependent upon n.

For generic β-Gaussian-Hermite ensembles with β= 1 (GOE), 2 (GUE), or 4 (GSE), the Dyson index is supplied by the joint probability density of the eigenvalues of Hn.For generic β-Gaussian-Hermite ensembles with β= 1 (GOE), 2 (GUE), or 4 (GSE), the Dyson index is supplied by the joint probability density of the eigenvalues of Hn.

$p_\beta(\lambda_1,\ldots,\lambda_n) = c_n \beta e^{-\frac{\beta}{4}\mathrm{tr}(H_n^2)} \prod_{1\le j<k\le n} |\lambda_j - \lambda_k|^\beta$ (3)

Where the normalizing constant ,

$$c_{n,\beta} = \frac{1}{2\pi^{n/2}\beta^{n/2+\beta n(n-1)/4}} \prod_{i=1}^{n} \frac{r(1+\frac{8}{2})}{r(1+\frac{8i}{2})} \qquad (4)$$

is dependent upon n and β .Dyson's β ensemble is another name for the distribution in (3). In certain discussions of this topic, the term is replaced with = 2/β, leading to the outcomes for GOE α= 2, GUE α= 1, and GSE α= 1/2.

Large n: Wigner's Semicircle Law

We will examine the distribution of the empirical eigenvalues of a real (nn) Wigner matrix, n-1/2Hn, as n draws nearer to infinity. Let IA be the function that indicates that event A has occurred, and let #{·} be the total number of items in the set being indicated.

The ESD of n-1/2Hn, Gn(λ), converges asymptotically to the non-random limiting distribution G(λ), according to Wigner's conclusion.

$$G_n(\lambda) = \frac{1}{n}\#\{i : \lambda_i \le \lambda\} = \frac{1}{n}\sum_{i=1}^{n} I_{[\lambda i \le \lambda]} \xrightarrow{a.s} G(\lambda),\ n \to \infty, \qquad (5)$$

Where G(k) has density

$$g(\lambda) = \frac{1}{2\pi}\sqrt{4-\lambda^2}\ ,\ |\lambda| \le 2\ . \qquad (6)$$

and zero for $|\lambda| > 2$. This limiting density, which is a semicircle of radius 2, is known as Wigner's semicircle law. In free probability theory, Wigner's semicircle rule may be seen as the standard Gaussian's matrix counterpart.

The kth Catalan number is the 2k-th moment of g(λ),

$$C_K = \frac{1}{K+1}\binom{2K}{K} \qquad (7)$$

and, by symmetry, the 2k + 1-st moment is zero, k = 0,1,2,..., where $C_0 = 1$ by convention. Numbers 1, 1, 2, 5, 14, 42, 132,... are called Catalan numbers because they follow the recursion formula $C_{k+1} = \sum_{i=1}^{K} C_{i-1}\, C_{k-i}$. It turns out that the only distribution for which the Catalan numbers serve as even moments is Wigner's semicircle law.

The Method of Moments: This was Wigner's first evidence (1955). Let gn(λ) be n1/2Hn's empirical spectral density function. This method takes use of the ability of expressing the kth instant of gn(λ) as

$\int_{-2}^{2} \lambda^k g_n(\lambda)\, d\lambda = \frac{1}{n}\,\mathrm{tr}\{(n^{-1/2}H_n)^k\} = \frac{1}{n^{1+k/2}}\,\mathrm{tr}\{H_n^k\}$.

As n →∞ starts going down, the moments of gn(λ), which were given above as the normalised trace of powers of Hn, converge to the Catalan numerals, which are the even moments of the semicircle law g(λ).

The Stieltjes Transform Method:The finite-n Stieltjes transform of n1/2 Hn can be written as

$S_n(z) = \int_{-\infty}^{\infty} \frac{g_n(\lambda)}{\lambda - z}\, d\lambda = \frac{1}{n}\,\mathrm{tr}\{(n^{-1/2}H_n - zI_n)^{-1}\}$,

For a simple (nn) Wigner matrix, convergence to the semicircle law is seen in Figure 1 above. To determine the eigenvalues of Hn, we first sampled n = 1,000 iid standard Gaussian deviations (left panel) and n = 25,000 (right panel). For both scenarios, we provide histograms of the Hn eigenvalues.

Large n: Largest Eigenvalue

the circumstances that must be met for the highest eigenvalue λ1 of the normalised Wigner matrix Hn(n-1/2) to converge to a constant as n →∞. Mean zero and a finite fourth moment for entries off the diagonal and a finite second moment for entries on the diagonal were prerequisites.

Single Wishart Matrix

A random r-vector X is of relevance in multivariate statistics if it follows a distribution with a mean vector μ and a covariance matrix Σ of the form where

$$\mu = E\{X\},\ \Sigma = E\{(X-\mu)(X-\mu)\tau\}. \qquad (8)$$

That X must also be Gaussian is an assumption. Numerous applications of multivariate analysis make use of dimensionality reduction and the study of functions of Σ, including its eigenvalues and associated eigenvectors.

Usually, Σ must be calculated using a sample of data since it is unknown. The standard estimate of is given by where X is an independent random variable chosen from the same distribution as the r-vectors Xi,i = 1, 2,..., n.

$$\hat{\Sigma} = n^{-1}\sum_{i=1}^{n}(X_i - \bar{X})(X_i - \bar{X})^{T} = n^{-1}X_c X_c^{T}, \qquad (9)$$

Where$\bar{X} = n^{-1}\sum_{i=1}^{n} X_i$ is the sample mean vector and is the population mean vector that may be estimated using the sample mean. X = (X1,⋯ , Xn) and Xc = X(In −n−1Jn), where Jn = 1n 1_n^T and 1n is an n-vector of 1s. In order to examine how the eigenvalues of n change under various assumptions for the number of variables r and the number of observations n, we may convert b into an unbiased estimator of by replacing 1/n with 1/r(n1).

A Spiked Covariance Matrix

As a specific alternative to the "null" model of a white Wishart distribution, where = Ir, the "non-null" idea of a "spiked" covariance model is presented. The bulk of the eigenvalues of the covariance matrix in this model are 1. The

spiking covariance model has shown promise in a variety of fields, including mathematical finance, wireless communication, signal processing, and speech recognition.

Assume m, the number of spikes, is known and that the first m eigenvalues are unique. Let Jm = {λ1,⋯ ,λm}. In the null model, λ1 = λ2 = ⋯ = λm = 1.The covariance matrix, m, of a population that is not null is a change to the identity matrix with a finite number of rows. One alternative to using the spiking covariance model to characterise the non-null case is to rescale it. The lowest eigenvalues (λm+1,...,λr) don't take the value 1; instead, they take the value σ2.

Two Wishart Matrices

Fixed r, Finite n: Exact Distribution

Real case. Let $X_i \overset{iid}{\sim} N_r(0,\Sigma)$, i = 1,2,...,n, and let X = (X_1,⋯ ,X_n) be an (r ×n)-matrix. LetA = $XX^\tau \sim W_r(n,\Sigma)$. we have another (r×r)-matrix B ~W_r(m,Σ) that is independent of A. We may select Σ = Ir without sacrificing generality if our focus is on the eigenvalues of A-1B, whose distribution does not rely on.

We now have two white Wishart matrices, A ~ Wr(n,Ir) and B ~ Wr(m,Ir), where A, B, and their product A+B are invertible if and only if m, n≥ r. The following generalized eigenvalue issue (for λ) is of relevance to ourselves:

$$|B-\lambda(A+B)| = 0. \quad (10)$$

The eigenvalues of the matrix (A + B)-1B are of importance to us. It follows that 0<λ<1 in (10) because A is positive definite. This is a different way to represent the eigenequation (10):

$$|B-\theta A| = 0, \quad (11)$$

and, in this form, we are interested in the eigenvalues of $A^{-1}B$ The eigenvalues λ and θ are related by $\lambda = \theta/(1+\theta)$ or $\theta = \lambda/(1-\lambda)$.

The eigenvalues of the generalised eigenequation (10) are exactly distributed in a joint manner by

$$p(\lambda_1,...,\lambda_r) = c_{m,n,r} \prod_i \left[w_{a,b}(\lambda_i)\right]^{1/2} \prod_{i<j} |\lambda_i - \lambda_j|, \quad (12)$$

where

$$w_{a,b}(\lambda) = \lambda^a(1-\lambda)^b,\ a = n-r-1,\ b = m-r-1, \quad (13)$$

is a normalising constant that relies on m, n, and r, and is a weight function for the Jacobi family of orthogonal polynomials.

For a more general form of (12), we get

$$P\beta(\lambda_1,...,\lambda_r) = c_{m,n,r,\beta} \prod_i \left[w_{r,m,n,\beta}(\lambda_i)\right]^{1/2} \prod_{i<j} |\lambda_i - \lambda_j|^\beta, \quad (14)$$

Where

$$w_{r,m,n,\beta}(\lambda) = \lambda^a(1-\lambda)^b,\ a = \beta(n-r+1)-2,\ b = \beta(m-r+1)-2, \quad (15)$$

and $c_{m,n,r,\beta}$ is a normalizing constant that depends upon m, n, r, and β. The values of are the same as before:β= 1 for reals, β=2 for complexes, and β= 4 for equations.

Setting $\lambda_i = \theta_i/(1+\theta_i)$, the joint distribution of the eigenvalues of the generalized eigenequation (12) is given by

$$p(\theta_1,...,\theta_r) = c_{m,n,r} \prod_i \left[w_{a,b}(\theta_i)\right]^{1/2} \prod_{i<j} |\theta_i - \theta_j|, \quad (16)$$

where

$w_{a,b}(\theta) = \theta^a(1+\theta)^b$, a = n−r−1, b = m + n. (17)

By substituting θ = (1 + x)/2 for in Equations (16) and (17), we get the Jacobi orthogonal ensemble.

$$p(x_1,\ldots,x_r) = c_{m,n,r}\prod_i [w_{a,b}(x_i)]^{1/2}\prod_{i<j}|x_i - x_j|, \quad (18)$$

where

$$w_{a,b}(x) = (1-x)a(1+x)b,\ a = n-r-1,\ b = m-r-1, \quad (19)$$

is the weight function for the Jacobi family of orthogonal polynomials .

Applications

Example : 4.1

The Patience sorting algorithm was developed from a British card game played by a single player. John Hammersley, seeing the potential in this, created the ensuing method to determine how long the largest rising subsequence is. Subadditive ergodic theory was also inspired by this finding.

The initial situation involves a "deck" of cards bearing the digits 1, 2, 3,..., n. After shuffling the cards, one is drawn at random and placed in a pile according to the rules below. Only cards with a value lower than the card on top can be added to a pile that already contains face-down cards. In the event that it isn't, a new pile is created to the right of the existing ones. It is possible to stack threes on top of fives, but a six requires you to start a new stack. Until all of the cards have been dealt and piled, the game will continue. In this game, you have to get rid of as many piles as possible.

Example : 4.2

Assume the previous game's order of cards was 2, 5, 1, 3, 4, 8, 6, 7. The 2 should be used to initiate the first pile; the 5 is larger than the 2, so it should initiate the second pile; the 1 should be placed atop the 2 and the 3 should be placed atop the 5; the 4 should initiate the third pile; the 8 should initiate the fourth pile; the 6 should be placed atop the 8; and the 7 should initiate the final pile.Thepilesareasfollows:

1	3		6	
2	5	4	8	7

The best approach is the "greedy" one, in which each card is placed on the leftmost pile possible. As with the longest rising subsequence of the previous permutation, the outcome in this case is five heaps. In most cases, the optimum greedy technique will result in a number of piles that is equal to the longest rising subsequence.

Example : 4.3

Cards may not be stacked in ascending subsequence order at the top of their respective heaps if they are not in permutation order.Here's a look at the numbers 8, 6, 1, 3, 4, 7, 5, 2, 8, and 6.Thepilesare:

1			
6	2		5
8	3	4	7

It's simple to see that the numbers bolded (1, 2, 4, 5) do not form a continuous subsequence of the main sequence, which progresses from least to largest. But the lengths of the subsequences 1, 3, 4, 5 or 1, 3, 4, 7 also equal 4, hence the number of piles is also 4. It turns out that there is a highly fast technique for determining the length of the longest rising subsequence, and that this corresponds to patience sorting$L_n=l_n(\pi)$.

Example : 4.4

Distances between the Riemann zeta function's successive zeros. By summing inverse powers of the positive integers, Riemann's zeta function is defined.

$$\zeta(s) = \sum_{n=1}^{\infty} n^{-s} = 1 + \frac{1}{2^8} + \frac{1}{3^8} + \frac{1}{4^8} + \dots \quad (20)$$

Set s = 2, and Leonhard Euler's famous finding that ζ(2) = π2/6 holds. The zeta function, as Euler showed, may also be represented as a product over the primes.

$$\zeta(s) = \prod_P (1 - p^{-s})^{-1} = \frac{1}{\left(1-\frac{1}{2^8}\right)\left(1-\frac{1}{3^8}\right)\left(1-\frac{1}{5^8}\right)\left(1-\frac{1}{7^8}\right)\dots} \quad (21)$$

The product of Euler is a well-known formula. As a result, the zeta function has characteristics with the pattern of prime numbers. But the storey has more to it. Since the zeta function has zeros on the complex plane, Riemann proved that it may be expressed as a product over those zeros.

$$\zeta(s)=f(s)\ (1 \frac{8}{p^1})\ (1 \frac{8}{p^2})\ (1 \frac{8}{p^3})\dots. \quad (22)$$

where ϱ1, ϱ2,... are the complex integers for which ζ(s) = 0, and f (s) is a straightforward "fudge factor."

CONCLUSION

We calculate the eigenvalues of a white Wishart matrix, the Markov-Pastur semicircle laws, the Tracy-Widom distributions, and Wishart-matrix simulations. Despite the book's focus on Gaussian ensembles, both Laguerre ensembles and Wishart matrices are mentioned for the crucial roles they play in mathematical statistics. All the best papers ever written on RMT are collected here.

REFERENCES

1. AKEMANN, G., BAIK, J., and DI FRANCESCO, P. (2011). The Oxford Handbook of Random Matrix Theory, Oxford University Press.
2. CAPITAINE, M., DONATI-MARTIN, C., and FERAL, D. (2009). The largest eigenvalues of finite rank deformation of large Wigner matrices, The Annals of Probability, 37, 1–47.
3. DESHPANDE, Y. and MONTANARI, A. (2014). Information-theoretically optimal sparse PCA, IEEE International Symposium on Information Theory, 2197–2201.
4. EDELMAN, A. and RAO, N.R. (2005). Random matrix theory, Acta Numerica, 1–65.
5. HAN, X., PAN, G., and ZHANG, B. (2016). The Tracy–Widom law for the largest eigenvalue of F type matrices, The Annals of Statistics, 44, 1564–1592.

6. JOHANSSON, K. (2002). Non-intersecting paths, random tilings, and random matrices, Probability Theory and Related Fields, 223, 225–280.
7. KIECHERBAUER, T., MARKLOF, J., and SOSHNIKOV, A. (2001). Random matrices and quantum chaos, Proceedings of the National Academy of Sciences, 98, 10531-10532.
8. NADLER, B. (2008). Finite sample approximation results for principal component analysis: A matrix perturbation approach, The Annals of Statistics, 36, 2791–2817.
9. ONATSKI, A., MOREIRA, M.J., and HALLIN, M. (2013). Asymptotic power of sphericity tests for highdimensional data, The Annals of Statistics, 41, 1204–1231.
10. PAUL, D. (2007). Asymptotics of sample eigenstructure for a large dimensional spiked covariance model, Statistica Sinica, 17, 1617–1642.
11. RAM´IREZ, J., RIDER, B., and VIR´AG, B. (2008). Beta ensembles, stochastic Airy spectrum, and a diffusion, available at arXiv:math/0607331v3.
12. TAO, T. and VU, V. (2010). Random matrices: universality of local eigenvalue statistics up to the edge, Communications in Mathematical Physics, 298, 549–572.
13. WANG, Q. and YAO, J. (2017). Extreme eigenvalues of large-dimensional spiked Fisher matrices with application, The Annals of Statistics, 45, 415–460.

TABLE1

β	Ensemble	TRI	SRS	H_{ij}	U
1	GOE	Yes	Yes	real	orthogonal
2	GUE	No	NA	complex	unitary
4	GSE	Yes	No	real-quaternion	symplectic

Table 2

Families of orthogonal polynomials and their weight functions w(x).

Case	w(x)	Interval	OrthoPoly
Gaussian	e^{-x2}	$(-\infty,\infty)$	Hermite
Wishart	$x^a e^{-x}$	$[0,\infty)$	Laguerre
Two Wisharts	$x^a(1-x)^b$	(0,1)	Jacobi

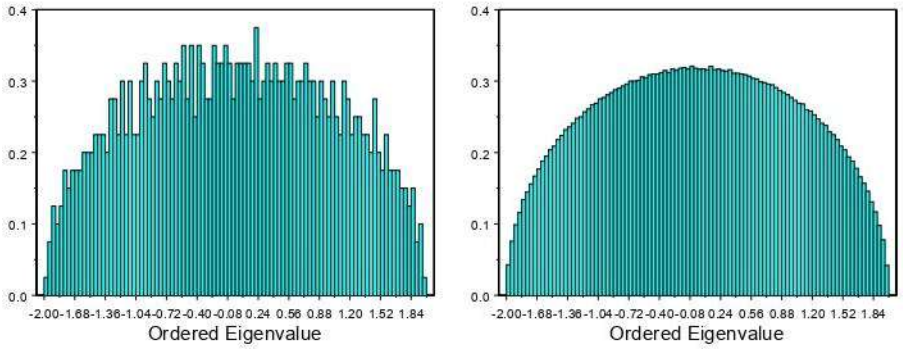

Fig. 1. Illustration of the convergence to Wigner's Semicircle Law. Normalized histograms of the eigenvalues from a single (n×n) Wigner matrix. Left panel: n = 1,000. Right panel: n = 25,000. For each n, there are 100 bins.

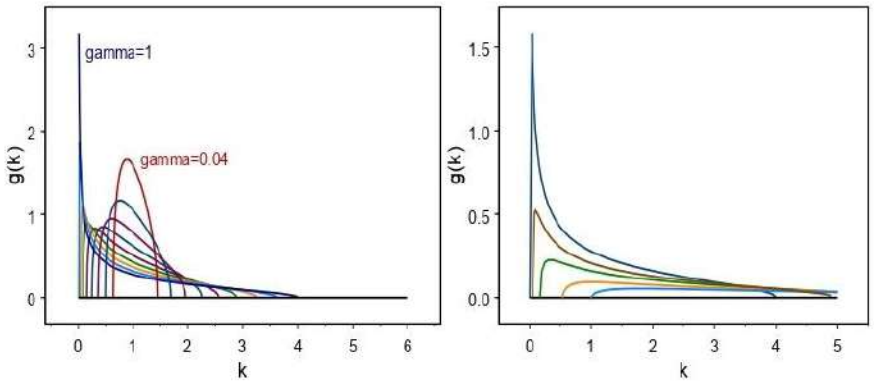

Fig. 2. Density of eigenvalues from the Mar˘cenko-Pastur Law.
Left panel: $\gamma = 0.04,0.09,0.16,0.25,0.36,0.49,0.64,0.81,1$ (i.e., $r \leq n$).
Right panel: $\gamma = 1,1.5,2,3,4$ (i.e., $r \geq n$).

The spiked covariance matrix is given by $\Sigma_m = \text{diag}\{\lambda_1,...,\lambda_m,1....,1\}$, $\lambda_1 > \lambda_2 > \cdots > \lambda_m > 1$,

Vol.15 / Issue 83 / Apr / 2024 International Bimonthly (Print) – Open Access ISSN: 0976 – 0997

REVIEW ARTICLE

Comprehensive Review: to Enhance Absorption and Bioavailability of Herbal Drug by Topical and Oral Route using Phytosome

Manisha Katkade[1]*, Rahul shivarkar[2] and Shashikant Dhole[3]

[1]Student, Department of Quality Assurance, PES Modern College of Pharmacy, (for Ladies) (Affiliated to University of Pune) Pune, Maharashtra, India.
[2]Assistant Professor, Department of Pharmacognosy, PES Modern College of Pharmacy, (for Ladies) (Affiliated to University of Pune) Pune, Maharashtra, India.
[3]Principal, Department of Pharmaceutics, PES Modern College of Pharmacy, (for Ladies) (Affiliated to University of Pune) Pune, Maharashtra, India.

Received: 11 Nov 2023 Revised: 09 Jan 2024 Accepted: 25 Mar 2024

***Address for Correspondence**
Manisha Katkade
Student,
Department of Quality Assurance,
PES Modern College of Pharmacy, (for Ladies) (Affiliated to University of Pune)
Pune, Maharashtra, India.
Email: manishakatkade0704@gmail.com

ABSTRACT

Phytopharmaceuticals or herbal drugs have a significant therapeutic effect on healthcare System. But due to poor lipophilicity and high polarity the active constituents are poorly absorbed resulting in poor bioavailability. These problems can be over comed by formulating a suitable novel preparation of the herbal extract i.e., Phytosome. Phytosome are one of the novel drug delivery system containing hydrophilic bioactive phyto constituents of herbs which are surround and bound by phospholipids. Phytosome technology is promising targeting novel drug delivery with improved efficacy, quality and target ability of active plant constituents. Novel herbal formulation techniques have assured the researchers to deliver the plant based secondary metabolites to their systemic targets for specific effect. The recent development and conducted works of various researchers have been studied thoroughly to establish the transdermal route as a potential way to deliver phytoconstituents to their specific targets. Phytosome can before emulated both topically and orally. Phytosome given by oral route increases the bioavailabilty of herbal drug. This review highlights the mechanism of action of phytosome by topical and oral route and also highlights unique properties of phyto-phospholipid complex along with their application in the novel natural drug delivery.

Keywords: transdermal, formulation, phytosome, therapeutic, plant

INTRODUCTION

The capability of the dosage form to deliver the medicament to its specific site of action at a rate and amount sufficient to achieve the desired curative effects is critical to the efficacy of any drug, whether it is comes from a plant, animal, or synthetic drug. There are numerous innovative drug delivery systems and methods can be supplied through various channels to allow the medication to pass through the barrier at appropriate and safe dosages. Phytopharmaceuticals or herbal extracts(Drugs) have a significant therapeutic effect on healthcare systems. The herbal extracts and its active constituents show excellent pharmacological in vitro effects, they still have very poor in vivo biological effects because of their considerable molecular weight and low lipid solubility, it leads to low systemic availability[1]. Additionally, combination of plant extracts into delivery channels will help improve and bulk dosing of these phytochemicals, as the activity of the herbal medicines depends on the overall synergism effect of all the constituents. Hence, integrating innovative delivery systems with traditional medicines is very important, especially for treating chronic diseases like asthma, diabetes, osteoporosis, and age-related diseases like dementia[2]. Novel drug delivery system is a novel approach to drug delivery which addresses the limitations of the traditional drug delivery systems. Phytosome is a novel patented technology which is developed to incorporate standardized plant extracts into phospholipids to form a lipid soluble molecular complexes, with improved bioavailability and absorption, which is called as "phytosome''. The term "Phyto" means plant, and "some" i.e., cell-like. Phytosome formed from the reaction of stoichiometric amount of phospholipid with standardized herbal extract or polyphenolic constituents in an aprotic solvent. Phytosome shows better stability due to formation of chemical bonds between phosphatidylcholine molecules and phytoconstituents[3]. The phytosome technology was first developed by the Indena S.p. A, Italy. The polyphenols active pharmaceutical ingredients are slightly soluble in both water and lipids.

This phenomenon makes the polyphenolic APIs difficult to be formulated into commercial medicines. In 1991, Bombardelli and Spelta have formulated a new drug delivery system and named it phytosome[4]. A phyto-phospholipid complex (Phytosome) is the promising emerging technique applied to pharmaceuticals for the enhancement of bioavailability of herbal extracts and phyto constituents. Phytosome are the advanced forms of herbal formulations contains the bioactive phyto constituents of herbal extract and it has good ability to transition from a hydrophilic into the lipophilic environment of the cell membrane, it exhibit better pharmacokinetic and pharmacodynamic profile than conventional herbal extracts. Phytosome formulated in the form of various dosage forms like suspensions, capsules, creams, gels etc[5]. The Phytosome increases the absorption of active ingredients of herbal extract ,when topically applied on the skin, And it also improves systemic bioavailability when administered orally[5]. Nanoparticles and Nanomaterials are Significant advancements have gained attention for the design of delivery methods because of their superior biological and chemical performance. Nano carriers includes safe and inert materials investigated for their potential role in medication(Drug) delivery and unique characteristics. A nano liposomal delivery system i.e.,Phytosome. is one such system for improved site-specific delivery of phytochemicals with enhanced absorption for the topical and oral route[6]. The updated pharmacokinetic and therapeutic parameters of phytosome are becoming beneficial in medical and cosmetic industries[8].

STRUCTURE OF PHYTOSOME

The structure of phytosome is majorly composed of standardized polyphenolic plant extract incorporated into phospholipids, mainly phosphatidylcholine(PC)[8]. The phytosome in the form of lipid vesicles are the result of a H-bond interaction between the polyphenolic moiety of the bioactive herbal extracts and the phosphate group of phospholipids matrix in non-polar solvents[9]. The water-soluble polyphenolic rings of phytochemicals (i.e., flavonoids and terpenoids) having a high affinity to chemically bind towards to the hydrophilic moiety of phospholipids (i.e., choline) to form the body of phytosome, while the phosphatidyl lipophilic moiety of the phospholipids forms a tail to incorporate the water-soluble choline bound phytoconstituents[10-11]. The encapsulated form(Capsule) of poorly soluble polyphenolic compounds into the phytosomal delivery system has a significant effect on the enhancement of their absorption, and it leading to better penetration and absorption across the biological membrane and enhanced bioavailability [12].

The potential role of Phytosome is in the improvement of herbal-originated polyphenolic compounds used for the treatment of several diseases and makes this nanotechnology a promising tool for the development of new formulations[13].

COMPONENTS

Phospholipids

Phospholipids which are extracted from soy, mainly phosphatidylcholine(PC), are lipophilic substances and readily complex polyphenolics. In this context, phosphatidylcholine(PC) are the major molecular building block of cell membranes and it is miscible in both water and in oil/lipid environments, and is well absorbed orally, and it has the potential to act as a chaperon for polyphenolics, accompanying them through biological membranes[14]. Phospholipids are majorly present in egg yolk and plant seeds. Phospholipids can be divided into glycerophospholipids and sphingomyelins depending on the backbone. Additionally, glycerophospholipids include phosphatidylcholine(PC),phos-phatidylethanolamine(PE), phosphatidylserine (PS), phosphatidyl- glycerol (PG) and phosphatidic acid (PA)[15] . PC, PS, and PE are the major phospholipids used to prepare complexes which are composed of a hydrophilic head group and two hydrophobic hydrocarbon chains[16]. Among these three phospholipids, PC is the most frequently used to prepare phospholipid complexes(Phytosome). The benefits of PC include it shows amphipathic properties that give it moderate solubility in water and lipid media. Also PC is an essential component of cell membranes, and accordingly it also exhibits robust biocompatibility and low toxicity[17].

Phyto-active constituents

The active constituents of herbal extracts identified by the researchers are generally defined based on robust *in vitro* pharmacological effects, rather than on *in vivo* activities. Most of these phyto active constituents are polyphenols. Some of the biologically active polyphenolic constituents of plants shows affinity towards the aqueous phase and cannot pass through biological membranes, such as hesperidin. And others have high lipophilic properties and cannot dissolve in aqueous gastrointestinal fluids, such as curcumin and rutin[17].

Solvents

Different solvents have been utilized by different researchers as the reaction medium for formulation of phyto-phospholipid complexes(Phytosome). Traditionally, aprotic solvents, such as aromatic hydrocarbons, methylene chloride, halogen derivatives, ethyl acetate, or cyclic ethers etc. have been used to prepare Phytosome but they have been largely replaced by protic solvents like ethanol[18-19]. Protonic solvents, for e.g., ethanol and methanol, have been more recently been successfully utilized to prepare phospholipid complexes. For example, the Xiao prepared silybin-phytosome using ethanol as a protonic solvent; subsequently, the protonic solvent was removed under vacuum at 40 °C[20].

Stoichiometric ratio of active constituents and phospholipids

Normally, Phytosome are employed by reacting a synthetic or natural phospholipid with the active constituents in a molar ratio ranging from 0.5 to 2.0 [21]. Whereas, a stoichiometric ratio of 1:1 is considered as the most efficient ratio for preparing phospholipid complexes[22]. For example, quercetin-phospholipid complexes(Phytosome) were prepared by mixing Lipoid S 100 and quercetin at a molar ratio of 1:1[23]. However, different stoichiometric ratios of active constituents and phospholipids have been used to prepare different Phytosome.

DIFFERENT METHODS OF PREPARATION

The methods used for phytosome preparation are described by the, Jiang *et al* [24], Maiti *et al* [25] and Maiti *et al*[26]. In the 2006, Yanyu *et al* prepared a silybin-phospholipid complex using ethanol as a reaction medium. Silybin and phospholipids were mixed into the medium, after the organic solvent was removed under vacuum condition, and a silybin Phytosome was formed[27]. Common stages in formulation of Phytosome are described in following Figure 1 Various methods of preparation of phytosome are as follows:-

Anti-solvent precipitation process

Take Specific amount of herbal extract and phospholipids and refluxed it with 20 ml of organic solvents such as acetone at specific experimental conditions below 50°C for 2-3 hrs. Then concentrate reaction mixture to minimum volume up to 10 ml and then add solvent with low polarity such as n-hexane with stirring, precipitates are obtained and filter it. Filtered precipitates are stored in desiccators or freezer. The dried precipitates are grinded and powdered complex are stored in dark amber colored glass bottle at room temperature [28].

Rotary evaporation process

Take Specific weight of herbal extract and phospholipids were mixed in 30 ml water miscible organic solvent such as acetone in round bottom glass container and stir it for 2 hours at a temperature less than 50°C in rota evaporator. Anti solvent such as n-hexane added to thin film which is obtained after uninterrupted stirring using a stirrer[29]. Precipitate of phytosome which obtained can be stored in amber colored glass container at controlled temperature under specified humidity.

Solvent ether-injection process

This process involves reaction of lipids dissolved in organic solvent with herbal extracts in aqueous phase. Phospholipids are solubilised in diethyl ether and are slowly injected drop wise in an aqueous solution of the phytoconstituents which is to be encapsulated to form phytosome. It results in the formation of cellular vesicles on subsequent solvent removal, leading to complex formation(Phytosome)[30]. Structure of phytosome depends upon concentration, when the concentration is less amphiphiles in mono state are produced, but variety of structures with different shapes *i.e.,* cylindrical, disc, round and cubic or hexagonal vesicles may be formed on increasing the concentration [31].

NOVEL METHODS

Novel methods for the phospholipid complexation which include supercritical fluids which include gas solvent technique, compressed solvent process and supercritical solvent method[31]. Traditional(Conventional) methods have several drawbacks, such as its including multistep processes, difficulty extraction, and time consumption. Supercritical fluid methods are used to change the size, morphology and shape of material of interest. Along with other benefits like as a single-step process, the capacity to process thermolabile substances, and eco-friendly technology, high product purity, crystal polymorphism controls Supercritical fluid (typically CO2) used as an anti-solvent in the Gas anti-solvents technique (GAS), Supercritical antisolvent technique (SAS), and Solution enhanced dispersion by supercritical fluids (SEDS) techniques, also Rapid expansion of supercritical solutions (RESS) uses it as a solvent [32].

Gas anti-solvents approach (GAS)

Supercritical CO2 gas usage is not necessary when using CO2 as an antisolvent. To accomplish homogeneous mixing, it is injected into the solution in a closed chamber, preferably from the bottom. Solutes precipitate because of the decreased solubilization power of the organic solvent brought on by the dissolution of CO2 gas. To get rid of any remaining solvent, the particles are rinsed with more antisolvent. If not, the solutes could resolubilize during the depressurization step, endangering the stability of the product. When scaled up to industrial levels, the gas antisolvent technology outperforms the solvent antisolvent technique in terms of results[33].

Supercritical antisolvent precipitation (SAS)

Submicrometer-sized particles with a restricted size distribution are produced by removing the solvent from the gas phase by reducing the pressure in the SAS. The supercritical state of CO2 is required. The solution and CO2 , both are injected from the top into a closed chamber. In contrast to GAS, this method has a proven record of widespread success[34].

Mechanism of Action of Phytosome by Topical and Oral Route

One of the most significant advances in the study of transdermal drug delivery systems (TDDS) is the increased bioavailability of phytoconstituents through the transdermal route. Therapeutic agents are delivered via the skin to the systemic circulation in TDDS. Due to its lipophilicity, the stratum corneum, the outermost horny layer, presents the main obstacle to medication transport. The phytoconstituent's phytosomal form aids in avoiding this barrier feature. The following summarizes the fruitful research experience of approximately twenty years of study by several researchers and shows that the phytosome technology is potent enough to be applied transdermally to increase the bioavailability of phytoconstituents[35]. The skin is an excellent site for the administration of pharmaceutical agents or medication for both local and systemic impacts and it serves as a strong barrier to the permeability of the majority of substances[36] [Figure 2]. The transdermal permeability can be increased when the active ingredients are lipophilic and they have a low molecular weight. Bombardelli et al. noted in 1991 that phospholipids had a strong affinity for particular types of flavonoids. By complexing phospholipid with extremely polar plant derivatives—that is, complexes between a pure phospholipid and a pure active principle—they created a novel class of molecules known as phytosome. He first obtained some pharmacological information and established some chemico-physical characteristics of phytosome of escin, quercetin, catechin, and glycyrrhetinic acid. He stated right away that phytosome are an effective way to transport phytoconstituents over the skin[37]. Yanyu et al. (2006) looked at how, in silymarin phytosome in experimental models, the well-known calming effect of silymarin is enhanced by a factor of more than six. Because the complex has a stronger affinity for skin phospholipid[38], the phytosome form's activity is improved as compared to the free active principle. According to Kidd's (2009) findings, the phospholipid complex's liposomal-like characteristics are connected to the hydration of the superficial corneous layer. Because of their transdermic effect, ginselect phytosome facilitate the skin's absorption of the ginseng saponin found in the phospholipid complex[39] Phytosome offer a number of possible benefits over traditional topical formulations in topical treatments. Phytosome promote the transport of herbal active ingredients to tissues and improve skin absorption and bioavailability [40]. Additionally, phytosome strengthen collagen structure, the balance of enzymes, and moisture in the skin [41]. When compared to other free chemicals, the potency of phytosome was enhanced due to their strong affinity for skin phospholipids [42]. As was already indicated, topical uses of phytosome formulation are confronted with a number of challenges. For instance, the SC, or thick outer layer of the epidermis, is one of the most significant obstacles to the transdermal administration of phytochemicals [43]. There are two main routes that bioactive compounds might pass through the SC: intracellular or intercellular[Figure 3]. Sweat can facilitate the entry of cells into one another.

Sweat glands, sebaceous glands, or hair follicles can all be used for intercellular penetration, while corneocytes and the intercellular lipid matrix are the primary routes for intracellular penetration[44-45]. According to reports, increasing the drug's diffusion coefficient can boost biomolecule concentrations and improve the way these molecules are partitioned between the SC layer and the molecules themselves. Taken together, these factors can increase the biomolecule permeability to the SC for transdermal application [46]. Topical medicines with lipophilic and low molecular weight active components have the potential to enhance transdermal permeability. Due to their hydrophilic character, polyphenols, which make up the majority of the phytocompounds that have been extensively researched, have poor bioavailability and lipid solubility, which limits their in vivo activity[47]. Several flavonoid compounds can be strongly bound by the phospholipid moieties of phytosome with a high affinity [48]. Many herbal extracts, including ginseng, hawthorn, grape seed, green tea, milk thistle, and grape seed, work better when loaded into phytosome than when they are in a liposomal formulation. Because the phospholipid molecules in Phytosome interact with the active phytoconstituents, enhancing their stability, the formation of polyphenol-based phytochemicals phytosome nanoparticles improves the application of conventional herbal materials. Moreover, the phytosome–herbal combination has a greater affinity for the phospholipid moiety of the epidermis, hence enhancing the topical formulation's lipid solubility[49]. Topical dosage forms: A topical formulation of the Phytosome complex is also possible. Dispersing the phospholipidic complex in a tiny amount of the lipidic phase and adding it to the already-created emulsion at low temperatures (not higher than 40°C) is the optimal method for incorporating the Phytosome complex in emulsion. The primary lipidic solvents used in topical preparations are soluble in the

Phytosome complexes. The Phytosome complex may also be disseminated into the watery phase and then added to the final formulation at a temperature lower than 40°C in formulations with a limited amount of lipids[50]. For topical use, phytosome have been developed as gel and cream According to Djekic et al., a hydrogel loaded with 18-GA phytosome was created by dispersing the phytosome and carbomer in water. 10% sodium hydroxide was then added to neutralize the formula. Hydrogel was formed later by adding humectant.

It is possible to manufacture Phytosome complexes for oral or topical use. To achieve the optimal results from this technological advancement in terms of formulation manageability and improved bioavailability (such as the proper disintegration and dissolving time of oral forms)

It has long been accepted that the best way to administer drugs is orally. Nowadays, there is continuous research being done on nano-formulations to improve absorption, increase bioavailability, and boost therapeutic efficacy. Formulation scientists have been drawn to lipid-based nano formulations because of their improved bioavailability and comparatively greater safety profile. The bioactives or medications can also be shielded from the urge of the gastrointestinal system by using these delivery methods. They also help hydrophobic medications that are trapped in lipid matrices to be absorbed. Lipid excipients have been shown to both increase the bioavailability of bioactives administered orally and decrease P-glycoprotein-mediated efflux[51]. Phytosome are advanced form which shows improvement in bioavailability of phytoconstituents. Polyphenolic phytoconstituents are complexed with phosphatidylcholine In 1:1 or 1:2 ratio, phytosome are formed. This is a novel patented technology of Indena, through which water soluble actives of plant origin can be delivered (mainly polyphenols). Most of the phytoconstituents (anthocyanidins,tannins, flavanoids and terpenoids) can penetrate lipoidal biological membranes due to their larger size and hydrophilicity. Phytosome are able to cross the hydrophilic and hydrophobic environments to successfully reach the human circulation system[51].

Phospholipid complex and their absorption by oral route

Phospholipid complexes are absorbed from the GIT through enterocyte based transport, and the drug transport to the systemic circulation via intestinal lymphatic system which has widespread network throughout the body. The major advantage of lymphatic transport i.e., to bypass the first-pass metabolism and applicable for targeted drug delivery. After oral administration of dosage form, the possible mechanism by which lipids affect drug bio availability is shown in Figure 4. Schematic diagram representing the possible mechanism by which phyto-phospholipid complex(Phytosome) entry into the intestine from unstirred water layer is both by direct solubilization through enterocytes or by endocytosis, inhibiting drug efflux by blocking transporter proteins, paracellular transport in lateral tight junctions, formation of chylomicron production and entering lymphatic port. Several researchers have proposed various processes for lipid absorption. Yeap et al. proposed that enterocytes play a role in lipid absorption. The paracellular transfer of phosphotidylcholine across lateral tight junctions was discovered by Stremmel et al.[51]. According to Holm et al., bile salts and other lipid emulsifiers can inhibit drug efflux by preventing the action of transporter proteins like CYP 450 and/or P-gp[52]. According to Jain et al., endocytosis facilitates medication absorption[53]**.** Green tea extract was formulated as Green Select Phytosome. and these were converted into oral coated tablets by Pierro et al. (2009). Clinical trial studies done on obese patients demonstrated that phytosome coated tablets were capable of weight loss when administered orally to patients [54]. **In 2014. Keerthi B *et al*,** Formulated and evaluated capsules of Ashwagandha Phytosome.

Oral Dosage Forms

Soft gelatin capsules

When creating Phytosome® complexes, soft gelatin capsules are a great option.To create solutions that may be put inside soft gelatin capsules, the Phytosome® complex can be distributed across greasy media. You can use semi-synthetic or vegetable oils for this. Granulometry of 100% < 200 μm is recommended by Indena for optimal capsule manufacture. First feasibility trials should be carried out to determine the most appropriate vehicle because, based on Indena's experience, not all Phytosome complexes react in the same way when distributed in oily vehicles and when the oily suspension is packed in the soft gelatin capsules[51].

Hard gelatin capsules

The Phytosome complex can be formulated in the form of hard gelatin capsules as well. Even though the phytosome complex's apparent low density appears to limit the amount of powder that can be placed into a capsule (typically no more than 300 mg for a size 0 capsule), a direct volumetric filling procedure (without pre compression) can be used. However, the amount of powder that can be put in a capsule using a piston tamp capsule filling method can be increased; however, pre compression may have an impact on the disintegration time. It is recommended by Indena to closely monitor the relevant parameters while developing new products and processes. To determine the optimal production technique, a preliminary dry granulation procedure isadvised[51].

Tablets

The best production method for producing tablets with greater unitary dosages and appropriate technological and biopharmaceutical characteristics is dry granulation. However, a direct compression process can only be used for low unitary doses due to the Phytosome complex limited flowability, potential stickiness, and low apparent density. It should be noted that whenever a direct compression process is used, the Phytosome complex should be diluted with 60–70% of excipients in order to maximize its technological properties and produce tablets with the proper technological and biopharmaceutical characteristics. However, because water and heat (granulation/drying) have a detrimental influence on the stability of the phospholipid complex, moist granulation should be avoided[51].

PROPERTIES OF PHYTOSOME

Hepatoprotective properties

The majority of PHYTOSOME® research focuses on the liver-protecting flavolignans found in Silybum marianum Gaertner. There are several flavonoids in milk thistle (Silybum marianum) fruit that have hepatoprotective properties [55-56]. Sily Research has demonstrated the efficacy of silymarin in the treatment of several kinds of liver conditions, such as cirrhosis, hepatitis, fatty infiltration of the liver (fatty liver caused by chemicals and alcohol), and bile duct inflammation [57-59]. Silymarin's antioxidant properties significantly improve the liver's tolerance to harmful incidents [60]. Based on three patterns of covalent interaction between its flavonol and lignan elements, silymarin has a complex composition.. Silymarin's primary and more potent component is silybin, which is a combination of two diastereomers [61]. Silybin maintains glutathione in the liver to protect It. In numerous human disease models, silybin has been found to be effective; however, due to its extremely poor oral bioavailability, the clinical application of these results has been prevented. In a pharmacokinetic study [62], the oral bioavailability of silybin was significantly increased when administered as silybin–phospholipid complex. The increased lipophilicity of the silybin–phospholipid complex has been claimed to explain the improved bioavailability. Silybin protects the liver by conserving glutathione in the parenchymal cells, while phosphatidylcholine aids in the repair and replacement of cell membranes.

Anti-inflammatory properties

The anti-inflammatory properties of Phytosome complexes better than their uncomplexed herbal extracts. Phytosome complexes were tested for their anti-inflammatory properties in animals using croton oil-induced dermatitis, an inflammation model that includes both tissue and vascular damage [63]. Results using silymarin, a flavanolignan with anti-phlogistic activity and a free radical scavenger, and glycyrrhetinic acid phytosome from glycyrrhiza glabra, a potent anti-inflammatory and anti-allergic triterpenoid, were reviewed. The ultimate aim was the decrease of edema, and the materials were delivered topically as micro dispersion in water. Although phospholipids by themselves have no anti-inflammatory properties, it was shown that their interaction with glycyrrhetinic acid increased this property's duration. As a result, 18-beta-glycyrrhetinic acid's anti-edematous effect diminished with time and almost stopped after 24 hours, during which its phosphatidyl complex continued to cause an 80% decrease in edema. In the croton oil test in mice, the silymarin complex demonstrated a higher degree of edema reduction (76% after 6 hours) in comparison to that with the free form (33% even after 12 hours) (Fig. 4). Therefore, compared to the free phytoconstituent, the PHYTOSOME was almost twice as effective. The 18-beta-

glycyrrhetinic acid compound showed strong effectiveness against UVA-induced erythema in a different research[64].

Anti-cancer properties

Alhakamy and a colleague investigated the use of quercetin phytosome functionalized by scorpion venom in the treatment of breast cancer. Pharmacologically active taxifolin (dihydroquercetin) is known for its anti-inflammatory, antibacterial, antiangiogenic, liver-protective, and anticancer characteristics. However, due to its hydrophilic nature, its application was limited. In this work, phospholipids and taxifolin-rich ethyl acetate were mixed, and the resulting Phytosome were tested ex vivo against MCF-7 cell lines. The Phytosome have a lower IC50 value and increased cytotoxic activity[65]. The MCF-7 cell line is susceptible to the anticancer effects of Phytosome loaded with aloe vera extract. Phosphatidylcholine(98% w/w) is the main constituent found in lecithin. Phosphatidylcholine nanoparticles have been shown to have mitogenic effects on MCF-7 breast cancer cells[66]. Specifically, the nanoparticles, when dispersed in a pH 7.0 buffer, alter the plasma membrane of the cancer cells, affecting the proliferation of the cells and the epidermal growth factor receptor (EGFR). Furthermore, Alkamy et al. discovered that Phytosome enriched with thymoquinone have anticancer properties against human lung cancer cells (A549 cell line). The work highlights the significance of this innovative phytosome method supporting cytotoxicity against lung cancer cells and a prolonged release profile[67]. Resveratrol inhibits the action of aromatase, has antiangio genesis and apoptotic properties, and is useful in the treatment of breast cancer. Two complementary anticancer drug combinations from fungal and herbal sources were chosen, synthesized in a multi compartment nano carrier system, and then encapsulated in a resveratrol phytosome for use in this investigation.

Anti aging

The most visible organ, the skin, performs vital tasks including controlling body temperature and sensing pressure, temperature, and pain. It also serves as a vital barrier against harmful substances and pollutants, which makes aging apparent[68-69].Thinning, sagging, age spots appearing, and dry skin are all signs of aging. Anti-aging solutions are in high demand as a result of the growing desire to look or feel young[70]. Free radicals are extremely reactive oxygen molecules that interact with collagen molecules to cause a loss of tone in the elasticity of the skin, which starts the aging process. Free radical-induced oxidative damage is prevented or slowed down by antioxidants [71].Antioxidant effects are very helpful in cosmetic compositions. The primary cause of this action in herbs is the redox characteristics of phenolic compounds, which enable them to function as hydrogen donors, reducing agents, and singlet oxygen quenchers[72]. Antioxidant polyphenols found in a wide variety of fruits, vegetables, whole grains, and herbs scavenge and remove free radicals. Natural skincare products are rapidly absorbed by the skin's outer layers and are hypoallergenic in nature[73].

Thus, anti-aging medicines can be produced from plants that contain antioxidants. Orange peel (Citrus auranticum, Rutaceae) extract has excellent skin-whitening, anti-oxidant, and anti-acne properties. Phenolic substances such as flavonoids and phenolic acids are abundant in the peel and seeds of citrus fruits. When compared to seeds, the peels have a higher flavonoid content [74]. Phenolic chemicals, or flavonoids, are present in liquorice (Glycyrrhiza glabra, Fabaceae) [75].Because phenolic components are present in high concentrations and have considerable ROS scavenging, hydrogen-donating, and reducing properties, liquorice ethanol extract has good anti-oxidant action[76]. It enhances the skin's hydration and viscoelastic qualities[77]. Because the chemical elements in the herbs work synergistically, polyherbal compositions have a high therapeutic impact [78].Licorice extract and orange peel extract have each been utilized for their possible cosmetic benefits. Thus, an effort was made to investigate how extracts together affect the aging of the skin.

Anti oxidant

In 2006 & 2007, Maiti et al, developed naringenin and curcumin Phytosome in two different studies and reported that antioxidant activity of the phytosomal complex has better therapeutic efficacy.A naturally occurring flavanone with a wide range of biological action is naringenin. Naringenin has to be administered frequently in order to maintain an effective plasma concentration because of its quick clearance. In comparison to free naringenin, we

assessed the therapeutic potential of the naringenin-phospholipid complex under oxidative stress conditions. At a dosing level of 100 mg kg-1 (p.o.), naringenin-phospholipid complex was produced and its antioxidant activity evaluated in rats intoxicated with carbon tetrachloride. Serum levels of total bilirubin, alkaline phosphatase, glutamate pyruvate transaminase, and glutamate oxaloacetate transaminase were measured in liver function tests.To evaluate the antioxidant capability at the same dose level, indicators for liver function, such as glutathione peroxidase, superoxide dismutase, catalase, and thiobarbituric acid reactive compounds, were evaluated. Naringenin's plasma levels was also evaluated. Compared to free naringenin at the same dosage level, the naringenin-phospholipid complex was found to considerably protect the liver for a longer period of time and to increase the antioxidant activity of the biomolecule. Naringenin's phospholipid complex demonstrated superior antioxidant activity compared to the free compound throughout an extended period of action, potentially decreasing the molecule's rapid excretion from the body[79]. A novel formulation of Curcumin with phospholipid was developed to overcome the limitation of absorption and to investigate the protective effect of curcumin-phospholipid complex on carbon tetrachloride induced acute liver damage in rats.

The antioxidant activity of curcumin-phospholipid complex(Curcumin Phytosome) (equivalent of curcumin 100 and 200 mg/kg body weight) and free curcumin (100 and 200 mg/kg body weight) was evaluated by measuring various enzymes in oxidative stress condition. Curcumin-phospholipid complex significantly protected the liver by restoring the enzyme levels of liver glutathione system and that of superoxide dismutase, catalase and thiobarbituric acid reactive substances with respect to carbon tetrachloride treated group ($P < 0.05$ and < 0.01). The complex provided better protection to rat liver than free curcumin at same doses. Serum concentration of curcumin obtained from the complex (equivalent to 1.0 g/kg of curcumin) was higher (Cmax 1.2 microg/ml) than pure curcumin (1.0 g/kg) (Cmax 0.5 microg/ml) and the complex maintained effective concentration of curcumin for a longer period of time in rat serum. The results demonstrated that, at the same dosage level, curcumin-phospholipid complex exhibits greater hepato protective action than free curcumin due to its superior antioxidant capacity[80]. In two distinct experiments, Maiti et al. synthesized the phytosome of naringenin, a flavonoid from grapefruit, Vitis vinifera, and curcumin, a flavonoid from turmeric, Curcuma longa. In every measured dosage range, the complex's antioxidant efficacy outperformed that of pure curcumin by a significant margin. In the other study, the naringenin phytosome that had been generated outperformed the free compound in terms of antioxidant activity. This difference in antioxidant activity may have been caused by a slower rate at which the molecule was removed from the body[81].

CHARACTERIZATION TECHNIQUES

Particle size determination

The particle size of the phytosome is determined by Dynamic Light Scattering (NANO ZS Malvern instrument) . And Particle size measurement was performed as following 1/100 (v/v) dilution of phytosomal suspension in redistilled water at 25°C[82].

Zeta Potential Determination

Zeta potential is estimated on the basis of the electro phoretic mobility under an electric field. Zeta potential was measured by using the NANO ZS Malvern instrument at 25°C following the same dilution in 1 mM NaCl solution[82].

Percentage yield

The prepared phytosome were dried properly and then weighed accurately. This weight was divided by the total weight of drugs non volatile recipients[82].

$$\text{Percent yield} = \frac{\text{weight of phytosomes formed}}{\text{weight of drugs and nonvolatile excipients}} \times 100$$

Drug entrapment efficiency

Take 100 mg of prepared Phytosome were dried properly and dispersed it in 50 ml distilled water. The content was stirred for 2 hrs and then filtered through Whatman filter paper of pore size of 45 μm. Then dilute it and analyzed spectro photometrically at λ max 266. The amount of drug entrapped is calculated from the standard calibration curve[82].

$$\text{Entrapment efficiency} \frac{\text{actual amount of drug in phytosomal formulation}}{\text{theoretical amount of drug in phytosomal formulation}} \times 100$$

Determination of drug content

To determine the drug content of phytosome complex, dissolve accurately weighed 10 mg of a complex in 10 ml methanol. After dilution, the absorbance was determined by UV – Spectrophotometer at 426nm and drug content was determined[83].

Field emission scanning electron microscopy

The Field emission scanning electron microscopy used to determine surface morphology of the Phytosome by using (FE-SEM; FEI Quanta FEG 200, Netherlands). The powdered sample, was placed on a metal stub of an electron magnifying device and coated with gold using a particle spray. A digital representation of the sample was obtained by examining the tip at different magnifications in an irregular manner. Using Image J software, FE-SEM images were used to measure the phytosome diameters randomly[84].

Transmission electron microscopy

The morphological properties of phytosome were assessed through the use of transmission electron microscopy (JOEL Ltd., Tokyo, Japan; TEM-100S Microscope). The samples undergo a 10-minute sonication after being diluted with ethanol at a ratio of 1:20. A carbon-glazed grid was coated with a drop of phytosome, which was then allowed to form a thin film. Using a TEM, phytosome images were captured[84].

Spectroscopic Evaluation of Phytosome

Ultraviolet spectra (UV-spectra)

The Samples that reflect different absorption in the UV wavelength range can be used to characterize own structural properties. Most studies have revealed that there is no differences in the UV absorption characteristics of constituents before and after complexation. Xu et al. prepared the luteolin-phospholipid complexes(Phytosome) and found that the characteristic peaks of luteolin remained present[85]. Therefore, we conclude that the chromophores of the compounds are not affected by being complexed with phospholipids.

Fourier transform infrared spectroscopy (FTIR)

FTIR is a powerful method for the structural analysis, and yields different functional groups that show distinct characteristics in band number, position, shape, and intensity. The formation of the phyto-phospholipid complexes(Phytosome) can be verified by comparing the spectroscopy of phospholipid complexes to that of physical mixtures. The Separate studies may show different results. In fact, Das and Kalita prepared the Rutin Phytosome. The FTIR of a physical mixture of rutin and phyto-phospholipid complexes was superimposable with the pure rutin[86]. When Mazumder et al. prepared the sinigrin-phytosome complexes, the FTIR of phytosome complex showed the different peaks from that of sinigrin, phospholipids and their mechanical mixtures[87].

Differential scanning calorimetry

In DSC, the interactions can be observed by comparing the transition temperature, appearance of new peaks, melting points, disappearance of original peaks, and changes in the relative peaks area. Phyto-phospholipid complexes(Phytosome) usually display the radically different characteristic peaks compared to those of a physical

mixture. It is concluded that, in addition to the two fatty chains of phospholipids, the strong interactions occur in the active ingredients and the polar part of phospholipids also inhibits free rotation. Das and Kalita prepared the phyto-phospholipid complexes rutin and the resulting DSC thermogram showed two characteristic peaks that were lower than that of the physical mixture and the peaks of rutin and PC disappeared[88].

X-ray diffraction

At present, the X-ray diffraction is an effective method to examine the microstructure of both crystal materials and some amorphous materials. The X-ray diffraction is usually performed on either active constituents or active constituent phyto-phospholipid complexes, PCs and their physical mixtures. X-ray diffraction of an active constituent and physical mixture shows the intense crystalline peaks that indicate a high crystal form. By contrast, the active constituent phyto-phospholipid complexes do not exhibit the crystalline peak, which suggests that the constituents in complex with phospholipids exhibit a molecular or amorphous form. The conclusion, that phyto-phospholipid complexes exhibit superior hydrophilicity and lipophilicity in comparison to active components[89].

Nuclear magnetic resonance (NMR)

The ^{1}H NMR and ^{13}C NMR techniques plays an very important role in the identification of the structures of the complexes. As mentioned above, interactions between polyphenols and phospholipids are created by the hydrogen bonds rather than chemical bonds. Angelico et al. established based on NMR data that the hydrogen bonds can form between some polar phenolic functional groups of silybin A and phospholipids[90]. The spectra of the different phyto-phospholipid complexes suggest that the hydrophobic side of lipids can act to cover the envelope on the central choline-bioactive parts of these complexes.

Recent Advancements of Phytosome

The virus appeared to spread globally in December 2019 and was declared a pandemic by the World Health Organization (WHO) on March 11, 2020. The SARS-CoV-2 coronavirus is responsible for it, as it has caused an unusually high number of infections and deaths (4.9 million) from acute severe respiratory syndromes across the globe[91]. Quercetin is a flavanol that the human body is not capable of producing. It is slightly soluble in lipids and popular dietary supplement that may offer protection from a number of illnesses. Quercetin phytosome is used as a supplement in COVID-19. The adequate potency of quercetin as a 3CLpro has only recently been confirmed. Recently, quercetin's oral bioavailability in humans has been evaluated by the use of a phospholipid delivery form called Quercetin Phytosome. Pharmacokinetics research revealed that total quercetin had a 20-fold increased bioavailability when its conjugated form, glucuronide, was hydrolyzed. In addition, it was reported that the body can create free systemic quercetin in response to a specific type of glucuronidase. In a therapeutic context, quercetin in a bioavailable form, like Quercetin Phytosome, should be considered as an effective way to treat COVID-19 while also considering its anti-inflammatory and thrombin-inhibitory properties[92]. Mariangela Rondanelli et al

examined the potential impacts of quercetin Phytosome (250 mg twice a day) multivitamin supplements for three months as a defense against symptomatic COVID-19. There are total of 120 individuals (63 men and 57 women, aged 49 and 12) includes there were 60 in the supplements group and 60 in the placebo group.There were no statistically significant differences seen between the groups with regarding gender, smoking, or chronic illness. Participants completed brief COVID-19 diagnostic examinations every three weeks. During the course of our trial, 5 out of 60 subjects in the quercetin group and 4 out of 60 in the control group had COVID-19. Complete clinical recovery was observed at 7 and 15 days in the quercetin and placebo groups, respectively. After five months, the analysis showed that participants who took quercetin supplements had a 99.8% COVID-free survival function (risk of infection), while those in the control group had a 96.5% risk.In order to prevent being infected with COVID-19, patients who took the supplement had a protection factor 14% higher than those who took a placebo, based on the value of EXP(B)[93]. Researchers conduct a lot of research, and the most recent studies show that phytosome technology is an innovative method to improve plant extract absorption and bioavailability while significantly reducing the dose level. Due to

their possible pharmacological effects, some plant extracts such as silymarin, grape seed extract, quercetin, curcumin, hesperetin, ginkgo biloba extract, Andrographolide, among others are receiving increased attention these days [94-95].Newer studies have been made possible by the technique's use and the increasing demand for herbal medicines in the current medical environment for the therapy of numerous diseases. Here is a brief summary of some of the important studies done by different researchers. In **1992 & 1994**, **Schandalik** *et al***,** used nine human volunteer patients and tested the hepatoprotective activity of silymarin and reported that the phytosomal form of silybin possess four times greater passage through the liver [96-97]. *et al***,** In **1993**, using 232 patients with chronic hepatitis. He also reported the better bioavailability of silymarin phytosome than the uncomplexed form[98]. In **1999, Grange** *et al***,** conducted series of experiments on silymarin Phytosome and reported the better fetoprotectant activity of the Silymarin Phytosome. In **2002**, **Busby** *et al,* also reported the better fetoprotectant activity of silymarin phytosome than uncomplexed silymarin against ethanol-induced behavioural deficit. In **2001**, **Jhiang** et al. Prepared Herba Epimedii flavonoid phytosome (EPF) by using a solvent evaporation approach, and a dissolution study was used to examine the accumulative dissolution of various ratios of EPF-PVP precipitate. According to the study, the precipitate dissolved much more quickly than both the physical mixture and the Herba Epimedii extract tablets [99]. According to **Bombardelli** et al. **(2005),** silymarin Phytosome had much greater specific activity and a more enduring effect compared to the individual constituent in terms of the percentage decrease of edema, myeloperoxidase activity inhibition, antioxidant activity, and free radical scavenging activity[100].

Some Patented Technologies Related to Phytosome

There are number of innovative processes and the formulation research studies in the field of Phytosome carried out by the academic scientists as well as in industrial laboratories. Some patents for Phytosome and the other related technologies along with their applications and innovations are listed in Table 1.

CONCLUSION

Phytosome are the novel formulations which offers improved bioavailability of water-soluble herbal constituents through skin and gastrointestinal tract. Phytosome are one of the phospholipid-based drugs delivery system with a better absorption and stability profile as compared to other drug delivery systems. Phytosome have improved pharmacokinetic and pharmacological parameter, which enable them to be used for different therapeutic purposes like cardiovascular, anti-inflammatory, anticancer, immune modulator, antidiabetic etc. Phytosome or herbosomes are advanced and novel form of botanicals and phytoconstituents that are better absorbed both orally, topically and transdermally. The formulation methods and characterization techniques of Phytosome has been well established. Many areas of Phytosome are to be reported in the future in the prospect of pharmaceutical application. The phytosome technology forms a link between the conventional delivery system of phyto constituents and novel drug delivery systems. This review is an attempt to present a concise profile of Phytosome as a delivery system includimg mechanism of action of phytosome by topical and oral route.

REFERENCES

1. Priya, V.M.H. and Kumaran, A., 2023. Recent Trends in Phytosome Nanocarriers for Improved Bioavailability and Uptake of Herbal Drugs. *Pharmaceutical Sciences*, *29*(3), pp.298-319.
2. Shelke SS. Phytosome - a new herbal drug delivery system. Int J Res Pharm Biomed Sci. 2012;3(4):1710- 15.
3. Vaishnavi, A & Arvapalli, Swarupa & Rishika, Ps & Jabeen, Syeda & Karunakar, B & Sharma, J. (2021). A Review on Phytosome: Promising Approach for Drug Delivery of Herbal Phytochemicals. 10.35629/7781-0601289296.
4. Saha, Sanjay & Sarma, Anupam & Saikia, Pranjal & Chakraborty, Tapash. (2013). Phytosome: A Brief Overview. 2. 12-20.

5. Semalty A, Semalty M, Rawat MS, Franceschi F. Supramolecular phospholipids-polyphenolics interactions: the PHYTOSOME strategy to improve the bioavailability of phytochemicals. *Fitoterapia*. 2010;81(5):306-314. doi: 10.1016/j.fitote.2009.11.001
6. Bhagyashree HAP. Phytosome as a novel biomedicine: a microencapsulated drug delivery system. J Bioanal Biomed. 2015;07(01):6-12. doi:10.4172/1948- 593x.1000116
7. Patel J, Patel R, Khambholja K, Patel N. An overview of Phytosome as an advanced herbal drug delivery system. Asian J Pharm Sci. 2009;4(6):363-71.
8. Lu, M.; Qiu, Q.; Luo, X.; Liu, X.; Sun, J.; Wang, C.; Lin, X.; Deng, Y.; Song, Y. Phyto-phospholipid complexes (Phytosome): A novel strategy to improve the bioavailability of active constituents. Asian J. Pharm. Sci. **2018**, 14, 265–274. [CrossRef] [PubMed]
9. Shakeri, A.; Sahebkar, A. Opinion Paper: Phytosome: A Fatty Solution for Efficient Formulation of Phytopharmaceuticals. Recent Patents Drug Deliv. Formul. **2016**, 10, 7–10. [CrossRef]
10. Rathore, P.; Swami, G. Planterosomes: A potential phyto-phospholipid carriers for the bioavailability enhancement of herbal extracts. Int. J. Pharm. Sci. Res. **2012**, 3, 737.
11. Jain, N.; Gupta, B.P.; Thakur, N.; Jain, R.; Banweer, J.; Jain, D.K.; Jain, S. Phytosome: A novel drug delivery system for herbal medicine. Int. J. Pharm. Sci. Drug Res. **2010**, 2, 224–228.
12. Yang, B.; Dong, Y.; Wang, F.; Zhang, Y. Nanoformulations to Enhance the Bioavailability and Physiological Functions of Polyphenols. Molecules **2020**, 25, 4613. [CrossRef] [PubMed]
13. Alharbi, W.S.; Almughem, F.A.; Almehmady, A.M.; Jarallah, S.J.; Alsharif,W.K.; Alzahrani, N.M.; Alshehri, A.A. Phytosome as an Emerging Nanotechnology Platform for the Topical Delivery of Bioactive Phytochemicals. Pharmaceutics **2021**, 13, 1475.https://doi.org/10.3390/ pharmaceutics13091475
14. Kidd PM. Phosphatidylcholine: a superior protectant against liver damage. Altern Med Rev 1996;1:258–74.
15. Li J ,Wang X ,Zhang T ,et al.A review on phospholipids and their main applications in drug delivery systems. Asian J Pharma Sci 2015;10(2):81–98.
16. Suriyakala PC ,Babu NS ,Rajan DS ,Prabakaran L . Phospholipids as versatile polymer in drug delivery systems. Int J Pharm Sci 2014;6(1):8–11.
17. Lu, M.; Qiu, Q.; Luo, X.; Liu, X.; Sun, J.; Wang, C.; Lin, X.; Deng, Y.; Song, Y. Phyto-phospholipid complexes (Phytosome): A novel strategy to improve the bioavailability of active constituents. Asian J. Pharm. Sci. **2018**, 14, 265–274. [CrossRef] [PubMed]
18. Khan J ,Alexander A ,Saraf S ,Saraf S . Recent advances and future prospects of phyto-phospholipid complexation technique for improving pharmacokinetic profile of plant actives. J Control Release 2013;168(1):50–60 .
19. Shakeri A ,Sahebkar A . Phytosome: a fatty solution for efficient formulation of phytopharmaceuticals. Recent Pat Drug Deliv Formul 2016;10(1):7–10.
20. Xiao Y ,Song Y ,Chen Z ,Ping Q . The preparation of silybin-phospholipid complex and the study on its pharmacokinetics in rats. Int J Pharma 2006;307(1):77–82.
21. Tripathy S ,Patel DK ,Barob L ,Naira SK . A review on Phytosome, their characterization, advancement & potential for transdermal application. J Drug Deliv Ther 2013;3(3):147–52.
22. Chauhan NS ,Rajan G ,Gopalakrishna B . Phytosome: a potential phyto-phospholipid carriers for herbal drug delivery. J Pharm Res 2009;2(7):1267–70.
23. Zhang K ,Zhang M ,Liu Z ,et al.Development of quercetin-phospholipid complex to improve the bioavailability and protection effects against carbon tetrachloride-induced hepatotoxicity in SD rats. Fitoterapia 2016;113:102–9.
24. C. Marena, M. Lampertico. Preliminary clinical development of silipide: A new complex of silybin in toxic liver disorders. Planta Med., 1991, 57: A124-A125.
25. Y. N. Jiang, Z. P. Yu, Z. M. Yan, *et. al*. Preparation of herba epimedii flavanoid and their pharmaceutics. Zhongguo Zhong Yao, 2001, 26: 105-108.
26. K. Maiti, K. Mukherjee, A. Gantait, *et al.* Curcumin phospholipid complex: preparation, therapeutic evaluation and pharmacokinetic study in rats. Int. J. pharm., Sept. 2006. (In Press)

27. K. Maiti, K. Mukherjee, A. Gantait, *et al*. Enhanced therapeutic potential of naringenin-phospholipid complex in rats. J. Pharm. Pharmacol., 2006, 58: 1227-1233.
28. X. Yanyu, S. Yunmei, C. Zhipeng, *et al*. The preparation of silybin-phospholipid complex and the study on its pharmacokinetics in rats. Int. J. Pharm., 2006, 307: 77-8
29. Rathore P, Swami G. Planterosomes: Potential phytophospholipid carriers for the bioavailability enhancement of herbal extracts. Int J Pharm Sci and Res. 2015;3(3):737-755.
30. Singh RP, Parpani S, Narke R, Chavan R. Phytosome: Recent advance research for novel drug delivery system. Asian J Pharm Res and Dev. 2014;2(3):15-29.
31. Khan J, Alexander A, Saraf A, Swarnlata SS. Recent advances and future prospects of phytophospholipid complexation technique for improving pharmacokinetic profile of plant actives. J Controlled Rel. 2013;168: 50-60
32. Kumar S, Baldi A, Sharma DK (2020) Phytosome: A Modernistic Approach for Novel Herbal Drug Delivery - Enhancing Bioavailability and Revealing EndlessFrontier of Phytopharmaceuticals. J Develop Drugs 9:2. doi: 10.4172/2329-6631. 1000195
33. Li J, Wang X, Zhang T, Wang C, Huang Z, Luo X, Deng Y. A review on phospholipids and their main applications in drug delivery systems. Asian J. Pharm. Sci. 2015;10(2):81-98.
34. Sheth P, Sandhu H. Amorphous solid dispersion using supercritical fluid technology. In: Shah N, Sandhu H, Choi DS, Chokshi H, Malick AW, editor. Amorphous Solid Dispersions. New York: Springer; 2014.
35. Patel, Pavan & Modi, Chirag & Patel, Harshad & Patel, Urvesh & Ramchandani, Divya & Patel, Harsh & Paida, Bhulesh. (2023). Phytosome: An Emerging Technique for Improving Herbal Drug Delivery. The Journal of Phytopharmacology. 12. 51-58. 10.31254/phyto.2023.12108
36. Patel, Dilip. (2013). A REVIEW ON PHYTOSOME, THEIR CHARACTERIZATION, ADVANCEMENT & POTENTIAL FOR TRANSDERMAL APPLICATION. Journal of Drug Delivery and Therapeutics. 3. 147-152.
37. Alharbi,W.S.; Almughem, F.A.; Almehmady, A.M.; Jarallah, S.J.; Alsharif,W.K.; Alzahrani, N.M.; Alshehri, A.A. Phytosome as an Emerging Nanotechnology Platform for the Topical Delivery of Bioactive Phytochemicals. Pharmaceutics **2021**, 13, 1475. https://doi.org/10.3390/ pharmaceutics13091475
38. Bombardelli E and Spelta M, Phospholipid-polyphenol complex: A new concept in skin care ingredients, Cosmetics Toiletries, 1991, 106, 69-76.
39. . Xiao Yanyu, Song Yunmei, Chen Zhipeng, Ping Qineng, The preparation of silybin–phospholipid complex and the study on its pharmacokinetics in rats, International Journal of Pharmaceutics, 2006, 307, 77–82.
40. Kidd PM, Bioavailability and activity of phytosome complexes from botanical polyphenols: The silymarin, curcumin, Green tea and Grape seed extracts, Alternative Medicines Review, 2009, 14 (3), 226-246
41. Dini, I.; Laneri, S. The New Challenge of Green Cosmetics: Natural Food Ingredients for Cosmetic Formulations. Molecules **2021**,26, 3921. [CrossRef] [PubMed]
42. Gupta, A.; Ashawat, M.; Saraf, S.; Saraf, S. Phytosome: A novel approach towards functional cosmetics. J. Plant Sci. **2007**,2, 644–649.
43. Chanchal, D.; Swarnlata, S. Novel approaches in herbal cosmetics. J. Cosmet. Dermatol. **2008**, 7, 89–95. [CrossRef]
44. Tessema, E.N.; Gebre-Mariam, T.; Neubert, R.H.;Wohlrab, J. Potential Applications of Phyto-Derived Ceramides in Improving Epidermal Barrier Function. Skin Pharmacol. Physiol. **2017**, 30, 115–138. [CrossRef]
45. Haque, T.; Talukder, M.U. Chemical Enhancer: A Simplistic Way to Modulate Barrier Function of the Stratum Corneum. Adv.Pharm. Bull. **2018**, 8, 169–179. [CrossRef] [PubMed]
46. Patzelt, A.; Antoniou, C.; Sterry,W.; Lademann, J. Skin penetration from the inside to the outside: A review. Drug Discov. Today Dis. Mech. **2008**, 5, e229–e235. [CrossRef]
47. Kim, B.; Cho, H.-E.; Moon, S.H.; Ahn, H.-J.; Bae, S.; Cho, H.-D.; An, S. Transdermal delivery systems in cosmetics. Biomed.Dermatol. **2020**, 4, 1–12. [CrossRef]
48. Lu, M.; Qiu, Q.; Luo, X.; Liu, X.; Sun, J.; Wang, C.; Lin, X.; Deng, Y.; Song, Y. Phyto-phospholipid complexes (Phytosome): A novel strategy to improve the bioavailability of active constituents. Asian J. Pharm. Sci. **2018**, 14, 265–274. [CrossRef] [PubMed]

49. Bombardelli, E.; Spelta, M. Phospholipid-polyphenol complexes: A new concept in skin care ingredients. Cosmet. Toilet. **1991**,106, 69–76.
50. Tripathy, S.; Patel, D.K.; Barob, L.; Naira, S.K. A review on Phytosome, their characterization, advancement & potential for transdermal application. J. Drug Deliv. Ther. **2013**, 3, 147–152. [CrossRef]
51. Suresh, E (2019) *Development of Mucuna Pruriens Phytosomal Capsule for Oral Application.* Masters thesis, College of Pharmacy, Madurai Medical College, Madurai
52. Gupta, Ranjana & Agrawal, Anant & Anjum, Meraj & Dwivedi, Harinath & Mamman, Koshy & Saraf, Shubhini. (2014). Lipid Nanoformulations for Oral Delivery of Bioactives: An Overview. Current Drug Therapy. 10.2174/1574885509666140805005207.
53. *Veena S.Kasture, Vijay.P.Sonar, Poonam P.Patil, Deepak S. Musmade;* Quantitative Estimation of L-Dopa from Polyherbal Formulation by usingRP-HPLC, Am.J.PharmTech Res.2014:4(3),ISSN:2249-3387.
54. *Chirstopher A.Lieu, Kala Venkiteswaran, Timothy P.Gilmour, Anand N.Rao, Andrew C.Petticoffer, Erin V.Gilbert, Milind Deogaonkar, Bala V.Manyam, and Thyagarajan Subhramanian;* The Antiparkinsonian and AntidyskineticMechanism of *Mucuna pruriens* in the MPTP-Treated NonhumanPrimate,Volume-2012,Article ID 840247,10 pages.
55. Pierro FD, Menghi AB, Barreca A, Lucarelli M, Calandrelli A. GreenSelect Phytosome as an Adjunct to a Low-Calorie Diet for Treatment of Obesity: A Clinical Trial. Altern Med Rev 2009; 14:
56. Hikino H, Kiso Y, Wagner H, Fiebig M. Antihepatotoxic actions of flavolignans from *Silybum marianum* fruits. Planta Med 1984;50:248–50.
57. Wellington K, Jarvis B. Silymarin: a review of its clinical properties in the management of hepatic disorders. BioDrugs 2001;15:465–89.
58. Canini F, Bartolucci L, Cristallini E, Gradoli C, Rossi A, Ribacchi R, et al. L'impiego della silimarina nel trattamento della steatosi epatica alcolica.Clin Ter 1985;114.
59. Boari C, Montanari FM, Galletti GP, Rizzoli D, Baldi E, Caudarella R, et al. Epatopatie tossiche professionali. Minerva Med 1981;72:2679–88.
60. Ferenci P, Dragosics B, Dittrich H, Frank H, Benda L, Lochs H, et al.Randomized controlled trial of silymarin treatment in patients withcirrhosis of the liver. J Hepatol 1989;9:105–13.
61. Valenzuela A, Aspillaga M, Vial S, Guerra R. Selectivity of silymarin on the increase of the glutathione content in different tissues of the rat.Med 1989;55:420–2.
62. Hikino H, Kiso Y, Wagner H, Fiebig M. Antihepatotoxic actions of flavolignans from *Silybum marianum* fruits. Planta Med 1984;50:248–50.
63. Yanyu X, Yunmei S, Zhipeng C, Quineng P. The preparation of silybin– phospholipid complex and the study on its pharmacokinetics in rats. Int J Pharm 2006;307:77–82.
64. Bombardelli E, Cristoni A, Morazzoni P. Phytosome in functional cosmetics. Fitoterapia 1994;65:387–401.
65. Bombardelli E, Spelta M. Phospholipid–polyphenol complexes: a new concept in skin care ingredients. Cosmet Toilet 1991;106:69–76.
66. Kumar S, Baldi A, Sharma DK. In vitro antioxidant assay guided ex vivo investigation of cytotoxic effect of Phytosome assimilating taxifolin rich fraction of *Cedrus deodara* bark extract on human breast cancer cell lines (MCF7). J Drug Deliv Sci Technol. 2021;63:102486. doi:10.1016/j.jddst.2021.102486
67. .Murugesan MP, Venkata Ratnam M, Mengitsu Y, Kandasamy K. Evaluation of anti-cancer activity of Phytosome formulated from *Aloe vera* extract. Mater Today Proc. 2021;42:631-6. doi:10.1016/J. MATPR.2020.11.047
68. Alhakamy NA, Badr-Eldin SM, Fahmy UA, Alruwaili NK, Awan ZA, Caruso G, et al. Thymoquinone-loaded soy-phospholipid-based Phytosome exhibit anticancer potential against human lung cancer cells. Pharmaceutics. 2020;12(8):761. doi:10.3390/ pharmaceutics12080761 \
69. Anti-aging, http://jp.indena.com/pdf/jp/anti_aging.pdf (Date accessed12July2014).
70. Serri R, Iorizzo M. Combating aging skin. Clin Dermatol. 2008;26(2):105.
71. Damle, M., Mallya, R. Development and Evaluation of a Novel Delivery System Containing Phytophospholipid Complex for Skin Aging. *AAPS PharmSciTech* **17**, 607–617 (2016). https://doi.org/10.1208/s12249-015-0386-x

72. Korać RR, Khambholja KM. Potential of herbs in skin protection from ultraviolet radiation. Pharmacogn Rev.2011;5(10):164–73.
73. Caragay AB. Cancer-preventive foods and ingredients. Food Technol.1992;46(4):65–8.
74. Mukherjee PK, Rai S, Kumar V, et al. Plants of Indian origin in drug discovery. Expert Opin Drug Discov.2007;2:633–57.
75. Yusof S, Mohd Ghazali H, Swee KG. Naringin content in local citrus fruits. Food Chem.1990;37:113–21.
76. Obolentseva GV, LitvinenkoVI, Ammosov AS,etal.Pharmacological and therapeutic properties of licorice preparations(a-review).Pharm Chem J.1999;33:24–31.
77. Visavadiya NP, Soni B, Dalwadi N.Evaluation of antioxidant and anti-atherogenic properties of Glycyrrhiza glabra root using in vitro models.Int J Food Sci Nutr.2009;60(2):135–49.
78. Ahshawat MS, Saraf S, Saraf S. Preparation and characterization of herbal creams for improvement of skin viscoelastic properties. Int J CosmetSci.2008;30(3):183–93.
79. Rafeeuddin M, Rao NV, Shanta Kumar SM, et al. Comparative efficacy of four Ayurvedic antidiabetic formulations in alloxan-induced diabetic rabbits. Acta Pharma Sci. 2009; 51
80. Maiti K, Mukherjee K, Gantait A, Saha BP, Mukherjee PK, Enhanced therapeutic potential of naringenin-phospholipid complex in rats, Journal of Pharmacy & Pharmacology, 2006, 58 (9),1227-33.
81. Maiti K, Mukherjee K, Gantait A, Saha BP, Mukherjee PK, Curcumin-phospholipid complex: Preparation, therapeutic evaluation and pharmacokinetic study in rats, International Journal of Pharmaceutics, 2007, 330, 155-163
82. Sindhumol, P.G. & Thomas, M. & Mohanachandran, P.S.. (2010). Phytosome: A novel dosage form for enhancement of bioavailability of botanicals and neutraceuticals. International Journal of Pharmacy and Pharmaceutical Sciences. 2. 10-14.
83. Sharma S, Sahu AN. Development, Characterization, and Evaluation of Hepatoprotective Effect of Abutilon indicum and Piper longum Phytosome. Pharmacognosy Research. 2016 Jan-Mar;8(1):29-36. DOI: 10.4103/0974-8490.171102. PMID: 26941533; PMCID: PMC4753757.
84. Sachin K S, Adlin Jino Nesalin J, Tamizh Mani T, "Preparation and Evaluation of Curcumin Phytosome by Rotary Evaporation Method," *SSRG International Journal of Pharmacy and Biomedical Engineering*, vol. 6, no. 1, pp. 29-34, 2019
85. Nandhini S, Ilango K. Development and characterization of a nano-drug delivery system containing vasaka phospholipid complex to improve bioavailability using quality by design approach. *Res Pharm Sci*. 2020;16(1):103-117. Published 2020 Dec 30. doi:10.4103/1735-5362.305193
86. Xu K, Liu B, Ma Y, et al. Physicochemical properties and antioxidant activities of luteolin-phospholipid complex. *Molecules.* 2009;14(9):3486–3493. [PMC free article] [PubMed] [Google Scholar]
87. Das MK, Kalita B. Design and evaluation of phyto-phospholipid complexes (Phytosome) of rutin for transdermal application. *J J Appl Pharm Sci.* 2014;4(10):51–57. [Google Scholar]
88. Mazumder A, Dwivedi A, Preez JLD, Plessis JD. *In vitro* wound healing and cytotoxic effects of sinigrin-phytosome complex. *Int J Pharm.* 2015;498(1–2):283–293. [PubMed] [Google Scholar]
89. Hao H, Jia Y, Han R, Amp IA. Phytosome: an effective approach to enhance the oral bioavailability of active constituents extracted from plants. *J Chin Pharm Sci.* 2013;22(5):385–392. [Google Scholar]
90. Ghanbarzadeh B, Babazadeh A, Hamishehkar H. Nano-phytosome as a potential food-grade delivery system. *Food Biosci.* 2016;15:126–135. [Google Scholar]
91. Angelico R, Ceglie A, Sacco P, Colafemmina G, Ripoli M, Mangia A. Phyto-liposomes as nano shuttles for water-insoluble silybin–phospholipid complex. *Int J Pharm.* 2014;471(1–2):173–181. [PubMed] [Google Scholar]
92. Rondanelli, M.; Perna, S.; Gasparri, C.; Petrangolini, G.; Allegrini, P.; Cavioni, A.; Faliva, M.A.; Mansueto, F.; Patelli, Z.; Peroni, G.; et al. Promising Effects of 3-Month Period of Quercetin Phytosome® Supplementation in the Prevention of Symptomatic COVID-19 Disease in Healthcare Workers: A Pilot Study. *Life* **2022**, *12*, 66. https://doi.org/10.3390/life12010066
93. F.D. Dipierro, A. Khan, A. Bertuccioli, P. Maffioli, G. Derosa, S. Khan, B.A. Khan, R. Nigar, I. Ujjan, B.R. Devrajani, Quercetin Phytosome® as a potential candidate for managing COVID-19, Minerva Gastroenterol. 67 (2) (2021) 190–195, https://doi.org/10.23736/s2724-5985.20.02771-3

94. Gaikwad SS, Morade YY, Kothule AM, Kshirsagar SJ, Laddha UD, Salunkhe KS. Overview of Phytosome in treating cancer: Advancement, challenges, and future outlook. *Heliyon*. 2023;9(6):e16561. Published 2023 May 24. doi:10.1016/j.heliyon.2023.e16561
95. Wellington K, Jarvis B, Silymarin: a review of its clinical properties in the management of hepatic disorder, Bio Drugs, 2001, 15, 465-89.
96. Hikino H, Kiso Y, Wagner H, Fiebig M, Antihepatotoxic actions of flavonolignans from Silybum marianum fruits, Planta Medica, 1984, 50,248-250.
97. Schandalik R, E. Perucca, Pharmacokinetics of silybin following oral administration of silipide in patients with extrahepatic biliary obstruction, Drugs under Experimental & Clinical Research, 1994, 20, 37-42.
98. Schandalik R, Gatti G, Perucca E, Pharmacokinetics of silybin in bile following administration of silipide and silymarin in cholecystectomy patients, Arzneimittelforschung, 1992, 42, 964-68.
99. Mascarella S, Therapeutic and antilipoperoxidant effects of silybin-phosphatidylcholine complex in chronic liver disease, Preliminary results, Current Therapeutic Research, 1993, 53 (1), 98-102.
100. Jiang YN, Yu ZP, Yan ZM, Chen JM, Studies on preparation of herba epimedii flavanoid Phytosome and their pharmaceutics, Zhongguo Zhong Yao Za Zhi, 2001, 26 (2), 105-8.
101. Bombardelli E, Spelta M, Loggia Della R, Sosa S, Tubaro A. Aging Skin: Protective effect of silymarin-Phytosome, Fitoterapia, 1991; 62(2), 115-22, Rev 2005; 10(3), 193-203.
102. G S, Ravi &Rompicherla, Narayana Charyulu& Dubey, Akhilesh & Hebbar, Srinivas & Mathias, Avril. (2018). Phytosomes: A Novel Molecular Nano Complex Between Phytomolecule and Phospholipid as a Value added Herbal Drug Delivery System. International Journal of Pharmaceutical Sciences Review and Research. 51. 84-90.

Table 1: Some patented technologies related to Phytosome.[101]

Title of Patent	Innovation	Patent Number
Phospholipid complexes of olive fruits or leaf extracts having improved bioavailability	Phospholipids complexes of olive fruits or leaf extracts or compositions having improved bioavailability.	EP/1844785
Fatty acid monoesters of sorbityl furfural and compositions for cosmetic and dermatological use	Fatty acid monoesters of sorbityl furfural and compositions for cosmetic and dermatological use.	EP1690862
Treatment of skin and wound repair with thymosin β4.	Compositions and methods for treatment of skin utilizing thymosin β4.	US/2007/0015698
An anti-oxidant preparation based on plant extracts for the treatment of circulation and adiposity problems	An anti-oxidant preparation based on plant extracts for the treatment of circulation and adiposity problems Preparation based on plant extracts which has an antioxidant effect and is particularly useful in treatment of circulation problems such as phlebitis, varicose veins, arteriosclerosis, haemorrhoids and high blood pressure.	EP1214084
Compositions comprising gingko biloba derivatives for the treatment of asthmatic and allergic conditions	Compositions containing fractions deriving from ginkgo biloba, useful for the treatment of asthmatic and allergic conditions.	EP1813280
Cosmetic and dermatological composition for the treatment of aging or photo damaged skin	Composition for topical treatment of the skin comprises a substance that stimulates collagen synthesis and a substance that enhances the interaction between extracellular matrix and fibroblasts Cosmetic or dermatological composition for topical treatment.	EP1640041

Soluble isoflavone compositions	Isoflavone compositions exhibiting improved solubility (Example: light transmittance), taste, color, texture characteristics and methods for making.	WO/2004/045541

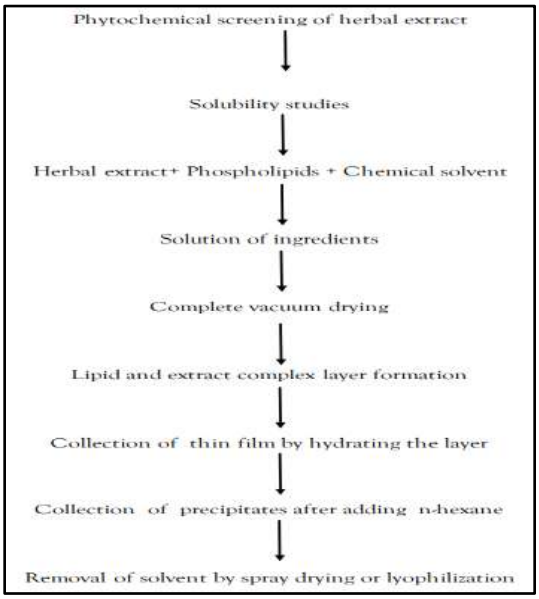

Figure 1.Common stages in formulation of Phytosome

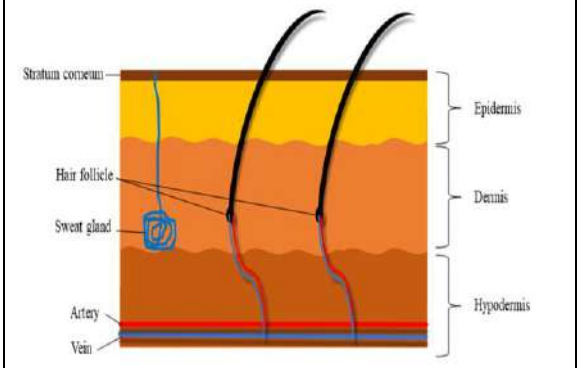

Figure 2. Simplified structure of the skin and its barriers.

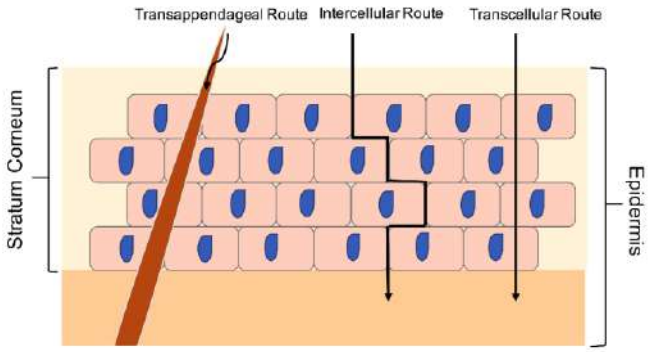

Figure 3. Mechanism of transdermal drug delivery.

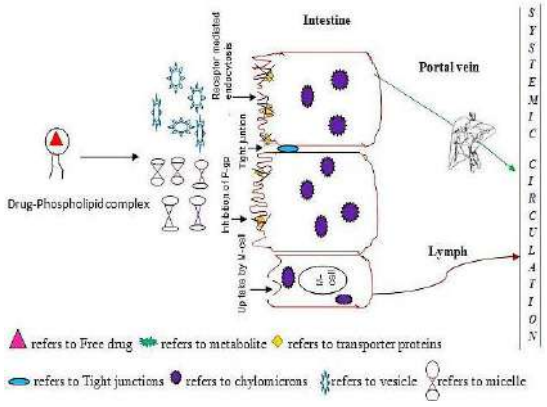

Figure 4.Schematic diagram representing the possible mechanism of phyto-phospholipids complex absorption

RESEARCH ARTICLE

Accurate Equitable Domination in Graphs

P.Nataraj[1]* , A. Wilson Baskar[2] and V.Swaminathan[3]

[1]Assistant Professor, Department of Mathematics, Sri Sai Ram Engineering College, (Affiliated to Anna University), Chennai, Tamil Nadu, India.
[2]Associate Professor, Department of Mathematics, Saraswathi Narayanan College, (Affiliated to Madurai Kamaraj University), Madurai, Tamil Nadu, India.
[3]Reader (Retd.), Saraswathi Narayanan College, (Affiliated to Madurai Kamaraj University), Madurai, Tamil Nadu, India.

Received: 30 Dec 2023 Revised: 09 Jan 2024 Accepted: 12 Jan 2024

***Address for Correspondence**
P.Nataraj
Assistant Professor,
Department of Mathematics,
Sri Sai Ram Engineering College,
(Affiliated to Anna University),
Chennai, Tamil Nadu, India.
Email: nataraj.maths@sairam.edu.in

ABSTRACT

A subset $D \subseteq V(G)$ is called an accurate equitable dominating set of G if $V - D$ does not contain an equitable dominating set of cardinality$|D|$. The minimum cardinality of an accurate equitable dominating set is the called the accurate equitable domination number of G and is denoted by $\gamma_{ae}(G)$. The upper accurate equitable domination number $\Gamma_{ae}(G)$ is the maximum cardinality of a minimal accurate equitable dominating set. In this paper we initiate the study of this parameter.

Keywords: Equitable domination, Accurate domination, Accurate equitable domination.

INTRODUCTION

In a simple graph G a subset S of the vertex set V of G is called a dominating set if a every vertex in the complement of S with respect to V is adjacent with some vertex of S. The cardinality of a minimum dominating set is called the domination number and is denoted by $\gamma(G)$. Two vertices x, y are said to be degree equitable if $|\deg_G(x) - \deg_G(y)| \leq 1$. If $x \in V(G)$, then the open equitable neighbourhood of x consists of those vertices which are adjacent with x and degree equitable with x. The closed equitable neighbourhood of x is the open neighbourhood of x together with x. If T is a subset of V then the open equitable neighbourhood of T is the union of the open equitable neighbourhoods of elements of T and the closed equitable neighbourhood of T is the union of the open equitable

neighbourhood of T and T. For a subset X of V the private equitable neighbour of v with respect to the X consists of those vertices in the closed equitable neighbourhood of v - the closed equitable neighbourhood of $X-\{v\}$. The maximum value of equitable degree of a vertex v in the G is denoted by $\Delta_e(G)$ and the minimum value by $\delta_e(G)$. A subset S of the vertex set V is called an equitable dominating set of G if every vertex in the complement of S with respect to the V is equitably dominated by the some vertex of S. The minimum cardinality of an equitable dominating set of G is denoted by $\gamma_e(G)$. If S is a dominating set of G with the property that the complement of S with respect to the V does not contain any dominating set of cardinality $|S|$, then S is called an accurate dominating set and the minimum cardinality in referred to as the accurate domination number of G and is denoted by $\gamma_a(G)$[7].

Definition 1. Suppose S is a subset of V of G such that S is an equitable dominating set and $V-S$ does not contain an equitable dominating set of G with cardinality $|S|$. Then S is called an accurate equitable dominating set of G and its minimum cardinality is called the accurate equitable domination number of G and is denoted by $\gamma_{ae}(G)$. The maximum cardinality of a minimal accurate equitable dominating set of G is denotes by $\Gamma_{ae}(G)$.

$\gamma_{ae}(G)$Of Some Standard Graphs

i) $\gamma_{ae}(K_n)=\left\lfloor\frac{n}{2}\right\rfloor+1$, for $n\geq 3$

ii)$\gamma_{ae}(P_n)=\begin{cases}\frac{n}{3}, & n\equiv 0(\text{mod}3)\\ \left\lceil\frac{n}{3}\right\rceil+1, & n\equiv 1\ or\ 2(mod\ 3)\end{cases}$

iii) $\gamma_{ae}(C_n)=\begin{cases}\left\lceil\frac{n}{3}\right\rceil+2, & n\equiv 0(\text{mod}3),\\ \left\lceil\frac{n}{3}\right\rceil+1, & n\neq\equiv 0(\text{mod}3)\end{cases}$

iv)$\gamma_{ae}(W_n)=\begin{cases}3, & \text{if } n=4\\ 1, & \text{if } n=5\\ \gamma_{ae}(C_{n-1})+1, & \text{if } n\geq 6\end{cases}$

v) $\gamma_{ae}\left(K_{m,n}\right)\begin{cases}min(m,n), if\ |m-n|\leq 1\\ m+n, if\ |m-n|\geq 2\end{cases}$

vi) $\gamma_{ae}\left(K_{1,n}\right)=n+1$, for $n\geq 3$

Bounds On $\gamma_{ae}(G)$

Remark 1. Every accurate equitable dominating set is an equitable dominating set.

Remark 2. An accurate equitable dominating set may or may not be a minimal equitable dominating set.

Proposition 1. For any graph $G, \gamma_e(G)\leq\gamma_{ae}(G)$.

Proposition 2. If G contains an equitable isolate, then a minimal equitable dominating set of G is an accurate equitable dominating set of G.

Proof. Let v be an equitable isolate of G. Then, $v\in D$ for every equitable dominating set D of G. Thus, $|V-D|$ cannot have an equitable dominating set of cardinality$D$.

Corollary1. If G contains an equitable isolate, then $\gamma_{ae}(G)=\gamma_e(G)$

Proposition 3. For any graph $G, \gamma_{ae}(G)\leq n-\gamma_e(G)+1$

Proof. Let D be a minimum equitable dominating set of G. Then, for any $v\in V-D$, $(V-D)\cup\{v\}$ is an accurate equitable dominating set of G. Hence, $\gamma_{ae}(G)\leq|\ (V-D)\cup\{v\}\ |\leq n-\gamma_e(G)+1$.

Corollary 2. If G contains equitable isolates, then $\gamma_{ae}(G) \leq \frac{n+1}{2}$

Proposition4. Let G be a simple graph with maximum equitable degree Δ_e, then $\frac{n}{\Delta_e + 1} \leq \gamma_{ae}(G) \leq \frac{n\Delta_e}{\Delta_e + 1} + 1$

Proof. Let D be a γ_e - set of G. Each vertex $v \in V(G)$ can equitable dominate at most $\Delta_e + 1$ vertices. Hence, $\gamma_e(G) \geq \frac{n}{\Delta_e+1}$. Now, since $\gamma_e(G) \leq \gamma_{ae}(G)$, the lower bound holds. Now by **Proposition 3**

$$\gamma_{ae}(G) \leq n - \gamma_e(G) + 1$$
$$\leq n - \frac{n}{\Delta_e + 1} + 1$$
$$\leq \frac{n\Delta_e}{\Delta_e + 1} + 1$$

Proposition 5. For any graph G with $n \geq 2$, an equitable dominating set D such that $|D| = \left\lfloor \frac{n}{2} \right\rfloor + 1$, then D is an accurate equitable dominating set.

Proof. Let D be an equitable dominating set with $|D| = \left\lfloor \frac{n}{2} \right\rfloor + 1$. Then $|V - D| \leq \frac{n}{2}$. Hence D is an accurate equitable dominating set.

Proposition 6. Let T be a tree with s cut vertices. Then, $\gamma_{ae}(T) \leq s + 1$. Equality holds if and only if each cut vertex is adjacent to a pendent vertex.

Proof. Let S be the set of all cut vertices of T with $|S| = s$. Let u be a pendent vertex of G. Then $S \cup \{u\}$ is an accurate equitable dominating set of T.
Suppose $\gamma_{ae}(T) = s + 1$. If there exists a cut vertex $v \in S$ such that v is not adjacent to any of the end vertices, then S is an accurate equitable dominating set, a contradiction. Converse is obvious.

Definition 2 [9] For a simple graph G with the vertex set $V(G)$, a subset S of $V(G)$ is called a maximal equitable dominating set of G, if the complement of S with respect to the V not an equitable dominating set of G. If such a set has a minimum cardinality then that cardinality is called the maximal equitable domination number of G and is denoting $\gamma_e^m(G)$.

Proposition 7. For any graph $G, \gamma_{ae}(G) \leq \gamma_e^m(G)$, equality holds if $G = C_n$.

Definition 3 [1] Suppose S is a subset of the vertex set V of a simple graph G, S is called an equitable total dominating set of G if S is an equitable dominating set of G and the subgraph included by S has no isolates. The minimum cardinality of such a set is called the equitable total domination number of G and is denoted by $\gamma_e^t(G)$.

Proposition 8. If a simple graph G has a pendent vertex, then $\gamma_{ae}(G) \leq \gamma_e^t(G) + 1$.

Proof. Let G be a graph and let $v \in V(G)$ be a pendent vertex and $u \in V(G)$ be its support vertex. Let D be a γ_e^t - set of G.

Case 1: Suppose $v \in D$. Then, u is also in D. Hence D is an accurate equitable dominating set of G. Thus, $\gamma_{ae}(G) \leq |D| = \gamma_e^t$.

Case 2: Suppose $v \notin D$. Then, $u \in D$. Hence $D \cup \{v\}$ is an accurate equitable dominating set of G. Thus, $\gamma_{ae}(G) \leq |D \cup \{v\}| = \gamma_e^t + 1$.

When $G = P_4, \gamma_{ae}(P_4) = 3 = 2 + 1 = \gamma_e^t + 1$.

Graphs With $\gamma_{ae} = \gamma_e$

Definition 4. Suppose H is a simple graph. Suppose one pendent vertex is attached with every vertex of H then the resulting graph is called the corona of H and is denoted by $H \circ K_1$.

Proposition 9. Let $G = (V, E)$ be a graph. Then $\gamma_{ae}(G) = \gamma_e(G)$ if and only if there exists a set $S \in D_{\gamma_e}(G)$ such that $S \cap S' \neq \emptyset$ for every set $S' \in D_{\gamma_e}(G)$, where $D_{\gamma_e}(G) = \{S \mid S \text{ is a } \gamma_e - \text{set}\}$.

Proof. Let G be a graph with $\gamma_{ae}(G) = \gamma_e(G)$. Let S be a minimum accurate equitable dominating set of G. Since S is an equitable dominating set and $|S| = \gamma_{ae}(G) = \gamma_e(G)$, $S \in D_{\gamma_e}$. Let S' be an arbitrary minimum equitable dominating set of G. If $S \cap S' = \emptyset$, then $S' \subseteq V(G) - S$, which implies S' is an equitable dominating set of G of cardinality $|S|$, a contradiction. Hence, $S \cap S' \neq \emptyset$.
Conversely, let $S \in D_{\gamma_e}(G)$ such that $S \cap S' \neq \emptyset$ for every set $S' \in D_{\gamma_e}(G)$. Then, S is an accurate equitable dominating set of G. Therefore, $\gamma_{ae}(G) \leq |S| = \gamma_e(G) \leq \gamma_{ae}(G)$. Thus, we must have $\gamma_{ae}(G) = \gamma_e(G)$.

Corollary 3. If $G = H \circ K_1, H \neq K_1$, then $\gamma_{ae}(G) = \gamma_e(G)$

CONCLUSION

In this paper we initiated the study of a new parameter accurate equitable domination number of graph and obtained some results. More results on this parameter can be obtained using other domination parameters.

REFERENCES

1. B. Basavanagoud, V. R. Kulli and Vijay V. Teli, Equitable total domination in graphs. J.Comp. Math. Sci., 5(2)(2014), 235-241.
2. K.M.Dharmalingam, V.Swaminathan, Degree equitable domination in graphs, Kragujevac Journal of Mathematics, 35 (1) (2011), 191 - 197.
3. F.Harary, Graph Theory, Addison-Wesley, 1969.
4. T.W.Haynes, S.T.Hedetniemi, P.J.Slater, Fundamentals of Domination in Graphs, Marcel Dekker, New York (1998)
5. T.W.Haynes, S.T.Hedetniemi, P.J.Slater, Domination in graphs : Advanced topics, Marcel Dekker, New York (1998)
6. J.Cyman, M.A.Henning, J.Topp, On Accurate domination in graphs, Discussiones Math. Graph Theory, 39 (2019), 615-627.
7. V.R.Kulli, M.B.Kattimani, The accurate domination number of a graph, Technical Report 2000:01, Dept.Mathematics, Gulbarga University, Gulbarga, India(2000).
8. W.Meyer, Equitable Coloring, American Mathematical Monthly, 80, 1973, 920 - 922.
9. P.N. Vinay Kumar, D.SonerNandappa, The Maximal Equitable Domination of a Graph, J. Comp. Math. Sci. Vol. 2 (4), 617 - 620 (2011).

Vol.15 / Issue 83 / Apr / 2024 International Bimonthly (Print) – Open Access ISSN: 0976 – 0997

RESEARCH ARTICLE

Anti-Hyperglycemic Effect of Siddha *Varmam* Formulation *Neerizhivu Kudineer* in Streptozotocin Induced Diabetics Rats

Thirunarayanan G[1]*, Suvedha P[2] and Jayalakshmi J[3]

[1]Medical Officer, National Institute of Siddha, Tambaram Sanatorium, Chennai, Tamil Nadu, India.
[2]PG Scholar, Department of Kuzhandhai Maruthuvam, National Institute of Siddha, Tambaram Sanatorium, Chennai, Tamil Nadu, India.
[3]Professor, Sivaraj Siddha Medical College, Salem and Ph.D Scholar (Part Time), National Institute of Siddha, Chennai, Tamil Nadu, India.

Received: 19 Oct 2023 Revised: 29 Dec 2023 Accepted: 19 Mar 2024

***Address for Correspondence**
G.Thirunarayanan,
Medical Officer,
National Institute of Siddha,
Tambaram Sanatorium, Chennai,
Tamil Nadu, India.
Email: thirunarayanan.dr@gmail.com

ABSTRACT

Varmam is a part of the Siddha system of medicine and it is well known for its therapeutic action in various health conditions. *Varmam* can work well in various lifestyle disorders like diabetes and hypertension. These life style disorders can be treated with both *Varmam* internal medicine and *Varmam* therapies. The Trail drug *Neerizhivu Kudineer* is an herbal formulation quoted in ancient Varma text for *Neerizhivu* (Diabetes mellitus). The study aims to determine the anti-hyperglycemic effect of Siddha *Varmam* formulation *Neerizhivu Kudineer* in streptozotocin induced diabetic rats. *Neerizhivu Kudineer* were analysed for anti-Hyperglycemic activity at the doses of 100 and 200 mg/kg orally continue for 28 days, with reference to the fasting blood glucose (FBG) and blood glycosylated haemoglobin (HbA1c) in the STZ induced diabetic. other factors like triglyceride (TG), total cholesterol (TC), serum biochemical parameters (AST, ALT, ALP), lipid peroxidation (MDA), HDL, total protein, body weight and liver antioxidants enzymes (GSH, SOD, CAT) levels were also analyzed in the STZ induced diabetic rats. The results of this study reveal that the traditional *Varmam* internal medicine *Neerizhivu Kudineer* has an anti-hyperglycemic effect and it can help in the reduction of blood glucose levels in patients suffering from diabetes mellitus.

Keywords: *Neerizhivu Kudineer*, *Neerizhivu noi,* Diabetes mellitus, Varma Maruthuvam, Siddha system of medicine.

INTRODUCTION

Varmam Maruthuvam is part Siddha system of medicine and it is one of the oldest traditional medicines in the world. *Varmam* Medicines are widely used in southern parts of India, predominantly in Tamilnadu[1]. *Neerizhivu* is a disease that has been given much importance both in the past and the present. *Neerizhivu* is a clinical or health condition characterized by frequent urination with more volume, invasion of ants and house flies at the place of urination, smelly urine with a sweet odour while it gets boiled, gradual loss of weight with the reduction in power of the human body and seven thathus[2]. The symptoms of *Neerizhivu* can be correlated with Diabetes in modern terms. Certain symptoms such as a burning sensation in the palm and soles, delayed wound healing etc., are the classic indicators of this *Neerizhivu* (Diabetes mellitus). Diabetes currently affects more than 62 million Indians, which is more than 7.1% of the adult population [3]. The average age of onset of *Neerizhivu* Noi is 42.5 years. Nearly one million Indians die due to *Neerizhivu* Noi every year[4]. According to the Indian Heart Association, India is projected to be home to 109 million individuals with *Neerizhivu* No by 2035[5].Siddha and *Varmam* Maruthuvam have various herbal and herbo mineral formulations which are giving remarkable changes in the management of *Neerizhivu* (Diabetes mellitus). One among these herbal formulations is *Neerizhivu Kudineer* mentioned in *Varmam* literature. The ingredients in *Neerizhivu Kudineer* have been used in the treatment of diabetes mellitus by common people as home remedies. Even though many herbal formulations are being used for its therapeutic action in day-to-day practices, it also has to be evaluated scientifically. Hence here it is tried to evaluate the anti-hyperglycemic effect of Siddha *Varmam* formulation *Neerizhivu Kudineer* in streptozotocin-induced diabetics rats.

MATERIALS AND METHODS

Ingredients of *Neerizhivu Kudineer* [6, 7]
Show the table No. 1: Drug Description

Collection, Identification and Authentication of the Drug
The drugs mentioned in the Table No.1 were collected from Tirunelveli and Kanyakumari district, Tamilnadu, India. Collected raw drugs were identified and authenticated by Botanist of Government Siddha Medical College, Palayamkottai, Tirunelveli, Tamilnadu.

Purification and Preparation of the Drug
The ingredients of this *Neerizhivu Kudineer* were purified according to the proper methods described in Siddha Classical Literature.

Animals
Healthy Wistar albino rats (weighing 185±10 g) of either sex were used in the study. Rats were kept in standard laboratory conditions i.e., 12 h light/dark cycles at 25-28 °C, relative humidity 55–60 % and were fed with a standard pellet diet and water. The animals were acclimatized to laboratory conditions for one week before the experiment.

Drugs and Chemicals
Streptozotocin was purchased from HI Media Laboratories Pvt. Ltd. India and glibenclamide (reference drug) was from Sanofi India Ltd. India. Trichloroacetic acid (TCA) from Merck Ltd., Mumbai, India; thiobarbituric acid (TBA), 5,5′-dithio bis-2-nitro benzoic acid (DTNB), phenazonium methosulfate (PMS), nicotinamide adenine dinucleotide (NADH) and reduced glutathione (GSH) from SISCO Research Laboratory, Mumbai, India; potassium dichromate, glacial acetic acid from Ranbaxy, Mumbai; and all the other reagents kits used were from Span Diagnostics Ltd. India.

Oral Glucose Tolerance Test (OGTT)

The OGTT was performed in overnight fasted Wistar albino rats. Rats were divided into three groups (n=6). Group I served as normal control (received distilled water 5 ml/kg b.w. p.o.), groups II and III received Siddha preparation *Neerizhivu Kudineer* at the doses of 100 and 200 mg/kg b.w. p.o. respectively. All the animals received glucose (2 g/kg b.w., orally) 30 min after drugs administration. Blood sample was withdrawn from the tail vein at 0, 30, 60, 120 and 240 min. after glucose administration[8]and blood glucose level was measured using a single touch glucometer (Contour TS, Bayer Health Care.).

Induction of Diabetes in Rats

The rats were rendered diabetic by a single intraperitoneal dose of 50 mg/kg b.w. STZ freshly dissolved in ice cold 0.1 M citrate buffer (pH 4.5)[9]. After 72 h, fasting blood glucose (FBG) levels were measured and only those animals showing blood glucose levels≥ 250 mg/dl were used for the present investigation [10].The day on which hyperglycemia had been confirmed was designated as day 0 [11].

Treatment Schedule and Estimation of Fasting Blood Glucose (FBG) Level

After induction of experimental diabetes, the rats were divided into five groups (n=6). Except for group I, which served as normal (non-diabetic) control, all other groups were comprised of diabetic rats. Group II served as diabetic (STZ) control. Groups III and IV received *Neerizhivu Kudineer* (100 and 200 ml/kg b.w., p.o. respectively) and group V received reference drug glibenclamide (0.5 mg/kg b.w., p.o) daily for 28days [12].

Treatment Protocol

Group I (Normal control): Normal Rats + Normal saline (5 ml/kg b.w.)
Group II (Diabetic control): Diabetic Rats + Normal saline (5 ml/kg b.w.)
Group III (Test low dose): Diabetic Rats + *Neerizhivu Kudineer* (100 ml/kg b.w.)
Group IV (Test high dose): Diabetic Rats + *Neerizhivu Kudineer* (200 ml/kg b.w.)
Group V (Standard): Diabetic Rats + Glibenclamide (0.5 mg/kg b.w.)
FBG level was measured on days 0, 14, 21 and 28by using a one-touch glucometer. After 24 hours of the last dose and 18 hours of fasting, blood was collected from all rats in each group by cardiac puncture for estimation of glycosylated hemoglobin (HbA1C), serum lipid profile and serum biochemical parameters and then the animals were sacrificed for collection of liver tissue to check the different endogenous antioxidant parameters.

Body Weight

The body weight of rats from each group was measured on days 0, 14, 21 and 28. Weight was measured using standard digital weight balance to get accuracy.

Estimation of Glycosylated Hemoglobin (HbA1c)

Glycosylated hemoglobin was analyzed by using a commercially available kit (Beacon Diagnostic Pvt. Ltd. India) which is based on the principle of the ion exchange resin method.

Estimation of Liver Biochemical Parameters and Antioxidant Status

All animals were sacrificed after 24 hr of the last dose by overdose of diethyl ether. Blood samples were collected and the liver was excised, washed in ice-cold phosphate buffer saline, blotted and weighed. 10% w/v of liver homogenate was prepared in 0.15 M Tris-HCl buffer (pH 7.4). The homogenate was centrifuged at 2000×g for 20 minutes at 4°C to remove the cell debris and then the supernatant was centrifuged (REMI C-24) at 12000×g for 1 hour at 4°C. The supernatant was obtained and used for the determination of Lipid peroxidation and endogenous antioxidant enzymes like superoxide dismutase (SOD), catalase (CAT) and non-enzymatic antioxidant i.e. reduced glutathione (GSH).

Estimation of Lipid Peroxidation Level (TBARS)

Lipid peroxidation (LPO) was assayed according to the method of Ohkawa et al. (1979). To 1 ml of tissue homogenate, 1 ml of normal saline (0.9%, w/v) and 2.0 ml of 10% trichloroacetic acid were added and mixed well. The mixture was then centrifuged (3000 × g) at room temperature for 10 min to separate proteins. 0.5 ml 1.0%thiobarbituric acid was added to 2 ml of supernatant followed by heating at 95 ◦C for 60 min to generate the pink-colored malondialdehyde (MDA). The absorbance of the samples was measured at 532 nm using a spectrophotometer (Beckman DU 64). The level of lipid peroxides i.e. thiobarbituric acid reactive substances (TBARS) was estimated and expressed as mM of MDA/mg wet tissue using the extinction coefficient of 1.56 ×105M−1 cm −1.

Superoxide Dismutase (SOD) Activity Assay

Superoxide dismutase (SOD) activity was assayed according to the method of Murklund and Murklund[14]. The liver homogenate was prepared in Tris buffer and centrifuged for 40 min at 10,000 r.p.m. at 4 ◦C. The supernatant was used for the enzyme assay. 2.8 ml Tris–EDTA (composed of 49.78 mM Tris, 0.0012 mM EDTA; pH 8.5) and 100 µl pyrogallol (2 mM) were taken in the cuvette and measured the auto-oxidation of pyrogallol by measuring the absorbance for 3 min (reading taken at 30 s interval for 3 min) at 420 nm wavelength. Then 2.8 ml Tris– EDTA (pH −8.5), 100 µl pyrogallol and 50 µl tissue homogenate were taken and scanned for 3 min at the same wavelength. One unit of SOD activity is the amount of the enzyme that inhibits the rate of auto-oxidation of pyrogallol by 50% and was expressed as Units/mg protein/min. The enzyme unit can be calculated by using the following equations: [50% inhibition =1 U].

Estimation of Catalase (CAT) Activity

Catalase activity was measured based on the ability of the enzyme to break down H2O2. Catalase (CAT) was assayed and expressed as moles of H2O2 decomposed KU/min/mg of tiss[13]. A 10 µl sample was taken in a tube containing 3 ml of H2O2 in phosphate buffer (M/15 phosphate buffer; pH −7.0). The time required for 0.05 optical density changes was observed at 240 nm against a blank containing the enzyme source in H2O2-free phosphate buffer. One unit of CAT activity is the amount of enzyme that liberates half the peroxide oxygen from H2O2 solution of any concentration in 100 s at 25 ◦C which is determined by CAT activity expression:

KU of H2O2 consumed/min (units/mg)

E is the optical density at 240 nm and is the time required for a decrease in the absorbance.

Estimation of Reduced Glutathione (GSH) Level

Non-enzymatic antioxidant i.e. reduced glutathione (GSH) was determined by the method of Ellman (1959)[15]. GSH was estimated spectrophotometrically by the determination of DTNB (dithiobis-2-nitrobenzoic acid) reduced by SH groups, expressed as µg/mg wet tissue. To 0.1 ml of tissue homogenate, 2.4 ml of 0.02 M EDTA solution was added and kept in an ice bath for 10 min. Then 2 ml of distilled water and 0.5 ml of 50% (w/v) trichloro acetic acid were added. This mixture was kept on ice for 10–15 min and then centrifuged at 3000 ×g for 15 min. To 1 ml of supernatant, 2.0 ml of Tris buffer (0.4 M) was added. Then 0.05 ml of DTNB solution (Ellman's reagent; 0.01 M DTNB in methanol) was added and vortexed thoroughly. OD was read (within 2–3 min after the addition of DTNB) at 412 nm in a spectrophotometer against a reagent blank. Appropriate standards were run simultaneously.

Estimation of Serum Biochemical Parameters

Collected blood was analyzed for various Serum biochemical parameters like Serum Aspartate transaminase (AST), Alanine transaminase (ALT) and Serum alkaline phosphatase (ALP). Total protein and lipid profiles. All the analyses were performed by using commercially available kits from Span Diagnostics Ltd. India.

Statistical Analysis

All the results are shown as mean ±SEM. The results were analyzed for statistical significance by one-way analysis of variance (ANOVA) followed by NewmannKeuls multiple range tests. using Graph Pad Prism 5.0 software (Graph Pad Software, USA). P values of < 0.05 were considered as statistically significant.

RESULTS

Oral Glucose Tolerance Test

Table 2 shows glucose loading to the normal rats increased blood glucose levels from 68 ± 1.8 to 169 ± 3.45 at 60 min and returned to normal at 240 min. Administration of *Neerizhivu Kudineer* at the doses of 100 and 200 ml/kg significantly ($p < 0.01$) improved glucose tolerance in a dose-dependent manner at 120 min.

Body Weight

The body weights of normal and diabetic rats were summarized in Table 3. The final body weights were significantly ($p < 0.01$) decreased in the diabetic control group as compared to a normal control group. Administration of *Neerizhivu Kudineer* at the doses of 100 and 200 ml/kg significantly ($p < 0.01$) improved the body weight when compared to the diabetic control group.

Fasting Blood Glucose Level

There was a significantly ($p < 0.01$) elevated FBG level in STZ-induced diabetic rats as compared to the normal control group. Administration of *Neerizhivu Kudineer* in diabetic rats at the doses of 100 and 200 ml/kg significant ($p < 0.01$) reduced the FBG level towards normal as compared to the diabetic control group (Table 4).

Estimation of Serum Lipid Profiles

Serum lipid profiles like total cholesterol and triglyceride in STZ-induced diabetic rats were significantly ($p < 0.001$) elevated and the HDL level significantly ($p < 0.01$) decreased compared to the normal control group. Treatment with *Neerizhivu Kudineer* at the doses of 100 and 200 ml/kg significantly ($p < 0.01$) reduced the total cholesterol and triglyceride levels and significantly ($p < 0.01$) increased the HDL level when compared to the diabetic control group (Table 5).

Estimation of Glycosylated Hemoglobin (HbA1c)

Glycosylated haemoglobin level in STZ-induced diabetic rats was significantly ($p < 0.01$) increased compared to the normal control group. Treatment with *Neerizhivu Kudineer* at the doses of 100 and 200 ml/kg significantly ($p < 0.01$) reduced the HbA1c level when compared to the diabetic control group (Table 6).

Estimation of Serum Biochemical Parameters

Biochemical parameters like AST, ALT and SALP in STZ-induced diabetic rats were significantly ($p < 0.01$) elevated and the total protein content was significantly ($p < 0.001$) decreased compared to the normal control group. Treatment with *Neerizhivu Kudineer* at the doses of 100 and 200 ml/kg significantly ($p < 0.001$) reduced the AST, ALT and SALP levels and significantly ($p < 0.01$) increased the total protein level as compared to the diabetic control group (Table 7)

Estimation of Tissue Antioxidant Parameter

Lipid peroxidation results in the formation of ROS species and subsequently elevates the level of malondialdehyde (MDA) in the liver tissue of STZ-induced diabetic rats. In the present study the MDA level was significantly ($p < 0.01$) increased in STZ-induced diabetic rats compared to the normal control group. Interestingly, treatment with *Neerizhivu Kudineer* at the doses of 100 and 200 ml/kg significantly ($p < 0.01$) reduced the MDA levels compared to the diabetic control group (Table 8). The levels of catalase reduced GSH and SOD were significantly ($p < 0.001$) decreased in STZ-induced diabetic rats compared to the normal control group. Administration of *Neerizhivu Kudineer* at the doses of 100 and 200 ml/kg significantly ($p < 0.01$) increased GSH, SOD and catalase levels in the liver of STZ-induced diabetic rats compared to the diabetic control group (Table 8).

DISCUSSION

This study is aimed to investigate the anti-hyperglycemic activity of *Varmam* preparation *Neerizhivu Kudineer* in STZ-induced diabetic rats. It was observed that there was significant increase in the fasting blood glucose (FBG), blood glycosylated haemoglobin (HbA1c), triglyceride (TG), total cholesterol (TC), serum biochemical parameters (AST, ALT, ALP), lipid peroxidation (MDA) and significantly decreased in the HDL, total protein, body weight and liver antioxidants enzymes (GSH, SOD, CAT) levels in the STZ induced diabetic rats when compared to normal control group. The *Varmam* preparation *Neerizhivu Kudineer* has shown the presence of alkaloids, flavonoids, steroids and triterpenoids when phytochemical screening was done. Hence, the present study was carried out to evaluate the antidiabetic activity of the *Varmam* preparation *Neerizhivu Kudineer* on streptozotocin-induced diabetic rats. Here *Varmam* preparation of *Neerizhivu Kudineer* at doses of 100 and 200 ml/kg orally continued for 28 days on streptozotocin-induced diabetic rats has revealed that the increase in blood glucose level was observed normal in glucose-loaded rats than in *Neerizhivu Kudineer* treated rats during oral glucose tolerance test (OGTT) and significantly reduced the glycosylated haemoglobin(HbA1c). Diabetic rats treated with *Neerizhivu Kudineer* showed significant improvement in body weight, further there was a significant reduction in serum triglycerides, total cholesterol and an increase in HDL.

Twenty-Eight days of treatment with *Varmam* preparation *Neerizhivu Kudineer* has restored the serum hepatic biochemical parameters toward the normal values in a dose-dependent manner, thereby alleviating liver damage caused by STZ-induced diabetes and also inhibited hepatic lipid peroxidation revealed by the reduction of TBARS levels towards normal with significant increase in the hepatic SOD, catalase and GSH activities in the diabetic rats. This result clearly shows that *Varmam* preparation *Neerizhivu Kudineer* contains a free radical scavenging activity, which could exert a beneficial action against pathological alteration caused by the presence of superoxide radicals and hydrogen peroxide radicals. It is observed that *Neerizhivu Kudineer* treated group has normalized elevated blood glucose level, glycosylated haemoglobin and body weight, further, it restored serum and liver biochemical parameters towards normal values when compared to the diabetic control group. These activities of *Varmam* preparation *Neerizhivu Kudineer* are due to the presence of the above-mentioned phyto constituents and it is assumed that the *Varmam* preparation *Neerizhivu Kudineer* may be responsible for the stimulation of insulin release and also for the observed restoration of metabolic activity.

CONCLUSION

This study reveals the anti-hyperglycaemic action of *Varmam* medicine *Neerizhivu Kudineer*. *Neerizhivu Kudineer* has a favourable effect not only on blood glucose levels but also on glycosylated haemoglobin, serum lipids, antioxidants, serum biochemical parameters and body weight. This *Varmam* preparation *Neerizhivu Kudineer* can act as an antidiabetic agent in treating diabetic complications.

REFERENCES

1. T.KananRajaram, Basic Concept of Therapeutic *Varmam*, National Conference on Siddha Varma-2019, TN. Dr. M.G.R. Medical University, Chennai, Conference Proceedings, PP. 1-3, 2019.
2. KuppusamyMuthaliya, Siddha Maruthuvam–Pothu, Department of Indian Medicine and Homeopathy, Chennai –16, pp. 493,509, 2016.
3. https://news.biharprabha.com/2014/02/diabetes-can-be-controlled-in-80-percent-of-cases-in-india/ 2014.
4. https://www.bloomberg.com/news/articles/2010-11-07/india-s-deadly-diabetes-scourge-cuts-down-millions-rising-to-middle-class. 2010.
5. http://indianheartassociation.org/why-indians-why-south-asians/overview/ 2015.
6. T.Mohanraj,Varmaodivumurivusara soothiram-1200, A.T.S.V.S. Munchirai.,Pg:67,273.
7. T.KannanRajaram ,Varma MarunthuSeimuraigal,A.T.S.V.S. Munchirai., Pg:83,84.

8. Haldar, P.K., Kar, B., Bhattacharya, S., Bala, A., Suresh Kumar, R.B., Antidiabetic activity and modulation of antioxidant status by *sansevieriaroxburghiana*rhizome in streptozotocin-induced diabetic rats. DiabetologiaCroatica 39(4), 115-123, 2010.
9. Hemalatha, S., Wahi, A.K., Singh, P.N., Chansouria, J.P.N.,Hypoglycemic activity of WithaniaCoaculantsDunal in streptozotocin induced diabetic rats. Journal of Ethnopharmacolgy 93, 261-264,2004.
10. Ewart, R.B.L., Kornfeld, S., Kipnis, D.M., Effect of lectins on hormone releasefrom isolated rat islets of Langerhans. Diabetes 24, 705-714, 1975.
11. Schnedl WJ, Ferber S, Johnson JH, Newgard CB, STZ transport and cytotoxicity.
12. Specific enhancement in GLUT2-expressing cells. Diabetes 43 (11):1326-1333, 1994.
13. Naskar, S., Mazumder, U.K., Pramanik, G., Gupta, M., Suresh Kumar, R.B. Bala, A., Islam, A, Evaluation of antihyperglycemic activity of *Cocosnucifera*Linn. On streptozotocin induced type 2 diabetic rats. Journal of Ethnopharmacology 138, 769- 773, 2011.
14. Aebi, H., Catalase. In: Packer, L. (Ed.), Methods in Enzymatic Analysis, vol.II. Academic Press, New York, pp. 673-684, 1974.
15. Murklund, S., Murklund, G., Involvement of the superoxide anion radical in the antioxidation of pyrogallol and a convenient assay for superoxide dismutase. European Journal of Biochemistry 47, 469-474, 1974.
16. Ellman, G.L., Tissue sulfhydryl groups. Archives of Biochemistry and Biophysics 82, 70-77, 1959.

Table No. 1: Drug Description

S.No	Drugs	Botanical Name	Family	Parts Used
1.	*AlamVithai*	*Ficus benghalensis*	Moraceae	Seed
2.	*VilamPisin*	*Limonia acidissima*	Rutaceae	Gums

Table 2.Effect of *Neerizhivu Kudineer* on Blood glucose(mg/dl) in oral glucose tolerance test (OGTT).

Groups	0 min	30 min	60 min	120 min	240 min
Normal control	68 ± 1.8	112 ± 2.25	169± 3.45	126 ± 2.36	72.75 ± 1.95
Neerizhivu Kudineer **100mg/kg**	61 ± 1.75	90 ± 1.98a**	95 ± 2.05 a**	88.45 ± 2.46 a**	65.47 ± 2.33 a**
Neerizhivu Kudineer **200mg/kg**	52.25 ± 1.38	84.15 ± 2.12a**	69.28 ± 1.35 a**	62.20± 1.24 a**	58.10± 1.02 a**

Each value is expressed as Mean ± SEM, where n = 6. a Normal control vs. all treated group, $^{**}P < 0.01$

Table 3. Effect of *Neerizhivu Kudineer* on fasting blood glucos(mg/dl) level in STZ-induced diabetic rats.

Groups	Before STZ	Day 0	Day 14	Day 21	Day 28
Normal control	75.34 ± 2.14	76.90 ± 2.45	70.70 ± 1.85	65.75 ± 1.56	63.65 ±1.30
Diabetic control (STZ 50 mg/kg)	72.35 ± 1.97	345.20 ± 6.38a**	360.10 ± 6.55 a**	376 ± 6.69 a**	385.25 ± 6.85 a**
Diabetic + *Neerizhivu Kudineer* (100 ml/kg)	68.74 ± 1.88	324.30 ± 6.18b**	224.45 ± 5.86 b**	116.40 ± 2.65 b**	98.36 ± 2.06 b**
Diabetic + *Neerizhivu Kudineer* (200 ml/kg)	76.28 ± 1.62	314.46 ± 5.75 b**	175.45 ± 3.60 b**	103.28 ± 1.95 b**	84.55 ± 1.22 b**
Diabetic + Glibenclamide (0.5 mg/kg)	73.37 ± 1.08	290.15 ± 5.45 b**	150.30 ± 1.65 b**	95.75 ± 2.08 b**	66.54 ± 1.63 b**

Each value is expressed Mean ± SEM, where n=6. a Normal control group vs. diabetic control group, b Diabetic control group vs. all treated group, $^{**}p < 0.001$.

Table 4. Effect of *Neerizhivu Kudineer* on body weight (grams) in STZ- induced diabetic rats.

Groups	Day 0	Day 14	Day 21	Day 28
Normal control	175 ± 3.28	172.5 ± 4.80	175.6 ± 5.12	180.4 ± 5.40
Diabetic control (STZ 50 mg/kg)	160 ±3.15	158.5 ± 4.20 a**	142.5 ± 3.80 a**	140.4 ± 3.70 a**

Diabetic + *Neerizhivu Kudineer* (100 ml/kg)	162.5 ± 3.22	158.20± 3.34 b**	155.10 ± 3.45 b**	152.20±3.26 b**
Diabetic + *Neerizhivu Kudineer* (200 ml/kg)	164.2 ± 3.75	161.30± 3.48 b**	158.7 ± 2.92 b**	156.6 ± 2.78 b**
Diabetic + Glibenclamide (0.5 mg/kg)	170.2 ± 3.45	166.25± 3.36 b**	163.20± 3.45 b**	161.2 ±3.28 b**

Each value is expressed as Mean ± SEM, where n=6. a Normal control group vs. diabetic control group, b Diabetic control group vs. all treated group, **$p < 0.001$.

Table 5. Effect of *Neerizhivu Kudineer* on serum lipid profiles (mg/dl)in STZ-induced diabetic rats.

Groups	Total cholesterol	Triglyceride	HDL
Normal control	45.90 ± 3.20	66.75 ± 3.60	64.30 ± 3.40
Diabetic control (STZ 50 mg/kg)	112.7 ± 4.63 a**	155.1 ± 4.95 a**	30.15 ± 1.75 a**
Diabetic + *Neerizhivu Kudineer*(100 ml/kg)	53.45 ± 2.53 b**	86.85 ± 2.86b**	43.35 ± 1.78 b**
Diabetic + *Neerizhivu Kudineer*(200 ml/kg)	49.80 ± 2.25b**	74.35 ± 2.67b**	55.30 ± 1.85b**
Diabetic + Glibenclamide (0.5 mg/kg)	47.25 ± 1.80 b**	70.30 ± 2.55 b**	60.35 ± 1.96 b**

Each value is expressed as Mean ± SEM, where n=6. a Normal control group vs. diabetic control group, b Diabetic control group vs. all treated group, **$p < 0.001$.

Table 6. Effect of *Neerizhivu Kudineer* on glycosylated hemoglobin in STZ-induced diabetic rats.

Groups	HbA1c (%)
Normal control	7.38 ± 0.85
Diabetic control (STZ 50 mg/kg)	16.40 ±1.70 a**
Diabetic + *Neerizhivu Kudineer*(100 ml/kg)	9.15 ± 1.45b**
Diabetic + *Neerizhivu Kudineer*(200 ml/kg)	8.24 ± 1.36 b**
Diabetic + Glibenclamide(0.5 mg/kg)	7.70 ± 1.27 b**

Each value is expressed as Mean ± SEM, where n=6. a Normal control group vs. diabetic control group, b Diabetic control group vs. all treated group, **$p < 0.001$.

Table 7. Effect of *Neerizhivu Kudineer* on serum biochemical parameters and total protein in STZ induced diabetic rats.

Groups	AST (IU/L)	ALT (IU/L)	ALP (IU/L	Total protein (g/dl)
Normal control	86.20 ± 2.75	73.95 ± 2.60	4.25 ± 0.55	8.14 ± 0.38
Diabetic control (STZ 50 mg/kg)	126.95 ± 3.45 a**	128.15 ± 3.65 a**	16.32 ± 1.05 a**	4.28 ± 0.52 a**
Diabetic + *Neerizhivu Kudineer* (100 ml/kg)	108.66 ± 3.12b**	101.65 ± 2.55 b**	7.70 ± 0.69 b**	6.80± 0.58 b**
Diabetic + *Neerizhivu Kudineer* (200 ml/kg)	96.90 ± 2.36b**	88.85 ± 2.24 b**	5.05 ± 0.60 b**	7.12 ± 0.68 b**
Diabetic + Glibenclamide(0.5 mg/kg)	92.65 ± 2.16 b**	82.60± 1.85 b**	4.48 ± 0.55 b**	7.56± 0.76 b**

Each value is expressed as Mean ± SEM, where n=6. a Normal control group vs. diabetic control group, b Diabetic control group vs. all treated group, **$p < 0.001$.

Table 8. Effect of *Neerizhivu Kudineer* on lipid peroxidation (MDA), reduced glutathione (GSH) superoxide dismutase (SOD)and catalase (CAT) in STZ- induced diabetic rats.

Groups	**MDA (mM of MDA/mg tissue)**	**GSH (µg GSH/mg tissue)**	**SOD (mU/min/mg tissue)**	**CAT (KU/min/mg tissue)**
Normal control	92.15 ± 2.60	3.55 ± 0.26	2.78 ± 0.13	4.15 ± 0.36
Diabetic control (STZ 50 mg/kg)	158.90 ± 4.12 a**	1.75 ± 0.14 a**	1.45 ± 0.12 a**	1.80 ± 0.15 a**
Diabetic + *Neerizhivu Kudineer* (100 ml/kg)	128.40 ± 3.15b**	2.72 ± 0.22 b**	1.90 ± 0.09 b**	2.60 ± 0.26 b**
Diabetic + *Neerizhivu Kudineer* (200 ml/kg)	115.90 ± 3.45 b**	2.95 ± 0.18 b**	2.40 ± 0.16 b**	3.66 ± 0.25 b**
Diabetic + Glibenclamide (0.5 mg/kg)	104.15 ± 1.25 b**	3.45 ± 0.26 b**	2.70 ± 0.15 b**	3.80 ± 0.26 b**

Each value is expressed as Mean ± SEM, where n=6. a Normal control group vs. diabetic control group, b Diabetic control group vs. all treated group, **$p < 0.001$.

RESEARCH ARTICLE

In silico Analysis to Validate the Activity of Quinazolinone Derivatives against Type 2 Diabetes Mellitus - A Computational Drug Discovery Study

Mincy Mathew[1]*, D.Kilimozhi[2], Santhosh M Mathews[3] and Anton Smith[4]

[1]Research Scholar, Department of Pharmacy, Faculty of Engineering and Technology (Affiliated to Annamalai University,Chidambaram) Annamalai Nagar, Tamil Nadu, India.
[2]Associate Professor, Department of Pharmacy, Faculty of Engineering and Technology,(Affiliated to Annamalai University,Chidambaram) Annamalai Nagar, Tamil Nadu, India.
[3]Professor, Department of Pharmaceutics, Pushpagiri College of Pharmacy, (Affiliated to Kerala University of Health Sciences) Kerala, India.
[4]Professor, Department of Pharmacy, Faculty of Engineering and Technology, (Affiliated to Annamalai University,Chidambaram) Annamalai Nagar, Tamil Nadu, India.

Received: 11 Nov 2023 Revised: 09 Jan 2024 Accepted: 17 Mar 2024

***Address for Correspondence**
Mincy Mathew
Research Scholar,
Department of Pharmacy,
Faculty of Engineering and Technology
(Affiliated to Annamalai University,Chidambaram)
Annamalai Nagar, Tamil Nadu, India.
Email: min_cmath@yahoo.co.in

ABSTRACT

Type 2 Diabetes Mellitus (T2DM) is an escalating worldwide health concern, demanding the development of innovative therapeutic strategies or potential drug candidates. This research employed an *insilico* analysis to validate the antidiabetic activity of novel quinazolinone derivatives against multiple T2DM-associated biomolecules such as alpha-amylase, insulin-like growth factor 1 receptor, sulfonylurea receptor -1, glycogen phosphorylase, lysosomal acid-alpha-glucosidase, glycogen synthase kinase-3 beta, dipeptidyl peptidase, and peroxisome proliferator-activated receptor gamma. Data mining, molecular modeling, molecular property calculation, pharmacokinetic-pharmacodynamic studies, molecular docking, and molecular dynamic simulations are the computational approaches encompassed for the study. QZ2 is identified as a promising candidate, exhibiting low toxicity, high drug-likeness, and favorable pharmacokinetics with remarkable binding affinities with peroxisome proliferator-activated receptor gamma (4PRG: -10.8 kcal/mol) and sulfonylurea receptor-1 (6JB3: -9.2 kcal/mol). The findings offer critical insights into potential antidiabetic compounds, guiding future in vitro, and in vivo experimental investigations and further applications as therapeutics for T2DM.

Keywords: Diabetes; Quinazolinone; Molecular modeling; Molecular docking; Molecular dynamic simulation.

INTRODUCTION

Diabetes mellitus is a metabolic disorder characterized by hyperglycemia, resulting from either insufficient insulin production by the pancreas or impaired insulin responsiveness within the body. In 2019, the statistical projection indicated that the prevalence of diabetes in India encompassed approximately 77 million individuals, and projections indicate that this figure is poised to surge, reaching an anticipated 134 million cases by the year 2045 [1]. Type 2 Diabetes Mellitus (T2DM), recognized as the ninth most prevalent cause of mortality worldwide, is linked to a spectrum of multiorgan complications, encompassing both microvascular and macrovascular issues, resulting in premature morbidity and mortality, emphasizing the urgent need for comprehensive research and interventions. Its increasing global incidence and the associated burden on healthcare systems underscore the urgent need for effective treatment strategies [2]. An effective control of blood sugar, blood pressure, and blood lipid levels can serve as a preventive measure, delaying the onset of complications associated with Diabetes. Despite their diverse and distinct functions, the biomolecules alpha-amylase, insulin-like growth factor 1 receptor, sulfonylurea receptor -1, glycogen phosphorylase, lysosomal acid-alpha-glucosidase, glycogen synthase kinase-3 beta, dipeptidyl peptidase, and peroxisome proliferator-activated receptor gamma play crucial roles in diabetes and insulin regulation, alpha-amylase plays a role in carbohydrate metabolism, affecting glucose levels [3].

Insulin-like growth factor 1 receptor is implicated in the insulin signaling pathway, impacting growth and metabolism [4]. Sulfonylurea receptor-1 is a key component in the regulation of insulin secretion [5]. Glycogen phosphorylase and glycogen synthase kinase-3 beta influence glycogen storage and release, which is crucial in glucose homeostasis [6] [7]. Lysosomal acid-alpha-glucosidase is essential for glycogen breakdown, a process linked to certain types of diabetes [8]. Dipeptidyl peptidase is involved in regulating the activity of incretin hormones, which impact insulin secretion [9]. Peroxisome proliferator-activated receptor gamma plays a role in insulin sensitivity and glucose metabolism [10]. In various ways, these biomolecules contribute to the intricate network of processes related to diabetes and insulin regulation in the human body. Many heterocyclic compounds both natural and synthetic exhibit antidiabetic activity. The fundamental structural scaffolds of such pharmacological agents encompass thiazolidinone, azole, chalcone, pyrrole, pyrimidine, and various others [11]. Diverse drug classes employ distinct mechanisms for regulating blood glucose levels. However, synthetic drugs are all associated with a plethora of adverse effects. Hence, it is essential to explore novel compounds that can more effectively combat diabetes with fewer side effects. Quinazolinone represents a fused nitrogen-containing heterocyclic ring structure. The quinazolinone moiety has been associated with a wide spectrum of pharmacological activities, including anticancer, anticonvulsant, antimalarial, antifungal, antibacterial, anti-inflammatory, antidiabetic, and hypolipidemic effects.

There are some approved drugs in the market as anticancer agents such as EGFR inhibitors, antihypertensive as alpha receptor blockers, etc. which contain quinazolinone as a core heterocyclic moiety [12]. Traditional drug discovery approaches are often time-consuming and resource-intensive, making it imperative to explore innovative methods to expedite the identification of potential therapeutics. Computational drug discovery, an indispensable tool in modern pharmaceutical research, offers an efficient and cost-effective means to assess the activity of novel molecules against target molecules. *In silico* analysis, as a key component of this approach, enables the prediction and validation of molecular interactions, thereby streamlining the drug discovery process. The study delves into the realm of computational drug discovery, to validate the activity of novel molecules against T2DM. For this, we designed various quinazolinone nucleus derivatives and performed various *in silico* analyses. By harnessing the power of computational approaches, we aim to accelerate the identification of promising drug candidates with antidiabetic activity with a reduced reliance on resource-intensive laboratory experiments.

MATERIALS AND METHODS

The research methodology includes a series of computational approaches such as Data mining, Molecular modeling, Molecular Property Calculation, Molecular docking, and Molecular Dynamic simulation to identify the potential molecule. Background studies and data mining were performed on the disease, related targets, and therapeutic drug molecules. Targets and their standard drug molecules were identified and considered for the study.

TARGETS

Alpha-amylase, Insulin-like growth factor 1 receptor (IGF1R), sulfonylurea receptor -1 (SUR1), glycogen phosphorylase, lysosomal acid-alpha-glucosidase, glycogen synthase kinase-3 beta, dipeptidyl peptidase, and peroxisome proliferator-activated receptor gamma are the target molecules selected for the study. The 3D structures of the selected targets were obtained from the Protein Data Bank (PDB) (https://www.rcsb.org/) [13]. The selected PDBIDs of the protein molecules for the study are included in Table 1.

LIGANDS

Molecular Modeling

In this study, we employed various computational tools to assess the druggability of the proposed ligand molecules. ACD/ChemSketch was utilized to draw chemical structures and generate SMILE notation for the derivatives. A total of 11 novel ligand molecules - QZ1, QZ2, QZ3, QZ4, QZ5, QZ6, QZ7, QZ8, QZ9, QZ10, and QZ11 were modeled using the Avogadro Tool [14]. The modeled structures were optimized, validated, and used for further *in silico* analysis. Also, standard therapeutic drug molecules were used to assess and compare interactions and binding affinities with the docking results of the novel ligand molecules.

Molecular Property Calculations

Molecular property calculation plays a crucial role in drug discovery to assess and predict the pharmacokinetic and pharmacodynamic attributes of potential drug candidates. These calculations provide valuable insights into a compound's solubility, stability, bioavailability, toxicity, and interactions with biological targets, aiding in the selection and optimization of lead compounds with the highest likelihood of success in the development of safe and effective drugs. By leveraging molecular property data, we can streamline the drug discovery process, reduce the risk of failure in clinical trials, and accelerate the development of innovative treatments. Molinspiration Cheminformatics software was used to evaluate adherence to Lipinski's rule of five and drug-likeness properties [15]. Swiss ADME (http://www.swissadme.ch/) &PkCSM software (https://biosig.lab.uq.edu.au/pkcsm/) were employed to compute physicochemical properties, predict ADME parameters, assess pharmacokinetic properties, and determine drug-like qualities [16][17]. Additionally, we employed OSIRIS Property Explorer (https://openmolecules.org/propertyexplorer/) to anticipate properties associated with high risks of undesired effects, such as mutagenicity or suboptimal intestinal absorption.

Screening of Ligands

The molecular properties of ligands were screened under Lipinski's rule of five and ADMET properties. Lipinski's Rule of Five is a set of 5 rules used in drug discovery and medicinal chemistry to evaluate the drug-likeness and potential for oral bioavailability of chemical compounds [18]. The rule criteria include,

1. *Molecular Weight: should be less than 500 daltons (Da).*
2. *Lipophilicity (LogP): should be less than 5.*
3. *Hydrogen Bond Donors: should have no more than 5 hydrogen bond donor atoms (nitrogen and oxygen).*
4. *Hydrogen Bond Acceptors: should have no more than 10 hydrogen bond acceptor atoms (nitrogen and oxygen).*
5. Molar refractivity: should be between 40-130.

ADMET calculations involve assessing the absorption, distribution, metabolism, excretion, and toxicity properties of a pharmaceutical compound [19]. The process plays a crucial role in drug discovery and development by helping to predict the behavior of compounds within the body.

MOLECULAR DOCKING STUDIES

The molecular interaction analysis (molecular docking) of the targets and ligand molecules was performed using Autodock Vina software (v.1.2.0.) [20]. The objective was to predict the bound conformation and the binding affinity of the considered ligands with the respective receptors. The selected targets, alpha-amylase (1B2Y), Insulin-like growth factor 1 receptor (2OJ9), sulfonylurea receptor -1 (6JB3), glycogen phosphorylase (3DD1), lysosomal acid-alpha-glucosidase (5NN8), glycogen synthase kinase-3 beta (1UV5), dipeptidyl peptidase (4CDC), peroxisome proliferator-activated receptor gamma (4PRG) was docked with the modeled molecules and their corresponding standard drug molecules. The protein preparation was performed using the Swiss PDB viewer. The process includes the addition of missing residues, the addition of non-polar hydrogen, and Kollman charges. The target structure was saved in .pdbqt format. The grid box for each protein was generated by the AutoDock vina grid box generation application and molecular docking was performed. Autodock Vina will compute the binding affinity (Kcal mol-1) and generate the best 10 binding poses of each ligand with the receptor. This calculation relied on the ligand's conformation at the binding site and the Root Mean Square Deviation (RMSD) between the initial and docked structures.

Interaction Analysis

Interaction analysis of the receptor-ligand complex was performed using Discovery Studio Biovia 2017 (https://discover.3ds.com/discovery-studio-visualizer-download). Poses with the best binding affinity and H-bond interaction were selected and subjected to Molecular Dynamic Simulation to validate the interaction stability.

MOLECULAR DYNAMICS SIMULATION

Molecular dynamic simulations of the selected protein-ligand complexes were performed using the GROMACS version 2020.6 MD package [21]. The process commenced with the removal of crystal water from the protein and ligand complex. Following this, the topology files of protein and ligands were created separately by using the Charmm36 force field (Charmm36-jul 2021.ff) and CGenFf server respectively. Subsequently, the systems were solvated within a dodecahedron box utilizing the transferable intermolecular potential with a three-point (TIP3P) water model. To maintain neutrality, Na+ and Cl- ions were added. Energy minimization was conducted using the steepest descent integrator to resolve any steric conflicts between the proteins and water molecules. After energy minimization, ligand restraining, and temperature coupling were performed. The systems underwent a two-step equilibration process: primarily volume equilibration in the NVT ensemble (constant number of particles, volume, and temperature) and then pressure equilibration in the NPT ensemble (constant number of particles, system pressure, and temperature). Both equilibration steps consisted of 100,000 steps, resulting in a cumulative simulation time of 200 picoseconds (ps). A constant pressure of 1 atm and a temperature of 300 K were maintained. Following, a production molecular dynamics run was conducted, consisting of 50,000,000 steps, equivalent to 100 nanoseconds (ns).

Trajectory Plot Generation And Analysis

MD simulation result analysis encompassed the analysis of trajectory plots and receptor-ligand interactions. The trajectory plots were generated and analyzed using Xmgrace. RMSD, RMSF, RoG, H-bond interaction distribution, and SASA were analyzed to assess the stability of the interaction between the biomolecules [22]. RMSD measures the deviation or difference between the coordinates of atoms in a given structure and a reference structure. It provides a quantitative measure of the molecule's confirmation changes over time during a simulation. This is essential for assessing the stability and structural changes of biomolecules or ligand-receptor complexes. RMSF provides insight into the flexibility and stability of individual atoms or residues within a biomolecular system and helps to identify regions of significant structural variability. By understanding RMSF, we can pinpoint critical regions that undergo conformational changes, aiding in the interpretation of protein dynamics and interactions. The protein compactness

was studied by plotting the radius of gyration (Rg). The number of Hydrogen bonds formed between the protein and ligands for 100 ns was depicted. For visualizing the post-MD simulation complexes and interaction, various tools, including DS Visualizer, Visual Molecular Dynamics, and Pymol, were employed. Protein compactness and overall shape of a biomolecule were evaluated using the radius of gyration (Rg) plot. Furthermore, the number of hydrogen bonds formed between the protein and ligands during the 100 ns period was illustrated in the H-bond distribution plot. Solvent Accessible Surface Area (SASA) plots provide insights into the structural dynamics and accessibility of specific regions, aiding in the characterization of biomolecular interactions and conformational changes. The gmx_MMPBSA package of GROMACS is used to calculate the binding free energy. CHARMM force field is used for this computational approach. Using the command "gmxmmpbsa, "the binding free energy of a complex was calculated from 200 frames extracted from the 100 ns MD trajectory.

RESULT

The *in silico* analysis was conducted to validate the anti diabetic activity of the newly modeled molecules against multiple targets that contribute to an intricate network of processes associated with diabetes and insulin regulation in the human body. The study focused on various proteins that play a role in the complex network of processes associated with diabetes and the regulation of insulin in the human body (Table 1).

Designing Of the Novel Molecules and Structure Modeling

A total of 11 quinazolinone derivatives were modeled and structures were optimized. The structure of the novel molecules is included in Table 2. These structures were modeled in 2D .sdf file format and subjected to further analysis.

Molecular Properties and ADMET Prediction.

Molecular and ADMET properties were calculated using various software and molecules were screened based on Lipinski's rule (Table 3). Table 3: The molecular descriptors include miLogP (predicted octanol-water partition coefficient), TPSA (topological polar surface area), nAtoms (number of atoms), MW (molecular weight), nON (number of oxygen atoms), nOHNH (number of hydroxyl and amine groups), nViolations (number of Lipinski rule violations), nRotb (number of rotatable bonds), and Volume. Seven of the eleven modeled molecules satisfied Lipinski's rule of five. QZ1, QZ2, QZ6, QZ7, QZ8, QZ9, and QZ11 were considered for next-level analysis, i.e., Toxicity Risk, Drug Likeness, and Solubility predictions (Table 4, 5, 6, 7). Table 4: The toxicity prediction of the modeled molecules: Toxicity Risk (Mutagenic, Tumorigenic, Irritant); Reproductive effect; Drug Likeness; Drug score; Solubility (Clog P - lipophilicity& Clog S - aqueous solubility). Out of the seven considered molecules, QZ11 shows a high tumorigenic property. As a result, the subsequent analysis was carried out using the remaining six molecules. The pharmacokinetics (ADME), and pharmacodynamic properties were calculated by using various software (Table 5& 6). Table 5: The prediction of Absorption, Blood-brain barrier (BBB) permeability, Bioavailability, Human intestinal absorption, and Caco2 permeability. Table 6: The prediction of P-glycoprotein, Cytochrome P450 activity of modeled molecules whether they acting as substrates or inhibitors. Table 7: The prediction of P-glycoprotein, Cytochrome P450 activity of modeled molecules whether they acting as substrates or inhibitors.

Molecular Docking by AutoDock Vina

The molecular interaction analysis of the human proteins and the ligand molecules were performed using Autodock Vina. Standard drug molecules for each receptor were also considered for the study, to perform comparative analysis. The dock results of the eight receptor-ligand complexes were analyzed, screened, and ranked based on the binding affinity and hydrogen bonding interactions (Table 8). Table 8: Dock result of multiple therapeutic targets-standard drug and modeled molecules. RECEPTORS (PDB ID): Alpha-amylase (1B2Y), Insulin-like growth factor 1 receptor (2OJ9), Sulfonylurea receptor -1 (6JB3), Glycogen phosphorylase (3DD1), Lysosomal acid-alpha-glucosidase (5NN8), Glycogen synthase kinase-3 beta (1UV5), Dipeptidyl peptidase (4CDC), Peroxisome proliferator-activated receptor gamma (4PRG). The results of the eight receptor-ligand docking show a binding affinity ranging from -4.8

kcal/mol to -10.8 kcal/mol. The selected receptor-ligand complexes were considered for further analysis (Figure 1 & 2).

Molecular Dynamic Simulation

To confirm the stability of the interactions, Molecular dynamic simulations of the top-ranked ligand poses were performed to validate the interaction stability. Following the MD simulation, we analyzed the trajectory and interactions to gain insights into the protein's spatial fluctuations and changes in interactions. The outcomes encompass a spectrum of interactions, including both stable and unstable ones. Some ligands maintain interactions with the same amino acid residues as initially observed in the molecular docking results. Conversely, others exhibit different interactions, primarily influenced by fluctuations in energy and shifts in conformational geometry (Table 9). Table 9: Molecular Docking and Molecular Dynamic simulation interaction result of Peroxisome proliferator-activated receptor gamma (4PRG) and Sulfonylurea receptor -1 (6JB3). Following molecular dynamic simulation, a thorough examination of interaction and trajectory was performed (Figure 3 and Figure 4) to validate the stability of the receptor- ligand interaction. Two complexes 4PRG - QZ2 and 6JB3-QZ2 were subjected to MMPBSA calculation. The score was found to be -41.3 kcal/mol for 4PRG - QZ2 complex and -21.26 kcal/mol for 6JB3 – QZ2 complex.

DISCUSSIONS

The *insilico* analysis employed in this study aimed to validate the antidiabetic activity of novel quinazolinone analogs against multiple targets associated with Type 2 Diabetes Mellitus (T2DM) disease. The urgency of effective treatment strategies for T2DM is underscored by its increasing global prevalence and the associated burden on healthcare systems [23]. The study specifically focused on biomolecules involved in the intricate network of processes related to diabetes and insulin regulation. The selected targets, including alpha-amylase, insulin-like growth factor 1 receptor, sulfonylurea receptor -1, glycogen phosphorylase, lysosomal acid-alpha-glucosidase, glycogen synthase kinase-3 beta, dipeptidyl peptidase, and peroxisome proliferator-activated receptor gamma, play significant roles in various activities related to diabetes and insulin regulation. Quinazoline derivatives were modeled and considered as ligands for the study based on their potential to interact with these targets and modulate their activities. The initial screening of ligands based on Lipinski's rule of five and ADMET properties resulted in the selection of six promising novel molecules for further analysis. The miLogP values, indicative of lipophilicity, range from 3.09 (QZ2) to 6.62 (QZ10), suggesting varying degrees of hydrophobicity among the molecules [24]. The Topological Polar Surface Area (TPSA) values, associated with molecular polarity, exhibit considerable diversity, with QZ2 having the highest TPSA (85.16 $Å^2$), emphasizing its potential for interactions with polar biological targets [25]. Notably, the number of violations against Lipinski's rule (nViolations) is generally low across all molecules, implying their adherence to drug-likeness criteria. The number of rotatable bonds (nRotb) varies, with QZ6, QZ8, QZ9, and QZ11 having a higher count, potentially influencing their conformational flexibility [26].

Molecular weights (MW) span a broad range, with QZ1 (327.39 g/mol) being the lightest and QZ5 (485.18 g/mol) the heaviest. The number of oxygen atoms (nON) and hydroxyl/amine groups (nOHNH) is relatively consistent among the molecules, indicating a structural similarity in terms of oxygen-containing functional groups. The toxicity and drug-likeness predictions from Osiris Property Explorer for the designed quinazolinone derivatives reveal a generally favorable profile. All compounds, except QZ11, demonstrate low risks in mutagenic, tumorigenic, irritant, and reproductive effect categories. QZ11 exhibits high tumorigenic risk, indicating a potential safety concern. In terms of drug-likeness, QZ2 stands out with the highest drug likeness score (4.73) and favorable physicochemical properties (Clog P, Clog S), suggesting its potential suitability as a drug candidate. Overall, most of the compounds exhibit low toxicity risks and favorable drug-likeness properties, emphasizing QZ2 as a particularly promising candidate for further consideration in antidiabetic drug development. The subsequent pharmacokinetic and pharmacodynamic evaluations were crucial in identifying potential lead compounds with favorable drug-like properties [27]. The ADMET, bioavailability, pharmacokinetic properties, and toxicity predictions reveal significant insights to the research study. Notably, QZ2 demonstrates high gastrointestinal absorption, favorable water

solubility, and remarkable human intestinal absorption, suggesting its potential as an orally administered drug [28]. QZ2 also exhibits interactions with important targets involved in diabetes regulation. However, caution is warranted due to its prediction as a P-glycoprotein substrate. Additionally, QZ2 displays promising pharmacokinetic attributes, including steady-state volume of distribution and BBB permeability. Despite its predicted CYP3A4 inhibition and AMES toxicity, further experimental validation is crucial to confirm the translational potential of QZ2 as a potential antidiabetic drug candidate. The overall findings highlight the importance of integrating computational predictions to guide the selection of lead compounds for subsequent experimental investigations. The molecular docking studies provided insights into the binding affinities and interactions between the ligands and target proteins [29]. As a result of the interaction analysis, QZ2 stands as a promising candidate, exhibiting remarkable binding affinities and consistent stability in interactions with the selected targets, particularly Peroxisome proliferator-activated receptor gamma (4PRG) and Sulfonylurea receptor-1 (6JB3). QZ2 exhibits a binding affinity of -10.8 kcal/mol to 4PRG and -9.2 kcal/mol to 6JB3. In the 4PRG-QZ2 complex, the ligand interacts with amino acid residues GLU 343, SER 342, and MET 364. In the 6JB3-QZ2 complex, the interaction formed with ASN 1296 and ASN B 547 residues during molecular docking. The stability of these interactions was validated through Molecular Dynamics (MD) simulations over a 100 ns period [30]. Notably, in the 4PRG-QZ2 complex, the ligand maintains a stable interaction with GLU 343 and SER 342 residues, persisting even after a 100 ns MDS (Figure 2). Similarly, in the case of the 6JB3-QZ2 complex, it sustains stability with ASN 1296 throughout a 100 ns MD simulation study (Figure 3).

The analysis of trajectory plots, including RMSD, RMSF, RoG, H-bond interactions, and SASA, offered a comprehensive understanding of the ligand-protein dynamics [31]. For the 4PRG-QZ2 complex, the RMSD plot recorded a minimum value at 0.1 ns (0.134272 nm) and a maximum at 7.30 ns (0.270155 nm). The plot indicates that the protein maintains relative stability in the time from 50.9 ns to 100 ns. The protein encompasses residues from GLU 207 to LEU 476. The RMSF plot for the 4PRG-QZ2 complex reveals fluctuations ranging from 0.0389 nm to 0.5574 nm across the entire protein. Notably, Leu 476 displays the highest fluctuation at 0.5574 nm. The radius of gyration (RoG) plot for 4PRG-QZ2 suggests a deviation in Rg from 1.93337 nm (at 7.4 ns) to 1.99864 nm (at 1.9 ns), with an average of 1.962889 nm. During the 100 ns molecular dynamics (MD) simulation, a maximum of 3 hydrogen bonds were observed. The solvent-accessible surface area (SASA) plot of the 4PRG-QZ2 complex indicates structural fluctuations ranging from 143.172 nm2 (at 11.9 ns) to 158.389 nm2 (at 0.9 ns). The SASA value is 141.402 nm2 at 0 ns and 151.442 nm2 at 100 ns. In the case of the 6JB3-QZ2 complex, the RMSD values depicted in the plot exhibit a range with a minimum of 0.2364022 nm observed at 0.1 ns and a maximum of 0.50818 nm at 50.80 ns. This graphical representation suggests that the protein maintains relative stability between 56.6 ns and 100 ns. The residue count spans from VAL 215 to TYR 1326. The RMSF plot for the 6JB3-QZ2 complex reveals fluctuations across the entire protein, ranging from 0.0498 nm to 0.4765 nm. Notably, TYR 1326 experiences the highest fluctuation at 0.4765 nm.

Examining the radius of gyration (RoG) plot for 6JB3-QZ2, it is observed that the Rg deviation varies from 2.74061 nm at 26.4 ns to 2.78635 nm at 80.7 ns, averaging at 2.763852 nm. Throughout the 100 ns molecular dynamics simulation, a maximum of 2 hydrogen bonds are observed. The SASA plot for the 6JB3-QZ2 complex indicates structural fluctuations ranging from 298.411 nm^2 at 91.3 ns to 319.825 nm^2 at 41.4 ns. The SASA value at the initial time point (0 ns) is 300.78 nm^2, and after the simulation (100 ns), it is 300.516 nm^2. The results collectively highlight QZ2 as a promising candidate with potential antidiabetic activity, demonstrating stable interactions with key biomolecules associated with T2DM. However, further experimental validation is essential to confirm the in silico findings and assess the translational potential of QZ2 as a therapeutic agent for T2DM. In conclusion, this computational drug discovery study provides valuable insights into the design and evaluation of novel quinazolinone derivatives for their potential antidiabetic activity. The integration of in silico analyses, including molecular docking and MD simulations, offers a systematic approach to identifying lead compounds with the desired pharmacological properties. The findings lay the foundation for future experimental investigations and the development of innovative therapeutics for Type 2 Diabetes Mellitus.

CONCLUSION

The research study undertook, *in silico* analysis, to validate the antidiabetic potential of quinazolinone derivatives against multiple Type 2 Diabetes Mellitus (T2DM) targets. The modeled quinazolinone derivative molecules were analyzed against key biomolecules - alpha-amylase, insulin-like growth factor 1 receptor, sulfonylurea receptor -1, glycogen phosphorylase, lysosomal acid-alpha-glucosidase, glycogen synthase kinase-3 beta, dipeptidyl peptidase, and peroxisome proliferator-activated receptor gamma, which are associated with diabetes and insulin regulation. The Computational approaches to molecular docking and dynamics identified QZ2 as a promising candidate with low toxicity, high drug-likeness, and favorable pharmacokinetic attributes. Noteworthy binding affinities were observed with Peroxisome proliferator-activated receptor gamma (4PRG, -10.8kcal/mol) and sulfonylurea receptor-1 (6JB3, -9.2 kcal/mol). These findings contribute valuable insights into the antidiabetic potentiality of the QZ2 for future *in vitro*, and *in vivo* experimental investigations and the development of innovative therapeutics for T2DM.

REFERENCES

1. American Diabetes Association. Diagnosis and classification of diabetes mellitus. Diabetes care. 2010 Jan 1;33(Supplement_1):S62-9.
2. Pradeepa R, Mohan V. Epidemiology of type 2 diabetes in India. Indian journal of ophthalmology. 2021 Nov;69(11):2932.
3. Poovitha S, Parani M. In vitro and in vivo α-amylase and α-glucosidase inhibiting activities of the protein extracts from two varieties of bitter gourd (Momordicacharantia L.). BMC complementary and alternative medicine. 2016 Jul;16(1):1-8.
4. Cheng CL, Gao TQ, Wang Z, Li DD. Role of insulin/insulin-like growth factor 1 signaling pathway in longevity. World journal of gastroenterology: WJG. 2005 Apr 4;11(13):1891.
5. Pratt EB, Yan FF, Gay JW, Stanley CA, Shyng SL. Sulfonylurea receptor 1 mutations that cause opposite insulin secretion defects with chemical chaperone exposure. Journal of Biological Chemistry. 2009 Mar 20;284(12):7951-9.
6. Wang L, Li J, Di LJ. Glycogen synthesis and beyond, a comprehensive review of GSK3 as a key regulator of metabolic pathways and a therapeutic target for treating metabolic diseases. Medicinal Research Reviews. 2022 Mar;42(2):946-82.
7. Kanungo S, Wells K, Tribett T, El-Gharbawy A. Glycogen metabolism and glycogen storage disorders. Annals of translational medicine. 2018 Dec;6(24).
8. Adeva-Andany MM, González-Lucán M, Donapetry-García C, Fernández-Fernández C, Ameneiros-Rodríguez E. Glycogen metabolism in humans. BBA clinical. 2016 Jun 1;5:85-100.
9. Godinho R, Mega C, Teixeira-de-Lemos E, Carvalho E, Teixeira F, Fernandes R, Reis F. The place of dipeptidyl peptidase-4 inhibitors in type 2 diabetes therapeutics: a "me too" or "the special one" antidiabetic class? Journal of diabetes research. 2015 Oct;2015.
10. Blaschke F, Takata Y, Caglayan E, Law RE, Hsueh WA. Obesity, peroxisome proliferator-activated receptor, and atherosclerosis in type 2 diabetes. Arteriosclerosis, thrombosis, and vascular biology. 2006 Jan 1;26(1):28-40.
11. Farwa U, Raza MA. Heterocyclic compounds as a magic bullet for diabetes mellitus: a review. RSC advances. 2022;12(35):22951-73.
12. Alsibaee AM, Al-Yousef HM, Al-Salem HS. Quinazolinones, the Winning Horse in Drug Discovery. Molecules. 2023 Jan 18;28(3):978.
13. Berman HM, Westbrook J, Feng Z, Gilliland G, Bhat TN, Weissig H, Shindyalov IN, Bourne PE. The protein data bank. Nucleic acids research. 2000 Jan 1;28(1):235-42.
14. Hanwell MD, Curtis DE, Lonie DC, Vandermeersch T, Zurek E, Hutchison GR. Avogadro: an advanced semantic chemical editor, visualization, and analysis platform. Journal of cheminformatics. 2012 Dec;4(1):1-7.
15. Srivastava R. Theoretical studies on the molecular properties, toxicity, and biological efficacy of 21 new chemical entities. ACS omega. 2021 Sep 15;6(38):24891-901.

16. Daina A, Michielin O, Zoete V. SwissADME: a free web tool to evaluate pharmacokinetics, drug-likeness and medicinal chemistry friendliness of small molecules. Scientific reports. 2017 Mar 3;7(1):42717.
17. Pires DE, Blundell TL, Ascher DB. pkCSM: predicting small-molecule pharmacokinetic and toxicity properties using graph-based signatures. Journal of medicinal chemistry. 2015 May 14;58(9):4066-72.
18. Lipinski CA, Lombardo F, Dominy BW, Feeney PJ. Experimental and computational approaches to estimate solubility and permeability in drug discovery and development settings. Advanced drug delivery reviews. 1997 Jan 15;23(1-3):3-25.
19. Guan L, Yang H, Cai Y, Sun L, Di P, Li W, Liu G, Tang Y. ADMET-score–a comprehensive scoring function for evaluation of chemical drug-likeness. Medchemcomm. 2019;10(1):148-57.
20. Trott O, Olson AJ. AutoDock Vina: improving the speed and accuracy of docking with a new scoring function, efficient optimization, and multithreading. Journal of computational chemistry. 2010 Jan 30;31(2):455-61.
21. Valdés-Tresanco MS, Valdés-Tresanco ME, Valiente PA, Moreno E. gmx_MMPBSA: a new tool to perform end-state free energy calculations with GROMACS. Journal of chemical theory and computation. 2021 Sep 29;17(10):6281-91.
22. Akash S, Bayıl I, Hossain MS, Islam MR, Hosen ME, Mekonnen AB, Nafidi HA, Bin Jardan YA, Bourhia M, Bin Emran T. Novel computational and drug design strategies for inhibition of human papillomavirus-associated cervical cancer and DNA polymerase theta receptor by Apigenin derivatives. Scientific Reports. 2023 Oct 2;13(1):16565.
23. Khan MA, Hashim MJ, King JK, Govender RD, Mustafa H, Al Kaabi J. Epidemiology of type 2 diabetes–global burden of disease and forecasted trends. Journal of epidemiology and global health. 2020 Mar;10(1):107.
24. Kharwar R, Bhatt M, Patel K, Patel S, Daxini N. A computational approach to identify natural putative inhibitors to combat monkeypox. In Nanotechnology and In Silico Tools 2024 Jan 1 (pp. 285-308). Elsevier.
25. Prasanna S, Doerksen RJ. Topological polar surface area: a useful descriptor in 2D-QSAR. Current medicinal chemistry. 2009 Jan 1;16(1):21-41.
26. Torres PH, Sodero AC, Jofily P, Silva-Jr FP. Key topics in molecular docking for drug design. International journal of molecular sciences. 2019 Sep 15;20(18):4574.
27. Tuntland T, Ethell B, Kosaka T, Blasco F, Zang RX, Jain M, Gould T, Hoffmaster K. Implementation of pharmacokinetic and pharmacodynamic strategies in early research phases of drug discovery and development at Novartis Institute of Biomedical Research. Frontiers in pharmacology. 2014 Jul 28;5:174.
28. Azman M, Sabri AH, Anjani QK, Mustaffa MF, Hamid KA. Intestinal absorption study: Challenges and absorption enhancement strategies in improving oral drug delivery. Pharmaceuticals. 2022 Aug 8;15(8):975.
29. Challapa-Mamani MR, Tomás-Alvarado E, Espinoza-Baigorria A, León-Figueroa DA, Sah R, Rodriguez-Morales AJ, Barboza JJ. Molecular Docking and Molecular Dynamics Simulations in Related to Leishmaniadonovani: An Update and Literature Review. Tropical Medicine and Infectious Disease. 2023 Sep 26;8(10):457.
30. Al-Karmalawy AA, Dahab MA, Metwaly AM, Elhady SS, Elkaeed EB, Eissa IH, Darwish KM. Molecular docking and dynamics simulation revealed the potential inhibitory activity of ACEIs against SARS-CoV-2 targeting the h ACE2 receptor. Frontiers in Chemistry. 2021 May 4;9:661230.
31. Rahman MM, Saha T, Islam KJ, Suman RH, Biswas S, Rahat EU, Hossen MR, Islam R, Hossain MN, Mamun AA, Khan M. Virtual screening, molecular dynamics and structure–activity relationship studies to identify potent approved drugs for Covid-19 treatment. Journal of Biomolecular Structure and Dynamics. 2021 Nov 2;39(16):6231-41.

Table 1: Proteins selected for the study; corresponding PDB IDs and the therapeutic drug molecules.

Sl No:	Protein Name	PDB ID	Standard Drugs
1	Alpha-amylase	1B2Y	ACARBOSE
2	Insulin-like growth factor 1 receptor (IGF1R)	2OJ9	METFORMIN
3	Sulfonylurea receptor -1 (SUR1)	6JB3	REPAGLINIDE
4	Glycogen phosphorylase	3DD1	METFORMIN

5	Lysosomal acid-alpha-glucosidase	5NN8	ACARBOSE
6	Glycogen synthase kinase-3 beta	1UV5	AR-AO14418
7	Dipeptidyl peptidase	4CDC	SITAGLIPTIN
8	Peroxisome proliferator-activated receptor gamma	4PRG	PIOGLITAZONE

Table 2: Structure of the proposed derivatives drawn by ACD/ChemSketch

Sl. No:	Sample code	Proposed Derivatives	Name of the Compound
1.	QZ1		3-[(*E*)-benzylideneamino]-2-phenyl-2,3-dihydroquinazolin-4(1*H*)-one
2.	QZ2		2-(4-hydroxyphenyl)-3-{(*E*)-[(4-hydroxyphenyl)methylidene]amino}-2,3-dihydroquinazolin-4(1*H*)-one
3	QZ3		2-(4-chlorophenyl)-3-{(*E*)-[(4-chlorophenyl)methylidene]amino}-2,3-dihydroquinazolin-4(1*H*)-one
4	QZ4		2-(3-chlorophenyl)-3-{(*E*)-[(3-chlorophenyl)methylidene]amino}-2,3-dihydroquinazolin-4(1*H*)-one
5	QZ5		2-(4-bromophenyl)-3-{(*E*)-[(4-bromophenyl)methylidene]amino}-2,3-dihydroquinazolin-4(1*H*)-one
6	QZ6		2-(4-ethoxyphenyl)-3-{(*E*)-[(4-ethoxyphenyl)methylidene]amino}-2,3-dihydroquinazolin-4(1*H*)-one

7	QZ7		2-(4-methylphenyl)-3-{(*E*)-[(4-methylphenyl)methylidene]amino}-2,3-dihydroquinazolin-4(1*H*)-one
8	QZ8		2-(2,4-dimethoxyphenyl)-3-{(*E*)-[(2,4-dimethoxyphenyl)methylidene]amino}-2,3-dihydroquinazolin-4(1*H*)-one
9	QZ9		2-(3,4-dimethoxyphenyl)-3-{(*E*)-[(3,4-dimethoxyphenyl)methylidene]amino}-2,3-dihydroquinazolin-4(1*H*)-one
10	QZ10		2-(2,4-dichlorophenyl)-3-{(*E*)-[(2,4-dichlorophenyl)methylidene]amino}-2,3-dihydroquinazolin-4(1*H*)-one
11	QZ11		2-(N,N-dimethylaminophenyl)-3-{(*E*)-[(N,N-dimethylaminophenyl)methylidene]amino} -2,3-dihydroquinazolin-4(1*H*)-one

Table 3: Predicted Lipinski Parameters and Molecular Properties of the Designed Molecules

Sl No:	Molecule	miLogP	TPSA	nAtoms	MW	nON	nOHNH	nViolations	nRotb	Volume
1	QZ1	4.05	44.70	25	327.39	4	1	0	3	300.28
2	QZ2	3.09	85.16	27	359.38	6	3	0	3	316.31
3	QZ3	5.41	44.70	27	396.28	4	1	1	3	327.35
4	QZ4	5.36	44.70	27	396.28	4	1	1	3	327.35
5	QZ5	5.67	44.70	27	485.18	4	1	1	3	336.05
6	QZ6	4.82	63.17	31	415.49	6	1	0	7	384.97
7	QZ7	4.95	44.70	27	355.44	4	1	0	3	333.40
8	QZ8	4.13	81.64	33	447.49	8	1	0	7	402.46
9	QZ9	3.34	81.64	33	447.49	8	1	0	7	402.46
10	QZ10	6.62	44.70	29	465.17	4	1	1	3	354.42
11	QZ11	4.25	51.18	31	413.52	6	1	0	5	392.09

Table 4: Predicted Toxicity Risk, Drug Likeness, Solubility Data by Osiris Property Explorer

Sl. No:	Compound	Mutagenic	Tumorigenic	Irritant	Reproductive effect	Drug Likeness	Drug score	Clog P	Clog S
1	QZ1	LOW RISK	LOW RISK	LOW RISK	LOW RISK	4.59	0.84	3.7	-4.63
2	QZ2	LOW RISK	LOW RISK	LOW RISK	LOW RISK	4.73	0.86	3.01	-4.04
3	QZ6	LOW RISK	LOW RISK	LOW RISK	LOW RISK	3.54	0.71	4.37	-5.27
4	QZ7	LOW RISK	LOW RISK	LOW RISK	LOW RISK	3.12	0.75	4.39	5.32
5	QZ8	LOW RISK	LOW RISK	LOW RISK	LOW RISK	3.38	0.74	3.42	-4.7
6	QZ9	LOW RISK	LOW RISK	LOW RISK	LOW RISK	3.53	0.47	3.49	-4.7
7	QZ11	LOW RISK	HIGH RISK	LOW RISK	LOW RISK	6.37	0.76	3.42	-4.7

Table 5: Predicted Absorption, BBB permeability, Bioavailability, Human intestinal absorption, and Caco2 permeability by Swiss ADME.

Sl No:	Compound	GI Absorption	BBB Permeant	Bioavailability	HIA (% absorbed)	Caco2 Permeability (log Papp in 10-6 cm/s)
1	QZ1	HIGH	YES	0.55	100	1.4
2	QZ2	HIGH	NO	0.55	93.963	1.076
3	QZ6	HIGH	YES	0.55	99.06	1.168
4	QZ7	HIGH	YES	0.55	99.199	1.133
5	QZ8	HIGH	NO	0.55	100	1.283
6	QZ9	HIGH	NO	0.55	100	1.248

Table 6: Predicted P-glycoprotein and Cytochrome P450 activity

Sl No:	Sample Code	P-gp Substrate	P-gp I Inhibitor	P-gp II Inhibitor	CYP2D6 Substrate	CYP3A4 Substrate	CYP1A2 Inhibitor	CYP2C19 Inhibitor	CYP2C9 Inhibitor	CYP2D6 Inhibitor	CYP3A4 Inhibitor
1	QZ1	Yes	Yes	Yes	No	Yes	Yes	Yes	Yes	No	No
2	QZ2	Yes	No	Yes	No	Yes	Yes	Yes	Yes	No	Yes
3	QZ6	No	Yes	Yes	No	Yes	Yes	Yes	Yes	No	Yes
4	QZ7	No	Yes	Yes	No	Yes	Yes	Yes	Yes	No	No
5	QZ8	No	Yes	Yes	No	Yes	Yes	Yes	Yes	No	Yes
6	QZ9	No	Yes	Yes	No	Yes	Yes	Yes	Yes	No	Yes

Table 7: Predicted total clearance and whether the molecule is a renal OCT2 substrate, AMES toxicity, human maximum tolerated dose, oral rat acute and chronic toxicity, hERG inhibition, hepatotoxicity, and skin sensitization.

SI No:	Sample Code	Total Clearance (log/ml/min/kg)	Renal OCT2 Substrate	AMES Toxicity	Max. Tolerate Dose (log mg/kg/day)	hERG I Inhibitor	hERG II Inhibitor	Oral Rat Toxicity (LD_{50}) (mol/kg)	Hepato-toxicity	Skin Sensitisation

1	QZ1	0.707	No	Yes	0.54	No	Yes	2.243	Yes	No
2	QZ2	0.483	No	Yes	0.402	No	Yes	2.71	No	No
3	QZ6	0.799	No	No	0.67	No	Yes	2.757	No	No
4	QZ7	0.759	No	Yes	0.406	No	Yes	2.61	Yes	No
5	QZ8	0.807	No	No	0.581	No	Yes	2.841	No	No
6	QZ9	0.63	No	No	0.557	No	Yes	3.006	No	No

Table 8: Autodock Vina Dock score of various receptor-ligand complexes.

SI NO	Ligand	Dock Score (kcal/mol) - Various Receptor Molecules (PDB ID)							
		1B2Y	2OJ9	6JB3	3DD1	5NN8	1UV5	4CDC	4PRG
1	Acarbose	-8.9	-	-	-	-8.5	-	-	-
2	Metformin	-	-4.8	-	-5.9	-	-	-	-
3	Repaglinide	-	-	-8.6	-	-	-	-	-
4	Ar-AO14418	-	-	-	-	-	-8	-	-
5	Sitagliptin	-	-	-	-	-	-	-8.6	-
6	Pioglitazone	-	-	-	-	-	-	-	-9.2
7	QZ1	-8.4	-8.6	-8.7	-8.3	-7.4	-8.7	-7.8	-9.2
8	QZ2	-8.4	-8.4	-9.2	-8	-7.7	-9.2	-9.2	-10.8
9	QZ6	-7.8	-8.3	-8.4	-7.6	-7.2	-8.1	-7.1	-8.4
10	QZ7	-8.3	-8.9	-9	-7.9	-7.8	-8.8	-9	-8.5
11	QZ8	-7.7	-7.2	-8.1	-7.4	-6.9	-9.1	-7.6	-10.4
12	QZ9	-8.1	-7.6	-8.7	-7.2	-7.6	-9	-7.2	-9.1

Table 9: Molecular Docking and Molecular Dynamic Simulation Interaction Result of Receptor-ligand complexes.

Sl No:	Complex (Receptor-Ligand)	Molecular Docking H-bond Interaction (Distance in Å)	OtherInteracting residues in Molecular Docking (Type of Interaction)	Binding Affinity (kcal/mol)	Molecular Dynamic Simulation H-bond interaction
1	4PRG - QZ2	GLU 343 (2.6574), SER 342 (2.9249), MET 364 (2.7415)	LEU 228, LEU 333, ARG 288, LEU 330, ILE 341 (Pi-Alkyl)	-10.8	LEU 340, GLU 343, SER 342

			CYS 285 (Pi-Sulfur) ILE 281 (Carbon Hydrogen Bond)		
2	6JB3 - QZ2	ASN 1296 (2.5053), ASN B 547 (2.5715)	ASN 1293, VAL 587 (Pi-Sigma) PRO 551 (Pi-Alkyl) TRP 1297, PHE 591 (Pi-Pi T-shaped)	-9.2	ASN 1293, ASN 1296

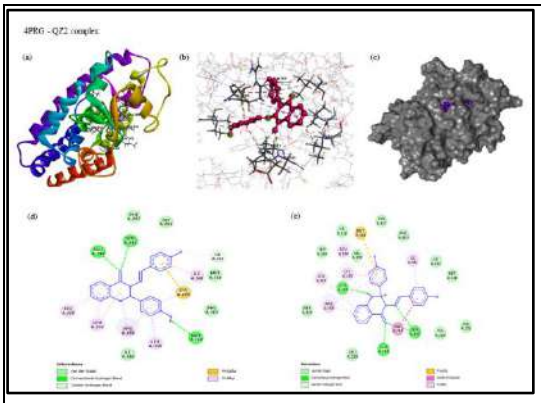

Figure 1: Molecular docking and dynamic simulation interaction diagrams of 4PRG-QZ2 complex. (a) 3D ribbon structure view of 4PRG-QZ2 interaction dock whole complex. (b) 3D line structure view of interacted fragment of 4PRG-QZ2 dock complex (pink – ligand).(c) Solid structural view of 4PRG-QZ2 docked complex. (d) 3D diagram of 4PRG-QZ2 interaction MD whole complex. (e) 3D diagram of 4PRG-QZ2 interacted fragment of MD complex. (f) 2D diagram of 4PRG-QZ2 interaction of MD complex.

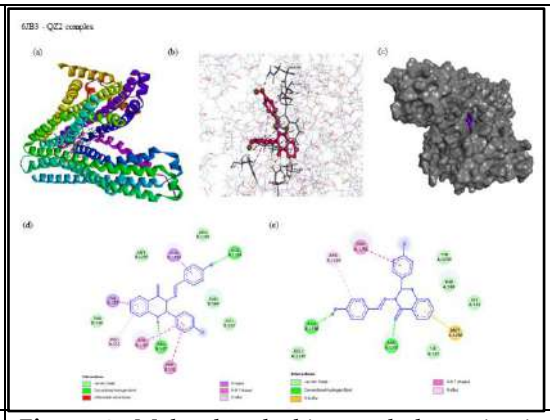

Figure 2: Molecular docking and dynamic simulation interaction diagrams of 6JB3-QZ2 complex. (a) 3D ribbon structure view of 6JB3-QZ2 interaction dock whole complex. (b) 3D line structure view of interacted fragment of 6JB3-QZ2 dock complex (pink – ligand).(c) Solid structural view of 6JB3-QZ2 docked complex. (d) 3D diagram of 6JB3-QZ2 interaction MD whole complex. (e) 3D diagram of 6JB3-QZ2 interacted fragment of MD complex. (f) 2D diagram of 6JB3-QZ2 interaction of MD complex.

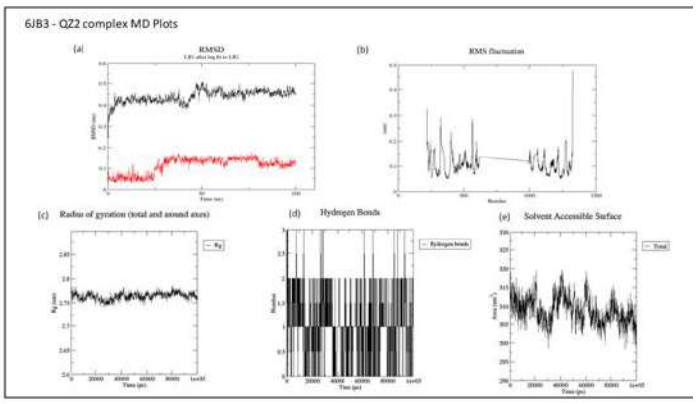

Figure 3: Trajectory plots of 4PRG-QZ2 complex (a) RMSD plot of 4PRG-QZ2 complex (b) RMSF plot of 4PRG-QZ2 complex (c) RoG plot of4PRG-QZ2 complex (d) H-bond distribution plot of 4PRG-QZ2 complex. (e) SASA plot of 4PRG-QZ2 complex.

RESEARCH ARTICLE

Max-Min and Min-Max Operators on Quin – Terranean Fuzzy Numbers

P.Rajarajeswari[1]* and T.Thirunamakkani[2]

[1]Associate Professor, Department of Mathematics, Chikkanna Government Arts College, Tirupur (Affiliated to *Bharathiar University, Coimbatore)* Tamil Nadu, India.
[2]Research Scholar, Department of Mathematics, Chikkanna Government Arts College, Tirupur (Affiliated to *Bharathiar University, Coimbatore)* Tamil Nadu, India.

Received: 15 Nov 2023 Revised: 16 Jan 2024 Accepted: 14 Mar 2024

***Address for Correspondence**
P. Rajarajeswari
Associate Professor, Department of Mathematics,
Chikkanna Government Arts College, Tirupur
(Affiliated to *Bharathiar University, Coimbatore)*
Tamil Nadu, India.
Email: p.rajarajeswari29@gmail.com

ABSTRACT

In comparison to Intuitionistic Fuzzy Set, Pythagorean Fuzzy Set and Fermatean Fuzzy Set, Quin-Terranean Fuzzy Set is a more advanced set that yields beneficial outcomes. The Quin-Terranean fuzzy set is the best measure for handling uncertainty. In this paper, we have defined some new operators namely, Max – Min ($\vee_{\tilde{Q}}$), Min – Max ($\wedge_{\tilde{Q}}$) operators and Average operator (@) on Quin – Terranean Fuzzy Numbers. Several properties of these Max – Min ($\vee_{\tilde{Q}}$) and Min – Max ($\wedge_{\tilde{Q}}$) operators as well as in combination with some basic operation already defined on Quin – Terranean Fuzzy Numbers such as complement and model operators $\boxplus,\boxtimes,\ominus,\oslash$ are also studied. In addition, several properties of the Average operator (@) in combination with Max – Min ($\vee_{\tilde{Q}}$), Min – Max ($\wedge_{\tilde{Q}}$) operators and model operators on Quin-Terranean Fuzzy numbers are also analyzed.

Keywords: Quin – Terranean fuzzy Number, Algebraic operations on Quin – Terranean fuzzy Numbers, Max – Min operator, Min – Max operator and Average operator on Quin – Terranean fuzzy Numbers.

INTRODUCTION

The idea of Fuzzy Set Theory, a development of classical set theory, was first put forward in 1965 by Zadeh [15]. For the simple computation of MIN and MAX operations for more than two upper semi-continuous Fuzzy Numbers, Dug Hun Hong and Kyung Tae Kim [2] suggested a new approach using the α-cut representation. They represented Non-continuous Fuzzy Numbers using this technique. This method allows the computation of the MIN and MAX operations for more than two Fuzzy Numbers to be done simultaneously rather than step-by-step as it is with Chiu and Wang's method. Based on Zadeh's extension principle, the max-min composition operators have a wide range of

desired results. In 2020, for two Triangular Fuzzy Numbers defined on R, Kim Hyun *et al*. [5] determined Zadeh's max-min composition operators. To implement the decisions of a decider, in 2020, Ferdinando Di Martino and Salvatore Sessa [3] suggested a new method based on the greatest (resp., smallest) eigen fuzzy set (GEFS, resp., SEFS) of a fuzzy relation R with respect to the max-min (resp., min-max) composition. They have generated the fuzzy relations RMAX (resp., RMIN), where any entry R_{MAXij} (resp., R_{MINij}) expresses how much the efficacy produced on the i^{th} characteristic is equal to or greater (resp., lesser) than that one produced by the j^{th} characteristic. This information comes from the evaluators assessments of how much a characteristic is improved with respect to others. To increase the performances of each characteristic, the GEFS of R_{MAX} (resp. SEFS of R_{MIN}) are calculated. They have also suggested a method to evaluate the tourism enhancement policies in the historical centre of a significant Italian city in as a result of earlier applications based on GEFS and SEFS.

In 1986, Atanassov [1] proposed the extended notion of Fuzzy Set Theory termed as Intuitionistic Fuzzy Set (IFS) to manage instances when Fuzzy Sets are insufficient. He outlined the IFS's functions and examined their characteristics. In 2017, Ion Iancu [4] suggested a group of Intuitionistic Fuzzy similarity measures whose expressions take the hesitancy degree into consideration. This group is an expansion of a few well-known measurements. They focused in two main directions to evaluate the effectiveness of these measures: the first demonstrates the reasonableness of the suggested measures, and the second discusses the potential applications to some real-world issues. With regard to the max-min product composition operator, in 2014, Melliani *et al*. [6] expanded the LU-factorization to the Intuitionistic Fuzzy Square Matrix. They provided algorithms to find two Intuitionistic Fuzzy (lower and upper) triangular matrices L and U for an Intuitionistic Fuzzy Square Matrix A such that A = LU and a result is provided for the existence and uniqueness of this decomposition. They have also suggested a method using LU-factorization to find the square system of solutions to Intuitionistic Fuzzy Relation Equations (IFRE). They have also provided an example to highlight their work.

Yager [12] presented the Pythagorean Fuzzy Set (PFS) in 2014, an extension of the IFS in which the sum of the squares representing the acceptance and non-acceptance of a proposition is less than or equal to one. In 2022, Snehaa and Sandhiya [11] studied the idea of Pythagorean Fuzzy Sets, along with some definitions the score and accuracy function of Fuzzy sets.They analyzed few Pythagorean Fuzzy Set properties. They have established the notion of a relation known as Pythagorean Fuzzy Relation, which is supported by numerical examples. They have also proposed a career placement decision-making process based on the Pythagorean Fuzzy Relation known as min-max-min composition which can be used to assess the appropriate suitability of careers for applicants based on skills and academic performance.

Senapathi and Yager [13] generated the Fermatean Fuzzy Set (FFS) in 2019, which is a Fuzzy Set where the sum of the cubes representing the acceptance and non-acceptance degrees is less than or equal to one. In 2019, Three additional operations—subtraction, division, and Fermatean arithmetic mean operations over Fermatean Fuzzy Numbers—were introduced by Tapan Senapati and Ronald Yager [14]. They have given a lot of information on their properties. To solve the problem of multi-criteria decision-making, they created a Fermatean Fuzzy Weighted Product Model. To support the theory they created and to demonstrate its applicability, they also offered a real-world example of selecting. In comparison to IFS, PFS, and FFS, the Quin-Terranean Fuzzy Set (QTFS) [8], an innovative concept we proposed in 2023, is the most significant and practical method to address uncertainty and contingency. Fundamental set theory operations including complement, intersection, and union were developed for Quin-Terranean Fuzzy sets. Regarding these activities, a number of the qualities are explored. The De Morgan's rule, associative property, commutative property, and distributive property have all been demonstrated to be satisfied by the Quin-Terranean Fuzzy set.

Preliminaries

In this session, the basic definitions, operations and properties related to the paper are given.

Definition 2.1[13]

The Pythagorean fuzzy sets defined on a non-empty set X as objects having the form $\mathcal{P} = \{\langle x, \alpha_P(x), \beta_P(x)\rangle : x \in X\}$, where the function $\alpha_P(x): X \to [0,1]$ and $\beta_P(x): X \to [0,1]$, denote the degree of membership and degree of non-membership of each element $x \in X$ to the set $\mathcal{P}$ respectively, and $0 \leq (\alpha_P(x))^2 + (\beta_P(x))^2 \leq 1$ for all $x \in \mathcal{X}$. For any Pythagorean fuzzy set $\mathcal{P}$ and $x \in X$, $\pi_P(x) = \sqrt{1 - (\alpha_P(x))^2 - (\beta_P(x))^2}$ is called the degree of indeterminacy of x to $\mathcal{P}$.

Definition 2.2[13]

Let X be a universe of discourse. A Fermatean fuzzy set $\mathcal{F}$ in X is an object having the form

$\mathcal{F} = \{\langle x, \alpha_{\mathcal{F}}(x), \beta_{\mathcal{F}}(x)\rangle : x \in X\}$,

where $\alpha_{\mathcal{F}}(x): X \to [0,1]$ and $\beta_{\mathcal{F}}(x): X \to [0,1]$, including the condition

$0 \leq (\alpha_P(x))^3 + (\beta_P(x))^3 \leq 1$,

for all $x \in X$. The $\alpha_{\mathcal{F}}(x)$ and $\beta_{\mathcal{F}}(x)$ denote, respectively, the degree of membership and the degree of non-membership of the element x in the set $\mathcal{F}$.

For any FFS $\mathcal{F}$ and $x \in X$,

$\pi_{\mathcal{F}}(x) = \sqrt[3]{1 - (\alpha_P(x))^3 - (\beta_P(x))^3}$

is identified as the degree of indeterminacy of x to $\mathcal{F}$.

Definition 2.3 [8]

Let $\boldsymbol{X}$ denotes a universe of discourse. A Quin – Terranean fuzzy set $\tilde{\boldsymbol{Q}}$ in $\boldsymbol{X}$ is the element possess the configuration $\tilde{\boldsymbol{Q}} = \{\langle \tilde{\boldsymbol{x}}, \boldsymbol{\sigma}_{\tilde{Q}}(\tilde{\boldsymbol{x}}), \boldsymbol{\delta}_{\tilde{Q}}(\tilde{\boldsymbol{x}})\rangle : \forall\, \tilde{\boldsymbol{x}} \in \boldsymbol{X}\}$,

where $\boldsymbol{\sigma}_{\tilde{Q}}(\tilde{\boldsymbol{x}}): \boldsymbol{X} \longrightarrow [\boldsymbol{0}, \boldsymbol{1}]$ and $\boldsymbol{\delta}_{\tilde{Q}}(\tilde{\boldsymbol{x}}): \boldsymbol{X} \longrightarrow [\boldsymbol{0}, \boldsymbol{1}]$ represents the degree of dependence and degree of non – dependence of the element respectively, satisfying the condition $\boldsymbol{0} \leq \left(\boldsymbol{\sigma}_{\tilde{Q}}(\tilde{\boldsymbol{x}})\right)^{\boldsymbol{4^5}} + \left(\boldsymbol{\delta}_{\tilde{Q}}(\tilde{\boldsymbol{x}})\right)^{\frac{5}{4}} \leq \boldsymbol{1}, \forall \tilde{\boldsymbol{x}} \in \boldsymbol{X}$.

For any Quin – Terranean fuzzy set $\tilde{\boldsymbol{Q}}$ and $\forall \tilde{\boldsymbol{x}} \in \boldsymbol{X}$, $\boldsymbol{\varphi}_{\tilde{Q}}(\tilde{\boldsymbol{x}}) = \left\{\boldsymbol{1} - \left(\boldsymbol{\sigma}_{\tilde{Q}}(\tilde{\boldsymbol{x}})\right)^{\boldsymbol{4^5}} - \left(\boldsymbol{\delta}_{\tilde{Q}}(\tilde{\boldsymbol{x}})\right)^{\frac{5}{4}}\right\}^{\frac{4}{5}}$ is the degree of hesitance of $\tilde{\boldsymbol{x}}$ to $\boldsymbol{X}$.

Definition 2.4 [7]

A Quin – Terranean fuzzy number $\tilde{\boldsymbol{Q}}$ is defined as,

(a) a Quin – Terranean fuzzy subset of the real line

(b) normal, that is, there exist $\tilde{x}_0 \in R$ such that $\sigma_{\tilde{Q}}(\tilde{x}_0) = \boldsymbol{1}$ and $\delta_{\tilde{Q}}(\tilde{x}_0) = \boldsymbol{0}$.

(c) a convex set for the acceptance function $\sigma_{\tilde{Q}}(\tilde{x})$, that is,

$$\sigma_{\tilde{Q}}(\boldsymbol{\lambda}\tilde{x}_1 + (1-\lambda)\tilde{x}_2) \geq \boldsymbol{min}\left(\sigma_{\tilde{Q}}(\tilde{x}_1), \sigma_{\tilde{Q}}(\tilde{x}_2)\right) \quad \forall\, \tilde{x}_1, \tilde{x}_2 \in R, \lambda \in [0,1]$$

(d) a concave set for the non-acceptance function $\delta_{\tilde{Q}}(\tilde{x})$, that is,

$$\delta_{\tilde{Q}}(\boldsymbol{\lambda}\tilde{x}_1 + (1-\lambda)\tilde{x}_2) \leq \boldsymbol{max}\left(\delta_{\tilde{Q}}(\tilde{x}_1), \delta_{\tilde{Q}}(\tilde{x}_2)\right) \quad \forall\, \tilde{x}_1, \tilde{x}_2 \in R, \lambda \in [0,1].$$

and satisfies the condition, $\boldsymbol{0} \leq \left(\boldsymbol{\sigma}_{\tilde{Q}}(\tilde{\boldsymbol{x}})\right)^{\boldsymbol{4^5}} + \left(\boldsymbol{\delta}_{\tilde{Q}}(\tilde{\boldsymbol{x}})\right)^{\frac{5}{4}} \leq \boldsymbol{1}$.

A doublet expressed by $\tilde{\boldsymbol{Q}} = \langle \sigma_{\tilde{Q}}(\tilde{x}), \delta_{\tilde{Q}}(\tilde{x})\rangle$ is known as Quin – Terranean fuzzy number. The Zero and one Quin – Terranean fuzzy number is denoted by (0,0) and (1,0) respectively.

Definition 2.5 [9]

Let $\tilde{\mathbb{Q}} = \langle \sigma_{\tilde{\mathbb{Q}}}(\tilde{x}), \delta_{\tilde{\mathbb{Q}}}(x)\rangle$, $\tilde{\mathbb{Q}}_1 = \langle \sigma_{\tilde{\mathbb{Q}}1}(\tilde{x}), \delta_{\tilde{\mathbb{Q}}1}(x)\rangle$ and $\tilde{\mathbb{Q}}_2 = \langle \sigma_{\tilde{\mathbb{Q}}_2}(\tilde{x}), \delta_{\tilde{\mathbb{Q}}_2}(\tilde{x})\rangle$ be three Quin – Terranean Fuzzy Numbers and $\lambda > 0$, then their operations are expressed as follows:

(i) $\tilde{\mathbb{Q}}_1 \boxplus \tilde{\mathbb{Q}}_2 = \langle \left\{\left(\sigma_{\tilde{\mathbb{Q}}_1}(\tilde{x})\right)^{4^5} + \left(\sigma_{\tilde{\mathbb{Q}}_2}(\tilde{x})\right)^{4^5} - \left(\sigma_{\tilde{\mathbb{Q}}_1}(\tilde{x})\right)^{4^5}\left(\sigma_{\tilde{\mathbb{Q}}_2}(\tilde{x})\right)^{4^5}\right\}^{\frac{1}{4^5}}, \delta_{\tilde{\mathbb{Q}}_1}(\tilde{x})\delta_{\tilde{\mathbb{Q}}_2}(\tilde{x})\rangle$

(ii) $\tilde{\mathbb{Q}}_1 \boxtimes \tilde{\mathbb{Q}}_2 = \langle \sigma_{\tilde{\mathbb{Q}}_1}(\tilde{x})\sigma_{\tilde{\mathbb{Q}}_2}(\tilde{x}), \left\{\left(\delta_{\tilde{\mathbb{Q}}_1}(\tilde{x})\right)^{\frac{5}{4}} + \left(\delta_{\tilde{\mathbb{Q}}_2}(\tilde{x})\right)^{\frac{5}{4}} - \left(\delta_{\tilde{\mathbb{Q}}_1}(\tilde{x})\right)^{\frac{5}{4}}\left(\delta_{\tilde{\mathbb{Q}}_2}(\tilde{x})\right)^{\frac{5}{4}}\right\}^{\frac{4}{5}}\rangle$

(iii) $\lambda\widetilde{\mathbb{Q}} = \langle\left\{1-\left(1-\left(\sigma_{\widetilde{\mathbb{Q}}}(\tilde{x})\right)^{4^5}\right)^{\lambda}\right\}^{\frac{1}{4^5}}, \delta_{\widetilde{\mathbb{Q}}}(\tilde{x})^{\lambda}\rangle$

(iv) $\widetilde{\mathbb{Q}}^{\lambda} = \langle\sigma_{\widetilde{\mathbb{Q}}}(\tilde{x})^{\lambda}, \left\{1-\left(1-\left(\delta_{\widetilde{\mathbb{Q}}}(\tilde{x})\right)^{\frac{5}{4}}\right)^{\lambda}\right\}^{\frac{4}{5}}\rangle.$

Definition 2.6 [10]

Let $T_1 = \langle\sigma_{T_1}, \delta_{T_1}\rangle$ and $T_2 = \langle\sigma_{T_2}, \delta_{T_2}\rangle$ be two Quin-Terranean Fuzzy numbers, then,

(i) $T_1 \ominus T_2 = \langle\left\{\frac{{\sigma_{T_1}}^{4^5}-{\sigma_{T_2}}^{4^5}}{1-{\sigma_{T_2}}^{4^5}}\right\}^{\frac{1}{4^5}}, \frac{\delta_{T_1}}{\delta_{T_2}}\rangle$, if $\sigma_{T_1} \geq \sigma_{T_2}$, $\delta_{T_1} \leq min\left\{\delta_{T_2}, \frac{\delta_{T_2}\varphi_1}{\varphi_2}\right\}$;

(ii) $T_1 \oslash T_2 = \langle\frac{\sigma_{T_1}}{\sigma_{T_2}}, \left\{\frac{{\delta_{T_1}}^{\frac{5}{4}}-{\delta_{T_2}}^{\frac{5}{4}}}{1-{\delta_{T_2}}^{\frac{5}{4}}}\right\}^{\frac{4}{5}}\rangle$, if $\sigma_{T_1} \leq min\left\{\sigma_{T_2}, \frac{\sigma_{T_2}\varphi_1}{\varphi_2}\right\}$, $\delta_{T_1} \geq \delta_{T_2}$.

MAIN RESULT

In this section, we define Max – Min ($\vee_{\tilde{Q}}$), Min – Max ($\wedge_{\tilde{Q}}$) operators and Average operator (@) on Quin – Terranean Fuzzy Numbers. Several properties of these Max – Min ($\vee_{\tilde{Q}}$) and Min – Max ($\wedge_{\tilde{Q}}$) operators as well as in combination with the basic operation of complement and model operators such as $\boxplus,\boxtimes,\ominus,\oslash$ on Quin – Terranean Fuzzy Numbers are also studied. In addition, several properties of the Average operator (@) in combination with Max – Min ($\vee_{\tilde{Q}}$), Min – Max ($\wedge_{\tilde{Q}}$) operators and model operators on Quin-Terranean Fuzzy numbers are also analyzed.

Max –min and Min – max operations on Quin Terranean fuzzy numbers

Definition 3.1.1

Let $\tilde{\boldsymbol{L}} = \langle\boldsymbol{\sigma}_{\tilde{L}}(\boldsymbol{x}), \boldsymbol{\delta}_{\tilde{L}}(\boldsymbol{x})\rangle$, $\tilde{\boldsymbol{M}} = \langle\boldsymbol{\sigma}_{\tilde{M}}(\boldsymbol{x}), \boldsymbol{\delta}_{\tilde{M}}(\boldsymbol{x})\rangle$ be two Quin – Terranean fuzzy numbers, then the max – min ($\vee_{\tilde{Q}}$) and min – max ($\wedge_{\tilde{Q}}$) operation on Quin – Terranean fuzzy numbers are defined as,

$\tilde{\boldsymbol{L}}\vee_{\tilde{Q}}\tilde{\boldsymbol{M}} = \langle\boldsymbol{max}\left(\boldsymbol{\sigma}_{\tilde{L}}(\boldsymbol{x}), \boldsymbol{\sigma}_{\tilde{M}}(\boldsymbol{x})\right), \boldsymbol{min}\left(\boldsymbol{\delta}_{\tilde{L}}(\boldsymbol{x}), \boldsymbol{\delta}_{\tilde{M}}(\boldsymbol{x})\right)\rangle$ and

$\tilde{\boldsymbol{L}}\wedge_{\tilde{Q}}\tilde{\boldsymbol{M}} = \langle\boldsymbol{min}\left(\boldsymbol{\sigma}_{\tilde{L}}(\boldsymbol{x}), \boldsymbol{\sigma}_{\tilde{M}}(\boldsymbol{x})\right), \boldsymbol{max}\left(\boldsymbol{\delta}_{\tilde{L}}(\boldsymbol{x}), \boldsymbol{\delta}_{\tilde{M}}(\boldsymbol{x})\right)\rangle$.

Properties of max –min ($\vee_{\tilde{Q}}$) and min – max ($\wedge_{\tilde{Q}}$) operations on Quin Terranean fuzzy numbers

The several properties of the max –min and min – max operations on Quin Terranean fuzzy numbers are given as follows,

Theorem 3.2.1: Let $\tilde{\boldsymbol{L}} = \langle\boldsymbol{\sigma}_{\tilde{L}}(\boldsymbol{x}), \boldsymbol{\delta}_{\tilde{L}}(\boldsymbol{x})\rangle$, $\tilde{\boldsymbol{M}} = \langle\boldsymbol{\sigma}_{\tilde{M}}(\boldsymbol{x}), \boldsymbol{\delta}_{\tilde{M}}(\boldsymbol{x})\rangle$ be two Quin – Terranean fuzzy numbers, then the following properties holds,

Idempotent Property:

(i) $\tilde{\boldsymbol{L}}\vee_{\tilde{Q}}\tilde{\boldsymbol{L}} = \tilde{\boldsymbol{L}}$

(ii) $\tilde{\boldsymbol{L}}\wedge_{\tilde{Q}}\tilde{\boldsymbol{L}} = \tilde{\boldsymbol{L}}$

Commutative property:

(iii) $\tilde{\boldsymbol{L}}\vee_{\tilde{Q}}\tilde{\boldsymbol{M}} = \tilde{\boldsymbol{M}}\vee_{\tilde{Q}}\tilde{\boldsymbol{L}}$

(iv) $\tilde{\boldsymbol{L}}\wedge_{\tilde{Q}}\tilde{\boldsymbol{M}} = \tilde{\boldsymbol{M}}\wedge_{\tilde{Q}}\tilde{\boldsymbol{L}}$

Demorgan Rule:

(v) $\left(\tilde{\boldsymbol{L}}\vee_{\tilde{Q}}\tilde{\boldsymbol{M}}\right)^{\boldsymbol{c}} = \left(\tilde{\boldsymbol{L}}\right)^{\boldsymbol{c}}\wedge_{\tilde{Q}}\left(\tilde{\boldsymbol{M}}\right)^{\boldsymbol{c}}$

(vi) $\left(\tilde{\boldsymbol{L}}\wedge_{\tilde{Q}}\tilde{\boldsymbol{M}}\right)^{\boldsymbol{c}} = \left(\tilde{\boldsymbol{L}}\right)^{\boldsymbol{c}}\vee_{\tilde{Q}}\left(\tilde{\boldsymbol{M}}\right)^{\boldsymbol{c}}$

Proof:

(i) Proof follows from the definition 3.11 (iii)

(ii) Proof follows from the definition 3.11 (iv)

(iii) L.H.S = $\tilde{\boldsymbol{L}}\vee_{\tilde{Q}}\tilde{\boldsymbol{M}} = \langle\boldsymbol{max}\left(\boldsymbol{\sigma}_{\tilde{L}}(\boldsymbol{x}), \boldsymbol{\sigma}_{\tilde{M}}(\boldsymbol{x})\right), \boldsymbol{min}\left(\boldsymbol{\delta}_{\tilde{L}}(\boldsymbol{x}), \boldsymbol{\delta}_{\tilde{M}}(\boldsymbol{x})\right)\rangle$

$= \langle\boldsymbol{max}\left(\boldsymbol{\sigma}_{\tilde{M}}(\boldsymbol{x}), \boldsymbol{\sigma}_{\tilde{L}}(\boldsymbol{x})\right), \boldsymbol{min}\left(\boldsymbol{\delta}_{\tilde{M}}(\boldsymbol{x}), \boldsymbol{\delta}_{\tilde{L}}(\boldsymbol{x})\right)\rangle = \tilde{\boldsymbol{M}}\vee_{\tilde{Q}}\tilde{\boldsymbol{L}} = \boldsymbol{R.H.S.}$

(iv) L.H.S = $\tilde{\boldsymbol{L}}\wedge_{\tilde{Q}}\tilde{\boldsymbol{M}} = \langle\boldsymbol{min}\left(\boldsymbol{\sigma}_{\tilde{L}}(\boldsymbol{x}), \boldsymbol{\sigma}_{\tilde{M}}(\boldsymbol{x})\right), \boldsymbol{max}\left(\boldsymbol{\delta}_{\tilde{L}}(\boldsymbol{x}), \boldsymbol{\delta}_{\tilde{M}}(\boldsymbol{x})\right)\rangle$

$= \langle \boldsymbol{min}(\sigma_{\tilde{M}}(x), \sigma_{\tilde{L}}(x)), \boldsymbol{max}(\delta_{\tilde{M}}(x), \delta_{\tilde{L}}(x)) \rangle = \tilde{M} \wedge_{\tilde{Q}} \tilde{L} = \boldsymbol{R.H.S}.$

(v) L.H. S $= (\tilde{L} \vee_{\tilde{Q}} \tilde{M})^{c} = \langle \boldsymbol{max}(\sigma_{\tilde{L}}(x), \sigma_{\tilde{M}}(x)), \boldsymbol{min}(\delta_{\tilde{L}}(x), \delta_{\tilde{M}}(x)) \rangle^{c}$

$= \langle \boldsymbol{min}(\delta_{\tilde{L}}(x), \delta_{\tilde{M}}(x)), \boldsymbol{max}(\sigma_{\tilde{L}}(x), \sigma_{\tilde{M}}(x)) \rangle$

$= \langle \delta_{\tilde{L}}(x), \sigma_{\tilde{L}}(x) \rangle \wedge_{\tilde{Q}} \langle \delta_{\tilde{M}}(x), \sigma_{\tilde{M}}(x) \rangle$

$= (\tilde{L})^{c} \wedge_{\tilde{Q}} (\tilde{M})^{c} = \boldsymbol{R.H.S}$

(vi) L.H. S $= (\tilde{L} \wedge_{\tilde{Q}} \tilde{M})^{c} = \langle \boldsymbol{min}(\sigma_{\tilde{L}}(x), \sigma_{\tilde{M}}(x)), \boldsymbol{max}(\delta_{\tilde{L}}(x), \delta_{\tilde{M}}(x)) \rangle^{c}$

$= \langle \boldsymbol{max}(\delta_{\tilde{L}}(x), \delta_{\tilde{M}}(x)), \boldsymbol{min}(\sigma_{\tilde{L}}(x), \sigma_{\tilde{M}}(x)) \rangle$

$= \langle \delta_{\tilde{L}}(x), \sigma_{\tilde{L}}(x) \rangle \vee_{\tilde{Q}} \langle \delta_{\tilde{M}}(x), \sigma_{\tilde{M}}(x) \rangle = (\tilde{L})^{c} \vee_{\tilde{Q}} (\tilde{M})^{c}$

$= \boldsymbol{R.H.S}$

Theorem 3.2.2: Let $\tilde{L} = \langle \sigma_{\tilde{L}}(x), \delta_{\tilde{L}}(x) \rangle$, $\tilde{M} = \langle \sigma_{\tilde{M}}(x), \delta_{\tilde{M}}(x) \rangle$ and $\tilde{R} = \langle \sigma_{\tilde{R}}(x), \delta_{\tilde{R}}(x) \rangle$ be three Quin – Terranean fuzzy numbers, then we have,

Associative Property:

(i) $\tilde{L} \vee_{\tilde{Q}} (\tilde{M} \vee_{\tilde{Q}} \tilde{R}) = (\tilde{L} \vee_{\tilde{Q}} \tilde{M}) \vee_{\tilde{Q}} \tilde{R}$

(ii) $\tilde{L} \wedge_{\tilde{Q}} (\tilde{M} \wedge_{\tilde{Q}} \tilde{R}) = (\tilde{L} \wedge_{\tilde{Q}} \tilde{M}) \wedge_{\tilde{Q}} \tilde{R}$

Distributive Property:

(iii) $\tilde{L} \wedge_{\tilde{Q}} (\tilde{M} \vee_{\tilde{Q}} \tilde{R}) = (\tilde{L} \wedge_{\tilde{Q}} \tilde{M}) \vee_{\tilde{Q}} (\tilde{L} \wedge_{\tilde{Q}} \tilde{R})$

(iv) $\tilde{L} \vee_{\tilde{Q}} (\tilde{M} \wedge_{\tilde{Q}} \tilde{R}) = (\tilde{L} \vee_{\tilde{Q}} \tilde{M}) \wedge_{\tilde{Q}} (\tilde{L} \vee_{\tilde{Q}} \tilde{R})$

Proof:

(i) L.H.S $= \tilde{L} \vee_{\tilde{Q}} (\tilde{M} \vee_{\tilde{Q}} \tilde{R})$

$= \langle \sigma_{\tilde{L}}(x), \delta_{\tilde{L}}(x) \rangle \vee_{\tilde{Q}} \langle \boldsymbol{max}(\sigma_{\tilde{M}}(x), \sigma_{\tilde{R}}(x)), \boldsymbol{min}(\delta_{\tilde{M}}(x), \delta_{\tilde{R}}(x)) \rangle$

$= \langle \boldsymbol{max}\left(\sigma_{\tilde{L}}(x), \boldsymbol{max}(\sigma_{\tilde{M}}(x), \sigma_{\tilde{R}}(x))\right), \boldsymbol{min}\left(\delta_{\tilde{L}}(x), \boldsymbol{min}(\delta_{\tilde{M}}(x), \delta_{\tilde{R}}(x))\right) \rangle$

$= \langle \boldsymbol{max}(\sigma_{\tilde{L}}(x), \sigma_{\tilde{M}}(x), \sigma_{\tilde{R}}(x)), \boldsymbol{min}(\delta_{\tilde{L}}(x), \delta_{\tilde{M}}(x), \delta_{\tilde{R}}(x)) \rangle$

$= \langle \boldsymbol{max}\left(\boldsymbol{max}(\sigma_{\tilde{L}}(x), \sigma_{\tilde{M}}(x)), \sigma_{\tilde{R}}(x)\right), \boldsymbol{min}\left(\boldsymbol{min}(\delta_{\tilde{L}}(x), \delta_{\tilde{M}}(x)), \delta_{\tilde{R}}(x)\right) \rangle$

$= \langle \boldsymbol{max}(\sigma_{\tilde{L}}(x), \sigma_{\tilde{M}}(x)), \boldsymbol{min}(\delta_{\tilde{L}}(x), \delta_{\tilde{M}}(x)) \rangle$

$\vee_{\tilde{Q}} \langle \sigma_{\tilde{R}}(x), \delta_{\tilde{R}}(x) \rangle = (\tilde{L} \vee_{\tilde{Q}} \tilde{M}) \vee_{\tilde{Q}} \tilde{R} = \boldsymbol{R.H.S}.$

(ii) L.H.S $= \tilde{L} \wedge_{\tilde{Q}} (\tilde{M} \wedge_{\tilde{Q}} \tilde{R})$

$= \langle \sigma_{\tilde{L}}(x), \delta_{\tilde{L}}(x) \rangle \wedge_{\tilde{Q}} \langle x, \boldsymbol{min}(\sigma_{\tilde{M}}(x), \sigma_{\tilde{R}}(x)), \boldsymbol{max}(\delta_{\tilde{M}}(x), \delta_{\tilde{R}}(x)) \rangle$

$= \langle \boldsymbol{min}\left(\sigma_{\tilde{L}}(x), \boldsymbol{min}(\sigma_{\tilde{M}}(x), \sigma_{\tilde{R}}(x))\right), \boldsymbol{max}\left(\delta_{\tilde{L}}(x), \boldsymbol{max}(\delta_{\tilde{M}}(x), \delta_{\tilde{R}}(x))\right) \rangle$

$= \langle \boldsymbol{min}(\sigma_{\tilde{L}}(x), \sigma_{\tilde{M}}(x), \sigma_{\tilde{R}}(x)), \boldsymbol{max}(\delta_{\tilde{L}}(x), \delta_{\tilde{M}}(x), \delta_{\tilde{R}}(x)) \rangle$

$= \langle \boldsymbol{min}\left(\boldsymbol{min}(\sigma_{\tilde{L}}(x), \sigma_{\tilde{M}}(x)), \sigma_{\tilde{R}}(x)\right), \boldsymbol{max}\left(\boldsymbol{max}(\delta_{\tilde{L}}(x), \delta_{\tilde{M}}(x)), \delta_{\tilde{R}}(x)\right) \rangle$

$= \langle \boldsymbol{min}(\sigma_{\tilde{L}}(x), \sigma_{\tilde{M}}(x)), \boldsymbol{max}(\delta_{\tilde{L}}(x), \delta_{\tilde{M}}(x)) \rangle$

$\wedge_{\tilde{Q}} \langle \sigma_{\tilde{R}}(x), \delta_{\tilde{R}}(x) \rangle = (\tilde{L} \wedge_{\tilde{Q}} \tilde{M}) \wedge_{\tilde{Q}} \tilde{R} = \boldsymbol{R.H.S}.$

(iii) L.H.S $= \tilde{L} \wedge_{\tilde{Q}} (\tilde{M} \vee_{\tilde{Q}} \tilde{R})$

$= \langle \sigma_{\tilde{L}}(x), \delta_{\tilde{L}}(x) \rangle \wedge_{\tilde{Q}} \langle \boldsymbol{max}(\sigma_{\tilde{M}}(x), \sigma_{\tilde{R}}(x)), \boldsymbol{min}(\delta_{\tilde{M}}(x), \delta_{\tilde{R}}(x)) \rangle$

$= \langle \boldsymbol{min}\left(\sigma_{\tilde{L}}(x), \boldsymbol{max}(\sigma_{\tilde{M}}(x), \sigma_{\tilde{R}}(x))\right), \boldsymbol{max}\left(\delta_{\tilde{L}}(x), \boldsymbol{min}(\delta_{\tilde{M}}(x), \delta_{\tilde{R}}(x))\right) \rangle$

and $\tilde{L} \wedge_{\tilde{Q}} \tilde{M} = \langle \boldsymbol{min}(\sigma_{\tilde{L}}(x), \sigma_{\tilde{M}}(x)), \boldsymbol{max}(\delta_{\tilde{L}}(x), \delta_{\tilde{M}}(x)) \rangle$,

$\tilde{L} \wedge_{\tilde{Q}} \tilde{R} = \langle \boldsymbol{min}(\sigma_{\tilde{L}}(x), \sigma_{\tilde{R}}(x)), \boldsymbol{max}(\delta_{\tilde{L}}(x), \delta_{\tilde{R}}(x)) \rangle$

R.H.S $= (\tilde{L} \wedge_{\tilde{Q}} \tilde{M}) \vee_{\tilde{Q}} (\tilde{L} \wedge_{\tilde{Q}} \tilde{R})$

$= \left\langle \begin{matrix} \boldsymbol{max}\left(\boldsymbol{min}(\sigma_{\tilde{L}}(x), \sigma_{\tilde{M}}(x)), \boldsymbol{min}(\sigma_{\tilde{L}}(x), \sigma_{\tilde{R}}(x))\right), \\ \boldsymbol{min}\left(\boldsymbol{max}(\delta_{\tilde{L}}(x), \delta_{\tilde{M}}(x)), \boldsymbol{max}(\delta_{\tilde{L}}(x), \delta_{\tilde{R}}(x))\right) \end{matrix} \right\rangle$

$= \langle \boldsymbol{min}\left(\sigma_{\tilde{L}}(x), \boldsymbol{max}(\sigma_{\tilde{M}}(x), \sigma_{\tilde{R}}(x))\right), \boldsymbol{max}\left(\delta_{\tilde{L}}(x), \boldsymbol{min}(\delta_{\tilde{M}}(x), \delta_{\tilde{R}}(x))\right) \rangle$

Hence L.H.S = R.H.S, therefore, $\tilde{L} \wedge_{\tilde{Q}} (\tilde{M} \vee_{\tilde{Q}} \tilde{R}) = (\tilde{L} \wedge_{\tilde{Q}} \tilde{M}) \vee_{\tilde{Q}} (\tilde{L} \wedge_{\tilde{Q}} \tilde{R})$.

(iv) L.H.S $= \tilde{L} \vee_{\tilde{Q}} (\tilde{M} \wedge_{\tilde{Q}} \tilde{R})$

$= \langle \sigma_{\tilde{L}}(x), \delta_{\tilde{L}}(x) \rangle \vee_{\tilde{Q}} \langle \boldsymbol{min}(\sigma_{\tilde{M}}(x), \sigma_{\tilde{R}}(x)), \boldsymbol{max}(\delta_{\tilde{M}}(x), \delta_{\tilde{R}}(x)) \rangle$

$= \langle \boldsymbol{max}\left(\sigma_{\tilde{L}}(x), \boldsymbol{min}(\sigma_{\tilde{M}}(x), \sigma_{\tilde{R}}(x))\right), \boldsymbol{min}\left(\delta_{\tilde{L}}(x), \boldsymbol{max}(\delta_{\tilde{M}}(x), \delta_{\tilde{R}}(x))\right) \rangle$

and $\tilde{L} \vee_{\tilde{Q}} \tilde{M} = \langle max(\sigma_{\tilde{L}}(x), \sigma_{\tilde{M}}(x)), min(\delta_{\tilde{L}}(x), \delta_{\tilde{M}}(x)) \rangle$,

$\tilde{L} \vee_{\tilde{Q}} \tilde{R} = \langle max(\sigma_{\tilde{L}}(x), \sigma_{\tilde{R}}(x)), min(\delta_{\tilde{L}}(x), \delta_{\tilde{R}}(x)) \rangle$

R.H.S = $(\tilde{L} \vee_{\tilde{Q}} \tilde{M}) \wedge_{\tilde{Q}} (\tilde{L} \vee_{\tilde{Q}} \tilde{R})$

$= \langle \begin{matrix} min\left(max(\sigma_{\tilde{L}}(x), \sigma_{\tilde{M}}(x)), max(\sigma_{\tilde{L}}(x), \sigma_{\tilde{R}}(x))\right), \\ max\left(min(\delta_{\tilde{L}}(x), \delta_{\tilde{M}}(x)), min(\delta_{\tilde{L}}(x), \delta_{\tilde{R}}(x))\right) \end{matrix} \rangle$

$= \langle max\left(\sigma_{\tilde{L}}(x), min(\sigma_{\tilde{M}}(x), \sigma_{\tilde{R}}(x))\right), min\left(\delta_{\tilde{L}}(x), max(\delta_{\tilde{M}}(x), \delta_{\tilde{R}}(x))\right) \rangle$

Hence L.H.S = R.H.S, therefore, $\tilde{L} \vee_{\tilde{Q}} (\tilde{M} \wedge_{\tilde{Q}} \tilde{R}) = (\tilde{L} \vee_{\tilde{Q}} \tilde{M}) \wedge_{\tilde{Q}} (\tilde{L} \vee_{\tilde{Q}} \tilde{R})$.

Theorem 3.2.3

Let $\tilde{L} = \langle \sigma_{\tilde{L}}(\tilde{x}), \delta_{\tilde{L}}(\tilde{x}) \rangle$, $\tilde{M} = \langle \sigma_{\tilde{M}}(\tilde{x}), \delta_{\tilde{M}}(\tilde{x}) \rangle$ and $\tilde{R} = \langle \sigma_{\tilde{R}}(\tilde{x}), \delta_{\tilde{R}}(\tilde{x}) \rangle$ be three Quin – Terranean Fuzzy numbers, then,

(i) $(\tilde{L} \wedge_{\tilde{Q}} \tilde{M}) \boxplus \tilde{R} = (\tilde{L} \boxplus \tilde{R}) \wedge_{\tilde{Q}} (\tilde{M} \boxplus \tilde{R})$

(ii) $(\tilde{L} \vee_{\tilde{Q}} \tilde{M}) \boxplus \tilde{R} = (\tilde{L} \boxplus \tilde{R}) \vee_{\tilde{Q}} (\tilde{M} \boxplus \tilde{R})$

(iii) $(\tilde{L} \wedge_{\tilde{Q}} \tilde{M}) \boxtimes \tilde{R} = (\tilde{L} \boxtimes \tilde{R}) \wedge_{\tilde{Q}} (\tilde{M} \boxtimes \tilde{R})$

(iv) $(\tilde{L} \vee_{\tilde{Q}} \tilde{M}) \boxtimes \tilde{R} = (\tilde{L} \boxtimes \tilde{R}) \vee_{\tilde{Q}} (\tilde{M} \boxtimes \tilde{R})$

Proof:

For the three Quin – Terranean Fuzzy numbers $\tilde{L} = \langle \sigma_{\tilde{L}}(\tilde{x}), \delta_{\tilde{L}}(\tilde{x}) \rangle$, $\tilde{M} = \langle \sigma_{\tilde{M}}(\tilde{x}), \delta_{\tilde{M}}(\tilde{x}) \rangle$ and $\tilde{R} = \langle \sigma_{\tilde{R}}(\tilde{x}), \delta_{\tilde{R}}(\tilde{x}) \rangle$, we get,

(i) L.H.S = $(\tilde{L} \wedge_{\tilde{Q}} \tilde{M}) \boxplus \tilde{R}$

$= \langle min\{\sigma_{\tilde{L}}(\tilde{x}), \sigma_{\tilde{M}}(\tilde{x})\}, max\{\delta_{\tilde{L}}(\tilde{x}), \delta_{\tilde{M}}(\tilde{x})\} \rangle \boxplus \langle \sigma_{\tilde{R}}(\tilde{x}), \delta_{\tilde{R}}(\tilde{x}) \rangle$

$= \langle \{min\{\sigma_{\tilde{L}}(\tilde{x})^{4.5}, \sigma_{\tilde{M}(\tilde{x})}{}^{4.5}\} + (\sigma_{\tilde{R}}(\tilde{x}))^{4.5} - min\{\sigma_{\tilde{L}}(\tilde{x})^{4.5}, \sigma_{\tilde{M}}(\tilde{x})^{4.5}\}(\sigma_{\tilde{R}}(\tilde{x}))^{4.5}\}^{\frac{1}{4.5}}, max\{\delta_{\tilde{L}}(\tilde{x}), \delta_{\tilde{M}}(\tilde{x})\}\delta_{\tilde{R}}(\tilde{x}) \rangle$

$= \langle \{\left(1 - (\sigma_{\tilde{R}}(\tilde{x}))^{4.5}\right) min\{\sigma_{\tilde{L}}(\tilde{x})^{4.5}, \sigma_{\tilde{M}}(\tilde{x})^{4.5}\} + (\sigma_{\tilde{R}}(\tilde{x}))^{4.5}\}^{\frac{1}{4.5}}, max\{\delta_{\tilde{L}}(\tilde{x})\delta_{\tilde{R}}(\tilde{x}), \delta_{\tilde{M}}(\tilde{x})\delta_{\tilde{R}}(\tilde{x})\} \rangle$

R.H.S = $(\tilde{L} \boxplus \tilde{R}) \wedge_{\tilde{Q}} (\tilde{M} \boxplus \tilde{R})$

$= \langle \{(\sigma_{\tilde{L}}(\tilde{x}))^{4.5} + (\sigma_{\tilde{R}}(\tilde{x}))^{4.5} - (\sigma_{\tilde{L}}(\tilde{x}))^{4.5}(\sigma_{\tilde{R}}(\tilde{x}))^{4.5}\}^{\frac{1}{4.5}}, \delta_{\tilde{L}}(\tilde{x})\delta_{\tilde{R}}(\tilde{x}) \rangle \wedge_{\tilde{Q}}$

$\langle \{(\sigma_{\tilde{M}}(\tilde{x}))^{4.5} + (\sigma_{\tilde{R}}(\tilde{x}))^{4.5} - (\sigma_{\tilde{M}}(\tilde{x}))^{4.5}(\sigma_{\tilde{R}}(\tilde{x}))^{4.5}\}^{\frac{1}{4.5}}, \delta_{\tilde{M}}(\tilde{x})\delta_{\tilde{R}}(\tilde{x}) \rangle$

$= \langle min \Big\{ \{(\sigma_{\tilde{L}}(\tilde{x}))^{4.5} + (\sigma_{\tilde{R}}(\tilde{x}))^{4.5} - (\sigma_{\tilde{L}}(\tilde{x}))^{4.5}(\sigma_{\tilde{R}}(\tilde{x}))^{4.5}\}^{\frac{1}{4.5}}, \{(\sigma_{\tilde{M}}(\tilde{x}))^{4.5} + (\sigma_{\tilde{R}}(\tilde{x}))^{4.5}$

$- (\sigma_{\tilde{M}}(\tilde{x}))^{4.5}(\sigma_{\tilde{R}}(\tilde{x}))^{4.5}\}^{\frac{1}{4.5}} \Big\}, max\{\delta_{\tilde{L}}(\tilde{x})\delta_{\tilde{R}}(\tilde{x}), \delta_{\tilde{M}}(\tilde{x})\delta_{\tilde{R}}(\tilde{x})\} \rangle$

$= \langle min \Big\{ \{\left(1 - (\sigma_{\tilde{R}}(\tilde{x}))^{4.5}\right)(\sigma_{\tilde{L}}(\tilde{x}))^{4.5} + (\sigma_{\tilde{R}}(\tilde{x}))^{4.5}\}^{\frac{1}{4.5}}, \{\left(1 - (\sigma_{\tilde{R}}(\tilde{x}))^{4.5}\right)(\sigma_{\tilde{M}}(\tilde{x}))^{4.5}$

$+ (\sigma_{\tilde{R}}(\tilde{x}))^{4.5}\}^{\frac{1}{4.5}} \Big\}, max\{\delta_{\tilde{L}}(\tilde{x})\delta_{\tilde{R}}(\tilde{x}), \delta_{\tilde{M}}(\tilde{x})\delta_{\tilde{R}}(\tilde{x})\} \rangle$

$= \langle \{\left(1 - (\sigma_{\tilde{R}}(\tilde{x}))^{4.5}\right) min\{\sigma_{\tilde{L}}(\tilde{x})^{4.5}, \sigma_{\tilde{M}}(\tilde{x})^{4.5}\} + (\sigma_{\tilde{R}}(\tilde{x}))^{4.5}\}^{\frac{1}{4.5}}, max\{\delta_{\tilde{L}}(\tilde{x})\delta_{\tilde{R}}(\tilde{x}), \delta_{\tilde{M}}(\tilde{x})\delta_{\tilde{R}}(\tilde{x})\} \rangle$

= L.H.S.

∴, $(\tilde{L} \wedge_{\tilde{Q}} \tilde{M}) \boxplus \tilde{R} = (\tilde{L} \boxplus \tilde{R}) \wedge_{\tilde{Q}} (\tilde{M} \boxplus \tilde{R})$.

Hence, (i) proved.

(ii) L.H.S = $(\tilde{L} \vee_{\tilde{Q}} \tilde{M}) \boxplus \tilde{R}$

$= \langle max\{\sigma_{\tilde{L}}(\tilde{x}), \sigma_{\tilde{M}}(\tilde{x})\}, min\{\delta_{\tilde{L}}(\tilde{x}), \delta_{\tilde{M}}(\tilde{x})\} \rangle \boxplus \langle \sigma_{\tilde{R}}(\tilde{x}), \delta_{\tilde{R}}(\tilde{x}) \rangle$

$= \langle \{max\{\sigma_{\tilde{L}}(\tilde{x})^{4.5}, \sigma_{\tilde{M}}(\tilde{x})^{4.5}\} + (\sigma_{\tilde{R}}(\tilde{x}))^{4.5} - max\{\sigma_{\tilde{L}}(\tilde{x})^{4.5}, \sigma_{\tilde{M}}(\tilde{x})^{4.5}\}(\sigma_{\tilde{R}}(\tilde{x}))^{4.5}\}^{\frac{1}{4.5}}, min\{\delta_{\tilde{L}}(\tilde{x}), \delta_{\tilde{M}}(\tilde{x})\}\delta_{\tilde{R}}(\tilde{x}) \rangle$

$= \langle \{\left(1 - (\sigma_{\tilde{R}}(\tilde{x}))^{4.5}\right) max\{\sigma_{\tilde{L}}(\tilde{x})^{4.5}, \sigma_{\tilde{M}}(\tilde{x})^{4.5}\} + (\sigma_{\tilde{R}}(\tilde{x}))^{4.5}\}^{\frac{1}{4.5}}, min\{\delta_{\tilde{L}}(\tilde{x})\delta_{\tilde{R}}(\tilde{x}), \delta_{\tilde{M}}(\tilde{x})\delta_{\tilde{R}}(\tilde{x})\} \rangle$

R.H.S = $(\tilde{L} \boxplus \tilde{R}) \vee_{\tilde{Q}} (\tilde{M} \boxplus \tilde{R})$

$= \langle \{(\sigma_{\tilde{L}}(\tilde{x}))^{4.5} + (\sigma_{\tilde{R}}(\tilde{x}))^{4.5} - (\sigma_{\tilde{L}}(\tilde{x}))^{4.5}(\sigma_{\tilde{R}}(\tilde{x}))^{4.5}\}^{\frac{1}{4.5}}, \delta_{\tilde{L}}(\tilde{x})\delta_{\tilde{R}}(\tilde{x}) \rangle \vee_{\tilde{Q}}$

$\langle \{(\sigma_{\tilde{M}}(\tilde{x}))^{4.5} + (\sigma_{\tilde{R}}(\tilde{x}))^{4.5} - (\sigma_{\tilde{M}}(\tilde{x}))^{4.5}(\sigma_{\tilde{R}}(\tilde{x}))^{4.5}\}^{\frac{1}{4.5}}, \delta_{\tilde{M}}(\tilde{x})\delta_{\tilde{R}}(\tilde{x}) \rangle$

$=$

$\langle max\left\{\{(\sigma_{\tilde{L}}(\tilde{x}))^{4^5}+(\sigma_{\tilde{R}}(\tilde{x}))^{4^5}-(\sigma_{\tilde{L}}(\tilde{x}))^{4^5}(\sigma_{\tilde{R}}(\tilde{x}))^{4^5}\}^{\frac{1}{4^5}},\{(\sigma_{\tilde{M}}(\tilde{x}))^{4^5}+(\sigma_{\tilde{R}}(\tilde{x}))^{4^5}-\right.$

$\left.(\sigma_{\tilde{M}}(\tilde{x}))^{4^5}(\sigma_{\tilde{R}}(\tilde{x}))^{4^5}\}^{\frac{1}{4^5}}\right\}, min\{\delta_{\tilde{L}}(\tilde{x})\delta_{\tilde{R}}(\tilde{x}),\delta_{\tilde{M}}(\tilde{x})\delta_{\tilde{R}}(\tilde{x})\}\rangle$

$= \langle max\left\{\{\left(1-(\sigma_{\tilde{R}}(\tilde{x}))^{4^5}\right)(\sigma_{\tilde{L}}(\tilde{x}))^{4^5}+(\sigma_{\tilde{R}}(\tilde{x}))^{4^5}\}^{\frac{1}{4^5}},\{\left(1-(\sigma_{\tilde{R}}(\tilde{x}))^{4^5}\right)(\sigma_{\tilde{M}}(\tilde{x}))^{4^5}\right.$

$\left.+(\sigma_{\tilde{R}}(\tilde{x}))^{4^5}\}^{\frac{1}{4^5}}\right\}, min\{\delta_{\tilde{L}}(\tilde{x})\delta_{\tilde{R}}(\tilde{x}),\delta_{\tilde{M}}(\tilde{x})\delta_{\tilde{R}}(\tilde{x})\}\rangle$

$=\langle\{\left(1-(\sigma_{\tilde{R}}(\tilde{x}))^{4^5}\right)max\{\sigma_{\tilde{L}}(\tilde{x})^{4^5},\sigma_{\tilde{M}}(\tilde{x})^{4^5}\}+(\sigma_{\tilde{R}}(\tilde{x}))^{4^5}\}^{\frac{1}{4^5}}, min\{\delta_{\tilde{L}}(\tilde{x})\delta_{\tilde{R}}(\tilde{x}),\delta_{\tilde{M}}(\tilde{x})\delta_{\tilde{R}}(\tilde{x})\}\rangle$ = L.H.S.

$\therefore, \left(\tilde{\boldsymbol{L}}\vee_{\tilde{\boldsymbol{Q}}}\ \tilde{M}\right)\boxplus\tilde{R}=\ \left(\tilde{\boldsymbol{L}}\boxplus\tilde{R}\right)\vee_{\tilde{\boldsymbol{Q}}}\ \left(\tilde{M}\boxplus\tilde{R}\right).$

Hence, (ii) proved.

(iii) L.H.S = $\left(\tilde{\boldsymbol{L}}\wedge_{\tilde{\boldsymbol{Q}}}\tilde{M}\right)\boxtimes\tilde{R}$

$= \langle min\{\sigma_{\tilde{L}}(\tilde{x}),\sigma_{\tilde{M}}(\tilde{x})\}, max\{\delta_{\tilde{L}}(\tilde{x}),\delta_{\tilde{M}}(\tilde{x})\}\rangle\boxplus\langle\sigma_{\tilde{R}}(\tilde{x}),\delta_{\tilde{R}}(\tilde{x})\rangle$

$=\langle min\{\sigma_{\tilde{L}}(\tilde{x}),\sigma_{\tilde{M}}(\tilde{x})\}\sigma_{\tilde{R}},\left\{max\left\{\delta_{\tilde{L}}(\tilde{x})^{\frac{5}{4}},\delta_{\tilde{M}}(\tilde{x})^{\frac{5}{4}}\right\}+(\delta_{\tilde{R}}(\tilde{x}))^{\frac{5}{4}}-max\left\{\delta_{\tilde{L}}(\tilde{x})^{\frac{5}{4}},\delta_{\tilde{M}}(\tilde{x})^{\frac{5}{4}}\right\}(\delta_{\tilde{R}}(\tilde{x}))^{\frac{5}{4}}\right\}^{\frac{4}{5}}\rangle$

$=\langle min\{\sigma_{\tilde{L}}(\tilde{x})\sigma_{\tilde{R}}(\tilde{x}),\sigma_{\tilde{M}}(\tilde{x})\sigma_{\tilde{R}}(\tilde{x})\},\left\{\left(1-(\delta_{\tilde{R}}(\tilde{x}))^{\frac{5}{4}}\right)max\left\{\delta_{\tilde{L}}(\tilde{x})^{\frac{5}{4}},\delta_{\tilde{M}}(\tilde{x})^{\frac{5}{4}}\right\}+(\delta_{\tilde{R}}(\tilde{x}))^{\frac{5}{4}}\right\}^{\frac{4}{5}}\rangle$

R.H.S = $\left(\tilde{\boldsymbol{L}}\boxtimes\tilde{R}\right)\wedge_{\tilde{\boldsymbol{Q}}}\left(\tilde{M}\boxtimes\tilde{R}\right)$

$= \langle\sigma_{\tilde{L}}(\tilde{x})\sigma_{\tilde{R}}(\tilde{x}),\left\{(\delta_{\tilde{L}}(\tilde{x}))^{\frac{5}{4}}+(\delta_{\tilde{R}}(\tilde{x}))^{\frac{5}{4}}-(\delta_{\tilde{L}}(\tilde{x}))^{\frac{5}{4}}(\delta_{\tilde{R}}(\tilde{x}))^{\frac{5}{4}}\right\}^{\frac{4}{5}}\rangle\ \wedge_{\tilde{\boldsymbol{Q}}}$

$\langle\sigma_{\tilde{M}}(\tilde{x})\sigma_{\tilde{R}}(\tilde{x}),\left\{(\delta_{\tilde{M}}(\tilde{x}))^{\frac{5}{4}}+(\delta_{\tilde{R}}(\tilde{x}))^{\frac{5}{4}}-(\delta_{\tilde{M}}(\tilde{x}))^{\frac{5}{4}}(\delta_{\tilde{R}}(\tilde{x}))^{\frac{5}{4}}\right\}^{\frac{4}{5}}\rangle$

$= \langle min\{\sigma_{\tilde{L}}(\tilde{x})\sigma_{\tilde{R}}(\tilde{x}),\sigma_{\tilde{M}}(\tilde{x})\sigma_{\tilde{R}}(\tilde{x})\},\left\{\left(1-(\delta_{\tilde{R}}(\tilde{x}))^{\frac{5}{4}}\right)max\left\{\delta_{\tilde{L}}(\tilde{x})^{\frac{5}{4}},\delta_{\tilde{M}}(\tilde{x})^{\frac{5}{4}}\right\}+(\delta_{\tilde{R}}(\tilde{x}))^{\frac{5}{4}}\right\}^{\frac{4}{5}}\rangle$ = L.H.S.

$\therefore, \left(\tilde{\boldsymbol{L}}\wedge_{\tilde{\boldsymbol{Q}}}\tilde{M}\right)\boxtimes\tilde{R}=\ \left(\tilde{\boldsymbol{L}}\boxtimes\tilde{R}\right)\wedge_{\tilde{\boldsymbol{Q}}}\left(\tilde{M}\boxtimes\tilde{R}\right).$

Hence, (iii) proved.

Hence, $\left(\tilde{\boldsymbol{L}}\wedge_{\tilde{\boldsymbol{Q}}}\tilde{M}\right)\boxtimes\tilde{R}=\ \left(\tilde{\boldsymbol{L}}\boxtimes\tilde{R}\right)\wedge_{\tilde{\boldsymbol{Q}}}\left(\tilde{M}\boxtimes\tilde{R}\right).$

(iv) L.H.S = $\left(\tilde{\boldsymbol{L}}\vee_{\tilde{\boldsymbol{Q}}}\tilde{M}\right)\boxtimes\tilde{R}$

$= \langle max\{\sigma_{\tilde{L}}(\tilde{x}),\sigma_{\tilde{M}}(\tilde{x})\}, min\{\delta_{\tilde{L}}(\tilde{x}),\delta_{\tilde{M}}(\tilde{x})\}\rangle\boxplus\langle\sigma_{\tilde{R}}(\tilde{x}),\delta_{\tilde{R}}(\tilde{x})\rangle$

$=\langle max\{\sigma_{\tilde{L}}(\tilde{x}),\sigma_{\tilde{M}}(\tilde{x})\}\sigma_{\tilde{R}}(\tilde{x}),\left\{min\left\{\delta_{\tilde{L}}(\tilde{x})^{\frac{5}{4}},\delta_{\tilde{M}}(\tilde{x})^{\frac{5}{4}}\right\}+(\delta_{\tilde{R}}(\tilde{x}))^{\frac{5}{4}}-min\left\{\delta_{\tilde{L}}(\tilde{x})^{\frac{5}{4}},\delta_{\tilde{M}}(\tilde{x})^{\frac{5}{4}}\right\}(\delta_{\tilde{R}}(\tilde{x}))^{\frac{5}{4}}\right\}^{\frac{4}{5}}\rangle$

$=\langle max\{\sigma_{\tilde{L}}(\tilde{x})\sigma_{\tilde{R}}(\tilde{x}),\sigma_{\tilde{M}}(\tilde{x})\sigma_{\tilde{R}}(\tilde{x})\},\left\{\left(1-(\delta_{\tilde{R}}(\tilde{x}))^{\frac{5}{4}}\right)min\left\{\delta_{\tilde{L}}(\tilde{x})^{\frac{5}{4}},\delta_{\tilde{M}}(\tilde{x})^{\frac{5}{4}}\right\}+(\delta_{\tilde{R}}(\tilde{x}))^{\frac{5}{4}}\right\}^{\frac{4}{5}}\rangle$

R.H.S = $\left(\tilde{\boldsymbol{L}}\boxtimes\tilde{R}\right)\vee_{\tilde{\boldsymbol{Q}}}\ \left(\tilde{M}\boxtimes\tilde{R}\right)$

$= \langle\sigma_{\tilde{L}}(\tilde{x})\sigma_{\tilde{R}}(\tilde{x}),\left\{(\delta_{\tilde{L}}(\tilde{x}))^{\frac{5}{4}}+(\delta_{\tilde{R}}(\tilde{x}))^{\frac{5}{4}}-(\delta_{\tilde{L}}(\tilde{x}))^{\frac{5}{4}}(\delta_{\tilde{R}}(\tilde{x}))^{\frac{5}{4}}\right\}^{\frac{4}{5}}\rangle\vee\ \langle\sigma_{\tilde{M}}(\tilde{x})\sigma_{\tilde{R}}(\tilde{x}),\left\{(\delta_{\tilde{M}}(\tilde{x}))^{\frac{5}{4}}+(\delta_{\tilde{R}}(\tilde{x}))^{\frac{5}{4}}-(\delta_{\tilde{M}}(\tilde{x}))^{\frac{5}{4}}(\delta_{\tilde{R}}(\tilde{x}))^{\frac{5}{4}}\right\}^{\frac{4}{5}}\rangle$

$= \langle max\{\sigma_{\tilde{L}}(\tilde{x})\sigma_{\tilde{R}}(\tilde{x}),\sigma_{\tilde{M}}(\tilde{x})\sigma_{\tilde{R}}(\tilde{x})\}, min\left\{\left\{\left(1-(\delta_{\tilde{R}}(\tilde{x}))^{\frac{5}{4}}\right)(\delta_{\tilde{L}}(\tilde{x}))^{\frac{5}{4}}+(\delta_{\tilde{R}}(\tilde{x}))^{\frac{5}{4}}\right\}^{\frac{4}{5}},\left\{\left(1-(\delta_{\tilde{R}}(\tilde{x}))^{\frac{5}{4}}\right)(\delta_{\tilde{M}}(\tilde{x}))^{\frac{5}{4}}+(\delta_{\tilde{R}}(\tilde{x}))^{\frac{5}{4}}\right\}^{\frac{4}{5}}\right\}\rangle$

$= \langle max\{\sigma_{\tilde{L}}(\tilde{x})\sigma_{\tilde{R}}(\tilde{x}),\sigma_{\tilde{M}}(\tilde{x})\sigma_{\tilde{R}}(\tilde{x})\},\left\{\left(1-(\delta_{\tilde{R}}(\tilde{x}))^{\frac{5}{4}}\right)min\left\{\delta_{\tilde{L}}(\tilde{x})^{\frac{5}{4}},\delta_{\tilde{M}}(\tilde{x})^{\frac{5}{4}}\right\}+(\delta_{\tilde{R}}(\tilde{x}))^{\frac{5}{4}}\right\}^{\frac{4}{5}}\rangle$ = L.H.S.

$\therefore, \left(\tilde{\boldsymbol{L}}\vee_{\tilde{\boldsymbol{Q}}}\tilde{M}\right)\boxtimes\tilde{R}=\ \left(\tilde{\boldsymbol{L}}\boxtimes\tilde{R}\right)\vee_{\tilde{\boldsymbol{Q}}}\ \left(\tilde{M}\boxtimes\tilde{R}\right).$

Hence, (iv) proved.

Hence, $\left(\tilde{\boldsymbol{L}}\vee_{\tilde{\boldsymbol{Q}}}\tilde{M}\right)\boxtimes\tilde{R}=\ \left(\tilde{\boldsymbol{L}}\boxtimes\tilde{R}\right)\vee_{\tilde{\boldsymbol{Q}}}\left(\tilde{M}\boxtimes\tilde{R}\right).$

Theorem 3.2.4

Let $\tilde{\boldsymbol{L}}=\{\langle\sigma_{\tilde{L}},\delta_{\tilde{L}}\rangle:\forall\tilde{\boldsymbol{x}}\in\boldsymbol{X}\}$ and $\tilde{M}=\{\langle\sigma_{\tilde{M}},\delta_{\tilde{M}}\rangle:\forall\tilde{\boldsymbol{x}}\in\boldsymbol{X}\}$ represents two Quin-Terranean fuzzy numbers, then,

(i) $\left(\tilde{\boldsymbol{L}}\vee_{\tilde{\boldsymbol{Q}}}\tilde{M}\right)\ominus\left(\tilde{\boldsymbol{L}}\wedge_{\tilde{\boldsymbol{Q}}}\tilde{M}\right)=\tilde{\boldsymbol{L}}\ominus\tilde{M}$ if $\sigma_{\tilde{L}}\geq\sigma_{\tilde{M}},\ \delta_{\tilde{L}}\leq min\left\{\delta_{\tilde{M}},\frac{\delta_{\tilde{M}}\varphi_1}{\varphi_2}\right\}.$

(ii) $\left(\tilde{\boldsymbol{L}}\wedge_{\tilde{\boldsymbol{Q}}}\tilde{M}\right)\ominus\left(\tilde{\boldsymbol{L}}\vee_{\tilde{\boldsymbol{Q}}}\tilde{M}\right)=\tilde{M}\ominus\tilde{\boldsymbol{L}}$ if $\sigma_{\tilde{L}}\geq\sigma_{\tilde{M}},\ \delta_{\tilde{L}}\leq min\left\{\delta_{\tilde{M}},\frac{\delta_{\tilde{M}}\varphi_1}{\varphi_2}\right\}.$

(iii) $\left(\tilde{\boldsymbol{L}}\wedge_{\tilde{\boldsymbol{Q}}}\tilde{M}\right)\oslash\left(\tilde{\boldsymbol{L}}\vee_{\tilde{\boldsymbol{Q}}}\tilde{M}\right)=\tilde{\boldsymbol{L}}\oslash\tilde{M}$ if $\sigma_{\tilde{L}}\leq min\left\{\sigma_{\tilde{M}},\frac{\sigma_{\tilde{M}}\varphi_1}{\varphi_2}\right\}\ ,\ \delta_{\tilde{L}}\geq\delta_{\tilde{M}}.$

(iv) $\left(\tilde{L}\vee_{\tilde{Q}}\tilde{M}\right)\oslash\left(\tilde{L}\wedge_{\tilde{Q}}\tilde{M}\right)=\tilde{L}\oslash\tilde{M}$ if $\sigma_{\tilde{L}}\leq min\left\{\sigma_{\tilde{M}},\frac{\sigma_{\tilde{M}}\varphi_1}{\varphi_2}\right\}$, $\delta_{\tilde{L}}\geq\delta_{\tilde{M}}$.

Proof:

Consider two Quin-Terranean fuzzy numbers $\tilde{L}=\langle\sigma_{\tilde{L}},\delta_{\tilde{L}}\rangle$ and $\tilde{M}=\langle\sigma_{\tilde{M}},\delta_{\tilde{M}}\rangle$.

(i) Since, $\sigma_{\tilde{L}}\geq\sigma_{\tilde{M}}$, $\delta_{\tilde{L}}\leq min\left\{\delta_{\tilde{M}},\frac{\delta_{\tilde{M}}\varphi_1}{\varphi_2}\right\}$, then,

L.H.S= $\left(\tilde{L}\vee_{\tilde{Q}}\tilde{M}\right)\ominus\left(\tilde{L}\wedge_{\tilde{Q}}\tilde{M}\right)$

$=\langle\max\{\sigma_{\tilde{L}},\sigma_{\tilde{M}}\},\min\{\delta_{\tilde{L}},\delta_{\tilde{M}}\}\rangle\ominus\langle\min\{\sigma_{\tilde{L}},\sigma_{\tilde{M}}\},\max\{\delta_{\tilde{L}},\delta_{\tilde{M}}\}\rangle$

$=\langle\left\{\frac{(\max\{\sigma_{\tilde{L}},\sigma_{\tilde{M}}\})^{4^5}-(\min\{\sigma_{\tilde{L}},\sigma_{\tilde{M}}\})^{4^5}}{1-(\min\{\sigma_{\tilde{L}},\sigma_{\tilde{M}}\})^{4^5}}\right\}^{\frac{1}{4^5}},\frac{\min\{\delta_{\tilde{L}},\delta_{\tilde{M}}\}}{\max\{\delta_{\tilde{L}},\delta_{\tilde{M}}\}}\rangle$

$=\langle\left\{\frac{\max\{\sigma_{\tilde{L}}{}^{4^5},\sigma_{\tilde{M}}{}^{4^5}\}-\min\{\sigma_{\tilde{L}}{}^{4^5},\sigma_{\tilde{M}}{}^{4^5}\}}{1-\min\{\sigma_{\tilde{L}}{}^{4^5},\sigma_{\tilde{M}}{}^{4^5}\}}\right\}^{\frac{1}{4^5}},\frac{\delta_{\tilde{L}}}{\delta_{\tilde{M}}}\rangle$

$=\langle\left\{\frac{\sigma_{\tilde{L}}{}^{4^5}-\sigma_{\tilde{M}}{}^{4^5}}{1-\sigma_{\tilde{M}}{}^{4^5}}\right\}^{\frac{1}{4^5}},\frac{\delta_{\tilde{L}}}{\delta_{\tilde{M}}}\rangle$

$=\tilde{L}\ominus\tilde{M}=$ R. H. S.

$\therefore,\left(\tilde{L}\vee_{\tilde{Q}}\tilde{M}\right)\ominus\left(\tilde{L}\wedge_{\tilde{Q}}\tilde{M}\right)=\tilde{L}\ominus\tilde{M}$.

Hence, (i) proved.

(ii) Similarly, we can prove $\left(\tilde{L}\vee_{\tilde{Q}}\tilde{M}\right)\oslash\left(\tilde{L}\wedge_{\tilde{Q}}\tilde{M}\right)=\tilde{L}\oslash\tilde{M}$ if $\sigma_{\tilde{L}}\leq min\left\{\sigma_{\tilde{M}},\frac{\sigma_{\tilde{T}_2}\varphi_1}{\varphi_2}\right\}$, $\delta_{\tilde{L}}\geq\delta_{\tilde{M}}$.

(iii) Since, $\sigma_{\tilde{L}}\leq min\left\{\sigma_{\tilde{M}},\frac{\sigma_{\tilde{M}}\varphi_1}{\varphi_2}\right\}$, $\delta_{\tilde{L}}\geq\delta_{\tilde{M}}$, then,

L.H.S = $\left(\tilde{L}\wedge_{\tilde{Q}}\tilde{M}\right)\oslash\left(\tilde{L}\vee_{\tilde{Q}}\tilde{M}\right)=\langle\min\{\sigma_{\tilde{L}},\sigma_{\tilde{M}}\},\max\{\delta_{\tilde{L}},\delta_{\tilde{M}}\}\rangle\oslash\langle\max\{\sigma_{\tilde{L}},\sigma_{\tilde{M}}\},\min\{\delta_{\tilde{L}},\delta_{\tilde{M}}\}\rangle$

$=\langle\frac{\min\{\sigma_{\tilde{L}},\sigma_{\tilde{M}}\}}{\max\{\sigma_{\tilde{L}},\sigma_{\tilde{M}}\}},\left\{\frac{(\max\{\delta_{\tilde{L}},\delta_{\tilde{M}}\})^{\frac{5}{4}}-(\min\{\delta_{\tilde{L}},\delta_{\tilde{M}}\})^{\frac{5}{4}}}{1-(\min\{\delta_{\tilde{L}},\delta_{\tilde{M}}\})^{\frac{5}{4}}}\right\}^{\frac{4}{5}}\rangle$

$=\langle\frac{\sigma_{\tilde{L}}}{\sigma_{\tilde{M}}},\left\{\frac{\max\left\{\delta_{\tilde{L}}{}^{\frac{5}{4}},\delta_{\tilde{M}}{}^{\frac{5}{4}}\right\}-\min\left\{\delta_{\tilde{L}}{}^{\frac{5}{4}},\delta_{\tilde{M}}{}^{\frac{5}{4}}\right\}}{1-\min\left\{\delta_{\tilde{L}}{}^{\frac{5}{4}},\delta_{\tilde{M}}{}^{\frac{5}{4}}\right\}}\right\}^{\frac{4}{5}}\rangle$

$=\langle\frac{\sigma_{\tilde{L}}}{\sigma_{\tilde{M}}},\left\{\frac{\delta_{\tilde{L}}{}^{\frac{5}{4}}-\delta_{\tilde{M}}{}^{\frac{5}{4}}}{1-\delta_{\tilde{M}}{}^{\frac{5}{4}}}\right\}^{\frac{4}{5}}\rangle$

$=\tilde{L}\oslash\tilde{M}=$ R. H. S.

$\therefore,\left(\tilde{L}\wedge_{\tilde{Q}}\tilde{M}\right)\oslash\left(\tilde{L}\vee_{\tilde{Q}}\tilde{M}\right)=\tilde{L}\oslash\tilde{M}$.

Hence, (iii) proved.

(iv) Similarly, we can prove, $\left(\tilde{L}\vee_{\tilde{Q}}\tilde{M}\right)\oslash\left(\tilde{L}\wedge_{\tilde{Q}}\tilde{M}\right)=\tilde{L}\oslash\tilde{M}$ if $\sigma_{\tilde{L}}\leq min\left\{\sigma_{\tilde{M}},\frac{\sigma_{\tilde{M}}\varphi_1}{\varphi_2}\right\}$, $\delta_{\tilde{L}}\geq\delta_{\tilde{M}}$.

Theorem 3.2.5

Let $\tilde{L}=\langle\sigma_{\tilde{L}},\delta_{\tilde{L}}\rangle$ and $\tilde{M}=\langle\sigma_{\tilde{M}},\delta_{\tilde{M}}\rangle$ represents two Quin-Terranean fuzzy numbers, then,

(i) $\left(\tilde{L}\wedge_{\tilde{Q}}\tilde{M}\right)\vee_{\tilde{Q}}\tilde{M}=\tilde{M}$

(ii) $\left(\tilde{L}\vee_{\tilde{Q}}\tilde{M}\right)\wedge_{\tilde{Q}}\tilde{M}=\tilde{M}$

(iii) $\left(\tilde{L}\ominus\tilde{M}\right)\boxplus\tilde{M}=\tilde{L}$ if $\sigma_{\tilde{L}}\geq\sigma_{\tilde{M}}$, $\delta_{\tilde{L}}\leq min\left\{\delta_{\tilde{M}},\frac{\delta_{\tilde{M}}\varphi_1}{\varphi_2}\right\}$.

(v) $\left(\tilde{L}\oslash\tilde{M}\right)\boxtimes\tilde{M}=\tilde{L}$ if $\sigma_{\tilde{L}}\leq min\left\{\sigma_{\tilde{M}},\frac{\sigma_{\tilde{M}}\varphi_1}{\varphi_2}\right\}$, $\delta_{\tilde{L}}\geq\delta_{\tilde{M}}$.

Proof:

Consider two Quin-Terranean fuzzy numbers $\tilde{L}=\langle\sigma_{\tilde{L}},\delta_{\tilde{L}}\rangle$ and $\tilde{M}=\langle\sigma_{\tilde{M}},\delta_{\tilde{M}}\rangle$.

(i) L.H.S = $\left(\tilde{L}\wedge_{\tilde{Q}}\tilde{M}\right)\vee_{\tilde{Q}}\tilde{M}$

$=\langle\min\{\sigma_{\tilde{L}},\sigma_{\tilde{M}}\},\max\{\delta_{\tilde{L}},\delta_{\tilde{M}}\}\rangle\vee_{\tilde{Q}}\langle\sigma_{\tilde{M}},\delta_{\tilde{M}}\rangle$

$=\langle\max\{\min\{\sigma_{\tilde{L}},\sigma_{\tilde{M}}\},\sigma_{\tilde{M}}\},\min\{\max\{\delta_{\tilde{L}},\delta_{\tilde{M}}\},\delta_{\tilde{M}}\}\rangle$

$=\langle\sigma_{\tilde{M}},\delta_{\tilde{M}}\rangle$

$=\tilde{M}$ = R.H.S.

$\therefore, (\tilde{L} \wedge_{\tilde{Q}} \tilde{M}) \vee_{\tilde{Q}} \tilde{M} = \tilde{M}.$

Hence, (i) proved.

(ii) L.H.S = $(\tilde{L} \vee_{\tilde{Q}} \tilde{M}) \wedge_{\tilde{Q}} \tilde{M}$

$= \langle \max\{\sigma_{\tilde{L}}, \sigma_{\tilde{M}}\}, \min\{\delta_{\tilde{L}}, \delta_{\tilde{M}}\} \rangle \cap \langle \sigma_{\tilde{M}}, \delta_{\tilde{M}} \rangle$

$= \langle \min\{\max\{\sigma_{\tilde{L}}, \sigma_{\tilde{M}}\}, \sigma_{\tilde{M}}\}, \max\{\min\{\delta_{\tilde{L}}, \delta_{\tilde{M}}\}, \delta_{\tilde{M}}\} \rangle$

$= \langle \sigma_{\tilde{M}}, \delta_{\tilde{M}} \rangle$

$= \tilde{M}$ = R.H.S.

$\therefore, (\tilde{L} \vee_{\tilde{Q}} \tilde{M}) \wedge \tilde{M} = \tilde{M}.$

Hence, (ii) proved.

(iii) Since, $\sigma_{\tilde{L}} \geq \sigma_{\tilde{M}},\ \delta_{\tilde{L}} \leq min\left\{\delta_{\tilde{M}}, \frac{\delta_{\tilde{M}} \varphi_1}{\varphi_2}\right\}$, then

L.H.S = $(\tilde{L} \ominus \tilde{M}) \boxplus \tilde{M} = \langle \left\{ \frac{{\sigma_{\tilde{L}}}^{4^5} - {\sigma_{\tilde{M}}}^{4^5}}{1 - {\sigma_{\tilde{M}}}^{4^5}} \right\}^{\frac{1}{4^5}}, \frac{\delta_{\tilde{L}}}{\delta_{\tilde{M}}} \rangle \boxplus \langle \sigma_{\tilde{M}}, \delta_{\tilde{M}} \rangle$

$$= \langle \left\{ \left[\left(\frac{{\sigma_{\tilde{L}}}^{4^5} - {\sigma_{\tilde{M}}}^{4^5}}{1 - {\sigma_{\tilde{M}}}^{4^5}} \right)^{\frac{1}{4^5}} \right]^{4^5} + {\sigma_{\tilde{M}}}^{4^5} - \left[\left(\frac{{\sigma_{\tilde{L}}}^{4^5} - {\sigma_{\tilde{M}}}^{4^5}}{1 - {\sigma_{\tilde{M}}}^{4^5}} \right)^{\frac{1}{4^5}} \right]^{4^5} {\sigma_{\tilde{M}}}^{4^5} \right\}^{\frac{1}{4^5}}, \frac{\delta_{\tilde{L}} \delta_{\tilde{M}}}{\delta_{\tilde{M}}} \rangle$$

$$= \langle \left\{ \left(\frac{{\sigma_{\tilde{L}}}^{4^5} - {\sigma_{\tilde{M}}}^{4^5}}{1 - {\sigma_{\tilde{M}}}^{4^5}} \right) + {\sigma_{\tilde{M}}}^{4^5} - \left(\frac{{\sigma_{\tilde{L}}}^{4^5} - {\sigma_{\tilde{M}}}^{4^5}}{1 - {\sigma_{\tilde{M}}}^{4^5}} \right) {\sigma_{\tilde{M}}}^{4^5} \right\}^{\frac{1}{4^5}}, \delta_{\tilde{L}} \rangle$$

$$= \langle \left\{ \frac{{\sigma_{\tilde{L}}}^{4^5} - {\sigma_{\tilde{M}}}^{4^5} + {\sigma_{\tilde{M}}}^{4^5} - {\sigma_{\tilde{M}}}^{4^5} {\sigma_{\tilde{M}}}^{4^5} - {\sigma_{\tilde{L}}}^{4^5} {\sigma_{\tilde{M}}}^{4^5} + {\sigma_{\tilde{M}}}^{4^5} {\sigma_{\tilde{M}}}^{4^5}}{1 - {\sigma_{\tilde{M}}}^{4^5}} \right\}^{\frac{1}{4^5}}, \delta_{\tilde{L}} \rangle$$

$$= \langle \left\{ \frac{{\sigma_{\tilde{L}}}^{4^5} \left(1 - {\sigma_{\tilde{M}}}^{4^5}\right)}{\left(1 - {\sigma_{\tilde{M}}}^{4^5}\right)} \right\}^{\frac{1}{4^5}}, \delta_{\tilde{L}} \rangle = \langle \left\{ {\sigma_{\tilde{L}}}^{4^5} \right\}^{\frac{1}{4^5}}, \delta_{\tilde{L}} \rangle = \langle \sigma_{\tilde{L}}, \delta_{\tilde{L}} \rangle$$

$= \tilde{L}$ = R.H.S.

$\therefore, (\tilde{L} \ominus \tilde{M}) \boxplus \tilde{M} = \tilde{L}$.

Hence, (iii) proved.

(iv) Since, $\sigma_{\tilde{L}} \leq min\left\{\sigma_{\tilde{M}}, \frac{\sigma_{\tilde{M}} \varphi_1}{\varphi_2}\right\}$, $\delta_{\tilde{L}} \geq \delta_{\tilde{M}}$, then,

L.H.S = $(\tilde{L} \oslash \tilde{M}) \boxtimes \tilde{M} = \langle \frac{\sigma_{\tilde{L}}}{\sigma_{\tilde{M}}}, \left\{ \frac{{\delta_{\tilde{L}}}^{\frac{5}{4}} - {\delta_{\tilde{M}}}^{\frac{5}{4}}}{1 - {\delta_{\tilde{M}}}^{\frac{5}{4}}} \right\}^{\frac{4}{5}} \rangle \boxtimes \langle \sigma_{\tilde{M}}, \delta_{\tilde{M}} \rangle$

$$= \langle \frac{\sigma_{\tilde{L}} \sigma_{\tilde{M}}}{\sigma_{\tilde{M}}}, \left\{ \left[\frac{{\delta_{\tilde{L}}}^{\frac{5}{4}} - {\delta_{\tilde{M}}}^{\frac{5}{4}}}{1 - {\delta_{\tilde{M}}}^{\frac{5}{4}}} \right]^{\frac{4}{5}} \right\}^{\frac{5}{4}} + {\delta_{\tilde{M}}}^{\frac{5}{4}} - \left\{ \left[\frac{{\delta_{\tilde{L}}}^{\frac{5}{4}} - {\delta_{\tilde{M}}}^{\frac{5}{4}}}{1 - {\delta_{\tilde{M}}}^{\frac{5}{4}}} \right]^{\frac{4}{5}} \right\}^{\frac{5}{4}} {\delta_{\tilde{M}}}^{\frac{5}{4}} \rangle$$

$$= \langle \sigma_{\tilde{L}}, \left[\frac{{\delta_{\tilde{L}}}^{\frac{5}{4}} - {\delta_{\tilde{M}}}^{\frac{5}{4}} + {\delta_{\tilde{M}}}^{\frac{5}{4}} - {\delta_{\tilde{M}}}^{\frac{5}{4}} {\delta_{\tilde{M}}}^{\frac{5}{4}} - {\delta_{\tilde{L}}}^{\frac{5}{4}} {\delta_{\tilde{M}}}^{\frac{5}{4}} + {\delta_{\tilde{M}}}^{\frac{5}{4}} {\delta_{\tilde{M}}}^{\frac{5}{4}}}{1 - {\delta_{\tilde{M}}}^{\frac{5}{4}}} \right]^{\frac{4}{5}} \rangle$$

$$= \langle \sigma_{\tilde{L}}, \left\{ \frac{{\delta_{\tilde{L}}}^{\frac{5}{4}} \left(1 - {\delta_{\tilde{M}}}^{\frac{5}{4}}\right)}{\left(1 - {\delta_{\tilde{M}}}^{\frac{5}{4}}\right)} \right\}^{\frac{4}{5}} \rangle = \langle \sigma_{\tilde{L}}, \left\{ {\delta_{\tilde{L}}}^{\frac{5}{4}} \right\}^{\frac{4}{5}} \rangle = \langle \sigma_{\tilde{L}}, \delta_{\tilde{L}} \rangle$$

$= \tilde{L}$ = R.H.S.

$$\therefore, (\tilde{L} \ominus \tilde{M}) \boxplus \tilde{M} = \tilde{L}\ .$$

Hence, (iv) proved.

Theorem 3.2.6

Let $\tilde{L} = \langle \sigma_{\tilde{L}}, \delta_{\tilde{L}} \rangle$, $\tilde{M} = \langle \sigma_{\tilde{M}}, \delta_{\tilde{M}} \rangle$ and $\tilde{R} = \langle \sigma_{\tilde{R}}, \delta_{\tilde{R}} \rangle$ represents three Quin-Terranean fuzzy numbers, then,

(i) $(\tilde{L} \wedge_{\tilde{Q}} \tilde{M}) \ominus \tilde{R} = (\tilde{L} \ominus \tilde{R}) \wedge_{\tilde{Q}} (\tilde{M} \ominus \tilde{R})$, if

$$\sigma_{\tilde{R}} \leq min\{\sigma_{\tilde{L}}, \sigma_{\tilde{M}}\}, max\{\delta_{\tilde{L}}, \delta_{\tilde{M}}\} \leq \left\{\delta_{\tilde{R}}, \frac{\delta_{\tilde{R}} \varphi_1}{\varphi_3}, \frac{\delta_{\tilde{T}_3} \varphi_2}{\varphi_3}\right\}, \frac{min\left\{{\sigma_{\tilde{L}}}^{4^5}, {\sigma_{\tilde{M}}}^{4^5}\right\} - {\sigma_{\tilde{T}_3}}^{4^5}}{\left(1 - {\sigma_{\tilde{R}}}^{4^5}\right)} + \frac{max\left\{{\delta_{\tilde{L}}}^{\frac{5}{4}}, {\delta_{\tilde{M}}}^{\frac{5}{4}}\right\}}{{\delta_{\tilde{R}}}^{\frac{5}{4}}} \leq 1;$$

(ii) $\left(\tilde{L}\vee_{\tilde{Q}}\tilde{M}\right)\ominus\tilde{R}=\left(\tilde{L}\ominus\tilde{R}\right)\vee_{\tilde{Q}}\left(\tilde{M}\ominus\tilde{R}\right)$,

(iii) if $\sigma_{\tilde{R}}\le min\{\sigma_{\tilde{L}},\sigma_{\tilde{M}}\},max\{\delta_{\tilde{L}},\delta_{\tilde{M}}\}\le\left\{\delta_{\tilde{R}},\frac{\delta_{\tilde{R}}\varphi_1}{\varphi_3},\frac{\delta_{\tilde{R}}\varphi_2}{\varphi_3}\right\},\frac{max\left\{{\sigma_{\tilde{L}}}^{4^5},{\sigma_{\tilde{M}}}^{4^5}\right\}-{\sigma_{\tilde{T}_3}}^{4^5}}{\left(1-{\sigma_{\tilde{R}}}^{4^5}\right)}+\frac{min\left\{\delta_{\tilde{L}}^{\frac{5}{4}},\delta_{\tilde{M}}^{\frac{5}{4}}\right\}}{\delta_{\tilde{R}}^{\frac{5}{4}}}\le 1$;

(iv) $\left(\tilde{L}\wedge_{\tilde{Q}}\tilde{M}\right)\oslash\tilde{R}=\left(\tilde{L}\oslash\tilde{R}\right)\wedge_{\tilde{Q}}\left(\tilde{M}\oslash\tilde{R}\right)$ if $\delta_{\tilde{R}}\le min\{\delta_{\tilde{L}},\delta_{\tilde{M}}\},max\{\sigma_{\tilde{L}},\sigma_{\tilde{M}}\}\le\left\{\sigma_{\tilde{R}},\frac{\sigma_{\tilde{R}}\varphi_1}{\varphi_3},\frac{\sigma_{\tilde{R}}\varphi_2}{\varphi_3}\right\},\frac{max\left\{\delta_{\tilde{L}}^{\frac{5}{4}},\delta_{\tilde{M}}^{\frac{5}{4}}\right\}-\delta_{\tilde{T}_3}^{\frac{5}{4}}}{\left(1-\delta_{\tilde{R}}^{\frac{5}{4}}\right)}+\frac{min\left\{{\sigma_{\tilde{L}}}^{4^5},{\sigma_{\tilde{M}}}^{4^5}\right\}}{{\sigma_{\tilde{R}}}^{4^5}}\le 1$;

(v) $\left(\tilde{L}\vee_{\tilde{Q}}\tilde{M}\right)\oslash\tilde{R}=\left(\tilde{L}\oslash\tilde{R}\right)\vee_{\tilde{Q}}\left(\tilde{M}\oslash\tilde{R}\right)$, if $\delta_{\tilde{R}}\le min\{\delta_{\tilde{L}},\delta_{\tilde{M}}\},max\{\sigma_{\tilde{L}},\sigma_{\tilde{M}}\}\le\left\{\sigma_{\tilde{R}},\frac{\sigma_{\tilde{R}}\varphi_1}{\varphi_3},\frac{\sigma_{\tilde{R}}\varphi_2}{\varphi_3}\right\},\frac{min\left\{\delta_{\tilde{L}}^{\frac{5}{4}},\delta_{\tilde{M}}^{\frac{5}{4}}\right\}-\delta_{\tilde{T}_3}^{\frac{5}{4}}}{\left(1-\delta_{\tilde{R}}^{\frac{5}{4}}\right)}+\frac{max\left\{{\sigma_{\tilde{L}}}^{4^5},{\sigma_{\tilde{M}}}^{4^5}\right\}}{{\sigma_{\tilde{R}}}^{4^5}}\le 1$;

Proof:

Let $\tilde{L}=\langle\sigma_{\tilde{L}},\delta_{\tilde{L}}\rangle$, $\tilde{M}=\langle\sigma_{\tilde{M}},\delta_{\tilde{M}}\rangle$ and $\tilde{R}=\langle\sigma_{\tilde{R}},\delta_{\tilde{R}}\rangle$ be three Quin-Terranean fuzzy numbers.

(i) Since, $\sigma_{\tilde{R}}\le min\{\sigma_{\tilde{L}},\sigma_{\tilde{M}}\},max\{\delta_{\tilde{L}},\delta_{\tilde{M}}\}\le\left\{\delta_{\tilde{R}},\frac{\delta_{\tilde{R}}\varphi_1}{\varphi_3},\frac{\delta_{\tilde{R}}\varphi_2}{\varphi_3}\right\},\frac{min\left\{{\sigma_{\tilde{L}}}^{4^5},{\sigma_{\tilde{M}}}^{4^5}\right\}-{\sigma_{\tilde{T}_3}}^{4^5}}{\left(1-{\sigma_{\tilde{R}}}^{4^5}\right)}+\frac{max\left\{\delta_{\tilde{L}}^{\frac{5}{4}},\delta_{\tilde{M}}^{\frac{5}{4}}\right\}}{\delta_{\tilde{R}}^{\frac{5}{4}}}\le 1.$

L.H.S = $\left(\tilde{L}\wedge_{\tilde{Q}}\tilde{M}\right)\ominus\tilde{R}=\langle\min\{\sigma_{\tilde{L}},\sigma_{\tilde{M}}\},\max\{\delta_{\tilde{L}},\delta_{\tilde{M}}\}\rangle\ominus\langle\sigma_{\tilde{R}},\delta_{\tilde{R}}\rangle$

$=\langle\left\{\frac{min\left\{{\sigma_{\tilde{L}}}^{4^5},{\sigma_{\tilde{M}}}^{4^5}\right\}-{\sigma_{\tilde{R}}}^{4^5}}{\left(1-{\sigma_{\tilde{R}}}^{4^5}\right)}\right\}^{4^5},\frac{\max\{\delta_{\tilde{L}},\delta_{\tilde{M}}\}}{\delta_{\tilde{R}}}\rangle$

$=\langle min\left\{\left(\frac{{\sigma_{\tilde{L}}}^{4^5}-{\sigma_{\tilde{R}}}^{4^5}}{1-{\sigma_{\tilde{R}}}^{4^5}}\right)^{\frac{1}{4^5}},\left(\frac{{\sigma_{\tilde{M}}}^{4^5}-{\sigma_{\tilde{R}}}^{4^5}}{1-{\sigma_{\tilde{R}}}^{4^5}}\right)^{\frac{1}{4^5}}\right\},max\left\{\frac{\delta_{\tilde{L}}}{\delta_{\tilde{R}}},\frac{\delta_{\tilde{M}}}{\delta_{\tilde{R}}}\right\}\rangle.$

$\left(\tilde{L}\ominus\tilde{R}\right)\wedge_{\tilde{Q}}\left(\tilde{M}\ominus\tilde{R}\right)=\langle\left\{\left(\frac{{\sigma_{\tilde{L}}}^{4^5}-{\sigma_{\tilde{R}}}^{4^5}}{1-{\sigma_{\tilde{R}}}^{4^5}}\right)^{\frac{1}{4^5}}\right\},\frac{\delta_{\tilde{L}}}{\delta_{\tilde{R}}}\rangle\wedge_{\tilde{Q}}\langle\left(\frac{{\sigma_{\tilde{M}}}^{4^5}-{\sigma_{\tilde{R}}}^{4^5}}{1-{\sigma_{\tilde{R}}}^{4^5}}\right)^{\frac{1}{4^5}},\frac{\delta_{\tilde{M}}}{\delta_{\tilde{R}}}\rangle$

$=\langle min\left\{\left(\frac{{\sigma_{\tilde{L}}}^{4^5}-{\sigma_{\tilde{R}}}^{4^5}}{1-{\sigma_{\tilde{R}}}^{4^5}}\right)^{\frac{1}{4^5}},\left(\frac{{\sigma_{\tilde{M}}}^{4^5}-{\sigma_{\tilde{R}}}^{4^5}}{1-{\sigma_{\tilde{R}}}^{4^5}}\right)^{\frac{1}{4^5}}\right\},max\left\{\frac{\delta_{\tilde{L}}}{\delta_{\tilde{R}}},\frac{\delta_{\tilde{M}}}{\delta_{\tilde{R}}}\right\}\rangle$

$\therefore,\left(\tilde{L}\wedge_{\tilde{Q}}\tilde{M}\right)\ominus\tilde{R}=\left(\tilde{L}\ominus\tilde{R}\right)\wedge_{\tilde{Q}}\left(\tilde{M}\ominus\tilde{R}\right)$

Hence, (i) proved.

(ii) Similarly we can prove $\left(\tilde{L}\vee_{\tilde{Q}}\tilde{M}\right)\ominus\tilde{R}=\left(\tilde{L}\ominus\tilde{R}\right)\vee_{\tilde{Q}}\left(\tilde{M}\ominus\tilde{R}\right)$, if $\sigma_{\tilde{R}}\le min\{\sigma_{\tilde{L}},\sigma_{\tilde{M}}\},max\{\delta_{\tilde{L}},\delta_{\tilde{M}}\}\le\left\{\delta_{\tilde{R}},\frac{\delta_{\tilde{R}}\varphi_1}{\varphi_3},\frac{\delta_{\tilde{R}}\varphi_2}{\varphi_3}\right\},\frac{max\left\{{\sigma_{\tilde{L}}}^{4^5},{\sigma_{\tilde{M}}}^{4^5}\right\}-{\sigma_{\tilde{R}}}^{4^5}}{\left(1-{\sigma_{\tilde{R}}}^{4^5}\right)}+\frac{min\left\{\delta_{\tilde{L}}^{\frac{5}{4}},\delta_{\tilde{M}}^{\frac{5}{4}}\right\}}{\delta_{\tilde{R}}^{\frac{5}{4}}}\le 1.$

(iii) Since, $\delta_{\tilde{R}}\le min\{\delta_{\tilde{L}},\delta_{\tilde{M}}\},max\{\sigma_{\tilde{L}},\sigma_{\tilde{M}}\}\le\left\{\sigma_{\tilde{R}},\frac{\sigma_{\tilde{R}}\varphi_1}{\varphi_3},\frac{\sigma_{\tilde{R}}\varphi_2}{\varphi_3}\right\},\frac{max\left\{\delta_{\tilde{L}}^{\frac{5}{4}},\delta_{\tilde{M}}^{\frac{5}{4}}\right\}-\delta_{\tilde{R}}^{\frac{5}{4}}}{\left(1-\delta_{\tilde{R}}^{\frac{5}{4}}\right)}+\frac{min\left\{{\sigma_{\tilde{L}}}^{4^5},{\sigma_{\tilde{M}}}^{4^5}\right\}}{{\sigma_{\tilde{R}}}^{4^5}}\le 1.$

L.H.S = $\left(\tilde{L}\wedge_{\tilde{Q}}\tilde{M}\right)\oslash\tilde{R}=\langle\min\{\sigma_{\tilde{L}},\sigma_{\tilde{M}}\},\max\{\delta_{\tilde{L}},\delta_{\tilde{M}}\}\rangle\oslash\langle\sigma_{\tilde{R}},\delta_{\tilde{R}}\rangle$

$=\langle\frac{min\{\sigma_{\tilde{L}},\sigma_{\tilde{M}}\}}{\sigma_{\tilde{R}}},\left\{\frac{max\left\{\delta_{\tilde{L}}^{\frac{5}{4}},\delta_{\tilde{M}}^{\frac{5}{4}}\right\}-\delta_{\tilde{R}}^{\frac{5}{4}}}{\left(1-\delta_{\tilde{R}}^{\frac{5}{4}}\right)}\right\}^{\frac{4}{5}}\rangle$

$=\langle min\left\{\frac{\sigma_{\tilde{L}}}{\sigma_{\tilde{R}}},\frac{\sigma_{\tilde{M}}}{\sigma_{\tilde{R}}}\right\},max\left\{\left(\frac{\delta_{\tilde{L}}^{\frac{5}{4}}-\delta_{\tilde{R}}^{\frac{5}{4}}}{\left(1-\delta_{\tilde{R}}^{\frac{5}{4}}\right)}\right)^{\frac{4}{5}},\left(\frac{\delta_{\tilde{M}}^{\frac{5}{4}}-\delta_{\tilde{R}}^{\frac{5}{4}}}{\left(1-\delta_{\tilde{R}}^{\frac{5}{4}}\right)}\right)^{\frac{4}{5}}\right\}\rangle$

R.H.S= $\left(\tilde{L}\oslash\tilde{R}\right)\wedge_{\tilde{Q}}\left(\tilde{M}\oslash\tilde{R}\right)$

$=\langle\frac{\sigma_{\tilde{L}}}{\sigma_{\tilde{R}}},\left(\frac{\delta_{\tilde{L}}^{\frac{5}{4}}-\delta_{\tilde{R}}^{\frac{5}{4}}}{\left(1-\delta_{\tilde{R}}^{\frac{5}{4}}\right)}\right)^{\frac{4}{5}}\rangle\wedge_{\tilde{Q}}\langle\frac{\sigma_{\tilde{M}}}{\sigma_{\tilde{R}}},\left(\frac{\delta_{\tilde{M}}^{\frac{5}{4}}-\delta_{\tilde{R}}^{\frac{5}{4}}}{\left(1-\delta_{\tilde{R}}^{\frac{5}{4}}\right)}\right)^{\frac{4}{5}}\rangle$

$= \langle min\left\{\frac{\sigma_{\tilde{L}}}{\sigma_{\tilde{R}}}, \frac{\sigma_{\tilde{M}}}{\sigma_{\tilde{R}}}\right\}, max\left\{\left(\frac{\delta_{\tilde{L}}{}^{\frac{5}{4}} - \delta_{\tilde{R}}{}^{\frac{5}{4}}}{\left(1-\delta_{\tilde{R}}{}^{\frac{5}{4}}\right)}\right)^{\frac{4}{5}}, \left(\frac{\delta_{\tilde{M}}{}^{\frac{5}{4}} - \delta_{\tilde{R}}{}^{\frac{5}{4}}}{\left(1-\delta_{\tilde{R}}{}^{\frac{5}{4}}\right)}\right)^{\frac{4}{5}}\right\}\rangle$

$\therefore, (\tilde{L} \wedge_{\tilde{Q}} \tilde{M}) \oslash \tilde{R} = (\tilde{L} \oslash \tilde{R}) \wedge_{\tilde{Q}} (\tilde{M} \oslash \tilde{R})$

Hence, (iii) proved.

(iv) Similarly we can prove $(\tilde{L} \vee_{\tilde{Q}} \tilde{M}) \oslash \tilde{R} = (\tilde{L} \oslash \tilde{R}) \vee_{\tilde{Q}} (\tilde{M} \oslash \tilde{R})$, if $\delta_{\tilde{R}} \leq min\{\delta_{\tilde{L}}, \delta_{\tilde{M}}\}, max\{\sigma_{\tilde{L}}, \sigma_{\tilde{M}}\} \leq \left\{\sigma_{\tilde{R}}, \frac{\sigma_{\tilde{R}}\varphi_1}{\varphi_3}, \frac{\sigma_{\tilde{R}}\varphi_2}{\varphi_3}\right\}, \frac{min\left\{\delta_{\tilde{L}}{}^{\frac{5}{4}}, \delta_{\tilde{M}}{}^{\frac{5}{4}}\right\} - \delta_{\tilde{T}_3}{}^{\frac{5}{4}}}{\left(1-\delta_{\tilde{R}}{}^{\frac{5}{4}}\right)} + \frac{max\left\{\sigma_{\tilde{L}}{}^{4^5}, \sigma_{\tilde{M}}{}^{4^5}\right\}}{\sigma_{\tilde{R}}{}^{4^5}} \leq 1.$

Quin-Terranean Arithmetic mean operations over Quin-Terranean fuzzy numbers

In this section, Quin-Terranean Arithmetic mean operation over Quin-Terranean fuzzy numbers is defined.

Definition 3.3.1

Let $\tilde{L} = \langle \sigma_{\tilde{L}}, \delta_{\tilde{L}} \rangle$, $\tilde{M} = \langle \sigma_{\tilde{M}}, \delta_{\tilde{M}} \rangle$ represents two Quin-Terranean fuzzy numbers, then the average operator on $\tilde{L}$ and $\tilde{M}$ is characterized as

$$\tilde{L}@\tilde{M} = \langle \frac{\sigma_{\tilde{L}}{}^{4^5} + \sigma_{\tilde{M}}{}^{4^5}}{2}, \frac{\delta_{\tilde{L}}{}^{\frac{5}{4}} + \delta_{\tilde{M}}{}^{\frac{5}{4}}}{2} \rangle$$

Properties of Quin-Terranean Arithmetic mean operations on Quin Terranean fuzzy numbers

The several properties of the max –min and min – max operations on Quin Terranean fuzzy numbers are given as follows,

Theorem 3.4.1

Let $\tilde{L} = \langle \sigma_{\tilde{L}}, \delta_{\tilde{L}} \rangle$, $\tilde{M} = \langle \sigma_{\tilde{M}}, \delta_{\tilde{M}} \rangle$ and $\tilde{R} = \langle \sigma_{\tilde{R}}, \delta_{\tilde{R}} \rangle$ represents three Quin-Terranean fuzzy numbers, then,

(i) $(\tilde{L} \wedge_{\tilde{Q}} \tilde{M})@\tilde{R} = (\tilde{L}@\tilde{R}) \wedge_{\tilde{Q}} (\tilde{M}@\tilde{R})$

(ii) $(\tilde{L} \vee_{\tilde{Q}} \tilde{M})@\tilde{R} = (\tilde{L}@\tilde{R}) \vee_{\tilde{Q}} (\tilde{M}@\tilde{R})$

Proof:

Let $\tilde{L} = \langle \sigma_{\tilde{L}}, \delta_{\tilde{L}} \rangle$, $\tilde{M} = \langle \sigma_{\tilde{M}}, \delta_{\tilde{M}} \rangle$ and $\tilde{R} = \langle \sigma_{\tilde{R}}, \delta_{\tilde{R}} \rangle$ represents three Quin-Terranean fuzzy numbers, then,

(i) L. H. S $= (\tilde{L} \wedge_{\tilde{Q}} \tilde{M})@\tilde{R}$

$= \langle \min\{\sigma_{\tilde{L}}, \sigma_{\tilde{M}}\}, \max\{\delta_{\tilde{L}}, \delta_{\tilde{M}}\} \rangle @ \langle \sigma_{\tilde{R}}, \delta_{\tilde{R}} \rangle$

$= \langle \min\left\{\frac{\sigma_{\tilde{L}}{}^{4^5} + \sigma_{\tilde{R}}{}^{4^5}}{2}, \frac{\sigma_{\tilde{M}}{}^{4^5} + \sigma_{\tilde{R}}{}^{4^5}}{2}\right\}, \max\left\{\frac{\delta_{\tilde{L}}{}^{\frac{5}{4}} + \delta_{\tilde{R}}{}^{\frac{5}{4}}}{2}, \frac{\delta_{\tilde{M}}{}^{\frac{5}{4}} + \delta_{\tilde{R}}{}^{\frac{5}{4}}}{2}\right\} \rangle$

$= \langle \frac{\sigma_{\tilde{L}}{}^{4^5} + \sigma_{\tilde{R}}{}^{4^5}}{2}, \frac{\delta_{\tilde{L}}{}^{\frac{5}{4}} + \delta_{\tilde{R}}{}^{\frac{5}{4}}}{2} \rangle \wedge_{\tilde{Q}} \langle \frac{\sigma_{\tilde{M}}{}^{4^5} + \sigma_{\tilde{R}}{}^{4^5}}{2}, \frac{\delta_{\tilde{M}}{}^{\frac{5}{4}} + \delta_{\tilde{R}}{}^{\frac{5}{4}}}{2} \rangle$

$= (\tilde{L}@\tilde{R}) \wedge_{\tilde{Q}} (\tilde{M}@\tilde{R})$ = R. H. S

$\therefore, (\tilde{L} \wedge_{\tilde{Q}} \tilde{M})@\tilde{R} = (\tilde{L}@\tilde{R}) \wedge_{\tilde{Q}} (\tilde{M}@\tilde{R})$.

Hence, (i) proved.

(ii) L. H. S $= (\tilde{L} \vee_{\tilde{Q}} \tilde{M})@\tilde{R} = \langle \max\{\sigma_{\tilde{L}}, \sigma_{\tilde{M}}\}, \min\{\delta_{\tilde{L}}, \delta_{\tilde{M}}\} \rangle @ \langle \sigma_{\tilde{R}}, \delta_{\tilde{R}} \rangle$

$= \langle \max\left\{\frac{\sigma_{\tilde{L}}{}^{4^5} + \sigma_{\tilde{R}}{}^{4^5}}{2}, \frac{\sigma_{\tilde{M}}{}^{4^5} + \sigma_{\tilde{R}}{}^{4^5}}{2}\right\}, \min\left\{\frac{\delta_{\tilde{L}}{}^{\frac{5}{4}} + \delta_{\tilde{R}}{}^{\frac{5}{4}}}{2}, \frac{\delta_{\tilde{M}}{}^{\frac{5}{4}} + \delta_{\tilde{R}}{}^{\frac{5}{4}}}{2}\right\} \rangle$

$= \langle \frac{\sigma_{\tilde{L}}{}^{4^5} + \sigma_{\tilde{R}}{}^{4^5}}{2}, \frac{\delta_{\tilde{L}}{}^{\frac{5}{4}} + \delta_{\tilde{R}}{}^{\frac{5}{4}}}{2} \rangle \vee_{\tilde{Q}} \langle \frac{\sigma_{\tilde{M}}{}^{4^5} + \sigma_{\tilde{R}}{}^{4^5}}{2}, \frac{\delta_{\tilde{M}}{}^{\frac{5}{4}} + \delta_{\tilde{R}}{}^{\frac{5}{4}}}{2} \rangle$

$= (\tilde{L}@\tilde{R}) \vee_{\tilde{Q}} (\tilde{M}@\tilde{R})$ = R. H. S

$\therefore, (\tilde{L} \vee_{\tilde{Q}} \tilde{M})@\tilde{R} = (\tilde{L}@\tilde{R}) \vee_{\tilde{Q}} (\tilde{M}@\tilde{R})$.

Hence, (ii) proved.

Theorem 3.4.2

Let $\tilde{L} = \langle \sigma_{\tilde{L}}, \delta_{\tilde{L}} \rangle$ and $\tilde{M} = \langle \sigma_{\tilde{M}}, \delta_{\tilde{M}} \rangle$ represents two Quin-Terranean fuzzy numbers, then,

$\left((\tilde{L} \wedge_{\tilde{Q}} \tilde{M}) \boxplus (\tilde{L} \vee_{\tilde{Q}} \tilde{M})\right) @ \left((\tilde{L} \wedge_{\tilde{Q}} \tilde{M}) \boxtimes (\tilde{L} \vee_{\tilde{Q}} \tilde{M})\right) = \tilde{L}@\tilde{M}$.

Proof:

We have, $\min(a,b)+\max(a,b)=a+b$ and

$\min(a,b).\max(a,b)=a.b$

Where a, b are two real numbers.

Consider L.H.S,

$(\tilde{L}\wedge_{\tilde{Q}}\tilde{M})\boxplus(\tilde{L}\vee_{\tilde{Q}}\tilde{M})=\langle\min\{\sigma_{\tilde{L}},\sigma_{\tilde{M}}\},\max\{\delta_{\tilde{L}},\delta_{\tilde{M}}\}\rangle\boxplus\langle\max\{\sigma_{\tilde{L}},\sigma_{\tilde{M}}\},\min\{\delta_{\tilde{L}},\delta_{\tilde{M}}\}\rangle$

$=\langle\left\{min\{{\sigma_{\tilde{L}}}^{4^5},{\sigma_{\tilde{M}}}^{4^5}\}+max\{{\sigma_{\tilde{L}}}^{4^5},{\sigma_{\tilde{M}}}^{4^5}\}-min\{{\sigma_{\tilde{L}}}^{4^5},{\sigma_{\tilde{M}}}^{4^5}\}max\{{\sigma_{\tilde{L}}}^{4^5},{\sigma_{\tilde{M}}}^{4^5}\}\right\}^{\frac{1}{4^5}},\max\{\delta_{\tilde{L}},\delta_{\tilde{M}}\}\min\{\delta_{\tilde{L}},\delta_{\tilde{M}}\}\rangle$

$=\langle\{{\sigma_{\tilde{L}}}^{4^5}+{\sigma_{\tilde{M}}}^{4^5}-{\sigma_{\tilde{L}}}^{4^5}{\sigma_{\tilde{M}}}^{4^5}\}^{\frac{1}{4^5}},\delta_{\tilde{L}}\delta_{\tilde{M}}\rangle$

$(\tilde{L}\wedge_{\tilde{Q}}\tilde{M})\boxtimes(\tilde{L}\vee_{\tilde{Q}}\tilde{M})=\langle\min\{\sigma_{\tilde{L}},\sigma_{\tilde{M}}\},\max\{\delta_{\tilde{L}},\delta_{\tilde{M}}\}\rangle\boxtimes$
$\langle\max\{\sigma_{\tilde{L}},\sigma_{\tilde{M}}\},\min\{\delta_{\tilde{L}},\delta_{\tilde{M}}\}\rangle$

$=\langle\min\{\sigma_{\tilde{L}},\sigma_{\tilde{M}}\}\max\{\delta_{\tilde{L}},\delta_{\tilde{M}}\},\left\{\max\left\{\delta_{\tilde{L}}^{\frac{5}{4}},\delta_{\tilde{M}}^{\frac{5}{4}}\right\}+\min\left\{\delta_{\tilde{L}}^{\frac{5}{4}},\delta_{\tilde{M}}^{\frac{5}{4}}\right\}-\max\left\{\delta_{\tilde{L}}^{\frac{5}{4}},\delta_{\tilde{M}}^{\frac{5}{4}}\right\}\min\left\{\delta_{\tilde{L}}^{\frac{5}{4}},\delta_{\tilde{M}}^{\frac{5}{4}}\right\}\right\}^{\frac{4}{5}}\rangle$

$=\langle\sigma_{\tilde{L}}\sigma_{\tilde{M}},\left\{\delta_{\tilde{L}}^{\frac{5}{4}}+\delta_{\tilde{M}}^{\frac{5}{4}}-\delta_{\tilde{L}}^{\frac{5}{4}}\delta_{\tilde{M}}^{\frac{5}{4}}\right\}^{\frac{4}{5}}\rangle.$

Therefore,

$L.H.S=\left((\tilde{L}\wedge_{\tilde{Q}}\tilde{M})\boxplus(\tilde{L}\vee_{\tilde{Q}}\tilde{M})\right)@\left((\tilde{L}\wedge_{\tilde{Q}}\tilde{M})\boxtimes(\tilde{L}\vee_{\tilde{Q}}\tilde{M})\right)$

$=\langle\{{\sigma_{\tilde{L}}}^{4^5}+{\sigma_{\tilde{M}}}^{4^5}-{\sigma_{\tilde{L}}}^{4^5}{\sigma_{\tilde{M}}}^{4^5}\}^{\frac{1}{4^5}},\delta_{\tilde{L}}\delta_{\tilde{M}}\rangle@$

$\langle\sigma_{\tilde{L}}\sigma_{\tilde{M}},\left\{\delta_{\tilde{L}}^{\frac{5}{4}}+\delta_{\tilde{M}}^{\frac{5}{4}}-\delta_{\tilde{L}}^{\frac{5}{4}}\delta_{\tilde{M}}^{\frac{5}{4}}\right\}^{\frac{4}{5}}\rangle$

$=\langle\frac{{\sigma_{\tilde{L}}}^{4^5}+{\sigma_{\tilde{M}}}^{4^5}}{2},\frac{\delta_{\tilde{L}}^{\frac{5}{4}}+\delta_{\tilde{M}}^{\frac{5}{4}}}{2}\rangle=\tilde{L}@\tilde{M}=\text{R.H.S}$

Hence the proof.

CONCLUSION

In this paper, we have defined various operators namely, Max – Min ($\vee_{\tilde{Q}}$), Min – Max ($\wedge_{\tilde{Q}}$) operators and Average operator (@) on Quin – Terranean Fuzzy Numbers. Several properties of these Max – Min ($\vee_{\tilde{Q}}$) and Min – Max ($\wedge_{\tilde{Q}}$) operators as well as in combination with the basic operation of complement and model operators such as $\boxplus,\boxtimes,\ominus,\varnothing$ already defined on Quin – Terranean Fuzzy Numbers are also studied. Additionally, several properties of the Average operator (@) in combination with Max – Min ($\vee_{\tilde{Q}}$), Min – Max ($\wedge_{\tilde{Q}}$) operators and model operators on Quin-Terranean Fuzzy numbers are also analyzed. Quin-Terranean Fuzzy Numbers have more applications, and it would be possible to study their features. Furthermore, these operations on Quin-Terranean Fuzzy Numbers have applications in numerous other fields, such as decision-making, agriculture, and healthcare, etc which will be planned as a future work.

REFERENCES

1. Krassimir T. Atanassov, "Intuitionistic Fuzzy Sets", Fuzzy Sets and Systems, 20, 87-96, 1986.
2. Dug Hun Hong and Kyung Tae Kim, "An Easy Computation of Min and Max Operations for Fuzzy Numbers", Journal of Applied Mathematics and Computing, 2006, 21(1-2), 555-561.
3. Ferdinando Di Martino and Salvatore Sessa, "Eigen Fuzzy Sets and their Application to Evaluate the Effectiveness of Actions in Decision Problems", mathematics, 2020,8,1999; doi:10.3390/math8111999.
4. Ion Iancu, "Intuitionistic Fuzzy Similarity measures based on min-max operators", Pattern Analysis and Applications, 2019, 22, 429-438, https://doi.org/10.1007/s10044-017-0636-5.
5. Kim Hyun, Yun Yong Sik and Park Jin Won, "A Zadeh's max-min composition operator for two triangular fuzzy numbers defined on R", Journal for History of Mathematics, 2020, 33(5), 277-287.
6. S.Melliani, M. Elomari, L. S. Chadli and R. Ettoussi, "Resolution of a system of the max-min product

7. Intuitionistic fuzzy relation equations using LU-factorization", Notes on Intuitionistic Fuzzy Sets, 2014, 20(5), 36-49.
8. P. Rajarajeswari, T. Thirunamakkani, "Application of Quin-Terranean Fuzzy Set in Transportation Problem under Fuzzy Environment", 2023, XCVI(12), 171-181.
9. Quin – Terranean Fuzzy set. *Accepted. Bulletin of Calcutta Mathematical Society.*
10. Algebraic operations on Quin-Terranean Fuzzy Number. *Accepted*. *Indian Journal of Natural Sciences*. Special algebraic operations on Quin-Terranean Fuzzy Number. *Accepted*. *Indian Journal of Natural Sciences*.
11. R.Snehaa and S. Sandhiya, "Pythagorean Fuzzy Set and Its Application in Career Placements Using Min-Max-Min Composition", Journal of Algebraic Statistics, 2022, 13(2), 2234-2239.
12. R.R. Yager, "Generalized orthopair fuzzy sets", IEEE Transaction on Fuzzy Systems, 25(5), 1222- 1230,2017.
13. Tapan Senapati, Ronald R. Yager, "Fermatean fuzzy sets", Journal of Ambient Intelligence and Humanized Computing, http:/doi.org/10.1007/s12652-019-01377-0,2019.
14. Tapan Senapati, Ronald R. Yager, "Some new operations over Fermaean Fuzzy Numbers and Application of Fermatean fuzzy WPM in Multi Criteria Decision Making", Informatica, Vol.30,No.2,391-412,2019.
15. L. A. Zadeh, "Fuzzy Sets", Information and Control, 8, 338-353, 1965.

Indian Journal of Natural Sciences *www.tnsroindia.org.in ©IJONS*

Vol.15 / Issue 83 / Apr / 2024 *International Bimonthly (Print) – Open Access* *ISSN: 0976 – 0997*

RESEARCH ARTICLE

Artificial Intelligence's Place in Radiology: Current uses and Future Prospects

Naresh Kumar[1]*, Bimal Nepal[2] and Dinesh Kumar[3] and Manvee Rai[4]

[1]Assistant Professor, Department of Radiology, School of Health Science, Om Sterling Global University, Hisar, Haryana, India.
[2]Research Scholar, Department of Radio Imaging Technology, College of Paramedical Sciences, Teerthanker Mahaveer University, Uttar Pradesh, India.
[3]Associate Professor, School of Pharmacy, Desh Bhagat University, Punjab, India.
[4]Assistant Professor, School of Paramedical Sciences ,Lifeline Educational Institute Sameda,Azamgarh U.P

Received: 30 Dec 2023 Revised: 09 Jan 2024 Accepted: 27 Mar 2024

***Address for Correspondence**
Naresh Kumar
Assistant Professor,
Department of Radiology,
School of Health Science,
Om Sterling Global University,
Hisar, Haryana, India.
Email: nareshkumar59239@gmai.com

ABSTRACT

This review explores how artificial intelligence (AI) has transformed radiology, redefining how medical images are analyzed and used. We delve into current AI applications, including image segmentation, lesion detection, disease classification, and image enhancement, all powered by advanced machine learning and deep learning techniques. Real-world case studies highlight AI's impact on diagnostic accuracy and operational efficiency. We also explain the core methodologies driving these radiological advancements, including deep learning architectures and convolutional neural networks. While AI holds promise, ethical concerns, biases in training data, and potential overreliance on automation necessitate careful consideration and collaboration between AI and human experts. Looking forward, we envision AI contributing to personalized treatment strategies through innovations like multimodal fusion and image-guided interventions. However, successful integration requires addressing challenges such as data quality and regulatory compliance, and ongoing training of radiologists to fully leverage AI's potential in clinical practice. We aim to illuminate the path that radiology has embarked upon—one where the collaboration between human expertise and AI-driven insights stands set to redefine the boundaries of radiologic imaging and patient care. In conclusion, this review underscores AI's transformative role in radiology, discussing current applications, methodologies, challenges, and prospects. This synergy

between AI and human expertise has the capability to reshape medical imaging and enhance health care service.

Keywords: Artificial Intelligence (AI), Convolutional Neural Networks (CNNs), natural language processing (NLP),Natural Language Processing (NLP), picture archiving and communication systems (PACS).

INTRODUCTION

AI refers to the emulation of human intelligence processes by machines, particularly computer systems. Among these processes are learning, logical reasoning, problem-solving, perception, and language comprehension**[1].** In recent years, Artificial intelligence (AI) is developing quickly, and this has caused a paradigm shift in the field of radiology [2].As medical imaging technologies continue to produce increasingly intricate datasets, the incorporation of AI-driven methodologies has enabled a more nuanced and efficient interpretation of these images[3, 4]. Radiologists have long grappled with the intricate task of analyzing a wealth of medical images, extracting critical information to aid accurate diagnoses and treatment plans[5, 6, 7, 8, 9]. However, this task has grown in complexity as imaging modalities evolve and generate voluminous data that demands precise and swift analysis[10, 11].The utilization of AI methods, especially machine learning and deep learning algorithms, has appeared as a ground-breaking solution. By harnessing the computational power of AI, radiologists are now empowered to decipher patterns, detect anomalies, and enhance the diagnostic process with unprecedented accuracy[12, 13, 14]. Beyond the realm of diagnostics, AI's impact resonates across various facets of radiology. From the early detection of diseases to the fine-tuning of treatment strategies, the synergy between AI and medical imaging has far-reaching implications for patient care[15, 16].Nevertheless, this technological amalgamation comes with its set of difficulties.

Ethical considerations, data privacy concerns, and the potential for bias within AI algorithms underscore the need for a comprehensive exploration of the interplay between AI and radiology. A notable advancement involves the utilization of contemporary computer vision techniques, driven by deep learning, in the realm of medical applications. This progress is particularly concentrated on enhancing medical imaging, medical video analysis, and facilitating clinical deployment. One notable instance is the application of computer vision in the medical domain, as depicted in consider Fig 1, depicting a deep learning setup designed to extract valuable information simultaneously from two sources: images, typically analyzed using convolutional networks, and non-image data, typically managed by more versatile deep networks. The acquired explanation may encompass pathology diagnostics, symptoms, clinical forecasting, and various amalgamation. Fig 2 illustrates that CNNs can learn to generate images through training. Tasks vary, spanning from regression between images (as shown) to enhancing image resolution, creating new images, and various other objectives. Computer vision in clinical settings covers a wide range of tasks, including screening, diagnosis, condition detection, outcome prediction, and segmentation for identifying abnormalities within organs at the cellular level. It also involves monitoring diseases and providing support for clinical research. By generating accurate diagnostic results, they prevent human errors, ultimately saving lives and reducing expenses. Predictive and early diagnostics benefit from AI-enabled assistants that generate scan reports with high accuracy.AI is presently utilized in the research and development sphere, specifically in mining data from medical records. Cognitive technologies support healthcare organizations by utilizing extensive data resources to improve diagnostic capabilities[17].

The background and significance

The background and significance of the role of AI in radiology lies at the intersection of technological innovation and the evolving demands of modern healthcare. Historically, radiologists have relied on their expertise to analyse medical images and provide critical insights for diagnosis and treatment. But with the introduction of cutting-edge imaging technologies like computed tomography (CT), magnetic resonance imaging (MRI), and positron emission tomography (PET), data generation has increased dramatically, making it more challenging for radiologists to

effectively process and interpret this data. This surge in data has created a bottleneck in the diagnostic process, leading to delays and the potential for missed diagnoses[18, 19,20]. In response, artificial intelligence (AI) technologies-in particular, machine learning and deep learning algorithms—have become a potent remedy. These algorithms have the capability to analyze extensive datasets and detect subtle patterns that might elude human observation. This ability has paved the way for breakthroughs in image segmentation, lesion detection, and disease classification. AI-driven image enhancement techniques further contribute to the extraction of clinically relevant information, facilitating more accurate and timely diagnoses[21]. The significance of this integration extends beyond diagnostic accuracy. AI's potential to streamline workflow processes, reduce interpretation times, and enhance efficiency holds the promise of addressing the challenges posed by the data deluge. Moreover, AI introduces the concept of predictive analytics, where algorithms can forecast disease progression and tre-atment responses, offering personalized and targeted interventions[22,23]. In essence, the integration of AI in radiology not only addresses the pressing challenges of data overload but also ushers in a new era of precision medicine. By augmenting radiologists' capabilities, AI has the capability to transform healthcare delivery, providing more accurate diagnoses, improved patient outcomes, and ultimately contributing to a more efficient and effective healthcare system. As such, understanding the background and significance of AI's role in radiology is crucial to navigating its benefits and hurdles in the swiftly changing environment of medical imaging[24 – 28].

Current Applications

In the present landscape of radiology, the integration of artificial intelligence (AI) has permeated various dimensions, propelling the field into new realms of accuracy and efficiency. AI's current applications encompass a spectrum of tasks, each addressing critical challenges within medical imaging.

Image Segmentation

AI algorithms excel at precisely delineating anatomical structures and identifying regions of interest within medical images. For instance, in brain MRI scans, AI-driven segmentation accurately separates different brain regions, aiding in the assessment of neurodegenerative disorders.

Lesion Detection

The ability of AI to detect subtle abnormalities is a game-changer. In mammography, AI-powered systems assist radiologists in spotting early signs of breast cancer by highlighting potential lesions that might otherwise be missed, thus enhancing diagnostic sensitivity.

Disease Classification

AI's capacity for pattern recognition has found prominence in disease classification. In the case of lung nodules detected in CT scans, AI algorithms can differentiate benign from malignant nodules with remarkable accuracy, expediting the diagnostic process and minimizing unnecessary interventions.

Image Enhancement

AI has the capacity to enhance image quality, particularly in cases of noisy or degraded images. This technology aids in reducing artifacts in MRI images, leading to improved visualization of soft tissue structures[29 – 33]. Furthermore, the integration of AI augments the radiologist's workflow. AI-powered tools can prioritize the order in which images are reviewed, reducing interpretation time. Moreover, AI-driven systems can flag cases that require immediate attention, ensuring that critical findings are swiftly brought to the radiologist's notice[21].

METHODOLOGIES AND TECHNIQUES

The incorporation of AI into radiology depends on a range of advanced methodologies and techniques, each designed to harness the intricacies of medical imaging data. Prominent among these are machine learning, deep

learning, convolutional neural networks (CNNs), and natural language processing (NLP), each delivering distinct capabilities to enhance diagnostics across various imaging modalities.

Machine Learning

This foundational AI technique involves training algorithmsto discern patterns within data and formulate forecasts or choices. In radiology, it can be used to develop predictive models for disease outcomes based on historical patient data[34, 35].

Deep Learning

it is a kind of machine learning, uses layers of neural networks to analyse complicated patterns. Deep learning excels at feature extraction, enabling radiologists to uncover intricate details in images that might elude traditional methods[36, 37].

Convolutional Neural Networks (CNNs)

A cornerstone of deep learning, CNNs are particularly well-suited for image analysis. Through the hierarchical analysis of visual characteristics, CNNs have shown impressive achievements in endeavors such as image categorization, identifying abnormalities, and dividing images into segments across various modalities including X-ray, MRI, CT, and PET scans [38, 39,40].

Natural Language Processing (NLP)

While NLP is more commonly associated with text analysis, its integration with radiology involves interpreting unstructured text data, such as radiology reports. NLP algorithms can extract relevant information from these reports, aiding in the correlation of clinical findings and image data[41, 42]. Collectively, these AI techniques and their application to diverse imaging modalities converge to transform the radiological landscape. By unlocking deeper insights and refining diagnostic accuracy, they underscore the potential of AI to augment radiologists' capabilities, ultimately translating to improved patient care.

CHALLENGES AND LIMITATIONS

Challenges:

1. **Workflow Disruption:** Incorporating new AI tools can disrupt established clinical workflows, potentially leading to initial inefficiencies as radiologists adapt to these changes[43, 44, 45].
2. **Integration with Existing Systems:**It takes meticulous coordination and technological know-how to ensure that AI is seamlessly integrated with current PACS and electronic health records (EHR) [44, 46].
3. **Data Compatibility:** AI models demand a large, diverse dataset for training. However, compatibility issues between AI algorithms and various imaging devices and formats can hinder effective model training[47, 48].
4. **Model Validation:** The dynamic nature of medical data necessitates continuous validation of AI models to ensure their accuracy and reliability over time.

Limitations

While the integration of AI in radiology presents ground-breaking possibilities, it is accompanied by an array of challenges and limitations that warrant careful consideration.

1. **Data Quality:** AI's efficacy relies heavily on high-quality, diverse, and well-curated data. However, medical imaging datasets can sometimes be incomplete, noisy, or biased, potentially compromising the performance and generalization of AI models.
2. **Interpretability:** Deep learning models, though highly effective, frequently serve as "black boxes, "It makes it difficult to grasp how they come to their conclusions. This lack of interpretability hinders radiologists from fully trusting and comprehending AI-generated results[49, 50].

3. **Bias:** Pre-existing biases within training data can inadvertently perpetuate biases in AI outputs. If AI models are trained on imbalanced datasets, they might exhibit disparities in performance across demographic groups, leading to inequitable healthcare outcomes[50, 51].
4. **Regulatory Compliance:** Incorporating AI into medical practice is subject to stringent regulatory frameworks to ensure patient safety and data privacy. Compliance with these regulations, like the Health Insurance Portability and Accountability Act (HIPAA) in the United States, requires meticulous design, validation, and monitoring of AI algorithms[50, 52].
5. **Role in Replacing Radiologists:** A prevailing concern is the perception that AI might replace radiologists entirely. While AI can expedite routine tasks, it's essential to recognize that the nuanced judgment, clinical context, and empathy that radiologists provide cannot be replicated by machines[53, 54, 55].
6. **Collaboration between AI and Human Experts**: The optimal approach lies in harnessing AI as a collaborative tool rather than a replacement. AI can assist radiologists by automating time-consuming tasks, allowing them to concentrate on intricate analyses and decision-making.
7. **Skill Gap and Training:** Integrating AI into radiology necessitates training radiologists to understand AI concepts and outputs. Bridging this knowledge gap is essential to maximize AI's potential and foster effective collaboration between humans and machines.
8. **Ethical Dilemmas:** The ethical considerations of AI in radiology extend to issues such as patient consent, transparency, and accountability. Ensuring patients are informed about AI's role in their diagnoses and treatment plans is crucial for maintaining trust[50].

Navigating these challenges requires a multidisciplinary approach involving radiologists, data scientists, ethicists, and regulators. The goal is to harness AI's capabilities while mitigating risks, preserving human expertise, and ultimately providing safer, more accurate, and equitable patient care. Recognizing AI as a complementary tool, one that augments human insight, paves the way for a harmonious future where technology enhances rather than replaces radiological expertise.

OPPORTUNITIES

1. **Efficiency Gains:** AI can automate regular work like image pre-processing and preliminary analysis, enabling doctors in radiology department to concentrate on more complicated cases and interpretations[50, 56].
2. **Enhanced Diagnosis:** AI's pattern recognition capabilities can lead to earlier and more accurate disease diagnoses, ultimately improving patient outcomes[50, 57].
3. **Predictive Analytics:** AI can predict disease progression and treatment responses, aiding in personalized treatment planning[58, 59].
4. **Standardization:** AI can assist in standardizing the interpretation of images, potentially reducing variability in diagnoses across different radiologists.

STRATEGIES FOR EFFECTIVE INTEGRATION:

1. **Clinical Engagement:** Involving radiologists and other healthcare professionals early in the AI implementation process ensures that AI tools align with clinical needs and workflows[59].
2. **Interoperability:** Implementing AI solutions that are compatible with various imaging devices, PACS, and EHR systems ensures seamless integration[60, 61].
3. **Training and Education:** Radiologists need training to understand AI outputs, interpret results, and collaborate effectively with AI algorithms[62, 63].
4. **Model Validation and Monitoring:** Continuous validation and monitoring of AI models are critical to ensure consistent and accurate performance. Regular updates should address evolving clinical needs and changing data patterns.
5. **Ethical Considerations:** Addressing patient consent, data privacy, and the ethical implications of using AI-generated insights is crucial to building trust and maintaining ethical standards[64, 65].
6. **Gradual Implementation:** Phased deployment of AI solutions allows radiologists to gradually adapt to changes, minimizing disruption to clinical workflows[62].

7. **Collaboration:** Collaborative efforts between radiologists, data scientists, engineers, and regulatory experts facilitate a comprehensive approach to AI integration[66, 67,68].

FUTURE DIRECTIONS

The field of radiology is on a dynamic trajectory with the evolution of artificial intelligence (AI), presenting a landscape filled with transformative possibilities. Several key trends emerge as we look towards the future multimodal imaging fusion, which harnesses AI to combine data from various imaging methods for a more comprehensive understanding of disease, explainable AI, which enhance transparency and trust by revealing how algorithms make decisions, federated learning, enabling AI training across institutions while preserving data privacy, AI-powered image guided interventions for real-time precision during procedures, precision medicine through AI's analysis of diverse patient data, automated report generation for efficient communication in health care, predictive analytics to forecast disease progression, and global accessibility via cloud-based AI platforms. Interdisciplinary collaboration, and addressing ethical and regulatory challenges will be essential as we embark on this transformative journey, promising a revolution in patient care and personalized medicine within the field of regulatory[69, 70,71,72].

CONCLUSION

In summary, this review paper underscores the pivotal role of artificial intelligence in radiology department. It addresses the challenges of complex radio imaging data and the need for innovative solutions, with AI integration enhancing diagnostic accuracy and workflow efficiency. AI's current applications in radiology, such as image segmentation and disease classification, are showcased with real-world examples. However, challenges like data quality, interpretability, and bias must be addressed. Understanding between radiologists and AI developers is crucial, leveraging human expertise with AI insights. The future of AI lies in radiology includes trends like multimodal imaging fusion and personalized treatments, promising precision medicine and improved patient care. Ultimately, AI has the future that lies in potential to revolutionize radiology, leading for diagnoses and streamlined workflow, benefiting the patient.

ACKNOWLEDGEMENT

We extend our sincere appreciation to Bimal Nepal, Research scholar, Department of Radio Imaging Technology, for their invaluable contributions and unwavering support throughout the development of this review paper. Their insights and dedicated efforts significantly enriched the content and quality of this work.

REFERENCES

1. Du-Harpur X, Watt FM, Luscombe NM, Lynch MD. What is AI? Applications of artificial intelligence to dermatology. British Journal of Dermatology. 2020 Sep 1;183(3):423-30.
2. Kotovich D, Twig G, Itsekson-Hayosh Z, Klug M, Ben-Simon A, Yaniv G, Konen E, Tau N, Raskin D, Chang PJ, Orion D. The impact on clinical outcomes after one year of implementation of an artificial intelligence solution for the detection of intracranial hemorrhage.
3. Rajkomar A, Dean J, Kohane I. Machine learning in medicine. New England Journal of Medicine. 2019 Apr 4;380(14):1347-58.
4. Hosny A, Parmar C, Quackenbush J, Schwartz LH, Aerts HJ. Artificial intelligence in radiology. Nature Reviews Cancer. 2018 Aug;18(8):500-10.
5. Esteva A, Kuprel B, Novoa RA, Ko J, Swetter SM, Blau HM, Thrun S. Dermatologist-level classification of skin cancer with deep neural networks. nature. 2017 Feb;542(7639):115-8.

6. Brinker TJ, Hekler A, Enk AH, Klode J, Hauschild A, Berking C, Schilling B, Haferkamp S, Schadendorf D, Holland-Letz T, Utikal JS. Deep learning outperformed 136 of 157 dermatologists in a head-to-head dermoscopic melanoma image classification task. European Journal of Cancer. 2019 May 1;113:47-54.
7. Balayla J, Shrem G. Use of artificial intelligence (AI) in the interpretation of intrapartum fetal heart rate (FHR) tracings: a systematic review and meta-analysis. Archives of gynecology and obstetrics. 2019 Jul 1;300:7-14.
8. Milea D, Najjar RP, Jiang Z, Ting D, Vasseneix C, Xu X, Aghsaei Fard M, Fonseca P, Vanikieti K, Lagrèze WA, La Morgia C. Artificial intelligence to detect papilledema from ocular fundus photographs. New England Journal of Medicine. 2020 Apr 30;382(18):1687-95.
9. Ting DS, Pasquale LR, Peng L, Campbell JP, Lee AY, Raman R, Tan GS, Schmetterer L, Keane PA, Wong TY. Artificial intelligence and deep learning in ophthalmology. British Journal of Ophthalmology. 2019 Feb 1;103(2):167-75.
10. O'neill TJ, Xi Y, Stehel E, Browning T, Ng YS, Baker C, Peshock RM. Active reprioritization of the reading worklist using artificial intelligence has a beneficial effect on the turnaround time for interpretation of head CT with intracranial hemorrhage. Radiology: Artificial Intelligence. 2020 Nov 18;3(2):e200024.
11. Davis MA, Rao B, Cedeno PA, Saha A, Zohrabian VM. Machine learning and improved quality metrics in acute intracranial hemorrhage by noncontrast computed tomography. Current Problems in Diagnostic Radiology. 2022 Jul 1;51(4):556-61.
12. Kundisch A, Hönning A, Mutze S, Kreissl L, Spohn F, Lemcke J, Sitz M, Sparenberg P, Goelz L. Deep learning algorithm in detecting intracranial hemorrhages on emergency computed tomographies. PLoS One. 2021 Nov 29;16(11):e0260560.
13. Topol EJ. High-performance medicine: the convergence of human and artificial intelligence. Nature medicine. 2019 Jan;25(1):44-56.
14. Yeung S, Downing NL, Fei-Fei L, Milstein A. Bedside computer vision-moving artificial intelligence from driver assistance to patient safety. N Engl J Med. 2018 Apr 5;378(14):1271-3.
15. Hemphill III JC, Greenberg SM, Anderson CS, Becker K, Bendok BR, Cushman M, Fung GL, Goldstein JN, Macdonald RL, Mitchell PH, Scott PA. Guidelines for the management of spontaneous intracerebral hemorrhage: a guideline for healthcare professionals from the American Heart Association/American Stroke Association. Stroke. 2015 Jul;46(7):2032-60.
16. Goldstein JN, Gilson AJ. Critical care management of acute intracerebral hemorrhage. Current treatment options in neurology. 2011 Apr;13:204-16.
17. Esteva A, Chou K, Yeung S, Naik N, Madani A, Mottaghi A, Liu Y, Topol E, Dean J, Socher R. Deep learning-enabled medical computer vision. NPJ digital medicine. 2021 Jan 8;4(1):5.
18. Krupinski EA. The future of image perception in radiology: synergy between humans and computers. Academic radiology. 2003 Jan 1;10(1):1-3.
19. George G, Lal AM. A personalized approach to course recommendation in higher education. International Journal on Semantic Web and Information Systems (IJSWIS). 2021 Apr 1;17(2):100-14.
20. Patyal S, Tejasvi B. Artificial intelligence with radio-diagnostic modalities in forensic science-a systematic review. InCEUR Workshop Proc 2021.
21. Bouarara HA. Recurrent neural network (RNN) to analyse mental behaviour in social media. International Journal of Software Science and Computational Intelligence (IJSSCI). 2021 Jul 1;13(3):1-1.
22. Goldenberg SL, Nir G, Salcudean SE. A new era: artificial intelligence and machine learning in prostate cancer. Nature Reviews Urology. 2019 Jul;16(7):391-403.
23. Ahmad Z, Rahim S, Zubair M, Abdul-Ghafar J. Artificial intelligence (AI) in medicine, current applications and future role with special emphasis on its potential and promise in pathology: present and future impact, obstacles including costs and acceptance among pathologists, practical and philosophical considerations. A comprehensive review. Diagnostic pathology. 2021 Dec;16:1-6.
24. Collado-Mesa F, Alvarez E, Arheart K. The role of artificial intelligence in diagnostic radiology: a survey at a single radiology residency training program. Journal of the American College of Radiology. 2018 Dec 1;15(12):1753-7.

25. Obermeyer Z, Emanuel EJ. Predicting the future—big data, machine learning, and clinical medicine. The New England journal of medicine. 2016 Sep 9;375(13):1216.
26. Kruskal JB, Berkowitz S, Geis JR, Kim W, Nagy P, Dreyer K. Big data and machine learning—strategies for driving this bus: a summary of the 2016 intersociety summer conference. Journal of the American College of Radiology. 2017 Jun 1;14(6):811-7.
27. Jha S, Topol EJ. Adapting to artificial intelligence: radiologists and pathologists as information specialists. Jama. 2016 Dec 13;316(22):2353-4.
28. Recht M, Bryan RN. Artificial intelligence: threat or boon to radiologists?. Journal of the American College of Radiology. 2017 Nov 1;14(11):1476-80.
29. Richardson ML, Garwood ER, Lee Y, Li MD, Lo HS, Nagaraju A, Nguyen XV, Probyn L, Rajiah P, Sin J, Wasnik AP. Noninterpretive uses of artificial intelligence in radiology. Academic Radiology. 2021 Sep 1;28(9):1225-35.
30. Chartrand G, Cheng PM, Vorontsov E, Drozdzal M, Turcotte S, Pal CJ, Kadoury S, Tang A. Deep learning: a primer for radiologists. Radiographics. 2017 Nov;37(7):2113-31.
31. Gulshan V, Peng L, Coram M, Stumpe MC, Wu D, Narayanaswamy A, Venugopalan S, Widner K, Madams T, Cuadros J, Kim R. Development and validation of a deep learning algorithm for detection of diabetic retinopathy in retinal fundus photographs. jama. 2016 Dec 13;316(22):2402-10.
32. Liu Y, Gadepalli K, Norouzi M, Dahl GE, Kohlberger T, Boyko A, Venugopalan S, Timofeev A, Nelson PQ, Corrado GS, Hipp JD. Detecting cancer metastases on gigapixel pathology images. arXiv preprint arXiv:1703.02442. 2017 Mar 3.
33. Rajpurkar P, Irvin J, Ball RL, et al. Deep learning for chest radiograph diagnosis: a retrospective comparison of the CheXNeXt algorithm to practicing radiologists. PLoS Med 2018; 15(11):e1002686. 6. Choy G, Khalilzadeh O, Michalski M, et al. Current applicat.
34. Caixinha M, Nunes S. Machine learning techniques in clinical vision sciences. Current eye research. 2017 Jan 2;42(1):1-5.
35. Duda RO, Hart PE, Stork DG. Pattern classification 2nd edition. New York, USA: John Wiley&Sons. 2001;35.
36. Krizhevsky A, Sutskever I, Hinton GE. Imagenet classification with deep convolutional neural networks. Advances in neural information processing systems. 2012;25.
37. Maier A, Syben C, Lasser T, Riess C. A gentle introduction to deep learning in medical image processing. Zeitschrift für Medizinische Physik. 2019 May 1;29(2):86-101.
38. Long J, Shelhamer E, Darrell T. Fully convolutional networks for semantic segmentation. InProceedings of the IEEE conference on computer vision and pattern recognition 2015 (pp. 3431-3440).
39. Simonyan K, Zisserman A. Very deep convolutional networks for large-scale image recognition. arXiv preprint arXiv:1409.1556. 2014 Sep 4.
40. Gonzalez RC. Deep convolutional neural networks [Lecture Notes]. IEEE Signal Processing Magazine. 2018 Nov 14;35(6):79-87.
41. Hearst MA. Untangling text data mining. In: Proceedings of the 37th annual meeting of the Association for Computational Linguistics on Computational Linguistics. College Park, Md: Association for Computational Linguistics, 1999
42. Pons E, Braun LM, Hunink MM, Kors JA. Natural language processing in radiology: a systematic review. Radiology. 2016 May;279(2):329-43.
43. Prevedello LM, Erdal BS, Ryu JL, Little KJ, Demirer M, Qian S, White RD. Automated critical test findings identification and online notification system using artificial intelligence in imaging. Radiology. 2017 Dec;285(3):923-31.
44. Yates EJ, Yates LC, Harvey H. Machine learning "red dot": open-source, cloud, deep convolutional neural networks in chest radiograph binary normality classification. Clinical radiology. 2018 Sep 1;73(9):827-31.
45. Lee EJ, Kim YH, Kim N, Kang DW. Deep into the brain: artificial intelligence in stroke imaging. Journal of stroke. 2017 Sep;19(3):277.
46. Syed AB, Zoga AC. Artificial intelligence in radiology: current technology and future directions. InSeminars in musculoskeletal radiology 2018 Nov (Vol. 22, No. 05, pp. 540-545). Thieme medical publishers.

47. Syeda-Mahmood T. Role of big data and machine learning in diagnostic decision support in radiology. Journal of the American College of Radiology. 2018 Mar 1;15(3):569-76.
48. Dimitrov DV. Medical internet of things and big data in healthcare. Healthcare informatics research. 2016 Jul 1;22(3):156-63.
49. Hleg AI. Ethics guidelines for trustworthy AI. B-1049 Brussels. 2019 Apr.
50. Sharma S. Artificial intelligence for fracture diagnosis in orthopedic X-rays: current developments and future potential. SICOT-J. 2023;9.
51. Gotterbarn DW, Brinkman B, Flick C, Kirkpatrick MS, Miller K, Vazansky K, Wolf MJ. ACM code of ethics and professional conduct.
52. Act A. Health insurance portability and accountability act of 1996. Public law. 1996 Aug 21;104:191.
53. Sardanelli F, Hunink MG, Gilbert FJ, Di Leo G, Krestin GP. Evidence-based radiology: why and how?. European radiology. 2010 Jan;20:1-5.
54. Dodd JD. Evidence-based practice in radiology: steps 3 and 4—appraise and apply diagnostic radiology literature. Radiology. 2007 Feb;242(2):342-54.
55. Pesapane F, Codari M, Sardanelli F. Artificial intelligence in medical imaging: threat or opportunity? Radiologists again at the forefront of innovation in medicine. European radiology experimental. 2018 Dec;2:1-0.
56. Gulshan V, Peng L, Coram M, Stumpe MC, Wu D, Narayanaswamy A, Venugopalan S, Widner K, Madams T, Cuadros J, Kim R. Development and validation of a deep learning algorithm for detection of diabetic retinopathy in retinal fundus photographs. jama. 2016 Dec 13;316(22):2402-10.
57. Gale W, Oakden-Rayner L, Carneiro G, Bradley AP, Palmer LJ. Detecting hip fractures with radiologist-level performance using deep neural networks. arXiv preprint arXiv:1711.06504. 2017 Nov 17.
58. Zhou SK, Greenspan H, Shen D, editors. Deep learning for medical image analysis. Academic Press; 2017 Jan 18.
59. Park SH, Han K. Methodologic guide for evaluating clinical performance and effect of artificial intelligence technology for medical diagnosis and prediction. Radiology. 2018 Mar;286(3):800-9.
60. Tang A, Tam R, Cadrin-Chênevert A, Guest W, Chong J, Barfett J, Chepelev L, Cairns R, Mitchell JR, Cicero MD, Poudrette MG. Canadian Association of Radiologists white paper on artificial intelligence in radiology. Canadian Association of Radiologists Journal. 2018 May;69(2):120-35.
61. Dumontier M, Baker CJ, Baran J, Callahan A, Chepelev L, Cruz-Toledo J, Del Rio NR, Duck G, Furlong LI, Keath N, Klassen D. The Semanticscience Integrated Ontology (SIO) for biomedical research and knowledge discovery. Journal of biomedical semantics. 2014 Dec;5:1-1.
62. Collado-Mesa F, Alvarez E, Arheart K. The role of artificial intelligence in diagnostic radiology: a survey at a single radiology residency training program. Journal of the American College of Radiology. 2018 Dec 1;15(12):1753-7.
63. Schuur F, Rezazade Mehrizi MH, Ranschaert E. Training opportunities of artificial intelligence (AI) in radiology: a systematic review. European Radiology. 2021 Aug;31:6021-9.
64. Jaremko JL, Azar M, Bromwich R, Lum A, Alicia Cheong LH, Gibert M, Laviolette F, Gray B, Reinhold C, Cicero M, Chong J. Canadian Association of Radiologists (CAR) Artificial Intelligence Working Group. Canadian association of radiologists white paper on ethical and legal issues related to artificial intelligence in radiology. Can Assoc Radiol J. 2019 May 1;70(2):107-18.
65. Miller DD. The medical AI insurgency: what physicians must know about data to practice with intelligent machines. NPJ digital medicine. 2019 Jun 28;2(1):62.
66. Shah P, Kendall F, Khozin S, Goosen R, Hu J, Laramie J, Ringel M, Schork N. Artificial intelligence and machine learning in clinical development: a translational perspective. NPJ digital medicine. 2019 Jul 26;2(1):69.
67. Ghesu FC, Georgescu B, Grbic S, Maier A, Hornegger J, Comaniciu D. Towards intelligent robust detection of anatomical structures in incomplete volumetric data. Medical image analysis. 2018 Aug 1;48:203-13.

68. Martín-Noguerol T, Paulano-Godino F, López-Ortega R, Górriz JM, Riascos RF, Luna A. Artificial intelligence in radiology: relevance of collaborative work between radiologists and engineers for building a multidisciplinary team. Clinical Radiology. 2021 May 1;76(5):317-24.
69. Mun SK, Wong KH, Lo SC, Li Y, Bayarsaikhan S. Artificial intelligence for the future radiology diagnostic service. Frontiers in molecular biosciences. 2021 Jan 28;7:614258.
70. Pichler BJ, Judenhofer MS, Wehrl HF. PET/MRI hybrid imaging: devices and initial results. European radiology. 2008 Jun;18:1077-86.
71. Nensa F, Bamberg F, Rischpler C, Menezes L, Poeppel TD, Fougère CL, Beitzke D, Rasul S, Loewe C, Nikolaou K, Bucerius J. Hybrid cardiac imaging using PET/MRI: a joint position statement by the European Society of Cardiovascular Radiology (ESCR) and the European Association of Nuclear Medicine (EANM). European Journal of Hybrid Imaging. 2018 Dec;2(1):1-23.
72. Prior F, Almeida J, Kathiravelu P, Kurc T, Smith K, Fitzgerald TJ, Saltz J. Open access image repositories: high-quality data to enable machine learning research. Clinical radiology. 2020 Jan 1;75(1):7-12.

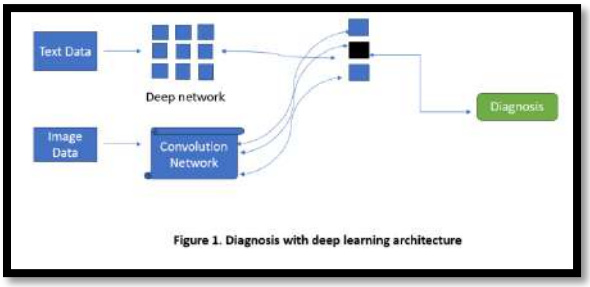

Figure 1. Diagnosis with deep learning architecture

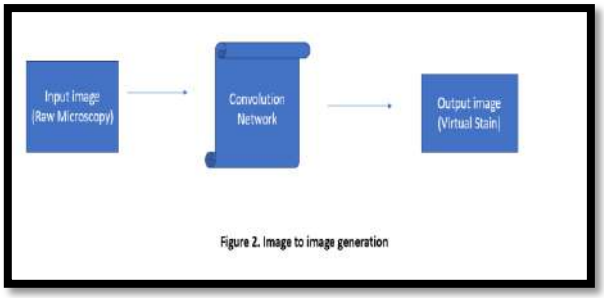

Figure 2. Image to image generation

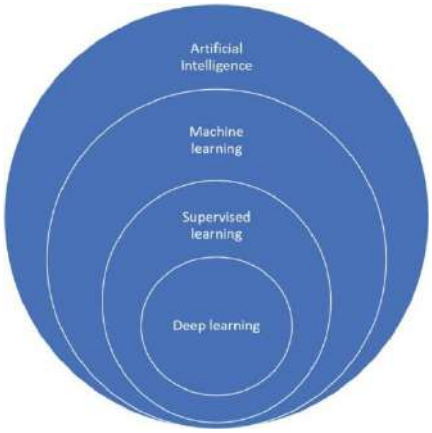

Figure 3: Components of Artificial Intelligence

RESEARCH ARTICLE

The Prevalence of Anemia, along with its Associated Factors and Treatment

Umme Ayman[1]*, Pallavi P[1], Sophy Thomas[1], Rahamtullah Khan[1], Manikanta BD[1] and Shailesh yadav[2]

[1]Pharm.D. Intern, Department of Pharmacy Practice, Mallige College of Pharmacy, (Affiliated to Rajiv Gandhi University of Health Sciences) Bengaluru, Karnataka, India.
[2]HOD, Associate Professor, Department of Pharmacy Practice, Mallige College of Pharmacy, (Affiliated to Rajiv Gandhi University of Health Sciences) Bengaluru, Karnataka, India.

Received: 30 Jan 2024 Revised: 09 Feb 2024 Accepted: 03 Apr 2024

***Address for Correspondence**
Umme Ayman
Pharm.D. Intern,
Department of Pharmacy Practice,
Mallige College of Pharmacy,
(Affiliated to Rajiv Gandhi University of Health Sciences)
Bengaluru, Karnataka, India.
Email: ainuainu75@gmail.com

ABSTRACT

Anemia constitutes a formidable public health challenge that frequently goes undetected or untreated. Despite advancements in healthcare, it still afflicts a quarter of the global populace. This study aims to demonstrate the prevalence, severity, types, available treatment alternatives, and correlated factors of anemia among hospitalized inpatients at a tertiary care hospital in Bengaluru, Karnataka. We undertook a cross-sectional observational study design at a tertiary care hospital. To gather data, we looked at the medical records of the clinical, biochemical, and medication profiles of recently registered patients in the hospital from April 2022 to July 2022. The chi-square and p-value were employed to identify the association between anemia and associated factors. The study found that 15.31% of the population had anemia, with 35.9% mild, 47.1% moderate, and 17.1% severe anemia. Of the total anemic cases, 52.4% were males, while 47.6% were females, and more than half of the patients had normocytic anemia, i.e., normocytic 62.5%, microcytic 31.3%, and macrocytic 6.3%. As individuals grow older, the probability of developing anemia rises. Therefore, it is advisable to incorporate regular anemia screening into routine check-ups, particularly for high-risk groups who may have additional health concerns. Early recognition and intervention by healthcare providers can also lessen the number of untreated and under diagnosed anemic patients. Educating the public about iron- and vitamin-rich (vitamin B12 and B9) sources of plant- and animal-based foods is an efficient strategy for reducing anemia prevalence in both vegetarian and non-vegetarian communities.

Keywords: Anemia, gender, hemoglobin, prevalence, treatment.

INTRODUCTION

Anemia implies a decrease in erythrocyte production and quality, substantially impairing the body's ability to provide O_2 to its tissues[1]. It is a symptom rather than a diagnosis, and its cause, severity, and multiple disorders, such as cardiovascular illness, influence symptoms. Once the Hb drops below 7.0 g/dL, symptoms like tiredness, weakness, and lethargy are common. Men, women, and children commonly lie within the range of 13.5–18.0 g/dL, 12–15 g/dL, and 11–16 g/dL, respectively. Pregnancy values vary depending on the trimester but are often larger than 10.0 g/dL[2]. The corrected reticulocyte count categorizes anemia into two main types: hypoproliferative (below2%) and hyperproliferative (above2%). Microcytic (MCV is above 80 fl), normocytic (MCV is betwixt80 and 100 fl), and macrocytic (MCV is below 100 fl) anemias are additional classifications based on the mean corpuscular volume[2]. The WHO has identified that roughly two billion populaces worldwide suffer from anemia, with iron deficiency being the leading cause in 50% of cases. Anemia is less common than iron deficiency by a factor of 2.5, with developing countries experiencing higher rates of anemia. Children under 5 have an estimated anemia prevalence of 39%, while the figures stand at 48% for children aged 5–14, 42% for women aged 15–59, 30% for men aged 15–59, and 45% for adults over 60 years. These statistics have significant health and economic implications for low- and middle-income countries[4]. Anemia can be upshot from reduced erythrocyte synthesis oran increased loss of blood via hemolysis, bleeding, or a combination of both. Nutritional, viral, or genetic factors may affect these. Hemoglobinopathies like sickle cell and thalassemia result from hereditary factors, while infectious disorders like malaria and schistosomiasis are common causes of anemia. Nutritional anemia results from a lack of minerals needed for hemoglobin production and erythropoiesis, including iron, vitamin B9, cobalamin, retinol, and protein-energy malnutrition. Iron deficiency is responsible for half of all anemias. Exposure to minor levels of trace elements, such as Zn and Cu, and hazardous heavy metals, such as lead, can potentially aggravate anemia[5]. Anemia is treatable by drug-based (iron tablets, folic acid, B12, and blood transfusions) and non-drug-based (vegetables, fruits, rosella beverages, and Moringa leaf juice) methods[6]. The main area of concern is the underlying etiology of anemia. For acute blood loss, blood transfusions, oxygen, and IV fluids are used, with a target of 7 g/dL for most patients. Oral or IV iron, B12, and folate all address nutritional deficiencies. Oral iron supplements are the most popular way to replenish iron, with the amount based on age, estimated iron deficiency, needed rate of correction, and tolerance to adverse effects. Bone marrow transplantation is required for a plastic anemia, while erythropoietin is effective for chronic diseases. Treatment of underlying diseases is necessary for autoimmune and rheumatological disorders. Increased red blood cell destruction results in hemolytic anemia, which calls for splenectomy, medicine, and mechanical valves. Hemoglobinopathies, namely sickle cell disease, necessitate blood transfusions, red cell exchange transfusions, and hydroxyurea. Bleeding that might be deadly is treated with antifibrinolytic medications[2].

MATERIALS AND METHODS

We undertook across-sectional observational study designat Mallige Medical Center, a multi-specialty tertiary care hospital in Bengaluru. The data available originated from the medical records of the clinical, biochemical, and pharmaceutical profiles of new patients admitted to the hospital between January 2022 and April 2022. The BMI was determined for each patient via available parameters. The inclusion and exclusion criteria are as follows: The study comprised all newly registered patients attending the hospital's inpatient department who were at least 18 years of age and older and whose records included a clinical history, complete blood count calculation, and medication chart during the study period. Patients who had just undergone surgery, pregnant women, and nursing mothers served as exclusion criteria. Before collecting any data, there view board of Mallige College of Pharmacy granted ethical approval and provided a letter of concurrence to Mallige Medical Center. The patient or a bystander was fully informed of the aim and purpose of the study, as required. A precise sample size of 1,110 patients who met established criteria was determined utilizing the single population proportion formula. To analyze the data, we

employed Microsoft Excel for statistical tabulation. We ensured that the data was accurate and free of any missing values. We then manually reviewed the results with tallies and a scientific calculator. We performed a rigorous statistical analysis using the chi-square test with a significance level of 0.05 to determine the correlation between the independent and dependent variables.

RESULTS

Out of 1,110 respondents analyzed based on inclusion and exclusion criteria, 170 were acknowledged as anemic, resulting in an overall prevalence rate of 15.31%. Out of 170 patients, the percentages of mild, moderate, and severe anemia were 35.88%, 47.06%, and 17.06%, respectively. The distribution of various types of anemia among the study population showed 31.18% with microcytic anemia, 62.35% with normocytic anemia, and 6.48% with macrocytic anemia. Table 4 shows that 170 out of 1,110 patients had anemia, of whom 52.35% were male patients (n = 89) and 47.65% were female patients (n = 81). Among all age groups, young adult patients (18–30 years) had the lowest prevalence of anemia (4.12%). Furthermore, quadragenarians (41–50 years, 12.35%) and the elderly (81 years and older, 12.35%) had the lowest rates of anemia. According to our findings, the age category of 61–70 years had the highest proportion of anemia (22.94%). Anemia was higher among urban residents (81.20%) than rural residents (18.80%). Most patients had a normal BMI (57.65%), while 17.06% were underweight, 16.47% were obese, and 8.82% were overweight. About 89 (52.35%) of the anemic patients were vegetarians, whereas the other 81 (47.65%) were non-vegetarians. The prevalence of blood type A (31.18%) surpasses that of blood type B (30%), blood type AB (19.41%), and blood type O (19.41%) among anemic subjects. Age and anemia were significantly correlated (x^2= 63.476, p = 0.00001). There was an association between BMI and anemia (x^2 = 11.34, p = 0.01002). It has been observed that anemia had a significant correlation with the blood group (x^2 = 9.57, p = 0.0226), but not statistically. Anemia had no significant association with gender (x^2 = 1.215, p = 0.2704), residence (x^2 = 0.711, p = 0.3991),or diet (x^2 = 0.896, p = 0.3438). Hypertension was discovered to be the most common co-morbidity in 170 anemic patients, accounting for 61.17%, followed by diabetes mellitus (41.76%), and others (i.e., 20%), including seizures, Crohn's disease, tuberculosis, obstructive sleep apnea, osteoporosis, and CAD (18.24%). Most patients who were mildly anemic received vitamin B supplements; just 3.28% received blood transfusions, and more than half (57.37%) did not get any treatment. Vitamin B supplements were administered to 37.5% of patients with moderate anemia, while blood transfusions were given to 20%, erythropoietin to 5%, vitamin B and iron supplements to 5%, and only iron supplements to 2.5%. Around 30% of moderately anemic patients went untreated. About 86.2% of severely anemic patients received blood transfusions, with 6.9% receiving vitamin B and iron supplements, 3.4% receiving iron supplements, and the remaining 3.4% receiving vitamin B supplements.

DISCUSSION

The study found a 15.31% overall prevalence of anemia. The observed prevalence is greater than the anemic prevalence of 15%reported at Hawas University in southern Ethiopia[7]. In contrast to the study done at the Gilgel Gibe Field Research Center in Ethiopia (40.9%), the prevalence found in this study is lower. This difference could be due to sample size, geographical variation, or socio-demographic variation[8].Contrary to research done at Hawas University in southern Ethiopia, where a large percentage of individuals had mild anemia (58.5%), the majority of cases in this study had moderate anemia (47.06%)[7]. 17.06% of the participants had severe anemia, a rate greater than Yaounde-Cameroon's detection rate (0.8%)[3] but lower than Hawas University's research in southern Ethiopia, which found 22.5%of participants to have severe anemia[7]. Age-related categories of anemia patients revealed that those over 51 had the highest prevalence (75.88%) of cases. Anemia and age were statistically linked, with severe cases being more prevalent in those aged 61 and above, who may also be affected by other health issues like hypertension, diabetes mellitus, and chronic kidney disease, all of which can impact the production of red blood cells. Anemia is more likely to occur as people get older because of various health conditions that may also be present. Males were slightly more common than females among the 170 anemic patients (52.35% vs. 20.3%), whereas research done in

New Jersey, USA,found the opposite to be true (79.6% vs. 20.3%) than males(20.3%)[7]. Females are more likely to acquire anemia because of menstruation and childbirth. Gender was not significantly associated with anemia, which might be because, as age increases, both sexes are more likely to have comorbid conditions that increase the risk of anemia. Urban residents had a greater rate of anemia (81.20%) than rural residents (18.80%). The Gilgel Gibe Field Research Center in Ethiopia conducted a similar study that found that rural individuals were more susceptible to anemia than urban ones[8]. Anemia and residence had no significant association. The discrepancy in our results could be because our study was conducted solely in an urban setting, which makes it difficult to determine the exact distribution of anemia in urban and rural areas. The results of the study show a notable correlation between BMI and anemia. The majority of patients had a normal BMI (57.65%), followed by underweight (17.06%) and obese (16.47%) patients. Malnutrition is a common cause of low blood counts in underweight patients[10], while obesity can interfere with iron hemostasis, leading to anemia[11].The study unequivocally demonstrates no significant link between diet and anemia. It is interesting to note that of the participants, 52.35% followed a vegetarian diet, while 47.65% were non-vegetarians. Vegetarians forego meat and eggs, which can result in iron and vitamin B12 deficiencies and, eventually, anemia[13].Among 170 patients with anemia, hypertension was the most common complication, affecting 61.17% of patients. Diabetes mellitus was also prevalent in 41.76% of patients, while CAD was prevalent in 18.24%. A similar study conducted in Camden, New Jersey, USA, found that the most common complications were hypertension (59.3%), hypothyroidism (29.3%), and diabetes mellitus (19.4%)[12] There was a note worthy association between blood type and anemia. Among the 170 anemic patients studied, individuals with blood types A(31.18%) and B (30%) were observed to possess a higher susceptibility to anemia in contrast to those with blood types AB and O. Additionally, a similar study performed in North India revealed that the prevalence of anemia was maximum in blood type O(39.24%). Following this, blood type Baccounts for 42.20%, then blood type A for 13.3%, and blood type AB for 5.25%[14]. More than 50% of patients with mild anemia and 30% of those with moderate anemia were not appropriately diagnosed or treated. Although mild anemia is not a serious concern, if left untreated, it can cause serious health problems like tiredness and cardiac issues like arrhythmias, which may present a high risk of complications and, in rare cases, even death[15].

CONCLUSION

As individuals grow older, the probability of developing anemia rises. Therefore, it is advisable to incorporate regular anemia screening into routine check-ups, particularly for high-risk groups who may have additional health concerns. Early recognition and intervention by healthcare providers can also lessen the number of untreated and under diagnosed anemic patients. Educating the public about iron- and vitamin-rich (vitamin B12 and B9) sources of plant- and animal-based foods is an efficient strategy for reducing anemia prevalence in both vegetarians and non-vegetarians.

ABBREVIATIONS

BMI: body mass index;
CAD: coronary artery disease;
CHF: congestive heart failure;
CKD: chronic kidney disease;
COPD: chronic obstructive pulmonary disease;
CVA: cerebrovascular accident;
Hb: hemoglobin;
MCV: mean corpuscular volume;
WHO: World Health Organization

ACKNOWLEDGMENTS

Above all, we express our immense gratitude to the Almighty for his unwavering support throughout our journey and for blessing us with sound health and the fortitude to complete this research study.

Financial assistance and sponsorship
None

Potential Conflict of Interest
There are no conflicting interests**.**

REFERENCES

1. BetregiorgisZegeye, Bight OpokuAhinkorah, Edward KwabenaAmeyaw, Abdul-Aziz Seidu, MphoKeetile, SanniYaya, "Determining Prevalence of Anemia and Its Associated Factors in Cameroon: A Multilevel Analysis", BioMed Research International, vol. 2021, Article ID 9912549, 12 pages, 2021. https://doi.org/10.1155/2021/9912549
2. Turner, J. (2023, August 8). Anemia. StatPearls - NCBI Bookshelf. https://www .ncbi.nlm.nih.go v/books/NBK49 9994/
3. Aggarwal, A., Aggarwal, A., Goyal, S., & Aggarwal, S. (2020). Iron-deficiency anemia among adolescents: A global public health concern. *International Journal of Advanced Community Medicine*, 3(2), 35–40. https://doi.org/10.33545/comed.2020.v3.i2a.148
4. Gerardo Alvarez-Uria, Praveen K. Naik, ManoranjanMidde, Pradeep S. Yalla, RaghavakalyanPakam, "Prevalence and Severity of Anaemia Stratified by Age and Gender in Rural India", Anemia, vol. 2014, Article ID 176182, 5 pages, 2014. https://doi.org/10.1155/2014/176182
5. Shaban L, Al-Taiar A, Rahman A, Al-Sabah R, Mojiminiyi O. Anemia and its associated factors among Adolescents in Kuwait. Sci Rep. 2020 Apr 3;10(1):5857. doi: 10.1038/s41598-020-60816-7. PMID: 32246050; PMCID: PMC7125127.
6. Putri, S. Z., Budu, B., Gemini, G., &Natsir, R. (2021). Non-Pharmacological Interventions for Anemia Treatment: Systematic Review. Muhammadiyah International Public Health and Medicine Conference, 1(1), 283–312. https://doi.org/10.53947/miphmp.v1i1.56
7. Mengesha MB, Dadi GB. Prevalence of anemia among adults at Hawassa University referral hospital, Southern Ethiopia. BMC Hematol. 2019 Jan 8;19:1. doi: 10.1186/s12878-018-0133-0. PMID: 30637107; PMCID: PMC6323856.
8. Tesfaye TS, Tessema F, Jarso H. Prevalence of Anemia and Associated Factors Among "Apparently Healthy" Urban and Rural Residents in Ethiopia: A Comparative Cross-Sectional Study. J Blood Med. 2020 Mar 11;11:89-96. doi: 10.2147/JBM.S239988. PMID: 32210654; PMCID: PMC7073428.
9. Jingi, A. M., Kuate-Mfeukeu, L., Hamadou, B., Ateba, N. A., Nganou, C. N., Amougou, S. N., Guela-Wawo, E., &Kingue, S. (2018). Prevalence and associates of anemia in adult men and women urban dwellers in Cameroon: a cross-sectional study in a Sub-Saharan setting. Annals of Blood, 3, 34. https://doi.org/10.21037/aob.2018.05.04
10. Gandhi SJ, Hagans I, Nathan K, Hunter K, Roy S. Prevalence, Comorbidity and Investigation of Anemia in the Primary Care Office. J Clin Med Res. 2017 Dec;9(12):970-980. doi: 10.14740/jocmr3221w. Epub 2017 Nov 6. PMID: 29163729; PMCID: PMC5687900.
11. Marcin, Ashley. "Underweight Health Risks: What You Should Know." Healthline, 15 May 2017, www.healthline.com/health/underweight-health-risks#malnutrition.
12. Alshwaiyat NM, Ahmad A, Wan Hassan WMR, Al-Jamal HAN. Association between obesity and iron deficiency (Review). ExpTher Med. 2021 Nov;22(5):1268. doi: 10.3892/etm.2021.10703. Epub 2021 Sep 7. PMID: 34594405; PMCID: PMC8456489.

13. Vann, Madeline R., et al. "Anemia Risk for Vegans and Vegetarians." EverydayHealth.Com, www.everydayhealth.com/anemia/anemia-risk-for-vegans-and-vegetarians.aspx. Accessed 11 Aug. 2023.
14. Pratima V, Shraddha S, Ashutosh K, Archna G and Ahilesh K. Prevalence of Anaemia in adults with respect to Socio-Demographic status, Blood groups and religion in North Indian population. *Int J Biol Med Res*. 2012;3(4):2441-2447.
15. Anemia - Symptoms and causes - Mayo Clinic. (2023, May 11). Mayo Clinic. https://www. mayoclinic.org/diseases-conditions/anemia/symptoms-causes/syc-20351360

Table 1. The WHO recommends hemoglobin values (g/dL) to determine anemia's severity in various populations[3].

Subject group	Normal	Mildly anemic	Moderately anemic	Severely anemic
Infants aged 6–59 months	≥ 11	10–10.9	7–9.9	<7
Children aged 5–11 years	≥ 11.5	11–11.4	8–10.9	<8
Adolescents aged 12–14 years	≥ 12	11–11.9	8–10.9	<8
Non-pregnant females aged 15 years and above	≥ 12	11–11.9	8–10.9	<8
Gestational females	≥ 11	10–10.9	7–9.9	<7
Males aged 15 years and above	≥ 13	11–12.9	8–10.9	<8

Table 2. Prevalence and severity of anemia

Grading of anemia severity	No. of Cases	Percentage (%)
Mild	61	35.88
Moderate	80	47.06
Severe	29	17.06
Total	170	100

Table 3. Grading ofanemia types among patients

Anemic types	No. of Cases	Percentage (%)
Microcytic	53	31.18
Normocytic	106	62.35
Macrocytic	11	6.47
Total	170	100

Table 4. Anemia-related factors among inpatients at a tertiary care hospital in Bengaluru (n=170)

Characteristics	Anemic subjects (n=170)	Percentage (%)	Chi-square(x^2)	P-value
Gender				
Male	89	52.35	1.215	0.2704
Female	81	47.65		
Age category				
18–30years	7	4.12	63.476	0.00001
31–40years	13	7.65		
41–50years	21	12.35		
51–60years	38	22.35		
61–70years	39	22.94		

71–80years	31	18.24		
81 years and older	21	12.35		
Residence				
Urban	138	81.20	0.711	0.3991
Rural	32	18.80		
BMI category				
Underweight (less than 18.5)	29	17.06	11.34	0.01002
Healthy weight (18.5 to 24.9)	98	57.65		
Overweight (25 to 29.9)	15	8.82		
Obese (more than or equal to 30)	28	16.47		
Diet				
Vegetarian	89	52.35	0.896	0.3438
Non-Vegetarian	81	47.65		
Blood types				
A	53	31.18	9.57	0.0226
B	51	30		
AB	33	19.41		
O	**33**	**19.41**		

Table 5. Prevalence of anemia based on co-morbidities

Co-morbidities	Anemic subjects (n =170)	Percentage (%)
Hypertension	104	61.17
Diabetes mellitus	71	41.76
COPD/Asthma	27	15.88
Thyroid illness	23	13.53
CKD	13	7.64
Malignancy	1	0.6
Rheumatological disease	1	0.6
CHF	1	0.6
CAD	31	18.24
CVA	9	5.3
Others	34	20
None	26	15.3

Table 6.Type of anemia and different options of treatment, showing the percentage distribution

Anemia Status	Vitamin B Supplements,n(%)	Iron Supplements,n(%)	Vitamin B + Iron,n(%)	Blood Transfusion,n(%)	Erythropoietin,n(%)	None,n(%)	Total, n(%)
Mild Anemia							
Microcytic	5 (8.19)	–	–	–	–	8 (13.11)	13 (21.3)

Normocytic	18 (29.5)	–	1 (1.63)	2 (3.28)	–	26 (42.62)	47 (77)
Macrocytic	–	–	–	–	–	1 (1.63)	1 (1.63)
Total	23 (37.7)	–	1 (1.63)	2 (3.28)	–	35 (57.37)	61 (100)
Moderate Anemia							
Microcytic	7 (8.75)	1 (1.25)	3 (3.75)	6 (7.5)	2 (2.5)	6 (7.5)	25 (31.25)
Normocytic	19 (23.75)	1 (1.25)	1 (1.25)	10 (12.5)	2 (2.5)	17 (21.25)	50 (62.5)
Macrocytic	4 (5)	–	–	–	–	1 (1.25)	5 (6.2)
Total	30 (37.5)	2 (2.5)	4 (5)	16 (20)	4 (5)	24 (30)	80 (100)
Severe Anemia							
Microcytic	–	1 (3.4)	–	11 (38)	–	–	12 (41.37)
Normocytic	1 (3.4)	–	–	8 (27.58)	–	–	9 (31.03)
Macrocytic	–	–	2 (6.9)	6 (20.68)	–	–	8 (27.6)
Total	**1 (3.4)**	**1 (3.4)**	**2 (6.9)**	**25 (86.2)**	–	–	**29 (100)**

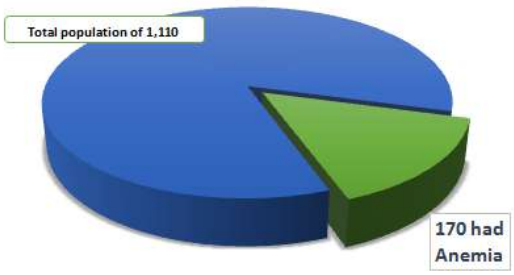

Figure 1.Prevalence of anemia

REVIEW ARTICLE

Orodispersible Tablets: A Review

G.S.Sharma[1]*, Namami Dutt[2] ,R. Shireesh Kiran and T. Rama Rao

[1]Associate Professor, Department of Pharmaceutics, CMR College of Pharmacy, (Affiliated to *Jawaharlal Nehru Technological University, Hyderabad)* Telangana, India.
[2]Student, Department of Pharmaceutics, CMR College of Pharmacy, (Affiliated to *Jawaharlal Nehru Technological University, Hyderabad)* Telangana, India.
[3]Associate Professor, Department of Pharmaceutics, CMR College of Pharmacy, (Affiliated to *Jawaharlal Nehru Technological University, Hyderabad)* Telangana, India.
[4]Professor, CMR College of Pharmacy, (Affiliated to Jawaharlal Nehru Technological University, Hyderabad) Telangana, India.

Received: 13 Dec 2023 Revised: 29 Jan 2024 Accepted: 27 Mar 2024

***Address for Correspondence**
G.S.Sharma
Associate Professor,
Department of Pharmaceutics,
CMR College of Pharmacy,
(Affiliated to *Jawaharlal Nehru Technological University, Hyderabad)*
Telangana, India.
Email: sharmampharm@gmail.com

ABSTRACT

Orodispersible tablets (ODTs) are becoming more and more popular among innovative oral drug delivery systems because they enhance patient compliance and offer a few more benefits over other oral formulations. ODTs are solid unit dose forms that quickly disappear or break down in the tongue without requiring water or chewing. In particular, elderly as well as pediatric patients who faces trouble in consuming traditional medications might benefit from the use of ODTs. This review outlines the different ideal properties, selection of drug candidate, types of super disintegrants used, limitations, the disintegrants used, technology created for ODTs. Scientists have used a variety of techniques to create orodispersible tablets. Nonetheless, the compression approach is the most often used way of preparation. The cotton candy process, melt granulation, phase-transition process, sublimation, freeze-drying, and quick film formation are other unique techniques. ODTs are also assessed in the areas of hardness, friability, content uniformity, weight uniformity, disintegration test, and dissolution test of solid dosage forms and various applications of oral dispersible tablets.

Keywords: ODTs, Patient compliance, Super disintegrants, Compression technique, Dissolution test.

INTRODUCTION

Pharmaceutical tablets are characterized as biconvex, flat, or solid plates that are compressed, either with or without diluents, to make a pharmaceutical or drug combination. This is in accordance with the Indian Pharmacopoeia. The quantity of medication and the preferred route of administration have a significant impact on their size, weight, and form. The most popular and advised method of delivering medication, including both liquid and solid dose forms, is orally. ODTs are taken without water and dissolved with saliva. Unless pre-gastric absorption shields it, the active component dissolves quickly in saliva regardless of membrane contact. This study aims to investigate the state of ODT technology at the moment, as well as the ODT characterization and sustainability of drug candidates. Other names for ODTs include orodispersible tablets, fast-acting tablets, mouth dissolving medications."Orodispersible tablet" is the word used by the European Pharmacopoeia to characterize tablets that, after being ingested, dissolve rapidly in the mouth (three minutes). ODT is described as "a solid dosage form containing a medicinal substance or active ingredient which disintegrates rapidly, usually within a matter of seconds, when placed upon the tongue".

PROPERTIES OF ORODISPERSIBLE TABLETS (6, 7)

- It doesn't need water to swallow.
- Dissolves or disintegrates in the oral cavity within less time.
- Show less susceptibility to external factors like temperature and humidity.
- A significant drug loading.
- ODTs must possess flexibility and compatibility with the existing processing and packaging machinery.
- ODTs must also be strong enough to withstand the rigorous demands of manufacturing and post-production processes.

ADVANTAGES OF ORALDISPERSIBLE TABLETS (8, 9, 10)

- Improved stability
- Suitable for patients and prescribers, this medication offers greater convenience and compliance for controlled/long-term usage.
- It promotes patient compliance.
- Reduces antimicrobial resistance.
- Makes distribution and procurement logistics easier to manage.
- There are the recommended dose form for faster drug administration and higher bioavailability without going through the stomach.
- They may be used to treat a variety of patients, such as the handicapped, travelers, and those who are always on the go and don't always have access to water. They are quite useful.

DISADVANTAGES OF ORALDISPERSIBLE TABLETS (11)

- It may be necessary to provide the medication more often
- Possibility of dose dumping
- Reduced ability to make precise dosage adjustments
- Lack of mechanical strength
- Intervention with rapid pharmacological treatment is not feasible.
- Diminished possibility of precise dosage modification.

SELECTION OF THE DRUGS FOR ODTS (12)

- Medications can diffuse and divide into the GIT top epithelium (log P>1/2); ODT formulations are ideal for those that are efficient to penetrate oral cavity.
- Patients who are taking ach medications at the same time possibly not a suitable candidate for these medications.

- ODT formulations may not be suitable for patients with reduced salivary flow leading to dry mouth

TYPES OF SUPERDISINTEGRANTS USED (13)

- Cross povidone
- Micro crystalline cellulose
- Sodium starch glycolate
- Sodium carboxymethyl cellulose or croscarmellose sodium
- Calcium carboxymethyl cellulose

FACTORS CONSIDERED FOR SELECTION OF SUPER DISINTEGRANTS (14)

- When the medicine is taken orally and then mixed with saliva, it should cause the tablet to dissolve.
- It should possess a smooth flow since it enhances the overall blend's capacity for flow.
- It should be compatible enough to generate fewer brittle tablets.

LIMITATIONS OF ORODISPERSIBLE TABLETS (15, 16)

- When making ODTs, the soluble diluents often give hydroscopic dosages, which can cause stability issues.
- The tablets are unpleasant to take in the oral cavity if improperly prepared.
- ODTs are not appropriate for drugs that react to light.

CHALLENGES IN THE FORMULATION OF ODTS (17, 18, 19)

Mechanical strength and disintegration time

Generally speaking, oral dispersible tablets dissolve in less than one minute. There's a greater likelihood that ODTs may break during packing, transit, or patient handling because many of them are brittle. Naturally, the disintegration process will be slowed down by increasing the mechanical strength.

Taste masking

Many medications have an unpleasant taste. Consequently, to stop bitter medications from leaving the tongue feeling tasted, excellent flavor masking is needed.

Size of tablets

The medication ease of use is determined by its size. Tablets bigger than 8 mm are said to be the simplest to manage, and tablets smaller than 7-8 mm are said to be the most easily ingested. That makes it difficult to design a tablet that is portable and manageable in terms of size.

Amount of drug

Generally speaking, the USP advises that the weight of the ODT pill not go beyond 500 mg. Smaller than 60 mg of soluble medication and smaller than 400 mg of insoluble medication should be administered by lyophilized dosage form. This characteristic is especially difficult to work with when creating oral films or wafers that disintegrate rapidly.

Hygroscopicity

In typical temperature and humidity conditions, a number of dosage forms intended for oral dissolution become hygroscopic and lose their physical integrity.

TECHONOLOGIES FOR PREPARING ORODISPERSIBLE TABLETS (20, 21, 22, 23)

1. Freeze-drying or lyophilisation
2. Melt granulation
3. Cotton candy process

4. Phase transition
5. Fast dissolving films
6. Direct compression.

Freeze drying or lyophilisation

The process of freeze drying or lyophilisation involves removing the solvent from a frozen pharmaceutical suspension or solution that includes excipients to aid in the formation of structures. These pills disintegrate fast due to their porous and generally thin structure. Excipients with a glassy, amorphous porous structure and the medicinal ingredient created by freeze drying both improve solubility.

Melt granulation

Pharmaceutical powders can be efficiently agglomerated using the melt granulation process by using a melt-able binder. This approach has the benefit of not using organic solvents or water, as compared to traditional granulation. To finish this process, high shear mixers are employed. The heat generated by the impeller blades' friction or a heating jacket in these mixers elevates the product temperature over the melting point of the binder.

Cotton candy process

This process is named for the unique spinning mechanism it uses to create crystalline structures that resemble cotton candy and floss. Another name for it is the candy floss approach. In order to create a matrix of polysaccharides, or saccharides, cotton candy is made by spinning and flash melting at the same time. Partially recrystallized matrix is used to improve flow characteristics and compressibility. Subsequently, After the candy floss matrix is pulverized, it is blended with the components for the active as well excipient ingredients, and compressed into ODT. The process results in enhanced mechanical strength and the capacity to manage large dosages of medication.

Phase transition

An innovative method for producing ODTs with the right amount of hardness by utilizing the sugar alcohol phase transition. By compressing and heating two sweeteners and alcohol tablets—one having a significant melting point and the other having a low point of melting—ODTs are produced using this process. Because of the stronger linkages created by heating the particles, the tablets are more durable than they otherwise would have been because of their incompatibility.

Fast dissolving films

It's a novel field of oral dispersible tablets facilitates supplement and drug intake. Medication as well as flavor-masking substances that are permitted to solidify as a film as soon as the solvent disappears. For bitter medications, the film can contain coated drug micro-particles or resin adsorbate. This film quickly melts or dissolves when ingested, releasing the medication in suspension or solution.

Direct compression

ODTs, it can be produced with standard tablet production and packaging equipment and because tableting excipients with better flow, compressibility, and disintegration qualities are readily available. These include sugar-based excipients, effervescent agents, and tablet disintegrants.

Superdisintegrants

Superdisintegrant additions primarily influence the pace of disintegration and, thus, the dissolution in many direct compression-based ODT methods. Additional formulation elements like effervescent agents and water-soluble excipients speed up the disintegration process even further.

Effervescent agents

The patented Orasolv technology (OT) is based on the evolution of CO2 as a disintegrating mechanism and is widely applied in the development of over-the-counter medications. The product has a mild effervescent quality and contains micro-particles. The effervescent ingredient is activated by saliva, which leads to the tablet disintegrating.

ADVANCEMENTS IN ODT TECHNOLOGIES (24, 25, 26, 27, 28)

1. **Zydis technology:** This process encircles the tablet with a rapidly dissolving carrier substance. so that when it gets to the mouth, it will swiftly decompose. To guarantee product stability, these pills include a range of adjuvants. Since the pill was frozen and dried, it is immune to germs. Usually, these pills are kept safe from ambient moisture via blister packs.
2. **Orasolv technology:** CIMA laboratories created this technique. Emulsifying disintegrating agent and flavor masking agent are used to disguise the disagreeable taste of API. To prepare tablets, additional standard equipment is used. To ensure rapid breakdown and softness upon completion, the tablets must to be crushed using a minimal compression force. Furthermore, to maintain the stability of these unpleasant dosage forms over the course of their shelf life, much caution must be used when storing them.
3. **Durasolv technology:** The approach was also created by CIMA Labs.The ingredients in composition are the medication, lubricant, and fillers. The same conventional tools used to produce tablets may also be used to make tablets with Durasolv technology. Additionally, these goods don't require specific packing for storage. This method is usually applicable to medications that have a modest quantity of active component.
4. **Flashtab technology:** This technique is yet another cutting-edge way to make oro-dispersible pills. Prographarm labs is the company that created the flashtab technology. Micro crystals are the form of active component utilized in the formulation. The production process can employ a variety of conventional tablet-making methods.
5. **Pharma burst technology:** As the name implies, the goal of this technique is to release the drug into the mouth right away. SPI Pharma, New Palace, provided protection for this tactic. This process produces a product that instantly releases the medication from its dose form by combining several specific excipients. One of the unique components utilized to create a powerful, quickly-melting tablet is mold able saccharine.

EVALUATION OF ORODISPERSIBLE TABLETS (29, 30, 31, 32, 33, 34, 35)

Content uniformity

Tablets with a content uniformity test score of fewer than 25 milligrams, or 25% of a tablet, must pass. All 10 random dose units have the same quantity of active component, as determined by the test procedure. A preparation is considered successful if each individual piece of information accounts for 85–15% of the average.

Weight uniformity

Twenty tablets are weighed individually, their average weights are determined, and the weights of each tablet are compared to the average weight in order to perform the weight variation test.

Hardness

Measuring the force required to break a tablet across its diameter yields the tablet's hardness.The hardness of the tablet controls its resilience to abrasion, cracking, and chipping during handling, storage, and preparation for use. ODTs often keep their hardness lower than that of normal tablets since a higher hardness causes the tablet to dissolve more slowly.

Friability test

The weight loss of a tablet within its container due to fine particle removal from the surface is known as friability. Tablets can be tested for friability using the Roche Friabilator.

Water absorption ratio

Three Folds of tissue paper were put into a small Petri dish that held six milliliters of water. The predicted duration for full soaking was calculated by placing a tablet on the paper. Next, a weight was taken off the moist pill.

Disintegration time

The experiment was conducted on six tablets using the apparatus described in I.P.-1996. Distilled water at 37°C ± 2°C served as the disintegration medium, and the time it took for the tablet to completely disintegrate with no palatable mass remaining in the apparatus was measured in seconds.

Dissolution test

This test is significant because it provides the drug-release profile. They are both USP dissolution test equipment that you may use. Rapid dissolution characterizes orodispersible tablets. Orodispersible tablet fragments or fractured tablet masses can become trapped at the inside top of the spindle of the USP Type I basket device, not withstanding its effectiveness. A poor and ineffective agitating technique might result in an inaccurate dissolving profile. Type II is recommended because of its repeatable-dissolution profile.

Moisture-uptake studies

This study on orodispersible pills is noteworthy. This investigation aims to assess the stability of the pills. The necessary humidity was attained by storing a saturated sodium chloride solution in the bottom of the desiccators for three days. Weighing the pills, we record the weight increase as a percentage.

Packaging

During manufacture and storage, packaging must be handled carefully to preserve the dose of other fast-dissolving dosage forms. Depending on the application and marketing goals, the oral delivery system can be packaged in a single pouch, blister card with multiple units, multiple unit dispenser, or continuous roll dispenser.

APPLICATIONS OF ORALDISPERSIBLE TABLETS (36)

1. The goal is to create dose forms that dissolve orally while utilizing already available disintegrants
2. To significantly enhance the ODTs' current technology.
3. To get ODTs by optimizing the mix of excipients or disintegrates.
4. To design and choose appropriate packaging materials and reasonably priced products.

FUTURE PROSPECTIVE FOR ORODISPERSIBLE TABLETS (37)

Many ODT producers face hurdles in the future related to cost reduction through the use of standard equipment, flexible packaging, capacity to hide taste. Orodispersible tablets can be a good option for medications like protein and treatments based on peptides, which are not very bio-available when taken as traditional medicines since they often break down quickly in GIT. Furthermore, the possibility exists to produce controlled release oral drug delivery systems (ODTs) utilizing diverse drug carriers.

CONCLUSION

The most exciting new approaches to medicine delivery is the use of orodispersible tablets. Traditional solid dosage forms may not be as effective as ODTs. ODTs functions like solution inside the body and upon administration, as a solid dose form external to the body. Time to action, bioavailability, convenience, and patient compliance have all increased as a consequence. This dose form should be used carefully because of its low mechanical strength. Future drug production may employ ODT for a great deal more kinds of medications. This medication delivery technique may result in improved patient compliance and ultimately higher clinical output because of the broad relevance of ODT. The development of several new medication classes in the form of ODT is possible.

REFERENCES

1. Leon, Lachman, Herbert A., Lieberman, Joseph L., Kanig. (1990). The theory and Practice of Industrial Pharmacy. Varghese publication house., 3rd edition, 293-373.
2. P. A., Hannan, J. A., Khan, and S., Saullah. (2016). Oral Dispersible System. A New Approach in Drug Delivery System. Indian J. Pharm Sci., 78(1): 2–7.
3. Srikond, VS., Janaki, RN., and Joseph, AF. (2000). Recent technological advances in oral drug delivery – Review. Pharm. Sci. Technol.Today., 3:138-145.
4. Fu, Y., Yang, S., Jeong, SH., Kimura, S., Park, K. (2004). Orally fast disintegrating tablets: Developments, technologies, taste-masking and clinical studies. Crit. Rev. The Drug Carrier Syst., 21(6):433-76.
5. MNK., Reddy, MA., Hussain, TR., Rao, TR., Krishna, V., Pavani. Formulation and evaluation of naproxen oral disintegrating tablets. Int. J. Pharm. Biol. Sci., 2:303-316
6. Patel, VN., Gupta, MM. (2013). Emerging trends in oral dispersible tablet. Journal of Drug Delivery and Therapeutics., 3(2):15.
7. Chiman, B., Isha, S. (2013). Development of fast disintegration tablets as oral drug delivery system - A review. Indian. J. Pharm. Biol. Res.,1(3):80-99.
8. Guptam, DK., Mauryam, A., Varshney, MM. (2020). Orodispersible tablets: An overview of formulation and technology. World Journal of Pharmacy and Pharmaceutical Sciences., 9(10): 1406-18.
9. Slowson, M., Slowson, S. (1985). What to do when patients cannot swallow their medications". Pharm. Times., 51: 90-6.
10. Seager, H. (1998). Drug-deliver Products and the Zydis Fast-dissolving Dosage Form. J. Pharm. and Pharmacol., 50: 375-82.
11. Ashish, P., Harsoliya, MS., Pathan, JK., Shruti, S. (2011). A review- Formulation of mouth dissolving tablet. Int. J. Pharm.Clin Sci., 1(1):1-8.
12. Prateek, S., Ramdayal, G., Kumar, SU., Ashwani, C., Ashwini, G., Mansi, S. (2012). Fast dissolving tablets: Anew venture in drug delivery. Am. J. Pharm.Tech. Res.,2(4):252-79.
13. CODEN. (2009). International Journal of PharmTech Research (USA): IJPRIF ISSN: 0974-4304.1(4):1079-1091.
14. Pahwa, R., and Gupta, N. (2011). Superdisintegrants in the Development of Orally Disintegrating Tablets: A Review. Int. J. Pharm. Sci. Res., 2: 2767-2780.
15. Abhay, Asthana., Swati, Agarwal., Gaytri, Asthana. (2013). Oral Dispersible Tablets: Novel Technology and Development. International Journal of Pharmaceutical Sciences Review and Research., 20(1): 193-199.
16. Kumar V., Dinesh, Sharma, Ira., Sharma, Vipin. (2011).A comprehensive review on fast dissolving tablet technology. Journal of Applied Pharmaceutical Science., 01(05): 50-58.
17. Deshpande, KB., Ganesh, NS. (2011). Orodispersible tablets: An overview of formulation and technology. Int. J. Pharm. Biol. Sci., 2(1):726-34.
18. Kumar, E., Bhagyashree, J. (2013). Mouth dissolving tablets – A comprehensive review. Int. J. Pharm. Res. Rev., 2(7):25-41.
19. Chiman, B., Isha, S. (2013). Development of fast disintegration tablets as oral drug delivery system - A review. Indian. J. Pharm. Biol. Res., 1(3):80-99.
20. Rakesh, P., Mona, P., Prabodh, SC., Dhirender, K., Sanju, N. (2010). Orally disintegrating tablets - Friendly to pediatrics and geriatrics. Arch. Appl. Sci. Res., 2(2):35-48.
21. Patil, MR., Gujarathi, Nayan, A., Rane, Bhushan, R. (2014). Formulation and evaluation of mouth dissolving tablet: Review article. Pharm. Sci. Monit., 5(2):7-20.
22. Deepak, H., Geeta, A., Hari, Kumar, SL. (2013). Recent trends of fast dissolving drug delivery system - An overview of formulation technology. Pharmacophore; 4(1):1-9.
23. Velmurugan, S., Vinushitha, S. (2010). Oral disintegrating tablets: An overview. Int. J. Chem. Pharm. Sci., 1(2):1-12.
24. Roshan, Kenneth., Keerthy, H S. (2021). "Orodispersible Tablets: A Compendious Review." Asian. J. pharm. Res. dev., 9:66-75.

25. Garud, SS., Derle, DV., Valavi, AB., Sheikh, SJ., Derle, ND. (2014). A review on: Orodispersible tablet (ODT) technology-A novel approach to develop the super generics. Int. J. Pharm. Sci. Rev. and Res., 26:231-236.
26. Ghosh, T., Ghosh, A., Prasad, D. (2011). A review on new generation orodispersible tablets and its future prospective. Int j. pharm. sci., 3:1-7.
27. Beri, C., Sacher, I. (2013). Development of fast disintegrating tablets as oral drug delivery system-A review. Indian. J. pharm.boi.l res., 1:80-99.
28. Raavi, PK., Kulkarni, PK., Dixit, M., Krishna, LNV., Lavanya, D. (2011). A Review On: Blazing Trends In Fast Dissolving Tablets. IJDFR., 2:82-101.
29. Kumar, SS., Ravendra, V., Vikash, C., Prakash, SS. (2014). Orally disintegrating tablets: A dosage form that extends the market exclusivity and patent protection. World. J. Pharm. Sci., 3(7):526-46.
30. Shubhra, S., Kumar, YS. (2014). Fast dissolving tablets: A strategy to improve solubility of poorly soluble compounds. Glob. J. Pharmacol., 8(4):584-91.
31. Pooja, A., Arora, SV. (2013). Orodispersible tablets: A comprehensive review. Int. J. Res.Dev. Pharm.Life .Sci., 2(2):270-84.
32. Puneet, M., Kumar, SP., Rishabha, M. (2014). A review on recent advances of oral mouth dissolving tablet. J. Drug. Discov. Ther., 2(18):17-22.
33. Alam, MD., Nayyar, P., Kumar, SP. (2014). Novel technology for formulation and evaluation of mouth dissolving tablet - A review. Adv. Biol. Res., 8(5):180-6.
34. Deepika, J., Mishra, A. (2014). A review-Formulation and development of orodispersible tablet. Int. J. Pharm. Erudition., 4(1):21-38.
35. Dey, P., Maiti, S. (2010). Orodispersible tablets: A new trend in drug delivery. J. Nat. Sci. Biol. Med., 1(1):2-5.
36. Saurabh, Thapliyal., Dr. Ganesh, Bhatt., and Garima, Kandpal. (2018). Oro dispersible tablets: a review, World Journal of Pharmaceutical Research., 7(13): 146-162.
37. Tanmoy. G., Amitava, G., Devi, P. (2011). A review on new generation orodispersible tablets and its future prospective. Int. J. Pharm. Sci., 3(1):1-7.

REVIEW ARTICLE

An Update Review on Iridoid Glycosides: Major Focus on Phytochemical and Pharmacological Versatility

Monika[1] and Neeraj Kumar[2]*

[1]Assistant Professor (Research Scholar), School of Pharmaceutical Sciences, Shri Guru Ram Rai University, Uttarakhand, India.
[2]Professor, School of Pharmaceutical Sciences, Shri Guru Ram Rai University, Uttarakhand, India.

Received: 29 Dec 2023 Revised: 19 Jan 2024 Accepted: 14 Mar 2024

***Address for Correspondence**
Neeraj Kumar
Professor,
School of Pharmaceutical Sciences,
Shri Guru Ram Rai University, Uttarakhand, India.
E mail: neeraj_sidana2007@rediffmail.com

ABSTRACT

The review covers about active substances that found the plant world are called iridoids. Various plants, especially those in the Gentianaceae, Loganiaceae, and Rubiaceous families, contain a group of naturally occurring substances known as iridoids. Numerous biological actions and potential health advantages of these substances are well-known. In traditional medicine and pharmaceutical research, iridoids are of interest because they frequently demonstrate antioxidant, anti-inflammatory, and antibacterial effects.Iridoids have been investigated for their possible function in boosting the immune system, promoting digestive health, and assisting in the management of many chronic conditions. These are the varieties of monoterpenoid, also present in some mammals, in the general form of cyclo-pentanepyran. They come from the biosynthesis of 8-oxogeranial and are normally present in plants as glycosides, frequently linked to glucose. Iridoids are bicyclic cis-fused cyclo-pentanepyrans from a structural perspective. Oleuropein and amaro-gnetin are examples of secoiridoids, which are created when a bond in the cyclopentane ring is broken. Iridoids' metabolites are a topic of interest to researchers due to their versatile spectrum of biological activities like neuro defensive, hepatoprotective, anticancer, anti-inflammatory, Anti-Diabetic and lipid lowering activities along with advantages like offering a fresh approach for the creation of new drugs and research focusing. Iridoids have the potential to become new natural medications and supplements because of their bioactive qualities, but additional study is vital to fully comprehend their modes of action and possible uses. In order for a rational consumer of information to be useful in the creation of therapeutic options, the present review's goal is to give extensive information about iridoids and its biological activity.

Keywords: Iridoids, Oleuropein, hypoglycemic, hepatoprotective, hypolipidemic.

INTRODUCTION

The acetal derivatives of iridodial, which is essentially extracted from the ant's defense secretions, are what make up the group of naturally occurring monoterpenoids known as iridoids. They are generally dicotyledons plants that are more common in the plantae kingdom, including the Scrophulariaceae, Oleaceae, Labiate, Rubiaceous, Gentianaceae, Alliaceae, Loganiaceae, and Verbenaceae families.[1]. These are the components, usually found in the fresh leaves and juvenile stems of plants, but sometimes rarely in the fruits and sprouts, that belong to the broad and extended class of cyclopentane pyran monoterpenes. There are several traditional medications that include iridoids that are used as antipyretics, sedatives, hypotensive agent, bitter tonics, cough medicines, and treatments of wounds and skin conditions. These underlying facts motivated researchers to examine the bioactivities of these phytochemicals. [2,3]. Iridoids possess an ample range of bioactivity like choleretic, neuroprotective, anti-inflammatory, antitumor, antioxidant, cardiovascular, antihepatotoxic, hypolipidemic, hypoglycemic, antispasmodic, antimicrobial, antiviral, immunomodulator, anti-leishmanial, antiallergic and molluscicide.[4] Based on their biosynthesis, chemical and structural characteristics, iridoids have been divided into many subgroups. Four subgroups are distinguished based on the iridoid's structural characteristics: iridoid-glycosides, secoiridoids glycosides, non-glucose iridoids, and bis iridoids. They are naturally more active and include hemiacetal hydroxyl groups. Moreover, they mostly take the shape like glycosides and are link to glucose at the C-1 (-OH) group. Because glycosides have alike qualities like tough ability to modify and facile absorption, they are chosenfor a lead compound. [5,6]. The topic Iridoids have gained attention as an active component that treats a diversity of diseases and disorders as a result of prior studies demonstrating their remarkable biological activity, including hepato-protective, anticancer, hypoglycemic, hyper-lipidemic, anti-inflammatory, and effects on various diseases. [7,8] This review's goal is to provide a stronger basis for the creation of novel medicines and research by focusing on iridoids and their biological activity broadly. This will enable future investigation into the chemicals' therapeutic potential.

Main Body

Biological Activity of Iridoids

Neuroprotective Effects

The body's coordination center, the CNS, acts as the body's remote control for neuronal activity (sending and receiving messages) and movement. Hence, neurological illness results in functional abnormalities in the brain and spine. [9]The causes of neurodegeneration include several elements. Many studies have sought to identify natural medicines that might enhance neuroplasticity in the hopes of avoiding memory loss due to ageing, postponing ageing, and lowering the prevalence of neurodegenerative disorders.[10]

Alzheimer's Disease: Most prevalent type of disorder which is caused by a degenerative brain illness with unclear etiology that often strikes people in their late middle or advanced years. It causes increasing memory loss, poor thinking, disorientation, and changes in personality and mood.[11]. Its disease is indicated by gradual neuronal death, and a deterioration of memory and cognition as a result. The brain's beta amyloid peptide plaques, which produce gliosis, which results in inflammation activation and ultimately cell death, are the primary cause of the gradual cognitive deficiencies.[12]

Mechanism of actions involved

Cholinesterase inhibitions: System acts by inhibiting the acetylcholinesterase enzyme. However, some drugs demonstrated an upsurge in the action of choline acetyltransferase and reversed its depletion, the cause of reduced interneuron connections and shortening of neurite outgrowth. [13]

Improving mitochondrial function: By assisting in mitochondrial dysfunction and the reduction in activity of monoamine oxidase. It also helps in shielding the midbrain neurons from MPTPinduced neurotoxicity.

Filteringdopamine system: Dopamine is a catecholamine neurotransmitter in brain. Iteffects on an increase in DA and DOPAClevel, which helpto slow down Dopamine conversion in nigrostriatal dopaminergic pathway and avert

the harm of TH-positive cells. The crucial mechanism involved is possibly connected with up-regulating the creation of a glial cell-derived neurotrophic factor in the striatum.[14].

Preventing inflammation: It act byinhibiting microglial cell initiation, the construction of proinflammatory cytokines.Glial cells in the midbrain shows dose-dependent rescued dopamine neurons from chemical induced neurotoxicity. In addition, it also exhibited neuroprotective effects in the D-gal-induced ageing of mice's brains, and its mode of action may be partially explained by the marked decline in inflammatory cytokines.[15-16]

Anti-apoptotic Pathway: By conquering activation of ERK and by monitoring the generation of NO & NOS in rotenone-activated primary cells, it helps in preventing the death of midbrain neurons[17-20]

Parkinson's Disease: Tremor, bradykinesia, and postural instability are symptoms of this slowly progressing neurodegenerative illness that affects the basal ganglia.[21]
In Parkinson disease there is –
i.) Degeneration of dopaminergic neurons at the fibers nerve endsthat go from the substantia nigra to the striatum causes dopamine to no longer be produced.
ii.) Characteristic alterations in depigmentation are caused by the loss of the neurons that carry melanin.
iii.) Lewy bodies' formation (a sticky protein lump that disrupt the normal functions of the brain).
iv.) Akinesia, stiffness, and bradykinesia are symptoms of dopamine deficiency.[22]

Mechanism of Action of Iridoids in PD
The improved locomotor function by increase in striatal dopamine, TH-positive neurons anddopamine transporter levels. Notably, it raised GDNF protein levels, this elevates GDNF expression is thought to have restored dopaminergic neuron function. [23-26]

Anti –inflammatory Activity
Iridoids' primary health-improving properties are their anti-oxidative and anti-inflammatory properties. Iridoids' ability to suppress proinflammatory cytokines, COX-2,PGE2, and TBX2 accounts for their anti-inflammatory properties. While certain iridoids, such as the hydrolyzed derivative of harpagiferid, are chemically (and physically) comparable to celecoxib, a selective COX-2 inhibitor, and PGE2.In response to inflammation, neutrophils produce a number of hazardous substances, including ROS, that have the natural ability to engulf and kill a variety of bacteria (Reactive oxygen species). Both acute and chronic illnesses have been linked to excessive levels of ROS generated by activated neutrophils through NADPH oxidase. So, it's crucial to prevent inflammatory regions from producing too much ROS from leukocytes.[27-28]One such iridoid is the root of *Gentiana straminea*, which contains the anti-inflammatory agent Loganic acid, which is extensively found in the *Gentianaceae* family. While LA has a high level of COX inhibition and a better affinity for COX-2 than COX-1, it may not have serious adverse effects such an increased risk of gastrointestinal ulcers. Moreover, because of its strong affinity for COX-2. Moreover, it inhibits the production of superoxide in human neutrophils caused by theformyl-methionyl-leucyl-phenylalanine, "a powerful chemotactic factor for human neutrophils".[29]

Hypoglycemic and Hyperlipidemic effect
A series of conditions known together as diabetes are characterized by elevated blood sugar levels. Disease that affects the majority of the people on a daily basis. It is found that Type-2 diabetes is the one that affects the greatest number of individuals. It is a chronic illness that is linked to lifestyle choices and is accompanied by a number of problems.[30]
Pathogenesis of type -2 DM

- Insulin resistance due to Genetic predisposition and Obesity Lifestyle factors.
- dysfunction of islet β cell
- Increase hepatic glucose output
- Decrease peripheral glucose uptake[31]

Study reveals that decisive gears of the insulin resistance syndrome and criticalissues for heart related disorders are hyperlipidemia and hyperinsulinemia. In various studies, it was revealing that iridoids efficaciously reduce hyperlipidemia and hyperglycemia.It was also discovered that few iridoids play a significant part in a few metabolic diseases. One such iridoid, oleuropein, had a hypoglycemic impact as well as an increase in glucose tolerance *in vivo*. Its mode of action was recently clarified by revealing its potential and positive effects by lowering oxidative stress and boosting the body's own antioxidant defenses. Thus, study reveals a new mechanism of treatment of hypoglycemic effect through antioxidant action [32]. However, Iridoidsseparated from the leaves of *G. Jasminoides* (Rubiaceous) shows that deacetylasperulosidic acid methyl ester had hypoglycemic effect and decreased blood glucose levels in normal mice.[33-34]

Mechanism of Action of hypoglycemia[35]

- Insulin stimulus
- Increase and Improve insulin sensitivity andresistance
- Restoration of pancreas
- Action on metabolism of glucose
- Regulating flora of intestine

Hepatoprotective Activity

The liver, the body's biggest and most important organ, is responsible for a number of vital biological processes, including metabolism, detoxification, the synthesis of proteins, and the production of biochemicals required for development and digesting. The organ's function exposes it to harm from many types of metabolic products, toxins, endotoxins, viruses, or medications. [36]Oxidative stress is the main factor to take into for liver disease. Damage to the liver is mostly caused by increase in the reactive oxygen or nitrogen and also in decrease in antioxidant molecules. It is depleted by highly reactive metabolites. Glutathione is required for the cleansing and to remove toxins of glutathione-S-transferase and also leads to causes cells to die. [37] Antioxidant is the function to perform in this situation. Iridoids take the lead thanks to their antioxidant capacity. The activity is both direct and indirect, by removing reactive oxygen species and by activating the anti-oxidant defenses within the body.[38-40] Iridoid, guards the liver against steatosis, fibrosis, and necrosis. According to various studies, they lower liver/body weight ratio, bilirubin, ALT, AST, and ALP. Iridoids also limits the fibrosis process by decreasing the accumulation of collagen in the liver and the inflammation by loweringIL-1, TNF, IL-18, IL-6 and COX-2 in a dosedependent way.On the basis of above result a conclusion is drawn that iridoids' hepatoprotective effect are because of their facilitation of drug metabolism, enhancement of mitochondrial dysfunction, decrease in oxidative stress and by suppression mitogen activated protein kinase signaling pathway. [41]

Antioxidant Activity

Each and every cell in the body depends on oxygen. Cells cannot produce energy without oxygen;therefore, metabolism is less efficient. Cellular functions such controlling gene expression, signal transmission, cell growth and development and cell death depend on it for survival. The body needs oxygen for oxidative phosphorylation because it facilitates the aerobic metabolism of glucose, which produces the energy needed by the body. Then, the formation of reactive oxygen species occurs. Now, in order to adapt to the environment, the body develops a self-antioxidant defense system, which includes vitamins, coenzyme Q, lipoic acid, glutathione (GSH), and other substances, all of which work together to prevent ROS from being produced. ROS can be eliminated even by antioxidant enzymes. In a typical physiological circumstance, there is a continual fluctuation in the creation and removal of ROS. Although it triggers an event that results in an excess of ROS and a lack of antioxidants, which leads to oxidative stress, when subjected to detrimental external stimuli.[42]This oxidative stress causes cell necrosis and apoptosis by destroying the structure and functionality of several macromolecules. The research study shows thatan iridoid(Aucubin) is a potent antioxidant. It either directly lowers levels of ROS, Malondialdehyde, and 4-hydroxynonenal, as well as efficiently remove oxygen, free hydroxy and 1,1-diphenyl-2-picrylhydrazyl radicals, or it does the opposite by raising the antioxidative activities of Superoxide dismutase, catalase, andGlutathione peroxidase. By balancing

oxidation and the antioxidant defense system better, therefore iridoids shows anincreased antioxidant ability to prevent damage to the gastric mucosa, endothelium, cardiac remodeling, and diabetic encephalopathy.[43-45]

Anti-tumor Activity

A tumor is an atypical mass of tissue that progresses as result of excessive cell growth, division, and survival rather than demise. Both benign and malignant tumors exist. It is among the world's major causes of death. Studies reveal that Gentipicroside, Valjatrate E, and Sertiamarin B are a few iridoids that do have anti-tumor effect. [46].Gentiopicroside has been reported to show antitumor activity against ovarian cancer cell line (SKOV3). Its anticancer effects were determined usingMethyl Thiazolyl Tetrazolium, Apoptosis by4', 6-diamidino-2-phenylindole annexin V or propidium iodide (PI) double staining, Mitochondrial membrane potential (MMP) andprotein expression by western blotting.[47] All resultsuggests that gentiopicroside may prove to be an effective lead chemical in the treatment and management of ovarian cancer. [48]

The Sertiamarin B, a new seco-iridoid,a chemical component which is identified from *Swertia mussotii*'s aerial part. Four human tumor cell lines (HCT-116, HepG2, MGC-803 and A549)exposed to it showed anti-tumor action. It demonstrated substantial cytotoxic activity against the MGC-803 cell line (IC50 = 3.61), and its ability to efficiently suppress cell growth raises the possibility that it might serve as a novel gastric cancer treatment agent. [49]

Anti-bacterial Activity

According to studies on iridoids various researchers demonstrated that they have antibacterial properties. Isoplumericin, plumericin, galioside, and gardenoside are a few of them; they have all been linked to anti-bacterial action.An intriguing action on *Staphylococcus aureus* was discovered when an iridoid (seco-iridoid glycoside)gentipicroside showed significant efficacy (MIC 6.3103 mg/ml). Likewise, Sweroside (an iridoid) isolated from the rootstock of *Scabiosa columbria* (Dipsacaceae) was used against *B. cereus, B. pumulus, B. subtilis, M. kristinae, S. aureus, E. coli, K. pneumoniae, P. aerugenosa, E. cloacae*and it showed good antibacterial activity. A group of various non-glycosidic iridoids likemussaenin A, gardendiol, isoboonein, and rehmaglutin D showed a potent anti-bacterial action. It shows that all glycosidic and non-glycosidic iridoids have antibacterial action similar to chloramphenicol.[50]

CONCLUSION

Iridoids are a substance that is extensively dispersed across the plant world; as previously indicated, it is particularly common among dicotyledons plants. Research in contemporary pharmacology have demonstrated their biological and pharmacological activity, high therapeutic value, and usefulness in the treatment of tumors, hepatoprotection, antimicrobial, neuroprotection, antioxidant, hyperlipidemia, and inflammation. Many biological functions of iridoids were investigated in this review paper. Iridoids' kinds, structure, and how the placement of different functional groups alters how active they are all discussed. Oleuropein, *C. officinalis*, and *G. jasminoides* are used as hypoglycemic agents. Catalpol and picroliv are used for hepatoprotective activity. Aucubin is used as an anti-oxidant. Gentiopicroside and Sertiamarin B are used in anti-tumor activity. Aucubin and Sweroside are used as anti-oxidants. Iridoids like catalpol are used for neurodegenerative diseases like Parkinson. This shows that the iridoids' versatility and current study on their activity have been important in luring scientists to learn more about iridoids in order to unlock these chemicals' untapped potential. This leads us to the conclusion that the iridoids group may prove to be a medicine with significant therapeutic potential and that more research into this area may lead to the creation of treatments with greater efficacy.

Abbreviations

CNS	Central Nervous System
MPTP	1-methyl-4-phenyl-1,2,3,6-tetrahydropyridine
DA	Dopamine

DOPAC	3,4-Dihydroxyphenylacetic acid
ERK	Extracellular signal-regulated kinase
PD	Parkinson's Disease
GDNF	Glial cell-derived neurotrophic factor
COX	Cyclooxygenase
PGE2	Prostaglandin E2
TBX2	Thromboxane-B2
ROS	Reactive oxygen species
DM	Diabetes Mellitus
ALT	Alanine aminotransferase
AST	Aspartate aminotransferase
ALP	Alkaline phosphatase
DPPH	1,1-diphenyl-2-picrylhydrazyl

REFERENCES

1. L. X. Guo, J. H. Liu, and F. Yin,"Regulation of insulin secretion by geniposide: possible involvement of phosphatidylinositol 3- phosphate kinase," European Review for Medical and Pharmacological Sciences, vol. 18, no. 9, pp. 1287–1294, 2014.
2. J. Yan, C. Wang, Y. Jin *et al*., "Catalpol ameliorates hepatic insulin resistance in type 2 diabetes through acting on AMPK/NOX4/PI3K/AKT pathway," Pharmacological Research, vol. 130, pp. 466–480, 2018.
3. P. Jiang, L. Xiang, Z. Chen *et al*., "Catalpol alleviates renal damage by improving lipid metabolism in diabetic db/db mice," American Journal of Translational Research, vol. 10no. 6, pp. 1750–1761, 2018.
4. J. Liu, H. R. Zhang, Y. B. Hou, X. L. Jing, X. Y. Song, and X. P. Shen, "Global gene expression analysis in liver of db/db mice treated with catalpol," Chinese Journal of Natural Medicines, vol. 16, no. 8, pp. 590–598, 2018.
5. C. Liu, Y. Hao, F. Yin, Y. Zhang, and J. Liu, "Geniposide protects pancreatic β cells from high glucose-mediated injury by activation of AMP-activated protein kinase," Cell Biology International, vol. 41, no. 5, pp. 544–554, 2017.
6. L. X. Guo, J. H. Liu, X. X. Zheng, Z. Y. Yin, J. Kosaraju, and K. Y. Tam, "Geniposide improves insulin production and reduces apoptosis in high glucose- induced glucotoxic insulinoma cells," European Journal of Pharmaceutical Sciences, vol. 110, pp. 70–76, 2017.
7. Q. L. Yang, F. Yang, J. T. Gong *et al*., "Sweroside ameliorates α-naphthylisothiocyanate-induced cholestatic liver injury in mice by regulating bile acids and suppressing proinflammatory responses," Acta PharmacologicaSinica, vol. 37, no. 9, pp. 1218–1228, 2016.
8. K. Karłowicz-Bodalska, S. Han, A. Bodalska, J. Frezer, and M. Smoleński, "Przeciwzapalnewłaściwościwybranychroślinzawierającychzwiązkiirydoidowe. Anti-inflammatory properties of selected plants containing iridoid compounds," PostępyFitoterapii, vol. 18, no. 3, pp. 229–234, 2017.
9. N. Yamabe, J. S. Noh, C. H. Park *et al*., "Evaluation of loganin, iridoid glycoside from Corni Fructus, on hepatic and renal glucolipotoxicity and inflammation in type 2 diabetic db/db mice," European Journal of Pharmacology, vol. 648, no. 1-3, pp. 179–187, 2010
10. R. Chander, N. K. Kapoor, and B. N. Dhawan, "Picroliv, picroside-I and kutkoside from Picrorhizakurrooa are scavengers of superoxide anions," Biochemical Pharmacology, vol. 44, no. 1, pp. 180–183, 1992.
11.] C. Girish and S. C. Pradhan, "Hepatoprotective activities of picroliv, curcumin, and ellagic acid compared to silymarin on carbon-tetrachloride-induced liver toxicity in mice," Journal of Pharmacology and Pharmacotherapeutics, vol. 3, no. 2, pp. 149–155, 2012.
12. K. Dai, X. J. Yi, X. J. Huang *et al*., "Hepatoprotective activity of iridoids, seco-iridoids and analog glycosides from Gentianaceae on HepG2 cellsviaCYP3A4 induction and mitochondrial pathway," Food & Function, vol. 9, no. 5, pp. 2673–2683, 2018.

13. McCormack JG, Westergaard N, Kristiansen M, Brand CL, Lau J. Pharmacological approaches to inhibit endogenous glucose production as a means of anti-diabetic therapy. Curr Pharm Des 2001; 7: 1451–74.
14. Maiese K, Chong ZZ, Shang YC. Mechanistic insights into diabetes mellitus and oxidative stress. Curr Med Chem 2007; 14: 1729–38
15. Nordlie RC, Foster JD, Lange AJ. Regulation of glucose production by the liver Annu Rev Nutr 1999; 19: 379–406.
16. B. Dinda, S. Debnath, Iridoids, in: K.G. Ramawat, J.M. Merillon (Eds) Natural Products: phytochemistry,botanyand metabolism of alkaloids, phenolics and terpenes, Springer, Berlin, 2013, pp. 3009-3067.
17. Alzheimer's Association, Alzheimer's disease facts and figures, Alzheimer's Dement. 14 (2018) 367-429
18. K. Hoglund, H. Salter, Molecular biomarkers of neurodegeneration, Expert Rev. Mol. Daign. 13 (2013) 845-861.
19. E. Esposito, S. Cuzzocrea,New therapeutic strategy for Parkinson's and Alzheimer's disease, Curr. Med. Chem. 17 (2010) 2764-2774.
20. R.E. Tanzi, L. Bertram, Twenty years of the Alzheimer's disease amyloid hypothesis: a genetic perspective, Cell 120 (2005) 545-555.
21. J.Z. Huang, *et al*., Catalpol preserves neural function and attenuates the pathology of Alzheimer's disease in mice, Mol. Med. Rep. 13 (2016) 491-496
22. H. Zhang, *et al*., Geniposide alleviates amyloid-induced synaptic injury by protecting axonal mitochondrial trafficking, Front. Cell Neurosci. 10(2016) 309.
23. J. Jaankovic, L. Giselle Aguilar, Current approaches to the treatment of Parkinson's disease, Neuropsychiatry Dis. Treat. 4 (2008) 743-757.
24. Li, C.M.; Luo, Y.W.; Tian, B.Y. Research Progress on Mass Spectral Fragmentation of Iridoids. J. Hebei Norm. Univ. (Nat Sci. Edit). 2015, 39, 522–526.
25. Pei, Y.H.; Lou, H.X. Natural Medicinal Chemistry; People's Health Publishing House: BeiJing, China. 2016; pp. 192–195.
26. Bianco, A. Recent developments in iridoids chemistry. Pure Appl. Chem. 1994, 66, 2335–2338.
27. Zheng, L.S.; Liu, X.Q. Research progress of iridoids. Res. Dev. Nat. Prod. 2009, 21, 702–711. 5. Ren, Z.J.; Zhang, L.M.; He, K.Z. Extraction Technology and Pharmacological Research Progress of Main Components of Gardenia jasminoides Ellis. Res. Dev. Nat. Prod. 2005, 17, 831–836
28. Akihisa, T.; Matsumoto, K.; Tokuda, H.; Yasukawa, K.; Seino, K.I.; Nakamoto, K.; Kimura, Y. Anti- inflammatory and potential cancer chemopreventive constituents of the fruits of Morindacitrifolia (Noni). J. Nat. Prod. 2007, 70, 754–757
29. Dong, J.E.; Zhang, J. Advances in the Research of Iridoids Occurring in Plants. J. Northwest For. Univ. 2004, 19, 131–135.
30. El-Naggar, L.J.; Beal, J.L.; Iridoids. A review. J. Nat. Prod. 1980, 43, 649–707
31. Li, J.; Huang, X.; Du, X.; Sun, W.J.; Zhang, Y.M. Study of chemical composition and antimicrobial activity of leaves and roots of Scrophularianingpoensis. Nat. Prod. Res. 2009, 23, 775–780.
32. Bai, M.; Li, S.F.; Liu, S.F.; Wang, X.B.; Huang, X.X.; Song, S.J. Iridoid glycoside and lignans from a wild vegetable (Patrinia villosa, Juss.) with antioxidant activity. J. Food Biochem. 2018, 42, e1251.
33. Lv, T.; Xu, M.; Wang, D.; Zhu, H.T.; Yang, C.R.; Zhang, T.T.; Zhang, Y.J. The chemical constituents from the roots of Gentiana crassicaulisand their inhibitory effects on inflammatory mediators NO and TNF-α. Nat. Prod. Bioprospect. 2012, 2, 217–221
34. Dinda, B. Pharmacology of Iridoids. Pharmacology and Applications of Naturally Occurring Iridoids. Springer, Cham, 2019. pp. 1–15. doi:10.1007/978-3-030-05575-2_1.
35. Tian, C.; Zhang, T.; Wang, L.; Shan, Q.; Jiang, L. The hepatoprotective effect and chemical constituents of total iridoids and xanthones extracted from Swertia mussotii Franch. J. Ethnopharmacol. 2014, 154, 259–266.
36. Jiefang, K.; Chen, G.; Rodolfo, T. Hypoglycemic, hypolipidemic and antioxidant effects of iridoid glycosides extracted from Corni fructus: Possible involvement of the PI3K–Akt/PKB signaling pathway. RSC Adv. 2018, 8, 30539–30549.

37. Chen, Y.; Liu, D.C. Research progress on mechanism of hypoglycemic Chinese medicine. Chin. J. Clin. Ration. Drug Use. 2017, 10, 159–161.
38. Ma, W.W.; Tao, Y.; Wang, Y.Y.; Peng, I.F. Effects of Gardenia jasminoides extracts on cognition and innate immune response in an adult Drosophila model of Alzheimer's disease. Chin. J. Nat. Med. 2017, 15, 899–904.
39. Yu, D.; Zhang, Y.; Guo, L.; Zhang, Q.; Zhu, H. Study on the Absorption Mechanism of Geniposide in the Chinese Formula Huang-Lian-Jie-Du-Tang in Rats. AAPS PharmSciTech. 2017, 18, 1382–1392.
40. Xu, G.L.; Li, H.L.; He, J.C.; Feng, E.F.; Shi, P.P.; Liu, Y.Q.; Liu, C.X. Comparative pharmacokinetics of swertiamarin in rats after oral administration of swertiamarin alone, Qing Ye Dan tablets and co- administration of swertiamarin and oleanolic acid. J. Ethnopharmacol. 2013, 149, 49–54.
41. Wojtunik-Kulesza, K.A.; Kasprzak, K.; Oniszczuk, T.; Oniszczuk, A. Natural Monoterpenes: Much More than Only a Scent. Chem. Biodivers. 2019, 16, e1900434. [CrossRef]
42. Wang, D.-S.; Dickson, D.W.; Malter, J.S. beta-Amyloid degradation and Alzheimer's disease. J. Biomed. Biotechnol. 2006, 2006, 58406.[CrossRef]
43. Hou, Y.C.; Tsai, S.Y.; Lai, P.Y.; Chao, P.D.L. Metabolism and pharmacokinetics of genipin and geniposide in rats. Food Chem. Toxicol. 2008, 46, 2764–2769
44. Modaressi, M.; Delazar, A.; Nazemiyeh, H.; Fathi-Azad, F.; Smith, E.; Rahman, M.; Gibbons, S.; Nahar, L.; Sarker, S.D. Antibacterial Iridoid Glucosides from Eremostachys laciniata. Phytother. Res. PTR 2009, 23, 99– 103
45. Zhang, L.; Weimin, L.I. Retrospective Study of the Efficacy of Acarbose Combined with Metformin in the Treatment of Type 2 Diabetes Complicated with Hyperlipidemia. China Pharm. 2017, 20, 284–286.
46. R. Wang, D. Xiao, Y. H. Bian, X.Y. Zhang, B.J. Li, L.S. Ding, S.L. Peng, Minor iridoids from the roots of Valeriana wallichii, J. Nat. Prod. 71 (2008) 1254–1257.
47. Y.P. Tang, X. Liu, B. Yu, Iridoids from the rhizomes and roots of Valeriana jatamansi, J. Nat. Prod. 65 (2002) 1949–1952.
48.] C.F. Wang, Y. Xiao, B.Y. Yang, Z.B. Wang, L.H. Wu, X.L. Su, A. Brantner, H.X. Kuang, Q.H. Wang, Isolation and screened neuroprotective active constituents from the roots and rhizomes of Valeriana amurensis, Fitoterapia 96 (2014) 48–55.
49. Miura, T.; Nishiyama, Y.; Ichimaru, M.; Moriyasu, M.; Kato, A. Hypoglycemic activity and structure-activity relationship of iridoidal glycosides. Biol. Pharm. Bull. 1996, 19, 160–161. [CrossRef] [PubMed
50. Shi, X.J.; Yu, H.N.; Zhan, Z.J.; Shan, W.G. Studies on the glycoside's constituents from the rhizome of Gardenia jasminoides. J. Zhejiang Univ. Technol. 2010, 38, 142–144

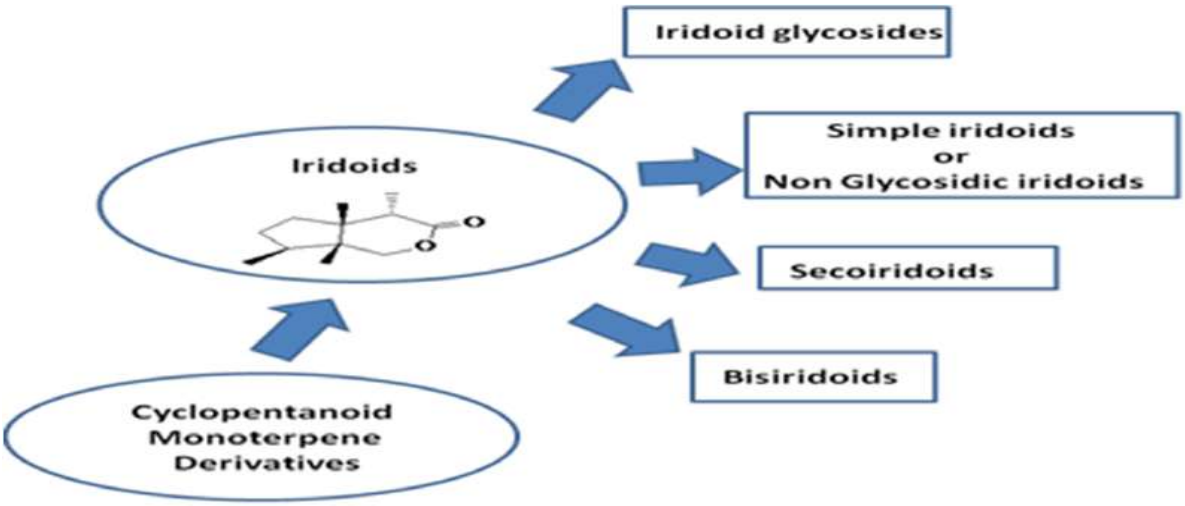

Fig1.: Chemistry and classification of iridoids.

Indian Journal of Natural Sciences www.tnsroindia.org.in ©IJONS

Vol.15 / Issue 83 / Apr / 2024 International Bimonthly (Print) – Open Access ISSN: 0976 – 0997

REVIEW ARTICLE

Application of Nanotechnology in Healthcare Sector: A Perspective Review

V.Sireesha[1]*, N. Chaitanya[2], K. Megana[2] and Meghana.Ch[2]

[1]Assistant Professor, CMR College of Pharmacy, Medchal, (Affiliated to Jawaharlal Nehru Technological University), Hyderabad, Telangana, India.
[2]Pharm D Student, CMR College of Pharmacy, Medchal, (Affiliated to Jawaharlal Nehru Technological University), Hyderabad, Telangana, India.

Received: 06 Dec 2023 Revised: 12 Jan 2024 Accepted: 13 Mar 2024

***Address for Correspondence**
V. Sireesha,
Assistant Professor,
CMR College of Pharmacy,
Medchal, (Affiliated to Jawaharlal Nehru Technological University),
Hyderabad, Telangana, India.
Email: *sireeshaganesh59@gmail.com,*

ABSTRACT

Nanotechnology is a fast-developing area as nanomedicine in engineering and medicine that holds the key for improving medical care in many areas. Nanoparticles have possible applications in diagnosis, targeted medicine products, pharmaceutical products, and biomedical implants. A detailed discussion of the use of nanotechnology in different sectors, including medicine and health, Drug delivery, for treating cancer and cardiovascular disease and diagnosis. Our article discusses about the use of different nanotubes in the delivery of drugs for the treatment of cancer. This article explains how nanotechnology is used in dentistry, nutrition, Covid vaccinations, and HIV/AIDS. Thus our Perspective review gives brief and well organized review on Nanotechnology that should be valuable to researchers, engineers and scientists for future research project.

Keywords: Nanotechnology, nanodevices, nanometer scale, Nanomedicine, Nanomatrials, Polyethylene glycol

INTRODUCTION

The idea and concept of Nanotechnology was introduced by the American physicist and Nobel Prize laureate Richard Feynman in 1959. Nanotechnology is the branch of science that manipulates matter on a scale close to the atomic level to create new materials, structures that function well at the Nanoscale. The development and advancement of numerous scientific fields, including medical, industry, energy, materials science and engineering, depend on this technology [1]. A typical dimensional range for nanoscale constructions is between 1 and 100 nano

meters. Nanomaterials can be produced as atomic-scale structural Manipulation is possible [2]. So these Nanomaterials are unique as they provide large surface area to volume ratio.Utilizing materials with distinctive features at the nanoscale is known as Nanotechnology. The use of Nanomaterials can be found in sunscreen, cosmetics, sporting goods, tyres, electronics and several other items. The use of Nanomaterials in every day products can be divided into 2 types:

a. Nanomaterials can be merged or added to pre-existing product to improve the performance.
b. Nanomaterials such as Nanocrystals and Nanoparticles can be used directly to create advanced and powerful devices[3].

Types of Nanoparticles

Several Nanoparticles and Nanomaterials have been investigated and approved for clinical use. These are tiny macromolecules used in medicinal Nanotechnology. Nanomaterials and Nanodevices are the two main categories of nanotools used in pharmaceutical research. Nanoparticles, dendrimers, micelles, drug conjugates, metallic Nanoparticles, etc. make up Nanostructures[4]. Some common types of Nanoparticles are discussed below

Micelles

These are amphiphilic surfactant molecules formed by combination of Lipids and other amphiphilic molecules. Hydrophobic therapeutic drugs can be included into micellar spherical vesicles, which spontaneously aggregate and self-assemble into a hydrophilic outer monolayer and a hydrophobic core in water conditions. As the special qualities of micelles, hydrophobic medications are made more soluble, increasing their bioavailability. Micelles have diameters ranging from 10 to 100 nm. Micelles can be used as therapeutic, imaging, contrast, and drug delivery agents, among other things[5]

Liposomes

Liposomes are spherical vesicles made of lipid bilayers that range in size from 30 nm to several microns. Hydrophilic therapeutic compounds can be incorporated into the liposomal membrane layer of liposomes, while hydrophobic agents can be incorporated into the aqueous phase [6]. One of the top nanosystems being developed for targeted medication delivery to treat different malignancies and cardiovascular illnesses is the nano-liposome. Doxil is the first FDA approved nano-liposome for treating breast cancer, it enhances the effective drug concentration in malignant effusion without the need to increase overall dose [7].

Dendrimers

Dendrimers are macromolecules that have an external functional group and branched repeating units that extend from a central core [8]. Because therapeutic substances can be bonded to the surface groups or enclosed within the internal space of dendrimers, dendrimers are extremely biodegradable and bioavailable [9]. Dendriplexes, which are polyamidoaminedendrimer-DNA complexes, have been studied as potential vectors for delivering drugs, and they show promise in promoting targeted drug delivery, successive gene expression, and enhanced medication efficacy [10]. Because of their transformable characteristics, dendrimers are a potential class of particulate systems for biological applications, including drug administration and imaging [11].

Carbon nanotubes

Carbon nanotubes are spherical molecules made of graphene, a single layer of carbon atoms wrapped up into sheets [12]. Carbon nanotubes can reach remarkably high loading capacities as drug carriers because of their large exterior surface area. Additionally, carbon tubes are attractive as biological sensors and imaging contrast agents due to their distinct optical, mechanical, and electrical properties [13].

Metallic nanoparticles

Gold and iron oxide are examples of metallic nanoparticles. Hydrophilic polymers like PEG with a magnetic core (4-5 nm) make up iron oxide nanoparticles[14]. Metallic nanoparticles have been applied as drug delivery vehicles, optical biosensors, laser-based therapy, and imaging contrast agents[15].

Quantum dots

Quantum dots (QDs) are fluorescent semiconductor nanocrystals that range in size from 1 to 100 nm. They have demonstrated promise for usage in a number of biomedical applications, including cellular imaging and drug administration. Quantum dots are used in medical imaging because of their unique optical characteristics, small size, high brightness, and stability [16].

Nano-Tube

The identification of different volatile organic chemicals in breath samples from patients with stomach and lung cancer, respectively, has been done using silicon nanowires and carbon nanotubes[17].

Nanobots

Robots of a nanometre (109 m) scale are also known as nano robotics, and they have been used in healthcare, early cancer diagnosis, targeted medication administration for treatment, and pharmacokinetic monitoring of diabetes. Nanobotsdentrifices (dentifrobots), for example, can cover all subgingival surfaces when used as toothpaste or mouthwash, metabolizing any organic material trapped there into safe and odorless fumes. Using correctly configured dentifrobots, pathogenic bacteria that are present in dental plaque are found and eliminated.

Nanowires

Carbon nanotubes, metal oxides, or silicon can be used to create nanowires (NW), which are nanosized channels that permit the passage of electrical current at very low amplitudes. Because of their tiny size and tiny diameter, which is typically 10 nm, they are extremely sensitive to even the smallest change in electrical characteristics. In order to use antibodies as detectors, one option is to attach them to the surface of nanowires. When the antibodies engage with the biomolecules of the target, this causes a conformational change that is detected as an electrical signal on the nanowire. As a result, when multiple nanowires with various antibodies attached are combined into a single device, they can be used as detectors for illnesses like cancer.

Application of Nanotechnology

Nanotechnology have a significant impact in almost all industries. Nanomaterials are directly used to create advanced and powerful devices. Nanomaterials serve as a beneficial use in sunscreen, cosmetic, sporting goods, tyres, electronics[19]. Additionally Nanotechnologies have revolutionized advances in medicine, specifically in diagnostic methods, imaging and drug delivery.The different fields that find potential applications of nanotechnology are as follows:

Nanotechnology in health and medicine

Nanomedicine is the branch of Nanotechnology and is used for the application of nanotechnology to the fields of medicine and healthcare [20]. It has been utilized to treat some of the most prevalent illnesses, such as cancer, musculoskeletal, psychiatric, neurodegenerative and cardiovascular conditions [21]. Early disease detection and prevention, better disease diagnosis, appropriate therapy, and follow-up are all made feasible by nanomedicine. Nanomaterials and nano electrical biosensors are used in nanomedicine. Nanomaterials and the use of nanotechnology allows for the replication or repair of damaged tissue. Tissue engineering, which could revolutionize organ transplantation or the use of artificial implants, uses so-called artificially activated cells. Carbon nanotubes can be used to create advanced biosensors with unique properties. The development of sensors for cancer diagnosis is also being done using this technology. In order to track and image stem cells, promote their differentiation into particular cell lineages, and eventually comprehend their biology, nanotechnology can be a useful tool[22].

In Drug delivery

Nanoparticles are employed in nanotechnology to deliver drugs to precise sites. As the active substance is exclusively deposited in the morbid zone, this procedure uses the required drug dose and considerably reduces adverse effects. Targeted medication delivery has seen a sharp rise in the use of nanotechnology in recent years, particularly in the medical fields. To transport medications, heat, light, or other things, to particular types of cells

such as cancer cells, nanotechnology is currently being explored.One of the top nanosystems being developed for targeted medication delivery to treat different malignancies and cardiovascular illnesses is the nano-liposome. Drug delivery systems should be carefully designed, using lipid- and polymer-based nano-particles to enhance the pharmacological and therapeutic effects of medications[23].Thus Nanoparticles find their use in medication encapsulation, block co-polymer-derived micelles, they deliver tiny medication molecules where they are needed. For the active release of medications, nano electromechanical systems are also used. A tailored medication lowers drug consumption and medical costs, making patient care more affordable for medications made with nanotechnology[24].

Need for Nanotechnology in drug delivery

1. Side effects can be reduced significantly.
2. Drug efficiency is ensured by specifically targeting and killing harmful and cancerous cells.
3. Minimised irritant reactions and improved penetration within the body due to their small size.
4. Improved drug bioavailability.
5. Provide sustained release/controlled release/prolonged release of the drug.
6. Tissue damage can be prevented by administering under regulated conditions.
7. Nanoparticles are used to administer the medication mare effectively for treatment of head and neck cancer.

For example: Doxorubicin which is highly toxic can be delivered directly to tumour cells using liposomes without effecting heart or kidney[25].

Diagnosis and Imaging

The greatest contribution of nanotechnologies to medicine has been the development of more potent contrast agents for nearly all imaging models. This is because nanomaterials have improved permeability and retention effects in tissues, as well as lower toxicity. The development of nano-enabled imaging diagnostic tools and nano-sensors is a focus of nanotechnology in biomedical engineering. Iron oxide (Fe2O3) nanoparticles have been used as contrast agents to improve magnetic resonance imaging for many years, Approved by US FDA The management of disease prognosis, which is important in determining the survival rate of patients, is enhanced by this. Nanoparticles are being used for molecular and biochemical sensing in cancer research, To find infections on-site, many different nanoparticles have been utilized. One of the most popular nanoparticles for rapid diagnostics is gold nanoparticle (AuNP)[26]. Nanodevices have been investigated for the detection of blood biomarkers and toxicity to adjacent healthy tissues. These biomarkers include tumour-shedding exosomes, circulating tumour nucleic acids, related proteins or cell surface proteins, circulating tumour nucleic acids, and cancer-associated circulating tumour cells. These biomarkers not only aid in the early detection of cancer, which is well recognized, but also in the monitoring of treatment and recurrence. Nano-enabled sensors allow high sensitivity, specificity, and multiplexed readings. Next-generation technology combines capture with genetic analysis to shed more light on a problem[27,28].

In cancer diagnosis and tumour hunting

Nanotechnology provides a speedier and more accurate initial diagnosis in addition to a continuous evaluation of cancer patient care through the use of novel molecular contrast fluids and materials[29].Chemical modifications of surface of Nanoparticles improve targeted delivery. One of the best modification is incorporating PEG, which avoids detection of Nanoparticle as foreign objects by the body's immune system, thus allowing them to circulate in blood stream until they reach tumour.

For **example**: application of hydrogel in breast cancer is the innovative technology and the Herceptin is a type of monoclonal antibody. To meet the requirement for nutrients and oxygen for cancer cell survival and growth, solid tumours frequently develop an aberrant, excessive vasculature. Therefore, blocking tumour vasculature is a promising therapeutic approach to starve tumour cells. It is essential, nevertheless, that such a therapy be able to recognize and block tumour blood arteries while ignoring those in healthy tissues. Design for a tumour-hunting

nanorobot that incorporates DNA origami and thrombin in a capsule. In animal models, the DNA robots specifically cause intravascular thrombosis (blood clotting) in tumours, causing necrosis and inhibiting tumour growth[30].

In treating Cardiovascular disease

Another area where the characteristics of nanoparticles may be used is in the treatment of cardiovascular disorders. The main cause of mortality worldwide is cardiovascular disease, and sedentary lifestyles are to blame for the worrisome rise in death rates[31]. permanent disabilities are caused by these illnesses. Novel therapeutic and diagnostic approaches for the treatment of cardiovascular disorders are made possible by nanotechnologies.Novel formulation of block copolymer micelles are made using PEG and poly(propylene sulphide) this supresses the level of cytokines which helps in managing atherosclerosis[32].

Nutrition

Many antioxidant nutrients and food ingredients lose some of their potency while traveling to the target tissues. Nano-concepts can be used in nutrient delivery to improve everyone's health and fitness, not only athletes, especially when it comes to weight control. Nanotechnology can be used to study microorganisms and change the flavour, colour, and quality of food. These ideas can help advance the research of physiology, nutrition metabolism, and dietary problems[33,34]

Dentistry

Nano-dentistry is a contemporary field in development that has the potential to use mechanical nana-robotic dentifrices for oral health care. This can be used in conjunction with local anaesthetic to treat hypersensitive tooth conditions and perform orthodontic corrections. The use of Silver Nanofluoride (NSF) in newborn dental care has also been demonstrated to be effective by recent research [35].

Energy and Environment

Fuel cells made of carbon nanotubes are used to power cars because they can store hydrogen. Photovoltaic systems use nanotechnology to become more affordable, lightweight, and effective. These systems can also reduce engine pollution through the use of nanoporous filters and mechanically clean exhaust with the aid of catalytic converters made of nanoscale noble metal particles, catalytic coatings for cylinder walls, and catalytic nanoparticles added to fuel[36,37].

Risks Associated with nanotechnology

While nanotechnology has generated a lot of interest in the general public, there have also been a lot of discussions about the safety of nanotechnologies and potential health dangers linked with their use. The use of nanomaterials presents new difficulties, particularly in terms of foreseeing, comprehending, and controlling any possible health hazards. Low-solubility nanoparticles are more hazardous and toxic on a mass by mass basis than larger particles[38]. The body can absorb nanoparticles through the skin, by food, inhalation, or injection during medical operations.Due to their great mobility, nanoparticles may be able to pass through the blood-brain barrier after they have entered the body. Through phagocyte overpopulation and nanoparticles may impact the immune system of the organism. Stress and inflammation responses could be set off, weakening defenses against more dangerous obstacles[39,40]. Significant energy requirements for nanoparticle production and may damage the environment by releasing hazardous and enduring nanoparticles into it. Low rates of recovery and limited possibility for recycling[41].

CONCLUSION

Nanotechnology emerges as a groundbreaking force with transformative potential across multiple sectors, especially in healthcare. Nanoparticles' versatility in drug delivery, imaging diagnostics, and therapeutic applications promises revolutionary advancements. However, challenges regarding safety and environmental impact necessitate ongoing

exploration. Overall, this comprehensive review underscores nanotechnology's immense promise while highlighting the need for responsible integration and further research for its sustainable use and maximal benefit.

REFERENCES

1. Sim S, Wong NK. Nanotechnology and its use in imaging and drug delivery. Biomed Rep. 2021 May;14(5):42.
2. Belkin A, Hubler A and Bezryadin A: Self-assembled wiggling nano-structures and the principle of maximum entropy production. Sci Rep. PubMed/NCBI. 5(8323)2015.
3. Allhoff F, Patrick L and Daniel M: What is Nanotechnology and Why Does it Matter? From Science to Ethics. John Wiley & Sons, pp3-5, 2010.
4. Anjum S, Ishaque S, Fatima H, Farooq W, Hano C, Abbasi BH, Anjum I. Emerging Applications of Nanotechnology in Healthcare Systems: Grand Challenges and Perspectives. Pharmaceuticals (Basel). 2021 Jul 21;14(8):707.
5. Katsuki S, Matoba T, Koga JI, Nakano K and Egashira K. Anti-inflammatory Nanomedicine for Cardiovascular Disease. PubMed/NCBI View Article : Google Scholer 4(87)2017.
6. Lombardo D, Kiselev MA and Caccamo MT: Smart Nanoparticles for Drug Delivery Application: Development of Versatile Nanocarrier Platforms in Biotechnology and Nanomedicine. J Nanomater. 12:1–26. 2019.
7. Matoba T, Koga JI, Nakano K, Katuski S and Egashira K. Anti-inflammatory Nanomedicine for Cardiovascular Disease. PubMed/NCBI View Aricle : Google Scholar. 4(87)2017.
8. Morgam MT, Carnahan MA, Finkelstein S, Prata CA, Degoricija L, Lee SJ and Grinstaff MW. Dendritic supramolecular assemblies for drug delivery. PubMed/NCBI View Article : Google Scholar. 97:4309-4311.
9. Tririveedhi V, kitchens KM, Nevels KJ, Ghandehari H and Butko P. Kinetic analysis of the interaction between poly(amidoamine) dendrimers and model lipid membranes. PubMed/NCBI View Article : Google Scholar. BiochimBiophys Act. 1808:209-218.2011.
10. Kukowska-Latallo JF, Bielinska AU, Johnson J, Spindler R, Tomalia DA and Baker JR. Efficient trasfer of genetic material into mammalian cells using Starburst polyamidoaminedendrimers. PubMed/NCBI View Article : Google Scholer. 93:4897-4902. 1996.
11. Svenson S and Tomalia DA. Dendrimers in biomedical applications - reflections on the field. PubMed/NCBI View Article : Google Scholar. 57:2106-2129. 2005.
12. Nune SK, Gunda P, Thallapally PK, Lin YY, Forrest ML and Berkland CJ. Nanoparticles for biomedical imaging. PubMed/NCBI View Aricle : Google Scholar. 6:1175-1194. 2009.
13. Dai HJ, Hafner JH, Rinzler AG, Colbert DT nad Smalley RE. Nanotubes as nanoprobes in scanning probe microscopy. Google Scholar. 384:147-150. 1996.
14. Shi Kam NW, Jessop TC, Wender PA and Dai H. Nanotube molecular transporters:Internationalization of carbon nanotube-protein conjugates into Mammalian cells. PubMed/NCBI View Article : Google Scholar. 126:6850-6851. 2004.
15. Mulder CE, Strijkers GJ, Van Tilborg GA, Cormode DP, Fayad ZA and Nicolay K. Nanoparticulate assemblies of amphiphiles and diagnostically active materials for multimodality imaging. PubMed/NCBI View Article:Google Scholar. 42:904-914. 2009.
16. Probst CE, Zrazhevskiy P, Bagalkot V and Gao X. Quantum dots as a platform for nanoparticle drug delivery vehicle design. PubMed/NCBI View Article : Google Scholar. 65:703-718. 2013.
17. Ricardo PN e Lino F. Stem cell research meets nanotechnology. Revista Da Sociedade Portuguesa D Bioquimica, CanalBQ. 7: 38-46. 2010.
18. Kong, X., Gao, P., Wang, J. *et al.* Advances of medical nanorobots for future cancer treatments. J HematolOncol **16**, 74 (2023).
19. Patrick L, Allhoff F and Daniel M: What is Nanotechnology and Why Does it Matter? From Science to Ethics. John Wiley & Sons, pp3-5, 2010.
20. Nikalje AP (2015) Nanotechnology and its Applications in Medicine. Med chem 5: 081-089. doi:10.4172/2161-0444.1000247

21. Lombardo D, Kiselev MA and Caccamo MT. Smart Nanoparticles for Drug Delivery Application: Development of Versatile Nanocarrier Platforms in Biotechnology and Nanomedicine. J Nanomater. 12:1–26. 2019
22. Ricardo PN e Lino F (2010) Stem cell research meets nanotechnology. Revista Da Sociedade Portuguesa D Bioquimica, CanalBQ 7: 38-46.
23. Allen TM, Cullis PR (2004) Drug delivery systems: entering the mainstream. Science 303: 1818-1822.
24. Allen TM, Cullis PR (2004) Drug delivery systems: entering the mainstream. Science 303: 1818-1822.
25. Cavalcanti A, Shirinzadeh B, Freitas RA, Hogg T (2008) Nano robot architecture for medical target identification. Nanotechnology 19: 15
26. Kiselev MA, Lombardo D and Caccamo MT: Smart Nanoparticles for Drug Delivery Application: Development of Versatile Nanocarrier Platforms in Biotechnology and Nanomedicine. J Nanomater. 12:1–26. 2019.
27. HA Owida, JI Al-Nabulsi, NM Turab, et al. Nanotechnology role development for COVID-19 pandemic management. Journal of Nanotechnology 2022 (2022): 1-12..
28. Thakor AS, Gambhir SS: Nanooncology: the future of cancer diagnosis and therapy. CA Cancer J Clin. 2013, 63:395-418. 10.3322/caac.21199
29. Zhou W, Gao X, Liu D, Chen X: *Gold nanoparticles for in vitro diagnostics*. Chem Rev. 2015, 115:10575-636. *10.1021/acs.chemrev.5b00100*
30. Bharali DJ, Mousa SA: *Emerging nanomedicines for early cancer detection and improved treatment: current perspective and future promise*. PharmacolTher. 2010, 128:324-35. *10.1016/j.pharmthera.2010.07.007*
31. KeyueShenTumorhuntingnanorobots.Sci.Transl.Med.10,eaas8968(2018).DOI:
32. *McGill HC Jr, McMahan CA and GiddingSS.Preventing heart disease in the 21st century: Implication of the Pathobiological Determinants of Atherosclerosis in Youth (PDAY) study. PubMed/NCBI View Article : Google Scholar. 117:1216-1227. 2008.*
33. Wu T, Chen X, Wang Y, Xiao H, Peng Y, Lin L, Xia W, Long M, Tao J and Shuai X. Aortic plaque-targeted andrographolide delivery with oxidation-sensitive micelle effectively treats atherosclerosis via simultaneous ROS capture and anti-inflammation. Nanomedicine (Lond). PubMed/NCBI View Article : Google Scholar. 14:2215–2226. 2018.
34. Frederick A Adrah, Mawulorm KI Denu, MaameAraba E Buadu. Nanotechnology Applications in Healthcare with Emphasis on Sustainable Covid-19 Management. Journal of Nanotechnology Research. 5 (2023): 06-13.
35. S Modi, et al. Recent trends in fascinating applications of nanotechnology in allied health sciences. Crystals 12 (2022): 39.
36. MS Dhaliwal, KS Nat, GS Waraich. Silver Nanoparticles and Its Application in Pediatric Dentistry: A Review
37. Shinn E, Hübler A, Lyon D, Perdekamp M, Bezryadin A and Belkin A: Nuclear energy conversion with stacks of graphenenanocapacitors. Complexity. 18:24–27. 2012..
38. Kurtoglu ME, Longenbach T, Reddington P and Gogotsi Y: Effect of calcination temperature and environment on photocatalytic and mechanical properties of ultrathin sol-gel titanium dioxide films. J Am Ceram Soc. 94:1101–1108. 2011.
39. Sahaym U and Norton M: Advances in the application of nanotechnology in enabling a hydrogen economy. J Mater Sci. 43:5395–5429. 2008.
40. Singh P: Impacts of nanotechnology on environmental (Review). Int Arch App Sci Technol. 9:14–16. 2018.
41. Chandarana M, Curtis A and Hoskins C: The use of nanotechnology in cardiovascular disease. ApplNanosci. 8:1607–1619. 2018.
42. Dreher KL: Health and environmental impact of nanotechnology: Toxicological assessment of manufactured nanoparticles. PubMed/NCBI View Article : Google Scholar. Toxicol Sci. 77:3–5. 2004.

Indian Journal of Natural Sciences *www.tnsroindia.org.in ©IJONS*

Vol.15 / Issue 83 / Apr / 2024 *International Bimonthly (Print) – Open Access* *ISSN: 0976 – 0997*

RESEARCH ARTICLE

Optimization and Partial Purification of Protease from *Bacillus Subtilis* AD20 Isolated from Dairy Effluent

Deepika Jothinathan[1]*, Anjali Kumari[1], Lavanyasri Rathinavel[2]

[1]Department of Biotechnology, SRM Arts and Science College, Kattankulathur, (Affiliated to University of Madras) India.
[2]Department of Biotechnology, Mercy College,(Affiliated to Calicut University) India.

Received: 22 Feb 2024 Revised: 07 Mar 2024 Accepted: 20 Mar 2024

***Address for Correspondence**
Deepika Jothinathan
Department of Biotechnology,
SRM Arts and Science College,
Kattankulathur, (Affiliated to University of Madras) India.
Email: deepikabt@srmasc.ac.in

ABSTRACT

Among the total worldwide enzyme market, 40% of the total protease is produced by microbial protease. The study aims to produce, purify and determine the properties of the protease from a bacterium isolated from diary effluent. The dairy effluent sample was collected from the dairy industry and bacteria were isolated by serial dilution on skim milk agar. The isolated bacteria were screened on skim milk agar for proteolytic activity. Based on the results of primary screening, different bacterial species were separated from the dairy effluent sample. The bacterial strain with the greater zone of clearance was selected for protease production in complex media. The protease positive bacterium was determined by 16S rRNA sequence analysis as *Bacillus subtilis* AD20. The optimisation studies with different parameters were investigated to produce the maximum extracellular protease. This enzyme was then partially purified with the help of 80% ammonium sulfate precipitation tailed by dialysis. The partially purified protease was studied by SDS- PAGE and Native-PAGE with Gelatin for their molecular weight determination and protease activity respectively. The findings of the characterization investigations indicated that the protease was most active at 55ºC and an acidic pH of 4. Among the tested substrates higher activity was evident with casein. In the presence of benzene, protease showed higher activity. According to results obtained it was understood that *Bacillus subtilis* AD20 produces protease that is temperature resistant i.e., thermostable and acidic. The comparison of enzyme activity with commercial detergent activity showed positive results. The washing performance studies were done which cleared the blood and dal stains.

Keywords: 16S rRNA, *Bacillus subtilis* AD20, Ammonium sulfate precipitation, Dialysis, SDS- PAGE and Native-PAGE

INTRODUCTION

Proteolysis, the process by which proteins are broken down into smaller polypeptides or individual amino acids, is catalyzed by the enzyme protease. These enzymes use a process called hydrolysis, in which water breaks peptide bonds, to cleave the bonds within proteins. Proteases are engaged in a variety of biological processes, such as cell signaling, protein catabolism, and the digestion of consumed or ingested proteins [1]. There are proteases in every kind of life. Proteases have undergone numerous independent evolutionary cycles and can catalyze the same reaction using entirely different catalytic pathways. Therefore, despite the fact that proteases are widely distributed, rapid growth, low cultivation area requirements and simplicity of genetic manipulation to produce new enzymes with altered properties that are desirable for their many uses, microorganisms are the preferred source of these enzymes [2]. Due to its high water use, the dairy industry is one of the most polluting in the food business. India's dairy business is predicted to expand quickly in light of the country's rising milk consumption. The waste production and associated environmental problems are also assumed to be amplified [3]. Dairy is one of the major industries causing water pollution. Many processes in the dairy manufacturing might contain pasteurization, cheese, cream, milk powder, etc. Large volumes of milk are handled by the dairy sector, and water is the main processing byproduct. Significant levels of organic milk products and minerals can be found in the milk's extracted water. Additionally, the plant's cleaning process produces caustic wastewater [4].

MATERIALS AND METHODS

Effluent collection

The positive strains for protease were isolated from dairy effluent which was collected from dairy industry, Chennai, Tamil Nadu.

Screening of Bacterial Strains for Protease Production

The protease producing bacterial strains were isolated from dairy effluent. Serial dilution was performed for the dairy effluent sample. The 10^{-7}, 10^{-8}, and 10^{-9} serially diluted samples were used for the spread plate technique in skim milk agar plates. The plates after overnight incubation, was observed for clear zone formation. A greater zone of clearance was used as a positive strain for further studies by separately inoculating the different stains in skim milk agar. The positive culture was preserved on sterile nutrient medium by quadrant streak plates and slants at 4˚C.

Identification of protease-producing by 16S rRNA sequencing

The microbial positive strains were characterized by 16S rRNA using sanger sequencing was performed in Elango Genetics Pvt Ltd.

Optimization of Culture Conditions for Protease Production

The optimal conditions for the growth of the positive cultures and growth curves were determined with different parameters (time durations, pH, carbon source, nitrogen source, and specific substrates).

Effect of Time Duration

The production medium was prepared in a flask and sterilized. The positive culture was inoculated and retained in a shaker incubator at 100 rpm at 37˚ C. Flasks were kept for incubation in a shaker incubator for 100 rpm at room temperature. The protein content and protease activity were recorded for every 24 hours for 92 hours (i.e., 4 days).

Effect of Different pH

The production medium was arranged with various pH i.e., 5.0, 6.0, 7.0, 8.0 and 9.0. After sterilization, the positive strain was inoculated and retained in a shaker incubator at 100 rpm at room temperature. The protein content and protease activity were recorded every 24 hours for 92 hours (i.e., 4 days).

Effect of Various Carbon Sources

The production medium was prepared with different 1% carbon sources i.e., starch, dextrose, sucrose, maltose, and fructose and inoculated a loop of positive strain in the media after sterilization. Then the flasks were incubated in a shaker incubator at 100 rpm at room temperature. The protein content and protease activity were recorded every 24 hours for 92 hours (i.e., 4 days).

Effect of Different Nitrogen Sources

The production media was prepared with different 1% different N_2 sources i.e., ammonium acetate, urea, peptone, casein, and yeast extract and inoculated a loop of positive strain in the media after sterilization. Then flasks were maintained in the same rpm and temperature used in the previous experiments. The protein content and protease activity were recorded every 24 hours for 92 hours (i.e., 4 days).

Effect of Various Substrates

The production medium was prepared with different 1 % substrates i.e., green gram husk, rice bran, sugarcane bagasse, grape waste, and kitchen waste and inoculated a loop of positive strain in the media after sterilization. The same conditions were maintained throughout the experiment. The protein content and enzyme activity were recorded every 24 hours for 92 hrs. (i.e., 4 days).

Estimation of Enzymatic Reaction

Using tyrosine (0.2–1.0 mg/L) as the standard, the protease activity method was used to determine the protease activity of the samples. A standard calibration curve was created using the response to the absorbance values of tyrosine standards that were developed in a range of concentrations. A UV Visible spectrophotometer was used to analyze the samples. The assay mixture was incubated for 10 minutes at 55° C in the water bath to measure the protease activity. 100 µl of 0.5% (w/v) casein in 50 mM Tris-HCl pH 7.2 (substrate) was added to 100 µl of enzyme solution (supernatant). To stop the process, 100 µl of 15% TCA was added in autoclaved distilled water to the enzyme-substrate solution. After 10 minutes in an ice bath, the mixture was centrifuged for 10 minutes at ambient temperature at 10,000 rpm. The pellet was then removed. 200 µl supernatant was taken in fresh micro fuge tube, then 1 ml NaOH (1N) and 200 µl Folin & Ciocalteu's Phenol reagent was added [5]. The control sample had the similar composition excluding the enzyme. The enzyme activity was documented for every parameter by UV Visible spectrophotometer at 660 nm after 1 hour incubation at room temperature.

Quantification of Protein Concentration

Using bovine serum albumin (BSA, 0.1 mg/ml) as the standard, the Bradford method was used to calculate the total protein concentration of a sample [6]. Aside from the enzyme, the makeup of the control sample was the same. The standard calibration curve was created in response to the absorbance values of the BSA standards, which were manufactured in various concentrations. The absorbance was measured in a UV visible spectrophotometer at 595 nm.

Mass Production of Crude Enzyme Extract

2 ml overnight culture was inoculated in 1-liter sterilized complex media and kept in a shaker at 100 rpm at 37°C for 3 days. Based on the previous experiments, the parameters that produced the maximum protease activity of the organism were chosen for mass production. To get the culture supernatant, the bacterial culture was centrifuged for 20 minutes at 5000 rpm and 4° C. After transferring the culture supernatant into the sterile flask, the pellet containing the cell debris was taken out.

Partial Purification of Enzyme

Ammonium sulfate was dissolved to 80% saturation (w/v) in the crude extracellular enzyme extract [7]. The ammonium sulfate has been gradually added into the culture filtrate by continuously stirring in a cold room. After dissolving, the flask was kept for overnight incubation for the precipitate formation of salt and protein at 4°C. After

collecting the precipitate using centrifugation at 10,000 rpm and 4° C for 10 minutes, the pellet was reconstituted in a brown bottle containing 50 ml of 50 mM Tris-HCl buffer at pH 7.2.

Preparation of Dialysis Membrane

The dialysis membrane was washed for 5 minutes in hot water. The enzyme solution was loaded in the dialysis membrane - 70 i.e., DEAE Cellulose column (width: 29.31 mm; diameter: 17.5 mm) which was dissolved with 50 mM Tris HCl buffer of pH 7.2. This membrane was dipped in 20 mM Tris HCl buffer (pH 7.2) for 6 hours and repeated for 2-3 times by changing the 20 mM tris HCl buffer.

Electrophoretic Studies

Sodium Dodecyl Sulphate- Polyacrylamide Gel Electrophoresis (SDS- PAGE)

The SDS-PAGE procedure was performed using Laemml's 1970 method [8]. After five minutes of heating the samples in boiling water at 100 °C, the molecular mass of protease was ascertained using separating gel with 10% acrylamide concentration and stacking gel with 5% acrylamide concentration. The electrophoresis was conducted after loading 25 µl of the sample-sample buffer mixture and 10 µl of the molecular weight marker onto the gel. The gel was passed through a resolving gel at 100 V and a stacking gel at 50 V for duration of 20 minutes. Coomassie staining was applied to the SDS-polyacrylamide gel for 30 minutes following the electrophoretic run. Finally, bands were evident after the gel was destained with the destaining solution and incubated for 12 hours.

Native Polyacrylamide Gel Electrophoresis (Native-PAGE)

The protease enzyme's approximate size was discovered using native PAGE. 0.1% gelatin was present in the polyacrylamide gel that was cast using 15% resolving gel. Using a typical gel loading buffer, the sample was loaded onto the gel. Due to the breakdown of gelatin in that area, a clearing was observed at the band responsible for protease activity when the enzyme sample was run on a polyacrylamide gel containing gelatin [9]. Under natural circumstances, the concentrated crude protease was electrophoresed [10]. Following electrophoresis, the gel was ran through three rounds of washing in 0.1% Tween 80 for thirty minutes each, and then it was cleaned with sterile distilled water. During two hours, the gel was immersed in 100 mM Tris HCl, pH 8.0, with 5 mM $CaCl_2$.

Characterization Studies of Protease

Impact of pH on Protease Activity and Stability

Protease activity was measured using a 50 mM Tris-HCl buffer at various pH levels for ten minutes at 55° C. Using conventional test settings, the optimal pH of the protease was ascertained by measuring its activity in the presence of buffers at various pH values (5.0, 5.0, 6.0, 7.0, 8.0, 9.0, and 10.0). Using spectrophotometry, the change in absorbance at 660 nm was recorded, and the relative activity was calculated.

Impact of Temperature on Protease Activity and Stability

The impact of varying temperatures on protease activity was examined through the use of 50 mM Tris-HCl buffer. Under normal assay environment, the optimal temperature of the protease was ascertained by measuring its activity at various temperatures (4, 25, 37, and 55° C). Prior to the test and for ten minutes throughout the test, the protease and the particular substrate, casein, were incubated at the appropriate temperatures. Using spectrophotometry, the change in absorbance at 660 nm was recorded, and the relative activity was calculated.

Substrate Specificity of Enzyme

By monitoring the enzyme's activity toward various substrates (BSA, casein, peptone, tryptone, and gelatin), the substrate specificity of the enzyme was ascertained. These various substrates were prepared in 50 mM Tris-HCl buffer at concentrations of 0.5% (w/v) according to normal assay conditions and the enzyme's activity was assessed by incubating them for 10 minutes at 55° C. Using spectrophotometry, the change in absorbance at 660 nm was recorded, and the relative activity was calculated.

Organic Solvents of Enzyme

The organic solvent specificity of the enzyme was estimated by measuring activity towards different solvents (Ethanol, Methanol, Benzene, and Dimethyl Sulfoxide). Using these various organic solvents, which were produced in 50 mM Tris-HCl buffer at solvent concentrations of 10% under standard test conditions, the enzyme activity was determined and the mixture was incubated for 10 minutes at 55° C. Using spectrophotometry, the change in absorbance at 660 nm was recorded, and the relative activity was calculated.

Analytical Methods of Partially Purified Protease by Skim Milk Assay

Protease activity was analyzed using skim milk 0.5% (w/v) with nutrient agar plates. Five wells were created, control (10 µl), 20 µl, 30 µl, 40 µl, and 50 µl partially purified protease was loaded in the well followed by 24 hours of incubation at room temperature.

Application of Proteases in detergents

Commercial Detergent Compatibility of the Partially Purified Protease

Using a concentration of 1%, different commercial detergents such as Ariel, Surf Excel, Tide and Rin were used to test the enzyme's stability in the presence of detergents. First, the enzymes that had been present in the detergent were heat-inactivated by boiling it for ten minutes. Skim milk agar wells were filled with the commercial detergents and the test enzyme solution.

Studies on Wash Performance

On a piece of white cotton fabric stained with dal and blood, the wash performance of the partly purified protease was investigated. After being stained with dal and human blood, the textile piece was allowed to dry for 12 hours. The pieces of stained cloth were placed on different Petri plates and exposed to the wash treatment experiments. The cloth pieces were removed from the incubator after an hour at room temperature, washed under tap water, allowed to dry, and then visually inspected to determine whether the stain had been effectively removed.

RESULTS AND DISCUSSION

Protease Production Screening

The positive strains were evaluated for protease production using 2 % skim milk agar. All positive strains were inoculated separately on skim milk agar to screen one bacterium with higher protease production. The single strain with a wider zone of clearance was used for further studies (Figure: 3.1).

Agarose Gel Electrophoresis of Isolated DNA and PCR Amplification

The DNA marker and the extracted DNA from the positive strain were seen on an agarose gel. A good DNA yield was shown by the brilliant appearance of the isolated DNA from the sample on lane 2 of the gel (Fig: 3.2).

Multiple sequence alignment of Isolated DNA

The BLAST results indicated that the obtained 16S rRNA gene sequence is matched with the maximum sequence homology with bacillaceae family. Phylogenetic trees were constructed by neighbor joining method. The tested strain showed maximum similarity with *Bacillus subtilis subsp. subtilis* strain KS6-27 and (Figure: 3.3) represents the phylogenetic tree of identified positive strain *Bacillus subtilis* AD20 constructed using mega 6.0 software with available strains in GenBank data (NCBI). The genbank accession number of the positive isolate is MT322145.

Augmentation of Culture Conditions for maximum Protease Production

Influence of pH on Protein Content and Enzyme Activity

The results showed that the pH significantly influenced the protein content and protease activity in *Bacillus subtilis* AD20. It was able to relate the maximum protein content of 146 µg/ml at pH 7 on 3rd day (Figure: 3.4.1a). At the same conditions, protease activity of 20,204.08 U/mg was obtained (Figure: 3.4.1b). The extracellular protein and

protease activity production at different pH revealed that at pH 7 protease activity was highly significant than other pH. Therefore, pH 7 was selected for further studies. This indicated that the specific strain was alkaliphilic in nature and optimum pH 7 for growth and enzyme production is an ideal character among alkaliphilic organisms [11, 12]. It is commonly recognized that the permeability of bacterial cell membranes and the availability of specific metabolic ions are influenced by the pH of the culture medium, and that these factors promote the development of cells and the synthesis of enzymes [13].

Effect of Different Time Duration on Protein Content and Protease Activity

The *Bacillus subtilis* AD20 produced a maximum protein content of 90.5 µg/ml on the 3rd day (Figure: 3.4.2a) and protease activity of 30,400 U/mg on the 3rd day at 55° C (Figure: 3.4.2b) of incubation. The protein content and protease activity showed that 55° C temperature on the 3rd day was highly significant than other days. Thus 3rd day was selected for further studies. As the incubation period extended, both cell growth and enzyme synthesis rose linearly, indicating that growth and enzyme production are naturally correlated [12, 14]. As previously reported, after 72 hours of incubation, the best growth and enzyme production were seen [15, 16].

Impact of Various Carbon Sources on Protein and Protease Activity

When dextrose was tested at 1 % for protease production in *Bacillus subtilis* AD20, it showed an enhanced protein content of 120 µg/ml on 3rd day and it induced maximum protease activity of 40,000 U/mg on 3rd day. Whereas minimum enzyme activity of 11,858.40 U/mg on 4th day in fructose and was not much significantly induced protease production. The protein content and protease activity production in different carbon sources revealed that dextrose was found highly significant than other carbon sources.

Impact of Various N_2 Sources on Protein content and Protease Activity

Five different 1 % nitrogen sources such as ammonium acetate, yeast extract, peptone, casein and urea were taken. Nitrogen source when tested at 1 % for enzyme production in *Bacillus subtilis* AD20 it showed a maximum protein content of 129 µg/ml on 3rd day with ammonium acetate. But with casein, higher protein content of 124 µg/ml on 3rd day and optimum protease activity of 23,621.62 U/mg was observed. Whereas, minimum protease activity of 4,496.12 U/mg on 1st day in urea and 5,368.42 U/mg in yeast extract recorded on the 4th day was observed. The protein content and protease production in different nitrogen sources revealed that casein was found highly significant than other nitrogen sources. Since nitrogen is the final building block of protein biosynthesis, its availability has a significant impact on the synthesis of enzymes. Additionally, the medium's pH can be impacted by the nitrogen source, which could have an impact on the enzyme's stability and activity [17]. The similar outcome was earlier reported by Gajju et al. (1996), who discovered that because organic nitrogen sources are rich in amino acids, Bacillus sp. were more adapted to them for the manufacture of enzymes [18]. A few essential amino acids, some carbohydrates and inorganic substances like phosphorus and calcium are also present in casein.

Impact of Various substrate on Protein and Protease Activity

Five different substrates such as 1 % green gram husk, rice bran, sugarcane bagasse, grape waste, and kitchen waste was taken. Rice straw, when tested at 1 % for protease production in Bacillus subtilis AD20 showed high protein content of 82 µg/ml on the 4th day and it induced maximum protease activity of 21,754.38 U/ml on 3rd day. The maximum protein content of 174 µg/ml on 3rd day in green gram husk was observed. Whereas minimum enzyme activity of 6,542.05 U/ml on 1st day in kitchen waste and 7,032.25 U/ml in grape waste recorded on the 4th day of incubation was seen. The protein content and protease production in different substrates revealed that rice straw was found highly significant than other carbon sources.

Protease Production in Laboratory Scale

In this work, ammonium sulfate precipitation (80% saturation) was used to partially purify the protease enzyme from *Bacillus subtilis* AD20. The amount of extracellular protease production by *Bacillus sp*. was estimated on a laboratory scale from optimized parameters. The protease activity reached a maximum of 790 U/ml on the 3rd day of incubation. The crude culture fitrate containing enzyme was exposed to the precipitation method like ammonium

sulfate to precipitate, partially purify and concentrate total protein. Finally, the precipitated enzyme was dialyzed and used for further analysis. The resulting partially purified protease had a specific activity of 24,687.5 U/mg. The molecular weight of protease was reported to be 35 kDa while the protease in literature was found to be 47 kDa [19]. The molecular mass of alkaline serine proteases normally comes in the array of 18 to 30 kDa [20]] with few exceptions.

Detection of Extracellular Protease Profile on SDS-PAGE

SDS-PAGE was used to analyze the samples obtained at the partially purified stage. Following an electrophoretic run, 15% of the gel was stained with SDS-polyacrylamide using G-250 Coomassie staining (Figure: 3.5). Because complex medium has a specific substrate under growth conditions, only two bands were seen on the gel. These two bands on the gel, which ranged in size from 40 kDa to 30 kDa, may be used to calculate the molecular weight of the enzymes.

Detection of Extracellular Protease Profile on Native-PAGE

On a 1% gelatin gel, the protein band that was corresponding for enzymatic activity demonstrated creating the halozone (Figure: 3.6). This process was performed after the ammonium sulfate precipitated protease was separated on Native-PAGE.

The protein marker bands are indicated by lane-2 arrows, while lane-1 indicates the clearance of protease bands (Figure: 3.6). Along the gel's side is a line that indicates each protein marker band's molecular weight. According on Native-PAGE analysis, the isolated proteases had a molecular weight of about 30 kDa. On the gelatin gel, there was just one clearing zone that could be seen, signifying a single kind of protease. A gel was cleared by partially purified protease in accordance with the protein marker's electrophoretic mobility. Proteases from bacteria typically have a molecular weight of 15–36 kDa [21]. The molecular weight of B. mojavensis protease was 30 kDa, greater than that of alkaline protease [22]. Both proteases, however, are not as large as the Bacillus sp. strain GX6638's serine version of enzyme HS (36 kDa) [23].

Physicochemical Properties of Partially Purified Protease

pH Optimum and Stability of Partially Purified Protease

The optimal pH for the activity of protease was pH 4 i.e., acidic pH. As pH goes on increasing, the relative activity of the enzyme goes on decreasing (Figure: 3.7). This optimal pH value is similar to the endoglucanase from Bacillus sp. [24]. The efficient operation of the enzyme was impacted as the pH value strayed from the ideal range. This might be attributed to either a lower affinity or reduced enzyme saturation with the substrate, or to the impact of pH on the stability of the enzyme [25].

Temperature Optimum and Stability

Higher temperatures are necessary for enzymes used in industries to remain active and stable, and temperature plays a vital role in maximizing enzyme activity. The partially purified protease of *Bacillus subtilis* AD20 showed a maximum enzyme activity at 55° C to determine its thermal stability, the enzyme was pre-incubated from 4° C to 55° C for 1 hour. It was stable from 24° C to 37° C with more 85.92 % to 90.37 % activity up to 60 minutes of incubation, respectively. Whereas, the protease at 55° C showed 100 % activity up to 1 hour (Figure: 3.8). On the other hand, the temperature optima of bacterial proteases are greater, reaching up to 85°C [26] and 115°C [27]. According to Bidochka and Khachatourians (1987), proteases function best at temperatures between 37 and 45°C [28].

Substrate Specificity of Partially Purified Protease

Among the specific substrates, casein was suitable for protease production. Peptone also showed good protease production when compared to others, but less then casein. The least protease production with the gelatin substrate (Figure: 3.9). It has been shown that the proteases from *Beauveria bassiana* and *Conidiobolus* sp. (*Cephalosporium* sp. KM388) are more active against casein than they are against bovine serum albumin. The catalytic process of an enzyme is modified by the presence of organic solvents due to the breaking of hydrogen bonds and hydrophobic interactions, as well as modifications in the protein's kinetics and structure.

Organic Solvent of Partially Purified Protease

Among all organic solvents, benzene was appropriate for enzyme production when compared to other organic solvents i.e., ethanol, methanol, and DMSO. The least favorable for protease production was methanol and DMSO (Figure: 3.10). The physicochemical properties of partially purified protease were optimized with pH 4 i.e., acidic pH, 55° C determines its thermal stability, casein as substrates, and organic solvent benzene with maximum relative activity among other parameters. According to Gupta and Khare (2007), Pseudomonas aeruginosa protease was found to be relatively less stable in the presence of a hydrophilic solvent and more stable in organic solvents such as benzene, isooctane, cyclohexane and n-dodecane [29]. We can therefore assume that the type of organic solvents used will determine how stable the enzyme is in organic solvents. This indicates that an enzyme's structure can occasionally be stabilized by substituting some of its water molecules with organic ones.

Partially Purified Enzyme Activity on Skim Milk with Different Concentration

The skim milk activity with different concentrations of partially purified protease was loaded and after incubation, the zone of clearance was observed. The 30 µl concentration showed a higher zone of clearance when compared with different other concentrations. The least zone was observed in 20 µl of concentration of partially purified protease (Figure: 3.11). The caseinolytic activity was also performed but no results were detected in the casein agar plates.

Application of Partially Purified Protease

Wash Performance Test

The comparison of washing of stained clothes with dal and blood after 12 hours of drying the stain was done. These clothes after incubation with distilled water and partially purified protease were observed. The clothes in partially purified protease were not having the outer stains and stains of both blood and dal was removed more than the distilled water (Figure: 3.12). Hence, the results showed that the enzyme can be used commercially for detergent purposes.

Comparison of Partially Purified Protease and Commercial Detergents

The activity of commercial detergent and partially purified protease was performed in skim milk agar. This showed the test sample was comparatively positive when compared to the detergent activity by the zone of clearance. This zone of clearance was higher in Ariel than the test sample, with the decreasing activity with the other detergents in the similar concentrations (Figure: 3.13). Protease from *Conidiobolus coronatus* was found to be stable and compatible when added to commercial detergents, according to Phadtare et al. (1993). There is an increasing need to investigate bacterial proteases for commercially viable applications in the detergent industry, as there are limited reports on the use of fungal proteases in this sector [30]. Protease from *Virgibacillus pantothenticus* that is stable in the presence of readily available detergents locally was reported by Gupta et al. (2008). Three hours of incubation at 40°C produced more than 50% activity in the protease [31].

CONCLUSION

In conclusion, the investigations resulted in a partial purification and characterization of the protease isolated from *Bacillus subtilis* AD20. The bacterially generated enzyme has an acidic and rather thermostable composition. In further research, chromatography can be used to purify it, and it can be immobilized on either organic or inorganic substrate for use in commercial operations. To increase its use in biotechnology, it can also be made by recombinant DNA technology. Future research should focus on X-ray crystallographic examinations of the proteases, since these will provide insight into the characteristics of the catalytic and structural metal-binding sites.

REFERENCES

1. John V, Liang Wenguang G, Scherpelz Kathryn P, Schilling Alexander B, Meredith Stephen C, Tang Wei-Jen. Molecular basis of substrate recognition and degradation by human pre-sequence protease. *A cell press journal,* (2014) *22*(7): 996-999. DOI: 10.1016/j.str.2014.05.003.
2. Motyan JA, Toth F, Tozser J. Research applications of proteolytic enzymes in molecular biology. *Biomolecules* (2013) *3*(4): 923–942. DOI: 10.3390/biom3040923.
3. Chopra AK, Mathur DK. Purification and Characterization of Heat-Stable Proteases from *Bacillus stearothermophilus* RM-67. *J Dairy Sci.* (1985) *68*: 3202-3211. DOI: 10.3168/jds.S0022-0302(85)81228-5.
4. Meer RR, Baker J, Bodyfelt FW, Griffiths MW. Psychrotrophic *Bacillus* species in fluid milk products a review. *J. Food Protect.* (1991) *54*: 969–979. DOI: 10.3389/fmicb.2017.00302.
5. Bakar MFA, Mohamed M, Rahmat A, Fry J. Phytochemicals and antioxidant activity of different parts of bambangan (*Mangifera pajang*) and tarap (*Artocarpus odoratissimus*). *Food chemistry* (2009) *113*(2), 479-483. https://doi.org/10.1016/j.foodchem.2008.07.081
6. Bradford MM. A rapid and sensitive method for the quantitation of microgram quantities of protein utilizing the principle of protein-dye binding. *Analytical biochemistry*, (1976) *72*(1-2), 248-254. https://doi.org/10.1016/0003-2697(76)90527-3
7. Naidu KS. Characterization and purification of protease enzyme. *Journal of Applied Pharmaceutical Science*, (2011) (Issue), 107-112.
8. Laemmli UK. Cleavage of structural proteins during the assembly of the head of bacteriophage T4. *Nature*, (1970) *227*(5259), 680-685.
9. Felicioli R, Garzelli B, Vaccari L, Melfi D, Balestreri E. Activity Staining of Protein Inhibitors of Proteases on Gelatin-Containing Polyacrylamide Gel Electrophoresis. *Analytical biochemistry* (1997) 244. 176-179. 10.1006/abio.1996.9917.
10. Davis BJ. Disc Electrophoresis II: Method and application to human serum proteins, *Ann. N. Y. Acad. Sci.* (1964) 121, 321–349.
11. Denizci AA, Kazan DİLEK, Abeln ECA, Erarslan A. Newly isolated *Bacillus clausii* GMBAE 42: an alkaline protease producer capable to grow under highly alkaline conditions. *Journal of Applied Microbiology*, (2004) *96*(2), 320-327. https://doi.org/10.1046/j.1365-2672.2003.02153.x
12. Johnvesly B, Naik GR. Studies on production of thermostable alkaline protease from thermophilic and alkaliphillic *Bacillus* sp JB-99 in a chemically defined medium. *Process Biochem* (2001) *37*:139-144. https://doi.org/10.1016/S0032-9592(01)00191-1
13. Ellaiah P, Adinarayana K, Pardasaradhi SV, Srinivasulu B. Isolation of alkaline protease producing bacteria from Visakhapatnam soil. *Ind J Microbiol* (2002) *42*:173-175.
14. Ariffin H, Abdullah N, Umi Kalsom MS, Shirai Y, Hassan MA. Production and characterization of cellulase by *Bacillus pumilus* EB3. *Int J Eng Technol* (2006) 3:47-53.
15. Amritkar N, Kamat M, Lali A. Expanded bed affinity purification of bacterial α-amylase and cellulose on composite substrate analogue-cellulose matrices. *Process Biochem* (2004) *39*:565-570. 10.1016/S0032-9592(03)00123-7
16. Heck JX, Hertz PF, Ayub MAZ. Cellulose and xylanase production by isolated amazon Bacillus strains using soybean industrial residue based solid-state cultivation *Brazilian J Microbiol* (2002) *33*:213-218. https://doi.org/10.1590/S1517-83822002000300005
17. Nizamudeen S, Bajaj B K. A novel thermo-alkalitolerant endoglucanase production using cost-effective agricultural residues as substrates by a newly isolated *Bacillus* sp NZ. *Food Technol Biotechnol* (2009) *47*:435-440.
18. Gajju H, Bhalla TC, Agarwal HO (1996) Thermostable alkaline protease from thermophilic *Bacillus coagulans* PB-77. *Ind J Microbiol 36*:153-155.
19. Firouzbakht Hossein, Zibaee Arash, Hoda Hassan, Sohani Mehdi. Purification and characterization of the cuticle-degrading proteases produced by an isolate of *Beauveria bassiana* using the cuticle of the predatory bug,

Andrallus spinidens Fabricius (Hemiptera: Pentatomidae). *Journal of Plant Protection Research* (2015). *55*: 179-186. 10.1515/jppr-2015-0024.

20. Gupta R, Beg QK, Lorenz P. Bacterial alkaline proteases: molecular approaches and industrial application. *Appl Microbial Biotechnol.* (2002) *59*:15-32 https://doi.org/10.1007/s00253-002-0975-y
21. Ghafoor A, Hasnain S. Purification and characterization of an extracellular protease from *Bacillus subtilis* EAG-2 strain isolated from ornamental plant nursery. *Polish Journal of Microbiology*, (2010) *59*(2), 107. DOI: 10.33073/pjm-2010-016
22. Beg QK, Gupta R. Purification and characterization of an oxidation-stable, thiol-dependent serine alkaline protease from *Bacillus mojavensis*. *Enzyme and Microbial Technology*, (2003) *32*(2), 294-304. https://doi.org/ 10.1016/S0141-0229(02)00293-4
23. Durham DR, Stewart DB, Stellwag EJ. Novel alkaline-and heat-stable serine proteases from alkalophilic *Bacillus* sp. strain GX6638. *Journal of Bacteriology*, (1987) *169*(6), 2762-2768. https://doi.org/10.1128/jb.169.6.2762-2768.1987
24. Endo K, Hakamada Y, Takizawa S, Kubota H. A novel alkaline endoglucanase from an alkaliphillic Bacillus isolate: enzymatic properties and nucleotide and deduced amino acid sequences. *Appl Microbiol Biotechnol* (2001) *57*:109-116. https://doi.org/10.1007/s002530100744
25. Dixon M, Webb EC. Enzyme kinetics In: Enzymes 3rd edition Academic Press New York San Francisco. A subsidiary of Harcourt Brace Jovanovich Publishers Longman Group (1979) p 47. https://doi.org/ 10.1590/S1517-83822013005000048
26. Rahman RNZA, Razak CN, Ampon K, Basri M, Zin WM, Yunus W, Salleh AB. Purification and characterization of a heat-stable alkaline protease from *Bacillus stearothermophilus* F1. *Applied microbiology and biotechnology* (1994) *40*, 822-827. https://doi.org/10.1007/BF00173982
27. Nakanishi T, Matsumura Y, Minamiura N, Yamamoto T. Action and specificity of Streptomyces alkalophilic proteinase. *Agric Biol Chem.* (1974) *38*:37–44. https://doi.org/10.1080/00021369.1974.10861520
28. Bidochka MJ, Khachatourians GG. Purification and properties of an extracellular protease produced by the entomopathogenic fungus *Beauveria bassiana. Applied and Environmental Microbiology*, (1987) *53*(7),1679-1684.https://doi.org/10.1128/aem.53.7.1679-1684.1987
29. Gupta A, Khare SK. Enhanced production and characterization of a solvent stable protease from solvent tolerant *Pseudomonas aeruginosa* PseA. *Enzyme and Microbial Technology*, (2007) *42*(1), 11-16. https://doi.org/ 10.1016/j.enzmictec.2007.07.019
30. Phadtare SU, Deshpande VV, Srinivasan MC. High activity alkaline protease from *Conidiobolus coronatus* (NCL 86.8.20): enzyme production and compatibility with commercial detergents. *Enzyme Microbial Technol* (1993) 15:72–76. https://doi.org/10.1016/0141-0229(93)90119-M
31. Gupta A, Joseph B, Mani A, Thomas G. Biosynthesis and properties of an extracellular thermostable serine alkaline protease from *Virgibacillus pantothenticus*. *World journal of Microbiology and Biotechnology* (2008) *24*, 237-243. https://doi.org/10.1007/s11274-007-9462-z

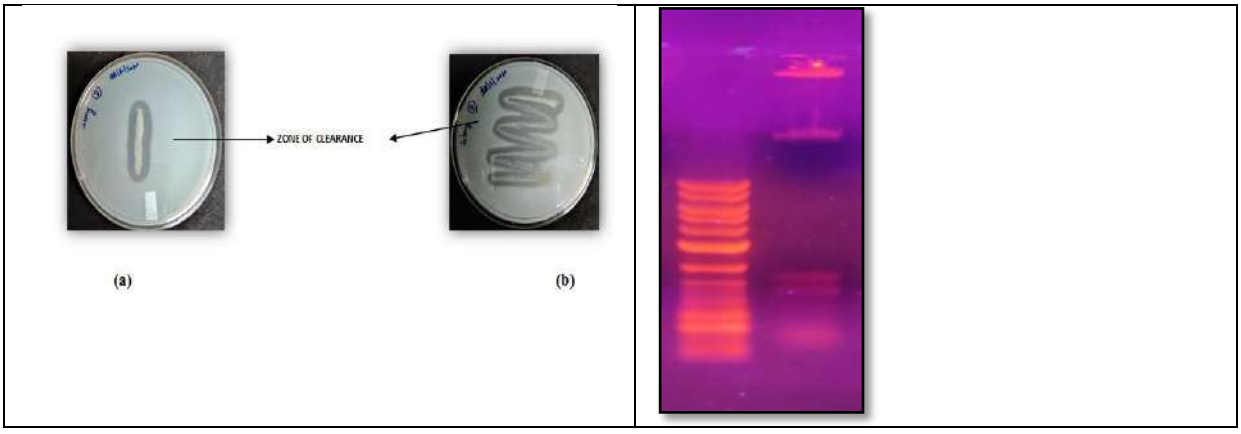

Figure 1. Screening of Single Positive Strain on 2 %Skim Milk Agar in (a) and (b)

Figure 2.a. Agarose Gel Electrophoresis of PCR product

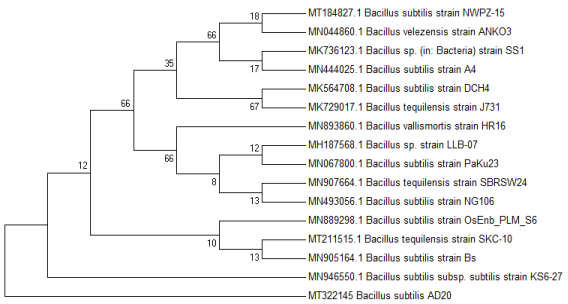

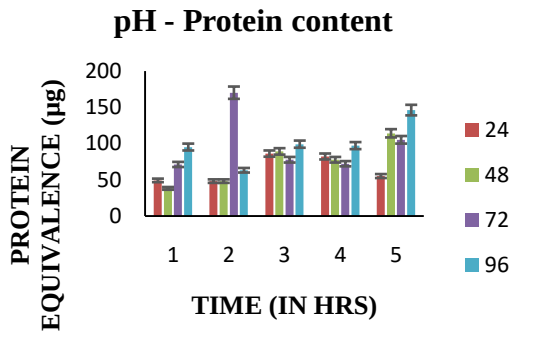

Figure 3. Phylogenetic position of *Bacillus subtilis* AD20 using neighbors-joining method with the related genus

Figure: 4.1 a. Effect of different pH on protein content in Bacillus subtilis AD20

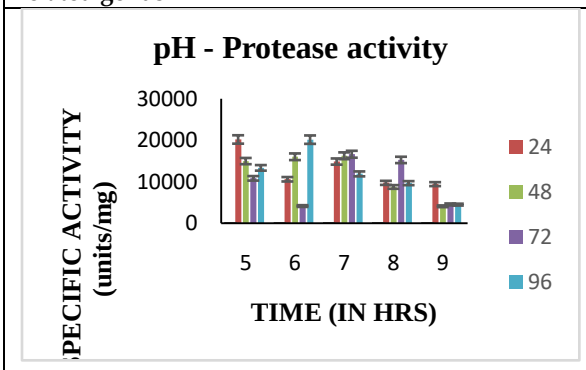

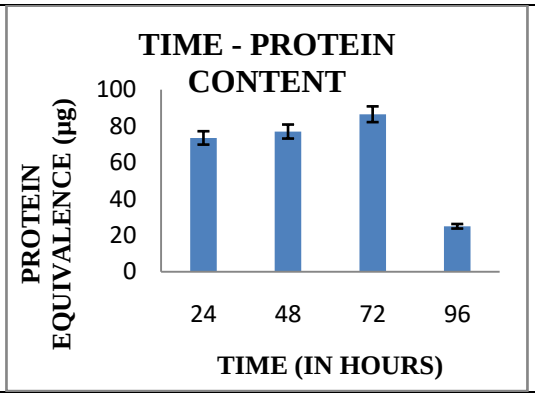

Figure: 4.1 b. Effect of different pH on protease activity in *Bacillus subtilis* AD20

Figure: 4.2a. Effect of time duration on protein content in *Bacillus subtilis* AD20

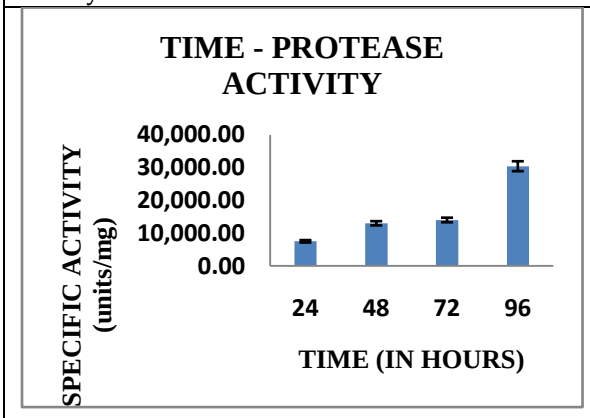

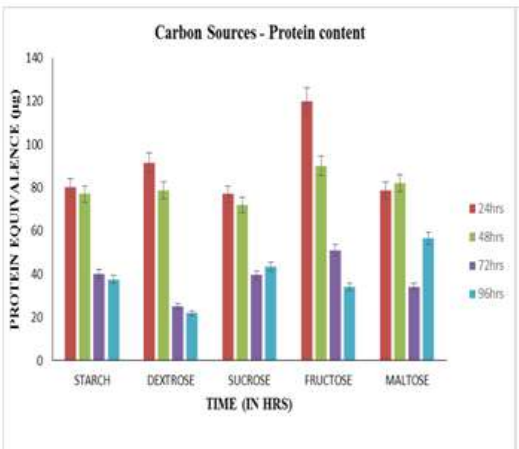

Figure: 4.2b. Effect of time duration on protease activity in *Bacillus subtilis* AD20

Figure: 4.3a. Effect of 1 % carbon source on protein content in *Bacillus subtilis* AD20

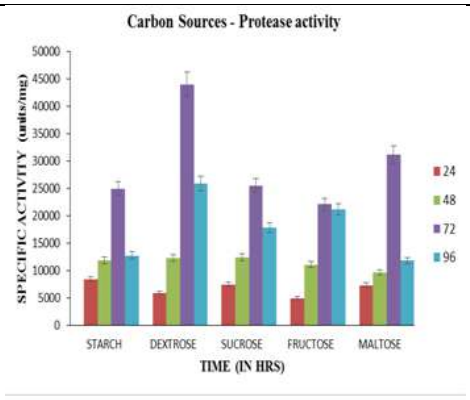

Figure: 4.3b. Effect of 1 % carbon source on protease activity in *Bacillus subtilis* AD20

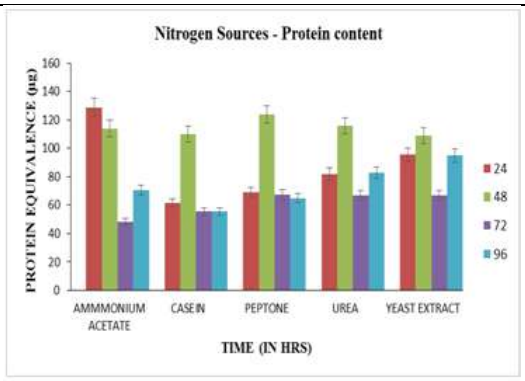

Figure: 4.4a. Effect of 1 % nitrogen source on protein content in *Bacillus subtilis* AD20

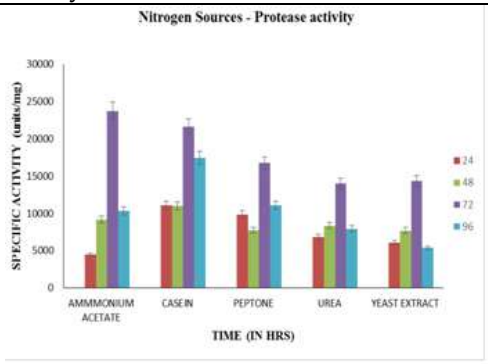

Figure: 4.4b. Effect of 1 % nitrogen source on protease activity in *Bacillus subtilis* AD20

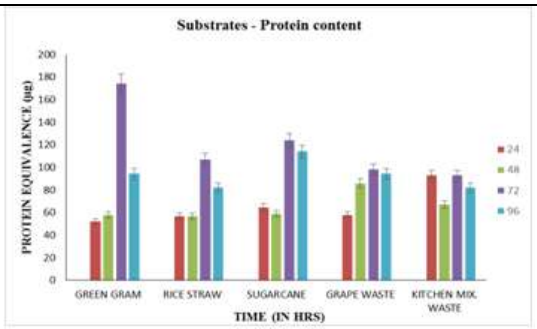

Figure: 4.5a. Effect of 1 % substrate on protein content in *Bacillus subtilis* AD20

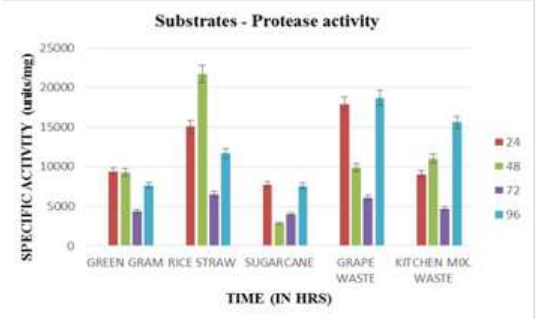

Figure: 4.5b. Effect of 1 % substrate on protease activity in *Bacillus subtilis* AD20

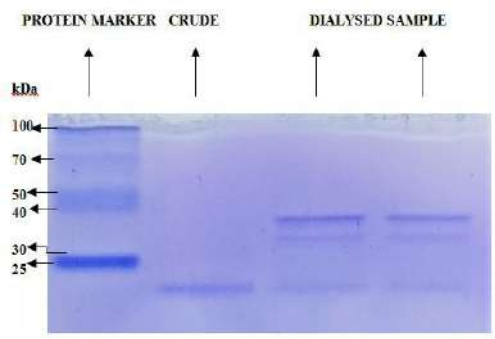

Figure: 5. SDS-PAGE with Coomassie Staining G-250

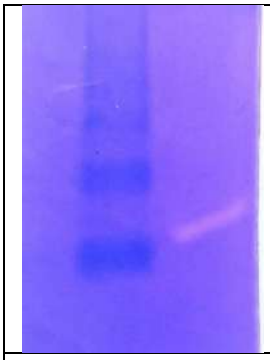

Figure: 6. Native-PAGE of Partially Purified Protease Action of *Bacillus subtilis* AD20 on 1 % Gelatin
Lane 1 - Marker, Lane 2 – partially purified enzyme

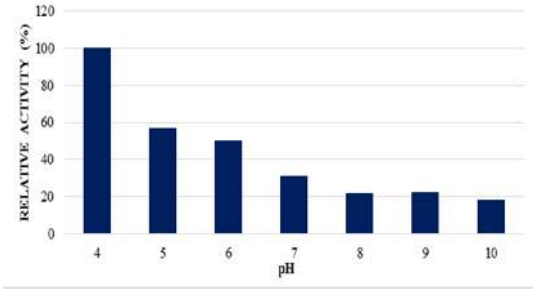

Figure: 7 Effect of pH on protease activity

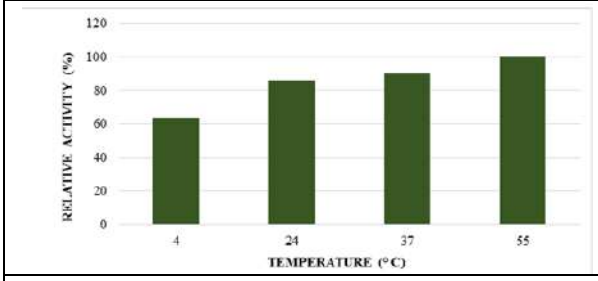

Figure: 8 Effect of temperature on protease activity

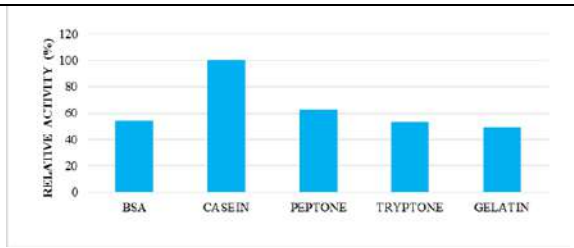

Figure: 9 Effect of substrate specificity on protease activity

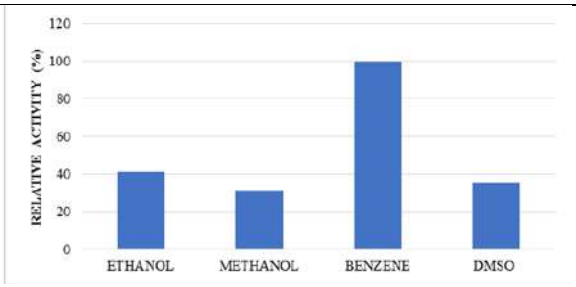

Figure: 10. Effect of organic solvents on protease activity

Figure: 11 Partially purified Protease activity in Skim Milk Agar 1st well- 50 µl, 2nd well- 40 µl, 3rd well- 30 µl, and 4th well- 20 µl partially purified protease

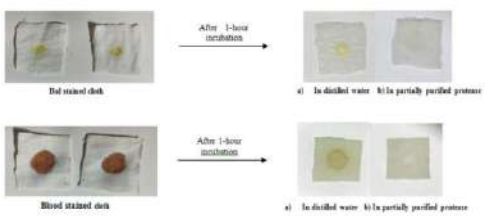

Figure:12 Wash Performance Study with Stained Clothes

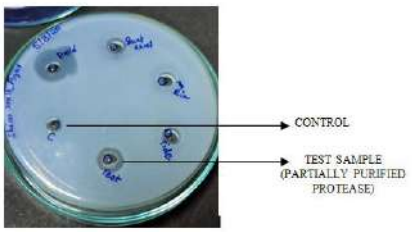

Figure: 13. Comparison of Protease Activity with the Commercial Detergent

Indian Journal of Natural Sciences www.tnsroindia.org.in ©IJONS

Vol.15 / Issue 83 / Apr / 2024 International Bimonthly (Print) – Open Access ISSN: 0976 – 0997

RESEARCH ARTICLE

Homomorphism in Bipolar Valued Vague Subnear Rings of a Nearring

S. Kamalaselvi[1] and B.Anandh[2]*

[1]Research Scholar, Department of Mathematics, Sudharsan College of Arts and Science (Affiliated to Bharathidasan University, Tiruchirappalli), Pudukkottai, Tamil Nadu, India.
[2]Assistant Professor, Department Mathematics, H. H. The Rajah's College (Affiliated to Bharathidasan University, Tiruchirappalli), Pudukkottai, Tamil Nadu, India.

Received: 29 Oct 2023 Revised: 10 Jan 2024 Accepted: 11 Mar 2024

***Address for Correspondence**
B.Anandh
Assistant Professor,
Department Mathematics,
H. H. The Rajah's College
(Affiliated to Bharathidasan University, Tiruchirappalli),
Pudukkottai, Tamil Nadu, India.
Email: drbaalaanandh@gmail.com

ABSTRACT

In this paper, bipolar valued vague subnearring of a nearring is studied by homomorphism and anti homomorphism and some properties are discussed. These properties are useful to further research.

Keywords: Fuzzy subset, vague subset, bipolar valued fuzzy subset, bipolar valued vague subset, bipolar valued vague subnearring, bipolar valued vague normal subnearring, intersection, image and preimage.

INTRODUCTION

In 1965, Zadeh [13] introduced the notion of a fuzzy subset of a Universal set. Vague set is an extension of fuzzy set and it is appeared as a unique case of context dependent fuzzy sets. The vague set was introduced by W.L.Gau and D.J.Buehrer [5]. W.R.Zhang [14, 15] introduced an extension of fuzzy sets named bipolar valued fuzzy sets in 1994 and bipolar valued fuzzy set was developed by Lee [6, 7]. Fuzzy subgroup was introduced by Azriel Rosenfeld [3]. RanjitBiswas [9] introduced the vague groups. Cicily Flora. S and Arockiarani.I [4] have introduced a new class of generalized bipolar vague sets. Anitha.M.S., et.al.[1] defined as bipolar valued fuzzy subgroups of a group. Sheena. K. P and K.Uma Devi [10] have introduced the bipolar valued fuzzy subbigroup of a bigroup. Shanthi.V.K and G.Shyamala[11] have introduced the bipolar valued multi fuzzy subgroups of a group. Yasodara.S, KE. Sathappan [12] defined the bipolar valued multi fuzzy subsemirings of a semiring. Bipolar valued multi fuzzy subnearring of a nearing has been introduced by S.Muthukumaran and B.Anandh [8]. Anitha.K., et.al.[2] defined as bipolar valued vague subsemirings of a semiring. Here, the concept of bipolar valued vague subnearring of a nearring is introduced

and estaiblished some results. Homomorphism and anti homomorphism are applied in bipolar valued vague subnearring of a nearring.

PRELIMINARIES

Definition 1.1. [13] Let X be any nonempty set. A mapping M : X → [0, 1] is called a fuzzy subset of X.

Definition 1.2. [5] A vague set A in the universe of discourse U is a pair [t_A, $1-f_A$],where t_A : U→ [0, 1] and f_A : U→ [0, 1] are mappings, they are called truth membership function and false membership function respectively. Here $t_A(x)$ is a lower bound of the grade of membership of x derived from the evidence for x and $f_A(x)$ is a lower bound on the negation of x derived from the evidence against x and $t_A(x) + f_A(x) \le 1$, for all x∈U.

Definition 1.3. [5] The interval [$t_A(x)$, $1-f_A(x)$] is called the vague value of x in A and it is denoted by $V_A(x)$, i.e., $V_A(x)$ = [$t_A(x)$, $1-f_A(x)$].

Example 1.4. A = { < a, [0.1, 0.2] >, < b, [0.3, 0.4] >, < c, [0.5, 0.6] >} is a vague subset of X = {a, b, c }.

Definition 1.5. [14] A bipolar valued fuzzy set (BVFS) A in X is defined as an object of the form A = { < x, $A^+(x)$, $A^-(x)$ >/ x∈X}, where A^+ : X→ [0, 1] and A^- : X→ [–1, 0]. The positive membership degree $A^+(x)$ denotes the satisfaction degree of an element x to the property corresponding to a bipolar valued fuzzy set A and the negative membership degree $A^-(x)$ denotes the satisfaction degree of an element x to some implicit counter-property corresponding to a bipolar valued fuzzy set A.

Example 1.6. A = { < a, 0.2, –0.3 >, < b, 0.4, –0.5 >, < c, 0.6, –0.7 >} is a bipolar valued fuzzy subset of X = {a, b, c }.

Definition 1.7. [4] A bipolar valued vague subset A in X is defined as an object of the form A = { ⟨ x, [$t_A^+(x)$, $1-f_A^+(x)$], [–1– $f_A^-(x)$, $t_A^-(x)$] ⟩ / x∈X }, where t_A^+ : X→ [0, 1], f_A^+ : X→ [0, 1], t_A^- : X→ [–1, 0] and f_A^- : X→ [–1, 0] are mapping such that $t_A(x) + f_A(x) \le 1$ and $-1 \le t_A^- + f_A^-$. The positive interval membership degree [$t_A^+(x)$, $1-f_A^+(x)$] denotes the satisfaction region of an element x to the property corresponding to a bipolar valued vague subset A and the negative interval membership degree [–1– $f_A^-(x)$, $t_A^-(x)$] denotes the satisfaction region of an element x to some implicit counter-property corresponding to a bipolar valued vague subset A. Bipolar valued vague subset A is denoted as A = { ⟨ x, $V_A^+(x)$, $V_A^-(x)$ ⟩ / x∈X }, where $V_A^+(x)$, = [$t_A^+(x)$, $1-f_A^+(x)$] and $V_A^-(x)$ = [–1– $f_A^-(x)$, $t_A^-(x)$].

Note that. [0] = [0, 0], [1] = [1, 1] and [–1] = [–1, –1].

Example 1.8. [A] = { < a, [0.5, 0,8], [–0.4, –0.1] >, < b, [0.22, 0.54], [–0.7, –0.2] >, < c, [0.11, 0.5], [–0.8, –0.5] > } is a bipolar valued vague subset of X = {a, b, c }.

Definition 1.9. [4] Let A = ⟨ V_A^+ , V_A^- ⟩ and B = ⟨ V_B^+ , V_B^- ⟩ be two bipolar valued vague subsets of a set X. We define the following relations and operations:

(i) A ⊂ B if and only if $V_A^+(u) \le V_B^+(u)$ and $V_A^-(u) \ge V_B^-(u)$, ∀ u∈X.

(ii) A = B if and only if $V_A^+(u) = V_B^+(u)$ and $V_A^-(u) = V_B^-(u)$, ∀ u∈X.

(iii) A∩B = { ⟨ u, rmin ($V_A^+(u)$, $V_B^+(u)$), rmax ($V_A^-(u)$, $V_B^-(u)$) ⟩ / u∈X }.

(iv) A∪B = { ⟨ u, rmax (V_A^+(u), V_B^+(u)), rmin (V_A^-(u), V_B^-(u)) ⟩ / u∈X }. Here rmin (V_A^+(u), V_B^+(u)) = [min { $t_A^+(x), t_B^+(x)$ }, min {1– $f_A^+(x)$, 1– $f_B^+(x)$}], rmax (V_A^+(u), V_B^+(u)) = [max {$t_A^+(x), t_B^+(x)$ }, max {1– $f_A^+(x)$, 1– $f_B^+(x)$ }], rmin (V_A^-(u), V_B^-(u)) = [min {–1– $f_A^-(x)$, –1– $f_B^-(x)$}, min {$t_A^-(x), t_B^-(x)$ }], rmax (V_A^-(u), V_B^-(u)) = [max {–1– $f_A^-(x)$, –1– $f_B^-(x)$ }, max {$t_A^-(x), t_B^-(x)$ }].

Definition 1.10. Let R be a nearring. A bipolar valued vague subset A of R is said to be a bipolar valued vague subnearring of R (BVVSNR) if the following conditions are satisfied,

(i) V_A^+(x–y) ≥ rmin{ V_A^+(x), V_A^+(y) }

(ii) V_A^+(xy) ≥ rmin{ V_A^+(x), V_A^+(y) }

(iii) V_A^-(x–y) ≤ rmax{ V_A^-(x), V_A^-(y) }

(iv) V_A^-(xy) ≤ rmax{ V_A^-(x), V_A^-(y) } for all x and y in R.

Example 1.11. Let R = Z_3 = { 0, 1, 2 } be a nearring with respect to the ordinary addition and multiplication. Then A = { < 0, [0.6, 0.8], [– 0.9, – 0.6] >, < 1, [0.5, 0.7], [– 0.8, –0.5] >, < 2, [0.5, 0.7], [– 0.8, – 0.5] > } is a BVVSNR of R.

Definition 1.12. Let R be a nearring. A BVVSNR A = ⟨V_A^+, V_A^-⟩ of R is said to be a bipolar valued vague normal subnearring (BVVNSNR) of R if V_A^+(x+y) = V_A^+(y+x), V_A^+(xy) = V_A^+(yx), V_A^-(x+y) = V_A^-(y+x) and V_A^-(xy) = V_A^-(yx) for all x and y in R.

Definition 1.13. Let R and R' be any two nearrings. Then the function f: R → R' is said to be an antihomomorphism if f(x+y) = f(y)+f(x) and f(xy) = f(y)f(x) for all x and y in R.

Definition 1.14. Let X and X' be any two sets. Let f : X→ X' be any function and let A = ⟨V_A^+, V_A^-⟩ be a bipolar valued vague subset in X, V = ⟨V_V^+, V_V^-⟩ be a bipolar valued vague subset in f(X) = X', defined by V_V^+(y) = $r\sup_{x\in f^{-1}(y)} V_A^+$(x) and V_V^-(y) = $r\inf_{x\in f^{-1}(y)} V_A^-$(x), for all x in X and y in X'. A is called a preimage of V under f and is defined as V_A^+(x) = V_V^+(f(x)), V_A^-(x) = V_V^-(f(x)) for all x in X and is denoted by f^{-1}(V).

SOME THEOREMS.

Theorem 2.1. Let R and R' be any two nearrings. The homomorphic image of a BVVSNR of R is a BVVSNR of R'.

Proof: Let f : R→ R' be a homomorphism. Let V = f(A) = ⟨V_V^+, V_V^-⟩, where A = ⟨V_A^+, V_A^-⟩ is a BVVSNR of R. We have to prove that V is a BVVSNR of R'. Now for f(x), f(y) in R', V_V^+(f(x)–f(y)) = V_V^+(f(x–y)) ≥ V_A^+(x–y) ≥ rmin{V_A^+(x), V_A^+(y)} = rmin{V_V^+(f(x)), V_V^+(f(y)) } which implies that V_V^+(f(x)–f(y)) ≥ rmin{V_V^+(f(x)), V_V^+(f(y))}. And V_V^+(f(x)f(y)) = V_V^+(f(xy)) ≥ V_A^+(xy) ≥ rmin{V_A^+(x), V_A^+(y)} = rmin {V_V^+(f(x)), V_V^+(f(y)) } which implies that V_V^+(f(x)f(y)) ≥ rmin{ V_V^+(f(x)), V_V^+(f(y)) }. Also V_V^-(f(x)–f(y)) = V_V^-(f(x–y)) ≤ V_A^-(x–y) ≤ rmax { V_A^-(x), V_A^-(y) } = rmax {V_V^-(f(x)), V_V^-(f(y))} which implies that V_V^-(f(x)–f(y)) ≤ rmax{ V_V^-(f(x)), V_V^-(f(y)) }. And V_V^-(f(x)f(y)) = V_V^-(f(xy)) ≤ V_A^-(xy) ≤ rmax{V_A^-(x), V_A^-(y)} = rmax{V_V^-(f(x)), V_V^-(f(y))} which implies that V_V^-(f(x)f(y)) ≤ rmax{ V_V^-(f(x)), V_V^-(f(y)) }. Hence V is a BVVSNR of R'.

Theorem. Let R and R' be any two nearrings. The homomorphic preimage of a BVVSNR of R' is a BVVSNR of R.

Proof. Let f : R → R' be a homomorphism. Let V = f(A) = $\langle V_V^+ , V_V^- \rangle$ where V is a BVVSNR of R'. We have to prove that A = $\langle V_A^+ , V_A^- \rangle$ is a BVVSNR of R. Let x and y in R. Now V_A^+ (x–y) = V_V^+ (f(x–y)) = V_V^+ (f(x)–f(y)) ≥ rmin { V_V^+ (f(x)), V_V^+ (f(y)) }= rmin {V_A^+ (x), V_A^+ (y)} which implies that V_A^+ (x–y) ≥ rmin{ V_A^+ (x), V_A^+ (y) }. And V_A^+ (xy) = V_V^+ (f(xy)) = V_V^+ (f(x)f(y)) ≥ rmin{ V_V^+ (f(x)), V_V^+ (f(y)) }= rmin { V_A^+ (x), V_A^+ (y)} which implies that V_A^+ (xy) ≥ rmin{ V_A^+ (x), V_A^+ (y) }. Also V_A^- (x–y) = V_V^- (f(x–y)) = V_V^- (f(x) –f(y)) ≤ rmax{ V_V^- (f(x)), V_V^- (f(y))} = rmax{V_A^- (x), V_A^- (y)} which implies that V_A^- (x–y) ≤ rmax{V_A^- (x), V_A^- (y) }. And V_A^- (xy) = V_V^- (f(xy)) = V_V^- (f(x)f(y)) ≤ rmax{V_V^- (f(x)), V_V^- (f(y))} = rmax{ V_A^- (x), V_A^- (y)} which implies that V_A^- (xy) ≤ rmax{ V_A^- (x), V_A^- (y)}. Hence A is a BVVSNR of R.

Theorem: Let R and R' be any two nearrings. The antihomomorphic image of a BVVSNR of R is a BVVSNR of R'.

Proof: Let f : R → R' be an antihomomorphism. Let V = f(A) = $\langle V_V^+ , V_V^- \rangle$ where A = $\langle V_A^+ , V_A^- \rangle$ is a BVVSNR of R. We have to prove that V is a BVVSNR of R'. Now for f(x), f(y) in R', V_V^+ (f(x) –f(y)) = V_V^+ (f(y–x)) ≥ V_A^+ (y–x) ≥ rmin { V_A^+ (x), V_A^+ (y) } = rmin { V_V^+ (f(x)), V_V^+ (f(y)) } which implies that V_V^+ (f(x) –f(y)) ≥ rmin{ V_V^+ (f(x)), V_V^+ (f(y)) }. And V_V^+ (f(x)f(y)) = V_V^+ (f(yx)) ≥ V_A^+ (yx) ≥ rmin { V_A^+ (x), V_A^+ (y)} = rmin {V_V^+ (f(x)), V_V^+ (f(y)) } which implies that V_V^+ (f(x)f(y)) ≥ rmin { V_V^+ (f(x)), V_V^+ (f(y)) }. Also V_V^- (f(x) –f(y)) = V_V^- (f(y–x)) ≤ V_A^- (y–x) ≤ rmax{ V_A^- (x), V_A^- (y)} = rmax {V_V^- (f(x)), V_V^- (f(y))} which implies that V_V^- (f(x) –f(y)) ≤ rmax{V_V^- (f(x)), V_V^- (f(y))}. And V_V^- (f(x)f(y)) = V_V^- (f(yx)) ≤ V_A^- (yx) ≤ rmax{ V_A^- (x), V_A^- (y)} = rmax{ V_V^- (f(x)), V_V^- (f(y)) } which implies that V_V^- (f(x)f(y)) ≤ rmax{ V_V^- (f(x)), V_V^- (f(y)) }. Hence V is a BVVSNR of R'.

Theorem: Let R and R' be any two nearrings. The antihomomorphic preimage of a BVVSNR of R' is a BVVSNR of R.

Proof: Let f : R → R' be an antihomomorphism. Let V = f(A) = $\langle V_V^+ , V_V^- \rangle$ where V is a BVVSNR of R'. We have to prove that A = $\langle V_A^+ , V_A^- \rangle$ is a BVVSNR of R. Let x and y in R. Now V_A^+ (x–y) = V_V^+ (f(x–y)) = V_V^+ (f(y) –f(x)) ≥ rmin{ V_V^+ (f(x)), V_V^+ (f(y)) } = rmin{ V_A^+ (x), V_A^+ (y) } which implies that V_A^+ (x–y) ≥ rmin{ V_A^+ (x), V_A^+ (y)}. And V_A^+ (xy) = V_V^+ (f(xy)) = V_V^+ (f(y)f(x)) ≥ rmin{V_V^+ (f(x)), V_V^+ (f(y)) } = rmin{ V_A^+ (x), V_A^+ (y)} which implies that V_A^+ (xy) ≥ rmin{V_A^+ (x), V_A^+ (y)}. Also V_A^- (x–y) = V_V^- (f(x–y)) = V_V^- (f(y) –f(x)) ≤ rmax{ V_V^- (f(x)), V_V^- (f(y)) } = rmax{V_A^- (x), V_A^- (y)} which implies that V_A^- (x–y) ≤ rmax{V_A^- (x), V_A^- (y)}. And V_A^- (xy) = V_V^- (f(xy)) = V_V^- (f(y)f(x)) ≤ rmax{ V_V^- (f(x)), V_V^- (f(y)) } = rmax{V_A^- (x), V_A^- (y)} which implies that V_A^- (xy) ≤ rmax { V_A^- (x), V_A^- (y) }. Hence A is a BVVSNR of R.

Theorem: Let R and R' be any two nearrings. The homomorphic image of a BVVNSNR of R is a BVVNSNR of R'.

Proof. Let f : R → R' be a homomorphism. Let V = f(A) = $\langle V_V^+ , V_V^- \rangle$ where A = $\langle V_A^+ , V_A^- \rangle$ is a BVVNSNR of R. We have to prove that V is a BVVNSNR of R'. By Theorem 2.1, V is a BVVSNR of R'. Now for f(x), f(y) in R', V_V^+ (f(x)+f(y)) = V_V^+ (f(x+y)) ≥ V_A^+ (x+y) = V_A^+ (y+x) ≤ V_V^+ (f(y+x)) = V_V^+ (f(y)+f(x)) which implies that V_V^+ (f(x)+f(y)) =

V_V^+ (f(y)+f(x)). And V_V^+ (f(x)f(y)) = V_V^+ (f(xy)) ≥ V_A^+ (xy) = V_A^+ (yx) ≤ V_V^+ (f(yx)) = V_V^+ (f(y)f(x)) which implies that V_V^+ (f(x)f(y)) = V_V^+ (f(y)f(x)). Also V_V^- (f(x)+f(y)) = V_V^- (f(x+y)) ≥ V_A^- (x+y) = V_A^- (y+x) ≤ V_V^- (f(y+x)) = V_V^- (f(y)+f(x)) which implies that V_V^- (f(x)+f(y)) = V_V^- (f(y)+f(x)). And V_V^- (f(x)f(y)) = V_V^- (f(xy)) ≥ V_A^- (xy) = V_A^- (yx) ≤ V_V^- (f(yx)) = V_V^- (f(y)f(x)) which implies that V_V^- (f(x)f(y)) = V_V^- (f(y)f(x)). Hence V is a BVVNSNR of R'.

Theorem: Let R and R' be any two nearrings. The homomorphic preimage of a BVVNSNR of R' is a BVVNSNR of R.

Proof: Let f : R → R' be a homomorphism. Let V = f(A) = ⟨ V_V^+ , V_V^- ⟩ where V is a BVVNSNR of R'. We have to prove that A = ⟨ V_A^+ , V_A^- ⟩ is a BVVNSNR of R. By Theorem 2.2, A = ⟨ V_A^+ , V_A^- ⟩ is a BVVSNR of R. Let x and y in R. Now V_A^+ (x+y) = V_V^+ (f(x+y)) = V_V^+ (f(x)+f(y)) = V_V^+ (f(y)+f(x)) = V_V^+ (f(y+x)) = V_A^+ (y+x) which implies that V_A^+ (x+y) = V_A^+ (y+x). And V_A^+ (xy) = V_V^+ (f(xy)) = V_V^+ (f(x)f(y)) = V_V^+ (f(y)f(x)) = V_V^+ (f(yx)) = V_A^+ (yx) which implies that V_A^+ (xy) = V_A^+ (yx). Also V_A^- (x+y) = V_V^- (f(x+y)) = V_V^- (f(x)+f(y)) = V_V^- (f(y)+f(x)) = V_V^- (f(y+x)) = V_A^- (y+x) which implies that V_A^- (x+y) = V_A^- (y+x). And V_A^- (xy) = V_V^- (f(xy)) = V_V^- (f(x)f(y)) = V_V^- (f(y)f(x)) = V_V^- (f(yx)) = V_A^- (yx) which implies that V_A^- (xy) = V_A^- (yx). Hence A is a BVVNSNR of R.

Theorem. Let R and R' be any two nearrings. The antihomomorphic image of a BVVNSNR of R is a BVVNSNR of R'.

Proof: Let f : R → R' be an antihomomorphism. Let V = f(A) = ⟨ V_V^+ , V_V^- ⟩ where A = ⟨ V_A^+ , V_A^- ⟩ is a BVVNSNR of R. We have to prove that V is a BVVNSNR of R'. By Theorem 2.3, V is a BVVSNR of R'. Now for f(x), f(y) in R', V_V^+ (f(x)+f(y)) = V_V^+ (f(y+x)) ≥ V_A^+ (y+x) = V_A^+ (x+y) ≤ V_V^+ (f(x+y)) = V_V^+ (f(y)+f(x)) which implies that V_V^+ (f(x)+f(y)) = V_V^+ (f(y)+f(x)). And V_V^+ (f(x)f(y)) = V_V^+ (f(yx)) ≥ V_A^+ (yx) = V_A^+ (xy) ≤ V_V^+ (f(xy)) = V_V^+ (f(y)f(x)) which implies that V_V^+ (f(x)f(y)) = V_V^+ (f(y)f(x)). Also V_V^- (f(x)+f(y)) = V_V^- (f(y+x)) ≤ V_A^- (y+x) = V_A^- (x+y) ≥ V_V^- (f(x+y)) = V_V^- (f(y)+f(x)) which implies that V_V^- (f(x)+f(y)) = V_V^- (f(y)+f(x)). And V_V^- (f(x)f(y)) = V_V^- (f(yx)) ≤ V_A^- (yx) = V_A^- (xy) ≥ V_V^- (f(xy)) = V_V^- (f(y)f(x)) which implies that V_V^- (f(x)f(y)) = V_V^- (f(y)f(x)). Hence V is a BVVNSNR of R'.

Theorem: Let R and R' be any two nearrings. The antihomomorphic preimage of a BVVNSNR of R' is a BVVNSNR of R.

Proof. Let f : R → R' be an antihomomorphism. Let V = f(A) = ⟨ V_V^+ , V_V^- ⟩ where V is a BVVNSNR of R'. We have to prove that A = ⟨ V_A^+ , V_A^- ⟩ is a BVVNSNR of R. By Theorem 2.4, A = ⟨ V_A^+ , V_A^- ⟩ is a BVVSNR of R. Let x and y in R. Now V_A^+ (x+y) = V_V^+ (f(x+y)) = V_V^+ (f(y)+f(x)) = V_V^+ (f(x)+f(y)) = V_V^+ (f(y+x)) = V_A^+ (y+x) which implies that V_A^+ (x+y) = V_A^+ (y+x). And V_A^+ (xy) = V_V^+ (f(xy)) = V_V^+ (f(y)f(x)) = V_V^+ (f(x)f(y)) = V_V^+ (f(yx)) = V_A^+ (yx) which implies that V_A^+ (xy) = V_A^+ (yx). Also V_A^- (x+y) = V_V^- (f(x+y)) = V_V^- (f(y)+f(x)) = V_V^- (f(x)+f(y)) = V_V^- (f(y+x)) = V_A^- (y+x) which implies that V_A^- (x+y) = V_A^- (y+x). And V_A^- (xy) = V_V^- (f(xy)) = V_V^- (f(y)f(x)) = V_V^- (f(x)f(y)) = V_V^- (f(yx)) = V_A^- (yx) which implies that V_A^- (xy) = V_A^- (yx). Hence A is a BVVNSNR of R.

REFERENCES

1. Anitha.M.S., Muruganantha Prasad &Arjunan. K, "Notes on Bipolar valued fuzzy subgroups of a group", *Bulletin of Society for Mathematical Services and Standards*, Vol. 2 No. 3 (2013), 52 –59.
2. Anitha.K, M.Muthusamy & K.Arjunan, " Bipolar valued vague subsemiring of a semiring", *Journal of Shanghai Jiaotong University,* Vol. 16, Issue 8 (2020), 129 – 135
3. Azriel Rosenfeld, fuzzy groups, Journal of mathematical analysis and applications 35(1971), 512-517.
4. Cicily Flora. S and Arockiarani.I, A new class of generalized bipolar vague sets, International Journal of Information Research and review, 3(11), (2016), 3058– 3065.
5. Gau W.L and Buehrer D.J, Vague sets, IEEE Transactions on systems, Man and Cybernetics, 23(1993), 610 – 614.
6. Lee K.M., "Bipolar valued fuzzy sets and their operations", *Proc. Int. Conf. on Intelligent Technologies, Bangkok, Thailand*, (2000), 307 – 312.
7. Lee K.M.., "Comparison of interval-valued fuzzy sets, intuitionistic fuzzy sets and bipolar valued fuzzy sets", *J. fuzzy Logic Intelligent Systems*, 14(2) (2004), 125 –129.
8. Muthukumaran.S & B.Anandh, "Some theorems in bipolar valued multi fuzzy subnearring of a nearing", *Infokara,* Vol.8, Iss. 11 (2019).
9. RanjitBiswas, Vague groups, International Journal of Computational Coginition, 4(2), (2006), 20 – 23.
10. Sheena. K. P and K.Uma Devi, "Bipolar valued fuzzy subbigroup of a bigroup" Wutan Huatan Jisuan Jishu, Vol. XVII, Issue III (2021), 134 -138.
11. Shyamala.G and Santhi.V.K "Some translations of bipolar valued multi fuzzy subgroups of a group", *Adalya journal*, volume 9, Issue 7 (2020), 111 -115.
12. Yasodara.S, KE. Sathappan, "Bipolar valued multi fuzzy subsemirings of a semiring", *International Journal of Mathematical Archive*, 6(9) (2015), 75 –80.
13. Zadeh.L.A , "Fuzzy sets", *Information and control* , Vol.8, 338-353 (1965).
14. W.R.Zhang, Bipolar Fuzzy sets and Relations, *a computational Frame work for cognitive modeling and multiple decision Analysis, proceedings of Fuzzy IEEE conferences*, (1994), 305– 309.
15. W.R.Zhang, Bipolar Fuzzy sets, *proceedings of Fuzzy IEEE conferences*, (1998), 835– 840.

RESEARCH ARTICLE

Ecotrail Energy Efficient Routing Algorithm (Eeera) for Green Internet of Things

A. Leolin Arockiadass[1]*, T. Kokilavani[2], A. Aloysius[3] and Y. Sunil Raj[4]

[1]Research Scholar, Department of Computer Science, St. Joseph's College (Autonomous), (Affiliated to Bharathidasan University) Tiruchirappalli, Tamil Nadu, India.
[2]Assistant Professor, Department of Computer Science, CHRIST University, Bengaluru, Karnataka, India.
[3]Assistant Professor, Department of Computer Science, St. Joseph's College (Autonomous), (Affiliated to Bharathidasan University), Tiruchirappalli, Tamil Nadu, India.
[4]Assistant Professor, Department of Data Science, St. Xavier's College (Autonomous), Palayamkottai (Affiliated to Manonmaniam Sundaranar University), Tirunelveli, Tamil Nadu, India.

Received: 22 Feb 2024 Revised: 06 Mar 2024 Accepted: 20 Mar 2024

***Address for Correspondence**
A. Leolin Arockiadass
Research Scholar,
Department of Computer Science,
St. Joseph's College (Autonomous),
(Affiliated to Bharathidasan University)
Tiruchirappalli, Tamil Nadu, India.
Email: leolin.arul@gmail.com

ABSTRACT

The advent of Green Internet of Things (G-IoT) heralds a transformative era in optimizing device utilization within smart environments, crucial for curtailing energy consumption and mitigating carbon emissions. This research addresses the pressing need for energy reduction, particularly at the network layer of the protocol stack, to foster eco-friendliness during data transmission. This work presents a novel routing algorithm, EcoTrial, leveraging Ant Colony Optimization (ACO) to bolster energy efficiency within G-IoT ecosystems. The simulation is conducted to evaluate EcoTrial's efficacy, revealing its superior performance compared to existing schemes. This pioneering approach not only advances sustainability goals but also diminishes environmental impact, thereby fostering the development of eco-conscious solutions in G-IoT environments.

Keywords: Green Internet of Things (G-IoT), Network Layer, Routing, Ant Colony Optimization (ACO), EcoTrial, Energy Efficiency

INTRODUCTION

Smart devices with inherent capability to autonomously gather, process and exchange data among themselves and their ability to actuate a decision/ action in a given environment has put the Internet of Things on the frontier top of the technological map. The ubiquitous nature of IoT devices augments the immense possibilities for innovation and efficiency in various applications such as smart city, smart agriculture etc. The steady evolution of these devices has resulted in a new era of connectivity, automation, and data-driven decision-making[1]. From smart homes and cities to industrial processes and healthcare systems, the impact of IoT is far-reaching. The Indian subcontinent is witnessing fast urbanization and it is evident from the mushrooming of small, medium and very large sized cities with dense populations. As a consequence there is a steep upsurge in environmental degradation and energy consumption. There is also the need to provide urban services such as traffic congestion, sanitation and waste management. As the volume of IoT data and the amount of data transmitted is mounting up, the implementation of efficient and intelligent procedures that can lead to a reduction in energy consumption become imperative. [2] Routing techniques play a major role in the reduction of energy consumption in IoT implementations [3,4,5]. Routing holds the responsibility of choosing optimal communication paths and speed of transmission. Further its responsibility extends to preserving connection longevity in low-power and cost-effective scenarios [6, 7, 8]. Enhancing energy efficiency involves the application of optimization algorithms, with nature-inspired algorithms playing a predominant role. Techniques such as Ant Colony Optimization (ACO) are employed in conjunction with energy reduction strategies and scheduling techniques, addressing challenges such as the Traveling Salesman Problem [9, 10]. The work aims at proposing an algorithm that optimizes energy usage in IoT networks which lead towards the advancement of the G-IoT environment. The objectives include studying existing energy efficiency techniques based on ACO, and proposing a novel algorithm based on the ACO scheme. The remainder of this article follows a structured organization, the section 2, presents the Review of Literature, Section 3 delves into the proposed optimization technique coupled with ACO, Section 4, presents the results and analysis and finally section 5, draws conclusions.

REVIEW OF LITERATURE

Routing techniques in IoT networks play a major role be it heterogeneous or homogeneous networks. In heterogeneous networks, nodes are grouped into clusters, and the source node determines the intermediary node acting as a proxy across radio access technologies [11]. Optimization coupled with routing algorithms enhance energy consumption in IoT networks. Pushpender Saraol have evaluated and compared routing protocols such as AODV, DSR, and Destination-Sequenced Distance-Vector Routing (DSDV) [12]. ACO is prominent among optimization algorithms associated with routing protocols. The N-EEABR algorithm, an improvement over conventional Energy Efficient Ant-Based Routing, optimizes transmission power for enhanced efficiency in ant colony routing in IoT networks, promoting energy conservation and waste prevention [13]. Algorithms such as ACO-BFC-Minkowski Static (ABMS) and ACO-BFC-Minkowski Dynamic (ABMD), show significant energy savings and extend the network lifetime in static IoT scenarios. These two meta-heuristic approaches are optimized with Swarm Intelligence for shortest path computation in static and dynamic IoT networks. Utilizing widely-used algorithms like Breadth-First Search (BFS) and Dijkstra, the routes are further optimized using ACO[14]. Based on the study, the fact emerges that hybrid ACO enhances the energy efficiency in G-IoT while making the environment greener. As a result this work highly recommends optimization algorithms such as EcoTrial to be used in G-IoT architectures as it provides effective optimization, speed and efficiency in finding solutions over other recent algorithms.

Proposed Work

The proposed approach reduces the energy utilization of EcoTrial which combines Ant Colony Optimization (ACO) with Electric Fields in Nature (EFN). In EcoTrial, routing nodes, akin to ants, create virtual trails in a network influenced by an electric field. These nodes establish and maintain virtual trails to other nodes. Electric fields are

formed between network nodes, where the source node carries a higher electric charge compared to the destination node. The strength of the electric field diminishes with increasing distance between nodes. Ant nodes prioritize trails representing the shortest path between source and destination, while also considering the influence of the electric field. They experience a force aligned with the electric field, influencing their routing decisions. As ant nodes traverse the network, they leave virtual "eco-trails" reflecting their chosen paths. The strength of these eco-trails is adjusted based on path quality factors such as energy consumption and latency. Furthermore, the electric field strength between nodes is updated based on traffic and energy consumption along the path.

The energy consumption of nodes during data transmission follows a linear model, as expressed by Equation 1, where E(s, d) denotes the energy consumed for transmitting from node s to node d, and is proportional to the distance D(s, d) between the nodes.

$E(s, d) = \alpha \propto D(s, d)$ eq. 1

Equation 1, shows the energy consumed E(s, d) for transmitting a packet from node s to node d is proportional to the distance D(s, d) between the nodes. Here s is assumed to have higher mass and d will be with lower mass, α is a proportionality constant and $\propto$ denotes proportionality. Figure 1, illustrates the connected components of an IoT network, depicting nodes as A, B, C, D, E, F, G, and H, with edges denoted by directed arrows and corresponding connections specified. The edges are connected with a directed arrows, where the connections can be represented as (A,B), (A,E), (B,C), (C,D), (D,E), (E,F), (F, G) and (G, H).

$E(s, d) = \beta / (D(s, d))^2$ eq. 2

Equation 2 models the electric fields between nodes as inverse-square forces, where the electric field strength between nodes s and d is inversely proportional to the square of their distance, denoted by β.

Figure 2, illustrates the movement of packets, the edges marked with red signifies the max strength of pheromone (1), while the dashed red marking signifies the presence of pheromone at an average of 0.5. Subsequently the other edges without red marking signifies the unused routes whose pheromone count will be 0. The probability of an ant at node s moving to node d is determined by a combination of eco-trails and electric field strengths, as expressed in Equation 3, with the weight factor 'w' controlling the balance between exploration and exploitation. A higher 'w' emphasizes eco-trails, while a lower 'w' emphasizes electric fields.

$P(s, d) = w * P\_eco(s, d) + (1 - w) * P\_electric(s, d)$ eq. 3

Eco-trail strengths are updated based on the energy consumption of paths taken by ants, as shown in Equation 4, 8where η represents the learning rate.

$\Delta P\_eco(s, d) = \eta * E(s, d)$ eq. 4

The probability of an ant moving to node d is determined by a combination of eco-trails and electric field strengths, as expressed in Equation 3, with the weight factor 'w' controlling the balance between exploration and exploitation. A higher 'w' emphasizes eco-trails, while a lower 'w' emphasizes electric fields. Eco-trail strengths are updated based on the energy consumption of paths taken by ants, as shown in Equation 4, where η represents the learning rate.

$R\_eco(s,d) = E\_init - E\_cnsm(s,d)$ eq. 5

Ants select paths with the highest probability to move from source node s to destination node d. The algorithm converges upon reaching a termination criterion, such as a predefined number of iterations or upon obtaining a stable/optimum route. To calculate the residual energy consumed, Equation 5 is utilized, where R_eco(s, d) represents the remaining energy at source node s after accounting for energy consumed along the path from node s to node d.

$R\_eco(s,d) = E\_init - \alpha \propto D(s, d)$ eq. 6

Finally, Equation 6 calculates the residual energy consumed, considering the initial energy at head node s and subtracting the energy consumed along the path, thus providing the remaining energy at head node s after the energy consumed along the EcoTrial path.

Algorithm: EcoTrail

nodes:=source, destination

electric field strengths:= nodes

no. ants=X, max. iterations=N, pheromone evaporation rate=r,

convergence criteria=c

```
While not converged and iterations < max_iterations:
   For each ant_node in the network:
      Choose the destination node based on an exploration-exploitation trade-off.
      Calculate the energy consumption for the chosen path.
    end
end

   Update the eco-trails:
   For each ant_node:
      Update the strength of the eco-trail based on the energy consumption of the
chosen path.
   end

   Update the electric fields:
   For each edge (u, v) in the network:
      Calculate the electric field strength based on the charge difference between
nodes u and v.
      Update the electric field strength on edge (u, v).
   end
Apply pheromone evaporation to eco-trails to prevent stagnation.
Check for convergence based on the specified criteria.
Choose the best path found based on eco-trails for routing.
Return the best path.
End
```

The algorithm introduces a novel method for achieving energy optimization within IoT networks, employing a graph representation with nodes (devices or sensors) and edges (connections). The approach algorithm starts by calculating the optimum route using Dijkstra's shortest path algorithm, while the weights are assigned for each edge. Further EcoTrail does the computation of energy required to be spent at each and every node (ni), during the transfer of packets (pi). The strength of the energy as well as the energy is computed. Now the presence of pheromone is verified with the chosen path, while the optimized route is selected. Once the path is chosen the pheromone count is increased with 0.1, which will be reduced in a similar manner if the path is not used for a specific duration. Figure 3, elaborates on the movement of packets which is supported by the EcoTrial algorithm. As described the process of routing starts with the preliminary assignments, followed by the computation of routes substantiated by computation of electric field strength after which the pheromone strength is verified. Passing these computations the

RESULTS AND ANALYSIS

The algorithm in question undergoes thorough testing within a simulated smart city environment facilitated by the Kooja simulator. Rigorous testing is conducted across various scenarios, including smart traffic, smart security systems, and smart waste management systems. The assessment of the algorithm's energy consumption spans multiple device configurations, starting with 10, 20, 30, and 40 sensors, respectively. Additionally, these evaluations consider the monitoring area as a pivotal parameter, analyzing energy, residual energy, and the overall performance of the algorithm. Figure 4, illustrates the amount of data generated by the devices in the G-IoT environment. Deploying 40 devices allows generation of data calculated in bits as 5000. Now considering the energy requirement for generating this huge amount of data is mandatory. Figure 5, presents the consumption of energy in watts (w) by different devices in G-IoT. Here the number of devices considered is 40. The peak representing the device in normal mode shows a maximum consumption between 150 to 400 w, in active and passive modes. On the optimization the results show significant energy savings of about 20 w to 110 w. The average consumption and savings can be

calculated as 350 w at the normal mode and 75 w in the optimal mode. Figure 5 illustrates the residual energy consumed by the node is watts for 1700 different iterations. EcoTrial demonstrates consistent energy retention at the end of each transfer while EcoTrial performs better by the reduced consumption of energy at an average of 250 w. Though differences between energy transfer and retrieval are highly independent, variations identified show that EcoTrial outperforms the existing proposals. Figure 7 discloses the performance of the proposed EcoTrial algorithm on considering the throughput it could provide. With a varied set of inputs, the algorithm's performance is calculated in terms of packets it could transmit. It is observed that on calculating the optimal route, the throughput it provides is reliable as it provides better performance by transmitting 3.5 packets at an average, which underscores the efficiency of EcoTrial.

CONCLUSION

The study delves into the expanding realm of Green Internet of Things (G-IoT), offering a crucial response to the dynamic landscape of smart applications. It aims to harmonize technological advancements with eco-conscious practices, envisioning a future where development is not only intelligent but also inherently green and resilient. Green Internet of Things (G-IoT) applications, particularly in power management, emphasize the significance of energy efficiency. The research underscores the pivotal role of network layer resources/devices in fostering environmental friendliness. Optimization algorithms, notably Ant Colony Optimization (ACO) based schemes, substantially enhance energy consumption efficiency in IoT networks. The proposed EcoTrail algorithm, drawing inspiration from ant colony behavior and electric fields, presents a novel approach to energy optimization. It outperforms existing optimization algorithms by achieving a higher level of optimization, up to 89% while reducing the energy consumption, and providing better throughput. By amalgamating eco-trails and electric fields, the algorithm facilitates effective routing decisions, thereby promoting energy conservation and waste prevention.

REFERENCES

1. Nižetić S, Šolić P, López-de-Ipiña González-de-Artaza D, Patrono L. Internet of Things (IoT): Opportunities, issues and challenges towards a smart and sustainable future. J Clean Prod. 2020 Nov 20;274:122877. doi: 10.1016/j.jclepro.2020.122877. Epub 2020 Jul 19. PMID: 32834567; PMCID: PMC7368922.
2. Dipra Mitr, Souradeep Sarkar, A comparative study of routing protocols, International, Journal of Advanced Science and Engineering, pp. 46 – 51, 2016, ISSN: 2455-9024
3. Sunil Raj Y, Albert Rabara S, Brito Ramesh Kumar, A Security Architecture for Cloud Data Using Hybrid Security Scheme, IEEE Xplore, 2021. ISBN: 978-1-6654-0118-0.
4. Sunil Raj Y, Albert Rabara S, Aurn Gnanaraj, Brito Ramesh Kumar, Novel Hybrid Technique Enhancing Privacy and Security, Computer Communication and Signal Processing, IFIP AICT 651, Springer Cham, Switzerland AG, 2022. ISBN: 978-3-031-11633-9
5. Sunil Raj Y, Albert Rabara S, An Integrated Architecture for IoT Based Data Storage in Secure Smart Monitoring Environment, International Journal of Scientific and Technology Research (IJSTR), Vol. 8(10), pp. 2213-2216, 2019. ISSN: 2277-8616
6. Shah Z, Levula A, Khurshid K, Ahmed J, Ullah I, Singh S. Routing Protocols for Mobile Internet of Things (IoT): A Survey on Challenges and Solutions. Electronics. 2021; 10(19):2320. https://doi.org/10.3390/electronics10192320
7. Saif Saad Hameed and Hadeel Mohammed Saleh, The impact of Routing Protocols and topologies on IOT Based Systems, J. Phys.: Conf. Ser. 1804, 2021.
8. Albreem, M.A.; Sheikh, A.M.; Alsharif, M.H.; Jusoh, M.; Yasin, M.N. Green Internet of Things (GIoT): Applications, practices, awareness, and challenges. IEEE Access 2021, 9, 38833–38858.
9. Kokilavani, T., George Amalarethinam, D.I. (2013). An Ant Colony Optimization Based Load Sharing Technique for Meta Task Scheduling in Grid Computing. In: Meghanathan, N., Nagamalai, D., Chaki, N. (eds)

Advances in Computing and Information Technology. Advances in Intelligent Systems and Computing, vol 177. Springer, Berlin, Heidelberg. https://doi.org/10.1007/978-3-642-31552-7_41.

10. Kokilavani, T., George Amalarethinam, D.I., Memory Constrained ANT Colony System for Task Scheduling in GRID Computing, International Journal of Grid Computing and Applications, Vol. 3 (3), pp. 11 - 20, 2012.Anukriti Sharma, Sharad Sharma, Dushyant Gupta, Ant Colony Optimization Based Routing Strategies for Internet of Things, EVERGREEN Joint Journal of Novel Carbon Resource Sciences & Green Asia Strategy, Vol. 10 (02), pp998-1009, 2023.
11. . Fan, Y., Xu, B., Zhang, L., Song, J., Zomaya, A., & Li, K.-C. (2023). Validating the integrity of convolutional neural network predictions based on zero-knowledge proof. Information Sciences, 625, 125–140. DOI: 10.1016/j.ins.2023.01.036.
12. Pushpender Sarao, Comparison of AODV, DSR, and DSDV Routing Protocols in a Wireless Network, Journal of Communications Vol. 13 (4), 2018, pp. 175 - 181.
13. Jianqiang He, Zhijun Teng, Fan Zhang, Research on Power Control Routing Algorithm for Wireless Sensor Networks Based on Ant Colony Optimization, 2022, Research Square. [https://doi.org/10.21203/rs.3.rs-2206732/v1].
14. Anukriti Sharma, Sharad Sharma, Dushyant Gupta, Ant Colony Optimization Based Routing Strategies for Internet of Things, EVERGREEN Joint Journal of Novel Carbon Resource Sciences & Green Asia Strategy, Vol. 10 (02), pp998-1009, 2023.

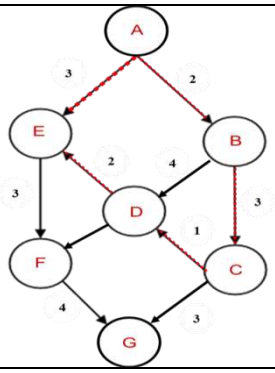

Figure 1. Trace of ECOTrials in IoT Network

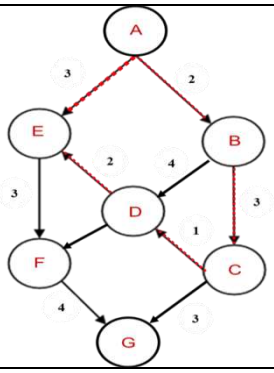

Figure 2. Trace of ECOTrials in IoT Network

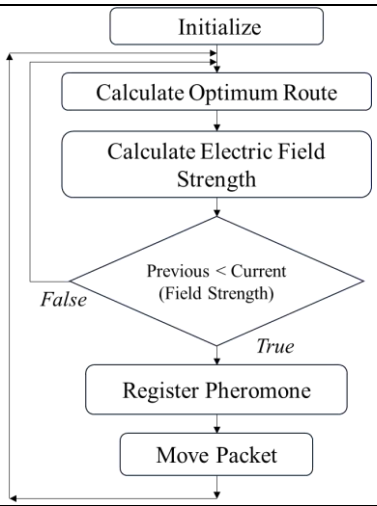

Figure 3. Proposed Approach to Enhance the Energy Efficiency

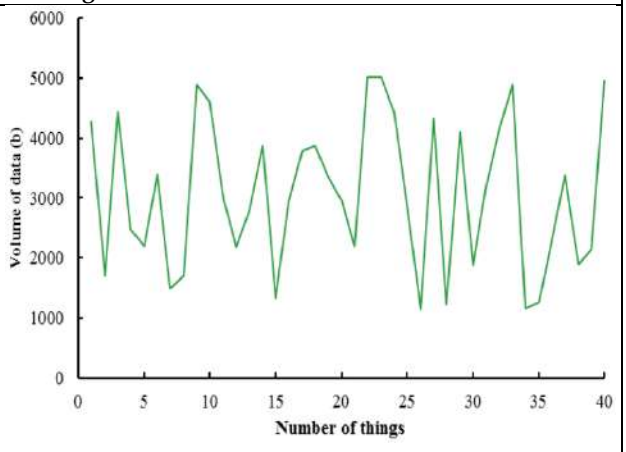

Figure 4. Data generated from the G-IoT

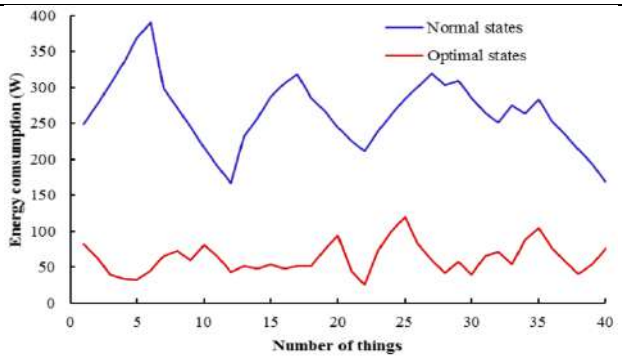

Figure 5. Different modes of devices in G-IoT

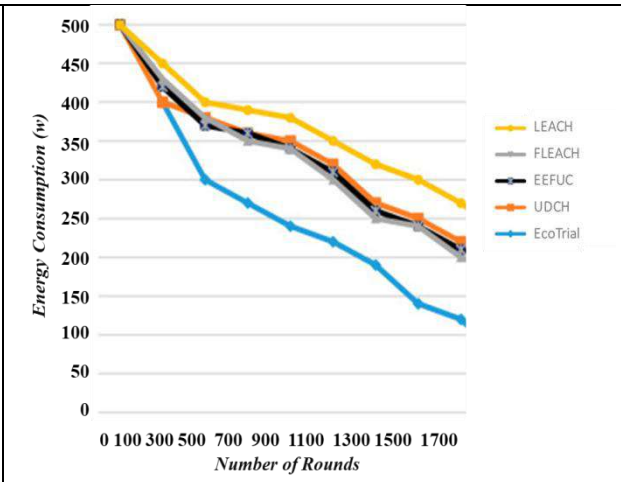

Figure 6. Average residual energy consumed

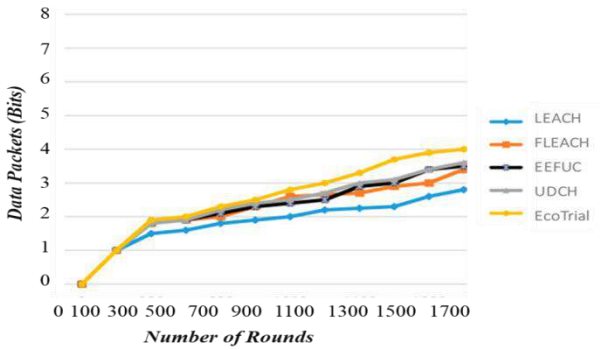

Figure 7. Performance of EcoTrial in terms of Throughput

RESEARCH ARTICLE

On Neutrosophic Λ_P- Neighbourhood and its Functions in Neutrosophic Topological Space

C. Reena[1]* and M. Karthika[2]

[1]Assistant Professor, Department of Mathematics, St. Mary's College (Autonomous), (Affiliated to Manonmaniam Sundaranar University, Abishekapatti, Tirunelveli) Thoothukudi, Tamil Nadu, India.
[2]Research Scholar, Reg.No. 21112212092004, Department of Mathematics, St. Mary's College (Autonomous), (Affiliated to Manonmaniam Sundaranar University, Abishekapatti, Tirunelveli)Thoothukudi, Tamil Nadu, India.

Received: 22 Feb 2024 Revised: 06 Mar 2024 Accepted: 20 Mar 2024

***Address for Correspondence**
C. Reena
Assistant Professor,
Department of Mathematics,
St. Mary's College (Autonomous),
(Affiliated to Manonmaniam Sundaranar University, Abishekapatti, Tirunelveli)
Thoothukudi, Tamil Nadu, India.
Email: reenastephany@gmail.com

ABSTRACT

The aim of this paper is to introduce the new notion of neutrosophic neighbourhood namely neutrosophicΛ_P-neighbourhood and neutrosophic Λ_P-quasi neighbourhood in neutrosophic topological space. Also, we introduce the neutrosophic continuous and irresolute functions along with their composition using neutrosophic Λ_P-open sets.

Keywords: neutrosophicΛ_P-open, neutrosophic Λ_P-closed, neutrosophic Λ_P-neighbourhood, neutrosophic Λ_P-continuous, neutrosophic Λ_P-irresolute.

INTRODUCTION

In mathematics, Zadeh[20] introduced the concept of fuzzy set between the real standard intervals in disclipine of logic and set theory. Atanassov[3] extended the intuitionistic fuzzy set which is a combination of membership and non-membership values. Smarandache[18] created the concept of neutrosophy and neutorsophic sets at the beginning of 20th century. Later Salama[15] and Alblowi initiated the neutrosophic sets in a topology entitled as neutrosophic topological space. G. C. Ray and Sudeep[11] proposed the definitions of neutrosophic point and neighbourhood structure. They have also explored the relation of quasi coincidence between neutrosophic sets and characterized the neutrosophic topological spaces by means of quasi-neighbourhood. In 2014, Salama[16] continued the studies on neutrosophic continuous functions. Recently, the authors[12] of this paper introduced a new notion of

neutrosophic sets namely neutrosophicΛ_P-open and neutrosophic Λ_P-closed sets. In this paper we have studied about novel concept of neutrosophic Λ_P-neighbourhood with quasi coincident. Also extended the neutrosophic continuous functions to neutrosophic Λ_P-continuous and neutrosophic Λ_P-irresolute functions with other existing continous functions in neutrosophic topological space. Also quoted the equivalent conditions and compositions of these functions.

PRELIMINARIES

Definition 2.1:[15]Let U be a non-empty fixed set. A **Neutrosophic set**K is an object having the form $K = \{\langle u,\ \mu_K(u), \sigma_K(u), \gamma_K(u)\rangle : u \in U\}$ where $\mu_K(u)$, $\sigma_K(u)$ and $\gamma_K(u)$ represents the degree of membership, the degree of indeterminacy and the degree of non-membership respectively of each element $u \in U$ to the set U. A neutrosophic set $K = \{\langle u,\ \mu_K(u), \sigma_K(u), \gamma_K(u)\rangle : u \in U\}$ can be identified to an ordered triple $\langle \mu_K(u), \sigma_K(u), \gamma_K(u)\rangle$ in $]^{-}0,1^{+}[$ on U.

Definition 2.2:[15]Let U be a non-empty set and $K = \{\langle u,\ \mu_K(u), \sigma_K(u), \gamma_K(u)\rangle : u \in U\}$ and $M = \{\langle u, \mu_M(u), \sigma_M(u), \gamma_M(u)\rangle : u \in U\}$ are neutrosophic sets, then

i. $K \subseteq M \Leftrightarrow \mu_K(u) \le \mu_M(u), \sigma_K(u) \le \sigma_M(u)$ and $\gamma_K(u) \ge \gamma_M(u) \forall u \in U$
ii. $K \cup M = \{\langle u, \max(\mu_K(u), \mu_M(u)), \max(\sigma_K(u), \sigma_M(u)), \min(\gamma_K(u), \gamma_M(u)) : u \in U\rangle\}$
iii. $K \cap M = \{\langle u, \min(\mu_K(u), \mu_M(u)), \min(\sigma_K(u), \sigma_M(u)), \max(\gamma_K(u), \gamma_M(u)) : u \in U\rangle\}$
iv. $K^C = \{\langle u, (\gamma_K(u), 1 - \sigma_K(u), \mu_K(u))\rangle : u \in U\}$
v. $0_{N_{tr}} = \{\langle u, 0, 0, 1\rangle : u \in U\}$ and $1_{N_{tr}} = \{\langle u, 1, 1, 0\rangle : u \in U\}$

Definition 2.3:[15]A **Neutrosophic topology** on a non-empty set U is a family $\tau_{N_{tr}}$ of neutrosophic sets in U satisfying the following axioms:

i. $0_{N_{tr}}, 1_{N_{tr}} \in \tau_{N_{tr}}$.
ii. $K_1 \cap K_2 \in \tau_{N_{tr}}$ for any $K_1, K_2 \in \tau_{N_{tr}}$.
iii. $\cup K_i \in \tau_{N_{tr}}$ for every $\{K_i : i \in I\} \subseteq \tau_{N_{tr}}$.

In this case the ordered pair $(U, \tau_{N_{tr}})$ is called a neutrosophic topological space. The members of $\tau_{N_{tr}}$ are neutrosophic open set and its complements are neutrosophic closed.

Definition 2.4:[6]A neutrosophic set $K = \{\langle u,\ \mu_K(u), \sigma_K(u), \gamma_K(u)\rangle : u \in U\}$ is called a **neutrosophic point** if for any element $v \epsilon U$, $\mu_K(v) = a, \sigma_K(v) = b, \gamma_K(v) = c$ and for $u = v$ and $\mu_K(v) = 0$, $\sigma_K(v) = 0, \gamma_K(v) = 1$ for $u \neq v$, where a, b, c are real standard or non standard sunsets of . A neutrosophic point is denoted by $u_{a,b,c}$. For the neutrosophic point $u_{a,b,c}, u$ will be called its support.

Definition 2.5[10]: Let $u_{a,b,c}$ be a neutrosophic point in a neutrosophic topological space $(U, \tau_{N_{tr}})$. Then a neutrosophic set N in U is said to be **neutrosophicneighbourhood**(N_{tr}nbhd) of $u_{a,b,c}$ if there exists a N_{tr}open set M such that $u_{a,b,c} \in M \subseteq N$.

Definition 2.6[1]: A neutrosophic point $u_{a,b,c}$ is said to be **neutrosophic quasi - coincident** with a neutrosophic set K, denoted by $u_{a,b,c} q K$ if $u_{a,b,c} \notin K^c$. If $u_{a,b,c}$ is not neutrosophic quasi – coincident with K, we denote it by $u_{a,b,c} \hat{q} K$.

Definition 2.7[1]: A neutrosophic set M is said to be neutrosophic quasi - coincident with a neutrosophic set K, denoted by MqK if $M \not\subseteq K^c$. If M is not neutrosophic quasi - coincident with K, we denote it by $M \hat{q} K$.

Definition 2.8[1]: A neutrosophic set N in U is said to be **neutrosophic quasi- neighbourhood**(N_{tr}Qnbhd) of $u_{a,b,c}$ if there exists a N_{tr}open set M such that $u_{a,b,c} q M \subseteq N$.

Definition 2.9[8]: Let $(U, \tau_{N_{tr}})$ be a neutrosophic topological space and S be a non-empty subset of U. Then, a neutrosophic relative topology on S is defined by

$\tau_{N_{tr}}^{S} = \{K \cap 1_{N_{tr}}^{S} : K \in \tau_{N_{tr}}\}$
where

$$1_{N_{tr}}^{S} = \begin{cases} < 1,1,0 >, & if\, s \in S \\ < 0,0,1 >, & otherwise \end{cases}$$

Thus, $(S, \tau_{N_{tr}}^{S})$ is called a neutrosophic subspace of $(U, \tau_{N_{tr}})$.

Definition 2.10:[5] Let U and V be two non-empty sets and $f_{N_{tr}} : U \longrightarrow V$ be a function. If$M = \{< v, \mu_M(v), \sigma_M(v), \gamma_M(v) >: v \in V\}$ is a neutrosophic set in V, then the **pre-image** of M under

under $f_{N_{tr}}$, denoted by $f_{N_{tr}}^{-1}(M)$, is the neutrosophic set in U defined by

$$f_{N_{tr}}^{-1}(M) = \{< u, f_{N_{tr}}^{-1}(\mu_M)(u), f_{N_{tr}}^{-1}(\sigma_M)(u), f_{N_{tr}}^{-1}(\gamma_M)(u) >: u \in U\}$$

If $K = \{< u, \mu_K(u), \sigma_K(u), \gamma_K(u) >: u \in U\}$ is a neutrosophic set in U, then the **image** of K under $f_{N_{tr}}$, denoted by $f_{N_{tr}}(K)$, is the neutrosophic set in V defined by

$f_{N_{tr}}(K) = \{< v, f_{N_{tr}}(\mu_K)(v), f_{N_{tr}}(\sigma_K)(v), \left(1 - f_{N_{tr}}(1 - \gamma_K)\right)(v) > : v \in V\}$where

$$f_{N_{tr}}(\mu_K)(v) = \begin{cases} sup_{u \in f_{N_{tr}}^{-1}(v)} \mu_K(u), & \text{if } f_{N_{tr}}^{-1}(v) \neq \emptyset \\ 0, & \text{otherwise} \end{cases}$$

$$f_{N_{tr}}(\sigma_K)(v) = \begin{cases} sup_{u \in f_{N_{tr}}^{-1}(v)} \sigma_K(u), & \text{if } f_{N_{tr}}^{-1}(v) \neq \emptyset \\ 0, & \text{otherwise} \end{cases}$$

$$\left(1 - f_{N_{tr}}(1 - \gamma_K)\right)(v) = \begin{cases} inf_{u \in f_{N_{tr}}^{-1}(v)} \gamma_K(u), & \text{if } f_{N_{tr}}^{-1}(v) \neq \emptyset \\ 1, & \text{otherwise} \end{cases}$$

Definition 2.11: Let $(U, \tau_{N_{tr}})$ and $(V, \rho_{N_{tr}})$ be neutrosophic topological spaces. Then the function $f_{N_{tr}} : (U, \tau_{N_{tr}}) \longrightarrow (V, \rho_{N_{tr}})$ is said to be **neutrosophic continuous**[15] (respectively, neutrosophic semi-continuous[4], neutrosophicα-continuous[2], neutrosophic regular-continuous[19], neutrosophicδ-continuous, neutrosophic b-continuous, neutrosophicΥ-continuous[13], neutrosophic$gb-$continuous[9], neutrosophicβ-continuous, neutrosophic $\Lambda_P{}^*$-continuous) if $f_{N_{tr}}^{-1}(M)$ is N_{tr}open(respectively N_{tr}semi-open, $N_{tr}\alpha$-open, N_{tr}r-open, $N_{tr}\delta$-open,$N_{tr}\,b$-open,$N_{tr}\,\Upsilon$-open,$N_{tr}\,gb$-open, $N_{tr}\,\beta$-open, $N_{tr}\,\Lambda_P{}^*$-open) in $(U, \tau_{N_{tr}})$ for every N_{tr}open set M in $\left(V, \rho_{N_{tr}}\right)$.

Definition 2.12:[12]A neutrosophic set K of a neutrosophic topological space $(U, \tau_{N_{tr}})$ is said to be **neutrosophicΛ_P-open** if there exist a N_{tr}pre-open set $E \neq 0_{N_{tr}}, 1_{N_{tr}}$ such that $K \subseteq N_{tr}\, cl(K \cap E)$. The complement of neutrosophic Λ_P-open set is neutrosophicΛ_P-closed. The class of neutrosophic Λ_P-open sets is denoted by $N_{tr}\,\Lambda_P O(U, \tau_{N_{tr}})$.
Theorem 2.13:[12] The union of an arbitrary collection of $N_{tr}\,\Lambda_P$-open sets is also $N_{tr}\,\Lambda_P$-open.

Theorem 2.14:[12]In any neutrosophic topological space $(U, \tau_{N_{tr}})$,

i. Every N_{tr}-open set is $N_{tr}\,\Lambda_P$-open.
ii. Every N_{tr} regular-open set is $N_{tr}\,\Lambda_P$-open.
iii. Every $N_{tr}\,\delta$-open set is $N_{tr}\,\Lambda_P$-open.
iv. Every N_{tr}semi-open set is $N_{tr}\,\Lambda_P$-open.
v. Every $N_{tr}\,\alpha$-open set is $N_{tr}\,\Lambda_P$-open.
vi. Every $N_{tr}\,\Lambda_P$-open set is $N_{tr}\,\Lambda_P{}^*$-open.

Remark 2.15:[12] The above theorem is also true for $N_{tr}\,\Lambda_P$-closed sets.

Theorem 2.16:[12]A neutrosophic set K in a neutrosophic topological space $(U, \tau_{N_{tr}})$ is $N_{tr}\,\Lambda_P$-open if and only if for every neutrosophic point $u_{a,b,c} \in K$, there exists a $N_{tr}\,\Lambda_P$-open set $M_{u_{a,b,c}}$ such that $u_{a,b,c} \in M_{u_{a,b,c}} \subseteq K$.

Definition 2.17:[12]Let $(U, \tau_{N_{tr}})$ be a neutrosophic topological space and K be a neutrosophic set in U.

i. The **neutrosophicΛ_P-interior** of K is the union of all $N_{tr}\,\Lambda_P$-open sets contained in K. It is denoted by $N_{tr}\,\Lambda_P\, int(K)$.

ii. The **neutrosophicΛ_P-closure** of K is the intersection of all N_{tr}-closed sets containing K. It is denoted by $N_{tr}\Lambda_P cl(K)$.

Theorem 3.10: A neutrosophic set K in a neutrosophic topological space $(U, \tau_{N_{tr}})$ is $N_{tr}\Lambda_P$-open if and only if for every neutrosophic point $u_{a,b,c} \in K$, K is a $N_{tr}\Lambda_P$-nbhd of $u_{a,b,c}$.
Proof: Let K be$N_{tr}\Lambda_P$-open in U. Then for each $u_{a,b,c} \in K$, $K \subseteq K$. Therefore K is a $N_{tr}\Lambda_P$-nbhd of $u_{a,b,c}$. Conversely, assume that for every $u_{a,b,c} \in K$, K is a $N_{tr}\Lambda_P$-nbhd of$u_{a,b,c}$. Then, there
exists a $N_{tr}\Lambda_P$-open set K in U such that $u_{a,b,c} \in M \subseteq K$. Therefore, by theorem 2.16, K is $N_{tr}\Lambda_P$-open.

Theorem 3.11: Every $N_{tr}\Lambda_P$-open set K in a neutrosophic topological space $(U, \tau_{N_{tr}})$ is a $N_{tr}\Lambda_P$-Qnbhd of every neutrosophic point quasi-coincident with K.
Proof: The proof is obvious since for every neutrosophic point $u_{a,b,c}qK$, we have $u_{a,b,c}qK \subseteq K$.

Theorem 3.12: Let K be a $N_{tr}\Lambda_P$-closed set in a neutrosophic topological space $(U, \tau_{N_{tr}})$ and $u_{a,b,c}qK^C$. Then there exists a $N_{tr}\Lambda_P$-Qnbhd$M$ of $u_{a,b,c}$ such that $K\hat{q}M$.
Proof: Since K is $N_{tr}\Lambda_P$-closed in U, K^C is $N_{tr}\Lambda_P$-open in U such that $u_{a,b,c}qK^C$. Then, by theorem 3.11, K^C is a $N_{tr}\Lambda_P$-Qnbhd of $u_{a,b,c}$. Hence there exists a$N_{tr}\Lambda_P$-open set M in Usuch that $u_{a,b,c}qK \subseteq K^C$ Again, by theorem 3.11, M is a $N_{tr}\Lambda_P$-Qnbhd of $u_{a,b,c}$ Also, since $M \subseteq K^C$, $K\hat{q}M$.

NEUTROSOPHIC Λ_P-NEIGHBOURHOOD
Definition 3.1: Let $u_{a,b,c}$ be a neutrosophic point in a neutrosophic topological space $(U, \tau_{N_{tr}})$. Then a neutrosophic set N in U is said to be

i. **neutrosophicΛ_P-neighbourhood**($N_{tr}\Lambda_P$-nbhd) of $u_{a,b,c}$ if there exists a $N_{tr}\Lambda_P$-open set M such that $u_{a,b,c} \in M \subseteq N$.
ii. **neutrosophicΛ_P-quasi neighbourhood**($N_{tr}\Lambda_P$-Qnbhd) of $u_{a,b,c}$ if there exists a $N_{tr}\Lambda_P$-open set M such that $u_{a,b,c}qM \subseteq N$.

Example 3.2: Let $U = \{a, b\}$ and $\tau_{N_{tr}} = \{0_{N_{tr}}, 1_{N_{tr}}, K\}$ where$K = \{< a, 0.6,0.4,0.2 >< b, 0.1,0.6,0.1 >\}$. Now, let us consider a neutrosophic point $a_{0.1,0.2,0.4}$ in U. Then there exists a $N_{tr}\Lambda_P$-open set $M = \{< a, 0.7,0.6,0.1 >< b, 0.4,0.8,0.1 >\}$ such that $a_{0.1,0.2,0.4} \in M \subseteq N$ where$N = \{< a, 0.8,0.7,0.1 >< b, 0.5,0.8,0.1 >\}$. Hence N is a $N_{tr}\Lambda_P$-nbhd of $a_{0.1,0.2,0.4}$.

Example 3.3: Let $U = \{a, b\}$ and $\tau_{N_{tr}} = \{0_{N_{tr}}, 1_{N_{tr}}, K\}$ where$K = \{< a, 0.7,0.6,0.1 >< b, 0.4,0.8,0.1 >\}$. Now, let us consider a neutrosophic point $a_{0.1,0.8,0.7}$ in U. Then there exists a $N_{tr}\Lambda_P$-open set$M = \{< a, 0.8,0.7,0.1 >< b, 0.7,0.8,0.1 >\}$ such that $a_{0.1,0.8,0.7}qM \subseteq N$ where $N = \{< a, 0.8,0.8,0.1 >< b, 0.7,0.8,0.1 >\}$. Hence N is a $N_{tr}\Lambda_P$-Qnbhd of $a_{0.1,0.8,0.7}$.

Theorem 3.4: Every N_{tr}nbhd of a neutrosophic point $u_{a,b,c}$ in a neutrosophic topological space $(U, \tau_{N_{tr}})$ is a $N_{tr}\Lambda_P$-nbhd of $u_{a,b,c}$.

Proof: Let N be a N_{tr}nbhd of a neutrosophic point $u_{a,b,c}$ in U. Then, there exists a N_{tr}open set M in U such that $u_{a,b,c} \in M \subseteq N$. Now, by theorem 2.14, M is $N_{tr}\Lambda_P$-open in U. Hence there exists a $N_{tr}\Lambda_P$-open set M in U such that $u_{a,b,c} \in M \subseteq N$. Therefore N is a $N_{tr}\Lambda_P$-nbhd of$u_{a,b,c}$.

Remark 3.5: The above theorem's converse need not hold.

Example 3.6: Let $U = \{a, b\}$ and $\tau_{N_{tr}} = \{0_{N_{tr}}, 1_{N_{tr}}, K\}$ where$K = \{< a, 0.5,0.5,0.1 >< b, 0.1,0.8,0.1 >\}$. Now, let us consider a neutrosophic point $a_{0.6,0.1,0.4}$ in U. Then there exists a $N_{tr}\Lambda_P$-open set

$M = \{< a, 0.7,0.7,0.1 >< b, 0.2,0.8,0.1 >\}$ such that $a_{0.6,0.1,0.4} \in M \subseteq N$ where $N = \{< a, 0.7,0.8,0.1 >< b, 0.3,0.8,0.1 >\}$. This implies N is a $N_{tr}\Lambda_P$-nbhd of $a_{0.6,0.1,0.4}$. However, N is not a N_{tr}nbhd of $a_{0.6,0.1,0.4}$.

Theorem 3.7: Every N_{tr}Qnbhdof a neutrosophic point $u_{a,b,c}$ in a neutrosophic topological space $(U, \tau_{N_{tr}})$ is a$N_{tr}\Lambda_P$-Qnbhd of $u_{a,b,c}$.

Proof: Let N be a N_{tr}Qnbhdof a neutrosophic point $u_{a,b,c}$ in U. Then, there exists a N_{tr}open set M in U such that$u_{a,b,c} qM \subseteq N$. Now, by theorem 2.14, M is $N_{tr}\Lambda_P$-open in U. Hence there exists a $N_{tr}\Lambda_P$-open set M in U such that $u_{a,b,c} qM \subseteq N$. Thus$N$ is a$N_{tr}\Lambda_P$-Qnbhd of $u_{a,b,c}$.

Remark 3.8: The above theorem's converse need not hold.

Example 3.9: Let $U = \{a, b\}$ and $\tau_{N_{tr}} = \{0_{N_{tr}}, 1_{N_{tr}}, K\}$ where$K = \{< a, 0.6,0.8,0.1 >< b, 0.4,0.6,0.3 >\}$. Now, let us consider a neutrosophic point $a_{0.1,0.1,0.5}$ in U. Then there exists a $N_{tr}\Lambda_P$-open set$M = \{< a, 0.7,0.8,0.1 >< b, 0.6,0.6,0.1 >\}$ such that$a_{0.1,0.1,0.5} qM \subseteq N$ where $N = \{< a, 0.8,0.8,0.1 >< a, 0.8,0.7,0.1 >\}$. This implies N is a$N_{tr}\Lambda_P$-Qnbhd of $a_{0.1,0.1,0.5}$. However, N is not a$N_{tr}\Lambda_P$-Qnbhd of $a_{0.1,0.1,0.5}$.

NEUTROSOPHIC Λ_P-CONTINUOUS FUNCTIONS

Definition 4.1: Let $(U, \tau_{N_{tr}})$ and $(V, \rho_{N_{tr}})$ be neutrosophic topological spaces. Then the function $f_{N_{tr}}: (U, \tau_{N_{tr}}) \longrightarrow (V, \rho_{N_{tr}})$ is said to be **neutrosophicΛ_P-continuous** if $f_{N_{tr}}^{-1}(M)$ is $N_{tr}\Lambda_P$-open in $(U, \tau_{N_{tr}})$ for every N_{tr}-open set M in $(V, \rho_{N_{tr}})$.

Example 4.2: Let $U = \{a, b\}, V = \{x, y\}, \tau_{N_{tr}} = \{0_{N_{tr}}, 1_{N_{tr}}, K, M\}and\rho_{N_{tr}} = \{0_{N_{tr}}, 1_{N_{tr}}, N\}$ where $K = \{< a, 0.7,0.8,0.4 >< b,1,1,0>$, $M=\{<a,0.5,0.6,0.5><b,0.6,\ 0.8,0.1>\}$ and$N=\{<x,0.8,0.9,0.1><y,1,1,0>\}$. Consider the collections $\mathcal{A}=\{A \ K \subset A, M^c \subset A\}$and $\mathcal{B} = \{B : K \subset B; B \not\subset M^c;\ M^c \not\subset B\}$ of neutrosophic sets in U. Then $N_{tr}\Lambda_P O(U, \tau_{N_{tr}}) = \{0_{N_{tr}}, K, M, \mathcal{A}, \mathcal{B}, 1_{N_{tr}}\}$. Define $f_{N_{tr}}: (U, \tau_{N_{tr}}) \longrightarrow (V, \rho_{N_{tr}})$ as $f_{N_{tr}}(a) = y$ and $f_{N_{tr}}(b) = x$. Then, $f_{N_{tr}}^{-1}(N) = \{< a, 1,1,0 >< b, 0.8,0.9,0.1 >\} \in \mathcal{A}$ which implies $f_{N_{tr}}^{-1}(N)$ is $N_{tr}\Lambda_P$-open in U. Hence $f_{N_{tr}}$ is $N_{tr}\Lambda_P$-continuous.

Theorem 4.3: Every N_{tr}-continuous function is $N_{tr}\Lambda_P$-continuous.

Proof: Let $f_{N_{tr}}: (U, \tau_{N_{tr}}) \longrightarrow (V, \rho_{N_{tr}})$ be a N_{tr}continuous function. Let M be a N_{tr}-open set in V. Since $f_{N_{tr}}$ is N_{tr}continuous, $f_{N_{tr}}^{-1}(M)$ is N_{tr}-open in U. By theorem 2.14(i), $f_{N_{tr}}^{-1}(M)$ is $N_{tr}\Lambda_P$-open in U. Hence $f_{N_{tr}}$ is $N_{tr}\Lambda_P$-continuous.

Remark 4.4: The above theorem's converse need not hold.

Example 4.5: Let $U = \{a, b\}, V = \{x, y\}, \tau_{N_{tr}} = \{0_{N_{tr}}, K, M, 1_{N_{tr}}\}and\rho_{N_{tr}} = \{0_{N_{tr}}, N, 1_{N_{tr}}\}$ where $K = \{< a, 0.3,0.4,0.9 >< b, 0.4,0.5,0.8 >\}, M = \{< a, 0.2,0.3,1 >< b, 0.3,0.4,0.9 >\}$ and $N = \{< x, 0.6,0.5,0.3 >< y, 0.7,0.6,0.2 >\}$. Consider the collections $\mathcal{A} = \{A : M \subset A \subset K^c\}$and $\mathcal{B} = \{B : B \subset M^C; B \not\subset K;\ K \not\subset B\}$ of neutrosophic sets in U.Then $N_{tr}\Lambda_P O(U, \tau_{N_{tr}}) = \{0_{N_{tr}}, K, M, \mathcal{A}, \mathcal{B}, 1_{N_{tr}}\}$. Define $f_{N_{tr}}: (U, \tau_{N_{tr}}) \longrightarrow (V, \rho_{N_{tr}})$ as $f_{N_{tr}}(a) = y$ and $f_{N_{tr}}(b) = x$.Then, $f_{N_{tr}}^{-1}(N) = \{< a, 0.7,0.6,0.2 >< b, 0.6,0.5,0.3 >\} \in Q$ which implies $f_{N_{tr}}^{-1}(N)$ is $N_{tr}\Lambda_P$-open but not N_{tr}open in U. Hence $f_{N_{tr}}$ is $N_{tr}\Lambda_P$-continuous but not N_{tr}-continuous.

Theorem 4.6: Let $f_{N_{tr}}: (U, \tau_{N_{tr}}) \longrightarrow (V, \rho_{N_{tr}})$ be a function between two neutrosophic topological spaces.

i. If $f_{N_{tr}}$ is N_{tr}regular-continuous, then $f_{N_{tr}}$ is $N_{tr}\Lambda_P$-continuous.
ii. If $f_{N_{tr}}$ is $N_{tr}\delta$-continuous, then $f_{N_{tr}}$ is $N_{tr}\Lambda_P$-continuous.
iii. If $f_{N_{tr}}$ is N_{tr}semi-continuous, then $f_{N_{tr}}$ is $N_{tr}\Lambda_P$-continuous.
iv. If $f_{N_{tr}}$ is $N_{tr}\alpha$-continuous, then $f_{N_{tr}}$ is $N_{tr}\Lambda_P$-continuous.
v. If $f_{N_{tr}}$ is $N_{tr}\Lambda_P$-continuous, then $f_{N_{tr}}$ is $N_{tr}{\Lambda_P}^*$-continuous.

Proof: Proof is obvious.

Remark 4.7: The above statements converse need not hold.

Example 4.8: Let $U=\{a,b\}, V=\{x,y\}, \tau_{N_{tr}}=\{0_{N_{tr}}, K, 1_{N_{tr}}\}$ and $\rho_{N_{tr}}=\{0_{N_{tr}}, M, 1_{N_{tr}}\}$ where $K=\{<a,0.7,0.6,0.8><b,0.6,0.8,0.9>$, $M=\{<a,0.6,0.4,0.9><b,0.5,0.7,0.1>\}$. Consider the collections $\mathcal{A}=\{A: K\subset A; A^C\subset K\}$, $\mathcal{B}=\{B: K\subset B; B\not\subset K^C\}$ of neutrosophic sets in U. Then, $N_{tr}RO(U,\tau_{N_{tr}})=\{0_{N_{tr}}, 1_{N_{tr}}\}$, and $N_{tr}\Lambda_P O(U,\tau_{N_{tr}})=\{0_{N_{tr}}, K, \mathcal{A}, \mathcal{B}, 1_{N_{tr}}\}$. Define $f_{N_{tr}}:(U,\tau_{N_{tr}})\longrightarrow(V,\rho_{N_{tr}})$ as $f_{N_{tr}}(a)=y$ and $f_{N_{tr}}(b)=x$. Then, $f_{N_{tr}}^{-1}(M)=\{<a,0.5,0.7,0.1><b,0.6,0.4,0.9>\}\in\mathcal{B}$ which implies $f_{N_{tr}}^{-1}(M)$ is $N_{tr}\Lambda_P$-open but not N_{tr} regular-open in U. Hence $f_{N_{tr}}$ is $N_{tr}\Lambda_P$-continuous but not N_{tr} regular-continuous.

Example 4.9: Let $U=\{a,b\}, V=\{x,y\}, \tau_{N_{tr}}=\{0_{N_{tr}}, K, 1_{N_{tr}}\}$ and $\rho_{N_{tr}}=\{0_{N_{tr}}, M, 1_{N_{tr}}\}$ where $K=\{<a,0.4,0.8,0.3><b,0.5,0.7,0.2>$, $M=\{<a,0.5,0.8,0.3><b,0.2,0.7,0.4>\}$. Consider the collections $\mathcal{A}=\{A: K^C\subset A\subset A\}$, $\mathcal{B}=\{B: K\subset B\subset 1_{N_{tr}}\}$ of neutrosophic sets in U. Then, $N_{tr}\delta O(U,\tau_{N_{tr}})=\{0_{N_{tr}}, K, 1_{N_{tr}}\}$ and $N_{tr}\Lambda_P O(U,\tau_{N_{tr}})=\{0_{N_{tr}}, K, \mathcal{A}, \mathcal{B}, 1_{N_{tr}}\}$. Define $f_{N_{tr}}:(U,\tau_{N_{tr}})\longrightarrow(V,\rho_{N_{tr}})$ as $f_{N_{tr}}(a)=y$ and $f_{N_{tr}}(b)=x$. Then, $f_{N_{tr}}^{-1}(M)=\{<a,0.2,0.7,0.4><b,0.5,0.8,0.3>\}\in\mathcal{A}$ which implies $f_{N_{tr}}^{-1}(M)$ is $N_{tr}\Lambda_P$-open but not $N_{tr}\delta$-open in U. Hence $f_{N_{tr}}$ is $N_{tr}\Lambda_P$-continuous but not $N_{tr}\delta$-continuous.

Example 4.10: Let $U=\{a,b\}, V=\{x,y\}, \tau_{N_{tr}}=\{0_{N_{tr}}, K, 1_{N_{tr}}\}$ and $\rho_{N_{tr}}=\{0_{N_{tr}}, M, 1_{N_{tr}}\}$ where $K=\{<a,0.4,0.5,0.6><b,0.6,0.3,0.8>$, $M=\{<x,0.3,0.4,0.7><y,0.5,0.2,0.9>\}$. Consider the collections $\mathcal{A}=\{A: 0_{N_{tr}}\subset A\subset K\}$, $\mathcal{B}=\{B: K^C\subset B\subset 1_{N_{tr}}\}$ and $\mathcal{C}=\{C: K\subset C\not\subset K^c\}$ of neutrosophic sets in U. Then, $N_{tr}\alpha O(U,\tau_{N_{tr}})=\{0_{N_{tr}}, 1_{N_{tr}}, K, M\}$, $N_{tr}SO(U,\tau_{N_{tr}})=\{0_{N_{tr}}, K, M, K^C, M^C, 1_{N_{tr}}\}$ and $N_{tr}\Lambda_P O(U,\tau_{N_{tr}})=\{0_{N_{tr}}, M, M^C, \mathcal{A}, \mathcal{B}, \mathcal{C}, 1_{N_{tr}}\}$. Define $f_{N_{tr}}:(U,\tau_{N_{tr}})\longrightarrow(V,\rho_{N_{tr}})$ as $f_{N_{tr}}(a)=y$ and $f_{N_{tr}}(b)=x$. Then, $f_{N_{tr}}^{-1}(M)=\{<a,0.5,0.2,0.9><b,0.3,0.4,0.7>\}\in\mathcal{A}$ which implies $f_{N_{tr}}^{-1}(M)$ is $N_{tr}\Lambda_P$-open. However, it is neither N_{tr} semi-open nor $N_{tr}\alpha$-open in U. Hence $f_{N_{tr}}$ is $N_{tr}\Lambda_P$-continuous but not N_{tr} semi-continuous and $N_{tr}\alpha$-continuous.

Example 4.11: Let $U=\{a,b\}, V=\{x,y\}, \tau_{N_{tr}}=\{0_{N_{tr}}, 1_{N_{tr}}, K\}$ and $\rho_{N_{tr}}=\{0_{N_{tr}}, 1_{N_{tr}}, M\}$ where $K=\{<a,0.7,0.6,0.8><b,0.6,0.8,0.9>\}$ and $M=\{<x,0.5,0.7,0.2><y,0.6,0.9,0.1>\}$. Consider the collections $\mathcal{A}=\{A: K^C\subset A\subset K\}, \mathcal{B}=\{B: K\subset B\subset 1_{N_{tr}}\}, \mathcal{C}=\{C: K^C\not\subset C; C\not\subset K^C; C\subset K\}$, $\mathcal{D}=\{D: K^C\not\subset D; D\not\subset K^C; D\not\subset K\}, \mathcal{E}=\{E: K^C\subset E\not\subset K\}$ and $\mathcal{F}=\{F: 0_{N_{tr}}\subset F\subset K^C\}$ of neutrosophic sets in U. Then, $N_{tr}\Lambda_P{}^* O(U,\tau_{N_{tr}})=\{0_{N_{tr}}, K, \mathcal{A}, \mathcal{B}, \mathcal{C}, \mathcal{D}, \mathcal{E}, \mathcal{F}, 1_{N_{tr}}\}$, and $N_{tr}\Lambda_P O(U,\tau_{N_{tr}})=\{0_{N_{tr}}, K, \mathcal{B}, \mathcal{F}, 1_{N_{tr}}\}$. Define $f_{N_{tr}}:(U,\tau_{N_{tr}})\longrightarrow(V,\rho_{N_{tr}})$ as $f_{N_{tr}}(a)=x$ and $f_{N_{tr}}(b)=y$. Then, $f_{N_{tr}}^{-1}(M)=\{<a,0.5,0.7,0.2><b,0.6,0.9,0.1>\}\in\mathcal{D}$ which implies $f_{N_{tr}}^{-1}(M)$ is $N_{tr}\Lambda_P{}^*$-open, but not $N_{tr}\Lambda_P$-open. Hence $f_{N_{tr}}$ is $N_{tr}\Lambda_P{}^*$-continuous, but not $N_{tr}\Lambda_P$-continuous.

Theorem 4.12: Let $f_{N_{tr}}:(U,\tau_{N_{tr}})\longrightarrow(V,\rho_{N_{tr}})$ be a function between two neutrosophic topological spaces. Then the following statements are equivalent:

i. $f_{N_{tr}}$ is $N_{tr}\Lambda_P$-continuous.
ii. The inverse image of every N_{tr}-closed set in $(V,\rho_{N_{tr}})$ is $N_{tr}\Lambda_P$-closed in $(U,\tau_{N_{tr}})$.
iii. $f_{N_{tr}}\left(N_{tr}\Lambda_P cl(K)\right)\subseteq N_{tr}cl\left(f_{N_{tr}}(K)\right)$ for every neutrosophic set K in U.
iv. $N_{tr}\Lambda_P cl\left(f_{N_{tr}}^{-1}(M)\right)\subseteq f_{N_{tr}}^{-1}\left(N_{tr}cl(M)\right)$ for every neutrosophic set M in V.

Proof:

(i)⟹(ii) Let $f_{N_{tr}}$ be a $N_{tr}\Lambda_P$-continuous function and M be a N_{tr} closed set in V. Then M^c is N_{tr} open in V. Since $f_{N_{tr}}$ is $N_{tr}\Lambda_P$-continuous, $f_{N_{tr}}^{-1}(M^C)$ is $N_{tr}\Lambda_P$-open in U which implies $(f_{N_{tr}}^{-1}(M))^C$ is $N_{tr}\Lambda_P$-open in U. Hence $f_{N_{tr}}^{-1}(M)$ is $N_{tr}\Lambda_P$-closed in U.

(ii)⟹(i) Let M be N_{tr} open in V. Then M^C is N_{tr} closed in V. By assumption, $f_{N_{tr}}^{-1}(M^C)$ is $N_{tr}\Lambda_P$-closed in U. That is, $(f_{N_{tr}}^{-1}(M))^C$ is $N_{tr}\Lambda_P$-closed in U. Hence $f_{N_{tr}}^{-1}(M)$ is $N_{tr}\Lambda_P$-open in U. Therefore, $f_{N_{tr}}$ is $N_{tr}\Lambda_P$-continuous.

(ii)⟹(iii) Let K be a neutrosophic set in U. Now, $K\subseteq f_{N_{tr}}^{-1}\left(f_{N_{tr}}(K)\right)$ implies $K\subseteq f_{N_{tr}}^{-1}(N_{tr}cl\left(f_{N_{tr}}(K)\right)$. Since $N_{tr}cl\left(f_{N_{tr}}(K)\right)$ is N_{tr} closed in V, by assumption $f_{N_{tr}}^{-1}\left(N_{tr}cl\left(f_{N_{tr}}(K)\right)\right)$ is a $N_{tr}\Lambda_P$-closed set containing K. Also,

$N_{tr}\Lambda_P cl(K)$ is the smallest $N_{tr}\Lambda_P$-closed set containing K. Hence, $N_{tr}\Lambda_P cl(K) \subseteq f_{N_{tr}}^{-1}(N_{tr}\, cl\left(f_{N_{tr}}(K)\right)$. Therefore, $f_{N_{tr}}\left(N_{tr}\Lambda_P cl(K)\right) \subseteq N_{tr}\, cl\left(f_{N_{tr}}(K)\right)$.

(iii)⟹(ii) Let M be a N_{tr} closed set in V. Then, by assumption $f_{N_{tr}}\left(N_{tr}\Lambda_P cl\left(f_{N_{tr}}^{-1}(M)\right)\right) \subseteq N_{tr}\, cl\left(f_{N_{tr}}\left(f_{N_{tr}}^{-1}(M)\right)\right) \subseteq N_{tr}\, cl(M) = M$ which implies $N_{tr}\Lambda_P cl\left(f_{N_{tr}}^{-1}(M)\right) \subseteq f_{N_{tr}}^{-1}(M)$. Also, $f_{N_{tr}}^{-1}(M) \subseteq N_{tr}\Lambda_P cl\left(f_{N_{tr}}^{-1}(M)\right)$. Hence $f_{N_{tr}}^{-1}(M)$ is $N_{tr}\Lambda_P$-closed in U.

(iii)⟹(iv) Let M be a neutrosophic set in V and let $K = f_{N_{tr}}^{-1}(M)$. By assumption, $f_{N_{tr}}\left(N_{tr}\Lambda_P cl(K)\right) \subseteq N_{tr}\, cl\left(f_{N_{tr}}(K)\right) = N_{tr}\, cl(M)$.This implies $N_{tr}\Lambda_P cl\left(f_{N_{tr}}^{-1}(M)\right) \subseteq f_{N_{tr}}^{-1}\left(N_{tr}\, cl(M)\right)$.

(iv)⟹(iii) Let $M = f_{N_{tr}}(K)$. Then, by assumption, $N_{tr}\Lambda_P cl(K) = N_{tr}\Lambda_P cl\left(f_{N_{tr}}^{-1}(M)\right) \subseteq f_{N_{tr}}^{-1}\left(N_{tr}\, cl(M)\right) \subseteq f_{N_{tr}}^{-1}\left(N_{tr}\, cl\left(f_{N_{tr}}(K)\right)\right)$.This implies $f_{N_{tr}}\left(N_{tr}\Lambda_P cl(K)\right) \subseteq N_{tr}\, cl\left(f_{N_{tr}}(K)\right)$

(iv)⟹(i) Let M be N_{tr} open in V. Then M^C is N_{tr} closed in V. By assumption, $f_{N_{tr}}^{-1}(M^C) = f_{N_{tr}}^{-1}\left(N_{tr}\, cl(M^c)\right) \supseteq N_{tr}\Lambda_P cl\left(f_{N_{tr}}^{-1}(M^C)\right)$.Also,we know that $f_{N_{tr}}^{-1}(M^c) \subseteq N_{tr}\Lambda_P cl\left(f_{N_{tr}}^{-1}(M^C)\right)$ Hence $f_{N_{tr}}^{-1}(M^C) = N_{tr}\Lambda_P cl\left(f_{N_{tr}}^{-1}(M^C)\right)$. Therefore, $f_{N_{tr}}^{-1}(M^C)$ is $N_{tr}\Lambda_P$-closed in U. That is, $\left(f_{N_{tr}}^{-1}(M)\right)^C$ is $N_{tr}\Lambda_P$-closed in U. Hence $f_{N_{tr}}^{-1}(M)$ is $N_{tr}\Lambda_P$-open in U. Thererfore $f_{N_{tr}}$ is $N_{tr}\Lambda_P$-continuous.

Theorem 4.13: A function $f_{N_{tr}}: (U, \tau_{N_{tr}}) \longrightarrow (V, \rho_{N_{tr}})$is $N_{tr}\Lambda_P$-continuous if and only if $f_{N_{tr}}^{-1}\left(N_{tr}\, int(M)\right) \subseteq N_{tr}\Lambda_P int\left(f_{N_{tr}}^{-1}(M)\right)$ for every neutrosophic set M in V.

Proof: Let $f_{N_{tr}}$ be a $N_{tr}\Lambda_P$-continuous function and M be a neutrosophic set in V. Then $N_{tr}\, int(M)$ is N_{tr} open in V. By assumption, $f_{N_{tr}}^{-1}\left(N_{tr}\, int(M)\right)$ is $N_{tr}\Lambda_P$-open in U. Now, $f_{N_{tr}}^{-1}\left(N_{tr}\, int(M)\right) \subseteq f_{N_{tr}}^{-1}(M)$ and $N_{tr}\Lambda_P int\left(f_{N_{tr}}^{-1}(M)\right)$ is the largest $N_{tr}\Lambda_P$-open set contained in $f_{N_{tr}}^{-1}(M)$. Hence $f_{N_{tr}}^{-1}\left(N_{tr}\, int(M)\right) \subseteq N_{tr}\Lambda_P int\left(f_{N_{tr}}^{-1}(M)\right)$. Conversely, let M be a N_{tr} open set in V. Then $f_{N_{tr}}^{-1}(M) = f_{N_{tr}}^{-1}\left(N_{tr}\, int(M)\right) \subseteq N_{tr}\Lambda_P int\left(f_{N_{tr}}^{-1}(M)\right)$. Also, $N_{tr}\Lambda_P int\left(f_{N_{tr}}^{-1}(M)\right) \subseteq f_{N_{tr}}^{-1}(M)$. This implies $f_{N_{tr}}^{-1}(M)$ is $N_{tr}\Lambda_P$-open in U. Hence $f_{N_{tr}}$ is $N_{tr}\Lambda_P$-continuous.

Theorem 4.14: Let $f_{N_{tr}}: (U, \tau_{N_{tr}}) \longrightarrow (V, \rho_{N_{tr}})$ be a function between two neutrosophic topological spaces. Then the following statements are equivalent:

i. $f_{N_{tr}}$ is $N_{tr}\Lambda_P$-continuous.
ii. For each neutrosophic point $u_{a,b,c}$, the inverse image of every N_{tr} nbhd of $f_{N_{tr}}(u_{a,b,c})$ is $N_{tr}\Lambda_P$-nbhd of $u_{a,b,c}$.
iii. For each neutrosophic point $u_{a,b,c}$ in U and every N_{tr} nbhd N of $f_{N_{tr}}\left(u_{a,b,c}\right)$, there exists a $N_{tr}\Lambda_P$-open set K in U such that $u_{a,b,c} \in K$ and $f_{N_{tr}}(K) \subseteq N$.

Proof:

(i)⟹(ii) Let $u_{a,b,c}$ be a neutrosophic point in U and let N be a N_{tr} nbhd of $f_{N_{tr}}(u_{a,b,c})$. Then there exists a N_{tr} open set M in V such that $f_{N_{tr}}\left(u_{a,b,c}\right) \in M \subseteq N$. Since $f_{N_{tr}}$ is $N_{tr}\Lambda_P$-continuous, $f_{N_{tr}}^{-1}(M)$ is $N_{tr}\Lambda_P$-open in U. Also, $u_{a,b,c} \in f_{N_{tr}}^{-1}\left(f_{N_{tr}}\left(u_{a,b,c}\right)\right) \in f_{N_{tr}}^{-1}(M) \subseteq f_{N_{tr}}^{-1}(N)$. Hence there exists a $N_{tr}\Lambda_P$-open set $f_{N_{tr}}^{-1}(M)$ such that $u_{a,b,c} \in f_{N_{tr}}^{-1}(M) \subseteq f_{N_{tr}}^{-1}(N)$. This implies $f_{N_{tr}}^{-1}(N)$ is $N_{tr}\Lambda_P$-nbhd of $u_{a,b,c}$.

(ii)⟹(iii) Let $u_{a,b,c}$ be a neutrosophic point in U and let N be a N_{tr} nbhd of $f_{N_{tr}}(u_{a,b,c})$. Then by assumption, $f_{N_{tr}}^{-1}(N)$ is $N_{tr}\Lambda_P$-nbhd of $u_{a,b,c}$. Then there exists a $N_{tr}\Lambda_P$-open set K in U such that $u_{a,b,c} \in K \subseteq f_{N_{tr}}^{-1}(N)$. Thus $u_{a,b,c} \in K$ and $f_{N_{tr}}(K) \subseteq f_{N_{tr}}\left(f_{N_{tr}}^{-1}(N)\right) \subseteq N$.

(iii)⟹(i) Let M be a N_{tr} open set in V and let $u_{a,b,c} \in f_{N_{tr}}^{-1}(M)$. Since M is N_{tr} open and $f_{N_{tr}}\left(u_{a,b,c}\right) \in M, M$ is a N_{tr} nbhd of $f_{N_{tr}}\left(u_{a,b,c}\right)$. Hence it follows (iii) that there exists a $N_{tr}\Lambda_P$-open set K in U such that $u_{a,b,c} \in K$ and $f_{N_{tr}}(K) \subseteq M$. This implies $u_{a,b,c} \in K \subseteq f_{N_{tr}}^{-1}\left(f_{N_{tr}}(K)\right) \subseteq f_{N_{tr}}^{-1}(M)$. By theorem 2.16,$f_{N_{tr}}^{-1}(M)$ is $N_{tr}\Lambda_P$-open in U. Therefore $f_{N_{tr}}$ is$N_{tr}\Lambda_P$ -continuous.

Definition 4.15: A neutrosophic topological space $(U, \tau_{N_{tr}})$ is said to be $\boldsymbol{N_{tr}T_{\Lambda_P}}$**-space** if every $N_{tr}\Lambda_P$-open set in $(U, \tau_{N_{tr}})$ is N_{tr} open.

Remark 4.16: The composition of two $N_{tr}\Lambda_P$-continuous functions need not be $N_{tr}\Lambda_P$-continuous.

Example 4.17: Let $U = \{a, b\}, V = \{x, y\}$and $W = \{p, q\}$. Consider the neutrosophic topologies $\tau_{N_{tr}} = \{0_{N_{tr}}, K, 1_{N_{tr}}\}$, $\rho_{N_{tr}} = \{0_{N_{tr}}, M, 1_{N_{tr}}\}$ and$\omega_{N_{tr}} = \{0_{N_{tr}}, N, 1_{N_{tr}}\}$ where$K = \{< a, 0.7,0.5,0.1 >< b, 0.8,0.6,0.2 >\}, M = \{< x, 0.2,0.4,0.8 >< y, 0.1,0.5,0.9 >\}$ and $N = \{< p, 0.2,0.2,0.2 >< q, 0.1,0.30.4 >\}$.Consider the collections $\mathcal{A} = \{A : 0_{N_{tr}} \subset A \subset K\}, \mathcal{B} = \{B : K \subset B \subset K^C\}, \mathcal{C} = \{C : R \not\subset K; K \not\subset C; C \subset K^C\}$ of neutrosophic sets in U and $\mathcal{D} = \{D : M \subset D \subset 1_{N_{tr}}\}$, the collection of neutrosophic sets in V. Then, $N_{tr}\Lambda_P O(U, \tau_{N_{tr}}) = \{0_{N_{tr}}, K, K^C, \mathcal{A}, \mathcal{B}, \mathcal{C}, 1_{N_{tr}}\}$ and $N_{tr}\Lambda_P O(V, \rho_{N_{tr}}) = \{0_{N_{tr}}, M, \mathcal{D}, 1_{N_{tr}}\}$. Define $f_{N_{tr}} : (U, \tau_{N_{tr}}) \to (V, \rho_{N_{tr}})$ as $f_{N_{tr}}(a) = x$and $f_{N_{tr}}(b) = y$. Then $f_{N_{tr}}^{-1}(M) = \{< a, 0.2,0.4,0.8 >< b, 0.1,0.5,0.9 >\}$ is $N_{tr}\Lambda_P$open in $(U, \tau_{N_{tr}})$. Also, define $g_{N_{tr}} : (V, \rho_{N_{tr}}) \to (W, \omega_{N_{tr}})$ as $g_{N_{tr}}(x) = q$ and$g_{N_{tr}}(y) = p$. Then $g_{N_{tr}}^{-1}(N) = \{< x, 0.1,0.3,0.4 >< y, 0.2,0.2,0.2 >\} \in \mathcal{D}$ which implies $g_{N_{tr}}^{-1}(N)$ is $N_{tr}\Lambda_P$-open in $(V, \rho_{N_{tr}})$. This implies that both $f_{N_{tr}}$ and $g_{N_{tr}}$ are $N_{tr}\Lambda_P$-continuous. Now, let $g_{N_{tr}} \circ f_{N_{tr}} : (U, \tau_{N_{tr}}) \to (W, \omega_{N_{tr}})$ be the composition of two $N_{tr}\Lambda_P$-continuous functions. Then, $g_{N_{tr}} \circ f_{N_{tr}}$ is not $N_{tr}\Lambda_P$-continuous since $(g_{N_{tr}} \circ f_{N_{tr}})^{-1}(N) = f_{N_{tr}}^{-1}(g_{N_{tr}}^{-1}(N)) = \{< a, 0.1,0.3,0.4 >< b, 0.2,0.2,0.2 >\}$ is not $N_{tr}\Lambda_P$-open in $(U, \tau_{N_{tr}})$.

Theorem 4.18: Let $(U, \tau_{N_{tr}}), (V, \rho_{N_{tr}})$ and$(W, \omega_{N_{tr}})$ be neutrosophic topological space and let $(V, \rho_{N_{tr}})$ be $N_{tr}T_{\Lambda_P}$-space. Then the composition $g_{N_{tr}} \circ f_{N_{tr}} : (U, \tau_{N_{tr}}) \to (W, \omega_{N_{tr}})$ of two$N_{tr}\Lambda_P$-continuous functions $f_{N_{tr}} : (U, \tau_{N_{tr}}) \to (V, \rho_{N_{tr}})$ and $g_{N_{tr}} : (V, \rho_{N_{tr}}) \to (W, \omega_{N_{tr}})$ is $N_{tr}\Lambda_P$-continuous.

Proof: Let N be any N_{tr}open set in W. Since $g_{N_{tr}}$ is $N_{tr}\Lambda_P$-continuous, $g_{N_{tr}}^{-1}(N)$ is $N_{tr}\Lambda_P$-open in V. Then, by assumption $g_{N_{tr}}^{-1}(N)$ is N_{tr}open in V. Also, since $f_{N_{tr}}$ is $N_{tr}\Lambda_P$-continuous, $f_{N_{tr}}^{-1}(g_{N_{tr}}^{-1}(N)) = (g_{N_{tr}} \circ f_{N_{tr}})^{-1}(N)$ is $N_{tr}\Lambda_P$-open in U. Hence $g_{N_{tr}} \circ f_{N_{tr}}$ is $N_{tr}\Lambda_P$-continuous.

Theorem 4.19: Let $f_{N_{tr}} : (U, \tau_{N_{tr}}) \to (V, \rho_{N_{tr}})$ be a $N_{tr}\Lambda_P$-continuous function and $g_{N_{tr}} : (V, \rho_{N_{tr}}) \to (W, \omega_{N_{tr}})$ be a N_{tr}continuous function. Then their composition $g_{N_{tr}} \circ f_{N_{tr}} : (U, \tau_{N_{tr}}) \to (W, \omega_{N_{tr}})$is $N_{tr}\Lambda_P$-continuous.

Proof: Let N be any N_{tr}open set in W. Since $g_{N_{tr}}$ is N_{tr}continuous, $g_{N_{tr}}^{-1}(N)$ is N_{tr}open in V.Also, since $g_{N_{tr}}$ is $N_{tr}\Lambda_P$-continuous, $f_{N_{tr}}^{-1}(g_{N_{tr}}^{-1}(N)) = (g_{N_{tr}} \circ f_{N_{tr}})^{-1}(N)$ is $N_{tr}\Lambda_P$-open in U. Hence $g_{N_{tr}} \circ f_{N_{tr}}$is $N_{tr}\Lambda_P$-continuous.

Theorem 4.20: Let $f_{N_{tr}} : (U, \tau_{N_{tr}}) \to (V, \rho_{N_{tr}})$ be a $N_{tr}\Lambda_P$-continuous function where $(U, \tau_{N_{tr}})$ is a $N_{tr}T_{\Lambda_P}$-space. If C is a subset of U, then the restriction $f_{N_{tr}}|_C : (C, \tau_{N_{tr}}^C) \to (V, \rho_{N_{tr}})$ is also $N_{tr}\Lambda_P$-continuous.

Proof: Let M be a N_{tr}open set in V. Since $f_{N_{tr}}$ is $N_{tr}\Lambda_P$-continuous, $f_{N_{tr}}^{-1}(M)$ is $N_{tr}\Lambda_P$-open in U. Now, since U is a $N_{tr}T_{\Lambda_P}$ −space, $f_{N_{tr}}^{-1}(M)$ is N_{tr}open in U. Hence ${f_{N_{tr}}|_C}^{-1}(M) = f_{N_{tr}}^{-1}(M) \cap 1_{N_{tr}}^C$ is N_{tr}open in C. By theorem 2.14, ${f_{N_{tr}}|_C}^{-1}(M)$ is $N_{tr}\Lambda_P$-open in C. Hence $f_{N_{tr}}|_C$ is $N_{tr}\Lambda_P$-continuous.

NEUTROSOPHIC $\boldsymbol{\Lambda_P}$-IRRESOLUTE FUNCTIONS

Definition 5.1: Let $(U, \tau_{N_{tr}})$ and $(V, \rho_{N_{tr}})$ be neutrosophic topological spaces. Then the function $f_{N_{tr}} : (U, \tau_{N_{tr}}) \to (V, \rho_{N_{tr}})$ is said to be **neutrosophic$\boldsymbol{\Lambda_P}$-irresolute** if $f_{N_{tr}}^{-1}(M)$ is $N_{tr}\Lambda_P$-open in $(U, \tau_{N_{tr}})$ for every $N_{tr}\Lambda_P$-open set M in $(V, \rho_{N_{tr}})$.

Example 5.2: Let $U = \{a, b\}, V = \{x, y\}, \tau_{N_{tr}} = \{0_{N_{tr}}, 1_{N_{tr}}, K,\}$ and $\rho_{N_{tr}} = \{0_{N_{tr}}, 1_{N_{tr}}, M\}$ where$K = \{< a, 0.6,0.3,0.5 >< b, 0.5,0.8,0.4 >\}$ and $M = \{< x, 0.5,0.2,0.7 >< y, 0.2,0.7,0.9 >\}$. Also, consider the collections $\mathcal{A} = \{A : K \subset A; K^C \subset A\}$ and $\mathcal{B} = \{B : M \subset B; M^C \subset B\}$of neutrosophic sets in U and V respectively. Then, $N_{tr}\Lambda_P O(U, \tau_{N_{tr}}) = \{0_{N_{tr}}, K, \mathcal{A}, 1_{N_{tr}}\}$ and $N_{tr}\Lambda_P O(V, \rho_{N_{tr}}) = \{< 0_{N_{tr}}, M, \mathcal{B}, 1_{N_{tr}}\}$. Now, let us define $f_{N_{tr}} : (U, \tau_{N_{tr}}) \to (V, \rho_{N_{tr}})$ as $f_{N_{tr}}(a) = x$and $f_{N_{tr}}(b) = y$. Then,$f_{N_{tr}}^{-1}(M) = \{< a, 0.5,0.2,0.7 >< b, 02,0.7,0.9 >\} \in \mathcal{A}$ and for each $B \in \mathcal{B}$, there exists some $A \in \mathcal{A}$ such that $f_{N_{tr}}^{-1}(B) = A$. Hence the inverse image of every $N_{tr}\Lambda_P$-open set in V is $N_{tr}\Lambda_P$-open in U. Therefore $f_{N_{tr}}$ is $N_{tr}\Lambda_P$-irresolute.

Theorem 5.3: Every $N_{tr}\Lambda_P$-irresolute function is $N_{tr}\Lambda_P$-continuous.
Proof: Let $f_{N_{tr}}:(U,\tau_{N_{tr}}) \longrightarrow (V,\rho_{N_{tr}})$ be a $N_{tr}\Lambda_P$-irresolute function and M be a N_{tr} open set in V. Then, by theorem 2.14, M is $N_{tr}\Lambda_P$-open in V. Since $f_{N_{tr}}$ is $N_{tr}\Lambda_P$-irreolsute, $f_{N_{tr}}^{-1}(M)$ is $N_{tr}\Lambda_P$-open in U. Hence $f_{N_{tr}}$ is $N_{tr}\Lambda_P$-continuous.

Remark 5.4: The above theorem's converse need not hold.
Example 5.5: Let $U=\{a,b\}, V=\{x,y\}, \tau_{N_{tr}}=\{0_{N_{tr}},1_{N_{tr}},K\}$ and $\rho_{N_{tr}}=\{0_{N_{tr}},1_{N_{tr}},M\}$ where$K=\{<a,0,0.2,0.6><b,0.2,0.1,0.7>\}$ and $M=\{<x,0.8,0.8,0.2><y,0.9,0.9,0.4>\}$ Consider the collections $\mathcal{A}=\{A: 0_{N_{tr}}\subset A\subset K\}$ and $\mathcal{B}=\{B: K\not\subset B; B\not\subset K; B\subset K^c\}$ of neutrosophic sets in U. Then, $N_{tr}\Lambda_P O(U,\tau_{N_{tr}})=\{0_{N_{tr}},K,K^c,\mathcal{A},\mathcal{B},\mathcal{C},1_{N_{tr}}\}$.Now, let us define $f_{N_{tr}}:(U,\tau_{N_{tr}}) \longrightarrow (V,\rho_{N_{tr}})$ as $f_{N_{tr}}(a)=x$and $f_{N_{tr}}(b)=y$. Then,$f_{N_{tr}}^{-1}(M)=\{<a,0.8,0.8,0.2><b,0.9,0.9,0.4>\}=K^c$ which implies $f_{N_{tr}}$ is $N_{tr}\Lambda_P$-continuous. However, the inverse image of a $N_{tr}\Lambda_P$-open set $D=\{<x,0.9,0.8,0.2><y,1,0.9,0.3>\}$ in V is not $N_{tr}\Lambda_P$-open in U. Hence $f_{N_{tr}}$ is $N_{tr}\Lambda_P$-continuous but not $N_{tr}\Lambda_P$-irresolute.

Theorem 5.6: Let $f_{N_{tr}}:(U,\tau_{N_{tr}}) \longrightarrow (V,\rho_{N_{tr}})$ be a$N_{tr}\Lambda_P$-continuous function where $(V,\rho_{N_{tr}})$ is a $N_{tr}T_{\Lambda_P}$-space. Then $f_{N_{tr}}$ is $N_{tr}\Lambda_P$-irresolute.
Proof: Let M be $N_{tr}\Lambda_P$-open in V. Then, by assumption M is N_{tr} open in V. Since $f_{N_{tr}}$ is $N_{tr}\Lambda_P$-continuous, $f_{N_{tr}}^{-1}(M)$ is $N_{tr}\Lambda_P$-open in U. Hence $f_{N_{tr}}$ is $N_{tr}\Lambda_P$-irresolute.

Theorem 5.7: If $f_{N_{tr}}:(U,\tau_{N_{tr}}) \longrightarrow (V,\rho_{N_{tr}})$ and $g_{N_{tr}}:(V,\rho_{N_{tr}}) \longrightarrow (W,\omega_{N_{tr}})$ are $N_{tr}\Lambda_P$-irresolute functions, then their composition $g_{N_{tr}}\circ f_{N_{tr}}:(U,\tau_{N_{tr}}) \longrightarrow (W,\omega_{N_{tr}})$ is also $N_{tr}\Lambda_P$-irresolute.
Proof: Let N be $N_{tr}\Lambda_P$-open in W. Since $g_{N_{tr}}$ is $N_{tr}\Lambda_P$-irresolute, $g_{N_{tr}}^{-1}(N)$ is $N_{tr}\Lambda_P$-open in V. Again, since $f_{N_{tr}}$ is $N_{tr}\Lambda_P$-irresolute, $f_{N_{tr}}^{-1}\left(g_{N_{tr}}^{-1}(N)\right)=\left(g_{N_{tr}}\circ f_{N_{tr}}\right)^{-1}(N)$ is $N_{tr}\Lambda_P$-open in U. Hence$g_{N_{tr}}\circ f_{N_{tr}}$ is $N_{tr}\Lambda_P$-irresolute.

Theorem 5.8: If $f_{N_{tr}}:(U,\tau_{N_{tr}}) \longrightarrow (V,\rho_{N_{tr}})$ is $N_{tr}\Lambda_P$-irresolute and $g_{N_{tr}}:(V,\rho_{N_{tr}}) \longrightarrow (W,\omega_{N_{tr}})$ is $N_{tr}\Lambda_P$-continuous, then $g_{N_{tr}}\circ f_{N_{tr}}:(U,\tau_{N_{tr}}) \longrightarrow (W,\omega_{N_{tr}})$ is $N_{tr}\Lambda_P$-continuous.
Proof: Let N be N_{tr}-open in W. Since $g_{N_{tr}}$ is $N_{tr}\Lambda_P$-continuous, $g_{N_{tr}}^{-1}(N)$ is $N_{tr}\Lambda_P$-open in V. Also, since $f_{N_{tr}}$ is $N_{tr}\Lambda_P$-irresolute, $f_{N_{tr}}^{-1}\left(g_{N_{tr}}^{-1}(N)\right)=\left(g_{N_{tr}}\circ f_{N_{tr}}\right)^{-1}(N)$ is $N_{tr}\Lambda_P$-open in U. Hence $g_{N_{tr}}\circ f_{N_{tr}}$ is $N_{tr}\Lambda_P$-continuous.

Theorem 5.9: Let $f_{N_{tr}}:(U,\tau_{N_{tr}}) \longrightarrow (V,\rho_{N_{tr}})$ be a function between two neutrosophic topological spaces. Then the following statements are equivalent:

i. $f_{N_{tr}}$ is $N_{tr}\Lambda_P$-irresolute.
ii. The inverse image of every $N_{tr}\Lambda_P$-closed set in $(V,\rho_{N_{tr}})$ is $N_{tr}\Lambda_P$-closed in $\left(U,\tau_{N_{tr}}\right)$.
iii. $f_{N_{tr}}\left(N_{tr}\Lambda_P cl(K)\right)\subseteq N_{tr}\Lambda_P cl\left(f_{N_{tr}}(K)\right)$ for every neutrosophic set K in U.
iv. $N_{tr}\Lambda_P cl\left(f_{N_{tr}}^{-1}(M)\right)\subseteq f_{N_{tr}}^{-1}\left(N_{tr}\Lambda_P cl(M)\right)$ for every neutrosophic set M in V.
v. $f_{N_{tr}}^{-1}\left(N_{tr}\Lambda_P int(M)\right)\subseteq N_{tr}\Lambda_P int\left(f_{N_{tr}}^{-1}(M)\right)$ for every neutrosophic set M in V.

Proof:
(i)⟹(ii) Let $f_{N_{tr}}$ be a $N_{tr}\Lambda_P$-irresolute function and M be a $N_{tr}\Lambda_P$-closed set in V. Then M^c is $N_{tr}\Lambda_P$-open in V. Since $f_{N_{tr}}$ is $N_{tr}\Lambda_P$-irresolute, $f_{N_{tr}}^{-1}(M^c)$ is $N_{tr}\Lambda_P$-open in U. That is, $(f_{N_{tr}}^{-1}(M))^c$ is $N_{tr}\Lambda_P$-open in U. Hence $f_{N_{tr}}^{-1}(M)$ is $N_{tr}\Lambda_P$-closed in U.
(ii)⟹(i) Let M be $N_{tr}\Lambda_P$-open in V. Then M^c is $N_{tr}\Lambda_P$-closed in V. By assumption, $f_{N_{tr}}^{-1}(M^c)$ is $N_{tr}\Lambda_P$-closed in U. That is, $(f_{N_{tr}}^{-1}(M))^c$is $N_{tr}\Lambda_P$-closed in U. Hence $f_{N_{tr}}^{-1}(M)$ is $N_{tr}\Lambda_P$-open in U. Therefore, $f_{N_{tr}}$ is $N_{tr}\Lambda_P$-irresolute.
(ii)⟹(iii) Let$K$be a neutrosophic set in U.Now, $K\subseteq f_{N_{tr}}^{-1}\left(f_{N_{tr}}(K)\right)$ which implies $K\subseteq f_{N_{tr}}^{-1}\left(N_{tr}\Lambda_P cl\left(f_{N_{tr}}(K)\right)\right)$. Since $N_{tr}\Lambda_P cl\left(f_{N_{tr}}(K)\right)$ is $N_{tr}\Lambda_P$-closed in V, by assumption $f_{N_{tr}}^{-1}\left(N_{tr}\Lambda_P cl\left(f_{N_{tr}}(K)\right)\right)$ is a $N_{tr}\Lambda_P$- closed set containing K.

Also, $N_{tr}\Lambda_P cl(K)$ is the smallest $N_{tr}\Lambda_P$-closed set containing K. Hence, $N_{tr}\Lambda_P cl(K) \subseteq f_{N_{tr}}^{-1}\left(N_{tr}\Lambda_P cl\left(f_{N_{tr}}(K)\right)\right)$. Therefore, $f_{N_{tr}}\left(N_{tr}\Lambda_P cl(K)\right) \subseteq N_{tr}\Lambda_P cl\left(f_{N_{tr}}(K)\right)$.

(iii)⟹(ii) Let M be a $N_{tr}\Lambda_P$-closed set in V. Then, by assumption $f_{N_{tr}}\left(N_{tr}\Lambda_P cl\left(f_{N_{tr}}^{-1}(M)\right)\right) \subseteq N_{tr}\Lambda_P cl\left(f_{N_{tr}}\left(f_{N_{tr}}^{-1}(M)\right)\right) \subseteq N_{tr}\Lambda_P cl(M) = M$implies $N_{tr}\Lambda_P cl\left(f_{N_{tr}}^{-1}(M)\right) \subseteq f_{N_{tr}}^{-1}(M)$. Also, $f_{N_{tr}}^{-1}(M) \subseteq N_{tr}\Lambda_P cl\left(f_{N_{tr}}^{-1}(M)\right)$. Hence $f_{N_{tr}}^{-1}(M)$ is $N_{tr}\Lambda_P$-closed in U.

(iii)⟹(iv) Let M be a neutrosophic set in V and let $K = f_{N_{tr}}^{-1}(M)$. By assumption, $f_{N_{tr}}\left(N_{tr}\Lambda_P cl(K)\right) \subseteq N_{tr}\Lambda_P cl\left(f_{N_{tr}}(K)\right) = N_{tr}\Lambda_P cl(M)$.This implies $N_{tr}\Lambda_P cl\left(f_{N_{tr}}^{-1}(M)\right) \subseteq f_{N_{tr}}^{-1}\left(N_{tr}\Lambda_P cl(M)\right)$.

(iv)⟹(iii) Let $M = f_{N_{tr}}(K)$. Then, by assumption, $N_{tr}\Lambda_P cl(K) = N_{tr}\Lambda_P cl\left(f_{N_{tr}}^{-1}(M)\right) \subseteq f_{N_{tr}}^{-1}\left(N_{tr}\Lambda_P cl(M)\right) = f_{N_{tr}}^{-1}\left(N_{tr}\Lambda_P cl\left(f_{N_{tr}}(K)\right)\right)$.This implies$f_{N_{tr}}\left(N_{tr}\Lambda_P cl(K)\right) \subseteq N_{tr}\Lambda_P cl\left(f_{N_{tr}}(K)\right)$.

(iv)⟺(v) This can be proved by taking complements.

(v)⟹(i) Let M be a $N_{tr}\Lambda_P$-open set in V. Then $f_{N_{tr}}^{-1}(M) = f_{N_{tr}}^{-1}\left(N_{tr}\Lambda_P int(M)\right) \subseteq N_{tr}\Lambda_P int\left(f_{N_{tr}}^{-1}(M)\right)$.Also, $N_{tr}\Lambda_P int\left(f_{N_{tr}}^{-1}(M)\right) \subseteq f_{N_{tr}}^{-1}(M)$. This implies $f_{N_{tr}}^{-1}(M)$ is $N_{tr}\Lambda_P$-open in U. Hence $f_{N_{tr}}$ is $N_{tr}\Lambda_P$-irresolute.

REFERENCES

1. Acikgoz A, Esenbel F.A, *A Look on Separation Axioms in Neutrosophic Topological Spaces,* AIP Conference Proceedings 2334, 020002, 2021.
2. Arockiarani I, Dhavaswwlan R, Jafari S, Parimala M, *On Some New Notions and Functions in Neutrosophic Topological Spaces,* Neutrosophic Sets and Systems, Vol 16, 16-19, 2017.
3. Atanassov K, *Intuitionistic Fuzzy Sets,* VII ITKR's Session, Sofia, 1983.
4. BhimrajBasumatary, Nijwm Wary, Jeevan Krishna Khaklary, Usha Rani Basumatary, *On Some Properties of Neutrosophic Semi Continuous and Almost Continuous Mapping,* Computer Modeling in Engineering and Sciences.
5. Dhavaseelan R, Jafari S, *Generalized Neutrosophic Closed Sets,* New Trends in Neutrosophic Theory and Applications, Vol II, 16-19, 2017.
6. Dhavaseelan R, Jafari S, Ozel C, Al-Shumrani M.A, *Generalized Neutrosophic Contra-Continuity,* New Trends in Neutrosophic Theory and Applications Vol II, 2017.
7. Iswarya P, Bageerathi K, *Some Neutrosohic Functions Associated with Neutrosophic Semi-Open Sets,* International Journal of Innovative Research in Science, Engineering and Technology, Vol 10(10), 13939-13946, 2021.
8. Karatas S, Kuru C, *Neutrosophic Topology,* Neutrosophic Sets and Systems, Vol 13, 90-95, 2016.
9. Maheswari C, Chandrasekar S, *Neutrosophicgb-closed sets and Neutrosophicgb-Continuity,* Neutrosophic Sets and Systems, Vol 46, 402-415, 2019.
10. Ray G.C, Sudeep Dev, *Neutrosophic point and its neighbourhood structure,* Neutrosophic Sets and Systems, Vol 43, 156-168, 2021.
11. Ray G.C, Sudeep Dev, *Relation of Quasi-coincidence for Neutrosophic Sets,* Neutrosophic Sets and Systems, Vol 46, 402-415, 2021.
12. Reena C, Karthika M, *On NeutrosophicΛ_P-Open Sets in Neutrosophic Topological Spaces,* Indian Journal of Pure and Applied Mathematics (Communicated).
13. Reena C, Yaamini K.S, *A New Notion of Neighbourhood and Continuity in Neutrosophic Topological Spaces,* Neutrosophic Sets and Systems, Vol 60, 74-87, 2023.
14. Renu Thomas, Anila S, *On NeutrosophicSemicontinuity in a Neutrosophic Topological Spae,* Journal of Emerging Technology and Innovative Research, Vol 6(6), 87-93, 2019.
15. Salama A.A, Alblowi S.A, *Neutrosophic Set and Neutrosophic Topological Spaces* IOSR Journal of Mathematics, Vol 3(4), 2012.

16. Salama A.A, Smarandache F, Kromov V, *Neutrosophic Closed Set and Neutrosophic Continuous Functions,* Neutrosophic Sets and Systems, Vol 4, 4-8, 2014.
17. Smarandache F, *A Unifying Field in Logics: Neutrosophic Logic, Set, Probability,* American Research Press, Rehaboth 1999.
18. Smarandache F, *Neutrosophy and Neutrosophic Logic, Set, Probability and Statistics,* First International Conference on Neutrosophy, University of Mexico, Gallup, NM 87301, USA, 2002.
19. Vijayalakshmi R, Praveen R, *Neutrosophic Regular Semi Continuous Functions,* Annals of Communications in Mathematics,Vol 4(3), 254-260, 2021, ISSN: 2582-0818.
20. Zadeh L.A, *Fuzzy Set,* Information and Control, Vol 8, 338-353, 1965.

Indian Journal of Natural Sciences *www.tnsroindia.org.in ©IJONS*

Vol.15 / Issue 83 / Apr / 2024 *International Bimonthly (Print) – Open Access* *ISSN: 0976 – 0997*

RESEARCH ARTICLE

A New Perspective of Connectedness and Hyperconnectedness in Soft Nano Topological Spaces

P.Anbarasi Rodrigo[1] and P.Subithra[2*]

[1]Assistant Professor, Department of Mathematics, St.Mary's College(Autonomous),(Affiliated to Manonmaniam Sundaranar University, Abishekapatti, Tirunelveli)Thoothukudi, Tamil Nadu, India.
[2]Research Scholar, Reg.No. 21212212092003, Department of Mathematics, St.Mary's College (Autonomous),(Affiliated to Manonmaniam Sundaranar University, Abishekapatti, Tirunelveli) Thoothukudi, Tamil Nadu, India.

Received: 22 Feb 2024 Revised: 06 Mar 2024 Accepted: 20 Mar 2024

***Address for Correspondence**
P.Subithra
Research Scholar,
Reg. No. 21212212092003
Department of Mathematics,
St.Mary's College(Autonomous),
(Affiliated to Manonmaniam Sundaranar University, Abishekapatti, Tirunelveli)
Thoothukudi, Tamil Nadu, India.
Email: p.subithra18@gmail.com

ABSTRACT

The article's primary focus is to introduce soft nano α^*-generalized separated sets and soft nano α^*-generalized connected spaces and delve into their characteristics and properties, elucidating their intricate relationship through apt examples. Further, it discuss about the equivalent conditions, union and preservation theorem. Following this examination, the article proceeds to investigate soft nano α^*-generalized hyperconnected spaces, particularly through the lens of soft nano α^*-generalized dense sets and explores their correlation with soft nano α^*-generalized connected spaces. Additionally, it presents equivalent conditions, preservation theorems and counterexamples to reverse implications offering a deeper understanding of the complexities involved.

Keywords: soft nano α^*-generalized separated sets, soft nano α^*-generalized connectedness, soft nano α^*-generalized dense sets, soft nano α^*-generalized nowhere dense sets, soft nano α^*-generalized hyper connectedness.

MSC Code: Primary 54D05, 54D99, Secondary 54A05

INTRODUCTION

Molodtsov [10] introduced the soft set theory in 1999 as a mathematical tool to address problems involving imprecise, indeterminacy and inconsistent data, to alleviate challenges in conventional theoretical approaches and proposed the fundamental results of soft set theory. Subsequently, in 2011, Muhammad Shabir and Munazza Naz [11] pioneered the concept of soft topological spaces defining them over an initial universe with a fixed set of parameters. Meanwhile in 2012, the notion of nano topology was unveiled by Lellis Thivagar and Carmel Richard [7], which is an extension of set theory to study the intelligent systems characterized by insufficient and incomplete information and it is defined in terms of approximations and boundary region of a subset of a universe using an equivalence relation on it. By taking inspirations from the above, in 2017, Benchalli et al. [5] introduced the notion of soft nano topological spaces using soft set equivalence relation on the universal set. Connectedness ensures continuity and integrity of spaces, allowing for the study of shapes and relationships critical for understanding complex structures. The notion of connectedness made its advent by the effort of R.L Wilder [14] in 1978. After that, the concept of connectedness was introduced in 2018, by S.Krishnaprakash, R.Ramesh and R.Suresh [6] in nano topology and in 2020, by P.G Patil and S.Benakanawari [12] in soft nano topology. Hyper connectedness explores intricate relationships among points, enabling deep analysis of complex structures and interconnections within spaces. In 1970, L.A. Steen and J.A.Seebach [9] pioneered the concept of hyper connectedness in topological spaces. Subsequently, nano hyperconnected spaces was introduced by M.LellisThivagar and I.Geetha Antoinette [8] in 2019. This paper communicates the role of soft nano α^*-generalized connected space through the lens of soft nano α^*-generalized separated sets and also elucidates the notion of soft nano α^*-generalized hyper connected spaces. A new class of sets namely soft nano α^*-generalized separated sets is ideated and exercised with theorems and appropriate examples. Furthermore, novel spaces including soft nano α^*-generalized connected spaces and soft nano α^*-generalized hyperconnected spaces are proposed and the essential characteristics, properties and equivalent conditions of these spaces are analysed, providing appropriate exemplifications for counter parts and the preservation theorem is also established.

Preliminaries

In this segment, we have outlined fundamental concepts and findings essential for advancing this work.

Definition 2.1: [3]Let $\mathcal{U}$ be a non-empty finite set of objects called the universe and $\mathfrak{W}$ be the set of parameters. Let $\mathcal{R}$ be a soft equivalence relation on $\mathcal{U}$. The triplet $(\tau_{\mathcal{R}}\mathcal{X}, \mathcal{U}, \mathfrak{W})$is said to be the soft approximation space. Let $\mathcal{X} \subseteq_{\mathcal{S}_t\mathcal{N}} \mathcal{U}$. Then

1. The **soft lower approximation** of $\mathcal{X}$ with respect to $\mathcal{R}$ and the set of parameters $\mathfrak{W}$ is the set of all objects, which can be for certain classified as $\mathcal{X}$ with respect to $\mathcal{R}$ and it is denoted by $(\mathcal{L}_{\mathcal{R}}(\mathcal{X}), \mathfrak{W})$. That is, $(\mathcal{L}_{\mathcal{R}}(\mathcal{X}), \mathfrak{W}) = \cup \{\mathcal{R}(k): \mathcal{R}(k) \subseteq_{\mathcal{S}_t\mathcal{N}} \mathcal{X}\}$, where $\mathcal{R}(k)$ denote the equivalence class determined by $k \in \mathcal{U}$.
2. The **soft upper approximation** of $\mathcal{X}$ with respect to $\mathcal{R}$ and the set of parameters $\mathfrak{W}$ is the set of all objects, which can be possibly classified as $\mathcal{X}$ with respect to $\mathcal{R}$ and it is denoted by $(\mathcal{U}_{\mathcal{R}}(\mathcal{X}), \mathfrak{W})$. That is, $(\mathcal{U}_{\mathcal{R}}(\mathcal{X}), \mathfrak{W}) = \cup \{\mathcal{R}(k): \mathcal{R}(k) \cap \mathcal{X} \neq \emptyset\}$
3. The **soft boundary region** of $\mathcal{X}$ with respect to $\mathcal{R}$ and the set of parameters $\mathfrak{W}$is the set of all objects, which can be classified neither inside $\mathcal{X}$ nor as outside $\mathcal{X}$ with respect to $\mathcal{R}$ and it is denoted by $(\mathcal{B}_{\mathcal{R}}(\mathcal{X}), \mathfrak{W})$. That is, $(\mathcal{B}_{\mathcal{R}}(\mathcal{X}), \mathfrak{W}) = (\mathcal{U}_{\mathcal{R}}(\mathcal{X}), \mathfrak{W}) - (\mathcal{L}_{\mathcal{R}}(\mathcal{X}), \mathfrak{W})$.

Definition 2.2: [3]Let $\mathcal{U}$ be a non-empty universal set and $\mathfrak{W}$ be the set of parameters. Let $\mathcal{R}$ be a soft equivalence relation on $\mathcal{U}$. Let $\mathcal{X} \subseteq_{\mathcal{S}_t\mathcal{N}} \mathcal{U}$. Let $(\tau_{\mathcal{R}}\mathcal{X}, \mathcal{U}, \mathfrak{W}) = \{\emptyset, (\mathcal{U}, \mathfrak{W}), (\mathcal{L}_{\mathcal{R}}(\mathcal{X}), \mathfrak{W}), (\mathcal{U}_{\mathcal{R}}(\mathcal{X}), \mathfrak{W}), (\mathcal{B}_{\mathcal{R}}(\mathcal{X}), \mathfrak{W})\}$. Then $(\tau_{\mathcal{R}}\mathcal{X}, \mathcal{U}, \mathfrak{W})$ is a Soft topology on $(\mathcal{U}, \mathfrak{W})$, called as the **soft nano topology** with respect to $\mathcal{X}$. Elements of Soft Nano topology are called **soft nano open sets**$(\boldsymbol{\mathcal{S}_t\mathcal{N} - Os})$ and $(\tau_{\mathcal{R}}\mathcal{X}, \mathcal{U}, \mathfrak{W})$ is called **soft nano topological space** $(\mathcal{S}_t\mathcal{N}TS)$. The complements of $\boldsymbol{\mathcal{S}_t\mathcal{N}\alpha^* g - Os}$ are called **soft nano closed sets**$(\boldsymbol{\mathcal{S}_t\mathcal{N} - Cs})$.

Definition 2.3: [2]A subset $(\mathcal{R}, \mathfrak{W})$ of a $\mathcal{S}_t\mathcal{N}TS(\tau_{\mathcal{R}}\mathcal{X}, \mathcal{U}, \mathfrak{W})$ is called soft nano α^*-generalized closed $(\boldsymbol{\mathcal{S}_t\mathcal{N}\alpha^* g - Cs})$ if $\mathcal{S}_t\mathcal{N}\alpha cl(\mathcal{R}, \mathfrak{W}) \subseteq_{\mathcal{S}_t\mathcal{N}} \mathcal{S}_t\mathcal{N}int^*(\mathcal{S}, \mathfrak{W})$ whenever $(\mathcal{R}, \mathfrak{W}) \subseteq_{\mathcal{S}_t\mathcal{N}} (\mathcal{S}, \mathfrak{W})$ and $(\mathcal{S}, \mathfrak{W}) \in \mathcal{S}_t\mathcal{N}\alpha O(\tau_{\mathcal{R}}\mathcal{X}, \mathcal{U}, \mathfrak{W})$. The class of all

$\mathcal{S}_t\mathcal{N}\alpha^*g-Cs$ in $(\tau_{\mathcal{R}}\mathcal{X},\mathcal{U},\mathfrak{W})$ is denoted by $\mathcal{S}_t\mathcal{N}\alpha^*gC(\tau_{\mathcal{R}}\mathcal{X},\mathcal{U},\mathfrak{W})$. The complement of $\mathcal{S}_t\mathcal{N}\alpha^*g-Cs$ are called $\boldsymbol{\mathcal{S}_t\mathcal{N}\alpha^*g-Os}$.

Definition 2.4: Let$(\tau_{\mathcal{R}}\mathcal{X},\mathcal{U},\mathfrak{W})$ and $(\sigma_{\mathcal{R}}\mathcal{Y},\mathcal{V},\mathcal{F})$ be two $\mathcal{S}_t\mathcal{N}TS$. Then $\mathfrak{f}:(\tau_{\mathcal{R}}\mathcal{X},\mathcal{U},\mathfrak{W})\to(\sigma_{\mathcal{R}}\mathcal{Y},\mathcal{V},\mathcal{F})$ is called

- $\boldsymbol{\mathcal{S}_t\mathcal{N}\alpha^*g}$ **−continuous**[3] if the inverse image of every $\boldsymbol{\mathcal{S}_t\mathcal{N}-Cs}$in $(\sigma_{\mathcal{R}}\mathcal{Y},\mathcal{V},\mathcal{F})$ is a$\mathcal{S}_t\mathcal{N}\alpha^*g-Cs$ in $(\tau_{\mathcal{R}}\mathcal{X},\mathcal{U},\mathfrak{W})$.
- $\boldsymbol{\mathcal{S}_t\mathcal{N}\alpha^*g}$ **−irresolute**[3] if the inverse image of every $\mathcal{S}_t\mathcal{N}\alpha^*g-Cs$ in $(\sigma_{\mathcal{R}}\mathcal{Y},\mathcal{V},\mathcal{F})$ is a$\mathcal{S}_t\mathcal{N}\alpha^*g-Cs$ in $(\tau_{\mathcal{R}}\mathcal{X},\mathcal{U},\mathfrak{W})$.
- $\boldsymbol{\mathcal{CS}_t\mathcal{N}\alpha^*g}$ **−continuous**[4] if the inverse image of every $\boldsymbol{\mathcal{S}_t\mathcal{N}-Os}$ in $(\sigma_{\mathcal{R}}\mathcal{Y},\mathcal{V},\mathcal{F})$ is a$\mathcal{S}_t\mathcal{N}\alpha^*g-Cs$ in $(\tau_{\mathcal{R}}\mathcal{X},\mathcal{U},\mathfrak{W})$.
- $\boldsymbol{\mathcal{CS}_t\mathcal{N}\alpha^*g}$ **−irresolute**[4] if the inverse image of every $\mathcal{S}_t\mathcal{N}\alpha^*g-Os$ in $(\sigma_{\mathcal{R}}\mathcal{Y},\mathcal{V},\mathcal{F})$ is a$\mathcal{S}_t\mathcal{N}\alpha^*g-Cs$ in $(\tau_{\mathcal{R}}\mathcal{X},\mathcal{U},\mathfrak{W})$.

Definition 2.5: [3] A $\mathcal{S}_t\mathcal{N}TS(\tau_{\mathcal{R}}\mathcal{X},\mathcal{U},\mathfrak{W})$ is called $\boldsymbol{\mathcal{S}_t\mathcal{N}\alpha^*gT_{1/2}}$ **−space** if every $\mathcal{S}_t\mathcal{N}\alpha^*g-Cs$ of $(\tau_{\mathcal{R}}\mathcal{X},\mathcal{U},\mathfrak{W})$ is a$\boldsymbol{\mathcal{S}_t\mathcal{N}-Cs}$ in $(\tau_{\mathcal{R}}\mathcal{X},\mathcal{U},\mathfrak{W})$.

Result 2.6: [2]

a) $\mathcal{S}_t\mathcal{N}\alpha^*gint(\mathcal{R},\mathfrak{W})=(\mathcal{R},\mathfrak{W})$ iff $(\mathcal{R},\mathfrak{W})$ is a $\mathcal{S}_t\mathcal{N}\alpha^*g-Os$ in $(\tau_{\mathcal{R}}\mathcal{X},\mathcal{U},\mathfrak{W})$.

b) $\mathcal{S}_t\mathcal{N}\alpha^*gcl(\mathcal{R},\mathfrak{W})=(\mathcal{R},\mathfrak{W})$ iff $(\mathcal{R},\mathfrak{W})$ is a $\mathcal{S}_t\mathcal{N}\alpha^*g-Cs$ in $(\tau_{\mathcal{R}}\mathcal{X},\mathcal{U},\mathfrak{W})$.

Remark 2.7:[2]For any subset $(\mathcal{R},\mathfrak{W})$ of a $\mathcal{S}_t\mathcal{N}TS$,

a) $\mathcal{S}_t\mathcal{N}\alpha^*gint(\mathcal{R},\mathfrak{W})^c=\left(\mathcal{S}_t\mathcal{N}\alpha^*gcl(\mathcal{R},\mathfrak{W})\right)^c$

b) $\mathcal{S}_t\mathcal{N}\alpha^*gcl(\mathcal{R},\mathfrak{W})^c=\left(\mathcal{S}_t\mathcal{N}\alpha^*gint(\mathcal{R},\mathfrak{W})\right)^c$

Remark 2.8: [3]A function $\mathfrak{f}:(\tau_{\mathcal{R}}\mathcal{X},\mathcal{U},\mathfrak{W})\to(\sigma_{\mathcal{R}}\mathcal{Y},\mathcal{V},\mathcal{F})$ is $\mathcal{S}_t\mathcal{N}\alpha^*g$ −continuous if and only if $\mathfrak{f}^{-1}(\mathcal{R},\mathcal{F})\in\mathcal{S}_t\mathcal{N}\alpha^*gO(\tau_{\mathcal{R}}\mathcal{X},\mathcal{U},\mathfrak{W})$ for every $(\mathcal{R},\mathcal{F})\in\mathcal{S}_t\mathcal{N}O(\sigma_{\mathcal{R}}\mathcal{Y},\mathcal{V},\mathcal{F})$.

Remark 2.9: [3]A function $\mathfrak{f}:(\tau_{\mathcal{R}}\mathcal{X},\mathcal{U},\mathfrak{W})\to(\sigma_{\mathcal{R}}\mathcal{Y},\mathcal{V},\mathcal{F})$ is $\mathcal{S}_t\mathcal{N}\alpha^*g$ −irresolute if and only if $\mathcal{S}_t\mathcal{N}\alpha^*gcl\left(\mathfrak{f}^{-1}(\mathcal{R},\mathcal{F})\right)\subseteq\mathfrak{f}^{-1}\left(\mathcal{S}_t\mathcal{N}\alpha^*gcl(\mathcal{R},\mathcal{F})\right)$ for each soft nano set $(\mathcal{R},\mathcal{F})$ in $(\sigma_{\mathcal{R}}\mathcal{Y},\mathcal{V},\mathcal{F})$.

Definition 2.10: [12]A $\mathcal{S}_t\mathcal{N}TS(\tau_{\mathcal{R}}\mathcal{X},\mathcal{U},\mathfrak{W})$ is called a soft nano connected space($\mathcal{S}_t\mathcal{N}-\mathcal{C}_nS$) if $(\mathcal{U},\mathfrak{W})$ cannot be represented as the union of two disjoint non-empty $\mathcal{S}_t\mathcal{N}-Os$.

Soft nano α^*-generalized separated sets

Separated sets in topology are vital for distinguishing points, characterizing topological properties and finding applications in geometry and analysis. They provide frameword for understanding topological structures and their properties. This segment conceptualizes the idea of soft nano α^*-generalized separated sets in soft nano topology and discuss their properties, validating their counterparts with illustrations and its equivalent conditions.

Definition 3.1: Two non-empty soft nano subsets $(\mathcal{R},\mathfrak{W})$ and $(\mathcal{S},\mathfrak{W})$ of a $\mathcal{S}_t\mathcal{N}TS(\tau_{\mathcal{R}}\mathcal{X},\mathcal{U},\mathfrak{W})$ are said to be soft nano α^*-generalized separated ($\mathcal{S}_t\mathcal{N}\alpha^*g-\mathcal{S}_p s$) if $(\mathcal{R},\mathfrak{W})\cap\mathcal{S}_t\mathcal{N}\alpha^*gcl(\mathcal{S},\mathfrak{W})=\mathcal{S}_t\mathcal{N}\alpha^*gcl(\mathcal{R},\mathfrak{W})\cap(\mathcal{S},\mathfrak{W})=\emptyset$.

The following set notations are consistently utilized in the examples of this article.
Let $\mathcal{U}=\{i,j,k,\ell\}$ and $\mathfrak{W}=\{m_1,m_2,m_3\}$. Then the soft nano sets are
$(\acute{\mathrm{K}}_1,\mathfrak{W})=\{(m_1,\emptyset),(m_2,\emptyset),(m_3,\emptyset)\}=\emptyset$
$(\acute{\mathrm{K}}_2,\mathfrak{W})=\{(m_1,\{i\}),(m_2,\{i\}),(m_3,\{i\})\}$
$(\acute{\mathrm{K}}_3,\mathfrak{W})=\{(m_1,\{j\}),(m_2,\{j\}),(m_3,\{j\})\}$
$(\acute{\mathrm{K}}_4,\mathfrak{W})=\{(m_1,\{k\}),(m_2,\{k\}),(m_3,\{k\})\}$
$(\acute{\mathrm{K}}_5,\mathfrak{W})=\{(m_1,\{\ell\}),(m_2,\{\ell\}),(m_3,\{\ell\})\}$

$(\acute{K}_6, \mathfrak{W}) = \{(m_1, \{i, j\}), (m_2, \{i, j\}), (m_3, \{i, j\})\}$
$(\acute{K}_7, \mathfrak{W}) = \{(m_1, \{i, k\}), (m_2, \{i, k\}), (m_3, \{i, k\})\}$
$(\acute{K}_8, \mathfrak{W}) = \{(m_1, \{i, \ell\}), (m_2, \{i, \ell\}), (m_3, \{i, \ell\})\}$
$(\acute{K}_9, \mathfrak{W}) = \{(m_1, \{j, k\}), (m_2, \{j, k\}), (m_3, \{j, k\})\}$
$(\acute{K}_{10}, \mathfrak{W}) = \{(m_1, \{j, \ell\}), (m_2, \{j, \ell\}), (m_3, \{j, \ell\})\}$
$(\acute{K}_{11}, \mathfrak{W}) = \{(m_1, \{k, \ell\}), (m_2, \{k, \ell\}), (m_3, \{k, \ell\})\}$
$(\acute{K}_{12}, \mathfrak{W}) = \{(m_1, \{i, j, k\}), (m_2, \{i, j, k\}), (m_3, \{i, j, k\})\}$
$(\acute{K}_{13}, \mathfrak{W}) = \{(m_1, \{i, j, \ell\}), (m_2, \{i, j, \ell\}), (m_3, \{i, j, \ell\})\}$
$(\acute{K}_{14}, \mathfrak{W}) = \{(m_1, \{i, k, \ell\}), (m_2, \{i, k, \ell\}), (m_3, \{i, k, \ell\})\}$
$(\acute{K}_{15}, \mathfrak{W}) = \{(m_1, \{j, k, \ell\}), (m_2, \{j, k, \ell\}), (m_3, \{j, k, \ell\})\}$
$(\acute{K}_{16}, \mathfrak{W}) = \{(m_1, \{i, j, k, \ell\}), (m_2, \{i, j, k, \ell\}), (m_3, \{i, j, k, \ell\})\} = (\mathcal{U}, \mathfrak{W})$

Example 3.2: Let $\mathcal{U} = \{i, j, k, \ell\}$, $\mathfrak{W} = \{m_1, m_2, m_3\}$ and $\mathcal{X} = \{j, \ell\} \subseteq \mathcal{U}$ with $\mathcal{U}\backslash\mathcal{R} = \{\{k\}, \{i, j, \ell\}\}$. Then $\mathcal{S}_t\mathcal{N}\alpha^*gC(\tau_{\mathcal{R}}\mathcal{X}, \mathcal{U}, \mathfrak{W}) = \{\emptyset, (\mathcal{U}, \mathfrak{W}), (\acute{K}_4, \mathfrak{W}), (\acute{K}_7, \mathfrak{W}), (\acute{K}_9, \mathfrak{W}), (\acute{K}_{11}, \mathfrak{W}), (\acute{K}_{12}, \mathfrak{W}), (\acute{K}_{14}, \mathfrak{W}), (\acute{K}_{15}, \mathfrak{W})\}$. Since $(\acute{K}_2, \mathfrak{W}) \cap \mathcal{S}_t\mathcal{N}\alpha^*gcl(\acute{K}_5, \mathfrak{W}) = (\acute{K}_2, \mathfrak{W}) \cap (\acute{K}_{11}, \mathfrak{W}) = \emptyset$ and $\mathcal{S}_t\mathcal{N}\alpha^*gcl(\acute{K}_2, \mathfrak{W}) \cap (\acute{K}_5, \mathfrak{W}) = (\acute{K}_7, \mathfrak{W}) \cap (\acute{K}_5, \mathfrak{W}) = \emptyset$, $(\acute{K}_2, \mathfrak{W})$ and $(\acute{K}_5, \mathfrak{W})$ are $\mathcal{S}_t\mathcal{N}\alpha^*g - \mathcal{S}_p s$.

Theorem 3.3: $\mathcal{S}_t\mathcal{N}\alpha^*g - \mathcal{S}_p s$ are inherently mutually exclusive.
Proof: Assume $(\mathcal{R}, \mathfrak{W})$ and $(\mathcal{S}, \mathfrak{W})$ be two $\mathcal{S}_t\mathcal{N}\alpha^*g - \mathcal{S}_p s$. By definition, $(\mathcal{R}, \mathfrak{W}) \cap \mathcal{S}_t\mathcal{N}\alpha^*gcl(\mathcal{S}, \mathfrak{W}) = \mathcal{S}_t\mathcal{N}\alpha^*gcl(\mathcal{R}, \mathfrak{W}) \cap (\mathcal{S}, \mathfrak{W}) = \emptyset$. Since $(\mathcal{R}, \mathfrak{W}) \cap (\mathcal{S}, \mathfrak{W}) \subseteq_{\mathcal{S}_t\mathcal{N}} (\mathcal{R}, \mathfrak{W}) \cap \mathcal{S}_t\mathcal{N}\alpha^*gcl(\mathcal{S}, \mathfrak{W})$, $(\mathcal{R}, \mathfrak{W}) \cap (\mathcal{S}, \mathfrak{W}) = \emptyset$. Hence $(\mathcal{R}, \mathfrak{W})$ and $(\mathcal{S}, \mathfrak{W})$ are mutually exclusive.

Theorem 3.4: For any two non-empty$\mathcal{S}_t\mathcal{N}\alpha^*g - Cs$ that are mutually exclusive, there exists $\mathcal{S}_t\mathcal{N}\alpha^*g$ −separation between them.
Proof: Suppose $(\mathcal{R}, \mathfrak{W})$ and $(\mathcal{S}, \mathfrak{W})$ be non-empty $\mathcal{S}_t\mathcal{N}\alpha^*g - Cs$ that are mutually exclusive. Then $(\mathcal{R}, \mathfrak{W}) \cap \mathcal{S}_t\mathcal{N}\alpha^*gcl(\mathcal{S}, \mathfrak{W}) = \mathcal{S}_t\mathcal{N}\alpha^*gcl(\mathcal{R}, \mathfrak{W}) \cap (\mathcal{S}, \mathfrak{W}) = (\mathcal{R}, \mathfrak{W}) \cap (\mathcal{S}, \mathfrak{W}) = \emptyset$. Hence $(\mathcal{R}, \mathfrak{W})$ and $(\mathcal{S}, \mathfrak{W})$ are $\mathcal{S}_t\mathcal{N}\alpha^*g - \mathcal{S}_p s$.

Remark 3.5: The reverse of the aforementioned theorem may not hold true, as demonstrated by the subsequent example.

Example 3.6: Let $\mathcal{U} = \{i, j, k, \ell\}$, $\mathfrak{WW} = \{m_1, m_2, m_3\}$ and $\mathcal{X} = \{j, \ell\} \subseteq \mathcal{U}$ with $\mathcal{U}\backslash\mathcal{R} = \{\{i\}, \{j, k\}, \{\ell\}\}$. Then $\mathcal{S}_t\mathcal{N}\alpha^*gC(\tau_{\mathcal{R}}\mathcal{X}, \mathcal{U}, \mathfrak{W}) = \{\emptyset, (\mathcal{U}, \mathfrak{W}), (\acute{K}_2, \mathfrak{W}), (\acute{K}_6, \mathfrak{W}), (\acute{K}_7, \mathfrak{W}), (\acute{K}_8, \mathfrak{W}), (\acute{K}_{12}, \mathfrak{W}), (\acute{K}_{13}, \mathfrak{W}), (\acute{K}_{14}, \mathfrak{W})\}$. Here $(\acute{K}_3, \mathfrak{W}) \cap \mathcal{S}_t\mathcal{N}\alpha^*gcl(\acute{K}_4, \mathfrak{W}) = (\acute{K}_3, \mathfrak{W}) \cap (\acute{K}_7, \mathfrak{W}) = \emptyset$ and $\mathcal{S}_t\mathcal{N}\alpha^*gcl(\acute{K}_3, \mathfrak{W}) \cap (\acute{K}_4, \mathfrak{W}) = (\acute{K}_6, \mathfrak{W}) \cap (\acute{K}_4, \mathfrak{W}) = \emptyset$. Hence $(\acute{K}_2, \mathfrak{W})$ and $(\acute{K}_5, \mathfrak{W})$ are mutually exclusive non-empty $\mathcal{S}_t\mathcal{N}\alpha^*g - \mathcal{S}_p s$ but not $\mathcal{S}_t\mathcal{N}\alpha^*g - Cs$.

Theorem 3.7: If $(\mathcal{S}_1, \mathfrak{W}), (\mathcal{S}_2, \mathfrak{W}) \in \mathcal{S}_t\mathcal{N}\alpha^*gO(\tau_{\mathcal{R}}\mathcal{X}, \mathcal{U}, \mathfrak{W})$ such that $(\mathcal{R}_1, \mathfrak{W}) = (\mathcal{S}_1, \mathfrak{W}) \cap (\mathcal{S}_2, \mathfrak{W})^c$ and $(\mathcal{R}_2, \mathfrak{W}) = (\mathcal{S}_1, \mathfrak{W})^c \cap (\mathcal{S}_2, \mathfrak{W})$, then $(\mathcal{R}_1, \mathfrak{W})$ and $(\mathcal{R}_2, \mathfrak{W})$ are $\mathcal{S}_t\mathcal{N}\alpha^*g - \mathcal{S}_p s$.

Proof: Since $(\mathcal{S}_1, \mathfrak{W}), (\mathcal{S}_2, \mathfrak{W}) \in \mathcal{S}_t\mathcal{N}\alpha^*gO(\tau_{\mathcal{R}}\mathcal{X}, \mathcal{U}, \mathfrak{W})$, $(\mathcal{S}_1, \mathfrak{W})^c, (\mathcal{S}_2, \mathfrak{W})^c \in \mathcal{S}_t\mathcal{N}\alpha^*gC(\tau_{\mathcal{R}}\mathcal{X}, \mathcal{U}, \mathfrak{W})$. Since $(\mathcal{R}_1, \mathfrak{W}) \subseteq_{\mathcal{S}_t\mathcal{N}} (\mathcal{S}_2, \mathfrak{W})^c$, $\mathcal{S}_t\mathcal{N}\alpha^*gcl(\mathcal{R}_1, \mathfrak{W}) \subseteq_{\mathcal{S}_t\mathcal{N}} \mathcal{S}_t\mathcal{N}\alpha^*gcl(\mathcal{S}_2, \mathfrak{W})^c = (\mathcal{S}_2, \mathfrak{W})^c$. Thus $\mathcal{S}_t\mathcal{N}\alpha^*gcl(\mathcal{R}_1, \mathfrak{W}) \cap (\mathcal{S}_2, \mathfrak{W}) = \emptyset$ which implies $\mathcal{S}_t\mathcal{N}\alpha^*gcl(\mathcal{R}_1, \mathfrak{W}) \cap (\mathcal{R}_2, \mathfrak{W}) = \emptyset$, since $(\mathcal{R}_2, \mathfrak{W}) \subseteq_{\mathcal{S}_t\mathcal{N}} (\mathcal{S}_2, \mathfrak{W})$. Similarly, by taking $(\mathcal{R}_2, \mathfrak{W}) \subseteq_{\mathcal{S}_t\mathcal{N}} (\mathcal{S}_1, \mathfrak{W})^c$, we get $(\mathcal{R}_1, \mathfrak{W}) \cap \mathcal{S}_t\mathcal{N}\alpha^*gcl(\mathcal{R}_2, \mathfrak{W}) = \emptyset$. Hence $(\mathcal{R}_1, \mathfrak{W})$ and $(\mathcal{R}_2, \mathfrak{W})$ are $\mathcal{S}_t\mathcal{N}\alpha^*g - \mathcal{S}_p s$.

Theorem 3.8: If $(\mathcal{R}_2, \mathfrak{W})$ and $(\mathcal{S}_2, \mathfrak{W})$ are $\mathcal{S}_t\mathcal{N}\alpha^*g - \mathcal{S}_p s$ such that $(\mathcal{R}_1, \mathfrak{W}) \subseteq_{\mathcal{S}_t\mathcal{N}} (\mathcal{R}_2, \mathfrak{W})$ and $(\mathcal{S}_1, \mathfrak{W}) \subseteq_{\mathcal{S}_t\mathcal{N}} (\mathcal{S}_2, \mathfrak{W})$, then $(\mathcal{R}_1, \mathfrak{W})$ and $(\mathcal{S}_1, \mathfrak{W})$ are $\mathcal{S}_t\mathcal{N}\alpha^*g - \mathcal{S}_p s$.

Proof: Let $(\mathcal{R}_2, \mathfrak{W})$ and $(\mathcal{S}_2, \mathfrak{W})$ are $\mathcal{S}_t\mathcal{N}\alpha^*g - \mathcal{S}_p s$. Then $(\mathcal{R}_2, \mathfrak{W}) \cap \mathcal{S}_t\mathcal{N}\alpha^*gcl(\mathcal{S}_2, \mathfrak{W}) = \mathcal{S}_t\mathcal{N}\alpha^*gcl(\mathcal{R}_2, \mathfrak{W}) \cap (\mathcal{S}_2, \mathfrak{W}) = \emptyset$.Since$(\mathcal{R}_1, \mathfrak{W}) \subseteq_{\mathcal{S}_t\mathcal{N}} (\mathcal{R}_2, \mathfrak{W})and(\mathcal{S}_1, \mathfrak{W}) \subseteq_{\mathcal{S}_t\mathcal{N}} (\mathcal{S}_2, \mathfrak{W})$,$(\mathcal{R}_1, \mathfrak{W}) \cap \mathcal{S}_t\mathcal{N}\alpha^*gcl(\mathcal{S}_1, \mathfrak{W}) \subseteq_{\mathcal{S}_t\mathcal{N}} (\mathcal{R}_2, \mathfrak{W}) \cap \mathcal{S}_t\mathcal{N}\alpha^*gcl(\mathcal{S}_2, \mathfrak{W}) =$

$\emptyset$ and $\mathcal{S}_t\mathcal{N}\alpha^*gcl(\mathcal{R}_1,\mathfrak{W}) \cap (\mathcal{S}_1,\mathfrak{W}) \subseteq_{\mathcal{S}_t\mathcal{N}} \mathcal{S}_t\mathcal{N}\alpha^*gcl(\mathcal{R}_2,\mathfrak{W}) \cap (\mathcal{S}_2,\mathfrak{W}) = \emptyset$. Hence $(\mathcal{R}_1,\mathfrak{W})$ and $(\mathcal{S}_1,\mathfrak{W})$ are $\mathcal{S}_t\mathcal{N}\alpha^*g - \mathcal{S}_p s$.

Theorem 3.9: The soft nano subsets $(\mathcal{R}_1,\mathfrak{W})$ and $(\mathcal{S}_1,\mathfrak{W})$ of a $\mathcal{S}_t\mathcal{N}TS(\tau_{\mathcal{R}}\mathcal{X},\mathcal{U},\mathfrak{W})$ are $\mathcal{S}_t\mathcal{N}\alpha^*g - \mathcal{S}_p s$ if and only if there exists $\mathcal{S}_t\mathcal{N}\alpha^*g - Os(\mathcal{R}_2,\mathfrak{W})$ and $(\mathcal{S}_2,\mathfrak{W})$ such that $(\mathcal{R}_1,\mathfrak{W}) \subseteq_{\mathcal{S}_t\mathcal{N}} (\mathcal{R}_2,\mathfrak{W})$ and $(\mathcal{S}_1,\mathfrak{W}) \subseteq_{\mathcal{S}_t\mathcal{N}} (\mathcal{S}_2,\mathfrak{W})$, $(\mathcal{R}_1,\mathfrak{W}) \cap (\mathcal{S}_2,\mathfrak{W}) = \emptyset$ and $(\mathcal{S}_1,\mathfrak{W}) \cap (\mathcal{R}_2,\mathfrak{W}) = \emptyset$.

Proof: Assume $(\mathcal{R}_1,\mathfrak{W})$ and $(\mathcal{S}_1,\mathfrak{W})$ are $\mathcal{S}_t\mathcal{N}\alpha^*g - \mathcal{S}_p s$. Then $(\mathcal{R}_1,\mathfrak{W}) \cap \mathcal{S}_t\mathcal{N}\alpha^*gcl(\mathcal{S}_1,\mathfrak{W}) = \mathcal{S}_t\mathcal{N}\alpha^*gcl(\mathcal{R}_1,\mathfrak{W}) \cap (\mathcal{S}_1,\mathfrak{W}) = \emptyset$. Take $(\mathcal{R}_2,\mathfrak{W}) = (\mathcal{U},\mathfrak{W})\backslash\mathcal{S}_t\mathcal{N}\alpha^*gcl(\mathcal{S}_1,\mathfrak{W})$ and $(\mathcal{S}_2,\mathfrak{W}) = (\mathcal{U},\mathfrak{W})\backslash\mathcal{S}_t\mathcal{N}\alpha^*gcl(\mathcal{R}_1,\mathfrak{W})$. Then $(\mathcal{R}_2,\mathfrak{W}),(\mathcal{S}_2,\mathfrak{W}) \in \mathcal{S}_t\mathcal{N}\alpha^*gO(\tau_{\mathcal{R}}\mathcal{X},\mathcal{U},\mathfrak{W})$ such that $(\mathcal{R}_1,\mathfrak{W}) \subseteq_{\mathcal{S}_t\mathcal{N}} (\mathcal{R}_2,\mathfrak{W})$ and $(\mathcal{S}_1,\mathfrak{W}) \subseteq_{\mathcal{S}_t\mathcal{N}} (\mathcal{S}_2,\mathfrak{W})$, $(\mathcal{R}_1,\mathfrak{W}) \cap (\mathcal{S}_2,\mathfrak{W}) = \emptyset$ and $(\mathcal{S}_1,\mathfrak{W}) \cap (\mathcal{R}_2,\mathfrak{W}) = \emptyset$.
Conversely, assume that $(\mathcal{R}_2,\mathfrak{W}),(\mathcal{S}_2,\mathfrak{W}) \in \mathcal{S}_t\mathcal{N}\alpha^*gO(\tau_{\mathcal{R}}\mathcal{X},\mathcal{U},\mathfrak{W})$ such that $(\mathcal{R}_1,\mathfrak{W}) \subseteq_{\mathcal{S}_t\mathcal{N}} (\mathcal{R}_2,\mathfrak{W})$ and $(\mathcal{S}_1,\mathfrak{W}) \subseteq_{\mathcal{S}_t\mathcal{N}} (\mathcal{S}_2,\mathfrak{W})$, $(\mathcal{R}_1,\mathfrak{W}) \cap (\mathcal{S}_2,\mathfrak{W}) = \emptyset$ and $(\mathcal{S}_1,\mathfrak{W}) \cap (\mathcal{R}_2,\mathfrak{W}) = \emptyset$. Then $(\mathcal{R}_1,\mathfrak{W}) \subseteq_{\mathcal{S}_t\mathcal{N}} (\mathcal{U},\mathfrak{W})\backslash(\mathcal{S}_2,\mathfrak{W})$ and $(\mathcal{S}_1,\mathfrak{W}) \subseteq_{\mathcal{S}_t\mathcal{N}} (\mathcal{U},\mathfrak{W})\backslash(\mathcal{R}_2,\mathfrak{W})$ where $(\mathcal{U},\mathfrak{W})\backslash(\mathcal{R}_2,\mathfrak{W}),(\mathcal{U},\mathfrak{W})\backslash(\mathcal{S}_2,\mathfrak{W}) \in \mathcal{S}_t\mathcal{N}\alpha^*gC(\tau_{\mathcal{R}}\mathcal{X},\mathcal{U},\mathfrak{W})$. Then $\mathcal{S}_t\mathcal{N}\alpha^*gcl(\mathcal{R}_1,\mathfrak{W}) \subseteq_{\mathcal{S}_t\mathcal{N}} (\mathcal{U},\mathfrak{W})\backslash(\mathcal{S}_2,\mathfrak{W})$ and $\mathcal{S}_t\mathcal{N}\alpha^*gcl(\mathcal{S}_1,\mathfrak{W}) \subseteq_{\mathcal{S}_t\mathcal{N}} (\mathcal{U},\mathfrak{W})\backslash(\mathcal{R}_2,\mathfrak{W})$. Since $(\mathcal{R}_1,\mathfrak{W}) \subseteq_{\mathcal{S}_t\mathcal{N}} (\mathcal{R}_2,\mathfrak{W})$ and $(\mathcal{S}_1,\mathfrak{W}) \subseteq_{\mathcal{S}_t\mathcal{N}} (\mathcal{S}_2,\mathfrak{W})$, $\mathcal{S}_t\mathcal{N}\alpha^*gcl(\mathcal{R}_1,\mathfrak{W}) \subseteq_{\mathcal{S}_t\mathcal{N}} (\mathcal{U},\mathfrak{W})\backslash(\mathcal{S}_1,\mathfrak{W})$ and $\mathcal{S}_t\mathcal{N}\alpha^*gcl(\mathcal{S}_2,\mathfrak{W}) \subseteq_{\mathcal{S}_t\mathcal{N}} (\mathcal{U},\mathfrak{W})\backslash(\mathcal{R}_2,\mathfrak{W})$. Thus $\mathcal{S}_t\mathcal{N}\alpha^*gcl(\mathcal{R}_1,\mathfrak{W}) \cap (\mathcal{S}_1,\mathfrak{W}) = \emptyset$ and $(\mathcal{R}_1,\mathfrak{W}) \cap \mathcal{S}_t\mathcal{N}\alpha^*gcl(\mathcal{S}_1,\mathfrak{W}) = \emptyset$. Hence $(\mathcal{R}_1,\mathfrak{W})$ and $(\mathcal{S}_1,\mathfrak{W})$ are $\mathcal{S}_t\mathcal{N}\alpha^*g - \mathcal{S}_p s$.

Soft nano α^*-generalized connectedness

Connectedness is a fundamental concept in topology, defining the continuity of a topological space. This property captures the idea of a single, cohesive entity, crucial for understanding the structure and behaviour of topological spaces in various mathematical and real world contexts. This segment underpins the origination of soft nano α^*-generalized connectedness, analyzing the structure and properties, making it a cornerstone of the field.

Definition 4.1: A $\mathcal{S}_t\mathcal{N}TS(\tau_{\mathcal{R}}\mathcal{X},\mathcal{U},\mathfrak{W})$ is called soft nano α^*-generalized connected space $(\mathcal{S}_t\mathcal{N}\alpha^*g - \mathcal{C}_n S)$ if $(\mathcal{U},\mathfrak{W})$ cannot be represented as the combination of two non-empty mutually exclusive $\mathcal{S}_t\mathcal{N}\alpha^*g - Os$ of $(\tau_{\mathcal{R}}\mathcal{X},\mathcal{U},\mathfrak{W})$. A subset of $(\tau_{\mathcal{R}}\mathcal{X},\mathcal{U},\mathfrak{W})$ is $\mathcal{S}_t\mathcal{N}\alpha^*g - \mathcal{C}_n$ if it is $\mathcal{S}_t\mathcal{N}\alpha^*g - \mathcal{C}_n$ as a subspace.

Example 4.2: Let $\mathcal{U} = \{i,j,k,\ell\}$, $\mathfrak{W} = \{m_1,m_2,m_3\}$ and $\mathcal{X} = \{i,k\} \subseteq \mathcal{U}$ with $\mathcal{U}\backslash\mathcal{R} = \{\{j\},\{k\},\{i,\ell\}\}$. Then $\mathcal{S}_t\mathcal{N}\alpha^*gO(\tau_{\mathcal{R}}\mathcal{X},\mathcal{U},\mathfrak{W}) = \{\emptyset,(\mathcal{U},\mathfrak{W}),(\acute{\mathrm{K}}_2,\mathfrak{W}),(\acute{\mathrm{K}}_4,\mathfrak{W}),(\acute{\mathrm{K}}_5,\mathfrak{W}),(\acute{\mathrm{K}}_7,\mathfrak{W}),(\acute{\mathrm{K}}_8,\mathfrak{W}),(\acute{\mathrm{K}}_{11},\mathfrak{W}),(\acute{\mathrm{K}}_{14},\mathfrak{W})\}$. Since $(\mathcal{U},\mathfrak{W})$ cannot be expressed as the combination of two non-empty mutually exclusive $\mathcal{S}_t\mathcal{N}\alpha^*g - Os$, $(\tau_{\mathcal{R}}\mathcal{X},\mathcal{U},\mathfrak{W})$ is $\mathcal{S}_t\mathcal{N}\alpha^*g - \mathcal{C}_n S$.

Remark 4.3 :A subset of $(\tau_{\mathcal{R}}\mathcal{X},\mathcal{U},\mathfrak{W})$ is $\mathcal{S}_t\mathcal{N}\alpha^*g$ −disconnected $(\mathcal{S}_t\mathcal{N}\alpha^*g - \mathcal{DC}_n)$ if and only if it is not $\mathcal{S}_t\mathcal{N}\alpha^*g - \mathcal{C}_n$.

Theorem 4.4: For any $\mathcal{S}_t\mathcal{N}TS(\tau_{\mathcal{R}}\mathcal{X},\mathcal{U},\mathfrak{W})$, the subsequent assertions are equivalent.

i) $(\tau_{\mathcal{R}}\mathcal{X},\mathcal{U},\mathfrak{W})$ is a $\mathcal{S}_t\mathcal{N}\alpha^*g - \mathcal{C}_n S$.
ii) $(\mathcal{U},\mathfrak{W})$ and $\emptyset$ are the only subsets of $(\mathcal{U},\mathfrak{W})$ which are both $\mathcal{S}_t\mathcal{N}\alpha^*g - Os$ and $\mathcal{S}_t\mathcal{N}\alpha^*g - Cs$ in $(\tau_{\mathcal{R}}\mathcal{X},\mathcal{U},\mathfrak{W})$.
iii) Each $\mathcal{S}_t\mathcal{N}\alpha^*g$ −continuous function of $(\tau_{\mathcal{R}}\mathcal{X},\mathcal{U},\mathfrak{W})$ into a $\mathcal{S}_t\mathcal{N}$ −discrete space $(\sigma_{\mathcal{R}}\mathcal{Y},\mathcal{V},H)$ with at least two points is a constant function.

Proof: i)⟹ii) Assume$(\mathcal{R},\mathfrak{W}) \in \mathcal{S}_t\mathcal{N}\alpha^*gCO(\tau_{\mathcal{R}}\mathcal{X},\mathcal{U},\mathfrak{W})$. Then $(\mathcal{R},\mathfrak{W})^c \in \mathcal{S}_t\mathcal{N}\alpha^*gCO(\tau_{\mathcal{R}}\mathcal{X},\mathcal{U},\mathfrak{W})$. Thus $(\mathcal{U},\mathfrak{W}) = (\mathcal{R},\mathfrak{W}) \cup (\mathcal{R},\mathfrak{W})^c$ and $\emptyset = (\mathcal{R},\mathfrak{W}) \cap (\mathcal{R},\mathfrak{W})^c$, where $(\mathcal{R},\mathfrak{W}),(\mathcal{R},\mathfrak{W})^c \in \mathcal{S}_t\mathcal{N}\alpha^*gO(\tau_{\mathcal{R}}\mathcal{X},\mathcal{U},\mathfrak{W})$. Since $(\tau_{\mathcal{R}}\mathcal{X},\mathcal{U},\mathfrak{W})$ is a $\mathcal{S}_t\mathcal{N}\alpha^*g - \mathcal{C}_n S$, either $(\mathcal{R},\mathfrak{W}) = \emptyset$ or $(\mathcal{R},\mathfrak{W}) = (\mathcal{U},\mathfrak{W})$.
ii)⟹i) Suppose$(\tau_{\mathcal{R}}\mathcal{X},\mathcal{U},\mathfrak{W})$ is $\mathcal{S}_t\mathcal{N}\alpha^*g - \mathcal{DC}_n$. Then $(\mathcal{U},\mathfrak{W}) = (\mathcal{R},\mathfrak{W}) \cup (\mathcal{S},\mathfrak{W})$ where $(\mathcal{R},\mathfrak{W})$ and $(\mathcal{S},\mathfrak{W})$ are non-empty mutually exclusive $\mathcal{S}_t\mathcal{N}\alpha^*g - Os$. Since $(\mathcal{R},\mathfrak{W}) = (\mathcal{U},\mathfrak{W})\backslash(\mathcal{S},\mathfrak{W})$, $(\mathcal{R},\mathfrak{W})$ is $\mathcal{S}_t\mathcal{N}\alpha^*g - Cs$. Since $(\mathcal{R},\mathfrak{W}) \in \mathcal{S}_t\mathcal{N}\alpha^*gCO(\tau_{\mathcal{R}}\mathcal{X},\mathcal{U},\mathfrak{W})$, by our assumption, either $(\mathcal{R},\mathfrak{W}) = \emptyset$ or $(\mathcal{R},\mathfrak{W}) = (\mathcal{U},\mathfrak{W})$ which implies either $(\mathcal{R},\mathfrak{W}) = \emptyset$ or $(\mathcal{S},\mathfrak{W}) = \emptyset$, leading to a contradiction. Hence $(\tau_{\mathcal{R}}\mathcal{X},\mathcal{U},\mathfrak{W})$ is a $\mathcal{S}_t\mathcal{N}\alpha^*g - \mathcal{C}_n S$.

ii)⟹iii) Let$\not{f}: (\tau_{\mathcal{R}}\mathcal{X}, \mathcal{U}, \mathfrak{W}) \to (\sigma_{\mathcal{R}}\mathcal{Y}, \mathcal{V}, H)$ be $\mathcal{S}_t\mathcal{N}\alpha^*g$ −continuous such that $(\sigma_{\mathcal{R}}\mathcal{Y}, \mathcal{V}, H)$ is a $\mathcal{S}_t\mathcal{N}$ −discrete space with at least two points. Then for each $(\mathcal{R}, H) \in (\sigma_{\mathcal{R}}\mathcal{Y}, \mathcal{V}, H)$, $(\mathcal{R}, H) \in \mathcal{S}_t\mathcal{N}CO(\sigma_{\mathcal{R}}\mathcal{Y}, \mathcal{V}, H)$. Since $\not{f}$ is $\mathcal{S}_t\mathcal{N}\alpha^*g$ −continuous, $\not{f}^{-1}(\mathcal{R}, H) \in \mathcal{S}_t\mathcal{N}\alpha^*gCO(\tau_{\mathcal{R}}\mathcal{X}, \mathcal{U}, \mathfrak{W})$. Hence $(\tau_{\mathcal{R}}\mathcal{X}, \mathcal{U}, \mathfrak{W})$ is covered by $\mathcal{S}_t\mathcal{N}\alpha^*g$ −clopen set $\{\not{f}^{-1}(\mathcal{R}, H): (\mathcal{R}, H) \in (\sigma_{\mathcal{R}}\mathcal{Y}, \mathcal{V}, H)\}$. Then by our assumption, $\not{f}^{-1}(\mathcal{R}, H) = \emptyset$ or $(\mathcal{U}, \mathfrak{W})$. If $\not{f}^{-1}(\mathcal{R}, H) = \emptyset$ for all $(\mathcal{R}, H) \in (\sigma_{\mathcal{R}}\mathcal{Y}, \mathcal{V}, H)$, then $\not{f}$ fails to be a function. Hence, there exists only one point $(\mathcal{R}, H) \in (\sigma_{\mathcal{R}}\mathcal{Y}, \mathcal{V}, H)$ such that $\not{f}^{-1}(\mathcal{R}, H) = (\mathcal{U}, \mathfrak{W})$ which shows that $\not{f}$ is a constant function.

iii)⟹ii) Let$(\mathcal{R}, \mathfrak{W}) \in \mathcal{S}_t\mathcal{N}\alpha^*gCO(\tau_{\mathcal{R}}\mathcal{X}, \mathcal{U}, \mathfrak{W})$. Suppose $(\mathcal{R}, \mathfrak{W}) \neq \emptyset$. Define $\not{f}: (\tau_{\mathcal{R}}\mathcal{X}, \mathcal{U}, \mathfrak{W}) \to (\sigma_{\mathcal{R}}\mathcal{Y}, \mathcal{V}, H)$ where $(\sigma_{\mathcal{R}}\mathcal{Y}, \mathcal{V}, H)$ is a $\mathcal{S}_t\mathcal{N}$ −discrete space with at least two points by $\not{f}(\mathcal{R}, \mathfrak{W}) = (\mathcal{S}, H)$, $\not{f}\big((\mathcal{U}, \mathfrak{W})\backslash(\mathcal{R}, \mathfrak{W})\big) = (\mathcal{T}, H)$. Then $\not{f}$ is $\mathcal{S}_t\mathcal{N}\alpha^*g$ −continuous. Therefore by hypothesis, $\not{f}$ is a constant function. Thus $(\mathcal{S}, H) = (\mathcal{T}, H)$ and hence $(\mathcal{R}, \mathfrak{W}) = (\mathcal{U}, \mathfrak{W})$.

Theorem 4.5: Every $\mathcal{S}_t\mathcal{N}\alpha^*g - \mathcal{C}_nS$ is $\mathcal{S}_t\mathcal{N} - \mathcal{C}_n$.

Proof: Suppose $(\tau_{\mathcal{R}}\mathcal{X}, \mathcal{U}, \mathfrak{W})$ is a $\mathcal{S}_t\mathcal{N}\alpha^*g - \mathcal{C}_nS$ but not $\mathcal{S}_t\mathcal{N} - \mathcal{C}_n$. Then there exists mutually exclusive non-empty $\mathcal{S}_t\mathcal{N} - Os(\mathcal{R}, \mathfrak{W})$ and $(\mathcal{S}, \mathfrak{W})$ such that $(\mathcal{U}, \mathfrak{W}) = (\mathcal{R}, \mathfrak{W}) \cup (\mathcal{S}, \mathfrak{W})$. Since every $\mathcal{S}_t\mathcal{N} - Os$ is a $\mathcal{S}_t\mathcal{N}\alpha^*g - Os$, $(\mathcal{R}, \mathfrak{W})$ and $(\mathcal{S}, \mathfrak{W})$ are mutually exclusive non-empty $\mathcal{S}_t\mathcal{N}\alpha^*g - Os$ such that $(\mathcal{U}, \mathfrak{W}) = (\mathcal{R}, \mathfrak{W}) \cup (\mathcal{S}, \mathfrak{W})$. Then the $\mathcal{S}_t\mathcal{N}\alpha^*g$ −disconnection of $(\tau_{\mathcal{R}}\mathcal{X}, \mathcal{U}, \mathfrak{W})$ presents a contradiction. Hence $(\tau_{\mathcal{R}}\mathcal{X}, \mathcal{U}, \mathfrak{W})$ is $\mathcal{S}_t\mathcal{N} - \mathcal{C}_n$.

Remark 4.6: Every $\mathcal{S}_t\mathcal{N} - \mathcal{C}_nS$ is $\mathcal{S}_t\mathcal{N}\alpha^*g - \mathcal{C}_n$ only if it is a $\mathcal{S}_t\mathcal{N}\alpha^*gT_{1/2}$ −space.

Theorem 4.7: For any $\mathcal{S}_t\mathcal{N}TS(\tau_{\mathcal{R}}\mathcal{X}, \mathcal{U}, \mathfrak{W})$, the subsequent assertions are equivalent.

i) $(\tau_{\mathcal{R}}\mathcal{X}, \mathcal{U}, \mathfrak{W})$ is a $\mathcal{S}_t\mathcal{N}\alpha^*g - \mathcal{C}_nS$.

ii) $(\mathcal{U}, \mathfrak{W})$ cannot be represented as the combination of two mutually exclusive non-empty $\mathcal{S}_t\mathcal{N}\alpha^*g - Cs$.

Proof: i)⟹ii) Suppose$(\mathcal{U}, \mathfrak{W}) = (\mathcal{R}, \mathfrak{W}) \cup (\mathcal{S}, \mathfrak{W})$ where $(\mathcal{R}, \mathfrak{W})$ and $(\mathcal{S}, \mathfrak{W})$ are two mutually exclusive non-empty $\mathcal{S}_t\mathcal{N}\alpha^*g - Cs$. Since $(\mathcal{R}, \mathfrak{W}) = (\mathcal{U}, \mathfrak{W})\backslash(\mathcal{S}, \mathfrak{W})$ and $(\mathcal{S}, \mathfrak{W}) = (\mathcal{U}, \mathfrak{W})\backslash(\mathcal{R}, \mathfrak{W})$, $(\mathcal{R}, \mathfrak{W}), (\mathcal{S}, \mathfrak{W}) \in \mathcal{S}_t\mathcal{N}\alpha^*gO(\tau_{\mathcal{R}}\mathcal{X}, \mathcal{U}, \mathfrak{W})$. Then $(\tau_{\mathcal{R}}\mathcal{X}, \mathcal{U}, \mathfrak{W})$ is $\mathcal{S}_t\mathcal{N}\alpha^*g - \mathcal{D}\mathcal{C}_n$, which leads to a contradiction of our assumption.

ii)⟹i) Suppose$(\tau_{\mathcal{R}}\mathcal{X}, \mathcal{U}, \mathfrak{W})$ is $\mathcal{S}_t\mathcal{N}\alpha^*g - \mathcal{D}\mathcal{C}_n$. Then $(\mathcal{U}, \mathfrak{W}) = (\mathcal{R}, \mathfrak{W}) \cup (\mathcal{S}, \mathfrak{W})$ where $(\mathcal{R}, \mathfrak{W})$ and $(\mathcal{S}, \mathfrak{W})$ are two mutually exclusive non-empty $\mathcal{S}_t\mathcal{N}\alpha^*g - Os$. Since $(\mathcal{R}, \mathfrak{W}) = (\mathcal{U}, \mathfrak{W})\backslash(\mathcal{S}, \mathfrak{W})$ and $(\mathcal{S}, \mathfrak{W}) = (\mathcal{U}, \mathfrak{W})\backslash(\mathcal{R}, \mathfrak{W})$, $(\mathcal{R}, \mathfrak{W}), (\mathcal{S}, \mathfrak{W}) \in \mathcal{S}_t\mathcal{N}\alpha^*gC(\tau_{\mathcal{R}}\mathcal{X}, \mathcal{U}, \mathfrak{W})$, which leads to a contradiction of our assumption.

Theorem 4.8:

i) If $\not{f}: (\tau_{\mathcal{R}}\mathcal{X}, \mathcal{U}, \mathfrak{W}) \to (\sigma_{\mathcal{R}}\mathcal{Y}, \mathcal{V}, H)$ is a $\mathcal{S}_t\mathcal{N}\alpha^*g$ −continuous surjection and $(\tau_{\mathcal{R}}\mathcal{X}, \mathcal{U}, \mathfrak{W})$ is $\mathcal{S}_t\mathcal{N}\alpha^*g - \mathcal{C}_n$, then $(\sigma_{\mathcal{R}}\mathcal{Y}, \mathcal{V}, H)$ is $\mathcal{S}_t\mathcal{N} - \mathcal{C}_n$.

ii) If $\not{f}: (\tau_{\mathcal{R}}\mathcal{X}, \mathcal{U}, \mathfrak{W}) \to (\sigma_{\mathcal{R}}\mathcal{Y}, \mathcal{V}, H)$ is a $\mathcal{S}_t\mathcal{N}\alpha^*g$ −irresolute surjection and $(\tau_{\mathcal{R}}\mathcal{X}, \mathcal{U}, \mathfrak{W})$ is $\mathcal{S}_t\mathcal{N}\alpha^*g - \mathcal{C}_n$, then $(\sigma_{\mathcal{R}}\mathcal{Y}, \mathcal{V}, H)$ is $\mathcal{S}_t\mathcal{N}\alpha^*g - \mathcal{C}_n$.

iii) If $\not{f}: (\tau_{\mathcal{R}}\mathcal{X}, \mathcal{U}, \mathfrak{W}) \to (\sigma_{\mathcal{R}}\mathcal{Y}, \mathcal{V}, H)$ is a $\mathcal{C}\mathcal{S}_t\mathcal{N}\alpha^*g$ −continuous surjection and $(\tau_{\mathcal{R}}\mathcal{X}, \mathcal{U}, \mathfrak{W})$ is $\mathcal{S}_t\mathcal{N}\alpha^*g - \mathcal{C}_n$, then $(\sigma_{\mathcal{R}}\mathcal{Y}, \mathcal{V}, H)$ is $\mathcal{S}_t\mathcal{N} - \mathcal{C}_n$.

iv) If $\not{f}: (\tau_{\mathcal{R}}\mathcal{X}, \mathcal{U}, \mathfrak{W}) \to (\sigma_{\mathcal{R}}\mathcal{Y}, \mathcal{V}, H)$ is a $\mathcal{C}\mathcal{S}_t\mathcal{N}\alpha^*g$ −irresolute surjection and $(\tau_{\mathcal{R}}\mathcal{X}, \mathcal{U}, \mathfrak{W})$ is $\mathcal{S}_t\mathcal{N}\alpha^*g - \mathcal{C}_n$, then $(\sigma_{\mathcal{R}}\mathcal{Y}, \mathcal{V}, H)$ is $\mathcal{S}_t\mathcal{N}\alpha^*g - \mathcal{C}_n$.

Proof: i) Suppose $(\sigma_{\mathcal{R}}\mathcal{Y}, \mathcal{V}, H)$ is not a $\mathcal{S}_t\mathcal{N} - \mathcal{C}_nS$. Then $(\mathcal{V}, H) = (\mathcal{R}, H) \cup (\mathcal{S}, H)$ such that $(\mathcal{R}, H)$ and $(\mathcal{S}, H)$ are mutually exclusive non-empty $\mathcal{S}_t\mathcal{N} - Os$ in $(\sigma_{\mathcal{R}}\mathcal{Y}, \mathcal{V}, H)$. Since $\not{f}$ is $\mathcal{S}_t\mathcal{N}\alpha^*g$ −continuous surjection, $(\mathcal{U}, \mathfrak{W}) = \not{f}^{-1}(\mathcal{V}, H) = \not{f}^{-1}\big((\mathcal{R}, H) \cup (\mathcal{S}, H)\big) = \not{f}^{-1}(\mathcal{R}, H) \cup \not{f}^{-1}(\mathcal{S}, H)$, where $\not{f}^{-1}(\mathcal{R}, H)$ and $\not{f}^{-1}(\mathcal{S}, H)$ are mutually exclusive non-empty $\mathcal{S}_t\mathcal{N}\alpha^*g - Os$ in $(\tau_{\mathcal{R}}\mathcal{X}, \mathcal{U}, \mathfrak{W})$. This contradicts the fact that $(\tau_{\mathcal{R}}\mathcal{X}, \mathcal{U}, \mathfrak{W})$ is $\mathcal{S}_t\mathcal{N}\alpha^*g - \mathcal{C}_n$. Hence $(\sigma_{\mathcal{R}}\mathcal{Y}, \mathcal{V}, H)$ is $\mathcal{S}_t\mathcal{N} - \mathcal{C}_n$.

Proofs of ii), iii) and iv) are similar to i).

Theorem 4.9: A $\mathcal{S}_t\mathcal{N}TS(\tau_{\mathcal{R}}\mathcal{X}, \mathcal{U}, \mathfrak{W})$ is a $\mathcal{S}_t\mathcal{N}\alpha^*g - \mathcal{C}_nS$ if and only if $(\mathcal{U}, \mathfrak{W})$ cannot be represented as a combination of any two $\mathcal{S}_t\mathcal{N}\alpha^*g - \mathcal{S}_ps$.

Proof: Assume $(\tau_{\mathcal{R}}\mathcal{X}, \mathcal{U}, \mathfrak{W})$ is a $\mathcal{S}_t\mathcal{N}\alpha^*g - \mathcal{C}_nS$. Suppose $(\mathcal{U}, \mathfrak{W}) = (\mathcal{R}, \mathfrak{W}) \cup (\mathcal{S}, \mathfrak{W})$ where $(\mathcal{R}, \mathfrak{W})$ and $(\mathcal{S}, \mathfrak{W})$ are $\mathcal{S}_t\mathcal{N}\alpha^*g - \mathcal{S}_ps$. Then $(\mathcal{R}, \mathfrak{W}) \cap \mathcal{S}_t\mathcal{N}\alpha^*gcl(\mathcal{S}, \mathfrak{W}) = \emptyset$ and $\mathcal{S}_t\mathcal{N}\alpha^*gcl(\mathcal{R}, \mathfrak{W}) \cap (\mathcal{S}, \mathfrak{W}) = \emptyset$, which implies

$\mathcal{S}_t\mathcal{N}\alpha^*gcl(\mathcal{S},\mathfrak{W}) \subseteq_{\mathcal{S}_t\mathcal{N}} (\mathcal{U},\mathfrak{W})\backslash(\mathcal{R},\mathfrak{W}) = (\mathcal{S},\mathfrak{W})$ and $\mathcal{S}_t\mathcal{N}\alpha^*gcl(\mathcal{R},\mathfrak{W}) \subseteq_{\mathcal{S}_t\mathcal{N}} (\mathcal{U},\mathfrak{W})\backslash(\mathcal{S},\mathfrak{W}) = (\mathcal{R},\mathfrak{W})$. Thus $(\mathcal{R},\mathfrak{W}),(\mathcal{S},\mathfrak{W}) \in \mathcal{S}_t\mathcal{N}\alpha^*g\mathcal{C}(\tau_{\mathcal{R}}\mathcal{X},\mathcal{U},\mathfrak{W})$. Since $(\mathcal{U},\mathfrak{W}) = (\mathcal{R},\mathfrak{W}) \cup (\mathcal{S},\mathfrak{W})$, $(\mathcal{R},\mathfrak{W}),(\mathcal{S},\mathfrak{W}) \in \mathcal{S}_t\mathcal{N}\alpha^*g\mathcal{O}(\tau_{\mathcal{R}}\mathcal{X},\mathcal{U},\mathfrak{W})$. Since $(\mathcal{R},\mathfrak{W})$ and $(\mathcal{S},\mathfrak{W})$ are $\mathcal{S}_t\mathcal{N}\alpha^*g - \mathcal{S}_p s$, they are non-empty and by theorem 3.3, they are mutually exclusive. Then the $\mathcal{S}_t\mathcal{N}\alpha^*g$ −disconnection of $(\tau_{\mathcal{R}}\mathcal{X},\mathcal{U},\mathfrak{W})$ presents a contradiction. Hence $(\mathcal{U},\mathfrak{W})$ is not a combination of any two $\mathcal{S}_t\mathcal{N}\alpha^*g - \mathcal{S}_p s$.

Conversely, assume that $(\mathcal{U},\mathfrak{W})$ is not a combination of any two $\mathcal{S}_t\mathcal{N}\alpha^*g - \mathcal{S}_p s$. Suppose $(\tau_{\mathcal{R}}\mathcal{X},\mathcal{U},\mathfrak{W})$ is $\mathcal{S}_t\mathcal{N}\alpha^*g - \mathcal{DC}_n$. Then $(\mathcal{U},\mathfrak{W}) = (\mathcal{R},\mathfrak{W}) \cup (\mathcal{S},\mathfrak{W})$ where $(\mathcal{R},\mathfrak{W})$ and $(\mathcal{S},\mathfrak{W})$ are two mutually exclusive non-empty $\mathcal{S}_t\mathcal{N}\alpha^*g - \mathcal{O}s$. Since $(\mathcal{R},\mathfrak{W}) = (\mathcal{U},\mathfrak{W})\backslash(\mathcal{S},\mathfrak{W})$ and $(\mathcal{S},\mathfrak{W}) = (\mathcal{U},\mathfrak{W})\backslash(\mathcal{R},\mathfrak{W})$, $(\mathcal{R},\mathfrak{W}),(\mathcal{S},\mathfrak{W}) \in \mathcal{S}_t\mathcal{N}\alpha^*g\mathcal{C}(\tau_{\mathcal{R}}\mathcal{X},\mathcal{U},\mathfrak{W})$. Then $(\mathcal{R},\mathfrak{W}) \cap \mathcal{S}_t\mathcal{N}\alpha^*gcl(\mathcal{S},\mathfrak{W}) = (\mathcal{R},\mathfrak{W}) \cap \mathcal{S}_t\mathcal{N}\alpha^*gcl\big((\mathcal{U},\mathfrak{W})\backslash(\mathcal{R},\mathfrak{W})\big) = (\mathcal{R},\mathfrak{W}) \cap \big((\mathcal{U},\mathfrak{W})\backslash(\mathcal{R},\mathfrak{W})\big) = \emptyset$. Similarly, $\mathcal{S}_t\mathcal{N}\alpha^*gcl(\mathcal{R},\mathfrak{W}) \cap (\mathcal{S},\mathfrak{W}) = \emptyset$. Thus $(\mathcal{R},\mathfrak{W})$ and $(\mathcal{S},\mathfrak{W})$ are $\mathcal{S}_t\mathcal{N}\alpha^*g - \mathcal{S}_p s$, which leads to a contradiction of our assumption. Hence $(\tau_{\mathcal{R}}\mathcal{X},\mathcal{U},\mathfrak{W})$ is a $\mathcal{S}_t\mathcal{N}\alpha^*g - \mathcal{C}_n S$.

Theorem 4.10: If $(\mathcal{R},\mathfrak{W})$ is $\mathcal{S}_t\mathcal{N}\alpha^*g - \mathcal{C}_n$ and $(\mathcal{S},\mathfrak{W}),(\mathcal{T},\mathfrak{W})$ are $\mathcal{S}_t\mathcal{N}\alpha^*g - \mathcal{S}_p s$ such that $(\mathcal{R},\mathfrak{W}) \subset_{\mathcal{S}_t\mathcal{N}} (\mathcal{S},\mathfrak{W}) \cup (\mathcal{T},\mathfrak{W})$, then $(\mathcal{R},\mathfrak{W})$ lies entirely in $(\mathcal{S},\mathfrak{W})$ or in $(\mathcal{T},\mathfrak{W})$.

Proof: Suppose $(\mathcal{R},\mathfrak{W}) \not\subset_{\mathcal{S}_t\mathcal{N}} (\mathcal{S},\mathfrak{W})$ and $(\mathcal{R},\mathfrak{W}) \not\subset_{\mathcal{S}_t\mathcal{N}} (\mathcal{T},\mathfrak{W})$. Let $(\mathcal{R}_1,\mathfrak{W}) = (\mathcal{R},\mathfrak{W}) \cap (\mathcal{S},\mathfrak{W})$ and $(\mathcal{R}_2,\mathfrak{W}) = (\mathcal{R},\mathfrak{W}) \cap (\mathcal{T},\mathfrak{W})$. Since $(\mathcal{R}_1,\mathfrak{W}) \subseteq_{\mathcal{S}_t\mathcal{N}} (\mathcal{S},\mathfrak{W})$, $(\mathcal{R}_2,\mathfrak{W}) \subseteq_{\mathcal{S}_t\mathcal{N}} (\mathcal{T},\mathfrak{W})$ and $(\mathcal{S},\mathfrak{W}),(\mathcal{T},\mathfrak{W})$ are $\mathcal{S}_t\mathcal{N}\alpha^*g - \mathcal{S}_p s$, $(\mathcal{R}_1,\mathfrak{W}) \cap \mathcal{S}_t\mathcal{N}\alpha^*gcl(\mathcal{R}_2,\mathfrak{W}) \subseteq_{\mathcal{S}_t\mathcal{N}} (\mathcal{S},\mathfrak{W}) \cap \mathcal{S}_t\mathcal{N}\alpha^*gcl(\mathcal{T},\mathfrak{W}) = \emptyset$. Similarly,$\mathcal{S}_t\mathcal{N}\alpha^*gcl(\mathcal{R}_1,\mathfrak{W}) \cap (\mathcal{R}_2,\mathfrak{W}) = \emptyset$.Thus $(\mathcal{R}_1,\mathfrak{W})$ and $(\mathcal{R}_2,\mathfrak{W})$ are $\mathcal{S}_t\mathcal{N}\alpha^*g - \mathcal{S}_p s$. Since $(\mathcal{R},\mathfrak{W}) \subset_{\mathcal{S}_t\mathcal{N}} (\mathcal{S},\mathfrak{W}) \cup (\mathcal{T},\mathfrak{W})$, $(\mathcal{R}_1,\mathfrak{W}) \cup (\mathcal{R}_2,\mathfrak{W}) = [(\mathcal{R},\mathfrak{W}) \cap (\mathcal{S},\mathfrak{W})] \cup [(\mathcal{R},\mathfrak{W}) \cap (\mathcal{T},\mathfrak{W})] = (\mathcal{R},\mathfrak{W}) \cap [(\mathcal{S},\mathfrak{W}) \cup (\mathcal{T},\mathfrak{W})] = (\mathcal{R},\mathfrak{W})$. Therefore $(\mathcal{R},\mathfrak{W}) = (\mathcal{R}_1,\mathfrak{W}) \cup (\mathcal{R}_2,\mathfrak{W})$ where $(\mathcal{R}_1,\mathfrak{W})$ and $(\mathcal{R}_2,\mathfrak{W})$ are $\mathcal{S}_t\mathcal{N}\alpha^*g - \mathcal{S}_p s$. Then by theorem 4.9, $(\mathcal{R},\mathfrak{W})$ is $\mathcal{S}_t\mathcal{N}\alpha^*g - \mathcal{DC}_n$, leading to a contradiction. Thus either $(\mathcal{R},\mathfrak{W}) \subset_{\mathcal{S}_t\mathcal{N}} (\mathcal{S},\mathfrak{W})$ or $(\mathcal{R},\mathfrak{W}) \subset_{\mathcal{S}_t\mathcal{N}} (\mathcal{T},\mathfrak{W})$.

Theorem 4.11: If $(\mathcal{R},\mathfrak{W})$ is $\mathcal{S}_t\mathcal{N}\alpha^*g - \mathcal{C}_n$ and $(\mathcal{R},\mathfrak{W}) \subset_{\mathcal{S}_t\mathcal{N}} (\mathcal{S},\mathfrak{W}) \subset_{\mathcal{S}_t\mathcal{N}}$ $\mathcal{S}_t\mathcal{N}\alpha^*gcl(\mathcal{R},\mathfrak{W})$, then $(\mathcal{S},\mathfrak{W})$ is $\mathcal{S}_t\mathcal{N}\alpha^*g - \mathcal{C}_n$.

Proof: Suppose $(\mathcal{S},\mathfrak{W})$ is $\mathcal{S}_t\mathcal{N}\alpha^*g - \mathcal{DC}_n$. Then by theorem 4.9, there exists two $\mathcal{S}_t\mathcal{N}\alpha^*g - \mathcal{S}_p s(\mathcal{S}_1,\mathfrak{W}),(\mathcal{S}_2,\mathfrak{W})$ such that $(\mathcal{S},\mathfrak{W}) = (\mathcal{S}_1,\mathfrak{W}) \cup (\mathcal{S}_2,\mathfrak{W})$. Since $(\mathcal{R},\mathfrak{W}) \subset_{\mathcal{S}_t\mathcal{N}} (\mathcal{S},\mathfrak{W}) = (\mathcal{S}_1,\mathfrak{W}) \cup (\mathcal{S}_2,\mathfrak{W})$, by theorem 4.10, $(\mathcal{R},\mathfrak{W}) \subset_{\mathcal{S}_t\mathcal{N}} (\mathcal{S}_1,\mathfrak{W})$ or $(\mathcal{R},\mathfrak{W}) \subset_{\mathcal{S}_t\mathcal{N}} (\mathcal{S}_2,\mathfrak{W})$. we can assume, without limiting generality that $(\mathcal{R},\mathfrak{W}) \subset_{\mathcal{S}_t\mathcal{N}} (\mathcal{S}_1,\mathfrak{W})$. Then $\mathcal{S}_t\mathcal{N}\alpha^*gcl(\mathcal{R},\mathfrak{W}) \cap (\mathcal{S}_2,\mathfrak{W}) \subset_{\mathcal{S}_t\mathcal{N}} \mathcal{S}_t\mathcal{N}\alpha^*gcl(\mathcal{S}_1,\mathfrak{W}) \cap (\mathcal{S}_2,\mathfrak{W}) = \emptyset$. Since $(\mathcal{S}_1,\mathfrak{W}) \cup (\mathcal{S}_2,\mathfrak{W}) = (\mathcal{S},\mathfrak{W}) \subset_{\mathcal{S}_t\mathcal{N}} \mathcal{S}_t\mathcal{N}\alpha^*gcl(\mathcal{R},\mathfrak{W})$, $(\mathcal{S}_2,\mathfrak{W}) \cap \mathcal{S}_t\mathcal{N}\alpha^*gcl(\mathcal{R},\mathfrak{W}) = (\mathcal{S}_2,\mathfrak{W})$. Thus $(\mathcal{S}_2,\mathfrak{W}) = \emptyset$ which is a contradiction, since $(\mathcal{S}_2,\mathfrak{W})$ is non-empty. Similarly, by taking $(\mathcal{R},\mathfrak{W}) \subset_{\mathcal{S}_t\mathcal{N}} (\mathcal{S}_2,\mathfrak{W})$, we encounter a contradiction to $(\mathcal{S}_1,\mathfrak{W}) \neq \emptyset$. Hence $(\mathcal{S},\mathfrak{W})$ is $\mathcal{S}_t\mathcal{N}\alpha^*g - \mathcal{C}_n$.

Theorem 4.12: If $(\mathcal{R},\mathfrak{W})$ is $\mathcal{S}_t\mathcal{N}\alpha^*g - \mathcal{C}_n$, then $\mathcal{S}_t\mathcal{N}\alpha^*gcl(\mathcal{R},\mathfrak{W})$ is $\mathcal{S}_t\mathcal{N}\alpha^*g - \mathcal{C}_n$.

Proof: Suppose $\mathcal{S}_t\mathcal{N}\alpha^*gcl(\mathcal{R},\mathfrak{W})$ is $\mathcal{S}_t\mathcal{N}\alpha^*g - \mathcal{DC}_n$. Then by theorem 4.9, $\mathcal{S}_t\mathcal{N}\alpha^*gcl(\mathcal{R},\mathfrak{W}) = (\mathcal{R}_1,\mathfrak{W}) \cup (\mathcal{R}_2,\mathfrak{W})$ where $(\mathcal{R}_1,\mathfrak{W})$ and $(\mathcal{R}_2,\mathfrak{W})$ are $\mathcal{S}_t\mathcal{N}\alpha^*g - \mathcal{S}_p s$. Since $(\mathcal{R},\mathfrak{W}) \subset_{\mathcal{S}_t\mathcal{N}} \mathcal{S}_t\mathcal{N}\alpha^*gcl(\mathcal{R},\mathfrak{W}) = (\mathcal{R}_1,\mathfrak{W}) \cup (\mathcal{R}_2,\mathfrak{W})$, by theorem 4.10, either $(\mathcal{R},\mathfrak{W}) \subset_{\mathcal{S}_t\mathcal{N}} (\mathcal{R}_1,\mathfrak{W})$ or $(\mathcal{R},\mathfrak{W}) \subset_{\mathcal{S}_t\mathcal{N}} (\mathcal{R}_2,\mathfrak{W})$. If $(\mathcal{R},\mathfrak{W}) \subset_{\mathcal{S}_t\mathcal{N}} (\mathcal{R}_1,\mathfrak{W})$, then $(\mathcal{R}_2,\mathfrak{W}) \subset_{\mathcal{S}_t\mathcal{N}} (\mathcal{R}_1,\mathfrak{W}) \cup (\mathcal{R}_2,\mathfrak{W}) = \mathcal{S}_t\mathcal{N}\alpha^*gcl(\mathcal{R},\mathfrak{W}) \subset_{\mathcal{S}_t\mathcal{N}} \mathcal{S}_t\mathcal{N}\alpha^*gcl(\mathcal{R}_1,\mathfrak{W})$. Also since $(\mathcal{R}_1,\mathfrak{W})$ and $(\mathcal{R}_2,\mathfrak{W})$ are $\mathcal{S}_t\mathcal{N}\alpha^*g - \mathcal{S}_p s$, $(\mathcal{R}_1,\mathfrak{W}) \cap \mathcal{S}_t\mathcal{N}\alpha^*gcl(\mathcal{R}_2,\mathfrak{W}) = \emptyset$ and $\mathcal{S}_t\mathcal{N}\alpha^*gcl(\mathcal{R}_1,\mathfrak{W}) \cap (\mathcal{R}_2,\mathfrak{W}) = \emptyset$. Then $(\mathcal{R}_2,\mathfrak{W}) \subseteq_{\mathcal{S}_t\mathcal{N}} (\mathcal{U},\mathfrak{W})\backslash\mathcal{S}_t\mathcal{N}\alpha^*gcl(\mathcal{R}_1,\mathfrak{W})$. Thus $(\mathcal{R}_2,\mathfrak{W}) \subset_{\mathcal{S}_t\mathcal{N}} \mathcal{S}_t\mathcal{N}\alpha^*gcl(\mathcal{R}_1,\mathfrak{W}) \cap \big((\mathcal{U},\mathfrak{W})\backslash\mathcal{S}_t\mathcal{N}\alpha^*gcl(\mathcal{R}_1,\mathfrak{W})\big) = \emptyset$ which leas to a contradiction, since $(\mathcal{R}_2,\mathfrak{W})$ is non-empty. Similarly, if we consider $(\mathcal{R},\mathfrak{W}) \subseteq_{\mathcal{S}_t\mathcal{N}} (\mathcal{R}_2,\mathfrak{W})$, then we encounter a contradiction to $(\mathcal{R}_1,\mathfrak{W}) \neq \emptyset$. Thus $\mathcal{S}_t\mathcal{N}\alpha^*gcl(\mathcal{R},\mathfrak{W})$ is $\mathcal{S}_t\mathcal{N}\alpha^*g - \mathcal{C}_n$.

Remark 4.13: If $(\mathcal{R},\mathfrak{W}) \subset_{\mathcal{S}_t\mathcal{N}} (\mathcal{S},\mathfrak{W}) \subset_{\mathcal{S}_t\mathcal{N}} (\mathcal{T},\mathfrak{W})$ such that $(\mathcal{R},\mathfrak{W})$ and $(\mathcal{T},\mathfrak{W})$ are both $\mathcal{S}_t\mathcal{N}\alpha^*g - \mathcal{C}_n$, then $(\mathcal{S},\mathfrak{W})$ is not necessarily $\mathcal{S}_t\mathcal{N}\alpha^*g - \mathcal{C}_n$.

Example 4.14: Let $\mathcal{U} = \{i,j,k,\ell\}$, $\mathfrak{W} = \{m_1,m_2,m_3\}$ and $\mathcal{X} = \{i,j\} \subseteq \mathcal{U}$ with $\mathcal{U}\backslash\mathcal{R} = \{\{i,j\},\{k,\ell\}\}$. Then $\mathcal{S}_t\mathcal{N}\alpha^*g\mathcal{O}(\tau_{\mathcal{R}}\mathcal{X},\mathcal{U},\mathfrak{W}) = \{\emptyset,(\mathcal{U},\mathfrak{W}),(\acute{\mathrm{K}}_2,\mathfrak{W}),(\acute{\mathrm{K}}_3,\mathfrak{W}),(\acute{\mathrm{K}}_6,\mathfrak{W}),(\acute{\mathrm{K}}_{12},\mathfrak{W}),(\acute{\mathrm{K}}_{13},\mathfrak{W})\}$. Even though $(\acute{\mathrm{K}}_2,\mathfrak{W})$ and $(\acute{\mathrm{K}}_{13},\mathfrak{W})$ are $\mathcal{S}_t\mathcal{N}\alpha^*g - \mathcal{C}_n$ and $(\acute{\mathrm{K}}_2,\mathfrak{W}) \subset_{\mathcal{S}_t\mathcal{N}} (\acute{\mathrm{K}}_6,\mathfrak{W}) \subset_{\mathcal{S}_t\mathcal{N}} (\acute{\mathrm{K}}_{13},\mathfrak{W})$, $(\acute{\mathrm{K}}_6,\mathfrak{W})$ is $\mathcal{S}_t\mathcal{N}\alpha^*g - \mathcal{DC}_n$.

Theorem 4.15: The combination of any two$\mathcal{S}_t\mathcal{N}\alpha^*g-\mathcal{C}_n s$ that have non-empty intersection is $\mathcal{S}_t\mathcal{N}\alpha^*g-\mathcal{C}_n$.
Proof: Let$(\mathcal{R},\mathfrak{W})$ and $(\mathcal{S},\mathfrak{W})$ be any two $\mathcal{S}_t\mathcal{N}\alpha^*g-\mathcal{C}_n s$ such that $(\mathcal{R},\mathfrak{W})\cap(\mathcal{S},\mathfrak{W})\neq\emptyset$. Suppose $(\mathcal{R},\mathfrak{W})\cup(\mathcal{S},\mathfrak{W})$ is $\mathcal{S}_t\mathcal{N}\alpha^*g-\mathcal{DC}_n$. Then by theorem 4.9, there exists two $\mathcal{S}_t\mathcal{N}\alpha^*g-\mathcal{S}_p s(\mathcal{R}_1,\mathfrak{W}),(\mathcal{S}_1,\mathfrak{W})$ such that $(\mathcal{R},\mathfrak{W})\cup(\mathcal{S},\mathfrak{W})=(\mathcal{R}_1,\mathfrak{W})\cup(\mathcal{S}_1,\mathfrak{W})$. Since $(\mathcal{R}_1,\mathfrak{W})$ and $(\mathcal{S}_1,\mathfrak{W})$ are $\mathcal{S}_t\mathcal{N}\alpha^*g-\mathcal{S}_p s$, $(\mathcal{R}_1,\mathfrak{W})$ and $(\mathcal{S}_1,\mathfrak{W})$ are non-empty and by theorem 3.3, $(\mathcal{R}_1,\mathfrak{W})\cap(\mathcal{S}_1,\mathfrak{W})=\emptyset$. Since $(\mathcal{R},\mathfrak{W})\subset_{\mathcal{S}_t\mathcal{N}}(\mathcal{R}_1,\mathfrak{W})\cup(\mathcal{S}_1,\mathfrak{W})$, by theorem 4.10, either $(\mathcal{R},\mathfrak{W})\subset_{\mathcal{S}_t\mathcal{N}}(\mathcal{R}_1,\mathfrak{W})$ or $(\mathcal{R},\mathfrak{W})\subset_{\mathcal{S}_t\mathcal{N}}(\mathcal{S}_1,\mathfrak{W})$. Also since $(\mathcal{S},\mathfrak{W})\subset_{\mathcal{S}_t\mathcal{N}}(\mathcal{R}_1,\mathfrak{W})\cup(\mathcal{S}_1,\mathfrak{W})$, either $(\mathcal{S},\mathfrak{W})\subset_{\mathcal{S}_t\mathcal{N}}(\mathcal{R}_1,\mathfrak{W})$ or $(\mathcal{S},\mathfrak{W})\subset_{\mathcal{S}_t\mathcal{N}}(\mathcal{S}_1,\mathfrak{W})$.
Case i) If $(\mathcal{R},\mathfrak{W})\subset_{\mathcal{S}_t\mathcal{N}}(\mathcal{R}_1,\mathfrak{W})$ and $(\mathcal{S},\mathfrak{W})\subset_{\mathcal{S}_t\mathcal{N}}(\mathcal{R}_1,\mathfrak{W})$, then $(\mathcal{R},\mathfrak{W})\cup(\mathcal{S},\mathfrak{W})=(\mathcal{R}_1,\mathfrak{W})$ and $(\mathcal{S}_1,\mathfrak{W})=\emptyset$ which is a contradiction to $(\mathcal{S}_1,\mathfrak{W})$ is non-empty.
Case ii) If $(\mathcal{R},\mathfrak{W})\subset_{\mathcal{S}_t\mathcal{N}}(\mathcal{S}_1,\mathfrak{W})$ and $(\mathcal{S},\mathfrak{W})\subset_{\mathcal{S}_t\mathcal{N}}(\mathcal{S}_1,\mathfrak{W})$, then $(\mathcal{R},\mathfrak{W})\cup(\mathcal{S},\mathfrak{W})=(\mathcal{S}_1,\mathfrak{W})$ and $(\mathcal{R}_1,\mathfrak{W})=\emptyset$ which is a contradiction to $(\mathcal{R}_1,\mathfrak{W})$ is non-empty.
Case iii) If $(\mathcal{R},\mathfrak{W})\subset_{\mathcal{S}_t\mathcal{N}}(\mathcal{R}_1,\mathfrak{W})$ and $(\mathcal{S},\mathfrak{W})\subset_{\mathcal{S}_t\mathcal{N}}(\mathcal{S}_1,\mathfrak{W})$, then $(\mathcal{R},\mathfrak{W})\cap(\mathcal{S},\mathfrak{W})\subset_{\mathcal{S}_t\mathcal{N}}(\mathcal{R}_1,\mathfrak{W})\cap(\mathcal{S}_1,\mathfrak{W})=\emptyset$ which implies $(\mathcal{R},\mathfrak{W})\cap(\mathcal{S},\mathfrak{W})=\emptyset$ which leads to a contradiction of our assumption.
Case iv) If $(\mathcal{R},\mathfrak{W})\subset_{\mathcal{S}_t\mathcal{N}}(\mathcal{S}_1,\mathfrak{W})$ and $(\mathcal{S},\mathfrak{W})\subset_{\mathcal{S}_t\mathcal{N}}(\mathcal{R}_1,\mathfrak{W})$, then $(\mathcal{R},\mathfrak{W})\cap(\mathcal{S},\mathfrak{W})\subset_{\mathcal{S}_t\mathcal{N}}(\mathcal{S}_1,\mathfrak{W})\cap(\mathcal{R}_1,\mathfrak{W})=\emptyset$ which implies $(\mathcal{R},\mathfrak{W})\cap(\mathcal{S},\mathfrak{W})=\emptyset$ which leads to a contradiction of our assumption. Hence $(\mathcal{R},\mathfrak{W})\cup(\mathcal{S},\mathfrak{W})$ is $\mathcal{S}_t\mathcal{N}\alpha^*g-\mathcal{C}_n$.

Soft nano α^*-generalized hyperconnectedness

Hyper connected spaces lack disconnected components, playing a crucial role in understanding strong connectivity properties and the structure of certain topological spaces. This segment introduces a novel form of hyper connectedness in soft nano topology namely soft nano α^*-generalized hyperconnectedness, elucidating its distinctive properties and implications for soft nano topological space analysis.

Definition 5.1: A subset $(\mathcal{R},\mathfrak{W})$ of a $\mathcal{S}_t\mathcal{N}TS(\tau_{\mathcal{R}}\mathcal{X},\mathrm{U},\mathfrak{W})$ is said to be
1) $\mathcal{S}_t\mathcal{N}\alpha^*g-$dense if $\mathcal{S}_t\mathcal{N}\alpha^*gcl(\mathcal{R},\mathfrak{W})=(\mathrm{U},\mathfrak{W})$
2) $\mathcal{S}_t\mathcal{N}\alpha^*g-$nowhere dense if $\mathcal{S}_t\mathcal{N}\alpha^*gint\big(\mathcal{S}_t\mathcal{N}\alpha^*gcl(\mathcal{R},\mathfrak{W})\big)=\emptyset$

Definition 5.2: A $\mathcal{S}_t\mathcal{N}TS(\tau_{\mathcal{R}}\mathcal{X},\mathrm{U},\mathfrak{W})$ is called soft nano α^*-generalized hyperconnected $(\mathcal{S}_t\mathcal{N}\alpha^*g-\mathcal{HC}_n)$ if every non-empty $\mathcal{S}_t\mathcal{N}\alpha^*g-Os$ of $(\tau_{\mathcal{R}}\mathcal{X},\mathrm{U},\mathfrak{W})$ is $\mathcal{S}_t\mathcal{N}\alpha^*g-$dense.

Example 5.3: Let $\mathrm{U}=\{i,j,k,\ell\}$, $\mathfrak{W}=\{m_1,m_2,m_3\}$ and $\mathcal{X}=\{i,k\}\subseteq\mathrm{U}$ with $\mathrm{U}\backslash\mathcal{R}=\{\{k\},\{j,\ell\}\}$. Then $\mathcal{S}_t\mathcal{N}\alpha^*gO(\tau_{\mathcal{R}}\mathcal{X},\mathrm{U},\mathfrak{W})=\{\emptyset,(\mathrm{U},\mathfrak{W}),(\acute{\mathrm{K}}_4,\mathfrak{W}),(\acute{\mathrm{K}}_7,\mathfrak{W}),(\acute{\mathrm{K}}_9,\mathfrak{W}),(\acute{\mathrm{K}}_{11},\mathfrak{W}),(\acute{\mathrm{K}}_{12},\mathfrak{W}),(\acute{\mathrm{K}}_{14},\mathfrak{W}),(\acute{\mathrm{K}}_{15},\mathfrak{W})\}$. Since every non-empty $\mathcal{S}_t\mathcal{N}\alpha^*g-Os$ of $(\tau_{\mathcal{R}}\mathcal{X},\mathrm{U},\mathfrak{W})$ is $\mathcal{S}_t\mathcal{N}\alpha^*g-$dense, $(\tau_{\mathcal{R}}\mathcal{X},\mathrm{U},\mathfrak{W})$ is $\mathcal{S}_t\mathcal{N}\alpha^*g-\mathcal{HC}_n$.

Theorem 5.4: For any $\mathcal{S}_t\mathcal{N}TS(\tau_{\mathcal{R}}\mathcal{X},\mathrm{U},\mathfrak{W})$, the subsequent assertions are equivalent.
i) $(\tau_{\mathcal{R}}\mathcal{X},\mathrm{U},\mathfrak{W})$ is $\mathcal{S}_t\mathcal{N}\alpha^*g-\mathcal{HC}_n$.
i) For every soft nano set $(\mathcal{R},\mathfrak{W})$ of $(\tau_{\mathcal{R}}\mathcal{X},\mathrm{U},\mathfrak{W})$, $(\mathcal{R},\mathfrak{W})$ is either $\mathcal{S}_t\mathcal{N}\alpha^*g-$dense or $\mathcal{S}_t\mathcal{N}\alpha^*g-$nowhere dense.
ii) Any pair of non-empty $\mathcal{S}_t\mathcal{N}\alpha^*g-Os$of $(\tau_{\mathcal{R}}\mathcal{X},\mathrm{U},\mathfrak{W})$ has non-empty intersection.
Proof: i)⟹ii) Let$(\mathcal{R},\mathfrak{W})$ be a soft nano set of $(\tau_{\mathcal{R}}\mathcal{X},\mathrm{U},\mathfrak{W})$, which is not $\mathcal{S}_t\mathcal{N}\alpha^*g-$nowhere dense. Then $\mathcal{S}_t\mathcal{N}\alpha^*gint\big(\mathcal{S}_t\mathcal{N}\alpha^*gcl(\mathcal{R},\mathfrak{W})\big)\neq\emptyset$. Since $(\tau_{\mathcal{R}}\mathcal{X},\mathrm{U},\mathfrak{W})$ is $\mathcal{S}_t\mathcal{N}\alpha^*g-\mathcal{HC}_n$ and $\mathcal{S}_t\mathcal{N}\alpha^*gint\big(\mathcal{S}_t\mathcal{N}\alpha^*gcl(\mathcal{R},\mathfrak{W})\big)\in\mathcal{S}_t\mathcal{N}\alpha^*gO(\tau_{\mathcal{R}}\mathcal{X},\mathrm{U},\mathfrak{W})$, $\mathcal{S}_t\mathcal{N}\alpha^*gint\big(\mathcal{S}_t\mathcal{N}\alpha^*gcl(\mathcal{R},\mathfrak{W})\big)$ is $\mathcal{S}_t\mathcal{N}\alpha^*g-$dense. Then $\mathcal{S}_t\mathcal{N}\alpha^*gcl\Big(\mathcal{S}_t\mathcal{N}\alpha^*gint\big(\mathcal{S}_t\mathcal{N}\alpha^*gcl(\mathcal{R},\mathfrak{W})\big)\Big)=(\mathrm{U},\mathfrak{W})\subseteq_{\mathcal{S}_t\mathcal{N}}\mathcal{S}_t\mathcal{N}\alpha^*gcl(\mathcal{R},\mathfrak{W})$, which implies $\mathcal{S}_t\mathcal{N}\alpha^*gcl(\mathcal{R},\mathfrak{W})=(\mathrm{U},\mathfrak{W})$ and hence $(\mathcal{R},\mathfrak{W})$ is $\mathcal{S}_t\mathcal{N}\alpha^*g-$dense.
ii)⟹iii) Suppose$(\mathcal{R},\mathfrak{W})$ and $(\mathcal{S},\mathfrak{W})$ be any two non-empty $\mathcal{S}_t\mathcal{N}\alpha^*g-Os$ of $(\tau_{\mathcal{R}}\mathcal{X},\mathrm{U},\mathfrak{W})$ such that $(\mathcal{R},\mathfrak{W})\cap(\mathcal{S},\mathfrak{W})=\emptyset$. Then $\mathcal{S}_t\mathcal{N}\alpha^*gcl(\mathcal{R},\mathfrak{W})\cap(\mathcal{S},\mathfrak{W})=\emptyset$. Since $(\mathcal{S},\mathfrak{W})\neq\emptyset$, $\mathcal{S}_t\mathcal{N}\alpha^*gcl(\mathcal{R},\mathfrak{W})\neq(\mathrm{U},\mathfrak{W})$ and hence $(\mathcal{R},\mathfrak{W})$ is not $\mathcal{S}_t\mathcal{N}\alpha^*g-$dense. Since $(\mathcal{R},\mathfrak{W})\in\mathcal{S}_t\mathcal{N}\alpha^*gO(\tau_{\mathcal{R}}\mathcal{X},\mathrm{U},\mathfrak{W})$, $(\mathcal{R},\mathfrak{W})=\mathcal{S}_t\mathcal{N}\alpha^*gint(\mathcal{R},\mathfrak{W})\subseteq_{\mathcal{S}_t\mathcal{N}}\mathcal{S}_t\mathcal{N}\alpha^*gint\big(\mathcal{S}_t\mathcal{N}\alpha^*gcl(\mathcal{R},\mathfrak{W})\big)$. Since $(\mathcal{R},\mathfrak{W})\neq\emptyset$, $\mathcal{S}_t\mathcal{N}\alpha^*gint\big(\mathcal{S}_t\mathcal{N}\alpha^*gcl(\mathcal{R},\mathfrak{W})\big)\neq\emptyset$. Then $(\mathcal{R},\mathfrak{W})$ is not $\mathcal{S}_t\mathcal{N}\alpha^*g-$nowhere dense. Hence $(\mathcal{R},\mathfrak{W})$ is neither $\mathcal{S}_t\mathcal{N}\alpha^*g-$ dense nor $\mathcal{S}_t\mathcal{N}\alpha^*g-$nowhere dense, which encounter contradiction to our assumption.

iii)⟹i) Suppose$(\tau_{\mathcal{R}}\mathcal{X}, \mathcal{U}, \mathfrak{W})$ is not $\mathcal{S}_t\mathcal{N}\alpha^*g - \mathcal{HC}_n$. Then there exists a non-empty $\mathcal{S}_t\mathcal{N}\alpha^*g - Os(\mathcal{T}, \mathfrak{W})$ of $(\tau_{\mathcal{R}}\mathcal{X}, \mathcal{U}, \mathfrak{W})$, which is not $\mathcal{S}_t\mathcal{N}\alpha^*g$ −dense. Then $\mathcal{S}_t\mathcal{N}\alpha^*gcl(\mathcal{T}, \mathfrak{W}) \neq (\mathcal{U}, \mathfrak{W})$. Thus $(\mathcal{U}, \mathfrak{W}) \backslash \mathcal{S}_t\mathcal{N}\alpha^*gcl(\mathcal{T}, \mathfrak{W})$ and $(\mathcal{T}, \mathfrak{W})$ are non-empty $\mathcal{S}_t\mathcal{N}\alpha^*g - Os$ of $(\tau_{\mathcal{R}}\mathcal{X}, \mathcal{U}, \mathfrak{W})$ such that $\big((\mathcal{U}, \mathfrak{W}) \backslash \mathcal{S}_t\mathcal{N}\alpha^*gcl(\mathcal{T}, \mathfrak{W})\big) \cap (\mathcal{T}, \mathfrak{W}) = \emptyset$, which encounter contradiction to our assumption. Hence $(\tau_{\mathcal{R}}\mathcal{X}, \mathcal{U}, \mathfrak{W})$ is $\mathcal{S}_t\mathcal{N}\alpha^*g - \mathcal{HC}_n$.

Remark 5.5: In a $\mathcal{S}_t\mathcal{N}TS(\tau_{\mathcal{R}}\mathcal{X}, \mathcal{U}, \mathfrak{W})$, if $\mathcal{S}_t\mathcal{N}\alpha^*gO(\tau_{\mathcal{R}}\mathcal{X}, \mathcal{U}, \mathfrak{W}) = \{\emptyset, (\mathcal{U}, \mathfrak{W})\}$, then $(\tau_{\mathcal{R}}\mathcal{X}, \mathcal{U}, \mathfrak{W})$ is $\mathcal{S}_t\mathcal{N}\alpha^*g - \mathcal{HC}_n$.

Theorem 5.6: If $\mathcal{S}_t\mathcal{N}\alpha^*gO(\tau_{\mathcal{R}}\mathcal{X}, \mathcal{U}, \mathfrak{W}) = \{\emptyset, (\mathcal{U}, \mathfrak{W}), (\mathcal{R}, \mathfrak{W})\}$, then $(\tau_{\mathcal{R}}\mathcal{X}, \mathcal{U}, \mathfrak{W})$ is $\mathcal{S}_t\mathcal{N}\alpha^*g - \mathcal{HC}_n$.
Proof: Since $(\mathcal{U}, \mathfrak{W})$ and $(\mathcal{R}, \mathfrak{W})$ are the only non-empty $\mathcal{S}_t\mathcal{N}\alpha^*g - Os$ of $(\tau_{\mathcal{R}}\mathcal{X}, \mathcal{U}, \mathfrak{W})$, $(\mathcal{U}, \mathfrak{W}) \cap (\mathcal{R}, \mathfrak{W}) = (\mathcal{R}, \mathfrak{W}) \neq \emptyset$. Then by theorem 5.4, $(\tau_{\mathcal{R}}\mathcal{X}, \mathcal{U}, \mathfrak{W})$ is $\mathcal{S}_t\mathcal{N}\alpha^*g - \mathcal{HC}_n$.

Theorem 5.7: Every $\mathcal{S}_t\mathcal{N}\alpha^*g - \mathcal{HC}_nS$ is $\mathcal{S}_t\mathcal{N}\alpha^*g - \mathcal{C}_n$.

Proof: Let $(\tau_{\mathcal{R}}\mathcal{X}, \mathcal{U}, \mathfrak{W})$ be $\mathcal{S}_t\mathcal{N}\alpha^*g - \mathcal{HC}_n$. Then by theorem 5.4, the intersection of any two non-empty $\mathcal{S}_t\mathcal{N}\alpha^*g - Os$ of $(\tau_{\mathcal{R}}\mathcal{X}, \mathcal{U}, \mathfrak{W})$ is non-empty. Thus $(\mathcal{U}, \mathfrak{W})$ cannot be expressed as the combination of any two mutually exclusive non-empty $\mathcal{S}_t\mathcal{N}\alpha^*g - Os$ of $(\tau_{\mathcal{R}}\mathcal{X}, \mathcal{U}, \mathfrak{W})$. Hence $(\tau_{\mathcal{R}}\mathcal{X}, \mathcal{U}, \mathfrak{W})$ is $\mathcal{S}_t\mathcal{N}\alpha^*g - \mathcal{C}_n$.

Remark 5.8: The reverse of the aforementioned theorem may not hold true, as demonstrated by the subsequent example.

Example 5.9: Let $\mathcal{U} = \{i, j, k, \ell\}$, $\mathfrak{W} = \{m_1, m_2, m_3\}$ and $\mathcal{X} = \{j, \ell\} \subseteq \mathcal{U}$ with $\mathcal{U} \backslash \mathcal{R} = \{\{i\}, \{j\}, \{k, \ell\}\}$. Then $\mathcal{S}_t\mathcal{N}\alpha^*gO(\tau_{\mathcal{R}}\mathcal{X}, \mathcal{U}, \mathfrak{W}) = \{\emptyset, (\mathcal{U}, \mathfrak{W}), (\acute{\mathrm{K}}_3, \mathfrak{W}), (\acute{\mathrm{K}}_4, \mathfrak{W}), (\acute{\mathrm{K}}_5, \mathfrak{W}), (\acute{\mathrm{K}}_9, \mathfrak{W}), (\acute{\mathrm{K}}_{10}, \mathfrak{W}), (\acute{\mathrm{K}}_{11}, \mathfrak{W}), (\acute{\mathrm{K}}_{15}, \mathfrak{W})\}$. Here $(\tau_{\mathcal{R}}\mathcal{X}, \mathcal{U}, \mathfrak{W})$ is $\mathcal{S}_t\mathcal{N}\alpha^*g - \mathcal{C}_n$ but not $\mathcal{S}_t\mathcal{N}\alpha^*g - \mathcal{HC}_n$, since only $(\mathcal{U}, \mathfrak{W})$ and $(\acute{\mathrm{K}}_{15}, \mathfrak{W})$ are $\mathcal{S}_t\mathcal{N}\alpha^*g$ −dense.

Theorem 5.10: In a $\mathcal{S}_t\mathcal{N}TS(\tau_{\mathcal{R}}\mathcal{X}, \mathcal{U}, \mathfrak{W})$, the subsequent assertions are equivalent.

a) $(\tau_{\mathcal{R}}\mathcal{X}, \mathcal{U}, \mathfrak{W})$ is $\mathcal{S}_t\mathcal{N}\alpha^*g - \mathcal{HC}_n$.
b) $\mathcal{S}_t\mathcal{N}\alpha^*g$ −interior of every proper $\mathcal{S}_t\mathcal{N}\alpha^*g - Cs$ of $(\tau_{\mathcal{R}}\mathcal{X}, \mathcal{U}, \mathfrak{W})$ is empty.

Proof: a) ⇒ b) Let $(\tau_{\mathcal{R}}\mathcal{X}, \mathcal{U}, \mathfrak{W})$ is $\mathcal{S}_t\mathcal{N}\alpha^*g - \mathcal{HC}_n$. If $(\mathcal{R}, \mathfrak{W})$ is a proper $\mathcal{S}_t\mathcal{N}\alpha^*g - Os$ in $(\tau_{\mathcal{R}}\mathcal{X}, \mathcal{U}, \mathfrak{W})$, then $(\mathcal{R}, \mathfrak{W})^c$ is a proper $\mathcal{S}_t\mathcal{N}\alpha^*g - Cs$ in $(\tau_{\mathcal{R}}\mathcal{X}, \mathcal{U}, \mathfrak{W})$. By remark 2.7 a), $\mathcal{S}_t\mathcal{N}\alpha^*gint(\mathcal{R}, \mathfrak{W})^c = \big(\mathcal{S}_t\mathcal{N}\alpha^*gcl(\mathcal{R}, \mathfrak{W})\big)^c$. Since $(\tau_{\mathcal{R}}\mathcal{X}, \mathcal{U}, \mathfrak{W})$ is $\mathcal{S}_t\mathcal{N}\alpha^*g - \mathcal{HC}_n$, $(\mathcal{R}, \mathfrak{W})$ is $\mathcal{S}_t\mathcal{N}\alpha^*g$ −dense which implies $\mathcal{S}_t\mathcal{N}\alpha^*gcl(\mathcal{R}, \mathfrak{W}) = (\mathcal{U}, \mathfrak{W})$. Therefore, $\mathcal{S}_t\mathcal{N}\alpha^*gint(\mathcal{R}, \mathfrak{W})^c = \emptyset$.b) ⇒ a) Assume that the $\mathcal{S}_t\mathcal{N}\alpha^*g$ −interior of every proper $\mathcal{S}_t\mathcal{N}\alpha^*g - Cs$ of $(\tau_{\mathcal{R}}\mathcal{X}, \mathcal{U}, \mathfrak{W})$ is empty. If $(\mathcal{R}, \mathfrak{W})$ is a proper $\mathcal{S}_t\mathcal{N}\alpha^*g - Cs$ in $(\tau_{\mathcal{R}}\mathcal{X}, \mathcal{U}, \mathfrak{W})$, then $(\mathcal{R}, \mathfrak{W})^c$ is a proper $\mathcal{S}_t\mathcal{N}\alpha^*g - Os$ in $(\tau_{\mathcal{R}}\mathcal{X}, \mathcal{U}, \mathfrak{W})$ and by our assumption, $\mathcal{S}_t\mathcal{N}\alpha^*gint(\mathcal{R}, \mathfrak{W}) = \emptyset$. By remark 2.7 b), $\mathcal{S}_t\mathcal{N}\alpha^*gcl(\mathcal{R}, \mathfrak{W})^c = \big(\mathcal{S}_t\mathcal{N}\alpha^*gint(\mathcal{R}, \mathfrak{W})\big)^c$. Then $\mathcal{S}_t\mathcal{N}\alpha^*gcl(\mathcal{R}, \mathfrak{W})^c = (\mathcal{U}, \mathfrak{W})$, for every proper $\mathcal{S}_t\mathcal{N}\alpha^*g - Os$ in $(\tau_{\mathcal{R}}\mathcal{X}, \mathcal{U}, \mathfrak{W})$and obviously, $\mathcal{S}_t\mathcal{N}\alpha^*gcl(\mathcal{U}, \mathfrak{W}) = (\mathcal{U}, \mathfrak{W})$. Thus $(\mathcal{R}, \mathfrak{W})$ is $\mathcal{S}_t\mathcal{N}\alpha^*g$ −dense for every non-empty $\mathcal{S}_t\mathcal{N}\alpha^*g - Os(\mathcal{R}, \mathfrak{W})$ of $(\tau_{\mathcal{R}}\mathcal{X}, \mathcal{U}, \mathfrak{W})$. Hence $(\tau_{\mathcal{R}}\mathcal{X}, \mathcal{U}, \mathfrak{W})$ is $\mathcal{S}_t\mathcal{N}\alpha^*g - \mathcal{HC}_n$.

Theorem 5.11: A$\mathcal{S}_t\mathcal{N}TS(\tau_{\mathcal{R}}\mathcal{X}, \mathcal{U}, \mathfrak{W})$ is $\mathcal{S}_t\mathcal{N}\alpha^*g - \mathcal{HC}_n$ if and only if the combination of any two non-universal $\mathcal{S}_t\mathcal{N}\alpha^*g - Cs$ is not universal.
Proof: Let $(\tau_{\mathcal{R}}\mathcal{X}, \mathcal{U}, \mathfrak{W})$ be $\mathcal{S}_t\mathcal{N}\alpha^*g - \mathcal{HC}_n$ and $(\mathcal{R}, \mathfrak{W})$,$(\mathcal{S}, \mathfrak{W})$ be two $\mathcal{S}_t\mathcal{N}\alpha^*g - Cs$ such that $(\mathcal{R}, \mathfrak{W}) \neq (\mathcal{U}, \mathfrak{W})$ and $(\mathcal{S}, \mathfrak{W}) \neq (\mathcal{U}, \mathfrak{W})$. Then $(\mathcal{R}, \mathfrak{W})^c$ and $(\mathcal{S}, \mathfrak{W})^c$ are non-empty $\mathcal{S}_t\mathcal{N}\alpha^*g - Os$. Since $(\tau_{\mathcal{R}}\mathcal{X}, \mathcal{U}, \mathfrak{W})$ is $\mathcal{S}_t\mathcal{N}\alpha^*g - \mathcal{HC}_n$, by theorem 5.4, $(\mathcal{R}, \mathfrak{W})^c \cap (\mathcal{S}, \mathfrak{W})^c \neq \emptyset$. This implies $\big((\mathcal{R}, \mathfrak{W}) \cup (\mathcal{S}, \mathfrak{W})\big)^c \neq \emptyset$ and hence $(\mathcal{R}, \mathfrak{W}) \cup (\mathcal{S}, \mathfrak{W}) \neq (\mathcal{U}, \mathfrak{W})$.
Conversely, let $(\mathcal{R}, \mathfrak{W})$,$(\mathcal{S}, \mathfrak{W})$ be two $\mathcal{S}_t\mathcal{N}\alpha^*g - Cs$ such that $(\mathcal{R}, \mathfrak{W}) \neq (\mathcal{U}, \mathfrak{W})$, $(\mathcal{S}, \mathfrak{W}) \neq (\mathcal{U}, \mathfrak{W})$ and $(\mathcal{R}, \mathfrak{W}) \cup (\mathcal{S}, \mathfrak{W}) \neq (\mathcal{U}, \mathfrak{W})$. Then $\big((\mathcal{R}, \mathfrak{W}) \cup (\mathcal{S}, \mathfrak{W})\big)^c \neq \emptyset$ which implies $(\mathcal{R}, \mathfrak{W})^c \cap (\mathcal{S}, \mathfrak{W})^c \neq \emptyset$, where $(\mathcal{R}, \mathfrak{W})^c$ and $(\mathcal{S}, \mathfrak{W})^c$ are non-empty $\mathcal{S}_t\mathcal{N}\alpha^*g - Os$. Then by theorem 5.4, $(\tau_{\mathcal{R}}\mathcal{X}, \mathcal{U}, \mathfrak{W})$ is $\mathcal{S}_t\mathcal{N}\alpha^*g - \mathcal{HC}_n$.

Theorem 5.12: $\mathcal{S}_t\mathcal{N}\alpha^*g$ −irresolute surjective image of a $\mathcal{S}_t\mathcal{N}\alpha^*g - \mathcal{HC}_nS$ is $\mathcal{S}_t\mathcal{N}\alpha^*g - \mathcal{HC}_n$.
Proof: Let $\not{f}: (\tau_{\mathcal{R}}\mathcal{X}, \mathcal{U}, \mathfrak{W}) \to (\sigma_{\mathcal{R}}\mathcal{Y}, \mathcal{V}, H)$ be a $\mathcal{S}_t\mathcal{N}\alpha^*g$ −irresolute surjection and $(\tau_{\mathcal{R}}\mathcal{X}, \mathcal{U}, \mathfrak{W})$ be $\mathcal{S}_t\mathcal{N}\alpha^*g - \mathcal{HC}_n$. Suppose $(\sigma_{\mathcal{R}}\mathcal{Y}, \mathcal{V}, H)$ is not $\mathcal{S}_t\mathcal{N}\alpha^*g - \mathcal{HC}_n$. Then there exists a non-empty $\mathcal{S}_t\mathcal{N}\alpha^*g - Os(\mathcal{R}, H)$ of $(\sigma_{\mathcal{R}}\mathcal{Y}, \mathcal{V}, H)$, which

is not $\mathcal{S}_t\mathcal{N}\alpha^*g$ −dense, that is $\mathcal{S}_t\mathcal{N}\alpha^*gcl(\mathcal{R},H) \neq (\mathcal{V},H)$. Since $\oint$ is $\mathcal{S}_t\mathcal{N}\alpha^*g$ −irresolute surjection, $\oint^{-1}(\mathcal{R},H) \in \mathcal{S}_t\mathcal{N}\alpha^*gO(\tau_{\mathcal{R}}\mathcal{X},\mathcal{U},\mathfrak{W})$ and by remark 2.9, $\mathcal{S}_t\mathcal{N}\alpha^*gcl\left(\oint^{-1}(\mathcal{R},H)\right) \subseteq_{\mathcal{S}_t\mathcal{N}} \oint^{-1}\left(\mathcal{S}_t\mathcal{N}\alpha^*gcl(\mathcal{R},H)\right) \neq \oint^{-1}(\mathcal{V},H)$, which implies $\mathcal{S}_t\mathcal{N}\alpha^*gcl\left(\oint^{-1}(\mathcal{R},H)\right) \neq (\mathcal{U},\mathfrak{W})$. Thus $\oint^{-1}(\mathcal{R},H)$ is a non-empty $\mathcal{S}_t\mathcal{N}\alpha^*g - Os$ of $(\tau_{\mathcal{R}}\mathcal{X},\mathcal{U},\mathfrak{W})$, which is not $\mathcal{S}_t\mathcal{N}\alpha^*g$ −dense. This encounters a contradiction to $(\tau_{\mathcal{R}}\mathcal{X},\mathcal{U},\mathfrak{W})$ is $\mathcal{S}_t\mathcal{N}\alpha^*g - \mathcal{HC}_n$. Hence $(\sigma_{\mathcal{R}}\mathcal{Y},\mathcal{V},H)$ is $\mathcal{S}_t\mathcal{N}\alpha^*g - \mathcal{HC}_n$.

CONCLUSION

This article delves into the realm of soft nano topology, shedding light on the significance of soft nano α^* −generalized connected spaces by introducing soft nano α^* −generalized separate sets. Their properties, equivalent conditions, interrelation with relevant examples and the intricacies of their preservation theorem are thoroughly explored. Additionally, the idea of soft nano α^* −generalized hyperconnected spaces are discussed along with its characteristics. Nowadays soft nano sets find diverse applications including machine reasoning, artificial neural networks, and databases for smart computing, among others. Soft nano topology, with its focus on connectedness and hyper connectedness, revolutionizes nanoscience by enabling precise control over molecular interactions, fostering innovations in diverse fields like medicine and electronics.

Conflict of Interest

"The authors declare no conflict of interests".

REFERENCES

1. Adiya K. Hussein, *S*-Hyperconnectedness*, IQSR Journal of Mathematics, 11(4) (2015), 66-72.
2. P. Anbarasi Rodrigo, P. Subithra, *Soft nano alpha star generalized closed sets in soft nano topological spaces,* Bulletin of the Calcutta Mathematical Society (communicated).
3. P. Anbarasi Rodrigo, P. Subithra, *Soft nano alpha star generalized continuous and irresolute functions in soft nano topological* spaces, proceedings of the International Conference on Applied Mathematics and Computing, (2023), 28-34, ISBN: 978-93-90956-07-4.
4. P. Anbarasi Rodrigo, P. Subithra ,*Contra functions on soft nano alpha star generalized closed sets in soft nano topological spaces,* Indian Journal of Pure and Applied Mathematics (communicated).
5. S.S. Benchalli, P.G. Patil, N.S. Kabbur, J. Pradeepkumar, *Weaker forms of soft nano open sets*, Journal of Computer and Mathematical Sciences, 8(11) (2017), 589-599.
6. S. Krishnaprakash, R. Ramesh and R. Suresh, *Nano-compactness and Nano-connectedness in nano topological space*, International Journal of Pure and Applied Mathematics, 119(13) (2018), 107-115.
7. M. Lellis Thivagar, Carmel Richard, *On Nano forms of weakly open sets*, International Journal of Mathematical and Statistics Invention, 1(1) (2012), 31-37.
8. M. Lellis Thivagar, I. Geetha Antoinette, *Note on nano hyper connected spaces*, South East Asian Journal of Mathematics and Mathematical Sciences, 15(1) (2019), 25-36.
9. Lynn Arthur Steen, J. Arthur Seebach, Jr., Counter examples in topology, Holt, Rinehart and Winston, 1970.
10. D. Molodtsov, *Soft set theory-First results*, Computers & Mathematics with Applications, 37 (1999), 19-31.
11. Muhammad Shabir, Munazza Naz, *On soft topological spaces*, Computers & Mathematics with Applications, 61 (2011), 1786-1799.
12. P.G. Patil, S. S. Benakanawari, *New version of soft nano compactness and soft nano connectedness*, Advances in Mathematics: Scientific journal, 9(4) (2020), 1787-1794.
13. P. Subbulakshmi, N.R. Santhi Maheswari, *Some new form of nano connectedness and nano compactness in nano topological spaces,* International Journal of Creative Research Thoughts, 11(4) (2023), 48-55.
14. R.L Wilder, *Evolution of the topological concept of connected*, The American Mathematical Monthly, 85(9) (1978), 720-726, JSTOR 2321676.

RESEARCH ARTICLE

Discrete Labeling of Some Trees

A.Punitha Tharani[1] and P.Saradha[2]*

[1]Associate Professor, Department of Mathematics, St. Mary's, College(Autonomous), Thoothukudi, Tamil Nadu, India, (Affiliated to Manonmaniam Sundaranar University, Abishekapatti, Tirunelveli), Tamil Nadu, India.

[2]Research Scholar (Register number: 21212212092005), Department of Mathematics, St.Mary's College (Autonomous), Thoothukudi, Tamil Nadu, India, (Affiliated to Manonmaniam Sundaranar University, Abishekapatti, Tirunelveli), Tamil Nadu, India.

Received: 22 Feb 2024 Revised: 06 Mar 2024 Accepted: 20 Mar 2024

***Address for Correspondence**
P.Saradha
Research Scholar (Register number: 21212212092005),
Department of Mathematics, St.Mary's College (Autonomous),
Thoothukudi, Tamil Nadu, India, (Affiliated to Manonmaniam Sundaranar University, Abishekapatti, Tirunelveli), Tamil Nadu, India.
Email: sara1998dha@gmail.com

ABSTRACT

In this paper we deal with Discrete labeling of some trees. We have previously defined discrete labeling which aims at providing the maximum output whenever the inputs are distinct with rational distribution of neighbours thereby exhibiting the stronger form of cordial labeling. This work serves as an aid in decision making. The discrete labels 0 and 1 are cordially assigned to the vertices such that the edges receive labels depending on the incident vertex labels using EX-OR operation with the condition that for every vertex the cardinality of neighbours labeled 0 and 1 differs by at most 1.This paper proposes the discrete labeling of some trees like H-graph, Perfect binary tree and Banana tree. We discuss various cases under which the above said graphs satisfy discrete labeling.

Keywords: Discrete, neighbours, H-graph, Perfect binary tree, Banana tree.

INTRODUCTION

Labeling of graphs is a function that maps the vertex set (edge set) to the set of labels. Here, the domain and co domain are the set of vertices and {0, 1} respectively. Motivated by the cordial labeling [1], we have previously defined a new type of labeling called "Discrete labeling" [2] which assigns labels using EX-OR operations. In our previous works, we have proved that certain standard graphs like path, star, comb, bistar, complete bipartite, broom and some special graphs are discrete. We have also found that friendship graphs, complete graphs, book graphs are

not discrete[2][3]. There are also graphs like cycle C_n , wheel $W_{1,n}$ which are discrete only for some n. We have found that certain standard and special graphs are discrete and obtained conditions under which some cycle related graphs admit discrete labeling. In this paper, we have obtained the discrete labeling of some trees. The graph $G(V,E)$ discussed here are simple, connected and undirected. The terminologies and symbols used in this paper are in accordance with [4].

METHODS

Definition 2.1: Let $G(V,E)$be a simple, connected, undirected graph.G is said to have a discrete labeling if there exist functions $d: V \to \{0,1\}$ and $e: E \to \{0,1\}$ defined by

$e(uv) = \begin{cases} 0 \ ; d(u) = d(v) \\ 1 \ ; \ d(u) \neq d(v) \end{cases} u, v \in V$for which

$|n_d(0) - n_d(1)| \leq 1$ ---(i)

$|n_e(0) - n_e(1)| \leq 1$and ---(ii)

$\left|n_{N(v)}(0) - n_{N(v)}(1)\right| \leq 1 \ \forall \ v \in V$, ---(iii)

where $n_d(x) and \ n_e(x)$ denote the number of vertices and edges with $d(u) = x$ and $e(uv) = x \ ; x \in \{0,1\}$ respectively and$n_{N(v)}(0) \ and \ n_{N(v)}(1)$ denote the number of neighbours of the vertex v labeled 0 and 1 respectively. A Graph G is discrete if it admits discrete labeling.[2]

RESULTS AND DISCUSSION

Theorem 3.1:

H-graph is discrete

Proof: The H-graph is the graph obtained from two copies of path P_n with the vertices $u_1, u_2, \dots, u_n$ and $v_1, v_2, \dots, v_n$ by joining the vertices $u_{\frac{n+1}{2}}$ and $v_{\frac{n+1}{2}}$ if n is odd and $u_{\frac{n}{2}+1}$ and $v_{\frac{n}{2}}$ if n is even.Thus the H-graph has $2n$ vertices and $2n-1$ edges.

Define a vertex function $f: V \to \{0,1\}$ by

$$f(u_1) = 0$$

$$f(u_{2i}) = f(u_{2i+1}) = \begin{cases} 1 & when\ i\ is\ odd \\ 0 & when\ i\ is\ even \end{cases}$$

Now let us label the vertices $v_i's$ as follows:

Case 1: When $n \equiv 0 \ mod \ 4$

$$f(v_1) = 0$$

$$f(v_{2i}) = f(v_{2i+1}) = \begin{cases} 1 & when\ i\ is\ odd \\ 0 & when\ i\ is\ even \end{cases}$$

Case 2: When $n \equiv 1 \ mod \ 4$

$$f(v_{2i}) = f(v_{2i-1}) = \begin{cases} 1 & when\ i\ is\ odd \\ 0 & when\ i\ is\ even \end{cases}$$

Case 3: When $n \equiv 2 \ mod \ 4$

$$f(v_1) = 1$$

$$f(v_{2i}) = f(v_{2i+1}) = \begin{cases} 0 & when\ i\ is\ odd \\ 1 & when\ i\ is\ even \end{cases}$$

Case 4: When $n \equiv 3 \ mod \ 4$

$$f(v_{2i}) = f(v_{2i-1}) = \begin{cases} 0 & when\ i\ is\ odd \\ 1 & when\ i\ is\ even \end{cases}$$

Now label the edges as 1 if the incident vertex labels are distinct and 0 otherwise. The number of vertices and edges labeled 0 and 1 and for every vertex the number of neighbouring vertices labeled 0 and 1 are listed below in Table 1 : It is observed from the table that $\left|n_f(0) - n_f(1)\right| = 0, \ |n_e(0) - n_e(1)| = 1, \left|n_{N_{v_i}}(0) - n_{N_{v_i}}(1)\right| \leq 1 \ for \ all \ 1 \leq i \leq n$ and $\left|n_{N_{u_i}}(0) - n_{N_{u_i}}(1)\right| \leq 1 \ for \ all \ 1 \leq i \leq n$.Hence H-graph admits Discrete labeling.

Theorem 3.2:

Perfect binary tree admits discrete labeling

Proof: A Perfect binary tree is a binary tree in which all the interior nodes have two children and all leaves have the same depth or same level. Hence the number of vertices and edges in a perfect binary tree of height h are $2^{h+1}-1$ and $2^{h+1}-2$ respectively. Let u denote the root vertex of the Perfect binary tree ,v_1, v_{2^1} denote the vertices in the first level ; v_{2^1+1} ,v_{2^1+2} …, $v_{2^1+2^2}$ denote the vertices in the second level;$v_{2^1+2^2+1}$,$v_{2^1+2^2+2}$, …. , $v_{2^1+2^2+2^3}$ denote the vertices in the third level. Proceeding like this, at the level h the vertices are $v_{2^1+2^2+\cdots+2^{h-1}+1}$,$v_{2^1+2^2+\cdots+2^{h-1}+2}$,… , $v_{2^1+2^2+\cdots+2^{h-1}+2^h}$.Define a vertex function $f: V \to \{0,1\}$ by

$$f(u) = 0$$
$$f(v_i) = \begin{cases} 0 & when\ i\ is\ odd \\ 1 & when\ i\ is\ even \end{cases}$$

and label the edges as 1 if the vertex labels are distinct and 0 otherwise. The number of vertices and edges labeled 0 and 1 and for every vertex the number of neighbouring vertices labeled 0 and 1 are listed below in Table 2 :

Hence we shall conclude that $|n_f(0) - n_f(1)| \le 1$, $|n_e(0) - n_e(1)| \le 1$,$\left|n_{N_{v_i}}(0) - n_{N_{v_i}}(1)\right| \le 1 for\ all\ i\ and\ |n_{N_u}(0) - n_{N_u}(1)| = 0$.

Theorem 3.3:

Banana Tree $B_{n,k}$ admits discrete labeling only when $n = 2$ for all k and when $n = 3$ and k is even.

Proof: An (n,k) banana tree is a graph obtained by connecting one leaf of each of n copies of a k-star graph with a single root vertex that is distinct from all stars. Thus in $B_{n,k}$,$|V| = nk + 1$ and $|E| = nk$. Let w denote the root vertex of $B_{n,k}$, $u_i (1 \le i \le n)$ denote the vertices of the stars attached to the root vertex, $v_i (1 \le i \le n)$ denote the central vertex of the stars and $x_{ij} (1 \le i \le n\ and\ 1 \le j \le k-2)$ denote the pendant vertices of the n stars respectively.

Necessary part: Case 1: When $n = 2$ and k is odd($k \ge 3$).

The vertex function $f: V \to \{0,1\}$ defined by

$$f(w) = 0$$
$$f(u_i) = \begin{cases} 0\ when\ i\ is\ odd \\ 1\ when\ i\ is\ even \end{cases}$$
$$f(v_i) = 1\ \forall\ i$$

$$f(x_{ij}) = \begin{cases} 0\ ; 1 \le j \le \frac{k-3}{2} \\ 1\ ; \frac{k-3}{2} + 1 \le j \le k-2 \end{cases}$$ when i is odd

$$f(x_{ij}) = \begin{cases} 1\ ; 1 \le j \le \frac{k-3}{2} \\ 0\ ; \frac{k-3}{2} + 1 \le j \le k-2 \end{cases}$$ when i is even

satisfies the discrete labeling. Now, assign the label 1 to the edges which are incident with distinct vertex labels and 0 otherwise. The number of vertices, edges and for every vertex the number of neighbours labeled 0 and 1 are tabulated below in Table 3:

Hence it is clear that $|n_f(0) - n_f(1)| = 1, |n_e(0) - n_e(1)| = 0$ and for every vertex, the number of neighbours labeled 0 and 1 differs by at most 1 which proves that $B_{n,k}$ when $n = 2$ and k is odd.

Case 2: When $n = 2,3$ and k is even.

The vertex function $f: V \to \{0,1\}$ defined by

$f(w) = 0$

$f(u_i) = \begin{cases} 0\ when\ i\ is\ odd \\ 1\ when\ i\ is\ even \end{cases}$

$f(v_i) = 1\ \forall\ i$

$$f(x_{ij}) = \begin{cases} 0\ ; 1 \le j \le \frac{k-2}{2} \\ 1\ ; \frac{k-2}{2} + 1 \le j \le k-2 \end{cases}$$

satisfies the discrete labeling. Now, assign the label 1 to the edges which are incident with distinct vertex labels and 0 otherwise. The number of vertices, edges and for every vertex the number of neighbours labeled 0 and 1 are

tabulated below in Table 4: Hence it is clear that $|n_f(0) - n_f(1)| = 1, |n_e(0) - n_e(1)| = 0$ and for every vertex, the number of neighbours labeled 0 and 1 differs by at most 1.Therefore, it can be concluded that $B_{n,k}$ is discrete when $n = 2,3$ and k is even.

Sufficient Part: Case 3: When k is odd for $n \geq 3$.
W.l.o.g , label the root vertex w as 0 and to maintain the desired absolute difference of vertices labeled 0 and 1 let $f(u_i) = \begin{cases} 0 \; when \; i \; is \; odd \\ 1 \; when \; i \; is \; even \end{cases}$. Now since u_i is of degree 2 and $f(w) = 0$, all $v_i's$ must be assigned the label 1 in order to satisfy $|n_{N(u_i)}(0) - n_{N(u_i)}(1)| \leq 1$. At this juncture , we are left with labeling n sets of $k - 2x_{ij}$'s. Keeping in mind that the neighbours of $v_i's$ are even, we are supposed to give equal number of 0's and 1's to the neighbours of v_i.Now when i is odd ,by the pre assigned vertex label $f(u_i) = 0, \frac{k-3}{2}$ vertices of x_{ij} must be labeled 0 and $\frac{k-1}{2}$ vertices of x_{ij} must be labeled 1.Similarly,When i is even, by the pre assigned vertex label $f(u_i) = 1, \frac{k-1}{2}$ vertices of x_{ij} must be labeled 0 and $\frac{k-3}{2}$ vertices of x_{ij} must be labeled 1 to satisfy $|n_{N(v_i)}(0) - n_{N(v_i)}(1)| \leq 1$. By labeling so, we find that the number of vertices labeled 0 and 1 are $1 + n\left(\frac{k-1}{2}\right)$ and $n + n\left(\frac{k-1}{2}\right)$ making the absolute difference $|n_f(0) - n_f(1)| = |1 - n| \geq |1 - 3| = 2$ violating the definition of discrete labeling.
Hence $B_{n,k}$ is not discrete when k is odd for all $n \geq 3$.

Case 4: When k is even for all $n \geq 4$.
First let us label the vertices optimally satisfying $|n_f(0) - n_f(1)| \leq 1$under $f: V \to \{0,1\}$.
Without loss of generality, label w as 0 and $f(u_i) = \begin{cases} 0 \; when \; i \; is \; odd \\ 1 \; when \; i \; is \; even \end{cases}$ .Since $u_i's$ are of degree two,all $v_i's$ must be assigned the label 1 to satisfy $|n_{N(u_i)}(0) - n_{N(u_i)}(1)| \leq 1$.Now for x_{ij} when i is odd ,label the first $\frac{k-2}{2}$ vertices 0 and next $\frac{k-2}{2}$ vertices 1.When i is even, label the first $\frac{k-4}{2}$ vertices with 1 and the remaining $\frac{k}{2}$ vertices with 0 which is the only possible way to label x_{ij} without violating $|n_f(0) - n_f(1)| \leq 1$.We notice that there are $\frac{nk+2}{2}$ vertices are labeled 0 and remaining $\frac{nk}{2}$ vertices are labeled 1 making $|n_f(0) - n_f(1)| = 1$.Now label the edges 1 whenever the vertex labels are distinct and 0 otherwise. On labeling the edges,we find that when n is even ,there are $n + \frac{n}{2}(k-3)$ edges labeled 0 and $n + \frac{n}{2}(k-1)$ edges labeled 1 and when n is odd,there are $\frac{n+1}{2}\left(\frac{k}{2}\right) + \frac{n-1}{2}\left(\frac{k-2}{2}\right)$ edges labeled 0 and $\frac{n+1}{2}\left(\frac{k}{2}\right) + \frac{n-1}{2}\left(\frac{k+2}{2}\right)$ edges labeled 1 making the absolute difference n and $n-1$ respectively which is obviously greater than or equal to 3 since $n \geq 4$ violating the definition.Hence,$B_{n,k}$ is not discrete when k is even for all $n \geq 4$.

CONCLUSION

We have discussed the Discrete labeling of some tree related graphs and found that not all trees are discrete.Further explorations are being done on characterisation of the class of graphs that admit discrete labeling. Also, this work can be extended by applying the adjacency condition of the vertices to the edges resulting in edge discrete labeling[5].

REFERENCES

1. Ibrahim Cahit, "Cordial Graphs: A Weaker Version of Graceful and Harmonious Graphs", *ArsCombinatoria*, Vol. 23(1987), 201-208.
2. A. PunithaTharani, P. Saradha, "Discrete Labeling of Some Graphs", *Indian Journal of Science and Technology* (Communicated for Publication)
3. A. PunithaTharani, P. Saradha, "Discrete Labeling of Some Cycle related Graphs", *Proceedings of National Seminar on Recent Trends in Pure and Applied Mathematics*, ISBN: 978-81-965805-3-7
4. D.B.West, *An Introduction to Graph Theory*, Prentice-Hall, (2002).

5. Prajapati, Udayan, Patel, Nittal, "Edge product cordial labeling of some graphs", *Journal of Applied Mathematics and Computational Mechanics*, Vol. 18(2019),69-76.
6. J. A. Gallian, A dynamic survey of graph labeling, *The Electronic Journal of Combinatorics*, Vol. 24(2021)
7. A. Lourdusamy, M.Seenivasan, "Vertex equitable labeling of graphs", *Journal of Discrete Mathematical Sciences & Cryptography*, Vol. 11(2008), 727-735.
8. U. M. Prajapati, K.K. Raval, "Different types of labeling of total path related graphs", *Journal of Xidian University*, Vol. 14(2020), 570-576.
9. Amit.H.Rokad, KalpeshM.Patadiya, "Cordial Labeling of Some Graphs", *Aryabhatta Journal of Mathematics and Informatics*, Vol. 9(2017), 589-597.
10. S Vaidya, LekhaBijukumar, "Some New Families of E-Cordial Graphs", *Journal of Mathematics Research,* Vol. 3, No. 4(2011), 105-111
11. Rajeswari, Parameswari, "On cordial magicness and cordial deficiency of paley digraphs", *2015 IEEE 9th International Conference on Intelligent Systems and Control(ISCO)*
12. S Dhanalakshmi, N Parvathi, "Mean Square Cordial Labeling on Star Related Graphs", *Journal of Physics Conference series 1377 012027,* 2019

Table 1: Vertex condition, Edge condition and neighbouring label condition of *H*- graph

Cases	$n_f(0)$	$n_f(1)$	$n_e(0)$	$n_e(1)$	$n_{N_{u_1}}(0)$	$n_{N_{u_1}}(1)$	$n_{N_{v_1}}(0)$	$n_{N_{v_1}}(1)$	$n_{N_{u_i}}(0)$ $2 \le i \le n-1$	$n_{N_{u_i}}(1)$ $2 \le i \le n-1$
$n = 0\ mod\ 8$	n	n	$n-1$	n	0	1	0	1	$1;\ i \neq u_{\frac{n}{2}+1}$ $2; i = u_{\frac{n}{2}+1}$	$1;\ i \neq u_{\frac{n}{2}+1}$ $1; i = u_{\frac{n}{2}+1}$
$n = 1\ mod\ 8$	n	n	$n-1$	n	0	1	0	1	$1;\ i \neq u_{\frac{n+1}{2}}$ $1;\ i = u_{\frac{n+1}{2}}$	$1;\ i \neq u_{\frac{n+1}{2}}$ $2;\ i = u_{\frac{n+1}{2}}$
$n = 2\ mod\ 8$	n	n	$n-1$	n	0	1	1	0	$1;\ i \neq u_{\frac{n}{2}+1}$ $1; i = u_{\frac{n}{2}+1}$	$1;\ i \neq u_{\frac{n}{2}+1}$ $2; i = u_{\frac{n}{2}+1}$
$n = 3\ mod\ 8$	n	n	$n-1$	n	0	1	1	0	$1;\ i \neq u_{\frac{n+1}{2}}$ $2;\ i = u_{\frac{n+1}{2}}$	$1;\ i \neq u_{\frac{n+1}{2}}$ $1;\ i = u_{\frac{n+1}{2}}$
$n = 4\ mod\ 8$	n	n	$n-1$	n	0	1	0	1	$1;\ i \neq u_{\frac{n}{2}+1}$ $1; i = u_{\frac{n}{2}+1}$	$1;\ i \neq u_{\frac{n}{2}+1}$ $2; i = u_{\frac{n}{2}+1}$
$n = 5\ mod\ 8$	n	n	$n-1$	n	0	1	0	1	$1;\ i \neq u_{\frac{n+1}{2}}$ $2;\ i = u_{\frac{n+1}{2}}$	$1;\ i \neq u_{\frac{n+1}{2}}$ $1;\ i = u_{\frac{n+1}{2}}$
$n = 6\ mod\ 8$	n	n	$n-1$	n	0	1	1	0	$1;\ i \neq u_{\frac{n}{2}+1}$ $2; i = u_{\frac{n}{2}+1}$	$1;\ i \neq u_{\frac{n}{2}+1}$ $1; i = u_{\frac{n}{2}+1}$
$n = 7\ mod\ 8$	n	n	$n-1$	n	0	1	1	0	$1;\ i \neq u_{\frac{n+1}{2}}$ $2;\ i = u_{\frac{n+1}{2}}$	$1;\ i \neq u_{\frac{n+1}{2}}$ $1;\ i = u_{\frac{n+1}{2}}$

$n_{N_{v_i}}(0)$	$n_{N_{v_i}}(1)$	$n_{N_{u_n}}(0)$	$n_{N_{u_n}}(1)$	$n_{N_{v_n}}(0)$	$n_{N_{v_n}}(1)$
$1; i \neq v_{\frac{n}{2}}$ $2; i = v_{\frac{n}{2}}$	$1; i \neq v_{\frac{n}{2}}$ $1; i = v_{\frac{n}{2}}$	0	1	0	1
$1; i \neq v_{\frac{n+1}{2}}$ $2;\ i = v_{\frac{n+1}{2}}$	$1; i \neq v_{\frac{n+1}{2}}$ $1; i = v_{\frac{n+1}{2}}$	1	0	1	0
$1; i \neq v_{\frac{n}{2}}$ $1; i = v_{\frac{n}{2}}$	$1; i \neq v_{\frac{n}{2}}$ $2; i = v_{\frac{n}{2}}$	1	0	0	1
$1; i \neq v_{\frac{n+1}{2}}$ $1;\ i = v_{\frac{n+1}{2}}$	$1; i \neq v_{\frac{n+1}{2}}$ $2; i = v_{\frac{n+1}{2}}$	0	1	1	0
$1; i \neq v_{\frac{n}{2}}$ $1; i = v_{\frac{n}{2}}$	$1; i \neq v_{\frac{n}{2}}$ $2; i = v_{\frac{n}{2}}$	0	1	0	1
$1; i \neq v_{\frac{n+1}{2}}$ $1; i = v_{\frac{n+1}{2}}$	$1; i \neq v_{\frac{n+1}{2}}$ $2;\ i = v_{\frac{n+1}{2}}$	1	0	1	0
$1; i \neq v_{\frac{n}{2}}$ $2; i = v_{\frac{n}{2}}$	$1; i \neq v_{\frac{n}{2}}$ $1; i = v_{\frac{n}{2}}$	1	0	0	1
$1; i \neq v_{\frac{n+1}{2}}$ $1; i = v_{\frac{n+1}{2}}$	$1; i \neq v_{\frac{n+1}{2}}$ $2;\ i = v_{\frac{n+1}{2}}$	0	1	1	0

Table 2:Vertex condition, Edge condition and neighbouring label condition of Perfect binary tree

$n_f(0)$	$n_f(1)$	$n_e(0)$	$n_e(1)$	$n_{N_u}(0)$	$n_{N_u}(1)$	$n_{N_{v_1}}(0)$
2^h	$2^h - 1$	$2^h - 1$	$2^h - 1$	1	1	2

$n_{N_{v_1}}(1)$	$n_{N_{v_2}}(0)$	$n_{N_{v_2}}(1)$	$n_{N_{v_{2i}}}(0)$ $2 \leq i \leq \frac{2^1 + 2^2 + \cdots . + 2^{h-1}}{2}$	$n_{N_{v_{2i}}}(1)$ $2 \leq i \leq \frac{2^1 + 2^2 + \cdots . + 2^{h-1}}{2}$
1	2	1	$2\ ; i\ even$ $1, i = 3,5, \ldots$	$1; i\ even$ $2; i = 3,5, \ldots$

$n_{N_{v_{2i-1}}}(0)$ $2 \leq i \leq \frac{2^1 + 2^2 + \cdots . + 2^{h-1}}{2}$	$n_{N_{v_{2i-1}}}(1)$ $2 \leq i \leq \frac{2^1 + 2^2 + \cdots . + 2^{h-1}}{2}$
$2\ ; i\ even$ $1; i = 3,5, \ldots$	$1; i\ even$ $2; i = 3,5, \ldots$

$n_{N_{v_{2i}}}(0)$ $\frac{2^1 + 2^2 + \cdots . + 2^{h-1}}{2} + 1 \leq i \leq \frac{2^1 + 2^2 + \cdots . + 2^h}{2}$	$n_{N_{v_{2i}}}(1)$ $\frac{2^1 + 2^2 + \cdots . + 2^{h-1}}{2} + 1 \leq i \leq \frac{2^1 + 2^2 + \cdots . + 2^h}{2}$	$n_{N_{v_{2i-1}}}(0)$ $\frac{2^1 + 2^2 + \cdots . + 2^{h-1}}{2} + 1 \leq i \leq \frac{2^1 + 2^2 + \cdots . + 2^h}{2}$	$n_{N_{v_{2i-1}}}(1)$ $\frac{2^1 + 2^2 + \cdots . + 2^{h-1}}{2} + 1 \leq i \leq \frac{2^1 + 2^2 + \cdots . + 2^h}{2}$

$1; i\ even$ $0; i\ odd$	$0; i\ even$ $1; i\ odd$	$1; i\ even$ $0; i\ odd$	$0; i\ even$ $1; i\ odd$

Table 3: Cardinality of vertices, edges and neighbours of $B_{n,k}$(k odd,$n = 2$)

Case (k odd)	$n_f(0)$	$n_f(1)$	$n_e(0)$	$n_e(1)$	$n_{N(w)}(0)$	$n_{N(w)}(1)$
$n = 2$	$\frac{kn}{2}$	$\frac{kn+2}{2}$	$\frac{kn}{2}$	$\frac{kn}{2}$	1	1

Case(k odd)	$n_{N(u_i)}(0)$	$n_{N(u_i)}(1)$	$n_{N(x_{ij})}(0)$	$n_{N(x_{ij})}(1)$
$n = 2$	1	1	0	1

Case(k odd)	$n_{N(v_i)}(0)$	$n_{N(v_i)}(1)$
$n = 2$	$\frac{k-1}{2}$	$\frac{k-1}{2}$

Table 4: Cardinality of vertices, edges and neighbours of $B_{n,k}$ (k even,$n = 2, 3$)

Case (k even)	$n_f(0)$	$n_f(1)$	$n_e(0)$	$n_e(1)$	$n_{N(w)}(0)$	$n_{N(w)}(1)$
$n = 2$	$\frac{kn}{2}$	$\frac{kn+2}{2}$	$\frac{kn}{2}$	$\frac{kn}{2}$	1	1
$n = 3$	$\frac{kn}{2}$	$\frac{kn+2}{2}$	$\frac{kn}{2}$	$\frac{kn}{2}$	2	1

Case(k even)	$n_{N(u_i)}(0)$	$n_{N(u_i)}(1)$	$n_{N(x_{ij})}(0)$	$n_{N(x_{ij})}(1)$
$n = 2$	1	1	0	1
$n = 3$	1	1	0	1

Case(k even)	$n_{N(v_i)}(0)$	$n_{N(v_i)}(1)$
$n = 2\ and$ $i\ odd$	$\frac{k}{2}$	$\frac{k-2}{2}$
$n = 2\ and$ $i\ even$	$\frac{k-2}{2}$	$\frac{k}{2}$
$n = 3\ and$ $i\ odd$	$\frac{k}{2}$	$\frac{k-2}{2}$
$n = 3\ and$ $i\ even$	$\frac{k-2}{2}$	$\frac{k}{2}$

RESEARCH ARTICLE

Cardinal Labeling of Some Standard and Special Graphs

A. Punitha Tharani[1] and S. Pratiksha[2]*

[1]Associate Professor, Department of Mathematics, St. Mary's College (Autonomous), Thoothukudi, Tamil Nadu, India,(Affiliated to Manonmaniam Sundaranar University, Abishekapatti, Tirunelveli), Tamil Nadu, India.

[2]Research Scholar (Register number: 21212212092004), Department of Mathematics, St.Mary's College (Autonomous), Thoothukudi-628 001, Tamil Nadu, India, (Affiliated to Manonmaniam Sundaranar University, Abishekapatti, Tirunelveli), Tamil Nadu, India.

Received: 22 Feb 2024 Revised: 06 Mar 2024 Accepted: 20 Mar 2024

***Address for Correspondence**
S. Pratiksha
Research Scholar (Register number: 21212212092004),
Department of Mathematics, St.Mary's College (Autonomous),
Thoothukudi-628 001, Tamil Nadu, India,
(Affiliated to Manonmaniam Sundaranar University,
Abishekapatti, Tirunelveli), Tamil Nadu, India.
Email: pratikshaprabhu32@gmail.com

ABSTRACT

Inspired from magic and graceful[1] labelings, we have introduced a new type of labeling wherein we optimally try to label the vertices and edges of a graph using their total count with no repetition under absolute difference operation. We call this as cardinal labeling and refer to those graphs as cardinal. This paper discusses the cardinal labeling for some standard and special graphs.

Keywords: Cardinal, standard graphs, complete graph, complete bipartite graph, special graphs, cardinality.

INTRODUCTION

Graph labeling in general is defined as assignment of elements to the vertices and edges of a graph under a defined function or condition. In our paper, the graphs are simple, connected and undirected and the elements used to label the vertex set (domain) and the edge set are natural numbers. For the graph G with $V(G)$ and $E(G)$ as the set of vertices and edges respectively, we define cardinal labeling and investigate it for certain standard and special graphs. The notations employed here are with reference to [2].

METHOD

Definition: Let $G(V,E)$be a simple connected undirected graph. Let $|V| = p, |E| = q$ and let $C = \{1,2,\dots,p+q\}$. G is said to admit cardinal labeling if the one-to-one function f from the vertex set V into the set C generates a one-to-one edge function f^*onto the set $C/f(V)$defined by $|f(u) - f(v)| = f^*(uv)\ \forall\ uv \in E$.A graph G is said to be cardinal if it admits cardinal labeling.Figure 1 illustrates the above definition. For this graph, |V|=4,|E|=5 and so we have $C = \{1,2,\dots,9\}$. We could see in the figure that all the members of C are uniquely assigned to the vertices and edges without repetition. Note that the edge labels are the absolute differences of the incident vertex labels. Cardinal labeling takes its origin by partly combination of vertex magic total labeling and graceful labeling. Unlike these two labelings, there is no constant preserved and the vertex and edge labels form a subset of natural numbers; i.e., no vertex or edge receive zero label.

RESULTS AND DISCUSSION

Cardinal Labeling of some Standard graphs

1.1 Theorem: Path $P_n$satisfies cardinal labeling.
Proof: Let $v_1, v_2, \dots, v_n$be the vertices of the path P_n where $|V| = n$, $|E| = n-1$ and $C = \{1,2,\dots,2n-1\}$. Label the vertices v_i ($i = 1,2,\dots,n$) of P_n by the function $f: V \to C$ given by

$$f(v_i) = \begin{cases} 2n-i & when\ i\ is\ odd \\ i-1 & when\ i\ is\ even \end{cases}$$

Next, label the edges of P_n by the induced function $f^*: E \to C/f(V)$ given by,
$f^*(v_iv_{i+1}) = \left|2n - i - \left((i+1)-1\right)\right| = 2(n-i), \quad i = 1,2,\dots,n-1$
If so done, all the vertices and the edges of P_n obtain distinct $|C| = 2n-1$ labels. Hence path $P_n$is cardinal.

1.2 Theorem: Star $K_{1,m}$is cardinal.
Proof: Let u denote the central vertex and let v_i $(i = 1, 2, \dots, m)$ denote its pendant vertices. Here $|V| = m+1$, $|E| = m$ and $C = \{1,2,\dots,2m+1\}$. Define $f: V \to C$ by
$f(u) = 2m+1$
$f(v_i) = 2m+1-i$, $i = 1, 2, \dots, m$
The induced edge function f^*onto the set $C/f(V)$ is given below.
$f^*(uv_i) = |2m-1-((2m-1)-i)| = i, \quad i = 1,2,\dots,m-1$
The resultant edge labels obtained by the absolute difference of the incident vertex labels are all distinct in C. Also vertices u and $v_i (i = 1, \dots, m)$ have distinct labels of C that are not given to $\{E\}$. The resulting labeling of the star graph is cardinal. Hence Star $K_{1,m}$is cardinal.

1.3 Theorem: Cycle graphC_n admits cardinal labeling.
Proof:C_n has n number of vertices and edges. Let u_i $(i = 1,2,\dots,n)$ be its vertices. We have $C = \{1,2,\dots,2n\}$. It is possible to cardinally label cycles if we define the vertex function $f: V \to C$ for the odd and even cases of n as follows.
Case 1: When n is odd

$$f(u_1) = 2n, \qquad f(u_n) = 2(n-1)$$
$$f(u_{2i}) = 2i-1, \qquad i = 1,2,\dots,\left\lfloor\frac{n}{2}\right\rfloor$$
$$f(u_{2i-1}) = 2n-(2i-1), \qquad i = 2,3,\dots,\left\lceil\frac{n-1}{2}\right\rceil$$

Case 2: When n is even

$$f(u_1) = 2n, \qquad f(u_n) = 2,$$
$$f(u_{2i}) = 2i-1, \qquad i = 1,2,\dots,\left\lceil\frac{n-1}{2}\right\rceil$$

$f(u_{2i-1}) = 2n - (2i - 1), \qquad i = 2,3,\ldots,\left\lceil\frac{n}{2}\right\rceil$

In both the cases, it is possible to get distinct edge labels of C_n if we label the edges using the condition $|f(u_i) - f(uj),\ i \neq j$.

The induced functions $f^*: E \to C/f(V)$ are discussed for the same.

Case (i) When n is odd

$$f^*(u_1u_2) = |2n - (2(1) - 1)| = 2n - 1$$
$$f^*(u_1u_n) = |2n - 2(n - 1)| = 2$$
$$f^*(u_{n-1}u_n) = |(n - 1) - 1 - (2(n - 1))| = n$$
$$f^*(u_iu_{i+1}) = \big|(i - 1) - \big(2n - (i + 1)\big)\big| = |2(i - n)|, \qquad i = 2,3,\ldots,n - 2$$

Case (ii) When n is even

$$f^*(u_1u_2) = |2n - (2 - 1)| = 2n - 1$$
$$f^*(u_1u_n) = |2n - 2| = 2(n - 1)$$
$$f^*(u_{n-1}u_n) = |2n - (n - 1) - 2| = n - 1$$
$$f^*(u_iu_{i+1}) = |i - 1 - (2n - (i + 1))| = 2(n - i), \qquad i = 2,\ldots,n - 2$$

Thus, all the vertices and edges receive distinct enumerations of the set C. Hence it may be concluded that the cycle admits cardinal labeling.

1.4 Theorem: Complete Bipartite graph $K_{m,n}$ satisfies cardinal labeling.

Proof: Let $u_i(i = 1,2,\ldots,m)$ and $v_i(i = 1,2,\ldots,n)$ be the vertices of $K_{m,n}$. We have $|V| = m + n$, $|E| = mn$ and $C = \{1,2,\ldots,m + (m + 1)n\}$. Let us define the vertex function f to C by

$$f(u_i) = i\,, \qquad i = 1,2,\ldots,m$$
$$f(v_i) = m + (m + 1)(n + 1 - i)\,, \qquad i = 1,2,\ldots,n$$

The edge labels are generated by simply finding the absolute difference of the respective vertex labels. Down below are the induced edge functions f^* onto $C/f(V)$.

$$f^*(u_iv_j) = \big|i - \big(r + (r + 1)(s + 1 - j)\big)\big| = (r - i) + (r + 1)(s + 1 - j),$$
$$i = 1,2,\ldots,r\,, \qquad j = 1,2,\ldots,s$$

On observation, we see that all the vertices and the edges receive definite labels from the set C. From this it becomes obvious that $K_{m,n}$ satisfies cardinal labeling.

1.5 Theorem: Complete graph K_n does not satisfy cardinal labeling for $n \geq 4$.

Proof: Cardinal labeling is true for the case when $n < 4$. Assume $n \geq 4$.

K_n has $n(= p)$ vertices and $\frac{n(n-1)}{2}$ $(= q)$ edges, thus $|C| = \frac{n(n+1)}{2}$. Now if we optimally apply the $p + q$ labels to distinct vertices and edges of the graph such that the definition of cardinal labeling is not violated, we see that at least $n - 3$ labels of the set C gets repeated. Since each vertex is adjacent to every other vertex in K_n, in order to obtain distinct edge labels, we have to remove $\Delta - 2$ edges from K_n. Otherwise $\Delta - 2$ number of labels gets repeated. In either case we arrive at a contradiction. Hence K_n $(n \geq 4)$ does not satisfy cardinal labeling.

***Cardinal Labeling of some Special graphs*[3]**

2.1 Bull graph

The bull graph is a cycle C_3 with two disjoint pendant edges which resembles a bull or a ram. It is a unit distance graph with 5 vertices and edges. For the bull graph, $C = \{1,2,\ldots,10\}$. It is possible to label the graph using C as shown in Figure 4.

2.2 Butterfly graph

The butterfly graph is a planar graph obtained by joining two copies of C_3 with a common vertex and is isomorphic to the friendship graph F_2. It has 5 vertices and 6 edges and so $C = \{1,2,\ldots,11\}$. Distinct vertex and edge labels could be allotted to the graph from C if we label as below (Figure 5)

2.3 Moser spindle graph

Named after Leo Moser, Moser Spindle graph is a planar unit distance graph with 7 vertices and 11 edges. Here $C = \{1,2, \ldots 18\}$. Figure 6 shows the possible way of labeling the graph cardinally.

2.4 Wagner graph

It is a 3-regular non planar graph with 8 vertices and 12 edges. It is the 8-vertex Möbius ladder graph. We have $C = \{1,2, \ldots ,20\}$. Figure 7 shows evidently that the graph is cardinal.

2.5 Observation

i) Petersen graph is not cardinal.

ii) Herschel graph does not admit cardinal labeling.

General results of Cardinal labeling

3.1 Observation

For a cardinal graph, the maximum label $|C|$can only be assigned as a vertex label. i.e. it is impossible to obtainlabel $|C|$under f^*.

3.2 Result

If all the vertices of a cardinal graph are labelled with odd labels of C, then the cardinality of the set C is odd.

Proof: By the above observation, maximum label $|C|$has to be given to one of the vertices of the cardinal graph G. Since all the labels of V are odd, $|C|$ is also odd.

3.3 Theorem

If all the vertices of a cardinal graph G have odd labels of C, then then the cardinality of the set C is odd and G is a tree.

Proof

We prove that $|C|$ is odd and G is a tree when $V(G)$ have odd vertex labels. The first part is evident from Result 3.2. Without loss of generality, we assume that $|V(G)| = n, n$ is odd, so n distinct odd labels of C are required to label every vertex of G odd. Since all the vertices are given odd labels, f^*can assign only distinct even labels of C to the edges of G. Further since G is cardinal and cardinality of the set C is odd, there can only be $n-1$ distinct even labels of C that could be given to its edges hence $|E(G)| = n-1$. Any graph $G(n, n-1)$ is certainly a tree, hence the result follows. The converse of theorem 3.3 is not true. i.e. i.e., If the cardinality of C is odd and if G is a tree, then all the vertices of G needn't bear odd labels only, for, it is possible to label path P_n cardinally with a combination of odd and even vertex labels.

Example:

Here P_5 is a tree and $|C| = 9$ but it could be observed that not all vertices obtain odd labels despite being cardinal (Figure 8).

3.4 Corollary: Any cardinal graph containing a cycle must have at least one even vertex label of C in that cycle.

Proof: We prove that if the cardinal graph has no even vertex labels then the graph cannot have cycles. Take a cardinal graph that has cycles and suppose that all its vertex labels are odd. Then by theorem 3.3, the cardinal graph is a tree contradicting the fact that the graph has cycles.

CONCLUSION

In this work, we have investigated the cardinal labeling for standard graphs like path, star and cycle and some special graphs. A few results have also been obtained as a result of employing the labeling to these graphs. Explorations are being made on some star related graphs and trees. We have planned to further extend our work on graphs obtained by arithmetic and set operations.

REFERENCES

1. Rosa A., "On certain valuations of the vertices of a graph", *In Theory of Graphs, International Symposium, Rome,* July 1966 (1967), pp. 349-355.
2. D.B.West, *An Introduction to Graph Theory*, Prentice-Hall, 2002.
3. Radu Mincu, Camelia Obreja, Alexandru Popa, "The Graceful Chromatic Number for Some Particular Classes of Graphs",in*21st International Symposium on Symbolic and Numeric Algorithms for Scientific Computing (SYNASC),* (2019).
4. J. A. Gallian, *A dynamic survey of graph labeling*, *The Electronic Journal of Combinatorics*, 24(2021), #DS6.
5. J. A. MacDougall, M. Miller, K. A. Sugeng, "Super Vertex-Magic Total Labelings of Graphs", in: *Proc. 15th Australian Workshop on Combinatorial Algorithms*, 2004, pp. 222-229.
6. A. Lourdusamy, M.Seenivasan, "Vertex Equitable Labeling of Graphs", *Journal of Discrete Mathematical Sciences and Cryptography*, 11(6) (2008), 727-735.

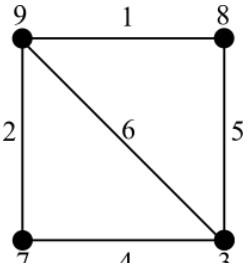

Figure 1: Diamond graph

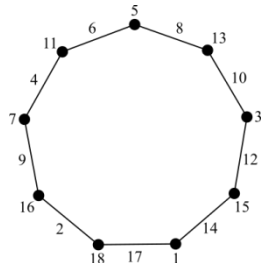

Figure 2: Odd Cycle C_9

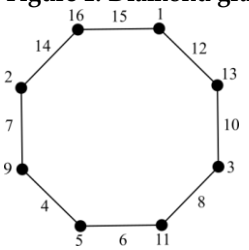

Figure 3: Even Cycle C_8

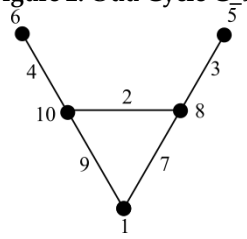

Figure 4: Bull graph

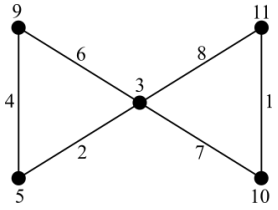

Figure 5: Butterfly graph

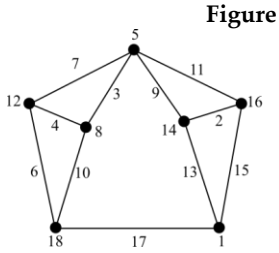

Figure 6: Moser Spindle graph

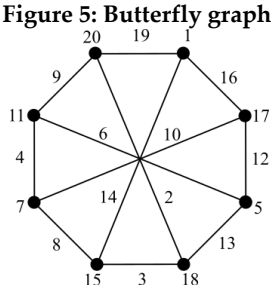

Figure 7: Wagner graph

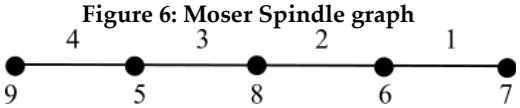

Figure 8: Path P_5

Vol.15 / Issue 83 / Apr / 2024 International Bimonthly (Print) – Open Access ISSN: 0976 – 0997

RESEARCH ARTICLE

Determinant of Some Cyclic Graphs using Incycle Vertices

Punitha Tharani A[1] and Anesha H R[2]*

[1]Associate Professor, Department of Mathematics, St. Mary's College (Autonomous), Thoothukudi,(Affiliated to Manonmaniam Sundaranar University), Abishekapatti, Tirunelveli , Tamil Nadu, India.
[2]Research Scholar (Reg. No.: 20212212092002), Department of Mathematics, St. Mary's College (Autonomous), Thoothukudi, (Affiliated to Manonmaniam Sundaranar University), Abishekapatti, Tirunelveli, Tamil Nadu, India.

Received: 30 Dec 2023 Revised: 09 Jan 2024 Accepted: 12 Mar 2024

***Address for Correspondence**
Anesha H R
Research Scholar (Reg. No.: 20212212092002),
Department of Mathematics,
St. Mary's College (Autonomous),
Thoothukudi,
(Affiliated to Manonmaniam Sundaranar University),
Abishekapatti, Tirunelveli, Tamil Nadu, India.
Email: aneshahr@gmail.com

ABSTRACT

The determinant of adjacency matrix of a graph is called the determinant of a graph. Various reduction procedures and formulae have been devised over the years to find the determinant of graphs. Sesquivalent spanning subgraph of a graph is a spanning sub graph in which all components are either cycles or edges. Harary F, gave a formula to find the determinant of a graph using sesquivalent spanning subgraphs. It is an inspiration for the concept of incycle vertices. Perfect matching of a graph, is a matching in which every vertex is covered. Perfect matching is also a sesquivalent spanning subgraph. A vertex is called an *incycle vertex* if it lies on some cycle in all possible sesquivalent spanning subgraphs of a graph, except the perfect matching. In this paper we have tried to find the determinant of some types of cycle related graphs, using the concept of incycle vertices.

Keywords: Sesquivalent, bicyclic graph, multicyclic graph, determinant, incycle vertex.

INTRODUCTION

Sesquivalent spanning subgraph of a graph is a spanning subgraph in which all components are either cycles or edges. Perfect matching of a graph is a matching in which every vertex is covered. Perfect matching is also a

sesquivalent spanning subgraph. A vertex is called an *incycle vertex* if it lies on some cycle in all possible sesquivalent spanning subgraphs of a graph, except the perfect matching. [1]If G is a graph whose adjacency matrix is $A(G)$ then

$$det(A(G)) = \sum(-1)^{r(\Gamma)}(2)^{s(\Gamma)}$$

where $c(\Gamma)$ is the number of components of Γ, $r(\Gamma) = |V(\Gamma)| - c(\Gamma)$ and $s(\Gamma) = |E(\Gamma)| - |V(\Gamma)| + c(\Gamma)$ and the summation is over all sesquivalent spanning subgraphs Γ of G. The above formula was given by Harary F, in 1962. The above formula is an inspiration for the concept of incycle vertices.

METHODS

In this paper we attempt to find the determinant of a few cycle related graphs. [2]A unicyclic graph is a tree with an edge that makes a cycle.[3]There are 3 types of bicyclic graphs. Consider two vertex disjoint cycles. The graph got by identifying a vertex in one cycle with a vertex of another cycle as v is called a ∞-graph. Throughout this paper we mean ∞-graph with trees attached to it when we say bicyclic graph with a common vertex$v$. We denote the set of all such graphs on n vertices by B_n^{++}.We have extended the concept of ∞-graphs to multicyclic graphs. Consider the graph got by identifying together,as v, one vertex from n disjoint cycles. Throughout this paper we mean this graph with trees attached to it when we say multicyclic graph with a common vertex$v$. We denote the set of all such graphs by M_n^{++}. We denote the set of all such graphs with only even cycles by $M_{n,e}^{++}$ and those with only odd cycles by $M_{n,o}^{++}$. Obviously, $M_{n,e}^{++} \cup M_{n,o}^{++} \subset M_n^{++}$. Some observations regarding incycle vertices are as follows.

Observation 2.1: Incycle vertices always lie on cycles but not all vertices on cycles are incycle vertices.
Example: $K_n, n > 4$. All vertices lie on cycles but no vertex is incycle vertex.

Observation 2.2: All non-singular graphs with cycle need not have an incycle vertex.
Example:Sunlet graph. Perfect matching is the only sesquivalent spanning subgraph.

Observation 2.3: Incycle vertices need not be unique.
Example:C_n. All vertices are incycle vertices.

Observation 2.4:Incycle vertices need not lie on every cycle in a graph.
Example: Wheel graph. It is possible to form a cycle with all rim vertices but the central vertex is the only incycle vertex.

Observation 2.5: Ifv is a vertex that lies on every cycle in a graph, then v belongs to the set of all incycle vertices of the graph.

Observation 2.6: If all cycles have a common vertex, then vertices from two different cycles cannot be incycle, as any sesquivalent spanning subgraph has at most one cycle.

INCYCLE VERTICES IN UNICYCLIC GRAPHS:
Theorem3.1: A unicyclic graph cannot have a unique incycle vertex.
Proof. Suppose a unicyclic graph has a unique incycle vertex, then it lies on a cycle in all sesquivalent spanning subgraphs. But there is only one cycle in a unicyclic graph. Therefore all vertices on that cycle lie on cycles in all sesquivalent spanning subgraphs, which implies all vertices on the cycle are incycle vertices.

Corollary 3.2: If a unicyclic graph has incycle vertices then total number of incycle vertices = the length of the cycle in the unicyclic graph.

Theorem 3.3: If a unicyclic graph has a sesquivalent spanning subgraph with cycle then all vertices on the cycle are incyclic.

Proof. The unicyclic graph has a sesquivalent spanning subgraph with cycle. The cycle can be odd or even. If the graph contains an odd cycle then no other sesquivalent spanning subgraph is possible. If the graph contains an even cycle then the only other possible sesquivalent spanning subgraphs are perfect matchings. In both cases there are no other cycles in other sesquivalent spanning subgraphs. Therefore all vertices on the cycle are incycle vertices.

Theorem 3.4: If a unicyclic graph has only one sesquivalent spanning subgraph then it has an odd cycle or it is the perfect matching.

Proof. Case 1: The unicyclic graph contains an odd cycle. It can have at most one sesquivalent spanning subgraph. The only possible sesquivalent spanning subgraphs are the perfect matching or one containing the odd cycle in it.

Case 2: The unicyclic graph contains an even cycle. The graph has more than one sesquivalent spanning subgraph iff it has a sesquivalent spanning subgraph with the even cycle as one of its components. If there exists a perfect matching in which at least one vertex is matched outside the cycle then no other sesquivalent spanning subgraph is possible.

Note 3.5: The converse is not true for all unicyclic graphs. In case of even unicyclic graph if all vertices in the cycle are matched within itself, in the perfect matching then it has 2 more sesquivalent subgraphs. But if an odd unicyclic graph has a sesquivalent subgraph with odd cycle in it or a perfect matching then it is unique. Also an odd unicyclic graph is non-singular iff it has a sesquivalent spanning subgraph.

Theorem 3.6: A non-singularunicyclic graph has no incycle vertices iff the perfect matching is the only sesquivalent spanning subgraph and $\left|Det\left(A(G)\right)\right| = 1$.

Proof. Let the unicyclic graph be non-singular. Therefore it has at least one sesquivalent spanning subgraph. Suppose it contains a cycle then by theorem 3.3 all vertices are incycle vertices, which is not possible. Hence the perfect matching is the only sesquivalent spanning subgraph. The converse follows from the definition of incycle vertices.

Theorem 3.7: If a unicyclic graph G has $k(\neq 0)$ incycle vertices, then

$$Det(A(G)) = \begin{cases} 0, & k \equiv 0(mod\ 4) \\ \pm 4, & k \equiv 2(mod\ 4) \\ \pm 2, & otherwise \end{cases}$$

Proof. Case 1: $k \equiv 0(mod\ 4)$. Ghas 3 sesquivalent spanning subgraphs. One with a cycle and two perfect matchings. $(-1)^{r(\Gamma)}(2)^{s(\Gamma)}$of the one with the cycle is twice the negative of that of the perfect matchings. Hence their sum is zero.

Case 2: $k \equiv 2(mod\ 4)$. Ghas 3 sesquivalent spanning subgraphs. One with a cycle and two perfect matchings. $(-1)^{r(\Gamma)}(2)^{s(\Gamma)}$of the one with the cycle is twice that of the perfect matchings. Hence their sum is -4 or 4.

Case 3: k is odd. G has only one sesquivalent spanning subgraph. It has an odd cycle in it. Hence its determinant is -2 or 2.

In conclusion, if G is a unicyclic graph, $\left|Det\left(A(G)\right)\right| \leq 4$.

INCYCLE VERTICES IN A BICYCLIC GRAPHS WITH ONE VERTEX IN COMMON:

Theorem 4.1: If $G \in B_n^{++}$ has an incycle vertex that is not the common vertex then the incycle vertex is not unique. In particular all vertices of that cycle are incyclic.

Proof. If a vertex is an incycle vertex then it lies on a cycle in all sesquivalent spanning subgraphs except the perfect matching. If a vertex other than v is incycle then that cycle is in every sesquivalent spanning subgraph other than the perfect matching. Therefore all its vertices including v are incyclic.

Theorem 4.2: If $G \in B_n^{++}$ has no incyclic vertex then the perfect matching is the only possible sesquivalent spanning subgraph and $\left|Det\left(A(G)\right)\right| \leq 1$.

Proof. If G has a sesquivalent spanning subgraph with cycle in it then at least v is an incycle vertex. If v is not an incycle vertex then G has no incycle vertices. Hence the perfect matching is the only sesquivalent spanning subgraph.If G has a sesquivalent spanning subgraph then its determinant is either -1 or 1. If G has no sesquivalent spanning subgraphs then its determinant is 0.

Corollary 4.3: If$G \in B_n^{++}$has no incycle vertices then determinant is 0,1 or -1

Theorem 4.4: Let $G \in B_n^{++}$and let G have no incyclic vertices. Then G is singular iff it has no sesquivalent spanning subgraph.

Proof. Let G be singular. From theorem 4.2G has at most one sesquivalent spanning subgraph. If G has a perfect matching then G is not singular. The converse is obvious.

Corollary 4.5: Let $G \in B_n^{++}$ and let$G$ have no incyclic vertices. Then G is singular if it has odd number of vertices.

Theorem 4.6: If $G \in B_n^{++}$, has $k(\neq 0)$ incycle vertices, then

$$Det(A(G)) = \begin{cases} 0, & k \equiv 0(mod\ 4) \\ \pm 4, & k \equiv 2(mod\ 4)\ or\ k = 1 \\ \pm 2, & otherwise \end{cases}$$

Proof. Case 1: $k \equiv 0(mod\ 4)$. Ghas 3 sesquivalent spanning subgraphs. One with an even cycle and two perfect matchings. $(-1)^{r(\Gamma)}(2)^{s(\Gamma)}$of the one with the cycle is twice the negative of that of the perfect matchings. Hence their sum is zero.

Case 2: $k \equiv 2(mod\ 4)$. Ghas 3 sesquivalent spanning subgraphs. One with an even cycle and two perfect matchings. $(-1)^{r(\Gamma)}(2)^{s(\Gamma)}$of the one with the cycle is twice that of the perfect matchings. Hence their sum is -4 or 4.

Case 3: $k \neq 1$ is odd. Ghas only one sesquivalent spanning subgraph. It has an odd cycle in it. Hence its determinant is -2 or 2.

Case 4: $k = 1$. Ghas 2 sesquivalent spanning subgraphs, both with an odd cycle in it. $(-1)^{r(\Gamma)}(2)^{s(\Gamma)}$for both are the same and their sum is -4 or 4.

Corollary 4.7: If $G \in B_n^{++}$ has an odd number of incycle vertices, then G is non-singular.

In conclusion, if $G \in B_n^{++}$, $\left|Det\left(A(G)\right)\right| \leq 4$.

INCYCLE VERTICES IN A MULTICYCLIC GRAPHS WITH ONE VERTEX IN COMMON:

Theorem 5.1: If $G \in M_n^{++}$ has no incycle vertex then the perfect matching is the only possible sesquivalent spanning subgraph and $\left|Det\left(A(G)\right)\right| \leq 1$.

Proof. If G has a sesquivalent spanning subgraph with cycle in it then at least v is an incycle vertex. If v is not an incycle vertex then G has no incycle vertices. Hence the perfect matching is the only sesquivalent spanning subgraph. If G has a sesquivalent spanning subgraph then its determinant is either -1 or 1. If G has no sesquivalent spanning subgraphs then its determinant is 0.

Corollary 5.2: If $G \in M_n^{++}$ has no incycle vertices then determinant is 0,1 or -1

Theorem 5.3: Let$G \in M_n^{++}$and let$G - v$ have no perfect matching. Then G has sesquivalent spanning subgraph iff there exists a maximum matching of $G - v$ in which exactly one neighbor of v is unmatched.

Proof. Let$G$ have a sesquivalent spanning subgraph. If it is a perfect matching then exactly one vertex was unmatched in $G - v$ and it must be a neighbour of v. If the sesquivalent spanning subgraph has a cycle, the cycle could not be odd. If the cycle is even then all vertices of that cycle should have been matched within itself except one. It is possible to get a maximum matching of $G - v$ in which exactly one neighbor of v is unmatched. Conversely, let there exist a maximum matching of $G - v$ in which exactly one neighbor of v is unmatched. Then by matching it with v in G we get a perfect matching that is a sesquivalent spanning subgraph.

Corollary 5.4:$G \in M_n^{++}$ is singular if in the maximum matching of $G - v$ there are more than one unmatched vertices.

Proof. By theorem 5.3, G has no sesquivalent spanning subgraph.

Theorem 5.5: Let $G \in M_{n,}^{++}$. If$G - v$ has no perfect matching and G has odd number of vertices then G is singular.
Proof. If G has odd number of vertices, $G - v$ has even number of vertices. As $G - v$ has no perfect matching at least 2 vertices are unmatched. By corollary 5.4, G is singular.

Multicyclic graphs having a vertex in common with only Even cycles:
Theorem 5.1.1: Let $G \in M_{n,e}^{++}$.If$G - v$ has a perfect matching then G has no sesquivalent spanning subgraphs and is singular.
Proof. If $G - v$ has a perfect matching then in every cycle of G at least one vertex is matched outside the cycle. Therefore G has no sesquivalent spanning subgraphs. Hence G is singular.

Theorem5.1.2: If $G \in M_{n,e}^{++}$ has incycle vertices. Then $G - v$ has no perfect matching.
Proof. Suppose $G - v$ has a perfect matching. Then G has no sesquivalent spanning subgraph and hence no incycle vertices, which is not possible.

Theorem 5.1.3: If $G \in M_{n,e}^{++}$ has incycle vertex then G has 3 sesquivalent spanning subgraphs.
Proof. Ghas incycle vertex. Then G has sesquivalent spanning subgraph with cycle. Consider a sesquivalent spanning subgraph with cycle. By removing the alternating edges in the cycle we get 2 perfect matchings. No other sesquivalent spanning subgraph with cycle is possible as all cycles are even.

Theorem 5.1.4: $G \in M_{n,e}^{++}$ cannot have exactly one incycle vertex. Number of incycle vertices is at least the number of vertices in the smallest cycle in G.
Proof. Suppose G has an incycle vertex. Then by theorem 5.1.3,G has exactly 3sesquivalent spanning subgraphs.Only one of it has a cycle in it. Therefore all the vertices in the cycle are incycle vertices. Hence G has either no incycle vertex or more than one incycle vertices.

Theorem 5.1.5: If $G \in M_{n,e}^{++}$ has $k(\neq 0)$ incycle vertices, then

$$Det(A(G)) = \begin{cases} 0, & k \equiv 0(mod\ 4) \\ \pm 4, & k \equiv 2(mod\ 4) \end{cases}$$

Proof. Case 1: $k \equiv 0(mod\ 4)$.By theorem 5.1.3, G has exactly 3 sesquivalent spanning subgraphs, one with cycle and 2 perfect matchings. One with an even cycle and two perfect matchings. $(-1)^{r(\Gamma)}(2)^{s(\Gamma)}$of the one with the cycle is twice the negative of that of the perfect matchings. Hence their sum is zero.
Case 2:$k \equiv 2(mod\ 4)$.By theorem 5.1.3, G has exactly 3 sesquivalent spanning subgraphs. One with an even cycle and two perfect matchings. $(-1)^{r(\Gamma)}(2)^{s(\Gamma)}$for the one with the cycle is twice that of the perfect matchings. Hence their sum is -4 or 4.

Theorem 5.1.6: Let $G \in M_{n,e}^{++}$. If G is non-singular, having incycle vertex then $|det(A(G))| = 4$.
Proof. Gcannot have odd number of incycle vertices as all cycles are even, by theorem 5.1.4. By theorem 5.1.5, if the number of vertices in the cycle is a multiple of 4 then the determinant is 0. But G is non-singular, hence the determinant is -4 or 4.
In conclusion if$G \in M_{n,e}^{++}$, $\left|Det\left(A(G)\right)\right| \leq 4$.

Multicyclic graphs having a vertex in common with only Odd cycles:
Theorem 5.2.1: If $G \in M_{n,o}^{++}$ has a perfect matching then G has exactly one sesquivalent spanning subgraph and $|det\ (A(G))| = 1$.
Proof. Gcannot have another perfect matching as all cycles in G are odd. Gcannot have sesquivalent spanning subgraphs with cycles in it, as there is no cycle which is matched within itself in the perfect matching. Therefore G has exactly one perfect matching and its determinant is -1 or 1.

Theorem 5.2.2: Let $G \in M_{n,o}^{++}$. Then either all sesquivalent spanning subgraphs of G have cycle in it or G has a perfect matching.

Proof. From previous theorem if G has a perfect matching, it has no other sesquivalent spanning subgraphs. If G has a sesquivalent spanning subgraph with cycle in it, then G cannot have a perfect matching as all cycles are odd.

Corollary 5.2.3: Let $G \in M_n^{++}$. If G has sesquivalent spanning subgraph with odd cycle in it then, G has no perfect matching.

Theorem 5.2.4: If$G \in M_{n,o}^{++}$ has more than one incycle vertices then G has exactly one sesquivalent spanning subgraph.

Proof. Ghas more than one incycle vertices. All vertices of at most one cycle are incycle. All cycles are odd, so if there exists a sesquivalent spanning subgraph with cycle then there is no perfect matching. Also there is at most one sesquivalent spanning subgraph corresponding to a cycle. So G has exactly one sesquivalent spanning subgraph.

Corollary 5.2.5: G $\in M_{n,o}^{++}$ has more than one sesquivalent spanning subgraphs iff$G$ has exactly one incycle vertex.

Proof. Let G have more than one sesquivalent spanning subgraphs. Then all sesquivalent spanning subgraphs have cycle in it, by theorem 5.2.2. But no two sesquivalent spanning subgraphs have the same cycle in it and hence G has only one incycle vertex. Conversely, let G have exactly one incycle vertex. Then G has at least two sesquivalent spanning subgraphs with cycle in it, corresponding to different cycles.

Theorem 5.2.6: If$G \in M_{n,o}^{++}$ has more than one incycle vertices then G is non-singularand $\left|Det\left(A(G)\right)\right| = 2$..

Proof. By theorem 5.2.4, G has exactly one sesquivalent spanning subgraph. $(-1)^{r(\Gamma)}(2)^{s(\Gamma)}$for it is -2 or 2. Hence G is non-singular.

Theorem5.2.7: Let $G \in M_{n,o}^{++}$. G is non-singulariff it has at least one sesquivalent spanning subgraph.

Proof. Let G be non-singular. Then G has at least one sesquivalent spanning subgraph. Conversely, let G have a sesquivalent spanning subgraph. If G has a perfect matching G cannot have any other sesquivalent spanning subgraphs. Then G is non-singular. If G has sesquivalent spanning subgraphs with cycle, then $(-1)^{r(\Gamma)}(2)^{s(\Gamma)}$ is of the same sign for all such subgraphs and hence their sum is greater than zero.

Theorem 5.2.8: Let $G \in M_{n,o}^{++}$and let $G - v$ have a perfect matching. G is non-singulariff it has at least one incycle vertex.

Proof. LetG be non-singular. As $G - v$ has a perfect matching, G cannot have a perfect matching. By theorem 5.2.7, G has at least one sesquivalent spanning subgraph with cycle. Hence G has at least one incycle vertex. Conversely, let G have at least one incycle vertex. Then G has sesquivalent spanning subgraph with cycle. By theorem 5.2.7, G is non-singular.

Corollary 5.2.9: $G \in M_{n,o}^{++}$is non-singular if G has incycle vertex.

Theorem 5.2.10: Let $G \in M_{n,o}^{++}$ and let $G - v$ have a perfect matching. Gisnon-singulariff there exists at least one cycle in which all vertices are matched within itself in $G - v$.

Proof. Let G be non-singular. As $G - v$ has a perfect matching, G cannot have a perfect matching. By theorem 5.2.7, G has at least one sesquivalent spanning subgraph with cycle, which is possible only if at least one cycle is matched within itself. Conversely, let there exist at least one cycle in which all vertices are mapped within itself. Then G has at least one incycle vertex. By corollary 5.2.9, G is non-singular.

Theorem 5.2.11: Let $G \in M_{n,o}^{++}$. If G is non-singular and $G - v$ has a perfect matching then G has exactly x sesquivalent spanning subgraphs, where x is the number of cycles that are matched within themselves in $G - v$.

Proof. G is non-singular, so G has sesquivalent spanning subgraph by theorem 5.2.7. $G - v$ has a perfect matching, so all sesquivalent spanning subgraphs have cycle in them. If a cycle is matched within itself in $G - v$ then G has a sesquivalent spanning subgraph with that cycle in it. In the same way G has a sesquivalent spanning subgraph with every cycle matched within itself in $G - v$. Hence the number of sesquivalent spanning subgraphs in G is equal to the number of cycles matched within itself in $G - v$.

Corollary 5.2.11:Let $G \in M_{n,o}^{++}$and let $G - v$ have a perfect matching. If G is non-singular then $det(A(G))$ is $\pm 2(x)$, where x is the number of cycles that are matched within themselves in $G - v$.

Proof. From previous theorem, G has x sesquivalent spanning subgraphs and all of them have cycle in it. $(-1)^{r(\Gamma)}(2)^{s(\Gamma)}$is either all -2 or 2 for every such subgraph. Their sum is $\pm 2(x)$.

Theorem 5.2.12: Let$G \in M_{n,o}^{++}|det(A(G))| > 2iffG$ has exactly one incycle vertex.

Proof. Let $|det(A(G))| > 2$. Suppose G has more than one incycle vertices, then by theorem 5.2.6, $|det(A(G)) = 2$. Conversely, let G have exactly one incycle vertex. Then by corollary 5.2.5, G has more than one sesquivalent spanning subgraphs, all with cycles in it. Each of the subgraph contributes -2 or 2 to the determinant. They are all of the same sign and hence $|det(A(G))| > 2$.

Multicyclic graphs having a vertex in common with both Odd and Even cycles:

Theorem 5.3.1: If :$G \in M_n^{++}$ has even number of incycle vertices then G has exactly 3 sesquivalent spanning subgraphs.

Proof. Ghas an even number of incycle vertices. Then G has a sesquivalent spanning subgraph with an even cycle. Consider that subgraph. By removing the alternating edges in that cycle we get 2 perfect matchings. No sesquivalent spanning subgraph with any other cycle is possible.

Theorem 5.3.2: Let$G \in M_n^{++}$has $k(\neq 0)$ incycle vertices, then

$$Det(A(G)) = \begin{cases} 0, & k \equiv 0(mod\ 4) \\ \pm 4, & k \equiv 2(mod\ 4) \end{cases}$$

Proof. Case 1: $k \equiv 0(mod\ 4)$.By theorem 5.3.1, G has exactly 3 sesquivalent spanning subgraphs, one with cycle and 2 perfect matchings. One with an even cycle and two perfect matchings. $(-1)^{r(\Gamma)}(2)^{s(\Gamma)}$for the one with the cycle is twice the negative of that of the perfect matchings. Hence their sum is zero.

Case 2: $k \equiv 2(mod\ 4)$. By theorem 5.3.1, G has exactly 3 sesquivalent spanning subgraphs. One with an even cycle and two perfect matchings. $(-1)^{r(\Gamma)}(2)^{s(\Gamma)}$for the one with the cycle is twice that of the perfect matchings. Hence their sum is -4 or 4.

Corollary 5.3.3: If a non-singular$G \in M_n^{++}$ has even number of incycle vertices then $|det(A(G))| = 4$.

Theorem 5.3.4: If $G \in M_n^{++}$ has an odd number of incycle vertices greater than 1 then $|det(A(G))| = 2$.

Proof.Ghas a sesquivalent spanning subgraph with an odd cycle and no other sesquivalent spanning subgraph with cycles in it. Gdoes not have a perfect matching. Hence the determinant is -2 or 2.

Theorem 5.3.5: If $G \in M_n^{++}$ has only one incycle vertex then G has more than one odd cycles.

Proof. Ghasonly one incycle vertex. Then G has at least two sesquivalent spanning subgraphs, all with distinct cycles in it. If a sesquivalent spanning subgraph has an even cycle in it, then it is the only sesquivalent spanning subgraph with cycle in it, by theorem 5.3.1. Therefore G has at least 2 odd cycles.

Theorem 5.3.6: Let $G \in M_n^{++}$. If $|det(A(G))| > 4$, then G has more than two odd cycles.

Proof. From theorem 5.3.2 and theorem 5.3.4 it is evident that G has exactly one incycle vertex. Gdoes not have any sesquivalent spanning subgraph with even cycle in it. Ghas no perfect matching either. By theorem 5.3.5, G has more than one odd cycles. Suppose$G$ has 2 odd cycles, then G has at most 2 sesquivalent spanning subgraphs, all with distinct cycles in it. Each of the subgraph contributes -2 or 2 to the determinant. They are all of the same sign and hence $\left|det\left(A(G)\right)\right| \leq 4$, which is not possible. Hence G has more than two odd cycles.

CONCLUSION

In this paper we have introduced the concept of incycle vertices. We have calculated the determinant of some cyclic graphs using incycle vertices. We arrive at the conclusion that $|det(A(G))| \leq 4$, where G is a multicyclic graph with

one vertex in common, having less than 3 odd cycles. Future study will be focused on solving the determinant of all types of bicyclic graphs and other graphs of similar structure.

REFERENCES

1. N. Biggs, *Algebraic Graph Theory*, Cambridge University Press, Cambridge, 1974.
2. Harold N. Gabow, Robert E. Tarjan,"A linear-time algorithm for finding a minimum spanning pseudoforest",*Information Processing Letters*,Volume 27, Issue 5,1988, 259-263.
3. Li, Jianxi& Chang, An &Shiu, Wai Chee, "On the nullity of bicyclic graphs",*MATCH - Communications in Mathematical and in Computer Chemistry*, 2008.
4. F. Harary, "The Determinant of the adjacency matrix of a graph", *SIAM Rev. 4*, 1961, 202–210.
5. Andreas Brandstädt, Van Bang Le, Jeremy P. Spinrad, *Graph Classes : A Survey*, Society for Industrial and Applied Mathematics, 1999.
6. Cvetković DM, Doob M, Sachs H,*Spectra of Graphs : Theory and Application*, Academic Press, 1980.
7. Lowell W. Beineke and Robin J. Wilson, *Topics in Algebraic Graph Theory*, Cambridge University Press, 2005.
8. Golumbic, Martin Charles, *Algorithmic graph theory and perfect graphs*,Academic Press New York, 1980.
9. Rara H.M., "Reduction procedures for calculating the determinant of the adjacency matrix of some graphs and the singularity of square planar grids", *Discrete Math.*, 1996, 151, 213-219.
10. Ma, H., Li, D. and Xie, C, "Non-Singular Trees, Unicyclic Graphs and Bicyclic Graphs", *Applied Mathematics*, 2019, 1-7.
11. SupotSookyang, SrichanArworn, Piotr Wojtylak, "Characterizations of Non-Singular Cycles, Path and Trees", *Thai Journal of Mathematics*, 2008.
12. Gong S-C., Zhang, J-L. and Xu G-H,"On the determinant of the distance matrix of a bicyclic graph", *arXiv:1308.2281v1*, 2013.

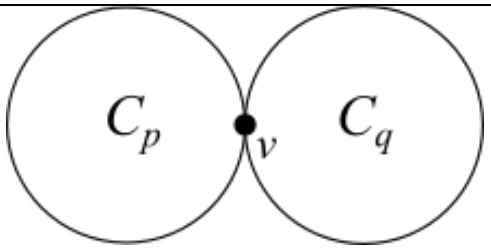

Figure 2.1: ∞-graph

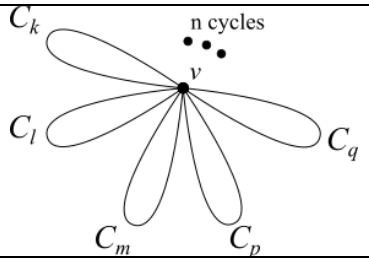

Figure 2.2: Graph got by identifying together one vertex from n disjoint cycles

Indian Journal of Natural Sciences www.tnsroindia.org.in ©IJONS

Vol.15 / Issue 83 / Apr / 2024 *International Bimonthly (Print) – Open Access* *ISSN: 0976 – 0997*

RESEARCH ARTICLE

Some New Families of Sum Divisor Cordial Graphs

K. Periasamy[1]* K. Venugopal[1] and P. Lawrence Rozario Raj[2]

[1]P.G. and Research Department of Mathematics, Dr. Kalaignar Government Arts College, Kulithalai, (Affiliated to Bharathidasan University), Tiruchirappalli, Tamil Nadu, India.
[2]P.G. and Research Department of Mathematics, St. Joesph's College (Affiliated to Bharathidasan University), Tiruchirappalli, Tamil Nadu, India.

Received: 30 Dec 2023 Revised: 09 Jan 2024 Accepted: 12 Mar 2024

***Address for Correspondence**
K. Periasamy
P.G. and Research Department of Mathematics,
Dr. Kalaignar Government Arts College,
Kulithalai,
(Affiliated to Bharathidasan University),
Tiruchirappalli, Tamil Nadu, India.
Email: kpsperiasamy87@gmail.com.

ABSTRACT

The eccentric graph of any graph G is a graph constructed from the vertices of G such that any two vertices are joined by an edge only when any one of them is an eccentric vertex of the other. It is denoted by G_{ecc}. In this paper, we investigate the sdc-labeling of $(K_n(e)K_n)_{ecc}$, $(S(K_{1,n})(e)S(K_{1,n})_{ecc}$, $(S(K_{1,n})(e)K_m)_{ecc}$ and $(C_n(e)C_n)_{ecc}$.

Keywords: Eccentric graph, sum divisor cordial graph, complete graph, cycle, subdivision of star graph.

INTRODUCTION

We start with an undirected, simple, finite graph. A graph G = (V,E), where V is the set of vertices with |V| = p and E is the set of edges with |E| = q, is referred to as a (p,q) graph G. The origins of graph theory are attributed to Leonhard Euler's 1736 examination of the well-known Königsberg bridge problem. Graph labeling is one of the main topics of graph theory. Graph labeling is the process of giving vertices, edges, or both of a graph labels, which are often represented by integers. One of the fascinating and active subfields of graph theory is labeling of graphs. Rosa presented the idea of grace in [10]. Graham et al. presented the idea of harmony in [6]. The graph labeling techniques in graph theory originated with graceful labeling and harmonic labeling. Another significant labeling style that incorporates elements of both graceful and harmonious is called cordial, and it was first established by Cahit in [2]. The idea of divisor cordial labeling of graphs was first presented by Varatharajan et al. in [12]. Lourdusamy et al. presented the idea of sum divisor cordial labeling in [8]. Eccentric graphs are one type of eccentricity-related graph study; these studies of graphs are fascinating and amazing. Akiyama et al. defined the unique kind of graph

operation known as the eccentric graph of graph in [1], and they also provided several intriguing characterizations of these kinds of graphs. There is only one graph structure driven by any graph action. However, nearly every graph has an eccentric graph operation that leads to multiple fascinating and amazing graph structures. Kaspar et al. discovered and described such intriguing graph topologies of eccentric graphs of specific classes of graphs in [7]. Ghosh et al. in[9] look into a few families of prime cordial eccentric graphs. The graphs under discussion are undirected, simple, and finite. The terms used in graph theory are referred to by Harary [5]. We refer to Tom M. Apostol [11] for the conventional terminology and notations in number theory, and Gallian [3] for the literature on graph labeling. Investigating the sdc-labeling of $(K_n(e)K_n)_{ecc}$, $(S(K_{1,n})(e)S(K_{1,n})_{ecc}$, $(S(K_{1,n})(e)K_m)_{ecc}$, and $(C_n(e)C_n)_{ecc}$ is the goal of this work.

Preliminaries

We will give brief summary of definitions which are useful for the present investigations.

Definition : A graph labeling is the assignment of unique identifiers to the edges and vertices of a graph.

Definition : Let G be a graph with vertex set V and edge set E. The eccentric graph of G is denoted by $G_{ecc} = (V,E')$, where $E' = \{ (u,v) : d_G(u,v) = ecc(u)$ or $d_G(u,v) = ecc(v)$ for $u,v \in V\}$.

Definition : Let $G = (V,E)$ be a simple graph and $f : V(G) \to \{1, 2, \ldots, |V(G)|\}$ be a bijection. For each edge uv, assign the label 1 if $2 \mid (f(u)+f(v))$ and the label 0 otherwise. The function f is called a sum divisor cordial labeling if $|e_f(0) – e_f(1)| \leq 1$. A graph which admits a sum divisor cordial labeling (sdc-labeling) is called a sum divisor cordial graph (sdc-graph).

Definition : An edge joining of two copies of any graph G is denoted by G(e)G.

Definition : An edge joining of two different graph G and H is denoted by G(e)H.

Main Results

Theorem 3.1 $(K_n(e)K_n)_{ecc}$ is sdc-graph for $n \geq 3$.

Proof.

Let G be $K_n(e)K_n$. G has 2n vertices and $n^2–n+1$ edges. Then the vertices of G are $v_1,v_2,v_3,\ldots,v_n, w_1,w_2,w_3,\ldots,w_n$. Let $(K_n(e)K_n)_{ecc}$ be the eccentric graph of $K_n(e)K_n$.

Then $(K_n(e)K_n)_{ecc}$ is $K_1 + \overline{K_{n-1}} + \overline{K_{n-1}} + K_1$, the vertices are $v_1, w_2, w_3, \ldots, w_n, v_2, v_3, \ldots, v_n, w_1$. In $(K_n(e)K_n)_{ecc}$, v_1 is adjacent to $w_2,w_3,\ldots,w_n$, w_1 is adjacent to $v_2, v_3, \ldots, v_n$, and also $w_2, w_3, \ldots,w_n$ and $v_2, v_3, \ldots,v_n$ are mutually adjacent. Then, $|V((K_n(e)K_n)_{ecc})| = 2n$ and $|E((K_n(e)K_n)_{ecc})| = n^2–1$.

Define $f : V((K_n(e)K_n)_{ecc}) \to \{1, 2, \ldots, 2n\}$ as follows.

$f(v_1) = 2$ and $f(w_1) = 1$,

$f(w_i) = i + n + 1$, for $i = 2,3,\ldots,n$.

$f(v_i) = i + 1$, for $i = 2,3,\ldots,n$.

Then $e_f(0) = e_f(1) = \frac{n^2-1}{2}$, when n is odd.

Then $e_f(0) = \frac{n^2-2}{2}$ and $e_f(1) = \frac{n^2}{2}$, when n even. Thus, $|e_f(0) – e_f(1)| \leq 1$.

Hence, $(K_n(e)K_n)_{ecc}$ is sdc-graph, for $n \geq 3$.

Illustration : 3.1

$K_4(e)K_4$ and sdc-labeling of $(K_4(e)K_4)_{ecc}$ are shown in figure 3.1

Theorem 3.2 $(S(K_{1,n})(e)S(K_{1,n}))_{ecc}$ is sdc-graph for $n \geq 2$.

Proof : Let G be $S(K_{1,n})(e)S(K_{1,n})$. $S(K_{1,n})(e)S(K_{1,n})$ has 4n+2 vertices and 4n+1 edges. Let $(S(K_{1,n})(e)S(K_{1,n}))_{ecc}$ be the eccentric graph of $S(K_{1,n})(e)S(K_{1,n})$. The vertices of $S(K_{1,n})(e)S(K_{1,n})$ are $v, v_{11}, v_{12}, \ldots, v_{1n}, v_{21}, v_{22}, \ldots, v_{2n}, w, w_{11}, w_{12}, w_{13}, \ldots, w_{1n}, w_{21}, w_{22}, w_{23}, \ldots, w_{2n}$. Then $(S(K_{1,n})(e)S(K_{1,n}))_{ecc}$ is $\overline{K_{n+1}} + \overline{K_n} + \overline{K_n} + \overline{K_{n+1}}$, the vertices are $v, v_{11}, v_{12}, \ldots, v_{1n}, v_{21}, v_{22}, v_{23}, \ldots, v_{2n}, w, w_{11}, w_{12}, \ldots, w_{1n}, w_{21}, w_{22}, \ldots, w_{2n}$. In $(S(K_{1,n})(e)S(K_{1,n}))_{ecc}$, $w, w_{11}, w_{12}, w_{13}, \ldots, w_{1n}$ are mutually adjacent to $v_{21}, v_{22}, v_{23}, \ldots, v_{2n}$; $v_{21}, v_{22}, v_{23}, \ldots, v_{2n}$ are mutually to $w_{21}, w_{22}, w_{23}, \ldots, w_{2n}$, and also $w_{21}, w_{22}, w_{23}, \ldots, w_{2n}$ and $v, v_{11}, v_{12}, v_{13}, \ldots, v_{1n}$ are mutually adjacent. Then, $|V((S(K_{1,n})(e)S(K_{1,n}))_{ecc})| = 4n+2$ and $|E((S(K_{1,n})(e)S(K_{1,n}))_{ecc})| = 3n^2+2n$. Define $f : V((S(K_{1,n})(e)S(K_{1,n}))_{ecc}) \rightarrow \{1, 2, \ldots, 4n+2\}$ as follows.

$f(w) = 1$ and $f(v) = 3n+2$

$f(w_{1i}) = i+1$, for $i = 1,2,\ldots,n$.

$f(w_{2i}) = i+2n+1$, for $i = 1,2,\ldots,n$.

$f(v_{2i}) = i+n+1$, for $i = 1,2,\ldots,n$.

$f(v_{1i}) = i+3n+2$, for $i = 1,2,\ldots,n$.

Then $e_f(0) = e_f(1) = \dfrac{3n^2+2n}{2}$, when n is even and $e_f(0) = \dfrac{3n^2+2n+1}{2}$ and

$e_f(1) = \dfrac{3n^2+2n-1}{2}$, when n odd. Thus, $|e_f(0) - e_f(1)| \leq 1$.

Thus, $(S(K_{1,n})(e)S(K_{1,n}))_{ecc}$ is sdc-graph for $n \geq 2$.

Illustration : 3.2

$S(K_{1,3})(e)S(K_{1,3})$ and sdc-labeling of $(S(K_{1,3})(e)S(K_{1,3}))_{ecc}$ are shown in figure 3.2

Theorem 3.3 $(S(K_{1,n})(e)K_m)_{ecc}$ is sdc-graph for $n \geq 2$ and $m \geq 3$.

Proof : Let G be graph $S(K_{1,n})(e)K_m$. G has 2n+m+1 vertices and $2n+1+\dfrac{m(m-1)}{2}$ edges.

Let $(S(K_{1,n})(e)K_m)_{ecc}$ be the eccentric graph of $S((K_{1,n})(e)K_m)$.

The vertices of G are $v, v_{11}, v_{12}, v_{13}, \ldots, v_{1n}, v_{21}, v_{22}, v_{23}, \ldots, v_{2n}, w_1, w_2, w_3, \ldots, w_n$.

Then $K_1 + \overline{K_n} + \overline{K_{m-1}} + \overline{K_{n+1}}$ by adding a vertex to the vertices of first set of vertices in $\overline{K_n}$ and set of vertices in $\overline{K_{m-1}}$, the vertices are $v, v_{11}, v_{12}, v_{13}, \ldots, v_{1n}, v_{21}, v_{22}, v_{23}, \ldots, v_{2n}, w_1, w_2, w_3, \ldots, w_m$. In $(S(K_{1,n})(e)K_m)_{ecc}$, w_1 is mutually adjacent to $v_{21}, v_{22}, v_{23}, \ldots, v_{2n}$; $v_{21}, v_{22}, v_{23}, \ldots, v_{2n}$ are mutually to $w_2, w_3, \ldots, w_m$, and also $w_2, w_3, \ldots, w_m$ and $v, v_{11}, v_{12}, v_{13}, \ldots, v_{1n}$ are mutually adjacent. Then, $|V((S(K_{1,n})(e)K_m)_{ecc})| = 2n+m+1$ and $|E((S(K_{1,n})(e)K_m)_{ecc})| = 2nm+m+n-1$.

Define $f : V((S(K_{1,n})(e)K_m)_{ecc}) \rightarrow \{1, 2, \ldots, 2n+m+1\}$ as follows.

Case 1 : n is odd and m is even.

$f(w_1) = 1$ and $f(v) = 2$

$f(w_i) = i+n+1$, for $i = 2,3,\ldots,m$.

$f(v_{1i}) = i+n+m+1$, for $i = 1,2,\ldots,n$.

$f(v_{2i}) = i+2$, for $i = 1,2,\ldots,n$.

Then $e_f(0) = \frac{2nm+m}{2}$ and $e_f(1) = \frac{2nm+m-2}{2}$, for n is odd and m is even.

Thus, $|e_f(0) - e_f(1)| \leq 1$.

Therefore, $(S(K_{1,n})(e)K_m)_{ecc}$ is sdc graph, for n is odd and m is even.

Case 2 : n is odd and m is odd or n is even and m is odd or n is even and m is even.

$f(w_1) = 1$ and $f(v) = 2n+m+1$

$f(w_i) = i+n$, for i = 2,3,…,m.

$f(v_{1i}) = i+n+m$, for i = 1,2,…,n.

$f(v_{2i}) = i+1$, for i = 1,2,…,n.

Then $e_f(0) = e_f(1) = \frac{2nm+m-1}{2}$, when m is odd and n is either odd or even.

Then $e_f(0) = \frac{2nm+m}{2}$ and $e_f(1) = \frac{2nm+m-2}{2}$, when n is even and m is even

Thus, $|e_f(0) - e_f(1)| \leq 1$.

Therefore, $(S(K_{1,n})(e)K_m)_{ecc}$ is sdc-graph for n is odd and m is odd or n is even and m is odd or n is even and m is even. Thus, $(S(K_{1,n})(e)K_m)_{ecc}$ is sdc-graph for $n \geq 2$ and $m \geq 3$.

Illustration : 3.3
$S(K_{1,3})(e)K_4$ and sdc-labeling of $(S(K_{1,3})(e)K_4)_{ecc}$ sdc-graph are shown figure 3.3.

Theorem 3.4 $(C_n(e)C_n)_{ecc}$ is sdc-graph for $n \geq 3$.
Proof. Let G be $C_n(e)C_n$ graph. G has 2n vertices and 2n+1 edges. The vertices of G are $v_1,v_2,\ldots,v_n, w_1,w_2,\ldots,w_n$. Let $(C_n(e)C_n)_{ecc}$ be the eccentric graph of $C_n(e)C_n$.

Case 1 : when n is even.
Then $(C_n(e)C_n)_{ecc}$ is $S_{n-1,n-1}$, the vertices of G_e are two centers $w_{\frac{n+2}{2}}$, $v_{\frac{n+2}{2}}$ and two set of pendent vertices $v_1,v_2,v_3,\ldots,$ $v_{\frac{n}{2}}, v_{\frac{n+4}{2}},\ldots,v_n$ and $w_1,w_2,w_3,\ldots, w_{\frac{n}{2}}, w_{\frac{n+4}{2}},\ldots,w_n$. Then, $|V((C_n(e)C_n)_{ecc})| = 2n$ and $|E((C_n(e)C_n)_{ecc})| = 2n-1$.

Define $f : V((C_n(e)C_n)_{ecc}) \rightarrow \{1, 2, \ldots, 2n\}$ as follows.

$f(v_{\frac{n+2}{2}}) = 1$, $f(v_1) = 3$ and $f(w_{\frac{n+2}{2}}) = 3$

$f(v_i) = i + 2$, for $i = 2,3,\ldots, \frac{n}{2}$.

$f(v_i) = i + 1$, for $i = \frac{n+4}{2}, \frac{n+6}{2},\ldots,n$.

$f(w_i) = i + n + 1$, for $i = 1,2,\ldots, \frac{n}{2}$.

$f(w_i) = i + n$, for $i = \frac{n+4}{2}, \frac{n+6}{2}, \ldots, n$.

Then $e_f(0) = n$ and $e_f(1) = n-1$. Thus, $|e_f(0) - e_f(1)| \leq 1$.

Therefore, $(C_n(e)C_n)_{ecc}$ is sdc-graph for n is even.

Case 2 : when n is odd.

Then $(C_n(e)C_n)_{ecc}$ is $\overline{K_{n-2}} + \overline{K_2} + \overline{K_2} + \overline{K_{n-2}}$, the vertices of G are $w_1, w_2, w_3, \ldots, w_{\frac{n-1}{2}}, w_{\frac{n+5}{2}}, \ldots, w_n$ of $\overline{K_{n-2}}$, $v_{\frac{n+1}{2}}, v_{\frac{n+3}{2}}$ of $\overline{K_2}$, $w_{\frac{n+1}{2}}, w_{\frac{n+3}{2}}$ of $\overline{K_2}$ and $v_1, v_2, v_3, \ldots, v_{\frac{n-1}{2}}, v_{\frac{n+5}{2}}, \ldots, v_n$ of $\overline{K_{n-2}}$. Then, $|V((C_n(e)C_n)_{ecc})| = 2n$ and $|E((C_n(e)C_n)_{ecc})| = 4n-4$.

Define $f : V((C_n(e)C_n)_{ecc}) \rightarrow \{1, 2, \ldots, 2n\}$ as follows.

$f(v_{\frac{n+1}{2}}) = 1$ and $f(v_{\frac{n+3}{2}}) = 2$, $f(w_{\frac{n+1}{2}}) = 3$ and $f(w_{\frac{n+3}{2}}) = 4$

$f(v_i) = n+2+i$, for $i = 1,2,\ldots, \frac{n-1}{2}$.

$f(v_i) = n+i$, for $i = \frac{n+5}{2}, \frac{n+7}{2}, \ldots, n$.

$f(w_i) = 4+i$, for $i = 1,2,\ldots, \frac{n-1}{2}$.

$f(w_i) = 2+i$, for $i = \frac{n+5}{2}, \frac{n+6}{2}, \ldots, n$.

Then $e_f(0) = e_f(1) = 2n - 2$. Thus, $|e_f(0) - e_f(1)| \leq 1$.

Therefore, $(C_n(e)C_n)_{ecc}$ is sdc-graph for n is odd.
Hence, $(C_n(e)C_n)_{ecc}$ is sdc-graph for $n \geq 3$.

Illustration 3.4. $C_5(e)C_5$ and sdc-labeling of $(C_5(e)C_5)_{ecc}$ are shown in figure 3.4.

CONCLUSIONS

It is confirmed that all of the intriguing and wonderful graph structures of a few more new families of eccentric graphs are sdc-graphs. The sdc-labeling of $(K_n(e)K_n)_{ecc}$, $(S(K_{1,n})(e)S(K_{1,n})_{ecc}$, $(S(K_{1,n})(e)K_m)_{ecc}$ and $(C_n(e)C_n)_{ecc}$ were the only topics we covered.

REFERENCES

1. J. Akiyama, K. Ando, and D. Avis. Eccentric graphs, Discrete Math., 56:1–6,1985.

2. I. Cahit, Cordial Graphs : A weaker version of graceful and harmonious Graphs, Ars Combinatoria, 23(1987), 201-207.
3. J.A. Gallian, A dynamic survey of graph labeling, The Electronic Journal of Combinatorics, 16(2014), # DS6.
4. S.W. Golomb, How to number a graph, in Graph Theory and Computing, R.C. Read, ed., Academic Press, New York (1972), 23-37.
5. F. Harary, Graph theory, Addison Wesley, Reading, Massachusetts (1972).
6. R. L. Graham and N. J. J. Sloane. On additive bases and harmonious graphs, SIAM J. Alg. Discrete Math., 1:382–404, 1980.
7. S. Kaspar, B. Gayathri, M. P. Kulandaivel, and N. Shobanadevi. Eccentric graphs of some particular classes of graphs, International Journal of Pure and Applied Mathematics, 16(119):145–152, 2018.
8. A. Lourdusamy and F. Patrick, Sum divisor cordial graphs, Proyecciones Journal of Mathematics, 35(1) (2016), 119-136.
9. Poulomi Ghosh and Anita Pal. Prime cordial labeling on eccentric graph of cycle and path, AdvancedModeling and Optimization, 19(1):133–139, 2017.
10. A. Rosa, On certain valuations of the vertices of a graph, Theory of Graphs (Internat. Sympos., Rome, 1966), Gorden and Breach, (1967), N.Y. and Dunod Paris (1967), 349-355.
11. Tom M Apostol. Introduction to Analytic Number Theory, Narosa, New Delhi,1998.
12. R. Varatharajan, S. Navanaeethakrishnan and K. Nagarajan, Divisor cordial graphs, International J. Math. Combin., 4(2011), 15-25.

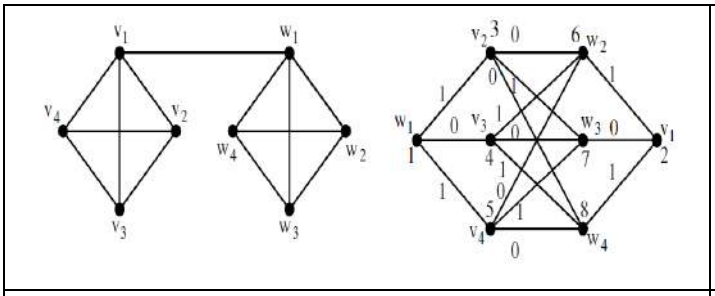

Figure 3.1

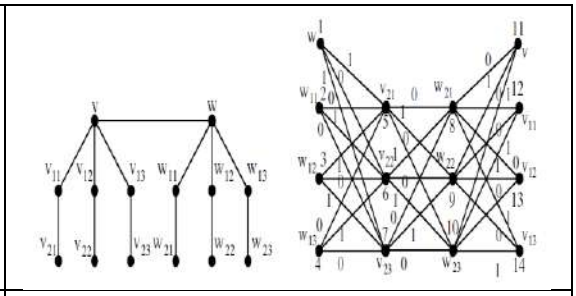

Figure 3.2

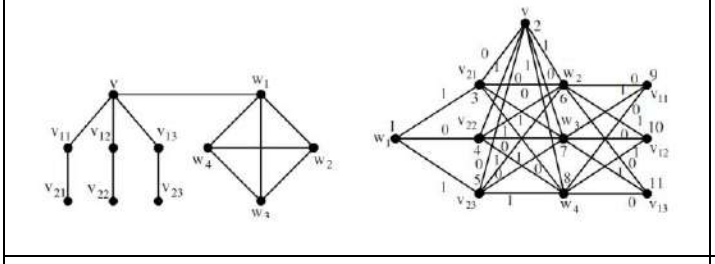

Figure 3.3

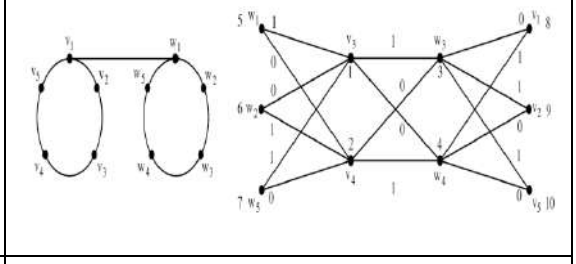

Figure 3.4

RESEARCH ARTICLE

Best Proximity Pair Theorem for Generalized Reich type Cyclic Meir-Keeler Contraction Mapping on Topological Spaces

S. Sahayarajjoseph Nirmalkumar[1] and S. Sujith[2]

[1]Reg. No : 20221282091006, Research Scholar, PG and Research Department of Mathematics, St.Xavier's College (Autonomous), Palayamkottai,(Affliated to Manonmaniam Sundaranar University), Abisekapatti-627012, Tirunelveli, Tamil Nadu, India.
[2]Assistant Professor, PG and Research Department of Mathematics,St.Xavier's College (Autonomous), Palayamkottai, (Affliated to Manonmaniam Sundaranar University), Abisekapatti-627012, Tirunelveli, Tamil Nadu, India.

Received: 30 Dec 2023 Revised: 09 Jan 2024 Accepted: 12 Mar 2024

***Address for Correspondence**
S. Sahayarajjoseph Nirmalkumar
Reg. No : 20221282091006,
Research Scholar,
PG and Research Department of Mathematics,
St.Xavier's College (Autonomous),
Palayamkottai,(Affliated to Manonmaniam Sundaranar University),
Abisekapatti-627012, Tirunelveli, Tamil Nadu, India.
Email: lssnirmal@gmail.com

ABSTRACT

In this paper, existence and uniqueness of best proximity pairs for generalized Reich type cyclic Meir-Keeler contraction mapping in arbitrary topological space is proved.

Keywords: cyclic contraction, cyclic Meir-Keeler contraction, cyclic topologically contraction, cyclic Reich type contraction, topological P-property.
AMS Subject Classification: 47H09, 47H10.

INTRODUCTION

In [3], Sankar Raj et al., introduced cyclic topologically r-contractive map and proved the existence and uniqueness of best proximity points. Later Sahayarajjoseph Nirmalkumar et al.[4], introduced cyclic topologically contraction map and proved the existence and uniqueness of best proximity points. For other best proximity point result on topological spaces , see[[5],[6]]. In this paper, we have verified the existence and uniqueness of best proximity point for the new class of generalized Reich type cyclic Meir-Keeler contraction maps on topological spaces. The notations below are used throughout the document:

Consider a topological space Y and a mapping $q: Y \to Y$. Fix $e_0 \epsilon Y$ .The orbit $O(e_0, q)$ of q starting at e_0 is defined as

$$O(e_0, q) := \{q^n(e_0): n \in \mathbb{N} \cup \{0\}\},$$

Where $q^0(e_0) = e_0$ and $q^n(e_0) = q(q^{n-1}e_0)$, for all $n \in \mathbb{N}$. Suppose that $\omega: Y \to Y$ is a function. Then the image of $O(e_0, q)$under ω is $\omega(O(e_0, q)) = \{\omega(q^n(e_0)): n \in \mathbb{N} \cup \{0\}\}$. The limit point set $\text{Lim}\{e_n\}$ of a sequence $\{e_n\}$ in a topological space Y is defined as

$$\text{Lim}\{e_n\} := \bigcap_{n=1}^{\infty} \overline{\{e_m: m \geq n\}},$$

Where $\overline{B}$ denote the closure of B in Y. It is easy to verify that if $q: Y \to Y$ is a continuous mapping and $x \in \text{Lim}\, O(e_0, q)$,then $\omega(x) \in \text{Lim}\, \omega(O(e_0, q))$

Main Result

Let us now define the concept of generalized Reich type cyclic Meir-Keeler contraction mapping [1] on a topological space

Definition 2.1. Let E and F be any two non-empty subsets of a topological space Y. A cyclic mapping $q: E \cup F \to E \cup F$ is called generalized Reich type cyclic topologically Meir-Keeler contraction map w.r.t a continuous function $\omega: Y \times Y \to \mathbb{R}$ for some $u \in E$ and for each $\epsilon > 0$,
there exists a $\delta > 0$ such that

$$R(u, v) < D_\omega(E, F) + \epsilon + \delta \quad \text{implies } | \omega(qu, qv) | < D_\omega(E, F) + \epsilon, \forall u \in E, \forall v \in F, \tag{2.1}$$

Where $(u, v) = \frac{1}{3} [| \omega(u, v) | + | \omega(qu, u) | + | \omega(qv, v) |]$.
Here's an example

Example 2.2. Consider $\mathbb{R}^2$ with its standard topology. Let $E := \{(0, t): 0 \leq t \leq 1\}$ and $F := \{(1, s): 0 \leq s \leq 1\}$. Let $q: E \cup F \to E \cup F$ be defined as

$$q(u, v) := \begin{cases} \left(1, \frac{v}{2}\right), & \text{if } u = 0, \\ \left(0, \frac{v}{2}\right), & \text{if } u = 1. \end{cases}$$

Let $\omega: \mathbb{R}^2 \times \mathbb{R}^2 \to \mathbb{R}$ be a mapping defined as $\omega((u, v), (w, z)) = vz$ forall $(u, v), (w, z) \in \mathbb{R}^2$.
ω is obviously a continuous function, not a metric on $\mathbb{R}^2$. Observe that $D_\omega(E, F) = 0$.
If for $u \in E$ and $v \in F$, $| \omega(u, v) | > D_\omega(E, F)$ then take $\epsilon = | \omega(u, v) | - D_\omega(E, F)$. It is easy to verify that for this $\epsilon > 0$ there exists $\delta > R(u, v)$ such that the function q satisfies the conditions of generalized Reich type cyclic topologically Meir-Keeler contraction map w.r.t ω.
Let us now show that the best proximity point in a topological space exists and is unique:

Proposition 2.3. Let E and F be non-empty and closed subsets of topological space Y. Let
$q: E \cup F \to E \cup F$ be a generalized Reich type cyclic topologically Meir-Keeler contraction map w.r.t a continous function $\omega: Y \times Y \to \mathbb{R}$. If $u \in E$ satisfies condition (2.1), then $| \omega(q^n u, q^{n+1} u) | \to D_\omega(E, F)$ as $n \to \infty$.

Proof. Suppose q is generalized Reich type cyclic topologically Meir-Keeler contraction map w.r.t a continuous function ω.Take $u \in E$ for which (2.1) holds.
Since either n or $n + 1$ is even, then for each $u \in E$, we have,
$\frac{1}{3} [| \omega(q^n u, q^{n-1} u) | + | \omega(q^{n+1} u, q^n u) | + | \omega(q^n u, q^{n-1} u) |] \geq D_\omega(E, F)$.
Consider the case, $\frac{1}{3} [| \omega(q^n u, q^{n-1} u) | + | \omega(q^{n+1} u, q^n u) | + | \omega(q^n u, q^{n-1} u) |] = D_\omega(E, F)$.
Then due to (2.1), we have $| \omega(q^{n+1} u, q^n u) | < D_\omega(E, F) + \epsilon$,
Which is equivalent to

$| \omega(q^{n+1}u, q^n u) | < \frac{1}{3}[| \omega(q^n u, q^{n-1}u) | + | \omega(q^{n+1}u, q^n u) | + | \omega(q^n u, q^{n-1}u) |] + \epsilon.$

Thus we have, $| \omega(q^{n+1}u, q^n u) | \leq | \omega(q^n u, q^{n-1}u) |$, as $\epsilon \to 0$.

Now consider the other case, that is

$$\frac{1}{3}[| \omega(q^n u, q^{n-1}u | + | \omega(q^{n+1}u, q^n u) | + | \omega(q^n u, q^{n-1}u) |] > D_\omega(E, F).$$

Set $\epsilon_1 = \frac{1}{3}[| \omega(q^n u, q^{n-1}u) | + | \omega(q^{n+1}u, q^n u) | + | \omega(q^n u, q^{n-1}u) |] - D_\omega(E, F) > 0$.

According to (2.1), for this ϵ_1, there exists δ_1 such that

$$| \omega(q^{n+1}u, q^n u) | < D_\omega(E, F) + \epsilon_1 \quad = \frac{1}{3}[| \omega(q^n u, q^{n-1}u) | + | \omega(q^{n+1}u, q^n u) | + | \omega(q^n u, q^{n-1}u) |].$$

Hence, $| \omega(q^{n+1}u, q^n u) | \leq | \omega(q^n u, q^{n-1}u) |$ for all $n \in \mathbb{N}$. (2.2)

Let $\alpha_n = | \omega(q^{n+1}u, q^n u) |$. Clearly $\{\alpha_n\}$ is a decreasing sequence bounded below by $D_\omega(E, F)$.

Therefore $\{\alpha_n\}$ converges to some α with $\alpha \geq D_\omega(E, F)$.

We now show that $\alpha = D_\omega(E, F)$ by assuming the contrary, that is $\alpha > D_\omega(E, F)$.

Set $\epsilon = \alpha - D_\omega(E, F) > 0$. Then there exists $\delta > 0$ for which (2.1) holds. Since $\{| \omega(q^{n+1}u, q^n u) |\} \to \alpha$, there exist a $n_0 \in \mathbb{N}$ such that

$$\alpha \leq \frac{1}{3}[| \omega(q^n u, q^{n-1}u) | + | \omega(q^{n+2}u, q^{n+1}u) | + | \omega(q^{n+1}u, q^n u) |] < \epsilon + D_\omega(E, F) + \delta, \forall n \geq n_0.$$

Thus, $| \omega(q^{n+2}u, q^{n+1}u) | < D_\omega(E, F) + \epsilon = \alpha, \ \forall n \geq n_0$. Which is contradiction .

Hence $\alpha = D_\omega(E, F)$.

Theorem 2.4. Let E, F be nonempty and closed subsets of a topological space Y and $\omega : Y \times Y \to R$ be a continuous mapping. Let $q : E \cup F \to E \cup F$ be a continuous generalized Reich type cyclic topologically Meir-Keeler contraction mapping w.r.t ω. Then for any $x \in E \cup F$, the set $\text{Lim } O(x, q)$ is either empty or consist of a point $\{u\}$, which satisfy $|\omega(u, qu)| = D_\omega(E, F)$.

Proof. Let $x \in E \cup F$. Let's say $\text{Lim } O(x, q)$ is nonempty, by continuity of q if $v \in \text{Lim } O(x, q)$,

$$q(v) \in \text{Lim } q(O(x, q)) \subseteq \text{Lim } O(x, q).$$

Define $\tau : E \cup F \to R$ by $\tau(u) := |\omega(u, qu)|$. Since q, ω are continuous, τ is also continuous. Hence,

$$\tau(v) \in \text{Lim } \tau(O(x, q)) \quad (2.3)$$

Suppose that $|\omega(q^n x, q^{n+1}x)| \neq D_\omega(E, F)$ for all $n \in \mathbb{N}$. Since q is generalized Reich type cyclic topologically Meir-Keeler contraction map w.r.t ω, from Proposition 2.3, we have $\{\tau(q^n x)\} \to D_\omega(E, F)$ asn $\to \infty$. i.e., $\text{Lim } \tau(O(x, q))$ is a singleton set. From (2.3), $\tau(v) = D_\omega(E, F)$. i.e., $|\omega(v, qv)| = D_\omega(E, F)$. i.e., v is a best proximity point q with respective ω. Suppose that $|\omega(q^{n_0} x, q^{n_0+1}x)| \neq D_\omega(E, F)$ for some $n_0 \in \mathbb{N}$. Then $\{\tau(q^n x)\}$ becomes an eventually constant sequence with the constant value $D_\omega(E, F)$. Hence $\text{Lim } \tau(O(x, q))$ is a singleton set. The same conclusion follows by the preceding argument.

Theorem 2.5. Let E, F be nonempty and closed subsets of a topological space Y and $\omega : Y \times Y \to R$ be a continuous mapping that satisfies the following requirements:

(1) $\omega(u, v) = \omega(v, u)$, for all $u \in E, v \in F$,

(2) $\omega(u_1, u_2) = 0 \Leftrightarrow u_1 = u_2$, for all $u_1, u_2 \in E$ (or $u_1, u_2 \in F$).

Let $q : E \cup F \to E \cup F$ be a continuous generalized Reich type cyclic topologically Meir-Keeler contraction mapping w.r.t ω. Suppose that the pair (E, F) has P-property w.r.t ω. Then for any $x \in E \cup F$, the set $\text{Lim } O(x, q)$ is either empty or $\text{Lim } O(x, q) \cap E$ is a singleton set $\{u\}$, which satisfy $|\omega(u, qu)| = D_\omega(E, F)$.

Proof. By Theorem 2.4, we conclude that the set $\text{Lim } O(x, q)$ is either empty or contains a best proximity point v (say) of q w.r.t ω. Now we show that the best proximity point, v, is unique. Without loss of generality, assume that v is in E. Suppose there exists two points u_0, v_0 in E such that $u_0, v_0 \in \text{Lim } O(x, q)$ satisfying

$|\omega(u_0, qu_0)| = D_\omega(E, F)$ (2.4)

$|\omega(v_0, qv_0)| = D_\omega(E, F)$ (2.5)

Since q is generalized Reich type cyclic topologically Meir-Keeler contraction mapping w.r.t ω and by Proposition 2.3, we have, $|\omega(qu_0, q^2u_0)| = D_\omega(E,F)$.

Hence, $|\omega(u_0, qu_0)| = |\omega(q^2u_0, qu_0)| = D_\omega(E,F)$. By P-property, we have $|\omega(u_0, q^2u_0)| = |\omega(qu_0, qu_0)| = 0$. Thus $u_0 = q^2u_0$. Similarly $v_0 = q^2v_0$.

Now by equation (2.2), we have,

$$|\omega(v_0, qu_0)| = |\omega(q^2v_0, qu_0)| \leq |\omega(qv_0, u_0)|. \quad (2.6)$$

Similarly, $|\omega(qv_0, u_0)| \leq |\omega(v_0, qv_0)|$ (2.7)

From (2.6) and (2.7), we get that

$$|\omega(v_0, qu_0)| = |\omega(u_0, qv_0)|. \quad (2.8)$$

Suppose that $|\omega(qu_0, v_0)| > D_\omega(E,F)$. Then $\epsilon_0 = |\omega(qu_0, v_0)| - D_\omega(E,F) > 0$.

Claim: For this ϵ_0, there exists a $\delta_0 > 0$ satisfying $R(qu_0, v_0) < D_\omega(E,F) + \epsilon_0 + \delta_0$.

Assume the contrary, Suppose for all $\delta_0 > 0$, $R(qu_0, v_0) \geq D_\omega(E,F) + \epsilon_0 + \delta_0$.

That is,

$$1/3\,[|\omega(qu_0, v_0)| + |\omega(q^2u_0, qu_0)| + |\omega(qv_0, v_0)|] \geq D_\omega(E,F) + \epsilon_0 + \delta_0$$
$$1/3\,[|\omega(qu_0, v_0)| + 2D_\omega(E,F)] \geq D_\omega(E,F) + \epsilon_0 + \delta_0$$
$$1/3\,|\omega(qu_0, v_0)| \geq (1 - 2/3)D_\omega(E,F) + \epsilon_0 + \delta_0$$
$$|\omega(qu_0, v_0)| \geq D_\omega(E,F) + 3\epsilon_0 + 3\delta_0$$
$$|\omega(qu_0, v_0)| \geq D_\omega(E,F) + 3(|\omega(qu_0, v_0)| - D_\omega(E,F) + 3\delta_0$$
$$-2|\omega(qu_0, v_0)| \geq -2D_\omega(E,F) + 3\delta_0$$
$$|\omega(qu_0, v_0)| \leq D_\omega(E,F) - 3/2\,\delta_0$$

As $\delta_0 \to 0$, $|\omega(qu_0, v_0)| < D_\omega(E,F)$ a contradiction.

Therefore, $R(qu_0, v_0) < D_\omega(E,F) + \epsilon_0 + \delta_0$. Then due to (2.1), we have,

$$|\omega(q^2u_0, qv_0)| < D_\omega(E,F) + \epsilon_0 = D_\omega(E,F) + |\omega(qu_0, v_0)| - D_\omega(E,F) = |\omega(qu_0, v_0)|.$$

That is, $|\omega(u_0, qv_0)| < |\omega(qu_0, v_0)|$, which is a contradiction to the equation (2.8).

Therefore, $|\omega(qu_0, v_0)| = D_\omega(E,F)$.

By using equation (2.4) and P-property, $|\omega(u_0, qu_0)| = |\omega(v_0, qu_0)| = D_\omega(E,F)$

$\Rightarrow |\omega(u_0, v_0)| = |\omega(qu_0, qu_0)| = 0$. Hence $u_0 = v_0$. i.e., the best proximity point of q w.r.t ω is unique in E.

REFERENCES

1. E. Karapinar and I.M. Erhan: Best proximity point on different type contractions, Appl. Math. Inf. Sci. 5 (3), 558-569, (2011).
2. S. Karpagam and Sushama Agrawal: Best proximity points theorems for cyclic Meir- Keeler contraction maps, Nonlinear Analysis, 74, 1040-1046, (2011).
3. V. Sankar Raj and T.Piramatchi: Best proximity point theorems in topological spaces, J. Fixed Point Theory Appl., 22 (1), Article 2 (2020).
4. S. Sahayarajjoseph Nirmalkumar and S. Sujith: Best proximity points for cyclic contraction mapping on topological spaces, AIP Conference Proceedings, 2829, 070001, (2023).
5. S. Sahayarajjoseph Nirmalkumar and S. Sujith: Best proximity points for generalized contraction mappings on topological spaces, Advances and Applications in Mathematical Sciences, 21, 6235-6250, (2022).
6. S. Sahayarajjoseph Nirmalkumar, S. Sujith, Best proximity points for cyclic Kannan-Chatterjea type contraction mappings on topological spaces, A conference proceedings of recent developments in pure and applied mathematics, 1, ISBN:978-93-5680-006-9, (2022).

Vol.15 / Issue 83 / Apr / 2024 International Bimonthly (Print) – Open Access ISSN: 0976 – 0997

RESEARCH ARTICLE

Analysis on Online Learning of Mathematics and Student's Attitude

A. Aruna[1] and PL. Meenakshi[2]

[1]Post Graduate Student, Department of Mathematics, Avinashilingam Institute for Home Science and Higher Education for Women, Tamil Nadu, India.
[2]Assistant Professor, Department of Mathematics, Avinashilingam Institute for Home Science and Higher Education for Women, Tamil Nadu, India.

Received: 30 Dec 2023 Revised: 09 Jan 2024 Accepted: 12 Mar 2024

***Address for Correspondence**
A. Aruna
Post Graduate Student,
Department of Mathematics,
Avinashilingam Institute for Home Science and Higher Education for Women,
Tamil Nadu, India.

ABSTRACT

The COVID-19 pandemic has resulted in significant effects in various sectors, digitalising the world. One of the most impacted sectors includes education, which resulted in the widespread adoption of remote learning policies like video classes, system-proctored tests etc. However, the shift to online classes has made learning more challenging for students as the accessibility to smartphones and systems is not even. It made understanding Mathematics even more challenging as it requires effective student-teacher interaction to understand the subject and cope with Mathematics and fewer students are enrolling in this field. This study aims to explain why students' interest in enrolling in Undergraduate Mathematics Courses in Coimbatore district has decreased after COVID-19.Itcontinues to investigate whether the 11th and 12th graders' interest in Mathematics has been impacted by their online math education. Also, the relationship between online learning of Mathematics and students' attitudes towards math is analysed.

Keywords: Online learning, COVID-19, Attitude, t-test.

INTRODUCTION

Mathematics is widely known as the "language of the universe" and includes a wide range of ideas, hypotheses, and applications that are essential to many academic disciplines as well as in daily life. Mathematics is the foundation of every innovation. It is widely used in almost every field. Its wide applications are seen in technologies, software, computers, art, economy, engineering, sports, and even in contemporary and ancient architectures. From basic algebra to sophisticated calculus, geometry to simple arithmetic, and all points in between, Mathematics offers the foundation for comprehending quantitative connections, resolving issues, and making wise judgments. Mathematics is a crucial subject in school and college curricula. It is a compulsory subject at the school level and a major subject at

a higher level. However, many students find Mathematics challenging, resulting in many of them failing in this subject. Despite the importance of Mathematics in research and development it does not attract many of the students to take it as a major. Most students find Mathematics difficult and online learning during COVID-19 made it a more and more difficult subject. It is found that in the aftermath of the pandemic enrolment of students in Mathematics is largely impacted negatively. This study aims to identify the online learning on student's attitudes towards Mathematics.

ONLINE LEARNING

Electronic devices like mobile, laptops, computers, etc.., are used for learning, a sort of educational activity with the support of the internet facilitating student-teacher interactions and instruction.Education around the world has been impacted by the development of online learning brought about by COVID-19. There will always be a process of interaction in every learning action, whether it takes place online or in person. The three types of interaction in the learning process are the interaction between

1. students and students,
2. students with teachers and
3. students with the material(Bernard et al., 2009).

Mathematicsis among the subjects that are affected by online learning. Here are some aspects that need to be considered regarding online learning of Mathematics during the pandemic and the student's attitudes towards the subject. The aspects are:

1. Challenges of Online Learning in Mathematics
2. Adaptation to Online Platforms
3. Students' attitude towards Mathematics
4. Long-term impact.

STUDENTS' ATTITUDE TOWARDS MATHEMATICS:

The term "attitude" describes a person's recurring beliefs, emotions, and actions that reveal their character and point of view. It is an amalgam of attitude, conviction, feeling, and action that mould reactions to different circumstances. A person's attitude greatly affects how they handle problems, relates to other people, and make decisions. Attitudes can be neutral, negative, or positive. It is essential for influencing general well-being, directing behaviours, and forming perceptions. A person's attitude is dynamic and subject to change in response to events, cultural standards, and personal development. To build healthy connections and succeed both personally and professionally, it is crucial to recognize and control one's attitude. The approach that students take to mathematics has a significant impact on both their academic achievement and interest in the subject. Students who take enjoyment in performing math-related assignments demonstrate a good attitude toward the subject. Therefore, it is essential to maintain a favourable attitude towards Mathematics to promote students' willingness to learn the subject and include it in Mathematics instruction. Conversely, a negative attitude towards Mathematics can lead to reluctance to learn and spend time on the subject, thus hindering their progress. Factors such as inappropriate instructional materials, poor instructional practices, classroom management, and class activities can significantly affect students' attitudes towards Mathematics.

REVIEW OF LITERATURE

Lazaros Anastasiadis and Poulcheria Zirinoglou (2022)

The study's goal is to determine how Greek students feel about studying analytics, AI algorithms, and big data. Four conceptual constructs are used in the study to examine the attitudes of the students: motivation, enjoyment, value, and self-confidence. The relationship between value and enjoyment, drive and value, and self-confidence and value were shown to have the greatest connections. Furthermore, the findings demonstrated that there was no big difference between male and female students' views about Mathematics.

I Putu Wisna Ariawan (2022)
The study demonstrated the effects of COVID-19 on the academic performance of Singaraja City public high school students enrolled in online mathematics courses. Some scams within the area of virtual math classes misled learners into thinking that their academic achievements were poor and that their abilities were compared to those of another.The results indicate that to eliminate the negative impact on learning teachers should put more effortinto neutralizing the effect in upcoming academic years.

Justice Enu, Osei K Agyman, Daniel Nkum (2015)
The purpose of the study was to investigate the factors impacting the mathematics performance of college students. The study concluded that the student's performance in mathematics is impacted by some issues like the style of instruction, which makes the student a passive participant in the learning process, and inadequate teaching and learning resources.

Nazir Haider Shah, Nadia Nazir (2023)
According to the study, anxiety had a higher mean score when compared to motivation, confidence, and importance in terms of students' attitudes towards mathematics. It indicates that students have anxiety before beginning a math lesson. It was determined that secondary school male and female students did not significantly differ in their mathematical performance and that male students had a greater attitude toward mathematics than female students. Anxiety, significance, getting around, and confidence all have a significant impact on mathematics success. The parameters of students' attitudes indicate that they will not change in the future with regard to their interest in mathematics; however, confidence and motivation will play a larger role than significance, and anxiety it will prevent students from interested in learning challenging subjects like mathematics.

THE PURPOSE OF THE STUDY
This study aims to explain why students' interest in enrolling in Undergraduate Mathematics Courses in Coimbatore district has decreased after COVID-19. It continues to investigate whether the 11th and 12th graders' interest in Mathematics has been impacted by their online math education. Also, the relationship between online learning of Mathematics and students' attitudes towards math is analysed.

LIMITATIONS OF THE STUDY
The focus of the study is limited to female undergraduate students of educational institutes who are not pursuing Mathematics as their major subject. The nature of the study is descriptive and qualitative, which means that it aims to provide an in-depth understanding of the research topic.

RESEARCH METHODOLOGY

An educational institute was selected for data collection, and the study population targeted ordinary-level students. As a result, the researchers randomly selected 50 students who participated in the study and had an average age of 18 years. To address the research question, a descriptive survey design was employed in the present study. The researchers constructed questionnaires based on the research questions, which were divided into two main themes:

1. Online learning of Mathematics, and
2. Students' attitude towards Mathematics.

The researchers deemed six items that are sufficient to analyse the relationship between online learning of Mathematics and students' attitudes. The students were given the surveys in English, using a 4-point Likert scale ranging from 4 (strongly agree) to 1 (strongly disagree).

DATA ANALYSIS
Data were analyzed using Microsoft Excel. The relation between students' attitudes toward mathematics and their online mathematics education was examined utilizing

1. independent sample t-tests.
2. Mean
3. Standard deviation

was utilized to describe the Online learning of Mathematics and student attitude.
Note: df – degree of freedom.

STUDENT'S ATTITUDE TOWARDS MATHEMATICS
ONLINE LEARNING MATHEMATICS

RESULT AND FINDINGS

To test the hypotheses, a t-test for independence with a significance level $\alpha = 0.05$ is used.
Null hypothesis H_0: There is no relationship between online learning and students' attitudes towards Mathematics.
Alternative hypothesis H_1: There is a relationship between online learning and students' attitudes towards Mathematics. By comparing the t-value and critical value 4.33277>1.9845So, we accept H_1.This study aimed to explore the correlation between online learning of Mathematics and students' attitudes towards the subject. The study proposed that online learning could impact attitudes towards math. The results show that there is, in fact, a link between students' attitudes toward mathematics and online learning. Table 1 displays the results of the Attitude Towards Mathematics Inventory as rated by the student-respondents. The table includes the mean score for each item and the overall mean rating.

1. The highest recorded mean score of 3.34 was achieved by the positive statement "I want to develop my mathematical skills",
2. The lowest recorded mean score of 1.74 was obtained by the negative statement "Mathematics is not necessary for our studies".
3. The overall mean Attitude towards Mathematics for all students is 2.7033.

Students find the subject something confusing and complicated. Despite these perceptions, they still see Math as important in our studies. Students see Mathematics in everyday living and it's important to everyone. The level of Online learning of Mathematics is presented in Table 2. Here the Highest mean value of 2.88 was obtained by the statement of the items, “Even if I have no idea about the subject matter, I am too lazy to approach the teacher when the math lessons are done online” and “Sometimes, internet network issues prevent me from properly participating in online math periods”. Table 3 shows that Online learning of Mathematics is related to student attitude. The relationship between Online learning of Mathematics and the student's attitude was measured using an independent sample t-test. According to the table,
The score of Online Learning is,

$$N=50, M=2.7033, SD=0.10077$$

and the score of the student's attitude is,

$$N=50,\ M=2.7933,\ SD=0.10686$$

Whereas,

$$t=4.33277>1.9845$$

So, there was a relationship between Online learning of Mathematics and the student's attitude. Furthermore, the Null hypothesis was rejected.

CONCLUSION

The purpose of the study was to investigate the impact of online learning on students' attitudes towards Mathematics during the pandemic. The results of the study showed a connection between online learning and students' negative outlook on mathematics. Consequently, online learning has affected students' attitudes and resulted in a low enrollment rate in Mathematics. So, the enrollment rate may rise if we reduce these explanations.

REFERENCES

1. Bernard, R.M.; Abrami, P.C.; Borokhovski, E.; Wade, A., Tamim, R. et al. (2009). A meta analysis of three interaction treatments in distance education .Review of Educational Research, 79(3), 1243-1289. DOI:10.3102 /00346543093 33844v1.
2. Delyanti Azzumarito Pulungan; Heri Retnawati; Amat Jaedun. STUDENTS DIFFICULTIES IN ONLINE MATH LEARNING DURING PANDEMIC COVID-19. Jurnal Program Studi Pendidikan Matematika. Volume 11, No. 1,2022, 305-318.
3. Fatima Daudu Suleiman; Muhd Rustam Muhd Rameli; Muhammad Ado (2020). Attitude of Nigerian Primary School Students towards Mathematics Subject. Journal of Research in Psychology; Vo. 2, No. 2. http://readersinsight.net/JRP.
4. Gabriel, M. Pagaram; Marife L. Loremas; Jenevieb D. Gultiano; Jonathan O. Etcuban. Mathematics Performance of Senior High School Students in Blended Learning Amidst the Covid-19 Pandemic. Journal of Positive School Psychology; Vol. 6, No. 6, 10593-10613.
5. Hummaira Qudsia; Sumaira Rehman; Muneeb Ahmed; Sidra Munawar (2022). Investigating student's satisfaction in online learning: the role of students' interaction and engagement in universities.https://doi.org/10.1080/10494820.2022.2061009.
6. I Putu Wisna Ariawan (2022). "The academic impact of online mathematics learning during COVID-19 for junior high school students". Jurnal Elemen; 8(1), 131-143, January 2022.
7. Lazaros Anastasiadis; Poulcheria Zirinoglou (2022).Student's attitudes toward Mathematics: The case of Greek students. International Journal of Education and Social Science; Vol. 9 No. 3,June 2022, 2415-1246.
8. Nazuha Muda @ Yusof; Zokree Abdul Karim; Ruzaidah A. Rashid; Zamzulani Mohamed. Factors Affecting Students' Achievement in Mathematics: Case Study in Terengganu. Jurnal Intelek. Volume 14 Issue 2(December 2019).
9. Scott, A. Chamberlin. A review of Instruments Created to Assess Affect in Mathematics. Journal of Mathematics Education. June 2010, Vol. 3, No. 1, pp.167-182.
10. Sebastian Geisler; Stefanie Rach; Katrin Rolka.The relation between attitudes towards mathematics and dropout from university mathematics- the mediating role of satisfaction and achievement. Educational Studies in Mathematics (2023) 112:359-381 https://doi.org/10.1007/s10649-022-10198-6. www.mjosbr.com www.researchgate.net

Table 1.Mean and standard deviation of student's responses in attitude towards Mathematics

Questions	Total	Strongly agree	Agree	Disagree	Strongly disagree	Mean	Standard deviation
Mathematics is very interesting to me and I enjoy Mathematics courses.	50	13	27	9	1	3.04	0.727
My mind goes blank and I am unable to think when working on Mathematics.	50	27	6	16	1	2.76	0.687
I love the study of Mathematics.							

	50	11	23	14	2	2.86	0.808
Mathematics is not necessary in our studies	50	1	5	24	20	1.74	0.723
I've never been good at Mathematics, and it's my least favourite subject.	50	7	16	21	6	2.48	0.886
I want to develop my mathematical skills.	50	20	27	3	0	3.34	0.593
					Overall Mean and SD	2.7033	0.10077

Table 2: Mean and standard deviation of student responses in Online learning of Mathematics.

Questions	Total	Strongly agree	Agree	Disagree	Strongly disagree	Mean	Standard deviation
I believe that my online learning math scores don't accurately represent my actual mathematics skills.	50	5	33	12	0	2.86	0.572
Even if I have no idea about the subject matter, I am too lazy to approach the teacher when the math lessons are done online.	50	7	31	11	1	2.88	0.659
Sometimes, internet network issues prevent me from properly participating in online math periods.	50	10	26	12	2	2.88	0.773
Math skills have decreased due to studying online.	50	6	26	16	2	2.72	0.730
Even though the mathematics lessons are done online, I frequently receive high marks.	50	10	24	13	3	2.82	0.825
Online math classes have potential sufficient opportunities for interactive learning and engagement.	50	7	20	19	4	2.60	0.833
				Overall	Mean and SD	2.7933	0.10686

Table 3 Analysis of Online Learning and Student's Attitude towards Mathematics.

	N	Mean	Standard deviation	df	t-value	Critical value	The result
Online learning	50	2.7033	0.10077				
				98	4.33277	1.9845	Reject H_0
Attitudes	50	2.7933	0.10686				

Vol.15 / Issue 83 / Apr / 2024 International Bimonthly (Print) – Open Access ISSN: 0976 – 0997

RESEARCH ARTICLE

A Diagnosis of Renal Disease using Multiclass with ERF Classifier Learning Techniques

K. Kottaisamy[1]* and S. Chidambaranathan[2]

[1]Research Scholar, Regno. 19221282291017, Dept. of Computer Applications, St. Xavier's College (Autonomous), Palayamkottai, (Affiliated to Manonmaniam Sundaranar University) Tirunelveli, Tamil Nadu, India.
[2]Associate Professor, Dept. of Computer Applications, St. Xavier's College (Autonomous), Palayamkottai (Affiliated to Manonmaniam Sundaranar University) Tirunelveli, Tamil Nadu, India.

Received: 30 Dec 2023 Revised: 09 Jan 2024 Accepted: 12 Mar 2024

***Address for Correspondence**
K. Kottaisamy
Research Scholar,
Regno. 19221282291017,
Dept. of Computer Applications,
St. Xavier's College (Autonomous), Palayamkottai,
(Affiliated to Manonmaniam Sundaranar University)
Tirunelveli, Tamil Nadu, India.
Email: kskottaisamy@gmail.com

ABSTRACT

Machine learning-based medical diagnostics will make early renal disease stage prediction viable in underdeveloped and developing nations. Multiclass classification algorithms are used to diagnose kidney illness using a real-time dataset. As a result, kidney failure sets in, making an early prediction of Chronic Renal Disease (CRD) vital even if it may be difficult. People with diabetes, hypertension, autoimmune diseases, or a family history of the condition should have priority screening for an early diagnosis of CRD. The suggested Ensemble Random Forest (ERF) with a multiclass classifier model was trained and tested in the study's research using the renal disease dataset. Finally, we considered how accurate the proposed model was at predicting the future. ERF with multi-class classification is used to classify data with 26 features, 20 features, 15 features, and 10 features to predict the Chronic renal stages. Finally, among the 26 characteristics, for the multiclass categorization. For all ten characteristics combined, the accuracy of the renal stage is 97%.

Keywords: Chronic Renal Disease, Diagnosis, Prediction, Multiclass Classification, Machine Learning, Hypertension, Diabetes.

INTRODUCTION

Biosciences have advanced to a greater level, generating vast amounts of data via electronic health records. This has created an urgent demand for knowledge generation from this massive volume of data. In this branch of biology, machine learning and data mining are crucial. Damaged kidneys that are unable to filter blood as well as they should are the outcome of CRD. People with lower socio-economic positions bear a disproportionate amount of the burden of CRD because they have a higher prevalence of the disease, less access to treatment, and worse outcomes. Therefore, it is crucial for equality that CRD is detected early and treated. CRD can be decreased or even prevented by doing tests such as urine tests, blood tests, and kidney scans, and consulting a doctor about additional symptoms of renal disease. The kidneys do not normally fail all at once in chronic renal disease. Instead, renal disease frequently advances slowly over time. If detected early, medications and lifestyle adjustments may help delay or prevent the course of CKD. CKD has five phases. The five phases of kidney disease are defined by the National Kidney Foundation (NKF). This enables clinicians to offer the best care possible because each stage necessitates a distinct set of tests and treatments. To ascertain the stage of renal illness, physicians utilize the Estimated Glomerular Filtration Rate (eGFR), a mathematical formula that takes into account an individual's age, gender, and serum creatinine level (ascertained by a blood test).An essential biomarker of renal function is creatinine, a byproduct of muscle activity. Blood creatinine levels grow when renal function decreases, whereas when the kidneys are functioning normally, they remove creatinine from the blood. The first stage of renal disease is linked to a high or normal GFR (GFR > 90 mL/min); the second stage is linked to CKD (GFR = 60–89 mL/min); the third stage is linked to moderate CKD (GFR = 45–59 mL/min); the fourth stage is linked to severe CKD (GFR 15 mL/min); and the fifth stage is linked to end-stage CKD.In this study, we created machine learning models utilizing important pathological categories that were specifically chosen to uncover clinical test characteristics that would help with the early and accurate diagnosis of CKD. Time and money will be saved for diagnostic screening with this method.

we investigated the accuracy rate of feature selection approaches in this work by lowering the dimensionality of the feature and merging heterogeneous classifiers to produce the ensemble model.The data employed in this study's response parameter are the various stages of chronic kidney disease based on eGFR, a variable that is categorical with five stages of development (i.e., 1, 2, 3A, 3B, 4, and 5). Several response rate categories bias the data for the above parameter in a negative direction. This work uses statistical models that capture the characteristics of the ordinal response factor to determine the factors impacting GFR to discover the optimum model that more precisely categorizes very unbalanced data. Our findings imply that when employing our suggested machine learning models to diagnose CKD, optimized datasets with key features perform well. Additionally, we assessed the characteristics of clinical tests using blood and urine tests as well as clinical indicators with low acquisition prices. The best-performing prediction model, the random forest classifier, produced excellent levels of CKD diagnosis accuracy using the optimized and pathologically categorized attribute set.

Conclusions: Using machine learning, we were able to produce effective predictive analytics for CKD screening that can be used to improve CKD screening processes and enable more effective and prompt treatment strategies.This document has the following structure. Section 2 demonstrates multiple machine learning Classifier methods for predicting chronic renal disease. Response variables, explanatory factors, and their characteristics are all part of the models and data for this study. The dataset is introduced and explained in Section 3 along with two original methods: preprocessing and model building. The results of a classification performance comparison between ensemble random forest machine learning techniques and generalized multi-class models are examined in Section 4. Finally, Section 5 offers a study analysis. Previously, multiple researchers employed chronic renal illness to test the precision of numerous machine-learning algorithms using methodologies. In their study,seven classifier algorithms were utilized by Chittora et al. [1]: the Chi²automatic interaction detector, Random Forest, ANN, C5.0, Logistic Regression (LR), Linear Support Vector classifier (LSVM) concluded penalty L1 & through penalty L2. The approach that produced the best accuracy was the linear model, which they determined after measuring the correctness, precision, recall, and AUC curve. The results have been calculated independently for each classifier using the least

absolute shrinking and selection operator regression, synthetic minority oversampling with complete attributes, Wrapper approach feature selection, and full features. According to this study, among all the classifiers, LSVM had the highest accuracy across all experiments. However, the aims for Logistics and KNN were not sufficiently met. Using pre-processing methods and datasets from the UCI Machine Learning repository such as label encoding and min-max normalizing, Sathyaraj et al. [2] presented a hybrid model that can accomplish better to detect kidney disease. Finally, they discovered that the Random Forest and AdaBoost algorithms consistently preserved a higher perfection rate. Wang et al.'s [3] regression model took into account six variables, including sex, age, smoking habit, haemoglobin, and urine protein level, to predict the risk of CKD. They tested with the XGBoost, Random Forest, and ResNet neural network regression models. Finally, XGBoost achieved the greatest result with an R2 score of 0.5523. To raise public awareness, Shirahatti et al. [4] proposed a classification system that uses ML algorithms to evaluate the likelihood of being impacted by CKD. Electronic Medical Records (EMR), Clinical history, and laboratory testing were used to gather the necessary data. They compared some machine learning methods, both with and without preprocessing, and determined that the random forest classifier achieved 100% accuracy.In underdeveloped and emerging nations, early detection of CKDwill be possible because of machine learning-based medical diagnostics. Renal disease is diagnosed with machine learning models using a real-time dataset. As a result, kidney failure sets in, and although early detection of CKD may be difficult, it is crucial. Prioritizing early detection of CKD requires screening those with diabetes, hypertension, autoimmune diseases, or a family history of the illness.

Machine learning may be applied to inpatient electronic medical data to find patterns associated with certain diseases and alert physicians to any abnormalities. The research findings indicate that enhancing the effectiveness of classification algorithms by feature selection can lead to a rise in the precision of chronic kidney disease prediction and diagnosis machine learning approaches including decision tree, random forest classifier, and extra tree. The trial's conclusions could help the medical field anticipate problems and make decisions early on to treat kidney illness and save lives. The experimental results for the proposed model appear to confirm the predicted degree of prediction accuracy [5]. Using the data from 551 patients, Xiao et al. [6] provided an approach to managing 9 machine learning classifiers: KNN, LR, Ridge regression, Random Forest ,Lasso regression, XGB, SVC, and Elastic Net. They applied machine learning, neural networks, and statistical approaches to analysis a variety of demographic information, including 13 blood and 5 additional indicators, to determine the disease's current stage. As a consequence, the suggested approach R-ACO-SVM achieved 99.50% accuracy and obtained good results when compared to the supplementary feature selection methods. Despite the significant number of missing values in the University of California Irvine (UCI) machine learning repository, Chen et al.'s [7] approach for diagnosing CKD makes use of machine learning techniques. They used feed-forward neural networks, random forest, naive Bayes classifiers, support vector classifiers, k-nearest neighbours, and logistic regression. They conducted their suggested model through about 10 simulations, and they discovered that logistic regression and random forest both had an accuracy of 99.83% on average. A patient's CKD status may be ascertained using machine learning algorithms. The dataset consists of 400 records of Indian patients from the Apollo Hospital in Tamil Nadu, along with 25 covariates. The dataset is divided into training and tested sections using a variety of machine learning methods. Early detection of renal issues lowers the risk of CKD. Algorithms are used to forecast kidney issues. The k-nearest neighbor, decision tree classifier, support vector classifier, logistic regression, random forest classifier, and extra tree classifier are some of the classification methods used on the Jupiter platform. The best and most effective method for detecting renal disease is this one. The random forest classifier is the best binary classifier for predicting renal illness when it comes to diagnosis[8][9].

MATERIAL AND METHODS

This study's main impartial is to investigate the accuracy of CKD detection using feature selection and machine learning methodologies. The identified classification method can provide predicted values for an early CKD diagnosis.

The Proposed Framework

The Recommended Framework Figure1.1 shows the suggested methodology for creating identification machine learning models and a comparison of them. The main objective of this learning is to provide a machine erudition approach using multiple classification algorithms for CKD identification. To diagnose CKD early, it can be helpful to find approaches with a high percentage of successfully classified examples and acknowledged classifiers. In this comparison analysis, the suggested method is compared to various state-of-the-art approaches.

Source of the Data & Description

The dataset for this study is based on patient data for chronic renal disease obtained from the Kidney Care Centre inNila Nursing HomeTamil Nadu, India. In addition to 13 numerical and 14 nominals, the dataset contains 1100 observations of individuals with the condition. The dataset, which quantifies the severity of the renal disease, consists of 275 observations at stage 1, 269 observations at stage 2, 133 observations at stage 3A, 109 observations at stage 3B, 145 observations at stage 4, and 169 observations at stage 5.Among the data variables in the dataset are those about Id, Age, Gender, Blood pressure, Anaemia, Blood Glucose Random, Specific gravity, Pus Cell, Albumin, Sugar, Diabetes mellitus, Packed Cell Volume, Sodium, Appetite, Hypertension, Bacteria, Red Blood Cells, Potassium, Pedal Edema, Red blood cell count, Serum creatinine, Blood Urea, Haemoglobin, Pus Cell Clumps, White blood cell count, Coronary Artery Disease, and CKD Stages.

Data preprocessing

The dataset is chosen for CKD prediction to facilitate data analysis and useful knowledge. To deploy a machine learning classifier for a chosen dataset, sufficient data must be available. The dataset has 27 attributes and is organized in attribute-relation file format. To use associative approaches, the dataset is transformed into a binomial format. Additionally, there are duplicate records and missing records. Category variables are converted to numeric values via label encoding.

Feature Selection

To reduce overfitting and increase projected accuracy, this class provides a meta-estimator that fits multiple randomized decision trees (extra-trees) to different dataset subsamples. The data set was split into two parts before modelling could start: The Train set (70%) was used to select and validate models, and the Test set (30%) contained data used to determine how effectively models generalized to new data. Data for instruction: The training dataset, which is derived from the main dataset, has 770 of the 1100 elements in the CKD main dataset. Information for testing: Out of the 1100 entries in the core CKD dataset, 330 were used in the testing.

Machine learning Model

This work focuses on developing a cataloguing model with feature selection based on evidence obtained to classify chronic kidney disease (CKD) using the Ensemble Random Forest classification technique. To function as an ensemble classification process, the random forest process builds a variety of decision trees. Random forests' hyper parameters bear striking similarities to decision trees' and bagging classifiers' hyper parameters. It is not necessary to combine a decision tree with a bagging classifier when using the random forest's classifier class. Using a random forest and the algorithm's regressor, regression jobs may be managed. While the trees are growing, the random forest improves the model's arbitrariness. Instead of looking for the main component when dividing a hub, it looks for the best part from an erratic subset of supply. As a result, there are many possibilities, the majority of which provide a better model. The training data sets' random subsets are used to build several decision trees. A vast collection of decision trees offers better outcome accuracy. The algorithm's runtime is reasonably quick and it takes into account missing data. The method is randomly generated by Random Forest, not the training set. The decision class is a type of class that decision trees produce.

Entropy

Entropy is a machine learning metric that quantifies the level of disorder or uncertainty in a system or dataset. It is a statistic that measures the amount of data in a dataset and is frequently used to evaluate the accuracy and quality of a model's predictions.

$Entropy = -p(a) * \log(p(a)) - p(b) * \log(p(b))$

Throughout the dataset, we have observations from Stages 1 through 5, including Stages 1, 2, Stages 3A and 3B. Then, according to the following equation:$E = -(P_j\ log2\ p_j + P_k\ log2\ p_k + P_l\ log2\ p_l + P_m\ log2\ p_m + P_n\ log2\ p_n + Po\ log2\ po$

Where P_j is the probability of selecting patients in Stage 1;

P_k denotes the probability of selecting patients in Stage 2;

P_l denotes the likelihood of selecting patients in Stage 3A.

P_m = Probability of selecting Stage 3B patients;

P_n = Probability of selecting Stage 4 patients and;

P_o= Probability of selecting Stage 5 patients.

Information Gain

After dividing a dataset on an attribute, the reduction in entropy is used to determine the information gain. The goal of building a decision tree is to locate the characteristic that provides the largest information gain (i.e., the most homogenous branches).The pattern detected in the dataset and the reduction in entropy is termed information gain. The following formula may be used to describe knowledge gain mathematically:

$$Information\ gain\ =\ E(parent) -\ [weighted\ average]E(children)$$

Each of our n datasets has m entries. The following pseudocode, which looks like Python, illustrates bootstrap sampling:

```
bootstrap_sample = bootstrap_sample (ckd_dataset, m):
Then, usingsub_dataset = [] in range(m) for i:
    add(random_one_element(ckd_dataset))to sub_dataset
sub_dataset should be returned
```

Pseudocode of an ensemble for multi-class classification using random forest:

```
mc_models = []
    for i in range (n_estimators):
    erfmodel = erf (max_depth=10, random state = i)
    mc_models.append(erfmodel)
ckdstage_prediction = []
    for erfmodel in mc_models:
    y_pred = mc_models.predict(x_test)
    ckdstage_prediction.append (y_pred)
```

Prediction of the Stages of CKD

We establish the important measures to evaluate the model's performance. We may develop measurement metrics to represent the performance of the classifiers in the digital diagnostics challenge using four essential characteristics.

Multi-Classification Confusion Matrix for Algorithms

```
r = assigned label
c = prediction classification
 for each instance of the input do
    K (r, c) + = 1
end for
```

K is the confusion matrix, where c and r stand for the matrix's column and row, respectively.

Accuracy of Classification

The created classifier model's accuracy may be designed using the equation below.

$$Accuracy = \frac{TN + TP}{\mathrm{TP} + \mathrm{FP} + \mathrm{TN} + \mathrm{FN}}$$

Where TP = Predicted is likewise positive and observation is positive

TN: Both the observed and the projected outcomes are negative.

FP = Predicted is positive while observation is negative

FN stands for "Observation is positive, but prediction is negative".

RESULTS AND DISCUSSION

After successfully the dataset through multi-classification machine learning algorithms,we acquired the accuracy numbers mentioned below. All metrics true positive, precision, or any other metric are calculated in multi-class classification in the same way they are in binary, with the exception that they must be calculated for each class. If we compute the true positive, false positive, true negative, and false negative given a class, we may virtually derive any metric for that class. In multi-class problems, precision has been calculated for each class, whereas in binary class problems, we only have one number. One global measure may be used to evaluate multi-class data and get micro, macro, and weighted precision. By adding micro, macro, and weighting, any metric from the confusion matrix may be transformed into a global metric. The figure 4.1 classifiers successfully predicted the CKD Stages at Stage 1 scoring 71 out of 74, and 4 of those indicated a poor result. The CKD Stage 2 is 66 out of 67, with 1 bad consequence anticipated. The CKD Stage 3A is 40 out of 42, and 2 outcomes were projected to be unfavourable. The CKD Stage 3B is 31 out of 33, and 2 outcomes were projected to be unfavourable. The CKD Stage 4 is 46 out of 51 and 5 outcomes were projected to be unfavorable. The CKD Stage 5 is 63 out of 63, meaning that not a single aspect in the report accurately indicated a bad result. The figure 4.2 classifiers successfully predicted the CKD Stages at Stage 1 scoring 72 out of 74, and Stage 2 was expected to be unsuccessful.

The CKD Stage 2 score is 67 out of 67, with 0 unfavourable outcomes foreseen. The CKD Stage 3A is 39 out of 42, and 3 outcomes were projected to be unfavourable. The CKD Stage 3B is 31 out of 33, and 2 outcomes were projected to be unfavourable. The CKD Stage 4 is 46 out of 51 and 5 outcomes were projected to be unfavorable. The CKD Stage 5 is 63 out of 63, meaning that not a single aspect in the report accurately indicated a bad result. The figure 4.3 classifiers successfully predicted the CKD Stages at Stage 1 scoring 72 out of 74, and Stage 2 was expected to be unsuccessful. The CKD Stage 2 is 66 out of 67, with 1 bad consequence anticipated. The CKD Stage 3A is 41 out of 42, and 1 unfavorable result was expected. The CKD Stage3B is 31 out of 33, and 2 outcomes were projected to be unfavourable. The CKD Stage 4 is 46 out of 51 and 5 outcomes were projected to be unfavorable. The CKD Stage 5 is 63 out of 63, meaning that not a single aspect in the report accurately indicated a bad result. The figure 4.4 classifiers correctly predicted the CKD Stages, with Stage 1 scoring 72 out of 74 and Stage 2 predicting a poor result. The CKD Stage 2 score is 67 out of 67, with 0 unfavourable outcomes foreseen. The CKD Stage 3A is 41 out of 42, and 1 unfavorable result was expected. The CKD Stage 3B is 31 out of 33, and 2 outcomes were projected to be unfavourable. The classifiers correctly predicted the CKD Stages, with Stage 4 being 46 out of 51 and 5 predicting a bad result. The classifiers successfully predicted the CKD Stages at Stage 5 had a score of 63 out of 63, and 0 of those predictions were incorrect across the board. The results of the validation accuracy for the multi-class classifier outlined above are summarized in Figure 4.5 overall in the CKD stage.

CONCLUSION

One of the difficult research issues in medical science nowadays seems to be the accurate prognosis of chronic renal disease. To identify which patients will exhibit which CKD symptoms at an early stage, this research proposes a prediction method. The models are trained and verified using the input parameters provided in the dataset, which include input parameters gathered from CKD patients. To perform the CKD diagnosis, multi-class classification with

ensemble random forest machine learning models is created. Out of the 26 CKD stages, the overall CKD stage accuracy for the 26 characteristics is 96.06%. Out of the 26 CKD stages, the overall CKD stage accuracy for the 20 characteristics is 96.36%. Out of the 26 CKD Stages, the accuracy of the CKD Stages for 15 features is 96.66% overall. Finally, for the multiclass classification out of the 26 CKD stages, the overall CKD stage accuracy for the 10 features is 97%.

ACKNOWLEDGEMENT

We sincerely thank the Nila Scan Centre, Virudhachalam or Vriddhachalam, Tamil Nadu for providing the resourceful data, Dr. J. Gandhi Mathi Rajarajan, MBBS., DMRD and S. Pappu Rajan, Kidney Care Centre for aiding me in the intellectual input, design, standardization and execution of this study.

REFERENCES

1. Chittora, P., Chaurasia, S., Chakrabarti, P., Kumawat, G., Chakrabarti, T., Leonowicz, Z., &Bolshev, V. (2021). Prediction of chronic kidney disease-a machine learning perspective. IEEE Access, 9, 17312-17334.
2. Janani, J., & Sathyaraj, R. (2021). Diagnosing Chronic Kidney Disease Using Hybrid Machine Learning Techniques. Turkish Journal of Computer and Mathematics Education (TURCOMAT), 12(13), 6383-6390.
3. Wang, W., Chakraborty, G., & Chakraborty, B. (2021). Predicting the risk of chronic kidney disease (CKD) using machine learning algorithm. Applied Sciences, 11(1), 202.
4. Shirahatti, A., Yadav, V., Vadde, N., Singh, A., Mahajan, P., & Sheikh, R. Prediction and preventive awareness of chronic kidney disease using machine learning algorithms.
5. Kottaisamy, M. K., & Chidambaranathan, S. (2023). Methods Of Recognizing Chronic Kidney Disease Using Machine Learning. Latin American Journal of Pharmacy, ISSN 0326 2383, Vol 42(3), 1025-1029.
6. Xiao, J., Ding, R., Xu, X., Guan, H., Feng, X., Sun, T., ... & Ye, Z. (2019). Comparison and development of machine learning tools in the prediction of chronic kidney disease progression. Journal of translational medicine, 17(1), 1-13.
7. Qin, J., Chen, L., Liu, Y., Liu, C., Feng, C., & Chen, B. (2019). A machine learning methodology for diagnosing chronic kidney disease. IEEE Access, 8, 20991-21002Debal, D.A., Sitote, T.M. Chronic kidney disease prediction using machine learning techniques. J Big Data 9, 109 (2022). https://doi.org/10.1186/s40537-022-00657-5
8. CHIDAMBARANATHAN, S., and K. KOTTAISAMY. "Comparative Study of Kidney Disease Prediction Using Classification Algorithms." Studies in Indian Place Names 40, no. 71 (2020): 923-926.
9. Kottaisamy, K., & Chidambaranathan, S. (2023). Machine Learning Model for Binary Classification Based Prediction of Chronic Renal Disease. *International Neurourology Journal*, *27*(4), 240-251.

Table 1: Multi-Class Classification using Ensemble Random Forest to classify datawith 26 features, 20 features, 15 features, and 10 features Classification Report

	Precision				Recall				F1-Score				Support			
Features	**26**	**20**	**15**	**10**	**26**	**20**	**15**	**10**	**26**	**20**	**15**	**10**	**26**	**20**	**15**	**10**
Stage 1	0.99	1.00	0.99	1.00	0.96	0.97	0.97	0.97	0.97	0.99	0.98	0.99	74	74	74	74
Stage 2	0.93	0.93	0.96	0.96	0.99	0.93	0.99	1.00	0.96	0.96	0.97	0.98	67	67	67	67
Stage 3A	0.95	0.95	0.95	0.95	0.95	0.95	0.98	0.98	0.95	0.94	0.96	0.96	42	42	42	42
Stage 3B	1.00	1.00	1.00	1.00	0.94	1.00	0.94	0.94	0.97	0.97	0.97	0.97	33	33	33	33
Stage 4	1.00	1.00	1.00	1.00	0.90	1.00	0.90	0.90	0.95	0.95	0.95	0.95	51	51	51	51
Stage 5	0.93	0.93	0.93	0.93	1.00	0.93	1.00	1.00	0.96	0.96	0.96	0.96	63	63	63	63
Accuracy	0.96	0.96	0.97	0.97		330	330	330	330							
Macro avg	0.97	0.97	0.97	0.97	0.96	0.96	0.96	0.97	0.96	0.96	0.97	0.97	33	33	33	33

													0	0	0	0
Weighted avg	0.96	0.97	0.97	0.97	0.96	0.96	0.97	0.97	0.96	0.96	0.97	0.97	330	330	330	330

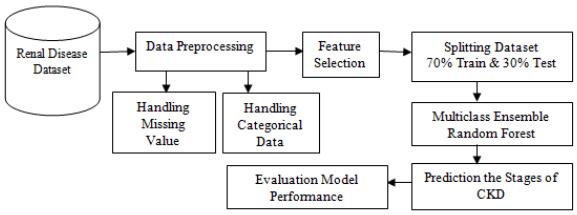

Figure 1: Proposed scheme multiclass with ERF classifier CKD stages.

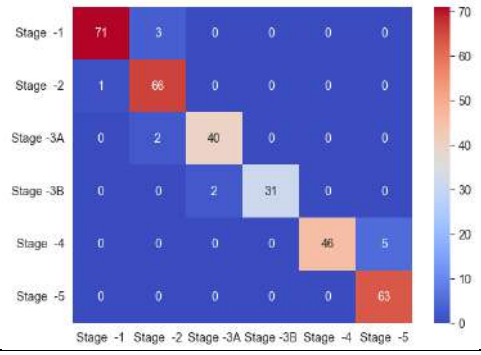

Figure 2: Report on Ensemble Random Forest classification with 26 features.

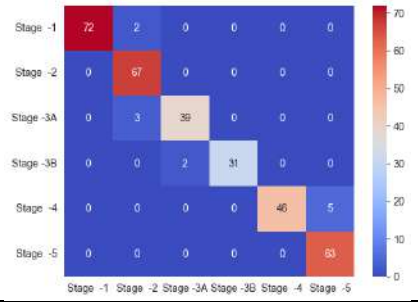

Figure 3: Report on Ensemble Random Forest classification with 20 features

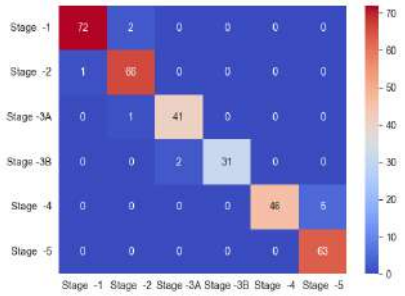

Figure 4: Report on Ensemble Random Forest classification with 15 features

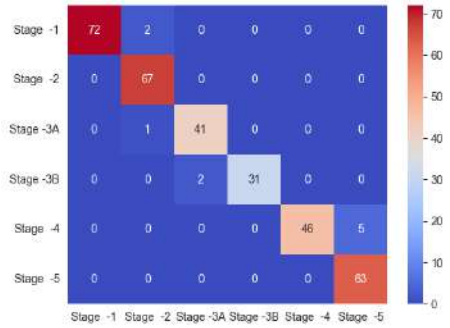

Figure 5 : Report on Ensemble Random Forest classification with 10 features

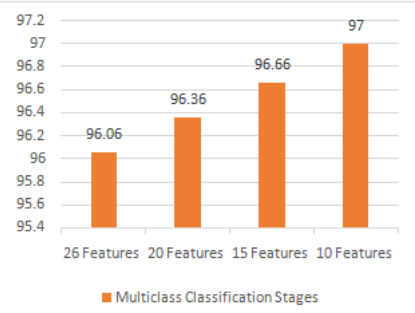

Figure 6 : Multiclass Classification CKD Stages Accuracy

Indian Journal of Natural Sciences www.tnsroindia.org.in ©IJONS

Vol.15 / Issue 83 / Apr / 2024 International Bimonthly (Print) – Open Access ISSN: 0976 – 0997

RESEARCH ARTICLE

Eccentricity Energy of Cover Pebbling Graphs

C. Muthulakshmi@Sasikala[1] and A. Arul Steffi[2]

[1]Associate Professor of Mathematics, Sri Paramakalyani College, Alwarkurichi, Tenkasi, India.
[2]Research Scholar of Mathematics, St. Xavier's College (Autonomous), Palayamkottai, Tirunelveli, India.

Received: 30 Dec 2023 Revised: 09 Jan 2024 Accepted: 12 Mar 2024

***Address for Correspondence**
C. Muthulakshmi@Sasikala
Associate Professor of Mathematics,
Sri Paramakalyani College,
Alwarkurichi, Tenkasi, India.
Email: kalasasispkc@gmail.com

ABSTRACT

Eccentricity matrix $E_{cp}(G)$ of cover pebbling graph G is defined from the weight of an edge $e = uv$ between two vertices u and v. Eccentricity eigen values of a graph G are the eigen value of its eccentricity matrix $E_{cp}(G)$. The eccentricity spectrum of a cover pebbling graph G consists of the eccentricity eigen values of its eccentricity matrix $E_{cp}(G)$. Eccentricity energy $E_{cp}(E)$ is summation of absolute values of eccentricity eigen values of the eccentricity matrix $E_{cp}(G)$. In this paper, we study the eccentricity energy $E_{cp}(E)$ of cover pebbling complete graph, cover pebbling path graph, cover pebbling bipartite graph.

Keywords: Eccentricity matrix, Eccentricity eigen values, Eccentricity energy, cover pebbling graph.

INTRODUCTION

Let $G = (V(G), E(G))$ be any simple and connected graph with n vertices and m edges. If $u, v \in V(G)$ and $uv \in E(G)$, a pebbling move is the removal of two pebbles from vertex u and placing one pebble on an adjacent vertex v throwing one pebble away. Define the weight of an edge $e, w(e)$ as follows.

$w(u, v) = 1$ if $uv \in E(G)$ and a pebbling move occurs between u and v.For a vertex v of G, the pebbling eccentricity of a vertex v is $e_p(v) = \max\{w(u, v); u \in V(G)\}$. The eccentricity matrix $E_{cp}(G) = (a_{ij})$ is defined as follows;

$$E_{cp}(G) = (a_{ij}) = \begin{cases} w(v_i, v_j) & \text{if } w(v_i, v_j) = \min\{e_p(v_i), e_p(v_j)\} \\ 0 & \text{otherwise} \end{cases}.$$

Eccentricity matrix of graphs are discussed by Wang in [7].Graph pebbling was first introduced by Lagarias and Saks and Chung [2] established various results concerning pebbling numbers. Sakunthala Srinivasan and Vimala Shanmugavel[5] introduced the concept of pebbling graph. Cover pebbling graphs were introduced in [4]. Energy of a graph is from Gutman[3]. In this paper, we combine the concepts of cover pebbling graphs and eccentricity matrix.

Preliminaries

Definition 2.1. In a simple graph, consisting of two vertices, a pebbling move [4] can be defined as the removal of two pebbles from the first vertex and placing one pebble on an adjacent vertex.

Definition 2.2. Define the weight of an edge e = uv between two vertices u and v as follows: w(e) = w(uv) = 1if uv ∈ E(G) and a pebbling move occurs between u and v. The number of pebbling move occurs between u and v is the weight of the edge connecting the vertices. Let $P_{ij} = v_i, v_{i+1}, v_{i+2}, \ldots, v_{j-1}, v_j$ be the shortest $v_i - v_j$ path. Then $w(P_{ij}) = \sum_{l=i}^{j-1} w(v_l, v_{l+1})$.

Definition 2.3. In a simple graph, consisting of two vertices, place a pebble on every vertex of the graph using sequence of pebbling moves is called a cover pebbling graph[4].

Definition 2.4. Energy graph E(G) is the total of absolute values of the eigen values $\lambda_1, \lambda_2 \cdots, \lambda_n$ of the adjacency matrix and it is expressed as $E(G) = \sum_{i=1}^{n} |\lambda_i|$.

Definition 2.5. The eccentricity energy of the cover pebbling graph G is defined by $E_{cp}(E) = \sum_{i=1}^{n} |\lambda_i|$ where $\lambda_1, \lambda_2 \cdots, \lambda_n$ are the eccentricity eigen values of eccentricity matrix of the corresponding cover pebbling graph G.

Definition 2.6. A complete graph is a simple graph in which any two vertices are adjacent and a complete graph with n vertices is denoted by K_n.

Definition 2.7. A path on n-vertices denoted by P_n is a sequence of vertices of which any two are adjacent if they are consecutive, and are nonadjacent otherwise.

Definition 2.8. A graph is bipartite if its vertices can be partitioned into two subsets X and Y so that every edge has one end in X and other end in Y. If |X| = n and |Y| = n, then complete bipartite graph is denoted by $K_{n,n}$.

Theorem 2.9. The cover pebbling number of complete graph K_n is $2n - 1$.[1]
Theorem 2.10. The cover pebbling number of path P_n is $2^n - 1$.[1]
Theorem 2.11. The cover pebbling number of complete bipartite graph $K_{n,n}$ is $6n - 3$.[6]

MAIN RESULTS

Example 3.1. Eccentricity energy of cover pebbling complete graph K_4. Now, $w(v_1, v_2) = 1, w(v_2, v_1) = 1, w(v_3, v_1) = 1, w(v_4, v_1) = 1, w(v_1, v_3) = 1, w(v_2, v_3) = 0, w(v_3, v_2) = 0, w(v_4, v_2) = 0, w(v_1, v_4) = 1, w(v_2, v_4) = 0, w(v_3, v_4) = 0, w(v_4, v_3) = 0, e_p(v_1) = 1, e_p(v_2) = 1, e_p(v_3) = 1, e_p(v_4) = 1.$

$$\min\{e_p(v_1), e_p(v_2)\} = 1 = w(v_1, v_2)$$

Hence $a_{12} = 1$.

$$\min\{e_p(v_1), e_p(v_3)\} = 1 = w(v_1, v_3).$$

Hence $a_{13} = 1$ and so on.

Also $a_{11} = a_{22} = a_{33} = a_{44} = 0$.

Eccentricity matrix $E_{cp}(G) = \begin{pmatrix} 0 & 1 & 1 & 1 \\ 1 & 0 & 0 & 0 \\ 1 & 0 & 0 & 0 \\ 1 & 0 & 0 & 0 \end{pmatrix}_{4\times 4}$

Characteristic equation is $\det(E_{cp}(G) - \lambda I) = 0$ i. e., $\lambda^2(\lambda^2 - 3) = 0$.

$\lambda = 0$ (two times) and $\lambda^2 = 3$.

$\lambda = \pm\sqrt{3}$
Eccentricity energy = $2\sqrt{3}$.

Theorem 3.2. Let K_n be the complete graph with n vertices and m edges. Then eccentricity energy of cover pebbling complete graph K_n is $2\sqrt{n-1}$ where $n > 2$.

Proof. Let K_n be the complete graph with n vertices $\{v_1, v_2, \cdots, v_n\}$ and m edges. Weight of an edge between v_1 to any other vertex is one. That is $w(v_1, v_2) = w(v_2, v_1) = 1$. In general, $w(v_1, v_i) = w(v_i, v_1) = 1$ where $i = 2,3, \cdots, n$. But weight of any edge between any two vertices v_i and v_j where $2 \le i, j \le n$ is zero. Now, $\min\{e_p(v_1), e_p(v_j)\} = w(v_1, v_j) = 1$ where $j = 2,3, \cdots, n$
$\min\{e_p(v_i), e_p(v_j)\} \ne w(v_i, v_j)$ where $2 \le i, j \le n$.
Eccentricity matrix for cover pebbling complete graph G is

$$E_{cp}(G) = \begin{pmatrix} 0 & 1 & & \cdots & 1 \\ 1 & 0 & 0 & \cdots & 0 \\ 1 & 0 & 0 & \cdots & 0 \\ \vdots & \vdots & \vdots & \ddots & \vdots \\ 1 & 0 & 0 & \cdots & 0 \end{pmatrix}_{n\times n}.$$

The characteristic equation is $\lambda^{n-2}\left(\lambda^2 - (n-1)\right) = 0$.
The eccentricity eigen values are 0 (n-2) times and $\lambda = \pm\sqrt{n-1}$. Eccentricity energy $E_{cp}(E) = 2\sqrt{n-1}$.

Example 3.3. Eccentricity energy of cover pebbling path graph P_4. Now,

$$w(v_1, v_2) = 7, w(v_2, v_1) = 7, w(v_3, v_1) = 10, w(v_4, v_1) = 11, w(v_1, v_3) = 10,$$
$$w(v_2, v_3) = 3, w(v_3, v_2) = 3, w(v_4, v_2) = 4, w(v_1, v_4) = 11, w(v_2, v_4) = 4,$$
$$w(v_3, v_4) = 1, w(v_4, v_3) = 1, e_p(v_1) = 11, e_p(v_2) = 7, e_p(v_3) = 10, e_p(v_4) = 11.$$
$$\min\{e_p(v_1), e_p(v_2)\} = \min(11,7) = 7 = w(v_1, v_2).$$

Hence $a_{12} = 7 = a_{21}$.

$$\min\{e_p(v_1), e_p(v_3)\} = \min(11,10) = 10 = w(v_1, v_3).$$

Hence $a_{13} = 10 = a_{31}$

$$\min\{e_p(v_1), e_p(v_4)\} = 11 = w(v_1, v_4).$$

Hence $a_{14} = 11 = a_{41}$. Other $a_{ij} = 0$ where $2 \le i, j, \le 4$.
Again $a_{11} = a_{22} = a_{33} = a_{44} = 0$.

Eccentricity matrix $E_{cp}(G) = \begin{pmatrix} 0 & 7 & 10 & 11 \\ 7 & 0 & 0 & 0 \\ 10 & 0 & 0 & 0 \\ 11 & 0 & 0 & 0 \end{pmatrix}_{4\times 4}$

Characteristic equation is $\det\left(E_{cp}(G) - \lambda I\right) = 0$
i. e., $\lambda^2\left(\lambda^2 - 270\right) = 0$.
$\lambda = 0$ (two times) and $\lambda = \pm\sqrt{270}$.
Eccentricity energy = $2\sqrt{270}$.

Theorem 3.4. Let P_n be a path on n vertices ($n \ge 3$). Then eccentricity energy of P_n is
$E_{cp}(E) = 2\sqrt{\sum_{j=1}^{n-2}\left(\sum_{i=1}^{j}(2^{n-i} - 1)\right)^2 + [\sum_{k=1}^{n-2}(2^{n-k} - 1) + 1]^2}$.

Proof. Let P_n be a path on n vertices $\{v_1, v_2, \cdots, v_n\}$ where $n \ge 3$.

$$w(v_1, v_2) = w(v_2, v_1) = 2^{n-1} - 1$$
$$w(v_1, v_3) = w(v_3, v_1) = 2^{n-1} - 1 + 2^{n-2} - 1$$
$$\vdots$$
$$w(v_1, v_n) = w(v_n, v_1) = 2^{n-1} - 1 + 2^{n-2} - 1 + \cdots + 2^{n-(n-2)} - 1 + 1$$
$$e_p(v_1) = 2^{n-1} - 1 + 2^{n-2} - 1 + \cdots + 2^{n-(n-2)} - 1 + 1$$
$$w(v_2, v_3) = w(v_3, v_2) = 2^{n-2} - 1$$

$\vdots$

$w(v_2, v_n) = w(v_n, v_2) = 2^{n-2} - 1 + 2^{n-3} - 1 + \cdots + 2^{n-(n-2)} - 1 + 1$

$e_p(v_2) = 2^{n-1} - 1$

$w(v_3, v_4) = 2^{n-3} - 1$

$\vdots$

$w(v_3, v_n) = w(v_n, v_3) = 2^{n-3} - 1 + 2^{n-4} - 1 + \cdots + 2^{n-(n-2)} - 1 + 1$

$e_p(v_3) = 2^{n-1} - 1 + 2^{n-2} - 1$

Similarly, $e_p(v_4) = 2^{n-3} - 1 + 2^{n-2} - 1 + 2^{n-1} - 1$.

In general, $e_p(v_i) = 2^{n-i+1} - 1 + 2^{n-i+2} - 1 + \cdots + 2^{n-1} - 1, 5 \le i \le n$.

Now,

$\min\left(e_p(v_1), e_p(v_2)\right) = \min\left(2^{n-1} - 1 + 2^{n-2} - 1 + \cdots + 2^{n-(n-2)} - 1 + 1, 2^{n-1} - 1\right) = 2^{n-1} - 1 = w(v_1, v_2)$.

So, $a_{12} = 2^{n-1} - 1$.

$\min\left(e_p(v_i), e_p(v_j)\right) = w(v_i, v_j) = a_{ij} = a_{ji}$, where $i = 1$ and $2 \le j \le n$ or $j = 1$ and $2 \le i \le n$.

For $i \ne 1$ and $2 \le j \le n$ or $j \ne 1$ and $2 \le i \le n$.

$$\min\left(e_p(v_i), e_p(v_j)\right) \ne w(v_i, v_j)$$

Hence $a_{ij} = 0 = a_{ji}$.

Also, $a_{ii} = 0$ where $i = 1,2,3, \cdots, n$.

Eccentricity matrix of cover pebbling path P_n is

$$E_{cp}(P_n) = \begin{pmatrix} 0 & 2^{n-1} - 1 & 2^{n-1} - 1 + 2^{n-2} - 1 & \cdots & a & b \\ 2^{n-1} - 1 & 0 & 0 & \cdots & 0 & 0 \\ 2^{n-1} - 1 + 2^{n-2} - 1 & 0 & 0 & \cdots & 0 & 0 \\ \vdots & \vdots & \vdots & \ddots & \vdots & \vdots \\ a & 0 & 0 & \cdots & 0 & 0 \\ b & 0 & 0 & \cdots & 0 & 0 \end{pmatrix}$$

where $a = \sum_{i=1}^{n-2}\left(2^{n-i} - 1\right)$ and $b = \sum_{i=1}^{n-1}\left(2^{n-i} - 1\right)$.

The characteristic equation is

$$\lambda^{n-2}\left(\lambda^2 - \left[\sum_{j=1}^{n-2}\left(\sum_{i=1}^{j}\left(2^{n-i} - 1\right)\right)^2 + \left[\sum_{k=1}^{n-2}\left(2^{n-k} - 1\right) + 1\right]^2\right]\right) = 0$$

$\lambda = 0$ $(n-2)$ times and

$$\lambda^2 = \sum_{j=1}^{n-2}\left(\sum_{i=1}^{j}\left(2^{n-i} - 1\right)\right)^2 + \left[\sum_{k=1}^{n-2}\left(2^{n-k} - 1\right) + 1\right]^2$$

$$\lambda = \pm\sqrt{\sum_{j=1}^{n-2}\left(\sum_{i=1}^{j}\left(2^{n-i} - 1\right)\right)^2 + \left[\sum_{k=1}^{n-2}\left(2^{n-k} - 1\right) + 1\right]^2}$$

Eccentricity energy, $E_{cp}(E) = 2\sqrt{\sum_{j=1}^{n-2}\left(\sum_{i=1}^{j}\left(2^{n-i} - 1\right)\right)^2 + \left(\sum_{k=1}^{n-2}\left(2^{n-k} - 1\right) + 1\right)^2}$.

Example 3.5. Eccentricity energy of cover pebbling complete bipartite graph $G = K_{2,2}$.

Eccentricity matrix $E_{cp}(G) = \begin{pmatrix} 0 & 3 & 4 & 1 \\ 3 & 0 & 0 & 0 \\ 4 & 0 & 0 & 0 \\ 1 & 0 & 0 & 0 \end{pmatrix}_{4\times 4}$

Characteristic equation is $\lambda^2(\lambda^2 - 26) = 0$.

$$\lambda = 0 \text{ (2 times)}, \lambda = \pm\sqrt{26}.$$

Eccentricity energy, $E_{cp}(E) = 2\sqrt{26}$.

Theorem 3.6. Let $K_{n,n}$ be the complete bipartite graph with $2n$ vertices where $n \ge 2$. The eccentricity energy of cover pebbling complete bipartite graph G is $E_{cp}(E) = 2\sqrt{n(4n^2 - 3)}$ where $n \ge 2$.

Proof. Let $K_{n,n}$ be the complete bipartite graph with vertex sets $X = \{u_1, u_2, \cdots, u_n\}$ and $Y = \{v_1, v_2, \cdots, v_n\}$. Eccentricity matrix of cover pebbling complete bipartite graph G is

$$E_{cp}(G) = \begin{pmatrix} 0 & 2n-1 & 2n & 1 & 2n & 1 & 2n & \cdots & 1 \\ 2n-1 & 0 & 0 & 0 & 0 & 0 & 0 & \cdots & 0 \\ 2n & 0 & 0 & 0 & 0 & 0 & 0 & \cdots & 0 \\ 1 & 0 & 0 & 0 & 0 & 0 & 0 & \cdots & 0 \\ 2n & 0 & 0 & 0 & 0 & 0 & 0 & \cdots & 0 \\ 1 & 0 & 0 & 0 & 0 & 0 & 0 & \cdots & 0 \\ 2n & 0 & 0 & 0 & 0 & 0 & 0 & \cdots & 0 \\ \vdots & \vdots & \vdots & \vdots & \vdots & \vdots & \vdots & \ddots & \vdots \\ 1 & 0 & 0 & 0 & 0 & 0 & 0 & \cdots & 0 \end{pmatrix}$$

The characteristic equation is $\lambda^{2n-2}\left(\lambda^2 - \left((2n-1)^2 + (n-1)(2n)^2 + (n-1)\right)\right) = 0$.

Eccentricity eigen values are $\lambda = 0(2n-2)$ times and $\lambda^2 = (2n-1)^2 + (n-1)(2n)^2 + (n-1)$.

$\lambda = \pm\sqrt{n(4n^2-3)}$.

Eccentricity energy , $E_{cp}(E) = 2\sqrt{n(4n^2-3)}$ where $n \geq 2$.

CONCLUSION

The eccentricity energy of cover pebbling complete graph, cover pebbling path and cover pebbling bipartite graph have been discussed. The eccentricity energy of cover pebbling cycle is an open problem.

REFERENCES

1. Betsy Crull, Tommy Cundiff et all, The cover pebbling number of graphs, Discrete Mathematics, Vol. 296, Issue 28 June 2005, Pages 15-23.
2. Chung F, 1989, Pebbling in Hypercubes, SIAM J. Discrete Math, 2(4), 461-472.
3. Gutman I, 1978, The Energy of a graph, Ber. Math Stat. Sekt. Forschungsz Graz, 103, 1-22.
4. Muthulakshmi@Sasikala C and Arul Steffi A, Adjancency Energy of Cover pebbling graphs, IJCRT, Vol. 11(2023), 2838-2853.
5. Sakunthala Srinivasan and Vimala Shanmugavel, 2021, J. Phys. Conf. Ser , 1850, 012089.
6. Sjostrant J, The cover pebbling theorem, Math Arxiv, Math.co 10410129.
7. Wang et al., The anti-adjacency matrix of a graph, Eccentricity matrix, Discrete applied Mathematics, Elsevier (2018).

Indian Journal of Natural Sciences www.tnsroindia.org.in ©IJONS

Vol.15 / Issue 83 / Apr / 2024 *International Bimonthly (Print) – Open Access* *ISSN: 0976 – 0997*

RESEARCH ARTICLE

Implementation of Time series Control charts using PCA and ARIMA Model

R. Sasikumar* and M.Sujatha

Department of Statistics, Manonmaniam Sundaranar University, Tirunelveli, Tamil Nadu, India.

Received: 30 Dec 2023 Revised: 09 Jan 2024 Accepted: 12 Mar 2024

***Address for Correspondence**
R. Sasikumar
Department of Statistics,
Manonmaniam Sundaranar University,
Tirunelveli, Tamil Nadu, India.
Email: sasikumarmsu@gmail.com

ABSTRACT

Public healthcare aims to promote and protect the health factors and environmental factors that contribute to the safety and overall health of persons and communities. It involves the analysis and management of data related to various health determinants, such as air; water, etc…environmental exposures, and healthcare services utilization. SPC (Statistical process control chart) is the procedure for monitoring the process and control with the help of statistical tools and techniques. ARIMA (Autoregressive integrated moving averages) control chart is a type of SPC time series chart that can be used to observe and handle processes over time. To determine the process signals out of control and trends or patterns that might be present in the data, process control charts are used, particularly ARIMA control charts are engaged. The secondary data contains various air pollutant factors like PM 2.5, PM 10, nitrogen dioxide(NO2), sulfur dioxide(SO2), carbon monoxide (CO) and other relevant pollutants from major cities in Tamil Nadu. This research contains three parts (i) Tirupur city identified as the most pollutant city (ii) the PCA (principal component analysis) technique used to determine the significant components (iii) estimating the parameters with ARIMA model. The results showed that the SCC (Special cause control chart) is more appropriate for auto-correlated data to evaluate the stability of the data since it provides a higher probability of coverage than individual control charts.

Keywords: ARIMA control charts, Public health, control charts, PCA

INTRODUCTION

Public health is the term used for protecting, upgrading, hopeful and administration of healthcare factors and environmental factors.To promote and protect community health, policymakers, researchers, and public health workers can use information about public health to make well-informed decisions, create evidence-based plans, and carry out actions.Air quality is one of the major determinants of public health. Most cities worldwide experience severe air-quality problems, and they have received rising attention in the past decade **(Vallero.D.A, 2014)**. Toxic air pollutants have two types: Physical and Chemical properties. Specified pollutants are those that are common in the United States and are known to be harmful to public health and the environment, as defined by the Clean Air Act of 1971. There are six major pollutants: lead, ozone, sulphur dioxide, nitrogen dioxide and Particular matters sizeunder 10 and 2.5 **(Mangayarkarasi, R, et al. 2021)**. **Particulate matter (PM)**: Airborne particles like small dust, filth and smoke are known as PM 10 and PM 2.5. When inhaled these particles, especially the tiny ones known as PM 2.5 and PM 10 can vary in size and composition and harm health. **Nitrogen oxide (NO_x)** is gases that are essentially created during the combustion process such as when fossil fuels are used in automobiles, power plants and industrial settings. They can have negative effects on the cardiovascular and respiratory systems. **Sulphur dioxide (SO_2):** The burning of fossil fuels emits gas that contains sulfur, such as coal and oil. It is a major provider of acid rain. **Carbon Monoxide (CO)**: The incomplete combustion of fossil fuels, largely in vehicles and industrial processes produced this colourless and odourless gas. **Ozone (O_3):** is a gas that protects humans from damaging UV rays. **Lead (Pb):** Lead is a poisonous heavy metal that was traditionally used in gasoline, paints and other products (**Kokilavani.S, et al. 2020)**. A quantitative metric of all the pollutants is known as the Air quality index (AQI).Higher AQI values denote a hazardous level of exposure for the general public **(Sasikumar.R, et al. 2022)**.

SPC is a methodology for process monitoring and control that makes use of statistical tools and techniques. One of the most important problem-solving instruments for monitoring stability in processes and enhancing capability through decreased variability is the control chart (**Montgomery D.C. 2009)**. This paper includes data from all the major cities of Tamil Nadu. Tirupur is identified as a major pollutant city. Due to a variety of anthropogenic activities and natural reasons, this city experiences air pollution problems. Autocorrelation in observations makes it difficult to identify "special causes". There is a large chance of false positives or negatives due to autocorrelation in observations, which makes it challenging to distinguish between "special causes" that are present and those that are not. **(Smeti et al.2007a)**. After selecting and adjusting an ARIMA model to the process, the residuals are examined using a conventional control chart. It makes reason to observe residuals instead of actual observations because residuals are uniformly distributed with an average of zero if the process is within control and stays independent of possible mean differences when the process differs from control **(Russo, et al 2012)**. Since several quality characteristics can be affected by the air, for this study we choose only two quality characteristics by using the PCA technique. Principal components are used to determine which variables or groups of variables have the greatest influence to detect a likelihood of an out-of-control signal in order to subsequently identify it as a primary operating source**(Souza. A. M. et al 2012)** This research paper aims to compare the traditional control charts and residuals from the fitted ARIMA control charts.

METHODOLOGY

The methods included in this study are

- Principal Component Analysis(PCA).
- Statistical Process Control charts.

Principal Component Analysis (PCA)

PCA is a dimensionality reduction technique that enables us to reduce the key information from a big collection of variables into a more approachable collection of main components, which are uncorrelated variables. We successfully minimize the dimensionality of the dataset while maintaining the most important data, by choosing the

principal components with the highest eigen values or the greatest proportion of variance explained **(Karamizadeh.S et al 2013)**

The steps that involve

- Standardization is the initial step, ensuring that each feature in the dataset has a mean (average) of 0 and a standard deviation of 1.The formula for standardization

$Z=X-\mu/\sigma$ (1)

where Z represents the standard value

X represents the values

μ represents the mean

σ represents the standard deviation

- Calculate the covariance matrix (C); Eigen values (L) and eigenvectors (λL).
- Select a subset of the top eigenvectors and their corresponding eigenvalues based on the explained variance. These eigenvectors become the principal components.

Control charts

Traditional control charts frequently make the assumption that observations pertaining to processes have an independent distribution with a constant mean and variance. Data autocorrelation makes it more difficult to distinguish between "special causes" that exist and those that do not, increasing the risk of incorrect results and/or false positives. **(Montgomery 2007)**.

Autocorrelation (ACF) and Partial autocorrelation function (PACF)

The term "autocorrelation" refers to a measure of interdependence between the observations. Data with a self-correlation are automatically correlated. The primary result of autocorrelation in data analysis on control charts is the production of far tighter than ideal control limits. This means that the prior approach needs to be modified to allow for the possibility of sufficient autocorrelation in the process data (**Elevli.S, et al 2016)**. Data autocorrelation can be detected using the ACF and PACF. The association between data points in a time series and the previous series is plotted using the ACF method. The relationship between the time series variables at time t and all other values at that time (t-1) is represented by the first lag. Once interval delays are taken into account, PACF computes the correlation between data points at time t and those at t-1 (**Russo, et al 2012)**.

Special cause control charts(SCC)

Establishing accurate control limits in control charts is one of the essential steps to ensure the statistical consistency of the process under analysis. If there are different levels of autocorrelation in the quality feature under investigation, the control charts derived using the independence assumption will display more false alarms. When data from control charts are evaluated, autocorrelation mostly results in considerably tighter control limits than planned. If the process data exhibits a significant amount of autocorrelation, the traditional approaches must be changed to consider this. In order to create control charts for auto-correlated data, there are two main methods. The first method uses traditional control charts but modifies the technique for calculating the process variance to estimate the actual process variation. As a result, the correlation in this chart is handled by positioning the control boundaries by the altered variability. The second effective approach for handling auto-correlated data is to employ a suitable time series model to explicitly characterize the correlative structure. Then, using that model, remove autocorrelation from the data and apply control charts to the residuals (**Montgomery 2007**). An SCC chart is the name for this form of control chart, which plots the residuals of the ARIMA model after fitting it to the process. This approach of graphics is compatible with all conventional process control instruments. The centre line is 0 because the mean of the residuals is nil. The residual's standard deviation σ_a is the standard deviation employed in this situation. The chart limits are determined by (i) the upper control limit of $3.\sigma_a$ (ii) the centre line of 0 and (iii) the lower control limit of $3.\sigma_a$.(**Perzy.M,et al 2015**).

Auto Regressive Integrated Moving Average(ARIMA)

The famous time series forecasting technique known as ARIMA is used to analyze and predict data that has temporal relationships. It combines moving average (MA), autoregressive (AR), and differencing (I) components. The use of the variable's historical values to forecast its future values is referred to as the AR component. It is predicated on the idea that a variable's present value is linearly related to its past values. The time series is made stationary by the employment of the I component, which stands for differencing. The stationarity assumption, which holds that the statistical properties of the data do not change over time, is an essential basis of time series analysis. Differencing is taking the current value and subtracting it from the previous value in order to get rid of seasonality and patterns. The MA element is for error terms of residuals (**Kovarik.M et al 2015**). The ARIMA model's order is determined by three variables: p, d, and q. the parameters p and q stand for the moving average components and the autoregressive components lagged error terms, respectively, while d stands for the order of differencing needed to prove stationarity.

$$Y(t) = C + \Phi_1 * Y_{(t-1)} + \Phi_2 * Y_{(t-2)} + \ldots + \Phi_p * Y_{(t-p)} + \theta_1 * \varepsilon_{(t-1)} + \theta_2 * \varepsilon_{(t-2)} + \ldots + \theta_p * \varepsilon_{(t-q)} + \varepsilon_{(t)}$$

where, the time series at time t is represented by Y(t).The expression C is constant.

- The autoregressive coefficients Φ_1, Φ_2... Φ_p indicate how dependent the time series is on earlier values.
- $Y_{(t-1)}$, $Y_{(t-2)}$... and $Y_{(t-p)}$ represent the time series' lagged values.
- The moving average coefficients denoting the reliance on previous error terms are represented by the values of θ_1, θ_2... θ_p.
- The lagged error terms are $\varepsilon_{(t-1)}$, $\varepsilon_{(t-2)}$... $\varepsilon_{(t-q)}$.

The current error term, denoted as $\varepsilon_{(t)}$,is presumed to have a normal distribution with a mean of zero and a constant variance.

Individual control charts

Individual control charts also denoted to as Shewhart control charts are a form of SQC tool used to track and manage a process's variability over time. They are frequently employed in projects aimed at process and quality enhancement. A central line, which often represents the process means. The upper and lower control limits, which specify the process's allowable range of variation, make up an individual control chart. The process's data points are charted over time, and any points that deviate from the control range are considered to be out of control.

The methodological aspects are described below: For this study, the secondary data were collected from the public sector Central Pollution Control Board (CPCB), which is the official portal of the Government of India. The data contains more than 15 cities. It contains various air pollutant factors like PM2.5, PM10 and others, such as nitrogen dioxide (NO2), sulfur dioxide (SO2), carbon monoxide (CO), Ozone (ug/m3), RH (%), WS (m/s), WD (deg), SR (W/mt2), BP (mmHg), VWS (m/s) and other essential pollutants. Only information from the most recent three months (January to March 2023) was used for this investigation. Each component is measured every one hour.

RESULT AND DISCUSSION

This paper first examines the state of Tamil Nadu air pollution data with a particular emphasis on its cities. Based on the dataset's pollution levels, chose one district to focus on for our study in the beginning. The technique which is used takes into account several pollution indicators and measures to identify the most contaminated district. The average pollution of the Tamil Nadu state is shown in Fig. 2. The most polluted days in Tamil Nadu will be January 14–16, 2023, according to Fig. 2. Any events or functions might happen at that time. The objective of the paper is to select the areas with the worst pollution. Then we can determine which district has the worst pollution by examining the data on pollution for each district. Multiple pollutants including PM2.5 and PM 10, NO2, SO2, CO, and other pertinent pollutants are taken into account when calculating the most polluted district. Figure 3 shows the average polluted district in Tamil Nadu from the last three months data. After this procedure, we determined Tripur City as the most pollutant district. So we choose Tirupur city for further analysis. Then, as a statistical method, we employ PCA to find and prioritize the most important air pollution-related components. This algorithm has several steps. To make sure that all of the variables are on the same scale, we first standardize the pollutant data. The analysis cannot

be dominated by variables with bigger degrees; hence standardization is essential. The covariance matrix is then computed using the standardized pollutant variables. The eigenvectors indicate the directions or patterns of variation in the pollutant data, and the eigenvalues represent the variance explained by each primary component. To find the primary components that best explain the variance, we order the eigen values in descending order. Each principal component's variance explanation shows how much of the total variability in the pollutant data that component was able to capture. We can also prioritize and concentrate our efforts on tackling the most significant pollutants or sources of pollution with the use of the PCA results (See Table 1 &Fig. 4), which are presented here. From Table 1 we conclude that PM 2.5 and PM 10 components of Tirupur city have significant impacts on air quality and are commonly monitored in air pollution studies. Descriptive statistics of PM2.5 and PM10 are given below in Table 2. There are significant data gaps in this report. Data that has been pre-processed by eliminating null values and substituting mean for the data. Python and Sigma XL software were used for this study.

Fitting of Individual control charts:

Control charts for people have been first recognised to determine the variation of the two variables PM 2.5 and PM10 components because the sample size utilised for the process monitoring is n=1. If the data are picked individually rather than in categories, the individual control charts are utilised to detect the presence of assignable causes as well as to establish the process level. Using the shifting range of two more observations, this type of graphic calculates the process variability. According to Fig. 5, both parameters are out of control since several points are outside the acceptable range and the oscillations of the points around the centreline are excessive and irregular.

Testing autocorrelation and trend

The control charts shown in Fig. 5 are based on the assumptions. First, we have to estimate the existence of autocorrelation. Fig. 6 represents the autocorrelations for the data. The straight lines are useful to estimate the non-zero correlation values of two standard deviation limits. **(a)** A bar extended outside the lines represents the statistical significance for both components. Since stationary series are required for the identification of the AR and MA components, it is important to check the data for trends before fitting the ARIMA model. ACF graphs in Fig. 6 are non-stationary because the autocorrelation is decreasing extremely slowly.

Fitting of ARIMA model

The final procedure model uses the difference in the d-th order transformation of the irregular variation in the "random walk" process to represent the stationary ARMA (p, q). In the ARMA (p, q) formula, the variables p and q represent the appropriate orders of the moving average and autoregressive components. To acquire an understanding, the PACF and ACF were examined. By utilizing substantial lags in ACF and PACF, we can select the significant ARIMA model. The procedures involved in creating an ARIMA control chart are the choice of a suitable model, estimation of the model parameters, and determination of control limits. The MSE and RMSE values of the model were used to choose the proper model. Less uncertainty in predicting mistakes is seen in improved ARIMA models' mean absolute error (MAE), mean squared error (RMSE), and mean absolute percentage error (MAPE). If the forecasts are accurate, the mean error (ME) and mean percentage error (MPE) should be very close to zero..The models chosen for the two components based on AIC values are listed in Table 3. For PM2.5 and PM10, respectively, ARIMA (1, 1, 3) and ARIMA (5, 1, 0) were defined as an appropriate models. The total amount of differences denoted as (d) for both models, since the data were differenced to provide stationarity. The resulting parameter estimates are shown in Table 4. A t-test and each estimated model coefficient are displayed. As a result of the coefficients' p-values being less than 0.05, the coefficients at the 5% level of significance are substantially different from 0.

Fitting of Special Cause Control charts(SCC)

Based on SCC tables for residuals The ARIMA model reveals that two PM2.5 and PM10 are beyond the set thresholds. Since some areas are outside of what can be controlled. This indicates that air pollution has not been under control for the last three months, and the cause of the change should be looked into. The IC control charts (Fig. 5) are unstable and uncontrollable. Traditional control charts demand that process observations be made in isolation from one another. The traditional control charts issue a high amount of false alarms when this criterion isn't met.The

effectiveness of these graphics is significantly affected by even extremely minor levels of autocorrelation in the observations. SCC charts, the classic control charts used to observe the residuals of the ARIMA model; they are more efficient in this situations because they offer a higher probability of detection than individual charts.

CONCLUSION

In this paper, the highest pollutant cities were determined by using several pollutant measures and indicators. Tirupur is identified as the most pollutant city in Tamil Nadu. The next procedure using statistical tools like PCA to get the primary air components with the greatest amount of variance explained, sort the eigenvalues in descending order. The amount of variability that each principal component can capture is shown by the variance explained. As a result of PCA the air pollutants PM 2.5 and PM 10 are selected as the most significant pollutant for Tirupur District.
Traditional control charts demanded that process observations be made in isolation from one another. The standard control charts issue a high number of false alerts when this requirement is not met. The performance of these charts is significantly impacted by even extremely low levels of autocorrelation in the observations. SCC charts, which are conventional control charts used to observe the ARIMA model's residuals, are more suitable related to environment since they give a better probability than individual charts. In this study, SCC charts for PM 2.5 and PM 10 are based on ARIMA (1, 1, 3) and ARIMA (5, 1, 0) models respectively. There are a few points out of control at the start of the second week of January and also at the March end. Compared to individual charts, residuals of fitted ARIMA model charts are valid for autocorrelation data. There must be many reasons like festivals, weekends, etc. To evaluate the performance and effectiveness of ARIMA control charts and individual control charts in monitoring and evaluating process stability, this study analysed and tracked the levels of air pollution in the Tirupur area. These findings demonstrated that the SCC chart, which offers a larger likelihood of coverage than individual control charts, is better appropriate for using auto-correlated data to assess the stability of the data. Even though it is essential to examine the assignable causes and try to recover the problem of the process. Quality of the air is important to the public health.

REFERENCES

1. Vallero, Daniel A. *Fundamentals of air pollution*. Academic Press, 2014.
2. Mangayarkarasi, R., et al. "COVID19: Forecasting Air Quality Index and Particulate Matter (PM2. 5)." *Computers, Materials & Continua* 67.3 (2021).
3. Kokilavani, S., Pangayarselvi, R., Ramanathan, S. P., DheebakaranGa, S. N., Maragatham, N., &Gowtham, R. "Forecasting of Monthly Rainfall Patterns for Coimbatore, Tamil Nadu, India." *Current Journal of Applied Science and Technology*, 39(8), 2020,69-76
4. Sasikumar. R, Indira. S and Sujatha. M. "Forecasting Air Quality Index using Time Series Modelling", '*TOWARDS RURAL SUSTAINABILITY Research and Development in Pandemic Era*", 2022, Pg.264
5. Ambikapathy, M., Rengasamy, M., Beerappa, R., Karunamoorthy, P., Basappa, N., Ambikapathy, M., &Taluk, D." Forecasting the levels of PM10 in Bangalore city using the seasonal auto-regressive integrated moving average (SARIMA) model"
6. Montgomery, D. C."*Statistical quality control* (Vol. 7)". New York: Wiley, 2007.
7. Smeti, E. M., Kousouris, L. P., Tzoumerkas, P. C., &Golfinopoulos, S. K."Statistical process control techniques on autocorrelated turbidity data from the finished water tank". In *Proceedings of An International Conference on Water Science and Technology Integrated Management on Water Resources, AQU, 2006*
8. Russo, S. L., Camargo, M. E., &Fabris, J. P. "Applications of control charts ARIMA for autocorrelated data". *Practical Concepts of Quality Control*, 2012, 31-53
9. SOUZA, A. M., Souza, F. M., &Menezes, R"Procedure to Evaluate Multivariate Statistical Process Control using ARIMA-ARCH Models (Theory and Methodology). *Journal of Japan Industrial Management Association*, 2012, *63*(2), 112-123.

10. Karamizadeh, S., Abdullah, S. M., Manaf, A. A., Zamani, M., &Hooman, A. An overview of principal component analysis. *Journal of Signal and Information Processing*, *4*(3B), 2013, 173."
11. Elevli, S., Uzgören, N., Bingöl, D., &Elevli, B. "Drinking water quality control: control charts for turbidity and pH". *Journal of Water, Sanitation and Hygiene for Development*, 2016, 6(4), 511-518.
12. Kovářík, M., Sarga, L., &Klímek, P. "Usage of control charts for time series analysis in financial management". *Journal of Business Economics and Management*, 2015,*16*(1), 138-158.
13. Pacella, M., &Anglani, A. (2008). "A Real-Time Condition Monitoring System by using Seasonal ARIMA Model and Control Charting". *MTISD Methods, Models and Information Technologies for Decision Support Systems*, *1*(1), 2008, 206-209.
14. Perzyk, M., &Rodziewicz, A. "Application of Special Cause Control charts to green sand process". *Archives of Foundry Engineering*.2015.
15. Samanta, B., & Bhattacherjee, A." An investigation of quality control charts for autocorrelated data." *Mineral Resources Engineering*, 2001, *10*(01), 53-69.
16. ÖZTÜRK, H., Murat, N., &Elevli, S. "Quality Control Charts For Monitoring Performance of Hospital Call Center". *Sigma Journal of Engineering and Natural Sciences*, 2019, *37*(4), 1396-1410.
17. Mohammed, M. A., Worthington, P., & Woodall, W. H."Plotting basic control charts: tutorial notes for healthcare practitioners". *BMJ Quality & Safety*, 2008, *17*(2), 137-145.
18. Ahmad, M. I., AL-Toubi, A. I., & Al-Saadi, M. S.." Monitoring Air Quality by Statistical Control Charts". ***วารสารวิทยาศาสตร์และเทคโนโลยีมหาวิทยาลัยมหาสารคาม***, 2014, 33(2), 157-159.
19. Smeti, E. M., Koronakis, D. E., & Golfinopoulos, S. K. "Control charts for the toxicity of finished water—modelling the structure of toxicity". *Water Research*, 2007, *41*(12), 2679-2689.
20. Kandananond, K. "Guidelines for applying statistical quality control method to monitor autocorrelated processes". *Procedia Engineering*, 2014, *69*, 1449-1458.
21. Vivancos, J. L., Buswell, R. A., Cosar-Jorda, P., &Aparicio-Fernandez, C. "The application of quality control charts for identifying changes in time-series home energy data". *Energy and Buildings*, 2020, 215, 109841.
22. Taskin, F., &Masud, M. S. "Application of Statistical Control Charts to detect unusual frequency of earthquakes in the world". *Journal of Data Science*, 2020, *18*(1), 44-55.
23. Alwan, L. C., & Roberts, H. V. "Time-series modelling for statistical process control". *Journal of Business &Economics*1988, *6*(1), 87-95.\
24. Moradnia, Maryam, et al. "Assessing Pregnant Women's Exposure to Toxic Metals via Indoor Dust and Biological Monitoring in Urine." (2023).

Table 1: Eigen values and variance explained

Components	Eigenvalues	Variance
PM2.5 (ug/m3)	68416.1191	82.26%
PM10 (ug/m3)	9193.5183	11.05%
NO (ug/m3)	3698.6877	4.45%
NO2 (ug/m3)	1002.0801	1.20%
NOx (ppb)	669.8080	0.81%
SO2 (ug/m3)	126.0290	0.15%
CO (mg/m3)	46.0467	0.06%
Ozone (ug/m3)	19.0137	0.02%
RH (%)	0.4251	0.00%
WS (m/s)	0.2279	0.00%
WD (deg)	0.0000	0.00%
SR (W/mt2)	0.0000	0.00%

Table 2: Descriptive Statistics

	PM 2.5	PM 10
Count	2160	2160
Mean	38.3362	55.4382
Std	18.5991	23.3344
Min	4.3700	6.5800
Max	196.0900	235.1700
25%	25.9950	40.1220
50%	37.0000	55.1850
75%	47.6575	65.7900

Table 3: Model comparison

Parameter	Model	RMSE	MAE	MAPE	MASE
PM 2.5	ARIMA(1,1,5)	8.0351	5.000	14.9541	1.0336
	ARIMA(1,1,3)	**8.0189**	**4.9573**	**14.7119**	**1.0247**
	ARIMA(4,1,1)	8.0283	4.9393	14.5958	1.0244
	ARIMA(2,1,1)	8.1711	4.92317	14.5075	1.0174
	ARIMA(3,1,1)	8.0407	4.9220	14.5856	1.01731
PM 10	ARIMA(4,1,0)	14.0399	7.1577	13.5114	1.1995
	ARIMA(5,1,0)	**14.0279**	**7.1936**	**13.6025**	**1.2055**
	ARIMA(3,1,.0)	14.0492	7.0800	13.3737	1.1865
	ARIMA(2,1,0)	14.0880	6.9796	13.1952	1.1697
	ARIMA (1,1,0)	14.1338	6.7747	12.7704	1.9353

Table 4: Parameter estimates

Parameter	Model	Model parameter	Estimate	Std Error	t	p
PM2.5	**ARIMA (1,1,3)**	AR(1)	0.7030	0.09	7.71	0.00
		MA(1)	0.7510	0.103	7.265	0.00
		MA(2)	0.3366	0.053	6.322	0.000
		MA(3)	-0.1483	0.077	1.910	0.05
		Constant	-0.0417	0.050	0.823	0.41
PM10	**ARIMA (5,1,0)**	AR (1)	-0.4183	0.043	9.572	0.00
		AR (2)	-0.3131	0.046	6.715	0.00
		AR (3)	0.2457	0.047	5.181	0.00
		AR (4)	-0.1846	0.046	3.964	0.00
		AR (5)	-0.0906	0.043	2.077	0.03
		Constant	-0.0863	0.1699	0.507	0.61

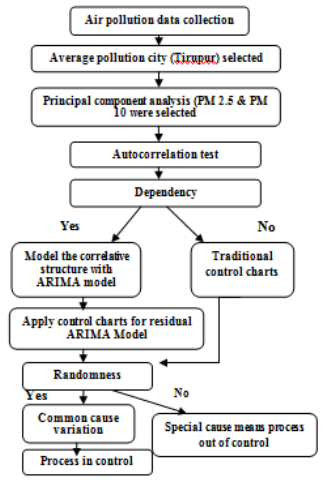

Fig. 1

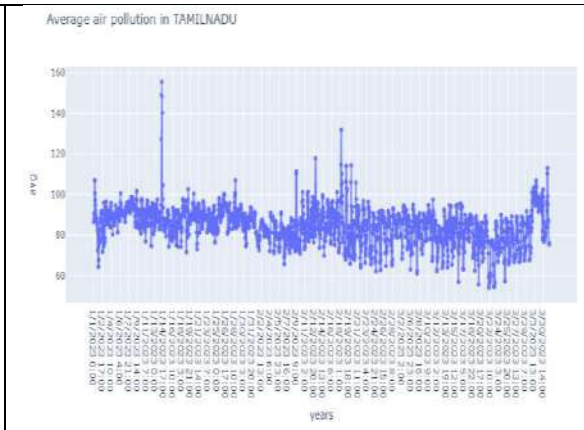

Fig.2 Average air pollution

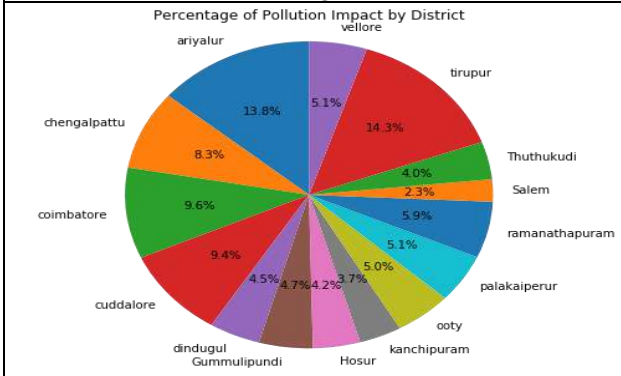

Fig.3 Pollution percentage

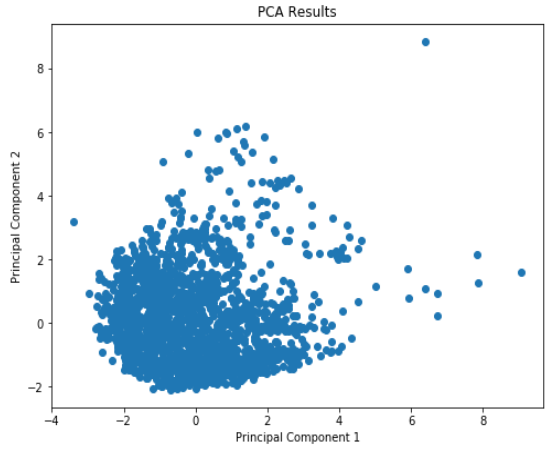

Fig. 4

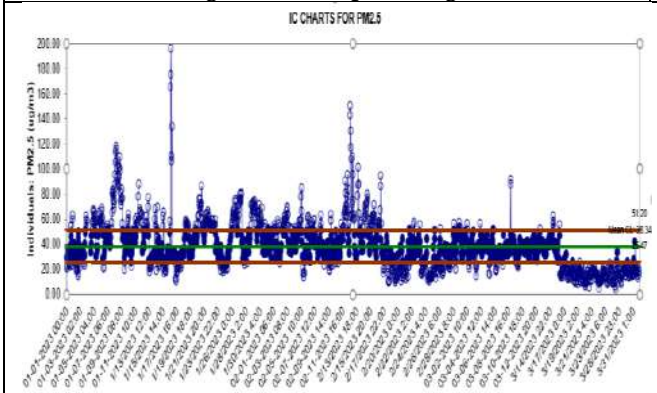

Fig.5(a) Individual control charts for PM 2.5

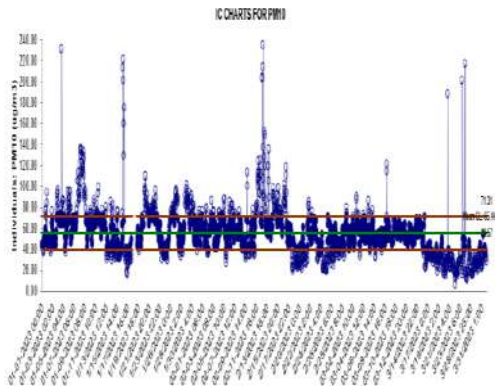

Fig.5(b) Individual control charts PM 10

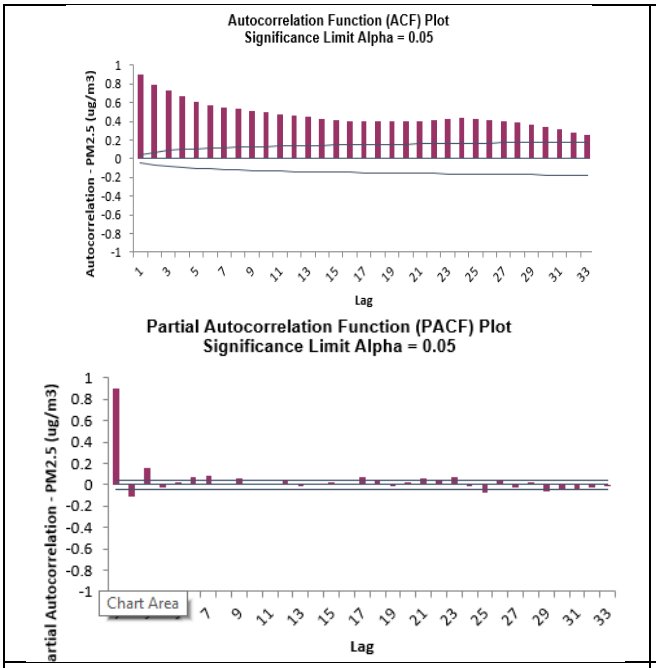

Fig. 6(a) ACF and PCF of PM 2.5

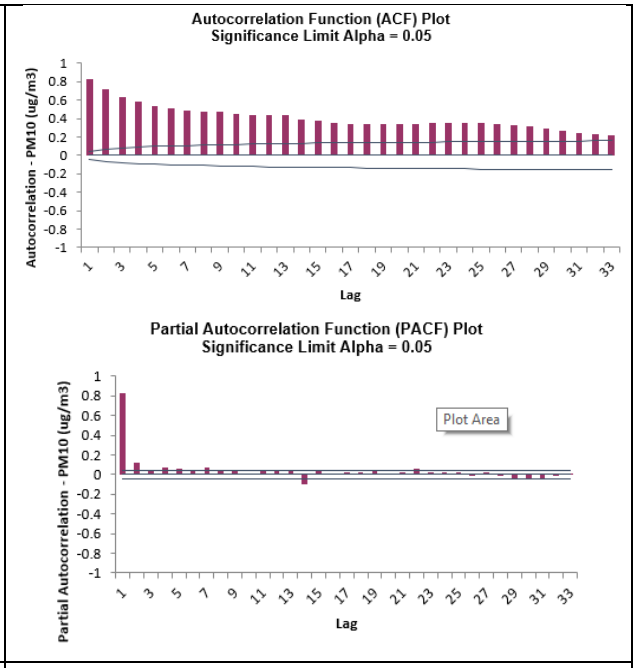

Fig.6(b) ACF & PCF of PM10

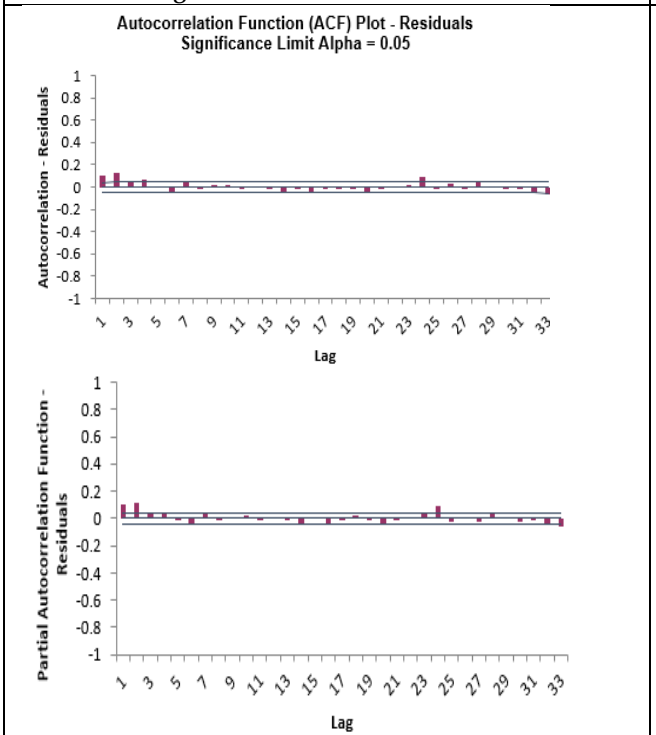

Fig.7(a) Estimated ACF & PCF for PM 2.5

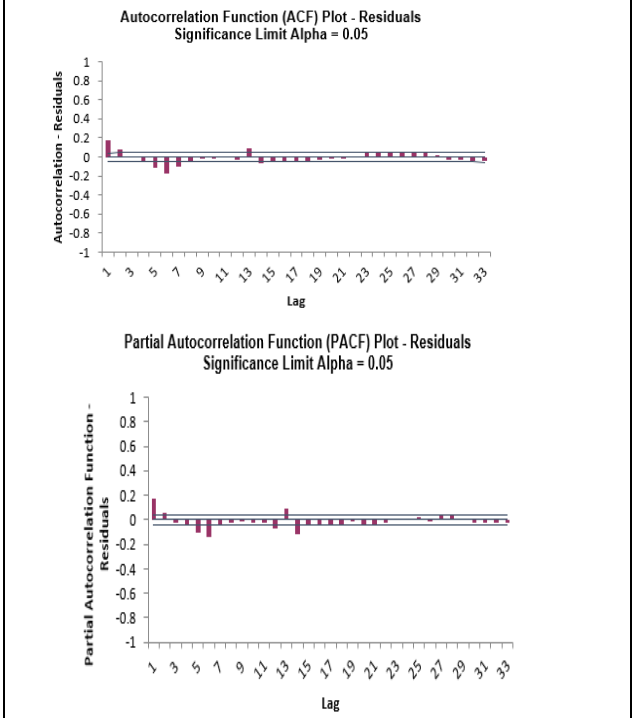

Fig.7(b) Estimated ACF & PCF for PM 10

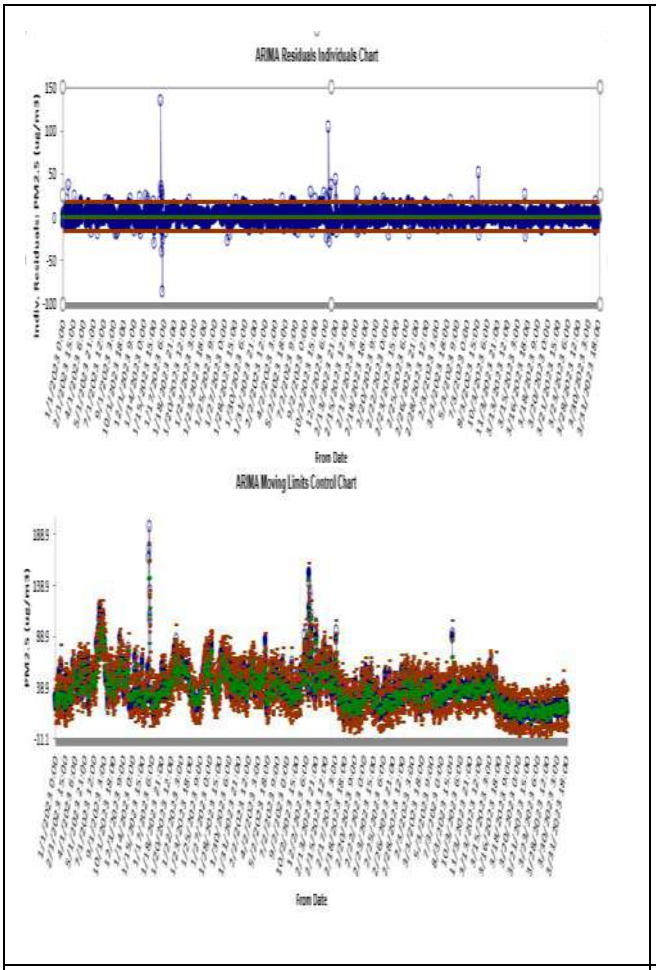

Fig.8 (a) Special cause control charts for PM 2.5

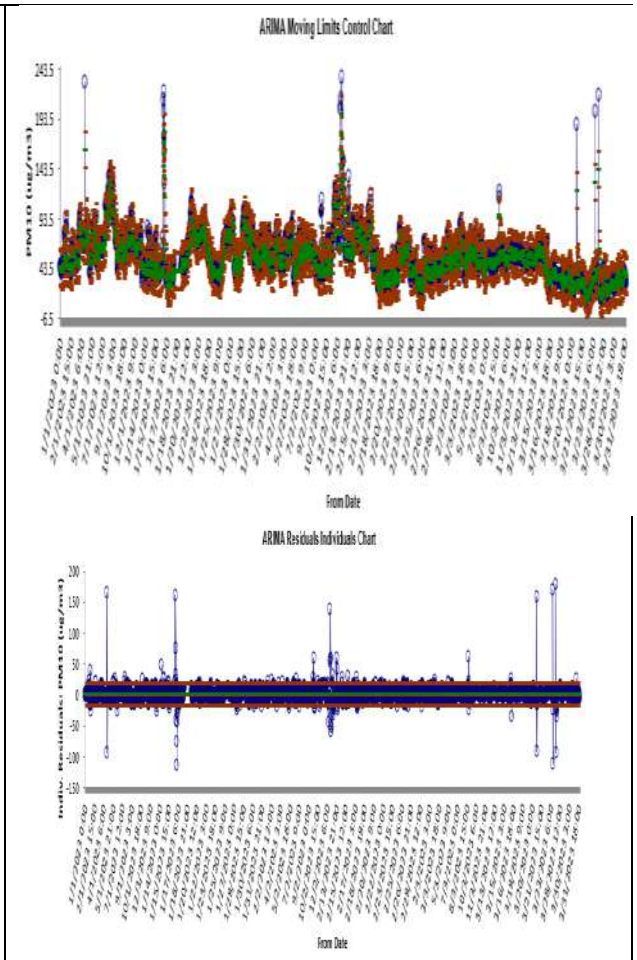

Fig.8(b)Special cause control charts PM10

RESEARCH ARTICLE

The Significance of Visual Design Principles in Enhancing Data Visualization: A Conceptual Perspective

M. Jebakumar

Assistant Professor, Department of Visual Communication, St. Xavier's College (Autonomous), Palayamkottai– 627002, Tamil Nadu, India.

Received: 30 Dec 2023 Revised: 09 Jan 2024 Accepted: 12 Mar 2024

***Address for Correspondence**
M. Jebakumar
Assistant Professor,
Department of Visual Communication,
St. Xavier's College (Autonomous),
Palayamkottai– 627002,
Tamil Nadu, India.
Email: jebakumarmp@gmail.com

ABSTRACT

Data visualization plays a crucial role in effectively communicating complex information and facilitating decision-making. The effectiveness of data visualization largely depends on the application of visual design principles. This research paper explores the significance of visual design principles in enhancing data visualization from a conceptual perspective. Through a case study approach, the paper examines three reports from reputable organizations: UNICEF, WHO, and the World Bank. By employing Gestalt Theory of Visual Perception and Cognitive Load Theory as the theoretical framework, the study analyses how the application of design principles such as simplicity, consistency, colour and contrast, hierarchy, and organization contribute to the effectiveness of data visualization. The results demonstrate that adhering to these principles significantly enhances the clarity, readability, and comprehension of complex data. The findings highlight the importance of incorporating visual design principles in data visualization to effectively communicate critical information and drive positive change. This conceptual perspective underscores the need for data visualization practitioners to prioritize the application of visual design principles in their work to maximize the impact of their visualizations.

Keywords: Data Visualization, Visual Design Principles, Gestalt Theory, Cognitive Load Theory, Data Science, Visual Communication, Data Communication

INTRODUCTION

Data visualization techniques are crucial in today's data-driven world due to the challenges posed by the vast amount of data being generated daily. These techniques enable individuals to quickly interpret and extract meaningful insights from complex datasets, facilitating faster and more accurate decision-making [1]. By choosing the right visualization techniques, such as charts, graphs, maps, and interactive dashboards, analysts can effectively convey desired insights. Visualizations also enhance comprehension and help in communicating insights to stakeholders, influencing them, and driving meaningful outcomes. Data visualization aids in data processing, identifying patterns, and developing ideas from large volumes of data. It enables better business understanding by presenting information in a visually appealing and informative manner[2]. Visual design principles play a crucial role in improving the effectiveness and understanding of data visualizations. These principles help in creating effective scientific visuals and improving the visual message. By utilizing principles such as hierarchy, contrast, alignment, and colour theory, data visualizations can be optimized for clarity, readability, and impact. These principles help in guiding the viewer's attention, simplifying complex information, and conveying insights more effectively[3]. In essence, the application of visual design principles is crucial for creating data visualizations that are not only visually appealing but also facilitate better comprehension and interpretation of the data presented. This research paper is to explore and understand the significance of visual design principles in enhancing data visualization from a conceptual perspective. By examining the various visual design principles and their application in data visualization, this study aims to shed light on how these principles contribute to the overall effectiveness and success of data visualization projects.

Review of the Literature

Visual design principles provide structured guidance on how to design compelling thumbnails for data stories and improve the overall effectiveness of data visualization. Kim et al. conducted a user study to understand the design choices for visualization thumbnails and found that different chart components play different roles in attracting reader attention and enhancing reader understandability[4]. They include determining the message before starting the visual, using appropriate colour combinations, and following established perceptual and cognitive principles[5]. Additionally, different chart components play different roles in attracting reader attention and enhancing reader understandability of visualization thumbnails. Design choices such as resizing, cropping, simplifying, and embellishing charts can make visualization thumbnails more inviting and interpretable[6].Data visualization is the graphical representation of information and data, using visual elements like charts, graphs, and maps to communicate complex data clearly and efficiently. It allows for quick decision-making and is crucial for businesses, researchers, and analysts when conveying their findings. By presenting data visually, it becomes easier for the audience to understand and interpret the underlying trends, patterns, and insights. Visualizations turn raw data into a story, making it easier to identify and understand significant information. Murchie and Diomede discuss the need or guidance on improving the visual aspects of science communication, including data visualization [7].Kelleher and Wagener emphasize the need for clear and concise visual representations of data, stating that well-designed visualizations can facilitate understanding and decision-making. They propose a set of guidelines for creating effective data visualizations, including the use of appropriate visual encodings, the consideration of the target audience, and the reduction of clutter [8]. Sainz Sujet emphasizes the importance of understanding the principles of data visualization for elegant and efficient design [9]. Few argues that the application of visual design principles is crucial for creating compelling and informative data visualizations. He suggests that effective visualizations should be aesthetically pleasing, easy to understand, and focused on conveying the most important information [10]. According to Fernandes and Steele, visual design principles play a vital role in creating effective data visualizations. They proposed that principles such as simplicity, coherence, and colour contrast contribute significantly to the clarity and understanding of the data being visualized. In their study, the authors demonstrated that adhering to these principles can improve the accuracy and speed of decision-making based on the visualized data [11]. Another critical aspect of visual design principles in data visualization is the use of Gestalt principles. As suggested by Nesbitt and Friedrich, Gestalt principles such as proximity, similarity, and continuation can be employed to guide the viewer's

attention and create a more coherent and organized visualization [12]. Harrower and Brewer proposed a colour scheme selection tool for data visualization, emphasizing the importance of colour consistency and contrast for effective visualization. They argued that appropriate colour schemes can significantly enhance the readability and understandability of data visualizations[13]. Balance and contrast are foundational design principles that contribute to the stability and clarity of visual presentations. Borkin et al. found that balanced compositions tend to be perceived as more professional and trustworthy, which is crucial for the credibility of data visualizations [14].

MATERIALS AND METHODS

The purpose of this paper is to conceptually examine and highlight the importance of applying established visual design principles to enhance the effectiveness of data visualizations. Specifically, it aims to review key visual design theories and principles, analyse how they facilitate extraction and comprehension of insights from data visualizations, and discuss their significance in the context of the growing reliance on data visualization across domains.

This research employed a case study approach to investigate the significance of visual design principles in enhancing data visualization from a conceptual perspective. Case studies were chosen as they allow for an in-depth examination of specific instances, providing rich insights into the application of visual design principles in data visualization[15].Three case studies were selected from World Wide Data Visualization Reports published by reputable organizations: the World Health Organization (WHO), the World Bank, and the United Nations International Children's Emergency Fund (UNICEF). These reports were chosen due to their extensive use of data visualization techniques to communicate complex information effectively.

This research employed Gestalt Theory of Visual Perception and Cognitive Load Theory. Gestalt Theory explores how people organize visual information into meaningful patterns and relationships[16]. Key principles such as figure-ground, similarity, proximity, closure, and continuity provide insight into how viewers interpret visual designs. These principles should inform choices made in data visualization regarding layout, colour, shapes, etc [17].The Cognitive Load theory suggests that there are limits to how much information can be processed effectively by the human brain at one time[18]. When these limits are exceeded, it can lead to cognitive overload, which hinders learning and retention. The integration of both theories provides a robust theoretical framework for examining the significance of visual design principles in enhancing data visualization.

RESULTS AND DISCUSSION

Case study 1: UNICEF Children Migration Report 2016

This report incorporates a diverse range of data visualization techniques to present statistics, trends, and narratives related to refugee and migrant children[19]. The report includes charts, graphs, maps, and infographics to present data on population demographics, education, health, and protection issues (see Fig. 1). These visual aids effectively support the narrative and provide a comprehensive understanding of the challenges faced by these vulnerable children. The application of design principles significantly enhances the effectiveness of data visualization in the UNICEF report. The following design principles were observed: The report utilizes a simple and clean design, ensuring that the visualizations are easily comprehensible. Complex data is simplified through the use of clear and concise visuals, making it accessible to a wide audience. The use of colour and contrast in the visualizations helps to highlight key information and draw attention to important data points. The colour palette is carefully chosen to create visual impact and facilitate quick understanding. The report effectively employs hierarchy and organization in its visual design to prioritize and structure information. This allows the audience to navigate through the content seamlessly and comprehend the data in a logical manner (See Fig. 2).The effective use of data visualization techniques, along with design principles such as simplicity, consistency, colour and contrast, hierarchy and organization aids in communicating complex information in a clear and engaging manner. This conceptual

perspective highlights the importance of incorporating visual design principles in data visualization to effectively communicate critical issues and drive positive change.

Case Study 2: WHO - World health statistics 2023

Data visualization in the WHO's report is primarily presented through graphs, charts, and infographics[20]. These visualizations effectively communicate global health trends and the progress of the SDGs. For instance, the use of line graphs to depict changes in health indicators over time, bar charts to compare health statistics across regions, and world maps to show geographical disparities in health outcomes (see Fig. 3).The design principles employed in the WHO's report include simplicity, clarity, consistency, and relevance. The report maintains a simple layout, which enhances readability and understanding. The use of clear, legible fonts and appropriate colour schemes contributes to the clarity of the report. Consistency in the use of visual elements, such as the same scales for axes in graphs, helps in easy comparison across different data sets. The relevance of the visuals to the data and the message they convey is also noteworthy (see Fig. 4).The results show that the effective use of design principles significantly enhances the data visualization in the WHO's report. Clear and simple visuals make it easier for readers to understand complex health data. Consistency in visual elements allows for easy comparison between different data sets. The relevance of the visuals to the data and message ensures that the intended information is effectively communicated.

Case study 3: World Bank – World Development Report 2023

This report effectively employs data visualization to convey complex information about migration and its impact on societies[21]. The report uses a variety of charts, graphs, and maps to illustrate key findings, such as:Global migration patterns and trends. The distribution of refugees and displaced persons,the economic and social impacts of migration on both sending and receiving countries (see Fig 5). Visualizations that adhere to these principles are more likely to communicate insights accurately and persuasively. Bar Chat (see Fig. 6) illustrating migration flows are more comprehensible when using consistent colour coding and appropriate legends. Similarly, charts and graphs that prioritize clarity and simplicity facilitate quicker comprehension of complex data relationships.The results demonstrate that well-designed data visualizations can effectively distil complex information related to migration and refugee movements into accessible and actionable insights. Through strategic application of design principles and the visualizations featured in the report succeed in conveying key messages and facilitating informed decision-making.

CONCLUSION

This research paper has explored the significance of visual design principles in enhancing data visualization from a conceptual perspective. Through a comprehensive review of the literature and an in-depth analysis of three case studies, it has become evident that the application of visual design principles plays a crucial role in creating effective and impactful data visualizations. The case studies examined in this paper, namely the UNICEF Children Migration Report 2016, the WHO World Health Statistics 2023, and the World Bank World Development Report 2023, have demonstrated how the strategic use of visual design principles can significantly improve the clarity, readability, and persuasiveness of data visualizations. By employing principles such as simplicity, consistency, colour and contrast, hierarchy, and organization, these reports have successfully communicated complex information in an accessible and engaging manner.

The findings of this study have several implications for the field of data visualization. Firstly, they underscore the importance of incorporating visual design principles into the creation of data visualizations, as they can greatly enhance the effectiveness and impact of the visualizations. Secondly, the results suggest that a thorough understanding of visual design principles is essential for professionals working in the field of data visualization, as it enables them to create visualizations that are not only aesthetically pleasing but also highly functional and informative. The integration of Gestalt Theory of Visual Perception and Cognitive Load Theory provides a robust theoretical framework for understanding the significance of visual design principles in data visualization. Gestalt

Theory highlights the importance of organizing visual information into meaningful patterns and relationships, while Cognitive Load Theory emphasizes the need to present information in a way that does not overwhelm the viewer's cognitive processing capacity. Moreover, this research highlights the need for further exploration and development of visual design principles specifically tailored to the field of data visualization. As the amount and complexity of data continue to grow, it is crucial to establish a set of best practices and guidelines that can help practitioners create visualizations that are both visually appealing and intellectually stimulating.

REFERENCES

1. M. F. B. b. M. Zanan and M. S. A. Aziz, "A Review On The Visual Design Styles In Data Storytelling Based On User Preferences And Personality Differences," in *2022 IEEE 7th International Conference on Information Technology and Digital Applications (ICITDA)*, Nov. 2022, pp. 1–7. doi: 10.1109/ICITDA55840.2022.9971409.
2. F. Yang, "Data Visualization," in *The International Encyclopedia of Health Communication*, John Wiley & Sons, Ltd, 2022, pp. 1–7. doi: 10.1002/9781119678816.iehc0756.
3. L. D. McGowan, R. D. Peng, and S. C. Hicks, "Design Principles for Data Analysis," *Journal of Computational and Graphical Statistics*, vol. 32, no. 2, pp. 754–761, Apr. 2023, doi: 10.1080/10618600.2022.2104290.
4. H. Kim *et al.*, "Towards Visualization Thumbnail Designs That Entice Reading Data-Driven Articles," *IEEE Transactions on Visualization and Computer Graphics*, pp. 1–16, 2023, doi: 10.1109/TVCG.2023.3278304.
5. M. Christen, P. Brugger, and S. I. Fabrikant, "Susceptibility of domain experts to color manipulation indicate a need for design principles in data visualization," *PLOS ONE*, vol. 16, no. 2, p. e0246479, Feb. 2021, doi: 10.1371/journal.pone.0246479.
6. S. R. Midway, "Principles of Effective Data Visualization," *PATTER*, vol. 1, no. 9, Dec. 2020, doi: 10.1016/j.patter.2020.100141.
7. K. J. Murchie and D. Diomede, "Fundamentals of graphic design—essential tools for effective visual science communication," *FACETS*, vol. 5, no. 1, pp. 409–422, Jan. 2020, doi: 10.1139/facets-2018-0049.
8. C. Kelleher and T. Wagener, "Ten guidelines for effective data visualization in scientific publications," *Environmental Modelling & Software*, vol. 26, no. 6, pp. 822–827, Jun. 2011, doi: 10.1016/j.envsoft.2010.12.006.
9. P. Sainz Sujet, "Review of Data Visualisation: A Handbook for Data Driven Design: Data Visualisation. A Handbook for Data Driven Design, by Andy Kirk, LA, Sage publications, 2019, 312 pp., $106.93 (hardcover), ISBN: 978-1-5264-6892-5," *Structural Equation Modeling: A Multidisciplinary Journal*, vol. 27, no. 2, pp. 330–332, Mar. 2020, doi: 10.1080/10705511.2019.1703709.
10. S. Few, *Show Me the Numbers: Designing Tables and Graphs to Enlighten*. Analytics Press, 2004.
11. A. Vande Moere, M. Tomitsch, C. Wimmer, B. Christoph, and T. Grechenig, "Evaluating the Effect of Style in Information Visualization," *IEEE Transactions on Visualization and Computer Graphics*, vol. 18, no. 12, pp. 2739–2748, Dec. 2012, doi: 10.1109/TVCG.2012.221.
12. K. V. Nesbitt and C. Friedrich, "Applying Gestalt principles to animated visualizations of network data," *Proceedings Sixth International Conference on Information Visualisation*, pp. 737–743, 2002, doi: 10.1109/IV.2002.1028859.
13. M. Harrower and C. A. Brewer, "ColorBrewer.org: An Online Tool for Selecting Colour Schemes for Maps," *The Cartographic Journal*, vol. 40, no. 1, pp. 27–37, Jun. 2003, doi: 10.1179/000870403235002042.
14. M. A. Borkin *et al.*, "What makes a visualization memorable?," *IEEE Trans Vis Comput Graph*, vol. 19, no. 12, pp. 2306–2315, Dec. 2013, doi: 10.1109/TVCG.2013.234.
15. S. M. Croucher and D. Cronn-Mills, *Understanding Communication Research Methods*, 1st edition. New York: Routledge, 2014.
16. J. Wagemans *et al.*, "A Century of Gestalt Psychology in Visual Perception I. Perceptual Grouping and Figure-Ground Organization," *Psychol Bull*, vol. 138, no. 6, pp. 1172–1217, Nov. 2012, doi: 10.1037/a0029333.
17. K. Koffka, *Principles Of Gestalt Psychology*. London: Routledge, 2013. doi: 10.4324/9781315009292.

18. F. Paas, A. Renkl, and J. Sweller, "Cognitive Load Theory: Instructional Implications of the Interaction between Information Structures and Cognitive Architecture," *Instructional Science*, vol. 32, no. 1, pp. 1–8, Jan. 2004, doi: 10.1023/B:TRUC.0000021806.17516.d0.
19. UNICEF, *Uprooted: The growing crisis for refugee and migrant children | UNICEF*. UNICEF, 2016. Accessed: Mar. 16, 2024. [Online]. Available: https://www.unicef.org/reports/uprooted-growing-crisis-refugee-and-migrant-children
20. World Health Organization, *World health statistics 2023: monitoring health for the SDGs*. World Health Organization, 2023.
21. United Nations, *World Development Report 2023: Migrants, Refugees, and Societies*. in World Development Report. The World Bank, 2023. doi: 10.1596/978-1-4648-1941-4.

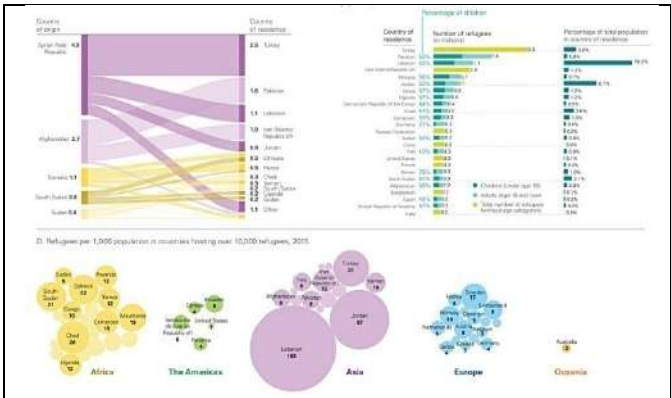

Fig. 1 – UNICEF –Top world's refugees – Data visualization (Page No.: 31)

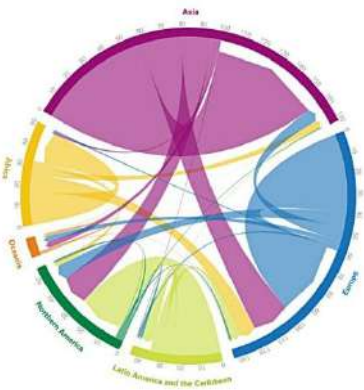

Fig. 2 – UNICEF – International migrants – Visual Principles (Page No.: 26)

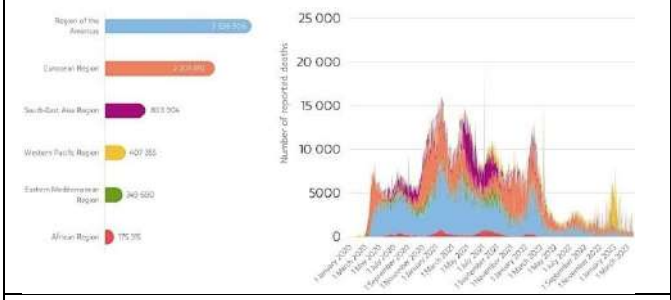

Fig. 3 – WHO - COVID-19 deaths by WHO region, to 11 March 2023 (Page No.:17)

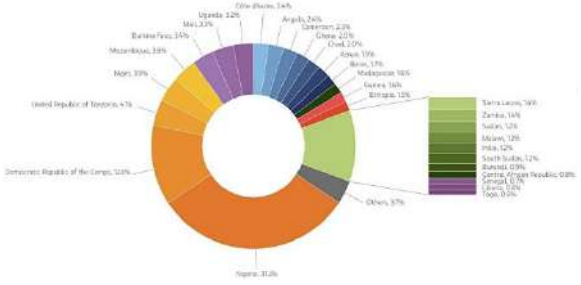

Fig. 4 – WHO - malaria cases and (b) deaths, by country, 2021 (Page No.:41)

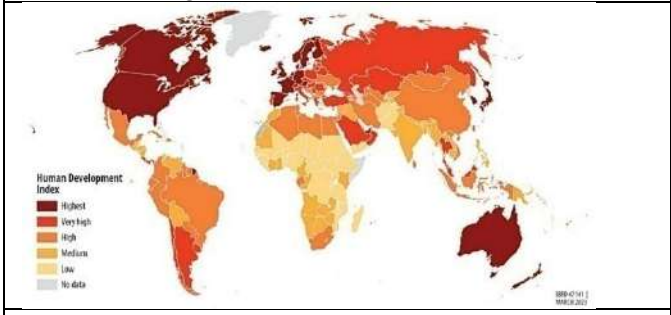

Fig. 5 – World Bank - Heat map-Human Development Insights (Page No.:52)

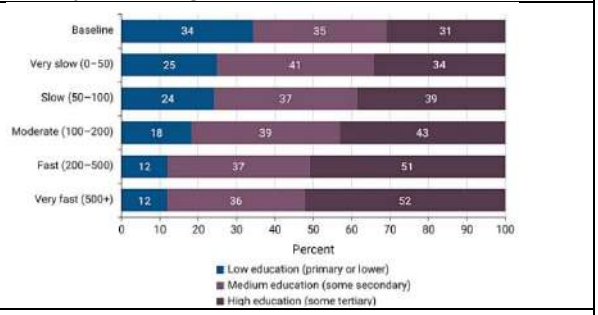

Fig. 6 – World Bank - migration flows (Page No.:260)

Indian Journal of Natural Sciences www.tnsroindia.org.in ©IJONS

Vol.15 / Issue 83 / Apr / 2024 International Bimonthly (Print) – Open Access ISSN: 0976 – 0997

RESEARCH ARTICLE

Investigations of Efficient Nonlinear Optical Tetra Glycine Ammonium Sulphate (TGAS) Crystal for Optoelectronic Applications

Josephine Gladiya M[1a], Anuradha G V[2], Sivashankar V[1*], Helina B[1]

[a]Research Scholar, 20211282132008

[1]Department of Physics, St. Xavier's College (Autonomous), Palayamkottai – 627 002, Tirunelveli, Tamilnadu, India.

[2]Department of Physics, Sri Parasakthi college for Women (Autonomous), Courtrallam, Tenkasi – 627 802, Tamilnadu, India

Affiliated to Manonmaniam Sundaranar University, Tirunelveli – 627 012, Tamilnadu, India

Received: 30 Dec 2023 Revised: 09 Jan 2024 Accepted: 12 Mar 2024

***Address for Correspondence**

Sivashankar V

Department of Physics,

St. Xavier's College (Autonomous),

Palayamkottai – 627 002,

Tirunelveli, Tamilnadu, India.

Email: tvsivashankar@yahoo.co.in

ABSTRACT

Current study focuses on synthesized Tetra glycine ammonium sulphate crystals (TGAS), which is grown by traditional solution growth approach and its unique properties. Single crystal as well as Powder XRD confirm the orthorhombic pattern of TGAS crystal. The lower cut off is 199 nm for TGAS crystal has been obtained from UV – Vis spectra and the crystal exhibit greater transparency in the visible zone. The high band gap value of 6.25 eV has been enumerated using Tauc's plot. The luminescent property has been confirmed by PL spectrum. The hardness and work hardening coefficient of 2.642 of TGAS crystal was obtained from Vickers hardness analysis. The TGAS crystal withstands the higher temperature of 240 °C.Using EDX analysis, every element found in the TGAS crystal in the predicted amounts was detected. The NLO property was confirmed by SHG analysis and the crystalline sample of TGAS is 1.17 time greater than KDP and the high Laser damage threshold of 2. 04 GW/ cm^2 has been obtained for the TGAS crystal. The enhanced and unique features of structural, optical, thermal, mechanical properties with greater SHG efficiency and Laser damage threshold for the TGAS crystal emphasize that TGAS is a superior candidate for fabricating Optoelectronic gadgets

Keywords: TGAS crystal, NLO, SHG, XRD

INTRODUCTION

Accentuately, Amino acids are the greatest torchbearers of crystal growth, as they're the organic compounds that comprises the astonishing optical, thermal and mechanical properties with greater Second Harmonic Generation (SHG) efficiency [1]. The quest for novel materials with enhanced characteristics is the leading lights of today's science and technology [2]. The new organic materials with wide transparency domain, greater thermal stability, higher mechanical hardness, relatively good Second harmonic generation efficiency is the desperate necessity in academic research as well as in technological aspects [3].In order to grow such novel materials with meticulous properties, Researchers used commercially available α – Glycine which is a stable and simplest of all amino acids [4,5]. Glycine is the Researcher's ecstasy, as it amuses the investigators with its eccentric and noteworthy characteristics [6]. Glycine is a non-polar achiral molecule, that can extensively incorporate with all the organic and inorganic compounds to produce novel materials with astonishing physiochemical properties [7]. Researchers have grown various glycine crystals utilizing organic and inorganic compounds, some are listed as follows: Gamma glycine crystals from cerous chloride [7], lithium nitrate [8], Manganese sulphate [9],Di glycine crystals [10], Tri glycine crystals [11]and Glycine doped crystals [12] have been reported and their unique properties have been scrutinized. Principal objective of this manuscript is to investigate and provide illuminationto the novel material of Tetra Glycine Ammonium sulphate (TGAS) single crystals and their astonishing properties are discussed for the first time. The single crystalline Tetra Glycine Ammonium Sulphate are(TGAS) grown by adapting conventional solution growth approach at ambient temperature. The various structural, spectral, mechanical, thermal, electrical and elemental characteristics of the proposed TGAS crystal have been briefly discussed.

Experimental Procedure

Single crystals of Tetra Glycine ammonium sulphate are grown by dissolving Glycine (Merck) of purity >=99% and Ammonium sulphate (Hi – media) of purity ≥99%in aa 4:1 ratio added to 100 milliliters of deionized water in a beaker.After that, the solutions in the vessel were agitated at a consistent temperature of 50 degrees for the next five hours. Following a Whatman filter paper filtering the saturated solution, the beaker was capped with perforated aluminum foil and allowed to slowly evaporate at room temperature. In less than 30 days, high-quality single crystals of Tetra Glycine Ammonium Sulphate (TGAS) were obtained. Theharvested crystal ofTGAS is depicted in Fig: 1

Characterization

To ascertain the lattice specifications and the structure of the TGAS crystal, a Bruker D8 Quest X-ray diffractometer of MoK_α radiation (λ = 0.710 Å) was employed. The crystal of TGAS was scrutinized bypowder XRD diffractometer Bruker AXS D8 Advance (PANalytical, Nickel filtered Cu K_α (λ= 1.540 Å) at 35 KV, 10mA).The optical transmission spectra for the TGAS crystal were collected viavarian Cary 5000 spectrometer in the region 190-1100 nm at room temperature.PL spectrum and it was recorded by photoluminescence spectrometer, Fluorolog HORIBA in 200 to 900 nm range with the wavelength of excitation about 250 nm. For hardness analysis, a diamond indenter-equipped Shimadzu Vickers microhardness tester connected to an incident light microscope was utilized. The thermal endurance of TGAS crystal was found by carrying out TG/DTA plot using a NETZSCH STA 409C/CD thermal analyzer with nitrogen atmosphere in 30-400^{o}Ctemperature at the heating rate 10^{o}C/min. The spectrum of EDX is collected employing a high-resolution scanning electron microscope (HRSEM), Thermo Scientific Apero S. A Q-switched Nd: YAG laser of model HG-4B was used with the repetition rate of 10 Hz and pulse width 6 ns in the Kurtz-Perry powder method. Using a high intensity Q-switched Nd:YAG laser with wavelength of 1064 nm and a pulse width of 10 ns, the LDT value of the grown TGAS crystal was determined. The antibacterial activity study is used to check the grown TGAS crystal's resistance to bacterial specimens.

RESULTS AND DISCUSSIONS

Single crystal XRD

Table 1 displays the acquired lattice specifications for the TGAS crystal. From the specifics, it is evident that the TGAS crystalline material crystallizes under orthorhombic system. The lattice specifications of previously reported Glycine ammonium sulphate crystals are compared with the parameters obtained for TGAS crystal are presented in table 1. It is apparent that the Tetra glycine ammonium sulphate crystal varies from previously reported Glycine ammonium sulphate crystal which crystallizes in a monoclinic system whereas TGAS crystallizes in an orthorhombic system.

PXRD Studies

The powder XRD spectrum of TGAS is illustrated in Fig.2. Utilizing the WinXMorph software, the corresponding Miller indices (hkl) were assigned for the TGAS crystal. The intense sharp diffraction peaks at2Θ = 19.025° and 25.293°indicates the (110) and (013) planes and medium intense peaks appears at 2Θ = 14.815°, 23.002°, 23.954°, 30.232°, 31.126°, 33.624°, 36.594°, 42.548°, 53.422°, 63.299° belongs to (002), (111), (112), (113), (022), (121), (212), (124), (304) and (135) planes respectively that confirms the existence of orthorhombic crystalline structure. The remarkable diffraction peaks reveal the exceptional crystallinity, high purity and good structural precision of the TGAS crystal [14]

FTIR Spectrum

Fig: 3 illustrates the FTIR spectra for the TGAS crystal. The intense and wide absorption peak at 3418 cm^{-1}denotes the OH stretching [15]. The peak at 2612 cm^{-1} belongs to C=O stretch [16]. The peak at 2229 cm^{-1} denotes the intense sulphate overtones and combinations [17]. The peak at 2173 cm^{-1} and 2057 cm^{-1}belongs to the CO stretching [18,19]. The peak at 1630 cm^{-1}denotes OH stretching [20] and the peak at 1590 cm^{-1} confirms COO^- ie, the stretching of carboxyl group [21]. The peak at 1488 cm^{-1} indicates the C=O vibration [22]. The peak at 1404 cm^{-1} indicates C-N vibration [23]. The peak at 1334 cm^{-1} indicates the in-plane bending of CH group [24]. The peaks at 1272 cm^{-1} and 1127 cm^{-1} indicates C-O band [25] and C-O-C stretching vibration [26]. The peak at 1041 cm^{-1} and 929 cm^{-1} indicates the presence of C-O stretching [27] and wagging vibration of OH group [28]. The peaks at 889 cm^{-1} and 833 cm^{-1} indicates the presence of C-O stretching [29] and OH stretching [30]. The peak at 685 cm^{-1} belongs to the torsion in hydrogen bonds of amide [31]. The peaks at 609 cm^{-1} and 503 cm^{-1} indicates the presence of OH bending vibration [32] and C-H out of plane bending vibration [33].

UV – Vis spectrum

The transmittance as well as absorbance spectra of TGAS crystal are displayed in the fig:4 and 5. From the plot, it is evident that the crystal possesses less absorbance in the complete UV, visible and near infrared zone. The lower cut-off for TGAS crystal is 199 nm. It is apparent that the transmittance spectrum of TGAS crystal shows greater transparency in the entire visible zone. The optical band gap was scrutinized from the Tauc's plot as illustrated in Fig.6. The band gap energy E_g of TGAS crystal is obtained to be 6.25 eV which is greater than the previously reported undoped Ammonium Sulphate which is 5.6 eV[34]

Photoluminescence Analysis

Fig 7 illustrates the PL spectrum for the TGAS crystal. The peaks of emission at 462 nm, 540 nm are due to the emission of visible light. The emission peak at 822 nm belongs to the IR light emission. The intense peak patterns reveal that the TGAS crystal has high ordered crystallinity, utmost purity and structural reliability, implying that TGAS crystal is a desirable luminescent material. The attainable PL emission conveys the crystal is an ideal choice for NLO applications[35].

Hardness Studies

The micro hardness number was enumerated and the hardness number variation (H_v) with the (P) applied load of TGAS crystal is illustrated in the fig:8 and hardness gradually rises with the rise in applied load. The work hardening efficacy (n) was enumerated using the Meyer's relation and the value of n is found to be 2.462 from the Fig.9. Since n is greater than 1.6, the proposed TGAS crystal is a softer medium [36].

Thermal Analysis

Fig: 10depicts the TG plot for the TGAS crystal. The TG curve depicts there is no change in weight upto 230 ℃. The first major weight loss of about 27.02% from 230 ℃ to 275 ℃ belongs to the sublimation and initial decomposition of TGAS crystal. The second weight loss of about 21.25% from 275 ℃ to 290 ℃ is due to further decomposition of TGAS crystal. The remaining sample melts and decomposes giving a weight loss percentage of about 17.05% from 290 ℃ to 400 ℃. The DTA curve for the TGAS crystal is depicted in fig11. The DTA exhibits an intense endothermic peak at 240 ℃ which is the decomposition point for the TGAS crystal. The outcomes suggests that the TGAS has a greater thermal stability of about 240 ℃ which is higher than the previously reported Gamma glycine crystal of ammonium sulphate as solvent [37], and it is apparent that the TGAS crystal can be effectively applied for fabrication of Optoelectronic devices[38].

EDX Spectrum

Fig11 illustrates the recorded Energy Dispersive X ray spectrum for the TGAS crystal. In the plot, S C, O and N peaks subsequently located at 0.1, 0.15, 0,2 and 0.25 keV. For the TGAS crystal, the identified elements viz, C, N, O and S are in expected proportions as their atomic distributions of C, N, O and S are 35.23%, 13.48%, 51.13% and 0.16% respectively. Hence, it is obvious that there is no detection of foreign element in the EDX spectrum of TGAS crystal, that implies that TGAS is a high purity crystal and can be utilized for fabricating Nonlinear optical devices[39].

Second Harmonic Generation Analysis

For measuring SHG efficacy, KDP was taken as a reference material. The incident wavelength is 1064 nm with emitted wavelength of light from the crystal is 532 nm (green laser light). The input energy is 0.5 J for both KDP and TGAS sample. The output energy is 8.75mJ for TGAS crystal and it is 7.5 mJ for KDP. Hence, the crystal of TGAS is 1.17 times that of KDP sample and it is greater than the previously reported Glycine ammonium sulphate crystals (0.90 times that of KDP)[13], since the SHG efficacy of TGAS crystal is high, it can be utilized for NLO applications[40]. Table 2 shows the obtained value of SHG efficacy for TGAS crystal.

Laser Damage Threshold studies

The equation for estimating the LDT of a TGAS crystal is Power density $(P)=E/\tau\pi r^2$, and the LDT value for the grown TGAS crystal was enumerated to be 2.04 GW/cm^2. Since it is more than LDT of KDP crystal (0.20) and Urea (1.50) [41] TGAS could be used for laser applications.

Antibacterial Activity

Antibacterial activity was carried out and the inhibition data were evaluated for the produced crystal of TGAS with the goal to obtain information about the bacteria and other microorganisms that tend to proliferate on the outermost layer of the crystal [42]. The examination of the antibacterial properties of the TGAS crystal involves two bacterial specimens viz., *Staphylococcus aureus* and *Pseudomonas aeruginosa.* The zones of inhibition areas for the grown crystal of TGAS and the standard sample are given in the figure 10. The data pertaining to the investigation of antibacterial activity is specified in the table 3. Considering the outcomes, it is apparent that the accomplished crystal of TGAS has lesser inhibitory effect on bacterial specimens, and it is therefore inferred that the crystal has less effective antibacterial properties [43]

CONCLUSION

Tetra glycine ammonium sulphate crystal was synthesized by utilizing Solution growth approach. The harvested crystal was examined with various spectral, structural, optical, thermal, mechanical, elemental, SHG and LDT analyses. Both the Single crystal and Powder XRD validates the presence of orthorhombic crystalline structure. UV-Vis spectra confirms the TGAS crystal has greater transparency in the complete visible zone with higher band gap value of 6.25 eV. Photoluminescence studies reveals that the TGAS crystal exhibits good luminescence. Hardness analysis reveals that the TGAS crystal is a softer medium. Thermal analysis conveys that the TGAS crystal possesses higher thermal durability of 240 °C. EDX spectra reveals that the TGAS crystal is a high purity material. The TGAS crystal possesses greater Second Harmonic generation efficacy of 1.17 times greater than KDP with greater LDT of 2.04 GW/ cm^2. The TGAS crystal is found to have less antibacterial activity. Thus, the TGAS crystal is found to exhibit greater transparency, higher band gap value, good structural perfection, high purity, good luminescence, greater mechanical and thermal stability, higher NLO efficiency and greater Laser damage threshold values, it could potentially be feasible to design optoelectronic gadgets utilizing the TGAS crystal.

Research Data Policy and Data Availability

The datasets generated or analyzed during the current study are included in this submitted article.

Author Contribution

Josephine Gladiya M: Conceptualization, methodology and writing - Original draft,
Anuradha G. V: Validation, Investigation and review,
Sivashankar V: Correction proof, Validation and review.
Helina B: review
All authors read and approved the final manuscript.

Ethics Declaration

Consent to Participate

All authors have given consent to participate

Funding and Competing Interest

The authors did not receive support from any organization for the submitted work. The authors declare no competing interests.

ACKNOWLEDGEMENTS

We are very grateful to the research support from various research institutions such as ACIC – St. Joseph's college, Trichy, Alagappa university, Karaikudi, BS Abdur Rahman Cresent Engineering College, Chennai, VIT, Vellore, and Department of chemistry, VOC college, Thoothukudi to carry out this research work.

REFERENCES

1. Reis IFS, Viana JR, de Oliveira Neto JG, Stoyanov SR, de M Carneiro JW, Lage MR, Dos Santos AO, Synthesis, characterization, and thermal and computational investigations of the L-histidine bis(fluoride) crystal, J Mol Model., 28(8),(2022) pp222. https://doi.org/10.1007/s00894-022-05168-x
2. Wellmann PJ, The search for new materials and the role of novel processing routes,Discov Mater., 1(1), (2021) pp 14. https://doi.org/10.1007/s43939-021-00014-y
3. Karuppusamy S, Muralidharan S, Babu KD, Sakthivel P, Choi D, Thermal, dielectric, mechanical and structural behavior of 2-amino 4-methylpyridinium 4-nitrophenolate 4-nitrophenol bulk single crystal,Heliyon, 9(7), (2023), e18260. https://doio.org/10.1016/j.heliyon.2023.e18260

4. Nate Schultheiss and Ann Newman, Pharmaceutical Cocrystals and Their Physicochemical Properties, *Crystal Growth & Design*,9 (6), (2009)pp 2950-2967. https://doi.org/10.1021/cg900129f
5. M. Anbu Arasi, M. Alagar, M. Raja Pugalenthi, Growth of γ-glycine single crystals using the tailored additive of potassium chloride and L-Proline and analyzing micro structural, optical, mechanical and electrical parameters, Chemical Physics Letters, 765, (2021), 138301, https://doi.org/10.1016/j.cplett.2020.138301
6. M. Esthaku Peter, P. Ramasamy, Growth of gamma glycine crystal and its characterisation, Spectrochimica Acta Part A: Molecular and Biomolecular Spectroscopy,75 (5), 2010, pp 1417-1421, https://doi.org/10.1016/j.saa.2010.01.011
7. M. Josephine Gladiya, G. V. Anuradha, V. Sivashankar, B. Helina, Characterizations of Gamma glycine crystals grown in aqueous solution of cerous chloride, European Chemical Bulletin, 12(6), (2023), pp 2704-2719, https://doi.org/10.31838/ecb/2023.12.6.243
8. R. Ashok Kumar, R. Ezhil Vizhi, N. Sivakumar, N. Vijayan, D. Rajan Babu, Crystal growth, optical and thermal studies of nonlinear optical γ-glycine single crystal grown from lithium nitrate,Optik, 123 (5), (2012), pp 409-413,https://doi.org/10.1016/j.ijleo.2011.04.019
9. Ghazaryan VV, Fleck M, Petrosyan AM, Glycine glycinium picrate--reinvestigation of the structure and vibrational spectra,Spectrochim Acta A Mol BiomolSpectrosc., 78(1), (2011), pp 128-32. https://doi.org/10.1016/j.saa.2010.09.009
10. Alexandru HV, Pure and doped triglycine sulfate crystals: growth and characterization, Ann N Y Acad Sci,1161, (2009), pp 387-396.https://doi.org/10.1111/j.1749-6632.2008.04080.x
11. V. Vijayalakshmi, P. Dhanasekaran, Growth and characterization of γ-glycine single crystals for photonics and optoelectronic device applications,Journal of Crystal Growth, 506, (2019), pp 117-121,https://doi.org/10.1016/j.jcrysgro.2018.09.048
12. M. Lawrence, J. Thomas Joseph Prakash, Growth and characterization of pure and glycine doped cadmium thiourea sulphate (GCTS) crystals, Spectrochimica Acta Part A: Mol. and Biomol. Spec.,91, (2012), pp 30-34,https://doi.org/10.1016/j.saa.2012.01.055
13. N. Rathna, V. John, T. Chithambarathanu, P.Selvarajan,Characterization of Glycine Ammonium Sulphate Crystals grown by Slow Evaporation Technique, IOSR Journal of Applied Physics, 02, (2017), pp 69-73. https://doi.org/10.9790/4861-17002026973
14. Ali A, Chiang YW, Santos RM, X-ray Diffraction Techniques for Mineral Characterization: A Review for Engineers of the Fundamentals, Applications, and Research Directions, *Minerals,* 12(2), (2022) pp 205. https://doi.org/10.3390/min12020205
15. Kang S, Xiao L, Meng L, Zhang X, Sun R, Isolation and Structural Characterization of Lignin from Cotton Stalk Treated in an Ammonia Hydrothermal System, *International Journal of Molecular Sciences,*13(11), (2012), pp 15209-15226.https://doi.org/10.3390/ijms131115209
16. S Umamaheswari, M.Murali, FTIR spectroscopic study of fungal degradation of poly(ethylene terephthalate) and polystyrene foam, Elixir Chemical Engineering, 64, 2013, pp 19159-19164.
17. Lisa-Marie Shillito, Matthew J. Almond, James Nicholson, Manolis Pantos, Wendy Matthews, Rapid characterisation of archaeological midden components using FT-IR spectroscopy, SEM–EDX and micro-XRD, Spectrochimica Acta Part A: Molecular and Biomolecular Spectroscopy, Vol 73, no 1, (2009),pp 133-139, https://doi.org/10.1016/j.saa.2009.02.004
18. Laiyuan Chen, Liwu Lin, Zhusheng Xu, Tao Zhang, Qin Xin, Pinliang Ying, Guoqiang Li, Can Li, Fourier Transform-Infrared Investigation of Adsorption of Methane and Carbon Monoxide on HZSM-5 and Mo/HZSM-5 Zeolites at Low Temperature, Journal of Catalysis, Vol 161, no 1, (1996), pp 107-114, https://doi.org/10.1006/jcat.1996.0167
19. J. Llorca, N. Homs, J. Araña, J. Sales, P. Ramírez de la Piscina, FTIR study of the interaction of CO and CO2 with silica-supported PtSn alloy, Applied Surface Science, Vol 134, no 1–4, 1998), pp 217-224, https://doi.org/10.1016/S0169-4332(98)00225-6
20. Krishnegowda, Jagadish & Abhilash, Mavinakere& Keerthiraj, Dr. Namratha & Shivanna, Srikantaswamy, Comparative Study on the Effects of Surface Area, Conduction Band and Valence Band Positions on the

Photocatalytic Activity of ZnO-M_xO_y Heterostructures, Journal of Water Resource and Protection, 11, (2019), pp 357-370. https://doi.org/10.4236/jwarp.2019.113021

21. M. Chai and M. Isa, The Oleic Acid Composition Effect on the Carboxymethyl Cellulose Based Biopolymer Electrolyte, Journal of Crystallization Process and Technology, Vol. 3, No. 1, (2013), pp. 1-4. https://doi.org/10.4236/jcpt.2013.31001
22. Rahim Molaei, Khalil Farhadi, Mehrdad Forough, Salaheddin Hajizadeh, Green Biological Fabrication and Characterization of Highly Monodisperse Palladium Nanoparticles Using Pistacia Atlantica Fruit Broth, *Journal of Nanostructures,*Vol 8, no 1, (2018), pp 47-54. https://doi.org/10.22052/JNS.2018.01.006
23. Das. D, Sen. K. & Maity. S, Studies on electro-conductive fabrics prepared by *in situ* chemical polymerization of mixtures of pyrrole and thiophene onto polyester, Fibers Polym**,** Vol 14, (2013),pp 345–351,https://doi.org/10.1007/s12221-013-0345-7
24. Miculescu, Florin &Maidaniuc, Andreea &Miculescu, Marian &Batalu, Dan & Ciocoiu, Robert & Voicu, Ş.I. & Stan, George & Thakur, Vijay, Synthesis and Characterization of Jellified Composites from Bovine Bone-Derived Hydroxyapatite and Starch as Precursors for Robocasting, ACS Omega, Vol 3, (2018),pp 1338-1349. https://doi.org.10.1021/acsomega.7b01855
25. Gwon, J.G, Lee, S.Y, Doh, G.H. and Kim, J.H, Characterization of chemically modified wood fibers using FTIR spectroscopy for biocomposites, J. Appl. Polym. Sci., Vol 116, (2010)pp 3212-3219. https://doi.org/10.1002/app.31746
26. Kurniawan Yuniarto, Yohanes Aris Purwanto, Setyo Purwanto, Bruce A. Welt, Hadi Karia Purwadaria, Titi Candra Sunarti, Infrared and Raman studies on polylactide acid and polyethylene glycol-400 blend, *AIP Conf. Proc.,* Vol 1725, no 1,(2016) pp 020101. https://doi.org/10.1063/1.4945555
27. Ibrahim, Maha & Fahmy, Tamer &Salaheldin, Ehab & Mobarak, Fardous& Youssef, Mohamed &Mabrook, Mohamed, Role of Tosyl Cellulose Acetate as Potential Carrier for Controlled Drug Release, Life Science Journal,Vol 12, (2015),pp127-133. https://doi.org/10.7537/marslsj121015.16
28. Jinyang Jiang, Qi Zheng, Yiru Yan, Dong Guo, Fengjuan Wang, Shengping Wu, Wei Sun, Design of a novel nanocomposite with C-S-H@LA for thermal energy storage: A theoretical and experimental study, Applied Energy, Vol 220, (2018), pp 395-407,https://doi.org/10.1016/j.apenergy.2018.03.134
29. Wang, Shen-Nan, Zhang, Fang-Da, Huang, An-Min and Zhou, Qun, Distinction of four Dalbergia species by FTIR, 2nd derivative IR, and 2D-IR spectroscopy of their ethanol-benzene extractives, Holzforschung, vol. 70, no. 6, (2016), pp. 503-510. https://doi.org/10.1515/hf-2015-0125
30. Thongam, D.D, Gupta, J. & Sahu, N.K, Effect of induced defects on the properties of ZnO nanocrystals: surfactant role and spectroscopic analysis, SN Appl. Sci.,Vol 1, (2019), pp 1030 https://doi.org/10.1007/s42452-019-1058-3
31. Juan C. Farias-Aguilar, Margarita J. Ramírez-Moreno, Lucia Téllez-Jurado, Heberto Balmori-Ramírez, Low pressure and low temperature synthesis of polyamide-6 (PA6) using Na0 as catalyst, Materials Letters, Vol 136, (2014), pp 388-392,https://doi.org/10.1016/j.matlet.2014.08.071
32. Wu, Shaokun, Mingyue He, Mei Yang, Biyao Zhang, Feng Wang, and Qianzhi Li. Near-Infrared Spectroscopy Study of Serpentine Minerals and Assignment of the OH Group, Crystals, Vol 11, no. 9, (2021), pp 1130. https://doi.org/10.3390/cryst11091130
33. Chang, C. Xu, J. Zhu, Haihua. Peng, Shunjin, - Jiang, Weijie, Electrochemical Properties of PANI as Single Electrode of Electrochemical Capacitors in Acid Electrolytes, The Scientific World Journal, Vol 940153, (2013), https://doi.org/10.1155/2013/940153
34. G. Marie Quintine sherly, G. Iswarya, Studies on growth and characterization of undoped ammonium sulphate and L-alanine doped ammonium sulphate semi organic crystals, International Journal of science and research, 8(4), (2019), pp 1005 – 1009.
35. A. Senthil, P. Ramasamy, Synthesis, growth and characterization of strontium bis (hydrogen l-malate) hexahydrate bulk single crystal: A promising semi-organic nonlinear optical material, Journal of Crystal Growth, 312(2), 2010, pp 276-281,https://doi.org/10.1016/j.jcrysgro.2009.10.021

36. J. Uma, V. Rajendran, Growth and properties of semi-organic nonlinear optical crystal: L-Glutamic acid hydrochloride, Progress in Natural Science: Materials International, 26(1), 2016, pp 24-31,https://doi.org/10.1016/j.pnsc.2016.01.013
37. S. Anbuchudarazhagan, S. Ganesan, Growth and characterization of Gamma glycine single crystal from Ammonium sulphate as solvent, Recent Research in science and technology, 2(6), (2010), pp 107-109.
38. Panpan Yu, Yonggang Zhen, Huanli Dong, Wenping Hu, Crystal Engineering of Organic Optoelectronic Materials, Chem, 5(11), 2019, pp 2814-2853,https://doi.org/10.1016/j.chempr.2019.08.019
39. Scimeca M, Bischetti S, Lamsira HK, Bonfiglio R, Bonanno E, Energy Dispersive X-ray (EDX) microanalysis: A powerful tool in biomedical research and diagnosis,Eur J Histochem, 62(1), (2018), 2841, https://doi.org/10.4081/ejh.2018.2841
40. S. Anbu Chudar Azhagan, S. Ganesan, Studies on the growth, structural, optical, SHG and thermal properties of γ-glycine single crystal: An organic nonlinear optical crystal, Optik, 124(20), (2013), pp 4452-4455,https://doi.org/10.1016/j.ijleo.2013.02.019
41. Vijayan N, Bhagavannarayana G, KanagasekaranT, Ramesh Babu R, GopalakrishnanR and Ramasamy P, Crystallization of benzimidazole by solution growth method and its characterization,Cryst. Res. Technol., 41, (2006), pp 784-789. https://doi.org/10.1002/crat.200510669
42. McDonnell G, Russell AD. Antiseptics and disinfectants: activity, action, and resistance, Clin Microbiol Rev., 12(1), (1999), pp 147-79, https://doi.org/10.1128/CMR.12.1.147
43. Wang TY, Zhu XY, Wu FG, Antibacterial gas therapy: Strategies, advances, and prospects, Bioact Mater., 23, (2022), pp 129-155. https://doi.org/10.1016/j.bioactmat.2022.10.008

Table 1: SXRD data for TGAS crystal

Parameters	**SXRD data for TGAS crystal**	**SXRD data for GAS Crystal**
Crystal structure	Orthorhombic	Monoclinic
A	90^{o}	90^{o}
B	90^{o}	92. 66^{o}
Γ	90^{o}	90^{o}
a(Å)	11.981(1) Å	8.262(3) Å
b(Å)	21.234(3) Å	10.074(2) Å
c(Å)	7.784(2) Å	8.632(2) Å
V(Å^{3})	1980.28(2)Å^{3}	717.39(4) Å^{3}
References	Present work	[13]

Table 2: Second harmonic efficiency data for TGAS crystal

S. No	**Name of the Sample**	**Output Energy (milli joule)**	**Input Energy (joule)**
1	KDP (Reference)	7.5	0.50
2	TGAS crystal	8.75	0.50

Table 3:Data forAntibacterial activity ofTGAS crystalline sample

Name of the Bacteria	**Zones of inhibition in TGAS crystal (mm)**	**Standard values of Zones of inhibitions (mm)**
Staphylococcus aureus	20	25
Pseudomonas aeruginosa	15	18

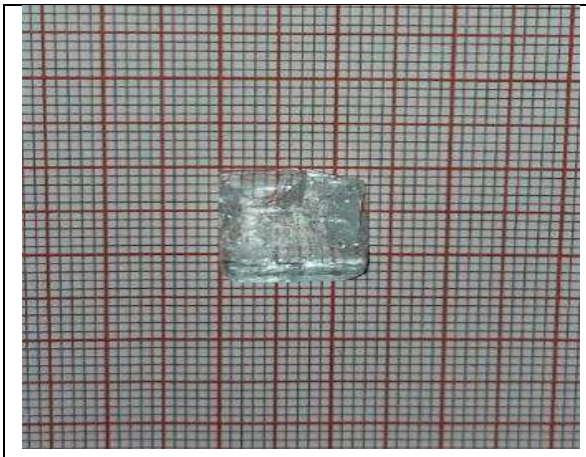

Fig 1: Grown TGAS crystal

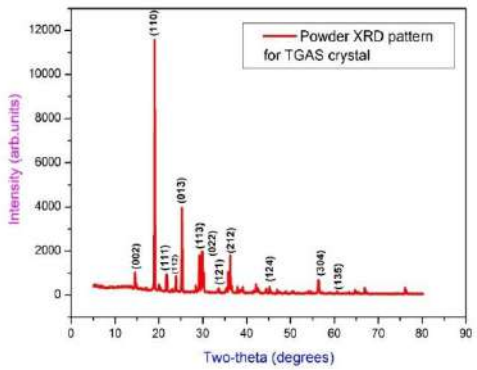

Fig.2. Powder XRD for TGAS crystal

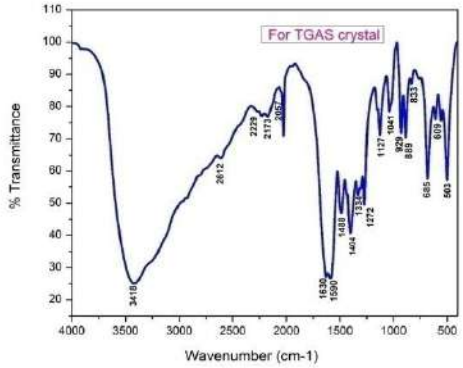

Fig: 3 FTIR spectrum for the TGAS crystal

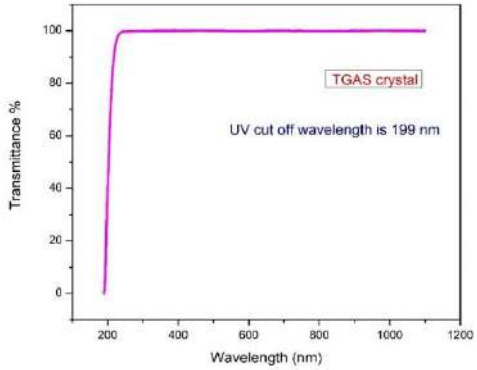

Fig 4: Transmittance spectrum for the TGAS crystal

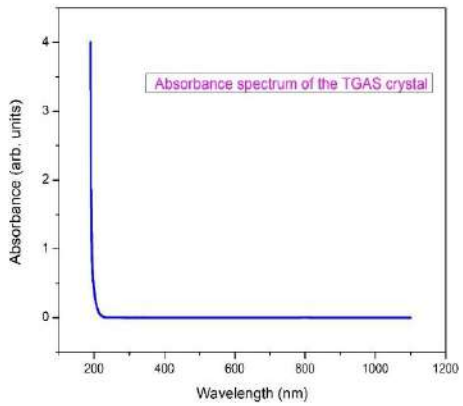

Fig 5: Absorbance spectrum for the TGAS crystal

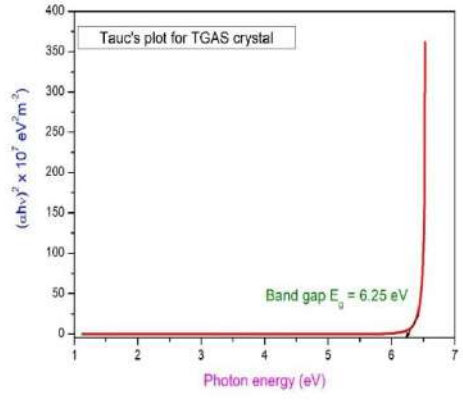

Fig 6: Tauc's plot for the TGAS crystal

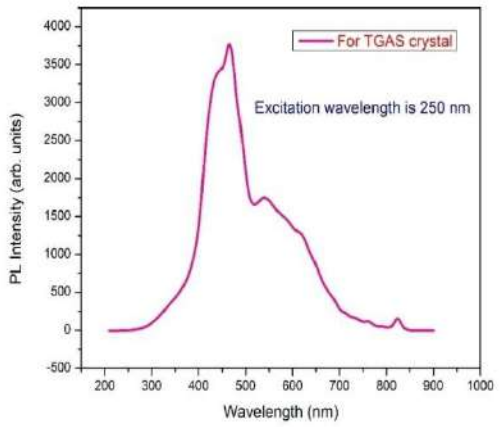

Fig 7: PL spectrum for the TGAS crystal

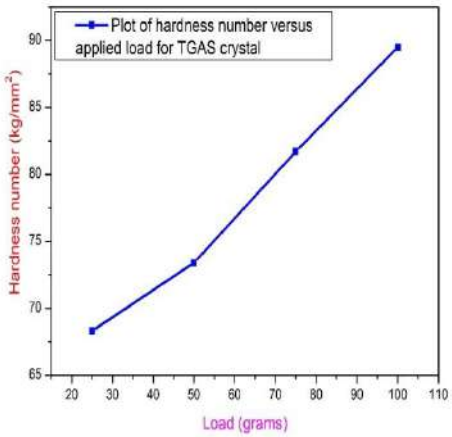

Fig. 8. Hardness with applied load variation for TGAS crystal

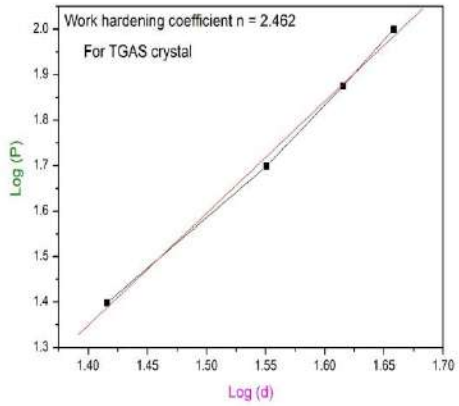

Fig. 9. Meyer's plot for TGAS crystal

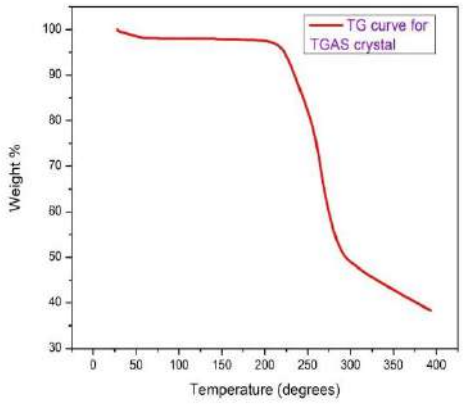

Fig 9: TG spectrum for TGAS crystal

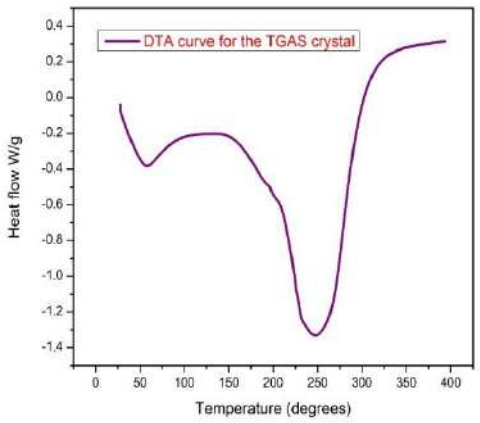

Fig 10: DTA curve for TGAS crystal

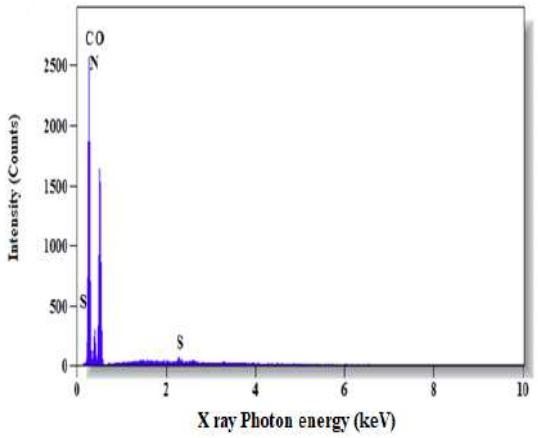

Fig 11: EDX spectrum for TGAS crystal

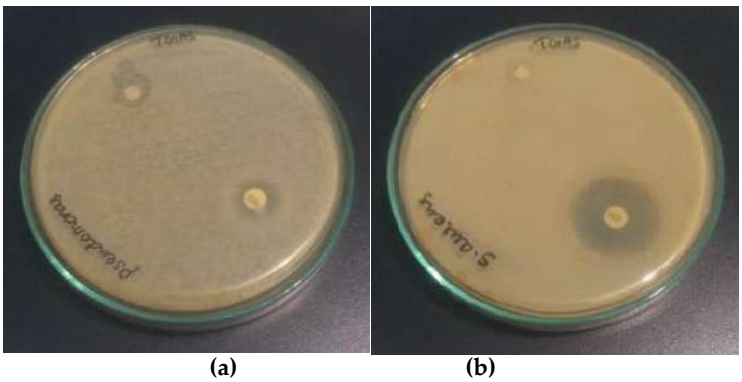

(a) **(b)**

Fig 12:The inhibition areas of LTMA crystal sample with bacterial pathogens: (a) Staphylococcus aureus (b) Pseudomonas aeruginosa

Indian Journal of Natural Sciences *www.tnsroindia.org.in ©IJONS*

Vol.15 / Issue 83 / Apr / 2024 *International Bimonthly (Print) – Open Access* *ISSN: 0976 – 0997*

RESEARCH ARTICLE

Impact of Artificial Intelligence in Automobile Industry in India

K.Kevin Selva[1*] and Dr.A.Natarajan[2]

[1]Student, PG Department of Data Science, St. Xavier's college, Palayamkottai – 627 002,TamilNadu, India.
[2]Assistant Professor, PG Department of Data Science, St. Xavier's college, Palayamkottai – 627 002, Tamil Nadu, India.

Received: 30 Dec 2023 Revised: 09 Jan 2024 Accepted: 12 Mar 2024

***Address for Correspondence**
K.Kevin Selva,
I[st] M.sc Data science,
Department of Data Science,
St. Xavier's college, Palayamkottai – 627 002,
Tamil Nadu, India.
Email: kevinselva2000@gmail.com

ABSTRACT

Artificial Intelligence (AI) is transforming a number of industries globally, and it has a significant and wide-ranging effect on the Indian automotive industry. Focusing on how AI is changing the Indian automotive industry, emphasizing the major areas in which AI technology is changing the scene. In this article we mostly discussed the consumer's interest in need of Autonomous Emergency Braking (AEB) and Driver Assistance System (ADAS)and other artificial intelligence system in Low/Mid- Range Cars and Other Automobiles for Safety and Business Reasons. Furthermore, AI is essential to India's development of connected and electric automobiles. Collecting data to give producers useful insights by analyzing industry trends and forecasting consumer preferences .In conclusion, the impact of AI on the automobile industry in India is profound and far-reaching, revolutionizing every aspect of the automotive value chain from design and manufacturing to sales and customer experience. As AI continues to evolve, it will be imperative for Indian automotive companies to embrace and harness its transformative potential to stay competitive in the rapidly evolving global automotive market.

Keywords: Artificial Intelligence, Automobile Industry, ADAS, AEB, Scope , Market trend, analysis.

INTRODUCTION

Artificial Intelligence(AI) is an alternative for human Intelligence in machines that are lined up to think like humans and implement the exact grasping techniques of human brain over various domain.AI encompasses the development of computer systems capable of performing tasks that typically require human intelligence, including learning, reasoning, problem-solving, perception, and decision-making[1]. AI serves for many purposes in a wide range of

sectors and fields since it can carry out operations that would typically require human intelligence Automotive industry is one of the biggest investors in AI. It is propelling a significant shift in how the auto industry will develop in the future. Players in the automotive sector are enhancing the quality of data essential for autonomous driving systems by utilizing machine learning techniques. This guarantees more accuracy and safety in the operation of self-driving cars. Technologies like ADAS monitors the area surrounding a car using a variety of technologies, including radar, cameras, and sensors. In considering this, ADAS gives drivers alerts and information in real time to help them steer clear of potential hazards like crashes. Depending on the ADAS tech's proficiency, the system can either fully take over control of the car to assist avoid any accidents, or it can alert the driver by sound, vibration, and display indications.[4] ADAS technology has up to five levels. Autonomous Emergency Braking (AEB) is defined as a system that constantly keeps track of the road ahead and will automatically halt the vehicle if the driver fails to take action. AEB works autonomously, with no input from the driver. The system can also add braking force if you are pressing the brake, but weaker than a vehicle needs to avoid a collision. Every AEB system monitors vehicles and most of the time, pedestrians and other obstacles. The goal of the AEB system is to avert or lessen serious crashes by applying the brakes when sudden dangers arise or if the driver is not taking appropriate action quickly enough and many other AI features can help towards safer and comfort driving experience and could make buyers towards AI integrated vehicles[5]. The growth of the Indian car market is encouraging. Owning a car is far more appealing to people than taking public transportation. Vehicle becomes sentiment for Indians as it results in Heavy traffic and pave way for accidents and loss of life. AI features can either recognize a threat to the car and engage the driver in order to prevent it from happening, or they can work automatically to steer the vehicle out of danger. When compared to low and mid-range vehicles, luxury cars are scarce in the Indian market.AI elements must be added to low- and mid-range vehicles in order to enhance passenger safety and satisfaction. Therefore, it is critical for manufacturers to understand that the Indian market will favor any vehicle with AI features that is within the affordability of the middle class. This article proves that buyers are interested and also ready to invest in artificial intelligence system in their cars and gives a prediction about the taste of future buyers.

Method Used For Analysis

The integration of Artificial Intelligence (AI) in the automotive sector has witnessed remarkable advancements, revolutionizing the industry's landscape. This article aims to provide a comprehensive overview of AI applications in automobiles, with a specific focus on leveraging gathered data for market analysis. In line with AI integration, the automobile sector is placing more and more focus on using collected data for insightful market analysis. A paradigm change has occurred with the advent of big data, allowing practitioners and scholars to identify important patterns and trends from enormous datasets. The convergence of AI and extensive datasets is driving transformative insights, shaping the future of the automotive industry. To obtain insightful information, a survey was conducted using Google Forms, and the raw data was gathered, cleaned, processed, visualized, and analyzed in Microsoft Excel.

Forecasting The Trend Of The Indian Automobile Market In Cars

The automobile market in India is one of the largest and fastest-growing in the world, playing a significant role in the country's economic development. With a diverse consumer base and a steadily increasing middle-class population, India has emerged as a crucial market for both domestic and international automotive manufacturers.

Market Overview

The Indian automobile market is characterized by a wide range of vehicles, including two-wheelers, four-wheelers, commercial vehicles, and electric vehicles, each contributing to the overall dynamism of the industry. The automobile Industry in India is a dynamic and evolving industry driven by consumer preferences, technological advancements, and government policies. As the country continues to urbanize and experience economic growth, the automotive sector is expected to play a crucial role in shaping India's mobility landscape.

Visualizing the past 20-Years Automobile(CARS) sales

Over the last 20 years, there has been an increase in car sales. The graph shows statistics from 2004 to 2023. The car business is developing far faster than expected, as seen by the jump from one lakh cars sold annually to about 40 lakh sales. Fig 1

India's Global Automobile Economy Share

India is a prominent player in the global automobile market, but compared to certain other big economies, its economic share in terms of car sales is not as high. A growing middle class, more urbanization, and expanding purchasing power are some of the reasons driving the steady growth of the Indian automotive market It's important to remember, nevertheless that India's economic contribution to global auto sales is not as significant as that of countries like China, USA, or the EU. The largest automobile market in the world, in terms of both sales and production, has been China at the end of last decade. Fig 2

Report on India's Top 10 Automobiles

As of January 2022, the list of the top-selling cars in the Indian market can change over time based on consumer preferences, new launches, and market trends. Here's a general overview of some popular and consistently well-selling cars in India. The specific rankings and models might have changed since then. Fig 3

BEV and Hybrid vehicle's performance in Indian market:

Sales of BEVs and hybrid automobiles have seen ups and downs, with a primary cause being consumers' confusion when selecting a vehicle type. The chart clearly showcases the sales fluctuations on BEV and Hybrid sales of 2023 market Fig 4

Data Analysis – Understanding Buyer's Mindset

This article intend to close the gap between buyers and manufacturers in this particular component. As seen previously, the market as a whole is expanding, but consumers are still having trouble selecting a car. Data from present and potential consumers to learn about their preferences and mindsets. Also to know if they were genuinely interested in having artificial intelligence (AI) systems installed in their vehicles.

List of questions placed to the audience and reason for the questions :

No.	Questions	Explanation
1.	Type of participant • Student • Working professional • Business and others	Understanding their role is crucial in order to comprehend their attitude
2.	Does the individual currently possess a car? • Yes • No	Future vehicle buyers may have different ideas about what kind of car to buy than someone who already owns one.
3.	The type of car model they would like to purchase in the future • Petrol/Diesel • Hybrid • BEV	The world is shifting towards electric vehicles (EVs), therefore we can analyze whether people are prepared to prefer EVs and hybrids over traditional gasoline and diesel vehicles.
4.	Preference of price range when they buy in future • Low(Upto 6L) • Mid(6-15L) • High(Above 15L)	The primary goal of this study is to apply artificial intelligence to low- and mid-range vehicles. By asking this question, we can ascertain what price range consumers are willing to invest in.
5.	Interested in installing AI feature in	After outlining the features of AI, participants are asked if they

	your car(Features like ADAS, ABS etc) • Yes • No	would want to have it in their cars. This helps us to understand the participant's interest in AI
6.	What will you prefer? • A car with AI features with a lakh higher than its actual price • A car without AI feature	To determine whether individuals are interested in investing for Artificial Intelligence

Examining the survey's findings:
The purpose of the survey is to determine consumer interest in AI integration into automobiles as well as the considerations that automakers should make when developing new models or making adjustments to current models. Fig 6

Types of People Participated
Results: The majority of students 53% who responded to the survey are prospective buyers. Fig 7

Current status of the participants
Results: As we previously stated, the proportion of persons without a car was higher since students were more involved than professionals in the workforce and other settings. Fig 8

Type of car variant they prefer when they buy in future
Results: Several factors contribute to why people may prefer petrol cars over electric vehicles (EVs). While the popularity of EVs is growing, there are still certain challenges and considerations that influence consumer choices. Here are some common reasons why individuals may currently prefer petrol cars:

- Infrastructure Concerns
- Price range anxiety
- Initial Cost
- Charging Time
- Longer Refuelling Time
- Limited Model Variety
- Limited Model Options
- Uncertain Resale Value
- Technological Concerns
- Less Government Incentives

Preference of price range when participants buy in future:
Results: The preference for mid-range cars over luxury cars among Indian consumers can be attributed to several economic, cultural, and practical factors. Here are some key reasons why many Indians tend to opt for mid-range cars:

- Affordability
- Fuel efficiency
- Average road Conditions
- Efficient resale Value
- Low maintenance Costs
- Demographic preferences
- Limited luxury infrastructure

While these factors contribute to the prevalence of mid-range cars in India, it's essential to note that the luxury car market is growing, and changing economic dynamics and consumer preferences may lead to shifts in purchasing patterns over time.

Preference of adding AI in cars:

Results: People appreciate and embrace AI (Artificial Intelligence) in their cars for several reasons, as it brings various benefits and enhances the overall driving experience. Here are some key reasons why individuals love AI in their cars: Fig 8

1. Enhanced Safety Features
2. Driver Assistance and Automation
3. Improved Navigation and Traffic Management
4. Voice-Activated Controls
5. Personalization and Customization

Are the participants willing to spend an additional one lakh rupees to deploy AI?

Results: The data indicates that most people are willing to invest in AI for their automobiles, which suggests that people are prepared to make the rapid transition from conventional to AI-enabled vehicles. Fig 9

Getting deeper into the data

We divided buyers into three categories: LOW, MID, and HIGH. According to our survey, 71% of Indians choose low- and mid-range cars over high- or luxury-class vehicles, indicating that low- and mid-range users dominate the market. However, the turning point came when individuals in all three categories expected their cars to include AI functions, and many of them were prepared to pay for them. Let's examine each category separately. Fig 10

Category -1:

Results: Here we can see that nearly 72% of the people from low budget range expecting AI feature to be installed in their cars and 61% are ready to invest a lakh more for it Fig 11

Category -2:

Results: Here we can see that mid budget people are also interested to have AI features in their car. 58% likes to have it and out of 58% nearly 60% likes to invest a lakh more for AI feature is quite impressive. Fig 12

Category -3:

Results: Over 80% of people who prefers to buy luxury cars needs AI in their cars. Out of 29% who voted as they prefer luxury cars than low are mid range cars ,more than 70% in high budget category are ready to invest more for AI in their cars says that any company which does not integrate AI cannot survive in Indian market Fig 13

CONCLUSION

The automotive industry has undoubtedly witnessed a significant transformation in the design, manufacturing, and user experience of automobiles due to the incorporation of Artificial Intelligence (AI). We have examined the several uses of AI in the automobile industry through our examination of the literature, as well as how it can revolutionize market analysis by utilizing collected data. This article provides a complete understanding of artificial intelligence (AI), how it has been implemented in the automotive industry, and Why we need to integrate AI into low- and mid-range cars in a way that benefits both the manufacturer and the customer. The role of the Indian market in the global economy and the most recent car sales data have been analyzed and visualized. AI has ushered in a period of innovation and growth, from improving safety features through Advanced Driver Assistance Systems (ADAS) to enabling autonomous driving capabilities. AI algorithms enable cars to comprehend complicated settings, make wise decisions, and instantly adjust to changing road conditions by utilizing enormous datasets. Moreover, market analysis in the automobile industry has been transformed by the combination of AI and collected data. When it comes to forecasting market trends, understanding customer behavior, and guiding decision-making processes, raw data is a strategic asset. Large-scale datasets powering machine learning algorithms give stakeholders a better understanding of market dynamics and help them formulate competitive strategies. In conclusion, artificial intelligence (AI) is having a significant and wide-ranging impact on the automotive sector. This signals the arrival of a time when intelligent cars will be able to anticipate and adapt to changing societal demands in addition to

managing highways. AI will surely continue to play a major role in determining the direction of mobility in the future, guiding the development of a safer, more intelligent, and environmentally friendly automobile ecosystem and by incorporating AI into low- and mid-range cars, any company that makes automobiles, especially cars, may increase their profits and thrive in the Indian market.

REFERENCES

1. Igor Koricanac, Impact of AI on the Automobile Industry in the U.S., Retrieved February 2024 from https://www.researchgate.net/publication/351554738_Impact_of_AI_on_the_Automobile_Industry_in_the_US
2. Team Geeks for geeks, Natural Language Processing overview, Retrieved February 2024 from https://www.geeksforgeeks.org/natural-language-processing-overview
3. TeamSpyne, AI effects and its future with automobile, Retrieved February 2024from https://www.spyne.ai/blogs/ai-in-automobile-industry
4. Team Synopsys, What is ADAS, Retrieved February 2024 from https://www.synopsys.com/automotive/what-is-adas.html
5. Kia, What is Autonomous Emergency Braking , Retrieved February 2024 from https://www.kia.com/dm/discover-kia/ask/what-is-autonomous-emergencybraking.html#:~:text= Autonomous%20Emergency%20Braking%20(AEB)%20is,impact%20of%20an%20unavoidable%20one.
6. Team Auto punditz, Indian car sales analysis for CY2023, from https://www.autopunditz.com/post/indian-car-sales-figures-february-2024
7. Pushkarsheth, List of countries by motor vehicle production, Retrieved February 2024 from https://public.flourish.studio/visualisation/551072
8. Team Auto punditz, Electic and Hybrid car sales analysis 2023,Retrieved February 2024 from https://www.autopunditz.com/post/electric-hybrid-cars-sales-analysis 2023#:~:text=92%2C344%20BEVs%20(Battery%20Electric%20Vehicle,continuous%20decline%20in%20H2%202023

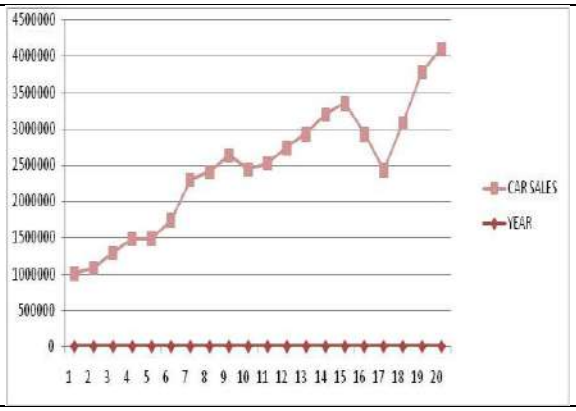

Fig1: Past twenty years car sales data (2004-2023)[6]

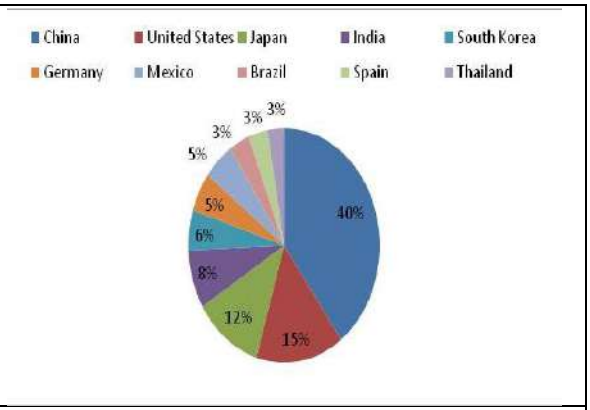

Fig2: Top automobile manufacturing countries in world[7]

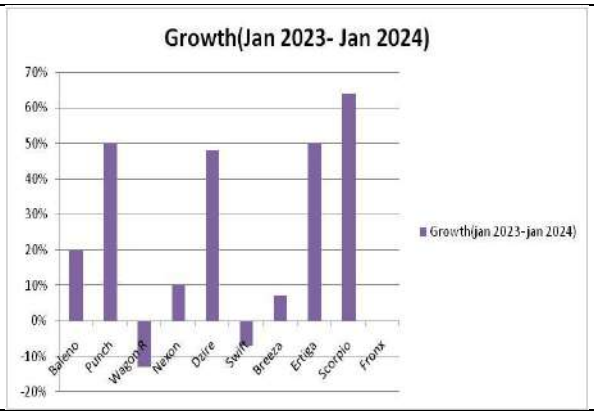

Fig3 : Sorting (left to right) from first to least selling cars in India.[6]

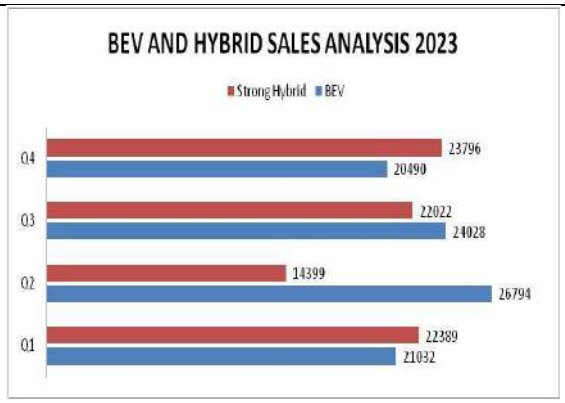

Fig4: Sales of BEV and Hybrid sales 2023[8]

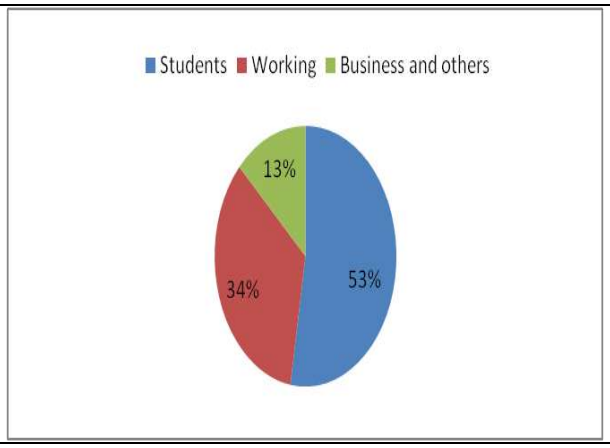

Fig5:Percentage of people involved in survey

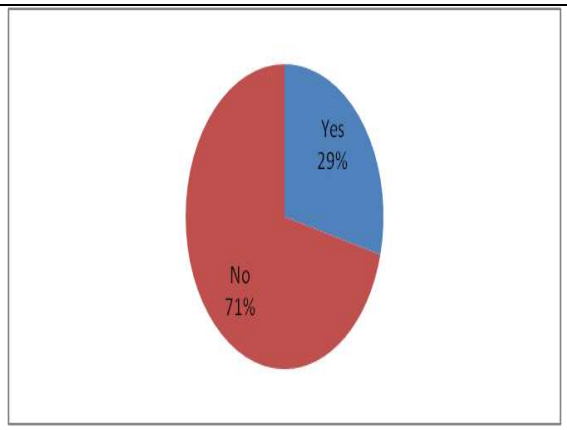

Fig6:Percentage of people who owns a car

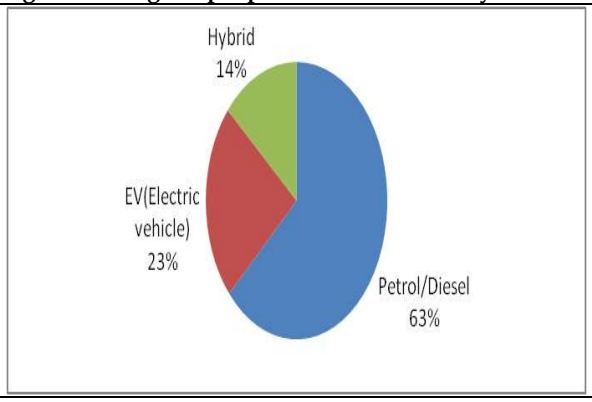

Fig7:Percentage of preference in choosing the type of vehicle

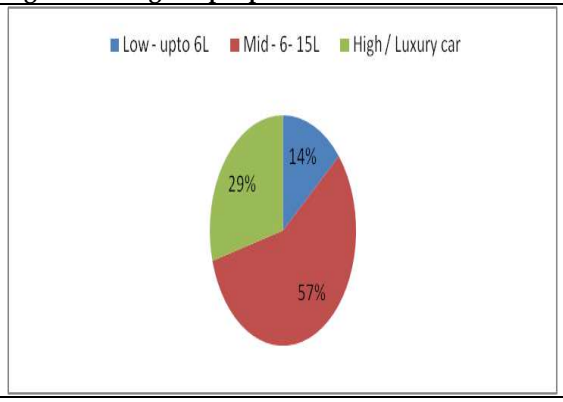

Fig 8:Percentage of preferences in price range

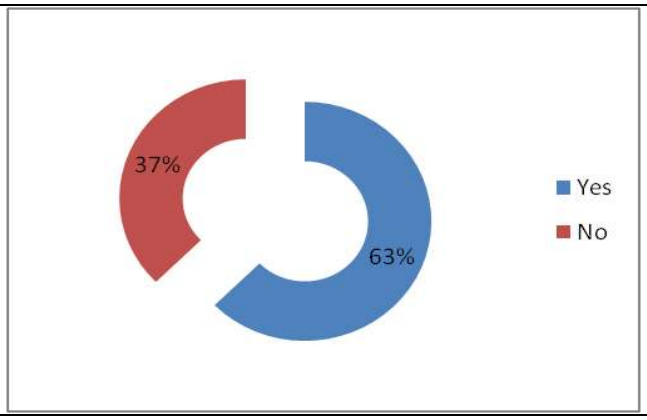

Fig 9: Percentage of preference in adding AI in cars

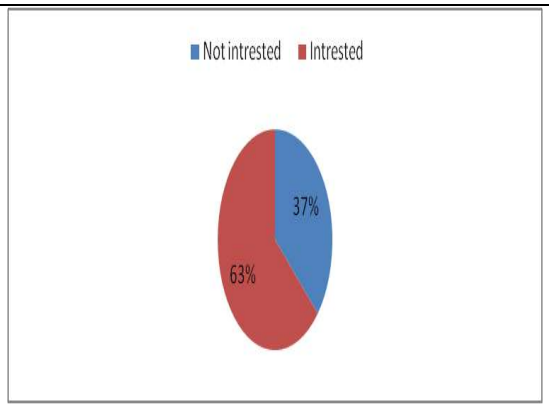

Fig10:Percentage of people interested in investing for AI

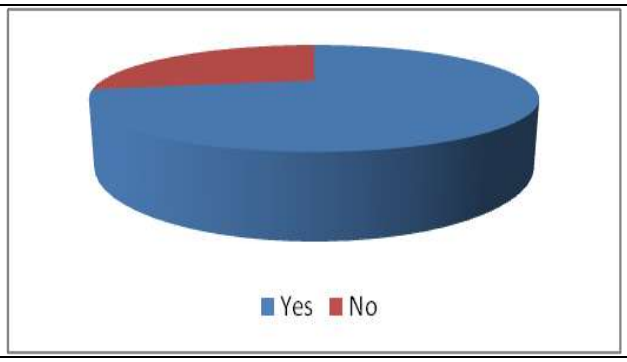

Fig11:Percentage of low budget buyer's interest in AI

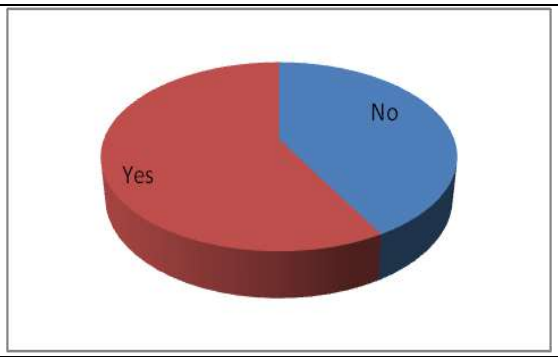

Fig12:Percentage of Mid budget buyer's interest in AI

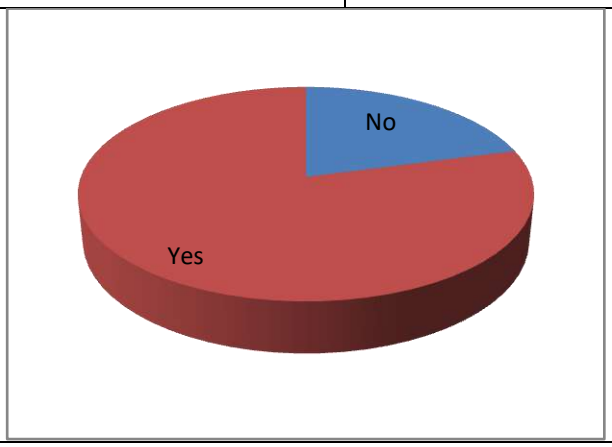

Fig13 :Percentage of High budget buyer's interest in AI

Vol.15 / Issue 83 / Apr / 2024 International Bimonthly (Print) – Open Access ISSN: 0976 – 0997

RESEARCH ARTICLE

Energy Management Strategy for Hybrid Energy Storage - Electric Vehicles Based on Intelligent Controllers

Gundu Venu[1]*, Giriprasad Ambati[2], Chamakura Krishna Reddy[3]

[1]Assistant Professor, Department of Electrical and Electronics Engineering, Malla Reddy Engineering College (Autonomous), (Affiliated to Jawaharlal Nehru Technological University Hyderabad), Telangana, India.
[2]Assistant Professor, Department of Electrical and Electronics Engineering, Vallurupalli Nageswar Rao Vignan Jyothi Institute of Engineering and Technology, (Affiliated to Jawaharlal Nehru Technological University), Hyderabad, Telangana, India.
[3]Assistant Professor, Department of Electrical and Electronics Engineering, BVRIT Hyderabad of Engineering for Women, Hyderabad, Telangana, India.

Received: 20 Dec 2023 Revised: 12 Jan 2024 Accepted: 13 Mar 2024

***Address for Correspondence**
Gundu Venu
Assistant Professor,
Department of Electrical and Electronics Engineering,
Malla Reddy Engineering College (Autonomous),
(Affiliated to Jawaharlal Nehru Technological University Hyderabad),
Telangana, India.
Email: gunduvenu83@mrec.ac.in

ABSTRACT

Developing an Energy Management Strategy (EMS) that takes into account the Electrical Vehicle's (EV's) power distribution between the battery and ultracapacitor helps lessen the EV's power usage and prolong battery life. Therefore, the goal of this paper is to create a Fuzzy Logic Controller-based EMS for EVs that takes battery degradation into account. The hybrid energy storage electric vehicle model is developed first for EMS verification. Battery deterioration modelling trials are complete in the meantime. After that, a Hybrid Energy Storage System's (HESS) power is distributed sensibly using a rule-based control strategy. By comparing the proposed EMS to the existing EMS and the findings, it becomes clear that the former uses less energy and causes less battery degradation. The features of the HESS serve as the basis for the experiment's design, execution, and modelling of battery deterioration. Based on the model, the proposed work tested in MATLAB/Simulink a rule-based EMS and a PMP energy management method that takes battery degradation into account. Considering battery deterioration, the

limited energy of hybrid energy storage electric vehicles is divided equitably and utilized to maximize energy management.

Keywords: electric vehicle; hybrid energy storage system; energy management strategy; fuzzy logic Controller; battery degradation

INTRODUCTION

The research and development of hybrid energy storage systems, which can increase the efficiency and power of electric vehicles, has been receiving greater attention recently. Both batteries and ultracapacitors play significant roles in a hybrid energy storage system. Lithium-ion battery shortages can be mitigated by using ultracapacitors because of their high-power density, rapid charge and discharge times, and multiple-cycle life [1]. On the other hand, the battery's power and efficiency would gradually degrade over time due to electrochemical processes and the battery's state [2]. In addition, the energy management system in a hybrid electric vehicle is responsible for controlling and balancing the power supplied by the car's power battery and ultracapacitor [3-4]. To maximize vehicle efficiency and prolong battery life, the energy management system must take battery degradation into account while providing the required power. Consequently, the primary difficulty of an energy management approach for hybrid energy storage electric vehicles is figuring out how to fairly divide the power from the power battery and the ultracapacitor. Hotspots in the study of energy management for hybrid energy storage electric cars include the design of energy management strategy, the construction of the battery decay model, and the matching of ultracapacitors and DC/DC converters. Battery ageing factors have been the basis for numerous models published by domestic and international academics depicting the decline in battery life and performance over time. The evaluation models are used to offer energy management techniques that take battery degradation into account [5].There are now three types of models used to describe the decline in lithium-ion battery capacity: mechanism models, equivalent models, and empirical models. The physical and chemical features of the battery provide the basis for the mechanism model, which aids in the investigation of the causes of battery capacity loss. Mechanism models are typically employed in battery research rather than control problems [6] due to the complexity of the model creation procedure and the difficulty of acquiring the electrochemical parameters included in the model. The correctness of the equivalent circuit model is affected by several external factors, and the electrical components are susceptible to losses.

The model accuracy requirements of this investigation can be met with the use of an empirical model, the establishment and computation of which are, however, rather straightforward [7]. Considering the battery capacity decline and the physical interaction of many parameters, a considerable amount of test data on battery life is employed for formula-fitting construction [8]. Battery state of charge, state of charge, and ultracapacitor state of charge are all examples of inputs. When discharging a battery or capacitor, the power is determined by the battery power distribution coefficient. Although this management strategy's foundation is straight forward to pick up, the control principles behind it necessitate extensive expertise. Complete utilization of composite power supply with pinpoint accuracy is unachievable. An onboard lithium-ion battery system's thermal safety and degradation were highlighted in recent research [9] that offered a universal algorithmic framework integrating a model-based state observer and a deep reinforcement learning-based optimizer. Rapid charging, thermal safety enforcement, increased battery life, and computational tractability are all areas where it has proven itself better. Optimizing energy management in rechargeable hybrid energy storage electric cars was the focus of [10], which also offered a battery model. This model predicts the rate of decline in battery health as the state of charge (SOC) and pack temperature are changed. The numerical multi-objective optimum control problem is solved by using SDP and PSO to strike a balance between power consumption and battery life while meeting the needs of the vehicle. Efficiencies in battery life and power consumption were analyzed.

Hybrid Energy Storage Electric Vehicle Modelling

In this paper, a closer look at the parallel hybrid energy storage system (HESS) is shown in Figure 1 which consists of a controller, motor, and ultracapacitor in addition to a battery and a DC/DC converter.

Vehicle Modelling

In order to simulate a hybrid electric car, it is necessary to analyze a simulation experiment involving energy management. That's why this research constructs a model car, complete with a driver model, a vehicle longitudinal dynamic model, a motor model, and a HESS model. While the other models are constructed using mathematical modelling, the motor model is generated by utilizing simulation results. In this paper, the UC module is connected to the DC bus via a bidirectional DC/DC converter, while the battery module is connected directly to the DC bus, resulting in a UC semi-active hybrid topology. The DC/DC converter can regulate the UC's output power to deliver the maximum amount of energy to the vehicle while keeping the system's overall power consumption to a minimum.

While the other models are constructed using mathematical modelling, the motor model is generated by utilizing experimental methods. In this research work, the UC module is connected to the DC bus via a bidirectional DC/DC converter, while the battery module is connected directly to the DC bus, resulting in a UC semi-active hybrid topology. Also, the DC/DC converter may regulate the UC's output power to deliver the vehicle's maximum power while minimizing the system's overall power draw and extending the battery's service life. The HESS model is calibrated using the battery, UC, and DC/DC factors and characteristics. It is the Rint equivalent circuit that is chosen by the battery model. The model's power battery has an open circuit voltage and internal resistance that vary with state-of-charge (SOC) and temperature, and whose values can be determined with experimentation. Power in the HESS is managed by a buck-boost bidirectional DC/DC converter, and a model of this converter is developed based on its operating principle and specifications.

Energy Management Strategy Based on Fuzzy Control

In energy management strategy, the primary function is to regulate power distribution in hybrid electric vehicles and all other electric vehicles that are operated with battery management. As a rule-based control approach, fuzzy control is very flexible and reliable. An important problem in developing energy management strategies is figuring out how to maintain the battery operating conditions in its optimal discharge state. Distribution of the discharge current from the battery and ultracapacitor will accomplish this purpose. It is possible to test the efficacy of the approach by plugging the multiplier for dispersed current into a battery decay model and determining the resulting battery decay rate. In this paper, the notion of the power distribution coefficient K symbolizes the importance placed on battery power, and picking the vehicle demand power, the ultracapacitor SOCuc, and the battery SOCb to achieve the best possible power distribution ratio. This allows for an examination of the fuzzy controller's power distribution coefficient.

$$K = \frac{P_b}{P_{req}} \quad (1)$$

$$P_b = P_{req}(1 - k) \quad (2)$$

where battery power (Pb), UC power (Pc), and vehicle power demand (Preq) are all inputs to the equation.

Based on the hybrid energy storage electric vehicle's operational characteristics, the following control ideas can be derived: when the required power is positive, the hybrid energy storage system outputs power; on the one hand, the ultracapacitor is used to protect the battery from discharging smoothly; on the other hand, it provides instantaneous power to the drive motor. Hybrid energy storage systems can recover energy whenever the power demand is negative. The ultracapacitor restores energy lost as a result of braking, and it also shields the battery from the destructive effects of high-current shocks. Power levels and amplitudes, as well as the emphasis placed on regulation, are distinct between the two modes of operation. It is necessary to design separate control methods for the two modes of operation of the composite power supply. Using the control concepts, it may categorize the control approach into two modes: driving and braking. Fuzzy controller 1 fairly divides the power during the discharge phase, and fuzzy controller 2 determines the charge phase power distribution.

Control Method

FLC evaluates input data in terms of logical variables with continuous values ranging from zero to one. The operation of the controller in a fuzzy logic control system is based on fuzzy rules generated using fuzzy set theory. Figure 3block diagram of Fuzzy logic controller. The fuzzification, defuzzification, input, and output variables make up FLC. The fuzzy sets are formed using seven membership functions for the inputs error E, change in error CE and the output (P_{loss}) are shown in Figures5 and 6 and Figure 4 depicts the output.

Simulation Results

Figure 5 depicts the ideal power distribution of the HESS with two distinct energy management strategies under UDDS operating conditions, demonstrating that both strategies can efficiently divide the power of batteries and the ultracapacitor. According to the findings, the PMP energy optimization management technique outperforms the fuzzy control strategy in terms of controlling battery degradation. The optimization method reduces the battery's peak current by 29.5 A, the cell deterioration rate after 300 cycles by 2.33 percent, and the energy consumption rate by 11.72-kilowatt hours per 100kilometers. To sum up, hybrid electric vehicles that employ a PMP-based energy management system that takes battery deterioration into account can significantly postpone battery decline and energy usage, save energy, and protect batteries.

CONCLUSIONS

The purpose of this work is to present an FLC-based energy management approach for hybrid electric vehicles that takes battery degradation into account, with the end objective of assessing the effect of battery decline on the power and economic benefits of electric vehicles. The hybrid electric vehicle model was first established to ensure the strategy's success. To prevent the battery from degrading too quickly and keep the vehicle's power performance stable, the fuzzy control method is utilized to intelligently divide the load between the ultracapacitor and the battery. Lastly, the proposed control method is verified using simulation.

REFERENCES

1. Fengyan Yi, Dagang Lu, Xingmao Wang, Chaofeng Pan, Yuanxue Tao, Jiaming Zhou,Changli Zhao. "Energy Management Strategy for Hybrid Energy Storage Electric Vehicles Based on Pontryagin’s Minimum Principle Considering Battery Degradation", Sustainability, 2022.
2. G. Sravanthi, T. Rama Subba Reddy, K. Mercy Rosalina. "Solar PV Integrated UPQC to Enhance Power Quality Problems of Distribution Power System Using Fuzzy Logic Controller", 2023 World Conference on Communication & Computing (WCONF), 2023.
3. R. Manivannan. "Research on IoT-Based Hybrid Electrical Vehicles energy management systems using Machine Learning-based algorithm", Sustainable Computing: Informatics and Systems, 2023.
4. Wei Zhou, Ziqi Zeng, Shijie Bao. "Intelligent Ventilation Management System of Laboratory Based on Fuzzy Logic", 2023 9th International Conference on Control, Automation and Robotics (ICCAR), 2023.
5. Saman Nasiri, Mostafa Parniani, Saeed Peyghami. "A multi-objective optimal power management strategy for enhancement of battery and propellers lifespan in all-electric ships", Journal of Energy Storage, 2023.
6. Wei Du, NikolceMurgovski, Fei Ju, Jingzhou Gao, Shengdun Zhao. "Stochastic Model Predictive Energy Management of Electric Trucks in Connected Traffic", IEEE Transactions on Vehicular Technology, 2022.
7. Hao Li, Haiqing Yang, Xingyue Li. "Investigation on the working performance of a non-dispersible grouting material for the crack repairment of underwater structures", Construction and Building Materials, 2023.
8. Rodolfo E. Haber. "IEEE Transactions on Systems Man and Cybernetics”, Part C (Applications and Reviews), 9/2007.
9. Mehmet Kubilay Eker, Ismail H. Altas. "A Fuzzy Voltage Regulator (FVR) for a Stand-alone Synchronous Generator", Electric Power Components and Systems, 2007.

10. Acharjee, P, and K Ali. "Load flow analysis using decoupled fuzzy load flow under critical conditions", International Journal of Engineering Science and Technology, 2011.

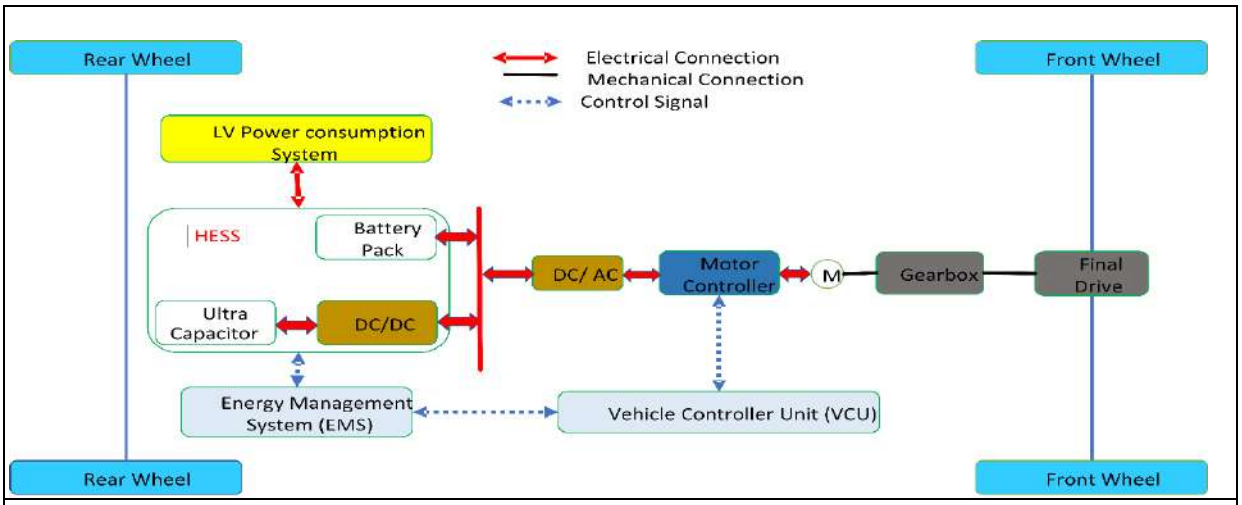

Figure 1. The configuration and detailed structure of a parallel hybrid electric vehicle.

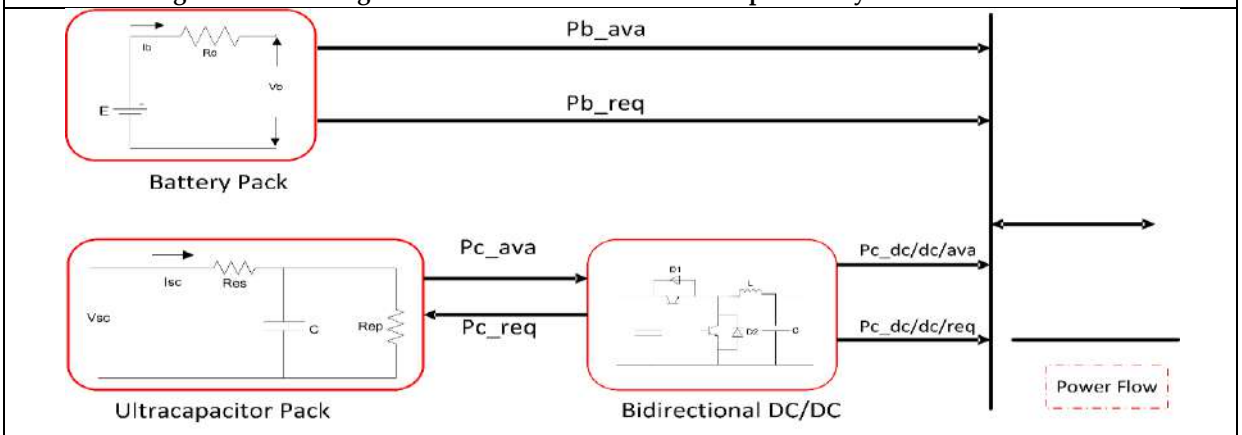

Figure.2 Modeling of Hybrid Energy Storage System

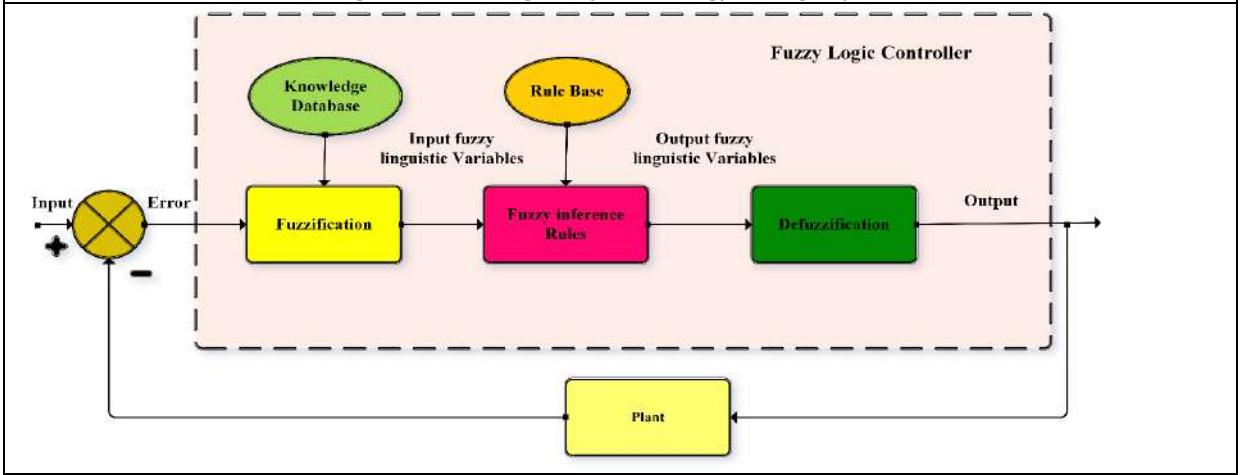

Figure 3.Block diagram of Fuzzy logic controller

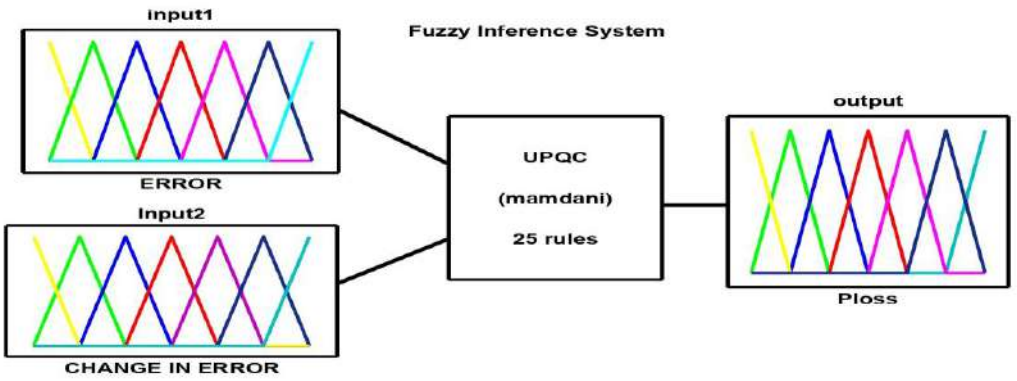

Figure 4. Fuzzy inference System

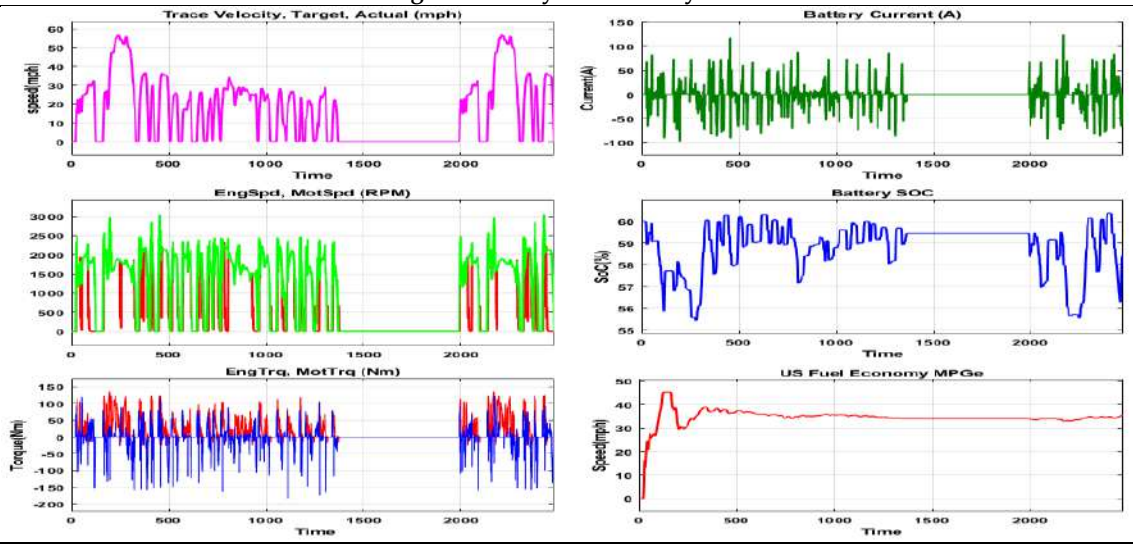

Figure 5. Result curve of speed and power distribution for the fuzzy control strategy.

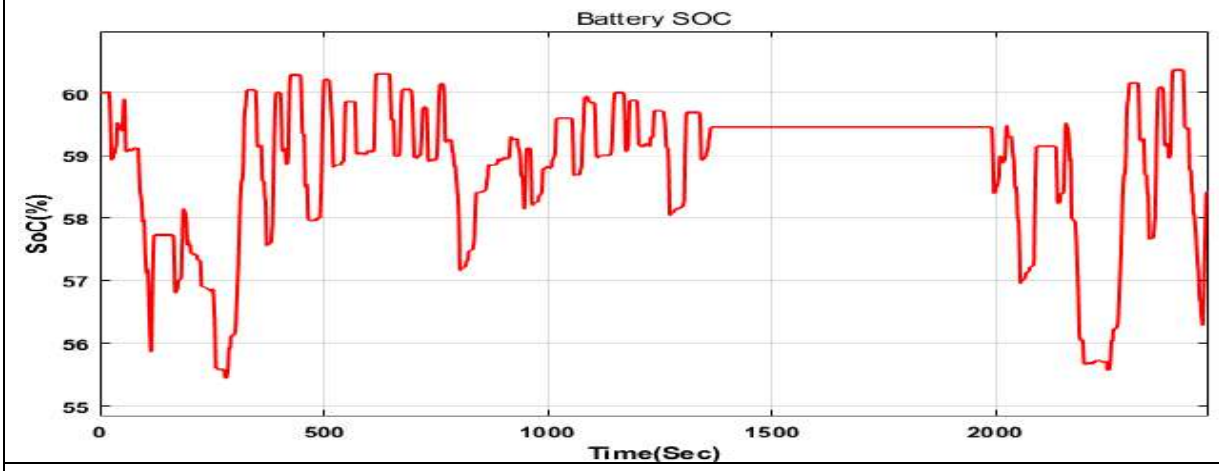

Figure 6. Simulation Result SOC

Vol.15 / Issue 83 / Apr / 2024 International Bimonthly (Print) – Open Access ISSN: 0976 – 0997

REVIEW ARTICLE

Current Evidences of Physiotherapy Interventions for Unilateral Neglect in Stroke Individuals: A Systematic Review

Nirmitee Honap[1] and Suraj B. Kanase[2]

[1]Department of Physiotherapy, Krishna Vishwa Vidyapeeth (Affiliated to Deemed to be University) Karad, Maharashtra , India
[2]Professor and HoD, Department of Neuro Physiotherapy, Krishna Vishwa Vidyapeeth (Affiliated to Deemed to be University) Karad, Maharashtra , India

Received: 24 Oct 2023 Revised: 09 Jan 2024 Accepted: 06 Mar 2024

***Address for Correspondence**
Suraj B. Kanase
Department of Neuro Physiotherapy,
Krishna Vishwa Vidyapeeth (Affiliated to Deemed to be University)
Karad, Maharashtra , India.
Email: drsurajkanase7@gmail.com

ABSTRACT

Neglect alone is the inability to respond to external stimuli, including visual, somatosensory, auditory, and kinesthetic sources. The incidence of stroke in the right hemisphere varies between 10% and 82%, and in the left hemisphere between 15% and 65%. Neglect is usually caused by a major stroke in the area of the middle cerebral artery, and the result of neglect will be more severe and persistent pain following damage to the right hemisphere. Different treatments and tools have been developed to measure and solve neglect. Recent data suggest that rehabilitation can be divided into two types of behavior: protecting the hemiplegic limb to reduce ipsilateral site preference or increasing awareness of the source of conflict to support the case. In particular, we recently performed a systematic review of the use of different physiotherapy modalities in the USN complex, including prismatic adaptation, optomotor stimulation, neck vibration, galvanic vestibular stimulation, non invasive brain stimulation, robotic learning, and smooth tracking. exercise. The aim of this review is to determine current physical therapy options for neglect in stroke patients. Articles were selected according to main subject headings and analyzed. Clinical studies have provided evidence that physical therapy is effective in improving symptoms of self-neglect in stroke patients.

Keywords: Unilateral Neglect, Stroke, Physiotherapy

INTRODUCTION

Stroke is the predominant cause of long-term disability worldwide. Consequences of stroke include motor and cognitive impairment, and survivors often develop impairments in activities of daily living (BADL) and independence in activities of daily living (IADL), life satisfaction, and depression. USN is a lack of response to contralateral stimulation that occurs in 25% to 48% of stroke patients. The ability of USN has been studied extensively and its presence has been shown to be associated with less BADL and IADL, fewer threats, longer hospital stays, and better outcomes. Activities to improve the UN are carefully designed, implemented and researched. [1] It is characterized by the inability to express or respond to stimuli from various sources such as visual, somatosensory, auditory and kinesthetic sources. The incidence of stroke is reported to be 10-82% in the right hemisphere and 15-65% in the left hemisphere. A variety of treatments and tools have been developed to evaluate and treat UN problems. Recent data suggest that rehabilitation can be divided into two types of actions: preservation of the hemiplegic limb to reduce ipsilateral preference or increasing awareness of the location of the problem to support the case. It is also difficult to declare which method is the best treatment recommendation because there is no evidence and, interestingly, doctors rarely use scientific evidence.[2]

Unilateral neglect (UN) is a medical term that refers to problems resulting from the failure to report, respond to, or refer to new or useful stimuli occurring on the side of the brain opposite the injury. UN affects 23.5% to 67.8% of stroke patients. However, the most commonly used tests (subtraction task and National Institutes of Health Stroke Scale (NIHSS) item 11) show greater than 30%. The United Nations is an initiative that addresses problems such as long-term homelessness, increased mobility, and decreased family responsibilities, which occur in 30-60% of the population 1 year after a stroke. Although there are many shortcomings in the work of the United Nations, a consensus has not been reached on effective and efficient strategies for measuring and solving this problem. The lack of valid research and effective treatment strategies illustrates the challenge of BM. The UN usually deals with multiple situations rather than the outcome of a single situation. Rather, it is a result of disruptions in the functional connectivity of brain regions associated with auditory, sensorimotor, and visual functions, especially in the fronto-parietal network. Therefore, the symptoms are diverse and can occur in different areas (visual, auditory, and sensorimotor) and locations (particularly inside and outside the body).[3] Neglect is often the result of a serious middle cerebral artery stroke.[4]After a right semicircular stroke, left spatial neglect is more severe, and after a left semicircular stroke, left spatial neglect is more severe and persistent than on the right.[5]

Spatial neglect has been studied extensively since the 1970s. The first study used a top-down approach, adding unconscious events to non-conscious events. However, the results of these original studies were mixed, which led to the development of alternative methods.[6] Recently, the United Nations has been interested in eliminating consciousness-based neuropsychological problems in space, but its impact has not yet been investigated. Although there is no consensus, active research has demonstrated the effectiveness of prismatic adaptation (PA), transcranial magnetic stimulation (TMS), and transcranial direct current stimulation (tDCS) interventions in the treatment of USN. Additionally, preliminary evaluation demonstrates the potential of electrical vestibular stimulation (GVS) and virtual reality (VR) methods in USN rehabilitation. Although many studies on SSN were published in the 20th and early 20th centuries, neuropsychological research has decreased in the last 10-15 years. The first reason could be twofold. Advances in neuroimaging and brain stimulation have recently led to an increase in the number of neurologists using these techniques. A new tool for studying the neural basis of spatial cognition in the healthy brain. Second, pharmacotherapy improves clinical and neuropsychological outcomes in stroke patients.[7] Many different methods have been used for a long time to improve the symptoms of neglect.

Many studies have been published on each method. Since this is not a medical negligence review, we will focus on the best treatments mentioned, although there are other good but less effective methods. Learn to treat this problem like eye patching,[8] caloric vestibular stimulation,[9]. Visuomotor imaging,[10] mirror therapy,[11] TENS, [12] photokinetic stimulation [13 – 15] and Constraint-induced movement therapy. [15 – 17] Specifically, we reviewed

research on the use of prism adaptation, noninvasive brain stimulation, and virtual reality in USN rehabilitation. Therefore, we use the words "neglect", "treatment", "prism adaptation", "tDCS", "vestibular stimulation", "TMS", "TBS" and "virtual reality" together.

METHODOLOGY

Search Strategy

We performed A systematic review for current physiotherapy interventions for unilateral neglect in stroke patients. For the purpose of this review, an electronic search for relevant articles was done using Google Scholar, PUBMED, MEDLINE, Pedro, Research Gate and CINHAL database from to 2013 to 2023 was done where in MeSH search terms such as cerebrovascular accident OR stroke; neglect; visuo-spatial neglect; visual neglect; unilateral neglect; and hemisphere neglect free words were used. The search was bounded to RCTs involving adults aged 19 or over. We included all RCTs that sought to identify the effectiveness of any type of physiotherapy intervention in Unilateral neglect in adult stroke patients diagnosed by clinical examination and/or classical neuropsychological tests. Only studies which reported only physiotherapy intervention were included. Observational studies and case reports, systematic reviews or meta-analyses, and cross-sectional studies were excluded. Additionally, searches for relevant books were performed manually. Articles were selected based on experience, self-awareness, and reflective practice.

Study selection

Review selection criteria include

1. Physiotherapy intervention for patients suffering from unilateral neglected stroke.
2. Effectiveness of physical therapy for unilateral neglect in stroke.
3. Research on stroke in adults.

Data extract

All stages of study selection were assessed against inclusion criteria. Study titles and abstracts were screened by reviewers. Relevant articles were reviewed in full text and included if they met the inclusion criteria. The following data were extracted from relevant articles, including purpose, study design, study population, study period, physiotherapy intervention, selected outcome measures, and main outcomes. Literature review (Table 1)

RESULT

The search identified 10 relevant studies. Inclusion criteria for further analysis were met. A new treatment method combining neck muscle vibration and transcranial stimulation appears directly in the routine treatment of patients with left hemi-neglect. HEMISTIM protocol of randomized trials led by Sarah Millot, Jean Marie et al., 2023. The purpose of this study was to evaluate immediate and long-term improvements through a novel relationship between left cervical muscle oscillation (NMV) and bipolar transcranial. Direct current stimulation (tDCS) of the posterior parietal cortex during occupational therapy in patients. He left USN. middle. Participants were divided into four groups: control, left NMV, sham left NMV-tDCS, or anodal tDCS left NMV. NMV and tDCS were used for the first 15 minutes of treatment, 3 days a week for 3 weeks. USN was assessed at baseline, at the end of the first study, after the first and third weeks of policy, and 3 weeks after policy end. The primary outcome of this study was change in functional scores on the Katherine Bergo Scale. Secondary outcomes included five tests examining USN neuropsychological variables. The vibrating stimulator is placed on the skin over the belly of each trapezius muscle and secured with a belt. The results of this multimodal approach also provide interesting insights into the hemispheric perspective and demonstrate the importance of right hemisphere or other "hemispheric" support. [18]

Thai Regina, Helio Rubens and others. the 2022 study, "Non-invasive brain stimulation reduces unilateral spatial neglect after stroke," examines the impact of physical therapy following anodal and cathodal transcranial direct current stimulation (A-tDCS and C-tDCS, respectively) on stroke recovery. Posterior USN This double-blind, randomized pilot study was conducted in patients with OSI after ischemic stroke. Randomization was stratified by

Behavioral Inventory-Inventory (BIT-C) and Catherine Belgo Scale (CBS). Twenty minutes of tDCS was followed by topical treatment for 7.5 weeks. The biggest advantage is the USN degree evaluated by BIT-C. Secondary outcomes were various CBS scores, stroke (National Institutes of Health Stroke Scale [NIHSS]), disability (modified Rankin Scale), autonomy (Barthel Index, Functional Independence Scale), and quality of life (five-dimensional EuroQol). personality survey). For the primary outcome, pairwise post hoc comparisons were performed using Bonferroni correction. The study results showed greater improvement in BIT-C scores after A-tDCS intervention compared to sham (mean difference [MD] = 18.4). There were no significant differences between groups in secondary outcomes. However, no improvements were observed in activities of daily living, stroke, dependency, independence, functional independence, or quality of life. Both stimulation methods have been shown to be safe. In conclusion, A-tDCS was shown to have a significant effect on physical therapy and reduce USN levels in the subacute phase of stroke. [19] Dr. Hyunse Choi and Dr. Bomin Lee conducted a study titled "Comprehensive Integrated Prism Adaptation and Neck Vibration Intervention for Unilateral Neglect in Chronic Stroke Patients" in 2022 to study the effectiveness of an integrated prism adaptation (PA) rehabilitation program. target.) and neck vibration (NV) due to unilateral neglect in stroke patients. 36 patients were divided into the PA NV group (group A, n=12), NV only group (group B, n=12), and PA only group (group C, n=12). The intervention was conducted for 50 minutes a day, 5 times a week, for 4 weeks. Traditional activities include joint mobility, functional training, and ADL training. Joint exercises include passive range of motion (ROM), assisted active range of motion, and resistance training.

Vocational training includes many activities such as assembling building blocks and assembling rings, as well as the next steps, including the role of the patient. ADL training includes eating, dressing, and using the bathroom. PA uses triangular glasses with a left-angled base that provides a 10° deviation of the visual axis to the right, so the user sees the object as if it has shifted 10° to the right. Vibratory stimulation is used for the neck extensor muscles. Vibratory stimulation is applied to the upper sternomastoid and osteomastoid muscles, located approximately 6 cm from the cervical spine. Allow the patient to rest for 30 seconds between each 2-minute dose increase. The Albert and Catherine Bergo scale was used to assess the impact of each intervention on personal neglect, and the modified Barthel index was used to assess the impact of ADL. After the intervention, all three groups experienced a decrease in neglect and improvements in activities of daily living (p < 0.05). Importantly, the reduction of neglect alone in group A (PA NV) was higher than in the other groups (p < 0.05); However, the improvement in ADL was not different between the three groups (p>0.05). This novel intervention involving PA NV is recommended for the treatment of chronic stroke patients with clinical failure. [20] Effects of mirror visual feedback on neglect in post-stroke patients: Kenneth Fong, K.H.Ting, et al (2022) conducted a preliminary randomized controlled trial in which a total of 21 subacute patients with left spatial neglect after right hemisphere stroke received a randomized clinical trial. For 3 groups: MVF, Sham 1 (view of the hemiplegic arm through a clear glass with both arms in motion) and Sham 2 (using a cover mirror). The 3-week treatment for each group included 12 physical exercises on the hemilegic arm, graded according to the severity of the injured arm.

A blind test was conducted before/after surgery and 3 weeks later. The results show that MVF does not have a significant effect on Simulation. However, as indicated by the diagonal line, MVF was significantly more effective than Sham 2 ($p = 0.022$). In contrast detection, MVF was slightly better than using a protective mirror at distinguishing numbers on the left and right sides of the page ($p = 0.013$; $p = 0.010$), indicating that MVF had little effect on reducing allocentricity. This study confirmed the superiority of MVF over using coverslips as a method to reduce spatial sloppiness and allocentric symptoms, but the results were not obtained. An alarm was seen when compared to two arms moving inside the transparent glass.[21] AlessioFacchin, GuisiFigliano and colleagues conducted a comparative study of prism-adapted optokinetic stimulation in unilateral spatial neglect rehabilitation in 2021. The aim of this study was to compare the effectiveness of two methods in an underserved patient group. Transitional design. PA and OCS were administered to 13 posttraumatic brain injury patients with unilateral spatial neglect. Each treatment was administered 10 times twice daily, with each patient receiving 2 treatments in a alternating sequence (e.g. PA followed by ACS or vice versa). Neuropsychological testing; It was conducted before the first session (T1), at the end of the first session/start of the second session (T2), at the end of the second session (T3) and 2 weeks after the end of treatment. (T4). Regardless of the type of training, both methods provide significant

improvements in T2 diagnosis. The results showed that PA or OCS had a significant effect on neglect in patients with right hemisphere brain injury, mainly in the first phase of treatment. There is no difference in treatment, so it can be used in treatment according to the patient's needs. [22] Effect of robotic training on the left side of hemi-spatial neglect in adults with stroke: A controlled study conducted in 2021 by Pilot and Park JH aimed to evaluate the effect of robot-assisted training on hemi-spatial neglect in adults with stroke. Participants were assigned to an experimental group (EG) (n = 12) receiving left hand robotics training or a control group (CG) (n = 12) receiving symptom care treatment. Each participant completed 20 sessions over 4 weeks. The Line Division Test (LBT), Albert Test, and Catherine Bergo Scale (CBS) were used to examine the impact of unilateral spatial neglect. Results were analyzed before and after 20 training sessions. After intervention, LBT showed improvement in the Albert test and CBS EG, while LBT and CBS showed improvement in the CG but did not improve in the Albert test. These results indicate that robotic training is effective in improving unilateral spatial dysfunction in adult stroke patients compared to non-stroke patients. The study concluded that the use of robotic limbs could help improve unilateral spatial neglect. [23] Efficacy of cervical taping in the treatment of unilateral spatial neglect in stroke patients: a pilot single-blind randomized controlled trial conducted in 2019 by Valentina Varalta and Daniele Munari.

The purpose of this study is to evaluate the effectiveness of therapeutic cervical taping in stroke patients. Visual-spatial ability, neck movement, and kinesthetic sensitivity in chronic stroke patients with hemispatial neglect. After randomization, 12 chronic stroke patients with hemispatial neglect underwent real (treatment group) or sham (control group) neckbanding for 30 consecutive days. The results are as follows: star removal test; neck range of motion; probation denial letter; Comb and razor control; Cervical spine joint dysfunction before and after one-month closure. Comparison between groups revealed a significant difference in neck joint error only after treatment ($p = 0.009$). Preliminary results support the hypothesis that neck taping may increase cervical kinesthetic sensitivity in chronic stroke patients with hemispatial neglect. Additional studies are needed to confirm our results and investigate the beneficial effects of therapeutic elastic tape on visuospatial abilities in stroke patients with hemispatial dysfunction[24] Kim SB, Lee KW, and Lee JH conducted a study on "The Effect of Combination Therapy of Robots and Low-Frequency Repetitive Transcranial Magnetic Stimulation on Hemispatial Neglect in stroke Patients" in 2018 to investigate the treatment of upper extremity pain by connecting robots together. Effects of cranial magnetic stimulation (rTMS) on unilateral spatial neglect in stroke patients. Patients with hemispatial neglect after right hemisphere stroke were divided into rTMS only group, robot only group and combined group.

Each group received a well-structured neglect treatment plus additional treatment for each group. The robotic group received robotic therapy, and the combined group received both treatments. The treatment effect was evaluated using the Visual Perception Test-3 (MVPT-3), Line Bisection Test, Asterisk Elimination Test, Katherine Bergo Scale (CBS), Korean version of Mini-Mental SE (MMSE), and Basel Index (K-). MBI). These parameters were measured before and after treatment. Ten patients were selected in each group. There were no remarkable differences in values between the three groups. After two weeks of treatment, MVPT-3, Linear Test, Star Elimination Test, CBS, MMSE, and K-MBI scores significantly improved in all groups. However, there was no significant difference in the rate of change between groups. It can be concluded that the combined effect of robotic therapy and low-frequency rTMS therapy in the treatment of hemispheric neglect does not differ depending on the treatment method. The results of this study showed no difference. Additional studies with larger patient groups are needed to evaluate the effectiveness of these treatments. [25] Volkening K, Kerkhoff G, Effects of repetitive galvanic vestibular stimulation on spatial neglect and vertical perception - a randomized controlled trial. They conducted the smallest randomized controlled trial. Twenty-four patients received 10 to 12 sessions per day, 5 days per week. The CL- and CR-GVS groups received 1.5 mA current stimulation for 20 min, whereas the Sham-GVS group received CL-GVS for only 30 s. Simultaneously, all patients were given clinical examples of visuomotor tasks (VMT) and visual training (VST). Test outcomes (ignorance test, visuo-tactile search, visual and tactile vertical) were assessed before the intervention, immediately after the intervention, and 2 and 4 weeks later. Results showed that neither our standard treatment nor the combination of standard treatment and GVS improved neglect symptoms. [26] Appropriate eye movement training promotes recovery from hearing and vision loss: a randomized controlled trial by Georg Kerkhoff and Stefan Reinhart Objective: To compare the effectiveness of CBT and visual stimulation (VST) on hearing and vision loss in

stroke patients. Fifty patients with left-sided hearing and visual impairment were excluded from the study. Twenty-four patients received CBT and 21 patients received VST. Five patients (4 VST, 1 SPT) were absent. Each group received one hour of neglect treatment for a total of five hours over five consecutive days. Outcome measures for visual impairment (digital clipping, visuomotor separation, sentence reading) and hearing impairment (intermediate vision) were assessed twice: before treatment, after treatment, and two weeks later. The SPT group showed good eye movements when following left-hand stimuli. The VST group systematically scanned identical but static stimuli. Both groups were divided into subgroups to study the effects of mild and severe neglect. Results: There were no differences between the two groups in pre-treatment demographic variables or level of neglect (hearing/visual). After treatment, the CBT group showed, on average, significant and sustained improvements in all visual and auditory measures. No significant changes in vision or hearing loss were noted after VST. Additionally, treatment effect sizes following PCT (Cohen's d) for visual and hearing impairment were greater than effect sizes following VST treatment, regardless of mild and severe neglect. The study concluded that contralateral smooth tracking training was more effective than combined treatment, resulting in mild and major neglect. [27]

DISCUSSION

This review summarizes 10 years of current data on physical therapy for neglect alone in stroke patients published in the published literature in clinical trials. Randomized controlled trials provide most of the evidence in this study. However, there are some differences between the recommendations and the research results. These differences may be due in part to the methods used in the studies reviewed, the types of research selected, the different characteristics of the studies examined, and/or the brand target or purpose of these studies. Therefore, there is a need for quality studies to evaluate the effectiveness of physical therapy alone in low-income stroke patients. The small number of articles reviewed may represent a limitation of this review. Finding other areas of conflict in stroke patients will expand our analysis and will not influence future recommendations and recommendations for physical therapy. However, Google Scholar and Pubmed were chosen because they are informative and support the purpose of the current review, which is to evaluate clinical trials for the treatment of this disease. Sarah Millot, Jean Marieet conducted a randomized controlled trial. et al combined neck muscle stimulation and transcranial direct current stimulation with respiratory rehabilitation in patients with left unilateral neglect - the HEMISTIM protocol. Findings suggest that using this modification in the treatment process may improve outcomes with rehabilitation. In fact, non-invasive brain stimulation is known to modulate cortical excitability and is therefore an ideal tool to promote long-term neuroplasticity. The results of the study "Non-invasive brain stimulation reduces unilateral spatial neglect after stroke", conducted by Tais Regina, Helio Rubens, showed that A-tDCS has a positive effect on the treated body, thereby reducing the risk of stroke USN19. in the subacute stage.

Hyun-Se Choi and Bo-Min Lee conducted a study on the effects of a combination of prism adaptation and neck vibration in the treatment of unilateral neglect in stroke cases. PA NV is also among its benefits. [20]. Effects of Specular Visual Feedback on Spatial Neglect After Stroke KH Ting, a preliminary randomized trial conducted by Kenneth Fong, concluded that optimal visual feedback using glass covers as a recording language reduced neglect and reduced allocentric symptoms. . Prismatic adaptation and optokinetic stimulation can be used in treatment on a case-by-case basis[21]. The results of the study conducted by AlessioFacchin, GuisiFigliano and colleagues in 2021 on the comparison of the transition from prisms to photodynamic excitation in the improvement of negativities in the blind spot well, revealed that PA or OKS believe that negligence. It was about events. It is certain that he is in the first stage of treatment for right brain damage. Because no difference was found between treatments[22]. Recently, left-handed robotic training affected hemispatial neglect in paralyzed adults. Park JH conducted a pilot and randomized controlled study in 2021. Results showed that EG had a small benefit compared to CG in all aspects of development; Therefore, robotic training may help improve the treatment of hemispatial neglect in adults with habitual neglect. Compared to conventional treatments for stroke. This study concluded that robotic support may help improve hemi-spatial neglect [23]. Effect of Neck Taping in the Treatment of Hemispatial Neglect in Patients with Habitual Stroke Valentina Varalta conducted a randomized controlled trial with Daniele, Munari. The main findings support the

argument that neck taping may increase cervicofacial kinesthetic sensitivity in stroke cases with hemispatial neglect. This study also noted that further research is needed to strengthen the results and investigate the positive effects of elastic band therapy on visuospatial ability in stroke with hemispatial neglect[24]. In 2018, SB Kim conducted a study on the effect of combined robotic therapy and low-frequency repetitive transcranial charismatic stimulation on hemi-spatial neglect in stroke patients and concluded that the combination of robotic therapy and low-frequency rTMS combination of hemi-spatial neglect. The treatment effect is no different from the effect of treatment alone. The results of this study do not prove the superiority of any of the three treatments. More studies involving more patients are needed to evaluate the effectiveness of these treatments. [25] Volkening K, Kerkhoff G, Keller I conducted a randomized sham-controlled study on the effects of repeated vestibular stream stimulation on spatial neglect and vertical perception. The results showed that neither standard treatment nor the combination of standard treatment and GVS significantly improved neglect symptoms. [26] Training to improve eye function promotes recovery from auditory and visual neglect The study was conducted by Georg Kerkhoff and Stefan Reinhart. This study concluded that contralateral, uniform learning would produce superior multimodal treatment in minor and major neglect conditions. [27]

CONCLUSION

The articles that were previously examined gave a summary of the most recent research on physiotherapy interventions for unilateral neglect in post-stroke patients. The evaluated studies provided evidence that the described physiotherapy techniques are useful in providing significant benefit to patients with unilaterally neglected stroke. If physical therapy includes neck muscle stimulation, direct transcranial stimulation, prismatic adaptation, optomotor stimulation, mirror visual feedback, repetitive vestibular galvanic stimulation, and robotic training, it may be useful to minimize neglect of the hemiplegic side.

CONFLICT OF INTEREST: None

ACKNOWLEDGEMENT

The authors would like to thank our colleagues from the department of neurosciences of Krishna college of physiotherapy

REFERENCES

1. Doron N, Rand D. Is Unilateral Spatial Neglect Associated With Motor Recovery of the Affected Upper Extremity Poststroke? A Systematic Review. Neurorehabil Neural Repair. 2019 Mar;33
2. Yang NY, Zhou D, Chung RC, Li-Tsang CW, Fong KN. Rehabilitation Interventions for Unilateral Neglect after Stroke: A Systematic Review from 1997 through 2012. Front Hum Neurosci. 2013 May 10;7:187. doi: 10.3389/fnhum.2013.00187. PMID: 23675339; PMCID: PMC3650319.
3. Fisher G, Quel de Oliveira C, Verhagen A, Gandevia S, Kennedy D. Proprioceptive impairment in unilateral neglect after stroke: A systematic review. SAGE Open Medicine. 2020 Aug;8:2050312120951073.
4. Hammerbeck U, Gittins M, Vail A, Paley L, Tyson SF, Bowen A. Spatial Neglect in Stroke: Identification, Disease Process and Association with Outcome During Inpatient Rehabilitation. Brain Sci. 2019 Dec
5. Beis JM, Keller C, Morin N, Bartolomeo P, Bernati T, Chokron S, Leclercq M, Louis-Dreyfus A, Marchal F, Martin Y, Perennou D. Right spatial neglect after left hemisphere stroke: qualitative and quantitative study. Neurology. 2004 Nov 9;63(9):1600-5.
6. Azouvi P, Jacquin-Courtois S, Luauté J. Rehabilitation of unilateral neglect: Evidence-based medicine. Annals of physical and rehabilitation medicine. 2017 Jun 1;60(3):191-7.

7. Gammeri R, Iacono C, Ricci R, Salatino A. Unilateral Spatial Neglect After Stroke: Current Insights. Neuropsychiatr Dis Treat. 2020 Jan 10;16:131-152. doi: 10.2147/NDT.S171461. PMID: 32021206; PMCID: PMC6959493.
8. Smania N, Fonte CS, Picelli A, Gandolfi M, Varalta V. Effect of eye patching in rehabilitation of hemispatial neglect. *Front Hum Neurosci*. 2013. doi: 10.3389/fnhum.2013.00527
9. Bottini G, Gandola M. Beyond the non-specific attentional effect of caloric vestibular stimulation: evidence from healthy subjects and patients. *Multisensory Res*. 2015;28(5–6):591–612. doi: 10.1163/22134808-00002504
10. Welfringer A, Leifert-Fiebach G, Babinsky R, Brandt T. Visuomotor imagery as a new tool in the rehabilitation of neglect: a randomised controlled study of feasibility and efficacy. *DisabilRehabil*. 2011;33(21–22):2033–2043. doi: 10.3109/09638288.2011.556208
11. Dohle C, Püllen J, Nakaten A, Küst J, Rietz C, Karbe H. Mirror therapy promotes recovery from severe hemiparesis: a randomized controlled trial. *Neurorehabil Neural Repair*. 2009;23(3):209–217. doi: 10.1177/1545968308324786
12. Pitzalis S, Spinelli D, Vallar G, Russo FD. Transcutaneous electrical nerve stimulation effects on neglect: a visual-evoked potential study. *Front Hum Neurosci*. 2013;7. doi: 10.3389/fnhum.2013.00111.
13. Kerkhoff G, Reinhart S, Ziegler W, Artinger F, Marquardt C, Keller I. Smooth pursuit eye movement training promotes recovery from auditory and visual neglect: a randomized controlled study. *Neurorehabil Neural Repair*. 2013;27(9):789–798. doi: 10.1177/1545968313491012
14. Machner B, Könemund I, Sprenger A, Von Der Gablentz J, Helmchen C. Randomized controlled trial on hemifield eye patching and optokinetic stimulation in acute spatial neglect. *Stroke*. 2014;45(8):2465–2468. doi: 10.1161/STROKEAHA.114.006059
15. von der Gablentz J, Könemund I, Sprenger A, et al. Brain activations during optokinetic stimulation in acute right-hemisphere stroke patients and hemispatial neglect: an fMRI study. *Neurorehabil Neural Repair*. 2019;33:581–592. doi: 10.1177/15459683198550
16. Kwakkel G, Veerbeek JM, Wegen EE, Wolf SL. Constraint-induced movement therapy after stroke. *Lancet Neurol*. 2015;14:224–234. doi: 10.1016/S1474-4422(14)70160-7
17. Corbetta D, Sirtori V, Castellini G, Moja L, Gatti R. Constraint-induced movement therapy for upper extremities in people with stroke. *Cochrane Database Syst Rev*. 2015
18. Millot S, Beis JM, Pierret J, Badin M, Sabau V, Bensoussan L, Paysant J, Ceyte H. Innovative Therapy Combining Neck Muscle Vibration and Transcranial Direct Current Stimulation in Association with Conventional Rehabilitation in Left Unilateral Spatial Neglect Patients: HEMISTIM Protocol for a Randomized Controlled Trial. Brain Sciences. 2023 Apr 18;13(4):678.
19. da Silva TR, de CarvalhoNunes HR, Martins LG, da Costa RD, de Souza JT, Winckler FC, Sartor LC, Modolo GP, Ferreira NC, da Silva Rodrigues JC, Kanda R. Non-invasive Brain Stimulation Can Reduce Unilateral Spatial Neglect after Stroke: ELETRON Trial. Annals of neurology. 2022 Sep;92(3):400-10.
20. Choi HS, Lee BM. A Complex Intervention Integrating Prism Adaptation and Neck Vibration for Unilateral Neglect in Patients of Chronic Stroke: A Randomised Controlled Trial. International Journal of Environmental Research and Public Health. 2022 Oct 18;19(20):13479.
21. Fong KN, Ting KH, Zhang X, Yau CS, Li LS. The Effect of Mirror Visual Feedback on Spatial Neglect for Patients after Stroke: A Preliminary Randomized Controlled Trial. Brain Sciences. 2022 Dec 20;13(1):3.
22. Facchin A, Figliano G, Daini R. Prism adaptation and optokinetic stimulation comparison in the rehabilitation of unilateral spatial neglect. Brain Sciences. 2021 Nov 11;11(11):1488.
23. Park JH. The effects of robot-assisted left-hand training on hemispatial neglect in older patients with chronic stroke: A pilot and randomized controlled trial. Medicine. 2021 Mar 3;100(9).
24. Varalta V, Munari D, Pertile L, Fonte C, Vallies G, Chemello E, Gandolfi M, Modenese A, Smania N, Picelli A. Effects of neck taping in the treatment of hemispatial neglect in chronic stroke patients: A pilot, single blind, randomized controlled trial. Medicina. 2019 Apr 17;55(4):108.
25. Kim SB, Lee KW, Lee JH, Lee SJ, Park JG, Lee JB. Effect of combined therapy of robot and low-frequency repetitive transcranial magnetic stimulation on hemispatial neglect in stroke patients. Annals of rehabilitation medicine. 2018 Dec 28;42(6):788-97.

26. Volkening K, Kerkhoff G, Keller I. Effects of repetitive galvanic vestibular stimulation on spatial neglect and verticality perception—a randomised sham-controlled trial. Neuropsychological rehabilitation. 2018 Oct 3;28(7):1179-96.
27. Kerkhoff G, Reinhart S, Ziegler W, Artinger F, Marquardt C, Keller I. Smooth pursuit eye movementtraining promotes recovery from auditory and visual neglect: a randomized controlled study. Neurorehabilitation and neural repair. 2013 Nov;27(9):789-98.

Table no. 1 Summary of review of literature

Sr no.	**Title of study**	Aim of study	Study design	Sample size	Study duration	Outcome measures	Intervention
1	**Innovative therapy combining neck muscle vibration and transcranial direct current stimulation in association with conventional rehabilitation in left unilateral neglect patients. Sarah millot,Jean Marie et.al(2023)**	To assess immediate and long term recovery induced by innovative association of left side neck muscle vibration and anodal transcranial direct current stimulation in patients with left unilateral spatial neglect	Randomized clinical trial	n=48	3 days a week for 3 weeks . Total 45 min of therapy	Catherine bergego scale Fluff test Gainottis drawing test Map of France test	Neck muscle stimulation using a vibrator placed over sternocleidomastoud followed by transcranial direct current stimulation
2	**Non invasive brain stimulation can reduce unilateral spatial neglect after stroke. Taisregina,Heli orubenset.al(2022)**	To examine the effects of physical therapy after anodal and cathodal transcranial direct current stimulation to improve visuospatial and functional impairment in individuals with unilateral neglect after stroke.	Randomized control trial	n=51 anodic group=15 cathodic group=15 sham grp=16	Total duration=7.5 weeks Total sessions =15 given 2 times per week	BIT-C – Behaviour inattention test-conventional CBS-Catherine bergego scale	A direct current was delivered by a battery-powered device using 2 pairs of surface saline-soaked sponge electrodes (5cm 5cm). Each side of the sponge was soaked in saline solution. The study mode was designed to encode the sham and active stimulation attempts using 5-digit codes

3	**A complex intervention integrating prism adaptation and neck vibration for unilateral neglect in patients of chronic stroke. Hyun se Choi,Bo min lee (2022)**	To investigate the effects of complex rehabilitative programme that integrates prism adaptation and neck vibration for unilateral neglect in patients of chronic stroke.	Single blind Randomized control trial	n=36 PA+NV = 12 Only NV=12 Only PA=12	50 Min per day 5 sessions per week for 4 weeks.	Alberts test Catherine Bergego test Barthel index	Prism adaptation using triangular prism goggles was given. In NV,vibratory stimuli was applied to neck extensors using a vibration stimulator.The patient was given 30s rest after every 2 min performance during the 20 min session.
4	**The effect of mirror visual feedback on spatial neglect for patients after stroke: A randomized controlled trial. Kenneth Fong,K.H.Tinge t.al (2022)**	To investigate the effects of mirror visual feedback on reduction of spatial neglect for patients with stroke	Randomized controlled trial	n=21	3 week treatment . 12 sessions-4 per week for 3 weeks each lasting for 30 min	Behavior al inattentio n test. Gap detection test. Catherine Bergego scale	In group 1,mirror was used and patient was asked to imitate the movements with the affected limb. In group 2, the mirror was covered by cloth repeating same procedure.
5	**Prism adaptation to optokinetic stimulation comparison in rehabilitation of unilateral spatial neglect. AlessioFacchin, GuisiFiglianoet .al (2021)**	To compare the effectiveness of these two methods in a group of unilateral neglect patients.	Randomized controlled trial	n= 12 prism adaptat ion=6 optokin etic stimula tion = 6	Each treatment was applied for 10 sessions – twice a day for 5 days a week	Letter cancellati on test Star cancellati on test Copy drawing test Sentence reading test	Prism adaptation was performed first followed by optokinetic stimulation. In the second group , treatment was reversed.
6	**The effects of robot assisted left hand training on hemispatial neglect in older patients with chronic stroke: A pilot and Randomized control trial. Park JH (2021)**	To investigate the effects of robot-assisted hand training on hemispatial neglect of older patients with chronic stroke.	Randomized control trial.	n=24 12=exp eriment al group 12=cont rol group	20 sessions 5 times a week for 4 weeks. Each session for 30 min	Line bisection test. Albert test. Catherine Bergego scale.	Robotic assisted training was given to left hand using AmadeoRobot.the motion was assisted by robot and the individuals level of function.

7	**Effect of neck taping in the treatment of hemispatial neglect in chronic stroke patients:A pilot single blind Randomized control trial. Valentina Varalta, Daniele Munari (2019)**	To assess the effect of therapeutic neck taping on visuospatial abilities,neck motion and kinesthetic sensibility in chronic stroke patients with hemispatial neglect.	Single blind Randomized control trial	n=12 6=treatment group 6=control group	30 days Tape was replaced every 4 days	Star cancellation test. Letter cancellation test. Comb and razor test.	The tape strip was applied from mastoid bone to clavicle with sternocleidomastoid kept in position of maximum stretching-15-25% stretch.
8	**Effect of combined therapy of robot and low frequency repetitive transcranial magnetic stimulation on hemispatial neglect in stroke patients. SB Kim, KW Lee (2018)**	To investigate the effect of upper limb rehabilitation combining robot with low frequency repetitive transcranial magnetic stimulation(Rtms)on unilateral spatial neglect in stroke patients.	Single Blind Randomized control trial	n=30 10=Rtms only group 10=robot	30 min a day 5 days a week for 2 weeks.	Motor free visual perception test. Line bisection test. Star cancellation test	
9	**Effects of repetitive galvanic vestibular stimulation on spatial neglect and verticality perception-a randomized controlled trial. KatherinaVolkening, Georg Kerkhoffet.al (2016)**	To compare the effects of repeated galvanic stimulation on spatial neglect and verticality perception.	Double blind Randomised controlled trial	n=24	10-12 sessions daily 5 days per week	Neglect test Visuo tactile search test	Participants received galvanic stimulation and simultaneously received a standard therapy of smooth pursuit eye movement training followed by visual scanning training.
10	**Smooth pursuit eye movements training promotes recovery from**	To compare the effects of SPT and visual scanning therapy on	Randomised controlled trial	n= 24 for SPT n=21 for VST	Each group received 1 hr session for 5	Digit Cancellation Visuoperceptual	The SPT group practiced smooth pursuit eye movements while trackinf stimuli moving leftward.

	auditory and visual neglect: A randomized controlled study. Georg Kerkhoff, Stefan Reinhart et.al (2013)	auditory and visual neglect in chronic stroke patients with neglect.			consecutive days for 3 weeks.	and motor line bisection Paragraph reading	The VST group systematically scanned the same but static stimuli.

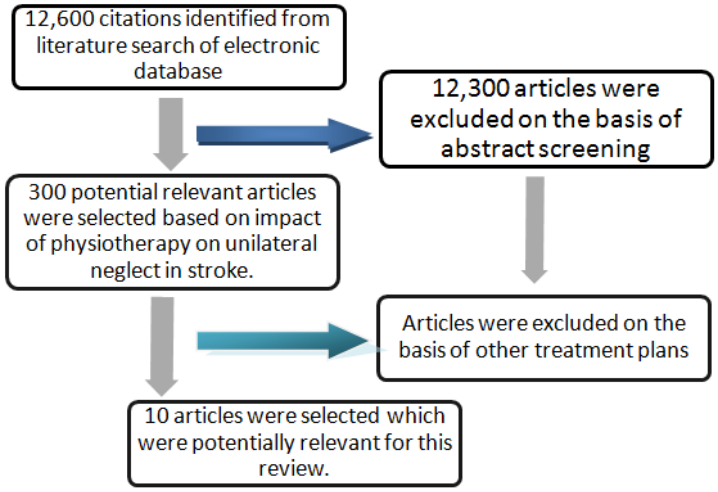

Figure no. 1 Flowchart depicting selection of database for the review.

Vol.15 / Issue 83 / Apr / 2024 *International Bimonthly (Print) – Open Access* *ISSN: 0976 – 0997*

RESEARCH ARTICLE

Evaluation of Salbutamol's Degree-Based and Degree-Splitting Topological Indices

R.Revathy*

Assistant Professor, Department of Mathematics, Sri S.Ramasamy Naidu Memorial College, Sattur (Affiliated to Madurai Kamaraj University) Madurai, Tamil Nadu, India

Received: 30 Dec 2023 Revised: 09 Jan 2024 Accepted: 09 Mar 2024

***Address for Correspondence**
R.Revathy
Assistant Professor,
Department of Mathematics,
Sri S.Ramasamy Naidu Memorial College, Sattur
(Affiliated to Madurai Kamaraj University)
Madurai , Tamil Nadu, India
Email :revathy7284@gmail.com

ABSTRACT

The drug Salbutamol aids in the lungs medium and broad airway enlargement. Treatment for acute episodes of bronchospasm caused by bronchial asthma, chronic bronchitis, and other long-term bronchopulmonary disorders including chronic obstructive pulmonary disease (COPD) usually involves its use. In this work, the degree-based and degree splitting topological indices of salbutamol are computed using both a Python software and manual calculation. Furthermore, QSAR analysis of the topological indices are discussed using SPSS

Keywords: Salbutamol, Topological indices, Degree Splitting graphs, Python Programming, SPSS

INTRODUCTION

A topological index of graph G is a numerical value that describes its topology. It reflects the theoretical characteristics of a chemical molecule when applied to its molecular structure. In this study, chemical structures of drugs used to treat asthma were subjected to well-known degree-based topological indices. Chemical structure is viewed as a graph, where the constituents are the vertices and the boundaries between them are the edges. Salbutamol is a member of the group of drugs known as bronchodilators, more specifically, 2-adrenergic agonists.This medicine is used to treat and prevent bronchospasm caused by respiratory illnesses like chronic bronchitis, asthma, and other breathing problems.

Preliminaries

In this section, certain well-known definitions and findings concerning various topological indices of graphs are described for quick reference while one reads the material presented in this paper.

Definition 2.1: The degree of a vertex v in G or simply d(v) is the number of edges of G incident with vertex v.

Definition 2.2: ABC (atom bond connectivity) index of a graph G defined in [2] as, ABC(G) (atombond connectivity) index of a graph G in as,

$$\mathrm{ABC(G)} = \sum_{pq\epsilon E\,(G)} \sqrt{\frac{d(u) + d(v) - 2}{d(u)d(v)}}$$

Definition 2.3: ABS (atom bond sum connectivity) index of a graph G defined

in [1] as $\mathrm{ABS(G)} = \sum_{pq\epsilon E\,(G)} \sqrt{\frac{d(u)+d(v)-2}{d(u)+d(v)}}$

Definition 2.4: ABS (atom bond sum connectivity) index of a graph G defined in [1] as$\mathrm{AZI(G)} = \sum_{pq\epsilon E\,(G)} \left(\sqrt{\frac{d(u)d(v)}{d(u)+d(v)-2}}\right)^3$

Definition 2.5:SAI (sum augmented index) is defined in [4] as,

$$\mathrm{SAI(G)} = \sum_{pq\epsilon E\,(G)} \left(\sqrt{\frac{d(u) + d(v)}{d(u) + d(v) - 2}}\right)^3$$

Definition 2.6: GA (geometric-arithmetic index)of a graph G is defined in [8]as

$$\mathrm{GA(G)} = \sum_{pq\epsilon E\,(G)} \frac{2\sqrt{d(u)d(v)}}{d(u) + d(v)}$$

Definition 2.7:AG (Arithmetic-geometric index) of a graph G is defined in [8]as

$$\mathrm{AG(G)} = \sum_{pq\epsilon\ E(G)} \frac{d(u) + d(v)}{2\sqrt{d(u)d(v)}}$$

Definition 2.8:GO1(first Gourava index) and GO2 (second Gourava index) of a graph G aredefined in [5] as,

$$GO1(G) = \sum_{pq\epsilon E\,(G)} \left[\left(d(u) + d(v)\right) + d(u)d(v)\right]$$

$$GO2(G) = \sum_{pq\epsilon E\,(G)} \left[\left(d(u) + d(v)\right)d(u)d(v)\right]$$

Definition 2.9:HGO1(first hyper Gourava index) and HGO2 (second hyper Gouravaindex)of a graph G are defined in [6] as,

$$HGO1(G) = \sum_{pq\epsilon\ E(G)} (d(u) + d(v) + d(u)d(v))^2$$

$HGO2(G) = \sum_{pq\epsilon\ E(G)} (d(u) + d\,(v)d(u)d(v))^2$.

Definition 2.10 : Let G= (V,E) be a graph with V= $S_1 \cup S_2 \ldots\ldots U T$ where each Si is a setof vertices having at least two vertices , having the same degree and T = V\USi.The Degree splitting of Graph denoted by DS(G) is obtained from G by adding new vertices $w_1, w_2 .. w_i$ and joining w_i to each vertex of S_i

Topological Indices of Salbutamol

The several topological indices of salbutamol are covered in this section. Salbutamol has 17 vertices and 17 edges in its chemical graph. The graph below displays salbutamol's chemical structure.

Theorem 1: ABC index of Salbutamolis ABC(G) = 12.6348

Proof: From definition 2.2

$$\mathrm{ABC(G)} = \sum_{pq\epsilon E\,(G)} \sqrt{\frac{d(u) + d(v) - 2}{d(u)d(v)}}$$

$$= 1\sqrt{\frac{1+2-2}{(1)(2)}} + 2\sqrt{\frac{1+3-2}{(1)(3)}} + 3\sqrt{\frac{1+4-2}{(1)(4)}} + 2\sqrt{\frac{2+2-2}{(2)(2)}} + 6\sqrt{\frac{2+3-2}{(2)(3)}} + 1\sqrt{\frac{2+4-2}{(2)(4)}} + 2\sqrt{\frac{3+3-2}{(3)(3)}}$$

= 12.6348

By using Python Programming, the ABC of Salbutamol is also calculated.

```
#ABC(G)
import math
foriinrange(1,8):
 a=int(input("enter a value:"))
 b=int(input("enter b value:"))

 if a==1and b==2:
  c=(a+b-2)/(a*b)
  print(c)
  c1_ans=math.sqrt(c)
  mul1=c1_ans*1
  print(mul1)


 if a==1and b==3:
   c=(a+b-2)/(a*b)
   print(c)
   c2_ans=math.sqrt(c)
   mul2=c2_ans*2
   print(mul2)

 if a==1and b==4:
   c=(a+b-2)/(a*b)
   print(c)
   c3_ans=math.sqrt(c)
   mul3=c3_ans*3
   print(mul3)


 if a==2and b==2:
   c=(a+b-2)/(a*b)
   print(c)
   c4_ans=math.sqrt(c)
   mul4=c4_ans*2
   print(mul4)
```

```
if a==2and b==3:
   c=(a+b-2)/(a*b)
   print(c)
   c5_ans=math.sqrt(c)
   mul5=c5_ans*6
   print(mul5)

if a==2and b==4:
   c=(a+b-2)/(a*b)
   print(c)
   c6_ans=math.sqrt(c)
   mul6=c6_ans*1
   print(mul6)

if a==3and b==3:
   c=(a+b-2)/(a*b)
   print(c)
   c7_ans=math.sqrt(c)
   mul7=c7_ans*2
   print(mul7)

final=mul1+mul2+mul3+mul4+mul5+mul6+mul7
print(final)
```

Output of the above program

```
enter a value:1
enter b value:2
0.5
0.7071067811865476

enter a value:1
enter b value:3
0.6666666666666666
1.632993161855452

enter a value:1
enter b value:4
0.75
2.598076211353316

enter a value:2
enter b value:2
0.5
1.4142135623730951

enter a value:2
enter b value:3
0.5
4.242640687119286
```

enter a value:2
enter b value:4
0.5
0.7071067811865476

enter a value:3
enter b value:3
0.4444444444444444
1.3333333333333333

12.635470518407578

Similarly, the other topological indices from Definition 2.3 to 2.9 are calculated by both analytically and using Python programming which are listed in the table below:

Topological Index	Topological Index of Salbutamol
ABC	12.6354
ABS	12.8266
AZI	116.6424
SAI	110.7916
GA	15.782
AG	18.3044
GO1	250
GO2	458
HGO1	7248
HGO2	15572

Topological Indices of Degree Splitting of Salbutamol

The different topological indices of Salbutamol's degree splitting are assessed in this section. The degree splitting graph of salbutamol consists of 21 vertices and 34 edges.

The topological indices from Definition 2.2 to 2.9 are calculated by both analytically and using Python programming which are listed in the table below:

Topological Index	Degree Splitting Topological Index of Salbutamol
ABC	22.6959
ABS	28.9427
AZI	433.2746
SAI	91.6532
GA	30.8491
AG	36.2013
GO1	1011
GO2	3360
HGO1	48111
HGO2	388584

Comparison Between Salbutamol & Degree Splitting Graph of Salbutamol

This section presents the correlation coefficient, as determined by a regression model, between Salbutamol's topological indices and its degree splitting graph. Using the SPSS software and the data in Tables 1 and 2, the linear and quadratic models are produced.

Best-fit values

Slope	22.42 ± 2.696
Y-intercept	-9224 ± 14649
X-intercept	411.4
1/Slope	0.04460

95% Confidence Intervals

Slope	16.20 to 28.64
Y-intercept	-43005 to 24558
X-intercept	-1281 to 1776

Goodness of Fit

R square	0.8963
Sy.x	41640

Is slope significantly non-zero?

F	69.18
DFn,DFd	1,8
P Value	< 0.0001
Deviation from horizontal?	Significant

Data

Number of XY pairs	10
Equation	Y = 22.42*X - 9224

CONCLUSION

Salbutamol's degree based topological indices and degree splitting topological indices are examined using degree-based indices. A graphical comparison of the computed findings for the chemical compounds stated above may be found in Figure 1. The creation of novel drugs to treat chronic bronchitis, bronchial asthma, and other long-term bronchopulmonary conditions may benefit from these discoveries.

REFERENCES

1. B. Furtula, A. Graovac, D. Vukiˇcevi´c, Atom-bond connectivity index of trees, Discrete Appl.Math. 157 (2009) 2828–2835.
2. Yan Yuan, Bo Zhou, NenadTrinajstic,On geometric-arithmetic index,J Math Chem (2010)47:833–841.
3. B. Furtula, A. Graovac, D. Vukiˇcevi´c, Augmented Zagreb index, J. Math. Chem.48 (2010) 370–380.
4. Shegehavalli V.S., Kanabur R. Arithmetic-geometric indices of path graph. J. Math. Comput.Sci. 2015, 16, 19–24
5. V.R.Kulli, The Gourava indices and coindices of graphs,International Journal of Mathematical Archive-8(12), 2017, 116-120.
6. V.R.Kulli, On Hyper Gourava Indices And Coindices, Annals of Pure and Applied Mathematics, 14(1) (2017).
7. A. Ali, B. Furtula, I. Redzepovi´c, I. Gutman, Atom-bond sum-connectivity index, J. MathChem. 60 (2022) 2081–2093.
8. V.R.Kulli, Sum augmented and multiplicative sum augmented indices of some nanostructures, Journal of

Mathematics and Informatics, 24 (2023) 27-31.

9. V.R.Kulli, KM. Niranjan, Venkanagouda M Goudar, S Raghu, Dupadahalli Basavaraja,Degree Based Topological indices of Fenofibrate, European Chemical Bulletin,2023,12(special issue 8),
10. R.Revathy, Difference Arithmetic Geometric Mean Index of Graphs, Indian Journal of Natural Sciences, ,Vol.14, Issue 82, Feb 2024

Table 1. Edge partition of Salbutamol

(d(u),d(v))/(u,v) ∈E(G)	Number of edges
(1,2)	1
(1,3)	2
(1,4)	3
(2,2)	2
(2,3)	6
(2,4)	1
(3,3)	2

Table 2. Edge Partition of degree Splitting of Salmabutamol

(d(u),d(v))/(u,v)∈(G)	Number of edges
(1,5)	1
(2,3)	2
(2,4)	2
(2,5)	3
(2,6)	6
(3,3)	2
(3,4)	5
(3,5)	1
(3,6)	6
(4,4)	6

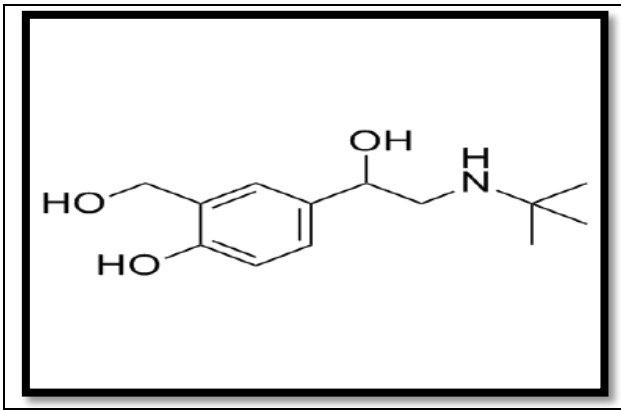

Figure 1 : Chemical Structure of Salbutamol

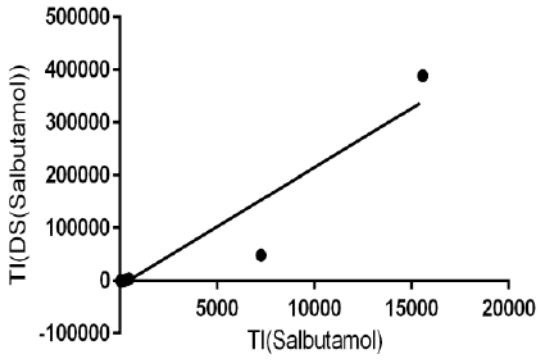

Figure 2 Best-fit values

Vol.15 / Issue 83 / Apr / 2024 International Bimonthly (Print) – Open Access ISSN: 0976 – 0997

RESEARCH ARTICLE

The Impact of COVID 19 Pandemic on the Professional Learning and Evaluation of Undergraduate Pharmacy Students

Srujankumar Reddy Pothula[1], Sravani Jollireddy[2], Dipak Dnyandeo Bharambe[3] and Mohanraj Rathinavelu[4]*

[1]Pharmacist, Department of Pharmacy, Bharat Heavy Electricals Limited Organisation (Electronics Division) Karnataka, India.
[2]Assistant Professor, Department of Pharmacy Practice, Oil Technological and Pharmaceutical Research Institute, (Affiliated to JNT University) Anantapur, Andhra Pradesh, India.
[3]Assistant Manager, Department of Clinical Pharmacy, P D Hinduja Hospital and Medical Research Center, Mumbai, Maharashtra, India.
[4]Associate Professor, Department of Pharmacy Practice, Raghavendra Institute of Pharmaceutical Education and Research (RIPER) (Affiliated to JNT University) Anantapur, Andhra Pradesh, India.

Received: 30 Dec 2023 Revised: 19 Jan 2024 Accepted: 27 Mar 2024

***Address for Correspondence**
Mohanraj Rathinavelu
Associate Professor,
Department of Pharmacy Practice,
Raghavendra Institute of Pharmaceutical Education and Research (RIPER)
(Affiliated to JNT University) Anantapur,
Andhra Pradesh, India.
Email: visitmoley@gmail.com

ABSTRACT

In the higher education teaching-learning process, evaluation is extremely important, it aids in the formation of judgmental values, educational status, and student accomplishment. The global pandemic of the Coronavirus has produced major change, bringing numerous difficulties to the higher education community. After four months in the midst of the global crisis, we've realized that the COVID-19 is here to stay, and we need to find ways to move forward. This crisis might be viewed as an opportunity to rebuild our long-standing educational systems and establish better, more up-to-date academic methods that are appropriate for today's learners. In this context, the current study investigated the perceptions of pharmacy students to the teaching and learning process in pharmacy education at undergraduate level, towards blended pedagogy by administering a standard validated questionnaire; and the educational outcomes with examination as indicators conducted as open-book examination and closed-book examination assessed the outcome through the results of end semester examination at undergraduate level in a self-financing, unaided, private pharmacy institute of south India. All the observations in our study were prolific in terms of teaching learning process through blended learning among students. In

addition, we observed that the end semester examination outcome is satisfactory in in terms of pass percentage, which had direct correlation with individual student outcome in terms of gender almost in most of cases. In conclusion, our study envisaged effective student engagement, with more facilitator-student interactions and adaptability; through blended learning which enabled, enhanced and transformed students to active learners.

Keywords: Assessment, Blended Pedagogy Coronavirus disease 2019, Open Book Examination, Pharmacy Students.

INTRODUCTION

The health, social and economic crises of the COVID-19 pandemic have thrown into sharp relief the disruptive forces acting on the global higher education (HE) sector [1,2]. With more than 3 million COVID 19 infection cases as of August 2020, India experienced an accelerated uptake of digital solutions, tools, and services, speeding up the transition towards digital education [3]. During the coronavirus crisis, the education sector has gone through a rapid transformation, Universities adopted e-learning was a cure-all to COVID-19 [4]. Considering the national scenario; India's apex regulatory body of higher education, University Grants Commission (UGC), mandated for all the universities to complete the 25% syllabus through online teaching mode and 75% face-to-face interaction (UGC, 2020) [5]. The COVID 19 pandemic have stalled the pharmaceutical education which highly pressed the priority to review, re imagine, and revisit the Indian pharmaceutical education which underwent a didactic change including the implementation of novel strategies of online education and complete curriculum revision by the Pharmacy Council of India (PCI). Across the globe blended learning is applied in pharmaceutical education, but it gained momentum in Indian pharmacy education during the global threat COVID 19 pandemic[6]. Therefore, for successful implementation of educational change implications of change need to be addressed with blended pedagogy enabling a greater access to course content, learning preparation in peers and interactions [7].

Additionally, the outcome of teaching-learning process is dependent and proportional to the third pillars in higher education which is called evaluation [8]. In Indian higher education at university level adapted open book examination (OBE) for students' evaluation but was not considered as gold standards. However, self-financing private institutes was not able to cope up with this OBE due to technical shortcoming, finance and student's perception. The sudden closure of institutions/universities has not only adversely impacted the learning of the students worldwide; unfortunately, the school closure situation coincided with the key assessment period of the students, and their exams were either postponed or have been cancelled that year. As a result, parents and teachers fail to assess a student's learning capabilities which can have long-term negative consequences for him or her. The studies conducted in the past have shown that while comparing students' scores for OBE and closed book examination (CBE), there was no statistical difference, even though students who took CBE had a slightly higher score. Hence, the current study was performed to investigate the perceptions of pharmacy students towards blended pedagogy in pharmaceutical education and outcome of teaching learning process during COVID 19 and post COVID 19 through examinations at undergraduate level in a self-financing, unaided, private pharmacy institute of south India.

MATERIALS AND METHODS

Research design and study

The current research applies a quantitative design where descriptive statistics are used for the student characteristics (age and gender variables), and features data to determine if they are significant in blended learning effectiveness and outcome evaluation.

This study is based on an experiment (online survey Google Form administered) in which learners participated during their on-line session (COVID 19) of B. Pharmacy program course teaching during academic year 2019-2020.

Research Instrument

The online self-regulated learning questionnaire [9] and the intrinsic motivation inventory [10] were adopted and applied to measure the constructs on self- regulation in the student characteristics and motivation in the learning outcome constructs. Other self-built instruments were used to study remaining variables (attitudes, computer competence, workload management, social and family support, satisfaction, knowledge construction, technology quality, and interactions).

Instrument reliability

Cronbach's alpha [11] (measure of internal consistency, that is, how closely related a set of items are as a group, test for reliability), one of the most important and pervasive statistics in research involving test construction and use [12]; was applied used to test reliability. All the scales and sub-scales had acceptable internal consistency reliabilities are within range and found to be significant within acceptable values, ranging from 0.70 to 0.95 [13-15].

Study participant

The experimental survey was performed online, by administering the validated questionnaire prepared through google form to students pursuing undergraduate program (B. Pharmacy) during the academic year 2019-2020 at an unaided self-financing private pharmacy institute (Raghavendra Institute of Pharmaceutical Education and Research RIPER Autonomous) in rural Andhra Pradesh and the responses were documented and analyzed in the Microsoft spread sheet.

Study procedure

The current quantitative online experimental survey of six months duration was performed in an unaided self-financing private autonomous pharmacy institute of rural Andhra Pradesh state. The study included students of both genders, pursuing undergraduate (B. Pharmacy) pharmacy program at the institute respectively, who showed willingness towards participation. Ethical approval was obtained from the institute before the start-up of study by submitting a detailed proposal with potential outcome.

Preparation of a validated questionnaire

A questionnaire was prepared to investigate the perception of students at undergraduate level towards blended pedagogy in pharmacy education by using the literatures [9,10] available in the core area.

Pilot study

A preliminary pilot pretesting of the questionnaire (comprising of 39 inventories) was done on 20 each randomly selected students from both undergraduate programs, with the purpose of identifying the practical and communication difficulties while surveying. Furthermore, the pilot testing allowed us to modify the ambiguous and unsuitable questions.

Assessment of reliability and internal consistency

The reliability and internal consistency of the questionnaire based on Cronbach's alpha coefficient value [12] were between 0.7 and 0.953 [13-15], and was found reliable for 28 inventories.

Final draft and standard

Furthermore, the questionnaire after its final drafting was reviewed by expert panel in subjects and curriculum for the face validity, content validity, and the relevance and comprehensiveness Thus, the validated questionnaire comprised of 28 inventories under 7 categories (online resources, interactions, quality of technology, self-management, students approach towards blended learning, motivation and satisfaction), along with the demography particulars of the students. Furthermore, the same validated questionnaire was administered to

students pursuing undergraduate program (B. Pharmacy) at our institute through Google Form due to the COVID 19 pandemic and lockdown in the academic year of 2019-2020, within the duration of February to June, 2020; who showed willingness towards the study. The responses were presented in 5-point Likert scale based on satisfaction, and the same was collected and analyzed using Microsoft spread sheet.

Program outcome evaluation (COVID 19 and post COVID 19)

It was observed that during COVID 19 pandemic, the institute (RIPER Autonomous) have convened two sessional examinations (I and II) in open book examination (OBE) mode and end semester examination in closed book examination (CBE) for undergraduate program (B. Pharmacy) students of academic year (AY) 2019-2020. The results of which, obtained from examination cell are collected and collated, and further evaluated for defining the outcomes as pass percentage in terms of course and program.

RESULTS AND DISCUSSION

The current study performed in an unaided private self-financing autonomous pharmacy institute of rural Andhra Pradesh to investigate the perception of pharmacy students towards blended pedagogy in pharmacy education, through an online experimental survey among students pursuing undergraduate pharmacy program (B. Pharmacy) during the academic year AY 2019-2020 for a period of six months. The study was performed by administering a validated self-administered questionnaire online, among a total of 501 undergraduate students (B. Pharmacy) at the institute through social networking applications.

Characteristics of study participants

Out of 448 administration, 430 respondents filled the form, which observed 2.79% of incomplete information, so the total completed responses obtained was 418. In our undergraduate student population of 418, 218 (52.15%) were female, and 200 (47.85%) were male. During the academic year AY 2019-2020 out of 418 complete responses, students of I year II semester 112 (with 41.07% male and 58.93% female) were more in comparison to students of other year and semesters, where students of II and III years were same in total (24.88% each) relatively equal gender distribution, observations of which is presented in Table 1.

Response towards online administration of validated self-administered questionnaire

Blended learning courses may be implemented in several ways[16,17]. Three categories described by Graham[16] cover a range of possibilities: enabling blends, enhancing blends, and transforming blends. Our study, observed an enhanced student perception towards online resources in terms of use ableness (68.6%), content (74.8%), and practical worth (62.5%); were facilitator purposely blended the teaching-learning process in to the course of the program, which involved a combination of face-to-face interactions with small group activities, through both synchronous and asynchronous computer-mediated interactions; and practice-oriented learning activities. Through which traditional classroom limitations were overcome, which transformed the passive learning environment to active learning environment. As discussed earlier the pedagogy facilitated by the teacher gained a didactic momentum, and were nothing out- of -box discussion was made, with face-to-face interactions and small group activities. Thus, high rate of teaching and learning experience was experienced by students through facilitation of student–faculty (78.88%) and student content interactions (70.4%), all the time during the course class, interactions was important to achieve enhanced blending. Blended learning approaches are being applied in pharmacy education programs across the learning continuum[18-20], but this have been adopted in India too due to the COVID 19 pandemic, which made the teaching learning process so interesting for students, with considerable limitations. The same was observed in our study, despite three-fourth of students experience quality materials and contents (75.4%) and enhanced face-to-face support (68.3%), the regular accessibility to technology was observed in one-half of the students, due to the rural and low-income backdrop of students. The learner satisfaction factor (self-management) is of high priority in blended learning, which provides them an opportunity to make a self-assessment, and identify their potentials and enables capacity building in terms of setting of strategies (72.7%), critical thinking (66.9%), time

management (75.8%) and maintaining an optimistic learning environment (68.81%). The students of our study (more than two-third on average) were able to map this clearly, showcasing a higher rate of satisfaction with blended pedagogy, build through an effective self-assessment (69.5%). Literature[21] suggests that there is a significant relationship between academic success and learner autonomy; academic success and motivation; and learner autonomy and motivation in terms blended learning (BL) environments. Blended learning refers to asynchronous distance mode learning coupled with face-to-face facilitation of pedagogy, whose success is highly influenced by student's autonomy (72.4%), interactions (78.8%), family and societal support (71.4%), and the standards of academic or course instructions (74.6%), our study observed all these indicators at highest level, with a considerably more workload (56.46%) which may not influence the success of blended learning, in turn it builds up stress among students. Hence, the facilitator has to take a heightened responsibility in guiding them in management of stress whatsoever it matters. The study observed a two-third satisfaction on an average in terms of all the indicators which influence the blended pedagogy (teacher 71.8%, course content 74.8%, technology transfer 58.7%, interactions 78.8%, and constructive knowledge 73.7%). In our study, all the observations were prolific in terms of teaching learning process through blended learning (reaction, learning, and behavior) among students, but the actual effectiveness of blended learning prevails on the extent of achieving the program outcomes, which has to be visualized through their performance in examinations, results of which are reported in Figure 1.

Matrix of course and outcomes

Evaluation has been supplied by C.E. Beeby (1977) [22] who described evaluation as "the systematic collection and interpretation of evidence leading as a part of process do a judgement of value with a view to action." Evaluation is an important component of the teaching-learning process. It helps teachers and learners to improve teaching and learning. Evaluation is a continuous process not a periodic exercise. In our study, we observed that the end semester examination outcome is satisfactory in in terms of pass percentage secured in respective courses, which had direct correlation with individual student outcome in terms of gender (were female secured appreciable pass percentage) almost in most of cases. On the other hand, pass percentage in some courses observed was lesser in male students likely in courses pharmaceutical organic chemistry (46%), biochemistry (54%), medicinal chemistry (55.22%), biopharmaceutics and pharmacokinetics (50.82%), and biotechnology (55.74%) respectively; which was highly influenced by internal examination results convened through open book examination, results of which are presented in Figure 2. This pandemic has made evaluation process handicapped for higher education and put us in wheel chair, though university grant commission (UGC) have suggested OBE has a mode of examination, the experience in Indian higher education is not enough prepared due to slow adoption to digitization and less equipped technocracy and utilization both in teachers and students. On a microscopic observation, student of our institute appears for online examination during the regular course of study in B. Pharmacy program; and the same was followed in midterm examination during pandemic where the outcome is good in almost all individual cases but less in few, findings of which is similar to other investigated studies.[23] The consideration of few may be due to their cognition as complicated production of questions and marking schemes, subjective marking and restriction of materials. In our experience and from our observations; when properly used, open-book examination is a beneficial assessment tool that proves to be popular among students because it eliminates the cueing effect, encouraging students to gain a deeper understanding of their learning material while also requiring the use of key skills such as critical thinking. We also strongly recommend effective evaluation process supports evident and productive decision-making process; which promotes teaching-learning process for which blended pedagogy is a gateway outweighing all complexities of pharmacy and pharmaceutical sciences teaching and learning (T and L) fulfilling classroom objectives.

CONCLUSION

In conclusion, our study envisaged effective student engagement, with more facilitator-student interactions and adaptability; through blended learning which enabled, enhanced and transformed students to active learners; and recognized that there are drawbacks to administering an online open book exam which prioritized further research in terms of efficacy and practicalities of online OBEs in Indian higher education.

ACKNOWLEDGEMENT

The authors would like to express sincere thanks to Prof. Dr. Yiragamreddy Padmanabha Reddy (Principal – Raghavendra Institute of Pharmaceutical Education and Research - RIPER Autonomous) for his valuable and constructive suggestions during the planning and development of this research work. His willingness to give his time so generously has been very much appreciated.

REFERENCES

1. Chronicle of Higher Education. How will the pandemic change higher education? The Chronicle of Higher Education. 2020. https://www.chronicle.com/article/how-will-the-pandemic-change-higher-education/. Accessed 7 July 2023.
2. Garcia M. Community colleges in crisis: how COVID-19 and race are reshaping higher education. The Boston Globe. 2020. https://www.bostonglobe.com/2020/07/20/opinion/community-colleges-crisis-how-covid-19-race-are-reshaping-higher-education/. Accessed 21 July 2023.
3. Sharma, AK. COVID 19: Creating a paradigm shift in India's Education System. 2020. https://economictimes.indiatimes.com/blogs/et-commentary/covid-19-creating-a-paradigm-shift-in-indias-education-system/. Accessed May 3, 2023.
4. Dhawan S. Online Learning: A Panacea in the Time of COVID-19 Crisis. Journal of Educational Technology Systems. 2020 Sep;49(1):5-22.
5. Report of the UGC committee on examinations and academic calendar for the universities in view of COVID-19 pandemic and subsequent lockdown. 2020. https://www.ugc.ac.in/pdfnews/4276446_UGC-Guidelines-on-Examinations-and-Academic-Calendar.pdf. Accessed 29 April 2023.
6. Mathivanan SK, Jayagopal P, Ahmed S, Manivannan SS, Kumar PJ, Raja KT, Dharinya SS, Prasad RG. Adoption of E-Learning during Lockdown in India. Int J Syst Assur Eng Manag. 2023;14(Suppl 1):575.
7. Priya KB, Rajendran P. Education: from disruption to recovery. UNESCO 2020.
8. Oliver, D. E., Casiraghi, A. M., Henderson, J. L., Brooks, A. M., &Mulsow, M. Teaching Program Evaluation Three Selected Pillars of Pedagogy. American Journal of Evaluation. 2008 Sep;29(3):330-339.
9. Barnard, L., Lan, W. Y., To, Y. M., Paton, V. O., & Lai, S. Measuring self-regulation in online and blended learning environments. Internet and Higher Education. 2009 Jan;12(1):1-6.
10. Deci, E. L., & Ryan, R. M. Intrinsic Motivation Inventory. Intrinsic and extrinsic motivation from a self-determination theory perspective: Definitions, theory, practices, and future directions. Contemporary Educational Psychology. 2020 Apr; 61:101860.
11. Cronbach, L. J. Coefficient alpha and the internal structure of tests. Psychometrika. 1951 Sep;16(3):297–334.
12. Cortina, J. M. What is coefficient alpha? An examination of theory and applications. Journal of Applied Psychology. 1993 Feb;78(1):98-104.
13. DeVellis R. Scale development: theory and applications: theory and application. Thousand Okas, CA: Sage; 2003.
14. Bland JM, Altman DG. Cronbach's alpha. BMJ. 1997 Feb 22;314(7080):572.
15. Nunnally J, Bernstein L. Psychometric theory. New York: McGraw-Hill Higher, INC; 1994.
16. Graham, Charles R. Blended learning systems: Definition, current trends, and future directions. 2005.
17. Yuen, A.H.K. Exploring teaching approaches in blended learning. Res. Pract. Technol. Enhanc. Learn. 2011 Jan; 6(1):3-23.
18. Visentin S., Ermondi G., Vallaro M., Scalet G., Caron G. Blended-learning for courses in Pharmaceutical Analysis. Part 2, Journal of e-Learning and Knowledge Society. 2013 Jan;9(1):93-102.
19. Edginton A, Holbrook J. A blended learning approach to teaching basic pharmacokinetics and the significance of face-to-face interaction. Am J Pharm Educ. 2010 Jun 15;74(5):88.

20. Motycka, C.A.; St. Onge, E.L.; Williams, J. Asynchronous versus synchronous learning in pharmacy education. Journal of Combinatorial Theory, Series A 2. 2013 Jan,2(1):63-67.
21. Güneş, S., &Alagözlü, N. The interrelationship between learner autonomy, motivation and academic success in asynchronous distance learning and blended learning environments. Novitas-ROYAL (Research on Youth and Language). 2020 Oct, 14(2), 1-15.
22. Beeby CE. The meaning of evaluation. Current issues in education. 1977;4(1):68-78.
23. Krasne S, Wimmers PF, Relan A, Drake TA. Differential effects of two types of formative assessment in predicting performance of first-year medical students. Adv Health Sci Educ Theory Pract. 2006 May;11(2):155-71.

Table 1. Demography of study participants

Program	Year and Semester	Gender distribution		Total	
		Male	Female	n	%
B. Pharmacy	I & II	46 (41.07%)	66 (58.93%)	112	26.79
	II & II	47 (45.19%)	57 (54.81%)	104	24.88
	III & II	54 (51.92%)	50 (48.08%)	104	24.88
	IV & II	53 (54.08%)	45 (45.92%)	98	23.44
Total		200 (47.85%)	218 (52.155)	418	100

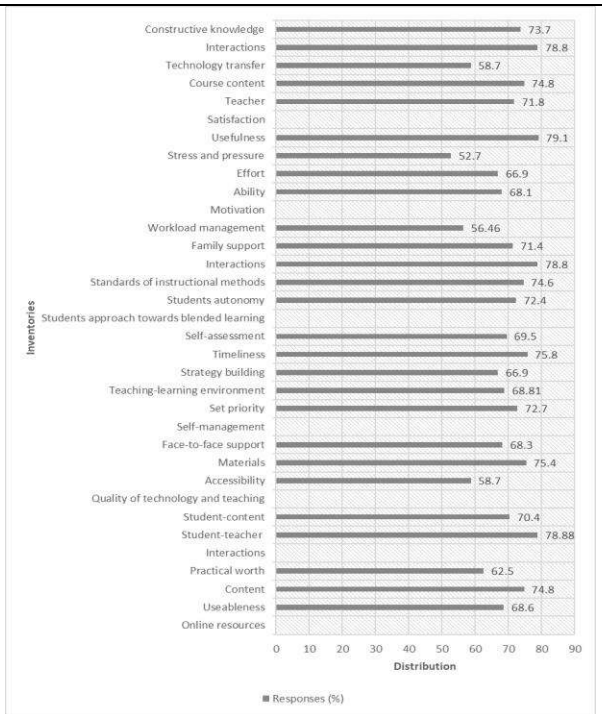

Figure 1. Perception of students towards standard self-administered questionnaire on blended learning

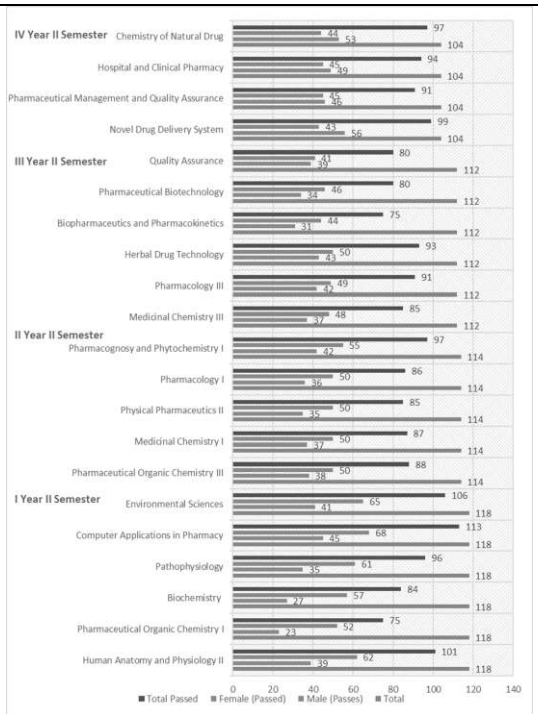

Figure 2. Matrix of program and course outcome

Indian Journal of Natural Sciences www.tnsroindia.org.in ©IJONS

Vol.15 / Issue 83 / Apr / 2024 International Bimonthly (Print) – Open Access ISSN: 0976 – 0997

RESEARCH ARTICLE

Assessing the Suitability of Groundwater for Irrigation in Pandavapura Taluk, Mandya District, Southern Karnataka, India

Madhu R[1]* and P Madesh[2]

[1]Research Scholar, Department of Studies in Earth Science, University of Mysore, Karnataka, India.
[2]Professor, Department of Studies in Earth Science, University of Mysore, Karnataka, India.

Received: 11 Nov 2023 Revised: 09 Jan 2024 Accepted: 27 Mar 2024

***Address for Correspondence**
Madhu R
Research Scholar,
Department of Studies in Earth Science,
University of Mysore,
Karnataka, India.
Email: madhu.r.geo@gmail.com

ABSTRACT

The groundwater suitability for irrigation in Pandavapura Taluk's comprehensive investigation employs a diverse set of hydrochemical indices to assess the quality of groundwater, including the Permeability Index, Salinity and Sodium Hazard Classification, Sodium Adsorption Ratio (SAR), Residual Sodium Carbonate (RSC), Sodium Ratio, Kelly's Ratio and Magnesium Adsorption Ratio (MAR). The research focuses on evaluating the groundwater's potential for sustainable agricultural use by examining key parameters related to water quality. The findings from this comprehensive analysis will provide valuable insights for farmers, policymakers, and water resource management authorities in Pandavapura Taluk, Mandya district.

Keywords: Irrigation, Groundwater, Pandavapura, water resource management, Mandya

INTRODUCTION

Water stands out as the most widely accessible and cost-effective raw material. Its diverse applications derive from its distinct physical and chemical characteristics. India's available water resources are insufficient to adequately irrigate the cultivatable land. As a result, it is essential to make concerted efforts to optimize the utilization of water resources for agricultural irrigation. Agriculture constitutes the primary livelihood for numerous communities in semi-arid regions, in Pandavapura taluk where agriculture is of paramount importance and its water supply relies on a combination of groundwater and a non-perennial river. To ensure successful crop growth and productivity, agriculture in these regions heavily depends on supplementary irrigation. However, the distribution of river water across the area is uneven. Therefore, groundwater serves as a primary irrigation water source due to its greater

reliability compared to surface water sources. **The monsoons play a vital role in replenishing the water resources** during June to October, as well as excessive extraction during the pre-monsoon period from February to May. Over-exploitation of groundwater, a common practice in many semi-arid areas, can lead to the depletion of aquifers and result in land subsidence, thereby diminishing both the availability and quality of groundwater. The chemical composition of irrigation water can directly impact plant growth through either toxicity or nutrient deficiencies, and indirectly by altering the accessibility of nutrients to plants. Irrigation water typically contains various dissolved salts. In the absence of proper management, considering the potential adverse effects on plants and soils, prolonged utilization of such water sources becomes unfeasible. This study aims to evaluate the suitability of groundwater for irrigation in the specified area.

Study Area

The study area, Pandavapura, lies between approximately 76°36' to 76°38' East longitude and 12°25' to 12°43' North latitude (Fig. 1), covering 529.9 square kilometers. It is depicted on topographical maps 57D/10, 57D/11, and 57D/14. Summers extend from February to May, while winters span mid-November to mid-February, the primary rainy season is from June to September with temperatures ranging from 16°C to 35°C. The average annual rainfall of about 650 millimeters. The area boasts a diverse composition of rock types, including migmatites, granodiorite tonalite gneiss, granite, metaultramafite, schist, metabasalt, and tuff from Archean to Proterozoic eras.

METHODS AND METHODOLOGY

The Pre-monsoon groundwater samples were collected from hand pumps and borewells across a systematically divided 10x10 square kilometer grid for comprehensive coverage. A total of 45 samples were carefully collected in clean polythene bottles, labeled, and borewells were pumped for 5-10 minutes to minimize iron pipe influence. GPS coordinates were recorded for accurate mapping in ArcGIS 10.8. Key parameters like TDS, pH, and EC were promptly measured in the field. In the lab, calcium, bicarbonate, carbonate, and chloride were assessed through titration, while calcium was determined by EDTA titration. Sodium and potassium were quantified using a flame photometer, and sulfate, fluoride, iron, and nitrate levels were determined through spectrophotometry. Data underwent processing in WATCHIT software, and thematic maps were generated using ArcGIS.

RESULT AND DISCUSSION

Groundwater Chemistry

The hydrochemical data for the pre-monsoon seasons are shown in Table.1. The pH range of 5.53 to 8.11 is attributed to natural geological features, atmospheric CO_2, microbial activity, human influence, and other environmental factors (Hitchon et al., 1999). Electrical conductivity (EC) reflects dissolved ions and salinity, affected by aquifer leaching, saline sources, or a combination (Hem 1991; Hounslow 1995). Pre-monsoon groundwater EC levels in this taluk range from 208 to 1600 µS/cm, while Total Dissolved Solids (TDS) vary from 105 to 689 mg/L, mainly comprising inorganic salts. Major ions influencing hydrochemical traits include Ca^{2+}, $Mg^{2+,}$ Na^{+}, Cl, SO_4^2, HCO_3, K, and NO_3, with concentrations falling within specific ranges (Li et al., 2016). Concentrations of $Ca^{2+,}$ $Mg^{2+,}$ and Na^{+} fall within the ranges of 24.8 to 237.6 mg/L, 6.8 to 92.34 mg/L, and 13.1 to 666 mg/L, respectively. Chloride (Cl) concentrations vary from 25.8 to 241.48 mg/L, while sulfate (SO_4) ranges from 1.8 to 432.3 mg/L. Bicarbonate (HCO_3) concentrations span from 43.7 to 735 mg/L, potassium (K^{+}) levels range from 0.8 to 154 mg/L, and nitrate (NO_3) concentrations vary between 0.01 and 115 mg/L (Table 1).

Irrigation Water Quality Parameter

The assessment of water suitability for irrigation is influenced by specific water quality standards established by various organizations and authorities (Ayers R 1994). Irrigation of flat land primarily depends on groundwater as its main source. The quality of irrigation water is influenced by a variety of factors, including soil composition, soil

texture, local geology, and agricultural practices (Abou El-Defan et al.,2016). Some factors that determine the quality of water used for irrigation are Kelly's Ratio, Magnesium Adsorption Ratio, Permeability Index, Salinity, Sodium Adsorption Ratio, Soluble Sodium Percentage and Sodium Ratio (Kshitindra Kr Singh et al., 2020).

Salinity Hazard Classification

Salinity Hazard Classification assesses and categorizes soil salt levels, crucial for agriculture. High salinity from saline irrigation reduces plant water absorption, harming crop growth and yield. If unaddressed, it leads to significant crop yield loss (Abou El-Defan et al., 2016). In 1954, Richards categorized irrigation water salinity into four groups, each with a letter grade (Table 2&3). This system sets thresholds for salinity hazard levels and guides decisions on soil management and mitigation strategies for land managers and agricultural practitioners. In the research area only 1 sample proved suitable for irrigation, whereas nearly 41 samples raised doubtful and three samples were deemed unfit for irrigation.

Sodium Ratio (SR)

The Sodium Ratio (SR), which is determined by comparing the concentration of dissolved sodium cations to the combined levels of calcium and magnesium ions in the irrigation water (Abou El-Defan et al., 2016). The sodium level is determined using the equation provided below.

$SR = (Na^{+})/(Ca^{2+} + Mg^{2+})$

In good water, this ratio should not exceed one (Table 4). All ion concentrations are expressed in meq/L. In the specified research area, only 10 out of the 45 samples were classified as inappropriate, while the remaining 35 samples were deemed suitable for agricultural purposes Fig.(2,3).

Soluble Sodium Percentage (SSP)

Sodium's vital for classifying irrigation water due to its effect on soil, reducing permeability. Na+ percentage gauges water suitability for irrigation (Wilcox, 1955). Groundwater quality is assessed based on Na% as follows: >20% (excellent), 20 – 40% (good), 40 – 60% (permissible), 60 – 80% (doubtful), and >80% (unsafe) (Table 5). The Na+% are determined through a formula, in which all ionic concentrations are expressed in meq/l.

$Na\% = (Na^{+} + K) / Ca^{2+} + Mg^{2+} + Na^{+} + K) \times 100$

Among 45 samples, 8 are excellent, 25 good, 5 permissible, and 1 unsafe Fig. (4).

Permeability Index (PI)

Soil permeability is influenced by sodium, calcium, magnesium, and bicarbonate levels, which also affect long-term irrigation water quality (Doneen 1964). Permeability is classified into three classes: I, II, and III (Table 6). The equation provided below is utilized to calculate the permeability index.

$$PI = \frac{Na + \sqrt{HCO_3}X100}{Ca + Mg + Na}$$

The concentrations of ions are uniformly expressed in meq/L. In the specified study area, 43 out of 45 samples were deemed suitable for agriculture, while the other two were unsuitable. Fig. (5).

Kelly's Ratio (KR)

Kelly's ratio (KR) assesses irrigation water suitability (Kelley 1963). A KR over one indicates unsuitability for irrigation (Aravinthasamy et al., 2020).

$KR = {}^{Na}/_{(Ca + Mg)}$

The Kelly's Ratio in the study region indicates that 35 samples were unsuitable, while the remaining 10 samples were within the acceptable range. (Table 7) & Fig. (6).

Sodium Absorption Ratio (SAR)

The SAR is crucial in evaluating water quality. Elevated salt levels in irrigation water can raise soil sodium levels, impacting permeability and causing water infiltration issues, leading to soil dispersion and cultivation challenges

(Keesari et al., 2016). SAR is calculated by comparing the sodium concentration to the square root of the calcium and magnesium concentrations in the water sample (Uma Mohan and Krishnakumar, 2021). The subsequent equation is employed for its calculation.

$$SAR = \frac{Na}{\sqrt{\frac{Ca+Mg}{2}}}$$

These concentrations are typically measured in units of meq/L. The USSL diagram was created to assess water quality Fig. (7, 8), Out of 45 samples, 37 were excellent, 5 good, 2 doubtful, and 1 unsuitable for irrigation. (Table 8, 9)

Residual Sodium Carbonate (RSC)

Residual Sodium Carbonate (RSC) measures potential sodium-related soil issues from bicarbonate (HCO_3) and carbonate (CO_3^{2-}) ions in irrigation water. It's computed by subtracting total calcium (Ca) and magnesium (Mg) ion concentrations from total bicarbonate and carbonate ions. A positive RSC signals excess sodium, leading to soil dispersion and reduced permeability during irrigation.

$$\mathrm{RSC} = (CO_3^- + \mathrm{HCO_3^-}) - (\mathrm{Ca^{2+}} + \mathrm{Mg^{2+}})$$

Negative RSC occurs when calcium and magnesium ions exceed bicarbonate and carbonate levels, indicating less sodium buildup in soil. This makes water suitable for irrigation and agriculture (Table 10). In the specified research area, 44 out of the 45 samples were classified as being in the good category, indicating their suitability for irrigation. Conversely, the remaining one sample fell into the poor category, signifying its unsuitability for irrigation. Fig. (09).

Magnesium Adsorption Ratio (MAR)

Calcium ions and magnesium ions are typically found in a natural equilibrium in the soil. However, this equilibrium can be disrupted on occasion when there is an elevated concentration of magnesium ions. An excess of magnesium ions can potentially hinder plant growth by increasing the alkalinity of the water. (Fallatah & Khattab, 2023). The calculation of the MAR was determined using a specific formula.

$$MAR = \frac{Mg\ X\ 100}{Ca + Mg}$$

The MAR in the study region indicates that 34 samples were suitable, while the remaining 11 samples were within the inappropriate for irrigation. (Table 11) & Fig. (10).

CONCLUSION

The suitability of groundwater for irrigation in semi-arid region pandavapura based on multiple parameters has yielded important insights. Sodium hazard classification results indicate that the majority of the samples fall into the doubtful category, with only a small percentage being classified as good. This classification suggests the need for careful monitoring and management to prevent potential harm to soil and crops. Furthermore, the sodium ratio and Kelly ratio results suggest that a significant portion of the groundwater samples is unsuitable for irrigation, emphasizing the importance of water quality management practices to mitigate the adverse effects on soil structure and crop growth. The Permeability Index highlights that the vast majority of samples (43 out of 45) are either highly suitable or suitable, demonstrating the water's ability to infiltrate and drain effectively in the soil. Additionally, the Sodium absorption ratio predominantly falls into the "excellent" category, which is an encouraging finding for irrigation practices. Residual sodium carbonate is generally good, with only a minor presence of "poor" samples, indicating acceptable conditions for irrigation. Finally, the Magnesium Absorption Ratio (MAR) results show that the majority of the samples are suitable for irrigation, although a portion falls into the "unsuitable" category. In summary, the groundwater in the study area exhibits a mixed suitability for irrigation, with certain parameters suggesting potential challenges. Effective management and monitoring practices, as well as the development of site-specific irrigation strategies, will be essential to ensure the sustainable use of groundwater for agricultural purposes in the region. This study serves as a valuable resource for local farmers and policymakers to make informed decisions regarding irrigation practices and water quality management.

ACKNOWLEDGMENTS

The authors express their gratitude for the assistance and guidance received from the Department of Studies in Earth Science at the University of Mysore in Mysuru. Additionally, they appreciate the University of Mysore for the fellowship provided.

REFERENCE

1. Aravinthasamy P, Karunanidhi D, Subba Rao N, Subramani T, Srinivasamoorthy K. Irrigation risk assessment of groundwater in a non-perennial river basin of South India: implication from irrigation water quality index (IWQI) and geographical information system (GIS) approaches. Arab J Geosci2020;13:1125.
2. Ayers R, Westcot D.Water quality for agriculture. 29th ed. Rome: Food, Agriculture Organization of the United Nations (FAO);1994.
3. Balasubramanian A, Nagaraju D. Water Chemistry Interpretation Techniques (WATCHIT-Software & its Application Manual) Version – 1 open File Report 01. Mysore: Centre for advanced Studies, Dept of Studies in EarthScience, University of Mysore.;2019.
4. Balasubramanian A. Hydrogeological investigations of Tambraparni River Basin, Tamil Nadu;1986.
5. Davis SN, De Weist RJM. Hydrogeology. Florida: KrinegarPulication Co:1966. p.476.
6. Doneen LD. Notes on water quality in Agriculture. Davis: Department of Water Sciences and Engineering, University of California;1964.
7. El-Defan A, El-Raies S, El-Kholy H, & Osman A. A summary of water Suitability Criteria for Irrigation. Jour.SoilSci.Agric.Eng 2016;7(12):981-989.
8. Fallatah O, Khattab, M. R. Evaluation of Groundwater Quality and Suitability for Irrigation Purposes and Human Consumption in Saudi Arabia. Water 2023;15(13):2352
9. Gupta, Suresh Kumar, Gupta IC. Management of saline soils and waters. Delhi: Oxford & IBH Publishing Co.; 1987
10. **Hem JD. Study and interpretation of the chemical characteristics of natural waters. 3rd ed. Jodhpur: Scientific Publishers;1991. p. 263.**
11. **Hitchon B, Perkins EH, Gunter WD. Introduction to groundwater geochemistry. Alberta: Geoscience Publishing Ltd;1999.**
12. **Hounslow AW. Water quality data analysis and interpretation. Florida: CRC Press;1995.**
13. KeesariTRamakumar KL, Chidambaram S, Pethperumal S, Thilagavathi R. Understanding the hydrochemical behavior of groundwater and its suitability for drinking and agricultural purposes in Pondicherry. South India-a step towards sustainable development.*Groundw. Sustain. Dev.* **2016**; *2*:143-153.
14. Kelly WP. Permissible Composition and concentration of irrigated water. In: Proceedings of the A.S.C.F;1940. p. 607.
15. **Li, P., Wu, J., Qian, H., Zhang, Y., Yang, N., Jing, L. and Yu, P. Hydrogeochemical characterization of groundwater in and around a wastewater irrigated forest in the southeastern edge of the Tengger Desert, Northwest China. . Expos. Health 2016;8(3):331-348.**
16. Richards, Lorenzo Adolph. Diagnosis and improvement of saline and alkali soils. Washinton Dc: U.S. Department of Agriculture 1954;pp.68-78.
17. Uma Mohan, Krishnakumar A. Assessment of Water Quality of Kallada River, Southern Westen Ghats, India: A Statistical Approach. Jour. Geosci. Res 2021;6(2):220-230
18. Wlicox LV. Classification and use of irrigation water. Washington DC: U.S. Dept. Agric;1996.

Table 1: Statistical assessment of physicochemical parameters in groundwater.

Parameter	Unit	Min	Max	Mean	Std. Deviation
pH	-	5.53	8.11	7.33	0.57
TDS	Mg/L	104	689	378.34	113.77
EC	µS/cm	208	1600	793.24	263.16
TH	Mg/L	122	852	388.51	141.06
SO_4	Mg/L	1.8	432.3	53.02	63.84
F	Mg/L	0.1	2.74	1.0384	0.44975
Fe	Mg/L	0.02	0.29	0.083	0.080
Mg	Mg/L	6.8	92.34	36.68	19.05
Cl	Mg/L	25.8	241.48	74.94	44.80
NO_3	Mg/L	0.01	115	18.88	26.63
HNO_3	Mg/L	43.7	735	278.48	119.10
K	Mg/L	0.8	154	12.873	28.83
Ca	Mg/L	24.8	237.6	92.036	40.411
Na	Mg/L	13.1	666	126.05	146.75

Table 2: Classes of irrigation water salinity (Richards, 1954).

Class	Description	Salinity	T.D.S.	Remarks
C1	Low Salinity	<25	<200	This irrigation method suits many crops and soils. Regular leaching is vital to remove excess salts, especially in poor or porous soils, which may require increased irrigation.
C2	Medium Salinity	0.25-0.75	200-500	This irrigation technique suits areas with stable leaching, where soil salt content doesn't rise significantly. It's ideal for plants tolerant to moderate salinity, suitable for widespread cultivation without special salinity controls.
C3	High Salinity	0.75-2.5	500-1500	**In areas with poor drainage, this irrigation method should not be used. Even if the drainage is adequate, special measures are needed to manage salinity, and only salt-tolerant plants can be grown.**
C4	Very High Salinity	>2.5	>1500	In most cases, this irrigation method should not be used. However, it may be used in special circumstances, such as when the soil is permeable, there is good drainage, and crops that can tolerate high salt levels are grown. In these cases, the irrigation water must be applied in excess to leach out salts.

Table:3 Salinity Hazard (after Davis and De Weiest, 1966; Wilcox, 1955)

Salinity Hazard Classification	Remarks on quality	Number. of Samples	Percentage
C1	Excellent	0	0
C2	Good	1	2.2
C3	Doubt	41	91.1
C4	unsuitable	3	6.7

Table 4: Sodium ratio (SR) classification (after Abou- El-Defan*et al.*, 2016)

Sl No.	Values meq/l	Remarks on quality	Numbers of Samples	percentage
1	>1	Unsuitable for agriculture	10	22.2
2	<1	Suitable for agriculture	35	77.8

Table 5: Soluble Sodium Percentage (SSP) classification (after Wilcox, 1954).

Category	S.S.P. Range (%)	No. of samples	Percentage
Excellent	<20	08	17.8
Good	20-40	25	55.6
Permissible	40-60	5	11.1
Doubtful	60-80	6	13.3
Unsafe	>80	1	2.2

Table 6: Permeability Index (Doneen, 1964)

Sl No.	Class	Remarks on quality	No of samples	Percentage
1	Class I (>75%)	Water is classified as having a high probability of providing irrigation benefits.	06	13.3
2	Class II (25-75%)	Water is classified as having a high probability of providing irrigation benefits	37	82.2
3	Class III (<25%)	Water is unsuitable with a 25% overall permeability	02	4.4

Table 7: Kelly's Ratio (Kelly, 1940)

Kelly's Ratio	Remarks	No of samples	Percentage
>1	Suitable	10	22.2
<1	Unsuitable	35	77.8

Table 8: Irrigation water classes and description as SAR values (after Abou-El-Defan*et al.*, 2016)

Class	Description	S.A.R. Value (meq/l)	Remarks
S1	Low Sodium water	<10	This irrigation method is safe to use on most soils, as it does not cause sodium to build up in the soil. However, sodium-sensitive crops may accumulate harmful levels of sodium if this irrigation method is used.
S2	Medium Sodium water	10-18	Fine-textured soils with a high CEC are at risk of becoming saline, especially if they do not have gypsum and are not leached regularly. This irrigation method can be used on coarse-textured or organic soils with good permeability, but it is not recommended for fine-textured soils.
S3	High Sodium water	18-26	This irrigation water is generally not recommended, as it could lead to high levels of exchangeable sodium in the soil, which can be harmful to plants. Most soils will require special management practices to mitigate these risks, such as good drainage, high leaching, and the addition of organic matter. However, this water may be safe to use in gypsiferous soils, which contain the mineral gypsum. Gypsum can help to replace exchangeable

			sodium with calcium, which is less harmful to plants.
S4	Very High Sodium water	>26	This water is too saline for most crops, but it may be possible to use it for irrigation of salt-tolerant crops in soils with high calcium levels or where gypsum is added to the water

Table 9: Sodium Hazard classification (Richards, 1954)

Sodium Hazard Class	S.A.R. range meq/l	Remark	No. of Samples	Percentage
S1	<10	Excellent	37	82.2
S2	10-18	Good	5	11.1
S3	18-26	Doubtful	2	4.4
S4	>26	Unsuitable	1	2.2

Table 10: Residual Sodium Carbonate (after Abou-El-Defan*et al.*, 2016)

Category	R.S.C. range (meq/l)	Water Quality	No. of samples	Percentage
Good	< 1.	Water probably safe for irrigation.	44	97.8
Medium	1.25-2.50	Water is marginally suitable for irrigation and can be used with certain conducts.	0	0
Poor	>2.50	Water is unsuitable for irrigation purposes.	1	2.2

Table 11: MAR Classification of the groundwater samples in the study area (after Gupta and Gupta, 1987)

MAR	Remarks	No of samples	Percentage
<50	Suitable	34	75.6
>50	Unsuitable	11	24.4

Table 12: Parameters indicating the quality of irrigation water in the research area.

Sample No.	Location	Lattitude	Longitude	SR	SSP	RSC	USSL salinity
1	Chikkayarahally	12.4396	76.5866	0.44	32	-2.98	C3
2	Anthanahalli	12.4690	76.5436	0.41	31.3	-8.57	C3
3	Bindahalli	12.4852	76.5490	0.16	14.9	-12.01	C4
4	Maligere	12.5021	76.5338	0.07	7.3	-3.26	C3
5	Dinka	12.5198	76.5457	0.54	35.4	-1.53	C3
6	Aralakuppe	12.4582	76.6163	0.10	9.8	-4.29	C3
7	Seethapura	12.4457	76.6131	0.13	11.4	-2.09	C3
8	Chaluvarasanakoppalu	12.4362	76.6382	0.45	32	-1.04	C3
9	Kyatanahalli	12.4638	76.6527	0.27	22	-0.12	C2
10	Kennalu	12.4725	76.6750	1.41	65.7	0.15	C3
11	Pandavapura	12.5042	76.6734	1.84	65.4	-0.36	C3
12	Hulkere	12.5026	76.6206	0.47	32.2	-3.14	C3
13	Chinakuruli	12.5383	76.6036	1.48	59.9	-6.53	C3
14	Kurubaramanchanahalli	12.5746	76.5782	0.32	25.1	-6.2	C3
15	Morasanahalli	12.5560	76.5966	2.26	69.6	-3.03	C3
16	Hiremaralli	12.5200	76.6933	4.59	83.9	5.76	C3
17	Kenchnalli	12.5344	76.6355	0.13	11.7	0.85	C3

18	Kerethanoor	12.5573	76.6443	1.97	67.6	-0.9	C3
19	Kodala	12.5928	76.6423	0.57	37	-2.98	C3
20	Marmalli	12.6156	76.6133	0.61	38.1	-4.01	C3
21	Kadaba	12.5873	76.6121	0.61	38.9	-1.01	C3
22	Gowdagere	12.6308	76.6641	0.65	39.8	-5.34	C3
23	Chikade	12.4977	76.6928	0.12	13	-0.6	C3
24	Talasasana	12.4879	76.7281	0.26	21	-4	C3
25	Dodda byadarahalli	12.5029	76.7464	0.51	34.4	0.83	C3
26	Agathahalli	12.5232	76.7800	1.33	57.2	-2.29	C3
27	Kanaganamaradi	12.5297	76.7294	0.47	34.2	-0.87	C3
28	Kurahatti	12.5568	76.7266	0.30	23.2	-3.59	C3
29	Kalenahalli	12.5690	76.7462	0.36	29.8	-4.18	C3
30	Madarahalli	12.5865	76.7278	0.32	25.5	-3.28	C3
31	Balenahalli	12.6315	76.7242	0.42	30.1	-1.63	C3
32	G.Hosahalli	12.6471	76.7264	0.55	36.2	-1.82	C3
33	Shamboonahalli	12.6377	76.7068	0.59	38.1	-0.42	C3
34	K.hosur	12.5389	76.6700	0.32	24.4	-4.09	C3
35	Madeshwarapura	12.5715	76.6796	1.47	60.1	-3.43	C3
36	Jakanahalli	12.6496	76.6809	0.46	31.7	-9.14	C3
37	Talekere	12.7045	76.6484	0.13	13.1	-12.69	C4
38	Melkote	12.6625	76.6505	0.47	32.6	-1.91	C3
39	Belatheguppe	12.5499	76.6902	3.33	78.2	-3.3	C4
40	Anunahalli	12.6071	76.6897	0.72	42.5	-2.69	C3
41	Basavanagudikopallu	12.5476	76.5668	0.73	42.6	-0.34	C3
42	Garudapura	12.6870	76.6744	0.08	7.6	-3.86	C3
43	shamboonahalli	12.4965	76.6464	1.05	51.3	-3.48	C3
44	Baby grama	12.4963	76.5899	0.41	29.4	-1.05	C3
45	Alphalli	12.4794	76.5935	0.24	20.9	-5.81	C3

Table 13: Parameters indicating the quality of irrigation water in the research area.

Location	Lattitude	Longitude	SAR	KR	Na%	MAR	PI	Na hazard
Chikkayarahally	12.4396	76.5866	2.47	0.44	31.97	38.00	50.16	S1
Anthanahalli	12.4690	76.5436	2.98	0.41	31.33	56.93	40.57	S1
Bindahalli	12.4852	76.5490	1.21	0.16	14.91	48.59	23.39	S1
Maligere	12.5021	76.5338	0.48	0.07	7.34	45.99	30.87	S1
Dinka	12.5198	76.5457	2.56	0.54	35.44	35.52	58.32	S1
Aralakuppe	12.4582	76.6163	0.59	0.1	9.83	8.92	31.20	S1
Seethapura	12.4457	76.6131	0.70	0.13	11.44	46.90	38.61	S1
Chaluvarasanakoppalu	12.4362	76.6382	2.08	0.45	31.99	36.71	58.07	S1
Kyatanahalli	12.4638	76.6527	0.83	0.27	22.04	49.18	70.20	S1
Kennalu	12.4725	76.6750	6.71	1.41	65.67	40.50	76.22	S1
Pandavapura	12.5042	76.6734	7.19	1.85	65.36	38.95	81.99	S1
Hulkere	12.5026	76.6206	2.50	0.47	32.20	47.50	51.09	S1
Chinakuruli	12.5383	76.6036	9.49	1.48	59.90	54.45	67.28	S2
Kurubaramanchanahalli	12.5746	76.5782	1.78	0.32	25.09	53.90	36.57	S1
Morasanahalli	12.5560	76.5966	14.63	2.27	69.57	32.21	77.36	S3
Hiremaralli	12.5200	76.6933	23.06	4.59	83.91	38.03	91.95	S4

Kenchnalli	12.5344	76.6355	0.65	0.13	11.74	46.32	48.62	S1
Kerethanoor	12.5573	76.6443	9.98	1.97	67.61	42.92	78.60	S2
Kodala	12.5928	76.6423	3.25	0.57	37.00	24.29	54.14	S1
Marmalli	12.6156	76.6133	3.87	0.61	38.05	41.22	52.92	S1
Kadaba	12.5873	76.6121	2.69	0.61	38.94	37.27	62.98	S1
Gowdagere	12.6308	76.6641	4.45	0.65	39.84	33.51	52.55	S1
Chikade	12.4977	76.6928	0.59	0.12	13.04	33.61	44.99	S1
Talasasana	12.4879	76.7281	1.56	0.26	21.02	30.21	40.45	S1
Dodda byadarahalli	12.5029	76.7464	2.13	0.51	34.37	39.73	67.85	S1
Agathahalli	12.5232	76.7800	8.07	1.33	57.24	50.49	69.33	S2
Kanaganamaradi	12.5297	76.7294	2.00	0.47	34.19	46.09	60.39	S1
Kurahatti	12.5568	76.7266	1.64	0.3	23.19	25.81	43.07	S1
Kalenahalli	12.5690	76.7462	2.19	0.36	29.78	39.34	44.45	S1
Madarahalli	12.5865	76.7278	1.82	0.32	25.51	19.43	44.83	S1
Balenahalli	12.6315	76.7242	2.30	0.42	30.07	38.64	52.59	S1
G.Hosahalli	12.6471	76.7264	2.35	0.55	36.16	52.21	58.92	S1
Shamboonahalli	12.6377	76.7068	2.65	0.59	38.13	25.86	64.20	S1
K.hosur	12.5389	76.6700	2.00	0.32	24.38	25.63	42.49	S1
Madeshwarapura	12.5715	76.6796	7.32	1.47	60.12	52.17	70.27	S2
Jakanahalli	12.6496	76.6809	3.08	0.46	31.69	59.63	40.37	S1
Talekere	12.7045	76.6484	0.97	0.13	13.14	11.62	17.23	S1
Melkote	12.6625	76.6505	1.92	0.47	32.58	52.38	56.38	S1
Belatheguppe	12.5499	76.6902	17.63	3.33	78.23	43.00	83.24	S3
Anunahalli	12.6071	76.6897	3.42	0.71	42.48	46.14	59.35	S1
Basavanagudikopallu	12.5476	76.5668	2.65	0.73	42.63	16.92	72.15	S1
Garudapura	12.6870	76.6744	0.43	0.08	7.62	53.15	30.79	S1
shamboonahalli	12.4965	76.6464	6.81	1.05	51.35	29.04	63.57	S2
Baby grama	12.4963	76.5899	2.04	0.41	29.39	51.04	54.76	S1
Alphalli	12.4794	76.5935	1.38	0.24	20.87	50.06	34.52	S1

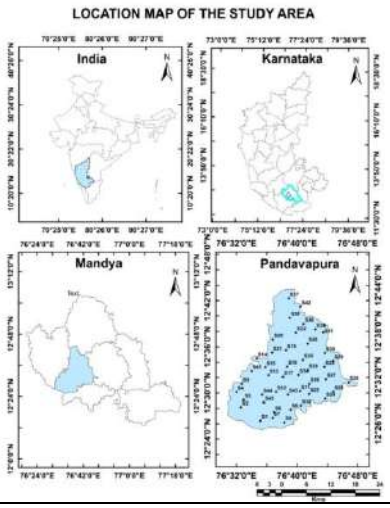

Fig.1. Location map of the study area

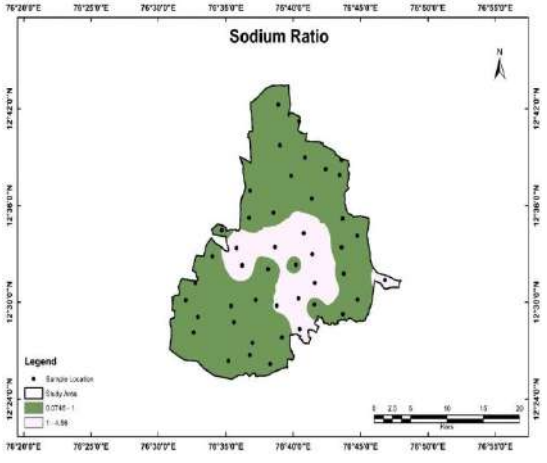

Fig.2. Spatial variation of Sodium Ratio

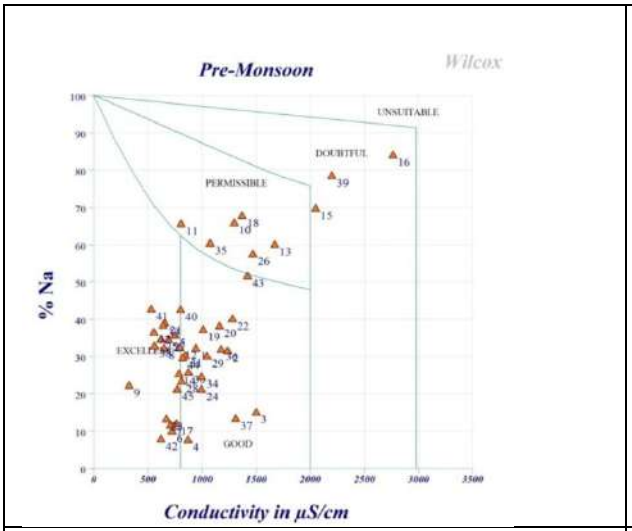

Fig.3. Wilcox diagram illustrating the quality of irrigation water (after Wilcox, 1955).

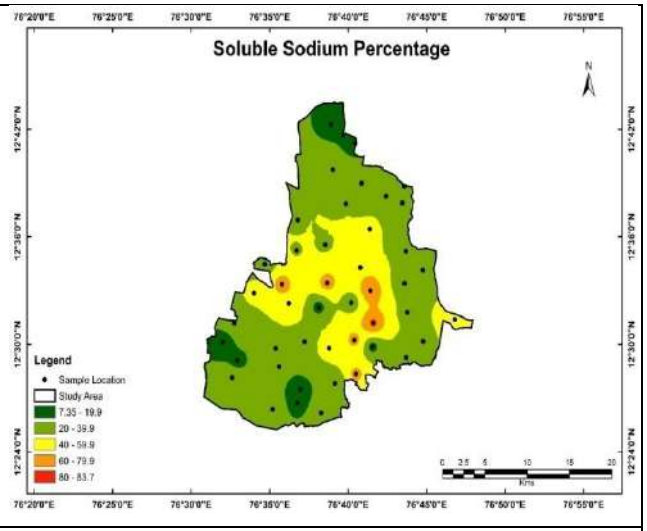

Fig.4. Spatial variation of Soluble Sodium Percentage (SSP)

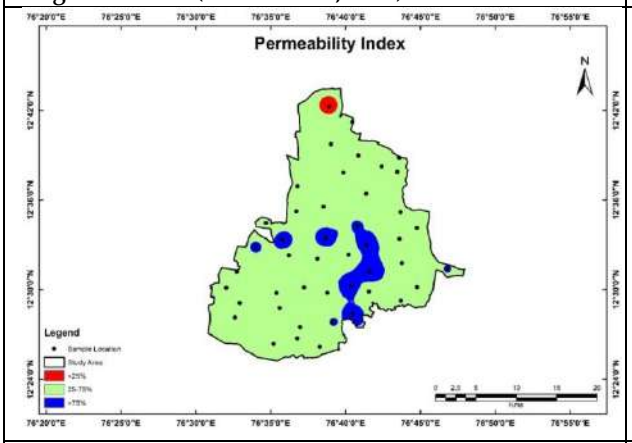

Fig.5. Spatial variation of Permeability Index (PI)

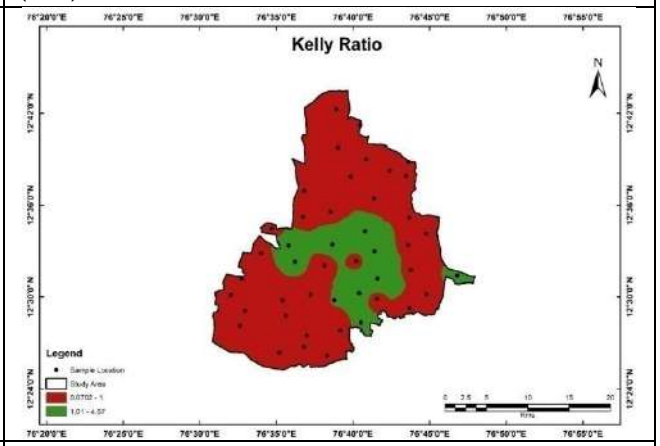

Fig.6. Spatial variation of Kelly Ratio (KR)

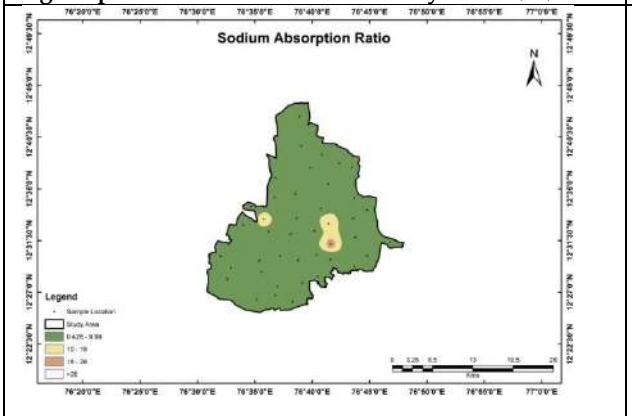

Fig.7. Spatial variation of Sodium Adsorption Ratio (SAR)

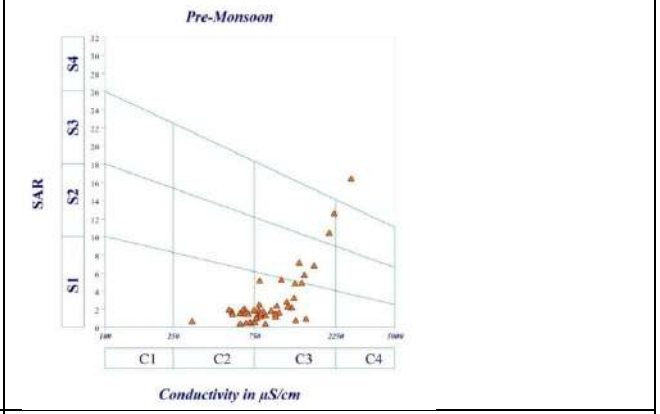

Fig.8. U.S.S.L. diagram showcasing the irrigation water quality of the groundwater samples within the research area (U.S.S.L.S., 1954).

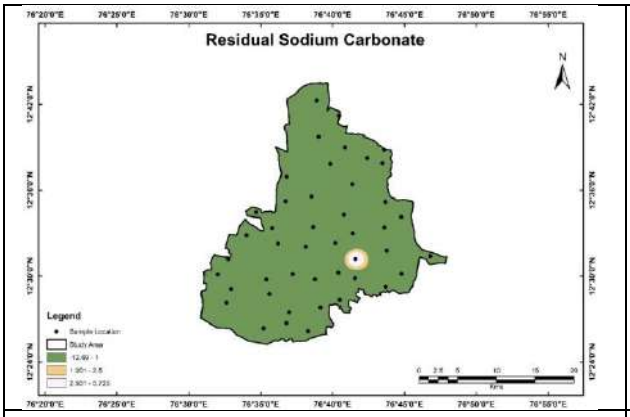

Fig.9. Spatial variation of Residual Sodium Carbonate (RSC)

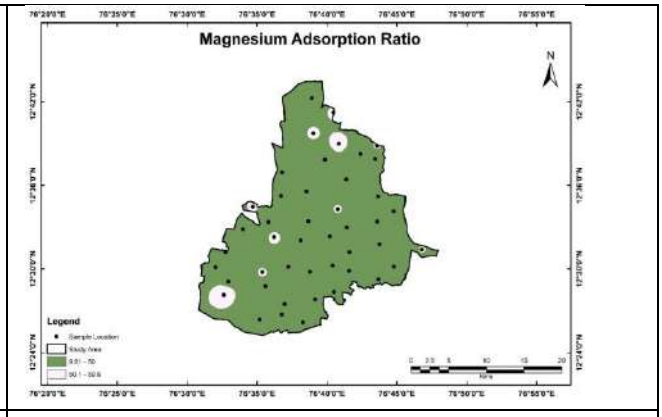

Fig.10. Spatial variation of Magnesium Adsorption Ratio (MAR)

Indian Journal of Natural Sciences *www.tnsroindia.org.in ©IJONS*

Vol.15 / Issue 83 / Apr / 2024 *International Bimonthly (Print) – Open Access* *ISSN: 0976 – 0997*

RESEARCH ARTICLE

Functional Recovery Following Early Strengthening After Middle Third Clavicle Fracture-A Single Case Study

Veluri Rakesh [1*], Arunachalam Ramachandran[2] and Anandhan Duraisamy[3]

[1*]Ph.D Scholar, Madhav College of Physiotherapy, Faculty of Medical Sciences, Madhav University, Pindwara, Sirohi, Rajasthan, India.
[2]Professor, Madhav College of Physiotherapy, Faculty of Medical Sciences, Madhav University, Pindwara, Sirohi, Rajasthan, India.
[3]Associate professor, Madhav College of Physiotherapy, Faculty of Medical Sciences, Madhav University, Pindwara, Sirohi, Rajasthan, India.

Received: 08 Nov 2023 Revised: 19 Jan 2024 Accepted: 14 Mar 2024

***Address for Correspondence**
Veluri Rakesh
Ph.D Scholar,
Madhav College of Physiotherapy,
Faculty of Medical Sciences,
Madhav University,
Pindwara, Sirohi, Rajasthan, India.
Email: dr.rakeshphysio91@gmail.com

ABSTRACT

Clavicle fractures are common injuries that can result in prolonged pain, or non-union, inadequate functional movements, if treated improperly. Often the rehabilitation gets delayed due to various reasons which when attested a better functional recovery may be attained. The objective of the report is to narrate novel implementation of early strengthening program within the period of six weeks for middle third clavicle fracture. The patient in this report, a 21 years old male, who had a middle third clavicle fractures, treated with early strengthening program followed by a surgical management showed convincing recovery in pain and function.

Keywords: Clavicle fracture**,** early strengthening, Rehabilitation.

INTRODUCTION

The clavicle is the most often broken bone in the human body, accounting for up to 5% to 10% of all fractures. [1,2] These injuries are especially common in younger patients and are frequently related with direct clavicle trauma, such as in contact sports and motor vehicle accidents. Males are more affected than females, and the prevalence decreases with age, yet traumatic falls in older patients generate a bimodal peak in the age distribution. [2]Fractures are the

most prevalent, which accounts for about 80% of all clavicle fractures.[3, 4]The gold standard is plate and screw fixation, often known as open reduction and internal fixation [ORIF].There is a surgical alternative. Plate fixation has the advantage of being less technically demanding than intramedullary fixation. [5] Plate mending research has provided promising outcomes. They claimed a unionization rate of 97% and a no unionization rate of 94%. [6] The rate of postoperative satisfaction in 232 midshaft clavicle fractures. They discovered that ORIF significantly decreased non-union and complication rates when compared to non-operative treatment for displaced midshaft clavicle fractures. [7] This study's main objective was to determine whether an early start-up strengthening program within six weeks would speed up functional recovery in a comparable manner to post-surgical treatment.

Patient Information

On November 27, 2022, a male, age 21, was involved in a bike accident. The patient was admitted to a nearby General Hospital due to loss of consciousness. Further medical examination was performed because the patient's vital signs were unstable and he was vomiting continuously. Due to such unfavourable medical condition, the underlying fracture was not diagnosed initially and the patient was managed conservatively for two weeks. Then he was admitted to an orthospeciality hospital, where he was diagnosed with a left medial one-third clavicle comminuted fracture through X-ray [Figure 1A]. The patient was successfully treated with open reduction and internal fixation [Figure 1B] and was discharged on the fifth post-operative day.

Physiotherapy Assessment

Following surgery, the patient was sling-immobilized advice his arm adducted for approximately one month. The Numerical Pain Rating Scale [NPRS] was initially used to assess the pain severity, which was 8/10. There was edema, left deltoid muscle atrophy, abrasions on the left forearm and hand, and a depressed shoulder with the arm adducted on examination. Palpatory examination revealed that the scar was adherent and had grade 1 tenderness. The active and passive range of motion and muscle power of the shoulder were slightly compromised during the examination using bubble inclinometer and push pull dynamometer, Functional outcome of an individual was measured using quick dash score[shown in table 1 & 2]. The patient reports difficulty with daily tasks such as lifting heavy objects, bathing, and overhead activities.

Time Line

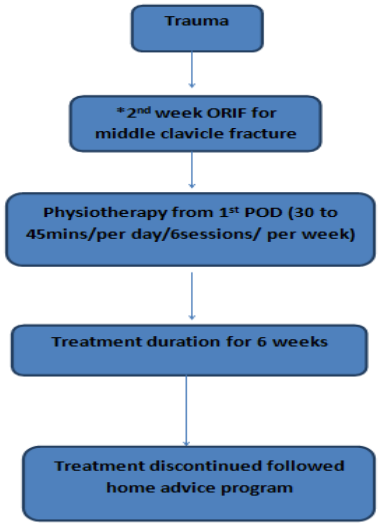

***Delayed due to unfavourable condition.**

Diagnostic Assessment
Show the figure 1 A] X-ray showing the mid third fracture. B]-X-ray Showing the open reduction with internal fixation[ORIF]

Therapeutic Intervention
StandardMedical management like medications, suturing, and wound care were offered by professionals. The main goal of physiotherapy sessions was to enhancement is to strengthen the shoulder muscles and daily tasks. The operative extremity was placed in a sling for two weeks immediately following surgery, so early active resisted range of motion of the elbow, wrist, and hand was encouraged.Intervention was offered for 30 to 45 minutes of one session/day, 6 sessions per week for 6 weeks.
W**eeks 1-2:**Daily 3 to 5 minutes of soft tissue mobilisation across the suture area; active elbow, wrist, and hand range of motion; and active shoulder range of motion with active assistance. The passive 90° flexion/abduction range of motion of the shoulder joint was encouraged.
Weeks 3 to 4: Soft tissue mobilisation across the suture region for 3 to 5 minutes. Internal and external shoulder flexion, abduction, and rotation exercises. Perform strengthening exercises for the elbow, wrist, and hand movements with dumbbells. Pendular and a wandexercise, Workouts with pulleys, ladders, and mariners wheel are encouraged.
Weeks 5 and 6: Scapular strengthening workout using dumbbells and theraband followed by scapula stabilisation exercises. Strength and functional training should be increased in preparation for a gradual return to activity.

DISCUSSION

Most previous studies have recommended sling immobilization and physical therapy following operative treatment of a clavicle fracture, using arm sling protection for two to six weeks after that followed by rehabilitation.[8,9,10]A Randomized controlled trail was done to compare open reduction and plate fixation versus non operative treatment for displaced mid shaft clavicular fracture. The results reveal that open reduction with internal fixation is expensive and associated with implant related complications, which are absent in non-operative treatment. They conclude that non operative treatment is more feasible choice for treating midshaft clavicular fracture. [7] A study was done by Karibasappa A G and Srinath S.R to find out the effectiveness of surgical versus conservative treatment for managing displaced midshaft clavicular fracture, they concluded that the group which received open reduction internal fixation with osteosynthesis showed good results as compared to the other group which received non-surgical treatment.[11]. Physiotherapy plays a vital part in healing quickly and returning to everyday activities by using fixation, immobilisation by braces in the first week, and gentle exercise in the sixth week following injury, followed by active exercise and muscular strength after 12 weeks.[12]

The main limitation of the current study is the lack of an objective tool to mark the recovery and the lack of long-term follow up. These aspects should be attested through robust research methods in future.Physical therapy is started as much as possible from the day one of the postoperative care in this trial, and it includes scar management and early strength training to improve the patient's ability to function. Scar management includes scar massage and soft tissue mobilisation. Early strengthening began after six weeks in a previous study, but in the current study, it began in the third week of the exercise regimen. As a result, early strength training will help to promote functional activities in the individual as soon as possible.

Patient Perspective
With a fractured collarbone, I've been in a lot of pain and under a lot of stress. My level of confidence has increased while receiving treatment, which helps me get through pain and return to my functional tasks.

Informed Consent

The patient agreed to provide his written, fully informed consent and his permission to record his thoughts on the course of treatment.

REFERENCES

1. Nordqvist A, Petersson C. The incidence of fractures of the clavicle. ClinOrthopRelat Res 1994;300:127–32
2. Postacchini F, Gumina S, De Santis P, Albo F. Epidemiology of clavicle fractures.J Shoulder Elbow Surg 2002;11:452–6.
3. Duan X, Zhong G, Cen S, Huang F, Xiang Z. Plating versus intramedullary pin or conservative treatment for midshaft fracture of clavicle: a meta-analysis of randomized controlled trials. *J Shoulder Elbow Surg*. 2011; 20[6]:1008-1015.
4. Abo El Nor T. Displaced mid-shaft clavicular fractures: surgical treatment with intramedullary screw fixation. *Arch Orthop Trauma Surg*. 2013; 133[10]:1395-1399.
5. Frigg A, Rillmann P, Perren T, Gerber M, Ryf C. Intramedullary nailing of clavicular midshaft fractures with the titanium elastic nail: problems and complications. *Am J Sports Med*. 2009; 37[2]:352-359.
6. Shen WJ, Liu TJ, Shen YS. Plate fixation of fresh displaced midshaft clavicle fractures. *Injury*. 1999; 30[7]:497-500.
7. Robinson CM, Goudie EB, Murray IR, et al. Open reduction and plate fixation versus nonoperative treatment for displaced midshaft clavicular fractures: a multicenter, randomized, controlled trial. *J Bone Joint Surg Am*. 2013; 95[17]:1576-1584.
8. Kirchhoff C, Banke IJ, Beirer M, Imhoff AB, Biberthaler P. Operative managementof clavicular non-union: iliac crest bone graft and anatomic locking compres-sion plate. OperOrthopTraumatol 2013;25:483–98.
9. Naimark M, Dufka FL, Han R, Sing DC, Toogood P, Ma CB, et al. Plate fixationof midshaft clavicular fractures: patient-reported outcomes and hardware-related complications. J Shoulder Elbow Surg 2016;25:739–46.
10. Rongguang A, Zhen J, Jianhua Z, Jifei S, Xinhua J, Baoqing Y. Surgical treatmentof displaced midshaft clavicle fractures: precontoured plates versus noncon-toured plates. J Hand Surg Am 2016;41:e263–6.
11. Karibasappa A G and Srinath S.R Surgical Versus Conservative Treatment in The Management of Displaced Mid Shaft Clavicular Fractures: A Clinical Study; International Journal of Scientific Research, 2014; 2277 – 8179.
12. Van der Meijden, O. A., Gaskill, T. R., & Millett, P. J. [2012]. Treatment of clavicle fractures: current concepts review. Journal of shoulder and elbow surgery, 21[3], 423- 429.

Table 1 -Pre and Post Outcomes for NPRS and Quick Dash disability

Outcome	1st day	3rd week	6th week
Numerical pain rating scale [NPRS]	8/10	4/10	2/10
Quick dash Disability	80%	40%	20%

Table 2 -Pre And Post Range Of Motion [ROM AND MMT]

MOVEMENT	LEFT SHOULDER								
	ACTIVE ROM			PASSIVE ROM			MANUAL MUSCLE TESTING [MMT]		
	1st Day	3rd Week	6th Week	1st Day	3rd Week	6th Week	1st Day	3rd Week	6th Week
FLEXION	60	110	170	80	120	180	2/5	4/5	5/5
EXTENSION	10	15	20	15	20	25	2/5	3/5	5/5
ABDUCTION	40	90	140	45	110	170	2/5	3/5	5/5
INTERNAL ROTATION	20	50	75	25	70	90	2/5	3/5	5/5
EXTERNAL ROTATION	10	35	50	15	60	75	2/5	3/5	5/5

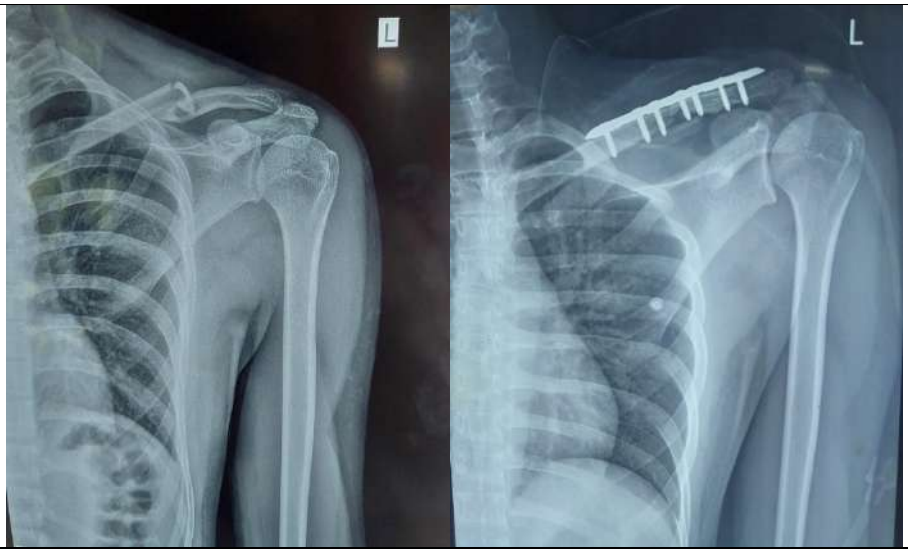

Figure 1. A] X-ray showing the mid third fracture. B]-X-ray Showing the open reduction with internal fixation [ORIF]

Indian Journal of Natural Sciences *www.tnsroindia.org.in ©IJONS*

Vol.15 / Issue 83 / Apr / 2024 *International Bimonthly (Print) – Open Access* *ISSN: 0976 – 0997*

RESEARCH ARTICLE

GC/MS Analysis of Methanolic Extract of *Pancratium triflorum* Roxb. bulbs

Rakkimuthu R[1]*, Neethu Krishna K[2], Sathishkumar P[3] , Ananda Kumar AM[3] and Sowmiya D[3]

[1]Assistant Professor and Head, PG and Research Department of Botany, Nallamuthu Gounder Mahalingam College, Pollachi (Affiliated to Bharathiar University), Coimbatore, Tamil Nadu, India.
[2]PG Student, PG and Research Department of Botany, Nallamuthu Gounder Mahalingam College, Pollachi (Affiliated to Bharathiar University), Coimbatore, Tamil Nadu, India.
[3]Assistant Professor, PG and Research Department of Botany, Nallamuthu Gounder Mahalingam College, Pollachi (Affiliated to Bharathiar University), Coimbatore, Tamil Nadu, India.

Received: 14 Nov 2023 Revised: 29 Jan 2024 Accepted: 16 Mar 2024

***Address for Correspondence**
Rakkimuthu R
Assistant Professor and Head,
PG and Research Department of Botany,
Nallamuthu Gounder Mahalingam College, Pollachi
(Affiliated to Bharathiar University), Coimbatore, Tamil Nadu, India.
Email: biorakki@gmail.com

ABSTRACT

This study presents the chemical composition of the methanolic extract obtained from *Pancratium triflorum* bulbs through gas chromatography and mass spectrometry analysis. Six distinct compounds were identified, namely 2,3-Anhydro-D-Galactosan, Triacontanoic Acid, Methyl Ester, 1-Hexadecyne, Eicosonoic Acid, Cis-9,10 Epoxyoctadecan-1-OL, and 2-Isopropyl-5-Methylcyclohexyl 3-(1-(4-Chlorophenyl)-3-Oxobutyl)-C. This comprehensive profiling provides insights into the molecular constituents of Pancratium triflorum, contributing to our understanding of its chemical composition and potential pharmacological applications. Further investigations into the biological activities of these identified compounds may unveil novel therapeutic possibilities associated with *Pancratium triflorum*.

Keywords: *Pancratium triflorum*, Bulb, GC-MS, Bioactive compounds, medicinal plant

INTRODUCTION

Pancratium triflorum. Roxb, a perennial herbaceous plant native to the Indian subcontinent, has a long-standing history of traditional use in various indigenous medicinal systems. Its cultural importance is underscored by its botanical nomenclature in which 'Pancratium' signifies 'all strength' and 'triflorum' refers to its characteristic three-flowered inflorescence [1]. In traditional practices, *Pancratium triflorum* is celebrated for its therapeutic attributes,

including its anti-inflammatory, diuretic, and analgesic properties [2]. However, despite its well-documented ethnobotanical uses, there exists a paucity of comprehensive scientific investigations exploring the phytochemical constituents and biological properties of this plant.Recent advancements in analytical techniques have provided the means to scrutinize the chemical composition of medicinal plants, thus shedding light on their pharmacological potential. Gas Chromatography-Mass Spectrometry (GC/MS) stands out as a powerful tool for the identification of bioactive compounds within plant extracts. This study employs GC/MS analysis to decipher the complex phytochemical profile of *Pancratium triflorum*. This research seeks to fill a significant knowledge gap and provide a solid foundation for further exploration of the medicinal and therapeutic potential of *Pancratium triflorum*.

The Amaryllidaceae family, to which *Pancratium triflorum* belongs, is well-known for the synthesis of alkaloids with diverse pharmacological properties. This is exemplified by the presence of lycorine, a prominent alkaloid known for its anti-inflammatory, cytotoxic, and antiviral activities, which is found in various Amaryllidaceae species [3]. Furthermore, the family Amaryllidaceae includes several species that have displayed notable antioxidant potential, which aligns with the increasing scientific interest in natural antioxidants as potential alternatives to synthetic antioxidants due to their lower toxicity and broader health benefits [4]. In light of the aforementioned, this research delves into the GC/MS analysis of *Pancratium triflorum* to uncover its phytochemical constituents. The outcomes of this study could pave the way for further investigations into the therapeutic applications of *Pancratium triflorum*. Roxb. and the development of antioxidant-based therapies.

MATERIALS AND METHODS

Plant Material and Extraction

Pancratium triflorum. bulbs were collected from karimkulam, palakkad district kerala. The plant material was identified and authenticated by botanical Survey of India, Coimbatore, and a voucher specimen (NGMPGB/20) was deposited in a herbarium. The bulbs were cleaned, shade-dried, and powdered for extraction

Preparation of Plant Extract

Powdered plant material (50 g) was w subjected to soxhlet extraction using methanol for 72 hours at room temperature. The extract was then filtered and concentrated under reduced pressure to obtain a crude methanolic extract of *Pancratium triflorum*.

GC-MS Analysis

The GC/MS analysis was performed using the Clarus 680 GC was used in the analysis employed a fused silica column, packed with Elite-5MS (5% biphenyl 95% dimethylpolysiloxane, 30 m × 0.25 mm ID × 250μm df) and the components were separated using Helium as carrier gas at a constant flow of 1 ml/min. The injector temperature was set at 260°C during the chromatographic run. The 1μL of extract sample injected into the instrument the oven temperature was as follows: 60 °C (2 min); followed by 300 °C at the rate of 10 °C min−1; and 300 °C, where it was held for 6 min. The mass detector conditions were: transfer line temperature 230 °C; ion source temperature 230 °C; and ionization mode electron impact at 70 eV, a scan time 0.2 sec and scan interval of 0.1 sec. The fragments from 40 to 600 Da. The spectrums of the components were compared with the database of spectrum of known components stored in the GC-MS NIST [5] (2008) library.

RESULTS AND DISCUSSION

The GC/MS analysis of the methanolic extract of *Pancratium triflorum*. revealed the presence of bioactive compounds. A total of 6 compounds were identified (Table 1). Notable compounds included carbohydrate derivatives, fatty acid derivatives, aliphatic hydrocarbons, eicosanoid derivatives, and structurally complex compounds. The Gas Chromatography-Mass Spectrometry (GC/MS) analysis of the methanolic extract of *Pancratium triflorum*. has unveiled a diverse array of bioactive compounds, contributing to the understanding of the plant's potential

pharmacological properties. In this study, a total of six compounds were identified, major compounds were Cis-9,10 Epoxyoctadecan-1-OL (39.240%) and 2-isopropyl-5-methylcyclohexyl 3-(1-(4-chlorophenyl)-3-oxobutyl)-c (35.494%) and minor compounds were shown in figure 1, each possessing distinctive chemical structures and, possibly, associated biological activities. These compounds are integral components of the plant's phytochemical composition and merit further investigation for their potential therapeutic applications.

Eicosonoic Acid, Cis-9,10 Epoxyoctadecan-1-OL, is a derivative of eicosanoids, which are signaling molecules involved in inflammation and immune responses [6]. The presence of this compound suggests that *Pancratium triflorum* may possess components with immunomodulatory properties. The compound 2-isopropyl-5-methylcyclohexyl 3-(1-(4-chlorophenyl)-3-oxobutyl)-c, a complex and structurally diverse compound, adds further intrigue to the phytochemical profile of *Pancratium triflorum*. Its structure implies the potential for multifaceted pharmacological activities, which may encompass anti-inflammatory, antioxidant, or even cytotoxic effects. One of the identified compound, 2,3-anhydro-d-galactosan, is a carbohydrate derivative. While carbohydrates are not typically associated with bioactive compounds, their presence in plant extracts could indicate potential interactions with other bioactive molecules, and they may play a role in the overall medicinal properties of the plant. Triacontanoic Acid, methyl ester, is a long-chain fatty acid derivative. Fatty acids and their derivatives are known for their various biological activities, including anti-inflammatory and antimicrobial properties [7]. This compound could contribute to the plant's anti-inflammatory potential. 1-Hexadecyne is an aliphatic hydrocarbon. Aliphatic hydrocarbons are commonly found in plant extracts and can exhibit diverse biological activities, including antioxidant properties [8]. This compound may contribute to the antioxidant potential of *Pancratium triflorum*. While these compounds have been identified, their specific pharmacological properties and the potential synergistic interactions among them remain to be explored. Additionally, the concentrations of these compounds in the plant extract and their bioavailability are essential factors that need further investigation.

CONCLUSION

The GC/MS analysis of *Pancratium triflorum*. revealed the presence of several bioactive compounds, including carbohydrate derivatives, fatty acid derivatives, aliphatic hydrocarbons, eicosanoid derivatives, and structurally complex compounds. This diverse range of compounds suggests the potential for a broad spectrum of pharmacological properties. Further research is required to elucidate the specific roles of these compounds and their potential for contributing to the medicinal and therapeutic properties of *Pancratium triflorum*. Roxb.

REFERENCES

1. Rao, R. S., & Rao, R. M. A comprehensive botanical, pharmacological and pharmacognostical review of *Pancratium triflorum*. Roxb. (Amaryllidaceae). International Journal of Pharmacy and Pharmaceutical Sciences, 6(8), 214-217, 2014.
2. Kirtikar, K. R., & Basu, B. D. Indian medicinal plants (Vol. 2). Bishen Singh Mahendra Pal Singh,1987.
3. Santos, S. A., Freire, C. S., Domingues, M. R., Silvestre, A. J., & Neto, C. P. A new approach for a detailed structural characterization of Amaryllidaceae alkaloids and their use in species differentiation. Phytochemistry Analysis, 23(2), 159-171, 2012.
4. Lopes, A. P., Oliveira, A., Rosa, D., Coutinho, J. A., Rodrigues, C., & Venâncio, F. Amaryllidaceae alkaloids as potential drugs for Alzheimer's disease: In silico and *in vitro* studies. European Journal of Medicinal Chemistry, 157, 296-309, 2018.
5. Hema R, Kumaravel S, Alagusundaram K. GC/MS Determination of bioactive components of Murraya koenigii. Journal of American Science.7(1):80-83, 2011.
6. Serhan, C. N., Chiang, N., & Van Dyke, T. E. Resolving inflammation: dual anti-inflammatory and pro-resolution lipid mediators. Nature Reviews Immunology, 8(5), 349-361, 2008.

7. Calder, P. C. Marine omega-3 fatty acids and inflammatory processes: Effects, mechanisms and clinical relevance. Biochimica et Biophysica Acta (BBA) - Molecular and Cell Biology of Lipids, 1851(4), 469-484, 2015.
8. El-Maghraby, A. M., Zaki, A. K., Wahby, I. A., & Amin, S. I. Antioxidant activity of some fatty acids on total lipid peroxidation and the chemical reactivity of alpha-linolenic acid. Chemistry and Physics of Lipids, 213, 13-20, 2018.

Table 1: Compounds identified in the methanolic extract of *Pancratium triflorum*

RT	Name of the compound	Molecular formula	Molecular weight	Peak area %	Compound nature
18.765	2,3-ANHYDRO-D-GALACTOSAN	$C_6H_8O_4$	144	5.567	Aldehyde
19.495	TRIACONTANOIC ACID, METHYL ESTER	$C_{31}H_{62}O_2$	466	6.154	Fatty acid methyl ester
20.566	1-HEXADECYNE	$C_{16}H_{30}$	222	5.774	Aliphatic hydrocarbon
21.171	EICOSANOIC ACID	$C_{20}H_{40}O_2$	312	7.771	Unsaturated fatty acid
22.411	CIS-9,10-EPOXYOCTADECAN-1-OL	$C_{18}H_{36}O_2$	284	39.240	Alcoholic compound
27.008	2-ISOPROPYL-5-METHYLCYCLOHEXYL 3-(1-(4-CHLOROPHENYL)-3-OXOBUTYL)-C	$C_{30}H_{33}O_6C1$	524	35.494	Benzopyrone Antioxidant, antimicrobial and anti-inflammatory activity

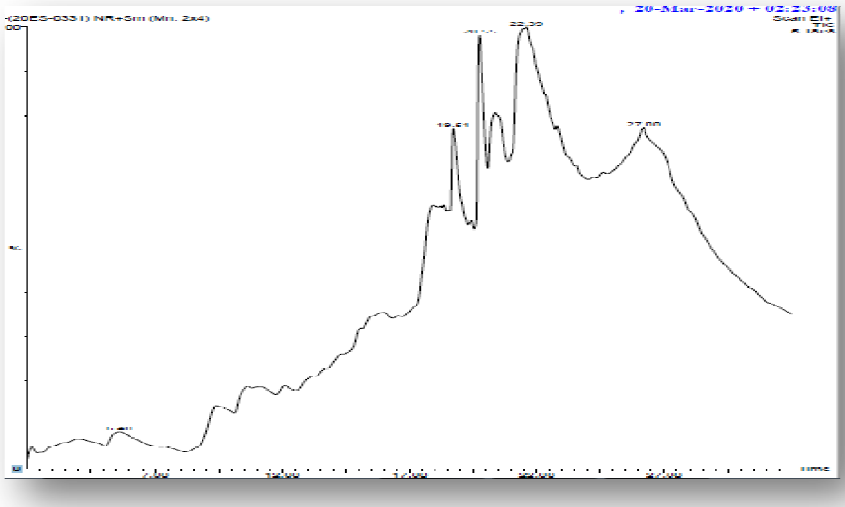

Figure 1 GC-MS chromatogram of methanolic extract of *Pancratium triflorum*

Indian Journal of Natural Sciences *www.tnsroindia.org.in ©IJONS*

Vol.15 / Issue 83 / Apr / 2024 *International Bimonthly (Print) – Open Access* *ISSN: 0976 – 0997*

RESEARCH ARTICLE

Novel Method of Controlling the Self Focusing and De-Focusing Length by using Non-Linear Kerr Material and Electro-Optic Materials

Rupali Maji

Assistant Professor, Department of Physics, New Alipore College (Affiliated of University of Calcutta), Kolkata, West Bengal, India.

Received: 18 Oct 2023 Revised: 09 Jan 2024 Accepted: 06 Mar 2024

***Address for Correspondence**
Rupali Maji
Assistant Professor,
Department of Physics,
New Alipore College (Affiliated of University of Calcutta),
Kolkata, West Bengal, India.
Email: rpl.maji@gmail.com

ABSTRACT

Nonlinear optical materials are used for several physical applications. In optical switching, lens less optical focusing and defocusing these non-linear materials can show its strong applications. The focal length of a material (if the material is used for self-focusing) depends on the applied power. Here in this chapter, a method of controlling the focal length of a nonlinear material based on the joint use of electro-optic material and a nonlinear crystal is proposed. The focal length of the nonlinear material depends upon the voltage applied to the electro-optic material. By changing this voltage/or field in the electro-optic material, the focal length can be varied and this technique can be used as a focal length controller. A suitable electro-optic material and a nonlinear material can be used this purpose.

Keywords: Nonlinear optical materials, field, voltage, controller

INTRODUCTION

When the refractive index of a material is depends on the applied electric field linearly is called Pockel effect and when it depends on the square of the applied field is called Kerr effect. The Kerr effect also called quadratic electro-optic effect [1]. The Kerr effect has a distinct from the Pockel's effect as has the induced index change is directly proportional to the square of the electric field instead of varying linearly with it. This refractive index variation is responsible for the nonlinear optical effects like self-focusing, self-phase modulation and modulation instability and is the basis for Kerr-lens mode locking. There are several applications of Kerr effects in optical switching, arithmetic and algebraic operations etc. [2, 3, 4, 5, 6, 7, and 8]. In the Kerr electro-optic effect, or DC Kerr effect, a slowly varying external electric field is applied across the sample material. Under the influence of the external signal the sample birefringent, with different indices of refraction for light polarized parallel or perpendicular the applied field. The

difference in index of refraction,Δn,($\Delta n=n-n_0$,where n and n_0 the refractive indices of the material with and without the applied of the external electric field respectively) is given by $\Delta n=\lambda KE^2$, where λ is the wavelength of the applied light, K is a material constant, and E is the strength of the electric field. This difference in index of refraction helps the material to act as a wave plate when the polarization of light is perpendicular of the applied electric field. If the material is kept between two 'crossed' linear polarizer's, no light come out when electric field is turned off, and almost all the light is transmitted for the application of the optimum value of the electric field. A higher value of the Kerr constant allow as a good transmission with a smaller applied electric field. In this particular work, the author shows by the use of Kerr material how one can control the focal length here the focal length of a non-linear material actually controlled by applied voltage, and the system is behaves like an optical lens.

Self-focusing and De-focusing of a Gaussian beam by the use of non-linear material

Due to a Kerr type of lensing, an intense optical pulse propagating in a non-linear medium experiences a self-focusing, where the beam diameter is decreased compared to of a weaker pulse. The physical mechanism is based on a Kerr nonlinearity with positive χ^2 .In this situation, the higher optical intensities of near to the beam axis, as compared to the off axis intensity, causes an increased refractive index in the inner part of the beam. This modified refractive index distribution acts like a focusing lens. The effect, occurring in the case of a negative χ^2 nonlinearity, self-defocusing, where a reduced refractive index is seen on the beam axis. A Kerr non-linear process which arises in a media exposed to intense electromagnetic radiation, and which produces a variation of the refractive index n as described by the formula $n=n_0+n_2I$, where n_0 and n_2 are the linear and non-linear components of the refractive index respectively, and I is the intensity of the light passing through it. The intensity distribution is taken spatially Gaussian, and the sign of the non-linear correction n_2 be either positive or negative, for self-focusing and defocusing [1, 9]. If the non-linear correction term n_2 is positive then in peripheral region the plane wave front takes a concave shape in the direction of the beam and is focused at the optical axis of the medium (Fig-1a).On the other hand if the n_2 is negative than central part of the beam goes faster than that of the peripheral region. Consequently, the plane wave front takes the shape of a convex shape direction of propagation and. Thus it defocused into the axis (Fig-1b).

Electro-optic material as an Amplitude modulator

Electro-optic modulator is an optical device in which an electrical signals exploiting the electro-optic effect and is used to modulate a proper beam of light. The modulation may be used to change the phase, frequency, amplitude, or polarization of the modulated beam. Modulation bandwidth at the gigahertz range is possible with the use of a laser based coherent controlled modulators. [10,11,12,13,14]. Certain materials change their optical properties when they are exposed to an electric field. This is caused by the forces that distort the positions and orientations of the molecules the material. The electro-optic effect gives the change in the refractive index from low frequency electric field to high one up to new range[15,16,17,18,19,20]. Some electric-optic materials are massively used as amplitude modulator such as Potassium di-deuterium phosphate (KD*P), Beta-barium borate (BBO), also Lithium niobate ($LiNb0_3$),Lithium Tantalite($LiTaO_3$) and Ammonium dihydrogen phosphate ($NH_4H_2PO_4$,ADP) etc. In addition to these there are also some organic types of special polymer modulators. A schematic diagram of $LiNb0_3$ based electro-optic modulator is shown in the fig 2.

Guassian beam

Gaussian beam has its transverse electric field and intensity distribution which is well approximated by Gaussian functions. Many lasers emits beams that has a Gaussian profile, for that reason the laser is said to be operating on the fundamental transverse mode, or "TEM_{00} mode" in the laser's optical resonator. When this beam is refracted by a diffraction-limited lens, a Gaussian beam is transformed into another Gaussian beam [13,14].

The beam profile of a Guassian beam is shown in fig 3. An integrated scheme of controlling the self-focusing length of a bulk non-linear medium by the use of electro-optic material

The refractive indices of the electro-optic modulator is [3.9]

$$n_{x'} = n_0 - \frac{1}{2} n_0^{\,3} r E_Z$$

(1)

$$n_{y'} = n_0 + \frac{1}{2} n_0^{\,3} r E_Z \quad (2)$$

Where 'r' is the material material constant. Ez, is the applied field along z direction.

First a linearly polarized wave polarized along the x-direction and (x' is one of the bi-axial direction of the Electro-optic material) traveling along the z-direction through electro-optic material is considered (fig 4), We have applied an external electric field Ez along the Z-direction (C-axis), then the output wave at Z=ℓ (where ℓ is the length of the electro-optic material along z) would be given by

$$\varepsilon_{X'}(\ell) = \varepsilon_{X'}(0)\exp\{i[\omega t - n_0(\omega/c)\ell + (\omega/2c)n_0^{\,3} r E_z \ell \quad (3)$$

Here $\varepsilon_{x'}(z)$ and $\varepsilon_{y'}(z)$ are the X' and Y' components of the electric field of the used light.

In a similar manner, a beam polarized along the Y-direction (where Y' is the other bi-axial direction of Electro-optic modulator) the output wave at Z=ℓ will be given by

$$\varepsilon_{y'}(\ell) = \varepsilon_{y'}(0)\exp\{i[\omega t - n_0(\omega/c)\ell + (\omega/2c)n_0^{\,3} r E_z \ell \quad (4)$$

Now consider an incident wave polarized along the y direction is taken then it can be decomposed into two linearly polarized waves along two orthogonal direction as X' and Y' as these two components will have equal amplitudes and will be in phase Z=0, i.e; at the input of the crystal. Thus the two components which were in phase at Z=o now develop a phase difference which is a function of the applied electric field (Ez).Thus the retardation at Z=ℓ between the two components will be

$\gamma=(\omega/c)n_0^3 r_{63} E_Z \ell = \omega n_0^3 r_{63} V/c$ (5)

Where V=Ezℓ is the voltage applied across the crystal. One can define the 'half wave'

Voltage $V_\pi$as the voltage required to develop a phase shift of π between the two orthogonal polarization components

So, $\gamma=\pi=(\omega/c)n_0^3 r_{63} V_\pi$ (6)

Or $V_\pi=\lambda_0/2n_0^3 r_{63}$

Substituting the values of ε_x and ε_y given by the equations (1) and (2), the expression of the total field (ε) becomes

$$\varepsilon=\frac{1}{2} A\exp\{i[\omega t-(n_0/c)\omega \ell+(\omega/2c)n_0^3 r_{63} E_Z \ell]\}[1-\exp(-i\gamma)] \quad (7)$$

Where $\gamma=(\omega/c)n_0^3 r_{63} E_Z \ell=\pi(V/V_\pi)$ (8)

Thus the intensity of the output beam is given by

$$I_0=\frac{1}{2}\mathrm{Re}[\varepsilon\varepsilon^*]=\frac{1}{2}A^2\sin^2\frac{1}{2}\gamma$$

$$=\frac{1}{2}A^2\sin^2[(\omega/2c)n_0^3 r_{63} V] \quad (9)$$

Where V=EzL is the applied voltage. The intensity of the input beam (I_i) is given by

$$I_i=\frac{1}{2}A^2 \quad (10)$$

$$\text{Thus} I_0/I_i=\sin^2(\frac{1}{2}\pi V/V_\pi) \quad (11)$$

I_0/I_i is the transmission coefficient of the electro-optic modulator.

If Vis very less than V_π

The $I_0/I_i \approx [\frac{\pi^2}{4}\frac{V^2(t)}{V_\pi^2}]$ (12)

Again the nonlinear refractive index of the Kerr type crystal is

$n=n_0+n_2I_0$. (13)

Putting the values of I_0 from equation (3.12) in equations (3.13)

$n=n_0+n_2I_i[\frac{\pi^2}{4}\frac{V^2(t)}{V_\pi^2}]$

$n-n_0=n_2I_i[\frac{\pi^2}{4}\frac{V^2(t)}{V_\pi^2}]$

$\Delta n=n_2I_i[\frac{\pi^2}{4}\frac{V^2(t)}{V_\pi^2}]$ (14)

We know the focal length (L_{sf}) of the Gaussian beam in a non-linear medium can be expressed as[1]

$L_{sf}=a\sqrt{n_0/2\Delta n}$ (15)

where a is the radius of the beam[1] (fig-5)

Now, putting the value of Δn from equation (14) we can get,

$$L_{sf}=a\sqrt{\frac{n_0}{2n_2I_i\frac{\pi^2}{4}\frac{V^2(t)}{V_\pi^2}}} \quad (16)$$

It is known that input intensity is I_i , where

$I_i=E_0^2$ (E_0 is the amplitude of the electric field strength of the light at the time of introduction in the modulator of the axis)

Thus the expression of the focal length can be written as,

$L_{sf}=\frac{aV_\pi}{\pi V(t)}\sqrt{\frac{2n_0}{n_2E_0^2}}$ (17)

$$L_{sf}=\frac{2V_\pi}{\pi V(t)}\frac{a}{E_0}\sqrt{\frac{n_0}{2n_2}} \quad (18)$$

Now E(r) can be written in a radial function (where r is the radial position in the circular beam)

as $E(r)=E_0\sqrt{1-r^2/a^2}$ (19)

For the mean value of the energy flux density, we obtain the expression

$\langle S\rangle=v\varepsilon E^2/2=[\varepsilon CE_0^2/(2n_0)](1-r^2/a^2)$

$=(\varepsilon_0 n_0 CE_0^2/2)(1-r^2/a^2)$ (20)

The energy flux of the beam is given by

$$P=\int_\sigma \langle S.\rangle d\sigma=\pi\varepsilon_0 n_0 cE_0^2\int_0^a(1-r^2/a^2)rdr \quad (21)$$

Where σ is the cross-sectional area of the beam. After integration the total energy flux (P) can be written as

$P=\pi\varepsilon_0 n_0 cE_0^2a^2/4$ (22)

$$E_0=\sqrt{\frac{P^2}{\pi\varepsilon_0 n_0 ca}} \tag{23}$$

Thus the self focal length

$$L_{sf}=\frac{V_\pi}{\pi V(t)}\frac{a^2\sqrt{\pi\varepsilon_0 n_0}c}{\sqrt{P}}\sqrt{\frac{n_0}{2n_2}} \tag{24}$$

RESULT

The result obtained in equation (24) can be used to obtain the focal length in Carbon bi sulphide, or in any other non-linear medium. For Carbon bisulphide, n_0=1.62, n_2=0.22*$10^{-19}$$m^2/w^2$, thus for a power P=10MW and beam radius a=1 cm,((the $LiNbo_3$ is used as Electro-optic modulator before the non-linear material) ℓ_{sf} become 6.92m (considering V_π=64V and V=64v also in equation (3.24))). Again if the applied voltage V=640V in $LiNbO_3$the ℓ_{sf} becomes 0.692 m.

CONCLUSION

From the above analytical treatment it is seen that if an electro-optic Pockel cell is used before a Kerr-cell which extends the self-focusing then one can easily control the focal length of the self-focusing system by applying the desired amount of voltage at the electro-optic material. Similarly the defocusing length can also be controlled by the same mechanism. The whole scheme may extend a tremendous application in optical communication through optical fiber. These mechanisms can help the coupling of desired amount of light intensity in an optical fiber from a source in case of data communication. To use it in the application domain one can use a suitable electro-optic material and a suitable simple Kerr non-linear medium.

REFERENCES

1. A.N.Matreev,Mir Publishers Moscow First Published (1988).
2. P. Kuila,A. Sinha,H.Bhowmik and S.Mukhopadhyay,"Theoretical study of using an amplitude modulation scheme with an electro-optic modulator for generation of the proper power shape function of an optical soliton pulse in a non-linear wave guide," Opt. Eng. 45(4),920060045 (2002).
3. A.Sinha,H.Bhoumik,P.Kuila and S.Mukhopadhyay, "New method of controlling the power of a Gaussian optical pulse through an electro-optic modulator and a non-linear wave guide for generation of solitons",opt. Eng,44(6)(065003)June(2005).
4. P.Mondal and S.Mukhopadhyay, "Analytical study to find the proper coupling energy from one optical wave guide to another with consideration of the non-linear correction factor", opt. Eng (USA),45(11),114605.114602.1-114605.5 (2006).
5. P.Mondal and S.Mukhopadhyay, "method of conducting an optical NAND logic operation controlled from a long distance," opt. Eng (USA),46(3),.035009 (2006).
6. P. Kuila,A. Sinha,S.Mukhopadhyay, "A Theoretical approach for generation of optical soliton pulse inside an optical fiber using electro-optic modulator", accepted for publication in journal of optics (2008).

7. 7)Cusack,J.Benedict,S.Benjamin,Shaddock,A.Daniel,Gray,B.Malcolm,Lam,Koy Ping,Whitecomb,E.Stan, "Electro-optic Modulator capable of Generating Simultaneous Amplitude and Phase Modulations",Appl.opt.Vol.43(26),5079-5091 (2004).
8. J.Nees,S.Williumson,G.Mourou, "100 GHz traveling wave electro-optic phase modulator",Appl.Phy .Lett,Vol.54,1962-1964 (1989).
9. "Optical electronics" A.Ghatak, K.Thayagarajan (Cambridge university press 2002.).
10. Abhijit Sinha,, and S. Mukhopadhyay, "Effect of higher order non-linearity in frequency variation of self-phase modulation in optical fiber communication", *Chinese Optics Letters*, **2(9)**, 500-502(2005).
11. G. Fibich and Alexander L. Gaeta "Critical power for self-focusing in bulk media and in hollow waveguides" Optics Letters, Vol. 25, Issue 5, pp. 335-337 (2000) doi.org/10.1364/OL.25.000335
12. D.Huang, M.lman, Lucio H. Acioli, H.A. Haus, and J.G. Fujimoto "Self-focusing-induced saturable loss for laser mode locking" Optics Letters, Vol. 17, Issue 7, pp. 511-513 (1992) .doi.org/10.1364/OL.17.000511
13. Abhijit Sinha, HariharBhowmik, PuspenduKuila, and S. Mukhopadhyay, "New method of controlling the power of a Gaussian optical pulse through an electro-optic modulator and a nonlinear wave guide for generation of solitons", Optical Engineering, **44(6)**, 065003(1 June, 2005).
14. PuspenduKuila, Abhijit Sinha, S. Mukhopadhyay, "An all-optical method of conducting some logic operations by interaction of two modulated Gaussian pulses," *Journal of Optics*, **35(4)**, 196-205 (2006).
15. Sidney A. "Self focusing of spherical Gaussian beams" Applied optics / Vol. 22, No. 5 / 1 March 1983.
16. A. Bencheikh, M. Bouafia, K. Ferria "new spherical aberration coefficient C4 for theGaussian laser beam" OpticaApplicata, Vol. XLI, No. 4, 2011.
17. Gee, C.M "17GHZ band width electro-optic modulator" Applied physics Letters, Vol 43, issue 11,PP 998-1000(1983)doi:10.1063/1.94211.
18. Girton, D.G "20GHZ electro-optic polymer Mach-Zehnder modulator "Applied physics letters, vol 58,issue 16 pp 1730-1732 (1991) doi:10.1063/1.105123.
19. Spickermann. R "GaAS/AlGaAs traveling wave electro-optic modulator with an electrical bandwidth >40GHZ"Electronics Letters.vol 32, issue 12,pp 1095-1096 (1996) doi:10.1049/el.1966745.
20. Miller, D.A.B "Novel hybrid optically bi stable switch the quantum well self electro-optic effect device" Applied physics letters , vol 45,issue 1 pp 13-15 (1984) doi: 10.1063/1.94985.

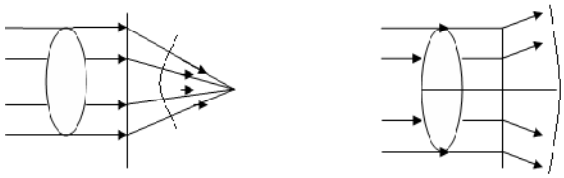

Fig-1 Focusing and defocusing in a non-linear medium. a)$n_2<0$, b)$n_2>0$

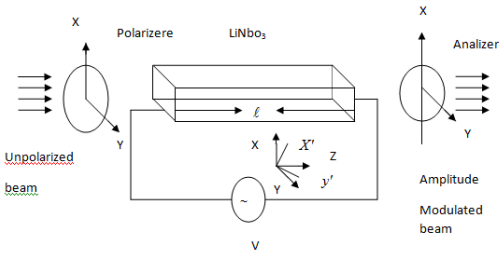

Fig-2 An electro-optic amplitude modulator using $LiNbo_3$

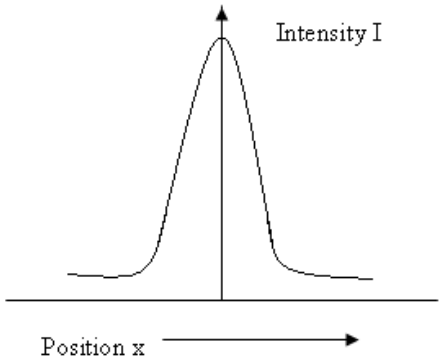

Fig-3 Profile of a Gaussian beam

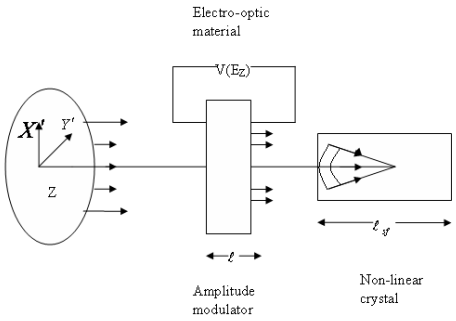

Fig-4 Scheme of controlling the focal length of Gaussian beam by use of E-o modulator and a Kerr type of non-linear material

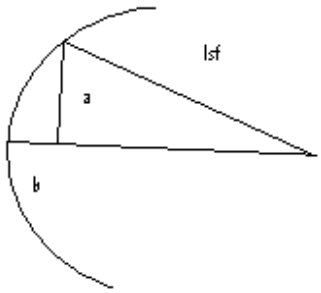

Fig-5 Calculation of self-focusing length.

Indian Journal of Natural Sciences *www.tnsroindia.org.in ©IJONS*

Vol.15 / Issue 83 / Apr / 2024 *International Bimonthly (Print) – Open Access* *ISSN: 0976 – 0997*

RESEARCH ARTICLE

Effect of Cold therapy for Reduction of Perineal Pain among Postnatal Mothers in Selected Hospitals, Assam

Bhagya Priya Phukan[1]*, Nongmeikapam Monika[2] and Zulanbeni C Kithan[3]

[1]Student(M.Sc Nursing), Department of Obstetrics and Gynaecological Nursing, Faculty of Nursing, Assam down town University, Assam, India.
[2]Professor, Department of Obstetrics and Gynaecological Nursing, Faculty of Nursing, Assam down town University, Assam, India.
[3]Lecturer , Faculty of Nursing, Assam down town University, Assam, India.

Received: 30 Dec 2023 Revised: 09 Jan 2024 Accepted: 17 Mar 2024

***Address for Correspondence**
Bhagya Priya Phukan
Student(M.Sc Nursing),
Department of Obstetrics and Gynaecological Nursing,
Faculty of Nursing,
Assam down town University,
Assam, India.
Email: nangbhagyapriyaphukan@gmail.com

ABSTRACT

Postpartum minor discomforts occur resulting from all systems adaptation. Perineal pain is one of the most common post partum minor discomforts. Cold therapy can help in reducing perineal pain after normal vaginal delivery. The main purpose of the study is to assess the effect of cold therapy for reduction of perineal pain among postnatal mothers in selected hospitals, Assam. With an evaluative approach, a pre-experimental, one group pretest-post-test design was adopted for the study among 60 samples by using purposive sampling technique. The study was conducted in Swahid Tilak Hemram Gunabhiram Civil Hospital, Morigaon and Bhurbandha Model Hospital, Morigaon, Assam. After obtaining consent from participants, pain score was assessed before application of cold therapy and it was applied for 15-20 min twice a day i.e immediately within 1 hour of normal vaginal delivery and subsequently after 8 hours for two consecutive days. The level of pain was assessed each day by using Numerical Pain Rating Scale. The study revealed that the mean postest level of pain (1.48) was lower than the mean pretest level of pain (7.73). The calculated t_{59}=39.36 and p-value=0.001 was significant at $p<0.05$, thus research hypothesis (H_1) was accepted. The result of Chi square test and Fisher's Exact test revealed that age is associated with the pretest level of perineal pain. The present study concluded that cold therapy application was proved to be significant in reducing perineal pain after normal vaginal delivery among postnatal mothers.

Keywords: Perineal pain, episiotomy wound, perineal tear, cold therapy, numerical pain rating scale

INTRODUCTION

Delivering a baby out of a relatively small opening can leave the vaginal and perineal muscle torn, with tears and sometimes the perineum is required to be given episiotomy and stitched. This causes a lot of perineal pain and discomfort [1]. Normal puerperium is 6 weeks post childbirth during which the pelvic organs reverts back to the near pre-pregnant state and the physiological changes of pregnancy are reversed [2]. WHO describes the postnatal period as most critical phase and yet most neglected period for the provision of quality care in the lives of mothers and babies; most death occur in the postnatal period [3]. Postpartum minor discomforts may occur resulting from all systems adaptation. Most common post partum minor discomforts include after pain, perineal pain, constipation, urinary distension, lactation problems. Immediate and effective care for these problems during intranatal and postnatal period can make the differences in postpartum adaptation [4]. It is the priority of the health care professionals to identify and value the morbidities resulting from a normal vaginal delivery, particularly the presence of pain. The identification of spontaneous perineal pain and the methods used for its relief are considered very important [5]. It is important that health care professional who attend to new postnatal mothers, should know how to assess and treat perineal pain. Considering the high rates of perineal trauma following vaginal deliveries, we as a midwife should need to provide cost-effective alternative treatment for perineal pain, based on scientific evidence. The researcher had been exposed to various hospitals and clinical settings where it was observed that women undergoing normal vaginal delivery with or without episiotomy had various degree of perineal pain and due to the pain the postnatal mothers find it difficult to do their daily activities of living and it interferes with caring the baby. The postnatal mothers, because of fear of pain do less voiding and passing of stool which leads to other issues during her stay in hospital. Non pharmacological treatment such as icepack covered with a soft covering can be used to reduce swelling and discomfort [6]. Cold therapy application is a very cost effective procedure and studies have shown the positive effect in relieving the discomfort of the perineal pain of the postnatal mothers. Moreover, this type of study has been done very less in the selected population. Therefore, the researcher felt the need to provide cold therapy application for perineal pain reduction after normal vaginal delivery among the postnatal mothers.

OBJECTIVES

1. To assess the level of perineal pain before cold therapy application among postnatal mothers in selected hospitals.
2. To assess the level of perineal pain after cold therapy application among postnatal mothers in selected hospitals.
3. To assess the effect of cold therapy for reduction of perineal pain among postnatal mothers in selected hospitals.
4. To find out the association between level of perineal pain before cold therapy application among postnatal mothers with the selected demographic variables.

MATERIALS AND METHODS

A pre experimental one group pre-test-post-test design was selected for the study. The study was conducted in Swahid Tilak Hemram Gunabhiram Civil Hospital, Morigaon and Bhurbandha Model Hospital Bhurbandha, Morigaon among 60 postnatal mothers. Ethical clearance certificate and formal permission was taken from the concerned authorities and participants to conduct the research study. The tools used for the study was demographic variables and Mc Caffery Numerical Pain Rating Scale. Non-probability Purposive sampling technique was used for selecting the postnatal mothers who had normal vaginal delivery with episiotomy or perineal tear. The pre-test was conducted before cold therapy application by using Mc Caffery Numeric Pain Rating scale and cold therapy was applied for 15-20 min twice a day i.e immediately within 1 hour of normal vaginal delivery and subsequently after 8 hours for two consecutive days. Observation was done before and after the intervention and postest pain score was

obtained once again for each selected samples. The data obtained were analyzed in terms of objective of the study by using descriptive and inferential statistics.

Inclusion criteria

The study includes those postnatal mothers

- Who are on the 1st postnatal day after normal vaginal delivery with episiotomy or perineal tear admitted in selected hospitals, Assam.
- Who are available during the time of data collection period.
- Who are having pain score of ≥ 4 in numerical pain rating scale.
- Who are able to communicate in English, Assamese.

Exclusion criteria

The study excludes the postnatal mothers

- Who are not willing to participate in the study.
- Who are receiving analgesic drug.
- Who are using any traditional method for reduction of perineal pain.
- Who are with any kind of mental health or medical related issues.

RESULT

With reference to the sample characteristics presented in Table 1, most of the postnatal mothers were in the age group of 21-25 years, i.e, 40 (66%), 30(50%) had higher secondary level of education, 35 (58%) were primi gravida, 27 (45%) of the postnatal mothers were from rural area, 35 (58%) had episiotomy wound, 46 (76%) birth weight of newborn was in between 2.5-3 kg. With reference to the level of perineal pain of the postnatal mothers pretest and posttest perineal pain score result indicates that 92% had pain score of 7-10 (severe pain). Whereas in the posttest 82% had pain score of 1-3 (mild pain). Hence posttest pain score remains lower than the pretest pain score. With reference to the effect of cold therapy for reduction of perineal pain after normal vaginal delivery among postnatal mothers presented in Table 2, the results shows that the mean postest pain score (1.48) was lower than the mean pretest pain score (7.73). The calculated t_{59} = 39.36 and p-value = 0.001 was significant at $p<0.05$. Therefore, cold therapy application was proved to significantly reduce the perineal pain among postnatal mothers.

With reference to the association between the pretest level of perineal pain before cold therapy application among postnatal mothers with the selected demographic variables. The data indicates that there is a significant association between the pretest level of perineal pain with the age (in years). Hence, the research hypothesis H_2 is accepted and null hypothesis H_{02} is rejected.

DISCUSSION

The findings of the present study had been discussed in relation with the objectives and hypotheses of the study under following headings;

To assess the of level of perineal pain before cold therapy application among postnatal mothers in selected hospitals. The findings of the present study revealed that out of 60 postnatal mother: majority 92% (55) had pain score between 7-10 (severe pain) and 8 % (5) had pain score between 4-6 (moderate pain) before the application of cold therapy. Similar study conducted by Sadashivsali A (2013) on effect of sitz bath versus gugguldhupan on pain related to episiotomy in postnatal mothers admitted in selected hospitals of Pune city, India. The sample size was 60 postnatal mothers, divided into two groups and convenience sampling technique was used. Group A consisted of 30 samples and received sitz bath as a treatment. Group B had another 30 samples who received gugguldhupan as a treatment. The study revealed that, 53.3 % postnatal mothers having severe episiotomy pain before giving sitz bath and

according to self assessment score maximum 63.3 % postnatal mothers having severe episiotomy pain before gugguldhupan [7].

To assess the of level of perineal pain after cold therapy application among postnatal mothers in selected hospitals

The present analysis revealed that out of 60 postnatal mother: majority 82% (49) had pain score between 1-3 (mild pain) and 18% (11) had 0 (no pain) after the application of cold therapy. Similar study conducted by Bini, Solomon JR, Ahita V (2019) on effectiveness of cold application on episiotomy pain among postnatal mothers in Kanyakumari district. The result revealed that experimental group in day 1 had pretest score of 53.33% very severe episiotomy pain and 46.67% worse episiotomy pain and on postest 73.34% severe pain and 13.33% very severe episiotomy pain. On day 2 the pretest pain score was 53.33% moderate pain and 46.67% severe pain which was reduced to 66.67% mild pain and 33.33% no episiotomy pain in postest. Whereas in the control group in day 1 pretest 53.33% very severe episiotomy pain and 46.67% worse episiotomy pain and on day 1 postest 90% had very severe pain, 6.67% had severe pain, 3.33% had worse episiotomy pain. On day 2 in pretest score 66.67% very severe pain and 33.33% severe pain and on postest 66.67 severe pain, 16.67% very severe pain, 16.67% moderate pain. There was a significant reduction in mean post-test episiotomy pain of the experimental group [8].

To assess effect of cold therapy for reduction of perineal pain among the postnatal mothers in selected hospitals.

Finding of the present study reveals that the mean postest level of pain (1.48) was lower than the mean pretest level of pain (7.73). The calculated t_{59} value was 39.36 and the tabulated valued of df for 0.05 significance was 0.001 was significant at $p<0.05$, thus the null hypothesis (H_{01}) was rejected and research hypothesis (H_1) was accepted. Therefore, cold therapy application was proved to significantly reduce the perineal pain after normal vaginal delivery among postnatal mothers.

Similar study conducted by Senol KD, Aslan E (2017) to determine the effects of cold application to the perineum on pain relief after vaginal birth in Turkey among 200 postnatal mothers. The samples were divided into experimental group and control group. Experimental group got application of crushed ice pack for 20 min in the postpartum 1st 2 hours and 4 hours after the first application. The result showed that the experimental group, the first visual analog scale score was 6.7$\pm$1.68; after cold gel pad application, the pain level decreased to 2.59$\pm$1.20 in both primiparous and multiparous mother. The result showed that both episiotomy and perineal laceration were strongly associated with the presence of perineal pain during immediate postpartum and at 3 months. It also showed that increased length of labor and decrease parity have been positively with postpartum perineal [9].

To find out the association between level of perineal pain before cold therapy application among postnatal mothers with the selected demographic variables.

The association findings of the present study revealed that there was a significant association between the pretest level of pain of pain with the age (in years). Hence, the research hypothesis H_2 is accepted and null hypothesis H_{02} is rejected. Similar study conducted by Mathias ADREA, Pitangui RCA, Vasconcelos AMA, Silva SS (2015) on perineal pain measurement in the immediate vaginal postpartum period in Petrolina and Juazerio among 147 women who had delivered baby through vaginal delivery. McGill Pain Questionnaire (MPQ) and numeric visual pain scale (NVS) was used to measure pain. The data was collected at a minimum of 6 hours and maximum of 24 hours after delivery. The study revealed that there was a significant association of pain with episiotomy ($p=0.002$), laceration (0.039) and parity (0.028). Thus the study concluded that there was significant association of pain with episiotomy, laceration, parity [10].

CONCLUSION

The present study was conducted to evaluate the effect of cold therapy for reduction of perineal pain among postnatal mothers. The findings of the study revealed that cold therapy is effective for reduction of perineal pain among postnatal mothers.

REFERENCES

1. Being the Parent. Easing-postpartum-perineal-pain. [Online]. [Accessed 2021 February 20]. Available from: https://www.beingtheparent.com/easing postpartum perineal pain.
2. Sharma B. J. Textbook of Obstetrics. 1st ed. New Delhi: Avichal Publishing Company 2017. p. 385
3. WHO. WHO recommendations on postnatal care of the mother and newborn [Online]. 2013. [Accessed 2021 Feb 20].
   Available from: https://www.who.int/maternal child adolescent/documents/postnatal care recommendation/en/
4. Shaban A.El.T.H, Ghoney G, Sayed El.AY. Effect of health teaching on postpartum minor discomfort. Beni-Suef University Journal of basic and applied science. 2018; 7(2):198-203. [cited- 2021 February 20] Available from: https://www.sciencedirect,com/article/pii/S2314853517302998
5. Fransisco A.A, Oliveria de V.J.M.S, Santos O.J, Silva B.M.F. Evaluation and treatment of perineal pain in vaginal postpartum 24(1): 94-100.
6. Babycenter. Postpartumperineal pain.[Online]. [Accessed 2021 Feb 20]. Available from: https://www.babycenter.com/baby/postpartum-health/postpartum-perineal-pain_256
7. Sadashivsali A**.** A comparative study on effect of sitz bath versus gugguldhupan on pain related to episiotomy in postnatal mothers admitted in selected hospital of Pune City, India. AA Rsch J of M 2014;1(20):286-300.
8. Bini, Solomon JR, Ahita V. Effectiveness of cold application on Episiotomy pain among postnatal mothers in selected hospitals at Kanyakumari district**.** Asian J. Nursing Education and Research.2019; 9(2):188-192.
9. Senol KD, Aslan E **.**The effect of cold application to the perineum on pain relief after vaginal birth. Asian Nurs Res (Korean Soc Nurs Sci) 2017:11(4):453-458.
10. Mathias ADREA et.al. Perineal pain measurement in the immediate vaginal postpartum period. Revista Dor 2015:12:267 271.

Table 1: Frequency and percentage distribution of demographic variables

n=60

Sl. No.	Demographic Variables	Frequency (f)	Percentage (%)
1	**Age (in years)**		
	a) ≤20	11	18
	b) 21-25	**40**	**67**
	c) ≥26	9	15
2	**Educational status**		
	a) Primary	-	-
	b) High school	17	28
	c) Higher secondary	**30**	**50**
	d) Graduation and above	13	22
	e) No formal education	-	-
3	**Gravida**		
	a) Primi gravida	**35**	**58**
	b) Multi gravida	25	42
4	**Area of residence**		

	a) Urban **b) Rural** c) Semiurban	20 **27** 13	33 **45** 22
5	**Type of perineal wound** a) Perineal tear wound **b) Episiotomy wound**	 25 **35**	 42 **58**
6	**Birth weight of newborn (in kg)** a) ≤ 2.4` b) **2.5 – 3.0** c) 3.1 - ≥3.5	 - **46** 14	 - **77** 23

Table 2: Frequency and percentage distribution of pretest and postest level of perineal pain among postnatal mothers

n=60

Level of perineal pain	Pre-test		Post-test	
	F	%	f	%
No pain	-	-	11	18
Mild pain	-	-	49	82
Moderate pain	5	8	-	-
Severe pain	55	92	-	-
Total	60	100	60	100

Table 3: Mean, Standard Deviation, Mean Difference, t test value, df, p value of pain score before and after cold therapy application among postnatal mothers.

n=60

Comparison of level of pain	Mean	SD	Mean Difference	t value	df	p value	Inferences
Pre-test	**7.73**	**1.006**	**6.25**	**39.36**	**59**	**0.001***	**S**
Post-test	**1.48**	**0.965**					

*** Significant at p<0.05 (t_{59}=39.36)** **S-Significant**

Table 4: Association between level of perineal pain before cold therapy application among postnatal mothers with the selected demographic variables

n=60

Sl. No	Demographic variables	Pre-test level of perineal pain		χ^2 Value	df	p value Fisher's exact test	Inference
		Moderate	Severe				
1	Age (in years) a. ≤ 20 b. ≥ 21	 3 2	 8 47	3.653	1	**0.038***	**S**
2	Educational status a. High school b. Higher secondary and above	 1 4	 16 39	0.186	1	1.00	NS

3	Gravida a. Primi gravida b. Multi gravida	3 2	32 23	0.006	1	1.00	NS
4	Area of residence a. Urban b. Others	1 4	19 36	0.436	1	0.656	NS
5	Type of perineal wound a. Perineal tear wound b. Episiotomy wound	2 3	23 32	0.006	1	1.00	NS
6	Birth weight of newborn (in kg) a. ≤ 3.0 b. ≥3.1	4 1	42 13	0.034	1	1.00	NS

*** Significant at p<0.05** **S-Significant NS-Non Significant**

Indian Journal of Natural Sciences *www.tnsroindia.org.in ©IJONS*

Vol.15 / Issue 83 / Apr / 2024 *International Bimonthly (Print) – Open Access* *ISSN: 0976 – 0997*

RESEARCH ARTICLE

Customer Perception towards Township Apartment

A. Pappu Rajan[1]*, P.J. Rosario Vasantha Kumar[2] and Sunil Raj Y[3]

[1]Associate Professor, Department of Management Studies, St. Joseph's Institute of Management, St. Joseph's College (Autonomous), (Affiliated to Bharathidasan University), Tiruchirappalli, Tamil Nadu, India.
[2]Librarian, St. Xavier's College (Autonomous) Palayamkottai, (Affiliated to Manonmaniam Sundaranar University), Tirunelveli, Tamil Nadu, India.
[3]Assistant Professor, Department of Data Science, St. Xavier's College (Autonomous) Palayamkottai, (Affiliated to Manonmaniam Sundaranar University), Tirunelveli, Tamil Nadu, India.

Received: 22 Feb 2024 Revised: 06 Mar 2024 Accepted: 20 Mar 2024

***Address for Correspondence**
A. Pappu Rajan
Associate Professor,
Department of Management Studies,
St. Joseph's Institute of Management, St. Joseph's College (Autonomous),
(Affiliated to Bharathidasan University),
Tiruchirappalli, Tamil Nadu, India.
Email: ap_rajan2001@jim.ac.in

ABSTRACT

Housing plays a crucial role in the economic, social, and civic development of both developed and developing countries. This study delves into the perceptions of middle-class individuals regarding living in apartment townships, particularly focusing on their understanding of affordable housing provided by developers in Chennai, India. By directly engaging with residents, the research aims to gain insights into their attitudes towards affordable housing options. The study specifically targets middle-income individuals who have had experience with apartment living in Chennai. Employing a descriptive research design, it seeks to analyze the market dynamics, enhance public comprehension of affordable housing concepts, and potentially generate more leads for banks. Objectives include assessing market demand, identifying potential risks for banks, and proposing mitigation strategies. Data collection involves simple random sampling from a database of builder projects in Chennai. Analysis is conducted using Microsoft Excel and IBM SPSS software, employing statistical measures such as means, descriptive statistics, and variance analysis to interpret primary data sources accurately.

Keywords: Segmentation, Customer perception, Marketing Research, Consumer Behavior

INTRODUCTION

A mediation model (Yingzi Xu et.al,2006) is used to links customer perceived service value to customer loyalty via customer satisfaction. The customer satisfaction (Boamah, Fredrick Ahenkora,2020) is impact of different combination of reliability, responsiveness, assurance and empathy with high service quality. Market Segmentation includes psychographics, lifestyles, values, behaviours, and multivariate cluster analysis routines of individual perceptions and experiences. According to Bharwana(2013) , service quality is very high impact on customers' satisfaction. Market segmentation Process has many difficulties that to be solved and it has described to be tackled to leading several management teams (Dibb, S. and Simkin, L,1997) through the analysis and strategy. As a result of the ongoing economic deregulation measures of the Government particularly those in the financial and banking sector, there have been market changes in the housing finance systems in India (P K, Manoj,2004).The House (Mondal et.al. 2020, Balanaga Gurunathan K and Nidhi Ahuja (2020) is the key need that the livelihood of a person as a proper house gives an individual security of the people. In this research gives over all view of customer perception towards township apartments and try to deal the important of the research in the filed of housing finance in particular to township apartments.

Conceptual Frame Work

Housing stands as a vital catalyst for economic, social, and civic development, constituting a significant component of developing nations' economies. The provision of public transport, parks, and local amenities is crucial for fostering community well-being within apartment complexes. While luxury amenities are valued, practicality and quality in personal and shared living spaces take precedence for most individuals (Hanif, 2015). Intense competition within the banking sector necessitates unwavering commitment to service excellence (Bose Ranjan, 2018). Urban density fluctuations and transportation demand dynamics influence housing preferences and purchasing behavior (Habibia& Asadi, 2011). Affordability has emerged as a central theme in housing policy and urban sustainability discussions (Mubiru &Ikiriza, 2021; Gupta, 2019). Economic models often focus on factors like transport accessibility and house prices in understanding housing markets (Matenge et al., 2016). High-rise living impacts various aspects of residents' lives, tempered by socioeconomic factors and neighborhood quality (Gifford, 2007). Location remains pivotal in the housing market, with proximity to employment and amenities driving demand (Aluko, 2011). The quality of economic output serves as a critical indicator for strategic business planning and consumer behavior (Ilieska, 2013). Understanding customer perceptions guides real estate developers in meeting buyer demands effectively (Misra et al., 2013; Engel et al., 2005). Open spaces within housing societies enhance residents' quality of life and property values (Kakkar & Supriya, 2014). Factors such as landownership, zoning, and public utilities are key considerations in apartment site selection for developers (Krisnaputri, 2016). As cities globally brace to accommodate an additional 3 billion people over the next two decades, the lack of resources poses a significant challenge to sustainable urban development.

Research Design

The study is focused on understanding the perceptions of middle-class individuals towards apartment township living and their comprehension of affordable housing provided by developers. It aims to delve into the depth of general awareness of affordable housing concepts prevalent in the market and evaluate the extent of market penetration achieved by builders. Conducted in Chennai, India, the research targets middle-income residents who have direct experience with apartment living. By engaging with this demographic, the study seeks to unravel the relationship between their demographic profiles and their perceptions of affordable housing.

The methodology employed incorporates a descriptive research design, allowing for a comprehensive analysis of various factors influencing perceptions, including physical, social, and economic attributes associated with apartment living. Additionally, the study endeavors to identify the preferences and requirements of respondents concerning ideal apartment living arrangements. Through this process, the research aims to contribute to a deeper understanding of the affordable housing market dynamics in Chennai.

The primary objective of the study is to provide insights into the affordable housing market, thereby facilitating enhanced understanding among both consumers and stakeholders, potentially leading to increased leads for HFFC (Housing Finance and Development Corporation). Apart from this overarching goal, the study also seeks to achieve several specific objectives. These include analyzing current market trends, assessing demand and supply dynamics, examining pricing mechanisms, and identifying potential risks faced by HFFC in the market. Furthermore, the research aims to propose mitigation strategies to address these risks effectively. To accomplish these objectives, the study employs a systematic approach to sample selection and data collection. The target population comprises individuals aged 20 to 60 years, belonging to the middle-income bracket, with monthly household incomes ranging from Rs. 5000 to Rs. 30000. These individuals must have been residents of Chennai and its surrounding areas for at least two years. The sampling technique employed is simple random sampling, drawing data from a comprehensive database of builder projects in Chennai. This ensures that the sample is representative of the broader population of interest. Data collection involves both primary and secondary sources. Primary data is collected through direct field visits and personal interviews using structured questionnaires. These interviews are conducted with randomly selected respondents residing in areas covered by builder projects listed in the database.

On the other hand, secondary data is gathered from HFFC's database, focusing on builder projects in specific areas such as Avadi and Ambattur, which cater to the affordable housing segment. The collected data is then subjected to rigorous analysis using appropriate statistical tools and software. Microsoft Excel is utilized for data input and initial organization, while IBM SPSS (Statistical Package for the Social Sciences) is employed for in-depth statistical analysis. Various statistical techniques are applied, including means comparison, descriptive statistics, variance analysis, and Chi-Square tests for goodness of fit. These analytical methods help in uncovering patterns, trends, and associations within the data, providing valuable insights into the perceptions and preferences of respondents. One of the critical aspects of the study is the examination of the relationship between respondents' demographic profiles and their perceptions of affordable housing. This involves testing the association between different demographic variables and the dependent variable of perception. By analyzing this relationship, the study aims to identify any significant demographic factors that influence individuals' perceptions of affordable housing. Furthermore, the research explores the concept of market potential in the affordable housing segment in Chennai.

It assesses the demand for affordable housing, considering factors such as population growth, income levels, and urbanization trends. Additionally, the study examines supply-side factors, including the availability of land, construction costs, and regulatory frameworks governing the housing sector. By analyzing both demand and supply dynamics, the research aims to provide a comprehensive understanding of the market landscape. Another important aspect of the study is the assessment of potential risks faced by HFFC in the affordable housing market. This involves identifying various risk factors, such as economic downturns, changes in government policies, and market competition. Subsequently, the research proposes mitigation strategies to manage these risks effectively and safeguard the interests of HFFC and other stakeholders. In summary, the study aims to contribute to a deeper understanding of the affordable housing market in Chennai by examining middle-class perceptions and preferences. Through a systematic research approach encompassing data collection, analysis, and interpretation, the study seeks to provide valuable insights for consumers, developers, policymakers, and financial institutions operating in the housing sector. By shedding light on market dynamics, potential risks, and mitigation strategies, the research aims to foster informed decision-making and promote sustainable growth in the affordable housing segment.

RESEARCH DISCUSSION

The researcher is tried to find the reason for choosing apartment as result of finding table 1.1 shows that 13 of respondents feel it is affordable, 45 of respondents feel it is proximity to transport and other amenities, 15 of respondents feel it is a socialistic thought who have responded for the survey. The researcher is tried to find the reason for shift from apartment as result of finding table 1.2 shows that 24 of the respondents shift due to rent or maintenance problem, 27 of the respondents shift due to independent living, 19 of the respondents shift due to

Quality issues and 14 of the respondents shift due to other reasons who have responded for the survey. Figure 1, presents the details on the reasons for the respondents to move form the apartment to another. The peak shows that most respondents would leave from the apartment due to the quality issues. H1:There is no significant difference between the perception of the people towards affordable apartment township living and their gender. As the P value is 0.094 which is lesser than 0.1 it shows that gender has influence on perception towards township apartments. Table 1.4 presents symmetric measures examining the relationship between gender and perception towards township living. Pearson's correlation coefficient for interval by interval variables is 0.034, while Spearman's rank correlation coefficient for ordinal by ordinal variables is 0.036. Both coefficients suggest a weak correlation between gender and perception towards township living. The asymptotic standard errors for both coefficients are 0.100. The approximate t-values are 0.335 for Pearson's correlation and 0.354 for Spearman's correlation. The p-values for both coefficients are notably high, with 0.738 for Pearson's correlation and 0.724 for Spearman's correlation, indicating that the observed correlations are not statistically significant at the 5% significance level. Thus, based on this analysis, there is insufficient evidence to support a significant relationship between gender and perception towards township living in the dataset. Figure 2, presents the symmetric measures where gender and perception towards township are considered. The peak shows the significance of the results, standard error and the values associated.

The Pearson's correlation coefficient of 0.034 indicates a positive relationship between gender and perception towards township living. Multiple hypotheses were tested, revealing that: a) educational qualifications have minimal impact on perception towards township apartments, b) salary influences perception towards such apartments, and c) employment type also affects perception. The questionnaire developed to assess customer attitudes towards apartment townships in the affordable housing segment proved valuable in gauging customer awareness and perception of available products. It can be utilized for future studies and market analyses to further understand individual perceptions. The sample population skewed male, with 61% male respondents compared to 39% female, reflecting the predominant male presence at HFFC branches. Age emerged as a significant determinant of perception, with those aged 20-30 exhibiting higher satisfaction with apartment townships than those aged 50-60. Educational qualifications, job type, and income were found to be interrelated factors influencing customer perception, with individuals of higher qualifications, income, and job status expressing less satisfaction with apartment townships. Conversely, those with moderate educational backgrounds, middle-class incomes, and decent jobs showed a more positive outlook. Among these factors, the locality and price of apartment townships exerted the most significant impact. Private sector banks should focus on enhancing customer satisfaction by offering housing loans with simplified procedures and transparent terms. Diversifying product offerings and leveraging various media channels for promotion is essential. Understanding and addressing customer grievances regarding home loans, including high-interest rates, through interest subsidies based on income categories, would benefit both customers and the organization. Banks should closely monitor customer preferences and collaborate with builders, DSAs, and masons to stay abreast of customer needs and generate more leads. Continuous promotion of products, including sponsoring builder community meetings, is vital for maintaining visibility and market presence.

CONCLUSION

The housing sector is an ever-expanding industry, heavily reliant on meeting customer needs and satisfaction for success. Any decrease in customer satisfaction and comfort within this sector could result in significant losses. Apartment townships have emerged as one of the fastest-growing segments within India's housing market, playing a pivotal role in revenue generation and contributing substantially to the country's GDP. Despite the industry's apparent success and sustained growth, there exists a notable challenge stemming from individual perceptions and viewpoints, which influence family members' attitudes towards the apartment township lifestyle. While younger demographics, such as teenagers, those in their early twenties, and thirties, often express a desire to reside in apartment townships, individuals aged forty and above typically exhibit strong reluctance toward embracing this lifestyle. Furthermore, there's a noticeable divide based on socioeconomic status and education level, with affluent and highly educated individuals displaying hesitancy while middle-class individuals with moderate educational

backgrounds show greater interest, relatively speaking.Our research has identified several key factors that significantly impact customers' inclination towards apartment townships. Privacy emerges as a primary concern, as residents may not enjoy the same level of privacy as they would in standalone houses. Despite the affordability of apartment townships, peace and proximity to amenities also play essential roles in shaping people's perceptions of this housing option. Therefore, it is imperative to focus efforts on addressing these concerns and improving customer satisfaction while working to alter perceptions of apartment townships.

REFERENCES

1. Yingzi Xu,Robert Goedegebuure,Beatrice van der Heijden(2007). *Customer Perception, Customer Satisfaction, and Customer Loyalty Within Chinese Securities Business: Towards a Mediation Model for Predicting Customer Behavior.* Journal of Relationship Marketing.Volume 5. Issue 4.Pp.79-104.
2. Boamah, Fredrick Ahenkora (September30,2020).*Customer Perception and Satisfaction Towards Service Providers.* Journal of Marketing and Consumer Research.
3. Fredrick Ahenkora Boamah, Nana Ama Asi Danso, Jonathan AseyeNutakor(2020). *Customer Perception and Satisfaction Towards Service Providers.* Journal of Marketing and Consumer Research. ISSN 2422-8451.Vol.71.
4. Bharwana, T. K., Bashir, M., & Mohsin, M. (2013). *Impact of service quality on customers' satisfaction: A study from service sector especially private colleges of Faisalabad, Punjab, Pakistan*. International Journal ofScientific and Research Publications, Volume 3. Issue 5.Pp.1-7
5. Dibb, S. and Simkin, L. (1997).*A program for implementing market segmentation.* Journal of Business & Industrial Marketing. Volume 12. Issue No. 1. pp. 51-65.
6. P K, Manoj. (2004). *Dynamic of Housing Finance in India. Bank Quest*. Indian Institute of Banking & Finance. Mumbai. India. 75. 19-25.
7. Mondal, Pranoy,Year, P. (2020). *Critical Analysis of Housing Finance Sector in India with Special Reference to the Assessment of Housing Shortage*.
8. Balanaga Gurunathan K, Nidhi Ahuja (2020). *Financial Performance of Housing Finance Companies in India*. Journal of Critical Reviews. ISSN- 2394-5125. Volume 7. Issue 13.
9. S. Hanif,S. T. Ahmad,S. S. Saleem(2015).*The Need to Build Upwards: a Study on perception of Vertical Apartment Housing Among Middle Income Group of Lahore*. Vidyabharati International Interdisciplinary Research Journal.ISSN 2319-4979. Volume 4. Issue 2.
10. Sumana Bose Ranjan(2018*).Study of Relationship between Perceptions and Expectations of Service Quality in Banks*.IOSR Journal of Economics and Finance.e-ISSN: 2321-5933.Pp 60-71.
11. S. Habibia,N. Asadi(2011).*Causes, results and methods of controlling urban sprawl. Procedia Engineering*.Elsevier.1877-7058.Pp.133–141.
12. Moses Mubiru, Pamela Ikiriza (2021). *Effect of Location Variations on Households' Social Affordability of Rental Accommodation in Informal Settlements of Kampala City*. International Journal of Scientific & Engineering Research. ISSN 2229-5518. Volume 12, Issue 6.
13. S.K. Gupta (2019).*Fusion Reviews on Human Living Beings in High-Rise/ or Tall Residential Buildings-Social Economical & Psychological Parameters*.International Journal of Engineering Research & Technology.ISSN: 2278-0181.Volume 8. Issue 06.
14. TendyMatenge, Rina Makgosa,Paul Mburu(2016). *Segmentation analysis of financial savings markets through the lens of psycho-demographics. Acta Commercii - Independent Research* Journal in the Management Sciences.ISSN:1684-1999.
15. Robert Gifford (2007). *The Consequences of Living in High-Rise Buildings. Architectural Science Review*. Volume 50. Issue 1. Pp.1-15
16. Aluko, O. (2011). *The effects of location and neighbourhood attributes on housing values in metropolitan Lagos*. Ethiopian Journal of Environmental Studies and Management, 4(2), 69-82
17. Karolina Ilieska(2013*).Customer Satisfaction Index – as a Base for Strategic Marketing Management.* TEM Journal. Volume 2.Issue 4.pp.327-33.

18. Mansi Misra,GaganKatiyar,A.K. Dey(2013).*Consumer perception and buyer behaviour for purchase of residential apartments in NCR*.International Journal of Indian Culture and Business Management.Volume 6. Issue No 1.
19. Engel, J.F., Blackwell, R.D. and Miniard, P.W. (2005). *Consumer Behavior (10th ed.). South Western College Pub*, Thompson India, ISBN-10: 0324271972, ISBN-13: 978-0324271973.
20. Anju Kakkar,Supriya(2014).*Socio-economic Benefits of Open Spaces:Towards Sustainable Housing*.International Journal of Environmental Research and Development.ISSN 2249-3131 Volume 4, Number 1.pp. 17-20.
21. Tywanda D. Tate1, Franklin M. Lartey, Phillip M. Randall (2019). *Relationship between Computer-Mediated Communication and Employee Engagement among Telecommuting Knowledge Workers*. Journal of Human Resource and Sustainability Studies. Volume.07 Issue No.02,Pp.20-29.
22. Dam, Leena B,Deshpande, Kalyani (2020). *Relationship Between Demographic Variables and Awareness on Cybersecurity Threats: An Empirical Analysis.* The Orissa Journal of Commerce, Vol 41, Issue 2, Pp. 112-122.
23. D.M.R.M Dissanayake, S. C. Premaratne(2020). *Association Mining Approach for Customer Behavior Analytics*.International Journal of Computer Science Engineering. ISSN: 2319-7323Volume 9. Issue 1.
24. D.M.R.M Dissanayake, S. C. Premaratne(2020). *Association Mining Approach for Customer Behavior Analytics*.International Journal of Computer Science Engineering.ISSN: 2319-7323 Volume 9. Issue 1.
25. Ali Abdulhussein Mohammed (2019),*Design and Implementation of a Prototype Data Mining Agent System*.International Journal of Computer Science and Mobile Computing, Volume 8. Issue. 3.Pp.240 – 248
26. Koyi Anusha, Yashaswini C, Manishankar S (2019). *Segmentation of Retail Mobile Market Using HMS Algorithm*. International Journal of Electrical and Computer Engineering. ISSN: 2088-8708.Volume. 6.Issue No. 4.pp. 1818~1827.
27. Deepika Saxena1, Neelam Dhall, R.K. Arora, Ms. Rashika Malik (2020). *Sustainable Development Through Green Banking: A Study on India Banking Sector.* International Journal of Recent Advances in Multidisciplinary Research. Volume 07, Issue 07 pp. 6089-6094.
28. Nedumaran, G. M, Manida. Baladevi, M (2020). *Impact on Customer Perceptions of Green Banking Process with Special Reference in Rajapalayam Taluk.* Available at SSRN: https://ssrn.com/abstract=3551974 or http://dx.doi.org/10.2139/ssrn.3551974
29. Nilam AtsirinaKrisnaputri,PurwanitaSetijanti,Happy Ratna S(2016).*SiteSelection Factors of Apartment on Developer Perspective*.International Journal of Engineering Research & Technology. ISSN: 2278-0181.Volume 5. Issue 01.
30. Molefe Maleka, TshaudiMotsima, Refilwe Matang, Patrick Lekgothoane (2016). *Comparing residents' perceptions in townships and suburbs regarding service delivery by municipality under administration. Problems and Perspectives in Management,*Volume 14,Issue 01.pp 137-144.

Table 1 Reason for choosing apartment

		Frequency	Percent	Valid Percent	Cumulative Percent
Valid	Affordable	13	13.0	13.0	13.0
	Proximity to transport and other amenities	45	45.0	45.0	58.0
	lifestyle and city living, better safety and security	15	15.0	15.0	73.0
	socialistic thought	27	27.0	27.0	100.0
	Total	100	100.0	100.0	

Table 2 Reason for shift from apartment

		Frequency	Percent	Valid Percent	Cumulative Percent
Valid	Rent or maintance problem	24	24.0	24.0	24.0
	wanted independent living	27	27.0	27.0	51.0
	Proximity problems	19	19.0	19.0	70.0

	Quality Issues	16	16.0	16.0	86.0
	others	14	14.0	14.0	100.0
	Total	100	100.0	100.0	

Table 3. Relationship between gender and Perception towards township apartments

			Asymptotic
	Value	**Df**	**Significant (2 Sided)**
Pearson Chi-Square	1.242[a]	4	.094
Likelihood Ratio	1.194	5	.094
Linear-by-Linear Association	.113	1	.073
N of Valid Cases	100		

Table 4 Symmetric Measures – Gender and perception towards township

Value			Asymptotic Standard Error	Approximate T[b]	Approximate Significance
Interval by Interval	Pearson's R	.034	.100	.335	.738[c]
Ordinal by Ordinal	Spearman Correction	.036	.100	.354	.724[c]
N of Valid Cases		100			

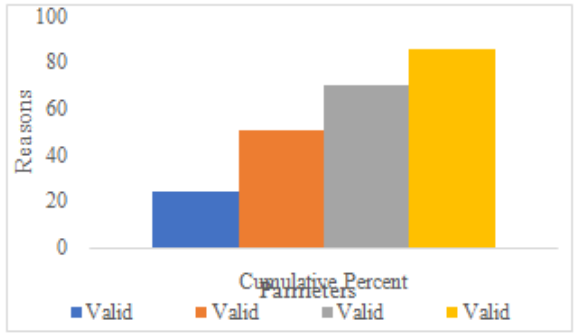

Figure 1. Reason for Shift between apartment

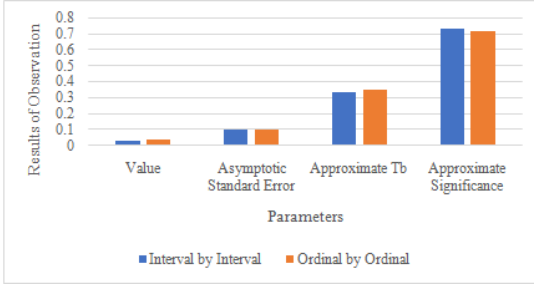

Figure 2. Symmetric Measures – Gender and perception towards township

Indian Journal of Natural Sciences *www.tnsroindia.org.in ©IJONS*

Vol.15 / Issue 83 / Apr / 2024 *International Bimonthly (Print) – Open Access* *ISSN: 0976 – 0997*

RESEARCH ARTICLE

For Multi-Valued Mappings, Fixed Point Theorems in Complex Valued b-Metric Spaces

Arul Xavier A* and Maria Joseph J

Department of Mathematics, St.Joseph's College, (Affiliated to Bharathidasan University Tiruchirappalli). Tiruchirappalli, Tamil Nadu, India.

Received: 22 Feb 2024 Revised: 06 Mar 2024 Accepted: 20 Mar 2024

***Address for Correspondence**
Arul Xavier A
Department of Mathematics,
St.Joseph's College,
(Affiliated to Bharathidasan University Tiruchirappalli).
Tiruchirappalli, Tamil Nadu, India.
Email: arulxavier3006@gmail.com,

ABSTRACT

This study establishes the complex-valued b-metric spaces on the fixed point theorem for two multi-valued mappings, which generalizes several papers in the present literature.

Keywords: Fixed point, contraction, complex-valued metric space, set-valued mapping, complete metric space, b-metric space.

INTRODUCTION

In mathematical analysis, the fixed point theory is crucial . In 1922, Stefan Banach[1] proposed contraction mapping principle which established foundation for many results fixed point theory. Subsequently, many researchers[2], [3][4]generalized the principle of Banach contracture mapping in metric and b-metric spaces. Regards, multi-valued transformations in b-metric spaces, Josephet.all[5]proved the fixed point theorem. Then Saleh AAl-Mezelet.all[6] proved fixed point, common fixed point theorem on multi-valued mappings in complex-valued metric spaces. This article, explores invariant point, common fixed point theorems on multiple valued transformations in complex-valued b-metric spaces.

Definition 1.1. Consider$\mathbb{C}$ stands for the collection of numbers in complex planebesides$z_1 , z_2 \in \mathbb{C}$. On $\mathbb{C}$,consider a partial order $\preccurlyeq$ as follows:

$z_1 \preccurlyeq z_2$ iff$Re(z_1) \leq Re(z_2)$ and $Im(z_1) \leq Im(z_2)$. Thus $z_1 \leq z_2$ if oneof the following holds:

1. $Re(z_1) = Re(z_2)$ and $Im(z_1) = Im(z_2)$;
2. $Re(z_1) < Re(z_2)$ and $Im(z_1) = Im(z_2)$;

3. $Re(z_1) = Re(z_2)$ and $Im(z_1) < Im(z_2)$;
4. $Re(z_1) < Re(z_2)$ and $Im(z_1) < Im(z_2)$;

We will write $z_1 \precnsim z_2$ if $z_1 \neq z_2$ and one of (2), (3), and (4) is satisfied; also we'll write $z_1 \prec z_2$ only if (4) is met.It shows that

i. $0 \preccurlyeq z_1 \precnsim z_2$ implies $|z_1| < |z_2|$;
ii. $z_1 \preccurlyeq z_2$ as well as$z_2 \prec z_3$ imply $z_1 \prec z_3$;
iii. $0 \preccurlyeq z_1 \preccurlyeq z_2$ implies $|z_1| < |z_2|$;
iv. if $a, b \in \mathbb{R}$, $0 \leq a \leq b$ and $z_1 \preccurlyeq z_2$ then $az_1 \prec bz_2$for all $z_1, z_2 \in \mathbb{C}$.

Definition1.2. Assume$X$ be a set of non-empty and$d: X \times X \to \mathbb{C}$ is knownas a complex metric on X, if for every$x, y, z \in X$, the conditions holds are

i. $0 \preccurlyeq d(x, y)$ with$d(x, y) = 0$ iff $x = y$,
ii. $d(x, y) = d(y, x)$,
iii. $d(x, y) \preccurlyeq d(x, z) + d(z, y)$.

The pair (X, d) is then referred toa metric space in complex- valued .

Definition 1.3. Assuming$\{x_n\}$ be a sequence in X and $x \in X$. On every $c \in \mathbb{C}$, and $0 \prec e$ there is $n_0 \in \mathbb{R}$in order toall $n \geq n_0, d(x_n, x) \prec c$, then assume that $x_n$converges to x. If $x_n \to x$, then we call x is the boundary point of x_n .We denotes limit by $\lim x_n = x$ or $x_n \to x$ when $n \to \infty$.

Definition 1.4. Let $\{x_n\}$ be a sequence in X. If for every $c \in \mathbb{C}$, with $0 \prec c$ there is $n_0 \in \mathbb{N}$ such that for all $n \geq n_0, d(x_n, x_{n+m}) \prec c$, then x_n is called Cauchysequence in (X, d). Every sequenceof Cauchy in entiremetric space(X, d) is convergent.

Definition 1.5. [1] Letting(X, d) be a metric space with complex-values and asequence $x_n$belongs to$X$. Thereforex_n converges to x iff $|d(x_n, x)| \to 0$ as $n \to \infty$.

Lemma 1.6. [1] Consider(X, d) be a metric space with complex-valued alsox_n be asequence in X. Thusx_nCauchy sequenceiff$|d(x_n, x_{n+m})| \to 0$ as $n \to \infty$.

Definition1.7.$\mathcal{H}: \mathcal{CB}(X) \times \mathcal{CB}(X) \to [0, \infty)$ is a function derived by $\mathcal{H}(A, B) = max\{\sup_{x \in A} D(x, A), \sup_{x \in B} D(x, B)\}$is the Hausdorff metric on $\mathcal{CB}(X)$ caused by the metric d on X here $D(x, A) = inf\{d(x, y) : y \in A\}$ for every$A \in \mathcal{CB}(X)$.

Definition 1.8. If $v = Tv$ (when $T : X \to X$ is a single-valued map) or $v \in Tv$ (while$T: X \to \mathcal{P}(X)$ is a a map with several values), there is av $in X$could be a fixed point of a map T.We states$T$ has an endpoint if there contains $v \in X$ such that $Tv = \{v\}$.The collection of invariant points of T is represents$\mathcal{F}(T)$ and the group of two multi-valued mappings, common fixed pointsT, S aredenotes$\mathcal{F}(T, S)$.

Definition 1.9. Two mappings with multiple values$T, S : X \to \mathcal{CB}(X)$, claims that$T, S$ fulfil the property of common approximate endpoint if there is a $\{x_n\} \subset X$ in the sense that
$\lim_{n \to \infty} \mathcal{H}(\{x_n\}, Tx_n) = \lim_{n \to \infty} \mathcal{H}(\{x_n\}, Sx_n) = 0$

Definition 1.10. For two mappings $T, S: X \to X$, we say that T, Sshare acommon arbitrary fixed point if there consists a sequence $\{x_n\} \subset X$ such that
$\lim_{n \to \infty} d(\{x_n\}, Tx_n) = \lim_{n \to \infty} d(\{x_n\}, Sx_n) = 0$
Throughout the paper, we assume that $\{a, b, c, d, e\} \subset [0,1)$.This article's fundamental theorem is as follows.

Theorem 1.11. Assume that(X, d) be an entire metric space besides$T, S: X \to \mathcal{CB}(X) are$ two multi-valued functions in order to every$x, y \in X$.

$\mathcal{H}(Tx,Ty) \leq$
$ad(x,y) + bD(x,Sx)D(y,Ty) + c\sqrt{D(y,Sx)D(x,Ty)} + dD(x,Sx)D(x,Ty) + eD(y,Sx)D(y,Ty).$
where $a+b+c+2d+2e < 1$. If and only if T, Scan satisfies the common approximate end point feature, hence they have a unique end point.

Theorem 1.12. Assuming an absolute metric space(X,d)also$T,S : X \to \mathcal{CB}(X)$be two multiple valued functions in the sense that each $x,y \in X$.
$\mathcal{H}(Tx,Ty) \leq ad(x,y) + b\frac{D(x,Sx)D(y,Ty)}{1+d(x,y)} + c\frac{\sqrt{D(y,Sx)D(x,Ty)}}{1+d(x,y)} + d\frac{D(x,Sx)D(x,Ty)}{1+d(x,y)} + e\frac{D(y,Sx)D(y,Ty)}{1+d(x,y)}.$
where $a+b+c+2d+2e < 1$. Then T,S having an endpoint uniquely, iffthey fulfils the common propertyof an approximate endpoint.
Now, we can present our key findings.

PRIMARY FINDINGS
Theorem 2.1. Let (W,d)be a entire valued space of b-metric with $s \geq 1$ also assume that$F,G: W \to \mathcal{CB}(W)$be two multiple valued functions in the sense that toevery$a,b \in W$.
$d(Fb,Ga) \leq k_1\, d(a,b) + k_2\, d(a,Ga)d(b,Fb) + k_3\, d(b,Ga)d(a,Fb) + k_4\, sd(a,Ga) + d(a,Fb) + k_5\, d(b,Ga)d(b,Fb)$
where $k_1 + k_2 + k_3 + 2k_4 s + 2k_5 < 1$. $k_i \geq 0, i = 1,2,3,4,5$. Thus$F,G$ having afixed point uniquely.

Proof. Letting$a_0 \in W$ be a random element and also$a_{2n-1} = Fa_{2n-2}$. We have

$d(a_{2n+1}, a_{2n}) = d(Fa_{2n}, Ga_{2n-1})$

$\leq k_1\, d(a_{2n}, a_{2n-1}) + k_2\, d(a_{2n-1}, Ga_{2n-1})d(a_{2n}, Fa_{2n}) + k_3 d(a_{2n}, Ga_{2n-1})d(a_{2n-1}, Fa_{2n}) + k_4\, sd(a_{2n-1}, Ga_{2n-1})d(a_{2n-1}, Fa_{2n}) + k_5\, d(a_{2n}, Ga_{2n-1})d(a_{2n}, Fa_{2n})$

$= k_1\, d(a_{2n}, a_{2n-1}) + k_2\, d(a_{2n-1}, a_{2n})d(a_{2n}, a_{2n+1}) + k_3 d(a_{2n}, a_{2n})d(a_{2n-1}, a_{2n+1}) + k_4\, sd(a_{2n-1}, a_{2n})d(a_{2n-1}, a_{2n+1}) + k_5\, d(a_{2n}, a_{2n})d(a_{2n}, a_{2n-1})$

$= k_1\, d(a_{2n}, a_{2n-1}) + k_2\, d(a_{2n-1}, Ga_{2n})d(a_{2n}, a_{2n+1}) + k_4\, sd(a_{2n-1}, a_{2n})\,(d(a_{2n-1}, a_{2n+1}) + d(a_{2n}, a_{2n+1}))$

$\leq k_1\, d(a_{2n}, a_{2n-1}) + k_2\, d(a_{2n}, a_{2n+1}) + k_4\, sd(a_{2n-1}, a_{2n})$
$(d(a_{2n-1}, a_{2n})d(a_{2n-1}, a_{2n+1}))$

$\leq k_1\, d(a_{2n}, a_{2n-1}) + k_2\, d(a_{2n}, a_{2n+1}) + k_4\, s(d(a_{2n-1}, a_{2n})d(a_{2n-1}, a_{2n+1}))$
$d(a_{2n+1-}, a_{2n}) = \frac{k_1 + k_4 s}{1 - k_2 - k_4 s} d(a_{2n-1}, a_{2n})$

$d(a_{2n-1}, a_{2n}) = d(Fa_{2n-2}, Ga_{2n-1})$

$\leq k_1\, d(a_{2n-2}, a_{2n-1}) + k_2\, d(a_{2n-1}, Ga_{2n-1})d(a_{2n-2}, Fa_{2n-2}) + k_3 d(a_{2n-2}, Ga_{2n-1})d(a_{2n-1}, Fa_{2n-2}) + k_4\, sd(a_{2n-1}, Ga_{2n-1})d(a_{2n-1}, Fa_{2n-2}) + k_5\, d(a_{2n-2}, Ga_{2n-1})d(a_{2n-2}, Fa_{2n-2})$

$= k_1\, d(a_{2n-2}, a_{2n-1}) + k_2\, d(a_{2n-1}, a_{2n})d(a_{2n-2}, a_{2n-1}) + k_3 d(a_{2n-2}, a_{2n})d(a_{2n-1}, a_{2n-1}) + k_4\, sd(a_{2n-1}, a_{2n})d(a_{2n-1}, a_{2n+1}) + k_5\, d(a_{2n-2}, a_{2n})d(a_{2n-2}, a_{2n-1})$

$= k_1\, d(a_{2n-2}, a_{2n-1}) + k_2\, d(a_{2n-1}, Ga_{2n})d(a_{2n-2}, a_{2n-1}) + k_5\, d(a_{2n-2}, a_{2n})d(a_{2n-2}, a_{2n-1})$

$\leq k_1\, d(a_{2n-2}, a_{2n-1}) + k_2\, d(a_{2n_1}, a_{2n}) + k_5\, sd(a_{2n-2}, a_{2n-1})$
$(d(a_{2n-1}, a_{2n})d(a_{2n-2}, a_{2n+1}))$

$\leq k_1\, d(a_{2n_2}, a_{2n-1}) + k_2\, d(a_{2n_1}, a_{2n}) + k_5\, s(d(a_{2n-2}, a_{2n-1})d(a_{2n-1}, a_{2n}))$

$$d(a_{2n-1}, a_{2n}) = \frac{k_1 + k_5\, s}{1 - k_2 - k_5\, s} d(a_{2n-2}, a_{2n_1})$$

Now taking, $\lambda = max\left\{\frac{k_1+k_4\, s}{1-k_2-k_4\, s}, \frac{k_1+k_5\, s}{1-k_2-k_5\, s}\right\} < 1$

We conclude that for each $n \in \mathbb{N}$, $d(a_{2n+1}, a_{2n}) \leq \lambda d(a_n, a_{n-1})$.By a conventionaltechnique, one can demonstrate that $\{a_n\}$ is Cauchy sequence.Because(W, d) is an entiremetric space, consists of$u \in W$ in order to$a_n \to u$.

Claim:*Fu and u* are identical to each other.

$d(u, Fu) = d(u, Ga_{2n-1}) + d(Ga_{2n-1}, Fu)$

$\leq d(u, Ga_{2n-1}) + k_1\, d(Ga_{2n-1}, u) + k_2\, d(Ga_{2n-1}, GGa_{2n-1})d(u, Fu) + k_3\, d(u, a_{2n-1})d(a_{2n-1}, Fu)$
$+ k_4\, sd(a_{2n-1}, Ga_{2n-1})d(a_{2n-1}, Fu) + k_5\, d(u, Ga_{2n-1})d(u, Fu)$

Assuming$n \to \infty$ from the above inequality, we get $d(u, Fu) \leq 0$.

Thus$Fu = u$.
Similarly,$Gu = u$ can deduce.Thus,it concludes u be the shared fixed point of F as well as$G$.

Corollary 2.1. Assume that a complete valued metric space(W, d)also letting$F, G: X \to \mathcal{CB}(W)$be two functions of multi-valued such that for all$a, b \in W$.

$$d(Fb, Ga) \leq k_1\, d(a, b) + k_2\, d(a, Ga)d(b, Fb) + k_4\, sd(a, Ga) + d(a, Fb) + k_5\, d(b, Ga)d(b, Fb)$$

where $k_1 + k_2 + 2k_4\, s + 2k_5 < 1$. $k_i \geq 0, i = 1,2,3,4,5$. Thus$F, G$ contains an invariant point commonly.

Theorem 2.2. An entire valued metric space(W, d) besides $s \geq 1$ also$F, G: W \to W$be two functions and $k_i \geq 0, i = 1,2,3,4,5$ be such that$k_1 + k_2 + k_3 + 2k_4\, s + 2k_5 < 1$.
Let $d(Fb, Ga) \preccurlyeq k_1\, d(a, b) + k_2 \frac{d(a,Ga)d(b,Fb)}{1+d(a,b)} + k_3 \frac{d(b,Ga)d(a,Fb)}{1+d(a,b)} + k_4\, s\frac{d(a,Ga)+d(a,Fb)}{1+d(a,b)} + k_5 \frac{d(b,Ga)d(b,Fb)}{1+d(a,b)}$
for all $a, b \in W$.Then $Fand\ G$ share a common fixed point.
Proof. We have $k_1 + k_2 + k_3 + k_4\, s + k_5 < k_1 + k_2 + k_3 + 2k_4\, s + 2k_5 < 1$.

$$\preccurlyeq k_1\, d(a, b) + k_2 \frac{d(a, Ga)d(b, Fb)}{1 + d(a, b)} + k_3 \frac{d(b, Ga)d(a, Fb)}{1 + d(a, b)} + k_4\, s\frac{d(a, Ga) + d(a, Fb)}{1 + d(a, b)} + k_5 \frac{d(b, Ga)d(b, Fb)}{1 + d(a, b)}$$
$$\preccurlyeq k_1\, d(a, b) + k_2\, d(a, Ga)d(b, Fb) + k_3\, d(b, Ga)d(a, Fb) + k_4\, sd(a, Ga)d(a, Fb) + k_5\, d(b, Ga)d(b, Fb)$$

By theorem 2.1 we declares that F &G shares a common fixed point. Trivially, uniqueness shown verbatim as per demonstration of corollary 2.1.

REFERENCES

1. S Banach., Sur les operations dans les ensembles abstraitsetleur application aux equations integrals, Fundam.Math.3, (1922), 133-181.https://doi.org/10.4064/fm-3-1-133-181
2. Tayyab Kamran, Maria Samreen and Qurat UL Ain (2017): A Generalization of b-metric space andsome fixed point theorems. Mathematics, 5(2), 19. https://doi.org/10.3390/math5020019
3. M Boriceanu (2009) Fixed point theory for multivalued generalized contraction on a set with twob-metricspaces. Stud Univ Babes- Bolyai Math LIV(3):1-14. http:// citeseerx.ist.psu.edu/viewdoc/download d?doi=10.1.1.576.5527&rep=rep1&type=pdf

4. A Arul Xavier ,J.Carmel Pushpa Raj,J.Maria Joseph, M.Marudai Common fixed point theorems in complex valued extended b-metric spaces under rational contractions. Journal of Physics confrerence series 1964(2021)022028.https://doi.org/10.1088/1742-6596/1964/2/022028
5. J Maria Joseph., D Dayana Roselin., M. Marudai: Fixed point theorems on multi-valued mappings in b-metric spaces. Springer Plus. 5 217, (2016). https://doi.org/10.1186/s40064- 016-1870-9.
6. Saleh A Al-Mezel., Hamed H Alsulami., ErdalKarapnar., FarshidKhojasteh: A note on fixed point results in complex-valued metric spaces. Journal of Inequalities and Applications. 2015 33, (2015). https://doi.org/10.1186/s13660-015-0550-6

Indian Journal of Natural Sciences *www.tnsroindia.org.in ©IJONS*

Vol.15 / Issue 83 / Apr / 2024 *International Bimonthly (Print) – Open Access* *ISSN: 0976 – 0997*

RESEARCH ARTICLE

A Nonlinear Mathematical Model for Asthma: Exploring the Impact of Environmental Pollution

N. Vasuki[1]* and D. Jasmine[2]

[1]Research Scholar, PG & Research Department of Mathematics, Bishop Heber College (Affiliated to Bharathidasan University), Trichy, Tamil Nadu, India.
[2]Assistant Professor, PG & Research Department of Mathematics, Bishop Heber College (Affiliated to Bharathidasan University), Trichy, Tamil Nadu, India.

Received: 22 Feb 2024 Revised: 06 Mar 2024 Accepted: 20 Mar 2024

***Address for Correspondence**
N. Vasuki
Research Scholar,
PG & Research
Department of Mathematics,
Bishop Heber College (Affiliated to Bharathidasan University),
Trichy, Tamil Nadu, India.
Email: vasu681999@gmail.com

ABSTRACT

This paper utilizes a nonlinear mathematical model to examine the effects of cigarette smoking and environmental pollution on the prevalence of asthma. To comprehend this relationship, we obtain an approximate analytical solution using the homotopy perturbation approach. This study indicates that smoking, both consciously and unconsciously, contributes to the expansion of asthma and that higher air pollution levels are associated with a higher prevalence of the condition. Furthermore, this study shows that an increased level of connection between smoking and susceptible people leads to a more lasting growth of asthma. We also carry out a numerical analysis to look at the influence of important parameters on the spread of asthma to verify the analytical findings. The main objective of the research is to investigate how smoking affects the prevalence of asthma.

Keywords: Environmental Pollution, Homotopy Perturbation Method (HPM),Asthma Prevalence.

INTRODUCTION

The development of descriptions of systems using mathematical terminology and concepts is known as mathematical modeling. It includes the process of building these models, which are instruments for understanding complex situations, predicting real-world phenomena, and assisting in decision-making. Applications of mathematical modeling can be found in many fields, such as engineering, scientific research, and even the study of

human behavior. It serves as a link between mathematics and the outside world. Many components of the nonlinear ordinary differential equation system are studied [1]. Fundamental differential equations are receiving a lot of attention these days. They will examine the analytics estimated outcome in this model [2].Chronic asthma is a respiratory condition marked by inflammation of the airways and an overabundance of mucus. It can cause symptoms like whooping, chest discomfort, coughing, and difficulty inhaling. Numerous things, including allergies, toxins in the environment, and exposure to compounds at work, might cause these symptoms. An ordinary differential equation model was first proposed by Perelson, Kirschner, and De Boer in 1993 [3, 4]. This model is significantly different at first. In many ways, this approach contributed significantly to the non-linear evolution. Stated differently, the nonlinear system beginning and endpoints are included [5,6]. The primary goal is to identify the nonlinear ODE's quantitative solutions [7].By simulating the interactions between these variables over time, mathematical models can help to understand asthma's mechanisms, predict disease progression, and evaluate potential treatment strategies. Such models play a crucial role in advancing our understanding of asthma and guiding clinical interventions. The homotopy perturbation method (HPM) is a powerful mathematical technique used to approximate solutions to a wide range of nonlinear differential equations [8,9]. It involves introducing a small parameter into the equations and expressing the solution as a series expansion in terms of this parameter. Through the systematic perturbation process, the solution is iteratively improved to obtain accurate approximations. An approach for obtaining numerical results is covered [10].

An Approach of Homotopy Perturbation Method

The limits of conventional perturbation methods have been discovered through the application of the HPM approach. Let's examine the non-linear differential equation

$$H_0(k) - f(m) = 0, m \in \phi$$

With boundary conditions

$$B_0(\mathrm{k}, \frac{\partial k}{\partial r}) = 0, r \in \Omega \quad (1)$$

when $f(m)$ is an identified mathematical function, B_0 is a boundary function, H_0 is a differential function, as well as ϕ , is a domain with Ω borders. The equation(1) is currently simplified into

$$X(k) + Y(k) - f(m) = 0$$

While applying HPM approaches, we obtain

$$D(l, p) = (1-p)[X(l) - \mathrm{X}(\mathrm{k}_0)] + p[\mathrm{H}_0(l) - f(m)] = 0 \quad (2)$$

$$D(l, p) = X(l) - X(k_0) + pX(k_0) + P[Y(l) - f(m)] = 0 \quad (3)$$

The origin of equation (1) is k_0, as well as its embedding parameter $p \in [0,1]$. Applying the limits in the equation (2) and (3), we obtain

$$D(l, 0) = X(l) - X(k_0) = 0$$

$$D(l, 1) = H_o(l) - f(m) = 0$$

At $p = 0$, the equation (3) gets linear, while at $p = 1$, it turns non-linear. The procedure shall conclude at zero whenever

$$X(l) - X(k_0) = 0 \text{ to } H_0(l) - f(m) = 0$$

The result is expressed in the following manner: the embedding parameter p remains extremely limited

$$l = l_0 + pl_1 + p^2 l_2 + ... \quad (4)$$

If p = 1, it represents an approximation to the equation (1)

$$k = p \xrightarrow{\lim} l = l_0 + l_1 + l_2 + ... \quad (5)$$

In the majority of scenarios, the series converges, Although the non linearfunction $H(l)$ determines the convergent level.

Example

We identify the differential equation of a system that is nonlinear by determining its exact solution

$$z = e^{2y}, z^1 = 2z_2^2 \quad (6)$$

If estimates for both terms in equation (4) are adequate, then we get

$$l = l_0 + pl_1 + p^2 l_2 + ... \quad (7)$$

If $l_{i,j}$, $i.j = 1,2,3....$ are as-yet-undetermined variables. Consequently, using equation (5)

$$z(y) = p \xrightarrow{\lim} l(y) = \sum_{r=0}^{r=2} l_r(\mathrm{y}) \quad (8)$$

The HPM allows us to build a homotopy of equation (6) in the manner described below

$$(1-p)(\dot{l}-k) + p(\dot{l}-2l_2^2) = 0 \quad (9)$$

These are the initial estimates $l(0) = 1 \& z(0) = 1$ (10)

By establishing equations (7)& (10) to equation (9) and remodeling according to the digits of p-terms, the result is

$$\dot{l}_0 + (\dot{l}_1 - 2l_{2,0}^2)p + (\dot{l}_2 - 4l_{2,0}\,1_{2,1})p^2 + ... = 0$$

To derive the unidentified variables $l_{i,j}$, $i, j = 1,2,3....$ we need to establish and resolve the system below

$$\dot{l}_0 = 0$$

$$\dot{l}_0 - 2l_{2,0}^2 = 0$$

$$\dot{l}_2 - 4l_{2,0}l_{2,1} = 0$$

$$l_0(y) = 1$$

$$l_1(y) = -\mathrm{e}^{-2y} + 8e^{-y} + 8y - 7$$

$$l_2(y) = \frac{1}{3}e^{-4y} - \frac{56}{9}e^{-3y} - 16e^{-2y}y + 6e^{-2y} + \frac{1}{3}e^{-4y} + \frac{272}{3}e^{-y} + 64e^{-y}y + \frac{112}{3}y - \frac{817}{9}$$

Hence based on equation (8)

$$z(y) = -3 + 6y + 4e^{-y}$$

Mathematical Model

Formulate the system as

$$\frac{dS}{dt} = \wedge - \delta S - \beta SC$$

$$\frac{dI}{dt} = \gamma C - \alpha I - \delta I$$

$$\frac{dC}{dt} = k - \gamma C - \theta C - \delta C$$

In this model, we divide the population into three categories: Sis the individuals who are susceptible to the disease, Ibe the number of individuals who are infected with a certain disease and C is the individuals who are categorized as smokers. This disease is primarily caused by smoking in public places. By applying the HPM, the system of equations changes to

$$\frac{dS}{dt} - \wedge + \delta S + \beta SC = 0$$

$$\frac{dI}{dt} - \gamma C + \alpha I + \delta I = 0$$

$$\frac{dC}{dt} - k + \gamma C + \theta C + \delta C = 0$$

Using the HPM, the above system can be solved as follows:

$$(1-p)(\frac{dS}{dt} - \wedge + \delta S) + hp(\frac{dS}{dt} + \wedge - \delta S - \beta SC) = 0$$

$$(1-p)(\frac{dI}{dt} - \gamma C + \alpha I + \delta I) + hp(\frac{dI}{dt} + \gamma C - \alpha I - \delta I) = 0$$

$$(1-p)(\frac{dC}{dt} - k + \gamma C + \theta C + \delta C) + hp(\frac{dC}{dt} + k - \gamma C - \theta C - \delta C) = 0$$

Compare the p-coefficient in the system described above

$$P^0 : \frac{dS_0}{dt} - \wedge + \delta S_0 = 0$$

$$p^0 : \frac{dI_0}{dt} - \gamma C_0 + \alpha I_0 + \delta I_0 = 0$$

$$p^0 : \frac{dC}{dt} - k + \gamma C_0 + \theta C_0 + \delta C_0 = 0$$

$$p^1 : \frac{dS_1}{dt} + \delta S_1 - \frac{dS_0}{dt} + \wedge - \delta S_0 + h\left(\frac{dS_0}{dt} + \wedge - \delta S_0 - \beta S_0 C_0\right) = 0$$

$$p^1 : \frac{dI_1}{dt} - \gamma C_1 + XI_1 - \frac{dI_0}{dt} + \gamma C_0 - XI_0 + h(\frac{dI_0}{dt} + \gamma C_0 - XI_0) = 0$$

$$p^1 : \frac{dC_1}{dt} + YC_1 - \frac{dC_0}{dt} + k - YC_0 + h(\frac{dC_0}{dt} + k - YC_0) = 0$$

The system above requires these initial & boundaries to have an approximate solution

$$\mathrm{S}(0) = 0, \mathrm{I}(0) = 0, \mathrm{C}(0) = 0 \text{ and}$$

$$\mathrm{S}(0) = 5500, \mathrm{I}(0) = 4000, \mathrm{C}(0) = 200$$

Applying initial conditions to the aforementioned system yields

$$S_0 = \frac{\wedge}{\delta}(1 - e^{-\delta t})$$

$$I_0 = \frac{k\gamma}{XY}(1 - e^{-Xt}) + \frac{k\gamma}{Y(X-Y)}(e^{-Xt} - e^{-Yt})$$

$$C_0 = \frac{k}{Y}(1-e^{-Yt})$$

The outcome, when applying the initial conditions, is as follows

$$S_1 = (5500 + \frac{1}{V^2} - \frac{U}{V}\left(\frac{1}{\delta} + \frac{1}{\delta - U}\right))\mathrm{e}^{-\delta t} + \frac{U}{V\delta} + \frac{U\,\mathrm{e}^{-Ut}}{V(\mu - U)} - \frac{Ut\,\mathrm{e}^{-\delta t}}{V} - \frac{\mathrm{e}^{-(U+\delta)t}}{V^2}$$

$$I_1 = 4000e^{-Xt} + \frac{200\gamma}{(X-Y)}(e^{-Yt} - e^{-Xt})$$

$$C_1 = 200e^{-Yt}$$

Using Homotopy Perturbation Method, we get the approximate solution of the model

$$\mathrm{S}(t) = \frac{\wedge}{\delta}(1-e^{-\delta t}) + (5500 + \frac{1}{V^2} - \frac{U}{V}\left(\frac{1}{\delta} + \frac{1}{\delta - U}\right))\mathrm{e}^{-\delta t} + \frac{U}{V\delta} + \frac{U\,\mathrm{e}^{-Ut}}{V(\mu - U)} - \frac{Ut\,\mathrm{e}^{-\delta t}}{V} - \frac{\mathrm{e}^{-(U+\delta)t}}{V^2}$$

$$\mathrm{I}(t) = \frac{k\gamma}{XY}(1-e^{-Xt}) + \frac{k\gamma}{Y(X-Y)}(e^{-Xt} - e^{-Yt}) + 4000e^{-Xt} + \frac{200\gamma}{(X-Y)}(e^{-Yt} - e^{-Xt})$$

$$C(t) = \frac{k}{Y}(1-e^{-Yt}) + 200e^{-Yt}$$

$$X = \alpha + \delta$$

$$Y = \gamma + \theta + \delta$$

$$U = h\beta \wedge k$$

$$V = (\gamma + \theta + \delta)\delta$$

Numerical Result

We separated people into three sections in order to examine the spread of the asthma illness. We employed numerical results to analyse the impact and spread of asthma in the model. The rate of variation of the susceptible people over duration and various values of $\beta, \wedge \text{and} h$ are examined in figure 1,4 &7.Next, the rate of variation of the diseased people over duration and various values of $\delta, \alpha \text{ and} \gamma$ are examined in figure 2,5 &8. For figure 3,6 and 9, we examine the behavior of the smoker population over time for various values of $\delta, \gamma \text{ and} \theta$ .Tables 1 and 2 provide a description of the model. More evident, consequently, whether the rate of variation of the diseased people over duration seems high.

CONCLUSION

To analyse how asthma spreads in a population of different type, we used a mathematical model in this study. The model takes into account how smoking affects an individual's risk of developing asthma. An approximate analytical solution for the spread of asthma in a population was found by analysing the model using a mathematical method known as the homotopy perturbation method. It is evident that individuals who are susceptible to infections become infected when exposed to a smoking environment consistently. Numerical models show that when smokers smoke often around others, the rate of variation of harmful pollutants rises over the duration. Therefore, it could be important to restrict the number of smokers entering the population to halt the spread of asthma.

REFERENCES

1. Hemeda, Homotopy Perturbation Method for solving systems of nonlinear coupled equation, Applied Mathematical sciences, 6(96): 4787-4800, 2012.
2. Murray A B, David M F, Lucink G H., and Zimmerman B, Secondhand cigarette smoke worsens systems in children with Asthma, Can. Med. Assoc. J., 135, pp.321 – 32, 1989.
3. Ghori Q.K, Ahme M, Siddiqui A.M, International Journal of Nonlinear Sciences and Numerical simulation, 8(2): 179-184, 2007.
4. Ahmed E, Elgazzar A.S, On fractional order differential equations model for nonlocal epidemics, Physics A, 379: 607-614, 2007.
5. Vazquez-Leal H,Generalized homotopy method for solving nonlinear differential equations, Computational and Applied Mathematics, 33(1): 275- 288, 2014.
6. Jafari M.A, Aminataei A, Improved homotopy perturbation method, International Mathematical Forum, 5(29-32): 1567-1579, 2010.
7. Boyd J.P, Pade approximant algorithm for solving nonlinear ordinary differential equation boundary value problems on an unbounded domain, Computers in Physics. 11(3): article 299,1997.
8. Yu L.T, Chen C.K, The solution of the blasius equation by the differential transformation method, Mathematical and Computer Modelling, 28(1): 101-111,1998.
9. He J.H, Approximate analytical solution of Blasius equation, Communications in Nonlinear Science and Numerical Simulation, 4(1): 75-78,1999.
10. He J.H,Homotopy perturbation technique, Computer Methods in Applied Mechanics and Engineering,178(3-4): 257-262,1999.
11. He J.H, Homotopy perturbation method for bifurcation of nonlinear problems, International Journal of Nonlinear Science and Numerical Simulation, 6(2), 207-208, 2005.

Table 1: Parameters and Description

Symbol	Description of Parameter
β	Frequency of interaction between smokers and susceptible
δ	Rate of natural death
α	Death rate due to disease
K	The rate at which new individuals become smokers
θ	The frequency of smokers quitting
$\wedge$	Interaction between pollution and those who are exposed
γ	Rate of infection among smokers

Table 2: Values of the asthma model's parameters

Symbol	The assigned value for a parameter
$\wedge$	0.014
α	0.018
K	60
θ	0.002
θ_1	0.0002
β	0.0002
$\wedge$	0.0001

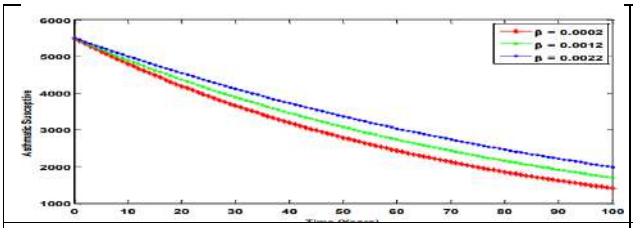

Figure 1:According to time, asthma is susceptibility for $\beta = 0.0002, 0.0012, 0.0022$

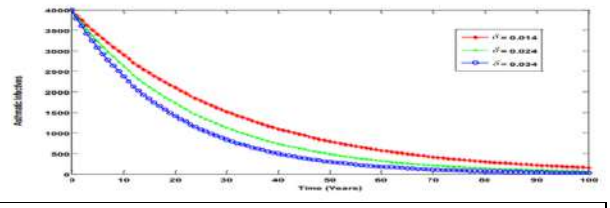

Figure 2: According to time, asthma is communicable for $\delta = 0.014, 0.024, 0.034$

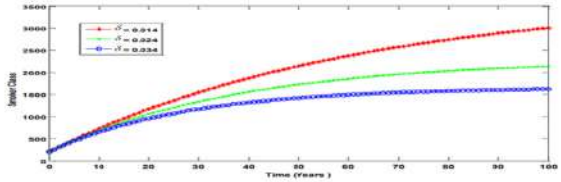

Figure 3: The evolution of the smoker population over time for $\delta = 0.014, 0.024, 0.034$

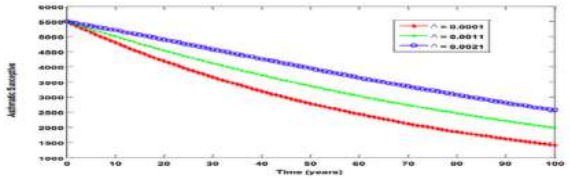

Figure 4:According to time, asthma is susceptibility for $\wedge = 0.0001, 0.0011, 0.0021$

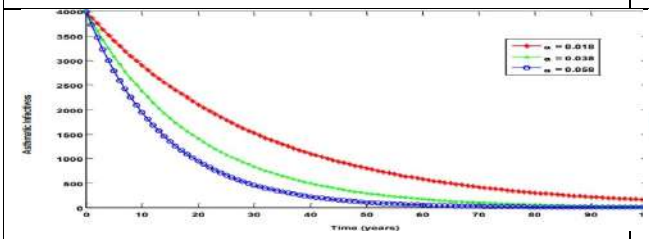

Figure 5:According to time, asthma is communicable for $\alpha = 0.018, 0.038, 0.058$

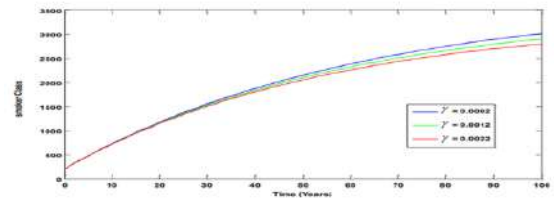

Figure 6:The evolution of the smoker population over time for $\gamma = 0.0002, 0.0012, 0.0022$

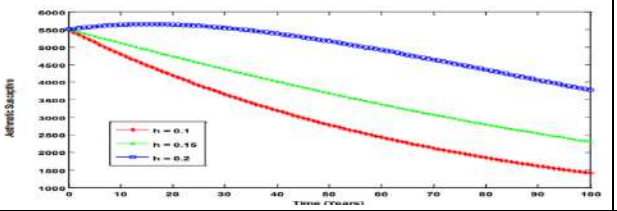

Figure 7:According to time, asthma is susceptibility for $h = 0.1, 0.15, 0.2$

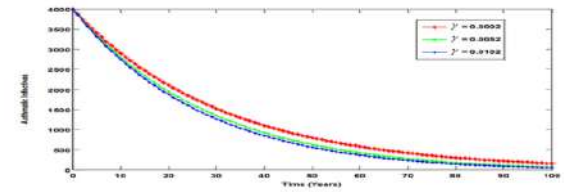

Figure 8:According to time, asthma is communicable for $\gamma = 0.0002, 0.0052, 0.0102$

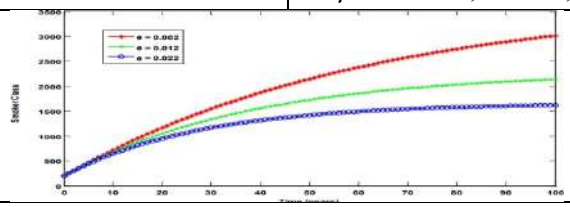

Figure 9: The evolution of the smoker population over time for $\theta = 0.002, 0.012, 0.022$

Indian Journal of Natural Sciences *www.tnsroindia.org.in ©IJONS*

Vol.15 / Issue 83 / Apr / 2024 *International Bimonthly (Print) – Open Access* *ISSN: 0976 – 0997*

RESEARCH ARTICLE

A Local and Global Stability Analysis of the Graves Disease Model

G. Lavanya and D. Jasmine

PG & Research Department of Mathematics, Bishop Heber College (Affiliated to Bharathidasan University), Trichy, Tamil Nadu, India.

Received: 30 Dec 2023 Revised: 09 Jan 2024 Accepted: 12 Mar 2024

***Address for Correspondence**
G. Lavanya
PG & Research
Department of Mathematics,
Bishop Heber College (Affiliated to Bharathidasan University),
Trichy, Tamil Nadu, India.
Email: lavanya.maths19@gmail.com

ABSTRACT

Graves' disease is a thyroid gland autoimmune disorder. We developed a novel mathematical model consisting of four nonlinear ordinary differential equations to describe the disease dynamics. The system of equation consist of variables such as Thyroid Stimulating Hormone (TSH), Free Thyroxine (FT4), thyroid gland volume (V) and TSH receptor autoantibodies (TRAB). The model was constructed by analyzing the underlying biological mechanisms and pathways involved in the pathogenesis of Graves' disease. Key interactions and feedback loops were translated into differential equations based on biochemical reaction kinetics. Analytical stability analysis was then conducted to study the dynamic behavior and equilibrium states of the system. To validate, the model was simulated in simbiology MATLAB. This work establishes a validated mathematical framework capturing the pathogenesis of Graves' disease. By proving and computationally verifying asymptotic stability of the disease state, the model can be further utilized to explore clinical interventions and treatment responses.

Keywords: Thyroid Stimulating Hormone (TSH), Free Thyroxine (FT4), thyroid gland volume (V) and TSH receptor autoantibodies (TRAB).

INTRODUCTION

Graves disease is an autoimmune condition characterized by the hyperactivity of the thyroid gland, causing it to produce excessive amounts of hormones. It ranks among the most prevalent thyroid conditions and stands as the primary cause of hyperthyroidism, a state characterized by the thyroid gland's excessive production of hormones[1,2,3,4]. It is responsible for 60% to 80% of instances of hyperthyroidism. In the US, hyperthyroidism represents 1.2% of the population overall, with an incidence of 20/100,000 to 50/100,000. People between the ages of

20 and 50 are most likely to have it. According to some research, women are more likely than males to have Graves' disease, with a lifetime risk of 3% compared to 0.5% for men. The 12-year incidence among women between the ages of 25 and 42 was as high as 4.6/1000, according to the Nurses' Health Study II (NHSII)[1]. Hormones that control metabolism are released by the thyroid, a little gland shaped like a butterfly that is located in front of the neck. When the thyroid gland is erratically attacked by the immune system, it generates excessive hormones, which causes a variety of problems throughout the body in Graves disease[2,3]. Once properly diagnosed, Graves' disease is quite manageable. In some instances, it may enter remission or resolve entirely after several months or years. However, if left untreated, it can lead to severe complications, including life-threatening situations. Prompt treatment is crucial to avoid such risks[4,5]. TSH stimulates thyroid follicular cells by attaching to TSH receptors (TSHR), which triggers the thyroid hormones production and dispersion into the bloodstream of triiodothyronine (T3) and thyroxine (T4)[5,6].

The immune system produces antithyroid stimulating receptor antibodies (TRAb) that circulate in the blood and mimic the action of TSH. Consequently, TSH levels drop below the normal range and become almost undetectable in the blood, while TRAb continuously stimulates the gland to produce and secrete hormones, leading to an overactive thyroid gland (hyperthyroidism) in otherwise healthy individuals[7]. Due to a complicated interaction between a genetic trait and environmental factors, Graves' illness is characterised by the development of TRAb and a loss of immunological tolerance to thyroid antigens. Though other organs like the eyes, pituitary, skin, and joints are also included, it is defined as an organ-specific autoimmune disease. Elevated levels of serum free thyroid hormones, specifically free T4 (FT4) and free T3 (FT3), along with undetectable blood TSH and the presence of serum TRAb at some time, are the laboratory confirmation of Graves' hyperthyroidism[7]. A simplified differential equation model were constructed to depict the functioning of the HPT axis in individuals with Hashimoto's thyroiditis. This model comprises four variables: the functional size of the thyroid gland, the concentration of serum TSH, serum FT4, and serum thyroid peroxidase antibody[8]. Similarly, Graves' disease was addressed through a set of differential equations. The initial mechanistic model, designed to predict relapse in Graves' disease patients, was constructed using an ordinary differential equation system to capture the dynamics of the condition[9].

METHODOLOGY

Construction of the Model

The given system of ordinary differential equations (ODEs) represents a mathematical model for Graves' disease, . The model describes the dynamics of thyroid stimulating hormone (TSH), thyroid-stimulating autoantibodies (TRAB), the volume of the thyroid gland (V) and free thyroxine (FT4). The equations governing the rates of change for these variables are as follows:

$$\frac{dTSH}{dt} = k_1 \frac{FT4}{K_a + FT4} - k_2 \frac{TSH}{K_b + TSH} - k_3 TSH + k_4$$

$$\frac{dFT4}{dt} = k_5 V \frac{Ab}{K_c + Ab} - k_6 FT4$$

$$\frac{dV}{dt} = k_7 + k_8 \frac{Ab}{V} - k_9 V$$

$$\frac{dAb}{dt} = \mathrm{k}_{prod} - k_{decay} Ab - k_{bind} Ab \frac{TSH}{K_d + TSH} \quad (1)$$

Where $k_1, k_2, k_3, k_4, k_5, k_6, k_7, k_8, k_9, k_{prod}, k_{decay}, k_{bind}, K_a, K_b, K_c, K_d > 0$ and $TSH(0) > 0, FT4(0) > 0, V(0) > 0$ and $Ab(0) > 0$

In first equation, The term $k_1 \frac{FT4}{K_a + FT4}$ represents the negative feedback regulation of TSH by FT4, where k_1 is the rate constant, and K_a is the Michaelis-Menten constant for this process. The second term represents the clearance or degradation of TSH, with k_2 as the rate constant and K_b as the Michaelis-Menten constant. The third term accounts for an additional clearance or degradation of TSH, with a rate constant k_3. The last term k_4, represents a constant production rate of TSH. In Second equation, the term $k_5 V \frac{Ab}{K_c + Ab}$ represents the production of FT4 stimulated by the thyroid-stimulating autoantibodies (TRAB), where k_5 is the rate constant, V is the volume of the thyroid gland, and K_c is the Michaelis-Menten constant for this process. The second term accounts for the clearance or degradation of FT4, with a rate constant k_6. In third equation, the first term k_7, represents a constant widening rate of thyroid gland. The second term accounts for the stimulation of thyroid growth by TRAB, where k_8 is the rate constant, and the term TRAB/V represents the concentration of TRAB relative to the thyroid gland volume. The third term, $-k_9 V$, represents a natural decay or shrinkage of the thyroid gland, with a rate constant k_9. In fourth equation, the first term, k_{prod}, represents a constant production rate of TRAB. The second term accounts for the natural decay or clearance of TRAB, with a rate constant k_{decay}. The third term represents the binding of TRAB to TSH, which effectively removes TRAB from the system. In this term, k_{bind} is the rate constant, and K_d is the Michaelis-Menten constant for the binding process.

Theorem 1. Using the initial conditions given in equation (1), the solutions $TSH(t), FT4(t), V(t), Ab(t)$ are non-negative for all time $t > 0$

Proof:

To prove the non-negativity of TSH(t), let's first analyze the differential equation:

$$\frac{dTSH}{dt} = k_1 \frac{FT4}{K_a + FT4} - k_2 \frac{TSH}{K_b + TSH} - k_3 TSH + k_4$$

Since all the parameters and initial conditions are positive,Now, to prove the non-negativity of $TSH(t)$,By the comparison theorem for differential equations. Let's define a new function $g(t) = e^{k_3 t} TSH(t)$. Taking the derivative of $g(t)$ with respect to t and check its sign:

$$\frac{dg(t)}{dt} = e^{k_3 t} \frac{dTSH}{dt} + k_3 e^{k_3 t} TSH(t)$$

Substituting the given differential equation into the above expression:

$$\frac{dg(t)}{dt} = e^{k_3 t} \left(k_1 \frac{FT4}{K_a + FT4} - k_2 \frac{TSH}{K_b + TSH} - k_3 \cdot TSH + k_4 \right) + k_3 e^{k_3 t} TSH(t)$$

We can simplify this expression:

$$\frac{dg(t)}{dt} = e^{k_3 t}\left(k_1 \frac{FT4}{K_a + FT4} - k_2 \frac{TSH}{K_b + TSH} + k_4\right)$$

Now, let's examine the terms in the brackets:

1. $k_1 \frac{FT4}{Km_1 + FT4} > 0$ since all parameters are positive.
2. $-k_2 \frac{TSH}{Km_2 + TSH}$ because $TSH > 0$ and the other parameters are positive.
3. $k_4 > 0$ as per our assumptions.

Therefore, $\frac{dg(t)}{dt} > 0$ for all t

Since $\frac{dg(t)}{dt} > 0$, $g(t)$ is an increasing function of t, which implies that $TSH(t)$ is also an increasing function of t because $e^{k_3 t} > 0$ for all t. Since $TSH(0) > 0$, and $TSH(t)$ is an increasing function of t, it follows that $TSH(t) > 0$ for all t. Therefore, we have proved the non-negativity of $TSH(t)$.

Similary, other equations can be proved.

Stability analysis

Theorem 2: The equilibrium E^* is locally asymptotically stable.

Here is an analytical proof of asymptotic stability for the given system of differential equations:

Let's define the state variables

$$x_1 = [TSH],\ x_2 = [FT4],\ x_3 = [V],\ x_4 = [TRAB]$$

Then we can rewrite the system as:

$$\frac{dx_1}{dt} = k_1 \frac{x_2}{K_a + x_2} - k_2 \frac{x_1}{K_b + x_1} - k_3 x_1 + k_4$$

$$\frac{dx_2}{dt} = k_5 x_3 \frac{x_4}{K_c + x_4} - k_6 x_2$$

$$\frac{dx_3}{dt} = k_7 + k_8 \frac{x_4}{x_3} - k_9 x_3$$

$$\frac{dx_4}{dt} = \mathrm{k}_{prod} - k_{decay} x_4 - k_{bind} x_4 \frac{x_1}{K_d + x_1}$$

To prove asymptotic stability, we find the equilibrium points by setting dx/dt = 0:

$$x_1^* = \frac{\left(k_1 k_5 k_{prod} - k_2 k_3 K_a K_b K_c\right)}{k_1 k_5 k_6 K_b K_c + k_2 k_3 k_4 K_a K_c + k_1 k_2 k_5 K_a K_b}$$

$$x_2^* = \frac{k_5 x_3 x_4^*}{k_6\left(K_c + x_4^*\right)}$$

$$x_3^* = \frac{k_7}{k_9}$$

$$x_4^* = \frac{k_{prod}}{k_{decay} + \frac{k_{bind} x_1^*}{K_d + x_1^*}}$$

At the equilibrium point, the Jacobian matrix is evaluated as follows:

$$J = \begin{vmatrix} -\frac{k_2 K_b}{(K_b + x_1^*)^2} - k_3 & \frac{k_1 K_a}{\left(K_a + x_2^*\right)^2} & 0 & 0 \\ 0 & -k_6 & \frac{k_5 x_4^*}{K_c + x_4^*} & \frac{k_5 K_c x_3^*}{\left(K_c + x_4^*\right)^2} \\ 0 & 0 & -\frac{k_8 x_4^*}{x_3^{*2}} - k_9 & \frac{k_8}{x_3^*} \\ -\frac{K_d k_{bind} x_4^*}{(K_d + x_1^*)^2} & 0 & 0 & -k_{decay} - \frac{k_{bind} x_1^*}{K_d + x_1^*} \end{vmatrix}$$

The trace of the Jacobian matrix is:

$$trace(J) = -k_3 - k_6 - k_9 - k_{decay} - \frac{k_2 K_b}{(K_b + x_1^*)^2} - \frac{k_8 x_4^*}{x_3^{*2}} - \frac{k_{bind} x_1^*}{K_d + x_1^*}$$

Which is negative since all rate constants and concentrations are positive.

The determinant of the Jacobian matrix is:

$$\det(J) = \left(\frac{k_2 K_b}{(K_b + x_1^*)^2} + k_3\right)\left(\frac{k_8 x_4^*}{x_3^{*2}} + k_9\right)\left(k_{decay} + \frac{k_{bind} x_1^*}{K_d + x_1^*}\right)$$
$$+ \left(\frac{k_1 K_a}{\left(K_a + x_2^*\right)^2}\right)\left(\frac{K_d k_{bind} x_4^*}{(K_d + x_1^*)^2}\right)\left[\left(\frac{k_5 x_4^*}{K_c + x_4^*}\right)\frac{k_8}{x_3^*} + \left(\frac{k_8 x_4^*}{x_3^{*2}} + k_9\right)\left(\frac{k_5 K_c x_3^*}{\left(K_c + x_4^*\right)^2}\right)\right]$$
$$> 0$$

According to the Routh-Hurwitz stability criterion, the equilibrium point is asymptotically stable since the trace of the matrix is negative and the determinant is positive.

Therefore, we have analytically proven that the given system of differential equations modeling thyroid hormone regulation is asymptotically stable around its equilibrium point.

Theorem 3. The equilibrium E^* is globally asymptotically stable with some conditions.

Proof. lets denote TSH as T, FT4 as F and Ab as A. let consider the positive definite function

$$U = \frac{1}{2}m_1\left(T-T^*\right)^2 + \frac{1}{2}m_2\left(F-F^*\right)^2 + \frac{1}{2}m_3\left(V-V^*\right)^2 + \frac{1}{2}m_4\left(A-A^*\right)^2$$

Differentiating the above the function with respect to time t, we have

$$\dot{U} = m_1\left(T-T^*\right)\dot{T} + m_2\left(F-F^*\right)\dot{F} + m_3\left(V-V^*\right)\dot{V} + m_4\left(A-A^*\right)\dot{A}$$

$$\dot{U} = -m_1\left(\frac{k_2K_b}{(K_b+T^*)^2}+k_3\right)\left(T-T^*\right)^2 + m_1\left(\frac{k_1K_a}{\left(K_a+F^*\right)^2}\right)\left(T-T^*\right)\left(F-F^*\right) - m_2(k_6)\left(F-F^*\right)^2$$

$$+m_2\left(\frac{k_5A^*}{K_c+A^*}\right)\left(F-F^*\right)\left(V-V^*\right) + m_2\left(\frac{k_5K_cV^*}{\left(K_c+A^*\right)^2}\right)\left(F-F^*\right)\left(A-A^*\right) -$$

$$-\left(\frac{k_8A^*}{V^{*2}}+k_9\right)m_3\left(V-V^*\right)^2 + m_3\frac{k_8}{V^*}\left(V-V^*\right)\left(A-A^*\right)$$

$$+m_4\left(\frac{K_dk_{bind}A^*}{(K_d+T^*)^2}\right)\left(A-A^*\right)\left(T-T^*\right) - m_4\left(k_{decay}+\frac{k_{bind}T^*}{K_d+T^*}\right)\left(A-A^*\right)^2$$

$\dot{U}$ will be negative definite

$$m_1\left(\frac{k_1K_a}{\left(K_a+F^*\right)^2}\right)^2 < \frac{2}{3}m_2k_6k_3$$

$$m_2\left(\frac{k_5A^*}{K_c+A^*}\right)^2 < \frac{2}{3}m_3k_6k_9$$

$$m_4\left(\frac{K_dk_{bind}A^*}{(K_d+T^*)^2}\right)^2 < \frac{2}{3}m_1k_3k_{decay}$$

$$m_2\left(\frac{k_5K_cV^*}{\left(K_c+A^*\right)^2}\right)^2 < \frac{4}{9}m_4k_6k_{decay}$$

$$m_3\left(\frac{k_8}{V^*}\right)^2 < \frac{2}{3}m_4k_9k_{decay}$$

Now $m_1 = 1, m_3 = 1, m_4 = 1$

$$\left(\frac{k_1 K_a}{\left(K_a + F^*\right)^2} \right)^2 < \frac{4}{9} k_6 \left(K_c + A^*\right)^2 \min\left\{ \frac{k_9}{k_5 (A^*)^2}, \frac{2}{3} \frac{k_{decay}}{K_c V^*} \right\}$$

$\dot{U}$ will be negative definite provided the above conditions are satisfied and hence E^* is globally asymptotically stable.

RESULTS AND DISCUSSION

Graves' disease involves a characteristic progression from normal thyroid hormone levels (euthyroidism) to overt hyperthyroidism. This progression typically follows a pattern marked by a decline in TSH (thyroid stimulating hormone) levels and an increase in FT4 (free thyroxine) levels. The drop in TSH is caused by negative feedback from the elevated circulating levels of thyroid hormones FT4 and FT3 (free triiodothyronine)[10,11]. Meanwhile, the rise in FT4 results from the overproduction of thyroid hormones by the overactive thyroid gland in Graves' disease. So the TSH decreases in response to the excess thyroid hormones, while the FT4 increases due to the gland's excessive hormone production and release. Let the Initial values of TSH 0.906 mU/L[13], FT4 36 pg/mL[7], thyroid volume (V) 30 mL[7,9], and antibody levels (Ab) 25 IU/mL[7,9] for the parameters values from the table.
We can plug in the initial conditions into the TSH rate equation:

$$0 = k_1(36)/\left(0.0434+36\right) - k_2(0.906)/\left(K_a+0.906\right) - 16.6355(0.906) + 30$$

$$k_1 = 15.0479 + k_2(0.906)/\left(K_a+0.906\right)$$

Lets assume:

$$k_2 = 0.5 \ /day \ , \ K_a = 1 \ mU/L \ \left(guess\right)$$

Then

$$k_1 = 15.0479 + 0.5(0.906)/\left(1+0.906\right) = 15.45 \ mU/L \ per \ \left(pg/mL \ x \ day\right)$$

In some cases, certain parameter values are calculated using the initial condition and known parameter values. For the remaining parameter values, an optimization approach is employed using the fmincon function in MATLAB. The upper and lower bounds for these parameters are set based on values reported in previous literature studies[10,12]. This optimization process simulates or estimates the unknown parameter values by finding the optimal solution within the specified bounds, leveraging the known information and the initial conditions.

CONCLUSION

A novel mathematical framework has been established to elucidate the pathophysiology of Graves' disease. This framework, formulated as a system of four nonlinear ordinary differential equations, integrates critical disease variables including thyroid-stimulating hormone (TSH), free thyroxine (FT4), thyroid gland volume (Fsize), and TSH receptor autoantibodies (TRAB). The development meticulously incorporates established biological mechanisms underlying Graves' disease pathogenesis. The system's dynamic behavior and equilibrium states were investigated through analytical stability analysis. Additionally, Lyapunov theory was employed to mathematically demonstrate the model's asymptotic stability. Parameter estimation utilized a combined approach, leveraging both clinical data and optimization techniques implemented using fmincon within the MATLAB environment. To ensure validity, the model underwent comprehensive simulation within simbiology MATLAB. This work represents a significant

contribution by establishing a validated mathematical framework that captures the essential features of Graves' disease pathogenesis. The model's utility extends beyond mere comprehension, it serves as a powerful tool to explore potential clinical interventions and analyze treatment responses. In conclusion, this research offers a valuable contribution to the field of Graves' disease by providing a robust mathematical modeling approach, paving the way for future investigations into optimized treatment strategies.

REFERENCES

1. Pokhrel B, Bhusal K. Graves Disease. Treasure Island (FL): StatPearls Publishing 2024. Available from: https://www.ncbi.nlm.nih.gov/books/NBK448195/
2. https://www.webmd.com/women/understanding-graves-disease-basic
3. *Burch, H. B. Management of Graves' disease: A review. JAMA, Internal Medicine. 2015; 314(23): 2544-2554.* https://doi.org/10.1001/jama.2015.16535
4. *https://www.healthline.com/health/graves-disease*
5. De Leo, S, Lee S Y, Braverman, L. E. Hyperthyroidism. The Lancet. 2016; 388(10047): 906-918. *https://doi.org/10.16/S0140-6736(16)00278-6*
6. *https://courses.washington.edu/pbio376/thyroid-disorders/thyroid-376.html*
7. Pandiyan B, Merrill SJ, Di Bari F, Antonelli A, Benvenga S. A patient-specific treatment model for Graves' hyperthyroidism. Theoritical Biology Medical Modelling. 2018 ;15(1):1. https://doi.org/10.1186/s12976-017-0073-6
8. Pandiyan B, Merrill S J. A homoclinic orbit in a patient-specific model of Hashimoto's thyroiditis. Differential Equations and Dynamical Systems. 2016; 28(2): 401-418. https://doi.org/10.1007/s1259-016-0335-5
9. Langenstein C, Schork D. Relapse prediction in Graves' disease. Towards mathematical modeling of clinical, immune and genetic markers. Reviews in Endocrine and Metabolic Disorders. 2016; 17(4): 571-581. https://doi.org/10.1007/s11154-016-9386-8
10. https://www.verywellhealth.com/understanding-thyroid-blood-tests-low-or-high-tsh-3233198
11. *Mo C, Chen H, Zhang Q, Guo Y, Zhong L. Central hyperthyroidism combined with Graves' disease: case series and review of the literature. European thyroid journal. 2023 Jul 28;12(4).* https://doi.org/10.1530/ETJ-22-0223
12. Sakane S. The prognostic application of thyroid volume determination in patients with Graves' disease. Nihon Naibunpi Gakkai Zasshi. 1990 May 20;66(5):543-56. Japanese. https://doi.org1 0.1507/end ocrine1927. 66.5_543
13. Yang B, Tang X, Haller MJ, Schatz DA, Rong L. A unified mathematical model of thyroid hormone regulation and implication for personalized treatment of thyroid disorders. Journal of Theoretical Biology. 2021 Nov 7;528:110853.*https://doi.org/10.1016/j.jtbi.2021.110853*

Table 1: Normal range and disease state

	Normal Range	Disease state	Source	Unit
TSH	0.4 - 4.0	< 0.4	Link(verywellhealth)	mU/L
FT4	7-18	>18	Literature(Mo C et al, 2023)	Pg/mL
V	10-18	-	Literature(Sakane 1990)	mL
Ab	0-1.75	>1.75	Literature(Mo C et al, 2023)	IU/L

Table 2: parameters description and values with units

	description	values	Units
k_1	Rate constant for TSH stimulation by FT4	15.45	$mU / L * day$
k_2	Rate constant for TSH auto-inhibition	0.5	$mU / L * day$
k_3	Rate constant for TSH degradation	16.6355	$pg / mL^2 * day$

k_4	Basal TSH production rate	30	$pg / mL^2 * day$
k_5	Rate of FT4 production stimulated by TSH and functional size of thyroid gland	0.0814	-
k_6	Rate constant for FT4 degradation	0.0183	$ml^3 / U * day$
k_7	constant widen rate of thyroid gland.	0.0289	-
k_8	Constant widen rate of thyroid gland stimulated by TRAb	0.2781	$U / mL * day$
k_9	constant decay or shrinkage rate of the thyroid gland	0.0316	$U / mL * day$
k_{prod}	Production rate constant for TRAb	3.1052	$1 / day$
k_{decay}	Decay/clearance rate of TRAb	0.0087	-
k_{bind}	Michaelis-Menten constant for TRAb binding to TSH.	0.0866	mU / L
K_a	Michaelis constant for FT4 stimulation of TSH	0.0434	$1 / day$
K_b	Michaelis constant for TSH auto-inhibition	1	$1 / day$
K_c	Michaelis constant for TSH stimulation of FT4	0.004	$1 / day$
K_d	Michaelis constant for TRAB binding to TSH	1	$1 / day$

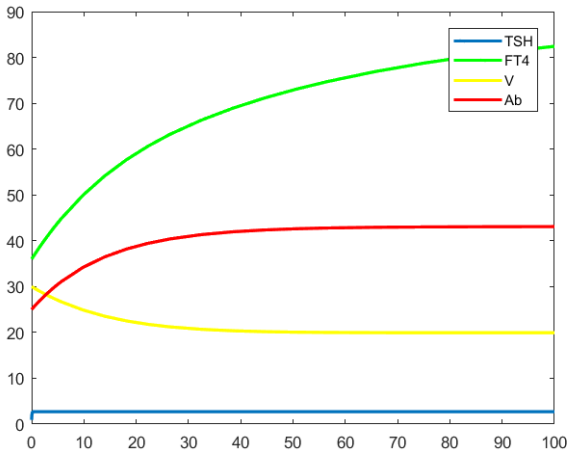

Fig 1: Graphical representation of the proposed model with initial values of TSH 0.906 mU/L, FT4 36 pg/mL, thyroid volume (V) 30 mL, and antibody levels (Ab) 25 IU/mL for the parameters values from the table 2.

Indian Journal of Natural Sciences www.tnsroindia.org.in ©IJONS

Vol.15 / Issue 83 / Apr / 2024 International Bimonthly (Print) – Open Access ISSN: 0976 – 0997

RESEARCH ARTICLE

Some New Results on Harary Energy of Graphs

M. Deva saroja[1] and V. Vinisha[2]

[1]Assistant Professor, Rani Anna Government College for Women, (Affliated to Manonmaniam Sundaranar University),Tamil Nadu, India.
[2]Research Scholar , Registration Number: 23111172092002,Rani Anna Government College for Women, (Affliated to Manonmaniam Sundaranar University) Tamil Nadu, India.

Received: 30 Dec 2023 Revised: 09 Jan 2024 Accepted: 12 Mar 2024

***Address for Correspondence**
M. Deva saroja
Assistant Professor,
Rani Anna Government College for Women,
(Affliated to Manonmaniam Sundaranar University),
Tamil Nadu, India.
Email: mdsaroja@gmail.com

ABSTRACT

In this paper, we compute the Harary energy of some graphs. Also, we obtained the Harary energy of regular graph obtained from join of complete graphs.

Keywords: Harary matrix, Harary energy, cocktail party graph, crown graph, friendship graph.
2020 Mathematics Subject Classification: 05C50

INTRODUCTION

Throughout the paper, all graphs wil be assumed to be simple and finite in order to simplify the analysis. There has been a lot of discussion about the concept of Energy of graph since 1978, when Ivan Gutman introduced it. A more detailed explanation of the concept energy can be found in [2,3]. The focus of this article is on Harary matrix[4], developed by Ivanciuc et al[5] in the 1970s. Assume that G is an undirected graph consisting of a vertices set $V(G) = \{n_1, n_2, \dots, n_p\}$ and edges set $E(G)$. In the case of this vertices n_j and n_k, the distance between them, denoted by D'_{jk}, can be considered to the length of the shortest path connecting this two vertices. The Harary matrix[4] $H(G) = [R_{jk}]$ of G is a $p \times p$ matrix, where

$$R_{jk} = \begin{cases} \frac{1}{D'_{jk}}, & if\ j \neq k \\ 0, & if\ j = k \end{cases}$$

A group of eigen values from $H(G)$ denoted by $\eta_1 \geq \eta_2 \geq \cdots \geq \eta_p$ are known as Harary eigenvalues and their collection is known as Harary spectrum of G. For more details on Harary eigenvalues, refer [6,7,8]. Harary energy of a graph G, referred to as $E_H(G)$, can be defined [9] as follows:

$$E_H(G) = \sum_{i=1}^{p} |\eta_i|$$

$H(G)$ is defined to have the characteristic polynomial of the form $P(G,\eta) = \det(\eta I - H(G))$. In this, I represents the unit matrix of order p. The eigen values of $H(G)$ are the roots of $P(G,\eta)$. Since, the Harary matrix $H(G)$ be a real symmetric with zero trace, the collection η_i's must be real with $\sum \eta_i = 0$.

PRELIMINARIES

Lemma 2.1. [10] If U, V, X and Y are all matrices with U non- singular, then we can write $\begin{vmatrix} U & V \\ X & Y \end{vmatrix} = |U||Y - XU^{-1}V|$

Lemma 2.2. [10] If U, V, X and Y are all matrices. Let $R = \begin{pmatrix} U & V \\ X & Y \end{pmatrix}$ if U and X are commutative matrices, then $|R| = |UY - XV|$

Lemma 2.3. [11] The adjacency matrix $A(K_q)$ of complete graph K_q, then $A^2(K_q) = (q-2)A(K_q) + (q-1)I_q$.

Definition 2.4. [12] Let us take a pair of complete graphs K_q with vertices set $\{p_i, i = 1,2,3,\dots,q\}$ and $\{r_j, j = 1,2,3,\dots,q\}$. Construct a graph by joining p_i to r_i , for $i = 1,2,3,\dots q$ and denote it by $J(K_q^q)$. It has $2q$ vertices and q^2 edges and is q-regular.

HARARY ENERGY OF SOME GRAPHS

Theorem 3.1. Let CP'_{2q} be the cocktail party graph. Then

$$S_pH(CP'_{2q}) = \begin{bmatrix} \left(\frac{4q-3}{2}\right) & \left(\frac{-3}{2}\right) & \left(\frac{-1}{2}\right) \\ 1 & q-1 & q \end{bmatrix}$$

and the Harary energy of CP'_{2q} is, $E_H(CP'_{2p}) = 4q - 3$ where $q \geq 2$

Proof : Let the cocktail party graph be CP'_{2q} then it has $2q$ vertices, $2q(q-1)$ edges and is $(2q-2)$ - regular. Let $\alpha = \{\alpha_1, \alpha_2, \alpha_3, \dots, \alpha_{2q}\}$ be the eigen values of Harary matrix of CP'_{2q}. Then the Harary matrix of CP'_{2q} has the form

$$H(CP'_{2q}) = \begin{bmatrix} A(K_q) & \frac{1}{2}I_q + A(K_q) \\ \frac{1}{2}I_q + A(K_q) & A(K_q) \end{bmatrix}$$

The corresponding characteristic polynomial is

$$\begin{aligned} |\alpha I_{2q} - H(CP'_{2q})| &= \begin{vmatrix} \alpha I_q - A(K_q) & -\left(\frac{1}{2}I_q + A(K_q)\right) \\ -\left(\frac{1}{2}I_q + A(K_q)\right) & \alpha I_q - A(K_q) \end{vmatrix} \\ &= \left|\left(\alpha I_q - A(K_q)\right)^2 - \left(\tfrac{1}{2}I_q + A(K_q)\right)^2\right| \text{ by lemma (2.2)} \\ &= \left|\left(\alpha^2 - \tfrac{1}{4}\right)I_q - (2\alpha+1)A(K_q)\right| \\ &= (2\alpha+1)^q \left|\frac{\left(\alpha^2 - \frac{1}{4}\right)}{(2\alpha+1)} I_q - A(K_q)\right| \\ &= (2\alpha+1)^q \left(\tfrac{2\alpha-1}{4} - (q-1)\right)\left(\tfrac{2\alpha-1}{4} + 1\right)^{q-1} \\ &= \left(\alpha - \left(\tfrac{-1}{2}\right)\right)^q \left(\alpha - \left(\tfrac{4q-3}{2}\right)\right)\left(\alpha - \left(\tfrac{-3}{2}\right)\right)^{q-1} \end{aligned}$$

Hence, the Harary spectrum of CP'_{2q} is

$$S_pH(D_1(K_{2q})) = \begin{bmatrix} \left(\frac{4q-3}{2}\right) & \left(\frac{-3}{2}\right) & \left(\frac{-1}{2}\right) \\ 1 & q-1 & q \end{bmatrix}$$

and the Harary energy of CP'_{2p} is, $E_H(CP'_{2q}) = 4q-3$ where $q \geq 2$

Theorem 3.2. Let $H'_{q,q}$ be the crown graph. Then

$$S_pH(H'_{q,q}) = \begin{bmatrix} \left(\frac{-3q+1}{6}\right) & \frac{9q-7}{6} & \frac{1}{6} & \left(\frac{-7}{6}\right) \\ 1 & 1 & q-1 & q-1 \end{bmatrix}$$

and the Harary energy is, $E_H(H'_{q,q}) = \frac{2(5q-4)}{3}$ where $q \geq 3$

Proof: Let $H'_{q,q}$ be the crown graph then it has $2q$ vertices, $q(q-1)$ edges and is $(q-1)$ –regular. Let $\eta = \{\eta_1, \eta_2, \eta_3, \dots, \eta_{2q}\}$ be the eigen value. Then, the Harary matrix of $H'_{q,q}$ is

$$H(H'_{q,q}) = \begin{bmatrix} \frac{1}{2}A(K_q) & \frac{1}{3}I_q + A(K_q) \\ \frac{1}{3}I_q + A(K_q) & \frac{1}{2}A(K_q) \end{bmatrix}$$

By lemma (2.3), we get the Characteristics polynomial is

$$\left(\eta - \left(\tfrac{-3q+1}{6}\right)\right)\left(\eta - \left(\tfrac{9q-7}{6}\right)\right)\left(\eta - \tfrac{1}{6}\right)^{q-1}\left(\eta - \left(\tfrac{-7}{6}\right)\right)^{q-1}$$

Hence, the spectrum

$$S_pH(H'_{q,q}) = \begin{bmatrix} \left(\frac{-3q+1}{6}\right) & \frac{9q-7}{6} & \frac{1}{6} & \left(\frac{-7}{6}\right) \\ 1 & 1 & q-1 & q-1 \end{bmatrix}$$

and the Harary energy is, $E_H(H'_{q,q}) = \frac{2(5q-4)}{3}$ where $q \geq 3$

Theorem 3.3. The complete bipartite graph $K_{q,q}$ has the spectrum

$$S_pH(K_{q,q}) = \begin{bmatrix} \left(\frac{-1}{2}\right) & \frac{-(q+1)}{2} & \frac{3q-1}{2} \\ 2(q-1) & 1 & 1 \end{bmatrix}$$

and the Harary energy of $K_{q,q}$ is, $E_H(K_{q,q}) = 3q-1$ where $q \geq 2$

Proof : Let the complete bipartite graph be $K_{q,q}$ and the eigen value of Harary matrix are $\gamma = \{\gamma_1, \gamma_2, \gamma_3, \dots, \gamma_{2q}\}$ respectively. Then, the Harary matrix of $K_{q,q}$ is

$$H(K_{q,q}) = \begin{bmatrix} \frac{1}{2}A(K_q) & I_p + A(K_q) \\ I_q + A(K_q) & \frac{1}{2}A(K_q) \end{bmatrix}$$

By lemma (2.3), we get

$$|\gamma I_{2q} - H(K_{q,q})| = \left(\gamma + \tfrac{1}{2}\right)^{2(q-1)}\left(\gamma + \left(\tfrac{q+1}{2}\right)\right)\left(\gamma - \left(\tfrac{3q-1}{2}\right)\right)$$

Therefore,

$S_pH(K_{q,q}) = \begin{bmatrix} \left(\frac{-1}{2}\right) & \frac{-(q+1)}{2} & \frac{3q-1}{2} \\ 2(q-1) & 1 & 1 \end{bmatrix}$ and $E_H(K_{q,q}) = 3q-1$ where $q \geq 2$

Theorem 3.4. Let the complete graph be K_q. Then

$$S_pH(K_q) = \begin{bmatrix} (-1) & q-1 \\ q-1 & 1 \end{bmatrix}$$

and the Harary energy of K_q is, $E_H(K_q) = 2(q-1)$ where $q \geq 2$

Proof : Let $\beta' = \{\beta'_1, \beta'_2, \beta'_3, \dots, \beta'_q\}$ be the eigen value of complete graph K_q . Then it has q vertices, $\frac{q(q-1)}{2}$ edges and is $(q-1)$- regular. Then the Harary matrix of K_q has the form

$H(K_q) = [A(K_q)]$.

By lemma (2.3), we get

$$(\beta' + 1)^{q-1}(\beta' - (q-1))$$

Hence,

$$S_pH(K_q) = \begin{bmatrix} (-1) & q-1 \\ q-1 & 1 \end{bmatrix}$$

and the Harary energy of K_q is, $E_H(K_q) = 2(q-1)$ where $q \geq 2$

Theorem 3.5. For any $q \geq 1$, the star graph $K_{1,q}$ has the spectrum

$$S_pH(K_{1,q}) = \begin{bmatrix} \left(\frac{-1}{2}\right) & \frac{\left(\frac{q-1}{2}\right) + \sqrt{\left(\frac{q-1}{2}\right)^2 + 4q}}{2} & \frac{\left(\frac{q-1}{2}\right) - \sqrt{\left(\frac{q-1}{2}\right)^2 + 4q}}{2} \\ q-1 & 1 & 1 \end{bmatrix}$$

and the Harary energy of $K_{1,q}$ is, $E_H(K_{1,q}) = \left(\frac{q-1}{2}\right) + \sqrt{\left(\frac{q-1}{2}\right)^2 + 4q}$

Proof : Let us take a star graph $K_{1,q}$ with vertices set $V' = \{v'_0, v'_1, v'_2, \ldots, v'_q\}$ where the vertex v'_0 has degree q and the eigen values of Harary matrix are $\mu = \{\mu_0, \mu_1, \ldots, \mu_q\}$ respectively. For this graph, the Harary matrix is

$$H(K_{1,q}) = \begin{bmatrix} 0 & 1 & 1 & 1 & \cdots & 1 & 1 \\ 1 & 0 & 1/2 & 1/2 & \cdots & 1/2 & 1/2 \\ 1 & 1/2 & 0 & 1/2 & \cdots & 1/2 & 1/2 \\ 1 & 1/2 & 1/2 & 0 & \cdots & 1/2 & 1/2 \\ \vdots & \vdots & \vdots & \vdots & \ddots & \vdots & \vdots \\ 1 & 1/2 & 1/2 & 1/2 & \cdots & 0 & 1/2 \\ 1 & 1/2 & 1/2 & 1/2 & \cdots & 1/2 & 0 \end{bmatrix}$$

On simplification, we get the characteristic polynomial

$\left(\mu + \frac{1}{2}\right)^{q-1}\left(\mu - \left(\frac{\left(\frac{q-1}{2}\right) \pm \sqrt{\left(\frac{q-1}{2}\right)^2 + 4q}}{2}\right)\right)$ and the spectrum would be

$$S_pH(K_{1,q}) = \begin{bmatrix} \left(\frac{-1}{2}\right) & \frac{\left(\frac{q-1}{2}\right) + \sqrt{\left(\frac{q-1}{2}\right)^2 + 4q}}{2} & \frac{\left(\frac{q-1}{2}\right) - \sqrt{\left(\frac{q-1}{2}\right)^2 + 4q}}{2} \\ q-1 & 1 & 1 \end{bmatrix}$$

Therefore, $E_H(K_{1,q}) = \left(\frac{q-1}{2}\right) + \sqrt{\left(\frac{q-1}{2}\right)^2 + 4q}$

Theorem 3.6. The spectrum and energy of the friendship graph F_q^3 is

$$S_pH(F_q^3) = \begin{bmatrix} 0 & -1 & \frac{q + \sqrt{q^2 + 8q}}{2} & \frac{q - \sqrt{q^2 + 8q}}{2} \\ q-1 & q & 1 & 1 \end{bmatrix}$$

and $E_H(F_q^3) = q + \sqrt{q^2 + 8q}$

Proof: Consider the friendship graph F_q^3 with vertices set $V' = \{v'_0, v'_1, v'_2, \ldots, v'_{2q}\}$ where $\deg(v'_0) = 2q$ and the eigen values of Harary matrix are $\eta' = \{\eta'_0, \eta'_1, \ldots, \eta'_{2q}\}$ respectively. Then the Harary matrix of F_q^3 is

$$H(F_q^3) = \begin{bmatrix} 0 & 1 & 1 & 1 & 1 & \cdots & 1 & 1 \\ 1 & 0 & 1 & 1/2 & 1/2 & \cdots & 1/2 & 1/2 \\ 1 & 1 & 0 & 1/2 & 1/2 & \cdots & 1/2 & 1/2 \\ 1 & 1/2 & 1/2 & 0 & 1 & \cdots & 1/2 & 1/2 \\ 1 & 1/2 & 1/2 & 1 & 0 & \cdots & 1/2 & 1/2 \\ \vdots & \vdots & \vdots & \vdots & \vdots & \ddots & \vdots & \vdots \\ 1 & 1/2 & 1/2 & 1/2 & 1/2 & \cdots & 0 & 1 \\ 1 & 1/2 & 1/2 & 1/2 & 1/2 & \cdots & 1 & 0 \end{bmatrix}$$

The characteristic polynomial becomes

$$\eta^{q-1}(\eta+1)^q\left(\eta-\left(\frac{q\pm\sqrt{q^2+8q}}{2}\right)\right)$$

Hence, the spectrum

$$S_pH(F_q^3)=\begin{bmatrix}0 & -1 & \frac{q+\sqrt{q^2+8q}}{2} & \frac{q-\sqrt{q^2+8q}}{2}\\ q-1 & q & 1 & 1\end{bmatrix} \text{ and } E_H(F_q^3)=q+\sqrt{q^2+8q}$$

Harary energy of regular graph obtained from join of complete graph

Theorem 4.1. Let $J(K_q^q)$ be the join of complete graph. Then the Harary spectrum of $J(K_q^q)$ is

$$S_pH(J(K_q^q))=\begin{bmatrix}\left(\frac{3q-1}{2}\right) & \frac{q-3}{2} & \left(\frac{-1}{2}\right) & \left(\frac{-3}{2}\right)\\ 1 & 1 & q-1 & q-1\end{bmatrix}$$

and the Harary energy of $J(K_q^q)$ is $E_H(J(K_q^q))=4(q-1)\,;q\geq 3$

Proof: Let $J(K_q^q)$ be the join of complete graph of order $2q$, $q=3,4,\dots,n$ and q^2 edges. Let the eigen value of Harary matrix be $=\{\lambda_1,\lambda_2,\lambda_3,\dots,\lambda_{2q}\}$. Then the Harary matrix of $J(K_q^q)$ has the form

$$H\left(J(K_q^q)\right)=\begin{bmatrix}A(K_q) & I_q+\frac{1}{2}A(K_q)\\ I_q+\frac{1}{2}A(K_q) & A(K_q)\end{bmatrix}$$

By lemma (2.3), we get the characteristic polynomial

$$\left|\lambda I_{2q}-H\left(J(K_q^q)\right)\right|=\begin{vmatrix}\lambda I_q-A(K_q) & -\left(I_q+\frac{1}{2}A(K_q)\right)\\ -\left(I_q+\frac{1}{2}A(K_q)\right) & \lambda I_q-A(K_q)\end{vmatrix}$$

$$=\left|(\lambda I_q-A(K_q))^2-(I_q+\tfrac{1}{2}A(K_q))^2\right| \text{ by lemma (2.2)}$$

$$=\left|(\lambda^2-1)I_q+\tfrac{3}{4}A^2(K_q)-(2\lambda+1)A(K_q)\right|$$

$$=\left|(\lambda^2-1)I_q+\tfrac{3}{4}((q-2)A(K_q)+(q-1)I_q)-(2\lambda+1)A(K_q)\right| \text{ by lemma (2.3)}$$

$$=\left(\lambda^2+\tfrac{3q}{4}-\tfrac{7}{4}\right)I_q-\left(2\lambda-\tfrac{3q}{4}+\tfrac{10}{4}\right)A(K_q)$$

Simplifying, we get

$$\left(\lambda-\left(\tfrac{3q-1}{2}\right)\right)\left(\lambda-\left(\tfrac{q-3}{2}\right)\right)\left(\lambda+\tfrac{1}{2}\right)^{q-1}\left(\lambda+\tfrac{3}{2}\right)^{q-1}$$

Hence, the Harary spectrum of $J(K_q^q)$ is

$$S_pH(J(K_q^q))=\begin{bmatrix}\left(\frac{3q-1}{2}\right) & \frac{q-3}{2} & \left(\frac{-1}{2}\right) & \left(\frac{-3}{2}\right)\\ 1 & 1 & q-1 & q-1\end{bmatrix} \text{ and } E_H\left(J(K_q^q)\right)=4(q-1) \text{ where } q\geq 3$$

ACKNOWLEDGEMENT

The author (V. Vinisha, Registration No: 23111172092002 , Research Scholar) would like to give the warmest thanks to the research supervisor for her guidance and support.

REFERENCES

1. J.A. Bondy and U.S.R. Murty, "Graph theory with applications", 1976, Elsevier Science.
2. I. Gutman, "The energy of a graph", Ber. Math. Stat. Sekt. Forschungsz. Graz, 103 (1978),1 – 22.

3. I. Gutman, "The energy of a graph: old and new results", Combinatorics and applications, A. Betten, A. Khoner, R. Laue and A. Wassermann, (Eds.), Springer, Berlin, (2001), 196-211.
4. O. Ivanciuc, T.S. Balaban and A.T. Balaban, "Reciprocal distance matrix, related local vertex invariants and topological indices", J. Math. Chem. 12 (1993), 309-318.
5. O. Ivanciuc, T. Ivnciuc and A.T. Balaban, "Quantative Structure- Property Relationship Evaluation of structural descriptors Derived from the distance and Reverse Wiener Matrices", Internet Electron. J. Mol. Des. 1 (2002), 467-487.
6. Z. Cui, B. Liu, "On Harary matrix, Harary index and Harary energy", MATCH Commun. Math. Comput. Chem. 68 (2012), 815-823.
7. K.C. Das, "Maximum eigenvalus of the reciprocal distance matrix", J. Math. Chem. 47 (2010), 21-28.
8. M. V. Diudea, O. Ivanciuc, S. Nikolic, N. Trinajstic, "Matrices of reciprocal distance, polynomials and derived numbers", MATCH Commun. Math. Comput. Chem. 35 (1997), 41-64.
9. A.D. Gungor, A.S. Cevik, "On the Harary energy and Harary Estrada index of a graph", MATCH Commun. Math. Comput. Chem. 64 (2010), 280-296.
10. Cvetkovic D.M, Doob M, Sachs H, "Spectra of graphs", Academic press, New york, 1980.
11. H.B. Walikar and S.R. Jog, "Spectra and energy of graphs obtained from complete graph", Graph theory and its applications Editors, R. Balakrishnan et al Narosa Publishing House New Delhi, India (2004).
12. M. Devasaroja, M.S. Paulraj, "Equienergetic regular graphs" Int Joul. Of Algori. Compu. and Math. Vol 3 No.3 (2010) 21-25.
13. R. Balakrishnan, "The Energy of a graph", Linear Algebra and its applications 384 (2004) 287-295.
14. Harishchandra S. Ramane, Raju B. Jummannaver, "Harary spectra and Harary energy of line graphs of regular graphs", Gulf Journal of Mathematics, Vol 4, Issue 1 (2016) 39-46.
15. B. Zhou, N. Trinajstic, "Maximum eigenvalues of the reciprocal distance matrix and the reverse Wiener matrix", Int. J. Quantum Chem. 108 (2008), 858-864.
16. K. Xu, K.C. Das, "On Harary index of graphs", Discr. Appl. Math. 159 (2011) 1631-1640.

Indian Journal of Natural Sciences *www.tnsroindia.org.in ©IJONS*

Vol.15 / Issue 83 / Apr / 2024 *International Bimonthly (Print) – Open Access* *ISSN: 0976 – 0997*

RESEARCH ARTICLE

Parameter Uniform Convergence of a Finite Element Method for a Singularly Perturbed Linear Reaction Diffusion System with Discontinuous Source Terms and Same Perturbation Parameter

Vinoth Maruthamuthu and Joseph Paramasivam Mathiyazhagan*

Department of Mathematics, Bishop Heber College, (Affiliated to Bharathidasan University), Tiruchirappalli, Tamil Nadu, India.

Received: 30 Dec 2023 Revised: 09 Jan 2024 Accepted: 12 Mar 2024

***Address for Correspondence**
Joseph Paramasivam Mathiyazhagan
Department of Mathematics,
Bishop Heber College,
(Affiliated to Bharathidasan University),
Tiruchirappalli, Tamil Nadu, India.
Email: paramasivam.ma@bhc.edu.in

ABSTRACT

A linear system of 'n' second order ordinary differential equations of reaction diffusion type with discontinuous source terms and same perturbation parameter is considered. On a piecewise uniform Shishkin mesh, a numerical system is built that employs the finite element method. The numerical approximations obtained by this approach are proven to be effectively almost second order convergent.

Keywords: singular perturbation problems, system of differential equations, reaction diffusion equations, overlapping boundary and interior layers, finite element method, Shishkinmesh, parameter uniform convergence, discontinuous source terms.

INTRODUCTION

Singularly perturbed differential equations are found in many disciplines of applicable mathematics. Many scholars have focused on the analytical and numerical treatment of these equations [1–22]. In general, simple numerical approaches do not give satisfactory approximations for these equations. As a result, one must seek for non-classical ways. Over the last three decades, there have been several publications published on non-classical approaches, the majority of which deal with second order problems. However, only a few authors have produced numerical approaches for singularly perturbed systems of ordinary differential equations [6–22]. In contrast to the work cited in reference [13], all singularly perturbed parameters remain consistent throughout our present paper. This consistency ensures a coherent framework for analysis and comparison across different sections or examples within our study.

By maintaining uniformity in these parameters, we aim to facilitate clearer and more accurate interpretations of our results and methodologies. In our current paper, inspired by the work of Miller [6], we delve into the discussion of approximate solutions generated through numerical methods. We emphasize the necessity for these solutions to be globally established at every point across the domain of the exact solution, particularly when representing a boundary layer with the chosen numerical approach. A fundamental consideration lies in the utilization of interpolation techniques to achieve this global establishment. Specifically, we advocate for the adoption of basic interpolation methods, such as piecewise linear interpolation. This approach facilitates the extension of the numerical solution beyond mesh points, thereby ensuring representation throughout the entire domain. Given our aspirations to tackle complex scenarios in higher dimensions, we opt to focus on finite-element subspaces utilizing piecewise polynomial basis functions. This choice enables us to maintain flexibility and precision in approximating solutions across diverse and intricate domains. A linear system of 'n' second order ordinary differential equations of the reaction diffusion type with discontinuous source terms is examined in the interval as a singularly perturbed system. Assume that there is just one discontinuity in the source terms at the position $d \in \Omega$.The jump at d in any function$\vec{\varphi}$is defined by$[\vec{\phi}](d) = \vec{\phi}(d+) - \vec{\phi}(d-)$.We look at the equation that follows

$$-E\vec{y}''(x) + A(x)\vec{y}(x) = \vec{f}(x) \; on \Omega^- \cup \Omega^+, \tag{1}$$

$\vec{y}$ given on$\{0,1\}$and$\vec{f}(d+) \neq \vec{f}(d-)$, where$\Omega^- = \{x : 0 < x < d\}, \Omega^+ = \{x : d < x < 1\}$.
Here$\vec{y}$is a column$n$vector,$E$and $A(x)$are$n \times n$matrices,E$= diag(\vec{\varepsilon})$, $\vec{\varepsilon} = (\varepsilon, \dots, \varepsilon)$with $0 < \varepsilon \leq 1$. For all $x \in \overline{\Omega}$, the following inequalities are assumed to satisfy components $a_{ij}(x)$ of $A(x)$ and $b_i(x)$ of $B(x)$

$$a_{ii}(x) > \sum_{\substack{j=1 \\ j \neq i}}^{n} \left| a_{ij}(x) + b_i(x) \right| \; for \; 1 \leq i \leq n \; and \; a_{ij}(x), b_i(x) \leq 0 \; for \; i \neq j \tag{2}$$

and, for some α,

$$0 < \alpha < \min_{\substack{x \in [0,2] \\ 1 \leq i \leq n}} \sum_{j=1}^{n} \left| a_{ij}(x) + b_i(x) \right|. \tag{3}$$

EVALUATION OF THE FINITE ELEMENT MODEL

Let V a given Hilbert space with scalar product$(\cdot,\cdot)$and a norm of $\|.\|_V$. $V$is usually a subspace of the Sobolev space $H_0^1(\Omega)$.Examine the weak formulation, find $\vec{y} \in H_0^1(\Omega)^n$in particular $y_i \in H_0^1(\Omega^- \cup \Omega^+)$ for $i = 1, \dots, n$ such that

$$\beta_i(y_i(x), z_i(x)) = f_i(v_i)(x) \; \forall \; z_i(x) \in H_0^1(\Omega^- \cup \Omega^+) \tag{4}$$

$$f_i(v_i)(x) = (f_i(x), v_i(x)),$$

where$(y_i(x), z_i(x)) = \int y_i(x) z_i(x) dx$.

$$\beta_i(y_i(x), z_i(x)) = -\varepsilon \left(y_i'(x), z_i'(x)\right) + \left(\sum_{j=1}^{n} \left(a_{ij}(x) y_j(x)\right), z_i(x) \right),$$

$f_i(z_i(d+)) \neq f_i(z_i(d-)), f_i(z_i)(x)$is a continuous linear functional on $H_0^1(\Omega^- \cup \Omega^+)^nand\beta_i(y_i(x), z_i(x))$arebilinear forms on $H_0^1(\Omega^- \cup \Omega^+)^n$.

Lemma 1 Suppose that the bilinear forms $\beta_i(y_i(x), z_i(x))$, $i = 1, \dots, n$, is continuous on $H_0^1(\Omega^- \cup \Omega^+)^n$ is coercive, that

$$\left|\beta_i(y_i(x), z_i(x))\right| \leq \gamma_1 \| y_i(x) \| \| z_i(x) \| \tag{5}$$

$$\beta_i(z_i(x), z_i(x)) \geq \alpha \| z_i(x) \|^2 \tag{6}$$

The constants $\alpha$and γ_1 are independent of y_i andz_i. For each continuous linear functional$f_i(\cdot)$, problem (4) has a unique solution.

Lemma 2 *Satisfies the coercive property with respect tothe bilinear functional* $\beta_i(y_i(x), z_i(x))$, $i = 1, \dots, n$,

$$\| z_i \|_\varepsilon^2 \leq \beta_i(z_i, z_i)$$

Proof: Each $i,\ i = 1, \dots, n$

$$\beta_i(z_i, z_i) = -\varepsilon\ \left(z_i^{'}, z_i^{'}\right) + \left(\sum_{j=1}^{n}(a_{ij}z_j), z_i\right)$$

$$= \varepsilon\ \ \| z_i \|_1^2 + \int_0^1 \left(\sum_{j=1}^{n}(a_{ij}z_j)\cdot z_i\right)dx$$

$$\geq \varepsilon\ \ \| z_i \|_1^2 + \alpha \| z_i \|_0^2.$$

FORMATION OF THE SHISHKIN MESH

We now build a piecewise uniform Shishkin mesh on $\Omega^- \cup \Omega^+$ with N mesh-intervals. Let $\Omega^N = \Omega^{-N} \cup \Omega^{+N}$ where$\Omega^{-N} = \{x_k\}_{k=1}^{\frac{N}{2}-1}$, $\Omega^{+N} = \{x_k\}_{k=\frac{N}{2}+1}^{N-1}$, $\overline{\Omega}^N = \{x_k\}_{k=0}^{N}$.The mesh $\overline{\Omega}^N$, which is piecewise uniform on [0,1], is produced by splitting [0,d] into three mesh-intervals, as shown below:

$$[0, \sigma\ ] \cup (\sigma\ , d - \sigma\ ] \cup (d - \sigma\ , d]$$

$$\sigma\ = \min\left\{\frac{d}{4}, \frac{2\sqrt{\varepsilon}}{\sqrt{\alpha}}\ln N\right\} \qquad (7)$$

Next, on the sub-interval$(\sigma\ , d - \sigma\ ]$, a uniform mesh of N/4 mesh-points is created; on each of the sub-intervals $(0, \sigma\ ]$ and $(d - \sigma\ , d]$ a uniform mesh of N/8 mesh-points is set. The remainder is produced by splitting [d, 1] into the following three mesh-intervals:

$$[d, d + \tau\ ] \cup (d + \tau\ , 1 - \tau\ ] \cup (1 - \tau\ , 1].$$

$$\tau\ = \min\left\{\frac{1-d}{4}, \frac{2\sqrt{\varepsilon}}{\sqrt{\alpha}}\ln N\right\} \qquad (8)$$

Next, on the sub-interval$(d + \tau\ , 1 - \tau\ ]$, a uniform mesh of N/4 mesh-points is created; on each of the sub-intervals $(d, d + \tau\ ]$ and $(1 - \tau\ , 1]$ a uniform mesh of N/8 mesh-points is set. It is convenient to take it in practice

$$N\ = 8\eta, \qquad \eta\ \geq 3, \qquad (9)$$

When$\sigma\ = \tau\ = \frac{1}{8N}$ are set to the left, the Shishkin mesh $\overline{\Omega}^N$ transforms into a classical uniform mesh with the transformation parameters $\sigma\ , \tau$ and a scale N^{-1} from 0to 1. The following inequalities apply to the meshΩ^N,

$$\begin{gathered}\delta_h \leq 2N^{-1} \quad for \quad 1 \leq h \leq N \\ \delta_h \geq N^{-1} \quad for \quad \frac{N}{8} \leq h \leq \frac{3N}{8}\ and\ \frac{5N}{8} \leq h \leq \frac{7N}{8} \\ \delta_h \leq N^{-1} \quad for \quad 1 \leq h \leq \frac{N}{8}\ \ and\ \ \frac{3N}{8} \leq h \leq \frac{N}{2} \\ \delta_h \leq N^{-1} \quad for \quad \frac{N}{2} \leq h \leq \frac{5N}{8}\ \ and\ \ \frac{7N}{8} \leq h \leq N\end{gathered} \qquad (10)$$

THE DISCRETE PROBLEM

In this section, a finite element approach with an appropriate Shishkin mesh is used to develop a numerical method for (4).Let for $i = 1, \dots, n$ and $k = 1,2, \dots, N\backslash\{N/2\}$, piecewise linear functional space$Z_{i,k} \subset H_0^1\left(\Omega^- \cup \Omega^+\right)^n$, that vanishes at $x = \{0,1\}$.This defines the finite element approach for the discrete two-point boundary value problem $Y_{i,k} \in Z_{i,k} \subset H_0^1(\Omega^- \cup \Omega^+)$, for $i = 1, \dots, n$,

$$\beta_i\left(Y_{i,k}(x), z_{i,k}(x)\right) = f_{i,k}\left(z_{i,k}\right)(x) \qquad \forall\ \ z_{i,k} \in Z_{i,k} \subset H_0^1(\Omega^- \cup \Omega^+) \qquad (11)$$

$$f_{i,k}\left(z_{i,k}\right)(x) = \left(f_{i,k}(x), z_{i,k}(x)\right).$$

$$\beta_i\left(y_{i,k}(x), z_{i,k}(x)\right) = -\varepsilon\ \left(y_{i,k}^{'}(x), z_{i,k}^{'}(x)\right) + \left(\sum_{j=1}^{n}\left(a_{ij}(x)y_{j,k}(x)\right), z_{i,k}(x)\right)$$

Lemma suggests that the discrete problem is stable and has a unique solution according to Lax-Migram.

INTERPOLATION ERROR BOUNDS

Lemma 3: *Define* $y_{i,k}^{*}$ *as the* $Z_{i,k}$*-interpolant of the solution* $y_{i,k}$ *of* (1) *on the fitted mesh* Ω^N. *Then*

$$\max_{i=1,\dots,n} \| y_{i,k}^{*} - y_{i,k} \|_{\Omega^N} \leq C(N^{-1} ln N)^2 ,$$

C is a constant that is independent of the parameter ε .

Proof:

The solution of this Lemma 3 is obtained by replacing with identical parameters according to the Lemma 5.1 in [13].

Lemma 4: Define $y_{i,k}^{*}$ as the $Z_{i,k}$ interpolant of the solution $z_{i,k}$ of (1) on the fitted mesh Ω^N. *Then*

$$\max_{i=1,\dots,n} \| y_{i,k}^{*} - y_{i,k} \|_{\varepsilon} \leq C(N^{-1} \ln N)^2,$$

C is a constant that is independent of the parameter ε .

Proof:

The solution of this Lemma 4 is obtained by replacing with identical parameters according to the Lemma 5.2 in [13].

Lemma 5: *Define* $y_{i,k}^{*}$ *as the* $Z_{i,k}$ *-interpolant of the solution* $y_{i,k}$ *of* (1) *on the fitted mesh* Ω^N. *Then*

$$\max_{i=1,\dots,n} \| y_{i,k}^{*} - y_{i,k} \|_{\varepsilon, \overline{\Omega}^N} \leq C (N^{-1} \ln N)^2.$$

C is a constant that is independent of the parameter.

Proof:

The solution of this Lemma 5 is obtained by replacing with identical parameters according to the Lemma 5.3 in [13].

INTERPOLATION ERROR ESTIMATE AND DISCRETIZATION ERROR

Lemma 6: *Define* $y_{i,k}$ *as the solution of (1) and* $Y_{i,k}$ *the solution of (4) Suppose that* $Z_{i,k} \subset H_0^1(\Omega^- \cup \Omega^{+N})$. *Then*

$$\max_{i=1,\dots,n} \left|\beta_i\left(Y_{i,k} - y_{i,k}, v_i\right)\right| \leq C (N^{-1} \ln N)^2 \quad \| z_{i,k} \|_{l^2(\Omega^{-N})},$$

C is a constant that is independent of the parameter ε .

Proof:

The solution of this Lemma 6 is obtained by replacing with identical parameters according to the Lemma 6.1 in [13].

Lemma 7: *Define* $y_{i,k}^{*}$ *as the* $Z_{i,k}$*-interpolant of the solution* $y_{i,k}$ *of (1) and* $Y_{i,k}$ *the solution of (4). Then*

$$\max_{i=1,\dots,n} \| Y_{i,k} - y_{i,k}^{*} \|_{\varepsilon, \overline{\Omega}^N} \leq C(N^{-1} \ln N)^2,$$

C is a constant that is independent of the parameter ε .

Proof: Since $Y_{i,k} - y_{i.k}^{*} \in Z_{i,k}$,

$$\| Y_{i,k} - y_{i,k}^{*} \|_{\varepsilon, \overline{\Omega}^N}^2 \leq C \beta_i\left(Y_{i,k} - y_{i,k}^{*}, Y_{i,k} - y_{i,k}^{*}\right)$$

$$\leq C\left[\beta_i\left(Y_{i,k} - y_{i,k}, Y_{i,k} - y_{i,k}^{*}\right) + \beta_i\left(y_{i,k} - y_{i,k}^{*}, Y_{i,k} - y_{i,k}^{*}\right)\right]$$

Using Lemma 4, with $z_i = Y_{i,k} - y_{i,k}^{*}$, then gives

$$\| Y_{i,k} - y_{i,k}^{*} \|_{\varepsilon, \overline{\Omega}^N}^2 \leq C (N^{-1} \ln N)^2 \| Y_{i,k} - y_{i,k}^{*} \|_{\varepsilon, \overline{\Omega}^N}.$$

Cancelling the common factor gives

$$\| Y_{i,k} - y_{i,k}^{*} \|_{\varepsilon, \overline{\Omega}^N} \leq C(N^{-1} \ln N)^2,$$

as required.

Theorem 1: *Define* $y_{i,k}$ *as a solution of (1) and* $Y_{i,k}$ *as a solution of (4). Then*

$$\max_{i=1,\dots,n} \| Y_{i,k} - y_{i,k} \|_{\varepsilon, \overline{\Omega}^N} \leq C(N^{-1} \ln N)^2,$$

C is a constant that is independent of the parameter ε .

Proof: Since

$$\| Y_{i,k} - y_{i,k} \|_{\varepsilon\ ,\Omega^N} \leq \| Y_{i,k} - y^*_{i,k} \|_{\varepsilon\ ,\overline{\Omega}^N} + \| y^*_{i,k} - y_{i,k} \|_{\varepsilon\ ,\overline{\Omega}^N},$$

the result follows by combining Lemmas (3) and (7).

Theorem 2: *Let $y_{i,k}$ be the solution of (1) and $Y_{i,k}$ the solution of (5). Then the following parameter uniform error estimate holds*

$$\max_{i=1,\dots,n} \| Y_{i,k} - y_{i,k} \|_{\varepsilon\ ,\overline{\Omega}^N} \leq C(N^{-1} \ln N)^2$$

C is a constant that is independent of the parameterε .

Proof:

The solution of this Theorem is obtained by replacing with identical parameters according to the Theorem 7.3in [13].

NUMERICAL ILLUSTRATIONS

Example: Consider the BVP

$-E\vec{u}''(x) + A(x)\vec{u}(x) = \vec{f}(x),\ for\ x \in (0,1), \vec{u}(0) = \vec{0},\ \vec{u}(1) = \vec{0}$where$E = diag\ (\varepsilon\ \ , \varepsilon\ \ ),\ A = \begin{pmatrix} 5 & -1 \\ -1 & 5(x+1) \end{pmatrix}, \vec{f} = (1 + x^2, 2)^T$. For various values of$\varepsilon\ , N = 8k,\ k = 2^r,\ r = 3, \cdots, 8,\ and\ \alpha = 1.9$.Based on the general methods outlined in Miller et al. [6], we applied the fitted mesh method to Example to compute the ε uniform order of convergence and the ε uniform error constant. The results of our computations are summarized in Table 1, which provides the following conclusions:

CONCLUSION

The research presented in this article builds upon the foundational concept pioneered by Miller et al. [6], who focused on convection-diffusion problems. In our paper, we extend this framework by establishing second order parameter uniform convergence for systems of n second order differential equations of reaction diffusion type with same perturbation parameter, incorporating discontinuous source terms. This advancement in methodology allows for a more robust treatment of complex systems, where discontinuities in source terms pose significant challenges. By achieving second order parameter uniform convergence, we enhance the accuracy and reliability of numerical solutions for such systems. Furthermore, our proposed method is not limited to one dimensional problems; it can be extended to tackle higher-dimensional scenarios. This scalability is crucial for addressing real world problems that often involve complex geometries and multi-dimensional phenomena.

REFERENCES

1. H.-G.Roos, M.Stynes, L.Tobiska, Numerical methods for singularly perturbed differential equations, Springer Verlag, 1996.
2. J.J.H.Miller, E.O'Riordan, G.I.Shishkin, Fitted Numerical Methods for Singular Perturbation Problems (Revised Edition), World Scientific Publishing Co., Singapore, New Jersey, London, Hong Kong, 2012.
3. P.A.Farrell,A.Hegarty,J.J.H.Miller,E.O'Riordan,G.I.Shishkin,RobustComputationalTechniquesforBoundaryLayers,AppliedMathematics & Mathematical Computation (Eds. R. J. Knops & K. W. Morton), Chapman & Hall/CRC Press, 2000.
4. P.A.Farrell,J.J.H.Miller,E.O'Riordan,G.I.Shishkin,Singularlyperturbeddifferentialequationswithdiscontinuoussourceterms,Proceedings of Workshop '98, Lozenetz, Bulgeria, Aug 27-31, 1998.
5. P.A.Farrell, E.O'Riordan, G.I.Shishkin,A class of singularly perturbed semi linear differential equations with interior layers, Mathematics of Computation, vol. 74, No. 252, June 7, 1759-1776, 1998.

6. J.J.H.Miller, E.O'Riordan, G.I.Shishkin, S.Wang, A parameter-uniform Schwarz method for a Singularly Perturbed reaction –diffusion problem with an interior layer, Applied Numerical Mathematics, 35,323-337,2000.
7. T.Linss, N.Madden, Analysis of a FEM for a coupled system of singularly perturbed reaction iffusion equations, Numer.Algor.50:283-291,2009.
8. T.Linss, N.Madden, A finite element analysis of a coupled system of singularly perturbed reaction diffusion equations., Appl. Math. Comput. 148(3), 869-880, 2004.
9. C. Xenophontos, L. Oberbroeckling, A numerical study on the finite element solution of singularly perturbed systems of reaction-diffusion problems, Applied Mathematics and Computation, 187, 1351-1367, 2007.
10. M.Paramasivam, S.Valarmathi, J.J.H.Miller, Second order parameter- uniform convergence for a finite difference method for a singularly perturbed linear reaction-diffusion system, Mathematical Communications, vol.15, No.2, 2010.
11. M.Paramasivam, S.Valarmathi, J.J.H.Miller, Second order parameter- uniform convergence for a finite difference method for a partially singularly perturbed linear reaction-diffusion system, Mathematical Communications, vol.18, No.2,271-295 2013.
12. M.Paramasivam, S.Valarmathi, J.J.H.Miller,Parameter-uniformconvergence for a finite difference method for a singularly perturbed linear reaction-diffusion system with discontinuous source terms, Int.J.Numer. Anal., vol.11, No.2,385-399 2014.
13. M.Vinoth, M.Paramasivam, Parameter uniform convergence of a finite element method for a singularly perturbed linear reaction diffusion system with discontinuous source terms, Ratio Mathematica, vol 50. 56-71, 2023
14. M.Vinoth, M.Paramasivam, Second order parameter uniform convergence of a finite element method for a system of 'n' singularly perturbed delay differential equations of reaction-diffusion type with discontinuous source terms, AIP Conference proceedings, 2649 (1), 2023.
15. M.Vinoth, M.Paramasivam, Parameter-uniform convergence of a finite element method for a partially singularly perturbed linear reaction-diffusion system, International Journal of Aquatic Science, vol 12, issue 02, 281, 2021.
16. M.Vinoth, M.Paramasivam, Second order parameter uniform convergence of a finite element method for a system of 'n' singularly perturbed delay differential equations, International Journal of Aquatic Science,vol 12, issue 02, 4549, 2021.
17. M.Vinoth, M.Paramasivam, Second order parameter uniform convergence of a finite element method for a system of 'n' partially singularly perturbed delay differential equations of reaction-diffusion type, Turkish journal of computer and mathematics education, vol. 12 No.11, 4954-4967, 2021.
18. Jichun Li., Uniform convergence of discontinuous finite element methods for singularly perturbed reaction-diffusion problems, Computers and Mathematics with Applications,vol.44,231-240 2002.
19. S.Dinesh, M.Paramasivam, A parameter uniform convergence for a system of two singularly perturbed initial value problems with different perturbation parameters and Robin initial conditions, Malaya Journal of Matematik, 4, 2021
20. S.Dinesh, M.Paramasivam, A parameter uniform numerical method for a singularly perturbed initial value problem with Robininitial condition, Malaya Journal of Matematik8(2),414-420,3,2020
21. R Praveena, M Joseph Paramasivam, First order parameter uniform numerical method for a system of two singularly perturbed delay differential equations with robin initial conditions, Journal of Algebraic Statistics 13 (2), 1063-1071, 2022.
22. S.Asha, M Joseph Paramasivam, A novel method for solving fully intuitionistic fuzzy transportation problems using singularly perturbed delay differential equations, AIP Conference Proceedings 2649 (1), 2023.

Table 1: $\boldsymbol{Values\ of\ \ D_{\varepsilon}^{N},\ D^{N},\ p^{N},\ p^{*}\ and\ C_{p^{*}}^{N}\ for\ \varepsilon_1 = \varepsilon_2 = \frac{\eta}{64}}$.

η	Number of mesh points N				
	64	128	256	512	1024
2^{0}	0.3142E-02	0.1550E-02	0.7695E-03	0.3833E-03	0.1913E-03
2^{-1}	0.4518E-02	0.2223E-02	0.1111E-02	0.5593E-03	0.2765E-03
2^{-2}	0.6386E-02	0.3168E-02	0.1577E-02	0.7869E-03	0.3929E-03
2^{-3}	0.8985E-02	0.4474E-02	0.2229E-02	0.1112E-02	0.5558E-03
2^{-4}	0.1260E-01	0.6311E-02	0.3150E-02	0.1573E-02	0.7860E-03
2^{-5}	0.1756E-01	0.8892E-02	0.4449E-03	0.2223E-02	0.1111E-02
2^{-6}	0.1756E-01	0.8892E-02	0.4449E-03	0.2223E-02	0.1111E-02
2^{-7}	0.1756E-01	0.8892E-02	0.4449E-03	0.2223E-02	0.1111E-02
D^{N}	0.1756E-01	0.8892E-02	0.4449E-03	0.2223E-02	0.1111E-02
P^{N}	0.9758E+00	0.9952E+00	0.1253E+01	0.1473E+01	
C_P^N	0.9633E+00	0.9453E+00	0.8898E+00	0.7031E+00	0.5032E+00
Computed order of $\vec{\varepsilon}$uniform convergence, $p^{*} = 1.293$					
Computed $\vec{\varepsilon}$-uniform error constant, $C_{P^{*}}^{N} = 0{:}8233$					

Indian Journal of Natural Sciences *www.tnsroindia.org.in ©IJONS*

Vol.15 / Issue 83 / Apr / 2024 *International Bimonthly (Print) – Open Access* *ISSN: 0976 – 0997*

RESEARCH ARTICLE

Study on Awareness about Recent Regulations in UPI among Users

R.Ragavi[1] and PL. Meenakshi[2]

[1]Post Graduate Student, Department of Mathematics, Avinashilingam Institute for Home Science and Higher Education for Women, Tamil Nadu, India.
[2]Assistant Professor, Department of Mathematics, Avinashilingam Institute for Home Science and Higher Education for Women, Tamil Nadu, India.

Received: 30 Dec 2023 Revised: 09 Jan 2024 Accepted: 12 Mar 2024

***Address for Correspondence**
R.Ragavi
Post Graduate Student,
Department of Mathematics,
Avinashilingam Institute for Home Science and Higher Education for Women,
Tamil Nadu, India.

ABSTRACT

Unified Payment Interface (UPI) is the most used digital payment method that keeps growing every year with new users due to its ease UPI is a secure and convenient way to make payments without carrying physical money. A recent study is focused on analyzing the awareness of the regulations set by NPCI (National Payment Corporation of India) that limit the number of transactions to 20 per 24 hours and the maximum payable amount to 1 lakh, cumulatively. The study was carried out with the primary data collected by simple random sampling with a sample size of 69 users. The study analyses the level of awareness among users about interchange fees and limits. Some statistical tools used are the chi-square test and percentage analysis. The analysis pointed out that around 51% of the users were aware of the number of transactions in a day and around 61% of the people had known the highest amount that can be sent.

Keywords: Digital Payment, UPI, NPCI, Awareness, Transactions.

INTRODUCTION

Unified Payment Interface (UPI) is one of the fastest-growing digital transaction methods that has gained prominence in recent years. People are getting more and more dependent on digital technologies, and many people prefer digital ways of payment then cash transactions due to its ease. Unified Payment Interface was developed by the National Payment Corporation of India (NPCI) in the year 2016, NPCI is an organization that settles retail payment in India. It is introduced by the Reserve Bank of India (RBI) and the Indian Banks Association (IBA). UPI enables the user to send and receive money from one bank account to another, facilitating person-to-person and person-to-merchant transactions. It is a real-time payment system, meaning the money will be exchanged

immediately without delay. It enables the user to send and receive money with unique UPI IDs which use VPA (Virtual Payment Address) to transfer the money securely to other bank accounts linked to that UPI ID. Since VPA is unique no fake ID can be created which makes it highly secure. It provides various banking features to the users like balance checking and amount transfer which reduces the need to visit banks or ATMs.

STATEMENT OF THE PROBLEM

As the economy advances, online transactions are gaining popularity rapidly. More and more individuals are opting for online payment methods like

1. UPI,
2. digital currencies,
3. cryptocurrencies and Internet banking

instead of cash due to their convenience. UPI transactions amount to **62%** of digital payment transactions in FY 2022-23. The study aims to investigate the potential impact of recent NPCI regulations on UPI usage.

OBJECTIVE OF THE STUDY

The objective of this study is to examine the level of awareness regarding recent limitations on the number of transactions that can be initiated in UPI and the maximum amount that can be transferred through UPI apps.

RESEARCH METHODOLOGY

A descriptive research design has been employed to analyze the awareness among UPI users. Random sampling method was used to take the sample and the sample size is 69. The data were collected from students. Structured methods of questionnaires have been employed to collect primary data from the respondents.

REVIEW OF LITERATURE

Dr.D. Durairaj & Princy Joseph (2019) UPI is more feasible than the mobile wallet if server-related issues are improved and if the right awareness about it is produced for young minds. It should attract the illiterate people of the society to use UPI to make it more inclusive. Rewarding UPI payments would sufficiently contribute to the growth of UPI. Amogh Das & Ashish Das (2022) Year-on-year growth and UPI transactions on a daily basis have improved and the number of transactions done from person to person and through person to merchant has increased significantly. Due to the government's intention to support UPI payments banks received monetary support. Putta Sai Kumar (2022) The level of satisfaction of customers with UPI is independent of the number of transactions done and the payments. The satisfaction level is not influenced by the complaints, issues, and transaction services provided by the banks.

Statistical Methods Used for Analysis

SPSS software was employed to analyze the data in the following methods.

1. Percentage Analysis
2. Chi-Square test
3. ANOVA table.

PERCENTAGE ANALYSIS

DISTRIBUTION OF UPI AWARENESS BASED ON AGE

Null hypothesis H_0: There is no significant relation between age and the level of awareness.

Alternative hypothesis H_1: There is a significant relation between age and the respondents' awareness level.

$\alpha = 0.05$ level of significance.

Interpretation

Number of transactions limit

P= 0.879 is greater than 0.05 hence null hypothesis is accepted. There is no significant relation between number of transaction limits and age.

Payment amount limit

P= 0.053 is higher than 0.05 hence null hypothesis is accepted. There is no significant relation between payment amount limit and age.

Prepaid Instruments

P = 0.597 is higher than 0.05, hence the null hypothesis is accepted and there is no significant relation between the level of awareness of prepaid instruments and age.

DISTRIBUTION OF AWARENESS ABOUT THE HIGHEST AMOUNT THAT CAN BE TRANSFERRED:

Null Hypothesis H_0: There is no significant relation between the number of transactions done by a person and the awareness.

Alternative hypothesis H_1: There is a significant relationship between the number of transactions done by a person and awareness.

$\alpha = 0.05$ has been considered as the level of significance.

Chi-Square Test

Interpretation

P value = 0.320

P value is greater than 0.05, hence null hypothesis is accepted.

There is no significant relation between some transactions done by individuals and the level of awareness about the highest amount limit.

FINDINGS OF THE SURVEY CARRIED OUT AMONG UPI USERS

94% of the people surveyed used UPI apps.

50.7% of the people surveyed used LESS than 5 transactions in a week.

20.9% of the people surveyed used LESS than 10 transactions in a week.

13.4% of the people surveyed used LESS than 15 transactions in a week.

14.9% of the people surveyed used MORE than 15 transactions in a week.

50.7% of the people surveyed were aware of the highest number of transactions that can be done through UPI in a day.

53.4% of the people surveyed used UPI transactions for merchant transfers of money.

60.9% of the people knew the highest limit that could be sent through UPI.

53.6% of the people surveyed have been denied to pay through UPI and requested to pay through other means at least once.

68.1 % of the people have used prepaid instruments.

5.8% of the users have encountered UPI fraud or lost money through UPI payments.

LIMITATIONS OF THE STUDY

1. The smaller size of the sample (69).
2. Less Geographical area covered.
3. The survey is limited only to the literates.

CONCLUSION

The recent regulations have not affected the growth of UPI payments. Most of the persons surveyed used UPI payments for merchant transfer thus helping to formalize the economy. 4% of the people surveyed have encountered UPI frauds thus with digitalizing the economy we have to increase online security and compliance.

REFERENCES

1. Dr. Bhuvaneshwari, M; Dr. Kamalasaravanan, S;Kanimozhi, V. A study on consumer behavior towards UPI (Unified Payment Interface) payment application based in Nilgiris district. An International Journal of Advance Research, Ideas and Innovation in Technology. (Volume-7, Issue 3-v713-1686)
2. Dr. Kamala Saravanan, S; Kala Devi; Aishwarya, C S. A Study on Usage of UPI Payments Services towards Merchants in Madurai. International Journal of Advance Research in Science, Communication and Technology (volume 2, Issue 9, June 2022).
3. https://www.npci.org.in ,NPCI – UPI statistics.
4. https://www.wikipedia.in , UPI.
5. www.forbes.in,UPI payments.
6. www.geeksforgeeks.org, Working of UPI.
7. www.jetir.org.in UPI.
8. www.researchsquare.com.
9. Vidhya, I V; Premshankar, C. Consumer Perception towards Cashless Economy with Special Reference to Unified Payment Interface. Shanlax International Journal of Economics, vol.11, no.2,2023

Indian Journal of Natural Sciences *www.tnsroindia.org.in ©IJONS*

Vol.15 / Issue 83 / Apr / 2024 *International Bimonthly (Print) – Open Access* *ISSN: 0976 – 0997*

RESEARCH ARTICLE

Detecting and Mitigating Cybersecurity Threats in Smart Grids using KMeans Clustering

Ramya Hyacinth Lourdusamy[1] and Gomathi Venugopal[2]

[1]Department of Electrical and Electronics Engineering, Loyola-ICAM College of Engineering and Technology, Chennai, India.
[2]Department of Electrical and Electronics Engineering, College of Engineering, Guindy, Anna University, Chennai, India.

Received: 30 Dec 2023 Revised: 09 Jan 2024 Accepted: 12 Mar 2024

***Address for Correspondence**
Ramya Hyacinth Lourdusamy
Department of Electrical and Electronics Engineering,
Loyola-ICAM College of Engineering and Technology,
Chennai, India.

ABSTRACT

In contemporary years, the integration of advanced digital meters, smart meters, and Phasor Measurement Units (PMUs) into power system networks has revolutionized real-time monitoring capabilities. These metering infrastructures are indispensable for facilitating decision-making processes and ensuring the smooth operation of power systems. However, their crucial role also renders them vulnerable to emerging threats, particularly in the realm of cybersecurity. One of the most pressing threats facing power system metering infrastructure is the occurrence of False Data Injection Attacks (FDIAs). These malicious attacks, resulting from the digital transformation of power systems, entail the injection of falsified data into the metering infrastructure. Such anomalies can severely compromise the reliability and stability of power system networks, undermining their integrity and posing significant operational risks. Traditional approaches to enhancing data reliability, such as statistical methods, have proven inadequate in effectively identifying and mitigating FDIAs. Consequently, there is a pressing need to leverage more advanced techniques, such as Machine Learning (ML), to combat this evolving threat landscape. This paper addresses the challenge of detecting FDIAs using ML algorithms and specifically, tailored to detect and mitigate FDIAs in power system networks. To evaluate the efficacy of our approach, the algorithm is tested using a dataset comprising real-time PMU data from the Australian Grid, artificially injected with false data. Additionally, the performance of the model is assessed in terms of precision and recall, providing valuable insights into its effectiveness in securing power system metering infrastructure against FDIAs.

Keywords: One of the most pressing threats facing power system metering infrastructure is the occurrence of False Data Injection Attacks (FDIAs).

INTRODUCTION

Data-driven systems [1] play a pivotal role in modern society, facilitating critical operations across various domains such as energy management, transportation, finance, and healthcare. These systems rely heavily on the integrity and accuracy of the data they process to make informed decisions and ensure reliable performance [2]. However, the proliferation of interconnected devices and the growing complexity of data networks have introduced new vulnerabilities, leaving these systems susceptible to malicious attacks. One such threat is the FDIA, a sophisticated form of cyberattack intended to undermine the integrity of data within a system[3]. In a false data injection attack, adversaries clandestinely inject fabricated or manipulated data into the system to deceive its operations and undermine its functionality. These attacks pose a significant threat to the reliability, security, and safety of data-driven systems, with potentially severe consequences ranging from financial losses [4] to operational disruptions [5] and even threats to public safety. Power systems equipped with advanced Information and Communication Technology are being transformed into a smart grid. Smart Grids are designed to enhance the reliability and efficiency of energy distribution [6]. Integrating and analysing data from these multiple modalities enables utilities and operators to enhance situational awareness, optimize operations, improve reliability, and support decision-making processes in power systems. The multimodal data collected from Smart meters, Phasor Measurement Units (PMUs) and other Advanced Metering Infrastructure (AMI) serves as the foundation for decision-making processes and control actions [7]. However, FDIAs can introduce inaccuracies into the data collected from sensors and meters, leading to incorrect load forecasting, faulty control decisions, and ultimately, disruptions in energy supply.

The impact of false data injection attacks can be particularly devastating in critical infrastructure sectors such as smart grids, where accurate data is essential for efficient energy distribution and grid stability [8]. In a smart grid context, for example, attackers may inject false data into sensor readings to manipulate load forecasts, disrupt energy distribution, or even cause widespread blackouts. Detecting and mitigating false data injection attacks present significant challenges due to the stealthy nature of these attacks and the complexity of data-driven systems. Traditional security measures such as firewalls and encryption may not be sufficient to defend against such threats, as attackers can exploit vulnerabilities in data processing algorithms and protocols to evade detection. Therefore, there is an urgent need for advanced anomaly detection techniques that can effectively identify and thwart false data injection attacks in real time. By detecting and mitigating FDIAs, the reliability of energy supply in Smart Grids can be safeguarded, ensuring uninterrupted power delivery to consumers [9]. Also, FDIAs can inject false data into Phasor Measurement Units (PMUs) and other monitoring devices, leading to misleading information about the state of the grid. This can undermine the stability of the Smart Grid, potentially causing voltage instability, frequency deviations, and even cascading failures [10]. This enhances the resilience of Smart Grids to cyber threats. With the increasing digitization of power systems, cybersecurity data becomes crucial for monitoring and protecting against cyber threats, such as malware, intrusion attempts, and denial-of-service attacks. The use of KMeans clustering—a popular unsupervised machine learning algorithm—for detecting false data injection attacks in data-driven systems is focussed in this article. By leveraging the inherent structure of the data and identifying deviations from normal patterns, a robust and efficient approach for safeguarding the integrity of data in critical infrastructure and other mission-critical applications is developed. Through empirical evaluation and analysis, the effectiveness and practical applicability of the proposed methodology in mitigating the threat posed by false data injection attacks are demonstrated.

REVIEW OF EXISTING LITERATURE

FDIAs involve injecting falsified data into sensors or measurement devices to manipulate system behaviour. Studies have investigated the impact of FDIAs on different types of systems, including power grids, water distribution networks, and industrial control systems. Research has focused on developing detection and mitigation techniques to counter FDIAs, ranging from statistical anomaly detection methods to machine learning-based approaches. Anomaly detection is a crucial component of cybersecurity, aiming to identify abnormal patterns or behaviours

indicative of malicious activity [11]. Traditional anomaly detection techniques include statistical methods such as mean-variance analysis, time-series analysis, and clustering-based approaches [12]. Statistical methods may struggle to distinguish between genuine anomalies and normal variations in system behaviour, leading to a high false positive rate [13]. These approaches often rely on predefined thresholds or assumptions about the distribution of data, which may not hold true in complex and dynamic systems. Statistical techniques may not be effective for detecting subtle and sophisticated attacks, such as those involving gradual changes in data over time.

More recent advancements in anomaly detection involve Machine Learning (ML) and data mining techniques, including supervised, unsupervised, and semi-supervised learning algorithms. ML models can learn patterns and relationships in data to identify anomalies. Common ML algorithms used for anomaly detection include support vector machines (SVMs), k-nearest neighbours (KNN), isolation forests, and autoencoders [14]. ML algorithms require labelled training data for supervised learning, which may be scarce or expensive to obtain, particularly for rare and complex anomalies. Unsupervised and semi-supervised ML algorithms may be used for problems involving unlabelled real-time data. ML models could be vulnerable to adversarial attacks [15], where attackers manipulate input data to circumvent detection by the anomaly detection system. Research has explored the application of deep learning models, such as autoencoders and recurrent neural networks, for detecting complex anomalies in high-dimensional data streams [16]. KMeans clustering, a popular unsupervised learning algorithm, has found various applications in cybersecurity, particularly in anomaly detection and intrusion detection systems [17]. Despite significant research efforts in detecting FDIAs, several gaps remain in the literature. These gaps indicate areas requiring additional investigation and development to bolster the effectiveness and robustness of FDIAs detection.

Some of the key gaps include

- Dynamic and Adaptive Detection: Existing detection techniques often rely on static thresholds or predefined models to identify anomalies. However, FDIAs can be highly adaptive and stealthy, evolving to evade detection. There is a need for dynamic and adaptive detection methods that can continuously learn and evolve in response to changing attack strategies.
- Scalability and Efficiency: Numerous detection algorithms encounter scalability challenges when utilized inlarge-scale systems with high-dimensional data streams, such as Smart Grids. Scalability becomes crucial for real-time detection in such scenarios. There is a need for scalable detection techniques that can handle the volume, velocity, and variety of data generated by modern cyber-physical systems.
- Multimodal Data Fusion: Smart Grids are complex electrical infrastructures that collect data from different meters not limited to Supervisory Control and Data Acquisition (SCADA), PMU, and Smart Meters. These meters have different sampling rates and capture parameters of different kinds. Thus, data obtained in real-time is multimodal data. Integrating information from multiple data sources can enhance the detection accuracy and resilience to attacks. However, there is limited research on effective techniques for multimodal data fusion in the context of FDIA detection.
- Adversarial Robustness: FDIA detection systems may be susceptible to adversarial attacks, where attackers tactically engineer input data to evade detection. Research is needed to develop detection techniques that are robust to adversarial perturbations and can withstand sophisticated evasion strategies employed by attackers.
- Real-world Evaluation: While numerous detection algorithms have been proposed in the literature, few have been extensively evaluated in real-world settings or deployed in operational environments. There is a lack of empirical studies that assess the performance, scalability, and practical utility of FDIAs detection techniques under realistic conditions.
- Cross-domain Adaptability: FDIAs detection methods developed for specific domains, such as power systems or industrial control systems, may not be directly applicable to other domains due to differences in data characteristics and system architectures. There is a need for cross-domain adaptable detection techniques that can be effectively deployed across diverse cyber-physical systems.

On the whole, previous research in these areas and the listed research gaps have laid the groundwork for developing more robust and effective cybersecurity solutions. By leveraging insights from past studies, detecting and mitigating cybersecurity threats including FDIAs using KMeans clustering is presented.

METHODOLOGY

The most popularly applied concept in distance-based ML approaches is the Euclidean distance. These values act as a tool for identifying malicious data. KMeans clustering helps to group a dataset with N entities into K −clusters. Clusters are formed by assigning data to the closest centroid by calculating distances. Thus, by calculating the distance between the data and the centroid, the ones with the largest distances are identified as anomalous data.
In this case, the data is grouped into binary clusters of normal/ anomalous data. The mathematical formulation is explained below: If the dataset is represented as $dt_1, dt_2, \dots, dt_n$, then they are grouped into k clusters $C = \{C_1, C_2, \dots, C_k\}$. The means of these clusters be represented as $\mu_1, \mu_2, \dots, \mu_k$; where μ_i is the mean of points in C_i. Normally, K −Means clustering follows two steps iteratively. They are the assignment step and the update step [18].

Assignment step
Every data point dt_p is assigned to a cluster with the closest mean. This is achieved by calculating the least square Euclidean distance.

$$C_i^{(t)} = \left\{ dt_p : \|dt_p - \mu_i^{(t)}\|^2 \le \|dt_p - \mu_j^{(t)}\|^2 \right\} \forall j, 1 \le j \le k \quad (1)$$

Thus, every data point dt_p is assigned only to one cluster C_i in the assignment step.

Update step
The centroid or mean of the cluster to which the data point dt_p was assigned in the previous step is recalculated and updated.

$$\mu_i^{(t+1)} = \frac{1}{\left|C_i^{(t)}\right|} \sum_{dt_j \in C_i^{(t)}} dt_j \quad (2)$$

The above two steps are repeated iteratively till the recalculated mean no longer changes. The data point that has the largest Euclidean distance is identified as the malicious data.

RESULTS AND DISCUSSION

Experimental Setup
Real-Time data obtained from 15 Phasor Measurement Units (PMUs) deployed at three different time zones in Australia that are sampled at three different sampling rates 30, 60 and 120 Hz at different offsets is considered for evaluating the methodology. Initially, the data in three different time zones with different offsets are aligned and the missing and duplicate data are removed. To ensure the availability of data at uniform intervals, missing values are interpolated using curve fitting techniques. Also, the measurements of PMU include voltage magnitudes, voltage angles and frequencies that are at different scales. Robust scaling is performed to prevent features with larger scales from dominating the analysis. In addition, dimensionality reduction using Principal Component Analysis (PCA) is performed as high-dimensional time series data test data is considered for analysis.
Let H denotes the Jacobian matrix obtained from the system configuration. Under conditions, when attack vector a is composed of a linear combination of the column vectors within H. That is a false data injection attack vector, $a = Hc$, is designed and injected along with the measurement vector, □□ ≔ □ + □. This intruder-attacked measurement surreptitiously escapes the bad data detection tests (Chi-square and Largest Normalised Residual Tests). For the sake of analysis, 5% of the measurement is intentionally corrupted.

Findings and Interpretations

The elbow method plot for the considered dataset is given in Figure 1. This demonstrates the correlation between the number of clusters (K) and the within-cluster sum of squares (WCSS).The elbow method aids in identifying the optimal number of clusters by pinpointing the juncture where the rate of decrease in WCSS begins to decelerate, signifying diminishing returns from further cluster additions. From Figure 1, it is evident that K for the considered data set could be taken as two or three. On applying K = 2, the scatter plot obtained is shown in Figure 2 and that obtained by considering K = 3 is shown in Figure 3. Outliers, which are observed away from the clustered data points on the scatterplot, are recognized as anomalous data and are excluded before being utilized as inputs for other decision-making operations related to power systems.

CONCLUSION

KMeans clustering contributes to addressing several of the gaps in detecting false data injection attacks (FDIAs) by leveraging its capabilities in unsupervised learning and pattern recognition. From the analysis, it is evident that KMeans Clustering is capable of:

- Dynamic and Adaptive Detection: KMeans can be used to dynamically cluster data points based on their similarity, allowing for the detection of evolving patterns and anomalies. By periodically re-training the KMeans model with new data, it can adapt to changes in system behaviour and identify emerging attack patterns.
- Scalability and Efficiency: KMeans is known for its scalability and efficiency, particularly when dealing with large-scale datasets. By efficiently partitioning data into clusters, KMeans helps to reduce the computational complexity of anomaly detection algorithms, enabling real-time detection in high-dimensional and high-volume data streams.
- Multimodal Data Fusion: KMeans clustering is applied to integrate information from multiple data modalities by clustering data points based on their combined features. By clustering multimodal data streams, KMeans can identify complex patterns and correlations that may indicate anomalous behaviour across different data sources.
- Adversarial Robustness: KMeans clustering is inherently robust to small perturbations in data, making it resistant to simple adversarial attacks. Additionally, ensemble approaches combining multiple KMeans models or incorporating robust clustering techniques can further enhance the resilience of FDIA detection systems against adversarial manipulation.
- Privacy Preservation: KMeans clustering can be applied to analyse data in a privacy-preserving manner by clustering data points based on their similarities while preserving individual privacy. Differential privacy techniques can be incorporated to ensure that sensitive information is not revealed during the clustering process.
- Real-world Evaluation: KMeans clustering provides a transparent and interpretable framework for analysing data and identifying clusters, making it suitable for real-world evaluation of FDIAs detection techniques. By applying KMeans to real-world datasets, researchers can assess the performance and practical utility of detection algorithms under realistic conditions.
- Cross-domain Adaptability: KMeans clustering is a domain-agnostic technique that can be applied across diverse cyber-physical systems and domains. By adapting the feature representation and clustering parameters, KMeans can be effectively deployed in different environments to detect FDIAs across various systems.
- In summary, KMeans clustering offers a versatile and scalable approach to addressing several of the gaps in FDIA detection. By leveraging its capabilities in unsupervised learning and pattern recognition, KMeans can contribute to the development of robust and efficient detection techniques for identifying and mitigating FDIAs in complex and dynamic cyber-physical systems.

REFERENCES

1. Strielkowski, W., Vlasov, A., Selivanov, K., Muraviev, K. and Shakhnov, V., 2023. Prospects and challenges of the machine learning and data-driven methods for the predictive analysis of power systems: A review. *Energies*, *16*(10), p.4025.
2. Basciftci, B., Ahmed, S. and Gebraeel, N., 2020. Data-driven maintenance and operations scheduling in power systems under decision-dependent uncertainty. *IISE transactions*, *52*(6), pp.589-602.
3. Liang, G., Zhao, J., Luo, F., Weller, S.R. and Dong, Z.Y., 2016. A review of false data injection attacks against modern power systems. *IEEE Transactions on Smart Grid*, *8*(4), pp.1630-1638.
4. Ahmed, M. and Pathan, A.S.K., 2020. False data injection attack (FDIA): an overview and new metrics for fair evaluation of its countermeasure. *Complex Adaptive Systems Modeling*, *8*, pp.1-14.
5. Tan, R., Nguyen, H.H., Foo, E.Y., Yau, D.K., Kalbarczyk, Z., Iyer, R.K. and Gooi, H.B., 2017. Modeling and mitigating impact of false data injection attacks on automatic generation control. *IEEE Transactions on Information Forensics and Security*, *12*(7), pp.1609-1624.
6. Petinrin, Joseph O., and Mohamed Shaaban. "Smart power grid: Technologies and applications." *2012 IEEE international conference on power and energy (PECon)*. IEEE, 2012.
7. Strielkowski, W., Vlasov, A., Selivanov, K., Muraviev, K. and Shakhnov, V., 2023. Prospects and challenges of the machine learning and data-driven methods for the predictive analysis of power systems: A review. *Energies*, *16*(10), p.4025.
8. Aoufi, S., Derhab, A. and Guerroumi, M., 2020. Survey of false data injection in smart power grid: Attacks, countermeasures and challenges. *Journal of Information Security and Applications*, *54*, p.102518.
9. Mahi-Al-rashid, A., Hossain, F., Anwar, A. and Azam, S., 2022. False data injection attack detection in smart grid using energy consumption forecasting. *Energies*, *15*(13), p.4877
10. Wang, Q., Tai, W., Tang, Y. and Ni, M., 2019. Review of the false data injection attack against the cyber-physical power system. *IET Cyber-Physical Systems: Theory & Applications*, *4*(2), pp.101-107.
11. Chattopadhyay, A. and Mitra, U., 2019. Security against false data-injection attack in cyber-physical systems. *IEEE Transactions on Control of Network Systems*, *7*(2), pp.1015-1027.
12. Sikder, M.N.K. and Batarseh, F.A., 2023. Outlier detection using AI: a survey. *AI Assurance*, pp.231-291.
13. Taha, A. and Hadi, A.S., 2019. Anomaly detection methods for categorical data: A review. *ACM Computing Surveys (CSUR)*, *52*(2), pp.1-35.
14. Toshniwal, A., Mahesh, K. and Jayashree, R., 2020, October. Overview of anomaly detection techniques in machine learning. In *2020 fourth international conference on I-SMAC (IoT in social, mobile, analytics and cloud)(I-SMAC)* (pp. 808-815). IEEE.
15. Chakraborty, A., Alam, M., Dey, V., Chattopadhyay, A. and Mukhopadhyay, D., 2018. Adversarial attacks and defences: A survey. *arXiv preprint arXiv:1810.00069*.
16. Gugulothu, N., Malhotra, P., Vig, L. and Shroff, G., 2018, July. Sparse neural networks for anomaly detection in high-dimensional time series. In *AI4IOT workshop in conjunction with ICML, IJCAI and ECAI* (pp. 1551-3203).
17. Yassin, W., Udzir, N.I., Muda, Z. and Sulaiman, M.N., 2013. Anomaly-based intrusion detection through k-means clustering and naives bayes classification.
18. Khaledian, E., Pandey, S., Kundu, P. and Srivastava, A.K., 2020. Real-time synchrophasor data anomaly detection and classification using isolation forest, kmeans, and loop. *IEEE Transactions on Smart Grid*, *12*(3), pp.2378-2388.

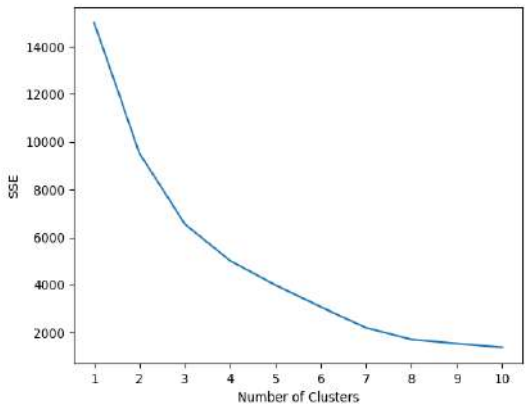

Figure 1. Elbow Method Plot obtained for the considered PMU dataset

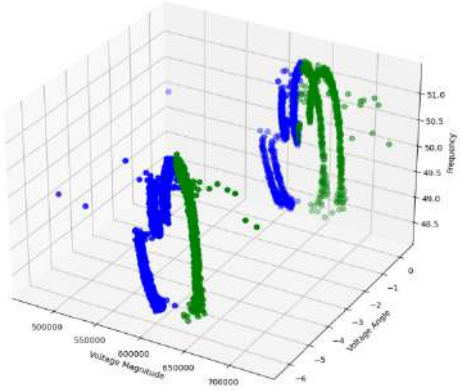

Figure 2. Scatterplot for K = 2

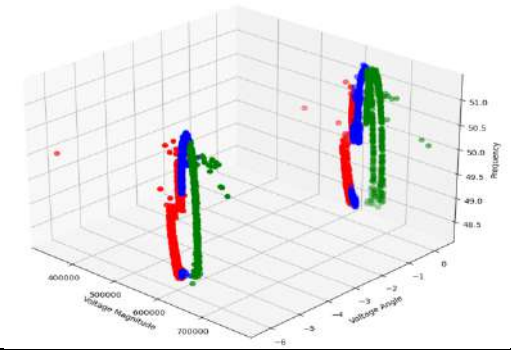

Figure 3. Scatterplot for K = 3

Indian Journal of Natural Sciences www.tnsroindia.org.in ©IJONS

Vol.15 / Issue 83 / Apr / 2024 *International Bimonthly (Print) – Open Access* *ISSN: 0976 – 0997*

RESEARCH ARTICLE

Pair Mean Cordial Labeling of Hexagonal Snake, Irregular Quadrilateral Snake and Triple Triangular Snake

R. Ponraj[1] and S. Prabhu[2]

[1]Department of Mathematics, Sri Paramakalyani College, Alwarkurichi-627 412, India.
[2]Research Scholar, Reg. No. : 21121232091003, Sri Paramakalyani College, Alwarkurichi-627 412, India.

Received: 30 Dec 2023 Revised: 09 Jan 2024 Accepted: 12 Mar 2024

***Address for Correspondence**
R. Ponraj
Department of Mathematics,
Sri Paramakalyani College,
Alwarkurichi-627 412, India.
Email: ponrajmaths@gmail.com

ABSTRACT

Consider a (p,q) graph $G=(V,E)$. Specify $\varrho=\begin{cases}\frac{p}{2} & even\ p\\ \frac{p-1}{2} & odd\ p,\end{cases}$ and $\Upsilon=\{\pm1,\pm2,\ldots.,\pm\varrho\}$ referred to as the label set. Let's consider a mapping $\lambda: V\to\Upsilon$ where, for every even p, distinct labels are assigned to the various elements of V in Υ, and for every odd p, distinct labels are assigned to the $p-1$ vertices of V in Υ, with a label that is repeated for the lone vertex. After that φ is referred to as a pair mean cordial labeling (PMC-labeling) if regarding every $\mu\nu$ edge within G, there is a label for $\frac{\varphi(\mu)+\varphi(\nu)}{2}\ if\ \varphi(\mu)+\varphi(\nu)$ is even and $\frac{\varphi(\mu)+\varphi(\nu)+1}{2}\ if\ \varphi(\mu)+\varphi(\nu)$ is odd ensue that $\left|\overline{\mathbb{S}}_{\varphi_1}-\overline{\mathbb{S}}_{\varphi_1^c}\right|\le 1$ in which $\overline{\mathbb{S}}_{\varphi_1}$and $\overline{\mathbb{S}}_{\varphi_1^c}$ are signify the quantity of edges designated with 1 and the quantity of edges that are unlabeled with 1 in that order. A pair mean cordial graph (PMC-graph) is defined as a graph G with PMC-labeling. In our study, we examine the PMC-labeling of several snake graphs.

Keywords: hexagonal snake, irregular quadrilateral snake, comb triangular graph, quadrilateral snake and triple triangular snake

INTRODUCTION

In our study, we consider a graph as a undirected, finite graph that has no looping and only one edge. Graph labeling is a well-known field of study in graph theory, with an extensive collection of literature and unresolved issues covering a wide range of graph kinds. Rosa[17] initially put up the graph labeling idea in the 1960s. We adhere to F. Harary [4] for different graphs, theoretical notations, and nomenclature and Gallian [3] provides a thorough analysis of different graph labeling techniques. I. Cahit [2] suggested the idea of cordial graphs and looking at the

cordial related graphs in [1,5-8,13-16,18-20]. Labeling graphs, and more specifically, cordial labeling graphs, was a topic of considerable interest. PMC-labeling is a notion that was first proposed to us in [9] and in [10-12], we looked at the pair mean cordiality of several family graphs. We examine PMC-labeling of several snake graphs, such as the hexagonal snake, irregular quadrilateral snake, comb triangular graph, double quadrilateral snake, alternate double quadrilateral snake, triple triangular snake and triple quadrilateral snake, in this article.

Preliminaries

Definition 2.1. The hexagonal snake HS_r is a graph that is created by taking a path $\mu_1\mu_2, \dots \mu_r$ of length r by adding μ_i and μ_{i+1} to three new vertices $\nu_i, \eta_i \; and \; \omega_i$, $1 \le i \le r-1$.

Definition 2.2. A graph known as the irregular quadrilateral snake IQ_r is produced by following a path with vertex set $V(IQ_r) = \{\mu_i, \nu_j, \omega_j \mid 1 \le i \le r \; and \; 1 \le j \le r-2\}$ and edge set
$E(IQ_r) = \{\mu_i\nu_i, \nu_i\omega_i, \omega_i\mu_{i+2} : 1 \le i \le r-2\} \cup \{\mu_i\mu_{i+1} : 1 \le i \le r-1\}$.

Definition 2.3. The double quadrilateral graph TQ_r is a graph that is created by taking a path $\mu_1\mu_2, \dots \mu_r$ of length r by adding μ_i and μ_{i+1} to new vertices $\nu_j, \zeta_j, \eta_j \; and \; \omega_j$ respectively and then adding $\nu_i \; and \; \zeta, \eta_j \; and \; \omega_j,$, $1 \le i \le r-1$.

Definition 2.4. A graph known as the alternate double quadrilateral snake $A(DQ_r)$ is produced by joining two alternative quadrilateral snakes which share a path.

Definition 2.5. The triple triangular graph TT_r is made by appending μ_i and μ_{i+1} to new vertices $\nu_i, \zeta_i, \eta_i \; and \; \omega_i$, $1 \le i \le r-1$ on a path of length r.

Definition 2.6. The triple quadrilateral graph TQ_r is a graph that is created by taking a path $\mu_1\mu_2, \dots \mu_r$ of length r by adding μ_i and μ_{i+1} to new vertices $\nu_j, \eta_j, \omega_j, \zeta_j, \xi_j \; and \; \delta_j$ respectively and then adding $\nu_i \; and \; \eta_i$, $\omega_i \; and \; \zeta_i$, $\xi_i \; and \; \delta_i$, $1 \le i \le r-1$.

3. Main Theorems

Theorem 3.1. [10]The quadrilateral snake Q_r is a PMC-graph for all $r \ge 2$.

Theorem 3.2. [10] The triangular snake T_r is a PMC-graph for all $r \ge 2$.

Theorem 3.3. The hexagonal snake HS_r is a PMC-graph for all $r \ge 2$.

Proof. Let $V(HS_r) = \{\mu_i \mid 1 \le i \le r+1\} \cup \{\nu_i, \zeta_i, \eta_i, \omega_i \mid 1 \le i \le r\}$.
Additionally $E(HS_r) = \{\mu_i\eta_i, \mu_i\nu_i, \eta_i\omega_i, \nu_i\zeta_i, \zeta_i\mu_{i+1}, \omega_i\mu_{i+1} | 1 \le i \le r\}$. Certainly, the hexagonal snake HS_r consists of $6r$ edges and $5r+1$ vertices.

Case (A): For odd r

Allocate the labels $-1, -6, \dots, \frac{-5r+3}{2}$ corresponding to $\mu_1, \mu_3, \dots, \mu_r$ and $4,9, \dots, \frac{5r-7}{2}$ to $\mu_2, \mu_4, \dots, \mu_{r-1}$ in that order. Fix the label 1 with μ_{r+1}. Designate the labels $2,7, \dots, \frac{5r-1}{2}$ according to $\nu_1, \nu_3, \dots, \nu_r$ and $-4, -9, \dots, \frac{-5r+7}{2}$ to $\nu_2, \nu_4, \dots, \nu_{r-1}$ in that order. Consequently, allocate the labels $-2, -7, \dots, \frac{-5r+11}{2}$ corresponding to $\zeta_1, \zeta_3, \dots, \zeta_{r-2}$ and $5,10, \dots, \frac{5r-5}{2}$ to $\zeta_2, \zeta_4, \dots, \zeta_{r-1}$ in that order. Fix the label $\frac{-5r-1}{2}$ with ζ_r. Designate the labels $3,8, \dots, \frac{5r+1}{2}$ according to $\eta_1, \eta_3, \dots, \eta_r$ and $-5, -10, \dots, \frac{-5r+5}{2}$ to $\eta_2, \eta_4, \dots, \eta_{r-1}$ in that order. Eventually, allocate the labels $-3, -8, \dots, \frac{-5r+9}{2}$ corresponding to $\omega_1, \omega_3, \dots, \omega_{r-2}$ and $6,11, \dots, \frac{5r-3}{2}$ to $\omega_2, \omega_4, \dots, \omega_{r-1}$ in that order. Fix $\frac{-5r+1}{2}$ with the vertex ω_r. Subsequently, the edges $\mu_i\eta_i, \mu_i\nu_i$ for $i = 1,3, \dots, r$, $\nu_i\zeta_i, \eta_i\omega_i$, for $i = 2,4, \dots, r-1$, $\zeta_i\mu_{i+1}, \omega_i\mu_{i+1}$, for $i = 1,3, \dots, r-2$ and $\eta_r\omega_r$ are designated with 1 and the remaining edges that are unlabeled with 1.

Case (B): For even r

Now designate the labels $-1, -6, \dots, \frac{-5r+8}{2}$ corresponding to $\mu_1, \mu_3, \dots, \mu_{r-1}$ and $4,9, \dots, \frac{5r-2}{2}$ to $\mu_2, \mu_4, \dots, \mu_r$ in that order. Fix the label 1 with μ_{r+1}. Allocate the labels $2,7, \dots, \frac{5r-8}{2}$ according to $\nu_1, \nu_3, \dots, \nu_{r-1}$ and $-4, -9, \dots, \frac{-5r+2}{2}$ to $\nu_2, \nu_4, \dots, \nu_r$ in that order. Consequently, designate the labels $-2, -7, \dots, \frac{-5r+8}{2}$ corresponding to $\zeta_1, \zeta_3, \dots, \zeta_{r-1}$ and $5,10, \dots, \frac{5r}{2}$ to $\zeta_2, \zeta_4, \dots, \zeta_r$ in that order. Allocate the labels $3,8, \dots, \frac{5r-4}{2}$ according to $\eta_1, \eta_3, \dots, \eta_{r-1}$ and $-5, -10, \dots, \frac{-5r}{2}$ to $\eta_2, \eta_4, \dots, \eta_r$

in that order. Eventually, designate the labels $-3,-8,\ldots,\frac{-5r+4}{2}$ corresponding to $\omega_1,\omega_3,\ldots,\omega_{r-1}$ and $6,11,\ldots,\frac{5r-8}{2}$ to $\omega_2,\omega_4,\ldots,\omega_{r-2}$ in that order. Fix 1 with the vertex ω_r. Subsequently, the edges $\mu_i\eta_i,\mu_i\nu_i,$, $\zeta_i\mu_{i+1},\omega_i\mu_{i+1}$ for $1\le i\le r-1$ *and i is odd,* $\nu_i\zeta_i,$ for $1\le i\le r$ *and i is even,* $\eta_i\omega_i$, $1\le i\le r-2$ *and i is even* and $\eta_r\omega_{r+1}$ are designated with 1 and the remaining edges that are unlabeled with 1. In each instance, $\overline{\mathbb{S}}_{\varphi_1}=3r=\overline{\mathbb{S}}_{\varphi_1^c}$.

Theorem 3.4. The irregular quadrilateral snake IQ_r is a PMC-graph for all $r\ge 2$.

Proof. Let $V(IQ_r)=\{\mu_i\mid 1\le i\le r\}\cup\{\nu_i,\omega_i\mid 1\le i\le r-2\}$. Additionally $E(IQ_r)=\{\mu_i\nu_i,\nu_i\omega_i,\omega_i\mu_{i+2}\mid 1\le i\le r-2\}\cup\{\mu_i\mu_{i+1}\mid 1\le i\le r-1\}$. Certainly, the irregular quadrilateral snake IQ_r consists of $4r-7$ edges and $3r-4$ vertices.

Case (A): For odd r

Allocate the labels $2,5,\ldots,\frac{3r-5}{2}$ corresponding to $\mu_1,\mu_3,\ldots,\mu_{r-2}$ and $-2,-5,\ldots,\frac{-3r+5}{2}$ to $\mu_2,\mu_4,\ldots,\mu_{r-1}$ in that order. Fix the label 1 with μ_r. Designate the labels $-1,-4,\ldots,\frac{-3r+7}{2}$ according to $\nu_1,\nu_3,\ldots,\nu_{r-2}$ and $4,7,\ldots,\frac{3r-7}{2}$ to $\nu_2,\nu_4,\ldots,\nu_{r-3}$ in that order. Consequently, allocate the labels $3,6,\ldots,\frac{3r-9}{2}$ corresponding to $\omega_1,\omega_3,\ldots,\omega_{r-4}$ and $-3,-6,\ldots,\frac{-3r+9}{2}$ to $\omega_2,\omega_4,\ldots,\omega_{r-3}$ in that order. Fix $\frac{3r-5}{2}$ with the vertex ω_r.

Case (B): For even r

Now designate the labels $2,5,\ldots,\frac{3r-8}{2}$ corresponding to $\mu_1,\mu_3,\ldots,\mu_{r-3}$ and $-2,-5,\ldots,\frac{-3r+8}{2}$ to $\mu_2,\mu_4,\ldots,\mu_{r-2}$ in that order. Fix the label 1 with μ_{r-1} and $\frac{-3r+4}{2}$ with μ_r. Allocate the labels $-1,-4,\ldots,\frac{-3r+10}{2}$ according to $\nu_1,\nu_3,\ldots,\nu_{r-3}$ and $4,7,\ldots,\frac{3r-4}{2}$ to $\nu_2,\nu_4,\ldots,\nu_{r-2}$ in that order. Consequently, designate the labels $3,6,\ldots,\frac{3r-6}{2}$ corresponding to $\omega_1,\omega_3,\ldots,\omega_{r-3}$ and $-3,-6,\ldots,\frac{-3r+9}{2}$ to $\omega_2,\omega_4,\ldots,\omega_{r-2}$ in that order. In each instance, the edges $\mu_i\nu_i,\omega_i\nu_i$ for $1\le i\le r-2$ are designated with 1 and the remaining edges that are unlabeled with 1. Subsequently, $\overline{\mathbb{S}}_{\varphi_1}=2r-4$ and $\overline{\mathbb{S}}_{\varphi_1^c}=2r-3$.

Theorem 3.5. The comb triangular graph CT_r is a PMC-graph for all $r\ge 2$.

Proof. Let $V(CT_r)=\{\mu_i,\nu_i,\omega_j\mid 1\le i\le r\ and\ 1\le j\le r-1\}$. Additionally $E(CT_r)=\{\mu_i\omega_i,\mu_{i+1}\omega_i,\mu_i\mu_{i+1},\mu_j\nu_j:\ 1\le j\le r\ and\ 1\le i\le r-1\}$. Certainly, comb triangular graph CT_r consists of $4r-3$ edges and $3r-1$ vertices.

Case (A): For odd r

Allocate the labels $-1,-4,\ldots,\frac{-3r+1}{2}$ corresponding to $\mu_1,\mu_3,\ldots,\mu_r$ and $4,7,\ldots,\frac{3r-1}{2}$ to $\mu_2,\mu_4,\ldots,\mu_{r-1}$ in that order. Designate the labels $2,5,\ldots,\frac{3r-5}{2}$ according to $\nu_1,\nu_3,\ldots,\nu_{r-2}$ and $-2,-5,\ldots,\frac{-3r+5}{2}$ to $\nu_2,\nu_4,\ldots,\nu_{r-1}$ in that order. Fix the label 1 with ν_r. Consequently, allocate the labels $3,6,\ldots,\frac{3r-3}{2}$ corresponding to $\omega_1,\omega_3,\ldots,\omega_{r-2}$ and $-3,-6,\ldots,\frac{-3r+3}{2}$ to $\omega_2,\omega_4,\ldots,\omega_{r-1}$ in that order.

Case (B): For even r

Designate the labels $-1,-4,\ldots,\frac{-3r+4}{2}$ corresponding to $\mu_1,\mu_3,\ldots,\mu_{r-1}$ and $4,7,\ldots,\frac{3r-4}{2}$ to $\mu_2,\mu_4,\ldots,\mu_{r-2}$ in that order. Fix the label 1 with μ_r. Allocate the labels $2,5,\ldots,\frac{3r-2}{2}$ according to $\nu_1,\nu_3,\ldots,\nu_{r-1}$ and $-2,-5,\ldots,\frac{-3r+2}{2}$ to $\nu_2,\nu_4,\ldots,\nu_r$ in that order. Consequently, designate the labels $3,6,\ldots,\frac{3r-6}{2}$ corresponding to $\omega_1,\omega_3,\ldots,\omega_{r-3}$ and $-3,-6,\ldots,\frac{-3r+6}{2}$ to $\omega_2,\omega_4,\ldots,\omega_{r-2}$ in that order. Fix the label $\frac{3r-2}{2}$ with ω_r. In each instance, the edges $\mu_i\nu_i,\nu_i\omega_i$, $1\le i\le r-1$ are are designated with 1 and the remaining edges that are unlabeled with 1. Eventually, $\overline{\mathbb{S}}_{\varphi_1}=2r-2$ and $\overline{\mathbb{S}}_{\varphi_1^c}=2r-1$.

Theorem 3.6. The double quadrilateral snake DQ_r is a PMC-graph for all $r\ge 2$.

Proof. Let $V(DQ_r)=\{\mu_i:1\le i\le r\}\cup\{\nu_i,\zeta_i,\eta_i,\omega_i\mid 1\le i\le r-1\}$.

Additionally $E(DQ_r)=\{u_iu_{i+1},\mu_i\nu_i,\nu_i\zeta_i,u_{i+1}\zeta_j,u_{i+1}\omega_i,u_i\eta_i,\eta_i\omega_i:1\le i\le r-1\}$. Eventually, the double quadrilateral snake DQ_r consists of $7r-7$ edges and $5r-4$ edges.

Case (A): For odd r

Allocate the labels $-1,-6,\ldots,\frac{-5r+13}{2}$ corresponding to $\mu_1,\mu_3,\ldots,\mu_{r-2}$ and $-3,-8,\ldots,\frac{-5r+9}{2}$ to $\mu_2,\mu_4,\ldots,\mu_{r-1}$ in that order. Put the label 1 with μ_r. Subsequently, designate the labels $3,8,\ldots,\frac{5r-9}{2}$ according to $\nu_1,\nu_3,\ldots,\nu_{r-2}$ and

$5,10,\ldots,\frac{5r-5}{2}$ to $v_2, v_4, \ldots, v_{r-1}$ in that order. Allocate the labels $-2,-7,\ldots,\frac{-5r+11}{2}$ corresponding to $\zeta_1,\zeta_3,\ldots,\zeta_{r-2}$ and $-4,-9,\ldots,\frac{-5r+7}{2}$ to $\zeta_2,\zeta_4,\ldots,\zeta_{r-1}$ in that order. Designate the labels $2,7,\ldots,\frac{5r-11}{2}$ according to $\eta_1,\eta_3,\ldots,\eta_{r-2}$ and $-5,-10,\ldots,\frac{-5r+5}{2}$ to $\eta_2,\eta_4,\ldots,\eta_{r-1}$ in that order. Eventually, allocate the labels $4,9,\ldots,\frac{5r-9}{2}$ corresponding to $\omega_1,\omega_3,\ldots,\omega_{r-2}$ and $6,11,\ldots,\frac{5r-13}{2}$ to $\omega_2,\omega_4,\ldots,\omega_{r-3}$ in that order. Fix 1 with the vertex ω_{r-1}. Consequently, the edges $\mu_i v_i, v_i\omega_i$, $1\le i\le r-1$, $u_i\eta_i, u_{i+1}\omega_i$, $i=1,3,\ldots,r-2$ and $\eta_i\omega_i, i=2,4,\ldots,r-2$ are labeled with 1 and the remaining edges are labeled with integers other than 1. Eventually, $\overline{\mathbb{S}}_{\varphi_1}=\frac{7r-7}{2}=\overline{\mathbb{S}}_{\varphi_1^c}$.

Case (B): For even r

Designate the labels $-1,-6,\ldots,\frac{-5r+8}{2}$ corresponding to $\mu_1,\mu_3,\ldots,\mu_{r-1}$ and $-3,-8,\ldots,\frac{-5r+4}{2}$ to $\mu_2,\mu_4,\ldots,\mu_r$ in that order. Consequently, allocate the labels $3,8,\ldots,\frac{5r-4}{2}$ according to $v_1,v_3,\ldots,v_{r-1}$ and $5,10,\ldots,\frac{5r-10}{2}$ to $v_2,v_4,\ldots,v_{r-2}$ in that order. Allocate the labels $-2,-7,\ldots,\frac{-5r+6}{2}$ corresponding to $\zeta_1,\zeta_3,\ldots,\zeta_{r-1}$ and $-4,-9,\ldots,\frac{-5r+12}{2}$ to $\zeta_2,\zeta_4,\ldots,\zeta_{r-2}$ in that order. Designate the labels $2,7,\ldots,\frac{5r-6}{2}$ according to $\eta_1,\eta_3,\ldots,\eta_{r-1}$ and $-5,-10,\ldots,\frac{-5r+10}{2}$ to $\eta_2,\eta_4,\ldots,\eta_r$ in that order. Eventually, allocate the labels $4,9,\ldots,\frac{5r-12}{2}$ corresponding to $\omega_1,\omega_3,\ldots,\omega_{r-3}$ and $6,11,\ldots,\frac{5r-8}{2}$ to $\omega_2,\omega_4,\ldots,\omega_{r-2}$ in that order. Fix 1 with the vertex ω_{r-1}. Consequently, the edges $\mu_i v_i, v_i\omega_i$, $1\le i\le r-1$, $u_i\eta_i, 1\le i\le r-1$ and i is odd , $u_{i+1}\omega_i$, $1\le i\le r-1$ *and* i is odd , and $\eta_i\omega_i, 1\le i\le r-2$ *and i is even* and $u_i\omega_{i-1}$ are designated with 1 and the remaining edges that are unlabeled with 1. Eventually, $\overline{\mathbb{S}}_{\varphi_1}=\frac{7r-8}{2}$ and $\overline{\mathbb{S}}_{\varphi_1^c}=\frac{7r-6}{2}$.

Theorem 3.7. The alternate double quadrilateral snake $A(DQ_r)$ is a PMC-graph for all $r\ge 3$.

Proof.

Case (A): Both the edges $\mu_{r-1}\mu_r$ and $\mu_1\mu_2$ are located on the double quadrilateral for even $r\ge 4$.

Then $V(A(DQ_r))=\{\mu_i \mid 1\le i\le r\}\cup\{v_i,\zeta_i,\eta_i,\omega_i \mid 1\le i\le\frac{r}{2}\}$.

Additionally $E(A(DQ_r))=\{u_iu_{i+1}\}\cup\{\mu_{2i-1}v_i, v_i\zeta_i, u_{2i}\zeta_j, u_{2i}\omega_i, u_{2i-1}\eta_i, \eta_i\omega_i : 1\le i\le\frac{r}{2}\}$. Presently, $A(DQ_r)$ includes $4r-1$ edges and $3r$ vertices. Designate the labels $-1,-4,\ldots,\frac{-3r+4}{2}$ corresponding to $\mu_1,\mu_3,\ldots,\mu_{r-1}$ and $-3,-6,\ldots,\frac{-3r}{2}$ to $\mu_2,\mu_4,\ldots,\mu_r$ in that order. Consequently, allocate the labels $3,6,\ldots,\frac{3r}{2}$ according to $v_1,v_2,\ldots,v_{r/2}$ and $-2,-5,\ldots,\frac{-3r+2}{2}$ to $\zeta_1,\zeta_2,\ldots,\zeta_{r/2}$ in that order. Designate the labels $2,5,\ldots,\frac{3r-2}{2}$ according to $\eta_1,\eta_2,\ldots,\eta r_{/2}$ and $4,7,\ldots,\frac{3r-4}{2}$ to $\omega_1,\omega_2,\ldots,\omega_{r-2/2}$ in that order. Fix 1 with the vertex $\omega r_{/2}$. Consequently, the edges $\mu_{2i-1}v_i, v_i\zeta_i, u_{2i-1}\eta_i$, $1\le i\le\frac{r}{2}$, $u_{2i}\omega_i, 1\le i\le\frac{r-2}{2}$ are are designated with 1 and the remaining edges that are unlabeled with 1. Eventually, $\overline{\mathbb{S}}_{\varphi_1}=2r-1$ and $\overline{\mathbb{S}}_{\varphi_1^c}=2r$.

Case (B): Both the edges $\mu_{r-1}\mu_r$ and $\mu_1\mu_2$ are not located on the double quadrilateral for odd $r\ge 4$.

Then $V(A(DQ_r))=\{\mu_i,v_j,\zeta_j,\eta_j,\omega_j : 1\le i\le r \text{ and } 1\le j\le\frac{r-2}{2}\}$. Additionally $E(A(DQ_r))=\{u_iu_{i+1}: 1\le r\le r\}\cup\{\mu_{2i}v_i, v_i\zeta_i, u_{2i+1}\zeta_j, u_{2i+1}\omega_i, u_{2i}\eta_i, \eta_i\omega_i : 1\le i\le\frac{r-2}{2}\}$. Presently, it includes $4r-7$ edges and $3r-4$ vertices. Fix 1 with the vertex μ_1. Designate the labels $-1,-4,\ldots,\frac{-3r+4}{2}$ corresponding to $\mu_2,\mu_4,\ldots,\mu_r$ and $-3,-6,\ldots,\frac{-3r+6}{2}$ to $\mu_3,\mu_5,\ldots,\mu_{r-1}$ in that order. Consequently, allocate the labels $3,6,\ldots,\frac{3r-6}{2}$ according to $v_1,v_2,\ldots,v_{r-2/2}$ and $-2,-5,\ldots,\frac{-3r+8}{2}$ to $\zeta_1,\zeta_2,\ldots,\zeta_{r-2/2}$ in that order. Designate the labels $2,5,\ldots,\frac{3r-8}{2}$ according to $\eta_1,\eta_2,\ldots,\eta_{r-2/2}$ and $4,7,\ldots,\frac{3r-4}{2}$ to $\omega_1,\omega_2,\ldots,\omega_{r-2/2}$ in that order. Consequently, the edges $\mu_{2i}v_i, v_i\zeta_i, u_{2i}\eta_i, u_{2i+1}\omega_i, 1\le i\le\frac{r-2}{2}$ are designated with 1 and the remaining edges that are unlabeled with 1. Eventually, $\overline{\mathbb{S}}_{\varphi_1}=2r-4$ and $\overline{\mathbb{S}}_{\varphi_1^c}=2r-3$.

Case (C): For odd $r\ge 3$, $\mu_{r-1}\mu_r$ and $\mu_1\mu_2$ are the edges that lie on and off the double quadrilateral, respectively. Let $(A(DQ_r))=\{\mu_i,v_j,\zeta_j,\eta_j,\omega_j : 1\le i\le r \text{ and } 1\le j\le\frac{r-2}{2}\}$.

Additionally $E(A(DQ_r))=\{u_iu_{i+1}: 1\le r\le r\}\cup\{\mu_{2i}v_i, v_i\zeta_i, u_{2i+1}\zeta_j, u_{2i+1}\omega_i, u_{2i}\eta_i, \eta_i\omega_i : 1\le i\le\frac{r-1}{2}\}$. Presently, it includes $4r-4$ edges and $3r-2$ vertices. Fix 1 with the vertex μ_1. Designate the labels $-1,-4,\ldots,\frac{-3r+7}{2}$

corresponding to $\mu_2, \mu_4, \ldots, \mu_{r-1}$ and $-3, -6, \ldots, \frac{-3r+3}{2}$ to $\mu_3, \mu_5, \ldots, \mu_r$ in that order. Consequently, allocate the labels $3,6, \ldots, \frac{3r-3}{2}$ according to $\nu_1, \nu_2, \ldots, \nu_{r-1/2}$ and $-2, -5, \ldots, \frac{-3r+5}{2}$ to $\zeta_1, \zeta_2, \ldots, \zeta_{r-1/2}$ in that order. Designate the labels $2,5, \ldots, \frac{3r-5}{2}$ according to $\eta_1, \eta_2, \ldots, \eta_{r-1/2}$ and $4,7, \ldots, \frac{3r-7}{2}$ to $\omega_1, \omega_2, \ldots, \omega_{r-3/2}$ in that order. Fix $\frac{-3r+7}{2}$ with the vertex $\omega_{r-1/2}$. Consequently, the edges $\mu_{2i}v_i$, $v_i\zeta_i$, $u_{2i}\eta_i, 1 \le i \le \frac{r-1}{2}$, $u_{2i+1}\omega_i, 1 \le i \le \frac{r-3}{2}$ are designated with 1 and the remaining edges that are unlabeled with 1. Eventually, $\overline{\mathbb{S}}_{\varphi_1} = 2r-2$ and $\overline{\mathbb{S}}_{\varphi_1^c} = 2r-2$.

Case (D): For odd $r \ge 3$, $\mu_{r-1}\mu_r$and $\mu_1\mu_2$ are the edges that lie off and on the double quadrilateral, respectively. Let $V(A(DQ_r)) = \{\mu_i, v_j, \zeta_j, \eta_j, \omega_j : 1 \le i \le r \text{ and } 1 \le j \le \frac{r-2}{2}\}$

Additionally $E(A(DQ_r)) = \{u_iu_{i+1} : 1 \le r \le r\} \cup \{\mu_{2i-1}v_i, v_i\zeta_i, u_{2i}\zeta_j, u_{2i}\omega_i, u_{2i-1}\eta_i, \eta_i\omega_i : 1 \le i \le \frac{r-1}{2}\}$. Presently, it includes $4r-4$ edges and $3r-2$ vertices. Fix 1 with the vertex μ_r. Designate the labels $-1, -4, \ldots, \frac{-3r+7}{2}$ corresponding to $\mu_1, \mu_3, \ldots, \mu_{r-2}$ and $-3, -6, \ldots, \frac{-3r+3}{2}$ to $\mu_3, \mu_5, \ldots, \mu_{r-1}$ in that order. Consequently, label $\nu_i, \zeta_i, \eta_i, \omega_i$, just as in case (C). The edges $\mu_{2i-1}v_i$, $v_i\zeta_i$, $u_{2i-1}\eta_i, 1 \le i \le \frac{r-1}{2}$, $u_{2i}\omega_i, 1 \le i \le \frac{r-3}{2}$ and $\eta_{r-1/2}, \omega_{r-1/2}$ are designated with 1 and the remaining edges that are unlabeled with 1.Eventually, $\overline{\mathbb{S}}_{\varphi_1} = 2r-2$ and $\overline{\mathbb{S}}_{\varphi_1^c} = 2r-2$.

Theorem 3.8. The triple triangular snake TT_r is not PMC-graph for all $r \ge 2$(except $r = 3$).

Proof. Let $V(TT_r) = \{\mu_i, v_j, \eta_j, \omega_j \mid 1 \le i \le r \text{ and } 1 \le j \le r-1\}$.

Additionally $E(TT_r) = \{\mu_i v_i, \mu_i\eta_i, \mu_i\omega_i, \mu_{i+1}v_i, \mu_{i+1}\eta_i, \mu_{i+1}\omega_i, \mu_i\mu_{i+1} : 1 \le i \le r-1\}$. Certainly, the triple triangular snake TT_r consists of $7r-7$ edges and $4r-3$ vertices.

Case (A): $r = 2$

Suppose the triple triangular snake TT_2 is PMC-graph. Accordingly, two possible outcomes exist if 1 is given to μv: both $\varphi(\mu) + \varphi(v) = 1$ and $\varphi(\mu) + \varphi(v) = 2$ can be utilized. As a result, there can be a maximum of 2 edges labeled with 1. That's $\overline{\mathbb{S}}_{\varphi_1} \le 2$. Subsequently, $\overline{\mathbb{S}}_{\varphi_1^c} \ge 5$. Eventually $\overline{\mathbb{S}}_{\varphi_1^c} - \overline{\mathbb{S}}_{\varphi_1} \ge 5-2 = 3 > 1$, which contradicts itself.

Case (B): $r = 3$

Allocate the labels $-1, -2, -3$ corresponding to μ_1, μ_2, μ_3 and 1,2,3 to ν_1, η_1, ω_1 in that order. Eventually, designate the labels $4, -4, 4$ according to ν_2, η_2, ω_2. Consequently, $\overline{\mathbb{S}}_{\varphi_1} = 7 = \overline{\mathbb{S}}_{\varphi_1^c}$.

Case (C): $r \ge 4$

Suppose the triple triangular snake TT_r is PMC-graph. Accordingly, two possible outcomes exist if 1 is given to μv: both $\varphi(\mu) + \varphi(v) = 1$ and $\varphi(\mu) + \varphi(v) = 2$ can be utilized. As a result, there can be a maximum of $2r+1$ edges labeled with 1. That's $\overline{\mathbb{S}}_{\varphi_1} \le 2r+1$. Subsequently, $\overline{\mathbb{S}}_{\varphi_1^c} \ge 7r-7-(2r+1) = 5r-8$. Eventually $\overline{\mathbb{S}}_{\varphi_1^c} - \overline{\mathbb{S}}_{\varphi_1} \ge 5r-8-(2r+1) = 3r-9 = 3 > 1$, which contradicts itself.

Theorem 3.9. The triple quadrilateral snake TQ_r is a PMC-graph for all $r \ge 2$(except $r = 3$).

Proof. Let $V(TQ_r) = \{\mu_i \mid 1 \le i \le r\} \cup \{v_i, \eta_i, \omega_i, \zeta_i, \xi_i, \delta_i \mid 1 \le i \le r-1\}$.

Additionally $E(TQ_r) = \{\mu_i\mu_{i+1}, \mu_i v_i, \mu_i\xi_i, \mu_i\omega_i, \mu_{i+1}\zeta_i, \mu_{i+1}\delta_i, \mu_{i+1}\eta_i, v_i\eta_i, \xi_i\delta_i, \omega_i\zeta_i : 1 \le i \le r-1\}$. Certainly, the triple quadrilateral snake TQ_r consists of $10r-10$ edges and $7r-6$ vertices.

Case (A): For even r

Fix the label 3 with μ_1. Next allocate the labels $9,16, \ldots, \frac{7r-10}{2}$ corresponding to $\mu_3, \mu_5, \ldots, \mu_{r-1}$ and $-4, -11, \ldots, \frac{-7r+20}{2}$ to $\mu_2, \mu_4, \ldots, \mu_{r-2}$ in that order. Fix the label $\frac{-7r+8}{2}$ with μ_r. Designate the labels $-1, -8, \ldots, \frac{-7r+12}{2}$ according to $\nu_1, \nu_3, \ldots, \nu_{r-1}$ and $6,13, \ldots, \frac{7r-16}{2}$ to $\nu_2, \nu_4, \ldots, \nu_{r-2}$ in that order. Fix 2 with the vertex η_1. Consequently, allocate the labels $10,17, \ldots, \frac{7r-8}{2}$ corresponding to $\eta_1, \eta_3, \ldots, \eta_{r-1}$ and $-5, -12, \ldots, \frac{-7r+18}{2}$ to $\eta_2, \eta_4, \ldots, \eta_{r-2}$ in that order. Designate the labels $-2, -9, \ldots, \frac{-7r+10}{2}$ according to $\omega_1, \omega_3, \ldots, \omega_{r-1}$ and $7,14, \ldots, \frac{7r-14}{2}$ to $\omega_2, \omega_4, \ldots, \omega_{r-2}$ in that order.

Eventually, allocate the labels $4,11,\ldots,\frac{7r-6}{2}$ corresponding to $\zeta_1,\zeta_3,\ldots,\zeta_{r-1}$and $-6,-13,\ldots,\frac{-7r+16}{2}$ to $\zeta_2,\zeta_4,\ldots,\zeta_{r-2}$ in that order. Designate the labels $-3,-10,\ldots,\frac{-7r+22}{2}$ according to $\xi_1,\xi_3,\ldots,\xi_{r-3}$ and $8,15,\ldots,\frac{7r-12}{2}$ to $\xi_2,\xi_4,\ldots,\xi_{r-2}$ in that order. Allocate the labels $5,12,\ldots,\frac{7r-18}{2}$ corresponding to $\delta_1,\delta_3,\ldots,\delta_{r-3}$ and $-7,-14,\ldots,\frac{-7r+14}{2}$ to $\delta_2,\delta_4,\ldots,\delta_{r-2}$ in that order. Fix the label $\frac{-7r+6}{2}$ with δ_{r-1}. Subsequently, the edges $\mu_i\nu_i,\nu_i\eta_i,\xi_i\delta_i$, for $1\le i\le r-1$, $\omega_i\,\zeta_i,\mu_{i+1}\zeta_j$ for $1\le i\le r-2$, $\mu_r\delta_{r-1}$ and $\mu_1\xi_1$ are designated with 1 and the remaining edges that are unlabeled with 1.

Case (B): For odd r

Fix the label 3 with μ_1. Next allocate the labels $9,16,\ldots,\frac{7r-17}{2}$ corresponding to $\mu_3,\mu_5,\ldots,\mu_{r-2}$ and $-4,-11,\ldots,\frac{-7r+13}{2}$ to $\mu_2,\mu_4,\ldots,\mu_{r-1}$ in that order. Fix the label $\frac{7r-11}{2}$ with μ_r. Designate the labels $-1,-8,\ldots,\frac{-7r+19}{2}$ according to $\nu_1,\nu_3,\ldots,\nu_{r-2}$ and $6,13,\ldots,\frac{7r-9}{2}$ to $\nu_2,\nu_4,\ldots,\nu_{r-1}$ in that order. Fix 2 with the vertex η_1. Consequently, allocate the labels $10,17,\ldots,\frac{7r-15}{2}$ corresponding to $\eta_1,\eta_3,\ldots,\eta_{r-2}$ and $-5,-12,\ldots,\frac{-7r+11}{2}$ to $\eta_2,\eta_4,\ldots,\eta_{r-1}$ in that order. Designate the labels $-2,-9,\ldots,\frac{-7r+17}{2}$ according to $\omega_1,\omega_3,\ldots,\omega_{r-2}$ and $7,14,\ldots,\frac{7r-7}{2}$ to $\omega_2,\omega_4,\ldots,\omega_{r-1}$ in that order. Eventually, allocate the labels $4,11,\ldots,\frac{7r-13}{2}$ corresponding to $\zeta_1,\zeta_3,\ldots,\zeta_{r-2}$and $-6,-13,\ldots,\frac{-7r+9}{2}$ to $\zeta_2,\zeta_4,\ldots,\zeta_{r-1}$ in that order. Designate the labels $-3,-10,\ldots,\frac{-7r+15}{2}$ according to $\xi_1,\xi_3,\ldots,\xi_{r-2}$ and $8,15,\ldots,\frac{7r-19}{2}$ to $\xi_2,\xi_4,\ldots,\xi_{r-3}$ in that order. Fix the label 1 with ξ_{r-1}. Allocate the labels $5,12,\ldots,\frac{7r-11}{2}$ corresponding to $\delta_1,\delta_3,\ldots,\delta_{r-2}$ and $-7,-14,\ldots,\frac{-7r+7}{2}$ to $\delta_2,\delta_4,\ldots,\delta_{r-1}$ in that order. Subsequently, the edges $\mu_i\nu_i,\nu_i\eta_i,\xi_i\delta_i$, for $1\le i\le r-1$, $\omega_i\,\zeta_i,\mu_{i+1}\zeta_j$ for $1\le i\le r-2$, $\mu_{r-1}\mu_r$ and $\mu_1\xi_1$ are designated with 1 and the remaining edges that are unlabeled with 1. In each instance, $\overline{\mathbb{S}}_{\varphi_1}=5r-5=\overline{\mathbb{S}}_{\varphi_1^c}$.

CONCLUSION

In this article, we have examined the PMC- labeling behavior of some snake graphs. There is unfinished business in terms of studying related theorems for other graphs.

REFERENCES

1. Beaulah Bell and R. Kala, Group Difference Cordial Labeling of some Snake Related Graphs, Mathematical Statistician and Engineering Applications, Vol 71 No. 3, pp. 1972 – 1984, 2022.
2. I. Cahit, Cordial Graphs: A weaker version of Graceful and Harmonious Graphs, Ars comb., 23, 201-207, 1987.
3. A. Gallian, A Dynamic Survey of Graph Labeling, Electronic Journal of Combinatorics, Vol. 18, pp. 1-219, 2011.
4. F. Harary, Graph Theory, Narosa Publishing House, New Delhi, 1988.
5. Pratik Shah and Dharamvirsinh Parmar, Integer Cordial Labeling of Alternate Snake Graph And Irregular Snake Graph, Applications and Applied Mathematics: An International Journal (AAM), Issue No. 10, pp. 59 – 71, 2022.
6. R. Patrias and O. Pechenik, Path cordial abelian groups, Australas. J. Combin., 80, pp 157-166, 2021.
7. A. Petrano and R. Rulete, On total product cordial labeling of some graphs, Internat. J. Math. Appl., 5(2B), pp 273-284, 2017.
8. A. C. Pedrano and Rulete, on the total product cordial labeling on the cartesian product of $P_m\times C_n$ and $C_m\times C_n$ and generalized peterson graph $P(m,n)$, Malaya J. Mat. 5(2), pp 194-201, 2017.
9. R. Ponraj and S. Prabhu, Pair mean cordial labeling of graphs, Journal of Algorithms and Computation 54, issue 1, pp 1-10, 2022.
10. R. Ponraj and S. Prabhu, Pair mean cordiality of some snake graphs, Global Journal of Pure and Applied Mathemtics, Vol. 18, No. 1, pp. 283-295, 2022.
11. R. Ponraj and S. Prabhu , Pair Mean Cordial labeling of some corona graphs, Journal of Indian Acad. Math., Vol.44, No. 1, pp 45-54, 2022.
12. R. Ponraj and S. Prabhu, Pair mean cordial labeling of graphs obtained from path and cycle, J. Appl. & Pure Math., Vol. 4 Number 3-4, 85-97, 2022..

13. U. M. Prajapati and R. M. Gajjar, Prime cordial labeling of generalized prism graph $Y_{m,n}$, Ultra Scientist, 27(3)A, pp 189-204, 2015..
14. U. M. Prajapati and R. M. Gajjar, Cordial labeling for complement of some graphs, Math. Today, 30, pp 99-118, 2015.
15. U. M. Prajapati and R. M. Gajjar, Cordiality in the context of duplication in Crown related graphs, J. Math. Comput. Sci., 6(6), 1058-1073, 2016.
16. U. M. Prajapati and N. B. Patel, Edge product cordial labeling of some graphs, J. Appl. Math. Comput. Mech., 18(1), pp 69-76, 2019.
17. A. Rosa, On certain valuations of the vertices of a graph, Theory of Graphs (Intl. Symp. Rome 1966), Gordon and Breach, Dunod, Paris, pp 349-355, 1967.
18. S.S. Sandhya, E. Ebin Raja Merly and S.D. Deepa, Heronian Mean Labeling of Triple Triangular and Triple Quadrilateral Snake Graphs, International Journal of Applied Mathematical Sciences, Volume 9, Number 2, pp. 177-186, 2016.
19. M. A. Seoud and A. E. I. Abdel Maqsoud, On cordial and balanced labeling of graphs, J. Egyptian Math. Soe., 7, pp 127-135, 1999.
20. M. A. Seoud and E. F. Helmi, On product cordial graphs, Ars Combin., 101, pp 519-529, 2011.

Indian Journal of Natural Sciences www.tnsroindia.org.in ©IJONS

Vol.15 / Issue 83 / Apr / 2024 International Bimonthly (Print) – Open Access ISSN: 0976 – 0997

RESEARCH ARTICLE

Some Properties of b# Interior and b#-Closure in Intuitionistic Topological Spaces

C. Velraj[1] and R. Jamuna Rani[2]

[1]Research Scholar, Register No. 20221172091005, Department of Mathematics, Rani Anna Govt. College for Women, Tirunelveli. Affiliated to MS University, Tirunelveli
[2]Asst. Professor and Head of the Dept. of Mathematics, Govt. Arts and Science College (Women), Sathankulam.

Received: 30 Dec 2023 Revised: 09 Jan 2024 Accepted: 12 Mar 2024

***Address for Correspondence**
C. Velraj
Research Scholar,
Department of Mathematics,
Rani Anna Govt. College for Women,
Tirunelveli.
Affiliated to MS University, Tirunelveli
Email: velraj.c79@gmail.com

ABSTRACT

This paper's main goal is to present intuitionistic topological spaces, specifically b#-closure and b#-interior. Numerous attributes and traits are listed.

Keywords: Intuitionistic b#interior, Intuitionistic b#closure.

INTRODUCTION AND PRELIMINARIES

Numerous generalizations of this core idea have been made since Zadeh[1] introduced fuzzy sets. The idea of "intuitionistic sets" presented by Coker[2] in 1996. All of the sets in this discrete version of the intuitionistic fuzzy set are completely crisp sets. He has investigated a few basic topological characteristics on intuitionistic sets. Because of their importance to general topology, open sets are currently a hot topic for study among academics all over the world. In intuitionistic topological spaces, semi open sets, pre open sets, and b-open sets were researched by Sasikala[4,5,6] and Navaneetha Krishnan. The b# open sets are researched by Velraj [7]. In topological spaces, Gnanambal Ilango[8] possesses the qualities of α-interior and α-closure. This work introduces and characterizes the features of intuitionistic b# open sets. Numerous pertinent papers have already been published in books. In this study, we described some of the features of b# interior and b# closure in intuitionistic topological spaces.

Definition1.1*cited from* [3]: A family τ of IS's in$\tilde{Y}$satisfyingthefollowingaxioms is called an intuitionistic topology.

(T1) $\tilde{\phi}, \tilde{Y} \in \tau$,
(T2) $\tilde{G}_1 \cap \tilde{G}_2 \in \tau$ for any $\tilde{G}_1, \tilde{G}_2 \in \tau$ and
(T3) $\cup \tilde{G}_i \in \tau$ for any arbitrary family $\{\tilde{G}_i : i \in J\} \subseteq \tau$.
Any IS in τ is referred to as an intuitionistic open set (IOS) in $\tilde{Y}$ and the pair $(\tilde{Y}, \tau)$ is called an intuitionistic topological space (ITS).
Definition 1.2*cited from*[3,9]: A subset $\tilde{S}$in $(\tilde{Y},\tau)$ is called
i) Intuitionistic regular open [3](IRO)*if* $\tilde{S} = int(cl(\tilde{S}))$
ii) Intuitionistic b# open [9](Ib#O) *if*$\tilde{S} = cl(int(\tilde{S})) \bigcup int(cl(\tilde{S}))$
Lemma 1.3*cited from* [10]:For a subset $\tilde{S}$ of an ITS $(\tilde{Y},\tau)$,
(i) $int(Ibcl(\tilde{S}))= Ibcl(int(\tilde{S}))= int(cl(int(\tilde{S})))$.
(ii) $cl(Ibint(\tilde{S}))= Ibint(cl(\tilde{S}))= cl(int(cl(\tilde{S})))$.
(iii) $Ibint(\tilde{S}) = Isint(\tilde{S}) \bigcup Ipint(\tilde{S})$.

Intuitionistic b# interior
We define intuitionistic b# interior and go over its characteristics in this section.
Definition 2.1. Consider the ITS$(\tilde{Y},\tau)$ .The union of all intuitionistic b#-open sets contained in $\tilde{U}$is called the intuitionistic b# interior of an intuitionistic set $\tilde{U}$and is denoted by Ib#$int(\tilde{U})$.
That is Ib#$int(\tilde{U})=\bigcup\{\tilde{V}: \tilde{V} \subseteq \tilde{U}$ and $\tilde{V}$ is Ib# open}.
The qualities of intuitionistic b# interior are provided in the following Propositions.
Proposition 2.2.
(i) Ib#$int(\tilde{\phi})=\tilde{\phi}$.
(ii) Ib#$int(\tilde{Y})= \tilde{Y}$.
(iii) Ib#$int(\tilde{U}) \subseteq \tilde{U}$.
(iv) If $\tilde{U}$ is Ib# open then Ib#$int(\tilde{U})= \tilde{U}$.
Proof: The definition provides proof.

Proposition 2.3. Let $(\tilde{Y},\tau)$ be an ITS. Then for any two sub sets $\tilde{C}$ and $\tilde{D}$ of $\tilde{Y}$, we get
(i) If $\tilde{C} \subseteq \tilde{D}$ then Ib#$int(\tilde{C}) \subseteq$ Ib#$int(\tilde{D})$.
(ii) Ib#int(Ib#$int(\tilde{C})$)= Ib#$int(\tilde{D})$.
(iii) Ib#$int(\tilde{C} \bigcup \tilde{D}) \subseteq$Ib#$int(\tilde{C}) \bigcap$ Ib#$int(\tilde{D})$.
(iv) Ib#$int(\tilde{C} \bigcup \tilde{D}) \supseteq$ Ib#$int(\tilde{C}) \bigcup$ Ib#$int(\tilde{D})$.
(v) Ib#$int(\tilde{C}) \subseteq$ Ib$int(\tilde{C})$.
(vi) Ib#$int(\tilde{C}) \subseteq Isint(\tilde{C}) \bigcup Ipint(\tilde{C})$.

Proof. Proof of (i), (iii), (iv) and (v) follows from the Definition.
Now to prove (ii). Using Proposition 2.2(iii), Ib#$int(\tilde{C}) \subseteq \tilde{C}$. Again Using (i), Ib#$int$(b#$int(\tilde{C})) \subseteq$ Ib#$int(\tilde{C})$. On the other hand let x∈Ib#$int(\tilde{C})$. This implies x∈$\tilde{D} \subseteq \tilde{C}$ for some Ib#-open set $\tilde{D}$. Now since $\tilde{D}$ is Ib#-open, Ib#-$int(\tilde{D})=\tilde{D}$. Since $\tilde{D} \subseteq \tilde{C}$, by (i), Ib#$int(\tilde{D}) \subseteq$Ib#$int(\tilde{C})$ that is $\tilde{D} \subseteq$Ib#$int(\tilde{C})$ that implies x∈$\tilde{D} \subseteq$Ib#$int(\tilde{C})$. This gives x∈Ib#int(Ib#$int(\tilde{C})$). Therefore Ib#$int(\tilde{C}) \subseteq$Ib#int(Ib#$int(\tilde{C})$). This proves (ii).
Now to prove (vi). By using Lemma 1.3(iii), $Ibint(\tilde{C})=Isint(\tilde{C}) \bigcup Ipint(\tilde{C})$. This together with (v) implies, Ib#$int(\tilde{C})$ $\subseteq$Ib$int(\tilde{C})= Isint(\tilde{C}) \bigcup Ipint(\tilde{C})$.This proves (vi).

It is possible to create examples to demonstrate that
(i) Ib#$int(\tilde{U}) \subseteq$ Ib#$int(\tilde{V})$ does not imply $\tilde{U} \subseteq \tilde{V}$.

(ii) $Ib^{\#}int(\widetilde{U} \bigcap \widetilde{V}) \neq Ib^{\#}int(\widetilde{U}) \bigcap Ib^{\#}int(\widetilde{V})$.

(iii) $Ib^{\#}int(\widetilde{U} \bigcup \widetilde{V}) \neq Ib^{\#}int(\widetilde{U}) \bigcup Ib^{\#}int(\widetilde{V})$.

(iv) $Ib^{\#}int(\widetilde{U}) \neq Ibint(\widetilde{U})$.

(v) $Ib^{\#}int(\widetilde{U}) \neq Isint(\widetilde{U}) \bigcup Ipint(\widetilde{U})$.

Example 2.4: Let $\widetilde{Y}$= {4,3,2,1} and τ={$\tilde{\phi}, \widetilde{Y_1}, \widetilde{Y_2}, \widetilde{Y_3}, \widetilde{Y}$} where $\widetilde{Y_1}$= <Y, {2,1},{4,3}>, $\widetilde{Y_2}$= <Y,{3}, {4,2,1}>, $\widetilde{Y_3}$= <Y,{3,2,1},{4}>. Let $\tilde{C}$= <Y, {4,3}, {1}> and $\tilde{D}$= <Y, {4,3,1}, {2}> be the intuitionistic subsets of ($\widetilde{Y}$, τ). Now $Ib^{\#}int(\widetilde{U}) = < Y, \{4,3\}, \{2,1\} >$ and $Ib^{\#}int(\widetilde{V}) = < Y, \{4,3\}, \{2,1\} >$. This shows that $Ib^{\#}int(\widetilde{U}) \subseteq Ib^{\#}int(\widetilde{V})$ does not imply $\widetilde{U} \subseteq \widetilde{V}$.

Example 2.5: Let $\widetilde{Y}$= {3,2,1} and τ={$\tilde{\phi}, \widetilde{Y_1}, \widetilde{Y_2}, \widetilde{Y_3}, \widetilde{Y}$}where $\widetilde{Y_1}$= <Y, {1},{3,2}>, $\widetilde{Y_2}$= <Y,{3}, {2,1}>, $\widetilde{Y_3}$= <Y, {3,1},{2}>. Let $\tilde{C}$ = <Y, {2,1}, {ϕ}> and $\tilde{D}$ = <Y, {3,2}, {ϕ}>be the intuitionistic subsets of ($\widetilde{Y}$, τ). $\tilde{C} \bigcap \tilde{D} = < X, \{2\}, \{\phi\} >$ $Ib\#int\left(\tilde{C} \bigcap \tilde{D}\right) = \phi$.Now, $Ib^{\#}int(\tilde{C}) = < Y, \{2,1\}, \{3\} >$ *and* $Ib^{\#}int(\tilde{D})$= <Y, {3,2},{1}>.$Ib^{\#}int(\tilde{C}) \bigcap Ib^{\#}int(\tilde{D})$ = <Y, {2},{3,1}>. Therefore, $Ib^{\#}int(\tilde{C} \bigcap \tilde{D}) \neq Ib^{\#}int(\tilde{C}) \bigcap Ib^{\#}int(\tilde{D})$.

Example 2.6: Let $\widetilde{Y}$= {4,3,2,1} and τ={$\tilde{\phi}, \widetilde{Y_1}, \widetilde{Y_2}, \widetilde{Y_3}, \widetilde{Y_4}, \widetilde{Y_5}, \widetilde{Y_6}, \widetilde{Y_7}, \widetilde{Y_8}, \widetilde{Y}$} where $\widetilde{Y_1}$= <Y, {3,2,1},{ϕ}>, $\widetilde{Y_2}$= <Y,{3,2}, {4}>, $\widetilde{Y_3}$= <Y, {2,1},{3}>, $\widetilde{Y_4}$= <Y, {2},{4,3}>, $\widetilde{Y_5}$= <Y, {3},{4,1}>, $\widetilde{Y_6}$= <Y,{ ϕ},{4,3,1}>, $\widetilde{Y_7}$= <Y, {1},{3}>, $\widetilde{Y_8}$= <Y, {ϕ},{4,3}>. Let $\tilde{C}$ = <Y, {4,3}, {1}> and $\tilde{D}$ = <Y, {4,1}, {ϕ}>be the intuitionistic subsets of ($\widetilde{Y}$, τ). $\tilde{C} \bigcup \tilde{D} = < X, \{4,3,1\}, \{\phi\} >$ $Ib\#int\left(\tilde{C} \bigcup \tilde{D}\right) = < Y, \{4,1\}, \{3\} >$. Now, $Ib^{\#}int(\tilde{C}) = < X, \{3\}, \{1\} >$ *and* $Ib^{\#}int(\tilde{D})$ = <Y, {4,1},{3}>.$Ib^{\#}int(\tilde{C})) \cup Ib^{\#}int(\tilde{D})$ = <Y, {4,3,1},{ϕ}>. Therefore $Ib^{\#}int(\tilde{C} \cup \tilde{D}) \neq Ib^{\#}int(\tilde{C}) \cup Ib^{\#}int(\tilde{D})$.

Example 2.7: Let us takethe ITS in Example 2.5. Let $\tilde{U}$ = <Y, {2,1}, {ϕ}>be an intuitionistic subset of ($\widetilde{Y}$, τ). Now, $Ib^{\#}int(\tilde{U}) = < Y, \{2,1\}, \{3\} >$ *and* $Ibint(\tilde{U})$= <Y,{2,1},{ϕ}>. This shows that $Ib^{\#}int(\tilde{U}) \neq Ibint(\tilde{U})$

Example 2.8: Let us take the ITS in Example 2.4. Let $\tilde{U}$ = <Y, {4,3}, {2}> be the intuitionistic subset of ($\widetilde{Y}$, τ).$Ib^{\#}int\left(\tilde{U}\right) = < Y, \{4,3\}, \{2,1\} >$.
Now $Isint\left(\tilde{U}\right) = < Y, \{4,3\}, \{2\} >$and $Ipint\left(\tilde{U}\right) = < Y, \{3\}, \{2\} >$.
Now $Isint(\tilde{U}) \cup Ipint\left(\tilde{U}\right) = < Y, \{4,3\}, \{2\} >$.
This shows that $Ib^{\#}int(\tilde{U}) \neq Isint(U) \cup Ipint\left(\tilde{U}\right)$.

Intuitionistic b$^{\#}$-Closure

This section presents the idea of intuitionistic b$^{\#}$-closure and discusses its characteristics.

Definition 3.1. Let $(\widetilde{Y}, \tau)$ *be an ITS*. The intersection of all intuitionistic b$^{\#}$-closed sets containing $\tilde{C}$is called the intuitionistic b$^{\#}$-interior of an intuitionistic set $\tilde{C}$ *in* (Y, τ), and is denoted by $Ib^{\#}cl(\tilde{C})$.

That is $Ib^{\#}cl(\tilde{C}) = \bigcap \{\tilde{D}: \tilde{C} \subseteq \tilde{D}$ and $\tilde{D}$ is Ib$^{\#}$-closed}.

Proposition 3.2. Let $(\widetilde{Y}, \tau)$ be an ITS. Then for any subset $\tilde{C}$ of $\widetilde{Y}$ we have

(i) $\widetilde{Y} \setminus Ib^{\#}int(\tilde{C}) = Ib^{\#}cl(\widetilde{Y} \setminus \tilde{C})$.

(ii) $\widetilde{Y} \setminus Ib^{\#}cl(\tilde{C}) = Ib^{\#}int(\widetilde{Y} \setminus \tilde{C})$.

Proof. By using Definition 2.1, $Ib^{\#}int(\tilde{C}) = \cup \{\tilde{D}: \tilde{D} \subseteq \tilde{C}$ and $\tilde{D}$ is Ib$^{\#}$-open}.

Accepting reciprocity on both ends, we obtain$\widetilde{Y} \setminus Ib^{\#}int(\tilde{C}) = \widetilde{Y} \setminus [\bigcup \tilde{D} : \tilde{D} \subseteq \tilde{C}$ and $\tilde{D}$ is Ib$^{\#}$-open}]= $\bigcap \{\widetilde{Y} \setminus \tilde{D}: \widetilde{Y} \setminus \tilde{C} \subseteq \widetilde{Y} \setminus \tilde{D}$ and $\widetilde{Y} \setminus \tilde{D}$ is Ib$^{\#}$-closed}= $Ib^{\#}cl(\widetilde{Y} \setminus \tilde{C})$. This proves (i).

Using(i), $\widetilde{Y} \setminus Ib^{\#}int(\widetilde{Y} \setminus \tilde{C}) = Ib^{\#}cl(\widetilde{Y} \setminus (\widetilde{Y} \setminus \tilde{C})) = Ib^{\#}cl(\tilde{C})$. This implies that $Ib^{\#}int(\widetilde{Y} \setminus \tilde{C}) = \widetilde{Y} \setminus Ib^{\#}cl(\tilde{C})$.

Preposition3.3.

(i) $Ib^{\#}cl(\tilde{\phi}) = \tilde{\phi}$,

(ii) $Ib^{\#}cl(\widetilde{Y}) = \widetilde{Y}$.

(iii) $\widetilde{U} \subseteq Ib^{\#}cl(\widetilde{U})$.

(iv) If $\widetilde{U}$ is Ib$^{\#}$closed then $Ib^{\#}cl(\widetilde{U}) = \widetilde{U}$.

Proof. The definition provides proof.

Proposition 3.4. Let $(\widetilde{Y}, \tau)$ be an ITS. Then for any two sub sets $\widetilde{C}$ and $\widetilde{D}$ of $\widetilde{Y}$ we have

(i) If $\widetilde{C} \subseteq \widetilde{D}$ then $Ib^{\#}cl(\widetilde{C}) \subseteq Ib^{\#}cl(\widetilde{D})$.

(ii) $Ib^{\#}cl(Ib^{\#}cl(\widetilde{C})) = Ib^{\#}cl(\widetilde{C})$.

(iii) $Ib^{\#}cl(\widetilde{C} \bigcup \widetilde{D}) \supseteq Ib^{\#}cl(\widetilde{C}) \bigcup Ib^{\#}cl(\widetilde{D})$.

(iv) $Ib^{\#}cl(\widetilde{C} \bigcap \widetilde{D}) \subseteq Ib^{\#}cl(\widetilde{C}) \bigcap Ib^{\#}cl(\widetilde{D})$.

(v) $Ib^{\#}cl(\widetilde{C}) \supseteq Ibcl(\widetilde{C})$.

(vi) $Ib^{\#}cl(\widetilde{C}) \supseteq Iscl(\widetilde{C}) \cap Ipcl(\widetilde{C})$.

Proof. Proof of (i), (iii), (iv) and (v) are follows from the Definition.

Now to prove (ii). By using Proposition 2.3(ii), $Ib^{\#}int(Ib^{\#}int(\widetilde{C})) = Ib^{\#}\text{-}int(\widetilde{C})$. Accepting reciprocity on both ends, we obtain $Ib^{\#}cl(Ib^{\#}cl(\widetilde{C})) = Ib^{\#}cl(\widetilde{C})$. This proves (ii).

Now to prove (vi). Since by Lemma 1.3(iii), implies that $Ibcl(\widetilde{C}) = Iscl(\widetilde{C}) \bigcap Ipcl(\widetilde{C}) \subseteq Ib^{\#}cl(\widetilde{C})$. This proves (vi)

It is possible to create examples to demonstrate that

(i) $Ib^{\#}cl(\widetilde{U}) \subseteq Ib^{\#}cl(\widetilde{V})$ does not imply $\widetilde{U} \subseteq \widetilde{V}$.

(ii) $Ib^{\#}cl(\widetilde{U} \bigcup \widetilde{V}) \neq Ib^{\#}cl(\widetilde{U}) \bigcup Ib^{\#}cl(\widetilde{V})$.

(iii) $Ib^{\#}cl(\widetilde{U} \bigcap \widetilde{V}) \neq Ib^{\#}cl(\widetilde{U}) \bigcap Ib^{\#}cl(\widetilde{V})$.

(iv) $Ib^{\#}cl(\widetilde{U}) \neq Ibcl(\widetilde{U})$.

(v) $Ib^{\#}cl(\widetilde{U}) \neq Iscl(\widetilde{U}) \bigcap Ipcl(\widetilde{U})$.

Example 3.5: Let us take the ITS in Example 2.6. Let $\widetilde{U}$ = <Y, {1}, {3,2}> and $\widetilde{V}$ = <Y, {1}, {4,3}> be the intuitionistic subsets of $(\widetilde{Y}, \tau)$. Now $Ib^{\#}cl(\widetilde{U}) = <Y, \{1\}, \{3\}>$ and $Ib^{\#}cl(\widetilde{V}) = <Y, \{1\}, \{3\}>$. This shows that $Ib^{\#}cl(\widetilde{U}) \subseteq Ib^{\#}cl(\widetilde{V})$ does not imply $\widetilde{U} \subseteq \widetilde{V}$.

Example 3.6: Let us take the ITS in Example 2.5. Let $\widetilde{C}$ = <Y, {3}, {1}> and $\widetilde{D}$ = <Y, {1}, {2}> be the intuitionistic subsets of $(\widetilde{Y}, \tau)$. $\widetilde{C} \cup \widetilde{D} = <Y, \{3,1\}, \{\phi\}>$. $Ib^{\#}cl(\widetilde{C} \cup \widetilde{D}) = \widetilde{Y}$. Now, $Ib^{\#}cl(\widetilde{C}) = <Y, \{3\}, \{2,1\}>$ *and* $Ib^{\#}cl(\widetilde{D})$ = <Y, {1},{3,2}>. $Ib^{\#}cl(\widetilde{C}) \cup Ib^{\#}int(\widetilde{D})$ = <Y, {3,1},{2}>. Therefore $Ib^{\#}cl(\widetilde{C} \cup \widetilde{D}) \neq Ib^{\#}cl(\widetilde{C}) \cup Ib^{\#}cl(\widetilde{D})$.

Example 3.7: Let us take the Example 2.4 Let $\widetilde{C}$ = <Y, {1}, {4,3}> and $\widetilde{D}$ = <Y, {2}, {4,3}> be the intuitionistic subset of $(\widetilde{Y}, \tau)$. $\widetilde{C} \bigcap \widetilde{D} = \phi$. $Ib^{\#}cl(\widetilde{C} \bigcap \widetilde{D}) = \phi$. Now, $Ib^{\#}cl(\widetilde{C}) = <Y, \{2,1\}, \{4,3\}>$ *and* $Ib^{\#}cl(\widetilde{D})$ = <Y, {2,1},{4,3}>. $Ib^{\#}cl(\widetilde{C}) \bigcap Ib^{\#}cl(\widetilde{D})$ = <Y, {2,1},{4,3}>. Therefore $Ib^{\#}cl(\widetilde{C} \bigcap \widetilde{D}) \neq Ib^{\#}cl(\widetilde{C}) \bigcap Ib^{\#}cl(\widetilde{D})$.

Example 3.8: Let us take the ITS in Example 2.6. Let $\widetilde{U}$ = <Y, {1}, {4,3,2}> be the intuitionistic subset of $(\widetilde{Y}, \tau)$. Now $Ib^{\#}cl(\widetilde{U}) = <Y, \{1\}, \{3\}>$. and $Ibcl(\widetilde{U}) = <Y, \{1\}, \{4,3,2\}>$. This shows that $Ib^{\#}cl(\widetilde{U}) \neq Ibcl(\widetilde{U})$.

Example 3.9: Let us take the ITS in Example 2.4. Let $\widetilde{U}$ = <Y, {4,3}, {2}> be the intuitionistic subset of $(\widetilde{Y}, \tau)$. $Ib^{\#}cl(\widetilde{U}) = <Y, \{2,1\}, \{4,3\}>$.

Now $Iscl(\widetilde{U}) = <Y, \{2,1\}, \{4,3\}>$ and $Ipcl(\widetilde{U}) = <Y, \{2\}, \{4,3,1\}>$.

Now $Iscl(\widetilde{U}) \cap Ipcl(\widetilde{U}) = <Y, \{2\}, \{4,3,1\}>$.

This shows that $Ib^{\#}cl(\widetilde{U}) \neq Iscl(\widetilde{U}) \cap Ipcl(\widetilde{U})$.

REFERENCES

1. Zadeh L.A, Fuzzy Sets, Inform and Control,8,(1965),338-353.
2. D.Coker, "Anoteonintuitionisticsetsandintuitionisticpoints",*TU.J.Math*.20-3(1996)343-351
3. D.Coker, (2000) "An introduction to intuitionistic topological spaces", Akdeniz Univ, Mathematics Dept. pp. 51 – 56.
4. G. Sasikala and M. Navaneetha Krishnan, "Study on Intuitionistic α-open sets and α-closed Sets" International Journal of Mathematical Archive (2017), 26-30.
5. G. Sasikala and M. Navaneetha Krishnan, "On Intuitionistic Preopen Sets", International Journal of Pure and Applied Mathematics, Vol.116, No. 24, 2017, 281-292.

6. G. Sasikala and M. Navaneetha Krishnan, "Study on Intuitionistic Semiopen Sets", IOSR Journal of Mathematics, Vol.12, No. 6, 2017, pp 79-84.
7. C. Velraj and R. Jamuna Rani, "b# - Open Sets and b# - Closed Sets in Intuitionistic Topological Spaces" ISBN:978-93-91563-72-1. Pages 168-173.
8. Gnanambal Ilango and T. A. Albinaa, "Properties of α-interior and α-closure in intuitionistic topological spaces", IOSR Journal of Mathematics. e-ISSN: 2278-5728, p-ISSN: 2319-765X. Volume 12, Issue 6 Ver. V (Nov. - Dec.2016), PP 91-95.
9. R. Usha Parameswari and P. Thangavelu, "On b # -open sets", International Journal of Mathematics Trends and Technology, 5(3) 2014, 202-218.
10. D. Andrijevic, On b-open sets, *Mat. Vesnik,*48 (1996), 59-64.

Indian Journal of Natural Sciences www.tnsroindia.org.in ©IJONS

Vol.15 / Issue 83 / Apr / 2024 *International Bimonthly (Print) – Open Access* *ISSN: 0976 – 0997*

RESEARCH ARTICLE

On the Computation of the Metric Dimension of Unit Graph

S.Nithya[1] and V.Prisci[2]

[1]Assistant Professor, St. Xavier's College (Autonomous), Palayamkottai-627002, Tamil Nadu, India.
[2]Reg.No.: 20211282092020, St. Xavier's college (Autonomous), Palayamkottai-627002.
[2]Manonmanium Sundaranar University, Abishekapatti, Tirunelveli-627012, Tamil Nadu, India.

Received: 30 Dec 2023 Revised: 09 Jan 2024 Accepted: 12 Mar 2024

***Address for Correspondence**
S.Nithya
Assistant Professor,
St. Xavier's College (Autonomous),
Palayamkottai-627002,
Tamil Nadu, India.
Email: nithyasxc@gmail.com

ABSTRACT

To determine the unit graph's metric dimension for finite commutative rings. We explore the metric dimension of the unit graph by finding the minimal cardinality of the resolving set. We examine the unit graph's metric dimension for both the product of the ring of integers modulo α, where α is prime and the ring of integers modulo n, where n is natural numbers. Finding the bare minimum of stations and pinpointing their locations will help address the navigation challenge in space stations. Here, we explore the novel notion of metric dimension in unit graph by calculating the minimum number of resolving set.

Keywords: Metric dimension, unit graph

INTRODUCTION

The unit graph $G(Z_n)$ was first introduced by R.P.Grimaldi in 1990 [1] and it was extended to $G(\mathcal{R})$ by N.Ashrafi and others [2]. Following that, a large number of mathematicians examined various aspects of unit graphs of commutative rings in terms of graph theory. Similar concepts has been studied in [3],[4]. Slater.P.J established the idea of metric dimension initially[5].In this paper, we discuss the metric dimension of the unit graph of integers modulo n and product of integers modulo α where α is prime.

METHODOLOGY

In this study, we will refer to the commutative ring with identity as $\mathcal{R}$. Consider a ring $\mathcal{R}$ with $U(\mathcal{R})$ as its set of unit elements. The graph $G(\mathcal{R})$ is said to be the *unit graph* with all the elements of $\mathcal{R}$ to be the vertices if for any two distinct vertices $s,t \in \mathcal{R}$, the vertices s and t are adjacent if and only if $s+t \in U(\mathcal{R})$. For an ordered subset $\Psi = \{\psi_1, \psi_2, \dots, \psi_k\}$ of vertices in a connected graph G and a vertex s of G, the metric representation ofs with respect to Ψ is the k-vector ordered set, $\zeta(s|\Psi) = \big(d(s,\psi_1), d(s,\psi_2), \dots, d(s,\psi_k)\big)$. The set Ψ is a resolving set for G if $\zeta(s|\Psi) = \zeta(t|\Psi)$ implies that$s = t$ for all pairs s,t of vertices of G. The minimum cardinality of the resolving set for G is represented by the metric dimension, $\beta(G)$.

RESULTS AND DISCUSSION

Theorem 3.1.*Let $\mathcal{R}$ be a ring. Then $\beta\big(G(\mathcal{R})\big) = |\mathcal{R}| - 1$ if and only if $\mathcal{R}$ is a division ring with Char $\mathcal{R} = 2$.*

*Proof :*The result follows from Theorem 3.4 of [2] and Lemma 2.2 of [6].

Theorem 3.2. *Let $\mathcal{R}$ be a ring with maximal ideal $\mathfrak{M}$ such that $\left|\frac{R}{\mathfrak{M}}\right| = 2$ or $n-1$. Then $\beta\big(G(\mathcal{R})\big) = |\mathcal{R}| - 2$ if and only if $\mathcal{R}$ is a local ring.*

Proof : The result follows from Theorem 3.5 of [2] and Corollary 2.1 of [6].

Theorem 3.3. *Let α be a prime number. If $n = 2\alpha$, then $\beta\big(G(\mathbb{Z}_n)\big) = 2$ or $n-1$.*

Proof. If $\alpha = 2$, then $\beta\big(G(\mathbb{Z}_4)\big) = 2$since $G(\mathbb{Z}_4)$ is a cycle. If $\alpha > 2$, then $G(\mathbb{Z}_{2\alpha})$ is isomorpic to a $\alpha - 1$ regular bipartite graph. Hence by Theorem 1 of [7], the result follows.

Theorem 3.4. *Let α be a prime number, then* $\beta\big(G(\mathbb{Z}_\alpha)\big) = \begin{cases} \frac{\alpha-1}{2}, & if\ \ \alpha > 2 \\ 1, & if \quad \alpha = 2 \end{cases}$.

Proof. If $\alpha = 2, \beta\big(G(\mathbb{Z}_2)\big) = 1$, since $G(\mathbb{Z}_2)$ is a path. If $\alpha > 2$, let $V_0 = \{0\}, V_j = \{j, \alpha - j\}, 1 \le j \le \frac{\alpha-1}{2}$ forms the distance similar classes. Consider $\Psi = \{j\}, 1 \le j \le \frac{\alpha-1}{2}$. Also, $0 \notin \Psi$ since $\zeta(0|\Psi) = (1,1,\dots,1)$ is a unique metric representation. Hence, by Theorem 2.1 of [6],$\beta\big(G(\mathbb{Z}_\alpha)\big) = \frac{\alpha-1}{2}$.

Theorem 3.5. *Let $\mathcal{R} \cong \mathbb{Z}_\alpha \times \mathbb{Z}_\beta$ where α and β are prime. If $\alpha = \beta, \alpha, \beta \ge 3$, then the metric dimension of the unit graph, $\beta\big(G(\mathcal{R})\big) \le \frac{3}{2}(\alpha - 1)$.*

Proof. Let us define$\Psi_1 = \{(0,1),(1,0),(\alpha-1,\alpha-1)\}, \Psi_2 = \{(2,3),(4,5),\dots,(\alpha-3,\alpha-2)\}$,
$\Psi_3 = \{(3,2),(5,4),\dots,(\alpha-2,\alpha-3)\}, \Psi_4 = \{(3,3),(5,5),\dots,(\alpha-2,\alpha-2)\}$.From the construction of the above sets, Ψ_1, Ψ_2, Ψ_3 and Ψ_4 are mutually disjoint to each other. Let $\Psi = \Psi_1 \cup \Psi_2 \cup \Psi_3 \cup \Psi_4$.

In Fig.1, for $(k,l),(m,n) \in \mathcal{R}, d\big((k,l),(m,n)\big) = \begin{cases} 2, & if\ k+m \in U(R)\ or\ l+n \in U(R) \\ 1, & otherwise \end{cases}$

The following metric representation are observed from Fig.1,

$\zeta\big((0,0)|\Psi\big) = (2,2,1,1,1,\dots,1,1,1,\dots,1,1,1,\dots 1), \zeta\big((0,2)|\Psi\big) = (2,1,1,1,1,\dots 2,1,1,\dots,1,1,1,\dots,2)$,
$\zeta\big((0,3)|\Psi\big) = (2,1,1,1,1,\dots,1,1,1,\dots,2,1,1,\dots,1), \dots, \zeta\big((0,\alpha-2)|\Psi\big) = (2,1,1,1,1,\dots,1,2,1,\dots 1,1,1,\dots 1)$,
$\zeta\big((0,\alpha-1)|\Psi\big) = (2,1,1,1,1,\dots,1,1,1,\dots,1,1,1,\dots,1), \zeta\big((1,1)|\Psi\big) = (1,1,2,1,1,\dots,1,1,1,\dots,1,1,1,\dots,1)$,
$\zeta\big((1,2)|\Psi\big) = 1,1,2,1,1,\dots,2,1,1,\dots,1,1,1,\dots 2), \dots, \zeta\big((1,\alpha-2)|\Psi\big) = (1,1,2,1,1,\dots,1,2,1,\dots 1,1,1,\dots 1)$,
$\zeta\big((1,\alpha-1)|\Psi\big) = (2,1,2,1,1,\dots,1,1,1,\dots,1,1,1,\dots,1), \zeta\big((2,0)|\Psi\big) = (1,2,1,1,1,\dots,1,1,1,\dots,2,1,1,\dots,2)$,
$\zeta\big((2,1)|\Psi\big) = (1,1,2,1,1,\dots,1,1,1,\dots,2,1,1,\dots 2), \zeta\big((2,2)|\Psi\big) = (1,1,1,1,1,\dots,2,1,1,\dots,2,1,1,\dots 2), \dots$,
$\zeta\big((2,\alpha-1)|\Psi\big) = (2,1,1,1,1,\dots,1,1,1,\dots 2,1,1,\dots 2), \zeta\big((\alpha-1,0)|\Psi\big) = (1,2,1,1,1,\dots,1,1,1,\dots,1,1,1,\dots,1)$,
$\zeta\big((\alpha-1,1)|\Psi\big) = (1,2,2,1,1,\dots,1,1,1,\dots,1,1,1,\dots,1)$,
$\zeta\big((\alpha-1,2)|\Psi\big) = (1,2,1,1,1,\dots,2,1,1,\dots,1,1,1,\dots 2), \dots$,
$\zeta\big((\alpha-1,\alpha-2)|\Psi\big) = (1,2,1,1,1,\dots,1,2,1,\dots,1,1,1,\dots 1)$.

By the definition, we have attained unique metric representations for the elements of $G(\mathbb{Z}_\alpha \times \mathbb{Z}_\alpha)$ Therefore, $\Psi$is a resolving set and $|\Psi| \le 3 + \alpha - 3 + \frac{\alpha-3}{2} = \frac{3}{2}(\alpha - 1)$.

Theorem 3.6. Let $\mathcal{R} \cong Z_\alpha \times Z_\beta$ where α and β are prime with $\alpha < \beta, \alpha = 3$, then $\beta\big(G(\mathcal{R})\big) \le \beta - 1$.

Proof. Let $\Psi = \{(1,1),(2,2),(1,3),(2,4),(1,5),(2,6),\dots,(1,\beta-2),(2,\beta-1)\}$.

In Fig.2, for any $(k,l),(m,n) \in \mathcal{R}, d\big((k,l),(m,n)\big) = \begin{cases} 2, & if\ k+m\ \in U(\mathcal{R})\ or\ l+n\ \in U(\mathcal{R}) \\ 1, & otherwise \end{cases}$

The following metric representations are observed from Fig.2,

$\zeta((0,0)|\Psi) = (1,1,1,1,1,1,\ldots,1,1)$, $\zeta((0,1)|\Psi) = (1,1,1,1,1,1,\ldots,1,2)$,

$\zeta((0,2)|\Psi) = (1,1,1,1,1,1,\ldots,2,1)$, …, $\zeta((0,-1)|\Psi) = (2,1,1,1,1,1,\ldots,1,1)$,

$\zeta((1,0)|\Psi) = (1,2,1,2,1,2,\ldots,1,2)$, $\zeta((1,2)|\Psi) = (1,2,1,2,1,2,\ldots,2,2)$, …,

$\zeta((1,-1)|\Psi) = (2,2,1,2,1,2,\ldots,1,2)$, $\zeta((2,0)|\Psi) = (2,1,2,1,2,\ldots,1,2,1)$

$\zeta((2,1)|\Psi) = (2,1,2,1,2,\ldots,1,2,2)$, …, $\zeta((2,-2)|\Psi) = (2,2,2,1,2,\ldots,1,2,1)$

By the definition, we have attained unique metric representations for the elements of $(\mathbb{Z}_3 \times \mathbb{Z})$. Therefore, Ψ is a resolving set and $|\Psi| \leq -1$.

Theorem 3.7. *Let* $\mathcal{R} \cong \mathbb{Z} \times \mathbb{Z}$ *where and are prime with* $<, > 3, \geq 2-3$, *then* $(()) \leq$.

Proof. Let us denote $\mathbb{Z}' = \mathbb{Z}\backslash\{0,1,-1\} = \{_{0,1},\ldots,_{-4}\}, \mathbb{Z}' = \mathbb{Z}\backslash\{0,1,-1\} = \{_{0,1},\ldots,_{-4}\}$. Now define $\Psi_1 = \{(0,1),(1,0),(-1,-1)\}, \Psi_2 = \{_{0,1},\ldots,_{-4}\}$ where $= (_{(-3)},), 0 \leq \leq -4$. From the Construction of the above sets, Ψ_1 and Ψ_2 are mutually disjoint to each other. Let $\Psi = \Psi_1 \cup \Psi_2$. The elements of $\mathcal{R}\backslash\Psi = \cup\mathcal{B}$ can be written as follows.Let $= \{(0,0),(1,1),(0,-1),(-1,0),(1,-1),(-1,1),(,0),(0,),(,1),(1,),(,-1),(-1,)\}$ where $0 \leq \leq -4, 0 \leq \leq -4$ and $\mathcal{B} = \{(_{(-3)},)\}$where $0 \leq , t \leq \beta - 4, s \neq t$. We now prove that Ψ is a resolving set for $G(\mathcal{R})$.

$d((0,0),(\alpha-1,\beta-1)) = 1, d((1,1),(\alpha-1,\beta-1)) = 2 \Rightarrow \zeta((0,0)|\Psi) \neq \zeta((1,1)|\Psi)$.

$d((0,\beta-1),(0,1)) = 2, d((\alpha-1,0),(0,1)) = 1 \Rightarrow \zeta((0,\beta-1)|\Psi) \neq \zeta((\alpha-1,0)|\Psi)$.

$d((1,\beta-1),(0,1)) = 2, d((\alpha-1,1),(0,1)) = 1 \Rightarrow \zeta((1,\beta-1)|\Psi) \neq \zeta((\alpha-1,1)|\Psi)$.

$d((0,\beta-1),(\alpha-1,\beta-1)) = 1, d((1,\beta-1),(\alpha-1,\beta-1)) = 2 \Rightarrow \zeta((0,\beta-1)|\Psi) \neq \zeta((1,\beta-1)|\Psi)$.

Similarly, $\zeta((0,\beta-1)|\Psi) \neq \zeta((\alpha-1,1)|\Psi), \zeta((\alpha-1,0)|\Psi) \neq \zeta((1,\beta-1)|\Psi)$,

$\zeta((\alpha-1,0)|\Psi) \neq \zeta((\alpha-1,1)|\Psi)$.

$d((0,0),(1,0)) = 2, d((0,\beta-1),(1,0)) = 1 \Rightarrow \zeta((0,0)|\Psi) \neq \zeta((0,\beta-1)|\Psi)$.

Similarly, $\zeta((0,0)|\Psi) \neq \zeta((\alpha-1,0)|\Psi)$.

$d((0,0),(\alpha-1,\beta-1)) = 1, d((1,\beta-1),(\alpha-1,\beta-1)) = 2 \Rightarrow \zeta((0,0)|\Psi) \neq \zeta((1,\beta-1)|\Psi)$.

Similarly, $\zeta((0,0)|\Psi) \neq \zeta((\alpha-1,1)|\Psi)$.

$d((1,1),(\alpha-1,\beta-1)) = 2, d((0,\beta-1),(\alpha-1,\beta-1)) = 1 \Rightarrow \zeta((1,1)|\Psi) \neq \zeta((0,\beta-1)|\Psi)$.

Similarly, $\zeta((1,1)|\Psi) \neq \zeta((\alpha-1,0)|\Psi)$.

$d((1,1),(0,1)) = 1, d((1,\beta-1),(0,1)) = 2 \Rightarrow \zeta((1,1)|\Psi) \neq \zeta((1,\beta-1)|\Psi)$.

Similarly, $\zeta((1,1)|\Psi) \neq \zeta((\alpha-1,1)|\Psi)$.

$\forall(a_i,0) \in \mathcal{R}\backslash\Psi$ and for any $b_j \in \mathbb{Z}_\beta$ there exists $(a_{\alpha-(i+\alpha-3)}, b_j) \in \Psi$ such that $d\left((a_i,0),(a_{\alpha-(i+\alpha-3)},b_j)\right) = 2 \Rightarrow \zeta((a_i,0)|\Psi) \neq \zeta((a_l,0|\Psi)), 0 \leq l \leq \alpha - 4$.

$\forall(0,b_j) \in \mathcal{R}\backslash\Psi$ and for any $a_i \in \mathbb{Z}_\alpha$ there exists $(a_i, b_{\beta-(j+\alpha-3)}) \in \Psi$ such that

$d\left((0,b_j),(a_i,b_{\beta-(j+\alpha-3)})\right) = 2 \Rightarrow \zeta\left((0,b_j)\middle|\Psi\right) \neq \zeta((0,b_m)|\Psi), 0 \leq m \leq \beta - 4$,

$\zeta\left((0,b_j)\middle|\Psi\right) \neq \zeta((a_i,0)|\Psi), \zeta\left((1,b_j)\middle|\Psi\right) \neq \zeta((1,a_m)|\Psi), 0 \leq m \leq \beta - 4$,

$\zeta((a_i,1)|\Psi) \neq \zeta((a_l,1)|\Psi), 0 \leq l \leq \alpha - 4, \zeta\left((1,b_j)\middle|\Psi\right) \neq \zeta((a_i,1)|\Psi)$.

$d((a_i,0),(\alpha-1,\beta-1)) = 1, d((a_i,1),(\alpha-1,\beta-1)) = 2 \Rightarrow \zeta((a_i,0)|\Psi) \neq \zeta((a_i,1)|\Psi)$.

Similarly, $\zeta\left((0,b_j)\middle|\Psi\right) \neq \zeta\left((1,b_j)\middle|\Psi\right), \zeta((a_i,0)|\Psi) \neq \zeta\left((1,b_j)\middle|\Psi\right), \zeta\left((0,b_j)\middle|\Psi\right) \neq \zeta((a_i,1)|\Psi)$.

$d\left((a_i,0),(a_{\alpha-(i+\alpha-3)},b_j)\right) = 2, d\left((0,0),(a_{\alpha-(i+\alpha-3)},b_j)\right) = 1 \Rightarrow \zeta((0,0)|\Psi) \neq \zeta((a_i,0|\Psi))$.

Similarly, $\zeta((0,0)|\Psi) \neq \zeta\left((0,b_j)\middle|\Psi\right), \zeta((0,0)|\Psi) \neq \zeta((a_i,1)|\Psi), \zeta((0,0)|\Psi) \neq \zeta\left((1,b_j)\middle|\Psi\right)$.

$d\left((a_i,0),(a_{\alpha-(i+\alpha-3)},b_j)\right) = 2, d\left((1,1),(a_{\alpha-(i+\alpha-3)},b_j)\right) = 1 \Rightarrow \zeta((a_i,0)|\Psi) \neq \zeta((1,1)|\Psi)$.

Similarly, $\zeta\left((0,b_j)\middle|\Psi\right) \neq \zeta((1,1)|\Psi), \zeta\left((1,b_j)\middle|\Psi\right) \neq \zeta((1,1)|\Psi), \zeta((a_i,1)|\Psi) \neq \zeta((1,1)|\Psi)$.

$d\left((a_i,0),(a_{\alpha-(i+\alpha-3)},b_j)\right)=2, d\left((\alpha-1,0),(a_{\alpha-(i+\alpha-3)},b_j)\right)=1 \Rightarrow \zeta((a_i,0)|\Psi) \neq \zeta((\alpha-1,0|\Psi))$.Similarly, $\zeta((a_i,0)|\Psi) \neq \zeta((\alpha-1,1)|\Psi)$.

$d((a_i,0),(0,1))=1, d((0,\beta-1),(0,1))=2 \Rightarrow \zeta((a_i,0)|\Psi) \neq \zeta((0,\beta-1)|\Psi)$.

Similarly, $\zeta((a_i,0)|\Psi) \neq \zeta((1,\beta-1)|\Psi), \zeta\left((0,b_j)\middle|\Psi\right) \neq \zeta((\alpha-1,0)|\Psi)$,

$\zeta\left((0,b_j)\middle|\Psi\right) \neq \zeta((\alpha-1,1)|\Psi), \zeta\left((0,b_j)\middle|\Psi\right) \neq \zeta((0,\beta-1)|\Psi), \zeta\left((0,b_j)\middle|\Psi\right) \neq \zeta((1,\beta-1)|\Psi)$.

$d\left((a_i,1),(a_{\alpha-(i+\alpha-3)},b_j)\right)=2, d\left((\alpha-1,0),(a_{\alpha-(i+\alpha-3)},b_j)\right)=1 \Rightarrow \zeta((a_i,1)|\Psi) \neq \zeta((\alpha-1,0|\Psi))$.

Similarly, $\zeta((a_i,1)|\Psi) \neq \zeta((\alpha-1,1)|\Psi), \zeta((a_i,1)|\Psi) \neq \zeta((0,\beta-1)|\Psi)$,

$\zeta((a_i,1)|\Psi) \neq \zeta((1,\beta-1)|\Psi), \zeta\left((1,b_j)\middle|\Psi\right) \neq \zeta((\alpha-1,0)|\Psi), \zeta\left((1,b_j)\middle|\Psi\right) \neq \zeta((\alpha-1,1)|\Psi)$,

$\zeta\left((1,b_j)\middle|\Psi\right) \neq \zeta((0,\beta-1)|\Psi), \zeta\left((1,b_j)\middle|\Psi\right) \neq \zeta((1,\beta-1)|\Psi)$.

$\forall (a_i,\beta-1) \in \mathcal{R}\backslash\Psi$ and for any $b_j \in \mathbb{Z}_\beta$ there exists $(a_{\alpha-(i+\alpha-3)},b_j) \in \Psi$ such that $d\left((a_i,\beta-1),(a_{\alpha-(i+\alpha-3)},b_j)\right)=2 \Rightarrow \zeta((a_i,\beta-1)|\Psi) \neq \zeta((a_l,\beta-1)|\Psi), 0 \leq l \leq \alpha-4$.

Similarly, $\zeta\left((\alpha-1,b_j)\middle|\Psi\right) \neq \zeta((\alpha-1,b_m)|\Psi), 0 \leq m \leq \beta-4$.

$d\left((a_i,\beta-1),(a_{\alpha-(i+\alpha-3)},b_j)\right)=2, d\left((\alpha-1,a_i),(a_{\alpha-(i+\alpha-3)},b_j)\right)=1 \Rightarrow \zeta((a_i,\beta-1)|\Psi) \neq \zeta\left((\alpha-1,b_j)\middle|\Psi\right)$.

Similarly, $\zeta((a_i,\beta-1)|\Psi) \neq \zeta((0,0)|\Psi), \zeta\left((\alpha-1,b_j)\middle|\Psi\right) \neq \zeta((0,0)|\Psi), \zeta((a_i,\beta-1)|\Psi) \neq \zeta((1,1)|\Psi), \zeta\left((\alpha-1,b_j)\middle|\Psi\right) \neq \zeta((1,1)|\Psi), \zeta((a_i,\beta-1)|\Psi) \neq \zeta((0,\beta-1)|\Psi), \zeta\left((\alpha-1,b_j)\middle|\Psi\right) \neq \zeta((0,\beta-1)|\Psi), \zeta((a_i,\beta-1)|\Psi) \neq \zeta((\alpha-1,0)|\Psi), \zeta\left((\alpha-1,b_j)\middle|\Psi\right) \neq \zeta((\alpha-1,0)|\Psi), \zeta((a_i,\beta-1)|\Psi) \neq \zeta((1,\beta-1)|\Psi), \zeta\left((\alpha-1,b_j)\middle|\Psi\right) \neq \zeta((1,\beta-1)|\Psi), \zeta((a_i,\beta-1)|\Psi) \neq \zeta((\alpha-1,1)|\Psi), \zeta\left((\alpha-1,b_j)\middle|\Psi\right) \neq \zeta((\alpha-1,1)|\Psi), \zeta((a_i,\alpha-1)|\Psi) \neq \zeta((a_i,0)|\Psi), \zeta((\alpha-1,a_i)|\Psi) \neq \zeta((a_i,0)|\Psi), \zeta((a_i,\alpha-1)|\Psi) \neq \zeta((a_i,1)|\Psi), \zeta((\alpha-1,a_i)|\Psi) \neq \zeta((a_i,1)|\Psi)$,
$\zeta((a_i,\alpha-1)|\Psi) \neq \zeta((0,a_i)|\Psi), \zeta((\alpha-1,a_i)|\Psi) \neq \zeta((0,a_i)|\Psi), \zeta((a_i,\alpha-1)|\Psi) \neq \zeta((1,a_i)|\Psi)$,
$\zeta((\alpha-1,a_i)|\Psi) \neq \zeta((1,a_i)|\Psi)$.

For any $a \in \mathbb{Z}_\alpha, d\left((a_i,b_j),(a,b_{\beta-(j+\alpha-3)})\right)=2 \Rightarrow \zeta\left((a_i,b_j)\middle|\Psi\right) \neq \zeta((a_l,b_m)|\Psi)$where $0 \leq l \leq \alpha-4, 0 \leq m \leq \beta-4$.

Similarly, $\zeta\left((a_i,b_j)\middle|\Psi\right) \neq \zeta((0,0)|\Psi), \zeta\left((a_i,b_j)\middle|\Psi\right) \neq \zeta((1,1)|\Psi), \zeta\left((a_i,b_j)\middle|\Psi\right) \neq \zeta((0,\beta-1)|\Psi)$,
$\zeta\left((a_i,b_j)\middle|\Psi\right) \neq \zeta((\alpha-1,0)|\Psi), \zeta\left((a_i,b_j)\middle|\Psi\right) \neq \zeta((1,\beta-1)|\Psi), \zeta\left((a_i,b_j)\middle|\Psi\right) \neq \zeta((\alpha-1,1)|\Psi)$.

$d\left((a_i,b_j),(1,0)\right)=1, d((a_i,0),(1,0))=2 \Rightarrow \zeta\left((a_i,b_j)\middle|\Psi\right) \neq \zeta((a_i,0)|\Psi)$.

$d\left((a_i,b_j),(0,1)\right)=1, d\left((0,b_j),(0,1)\right)=2 \Rightarrow \zeta\left((a_i,b_j)\middle|\Psi\right) \neq \zeta\left((0,b_j)\middle|\Psi\right)$.

$d\left((a_i,b_j),(\alpha-1,\beta-1)\right)=1, d((a_i,1),(\alpha-1,\beta-1))=2 \Rightarrow \zeta\left((a_i,b_j)\middle|\Psi\right) \neq \zeta((a_i,1)|\Psi)$.

$d\left((a_i,b_j),(\alpha-1,\beta-1)\right)=1, d\left((1,b_j),(\alpha-1,\beta-1)\right)=2 \Rightarrow \zeta\left((a_i,b_j)\middle|\Psi\right) \neq \zeta\left((1,b_j)\middle|\Psi\right)$.

$d\left((a_i,b_j),(0,1)\right)=1, d((a_i,q-1),(0,1))=2 \Rightarrow \zeta\left((a_i,b_j)\middle|\Psi\right) \neq \zeta((a_i,q-1)|\Psi)$.

$d\left((a_i,b_j),(1,0)\right)=1, d\left((\alpha-1,b_j),(1,0)\right)=2 \Rightarrow \zeta\left((a_i,b_j)\middle|\Psi\right) \neq \zeta\left((\alpha-1,b_j)\middle|\Psi\right)$.

Hence Ψ is a resolving set for $G(\mathcal{R})$.

We now prove that removal of any element from Ψ does not result in resolving set.If $\Psi'=\Psi\backslash(0,1)$, then $\zeta((0,0)|\Psi)=\zeta((\alpha-1,0)|\Psi)$.Similarly, if $\Psi'=\Psi\backslash(1,0)$, then $\zeta((0,0)|\Psi)=\zeta((0,\beta-1)|\Psi)$.If $\Psi'=\Psi\backslash(\alpha-1,\beta-1)$, then $\zeta((0,\beta-1)|\Psi)=\zeta((1,\beta-1)|\Psi)$.If $\Psi'=\Psi\backslash(a_{k \bmod (\alpha-3)},b_k)$ then $\zeta((0,\beta-b_k)|\Psi)=\zeta((0,\beta-1)|\Psi)$ where $0 \leq k \leq \beta-4$.Therefore, Ψ is a resolving set and $|\Psi| \leq \beta$.

CONCLUSION

For over a decade, there has been considerable research on the metric dimension of graphs. Metric dimension of zero divisor graph, total graph and other such graphs have been computed already. In this work, the metric dimension of unit graph is computed while the metric dimension of other algebraic graphs are up for research.

REFERENCES

1. Grimaldi R P. Graphs from rings, in Proceedings of the 20th Southeastern Conference on Combinatorics. Graph Theory and Computing (Boca Raton, FL, 1989), *Congress Proc*. 71, 95–103 (1990).
2. Ashrafi N,Maimani H R, Pournaki M R,Yassemi S. Unit graphs associated with rings.*Communications in Algebra*. 38(8) (2010), 2851-2871. Available from: https://doi.org/10.1080/00927870903095574
3. Nithya S, Elavarasi G. Extended annihilating-ideal graph of a commutative ring. *DiscussionesMathematicae-General Algebra and Applications*. 42(2), 279-291.Available from: https://doi.org/10.7151/dmgaa.1390
4. Nithya S, Elavarasi G.Partition and local metric dimension of an extended annihilating-ideal graph. *Palestine Journal of Mathematics*, 11(2022).
5. Slater P J, Leaves of trees, Congress. Number. 14(1975), 549-559.
6. Pirzada S,Raja R, Redmond S P. Locating sets and numbers of graphs associated to commutative rings. Journal of Algebra and its Applications. 13(7) (2014), 1450047, 18pp. Available from :https://doi.org/10.1142/S0219498814500479
7. Saputro S W, Baskoro E T, Salman A N M, Suprijanto D, Baˇca M. The metric dimension of regular bipartite graphs.*Bulletin Mathématique de La Société Des Sciences Mathématiques de Roumanie*. 54(102) (2011), 15-28. Available from: https://www.jstor.org/stable/43679200.

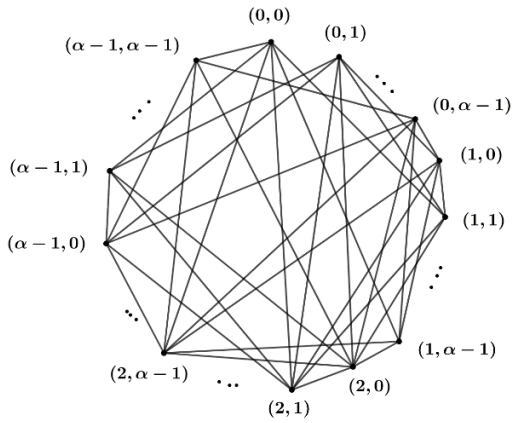

Figure 1: $G(\mathbb{Z}_\alpha \times \mathbb{Z}_\alpha)$

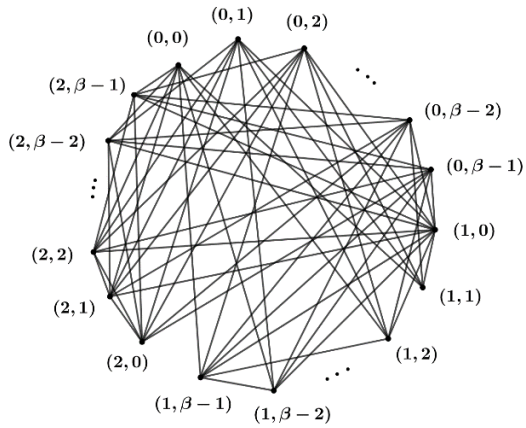

Figure 2: $G(\mathbb{Z}_3 \times \mathbb{Z}_\beta)$

Indian Journal of Natural Sciences *www.tnsroindia.org.in ©IJONS*

Vol.15 / Issue 83 / Apr / 2024 *International Bimonthly (Print) – Open Access* *ISSN: 0976 – 0997*

RESEARCH ARTICLE

Predictive Modeling for Breast Cancer Detection: A Logistic Regression Approach

Imran Qureshi

College of Computing and Information Sciences, UTAS, Al Musanna Sultanate of Oman

Received: 30 Dec 2023 Revised: 09 Jan 2024 Accepted: 12 Mar 2024

***Address for Correspondence**
Imran Qureshi
College of Computing and Information Sciences,
UTAS, Al Musanna Sultanate of Oman
Email: imranqureshi1210@gmail.com

ABSTRACT

A pestilence disease that kills people in large numbers annually is breast cancer. On a global scale, it ranks as the leading cancer killer of females. When it comes to health-related information classification, ML approaches are the way to go. Classification and analysis make heavy use of it to help in the decision-making process. As in this study, analysis of logistical regression is one of the many ML classification models used to analyses the WBCD… The study aims to determine how good the classifiers performed in classification of the datasets. To achieve this, we used all the features in our dataset through the RFE approach. To evaluate the replica's efficiency, k-fold cross validation metric was used. All experiments were conducted using Anaconda Jupiter notebooks in Python language. Empirical analysis shows that the logistic regression model has a very high prediction accuracy of 96.7 percent for tumor benign or malignant in breast cancer Wisconsin.

Keywords: Breast Cancer; WBCD; classifiers, Logistic regression

INTRODUCTION

Cancer is a spectrum of illnesses signified by clonal expansion of rogue cells that can arise from any organ or tissue in the body [1]. In 2018, the disease was responsible for about 9.6 million deaths. This disease is characterized by its heterogeneity and can be classified into various unique forms. Breast cancer, a form of cancer, is the second most mutual malignancy in females, following carcinoma of the lung [2]. Finding out how well and efficiently the classifiers classified the dataset is the main goal of this investigation. We used the Recursive Feature Elimination method to select all of the dataset's characteristics for achieving this goal. We measured the model's efficacy using the K-fold cross-validation metric. We executed every single investigation in the Anaconda environment using Jupiter Notebooks and the Python computer programming language. In 2018, Nigeria recorded a total of 115,000 ongoing cancer cases, which led to over 70,000 fatalities attributed to the illness. In addition, breast cancer accounted

for 22.7% of all cases, with a mortality rate of 16.4%. The breast cancer trend chart projected a significant rise in reported cases, estimating that by the year 2040, the number of active cases will nearly double from 26,310 in 2018 to around 50,921 [1]. Figure 1 illustrates a visual representation of breast cancer tumor sizes, with T1 representing tumors that are 2cm or smaller, and T4 representing tumors that have grown into the chest wall regardless of their size. Early identification of cancer increases the likelihood of effective therapy by 30%, whereas late discovery complicates the remedy process [4,5]. Medical practitioners apply many ways to detect preliminary carcinoma of the breast, involving surgical biopsy, which is approximately 100% accurate. [4], The Fine Needle Aspiration procedure involves visually interpreting the results, which have an accuracy rate ranging from 65% to 98% [6], and mammography with 63% to 97% accuracy [7]. Although it's expensive, the first method is the most dependable. The WBCD dataset will be evaluated in this study using ensemble ML classifiers based on FNA.

A form of AI called machine learning trains computers to acquire new skills by feeding them examples of information from actual real-world problems [8]. In recent decades, ML has been widely adopted to develop prediction models that allow better decision-making across different areas. This approach may be advantageous for the realm of cancer research due to which it can detect deviating patterns in datasets and utilize such unusual patterns in forecasts. To date, several papers have focused on enhancing computational analysis of FNA specimens over the last two decades [9]. To assess the WBCD dataset, this study employs a pair of ensemble machine learning classifiers: XG Boost and RF. In section 2, there is a summary of relevant studies. Section 3 provides an in-depth analysis of the cancer dataset utilized for the try out. The experimental procedure and the ideas of two ensemble machine learning classifiers that were studied are described in detail: section 4. In Section 5, the results and discussion of the experiment are given. This work contains sections 6 and, both of which offer advice, as well as a conclusion.

Related Work

Perhaps the most widely known application of machine learning is classification task. For example, many studies apply machine learning classifiers on various medical data sets such as WBCD dataset. Numerous studies have shown that the classifiers employed in those studies gave high classification accuracies. As one of the studies by Salama *et al*., their work was done under "Breast Cancer Diagnosis on Three Different Datasets Using Multi-Classifiers" using WEKA data mining system [10]. This study employed the WBCD dataset, one of the breast cancer data sets. Five types of AI classifications were used to do a binary classification job on the datasets: These are NB, MLP, J48 SMO and IBK. According to the results of these WBCD experiments, SMO classifier showed better performances with a mean classification accuracy of 94.5637 % and max value: 96.9957% as compared to IBK classification scheme Therefore, it was not difficult to yield an accuracy rate of 97.568 using J48 and M [11] have analyzed feature selection for breast cancer data from three separate datasets. In the study, binary classification was used when the CART classifier was adopted. That is, experiments showed nearly 94.84% classification rate for this classifier when it was used on WBCD without feature reduction. Lastly, after trying a variety of feature selection methods on the dataset, CART with exhaustive elimination produced a high accuracy. But the combination of these six descriptors results in 95.13% precision level. A set of machine learning classifiers such s Simple Logistic, RepTree and RBF Network were tested in [12]. The sample for this study was drawn from the Institute of Oncology, University Medical Center Ljubljana in Yugoslavia. The dataset has 286 rows and ten features. From the results of an experimental study, it is observable that Simple Logistic classifier yields better results in a binomial classification test with an accuracy percentage of 74.5%. Asri *et al*. [13] applied varied machine-learning algorithms in detecting and diagnosis of cancer risk for breast cancer. Performance evaluation was performed by comparing the performance of SVM, C4.5, NB and kNN algorithms with WBCD dataset for classification of cancer data correctly. The findings of the experimental results indicated highest level accuracy for SVMs had a nine percent error score rating as lowest. The research used the WEKA data mining tool. Therefore, I performed a review to assess and compare the power of machine learning algorithms used in breast cancer diagnosis. Three machine learning approaches utilised the analytical component of the study included support vector machines , random forests and Bayesian networks . For this experiment, the algorithms' performance was evaluated using WBCD dataset. The study used the WEKA data mining tool for simulation which indicated an accuracy rate of 97%. Second, the selected method may have a

substantial effect on the outcome of categorization. Support Vector Machine (SVM) can be compared to the sensitivity, detail and accuracy. Although, random forest had the highest likelihood of classification on breast cancer data. Ivančáková *et al*. [15] conducted a comparison of diverse machine learning methods using the Wisconsin Dataset. The dataset used had 569 unique records with 32 attributes. Six machine learning classifiers were used to simulate the study experiment. The dataset was partitioned into three different ratios (60:For the purposes of assessing, 40%, 70:30 and 80:20 were selected. I did some research to assess and compare the competencies of machine learning algorithms in detecting and identifying breast cancer. The study presented three machine learning methods: SVM, RF, and BN. The experiment confirmed the efficiency of the algorithm applied by using WBCD database. As for the WEKA data mining tool that was applied by the study, the accuracy of 97% as a result in testing phase. Moreover, the chosen method can have significant influence on the classification result. As for reliability, sensitivity and precision, SVM has performed better. On the other hand, random forests had the biggest likelihood of correctly classifying the breast cancer dataset. As the utilization of data mining methods, a model was constructed from breast cancer data by Shajahaan *et al*. [16]. The WBCD data set was also used to try various machine learning classifiers such as RF, CART, C4.5, ID3 and NB. In addition, the processes of simulated data were carried out with TANGARA and WEKA programs associated with data mining. The highest accuracy was demonstrated by the NB classifier with 97.42% obtained from experiment results, which is relatively perfect in this study. The work Amrane *et al*. [17] runs kNN and NB as two ML classifiers aimed at the classification of breast cancer. WBCD data were used to assess the accuracy of classifiers. In simulation results, the KNN classifier obviously outperforms all others with an accuracy of 97.51% as compared to 96.19%. In terms of the total running time, the NB classifier was quicker in comparison with kNN model. In their paper, Bayrak *et al*. [18] examined the performance of two machine learning algorithms – Artificial Neural Network and Support Vector Machine (SVM), used in breast cancer diagnosis. Based on the WBCD dataset, strategy effectiveness was evaluated using WEKA data mining tool in the experiment. In case the sequential minimal optimization algorithm is implemented for the dataset to be diagnosed and predicted, its parameters are optimal with 96.9957% accuracy. Ahmad *et al*. [19] use three ML algorithms (C4.5, ANN, and SVM) to model breast cancer onset predictors. An Iranian ICBC dataset was used in this analysis. The dataset has 1,189 cases, with 22 predictors and one dependent variable. When the records went missing, 547 were left in the list after pre-processing. On the accuracy point of view, SVM classifier performed better (95.7%) compare to C4.5's 93.6% and ANN had 94.7%. We performed all experiments using the only WEKA data mining tools. Lastly, with a view to discriminate and diagnose the levels of risk for breast cancer through machine learning algorithms, Showrov *et al*. [20 took several approaches such as C4.5, ANN and SVM that were used in order to predict if a patient will develop or not breast cancer. This study used a data set from the ICBC in Iran. Overall, the dataset had 1,189 total observations; of these there were 22 predictors and one was an outcome variable. At the conclusion of the pre-treatment stage, only 547 records were left due to missing data regarding the issues that disrupted a total number of 642 entries. In contrast to the C4.5 and ANN algorithms, our SVM algorithm yielded a better performance score of 95.7 compared to 93.6% while using binary tasks with two classifiers namely Naive Bayes and k-Nearest Neighbours. This performance from the experiment showed that kNN classifier accuracy was on 97.51% and NB got a high rating of 96.19%. On the contrary, scientists also revealed that while kNN was more accurate, its compute time would rise if there were a larger set of data in the experiment. The accuracy of C4.5 classifier in classification was measured by Sarkar and Nag [22] using the WBCD dataset. The classifier was used to solve a binary classification problem. For the classifier, experimental results were 96.71% accuracy. Java 7 programming language was used for the studies. Using C4.5 decision tree-based categorization systems, the study's authors found that their performance improved early stage detection in individuals with risk factors for breast cancer. This might also possibly save thousands of lives annually. Houfani and his colleagues did a study titled "Breast cancer classification using machine learning techniques: a comparative work [23], based on the WBCD database. The datasets were binary-classified using seven different artificial intelligence classifiers: SVM, RF, DT, MLP, LR, NB and kNN. According to the results of the experiment, classification accuracy varied from 95% for NB to 97.9% for MLP and LR classifiers. Among the classifiers tested, MLP and LR performed well. Two ensemble classifiers that are used in this study are RF and EGB. For the classifier's performance evaluation, we adopted RFE technique to reduce features in the dataset. There are two key areas where machine learning algorithms learn: supervised learning and unsupervised learning. In this case,

the issue is supervised learning that requires a dataset of labeled data examples in order to train the system so as it produces correct outcomes (classification). In this study we selected supervised learning classifiers.

MATERIALS AND METHODS

There are 699 occurrences in the breast cancer Wisconsin dataset, as stated in the publication. Ten characteristics make up the breast cancer dataset in Wisconsin. Among the characteristics included in the Wisconsin breast cancer dataset are the following: sample code number, lump thickness, cell size uniformity, cell shape consistency, and marginal adhesion. Dimensions of a single epithelial cell, Standard nucleoli, nuclei without chromatin, Mitoses
Table 1: Summary of the Dataset

METHODOLOGY

The suggested research approach consists of the following procedures: The breast cancer dataset from Wisconsin was obtained by gathering information using the UCI machine learning repository. [24]. Information preprocessing is used to handle missing values and prepare the dataset for logistical regression model training. The modeling process uses Python for logistic regression. Separating the dataset into a training set and a test s*et al*lows one to train a logistic regression model on the former and then assess its efficacy on the latter. K-fold cross-validation provides a more robust metric for evaluating the model's correctness and effectiveness on fresh data. Logistic regression, a statistical tool, aids in binary classification by estimating the likelihood of a binary result. Logistic regression allows one to make certain conclusions about the type of tumor, benign or malignant, from the Wisconsin data set on breast cancer provided some conditions are met. The logistic regression model is a derivation of the logistic function or the sigmoid function that indicates how input features correspond to the probability of binary outcome. The estimated probability must lie within the bounds of 0 and 1 for the logistic function to be valid. The model generates the log odds of the binary result by using coefficients to represent input variables. The model estimates the propensity towards binary result with logistic function based on log-odds. Logistic regression is often employed for training a model on labeled data, assessing the quality of the model and then using it to make forecasts on new instances. It is possible to assess the performance of a model using different measures such as accuracy, precision, recall and area under the ROC curve. But logistic regression is a great option when you need to figure out the relationship between input data and binary output, for it produces clear results that are popular in binary classification projects. As its mathematical representation, logistic regression makes use of the logistic function, which is

P(Y=1|X) = \frac{1}{1 + e^{-(\beta_0 + \beta_1X_1 + \beta_2X_2 + ... + \beta_pX_p)}} (1)

Where

P(Y=1|X)) is the probability of the binary outcome being 1 given the input features X.

e is the base of the natural logarithm.

\beta_0, \beta_1, \beta_2, ..., \beta_p are the coefficients estimated by the model.

X_1, X_2, ..., X_p are the input features.

A logistic function can be used for binary classification because it guarantees that the predicted probabilities range from 0 to 1. Given that logistic regression uses coefficients (\beta_0, \beta_1, \beta_2,... ,\beta_p) to depict the influence of input features on the estimated binary outcome rate.

Data Preprocessing

We used Jupyter Notebook, an integrated development environment (IDE) for Python, to generate the classifiers. We chose this option because Python is a robust programming platform that has been regularly used in previous studies of this kind.. Python offers numerous built-in libraries that are commonly utilised during the dataset pre-processing stage. The initial step undertaken was the importation of the dataset into the graphical user interface (GUI) in order to comprehend and visually represent the dataset. The results showed that 16 cancer reports had missing or partial information; thus, they were removed. The experiment utilized the remaining 683 data points. More so, the sample code number element was eliminated as it contains the patient's identifying number, which is superfluous for

classification. In addition, there are two parts to the experiment; the first part makes use of every characteristic in the dataset. Step two included applying Recursive Feature Elimination (RFE) to the dataset in order to reduce the number of features. The feature selection approach determined that five features were the best fit for the categorization problem. Among these traits are mitoses, normal nucleoli, uniform cell size and shape, and bland chromatin. In addition, we used the min-max normalization approach to rescale the features to values between 0 and 1, which helped reduce the dataset's intrinsic skewness. The following formula describes it [24].

Y=x-minimum(x)/max(x)-min(x) (2)

Classifier Evaluation

For the evaluation of this logistic regression model, we used a technique termed K-fold cross validation. To assess the logistic regression model, we used K-fold cross-validation. Likewise, a confusion matrix was adopted to assess the precision of correct and wrong guesses on test set. With these assessment frameworks, we evaluated the model generalizability outside of training information and its performance on novel observations. It has good accuracy to the extent that a logistic regression model can predict benign or malignant tumors in breast cancer Wisconsin dataset approximately up to 96.7%. The k-fold cross validation metric used to evaluate the proposed model was deemed to be a more reliable measure of accuracy, and the results therefore indicate that its variance in performance was moderate across different test folds. Physicians and organizations could evaluate whether the logistic regression model is of practical utility in predicting outcomes for women with breast cancer. These conclusions suggest that the logistic regression model has implementation capacity into forecasting tumor characteristics on which health care and medical decision-making can be built. Our model on the logistic regression model demonstrates a high level of accuracy, approximately 96.7%, in predicting benign or malignant tumors in the breast cancer Wisconsin data set.

Future Scope & Recommendations

But its efficacy or not could have been found out from other medical data sets and hence, its wide applicability to medicine also may be evaluated. Illuminating more features or creating new ones in the dataset could improve the prediction power of models and provide a better insight into the tumor properties. This model performance assessment used a method known as K-fold cross-validation. To assess the performance of the logistic regression model, we used K-fold cross-validation. We also investigated the accuracy and misjudgment of predictions on test set with confusion matrix. We evaluated the extrapolation ability of the model with these testing protocols, also enabling us to estimate its performance on new data.

REFERENCES

1. World Health Organization, "Breast Cancer: Prevention and Control," [Online]. Available: https://www.who.int/health-topics/cancer. [Accessed December 3, 2020].
2. U. C. S. W. Group *et al.*, "United States Cancer Statistics: 1999–2011 Incidence and Mortality Web-Based Report," Department of Health and Human Services, Centers for Disease Control and Prevention, and National Cancer Institute, Atlanta, GA, 2014.
3. National Cancer Institute, "SEER: Cancer Statistics Review," 2012. M. Çinar *et al.*, "Artificial Neural Networks and Support Vector Machines in Early Prostate Cancer Diagnosis," Expert Systems with Applications, vol. 36, no. 3, pp. 6357–6361, 2009.
4. L. R. Borges, "Examining the Wisconsin Breast Cancer Dataset and Applying Machine Learning for Breast Cancer Detection," Group, vol. 1, no. 369, 1989.
5. J. G. Elmore *et al.*, "Comparative Study of Screening Mammography Interpretations in International Community-Based Programs," Journal of the National Cancer Institute, vol. 95, no. 18, pp. 1384–1393, 2003.
6. R. W. Giard and J. Hermans, "Evaluating the Effectiveness of Aspiration Cytologic Examination of the Breast: A Statistical Analysis of Medical Literature," Cancer, vol. 69, no. 8, pp. 2104–2110, 1992.
7. J. G. Elmore, K. Armstrong, C. D. Lehman, and S. W. Fletcher, "A Review of Breast Cancer Screening," Jama, vol. 293, no. 10, pp. 1245–1256, 2005.

8. D. Michie, D. J. Spiegelhalter, C. Taylor *et al.*, "Advances in Machine Learning: Neural and Statistical Classification," vol. 13, 1994, pp. 1–298.
9. S. Saxena and K. Burse, "Review of Neural Network Techniques for Breast Cancer Data Classification," International Journal of Engineering and Advanced Technology, vol. 2, no. 1, pp. 234–237, 2012.
10. G. I. Salama, M. Abdelhalim, and M. A.-e. Zeid, "Investigating Breast Cancer Diagnosis Using Multi-Classifiers on Various Datasets," Breast Cancer (WDBC), vol. 32, no. 569, p. 2, 2012.
11. D. Lavanya and K. U. Rani, "Exploring Feature Selection and Classification in Breast Cancer Datasets," Indian Journal of Computer Science and Engineering (IJCSE), vol. 2, no. 5, pp. 756–763, 2011.
12. V. Chaurasia and S. Pal, "Employing Data Mining Techniques for Breast Cancer Survivability Prediction and Resolution," International Journal of Computer Science and Mobile Computing (IJCSMC), vol. 3, no. 1, pp. 10–22, 2014.
13. H. Asri *et al.*, "Utilizing Machine Learning Algorithms for Breast Cancer Risk Prediction and Diagnosis," Procedia Computer Science, vol. 83, pp. 1064–1069, 2016.
14. D. Bazazeh and R. Shubair, "Comparative Analysis of Machine Learning Algorithms for Breast Cancer Detection," in 2016 5th International Conference on Electronic Devices, Systems and Applications (ICEDSA), IEEE, 2016, pp. 1–4.
15. J. Ivanc˘akov ´ a, F. Babi ´ c, and P. Butka, "Evaluating Different Machine Learning Methods on the Wisconsin Dataset," in 2018 IEEE 16th World Symposium on Applied Machine Intelligence and Informatics (SAMI), IEEE, 2018, pp. 000 173–000 178.
16. S. S. Shajahaan, S. Shanthi, and V. ManoChitra, "Modeling Breast Cancer Data Using Data Mining Techniques," International Journal of Emerging Technology and Advanced Engineering, vol. 3, no. 11, pp. 362–369, 2013.
17. M. Amrane, S. Oukid, I. Gagaoua, and T. Ensarİ, "Classifying Breast Cancer with Machine Learning Techniques," in 2018 Electric Electronics, Computer Science, Biomedical Engineerings' Meeting (EBBT), IEEE, 2018, pp. 1–4.
18. E. A. Bayrak, P. Kırcı, and T. Ensari, "Machine Learning Methods Comparison for Breast Cancer Diagnosis," in 2019 Scientific Meeting on Electrical-Electronics & Biomedical Engineering and Computer Science (EBBT), IEEE, 2019, pp. 1–3.
19. L. G. Ahmad *et al.*, "Predicting Breast Cancer Recurrence Using Machine Learning Techniques," J Health Med Inform, vol. 4, no. 124, p. 3, 2013.
20. M. I. H. Showrov *et al.*, "Classifier Performance Comparison for Breast Cancer Dataset Classification," in 2019 4th International Conference on Electrical Information and Communication Technology (EICT), Khulna, Bangladesh, 2019, pp. 1-5.
21. M. Amrane, S. Oukid, I. Gagaoua, and T. Ensarİ, "Machine Learning Application in Breast Cancer Classification," 2018 Electric Electronics, Computer Science, Biomedical Engineering's' Meeting (EBBT), Istanbul, 2018, pp. 1-4.
22. S. K. Sarkar and A. Nag, "Breast Cancer Risk Identification through Decision Trees," International Journal of Advanced Research in Computer Science, vol. 8, no. 8, pp. 88–91, 2017.
23. D. Houfani *et al.*, "Machine Learning Techniques in Breast Cancer Classification: A Comparative Study," Medical Technologies Journal, vol. 4, no. 2, pp. 535–544.
24. UCI Breast Cancer Wisconsin (Original) Dataset," [Online]. Available: https://archive.ics.uci.edu/ml/datasets/Breast+Cancer+Wisconsin+%28Original%29, 2020. [Accessed December 24, 2020].

Table 1: Summary of the Dataset

S/N	Attribute	Domain
1	Sample code number	id number
2	Clump Thickness	1–10
3	Uniformity of Cell Size	1–10
4	Uniformity of Cell Shape	1–10
5	Marginal Adhesion	1–10
6	Single Epithelial Cell Size	1–10
7	Bare Nuclei	1–10
8	Bland Chromatin	1–10
9	Normal Nucleoli	1–10
10	Mitoses	1–10
11	Class	2 for Benign & 4 for Malignant
Class Distribution		Benign: 458 (65.5%); Malignant: 241 (34.5%)
Total Number of All Instances		699
Number of Missing Values		16

Table 2 : Papers using WBCD.

Ref	Classifiers	Accuracy
Lavanya and Rani [11]	CART + Exhaustive (FST)	95.13%
Chaurasia and Pal [12]	Simple Logistic	74.5%
Asri and his colleagues [13]	SVM	97.13
Bazazeh and Shubair [14]	SVM	97%
Shajahaan and his colleagues [16]	NB	97.42
Ahmad and his colleagues [19]	SVM	95.7%
Showrov and his colleagues [20]	SVM	96.72%
Amrane and his colleagues [21]	kNN	97.51%
Sarkar and Nag [22]	C4.5	96.71%
Houfani and his colleagues [23]	MLP & LR	97.9%
Sumbaly and his colleagues [30]	J48	94.36%
Bennett and Blue [31]	SVM	97.20%
Chaurasia and his colleagues [32]	NB	97.36%
Islam and his colleagues [33]	ANN	98.57%
Our Study	**XGBoost + RFE**	**99.02%**

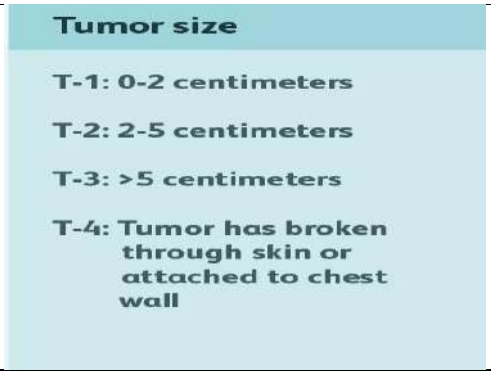

Figure: 1 Tumor Sizes

Indian Journal of Natural Sciences *www.tnsroindia.org.in ©IJONS*

Vol.15 / Issue 83 / Apr / 2024 *International Bimonthly (Print) – Open Access* *ISSN: 0976 – 0997*

RESEARCH ARTICLE

Modelling Threshold Logic Neuron as a Linear Filter for Pattern Classification

S. Arulraj[1] and M. Subbulakshmi. N. Murugan[2]

[1]Department of Mathematics, St. Xavier's College (Autonomous), Palayamkottai 627 002, Tamil Nadu, India.
[2]Research Scholar (Reg.No:20111282092006), PG and Research Department of Mathematics, St. Xavier's College (Autonomous), Palayamkottai 627 002, Tamil Nadu, India.
[1,2]Affiliated to Manonmaniam Sundaranar University, Abishekapatti, Tirunelveli 627 012, Tamil Nadu, India.

Received: 30 Dec 2023 Revised: 09 Jan 2024 Accepted: 12 Mar 2024

***Address for Correspondence**
S. Arulraj
Department of Mathematics,
St. Xavier's College (Autonomous),
Palayamkottai 627 002,
Tamil Nadu, India.
Email: arulrajsj@gmail.com

ABSTRACT

For the past few years, the thirst to explore the human brain and to design a machine to mimic human intelligence has paved the way for neural network models to spread their application in various domains of engineering. In this artificial intelligence-driven culture, neural networks play a significant role in solving the pattern classification problem. A literature review revealed that binary neurons are pattern dichotomizers in two-dimensional Boolean space. In this paper, we have extended the two-dimensional Boolean space to n-dimensional linearly separable Boolean space and implemented Threshold Logic Neuron as a pattern classifier. In the present context, the Threshold parameter and the weight vector have been fixed, and the binary threshold signal function is used as the neuronal activation function. Threshold Logic Neuron is employed to approximate a hyperplane, which acts as a tool to classify the given linear separable pattern set into two distinct classes.

Keywords: Threshold Logic Neuron, Pattern set, Threshold parameter, neuronal activation function, hyperplane.

INTRODUCTION

The father of the modern brain [7] referred to neurons as the mysterious butterflies of the soul, by beating its wings could provide insights into the secret of mental life. The organization of the human brain is far too complex to analyse and quantify in numeric terms. The history of neuroscience dates to the period of Greek civilization which sown the seed about the structure and function of the human brain [7]. The thirst to design an engineering system that can endure the Turing test [7] and model the complex structure of the human brain is ever ending process. The field of learning has expanded its horizon from humans to machines. In this 21st century machines do learn, make errors, and make corrections thanks to the advancement in the field of artificial intelligence. In [1] McCulloch and Pitts perceived that the brain consists of entities with logic-gating potential. The origin of the neural network is motivated by the information-processing entity of the brain called the neuron. In 1943 McCulloch and Pitts gave birth to the concept of the "Boolean brain" [7] and introduced the first neural network to form a mathematical model.The artificial neural network model [9] is represented as a mathematical model of a natural neural network. Artificial neural networks can be applied as a problem-solving tool in various fields like classification, pattern recognition, and optimization. Pattern recognition [2] involves the study of the process by which machines can learn from the environment and differentiate patterns of concern to predict appropriate and make rational decisions about the pattern classes.According to [6]CNNs extract features better than traditional algorithms in image classification, object detection, and speech recognition. [5] proposed a new CNN architecture for classification.A CNN was designed for pneumonia detection, using transfer learning and pattern recognition. [8] ANN can predict supercritical fluid heat transfer accurately in thermodynamics. [4] B. C. Geigerhas thrown light on the issue of estimating mutual information in deterministic NNs and addressed its consequences. In [7] Mc Culloch and Pitts proposed a highly simplified computational model of the brain, which is referred to as MP neuron and is used for pattern classification in 2D linearly separable Boolean space. In the present context, MP neuron is referred as Threshold Logic Neuron (TLN) with binary threshold signal function. Motivated by [7] we extend the two-dimensional linearly Boolean space to n-dimensional linearly separable Boolean space and employ TLN as a two-class pattern classifier.TLN is also used to approximate the hyperplane which is the decision surface to classify the linearly separable pattern set into two classes.

Preliminaries

The following notation discussed below are employed in this paper. $X = (x_1, x_2, \dots, x_n)^T$here X denotes the vector and $x_1, x_2, \dots, x_n$ denotes its component and T refers to the transpose of the vectors. The $\chi$is used to denote the pattern set taken into consideration.

Definition[7]

A Boolean $f(x_1, x_2, \dots, x_n): B^n \to \{0,,1\}$ is linearly separable, if there exist a hyperplane πin $\mathbb{R}^n$that strictly separates χ_0 fromχ_1 and $\pi \cap \{0,1\}^n = \emptyset$.

Architecture of TLN

The TLN consist of two parts. The first part receives the input signal x_i from various sources. These input signal travels through a weighted path $w_i$and neuronal activation a_l is generated, where l is the index of the TLN taken into consideration. The internal activation a_l is linear weighted summation of the input vectors, modified by the internal threshold parameter θ_l. That is,

$$a_l = \sum_{i=1}^{n} w_{i_l} x_i \qquad (1)$$

The activation a_l represent the inner product of the input vector $X = (x_1, x_2, \dots, x_n)^T$ and weight vector $W_l = (w_1, w_2, \dots, w_n)$

$a_l = X^T W_l = \sum_{i=0}^{n} w_{i_l} x_i$

(2)

Where $x_0 = +1$ and $w_0 = -\theta_l$.

In the second part, the neuronal activation a_l represented in (2) is now transferred to a signal function $\delta(.)$,which is

$$\delta(a_l) = \begin{cases} 0 \; if \; a_l < 0 \\ 1 \; if \; a_l > 0 \end{cases} \quad (3)$$

defined as follows:

In this study signal function $\delta(a_l)$, is Binary threshold signal function, which yields the output $y_l = 1$*for positive neuronal activity and yields output* $y_l = 0$ *for negative neuronal activity.*

Threshold Parameter (θ)

Consider the neuronal activation of TLN represented in the equation (2)

$$a_l = \sum_{i=0}^{n} w_{i_l} x_i$$

$$= \sum_{i=1}^{n} w_{i_l} x_i + w_0 x_0$$

$$= m_l + \theta_l$$

Where θ_l is the threshold parameter of TLN modelled by $w_0 = -\theta_l$ and $x_0 = 1$. Here, m_l refers to the neuronal activation from external sources of input. And $\theta_l$is threshold internal to the neuron. For the $\theta_l$consider the following cases.

Case 1: $\theta_l = 0$

In this case the net activation of the neuron is from external input sources. That is a_l refers to neuronal activation, when threshold is set to zero. That is the signal function $\delta(.)$ is always centered at 0. For neuronal activational value in the range $(-\infty, 0)$, the signal function yield output $y_l = 0$ and for the range $(0, \infty)$it yields output $y_l = 1$.

Case 2: $\theta_l = k \neq 0$

In this case, the threshold parameter θ_l, biases the neuron to yield output $y_l = 0$ for the net external inputs in range $(-\infty, +k)$, and yield output $y_l = 1$ for the net external inputs in range$(+k, \infty)$.

Measures of Activation

The activation a_l represented in equation (2) is simply the inner product of input vector $X = (x_0, x_1, \ldots, x_n)^T$ with the weight vector $W = (w_0, w_1, \ldots, w_n)^T$. That is,

$a_l = X^T W_l$

$= \sum_{i=0}^{n} w_{i_l} x_i$ where $w_0 = -\theta_l \& x_0 = 1$ (4)

This inner product depicts the similarities or dissimilarities measure between the input vector and the weight vector. *For larger neuronal activation, the similarity between the input vector and weight vector is large. Otherwise, it yields a relatively smaller neuronal activation which implies the input vector is dissimilar to weight vector.* We can interpret the TLN as Linear filter, as neuronal activation measures help to filter the input vector that are similar or dissimilar to weight vector respectively.

Problem Formulation

Space of Input pattern set An n-dimensional Boolean function is a map that assign each n-dimensional vector in domain spaceB^ninto unique element in the set {0,1}.

$f: B^n \rightarrow \{0,1\}$ (5)

The function given in (5) is a Boolean function.

For the present study, we restrict linearly separable Boolean function and domain $B_n$to its finite subset $\chi = \{X_1, X_2, \dots, X_p\}$, where χ is the input pattern set under consideration.
For the input pattern $\chi \subseteq B^n$, the corresponding Boolean function
$f_\chi(x_1, x_2, \dots, x_n): B^n \to \{0,1\}$ (6)

is defined such that.
$\chi_0 = f_\chi^{-1}(0) = \{(x_1, x_2, \dots, x_n) \in \chi | \forall\, x_i \neq 1; 1 \leq i \leq n\}$
$\chi_1 = f_\chi^{-1}(1) = \{(x_1, x_2, \dots, x_n) \in \chi |\, \forall\, x_i = 1; 1 \leq i \leq n\}$
This paper aims to classify the pattern set χinto two class χ_0 and χ_1 using TLN.

TLN: As Two Class Pattern Classifier

Now let us proceed further to approximate a hyperplane,πin $\mathbb{R}^n$that separatesχ_0 and χ_1 and $\pi \cap \chi = \emptyset$ using TLN which is illustrated below.
Let $\theta = \frac{2n-1}{2}$be the threshold parameters for the TLN. Let $W = (w_1, w_2, \dots, w_n)$ and $w_i = 1 \forall\, i = 1,2, \dots, n$. The pattern set $\chi = \chi_0 \cup \chi_1$ is the input pattern set of vectors to the threshold logic neuron (TLN) respectively. Now, let $\chi_0 = \chi_0^{'} \cup \chi_0^{''}$where.
$\chi_0^{'} = \{(x_1, x_2, \dots, x_n) \in \chi_0 | x_i = 0;\ \forall 1 \leq i \leq n\}$
$\chi_0^{''} = \{(x_1, x_2, \dots, x_n) \in \chi_0 |\, \forall\, x_i \neq 0;\ \forall 1 \leq i \leq n\}$
Let $X_j \in \chi_0$ which implies $X_j \in \chi_0^{'}$or$X_j \in \chi_0^{''}$. The suffix j is the index of the input vector taken into consideration.
Case 1: Let $X_j \in \chi_0^{'}$ be the input vector to the TLN. Let

$$\sum_{i=1}^{n} w_i x_{ji} = a_j \quad (7)$$

Where a_j is the inner product of the j^{th} input vector ${X_j}^T$ with the weight vector W.
Therefore $a_j = 0$. Let
$b_j = a_j - \theta$ (8)

$$\therefore\ b_j = 0 - \frac{2n-1}{2} < 0$$

Now, the activation b_j in equation (7) for the input vector X_j received from the aggregation part of the neuron is send to the Binary threshold signal function $\delta$where

$$\delta(b_j) = \begin{cases} 1 \ if\ b_j > 0 \\ 0 \ if\ b_j < 0 \end{cases} \quad (9)$$

$$\delta(b_j) = y_j = 0 \quad (10)$$

Where y_j is the output of input vector X_j.
Case 2: Let $X_j \in \chi_0^{''}$ be the input vector to the TLN. That is,

$$\sum_{i=1}^{n} w_i x_{ji} = a_j \quad (11)$$

Therefore $a_j \leq n-1$ since $X_j \in \chi_0^{''}$. Consider, For,
$b_j = a_j - \theta$
$b_j = n - 1 - \frac{2n-1}{2} < 0$
Now, the activation b_j for the j^{th} input X_j received from aggregation part of the TLN sent to the Binary threshold signal function δ, which yields final output y_j.
$\delta(b_j) = 0 \qquad (\because\ b_j < 0)$
i.e., $y_j = 0$ (12)

Thus equation (10) and (12) suffices that for $X_j \in \chi_0$. The TLN yield output $y_j = 0$. Let $X_j \in \chi_1$ be the input vector to the TLN and

$$a_j = \sum_{i=1}^{n} w_i x_{ij}$$

Hence, we get that $a_j = n$ since all the component of X_j input vector is 1. Now for,

$$b_j = n - \theta$$
$$= n - \frac{(2n-1)}{2}$$
$$= 0.5 > 0$$

The activation b_j for the j^{th} input vector X_j is send to the Binary threshold signal function δ which yields the final output.

$$\therefore \ \delta(b_j) = 1 \ (\because \ b_j > 0)$$
$$i.e. \delta(b_j) = y_j = 1 \quad (14)$$

From (10), (12) and (14) we observe that the weighted Σ of inputs yields a neuronal activation. That is,

$$y = X^T W = w_1 x_1 + w_2 x_2 + \cdots + w_0 x_0$$

Where $w_0 = -\theta$, that is the threshold parameter $\theta$is modelled by the weight w_0.The function $y(X) = 0$ is called the discriminant function of the neuron that is it is the equation of the required hyperplane π defined in equation,

$$x_1 + x_2 + \cdots - \frac{2n-1}{2} = 0 \quad (15)$$

Thus, TLN approximated the hyperplane π in $\mathbb{R}^n$ given in the equation (15) classifies the pattern set, χ into χ_0 and$\chi_1$that is, $\forall X \in \chi_0$ on one side of the plane and $\forall X \in \chi_1$ on the other side respectively with$\pi \cap \chi = \emptyset$.*Thus, we have illustrated that TLN is a two-class pattern classifier in n-dimensional linearly separable Boolean space.*

CONCLUSION

In the present paper, we have implemented Threshold Logic Neuron as a linear filter and classified the n-dimensional linearly separable Boolean pattern space into two class pattern spaces. This study can be extended to the linear classification of multi-class patterns. Also, multilayer network of neurons could be employed to solve pattern classification problems.

REFERENCES

1. Adonias, G. L., Yastrebova, A., Barros, M. T., Koucheryavy, Y., Cleary, F., & Balasubramaniam, S. Utilizing neurons for digital logic circuits: a molecular communications analysis. *IEEE transactions on nanobioscience*, 19(2), (2020) 224-236.
2. Basu, J. K., Bhattacharyya, D., & Kim, T. H. Use of artificial neural network in pattern recognition. *International journal of software engineering and its applications*, 4(2), (2010).
3. DEMİR, Y., & BİNGÖL, Ö. Detection of pneumonia from pediatric chest X-Ray images by transfer learning. Sigma, 41(6), (2023) 1264-1271.
4. Geiger, B. C., "On Information Plane Analyses of Neural Network Classifiers—A Review," in IEEE Transactions on Neural Networks and Learning Systems,33(12), (2022) 7039-7051.
5. Huang, S., Lee, F., Miao, R. *et al.* A deep convolutional neural network architecture for interstitial lung disease pattern classification. *Med Biol Eng Comput* 58, (2020) 725–737.
6. Huang, F., Tan, X., Huang, R., & Xu, Q. Variational convolutional neural networks classifiers. *Physica A: Statistical Mechanics and its Applications, 605*, (2022) 128067.
7. Kumar, S. Neural networks: a classroom approach. *Tata McGraw-Hill Education*, (2004).

8. KS, R. P., Krishna, V., & Bharadwaj, S. Effect of heat flux and mass flux on the heat transfer characteristics of supercritical carbon dioxide for a vertically downward flow using computational fluid dynamics and artificial neural networks. *Journal of Thermal Engineering*, 9(5), (2021) 1291-1306.

Indian Journal of Natural Sciences www.tnsroindia.org.in ©IJONS

Vol.15 / Issue 83 / Apr / 2024 *International Bimonthly (Print) – Open Access* *ISSN: 0976 – 0997*

RESEARCH ARTICLE

Edge Sum Divisor Cordial Labeling of Crown & Comb Graphs

A. Anto Cathrin Aanisha[1,2] and R. Manoharan[3]

[1]Sathyabama Institute of Science and Technology, Chennai, India
[2]Department of Education, DMI-St. John The Baptist University, Mangochi, Malawi
[3]Department of Mathematics, Sathyabama Institute of Science and Technology, Chennai, India

Received: 30 Dec 2023 Revised: 09 Jan 2024 Accepted: 12 Mar 2024

***Address for Correspondence**
A. Anto Cathrin Aanisha
Sathyabama Institute of Science and Technology,
Chennai, India
Department of Education,
DMI-St. John The Baptist University,
Mangochi, Malawi
Email: antocathrinaanisha@gmail.com

ABSTRACT

Let $\Omega = (W(\Omega), E(\Omega))$ be a graph which is having neither loop nor multiple edges, where $W(\Omega)$ represent node set and $E(\Omega)$ represent line set and let $h: E(\Omega) \rightarrow \{1, 2, \ldots |E(\Omega)|\}$ be a bijection. For each node u, give it a label of 1 if $2 \mid h(b_1) + h(b_2) + \ldots + h(b_s)$ and 0 if it doesn't where $b_1, b_2, \ldots b_s$ are edges that are incident with the node u. If the difference between nodes categorized 0 and 1 is less than or equal to 1, the function h is called ESDC labelling. A ESDC graph is one that has the ESDC labeling. In this paper, we prove that the crown graph $C_t \odot K_1$ and the comb graph $P_t \odot K_1$ ESDC graph are edge sum divisor cordial graphs when t is even.

Keywords: SDC graph, ESDC graph, Crown graph, Comb graph

INTRODUCTION

This paper only considers nontrivial and undirected graph. Graph labeling is one of the part of graph theory Graph labeling has direct application in a number of fields such as coding theory, the research of X-ray crystallography, communication networks and many more (Parthiban & Sharma, 2020).For the past 60 years, graph labeling has found popularity in the field of graph theory(Daisy *et al*., 2022).The effective connection between number theory and the structure of graphs is facilitated by graph labelling. Graph labeling is a mathematical concept that is concerned with assigning positive integers to nodes or lines or both. Vertex labelling is when the subject of labelling is a set of vertices. Edge labelling is the process of putting labels on a set of edges. And labelling is called "total labelling" if the

domain has both vertices and edges (Raheem *et al*., 2022).The cordial labelling is one of the graph's labelling options. As an extension of cordial labeling, prime cordial labelling, total cordial labelling, Fibonacci cordial labelling, etc have come into being (Raheem *et al*., 2022). DC labeling was initiated by (Varatharajan *et al*., 2011). Many graphs are divisor cordial graphs. Especially (Barasara & Thakkar, 2022) proved some ladder related graphs are divisor cordial graph. The practice of DC labelling has been expanded to SDC labelling, DDC labelling, PD – divisor cordial labelling, and other similar practices. The ESDC labeling is the topic of discussion in our paper. This discussion continues from where the Sum divisor cordial labelling left off. SDC labeling was initiated by (Lourdusamy & Patrick, 2016). After that he proved some graph which are satisfied the axioms of sum divisor cordial graph. Like some star and bistar related graphs are SDC graphs (Lourdusamy & Patrick, 2019). It has been demonstrated by a great number of authors that many graphs are SDC graph. And (Raheem *et al*., 2022) examined disconnected graphs, including disjoint union of paths and subdivided star SDC graphs. Recently (Adalja & Ghodasara, 2018)proved splitting graph, shadow graph, sunlet graph, shell graph are SDC graphs. Not all graphs are pleasant SDC graphs. Investigating sum divisor cordial labelling for the graphs or families of graphs that permit sum divisor cordial labelling is both very intriguing and challenging(Lourdusamy & Patrick, 2016).SDC graph is extended to ESDC graph. ESDC labeling was introduced by (Vijayalakshmi *et al*., n.d.). Already they proved that path, cycle, fan, wheel, closed helm, flower graph and friendship graphs are ESDC graph. In this paper, we prove that the crown graph C_t Θ K_1 and the comb graph P_t Θ K_1 ESDC graph are edge sum divisor cordial graphs when t is even.

Definition: 1.1

Consider Ω = (W(Ω), E(Ω)) be a graph which is having neither loop nor multiple lines, where W(Ω) represent node set and E(Ω) represent line set and let h: W(Ω) → {1, 2, . . . |W(Ω)|} be a bijection. For each line x, give it a label of 1 if h(x) divides h(y) or h(y) divides h(x) and 0 if not. If the difference between lines categorized 0 and 1 is less than or equal to 1, the function h is called DC labelling. A DC graph is one that has the DC labeling (Varatharajan *et al*., 2011).

Definition of SDC graph: 1.2

Let Ω = (W(Ω), E(Ω)) be a graph which is having neither loop nor multiple lines, where W(Ω) represent node set and E(Ω) represent line set and let h: W(Ω) → {1, 2, . . . |W(Ω)|} be a bijection. For each line x, give it a label of 1 if 2/(h(x)+h(y)) and 0 if not. If the difference between lines categorized 0 and 1 is less than or equal to 1, the function h is called SDC labelling. A SDC graph is one that has the SDC labeling(Lourdusamy & Patrick, 2016).

Definition of EDSC graph: 1.3

Let Ω = (W(Ω), E(Ω)) be a graph which is having neither loop nor multiple lines, where W(Ω) represent node set and E(Ω) represent line set and let h: W(Ω) → {1, 2, . . . |W(Ω)|} be a bijection. For each node u, give it a label of 1 if 2 | h(b_1)+ h(b_2)+...+ h(b_s) and 0 if it doesn't where b_1, b_2, . . . b_s are edges that are incident with the vertex u. If the difference between nodes categorized 0 and 1 is less than or equal to 1, the function h is called ESDC labelling. A ESDC graph is one that has the ESDC labeling (Vijayalakshmi *et al*., n.d.).

Definition of crown graph: 1.4

The crown C_t Θ K_1 is the graph formed by linking each vertex of a cycle with a pendant edge (Lourdusamy & Patrick, 2016).

Definition of comb graph: 1.5

The comb P_t Θ K_1 is the graph formed by adding a pendant edge to each vertex of a path(Lourdusamy & Patrick, 2016).

MAIN RESULT

Theorem: 2.1

The crown graph C_t Θ K_1 is an edge sum divisor cordial graph when t is even.

Proof:

Let Ω = C_t ▫ $K_1$where t is even.

Let W(Ω) = {u_x; 1≤x≤t and v_x; 1≤x≤t} be a node set and E(Ω)= {e_1, e_2, . . . e_{2t}}be a line set, where

e_x= u_{x+1} $v_{x+1;}$ 1≤x≤t-1

$e_t = v_1u_1$
$e_{t+x} = v_xv_{x+1}$; $1 \le x \le t-1$
$e_{2t} = v_tv_1$
Also $|W(\Omega)| = 2t$ and $|E(\Omega)| = 2t$
Define h: $E(\Omega) \rightarrow \{1, 2, \ldots |E(\Omega)|\}$ as follows:
$h(e_{t+2x-1}) = 4x-3$, $1 \le x \le \frac{t}{2}$;
$h(e_{2x-1}) = 4x-2$, $1 \le x \le \frac{t}{2}$;
$h(e_{t+2x}) = 4x$, $1 \le x \le \frac{t}{2}$;
$h(e_{2x}) = 4x-1$, $1 \le x \le \frac{t}{2}$;
Then induced vertex labels are
$h^*(v_{2x-1}) = 1$, $1 \le x \le \frac{t}{2}$;
$h^*(v_{2x}) = 0$, $1 \le x \le \frac{t}{2}$;
$h^*(u_{2x-1}) = 0$, $1 \le x \le \frac{t}{2}$;
$h^*(u_{2x}) = 1$, $1 \le x \le \frac{t}{2}$;
Considering the previously described labelling pattern, we have
$v_h(0) = v_h(1) = t$
Thus, $|v_h(0) - v_h(1)| = |t-t| = 0 \le 1$
Here $v_h(1)$ represents the number of nodes labeled with 1 and $v_h(0)$ represents the number of nodes labeled with 0 among all nodes in Ω.
Therefore, the crown graph $C_t \odot K_1$ is an edge sum divisor cordial graph when t is even.

Example: 2.2

The crown graph $C_t \odot K_1$, in which t=6 is shown in figure (a).
From figure (a), $|v_h(0) - v_h(1)| = |6-6| = 0 \le 1$.
So, we conclude that the crown graph $C_t \circ K_1$, where t= 6 is having ESDC labeling.
Hence the crown graph $C_t \circ K_1$, in which t=6 is an ESDC graph.

Example: 2.3

The crown graph $C_t \odot K_1$, in which t=4 is shown n figure (b).
From figure (b), $|v_h(0) - v_h(1)| = |4-4| = 0 \le 1$.
So, we conclude that the crown graph $C_t \circ K_1$, where t= 4 is having ESDC labeling.
Hence the crown graph $C_t \circ K_1$, in which t=4 is an ESDC graph.

Theorem: 2.4

The comb graph $P_t \odot K_1$ is an edge sum divisor cordial graph when t is even.

Proof:

Let $\Omega = P_t \odot K_1$ be the comb graph when t is even.
Let $W(\Omega) = \{u_x; 1 \le x \le t$ and $v_x; 1 \le x \le t\}$ be node set and $E(\Omega) = \{e_1, e_2, \ldots e_{2t-1}\}$ be a line set, where
Let $e_x = u_x v_x$; $1 \le x \le t$
and $e_{t+x} = v_x v_{x+1}$; $1 \le x \le t-1$
Also, $|V(\Omega)| = 2t$ and $|E(\Omega)| = 2t-1$
Define h: $E(\Omega) \rightarrow \{1, 2, \ldots . |E(\Omega)|\}$
$h(e_x) = t-1+x$; $1 \le x \le t$
$h(e_{t+x}) = x$; $1 \le x \le t-1$
Then induced vertex labels are
$h^*(v_{2x-1}) = 0$; $1 \le x \le \frac{t}{2}$
$h^*(v_{2x}) = 1$; $1 \le x \le \frac{t}{2}$
$h^*(u_{2x-1}) = 1$; $1 \le x \le \frac{t}{2}$
$h^*(u_{2x}) = 0$; $1 \le x \le \frac{t}{2}$
Considering the previously described labelling pattern, we have

$v_h(0)=v_h(1)= t$

Here $v_h(0)$ represents the number of nodes labeled with 0 and $v_h(1)$ represents the number of nodes with 1 in Ω.

Thus, $|v_h(0)- v_h(1)|=|t-t|=0\leq 1$

Hence comb graph $P_t \Theta K_1$ is edge sum divisor cordial labeling where t is even.

Example: 2.5

The comb graph $P_t \Theta K_1$, in which t=4 is shown in figure (c).

From figure (c), $|v_h(0)-v_h(1)|= |4-4|= 0\leq 1$.

So, we conclude that the comb graph $P_t \Theta K_1$, where t= 4 is having ESDC labeling.

Hence the comb graph $P_t \Theta K_1$, in which t=4 is an ESDC graph.

Example: 2.6

The comb graph $P_t \Theta K_1$, in which t=6 is shown in figure (d).

From figure (d), $|v_h(0)-v_h(1)|= |6-6|= 0\leq 1$.

So, we conclude that the comb graph $P_t \Theta K_1$, where t= 6 is having ESDC labeling.

Hence the comb graph $P_t \Theta K_1$, in which t=6 is an ESDC graph.

CONCLUSION

In this paper, we have shown that the crown graph $C_t \triangleright K_1$and comb graph $P_t \Theta K_1$ are an edge sum divisor cordial graph for t is even. Future research will also determine whether the crown graph $C_t \triangleright K_1$and the comb graph $P_t \Theta K_1$ are an edge sum divisor cordial graph or not when t is odd.

REFERENCES

1. Adalja, D. G., & Ghodasara, G. V. (2018). Sum Divisor Cordial Labeling of Snakes Related Graphs. *Journal of Computer and Mathematical Sciences*, *9*(7), 754–768. https://doi.org/10.29055/jcms/813
2. Barasara, C. M., & Thakkar, Y. B. (2022). *DIVISOR CORDIAL LABELING FOR LADDERS AND TOTAL GRAPH OF SOME GRAPHS*. *21*(7), 3577–3594.
3. Daisy, K. J., Sabibha, R. S., Jeyanthi, P., & Youssef, M. Z. (2022). K-Product Cordial Labeling of Powers of Paths. *Jordan Journal of Mathematics and Statistics*, *15*(4 Part A), 911–924. https://doi.org/10.47013/15.4.8
4. Lourdusamy, A., & Patrick, F. (2016). Sum divisor cordial graphs. *Proyecciones*, *35*(1), 119–136. https://doi.org/10.4067/S0716-09172016000100008
5. Lourdusamy, A., & Patrick, F. (2019). Sum divisor cordial labeling for path and cycle related graphs. *Journal of Prime Research in Mathematics*, *15*(1), 101–114.
6. Parthiban, A., & Sharma, V. (2020). A comprehensive survey on prime cordial and divisor cordial labeling of graphs. *Journal of Physics: Conference Series*, *1531*(1). https://doi.org/10.1088/1742-6596/1531/1/012074
7. Raheem, A., Javaid, M., Numan, M., & Hasni, R. (2022). Sum divisor cordial labeling of disjoint union of paths and subdivided star. *Journal of Discrete Mathematical Sciences and Cryptography*, *25*(8), 2467–2478. https://doi.org/10.1080/09720529.2020.1864935
8. Varatharajan, R., Navanaeethakrishnan, S., & Nagarajan, K. (2011). Divisor cordial graphs. *Int. J. Math. Comb.*, *2011*(4), 15–25.
9. Vijayalakshmi, G., Sheriff, M. M., Raj, P. L. R., Nadu, T., & Rowther, H. K. (n.d.). *Journal of Clinical Otorhinolaryngology , Head , and Neck Surgery*. *December 2022*, 407–417.

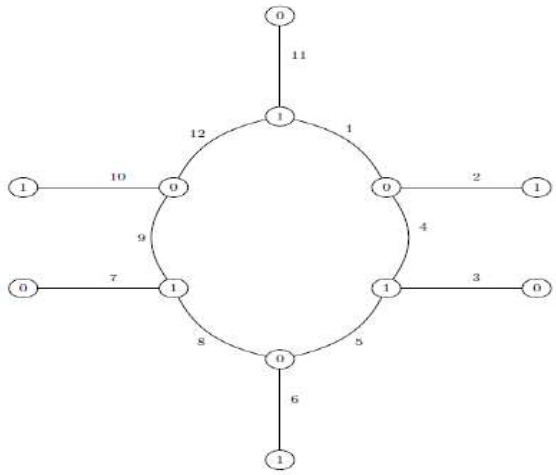

Figure (a)

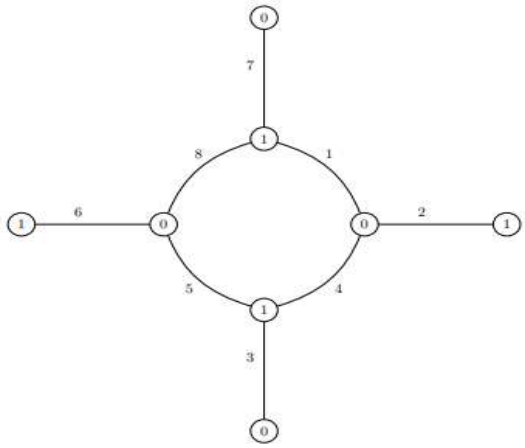

Figure (b)

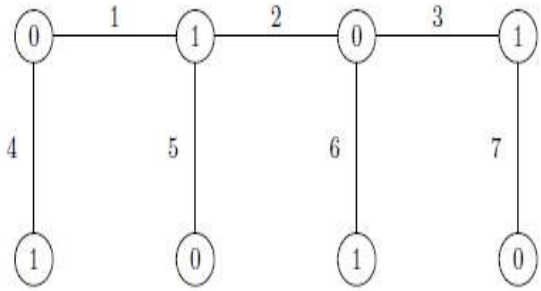

Figure (c)

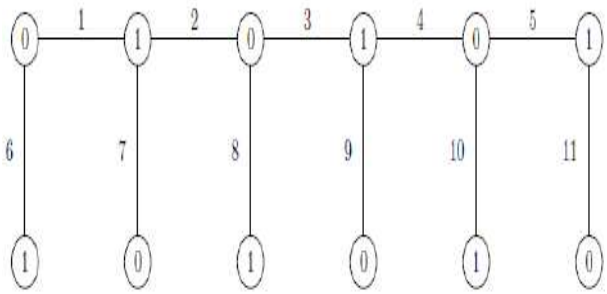

Figure (d)

Indian Journal of Natural Sciences *www.tnsroindia.org.in ©IJONS*

Vol.15 / Issue 83 / Apr / 2024 *International Bimonthly (Print) – Open Access* *ISSN: 0976 – 0997*

RESEARCH ARTICLE

Enhancing Data Science Resources Within The Academic Library

P.J. Rosario Vasantha Kumar[1]

Librarian, St. Xavier's College (Autonomous), Palayamkottai- 627 002

Received: 30 Dec 2023 Revised: 09 Jan 2024 Accepted: 12 Mar 2024

***Address for Correspondence**
P.J. Rosario Vasantha Kumar
Librarian,
St. Xavier's College (Autonomous),
Palayamkottai- 627 002
Email: rosario.kumar@gmail.com

ABSTRACT

The rise of data science as a pivotal interdisciplinary field has necessitated significant transformations within academic institutions, particularly in the resources and support provided by academic libraries. This research article explores the multifaceted role of academic libraries in enhancing data science resources and support within the university setting. Through an in-depth analysis of current practices, challenges, and opportunities, this article provides insights into the evolving landscape of data science within academic libraries. Drawing on literature review, case studies, and expert interviews, this article presents a comprehensive framework for optimizing data science resources and services within academic libraries. Key areas of focus include access to datasets, training and workshops, support for data management, access to software and tools, collaboration and partnerships, and research support services. By adopting a holistic approach to data science support, academic libraries can effectively meet the diverse needs of students, faculty, and researchers, and contribute to the advancement of data-driven research and innovation.

Keywords: Data Science, Academic Library, Resources, Support, Datasets, Training, Data Management, Software, Collaboration, Research Support

INTRODUCTION

In recent years, the exponential growth of data and the emergence of sophisticated analytical techniques have revolutionized various industries, research domains, and decision-making processes. The interdisciplinary field of

data science, which integrates statistics, computer science, domain expertise, and communication skills, has become increasingly central to addressing complex societal challenges and driving innovation across diverse sectors. As the demand for data-driven insights continues to soar, academic institutions are recognizing the importance of fostering a robust data science ecosystem to equip students, faculty, and researchers with the requisite skills and resources. Academic libraries, as vital repositories of knowledge and information within universities, play a pivotal role in supporting data science education, research, and practice. Traditionally, libraries have served as custodians of scholarly resources, providing access to books, journals, and databases. However, with the advent of data science, libraries are adapting their services and collections to meet the evolving needs of the academic community. This research article seeks to explore the multifaceted role of academic libraries in enhancing data science resources and support within the university setting.

LITERATURE REVIEW

The interdisciplinary realm of data science is swiftly emerging as one of the most dynamic areas of exploration both within academia and beyond its borders. Integrating principles from statistics and computer science, data science is propelling groundbreaking discoveries across various fields. Examples abound, including automated linguistic analysis facilitating timely interventions in online support forums (Kornfield *et al*., 2018), neuroimage processing predicting health outcomes (Lancaster, Lorenz, Leech, & Cole, 2018), and the study of environmental factors' impact on childhood cognitive development (Stingone, Pandey, Claudio, & Pandey, 2017). However, delving into such applications necessitates specialized skills and resources, encompassing computer programming and data visualization, which are indispensable for today's workforce (National Academies of Sciences, Engineering, and Medicine, 2018; Ridsdale *et al*., 2015).

Regrettably, many academic institutions lack comprehensive data science support, resulting in a growing roster of unmet needs (Barone, Williams, & Micklos, 2017; Galanek & Brooks, 2018; Garcia-Milian, Hersey, Vukmirovic, &Duprilot, 2018; Oliver, 2017), thereby hindering researchers from fully capitalizing on the big data revolution. Several factors contribute to this gap in skills and resources vital for harnessing data science applications. Firstly, while data science as a field has existed for decades (Donoho, 2017), its widespread recognition across academic domains is a recent phenomenon. Consequently, many researchers are just now realizing the imperative of skill development (Barone *et al*., 2017), often while holding positions—such as post-doctoral or faculty roles—where formal training proves especially challenging.

Engaging academic libraries in supporting data science endeavors presents a promising avenue for enhancing campus-wide data literacy (Martin, 2016; Maxwell, Norton, & Wu, 2018; Wang, 2013). Given their role as central hubs on college and university campuses, libraries naturally embody interdisciplinary collaboration, mirroring the ethos of data science. Moreover, the audience for academic libraries arguably surpasses that of any other campus unit, serving not only students but also staff and faculty. While the idea of libraries supporting aspects of data science is not novel—libraries have long championed data collection, management, and sharing best practices (Antell, Foote, Turner, & Shults, 2014)—some have also provided researchers with training in computational and statistical skills (e.g., North Carolina State University: https://www.lib.ncsu.edu/services/data-visualization, New York University Libraries: https://library.nyu.edu/departments/data-services/, Arizona State University: https://lib.asu.edu/data). Thus, the current landscape presents a ripe opportunity for academic libraries to explicitly address the growing demand for data science training.

Engaging academic libraries in supporting data science endeavors presents a promising avenue for enhancing campus-wide data literacy (Martin, 2016; Maxwell, Norton, & Wu, 2018; Wang, 2013). Given their role as central hubs on college and university campuses, libraries naturally embody interdisciplinary collaboration, mirroring the ethos of data science. Moreover, the audience for academic libraries arguably surpasses that of any other campus unit, serving not only students but also staff and faculty. While the idea of libraries supporting aspects of data science is not novel—libraries have long championed data collection, management, and sharing best practices (Antell, Foote, Turner, & Shults, 2014)—some have also provided researchers with training in computational and statistical skills (e.g., North Carolina State University: https://www.lib.ncsu.edu/services/data-visualization, New York University Libraries: https://library.nyu.edu/departments/data-services/, Arizona State University: https://lib.asu.edu/data). Thus, the current landscape presents a ripe opportunity for academic libraries to explicitly address the growing demand for data science training.

Access to Datasets

One of the primary roles of academic libraries in supporting data science is providing access to a diverse array of datasets for research purposes. Libraries acquire and curate datasets from various sources, including government agencies, research institutions, and commercial providers. These datasets cover a wide range of domains, including social sciences, natural sciences, healthcare, economics, and more. By offering access to datasets, libraries facilitate interdisciplinary research and foster innovation across diverse fields.

Training and Workshops

Many academic libraries offer training sessions, workshops, and tutorials on data science tools, techniques, and methodologies. These sessions are designed to help students, faculty, and researchers develop essential data literacy skills, such as data manipulation, visualization, statistical analysis, and machine learning. Moreover, libraries often collaborate with campus units, such as computer science departments, statistics departments, and interdisciplinary research centers, to deliver comprehensive training programs tailored to the needs of the academic community.

Data Management Support

Effective data management is essential for conducting robust and reproducible research. Academic libraries provide guidance and support to researchers in managing, organizing, and sharing their data in compliance with best practices and institutional policies. This includes assistance with data storage, metadata creation, data documentation, version control, and data preservation strategies. Moreover, libraries play a key role in advocating for open data initiatives and promoting data sharing and transparency within the research community.

Access to Software and Tools

Libraries often license and provide access to a variety of data science software and tools, including statistical analysis software, programming languages, data visualization platforms, and machine learning libraries. By offering these resources, libraries ensure that students and researchers have the necessary tools to analyze and interpret data effectively. Moreover, libraries may provide training and support services for these tools, helping users navigate complex software environments and leverage advanced functionalities.

Collaboration and Partnerships

Academic libraries collaborate with other campus units, such as research centers, computer science departments, and interdisciplinary programs, to strengthen data science initiatives. By forging partnerships and leveraging expertise

from diverse areas, libraries enhance their ability to support cutting-edge research and innovation in data science. Moreover, libraries may collaborate with external stakeholders, such as industry partners, government agencies, and non-profit organizations, to access additional resources, expertise, and funding opportunities for data science initiatives.

Research Support Services

Libraries offer a wide range of research support services tailored to the needs of data scientists and researchers. This includes assistance with literature searches, citation management, research impact analysis, data citation, and research data management planning. Librarians with expertise in data science and information retrieval play a pivotal role in guiding researchers through the complex landscape of scholarly communication and data discovery. Moreover, libraries may provide consultation services, workshops, and training sessions on research methodologies, data analysis techniques, and scholarly publishing practices. The impact of data science on academic libraries is profound and multifaceted, influencing various aspects of research, education, and scholarly communication. By embracing data science initiatives, academic libraries can effectively address the evolving needs of researchers, students, and faculty, ultimately enhancing the quality and impact of scholarly endeavors. Here are some key ways in which data science initiatives impact academic libraries:

The Impact Of Data Science On Academic Libraries

Facilitating Research Innovation: Data science initiatives enable academic libraries to support innovative research projects by providing access to diverse datasets, advanced analytical tools, and expertise in data analysis methodologies. This facilitates interdisciplinary collaboration and empowers researchers to explore complex research questions, leading to novel discoveries and insights across disciplines.

Enhancing Teaching and Learning Academic libraries play a crucial role in promoting data literacy and computational skills among students through workshops, training programs, and access to educational resources. By incorporating data science concepts into curriculum development, libraries help students develop critical skills for navigating the data-rich landscape and conducting rigorous research.

Promoting Open Science and Data Sharing Academic libraries advocate for open science principles by promoting data sharing, transparency, and reproducibility in research. By providing platforms for hosting and disseminating research data, libraries contribute to the advancement of open access initiatives and foster collaboration among researchers worldwide.

Supporting Scholarly Communication Data science initiatives in academic libraries enhance scholarly communication by enabling researchers to leverage data visualization techniques, interactive dashboards, and text mining tools to communicate their findings more effectively. This facilitates knowledge dissemination and encourages interdisciplinary collaboration within the academic community.

Bridging the Digital Divide Academic libraries play a crucial role in bridging the digital divide by providing equitable access to data science resources and support for students and researchers from diverse backgrounds. By promoting inclusivity and accessibility, libraries ensure that all members of the academic community have the opportunity to engage in data-driven research and education. Overall, the impact of data science initiatives in academic libraries is transformative, empowering researchers, students, and faculty to harness the power of data for discovery, innovation, and scholarly advancement. By embracing data science initiatives, academic libraries can fulfill their mission of supporting research, teaching, and learning in the digital age, ultimately contributing to the advancement of knowledge and society as a whole.

Rosario Vasantha Kumar

Challenges in Strengthening Data Science Resources within Academic Libraries

Enhancing data science resources within the academic library presents various challenges that must be addressed to effectively meet the evolving needs of researchers, students, and faculty.

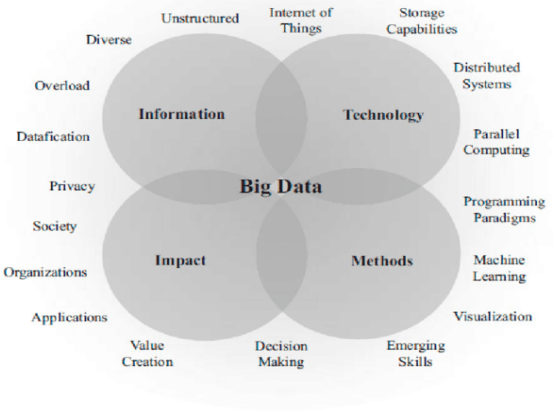

These Challenges Include

Lack of Specialized Expertise Academic libraries may face challenges in recruiting and retaining staff with specialized expertise in data science methodologies, tools, and technologies. Building a team of skilled professionals capable of providing comprehensive support for data science initiatives can be difficult, especially in competitive job markets.

Limited Funding and Resources Acquiring and maintaining data science resources, such as access to datasets, software licenses, and computational infrastructure, requires significant financial investment. Academic libraries may struggle to secure adequate funding to procure these resources, especially in the face of competing priorities and budget constraints.

Technological Complexity Data science tools and technologies are constantly evolving, requiring library staff to stay abreast of new developments and trends. Keeping up with the rapid pace of technological change can be challenging, particularly for libraries with limited technical expertise and resources. Data Management and Governance: Academic libraries must navigate complex data management and governance issues, including data privacy, security, and compliance with regulatory requirements. Ensuring the responsible and ethical use of data while also facilitating access and sharing presents a delicate balancing act for library staff.

Interdisciplinary Collaboration Data science is inherently interdisciplinary, requiring collaboration between researchers from diverse fields. Academic libraries must foster partnerships with other campus units, research centers, and external stakeholders to effectively support interdisciplinary data science initiatives. Overcoming institutional silos and promoting collaboration across departments can be challenging but is essential for success.

Promoting Data Literacy: Promoting data literacy among students, faculty, and researchers is essential for leveraging data science resources effectively. Academic libraries must develop and deliver data literacy programs, workshops, and educational resources to empower users with the skills and knowledge needed to navigate the data-rich landscape.

Infrastructure and Access Issues Ensuring equitable access to data science resources and infrastructure can be challenging, particularly for institutions with limited physical or technological resources. Addressing issues of accessibility, usability, and inclusivity is essential for ensuring that all members of the academic community can benefit from data science initiatives.

Resistance to Change Embracing data science initiatives may require cultural and organizational changes within academic libraries, including shifts in priorities, workflows, and decision-making processes. Overcoming resistance to change and fostering a culture of innovation and experimentation is essential for driving progress in enhancing data science resources within the academic library. Addressing these challenges requires strategic planning, collaboration, and investment in staff training and development. By overcoming these obstacles, academic libraries can effectively enhance their data science resources and support, ultimately advancing research, teaching, and learning within the academic community.

CONCLUSION

The integration of data science resources within academic libraries represents a significant leap forward in meeting the evolving needs of researchers, students, and faculty within the university setting. The transformative impact of data science initiatives on academic libraries is evident across various fronts, including research innovation, teaching and learning enhancement, promotion of open science, scholarly communication support, and bridging the digital divide. By embracing data science, libraries are not only adapting to the changing landscape of scholarly communication but also actively contributing to the advancement of knowledge and society as a whole. However, this journey toward enhancing data science resources within academic libraries is not without its challenges. From the necessity for specialized expertise to limited funding and resources, technological complexity, data management concerns, interdisciplinary collaboration barriers, and resistance to change, libraries face multifaceted obstacles that require strategic planning and concerted efforts to overcome. Yet, by addressing these challenges through collaboration, investment in staff training, and fostering a culture of innovation, libraries can effectively navigate the complexities of data science and continue to serve as vital hubs for research, teaching, and learning in the digital age.
Moving forward, it is imperative for academic libraries to remain agile and proactive in adapting to emerging trends and technologies in data science. By staying abreast of developments, forging partnerships, and advocating for the principles of open science and data literacy, libraries can play a pivotal role in empowering the academic community to leverage the power of data for discovery, innovation, and societal impact. Through these collective efforts, academic libraries will continue to fulfill their mission of supporting research, education, and scholarly communication in an increasingly data-driven world.

REFERENCES

1. Aarts, A. A., Anderson, J. E., Anderson, C. J., Attridge, P. R., Attwood, A., Axt, J., Open Sci Collaboration. (2015). Estimating the reproducibility of psychological science. Science, 349, aa4716. doi:10.1126/science.aac4716
2. Allaire, J. J., Xie, Y., McPherson, J., Luraschi, J., Ushey, K., Atkins, A., Chang,W. (2018). Rmarkdown: Dynamic documents for R. Retrieved from https://CRAN.R-project.org/package¼rmarkdown
3. Antell, K., Foote, J. B., Turner, J., & Shults, B. (2014). Dealing with data: Sciencelibrarians' participation in data management at association of researchlibraries institutions. College and Research Libraries, 75, 557–574. doi:10.5860/crl.75.4.557
4. Baker, J., Moore, C., Priego, E., Alegre, R., Cope, J., Price, L., … Wilson, G.(2016). Library carpentry: Software skills training for library professionals.Liber Quarterly, 26, 141–162. doi:10.18352/lq.10176Barba, L. A. (2018). Terminologies for reproducible research. CoRR. Retrievedfrom http://arxiv.org/abs/1802.03311
5. Barone, L., Williams, J., & Micklos, D. (2017). Unmet needs for analyzingbiological big data: A survey of 704 NSF principal investigators. PLoSComputational Biology, 13, e1005755. doi:10.1371/journal.pcbi.1005755

6. Burton, M., Lyon, L., Erdmann, C., & Tijernia, B. (2018). Shifting to data savvy:The future of data science in libraries. University of Pittsburgh. Retrievedfrom http://d-scholarship.pitt.edu/id/eprint/33891
7. Camerer, C. F., Dreber, A., Forsell, E., Ho, T.-H., Huber, J., Johannesson, M.,Wu, H. (2016). Evaluating replicability of laboratory experiments ineconomics. Science, 351, 1433–1436. doi:10.1126/science.aaf0918
8. Carey, M. A., & Papin, J. A. (2018). Ten simple rules for biologists learning toprogram. Plos Computational Biology, 14, e1005871. doi:10.1371/journal.pcbi.1005871.
9. Conrad, O., Bechtel, B., Bock, M., Dietrich, H., Fischer, E., Gerlitz, L.,Bohner,J. (2015). System for automated geoscientific analyses (SAGA) v. 2.1.4. Geoscientific Model Development, 8, 1991–2007. doi:10.5194/gmd-8-1991-2015
10. Donoho, D. (2017). 50 years of data science. Journal of Computational andGraphical Statistics, 26, 745–766. doi:10.1080/10618600.2017.1384734Environmental Systems Research Institute. (2018). ArcGIS. Retrieved from https://www.esri.com/en-us/store/arcgis-desktop
11. Galanek, J. D., & Brooks, D. C. (2018). Supporting faculty research withinformation technology. Research report. Educause Center for Analysis andResearch.Garcia-Milian, R., Hersey, D., Vukmirovic, M., &Duprilot, F. (2018). Datachallenges of biomedical researchers in the age of omics. Peer Journal, 6,e5553. doi:10.7717/peerj.5553
12. GRASS Development Team. (2017). Geographic resources analysis support system(GRASS GIS) software, version 7.2, Open Source. Geospatial Foundation. Retrieved from http://grass.osgeo.org
13. Huppenkothen, D., Arendt, A., Hogg, D. W., Ram, K., VanderPlas, J. T., &Rokem,A. (2018). Hack weeks as a model for data science education andcollaboration. Proceedings of the National Academy of Sciences, 115,8872–8877. doi:10.1073/pnas.1717196115
14. Ioannidis, J. P. A. (2005). Why most published research findings are false. PlosMedicine, 2, 696–701. doi: 10.1371/journal.pmed.0020124
15. Kerr, N. L. (1998). HARKing: Hypothesizing after the results are known.Personality and Social Psychology Review, 2, 196–217. doi:10.1207/s15327957pspr0203_4
16. Kluyver, T., Ragan-Kelley, B., Perez, F., Granger, B., Bussonnier, M., Frederic, J.,Willing, C. (2016). Jupyter notebooks – A publishing format forreproducible computational workflows. Paper presented at the Positioningand Power in Academic Publishing: Players, Agents and Agendas, 87. doi:10.3233/978-1-61499-649-1-87.Retrieved from http://ebooks.iospress.nl/publication/42900
17. Steeves, V. (2017). Reproducibility librarianship. Collaborative Librarianship, 9, 4.Retrieved from https://digitalcommons.du.edu/collaborativelibrarianship/vol9/iss2/4
18. Stingone, J. A., Pandey, O. P., Claudio, L., & Pandey, G. (2017). Using machinelearning to identify air pollution exposure profiles associated with earlycognitive skills among US children. Environmental Pollution, 230, 730–740.doi:10.1016/j.envpol.2017.07.023
19. Tenopir, C., Allard, S., Frame, M., Birch, B., Baird, L., Sandusky, R.,Lundeen,A. (2015). Research data services in academic libraries: Data intensive rolesfor the future? Journal of eScience Librarianship, 4, e1085. doi:10.7191/jeslib.2015.1085
20. Towns, J., Andrews, P., Boisseau, J., Roskies, R., Brown, J., Boudwin, K.,Wallnau, K. (2010). Project summary: XSEDE: eXtreme science and engineering discovery environment. Retrieved from http://hdl.handle.net/2142/42546
21. Valle, D., &Berdanier, A. (2012). Computer programming skills for environmentalsciences. Bulletin of the Ecological Society of America, 93, 373–389. doi:10.1890/0012-9623-93.4.373
22. Wang, M. (2013). Supporting the research process through expanded library dataservices. Program: Electronic Library and Information Systems, 47, 282–303.doi:10.1108/PROG-04-2012-0010
23. Wickham, H. (2016). Ggplot2: Elegant graphics for data analysis. New York:Springer-Verlag. Retrieved from http://ggplot2.org
24. Wilson, G. (2016). Software carpentry: Lessons learned. F1000Research, 3, 24.doi:10.12688/f1000research.3-62.v2
25. Xie, Y. (2014). Knitr: A comprehensive tool for reproducible research in R. In V.Stodden, F. Leisch & R. D. Peng (Eds.), Implementing reproduciblecomputational research. Boca Raton, FL: Chapman and Hall/CRC. Retrievedfrom http://www.crcpress.com/product/isbn/9781466561595

Indian Journal of Natural Sciences *www.tnsroindia.org.in ©IJONS*

Vol.15 / Issue 83 / Apr / 2024 *International Bimonthly (Print) – Open Access* *ISSN: 0976 – 0997*

RESEARCH ARTICLE

A Role of Artificial Intelligence In Smart Building

AR.A.Bhuvaneshwari[1*] and A.Natarajan[2]

[1]Professor, Department of Architecture, Sigma College of Architecture, Kuzhithurai-629168, Tamil Nadu.
[2] Assistant Professor, PG Department of Data Science, St. Xavier's College, Palayamkottai-627002,Tamil Nadu, India.

Received: 30 Dec 2023 Revised: 09 Jan 2024 Accepted: 12 Mar 2024

***Address for Correspondence**
AR. A. Bhuvaneshwari
Prof/Dept Of Architecture,
Sigma College Of Architecture,
Kuzhithurai, Tamil Nadu 629168
Email: natrajanbhuvana@gmail.com

ABSTRACT

Smart building uses artificial intelligence in various stages of construction of a building like designing, material selection, construction management, structures and maintenance. In this paper case study of five smart buildings of different countries using artificial intelligence has been analysed. The study reveals the usage of architectural intelligence to enhance design, project management, safety, and sustainability. With the evolution of artificial intelligence we can expect more innovations and efficiency in the building industry.

Keywords: Smart Buildings, Artificial Intelligence, Energy Efficiency.

INTRODUCTION

Artificial intelligence has made revolution in building industry in optimising designs, project management, predicting hazards, and optimising energy use. Artificial intelligence helps in making cost effective, safe and sustainable designs. It makes eco-friendly choices to attain sustainability.

Artificial Intelligence
Artificial intelligence is the intelligence of machines or software, as opposed to the intelligence of other living beings, primarily of humans. It is a field of study in computer science that develops and studies intelligent machines.

Smart Building
Smart buildings take advantage of many existing technologies and are designed or redesigned to allow for the integration of future technological developments. Internet of things (iot) sensors, building management, artificial intelligence (ai) and augmented reality are some of the techniques and technologies that can be used in these smart

homes to manage and improve their performance. Current standards for smart homes cover areas such as health, energy and security. this model can operate continuously through relationships with users or self-management. Smart home solutions should not only be about the relationship between buildings and their users, but also about the outside and places like smart cities and smart communities. Smart buildings are important for the low-cost economy in the future, and the use of information technology and smart buildings will be efficient and integrated. In the long term, smart home implementation will require multiple layers of software/hardware adaptability to achieve high-quality services and reduce energy/cost major improvements require new hardware, understanding of all system issues, and integration.

Study Of Role Of Ai In Smart Buildings Through Case Studies

The Shanghai Tower, China
The Edge, Amsterdam
The One Central Park, Sydney
The Biqbuilding, Hamburg.
The Museum Of The Future, Dubai.

Case Study1

The Shanghai Tower,China(2015)
Architect : Gensler
Structural Engineer: Thornton Tomasetti
Mep: Cosentini
Fire Protection And Life Safety: Rja Fire Protection Technology Consulting (Rja)
Building Façade: Aurecon Engineer Consulting (Shanghai) Co., Ltd. (Aurecon)

About Shangai Towers

Shangai world financial centre is the tallest building of china with a china green building three star rating. The shanghai tower is also a leed gold-rated building . It is the second tallest building of the world after burj khalifa in dubai.

AI Applications In Shangai Towers

The shanghai is the best example for usage of artificial intelligence in design and construction of sky scrapers. Few such applications are as follows.

Energy Efficiency

AI algorithm was used to study the building occupancy pattern and weather data to control the heat, cool and light of the building. It reduces the energy consumption of the building.

Structural Stability

AI was used to study the wind patterns as it was an important treat for structural stability. It created a unique, twisting form to reduce wind loads.

Selection Of Materials

AI was used to select material in the basis of structural stability and environmental impact. This helped with the sustainable principles of the tower.

Project Management

Artificial Intelligence was used to schedule construction activities, allocate resources efficiently, and monitor progress. It helped in achieving time and financial management.

Safety Measures

AI is used for sensing hazards and saving workers. They used sensors and cameras.

Customization
Ai was used in designing the interior space according to the tenants need. Ai was used in complete customization.

Case Study2
The Edge, Amsterdam(2015)
Architect :Plp Architects
Structural Engineer:Van Rossum
Mep:Deerns
Building Façade:Rollecate

About The Edge
The edge is an office building in amsterdam. It provides a better environment with sustainable properties. It is the world's highest breeam rating awarded to an office building.

AI Applications In Edge
The edge has been admired as the smartest building of the world. It has been rightly called as the computer with a roof. Its artificial intelligence application is as follows

Smart Office
Artificial intelligence suggests workers desk location based on temperature preference and meeting locations. On days when there are less employees expected some section might be shut down to reduce the cost of heating, cooling, lighting and cleaning. Artificial intelligence informs when to fill the coffee machine. It even informs when to clean up a busy bathroom, robots are used for office security.

Smart Parking
When we enter the garage a camera snap a photo of the license plate. It checks with the employees record and raised the gate. Sensor light brighten when one approaches and dims as we leave.

Case Study 3
The One Central Park, Sydney,(2014)
Architect: Ateliers Jean Nouvel
Structural Engineer: Robert Bird Group
Mep: Arup
Building Façade: Surface Design Pty Ltd

About The One Central Park
The one central park is a living architectural project in Australia. The building is visually appealing greenery in urban context.

AI Applications In One Central Park
The one central park has five green star rating. Artificial intelligence has been used for designing its greenery.

Green Facade
Artificial intelligence was used to face the challenges due to microclimate. Planting design and technology used were tested for long term planting success. For the façade wind and shade analysis were done to analyze the suitability of plant.in foyer and atrium lux level is recorded to determine low level light plant.

Case Study 4
The Biq Building, Hamburg,(2014):
Architect :splitterwerk

Bio energy façade: arup

About The Biqbuilding, Hamburg
The biq building is a four floor residential building. it is the first bio energy façade building. the project won the zumtobel group award 2014 .

AI Applications In Biq Building
The biq building has 129 glass panels to cultivate microalgae. Ai usage in this building is as follows.

Algae Growth
The residential building is made of algae bricks that produces oxygen and absorbs carbon dioxide. Ai used to control the building ventilation system and optimize the algae growth.

Case Study 5
The Museum Of Future, Dubai (2022)
Architectural Firm: Killa Design
Structural Engineer: Burahappold
Exterior Arabic Calligraphy: Emirati Artist Mattar Bin Lahej

About Future Museum
The museum of the future's has a unique form that represents image of the future. It has received leed platinum certification.

AI Applications In Future Museum
The calligraphy and the building's unusual appearance make it one of the most complex architectural projects ever completed. Artificial intelligence was used in the construction of the building.

Design Of The Building
If you don't have the skills, parametric design and design knowledge this will be an impossible task. Parametric design is a technique based on algorithmic reasoning that allows certain variables or parameters to change the outcome of the equation. Bim is a 3d model-based technology for construction professionals to collaboratively design and document projects.

Comparison Of Case Studies
Show Table 1

CONCLUSION

Ai using different algorithm produces multiple design options based on material selection and construction cost. This helps architects to explore multiple design considering key features like strength, sustainability and aesthetics. It makes revolution in the field of architecture by streamlining decision making and designing more efficient and sustainable buildings.

REFERENCES

1. Tian, W., Yang, S., Zuo, J., Li, Z., & Liu, Y. Relationship Between Built Form And Energy Performance Of Office Buildings In A Severe Cold Chinese Region. In Building Simulation (10, 1, 11–24). Tsinghua University Press, (2017).

2. Van Bueren, E.M., & Priemus, H. Institutional Barriers To Sustainable Construction. Environment And Planning B: Planning And Design, 29(1), 75–86 (2002).
3. Zhou, Y.K., Zheng, S.Q., & Zhang, G.Q. A Review On Cooling Performance Enhancement For Phase Change Materials Integrated Systems—Flexible Design And Smart Control With Machine Learning Applications. Building And Environment, 174, 106786, (2020).
4. World Green Building Council (Worldgbc), 2022, Https://Www.Worldgbc.Org/ What-Green-Building. (Accessed 4 October 2022).
5. Y. Liu, C. Yang, L. Jiang, S. Xie, Y. Zhang, Intelligent Edge Computing For Iot-Based Energy Management In Smart Cities, Ieee Netw. 33 (2) (2019) 111–117.
6. Zhou, Y.K., & Zheng, S.Q. Machine-Learning Based Hybrid Demand-Side Controller For High- Rise Office Buildings With High Energy Flexibilities. Applied Energy, 262, 114416, (2020)
7. Naganathan, H., Chong, W.O., & Chen, X. Building Energy Modeling (Bem) Using Clustering Algorithms And Semi-Supervised Machine Learning Approaches. Automation In Construction, 72, 187–194, (2016).

Table1: Comparison Of Case Studies

Example	**Location**	**Type Of Building**	**Ai Usage**
Shangai Towers	China	Mixed Use	Energy Efficiency, Structural Stability, Selection Of Materials, Project Management, Safety Measures, Customization
The Edge	Amsterdam	Office	Smart Office, Smart Parking
The One Central Park	Sydney	Mixed Use	Green Facade
The Biq Building	Hamburg	Residential	Algae Growth
The Museum Of Future	Dubai	Public	Design Of The Building.
Interference	Ai Is Used In Building Industry In Various Stages Right From Designing, Material Selection, Construction, Maintenance And Operation.		

Figure1: The Shanghai Tower, China

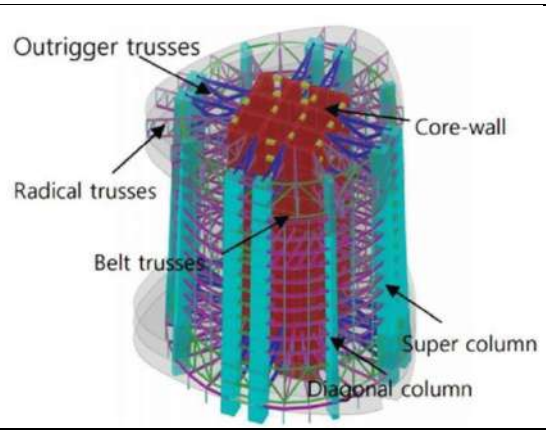

Figure2: Material

Figure 3: The Edge, Amsterdam

Figure 4: The One Central Park

Figure 5: Biq Building

Indian Journal of Natural Sciences *www.tnsroindia.org.in ©IJONS*

Vol.15 / Issue 83 / Apr / 2024 *International Bimonthly (Print) – Open Access* *ISSN: 0976 – 0997*

RESEARCH ARTICLE

LTE: Performance Investigation for The Mode of Interfacing in The Integrated Hetnets

[1]Burhanuddin Mohammad and [2]Imran Qureshi

[1,2]Lecturer, College of Computing and Information Sciences-IT Department, University of Technology and Applied Science-AlMusanna, Sultanate of Oman

Received: 30 Dec 2023 Revised: 09 Jan 2024 Accepted: 12 Mar 2024

***Address for Correspondence**
Burhanuddin Mohammad
Lecturer,
College of Computing and Information Sciences-IT Department,
University of Technology and Applied Science-
Al Musanna, Sultanate of Oman
Email: burhanuddin@act.edu.om

ABSTRACT

Networking techniques are advancing quickly especially in case of pertaining to wireless communication systems. Researchers are looking forward to make the wireless technology as the future of networking. Since the evolution of wireless technologies rapid proliferation has been observed in wireless technologies. Simultaneously heterogeneity in technological development is observed. This heterogeneity comes up due to the application for the specific group of users. Now the demand with the development of the various wireless technologies is to bring all the heterogeneous technologies under one Umbrella i.e. Long-Term Evolution. LTE is a key development in wireless technologies. And LTE is considering the heterogeneous wireless technologies to integrate them. This research paper proposed the possible research challenges while integrating the different wireless technologies. And we consider the two scenarios for designing the framework tight and loose coupling. We simulated the both scenarios and observed how well the system works. Our research indicates that Tight coupling is better than the loose coupling.

Keywords: WiMax, LTE, HetNets, WLAN, Integration of wireless networks.

INTRODUCTION

Various wireless technologies are emerged and became obsolete before implementations few are very good case in point are Adhoc networks, and measuring device networks. Such innovations have valuable societal implications and are restricted to particular consumers. The evolution of LTE will have a significant impact on the incorporation of such innovations. For the simple reason that it is compatible with packet switched innovations and allows high-

data-rate hybridized networking. In recent years WiMax (IEEE802.16e) gained great heed due to facilitate massive amounts of information assigns, high standards of services and support to movement and wider coverage area [6]. The 3rd Generation Partnership Project most presently specified the global LTE to meet the increasing working requirements of wireless internet access in cellphones . An attractive possibility for making the 4G paradigm a reality is the cooperation and amalgamation of multiple innovations [7]. Because the protocols and procedures for supporting quality of service in LTE connections are distinct. Integrating the innovations alongside the help of inter-networking needs standard adaption. If we were to use layer two strategy, for instance, the The WiMax network BS and LTE eN would need to have their medium access control layers adapted. An LTE user will only ever interface with their respective LTE serving gateway (S-GW) under a layer 3 architecture, where adaption is executed at the IP layer. This WiMax/LTE integrated network is best suited for it 3 technique. No changes to the WiMax base station or LTE user devices are necessary because an LTE S-GW is in charge of protocol adaption up to the IP layer [5]. And at this level integration and internetwork of Adhoc and wireless sensor network has no obligation because WiMax, Adhoc and Sensor network are already supporting the same routing protocols like AODV, OLSR, TORA and GRP.

Advancements in such modular design enabling consumers to modify swiftly among the heterogeneous networks would provide numerous beneficial to both end users and operators. By providing comprehensive LTE/WiMax/Adhoc/WSN services, users would be benefitted from the increased performance and tremendous data rate of such integrated services and unlimited applications. For now, the WiMax subscriber owns the necessary LTE connectivity infrastructure but not restricted and can be owned by any other party. For this integration and ownership . For seamless cooperation, appropriate guidelines and terms of service must be established [5]. Now it is the perfect moment to consider how to incorporate diverse technological innovations into the LTE network. In addition, we need to zero in on the problems and obstacles associated with doing investigation into the complete portable network's cooperation, execution, and activation. Wireless connectivity provide a number of significant investigation issues. There will be a plethora of new problems to solve as we attempt to include differing wireless innovations, which will inevitably bring their own set of difficulties. The subsequent investigation obstacles require attention and conversation.

Research Challenges

Framework for Integration

A seamless switching across different types of communication networks is a crucial need for the next generation wireless system. Radio access networks have different features and technologies to provide the services to the user. UMTS and WiMax provide the support for a scarce data transport capacity that allows for greater accessibility. WLAN supports the less degree of mobility with high data transmission bandwidth. And for coverage a large number of access points needed. A temporary network allows for a great deal of getting around, lacks a centralised design, and has a geometry that is constantly changing to accommodate different levels of data transfer. Variegated degrees of accessibility are accommodated via Zigbee or smart sensor networks, which need minimal data transfer and provide concentrated assistance. The standards and limits that allow different types of organizations to deliver their capabilities to users are well specified. Therefore, linking all of the disparate WiFi networks is an enormous undertaking that calls for an extremely complex foundational architecture. Several ports and couplings are covered here to facilitate the creation of an LTE foundation and the integration of various wireless networks. When planning a melding arrangement, it is possible to think about

Open Interface

Independent connections and transportation routes were required by the open communication. Even though it's the most basic interface, it's rather complicated to come together. It incorporates a significant postponement over changeover between sites and requires an additional authentication method. If we stick to the accessible interface, we'll end up with inadequate connectivity and data delays during transfer, which goes against the whole point of LTE. This means it should be reserved for use as a last resort and main adoption [5].

Tight/Close Interface

The principle of a network controller is derived from the notion of snug or intimate interconnection. During a transition, the link's access point that connects both systems acts as a radio network controller. Here, many radio technologies function as an integrated fundamental infrastructure. Substantial data transmission rates and smooth transitioning between connections are the foundation of LTE, and although the interface is a bit complicated, it provides these features [5].

Loose Interface

A disintegrating connection connects the WLAN network's AAA server to the WiMax framework using a shared authorization process. So, instead of modifying the WLAN and WiMax standards, users can have accessibility to capabilities through a loose integration.

Mobile IP based Interface

In order to facilitate the world of technology portability of points through the process of packet swapping idea, mobile IP is a top option for implementing the network connection. The care of address from the person's residence connection is used to identify cellphone users [8]. When moving clients on the move across different networks, mobile IP is the easiest and most effective way to do it missing affecting the functionality [9].

Clients can easily move across networks with the use of cell-phone IP [10]. However, information packet flipping across diverse networks is supported via packet wrapping in a standard arrangement [11].

Layered Protocols

Intensive and thorough investigation is required to develop a methodology as the foundation for Hspa-based networking in order to preserve the core of LTE and framework reliability. Due to the fact that various architectural styles employ distinct groups of methods. Investigators should prioritize the implementation of regulations for LTE-based combined networks.

Channel Allocation

Regulated broad range is being utilized by WiMax as well as other network operators. gratis levels are utilized by WLAN, Adhoc, WSN, and Zigbee connections. Channel allocation conflicts are a natural consequence of technology interconnection. Furthermore, it will generate a significant amount of distraction. A number of transmit placement strategies are at your disposal, including hybrid approaches, dynamic, and regular channels.

Handoff

Vertical handoff between between two different networks and horizontal handoff between the two different access points within the same network is available.

Security

Integrating diverse networks and LTE-based systems poses serious threats to security. Tradeoffs exist within safety and latency. We must find a way to solve this challenge better than everyone else. Completely coordinated safety features for networks are notoriously difficult to create all at once. However, we may go step-by-step. If you want your data exchange to be both quick and trustworthy, you may add layers of protection [36, 37, 38, 39, and 40].

Quality of Service

Quality of service concerns are less pressing when technologies are in their early stages of advancement. However, we must ensure that the system's fundamental performance remains intact. The standard of service may be categorized into two groups: those based on internal networks and those based on global networks [27], [28], and [29], respectively. The reason being that various networks offer varying levels of assistance, and the minimum requirement worldwide for excellence performance ought to match the highest level of the internally network's QoS.

Related Work

The goal of the future-oriented infrastructure is to standardize the building blocks and foundation for all portable and connected systems, regardless of their heterogeneity. Access to the network made available to users through the notion of everywhere, anytime, and using any gadget. As a result, integrating networks is seen as the next big hurdle for digital communication to overcome [22]. Since conversations over LTE began inside 3GPP in 2004, it cannot be a very fresh field. An example of this "unceasing toil" is the hundreds of engineers who are involved with the 3GPP standards panels. Long-Term Evolution is the innovative technology that will utilize MIMO antenna transmission to

push the boundaries of limit. The connection with the radio system and the construction of the radio infrastructure are both encompassed in LTE system layouts.

Media Independent changeover (MIH) is a continuing effort in the IEEE802.21 WG which involves many types of connections. Its goal is to create smooth changeover across numerous broadband networks, despite their equipment. [1, 2, 3, and 4]. Anyone can own the necessary LTE access network; what's important is that the right regulations and service level contracts be in place to ensure that users can roam and interact seamlessly with one another [5]. Because of its broad signal area, assistance with user independence, inherent quality of service, and high data rate capabilities, WiMax technology relying on the IEEE802.16e equipped has garnered a lot of interest from both consumers and broadband providers [34]. One possible way to achieve the 4G situation is by combining and interconnecting LTE and WiMax innovations [24].

The wireless connectivity Broadband Conformity Coalition, better known as WiFi [26], is responsible for verifying that devices that adhere to the IEEE 802.11 standard can communicate with one another. The maximum indoor visibility radius for a WiFi access point is around 100 meters [23]. The range of WiFi outside depends on factors like the weather and other external factors, although it may be as long as 300 meters [25]. From 11 Mbps to 54 Mbps, that's the range of WiFi data transmission speeds [3]. Known variously as Fixed WiMax and the IEEE802.16d protocol, it forms the basis of WiFi-WiMax integration. Additionally, the IEEE 802.16e regulation has not been implemented yet. In [30], the authors conduct a simulation research that demonstrates how connectivity impacts the efficiency of program technologies such as HTTP, FTP, email, and VoIP. In [31], we find a method for safely integrating wireless diverse networks. In [32], we find a standard infrastructure for adaptive radio-assisted integration of heterogeneous wireless networks. In reference [33], a method for vertical handoff in HetNet is described.

Simulation Environment

The objective of the investigation is to analyze the working of tight and loose coupling. And impact over the protocols of different layers. For application layer protocols Email, FTP, VOIP and http are considered. For individual network-based parameters WiMax and WLAN are considered. A hypothetical research with coupled WiMax/WLAN is conducted using the LTE Opnet version modeling. Twenty square kilometers constitute the space of the model. The experiment time is configured at 3600 seconds. The first graph shows the tightly coupled modeling situation. Simulation scenario for loose interface/ coupling is given in figure 2. Four application servers are connected with cloud and user from both scenarios for WiMax and WLAN are trying to download the files and services from the cloud. The users are mobile and speed is varying from 0-20m/s and following a random way point trajectory.

RESULT ANALYSIS AND DISCUSSION

Performance of Application Protocol

Implementation procedures provide the foundation for measuring the efficacy of networks for people who use it. Here we get into the topic in use protocols, specifically looking at Email, FTP, VOIP, and HTTP. The third figure through Figure 13 show the FTP's functionality. For the different kind of application tight coupling is showing better performance.

Performance of WiMax

Monitoring the efficiency for each person innovations and the effects of combining on these innovations are crucial during diverse system integration. See Figures 14 and 15 for WiMax effectiveness details. As a result of strong association, the WiMax layer duration is shown to be optimal. Keep in mind that the WiMax layer's strong productivity for informal coupling might be because of the regulation sessions.

Performance of WLAN

You can see how well the WLAN infrastructure is doing in Figures 16 and 17. Though WLAN delay is good in case of loose coupling but it has been due to the internal performance but not for the integrated network. If we are integrating the network then we have to consider all possible scenarios and outcomes.

CONCLUSION

In this paper WiMax and WLAN are integrated under the umbrella of LTE. We simulated the results for Loose and Tight interfacing/coupling for designing the framework for the HetNets. And we observed that tight coupling is good in comparison to loose coupling. We can consider this point when laying the groundwork for technology integration. Further discussion may include the designing of Framework in order to integrate wireless networks that are not homogeneous.

REFERENCES

1. Cordeiro, C.; Challapali, K.; Birru, D.; Sai Shankar, N.; , "IEEE 802.22: the first worldwide wireless standard based on cognitive radios," *New Frontiers in Dynamic Spectrum Access Networks, 2005. DySPAN 2005. 2005 First IEEE International Symposium on* , pp. 328-337, 8-11 Nov. 2005, doi: 10.1109/DYSPAN.2005.1542649 Url: http://ieeexplore.ieee.org/stamp/stamp.jsp?tp=&arnumber=1542649&isnumber=32916
2. Kumar, V.; Tyagi, N.; , "Media independent handover for seamless mobility in IEEE 802.11 and UMTS based on IEEE 802.21," *Computer Science and Information Technology (ICCSIT), 2010 3rd IEEE International Conference on* , Vol. 4, no., pp. 474-479, 9-11 July 2010, doi: 10.1109/ICCSIT.2010.5563797 Url: http://ieeexplore.ieee.org/stamp/stamp.jsp?tp=&arnumber=5563797&isnumber=5563533
3. Eastwood, L.; Migaldi, S.; Qiaobing Xie; Gupta, V.; , "Mobility using IEEE 802.21 in a heterogeneous IEEE 802.16/802.11-based, IMT-advanced (4G) network," *Wireless Communications, IEEE* , Vol. 15, no. 2, pp. 26-34, April 2008, doi: 10.1109/MWC.2008.4492975 Url: http://ieeexplore.ieee.org/stamp/stamp.jsp?tp=&arnumber=4492975&isnumber=4492967
4. De La Oliva, A.; Eznarriaga, L.; Bernardos, C.J.; Serrano, P.; Vidal, A.; , "IEEE 802.21: A shift in the Media Independence," *Future Network & Mobile Summit (FutureNetw), 2011* , vol., no., pp. 1-8, 15-17 June 2011Url: http://ieeexplore.ieee.org/stamp/stamp.jsp?tp=&arnumber=6095208&isnumber=6095189
5. Yahiya, Tara A.; Chaouchi, Hakima; , "On the Integration of LTE and Mobile WiMax Networks," *Computer Communications and Networks (ICCCN), 2010 Proceedings of 19th International Conference on* , vol., no., pp. 1-5, 2-5 Aug. 2010, doi: 10.1109/ICCCN.2010.5560067 Url: http://ieeexplore.ieee.org/stamp/stamp.jsp?tp=&arnumber=5560067&isnumber=5560011
6. Banivaheb, N.; Navaie, K.; , "Outage probability of hybrid cellular-adhoc CDMA networks," *Electrical Engineering (ICEE), 2011 19th Iranian Conference on* , vol., no., pp. 1-6, 17-19 May 2011 Url: http://ieeexplore.ieee.org/stamp/stamp.jsp?tp=&arnumber=5955592&isnumber=5955412
7. Ibanez, S.R.; Santos, R.A.; Licea, V.R.; Block, A.E.; Ruiz, M.A.G.; , "Hybrid WiFi-WiMax Network Routing Protocol," *Electronics, Robotics and Automotive Mechanics Conference, 2008. CERMA '08* , vol., no., pp. 87-92, Sept. 30 2008-Oct. 3 2008, doi: 10.1109/CERMA.2008.24 Url: http://ieeexplore.ieee.org/stamp/stamp.jsp?tp=&arnumber=4641052&isnumber=4641028
8. Chang, Alvin T. S. And He, Dan and Chuang, SiuNam and Cao, Jiannong," Towards a Programmable Mobile IP", published in Lecture Notes in Computer Science in the book title "Mobile Data Management", Springer Berlin Heidelberg, vol. 1987, year 2001, pp 210-221. doi:10.1007/3-540-44498-X_17. Url: http://dx.doi.org/10.1007/3-540-44498-X_17
9. Åhlund, Christer and Zaslavsky, Arkady," Multihoming with Mobile IP", published in Lecture Notes in Computer Science in book title High-Speed Networks and Multimedia Communications by Springer Berlin Heidelberg, vol. 2720, year 2003, pp 235-243. doi:10.1007/978-3-540-45076-4_24. Url: http://dx.doi.org/10.1007/978-3-540-45076-4_24

10. Gupta, Vipul and Montenegro, Gabriel, "Secure and mobile networking" published in journal Mobile Networks and Applications Vol. 3 issue 4 year 1998, pp 381-390. doi: 10.1023/A:1019153505523. Url: http://dx.doi.org/10.1023/A%3A1019153505523
11. 11. H. Fathi et. Al "IP-Based Wireless Heterogeneous Networks" published in book title "Voice over IP in Wireless Heterogeneous Networks" in series Signals and Communication Technology published by Springer Netherlands year 2009 pp 15-36, ISBN 978-1-4020-6630-6, doi: 10.1007/978-1-4020-6631-3_2. Url: http://dx.doi.org/10.1007/978-1-4020-6631-3_2
12. Qing-An Zeng and Dharma P. Agrawal. 2002. Handoff in wireless mobile networks. In "Handbook of wireless networks and mobile computing". John Wiley & Sons, Inc., New York, NY, USA pp: 1-25. Url: http://dl.acm.org/citation.cfm?id=512322
13. Jon Chung-Shien Wu, Chieh-Wen Cheng, Gin-Kou Ma, and Nen-Fu Huang. 2001. Intelligent handoff for mobile wireless internet. *Mob. Netw. Appl.* 6, 1 (January 2001), 67-79. doi:10.1023/A:1009817921307 Url: http://dx.doi.org/10.1023/A:1009817921307
14. Hoon-ki Kim, Soo-Hyun Park, and Jae-IL Jung. 2004. Dynamic channel reservation scheme for mobility prediction handover in future mobile communication networks. In *Proceedings of the Third Asian simulation conference on Systems Modeling and Simulation: theory and applications* (AsiaSim'04), Doo-Kwon Baik (Ed.). Springer-Verlag, Berlin, Heidelberg, 410-418. doi:10.1007/978-3-540-30585-9_46 Url: http://dx.doi.org/10.1007/978-3-540-30585-9_46
15. Jung, Jae-IL and Kim, Jaeyeol and You, Younggap," Mobility Prediction Handover Using User Mobility Pattern and Guard Channel Assignment Scheme" published in Lecture Notes in Computer Science by Springer Berlin Heidelberg, vol. 3262, year 2004, pp 155-164. doi: 10.1007/978-3-540-30197-4_16. Url: http://dx.doi.org/10.1007/978-3-540-30197-4_16
16. Ken Murray, Rajiv Mathur, and Dirk Pesch. 2003. Intelligent access and mobility management in heterogeneous wireless networks using policy. In *Proceedings of the 1st international symposium on Information and communication technologies* (ISICT '03). Trinity College Dublin 181-186. Url: http://dl.acm.org/citation.cfm?id=963637
17. MeriemKassar, Brigitte Kervella, Guy Pujolle, An overview of vertical handover decision strategies in heterogeneous wireless networks, Computer Communications, Volume 31, Issue 10, 25 June 2008, Pages 2607-2620, ISSN 0140-3664, 10.1016/j.comcom.2008.01.044. Url: http://www.sciencedirect.com/science/article/pii/S0140366408000492
18. MariemZekri, BadiiJouaber, DjamalZeghlache, A review on mobility management and vertical handover solutions over heterogeneous wireless networks, Computer Communications, Volume 35, Issue 17, 1 October 2012, Pages 2055-2068, ISSN 0140-3664, 10.1016/j.comcom.2012.07.011. Url: http://www.sciencedirect.com/science/article/pii/S0140366412002526
19. Qing Wei, Károly Farkas, Christian Prehofer, Paulo Mendes, Bernhard Plattner, Context-aware handover using active network technology, Computer Networks, Volume 50, Issue 15, 18 October 2006, Pages 2855-2872, ISSN 1389-1286, 10.1016/j.comnet.2005.11.002. Url: http://www.sciencedirect.com/science/article/pii/S1389128605003865
20. Moonjeong Chang, Hyunjeong Lee, Meejeong Lee, A per-application mobility management platform for application-specific handover decision in overlay networks, Computer Networks, Volume 53, Issue 11, 28 July 2009, Pages 1846-1858, ISSN 1389-1286, 10.1016/j.comnet.2009.02.018. Url: http://www.sciencedirect.com/science/article/pii/S1389128609000553
21. Jian Wang, Jeng-Yuan Yang, Irfan M. Fazal, Nisar Ahmed, Yan Yan, Hao Huang, Yongxiong Ren, Yang Yue, Samuel Dolinar, Moshe Tur & Alan E. Willner,"Terabit free-space data transmission employing orbital angular momentum multiplexing" published in Nature Photonics 6, 488–496 (2012) doi: 10.1038/nphoton. 2012.138 Url: http://www.nature.com/nphoton/journal/v6/n7/full/nphoton.2012.138.html
22. Salkintzis, A.K.; , "WLAN/3G interworking architectures for next generation hybrid data networks," *Communications, 2004 IEEE International Conference on* , Vol. 7, no., pp. 3984- 3988 Vol.7, 20-24 June 2004, doi: 10.1109/ICC.2004.1313299 Url: http://ieeexplore.ieee.org/stamp/stamp.jsp?tp=&arnumber=1313299&isnumber=29132

23. Jindal, S.; Jindal, A.; Gupta, N.; , "Grouping WI-MAX, 3G and WI-FI for wireless broadband," *Internet, 2005.The First IEEE and IFIP International Conference in Central Asia on* , vol., no., pp. 5 pp., 26-29 Sept. 2005, doi:10.1109/CANET.2005.1598202 Url: http://ieeexplore.ieee.org/stamp/stamp.jsp?tp=&arnumber=1598202&isnumber=33616
24. Ian F. Akyildiz, Xudong Wang, Weilin Wang, Wireless mesh networks: a survey, Computer Networks, Volume 47, Issue 4, 15 March 2005, Pages 445-487, ISSN 1389-1286, 10.1016/j.comnet.2004.12.001. Url: http://www.sciencedirect.com/science/article/pii/S1389128604003457
25. Dhawan, S.; , "Analogy of Promising Wireless Technologies on Different Frequencies: Bluetooth, WiFi, and WiMax," *Wireless Broadband and Ultra Wideband Communications, 2007. AusWireless 2007. The 2nd International Conference on* , vol., no., pp. 14, 27-30 Aug. 2007, doi: 10.1109/AUSWIRELESS.2007.27 Url: http://ieeexplore.ieee.org/stamp/stamp.jsp?tp=&arnumber=4299663&isnumber=4299641
26. Ibanez, S.R.; Santos, R.A.; Licea, V.R.; Block, A.E.; Ruiz, M.A.G.; , "Hybrid WiFi-WiMax Network Routing Protocol," *Electronics, Robotics and Automotive Mechanics Conference, 2008. CERMA '08* , vol., no., pp. 87-92, Sept. 30 2008-Oct. 3 2008, doi: 10.1109/CERMA.2008.24 Url: http://ieeexplore.ieee.org/stamp/stamp.jsp?tp=&arnumber=4641052&isnumber=4641028
27. Ehsan Pourfakhar, Amir Masoud Rahmani, A hybrid QoS multicast framework-based protocol for wireless mesh networks, Computer Communications, Volume 33, Issue 17, 15 November 2010, Pages 2079-2092, ISSN 0140-3664, 10.1016/j.comcom.2010.07.026. Url: http://www.sciencedirect.com/science/article/pii/S0140366410003543
28. Andrea Calvagna, Aurelio La Corte, Sabrina Sicari, Mobility and quality of service across heterogeneous wireless networks, Computer Networks, Volume 47, Issue 2, 4 February 2005, Pages 203-217, ISSN 1389-1286, 10.1016/j.comnet.2004.07.005. Url: http://www.sciencedirect.com/science/article/pii/S1389128604001951
29. Antonio Guerrero-Ibáñez, Juan Contreras-Castillo, Antoni Barba, Angélica Reyes, A QoS-based dynamic pricing approach for services provisioning in heterogeneous wireless access networks, Pervasive and Mobile Computing, Volume 7, Issue 5, October 2011, Pages 569-583, ISSN 1574-1192, 10.1016/j. pmcj. 2010.10.003. Url: http://www.sciencedirect.com/science/article/pii/S1574119210001148
30. Chowdhury, A.S.; Gregory, M.; , "Hybrid next generation mobile system analysis based on Internet applications," *Telecommunication Networks and Applications Conference (ATNAC), 2010 Australasian* , vol., no., pp.90-95, Oct. 31 2010-Nov. 3 2010, doi: 10.1109/ATNAC.2010.5680263 Url: http://ieeexplore.ieee.org/stamp/stamp.jsp?tp=&arnumber=5680263&isnumber=5679553
31. Jiannong Cao; Chisheng Zhang; Jun Zhang; Yueming Deng; Xin Xiao; Miao Xiong; Jie Zhou; Yang Zou; Gang Yao; Wei Feng; Liang Yang; Yao Yu; , "SHAWK: Platform for Secure Integration of Heterogeneous Advanced Wireless Networks," *Advanced Information Networking and Applications Workshops (WAINA), 2012 26th International Conference on* , vol., no., pp.13-18, 26-29 March 2012 doi:10.1109/WAINA.2012.118 Url: http://ieeexplore.ieee.org/stamp/stamp.jsp?tp=&arnumber=6185092&isnumber=6185080
32. Tang Long; Chi He-hua; Wu Jue-bo; , "Study on Heterogeneous Networks Integration Based on Cognitive Wireless Network," *Computational Intelligence and Software Engineering (CiSE), 2010 International Conference on* , vol., no., pp.1-5, 10-12 Dec. 2010,doi:10.1109/CISE.2010.5677267 Url: http://ieeexplore.ieee.org/stamp/ stamp.jsp?tp=&arnumber=5677267&isnumber=5676710
33. Fan Zhi-hui; Zhang Zhi-xue; Wang Hui; , "A Vertical Handoff Algorithm Application to the Integration of WLAN and WMAN Wireless Heterogeneous Networks," *Computational and Information Sciences (ICCIS), 2012 Fourth International Conference on* , vol., no., pp.803-806, 17-19 Aug. 2012, doi: 10.1109/ICCIS.2012.57 Url: http://ieeexplore.ieee.org/stamp/stamp.jsp?tp=&arnumber=6300745&isnumber=6299898
34. S. Toumpis, "Capacity bounds for three classes of wireless networks: Asymmetric, cluster, and hybrid," in Proceeding of the ACM MobiHoc,2004, pp. 133–144 Url: http://www.sigmobile.org/mobihoc/2004/presentations/p133-toumpis.pdf
35. Husain Shahnawaz, Sharma R., Mukesh Chand," A Rms Approach For Channel Allocation Under Hybrid Mode For Mobile Computing", presented in International Conference in Advanced Computing & Communication

Technologies ICACCT-2008,8-9 November organized by APIIT ,Panipat, India & Published in Proc. ISBN 81-87433-68-X,pp 588-590.

36. Shahnawaz, Husain; Gupta, S. C.; Mukesh, Chand; , "Denial of Service attack in AODV & friend features extraction to design detection engine for intrusion detection system in Mobile Adhoc Network," *Computer and Communication Technology (ICCCT), 2011 2nd International Conference on* , vol., no., pp.292-297, 15-17 Sept. 2011, doi: 10.1109/ICCCT.2011.6075162 URL: http://ieeexplore.ieee.org/stamp/stamp.jsp?tp=&arnumber=6075162&isnumber=6075092
37. Husain Shahnawaz, Gupta S.C., "Friend Features Extraction to Design Detection Engine for Intrusion Detection Systemin Mobile Adhoc Network", Published in International Journal of Computer Science & Information Technology, ISSN 0975-9646, Vol (2) Issue 4, 2011, pp 1569-1573 URL:http://www.ijcsit.com/docs/Volume%202/vol2issue4/ijcsit2011020440.pdf
38. Husain, S.; Gupta, S.C.; Chand, M.; Mandoria, H.L.; , "A proposed model for Intrusion Detection System for mobile Adhoc network," *Computer and Communication Technology (ICCCT), 2010 International Conference on* , vol., no., pp. 99-102, 17-19 Sept. 2010, doi: 10.1109/ICCCT.2010.5640420 URL: http://ieeexplore.ieee.org/stamp/stamp.jsp?tp=&arnumber=5640420&isnumber=5640373
39. Husain S.; Gupta, S.C.; , "Black Hole Attack in AODV & Unique Friend Features Extraction to Design Detection Engine for Intrusion Detection System in Mobile Adhoc Network**", published in** Journal of Engineering Science and Technology (JESTEC) Vol 7 issue 5, October 2012; ISSN : 1823-4690, pp 591-601. URL: http://jestec.taylors.edu.my/V7Issue5.htm
40. Husain Shahnawaz, Joshi R.C, Gupta S.C, "Design of Detection Engine for Wormhole Attack in Adhoc Network Environment" published in International Journal of Engineering and Technology (IJET), Vol. 4 issue 6, December 2012- January 2013, ISSN: 0975-4024, pp 381-395. URL:http://www.enggjournals.com/ijet/docs/IJET12-04-06-012.pdf

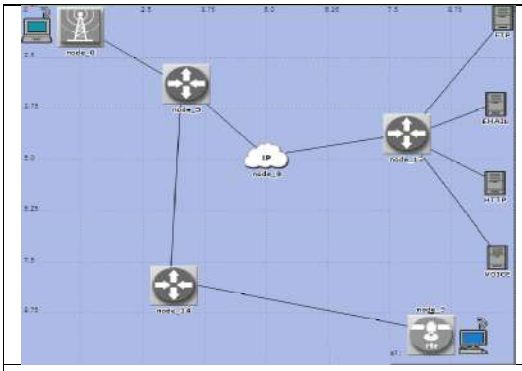

Figure 1: Tight Interface / Coupling

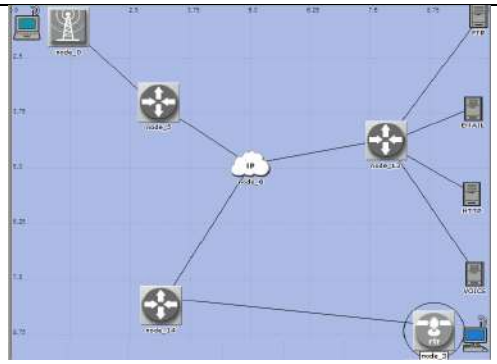

Figure 2: Loose Interface/Coupling

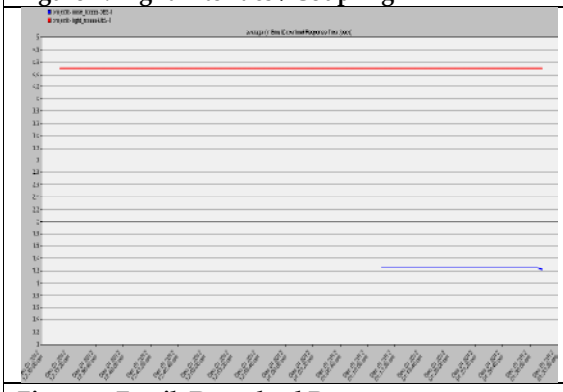

Figure 3: Email: Download Response

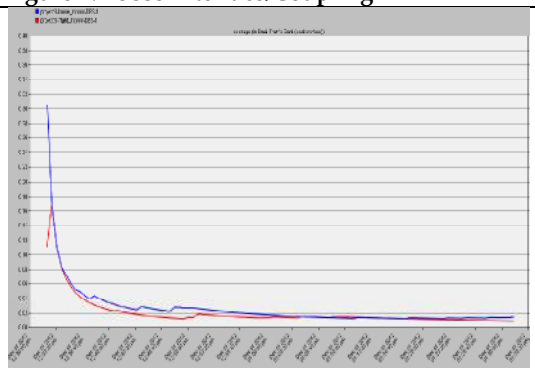

Figure4: Email: Traffic Sent

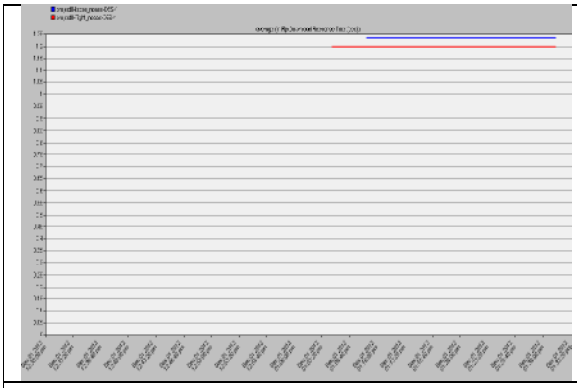

Figure 5: FTP: Download Response

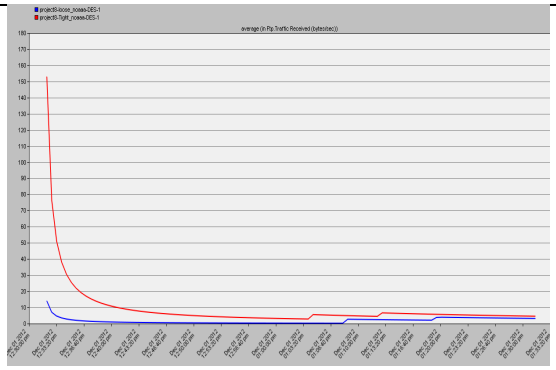

Figure 6: FTP: Traffic Received

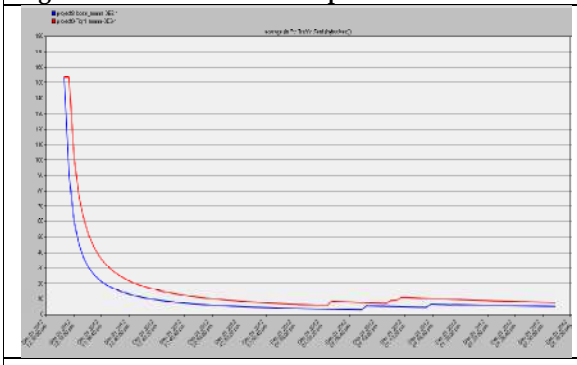

Figure 7: FTP: Traffic Sent

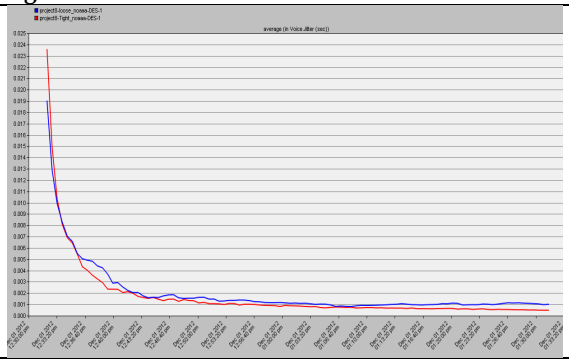

Figure 8: VOIP: Jitter

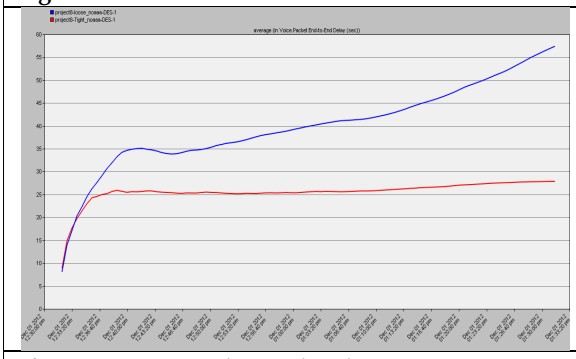

Figure 9: VOIP: End to End Delay

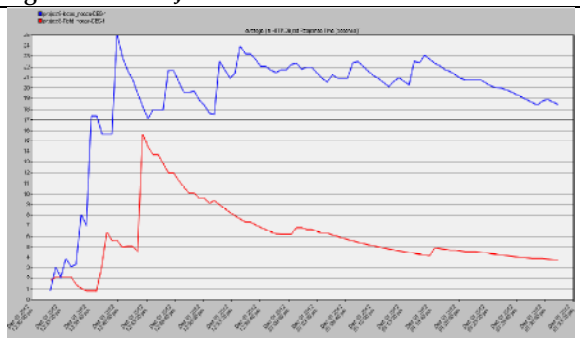

Figure 10: http: Object Response Time

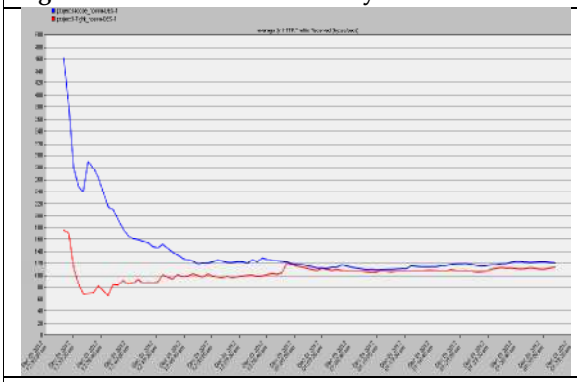

Figure 11: http: Traffic Received

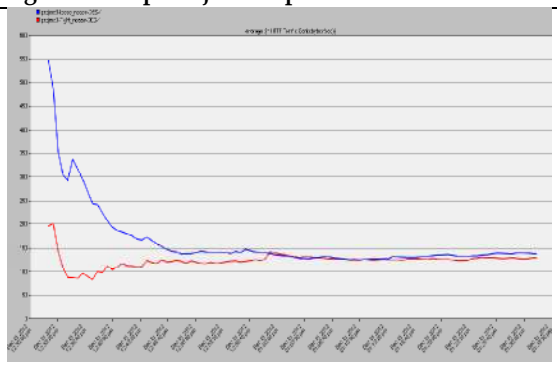

Figure 12: http: Traffic Sent

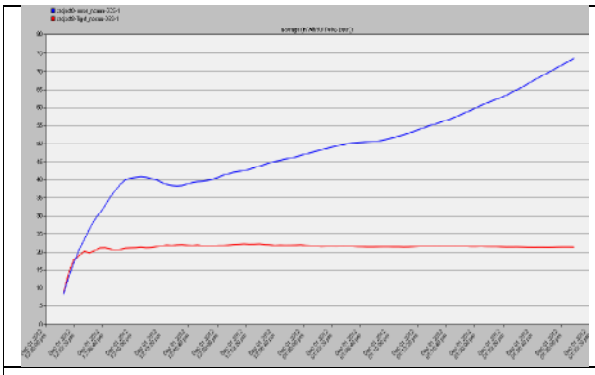

Figure 13: WiMax: Delay

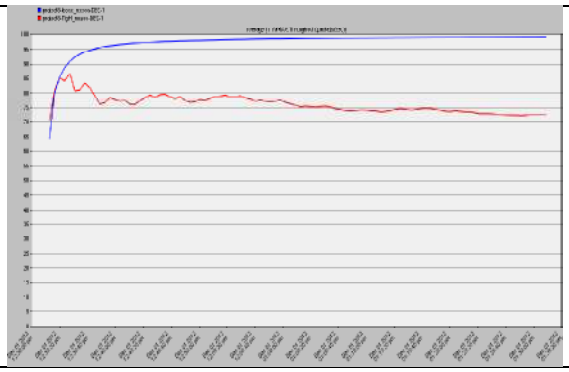

Figure 14: WiMax: Throughput

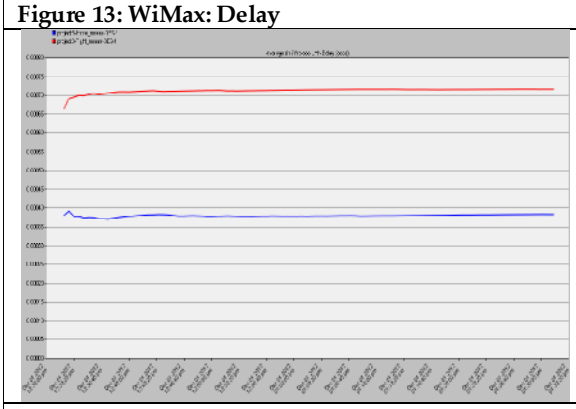

Figure15: WLAN: Delay

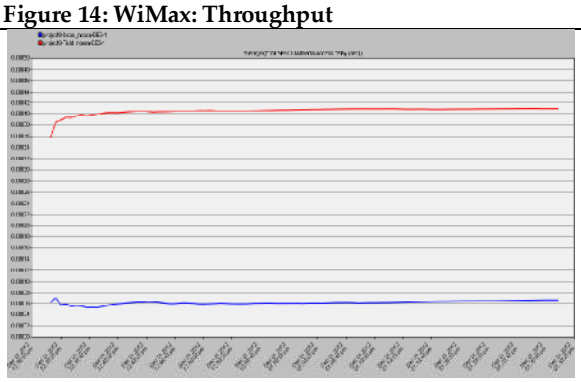

Figure 16: WLAN: Throughput

Indian Journal of Natural Sciences *www.tnsroindia.org.in ©IJONS*

Vol.15 / Issue 83 / Apr / 2024 *International Bimonthly (Print) – Open Access* *ISSN: 0976 – 0997*

RESEARCH ARTICLE

Descriptive Analytics On Healthcare Data –A Systematic Approach To Enhance Patient Engagement

Lavonya A[1], Sunil Raj Y[2], Charles S[3] and A Leolin Arockiadass[4]

[1]PG Student, Dept of Data Science, St. Xavier's College (Autonomous), Palayamkottai, India.
[2]Assistant Professor, Dept of Data Science, St. Xavier's College (Autonomous), Palayamkottai, India.
[3]Assistant Professor, Dept. of Computer Science, AL Musana Institute of Engineering & Technology, Sultanate of Oman, UAE
[4]Assistant Professor, Dept of Computer Science, St. Xavier's College (Autonomous), Palayamkottai, India.

Received: 30 Dec 2023 Revised: 09 Jan 2024 Accepted: 12 Mar 2024

***Address for Correspondence**
Sunil Raj Y
Assistant Professor,
Dept of Data Science,
St. Xavier's College (Autonomous),
Palayamkottai, India.
Email: ysrsjccs@gmail.com

ABSTRACT

Healthcare analytics leverages mathematical methodologies to analyze vast amounts of data, facilitating informed decision-making within the healthcare sector. By integrating data-driven insights, healthcare analytics enhances patient care outcomes and operational efficiencies across various healthcare settings. Its application spans from refining diagnostic processes to optimizing resource allocation and treatment strategies. The transformative impact of healthcare analytics parallels its counterparts in finance, marketing, and technology sectors, driving advancements in healthcare delivery. Despite its potential benefits, healthcare analytics faces challenges such as data privacy concerns and interoperability issues that necessitate innovative solutions. Addressing these challenges is essential to fully harness the potential of healthcare analytics in improving patient outcomes and organizational effectiveness.

Keywords: Data Analytics, Descriptive Analytics, Diagnostic Analytics, Predictive Analytics, Prescriptive Analytics, Healthcare Analytics

INTRODUCTION

Data analytics plays a crucial role in extracting valuable insights from raw data, with its applications expanding significantly due to the widespread adoption of smart devices, which furnish abundant information about monitored

assets. The temporal dimension of analytics empowers organizations to make informed decisions at specific junctures, profoundly impacting business performance metrics such as revenue, cost management, resource utilization, and operational efficiency. Integration of advanced analytical tools like machine learning (ML) and artificial intelligence (AI) further augments the efficacy of data analytics processes. Access to data at various managerial levels facilitates streamlined monitoring of processes. Depending on the timing of execution, data analytics finds diverse applications, broadly categorized as descriptive, diagnostic, predictive, and prescriptive analytics. Healthcare represents society's collective endeavor to ensure, finance, provide, and promote health, with a paradigm shift in the twentieth century towards wellness and preventive measures. Standardized protocols within healthcare aid in evaluating actions or situations influencing decision-making processes. As a multi-dimensional system, healthcare aims to diagnose and treat illnesses or disabilities, emphasizing the fundamental goal of fostering overall well-being. The following sections are organized as; background of the study, review of literature, analysis on the existing work, issues discussed and amble solutions for the issues and lastly the conclusion.

Background

Healthcare analytics, a specialized branch of data analytics, harnesses historical and current data to extract actionable insights, refine decision-making processes, and optimize outcomes within the healthcare domain. Beyond merely benefiting healthcare organizations, this analytical approach plays a pivotal role in enhancing the overall patient experience and advancing health outcomes. Given the vast reservoir of detailed records pervasive throughout the healthcare industry, a wealth of valuable data is readily available, presenting abundant opportunities for thorough analysis and interpretation.

Figure 1, presents a visual representation of how healthcare analytics fits within the field of data analytics. It illustrates how healthcare analytics is a specialized subset of data analytics, focusing specifically on the healthcare sector. Healthcare analytics, including descriptive, diagnostic, predictive, and prescriptive analytics, play a vital role in improving patient care for those with End Stage Renal Disease (ESRD). Descriptive analytics helps understand past trends, while diagnostic analytics identifies root causes of specific events. Descriptive analytics provides insights into historical events, addressing queries like the number of hospitalized patients or the percentage discontinuing home therapy. Diagnostic analytics delves into understanding causal factors behind events, addressing queries like why patients visited hospitals, abandoned home therapy, or failed to meet treatment targets [11]. Predictive analytics is a powerful tool in healthcare, leveraging historical data to forecast future events with notable accuracy. These can predict patient transitions, such as those likely to shift from home therapy to in-center care, facilitating resource allocation and patient support planning [12]. Healthcare analytics contributes significantly to improving patient outcomes by identifying trends and patterns for early disease detection and timely intervention, ultimately enhancing patient well-being. Personalized medicine is facilitated through the analysis of patient data, allowing for the development of tailored treatment plans that consider individual health characteristics, thus improving the efficacy of medical interventions and patient satisfaction [13]. Additionally, analytics plays a crucial role in fraud detection, ensuring fairness and accuracy in financial transactions, which is essential for maintaining trust and integrity within the healthcare system. Healthcare analytics significantly enhances the quality of patient services by providing insights into industry trends and practices. Descriptive analytics, known for its ability to unveil prevailing facts, is particularly suited for examining healthcare data.

REVIEW OF LITERATURE

Descriptive analytics involves the exploration and interpretation of historical data to identify patterns and trends. In the healthcare context, it encompasses various components such as data visualization, summarization, and reporting techniques. Studies by Jeremiah O A, *et al*. (2024) highlight the importance of understanding the foundational aspects of analytics in healthcare settings[14]. Numerous studies have demonstrated the diverse applications of descriptive analytics in healthcare. Research by F AI Zoubi, *et al*. showcases how descriptive analytics can be employed to monitor patient health, optimize resource allocation, and improve overall operational efficiency within healthcare

organizations [15].The dynamic nature of healthcare demands a constant evolution of analytic approaches. Research by Lee and Kim., 2023, explores emerging trends such as the integration of artificial intelligence and machine learning techniques with descriptive analytics, offering insights into potential advancements in the field. Sabah M, *et al*, 2022, have focused on Health data analytics and identified the improvements it makes towards patient care, faster diagnoses, preventive measures, more personalized treatment and provide more informed decision-making. Also, it was found that healthcare analytics could assist improving patient outcomes, enhancing care management, and address social determinants of health [7, 11]. As the health analytics grows eventually in the healthcare space, healthcare organizations could gather data from manifold sources, after which apply data analytics, and provide insights for the population.

METHODOLOGY

Healthcare analytics has emerged as a pivotal tool in improving patient care and operational efficiency within the healthcare domain. This proposed methodology outlines a structured approach to conducting research in healthcare analytics, aiming to address existing research issues and provide actionable solutions. The methodology integrates various analytical techniques and data-driven approaches to inform decision-making processes in healthcare settings. The first step in our proposed methodology is to identify and define the specific healthcare problem or challenge to be addressed through analytics. This may include issues such as optimizing resource allocation, improving patient outcomes, reducing costs, or enhancing operational efficiency. Once the problem is identified, relevant data sources need to be identified and collected. This may include electronic health records (EHRs), medical imaging data, administrative data, patient surveys, and other relevant sources. Data cleaning and preprocessing techniques are then applied to ensure data quality and consistency. EDA involves analyzing and visualizing the collected data to gain insights into underlying patterns, trends, and relationships. Descriptive statistics, data visualization techniques, and exploratory data mining methods are employed to identify potential correlations and associations within the data. Predictive modeling techniques, such as machine learning algorithms, are utilized to build predictive models based on the available data. These models can be used to forecast future healthcare outcomes, predict patient risk levels, or identify potential areas for intervention. Figure 2, describe the methodology used to analyze the patient engagement scenario for reducing the complication ratio and reducing the unnecessary visits. After the exploration of data, models are developed after which it is evaluated and validated using appropriate metrics and validation techniques. This ensures the reliability and generalizability of the models and their applicability to real-world healthcare scenarios. The insights gained from the analytics process are interpreted in the context of the healthcare problem being addressed. Key findings and actionable insights are identified, which can inform decision-making processes and drive improvements in patient care and healthcare operations. The validated models and insights are then implemented into healthcare practice, either through integration into existing systems or through the development of new tools and workflows. Close collaboration with healthcare stakeholders is essential to ensure successful implementation and adoption. Finally, the implemented solutions are continuously monitored and evaluated to assess their impact on healthcare outcomes and operations. Iterative refinements and improvements are made based on feedback and new data, ensuring ongoing optimization and effectiveness.

RESULTS AND DISCUSSION

The dataset chosen consists features of about 300k, which records the medical appointments of patients. The focus is to analyze whether the patients showed up for their appointments and the factors behind their response. The dataset consists of 15features, including appointment details, medical conditions, and appointment attendance status. Age and gender represent demographic information, while Appointment Registration and Appointment Date indicate scheduling details. The Status column distinguishes between patients who attended their appointments and those who missed them. Medical conditions such as diabetes, alcoholism, hypertension, handicap, smokers, tuberculosis, and whether the patient has a medical scholarship are also recorded. SMS_ Reminder indicates if the patient received reminder messages. Awaited Time represents the duration patients had to wait from registration to appointment.

This data allows for analysis of factors influencing appointment attendance and the effectiveness of SMS reminders. Figure 3 displays the count of patient show-ups categorized by various factors such as age, gender, medical conditions (diabetes, alcoholism, hypertension, handicap, smokers, tuberculosis), presence of medical scholarship, receipt of SMS reminders, and waiting time. This visualization provides insights into which demographics or conditions correlate with higher or lower attendance rates, aiding in the identification of factors influencing appointment attendance. Such analysis can inform targeted interventions to improve attendance and patient outcomes.

Figure 4 presents a gender distribution plot that depicts the count of appointments by gender, further segmented by appointment status (attended or missed). This visualization offers a comprehensive view of appointment attendance patterns across different genders. By visualizing the distribution of show-ups and no-shows within each gender category, healthcare providers can gain insights into potential gender-specific factors influencing appointment adherence. This understanding facilitates the development of targeted interventions to address any disparities and improve overall appointment attendance rates. Figure 5 displays a count plot based on the "Day Of The Week" variable, illustrating the distribution of appointments across different days of the week. This visualization provides insights into appointment scheduling patterns, revealing which days are most popular for appointments and which days have lower appointment volumes. Analyzing this information enables healthcare providers to optimize appointment scheduling and resource allocation, ensuring efficient and effective healthcare service delivery throughout the week.

Figure 6 depicts the percentage of missing values across different variables in the dataset. This visualization offers insights into the completeness of the data and highlights any variables with significant missing values. Understanding the extent of missing data is crucial for ensuring the reliability and validity of analytical results. By identifying variables with high percentages of missing values, researchers can prioritize data collection efforts or employ appropriate imputation techniques to mitigate the impact of missing data on subsequent analyses. Figure 7 illustrates the status of patients who turned up for their appointments, with each status. Also, the visualization provides a nuanced understanding of the various factors and circumstances influencing appointment attendance, highlighting the diverse pathways through which patients ultimately turn up for their scheduled appointments.

Comparison and Analysis

The descriptive analysis is conducted on the chosen patient data set where it is free from missing values. Among the chosen set of data about 69.75% of people showed-up and the remaining 30.24%did not show up for their appointments. The analysis shows that female patients have taken more appointments than male patients. There are around 200505 Females and out of them around 70.13% showed-up for their appointments and the remaining 29.87% did not show up. Out of 99495 males, 69% showed-up while 31% did not show up. The highest no of people showed-up was between the age group 41-61 and between the age group between 101-121 people did not show up for their appointments. The least number of appointments were made on Sunday while most of them are on Wednesday The observed results in figure 8, shows that the proposed methodology exhibits better based on the size of data chosen. As the impact the complication ratio is comparatively reduced to 98% while the existing proposal showed 92%. Also, the number of unnecessary visits of the patients is also reduced and it was up to 89%. This shows the importance of analytics in healthcare as it substantiates the assistants by enhancing the overall performance, while provide better service.

CONCLUSION

Healthcare analytics stands as a transformative tool in enhancing patient care and operational efficiency within the healthcare sector. The proposed methodology delineates a systematic approach to healthcare analytics research, aimed at tackling prevailing research challenges and furnishing actionable solutions. By amalgamating diverse analytical techniques and data-driven methodologies, informed decision-making in healthcare settings becomes

attainable. Initial findings from patient data analysis reveal that about 69.75% of individuals attended their appointments while 30.24% did not, underscoring the significance of attendance trends. Gender-based analysis demonstrates that female patients made more appointments (200,505) compared to males (99,495), with 70.13% of females showing up versus 69% of males. Age-group specific analysis indicates the highest attendance within the 41-61 age range, while those aged 101-121 exhibited lower attendance rates. Additionally, appointment distribution analysis highlights a preference for midweek appointments, with fewer appointments scheduled for Sundays. Therefore, it is evident that insights from the descriptive analytics drives informed decision-making. The implementation of validated solutions in healthcare, enable continuous refinement to optimize scheduling, and service delivery for improved patient outcomes and operational excellence.

REFERENCES

1. Stages of Data Analytics Maturity: Challenging Gartner's Model. Available at: https://www.linkedin.com/pulse/4-stages-data-analytics-maturity-challenging-gartners-taras-kaduk/, accessed January 30, 2018.
2. https://www.coursera.org/in/articles/healthcare-analytics
3. https://onlinestats.canr.udel.edu/key-components-of-data-analytics-for-healthcare/
4. Mohammed Badawy, Nagy Ramadan and Hesham Ahmed Hefny – "Healthcare predictive analytics using machine learning and deep learning techniques: a survey (2023)"
5. Metta Ongkasuwan, Wut Sookcharoen, "Data analytics for service and operation management improvement in medical equipment industry", 2018 5th International Conference on Business and Industrial Research (ICBIR),
6. Sabah Mohammed, Tai-Hoon Kim, Ruay-Shiung Chang, Carlos Ramos, "Guest Editorial: Data Analytics for Public Health Care," IEEE Journal of Biomedical and Health Informatics, Vol. 26 (4), 2022.
7. Sanket Patel, Decoding Healthcare Analytics: Definition, Types, and Importance, Digicorp, 2024.
8. Bombard Y, Baker G R, Orlando, et. al, Engaging Patients To Improve quality of care- A Systematic Review , Implementation science (2018)
9. Sabah Mohammed, Tai-Hoon Kim, RuayShiung Chang, Carlos Ramos. "Guest Editorial: Data Analytics for Public Health Care" , IEEE Journal of Biomedical and Health Informatics, 2022.
10. Metta Ongkasuwan, Wut Sookcharoen. "Data analytics for service and operation management improvement in medical equipment industry", 2018 5th International Conference on Business and Industrial Research (ICBIR), 2018
11. Batko K, Ślęzak A. The use of Big Data Analytics in healthcare. J Big Data. 2022;*9*(1):3. doi: 10.1186/s40537-021-00553-4. Epub 2022 Jan 6. PMID: 35013701; PMCID: PMC8733917.
12. Jiaqi Wang, Junyu Luo, Muchao Ye, Xiaochen Wang, Yuan Zhong, Aofei Chang, Guanjie Huang, Ziyi Yin, Cao Xiao, Recent Advances in Predictive Modeling with Electronic Health Records, arXiv, 2024.
13. Dinesh Kumar & Nidhi Suthar (2024) Predictive analytics and early intervention in healthcare social work: a scoping review, Social Work in Health Care, DOI: 10.1080/00981389.2024.2316700.
14. Jeremiah Olawumi Arowoogun, Oloruntoba Babawarun, Rawlings Chidi,Adekunle Oyeyemi Adeniyi and Chioma Anthonia Okolo, A comprehensive review of data analytics in healthcare management: Leveraging big data for decision-making, World Journal of Advanced Research and Reviews, 2024, 21(02), 1810–1821.
15. Al Zoubi F, Beaulé PE, Fallavollita P. Factors influencing delays and overtime during surgery: a descriptive analytics for high volume arthroplasty procedures. Front Surg. 2024 Jan 4;10:1242287. doi: 10.3389/fsurg.2023.1242287. PMID: 38249310; PMCID: PMC10797887.

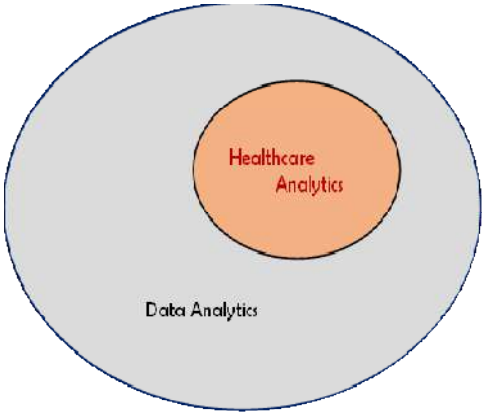

Figure 1: Healthcare analytics in the perspective of Data Analytics

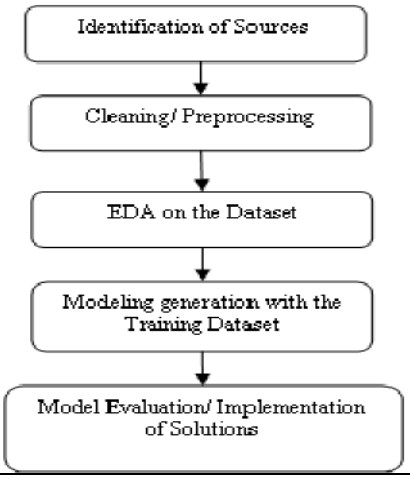

Figure 2. Methodology used for the Analysis of Healthcare Data

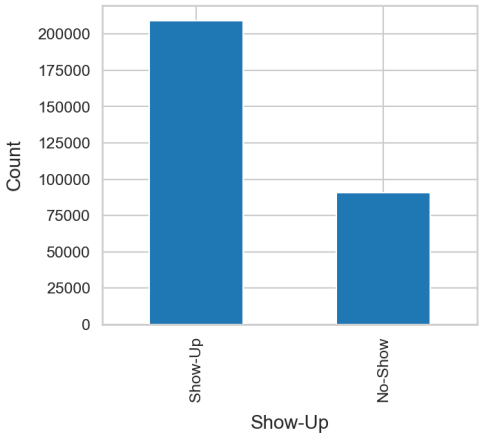

Figure 3: Count of Show-Upper category

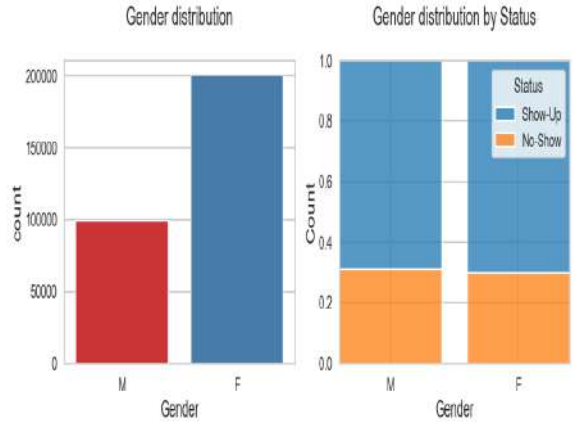

Figure 4: Gender Distribution Plot by count and by status

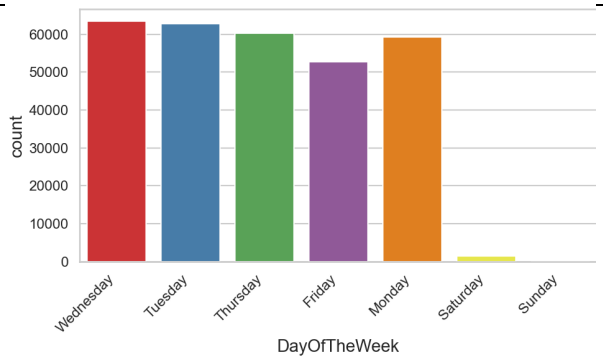

Figure 5: Count Plot based on Day Of The week

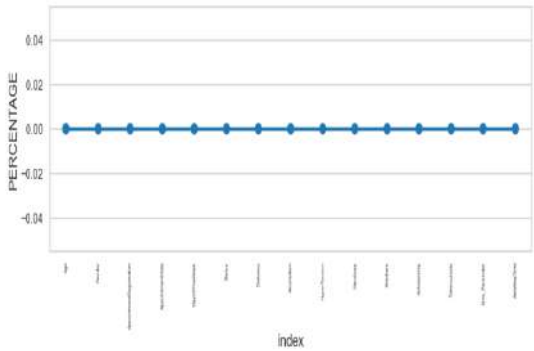

Figure 6:Percentage Of missing Values

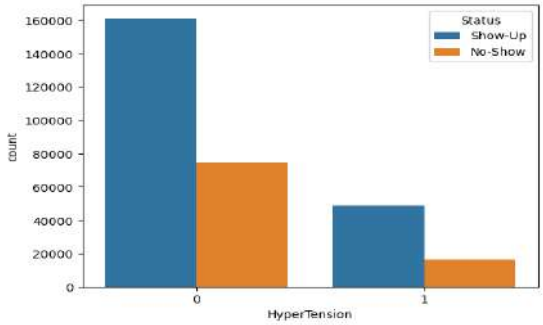

a) Status of persons showed up based on hypertension

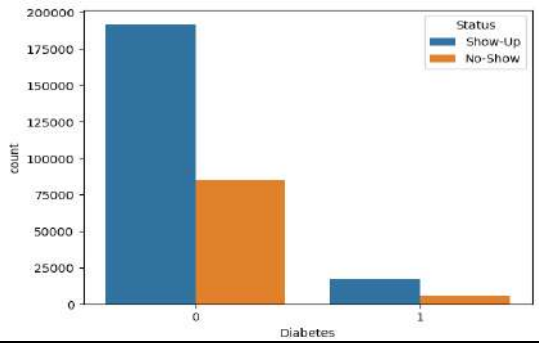

b) Status of persons showed up based on diabetes

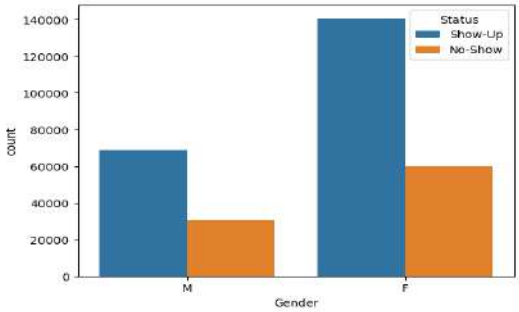

c) Status of persons showed up based on Gender

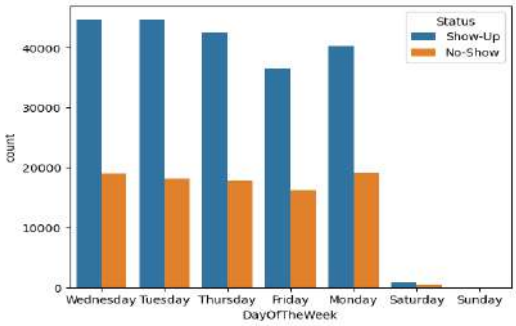

d) Status of persons showed up based on days of the week

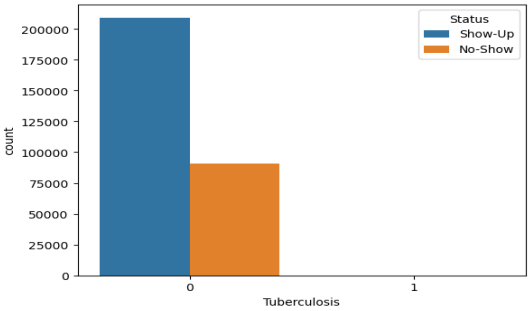

e) Status of persons showed up based on tuberculosis

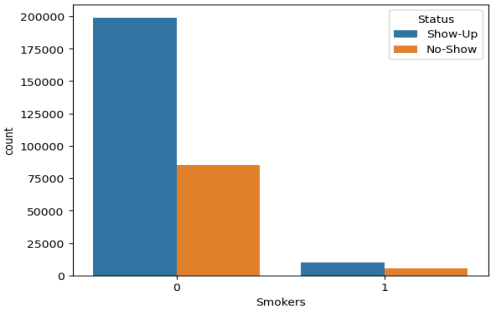

f) Status of persons showed up based on smokers

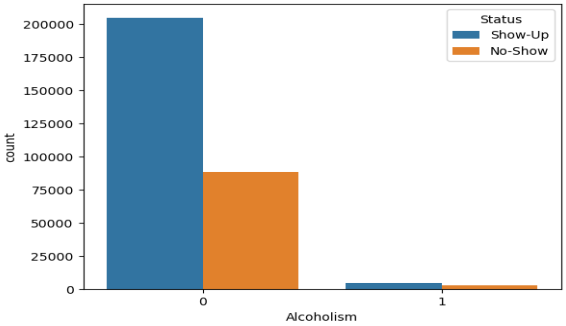

g) Status of persons showed up based on alcoholism

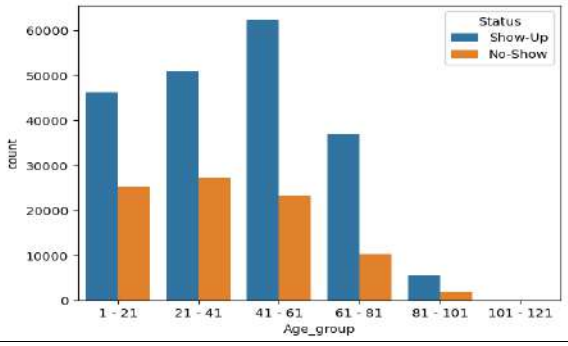

h) Status of persons showed up based on age group

Figure 7: Status of Patients showed up based on a) Hyper Tension, b) Diabetes, c) Gender, d) Days of the week, e) Tuberculosis, f) Smokers, g) Alcoholism, h) Age group

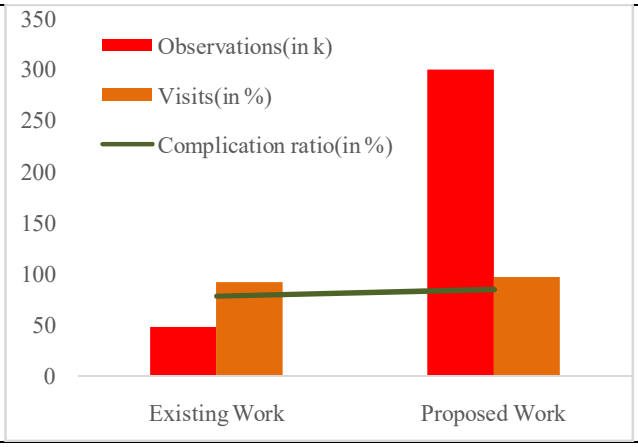

Figure 8. Comparison on the Observations - Reduction of Complication and Visits

Indian Journal of Natural Sciences *www.tnsroindia.org.in ©IJONS*

Vol.15 / Issue 83 / Apr / 2024 *International Bimonthly (Print) – Open Access* *ISSN: 0976 – 0997*

RESEARCH ARTICLE

BER Performance Evaluation of DWDM Optical Network at Various Channel Spacing

Poorna Lakshmi Uppalapati[1]*, Kotika Sai Kumar[2], Lingaiahgari Amulya[2] and Arige Sai Yashwanth[2]

[1]Professor and HoD, Department of Electronics and Communication Engineering, Vignana Bharathi Institute of Technology, Hyderabad, Telangana, India.
[2]Student, Department of Electronics and Communication Engineering, Vignana Bharathi Institute of Technology, Hyderabad, Telangana, India.

Received: 08 Nov 2023 Revised: 11 Jan 2024 Accepted: 09 Mar 2024

***Address for Correspondence**
Poorna Lakshmi Uppalapati
Professor and HoD,
Department of Electronics and Communication Engineering,
Vignana Bharathi Institute of Technology,
Hyderabad, Telangana, India
Email: uppalapati.poornalakshmi@vbithyd.ac.in

ABSTRACT

Dense Wavelength Division Multiplexing (DWDM) is a method of optical fiber transmission that employs densely spaced light frequencies and can simultaneously transport large amounts of data. This is a useful method to increase the system's capacity. In this work, we studied the 16 x 10 GBps DWDM communication network over a 50 km length Single-Mode Fiber (SMF) at various channel spacing, including 0.8 nm and 1.6 nm with bit rates of 10 Gbps.

Keywords: DWDM, Single-Mode Fiber, Dispersion-Compensating Fiber, Channel Spacing

INTRODUCTION

The development of optical communication technologies has been accelerated by the expansion of data-hungry applications and the unrelenting demand for higher network capacity [1]. Dense Wavelength Division Multiplexing (DWDM) has become a key option, enabling the simultaneous transmission of numerous data channels over a single optical fiber while utilizing various light wavelengths [2]. The performance of the DWDM optical network can fluctuate significantly when the channel spacing, which is the frequency difference between neighboring channels, varies [3, 4]. In This work, the Bit Error Rate (BER) of a DWDM optical network over a range of channel spacing values [5] is studied. A key indicator for evaluating the DWDM optical network is BER. It measures the proportion of wrongly received bits to all transmitted bits, demonstrating the robustness of the system against errors and the overall data integrity. It is possible to learn a lot about how the network reacts to changes in the spectral allocation of channels by methodically

analyzing the BER performance at various channel spacing configurations[6]. The study entails a thorough examination through simulation. The effect of various channel spacing values on the BER performance are investigated, revealing information on the network's capability to maintain dependable data transmission under various circumstances [7, 8, 9]. The results of the study are expected to aid in the optimization of DWDM optical networks and in the development of more reliable and effective communication systems that can handle the increasing demands of contemporary datacentric environments[10, 11].

Schematic of DWDM system

Fig. 1 shows DWDM communication system. Multiple data at the output of transmitters is given to multiplexer, which is used to combine multiple data and transmit over an optical fibre. The signal is then given to an EDFA (erbium-doped fibre amplifier). The optical demultiplexer output is given to respective receivers.

BER Performance Analysis

BER performance is evaluated for channel spacing of 0.8 nm and 1.6 nm for 2, 4, 8 and 16-channel DWDM optical network. PRBS generator generates pseudo random bit sequence used to modulate the light carrier in the transmitter section. The modulated carrier signals are multiplexed using Multiplexer and placed on an optical fiber channel. At the other end of the optical fiber the wavelength selection filter selects and receiver detects the electrical signal. Power normalizer is used to normalize the power levels. BER tester is used to analyse the Bit error rate. Here, we're using two channels operating at a data rate of 10 Gbps. RSoft Otsim is uesd for the simulation of DWDM network. Table 1 shows BER values for 2 channel.

DWDM with channel spacing 0.8 nm and Table 2 shows BER values for 2 channel DWDM with channel spacing 1.6 nm. Fig. 3 shows log(BER) value for two channel DWDM system with channel spacing 0.8 nm and 1.6 nm. BER values for DWDM system with 1.6 nm channel spacing are better than 0.8 nm channel spacing. The same can be seen for 4, 8 and 16 channel DWDM system.

Table 3 shows BER values for 4 channel DWDM with channel spacing 0.8 nm and Table 4 shows BER values for 4 channel DWDM with channel spacing 1.6 nm. Fig. 4 shows log (BER) value for four channel DWDM system with channel spacing 0.8 nm and 1.6 nm. Similarly, the BER performance is evaluated for channel spacing 0.8 nm and 1.6 nm for 8 channel and 16 channel DWDM. Table ?? shows BER values for 8 channel DWDM with channel spacing 0.8 nm and Table ?? shows BER values for 8 channel DWDM with channel spacing 1.6 nm. Fig. 5 shows log (BER) value for eight channel DWDM system with channel spacing 0.8 nm and 1.6 nm. Table 7 shows BER values for 16 channel DWDM with channel spacing 0.8 nm and Table 8 shows BER values for 16 channel DWDM with channel spacing 1.6 nm. Fig. 6 shows log (BER) value for sixteen channel DWDM system with channel spacing 0.8 nm and 1.6 nm. It can be observed that Bit Error Rate decreases as channel spacing is increased. At the chosen parameters, data rate 10 Gbps, NRZ modulation and link length 50 km the BER values are far better than threshold value 10−12. For a DWDM network with channel spacing 1.6 nm, the BER value is even better than 0.8 nm channel spacing so the data rate can be increased.

CONCLUSION

Through this simulation, how different channel spacings influence the performance of a 2,4,8,16 channel DWDM system has been studied. BER performance evaluated at channel spacing 0.8 nm and 1.6 nm. BER value is better for channel spacing 1.6 nm for all the 2,4,8 and 16 DWDM networks. The BER value for the chosen simulation parameters is far better than the trshold value of BER 10−12. Therefore the data rate can be allowed to increase. Further the DWDM network with more number of channels, channel spacing and data rate can be studied.

REFERENCES

1. M. Meena, D. Meena, Performance analysis of dwdm optical network with dispersion compensation techniques for 4× 8 gbps transmission system, ICTACT Journal on Microelectronics 4 (2) (2018) 613–617.
2. D. Sharma, Y. Prajapati, Performance analysis of dwdm system for different modulation schemes using variations in channel spacing, Journal of Optical Communications 37 (4) (2016) 401–413.
3. M. Klinkowski, M. Ruiz, L. Velasco, D. Careglio, V. Lopez, J. Comellas, Elastic spectrum allocation for time-varying traffic in flexgrid optical networks, IEEE journal on selected areas in communications 31 (1)(2012) 26–38.
4. O. Gerstel, M. Jinno, A. Lord, S. B. Yoo, Elastic optical networking: A new dawn for the optical layer?, IEEE communications Magazine 50 (2)(2012) s12–s20.
5. P. Kaur, A. Gupta, M. Chaudhary, Comparative analysis of inter satellite optical wireless channel for nrz and rz modulation formats for different levels of input power, Procedia Computer Science 58 (2015) 572–577.
6. M. U. A. Siddiqui, H. Abumarshoud, L. Bariah, S. Muhaidat, M. A.Imran, L. Mohjazi, Urllc in beyond 5g and 6g networks: An interference management perspective, IEEE Access (2023).
7. G. Mohan, C. S. R. Murthy, A. K. Somani, Efficient algorithms for routing dependable connections in wdm optical networks, IEEE/ACM transactions on Networking 9 (5) (2001) 553–566.
8. D. D. Pradhan, A. Mandloi, Performance analysis of backward multipumped raman amplifier in dwdm system, Procedia computer science 115 (2017) 182–187.
9. H. A. Mohammed, Performance evaluation of dwdm for radio over fiber system with dispersion compensation and edfa, International Journal of Computer Applications 72 (10) (2013).
10. H. Louchet, A. Hodzic, K. Petermann, Analytical model for the performance evaluation of dwdm transmission systems, IEEE Photonics Technology Letters 15 (9) (2003) 1219–1221.
11. L. Xu, T. Wang, A. Chowdhury, J. Yu, G.-k. Chang, K. Fukuchi, T. Ito, Spectral efficient transmission of 40gbps per channel over 50ghz spaced dwdm systems using optical carrier suppression, separation and optical duobinary modulation, in: National Fiber Optic Engineers Conference, Optica Publishing Group, 2006, p. NTuC2.

Table 1: 2-channel with spacing of 0.8.

Wavelength	BER Value
1552.52	7.68e-13
1553.32	8 6.87e-20

Table 2: 2-channel with spacing of 1.6.

Wavelength	BER Value
1552.52	6.13e-25
1554.12	6.87e-29

Table 3: 4-channel with spacing of 0.8.

Wavelength	BER Value
1552.52	9.37e-15
1553.32	1.13e-11
1554.12	4.15e-10
1554.92	8.12e-20

Table 4: 4-channel with spacing of 1.6.

Wavelength	BER Value
1552.52	7.50e-15
1554.12	7.65e-27
1555.72	6.23e-20
1557.32	1.4764e-32

Table 5: 8-channel with spacing of 0.8.

Wavelength	BER Value
1552.52	2.64e-15
1553.32	1.54e-12
1554.12	8.66e-11
1554.92	2.19e-12
1555.72	1.56e-11
1556.52	1.05e-10
1557.32	2.05e-10
1558.12	8.21e-18

Table 6: 8-channel with spacing of 1.6.

Wavelength	BER Value
1552.52	2.64e-15
1553.32	1.54e-12
1554.12	8.66e-11
1554.92	2.19e-12
1555.72	1.56e-11
1556.52	1.05e-10
1557.32	2.05e-10
1558.12	8.21e-18

Table 7: 16-channel with spacing of 0.8.

Wavelength	BER Value
1552.52	1.81e-15
1553.32	3.8e-13
1554.12	1.24e-10
1554.92	1.42e-20
1555.72	4.47e-12
1556.52	3.16e-11
1557.32	6.57e-11
1558.12	6.24e-12
1558.92	4.92e-11
1559.72	4.03e-12
1560.52	6.56e-12
1561.32	3.13e-10
1562.12	3.38e-11
1562.92	3.09e-09
1563.72	1.03e-10
1564.52	1.04e-14

Table 8: 16-channel with spacing of 1.6.

Wavelength	BER Value
1552.52	9.35e-22
1554.12	9.94e-27
1555.72	5.05e-20
1557.32	1.38e-29
1558.92	3.67e-24
1560.52	5.62e-21
1562.12	1.45e-22
1563.72	2.36e-25
1565.32	6.75e-20
1566.92	1.00e-25
1568.52	5.79e-21
1570.12	1.53e-16
1571.72	3.49e-19
1573.32	4.68e-15
1574.92	8.04e-18
1576.52	4.28e-20

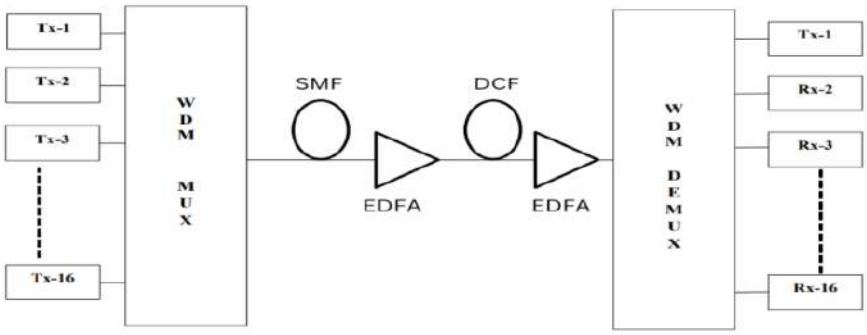

Figure 1: Schematic Diagram of DWDM System

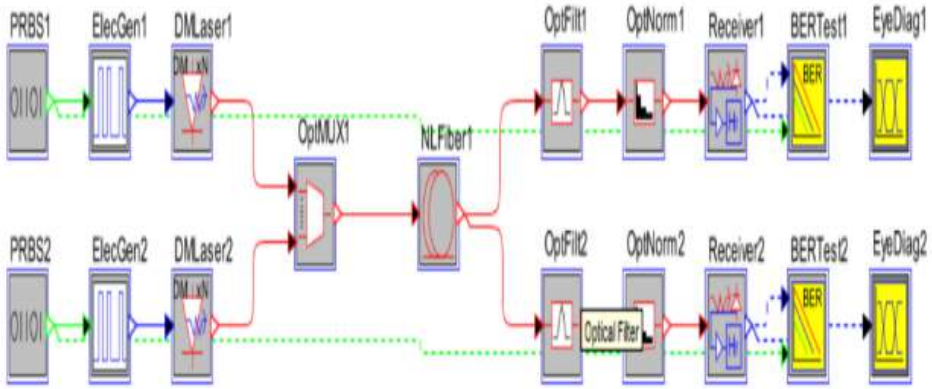

Figure 2: Simulation set up for 2-channel DWDM Optical fiber link

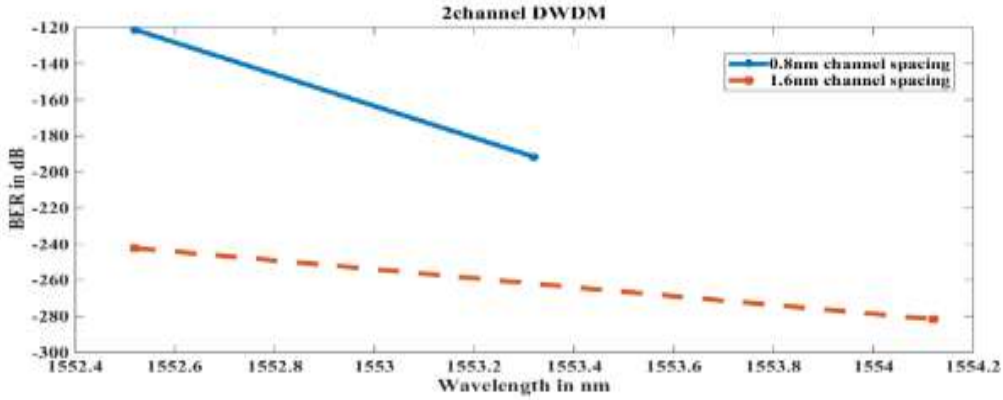

Figure 3: BER values for two channel DWDM with 0.8 and 1.6 spacing

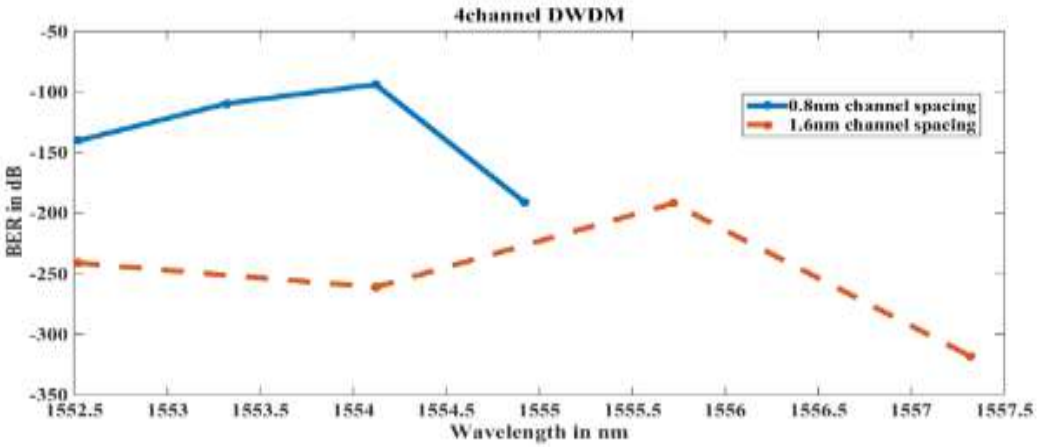

Figure 4: 4-channel Performance evaluation of BER between 0.8 and 1.6 spacing

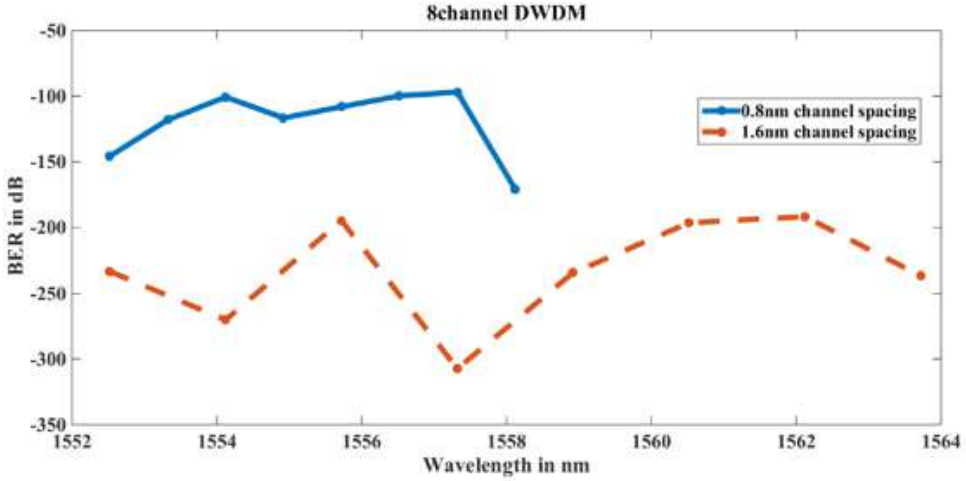

Figure 5: 8-channel Performance evaluation of BER between 0.8 and 1.6 spacing

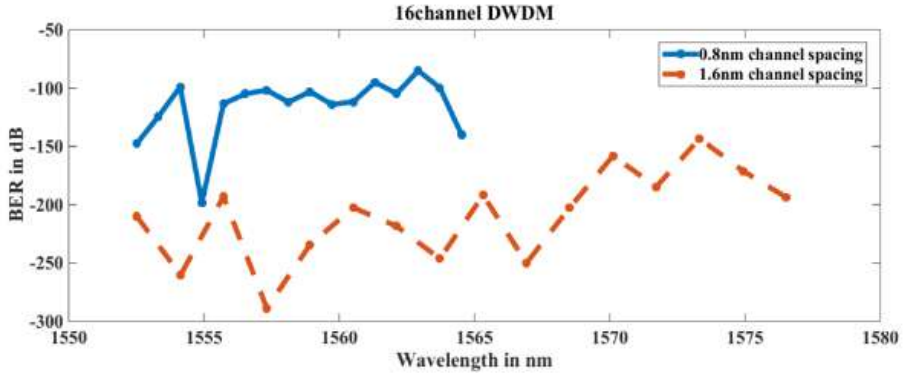

Figure 6: 16-channel Performance evaluation of BER with 0.8 and 1.6 nm channel spacing

Indian Journal of Natural Sciences *www.tnsroindia.org.in ©IJONS*

Vol.15 / Issue 83 / Apr / 2024 *International Bimonthly (Print) – Open Access* *ISSN: 0976 – 0997*

RESEARCH ARTICLE

Taxonomic Enumeration of Natural Dyes from India: Sir Thomas Wardle's Collection

Sudeshna Datta[1], Surendra Kumr Sharma[2], Manas Bhaumik[3] and Kangkan Pagag[4]*

[1]Botanist, Botanical Survey of India, Central National Herbarium, Howrah, West Bengal, India.
[2]Botanical Assistant, Botanical Survey of India, Central Botanical Laboratory, Howrah, West Bengal, India.
[3]Scientist-F, Botanical Survey of India, Industrial Section Indian Museum, Kolkata, West Bengal, India.
[4]Assistant Professor, Department of Botany, Sibsagar College, Joysagar (Autonomous), (Affiliated to Dibrugarh University), Assam, India.

Received: 18 Nov 2023 Revised: 19 Jan 2024 Accepted: 16 Mar 2024

***Address for Correspondence**
Kangkan Pagag
Assistant Professor,
Department of Botany, Sibsagar College, Joysagar (Autonomous),
(Affiliated to Dibrugarh University),
Assam, India.
Email: kpagag@gmail.com

ABSTRACT

The present study deals with archival data of Indian plants used by renowned British dyer & innovator Sir Thomas Wardle. He had used Indian plants singly or in combination which brought out various shades of colors on various fabrics viz. cotton, silk, wool. He had made sets of catalogues of samples dyed with natural dyes and one is deposited at Industrial Section Indian Museum, Kolkata. Therefore the present systematic taxonomic enumeration will help dyers or weavers or handloom industry in knowing dye yielding plants used in 19th century in India which may promote sustainable organic dye.

Keywords: Economic, colors, fabric, organic, sustainable.

INTRODUCTION

Sir Thomas Wardle (1831-1909), a remarkable British dyer and printer, innovator and entrepreneur who was erudite in dyeing of silk textiles and bringing out new innovations for it. He had a deep passion for silk and dyes. And due to this passion he was dedicated towards wild silks and dyes particularly Indian which created a platform for Indian dyes and silks in India & Europe. He was also a president of the Silk Association of Great Britain and contributed in setting up a silk factory in 1897. Sir Thomas Wardle studied wild silks of India (1880). He was reputed in bringing out different shades of color to textiles. He received a knighthood and many awards due to his marvelous feat of

researches. He was also granted a Fellowship of the Royal Society of Chemists. India at 19th century was rich in textile industry and many of the products or textiles were plants based. Indian Indigo was immensely popular in Europeans. Europe during those period was exported Indian textiles with Indian dyes. Thomas Wardle was drawn towards the richness of the natural dye yielding plants. He had experimented with many Indian dyes. In 1878 he had started the exploring the potentials of tinctorial powers and properties many of Indian dyes on the request of Government of India. The then Secretary of State for India had stated to him that if the natives of India could be taught how to dye their Tusser silk, a valuable industry could be created for their benefit (Wardle, 1887). These dyes were plant based, minerals as well as insects. To carry out such a huge task was very tedious and time consuming and it took many years to bring out the samples and present the report. He was helped by Mr Hugh Mccain who visited or brought out the information from the common locals or dyers also by providing raw materials of Indian dyes. Mr Hugh Mccain (1883) had published these details on Dyes of Bengal too. But he had just published the data he obtained from the field. It was Sir Wardle who made the album of the samples of the dyed textiles out of his experimentation. He chose different fabrics such as cotton, wool, muslin, silk, tussar for dyeing. He employed all the known methods of dyeing. He had used not only known mordants but used some of his private methods or mordants and as a result he subsequently discovered others. Since he was in business of dye and print he didn't reveal the methodology or percentage of mordant and dyes used. He used fustic also. He deposited the catalogue to the Government and published the report (1887). These albums of samples which were in possession of Industrial Section Indian Museum still attracts many researchers and dye experts from all over the globe. The samples are still vibrant in colour and which shows the efficacy of Indian dyes as well as working techniques of Wardle. According to Wardle some of the Indian dyes possessed distinct properties and in many cases superior to the dyes obtained from artificial sources. The set of 3000 samples are consists of fifteen volumes and arranged 09 samples per page with names of the dye and mordant used with common or scientific name of the plant. One will be mesmerized when goes through these samples which are the beautiful shades of pink, red, yellow, green, blue, brown etc. Therefore it reflects the importance of Indian dyes along with the techniques used in dyeing.

MATERIALS AND METHODS

The catalogues more than century old & prepared by Sir Thomas Wardle possessed by Industrial Section Indian Museum, Botanical Survey of India were consulted. Also the report submitted by Thomas Wardle (1887) to Government of India consulted & literature by M'cann (1883), were studied. Photographs taken. Enumeration of the plants was prepared with the current scientific nomenclature by consulting POWO (2023).

RESULT

Along with the plant dye, the role of mordants are very important in production of particular shades. Wardle had only written coded symbols for mordants which is yet to be deciphered. The plants used by him were the dye yielding plants of that period which included many common plants. The following is the enumeration of dye-yielding plants along with the scientific name, parts used and colour shades

Sl. No.	**Common Name**	**Scientific Name**	**Parts Used**	**Colour shades obtained**
1	Indigo	*Indigofera tinctoria* L.	Whole plant	Green, Blue, Blue-green
2	Madder	*Rubia cordifolia* L.	Bark, Root	Red, Brown, Maroon, Violet, Orange, Peach, Pink, Purple, Grey
3	Weld	*Reseda luteola* L.	Whole plant	Yellow, Grey, Green

4	Sapan wood	*Caesalpinia sappan* L.	Wood	Coral, Brown, Peach, Yellow, Red, Maroon, Orange
5	Sanders wood	*Pterocarpus santalinus* L. f.	Wood	Brown, Red
6	Annatto	*Bixa Orellana* L.	Seed	Yellow
7	Turmeric	*Curcuma longa* L.	Rhizome	Brown, Blue, Yellow, Off-white
8	Safflower	*Carthamus tinctorius* L.	Flower	Brown, Orange, Pink, Yellow, Red
9	Manjeeth	*Rubia manjith* Roxb.	Root	Brown, Yellow, Orange, Red, Maroon, Green, Magenta, Peach
10	Berberry	*Berberis lyceum* Royle & *Berberis tinctoria* Lesch.	Wood, Root	Yellow, Brown, Yellow-ochre, Off-white, Khaki
11	Peepal	*Ficus religiosa* L.	Bark	Ochre, Brown, Golden yellow, Yellow, Off-white
12	Pulha Babul, Kekir, Babool	*Vachellia nilotica* subsp. tomentosa (Benth.) Kyal & Boatwr. (syn. *Acacia Arabica*)	Bark, Pods	Brown, Yellow-ochre
13	Lodh	*Symplocos racemosa* Roxb.	Bark	Yellow-ochre, Brown, Off-white
14	Jigna	*Lannea coromandelica* (Houtt.) Merr. (syn. *Odina wodier*)	Bark	Brown
15	Himalayan Blue Pine	*Pinus wallichiana* A.B. Jacks (*Pinus excelsa)*	Bark	Brown
16	Chir pine	*Pinus roxburghii* Sarg. (Syn. *Pinus longifolia*)	Bark	Brown
17	Jack wood	*Cryptocarya glaucescens* R. Br.	Wood	Brown
18	Peach Tree	*Prunus persica* (L.) Batsch	Root bark	Brown
19	Daruharidra, Al roots, Bhartondi, Meddi tree	*Morinda citrifolia* L.	Root, Bark	Yellow, Brown, Off-white, ochre, Orange
20	Henna	*Lawsonia inermis* L.	Leaves	Yellow, Brown
21	Jangali badam	*Terminalia catappa* L.	Bark, Leaves	Yellow, Brown, Off-white, Yellow-ochre
22	Taira	*Libidibia coriaria* (Jacq.) Schltdl. (Syn. *Caesalpinia coriaria*)	Pods	Brown, Yellow-Brown
23	Chaikatha	*Piper retrofractum* Vahl (Syn. *Piper chaba*)	Not known	Brown, Yellow, Off-white
24	Ashna	*Terminalia tomentosa* Wight & Arn.	Bark	Brown
25	Tarwad, Tarota	*Senna auriculata* (L.) Roxb. (Syn. *Cassia auriculata*)	Bark, Leaves,Seeds	Brown, Yellow
26	Bokal	*Mimusops elengi* L.	Bark	Brown, Off-white
27	Madar	*Erythrina Americana* Mill. (Syn. *Erythrina fulgens*)	Bark	Brown, Yellow

28	Bihul	*Grewia optiva* J. R. Drumm. ex Burret (Syn. *Grewia oppositifolia*)	Leaves	Off-white, Brown
29	Jangli erandi	*Jatropha glandulifera* Roxb.	Leaves	Yellow, Brown, Off-white
30	Anjan	*Memecylon coeruleum* Jack (Syn. *Memecylon tinctorium*)	Leaves	Yellow, Brown
31	Gab	*Diospyros malabarica (Desr.) Kostel.*	Leaves, Fruits	Yellow, Off-white
32	Bhauri	*Symplocos theifolia* D. Don	Leaves	Off-white, Khaki, Golden, Yellow
33	Arjun	*Terminalia arjuna* (Roxb. ex DC.) Wight & Arn.	Bark	Yellow, Brown
34	Pomergranate rind	*Punica granatum* L.	Rind	Brown, Yellow-ochre, Steel gray, Blue-Black, Yellow
35	Anglithor	*Euphorbia tirucalli* L.	Not known	Yellow, Brown, Off-white, Green
36	Harsinghar	*Nyctanthes arbor-tristis* L.	Flowers	Yellow
37	Toon	*Cedrela toona* Roxb. ex Rottler & Willd. (Syn. *Cedrela toona*)	Flowers, Bark	Yellow, Green, Brown, Off-white, ochre
38	Palas	*Butea monosperma* (Lam.) Kuntze (Syn. *Butea frondosa*)	Flowers	Yellow-ochre, Brown, Yellow, off-white, Ochre, Red
39	Paras pipal	*Thespesia populnea* (L.) Sol. Ex Corrêa	Flowers, Dried capsules and calyces	Yellow-ochre, Yellow
40	Dhao ka phul, Dhauri	*Woodfordia fruticosa* (L.) Kurz (Syn. *Grislea tomentosa*)	Flowers, Leaves	Yellow-ochre, Red, Yellow
41	Mittikut	*Senegalia catechu* (L.f.) P.J. H Hunter & Mabb. (Syn. *Acacia catechu*)	Catechu	Brown, Yellow, Blue-brown, Brown-red, Blue, off-white
42	Mahuwa	*Madhuca longifolia* var. *latifolia* (Roxb.) A. Chev.	Bark	Brown
43	Mango	*Mangifera indica* L.	Bark, Fruit pulp	Brown, Yellow, Yellow-ochre, Off-white
44	Kachnar	*Bauhinia variegata* L.	Bark	Brown, Yellow-ochre, Moss green, Off-white
45	Harra	*Terminalia chebula* Retz.	Bark, Nut	Yellow-ochre, Yellow, Brown
46	Amla	*Phyllanthus emblica* L.	Fruits, Leaves	Brown, Yellow-ochre
47	Mountain ru	*Casuarina junghuhniana* Miq. (Syn. *Casuarina muricata*)	Bark	Yellow-ochre, Yellow, Grey
48	Genda	*Tagetes erecta* L.	Flowers	Brown, Yellow
49	Amaltas	*Cassia fistula* L.	Bark	Brown, Biscotti
50	Dhaura	*Terminalia anogeissiana* Gere & Boatwr.	Leaves	Brown

51	Rohun	*Soymida febrifuga* (Roxb.) A. Juss.	Bark	Yellow, Brown, Green, Off-white
52	Logwood	*Haematoxylum campechianum* L.	Extract	Violet, Blue, Brown, Grey
53	Barwood	*Baphia nitida* G. Lodd.	Not known	Yellow, Brown, Maroon, Red, Violet, Pink
54	Fustic	*Maclura tinctoria* (L.) D. Don ex G. Don	Extract	Brown, Yellow, Green
55	Kamela	*Mallotus philippensis* (Lam.)Müll.Arg.	Fruits	Yellow
56	Weniwel	*Coscinium fenestratum* (Gaertn.) Colebr.	Wood	Yellow
57	Rang	*Dicliptera tinctoria* (Nees) Kostel (Syn. *Peristrophe tinctoria)*		Yellow, Brown, Peach, Pink
58	Red Creeper	*Ventilago madraspatana* Gaertn.	Root bark with galls	Brown
59	Tartigyan	*Senna torra* (L.) Roxb.	Seeds	Brown
60	Pista	*Pistacia vera* L.	Flowers	Brown
61	Dhayati, Kapila	*Woodfordia fruticosa* (L.) Kurz.	Flowers	Yellow
62	Suranji	*Mammea suriga* (Buch.-Ham ex Roxb.) Kosterm (Syn. *Calysaccion longifolium)*	Root bark	Yellow
63	s.n.	*Amaranthus tricolor* L. (Syn. *Amaranthus polygamous*)	Stems	Yellow
64	Guljullil	*Delphinium saniculifolium* Boss.		Yellow
65	Cotton	*Gossypium herbaceum* L.	Flowers	Yellow, Brown
Some combinations of plants for extraction of dyes by Wardle				
66	Indigo and Weld	*Indigofera tinctoria* L., *Reseda luteola* L.	Whole plant	Prussian blue, Green, Blue
67	Indigo and Turmeric	*Indigofera tinctoria L., Curcuma longa* L.	Whole plant, Rhizomes	Yellow, Green, Blue-green, Blue.
68	Indigo and Berberry Wood	*Indigofera tinctoria* L., *Berberis lyceum* Royle/*Berberis tinctoria* Lesch.	Whole plant, Root	Green
69	Indigo and Logwood	*Indigofera tinctoria* L., *Haematoxylum campechianum* L.	Whole plant, Extract	Green, Blue-green
70	Indigo, Madder and Turmeric	*Indigofera tinctoria* L., *Rubia cordifolia, Curcuma longa* L.	Whole plant, Root, Rhizomes	Brown, Green
71	Indigo, Berberry Wood and Munjeet	*Indigofera tinctoria* L., *Berberis lyceum* Royle/*Berberis tinctoria* Lesch., *Rubia munjith* Roxb. ex Fleming	Whole plant, Root	Blue, Green
72	Indigo, Madder and Berberry Wood	*Indigofera tinctoria* L., *Rubia tinctorum* L., *Berberis lyceum* Royle/*Berberis tinctoria* Lesch.	Whole plant, Root	Green
73	Indigo, Madder and Sanderswood	*Indigofera tinctoria* L., *Rubia cordifolia* L., *Pterocarpus santalinus* L. f.	Whole plant, Root, Wood	Blue
74	Indigo, Logwood and Berberry Wood	*Indigofera tinctoria* L., *Haematoxylum campechianum* L., *Berberis lyceum* Royle	Whole plant, Extract, Root	Green

75	Indigo, Madder, Sanderswood and Turmeric	*Indigofera tinctoria* L., *Rubia cordifolia* L., *Pterocarpus santalinus* L.f., *Curcuma longa* L.,	Whole plant, Root, Wood, Rhizomes	Brown, Yellow, Green
76	Indigo, Berberry Wood, Turmeric and Munjeet	*Indigofera tinctoria* L., *Berberis lyceum* Royle/*Berberis tinctoria* Lesch., *Curcuma longa* L., *Rubia munjith* Roxb. ex Fleming	Whole plant, Root, Rhizomes, Root	Green
77	Indigo, Fustic, Madder and Barwood	*Indigofera tinctoria* L., *Maclura tinctoria* (L.) D. Don ex Steud., *Rubia cordifolia* L., *Baphia nitida* Lodd.	Whole plant, Extract, Root	Green, blue, olive green
78	Indigo, Berberry Wood, Logwood and Madder	*Indigofera tinctoria, Berberis lycium, Haematoxylum campechianum, Rubia cordifolia* L.	Whole plant, Root, extract, Root	Brown
79	Manjeeth and Palas	*Rubia munjith* Roxb. ex Fleming, *Butea monosperma* (Lam.) Kuntze	Root, Flowers	Brown, Yellow
80	Madder and Turmeric	*Rubia cordifolia* L., *Curcuma longa* L.	Root, Rhizomes	Brown
81	Madder and Sanderswood	*Rubia cordifolia* L., *Pterocarpus santalinus* L. f., *Butea monosperma* (Lam.) Kuntze	Root, Wood	Brown, Maroon, Orange
82	Welds and Turmeric	*Reseda luteola* L., *Curcuma longa* L.	Whole plant, Rhizomes	Yellow
83	Sapan wood and Madder	*Caesalpinia sappan* L., *Rubia cordifolia* L.	Wood, Root	Red
84	Madder, Turmeric and Welds	*Rubia cordifolia* L., *Curcuma longa* L., *Reseda luteola* L.	Root, Rhizomes, Whole plant	Orange, Red, Yellow
85	Madder, Berberry Wood and Logwood	*Rubia cordifolia* L., *Berberis lyceum* Royle/*Berberis tinctoria* Lesch., *Haematoxylum campechianum* L.	Root, extract	Brown
86	Ukulbir	*Datisca cannabina* L.	Wood	Brown, Yellow
87	Fir	*Abies* Mill.	Bark	Brown
88	Rasun Buti	Probably *Allium sativum*	Not known	Brown, Off-white
89	s.n.	*Leucus sp.*	Bark	Brown
90	Kauna	s.n.	Bark	Brown, Yellow, Off-white
91	Amlia sak	*Amaranthus sp./ Hibiscus sp.*	Not known	Ochre, White, Brown, Yellow, Yellow-ochre
92	Hinro	Scientific name undetected	Not known	Brown, Moss green, Red
93	Sakra beu	Scientific name undetected	Bark	Brown, Yellow, Off-white
94	Esfurkee patta	*Delphinium* sp.	Not known	Yellow
95	Ragira	*Amaranthus sp.*	Plants and Leaves	Yellow
96	Tamarix galls	*Tamarix sp.*	Galls	Black

97	Cochineal	*Dactylopius coccus* Costa	Not known	Red, Yellow, Pink, Orange, Violet, Peach, Maroon, Bluish grey, Brown, Blue, Purple, Magenta
98	Lac	*Scarlet resinous secretion of Laccifer lacca*	Not known	Orange, Red, Maroon, Violet, Purple, Peach, Yellow-red, Brown, Pink
99	Haematin	Dark brownish pigment containing iron in the ferric state	Not known	Blue, Grey, Brown, Violet, Green, Purple
100	Lac and Indigo	*Laccifer lacca, Indigofera tinctoria* L.	Whole plant	Red, Orange
101	Indigo and Cochineal	*Indigofera tinctoria* L., *Dactylopius coccus* Costa	Whole plant	Grey, Blue, Red, Purple, Brown, Maroon, Pink
102	Madder and Cochineal	*Rubia cordifolia* L., *Dactylopius coccus* Costa	Root	Brown, Purple, Maroon, Red, Blue, Violet, Orange
103	Cochineal and extract of Jackfruits wood	*Dactylopius coccus* Costa, *Artocarpus integrifolia* L.	Not known	Yellow, Pink
104	Munjeet and Cochineal	*Rubia munjith* Roxb. ex Fleming, *Dactylopius coccus* Costa	Root	Red
105	Lac and Turmeric	*Laccifer lacca, Curcuma longa* L.	Rhizomes	Orange
106	Haematin, Barwood	*Baphia nitida* Lodd.	Not known	Grey
107	Cochineal, Pista flower and Sapan Wood	*Dactylopius coccus* Costa, *Pistacia vera, Caesalpinia sappan* L.	Flowers	Red
108	Cochineal, Madder and Turmeric	*Dactylopius coccus* Costa, *Rubia cordifolia* L., *Curcuma longa* L.	Root, Rhizomes	Orange
109	Lac, Cochineal and Indigo	*Laccifer lacca, Dactylopius coccus, Indigofera tinctoria* L.	Whole plant	Red
110	Cochineal, Berberry Wood and Logwood	*Dactylopius coccus* Costa, *Berberis lyceum* Royle/*Berberis tinctoria* Lesch., *Haematoxylum campechianum* L.	Root	Red

CONCLUSION

The present paper was an attempt to bring out or highlight the hundred and thirty-six year old legacy of Indian natural dyes which were very popular, rich and for which the India is famous. These hundred years old information can be helpful or a source of guide to all the people who is in interested in Indian dyes or plant based dyes. Many textile designers can be benefitted with these information by utilizing it for their customers who are drawn towards organic plant based dyes.

ACKNOWLEDGEMENT

The authors are thankful to the Director, Botanical Survey of India for encouragement and facilities.

REFERENCES

1. M'cann, Hugh. W. 1883. *Report on the dyes and tans of Bengal*. Bengal Secretariat press. Calcutta. 238p.
2. POWO 2023. Plants of the World online. Facilitated by the Royal Botanic Gardens, Kew. Available at https://plantsoftheworldonline.org (Accessed on 18.4.2023).
3. Wardle Thomas, 1880. *The wild silks of India, principally Tusser*. George Edward Eyre and William Spottiswoode, London. 50 p.
4. Wardle Thomas, 1887. *Report on dyes and Tans of India*. Calcutta: Superintendent of Government of printing, India. 82 p.

Indian Journal of Natural Sciences *www.tnsroindia.org.in ©IJONS*

Vol.15 / Issue 83 / Apr / 2024 *International Bimonthly (Print) – Open Access* *ISSN: 0976 – 0997*

RESEARCH ARTICLE

Optimum Solution on Two Stage Flow Shop Scheduling Model with Identical Parallel Machines

Khushboo Malhotra[1,2], Deepak Gupta[2] , Sonia Goel[2*] and A. K. Tripathi[2]

[1]Department of Mathematics, D. A. V. College (Lahore), Ambala City.
[2]Department of Mathematics, Maharishi Markandeshwar Engineering College, MM (Deemed to be University), Mullana, Ambala.

Received: 30 Dec 2023 Revised: 09 Jan 2024 Accepted: 12 Jan 2024

***Address for Correspondence**
Sonia Goel
Department of Mathematics,
Maharishi Markandeshwar Engineering College,
MM (Deemed to be University),
Mullana, Ambala.
Email: sonia.mangla14@gmail.com

ABSTRACT

Efficient scheduling in manufacturing is crucial for optimizing production processes and minimizing costs. The type of FSSP considered in this study presents a challenging scenario. The present study gives a novel BB algorithm tailored for large problem instances. The proposed BB algorithm leverages the power of mathematical programming and MATLAB implementation to address large-scale instances of the problem, a critical need in contemporary manufacturing environments. This research aims to guide practitioners and researchers in selecting the most suitable method for optimizing make-span in manufacturing environments. The findings contribute to the ongoing efforts in the field of operations research and production scheduling. This study develops a Model for optimizing the elapsed time with two machines involving m identical parallel processors at first level and single processor at second level having utilization time of each task on each of the two machines. A MATLAB Code in R2018a is developed for introducing the proposed algorithm for very large number of tasks and machines. Numerical experiment has also been done for supporting the coding.

Keywords: Scheduling, Mathematical Model, MATLAB, Identical Parallel Machines.

INTRODUCTION

Efficient production scheduling is a cornerstone of modern manufacturing, as it directly impacts productivity, cost-effectiveness, and overall operational performance. Among the various scheduling problems that industries face, this problem which is considered in this study presents a complex and practically significant challenge. This scheduling scenario is particularly common in industries where optimizing the sequential processing of jobs through different stages is paramount. In this paper, we embark on a comprehensive exploration of scheduling techniques to address the FSSP with a focus on the specific configuration of identical parallel machines. The primary objective is to minimize the make-span, the total time required to complete all jobs, while respecting the constraints inherent to this problem. This study evaluates a novel Branch and Bound algorithm, specifically designed to tackle large problem instances. Leveraging the power of mathematical programming and implemented in MATLAB, this algorithm aims to provide an efficient solution to the scheduling problem, especially pertinent for manufacturing environments where the scale of the problem is substantial.

PRACTICAL SITUATION

The real life application of our model can be shown through the following illustration:

Pharmaceutical Manufacturing

Stage 1 (Parallel Machines) Multiple machines can be used for various stages of pharmaceutical tablet manufacturing, including mixing, granulation, and compression.

Stage 2 (Single Machine) A single machine, like a tablet coating machine, can be used in the second stage for coating tablets with the desired coating material.

Here the two-stage flow shop model is applied to optimize production processes, enhance quality control, and manage the flow of materials and products efficiently. The use of parallel machines in the first stage improves throughput, while the single machine in the second stage ensures precision and consistency in critical operations.

LITERATURE REVIEW

Efficient scheduling in manufacturing operations is vital to enhance productivity and reduce costs. Next, if Scheduling is done with the help of parallel machines then it would be a boon for manufacturing field. Hence in this study we are considering parallel processors. Parallel machine scheduling (PMS) means to perform tasks on multiple processors. Feifeng Zheng also did work in this field (Zheng, 2022). Malhotra et. al. also worked on FSSM with identical parallel processors (Malhotra, 2022). Many methodologies have been considered for obtaining performance measures.But here we are considering branch and bound in this paper. Branch and Bound algorithm is a classical technique often applied to various scheduling problems. In the context of flow shop scheduling, it has shown its potential for solving problems with smaller instances (Sullivan &Daganzo, 1986). Many researchers have worked on this BB method like (Gupta D., 2022), (Gupta D., 2020), (Malhotra K. 2022) , (Malhotra K., 2023) and many more. Researchers have explored variations of the two-stage flow shop scheduling problem, including considering job release times, due dates, and machine breakdowns. Hazzi et. al. also worked on two stage flow shop scheduling model (Hazzi , 2023). Liu and Pardalos also worked with parallel machines (Liu, 2023). Hnaien also studied on two stage flow shop scheduling model (Hnaien , 2023). A comprehensive survey by Hino and Morabito (2017) provides insights into different scheduling problems and their solution methods. Jemmali et. al. worked on two stage flow shop scheduling model (Jemmali , 2023). Parviznejad also studied the problem related to parallel machines (Parviznejad , 2021). Hidri also worked on parallel machine scheduling (Hidri , 2022).

PROBLEM DISCRIPTION

Let us assume that there are n jobs for performing on two machines E and F. Type E has m identical processors and Type F has single processor where ei and fi denote consumption time of task i on E and F processors respectively. It is not necessary to perform each job on all parallel machines of type E, one job can be performed partially on parallel

machines of type E and then after processing on first processor, it will be performed on second processor. Offered time of all similar processors t1j are also given. The purpose of the problem is to manage scheduling in such a way to complete project in minimum time. The model is represented as:

MATRIX FORM OF MODEL

The model of the problem is depicted in matrix form is given in Table 1 which is given below:

SOLUTION APPROACH

PROPOSED METHODOLOGY

We solve this problem as follows:

Step 1 :

Now check the condition

$$\sum_{j=1}^{m} t_{1j} = \sum_{j=1}^{n} e_i \quad (1)$$

and apply MODI method otherwise make arrangement to satisfy condition (1).

Step 2 :

Apply the formula

$$1' = \max_{i \in Jr} \left(\sum_{i=1}^{n} e_{ij} \right) + \min_{i \in Jr'} (fi) \quad (2)$$

$$1'' = \max_{i \in Jr} \left(e_{ij} \right) + \sum_{i=1}^{n} (fi) \quad (3)$$

a. Find l = max {l', l''}
b. Extract out l for all arrangement of tasks.
c. After that take minimum value from all l's. This will prepare branching tree.
d. In last, we have to generate In-Out table for the required sequence of tasks.

NUMERICAL APPROACH

The numerical problem is given in Table 2.

SOLUTION

We solved the problem in four Steps.

Step 1: See MODI method in Table 3:

Step 2: Apply branch and bound method and get the final table

The final In-Out Table of required sequence is given in Table 4. The above gantt chart is showing final In-Out table with six parallel machines of type E and single machine of type F. Here minimum make-span is 37.6620 hrs. Hence, the problems of small size where either the no. of jobs are less or the no. of equipotential parallel machines are less are easily solvable manually but for large sized problems we have generated MATLAB program in R2018a version for finding make-span for large sized problems. Table 5 is shown by taking more parallel machines at level 1 and more no of jobs also.

CONCLUSION

This study addresses the critical issue of efficient scheduling in manufacturing, focusing on the Two-Stage Flow Shop Scheduling problem with m identical parallel processors at the first level and a single processor at the second level. The development of a novel Branch and Bound algorithm specifically tailored for large-scale instances of the problem sets this research apart. The algorithm's implementation in MATLAB 2018a enables its application to real-

world manufacturing scenarios, where optimizing the make-span is essential for minimizing costs and improving production processes. The proposed Branch and Bound algorithm demonstrates its efficacy in handling large problem instances, showcasing the power of mathematical programming in addressing complex scheduling challenges. The numerical experiments conducted not only validate the efficiency of the proposed algorithm. The findings offer valuable insights into the strengths and weaknesses of each scheduling approach, guiding both practitioners and researchers in selecting the most suitable method for optimizing Two-Stage Flow Shop Scheduling in manufacturing environments. This research contributes to the broader field of operations research and production scheduling, enhancing our understanding of how diverse techniques can be employed to bolster manufacturing competitiveness. Overall, the study underscores the significance of tailored algorithmic approaches in addressing specific scheduling challenges within the manufacturing domain.

REFERENCES

1. Gupta, D., & Goel, S. (2018). Three stage flow shop scheduling model with m-equipotential machines. International Journal on Future Revolution in Computer Science & Communication Engineering 4(3), 269-274.
2. Gupta, D., & Goel, S. (2022). Branch and bound technique for two stage flow shop scheduling model with equipotential machines at every stage. International Journal of Operational Research ,44(4), 462-472
3. Gupta, D., & Goel, S.(2020). 'Nx2 Flow Shop Scheduling Problem With Parallel Machines At Every Stage, Processing Time Associated With Probabilities. Advances in Mathematics: Scientific Journal, 9(3), 1061–1069. DOI: 10.37418/amsj.9.3.31.
4. Gupta, D., Goel, S. & Mangla, N.(2022). Optimization of production scheduling in two stage Flow Shop Scheduling problem with m equipotential machines at first stage. International Journal of System Assurance Engineering and Management, 13(3), 1162-1169.
5. Hajji, M. K., Hadda, H., & Dridi, N. (2023). Makespan Minimization for the Two-Stage Hybrid Flow Shop Problem with Dedicated Machines: A Comprehensive Study of Exact and Heuristic Approaches. *Computation*, *11*(7), 137.
6. Hidri, L., &Elsherbeeny, A. M. (2022). Optimal Solution to the two-stage hybrid flow shop scheduling problem with removal and transportation times. *Symmetry*, *14*(7), 1424.
7. Jemmali, M., Hidri, L., &Alourani, A. (2022). Two-stage hybrid flowshop scheduling problem with independent setup times. *Int. J. Simul. Model*, *21*, 5-16.
8. Liu, S., Pei, J., Cheng, H., Liu, X., &Pardalos, P. M. (2019). Two-stage hybrid flow shop scheduling on parallel batching machines considering a job-dependent deteriorating effect and non-identical job sizes. *Applied Soft Computing*, *84*, 105701.
9. Malhotra, K., Gupta, D., Goel, S. &Tripathi, A. K.(2022).Bi-Objective Flow Shop Scheduling with Equipotential Parallel Machines. Malaysian Journal of Mathematical Sciences, 16(3), 451-470.
10. Malhotra, K., Gupta, D., Goel, S., & Tripathi, A. K. (2023, May). Scheduling Involving Equipotential Processors with Constraint as Fuzzy Utilization Time of Jobs. In *International Conference on Data Analytics and Insights* (pp. 491-503). Singapore: Springer Nature Singapore.
11. Naien, F., & Arbaoui, T. (2023). Minimizing the makespan for the two-machine flow shop scheduling problem with random breakdown. *Annals of Operations Research*, 1-24.
12. Parviznejad, P. S., &Asgharizadeh, E. (2021). Modeling and Solving Flow Shop Scheduling Problem Considering Worker Resource. *International Journal of Innovation in Engineering*, *1*(4), 1-17.
13. Sullivan, R. S., &Daganzo, C. F. (1986). A Lagrangian relaxation approach to the flow shop scheduling problem. Management Science, 32(9), 1093-1103.
14. Zheng, F., Jin, K., Xu, Y., & Liu, M. (2022). Unrelated Parallel Machine Scheduling with Job Splitting, Setup Time, Learning Effect, Processing Cost and Machine Eligibility. Asia-Pacific Journal of Operational Research, DOI:10.1142/S0217595922500233.

Table 1. Matrix Form

Jobs	Machine E	Machine F	
I	E_1 E_2 E_3 E_4 E_5 ..... E_m	Utilization Time (e_i)	Utilization Time (f_i)
(1)	e_{11} e_{12} e_{13} e_{14} e_{15}. . . . e_{1m}	e_1	f_1
(2)	e_{21} e_{22} e_{23} e_{24} e_{25}… e_{2m}	e_2	f_2
(3)	e_{31} e_{32} e_{33} e_{34} e_{35} ….. e_{3m}	e_3	f_3
.	.	.	.
.	.	.	.
.	..	.	.
.	..	.	.
(n)	e_{n1} e_{n2} e_{n3} e_{n4} e_{n5} e_{nm}	e_n	f_n
Available Time	t_{11} t_{12} t_{13} t_{14} t_{15} t_{1m}		

Table 2. Defined problem

Jobs	E_1	E_2	E_3	E_4	E_5	E_6	Processing time (e_i)	Processing time(f_i)
1	1	6	6	6	7	7	3.666	3.333
2	5	6	7	8	9	9	2.666	6
3	2	2	2	3	3	2	3	5.333
4	5	6	7	8	9	9	4.333	5.333
5	2	2	3	3	3	2	4.666	6
6	5	6	7	8	9	9	3.666	4.666
7	5	6	7	8	9	9	4.333	5.333
t_{1j}	9	9	8	7	6	5		

Table 3. Modi Method

Jobs	E_1	E_2	E_3	E_4	E_5	E_6	F
1	3.6660	0	0	0	0	0	3.333
2	2.6660	0	0	0	0	0	6.000
3	0	0	3.0000	0	0	0	5.333
4	0	4.3330	0	0	0	0	5.333
5	0	0	0	0	0	4.6660	6.000
6	0	1.6640	1.0010	0	0	0	4.666
7	0	0	4.3330	0	0	0	5.333
8	2.6680	1.0010	0.6670	7.0000	6.0000	0.3340	0

Table 4. In – Out table for best possible sequence

Jobs	E_1	E_2	E_3	E_4	E_5	E_6	F
6	-	0 – 1.6640	0-1.0010	-	-	-	1.6640-6.3300
2	0-2.666	-	-	-	-	-	6.3300-12.3300
8	2.666-5.334	1.664-2.665	1.0010-1.6680	0-7	0-6	0-0.3340	12.3300-12.3300
7	-	-	1.6680-6.0010	-	-	-	12.3300-17.6630
5	-	-	-	-	-	0.3340-5.000	17.630-23.6630
4	-	2.6650-6.9980	-	-	-	-	23.630-28.6630
3	-	-	6.0010-9.0010	-	-	-	28.6630-34.3290
1	5.3340-9.0000	-	-	-	-	-	34.3290-37.6620

Table 5. Matlab output table for proposed Algorithm

Number of Tasks	Number of Processors at level 1	Optimal Sequence of Jobs	Optimum Make span in Hrs.
4	6	4,3,5,2,1	26.6650
5	6	2,5,6,4,3,1	36.6650
7	6	6,2,8,7,5,4,3,1	37.6620
10	6	1,2,11,10,9,8,7,6,5,3,4	51.6630
15	6	9,10,2,13,12,15,1,14,7,3,5,6,8,11,4	115.9997
20	6	10,1,11,2,20,15,17,9,14,16,4,5,8,12,19,7,10,6,13,3	137.6583
30	6	26,24,1,11,18,17,29,28,20,12,15,9,16,2,4,5,8,19,23 27,30,7,10,22,25,14,6,21,13,3	195.6600
50	6	46,49,1,45,42,48,50,9,47,44,43,11,16,24,26,31,39,41,2,4,5,8, 12,15,17,19,20,23,27,30,32,34,35,38,7,10,22,25,37,40,14,29,6,21 36,3,13,18,33,28	328.6550
80	6	9,14,1,12,11,13,80,10,15,2,79,16,24,26,31,39,41,46,54,56,62,67,75 77,4,5,8,17,19,20,23,27,30,32,34,35,38,42,45,47,49,50,53,57,60,63 66,68,70,71,74,78,7,22,25,37,40,52,55,61,73,76,29,44,59,65,6,21 36,51,72,3,18,28,33,43,48,58,69,64	522.6420

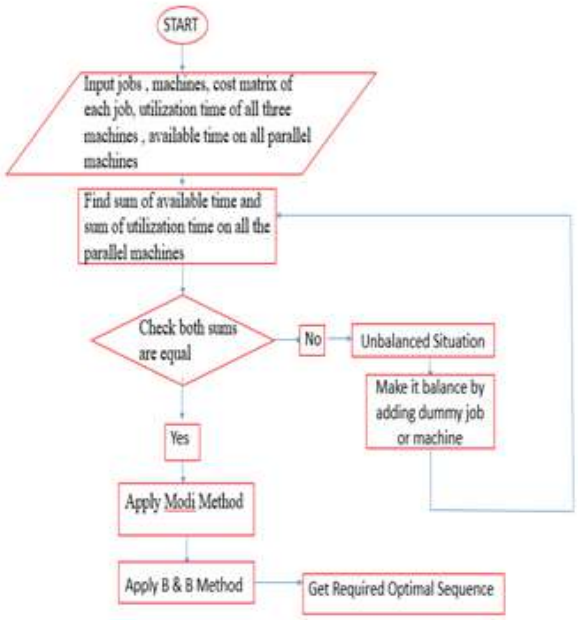

Figure. 1.Flow Chart Supporting Algorithm

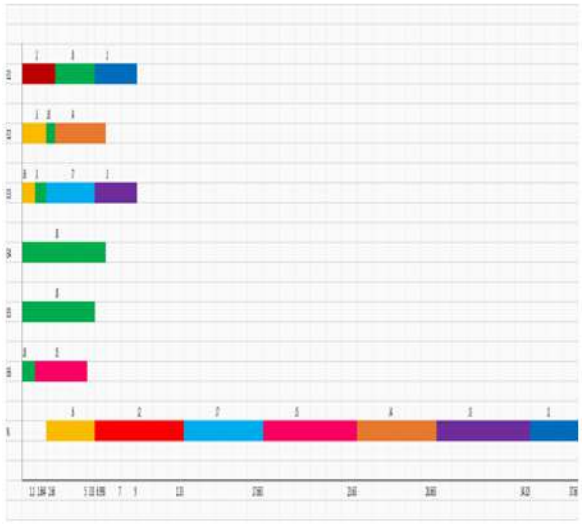

Figure. 2Gantt Chart showing the above problem

Indian Journal of Natural Sciences *www.tnsroindia.org.in ©IJONS*

Vol.15 / Issue 83 / Apr / 2024 *International Bimonthly (Print) – Open Access* *ISSN: 0976 – 0997*

RESEARCH ARTICLE

Insights into the Photo Catalytic Degradation of Phthalates: Current Trends and Future Applications for Environmental Remediation

Urvashi, Gunjan Chauhan*

Department of Chemistry, MMEC, Maharishi Markandeshwar (Deemed to be University), Mullana, Ambala Haryana 133207.

Received: 30 Dec 2023 Revised: 09 Jan 2024 Accepted: 12 Jan 2024

***Address for Correspondence**
Gunjan Chauhan
Department of Chemistry,
MMEC, Maharishi Markandeshwar (Deemed to be University),
Mullana, Ambala Haryana 133207.
Email: gunjan.chauhan@mmumullana.org

ABSTRACT

Esters of 1, 2-benzenedicarboxylic acid commonly known as phthalates have a wide variety of industrial, agricultural and many other applications. The most significant usage of phthalates is as plasticizers, i.e. increase the functionality and flexibility of polymeric materials. However, researches have shown that exposure to phthalates can lead to detrimental health effects, such as hormone disruption, increased risk of asthma and allergy, type II diabetes, insulin resistance, reproductive and developmental issues. This raises concerns about the safety and sustainability of their widespread use in almost every industry. Numerous regulatory bodies classified phthalates, a top priority pollutant, mandating the reduction and control of "**phthalate pollution**". The US Environmental Protection Agency (EPA) and European Union(EU) implemented regulations that require companies to monitor and limit the use of phthalates in consumer products, also prompting manufacturers to reformulate their products to reduce phthalate content and ensure compliance. The present study provides a clear perspective on the recent progress in the degradation of phthalates by photo catalytic degradation, also highlighting its potential for environmental remediation. Various researches have focused on exploring semiconductor-based photo catalysts, and their modifications to enhance degradation efficiency. Future prospects encompass the fabrication of novel photo catalysts, mechanistic understanding, scaling up processes for practical applications, also addressing challenges towards sustainable and efficient phthalates degradation.

Keywords: phthalate pollution, hormone disruption, development issues, photo catalytic degradation, semiconductor-based photo catalysts (SBP)

INTRODUCTION

The manufacturing, consumption, and disposal of plastics have resulted in the release of phthalates in environmental matrices, including the air, groundwater, sediments, waste water, streams and lakes [1]. Phthalates, which are also known as phthalic acid esters such as di(2-ethylhexyl) phthalate (DEHP), diisononyl phthalate (DINP), diisodecyl phthalate (DIDP), and di(2-propylheptyl) phthalate (DPHP) are used in poly vinyl chloride compounds (PVCs) to increase the flexibility and stability of plastics. In non-polyvinyl compounds (non-PVCs), phthalates such as dimethyl phthalate (DMP), diethyl phthalate (DEP), butyl benzyl phthalate (BBP), and di-butyl phthalate (DBP) used to improve the stability and solubility in cosmetic products like hair growth sprays, perfumes, nail polishes, cleansers, and shampoos[2-4].The plasticizers are frequently utilized as phthalates, readily and extensively released into the environment through a variety of processes, such as leaching, migration, evaporation during product use, the disposal of industrial and municipal solid wastes[5]. Environmental concerns have been raised due to the hepatotoxic, teratogenic, and carcinogenic properties of phthalates, which are caused by the large manufacturing units and usage of phthalate containing products[6].

The phthalates are used often to soften plastics in a variety of consumer goods, including office supplies, footwear, flooring, toys, coated paper and fabrics, recreational equipment, beds, cables and others[7].The exposure of bottled water to direct sunlight and the interaction of hot water with disposable plastic and paper cups both significantly raised the levels of phthalate in the drinking water (p value < 0.05)[8-10].A team of scientists and medical professionals with expertise in neurotoxicity and toxic chemicals, recently came to the conclusion that there is strong evidence connecting phthalate exposure to a higher risk of behavioural, attention, and learning issues in kids. It has been suggested that phthalates should be removed from goods that could expose vulnerable groups, such as pregnant women, and children[11].There is now increased focus on developing technology that can efficiently achieve degradation and removal of these compounds.In this review, phthalate photo catalysis degradation is reviewed in depth to reduce environmental contamination. This review paper explores the use of semiconductor photo catalysis as a viable option for phthalate removal. An overview of photo catalyst development is provided which covers a broad range of materials that have been reported in the literature. In addition, an overview of the effects of phthalates on human health, including the mechanisms of phthalate degradation and risk assessment are reviewed to provide the reader with a detailed insight into the photo catalytic removal mechanism.

PHTHALATES SOURCES AND CATEGORY

Phthalatesare used in the production of variety of consumer, industrial as well as personal care goods. Phthalates are generally utilized as plasticizers in the manufacturing industries to create (PVC). In the majority of cases, phthalates are added to the polymers to make them softer and more malleable[12].From the past two decades the European Union (EU) and United state Environmental Protection Agency (USEPA) has prohibited the use of six phthalates due to their potential hazards to health. The phthalates include (DEHP), (BBP), (DBP), (DINP), (DIDP), and (DNOP)[13].

Categories and applications of phthalates

Tere- and ortho-phthalates are the two types of phthalates that tend to be used most frequently. Numerous types of alcohols, including methanol, ethanol, and tridecyl alcohol, react with phthalic anhydride to form ortho-phthalates, which are then simply referred to as "**phthalates**"[14].The ortho-phthalates are classified into two categories: ortho-phthalates with a high molecular weight (HMW) such as DEHP, DNOP, DIBP,DIDP, and low molecular weight (LMW) include DMP, DEP, DBP listed in the table 1. The molecular structure of HMW phthalates has seven to thirteen carbon atoms, while LMW phthalates has three to six carbon atoms only[15].

Exposure routes of phthalates

Through food

Food is presumed to be the primary source of exposure and the majority of the population is exposed to phthalates through dietary supplements thus they have received increased attention. Phthalate regulations have been established for plastic packaging materials related to food, with limits of 1.5, 0.3, and 30 mg/kg for DEHP, DBP, and BBP, respectively[16]. Edwards et al. carried out a preliminary investigation in order to examine the amounts of ortho-phthalate and replacement plasticizer in food and food handling gloves from fast food restaurants in the United States. The highest quantities of DEHT were detected in gloves. The results indicated that the food samples consist of 70% DEHP and 81% DnBP. The average DEHT concentrations in burritos were much higher than in hamburgers (6000 μg/kg vs. 2200 μg/kg; $p < 0.0001$)[17].

Through air

Phthalate concentrations in indoor air are frequently high but can also vary based on the presence of phthalate[18]. Huang et al. conducted a study by taking gas and $PM_{2.5}$concentrations of 7 phthalates from 40 residences were measured during summer and winter. Higher air humidity led to more water absorption of aerosols in summer, facilitated mass transfer of phthalates from air to $PM_{2.5}$, and resulted in greater Kp of DiBP and DnBP in the summer. According to the results, the overall amounts of airborne phthalates (gas $PM_{2.5}$) significantly dropped from summer to winter[19].

Through water

Hot water in disposable plastic and paper cups raise the levels of phthalates in drinking water.DMP and DEHP were the main phthalate-containing chemicals, contributing more than 60% of the overall phthalate levels across all water sources[20]. Tehran, Spain, China and Iran, Abtahi et al. investigated the health risks associated with phthalate exposure from drinking water, and they also examined the presence of phthalates in bottled, tap, and water resources. The results showed that the average concentrations of total phthalates (±standard deviation: SD) were 0.76 ± 0.19, 0.96 ± 0.10, 1.06 ± 0.23, and 0.77 ± 0.06 μg/L in surface waters, ground waters, bottled water, and drinking water from the water distribution system, respectively. DMP and DEHP were the leading phthalate-containing chemicals, contributing more than 60% of the overall phthalate levels in all water sources[4].

Toxicity effects

The widespread use of plastics associated with the use of variety of substances such as additives and phthalates chemicals that are discharged into the environment, are among the primary effects of industrialization[21]. In 2021, an astounding 390.7 million metric tones of plastic has been manufactured globally, of which 9% was recycled, 12% was burned, and the remaining was disposed of directly into the landfills or the environment[22].Numerous of these substances bio accumulate in biological tissues and can have a deleterious effect on the health of people and animals by changing endocrine functions. Therefore, through skin contact, ingestion, or inhalation of these widely dispersed environmental toxicants, living organisms including people and animals are invariably exposed to endocrine disrupting chemicals (EDCs)[21].The hormone Society and the International Pollutants Elimination Network (IPEN) addressed the growing concern in the economy regarding the numerous health effects of hormone disruptive chemicals found in phthalates[23].

Toxic Effect on Aquatic Organisms

The harmful effects of phthalates concentrations are dependent on the type and toxicity of the phthalate. Phthalates are hazardous to the immune system, endocrine system, metabolism, and produce oxidative stress in the aquatic organisms. Exposure to phthalates in adult aquatic organisms causes damage to the liver, kidney, reproductive system, and other organs. It has been determined via numerous studies that phthalates exposure to aquatic organisms pose both acute and long-term health effects. Cong *et al.* conducted a study to examine the effects of (DMP) on adult zebrafish (*Danio rerio*). The research findings shows that the survival is dependent on the DMP dosage. Within 96 hours, only 20% of the fish died in the presence of 25 mg/L of DMP, while the remaining fish

managed to survive. 80% of the fish died with 100 mg/L DMP died within 96hours. In the 200 mg/L concentration of DMP, fatality happened in 96 hours at a rate of 100% [24] . Furthermore, exposure to DEP, DBP, BBP, and DEHP produce neurotoxicity by affecting the activity of genes present in aquatic organisms such as mRNA (messenger ribonucleic acid) and acetylcholinesterase (AchE). Chen et al. studied the effects of exposure to the different concentrations of Di-n-butyl phthalate (DBP) (20 μg L^{-1}, 100 μg L^{-1}, and 500 μg L^{-1}) on juvenile red snapper Lutjanus argentimaculatus, for a time period of 15 days. The study demonstrated that fish exposed to DBP shows that the ethoxyresorufin O-deethylase (EROD) activities and cytochrome P4501A (CYP1A) levels in the liver and lungs is dependent on time, concentration, and tissue [25].

Toxic Effects on Human Health

Exposure to phthalates with human body through the mouth, nose, or skin cause detrimental health effects. Both the male and female reproductive system is adversely affected. A Chinese study examine that the exposure to the phthalates metabolites: monomethyl phthalate (MMP), monoethyl phthalate (MEP), monobutyl phthalate (MBP), monobenzyl phthalate (MBzP), mono-2-ethylhexyl phthalate (MEHP), and mono-2-ethyl-5-oxohexyl phthalate (MEOHP) strongly impact the male semen quality [26, 27].Among the several types of phthalates, DEHP is the most commonly used and hazardous. Also has the potential to negatively affect human health and functions as an endocrine disruptor [28]. Another prospective study demonstrated increased phthalate concentrations will decrease the oocyte fertilization, mature oocyte and good-quality embryos. Thus, it appears that exposure to phthalates is associated with early puberty, preterm birth, and certain conditions that impact female fertility, including endometriosis and DMP. Furthermore, the unfavourable outcomes male foetuses face during pregnancy may be due to phthalate's exposure.

PHOTOCATALYSIS MECHANISM FOR SUSTAINABLE DEGRADATION OF PHTHALATES

The term "photo catalyst" refers to a semiconductor material that can accelerate a chemical reaction by the absorption of photons of energy (in ultraviolet or visible region) greater than or equal to 3.2 eV. The photochemical process initiates when photons with energy greater than or equal to the photo catalyst material ($h\upsilon \geq E_{gap}$) interacts with the surface of photo catalyst[29]. The simultaneous photochemical redox reactions can take place. As a result of this photo redox reaction the electron-hole (e^-/h^+) pairs are generated in the conduction(e_{cb}^-)and valence bands(h_{vb}^+) (equation) respectively[30].The produced $e_{cb}^- \; and \; h_{vb}^+$ are strong reducing and oxidizing agents[31]. The e_{cb}^- combine with oxygen molecule to form superoxide radical ($O_2^{-\cdot}$) whereas the h_{vb}^+ combine with water molecule to produce hydroxyl ($OH^{\cdot}$). The produced ($OH^{\cdot}$) with strong oxidation potential of 2.06 eV degrades pollutant molecule(X) such as phthalates, irrespective of the X selectivity. The pollutant molecule degradation mechanism is mentioned in equation (a-d)

$$Photocatalyst + h\upsilon \geq Egap \rightarrow h_{vb}^+ + e_{cb}^- \quad (a)$$

$$h_{vb}^+ + H_2O \rightarrow Photocatalyst + OH^{\cdot} + H^+ \quad (b)$$

$$e_{cb}^- + O_2 \rightarrow Photocatalyst + O_2^{-\cdot} \quad (c)$$

$$OH^{\cdot} + X \rightarrow intermediates \rightarrow CO_2 + H_2O + by\,products \quad (d)$$

Semiconductor-based photo catalysis

The semiconductor photo catalysts have drawn more attention in recent years, due to potential applications in the environmental purification and mitigation of organic as well as inorganic pollutants from water and air [32].The photo catalytical degradation is considered to be one of the best photochemical processes for mineralisation of the personal care products (PCPs) particularly phthalates. In 2022, Pang et al. fabricated two commercial catalysts TiO_2, ZnO for the degradation of the Diisobutyl phthalate (DiBP). The results show that greater than 90% of degradation takes place within 25 min. The generated super oxide radical •OH and $•O_2^-$ are essential components in the photo catalytic degradation of DiBP for both materials. This is the first research on semiconductor photo catalysis-induced phthalate DiBP disintegrate in water[33]. The alkaline earth metals are abundant and inexpensive in the earth's crust, their stannate perovskite oxides offer a wider range of potential applications in multiple fields. The band gap value, affordability, stability, and environmental friendliness of $MgSnO_3$ and $CaSnO_3$

which enable them to degrade phthalates.*Ye et al.* investigated the photocatalytic degradation performances of dimethyl phthalate (DMP) and diethyl phthalate (DEP) by the oxides of stannate perovskite $MgSnO_3$ and $CaSnO_3$under simulated sunlight. The photochemical examination results demonstrated that $MgSnO_3$ perovskite performed better when compared to $CaSnO_3$ perovskite. This is due to increased specific surface area, pore volume, average pore width, greater abundance of oxygen vacancies which facilitated the adsorption, transport, and activation of reactive oxygen species [34]. According to reports, PAEs that have an alkyl chain length of less than six such as DMP, DEP, and DBP are intrinsically harmful to aquatic life. Thus allows them to be easily absorbed by the skin and digestive system, and then subsequently transmitted to the majority of the body tissues, including the placenta[35]. Wang et al.'s research illustrated that phthalic acid esters dimethyl phthalate (DMP), diethyl phthalate (DEP), dibutyl phthalate (DBP) undergoes photo catalysis degradation by the UV, UV/TiO_2, and UV-Vis/Bi_2WO_6.The results indicate that, the UV/TiO_2 exhibited the highest degrading efficacy on a particular group of PAEs, achieving removal efficiencies of up to 93.03, 92.64, and 92.50% in 90 minutes for DMP, DEP, and DBP, respectively. However, the system UV-Vis/Bi_2WO_6 was completely inefficient for eliminating DEP and DMP[36]. Zhang et al. synthesized a Z-scheme nanocomposite rGO-(Bi_2O_3–TiO_2) for the removal of the Di(2-ethylhexyl) phthalate (DEHP) is a known carcinogen, teratogen, and mutagenic environmental contaminant. The findings show that, doping a composite Bi_2O_3–TiO_2 with 4% rGO, shows the best photo catalytic degradation of 89% within 90 minutes of continuous solar light irradiation. By considering the reaction parameters such as pH=6 of the solution and concentration of DEHP (10 mg L^{-1}). Therefore, the created hetero junction enhanced electron-hole separation rate in [rGO-(Bi_2O_3–TiO_2)]. Furthermore, the photo catalytic performance of Bi_2O_3–TiO_2 was 1.61 times stronger than that of pristine Bi_2O_3 and TiO_2.[37].

Abbreviations
DMP (dimethyl phthalate),
DEP(Diethyl phthalate),
DBP (Dibutyl Phthalate),
DEHP (Di-Ethyl-Hexyl-Phthalate),
BBP(Butyl-Benzyl-Phthalate),
DIBP (Diisobutyl phthalate)

CONCLUSION

Phthalates are one of the categories of emergent contaminants that have the greatest negative environmental impact due to their extensive use as well as constantly spilled into the reservoirs. The origins of phthalate contamination, its health effects, the exposure routes, and, photo catalytic mineralisation technique have all been covered in this analysis. This study provided a comprehensive summary of the disrupting-effects of phthalates on living organisms such as the human and animals. Currently, the effects of phthalates on aquatic organisms are better documented than the effects on human health. Therefore, there is need to evaluate this issue better and improve the negative impact of exposure to phthalates on the both vivo and vitro. The degradation of the phthalate's contaminants by advanced oxidation processes such as photo catalysis is important for environmental remediation. The review aims to provide information on how photo catalytic process has become a rapid and important strategy to mitigate the pollutants released from the overuse of the phthalates containing products.

REFERENCE

1. Wensing, M., E. Uhde, and T. Salthammer, Plastics additives in the indoor environment--flame retardants and plasticizers. Sci Total Environ, 2005. 339(1-3): p. 19-40.
2. Peijnenburg, W.J.G.M., Phthalates, in Encyclopedia of Ecology, S.E. Jørgensen and B.D. Fath, Editors. 2008, Academic Press: Oxford. p. 2733-2738.

3. De-la-Torre, G.E., et al., Release of phthalate esters (PAEs) and microplastics (MPs) from face masks and gloves during the COVID-19 pandemic. Environmental Research, 2022. 215: p. 114337.
4. Abtahi, M., et al., Health risk of phthalates in water environment: Occurrence in water resources, bottled water, and tap water, and burden of disease from exposure through drinking water in tehran, Iran. Environmental Research, 2019. 173: p. 469-479.
5. Luo, Q., et al., Migration and potential risk of trace phthalates in bottled water: A global situation. Water Research, 2018. 147: p. 362-372.
6. Quan, C.S., et al., Biodegradation of an endocrine-disrupting chemical, di-2-ethylhexyl phthalate, by Bacillus subtilis No. 66. Appl Microbiol Biotechnol, 2005. 66(6): p. 702-10.
7. Monti, M., et al., A review of European and international phthalates regulation: focus on daily use products: Marco Monti. Eur J Public Health. 2022 Oct 25;32(Suppl 3):ckac131.226. doi: 10.1093/eurpub/ckac131.226. eCollection 2022 Oct.
8. Abtahi, M., et al., Health risk of phthalates in water environment: Occurrence in water resources, bottled water, and tap water, and burden of disease from exposure through drinking water in tehran, Iran. Environ Res, 2019. 173: p. 469-479.
9. Liu, X., et al., Occurrence and risk assessment of selected phthalates in drinking water from waterworks in China. Environ Sci Pollut Res Int, 2015. 22(14): p. 10690-8.
10. Domínguez-Morueco, N., S. González-Alonso, and Y. Valcárcel, Phthalate occurrence in rivers and tap water from central Spain. Sci Total Environ, 2014. 500-501: p. 139-46.
11. Engel, S.M., et al., Neurotoxicity of Ortho-Phthalates: Recommendations for Critical Policy Reforms to Protect Brain Development in Children. Am J Public Health, 2021. 111(4): p. 687-695.
12. Wolff, M.S., et al., Prenatal phenol and phthalate exposures and birth outcomes. Environ Health Perspect, 2008. 116(8): p. 1092-7.
13. Erickson, B., European Union further restricts four phthalates. C&EN Global Enterprise, 2017. 95.
14. Kueseng, P., P. Thavarungkul, and P. Kanatharana, Trace phthalate and adipate esters contaminated in packaged food. J Environ Sci Health B, 2007. 42(5): p. 569-76.
15. Tsumura, Y., et al., Eleven phthalate esters and di(2-ethylhexyl) adipate in one-week duplicate diet samples obtained from hospitals and their estimated daily intake. Food Addit Contam, 2001. 18(5): p. 449-60.
16. Luo, Q., et al., Migration and potential risk of trace phthalates in bottled water: A global situation. Water Res, 2018. 147: p. 362-372.
17. Edwards, L., et al., Phthalate and novel plasticizer concentrations in food items from U.S. fast food chains: a preliminary analysis. Journal of Exposure Science & Environmental Epidemiology, 2022. 32(3): p. 366-373.
18. Marega, M., et al., Phthalate analysis by gas chromatography-mass spectrometry: Blank problems related to the syringe needle. Journal of chromatography. A, 2012. 1273.
19. Huang, L., et al., Airborne phthalates in indoor environment: Partition state and influential built environmental conditions. Chemosphere, 2020. 254: p. 126782.
20. Amiridou, D. and D. Voutsa, Alkylphenols and phthalates in bottled waters. Journal of Hazardous Materials, 2011. 185(1): p. 281-286.
21. Maradonna, F., L.N. Vandenberg, and R. Meccariello, Editorial: Endocrine-Disrupting Compounds in Plastics and Their Effects on Reproduction, Fertility, and Development. Front Toxicol, 2022. 4: p. 886628.
22. Zoeller, R.T., et al., The Path Forward on Endocrine Disruptors Requires Focus on the Basics. Toxicological sciences : an official journal of the Society of Toxicology, 2016. 149(2): p. 272.
23. Chavoshani, A., et al., Chapter 3 - Personal care products as an endocrine disrupting compound in the aquatic environment, in Micropollutants and Challenges, A. Chavoshani, et al., Editors. 2020, Elsevier. p. 91-144.
24. Cong, B., et al., The Impact on Antioxidant Enzyme Activity and Related Gene Expression Following Adult Zebrafish (Danio rerio) Exposure to Dimethyl Phthalate. 2020. 10(4): p. 717.
25. Chen, H., et al., Effects of di-n-butyl phthalate on gills- and liver-specific EROD activities and CYP1A levels in juvenile red snapper (Lutjanus argentimaculatus). Comp Biochem Physiol C Toxicol Pharmacol, 2020. 232: p. 108757.

26. Yang, P., et al., Phthalate exposure with sperm quality among healthy Chinese male adults: The role of sperm cellular function. Environmental Pollution, 2023. 331: p. 121755.
27. Liu, L., et al., Phthalates exposure of Chinese reproductive age couples and its effect on male semen quality, a primary study. Environ Int, 2012. 42: p. 78-83.
28. Mesquita, I., M. Lorigo, and E. Cairrao, Update about the disrupting-effects of phthalates on the human reproductive system. 2021. 88(10): p. 650-672.
29. Boroski, M., et al., Combined electrocoagulation and TiO(2) photoassisted treatment applied to wastewater effluents from pharmaceutical and cosmetic industries. J Hazard Mater, 2009. 162(1): p. 448-54.
30. Baruah, A., et al., 17 - Nanotechnology Based Solutions for Wastewater Treatment, in Nanotechnology in Water and Wastewater Treatment, A. Ahsan and A.F. Ismail, Editors. 2019, Elsevier. p. 337-368.
31. Solarska, R., A. Królikowska, and J. Augustyński, Silver nanoparticle induced photocurrent enhancement at WO3 photoanodes. Angew Chem Int Ed Engl, 2010. 49(43): p. 7980-3.
32. Gaya, U.I. and A.H. Abdullah, Heterogeneous photocatalytic degradation of organic contaminants over titanium dioxide: A review of fundamentals, progress and problems. Journal of Photochemistry and Photobiology C: Photochemistry Reviews, 2008. 9(1): p. 1-12.
33. Pang, X., et al., Kinetic modelling of the photocatalytic degradation of Diisobutyl phthalate and coupling with acoustic cavitation. Chemical Engineering Journal, 2022. 444: p. 136494.
34. Ye, Q., et al., Insights into photocatalytic degradation of phthalate esters over MSnO3 perovskites (M = Mg, Ca): Experiments and density functional theory. Journal of Environmental Management, 2022. 307: p. 114511.
35. Staples, C.A., et al., Aquatic toxicity of eighteen phthalate esters. Environmental Toxicology and Chemistry, 1997. 16(5): p. 875-891.
36. Wang, C., et al., Photodegradation Pathways of Typical Phthalic Acid Esters Under UV, UV/TiO(2), and UV-Vis/Bi(2)WO(6) Systems. Front Chem, 2019. 7: p. 852.
37. Zhang, Y., et al., Rapidly degradation of di-(2-ethylhexyl) phthalate by Z-scheme Bi2O3/TiO2@reduced graphene oxide driven by simulated solar radiation. Chemosphere, 2021. 272: p. 129631.
38. Zhou, W., et al., Ultrasonic fabrication of N-doped TiO2 nanocrystals with mesoporous structure and enhanced visible light photocatalytic activity. Chinese Journal of Catalysis, 2013. 34: p. 1250-1255.
39. Chin, Y.-H., et al., 3-D/3-D Z-Scheme Heterojunction Composite Formed by Marimo-like Bi2WO6 and Mammillaria-like ZnO for Expeditious Sunlight Photodegradation of Dimethyl Phthalate. 2022. 12(11): p. 1427.
40. Singla, P., O. Pandey, and K. Singh, Enhanced photocatalytic degradation of diethyl phthalate using Zn doped rutile TiO2. Indian Journal of Pure and Applied Physics, 2017. 55: p. 710-715.
41. Huang, W.-B. and C.-Y. Chen, Photocatalytic Degradation of Diethyl Phthalate (DEP) in Water Using TiO2. Water, Air, and Soil Pollution, 2009. 207: p. 349-355.
42. Meenakshi, G. and A. Sivasamy, Nanorod ZnO/SiC nanocomposite: An efficient catalyst for the degradation of an endocrine disruptor under UV and visible light irradiations. Journal of Environmental Chemical Engineering, 2016. 6.
43. Mphahlele, I.J., S.P. Malinga, and L.N. Dlamini, Combined Biological and Photocatalytic Degradation of Dibutyl Phthalate in a Simulated Wastewater Treatment Plant. 2022. 12(5): p. 504.
44. Akbari-Adergani, B., et al., Removal of dibutyl phthalate from aqueous environments using a nanophotocatalytic Fe, Ag-ZnO/VIS-LED system: modeling and optimization. Environ Technol, 2018. 39(12): p. 1566-1576.
45. Eslami, A., et al., Synthesis and characterization of a coated Fe-Ag@ZnO nanorod for the purification of a polluted environmental solution under simulated sunlight irradiation. Materials Letters, 2017. 197.
46. Xu, X.-R., et al., Degradation of n-butyl benzyl phthalate using TiO2/UV. Journal of Hazardous Materials, 2009. 164(2): p. 527-532.

Table 1 displays the categories, molecular formula, photocatalyst, % degradation and time period, experimental conditions, and uses of the phthalates

Compounds	Molecular Formula	Photocatalyst	% degradation and time period(min)	Experimental conditions	Uses	Ref
Dimethyl phthalate (DMP)	$C_{10}H_{10}O_4$	N/TiO_2 and N/TiO_2	N/TiO_2 (41%) and UN/TiO_2 (58%) within 5 hrs	DMP initial concentration: 15 mg/L Temperature: 22±2 °C Catalyst loading: 0.5 g/L.	Used in hair sprays, enteric coatings for medicines and rubber , solid rocket propellants, nail polish, artificial nails, insect repellents, and pesticides.	[38]
	$C_{10}H_{10}O_4$	20 wt % Bi_2WO_6/ZnO (20-BWZ)	86.6% within 90 min	DMP degradation under natural sunlight irradiation		[39]
Diethyl phthalate (DEP)	$C_{12}H_{14}O_4$	0.2 mol % of Zn doped TiO_2	100% within 200 min	mercury lamp =125 W catalyst load = 1 g/l. Zn doped TiO_2 calcined at 450 ^{0}C.	Directly added in cosmetic products and indirectly in fragrances. Also used as a solvent and alcohol denaturant.	[40]
		TiO_2 (anatase)	100% within 50 mins	initial concentration: 20 mg/L Catalyst loading: 0.2 g/L Temperature=25°C pH=4.0 Luminous intensity: 2.5×10−6 Einstein/L·s.		[41]
		ZnO/SiC	90%within 120 and under visible light irradiation the time for maximum degradation was nearly 660 min.	DEP initial concentration: 5, 10, 15 and 25 mg/L pH: ranging from 2 to 12.		[42]
Dibutyl Phthalate (DBP)	$C_{16}H_{22}O_4$	3% Ce/Gd-WS_2	75% within 60 min	initial concentration of catalyst = 5ppm pH= 7 catalyst loading =10 mg	Plastics such as PVC, adhesives, printing inks, sealants, grouting agents, perfumes, deodorants, hair sprays, nail polish, and insecticides.	[43]
		(Fe, Ag) co-	95% within	DBP initial		[44]

		doped ZnO	137.5 min	concentration: 15 mg/L pH: 3 Catalyst loading: 0.15 g/L.		
Di-Ethyl-Hexyl-Phthalate (DEHP)	$C_{24}H_{38}O_4$	rGO-(Bi_2O_3–TiO_2)	89% within 95 min	pH = 6 Concentration of DEHP =10 mg L^{-1} reaction temperature =25 °C catalyst dosage = 0.0834 mg L^{-1}	Diapers, food containers, plastic film for food packaging, blood bags, catheters, gloves, and medical equipment's such as tubes for fluids etc.	[37]
		Fe-Ag@ ZnO	90 % within 120 min	Catalyst loading: 20 mg/L. The authors reported that photocatalytic degradation of DEHP increased when operated at a higher and lower pH (as a result of acidic and basic catalytic hydrolysis).		[45]
Butyl-Benzyl-Phthalate (BBP)	$C_{19}H_{20}O_4$	TiO_2/UV	70% and 120 min	catalyst dosage = 2.0 g L^{-1} pH=7.0 concentration of BBP = 1 mg L−1 concentrations of the co-existing substances = 0.01 M	Perfumes, hair sprays, adhesives and glues, automotive products, vinyl floor coverings	[46]
Diisobutyl phthalate (DIBP)	$C_{16}H_{22}O_4$	P25 TiO_2 and ZnO	>90% and 30 min	catalyst loading = 20 mg concentration of DiBP = 10 mg L^{-1}	utilised as plasticizer in solid rocket propellants, nitrocellulose lacquers, elastomers, explosives, printing inks, adhesives and nail polish.	[33]

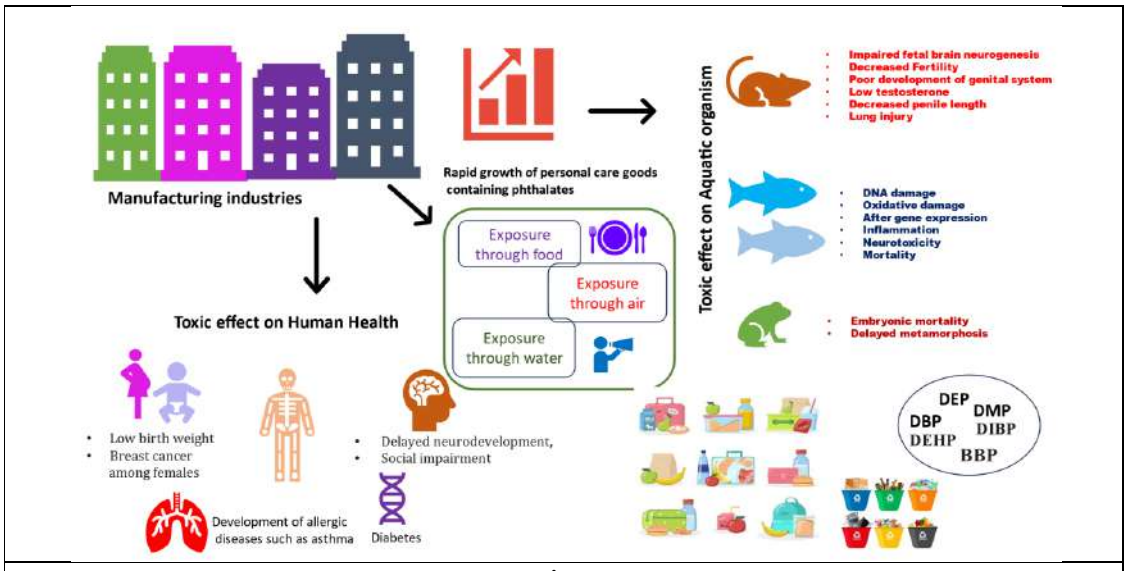
Manufacturing industries
Rapid growth of personal care goods containing phthalates
Exposure through food
Exposure through air
Exposure through water
Toxic effect on Human Health
Low birth weight
Breast cancer among females
Delayed neurodevelopment,
Social impairment
Development of allergic diseases such as asthma
Diabetes
Toxic effect on Aquatic organism
Impaired fetal brain neurogenesis
Decreased Fertility
Poor development of genital system
Low testosterone
Decreased penile length
Lung injury
DNA damage
Oxidative damage
After gene expression
Inflammation
Neurotoxicity
Mortality
Embryonic mortality
Delayed metamorphosis
DEP
DMP
DBP
DIBP
DEHP
BBP

Fig:1

Indian Journal of Natural Sciences *www.tnsroindia.org.in ©IJONS*

Vol.15 / Issue 83 / Apr / 2024 *International Bimonthly (Print) – Open Access* *ISSN: 0976 – 0997*

RESEARCH ARTICLE

Preparation of Graphene Oxide: Various methods and their comparison

Ajay Jakhar and Jyoti Sharma*

Department of Chemistry,MMEC, Maharishi Markandeshwar (Deemed to be University), Mullana-133207 (Ambala) Haryana, India.

Received: 30 Dec 2023 Revised: 09 Jan 2024 Accepted: 12 Jan 2024

***Address for Correspondence**
Jyoti Sharma
Associate professor,
Department of Chemistry,MMEC,
Maharishi Markandeshwar (Deemed to be University),
Mullana-133207 (Ambala) Haryana, India.
Email: jsharma117@gmail.com

ABSTRACT

Graphene oxide (GO), a versatile and extensively studied material, finds applications in a myriad of fields owing to its unique properties. This abstract provides a comprehensive overview of various methods for the preparation of graphene oxide, drawing insights from seminal and contemporary research. The Hummers' method, initially introduced in 1958, involves the oxidation of graphite using a mixture of potassium permanganate, sulfuric acid, and sodium nitrate. Brodie's method, a historical precursor to Hummers', employs nitric acid as the oxidizing agent. Building upon these foundational approaches, the Improved Hummers' method and chemical exfoliation of graphite have been proposed, allowing for adjustments in reaction conditions and alternative oxidants. Ultrasound-assisted methods utilize acoustic energy for exfoliation, while microwave-assisted exfoliation accelerates the process through targeted irradiation. Electrochemical exfoliation, on the other hand, involves the reduction of graphene oxide on an electrode. The review synthesizes these methods, highlighting their respective advantages and limitations, providing a valuable resource for researchers engaged in the synthesis of graphene oxide for diverse applications. As the field continues to evolve, this overview serves as a foundation for understanding and exploring novel techniques for graphene oxide preparation.

Keywords: Graphene Oxide, Hummers method, Exfoliation methods, Oxidizing agent and Microwave-assisted methods.

INTRODUCTION

When in 1859 Graphene oxide was synthesized by Brodie[1], there is a surge in its research after the introduction of electronic properties of Graphene by Giem and Novoselov[2] as it has a prominent role in the development of Graphene. On investigating the nomenclatures of Graphene and graphene oxide they show some similarities as they both are carbon nanomaterials howsoever graphene and GO are very different, Graphene is a single layer of SP^2 hybridized Carbon atoms whereas GO has a carbon structure with defects and oxygen containing functional groups which imparts to its SP^3 hybridization to a substantial degree. The presence of oxygenated groups in GO affects its electronic, mechanical and electrochemical properties. These polar functional groups of GO makes it strongly hydrophilic[3] making it easy for GO to link to other metals and nonmetallic nanoparticles by noncovalent or covalent chemical bonds which creates extraordinary optical and electrical properties for GO based nanocomposites[4,5] and stable GO dispersion for preparation of thin conductive films by drop-casting or spin coating[6]. The structure of GO and positioning of GO is been a topic of debate ever since and exact structure is yet to be found though the Lerf-Klinowski[7] model is been widely accepted Fig-1. In this model, Hydroxyl and epoxide functional groups are proposed to decorate the basal plane which are segregated into islands among the lightly oxidized, graphene-like regions while carboxylic acids or carbozlates, depending on the pH of the solution are present on the edges of the sheets. Electronic properties of GO sheets depend on degree of structural disorder from the presence of substantial amount of sp^3carbon fraction. GO films have a energy fap in the electron density making it typically insulating in its natural state[8], in sheet form GO exhibits high sheet resistance (R_s) about 10^{12}-Ωsq^{-1}[9]. GO also exhibits excellent photoluminescence[10] which occur from near-UV-to blue visible (vis) to near-infrared (IR) wavelength range which makes GO very useful in biosensing, optoelectronics applications.[11]

Electrochemical properties of GO are also fascinating as because of its favorable electron mobility and unique surface properties, such as one-atom thickness and high surface area, GO can accommodate the active species and facilitate their electron transfer at electrode surfaces as reported by Zuo et al[12], GO supports the efficient electrical wiring of the redox xenters of several heme-containing metalloproteins to the electrodes. Graphene oxide is an excellent candidate for fluorescence resonance energy transfer sensors for single stranded DNA monitoring, GO has unique interaction with nucleic acid makes it simple to identify and quantify a target DNA.[13] Abundance of oxygen containing functional groups it binds to various catalysts for hydrogen storage and generation, taking advantage of bandgap of GO it has wide application iin LEDs having GO interlayers reaching a high value in luminosity of 220% increase and 280% power efficiency in comparison to devices without GO.[14] In a comparative study of oxidation synthesis methods of Graphene Oxide Pumera et al[15] concluded in their study that permanganate-based oxidations such as Hummers and Tour methods introduced a greater amount of oxygen functionality and higher proportion of carbonyl and carboxylic acid groups than methods that utilize chlorate-based oxidants such as Staudenmaier , the Brodie, Hofmann methods but chlorate based oxidations methods has more uniform functionality and less extensive methods and materials. In this review we try our best to summarise the abundantly used methods for preparation of Graphene Oxide- Hummers Method, Brodie Method, Staudenmaier Method, Electrochemical Exfoliation methods, Microwave Exfoliation methods.

Methods for GO preparation

Protocols and procedures used in various methods are summarized in a brief manner as follows

Hummers method

In Hummers' method concentrated H_2SO_4 behaves as the intercalator and $KMnO_4$ acts as the oxidant[16-17] and the ratio of these are very crucial for preparation of good quality of Graphene oxide. Procedure used by Hummers is briefed in Fig-2 Formation of Graphene oxide from graphite can be divided into three individual steps as explained by Dimiev[18], where each step can be stopped and each intermediate product can be isolated and stored at appropriate conditions. First step involves formation of graphite intercalation compound with H_2SO_4(H_2SO_4-GIC) which is a crucial step for GO formation as this step allows diffusion of oxidizing agents into the interlayer spaces of

graphite, sodium nitrate has synergistic effect in the process. In second step GIC is converted to pristine oxidized graphite (PGO), this is rate determining step which takes hours to complete. In third step PGO is converted to GO with exposure with water.We can also modify the timing of reaction in Hummers' method for production of well exfoliated Graphene oxide as shown by Aixart[19], where they produced GO with reaction time as GO-30 min, GO-60 min, GO-120 min, GO-300 min, GO-540 min and concluded that with increase in reaction time and avoiding aggressive steps during end of reaction we can produce greater exfoliated GO with increased interlaminar spacing. Graphene oxide synthesized from Hummers' method contains higher amount of carbonyl and carboxyl groups when compared to GO from Brodies' method.

Brodies' Method

This method involves high vaccum conditions and samples are efficiently dried from residual water to yield correct C/O ratio (atomic percent).[20] Graphene oxide synthesized by Brodies' method[1](Procedure briefed in Fig-3) has high relative amount of epoxy and hydroxyl groups on the planar surface of graphene oxide flakes as compared to graphene oxide synthesized from Hummers' method. The GO produced from brodies method has as interlayer spacing of 7.0±0.35Å[21]and functional groups such as hydroxyl, epoxide, carboxyl and some alkyl groups are distributed randomly. Hydroxyl and epoxide groups are located on their basal planes close to each other and carboxyl and alkyl groups were located at the edges of the GO flakes, when characterised by EA, XRD, SEM, TEM, RAMAN, FTIR, ^{13}C NMR and XPS techniques.

Staudenmaier Method

In 1898 staudenmaier improved Brodies' reaction by adding sulfuric acid to increase the acidity of mixture and $KClO_3$ over the reaction process[22]. Detailed procedure is briefed in Fig-4. In this method $KClO_3$ acts as an oxidant[23]with fuming HNO_3 as reaction media and the product contains Carbon-to-oxygen ratio as 1.17, Raman Spectral I_D/I_Gratio as 0.89, charge transfer resistance $(R_{CT})^a$ (kΩ) 1.74. In 2013 Sheshmani et al[24]modified Staudenmaier method for preparation of Graphene Oxide where they examined the effect of HNO_3/H_2SO_4amount on interlayer spacing and its comparison. In this method oxidation of Graphite with Nitric acid and sulfuric acid in 1:3 ratio for 4 days was performed which resulted in a slightly expanded interlayer distance to 9.13A^o.

Electrochemical Exfoliation methods for GO preparation

Electrochemical exfoliation methods for the preparation of Graphene oxide (GO) involves the use of electrochemical techniques to exfoliate graphite and introduce oxygen containing functional groups. In the initial steps for exfoliation of graphite there is intercalation of ions which is followed by expansion induced by gaseous products. The use of high anodic potentials creates oxidized Graphene (Graphene Oxide) which is rich in oxygen functional groups and structural defects.

Direct electrochemical exfoliation of Graphite for GO

In this method graphite is directly exfoliated in electrolyte medium for the production of high quality of Graphene oxide. Most commonly used electrolyte for this method are as sulfuric acid[25], Poly(styrenesulfonate) (PSS)[26]. Su et al[25]synthesized graphene oxide using electrochemical exfoliation method of graphite in sulfuric acid and obtained high quality graphene oxide. In this work natural graphite flakes were employed as an electrode and a Pt wire used as grounded electrode in H_2SO_4. The obtained graphene sheets exhibited ultra transparency (~ 96% transmittance) and a resistance of <1KΩ/sq.

Ionic Liquid-assisted electrochemical exfoliation of Graphite

In this method ionic liquids are used in environmentally friendly electrolytes. In a study by Jamaluddin et al[27]produced surfactant-assissted exfoliated graphene oxide (sEGO) with 1-butyl-3-methyl-imidazolium (BMIM) and surfactant ionic liquids in presence of triple chain surfactant TC14 (sodium 1,4-bis(neopentyloxy)-3-(neopentylcarbonyl)-1,4-dioxobutane-2-sulfonate) where TC14 is substituted with BMIM generating surfactant ionic liquids to produce BMIM-TC14sEGO/NFC composites.

Aqueous Electrochemical exfoliation of Graphite for GO preparation

In this exfoliation aqueous medium electrolyte is used. As graphene prepared by Anurag et al[28] prepared Graphene in an electrolytic bath which contains 0.1 M Ferrous sulfate ($FeSO_4$), two graphite rods are used at 3 cm distance and consistent potential of 15-20 V was applied across the setup and the resulting exfoliated graphene exhibited at 267 nm which is recognised to π-π transition of C-O bonds. Qingtao et al[29] used aqueous medium electrolyte method for preparation of exfoliated graphene oxide films where graphite is treated with concentrated sulfuric acid and hydrogen peroxide at room temperature then this exfoliated graphite without removing H_2SO_4 contained in a container which have holes for electrochemical oxidization, purpose of holes in walls is to confine graphite particles in limited space which avoid shedding of graphite from the reacting region during the process. On characterization it was found that the reduced exfoliated graphene oxide have a high conductivity of 1022 s cm^{-1}.

Surfactant assisted exfoliation of graphite

Two types of surfactant can be used in this exfoliation technique anionic surfactant and cationic surfactant both were tried and tested by Yang et al[30] where graphite is mildly oxidized using improved hummers method[31]and exfoliation is performed using HCDDACI and HCSL with different concentrations and they concluded that anionic surfactant was more favourable than cationic surfactants. Surfactants have a great deal on the extent of exfoliation, surfactants affect the exfoliation of mildly oxidized graphite through intercalating into the lamellas to weaken or strengthen the interlayer force.

Microwave assisted exfoliation method for preparation of Graphene oxide

Preparation of graphene via Hummers method, Brodies method or Staudenmaier method is a long time taking processes which involves highly toxic materials. Microwave assisted method is really time saving method for preparation of Graphene Oxide, GO was manufactured in 2015 by Viana et al.[32] via this process, which involved magnetically mixing natural graphite, 70% nitric acid, and $KMnO_4$ in a glass flask for 10 minutes at ambient temperature. The graphite:HNO_3:$KMnO_4$ weight ratio was 1:2:1. Expanded graphite (EG) was made by transferring the acid dispersion to a crucible, heating it to 110°C for three hours, and then rinsing the resulting powder with deionized water until it became neutral. 2.2 ml of H_2SO_4 and 1.0 g of $KMnO_4$ are added to 1.0 g of EG for oxidation and exfoliation. The mixture is magnetically agitated for 30 minutes to create a green dispersion, and then deionized water and the dispersion are sonicated for two hours, turning the brown color of the combination into a bright yellow tint. The mixture is then rinsed with 10% HCl and deionized water until it becomes neutral, resulting in a brown powder which is precipitated GO.Wang et al[33]Weighed and transferred 0.125g graphite in a 500 ml volumetric flask and 10 ml H2SO4 was added followed by the addition of 0.923g KMnO4. Stirred the mixture for 5 min then placed in Microwave. The microwave for 3 cycle and 30 sec each cycle for a total reaction time of 150 sec. After each cycle, keep the volumetric flask in ice bath for rapid cooling. Now 15 ml 30% H2O2 added drop wise and continue the reaction for 2 min with stirring, then centrifuge the solution for 10 min at 13000 RPM. Discard the supernatant and wash the solid with 5% HCl solution followed with ultrapure water as long as the pH of the solution is neutralized. The product has been dispersed in 100 ml water with stirring for 5 min. and used the ultrasonic bath to exfoliate the suspension for half an hour. The solution is centrifuged for 15 min at 4500 rpm and finally dry the solid product overnight at room temperature.

CONCLUSION

After reviewing all the procedures and chemicals used in all processes we conclude that all procedures have their own benefits for the production of GO and in this time of global warming and pollution fast and facile green methods should be used for the production of GO on commercial scale as the method and procedure discussed in this review gives 100% yield as claimed by the authors which takes very small time as compared to well established previous methods like hummers method and brodies methods.

REFERENCES

1. Brodie BC. XIII. On the atomic weight of graphite. Philosophical transactions of the Royal Society of London. 1859 Dec 31(149):249-59.
2. Novoselov KS, Geim AK, Morozov SV, Jiang DE, Zhang Y, Dubonos SV, Grigorieva IV, Firsov AA. Electric field effect in atomically thin carbon films. science. 2004 Oct 22;306(5696):666-9.
3. Bissessur R, Scully SF. Intercalation of solid polymer electrolytes into graphite oxide. Solid State Ionics. 2007 May 15;178(11-12):877-82.
4. Wu Y, Luo Y, Qu J, Daoud WA, Qi T. Liquid single-electrode triboelectric nanogenerator based on graphene oxide dispersion for wearable electronics. Nano Energy. 2019 Oct 1;64:103948.
5. Yang W, Chata G, Zhang Y, Peng Y, Lu JE, Wang N, Mercado R, Li J, Chen S. Graphene oxide-supported zinc cobalt oxides as effective cathode catalysts for microbial fuel cell: High catalytic activity and inhibition of biofilm formation. Nano Energy. 2019 Mar 1;57:811-9.
6. Kim F, Cote LJ, Huang J. Graphene oxide: surface activity and two-dimensional assembly. Advanced Materials. 2010 May 4;22(17):1954-8.
7. Lerf A, He H, Forster M, Klinowski J. Structure of graphite oxide revisited. The Journal of Physical Chemistry B. 1998 Jun 4;102(23):4477-82.
8. Boukhvalov DW, Katsnelson MI. Modeling of graphite oxide. Journal of the American Chemical Society. 2008 Aug 13;130(32):10697-701.
9. Becerril HA, Mao J, Liu ZF, Stoltenberg RM, Bao ZN. ACS Nano, 2008, 2, 463;(b) ZF Liu, Q. Liu, XY Zhang, Y. Huang, YF Ma, SG Yin and YS Chen. Adv. Mater. 2008;20:3924.
10. Loh KP, Bao Q, Eda G, Chhowalla M. Graphene oxide as a chemically tunable platform for optical applications. Nature chemistry. 2010 Dec;2(12):1015-24.
11. Liu F, Choi JY, Seo TS. Graphene oxide arrays for detecting specific DNA hybridization by fluorescence resonance energy transfer. Biosensors and Bioelectronics. 2010 Jun 15;25(10):2361-5.
12. Zuo X, He S, Li D, Peng C, Huang Q, Song S, Fan C. Graphene oxide-facilitated electron transfer of metalloproteins at electrode surfaces. langmuir. 2010 Feb 2;26(3):1936-9.
13. Jakhar A, Sharma J, Sharma S, Krishan Sharma L. Graphene-Based Nano Materials: Biomedical Applications. Chemistry Select. 2023 Oct 6;8(37):e202302689.
14. Ajay A, Sharma J, Sharma S, Sharma LK. Graphene-based Materials for Advanced Electronics. In2023 2nd Edition of IEEE Delhi Section Flagship Conference (DELCON) 2023 Feb 24 (pp. 1-5). IEEE.
15. Chua CK, Sofer Z, Pumera M. Graphite oxides: effects of permanganate and chlorate oxidants on the oxygen composition. Chemistry–A European Journal. 2012 Oct 15;18(42):13453-9.
16. Hummers Jr WS, Offeman RE. Preparation of graphitic oxide. Journal of the american chemical society. 1958 Mar;80(6):1339.
17. Hou Y, Lv S, Liu L, Liu X. High-quality preparation of graphene oxide via the Hummers' method: understanding the roles of the intercalator, oxidant, and graphite particle size. Ceramics International. 2020 Feb 1;46(2):2392-402.
18. Dimiev AM, Tour JM. Mechanism of graphene oxide formation. ACS nano. 2014 Mar 25;8(3):3060-8.
19. Aixart J, Diaz F, Llorca J, Rosell-Llompart J. Increasing reaction time in Hummers' method towards well exfoliated graphene oxide of low oxidation degree. Ceramics International. 2021 Aug 1;47(15):22130-7.
20. Talyzin AV, Mercier G, Klechikov A, Hedenström M, Johnels D, Wei D, Cotton D, Opitz A, Moons E. Brodie vs Hummers graphite oxides for preparation of multi-layered materials. Carbon. 2017 May 1;115:430-40.
21. Jeong HK, Lee YP, Lahaye RJ, Park MH, An KH, Kim IJ, Yang CW, Park CY, Ruoff RS, Lee YH. Evidence of graphitic AB stacking order of graphite oxides. Journal of the American Chemical Society. 2008 Jan 30;130(4):1362-6.
22. Staudenmaier, L.: Method for the representation of graphitic acid. Reports of the German Chemical Society. 1898 May; 31(2):1481-7.

23. Dreyer DR, Todd AD, Bielawski CW. Harnessing the chemistry of graphene oxide. Chemical Society Reviews. 2014;43(15):5288-301.
24. Sheshmani S, Fashapoyeh MA. Suitable chemical methods for preparation of graphene oxide, graphene and surface functionalized graphene nanosheets. Acta ChimicaSlovenica. 2013 Dec 1;60(4).
25. Su CY, Lu AY, Xu Y, Chen FR, Khlobystov AN, Li LJ. High-quality thin graphene films from fast electrochemical exfoliation. ACS nano. 2011 Mar 22;5(3):2332-9.
26. Wang G, Wang B, Park J, Wang Y, Sun B, Yao J. Highly efficient and large-scale synthesis of graphene by electrolytic exfoliation. Carbon. 2009 Nov 1;47(14):3242-6.
27. Jamaluddin NA, Mohamed A, Bakar SA, Ardyani T, Sagisaka M, Saito H, Mamat MH, Ahmad MK, Khalil HA, King SM, Rogers SE. Fabrication and application of composite adsorbents made by one-pot electrochemical exfoliation of graphite in surfactant ionic liquid/nanocellulose mixtures. Physical Chemistry Chemical Physics. 2021;23(35):19313-28.
28. Anurag K, Kumar SR. Synthesis of graphene through electrochemical exfoliation technique in aqueous medium. Materials Today: Proceedings. 2021 Jan 1;44:2695-9.
29. Yu Q, Wei L, Yang X, Wang C, Chen J, Du H, Shen W, Kang F, Huang ZH. Electrochemical synthesis of graphene oxide from graphite flakes exfoliated at room temperature. Applied Surface Science. 2022 Oct 1;598:153788.
30. Hu Y, Su M, Xie X, Sun C, Kou J. Few-layer graphene oxide with high yield via efficient surfactant-assisted exfoliation of mildly-oxidized graphite. Applied Surface Science. 2019 Nov 15;494:1100-8.
31. Chen J, Yao B, Li C, Shi G. An improved Hummers method for eco-friendly synthesis of graphene oxide. Carbon. 2013 Nov 1;64:225-9.
32. Viana MM, Lima MC, Forsythe JC, Gangoli VS, Cho M, Cheng Y, Silva GG, Wong MS, Caliman V. Facile graphene oxide preparation by microwave-assisted acid method. Journal of the Brazilian Chemical Society. 2015;26:978-84.
33. Wang X, Tang H, Huang S, Zhu L. Fast and facile microwave-assisted synthesis of graphene oxide nanosheets. RSC advances. 2014;4(104):60102-5.

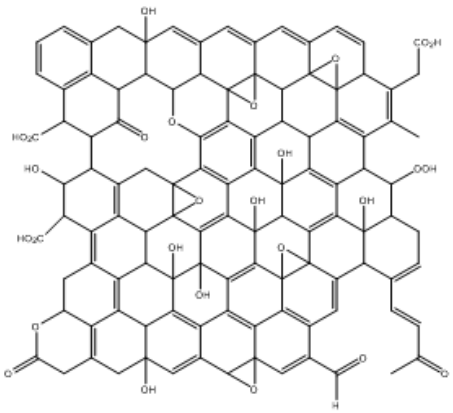

Fig-1 Lerf-Klinwoski Structure of Graphene Oxide

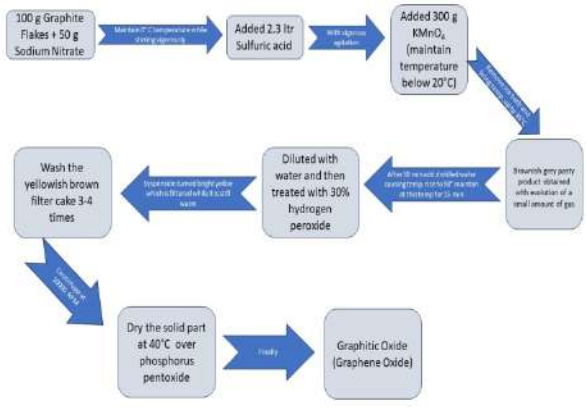

Fig-2 Hummers method briefed in flowchart

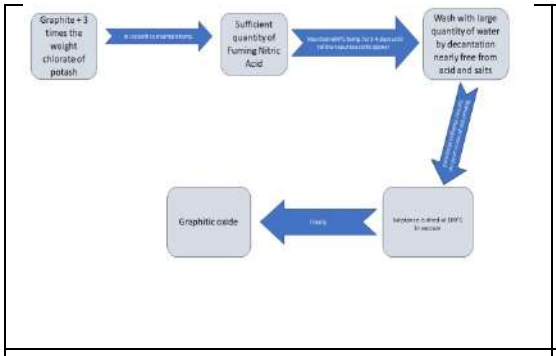

Fig-3 Brodies' Method for GO preparation

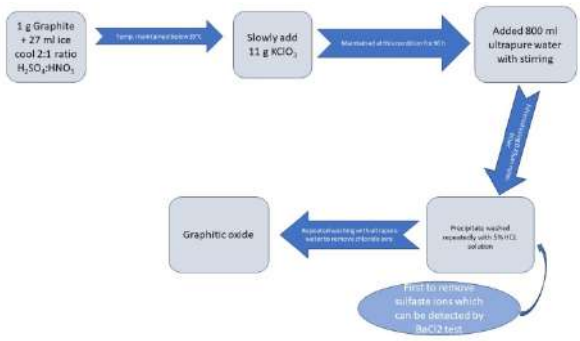

Fig-4 Procedure of Staudenmaiers' method

Indian Journal of Natural Sciences *www.tnsroindia.org.in ©IJONS*

Vol.15 / Issue 83 / Apr / 2024 *International Bimonthly (Print) – Open Access* *ISSN: 0976 – 0997*

REVIEW ARTICLE

A Review of House Dust Mites (HDMs) induced allergy, its Diagnosis and Treatment

Asha Poonia, Nisha Dhull, Sharda Kalra, Parvati Sharma, Vikash , Amit Kumar* & Kapish Samota

Faculty of Life Sciences, Chaudhary Bansi Lal University Bhiwani, Haryana, India.

Received: 30 Dec 2023 Revised: 09 Jan 2024 Accepted: 12 Jan 2024

***Address for Correspondence**
Amit Kumar
Faculty of Life Sciences,
Chaudhary Bansi Lal University Bhiwani,
Haryana, India.
Email: amitmehra455@gmail.com

ABSTRACT

Approximately 1–2% population of worldwide has allergic sensitization towards HDMs. Symptoms of HDMs allergens are usually respiratory related problems. Both innate and adaptive immune response activates against HDM allergens. Avoidance of allergens, pharmacotherapy treatment, Allergen immunotherapy (AIT) and probiotics are mainly used for treatment against respiratory allergies. Accurate diagnosis and designing of specific immunotherapeutic vaccine are mainly based on proper identification of allergens. This review describes the HDM characters, symptoms, diagnosis and treatments strategies with mechanism.

Keywords: House Dust Mites, pharmacotherapy, Allergen immunotherapy, probiotics, symptoms, desensitization, acaricides, India.

INTRODUCTION

House Dust Mites (HDM) are 0.2–0.4 mm in size tiny creatures. They are members of the suborder Astigmata in the class Arachnids in the kingdom Animalia. These pale creatures have a translucent body that ranges in size from 250 to 350 μm. They are a major indoor allergen source (Wong et al., 2011; Dey et al., 2019). They have a close relationship with people; high concentrations of HDM allergens are especially common in homes, carpets, and sleeping quarters. HDMs are primarily found in high-furniture areas like beds, chairs, and long-fiber carpets. They also feed on skin scales from human and pet activity, dander, and other materials such as household dust and plant particles (Tilak et al., 1994). In contrast to pollen, mite allergens specifically cause sleep disruptions, which lead to daytime lethargy and diminished bodily function (Brehler, 2023). Dermatophagoidespteronyssinus (Dp) and Dermatophagoidesfarinae (Df), two prominent pyroglyphid HDM species, are closely linked to allergic disorders (Dey et al., 2019). Due to their enzymatic activity, these mites take advantage of compromised epidermal skin

barriers in atopic dermatitis (AD) sufferers to get access to immune cells. The symptoms of AD are made worse by the HDM allergens, which cause both delayed and acute allergic reactions (Bussmann et al., 2006). While HDMs are most prevalent during the rainy season, their greatest influence is seen in the drier and cooler months. It has been determined that the ideal temperature range for their development is between 25 and 26°C (AICPAHH, 2000; Colloff, 2009; Mumcuoğlu and Özkan, 2020). Gaining an understanding of the complex interactions between HDMs and human habitats, as well as their propensity to cause allergies, is essential to understanding the dynamics of indoor allergen exposure and its effects on human health. With a short life cycle marked by fast reproductive turnover and a 7–10week life expectancy, house dust mites (HDMs) are made up of several primary species, including Dermatophagoidespteronyssius, Dermatophagoidesfarinae, and Blomia tropicalis.

Female HDMs can lay 40–80 eggs, which starts a life cycle that consists of five stages: mating, laying one or two eggs a day, and developing through larval stages (protonymphs, tritonymphs) until they become adults, either male or female (Yang and Zhu, 2017). This entire life cycle takes about a month to complete. 1-2 percent of people worldwide exhibit allergic sensitivity to HDMs, which primarily presents as respiratory symptoms. Asthma and rhinitis are common symptoms that are frequently ignored until they worsen. Sneezing, itching, watery eyes, wheezing, Headaches, exhaustion, and depression, Headaches, exhaustion, and inflammation around the neck area are among the symptoms. (Lyon, 1991). Hypersensitive people who inhale HDM allergens may experience acute bronchial asthma attacks, characterized by wheezing, dyspnea, and, in extreme situations, death (Sharma et al., 2011). Effective therapy and prevention efforts require an understanding of the prevalence of allergic sensitization to HDMs as well as the respiratory symptoms that are associated with it.

House Dust Mite Allergens: Optimizing Human Immune Responses"

Both innate and delayed type's immune response activates against HDM allergens (Bussmann et al., 2006). HDM allergens mainly affects the respiratory epithelial cells and mainly follows two different immunological pathways for allergenic effects: first, through the CD4 and TH2 cells that activate IgE dependent allergy responses and they also activate mast cells independently of IgE and second, through activating the innate immune system by proteases, immunological epitopes, structural polysaccharides chitin and compounds and ligands derived from mite-associated sources. Strong allergens stimulate the immune system's innate and adaptive components(Jacquet et al., 2013; Burks et al., 2013).

House Dust Mite (HDM) Diagnosis and treatment

Allergies pose difficulties in general care because they are frequently neglected until symptoms become severe. The diagnosis of HDM allergy has historically depended on a patient's history of HDM exposure, in addition to proof of HDM sensitization discovered by specific IgE testing and skin prick tests. To improve diagnosis accuracy, nasal challenge tests may be used (Pfaar et al., 2014; Calderon et al., 2015a). However, obtaining an accurate diagnosis demands increased knowledge at the primary care level. When clinical signs such as nasal obstruction, rhinorrhea, sneezing, and pruritus, particularly redness, are present, HDM allergy is diagnosed (Zhang et al., 2018). Improving diagnostic techniques and raising primary-level awareness are critical for addressing the complexities of HDM allergy diagnosis (Table 1).Currently, there are four primary therapeutic approaches available to treat respiratory allergic illnesses caused by HDM: (1) avoidance of allergens; (2) pharmacological intervention; (3) allergen immunotherapy (AIT); and (4) use of probiotics to combat respiratory allergies. Avoiding allergens and adopting AIT are only possible once the particular allergy has been identified.

Avoidance of allergens

Immunostimulatory proteins found in dust mite faeces, which are mostly found in most dust reservoirs in our homes—including mattresses, couches, carpets, and clothing—are the primary cause of allergies (Zuiani and Custovic 2020). The main strategies for managing HDM allergy include Allergen Avoidance, which include covering beds and carpets, keeping ventilation adequate, cleaning the house, using acaricides, and avoiding humid and hot environments (Mumcuoğluand Özkan ,2020).

Pharmacological intervention

When used in pharmacotherapy, allergen extracts from allergic patients increase their standard of life and give long-term symptom alleviation during subsequent natural exposure. When treating individuals with IgE-mediated allergy disorders, it is quite successful. About 85% of patients were prescribed oral antihistamines and nasal steroids for the treatment of rhinitis and asthma. Other medications, such as oral steroids, oral LABA, oral corticoids, cromones, anti-leukotrienes, and theophylline, were rarely prescribed to rhinitis and asthma patient(Trebuchon et al., 2014; Calderón et al., 2015b; Demoly et al., 2016). At present, allergen immunotherapy (AIT) completely replaces it. By giving certain allergens to patients, allergen immunotherapy (AIT) strengthens their immune systems and helps them recover from allergic disorders. Co-exposure to substances can result in complex physiopathology of allergic disease due to a variety of factors, including riskpathway,allergen/antigen structural features, dose and exposure duration of allergens, genetic susceptibility and stimulators of the innate immune response like bacterial infections (Akdis and Akdis, 2014). AIT begins with identifying a patient's particular allergen, which can be a very challenging task at times due to the cross-reactivity among allergens (Zhang et al., 2018). Allergen immunotherapy (AIT) is one measure of the condition's severity. The two main categories of AIT are SLIT and SCIT. The primary goal of subcutaneous immunotherapy (SCIT) and sublingual immunotherapy (SLIT) is the delivery of immunotherapy, namely allergen-specific immunotherapy or allergy-specific immunotherapy (Burks et al., 2013). For the majority of outcomes, SCIT and SLIT were more beneficial than placebo. Medication and symptom scores improved more with SCIT than with SLIT, and there were no changes in quality of life. One effective alternative for treating allergic rhinitis, including HDM-triggered AR, is allergen-specific immunotherapy (AIT). According to Eifan et al. (2013) and Fujita et al. (2012), allergen tolerance Th2 responses are suppressed when AIT activates Treg cells. By modifying the immune response to AIT, adjuvants also improve efficacy and safety.

The allergen immunotherapy AIT Mechanism

Events that occur at the cellular and molecular level during AIT can be divided into three categories.

1. Tregulatory (Treg) and B regulatory (Breg cells) promote switching of B cell class
2. Suppression of late-phase effector cells (Eosinophils & T-cells) and
3. Rapid desensitisation of mast cells and basophils

Treg and Breg cells promote B cell class switching

The effectiveness of AIT depends on the activation of Breg and Tregcells . Originating in the thymus, teg cells regulate both tissue-specific and systemic autoimmune. IL-10 is essential for effective immunotherapy since it is linked to T-cell tolerance in allergic disorders. Breg cells have potent regulatory and suppressor capabilities, especially IL-10-secreting B cells The release of IL-10 after AIT and spontaneous allergen exposure is caused by antigen-specific IL-10–secreting regulatory T (TR1) cells and IL-10–secreting regulatory B (BR1) cells(Van et al., 2013). T and B regulatory cells stimulate B cell class switching, which influences IgE production. Serum-specific IgE levels are momentarily elevated by AIT before declining with continued treatment. Improved clinical outcomes are correlated with elevated Specific IgG, particularly IgG4. By preventing the release of inflammatory mediators that are induced by allergens, blocking antibodies also hinders the formation of memory IgE with increased allergen exposure and reduces the ability of IgE to deliver allergens to T cells (Akdis and Akdis, 2014).

Suppression of late-phase effector cells (Eosinophils & T-cells)

AIT also inhibits late-phase effector cells linked to late-phase responses (LPR), including T cells and eosinophils. According to Van and Stevens (1989) and Akdis and Akdis (2014), AIT increases the concentration of allergen needed to cause instant reactions, or LPRs, which reflects underlying mucosal inflammation and correlates with clinical improvement. Reduced responses to AIT indicate that the LPR interaction is essential to its therapeutic efficacy. As demonstrated by reduced responses to non-stimulatory stimuli and improvements in bronchial, nasal, and conjunctival hyper-reactivity following AIT, the interaction between AIT and the LPR is essential to its therapeutic success (Akdis&Akdis, 2014).

Rapid desensitisation of mast cells and basophils

As part of allergen immunotherapy, mast cell and basophil desensitisation quickly is essential (AIT). After the first treatment with allergen supplements themast cells and basophil activity has significantly decreased, which makes them immune to environmental proteins—even when particular IgE is present (Akdis and Akdis, 2014). Despite high levels of specific IgE in treated participants, systemic anaphylaxis can occur early in the AIT process, especially after the initial injection of three-dimensional structure-intact allergens due to a decrease in sensitivity in mast cells and basophils. The degree of mediator release from these cells is changed by successful hypo-sensitization, which affects the activation thresholds that follow (Boonpiyathad et al., 2019).

Application of probiotics for respiratory allergies

The composition of the immune system is determined by the microflora in the gut, and probiotic-based microflora enrichment can be very important in preventing allergic reactions (Zuccotti et al., 2015; Ismail et al., 2013). The microbiota in the stomach suppresses the synthesis of T helper-1 (T1) cytokines and modifies their reaction. Additionally, the microbial fauna suppresses the T2 response and induces T regulatory cells (Smith-Norowitz and Bluth, 2016). Probiotics boost the production of IgA locally, which impacts mucosal defence. In order for adaptive T cell immunity to mature, they also promote the production of IL-17 (Isailovic et al., 2015). Thus, probiotics are also crucial in preventing HDM allergic reactions, based on recent research (Fassio and Guagnini, 2018). Heat-killed Lactobacillus plantarum Probiotics such as Lactobacillus plantarum, Lactobacillus paracasei, Lactobacillus rhamnosus, Bifidobacterium lactis BL-04, Lactobacillus acidophilus NCFM, and Clostridium butyricum are being utilised to treat allergic disorders.

House dust mite sensitization detection

Skin prick test

Due to its high sensitivity, the skin prick test with mite extracts is the best approach for determining house dust mite sensitization. The test outcome is dependent on the quality of the allergen extract, which must include all relevant components in sufficient quantities. Skin testing has traditionally been the gold standard for allergy diagnosis, offering quick results for discussion with patients and eliminating the need for follow-up meetings or laboratory reports (Heinzerling et al., 2013; Gureczny et al., 2023; Brehler, 2023).

In vitro tests (detection of specific IgE antibodies)

In vitro assays entail the use of common commercial techniques to identify certain IgE antibodies. For reliable findings, the allergen extract's purity is essential. It is possible to identify specific IgE in nasal secretions in cases of suspected local allergic rhinitis, though this has not been confirmed. Dermatophagoidespteronyssinus and farinae extracts are available for in vitro testing along with key allergens such as Der p 1, Der p 2, Der p 23, and Der p 10 (Weghofer et al., 2013; Haxel et al., 2017).

Provocation test

An allergy diagnosis must be confirmed by a nasal or conjunctival provocation test in circumstances when the patient's history is unclear. Subjective symptom scores and objective measures made with methods such as peak nasal inspiratory flow determination, acoustic rhinometry, anterior rhinomanometry, and 4-phase rhinomanometry are included in the evaluation (Haxel et al., 2017; Brehler et al., 2023).

Global and Indian Perspectives on Current Research and Future Prospects in Allergy Studies

Rigidity of the respiratory system affects almost one-third of the population in India, and its detrimental effects on quality of life have a major socioeconomic cost. According to epidemiological data, almost 25% of people in India have sensitivity to several allergies, such as rhinitis and asthma. A comprehensive approach is required to manage and comprehend the increasing prevalence of allergies, including eczema, angioedema, food and insect allergies, and anaphylaxis. Due to a lack of sophisticated multiplexed assay systems, there are few reports on developments in molecular allergology; nevertheless, India is now placing a higher priority on the creation of instruments and

approaches for improved allergy control. In order to understand immunological mechanisms and provide better treatments, molecular allergy research conducted in India focuses on the detection, identification, purification, and molecular characterization of individual allergen molecules, including recombinant allergens. Nevertheless, because there aren't enough qualified clinical allergists and well-equipped allergy centres, problems with applying allergen immunotherapy (AIT) still exist. To address regional differences in allergenicity, proper identification, purification, and molecular characterization of House Dust Mite (HDM) allergens are stressed. In comparison to Europe and the United States, Asia has a greater global burden of dust mite sensitization. All countries use different approaches, although diagnostic technologies like Immuno CAP, allergen microarrays, and skin prick testing are widely employed. As a treatment for IgE-mediated allergy illnesses, AIT is still widely used since it produces long-lasting immunological and clinical tolerance. Probiotics are being investigated as a potential substitute to lessen HDM symptoms, strengthen mucosal defences, and enhance allergy sufferers' quality of life. The best bacterial strains for reducing allergy symptoms are still being researched globally.

ACKNOWLEDGEMENT

I acknowledge University grant commission and Chaudhary Bansi Lal University Bhiwani for providing funds and laboratory facilities.

REFERENCES

1. AICPAHH, "Epidemiological and immunological studies," 2000.
2. Akdis, M. and Akdis, C. (2014). Mechanisms of allergen-specific immunotherapy: Multiplesuppressor factors at work in immune tolerance to allergens. . J Allergy Clin Immunol 2014;133:621-31.
3. Batard, T., Canonica, W. G., Pfaar, O., Shamji, M. H., O'Hehir, R. E., van Zelm, M. C., &Mascarell, L. (2023). Current advances in house dust mite allergen immunotherapy (AIT): Routes of administration, biomarkers and molecular allergen profiling. Molecular Immunology, 155, 124-134.
4. Boonpiyathad, T., van de Veen, W., Wirz, O., Sokolowska, M., Rückert, B., Tan, G., ... &Akdis, M. (2019). Role of Der p 1–specific B cells in immune tolerance during 2 years of house dust mite–specific immunotherapy. *Journal of Allergy and Clinical Immunology*, *143*(3), 1077-1086.
5. Brehler, R. (2023). Clinic and diagnostics of house dust mite allergy. Allergo Journal International, 32(1), 1-4.
6. Burks, A.W., Calderon, M.A., Casale, T., Cox, L., Demoly, P., Jutel, M., Nelson, H., Akdis, C.A. (2013). Update on allergy immunotherapy: American Academy of Allergy, Asthma & Immunology/European Academy of Allergy and Clinical Immunology/PRACTALL consensus report. J. Allergy Clin. Immunol;131(5):1288e1283–1296e1283.
7. Bussmann, C., Böckenhoff, A., Henke, H., Werfel, T., Novak, N. (2006). Does allergenspecificimmuno therapy represent a therapeutic option for patients with atopic dermatitis?. J Allergy Clin Immunol; 118 (6):1292-8).
8. Bussmann, C., Böckenhoff, A., Henke, H., Werfel, T., Novak, N. (2006). Does allergenspecificimmuno therapy represent a therapeutic option for patients with atopic dermatitis?. J Allergy Clin Immunol; 118 (6):1292-8).
9. Calderón, M.A., Kleine-Tebbe, J., Linneberg, A., De, Blay. F., Hernandez, Fernandez. de. Rojas. D., Virchow, J.C., Demoly,P. (2015b). House Dust Mite Respiratory Allergy: An Overview of Current Therapeutic Strategies. J Allergy Clin Immunol Pract; 3(6):843-55. doi: 10.1016/j.jaip.2015.06.019. Epub 2015 Sep 3. PMID: 26342746.
10. Calderón, M.A., Linneberg, A., Kleine-Tebbe, J., De, Blay. F., De, Rojas. D.H.F., Virchow, J.C., Demoly, P. (2015a). Respiratory allergy caused by house dust mites: what do we really know? J Allergy Clin Immunol. 2015;136:38–48.
11. Colloff, M. (2009). Dust mites (Vol. 29). Dordrecht: Springer.
12. Demoly, P., Emminger, W., Rehm D., Backer, V., Tommerup, L., Kleine-Tebbe, J. (2016). Effective treatment of house dust mite-induced allergic rhinitis with 2 doses of the SQ HDM SLIT-tablet: Results from a

randomized, double-blind, placebo-controlled phase III trial. J Allergy Clin Immunol.;137(2):444-451.e8. doi: 10.1016/j.jaci.2015.06.036. Epub 2015 Aug 17. PMID: 26292778.

13. Dey, D., Saha, G.K., Podder, S. (2019). A review of house dust mite allergy in India. Experimental and Applied Acarology. 78:1–14 https://doi.org/10.1007/s10493-019-00366-4.
14. Eifan, A.O., Calderon, M.A., Durham, S.R. (2013). Allergen immunotherapy for house dust mite: clinical efficacy and immunological mechanisms in allergic rhinitis and asthma. Expert OpinBiolTher;13:1543–56.
15. Fassio, F. and Guagnini, F. (2018). House dust mite-related respiratory allergies and probiotics: a narrative review. Clin Mol AllergY 16:15. https://doi.org/10.1186/s12948-018-0092-9.
16. Fujita, H., Meyer, N., Akdis, M., Akdis, C.A. (2012). Mechanisms of immune tolerance to allergens. Chem Immunol Allergy.; 96:30–8.
17. Gureczny, T., Heindl, B., Klug, L., Wantke, F., Hemmer, W., &Wöhrl, S. (2023). Allergy screening with extract-based skin prick tests demonstrates higher sensitivity over in vitro molecular allergy testing. Clinical and Translational Allergy, 13(2), e12220.
18. Haxel, BR. (2017). Relevance of nasal provocation testing in house dustmite allergy. HNO.65(10):811–7. 23.
19. Heinzerling L, Mari A, Bergmann KC, Bresciani M, Burbach G, Darsow U, Gjomarkaj M, Haahtela T, Bom AT, Locke R. The skin prick test–European standards. Clin Trans Allergy. 2013;3(1):3. doi: 10.1186/2045-7022-3-3.
20. Huang, H. J., Sarzsinszky, E., &Vrtala, S. (2023). House dust mite allergy: The importance of house dust mite allergens for diagnosis and immunotherapy. Molecular Immunology, 158, 54-67.
21. Isailovic, N., Daigo, K., Mantovani, A., Selmi, C. (2015). Interleukin-17 and innate immunity in infections and chronic infammation. J Autoimmun. 2015;60:1–11.
22. Ismail IH., Licciardi, P.V., Tang, M.L. (2013). Probiotic efects in allergic disease. J Paediatr Child Health. 2013;49:709–15.
23. Jacquet, A. (2013). Innate immune responses in house dust mite allergy. ISRN Allergy; 2013:735031.
24. Jacquet, A. (2021). Characterization of innate immune responses to house dust mite allergens: pitfalls and limitations. Frontiers in Allergy, 2, 662378.
25. Lyon, W.F. (1991). House dust mites," Ohio State University Extension Fact Sheet, HYG-2157-97.
26. Mumcuoğlu, K. and Taylan Özkan, A. (2020). Preventive measures to avoid contact with house dust mites and their allergen. Acarological Studies, 2 (1), 1-6. Retrieved from https://dergipark.org.tr/en/pub/acarol stud/issue/52206/659923
27. Pfaar, O., Demoly, P., Gerth, van., Wijk. R., Bonini, S., Bousquet, J., Canonica, G.W., Durham, S.R., Jacobsen, L., Malling, H.J., Mösges, R., Papadopoulos, N.G., Rak, S., Rodriguez, del., Rio. P., Valovirta, E., Wahn, U., Calderon, M.A. (2014). European Academy of Allergy and Clinical Immunology. Recommendations for the standardization of clinical outcomes used in allergen immunotherapy trials for allergic rhinoconjunctivitis: an EAACI Position Paper. Allergy ;69:854-67
28. Sharma, D., Dutta, B.K., Singh, A.B. (2011). Dust Mites Population in Indoor Houses of Suspected Allergic Patients of South Assam, India. International Scholarly Research Network ISRN Allergy Volume 2011, Article ID 576849, 7 pages doi:10.5402/2011/576849.
29. Smith-Norowitz, T.A. and Bluth, M.H. (2016). Probiotics and diseases of altered IgE regulation: a short review. J Immunotoxicol;13:136–40
30. Tilak, S.T., Jogdand, S.B., Singh, N.I. (1994). Allergy due to house dust mites, Forontr. Botany Special. 1. 16-52.
31. Trebuchon, F., Lhéritier-Barrand, M., David, M., Demoly, P. (2014). Characteristics and management of sublingual allergen immunotherapy in children with allergic rhinitis and asthma induced by house dust mite allergens. Clin Transl Allergy. https://doi.org/10.1186/2045-7022-4-15.
32. Van-Bever, H.P. and Stevens, W.J. (1989). Suppression of the late asthmatic reaction by hyposensitization in asthmatic children allergic to house dust mite (Dermatophagoidespteronyssinus). Clin Exp Allergy; 19:399-404.
33. Van-de. Veen. W., Stanic, B., Yaman, G., Wawrzyniak, M., Sollner, S., Akdis, D.G., Rückert, B., Akdis, C.A., Akdis, M. (2013). IgG4 production is confined to human IL-10-producing regulatory B cells that suppress antigen-specific immune responses. J Allergy Clin Immunol; 131: 1204-12.

34. Weghofer, M., Grote, M., Resch, Y., Casset, A., Kneidinger, M., Kopec, J., ... &Vrtala, S. (2013). Identification of Der p 23, a peritrophin-like protein, as a new major Dermatophagoidespteronyssinusallergen associated with the peritrophic matrix of mite fecal pellets. The Journal of Immunology, 190(7), 3059-3067.
35. Wong, S. F., Chong, A. L., Mak, J.W., Tan, J., Ling, S.J., Ho, T.M. (2011). Molecular identification of house dust mites and storage mites. Experimental and Applied Acarology, 55(2), 123–133. doi:10.1007/s10493-011-9460-6
36. Yang, L. and Zhu, R. (2017). Immunotherapy of house dust mite allergy. Hum Vaccin Immunother; 13(10):2390-2396. doi: 10.1080/21645515.2017.1364823.
37. Zhang, J., Chen, J., Newton, G. K. Perrior, T.R., Robinson, C. (2018). Allergen Delivery Inhibitors: A Rationale for Targeting Sentinel Innate Immune Signaling of Group 1 House Dust Mite Allergens through Structure-Based Protease Inhibitor Design. Molecular pharmacology, 94(3), 1007–1030. https://doi.org/10.1124/mol.118.112730
38. Zuccotti, G., Meneghin, F., Aceti, A., Barone, G., Callegari, M.L., Di-Mauro, A., Fantini, M.P., Gori, D., Indrio, F., Maggio, L., Morelli, L., Corvaglia, L. (2015). Probiotics for prevention of atopic diseases in infants: systematic review and meta-analysis. Allergy; 70:1356–71.
39. Zuiani, C and Custovic, A. (2020). Update on house dust mite allergen avoidance measures for asthma. *Current Allergy and Asthma Reports*, *20*, 1-8.

Table 1. Clinical Cases of Allergy: Identification and Customised Immunotherapeutic Treatments"

Case No.	Scenario of Clinical Cases	References
1.	The patient in the first scenario had many lesions spread across her body, especially on her hands, feet, scalp, and trunk. These lesions are suggestive of severe refractory atopic dermatitis. Using a diagnostic technique, the condition is identified thorough evaluation. The process of treatment consists of a combination of medicinal approaches, including systemic steroids, antihistamines, immune suppressants, moisturizers, emollients, and antibiotics. Notably, sublingual immunotherapy (SLIT) is advised since it effectively reduces adverse effects in patients.	Yang et al., 2022; Huang et al., 2023; Brehler, 2023
2.	In the second scenario the symptoms include a red rash around the neck, watery eyes, coughing, sneezing, and itching, all of which are indicative of an infection that has been linked to house dust mites (HDMs). To effectively manage the condition, the diagnosis entails determining the causing factors. Treatment options include corticosteroids and moisturizer lotions, with an emphasis on inhaling dust mite allergens.	Yang et al., 2022; Brehler, 2023; Batard et al., 2023
3.	The third scenario is about bronchial asthma brought on by a lifetime of exposure to allergens related to HDM. Oral antihistamines and nasal steroids are part of the pharmacotherapy suggested to effectively control the illness and relieve symptoms.	Zuiani, C. and Custovic, 2020
4.	The patient in the fourth case exhibits lesions and a rash suggestive of a long-term HDM infection. The preferred course of treatment is Allergy Immunotherapy (AIT), which offers long-term advantages beyond the course of the treatment and the ability to change the course of the allergic disease naturally.	Zuiani, C. and Custovic, 2020; Yang et al., 2022; Brehler, 2023; Batard et al., 2023
5.	Swelling and redness are indicative of mild to moderate allergic reactions in the fifth case. The recommended course of action is called Specific Allergen Immunotherapy (SCIT), which is designed to provide the patient with focused relief from allergic rhinitis and asthma. The significance of accurate diagnosis and customised treatment plans in the management of various allergy diseases is highlighted by these organized interventions. (Sources: a) SCIT for mild to	Yang and Zhu, 2017; Zuiani, C. and Custovic, 2020; Yang et al., 2022; Brehler, 2023; Batard et al., 2023

	moderate HDM infection, b) Inhalation therapy for HDM infection, c) AIT for chronic HDM infection	

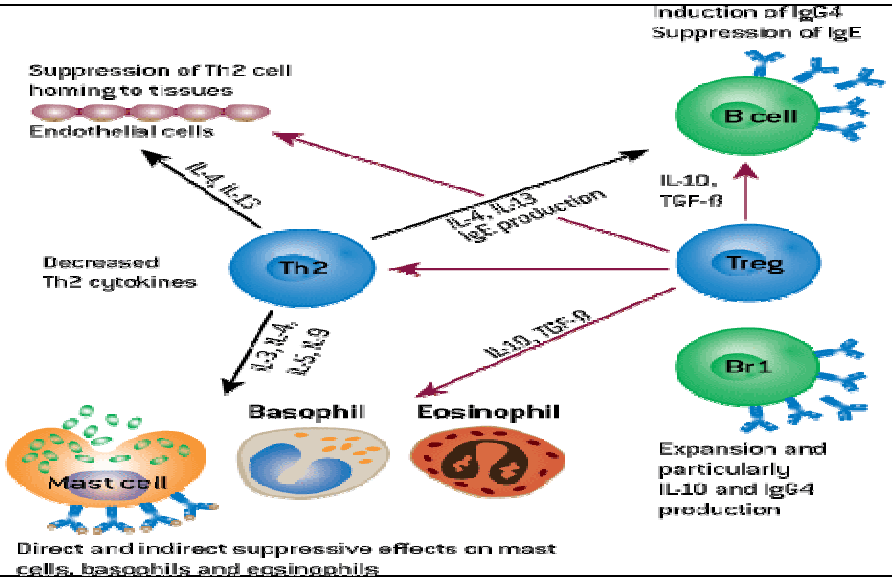

Fig.2. from (Akdis and Akdis, 2014). The complex regulation of allergic inflammation is carried out by Treg and Breg cells. The equilibrium between TH2/Treg cells is a critical factor in the development of allergic inflammation. Allergy-related disorders are impacted by TH2 immune response suppression by treg cells and associated cytokines. The regulatory effects of Treg cells are indicated by red arrows. These effects include reduction of IgE and induction of IgG4/IgA and B cell homing, as well as direct and indirect regulation of mast cells, basophils, and eosinophils and vascular endothelium. Breg cells also promote the generation of IgG4 and inhibit effector T cells.

Indian Journal of Natural Sciences *www.tnsroindia.org.in ©IJONS*

Vol.15 / Issue 83 / Apr / 2024 *International Bimonthly (Print) – Open Access* *ISSN: 0976 – 0997*

RESEARCH ARTICLE

A brief overview on Schiff Base Synthesis techniques

Gurdeep Sangwan, Jyoti Sharma*,Avinash Rani and Sonu Prasad

Department of Chemistry, MMEC, Maharishi Markandeshwar (Deemed to be) University, Mullana-133207 (Ambala) India.

Received: 30 Dec 2023 Revised: 09 Jan 2024 Accepted: 12 Jan 2024

***Address for Correspondence**
Jyoti Sharma
Associate professor,
Department of Chemistry,
MMEC, Maharishi Markandeshwar (Deemed to be) University,
Mullana-133207 (Ambala) India.
Email: jsharma117@gmail.com

ABSTRACT

This comprehensive review delves into the synthesis of Schiff bases, pioneered by Hugo Schiff in the 19th century, elucidating their significance in organic chemistry. Schiff bases, characterized by the C=N group, result from the condensation of primary amines with active carbonyl compounds. The review explores classical and environment friendly approaches, dissecting methods such as condensation with Lewis acid, use of molecular sieves, and azeotropic distillation. Additionally, non-conventional methods like water-based synthesis, microwave-assisted synthesis, ultrasound-promoted synthesis, and grindstone chemistry are discussed, emphasizing advancements in reaction efficiency, selectivity, and sustainability.

Keywords: Schiff bases, organic synthesis, condensation, environment friendly approaches, non-conventional methods, reaction efficiency.

INTRODUCTION

In the 19th century, Hugo Schiff pioneered the synthesis of Schiff bases, also known as imines[1]. ASchiff base is defined as an aldehyde containing a C=N group (azomethine -N=CH- group) as shown in Figure 1[2]. These are synthesized by a condensation reaction of primary amines and an active carbonyl compound (aldehydes/ ketones). Water is the by- product of this reaction. The general formula of Schiffbase is $RCH=NR_1$, where R & R_1 represents alkyl/aryl substituents [3]. Compounds featuring anazomethine group exhibit basic properties owing to the presence of unshared electron pairs on the nitrogen atom and the electron-donating characteristic of the double bond. Schiff bases, a subset of compounds with an azomethine group, display relatively weaker basic properties when compared to their corresponding amines. This disparity arises from the alteration in hybridization during the formation of the imine structure. While the nitrogen atom in amines undergoes sp^3 hybridization, the hybridization shifts to sp^2 in the

imine structure. As a consequence of this increased s character in hybridization, there is a significant reduction in basicity. Schiff bases are selective toward metal ions and form complexes by transferring electrons from the active ends they contain to the metal. Schiff bases are known as a good nitrogendonorlig and (—CH = N—). During the formation of the coordination compound, one or more electron pairs are donated to the metal ion by these ligands. Schiff bases can form highly stable 4-, 5-, and 6-ring complexes if they donate more than one electron pair. For this, a second functional group with a displaceable hydrogen atom must be found as close as possible to the azomethine group. This group is preferably the hydroxyl group or any S atom Schiff base compounds play a crucial role in both pharmaceutical and chemical industries, showcasing a spectrum of biological activities such as antimicrobial, antidyslipidemic, antitubercular, antihelmintic, anticonvulsant, anti-inflammatory, antiviral, antioxidant, and more[4]. These compounds have been a focal point in organic synthesis for decades. The classical condensation reactions involving primary amines and aldehydes or ketones have paved the way for the synthesis is of these valuable compounds. However, as the field advances, researchers are exploring novel methodologies to enhance reaction efficiency, selectivity, and environmental sustainability. In this article we are going to explore conventional and non-convential approaches for the preparation of Schiff base as shown in Figure 2.

Different methods of Schiff base synthesis

Conventional methods of Schiff base synthesis

Condensation in the presence of Lewis acid: The synthesis of the Schiff base is carried out by condensing amine with aldehyde in suitable solvent, such as ethanol at refluxing. There action is carried out in the presence of a catalyst: Lewis acid. The mechanism of the reaction is shown in figure 3[5]. This method is widely used in the synthesis of Schiff base. However, this method has a limitation of performing reaction at high temperature and longer duration. A Schiff base was synthesized through the reaction of an equi molar mixture of 4-amino benzene sulphon amide and substituted aromatic aldehydes or acetophenone. The individual reactants were dissolved in a minimal amount of ethanol, combined, and supplemented with 2 ml of glacial acetic acid. The resulting solution underwent reflux for 8 hours, followed by cooling to room temperature and pouring into ice-cold water. The solid precipitate obtained was collected via filtration, dried using an oven at 80 ºC, re dissolved in ethanol for re crystallization, and subsequently dried to yield the final product[6].

Using molecular sieves/ azeotropic distillation for water removal

In Schiff base synthesis, molecular sieves play a crucial role by serving as desiccants to remove water from the reaction mixture. The presence of water can adversely affect the reaction equilibrium and lead to hydrolysis of the desired imine product. To mitigate this, the water can be removed by using Dean–Stark apparatus azeotropically. Also, molecular sieves, commonly of 3 Å or 4 Å pore size, are introduced into the reaction vessel along with the aldehyde or ketone and primary amine. As the condensation reaction progresses, water is produced, and the molecular sieves continuously adsorb and remove it, promoting the formation of the Schiff base. This ensures a more efficient and higher-yielding synthesis. Following the completion of the reaction, the molecular sieves are removed, and the Schiff base product can be isolated through standard workup procedures. Proper care, including pre-drying of molecular sieves and choosing the appropriate pore size, contributes to the compliance of the reaction. Overall, molecular sieves serve as effective tools in facilitating Schiff base synthesis by maintaining a dry reaction environment. This process is also time consuming and the molecular sieves need to be dried at high temperature to make them moisture free. Kazuo Taugchi and F.H. Westheim utilized molecular sieves for the synthesis of ketimines, as described in their work [7]. In their experimental procedure, around 40 grams of Linde 5Å molecular sieves were introduced into a mixture comprising 0.10 moles of ketone (Cyelooctanone, Cycloheptanone, Cyclohexanone, camphor, keto acids, and Acetophenone) and 0.12 moles of aromatic amine(Anilines and m-Toluidine) dissolved in either 40 milliliters (about 1.35 oz) of benzene or ether. There action duration spanned 1 to 30 hours, during which the progress was monitored through infrared (IR)and nuclear magnetic resonance (NMR) spectroscopy to ensure the absence of ketones. The isolation process encompassed filtration, removal of the solvent, and subsequent purification utilizing vacuum distillation or crystallization techniques.

Non-conventional methods for Schiffbase synthesis

Water as green solvent

This includes the use of water as a solvent and environmentally benign catalysts to minimize the environmental impact. Using water as solvent is also safe because it is non- toxic and non-flammable. Rao and colleagues [8] showcased an efficient method for synthesizing Schiff bases in an aqueous environment, yielding superior results compared to conventional approaches. Notably, this technique obviates the need for acid catalysts. The Schiff bases produced exhibited high yields and could be easily separated through filtration. It is noteworthy that water efficiently facilitated the reactions. This innovative method significantly accelerated the reaction rate, achieving a nearly 300-fold increase. The procedure involved adding salicylaldehyde to a solution of 1,2-diaminobenzene in 10 milliliters of water, followed by stirring the mixture for 10 minutes at 25 ºC. The resulting yield was an impressive 95%, surpassing the 65% yield obtained through the traditional method.

Microwave-Assisted Synthesis

Microwave technology utilizes electromagnetic waves generated by a magnetron, typically at 2.45 GHz to avoid interference. During microwave irradiation, polarized molecules align with the electric field, inducing molecular motion and generating heat (dipolar polarization). Ionic conduction, involving charged compounds, also contributes to heat generation through oscillating trajectories. Temperature in the reaction mixture can peak at 250-300 °C, facilitating faster reactions based on the Arrhenius equation. Synthesis instruments often use sealed tubes for pressure buildup. Solvent choice is critical for microwave absorption and heat generation. In organo metallic chemistry, metals or metallic salts ensure microwave absorption, promoting reactions through localized temperature increases (hot spot theory)[9]. It presents advantages such as expedited reaction rates, higher yields, energy efficiency, and reduced reaction durations. By directly heating the reaction mixture, microwave irradiation facilitates rapid and efficient warming, leading to accelerated reactions and improved product quality. Microwaves have the capability to directly penetrate the reactants, inducing heat through molecular rotation and frictional heating. Mousumi Chakraborty et al[10] used microwave irradiation method, in which, reactant mixtures were subjected to microwave power at 300 W from 30 sec to 2 min and temperature was maintained at 80°C. The progress of the reaction at different time interval was monitored by TLC. On completion of reaction, the yellow coloured amorphous product **1** was separated, filtered, dried and re crystallized from methanol. There action occurred within very short time (30sec-2min).

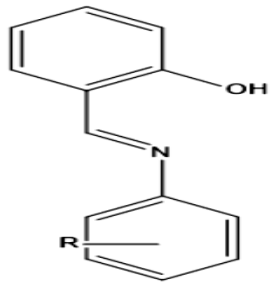

[1]

In another microwave-assisted synthesis, performed by Bhusnureet al, a mixture of 3,5-dichlorobenzaldehyde (0.001 mol), 3-amino-6-bromo-2-phenylquinazoline-4(3H) one (0.001 mol), andtwo drops of ß-ethoxyethanol as a wetting reagent was prepared in a beaker. The reaction mixture underwent irradiation within a modified MC767W (Electrolux) system at 200 W for approximately 3minutes, with intermittent cooling intervals, Reaction was monitored by TLC. After the 3-minutereaction period, the flask was cooled in ice water, diluted with ice-cold water, and the resulting Schiff bases was filtered, dried, and re crystallized from ethyl acetate. Using the same procedure, other compounds were synthesized within 3-5 minutes (180-300 seconds). Optimization involved varying the reaction time and microwave power from 180W to 600W. The conversion and yield was found to be better than that with the conventional method of synthesis[11].

Ultrasound-Promoted Synthesis

Sono-chemistry refers to the use of ultrasonic vibrations to enhance chemical reactivity. Ultrasound irradiation is a green technique used to speed up chemical processes, particularly inorganic synthesis. Ultrasonic waves, with frequencies above 20KHz, are particularly useful for chemical processes. As sound waves travel through a liquid medium, molecules oscillate due to cycles of rarefaction and compression. Under certain conditions, bubbles can emerge, leading to high local temperatures and pressures. Ultrasonic cavitation occurs when low pressure is applied to a liquid medium, causing cavities or bubbles to form and collapse. This technique is commonly used in laboratories using an ultrasonic bath or probe[12]. This technology is easier to handle and more convenient than older methods. With ultrasonic irradiation, many chemical processes can be carried out in milder conditions and with shorter reaction periods, yielding greater yields [13]. When compared to traditional heating, this can be seen as a processing help in terms of waste reduction and energy conservation. Hadi Kargar et al[14] have successfully synthesized and characterized two Schiff base compounds derived from 3-ethoxysalicylaldehyde and 2-aminopyridine derivatives under ultrasound irradiation. Compound **2** was prepared by placing a 1:1 M combination of 3-hydroxy-2-aminopyridine and 3-ethoxysalicylaldehyde in ethanol in an ultrasonic bath set at room temperature for five minutes. TLC was used to monitor the reaction's development. Subsequently, the mixture was exposed to air to gradually evaporate over a few days, allowing the products to settle. After characterization by NMR spectroscopic techniques and elemental analyses, the crystal structures of compounds were confirmed by single crystal X-ray analysis.

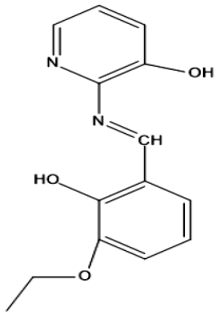

[2]

A Schiff base was synthesized by Ahmad Aziz and co-workers by condensing piperonal (15 mmol)and anthranilic acid (15 mmol) with acetic acid as a catalyst in methanol. The mixture was sonicated at 37KHz for 10 minutes at 25 °C in an ultrasonic bath, and the reaction progress was monitored using TLC. After completion, the reaction mixture was concentrated, cooled, and filtered. The resulting precipitates were washed with methanol, resulting in a yellow product. The structure of the Schiff base was confirmed through analysis of physical and spectroscopic data[15].

Grinding method

Many exothermic reactions can achieve high yields simply by grinding solid reactants together using a mortar and pestle, a method referred to as "grindstone chemistry." This technique, categorized under "green chemistry," involves initiating reactions through the act of grinding, where minimal energy transfer occurs through friction. Grindstone chemistry not only proves energy-efficient but also exhibits heightened reactivity and produces fewer waste products. These reactions are straight forward to manage, contribute to pollution reduction, are relatively cost-effective, and are considered more economical and environmentally friendly procedures in the field of chemistry. Solid-state reactions, facilitated by grindstone chemistry, demonstrate enhanced efficiency and selectivity compared to solution reactions, owing to the tightly arranged and regular molecular structure in crystals[16]. The solid-state synthesis of several types of benzylidene aniline derivatives without going through liquid phases was described by Schmeyers et al [17]. Equi molar mixtures of pure aniline derivative and aldehyde derivative were ground together in a mortar for two hours at room temperature to carry out the solid-solid reactions. The completion of the reaction was checked by IR spectroscopy in KBr. The water produced in there action was removed at 80°C under vacuum.

Chemical analysis was carried out by IR and NMR spectroscopy which gave the expected peaks and signals. In contrast to (acid catalyzed)imine synthesis in solution, these solid-solid condensations occur without the production of waste.

CONCLUSION

In summary, this comprehensive review explores the evolution of Schiff base synthesis methodologies from classical to innovative approaches. While classical methods have proven effective, the emerging techniques, including microwave-assisted and ultrasound- promoted synthesis, water as a green solvent, and grindstone chemistry, offer advantages such as expedited reactions, higher yields, and environment friendly procedures. The dynamic pursuit of sustainability, efficiency, and selectivity in Schiff base synthesis reflects the ongoing commitment of researchers to advance the field of organic and inorganic synthesis.

REFERENCES

1. H. Schiff, "Mittheilungen aus dem Universitätslaboratorium in Pisa: Eine neue Reihe organischer Basen," Justus Liebigs Ann. Chem., vol. 131, no. 1, pp. 118–119, Jan. 1864, doi: 10.1002/jlac.18641310113.
2. S. Hossain, P. K. Roy, and C. Zakaria, "Selected Schiff base coordination complexes and their microbial application: A review," Int. J. Chem. Stud., vol. 6, no. 1, pp. 19–31, Nov. 2017, doi: 10.1002/jlac.18641310113.
3. D. V. Saraf, P. A. Kulkarni, V. G. Deshpande, and S. I. Habib, "Heterocyclic schiff base cu(ii) metal complexes and their x-ray diffraction study," Eur. J. Pharm. Med. Res., vol. 4, no. 9, pp. 680–683, 2017.
4. R. Das, "Schiff bases: synthesis, applications and characterization using ft-nmr spectroscopy," J. Emerg. Technol. Innov. Res., vol. 5, no. 1, pp. 1435–1447, 2018.
5. S. Laxman Sangle, "Introduction to Schiff Base," in Schiff Base in Organic, Inorganic and Physical Chemistry, T. Akitsu, Ed., IntechOpen, 2023. doi: 10.5772/intechopen.108289.
6. Sonu, A. Kumar, and Sabiya Praveen and Himanshu Pal, "Synthesis and antimicrobial study of some new schiff bases of sulphonamides derivatives," Int. J. Res. Pharm. Chem., vol. 7, no. 3, pp. 216–220, 2017.
7. F. H. Westheimer and K. Taguchi, "Catalysis by molecular sieves in the preparation of ketimines and enamines," J. Org. Chem., vol. 36, no. 11, pp. 1570–1572, Jun. 1971, doi: 10.1021/jo00810a033.
8. A. Shameli, A. H. Raeisi, B. Pourhasan, H. Naeimi, and M. M. Ghanbari, "The One-Pot Three Components of Iodone, Schiff Base and Epoxide for Synthesis of Iodohydrins," Orient. J. Chem., vol. 28, no. 2, pp. 749–755, Jun. 2012, doi: 10.13005/ojc/280214.
9. A. Beillard, X. Bantreil, T.-X. Métro, J. Martinez, and F. Lamaty, "Alternative Technologies That Facilitate Access to Discrete Metal Complexes," Chem. Rev., vol. 119, no. 12, pp. 7529–7609, Jun. 2019, doi: 10.1021/acs.chemrev.8b00479.
10. M. Chakraborty, S. Baweja, S. Bhagat, and T. Chundawat, "Microwave Assisted Synthesis of Schiff Bases: A Green Approach," Int. J. Chem. React. Eng., vol. 10, no. 1, Jul. 2012, doi: 10.1515/1542-6580.2973.
11. O. G. Bhusnure, "Innovative Green synthesis of Schiff bases and their Antimicrobial Activity," J. Pharm. Res., vol. 9, no. 12, pp. 670–677, 2015.
12. R. P. Karad, Aakash Sanjeev Singare, Ennus Khaim Pathan, and Nanda Sheshrao Korde, "Ultrasonic assisted and conventional synthesis of schiff base and metal complexes: a comparative study," Int. Res. J. Mod. Eng. Technol. Sci., vol. 5, no. 4, Apr. 2023, doi: 10.56726/IRJMETS34663.
13. L. Ding, W. Wang, and A. Zhang, "Synthesis of 1,5-dinitroaryl-1,4-pentadien-3-ones under ultrasound irradiation," Ultrason. Sonochem., vol. 14, no. 5, pp. 563–567, Jul. 2007, doi: 10.1016/j.ultsonch.2006.09.008.
14. H. Kargar et al., "Ultrasound-based synthesis, SC-XRD, NMR, DFT, HSA of new Schiff bases derived from 2-aminopyridine: Experimental and theoretical studies," J. Mol. Struct., vol. 1233, p. 130105, Jun. 2021, doi: 10.1016/j.molstruc.2021.130105.

15. O.-U.-R. Abid et al., "Ultrasonic Assisted Synthesis, Characterization and Bioactivity Assessment of Novel Piperonal Based Schiff Base and Its Metal Complexes," Iran. J. Chem. Chem. Eng. IJCCE, vol. 39, no. 2, Apr. 2020, doi: 10.30492/ijcce.2020.33369.
16. H. Sachdeva, R. Saroj, S. Khaturia, and D. Dwivedi, "Operationally simple green synthesis of some Schiff bases using grinding chemistry technique and evaluation of antimicrobial activities," Green Process. Synth., vol. 1, no. 5, Jan. 2012, doi: 10.1515/gps-2012-0043.
17. J. Schmeyers, F. Toda, J. Boy, and G. Kaupp, "Quantitative solid–solid synthesis of azomethines," J. Chem. Soc. Perkin Trans. 2, no. 4, pp. 989–994, 1998, doi: 10.1039/a704633b.

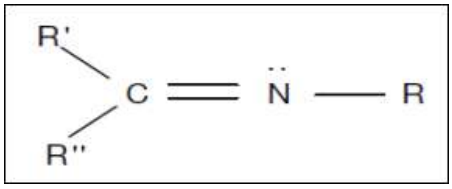

Figure 1: Structure of Schiff base

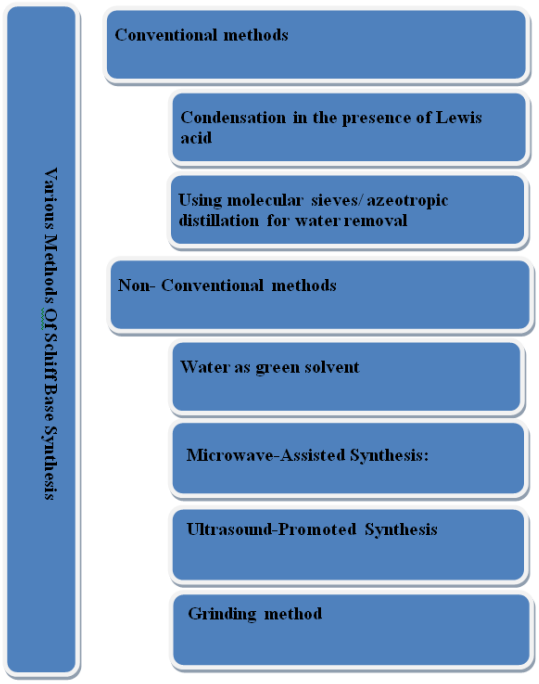

Figure 2:Different methods for Schiff base Synthesis

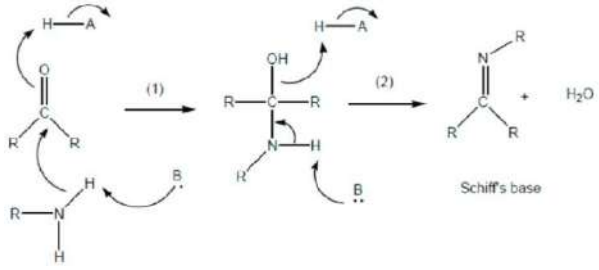

Figure 3

Indian Journal of Natural Sciences *www.tnsroindia.org.in ©IJONS*

Vol.15 / Issue 83 / Apr / 2024 *International Bimonthly (Print) – Open Access* *ISSN: 0976 – 0997*

RESEARCH ARTICLE

Chemistry of Iridium(III)-3-hydroxy-2-tolyl-4H-chromen-4-one: The Spectrophotometric Analysis, Radical Scavenging Activity and Computational Studies

Khushboo Devi, Nivedita Agnihotri*, Gulshan Kumar

Department of Chemistry, Maharishi Markandeshwar (Deemed to be University), Mullana, Ambala-133207, India.

Received: 30 Dec 2023 Revised: 09 Jan 2024 Accepted: 12 Jan 2024

***Address for Correspondence**
Nivedita Agnihotri
Department of Chemistry,
Maharishi Markandeshwar (Deemed to be University),
Mullana, Ambala-133207, India.
Email: niveditachem@mmumullana.org;

ABSTRACT

3-Hydroxy-2-tolyl-4*H*-chromen-4-one (HToC)has been utilized successfully for the microgram level analysis of iridium (III) employing a spectrophotometric determination technique. Iridium (III) instantaneously reacts with HToC in phosphoric acid medium to form a stable light yellow-coloured non-extractable complex. The Ir(III)-HToC complex evinces a maximum absorbance at 423nm when studied against a reagent blank prepared analogously and coheres to linearity up to 1.8 μg Ir (III) ml^{-1}. The accuracy and reproducibility of the method are confirmed by the corresponding values of relative standard deviation (%RSD) and the coefficient of variance as 0.0146% and 0.00146, respectively, at 423 nm. The stoichiometric constitution of the developed complex, as validated by the studied Mole Ratio and Job's continuous variation methods is 1:3 [Ir(III):HToC], indicating hence the octahedral geometry of the formed species. Study has been done for interference by various cations, anions and complexing agents to analyse selectivity of the method. It is observed that the majority of the ions/complexing agents do not interfere with the complex determination. Besides, electronic properties of the studied complex have been affirmed by subjecting it to the computational studies. The practicability of the procedure has been assessed by conducting analysis of numerous synthetic samples. Finally, the studied complex is exposed to the estimation of antioxidant capacity by employing DPPH radical scavenging method. Antioxidant capacity results propounded the better radical scavenging capacity of the developed complex than that of the ligand alone.

Keywords: Iridium(lll), spectrophotometric analysis,radical scavenging activity,computational studies, QTAIM, TDDFT

INTRODUCTION

Organic and inorganic compounds including transition metals especially the platinum group metals (PGMs)are qualitatively and quantitatively determined by using numerous analytical methods, such as volumetric titrations [1], atomic absorption spectrophotometry (AAS) [2], neutron activation analysis (NAA) [3], UV-VIS spectrophotometry [4], ion exchange chromatography [5], inductive coupled plasma optical emission spectroscopy (ICP-OES) [6], X-ray fluorescence spectrometry[7] and voltammetry [8]. Among the several methods for determining the metals in traces, UV-VIS spectrophotometric methods ofdetermination are the most generally employed due to less apparatus and methodology requirements. Spectrophotometric approaches are regarded relatively convenient for micro level determination and are widely utilized for the same reason. The elucidation of results in UV-VIS spectrophotometer can be operated to analyze the chemical elements, structure and composition of inorganic complexes[4]. The method is based on the basic principle of measurement of intensity of ultraviolet and visible light absorbed by the sample as a function of wavelength. Samples absorbs ultraviolet radiation at a wavelength of 180-380 nm or visible at a wavelength of 380-780 nm. The results are estimated in the form of transmittance or absorbance or UV-VIS spectrum of the complexes prepared as clear solutions. All PGMs including ruthenium, rhodium, palladium, osmium, iridium and platinum crop up naturally in the Earth's crust at very low concentrations [9].Iridium, one of the PGMs is known as a very hard, brittle and silvery-white metal. After osmium it is considered the second-densest (density 22.56 gcm^{-3}) naturally occurring metal[10]. The metal was discovered in 1803 by Smithson Tennant.

Its chemical name originated from the Greek goddess, Iris, an epitome of the rainbow [11]. Iridium forms compounds in variable oxidation states ranging from −3 to +9, the most common oxidation states being +1, +3 and +4. Iridium has extensive coordination chemistry. Iridium in its complexes is always low-spin. Octahedral complexes of Ir(III) and Ir(IV) are generally known[12]. Iridium and its complexes find extensive applications in various fields such as catalysis, medical imaging, electrodes for producing chlorine and other aggressive products, OLED, crucibles and ignition tips for spark plugs [13-15]. Radioisotope, iridium-192, is one of the most important source of energy used in industrial γ-radiography for non-destructive testing of metals and in the treatment of cancer using brachytherapy, a form of radiotherapy[16]. Iridium along with otherplatinum group metals play an important role in analytical chemistry producing a variety of complexes with a number of ligands carrying variable donor groups and studied by the spectrophotometric techniques. Coloured complexes of iridium are reported with hydrazine carbothioamide[17], p-methylphenylthiourea [18] and Schiff bases [19] but suffering with very poor sensitivity. However, 4*H*-1-benzopyrans were observed to show significant improvement when used as ligands over to the others[20,21]. For the same reason, in the present study, another benzopyran derivative, 3-hydroxy-2-tolyl-4*H*-chromen-4-one (HToC; figure1) has been employed as a noble reagent for trace determination of iridium in its trivalent oxidation state to give a very enhanced value of sensitivity as compared to the other mentioned reagents[17-19]. It has been searched out that the transition metal complexes with organic especially chelating ligands helped in enhancing the antioxidant potential while used in medicinal and pharmaceutical industries [22]. Chelation exhibited by the metal complexes is the key for this improved activity over the traditionally used synthetic antioxidants. On the same basis, in the present research the newly prepared Ir(III)-HToC chelate has been subjected to antioxidant potential and was found to betray the same [23].

Experimental section

MATERIAL AND METHODS FOR SPECTROPHOTOMETRIC ANALYSIS

Instrumentation and solutions

All the absorbance measurements were performed using UV-VIS spectrophotometer (double beam; EI-2375) with 1 cm identical quartz cuvettes. A 100 ml of the stock solution of iridium with a strength of 1 mg Ir(III) $ml^{-1}$and working solutions of the required concentration (100 and 10 μg ml^{-1}) were prepared by the reported method [20]. High purity chemicals of AR grade and deionized water were used for all the experiments. For the regulation of the ambient

acidity of the reaction medium, 0.5 M H_3PO_4 was prepared. Other required solutions were prepared to study the effects caused by foreign ions (cations, anions and complexing agents) from the respective sodium or potassium salts by dissolving in appropriate solvents.

Ligand solution

The chromogenic reagent, 3-hydroxy-2-tolyl-4*H*-chromen-4-one (HToC), carrying the carbonyl group and the hydroxyl group as the binding sites (figure 1) was synthesized by applying the reported methodology[24]. Itsfreshly prepared solution of strength 0.1% (w/v) was made by dissolving 0.05g of it in a small amount of ethanol, followed by dilution with the same solvent up to the mark in a 50 ml volumetric flask.

Spectrophotometric Determination

In order to achieve accurate and impeccable results, the spectrophotometric determination was carried out in the most optimized manner. By diluting the stock solution with appropriate amounts of double-deionized water, a working solution (10 μg ml^{-1}) of Ir(III) was prepared for analysis. For the process of complexation, 1 ml of the working solution of the metal ion in trivalent oxidationwas pipetted out in a 10 ml standard flask, 1 ml of the 0.1% chromogenic reagent solution in ethyl alcohol was added to develop complex in the presence of 0.035M H_3PO_4.After adding 1ml of ethanolic solution of 0.1% (w/v) HToC, a light yellow-coloured complex was formed instantaneously. The colour intensity of Iridium(III)-HToC complex was measured at 423nm against a comparable reagent blank solution. The precise amount of metal ion was calculated using the calibration curve constructed between absorbance and varying iridium(III) concentrations.

Antioxidant activity

The antioxidant capacity of Ir(III)-HToC was mannered by Radical Scavenging Activity (RSA) towards ***2,2-diphenyl-1-picrylhydrazyl analysis*** (DPPH) and the outcomes were observed by engaging a UV-VIS spectrophotometer. DPPH radical scavenging is the well known procedure to the evaluation of the antioxidant property of chemical compounds. The DPPH (methanolic solution) gives deep purple colour contributing an acute absorption band at 517 nm; where colour change of solution is indication of the reaction with the substance that has antioxidant capacity. Stock solution of 1 mg ml^{-1} of Ir(III)–HToC was prepared by dissolving 5 mg of it in 5 ml methanol. However, the stock solution of DPPH of strength 1.0 mM and the solution acting as a negative control were prepared similarly as reported [21,25]. A number of range of dilutions (500, 250, 125, 62.5 and 31.25 μg ml^{-1}) of complex were prepared from the stock solution of Ir (III)-HToC. To retain the RSA of the resultant complex and the ligand (HToC), lower dilutions of HToC of the same concentrations as those of Ir (III)-HToC complex were prepared consequently. This was accompanied by incubating the solutions at 37°C for 30 min in dark. The positive control, gallic acid of same concentrations were prepared simultaneously. Ultimately, the absorbance of each solution was spectrophotometrically determined at 517 nm against the prepared negative control, and the % radical scavenging activity was calculated as per the equation: % RSA = $[(A_{negativecontrol}-A_{sample})/ A_{negative\ control}] \times 100$, where $A_{negative\ control}$ denotes the absorbance of negative control and A_{sample} denotes absorbance of the antioxidant compounds (gallic acid, Ir (III)-HToC, HToC) [22-25].

Software details

The reagent HToC and Ir(III)-HToC complex were optimized at ground state (S_0) using density functional theory (DFT) at the B3LYP/ LANL2DZ level[26]. The absence of imaginary vibration frequencies analyzed the stability of molecular structures. The excitation energies were calculated using time-dependent DFT (TDDFT) methods. All DFT and TDDFT calculations were carried out using Gaussian 16 [27]. Quantum chemical parameters were utilized to investigate the electronic properties of the complex's most stable conformation. This was done to better understand the studied complex's chemistry. The electronic properties of HToC and Ir(III)-HToC complex, such as the ionization energy (I), electron affinity (A), electronegativity (χ), chemical potential (μ), absolute hardness (η), global softness (σ), and electrophillicity index (ω), were determined using the band gap energy ($E_{gap} = E_{HOMO} - E_{LUMO}$) and the HOMO/LUMO energies. Frontier molecular orbitals are used to determine these properties as main orbitals involved

in chemical stability. A molecule's reactivity can be explained by considering its chemical hardness, which is directly related to the HOMO–LUMO energy gap. A molecule with a greater E_{gap} or chemical hardness is less reactive [28-30]. The application of theoretical studies on the complex was further expanded by employing QTAIM analysis[31].

RESULTS AND DISCUSSION

A light yellow stable complex (>2 days) ofIr(III)-HToC was obtainedin aqueous phase upon interaction with the chromogenic reagent, HToC from an acidic medium provided by phosphoric acid.The complex was non extractable in any of the solvents, polar or nonpolar, when subjected to its extraction. The spectrophotometric determination procedures, computational studies and bioanalytical analysis of the complex are mentioned in succeeding discussion.

Spectrophotometric analysis

Absorption spectrum

Under aqueous conditions, the absorption curve of Ir(III)-HToC complex against blank had a paramount and consistent colour intensity in the range 420–425 nm in phosphoric acid medium. The spectrum of reagent blank when examined similarly against pure water indicated a minimal absorbance in the same region (figure 2). Thus, 423 nm wavelength was fixed for absorbance in case of all further parameters and against reagent blank for the analysis of Ir (III).

Effect of medium and acidity

Of the numerous acidic (HNO_3, H_2SO_4, HCl, $HClO_4$, H_3PO_4 and CH_3COOH) and basic media ($NaHCO_3$ and Na_2CO_3), resulting complex exhibits maximum and stable absorbance in phosphoric acid medium as is shown Table 1 and Figure 3.However, highly turbid solutions were obtained while using basic media for complexation.Phosphoric acid is observed as the appreciable complex forming medium and hence selected.The Ir (III)-HToC complex attained maximum absorbance(0.310) in the acidity range of 0.020-0.045M concentration of H_3PO_4. Therefore, acidity of the complexing medium is adjusted to 0.035M of H_3PO_4(Table 2; Figure 4A).

Conditions: Ir (III) =10 μg; Acidity of aqueous medium = 0.025M; HToC [0.1% (w/v)] in ethanol = 1ml; Solvent = water; aqueous phase = 10 ml; λ_{max} = 423 nm

Conditions: Ir (III) = 10 μg; Acidity of aqueous medium (using H_3PO_4) = variable; HToC [0.1%(w/v)] in ethanol =1ml; Solvent = water; aqueous phase = 10ml; λ_{max} = 423nm

Effect of Reagent (HToC) concentration

The metal ion starts forming a coloured species on addition of the reagent whose absorbance in aqueous phase increases with increase in HToC content. In the range of 0.5–1.4 ml of 0.1% (w/v) ethanolic solution of reagent, the absorbance attains a maximum value of 0.310. Decrease in colour intensity results if concentration of reagent is further increased (Table 3; Figure 4B). Therefore, 1ml of 0.1% HToC is selected for further studies.

Conditions: Ir (III) = 10 μg; Acidity of aqueous medium = 0.035M; HToC [0.1% (w/v)] in ethanol = variable; Solvent = water; aqueous phase = 10 ml; λ_{max} = 423 nm

Interference studies

To examine the tolerable value of the diverse ions, the foreign ion effect was studied under ideal conditions of the procedure while keeping a constant metal ion concentration (10 μg of iridium (III) in 10 mL aqueous volume) for each. The ions or complexing agents were added as their sodium or potassium salts, initially in large amounts but the reduced quantities if an error of >1% is noticed in certain cases(Table 4).Similarly, effect of cations on the colour intensity of iridium complex is also studied by taking 10 μg of iridium (III) per 10 mL aqueous phase and adding suitable amounts of different cations (Table 5). It is found that of the 33cations studied, none effected the absorbance of Ir(III)-HToC complex.

Conditions: **As mentioned in procedure**

Conditions: As mentioned in procedure *Initial oxidation state shown in parentheses.

Calibration curveand statistical analysis

Iridium(III) determination employing HToC as complexing reagent depends linearly on the metal ion concentration in the aqueous solution and is narrated by the regression equation as Y= 0.315X-0.007, where X in the equation denotes concentration of Ir(III) in μg ml^{-1} (R=0.9981). it has been observed from the calibration curve that Beer's law holds good over the Ir(III) concentration range of 0.0-1.8 μg ml^{-1}(figure 5A). Beyond this concentation, it starts deviating from linearity. The optimum concentration range for accurate determination, as evaluated from a Ringbom plot [32], however, is 0.3-1.6ppm of Ir (III) (figure 5B). The standard deviation was ± 0.0045 and relative standard deviation(RSD) = 0.0146% depicted that the developed method is precise and accurate. The method is highly sensitive as is indicated from its molar extinction coefficient as 5.960×10^4 l mol^{-1} cm^{-1}. The various analytical parameters have been placed in table 6.

Stoichiometry of Ir(III)-HToC complex

1:3 [Ir(III):HToC] ratio of metal to ligand in the developed complex is estimated by Job's continuous variations method [33,34]by mixing equimolar concentrations (1.040×10^{-3}M) of both the metal ion and reagent and measuring the absorbance at 3 divergent wavelengths 380, 423 and 450 nm as presented in figure 6A. The 1:3 complex ratio has further been confirmed by mole ratio methods [35]where in a clear break in the curves corresponding to mole ratio(reagent/metal) 3.0 suggests the metal to ligand ratio to be 1:3 (figure 6B). The above stoichiometric investigation supports the metal-ligand complex to have the optimized structure as

Computational results

Geometry optimization

After geometrical optimization, with the help of FMOs, a molecule's desired locations in the donor-acceptor connection between the ligand and the complex are precisely represented. Figure 8shows the optimized structure and electronic distribution of frontier molecular orbitals for chromogenic reagent (HToC) and its complex with Ir(III). E_{HOMO} and E_{LUMO} are generally used as reactivity markers in terms of a molecule's willingness to give and receive electrons under favourable conditions. The energy gaps for the HOMO and LUMO molecules account for the charge transfer interactions that occur within the molecule. The primary characteristic of this electronic absorption, associated with the transition from ground to the first excited state, is the single electron excitation from HOMO to LUMO. The energy gap (E_{gap}) between the HOMO (-8.28 eV) to LUMO (-5.92 eV) is 2.36 eV forthe reagent, while for complex it is determined to be 1.05 eV. HOMO and LUMO of the reagent are distributed over the whole molecule and therefore showed π-π* transition. The E_{gap} forreagent is more than that of complex.

Furthermore, the Ir(III)-HToCcomplex has a smaller dipole moment (0.359293) than that ofHToC (3.257415) indicating weak dipole-dipole interactions. Furthermore, according to other chemical descriptors such as chemical hardness/global hardness (χ), directly related to it, the HOMO–LUMO energy gap is larger for the reagent than its complex. A substance with a high chemical hardness grade is said to be stable. Similarly, the strength with which electrons are pulled to a covalent bond is determined by its electronegativity value. The inverse of global hardness, global softness serves as an additional metric to evaluate the low reactivity of the stable complex. Further, Table 7 shows that the interaction between the ligand and Ir(III) causes the chromogenic reagent's chemical hardness to decrease from 1.18 eV to 0.53 eV, indicating that the formed complex had lower kinetic stability and more chemical reactivity. Table 7 demonstrates that there was a significant charge transfer from the reagent to the metal due to its increased electro negativity compared to its metal complex. The energy stabilization that occurs when a system picks up an extra electronic charge from its surroundings, is measured by the electrophilicity index. The complex and ligand had electrophile and nucleophile properties, respectively, according to the computed electrophilicity index. Ultimately, the desire of a molecule to provide and receive electronic charge is known as its capacity for giving and receiving electrons, respectively.

QTAIM Study

By using Bader's topological QTAIM analysis, we examine the type and intensity of metal-ligand interactions [36]. The reagent(HToC) and Ir(III)-HToC complex's molecular graph is graphically represented in figure 9, showing the locations of bond critical points (BCPs) and the bond pathways that connect the oxygen atoms (O_{11}, O_{12}, O_{20}, O_{21}, O_{27}, and O_{34}) of the ligand with iridium metal. Table 8 provides topological metrics at BCPs of intermolecular interactions between the reagent and metal, including electron density (ϱ_{BCP}), laplacian ($\nabla^2\varrho_{BCP}$), total energy density (H_{BCP}), kinetic energy density (G_{BCP}), and potential energy density (V_{BCP}). Additionally, the sign of the H_{BCP} and $\nabla^2\varrho_{BCP}$ values can be used to determine the intensity of the intermolecular interactions. Thus, a strong interaction ($\nabla^2\varrho$BCP and $H_{BCP}< 0$), a medium strength interaction ($\nabla^2\varrho_{BCP}>0$ and $H_{BCP}< 0$), and a weak interaction ($\nabla^2\varrho_{BCP}$ and $H_{BCP}> 0$) may be distinguished. The findings presented in Table 8 indicate that the metal-ligand interaction strength is medium, as indicated by the positive values of $\nabla^2\varrho_{BCP}$ and the negative values of H_{BCP} for Ir-O bonds. A good criterion for figuring out the type of interaction is the ratio of $G_{BCP}/|V_{BCP}|$ [37]. Covalent, electrostatic with partially covalent, and non-covalent interactions are shown by the ratios of $0.5 < G_{BCP}/|V_{BCP}| > 0$, $1 < G_{BCP}/|V_{BCP}| 1$, and so on. The computed G_{BCP}/V_{BCP} value for Ir-O bonds is found to range between 0.5 and 1, as indicated in the Table 8. This indicates that the interactions are primarily electrostatic with a partial covalent nature.

Applications

Analytical Applications

For the micro amount of Ir (III), the proposed technique of spectrophotometric determination is simple, rapid and offers the advantage of high sensitivity ($\varepsilon = 5.960\times10^4$ l $mol^{-1}cm^{-1}$) and selectivity (free from interference of 23 anions/ complexing agents and 33 cations of analytical interest). The wide practicability of the procedure has been assessed by analysing different samples of varying compositions and the results obtained are quite satisfactory(Table9). The total operation for each determination requires not more than 5minutes.

*Figure in parantheses indicates the amount of metal ion in mg

** Average of duplicate analyses

Bioanalytical applications

DPPH radical scavenging capacity

The managementof antioxidants play a vital role for the preservation of biological systems. Scavenging free radicals and inhibiting chain reactions work as antioxidants by providing the free radical. Safer antioxidant has been created in the presented work. The antioxidant capacity at various concentrations of HToC and Ir (III) complex was analysed by detecting the de-colorization of DPPH. %RSA increases with enhanced concentrations of the compound under study. HToC and Ir (III)-HToC complex exhibited the highest scavenging activity of 59.3% and 70.04%, respectively, at 500 µg ml^{-1} concentration. It has also been noticed that the Ir (III)-HToC complex, a chelate, acted as better antioxidant as compared to reagent alone.The RSA can be ranked in the following order: gallic acid > Ir (III)-HToC complex > HToC. This indicates that the prepared complex has the potential to be highly influencial in the development of innovative, therapeutic approaches that rely on antioxidants.

CONCLUSION

In the reported work, spectrophotometric determination technique has been used to analyse iridium(III) at the microgram level using a new derivative from the family of benzopyrans, 3-hydroxy-2-tolyl-4H-chromen-4-one(HToC) aschromogenic reagent. In phosphoric acid medium, iridium (III) instantly interacts with HToC to generate a stable light yellow-coloured, non-extractable complex that coherently responded linearly upto 1.8 Ir (III) µg ml^{-1}. The corresponding values of the statistical parameters viz. %RSD, molar absorptivity, Sandell's sensitivity and corelation coefficient, validated the method's precision and accuracy. The procedures under study confirmed that the produced complex had stoichiometric constitution of 1:3[Ir (III):HToC].The molecular structural features are elucidated by TDDFT analysis and QTAIMevaluation. The method found its satisfactory importance in

numerous analytical applications in different synthetic mixtures of varying compositions. The antioxidant findings of the complex reveal itsbest potential to scavenge radicals.

ACKNOWLEDGEMENT

We acknowledge infrastructure support from Maharishi Markandeshwar (Deemed to be university), Mullana. No grant had been received for this work.

REFERENCES

1. Dion B., NemezL. C., Trokajlo P., Liang Y., Goldman D., Motnenko I. and Herbert D.E. (2023). a titration method for standardization of aqueous sodium chlorite solutions using thiourea dioxide.ACS Omega, 8 (42), 39616–39624.
2. Ingo O., Michael S., Heike S., William S.S. and Gust R. (2008). Atomic absorption spectrometric determination of iridium content in tumor cells exposed to an iridium metallodrug. J. Pharm.& Biomed. Anal., 47, 938.
3. Miura T., Linuma Y. and Sekimoto S. (2020). Precise determination of iridium by neutron activation analysis coupled with internal standard method. J. Radioanal.&Nucl. Chem.,324, 1007–1012.
4. PratiwiR.A. andNandiyanto A.B.D. (2022).How to Read and Interpret UV-VIS Spectrophotometric Results in Determining the Structure of Chemical Compounds. Indo. J. Edu. Res. Tech., 2(1), 1-20.
5. Chen Y.C., YaoS.J. and Dong-Qiang L. (2023).Parameter-by-parameter method for steric mass action model of ion exchange chromatography: Simplified estimation for steric shielding factor. J. Chromat. A,1687, 46365.
6. Zhang, G. and Tian, M. (2015). A rapid and practical strategy for the determination of platinum, palladium, ruthenium, rhodium, iridium and gold in large amounts of ultrabasic rock by inductively coupled plasma optical emission spectrometry combined with ultrasound extraction. Opt. Spectrosc., 118, 513–518.
7. Zhang Y., Yaxiong He, Zhou W., Guanqin Mo, Hui Chen and Tao Xu.(2023).Review on the elemental analysis of polymetallic deposits by total-reflection X-ray fluorescence spectrometry.App. Spectrosc. Rev. ,58, 428-441.
8. Locatelli C. (2013). Iridium and lead as vehicle emission pollutants: Their sequential voltammetric determination in vegetable environmental bio-monitors. Microchem. J.,106, 282–288.
9. Komendova R. (2019).Recent advances in the preconcentration and determination of platinum group metals in environmental and biological samples. Trends Anal. Chem., 19, 30474.
10. Greenwood N. N. and Earnshaw A. (1997). Chemistry of the Elements (2nd ed.). Oxford: Butterworth–Heinemann,1294 ,1113–1143.
11. Greenwood N. N. and Earnshaw A. (1997).A History of Iridium. Platinum Metals Review. Oxford: Butterworth–Heinemann, 31 (1), 32–4.
12. Yellowlees L.J. and Macnamara K.G.(2003).Iridium Compounds. Coord. Chem., 6,147–246.
13. Maenaka Y., Suenobu T. and Fukuzumi S. (2012). Catalytic interconversion between hydrogen and formic acid at ambient temperature and Pressure. Ener. Environ. Sci., 5, 7360–7367.
14. Cheung H., Tanke R.S. and Torrence G.P.(2000). "Acetic acid" Ullmann's Encyclopedia of Industrial Chemistry, Wiley.
15. Lee J., Chen H., Batagoda T., Coburn C., Djurovich P.I., Thompson M.E. and Forrest S. R. (2016).Deep blue phosphorescent organic light-emitting diodes with very high brightness and efficiency. Nat. Mater. 15, 92–98.
16. Liu Z. andSadler P.J.(2014). Organoiridium complexes: anticancer agents and catalysts. Acc. Chem. Res. 47 (4), 1174–1185.
17. Borgave S. S. and Barhate V. D. (2016). Extractive and spectrophotometric determination of Iridium(III) using 2-(5-bromo-2-oxoindolin-3-ylidene) hydrazine carbothioamide as an analytical reagent. J. Chem. Pharma. Res., 8(5), 584-589.
18. Kuchekar S., Bhumkar S., Aher H. and Han S.H. (2019). Solvent Extraction, Spectrophotometric determination of Iridium (III) using p-methylphenylthiourea as a chelating agent: Sequential Separation of Iridium(III), Ruthenium(III) and Platinum(IV), J. Mater Environ. Sci., 10(12),1200-1213.

19. Makhijani R. (2021). Development of Extractive Spectrophotometric Determination Of Iridium (III) Using Schiffs base As An Analytical Reagent. JETIR,8(6).
20. Mohmad M.,Agnihotri N., Kumar V., Kumar R., and Kaviani S.(2022). Iridium(III)-3-hydroxy-2-(3′-methyl-2′-thienyl)-4-oxo-4H-1-benzopyran complex: The analytical, in-vitro antibacterial and DFT studies. Inorg. Chem. Comm., 139,109-333.
21. Mohmad M., Agnihotri N., Kumar V., Kumar R., Kaviani S., Mohammad A., Mohammad W.S., Raj K. and Mahboob A.(2022). Radical scavenging capacity, antibacterial activity and quantum chemical aspects of the spectrophotometrically investigated iridium (III) complex with benzopyran derivative. Front. Pharmacol, 13,945323.
22. El-lateef H.M., El-dabea T., Khalaf M.M. and Abudief A.M. (2023). Recent overview of potent antioxidant activity of coordination compounds. Antioxidants, 12(2).
23. Rodriguez-arce E. and Saldias M. (2021). Antioxidant properties of flavonoid metal complexes and their potential inclusion in the development of novel strategies for the treatment against neurodegenerative diseases. Biomed. Pharmacothe., 143, 112236
24. Padgett C. W., Lynch W.E., Sheriff K., Dean R. and Zingales S. (2018). 3-Hydroxy-2-(4-methylphenyl)-4H-chromen-4-one. IUCr Data, 3, No. x181138
25. MohmadM., Agnihotri N., Kumar V., Kumar R., Kaviani S., Mohammad A., Mohammad W.S., Raj K., Kumar A., Sharma U., Javed S., Muthu S. and Kim Min.(2023). Preparation of a Pt(II)–3-Hydroxy-2-tolyl-4H-chromen-4-one Complex Having Antimicrobial, Anticancerous, and Radical Scavenging Activities with Related Computational Studies. ACS Omega,8(35), 31648-31660.
26. Kumar A., Trivedi M., Sharma R. K. and Singh G. (2017). Synthetic, spectral and structural studies of a Schiff base and its anticorrosive activity on mild steel in H_2SO_4. New J. Chemi., 41 (16), 8459-8468.
27. Frisch M. e., Trucks G., Schlegel H., Scuseria G., Robb. M., Cheeseman. J., Scalmani G., Barone V., Petersson G. and Nakatsuji H.(2016) Gaussian 16, revision C. 01. Gaussian, Inc., Wallingford CT: 2016.
28. Muscat J., Wander A. and Harrison N. (2001).On the prediction of band gaps from hybrid functional theory. Chem. Phys. Lett., 342 (3-4), 397-401.
29. Rienstra-Kiracofe J. C., Barden C. J., Brown S. T. and Schaefer H. F.(2001). Electron affinities of polycyclic aromatic hydrocarbons. J. Phys. Chem. A, 105 (3), 524-528.
30. Vektariene A., Vektaris G. and Svoboda J.(2009). A theoretical approach to the nucleophilic behavior of benzofused thieno [3, 2-b] furans using DFT and HF based reactivity descriptors. Arkivoc: Online J. Org. Chem., (7) 311-329.
31. Henkelman G., Arnaldsson A. and Jónsson H. (2006) A fast and robust algorithm for Bader decomposition of charge density. Comput. Mater. Sci., 36 (3), 354-360
32. Ringbom A. (1938). On the accuracy of colorimetric analytical methods I. Z. Anal. Chem., 115, 332–343.
33. Job P.(1928).Formation and stability of inorganic complexes in solution. Ann. Chem., 9, 113–203.
34. Vosburgh W.C., Cooper G.R. and Complex Ions I. (1941).The identification of complex ions in solution by spectrophotometric measurements. J. Am. Chem. Soc., 63, 437–442.
35. Yoe J.H. and Jones A.L. (1944). Colorimetric determination of iron with disodium-1,2- dihydroxybenzene-3,5-disulfonate. Ind. Eng. Chem. Anal. Ed., 16,111–115.
36. Popelier P. L. A. (2014). The QTAIM perspective of chemical bonding. The chemical bond: fundamental aspects of chemical bonding, 271-308.
37. Wick C. R. and Clark T. (2018). On bond-critical points in QTAIM and weak interactions. J. Mol. Model., 24,142 (1-9).

Table 1: Effect of medium on the absorbance of Ir (III)–HToC complex

Medium Used	Absorbance	Medium Used	Absorbance
H_3PO_4	0.310	HCl	0.118

HNO_3	0.119	H_2SO_4	0.176
CH_3COOH	0.085	$HClO_4$	0.126

Table 2: Effect of acidity on the absorbance of Ir (III) –HToC complex

H_3PO_4 (M)	0.005	0.010	0.015	0.020-0.045	0.05	0.06	0.075
Absorbance	0.09	0.19	0.293	0.310	0.255	0.210	0.175

Table 3: Effect of concentration of reagent on the absorbance of Ir (III)-HToC complex

Amount of HToC added (ml)	0.1	0.3	0.4	0.5-1.4	1.5	1.7	2.0
Absorbance	0.020	0.160	0.200	0.310	0.280	0.127	0.080

Table 4: Effect of anions or complexing agents on Ir(III)-HToC complex

Anions/ Complexing agent added	**Tolerance limit mg/10mL**	**Anions/ Complexing agent added**	**Tolerance limit mg/10mL**
Chloride	100	Phosphate	100
Bromide	100	Thiourea	100
Iodide	100	Sulphate	90
Nitrate	100	Ascorbic acid	90
Nitrite	100	Acetate	50
Sulphite	100	Fluoride	50
Carbonate	100	Oxalate	50
Bicarbonate	100	Dithionite	50
Sulfosalicylic acid	100	Tartrate	40
EDTA'Disodium salt'	100	H_2O_2 (30%)	1ml
Hydrazine sulfate	100	Glycerol	1ml
Thiocynate	100		

Table 5: Effect of cations on Ir (III)-HToC complex

Cations added*	**Tolerance limit mg/10mL**	**Cations added***	**Tolerance limit mg/10mL**
Cu(II)	10	Pd(II)	1
Zn(II)	10	Fe(II)	1
Mg(II)	10	Fe(III)	1
Mn(II)	10	Os(VIII)	1
Ca(II)	10	Zr(IV)	1
Sr(II)	10	Sn(II)	0.8
Ni(II)	10	W(VI)	0.5
Co(II)	10	Ti(IV)	0.5
Cr(III)	10	Au(III)	0.5
Cd(II)	10	V(V)	0.5
Se(IV)	8	Mo(VI)	0.5
Al(III)	7	Ru(III)	0.5
Ba(II)	7	Pt(IV)	0.5
Ce(IV)	5	Nb(V)	0.5

Pb(II)	5	As(V)	0.5
Ag(I)	5	Cr(VI)	0.1
Hg(II)	1		

Table 6: Analytical characteristics of Ir (III)-HToC complex

S.NO.	Characterstics	Specification
1	λ_{max}	420-425 nm
2	Molar absorptivity(Ɛ)	5.960×10^4 l $mol^{-1}cm^{-1}$
3	Sandell´s sensitivity(S)	0.0032 µg cm^{-2}
4	Beer´s law range (B.L.)	0.0-1.8 µg ml^{-1}
5	Ringbom´s ideal range	0.3-1.6 µg Ir (III) ml^{-1}
6	Linear regression equation	Y = 0.315X- 0.007
7	Correlationcoefficient	0.9981
8	Limit of detection (LOD)	0.036 µg ml^{-1}
9	Standard deviation	0.0045
10	%Relative Standard deviation	0.0146
11	Coefficient of variance	0.00146
12	Stoichiometry of the complex	1:3 (M:L)
13	Stability of the complex	>2 days

Table 7: Calculated HOMO-LUMO energy gap (E_{gap}) and quantum molecular descriptors in eV for the studied reagent and complex Ir(III)-HToC

Parameters studied	E_{HOMO} (eV)	E_{LUMO} (eV)	E_{gap} (eV)	I	A	χ (eV)	η (eV)	σ	ω
HToC	-8.28	-5.92	2.36	8.28	5.92	7.10	1.18	0.85	21.37
Ir(III)- HToC complex	-5.89	-4.83	1.05	5.89	4.83	5.36	0.53	1.90	27.29
I= Ionization potential; A= Electron affinity; χ = Electronegativity; η= chemical hardness; σ= chemical softness; ω= electrophilicity index HToC									

Table 8: Evaluated topological parameters (a.u) at BCP in the studied Ir(III)-HToC complex

Bond	ϱ_{BCP}	$\nabla^2\varrho_{BCP}$	H_{BCP}	G_{BCP}	V_{BCP}	$G_{BCP}/\lvert V_{BCP}\rvert$
Ir-O12	0.09334	0.5323	-0.0085	0.1380	-0.1466	0.94133697
Ir-O11	0.0937	0.5047	-0.0099	0.1326	-0.1425	0.93052632
Ir-O34	0.0975	0.5296	-0.0105	0.1391	-0.1496	0.92981283
Ir-O27	0.0936	0.5337	-0.0086	0.1384	-0.1470	0.9414966
Ir-O21	0.0939	0.5077	-0.0099	0.1333	-0.1432	0.93086592
Ir-O20	0.0894	0.5031	-0.0081	0.1306	-0.1387	0.94160058

Table 9: Analysis of synthetic mixtures by the studied method

S.No.	Composition of sample		Ir found** (µg / 10 ml)
	Matrix *	Ir added (µg / 10 ml)	
1	Cu(5), Zn(2), Se(0.1)	10	10.05
2	Mg(2), Mn(5), W(0.5)	5	4.95
3	Ca(5), Ni(2), Pb(0.1)	15	15.11

4	Co(5), Cr^{III}(2), Mo(0.1)	12	12.06
5	Zn(5), Pt(0.5), V(0.1)	7	7.08
6	Os(0.1), Ce (1), Fe(0.5)	10	10.07
7	Zr(0.5), Hg(0.1), Ti(5)	8	7.90
8	Ca(5), Cd(0.5), Ba(2)	5	4.95
9	Mn(5), Fe(0.1), Ag(0.1)	7	7.50
10	Mg(2), Sn(0.1), Pd(0.1)	12	11.94

Table 10: %RSA of Ir(III)-HToC complex

Concentration (µg ml^{-1})	%RSA		
	HToC#	Ir(III)-HToC##	Gallic acid###
31.2	34.8	37.2	47.6
62.5	38.1	42.5	52.2
125	45.8	58.1	65.7
250	54.5	65.1	74.3
500	59.3	70.4	80

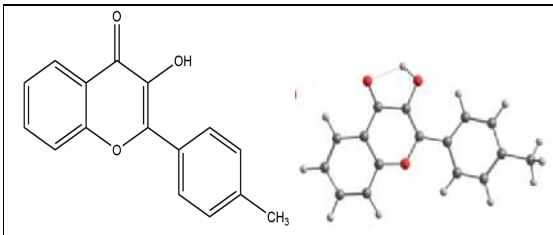

Figure 1. Structure of HToC

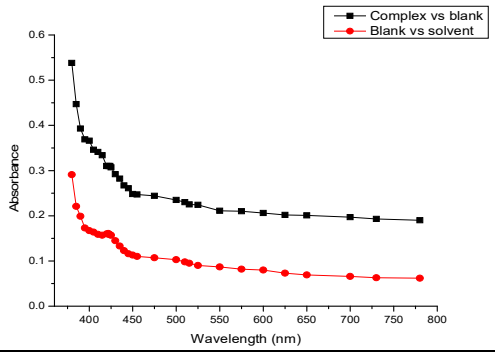

Figure 2. Absorbance spectrum of Ir (III)-HToC complex

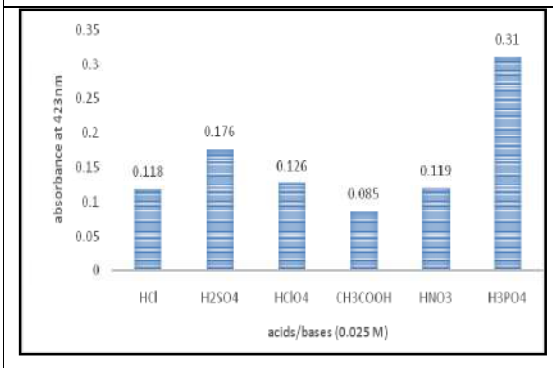

Figure 3. Effect of medium on the absorbance of Ir (III)–HToC complex

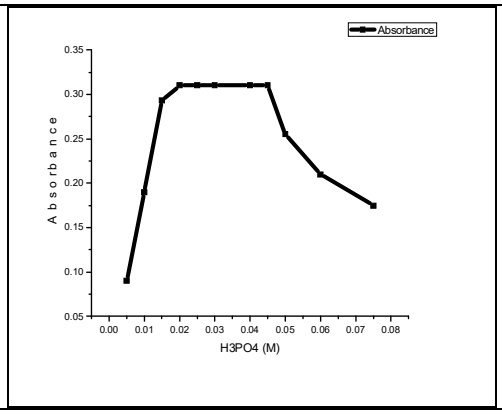

Figure 4. Effect of acidity[A] and reagent concentration

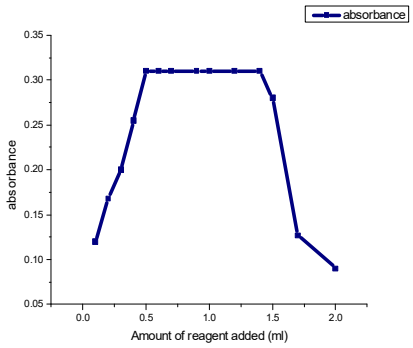

Figure 4. [B] on absorbance of Ir (III)–HToC complex

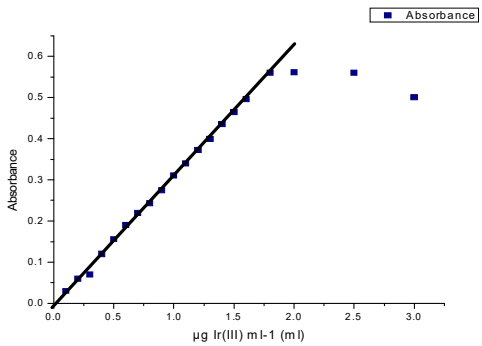

Figure 5. Beer's law range[A] andRingbom's plot

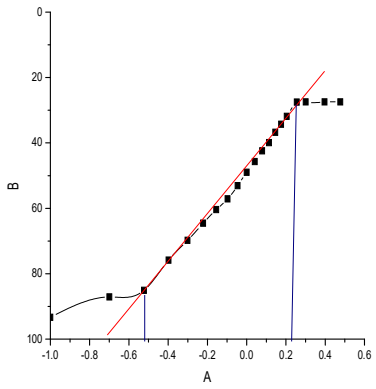

Figure 5. [B] for Ir (III)- HToC complex at 423nm

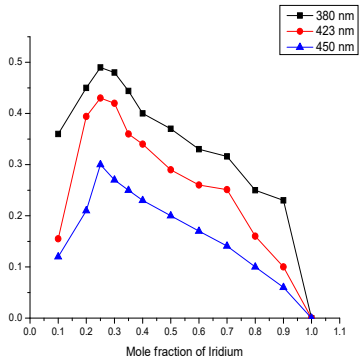

Figure 6. Stoichiometry of Ir (III): HToC [A] Jobs continuous variation

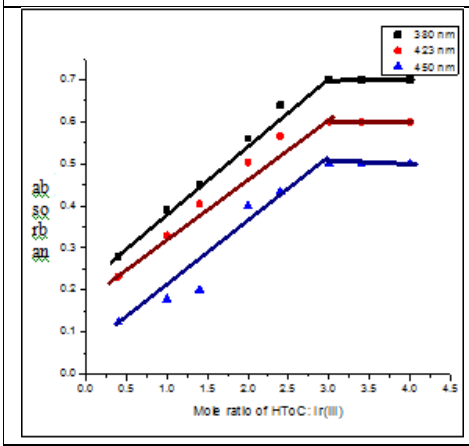

Figure 6. [B] Mole ratio method

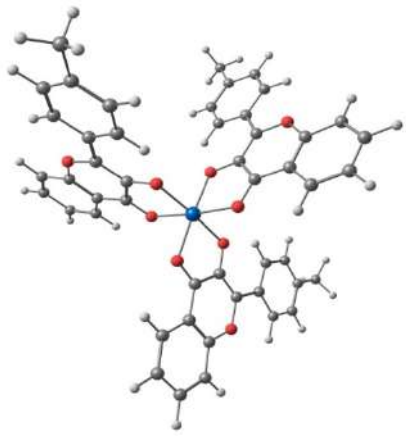

Figure 7. Structure of complex

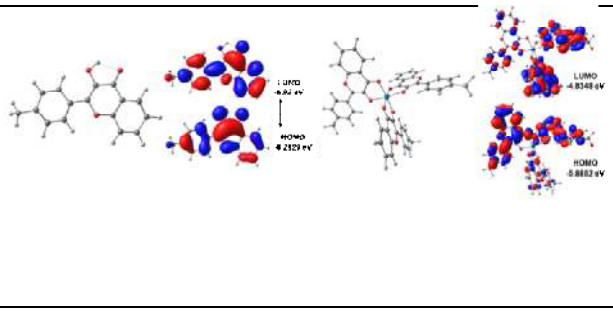

Figure 8. Optimized structures of HToC andIr(III)-HToC along with their frontier molecular orbitals

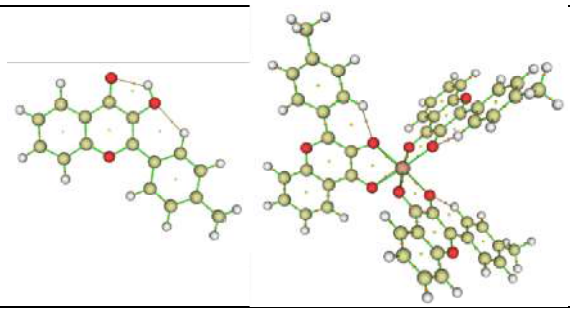

Figure 9. Molecular graph of reagentHToC and Ir(III)-HToC complex

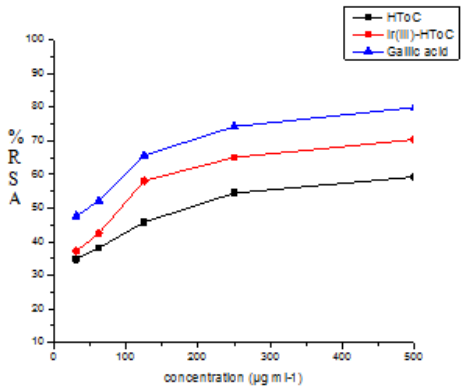

Figure 10.% RSA of gallic acid, Ir(III)–HToC complex and HToC

Indian Journal of Natural Sciences *www.tnsroindia.org.in ©IJONS*

Vol.15 / Issue 83 / Apr / 2024 *International Bimonthly (Print) – Open Access* *ISSN: 0976 – 0997*

REVIEW ARTICLE

Review of Covalent Organic Frameworks and their Applications

Shipra Sharma, Satvinder Khatkar, and Bhawna Pareek*

Department of Chemistry, Maharishi Markandeshwar (Deemed to be University), Mullana, Ambala, 133207, Haryana, India.

Received: 30 Dec 2023 Revised: 09 Jan 2024 Accepted: 12 Jan 2024

***Address for Correspondence**
Bhawna Pareek
Department of Chemistry,
Maharishi Markandeshwar (Deemed to be University),
Mullana, Ambala, 133207, Haryana, India.
Email: dr.bhawnapareek@gmail.com,

ABSTRACT

Covalent Organic Frameworks are two or three dimensional (2D or 3D) structures in which monomers are connected by covalent bonds. The extended crystalline solids can be formed by linkage of organic units by covalent bonds between light elements like (B, C, N, H, O) to form covalent organic frameworks (COFs). Gilbert N Lewis in 1916 describe the covalent bond and nature of bonding within the molecules and linkages of atom to form molecules. In 2005 Omar M. Yaghi and his coworkers discovered the first crystalline covalent organic framework COF-1. Different methods are used to make crystalline covalent organic frameworks like room temperature synthesis, solvothermal methods, microwave synthesis, ionothermal methods of synthesis etc. The most common method of synthesis is solvothermal method which is used for the formation of highly crystalline and stable covalent organic frameworks. Covalent organic frameworks are highly ordered crystalline porous structures having combination of both physical and chemical properties. The band gap of COFs can be tuned by different molecular building blocks. Due to their strong covalent bonds, high porosity, high solubility, high crystallinity and tunability COFs can be used in Hydrogen storage, Methane storage, Gas separation, Sensing, Catalysis, drug delivery system, CO_2 conversion etc. Covalent organic frameworks and COFs linked hybrid materials are very important in photodegradation of dyes and pollutants.

Keywords: Covalent Organic Frameworks, Covalent Bonds, Photodegradation, Crystalline porous structures etc.

INTRODUCTION

Covalent organic frameworks are highly crystalline material having two dimensional (2D) or three dimensional (3D) porous crystalline structures having high surface area and high thermal stability. Covalent organic framework has low density which is due to less dense elements present in organic linkers connected by strong covalent bonds. The first COF material was discovered by Yaghi and his coworkers in 2005 i.e COF-1. Covalent organic framework an emerging crystalline material having high porosity and crystallinity with tunable pore size and having large self-healing capacity. Covalent organic frameworks (COFs) are playing an important role in research now days due to their combined physical and chemical properties. Different methods are used in synthesis of COFs and number of methods have been developed for improving band structure and photocatalytic activities of Covalent Organic Frameworks.

Linkages

The building blocks of Covalent Organic Frameworks are made up of different linkages having Boron, Nitrogen, Sulphur and Oxygen having strong covalent bonds present in their molecular building units. These linkages introduced electron donor acceptor unit into conjugated system to extend light absorption towards visible light. The different building blocks of linkages are given below. (6)

1. Boron containing linkages
2. Triazine based linkages
3. Imine based linkages
4. Imide based linkages
5. Hydrazone based linkages
6. Azine based linkages

Boron containing linkages

Boroxine linkage, Boronate ester linkage, Boronated anhydride linkage can be synthesized by self condensation of Boronic acid(RBOH2) or co-condensation of boronic acid (RBOH2). Boron containing COFs are highly sentient of water and moisture so can be easily oxidized and hydrolyzed. Boron containing linkages have low density but have high photoconductivity, high crystallinity and large surface area and high thermal stability as compared to others linkages. Examples are COF-1.

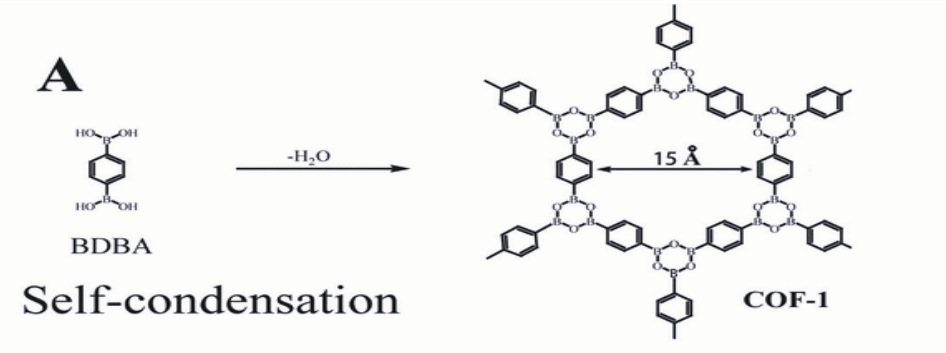

Triazine based linkages

Covalent triazine based frameworks (CTFs)which can be synthesized by cyclo-trimerization of nitriles under ionothermal condition and Friedel craft reaction. Triazine based COFs have superior stability as compared to boron-containing linkages but have low crystallinity due to presence of large

number of Nitrogen atoms and high degree of conjugation and high structural tunability e.g. CTF-1

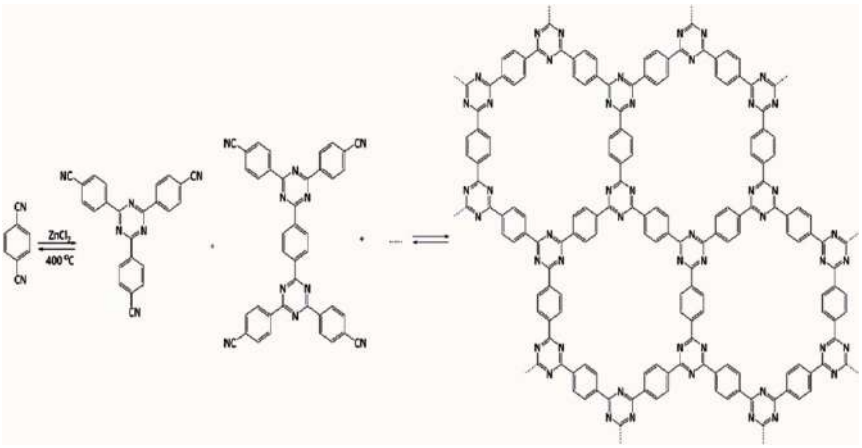

Imine based linkages

Imine based COFs are synthesized by co-condensation of amine with aldehydes in the presence of Lewis acid catalyst or an organic acid. Imine linked COFs show more stability in water, acidic or basic condition and organic solvent but inferior crystallinity. Imine liked COFs show low pi-delocalization due to high polarization of Nitrogen atom. Imine linked COFs can chelate with metal ion due to presence of large no of nitrogen atom e.g. 3D COF-300

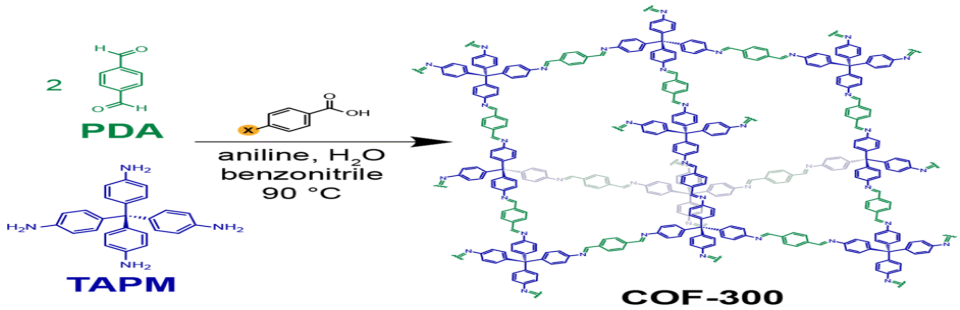

X = OH, OCH_3, CH_3, H, F, Cl, Br, I, CF_3, CN, NO_2

Imide based linkages

Imide linkage can be synthesized by condensation of amine with acetic anhydride up to 250°C temperature A series of crystalline polyimide COFs were fabricated via reversible imidization reaction by extending the building blocks and the large pore size of PI-COFs could be tuned. e.g. PI- COFs-1

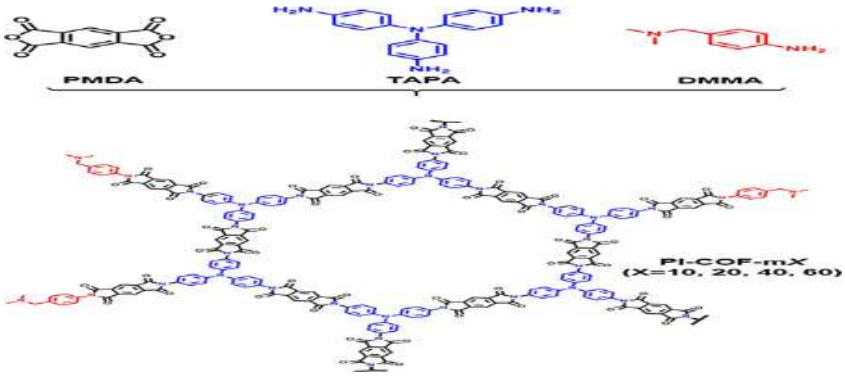

Hydrazone based linkages

Hydrazone linked COFs have been synthesized by co-condensation of aldehydes and hydrazides in presence of acetic acid as catalyst. Due to weak interlayer interactions in hydrazone linked COFs they can be exfoliated into thin film under mild conditions E.g. COF-42.

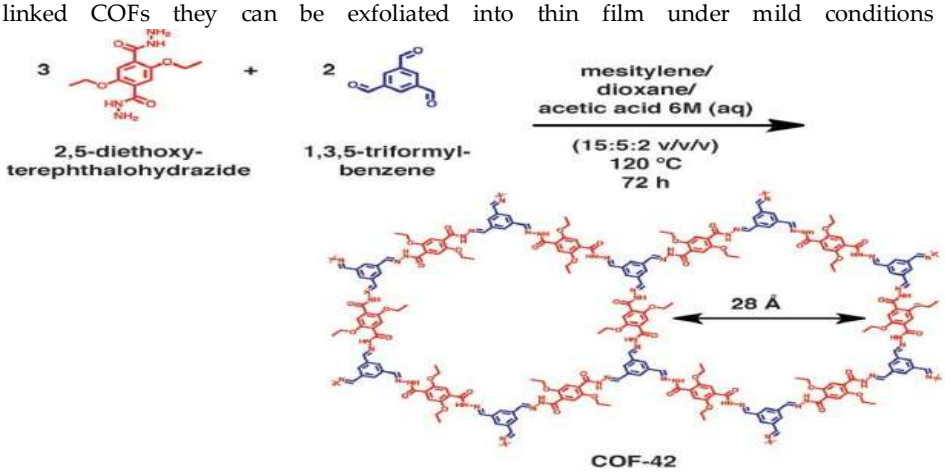

Azine based linkages

Azine based COF have linkage present in most of COF. It is result of short hydrazine monomer being used to connect two aldehydes form polygon skeleton. The azine linked COFs have permanent porosity and high surface area and high chemical stability. E.g. Py-Azine COF.Azine based covalent organic frameworks are used as metal free visible light photocatalyst in carbon di oxide reduction and hydrogen production.

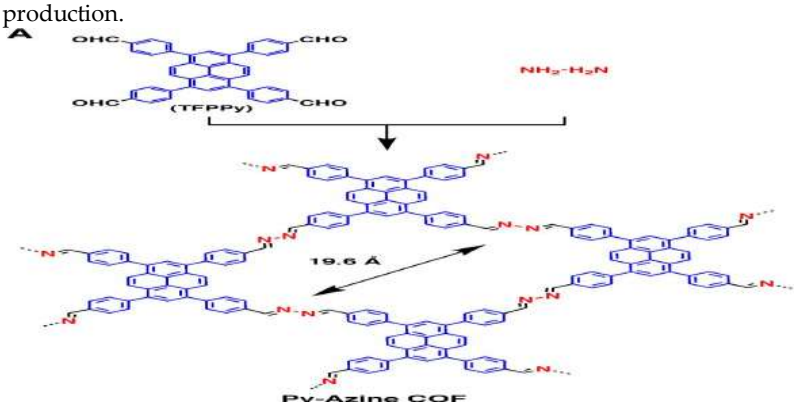

Methods of synthesis

Different methods for the synthesis iof Covalent Organic frameworks powders are Solvothermal Method, Ionothermal, Room temperature, Microwave synthesis.(6)

Solvothermal Synthesis

Most of the COFs are synthesized by Solvothermal Method. In this Method reaction is carried out under heating (80 to 120 C) in sealed vessel for 3 to 7 days. The selection of solvent is very important like 1,4 –dioxane/mesitylene), DMAC-o-Chlorobenzene have been utilized to fabricate COFs liked with organic linkers to fabricate crystalline framework in COF. Solvothermal method of synthesis is very time consuming process as the reaction rate of COF synthesis is very slow.

Ionothermal Method

In Ionothermal method Molten metal salt or ionic liquids are used as both solvent and catalyst to form solid at high temperature around 400°C and high pressure. Harsh condition like high temperature(around 400°C) and high pressure limits the application of Ionothermal method. e.g COFs prepared by Ionothermal method are Covalent Triazine framework.

Room Temperature Synthesis

Room temperature synthesis consist of two methods

a) Mechanochemical Grinding
b) Solvent Method

Mechanochemical Grinding

This method is used by pestle and mortar to prefer manual grinding. It is simple, rapid, facile, environment friendly, solvent free method carried out at room temperature. The change of colour indicate the formation of COFs.

Solvent Method

In this method liquid assisted mechanical grinding was used in which addition of catalyst solution increases the rate of chemical reaction.

Microwave assisted Synthesis

Microwave assisted method of synthesis has short reaction time, high product yield, low energy usage, cleaner products and controllable reaction temperature and pressure and 200 times faster than solvothermal method of synthesis and has large BET surface area as compared to solvothermal method.

Applications

COFs can be used in Hydrogen storage, Methane storage, Gas separation, Sensing, Catalysis, drug delivery system, CO_2 conversion etc.(2)

Drug delivery

Drug delivery using Covalent organic frameworks spotlight the encapsulation and decapsulation of drugs in a versatile way. Covalent organic frameworks are the good drug carriers and delivers drug to the target molecules in effective way which solve the many drug delivery problems.

Sensing

Covalent organic frameworks are used as a electrochemical sensor as well as biological sensors due to their unique structures and except physical and chemical properties. Detecting chemicals and biomolecules in the fields of environmental protection, health monitoring and for public benefits a large numbers of chemical and biomolecules are detected by detectable signals which can be electrical, thermal by the selective adsorption of analytes.

CO_2 Conversion

Covalent organic frameworks have essential role in carbon di oxide reduction and conversion.COFs could convert the CO_2 in high valuable product which is not harmful for environment. As COFs can transform the CO_2 into HCOOH, CH_3OH at different redox potentials.

Hydrogen production

Covalent organic frameworks can be used as the production and evolution of hydrogen through water splitting by using method photocatalysis and electrocatalysis which are highly dependent of different structure of COFs.

Gas Storage

Covalent organic frameworks have large numbers of pore structures and large surface area which further increses the storage of gas molecules in it. Also the tunable pore size increses their importance in the gas storage process as well as gas separation process.

Catalysis

COFs based photocatalytic reaction show superior photocatalytic activities which show their possible application in development of environmental friendly reaction using visible lights well as ultraviolet light. Photocatalysis of COFs shows many photocatalytic degradations of dyes, pesticides, and environmental pollution.

CONCLUSION

COFs are the class of highly porous crystalline materials having high photocatalytic properties and structural versatility and tunability which shows their large capacity to degrade aqueous pollutants like dyes, pesticides, antibiotics under visible light or sun light irradiation. COFs are useful in degradation of various pollutants but adsorption of pollutants is still under exploration. But literature review presented various photocatalytic application of COFs in water splitting, CO2 reduction, gas storage, degradation of aqueous pollutants and drug delivery system but still there are many challenges in formation of crystalline covalent organic frameworks and also to maintain the stability of COFs.

Declaration of Interest

The author declared that they do not have any conflict of interest.

REFERENCES

1. YangQ, Luo M, Liu K, Cao H, Yan H. Covalent organic frameworks for photo catalytic applications. Applied Catalysis B: Environmental.2020Nov5;276:119174.

2. Wang H, Wang H, Wang Z, Tang L, ZengG, Xu P, Chen M, Xiong T, Zhou C, LiX, HuangD. Covalent organic framework photo catalysts: structures and applications. Chemical Society Reviews.2020;49(12):4135-65.
3. Qian Y, Ma D. Covalent organic frame works: New materials platform for photocatalytic degradation of aqueous pollutants. Materials. 2021Sep27;14(19):5600.
4. LiX, KawaiK, FujitsukaM, Osakada Y. COF-based photo catalyst for energy and environment applications. Surfaces and Interfaces.2021Aug1;25:101249.
5. Wang GB, Li S, Yan CX, Zhu FC, Lin QQ, XieKH, GengY, DongYB. Covalent organic frameworks: emerging high-performance platforms for efficient photocatalytic applications. Journal of materials chemistry A. 2020;8(15):6957-83.
6. Sharma RK, Yadav P, Yadav M, Gupta R,Rana P,SrivastavaA, ZbořilR, Varma RS,Antonietti M, Gawande MB. Recent development of covalent organic frameworks (COFs): synthesis and catalytic(organic-electro-photo)applications. Materials Horizons. 2020;7(2):411-54.
7. López-MaganoA,DaliranS,OveisiAR, Mas-BallestéR, Dhakshinamoorthy A, Alemán J,Garcia H, Luque R. Recent advances in the use of covalent organic frameworks as heterogeneous photocatalysts in organic synthesis. Advanced Materials. 2022Dec23:2209475.
8. Machado TF, Serra ME, Murtinho D, ValenteAJ, NaushadM. Covalent organic frameworks: synthesis, properties and applications—an overview.Polymers.2021Mar22;13(6):970.
9. Ayed,C., Huang, W., Zhang, K.A.I., 2020. Covalent triazine framework with efficient photocatalytic activity in aqueous and solid media.Front.Chem.Sci.Eng.14,397e404.https://doi.org/10.1007/s11705-019-1884-2.
10. Banerjee,T.,Gottschling, K., Savasci, G.,Ochsenfeld,C.,Lotsch,B.V.,2018. H2 evolution with covalent organic framework photo catalysts. ACS Energy Lett.3,400e409.https://doi.org/10.1021/acsenergy lett.7b01123.
11. You J, Zhao Y, Wang L, Bao W. Recent developments in the photoc atalytic applications of covalent organic frameworks: A review. Journal of Cleaner Production. 2021 Apr 1;291:125822.
12. Kandambeth, S., Dey, K., Banerjee, R., 2019. Covalent organic frameworks: chemistry beyond the structure. J. Am. Chem. Soc. 141,1807e1822. https://doi.org/10.1021/jacs.8b10334.
13. Liu, P., Xing, L., Lin, H., Wang, H., Zhou, Z., Su, Z., 2017a. Construction of porous covalent organic polymer as photocatalysts for RhB degradation under visible light. Sci. Bull. 62,931e937.

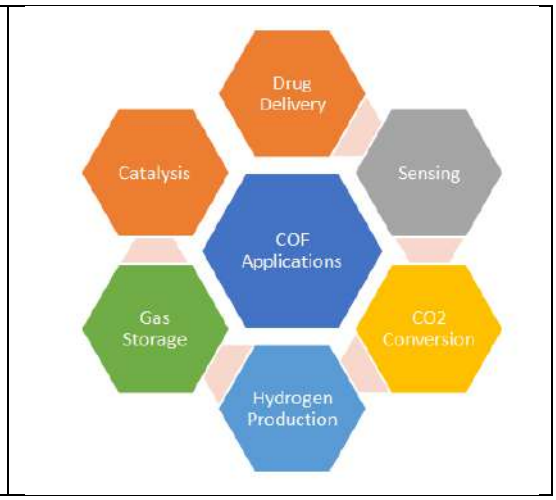

Indian Journal of Natural Sciences *www.tnsroindia.org.in ©IJONS*

Vol.15 / Issue 83 / Apr / 2024 *International Bimonthly (Print) – Open Access* *ISSN: 0976 – 0997*

RESEARCH ARTICLE

Catalytic role of Carbon Quantum Dots in Super Capacitor Applications Synthesis, Characterization, and Properties

Karamveer Sheoran and Samarjeet Singh Siwal*

Department of Chemistry, M.M. Engineering College, Maharishi Markandeshwar (Deemed to be University), Mullana-Ambala, Haryana, 133207, India.

Received: 30 Dec 2023 Revised: 09 Jan 2024 Accepted: 12 Jan 2024

***Address for Correspondence**
Samarjeet Singh Siwal
Department of Chemistry,
M.M. Engineering College,
Maharishi Markandeshwar (Deemed to be University),
Mullana-Ambala, Haryana, 133207, India.
Email: samarjeet6j1@gmail.com

ABSTRACT

Carbon quantum dots (CQDs) have emerged as promising materials in various technological applications due to their unique physicochemical properties. In the realm of energy storage, their role in super capacitors has garnered significant attention. This paper investigates the catalytic role of carbon quantum dots in enhancing the performance of SCs. The synthesis methodologies of CQDs and their subsequent characterization techniques are elucidated, emphasizing their structural, morphological, and surface properties. The electrochemical behavior and specific capacitance of SCs employing CQDs as active materials are thoroughly examined. The superior charge storage capability, high conductivity, and remarkable stability exhibited by CQD-based SCs are discussed in detail. Additionally, insights into the mechanisms underlying the enhanced electrochemical performance facilitated by CQDs are provided. This comprehensive analysis underscores the potential of CQDs in revolutionizing the development of efficient and high-performance super capacitors for advanced energy storage applications.

Keywords: Carbon quantum dots; Energy storage applications; Electrochemical performance; Physicochemical properties.

INTRODUCTION

The demand for sustainable energy supply, it's storage and environmental significance have been surging worldwide. Owing to unique features such as high power density, excellent cycle stability, elongated life cycle, and cost-effective, super capacitors (SCs) emerged as potential energy storage devices which grabs the focus of scientific

communities [1, 2].However, the relatively low energy density restricts the widespread application of SCs. Multitude efforts have been made by researchers towards the development of high energy density SCs but it still remains challenging. To boost the energy density of SCs, researchers can inflate either the specific capacitance or the voltage window. Nevertheless, the electrocatalytic performance of SCs are greatly depends on the nature and the type of materials for their electrodes and electrolytes[3]. Therefore, the electrochemical activity of the SCs can be improved with the fabrication of novel electrode materials. With regard to this, carbon quantum dots (CQDs) have arisen as a novel class of nanomaterials that hold great promise for SC applications. CQDs possess exclusive characteristics such as excellent biocompatibility, high stability, and ultra small particle size (<10 nm) resulting not only from quantum confinement but also due to edge effects and surface passivation [4, 5] which makes them suitable candidate for energy storage devices. CQDs can be utilized as electrolyte additives, active materials and conductive additives in SCs to enhance electrolyte features, electrical conductivity and to store energy respectively. The integration of CQDs into SC materials offers opportunities for improving the electrochemical performance and energy storage capabilities of SCs. This review summarized and discussed the potential of CQDs in revolutionizing the development of efficient and high-performance supercapacitors for advanced energy storage applications. We systematically elucidate synthetic approaches of CQDs along with different properties and catalytic role of CQDs in SCs. Recent research findings and case studies on CQDs-based SCs are presented to provide insights into their performance and potential applications. Finally, the challenges and future prospects of CQDs and it's composites for SC applications are discussed.

Synthesis methods of carbon quantum dots

Usually, CQDs have been synthesized with the utilization of "top-down" and "bottom-up" approaches where high dimensional carbon materials like graphene, graphite, carbon nanotubes, and graphene oxides (GO) are used as starting materials in case of top-down approach for the synthesis of CQDs by physical or chemical techniques whereas smaller carbon materials are utilized in case of bottom-up approach for the fabrication of CQDs by chemical reactions. Different top-down and bottom-up approaches are demonstrated in **figure 1**.

Top-down approach

Laser ablation, arc-discharge, ultrasonic, chemical exfoliation and electrochemical methods have been utilized in top-down approach for the synthesis of CQDs. In this section, we briefly discussed these techniques to fabricate CQDs.

Laser ablation

Laser ablation is widely used method for the fabrication of CQDs with diverse morphologies. This method was firstly purposed by Sun *et al.*[6]with the utilization of Nd:YAG laser source (1064 nm, 10 Hz) for the irradiation of carbon raw material followed by acid treatment. The obtained CQDs did not emit light initially; but when the surface was modified with two different oligomers i.e., poly(ethylene glycol) and poly(propionylethylenimine-*co*-ethylenimine), CQDs exhibited strong photoluminescence emission. After that CQDs of different sizes have been synthesized successfully under controlled nucleation. At the interface of solid target and surrounding liquid media of target, plasma pulse can be localized by using a high energy laser. This plasma pulse initiates rapidly expandable bubble. This bubble shrinks after the application of pressure from surrounding liquid and the nucleation of CQDs was slowly started by cooling core. With the adjustments of laser pulse width, CQDs with different cluster densities can be developed[7].CQDs were prepared by Li *et al*. [8] using simple laser ablation technique where dispersion of nano-carbon material in 50 mL of solvent was used as starting material. Nd:YAG pulsed laser was used for laser irradiation to obtain CQD. CQDs with narrow particle size distribution and outstanding fluorescence features can be fabricated by using laser ablation method. Though high cost and complicated process limits it's application in several fields.

Arc-discharge

In the arc-discharge method bulk carbon precursor undergo decomposition in anodic electrode in the presence of plasma generated in a sealed reactor[9].The temperature within the reactor reaches up to 3727 ℃, where vaporisation

of the carbon atoms occurred at anode and then reassembled at cathode which results in the formation of CQDs. Without the modification of surface, the obtained CQDs have higher oxygen content and highly fluorescent characteristics[10]. However, due to the presence of complex impurities, purification of CQDs produced by this technique is difficult [9].Xu *et al.*[11]prepared CQDs accidently while synthesizing single-walled carbon nanotubes (SWCNTs) with the utilization of arc discharge technique. At 365 nm, yellow, blue-green, and orange fluorescence were emitted by the as-prepared CQDs. The reports showed that the CQDs fabricated with the utilization of this method exhibits good water stability but have larger particle size distribution because of which the surface area of CQDs was decreased extensively and restrict electrocatalytic performance of the material.

Ultrasonic

Ultrasonic techniques are considered as convenient and simple method for the fabrication of CQDs. In this approach, low-and high-pressure waves are created in the solution by high-intensity ultrasound that generate collapsing bubbles with high temperatures(5500 K) and pressure (500 atm.).For the production of CQDs, high energy spot act as micro reactors for dehydration, polymerization and carbonization and then single nuclear burst of precursors have been used[12].A team of researchers synthesized Sn@CQDs@Sn via ultrasound method. The authors observed that the as-prepared CQDs are stable up to 90 cycles and reached maximum coulombic efficiency of 99% for energy storage device [13].

Chemical exfoliation

The electrochemical cleavage of different carbon materials like graphene, reduced graphene oxide, graphite rods, and CNTs results in the production of CQDs and this approach to synthesize CQDs is known as chemical exfoliation technique. In this technique, $OH^{\cdot}$ and $O^{\cdot}$ are produced ate the anode by the oxidation of water. These radicals work as electrochemical scissors to generate CQDs. The process of exfoliation generally occurs at edge points and become faster at the defective points[14]. This method is considered as promising facile and approach for the large scale formation of CQDs as no harsh conditions and strong acids are needed in this technique [15].

Electrochemical Methods

Electrochemical method is prominent and convenient method to fabricate CQDs owing to several merits such as abundance of raw materials, cost-effectiveness, and facile preparation under normal conditions of temperature and pressure. CQDs were prepared by Chi *et al.*[16] using electrochemical method using phosphate buffer solution (pH 7.0) where working electrode was graphite electrode, and Pt mesh and Ag/AgCl was counter and reference electrode respectively. The only demerit of this technique is it's tedious purification process.

Bottom-up approach

Hydrothermal, microwave and thermal pyrolysis techniques are involved in bottom-up approach for the fabrication of CQDs. Saccharides and citric acids are generally utilized as building blocks to prepare CQDs. With the modifications of experimental conditions, CQDs of desired size can be obtained in cost-effective way. This section briefly elucidates bottom-up approaches to fabricate CQDs.

Hydrothermal method

Hydrothermal technique of CQDs preparation involves the carbonization of organic precursors which are sealed under high temperature of up to 200 ℃ in Teflon-lined hydrothermal reactor. Carboxylic acid and amino groups were utilized as precursor for the formation of CQDs. Further studies on hydrothermal synthesis of CQDs revealed that monopotassium phosphate and glucose can also be utilized as precursor to prepare CQDs. For instance, Vandana and co-workers [17]synthesized CQDs via hydrothermal method by utilizing glucose as precursor. The as-synthesized CQDs were used as electrode material for SC and exhibited excellent specific capacitance of 647.5 F/g with decent energy density and power density of 93 Wh/kg and1430 W/kg respectively. Furthermore, the as-synthesized CQDs possess high stability of 2000 cycles.

Microwave method

In microwave synthesis, electromagnetic radiations of 1mm to 1 m wavelengths allow the interaction with precursor and results in CQDs generation within 10 min[18].The CQDs formed via microwave method exhibits several surface functional and broad size distributions because of abrupt heating of microwave resonance. CQDs were prepared by Kumar *et al.*[19]synthesized CQDs via microwave technique using solution of citric acid and urea as precursor. The CQDs were prepared within 300 sec. This technique is facile and scalable method but poor control over obtained particle size restricts the performance of CQDs in various fields.

Comparative analysis of synthesis methods and their impact on CQD properties

The synthetic methods for the formation of CQDs have some pros and cons which are summarized in **table 1**.

Properties and catalytic role of CQDs in supercapacitors

The electron transfer features of CQDs are regulated by the interactions between carbogenic core and functional groups. High surface area and available active sites of CQDs enhances the electron transfer process. The enhancement in the catalytic features of CQDs can be obtained with the doping of heteroatoms like S, B and N etc. The oxygenated functional groups present on edges also enhances the catalytic feature of CQDs[21]. This section summarizes the beneficial property and utilization of CQDs in SCs.

Electrochemical properties of carbon quantum dots

Electron transfer properties of CQDs can be regulated by the interactions of functional groups and carbogenic core. Doping of heteroatoms also influences electron transfer of CQDs [22]. The higher surface area and availability of profuse edge sites of CQDs facilitates the transfer of electrons. Particularly, abundant functional groups which are present on CQD's surface solidly nucleate and modify the pristine nanocrystals which results in intense electrostatic interactions. Consequently, stability and electrochemical activity of the material enhances due to the strengthening of contact between active material and conductor. CQDs can be combined with other materials to enhance the electrochemical performance of the material. For example, Zheng *et al.*[23] prepared molybdenum disulphide (MoS_2) based electrode materials and observe the electrochemical performance of modified electrodes. Briefly, the MoS_2 electrode was firstly modified with zinc sulphide (ZnS); (MoS_2@ ZnS) and then modified with CQDs by utilization of facile hydrothermal method. The obtained results indicate that CQDs/ MoS_2@ ZnS showed better electrocatalytic activitywith specific capacitance of 2899.5 F/g and capacitance retention of 76.1% over 3500 cycles while the obtained specific capacitance of MoS_2, ZnS and MoS_2@ ZnS was 1067.6 F/g, 423.4 F/g and 2176.1 F/g respectively. In another study, CQDs/NiAl-layered double oxide (CQDs/NiAl-LDH) composite nanosheet were prepared via one step solvo thermal method [24]. The as synthesized composite exhibited pore size and surface area of 7.1 nm and 77.9 m^2/g respectively. The authors revealed that the introduction of CQDs enhances the electrochemical performance of the composite by comparing the specific capacitance of their material with previously reported NiAl-LDH based materials. The as-prepared material hadspecific capacitance of 1794 F/g at current density of 2 A/g. It also showed high cycling stability of 1500 cycles with retention of nearly 93%. These results further proves that the special features such as porous structure, active sites, high charge transfer capacity, and easy accessibility to electrolytes of CQDs helps to achieve high stability, conductivity or electrochemical performance of the material which are highly beneficial in the field of supercapacitors.

CQDs in electrocatalysis

High surface area and fast electron transfer feature of CQDs make them suitable candidate for energy conversion and storage devices. To design multi component electrocatalysts using CQDs is easy because of the ease of surface modification or functionalisation. The modification of surface with different functional groups promotes the electron transfer process which in turn improves the electrocatalytic activity of CQDs[21].Samantara and team [25] prepared CQD composite (rGO/N-S-CQD) which was used as electrode material for SC and observed that the as-prepared CQDs exhibited decent energy and power density having cyclic stability over 5000 cycles. This showed that the doping of hetero atoms significantly increases the number of active sites for reactions of electrocatalytic devices.

CONCLUSION, EXISTENCE CHALLENGES AND FUTURE PROSPECTS

CQDs are considered as potential candidates for the application of next generation SCs. This review provides different synthetic approaches of CQDs, their electrocatalytic properties and the role of CQDs in electrocatalysis. Despite of numerous advantages of CQDs in SCs, the research on CQDs in SCs is still in infancy stage which indicates that several avenues are yet to explored. There are still plentiful chances to use CQDs and their composites in SCs. There are some specific challenges that need to clarified in near future for the advanced research of CQD based SCs. The challenges include the deep understanding of charge storage mechanism of CQDs and diversification of functionalization and purification of CQDs. By resolving these issues industrialization of CQDs in SCs can be achieved.

REFERENCES

1. Xiao, J., R. Momen, and C. Liu, Application of carbon quantum dots in super capacitors: A mini review. Electrochemistry Communications, 2021. 132: p. 107143.
2. Permatasari, F.A., et al. Carbon-Based Quantum Dots for Super capacitors: Recent Advances and Future Challenges. Nanomaterials, 2021. 11, DOI: 10.3390/nano11010091.
3. Arsalani, N., et al., Green Synthesized Carbon Quantum Dots/Cobalt Sulfide Nanocomposite as Efficient Electrode Material for Super capacitors. Energy & Fuels, 2021. 35(11): p. 9635-9645.
4. Dager, A., et al., Synthesis and characterization of Mono-disperse Carbon Quantum Dots from Fennel Seeds: Photoluminescence analysis using Machine Learning. Scientific Reports, 2019. 9(1): p. 14004.
5. Guo, R., et al., Functionalized carbon dots for advanced batteries. Energy Storage Materials, 2021. 37: p. 8-39.
6. Sun, Y.-P., et al., Quantum-Sized Carbon Dots for Bright and Colorful Photoluminescence. Journal of the American Chemical Society, 2006. 128(24): p. 7756-7757.
7. Rasal, A.S., et al., Carbon Quantum Dots for Energy Applications: A Review. ACS Applied Nano Materials, 2021. 4(7): p. 6515-6541.
8. Wang, Y. and A. Hu, Carbon quantum dots: synthesis, properties and applications. Journal of Materials Chemistry C, 2014. 2(34): p. 6921-6939.
9. Wang, X., et al., A Mini Review on Carbon Quantum Dots: Preparation, Properties, and Electrocatalytic Application. 2019. 7.
10. Dey, S., et al., Luminescence properties of boron and nitrogen doped graphene quantum dots prepared from arc-discharge-generated doped graphene samples. Chemical Physics Letters, 2014. 595-596: p. 203-208.
11. Xu, X., et al., Electrophoretic Analysis and Purification of Fluorescent Single-Walled Carbon Nanotube Fragments. Journal of the American Chemical Society, 2004. 126(40): p. 12736-12737.
12. Du, X.-Y., et al., The Rapid and Large-Scale Production of Carbon Quantum Dots and their Integration with Polymers. Angewandte Chemie International Edition, 2021. 60(16): p. 8585-8595.
13. Kumar, V.B., et al., In situ sonochemical synthesis of luminescent Sn@C-dots and a hybrid Sn@C-dots@Sn anode for lithium-ion batteries. RSC Advances, 2016. 6(70): p. 66256-66265.
14. Gu, S., et al., Optimization of graphene quantum dots by chemical exfoliation from graphite powders and carbon nanotubes. Materials Chemistry and Physics, 2018. 215: p. 104-111.
15. Tian, L., et al., The influence of inorganic electrolyte on the properties of carbon quantum dots in electrochemical exfoliation. Journal of Electroanalytical Chemistry, 2020. 878: p. 114673.
16. Zheng, L., et al., Electrochemiluminescence of Water-Soluble Carbon Nanocrystals Released Electrochemically from Graphite. Journal of the American Chemical Society, 2009. 131(13): p. 4564-4565.
17. Vandana, M., et al., Hydrothermal synthesis of quantum dots dispersed on conjugated polymer as an efficient electrodes for highly stable hybrid supercapacitors. Inorganic Chemistry Communications, 2020. 117: p. 107941.

18. Zhai, X., et al., Highly luminescent carbon nanodots by microwave-assisted pyrolysis. Chemical Communications, 2012. 48(64): p. 7955-7957.
19. Kumar, P., et al., Synthesis and modulation of the optical properties of carbon quantum dots using microwave radiation. Fullerenes, Nanotubes and Carbon Nanostructures, 2020. 28(9): p. 724-731.
20. Wang, R., et al., Recent progress in carbon quantum dots: synthesis, properties and applications in photocatalysis. Journal of Materials Chemistry A, 2017. 5(8): p. 3717-3734.
21. Hoang, V.C., K. Dave, and V.G. Gomes, Carbon quantum dot-based composites for energy storage and electrocatalysis: Mechanism, applications and future prospects. Nano Energy, 2019. 66: p. 104093.
22. Zheng, X.T., et al., Glowing Graphene Quantum Dots and Carbon Dots: Properties, Syntheses, and Biological Applications. Small, 2015. 11(14): p. 1620-1636.
23. Zheng, J., et al., Importance of carbon quantum dots for improving the electrochemical performance of MoS2@ZnS composite. Journal of Materials Science, 2019. 54(21): p. 13509-13522.
24. Wei, Y., et al., Carbon quantum dots/Ni–Al layered double hydroxide composite for high-performance supercapacitors. RSC Advances, 2016. 6(45): p. 39317-39322.
25. Samantara, A.K., et al., Sandwiched graphene with nitrogen, sulphur co-doped CQDs: an efficient metal-free material for energy storage and conversion applications. Journal of Materials Chemistry A, 2015. 3(33): p. 16961-16970.

Table 1:

Top- down Approach	Technique	Advantages	Disadvantages	Ref.
	Arc-discharge	CQDs with high oxygen content, high fluorescent	Costly, difficulty in purification and high variation in surface area	[10]
	Laser ablation	Controlled morphology, high water solubility	Process complications and high cost	[20]

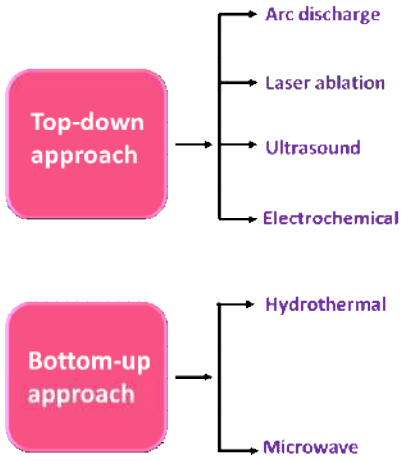

Figure 1: Pictorial presentation of different techniques involved in top-down and bottom-up approaches.

Graphical Abstract:

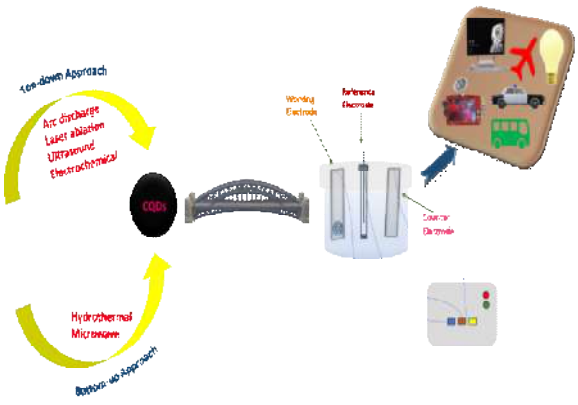

Indian Journal of Natural Sciences *www.tnsroindia.org.in ©IJONS*

Vol.15 / Issue 83 / Apr / 2024 *International Bimonthly (Print) – Open Access* *ISSN: 0976 – 0997*

RESEARCH ARTICLE

Spatial analysis of pH, EC and TDS levels in supply water through ArcGIS mapping in different blocks of Ambala district, in North India

Saloni Kamboj[1], Nirankar Singh[1]* and Brajesh Saxena[2]

[1]Department of Chemistry, Maharishi Markandeshwar Engineering College, Maharishi Markandeshwar (Deemed to be University), Mullana, Ambala-133207, India.
[2]ICAR-Central Soil Salinity Research Institute, Karnal-132001, India.

Received: 30 Dec 2023 Revised: 09 Jan 2024 Accepted: 12 Jan 2024

***Address for Correspondence**
Nirankar Singh
Department of Chemistry,
Maharishi Markandeshwar Engineering College,
Maharishi Markandeshwar (Deemed to be University),
Mullana, Ambala-133207, India.
Email: nirankar_singh11@yahoo.com

ABSTRACT

Groundwater quality is a major concern in various regions around the globe, and research on quality parameters is particularly important for irrigation and drinking purposes. A systematic study of selected water quality parameters was conducted in several blocks of the Ambala district in the winters and summers of 2021–2022. Arc GIS mapping software was utilized for the spatial analysis of water quality parameters including pH, EC and TDS. Globally, water resources are investigated in conjunction with the growth of agricultural practices, industrialization, urbanization, etc. The primary goal of this study was to employ Geographic Information System (GIS) software to map the supply water quality in the studied region. In order to create spatial distribution maps of water quality parameters including pH, EC, and TDS for Ambala district, twenty predefined locations were selected from the different blocks of Ambala district, for the collection of supply water samples. These samples were then subjected to quantitative analysis and results obtained were utilized for the ArcGIS mapping.

Keywords: GIS, Ground Water, Chemical Parameters, Mapping.

INTRODUCTION

Regardless of caste, religion, nationality, gender, or social standing, everyone has the human right to access clean drinking water (Mukherje et al., 2020; Satpathy et al., 2022). However, groundwater resources are depleting globally due to rapidly growing population urbanization and industrialization(Sajjad et al., 2023; Zahran et al., 2023). Tainted drinking water can have an adverse effect on health and lead to several illnesses like diarrhea, cholera, and typhoid

(Yasmeen et al., 2023; Misra et al., 2023). Comprehension of the current state of drinking water conditions is a fundamental prerequisite for any urban or rural area to get ready for healthy ecosystem sustainable growth(Shutaleva et al., 2020; Dutta et al., 2022). The appropriateness of ground water for drinking and other domestic uses has been investigated by various researchers using a variety of approaches and procedures (Gaagai et al., 2022). Contamination of groundwater and the variety of pollutants affecting water supplies are among the most significant environmental challenges of present time (Singh et al., 2022; Ismanto et al., 2023).

Although the inherent chemical quality of groundwater is generally found good, but various anthropogenic factors contribute to the high quantities of various elements (Saqib et al., 2023). The quality of groundwater can be significantly altered by heavily irrigated agricultural flows into the groundwater (Bodrud-Doza, et al., 2020; Balogun et al., 2022; Singh et al., 2023) An evaluation of the supply water quality has been attempted in this paper with reference to current state of pH, EC and TDS levels in the area. To ensure the quality of supply water for domestic, agriculture and industrial purposes, several parameters including the levels of pH, EC and TDS, are evaluated, and the results are compared to the acceptable/desirable values specified by the World Health Organization (WHO) and the BIS (Mazinder Baruah., 2022; Singh et al., 2024; Khapraet al., 2023). The present study offers preliminary results of pH, EC, TDS levels that can affect human health as well as the machinery systems used for domestic and industrials purposes in the study area. Learning the variations of pH,EC and TDS levels may aid in research advancement and reduce decision-making uncertainties (Prieto-Amparán et al., 2018; Mohamed et al., 2019). For the benefit of community welfare, the study offers baseline data on water quality, which may also be used in future planning for the regional water resources, human health, and machinery system.

Description of the study area

Ambala is a rapidly expanding district in the state of Haryana that covers a total geographic area of approximately 1574 square kilometers and located between latitude 30° 10'31° 35' N and longitude 76° 30' 77° 10' E Different sites selected from different blocks are shown in Figure 1 and 2. A pronounced continental climate prevails in Ambala for most of the year where winters are considerably cold, and summers very hot. The temperatures in May and June may reach to above 46°C, while in winters can drop as low as 2°C (Paul et al., 2014). Ambala experiences both a tropical and a semi-arid climate. Thirty percent of the yearly rainfall occurs between December and February, and seventy percent occurs between July and September months with average rainfall of 47.16 mm (Ambala City Population Census 2011, Haryana) The sediments are made up of medium- and fine-grained sand particles, as well as clays, silts, and gravels in the district's western and southwest regions. The district has thin clay and sand bed inter layers and is located beneath the Ghaggar River basin. The clays are typically sticky to silty with color from brown to yellowish. Ambala, the district headquarter, is roughly 43 km from Chandigarh (U.T.) and 215 km from New Delhi, the Indian capital(Singh, N. et al., 2019). The Tangri, Beghna, and Markanda seasonal streams transverse and drain the Indo-Gangetic alluvium that covers the district (Singh, R., 2014).

MATERIALS AND METHODS

Water samples were collected from 20 different sites in different blocks of Ambala district and analyzed for pH,EC, and TDS as per standard methods (APHA2012& BIS 2012). The sampling was conducted during winter and summer seasons (2021-2022) collecting 40 samples from different locations. All water samples were collected in polypropylene bottles pre-washed with distilled water and 10% nitric acid (HNO_3). Every sample was collected after running the tap for 5 minutes to avoid any major contamination from the pipes and the taps. A portion of each water sample was acidified with 98 % HNO_3 during analysis. The pH of groundwater samples was determined using a portable pH meter at the sampling locations.EC of the samples was determined using the EC 372 (Systronics, India),and the TDS of the samples water was quantified using the Water Quality Analyzer PE 138 (Elico Ltd., Hyderabad, India). Using the inverse distance weighted (IDW) interpolation technique in Arc GIS 10.3 software, the maps were created for observed data. Water quality data sets are spatially represented using the geographic information system (GIS) method to create maps and perform geographical comparisons of the data.

RESULTS AND DISCUSSION

The maps displaying the levels of pH, EC and TDS in supply water are shown in figures (Figure 3-8) covering six blocks in the Ambala district being utilized for both drinking and irrigation. Arc GIS software was used to create the maps of the collected data on supply water quality for this region.

pH variations

One of the key elements affecting water quality is pH, which decides the acidic or alkaline nature of water. (Table - 1).The pH values had a mean of 7.6 and varied from 6.9 to 8.4in winter 2021 and ranged 6.8 to 7.9 with a mean value of 7.3 in summer 2022.Values remained within the range according to WHO and BIS during both the seasons. Figure 3, shows the mapping of pH levels in different blocks of Ambala district during winter (2021) and summer (2022).

Electrical conductivity

Electrical conductivity, measures (μS/cm) the water capacity to conduct electrical current. Water may conduct electricity because it contains ions like sodium, potassium, and chloride etc. It is an indirect measure of total dissolved salts content. The amount of ions present, and the temperature of water are crucial components of the conductivity measurements. In present study the EC values ranged between 334 and 1885 (μS/cm) in year 2021 and 446 and 1576 (μS/cm) in year 2022, with corresponding mean values of 625.85 and 744.05 (μS/cm). The allowed EC value for drinking water, according to WHO (2011) standards, is 750 (μS/cm). EC values measured during 2021-2022 were found to be higher at some areas than the regulatory limits at some sites.EC values were are out of range in year 2021-2022.

Total dissolved solid (TDS)

Soluble solids are the mineral components that are dissolved in water. Natural water typically contains < 500 mgl^{-1} of dissolved solids, whereas water that contains greater than this amount is considered unsuitable for consumption as well as several industrial uses. Water containing a TDS content of < 300 $mgL^{-1}$is ideal for pulp paper, plastics, and textile dyeing. The total concentration of dissolved minerals in the water is broad indicator of the water's overall fitness for a variety of uses. Solar distillation, electro dialysis, ion exchange, and reverse osmosis methods are frequently used for removing TDS. TDS represents the amount of non-volatile chemicals in colloidal and molecularly dispersed form that are present in the water. Water contains a wide range of dissolved inorganic substances in varying concentrations because of surface and subsurface movements. It all comes down to the concentration of NaCl, which controls the conductivity and affects TDS. In 2021, TDS values ranged 200.4-1131 mgL^{-1} with a mean value 375.51 mgL^{-1}. In 2022, TDS values ranged from 267.6 – 945.6 mgL^{-1} with a mean value 448.21 mgL^{-1}. At some sites TDS values were out of range according to BIS and WHO Mapping of TDS levels for 2021 and 2022are shown in (Figure- 7 and 8).

CONCLUSION

In order to look into the water quality for irrigation and drinking, the criteria pertaining to groundwater quality were examined. To visualise the water quality data. Arc GIS software was utilized for mapping and analysis of data. In several blocks of the Ambala district, where industrial and agricultural practices predominate, high levels of EC and TDS were detected in winter and summer months of 2021-2022. The current finding can be utilized to check the suitability of water for irrigation and domestic consumption.

ACKNOWLEDGEMENTS

The authors are thankful to the officials at MM(DU),Mullana for providing research lab facilities to carry out this investigation.

REFERENCES

1. APHA, 2023. Standard Methods for the Examination of Water and Wastewater, 23rd ed. American Public Health Association, American Water Works Association, Water Environment Federation. https://doi.org/10.3769/radioisotopes.62.423.
2. Balogun, M.A., Anumah, A.O., Adegoke, K.A. and Maxakato, N.W., 2022. Environmental health impacts and controlling measures of anthropogenic activities on groundwater quality in Southwestern Nigeria. *Environmental Monitoring and Assessment*, (5), 194-384.https://doi.org/10.1007/s10661-022-09805-z.
3. BIS, I., 2012. 10500: 2012. Indian standard drinking water-specification (second revision), Bureau of Indian Standards, New Delhi.
4. Bodrud-Doza, M., Islam, S.D.U., Rume, T., Quraishi, S.B., Rahman, M.S. and Bhuiyan, M.A.H., 2020. Groundwater quality and human health risk assessment for safe and sustainable water supply of Dhaka City dwellers in Bangladesh. *Groundwater for sustainable development*, *10*, 100374.https://doi.org/10.1016/j.gsd.2020.100374
5. CGWB (2014). Dynamic ground water resources of India, (as on 31st March 2011). Central Ground Water Board Ministry of Water Resources, River Development & Ganga Rejuvenation Government of India.
6. Dutta, N., Thakur, B.K., Nurujjaman, M., Debnath, K. and Bal, D.P., 2022. An assessment of the water quality index (WQI) of drinking water in the Eastern Himalayas of South Sikkim, India. *Groundwater for Sustainable Development*, *17*, 100735.https://doi.org/10.1016/j.gsd.2022.100735
7. Gaagai, A., Aouissi, H.A., Bencedira, S., Hinge, G., Athamena, A., Heddam, S., Gad, M., Elsherbiny, O., Elsayed, S., Eid, M.H. and Ibrahim, H., 2023. Application of water quality indices, machine learning approaches, and GIS to identify groundwater quality for irrigation purposes: a case study of Sahara Aquifer, Doucen Plain, Algeria. *Water*, *15*(2), 289.https://doi.org/10.3390/w15020289
8. Ismanto, A., Hadibarata, T., Widada, S., Indrayanti, E., Ismunarti, D.H., Safinatunnajah, N., Kusumastuti, W., Dwiningsih, Y. and Alkahtani, J., 2023. Groundwater contamination status in Malaysia: level of heavy metal, source, health impact, and remediation technologies. *Bioprocess and BiosystemsEngineering*, *46*(3), 467-482.https://doi.org/10.1007/s00449-022-02826-5.
9. Khapra, R. and Singh, N., 2023. Physical, chemical, and biological evaluation of domestic laundry greywater discharges to attract reclamation strategies and reuse applications in urban settings. *Environmental Quality Management*.https://doi.org/10.1002/tqem.22110.
10. Mazinder Baruah, P. and Singh, G., 2022. Assessment of potability of minewater pumped out from Jharia Coalfield, India: an integrated approach using integrated water quality index, heavy metal pollution index, and multivariate statistics. *Environmental Science and Pollution Research*, 1-16.https://doi.org/10.21203/rs.3.rs-809314/v1
11. Misra, P. and Paunikar, V.M., 2023. Healthy Drinking Water as a Necessity in Developing Countries Like India: A Narrative review. *Cureus*, *15*(10). DOI: 10.7759/cureus.47247
12. Mohamed, A.K., Liu, D., Song, K., Mohamed, M.A., Aldaw, E. and Elubid, B.A., 2019. Hydrochemical analysis and fuzzy logic method for evaluation of groundwater quality in the North Chengdu Plain, China. *International Journal of Environmental Research and Public Health*, *16*(3), 302. https://doi.org/10.3390/ijerph16030302.
13. Mukherjee, S., Sundberg, T. and Schütt, B., 2020. Assessment of water security in socially excluded areas in Kolkata, India: An approach focusing on water, sanitation and hygiene. *Water*, *12*(3), 746. https://doi.org/10.3390/w12030746
14. Paul, S. and Singh, O.P., 2014.A study on trends in meteorological parameters over Punjab and Haryana.MAUSAM, 65(4), 603-608.
15. Prieto-Amparán, J.A., Rocha-Gutiérrez, B.A., Ballinas-Casarrubias, M.D.L., Valles-Aragón, M.C., Peralta-Pérez, M.D.R. and Pinedo-Alvarez, A., 2018. Multivariate and spatial analysis of physicochemical parameters in an irrigation district, Chihuahua, Mexico. *Water*, *10*(8), 1037.https://doi.org/10.33 90/w10081037.
16. Sajjad, M.M., Wang, J., Afzal, Z., Hussain, S., Siddique, A., Khan, R., Ali, M. and Iqbal, J., 2023. Assessing the Impacts of Groundwater Depletion and Aquifer Degradation on Land Subsidence in Lahore, Pakistan: A PS-

InSAR Approach for Sustainable Urban Development. *Remote Sensing*, *15*(22), 5418.https://doi.org /10.3390/rs15225418

17. Saqib, N., Rai, P.K., Kanga, S., Kumar, D., Đurin, B. and Singh, S.K., 2023. Assessment of Ground Water Quality of Lucknow City under GIS Framework Using Water Quality Index (WQI). *Water*, *15*(17), 3048.https://doi.org/10.3390/w15173048
18. Satpathy S, Jha R. Intermittent water supply in Indian cities: considering the intermittency beyond demand and supply. AQUA—Water Infrastructure, Ecosystems and Society. 2022 71(12), 1395-407.https://doi.org/10.2166/aqua.2022.149.
19. Shutaleva, A., Nikonova, Z., Savchenko, I. and Martyushev, N., 2020. Environmental education for sustainable development in Russia. *Sustainability*, *12*(18), 7742.https://doi.org/10.3390/su12187742
20. Singh, N. and Singh, D.P., 2019. Total Quality Management: An Important Growth Strategy For Small-Scale Scientific Instrument Industry Of Ambala. *Think India Journal*, *22*(14), 324-331.
21. Singh, N., Bala, R. and Poonia, T., 2023. Hydrochemistry of drinking water sources and water purifiers in relation to epidemiological study in Hisar, North-West India. *Environmental Quality Management*.https:// doi.org/10.1002/tqem.21977.
22. Singh, N., Kamboj, S., Siwal, S.S., Srivastav, A.L. and Naresh, R.K., 2024. Toxic, non-toxic, and essential elements in drinking water: sources and associated health issues in rural Asia. In *Water Resources Management for Rural Development*, Elsevier. 171-190.https://doi.org/10.1016/B978-0-443-18778-0.00012-X
23. Singh, N., Poonia, T., Siwal, S.S., Srivastav, A.L., Sharma, H.K. and Mittal, S.K., 2022. Challenges of water contamination in urban areas. In *Current directions in water scarcity research*, Elsevier (6, 173-202). https://doi.org/10.1016/B978-0-323-91838-1.00008-7
24. Singh, R., 2014. Challenges in recovery Phase related to Floods: Case Study of District Ambala, Haryana, India. 3(6), 92-98.
25. World Health Organization (WHO), Guidelines for Drinking-Water Quality, fourth ed., 2011. Geneva, Switzerland.
26. Yasmeen, Q. and Yasmeen, S., 2023. Impact of Drinking Water on People's Health and Water Borne Diseases: Impact of Drinking Water on People's Health. *Pakistan BioMedical Journal*, .31-35.https://doi.org/10.54393/pbmj.v6i07.867
27. Zahran, H., Ali, M.Z., Jadoon, K.Z., Yousafzai, H.U.K., Rahman, K.U. and Sheikh, N.A., 2023. Impact of Urbanization on Groundwater and Surface Temperature Changes: A Case Study of Lahore City. *Sustainability*, *15*(8), 6864.https://doi.org/10.3390/su15086864

Table 1: Grid locations and abbreviations of sampling sites selected from different locks of Ambala District in Haryana

Block Name	Site Name	Site Abbreviation	Latitude	Longitude
Barara	Holi	S_1	30.235277	77.071556
	Dosadka	S_2	30.290048	77.113397
	Mullana	S_3	30.275337	77.049278
	Sohana	S_4	30.280845	76.951791
Saha	Kalpi	S_5	30.294482	76.988794
	Saha	S_6	30.300613	76.967186
	Tepla	S_7	30.306392	76.946268
	Dhakola	S_8	30.280598	76.973487
Shahzadpur	Patherari	S_9	30.415204	77.027899
	Shahzadpur	S_{10}	30.446484	77.033943
	Bhundmajra	S_{11}	30.440053	77.038965

	Majra	S_{12}	30.442322	77.032984
Naraingarh	Bara-garh	S_{13}	30.460031	77.064972
	Badi – Basi	S_{14}	30.470678	77.072202
	Choti-Basi	S_{15}	30.462239	77.086309
	Chajal–Majra	S_{16}	30.458244	77.082691
Ambala	Sullar	S_{17}	30.316313	76.700875
	Ballana	S_{18}	30.320678	76.728512
	Ambala Cantonment	S_{19}	30.339599	76.830023
	Ambala City	S_{20}	30.378180	76.776695

Table 2.Chemical variation of parameters analyzedin supply water Samples during 2021- 2022

	2021			**2022**		
Sampling sites	pH	**EC (µS/cm)**	**TDS(mgL^{-1})**	pH	**EC (µS/cm)**	**TDS(mgL^{-1})**
S_1	7.9	344	206.4	7.9	446	267.6
S_2	7.7	334	200.4	7.8	549	329.4
S_3	7.8	360	216	7.9	526	315.6
S_4	7.7	345	207	7.8	546	327.6
S_5	7.7	478	286.8	7.3	1073	643.8
S_6	7.1	543	325.8	7.8	521	312.6
S_7	7.2	498	298.8	7.2	519	311.4
S_8	7.6	525	315	7.7	533	319.8
S_9	7.6	636	381.6	6.9	688	-
S_{10}	7.5	629	377.4	7.5	614	368.4
S_{11}	6.9	590	354	7.1	816	489.6
S_{12}	7.2	582	349.2	7.2	605	363
S_{13}	7.65	545	327	7.2	549	329.4
S_{14}	7.61	754	452.4	7.3	759	455.4
S_{15}	7.8	547	328.2	7.5	572	343.2
S_{16}	7.5	557	334.2	7.3	759	455.4
S_{17}	8.4	526	315.6	6.8	1027	616.2
S_{18}	8.1	471	282.6	7.1	1059	635.4
S_{19}	7.6	1885	1131	7	1144	686.6
S_{20}	7.4	1368	820.8	6.9	1576	945.6
Mean	7.60	625.85	375.51	7.36	744.05	448.21
Median	7.60	544	326.4	7.3	609.5	363
S.D.	0.3466	368.2	220.9	0.356001	291.1692	179.31
Min	6.9	334	200.4	6.8	446	267.6
Max	8.4	1885	1131	7.9	1576	945.6

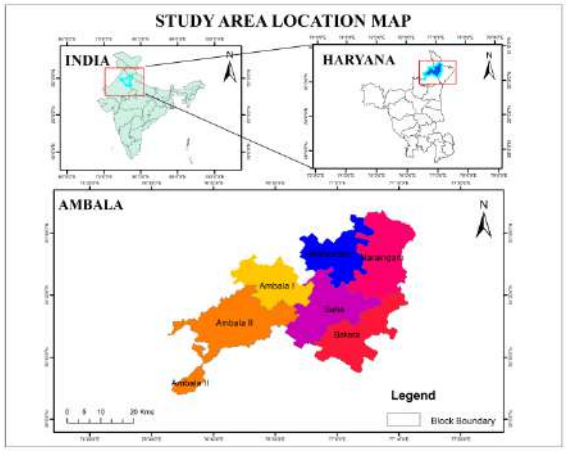

Figure 1: Location of Ambala, India and different blocks of Ambala Districts.

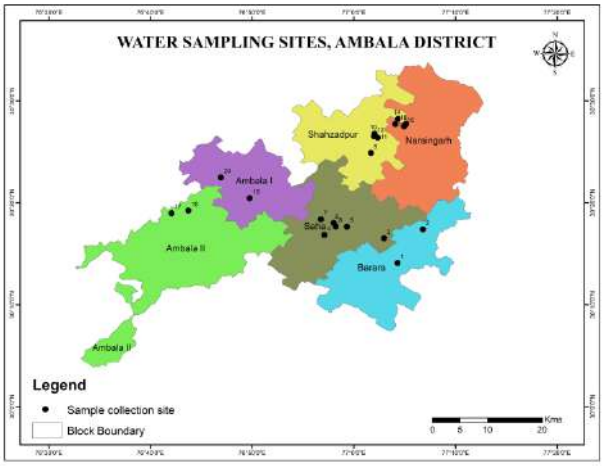

Figure 2: Water sampling sites in different blocks of Ambala.

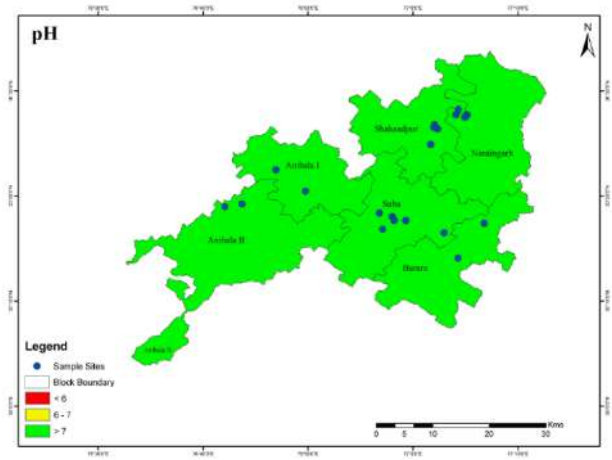

Figure 3. Mapping of pH in different blocks of Ambala district in 2021 (winter).

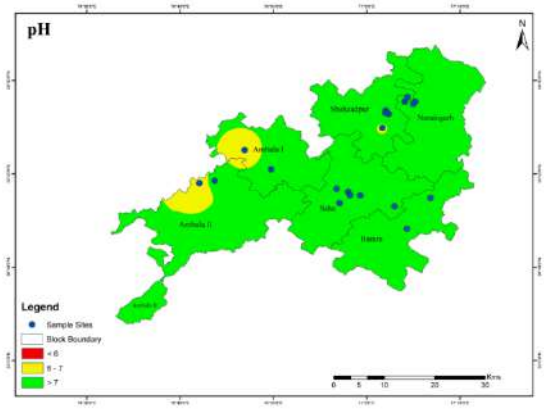

Figure 4. Mapping of pH in different blocks of Ambala district in 2022 (summer).

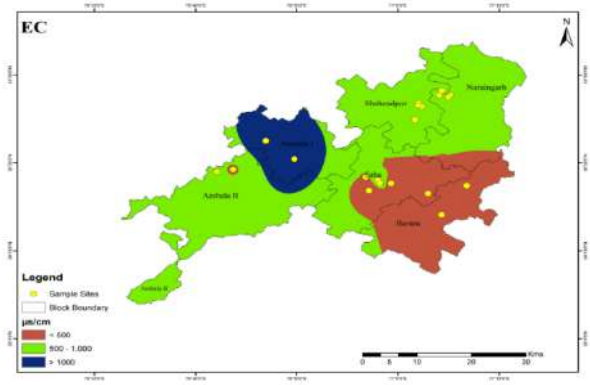

Figure -5 Mapping of EC in different blocks of Ambala district in winters 2021.

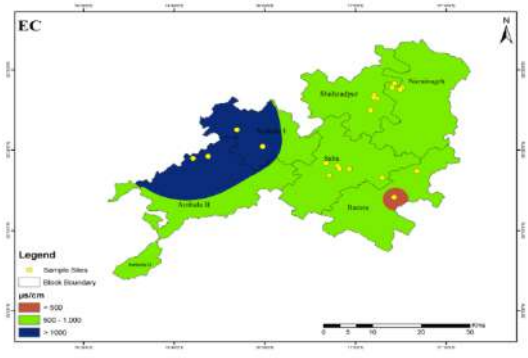

Figure -6 Mapping of EC in different blocks of Ambala district in summer 2022.

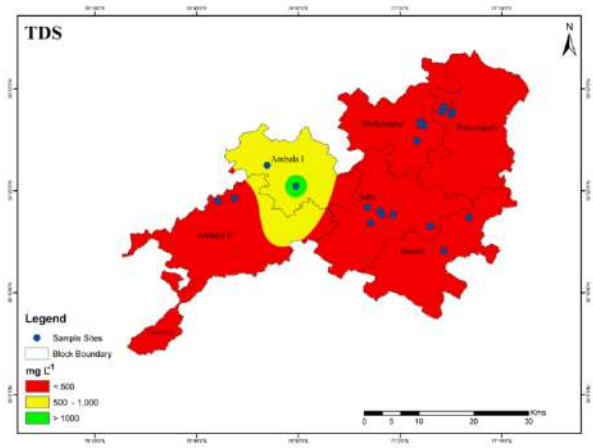

Figure-7 Mapping of TDS in different blocks of Ambala district in year 2021.

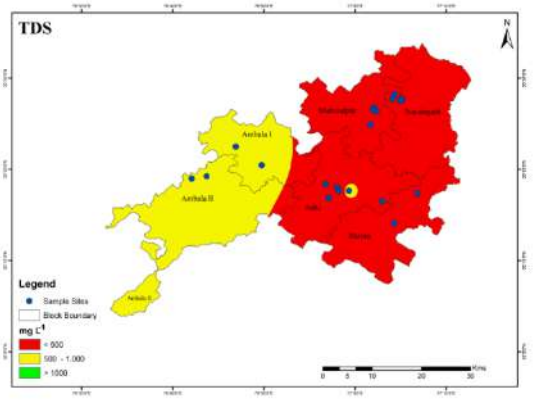

Figure8. Mapping of TDS in different blocks of Ambala district in year 2022.

Indian Journal of Natural Sciences *www.tnsroindia.org.in ©IJONS*

Vol.15 / Issue 83 / Apr / 2024 *International Bimonthly (Print) – Open Access* *ISSN: 0976 – 0997*

RESEARCH ARTICLE

Fluorine-Free Hydrophobic Coating on Polyurethane Foam for Oil Spill Absorption from Water Surface

Lipika and Arun K. Singh*

Department of Chemistry, M. M. Engineering College, Maharishi Markandeshwar (Deemed to be University), Mullana, Ambala, Haryana 133207, India.

Received: 30 Dec 2023 Revised: 09 Jan 2024 Accepted: 12 Jan 2024

***Address for Correspondence**
Arun K. Singh
Department of Chemistry,
M. M. Engineering College,
Maharishi Markandeshwar (Deemed to be University),
Mullana, Ambala, Haryana 133207, India.
Email: arunkumar.singh@mmumullana.org

ABSTRACT

In this study, polyurethane foam was functionalized by Fe_3O_4 nanoparticles and calcium stearate (CS) as a coating material to produce hydrophobic and magnetic material applicable in separating oil/water mixtures. Scanning electron microscopy (SEM), Fourier-transform infrared spectroscopy (FTIR) techniques-based analysis and water contact angle (WCA) measurement were performed to examine the surface characteristics properties of coated foam. With a water contact angle of 135º, the created foam demonstrated good hydrophobicity. The as-prepared coated foam exhibited good selective sorption capacity of oils and organic solvents from contaminated water surfaces. The prepared hydrophobic foam along with the incorporation of Fe_3O_4 nanoparticles was easily separable from treated oil/water mixtures with the use of simple conventional magnet. This study provides promising approach for the fabrication of hydrophobic and magnetic foam without use of any fluorinated coating materials.

Keywords: Hydrophobic; Oil/water mixtures, Magnetic foam, Absorption capacity

INTRODUCTION

The rapid growth in global industrialization is one of the significant reasons for the pollution in aquatic environment [1] [2]. For instance, oily contamination in aquatic body causes several adverse effects on aquatic ecosystem, leads to the water pollution and scarcity [3][4] [5]. In the recent past, several artificial surfaces with special wetting behavior such as hydrophobic and oleophilic behavior attracted wide attention for the remediation of oily contaminated water. Fabrication of such kind of super hydrophobic/ oleophilic surfaces resolves the adverse outcomes coming out from spilling of oil directly into the water and separation of oil from the water is the urgent need for the environment [6] [7].

Currently various other techniques are used to depart oil from the oil/ water emulsion but are time taken, difficult to proceed and causes secondary pollution [8]. Foam has been used widely in the process of separating oil/water mixtures because of its three-dimensional structure[9]. Foam technology, with its elastic form, high porosity, mechanical durability, and cost-effectiveness, has earned significant interest in improving absorption capacity and streamlining oil recovery processes [10] [11] [12] . Excellent reusability, outstanding absorption capacity, and superior anti-wetting qualities are essential for the ideal absorbent material for the oil recovery process [13]. Water quality deteriorates as a result of many toxins that are present in it as a result of excessive industrial activity[14]. Contaminated oily waste water presents a serious risk to the ecosystem when it is disposed of in fresh water[15] [17]. It is currently a big problem to remove greasy materials from the water[18]. To change the hydrophilic properties of polyurethane foam s into hydrophobic ones, dangerous substances as fluorinated have been employed [19][20][21].

However, fluorinated compounds required various toxic solvents for the fabrication of hydrophobic surfaces [22]. `To eliminate greasy waste from water in a way that is easy to use, affordable, and environmentally beneficial, the creation of a fluorine-free unique wettable surface has gained significance [22] [23] . Oil/water separation, anti-fouling, self-cleaning, anti-microbial, anti-scaling, and anti-fogging are only a few of the applications for which the creation of superhydrophobic surfaces has become increasingly important [24] [25] [26]. In this work, non-fluorinated calcium stearate and Fe_3O_4 magnetic nanoparticles were used to generate hydrophobic surface coating on polyurethane foam with excellent magnetic behavior. Fe_3O_4 magnetic nanoparticles (NPs) were synthesized via co-precipitation approach in a basic medium [10]. Calcium stearate based coating material was used in order to provide hydrophobicity and lowering the surface energy. In addition, functionalization of Fe_3O_4 was performed in order to provide magnetically separation ability in foam from treated water [27]. The selective oily or organic solvents separation ability of the as-prepared modified foam was examined in various oils-organic solvents/water mixtures.

Experimental section

Materials and methods

Calcium stearate and cyclohexanol was purchased from central drug house private limited. Toluene was supplied by the Molychem. Ferric chloride hexahydrate ($FeCl_3.6H_2O$, ≥ 97%), Ferrous sulfate heptahydrate ($FeSO_4{\cdot}7H_2O$, ≥ 98 %) and sodium hydroxide were purchased from the Loba chemie private limited. Commercial foam was purchased from local general store and rinsed with acetone and dried at room temperature for 30 min. Several oils and organic solvent were used to determine the absorption capacity such as diesel oil, engine oil, olive oil, soybean oil, n-hexane, n-heptane.

Fabrication of Magnetic polyurethane foam

The fabrication of water repellent coatings on polyurethane foam was accomplished with the help of dip coating technique. Initially, Ferrous sulfate heptahydrate and Ferric chloride hexahydrate is added in 40 ml of deionized water in molar proportion of 2:1 respectively and allowed to stirred for about 60 min. The sodium hydroxide is added to the mixture slowly until the pH of the solution reaches 11 and continued for stirring for 1 h for complete reaction. The clean small pieces of foam were done now dipped into the prepared magnetic mixture and allowed to stir for 15 min on magnetic stirrer. Finally, dipped polyurethane foam placed in hot air oven for 8 h and then dried at 60 ℃ for 1 h. Thus, obtained coated foam are considered as magnetic polyurethane foam.[28]

Fabrication of magnetic superhydrophobic foam

The calcium stearate coated polyurethane foam was fabricated by simple dip-coating approach by preparing the homogenous solution of 3% calcium stearate in toluene and cyclohexanol in volumetric ratio of 9:1. To decompose calcium stearate in the above mixture, heat the mixture along with continuous stirring up to 110º C. Subsequently, when the temperature decreases to 80º C, dipped the above prepared magnetic polyurethane foam into it for 5 sec and then kept for drying at 80º C for 1 h. Therefore, the fabricated foam is now regarded as magnetic hydrophobic foam.

Characterization

The surface morphological properties of the modified polyurethane foam were examined by field emission scanning electron microscopy along with energy dispersive X-ray technique [29]. FTIR spectrometer was utilized for the determination of chemical composition on the coated and uncoated foam in the range of 400 cm^{-1} to 4000 cm^{-1}[30]. The water repellent ability and coating durability will be examined through some scientific terms i.e., water contact angle/oil contact angle with the help of instrument known as goniometer which works on the principle of sessile liquid drop method [31].

RESULTS AND DISCUSSION

Surface morphology and chemical composition

An energy dispersive X-ray (EDS) detector and scanning electron microscopy (SEM) were utilized to investigate the elemental composition and surface morphology of coated and uncoated polyurethane foam [32] . The high-resolution FESEM spectroscopic tool has been used to investigate the surface morphology [33] and observe that the three-dimensional network-like structure of the magnetic PU foam was very porous and linked (Fig. 3a-b). High magnification SEM images made it evident that Fe_3O_4 nanoparticles were distributed randomly within the PU foam's porous structure, creating a hierarchical micro/nano structure [34]. Unmodified foam has a smoother surface than modified ones [9] . The foam have lower surface energy after being treated with calcium stearate coating solution which causes the surface to become hydrophobic[35]. The presence of Fe, Ca, and C was observed in the EDS spectra of the modified coated foam as compared to unmodified foam as shown in Fig. 3c-d. We observed two peaks at 2848 cm^{-1}, 2915cm^{-1} and1464$cm^{-1}$the FTIR spectra of modified foam, corresponding to the C-H stretching vibrations and absorption peak between 1500- 1700cm^{-1} due to symmetric and asymmetric stretching vibrations of coordinated carboxyl group in $Ca(CH_3(CH_2)_{16}COO)_2$[36]. Magnetic Fe_3O_4 nanoparticles have a characteristic peak that is linked to the absorption bands at around 555 cm^{-1} (Fig.4) [9].

Evaluation of super hydrophobicity of the coated material

The water repellent ability of coated magnetic hydrophobic foam was examined by measuring water contact angle with the help of contact angle goniometer instrument via sessile drop technique at room temperature.[37] Water contact angle was measured at several diverse angle and the average value of the contact angle were taken. The water contact angle of fabricated surface was found to be.

Application in oil/water separation

In order to examined the oil/water separation capability of the coated polyurethane sponge from oil/water mixture, absorption experiments were conducted. In this experiment work, n-hexane/water, n-heptane/water, toluene/water, diesel oil/water, engine oil/water, olive oil/water, soyabean oil/water were taken (1:1 v/v) in which water was dyed with methylene blue. The oil/water mixture in 1:1 ratio was stirred vigorously for 5 min. Now, weighed amount of coated foam dipped into the oil/water mixture with continuous stirring for 5 to 7 min. and then note down the absorbed weight of the foam to calculate the absorption capability of the coated foam. In addition, the whole experimental procedure was repeated three times to calculate the mean value of absorption capacity of the coated material [38]. The oil absorption capacity was calculated by the mathematical expression. [39] [40]. The absorption capacities of the prepared hydrophobic coated foam are summarized (Table 1 and Fig. 6) with respect different oils and organic solvents.

$$K = \frac{M_1 - M_0}{M_0}$$

Where, m_0= weight of foam before absorption

m_1= weight of foam after absorption

K= absorption capacity

CONCLUSION

A super hydrophobic/superoleophillic magnetic polyurethane (PU) foam was prepared by the functionalization with Fe_3O_4 nanoparticles and surface modification using calcium stearate based coating materials. Dip coating approach was adopted to prepare hydrophobic foam from unmodified. The developed modified foam exhibited good selective absorption capacity in the range of 13.9–50.7 g/g with respect to various oils or organic solvents from water surface. Thus results of the study inferred that as-prepared magnetic hydrophobic polyurethane foam showed excellent ability as adsorbent for oils and organic solvents from contaminated water surface.

ACKNOWLEDGEMENTS

The authors acknowledge the support from the Department of Chemistry, and Research & Development Cell of Maharishi Markandeshwar (Deemed to be University), Mullana, Ambala, Haryana, India.

REFERENCES

1. S. Liang et al., "A facile approach to fabrication of superhydrophilic ultrafiltration membranes with surface-tailored nanoparticles," Sep. Purif. Technol., vol. 203, no. March, pp. 251–259, 2018, doi: 10.1016/j.seppur.2018.04.051.
2. Q. Tian, F. Qiu, Z. Li, Q. Xiong, B. Zhao, and T. Zhang, "Structured sludge derived multifunctional layer for simultaneous separation of oil/water emulsions and anions contaminants," J. Hazard. Mater., vol. 432, no. February, 2022, doi: 10.1016/j.jhazmat.2022.128651.
3. J. Huang and Z. Yan, "Adsorption Mechanism of Oil by Resilient Graphene Aerogels from Oil-Water Emulsion," Langmuir, vol. 34, no. 5, pp. 1890–1898, 2018, doi: 10.1021/acs.langmuir.7b03866.
4. M. P. Sathianarayanan and K. Hemani, "Development of Bio-degradable Cotton Waste based Super Oleophilic and Super Hydrophobic Sorbent for Oil Spill Clean-up," J. Inst. Eng. Ser. E, vol. 102, no. 2, pp. 215–226, 2021, doi: 10.1007/s40034-021-00211-7.
5. W. Zhang et al., "Polyacrylamide-Polydivinylbenzene Decorated Membrane for Sundry Ionic Stabilized Emulsions Separation via a Facile Solvothermal Method," ACS Appl. Mater. Interfaces, vol. 8, no. 33, pp. 21816–21823, 2016, doi: 10.1021/acsami.6b07018.
6. H. P. Ngang, A. L. Ahmad, S. C. Low, and B. S. Ooi, "Preparation of thermoresponsive PVDF/SiO2-PNIPAM mixed matrix membrane for saline oil emulsion separation and its cleaning efficiency," Desalination, vol. 408, pp. 1–12, 2017, doi: 10.1016/j.desal.2017.01.005.
7. X. Gong et al., "Construct a stable super-hydrophobic surface through acetonitrile extracted lignin and nano-silica and its application in oil-water separation," Ind. Crops Prod., vol. 166, no. April, p. 113471, 2021, doi: 10.1016/j.indcrop.2021.113471.
8. Y. Sun et al., "Simultaneously achieving high-effective oil-water separation and filter media regeneration by facile and highly hydrophobic sand coating," Sci. Total Environ., vol. 800, 2021, doi: 10.1016/j.scitotenv.2021.149488.
9. P. Jiang, K. Li, X. Chen, R. Dan, and Y. Yu, "Magnetic and hydrophobic composite polyurethane sponge for oil-water separation," Appl. Sci., vol. 10, no. 4, 2020, doi: 10.3390/app10041453.
10. A. A. Alazab and T. A. Saleh, "Magnetic hydrophobic cellulose-modified polyurethane filter for efficient oil-water separation in a complex water environment," J. Water Process Eng., vol. 50, 2022, doi: 10.1016/j.jwpe.2022.103125.
11. Z. T. Li, F. A. He, and B. Lin, "Preparation of magnetic hydrophobic melamine sponge for oil-water separation,"Powder Technol., vol. 345, pp. 571–579, 2019, doi: 10.1016/j.powtec.2019.01.035.
12. Z. Yin et al., "An environmentally benign approach to prepare superhydrophobic magnetic melamine sponge for effective oil/water separation," Sep. Purif. Technol., vol. 236, 2020, doi: 10.1016/j.seppur.2019.116308.

13. F. Beshkar, H. Khojasteh, and M. Salavati-Niasari, "Recyclable magnetic superhydrophobic straw soot sponge for highly efficient oil/water separation," J. Colloid Interface Sci., vol. 497, pp. 57–65, 2017, doi: 10.1016/j.jcis.2017.02.016.
14. B. Zhao, L. Ren, Y. Du, and J. Wang, "Eco-friendly separation layers based on waste peanut shell for gravity-driven water-in-oil emulsion separation," J. Clean. Prod., vol. 255, 2020, doi: 10.1016/j.jclepro.2020.120184.
15. Q. Fan et al., "Bio-based materials with special wettability for oil-water separation," Sep. Purif. Technol., vol. 297, no. May, p. 121445, 2022, doi: 10.1016/j.seppur.2022.121445.
16. W. Bigui et al., "Fabrication of superhydrophilic and underwater superoleophobic quartz sand filter for oil/water separation," Sep. Purif. Technol., vol. 229, 2019, doi: 10.1016/j.seppur.2019.115808.
17. J. J. Li, Y. N. Zhou, and Z. H. Luo, "Polymeric materials with switchable superwettability for controllable oil/water separation: A comprehensive review," Prog. Polym. Sci., vol. 87, pp. 1–33, 2018, doi: 10.1016/j.progpolymsci.2018.06.009.
18. J. Usman et al., "An overview of superhydrophobic ceramic membrane surface modification for oil-water separation," J. Mater. Res. Technol., vol. 12, pp. 643–667, 2021, doi: 10.1016/j.jmrt.2021.02.068.
19. A. K. Singh and J. K. Singh, "Fabrication of zirconia based durable superhydrophobic-superoleophilic fabrics using non fluorinated materials for oil-water separation and water purification," RSC Adv., vol. 6, no. 105, pp. 103632–103640, 2016, doi: 10.1039/c6ra24460b.
20. Lipika and A. K. Singh, "Polydimethylsiloxane based sustainable hydrophobic/oleophilic coatings for oil/water separation: A review," Clean. Mater., vol. 6, no. April, p. 100136, 2022, doi: 10.1016/j.clema.2022.100136.
21. S. Barthwal and S. H. Lim, "A durable, fluorine-free, and repairable superhydrophobic aluminum surface with hierarchical micro/nanostructures and its application for continuous oil-water separation," J. Memb. Sci., vol. 618, no. August 2020, p. 118716, 2021, doi: 10.1016/j.memsci.2020.118716.
22. H. Zhang, C. Zhao, Y. Yang, Y. Sheng, and S. Peng, "Fluorine-free fabrication of a magnetic-responsive sponge as absorbent for highly efficient and ultrafast oil-water separation," Thin Solid Films, vol. 751, 2022, doi: 10.1016/j.tsf.2022.139205.
23. B. Du et al., "Superhydrophobic Surfaces with pH-Induced Switchable Wettability for Oil-Water Separation," ACS Omega, vol. 4, no. 15, pp. 16508–16516, 2019, doi: 10.1021/acsomega.9b02150.
24. Z. T. Li et al., "Effective preparation of magnetic superhydrophobic Fe 3 O 4 /PU sponge for oil-water separation," Appl. Surf. Sci., vol. 427, pp. 56–64, 2018, doi: 10.1016/j.apsusc.2017.08.183.
25. X. Wang, Z. Han, Y. Liu, and Q. Wang, "Micro-nano surface structure construction and hydrophobic modification to prepare efficient oil-water separation melamine formaldehyde foam," Appl. Surf. Sci., vol. 505, p. 144577, 2020, doi: 10.1016/j.apsusc.2019.144577.
26. P. Chauhan, A. Kumar, and B. Bhushan, "Self-cleaning, stain-resistant and anti-bacterial superhydrophobic cotton fabric prepared by simple immersion technique," J. Colloid Interface Sci., vol. 535, pp. 66–74, 2019, doi: 10.1016/j.jcis.2018.09.087.
27. H. Liu, S. Su, J. Xie, Y. Ma, and C. Tao, "Preparation of superhydrophobic magnetic stearic acid polyurethane sponge for oil-water separation," J. Mater. Res., vol. 35, no. 21, pp. 2925–2935, 2020, doi: 10.1557/jmr.2020.260.
28. A. K. Singh, K. Ketan, and J. K. Singh, "Simple and green fabrication of recyclable magnetic highly hydrophobic sorbents derived from waste orange peels for removal of oil and organic solvents from water surface," J. Environ. Chem. Eng., vol. 5, no. 5, pp. 5250–5259, 2017, doi: 10.1016/j.jece.2017.09.060.
29. N. Ahmad, S. Rasheed, K. Ahmed, S. G. Musharraf, M. Najam-ul-Haq, and D. Hussain, "Facile two-step functionalization of multifunctional superhydrophobic cotton fabric for UV-blocking, self cleaning, antibacterial, and oil-water separation," Sep. Purif. Technol., vol. 306, no. PA, p. 122626, 2023, doi: 10.1016/j.seppur.2022.122626.
30. S. Bayraktaroglu, S. Kizil, and H. Bulbul Sonmez, "A highly reusable polydimethylsiloxane sorbents for oil/organic solvent clean-up from water," J. Environ. Chem. Eng., vol. 9, no. 5, p. 106002, 2021, doi: 10.1016/j.jece.2021.106002.

31. A. K. Singh and J. K. Singh, "Fabrication of durable superhydrophobic coatings on cotton fabrics with photocatalytic activity by fluorine-free chemical modification for dual-functional water purification," New J. Chem., vol. 41, no. 11, pp. 4618–4628, 2017, doi: 10.1039/c7nj01042g.
32. A. K. Singh, K. Ketan, and J. K. Singh, "Graphical Abstract Highlights :," Biochem. Pharmacol., 2017, doi: 10.1016/j.jece.2017.09.060.
33. G. Guo, L. Liu, Q. Zhang, C. Pan, and Q. Zou, "Solution-processable, durable, scalable, fluorine-grafted graphene-based superhydrophobic coating for highly efficient oil/water separation under harsh environment," New J. Chem., vol. 42, no. 5, pp. 3819–3827, 2018, doi: 10.1039/c7nj05182d.
34. S. Liu, Q. Xu, S. S. Latthe, A. B. Gurav, and R. Xing, "Superhydrophobic/superoleophilic magnetic polyurethane sponge for oil/water separation," RSC Adv., vol. 5, no. 84, pp. 68293–68298, 2015, doi: 10.1039/c5ra12301a.
35. A. Verbič et al., "Designing UV-protective and hydrophilic or hydrophobic cotton fabrics through in-situ ZnO synthesis using biodegradable waste extracts," Appl. Surf. Sci., vol. 599, no. May, 2022, doi: 10.1016/j.apsusc.2022.153931.
36. H. Bai, L. Zhang, and D. Gu, "Calcium stearate nanoparticles as building blocks for mechanically durable superhydrophobic coatings," Mater. Chem. Phys., vol. 294, no. May 2022, p. 127040, 2023, doi: 10.1016/j.matchemphys.2022.127040.
37. A. K. Singh, S. Mishra, and J. K. Singh, "Underwater superoleophobic biomaterial based on waste potato peels for simultaneous separation of oil / water mixtures and dye adsorption," Cellulose, vol. 26, no. 9, pp. 5497–5511, 2019, doi: 10.1007/s10570-019-02458-1.
38. M. Peng et al., "Synthesis and application of modified commercial sponges for oil-water separation," Chem. Eng. J., vol. 373, pp. 213–226, 2019, doi: 10.1016/j.cej.2019.05.013.
39. C. F. Wang and S. J. Lin, "Robust Superhydrophobic/superoleophilic sponge for effective continuous absorption and expulsion of oil pollutants from Water," ACS Appl. Mater. Interfaces, vol. 5, no. 18, pp. 8861–8864, 2013, doi: 10.1021/am403266v.
40. A. K. Singh and J. K. Singh, "An efficient use of waste PE for hydrophobic surface coating and its application on cotton fibers for oil-water separator," Prog. Org. Coatings, vol. 131, no. December 2018, pp. 301–310, 2019, doi: 10.1016/j.porgcoat.2019.02.025.

Table 1:Absorption capacities of the prepared hydrophobic coated foam are summarized with respect different oils and organic solvents.

Sr.No	Organic solven	Viscosity (cP	Density (g/cm³	Average value (**g**g⁻¹
1.	n-hexane	0.31 at 25°C	0.66	13.9
2.	n-heptane	0.42 at 25°C	0.68	44.2
3.	Toluene	0.59 at 25°C	0.87	50.27
4.	Soyabean oil	50.09 at 25°C	0.91	14.7
5.	Diesel oil	3.45 at 25°C	0.82	36.95
6.	Engine oil	50 at 23°C	0.96	23.9
7.	Olive oil	84 at 20°C	0.91	34.2

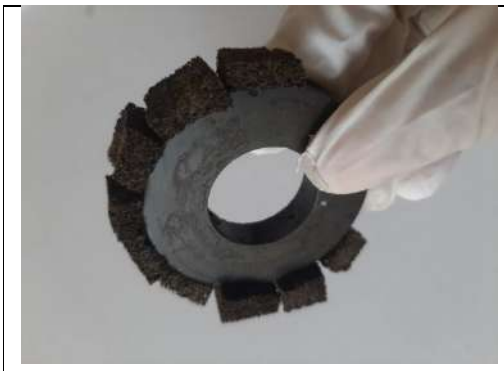

Fig.1 Digital photograph of magnetic polyurethane foam.

Fig.2 Digital photograph of magnetic and hydrophobic foam.

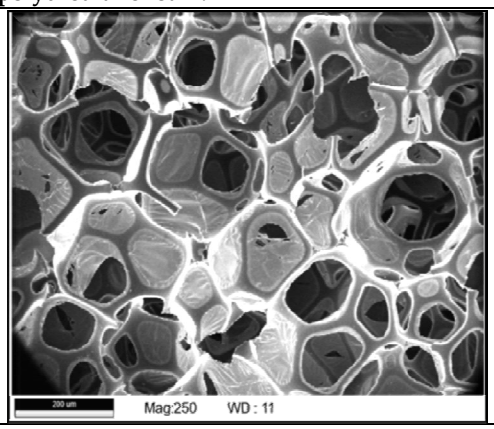

Fig.3a SEM image of unmodified polyurethane foam.

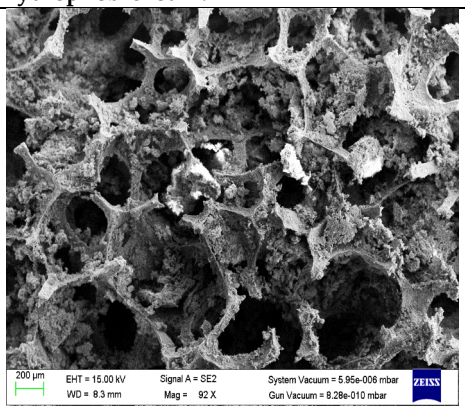

Fig.3b SEM image of modified magnetic hydrophobic polyurethane foam.

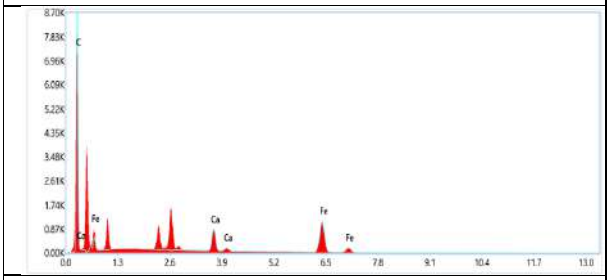

Fig. 3c EDS Spectra of coated magnetic hydrophobic polyurethane foam.

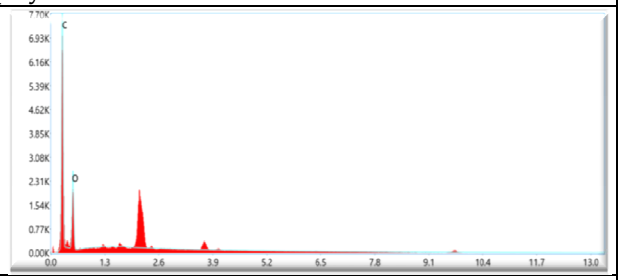

Fig. 3d EDS Spectra of uncoated hydrophilic polyurethane foam.

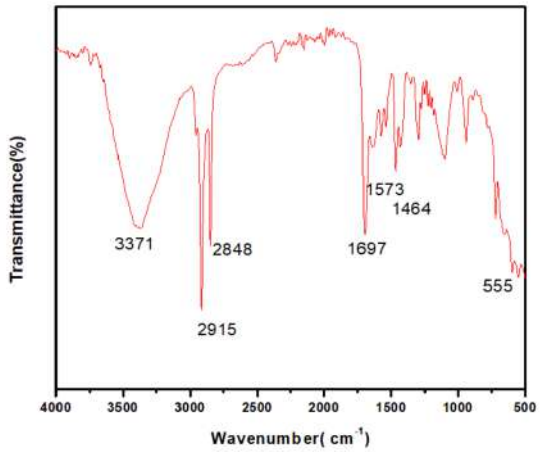

Fig.4 FTIR spectra of modified magnetic hydrophobic polyurethane foam.

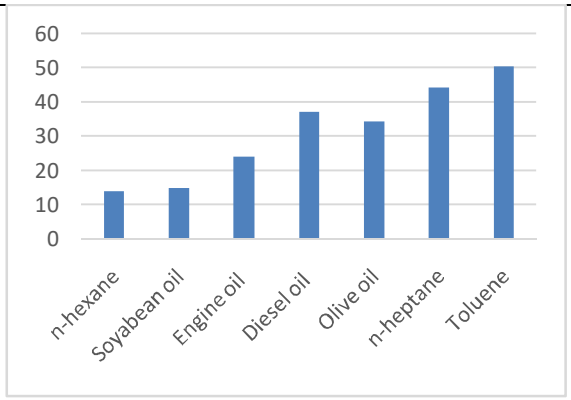

Fig.5 Pictorial representation of absorption capacities of different oils/solvent.

Indian Journal of Natural Sciences *www.tnsroindia.org.in ©IJONS*

Vol.15 / Issue 83 / Apr / 2024 *International Bimonthly (Print) – Open Access* *ISSN: 0976 – 0997*

RESEARCH ARTICLE

Gibberellic Acid Treated Seeds Improves Salinity Induced Inhibition of Germination and Seedling Growth of *Thespesia populnea* (L.) Soland. ex Correa, *Morinda citrifolia* L., and *Markhamia lutea* (Benth.) K.Schum

Preethi Jenifer Praticia.S [1] and Kanchana.M[2]*

[1]Research Scholar, Department of Botany, PSGR Krishnammal College for Women, (Affiliated to Bharathiar University), Coimbatore, Tamil Nadu, India.
[2]Associate Professor, Department of Botany, PSGR Krishnammal College for Women, (Affiliated to Bharathiar University), Coimbatore, Tamil Nadu, India.

Received: 08 Nov 2023 Revised: 11 Jan 2024 Accepted: 11 Mar 2024

***Address for Correspondence**
Kanchana.M
Associate Professor,
Department of Botany,
PSGR Krishnammal College for Women,
(Affiliated to Bharathiar University),
Coimbatore, Tamil Nadu, India.
Email: kanchana09psgrkcw@gmail.com

ABSTRACT

Salinity is one of the abiotic stresses affecting crop productivity, predominantly by inhibiting seed germination. It has been demonstrated that the accumulation of soluble solutes around the seeds increases the osmotic pressure, often leading to excessive uptake of ions and impairing germination. There is some evidence to show that *hormonal priming, primarilytreating seeds with*gibberellic acid (GA_3), is an effective strategy for regulating the germination percentage under saline stresses. Therefore, this study explored the impact of GA_3 application on *Thespesia populnea* (L.) Soland. ex Correa, *Morinda citrifolia* L., *Markhamia lutea* (Benth.) K. Schum seeds under saline conditions. Our results demonstrate that priming seeds with 0.2 g/L GA_3 slightly enhances the germination rate from 71% to 74%. However, the germination rate decreased considerably with the rapid development of shoots and length. In particular, the mass and length of shoots were notably better compared with untreated seeds.

Keywords: Germination Percentage, Gibberellic Acid , Priming, Tolerance,

INTRODUCTION

Salinity is a critical environmental stress affecting plant growth worldwide and one of the top ten threats to the world's soil resources [1];[2]. Previous studies have shown that salinity causes three basal issues for plants. First, excess salt in the soil decreases the osmotic potential, which leads to a reduction in water uptake by plants. Second, a higher amount of Na^+ and Cl_2 ion uptake distracts from the absorption of necessary minerals and imputes toxicity to plants [3]. The salinity has more adverse effects that reduce the growth, development, and yield of the crop by changing the activation of some pre-germination metabolic processes [4]. In this context, salinity affects the crop yield on over 800 million ha of arable land, which accounts for approximately 6% of the total terrestrial land and 10 million ha of agricultural land are destroyed by salt accumulation each year [5]. Seeds are more vulnerable to salinity-induced stress. Typically, seeds require more water intake during germination, which indirectly results in the accumulation of soluble solutes around the seeds, thereby increasing the osmotic pressure. In effect, the osmotic pressure change causes ion toxicity and leads to the assimilation of Na^+ ions [6]. Hence, the ionic imbalance affects the uptake and transport of other essential ions in target cells, which stops the metabolism [7]. Many efforts have been made to improve the salinity and osmotic tolerance of the crop through selective breeding techniques [8]. However, the success rate of crop productivity is limited, and commercialization has also been less successful [9]. To mitigate the changes resulting from salt environment stress, priming, wherein seeds are treated with a chemical substance under controlled conditions, has been considered one of the simplest and most cost-effective techniques [10]; [11].

Seed germination is a complex process that includes events starting with water uptake by the (quiescent) dry seed and culminating with the elongation of the embryonic axis and the emergence of the radicle [12]. Among multiple techniques, seed priming is one of the most effective strategies by which pre-germination can be activated through physiological and chemical processes [6]; [13]. Further, seed priming will improve uniform germination by *decreasing*the imbibition time [14]. Priming treatments can be done by treating seeds with plant growth regulators, buffer solutions, and other chemical substances, e.g., gibberellic acid (GA_3) [12]; [13]. Nevertheless, a practical priming approach is accomplished by treating the seeds with GA_3, which increases the germination of fewer vigorous seeds [15]. Indeed, GA_3 as a plant hormone is known to induce different physiological responses in plants, which are well suited for stimulating and improving germination, plant growth, and photosynthetic activity [16]. Considering the tendencies of growth reduction due to salinity and the progressive efficacy of exogenous GA_3 application on different morphological, physiological, and biochemical activities, it can be described that the application of GA_3 is practical to detract salinity stress and that its effectiveness is more dynamic in salt-tolerant plants [17].

Thespesia populnea (L.) Soland. ex Correa (Malvaceae) most probably originated from the Pacific and Indian Ocean coastlines, the Asian tropics, or even both. It is currently present in coastal locations across the tropics; it is planted in coastal communities and sporadically on land [18].One of the most significant sources of traditional remedies among Pacific Island civilizations is *Morinda citrifolia* L. (Rubiaceae), sometimes known as noni in the commercial sense. It grows widely throughout the Pacific. The diminutive evergreen tree or shrub is native to Australia and Southeast Asia (Indonesia), but it is now found throughout the entire tropical world. [19] and *Markhamia lutea* (Benth.) K. Schum (Bignoniaceae), this species natural habitat ranges from Tanzania and South Sudan to Ghana [20]. In this work, we specifically explored: (1) the germination activity and seedling growth through priming with GA_3in seeds of *Thespesia populnea* (L.) Soland. ex Correa (Malvaceae), *Morinda citrifolia* L. (Rubiaceae), and Markhamia *lutea* (Benth.) K.Schum (Bignoniaceae), and (2) seeds were also treated with two different concentrations of NaCl, characterising their tolerance during germination and early seedling growth.

MATERIALS AND METHODS

Seed Collection

The mature seeds of *Thespesia populnea* (L.) Soland. ex Correa (Malvaceae), *Morinda citrifolia* L. (Rubiaceae), and *Markhamia lutea* (Benth.) K. Schum (Bignoniaceae) were collected from September to December 2020 from the Western Ghats, Sadivayal area in Coimbatore district (11.0168°N, 76.9558°E). The collection site has a mean annual temperature of 26°C, ranging from 32°C in September to 19°C in December. Several hundred seeds were collected from 10 randomly chosen trees located within a 20-km radius by gently shaking the mature trees. Seeds were transported to the laboratory via road on the same day, visually inspected, and any unhealthy seeds or debris were removed. The seed surface was sterilised with a 5% sodium hypochlorite solution for 10 minutes and thoroughly washed with sterile distilled water 4–5 times. The seeds were then bench-dried for a day and subsequently stored in air-tight glass bottles under room temperature and humidity until used in the experiment. Experiments commenced within two weeks of collection.

Hormonal Priming

The seeds were primed by soaking in a 0.2 g/L GA_3 solution for 12 hours at 27°C in complete darkness, achieved by wrapping the Petri dishes with two layers of aluminium foil paper. After priming, seeds were removed and washed in running tap water, then rinsed three times with sterile distilled water. Seeds were blotted dry by placing them between filter papers. After drying, the seeds were kept in Petri dishes containing moist No. 1 Whatman filter paper at room temperature, 27°C. Control seeds (unprimed) are soaked in water for 12 hours, re-dried, and then placed in Petri dishes containing moist No. 1 Whatman filter paper in room temperature at 27°C.

A fully randomised factorial experiment consisting of three replicates of 25 seeds each from the control and primed groups was irrigated with equal volumes of NaCl solutions at two different concentrations: 50 and 100 mM. Physiological parameters such as seed germination percentage and mean germination time (MGT) were calculated by the formulae given below. The shoot and root lengths of all seedlings were measured using a transparent ruler. Shoots and roots were measured using a weighing balance. The separated shoots and roots were dried at 70°C for 12 h, and then dry weights were recorded [21]; [11].

Measurements of Germination Efficiency

Total germination (TG) was measured every day and terminated at day 14 after sowing (Kandil *et al*., 2012). It was computed as:

TG% $=\frac{n}{N}\times 100$, where n is the total germinated seeds, and N is the total seeds sown.

MGT was calculated according to Fuller *et al*.(2012)

$MGT=\frac{\sum(n\times d)}{N}$

Where n is the number of seeds germinated on each day, $d$is the number of days from the beginning of the test, and $N$is the total number of seeds germinated at the termination of the experiment.

The vigour index (VI) was measured using the formula of [9] :

VI= TG% × Seedling length (cm)/100

Statistical Analysis

All data collected from the experiments were subjected to two-way ANOVA using the Statistical Package for the Social Sciences (SPSS, version 20) software, and the difference between means was computed by Fisher's Post Hoc Least Significance Difference Test at $P< 0.05$.

RESULTS AND DISCUSSION

Germination Percentage and Mean Germination Time of the Study Seeds

Experimental results showed that both salinity and treatment with GA_3 noticeably affected the germination percentage as well as Mean Germination Time (MGT) of the three crops, *Thespesia populnea*, *Morinda citrifolia*, and *Markhamia lutea* at $P< 0.05$ (Figures 1–3). The synergistic effect of seed type, GA_3 treatment, and salt concentration also significantly affected the germination percentage as well as the MGT of *Thespesia populnea*, *Morinda citrifolia*, *and Markhamia lutea* at $P< 0.05$. Increasing the salinity concentrations in the germination medium negatively affected the germination percentage and delayed the germination time in all three species. However, the reduction was significantly more noticeable in the unprimed seeds than in the GA_3-primed ones (Figures 1–3). Notably, a high reduction was detected at the highest concentration of 100 mM NaCl. An increase in germination percentage was observed in the treated seeds at 50 mM NaCl salinity. While comparing the untreated seeds of *Markhamia lutea and* Morinda *citrifolia* with the treated ones, they were most affected due to the salinity stress. In addition, the germination rate was also significantly affected. The maximum germination rate was recorded for 0–2 g/L GA3-treated seeds of Thespesia *populnea* at the highest salinity levels (Figures 1–3). The results of the present study are consistent with [22], who showed that plants identified the accumulation of some inorganic ions or organic compounds to balance the osmotic potential against the initial issues of salinity, which causes inhibition of water uptake by the roots due to high ion content in the soil solution. When seeds are sown in varied concentrations of salinity, the germination rate is directly proportional to the time required for germination. 0.2 g/L GA_3 treated seeds show better germination at varied concentrations of salinity. GA_3 can potentially increase germination percentage due to the activation of some specific genes for α-amylase mRNA transcription and shut off the defensive effects of salinity stress on germination. The progressive growth in germination percentage with GA_3 might be due to the involvement of GA_3 in the activation of amylases, lipases, and proteases, as well as an increase in cell wall plasticity and improved water absorption [11]. Any increase in the activity of these enzymes may result in early, vigorous germination and better crop establishment.

In addition, RNA synthesis and acid phosphatase may also increase in the cotyledons and embryonic axes of the GA_3treated seeds compared with the untreated ones. The α-amylase plays a significant role in the hydrolysis of macromolecules such as proteins and starch in the aleurone cells. The stored content is converted into forms available for the development of the embryo by increasing the size and water potential through osmotic processes [23]. Besides, the signalling pathways of GA_3 tend to boost seed germination through the release of seed dormancy by counteracting the activity of abscisic acid (ABA). ABA will inhibit embryonic expansion during stressful situations by weakening the endosperm and inhibiting the expansion of embryonic cells [24]. Similar effects of GA_3 were observed on the germination of *Sorghum bicolor* [8], *Ricinus communis* [25], *Satureja thymbra [26*], *Delonix regia* [27], and on*Lathyrussativus* [28].

Effect of Salinity and Priming on the Seedling Growth Performance of the Three Seeds

Seeds exposed to higher salt concentrations during germination caused stress and decreased the seedling vigour index, shoot and root length, and shoot and root fresh and dry weights of all the experimental seedlings (Figures 1–3). The salinity levels are indirectly proportional to the growth of the seedlings. It was noticed that when salinity levels increased, seedling growth decreased significantly. However, priming with GA_3 had a stimulatory effect on maximum physiological characteristics up to a certain salinity level (50 mM NaCl). An exceptionally high number of seedlings were documented at primed seedlings (75%) irrigated with salinity levels up to 50 mM NaCl for *Thespesia populnea,* followed by *Morinda citrifolia* (64%) and *Markhamia lutea* (43%) (Figures 1–3).

The seedling growth of *Thespesia populnea*, *Morinda citrifolia*, and *Markhamia lutea* significantly decreased when grown in high salinity. Seedling vigour declined from the control (no salt) to the 50 mM NaCl medium. The maximum seedling vigour index was observed at 50 mM NaCl (43.10 for primed and 14.12 for unprimed), and the minimum seedling vigour index was at 100 mM NaCl (3.02 for primed and 1.12 for unprimed). Figures 1–3 show reductions in

seedlings were observed on all tested seedling traits: seedling length (SL), seed dry weight (SDW), seed fresh weight (SFW), root length (RL), root fresh weight (RFW), and root dry weight (RDW). When viewed in the context of ion uptake, high salinity in the growth medium reduces the water uptake capacity of the seedlings, which causes a reduction in growth rate. The mechanism by which salt tolerance affects the growth of a plant depends on the time scale, and the plant is exposed to a high salt environment. Na^+ and Cl^- ions can enter the cells and influence the metabolic activities in the cytosol and cell membranes via direct toxic effects [29]. [30] concluded that seed priming with GA_3 in *Calendula officinalis* L. and *Foeniculum vulgare* Mill. accelerated metabolic activity and increased radicle and plumule weight, especially under salt stress.

The roots of all the tree seeds were affected first due to direct contact with the saline growth medium, then the shoots of all tree seeds (Figures 1–3). This is because the roots were under osmotic salt pressure at the rhizopsheric region of the seedlings, which directly corroded the roots. The osmotic regulation, together with the toxic effects of Na^+ and Cl^- ions, decreases water uptake and causes an imbalance of essential nutrients at the time of seed germination (31). GA_3 caused a significant reduction in Na^+ content as well as decreased the range of other ions [32]. Similar results were also observed in stressed maize plants treated with GA3, showing a significant reduction in the accumulation of fewer Na^+ ions [33]. Most toxic effects of NaCl can be attributed to Na^+ toxicity, resulting in the dormancy of seeds and delayed germination. In addition, K^+ ions also play a vital role in stomatal regulation and preventing water loss and necrosis. Hence, it is essential to nullify the toxicity of the Na^+ ion, and nevertheless, it increases the uptake of K^+ ions to improve cellular function [34]

CONCLUSION

This study provided valuable information about *Thespesia populnea*, *Morinda citrifolia*, and *Markhamia lutea* seeds under salt stress and pretreatments with a growth hormone (GA_3). Seed priming with GA_3 significantly improved seed germination and seedling growth and alleviated the inhibitory effect of salt stress on germination and seedling growth of the investigated tree plants. Decreases in seed germination percentage and seedling growth with increasing salt stress were more apparent in the unprimed seeds than in the primed seeds. Furthermore, the roots of the studied tree plants were more affected than the shoots. Pre-treatment with GA_3 increased total seed germination percentage, decreased MGT, and increased seedling growth performances. In conclusion, this study showed the effectiveness of applying seed priming techniques in salt-stressed environments to reduce the harmful effects of salinity stress on seed germination and the early growth of the seedlings *in vitro*. Nevertheless, further research is necessary to see the performance of the three primed (GA_3) tree plants on vegetative growth and yield under field conditions.

Conflict of interest

The authors declares that there is no of conflict of interest

ACKNOWLEDGEMENT

The authors would like to acknowledge Nirmala College for Women, Coimbatore for providing the infrastructural facilities for the successful completion of the work.

REFERENCES

1. González-Orozco, C. E., Porcel, M., Velásquez, D. F. A., &Orduz-Rodríguez, J. O. (2020). Extreme climate variability weakens a major tropical agricultural hub. *EcologicaIndicators*, *111*106015. https://doi.org/10.1016/j.ecolind.2019.106015
2. Chutipaijit, S., Cha-um, S., & Sompornpailin, K. (2011). High contents of proline and anthocyanin increase protective response to salinity in *'Oryza sativa'* L. spp.'indica'. *Australian Journal of Crop Science*, *5*(10), 1191-1198.
3. Tester, M., & Davenport, R. (2003). Na+ tolerance and Na+ transport in higher plants. *Annals of botany*, *91*(5), 503-527.
4. Devika, O. S., Singh, S., Sarkar, D., Barnwal, P., Suman, J., &Rakshit, A. (2021). Seed priming: a potential supplement in integrated resource management under fragile intensive ecosystems. *Frontiers in Sustainable Food Systems*. https://doi.org/10.3389/fsufs.2021.654001
5. Machado, R. M. A., &Serralheiro, R. P. (2017). Soil salinity: effect on vegetable crop growth. Management practices to prevent and mitigate soil salinization. *Horticulturae*, *3*(2), 30.https://doi.org/10.3390/horticulturae3020030
6. Sinha, V. B., Grover, A., Yadav, P. V., &Pande, V. (2018). Salt and osmotic stress response of tobacco plants overexpressing Lepidiumlatifolium L. Ran GTPase gene. Indian Journal of Plant Physiology, 23(3), 494-498. DOI : 10.1007/s40502-018-0396-2
7. Borsai, O., Al Hassan, M., Boscaiu, M., Sestras, R. E., & Vicente, O. (2018). Effects of salt and drought stress on seed germination and seedling growth in Portulaca. *Romanian Biotechnological Letters*, *23*(1), 13340-13349. https://doi.org/10.19159/tutad.703369
8. Nimir, N. E. A., Zhou, G., Zhu, G., & Ibrahim, M. E. (2020). Response of some sorghum varieties to GA3 concentrations under different salt compositions. *Chilean journal of agricultural research*, *80*(4), 478-486. http://dx.doi.org/10.4067/S0718-58392020000400478
9. Elouaer, M. A., & Hannachi, C. (2012). Seed priming to improve germination and seedling growth of safflower (Carthamus tinctorius) under salt stress. *Eurasian Journal of BioSciences*, *6*(1), 76-84. https://doi.org/10.35229/jaes.958049
10. Marthandan, V., Geetha, R., Kumutha, K., Renganathan, V. G., Karthikeyan, A., &Ramalingam, J. (2020). Seed priming: a feasible strategy to enhance drought tolerance in crop plants. International Journal of Molecular Sciences, 21(21), 8258. https://doi.org/10.3390%2Fijms21218258
11. Chauhan, A., AbuAmarah, B. A., Kumar, A., Verma, J. S., Ghramh, H. A., Khan, K. A., &Ansari, M. J. (2019). Influence of gibberellic acid and different salt concentrations on germination percentage and physiological parameters of oat cultivars. *Saudi Journal of Biological Sciences*, *26*(6), 1298-1304. doi: 10.1016/j.sjbs.2019.04.014
12. Hussain, M., Farooq, M., & Lee, D. J. (2017). Evaluating the role of seed priming in improving drought tolerance of pigmented and non-pigmented rice. *Journal of Agronomy and Crop Science*, *203*(4), 269-276. https://doi.org/10.1111/jac.12195
13. Waqas, M., Korres, N. E., Khan, M. D., Nizami, A. S., Deeba, F., Ali, I., & Hussain, H. (2019). Advances in the concept and methods of seed priming. In *Priming and pretreatment of seeds and seedlings* (pp. 11-41). *Springer*, Singapore.http://dx.doi.org/10.1007/978-981-13-8625-1_2
14. Othman, Y., Al-Karaki, G., Al-Tawaha, A. R., & Al-Horani, A. (2006). Variation in germination and ion uptake in barley genotypes under salinity conditions. *World J. Agric. Sci*, *2*(1), 11-15.
15. Rhaman, M. S., Imran, S., Rauf, F., Khatun, M., Baskin, C. C., Murata, Y., &Hasanuzzaman, M. (2020). Seed priming with phytohormones: An effective approach for the mitigation of abiotic stress. *Plants*, 10(1), 37. doi: 10.3390/plants10010037
16. Fuller MP, Hamza JH, Rihan HZ, Al-Issawi M. 2012. Germination of primed seed under NaCl stress in wheat. *International Scholarly Research Notices*, http://dx.doi.org/ 10.5402/2012/167804
17. Ma, H. Y., Zhao, D. D., Ning, Q. R., Wei, J. P., Li, Y., Wang, M. M., ... & Liang, Z. W. (2018). A multi-year beneficial effect of seed priming with gibberellic acid-3 (GA3) on plant growth and production in a perennial grass,*Leymus chinensis*. *Scientific reports*, *8*(1), 1-9. https://doi.org/10.1038/s41598-018-31471-w

18. Parthasarathy, R., Ilavarasan, R., &Karrunakaran, C. M. (2009). Pharmacognostical Studies on *Thespesia populnea* Bark. *Research Journal of Pharmacognosy and Phytochemistry*, *1*(2), 128-131.
19. McClatchey, W. (2002). From Polynesian healers to health food stores: changing perspectives of *Morinda citrifolia* (Rubiaceae). *Integrative cancer therapies*, *1*(2), 110-120.https://doi.org/10.1177/1534735402001002002
20. Lacroix, D., Prado, S., Deville, A., Krief, S., Dumontet, V., Kasenene, J., &Bodo, B. (2009). Hydroperoxy-cycloartanetriterpenoids from the leaves of Markhamia lutea, a plant ingested by wild chimpanzees. *Phytochemistry*, *70*(10), 1239-1245.DOI: 10.1016/j.phytochem.2009.06.020
21. Yadav, P. V., Khatri, D., &Nasim, M. (2017). Salt and PEG induced osmotic stress tolerance at germination and seedling stage in Camelina sativa: A potential biofuel crop. J. Seed Sci, 10, 27-32.
22. Chauhan, B. S. (2016). Germination biology of Hibiscus tridactylites in Australia and the implications for weed management. *Scientific reports*, *6*(1), 1-6. https://doi.org/10.1038/srep26006
23. Ibrahim, H., Zhu, X., Zhou, G., Nimir, A. &Eltyb, N. Comparison of germination and seedling characteristics of wheat varieties from China and Sudan under salt stress. *Agron. J.* 108, 85–92 (2016). https://doi.org/10.2134/agronj15.0176
24. Miransari, M., & Smith, D. L. (2014). Plant hormones and seed germination. *Environmental and Experimental Botany*, *99*, 110-121. https://doi.org/10.1016/j.envexpbot.2013.11.005
25. Jiao, X., Zhi, W., Liu, G., Zhu, G., Feng, G., Eltyb Ahmed Nimir, N., ...& Zhou, G. (2019). Responses of foreign GA3 application on seedling growth of castor bean (Ricinus communis L.) under salinity stress conditions. *Agronomy*, *9*(6), 274.https://doi.org/10.3390/agronomy9060274
26. Ummahan, Ö. Z. (2022). The effect of salinity stress on germination parameters in *Satureja thymbra* L.(Lamiaceae). *International Journal of Secondary Metabolite*, *9*(1), 74-90.doi : https://doi.org/10.21448/ijsm.1025295
27. Yongkriat, K. O., Leksungnoen, N., Onwimon, D., &Doomnil, P. (2020). Germination and salinity tolerance of seeds of sixteen Fabaceae species in Thailand for reclamation of salt-affected lands. *Biodiversitas Journal of Biological Diversity*, *21*(5).doi:https://doi.org/10.13057/biodiv/d210547
28. Moghaddam, S. S., Rahimi, A., Pourakbar, L., &Jangjoo, F. (2020). Seed Priming with salicylic acid improves germination and growth of *Lathyrus sativus* L. under salinity stress. *YuzuncuYıl University Journal of Agricultural Sciences*, *30*(1), 68-79. https://doi.org/10.29133/yyutbd.624649
29. Zhu, G., An, L., Jiao, X., Chen, X., Zhou, G., & McLaughlin, N. (2019). Effects of gibberellic acid on water uptake and germination of sweet sorghum seeds under salinity stress. *Chilean journal of agricultural research*, *79*(3), 415-424. http://dx.doi.org/10.4067/S0718-58392019000300415
30. Zhang, H., Irving, L. J., McGill, C., Matthew, C., Zhou, D., & Kemp, P. (2010). The effects of salinity and osmotic stress on barley germination rate: sodium as an osmotic regulator. *Annals of botany*, *106*(6), 1027-1035.doi: 10.1093/aob/mcq204.
31. Hasanuzzaman, M., Nahar, K., & Fujita, M. (2013). Plant response to salt stress and role of exogenous protectants to mitigate salt-induced damages. Ecophysiology and responses of plants under salt stress, 25-87. DOI:10.1007/978-1-4614-4747-4_2
32. Ahmed Nimir, N. E., Lu, S., Zhou, G., Ma, B. L., Guo, W., & Wang, Y. (2014). Exogenous hormones alleviated salinity and temperature stresses on germination and early seedling growth of sweet sorghum. *Agronomy Journal*, *106*(6), 2305-2315.https://doi.org/10.2134/agronj13.0594
33. Kaya, C., Tuna, A. L., &Okant, A. M. (2010). Effect of foliar applied kinetin and indole acetic acid on maize plants grown under saline conditions. *Turkish Journal of Agriculture and Forestry*, *34*(6), 529-538. http://dx.doi.org/10.3906/tar-0906-173
34. Tavakkoli E, Rengasamy P, McDonald GK. 2010. High concentrations of Na+ and Cl– ions in soil solution have simultaneous detrimental effects on growth of faba bean under salinity stress *J. Exp. Bot.* 61(15):4449-4459 https://doi.org/10.1093/jxb/erq25

Table:1 Analysis of variance for morphological growth parameters of *Thespesia populnea*, *Morinda citrifolia*, and *Markhamia lutea* seeds primed with gibberellic acid and germinated using various concentrations of NaCl solutions

Source of Variation	Total Germination (%)	Mean Germination Time (days)	Seedling Vigour (SVI)	Shoot Length (cm)	Root Length (cm)	Shoot Fresh Weight (g)	Shoot Dry Weight(g)	Root Fresh Weight (g)	Root Dry Weight (g)
Treatment	8572.33*	50.94*	464*	18.08*	14.02*	4.35*	2.3*	2.49*	1.38*
seed type	2056.48*	55.40*	50*	9.75*	6.75*	5.38*	1.1*	5.41*	2.11*
Salt conc.	6097.71*	53.70*	14*	4.43*	4.3*	1.23*	1.3*	3.29*	3.01*
Treatment × seed type	354.73*	0.29*	1.3*	1.73*	5.4*	3.23*	0.52*	1.73*	4.01*
Treatment × salt conc.	1094.97*	0.90*	4.5*	2.13*	6.7*	6.11*	4.35*	2.49*	2.38*
seed type× salt conc.	363.09*	0.42*	1.2*	4.73*	8.1*	3.58*	3.72*	1.39*	3.59*
Treatment × seed type ×salt conc	706.73*	0.68*	8.2*	5.27*	7.9*	2.11*	0.91*	0.58*	0.27*
Error	14.73	0.8	1.82	3.72	0.054	0.0015	0.067	0.269	0.0084

*Significantly different at $P< 0.05$.

Table :2 Correlation analysis between germination and morphological growth parameters of *Thespesia populnea*, *Morinda citrifolia*, and *Markhamia lutea* seeds primed with gibberellic acid and germinated using various concentrations of NaCl solutions

	SL	RL	SFW	SDW	RFW	RDW	GR	MGT	SVI
SL	1	0.81	0.85	-0.75	-0.73	0.95	0.98	-0.59	0.96
RL		1	0.87	-0.99	-0.56	0.49	0.95	-0.54	0.72
SFW			1	0.93	0.72	0.72	0.41	-0.47	0.39
SDW				1	0.86	-0.76	0.75	-0.67	0.81
RFW					1	0.78	0.67	-0.73	0.77
RDW						1	0.49	-0.61	0.49
GR							1	0.72	0.73
MGT								1	0.59
SVI									1

SL: length of shoot, RL: length of root, SFW: shoot fresh weight, SDW: shoot dry weight, RFW: Root fresh weight, RDW: Root dry weight MGT: Mean germination time, GR: Germination rate, SVI: Seedling vigour index.

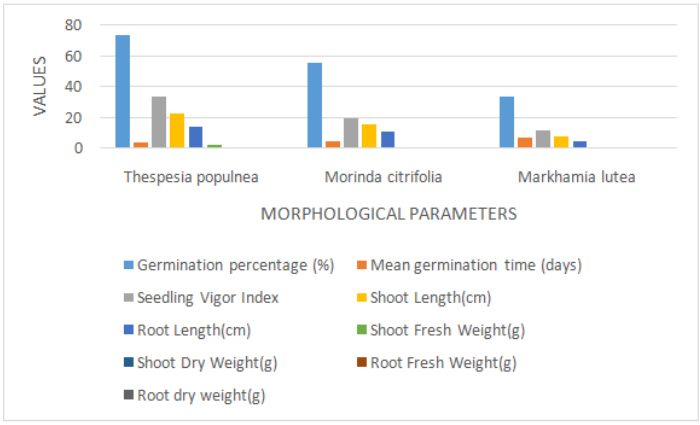

Fig :1 Effect of seed priming with gibberellic acid for morphological growth parameters of *Thespesia populnea*, *Morinda citrifolia*, and *Markhamia lutea*seeds primed after germinated under salinity stress (50mMNaCl concentration)

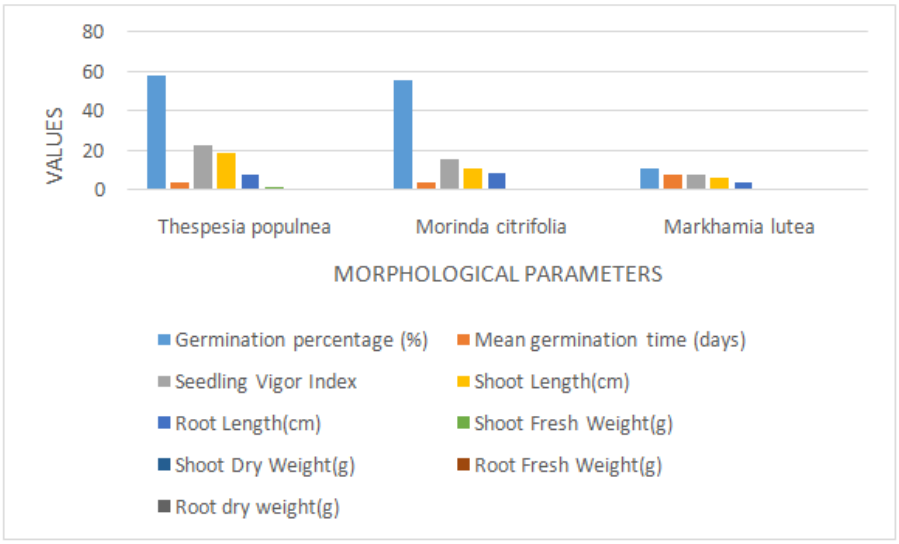

Fig: 2 Effect of seed priming with gibberellic acid for morphological growth parameters of *Thespesia populnea*, *Morinda citrifolia*, and *Markhamia lutea*seeds primed after germinated under salinity stress (100mMNaCl concentration)

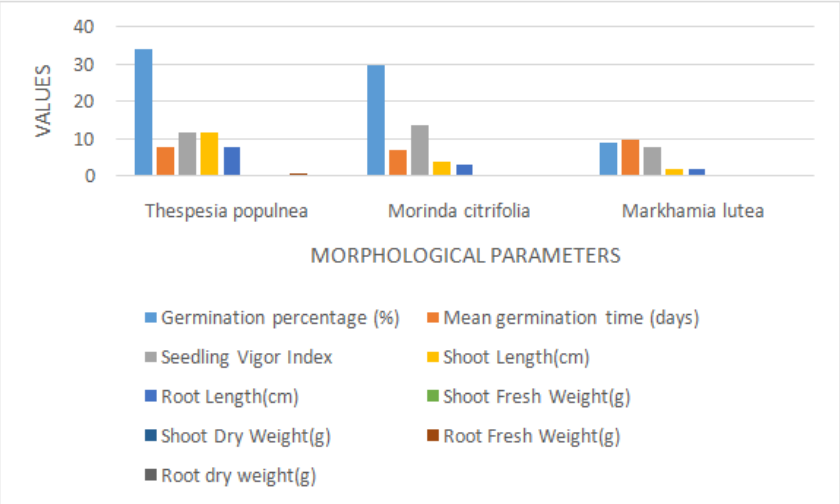

Fig: 3 Morphological growth parameters of *Thespesia populnea*, *Morinda citrifolia*, and *Markhamia lutea*unprimed seeds (without GA_3) after germinated under salinity stress (50mM and100mMNaCl concentration)

Indian Journal of Natural Sciences *www.tnsroindia.org.in ©IJONS*

Vol.15 / Issue 83 / Apr / 2024 *International Bimonthly (Print) – Open Access* *ISSN: 0976 – 0997*

RESEARCH ARTICLE

Method Development and Validation of Chloramphenicol in Commercially Available Milk by LC-MS/MS

Syed Rihana[1]*, Vidyadhara Suryadevara[2] and Venkata Rao Vutla[3]

[1]Assistant Professor, Department of Pharmaceutical Analysis, Chebrolu Hanumaiah Institute of Pharmaceutical Sciences, Guntur, Andhra Pradesh, India.
[2]Principal and Professor, Department of Pharmaceutics, Chebrolu Hanumaiah Institute of Pharmaceutical Sciences, Guntur, Andhra Pradesh, India.
[3]Professor, Department of Pharmaceutics, Chebrolu Hanumaiah Institute of Pharmaceutical Sciences, Guntur, Andhra Pradesh, India.

Received: 30 Dec 2023 Revised: 09 Jan 2024 Accepted: 27 Mar 2024

***Address for Correspondence**
Syed Rihana
Assistant Professor,
Department of Pharmaceutical Analysis,
Chebrolu Hanumaiah Institute of Pharmaceutical Sciences,
Guntur, Andhra Pradesh, India.
Email: rihanasyed687@gmail.com

ABSTRACT

A quantitative method for the determination of chloramphenicol in milk samples was developed based on the (quick, easy, cheap, effective, rugged, and safe) approach for lc-ms/ms chromatographic method for determination of chloramphenicol in milk using 0.1% formic acid in hplc grade water : acetonitrile as mobile phase at 0.6 ml/min with agilent eclipse plus c18 ,(5 µm ,4.6×150 mm) as column using triple quadrapole mass spectroscopy was developed. The developed method was validated and parameters were found to be within limits The validation experiments demonistrated system precision , system suitability , accuracy, linearity of experimental parameters. The retention time of system suitability are given chromatography–tandem mass spectrometry (LC–MS/MS). Homogenized milk samples were extracted with acetonitrile. Validation results demonstrated that this method fulfills criteria for the determination of chloramphenicol in milk. The present study was carried out to validate a simple ,precise and accurate lc-ms/ms chromatographic method for determination of chloramphenicol in milk using 0.1% formic acid in hplc grade water : acetonitrile as mobile phase at 0.6 ml/min with agilent eclipse plus c18 ,(5 µm ,4.6×150 mm) as column using triple quadrapole mass spectroscopy was developed. The developed method was validated and parameters were found to be within limits

Keywords: Chloramphenicol; LC–MS/MS; Milk; Liquid-Liquid Extraction (LLE)

INTRODUCTION

Antibiotics, also called anti-bacterials, are a type of antimicrobial drug used in the treatment and prevention of bacterial infections. They may either kill or inhibit the growth of bacteria. A limited number of antibiotics also possess antiprotozoal activity. Antibiotics are used in different food commodities to promote the growth rate and efficacy, for a lactation property, etc. Antibiotics in milk samples, which might pose a potential risk for human health due to their sub acute and chronic toxicity. Antibiotics in milk yields to severe acute and long term health effects like cancer, leukemia, grey baby syndrome in infants, Aplastic anemia, Bone marrow suppression, Neurotoxic reactions, Hypersensitivity reactions.When we consume the milk that contains more amount of antibiotics it leads to acute and chronic health problems. So, antibiotic usage should be reduced. Chloramphenicol is a broad-spectrum antibiotic suitable for the treatment of variety of infectious organisms (Bayo et al. 1994). The compound has been bannedin several countries, including the European Union, for treatment of food-producing animals. The European Commission defined aminimum required performance limit for chloramphenicol in food of animal origin at a level of 0.3 μg kg−1. However, data from p a s t years from Rapid Alert System for Food and Feed indicated contamination of incidents in various matrices with chloramphenicol (456 cases) in which 49 were in dairy products. Different analytical methods have been developed for the determination of chloramphenicol in milk using ELISA (Ferguson et al. 2005; Shi et al. 2010; Tao et al. 2012; van der Water and Haagsma 1991), gas chromatography (Kijak 1994.; Pfenning et al. 1998), and liquid chromatography(Ali et al. 2009; Bayo et al. 1994; Berendsen et al. 2013; Guy et al. 2004; Rezende, Fleury Filho, and Rocha 2012; Rodziewicz and Zawadzka 2008; Shi et al. 2010). Most of these methods are based on LLE (Dubourg et al. 1987; Perez et al. 2002; Petz and Lebens 1983; Ramsey et al. 1998; Rezende et al. 2012; Wal, Peleran, and Bortes 1980), solid phase extraction (SPE) (Guy et al. 2004; Rejtharová and Rejthar 2009), or combination of both (Sniegocki, Posyniak, and Z˙mudzki 2007). In recent years, a fast and inexpensive approach for the determination of pesticide residues in fruit and vegetable samples, named QuEChERS was developed by Anastassiades et al. (2003). However, few studies have been reported for the determination of different class of veterinary drugs in samples of animal originsuch bovine milk and liver (Kinsella et al. 2009), and shrimp (Villar-Pulido et al. 2011). Only one paper reported the determination of forbidden compounds such as chloramphenicol in honey (Pan et al. 2006). The goal of this work was to develop a simple and low-cost procedure LLE methods for the determination of chloramphenicol in milk.

EXPERIMENTAL

Reagents and Materials

Acetonitrile was obtained from Merck (HPLC)graded.. Ammonium formate obtained from Merck which is Ar grade. Water which is obtained from rankem which is HPLC graded. Formic acid was obtained from Merck (Emsure). All reagents were of analytical grade or higher The liquid chromatographic system consists of the following components: the hplc system shimadzu consisting of quaternary pump, degasser, auto sampler, thermo stated column oven compartment, isocratic elution with mass detector, computer & printer and mass spectrometer consists of the following components: the mass system, mass detector, roughing pump, syringe pump and a gas generator. Chromatographic analysis was performed using lab solutions software on a column agilent eclipse plus C18, 5 μm ,4.6×150mm.

Certified Reference Standards

During method validation, a blank matrix will be spiked with the analyte of interest using solutions of reference standard. It is important that the quality of the reference standard is ensured, as the quality (purity) may affect the outcome of the analysis, and therefore the outcome of the study data. Therefore the reference standards used for the analytical validation and analysis should be obtained from an authentic and traceable source. Suitable reference standards, include certified standards such as chloramphenicol d5(sigma Aldrich,Dr.ehrenstorfer), commercial available standards. Suitability of the reference standard should be scientifically justified. They should be stored in frost free refrigerator below -10oc in order to prevent undesirable reactions.

COLLECTION OF SAMPLES

Different brands of milk samples were collected from dairy in hyderabad . The milk samples were homogenized, extracted and analyzed as per the sample preparation procedure. On the basis of analysis the compound were not detected and their results are reported.

SAMPLE PREPARATION

Liquid-Liquid Extraction (LLE)

Take 2 ml of homogenized sample were weighed and transferred in to 50 ml centrifuge tube

To this add internal standard to all samples, spiked samples too then extract with ethyle acetate. For separation of compound. Then vortex for 5 minutes & centrifuge for 10 minutes. Transfer the 1 ml of supernated liquid into ria vials then it undergone to the nitrogen stream turbo evaporator for 15 minutes.It was reconstitute with diluents then clean up with hexane.Finaly centrifuge it for 5 minutes and transfer the bottom layer of the sample in to instrument vails then inject the sample to lc-ms/ms Selection of initial conditions for method development Determination of

solubility of chloramphenicol

Chloramphenicol is freely soluble in methanol and chloroform.

Selection of stationary phase and mobile phase

For selection of stationary phase, two different columns C18 and C8 were used in order to get optimum results and various solvent systems such as acetonitrile, buffers and methanol. buffer were used in various ratios.

Preparation of calibration curve standards

Prepare calibration curve standards in samples from the above working standard solution as shown in below table and process the samples.

EXTRACTION PROCEDURE

Take 2 ml of homogenized sample in 50 ml centrifuge tube. Extract the sample with 10 ml ethyl acetate

vortex for 5 minutes, then centrifuge at 4000 rpm. Transfer about 1 ml of supernated liquid & evaporate under nitrogen stream. By using turbo evaporater Reconstitute with 0.2 ml of diluent then vortex for 5 minutes, Clean up the sample by adding 1 ml of hexane. Transfer the bottom layer in to auto sampler vial & inject in to lc-ms/ms

Preparation of QC stock dilutions

Prepare QC stock dilution standards in samples from the above working standard solution as shown in below table and process the samples

Preparation of QC stock solutions

Preparation of 0.3ppb QC stock solution: Weigh 10gm of sample and spiked with 0.060ml of 10 ppb mix into sample and followed the sample preparation procedure.

Preparation of 0.5ppb QC stock solution

Weigh 10gm of sample and spiked with 0.100ml of 10.0 ppb mix into sample and followed the sample preparation procedure.

Preparation of 1ppb QC stock solution

Weigh 10gm of sample and spiked with 0.200ml of 10.0 ppb mix into sample and followed the sample preparation procedure.

RESULTS AND DISCUSSION

DATA PROCESSING

Acquired chromatograms using the computer based chemstation software,process the data by peak area method. The concentration of the unknown is calculated by using regression analysis.

$$y = mx + c$$

Where, x = concentration of analyte m =slope of calibration curve

y = peak area of analyte

c = y-axis intercept of the calibration curve Calculation

Concentration µg/kg = concentration found x volume of extract made up/wt.of sample taken for analysis.

Use a regression equation with an appropriate weighting factor for determining the detector response/ concentration relationship. Include standard a and standard i in preparation of calibration curve The representative calibration curve for regression analysis is illustrated. Linearity was established using matrix-matched calibration curves. five calibration curves were prepared at levels of Matrix blank, 0.1ppb, 0.3ppb, 0.5ppb, 1ppb and 2ppb, in milk.

These curves were prepared and plot a graph through software against the concentration of the each Analyte and its response. The Correlation Coefficient (R2) ≥ 0.99.

SYSTEM SUITABILITY

System suitability shall perform by injecting six replicates of known concentration of 1.00 ppb aqueous standard solution of Chloramphenicol & Chloramphenicol d5 .% RSD of area was >20% and retention time was within ±2 min. Mean= no. of observations /total no. of runs .

Standard deviation= $\frac{}{i=1}$ % cv= std.dev/mean volume*10.

PRECISION

The precision of the analytical method describes the closeness of repeated individual measures of analyte. Precision is expressed as the coefficient of variation (CV). The statistical method for estimation of the precision should be predefined and calculated according standard practice. Method precision was performed by injecting six spiked samples at 0.3 ppb,0.5 ppb and 1 ppb. % RSD of area≤20% and % Accuracy (Recovery) was injecting the spiked sample at 0.3ppb, 0.5ppb and 1ppb levels. Acceptance criteria in between 80-120%.

Formula: Precision=standard deviation /mean volume* 100

Accuracy

The accuracy of an analytical method described the closeness of the determined value obtained by the method to the true concentration of the analyte (expressed in percentage). Accuracy should be assessed on samples spiked with known amounts of the analyte, to the quality control samples (QC samples).During method validation accuracy should be determined by replicate analysis using a minimum of 6 determinations at a minimum of 3 concentration levels which are covering the calibration curve range. The QC samples are analyzed against the calibration curve, and the obtained concentrations are compared with the nominal value .Method accuracy was performed by injecting six spiked samples at 0.3,0.5,1.00ppb. % RSD of area ≤20% and % Accuracy (Recovery) was injecting the spiked sample at 0.3ppb, 0.5ppb and 1ppb levels. Acceptance criteria in between 80-120%.

Accuracy=mean volume /set volume*100

BATCH ANALYSIS

Batch analysis was performed by collecting different brands of milk samples from Diary forms and they are analyzed by using the LLE method and the results are tabulated below. The results are expressed in ppb level i.e; (µg/kg)

The present study was carried out to validate a simple ,precise and accurate lc-ms/ms chromatographic method for determination of chloramphenicol in milk using 0.1% formic acid in hplc grade water : acetonitrile as mobile phase at 0.6 ml/min with agilent eclipse plus c18 ,(5 µm,4.6×150 mm) as column using triple quadrapole mass spectroscopy was developed. The developed method was validated and parameters were found to be within limits. The validation experiments demonstrated system precision , system suitability , accuracy, linearity of experimental

parameters. The retention time of system suitability are givin in table – 5.12 , precision results are found in table – 5.14 for 0.3 ppb,0.5 ppb and 1 ppb. the chromatograms for the precision study were shown .

CONCLUSIONS

A simple, sensitive, and high-throughput method for chloramphenicol determination in milk samples was developed and validated. The developed LLS technique for the determination of chloramphenicol allows extraction and clean-up to be carried out in simple steps, without additional purification of the extracts. Good values for validation parameters such as linearity, recovery. The method was developed and validated for the estimation of chloramphenicol in different brands of milk by lc-ms/ms. Milk samples were collected from Dairy forms in hyderabad and were analyzed. On the basis of analysis I conclude that chloramphenicol were not detected in milk so it is beyond the limit in milk. so we are in safe zone. Antibiotics are used in different food commodities to promote the growth rate and efficacy, for a lactation property, etc. Antibiotics in milk yields to severe acute and long term health effects like cancer, leukemia, grey baby syndrome in infants, Aplastic anemia, Bone marrow suppression Neurotoxic reactions, Hypersensitivity reactions. When we consume the milk that contain more amount of antibiotics it leads to acute and chronic health problems. So antibiotic usage should be reduced.

REFERENCES

1. Ali, I., H. Y. Aboul-Enein, V. K. Gupta, P. Singh, and U. Negi. 2009. Analyses of chloramphenicol in biological samples by HPLC. Anal. Lett. 42 (10): 1368–1381.
2. Anastassiades, M., S. J. Lehotay, D. Stajnbaher, and F. J. Schenk. 2003. Fast and easy multiresidue method employing acetonitrile extraction/partitioning and "dispersive solid- phase extraction" for the determination of pesticide residues in produce. J. AOAC Int. 86:412–431.
3. Bayo, J., M. A. Moreno, J. Prieta, S. Diaz, G. Suarez, and L. Dominguez. 1994. Determination of chloramphenicol in bovine milk by liquid chromatography/tandem mass spectrometry. J. AOAC Int. 77: 854–862.
4. .Berendsen, B., M. Pikkemaat, P. Römkens, R. Wegh, M. van Sisseren, L. Stolker, and M. Nielen. 2013. Occurrence of chloramphenicol in crops through natural production by bacteria in soil. J. Agric. Food Chem. 61 (17): 4004–4010.
5. Commission Decision of 12 August 2002 implementing Council Directive 96/23/EC concerning the performance of analytical methods and the interpretation of results. Official Journal of the European Communities, L 221/8 (2002).
6. Dubourg, D., M. C. Saux, M. A. Lefebvre, and J. B. Fourtillan. 1987. Assay of chloramphenicol in biological media by high performance liquid chromatography with UV absorbance as the detection mode. J. Liq. Chromatogr. 10 (5): 92/1940.
7. EURACHEM/CITAC Guide. 2000 Use of uncertainty information in compliance assessment, 2nd edition. ISBN0 948926 15 5.
8. Ferguson, J., A. Baxter, P. Young, G. Kennedy, Ch. Elliott, S. Weigel, R. Gatermann,
9. H. Ashwin, S. Stead, and M. Sharman. 2005. Detection of chloramphenicol and chloramphenicol glucuronide residues in poultry muscle, honey, prawn and milk using a surface plasmon resonance biosensor and Qflex® kit chloramphenicol. Anal. Chim. Acta 529 (1-2 January 24): 109–113.
10. Guy, P. A., D. Royer, P. Mottier, E. Gremaud, A. Perisset, and R. H. Stadler. 2004. Quantitative determination of chloramphenicol in milk powders by isotope dilution liquid chromatography coupled to tandem mass spectrometry. J. Chromatogr. A. Oct 29; 1054(1–2): 365–371.
11. ISO 11843. ISO-11843-2:2000(E), 2000, 1.
12. Kijak, P. J. 1994. Confirmation of chloramphenicol residues in bovine milk by gas chromatography/mass spectrometry. J. AOAC Int. 77: 34–40.

13. Kinsella, B., S. J. Lehotay, K. Mastovska, A. R. Lightfield, A. Furey, and M. Danaher. 2009. New method for the analysis of flukicide and other anthelmintic residues in bovine milk and liver using liquid chromatography–tandem mass spectrometry. Anal. Chim. Act., 637: 196–207.
14. Martins Junior, A. H., O. V. Bustillos, and M. A. F. Pires. 2006. Determinacaõ de resíduos de cloranfenicol em amostras de leite e mel industrializados utilizando a técnica de spectrometria de massas em "tandem" (CLAE-EM/EM). Quim Nova. 29: 586–592.
15. 15. Matuszewski, B. K., M. L. Constanzer, and C. M. Chavez-Eng. 2003. Strategies for the assessment of matrix effect in quantitative bioanalytical methods based on HPLC-MS/MS. Anal Chem. Jul 1; 75 (13): 3019–3030.
16. KD Tripathi. Essentials of medical pharmacology, 6th Ed. Pages 694 - 704
17. Journal of Agricultural and Food Chemistry April 2008, 56 (10), pages 3509–3516.
18. The nutrition society, Volume 13, Issue 2December 2000, pages 279-299.
19. Clinical Microbiological Review. April 2003 vol. 16, pages 175-188.
20. European food safety authority. Journal 2014; 12(11):3907 pages 145 -157.
21. Ramana Rao G, Murthy SSN, Khadgapathi P. High performance liquid chromatography and its role in pharmaceutical analysis. Eastern Pharmacist 1986; 29(346): 53.
22. Sastry CSP, Prasad TNV, Rao EV. Recent applications of high performance liquid chromatography in pharmaceutical analysis (Review). Indian J Pharm Education 1987; 21: 37.
23. Snyder LR, Kirkland JJ, Glajch JL. Practical HPLC method development, 2nd Ed. New York: Wiley Inter Science; 1997.
24. Dr. S. Ravi Shankar, Pharmaceutical Analysis, pages 18.1 – 15
25. Gurdeep R. Chatwal, Sham k Anand, Instrumental methods of analysis 1st Ed, 1979, pages 2.272 -96.

Table 1.1:Preparation of diluents working standard solution

Stock conc.(ppm)	Volume of stock standard(ml)	Volume of methanol (ml)	Final volume(ml)	Final conc.(ppb)
10.000	0.100	0.900	1.000	1000.00
1.0	0.100	9.900	10.000	10.00
0.01	0.100	0.900	1.000	1.00

Table 1.2:Preparation of calibration curve standards

Working standard Conc.(ppb)	Volume of standard (ml)	Sample weight(gm)	Final conc.(ppb)	Level
10.00	0.400	2.0	2.00	Cc-5
10.00	0.200	2.0	1.00	Cc-4
10.00	0.100	2.0	0.50	Cc-3
10.00	0.060	2.0	0.30	Cc-2
1.00	0.200	2.0	0.10	Cc-1
0.00	0.00	2.0	0.00	Blank

Table 1.3:Preparation of qc stock dilutions

Working standard Conc.(ppb)	Volume of standard(ml)	Sample weight(gm)	Final conc.(ppb)	Level
10.00	0.200	2.0	1.00	Qc-1.0ppb
10.00	0.100	2.0	0.50	Qc-0.5ppb
10.00	0.060	2.0	0.30	Qc-

				0.3ppb

Table1.4:Mrm parameters

Compound name	Precursorion ms 1 response	Production ms 2 response	D well time (m.sec)	Q1Prebase(v)	CE	Q3 Prebase	RT	Polarity
Chloramphenicol	321	152.05	100	11	15	16	2.5	Negative
				15	27	11		
		121						
				20	10	11		
		257						
Chloramphenicol D5	326	157	100	15	16	15	2.5	Negative
		262.05		15	11	17		
		126		11	28	12		

Table1.5:Linearity For Correlation Coefficient

Compound name	R-value	R-2value
Chlorampenicol-01	0.998	0.997
Chlorampenicol-02	0.998	0.997
Chlorampenicol-03	0.998	0.997

Table 1.6:Linearity for the ion of 321>152

Linearity	Area	Actual concentration(ppb)	Obtained concentration(ppb)	Accuracy(%)
Cc1	26159	0.1	0.090	90.50
Cc2	78530	0.3	0.315	104.90
Cc3	118354	0.5	0.542	108.40
Cc4	213877	1	0.971	97.1
Cc5	406442	2	1.981	99.1

Table 1.7:Linearityfortheionof321>121.10

Linearity	Area	Actual concentration(ppb)	Obtained concentration(ppb)	Accuracy(%)
Cc1	8136	0.1	0.089	89.5
Cc2	26742	0.3	0.320	106.70
Cc3	39766	0.5	0.537	107.50

Cc4	73195	1	0.974	94.4
Cc5	139205	2	1.979	99.0

Table 1.8: Chloramphenicol d5(istd area)326.00>157.10

Linearity	Area
Cc1	43942
Cc2	41903
Cc3	37333
Cc4	38070
Cc5	35721

Table1.9: System Suitability RT

Compound name	Run-01	Run-02	Run-03	Run-04	Run -05	Run -06	Mean	Stdev	%cv
Chlorampenicol-01	2.468	2.471	2.469	2.469	2.47	2.471	2.47	0.00	0.05
Chlorampenicol-02	2.466	2.468	2.468	2.469	2.468	2.469	2.47	0.00	0.04
Chlorampenicol-d5(ISTD)	2.444	2.446	2.446	2.445	2.447	2.447	2.45	0.00	0.05

Table1.10: System Suitability Area

Compound name	Run-01	Run-02	Run -03	Run-04	Run-05	Run-06	Mean	Stdev	%cv
Chloramphenicol	129120	137425	130284	135798	141049	142409	136014.1	5452.4	4.01
Chloramphenicold5	192503	201701	186462	195438	202405	205943	197408.6	7266.3	3.68

Table 1.11:PrecisionAt 0.3ppb

Compound Name	RUN -01	RUN -02	RUN -03	RUN -04	RUN -05	RUN -06	Mean	Stdev	%CV
Chlorampenicol-01	71515	64978	70498	67426	67922	68186	68420.83	2325.31	3.40
Chlorampenicol-02	23728	23823	23628	22716	23365	23826	23514.33	426.76	1.81
Chlorampenicol-d5(ISTD)	36664	36015	37608	36908	35007	37909	36685.17	1064.41	2.90

Table1.12:Precision at 0.5ppb

Compound Name	RUN-01	RUN-02	RUN-03	RUN-04	RUN-05	RUN-06	Mean	Stdev	%CV

Chlorampenicol-01	95819	83493	82479	89550	86408	89536	87880.83	4881.44	5.55
Chlorampenicol-02	33037	28350	26599	29346	30279	31321	29822.00	2261.56	7.58
Chlorampenicol-d5(ISTD)	34430	31036	28798	30334	31871	33005	31579.00	1991.27	6.31

Table 1.13:Precisionat 1 ppb

Compound Name	RUN-01	RUN-02	RUN-03	RUN-04	RUN-05	RUN-06	Mean	Stdev	%CV
Chlorampenicol-01	155964	160452	156810	151250	156826	150565	155311.17	3752.73	2.42
Chlorampenicol-02	55295	54333	53281	50339	52349	51988	52930.83	1767.66	3.34
ChloramphenicolD5(ISTD)	29840	29801	28967	27651	31003	28714	29329.33	1149.88	3.92

Table 1.14:Accuracy At0.3ppb

Compound Name	RUN-01	RUN-02	RUN-03	RUN-04	RUN-05	RUN-06	Mean	Accuracy
Chlorampenicol-01	0.328	0.302	0.315	0.306	0.326	0.302	0.31	104.39
Chlorampenicol-02	0.325	0.332	0.315	0.309	0.335	0.315	0.32	107.28
Chlorampenicol-03	0.328	0.322	0.327	0.306	0.331	0.301	0.32	106.39

Table1.15: Accuracy At 0.5ppb

Compound Name	RUN-01	RUN-02	RUN-03	RUN-04	RUN-05	RUN-06	Mean	Accuracy
Chlorampenicol-01	0.474	0.458	0.488	0.504	0.462	0.462	0.47	94.93
Chlorampenicol-02	0.484	0.46	0.465	0.488	0.479	0.478	0.48	95.13
Chlorampenicol-03	0.474	0.462	0.469	0.501	0.469	0.478	0.48	95.10

Table 1.16:Accuracy At1 ppb

Compound Name	RUN-01	RUN-02	RUN-03	RUN-04	RUN-05	RUN-06	Mean	Accuracy
Chlorampenicol-01	0.903	0.93	0.935	0.945	0.873	0.906	0.92	91.53

Chlorampenicol-02	0.939	0.923	0.932	0.922	0.855	0.917	0.91	91.47
Chlorampenicol-03	0.892	0.898	0.915	0.964	0.882	0.899	0.91	90.83

Table1.17:BATCH ANALYSIS REPORT

Compound name	Sample-01	Sample-02	Sample-03	Sample-04	Sample-05
Chloramphenicol	BLQ	BLQ	BLQ	BLQ	BLQ

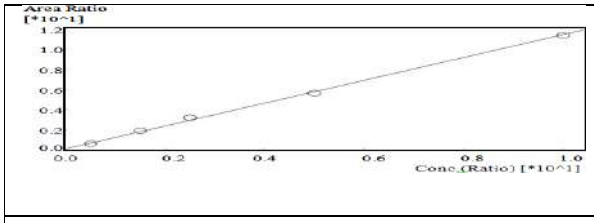

Fig .1 Calibration Curve for the Ion of 321>152

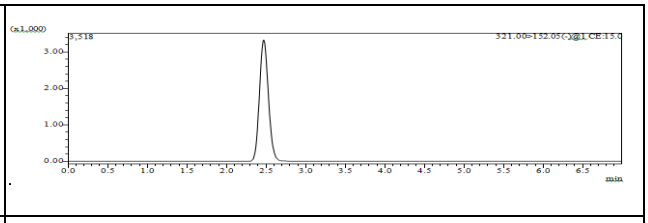

Fig2:Chromatogram For Linearity

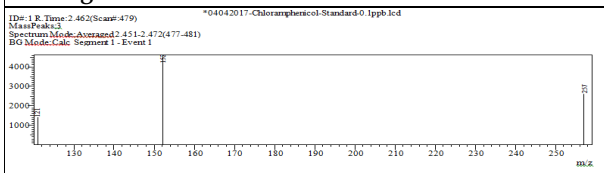

Fig3:Mass Spectrum For Linearity

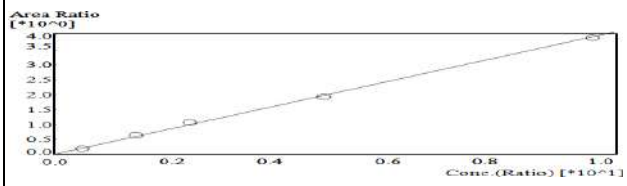

Fig4:CalibrationCurvefor321>121.10

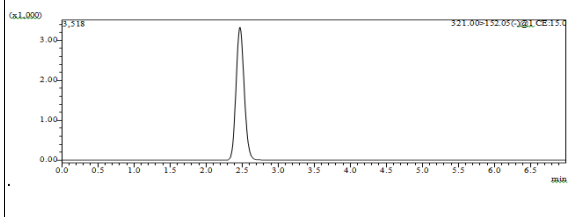

Fig 5: Chromatogram for linearity at 321>121

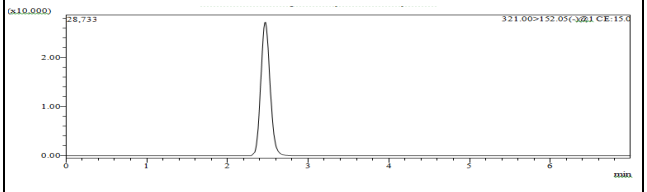

Fig6:Chromatogram for System Suitability

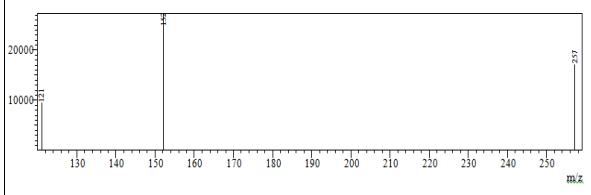

Fig7:Masss Spectrum For System Suitability

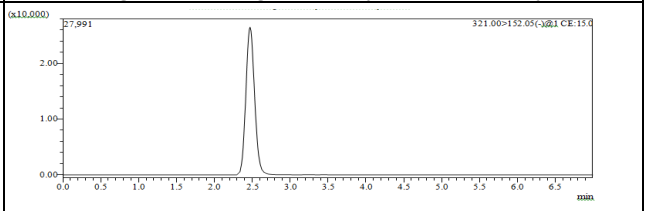

Fig.8:Chromatogram for System Suitability

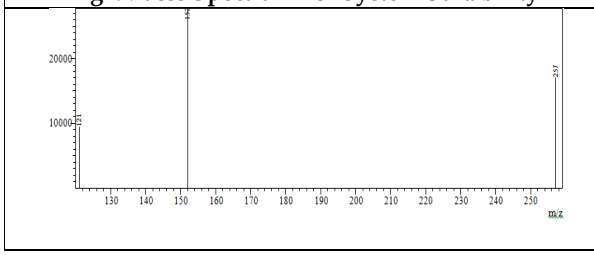

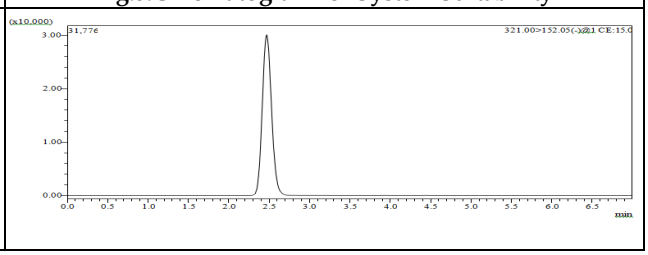

Fig.9:Mass Spectrum For System Suitability	**Fig10: Chromatogram For System Suitability**
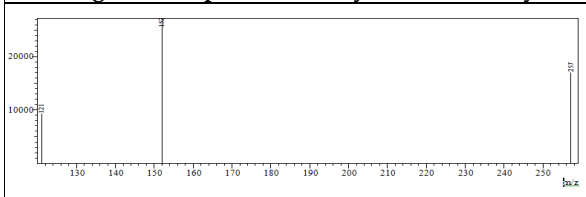	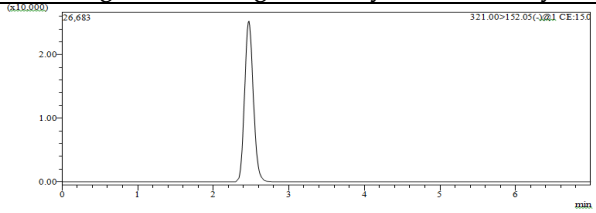
Fig11: Mass Spectrum For System Suitability	**Fig12: Chromatogram For System Suitability**
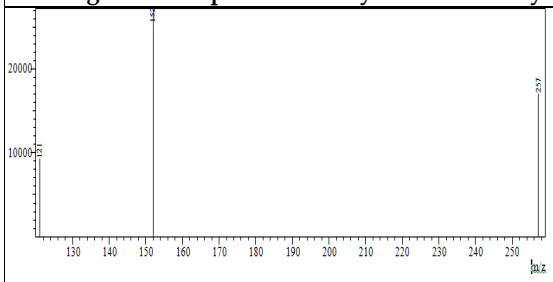	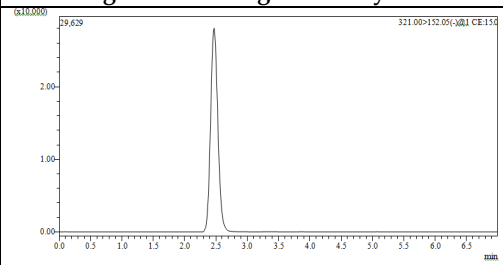
Fig13: Mass Spectrum For System Suitability	**Fig14: Chromatogram For System Suitability**
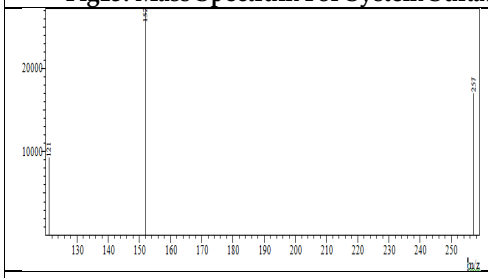	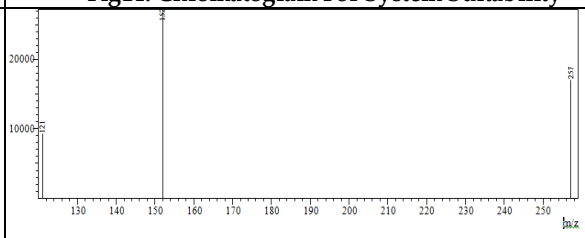
Fig15: Mass Spectrum For System Suitability	**Fig16: Mass spectrum for precision**
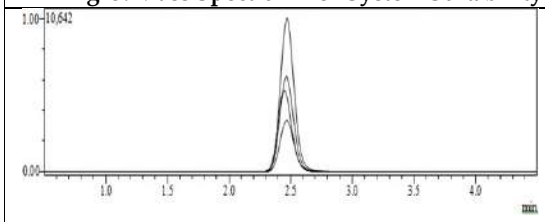	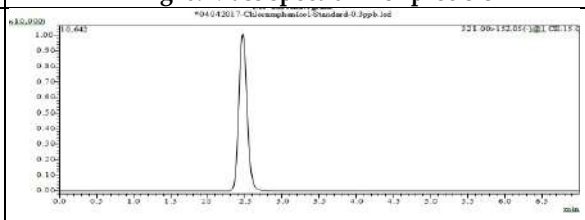
Fig17: Chromatogram for precision	**Fig18: Chromatogram for accuracy(0.3 ppb)**
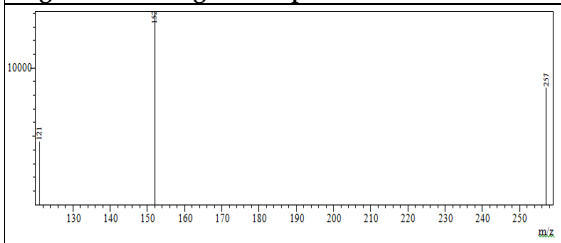	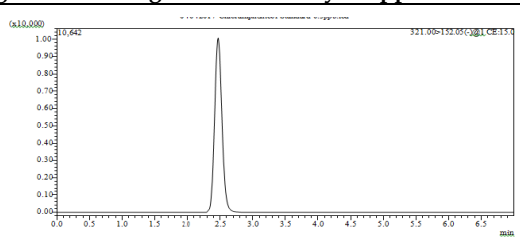
Fig19: Mass Spectrum For Accuracy	**Fig 20 :Chromatogram For Accuracy(At 0.5Ppb)**

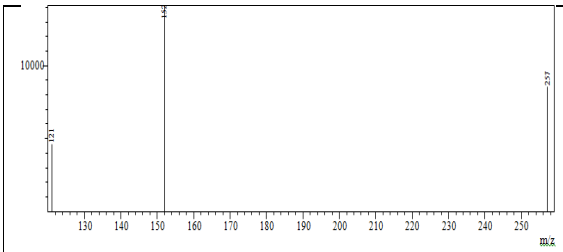

Fig21: Mass Spectrum For Accuracy(At 0.5Ppb)

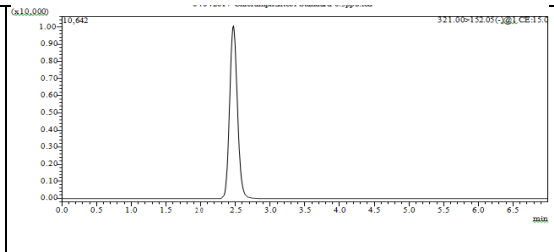

Fig22: Chromatogram For Accuracy(At1Ppb)

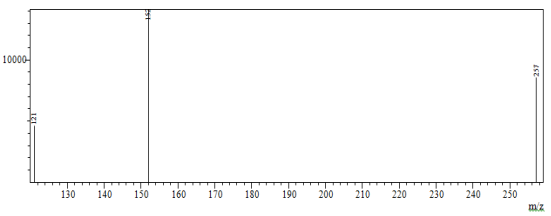

Fig.23:MassSpectrumForAccuracy(At 1Ppb)

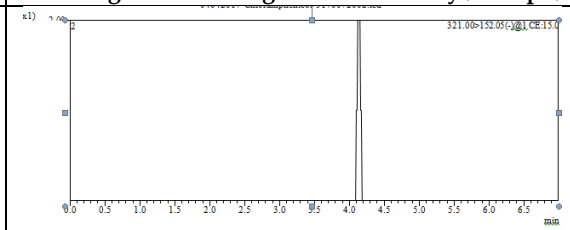

Fig24:Chromatogram for SAMPLE-01

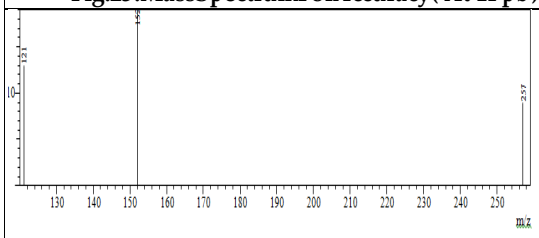

Fig25 : Mass Spectrum for SAMPLE-01

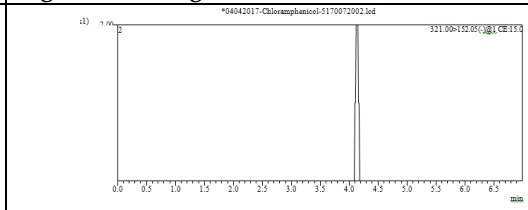

Fig26:ChromatogramforSAMPLE-02

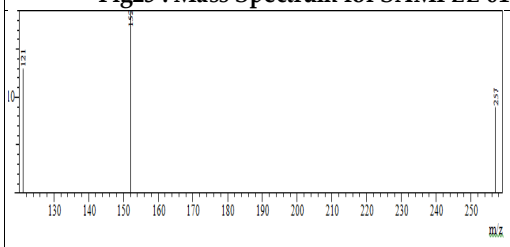

Fig27:Mass Spectrum for SAMPLE-02

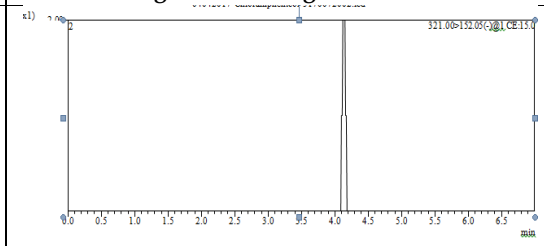

Fig.28:Chromatogram for SAMPLE-03

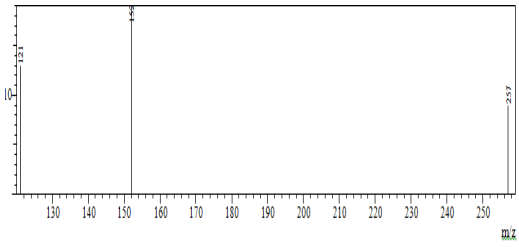

Fig29: Mass Spectrum for SAMPLE-03

Indian Journal of Natural Sciences *www.tnsroindia.org.in ©IJONS*

Vol.15 / Issue 83 / Apr / 2024 *International Bimonthly (Print) – Open Access* *ISSN: 0976 – 0997*

RESEARCH ARTICLE

Foliar-applied Alfa-Tocopherol and Brassinolide Enhance Salt Tolerance, Growth Improvement, and Pigment Composition in *Vigna radiata* L. (Co-6) Variety Grown under NaCl Stress

Aamir Abdullah[1] and R. Somasundaram[2]*

[1]Ph.D, Research Scholar, Stress Physiology Lab, Department of Botany, Annamalai University, Annamalai Nagar, Chidambaram, Tamil Nadu, India.
[2]Professor Stress Physiology Lab, Department of Botany, Annamalai University, Annamalai Nagar, Chidambaram, Tamil Nadu, India.

Received: 30 Dec 2023 Revised: 09 Jan 2024 Accepted: 27 Mar 2024

***Address for Correspondence**
R. Somasundaram
Professor Stress Physiology Lab,
Department of Botany,
Annamalai University,
Annamalai Nagar, Chidambaram, Tamil Nadu, India.
Email: botanysundaram@gmail.com

ABSTRACT

Soil salinity is a key environmental constraint that reduces the growth development and production of essential crops globally and other abiotic stresses. Therefore, certain strategies, such as the use of plant growth regulators might be useful ways to ameliorate the adverse consequences of NaCl-induced stress on agricultural crops. In this view, the present Experimental pot culture study was conducted to determine the efficacy of foliar applicationof Alfa-Tocopherol (200mg/L) Brassinolide (4mg/L), (Alfa-Toc + NaCl), and (BL + NaCl) on (*Vigna radiata* L. Co-6 variety), under NaCl (80mM) concentration. however, NaCl was applied by soil drenching. The plant samples were collected after the 25th,35th,and 45th, Days after sowing (DAS), to investigate the different physiological parameters such as root length, stem length, biomass, and pigment composition, in all applied treatments. Salt stress reduces plant growth pigment composition and biomass, Application of Alpha-Tocopherol and Brassinolide on leaves mitigates the negative effects of salt stress supporting the recovery of physiological aspects and improving pigment composition. Overall, in *Vigna radiata*L. (Co–6 var), Alfa-Toc and BL foliar spray mitigated the negative effects caused by NaCl stress, and it can be concluded that these plant growth regulators induce the tolerance to stress in the plants.

Keywords: Alfa-tocopherol, brassinolide, salt stress, pigment composition, NaCl.

INTRODUCTION

Salinity is the main environmental factor affecting plant production and development. [1] In the modern world, soil salinity has emerged as a significant issue for agriculture. [2]. Approximately 800 million hectares of land globally are impacted by salinity (397 million hectares) or sodicity (434 million hectares).[3.4]. Almost all of the biochemical and physiological processes that occur in plants are impacted by the intricate mechanism of salt stress. [5] The impact of salt stress arises from the reduced osmotic potential in the soil solution, leading to water scarcity. This stress triggers a domino effect, causing imbalances in nutrients, specific ion impacts, or a blend of these factors.[6]. Salt stress may result in membrane disorder, toxic metabolite production, photosynthetic reduction, ROS production, and reduced nutrition acquisition, all of these may result to cell and plant death. [7,8]. Stress due to salinity raises Na^+ and Cl^- concentrations in the root, stem, and leaves, while the leaves accumulate the most ions, followed by the stem and root, demonstrating a positive association between Na^+ and Cl^- concentration[9]. With the increase in salinity stress, a linear decrease in the levels of total chlorophyll, chlorophyll *a*, chlorophyll *b*, carotenoids, and xanthophylls as well as the intensity of chlorophyll fluorescence was found in *Vigna radiata*L. [10]High salt levels in the soil disrupt water balance in plants, lowering leaf water potential and affecting crucial plant functions like growth, nutrient uptake, and photosynthesis.[11]. salinity causes excessive accumulation of reactive oxygen species (ROS) such as superoxide ($O_2^{\bullet -}$), hydrogen peroxide (H_2O_2), hydroxyl radical ($OH^{\bullet}$), and singlet oxygen ($^1O_2$) which can cause peroxidation of lipids, oxidation of protein, inactivation of enzymes, DNA damage, and interact with other vital constituents of plant cells. [12]. In south and southeast Asia, mungbean *Vigna radiata* L. is one of the major pulse crops. Approximately 90% of the world's production occurs in South Asia, with India being the primary producer. [13] Mungbean seeds are a good source of dietary protein for humans including marginal people, and mostly vegetarian people, they are rich sources of vitamins and minerals [14,15].

Salinity affects the mungbean plants showing a significant reduction in whole plant growth, biomass, and variation in leaf color, and photosynthesis, reducing nodule respiration, nitrogen fixation, and root hair formation[16].Alpha-tocopherol acts as a crucial plant growth regulator, shielding photosystems from photo-inhibition and safeguarding chloroplast membrane lipids during salinity stress.[17].α-Toc is effective in eliminating free radicals and preventing membrane lipid peroxidation in soybean. [18]. Using alpha-tocopherol externally has proven highly effective in boosting growth and yield-related characteristics in *Calendula officinalis*. [19].Alpha-tocopherol application externally to *Helianthus annuus*, regulated protein content and sugar levels, ultimately enhancing yield. It also led to improved chlorophyll content, growth, and development in *Vigna radiata* L. [20,21].Brassinolide is an important plant growth regulator enhancing the growth development, photosynthesis, photomorphogenesis, chlorophyll, and pigment composition in plants. [22]. Brassinolide acts as a guardian, easing the detrimental effects of salt stress on plants by safeguarding stomatal conductance, maintaining membrane integrity, preserving leaf hydration, and balancing the ionic composition. [23,24]. Application of Brassinolide applied 1mg/L^{-1} contributed significantly in improving the floral characteristics, highest average No. of racemes, and fertility percentage in *Vigna radiata* L.[25].

MATERIALS AND METHODS

Seed collection and Chemical reagents.

Vigna radiata L. (Green gram seeds Co-6 variety) were purchased from Tamil Nadu Agricultural University Coimbatore, Tamil Nadu, India. Chemical regulators Alfa-tocopherol and Brassinolide and analytical reagent NaCl were purchased from Sisco Research Laboratories [SRL]- Chennai-600117.

Experimental design.

The Experimental study was conducted within the Botanical Garden of Annamalai University, situated in Chidambaram, Tamil Nadu. The specific geographic location was identified by coordinates 11°23'23.1"N/ 79°43'05.3"E. Healthy seeds of *Vigna radiata* L. (Co-6) variety were used for the research, were surface sterilized with

0.2% mercuric chloride($HgCl_2$) solution for 2 minutes and washed extensively with sterile double distilled water (ddH_2o). *Vigna radiata* L.Seeds were distributed and sown in 90 pots which were subsequently separated into six groups. Each pot was filled with a mixture of Red soil, sand, and farm yard manure in a ratio of (1:1:1). Plants were treated in Control, NaCl (80mM) Alfa-Toc (200mg/L) Brassinolide (4mg/L), NaCl (80mM) + Alfa-Toc(200mg/L), and NaCl (80mM) + BL (mg/L). To maintain particular salinity levels in pots, the soil samples from each pot were checked with Electrical Conductivity Meter at regular intervals. Plants were harvested for analyzing morphological and chlorophyll pigment analysis at the 25^{th}, 35^{th}, and45^{th}, days after sowing [DAS].

Root length

Root length was measured from the point where the root and shoot meet to the tap root. The length of the lateral roots was taken together to get the total length of the root. The length of the roots was measured in cm plant $^{-1}$.

Stem length

The length of the stem was measured from the tip to the point where the stem meets the root. And The length of the stems is given in cm plant $^{-1}$.

Fresh weight

The roots and shoots of the plant were washed and cleaned with tap water, and gently dried with tissue paper. After drying automatic balance (Model: XK3190-A7M) was used to measure the fresh weights of the roots and shoots. The values were measured and expressed in gm plant $^{-1}$.

Dry weight

After getting the fresh weight of plants, they were dried in a hot air oven at 60°C for 48 hours. After the plants were dry, their weights were measured, and they were kept in the same oven until their dry weights were the same. The values were expressed in gm plant $^{-1}$.

Leaf Area

The total leaf area was measured using LICOR Photo Electric area meter (Model L1-3100 Lincoln, USA.) and expressed in cm^2 plant $^{-1}$.

Chlorophyll pigment and carotenoid contents

Fresh leaf samples of 500 mg were taken from the plants and crushed with a pestle and mortar added 10 ml of 80% acetone. The mixture was then centrifuged at 800 rpm for 15 minutes. The extraction process was repeated, and the upper supernatant was collected, and mixed, with 20 ml of acetone to make a final volume of 20 ml. The spectrophotometer was used to measure absorption at 645, 663, and 480, nm against a blank of 80% acetone. The chlorophyll and carotenoids in the leaves were taken out and their amounts were measured using Arnon's method (1949). The findings are given in mg/gram of fresh weight.

RESULT AND DISCUSSION

Root length.

NaCl in *Vigna radiata* L. causes the stress declining the growth. In this experimental study, it was found that the plants treated with NaCl showed much decline in root length growth as compared to the control. However, plants treated with Alfa-Toc and Brassinolide show enhanced root growth than NaCl and control-treated plants. NaCl + BL and NaCl + Alfa-Toc treated plants also show increased root length than NaCl treated plants. (Fig-1)Plant development is negatively impacted by salinity due to low osmotic potential in soil solutions and nutritional imbalances. [26] Salinity causes regulated biophysical constraints on cell growth, which hinder root uptake and development. [27]. Other plants also show decreased root length with an increase in salinity like Tomato [28]*Brassica napus* [29]foliar application of Alfa-toc leads to notable increases in the growth of roots in sunflower *Helianthus*

annuus L. [30].and *Glycine max* [31]Applying brassinolide via foliar spray notably countered the detrimental effects of salt stress, fostering increased root length in both wheat and *Vigna radiata* L.[32,33].

Stem length.

Salt stress hampers the growth and development of plants by restricting cell division and expansion, which hampers photosynthesis and results in shortened stem.[34] As per our results, the stem length of plants treated with NaCl declined much compared to the control, while the plants treated with Alfa-Toc and BL showed increased stem length compared to the control, the plants treated with Alfa-Toc+ NaCl and BL + NaCl showed enhanced growth than plants treated with NaCl alone. (Fig-2) High salinity levels have a substantial negative effect on plant growth by inducing osmotic stress and disrupting the balance of ions and nutrients. These disruptions have adverse consequences on the plant's essential physiological and biochemical processes necessary for its overall well-being and development.[35].Salt levels have been associated with a decrease in the growth of stem in sugar beet (*Beta vulgaris* L.) [36].and a similar outcome has been observed in sorghum[37]. Foliar applications of α-tocopherol increased growth traits such as stem length and ameliorated the salinity stress effects in faba beans [38].Alpha-tocopherol rejuvenates plant growth by neutralizing singlet oxygen species, acting as a shield for photosystems, particularly in saline environments. [39]. Brassinosteroids (BRs) are commonly occurring plant hormones crucial for both plant growth and managing stress [40]. Application of brassinolide (BL) treatments prompts elongation, cell division, and differentiation, ultimately supporting the growth of plants. [41]BL application has been associated with an increase in stem length in both sunflower [42] and cowpea.[43].

Fresh weight and dry weight.

The fresh weight and dry weight decrease under the saline treatments. In this study, the plants treated with NaCl show a drastic decline in weight compared to the control. In comparison, the plants treated with Alfa-Toc and BL show increased fresh and dry weights. However, plants treated with Alfa-Toc + NaCl and BL + NaCl show increased growth than NaCl-treated plants.(Fig-3,4). The application of NaCl treatment showed adverse effects on both the fresh weight and dry weight of *Brassica juncea*. [44].*Lactuca sativa* [45] and Sorghum plants [46]. Our results agree with the results found in*Zea mays*[47], and wheat [48], and many others who observed the marked decreasein all the growth parameters. Application of Alfa-tocopherol at a concentration of 200mg/L^{-1} via foliar spray boosted both the fresh and dry weight of *Vigna radiata* L. [49] Alfa-toc also increased the fresh and dry weight of plants like carrot (*Daucus carota* L.). [50] *Glycine max* L. [51] and *Safflower* [52]The effects of salt are mitigated and the fresh and dry weight is increased by brassinolide foliar spray in *barley*[53]The treatment resulted in enhanced growth and higher dry and fresh weights in both *Medicagosativa* L. (alfalfa) and *Brassica juncea* plants. [54,55]and *Triticum aestivum* L. [56].

Leaf Area.

Leaf Area decreased inthe *Vigna radiata* L. in NaCl-treated plants when compared to the control, However, plants treated with Alfa-Toc and BL have found increased Leaf- Area compared to the control, plants treated with Alfa-Toc + NaCl and Bl + NaCl show increased leaf area than NaCl treated plants but lesser than control plants. (Fig-5)Many types of plants have shown that salt significantly affects leaf area. [57]. with increasing salt stress decreased leaf-Area has been found in many plants Like, sugar beet (*Beta vulgaris* L.) [58].Rice (*Oryza sativa*) [59]. Barley (*Hordeum vulgare* L.) [60]. The application of Alfa-Tocopherol through foliar has been observed to alleviate the effects caused by salt stress and enhance growth parameters, like leaf area, in *Helianthus annuus*L. [61]. Enhanced leaf area by Alfa-Toc application has been also found in *Vicia faba*L. [62]Application of Brassinolide externally has been demonstrated to boost both the height of the plant and the area of its leaves in maize, and same plant [63,64] and helps in mitigating the salt stress effects on plants.

Chlorophyll pigments.

Salinity causes a reduction in photosynthetic pigment concentrations due to a reduction in water potential. NaCl prevents the uptake of Nitrogen which is an important constituent of Chlorophyll. [65]. Declining the content of Chlorophyll, a and b, and total chlorophyll in *Vicia faba,* and *Vigna unguiculata* L. [66,67].In our experimental study,

the chlorophyll content of plants treated with NaCl showed a decline compared to the control, However, plants treated with Alfa-Toc and BL show enhanced chlorophyll content compared to control, and the plants treated with Alfa-toc+ NaCl and BL+ NaCl show a bit increased content than NaCl Treated plants. (Fig-6,7,8) our results are in accordance with the results found in *Hibiscus rosa sinensis* L[68].*Zea mays* [69]. *Oryza sativa*. [70] *Vigna radiata* L. [71]. Alfa-Toc and Brassinolide assists in reducing the harmful impact of salt stress and improving the levels of photosynthetic pigments.

Carotenoid content

Carotenoids are supposed to be helpful in protection of the photosynthetic system of those plants that generally grown under extreme environmental conditions by enhancing the process of ROS scavenging.[72]. As per our results, the plants treated with Alfa-Toc and BL have high carotenoid content compared to the control, however, plants treated with NaCl have less carotenoid content compared to control, and the plants treated with Alfa-Toc + NaCl and BL + NaCl have high carotenoid content than NaCl treated plants. (Fig-9) Brassinolide application enhances the content of carotenoids in plant leaves [73]Carotenoids can deactivate singlet oxygen by absorbing it, causing them to enter a triplet state that dissipates through thermal decay, effectively neutralizing its effects. [74]Alfa-Toc plays a significant role in plants by increasing the carotenoid content, as observed in *Triticum aestivum*. [75].

CONCLUSION

High salt levels pose a substantial environmental challenge, particularly constraining plant productivity, especially in dry and semi-dry climates. In the present study,NaCl causes negative impacts on physiological, biochemical, and pigment composition in *Vigna radiata* L. (Co-6) variety.Application of brassinolide and Alfa-tocopherol helps in mitigating the negative impacts of salinity stress,andplays an eminent role in enhancing growth, development, and pigment composition in green gram(*Vigna radiata* L. Co-6 variety)Therefore, spraying these two Plant growth regulators might be a suitable approach in Ameliorating the salt stress in *Vigna radiata* L and in enhancing biomass and pigment composition.

ACKNOWLEDGMENT

We humbly and sincerely thank to the Head of the department, Department of Botany for providing facilities and full support to carry out this research work.

REFERENCES

1. Allakhverdiev, S. I., Nishiyama, Y., Suzuki, I., Tasaka, Y., & Murata, N. (1999). Genetic engineering of the unsaturation of fatty acids in membrane lipids alters the tolerance of Synechocystis to salt stress. *Proceedings of the National Academy of Sciences*, *96*(10), 5862-5867.
2. Noreen, S., Sultan, M., Akhter, M. S., Shah, K. H., Ummara, U., Manzoor, H., Ulfat, M., Alyemeni, M.N. and Ahmad, P. (2021). Foliar fertigation of ascorbic acid and zinc improves growth, antioxidant enzyme activity and harvest index in barley (*Hordeum vulgare* L.) grown under salt stress. Plant Physiology and Biochemistry, 158: 244-254.
3. Eynard, A., Lal, R., & Wiebe, K. (2005). Crop response in salt-affected soils. *Journal of sustainable agriculture*, *27*(1), 5-50.
4. Munns, R. (2005). Genes and salt tolerance: bringing them together. *New Phytologist*, *167*(3), 645-663.

5. Nabati, J., Kafi, M., Nezami, A., Moghaddam, P. R., Ali, M., & Mehrjerdi, M. Z. (2011). Effect of salinity on biomass production and activities of some key enzymatic antioxidants in kochia (*Kochiascoparia*). *Pakistan Journal of Botany*, *43*(1), 539-548.
6. Evelin, H., Kapoor, R., & Giri, B. (2009). Arbuscular mycorrhizal fungi in alleviation of salt stress: a review. *Annals of botany*, *104*(7), 1263-1280.
7. Sun, J. K., Li, T., Xia, J. B., Tian, J. Y., Lu, Z. H., & Wang, R. T. (2011). Influence of salt stress on ecophysiological parameters of *Periploca sepium* Bunge. *Plant, Soil and Environment*, *57*(4), 139-144.
8. Chartzoulakis, K., & Psarras, G. (2005). Global change effects on crop photosynthesis and production in Mediterranean: the case of Crete, Greece. *Agriculture, ecosystems & environment*, *106*(2-3), 147-157.
9. Khan, M. A., Ungar, I. A., & Showalter, A. M. (2000). Effects of salinity on growth, water relations and ion accumulation of the subtropical perennial halophyte, *Atriplex griffithii* var. stocksii. *Annals of Botany*, *85*(2), 225-232.
10. Saha, P., Chatterjee, P., & Biswas, A. K. (2010). NaCl pretreatment alleviates salt stress by enhancement of antioxidant defense system and osmolyte accumulation in mungbean (*Vignaradiata* L. Wilczek).
11. Khan, M. M., Al-Mas'oudi, R. S., Al-Said, F., & Khan, I. (2013, October). Salinity effects on growth, electrolyte leakage, chlorophyll content and lipid peroxidation in cucumber (*Cucumis sativus* L.). In *International Conference on Food and Agricultural Sciences Malaysia: IACSIT Press* (Vol. 55, pp. 28-32).
12. Parvaiz, A., & Satyawati, S. (2008). Salt stress and phyto-biochemical responses of plants-a review. *Plant soil and environment*, *54*(3), 89.
13. Nair, R. M., Schafleitner, R., Kenyon, L., Srinivasan, R., Easdown, W., Ebert, A. W., & Hanson, P. (2012). Genetic improvement of mungbean. *Sabrao J. Breed. Genet*, *44*(2), 177-190.
14. Nair, R., Schafleitner, R., Easdown, W., Ebert, A., Hanson, P., D'arros, H. J., & Donough, H. K. J. (2014). Legume improvement program at AVRDC-The World Vegetable Center: Impact and future prospects. *Ratarstvo i povrtarstvo*, *51*(1), 55-61.
15. Keatinge, J. D. H., Easdown, W. J., Yang, R. Y., Chadha, M. L., & Shanmugasundaram, S. (2011). Overcoming chronic malnutrition in a future warming world: the key importance of mungbean and vegetable soybean. *Euphytica*, *180*, 129-141.
16. Sehrawat, N., Bhat, K. V., Kaga, A., Tomooka, N., Yadav, M., & Jaiwal, P. K. (2014). Development of new gene-specific markers associated with salt tolerance for mungbean (Vigna radiata L. Wilczek). *Spanish Journal of Agricultural Research*, *12*(3), 732-741.
17. Bose, J., Rodrigo-Moreno, A., & Shabala, S. (2014). ROS homeostasis in halophytes in the context of salinity stress tolerance. *Journal of experimental botany*, *65*(5), 1241-1257.
18. Clément, S. A., Tan, C. C., Guo, J., Kitta, K., & Suzuki, Y. J. (2002). Roles of protein kinase C and α-tocopherol in regulation of signal transduction for GATA-4 phosphorylation in HL-1 cardiac muscle cells. *Free Radical Biology and Medicine*, *32*(4), 341-349.
19. Soltani, Y., Saffari, V. R., Moud, A. A. M., & Mehrabani, M. (2012). Effect of foliar application of α-tocopherol and pyridoxine on vegetative growth, flowering, and some biochemical constituents of *Calendula officinalis* L. plants. *African Journal of Biotechnology*, *11*(56), 11931-11935.
20. Sadiq, M., AKRAM, N. A., & Ashraf, M. (2017). Foliar applications of alpha-tocopherol improve the composition of fresh pods of *Vigna radiata* subjected to water deficiency. *Turkish Journal of Botany*, *41*(3), 244-252.

21. Maity, U., & Bera, A. K. (2009). Effect of exogenous application of brassinolide and salicylic acid on certain physiological and biochemical aspects of green gram (*Vigna radiata* L. Wilczek). *Indian Journal of Agricultural Research*, *43*(3), 194-199.
22. Nolan, T. M., Vukašinović, N., Liu, D., Russinova, E., & Yin, Y. (2020). Brassinosteroids: multidimensional regulators of plant growth, development, and stress responses. *The Plant Cell*, *32*(2), 295-318.
23. Karlidag, H., Yildirim, E., & Turan, M. (2011). Role of 24-epibrassinolide in mitigating the adverse effects of salt stress on stomatal conductance, membrane permeability, and leaf water content, ionic composition in salt-stressed strawberry (Fragaria× ananassa). *Scientia horticulturae*, *130*(1), 133-140.
24. Jin-Huan, L., Anjum, S. A., Mei-Ru, L., Jian-Hang, N., Ran, W., Ji-Xuan, S., & San-Gen, W. (2015). Modulation of morpho-physiological traits of Leymus chinensis (Trin.) through exogenous application of brassinolide under salt stress. *JAPS: Journal of Animal & Plant Sciences*, *25*(4).
25. khashan, a. a., & hamedi al-hilfy, i. h. (2020). floral characteristics of mung bean (*vigna radiata* L.) as affected by planting dates and brassinolide spraying. *plant archives (09725210)*, *20*(1).
26. Munns, R., & Tester, M. (2008). Mechanisms of salinity tolerance. *Annu. Rev. Plant Biol.*, *59*, 651-681.
27. Neumann, P. M. (1995). Inhibition of root growth by salinity stress: toxicity or an adaptive biophysical response In *Structure and Function of Roots: Proceedings of the Fourth International Symposium on Structure and Function of Roots, June 20–26, 1993, Stará Lesná, Slovakia* (pp. 299-304). Springer Netherlands.
28. Snapp, S. S., & Shennan, C. (1992). Effects of salinity on root growth and death dynamics of tomato, Lycopersicon esculentum Mill. *New phytologist*, *121*(1), 71-79.
29. Arif, M. R., Islam, M. T., & Robin, A. H. K. (2019). Salinity stress alters root morphology and root hair traits in Brassica napus. *Plants*, *8*(7), 192.
30. Lalarukh, I., Wang, X., Amjad, S. F., Hussain, R., Ahmar, S., Mora-Poblete, F., ... & Datta, R. (2022). Chemical role of α-tocopherol in salt stress mitigation by improvement in morpho-physiological attributes of sunflower (Helianthus annuus L.). *Saudi Journal of Biological Sciences*, *29*(3), 1386-1393.
31. Mostafa, M. R., Mervat, S. S., Safaa, R. E. L., Ebtihal, M. A. E., & Magdi, T. A. (2015). Exogenous α-tocopherol has a beneficial effect on Glycine max (L.) plants irrigated with diluted seawater. *The Journal of Horticultural Science and Biotechnology*, *90*(2), 195-202.
32. Lal, B., Bagdi, D. L., & Dadarwal, B. K. (2019). Role of brassinolide in amelioration of salinity induced adverse effects on growth, yield attributes and yield of wheat. *Journal of Pharmacognosy and Phytochemistry*, *8*(5), 1790-1793.
33. fariduddin, q. a. z. i., hayat, s. h. a. m. s. u. l., ali, b. a. r. k. e. t., & Ahmad, A. Q. I. L. (2006). Effect of 28-homobrassinolide on the nitrate reductase, carbonic anhydrase activities and net photosynthetic rate in Vigna radiata. *Acta Botanica Croatica*, *65*(1), 19-23.
34. Zhao, S., Zhang, Q., Liu, M., Zhou, H., Ma, C., & Wang, P. (2021). Regulation of plant responses to salt stress. *International Journal of Molecular Sciences*, *22*(9), 4609.
35. Zhang, M., Fang, Y., Ji, Y., Jiang, Z., & Wang, L. (2013). Effects of salt stress on ion content, antioxidant enzymes and protein profile in different tissues of Broussonetia papyrifera. *South African journal of botany*, *85*, 1-9.
36. Jamil, M., Rehman, S., & Rha, E. S. (2007). Salinity effect on plant growth, PSII photochemistry and chlorophyll content in sugar beet (*Beta vulgaris* L.) and cabbage (*Brassica oleracea capitata* L.). *Pak. J. Bot*, *39*(3), 753-760.
37. Francois, L. E., Donovan, T., & Maas, E. V. (1984). Salinity Effects on Seed Yield, Growth, and Germination of Grain Sorghum 1. *Agronomy Journal*, *76*(5), 741-744.

38. Semida, W. M., Taha, R. S., Abdelhamid, M. T., & Rady, M. M. (2014). Foliar-applied α-tocopherol enhances salt-tolerance in Vicia faba L. plants grown under saline conditions. *South African Journal of Botany*, *95*, 24-31.
39. Zandi, P., & Schnug, E. (2022). Reactive oxygen species, antioxidant responses and implications from a microbial modulation perspective. *Biology*, *11*(2), 155.
40. Ahanger, M. A., Mir, R. A., Alyemeni, M. N., & Ahmad, P. (2020). Combined effects of brassinosteroid and kinetin mitigates salinity stress in tomato through the modulation of antioxidant and osmolyte metabolism. *Plant Physiology and Biochemistry*, *147*, 31-42.
41. Gabr, M. A., Fathi, M. A., Azza, I. M., & Mekhaeil, G. B. (2011). Influences of some chemical substances used to induce early harvest of 'Canino'apricot trees. *Nature and Science*, *9*(8), 59-65.
42. Kurepin, L. V., Joo, S. H., Kim, S. K., Pharis, R. P., & Back, T. G. (2012). Interaction of brassinosteroids with light quality and plant hormones in regulating shoot growth of young sunflower and Arabidopsis seedlings. *Journal of Plant Growth Regulation*, *31*, 156-164.
43. El-Mashad, A. A. A., & Mohamed, H. I. (2012). Brassinolide alleviates salt stress and increases antioxidant activity of cowpea plants (*Vigna sinensis*). *Protoplasma*, *249*, 625-635.
44. Shah, S. S., Mohammad, F. I. D. A., Shafi, M., Bakht, J. E. H. A. N., & Zhou, W. E. I. J. U. N. (2011). Effects of cadmium and salinity on growth and photosynthesis parameters of Brassica species. *Pakistan Journal of Botany*, *43*(1), 333-340.
45. Al-Maskri, A. H. M. E. D., Al-Kharusi, L., Al-Miqbali, H., & Khan, M. M. (2010). Effects of salinity stress on growth of lettuce (Lactuca sativa) under closed-recycle nutrient film technique. *Int. J. Agric. Biol*, *12*(3), 377-380.
46. Nxele, X., Klein, A., & Ndimba, B. K. (2017). Drought and salinity stress alters ROS accumulation, water retention, and osmolyte content in sorghum plants. *South African journal of botany*, *108*, 261-266.
47. Li, G., Peng, X., Wei, L., & Kang, G. Salicylic acid increases the contents of glutathione and ascorbate and temporally regulates the related gene expression in salt-stressed wheat seedlings. Gene, 2013, 529(2), 321-325.
48. Dong, Y., Wang, W Hu, G., Chen, W., Zhuge, Y., Wang, Z., & He, M. R. Role of exogenous 24-epibrassinolide in enhancing the salt tolerance of wheat seedlings. Journal of Soil Science and Plant Nutrition, 2017, 17(3), 554-569.
49. Sadiq, M., AKRAM, N. A., & Ashraf, M. (2017). Foliar applications of alpha-tocopherol improve the composition of fresh pods of *Vigna radiata* subjected to water deficiency. *Turkish Journal of Botany*, *41*(3), 244-252.
50. Hameed, A., Akram, N. A., Saleem, M. H., Ashraf, M., Ahmed, S., Ali, S., ... & Alyemeni, M. N. (2021). Seed treatment with α-tocopherol regulates growth and key physio-biochemical attributes in carrot (*Daucus carota* L.) plants under water limited regimes. *Agronomy*, *11*(3), 469.
51. Mostafa, M. R., Mervat, S. S., Safaa, R. E. L., Ebtihal, M. A. E., & Magdi, T. A. (2015). Exogenous α-tocopherol has a beneficial effect on Glycine max (L.) plants irrigated with diluted sea water. *The Journal of Horticultural Science and Biotechnology*, *90*(2), 195-202.
52. Furuya, T., Yoshikawa, T., Kimura, T., & Kaneko, H. (1987). Production of tocopherols by cell culture of safflower. *Phytochemistry*, *26*(10), 2741-2747.
53. Dabariya, S., & Bagdi, D. L. (2019). Impact of brassinolide in amelioration of salinity induced adverse effects on growth, yield attributes, and yield of barley. *Journal of Pharmacognosy and Phytochemistry*, *8*(6), 1536-1539.
54. Zhang, S., Hu, J., Zhang, Y., Xie, X. J., & Knapp, A. (2007). Seed priming with brassinolide improves lucerne (Medicago sativa L.) seed germination and seedling growth in relation to physiological changes under salinity stress. *Australian Journal of Agricultural Research*, *58*(8), 811-815.

55. Hayat, S., Maheshwari, P., Wani, A. S., Irfan, M., Alyemeni, M. N., & Ahmad, A. (2012). Comparative effect of 28 homobrassinolide and salicylic acid in the amelioration of NaCl stress in *Brassica juncea* L. *Plant physiology and biochemistry*, *53*, 61-68.
56. Mandavia, C., Cholke, P., Mandavia, M. K., Raval, L., & Gursude, A. (2014). Influence of brassinolide and salicylic acid on biochemical parameters of wheat (*Triticum aestivum* L.) under salinity stress. *Indian Journal of Agricultural Biochemistry*, *27*(1), 73-76.
57. Longstreth, D. J., & Nobel, P. S. (1979). Salinity effects on leaf anatomy: consequences for photosynthesis. *Plant physiology*, *63*(4), 700-703.
58. Jamil, M., Rehman, S., & Rha, E. S. (2007). Salinity effect on plant growth, PSII photochemistry and chlorophyll content in sugar beet (*Beta vulgaris* L.) and cabbage (*Brassica oleracea capitata* L.). *Pak. J. Bot*, *39*(3), 753-760.
59. Yeo, A. R., Lee, Λ. S., Izard, P., Boursier, P. J., & Flowers, T. J. (1991). Short-and long-term effects of salinity on leaf growth in rice (Oryza sativa L.). *Journal of Experimental Botany*, *42*(7), 881-889.
60. Belkhodja, R., Morales, F., Abadia, A., Medrano, H., & Abadia, J. (1999). Effects of salinity on chlorophyll fluorescence and photosynthesis of barley (*Hordeum vulgare* L.) grown under a triple-line-source sprinkler system in the field. *Photosynthetica*, *36*(3), 375-387.
61. Lalarukh, I., Wang, X., Amjad, S. F., Hussain, R., Ahmar, S., Mora-Poblete, F., ... & Datta, R. (2022). Chemical role of α-tocopherol in salt stress mitigation by improvement in morpho-physiological attributes of sunflower (*Helianthus annuus* L.). *Saudi Journal of Biological Sciences*, *29*(3), 1386-1393.
62. Semida, W. M., Taha, R. S., Abdelhamid, M. T., & Rady, M. M. (2014). Foliar-applied α- tocopherol enhances salt-tolerance in Vicia faba L. plants grown under saline conditions. *South African Journal of Botany*, *95*, 24-31.
63. Anjum, S. A., Wang, L. C., Farooq, M., Hussain, M., Xue, L. L., & Zou, C. M. (2011). Brassinolide application improves the drought tolerance in maize through modulation of enzymatic antioxidants and leaf gas exchange. *Journal of Agronomy and crop science*, *197*(3), 177-185.
64. Nasser, S. E. D. M., & Sarhan, I. A. (2023, April). Effect of Foliar Nutrition with Brassinolide on Vegetative Growth Characteristics of Several Sesame Cultivars. In *IOP Conference Series: Earth and Environmental Science* (Vol. 1158, No. 6, p. 062034). IOP Publishing.
65. Kaya, C.Sonmez, O., Aydemir, S., Tuna, A. L., & Cullu, M. A. (2009). The influence of arbuscular mycorrhizal colonisation on key growth parameters and fruit yield of pepper plants grown at high salinity. *Scientia horticulturae*, *121*(1), 1-6.
66. Qados, A. M. A. (2011). Effect of salt stress on plant growth and metabolism of bean plant Vicia faba (L.). *Journal of the Saudi Society of Agricultural Sciences*, *10*(1), 7-15.
67. Taffouo, V. D., Kouamou, J. K., Ngalangue, L. T., Ndjeudji, B. A. N., & Akoa, A. (2009). Effects of salinity stress on growth, ions partitioning and yield of some cowpea (*Vigna unguiculata* L. Walp.) cultivars. *International Journal of Botany*, *5*(2), 135-143.
68. El-Quesni, F. E., Abd EL-Aziz, N., & Maga, M. K. (2009). Some studies on the effect of Ascorbic Acid and α-tocopherol on the growth and some chemical composition of *Hibiscus rosa sinensis* L. at Nurbaria. *Ozean J. Appl. Sci*, *2*(2), 159-167.
69. Ali, Q., Tariq Javed, M., Haider, M. Z., Habib, N., Rizwan, M., Perveen, R., ... & Al-Misned, F. A. (2020). α-Tocopherol foliar spray and translocation mediates growth, photosynthetic pigments, nutrient uptake, and oxidative defense in maize (*Zea mays* L.) under drought stress. *Agronomy*, *10*(9), 1235.

70. Mohammed, A. R., & Tarpley, L. (2013). Effects of enhanced ultraviolet-B (UV-B) radiation and antioxidative-type plant growth regulators on Rice (*Oryza sativa* L.) leaf photosynthetic rate, photochemistry and physiology. *Journal of Agricultural Science*, *5*(5), 115.
71. Mir, B. A., Khan, T. A., & Fariduddin, Q. (2015). 24-epibrassinolide and spermidine modulate photosynthesis and antioxidant systems in *Vigna radiata* under salt and zinc stress. *Int J Adv Res*, *3*(5), 592-608.
72. Siefermann-Harms, D. (1987). The light-harvesting and protective functions of carotenoids in photosynthetic membranes. *Physiologia Plantarum*, *69*(3), 561-568.
73. Sharma, A., Kumar, V., Singh, R., Thukral, A. K., & Bhardwaj, R. (2016). Effect of seed pre-soaking with 24-epibrassinolide on growth and photosynthetic parameters of *Brassica juncea* L. in imidacloprid soil. *Ecotoxicology and Environmental Safety*, *133*, 195-201.
74. d'Alessandro, S., & Havaux, M. (2019). Sensing β-carotene oxidation in photosystem II to master plant stress tolerance. *New Phytologist*, *223*(4), 1776-1783.
75. zaman, s. a. r., & ozdemir, f. a. (2022). Effect of Thermopriming and Alpha-Tocopherol Spray in Triticum Aestivum L. under Induced Drought Stress: A Future Perspective of Climate Change in the Region. *Sains Malaysiana*, *51*(4), 977-991.

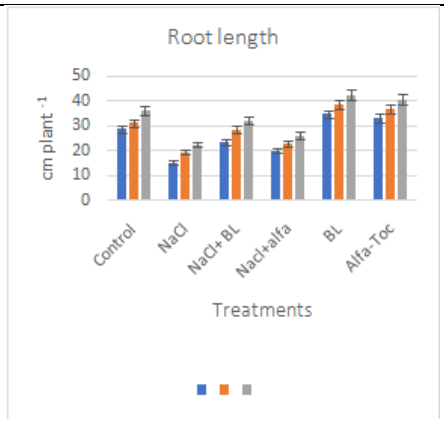

Fig. 1. Effect of exogenous application of Alfa-Toc and BL on Root length of Vigna radiata L. [CO-6 variety] under 80mM NaCl stress. Values represented in Bars are the mean of three replicates [n=3] and [±] standard error.

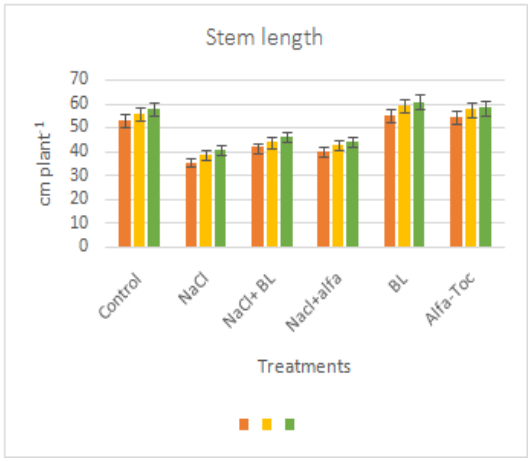

Fig. 2. Effect of exogenous application of Alfa-Toc and BL on stem length of *Vigna radiata* L. [CO-6 variety] under 80mM NaCl stress. Values represented in Bars are the mean of three replicates [n=3] and [±] standard error.

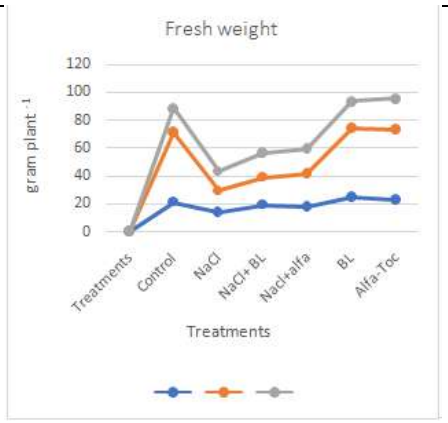

Fig. 3. Effect of exogenous application of Alfa-Toc and BL on Fresh weight of Vigna radiata L. [CO-6 variety] under 80mM NaCl stress. Values represented in Bars are mean of three replicates [n=3] and [±] standard error.

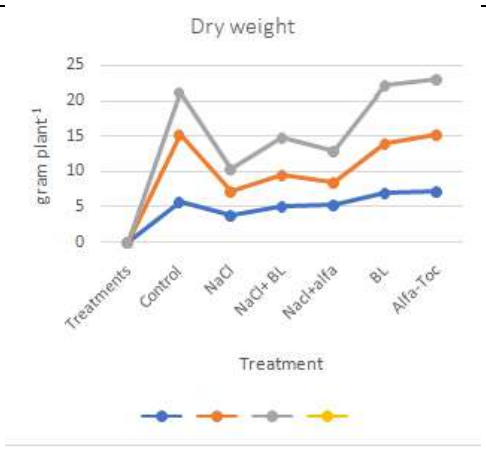

Fig. 4. Effect of exogenous application of Alfa-Toc and BL on Dry weight of Vigna radiata L. [CO-6 variety] under 80mM NaCl stress. Values represented in Bars are mean of three replicates [n=3] and [±] standard error.

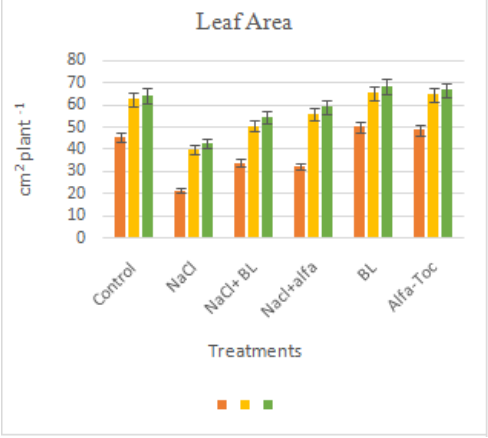

Fig. 5. Effect of exogenous application of Alfa-Toc and BL on leaf area of *Vigna radiata* L. [CO-6 variety] under 80mM NaCl stress. Values represented in Bars are the mean of three replicates [n=3] and [±] standard error.

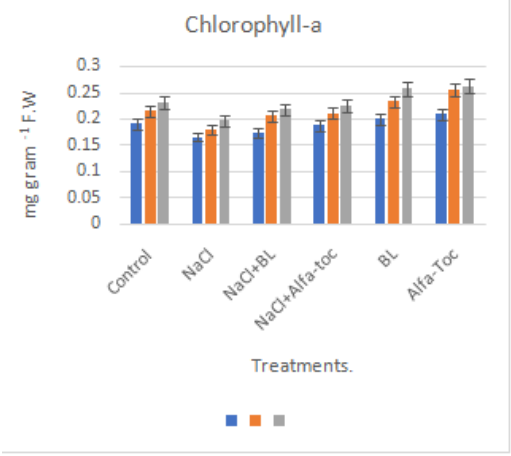

Fig. 6. Effect of exogenous application of Alfa-Toc and BL on Chlorophyll-a of *Vigna radiata* L. [CO-6 variety] under 80mM NaCl stress. Values represented in Bars are the mean of three replicates [n=3] and [±] standard error.

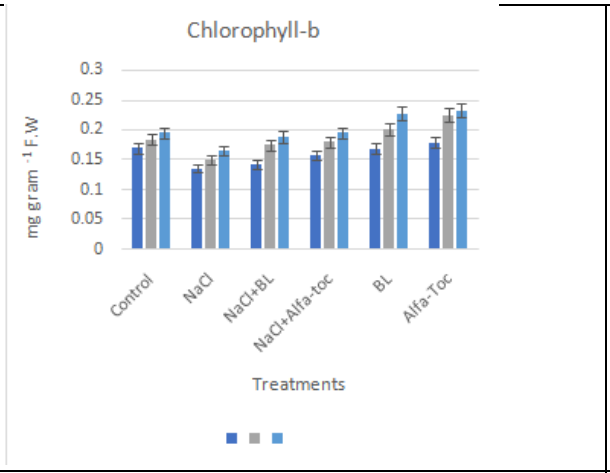

Fig. 7. Effect of exogenous application of Alfa-Toc and BL on Chlorophyll-b of *Vigna radiata* L. [CO-6 variety] under 80mM NaCl stress. Values represented in Bars are the mean of three replicates [n=3] and [±] standard error.

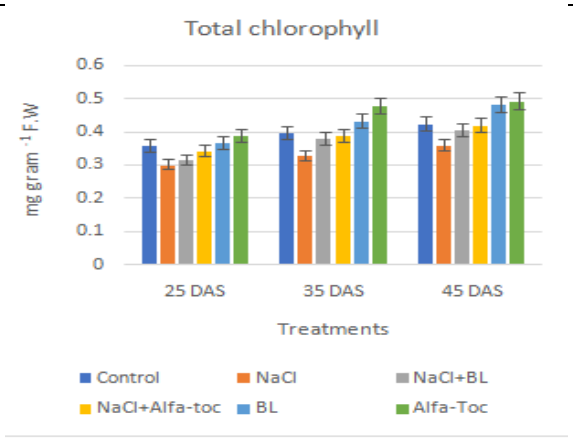

Fig. 8. Effect of exogenous application of Alfa-Toc and BL on Total Chlorophyllof *Vigna radiata* L. [CO-6 variety] under 80mM NaCl stress. Values represented in Bars are the mean of three replicates [n=3] and [±] standard error.

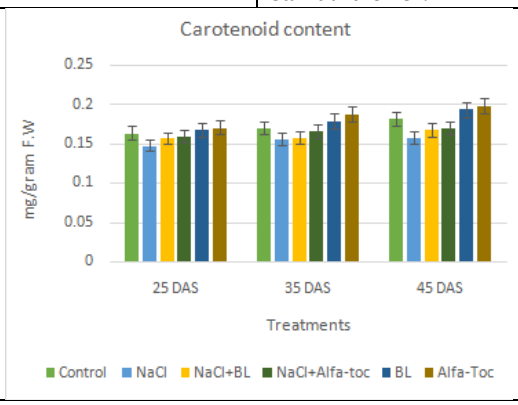

Fig. 9. Effect of exogenous application of Alfa-Toc and BL on carotenoid content of *Vigna radiata* L. [CO-6 variety] under 80mM NaCl stress. Values represented in Bars are the mean of three replicates [n=3] and [±] standard error.